TRANSACTIONS

of the

American Institute of Electrical Engineers

UNIVERSITY OF ILLINOIS
AT CHICAGO
801 S. MORGAN
CHICAGO, IL 60607

文能足事

TK
1
A59
v.70
pt.1
1951
DER
etc

TRANSACTIONS

OF THE

AMERICAN INSTITUTE

OF

ELECTRICAL ENGINEERS

VOLUME 70

1951

PART I

PUBLISHED BY THE
AMERICAN INSTITUTE OF ELECTRICAL ENGINEERS
33 WEST 39TH STREET
NEW YORK 18, N. Y., U. S. A.

COPYRIGHT 1951
BY THE
AMERICAN INSTITUTE OF ELECTRICAL ENGINEERS

Printed in the United States of America by
The Mack Printing Company, Easton, Pa.

Preface

The 1951 TRANSACTIONS (volume 70) of the American Institute of Electrical Engineers will be published in two parts.

Part I contains technical program papers and related discussions presented at these meetings:

1. Winter General Meeting, New York, N. Y., January 22–26, 1951.
2. Southern District Meeting, Miami, Fla., April 11–13, 1951.
3. North Eastern District Meeting, Syracuse, N. Y., May 2–4, 1951.
4. Great Lakes District Meeting, Madison, Wis., May 17–19, 1951.
5. Summer General Meeting, Toronto, Ont., Canada, June 25–29, 1951.

Twenty-four Summer General Meeting papers are included in Part I. The remainder of the Summer General Meeting papers will be included in Part II together with the approved papers and related discussions presented at the Pacific General Meeting and the Fall General Meeting.

The TRANSACTIONS now contains a new section entitled Discussions From Abroad, which has been established to permit members residing outside of the United States (exclusive of Canada) to submit discussions which could not otherwise be received before the closing dates.

Full correlation of all material in this volume has been accomplished by means of the multi-entry index beginning on page 1110. Reference to any of the several subject entries for a technical paper will lead directly to the paper and to any published discussion on that paper. The original number assigned each paper by the Technical Program Committee is given in the author index.

Statements and opinions given in papers and discussions published in TRANSACTIONS are the expressions of contributors for which the American Institute of Electrical Engineers assumes no responsibility.

Part II of Volume 70 is expected to be available for distribution early in 1952.

The Power Interruption Testing of Lightning Arresters

OTTO ACKERMANN
ASSOCIATE AIEE

A LIGHTNING arrester is a device which permits a practically unrestricted flow of electric current between its line and ground terminals when the terminal voltage becomes a certain multiple of its rated voltage, and which interrupts the flow of current when the overvoltage has passed. The interruption preferably should take place when the power current goes through zero for the first time after the overvoltage has disappeared. In this phase of their operating cycle lightning arresters perform as circuit breakers.

This observation applies to valve-type and expulsion-type lightning arresters alike. Their difference as interrupting devices lies in the manner in which they influence the power follow current before current zero occurs. Valve-type lightning arresters have a nonlinear resistance characteristic chosen so that the resistance at rated voltage is very large compared to the reactance of any ordinary power source. Therefore the power current flowing through a valve type arrester is practically in phase with the generated voltage. For this reason the current flow is rather easily interrupted at current zero. The interruption is accomplished by a series gap structure which consists of a number of closely spaced metal electrodes. The more the current is restricted by the valve section the easier is the duty on the gap section as an interrupting device. Power follow currents in valve type lightning arresters are of the order of 10 to 100 amperes.

Some types of expulsion lightning arresters, particularly those for transmission line protection, constitute the other extreme in the spectrum of interruption processes. The arc drop in such devices is so low that the power follow current is determined almost entirely by the system itself. In most cases the system short-circuit current is preponderantly reactive; hence current zero occurs near the crest of the generated voltage. The recovery conditions therefore are severe. The clearing action takes place entirely in the arc channel of the expulsion device and at its electrodes; the series gap is not counted upon to contribute to the extinction process. It merely serves to insulate the expulsion device from the line while normal service voltage only is present.

In some expulsion lightning arresters for distribution service, the arc voltage developed in the deionizing channel becomes an appreciable part of the service voltage. In these cases therefore the expulsion lightning arrester actually limits the power follow current and it becomes in this respect more like a valve-type lightning arrester, with one fundamental difference however always remaining. In expulsion lightning arresters the series gap plays no part in the current interruption while in valve-type lightning arresters the series or quench gap takes over at least part of the interrupting duty. That the series gap of expulsion lightning arresters cannot be expected to assist in the current interruption becomes evident if one considers the recovery characteristics of rod gaps on which very interesting information has been presented recently.[1]

When testing lightning arresters for their power current interrupting ability, the discharge usually is started by a surge generator. The surge however is not always followed by power current. The establishment and the severity of the latter depends on the following factors:

1. Amplitude and wave shape of the surge.
2. Relations between surge and power circuit impedances.
3. Timing of the surge with respect to the 60-cycle voltage.
4. Voltage and current output of the power source.
5. Power factor between generated voltage and bolted fault current.
6. Circuit recovery voltage.
7. Characteristics of the interrupting device.

The importance of these features in duty-cycle testing of lightning arresters has long been realized and they have found recognition in the various standards.[2,3,4,5] Therefore, adequate test circuits must contain means for controlling these factors.

A basic circuit which incorporates these features is shown in Figure 1. The circuit consists essentially of three sections:

1. The power source with series reactance L_1, resistance R_0 and shunt capacity C_2 to control short-circuit current and recovery voltage.
2. The surge circuit comprising surge generator, test piece, and separating gap.
3. The impulse timing circuit.

Besides having adequate 60-cycle power and a high-voltage d-c source available, the construction of the circuit sections (1) and (2) is mainly a matter of procuring and inserting the required ohmic, reactive, and capacitive impedances. In the case of timing the surge, however, various means can be employed. A special circuit which is very effective for this purpose, has been developed and is widely used in the laboratories of the company with which the author is associated. It is shown in the left-hand lower portion of Figure 1.

The key to the circuit is the three electrode gap "A-B". When the surge generator is charged, the full voltage of the first capacitor unit appears across the

Paper 51-1, recommended by the AIEE Protective Devices Committee and approved by the AIEE Technical Program Committee for presentation at the AIEE Winter General Meeting, New York, N. Y., January 22–26, 1951. Manuscript submitted July 14, 1950; made available for printing November 3, 1950.

OTTO ACKERMANN is with the Westinghouse Electric Corporation, East Pittsburgh, Pa.

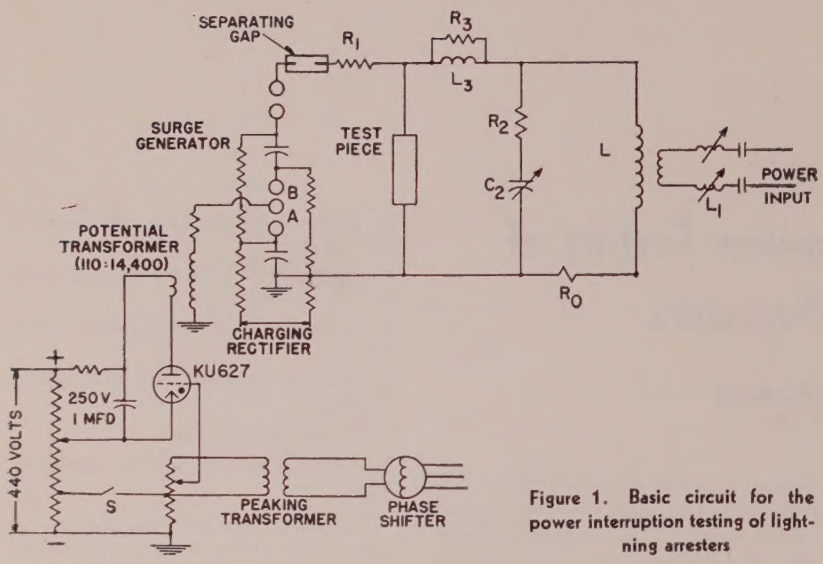

Figure 1. Basic circuit for the power interruption testing of lightning arresters

gap "A" since the center electrode is grounded through an unenergized transformer. This gap is adjusted to spark over at a potential 10 to 20 per cent above the surge generator charging voltage. The necessary increment in voltage, which must be opposite to the polarity of the charging source, is obtained by shock excitation of the potential transformer. Gap "B" must be set so that the transformer surge alone does not break it down; this should be checked with the surge generator de-energized. On the other hand, the setting of gap "B" must be smaller than that of gap "A". With the gaps co-ordinated in this manner, "A" will spark first and "B" will follow within a matter of a microsecond. The signal impulse in the potential transformer is produced by the discharge of a capacitor which in turn is timed by a thyratron tube. The grid of the latter normally is kept at a d-c potential so low that even the continuously superimposed voltage from the peaking transformer will not unblock it. However, if the bias level is decreased by closing the switch "S", the first following peaking impulse of the proper polarity will open the valve. The peaking transformer is energized from a phase shifter which ties in with the power supply to the lightning arrester under test.

The surge circuit consists of the surge generator capacitors, the series resistance R_1, the test piece, and the separating gap. The function of the latter is to insulate the surge generator from the power circuit after the surge discharge. An ordinary rod gap, set as high as the surge generator voltage will permit, is sufficient in many cases. In others it is necessary to employ a regular deionizing gap. A device similar to the test piece itself often answers the purpose.

The resistor R_1, which stands for the total damping and series resistance, has the purpose of regulating intensity, duration, and wave shape of the discharge. Heavy oscillatory surges should normally be avoided since they may constitute an unusually favorable condition for the device to clear because of the expulsion action created by the surge or because of the introduction of a current zero before power follow current is established. Unidirectional surges of moderate current are most likely to produce power follow.

Because of the various circuit conditions which may or may not produce power follow,[6] it is not safe to credit a device with unusually good performance characteristics, if no power follow current can be obtained even though circuit conditions may have been varied to some extent; for one can be almost certain that within the unlimited combinations of surge and power occurring in the field, power follow current will be established under some possibly not even rare conditions. Then the device whose design has grown around no power follow test conditions may find itself in a situation which it is not equipped to handle. In the testing of protective devices one therefore should explore all reasonable means to make the test piece take power follow, such as controlled timing and variation of length and intensity of the surge current.

In order to obtain the maximum severity discharge from a given power source, the various standards stipulate that the current flow be started as early as possible in the cycle of the generated voltage. Starting the discharge at the zero point of the generated voltage theoretically produces the longest duration of power follow current up to the next current zero, and it also will produce the highest current peak. The subject is treated more fully in the Appendix where it is shown that, while the current will reach its highest crest under that condition, it will remain near zero for the longest possible time at its beginning. This, together with the fact that the generated voltage is lowest during that time, renders it difficult and, in lightning arresters with very effective deionizing action even impossible, to start power follow at the zero of generated voltage. The most consistently operating setup usually is one in which the discharge is initiated 20 to 30 degrees after that moment.

The deductions drawn in the Appendix also serve to highlight the decisive influence of even moderate ohmic resistance—and for that matter, of arc voltage—on the development of power follow current. If a current has zero per cent power factor, which implies that there be

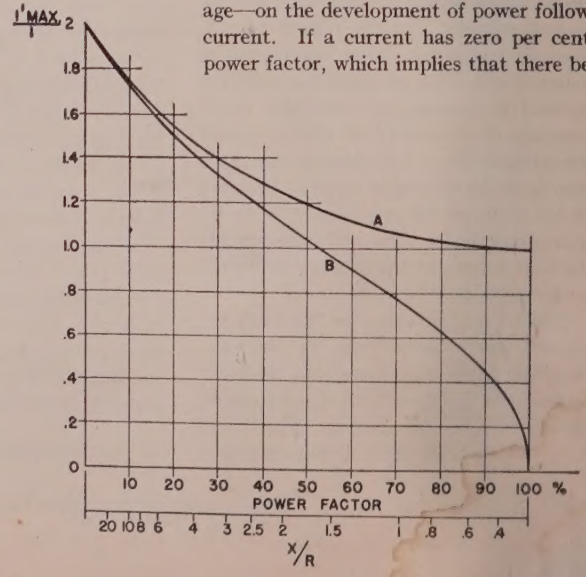

Figure 2. Ratio of maximum possible peak current to symmetrical crest current as a function of power factor

A—Symmetrical current remaining constant; peak current = $I_{rms} \times \sqrt{2} \times A$

B—Resistance being added to fixed circuit reactance X; peak current = $(E_{rms}/X)\sqrt{2}$ B

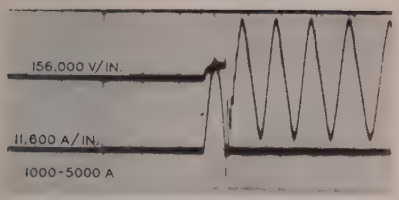

Figure 3(A). Magnetic oscillogram of a line-type expulsion lightning-arrester operation

no losses at all in the circuit and hence no decrement in the d-c component, and if the discharge is started at the zero point of the generated voltage, the peak current will be twice the symmetrical crest value. This is the condition represented by the start of both curves "A" and "B" in Figure 2. If the power factor is increased while the symmetrical rms current is maintained by corresponding adjustments in the circuit reactance, the obtainable current peak decreases as shown by curve "A". This illustrates how the severity of tests at plants set for the same symmetrical current output can be affected by the power factor. If, on the other hand, the reactance of the power source remains fixed and the power factor is increased by adding resistance, the obtainable peak current changes as shown by curve "B". This curve illustrates for instance how drastically even moderate circuit or ground resistance reduces the service duty of an expulsion lightning arrester below what would be expected on the basis of bolted fault calculations made by considering the circuit reactance only which is done quite frequently. It also illustrates in an approximate manner the beneficial effect of high arc drop in expulsion lightning arresters. A rigid analytical treatment of this subject has been presented by Boehne a decade ago.[7]

The curves "A" and "B" in Figure 2 are drawn up for the power follow current being started at the zero point of the generated voltage. As mentioned before, this is a somewhat hypothetical case because lightning arresters are likely to suppress power current under that condition. If the discharge is initiated β electrical degrees later, the crest current ratio at zero power factor, instead of being equal to 2, will be $1 + \cos \beta$, which is 1.985, 1.94, and 1.87 for $\beta = 10$, 20, and 30 degrees respectively. The curves "A" and "B" for the various timing angles would therefore start at the values quoted above, which are only little below 2, but, for 100 per cent power factor would all end up at the same points as the original curves. It is evident that the deviations from the original curves are small and that the latter can be used with little error for the purpose of this analysis. One of its objects is to show that for strictly comparative tests it is not enough to have the power sources adjusted for the same symmetrical rms current, but that the power factors also should be held within reasonably narrow limits. At 10 per cent power factor for instance, the crest current ratio is close to 1.75, while at 40 per cent power factor it is 1.28.

Air core reactors are the most suitable primary means for controlling the test current. They are represented by L_1 in Figure 1. The power factor is increased by inserting the resistance R_0. R_0 as well as L_1 may be placed in either the input or the output side of the power transformer.

The recovery voltage also must be subject to control as the natural frequency of unmodified test circuits usually is too high to be representative of the service conditions for which protective devices, particularly of the expulsion type, are designed. The frequency of the recovery voltage is controlled by the variable capacity C_2, and its amplitude by R_2[8] and by R_0, the latter affecting the phase angle and thereby the instantaneous value of the generated voltage to which the circuit tries to recover.

It has long been established by studies on the recovery conditions on power systems[9,10,11] that the recovery voltages encountered usually are not of a single frequency. The main features of their rather variable pattern have been described by giving voltage and time for first and second crest[9] or by the time to 90 per cent of normal, and to maximum voltage.[10] While circuits of such characteristics can readily be set up on analogue computers, it commonly is impractical to duplicate them in power laboratory tests. It is, of course, essential that the recovery conditions encountered in the field be known, but they need not necessarily be duplicated in testing. It is in general satisfactory if the test circuit comes reasonably close to field conditions, or better yet if it is somewhat more severe so as to demonstrate an operating margin. It usually is not too difficult to set up a circuit which although having only one recovery frequency, fulfills these requirements sufficiently well.[8] The time T from current zero to recovery voltage crest can be predicted with fair accuracy by considering it to be equal to one half cycle of the natural frequency of the circuit:

$$T = 3.14 \times \sqrt{LC_2}$$

where L is the reactance of the power supply in henries. Expressing L in terms of the reactive short circuit current I and of the plant voltage E, the shunt capacity required in the case of 60-cycle power becomes

$$C_2 = T^2 \times 38.2 \times I/E \times 10^{-6} \text{ mfd}$$

T being expressed in microseconds.

The addition of such capacity to the test circuit always poses certain difficulties. Being in parallel to the test piece it increases appreciably the demand on the surge generator output required to produce sparkover and, after sparkover, it may cause the same type of oscillatory currents as the surge generator capacitors which, as explained earlier, may interfere with the normal functioning of the lightning arrester. Therefore the capacitor C_2 should be separated from the test piece by a resistance R_2 or by a small reactance L_3. The resistor R_2 must be kept below certain values because of its effect

Figure 3(B). Cathode-ray oscillogram of the voltage of the same operation as Figure 3(A)

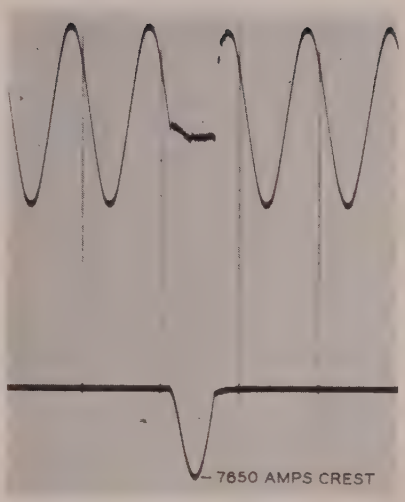

Figure 4. Operation of an expulsion lightning arrester on a 70 per cent power factor circuit with $E/X = 7{,}500$ amperes rms; showing a low crest current despite maximum severity timing

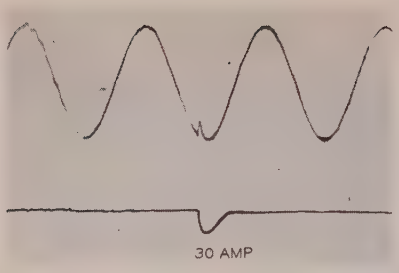

Figure 5. Power follow in a valve-type lightning arrester

on the recovery voltage.[8] In a surge circuit with negligible reactance, R_1 and R_2 determine the initial voltage available for the sparkover of the test piece. If this is insufficient, additional impedance to the drain of surge energy may be provided by the reactance L_3. It is important, however, that the C_2 L_3 circuit be kept from oscillating particularly in tests with low power follow currents because of the possibility of establishing unrealistic current zeros. To eliminate oscillations in the L_3 C_2 loop, R_2 must be about twice, or R_3 about one half times,

$$\sqrt{L_3/C_2}$$

if either resistor is used alone.

From the foregoing discussion it is evident that before power voltage is applied, a certain amount of testing and circuit adjustments are required in order to assure that the test piece sparks over consistently. It occasionally happens that despite these preparations the lightning arrester refuses to operate when the power supply circuit is closed in. The cause for this behavior usually is found in the resultant lowering of the total circuit impedance. In this case the preliminary tests should be made with the primary of the power transformer shorted, or with the power source circuit fully connected but de-energized.

In order to properly evaluate tests it is essential that voltages and currents be recorded adequately. The location as well as the characteristics of the measuring devices must be given proper consideration. The measurement of the recovery voltage deserves particular attention because changes in this quantity sometimes have a decisive influence on the performance of the protective device. Magnetic oscillographs as well as potential transformers can be relied upon for faithful recording as long as the measured frequencies are below, and not too close to either the response limit of the vibrator element or the resonant frequency of the measuring circuit. Oscillations which can be read clearly on the magnetic record usually are far enough from these limitations and are therefore reliable. The magnetic and cathode-ray voltage records of Figures 3 (A) and (B) for instance agree very closely although the recorded frequency is close to 1,000 cycles. The cathode-ray oscillogram is taken over a capacity divider and is recorded on a film drum of 18-inch periphery rotating at 6,000 rpm. As the film is exposed for several revolutions of the drum the lines overlap, but they can readily be traced through.

Figure 4 shows the test of a 9-kv expulsion type lightning arrester on a circuit whose reactance would permit a current of 7,500 amperes rms but which had a resistance $R_0=0.83$ ohm added, making the power factor about 70 per cent. The discharge was initiated by a surge about 10 degrees from voltage zero. The current reached a crest of 7,650 amperes which makes the crest current ratio $7{,}650/7{,}500\times1.41=0.72$. In spite of the not strictly accountable effects of the arc voltage this is in good agreement with the value predicted by curve "B" in Figure 2.

Figure 5 shows the power follow in a valve-type lightning arrester. There is no voltage recovery surge because voltage and current go through zero at practically the same instant. Because of the current limiting effect of the valve element, the follow current is independent of the available short-circuit current.

Figure 6 is the record of the failure of an experimental expulsion lightning arrester. The sharp break in arc voltage in the first half cycle of power follow indicates clearly that this was the crucial moment and that the integrated effects of current and arc voltage up to that point only were responsible for failure of the device.

The decisive features in performance tests however are not always as plainly evident as on the records cited in the foregoing. Painstaking analysis of sometimes seemingly insignificant details in oscillograms, the appreciation of the functions of the various branches of test circuits, and the critical inspection of the

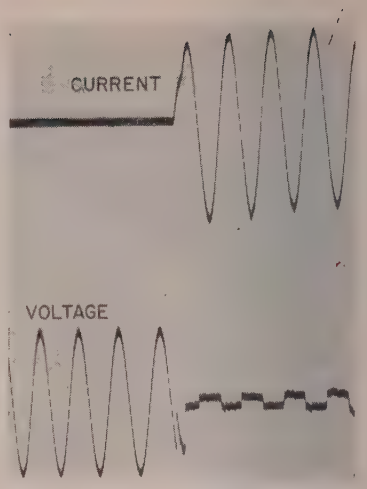

Figure 6. Failure to interrupt power follow of an experimental expulsion lightning arrester

test piece must combine to get full value out of test efforts which are a major and usually quite expensive part of the engineering endeavor in the development and the application of protective devices. Their number has increased considerably in the last decade or two. With regard to their merits, staged tests cannot furnish unequivocal answers as long as the range and the effects of the many variables which influence test performance are not considered sufficiently. A broad analysis of some of these variables, in particular of impulse timing and of the power factor has been the object of this paper.

Appendix I. Power Factor and Obtainable Crest Current

The equation for an asymmetrically started short-circuit current is

$$i=i_{ac}+i_{dc} \qquad (1)$$

Designating the time of start by the angle α to the next following zero of the symmetrical current, and the crest value of the symmetrical current by I,

$$_{ac}=I\ \sin\ (2\pi ft-\alpha) \qquad (2)$$

The initial value I_{dc} of the d-c component is equal and opposite to the instantaneous value of the a-c component at time $t=0$. Therefore, employing equation 2

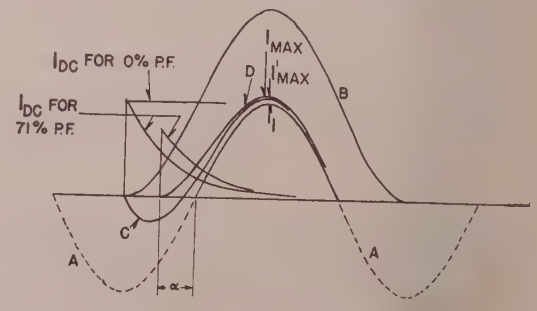

Figure 7. Course of power follow current for various initiation times and power factors

$$I_{dc} = -I \sin(-\alpha) = I \sin \alpha \quad (3)$$

The course of the d-c component is given by

$$i_{dc} = I_{dc} \epsilon^{-\frac{t}{T}} \quad (4)$$

The time constant being

$$T = \frac{X}{R 2\pi f} \quad (5)$$

where X and R are the total circuit impedance and resistance in ohms.

It is to be noted that the time constant T of the d-c component is related directly to the power factor of the circuit if the difference between a-c and d-c resistance is neglected. Therefore

$$\frac{X}{R} = \tan \varphi \quad (6)$$

φ being the phase angle between voltage and current. Equation 1 therefore takes the form

$$i = I[\sin(2\pi ft - \alpha) + \sin \alpha \epsilon^{-t 2\pi f R/X}] \quad (7)$$

This is illustrated for a few cases in Figure 7. In this figure curve "A" represents the course of the symmetrical current. If the short circuit is started at the time of symmetrical current zero, the current will follow curve "A" irrespective of its power factor. If the current is started one quarter cycle ahead of this point and if the power factor is zero, the current will follow curve "B," the d-c component in this hypothetical case remaining constant. If the power factor is 71 per cent ($X/R = 1$) and the current again is started one quarter cycle ahead of normal current zero, the course of the current is represented by curve "C." It is noted that in this case the current first develops a small negative loop.

If seeking the starting point from which the current would reach its highest possible crest, inspection of Figure 7 indicates, and it can be proved rigidly, that this point should be as far as possible ahead of the symmetrical current zero without developing a negative loop. This condition is met when the current starts out tangentially to the time axis, in other words, when $di/dt = 0$. Differentiating equation 7 in this manner results in

$$2\pi f \times \cos(2\pi ft - \alpha) - 2\pi fR/X \sin \alpha \times \epsilon^{-t 2\pi f R/X} = 0 \quad (8)$$

For $t = 0$ this reduces to

$$\frac{\sin \alpha}{\cos \alpha} = \tan \alpha = \frac{X}{R} = \tan \varphi \quad (9)$$

In other words, the starting point for obtaining maximum crest current lies φ degrees ahead of normal current zero and therefore coincides with the zero point of the voltage cycle.

For 71 per cent power factor this case is represented by curve "D" in Figure 7.

The maximum current crest for any power factor now can be calculated by combining equations 7 and 9. It is obvious that the actual crests I_{max} occur slightly ahead of the symmetrical current peak values I, but also that the amplitude I_{max}' at the time of symmetrical peak is very close to the absolute maximum. Since the expression for I_{max}' is much simpler than that for I_{max}, the former is used to present the relation between power factor and maximum crest current. The time t becomes

$$t = \frac{\varphi + \pi/2}{2\pi f} \quad (10)$$

thus reducing equation 7 to

$$I_{max}' = I\left(1 + \sin \varphi \epsilon^{-\left(\varphi + \frac{\pi}{2}\right)\cot \varphi}\right) \quad (11)$$

The ratio $I_{max}' : I$ as a function of the power factor cos φ is shown in Figure 2. If the actual symmetrical rms current I_{rms} and its power factor are known the possible peak current is

$$I_{max}' = I_{rms} \sqrt{2} A \quad (12)$$

as read from curve "A" in Figure 2.

Curve "B" presents the effect of adding resistance to a circuit of given reactance X. The symmetrical peak current is

$$I = \frac{E\sqrt{2}}{\sqrt{X^2 + R^2}} = \frac{E\sqrt{2}}{X\sqrt{1 + \cot^2 \varphi}} \quad (13)$$

where E is the rms value of the generated voltage. Substituting this in equation 11 and noting that $\sqrt{2}E/X$ now is to remain constant, one obtains the equation for curve "B." Hence, if the circuit reactance is known, the maximum crest current obtainable when resistance is introduced in the circuit is

$$I_{max}' = \frac{E\sqrt{2}}{X} B \quad (14)$$

References

1. Dielectric-Recovery Characteristics of Power Arcs in Large Air Gaps, **G. D. McCann, J. E. Conner, H. M. Ellis.** *AIEE Transactions*, volume 69, part I, 1950, pages 616–25.

2. Lightning Arresters for A-C Power Circuits. *AIEE Standard Number 28*, April 1944.

3. Report on Standard for Valve and Expulsion Type Lightning Arresters. *AIEE Standard Number 28A*, February 1950.

4. Standard for Lightning Arresters. *Standard Number 44–89*, National Electrical Manufacturers' Association (New York, N. Y.), 1944.

5. Standard for Expulsion Type Distribution Lightning Arresters. *Standard Number 45–95*, National Electrical Manufacturers' Association (New York, N. Y.), 1945.

6. Surging Lightning Arresters Connected to Power Voltage, **A. D. Forbes.** *Electric Journal* (East Pittsburgh, Pa.), April 1935.

7. The Geometry of Arc Interruption, **E. W. Boehne.** *AIEE Transactions*, volume 60, 1941, pages 524–32.

8. *Discussion* by **A. M. Opsahl** of reference 10, page 181.

9. Protector Tubes for Power Systems, **H. A. Peterson, W. S. Rudge, Jr., A. C. Monteith, L. R. Ludwig.** *Electrical Engineering* (*AIEE Transactions*), volume 59, May 1940, pages 282–92.

10. Voltage-Recovery Characteristics of Distribution Systems, **R. L. Witzke.** *AIEE Transactions*, volume 69, part I, 1949, pages 172–87.

11. Short Circuit Currents and Recovery Voltages on Rural Distribution Systems, **W. H. Eason, I. B. Johnson, J. W. Kalb, H. A. Peterson.** *AIEE Transactions*, volume 69, part II, 1949, pages 930–38.

Discussion

M. G. Leonard (Westinghouse Electric Corporation, Sharon, Pa.): Mr. Ackermann's paper makes a very important contribution to the subject of how to test lightning arresters and what equipment is necessary to make these tests as valuable as possible. A few questions might be raised, however, by this paper, to which we would like to suggest answers. Some of these are as follows:

(1) Can lightning arresters be tested in the field to determine whether they are functioning properly?

Mr. Ackermann's paper makes it clear that if significant test results are expected, the equipment required for testing is necessarily rather complicated. It seems to be impractical under most conditions to make such tests on apparatus in the field. It may be possible in some cases to set up apparatus in the Repair Shop for this purpose, but even here it is not often economically justified. It is unfortunate that a simple test, such as could be obtained by measuring the 60-cycle breakdown strength, does not give a significant result in regard to the general performance of the lightning arrester, but this is quite obviously the case.

(2) Is the testing made under laboratory conditions as described adequate to predict field performance?

The answer to this is "yes." This is demonstrated by the fact that lightning arresters which have been proved under these laboratory tests have also proved to be adequate in the field. In fact, the laboratory tests are usually more severe in such factors as rate-of-rise of recovery voltage and point-of-timing of the surge wave than conditions experienced in the field. The only qualification to this answer is in regard to the application of other tests which brings us to our next question.

(3) Is this the most important part of laboratory testing of lightning arresters?

The answer is that although it is highly important, other tests are equally important. For example, the surge current capacity as determined by tests which simulate direct strokes of lightning, is extremely important. This is true partly because of the inherent destructive effects of the lightning surge, and partly because current magnitude is unpredictable as contrasted to the 60-cycle current, which can generally be approximated for any given installation. All of the other tests which are used to prove the performance of the device must, of course, be taken into account. These other tests are not as complicated in general as the power testing, and it was for this reason that Mr. Ackermann confined himself to the one field. Our purpose here is to point out that other testing must be considered and may be of equal importance.

H. O. Stoelting (Line Material Company, Milwaukee, Wis.): Mr. Ackermann has

resters, particularly of the expulsion type. All of the variables are of importance in the development of a lightning arrester which is satisfactory in service.

As discussed in the paper, the severity of duty cycle tests on expulsion lightning arresters is particularly affected by the power factor of follow current, more preferably termed the X/R ratio of the power circuit.

Although the importance of power factor is recognized in the lightning arrester standards, the severity of service conditions is not known so the standards specify that tests be made at power factors not over 40 per cent. This permits tests to be made, at the option of the designer, ranging in power factor from near zero up to 40 per cent.

As pointed out in the paper, the ratio of maximum asymmetric crest current to symmetric crest current can range from two at zero power factor to 1.28 at 40 per cent power factor. Thus there is a considerable range in severity of the duty cycle tests as permitted by the standards.

In order to make tests in all laboratories on a common basis it will be necessary to specify X/R of the test circuits much more closely than is done in the present standards. The ratio should be based on conditions that exist in service. This requires a survey of the power industry.

The beneficial effect of high arc voltage of expulsion lightning arresters in limiting the maximum follow current through the lightning arresters is extremely variable. The arc drop is dependent on the magnitude and duration of surge current as well as on timing, X/R of the power circuit, and magnitude of the follow current available.

The arc voltage of a lightning arrester also may vary with the number of unit operations. As the arcing channel is enlarged by erosion the arc voltage becomes lower and the current limiting action is reduced.

As a result of the variable nature of arc voltage the current limiting action of expulsion lightning arresters will vary over a wide range. Therefore, lightning arresters must be tested on circuits having follow currents available equal to the maximum rating of the lightning arrester. It is not sufficient to test at lower currents and extrapolate these data to the higher current ranges.

The various standards define an expulsion lightning arrester operating according to specifications on a circuit having a symmetrical fault current of 10,000 amperes as "unlimited" in rating. The choice of the term "unlimited" is unfortunate as it creates the impression that a lightning arrester can be used anywhere without regard to the follow current available. This is not necessarily true. A lightning arrester which operates properly at 10,000 amperes may fail on a circuit having available 15,000 or 20,000 amperes.

Although a high arc voltage aids the operation of an expulsion lightning arrester in so far as it assists in limiting the maximum current through the lightning arrester, it may have a deleterious effect by increasing the recovery voltage of a circuit. This is particularly true when there is a sudden rise in arc voltage at the moment of arc extinction.

Although the various lightning arrester standards recognize the importance of rates

specified as very little is known about the range of voltages that can exist under service conditions. This is another case of where a study of field conditions will assist in the writing of lightning arrester standards which will assure lightning arresters that operate satisfactorily in service.

T. J. Carpenter (General Electric Company, Pittsfield, Mass.): In comparing lightning arrester performance by laboratory power tests, the effect of power factor and impulse timing are of primary importance, as stressed by the author of this paper. This is particularly true when testing expulsion lightning arresters. The life of all expulsion lightning arresters is limited and depends on the current magnitude and duration, because some of the arc chamber material is removed by erosion on each power current operation. Consequently, the interrupted current will approach that of the available short-circuit current during the erosion life of expulsion lightning arresters, including those that limit the current for the first few operations.

Figure 1 of this discussion shows the relation of the available circuit crest current as a function of the impulse timing and power factor in greater detail than curve A of Figure 2 of the paper. Only the range of power factors recommended by AIEE Standard *28A*[1] is included. The basic equation from which the curves of Figure 1 were calculated is the same as that derived in the Appendix, equation 7 of the paper, but with the voltage as the reference base. The closing angle θ is the angle between the voltage angle ϕ, the current is symmetrical; and when closing angle θ equals zero, the current is maximum. It should also be pointed out that the duration of the current increases as the power factor and closing angle θ decrease.

The conditions which determine the establishment of lightning arrester power follow current in the field and in laboratory tests differ as stated by the author. One essential difference is that impulse surges used in laboratory tests are produced by lumped capacitance impulse generators. Follow current will be more difficult to start with a lumped capacitance generator because the capacitance of the impulse generator and the inductance of the power source produce an oscillatory component of current. Even with conventional impulse wave shapes, the resultant lightning arrester current may pass through zero several times during the build up of follow current, due to the oscillatory component current of the branch circuit. With the same polarity impulse and power voltage, the current component due to the stored energy in the reactive power circuit and the component from the power circuit are opposite in polarity. This produces a period of low resultant current, and the lightning arrester gap may interrupt this current at the next current zero, thus preventing the establishment of lightning arrester follow current. With opposite polarity impulse and power voltage, the component currents are additive, and power current is more easily established. Although follow current may be difficult to start in some laboratory tests, this can generally be accomplished by varying the impulse current magnitude and wave form, timing angle, and relative polarities.

The adjustment of the three electrode gap A-B, Figure 1 of the paper, can be made less critical and independent of generator polarity by holding the center electrode at half potential by a high resistance divider. The initiating pulse can be applied through a low capacity high-voltage capacitor con-

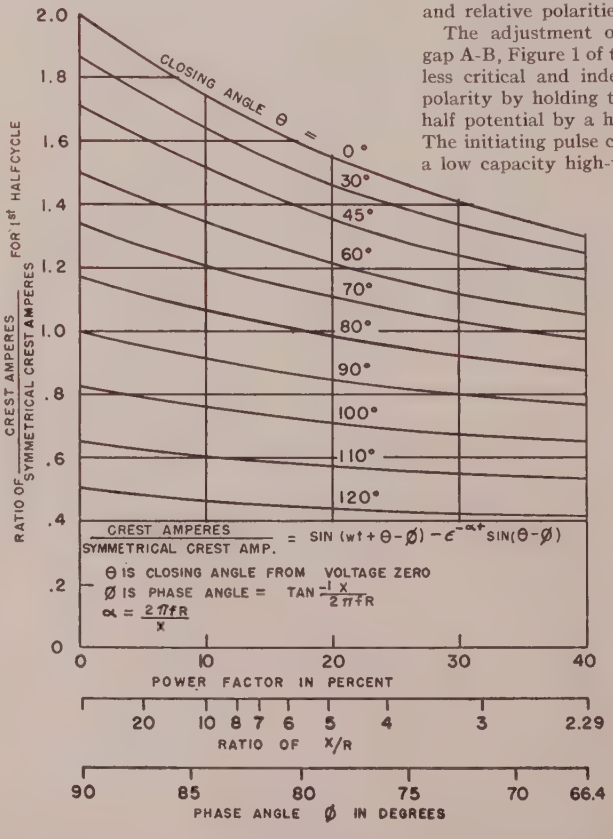

Figure 1. Ratio of maximum peak current to symmetrical crest current as a function of power factor

electrode gap A-B.

Reference

1. See Reference 3 of the paper.

Otto Ackermann: I wish to thank the gentlemen who have entereddiscussions, particularly because their contributions are furnishing welcome emphasis to the principal theme of my paper, namely the effect of power factor and timing on the test severity. In addition, Mr. Carpenter has introduced the question of the effect of surge voltage polarity on the establishment of power follow current. As far as valve-type lightning arresters are concerned, I have not treated the subject at all in my paper because there already exists a well founded understanding (see reference 2 of the paper) and standardized practice (see reference 1 of the paper). The latter consists in testing with surge and instantaneous power voltage of the same polarity.

With regard to expulsion lightning arresters, I simply mentioned that oscillatory surges or surge current reversal in the lightning arrester should be avoided. The reason for this is that the lightning arrester tries to seal off when the sum of the currents I' and I'', shown in Figure 2 of this discussion, becomes zero. Whether it will be successful depends on the course of the recovery voltage. The latter has three components:

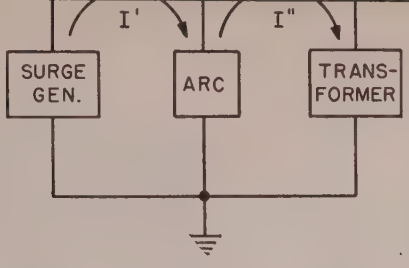

Figure 2. Condition for arc current zero; $I' = I''$

(1) The transformer electromotive force.

(2) The charge left on the surge generator. At the first current zero, this charge is opposite to what it was initially in accordance with the well-known phase relations between voltage and current in an oscillatory circuit.

(3) The voltage originating from stored magnetic energy. This tries to maintain the currents I' and I'' shown in Figure 2. I'' is the current built up in the transformer by the initial surge before lightning arrester sparkover and then by the sum of arc voltage and transformer electromotive force during the time of arcing. At the moment of zero arc current I' and I'' are equal. With the arc interrupted, they continue to flow as one in the surge generator-transformer to overcome the total circuit resistance. As the current I'' depends almost entirely on the relation between arc voltage and transformer electromotive force, the magnetic energy voltage component is extremely variable. At a given arc polarity, its direction however is the same whether the transformer electromotive force is opposite to, or just smaller than, the arc voltage.

While the transformer electromotive force remains almost unchanged during the surge discharge, the polarity of the surge generator charge and probably that of the stored magnetic energy component alternate repeatedly during any one oscillatory surge discharge. Since their combined effect determines the character of the recovery voltage at each current zero, more and less favorable interrupting conditions apparently alternate within the course of any one surge. If the conditions ever are favorable enough to interrupt the discharge, the development of regular power follow will thereby be stopped no matter whether the surge polarity initially was equal or opposite to the transformer electromotive force.

It therefore appears to me that Mr. Carpenter's observations regarding a polarity effect when working with oscillatory surges cannot be generalized. The effect rather must be the result of special characteristics of circuit and test piece. It has however furnished the occasion for this added probing into a rather involved subject and thereby, I hope, has helped its further clarification.

A 2,000,000-Kva Transformer Core

W. C. SEALEY
FELLOW AIEE

Synopsis: The largest 60-cycle transformer core ever made now is in successful operation on a 300,000,000-volt betatron. If this core were used for an oil immersed power transformer, windings for continuous operation at 2,000,000 kva could be placed on it. Construction of this core is a demonstration of the feasibility of constructing transformers many times as large as those now being built. The advantages of larger transformers are lower cost per kilovolt-ampere and less loss per kilovolt-ampere transformed resulting in higher efficiency. The present limitation in the size of transformers is shipping clearances. When transformers larger than those which can be shipped are needed, they can be constructed by assembling them in the field using construction and methods similar to those employed for this large core.

THE largest 60-cycle transformer core made to date was constructed for a 300,000,000-volt betatron. Since the core operates at 60 cycles, the mechanical and electrical construction used is typical of the construction required for a 60-cycle power transformer core of the same physical size. The size of power transformer cores is normally limited by the requirement that they be shipped from factory to destination by railroad. The size and weight of this particular core was far beyond the possibilities of rail shipment and, consequently, it was assembled and erected in the field.

A betatron is a high-voltage transformer in which the primary winding is a wound transformer coil and the secondary winding is a stream of electrons flowing around in a circle inside of a doughnut-shaped porcelain vacuum tube. Other betatrons have been built for lower voltages, the greatest number having been constructed in the 20,000,000-to 25,000,000-volt range, although units of lower and higher voltage also have been made. This 300,000,000-volt betatron at the University of Illinois is by far the largest and highest voltage betatron which has been constructed. The main magnet of this betatron is the core of a shell-type transformer. It was designed by power transformer engineers and erected in the field under the supervision of transformer erection engineers.

Paper 51-2, recommended by the AIEE Transformers Committee and approved by the AIEE Technical Program Committee for presentation at the AIEE Winter General Meeting, New York, N. Y., January 22-26, 1951. Manuscript submitted October 2, 1950; made available for printing November 3, 1950.

W. C. SEALEY is with the Allis-Chalmers Manufacturing Company, Milwaukee, Wis.

Construction

The main core of this betatron is a shell-type transformer core of 0.014-inch thick silicon steel of transformer grade having a stack height of 75 inches, a length of 280½ inches, and a height of 154 inches. Including the end frames, the dimensions are 287 inches long by 196 inches wide by 212 inches high. The total weight of 0.014-inch thick (29 gauge) transformer steel in the completed core is 575,000 pounds.

The core was stacked with the planes of the laminations horizontal as a matter of convenience using temporary bracing to support the core. In its final position the planes of the laminations are vertical, in which position the laminations have ample strength to be self-supporting.

The main core of the betatron is the core of a shell-type transformer. Because of its large size and weight, departures from conventional construction commonly used for transformer cores were necessary. The changes which were made are typical of the changes which are applicable to large power transformer cores.

The largest punching size required was 47 inches wide and 107 inches long. Because the core steel was available in only 30-inch wide coils, the core is made in layers such as shown in Figure 2 in which the width is made of two laminations instead of a single lamination. A 1/2-inch core duct is provided in the center of the core for cooling. Air at high pressure is forced through the core duct in order to keep the operating temperature of the core low.

In a transformer core the eddy currents which flow between sheets are limited by the interlamination resistance. In ordinary size cores it is feasible to make the interlamination resistance sufficiently high so that this current is negligible. However, the per cent loss caused by this current increases as the square of linear dimensions of the core.

In addition, in this particular core the voltage produced by the flux change is twice its normal value. This occurs because the flux in the core is biased in a negative direction by direct current applied to a winding on the core. The result is a rate of flux change which is twice the normal rate for a 60-cycle core since the change from maximum negative to maximum positive flux density occurs in half the time of that of a 60-cycle transformer core.

To keep these stray currents at a low value, sheets of 5-mil paper were inserted every 1/4 inch of core stack in the core to give the effect of a large number of small cores instead of one large core. With this construction each individual section acts like a small individual core and the losses in it are not affected by the voltages in the remaining sections.

The steel of the core is clamped between end frames which hold the core in position and provide a mounting for the auxiliary cores of the betatron similar to the mounting which would be necessary for clamping the coils of a power transformer.

The end frames are clamped together by the use of tie bolts and jack bolts as shown in Figure 3. These bolts are tightened to apply the desired pressure to the core iron. As with other large cores it is desirable to avoid the use of bolts through the core iron. Such through bolts must be insulated and are a potential source of trouble if the insulation be-

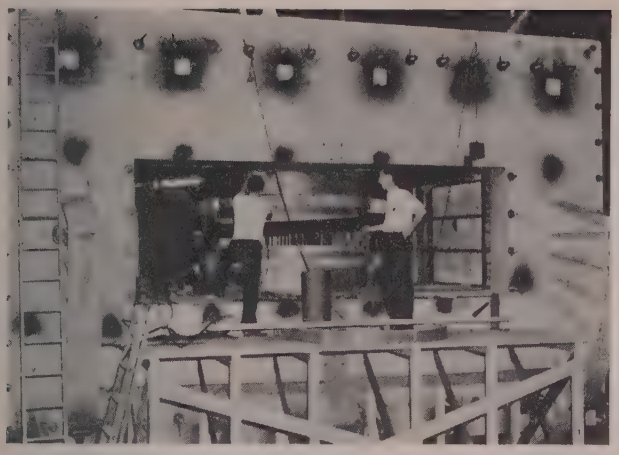

Figure 1 (left). A 300,000,000-volt betatron core

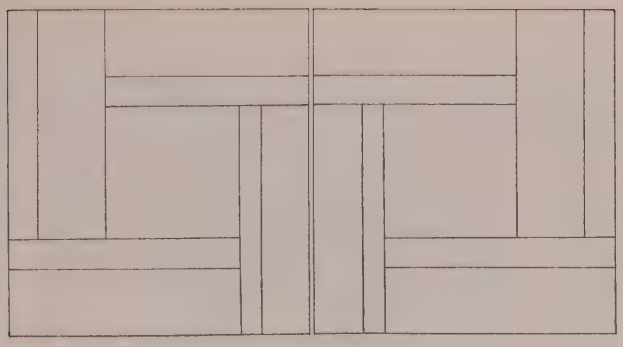

Figure 2 (above). Core construction showing one layer of laminations

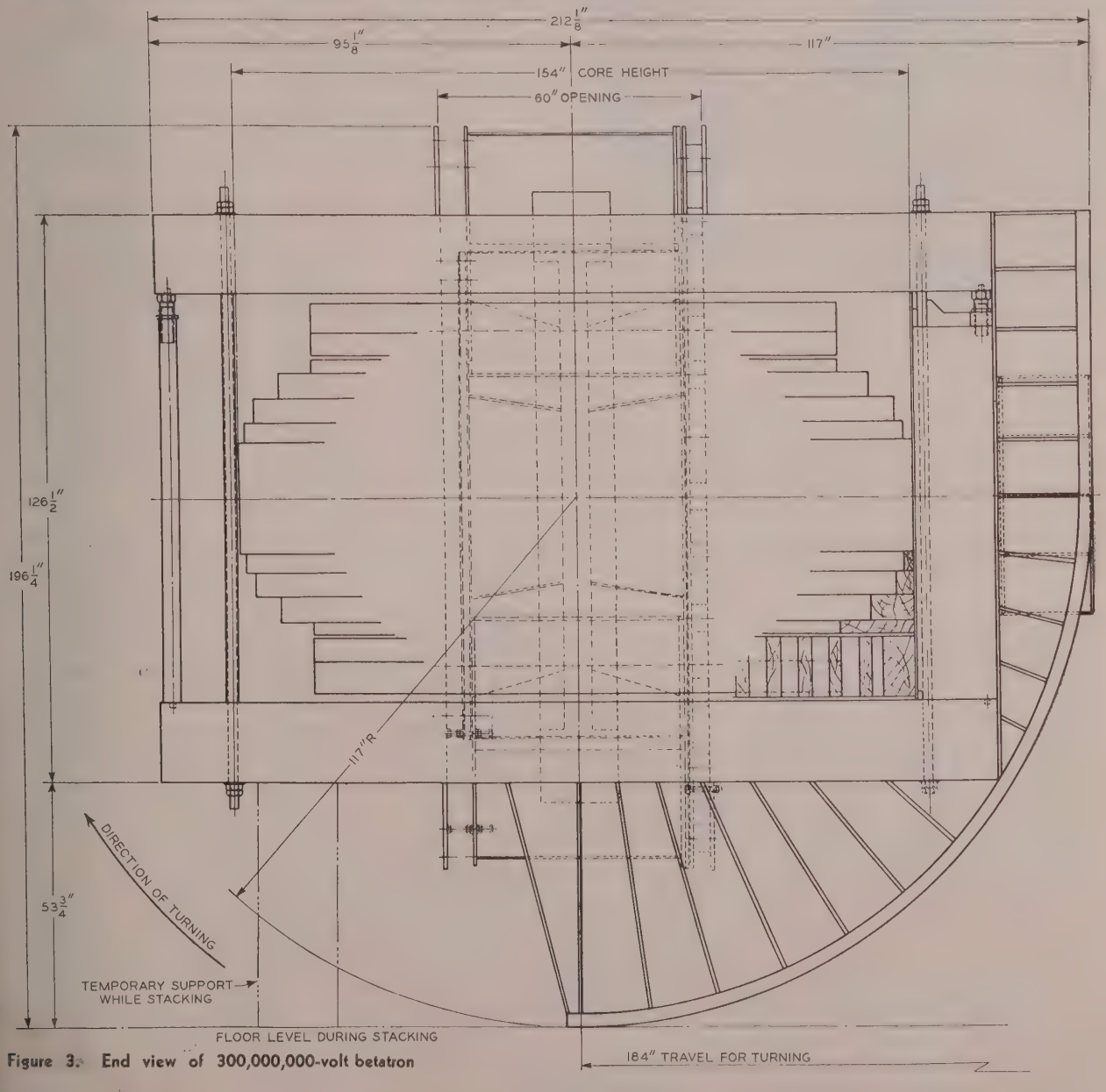

Figure 3. End view of 300,000,000-volt betatron

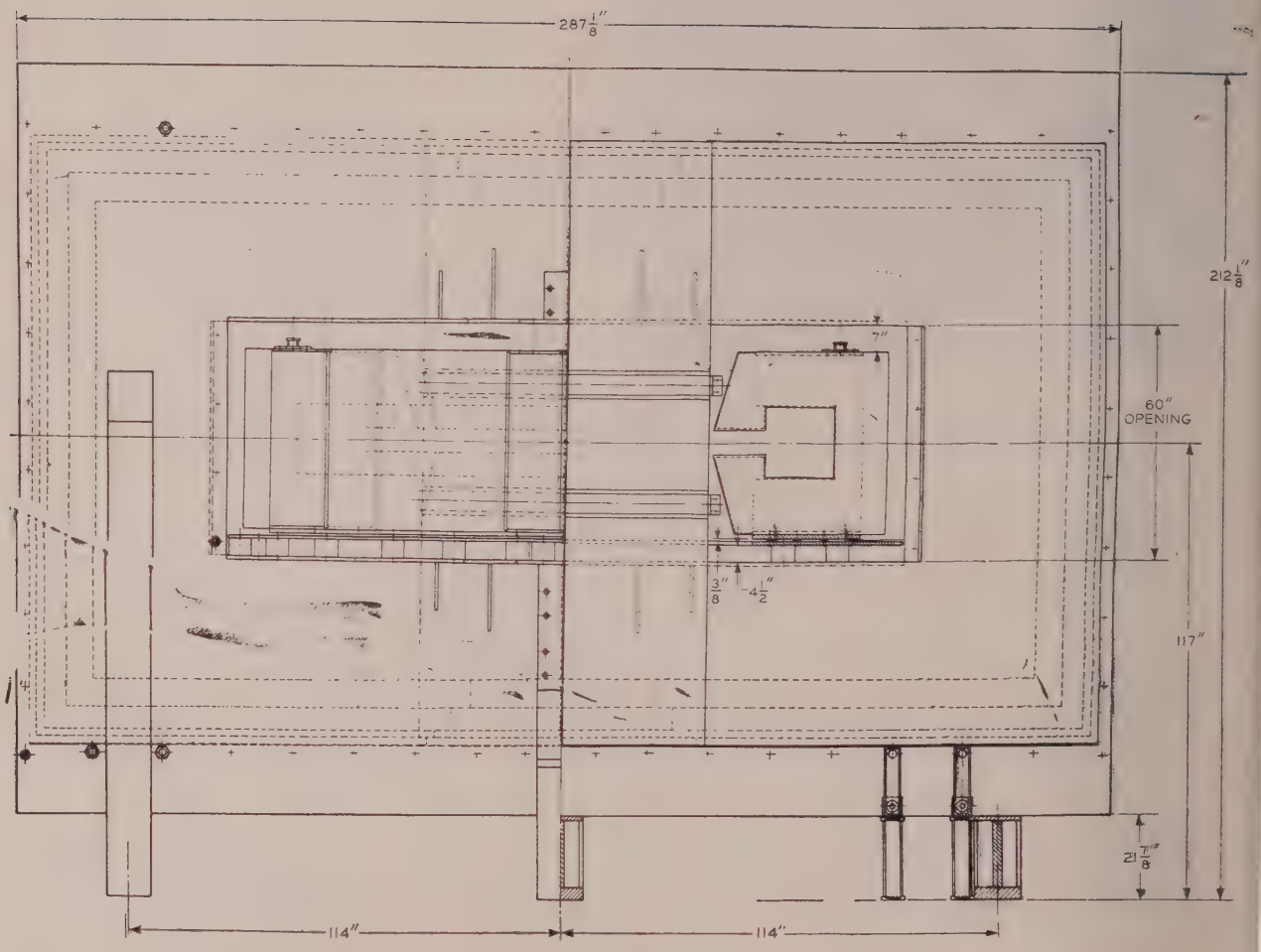

Figure 4. Side view of 300,000,000-volt betatron

comes damaged and breaks down. In addition, core bolts involve the mechanical difficulty of punching holes in the laminations and keeping them lined up in core material which is never perfectly flat. These difficulties increase as the size of the core is increased, and are avoided by the use of the combination of tie bolts and jack bolts. The type of construction used is applicable to power transformer cores much larger in size than the one constructed.

Erection

For ease in construction, the core was stacked with the planes of the laminations horizontal, with the laminations supported by the end frames and temporary bracing which was later removed. To place the core in its final operating position, it was necessary that the planes of the punchings be made vertical requiring rotating the entire core through 90 degrees. In a factory, such changes in position are normally made with heavy lifting equipment such as overhead cranes.

To avoid the necessity for such equipment, rockers were made a part of the end frame, so that the core could be stacked flat in the usual position and rolled to the upright position after assembly. The center rocker was removed after moving the core to position, but the outside rockers remained as a part of the end frame.

The rather spectacular turning over operation was accomplished by the usual rigging means. Since the center of the rocker was placed at approximately the center of gravity of the unit, no great force was necessary for this operation. It would not be difficult to develop a simpler method of turning over to replace the conventional rigging means.

Application of Core to Power Transformers

This betatron core could be used for a 60-cycle power transformer. Designs have been laid out to fit in this core and the curve of Figure 5 has been plotted showing how the kilovolt-amperes obtainable varies with the voltage of the winding of the transformer. The kilovolt-amperes obtainable varies from 2,100,000 kva at 15 kv to 1,200,000 kva for a 230-kv transformer. As would be expected the highest kilovolt-amperes are obtained with the lowest voltage rating because of the better insulation space factor at the lower voltage rating. A 2,000,000-kva single-phase transformer is far larger than any unit which has been built.

However, the construction of such a unit is entirely practicable by fabricating the parts in the factory and performing the assembly work in the field. The construction of this core demonstrates the practicability of assembling the heaviest part which is the core in the field. Cores employing similar construction can be made for considerably larger transformers.

Such cores would be arranged as shown in Figure 6 with the plane of the laminations vertical so that the laminations are self supporting. The end frame con-

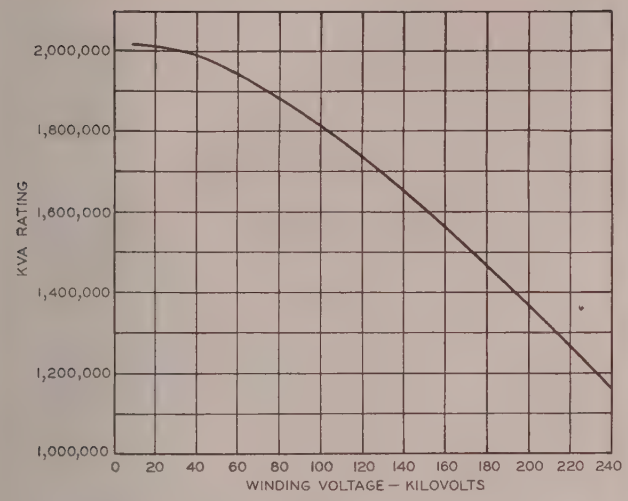

Figure 5 (above). Variation of kilovolt-amperes obtainable in betatron core with winding voltage

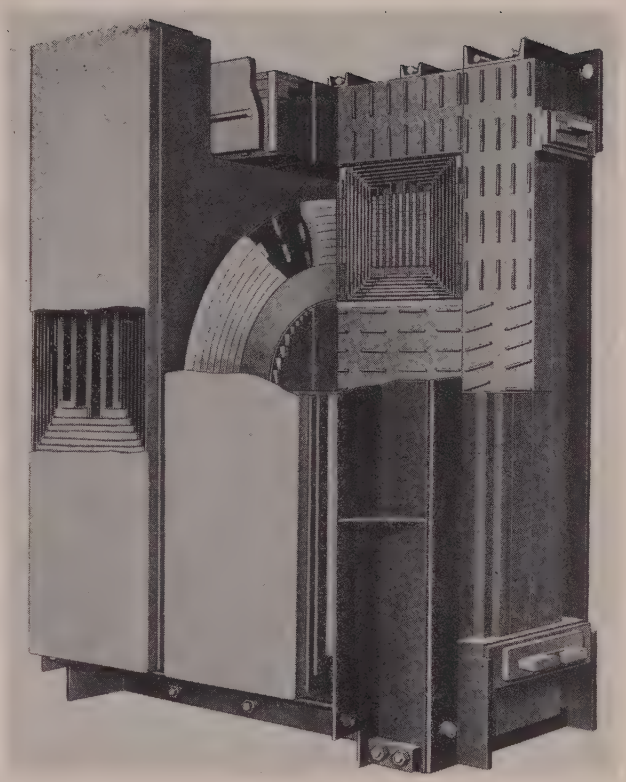

Figure 6 (right). Typical core and coil construction for a 2,000,000-kva power transformer

struction employed would be similar to that employed for the betatron but modified to provide the necessary clamping for the coils. In order to provide the maximum mechanical strength for the coils, it is desirable to wind such large coils on a circular mold, so that the resulting coil is a circular disk, providing maximum strength for winding, assembling, and to resist short-circuit stresses. The most desirable procedure would be to assemble the coils and insulation in the factory either in a single group or in more than one group with the required insulation. In the field the coils would be put in place and the core built into the coils. The tank could be made in sections with provision for welding the sections together after the core and coils had been assembled and turned into position. The tank would be constructed to withstand full vacuum to facilitate dryout after completion.

The disadvantages of such a large transformer are, of course, the large investment contained in a single unit together with difficulties of providing associated equipment for the circuits. The advantages of such a unit are the increased efficiency and decrease in weight obtainable. For example, the losses of a 2,000,000-kva unit would be half of the losses of 16 125,000-kva transformers to transmit the same amount of power. The weight of material required for the 2,000,000-kva transformer would be half of the material required for construction of 16 125,000-kva units. This does not mean that the cost of the 2,000,000-kva unit would be half that of the 16 units but with proper erection techniques, the saving in cost should be substantial.

Conclusions

The construction of a 60-cycle transformer core sufficiently large for a 2,000,000-kva transformer demonstrates the practicability of building transformer cores several times the size of those now being used for power transformers. It also demonstrates the effectiveness of the construction used to secure electrical and mechanical performance in a large core. It demonstrates the practicability of constructing transformers several times as large as those now being made.

Although the cost of field erection on a per-pound basis of material is greater than that of factory construction, the saving in weight and the improvement in efficiency inherent in a larger unit for transforming a given kilovolt-ampere, may at some future date make the construction of transformers much larger than can be shipped by rail an economical procedure.

No Discussion

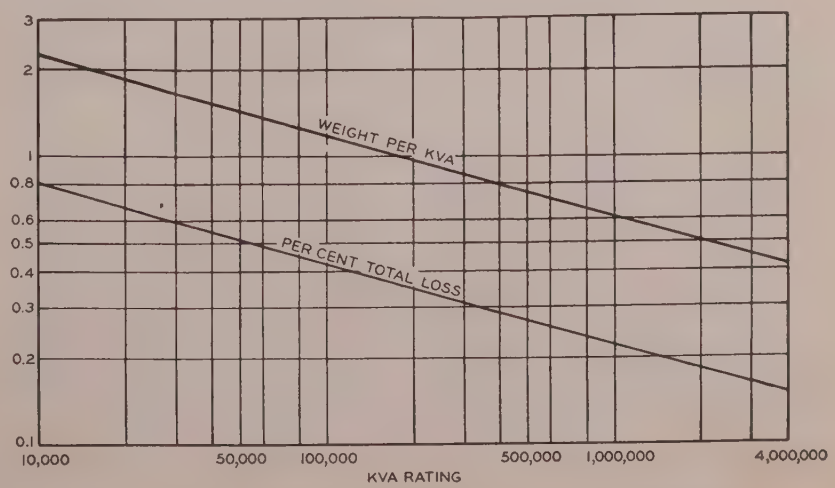

Figure 7. Typical variation of transformer loss and weight, with transformer size

Marking of Varmeters

AIEE COMMITTEE REPORT

A SURVEY of operating practices with respect to the marking of varmeters has been made under the sponsorship of the Instruments and Measurements Committee. Although the results show a wide divergence of practice, the "In" and "Out" markings are most commonly used, with "In" at the left of the scale. These markings are recommended as standard.

This report contains the results of an investigation by an Instruments and Measurements Subcommittee on the Marking of Varmeters and Related Instruments, first appointed in 1946. At the time this Subcommittee was appointed, the recommended change of the sign of inductive reactive power from negative to positive had not been adopted. The conflict still existed between the use of the negative sign in technical discussions and calculations, and the use of the positive sign in actual practice. The Subcommittee on the Marking of Varmeters was supposed to find a solution which might make the change in sign unnecessary.

When the change in sign was formally approved by the Standards Committee, the original reason for the existence of the Subcommittee was eliminated. However the Instruments and Measurements Committee decided that the Subcommittee should be continued, with the assignment to determine present operating practices on the marking of varmeters.

Paper 51-3, recommended by the AIEE Instruments and Measurements Committee and approved by the AIEE Technical Program Committee for presentation at the AIEE Winter General Meeting, New York, N. Y., January 22-26, 1951. Manuscript submitted October 16, 1950; made available for printing November 3, 1950.

This report was prepared by the AIEE Subcommittee on Marking of Varmeters and Related Instruments of the AIEE Instruments and Measurements Committee.

Personnel of the AIEE Subcommittee on Marking of Varmeters and Related Instruments: A. B. Craig, *Chairman;* A. L. Brownlee; A. L. Carvill; W. G. Knickerbocker; A. E. Knowlton; F. A. Redding; F. B. Silsbee, and H. B. Smith.

A questionnaire regarding present practices was circulated to operating companies in December 1948. The replies are the basis for this report and its recommendations.

Replies to Questionnaire

The questionnaire was sent to 106 operating companies in order to obtain the desired data on current practice.

The questionnaire was in the form of a diagram of an imaginary system showing probable varmeter locations and assumed direction of quadergy* flow, with spaces provided for the indication of the scale marking of each instrument and the direction of deflection under the assumed conditions, see Figure 1.

Following is a summary of the replies received from the 48 companies replying, which constitute about 45 per cent of the 106 questionnaires sent.

Type of Marking

Types of scale markings are listed in Table I together with the number of companies reporting the use of each type in one or more locations.

Attention is called to the fact that although reports were received from only 48 companies, the summation of the number of companies using each type of marking is 67. This indicates that a number of companies use more than one type of marking.

"In" and "Out" markings are the most common and are used by about 52 per cent of the companies reporting. Sixteen companies (33 per cent) use this marking exclusively. Three of the 10 companies reporting the use of "Lag" and "Lead" indicate that the instruments are power factor meters rather than varmeters.

Twenty-five of the companies use left-hand zero instruments at certain locations instead of the center or off-center zero type. Table II is a list of the left-hand zero scales reported and the number of companies using each marking.

The use of left-hand zero instruments is distributed as shown in Table III.

Reference Point

Table IV shows how the companies divided with respect to the point used as a reference for the markings of the varmeters at various locations.

Nine of the reporting companies use the station bus as a reference in all cases. The majority (about 65 per cent), however, use the generator as a reference point for the generator varmeters and the bus as a reference for those in the lines.

Direction of Deflection

Table V shows the number of companies reporting right- or left-hand de-

Table I. Center and Off-Center Zero Instruments

Category	Scale Marking	Companies Using		Per Cent
1	In-O-Out	28		
	Out-O-In	7	35	52
2	Lead-O-Lag	6		
	Lag-O-Lead	4	10	15
3	To-O-From	2		
	From-O-To	3	5	7½
4	Minus-O-Plus	3		
	Plus-O-Minus	1	4	6
5	Buck-O-Boost (syn. cond.)	1		
	Boost-O-Buck (gen. and syn. cond.)	1	2	3
6	Received-O-Delivered	2		3
7	Under Excited-O-Over Excited (gen., syn. cond., syn. conv.)	1		1½
8	Value-O-Value	5		7½
9	To Specific Point-O-To Specific Point	3		4½
		67		100

Quadergy: In describing the operation of an a-c system with reactive loads, it has been found convenient to assume the existence of this quantity, which is analogous to energy, which is inherently positive and which is assumed to flow out of a properly excited source and into an inductive load. A proposed definition of quadergy is: "The quadergy which has been supplied by a source to a load during a time interval is the integral with respect to time of the reactive power at the points of entry of the load taken over the time interval. The value of quadergy is given in varhours when the reactive power is in vars and the time is in hours."

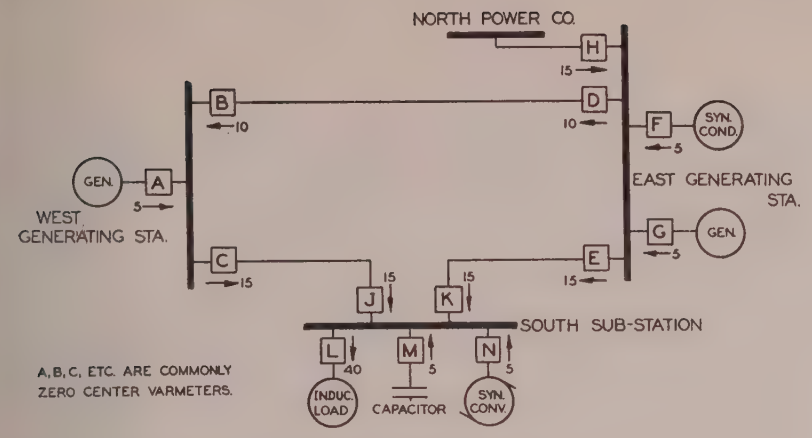

DIRECTION OF QUADERGY FLOW IS SHOWN BY ARROWS.

REFERENCE – BUS IN ALL CASES

WEST STATION			EAST STATION			SOUTH SUB-STATION		
METER	IN	OUT	METER	IN	OUT	METER	IN	OUT
A	5		D		10	J	15	
B	10		E		15	K	15	
C		15	F	5		L		40
			G	5		M	5	
			H	15		N	5	
	15	15		25	25		40	40

REFERENCE – GENERATOR AND BUS

A		5	D		10			
B	10		E		15			
C		15	F	5		SAME AS ABOVE		
			G		5			
			H	15				

Figure 1. Quadergy flow in an imaginary system

flection of center or off-center zero instruments in each of the positions listed in the questionnaire.

All companies reporting do not use varmeters at every point shown in the questionnaire. The number of companies reporting no instruments at various points is given below:

Inductive load	6
Capacitor	12
Synchronous converter	10
Synchronous condenser	4
Lines	2

Table II

Scale	Number of Companies
O-in	9
O-out	10
O-lag	1
O-to	3
O-from	4
O-plus	1
O-delivered	1
O-value only	4
O-to specific point	3
	36

Several companies, although reporting that varmeters are not used at some of the points shown, indicated the probable scale marking if they should use varmeters at these points.

Discussion

In general, the replies show a wide divergence of practices which apparently depend largely upon individual preferences. The points on which the greatest number of companies are in agreement are, the use of In-O-Out markings ("In" on the left), the use of the station bus as a reference point for line varmeter markings and the use of the generator as a reference point for the generator varmeter.

However another practice followed by nine of the reporting companies specifies the use of the bus as a reference point in all cases. This method presents the advantage that the sum of the "In" varmeter readings on a particular bus should always equal the sum of the "Out" readings. (See log sheet, Figure 1).

It is interesting to note that 67 per cent of the companies replying, in their load dispatching evidently make use of the concept that there is a quantity which flows from one part of the system to another, and in so doing goes "in" and "out", "to" or "from", and is "received" and "delivered". These are the companies listed in categories 1, 3, 6, and 9 of Table I. This fact seems to the Committee to justify the introduction by the AIEE Committee on Instruments and Measurements into engineering parlance, of the new word "quadergy" to designate this quantity. Reactive power is the measure of the rate of flow of the quantity, but strictly speaking, reactive power does not "flow" but merely is maintained at the load terminals by the action of the power system.

The results of the survey indicate that the establishment of a standard for the marking of varmeters is desirable. There-

Table III

Location	Number of Companies
Generator	3
Inductive load	22
Capacitor	21
Synchronous converter	1
Synchronous condenser	2

Table IV

Location	Number of Companies: Reference Point: Machine or Load	Reference Point: Station Bus
Generator	29	14
Inductive load	8	23
Capacitor	11	17
Synchronous converter	15	22
Synchronous condenser	18	20
Tie line	3 (other station)	39
Line to substation		
Station meter	4	37
Substation meter	6	35

Table V

Location	Direction of Quadergy Flow	Number of Companies: Deflection Left	Right
Generator	From generator	10	33
Inductive load	To load	6	10
Capacitor	From capacitor	8	2
Synchronous converter	From converter	15	21
Synchronous condenser	From condenser	14	27
Tie line	To station bus	35	9
Line out to substation	From station bus	7	35
Line into substation	In to substation	30	11
Incoming line	To station bus	2	39

fore in conformance with the present practice of the greatest number of reporting companies, the Committee recommends that the "In" and "Out" marking be adopted as standard, and in center zero or off-center zero instruments, that "In" be on the left.

The Committee calls attention to the advantages of uniformity and of a quantitative check on log sheets, which can be obtained by the use of the bus as a standard reference point.

Discussion

Ralph M. Rowell (General Electric Company, West Lynn, Mass.): The Subcommittee has done an excellent job in co-ordinating a large number of reports from various sources on a subject as controversial as that pertaining to the marking of varmeters. It is particularly gratifying to note the large percentage favoring the "In-O-Out" marking, which we have favored and have used now for several years.

Lack of standardization of these markings has been distressing both to the instrument manufacturer and to the user alike, and numerous complaints arise when a standardized marking does not fit in with a particular company's special requirements. We feel that this Subcommittee's recommendations will go a long way toward standardizing the marking of these instruments throughout the industry, and, while many special types of markings have been reported in the questionnaire, it seems likely that a majority of the companies using these will fall in line with the new recommendation once it becomes standardized by instrument manufacturers.

While the Subcommittee does not definitely recommend the use of the station bus as a reference point for deciding the direction of indication, the report does state some of its advantages. However, we feel that these claimed advantages are not all realistic. While it is true that complete varmetering of a system, including generators, tie lines, sychronous condensers, and so forth, by this method could furnish a convenient check on the summation of "In" and "Out" values, there are actually few systems which are so complete as to cover all these points. If one point in a system is omitted, such a check is no longer possible.

On the other hand, we must point out the advantages of using the machine as a reference point except as in the case of a tie line, where the bus would be more suitable. Generator instruments usually are grouped on a single panel and to the operator represent conditions which apply to that particular generator. Thus, in the usual case of an inductive load with the generator furnishing the reactive power to the load, it would seem logical to have this instrument read "Out," indicating that the reactive power or "quadergy" is flowing out of the machine to the bus.

If the bus is used as a reference in this case, as shown in Figure 1 of the report, generator varmeters A and G would read "In" and would be confusing to the operator. A large majority of companies have indicated a preference for right scale deflection on generator instruments with quadergy flow from the generator to the bus. This preference would agree with the "Out" reading recommended for the right side of varmeter scales. It also would be consistent with the direction of indication of the other instruments on the generator switchboard.

While it may be difficult to standardize on the direction of these instruments, we would recommend that the use of the machine as a reference point be considered, except in case of feeders or tie lines, where the bus would be acceptable.

H. Bany (General Electric Company, Philadelphia, Pa.): I have noted the final paragraph of this report:

"The Committee calls attention to the advantages of uniformity and of a quantitative check on log sheets, which can be obtained by the use of the bus as a standard reference point."

Admittedly, there are advantages in having one standard reference point for vars, such as the bus, but it would seem that this same principle would be applicable to watts as well as to vars. However, it probably would be a little difficult to have the bus adopted as the reference point for watts, which would mean that for a generator delivering load into the bus the wattmeter would show "watts in." Hence, from a practical standpoint, to agree in general with the practice on wattmeters, we have been marking varmeters furnished with switchgear in accordance with the following rules and these seem to meet the approval of most of our customers:

"In applying varmeters to different types of circuits, these fall into two separate classifications, as follows:

"1. When the apparatus is located in the station or the installation itself, these individual pieces of apparatus are considered as the point of reference, and so the varmeter is connected to read "Out" when these machines or other pieces of apparatus are delivering magnetizing vars to the system, as in the case of overexcited synchronous generators.

"2. For incoming and outgoing lines or feeders the station bus is considered as the point of reference and the varmeters are connected in the opposite direction, that is, to read "In" when magnetizing vars are supplied to the station bus."

G. S. Lunge (General Electric Company, Schenectady, N. Y.): The Subcommittee is to be congratulated on concurring with the opinion of the majority of those returning the questionnaire regarding "In-Out" scale marking of all center zero or displaced zero varmeters.

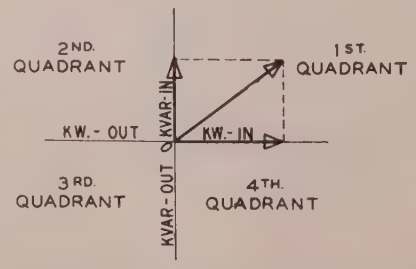

Figure 1. Vector diagram showing active, reactive, and apparent power relationships

It appears regrettable, however, that in the only other recommendation it made, the Subcommittee disagreed with the opinion of the majority of the 48 reporting companies, 65 per cent of whom favor using the (reactive power) generator as a reference point for the generator varmeter and the bus as a reference point for the varmeters in the lines.

To use the bus as a reference point for all varmeters in the station, as advocated by the subcommittee at the end of its report, means that:

1. Generator varmeters will deflect farther and farther downscale (to the left) the greater their kilovar output becomes, in contrast to their wattmeters, a-c ammeters, and field ammeters, which will all deflect farther and farther upscale as the load on the machine is increased.
2. To be consistent, wattmeters should be marked similarly if it is really of value to be able to equate the totals of the "In" and "Out" readings quickly for each bus in a station as recorded on log sheets. This would mean that all generator wattmeters would be marked "In" and normally would deflect to the left, if they are to correspond to tie-line wattmeters marked "In-O-Out."
3. Every circuit coming to, or leaving, the bus would need to be equipped with a varmeter, if it is to be possible to balance the totals of the "In" and "Out" readings for that bus.

It appears doubtful whether any of the three foregoing consequences would be tolerated generally by operating companies.

Perhaps an even larger majority of those answering the questionnaire would have rejected the proposal to use the bus as reference point in all cases, if the lower half of the tabulation in Figure 1 of the report had been entitled "Reference: Var Source or Station." Then meters F, M, and N would have read "Out" as, indeed, they should, if they are to deflect similarly to meters A and G, which also are metering sources of quadergy.

B. R. Nevins (Philadelphia Electric Company, Philadelphia, Pa.): The recommendation of the Subcommittee that varmeter scales of the center zero or off-center zero type be marked "In-O-Out" apparently is based entirely on the fact that answers to the 1948 questionnaire indicate that 28 of the 67 companies replying currently use this scale marking, with the rest of the answers spread thinly over 13 other scale markings.

We do not believe the raw fact that a plurality or even a majority survey result of current practice necessarily reflects the best modern practice. In a survey "by companies" a majority answer may well represent a very small percentage of application by the companies replying. New concepts

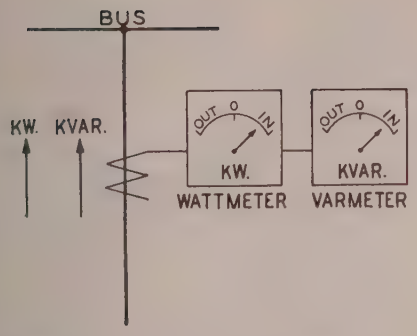

Figure 2 (A). Tie line feeding active and reactive power into the bus. Tie line is acting like an overexcited generator on the bus

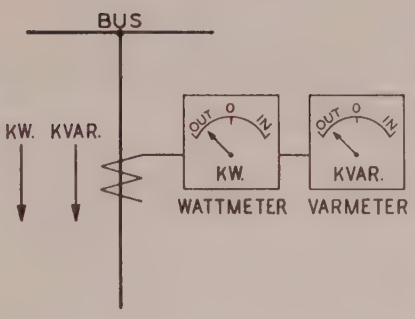

Figure 2 (C). Tie line taking active and reactive power from the bus. The tie line is acting like an induction motor load on the bus

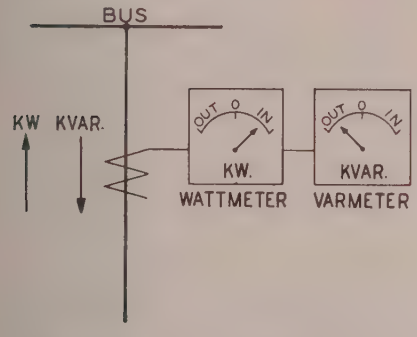

Figure 2 (B). Tie line feeding active power into the bus and taking reactive power from the bus. Tie line is acting like an underexcited generator on the bus

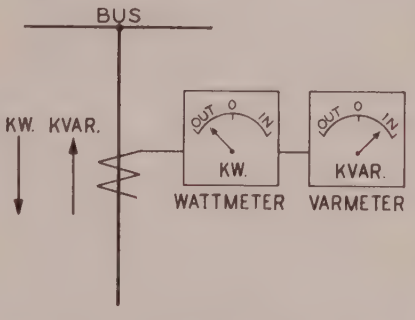

Figure 2 (D). Tie line taking active power from the bus and feeding reactive power into the bus. The tie line is acting like an overexcited synchronous motor on the bus

may have been accepted since the practices under question were established. Some or most of the companies representing the plurality or majority may sense the inadequacy of their practice, but lacking constructive suggestion for a change do not reflect this inadequacy in their answers to a questionnaire. For these reasons, and in the belief that we have a constructive suggestion based on sound theoretical and practical argument, we take this opportunity to disagree with the Committee Report.

It is our opinion that marking both wattmeter and varmeter scales "Out-O-In" and using the bus as the reference point is completely in accord with modern concepts of watts and vars both electrically and analytically, and correlates the visual indication with another universally accepted practice that positive quantities be indicated to the right, or upward, and negative quantities to the left, or downward.

Using active power into the bus as the reference vector, the apparent power (kilovolt amperes) for a tie line may occupy any position in any of the four quadrants shown in Figure 1 of this discussion. The apparent power vector shown in the first quadrant may be resolved into two components, one along the horizontal axis, which is the active power indicated by the wattmeter, and another along the vertical axis, which is the reactive power indicated by the varmeter. From this it follows that active and reactive power, although at right angles to each other, are in themselves algebraic quantities and both should be considered as such. On this basis, both active and reactive power may be positive or negative independently of each other with respect to some reference point in the circuit.

It is logical to take as a reference point the bus to which the various equipment in a station connects and to assume that active and reactive power are positive quantities (analytically) when flowing toward or "In" the bus and negative when flowing away from or "Out" of the bus. On this basis Kirchhoff's laws will apply separately to the active and reactive power, that is, the total active power flowing "In" to the bus will equal the total active power flowing "Out" of the bus and the total reactive power flowing "In" to the bus will equal the total reactive power flowing "Out" of the bus.

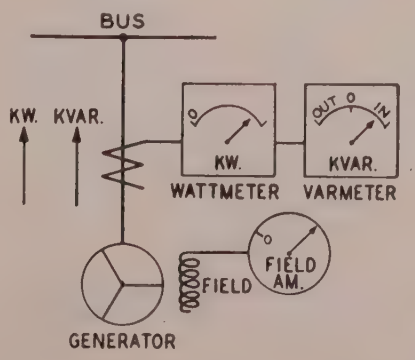

Figure 3 (A). Overexcited generator feeding active and reactive power to the bus

Considerable confusion has prevailed at various times in interpreting the readings of varmeters largely because reactive power was considered as four kinds corresponding to the four quadrants of a tie-line power factor meter, rather than as a positive or negative algebraic quantity, which it really is. The principles outlined in the preceding paragraph were applied to our system in 1942, with the result that confusion was eliminated. The ease and accuracy with which active and reactive power flow in the system can be established at any time has so pleased our system operators and other Operating Department people that they probably would oppose any suggested change.

Figures 2 through 6 of this discussion indicate the various applications of varmeters on our system, and conclusively show that our recommended marking and reference point do not provoke any of the discussion as to illogical relative indications between various meters. The one exception where there is an apparently illogical indication is in the case of an outgoing radial line. However, if the 0 left wattmeter is treated as a nondirectional or arithmetic instrument (like the ammeter), mental compatability is achieved.

We have no comment concerning the recommendation that a new term "quadergy" be added to engineering parlance to designate the concept that there is a quadrature quantity analogous to energy which flows from one part of a system to another. We do not feel the need for the term, but if others do we can see no harm that could result from its adoption.

We do, however, strongly recommend that the Subcommittee reconsider its recommendations with regard to varmeter marking in view of the argument herein presented.

H. B. Smith (Niagara Mohawk Power Corportation, Buffalo, N. Y.): In order to make my position clear at the start, I shall state that with respect to this report, I am a dissenter.

My first experience with the confusion and errors that may result from most meter-marking systems (including the one recommended in this report) was in early 1932. A system-wide power flow and voltage survey had been made, and I was asked to assemble and correlate the readings. I finally had to give up. The ambiguities and

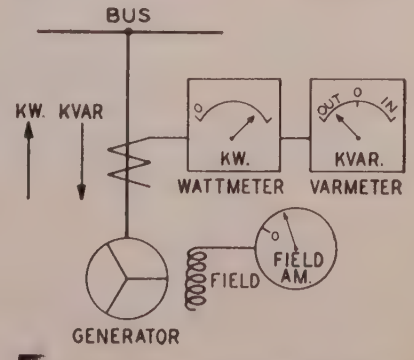

Figure 3 (B). Underexcited generator feeding active power into the bus and taking reactive power from the bus

confusion in the readings due to local ground rules, and so forth, regarding "In and Out," "Plus and Minus," and other markings, made the survey worthless. As a remedy I proposed a method of standardization of kilowatt, reactive kilovolt-ampere, and power factor designations and applications. This standardization was adopted by operating companies of Niagara Hudson late in 1932, and was presented to the profession as part of an AIEE paper by J. A. Johnson.[1]

Briefly, this standardization had two important concepts:

1. We can and should deal with only one kind of reactive power.
2. All power and reactive power flow should be indicated, transmitted, or recorded as a flow between two points.

This standardization is demonstrated most easily and quickly by Figures 7 and 8 of this discussion.

It will be noted that in (A) the meter view, (B) the oral reading, (C) the log sheet recording, and (D) the flow diagram, the power and reactive power appears as a flow between the two terminals of the circuit under consideration, and the names of these terminals are given. It is not necessary to use or remember any rules regarding reference points.

Figure 8 of this discussion shows how this method of standardization can be applied to power factor meters (including the 4-quadrant power factor meter). A power factor meter really indicates direction of flow of vars, besides giving the ratio of watts to volt-amperes.

This standardization works, as would any standardization, if correctly and consistently applied. The advantage of this standardization over the one recommended in the Subcommittee Report is that it does not require the memorizing of any rules regarding reference points, and so forth, thus there is much less possibility of errors and confusion. It is a standard that can be applied universally and consistently.

From the Subcommittee Report it appears that the main reason for the recommendation is that it is the system already in use by the majority of operating companies.

In my mind there is little justification in recommending a standard simply because it agrees with present practice of a majority of companies. The majority can be wrong. Furthermore, as I see it, the Subcommittee Report makes no recommendation regarding retaining or eliminating "Lead" or "Lag" markings on varmeters and related instruments (power factor meters). Such a recommendation is decidedly within the scope of the title of the Subcommittee. In fact, the recommendation of standardizing on "In" and "Out" for varmeter marking is incomplete until it also is recommended that one kind of vars be standardized upon (as in the Niagara Mohawk standardization). It follows, then, that the kind of vars ("Lead" or "Lag") to be standardized upon must be recommended also.

I should like to propose that the AIEE adopt a standardized method of marking and dealing with reactive power and associated instruments, as shown in Figures 7 and 8 of this discussion.

Referring to the second sentence in the AIEE Subcommittee Report entitled "The Sign of Reactive Power,"[2] this standardization . . . "provides definiteness in technical discussions,. . . in network calculator investigations and in recording system power readings for dispatching and similar operating purposes."

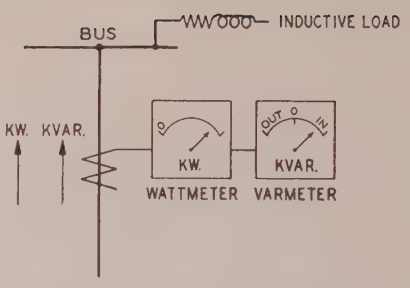

Figure 5 (A). Incoming line supplying a bus which in turn supplies an inductive load

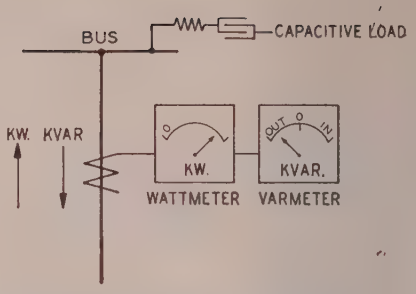

Figure 5 (B). Incoming line supplying a bus which in turn supplies a capacitive load

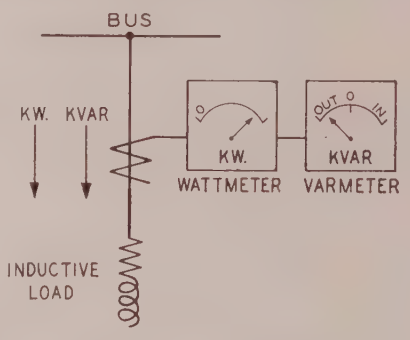

Figure 6 (A). Outgoing or radial line supplying an inductive load

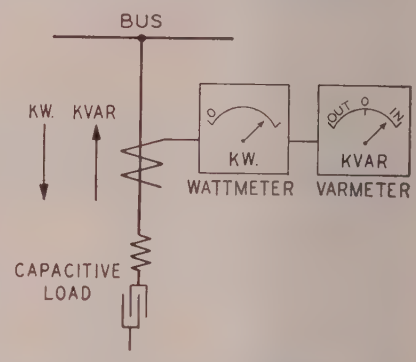

Figure 6 (B). Outgoing or radial line supplying capacitive load

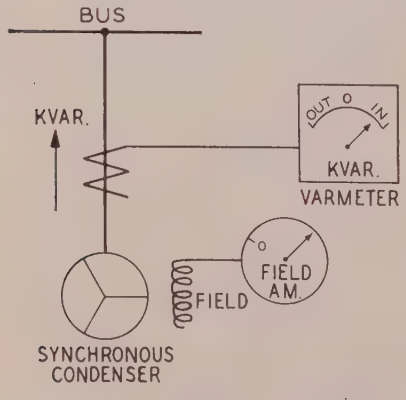

Figure 4 (A). Overexcited synchronous condenser feeding reactive power in the bus

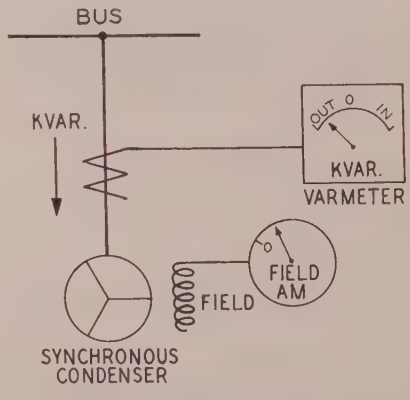

Figure 4 (B). Underexcited synchronous condenser taking reactive power from the bus

REFERENCES

1. Operating Aspects of Reactive Power, J. Allen Johnson. *AIIE Transactions*, volume 52, September–December Section, 1933, pages 752–57.

2. The Sign of Reactive Power, AIEE Committee Report. *Electrical Engineering*, volume 65, November 1946, pages 512–16.

A. E. Knowlton (*Electrical World*, New York, N. Y.): It is evident from the discussion already presented that there was not and is not complete unanimity in the Subcommittee's recommendations concerning the "In" and "Out" marking. As I see this sentiment it stems from much the same 2-alternative status which resulted in diversity of opinion about other aspects of algebraic signs, phase angles, and reactive power. It may be recalled that the standards were even reversed after adoption in two such cognate segments of the art. For one, the signs or lead-lag discrimination of the phase-angle of current transformers first was adopted as the opposite to that of the voltage transformer, but later it was changed to be the same. For another, the algebraic sign of inductive reactive power first was adopted as negative and later changed to positive. It had to be one or the other, and there was ample support at the outset for either alternative. That did not deter standardization and with it the expectation of ultimate uniform conformity.

This atmosphere surrounds the matter of systematic and uniform marking of varmeters. The same serious effort to apply the present recommendations may even result in

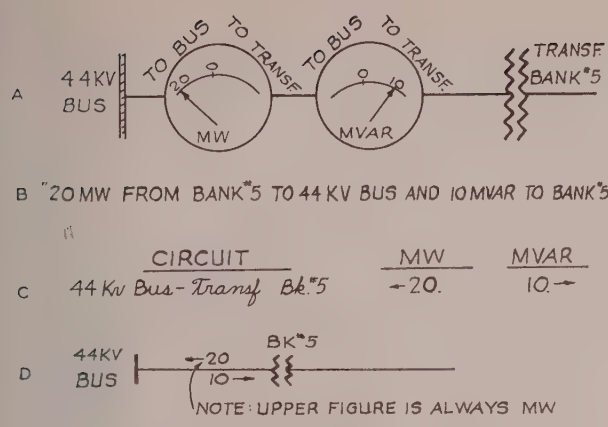

Figure 7. Niagara Hudson meter marking—mw and mvar meters

(A) meter view (B) oral reading (C) log sheet recording (D) flow diagram

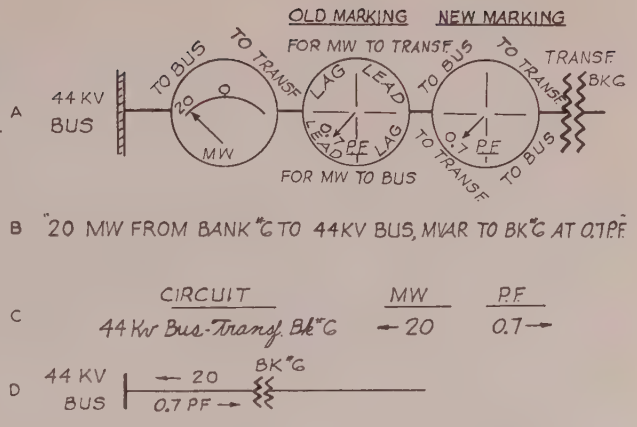

Figure 8. Niagara Hudson meter marking—mw and PF meters

(A) meter view (B) oral reading (C) log sheet recording (D) flow diagram

later substitution of a different concept. If such sentiment for a change prevails, that fact in itself will constitute convergence toward the unanimity that a standard should earn if it is worthy of the name.

A. B. Craig: Mr. Smith stresses the point that "we can and should deal with only one kind of reactive power."

Since the introduction of the term "quadergy" we are dealing with only one kind of reactive power. Reactive power is a measure of the rate of flow of quadergy, which is described as being "inherently positive, and which is assumed to flow out of a properly excited source and into an inductive load." With the acceptance of the term "quadergy" it appears that we have, as Mr. Smith recommends, standardized on one kind of vars.

While the original assignment of the Subcomittee was concerned with the "Marking of Varmeters and Related Instruments," it was found advisable during the investigation to limit the report to the marking of varmeters, since the trend seemed to be toward the use of this type of meter.

Messrs. Rowell and Lunge have commented on the fact that the Subcommittee calls attention to the advantages obtained by the use of the station bus as a standard reference point. They have pointed out some of the disadvantages of this practice. The comments of Mr. Bany of the General Electric Company are similar.

It should be noted that the Subcommittee made no recommendation relative to the choice of a reference point. Attention was merely called to the advantages to be obtained by the use of the station bus. Nine companies considered these advantages important enough to justify using this method. However, as pointed out in the discussions, there are some disadvantages to be considered, and the final choice of a reference point must take into consideration all the factors.

Mr. Nevins of the Philadelphia Electric Company, one of the nine companies using the bus as a reference in all cases, approved of the use of "In" and "Out" markings, but believes "In" should be on the right instead of on the left of the scale. The practice of this company is to consider vars in to the bus as positive and vars out as negative. They therefore prefer "Out" readings toward the left to indicate a negative quantity and "In" readings toward the right to indicate a positive quantity.

Table 1 in the report shows that very few companies use "Plus" and "Minus" markings on varmeters, and these few are not in complete agreement that "Plus" should be on the right. Of the companies using "In" and "Out," 80 per cent have "In" on the left.

Mr. Knowlton of the *Electrical World* points out that the situation has arisen before in which there has been a diversity of opinion regarding a committee's recommendations, but this fact has not prevented standardization.

As he indicates, it is sometimes necessary to make an arbitrary decision in these cases, so that experience may be obtained in applying the recommended standard, which will be helpful in reaching ultimate agreement.

Summarizing the discussions received, there has been one objection to the use of "In" and "Out" markings, one objection to the use of "In-O-Out" instead of "Out-O-In," and several objections to calling attention to the advantages of using the bus as a reference in all cases.

However, all these discussions and comments, together with any others that may be received, will be studied by the members of the Subcommittee. If in the opinion of the Subcommittee any changes or modifications of the report are desirable, recommendations to that effect will be made to the Instruments and Measurements Committee.

Deterioration of Transformer Oil and Paper Insulation by Temperatures

F. J. VOGEL
FELLOW AIEE

C. C. PETERSEN
ASSOCIATE AIEE

L. W. MATSCH
MEMBER AIEE

SEVERAL years ago, the question arose of overloading transformers for short periods of time. This in turn brought up the question of insulation deterioration with both temperature and time.

It is a subject which is as old as the electrical industry, but nevertheless one which has no end. Because it fringes on the edge of chemistry and other subjects not at the finger tips of the electrical engineer, it is not understood as well as it should be. During the war, materials which were not oil proof and which accelerated deterioration, were often used, showing that design engineers for some manufacturers were not aware of the problem. In earlier days this was common throughout the industry, as a number of materials, impregnants, and varnishes were used which accelerated deterioration.

The effect of different materials also is affected by the use of inert gas over the oil. Since most transformers now are either sealed or protected from oxygen, this is the most important condition. The use of this protection again raised the question of the rate of insulation deterioration with short-time overloads as stated before.

There have been a number of papers on the subject of fairly recent date. One of these papers reported a joint investigation[1] which was made because of some difference in opinion based on the results of different observers. The results of this investigation could lead to conclusions at variance with some previously obtained data.[2,3] In this case, curiosity as to the cause was naturally aroused, and to satisfy this, the work reported in this paper was done. At the same time some other questions arose, and these were investigated.

These questions were as follows: if air or oxygen is not present, does oil itself deteriorate due to temperature and time? The belief has been expressed that changes would be small. Also, the catalytic nature of copper is known, so tests with both tough pitch and oxygen-free copper were made in combination with oil sealed from oxygen or air. The effect on the oil of silicon steel, with both a common core plate enamel, and a so-called "glass" coating also was tested. Since the reason for the reported differences stated previously was perhaps in the papers tested, tests were made with manila paper, kraft paper, and rag paper under oil. Also, varnish treated samples and other combinations were tested.

The results of the tests indicated that some changes took place even in the oil alone, but that in some cases it was accelerated by the presence of other materials. There were distinct differences due to the materials, as the oxygen free copper, "glass" covered iron, and kraft or rag papers led to the least deterioration. It also was noted that the latter papers tended to absorb the high power factor materials resulting from the oil deterioration.

This reduced the power factor of the oil and increased the power factor of the paper. The results do not, however, indicate any changes in the present recommendations for loading transformers, but do throw some light on the changes which take place.

Paper 51-4, recommended by the AIEE Transformers Committee and approved by the AIEE Technical Program Committee for presentation at the AIEE Winter General Meeting, New York, N. Y., January 22–26, 1951. Manuscript submitted August 18, 1950; made available for printing November 3, 1950.

F. J. Vogel, C. C. Petersen, and L. W. Matsch are all with the Illinois Institute of Technology, Chicago, Ill.

Preparation of Samples

Six of each type sample were prepared, three to be aged at 105 degrees centigrade, and three to be aged at 120 degrees centigrade. Each sample comprised a 1 by 8 inch Pyrex test tube into which were placed various transformer materials covered with a standard type of transformer oil, and which was sealed after suitable treatment.

The types of samples follow:

1. (a) Untreated kraft paper, 12 strips.
   (b) Untreated manila rope paper, 12 strips.
   (c) Untreated rag stock paper, 12 strips.
2. (a) Tough-pitch copper.
   (b) Oxygen-free copper.
3. Control sample—oil alone.
4. Kraft paper wrapped around oxygen-free copper, tied, dipped in phenolalkyd varnish, and baked in accordance with instructions of one of the large electrical manufacturers.
5. (a) Hot-rolled silicon steel, coated with a standard core plate enamel; 4 strips.
   (b) Cold-rolled silicon steel, coated with glass; 4 strips.
6. (a) Untreated manila paper and 4 strips hot-rolled silicon steel, coated with a standard core plate enamel.
   (b) Untreated manila paper and 4 strips cold-rolled silicon steel, coated with glass.

The dimensions, in inches, of the materials are:

Kraft and manila papers—$1/2 \times 10 \times 0.003$
Rag stock paper—$1/2 \times 10 \times 0.004$
Tough-pitch copper—$1/4 \times 1/4 \times 3^1/_8$
Oxygen-free copper—$3/8 \times 1/8 \times 3$
Silicon steel—$1/2 \times 3 \times 0.014$

In preparing the sealed samples, the dry material was placed in the open test tube, the tube was sealed to an exhaust manifold and a vacuum of 1/4 inch of mercury was applied for 4 hours. Transformer oil at room temperature, was allowed to run slowly into the evacuated tube. The oil adhering to the neck of the tube was volatilized, while still under vacuum, by application of heat. Dry nitrogen was introduced into the tube, and the tube was sealed, taking care not to heat the oil.

After an aging period of one year, the samples were permitted to cool to room temperature. Sixty-cycle power factor measurements were made on the oil of each type sample, using a gradient of 27 volts per mil. Measurements were made at room temperature and at 100 degrees centigrade.

Tensile strength tests were made on the paper strips using a 3/8-inch throat 1 inch long cut in each paper strip. In most cases, seven measurements were averaged to determine the strength of a particular sample. For comparative purposes, tensile strength was measured on oil soaked paper strips which were not aged. Some samples were tested in accordance with the American Society of Testing Materials' tentative method of test, *D-663-44T*.[4]

Results of Tests

The results of the tests on the oil alone are given in Table I. The results of the tests indicate a definite change in the molecular structure of the oil, due to the change in power factor. It is to be noted that there was little change in acidity, and little change in oil color.

Table I. Oil Only

Test	Original	Sample Aged at 105° C
Acidity	0.035	0.04
Power factor—room temp.	0.0007	0.0032
Power factor—100° C	0.00125	0.0066
Power factor—room temp. after cooling		0.0027
Color		No change

Table II. Oil with Tough Pitch Copper

Test	Sample Aged at 105° C	Sample Aged at 120° C
Acidity	small*	small*
Power factor—room temp.	0.0123	0.068
Power factor—100° C	0.153–0.195	0.245
Color oil	little change	yellowed slightly

* Less than 0.03.

Table III. Oil with Oxygen—Free Copper

Test	Sample Aged at 105° C	Sample Aged at 120° C
Acidity	0.03	0.03
Power factor—room temp.	0.0076	0.044
Power factor—100° C	0.134–0.154	0.144
Color oil	little change	little change

Test	Original	Sample Aged at 105° C	Sample Aged at 120° C
Oil power factor—room temp.		0.0001	0.0085–0.0019
Oil power factor —100° C		0.0019	0 0016
Tensile strength of paper, lbs.	16	12	2
Oil color		little change	yellow
Paper color—room temp.	tan	tan	nearly black
Paper power factor	0.005 approx.	0.024	0.573

Table V. Oil and Untreated Manila Paper

Test	Original	Sample Aged at 105° C	Sample Aged at 120° C
Oil acidity		0.25	0.59
Oil power factor—room temp.		0.0002	0.025–0.0123*
Oil power factor —100° C		0 0017	0 0032
Tensile strength of paper, lbs.	20	2.8	2.3
Color oil		little change	discolored and cloudy
Color paper	yellow	nearly black	black
Paper power factor		0.417	0 542

* When the sample was opened, the oil bubbled and emitted an odor of charred paper. The power factor of the oil changed, and even decreased with heating to 100 degrees centigrade. The power factor of the same sample, after cooling, decreased ultimately to 0.01 per cent.

Table VI. Oil and Rag Paper

Test	Original	Sample Aged at 105° C	Sample Aged at 120° C*
Oil acidity		0 06	0.36
Oil power factor—room temp.		0.0001	0.0001
Oil power factor—100° C		0.0011	0.0014
Tensile strength of paper, lbs.	22	8.3	5.7
Color oil		little change	little change–fairly clear
Color paper	blue	tan	nearly black
Paper power factor	0.005 approx.	0.0125	

* The sample aged at 120 degrees centigrade had an odor of charred paper when opened.

Table VII. Oil and Silicon Steel and Core Plate Enamel

Test	Sample Aged at 105° C	Sample Aged at 120° C
Oil power factor—room temp.	0.00082	0.0023
Oil power factor—100° C	0.0153	0.037 to 0.0017 after 16 hours
Color oil	little change	little change—sour smell

Table VIII. Oil and Glass-Coated Silicon Steel

Test	Sample Aged at 105° C (A)	Sample Aged at 105° C (B)	Sample Aged at 120° C (A)	Sample Aged at 120° C (B)
Oil power factor—room temp.	0.0066	0.0041–0.0011	0.0005	0.0469
Oil power factor—100° C	0.129	0.0300	0.0117	0.0044
Oil cooled to room temp. after 78 hours				0.0001
Color oil	No change		No change	

(A) and (B) refer to two separate samples.

Table IX. Oil, Silicon Steel and Core Plate Enamel, and Untreated Manila Paper

Test	Sample Aged at 105° C	Sample Aged at 120° C
Oil acidity	0.28	0.28
Oil power factor—room temp.	0.0003	0.0603
Oil power factor—100° C	0.0227	0.0028
Oil power factor—cooled to room temp.		0.0004 after 16 hours
Tensile strength of paper, lbs.	4.1	2.2
Color oil	badly yellowed	yellow and much sediment
Color paper and steel	both darkened	both black; oil frothed when opened; charred odor

Table X. Oil, Silicon Steel with Glass Coating and Untreated Manila Paper

Test	Sample Aged at 105° C	Sample Aged at 120° C
Oil acidity	0.06	0.45
Oil power factor—room temp.	0.0003	0.0016–0.0009 after 1 hour
Oil power factor—100° C.	0.0010	0.0024
Tensile strength of paper, lbs.	2.3	1.9
Color oil	slightly yellow	yellow
Color paper and steel	paper darkened	black
	steel black	oil frothed when opened

Table XI. Oil, Oxygen Free Copper, Synthetic Varnish on Kraft Paper

Test	Sample Aged at 105° C	Sample Aged at 120° C
Acidity	0.85	1.06
Power factor—room temp.	0.0211	0.0167
Power factor—100° C.	0.0364	0.0302
Oil condition	yellow and sediment	yellow, much sediment; charred paper odor

The test results on oil with tough-pitch copper and oxygen free copper are shown in Tables II and III. The presence of the copper, even when oxygen free, resulted in a considerable increase in power factor. The acidity, in both cases, was little changed.

The test results with the untreated papers are given in Tables IV, V, and VI. Note that the power factor of the oil after the test changed with exposure to air, the higher values given being values obtained soon after opening the samples, and the latter after approximately 16 hours exposure. Evidently some of the deterioration products were highly volatile, and the paper absorbed the high power factor materials.

It is of interest that the kraft and rag papers seemed much more stable than the manila paper. The presence of any paper seemed to reduce the power factor of the oil, but increased acidity, as indicated by Table I.

It is very apparent that the tests made using manila paper showed markedly increased acidity and power factor over those using the rag paper.

Since the co-operative tests, previously referred to, used manila paper only, it is seen that they are not representative of what might happen with transformers using some rag and kraft materials. It also is believed that it would be advantageous to remove the volatile deterioration products, particularly those produced by the manila paper, during operation.

The series of tests made with steel, and steel and manila paper are given in Tables VII, VIII, IX, and X. In these tests, it still appears that the effect of the steel and coatings is to create a volatile material resulting in the high values of power factor which decrease markedly on exposure to air. They also show that the deterioration was affected greatest by the core plate enamel, and the products causing the high power factor were eliminated by heating or exposure to the atmosphere.

The results of the tests using impregnating materials are shown in Tables XI and XII.

The treated paper was extremely brittle, showing very little strength.

Discussion and Conclusions

Even without the presence of oxygen, some change in the oil was indicated by the change in power factor of the oil. This also occurred in the presence of copper, iron, and the glass coating.

The papers seemed to absorb some of this high power factor material from the oil. The oil then remained with a low power factor and the power factor of the paper increased tremendously. It was noted that deterioration products causing the high power factors seemed to be volatile, as the power factors of the oil decreased with exposure to air.

As in the previous tests, the paper was found to be very brittle. Higher strength values after test than given here were reported before,[1] but the length of samples were shorter in these tests and it was more difficult to avoid clamping difficulties in the tensile strength tests.

It is to be noted that both the kraft and rag papers resist heat much better than manila paper. It is believed that new manila paper has a little stretch, and this enables it to be taped on rectangular conductors faster and with less breakage. However, transformers use the kraft and rag materials where the heating is less, and the manila directly against hot copper.

It seems that the presence of the varnishes or enamels affect the oil adversely. In the case of the steel core plate enamel, sediment, gas and discoloration were produced. This also occurred with the phenol-alkyd varnish, which was represented as being an oilproof and satisfactory varnish for transformer impregnation. The test on the black treated tape was included because even though it is not usually claimed to be oilproof, it is sometimes used even today.

Table XII. Oil and Black Treated Tape

Test	Sample Aged at 105° C	Sample Aged at 120° C
Acidity	0.78	1.15
Power factor—room temp.	0.52	practically unity
Oil color	black	black

It is interesting that there are two other papers reporting tests on transformer assemblies.[5,6] In the case of one of these,[5] it is believed that these tests form a rough explanation of why some of the results took place. In the case of the other reference,[6] the statement that the condition of the oil is affected by the materials used and that in turn the materials are affected by the oil could be inferred, and is confirmed by the results of these tests. Since the oil deterioration or change may not be wholly one of oxidation, one might be led to question the effect of inhibitors, as raised in the latter paper.[6] The best idea might be to prevent oxidation, and remove the deterioration products evidently produced by the oil and paper.

When this work was started, it was thought that it might have some application to the previous work on transformer insulation life. As a result of it, the authors believe the mathematical and experimental foundations are not too well founded, but that the recommendations as made and used are satisfactory in giving usable results. More care in the selection of materials and in the removal of deterioration products will lead to longer transformer life.

References

1. Preliminary Report on Laboratory Aging Tests on Class A Insulation, **AIEE Committee Report.** *AIEE Transactions*, volume 66, 1947, pages 879–83.

2. Temperature Limits Set by Oil and Cellulose Insulation, **Charles F. Hill.** *Electrical Engineering* (*AIEE Transactions*), volume 58, September 1939, pages 484–91.

3. Emergency Overloads for Oil-Insulated Transformers, **F. J. Vogel, T. K. Sloat.** *Electrical Engineering* (*AIEE Transactions*), volume 61, September 1942, pages 669–73.

4. Acid and Base Numbers of Petroleum Products by Color Indicator Titration. *D-663-44T*, American Society for Testing Materials (Philadelphia, Pa.).

5. Controlled Temperature and Insulation Protection in the Operation of Power Transformers, **W. W. Satterlee, R. D. Reed.** *AIEE Transactions*, volume 69, part I, 1949, pages 753–59.

6. Transformer Oil, **E. D. Treanor, E. L. Raab.** *AIEE Transactions*, volume 69, part II, 1950, pages 1060–70.

Discussion

W. W. Satterlee (Westinghouse Electric Corporation, Sharon, Pa.): The authors have presented an interesting subject and one which, as they state, seems to have no end. This in itself is a good point since, should an end come to investigations of this kind, an end also would come to the improvement of the equipment to which these investigations are directed.

While World War II did make it necessary to use many substitute materials, and this condition seems to be rapidly coming again, it is believed that the use of other than oil-proof materials was not caused by a lack of a knowledge of the problem, but rather by the necessity of using the best materials available.

Although the authors state that most transformers now are either sealed or protected from oxygen, it should be realized that sealed transformers are effectively protected from oxygen.

It is well known that the deterioration of oil is accelerated, especially at elevated temperatures, by the presence of some insulating materials and by some varnishes used in the construction of transformers. It is reasonable to believe that some impurities may act as inhibitors.

As the paper states, some changes took place in oil alone, but the changes were accelerated by the presence of other materials. Also, as might be expected oxygen-free copper, glass-coated core steel, and kraft and rag papers led to the least deterioration. Probably one reason for this is because such materials are relatively free of soluble impurities. It is realized that the behavior of these materials would be quite different if air were present.

While the tests made are strictly of a laboratory nature, the following comments seem evident. Can the results obtained be expected to represent or to be comparable to actual conditions of operation? Was the degree to which the test tubes were evacuated sufficient to clear them of oxygen? In evacuating the tubes to 1/4-inch of mercury, it seems that there might have been sufficient oxygen remaining to cause some of the changes noted, particularly in the cases of oil alone. It would seem that the acidity of 0.035 as given for the original or new oil in Table I of the paper is high; that it should have been more of the order of 0002. In the conclusions, the authors cite an earlier study (see reference 5 of the paper), and state: "It is believed that these tests form a rough explanation of why some of the results took place." This is probably true, but it was, in general, well known before the tests referred to in the 1949 paper were started. Two purposes of the tests covered in that paper are to learn to what degree the deterioration of oil and insulating materials occurs, and how well the different types of oil and insulation protection function.

Regarding inhibitors, I do not believe that the results shown in the present paper indicate that the use of inhibitors might not be beneficial.

I agree that in the design and operation of modern transformers, it is best to prevent oxidation and to remove the products of deterioration which are formed gradually by the slow decomposition of insulating materials. Thermosiphon filters will perform this function.

With reference to statements in the last paragraph of the paper, it is evident that the work described is related to previous work on the life of insulation, and that the selection of materials and the removal of deteriorating products do lead to longer transformer life.

P. L. Bellaschi (Consulting Engineer, Portland, Oreg.): In the face of the current emergency, fullest utilization of all equipment again is becoming a matter of pressing necessity and good economics alike. The problem is one of utilizing the equipment effectively up to maximum load capability without encroaching disadvantageously on the inherent economic life of the equipment, taking advantage fully of present-day design and of developments and findings during the past decade.

A first requirement to fulfill in order to operate modern transformers at higher temperatures obviously is to exclude the oxygen and moisture in the atmosphere from the oil and insulation. This can be accomplished readily by such well-known preventive measures as complete sealing of the transformer tank, the use of an inert (nitrogen) gas, or other similar measures.

Sustained operating temperatures of the copper in the winding in excess of 120 degrees centigrade almost certainly will result in material thermal decomposition of the cellulose insulation adjacent to the winding, such as the turn-to-turn insulation. On the other hand, studies conducted on insulation as such and on complete transformers at temperatures well up to 105 degrees centigrade point definitely to the feasibility of good economic life of the insulation at these temperatures, more so when residues originally present in the insulation body or liberated as the result of operating at the higher temperatures are given ample opportunity to escape from the insulation subject to the higher temperatures and to become absorbed elsewhere. The removal of these residue products and the continuous purification of the insulation by such means as thermosiphon filter circulation of the oil through activated clay or alumina—in combination with inhibitors if need be—will permit the operation of modern transformers at temperatures above levels now recognized in the present operating guides.

Through these or other equally effective measures, the possibility of operating transformers continuously or for long periods of time at temperatures estimated at least 5 degrees centigrade above present so-called normal 95 degrees centigrade hottest-spot copper, appear feasible and economical. Other current-carrying parts, such as leads, bushings, and tap-changing equipment, all will require proper proportioning if full advantage is to be taken of the increased load capability available in the transformer proper.

The proposal outlined essentially is to liberalize the present operating guides in view of the critical situation, taking the fullest advantage of the inherently better load capability obtainable from transformers of modern design. No change in the standards proper is proposed here. By such measures, it is estimated that for the same equipment the effective kilovolt-ampere loading can be increased at least 5 per cent with a corresponding, if not greater, saving in critical materials such as copper, iron, oil, and insulation.

F. J. Vogel: We wish to thank Messrs. Satterlee and Bellaschi for their discussions.

The use of materials which are not oil-proof may have been caused by the lack of materials, but in some cases it resulted from errors in choice.

Previous tests were made with extreme care in the materials used and in the processing. In these tests, it was intended to use various common materials and also representative processing. Transformers when oil-filled under vacuum are not commonly evacuated to even 1/4 inch of mercury. The oil was drawn from a drum supplied by one of the manufacturers, and no doubt would have been used as received in the field. The amount of oxygen left in the oil by the processing would have been an extremely small percentage.

With respect to the use of inhibitors, I also do not claim that they are proved not to be beneficial. I do believe that there is no evidence that they are beneficial in the presence of usual insulating materials and the absence of air. In order to prove the benefit of inhibitors under these conditions, tests similar to those described in the paper would be required, so that a direct comparison could be made. Further, I do not believe this has been done. I think it should be.

I have long thought that hottest-spot operation at 120 degrees centigrade, with proper oil maintenance, might be reasonable. Even the increase from 95 degrees centigrade normal hottest spot to 100 degrees centigrade perhaps would be acceptable. The use of the word "normal" is assumed to put the average ambient at 30 degrees centigrade and permit ambients to be at 40 degrees centigrade at times. Extra cooling is very cheap, and it is possible to gain more in many cases by additional fans, radiators, forced cooling, and similar devices.

Tables of Green's Functions, Fourier Series, and Impulse Functions for Rectangular Co-ordinate Systems

J. J. SMITH
MEMBER AIEE

TABLES of Green's functions, Fourier series, and impulse functions are given in this paper. They have been prepared to materially reduce the work in solving partial differential equations encountered in engineering and physics. They allow us to solve such equations by obtaining results directly from these tables which can be used in a similar way to tables of integrals.

The Green's function,[1,2] which is the potential due to a single point charge within a given space with assigned conditions on the boundaries of the space, is used as the fundamental solution connected with that space. This is due to the fact that when the Green's function for any space is known, the solution for other conditions usually encountered can generally be found by the use of auxiliary theorems. This makes it possible to avoid the necessity of solving the differential equation itself for different types of conditions, as is commonly done in textbooks at the present time. This crystallization of the solution into a single function, the Green's function, together with the ensuing possibility that such results may be tabulated fairly simply, results in a great economy of labor in connection with the solution of such partial differential equations.

Fourier series are, of course, connected closely with the solution of partial differential equations, so it is natural to expect that the quantities which have been tabulated for the Green's function also should be available for use as a tabulation for Fourier series. As will be noted from the tables, the same fundamental expression serves in both cases.*

With regard to impulse functions,[3] these have been coming into use in the literature for quite a long time and have been used by many authors. They are not recognized as functions by the mathematicians at the present time. They are extremely useful because although they may appear very complex as mathematical expressions, they represent an extremely simple physical concept which is that their value is zero at all points except the point at which there is an impulse. Thus, the integral of the impulse function between any two points, (1) which do not include this impulse is zero, and (2) which do include the impulse is unity.

As would be expected, they are very closely allied to Fourier series and also to Green's functions. Thus the expressions already worked out for the Green's functions may be directly used for tabulation of impulse functions.

Paper 51-6, recommended by the AIEE Basic Sciences Committee and approved by the AIEE Technical Program Committee for presentation at the AIEE Winter General Meeting, New York, N. Y., January 22–26, 1951. Manuscript submitted November 16, 1948; made available for printing November 14, 1950.

J. J. Smith is with the General Electric Company, Schenectady, N. Y.

Note: Possibly, it would be a more correct use of terminology to call the series tabulated "trigonometrical series" since the term Fourier series seems to be reserved for series of sines and cosines when the harmonics are integral multiples of the fundamental. However, since later tables will include series of Bessel's functions and Legendre functions, some title is needed to include all of these in one expression, it would appear that perhaps the best title to use for all of these series is the general one of Fourier series, although the terminology may not be in agreement with that presently used.

Explanation of Method

These tables are based on a paper by the author[4] and may readily be checked by substituting appropriate sine and cosine functions in the formulas given in that paper. The tables only cover applications to rectangular co-ordinates. While tables covering both cylindrical and spherical co-ordinates have been prepared, lack of space prohibits their inclusion at the present time. It is hoped to publish them later.

The results in this paper are presented in the following order:

(a). Green's function due to steady state plane, line, and point source in 1, 2, and 3 dimensions respectively in sections I to III.
(b). Green's function due to instantaneous plane, line, and point source in 1, 2, and 3 dimensions respectively in sections IV to VI.
(c). Fourier series for $f(x)$ in terms of sin $\alpha_p x$ and cos $\alpha_p x$ with given linear conditions at each end of interval in section VII.
(d). Impulse functions in terms of sin $\alpha_p x$ and cos $\alpha_p x$ with given linear conditions at each end of interval in section VIII.
(e). The results in (a), (b), (c), and (d) above are given in terms of quantities designated X_{1p}, $X_{1p}{}^*$, Y_{1q} . . . . The values of these symbols and a statement of what these symbols mean will be found in the section entitled "Equations for Finding the Values of X_{1p}, $X_{1p}{}^*$, Y_{1q} . . . ."
(f). A brief reference to some theorems for deriving from the Green's function (tabulated here) the solution of other problems is given in Appendix I.
(g). A few brief examples of the use of these tables in specific problems are given in Appendix II.

I. Green's Function Steady State One Dimension

A steady-state plane source Q is placed at the point x_1 in the space whose boundaries are given by $x=l_1$, $x=l_2$. The condition (cond.) at the boundaries is given by equations of the type $\partial v/\partial n+hv=0$. The resulting potential v is given below.

The Differential Equations and Boundary Conditions are as Follows:

$$\frac{\partial^2 v}{\partial x^2}=g_0\rho$$

with condition at $x=l_1$,

$\left(h_1v-\frac{\partial v}{\partial x}\right)$, v, or $\frac{\partial v}{\partial x}=0$

or if $l_1=-\infty$, $v=0$, and $l_2>l_1$, condition at $x=l_2$,

$\left(h_2v+\frac{\partial v}{\partial x}\right)$, v, or $\frac{\partial v}{\partial x}=0$

or if $l_2=\infty$, $v=0$,

and Limit v $=$ Limit v
$x=x_1+0$ $\quad x=x_1-0$

$\rho=0$ when $x\neq x_1$

and $\int_{x_1-0}^{x_1+0}\rho dx=Q$

These equations have the following solution:

$v=g_0QX_{1p}^*$ (condition at $x=l_1$, condition at $x=l_2$)

where $\alpha_p^2=0$.

This solution may seem more complicated than necessary since it involves the limiting process of putting $\alpha_p=0$. To avoid this, however, would require adding new symbols which does not seem necessary.

As an illustration the potential due to a plane source Q at x_1 where the boundary conditions are $v=0$ at $x=l_1$ and $\partial v/\partial x=0$ at $x=l_2$ is found to be

$v=g_0Q\operatorname*{Lim}_{\alpha\to 0}X^*_{1p}\ (v,\ \partial v/\partial x)$

$v=g_0Q[(x-l_1)[1-H(x,x_1)]+(x_1-l_1)H(x,x_1)]$

II. Green's Function Steady State Two Dimensions

A steady-state line source Q is placed at the point x_1, y_1 in the space whose boundaries are given by $x=l_1$, $x=l_2$, $y=m_1$, $y=m_2$. The condition at the boundaries is given by equations of the type $\delta v/\delta n+hv=0$. The resulting potential v is given below.

The differential equations and boundary conditions are as follows:

$\partial^2v/\partial x^2+\partial^2v/\partial y^2=g_0\rho$

with

Condition at $x=l_1$, $(h_1v-\delta v/\delta x)$, v, or $\delta v/\delta x=0$, or if $l_1=-\infty$, $v=0$
Condition at $x=l_2$, $(h_2v+\delta v/\delta x)$, v, or $\delta v/\delta x=0$, or if $l_2=\infty$, $v=0$
} where $(l_2>l_1)$

Condition at $y=m_1$, $(h_3v-\delta v/\delta y)$, v, or $\delta v/\delta y=0$, or if $m_1=-\infty$, $v=0$
Condition at $y=m_2$, $(h_4v+\delta v/\delta y)$, v, or $\delta v/\delta y=0$, or if $m_2=\infty$, $v=0$
} where $(m_2>m_1)$

Limit v $=$ Limit v; $\quad$ Limit v $=$ Limit v
$x=x_1+0$ $\quad x=x_1-0$ $\quad y=y_1+0$ $\quad y=y_1-0$

$\rho=0$ when $x\neq x_1$, $y\neq y_1$ and $\int_{y_1-0}^{y_1+0}\int_{x_1-0}^{x_1+0}\rho dx\,dy=Q$

These equations have the following solutions:

$v=g_0QX_{1p}$ (cond. at $x=l_1$, cond. at $x=l_2$) $\quad Y_{1q}^*$ (cond. at $y=m_1$, cond. at $y=m_2$)

where $\beta_q^2=\alpha_p^2$ or

$v=g_0QX_{1p}^*$ (cond. at $x=l_1$, cond. at $x=l_2$) $\quad Y_{1q}$ (cond. at $y=m_1$, cond. at $y=m_2$)

where $\alpha_p^2=\beta_q^2$ or the double summation form

$v=\frac{g_0Q}{\alpha_p^2+\beta_q^2}X_{1p}$ (cond. at $x=l_1$, cond. at $x=l_2$) $\quad Y_{1q}$ (cond. at $y=m_1$, cond. at $y=m_2$)

III. Green's Function Steady State Three Dimensions

A steady-state point source Q is placed at the point x_1, y_1, z_1 in the space whose boundaries are given by $x=l_1$, $x=l_2$, $y=m_1$, $y=m_2$, $z=n_1$, $z=n_2$. The condition at the boundaries is given by equations of the type $\delta v/\delta n+hv=0$. The resulting potential v is given below.

The differential equations and boundary conditions are as follows:

$\partial^2v/\partial x^2+\partial^2v/\partial y^2+\partial^2v/\partial z^2=g_0\rho$

Condition at $x=l_1$, $(h_1v-\partial v/\partial x)$, v, or $\partial v/\partial x=0$, or if $l_1=-\infty$, $v=0$
Condition at $x=l_2$, $(h_2v+\partial v/\partial x)$, v, or $\partial v/\partial x=0$, or if $l_2=\infty$, $v=0$
} where $(l_2>l_1)$

Condition at $y=m_1$, $(h_3v-\partial v/\partial y)$, v, or $\partial v/\partial y=0$, or if $m_1=-\infty$, $v=0$
Condition at $y=m_2$, $(h_4v+\partial v/\partial y)$, v, or $\partial v/\partial y=0$, or if $m_2=\infty$, $v=0$
} where $(m_2>m_1)$

Condition at $z=n_1$, $(h_5v-\partial v/\partial z)$, v, or $\partial v/\partial z=0$, or if $n_1=-\infty$, $v=0$
Condition at $z=n_2$, $(h_6v+\partial v/\partial z)$, v, or $\partial v/\partial z=0$, or if $n_2=\infty$, $v=0$
} where $n_2>n_1$

Limit v $=$ Limit v; $\quad$ Limit v $=$ Limit v; $\quad$ Limit v $=$ Limit v
$x=x_1+0$ $\quad x=x_1-0$ $\quad y=y_1+0$ $\quad y=y_1-0$ $\quad z=z_1+0$ $\quad z=z_1-0$

$\rho=0$ when $x\neq x_1$, $y\neq y_1$, $z\neq z_1$ and $\int_{z_1-0}^{z_1+0}\int_{y_1-0}^{y_1+0}\int_{x_1-0}^{x_1+0}\rho dx\,dy\,dz=Q$

These equations have the following solutions:

$v=g_0QX_{1p}$ (cond. at $x=l_1$, cond. at $x=l_2$) $\quad Y_{1q}$ (cond. at $y=m_1$, cond. at $y=m_2$) $\quad Z_{1u}^*$ (cond. at $z=n_1$, cond. at $z=n_2$)

where $\gamma_u^2=\alpha_p^2+\beta_q^2$, or

$v = g_0 Q X_{1p}$ (cond. at $x=l_1$, cond. at $x=l_2$) Y_{1q}^* (cond. at $y=m_1$, cond. at $y=m_2$) Z_{1u} (cond. at $z=n_1$, cond. at $z=n_2$)

where $\beta_q^2 = \alpha_p^2 + \gamma_u^2$, or

$v = g_0 Q X_{1p}^*$ (cond. at $x=l_1$, cond. at $x=l_2$) Y_{1q} (cond. at $y=m_1$, cond. at $y=m_2$) Z_{1u} (cond. at $z=n_1$, cond. at $z=n_2$)

where $\alpha_p^2 = \beta_q^2 + \gamma_u^2$, or the triple summation form

$$v = \frac{g_0 Q}{\alpha_p^2 + \beta_q^2 + \gamma_u^2} X_{1p} \text{ (cond. at } x=l_1, \text{ cond. at } x=l_2) \quad Y_{1q} \text{ (cond. at } y=m_1, \text{ cond. at } y=m_2) \quad Z_{1u} \text{ (cond. at } z=n_1, \text{ cond. at } z=n_2)$$

IV. Green's Function Instantaneous Source One Dimension

An instantaneous plane source Q_1 at the time t_1 is placed at the point x_1 in the space whose boundaries are $x=l_1$, $x=l_2$. The conditions at the boundaries are given by the equations of the type $\partial v/\partial n + hv = 0$. The resulting potential v is given for the following cases: **Case I.** Conditions corresponding to the heat equation. **Case II.** Conditions corresponding to the wave equation in a dissipative medium. **Case III.** Conditions corresponding to the wave equation in a nondissipative medium.

The differential equations and boundary conditions are as follows:

$\partial^2 v/\partial x^2 = g_1 \partial v/\partial t + g_0 \rho_1$ **Case I**

$\partial^2 v/\partial x^2 = g_2 \partial^2 v/\partial t^2 + g_1 \partial v/\partial t + g_0 \rho_1$ **Case II**

$\partial^2 v/\partial x^2 = g_2 \partial^2 v/\partial t^2 + g_0 \rho_1$ **Case III**

Condition at $x=l_1$, $(h_1 v - \partial v/\partial x)$, v, or $\partial v/\partial x = 0$, or if $l_1 = -\infty$, $v=0$
Condition at $x=l_2$, $(h_2 v + \partial v/\partial x)$, v, or $\partial v/\partial x = 0$, or if $l_2 = \infty$, $v=0$ } $(l_2 > l_1)$

Limit v = Limit v and $\rho_1 = 0$ when $x \neq x_1$ and $t \neq t_1$.
$x=x_1+0$ $x=x_1-0$

$\int_{t_1-0}^{t_1+0} \int_{x_1-0}^{x_1+0} \rho_1 dx dt = Q_1$ and $v=0$ when $t < t_1$.

These equations have the following solutions:

$v = g_0 Q_1 X_{1p}$ (cond. at $x=l_1$, cond. at $x=l_2$)T where

$T = \epsilon^{-\alpha_p^2 (t-t_1)/g_1} H(t, t_1)/g_1$ **Case I**

$T = \epsilon^{-g_1 (t-t_1)/2g_2} \sin [(t-t_1)\{g_2 \alpha_p^2 - g_1^2/4\}^{1/2}/g_2] H(t, t_1)/[g_2 \alpha_p^2 - g_1^2/4]^{1/2}$ **Case II**

$T = \sin [\alpha_p (t-t_1)/g_2^{1/2}] H(t, t_1)/\alpha_p g_2^{1/2}$ **Case III**

V. Green's Function Instantaneous Source Two Dimensions

An instantaneous line source Q_1 at the time t_1 is placed at the point x_1, y_1 in the space whose boundaries are $x=l_1$, $x=l_2$, $y=m_1$, $y=m_2$. The conditions at the boundaries are given by equations of the type $\partial v/\partial n + hv = 0$. The resulting potential v is given for the following cases: **Case I.** Conditions corresponding to the heat equation. **Case II.** Conditions corresponding to the wave equation in a dissipative medium. **Case III.** Conditions corresponding to the wave equation in a nondissipative medium.

The differential equations and boundary conditions are as follows:

$\partial^2 v/\partial x^2 + {}^2\partial v/\partial y^2 = g_1 \partial v/\partial t + g_0 \rho_1$ **Case I**

$\partial^2 v/\partial x^2 + \partial^2 v/\partial y^2 = g_2 \partial^2 v/\partial t^2 + g_1 \partial v/\partial t + g_0 \rho_1$ **Case II**

$\partial^2 v/\partial x^2 + \partial^2 v/\partial y^2 = g_2 \partial^2 v/\partial t^2 + g_0 \rho_1$ **Case III**

Condition at $x=l_1$, $(h_1 v - \partial v/\partial x)$, v, or $\partial v/\partial x = 0$, or if $l_1 = -\infty$, $v=0$
Condition at $x=l_2$, $(h_2 v + \partial v/\partial x)$, v, or $\partial v/\partial x = 0$, or if $l_2 = \infty$, $v=0$ } where $(l_2 > l_1)$
Condition at $y=m_1$, $(h_3 v - \partial v/\partial y)$, v, or $\partial v/\partial y = 0$, or if $m_1 = -\infty$, $v=0$
Condition at $y=m_2$, $(h_4 v + \partial v/\partial y)$, v, or $\partial v/\partial y = 0$, or if $m_2 = \infty$, $v=0$ } where $(m_2 > m_1)$

Limit v = Limit v; Limit v = Limit v
$x=x_1+0$ $x=x_1-0$ $y=y_1+0$ $y=y_1-0$

and $\rho_1 = 0$ when $x \neq x_1$, $y \neq y_1$, and $t \neq t_1$, and $\int_{t_1-0}^{t_1+0} \int_{y_1-0}^{y_1+0} \int_{x_1-0}^{x_1+0} \rho_1 \, dx \, dy \, dt = Q_1$, and $v=0$ when $t > t_1$.

These equations have the following solutions:

$v = g_0 Q_1 X_{1p}$ (cond. at $x=l_1$, cond. at $x=l_2$) Y_{1q} (cond. at $y=m_1$, cond. at $y=m_2$)T

where

$T = \epsilon^{-(\alpha_p^2 + \beta_q^2)(t-t_1)/g_1} H(t, t_1)/g$ **Case I**

$T = \epsilon^{-g_1 (t-t_1)/2g_2} \sin [(t-t_1)\{g_2(\alpha_p^2 + \beta_q^2) - g_1^2/4\}^{1/2}/g_2] H(t, t_1)/[g_2(\alpha_p^2 + \beta_q^2) - g_1^2/4]^{1/2}$ **Case II**

$T = \sin [(t-t_1)(\alpha_p^2 + \beta_q^2)^{1/2}/g_2^{1/2}] H(t, t_1)/[g_2(\alpha_p^2 + \beta_q^2)]^{1/2}$ **Case III**

VI. Green's Function Instantaneous Source Three Dimensions

An instantaneous point source Q_1 at the time t_1 is placed at the point x_1, y_1, z_1 in the space whose boundaries are $x=l_1$, $x=l_2$, $y=m_1$, $y=m_2$, $z=n_1$, $z=n_2$. The conditions at the boundaries are given by equations of the type $\partial v/\partial n+hv=0$. The resulting potential v is given for the following cases: **Case I.** Conditions corresponding to the heat equation. **Case II.** Conditions corresponding to the wave equation in a dissipative medium. **Case III.** Conditions corresponding to the wave equation in a nondissipative medium.

The differential equations and boundary conditions are as follows:

$$\partial^2 v/\partial x^2+\partial^2 v/\partial y^2+\partial^2 v/\partial z^2=g\partial_1 v/\partial t+g_0\rho_1 \qquad \text{Case I}$$

$$\partial^2 v/\partial x^2+\partial^2 v/\partial y^2+\partial^2 v/\partial z^2=g_2\partial^2 v/\partial t^2+g_1\partial v/\partial t+g_0\rho_1 \qquad \text{Case II}$$

$$\partial^2 v/\partial x^2+\partial^2 v/\partial y^2+\partial^2 v/\partial z^2=g_2\partial^2 v/\partial t^2+g_0\rho_1 \qquad \text{Case III}$$

Condition at $x=l_1$, $(h_1 v-\partial v/\partial x)$, v, or $\partial v/\partial x=0$, or if $l_1=-\infty$, $v=0$
Condition at $x=l_2$, $(h_2 v+\partial v/\partial x)$, v, or $\partial v/\partial x=0$, or if $l_2=\infty$, $v=0$ } where $(l_2>l_1)$

Condition at $y=m_1$, $(h_3 v-\partial v/\partial y)$, v, or $\partial v/\partial y=0$, or if $m_1=-\infty$, $v=0$
Condition at $y=m_2$, $(h_4 v+\partial v/\partial y)$, v, or $\partial v/\partial y=0$, or if $m_2=\infty$, $v=0$ } where $(m_2>m_1)$

Condition at $z=n_1$, $(h_5 v-\partial v/\partial z)$, v, or $\partial v/\partial z=0$, or if $n_1=-\infty$, $v=0$
Condition at $z=n_2$, $(h_6 v+\partial v/\partial z)$, v, or $\partial v/\partial z=0$, or if $n_2=\infty$, $v=0$ } where $(n_2>n_1)$

Limit v = Limit v; Limit v = Limit v; Limit v = Limit v
$x=x_1+0$ $x=x_1-0$ $y=y_1+0$ $y=y_1-0$ $z=z_1+0$ $z=z_1-0$

$\rho_1=0$ when $x\neq x_1$, $y\neq y_1$, $z\neq z_1$, and $t\neq t_1$, and $\int_{t_1-0}^{t_1+0}\int_{z_1-0}^{z_1+0}\int_{y_1-0}^{y_1+0}\int_{x_1-0}^{x_1+0}\rho_1 dxdydzdt=Q_1$

These equations have the following solutions:

$v=g_0Q_1X_{1p}$ (cond. at $x=l_1$, cond. at $x=l_2$) Y_{1q} (cond. at $y=m_1$, cond. at $y=m_2$) Z_{1u} (cond. at $z=n_1$, cond. at $z=n_2$)T where

$$T=\epsilon^{-(\alpha p^2+\beta q^2+\gamma u^2)(t-t_1)/g_1}H(t,t_1)/g_1 \qquad \text{Case I}$$

$$T=\epsilon^{-g_1(t-t_1)/2g_2}\sin\,[(t-t_1)\{g_2(\alpha_p{}^2+\beta_q{}^2+\gamma_u{}^2)-g_1{}^2/4\}^{1/2}/g_2]H(t,t_1)/[g_2(\alpha_p{}^2+\beta_q{}^2+\gamma_u{}^2)-g_1{}^2/4]^{1/2} \qquad \text{Case II}$$

$$T=\sin\,[(t-t_1)(\alpha_p{}^2+\beta_q{}^2+\gamma_u{}^2)^{1/2}/g_2{}^{1/2}]H(t,t_1)/[g_2(\alpha_p{}^2+\beta_q{}^2+\gamma_u{}^2)]^{1/2} \qquad \text{Case III}$$

VII. Fourier Series

Expansions of $f(x)$ in $\sin\alpha_p x$ and $\cos\alpha_p x$ with given linear relations at each end of the interval

$$f(x)=\int_{l_1}^{l_2} f(x_1)X_{1p}\left(h_1v-\frac{\partial v}{\partial x},\ h_2v+\frac{\partial v}{\partial x}\right)dx_1$$

$$f(x)=\int_{l_1}^{l_2} f(x_1)X_{1p}\left(h_1v-\frac{\partial v}{\partial x},\ v\right)dx_1$$

$$f(x)=\int_{l_1}^{l_2} f(x_1)X_{1p}\left(h_1v-\frac{\partial v}{\partial x},\ \frac{\partial v}{\partial x}\right)dx_1$$

$$f(x)=\int_{l_1}^{l_2} f(x_1)X_{1p}\left(v,\ h_2v+\frac{\partial v}{\partial x}\right)dx_1$$

$$f(x)=\int_{l_1}^{l_2} f(x_1)X_{1p}(v,\ v)dx_1$$

$$f(x)=\int_{l_1}^{l_2} f(x_1)X_{1p}\left(v,\ \frac{\partial v}{\partial x}\right)dx_1$$

$$f(x)=\int_{l_1}^{l_2} f(x_1)X_{1p}\left(\frac{\partial v}{\partial x},\ h_2v+\frac{\partial v}{\partial x}\right)dx_1$$

$$f(x)=\int_{l_1}^{l_2} (fx_1)X_{1p}\left(\frac{\partial v}{\partial x},\ v\right)dx_1$$

$$f(x)=\int_{l_1}^{l_2} f(x_1)X_{1p}\left(\frac{\partial v}{\partial x},\ \frac{\partial v}{\partial x}\right)dx_1$$

$$f(x)=\int_{l_1}^{\infty} f(x_1)X_{1p}\left(h_1v-\frac{\partial v}{\partial x},\ \infty\right)dx_1$$

$$f(x)=\int_{l_1}^{\infty} f(x_1)X_{1p}(v,\ \infty)dx_1$$

$$f(x)=\int_{l_1}^{\infty} f(x_1)X_{1p}\left(\frac{\partial v}{\partial x},\ \infty\right)dx_1$$

$$f(x)=\int_{-\infty}^{\infty} f(x_1)X_{1p}(-\infty,\ \infty)dx_1$$

The terms in the bracket after X_{1p} indicate the conditions satisfied by the Fourier series at the ends of the interval. For instance, $X_{1p}(v,\ dv/dx)$ has $v=0$ at $x=l_1$ and $dv/dx=0$ at $x=l_2(l_1<l_2)$. On writing out

$$\int_{l_1}^{l_2} f(x_1)X_{1p}\left(v,\ \frac{dv}{dx}\right)dx_1$$

it will be found to satisfy conditions similar to those satisfied by v.

When v and dv/dx have the same values respectively at the ends of the interval $(-\pi<x<\pi)$ the corresponding series is

$$f(x)=\int_{-\pi}^{\pi} f(x_1)X_{2p}\left([v]_{x=-\pi}=[v]_{x=\pi},\ \left[\frac{dv}{dx}\right]_{x=-\pi}=\left[\frac{dv}{dx}\right]_{x=\pi}\right)dx_1$$

VIII. Impulse Functions

Impulse functions in terms of $\sin\alpha_p x$ and $\cos\alpha_p x$ with given linear relations at each end of the interval*

$$dH(x,\ x_1)/dx=X_{1p}\left(h_1v-\frac{\partial v}{\partial x},\ h_2v+\frac{\partial v}{\partial x}\right)$$

$$dH(x,\ x_1)/dx=X_{1p}\left(h_1v-\frac{\partial v}{\partial x},\ v\right)$$

$$dH(x,\ x_1)/dx=X_{1p}\left(h_1v-\frac{\partial v}{\partial x},\ \frac{\partial v}{\partial x}\right)$$

$$dH(x,\ x_1)/dx=X_{1p}\left(v,\ h_2v+\frac{\partial v}{\partial x}\right)$$

$$dH(x,\ x_1)/dx=X_{1p}(v,\ v)$$

$$dH(x,\ x_1)/dx=X_{1p}\left(v,\ \frac{\partial v}{\partial x}\right)$$

$$dH(x,\ x_1)/dx=X_{1p}\left(\frac{\partial v}{\partial x},\ h_2v+\frac{\partial v}{\partial x}\right)$$

* Later studies indicate the desirability of distinguishing between these values of $dH(x,\ x_1)/Hx$. A suggested notation for the first one is $H'\left(x,\ x_1;\ l_1,\ l_2;\ h_1v-\frac{\partial v}{\partial x},\ h_2v+\frac{\partial v}{\partial x}\right)$ this notation indicating that it is the impulse function with respect to x with the impulse at x_1, that it extends over the interval l_1 to l_2 $(l_2>l_1)$ and that at $x=l_1$ it satisfies the condition $h_1H'-\frac{\partial H'}{\partial x}=0$ at $x=l_1$ and $h_2H'+\frac{\partial H'}{\partial x}=0$ at $x=l_2$. The modification of this notation for the other equations is obvious.

$$dH(x, x_1)/dx = X_{1p}\left(\frac{\partial v}{\partial x}, \frac{\partial v}{\partial x}\right)$$

$$dH(x, x_1)/dx = X_{1p}\left(h_1 v - \frac{\partial v}{\partial x}, \infty\right)$$

$$dH(x, x_1)/dx = X_{1p}(v, \infty)$$

$$dH(x, x_1)/dx = X_{1p}\left(\frac{\partial v}{\partial x}, \infty\right)$$

$$dH(x, x_1)/dx = X_{1p}(-\infty, \infty)$$

The terms in the bracket after X_{1p} indicate the conditions satisfied by it (the impulse function) at the ends of the interval.

For instance, $X_{1p}(v, dv/dx)$ has $v=0$ at $x=l_1$ and $dv/dx=0$ at $x=l_2$ $(l_1<x<l_2)$. On writing out $X_{1p}(v, dv/dx)$ it will be found to satisfy conditions with respect to x similar to those satisfied by v.

When v and dv/dx have the same values respectively at the ends of the interval $(-\pi<x<\pi)$ the corresponding impulse function is

$$dH(x, x_1)/dx = X_{2p}\left([v]_{x=-\pi} = [v]_{x=-\pi}, \left[\frac{dv}{dx}\right]_{x=-\pi} = \left[\frac{dv}{dx}\right]_{x=\pi}\right)$$

These expressions for the impulse function have the property

$$\int_a^b f(x_1)\frac{dH(x, x_1)}{dx}dx_1 = 0$$

when $l_1<a<b<x_1<l_2$

$$\int_a^b f(x_1)\frac{dH(x, x_1)}{dx}dx_1 = f(x)$$

when $l_1<a<x_1<b<l_2$

$$\int_a^b f(x_1)\frac{dH(x, x_1)}{dx}dx_1 = 0$$

when $l_1<x_1<a<b<l_2$

So that by use of the impulse function, we get a more general expression than Fourier series which latter corresponds to the case $a=l_1$ and $b=l_2$.

IX. Equations for Finding the Values of X_{1p}, X_{1p},* and So Forth

Notes on the use of these tables

Symbols: In the solution of the differential equation terms such as the following will be found:

X_{1p} (condition at $x=l_1$, condition at $x=l_2$)

This means that for any given problem $x=l_2(l_2>l_1)$ and then find the corresponding value from the table. For instance, if the condition at $x=l_1$ is $h_1v-dv/dx=0$ and the condition at l_2 is $v=0$, then X_{1p} (condition at $x=l_1$, condition at $x=l_2$) is simply $X_{1p}(h_1v-dv/dx, v)$. The value of this quantity is found directly in the appropriate part of the table.

In certain cases there will be found in the parentheses just a number which does not include v. This simply means that at the boundary corresponding to this number, the boundary conditions are determined by the equation itself and thus are not at our disposal. An example of this is the symbol $X_{1p}(v, \infty)$. This corresponds to the condition $v=0$ when $x=l_1$, and the boundary corresponding to l_2 is at ∞.

Another type of boundary condition frequently met is where the value of v and dv/dx are the same for $x=+\pi$ and $x=-\pi$.

This symbol is denoted by

$$X_{2p}\left([v]_{x=-\pi} = [v]_{x=\pi} \times \left[\frac{dv}{dx}\right]_{x=-\pi} = \left[\frac{dv}{dx}\right]_{x=\pi}\right)$$

Summation Signs: In the tables where infinite series of the forms $\sum_p A_p$ and so forth occur, if there is a root corresponding to $p=0$, we always take

$$A_0 = 1/2 \operatorname*{Limit}_{p\to 0} A_p$$

some authors denote this using $\sum_p'$ but the addition of the $'$ hardly seems necessary.

It will also be noted in the tables that dots are written in expressions such as $\sum_p \ldots A_p$. This simply means that if we have two or more terms after the summation sign in the solution of this type, such as $\sum_p \ldots A_p$ and $\sum_p \ldots B_q$, we write the resultant term $\sum_p \sum_q A_q B_q$; it is not necessary to write it in the form $\sum_p A_p \sum_q B_q$.

Problems Dealing With Heat Flow: In problems dealing with the flow of heat due to an instantaneous point source, the equation is written in the form

$$\nabla^2 v = \frac{1}{K}\frac{\partial v}{\partial t} - \frac{\rho_1}{C}\frac{dH(t, 0)}{dt} = g_1\frac{\partial v}{\partial t} + g_0\rho_1$$

This equation differs from the one usually given in textbooks.

$$\nabla^2 v = \frac{1}{K}\frac{\partial v}{\partial t}$$

source is introduced at a given point at the time $t=0$. A derivation and explanation of this modified heat equation will be found in a paper by J. J. Smith.[5]

Use of the Unit Function in These Tables: The terms $1-H(\xi, \xi_1)$ and $H(\xi, \xi_1)$ appearing in the expressions marked with asterisks, that is, X^*, Y^*, and so forth, are to be understood as follows:

$H(\xi, \xi_1)=0$ when $\xi<\xi_1$

$H(\xi, \xi_1)=1$ when $\xi>\xi_1$

Thus the following formula, typical of many given in the tables

$$A^* = A_1[1-H(\xi, \xi_1)] + A_2H(\xi, \xi_1)$$

is equivalent to the equations

$A^*=A_1$ when $\xi<\xi_1$

$A^*=A_2$ when $\xi>\xi_1$

In mathematical textbooks it is usually found that when this type of equation arises, the quantities A_1 and A_2 are related in such a manner that A_2 is obtained from A_1 by interchanging ξ and ξ_1. The result is written in such cases in these textbooks in the following manner.

$A^*=A_1$ where $\xi>\xi_1$,

when $\xi<\xi_1$ interchange ξ and ξ_1.

In the following tables the equation between A^* and A_1 and A_2 by means of $H(\xi, \xi_1)$ is used exclusively (although it requires more space for writing than the usual mathematical method) since this is the form in which the result is obtained using the operational calculus method of derivation.

Problems in Which v and dv/dx Are the Same at Each End of the Interval: The present tables have been drawn up conforming to the pattern that the condition at the end of the interval is of the type

$$hv - \frac{dv}{dx} = 0$$

In many problems the condition may be of the form

$$[v]_{x=-\pi} = [v]_{x=\pi}$$

and

$$\left[\frac{dv}{dx}\right]_{x=-\pi} = \left[\frac{dv}{dx}\right]_{x=\pi}$$

When these conditions are given for any coordinate then the value of X_{1p}, Y_{1q}, or Z_{1u} for that particular co-ordinate should be replaced by the corresponding value for that co-ordinate of X_{2p}, Y_{2q}, and Z_{2u}.

$$X_{1p}\left(-\frac{\partial v}{\partial x}+h_1 v,\ \frac{\partial v}{\partial x}+h_2 v\right)=\sum_{\alpha p}\ldots\ldots\frac{2(\alpha_p^2+h_2^2)[h_1\sin\alpha_p(x-l_1)+\alpha_p\cos\alpha_p(x-l_1)][h_1\sin\alpha_p(x_1-l_1)+\alpha_p\cos\alpha_p(x_1-l_1)]}{(\alpha_p^2+h_1h_2)(h_1+h_2)+(l_2-l_1)(\alpha_p^2+h_1^2)(\alpha_p^2+h_2^2)}$$

$\alpha_1, \alpha_2, \ldots\ldots$ are the roots of $\tan\alpha(l_2-l_1)=\alpha(h_1+h_2)/(\alpha^2-h_1h_2)$

$$X_{1p}\left(-\frac{\partial v}{\partial x}+h_1 v,\ v\right)=\sum_{\alpha p}\ldots\ldots\frac{2[h_1\sin\alpha_p(x-l_1)+\alpha_p\cos\alpha_p(x-l_1)][h_1\sin\alpha_p(x_1-l_1)+\alpha_p\cos\alpha_p(x_1-l_1)]}{h_1+(l_2-l_1)(\alpha_p^2+h_1^2)}$$

$\alpha_1, \alpha_2, \ldots\ldots$ are the roots of $\tan\alpha(l_2-l_1)=-\alpha/h_1$

$$X_{1p}\left(-\frac{\partial v}{\partial x}+h_1 v,\ \frac{\partial v}{\partial v}\right)=\sum_{\alpha p}\ldots\ldots\frac{2[h_1\sin\alpha_p(x-l_1)+\alpha_p\cos\alpha_p(x-l_1)][h_1\sin\alpha_p(x_1-l_1)+\alpha_p\cos\alpha_p(x_1-l_1)]}{h_1+(l_2-l_1)(\alpha_p^2+h_1^2)}$$

$\alpha_1, \alpha_2, \ldots\ldots$ are the roots of $\tan\alpha(l_2-l_1)=h_1/\alpha$

$$X_{1p}\left(v,\ \frac{\partial v}{\partial x}+h_2 v\right)=\sum_{\alpha p}\ldots\ldots\frac{2(\alpha_p^2+h_2^2)\sin\alpha_p(x-l_1)\sin\alpha_p(x_1-l_1)}{h_2+(l_2-l_1)(\alpha_p^2+h_2^2)}$$

$\alpha_1, \alpha_2, \ldots\ldots$ are the roots of $\tan\alpha(l_2-l_1)=-\alpha/h_2$

$$X_{1p}(v,\ v)=\sum_{\alpha p}\ldots\ldots\frac{2\sin\alpha_p(x-l_1)\sin\alpha_p(x_1-l_1)}{l_2-l_1}$$

$\alpha_1, \alpha_2, \ldots\ldots$ are the roots of $\tan\alpha(l_2-l_1)=0$. Hence

$\alpha_p=p\pi(l_2-l_1)$ where $p=0, 1, 2, \ldots\ldots$

$$X_{1p}\left(v,\ \frac{\partial v}{\partial x}\right)=\sum_{\alpha p}\ldots\ldots\frac{2\sin\alpha_p(x-l_1)\sin\alpha_p(x_1-l_1)}{l_2-l_1}$$

$\alpha_1, \alpha_2, \ldots\ldots$ are the roots of $\tan\alpha(l_2-l_1)=\infty$. Hence

$\alpha_p=(2p+1)\pi/2(l_2-l_1)$ where $p=0, 1, 2, \ldots\ldots$

$$X_{1p}\left(\frac{\partial v}{\partial x},\ \frac{\partial v}{\partial x}+h_2 v\right)=\sum_{\alpha p}\ldots\ldots\frac{2(\alpha_p^2+h_2^2)\cos\alpha_p(x-l_1)\cos\alpha_p(x_1-l_1)}{h_2+(l_2-l_1)(\alpha_p^2+h_2^2)}$$

$\alpha_1, \alpha_2, \ldots\ldots$ are the roots of $\tan\alpha(l_2-l_1)=h_2/\alpha$

$$X_{1p}\left(\frac{\partial v}{\partial x},\ v\right)=\sum_{\alpha p}\ldots\ldots\frac{2\cos\alpha_p(x-l_1)\cos\alpha_p(x_1-l_1)}{l_2-l_1}$$

$\alpha_1, \alpha_2, \ldots\ldots$ are the roots of $\tan\alpha(l_2-l_1)=\infty$ Hence

$\alpha_p=(2p+1)\pi/2(l_2-l_1)$ where $p=0, 1, 2, \ldots\ldots$

$$X_{1p}\left(\frac{\partial v}{\partial x},\ \frac{\partial v}{\partial x}\right)=\sum_{\alpha p}\ldots\ldots\frac{2\cos\alpha_p(x-l_1)\cos\alpha_p(x_1-l_1)}{l_2-l_1}$$

$\alpha_1, \alpha_2, \ldots\ldots$ are the roots of $\tan\alpha(l_2-l_1)=0$. Hence

$\alpha_p=p\pi/(l_2-l_1)$ where $p=0, 1, 2, \ldots\ldots$

$$X_{1p}\left(-\frac{\partial v}{\partial x}+h_1 v,\ \infty\right)=\frac{2}{\pi}\int_0^\infty d\alpha_p\ldots\ldots\frac{[h_1\sin\alpha_p(x-l_1)+\alpha_p\cos\alpha_p(x-l_1)][h_1\sin\alpha_p(x_1-l_1)+\alpha_p\cos\alpha_p(x_1-l_1)]}{\alpha_p^2+h_1^2}$$

$$X_{1p}(v,\ \infty)=\frac{2}{\pi}\int_0^\infty d\alpha_p\ldots\ldots\sin\alpha_p(x-l_1)\sin\alpha_p(x_1-l_1)$$

$$X_{1p}\left(\frac{\partial v}{\partial x},\ \infty\right)=\frac{2}{\pi}\int_0^\infty d\alpha_p\ldots\ldots\cos\alpha_p(x-l_1)\cos\alpha_p(x_1-l_1)$$

$$X_{1p}(-\infty,\ \infty)=\frac{1}{\pi}\int_0^\infty d\alpha_p\ldots\ldots\cos\alpha_p(x-x_1)$$

$$X_{2p}\left([v]_{x=-\pi}=[v]_{x=\pi},\left[\frac{dv}{dx}\right]_{x=-\pi}=\left[\frac{dv}{dx}\right]_{x=\pi}\right)=\frac{1}{\pi}\sum_{\alpha p}\ldots\cos\alpha_p(x-x_1)$$

where $\alpha_p = 0, 1, 2, \ldots$

$$X_{1p}\left(-\frac{\partial v}{\partial x}+h_1 v,\ \frac{\partial v}{\partial x}+h_2 v\right)=\frac{[h_1 \sinh \alpha_p(x-l_1)+\alpha_p \cosh \alpha_p(x-l_1)][h_2 \sinh \alpha_p(l_2-x_1)+\alpha_p \cosh \alpha_p(l_2-x_1)]}{\alpha_p(\alpha_p^2+h_1h_2)\sinh \alpha_p(l_2-l_1)+\alpha_p^2(h_1+h_2)\cosh \alpha_p(l_2-l_1)}[1-H(x, x_1)]+$$

$$\frac{[h_2 \sinh \alpha_p(l_2-x)+\alpha_p \cosh \alpha_p(l_2-x)][h_1 \sinh \alpha_p(x_1-l_1)+\alpha_p \cosh \alpha_p(x_1-l_1)]}{\alpha_p(\alpha_p^2+h_1h_2)\sinh \alpha_p(l_2-l_1)+\alpha_p^2(h_1+h_2)\cosh \alpha_p(l_2-l_1)}H(x, x_1)$$

$$X_{1p}\left(-\frac{\partial v}{\partial x}+h_1 v,\ v\right)=\frac{\sinh \alpha_p(l_2-x_1)[h_1 \sinh \alpha_p(x-l_1)+\alpha_p \cosh \alpha_p(x-l_1)]}{\alpha_p h_1 \sinh \alpha_p(l_2-l_1)+\alpha_p \cosh \alpha_p(l_2-l_1)}[1-H(x, x_1)]+$$

$$\frac{\sinh \alpha_p(l_2-x)[h_1 \sinh \alpha_p(x_1-l_1)+\alpha_p \cosh \alpha_p(x_1-l_1)]}{\alpha_p h_1 \sinh \alpha_p(l_2-l_1)+\alpha_p \cosh \alpha_p(l_2-l_1)}H(x,x_1)$$

$$X_{1p}\left(-\frac{\partial v}{\partial x}+h_1 v,\ \frac{\partial v}{\partial x}\right)=\frac{\cosh\ \alpha_p(l_2-l_1)[h_1 \sinh \alpha_p(x-l_1)+\alpha_p \cosh \alpha_p(x-l_1)]}{\alpha_p^2 \sinh \alpha_p(l_2-l_1)+\alpha_p h_1 \cosh \alpha_p(l_2-l_1)}[1-H(x, x_1)]+$$

$$\frac{\cosh \alpha_p(l_2-x)[h_1 \sinh \alpha_p(x_1-l_1)+\alpha_p \cosh \alpha_p(x_1-l_1)]}{\alpha_p^2 \sinh \alpha_p(l_2-l_1)+\alpha_p h_1 \cosh \alpha_p(l_2-l_1)}H(x, x_1)$$

$$X_{1p}\left(v,\ \frac{\partial v}{\partial y}+h_2 v\right)=\frac{\sinh \alpha_p(x-l_1)[h_2 \sinh \alpha_p(l_2-x_1)+\alpha_p \cosh \alpha_p(l_2-x_1)]}{\alpha_p h_2 \sinh \alpha_p(l_2-l_1)+\alpha_p^2 \cosh \alpha_p(l_2-l_1)}[1-H(x, x_1)]+$$

$$\frac{\sinh \alpha_p(x_1-l_1)[h_2 \sinh \alpha_p(l_2-x)+\alpha_p \cosh\ (l_2-x)]}{\alpha_p h_2 \sinh \alpha_p(l_2-l_1)+\alpha_p^2 \cosh \alpha_p(l_2-l_1)}H(x, x_1)$$

$$X_{1p}(v, v)=\frac{\sinh \alpha_p(x-l_1)\sinh \alpha_p(l_2-x_1)}{\alpha_p \sinh \alpha_p(l_2-l_1)}[1-H(x,\ x_1)]+\frac{\sinh \alpha_p(x_1-l_1)\sinh \alpha_p(l_2-x)}{\alpha_p \sinh \alpha_p(l_2-l_1)}H(x, x_1)$$

$$X_{1p}\left(v,\ \frac{\partial v}{\partial x}\right)=\frac{\sinh \alpha_p(x-l_1)\cosh \alpha_p(l_2-x_1)}{\alpha_p \cosh \alpha_p(l_2-l_1)}[1-H(x,\ x_1)]+\frac{\sinh \alpha_p(x_1-l_1)\cosh \alpha_p(l_2-x)}{\alpha_p \cosh \alpha_p(l_2-l_1)}H(x, x_1)$$

$$X_{1p}\left(\frac{\partial v}{\partial x},\ \frac{\partial v}{\partial x}+h_2 v\right)=\frac{\cosh \alpha_p(x-l_1)[h_2 \sinh \alpha_p(l_2-x_1)+\alpha_p \cosh \alpha_p(l_2-x_1)]}{\alpha_p \sinh \alpha_p(l_2-l_1)+\alpha_p h_2 \cosh\ (l_2-l_1)}[1-H(x, x_1)]+$$

$$\frac{\cosh \alpha_p(x_1-l_1)[h_2 \sinh \alpha_p(l_2-x)+\alpha_p \cosh \alpha_p(l_2-x)]}{\alpha_p^2 \sinh \alpha_p(l_2-l_1)+\alpha_p h_2 \cosh \alpha_p(l_2-l_1)}H(x, x_1)$$

$$X_{1p}\left(\frac{\partial v}{\partial x},\ v\right)=\frac{\cosh \alpha_p(x-l_1)\sinh \alpha_p(l_2-x_1)}{\alpha_p \cosh \alpha_p(l_2-l_1)}[1-H(x,\ x_1)]+\frac{\cosh \alpha_p(x_1-l_1)\sinh \alpha_p(l_2-x)}{\alpha_p \cosh \alpha_p(l_2-l_1)}H(x, x_1)$$

$$X_{1p}\left(\frac{\partial v}{\partial x},\ \frac{\partial v}{\partial x}\right)=\frac{\cosh \alpha_p(x-l_1)\cosh \alpha_p(l_2-x_1)}{\alpha_p \sinh \alpha_p(l_2-l_1)}[1-H(x,\ x_1)]+\frac{\cosh \alpha_p(x_1-l_1)\cosh \alpha_p(l_2-x)}{\alpha_p \sinh \alpha_p(l_2-l_1)}H(x, x_1)$$

$$X_{1p}\left(-\frac{\partial v}{\partial x}+h_1 v,\ \infty\right)=\frac{\epsilon^{-\alpha_p x_1}[h \sinh \alpha_p(x-l_1)+\alpha_p \cosh \alpha_p(x-l_1)]}{\alpha_p(h_1+\alpha_p)\epsilon^{-\alpha_p l_1}}[1-H(x, x_1)]+\frac{\epsilon^{-\alpha_p x}[h_1 \sinh \alpha_p(x_1-l_1)+\alpha_p \cosh \alpha_p(x_1-l_1)]}{\alpha_p(h_1+\alpha_p)\epsilon^{-\alpha_p l_1}}H(x, x_1)$$

$$X_{1p}(v,\ \infty)=\frac{\epsilon^{-\alpha_p x_1}\sinh \alpha_p(x-l_1)}{\alpha_p \epsilon^{-\alpha_p l_1}}[1-H(x, x_1)]+\frac{\epsilon^{-\alpha_p x}\sinh \alpha_p(x_1-l_1)}{\alpha_p \epsilon^{-\alpha_p l_1}}H(x, x_1)$$

$$X_{1p}\left(\frac{\partial v}{\partial x},\ \infty\right)=\frac{\epsilon^{-\alpha_p x_1}\cosh \alpha_p(x-l_1)}{\alpha_p \epsilon^{-\alpha_p l_1}}[1-H(x, x_1)]+\frac{\epsilon^{-\alpha_p x}\cosh \alpha_p(x_1-l_1)}{\alpha_p \epsilon^{-\alpha_p l_1}}H(x, x_1)$$

$$X_{1p}(-\infty,\ \infty)=\frac{\epsilon^{-\alpha_p(x_1-x)}}{2\alpha_p}[1-H(x, x_1)]+\frac{\epsilon^{-\alpha_p(x-x_1)}}{2\alpha_p}H(x, x_1)$$

$$X_{2p}\left([v]_{x=-\pi}=[v]_{x=\pi},\left[\frac{dv}{dx}\right]_{x=\pi}=\left[\frac{dv}{dx}\right]_{x=\pi}\right)=\frac{[1-H(x, x_1)]\cosh \alpha_p(\pi+x-x_1)}{2\alpha_p \sinh \alpha_p\pi}+\frac{H(x, x_1)\cosh \alpha_p(\pi-x+x_1)}{2\alpha_p \sinh \alpha_p\pi}$$

Expressions for Y_{1q}, Y^*_{1q}, Z_{1u}, Z^*_{1u}: For the normal use of these tables, it is desirable to have the expression for these quantities written out in full. However, in order to conserve space, we are giving below substitutions by which the values of these quantities can be derived from the values already given for X_{1p}, X^*_{1p}. Y_{1q}, or Z_{1u} are derived from X_{1p} by substituting the values given in Table I under the heading for one of these terms for the value given under the column headed by X_{1p}.

Table I

X_{1p} or X_{1p}^*	Y_{1q} or Y_{1q}^*	Z_{1u} or Z_{1u}^*
x	y	z
x_1	y_1	z_1
l_1	m_1	n_1
l_2	m_2	n_2
h_1	k_1	h_3
h_2	k_1	h_4
α_p	β_q	γ_u

Similar substitutions can be used to derive Y_{1q} and Z_{1u} from X_{2p}.

Appendix I. General Theorems on the Use of Green's Function

Steady State Problems in Three Dimensions

In electrostatic and other steady state problems, the Green's Function is defined for the space considered as the potential at any point (x, y, z) in the space due to a positive charge Q placed at the point (x_1, y_1, z_1) the boundary surfaces being (a) insulated, (b) held at zero potential, (c) or conditions equivalent to radiation holding at these sur-

faces. When the Green's Function $G(x, y, z; x_1, y_1, z_1)$ is known, the potential resulting from a potential distribution $f(x, y, z)$ which is given over some of the faces of the space, the behavior on the other faces being given by boundary conditions of the usual type, and no other charges being present inside the space, can be obtained from the formula[6]

$$V=\frac{1}{4\pi Q}\int_S\int f(x, y, z)\times \frac{dG(x, y, z; x_1, y_1, z_1)}{dn_1}\,dS$$

the surface integral being taken over the faces on which the potential is given, and $G(x, y, z; x_1, y_1, z_1)$ being the Green's function which corresponds with the condition $v=0$ over these.

Instantaneous Point Source

In problems in the flow of heat, use is made of the concept of a quantity of heat Q suddenly generated at a point. This is called an instantaneous point source.[6,7]

In transient problems the Green's function is defined for a space considered as the condition at the time t at any point (x, y, z) in the space due to an instantaneous point source of strength Q placed at the time $t=0$ at the point (x_1, y_1, z_1) the boundary surfaces being (a) insulated, (b) held at zero, or (c) conditions equivalent to radiation taking place at these surfaces.

When the Green's function $G(x, y, z; x_1, y_1, z_1; t)$ is known, the condition resulting from an initial volume distribution $f(x, y, z)$ and a given surface distribution $\phi(x, y, z)$ which is given over some of the surfaces of the space, the behavior on the other surfaces being given by boundary conditions of the usual type can be obtained from the formula[8]

$$V=\frac{1}{Q}\int\int_v\int G(x, y, z; x_1, y_1, z_1; t)\, f(x_1, y_1, z_1)dx_1\,dy_1\,dz_1+\int_0^t\int_s\int \frac{dG(x, y, z; x_1, y_1, z_1; t-\tau)}{dn_1}\,\phi(x_1, y_1, z_1)\times ds\,d\tau$$

the surface integral being taken over the faces on which the potential is given and the Green's function being that which corresponds with the condition $v=0$ over these faces.

The bare outlines of these theorems are given in the above. For further detailed instructions as to their application, the references given should be consulted.

It may also be well to point out that similar formula are needed for application to the wave equation.

Appendix II

The following simple examples have been chosen to illustrate the use of these tables in solving problems in three different types of problems. It will be noted that in all cases the appropriate Green's function is first obtained from the tables. Then by use of the theorems in Appendix I, or otherwise, the solutions corresponding to given boundary conditions or initial conditions are found from these Green's functions.

Example 1. Required the Green's function corresponding to a continuous line charge at (x_1, y_1) in the infinite positive half plane bounded by the x axis which is maintained at zero potential. Here the terminal conditions are given by

$l_1=-\infty$ and $v=0$ when $y=0$

$l_2=+\infty \quad m_2=\infty$

Use Green's function II and obtain

$$v=g_0QX_{1p}(-\infty, \infty)Y_{1q}{}^*(v, \infty)$$

$$=\frac{g_0Q}{\pi}\int_0^\infty d\alpha\cos\alpha(x-x_1)\times \frac{\{[1-H(y, y_1)]\epsilon^{-\alpha y_1}\sinh\alpha y+H(y, y_1)\epsilon^{-\alpha y}\sinh\alpha y\}}{\alpha}$$

Example 2. Assume electricity is flowing in a thin plane sheet of infinite extent bounded by the x axis and that the value of the potential function is given for every point along the x axis. Required the potential at any point of the sheet.

Using the result in example 1 and the 2-dimensional analogue corresponding to the first theorem in Appendix I, we obtain

$$v=\frac{g_0Q}{4\pi Q}\frac{1}{\pi}\int_0^\infty d\alpha\cos\alpha(x-x_1)\times\int_{-\infty}^{\infty} f(x_1)\epsilon^{-\alpha y}dx_1$$

and on putting $g_0=4\pi$ and making appropriate changes in notations, this is identical with the result given by Byerly.[9]

Example 3. Required the Green's function due to an instantaneous heat source at $t=0$, at the point x_1 in the 1-dimensional space with boundaries at $x=0$ and at $x=a$, which are held at zero temperature. Use Green's function IV and obtain

$$v=g_0QX_{1p}(v, v)\epsilon^{-p^2\pi^2t/a^2g_1}H(t, 0)/g_1$$

$$v=\frac{2g_0QH(t, 0)}{ag_1}\sum_p \sin\frac{p\pi x}{a}\sin\frac{p\pi x_1}{a}\times\epsilon^{-p^2\pi^2t/a^2g_1}$$

and on putting $g_1=1/\kappa$ and appropriate changes in notation, this is identical with the result given by Carslaw.[10]

Example 4. The same space as in example 3 with boundaries at $x=0$ and $x=a$. However, now the initial temperature is given by $f(x)$ and the surfaces $x=0$ and $x=a$ are kept at $\phi_1(t)$ and $\phi_2(t)$. Required the temperature at the point x at a subsequent time t.

This example is an illustration of the application of the second theorem referred to in Appendix I using the result obtained in example 3. The result will be found worked out in Carslaw[10] and as it does not involve anything more complicated than the application of integration to the Green's function, it will not be worked out further here.

Since the differential equations for temperature in heat problems are identical with those for potential in a cable with R and C, we may in turn use the result in this example in Carslaw by putting $f(x)=0$, $\phi_1(t)=V$ and $\phi_2(t)=0$ to obtain the voltage along a cable to which a voltage V is applied at $t=0$, the other end $x=a$ being maintained at $v=0$ and the result checked with that given by Heaviside.[11]

Example 5. This example illustrates the application to a moving point source. The Green's function due to an instantaneous point source of heat at x_1 at the time t_1 in the space whose boundaries all lie at ∞ is given by Green's function VI as

$$v=\frac{g_0Q_1}{\pi g_1}YZ\int_0^\infty \cos\alpha(x-x_1)\times H(t, 0)d\alpha\,\epsilon^{-(\alpha^2+\beta^2+\gamma^2)(t-t_1)/g}$$

where

$$YZ=\frac{1}{\pi^2}\int_0^\infty\int_0^\infty \cos\beta(y-y_1)\times\cos\gamma(z-z_1)d\beta d\gamma$$

Now consider a case in which a continuous point source that was at the point x_0 at $t=t_0$ and is moving with uniform velocity u so that $x_1=x_0+u(t_1-t_0)$. Substituting this in the expression for the Green's function, we find for the temperature v, due to a continuous point source moving with uniform velocity

$$v_1=\frac{g_cQ_1}{\pi g_1}YZ\int_{-\infty}^t\int_0^\infty dx dt_1\times\cos(x-x_0-u[t_1-t_0])\epsilon^{-(\alpha^2+\beta^2+\gamma^2)(t-t_1)/g_1}$$

This example would probably be of greater interest if applied to moving electrical charges but since in application to these, more complicated problems arise than can be considered in this brief discussion, they will be dealt with more fully in a subsequent paper.

Examples of Fourier Series and Impulse Functions

Example 1. Required a Fourier series S for $f(x)$ or an impulse function I in terms of sine and cosine functions over the interval $l_1<x<l_2$ with the following boundary conditions

$S=0$ at $x=l_1$ and at $x=l_2$

or $I=0$ at $x=l_1$ and at $x=l_2$

We have from the tables

$$S=f(x)=\int_{l_1} f(x_1)X_{1p}(v, v)dx_1$$

or $I=X_{1p}(v, v)$

where

$$X_{1p}(v, v)=\frac{2}{l_2-l_1}\sum_p \sin\frac{p\pi(x-l_1)}{l_2-l_1}\sin\frac{p\pi(x_1-l_1)}{l_2-l_1}$$

Example 2. Required a Fourier integral S for $f(x)$ or an impulse function I in terms of sine and cosine functions over the interval $l_1<x<\infty$ with the boundary conditions

$dS/dx=0$ at $x=l_1$

or $dI/dx=0$ at $x=l_1$

Note that in this case the boundary condition at $x=\infty$ is not at our disposal. We have from the tables

$$S=f(x)=\int^{\infty} f(x_1)X_{1p}\left(\frac{dv}{dx},\ \infty\right)dx_1$$

or $$I=X_{1p}\left(\frac{dv}{dx},\ \infty\right)$$

where

$$X_{1p}\left(\frac{dv}{dx},\ \infty\right)=\frac{2}{\pi}\int_0^{\infty}\times$$
$$\cos\ \alpha(x-l_1)\ \cos\ \alpha(x_1-l_1)d\alpha$$

References

1. The Conduction of Heat (book), **H. S. Carslaw.** MacMillan and Company, London, England, second edition, 1921, page 169.

2. Electricity and Magnetism (book), **James C. Maxwell.** Oxford Clarendon Press, London, England, volume 1, third edition, paragraph 97b, page 133.

3. How to Say "No" in Mathematics, **J. J. Smith.** *Journal*, Franklin Institute, (Philadelphia, Pa.), volume 240, August 1945, page 113.

4. The Extension of the Heaviside Expansion Theorem to the Equations of Engineering and Physics in Curvilinear Orthogonal Coordinates, **J. J. Smith.** *Journal*, Franklin Institute (Philadelphia, Pa.), volume 238, October 1944, page 245.

5. An Analogy between Pure Mathematics and the Operation Mathematics of Heaviside, **J. J. Smith.** *Journal*, Franklin Institute (Philadelphia, Pa.), December 1925, page 789.

6. Fourier Series, **W. E. Byerly.** Ginn and Company, Boston, Mass., page 93.

7. See reference 1, page 150.

8. See reference 1, page 171.

9. See reference 6, page 70.

10. See reference 1, page 180.

11. Electromagnetic Theory, **O. Heaviside.** *The Electrician* (London, England), volume 2, equation 43, page 139.

No Discussion

Operational Study of a Highway Mobile Telephone System

LOUIS A. DORFF
NONMEMBER AIEE

SUBSTANTIAL progress has been made during the past few years in establishing mobile telephone service for vehicles. This mobile telephone service, inaugurated in St. Louis on June 17, 1946, is given through two types of systems. Urban mobile telephone systems serve the metropolitan areas and many of the cities of 100,000 population and over, and highway mobile telephone systems serve intercity highways, waterways, and cities along these routes which do not have independent urban facilities. These highway systems have been rapidly expanding into large area coverage systems blanketing complete states. The urban mobile telephone systems operate on channels in the 152 to 162-megacycle band, while the highway systems have been allocated channels in the 30- to 44-megacycle band.

As of May 31, 1950, highway mobile telephone service in the United States has expanded to include 110 base transmitting stations, serving about 3,500 mobile units and handling approximately 81,000 completed calls per month. These highway systems already cover many of our major highways in both the east and the west. In the middle west, statewide coverage systems have been established in Michigan, Wisconsin, Minnesota, Illinois, Missouri, Kansas, Oklahoma, Arkansas, and Texas. Existing highway service base stations in the United States are shown on Figure 1.

When highway service was first inaugurated in Green Bay, Wis., August 28, 1946, it was planned to operate all stations throughout the United States on a single channel of two frequencies, one for transmission to the mobile unit and the other for transmission from the mobile unit. This would allow a vehicle equipped with the normal single-channel radio set to travel anywhere in continental United States and make or receive calls. During the testing of these systems, however, considerable sky-wave interference was experienced between systems separated geographically by more than 1,000 miles. A study of the situation indicated that the most satisfactory method of reducing this interference would be to use different frequencies in different parts of the country. The country was therefore divided into zones 800 to 1,200 miles in extent and a particular pair of channel frequencies was assigned to each for its exclusive use. A frequency zoning plan comprising seven zones was adopted and is shown on Figure 2. With this plan all stations within a particular zone operate on the same channel frequencies. Vehicles moving from one zone to another may be equipped with an additional oscillator unit with relay-switched crystals, which is controlled by a manual channel selector mounted alongside the unit holding the handset. As the mobile subscriber moves into a different zone, he must manually switch the frequency of his mobile radio equipment. Areas such as St. Louis, Mo., and Buffalo, N. Y., located on zone boundaries, have base stations operating on the channel frequencies of each zone. The channel switch mounted on the right-hand side of the handset holder as shown in Figure 3, is capable of manual switching to as many as six different channels in the highway service band of frequencies. The added oscillator and crystal unit serving both the transmitter and receiver is shown at the left of the radio transmitter in Figure 4.

The provision of highway mobile telephone service presented problems of considerable greater complexity than did urban mobile service. One important difference is the need for continuous coverage over the entire length of hundreds and ultimately thousands of miles of highway, or thousands of square miles of area, as against coverage of a limited urban or metropolitan area. This, of course requires many base stations established miles apart along the highway or covering the desired large area. Each of these base stations is operated as a separate entity and with a particular point of contact with the land wire telephone plant, but each must also function smoothly as a part of the whole system to the end that a mobile unit may travel anywhere in the entire service area and yet be reached promptly and satisfactorily. Operation on a single channel within a given zone, complicates the problem of complete coverage of an area. It is obvious, that to provide complete and continuous radio coverage of a highway or area, there must be areas of overlapping coverage.

Consider for example, the two adjacent base stations *A* and *B* with transmitters and receivers disposed as shown on Figure 5(A). The irregular line surrounding each station is the boundary of the radio coverage area. A portion of the highway is covered by both stations. With both stations on the same channel, as is the case in highway telephone systems, a large portion of the overlapping area becomes an area of interference any time both stations are on the air. Now con-

Paper 51-7, recommended by the AIEE Radio Communications Systems Committee and approved by the AIEE Technical Program Committee for presentation at the AIEE Winter General Meeting, New York, N. Y., January 22–26, 1951. Manuscript submitted July 25, 1950; made available for printing November 14, 1950.

L. A. Dorff is with the Bell Telephone Laboratories, Inc., New York, N. Y.

The author wishes to express his appreciation for the assistance of R. E. Johnson, E. Thoet, and P. B. Howell, members of the study committee and all of the American Telephone and Telegraph Company. Also appreciation is extended to members of the Engineering, Plant, Training, and Traffic Departments of the Illinois Bell Telephone Company and Long Lines Department of the American Telephone and Telegraph Company, who carried on the study in their areas; and especially those operators of both companies who acted as observers, without whose co-operation the study would have been impossible.

Figure 1. Base stations of the highway mobile telephone service

sider Figure 5(B) with vehicles at "X" and "Y." Since neither vehicle is in the overlap area both could operate at the same time, "X" with station *A*, and "Y" with station *B*. Consider one further step shown on Figure 5(C). Here a vehicle is located at "X" in the overlap area of the two stations. When "X" attempts to make a call it will no doubt bring in both operators because its transmitter opens the squelch circuits and operates signalling relays in receivers associated with both stations. One operator will handle the call, but each time the mobile unit at "X" operates its transmitter, it will bring in the other operator, giving her a "false signal." Should the operator at *B* set up a call in her own area, operation of the *B*-base transmitter will in all probability cause interference to mobile unit "X" receiving transmission from base transmitter *A*.

This difficulty was recognized at the outset, so to prevent all probability of causing interference between adjacent areas, it was decided to keep station *B* off the air whenever station *A* was handling a call and vice versa. This was accomplished by providing the operator at each base station with a busy lamp, which lighted whenever the adjacent area base transmitter was on the air. When this lamp was lighted, the operators were instructed not to handle any calls through their stations. This became known as the "*A* On-*B* Off" method of operation. While this method did theoretically prevent all interference, should the mobile unit happen to be in the overlap area of two adjacent stations, Figure 5(C), it also prevented many calls from being placed in situations like that shown in Figure 5(B). This method of operation however delayed many calls and reduced the traffic handling capacity of the system materially, since whenever one base station was on, adjacent stations to the right and left were artificially busy.

It was evident that when the linear systems developed into area coverage systems, the use of this method of operation would become seriously inefficient in the use of the radio channel and station equipment available. For example consider Figure 6 which shows the base stations in the state of Oklahoma. There are a total of six stations located at Enid, Tulsa, Oklahoma City, McAlester, Ardmore, and Lawton. In effect, five of them surround Oklahoma City and their coverage areas, as shown, overlap that of Oklahoma City. Therefore, if the "*A* On-*B* Off" method of operation were used, each time Oklahoma City handled a call to a mobile unit, all the other surrounding overlapping stations would have to keep their transmitters off the air. This would mean that one call in the Oklahoma City station area could prevent the handling of any other calls in an area of about 58,000 square miles, practically the rest of the state of Oklahoma. This of course would not be efficient use of equipment or radio channel space and would in addition result in poor service.

This was most provoking to the radio systems engineer, especially since it was more than likely that the particular call deactivating this tremendous area, would originate from a vehicle in the center of Oklahoma City and the operation of any or all of the other base stations in the state would cause no interference. Something had to be done to improve the efficiency of the system before such situations became prevalent.

Ideas for solving this problem ranged from a few high-powered transmitters with their antennas on very high towers covering large areas to low-powered transceivers located every quarter mile, and connected through an elaborate network of land wire to complex switching arrangements which would follow the vehicle from transceiver to transceiver. Most of the ideas were ruled out as being noneconomical for application to present systems, or as having a too limited traffic capacity. Information and experience as to the calling habits of highway telephone customers and the detailed functioning of the new systems under service conditions,

was needed for proper evaluation of these proposals. This kind of information is generally available to the designers, the traffic engineers, and operating method people of fixed telephone systems, based on years of study of the calling habits of the telephone user. While the necessary information on mobile systems based on experience would in time become available, it was agreed that much could be gained if somehow the gathering of the necessary information could be accelerated to a point where it would be available in months rather than years.

The answer appeared to lie in a detailed operational study of a large working system. The Illinois state-wide highway telephone system was chosen for the study, since it was the oldest in point of service, the busiest, gave a typical example since it had both land and water vehicles with average spacing of base transmitter locations, and it included Chicago, the second largest city in the country and one having a large confluence of road and waterway systems. The layout and coverage areas of this system are shown on Figure 7.

The main objectives of the study were:

1. To learn as much as possible about the general operation and equipment functioning relationships of a large mobile telephone system.

2. To evolve the most efficient traffic operating method.

3. To learn something of the telephone habits of mobile service customers.

4. To determine what relation if any, there might be between the density of vehicular traffic and mobile telephone traffic.

5. To determine the need for additional equipment or new practices to improve the service.

Trained observers with specially built observing equipment were located at each of the seven base operating locations. A closeup view of the front panel of one of these observing boxes is shown in Figure 8. The box was equipped with lamps, a clock, and a monitoring circuit whereby the observer could follow and time the operations of the mobile service operator. The box also contained a stop clock and two lamps associated with each base receiver by which the observer could record which base receivers were activated, and the period each receiver was selected for use by the base station receiver selector. By monitoring the radio channel she could record the telephone number of the called and calling customers, comments of the customers on the service, their location, which they were asked to give during the period of the study, and whether or not the call encountered any interference. Lamps also kept her informed of the busy status of the adjacent areas.

During the study a provisional operating method was used, designed to handle calls in areas adjacent to a busy area provided the vehicle in the busy area was not in the overlap area. The method was based on the premise that if a mobile unit was in the overlap area, it would be in range of base receivers of both areas, and both operators should be able to hear the mobile unit each time it operated its transmitter. Normally the answer of the mobile service operator to a received signal on the radio channel, causes the base transmitter to be activated. However where the mobile unit may be in the overlap area, it was desirable that only one transmitter be operated in order to avoid interference. Therefore if an operator received a channel signal during a period when the adjacent area was busy (adjacent area busy lamp lighted), she had to determine before activating her transmitter, whether the signal was from a unit in her own area or from an operating unit in the adjacent area. To do this she had to be able to monitor her base receivers without activating her transmitter. This was accomplished readily by providing her with a monitoring jack, which gave her access to all her receivers, and through which she could monitor whichever receiver was activated by a mobile call.

By monitoring the receivers, she could determine if the adjacent area mobile unit was in range of her station. If she heard conversation, the provisional practice instructed her to leave a switchboard cord in the monitoring jack until the adjacent area call was completed, thereby preventing a new signal (false signal) each time the mobile unit transmitted. If she heard no conversation after a reasonable period of monitoring, she could assume her signal did not originate from the adjacent area unit, but from one in her own area. Since the adjacent area unit was not then activating any of her receivers, she could further assume it was not in the overlap area. Therefore she was instructed to plug a switchboard cord into the line jack, place her base transmitter on the air, and proceed with the call. In the "*A* On-*B* Off" method of operation this call would not have been delayed until the adjacent area became idle and the busy lamp went out.

The mobile service operators also were instructed to handle outgoing calls to mobile units regardless of whether or not the adjacent area was busy. This was done on the assumption that if a mobile unit operating in the adjacent area was in the overlap area of the two base trans-

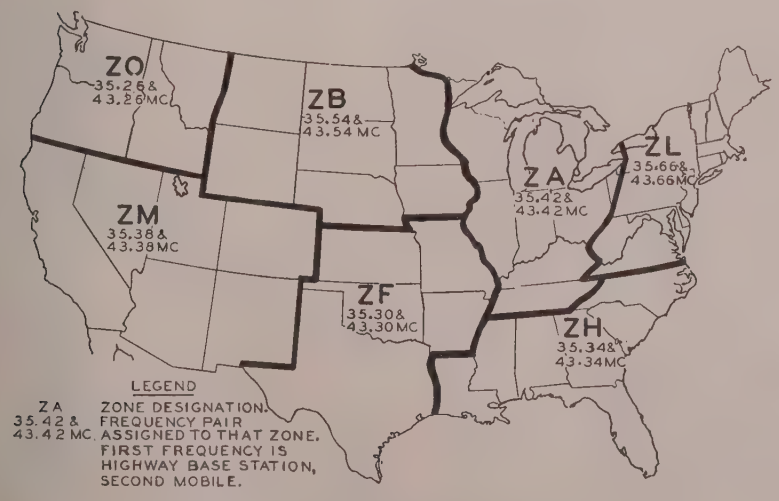

Figure 2. Frequency zoning plan for highway mobile telephone service

Figure 3. Mobile telephone control unit with channel selector mounted at the right

Figure 4. Multi-frequency highway mobile telephone equipment. Oscillator and crystal unit at left

mitters, it would have brought in a line lamp and the operator would be in the monitoring jack, and therefore knew no call could be handled without interference to the adjacent area call.

With the "*A* On-*B* Off" method no interference between calls in adjacent areas could occur since this condition was nonexistent, however under the provisional method, since calls were concurrent in adjacent areas under conditions as described previously, interference would occur at times due to changes in the position of the mobile units in the adjacent areas after the calls were initiated.

While the provisional operating method required the operator to monitor on all incoming calls during periods of adjacent area busy, it saved operating effort in preventing many false signals and showed real promise of increased efficiency. Since a change in operating method involved no added development or equipment, and could be applied with relative ease and economy, the efficiency of the operating method used in the study was examined first.

In the following paragraphs where interference is indicated, in so far as possible it refers to adjacent area interference. It does not always mean that detrimental interference actually occurred, but only indicates that it could have taken place. Interference as considered here, ranged from the momentary selection of a base receiver during a period when the local mobile unit was listening, which could be the local customer depressing his push-to-talk button while listening, and sometimes was, to those cases where the conversation from the adjacent area unit "captured" the base receiver from the local unit interrupting his conversation.

During the period of the study, approximately 6,800 messages or completed calls were observed. Of these, 3,400, or 50 per cent, were initiated during periods when one or more of the adjacent areas were busy. This means that there was a 100 per cent increase in the number of messages handled without long delay. Under the "*A* On-*B* Off" method, these messages would have encountered serious delay or might not have been handled at all.

A sample analysis of a typical hour for the whole system indicated that there would have been insufficient channel time at each station when all adjacent stations were idle, to carry the traffic actually handled, even if the calls were timed to follow one after the other. Completing calls without long delays gives a greatly improved service which could not otherwise be realized without providing an additional channel at each station. In one station, Ottawa, surrounded by four other stations, as many as 74 per cent of the messages were handled during an adjacent area busy condition.

As expected, some interference did take place. For the period of the study this amounted to about 3 per cent of the total 6,800 completed calls observed. During the first three weeks of the study period, before the operators were thoroughly familiar with the new practice, interference was noted on 4.3 per cent of the completed calls. During the last three weeks this figure had fallen to 1.5 per cent. It is expected that with well-trained operators the amount of interference in areas similar to Illinois should be between 1 and 2 per cent.

In the Chicago area the percentage of interference was comparatively high, 8.5 per cent, and showed little improvement with time as did the other areas. In order to ascertain as definitely as possible the cause of this, a special analysis of the Chicago area was made. Each case of interference was arbitrarily placed into one of three categories as to degree.

First Degree: Interference causing a definite interruption, or one where comments were made by the customers.

Second Degree: Interference where adjacent area conversation was heard but did not interrupt the call, or if noticed by the customers it was not commented upon.

Third Degree: Momentary selection of a base receiver presumably by a mobile unit in the adjacent area.

Table I. Chicago Interference Study—Summary of Possible Causes

Cause	Per Cent of Total
Operating irregularities	19
Range of receiver beyond transmitter range	75
5000 East End (south)	9.0
Munster (southeast)	1.5
Lockport (southwest)	42.0
Wheaton (west)	4.5
Lake Forest (north)	18.0
Miscellaneous	6

It was found that 31 per cent of the cases of interference were of first degree nature, 51 per cent second degree, and 18 per cent third degree. This indicates that about one-third of the cases of interference recorded were serious enough to cause comment or stop the call. Possibly not more than one-half of all cases recorded would be noticed by the customers.

What were the probable causes of interference? Again the Chicago cases were analyzed with the result shown in Table I.

Seventy-five per cent of the causes were attributed to the excess in range of the base receivers to that of the base transmitter. One receiver, Lockport, located in the southwest corner of the Chicago transmitter coverage area to fill a receiver "hole" in an important area, was the largest single contributor of in-

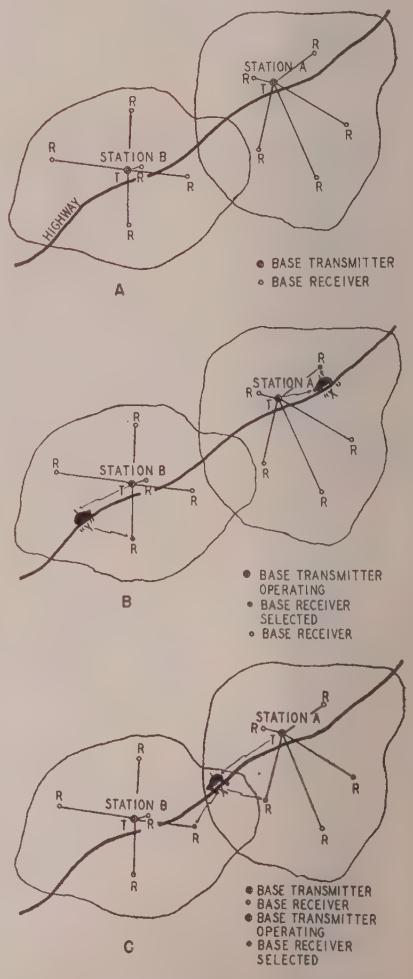

Figure 5. Elementary highway mobile telephone service coverage map, illustrating interference problems

terference (42 per cent). Its location unfortunately caused it to have a deep coverage in the Ottawa area. This condition was aggravated by the fact that this general area is one of heavy traffic density because of calls from river-craft on the Chicago Sanitary and Ship Canal and the Calumet-Sag Channel. While the Lake Forest receiver contributed 18 per cent of all causes, examination of the data showed it was due in a large part to the lack of the adjacent area busy lamp associated with the Milwaukee area to the north, which was being installed during the study period.

Operating irregularities, mainly due to unfamiliarity with the new method, accounted for 19 per cent of the interference cases. In large areas like Chicago, more different operators are involved than in the smaller centers and the introduction of a new method always requires more time to reach full operating proficiency. It was found, however, that all mobile service operators needed some special instruction in the physical functioning of a radio system, to better understand conditions that arise and how to handle them.

A miscellaneous 6 per cent of the interference cases resulted from causes such as the adjacent area test transmitters, used for testing and checking the base receivers, reaching beyond their own area; mobile customers momentarily depressing their transmit button while listening, (this is actually not adjacent area interference but only appears to be); and probably some long range interference from distant points in the same zone. The latter were eliminated from the data whenever they were recognized.

The relation of vehicle density to mobile telephone traffic was explored by a study of the mobile unit location and receiver used data. Referring to the system layout of Figure 7 and considering all areas, it was found that approximately 60 per cent of the mobile service traffic was handled through the base receiver located in the major city (base transmitter location) of each area, except in the case of Ottawa where only 19 per cent of the traffic was handled by the base receiver located in Ottawa. The major cities also represented the highest concentration of road traffic. In the case of the Ottawa area, the Illinois river provided most of the traffic, and the calls were spread between the three base receivers along the river. A high percentage of the Chicago traffic also was handled on the Lockport receiver for the same reason. Considering distance from the base transmitter, about 75 per cent of the calls were within a 15-mile radius, with about 80 per cent within a 20-mile radius, except for Ottawa where only 50 per cent were within 20 miles.

It is believed the success of the operating method used, is directly related to the fact that a high percentage of the calls occur within a 20-mile radius of the base transmitter. While the number of areas studied was too small to be conclusive, it appeared that the percentage of interference trouble at any station was directly associated with the percentage of traffic beyond the 20-mile radius in a system where the base stations were approximately 50 miles apart. On Figure 9 are

Figure 6. Oklahoma highway mobile telephone system and coverage map

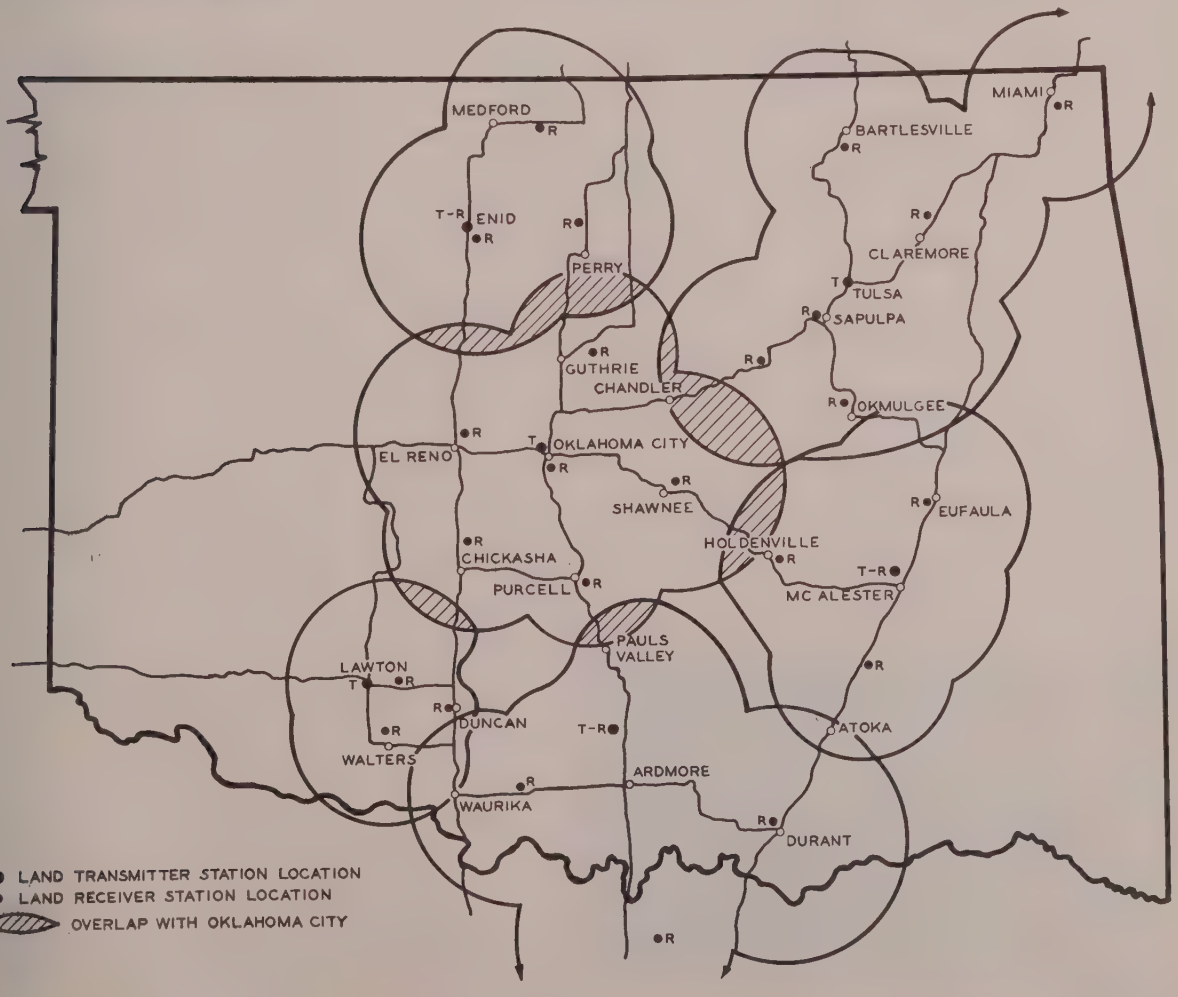

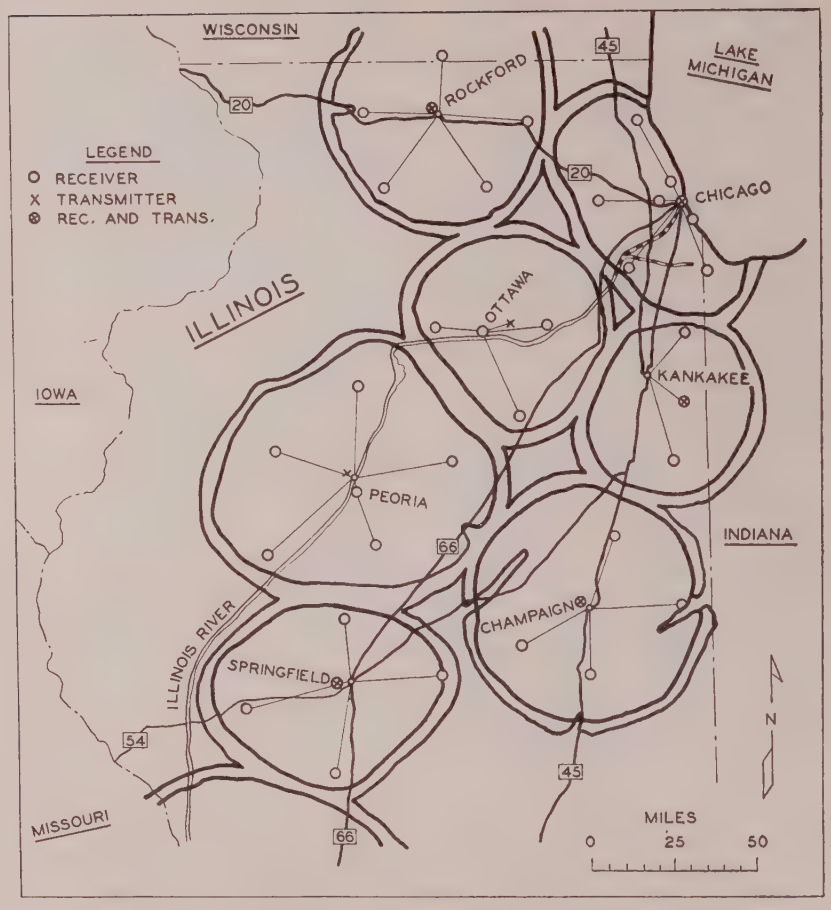

Figure 7. Illinois highway mobile telephone system and coverage map

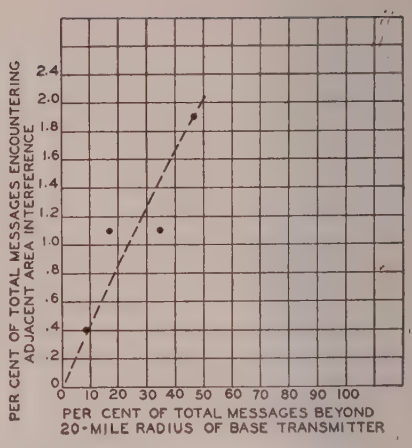
PER CENT OF TOTAL MESSAGES ENCOUNTERING ADJACENT AREA INTERFERENCE
0 .2 .4 .6 .8 1.0 1.2 1.4 1.6 1.8 2.0 2.4
0 10 20 30 40 50 60 70 80 90 100
PER CENT OF TOTAL MESSAGES BEYOND 20-MILE RADIUS OF BASE TRANSMITTER

Figure 9. Relation between expected interference in any base station and percentage of completed calls made in outlying portions of its coverage area

plotted points for four areas showing the relation of the percentage of total messages encountering adjacent area interference to the percentage of the total messages occurring beyond a 20-mile radius from the base transmitter. The dotted line indicates the trend, showing an increase in adjacent area interference as the percentage of calls beyond the 20-mile radius increases. Of course, if the base transmitters were closer together than 50 miles these figures would not hold for the 20-mile radius but would apply to a lesser radius, which like the 20-mile radius in this study, would lie well away from the overlap areas of the adjacent stations.

Conclusions

As a result of this study the following conclusions were reached.

1. It was decided to adopt the new operating method, which allowed calls to be made during adjacent area busy conditions provided the adjacent area mobile unit was not within the range of any of the base receivers, since it provided a ready and economical means of increasing the efficiency of use of the mobile system equipment and channel space. While it increased the interference over the old method from a theoretical zero to 1 to 2 per cent, it increased the call carrying capacity by as much as 100 per cent thereby decreasing the delays encountered, and improving the over-all service to the customer. Soon after the introduction of this method to the New York-Buffalo Highway system in 1949, it showed a 10 per cent decrease in delays on traffic to the mobile units, while at the same time the total traffic on the channel increased 20 per cent.

2. For good system operation base receivers should be so engineered and maintained that their location and adjustment provides a coverage area which does not extend beyond that of the base transmitter. When attempting to handle simultaneous calls in adjacent areas this requirement is of even greater importance. It aids in preventing adjacent area interference, and improves service by making it impossible for the mobile customer to signal an operator who cannot reach him, causing an apparent "don't answer" to the customer and a "false" signal to the operator. While too much emphasis cannot be placed on this conclusion, in all fairness to the field engineer who is charged with laying out these systems it should be pointed out that this objective is difficult to realize in practice. This is especially true in flat country, where the transmitter and receiver coverages are approximately circular. Filling a transmitter circle with receiver circles cannot be done without either excessive receiver coverage or pie-shaped "holes" around the transmitter fringe. However this should not prevent him from doing the best

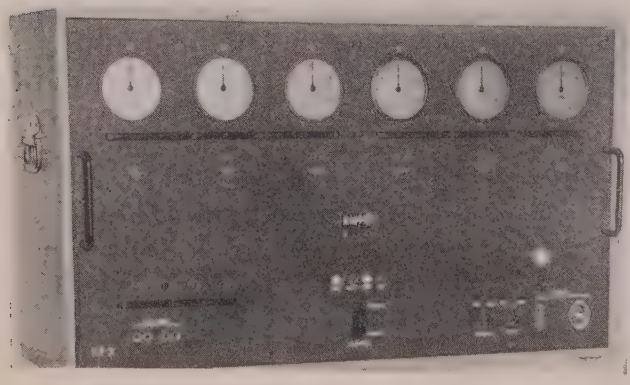

Figure 8. Observing box used for operational study of highway mobile telephone service

possible job of covering all important areas within the transmitter circle, without excessive receiver coverage in the adjacent areas. Development work toward better solutions of this problem is still underway. The provision of an adjustable output test transmitter is a real aid in the maintenance of base receiver adjustments. With it, receiver adjustment can be checked easily at frequent intervals and the test transmitter also can be kept from reaching into the adjacent area causing interference.

3. Further education of customers, maintenance forces, and installers was necessary to prevent interference and undesired radiation from mobile units.

4. All operators should receive special instruction for mobile service work to better cope with irregularities which arise due to vicissitudes of the radio system.

No Discussion

Ice Testing and Its Influence Upon Switch Design

G. E. HEBERLEIN
MEMBER AIEE

E. J. FIELD
ASSOCIATE AIEE

Synopsis: Requirements for disconnecting switches to operate when ice-coated demand special attention to details of design and to methods of testing the performance of a given design. In order for an ice test to provide a true criterion of the performance of a design, the icing program must be preceded by a wetting period above freezing temperatures, the simulated rain must be uniform over the test area, and the volume of water must be in balance with the ambient temperature in order to permit continuous wetting of the surfaces upon which ice is forming. Operation tests should be made at 20 degrees Fahrenheit and adequate time should be allowed after ending the spraying to equalize the masses of ice and metal at this temperature. Based upon the observed results of almost 100 individual ice tests, it is found that rounded contours, generous clearances, dry sealed bearings, small radii of all rotating members, sealed and enclosed hinge contacts, high-pressure line contacts, optimum clearance at linkage points, and absence of compression points are all required to maximize the ability of a disconnecting switch to be operated when coated with ice.

OUTDOOR disconnecting and horn gap switches are by the very nature of their application subjected to adverse weather conditions, including the formation of glaze ice. The thickness of glaze ice that is likely to occur in various sections of the United States has been determined from utility companies and from the records of the United States Weather Bureau. A loading map in the Standard Handbook for Electrical Engineers[1] discloses that about 40 per cent of the United States is subject to heavy ice conditions. At rare intervals radial ice may form as thick as one inch or more, as is illustrated by Figure 1, showing the results of an ice storm that occurred during the winter of 1949–50. The remaining sections of the country either experience no ice or are subject to medium and light glaze conditions. The term "glaze ice" as used here defines ice which has been formed at freezing temperatures upon surfaces that have been continuously wetted during freezing by a rain having a temperature slightly above the freezing point. In appearance it is a relatively clear and smooth coating of ice. It does not include wet snow or wet sleet which cling to surfaces upon which they fall and later freeze into a relatively solid mass. These latter forms of ice are neither as dense nor as strong mechanically as is glaze ice.

With modern concepts of continuity of service, it is of increasing importance to companies in the business of transmitting and distributing electrical power to be able to operate disconnecting switches under any weather conditions, including glaze ice. Hence, it is necessary for the designer to incorporate into the design of disconnecting switches features that will maximize their ability to operate under these conditions. Intelligent testing and effective designing demand a knowledge of the characteristics of ice and the manner in which these characteristics are related to ambient conditions both during and after ice formation. An additional requirement is for the icing and testing procedure itself to be standardized in order that true comparisons may be made between the results of different tests, and in order that the condition of ice experimentally imposed upon a switch may be as severe as that encountered in nature.

Testing

There are two slightly different basic requirements for ice testing. One requirement is to artificially simulate natural ice forming conditions so that a test under the simulated conditions measures the ability of a switch to cope with natural phenomena. This is termed a performance test. A second and even more important requirement is for a set of conditions that can be readily duplicated from test to test. The conditions must impose a severe test upon the equipment but will not necessarily exactly imitate natural phenomena. Since this set of conditions is controlled and reproducible, it is used to compare the performance of different designs and is termed a comparative test. Because it does not follow a temperature and precipitation program imitating nature, a comparative test requires less time than a performance test, but since the final temperature is equalized and is lower, the comparative test imposes a greater hardship on the switch. It follows, therefore, that if a design performs satisfactorily under comparative test conditions as detailed later in this paper, it also will perform satisfactorily under performance test conditions. The reverse is not always true.

The properties and physical characteristics of ice have been studied by a number of researchers whose findings have been commented upon and summarized by H. T. Barnes.[2] Table I reports the properties of ice pertinent to a program of ice testing. A knowledge of these properties is essential to the preparation of significant tests and to the intelligent interpretation of results. Ice behaves like other brittle solids in that it has greater strength in shear and compression than it has in tension. Mr. Barnes does not report shear strength but calculations based upon data taken from tests reported in this paper show that the shear strength of clear ice at 24 degrees Fahrenheit falls within the limits of 255 to 285 pounds per square inch.

Paper 51-8, recommended by the AIEE Switchgear Committee and approved by the AIEE Technical Program Committee for presentation at the AIEE Winter General Meeting, New York, N. Y., January 22–26, 1951. Manuscript submitted October 18, 1950; made available for printing November 14, 1950.

G. E. Heberlein and E. J. Field are both with the Railway and Industrial Engineering Company, Greensburg, Pa.

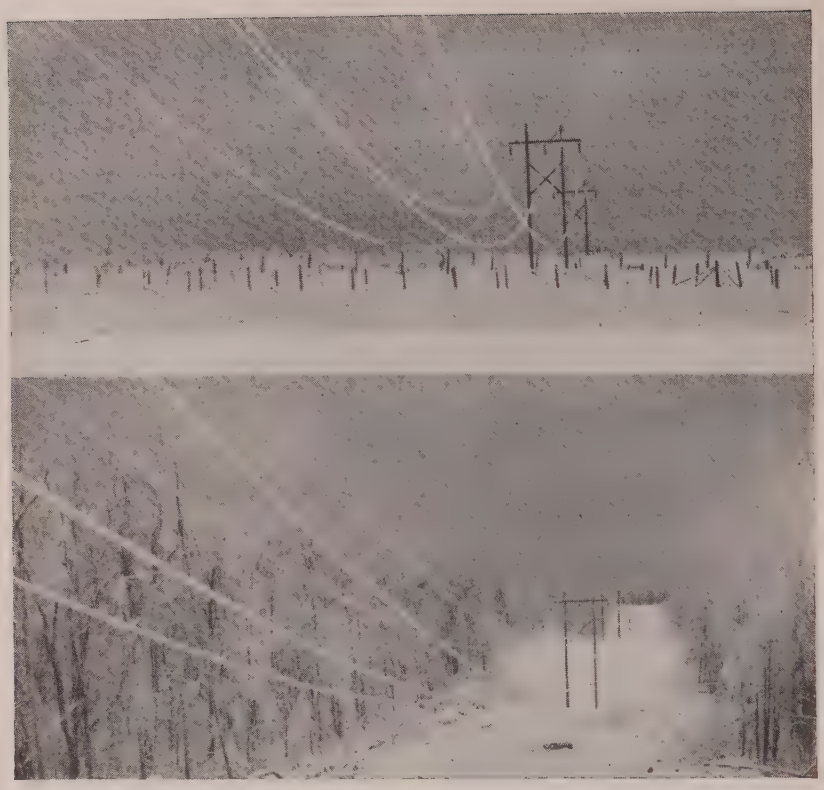

Figure 1. Two views of 1 1/4-inch radial ice formation on 110-kv transmission line between DuBois and Ridgeway, Pa.

The rate of water precipitation during ice formation and the velocity of the air during the same period influence the strength of the ice only to the extent to which they contribute directly to the amount of air inclusions contained in the frozen mass. The strongest ice is clear ice that is free from air inclusions. At a given temperature, ice will be found to be progressively weaker as the amount of air is increased. A rough visual index to the amount of air inclusion is the color or clarity of the ice. When entirely free of air, it has a window glass clarity. As the amount of air becomes progressively greater, the ice takes on a cloudy or milky appearance, which increases in intensity in proportion to the air content. The maximum amount of air inclusion and consequently the weakest ice has been found to form when the ambient temperature and the rate of precipitation are balanced at a point which causes all of the moisture striking a surface to freeze without any of it running off. On the other hand, the clearest, most dense, and consequently strongest, ice is formed when the ambient temperature and rate of moisture precipitation are of such values that only a small amount of the moisture striking a surface freezes; in other words, the growing film of ice is being continually washed by water and the growth of ice itself is occurring at the boundary line between ice already formed and the water film.

The strength of clear ice is related to its hardness which, in turn, is directly related to temperature. Ice has almost zero mechanical strength at the freezing point. As the temperature drops, strength increases very rapidly until 20 degrees Fahrenheit is reached. For temperatures lower than 20 degrees Fahrenheit, there is very little further increase in strength. This is illustrated in more detail in Figure 2.[2] The strength and temperature relationship of ice brands as a fallacy a kind of tough resilient ice popularly referred to as "rubber ice," which is purported to occur at or near the freezing point.

Tests verify the conclusions to be drawn from Figure 2, namely, that for any given thickness of clear ice, its strength and hence the resistance it offers to the operation of a switch increases as temperature decreases. For the same reason tests conducted near the freezing point impose a minimum hardship upon operation and cannot be regarded as either significant or conclusive.

The temperature at any particular point in the curve on Figure 2 is the temperature of the entire mass of ice at the time of test. It is not related in any way to the ambient temperature prevailing at the time of ice formation. To support this claim, it may be pointed out that regardless of ambient conditions and regardless of the temperature of the falling moisture, the actual formation of ice at the boundary between water and ice is occurring at a constant temperature of 32 degrees Fahrenheit. For this reason, it is important that at the conclusion of ice build-up, the investigator allow adequate time to elapse for equalizing of the entire ice mass and testing equipment at the temperature at which the particular test is to be performed. It is advisable that the temperature at the time of test be 20 degrees Fahrenheit, because lower temperatures introduce very little gain in ice strength. Higher temperatures approach the steep slope portion of the curve where consistent comparisons cannot be depended upon because small differences in temperature introduce wide differences in hardness.

Taking into consideration the facts presented in the foregoing paragraphs a procedure has been established for testing the operating ability of ice coated gang operated disconnecting switches. The procedure, as outlined in the following, provides a reliable means of duplicating in a series of tests a coating of glaze ice that imposes a rigorous test upon switches. It is suggested as a basis from which to prepare a standardized procedure as a comparative test for users and manufacturers.

1. Switches to be tested are to have all exposed surfaces free of grease, wax, or oil. All surfaces should be in a condition resulting from normal production and not specially cleaned or polished.

2. Test to be made upon 3-pole switches complete with standard mechanical control parts and operating handle.

(a) For comparison of different designs, like voltage and current ratings shall be tested. Also, the same type of control shall be used,

Table I. Physical and Mechanical Properties of Ice

Coefficient of cubical expansion (10° C to 0° C)—0.00016/° C
Tensile strength— 98–112 pounds per square inch*
142–223 pounds per square inch†
Crushing strength—327–1,000 pounds per square inch
Modulus of elasticity, between 0° F and 23° F—0.392×10^6 pounds per square inch
Dielectric constant—between 60 and 78 (86.4 at 1,000 cycles)
Resistance 7.22×10^7 ohms per centimeter
Breakdown voltage 0.011×10^6 volts per cubic centimeter
Density—0.91676 at 0° C (maximum water density, 1.0, occurs at 4° C)
Latent heat of fusion—79.67 calories per cubic centimeter
Specific heat—0.49 at 0° C

* Hess.

† American Civil Engineers' Pocket Handbook.

that is, direct connected or fourth bearing, guide plates.

(b) Crank of fourth bearing, when used, shall be parallel to the switch bearing cranks. Toggle connections shall not be used for comparative testing.

3. Water to be introduced in a manner to cause it to descend upon the switch at any angle not exceeding 45 degrees off of vertical. The water to be in the form of finely divided drops spread uniformly over the area occupied by the switch, interphase connecting rods, operating rods, and operating mechanism.

4. Spray for preliminary period of one hour. Test chamber temperature not to be less than 40 degrees Fahrenheit nor greater than 70 degrees Fahrenheit.

5. Over period not exceeding three hours, drop the test chamber temperature to 25 degrees Fahrenheit, ± 5 degrees Fahrenheit, meanwhile continuing spraying.

6. Continue spraying at 25 degrees Fahrenheit, ± 5 degrees Fahrenheit, until desired ice thickness is obtained. The formed ice shall be windowpane clear in appearance and shall be free of crevices and knobular crystal clusters.

7. After cessation of spray, the switch shall stand for three hours at 20 degrees Fahrenheit, ± 2 degrees Fahrenheit, to equalize temperatures throughout the ice and metal masses.

8. Operate the switch at 20 degrees Fahrenheit, ± 2 degrees Fahrenheit.

9. The thickness and uniformity of ice formation shall be determined by measuring at six points the thickness of the solid ice formed on the upper surface of two $1^1/_4$ inch diameter sample bars placed with their axes parallel to the ground and with their lengths traversing the entire area occupied by a plane projection of the switch and mechanical control parts.

10. The minimum thickness when measured in accordance with item 9 shall be 3/4 inch.

Table II. Operating Resistance of Various Members of a 3-Pole 600-Ampere, 34.5-Kv Air-Break Disconnecting Switch When Coated with 1-inch of Clear Ice at 24 Degrees Fahrenheit

Component	Maximum Resisting Moment Measured on Vertical Operating Pipe, Inch Pounds
Locking plate (for torsional operating mechanism)	500
Guide plates (2)	4,000
Interconnecting rods and bearing cranks	5,000
Switch mechanism (3-poles)	
To initiate motion of rotating insulator	4,500
To fracture ice at hinge and contact ends	7,000
To continue to turn blade and lift clear of contact—without arcing horns	5,000
with arcing horns	8,000
Total, based on using arcing horns	29,000

Attempts to test the strength of an ice coating by some simple means, such as striking with a hammer, are unreliable because too much variation in impact energy and angle of impact is possible. The most reliable measure of strength is to ascertain that the temperature is equalized at 20 degrees Fahrenheit and that the ice is clear and, therefore, free of air inclusions. At normal atmospheric pressure, clear ice can have only one strength characteristic at a given temperature.

Test Findings and Their Application to Switch Design

Early tests of disconnecting switches were in the nature of "go," "no-go" tests. That is to say, after the switch had been coated with ice, an attempt was made to operate it and it either worked or it did not. With this kind of testing, it is not known by how wide a margin the switch fails or succeeds. However, an investigator can observe the principal ways in which ice interferes with operation and design can be directed accordingly. An early design resulting directly from ice tests is the basic principle of blade motion, which causes the blade to first rotate on its axis to release contact pressure, and then to lift out of contact. Carl G. Koppitz introduced this new and novel principle in the early 1920's[3] and its soundness is testified to by the fact that practically all switch designs manufactured today incorporate Mr. Koppitz' basic principle of blade motion. These early tests also disclosed the importance of wide clearances between parts having relative motion.

Some considerations for proper design are apparent from a knowledge of the mechanical properties of ice. For example, since its crushing strength may be as much as seven times its tensile strength a design should avoid any point where ice can be brought under compression and thereby resist motion of the mechanism. Since ice is least strong in tension, it is desirable for a design to cause ice to resist motion only in tension. However, this is not practical because rotating members emerge from stationary bearings and an ice shear point exists at the boundary between rotating and stationary parts. The next best thing is to minimize such bearing points as well as the radius of the rotating member, which is exposed to the formation of ice. To express a basic principle, never use two exposed bearing points when one will do. For example, where the rotating blade joins with the stationary hinge, a double bearing con-

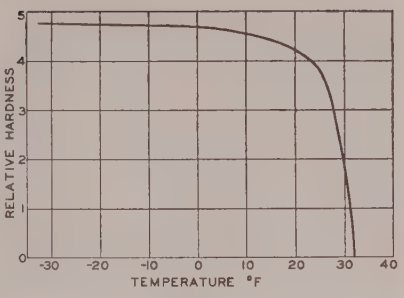

Figure 2. Relationship between strength and temperature for clear ice

struction spanning the section of blade on which is mounted the blade trunnion doubles the ice which must be sheared when the blade is rotated. Good design can avoid this type of construction.

A practice in more recent tests is to measure the actual effort in inch pounds of operating moment required on the vertical operating pipe to overcome the resistance offered by deposits of ice on various elements of a 3-pole switch. By separately mounting the individual sections of a switch and selectively shielding areas that are to remain clear of ice, the resistance offered by deposits of ice on the different parts of a 3-pole switch has been determined. Table II lists for each part of a switch the average of a number of tests to determine the interference to switch operation caused by ice on the part. It is to be noted that a summation of the resisting moments offered by the individual ice coated parts amounts to 29,000-inch pounds, which is adequate to positively lock a switch against operation. Actually, this same 3-pole switch and the control parts enumerated in the table required only 9,000-inch pounds to operate when all parts had been subjected to ice formation amounting to one inch of clear radial ice. This apparent paradox is explained in part by the fact that ice is brittle and the fact that there is some elastic deflection of parts, for example, the torsional twist of the operating rod within its elastic limit. More of the explanation lies in the fact that the brittleness of ice has been utilized by the designer in establishing optimum clearances at all linkage points so that motion is not transmitted to all parts of the switch simultaneously. Instead, when the operator applies effort to the operating mechanism, motion occurs in sequence from part to part like the starting of a train of cars. Thus, almost all of the operating effort is available to fracture the ice impeding each of the individual parts. A design employing precision connections in the several linkages existing between the

Figure 3. Representative crystal clear ice resulting from recommended artificial storm conditions

Figure 4. Three-pole switch artificially coated with 2 1/4 inches of hard ice

operating handle and the switch blade would cause all of the resisting moments to be effective simultaneously and it would be impossible to operate the switch under any appreciable ice coated condition.

When a good bond exists between ice and the surface of a cylindrical part on which it is formed, the resistance to rotation introduced by the ice is a product of the unit shear strength of ice, the area of the cylindrical boundary existing between ice and part, and the radial distance between the axis of rotation and the ice boundary. Since the shear area is proportional to the diameter of the cylindrical part, and since the radius over which the moment is effective is one-half the diameter, it follows that the resisting moment of the ice sheath is directly proportional to the square of the diameter. Hence, the resistance offered by a sheath of ice on a cylindrical part increases rapidly with increase in diameter. This fact applied to bearing design dictates the smallest possible diameter of shaft consistent with adequate mechanical strength. Furthermore, small clearances between a rotating flange and a stationary housing must be avoided because ice will form in the clearance space and add appreciably to the area of ice which will be in shear.

To demonstrate the principles expressed in the foregoing paragraph, six different designs of bearings were mounted on a plate, which was exposed to a standard ice forming procedure until partially coated with 5/8-inch of clear ice. The artificial rain was projected upon the bearings at an angle of 45 degrees, to simulate a driving rain storm. No ice formed on the lee side of the bearings. Table III tabulates both the effort required to start rotation and the effort required to continue rotating the bearings after the resisting ice fractured. The effort required to start rotation relates directly to the area of ice which covers portions of the bearings and offers resistance to rotation. Consistent with theory, the greatest resisting moments occurred with either largest radii or the largest areas in shear. After rotation has started, continued resistance is due primarily to ice formed within a bearing because of water which penetrates to the interior. Some resistance is attributable to the debris from shattered ice that is trapped in small clearance spaces. It is significant to note that the bearing requiring the least effort to start rotation, as well as the least effort to continue rotation, is a design that minimizes both the area of shear ice and the radius over which it is effective. This design incorporates fully sealed construction to exclude moisture and dry type bearings to avoid corrosion due to lubricant breakdown.

Tests were performed upon 32 additional bearings, design *F* in Table III, to demonstrate the resistance to rotation caused by internal ice. These bearings have an upper and a lower set of balls and races. Measured amounts of water were intentionally introduced to the interior of the housings and the bearings then were exposed to a freezing temperature. All force measurements are made at 24 degrees Fahrenheit. Test results disclose that a clean, dry, sealed bearing turns freely with less than 25-inch pounds of applied force. With only sufficient ice to fill the spaces between balls and races of the lower race, 400-inch pounds are required to turn a single bearing. With 1 3/4 ounces of water, 600- to 1,000-inch pounds are required, which means as much as 3,000-inch pounds for a 3-pole switch. These facts disclose the importance of a water proof sealed bearing such as has been adopted for the bearing used on the switch shown in Figure 6.

Economical design requires that parts be proportioned in a manner that will work the metals used as fully as possible consistent with acceptable safety factors. For a switch that is designed to operate

Table III. Operating Moment Required for Different Bearing Designs at 24 Degrees Fahrenheit after Exposure to Artificial Ice Forming Conditions

Maximum Ice Thickness, 5/8 Inch

Bearing	Type of Construction	Operating Moment To Start Rotation, Inch Pounds	Operating Moment To Continue Rotation, Inch Pounds
A	Unsealed and dry	624	574
B	Unsealed and dry	755	126
C	Semisealed and lubricated	1,175	130
D	Semisealed and lubricated	1,000	125
E	Semisealed and lubricated	545	27
F	Fully sealed and dry	136	27

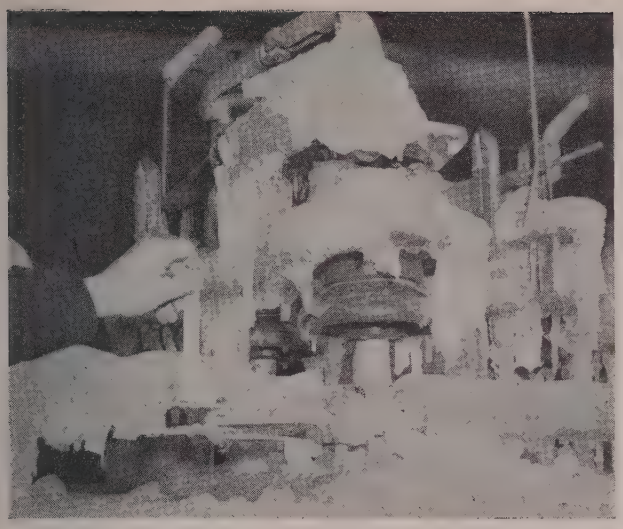

Figure 5 (left). Same switch as Figure 4, but immediately after opening and reclosing

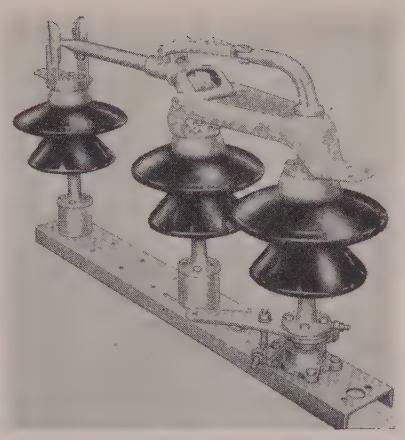

Figure 6 (right). The type *TTR-49* switch, a design incorporating the features proven to be necessary for maximum ability to operate when ice coated

effectively when ice coated, there is a further incentive for the thrifty use of metal because, generally speaking, the more weight of metal used, the larger are the areas of finished parts, and the larger the areas, the greater the opportunity for ice to interfere with operation. For the same reason, only high strength materials are desirable for switch mechanism parts. When severe operating effort is applied to a switch, heavily coated with ice, the strain upon mechanism parts may be severe. Careful attention to mechanical design is demanded in order to meet both the requirement for strength and the requirements for minimum areas and radii. These factors usually are not taken into consideration in switch design but they must be for best performance.

The modern trend in switch design is to eliminate the flexible connection formerly used at the hinge end of the blade. Thinking again in terms of ice operation, the method of current conduction used to substitute for the hinge end flexible connection should be of the enclosed and sealed type of contact design, rather than an exposed, shuntless contact similar to the main switch contact. The latter offers additional opportunity for ice to impede the motion of switch mechanism.

A design, incorporating all of the desirable features learned from the analysis of ice studies and tests, and five other present-day designs were subjected to operation tests, using the standard procedure for ice testing suggested previously. Tests on these switches differ from suggested procedure only in the fact that final ice thickness is either 7/8 or one inch. Figure 3 illustrates the type of clear ice resulting from the standard icing procedure. Note that even though the switch tie castings are covered by a solid sheath of ice one-inch thick, markings on the castings are readily discernible. Table IV summarizes the results of these tests performed upon the various designs. All designs have the same voltage and current ratings. The operations were performed at 22 degrees Fahrenheit ±2 degrees Fahrenheit. Operating rods, interphase connecting links, and rotating insulator bearings were shielded to confine the test to the switch mechanism.

Designs *B* and *E* were incapable of being completely opened because of construction at the hinge end permitting ice to be placed under compression between parts of the mechanism. In the case of design *B*, the pressure was so great that the ice under compression was completely pulverized but since it had no place to go, the pulverized ice remained in position to impede operation. In support of the principle of thrifty use of metal, it is to be noted that designs *C* and *F*, which are the two using the greatest weight of metal in the mechanism, required high efforts for operation. As a further demonstration of the principle, design *D* was so severely damaged in the opening operation that two poles would not make contact when the operator tried to reclose the switch. Damage consisted of deformation of the blade trunnion, caused when the forked link of the mechanism tried to twist the blade against the resisting moment existing at the ice locked contacts. Design *E* erred on the side of not using adequate material. Even though operating against only 7/8 inch of ice, a key part of the mechanism deformed and fractured on two of the three poles.

Except for design *E*, design *A* uses the least material, but the material is used so effectively that successful operation was achieved with no visible damage to parts. In an effort to find the ultimate capacity of this design to operate under an ice coating without damage to parts, it was coated again with solid ice, this time $2^1/_4$ inches thick. Figure 4 shows the extent

Table IV. Resistance to Operation of Ice Covered Switches Having Different Mechanism and Contact Designs

Switch Design	Weight of Switch Mechanism and Blade Pounds	Ice Thickness, Inches	Hinge End Contact	Operating Effort for 3-Pole Switch: To Release Contact Pressure, Inch Pounds	Operating Effort for 3-Pole Switch: To Raise Blade, Inch Pounds
A*	34	1	Enclosed, sealed continuous contact	6,600	9,000
B	39	7/8	Enclosed, unsealed continuous contact	6,900	14,000**
C	46	1	Exposed, make and break contacts	12,300	9,900
D	41	1	Exposed, make and break contacts	13,700	11,800
E	25	7/8	Flexible braid	4,000	11,200†
F	45	1	Exposed, make and break contacts	13,200	7,100

* Railway and Industrial Engineering Company type *TTR-49*, same as illustrated in Figure 6.

** 8,400-inch pounds moved the blade out of the contacts but the maximum available effort of 14,000-inch pounds opened the blade only 50 degrees.

† 11,200-inch pounds opened blade to 75-degree position. More effort was not applied because the mechanism driving crank fractured on one pole.

of this coating as it appeared on the switch prior to operation. By means of a heavy pipe inserted in the handle socket of the operating mechanism, increasing force was applied on the operating rod until the 3-pole switch opened. Figure 5 shows the appearance of the switch immediately after it had been opened and then reclosed. Note that when the ice is as thick as that used for this test, it spalls off of mechanism parts in large sections. Detailed examination of all poles of the switch after the remaining ice had melted off, disclosed absolutely no damage whatever to any mechanism parts.

Summary

A plan to design outdoor disconnecting switches to operate when covered with glaze ice presents a need for a rigorous and reproducible procedure for ice testing different types of designs. Formulation of a testing procedure must be preceded by a knowledge of the properties and characteristics of ice itself in order that the method will be reliable and in order that the results of tests will be intelligently interpreted. The results of tests made in accordance with the procedure suggested in this paper have been used to guide the design of the switch illustrated in Figure 6. The features of design necessary to achieve operation of an ice covered switch with minimum effort and without damage to the switch mechanism may be summarized as follows:

1. Dry type, rotating insulator bearings, positively sealed against moisture penetration.

2. Liberal clearances between all parts having relative motion—for example, between insulator driving crank and switch base, and between forked link and tie casting.

3. Rounded contours on switch mechanism parts to facilitate clearing fractured ice from the parts when the switch is being operated.

4. No opportunity for ice to be brought under compression between two or more parts of the switch mechanism.

5. Use of noncorrosive alloys, having a high yield strength, and proportioning of parts to work the alloy to its full capacity, thus minimizing size.

6. Release of main contact pressure prior to lifting the blade from the contacts.

7. Enclosed, sealed continuous contact current path at the hinge end.

8. Small radii on the portion of rotating members adjacent to their stationary bearings.

9. Avoidance of exposed dual bearings.

Generally speaking, no single feature of design has a decisive effect upon the ice operating ability of a switch, although some features have a greater influence than others. The studies and tests reported show that it is attention to detail in all of the features enumerated above that is necessary to produce a design which is effective in overcoming the resistance to operation imposed by ice.

References

1. Standard Handbook for Electrical Engineers, **A. E. Knowlton.** McGraw-Hill Book Company, New York, N. Y., section 4-774, 1949.

2. Ice Engineering, **Howard T. Barnes.** Renouf Publishing Company, Montreal, Canada, 1928.

3. High Tension Switch Mechanism, **Carl G. Koppitz.** United States Patent 1,560,998, 1925.

Discussion

W. B. Morton (Pennsylvania Power and Light Company, Allentown, Pa.): The high-temperature freeze techniques covered by this paper were promoted at the instigation of engineers of the Pennsylvania Power and Light Company, as a result of years of investigation into the vagaries of sleet formation and much experimentation with various kinds of sleet-melting devices on a transmission system covering 9,500 square miles of territory that is highly vulnerable to sleet formation. It was discovered in these investigations that no disconnecting switches on the Pennsylvania Power and Light Company system, of any manufacturer, were entirely immune to freezing fast and becoming inoperable in service, despite elaborate ice testing by the manufacturers in the laboratory.

This experience led to one obvious conclusion—that current experimental practices were inadequate to produce the conditions of ice formation actually experienced under field conditions. Thus, a new concept of ice-freezing technique was developed and promoted by Pennsylvania Power and Light Company engineers with results outlined in the paper. This detailed procedure is written into all Pennsylvania Power and Light Company disconnecting switch specifications.

The paper should lay more emphasis on the important fact that this new concept of ice testing differs from all previous ones in that it is based on a high-temperature slow freeze, in contrast to the previous universally accepted, but erroneous, thinking that low-temperature quick freezing is a true criterion of field conditions. Moreover, an important consideration early discovered in the Pennsylvania Power and Light Company investigations is the necessity for thoroughly spraying the equipment for at least an hour prior to the test with precooled water, artificially agitated (as a sleet storm usually is preceded by rain before reaching the sleet stage), to insure that water has penetrated all crevices and interstices. This penetration under field conditions is one of the major causes of some switch failures that are not detected in the obsolete laboratory "quick freeze, low temperature" testing.

The paper also should emphasize that the needed revisions to the AIEE standards for disconnecting switches should require that they be ice tested in both open and closed positions. Also, an impact test is desirable not to determine the strength of the ice, but to determine the adhering qualities.

J. B. Owens (Westinghouse Electric Corporation, East Pittsburgh, Pa.): In this excellent paper the authors have described two fundamentally different ice tests for outdoor air switches. One test, which is termed a "performance test," is designed to duplicate the conditions which actually occur in the field during a severe ice storm. The second test, which is termed a "comparative test," does not attempt to follow a temperature and precipitation program which duplicates nature. This test is designed to utilize a set of conditions which can be duplicated readily from test to test.

There is still a wide difference of opinion as to the particular set of natural conditions which produce the greatest difficulty in switch operation. It will therefore be very difficult to design a single performance test which will be acceptable to all members of the industry. However, there is a great need for a standardized comparative test which will give consistent results and will provide fair comparisons between various designs. Such a test should not depart radically from natural conditions; however, reasonable departures should be acceptable provided the resulting ice coating is of high strength, is well bonded to the switch, and is well distributed over the entire switch and operating mechanism.

Experience in ice testing in the cold room in East Pittsburgh indicates that the comparative test outlined by the authors will give a reasonable test on air switches with an ice coating comparable to that produced by nature. The suggestion that the actual operation always be performed with the entire iced switch equalized to 20 degrees Fahrenheit is an excellent one, since this tends to produce more consistent results and fairer comparisons between tests.

The only item of the testing program which appears to prolong the test unnecessarily is the temperature during preliminary spraying. This spraying is highly desirable, since it gets water into all the crevices of the switch structure before freezing begins. However, it seems unnecessary to maintain the test chamber temperature above 40 degrees Fahrenheit during this 1-hour period. As long as the temperature is above 32 degrees Fahrenheit the desired result is obtained, and by doing this spraying in the vicinity of 35 degrees Fahrenheit, the total testing time measured from the beginning of the spraying is reduced.

In listing the design features necessary to achieve operation of an ice-covered switch with minimum effort, the authors mentioned the release of contact pressure before blade rise begins. They overlooked, however, the importance of enclosing the mechanism which provides this blade motion. While they mention the difficulties induced by ex-

posed bearings, they depict a switch in which the blade-actuating linkage is mounted directly on top of the switch with at least three exposed bearings. J. B. Owens[1] depicts a switch which embodies the same blade motion as the switch described here and at the same time provides total enclosure and complete ice protection for the blade-actuating mechanism.

The authors are to be congratulated for the thoroughness of their analysis of the ice testing problem. We heartily endorse their proposed program of developing a standardized testing procedure for comparison of switch designs.

REFERENCE

1. ICE TESTING OF OUTDOOR DISCONNECTING SWITCHES TO SIMULATE FIELD CONDITIONS, J. B. Owens. *AIEE Transactions*, volume 69, part II, 1950, pages 1488–92.

S. C. Killian (Delta-Star Electric Company, Chicago, Ill.): The operation of the outdoor air switch under artificial ice is rapidly generating a whole new literature. Several articles and AIEE papers in the past year have dealt with this question and, like any good discussion, this variety of opinion ultimately will produce some sort of testing standard and the industry will be the better for it. The Delta-Star Electric Company recently has installed an ice chamber for switch testing also, and as more of this type of equipment becomes available, a wider cross section of data will be available.

The authors of this paper are to be commended for their precise outlining and also for the introduction of several new requirements into the test program, such as a resting period between the cessation of spray and actual operation, a limited temperature at which switch operation must take place, and the introduction of sample bars to measure ice thickness.

I do not believe that the authors are justified in their statement that "rubber ice," a high-strength thin ice formed at some optimum temperature, is to be ignored. I am sure that we should hesitate to guarantee that we have duplicated in the laboratory every combination of circumstances in nature, such as temperature of the equipment, temperature of the precipitation, rate of precipitation, condition of the precipitate, wind velocity, and many other possible variables. We know that in nature very tough ices form under what seems to be some optimum condition, and we should admit that we are testing under some set of standard conditions which is the best we can do, but this does not necessarily include everything that Mother Nature might drop on us.

With the elimination of the flexible braid from vertical break switches, the construction of the hinge contact becomes very important. A variety of hinge contact designs is now available. Besides the ice angle, other extremely important points, such as minimum number of parts, minimum number of current interchange surfaces, avoidance of small spring members, and accessibility for inspection, must be considered. For the small gain in reducing operating effort under ice, we should not apparently sacrifice all three of the latter precepts and have permanently locked from view the very troubles which the use of additional current interchange members and small springs may likely produce. An exposed hinge contact, on the other hand, increases operating effort only slightly because of the short moment arms involved and does allow the use of minimum current interchange members, large springs, a better noncramped contact design, and accessibility for inspection at all times.

There certainly is no doubt that ice formation is important in design. But let us not grow so enthusiastic about this urge toward ice-test standardization that we lose sight of many other extremely important factors in switch design.

A. H. Powell and **H. R. Harrison** (General Electric Company, Philadelphia, Pa.): Apparently increasing attention has recently been paid to ice problems on switches by both user and manufacturer. Some users are including requirements in their specifications, while others indicate, in a general way, the need for switches which will operate under ice conditions. The authors are to be commended for the comprehensive manner in which they have approached the ice problem, for much new and interesting data have been accumulated.

Some suggested procedures for making tests so that results can be easily duplicated are given in the paper, along with observations about the formation of ice and its characteristics. Several comments on these items appear to be in order.

The superiority of tests on a 3-pole switch as compared to a single-pole switch is questionable, for it would be difficult to obtain a uniform thickness of coating of ice on all three poles because of the larger projected area to be covered by the spray, unless the freezing room and facilities were large and a sufficient number of spray heads were used to assure formation of ice uniformly. This seems to be the case in the pictures (Figures 3 and 4), where the nearest poles apparently have considerably more ice on them than the pole farthest away.

Water introduced at an angle from above the specimen to be tested will result in ice formation on only one side of the switch. The paper describes tests on bearings where the water was projected at an angle of 45 degrees and no ice was formed on the lee side of the bearings. The water should be projected from spray heads or nozzles on each side so the ice formed will be uniform on both sides of the switch. The configuration of the spray head should be specified, together with the water pressure and the temperature of the water at the spray head. Adequate preliminary spraying is necessary, but the suggested period of one hour is questionable. After the switch parts are thoroughly wet, they cannot be made to absorb any more moisture by continued wetting. Tests we have made show that the temperature of the room during the freezing period should be lower than +20 to +30 degrees Fahrenheit. Before standards are established, tests should be made to obtain more data as to the correct temperature for strongest ice formation. Also, the authors state, ice has a greater strength in shear than in tension. However, we have found that ice has very little strength in shear and will break readily in shear upon impact. Switches should be designed with this in mind.

As a general comment, it appears that two items have been overlooked in the paper. First, the need for tests with the switch frozen open, and then closed. This might be the more common case in actual practice. Second, the effect of ice accumulation on high-voltage switches, 115 kv and above. These switches present a more severe condition than is met with the 34.5-kv switch covered in the paper under discussion, because of the longer blades and the difficulty in obtaining sufficient operating torques to break the ice. This is especially true when the switches are motor-operated, as is more often the case with high-voltage than with low voltage switches, 69 kv and below. It would seem, therefore, that these two problems must be checked more thoroughly before attempting to prepare any standardized testing procedures.

If switches must be operated under ice formation frequently enough so that the subject is of sufficient importance to the user, it is suggested that appropriate committees be set up to study the problem and to recommend standards. The manufacturer and user then will have a common understanding of the problem so that the switches can be designed adequately and tested properly.

G. E. Heberlein and **E. J. Field:** The authors appreciate the interest shown in the subject of this paper. Some of the discussions indicate that we need to clarify further some of the objectives and findings that are reported in the paper.

The excellent work done by Mr. Morton and his associates resulted in the only standard to reach our attention that was adequate to serve as a tentative industry standard, while the subject of ice testing was being explored further. We are in agreement with their high-temperature concept of spraying at elevated temperatures to saturate the equipment prior to freezing. Mr. Owens refers to this point too, but we do believe that a starting temperature above 40 degrees Fahrenheit imposes a greater hardship on the switch. Any decreasing air pressure within cavities accompanying a decreasing temperature tends to draw in moisture. This influence will be greater at higher starting temperatures.

The paper calls attention to a new concept of ice formation, which is to maintain a balance between the variables—room temperature, water volume, size of drops, and air flow velocity—such that, regardless of ambient temperature, the surfaces upon which ice is forming are continually washed by falling water. Ice formation then takes place at the boundary existing between the ice and the enveloping moisture film, and this boundary retains a constant temperature of 32 degrees Fahrenheit. Proper balance of the variables permits crystal clear ice to be formed at any subfreezing ambient, at least down to the minus-10-degree limit of our test chamber. As pointed out in the paper, the strength of the air-free ice is then related directly to its equalized temperature.

Air agitation of the falling moisture can serve the useful function of creating a more uniform precipitation pattern. This result also can be achieved by proper design of orifices and the arrangement of nozzles over

the test area. Either method can be utilized.

Ice tests have disclosed interesting facts relating to hinge-end mechanism and contact designs, discussed by Mr. Owens and Mr. Killian. Enclosing the mechanism that imparts a rotating motion to the blade does reduce the effort required for this phase of operation, but this gain is offset by an increase in effort required for the subsequent blade-lifting phase of the opening operation. The effect of exposed contacts is illustrated in Table IV of the paper. For the initial contact-releasing phase of operation, designs C, D, and F require essentially double the effort of designs A and B. These test results are consistent with theory, since the latter designs present only half the area of ice that must be sheared by the operating effort. In addition to reducing operating effort, an enclosed hinge contact lends itself to a simplicity of design that appreciably reduces the number of parts involved.

Messrs. Powell and Harrison call attention to single-pole testing. A designer can derive much valuable data from single-pole tests, but only 3-pole tests can provide a direct measurement of the interference introduced by ice formations covering a complete switch, inclusive of its operating control and interpole connections. Uniform ice coverage over extended areas can be accomplished by methods already described, but in order to confine the dimensions of test facilities within practical bounds, it may be desirable to limit 3-pole testing to classifications below 220 kv.

The 45-degree bearing test described in the paper was an intentional effort to simulate on one side ice build-up such as could be caused by a driving rain. Using our concept of balancing the variables, auxiliary angle sprays are unnecessary to fully surround the test equipment with ice.

Since the majority of the disconnecting switches in service are installed "normally closed," it is natural to place greater design emphasis on ability to operate from a closed position. We agree, however, that closing tests from a frozen open position should not be overlooked. The same standardized test procedure is applicable to either type of test.

The many closing tests that we have performed disclose few design considerations that differ from those of an opening operation. Each of the performance features enumerated in the summary of the paper is applicable to closing operations as well as to opening operations.

Thermal Transients on Buried Cables

F. H. BULLER
MEMBER AIEE

IN THE early days of the electrical industry, most engineers were not greatly concerned with transient ratings. If equipment performed as required under continuous load, they were satisfied and equipment was rated accordingly.

Now, there are many cases where apparatus does operate for long periods at full load, or substantially so. Obvious examples are certain types of ventilating fans and pumps, marine propulsion equipment, and base load generating stations. Such equipment, and the cables serving it, must, of course, be rated on a continuous basis; but most power cables handle diverse and fluctuating loads, and rarely if ever reach temperatures corresponding to peak loads continuously maintained.

It is, of course, very conservative to rate such cables on a continuous basis; but, while this procedure can sometimes be justified on the basis of potential load growth, the importance of continuous service on a particular circuit, or some consideration of that nature, it gives rise to increased investment cost, and can only be justified for particular applications and not as a general policy.

The existence of thermal transients on cable circuits, and the possibility of using the thermal time lag of such circuits to realize economies without violating existing temperature rules were recognized a long time ago. In England, transient heating tests are reported in the literature as far back as 1911;[1] and in 1923 Melsom and Booth published a technique for calculating transient ratings on low-voltage cables in air,[2] obviously with copper economy in mind. In 1927, S. Whitehead[4] gave a formula for transient heating of buried cables. It was an interesting, but not altogether satisfactory, variation on the exponential integral formula. In 1938 Whitehead and Hutchings[5] presented this formula as part of the recommended technique for transient ratings of buried cables, under the auspices of the British Electrical and Allied Industries Research Association.

American practice has tended to stress the cyclic character rather than the transient character of fluctuating loads, when attempting to gain economies by allowing for load fluctuations. British engineers were doubtless discouraged from so doing by a series of tests, reported in 1923[3] which show surprisingly little temperature difference between cyclic and continuous load, heating even at low load factors. These tests were based on directly buried cables, and on small cables drawn into very light duct structures, not deeply buried. These results do not necessarily apply directly to American practice, which involves almost exclusively the use of massive duct banks, deeply buried and heavily loaded with large cables, and which, until very recently, involved practically no buried cable. American correction factors for different load factors were first widely publicized in 1933[11] although they had been in general use for sometime before that.

Despite the stressing of the cyclic feature of fluctuating loads, American engineers by no means neglected transients per se. In 1929, N. P. Bailey published a formula for transient heating of buried cables.[6] W. B. Kirke in 1930 published a transient technique for use on cables in ducts; but he seems to have considered the soil component of the transient to be negligible.[7] E. A. Church in 1931[8] and again in 1935[13] presented a very interesting theory, based on Fourier analysis, covering both transient and cyclic loads on duct cables. He seems to have been inclined to include the thermal constants of the duct bank itself but to neglect those of the soil in obtaining his results.

In 1931 Shanklin and Buller,[9,10] published an exhaustive transient analysis for cables in air, primarily intended to solve the oil demand problem; they gave a simple (and approximate) correction factor to allow for the effect of the earth in the case of buried cable and duct cable. Miller and Wollaston,[12*] in a slightly different approach to the same problem in 1933 omitted the earth component of the transient from their mathematical work, and suggest that an empirical correction be used to take care of it.

About 1935, a more active interest in thermal transients per se, as distinct from their use in oil demand calculations, became apparent. This is emphasized by the publications of Church[13] and Kidder.[14] In 1942 Eaches,[15,16] made recommendations which carried weight with at least one major utility. Very little work on this subject seems to have been done during the war however, doubtless due to pressure of more urgent matters.

Since the war, thermal transients on buried cables, pipes, and other cylindrical heat sources have assumed a very considerable importance in many fields; transcontinental transmission of petroleum by pipe line, and heat pumps, as well as buried cables. Moreover, in the cable industry, interest in this matter has been stimulated by the increased use of pipe cable, and by the serious consideration of buried cable in many cases where duct cable was formerly used exclusively. Questions have been raised about thermal transients and the effect of cyclical loads on such cables. Do the old formulas, which are known to be reasonably satisfactory for duct cables, apply equally well to pipe cable?

In 1947, Carslaw and Jaeger's important book[17] on heat conduction was pub-

Paper 51-9, recommended by the AIEE Insulated Conductors Committee and approved by the AIEE Technical Program Committee for presentation at the AIEE Winter General Meeting, New York, N. Y., January 22–26, 1951. Manuscript submitted August 31, 1950; made available for printing November 14, 1950.

F. H. BULLER is with the General Electric Company, Schenectady, N. Y.

* F. O. Wollaston published a refinement[23] of this method in 1949, for cases where 3-conductor cables are involved.

lished; this book contains much material bearing on the subject of underground heat conduction of line and cylindrical sources, as does Ingersoll and Zobel's book,[19] and Ingersoll and Plass' paper[18] published in 1948. H. L. Knudsen[20] offered another solution in the same year. The technique of numerical analysis as presented by Dusinberre although entirely different from any of the other methods of handling the problem which will be discussed herein, is well worthy of consideration, especially in extending existing and proposed solutions to cover more complex conditions.

From the foregoing discussion, it should be evident that thermal transients on buried cables are a matter of importance from many points of view. Not only are the copper size and the economics of the system affected materially by these transient phenomena when an overload rating is required, as is so often the case nowadays; but any logical theory of cyclic loading and effect of load factor on rating should be based on a sound thermal transient theory. Again, oil demand is a direct function of the temperature transient; and by using a suitable formula, the mutual heating between adjacent buried cables during the transient period can be determined if required.

Comparison of Available Formulas

With all this background of interest and investigation, it is reasonable to expect that there will be a good many formulas and techniques for calculating thermal transients on buried cables. Such, indeed, proves to be the case. It is proposed to examine these formulas, to determine the advantages and limitations of each, and to establish a criterion by which their relative accuracy can be judged.

The formulas, in general, are found to fall into two groups: semiempirical formulas and Bessel cable* formulas.

* This terminology is due to Oliver Heaviside, who defines a Bessel cable as a cable in which conductance and capacitance (thermal or electrical) per unit length are directly proportional to the distance from a fixed point on the cable, which may conveniently be called the origin. While practical cables are not built in this way, the equations of the Bessel cable are identical with those for radial conduction in a homogeneous medium. Thus the term "Bessel cable" may be regarded as a convenient way of referring to a field in a homogeneous medium in which conduction is radial.

List of Symbols

W_0 = loss in cable or pipe, watts per centimeter assumed to be applied at time $t=0$

T_r = surface temperature rise of cable or pipe, degrees centigrade

T_c = copper temperature rise, degrees centigrade

R and R_n = empirically determined coefficients used in formula 1 and formula 2 respectively

α and α_n = empirically determined exponents, used in formula 1 and formula 2 respectively

p' = soil thermal resistivity, degree centigrade centimeter per watt

q = soil thermal capacity, watt-hour per degree centigrade per cubic centimeter

k = soil thermal diffusivity, $=1/p'q$ centimeter squared per hour

t = time, hours

r = radius of cable or pipe surface, centimeters

D = depth of burial, centimeters

Q = total thermal capacity of buried cable, or, in the case of pipe cable, of the pipe and its contents, watt-hour per degree centigrade per centimeter

Q_1 = thermal capacity of conductors, plus 1/2 of thermal capacity of insulation of buried cable or pipe cable, watt-hour per degree centigrade per centimeter (See Figure 1)

Q_2 = thermal capacity of finish (sheath and armor, jacket, and so forth of buried cable or skid wire and shield of pipe cable) plus 1/2 of thermal capacity of insulation; plus thermal capacity of oil or gas in pipe, in the case of a pipe cable, watt-hours per degree centigrade centimeter (See Figure 1)

R_1 = insulation thermal resistance of buried cable; insulation thermal resistance plus 1/2 of thermal resistance from cable to pipe (pipe cable), degree centigrade centimeter per watt (See Figure 1)

R_2 = thermal resistance of finish (jacket, armor, etc.) of buried cable; 1/2 of thermal resistance from cable to pipe (pipe cable), degree centigrade centimeter per watt (See Figure 1)

x = distance (greater than r) from the center of a cable buried in the earth, centimeters

β and ψ variables of integration, used in defining the integrals in formulas 3A, 4A, and 5

p_1 and p_2 = exponents, defined in Appendix II

T_1 and T_2 = coefficients, defined in Appendix II

$p = d/dt$ (the Heaviside operator)

$M_1 = Q_1/2\pi qr^2$

$M_2 = Q_2/2\pi qr^2$

$N_1 = p'/2\pi R_1$

$N_2 = p'/2\pi R_2$

$\sigma = x/r$

$\theta = u^2/p'q$

$u = \sqrt{pp'q} = j\lambda$

$\phi = \lambda r = -jur$

J_0, J_1, Y_0, Y_1, I_0, I_1, K_0, K_1 are Bessel functions, defined as in reference 17c.*

$F_0(\phi) = M_1M_2N_2\phi^3 - (M_1+M_2)N_1N_2\phi$

$F_1(\phi) = M_1M_2\phi^4 - (M_1N_2 + M_2N_1 + M_1N_1)\phi^2 + N_1N_2$

* Note that the functions designated by Y_0 and Y_1 in that reference are the same as those designated by N_0 and N_1 in reference 24.

Semiempirical Formulas

The Simple Exponential Formula

$$T_r = W_0R(1-\epsilon^{-\alpha t}) \qquad (1)$$

This is the earliest, simplest, and least exact of the available formulas. It gives cable surface temperature T_r only, and if copper temperature T_c is required, additional terms must be used.

It is satisfactory for use when the change in earth temperature contributes little to the transient under consideration, for example, short time temperature transients, and especially oil demand transients for cable in ducts. (Oil demand transients depend on rate of change of temperature and hence are less affected by the relatively slow soil heating components than are the temperature transients themselves.) On the other hand, the equation is open to question when used on directly buried cables.

Exponential Series Formulas

These are of the form

$$T_r = W_0\sum R_n(1-\epsilon^{-\alpha_n t}) \qquad (2)$$

This type of formula is attractive from the theoretical standpoint, since it is known[9,10] that the solution for the finite Bessel cable comes out in this form, and since the problem of soil heating is the problem of an infinite Bessel cable, and its image. Presumably therefore, it should be possible to obtain an analytical solution in this form.

N. P. Bailey[6] attempted to do this in his analysis; and while he was not entirely successful, his method is worthy of study from the mathematical standpoint by those who are interested in this form of solution.

The two principal champions of this formula, as a semiempirical form, are Dr. R. J. Wiseman and J. H. Neher. The problem is of course to evaluate the empirical coefficients R_n and the exponents α_n. Wiseman's technique involves the division of the cable (or pipe) and everything inside it into two zones, and the earth outside the cable into four zones, proportioned in a particular way. Each zone is treated as an independent unit, and coupling between zones is neglected. The constants are determined for each zone separately. While, from the theoretical standpoint, such coupling should be included, it is reported that this technique has worked satisfactorily in some cases.

Mr. Neher fits an exponential series to a curve obtained, preferably, from test data, and uses an ingenious method to provide coupling between the soil constants thus obtained and the cable (or

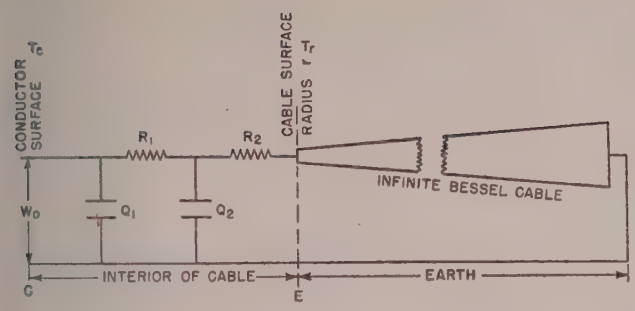

Figure 1 (above). Equivalent circuit of cable buried in infinite earth

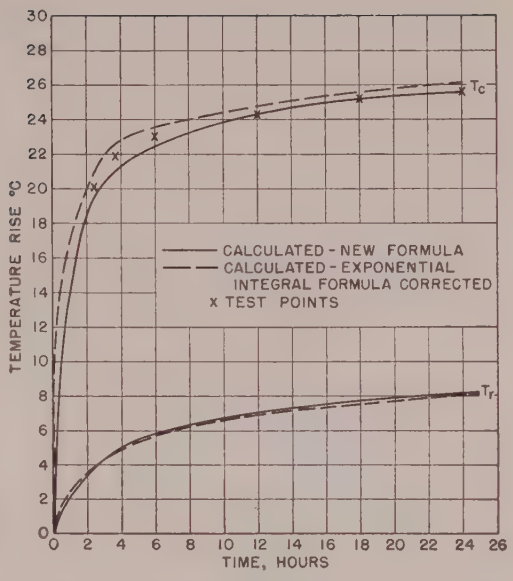

Figure 2 (right). Calculated and test results on 3-inch buried cable

pipe) constants. This method should work well if the necessary test data are available. In their absence, Mr. Neher recommends the use of the Ingersoll integral formula as a substitute. Thus, in such cases, the accuracy of the Neher technique depends, in the last analysis, on the accuracy of the Ingersoll integral formula.

Bessel Cable Formulas

The Exponential Integral and the Ingersoll Integral Formulas

The exponential integral formula takes the form

$$T_r=\frac{W_0p'}{4\pi}\left[-Ei\left(\frac{-r^2}{4kt}\right)+Ei\left(\frac{-D^2}{kt}\right)\right] \quad (3)$$

and the Ingersoll integral formula takes the form

$$T_r=\frac{W_0p'}{2\pi}\left[I\left(\frac{r}{2\sqrt{kt}}\right)-I\left(\frac{D}{\sqrt{kt}}\right)\right] \quad (4)$$

Here $-Ei(-x)$ is the exponential integral

$$\int_x^\infty \frac{\epsilon^{-\beta}}{\beta}d\beta \quad (3A)$$

and $I(x)$ is the Ingersoll integral

$$\int^\infty \frac{\epsilon^{-\beta^2}}{\beta}d\beta \quad (4A)$$

Formulas 3 and 4, in spite of the fact that they look different, may be proved to be identical.[17] Thus they can be treated as a single formula for purposes of this discussion. (Ingersoll did not originate formula 4; but so far as the writer knows, he was the first to calculate tables of the value of the integral (See reference 19 pages 253 and 254). Tables of the exponential integral will be found in reference 22.)

These formulas are extremely valuable and important. It is known[18] that they are very accurate for long times, and further that the effect of the image (the second term in the equation in each case) is negligible for short times (up to, say, 24 hours).

The formulas are, however, based on the assumption of a line source, the dimensions of the cable being taken into account by calculating the effect of the line source at a distance r, equal to the radius of the cable. This is tantamount to replacing the actual cable by a cylinder of soil of radius r. This approximation turns out to be not nearly as wild as it sounds, but is subject to further investigation for short values of time.

Here again the formula gives only the temperature at the surface of the cable, T_r, and does not give the copper temperature directly. If the copper temperature is required it is necessary to add some extra terms, making allowance for coupling in some way. The Neher technique is one way of handling this.

By utilizing these formulas for long times, the problem is reduced to finding a suitable formula for short times (up to 24 hours) and then checking it against these formulas to determine to what extent they should be corrected.

An interesting variation of these formulas, involving a cylinder source was proposed by Whitehead.[4] It was obtained by superposition of a series of line sources located on the surface of a cylinder of radius r. It took the form

$$T_r=\frac{W_0p'}{4\pi}\left[\int_0^t \epsilon^{-r^2/2k\psi}I_0\left(\frac{r^2}{2k\psi}\right)d\psi-\int_0^t \epsilon^{-(4D^2+r^2)/4k\psi}I_0\left(\frac{Dr}{k\psi}\right)d\psi\right] \quad (5)$$

It was presented in reference 5 with the integrals worked out in series form; and it amounts to an exponential integral formula with a correction factor.

The superposition of a group of line sources on the surface of a cylinder of radius r gives a thin cylindrical shell, situated in the middle of an infinite earth and filled with earth. The image of this shell can be included by the use of the second term in the foregoing formula. It should give better results than the exponential integral formula for the case of a cable heated from the sheath; but where most of the heat, or all of it, comes from the conductor, the exponential integral formula, uncorrected, is probably the more accurate.

*The Carslaw and Jaeger Formulas**

These formulas take the form

$$T_r=-\frac{W_0p'r}{\pi^2}\int_0^\infty (1-\epsilon^{-\lambda^2t/p'q})\times\frac{J_0(\lambda x)\,Y_1(\phi)-Y_0(\lambda x)J_1(\phi)}{\phi^2[J_1^2(\phi)+Y_1^2(\phi)]}\,d\lambda \quad (6)$$

$$T_r=-\frac{W_0p'r}{\pi^2}\int_0^\infty (1-\epsilon^{-\lambda^2t/p'q})\times\frac{\{J_0(\lambda x)\,[Y_1(\phi)-M_1\phi\,Y_0(\phi)]-Y_0(\lambda x)\,[J_1(\phi)-M_1\phi J_0(\phi)]\}}{\phi^2\{[Y_1(\phi)-M_1\phi\,Y_0(\phi)]^2+[J_1(\phi)-M_1\phi J_0(\phi)]^2\}}\,d\lambda \quad (7)$$

Here

$$M_1=\frac{Q_1}{2\pi qr^2} \text{ and } \phi=\lambda r$$

The preceding formulas are for the temperature at a distance x from the center of a cable or pipe of radius r, buried in the center of an infinite earth. To get the cable temperature, substitute r for x in the formulas. To get the temperature at r due to the image, substitute $2D$ for x in the formulas and reverse the sign of W_0. The temperature of a cable buried at depth D is of course the algebraic sum of the cable temperature and the temperature due to the image.

* These formulas will be found in reference 17, pages 283, 284. The notation used therein has been changed to line up with reference 10.

Formula 6 is the temperature transient equation for a cylindrical source of zero thermal capacity; and formula 7 is the equation for a cylindrical source with thermal capacity Q_1.

Both these formulas give the surface temperature of the cable or pipe, T_r under the conditions specified above. Formula 6 involves no coupling with anything inside the pipe, and formula 7 allows for coupling with the thermal capacity Q_1. Neither of these formulas gives the copper temperature directly.

The Knudsen Formula

All of the foregoing formulas involve certain simplifying assumptions. Formulas 3 and 4 involve the assumption that the actual contents of the cable or pipe are replaced by a cylinder of earth which has the same thermal constants as the outside earth. Formula 6 neglects the contents of the cable or pipe altogether; while formula 7 takes the thermal capacity of these contents into account (as a lumped constant) but neglects entirely their distribution, and also any thermal resistance inside the pipe.

Actually, if we have a buried single-conductor cable, we have two Bessel cables in series; a finite Bessel cable representing the actual cable, with inside radius equal to that of the conductor, outside radius r, and a lumped thermal capacity Q_c at the conductor, coupled to the second Bessel cable, which represents the earth, through an impedance

$$\frac{R_2}{pQ_2R_2+1}$$

representing the thermal resistance of the sheath (and armor if any) and the thermal capacity of these elements. A 3-conductor buried cable, or a buried pipe cable, is approximately represented by such a pair of Bessel cables in series.

Hans Lottrup Knudsen of the University of Copenhagen (Denmark) has developed a theoretical formula for two such Bessel cables in series. He did not see fit to use an infinite Bessel cable to represent the earth; instead he used a finite Bessel cable, of radius Ar, where A is some arbitrary constant. He stated in his paper[20] that $A=2$ should be satisfactory.

A numerical check showed that the results obtained using various values of A differed considerably. The results obtained from this formula tended to approach those obtained from formula 3 as A was increased. It is evident that while Knudsen's fundamental assumptions are very accurate, his approximation is not satisfactory. Moreover, the formula is exceedingly difficult to apply, even in the form recommended by Knudsen.

A New Formula

All the foregoing formulas seem to be open to some questions, either in the fundamental assumptions on which they are based, or in the simplifying assumptions made in the course of development. It would seem that a new formula is desirable, which would fulfill the following conditions:

(A) It should be based on fundamental assumptions which represent closely the actual conditions met in practice.

(B) It should give both copper and surface temperatures directly, without additional approximations.

(C) If too complicated for everyday design calculations, it should be capable of serving as a criterion, against which design formulas can be checked.

Such a formula has been derived by the writer. The fundamental assumptions are those shown in Figure 1. The derivation will be found in Appendix II. The formula takes the forms shown in equations 8, 8A, 8B, 8C, 8D, and 9.

It will be noted that these formulas are based on a simple circuit consisting of lumped constants, in series with an infinite Bessel cable; see Figure 1. This simplifying assumption of lumped constants arranged in this particular way has been found to work very well as an accurate approximation for radial heat conduction in the case of a cable in air, and serves as the basis of a practical design formula for such cables (see references 9 and 10 for the corresponding exact Bessel cable formulas). It should work at least equally well if the cable is buried. On the other hand, it greatly simplifies the result that would be obtained if the actual cable were replaced by a Bessel cable as proposed by Knudsen. Thus condition (A) is met for all practical purposes.

Condition (B) is obviously met by using formula 9 for the copper temperature, and using formulas 8 and 8D as follows:

1. To obtain the surface temperature of the cable due to its own heating, use formula 8D.

2. Substitute $2D$ for x in formulas 8C and 8, and reverse the sign to get the effect of the image.

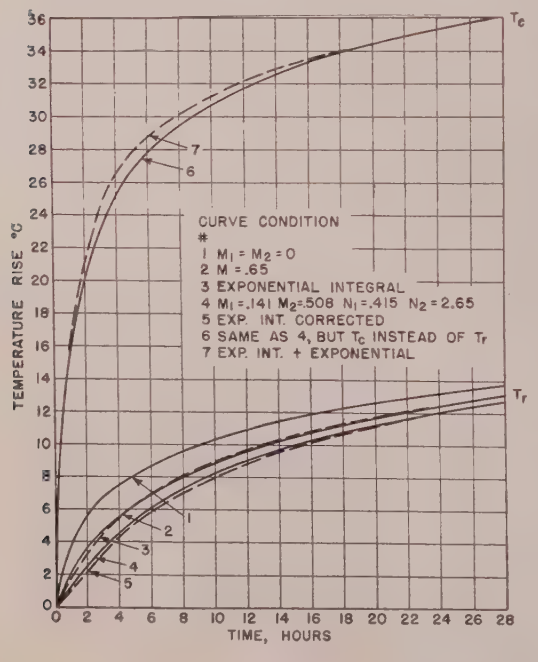
TEMPERATURE RISE °C
TIME, HOURS
T_c
T_r
CURVE CONDITION
#
1 $M_1 = M_2 = 0$
2 M = .65
3 EXPONENTIAL INTEGRAL
4 $M_1 = .141$ $M_2 = .508$ $N_1 = .415$ $N_2 = 2.65$
5 EXP. INT. CORRECTED
6 SAME AS 4, BUT T_c INSTEAD OF T_r
7 EXP. INT. + EXPONENTIAL

Figure 3 (left). Calculated results on 8⅝-inch pipe cable comparison of exponential integral formula with new formula, and effect of varying M and N

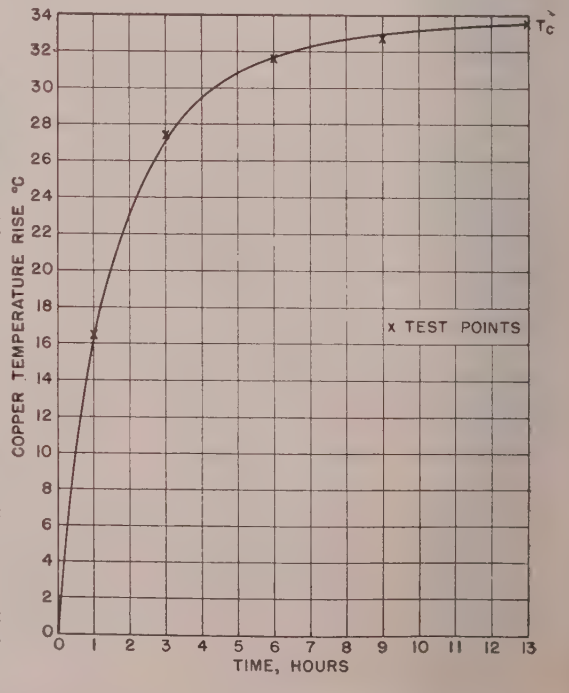

Figure 4 (right). Duct cable

Comparison of exponential integral formula plus exponential terms with test curve is calculated

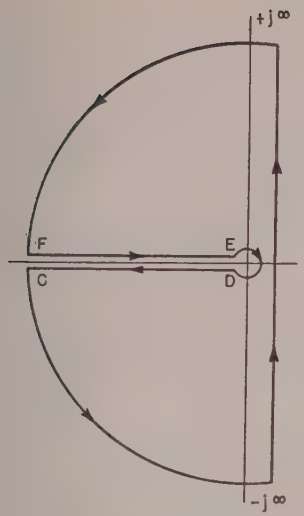

Figure 5. Inversion theorem path of integration

3. Add the results algebraically.

With regard to condition (C), it is unfortunate that the integrals are too complicated to be evaluated in formal terms. Fortunately they converge quite rapidly; and for values of ϕ greater than ten, they can be evaluated as exactly as desired by using the asymptotic forms of the Bessel functions. This will very rarely be necessary, however, since such evaluation gives a negligible correction factor.

Mechanical or numerical integration is necessary to evaluate the integrals over the interval $\phi=0$ to $\phi=10$. The actual work of calculating a transient curve of T_c and T_r for one cable or pipe size consumes about 16 hours.

Thus, though the formulas are hardly suited for everyday design calculations, they should be satisfactory as a criterion against which other formulas can be checked. In this respect they are analogous to a laboratory standard instrument, which is used to check the readings of more simple, rugged and versatile but less accurate test and switchboard instruments.

$$T_x=-\frac{W_0p'}{\pi^2}\int_0^\infty(1-\epsilon^{-\phi^2t/p'qr^2})\times \frac{\{F_1(\phi)[J_0(\sigma\phi)Y_1(\phi)-Y_0(\sigma\phi)J_1(\phi)]+F_0(\phi)[J_0(\sigma\phi)Y_0(\phi)-Y_0(\sigma\phi)J_0(\phi)]\}N_1N_2}{\phi^2\{[F_1(\phi)J_1(\phi)+F_0(\phi)J_0(\phi)]^2+[F_1(\phi)Y_1(\phi)+F_0(\phi)Y_0(\phi)]^2\}}d\phi \quad (8)$$

$$T_c=\frac{2W_0p'}{\pi^2}\int_0^\infty\times \frac{(N_1N_2)^2(1-\epsilon^{-\phi^2t/p'qr^2})}{\phi^3\{[F_1(\phi)J_1(\phi)+F_0(\phi)J_0(\phi)]^2+[F_1(\phi)Y_1(\phi)+F_0(\phi)Y_0(\phi)]^2\}}d\phi \quad (9)$$

where

$$F_1(\phi)=M_1M_2\phi^4-(M_1N_2+M_2N_1+M_1N_1)\phi^2+N_1N_2 \quad (8A)$$

$$F_0(\phi)=M_1M_2N_2\phi^3-(M_1+M_2)N_1N_2\phi \quad (8B)$$

$$\sigma=x/r \quad (8C)$$

T_x = temperature in the earth, at a distance x from the center of the cable

T_c = copper temperature

To get T_r, substitute r for x in equation 8C, which gives $\sigma=1$. Substituting this value in formula 8 gives:

$$T_r=\frac{2W_0p'}{\pi^2}\int_0^\infty \frac{N_1N_2F_1(\phi)(1-\epsilon^{-\phi^2t/p'qr^2})}{\phi^3\{[F_1(\phi)J_1(\phi)+F_0(\phi)J_0(\phi)]^2+[F_1(\phi)Y_1(\phi)+F_0(\phi)Y_0(\phi)]^2\}}d\phi \quad (8D)$$

To get the effect of the image, substitute $x=2D$ in formula 8C, and $\sigma=2D/r$ in formula 8.

Results of Calculations

Comparison with Test Results

Test data for periods of less than 24 hours on cable transients are available in reference 3. Figure 2 shows how the formula compares with these test data. The agreement is acceptable; and it might have been even closer if the thermal resistivity and diffusivity of the soil had been more exactly known. These constants were unfortunately not given in reference 3, and it was necessary to estimate them from the test data presented.

Effect of Varying Constants

Figure 3 shows the results of calculations made on a pipe cable installation with a pipe $8^5/_8$ inch outside diameter under the following conditions:

(A) $M_1=M_2=0$

(B) $M=0.65N_1=N_2=\infty$

(C) $M_1=0.141$ $M_2=0.509$
$N_1=0.415$ $N_2=2.65$

(D) By formula 3

(E) By formula 10 (see below)

Taking case (C) as the standard of accuracy, it will be seen

1. That the exponential integral formula gives good results.

2. That the use of the exponential integral with correction factor gives excellent results.

3. That the use of an M value corresponding to the total thermal capacity of the pipe contents (formula 7) gives results that check very closely with the exponential integral formula (which corresponds approximately to a value of $M=0.500$).

4. The value $M=0$ (formula 6) gives too high a rate of temperature rise.

5. After 24 hours, the exponential integral formula agrees very closely with the new formula.

6. The effect of the image during the first 24 hours is negligible.

The corrected exponential integral formula and the new formula also are compared in Figure 2, where the surface temperature T_r of a 3-inch cable is calculated. It will be seen that the corrected exponential integral still gives good agreement with the new formula.

Working Formulas

As was suspected, the formulas for copper and sheath temperatures turn out to be too complicated for use as design formulas. However, they do give a valuable check on the accuracy to be expected of the simpler formulas.

Using the new formulas in this way, we can arrive at the following working formula (see Figures 2 and 3 for direct comparison).

$$T_r=\frac{W_0p'}{4\pi}\left[-Ei\left(\frac{-r^2}{4kt}\right)+Ei\left(\frac{-D^2}{kt}\right)\right]\times\left[1-\frac{p'Q}{4\pi t}\epsilon^{-r^2/4kt}\right] \quad (10)$$

For copper temperatures

$$T_c=T_r+w_0(R_1+R_2+T_1+T_2) \quad (11)$$

For the evaluation of T_1 and T_2, see Appendix II.

These formulas are easy to use, and give acceptably accurate results for most practical purposes. The author is prepared to provide a worked example, if desired.

Cables in Ducts

The new formulas do not apply to cables in ducts. Neither the duct radius itself, nor the equivalent periphery of the duct bank seems to give accurate results. The calculations on which this statement is based were made on a 6-duct bank with only one cable loaded, and it is possible that a fully loaded duct bank might give a more satisfactory correlation.

This is probably because the structure of the duct bank so distorts the heat

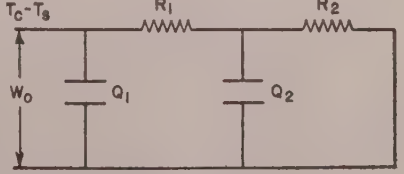

Figure 6. Equivalent circuit for calculation of exponential terms in formula 10

field, particularly in the critical region in the neighborhood of the cable, that the fundamental assumptions on which the formulas are based do not hold. While it might be possible to find some equivalent radius that would make the formulas fit reasonably well, it does not seem worthwhile to try to adapt a complicated mathematical derivation to conditions to which it is known to be unsuited.

The best plan is to use formula 3 for T_r, using a value of r equal to the periphery of the duct assembly divided by π, and then to get T_c from T_r by using formula 11. The results of this procedure are shown in Figure 4 for a particular test.

Conclusions

1. All present formulas and techniques for calculating temperature transients on buried cables have theoretical limitations.
2. A more accurate formula has been developed herein in which these theoretical limitations are overcome. While too complicated for an everyday working formula, it forms an acceptable standard of comparison against which such formulas can be checked.
3. The exponential integral formula, with a simple correction factor, is an excellent working formula for the calculation of T_r.
4. Copper temperatures may be calculated with fair accuracy by adding the effect of the thermal resistances and capacitances inside the cable directly as though they acted independently, and neglecting coupling between the earth part of the circuit, and the interior of the cable.
5. The new formula does not apply to cables in ducts. Formulas are given which appear to be reasonably accurate for such cables on the basis of known test results.

Two Possible Lines of Further Investigation

While the formulas developed herein are more exact than any given previously, and while the test data seem to indicate that they are close enough for almost any practical purpose, there are doubtless investigators who feel that the circuit of Figure 1 is too rough an approximation. It is, of course, always possible to improve this circuit by adding more elements of resistance and capacity; and, in the limit, it is possible to go to a finite Bessel cable as proposed by Knudsen. While the increased precision of such a treatment is probably not worth the great extra complication involved, it presents an interesting mathematical problem, which someone may desire to solve.

A more important practical point is the following one: every Bessel cable formula in the present paper is based on the assumption of a homogeneous earth with an isothermal surface. While the error introduced by the departure of the surface from the isothermal is practically negligible even in the steady state, and is even smaller in short time transient calculations, variations of soil thermal resistivity and specific heat may not be negligible. It is known that the moisture content of the soil increases with depth, although the law relating moisture content to depth does not appear to have been established; and furthermore moisture migration toward the cable (by seepage into the back-filled cable trench) or away from it (due to heating) produces further departures from homogeneity.

Differential equations with variable coefficients are notoriously refractory; probably the best method of attacking this problem is by some form of numerical analysis.[21] In any case a comparison of the calculated results obtained herein with test results indicates that these effects are probably secondary in character and can be safely neglected for reasonably conservative loading.

Appendix I. Derivation of Equations 8 and 9

The differential equation of cylindrical conduction in a homogeneous medium is[10]

$$\frac{\partial T}{\partial t}=\frac{1}{p'q}\left[\frac{\partial^2 T}{\partial x^2}+\frac{1}{x}\frac{\partial T}{\partial x}\right] \tag{12}$$

Expressed in Heaviside form, this equation becomes

$$\frac{d^2T}{dx^2}+\frac{1}{x}\frac{dT}{dx}-pp'qT=0 \tag{13}$$

The solution of this equation is

$$T=AI_0(ux)+BK_0(ux) \tag{14}$$

where $u=\sqrt{pp'q}$. Now, the heat flow is given by the equation

$$-W=\frac{2\pi x}{p'}\frac{\partial T}{\partial x}$$

So that

$$W=-\frac{2\pi ux}{p'}[AI_1(ux)-BK_1(ux)] \tag{15}$$

If the boundary condition at $x=\infty$ is $T=0$, then $A=0$, and

$$T=BK_0(ux)$$

$$W=\frac{2\pi ux}{p'}BK_1(ux) \tag{16}$$

Referring to Figure 1, let $T=T_r$ and $W=W_r$ at the point E. Then

$$T_r=BK_0(ur)$$

$$W_r=\frac{2\pi ur}{p'}BK_1(ur) \tag{17}$$

The thermal impedance of the circuit consisting of the series resistances R_1 and R_2, and the parallel capacitances Q_1 and Q_2 may readily be evaluated by the Heaviside technique, which treats a capacitance as though it were a resistance of value $1/pQ$. Proceeding in this way we find that, at the point C

$$W_0=B[p(Q_1+Q_2+pQ_1Q_2R_1)K_0(ur)+\frac{2\pi ur}{p'}K_1(ur)(1+pQ_2R_2+pQ_1R_1+pQ_1R_2+p^2Q_1Q_2R_1R_2)]$$

or

$$B=\frac{W_0}{[p^2Q_1Q_2R_1+p(Q_1+Q_2)]K_0(ur)+[p^2Q_1Q_2R_1R_2+p(Q_1R_1+Q_2R_2+Q_1R_2)+1]\frac{2\pi ur}{p'}K_1(ur)}$$

giving

$$T_c=\frac{W_0[(pQ_2R_1R_2+R_1+R_2)\frac{2\pi ur}{p'}K_1(ur)+(1+pQ_2R_1)K_0(ur)]}{[p^2Q_1Q_2R_1+p(Q_1+Q_2)]K_0(ur)+[p^2Q_1Q_2R_1R_2+p(Q_1R_1+Q_2R_2+Q_1R_2)+1]\frac{2\pi ur}{p'}K_1(ur)}$$

Now substitute $p=u^2/p'q$, and write

$$M_1=\frac{Q_1}{2\pi qr^2}\quad M_2=\frac{Q_2}{2\pi qr^2}\quad N_1=\frac{p'}{2\pi R_1}\quad N_2=\frac{p'}{2\pi R_2}$$

Then

$$T_c=\frac{\frac{W_0p'}{2\pi}[\{M_2(ur)^2+N_1+N_2\}urK_1(ur)+\{M_2N_2(ur)^2+N_1N_2\}K_0(ur)]}{[M_1M_2(ur)^4+(M_1N_2+M_2N_1+M_1N_1)(ur)^2+N_1N_2]urK_1(ur)+[M_1M_2N_2(ur)^4+(M_1+M_2)N_1N_2(ur)^2]K_0(ur)} \tag{18}$$

Also

$$T_r=\frac{\frac{W_0p'}{2\pi}N_1N_2K_0(ur)}{[M_1M_2(ur)^4+(M_1N_2+M_2N_1+M_1N_1)(ur)^2+N_1N_2]urK_1(ur)+[M_1M_2N_2(ur)^4+(M_1+M_2)N_1N_2(ur)^2]K_0(ur)} \tag{19}$$

And at the point x, out in the earth, since $T_x=BK_0(ux)$

$$Tx=\frac{\frac{W_0p'}{2\pi}N_1N_2K_0(ux)}{[M_1M_2(ur)^4+(M_1N_2+M_2N_1+M_1N_1)(ur)^2+N_1N_2]urK_1(ur)+[M_1M_2N_2(ur)^4+(M_1+M_2)N_1N_2(ur)^2]K_0(ur)} \tag{20}$$

Now, it is evident that equation 18 can be written

$$T_c=\frac{W_0p'}{2\pi}\frac{F(ur)}{G(ur)} \tag{21}$$

In general, $F(ur)$ and $G(ur)$ are complex quantities; and, unfortunately there do not appear to be any roots of the equation $G(ur)=0$, so that the Heaviside expansion the-

orem cannot be applied to evaluate equations 18 to 20 as a function of time. It is necessary to go to the Laplace Transform, and to use the Inversion Theorem to do this.

There is more than one Laplace Transform notation. In order to simplify correlation with the work of those authors, we will use the notation employed by Carslaw and Jaeger; and we also will use their Bessel function notation. Note that their Y functions are the same as the Jahnke and Emde N functions. In this notation

$$T_c=\frac{W_0p'}{2\pi}\frac{1}{p}\frac{F(ur)}{G(ur)}=\frac{W_0p'}{2\pi}v \tag{22}$$

This equation gives T_c in the operational form, that is, as a function of p. The expression $(1/p)[F(ur)/G(ur)]$ is called the Laplace Transform of the equation for T_c. To get T_c as an explicit function of time, it is necessary to obtain the inverse transform of $(1/p)[F(ur)/G(ur)]$. This is done by the use of two theorems. The first is the one called Theorem IV by Carslaw and Jaeger (reference 17, page 242)

$$\frac{1}{p}\frac{F(ur)}{G(ur)}=L\left\{\int_0^t v(t')dt'\right\} \tag{23}$$

and the second, called the Inversion Theorem, states that

$$v(t')=\frac{1}{2\pi j}\int_{\gamma-j\infty}^{\gamma+j\infty}\epsilon^{\theta t}L\{\theta\}d\theta \tag{24}$$

The expression $L\{v(t')\}$ should be read "The Laplace Transform of $v(t')$." Writing $\theta=u^2/p'q$, and $L\{\theta\}=F(ur)/G(ur)$, and substituting in equation 24 gives

$$v(t')=\frac{1}{2\pi r^2 j}\int_{\gamma-j\infty}^{\gamma+j\infty}ur\left[\epsilon^{(ur)^2t'/p'qr^2}\right]\frac{F(ur)}{G(ur)}\times d(ur) \tag{25}$$

and

$$T_c=\frac{W_0}{2\pi^2qr^2j}\int_0^t v(t')dt' \tag{26}$$

This is an integral in the complex plane. Since there is a singularity at $u=0$, the part of integration shown in Figure 5 is used. The contour integral around this path, designated by the symbol $\oint$ becomes

$$\oint=\int_{FE}+\int_{DC}+\oint_{ED} \tag{27}$$

The integrals on the right-hand side of this equation are respectively the line integral along the line FE, the line integral along the line DC, and the integral around the small circle ED enclosing the singularity at the origin. Now, by the theory or residues,

$$\oint_{ED}=2\pi j\operatorname*{Res}_{u=0}\left[ur\,\epsilon^{u^2t/p'q}\frac{F(ur)}{G(ur)}\right]$$

$$=2\pi j\left[\frac{F(ur)\epsilon^{u^2t/p'q}}{\dfrac{\partial}{\partial u}\dfrac{G(ur)}{ur}}\right]_{u=0}$$

By evaluation of this expression, it is found that $\oint_{ED}=0$. To obtain the line integrals $\int_{FE}$ and $\int_{DC}$, substitute $u=j\lambda$, and use the formulas

$$\left.\begin{aligned}K_0(jz)&=\frac{-j\pi}{2}[J_0(z)-jY_0(z)]\\K_1(jz)&=\frac{-\pi}{2}[J_1(z)-jY_1(z)]\end{aligned}\right\} \tag{28}$$

Substitute these expressions into equation 18, and rationalize the denominator, for each of these integrals. The sum of the two integrals will be found to be

$$-\frac{2W_0}{\pi^3qr^2}\int_0^\infty\frac{(N_1N_2)^2\lambda r\epsilon^{-(\lambda r)^2t/p'qr^2}}{[\{M_1M_2(\lambda r)^4-(M_1N_2+M_2N_1+M_1N_1)(\lambda r)^2+N_1N_2\}\lambda rJ_1(\lambda r)+\{M_1M_2(\lambda r)^2-(M_1+M_2)N_1\}N_2(\lambda r)^2\times J_0(\lambda r)]^2+[\{M_1M_2(\lambda r)^4-(M_1N_2+M_2N_1+M_1N_1)(\lambda r)^2+N_1N_2\}\lambda rY_1(\lambda r)+\{M_1M_2(\lambda r)^2-(M_1+M_2)N_1\}N_2(\lambda r)^2\times Y_0(\lambda r)]^2}\cdot d(\lambda r)$$

This is the expression for $v(t')$. To get T_c from equation 22, this expression must be integrated with respect to time, between time t and zero. Performing this integration, and writing

$$\lambda r=\phi$$

$$M_1M_2(\lambda r)^4-(M_1N_2+M_2N_1+M_1N_1)(\lambda r)^2+N_1N_2=F_1(\phi)$$

$$M_1M_2N_2(\lambda r)^3-(M_1+M_2)N_1N_2(\lambda r)=F_0(\phi)$$

gives

$$T_c=\frac{+2W_0p'}{\pi^3}\int_0^\infty\frac{(N_1N_2)^2(1-\epsilon^{-\phi^2t/p'qr^2})}{\phi^3[\{F_1(\phi)J_1(\phi)+F_0(\phi)J_0(\phi)\}^2+\{F_1(\phi)Y_1(\phi)+F_0(\phi)Y_0(\phi)\}^2]}d\phi \tag{29}$$

By following the same procedure, it can be shown that at a distance x from the center of the cable, x being greater than r

$$T_x=\frac{-W_0p'}{\pi^3}\int_0^\infty\frac{\{F_1(\phi)[J_0(\sigma\phi)Y_1(\phi)-Y_0(\sigma\phi)J_1(\phi)]+F_0(\phi)[J_0(\sigma\phi)Y_0(\phi)-Y_0(\sigma\phi)J_0(\phi)]\}N_1N_2\left(1-\epsilon^{-\frac{\phi^2t}{p'qr^2}}\right)}{\phi^2[\{F_1(\phi)J_1(\phi)+F_0(\phi)J_0(\phi)\}^2+\{F_1(\phi)Y_1(\phi)+F_0(\phi)Y_0(\phi)\}^2]}d\phi \tag{30}$$

And, by substituting $x=r$ in equation 30, it is found that, when

$$x=r$$

$$T_r=+\frac{2W_0p'}{\pi^3}\int_0^\infty\frac{F_1(\phi)N_1N_2(1-\epsilon^{-\phi^2t/p'qr^2})d\phi}{\phi^3[\{F_1(\phi)J_1(\phi)+F_0(\phi)J_0(\phi)\}^2+\{F_1(\phi)Y_1(\phi)+F_0(\phi)Y_0(\phi)\}^2]} \tag{31}$$

The foregoing equations refer to a cable situated in the center of an infinite earth. To make proper allowance for the actual depth of burial in the case of a practical cable installation, introduce an image at a distance $2D$ from the center of the cable. This can be done by substituting $2D$ in equation 30, reversing the sign of this equation, and adding the result to equations 29 and 31.

In the foregoing equations, W_0 is in watts per centimeter length. If W_0 is given in watts per foot, divide by 30.5 to get watts per centimeter.

Appendix II. Solution for the Circuit in Figure 6

In Heaviside notation, the operational equation for this circuit is

$$T=\frac{W_0(pQ_2R_1R_2+R_1+R_2)}{p^2Q_1Q_2R_1R_2+p(Q_1R_1+Q_2R_2+Q_1R_2)+1}$$

This expression is derived in the usual manner, by treating Q_1 and Q_2 as though they were resistances, of value $1/pQ_1$ and $1/pQ_2$ respectively, and combining these "resistances" with the actual resistances R_1 and R_2 in series-parallel, as shown in Figure 6.

By using the Expansion Theorem on the above expression, it is found that T_c-T_s, the conductor rise over the cable surface temperature, T_r, is

$$T_c-T_s=W_0(R_1+R_2+T_1+T_2)$$

where

$$T_1=\frac{(p_1Q_2R_1R_2+R_1+R_2)\epsilon^{p_1t}}{2p_1{}^2Q_1Q_2R_1R_2+p_1(Q_1R_1+Q_2R_2+Q_1R_2)}$$

T_2 is the same expression, with p_2 substituted for p_1

$$p_1=\frac{-(Q_1R_1+Q_2R_2+Q_1R_2)}{2Q_1Q_2R_1R_2}+\sqrt{\left(\frac{Q_1R_1+Q_2R_2+Q_1R_2}{2Q_1Q_2R_1R_2}\right)^2-\frac{1}{Q_1Q_2R_1R_2}}$$

$$p_2=\frac{-(Q_1R_1+Q_2R_2+Q_1R_2)}{2Q_1Q_2R_1R_2}-\sqrt{\left(\frac{Q_1R_1+Q_2R_2+Q_1R_2}{2Q_1Q_2R_1R_2}\right)^2-\frac{1}{Q_1Q_2R_1R_2}}$$

References

1. Heating of Cables with Current, **Melsom, Booth.** *Journal*, Institution of Electrical Engineers (London, England), volume 47, May 1911, page 711.

2. The Rating of Cables for Intermittent or Fluctuating Loads, **Melsom, Booth.** *Journal*, Institution of Electrical Engineers (London, England), volume 61, March 1923, page 363.

3. Permissible Loading of British Standard Impregnated Paper Insulated Electric Cables, **Melsom, Fawssett.** *Journal*, Institution of Electrical Engineers (London, England), volume 61, May 1923, page 517.

4. Determining Temperature Distribution, **S. Whitehead.** *Electrician* (London, England), volume 99, August 19, 1927, page 225.

5. Current Rating of Cables for Transmission and Distribution, **S. Whitehead, E. E. Hutchings.** *Journal*, Institution of Electrical Engineers (London, England), volume 83, Appendix 3, 1938, pages 551–52.

6. Heat Flow from Underground Electric Power Cables, **N. P. Bailey.** *AIEE Transactions*, volume 48, January 1929, pages 156–65.

7. The Calculation of Cable Temperature in Subway Ducts, **W. B. Kirke.** *AIEE Journal*, volume 49, part II, 1930, page 855–59.

8. Temperatures in Electric Power Cables under Variable Loading, **E. A. Church.** *AIEE Transactions*, volume 50, September 1931, pages 982–92.

9. Characteristics of Oil-Filled Cable, **G. B. Shanklin, F. H. Buller.** *AIEE Transactions*, volume 50, December 1931, pages 1411–20.

10. The Theory of Oil-Filled Cable, **G. B. Shanklin, F. H. Buller.** *General Electric Review* (Schenectady, N. Y.), volume 34, July 1931, page 416; September 1931, page 523.

11. Current Carrying Capacity of Impregnated Paper Insulated Cable. *Publication A-14*, Edison Electric Institute (New York, N. Y.), July 1933.

12. Thermal Transients and Oil Demands on Cables, **K. W. Miller, F. O. Wollaston.** *AIEE Transactions*, volume 52, March 1933, pages 98–113.

13. Economical Loading of Underground Cables, **E. A. Church.** *Electrical Engineering* (*AIEE Transactions*), volume 54, November 1935, pages 1166–72.

14. Notes on Emergency Ratings, **A. H. Kidder.** *Electrical Engineering* (*AIEE Transactions*), volume 58, November 1939, pages 599–610.

15. Calculation of Emergency Ratings for Underground Cables, **A. R. Eaches.** *Report*, Philadelphia Electric Company (Philadelphia, Pa.), 1942.

16. Comparison of Thermal Characteristics of Terra Cotta Ducts in Concrete Envelope and Extruded Concrete Ducts Without Envelope, **A. R. Eaches.** *Report*, Philadelphia Electric Company (Philadelphia, Pa.), March 16, 1942.

17. Conduction of Heat in Solids (book), **Carslaw, Jaeger.** Oxford University Press (London, England), 1947.

18. Theory of the Ground Pipe Heat Source for the Heat Pump, **Ingersoll, Plass.** *Journal*, American Society of Heating and Ventilating Engineers (New York, N. Y.), volume 20, July 1948, page 119.

19. Heat Conduction (book), **Ingersoll, Zobel.** McGraw-Hill Book Company, New York, N. Y., 1948.

20. Temperature in Oil-Filled Cables Buried in Earth, **H. L. Knudsen.** *Paper 478-11*, Institution of Civil Engineers (London, England), 1949.

21. Numerical Analysis of Heat Flow, **G. M. Dusinberre.** McGraw-Hill Book Company, New York, N. Y., 1949.

22. Tables of Functions, **Jahnke, Emde.** Dover Publications, New York, 1945.

23. Transient Temperature Phenomena of 3-Conductor Cables, **F. O. Wollaston.** *AIEE Transactions*, volume 68, part II, 1949, pages 1284–97.

Discussion

W. A. Del Mar (Phelps Dodge Copper Products Corporation, Yonkers, N. Y.): Mr. Buller has performed a valuable service in establishing a standard whereby the accuracy of more workable methods of calculation may be evaluated. In case anyone should be alarmed by the complexities of Mr. Buller's "short method," and the still shorter method of Mr. Wiseman, they can have recourse to an electronic analogue computer which will enable the same calculations to be made in a matter of minutes without the risk of error which is inseparable from long calculations.

J. H. Neher (Philadelphia Electric Company, Philadelphia, Pa.): Mr. Buller has given us a very complete summary of the attempts by various investigators to derive mathematical expressions for the transient temperature rise over a whole or a part of the thermal circuit of a buried cable system with a constant load suddenly applied, even to developing formulas of his own which are equally incomprehensible. While he is to be commended for his attempts to develop simplified mathematical expressions for these relationships, however, I am convinced that the formulas thus derived still have the infirmity of many of their predecessors; that is, an invalid assumption that the temperature rise at the juncture of two thermal networks can be accurately represented without accounting for the mutual effect of each on the other at that juncture.

In order to obtain a proper appreciation of the problem, it is advantageous to consider the heat transfer system as a thermal network consisting of shunt thermal capacities interspersed between series thermal resistances as shown in Figure 1 of this discussion. It will be evident that the accuracy of such a representation may be increased at will, by increasing the number of lumped capacities and associated resistances used to represent a given section in which the capacity involved is actually distributed. By reference to the figure, it is readily seen that heat entering C_1 produces a charge therein and a temperature change which causes some heat to flow through H_1 and some to enter and modify the charge on C_2, and so on successively through the network. It is therefore apparent that the temperature rise at each junction point in the network is dependent upon the characteristics of the portions of the network both preceding and succeeding the juncture in question. It is, therefore, seen that little confidence can be placed in calculations obtained by simple superposition of independent responses of such interdependent portions, particularly at points of physical discontinuity in the thermal network. While Mr. Buller clearly recognizes this principle in his discussion, he has not abided by it in his simplified formula in considering the portion within the pipe or duct perimeter separately as the first portion, and adding it to the earth as the second portion.

The result is that for very short times his procedure is satisfactory because only the first portion is effectively involved and this rise can be calculated by the network formula which he has given. For very long times it is also satisfactory because the rate of temperature rise is so slow that the error introduced into the temperature rise of the second part by mismatch of the first part which can be considered as an error in the time scale is of no significance, and the temperature rise across the first part has now become substantially steady state. His system breaks down, however, in the transition time zone, so to speak, and this is important because most problems of emergency load ratings deal with the intermediate time zone. Although he attempts to correct the temperature rise of the second part by applying a correction to the exponential integral formula, the correction factor which he gives is mathematically unsound, and is applicable by the author's admission only to the case of buried cables and pipe type cable lines. While it may give the temperature rise at the cable or pipe surface for these cases with sufficient accuracy, it obviously does not correct the temperature rise of the conductor above the cable or pipe surface. A further inadequacy of the formulas is that they cannot be applied to the very important case of cables in duct.

I do not wish to infer that the exponential integral formula is unsuitable for calculating transient temperature rises in the earth portion of the thermal circuit. This formula rigorously takes account of the effect of the image, but since it is theoretically correct for all values of time only for a line source of heat flow in a homogeneous medium its use is accordingly restricted to

Figure 1. Basic thermal networks and equations for calculating transient cable temperatures

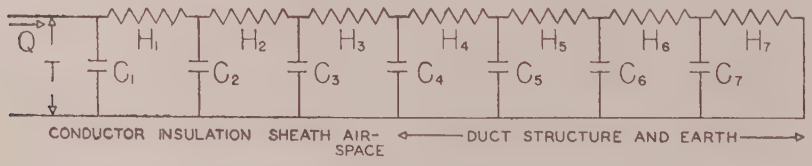

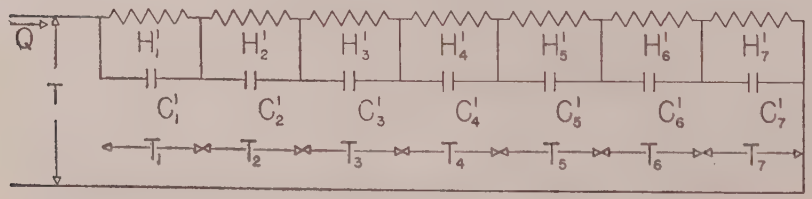

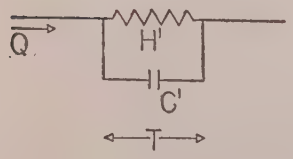

$$T = QH'\left(1 - e^{\frac{-t}{H'C'}}\right) \qquad (1)$$

$$T_f = T_0 e^{\frac{-\Delta t}{H'C'}} + Q_{\Delta t}\left(1 - e^{\frac{-\Delta t}{H'C'}}\right) \qquad (2)$$

$$\phi = A\left(1 - e^{-at}\right) \qquad (3)$$

those applications which may be so treated within the required degree of accuracy. In the present instance the medium is homogeneous only from the cable or pipe surface outwards. The formula therefore can be used to determine the temperature rise at a point some distance out in the earth, since from this view point the system is essentially homogeneous. But this is not so at the cable or pipe surface where the discontinuity commences and the formula gives the correct result only after sufficient time has elapsed to nullify for practical purposes the effect of this discontinuity.

I am of the opinion that the only satisfactory solution of the transient temperature problem can be obtained by setting up the equivalent thermal network of the system and solving this network as a whole. There is no reason why the cable in duct problem cannot be so treated as well as buried cables or pipe type cable systems by the proper selection of the constants of the network.

The accurate mathematical solution of this network presents considerable difficulty, since it requires the solution for the roots of a power equation, the power of which is equal to the number of sections in the network. Such a solution will yield a series of terms each of the form given in equation 3 of Figure 1 of this discussion and which may be represented by an equivalent thermal network of the series form as shown. In this form the temperature rises across the component parts are directly additive although each component part no longer has any physical significance. The step-by-step transformation which I originated some time ago and to which Mr. Buller has kindly referred was intended to avoid the solution of the power equation. This method also has infirmities, however, which it now appears practical to avoid by the use of some sort of computer which would permit accurate physical representation of the heat flow circuit, without need for concern about the mathematical complexities which might prevent a rigorous calculation of its response.

L. R. Ingersoll (University of Wisconsin, Madison, Wis.): I have followed with interest the recent attacks on the buried cable problem because of its similarity to the problem of the ground pipe heat exchanger for the heat pump. (It is obviously, however, more complicated than the latter because of sheath and duct considerations.) It has seemed to me that the most satisfactory treatment would involve a simple approximate solution, such as is available with the line source equation (that is, "exponential integral"), followed by a rigorous analysis which would doubtless involve mathematical complications of a distinctly higher order.

This is essentially what Mr. Buller has done and in a very scholarly manner. While doubtless not the "last word" it is a notable contribution and goes far towards solving the problem. The comparison of calculated and test results is highly satisfactory.

One small point might be mentioned: The statement following formula (4A) to the effect that (3A) and (4A) are identical should not be (and doubtless is not intended to be) taken too literally. To make these two formulas identical, (3A) must be multiplied by one-half, and the x in the limit should be squared.

Robert J. Wiseman (The Okonite Company, Passaic, N. J.): Mr. Buller has written an interesting paper on the history of the attempts to provide a method for calculating the transient temperature of a buried cable. It shows an active interest for many years, but in more recent times the desire to appreciate what kind of a transient temperature curve occurs has been intensified by the increasing use of pipe type cable systems. It is noted that there have been two approaches to the problem, one quite theoretical and the other empirical. As shown in Mr. Buller's paper, the theoretical approach is highly mathematical, involving exponential integrals and Ingersoll integrals. This did not appeal to some of us as it seemed to make it difficult to visualize and also there are not too many engineers who are acquainted with ready applications of these integrals. Therefore, we sought a simpler solution of the problem and we arrive at what Mr. Buller calls the semi-empirical approach.

I became interested in this problem about 15 years ago and nine years ago I had some thermal transient tests made by Dr. Paschkis of Columbia University. Steady load and intermittent load tests were made. We obtained the well-known temperature-time curves as shown in Figures 2 and 3 of Mr. Buller's paper. Recognizing it as a form of exponential series, I applied the formula and found by trial and error that I could duplicate the curves by assuming a cylindrical field around the pipe and dividing it into four zones. The total thermal resistance would be the same as the calculated value assuming that the commonly used law of images formula is correct. Incidentally, I am not too sure that this law is correct practically. After determining the diameter of the cylinder which gives the same thermal resistance as for the image law, I found if we divide the zones such that their areas are in the ratio of 1, 4, 16, and 64, that is, if the zone next to the pipe has an area A, then the next outer zone would have an area 4A, the third zone 16A and the outer zone 64A. This permits calculation of the diameter of each zone from which we can obtain the thermal resistance and also knowing the area we can compute the thermal capacity of each zone. It is then easy to express the thermal transient temperature of each zone by

$$\Delta T_n = T_n\left[1-\epsilon^{\frac{3600t}{R_{th}C_{th}}}\right]$$

where t is expressed in hours.

The sum of all four zones gives the thermal transient temperature for the surroundings and is comparable to the exponential integral or the Bessel functions that Mr. Buller uses.

Inside the pipe I divide the thermal circuit into two zones; the first one consists of the conductor and the insulation on one cable and the other is the surrounding medium (oil or gas) and pipe. These also are expressed as exponentials and their sum gives the thermal transient temperature. This differs only slightly from Mr. Buller where he also uses two zones but takes the conductor and half the insulation for one zone and the remaining insulation plus surrounding medium (oil or gas) and pipe as the other zone. I believe we both will arrive at the same results. Adding the thermal transients for the six zones, we arrive at the transient temperature for the conductor.

I have always felt that the exponential integral as given in formula 3 in Mr. Buller's paper was a good theoretical solution of the problem. It is very difficult to check these formulas in the field as it requires long time tests and the earth is subject to changing climatic conditions. Therefore, it is difficult to prove in a formula to a high degree of accuracy. If we compare Curves 4 and 5 and Curves 6 and 7, they are so closely the same that I do not see where Buller's formula is any better than the exponential integral and the difference is within the accuracy that we know our thermal constants to have, so practically both curves are the same. We are not concerned with differences in a transient of fractions of a degree or even one or two degrees. The system is subject to so many variables which can change from day to day that whatever we take for constants can differ 15 per cent or more and not influence calculations very much. To me, we must approach these problems in a realistic manner. It is nice to be able to have a pure theoretical approach to fall back on, but it is not a tool that can be used every day. Also we must try to visualize what is taking place. Anyone of the integral formulas as you look at them are just formulas with no indication of what kind of a curve they give. Everyone that has anything to do with curves involving time knows the shape of the curve where an exponential formula is used.

I wish Mr. Buller had given the construc-

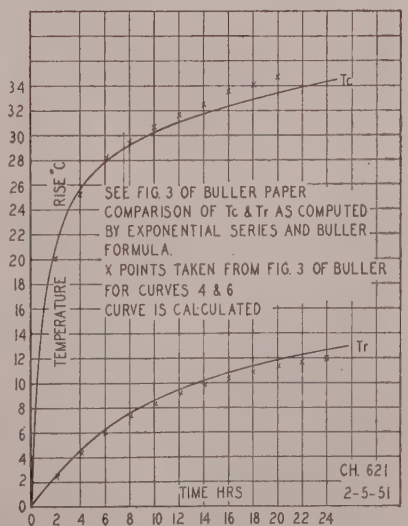
Tc
Tr
SEE FIG. 3 OF BULLER PAPER
COMPARISON OF Tc & Tr AS COMPUTED
BY EXPONENTIAL SERIES AND BULLER
FORMULA.
X POINTS TAKEN FROM FIG. 3 OF BULLER
FOR CURVES 4 & 6
CURVE IS CALCULATED
RISE °C
TEMPERATURE
TIME HRS
CH. 621
2-5-51
0 2 4 6 8 10 12 14 16 18 20 22 24
0 2 4 6 8 10 12 14 16 18 20 22 24 26 28 30 32 34

Figure 2. Comparison of T_c and T_r as computed by exponential series and Buller formula

Table I

Material	Thermal Resistivity, °C. Per Watt Per Cm	Thermal Capacity, Watt Seconds Per °C. Per Cm
Copper	0.26 (rarely used)	3.56
Paper	500	1.91
Oil	100	1.37
Pipe (steel)	2.2 (rarely used)	3.92

tion and constants of the circuits he used to calculate Figures 2 and 3. I did find out for Figure 3 that he used three single-conductor, 1,500,000 circul mil cables, 138 kv, in a $8^5/_8$ inch pipe, an earth thermal resistivity of 58 thermal ohms per centimeter and a thermal capacity for the earth of 2.46 watt seconds per degree centigrade per centimeter. Taking the values given in Table I of this discussion for thermal constants of the pipe system and the pipe buried 3 feet in the ground (to center of pipe) I set up the six zones on my method to obtain the exponential series.

The equation with all zones is

$$\Delta T = \underset{(a)}{1.53(1-\epsilon^{-0.964t})} + \underset{(b)}{0.63(1-\epsilon^{-0.928})} + \underset{(c)}{0.66(1-\epsilon^{-0.178t})} + \underset{(d)}{0.64(1-\epsilon^{-.0469t})} + \underset{(f)}{0.635(1-\epsilon^{-.01146t})} + \underset{(g)}{0.635(1-\epsilon^{-.00276t})}$$

per watt per foot per conductor

Term "a" is for the conductor and insulation; term "b" is for the oil zone and pipe; term "c" is for the earth zone next to the pipe; term "d" is the next outer zone; term "f" is the third zone; and term "g" is the outermost zone. Note that for zones "a" and "b" the rate of rise is rather rapid, zone "c" much slower and each succeeding zone is still slower. This helps to visualize what is taking place. It indicates that zones "f" and "g" have very little influence on the temperature rise during the early stages of heating; in fact, zone "g" will have little effect for several days.

As I do not know what load Mr. Buller used, I have assumed 10 watts per foot per conductor. Figure 2 of this discussion shows curves for T_c and T_r calculated by the above formula. T_c is the curve for the sum of all six terms and T_r is the curve for the sum of the last four terms. For comparison I have noted on the curves points for various times read as well as I can from Curves 4 and 6 of Figure 3 of Mr. Buller's paper. The agreement is good. I seem to be in error about one degree for T_c and less than a degree for T_r. Practically my results are as good as his without going through the long process he uses.

We can thank Mr. Buller for the interesting history of the subject, but I am not able to say that he has improved our knowledge of it by his formula over that which we already have.

F. H. Buller: As Mr. Del Mar points out in his discussion, the electronic analogue computer will save much labor as compared with any of the formulas presented, especially if a number of different types of transients have to be studied. It should be pointed out that formulas 8, 8D, and 9 are suitable for checking the performance of such a computer whenever such a check may be deemed necessary.

Incidentally, the figure of 16 hours for the calculation of a transient curve of T_c and T_r refers to the more elaborate formulas 8, 8D, and 9. The simplified formulas 10 and 11, usually require only 2 to 3 hours to give the same results.

Mr. Neher has again drawn attention to an important point which was mentioned specifically in the text of the paper; namely that in any rigorous mathematical analysis of this problem it is essential that the coupling between the cable, or the pipe and its contents, and the earth be fully taken into account. This is the reason why the rather complicated formulas 8, 8D, and 9 were developed—to provide rigorous mathematical equations in which this coupling is fully and properly allowed for. These formulas are admittedly not easy to understand completely; and even when fully understood cannot be used without laborious calculations. This point is strongly emphasized when a man of Mr. Neher's very considerable attainments labels them incomprehensible. It was for these reasons that the simpler approximate working formulas 10 and 11 were worked out and presented in this paper; and one gathers that it is these two formulas that Mr. Neher feels are open to question.

A point that Mr. Neher seems to have overlooked is the fact that these formulas as they stand are semiempirical in character; that is to say the correction factor applied to the exponential integral formula is empirical, and so is the technique of simple superposition of independent responses of interdependent portions of the network. No one claims that this procedure is mathematically rigorous; and as an empirical procedure all that is required of it is that it check test in the range in which it is used; or alternatively if tests are not available that it check with another formula which is known to be more rigorous mathematically over this range.

Figures 2 and 3 of the paper show clearly how well the semiempirical formulas 10 and 11 check test, and how well they check with the more rigorous mathematical formulas 8, 8D, and 9, in the case of a buried cable and the case of a representative oil pipe cable line.

Observe in Figure 3, how closely the approximate formula agrees with the exact formula in the case of T_r, the pipe temperature. There is hardly any divergence between these curves for short times, and they come together for long times.

In the case of T_c, the conductor temperature, the agreement is also good enough to be satisfactory for all practical purposes. So it is difficult to understand or accept Mr. Neher's contention that the formula "breaks down for intermediate times."

Now as to the neglect of coupling between the interior of the pipe and the earth portion of the circuit. The error resulting from such neglect can be seen in the curves for T_c in Figures 2 and 3. It is obviously not serious. Of course one can imagine a theoretical condition where even this error would be objectionable. If Mr. Neher should be faced with such a condition, he should certainly use the rigorous formulas 8, 8D, and 9, in spite of the additional labor involved.

Nr. Neher did not raise the question as to whether formulas 10 and 11 are suitable for use with gas filled pipe cable lines. This point is still under investigation; and the tools for this investigation are all available in the present paper. It is possible that the empirical formula for this case may involve a different correction factor for the exponential integral formula; whether this proves to be the case or whether the present factor will be found to apply with acceptable accuracy to gas filled pipes also, the value of Formulas 8, 8D, and 9 will be emphasized once again. It is possible now that they are available to use them to check formulas 10 and 11 under any conditions to which they apply, or to check any other approximate or empirical formulas in cases where there is any doubt.

When we come to the question of cable in ducts the situation is far more difficult, since the arrangement of thermal resistances and thermal capacitance at the "transition point" is extremely complicated and since moreover any mathematical theory seems to involve the use of "equivalent" isothermals which it is practically impossible to establish accurately a priori. For this reason it seemed advisable to make it clear that the rigorous formulas 8, 8D, and 9 do not apply to this case. For some reason, however, formulas 10 and 11 seem to check test remarkably well for this case also (see Figure 4). These formulas are admittedly liable to be less accurate for cable in ducts than for the case of buried cable in pipes, and must be used with caution until further evidence is available, where cable in ducts is involved.

Unfortunately, these comments apply with equal force to any known type of computer. It is perfectly true as Mr. Neher says that in theory at least the problem of cable in duct can be solved by setting up the equivalent thermal network of the system and solving this network as a whole if the required constants can be properly selected. This, in fact, is the whole point. The basic difficulty lies not in the operation of the computer but in its setup. If the number and location of the transition points are not accurately known and if the constants at these points are in doubt, the accurate setting up of the computer would seem to be impossible. Thus any solution for a cable in ducts must be recognized as rather a rough approximation; and while doubtless it is possible to make better approximations than the one represented by formulas 10 and 11 for this case, it does not yet appear to have been done either on a computer or in any other way.

Professor Ingersoll's very courteously worded discussion includes a point which should be clarified. Actually, it is formulas 3 and 4, rather than 3A and 4A which give the results which are identical. A comparison of these four formulas (3, 4, 3A, and 4A) will make it clear that the point brought up by Professor Ingersoll has actually been taken care of. Formula 3 has a factor 4π in the denominator and a parameter $r^2/4\ kt$; whereas formula 4 has a factor 2π in the denominator and a parameter $r/2\sqrt{kt}$.

Doctor Wiseman's discussion is of interest principally because it illustrates two points to perfection; namely how desirable it is to have available formulas such as 8, 8D, and 9 as a check against less exact formulas, and how they can be used as a check.

Take his reference to Figure 3 in the paper. Curve 3 is the curve for the exponential integral formula—not curve 5. Curve 3 did not fit too well—and by comparing curves 3 and 4 it is possible to determine the sort of empirical correction factor that will improve the fit. And when the correction factor was finally established, and curve 5 derived by its use, a direct comparison of curves 4 and 5 showed how good the final formula 10 actually is—something that was not known previously in the absence of test data covering the first 24 hours of

heating for this particular pipe cable.

Again, a comparison of curves 6 and 7 shows how much error is introduced by the lack of coupling between the region inside of the pipe and the region outside; and by showing that this error is small this comparison proved that the use of formulas 10 and 11 should be perfectly satisfactory in practice in spite of the theoretical objection raised by Mr. Neher.

Next, Dr. Wiseman offers an empirical technique which he himself has developed. In involves taking a cylinder of earth of the right outside diameter to give the proper steady-state response and then dividing it into six zones, in accordance with an empirical rule. These zones are then represented by lumped constants, instead of distributed constants, and are calculated individually, with no allowance for coupling between zones.

Dr. Wiseman has thus made three important approximations.

1. He has substituted an arbitrary "equivalent" heat field for the actual heat field in the earth. How nearly equivalent is it on transients?

2. He has substituted lumped constants for distributed constants. This has been shown to be permissible inside the pipe; how good an approximation is it in the earth, where the zones are much thicker than in the pipe?

3. He has neglected coupling between zones, not in one place, as was done with reasonable success in formula 11 of the paper, but in no less than five places. How much is the error increased by so doing?

These questions, and any other questions that may be raised concerning the validity of Dr. Wiseman's methods can be answered by using formulas 8, 8D, and 9. This, Dr. Wiseman has done in his Figure 2. His guess as to the load used in the paper was fairly good—the actual load was 9.15 watts per foot per conductor instead of 10. Thus, in order to be directly comparable with the results presented in the paper, the values shown on Dr. Wiseman's curves must be reduced by about 9 per cent. At 20 hours, Dr. Wiseman would obtain a conductor rise of $33.4 \times 0.915 = 30.6$ degrees centigrade with a loss of 9.15 watts per foot of conductor; the value obtained from Figure 3 of the paper is 34.9 degrees centigrade. Thus the error involved in Dr. Wiseman's approximations is 4.3 degrees centigrade or 14 per cent at this point, and it is on the unsafe side. This information was obtained without going to the expense of either building or renting a transient computing device or of making a field test which is even more expensive and moreover very difficult to arrange for, since it is hard to get the use of an important cable line for a period of time long enough to make such tests.

It is thus apparent that the opinion expressed by Dr. Wiseman in the last paragraph of his discussion is hardly justified; and that he would be well advised to use these formulas in improving and refining his own empirical methods.

(For additional discussion, see section in back of this volume "Discussions From Abroad")

Radial and Tangential Stresses in Impregnated Paper Insulation

J. B. WHITEHEAD
FELLOW AIEE

THE weakest points in the impregnated paper insulation of underground power cables are in the oil channels between successive turns of paper tape. Not only has the oil a lower dielectric strength than the adjacent paper, but the relation of values of dielectric constant is such as to throw the greater proportion of the local stress into the oil channel. Many experiments have shown that in insulation originally free of air or gas pockets, themselves sure causes of trouble, the large proportion of incipient failures are found in the oil channels.

In general the maximum stress on the insulation occurs at the conductor surface, and were it not for the occasional occurrence of other causes of failure, and the normal variations of structure and condition of the constituent materials, it would be expected that all failures would originate in an oil channel adjacent to the conductor surface.

An average value of the stress at the surface of the circular conductor of a single conductor cable may be readily computed from the dimensions of the cable and the value of the applied voltage. In a previous paper[1] under another title a method is given for deriving the stress in the oil channel in terms of the average stress computed in this way. But since the dielectric of the cable is not uniform and this average value depends on the oil stress being computed, the method is not rigidly beyond question. The present paper gives a more direct analytical method for computing the stresses in the oil channels.

Paper 51-10, recommended by the AIEE Insulated Conductors Committee and approved by the AIEE Technical Program Committee for presentation at the AIEE Winter General Meeting, New York, N. Y., January 22–26, 1951. Manuscript submitted May 15, 1950; made available for printing November 14, 1950.

J. B. Whitehead is with The Johns Hopkins University, Baltimore, Md.

Oil Stresses in the Single Conductor Cable

We make two assumptions in order to simplify our analysis:

1. That the pattern of overlay of tapes repeats itself regularly through the insulation wall.

2. That the electric stress in the central region of the oil channel and immediately overlying paper tapes is radial and uniform.

Under the first assumption the insulation wall may be considered as made up of a number of coaxial cylindrical capacitors, each having the same radial thickness, the same number of paper layers, the same overlay of tapes, and the same width of oil channel. Also for any one type of paper, the dielectric constants of paper and oil will have the same values in all the constituent capacitors.

Assumption (2) is warranted* by the fact that the oil channel is usually from 10 to 20 times as wide as it is thick.

Let us then consider a very narrow wedge-shaped tube of electrostatic induction, beginning on a very small area of the conductor surface at the center of an oil channel. And let the area be so small that the boundary surface of the tube will pass radially through the entire wall of the insulation to the outermost paper layer without leaving the central regions of the successive oil channels, in which the electric stress is assumed to be radial. The tube will then be made up of a number of small capacitors in series. Each capacitor will consist of a small area of oil channel in series with similar areas of several layers of paper as determined by the overlay in assembly. These capacitors will be similar in all respects except as to cross sectional area, which, however, bears a simple relation to the radial distance from the center of the conductor. Figure 1 shows an exaggerated view of a radial cross section of such a tube of induction. It has uniform thickness normal to the plane of the paper.

In Figure 1

a_1 = radius of the circular conductor
$a_1, a_2, a_3 \ldots a_x$ = radii of the inner surfaces of the successive oil films proceeding outwards
$S_1, S_2, S_3 \ldots S_x$ = areas of the intersections of the tube of induction with the inner surfaces of the successive oil films, a_1, a_2, and so forth
K_o and K_p = dielectric constants of the oil and the impregnated paper respectively
V_0 = potential of the conductor
$V_1, V_2, V_3 \ldots V_x$ = potentials of the outer surfaces of the respective constituent capacitors
$F_1, F_2, F_3 \ldots F_x$ = uniform values of the radial electric stress over the inner surfaces, $S_1, S_2, S_3 \ldots S_x$
t = thickness of the paper
n = number of layers of paper tape in the radial wall thickness of each of the typical cylindrical capacitors

The innermost capacitor of our tube of induction will consist of an oil layer of

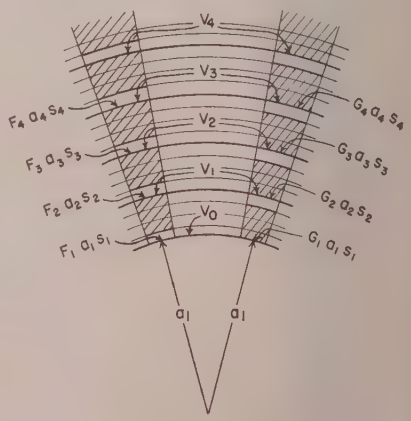

CHARACTERISTIC CAPACITORS

LEFT: OIL GAP IN FIRST LAYER
RIGHT: OIL GAP IN FOURTH LAYER

Figure 1. Ideal tubes of electrostatic induction through insulation of single conductor cable

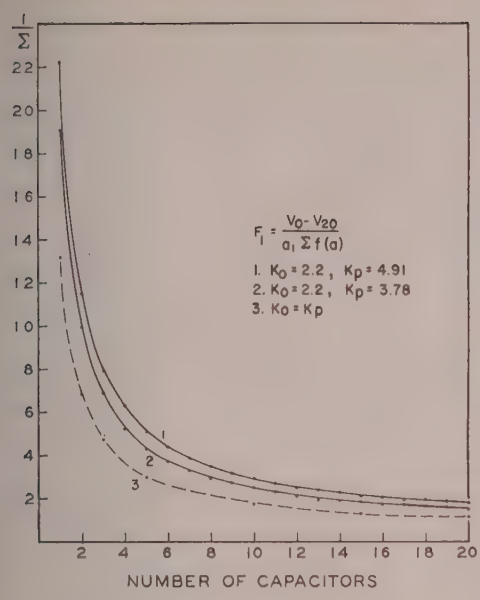

Figure 2 (left). Variation of maximum oil stress with number of layers of paper

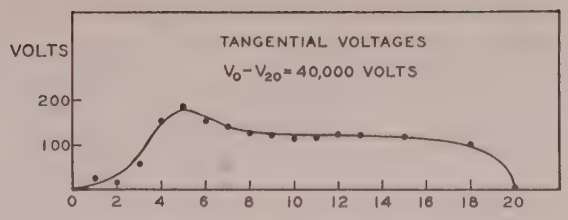

Figure 3 (upper right). Variation of tangential voltage with radial thickness of paper

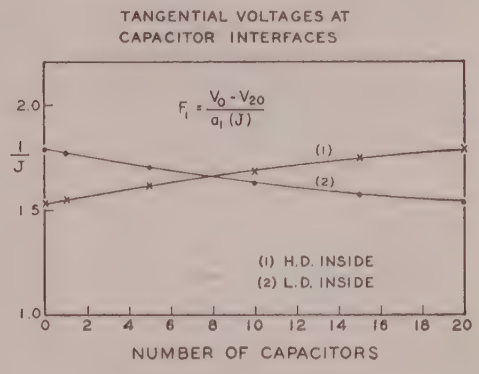

Figure 4 (lower right). Graded cable

Variation of maximum oil stress with relative radial depths of a dense and of a less dense paper

thickness t in series with $(n-1)$ layers of paper. The voltage over the capacitor is $V_0 - V_1$, and let the voltage over the oil be v_o and let that over the paper be v_p.

Then

$$\frac{v_o}{v_p} = \left(\frac{K_p}{K_o} \frac{\log \frac{a_1+t}{a_1}}{\log \frac{a_1+nt}{a_1+t}} \right) \equiv A \qquad (1)$$

Also

$$v_o + v_p = V_0 - V_1 \qquad (2)$$

$$v_o = (V_0 - V_1) - v_p$$

$$= (V_0 - V_1) - \frac{v_o}{A} \qquad (3)$$

$$= \frac{A}{1+A} (V_0 - V_1) \qquad (4)$$

The radial stress in the oil at the surface of the conductor is:

$$F_1 = \frac{v_o}{a_1 \log \frac{a_1+t}{a_1}} \qquad (5)$$

$$= \frac{V_0 - V_1}{a_1 \left[\frac{K_o}{K_p} \log \frac{a_1+nt}{a_1+t} + \log \frac{a_1+t}{a_1} \right]}$$

$$\equiv \frac{V_0 - V_1}{a_1 [f(a_1)]} \qquad (6)$$

Similarly:

$$F_2 = \frac{V_1 - V_2}{a_2 \left[\frac{K_o}{K_p} \log \frac{a_2+nt}{a_2+t} + \log \frac{a_2+t}{a_2} \right]} \quad \frac{V_1 - V_2}{a_2 [f(a_2)]}$$

$$F_r = \frac{V_{r-1} - V_r}{a_r \left[\frac{K_o}{K_p} \log \frac{a_r+nt}{a_r+t} + \log \frac{a_r+t}{a_r} \right]} \quad \frac{V_{r-1} - V_r}{a_r [f(a_r)]}$$

where r is the total number of typical capacitors and n and t have constant values.

Whence:

$$V_0 - V_r = F_1 a_1 [f(a_1)] + F_2 a_2 [F(a_2)] + \ldots F_r a_r [(f(a_r)] \qquad (7)$$

But:

$$K_1 F_1 S_1 = K_2 F_2 S_2 = \ldots K_x F_x S_x = K_r F_r S_r$$

$$K_1 = K_2 = \quad K_r = K_o$$

$$F_2 = F_1 \frac{S_1}{S_2} = F_1 \frac{a_1}{a_2}; \quad F_x = F_1 \frac{S_1}{S_x} = F_1 \frac{a_1}{a_x}$$

Thus:

$$V_0 - V_r = F_1 a_1 [f(a_1) + f(a_2) + f(a_3) + \ldots + f(a_r)]$$

$$F_1 = \frac{V_0 - V_r}{a_1 \sum_{x=1}^{r} f(ax)} \qquad (8)$$

From equation 8 the values of F_1 of the stress in an oil channel at the surface of the conductor may be computed. Also, with F_1 known, the values F_2, F_3,..., as well as the radial stresses at any point along the tube of induction follow at once since the product of KFS is constant throughout the tube. If in equation 8 K_o and K_p have the same value, the expression for F_1 reduces to that for the stress at the conductor surface when the insulation of a cylindrical conductor is of uniform value of K throughout.

There is apparently no simple method available for writing immediately the value of the summation in the denominator of equation 8. There is no trouble, however, in evaluating the single terms; a 5-place table for the natural logarithms is desirable. For the example given in a later paragraph computations have been made for the summation of 20 terms, that is, a cable with 20 characteristic capacitors in its wall of insulation. Figure 2 shows how the maximum oil stress varies with the number of characteristic capacitors.

Stress in Impregnated Paper at Surface of Conductor

If in Figure 1 the positions of oil channel and adjacent paper layers be reversed so that our tube of electrostatic induction now leaves the conductor surface and passes through $n-1$ paper layers before meeting an oil channel, we can proceed by similar analysis to the following expressions for the radial stresses (G_1, G_2, G_3...G_r) at the conductor surface and at the inner paper surfaces of the successive characteristic capacitors:

$$G_1 = \frac{V_0 - V_1}{a_1 \left[\log \frac{a_1+(n-1)t}{a_1} + \frac{K_p}{K_o} \log \frac{a_1+nt}{a_1+(n-1)t} \right]} \equiv \frac{V_0 - V_1}{a_1 [\varphi(a_1)]} \qquad (9)$$

$$G_2 = \frac{V_1 - V_2}{a_2 \left[\log \frac{a_2+(n-1)t}{a_2} + \frac{K_p}{K_o} \log \frac{a_2+nt}{a_2+(n-1)t} \right]} \equiv \frac{V_1 - V_2}{a_2 [\varphi(a_2)]}$$

$$G_r = \frac{V_{r-1} - V_r}{a_r \left[\log \frac{a_r+(n-1)t}{a_r} + \frac{K_p}{K_o} \log \frac{a_r+nt}{a_r+(n-1)t} \right]} \equiv \frac{V_{r-1} - V_r}{a_r [\varphi(a_r)]}$$

whence:

$$V_0 - V_r = G_1 a_1 [\varphi(a_1)] + G_2 a_2 [\varphi(a_2)] + \ldots G_r a_r [\varphi(a_r)]$$
$$= G_1 a_1 [\varphi(a_1) + \varphi(a_2) + \varphi(a_3) + \ldots \varphi(a_r)]$$

$$G_1 = \frac{V_0 - V_r}{a_1 \left[\sum_{x=}^{r} \varphi(a_x) \right]} \qquad (10)$$

Computations of the summations in the denominator of equation 10 have been made for values of x from whole numbers 1 to 20, and utilized in the example below.

Example

As an example some of the stress values have been computed for a single-conductor cable having the following characteristics: conductor of circular cross section, diameter $d=0.5$ inch; number of paper layers, 80; paper 0.005-inch thick, 1-inch wide, overlap 25 per cent; $n=4$; dielectric constant, oil $K_o=2.2$; impregnated paper $K_p=4.05$.[2]

The stress F_1 in an oil channel at the conductor surface may be computed from equation 8, in which the summation is to be taken from $r=1$ to $r=20$, since there are 20 characteristic capacitors each four layers thick in the insulation wall. The value of the summation in equation 8 is 0.6266. Consequently

$$F_1 = \frac{V_0 - V_r}{0.25 \times 0.6266} = \frac{V_0 - V_r}{0.1567}$$

if $V_0 - V_r$ be taken at 40,000 volts, the value of F_1 is 255 volts per mil.

Similarly, the value of the summation in the denominator of equation 10, from $r=1$ to $r=20$, is 1.124. Consequently, the value of the stress at the conductor surface in a paper tape and at a point about 0.25 inch from an adjacent oil channel is:

$$G_1 = \frac{V_0 - V_r}{0.25 \times 1.124} = \frac{V_0 - V_r}{0.281}$$

which at 40,000 volts is 142 volts per mil.

If the insulation were uniform throughout and b the over-all radius, the stress at the conductor surface computed from the dimensions alone, would be

$$F = \frac{V_0 - V_r}{a_1 \log \frac{b}{a_1}} = \frac{V_0 - V_r}{0.25 \times 0.9555} = \frac{V_0 - V_r}{0.2388}$$

which at 40,000 volts is about 167 volts per mil, and so intermediate to the values of F_1 and G_1 above.

The values of the stress at any point in the insulation may be readily computed from the values of F_1 and G_1, using the properties of the tube of induction. Thus the stresses F_{20} and G_{20} in the oil and in the paper of the outermost capacitors are $F_{20}=99.6$, $G_{20}=54.6$ volts per mil.

Thus the radial stress in the insulation at the conductor surface varies widely from point to point being a maximum in an oil channel, where in the case here considered it is 82.5 per cent higher than the stress in the paper only 0.25 inch distant. Similar differences occur at all radial levels through the insulation wall, result in inequalities of the radial voltage distribution, and thus introduce longitudinal or "tangential" voltages in the interfaces between paper layers.

Radial and Tangential Stresses

The voltages between conductor and outerface of any characteristic capacitor $x(x=1$ to 20) along our two tubes of induction, from equations 6 and 9 are:

$$V_0 - V_x = F_1 a_1 \sum_{1}^{x} f(a_x) \qquad (11)$$

$$V_0 - V_x = G_1 a_1 \sum_{1}^{x} \varphi(a_x) \qquad (12)$$

Substituting the values of F_1 and G_1 for the example used above, we have:

$$V_0 - V_x = \frac{V_0 - V_{20}}{0.6266} \sum_{1}^{x} f(a_x), \text{ and}$$

$$V_0 - V_x = \frac{V_0 - V_{20}}{1.124} \sum_{1}^{x} \varphi(a_x)$$

The values of the two summations have been completed for all values of x, that is, all whole numbers from 1 to 20. The values for $x=5$, where the maximum tangential stress occurs, are 0.2210 for the f series and 0.4018 for the φ series. Giving $V_1 - V_{20}$ the value 40,000 volts, we find the tangential voltage along the interface of the fifth and sixth capacitors, and between oil channel and a point 0.25 inch distant between paper tapes is 188 volts. For the interface between the first and second capacitors the tangential voltage is about 20 volts, for capacitors beyond the fifth the average value up to the fifteenth is about 120 volts falling then to 0 at the cable sheath. See Figure 3.

The values given in the foregoing pertain to the interfaces between successive characteristic capacitors. Higher values are developed within the capacitors themselves. Thus the radial stresses in an oil gap and in a paper tape at the conductor surface, by equations 8 and 10, and again using our example are:

$$F_1 = \frac{V_0 - V_{20}}{a_1(0.6266)} = 255 \text{ volts/mil, and}$$

$$G_1 = \frac{V_0 - V_{20}}{a_1(1.124)} = 142 \text{ volts/mil}$$

The average stresses in the oil channel and first tape are roughly 99 per cent of these values, so that the voltages over the 0.005 inch thick channel and tape are roughly 1,280 and 702 volts respectively, with a difference of 578 volts along the interface from the center of the oil channel to a point about 0.25 inch away between the first and second tapes. For the corresponding interfaces in the outlying capacitors the values fall off to about 222 volts in the twentieth or outermost capacitor.

Thus the maximum tangential stress in the example cited is 578 volts over a distance of 0.25 inch, or slightly over 2 volts per mil. Not a high value, as compared with the radial stresses mentioned herein, but quite high enough to set up over a paper interface a path for "dendrites" or tree-patterns, if serious trouble arises in the oil channel itself.

Oil Stresses in Graded Cables

The foregoing method of analysis lends itself readily to the computation of the stresses in the oil channels of a "graded" cable, that is, a cable with more than one grade of paper in its insulation, the several grades having different values of density and of dielectric constant.

In order to simplify our written expressions and computations we will fix the values of several variables and consider the simple case of a single-conductor cable of circular cross section already utilized in the example above, but now insulated with two grades of paper with different radial depths in assembly and in different relative positions. Further, we use these values of dielectric constant:

Dielectric constant of denser paper	$K_d=4.91$
Dielectric constant of less dense paper	$K_l=3.78$
Dielectric constant of oil	$K_o=2.2$

Also let

V_0 = potential of central conductor
V_1 = potential of outer surface of first capacitor
V_{20} = potential of outer surface of twentieth capacitor, usually 0. See Figure 1
x = number of capacitors of inside paper
F_1, F_2 = potential gradients on inside surfaces of successive oil channels.

Then recalling equations 6 to 8, and for the case high density paper inside, we have:

$$V_0 - V_1 = F_1 a_1 \left(\log \frac{a_1 + t}{a_1} + \frac{K_o}{K_d} \log \frac{a_1 + nt}{a_1 + t} \right)$$

$$V_1 - V_2 = F_2 a_2 \left(\log \frac{a_2+t}{a_2} + \frac{K_o}{K_d} \log \frac{a_2+nt}{a_2+t} \right)$$

$$V_{x-1} - V_x = F_x a_x \left(\log \frac{a_x+t}{a_x} + \frac{K_o}{K_d} \frac{a_x+nt}{a_x+t} \right)$$

$$V_x - V_{x+1} = F_{x+1} a_{x+1} \left(\log \frac{a_{x+1}+t}{a_{x+1}} + \frac{K_o}{K_l} \log \frac{a_{x+1}+nt}{a_{x+1}+t} \right)$$

$$V_{19} - V_{20} = F_{20} a_{20} \left(\log \frac{a_{20}+t}{a_{20}} \right) + \frac{K_o}{K_l} \left(\log \frac{a_{20}+nt}{a_{20}+t} \right)$$

Whence:

$$V_0 - V_{20} = \sum_{r=1}^{20} F_r a_r \left(\log \frac{a_r+t}{a_r} \right) + \sum_{r=1}^{X} F_r a_r \frac{K_o}{K_d} \left(\log \frac{a_r+nt}{a_r+t} \right) + \sum_{r=x+1}^{20} F_r a_r \frac{K_o}{K_l} \left(\log \frac{a_r+nt}{a_r+t} \right) \quad (13)$$

For the case low density paper inside the equations are identical throughout, except that the two ratios of dielectric constants exchange places.

The several summations in equation 13 have been computed for the cable of our example, and for various values of x between 1 and 20; that is, for different proportions of denser and less dense paper; first with high density paper inside, then with low density paper inside.

In view of our special interest in the value of the stress in an oil channel at the conductor surface, and remembering the relations throughout a tube of induction, we may write:

$$F_1 = \frac{V_0 - V_{20}}{a_1(J)} \quad (14)$$

where:

$$J \equiv \sum_{r=1}^{20} \log \left(\frac{a_r+t}{a_r} \right) + \sum_{r=1}^{x} \frac{2.2}{4.91} \log \left(\frac{a_r+nt}{a_r+t} \right) + \sum_{r=x+1} \frac{2.2}{3.78} \left(\frac{a_r+nt}{a_r+t} \right)$$

Again we note that in the expression for F_1 in equation 14, the quantity J, if the dielectric of the insulation is uniform throughout, reduces to $\log b/a$, in which b is the over-all radius of the insulation. In our case the value of b/a, is 2.6, for which $J = 0.956$, and at 40,000 volts, $F_1 = 167$ volts per mil.

Table I

High Density Paper Inside			Low Density Paper Inside		
x	J	F_1 Volts/Mil	x	J	F_1 Volts/Mil
0	0.6535	245	0	0.5581	287
1	0.6460	248	1	0.5657	283
5	0.6199	258	5	0.5917	271
10	0.5953	269	10	0.6163	260
15	0.5747	279	15	0.6369	249
20	0.5581	287	20	0.6535	245

The values of J are given in Table I for the two cases, high density paper inside and low density paper inside. These values hold only for the conditions of our example, except as to voltage to which any value may be given. In Table I values of F_1 are based on $V_0 - V_{20} = 40{,}000$ volts.

The results in Table I are plotted in Figure 4 with $1/J$ as ordinates, and x, the number of characteristic capacitors of either paper as abscissae. The ordinates are thus proportioned to F_1, the radial stress in an oil channel at the conductor surface. We may note the following striking facts: as between two papers of different densities, the lowest value of maximum oil stress is obtained in using all low density paper. Replacing any proportion of low density paper with high density paper results in an increase in the value of oil stress. This result obtains whether the added high density paper is outside or inside the low density paper. Similarly, the substitution of low density paper for any proportion of an original all high density insulation will result in a lowering of the maximum oil stress; and wherever in the insulation wall the substitution may be made.

Thus, in a graded cable, with two papers of different density, from the standpoint of maximum oil stress alone, nothing is gained by substituting high density for low density paper, either inside or outside the latter; in fact the maximum oil stress is increased. Dividing the radial depth of the insulation roughly half and half between the two papers, the effect on maximum oil stress is nearly the same whichever paper is inside. In our example, in this division, the oil stress at the conductor surface is roughly 265 volts per mil, while the stress with all low density paper is 245 volts per mil, with all high density paper 287 volts per mil.

Thus while a high density paper inside a low density paper, owing to its higher over-all or measured dielectric constant, shifts a greater proportion of the over-all voltage to the outer low density paper, and so reduces the computed average stress at the conductor surface, this is not sufficient to offset the increase in the stress in the oil channel due to the increase in the dielectric constant of the adjacent (high density) paper. In an earlier paragraph it was shown that in a particular case the average stress at the conductor surface was approximately 167, that in an oil channel, 259, and that in the adjacent paper 142 volts per mil.

The relations here described account for the now well-known[3] fact that the use of a higher density paper in a cable reduces its breakdown strength; and further that failure in a well constructed cable begins[4] in an oil channel.

It is to be emphasized that the formulas and conclusions as described herein are based on the assumption of uniform materials, regularly assembled and retained in position, free of gas pockets, foreign substances, and irregular pressure strains.

The conclusions therefore pertain to an optimum condition; the lowest stress values obtainable with given materials and design. The stranding of the conductor will increase local stresses. Imperfections of the types mentioned also will introduce higher values of local stresses.

Summary

An analytical method for computing the stress at any point in the impregnated paper insulation of high voltage power cables is developed. The method is extended to the evaluation of both radial and tangential stresses, and to those arising in graded cables. The limitations in the use of high density paper are explained.

References

1. Oil Stresses in Impregnated-Paper Insulation, **J. B. Whitehead.** *Electrical Engineering* (*AIEE Transactions*), volume 64, August 1945, pages 555–57.

2. The Dielectric Losses in Impregnated Paper, **J. B. Whitehead.** *AIEE Transactions*, volume 52, June 1933, pages 667–81 and 689–92.

3. The Dielectric Strength and Life of Impregnated-Paper Insulation, I, **J. B. Whitehead.** *AIEE Transactions*, volume 59, 1940, pages 715–20

4. The Dielectric Strength and Life of Impregnated-Paper Insulation, IV, **J. B. Whitehead, J. M. Kopper.** *Electrical Engineering* (*AIEE Transactions*), volume 64, April 1945, pages 171–77.

Discussion

L. C. Ebel and **L. F. Roehmann** (Anaconda Wire and Cable Company, Hastings-on-Hudson, N. Y.): The author states that "were it not for the occasional occurrence of

other causes of failure, and the normal variations of structure and condition of the constituent materials, it would be expected that all failures would originate in an oil channel adjacent to the conductor surface." Thus, it seems that, other things being equal, an electrically stronger cable could be made by using maximum oil stress as a primary design criterion.

The author has used for purposes of illustration a 75/25 overlay pattern, giving the sequence of oil, three paper tapes, oil, three paper tapes, and so forth, in a radial line. Similar calculations may be made for other overlay patterns, such as 70/30, 60/40, 50/50, with interesting results. If, for instance, we choose such an overlay pattern that, following the author's example, $n=80$ (that is, one oil layer followed by 79 paper layers) and consequently $r = 1$, then F_1, the maximum stress in the oil channel at the surface of the conductor, is calculated as 303 volts per mil. This compares with 255 volts per mil in the author's example ($n=4$; $r=20$). This comparison would seem to indicate an advantage, for reducing maximum oil stress, of overlay patterns having n small and r large. In fact, the maximum oil stress may be reduced to 167 volts per mil if $n=1$ and $r=80$ (complete registration of the tapes throughout the insulation).

Thus, it appears that the long-time dielectric strength of a wall of taped insulation, such as in cable, is not merely a function of the stress in the oil channels. For example, a 50/50 overlay gives the longest path along the surface of the tapes from conductor to ground, that is, surface tracking path, but only half the tapes (with dielectric strength higher than that of an equivalent thickness of oil) are interposed, in a radial line, between conductor and ground. Other overlay patterns vary this relation between length of tracking path and radial thickness of tape.

The author states that assumption (b) "is warranted by the fact that the oil channel is usually from ten to twenty times as wide as it is thick." For 5-mil tapes this means butt spaces from 50 to 100 mils wide, which do not occur in a well-made cable. Very many dissections made in our laboratory show butt spaces from 0.5 per cent to 4 per cent of the tape width, with values of 1 to 2 per cent predominating. For a $^3/_4$-inch (750-mil) wide tape, 1 per cent is 7.5 mils. The butt space widths observed in our laboratory are but a small fraction of those on which the assumption of purely radial stress is based.

Figure 2 of the paper is not clear. It is apparently a plot of

$$\frac{1}{\sum_{x=1}^{r} f(a_x)}$$

for various values of r, but always with $n=4$. Then the title more appropriately would be "Variations of Maximum Oil Stress at Conductor with Number of 4-Layer Capacitors."

L. Meyerhoff (General Cable Corporation, Bayonne, N. J.): In this latest addition to his long list of valuable papers on impregnated paper insulation Dr. Whitehead analyzes mathematically the stresses in various parts of such insulation, and emphasizes that the highest stresses occur in the oil films. To simplify the mathematics involved he makes certain assumptions. However, his mathematics can be further simplified and his point made stronger if his assumptions are made to accord more nearly with actual conditions.

In deriving the expressions for stress in the oil film and in the impregnated paper, the assumption is made that in a given radial line there is a regularly recurring pattern of oil and paper in each group of n layers. Since the geometry differs at each radial distance from the conductor, a new equation is required for each group and the equation is different when the oil film is next to the conductor than when a paper film is next to the conductor.

Actually, no significant error is introduced if for the purpose of computing average dielectric constant the dielectric in each group is considered as made up of a rectangular instead of a cylindrical mass. On this basis the average dielectric constant for both cases in the first example would be simply

$$K=\frac{4}{\frac{1}{2.2}+\frac{3}{4.05}}=3.35$$

The stress in the oil film next to the conductor will be

$$F_1=\frac{K(V_0-V_r)}{K_0 a_1 \log\frac{b}{a_1}}$$

$$=\frac{3.35\times 40000}{2.2\times 0.25\times 0.9555}=255$$

(Whitehead's value is 255.)

The stress in the paper next to the conductor will be

$$G_1=\frac{K(V_0-V_r)}{K_p a_1 \log\frac{b}{a_1}}$$

$$=\frac{3.35\times 40000}{4.05\times 0.25\times 0.9555}=139$$

(Whitehead's value is 142.)

However, actual conditions would be more nearly represented on the assumption that the dielectric is a homogeneous mass consisting of impregnated paper and oil in the proportions actually obtaining in the insulation. For normal cable insulation this would be about 7 parts impregnated paper to 1 part oil, instead of 3 parts to 1 part oil, as assumed in Whitehead's example. On this basis average dielectric constant would be

$$K=\frac{8}{\frac{1}{2.2}+\frac{7}{4.05}}=3.67$$

and F_1 and G_1 will be, respectively, 279 and 152 volts per mil.

A similar method of computation could be employed in the case of graded paper insulation. The average dielectric constants, K_1 and K_2, of the two kinds of insulation would first be computed as for K, above. Using these values of K_1 and K_2 and the applicable radii, the effective over-all dielectric constant of the insulation can be calculated by means of the following equation:

$$K_{eff}=\frac{\log\frac{b}{a_1}}{\frac{\log\frac{a_x}{a_1}}{K_1}+\frac{\log\frac{b}{a_x}}{K_2}}$$

where a_x is the radius at the dividing line between the two kinds of insulation. The stress in the oil film and in the paper next to the conductor can then be calculated by use of the equations given previously for F_1 and G_1, substituting K_{eff} for K.

Such a computation has been carried out for the oil films in Whitehead's second example, on the basis of 3 parts paper to 1 part oil and on the basis of 7 parts paper to 1 part oil, with results shown in Table I (below).

There can be no question, as Dr. Whitehead points out, that the denser the paper the higher the stress in the oil films and that the substitution of denser paper for the less dense anywhere in the insulation and in any amount increases the stress in the oil film next to the conductor. This follows directly from the fact that the addition of the denser paper increases the over-all dielectric constant of the insulation. The increased stress in the oil film can be expected to result in reduced dielectric strength, other things being equal.

Whitehead has shown that in his laboratory models the dielectric strength bears an inverse proportionality relationship to paper density. However, the situation in practical cables apparently is somewhat different, because of certain mechanical factors, as is pointed out in Mr. R. W. Atkinson's discussion.

R. W. Atkinson (General Cable Corporation, Bayonne, N. J.): Dr. Whitehead shows that, as the density of the paper used over a cylindrical conductor is increased, the stress in the oil is increased and that this is true whether all of the paper is changed or only part of it and regardless of which layers are varied. He correlates this with his previous extensive experimental data on straight cylindrical conductors insulated with saturated paper tape where he shows that, under all of the test conditions used, the dielectric breakdown was determined by the stress in the oil, not that in the paper. He now

Table I

	High Density Paper Inside				Low Density Paper Inside		
X	F_1-Whitehead	F_1-3/1	F_1-7/1	X	F_1-Whitehead	F_1-3/1	F_1-7/1
0	245	243	263	0	287	285	323
1	248	246	267	1	283	282	318
5	258	257	282	5	271	269	299
10	269	268	298	10	260	258	283
15	279	277	310	15	249	250	272
20	287	285	323	20	245	243	263

derives that, for a given average stress, the stress in the oil increases in direct proportion to the over-all dielectric constant of the composite dielectric.

It is significant that much of the initial interest in Dr. Whitehead's experimental work was because many of us expected to find in it a measure of the increase in dielectric strength of paper as the density increases. When the data showed the opposite result there was much puzzlement and confusion. When further experiments under other conditions confirmed the first results—more confusion and argument.

Why was it that, during the period when all manufacturers of paper power cables were using paper of higher and higher density, the dielectric strength of their cables progressively increased? Many explanations have been offered. Of course, part of the gain resulted from improvements in manufacturing technique. But there still remained an important part that was directly correlated with the increase in paper density.

I have no doubt that the explanation for this apparent paradox is a very simple one—that the gain is related not to the electrical properties of the paper, but to its physical properties. The paper of low density is physically weak and was unable to retain its integrity and thus unable, under the conditions imposed by cable fabrication and handling, to perform effectively its function as a barrier between oil films. In Dr. Whitehead's laboratory samples which were not subject to bending, this low physical strength was not a handicap. On the other hand, the paper of high density possessed such physical properties that it was possible to realize in commercial manufacture the full electrical strength of the composite dielectric.

For long it seemed regrettable that there were no data published substantiating the practical experience record just cited; mature consideration shows, however, that there is really no merit to this thought. On cables made with present-day paper of relatively high density, dielectric strength is obtained on test lengths of commercial cables that is entirely in line with Dr. Whitehead's data on laboratory samples wound on rigid mandrels. No one every succeeded in producing this result on a commercial scale with paper of low density such as produced the best results (on straight, rigid samples) for Dr. Whitehead.

The gain obtained in dielectric strength with each increase in paper density was attributed to improved electrical properties of the denser paper. This was true in the United States and in Europe, and I know of no one ever taking exception to this explanation until Dr. Whitehead's data were obtained. Thus, we owe to Dr. Whitehead's experiments and to his persistence in emphasizing their significance, the fact that this long-accepted fallacy has not persisted. Failure to obtain on a cable insulated with low density paper, the values obtained by Whitehead on a rigid mandrel insulated with the same paper, is not a conflict with Whitehead but rather a measure of the effect of the mechanical weakness of the paper upon the electrical strength of the cable. That relatively better results may be obtained, using the same manufacturing controls on a cable insulated with high density paper, is simply evidence that the controls or procedure that are inadequate for the low density paper may suffice for the stronger high density paper.

It must be recognized that these comments are related to power frequency stresses in certain cases. It has not been established that the surge strength of the impregnated insulation is not directly related to the electrical properties of the paper; such evidence as there is indicates that there is such a direct relationship.

Edwin J. Merrell (Phelps Dodge Copper Products Corporation, Yonkers, N. Y.): The author has covered ably many of the various voltage stresses in oil-impregnated paper-tape insulation, which should be taken into account when designing electric cable dielectrics. He has based his analysis on the assumption of radial and uniform electrical stress in the central region of the oil channel, and the observation that many experiments have located incipient failures in these oil channels. He does not note specifically whether these incipient failures are at the center of the oil space or at one side.

I wonder if the author has given consideration to the stress relations along the edges of the paper tapes. While the tubes of induction are radial at the center of the oil channels, they are not radial near the paper edges or within the paper tapes because of the complex pattern of paper fibers and oil. Are not the critically weak areas inherently those at these interfaces or close thereto with the probability of rupture at the mutual surface, because of overflux concentration resulting from the difference in permittivities?

Improvement of the intrinsic dielectric strength of these interfaces has been of concern for many years. For example, densified paper eliminated the characteristic windows of low-density paper and achieved a labyrinth within the dimensions of the tape. Thorough degasification of dielectric materials has reduced the gas phase at the interface to minute proportions, and application of high operating pressure has increased the 60-cycle dielectric strength significantly above that obtainable at atmospheric pressure. The most recent step has been the use of very thin tapes in the maximum stress zone, thereby reducing the radial length of these interfaces, which results in an additional increment of dielectric strength.

L. I. Komives (The Detroit Edison Company, Detroit, Mich.): We agree with Dr. Whitehead's statement that "in a graded cable, with two papers of different density, from the standpoint of maximum oil stress alone, nothing is gained by substituting high density for low density paper, either inside or outside the latter; in fact the maximum oil stress is increased." Some laboratory tests which we made about ten years ago seem to prove this point. In Table I of an AIEE paper by Faucett and others[1] the samples from cable type *A* stood up better on comparatively short time a-c testing (100 hours or so at 233 *V*/mil average stress) than samples from type *B*. Samples from type *C* were even better than the other two. It should be noted that the type-*A* cable was constructed of paper tapes having the same thickness and density, while in type *B* a number of thinner tapes with much higher density were used near the conductor, and in type *C* thinner tapes with lower density than those in *B* but higher than in *A* were used near the conductor. The success of type-*C* cable on this short-time test was attributed to the somewhat thinner tapes, equivalent to a lower total stress across the butt space.

To our sorrow, we had to abandon the type-*C* construction and choose a cable having higher density tapes near the conductor, because type-*C* cable had an impulse strength lower than required by the AIEE standards. It is possible that the AIEE standards are too high for certain installations; however, under all conditions a certain minimum impulse strength is very desirable.

On Figure 3 of Dr. Whitehead's paper the point of maximum tangential voltage seemed to check with our observations of tree formations upon examination of samples subjected to prolonged ionization.

REFERENCE

1. 120-KV COMPRESSION-TYPE CABLE, **I. T Faucett, L. I. Komives, H. W. Collins, R. W. Atkinson.** *Electrical Engineering* (*AIEE Transactions*), volume 61, September 1942, pages 652–57.

William A. Del Mar (Phelps Dodge Copper Products Corporation, Yonkers, N. Y.): Dr. Whitehead has developed a very ingenious mathematical method of calculating the stress in an oil film adjacent to the conductor of a cylindrical cable, and his paper is devoted essentially to that restricted subject.

If that were all that the paper signifies, there would be little in it to which exception could be taken. The only limitation that I would suggest is that the method is correct only for stresses below the ionization point of the oil, as with higher stresses the maximum stress does not occur at the conductor surface, but at some depth in the insulation, because of the re-entrant shape of the volt-ampere characteristic of the insulation at high stresses. This was shown by P. L. Hoover, in 1926,[1] to apply to both direct and alternating potentials.

However, the whole significance of the calculation of maximum stresses in the oil relates to stresses at which ionization does occur, and this immediately relates the calculation of stress to the breakdown voltage.

While Dr. Whitehead mentions breakdown strength only once in his paper, it is safe to assume that anyone trying to apply his calculations to cable design would use it in connection with breakdown strength.

Dr. Whitehead certainly encourages this where he says that "the use of a higher density paper in a cable reduces its breakdown strength." I think that he meant to say its "breakdown voltage."

In my discussion I shall use the expression "dielectric strength" to designate the characteristic of the insulation which resists breakdown and which is due principally to the baffle action of the paper fibers against ion emission from oil or copper.

As a matter of fact, the breakdown voltage of a cable is a function both of the stress and of the dielectric strength as thus defined. The stress in the oil is greater the higher the paper density, but so is the dielectric strength of the cable.

These effects, therefore, tend to balance

one another, and which of them will predominate depends on several circumstances, one of which is the time of application of the voltage. The importance of this distinction will appear later.

I think that Dr. Whitehead should exclude impulse voltages from his conclusions, as I do not believe that oil ionization is nearly as great a factor as dielectric strength in microsecond insulation failures.

Every cable manufacturer knows that high impulse strength is attainable by putting a few layers of very high density paper at the conductor. This gives 20 to 25 per cent increase in impulse breakdown on average new cable; yet, according to Dr. Whitehead's formulas, the effect of these special papers is to increase the stress and, therefore, inferentially, to reduce the breakdown voltage.

This may be explained partly by a surface effect at the conductor. This was illustrated very well in a paper by E. Jona, in 1904,[2] in which he tells of comparative tests of flat condensers made with high-density papers sandwiched between low-density papers, and vice versa, the number of sheets of each sort being the same in both cases. On voltage time test, the capacitors with low-density paper adjacent to the electrodes failed at 260 kilovolts per centimeter (660 volts per mil), while those with the high-density paper at the electrodes failed at 300 kilovolts per centimeter (762 volts per mil).

This phenomenon is not completely understood, but it may be due to the fact that the baffle effect of the paper fibers is most effective at the starting point of ion emission from the electrodes. Use is made of this by having high-density paper as a backing for aluminum conductor shields.

However, this is not the whole story, as C. M. Foust and J. A. Scott[3] give the following values for new oil filled cables having a conductor diameter of 1.89 inch and insulation thickness 0.5 inch, in which the entire insulation, or large proportions thereof, were made with papers of different densities.

Table II

Paper Density	Average Impulse Breakdown, Kv
All 0.8	639
All 1.0 to 1.1	747
40% 1.0 to 1.1 inside 60% 0.8 outside	923

Now leaving the matter of impulse tests and returning to the more general subject, I will again quote Dr. Whitehead where he says: "It is a well-known fact that the use of a higher density paper in a cable reduces its dielectric strength." Cable manufacturers had the opposite experience, and Dr. Whitehead called upon the manufacturers to explain the discrepancy. The discussion that follows is an answer to that call.

I do not question the accuracy of Dr. Whitehead's test data, I only challenge the too general deductions he has made from them.

Dr. Whitehead appears to have derived his belief in the virtues of low-density paper largely from his tests of $2^1/_2$-inch brass rods insulated with 60 mils of void-free impregnated paper, in 15 layers of 4 mils each. Here, there was little difference in stress in all the paper layers, as the diameter ratio, and consequently the ratio of maximum to minimum stress, was only 1.05. This means that all the oil spaces ionized simultaneously and equally, or substantially so, and that failure resulted from a general condition existing throughout the sample and dependent only on the average stress in the oil. The action in a cable with insulation of thickness suitable for high-voltage operation is quite different. Here the oil of the inner layers ionizes when the stress reaches a critical value, but that in the outer layers does not ionize. This is where it is important to distinguish between breakdown voltage and breakdown strength, as in such a cable the outward attack by the jets of ionized interior oil is countered by the overlying paper fibers to a degree which is greater the higher their Gurley density. That, I believe, is the principal reason for the discrepancy between the universal experience with cables and Dr. Whitehead's test data.

However, explanations on paper are not fully convincing, and I therefore had some tests made to check their validity.

It had been suggested, in some vague way, that the improvement in dielectric strength obtained by manufacturers, when they used higher density paper, might have resulted from other more or less simultaneous improvements in materials or technique. In order to check this, I had three cables of the following description made in the laboratory, with papers of widely different densities, chosen to obtain a wide spread of "stresses in oil." Great care was taken to obtain mechanical perfection and uniformity.

Conductor, 4/0 A.W.G., 19 strands
Insulation, 220 mils of paper (solid type)
Ratio $D/d = 1.83$
Shielded and lead sheathed

The cables, in duplicate, were subjected to 80,000 volts, 60 cycles, with the results shown in Table III. The duplicates checked quite closely.

Table III

Cable	Gurley Density, Seconds	Average Life at 80 Kv, Minutes	Volts Per Mil on Basis of 1-Hour Equivalent 6th Root
A	32	60	364
B	225*	150	422
	32†		
C	225	509	518

*22 inside tapes.
†15 outside tapes.

This is supported by D. M. Robinson, who, in his 1935 paper,[4] shows voltage-time curves which quite definitely support the view that high-density paper favors high breakdown voltage.

While I believe that the preceding explanation accounts for the major part of this discrepancy between Dr. Whitehead's tests and the manufacturers' experience, other factors may have some influence.

Thus, in the case of voltages insufficient to produce jets of ionized fluid, but sufficient to create tangential stresses along the paper tapes, ionization has the choice between a long zigzag path on tape surfaces and a short radial path through the paper. Which path it will take depends both on the paper density and the tape stagger, and here the higher dielectric strength of high-density paper acts to obstruct failure by the shorter path.

Where high dielectric strength is desired, Dr. Whitehead's calculations suggest that high-density paper should not be used either inside or out. This may be justified in the case of his wholly geometrical conception, from which he excludes "irregular pressure strains," but actual papers have mechanical as well as electrical characteristics, and pressure strains do exist. These characteristics lead to distinct advantages when high-density paper is placed over the low-density paper, as shown by styrene wafers of the two constructions. After load cycles, there is a distinct area of cleavage between the two types of paper when the high-density paper is inside, whereas there is tight fit between the two types of paper when the high-density paper is outside. This area of cleavage has been shown experimentally to be an invitation to ionization and consequent deterioration, in conventionally graded cable, which shows in deterioration of power factor and decrease in impulse strength, after continued load cycles.

Finally, cable failure in laboratory tests does not necessarily start near the interior conductor. For example, while load cycle tests of "graded" cables always show dendrites on the inner faces of the tapes, "reverse-graded" cables often show them on the outside faces, indicating that failure was initiated near the outer shield rather than near the inner conductor. This does not check with Dr. Whitehead's Figure 4, according to which the stress is not only less at the outer layers of a reverse-graded cable than at the outer layers of a cable graded with high-density paper inside, but also is less than that at the inner layers of the reverse-graded cable.

My conclusion is, therefore, that while Dr. Whitehead has presented a very elegant mathematical study of stress in the geometrical picture of a cable, the practical application of such a study to the estimation of breakdown voltages of actual cables is far more complicated than the paper seems to imply.

References

1. The Mechanism of Breakdown of Dielectrics, **P. L. Hoover.** *AIEE Transactions*, volume 45, June 1926, pages 983–97.

2. Insulating Materials in High Tension Cables, **E. Jona.** *Transactions*, International Electrical Congress (St. Louis, Mo.), volume 2, 1904, pages 550–71.

3. Some Impulse-Voltage Breakdown Tests on Oil-Treated Paper-Insulated Cables, **C. M. Foust, J. A. Scott.** *Electrical Engineering* (*AIEE Transactions*), volume 59, July 1940, pages 389–94.

4. The Breakdown Mechanism of Impregnated Paper Cables, **D. M. Robinson.** *Journal*, Institution of Electrical Engineers (London, England), volume 77, 1935, pages 90–103.

J. B. Whitehead: The discussion seems to agree on the following:

1. The method of the paper for computing stresses in a new cable is correct and independent of the dimensions of the cable section and of the materials used.

2. The conclusion from the method that

the use of higher density paper in any amount or location results in higher values of oil stress in a new cable is correct.

3. Laboratory experiments at Johns Hopkins University on cable insulation 16 layers thick indicate that most failures start in an oil channel and that the short-time life of the sample decreases with increasing paper density.

4. In recent years cable manufacturers have found that the use of high density paper results in a "better" cable, having higher dielectric strength.

The apparent conflict between theory and practice as indicated between (2) and (4) undoubtedly is due to the fact that in the process of cable manufacture some other elements bearing on breakdown are introduced.

Mr. Atkinson thinks a part of these are the physical weakening of the paper on assembling and bending, and that increased care and improvement in materials has at least partly accounted for the improvement since the introduction of high-density paper. Also, he apparently thinks that the case for high-density paper, as based on its electrical properties, is not yet clearly proved. Mr. Komives seems to be of a similar opinion. Mr. Del Mar is the ardent champion of higher density paper, and apparently feels that aside from its mechanical properties, a case can be made for it on its electrical properties as well. With this I disagree. But I think we would reach a common ground at once if we agree on a definition of "failure," "breakdown," and "dielectric strength." Everyone is familiar with the time element in the complete breakthrough of insulation. But to my mind a cable is on the way out, that is, to complete failure, as soon as gaseous ionization begins, either in an oil channel or in a tear in a paper tape. The time element is caused by the more or less rapid boring action of the gaseous spark through the paper fiber, until an avalanche of complete rupture sets in, and it seems to me Mr. Del Mar is thinking more of these later periods of the progressive failure than of the initial fatal step.

Incidentally, Mr. Del Mar appears to have forgotten the test samples of the Johns Hopkins experiments. In these the conductor was 1.0 inch (not 2.5 inches) in diameter, and there were 16 layers of 0.005-inch paper. The ratio of maximum stress was 1.15 and not 1.05, as stated by Mr. Del Mar.

So I think that it is safe to say that if we have two otherwise similar cables, both undamaged in assembly, one of lower and the other of higher density paper, the latter would start gaseous ionization at a lower voltage, but would run longer than the former after it, too, had started gaseous ionization at a higher voltage. How much higher and how much longer are the open questions, which will require for answers very much more extensive study than any heretofore published; witness the apparently conflicting experimental tests now reported by Mr. Del Mar and those by Mr. Komives.

In view of the foregoing, under impulse test the cable with higher density paper should have the higher dielectric strength.

Messrs. Meyerhoff and Ebel and Roehmann point out interesting variations in the numerical values of stress resulting from the use of approximate methods, and for examples other than that in the paper. All agree as to the general validity of the method of the paper.

Answering Mr. Merrell, the maximum flux density and the maximum stress within the oil gap are along the central radius. I do not think these quantities are any greater at the edges of the tapes, nor do I know of any attempt to discuss the conditions within the mass of the tape. Most of our failures started in the oil (see reference 4 of the paper).

In closing it is interesting to note the tests of Hopkins, Walters, and Scoville (reported at this Winter General Meeting) on rolled capacitors of kraft paper and pentachlor diphenyl, showing a clear decrease of initial internal corona of about 15 per cent with increase of density of the paper from 0.7 to 1.3.

The 300/315 Kv Extra-High-Voltage Transmission System of the American Gas and Electric Company

PHILIP SPORN
FELLOW AIEE

E.L. PETERSON
MEMBER AIEE

I. W. GROSS
FELLOW AIEE

H. P. ST. CLAIR
FELLOW AIEE

THIS paper, one of a series designed to give a full report on the previously discussed[1] American Gas and Electric Company 500-kv test project, gives a description of the extra-high-voltage transmission system which, based on that investigation, has been designed to provide the increase in transmission requirements of the American Gas and Electric Company power system. It, therefore, presents the fruits of a major and extensive research project in transmission made available to the practical job of providing additional and much greater transmission capabilities for a rapidly expanding and growing power system. It is worth noting that the considerations that led to the projection of the original research project were not only kept in mind throughout the carrying out of that research program, but were kept equally in the forefront in the translation of the results of the program. The resulting system, it is believed, is in consequence unique not so much from the standpoint that the voltage is higher than any that has been utilized or projected heretofore in the United States, but more notably by the fact that the basic ideas and the designs developed have been based on detail data and much information unavailable previously and made available directly by the research. Aided by this, the margins of safety in insulation strength, and in factors of safety in general could, therefore, be brought down, and was brought down, to within relatively narrow limits of the zones of absolute requirements. This and the extensive economic analysis carried out as a basis for the design of the system as a whole made it possible to project a system not only technically but likewise economically sound.

While all of this will be presented in this paper, only a small portion of the system projected is now in actual construction stage: of necessity details of other parts of it remain still to be worked out as the construction program develops.

The main essentials, however, have been determined and these, it is believed will remain substantially unaltered.

The Basic Need for Extra High Voltage

The basic need for higher voltage transmission has been discussed on a previous occasion.[2] It may, however, be interesting and pertinent to summarize the need not for the general case but for the particular case presented by a power system such as the subject system. As is well known, the American Gas and Electric Company system, because of the availability of coal and water resources, possesses, to an unusual degree, flexibility in the location of its power generation facilities; the problem of transmission of very large blocks of power, therefore, over long distances of the order of 250 to 500 miles is not encountered.

Nevertheless, the growth in system peak from a value of approximately 1,000,000 kw in 1940 to a figure of 2,250,000 kw by 1950, with an expected doubling of that peak, that is, to 4,500,000 kw within the next 12 years, has brought sharply into focus the need of larger and technically improved transmission facilities to keep unit costs down with the growth in system size. This is sharpened by the development of larger and larger units at steam-electric generating stations to the point where units of 200 megawatts net capability to feeders have been projected and are in process of construction on the subject system.

The need for greater transmission capacity is brought about by the following factors:

1. The necessity of carrying larger blocks of load to load centers even though the distances involved preclude classing the lines as long distance transmission lines.

2. The necessity of shifting generation from one plant to another both for emergency and for economy reasons.

3. The required ability to transmit loads from points of overbalance between generation and load and points of deficiency during relatively brief but frequently occurring periods as a result of carrying on expansion and construction in relatively large blocks at successively different points on the system.

4. The need to restore flexibility in the basic transmission system which to a considerable degree has been lost due to system loads and generating units outgrowing the present 138-kv system.

5. The fact that necessary expansion of transmission capability at the present 138-kv level is becoming more difficult all the time because of the multiplicity of rights-of-way required. These difficulties, it appears almost certain, will grow into almost insurmountable obstacles as densities of load and of population increase, and particularly as centers of transmission originally developed in relatively sparsely settled areas become more thickly populated.

6. The obligation to provide for the needs of national defense.

7. The pressing, almost imperative need to take measures designed to counterbalance in part or in whole the natural increase in cost at a given voltage as system size grows and as areas grow and develop, and the abnormal increases in cost as a result of the postwar rise in cost of basic materials, labor, and equipment.

Paper 51-11, recommended by the AIEE Transmission and Distribution Committee and approved by the AIEE Technical Program Committee for presentation at the AIEE Winter General Meeting, New York, N. Y., January 22–26, 1951. Manuscript submitted October 24, 1950; made available for printing November 15, 1950.

PHILIP SPORN, E. L. PETERSON, I. W. GROSS, and H. P. ST. CLAIR all are with the American Gas and Electric Service Corporation, New York, N. Y.

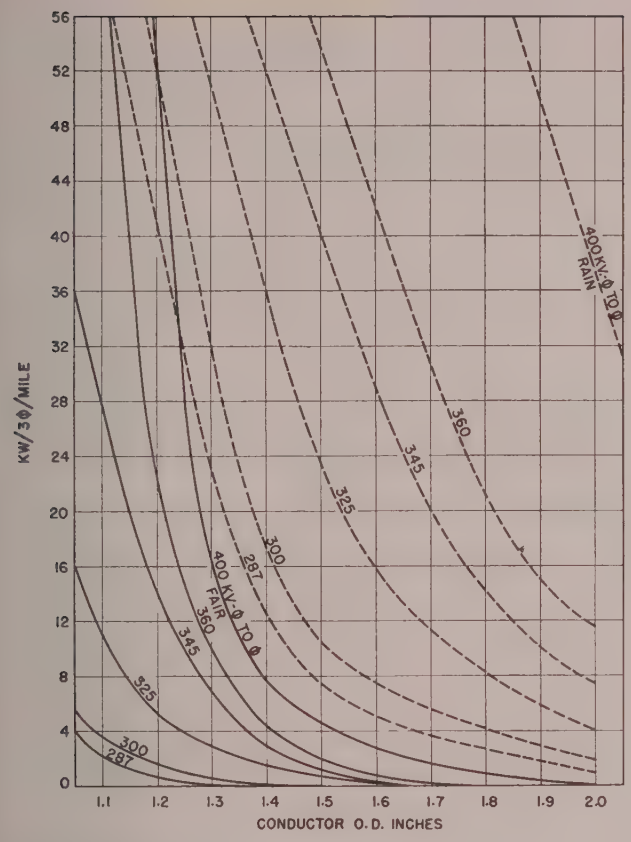

Figure 1 (left). Typical 3-phase corona loss versus conductor diameter and line voltage

——Fair weather average
------Rain

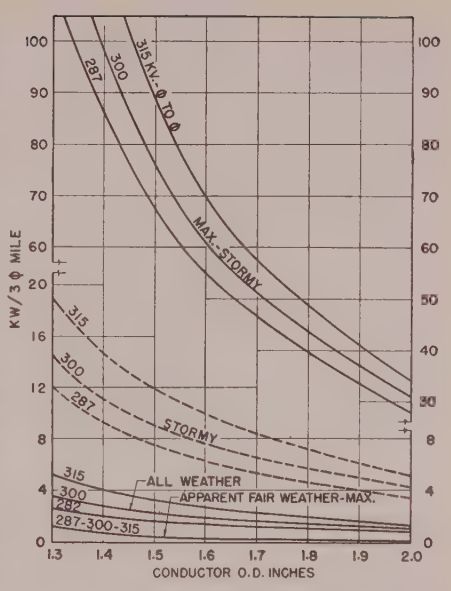

Figure 2 (right). Typical 3-phase corona loss versus conductor diameter at line-to-line voltages of 287, 300, and 315 kv under various weather conditions

Considerations in the Selection of Voltage Level

With the development and superposition of higher voltage transmission an inescapable requirement, the central question on which intensive study and research has been focused for the past several years, was the transmission voltage level to be used. It is believed that it will be of interest to describe some of the many considerations that have entered into the selection of this voltage. The final answer, of course, represents an approximate balance between opposing factors, such as those relating to technical difficulties and economic considerations, as well as practical performance.

Looking back over past experience, one notes that the present voltage, 138 kv, has taken care of system growth over a period of more than 30 years. It seems reasonable, therefore, to expect that the new voltage level should be capable of meeting internal system requirements for at least as long, certainly not less than 30 years, based upon the best load predictions it is possible to make at the present time.

In addition to adequacy from the standpoint of internal system requirements, consideration in voltage selection also was given to interconnection capacity between systems and areas. As the neighboring systems grow in size, both in total load and in size of individual generating units, it is logical that capacity of interconnections between systems should be increased on a similar scale. Adequate capacity in this respect is not only important from the standpoint of emergency arrangements, staggering of generating capacity, and so forth, but also from the standpoint of national defense.

Other considerations which were brought into the problem of voltage selection had to do with keeping lines in service. One of these is the sleet problem which is a very serious one in a large part of the territory covered by the American Gas and Electric Company system. The solution of this problem by outright melting of sleet on 138-kv circuits has been developed and on repeated occasions is being used successfully.[16] Based upon this experience and upon weather records in the area concerned, it has been concluded that the design of the new high-voltage system must be such as to permit sleet melting, if not in the first stages, at least in the system as it becomes fairly well developed. Obviously, since both the conductor diameter and the conductivity necessarily go up as the voltage level is increased, the sleet-melting problem will likewise become more and more difficult and may constitute a practical limit to the voltage level selected.

Another important consideration in keeping lines in service is the use of hot-line maintenance procedure. On the present 138-kv system this is considered a necessary routine and in order to maintain maximum service continuity on the higher voltage system, it will be highly desirable to be able to retain this practice. While it may not be feasible to continue such practices if and when much higher voltages are used, nevertheless, it is believed entirely practicable to use hot-line maintenance in the range of voltages under consideration for this project.

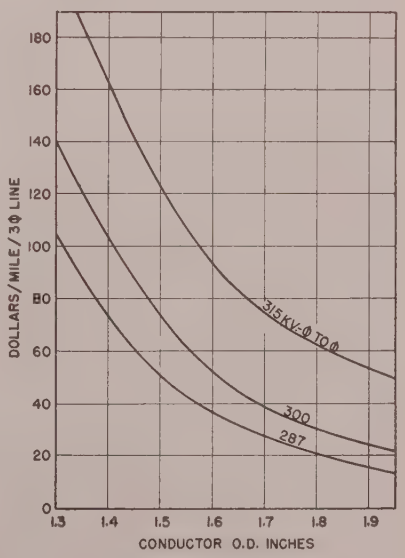

Figure 3. Increased capitalized cost of corona loss and generating facilities for each 0.05-inch increase in conductor diameter at various conductor diameters

Tied in with the limitations in the selection of voltage brought about by sleet melting and hot-line maintenance, are the practical questions and economic implications of double-circuit versus single-circuit lines. While it is not necessarily a foregone conclusion that 345-kv or even 360-kv double-circuit lines could not be built from a practical standpoint, at the same time, at these voltages, a double-circuit line would in effect tie up an excessively large transmission capability on one right-of-way. For example, on 100-to-150 mile sections at 360 kv, this capacity would approach 1,000,000 kw. On the other hand, a 315-kv double-circuit line appears to offer all the advantages of sleet-melting feasibility and hot-line maintenance procedures, and at the same time does not involve so great a capacity concentrated in any one route that the voltage would have to be rejected for that reason.

That corona and radio influence effects were factors to be considered in choosing a satisfactory transmission voltage were early recognized and steps taken over three years ago to investigate these features by organizing and carrying out an extensive field research.[2–8] Basically, corona produces two adverse effects: First, energy loss which must be kept within economic limits, and second, radio influence in areas adjacent to the line, which again must be held within tolerable limits, keeping in mind the type and character of populated areas where high-voltage lines will most likely be built.

Both of these features, corona and radio influence, increase rapidly as line voltage is raised for any size, type, and

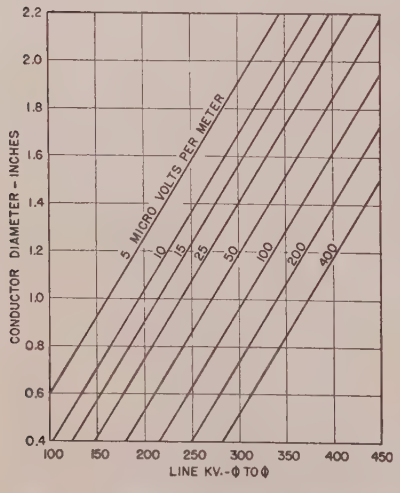

Figure 4. Typical radio influence effects 100 feet from under conductor for various line to line voltages and conductor diameters. Fair weather conditions

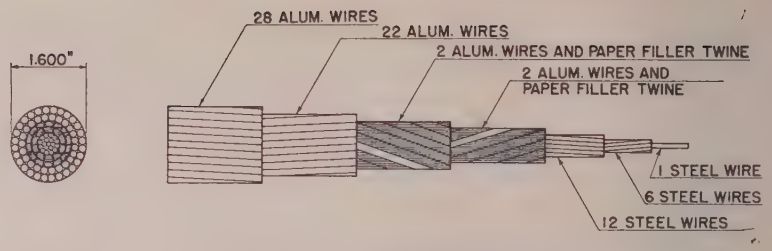

Figure 5. 1.60-inch outside diameter expanded steel reinforced aluminum cable

1,269,000 cm aluminum; 798,000 cm copper equivalent; 1.833 pounds/foot; 41,970 pounds tensile strength

arrangement of conductors within practical limits. Just how they increase is covered by the results of the Tidd field research project in companion papers.[9–10] The method of evaluating these features in the transmission system here described is covered in considerable detail later in this paper.

Final Determination of System Voltage

In the process of determining a final voltage level for the new transmission system, it was necessary to follow through each of the general considerations mentioned previously with a definite quantitative evaluation of all of the important factors. As the entire project hinged on these evaluations, some of them are described in detail here.

While estimated future loads constitute a quantitative factor in the determination of the best transmission voltage at the same time on an interconnected network type of system where line loading requirements arise from a variety of conditions, as compared with straightforward bulk power transmission, the evaluation of this factor does not lend itself to a simple direct solution. For this reason the approach has been to examine by means of rather extensive network analyzer studies the performance of the future system as plans were developed, using voltage levels from 287 kv to 360 kv or higher. For each voltage, critical system conditions such as generator unit outages, interconnection loadings, and so forth, were varied to test the capability of various transmission elements under the heaviest assumed loads. Also, since these studies were carried out over a period of several years, important economic development and concept occurred which required changes from time to time in basic ideas as to the future system plan —changes both in plant locations, size of units, and so forth, as well as in the transmission and switching layout. From all of these studies it was possible to judge fairly well the adequacy of a given voltage to handle future load requirements, even though quantitative exactness was not obtainable.

As an example of one of the earlier studies, Figure 8 shows one power-flow diagram of a projected 4,500,000-kw 360-kv system. Other studies were made at voltages of 345 kv, 330 kv, 287 kv, and more recently at 300 and 315 kv. A typical power flow diagram taken from studies of a 6,000,000-kw system at 300 kv is shown in Figure 9.

For a system such as the one studied, while the over-all length of the high-voltage system will be quite large, the effective transmission distance involved in any one line element will be moderate. For example as shown in Figures 8 and 9, these distances vary from a maximum of about 175 miles down to 50 miles or less. The load carrying capability per circuit of these lines will, therefore, range from around 1.5 times surge impedance loading for the longest line, up to at least $2^1/_2$ times surge impedance loading for the shortest. At 287 kv this gives 300 to 500 megawatts, whereas at 345 kv it would be 450 to 750 megawatts. This means that the 175-mile line capability limit is stability and the ability to hold voltage and supply the reactive loss in the line (approximately 125,000 reactive kilovolt-amperes at 345 kv and 450 megawatts), whereas the 50-mile line limit may be a matter of thermal capacity of conductors as well as reactive loss. For example, the line currents associated with these limits for the 50-mile line loading would be about 1,000 amperes and 1,250 amperes, respectively, for 287 kv and 345 kv.

The conclusions drawn from the power flow studies were that for the loads assumed, adequate transmission capacity was provided by any of the voltages tried, ranging from 287 kv to 360 kv; but the main difference was that 287 kv required double circuits on some of the lines, whereas single circuits were adequate throughout with 345 kv or 360 kv. This, naturally, brought out the fact that

the capability of a 287-kv double-circuit line exceeds that of a 345-kv single circuit by 38 per cent and 360 kv by 27 per cent. As the studies progressed with ever-increasing goals of future loads, the possibilities of double-circuit lines become more and more attractive.

Concurrent with future system power flow studies, economic studies, investigations of corona, and radio influence also were being carried on intensively, and the results, particularly as to radio influence, played a very important if not decisive part in the final selection of voltage level. Corona losses as such are of interest and the economics of corona loss will be discussed later, but they were definitely not a determining factor in selecting the system voltage.

To facilitate evaluation of the radio influence factor, a summary of representative data accumulated from the American Gas and Electric 500-kv test project, from field tests on operating lines, and from laboratory tests, is shown in Figure 4. A study of this figure gives the information shown in Table I.

In each case in the table it is assumed the operating voltage is 5 per cent above rated.

From this data it was immediately evident that an excessively large and unwieldy single conductor would be necessary with a voltage level as high as 360 kv, or even 345 kv, if radio influence were to be maintained at a reasonably low level. Bundle conductors were considered, but ruled out rather early in the project because of complication and expense introduced in stringing, sleet melting, hot-line maintenance, high tower costs, and so forth.

These results, therefore, tended to discourage the adoption of the higher voltage single-circuit idea and to favor more than ever the use of double-circuit lines at a more moderate voltage.

With the upper limit of voltage fairly well established, a further examination of previously discussed limitations of sleet melting, hot-line maintenance, and other factors led to the conclusion that the new transmission lines should be double-circuit construction rated tentatively at 300 kv (315 kv maximum), and using a 1.6-inch diameter conductor and all other design features suitable for a 315-kv nominal rating, 330-kv maximum. As will be described later, all insulation requirements, including line units, transformer basic impulse insulation levels, and so forth, have been based on the 315-330 kv level.

While the final decision on voltage level was thus based largely on radio influence and other considerations described previously, corona losses and their economics were also carefully analyzed. Obviously, any economic evaluation to be significant must be based on

Table I

Rated Line, kv	Cond. Diam. Inches	Approx. Radio Influence, Microvolts Per Meter
138	0.5	15
230	1.15	15
287	1.4	25
300	1.6	17
315	1.6	25
345	1.8	25
360	1.9	25

annual integrated energy losses under all types of weather, since stormy weather losses are many times greater than fair weather. From tests made at the American Gas and Electric test site, the data in Figure 1 have been compiled to show typical corona losses to be expected for a conductor size from 1.1 to 2.0 inches in diameter, and for line voltages from 287 to 400 kv line to line, under fair weather and rain. Similar typical data under apparent fair weather, all weather, stormy, and maximum stormy weather are given in Figure 2, in the voltage range of 287 to 315 kv, and for conductor diameters from 1.3 to 2.0 inches. The large increase in corona loss as the conductor diameter is decreased and the voltage increased is evident.

With a conductor outside diameter of 1.6 inches and a line voltage of 315 kv, the maximum apparent fair weather loss is 0.2, the all weather loss 1.8, the storm weather loss 10, and the maximum storm weather loss 69 kw per 3-phase mile of line.

While widespread storm conditions involving considerable line mileage could produce corona loss increasing system demand, it does not appear that the increase would be significant or burdensome with a 1.6-inch, or even a somewhat smaller conductor. The high probability of diversity between the rather infrequent occurrence of such a system condition simultaneously with a monthly or yearly peak system demand would seem to preclude evaluating such a loss in terms of investment in generating capacity.

To evaluate the economics of decreased corona loss by increasing the conductor diameter in successive steps of 0.05 inch, Figure 3 has been developed from the data in Figure 2. On a 315-kv line, for example, an increase in conductor diameter from 1.6 to 1.65 inches shows the annual savings in corona loss (using energy at $0.0025 per kilowatt-hour, and annual charges at 16.25 per cent) would justify an increased investment of only $94 per mile. Since this amount would be far less than the actual cost of installing

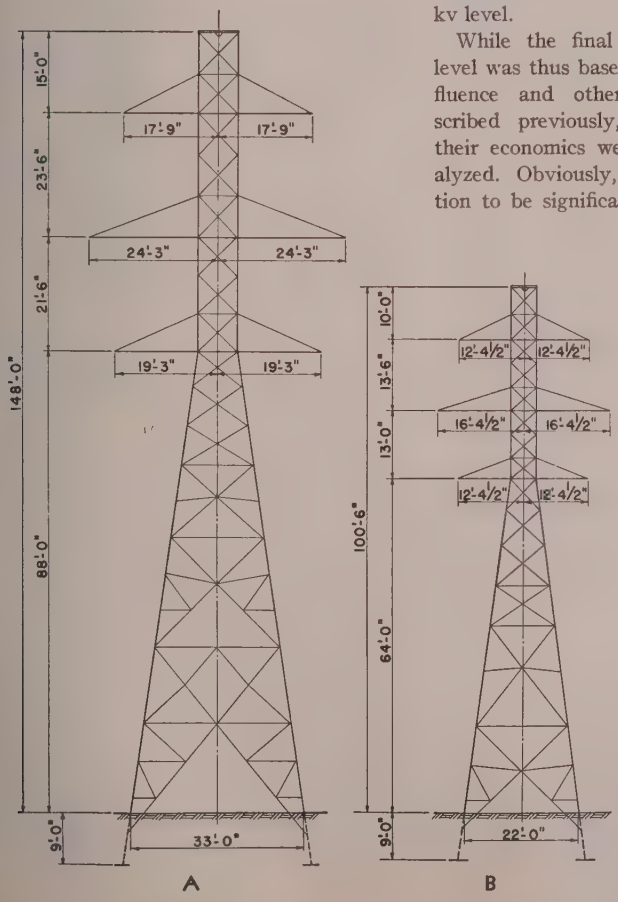

Figure 6. Outline of double-circuit tower
A—300/315-kv type
B—138-kv type

the increased conductor diameter, it is obvious that the annual integrated corona loss is not a determining economic factor.

Determination of Various System Features

From the very beginning of the project a great deal of research and study was being given to all of the features of the high-voltage system, including line and transformer insulation, tower design, switching layouts, conductor conductivity, relaying, and many others. However, it was impossible to bring most of these to final decisions until the voltage level had been decided. The determination of some of these features will be discussed below.

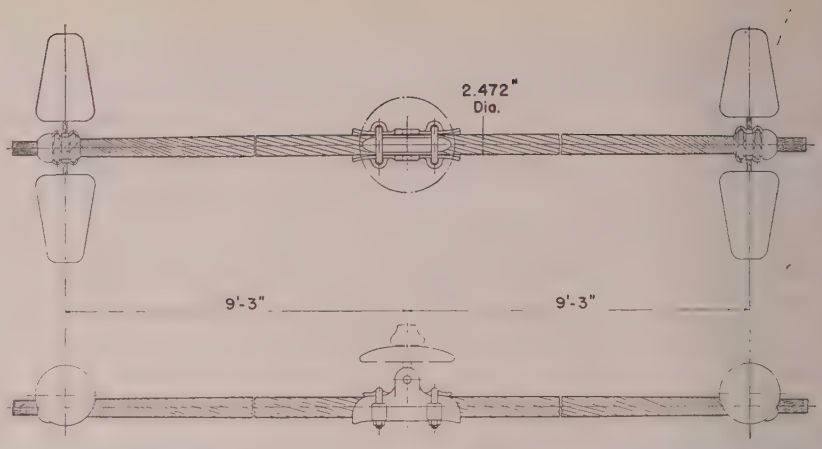

Figure 7. Stockbridge dampers over tapered armor rods on 1.60 inch outside diameter steel reinforced aluminum cable. Dampers have been designed to shield ends of armor rods from corona

Conductors

While the conductor diameter of 1.6 inches was determined principally by radio influence requirements as described before, the conductivity required is based upon at least three considerations: First, the thermal requirements to carry the maximum load that a circuit would ever be expected to carry; second, the economics of resistance losses, taking into account both the capacity losses and the annual energy losses involved; and, third, the feasibility of melting sleet.

As pointed out previously, the shorter line sections at least should be capable of carrying not less than $2^1/_2$ times surge impedance loading, which at 315 kv would be 625,000 kw, or a current of approximately 1,150 amperes. A study of loss economics, based upon reasonable line loading assumptions, indicated, however, that substantially higher conductivity than that required for the 1,150-ampere thermal limit would be justified. At this point, a conductor of 850,000-circular mil copper equivalent was seriously considered, subject to a study of the sleet-melting problem. Extensive network analyzed studies were made, in addition to actual ice melting tests by the conductor manufacturer on different conductor sizes. From all of these it was concluded that the conductor should be brought down to 800,000-circular mil copper equivalent as a compromise in the interest of successful sleet melting, which it is believed, can be accomplished in spite of some difficult problems. It is planned, of course, to utilize 138-kv sources applied directly to 315-kv lines, which will have to be short circuited at the far ends of 60- to 75-mile sections.

The final conductor design, Figure 5, will be 1,269,300 circular mil steel-reinforced aluminum cable, or 798,300 circular mil copper equivalent, 1.6-inch diameter, and 1,883.6 pounds per thousand feet. It will have two layers of 0.1546-inch diameter aluminum strands, 28 and 22 strands in the first and second layers respectively, and a steel core of 19 strands of 0.0874 inch. The 1.6-inch diameter was obtained by incorporating between the aluminum and the steel core, a filler, consisting of two layers of twisted treated paper twine, 12 strands in the outer and eight in the inner layer, and in addition, two aluminum wires in each paper layer to increase the compression strength of the cable. The ultimate strength will be 41,970 pounds.

Table II

Number of Circuit Breaker Arc Restrikes	Switching Surge-Times Max. Normal Voltage to Ground
0	$2-2^1/_2$
1	2.8
2	3.2
3	3.3

System Overvoltages

A knowledge of the magnitude of both 60-cycle and switching surge overvoltages on the system is necessary if insulation is to be applied on the most economical basis. Transient analyzer studies and calculations were therefore made to determine these.

The interconnected network type of system, such as herein described, does not present the severe 60-cycle overvoltage possibilities inherent in systems with long 1-way bulk power transmission lines, particularly where hydro-generator overspeeding must be added to the other causes of overvoltage. The studies on the proposed high-voltage system indicated no more than 18 per cent 60-cycle overvoltage, that is, above a maximum operating level of 330 kv.

Switching surges, or transient overvoltages accompanying one or more restrikes in a circuit breaker during the interruption of line charging current, were a matter of some concern. Transient analyzer studies were made to simulate the most severe switching operations that can take place, including line sections of considerable length switched on high or low side of transformers, and with simulated restrikes from 0 to 3. From these studies, switching surge voltages were found to be of the order given in Table II.

Although an essentially nonrestriking type of circuit breaker may be used, nevertheless it was felt that it would be wise to allow for one restrike, which would mean a switching surge transient of 2.8 times normal line-to-ground voltage.

Line Insulation

There are three types of overvoltages which must be considered in determining line insulation requirements. First, nominal frequency or 60-cycle voltages under both normal operating and line fault conditions. Second, overvoltages of short duration due to switching surge phenomena; and third, overvoltages due to lightning against which it may not always be possible to completely insulate, even with a well shielded line and low tower footing resistances. A fundamental engineering approach was made to the 60-cycle and switching surge problems rather than the somewhat arbitrary and rule-of-thumb method of supplying insulation on a three to five times normal line-to-ground voltage basis.

60-Cycle Requirements: As the 300/315 kv system will be solidly grounded the

Table III. Basis for Determining Line Insulators for 315-Kv Rated System

(Factors or Margins Added to Obtain Requirements)

	Factors For		
	60 Cycle Rms-Wet*		Switching† Surges
Max. operating voltage times rated	1.05		1.05
Line faults	1.20		
Switching surge			2.8**
Critical impulse to switching surge			1.15
Contaminated atmosphere	1.40		1.10
Wet Flashover vs. dry			1.0
Withstand vs. Flashover	1.15		1.15
Nonstandard atmosphere	1.10		1.10
Factor of safety	1.50		1.15
Use of grading shields	1.00		1.00
Crest factor			1.414
Defective insulator	1 unit		1 unit
Hot-line maintenance	1 unit		1 unit
Over-all factor	3.35+2 units		7.7+2 units
Applied to	60 Cy. rms-Flashover		Critical pos. impulse Flashover
Resultant no. $5^3/_4$″×10″ Units	$17^1/_3$		$17^1/_3$
Insulators selected	18		18

* Based on wet 60-cycle Flashover-rms.
†Based on critical impulse and crest of 60 cycle.
** Based on one arc restrike in circuit breaker.

60-cycle requirements will be based on the rated line-to-ground voltage. During system faults this voltage will increase momentarily until the fault is cleared. Calculations on the ultimate system in question indicated this might increase to 1.18 times normal. A rounded figure of 1.20 was used in this study.

Other considerations include margins, or factors, for such features as contaminated atmosphere, insulator withstand voltage versus flashover, nonstandard atmospheric conditions, and an over-all factor of safety of 50 per cent. The factors used for the various items are given in the first column of numbers in Table III. Applying these factors to the published values of wet flashover of standard $5^3/_4$ by 10 inches insulators gave the required number of units. One extra unit was then added to provide against a unit in a string becoming defective in service, and another unit was added as an additional protection for hot-line maintenance. This resulted in $17^1/_3$ units, or the practical figure of 18 units. The wet flashover voltage of 18 units is 3.8 times the 60-cycle rms line-to-ground voltage of a rated 315-kv system.

Switching Surge Requirements: While it may be expected that so-called no-restrike circuit breakers will rarely have a voltage restrike, some insurance should be provided in case occasionally during their life a restrike should occur. Assuming, therefore, that one restrike might occasionally occur, insulation should be provided for this condition. Again using selected factors for environmental and operational features as shown in the last column of Table III, a value of 18 $5^3/_4$-inch units also was indicated for switching surge requirements. A similar approach to the switching surge requirements based on the insulators having the same flashover if the crest of the 60-cycle and switching surge voltages were the same, and a factor of safety of 25 per cent instead of the 15 per cent used on the critical impulse basis also indicated 18 insulators as needed. Thus both 60-cycle and switching surge considerations gave the same results, namely, 18 $5^3/_4$-inch insulators per string.

Line Lightning Performance

Assuming 18 $5^3/_4$-inch insulator units, tower footing resistances not to exceed 20 ohms, and a ground wire separation in midspan of 48 feet, the line lightning flashovers per 100 miles of line per year has been determined for an isoceraunic level of 45 as 0.3, or one in three years. Most of such lightning flashovers, although infrequent, would not be expected to cause a service interruption since high-speed reclosing circuit breakers will be used, and the timing of the lightning on the 60-cycle wave will not always produce dynamic current flow.

Comparison with Insulation of Other High Voltage Lines

In Table IV is given a comparison of the line insulation and characteristics with some published data on two other high-voltage lines.

Assuming insulator string flashover is 15 per cent higher than the withstand voltage, the comparisons given in Table V are of interest. The insulator dry flashover is not considered of particular importance. The impulse flashover is related only to lightning performance of a line, not to its 60-cycle voltage requirements. Provision against wet flashover are of the same order for all three lines namely 4.5 to 3.8 kv per kilovolt of line rating. If the American Gas and Electric system is limited to 300-kv rated voltage instead of 315, the ratio becomes 4.0 the same as the Swedish line. At 315 kv, however, the insulation will be stressed 5 per cent higher.

Tower Design

Tower design is based on a number of factors such as conductor loading assumptions, height of conductors above the ground, angle of sideswing of the insulator strings, and clearance of the conductors to the tower members under maximum assumed insulator string deflection.

Studies on system load requirements resulted in a decision to utilize double-circuit towers on the first link of the high-voltage network. This first line will extend from Philip Sporn Station to the Kanawha Station near Glasgow, West Virginia, a distance of 63 miles. One circuit only is to be installed at the present time. This line will traverse rolling and mountainous sections of country, with spans up to 3,000 feet or more.

One of the prime considerations in mechanical line design is the choosing of the conductor tension. On our first line which as noted previously, traverses rugged country, a value of 13,500 pounds was chosen for a loading condition of 1/2-inch ice and 8-pounds wind. This load is only $32^1/_2$ per cent of the tensile strength of the cable, but was chosen to give the most economical tower weight per mile of line for this particular topography where advantage can be taken of the rolling nature of the profile without resorting to high conductor tension. In flat country, on the other hand, higher tensions are indicated.

Only a single ground wire will be used. This will be installed at the center of the tower and will be a standard steel-reinforced aluminum cable of 159,000 circular mils.

The minimum clearance from the bottom conductor to ground will be 35 feet. The minimum length of crossarms was determined by the assumed clearance to steel of 7 feet–9 inches under a sideswing deflection of 35 degrees. The vertical separation of the crossarms also was determined by this same condition plus the clearance requirements for offsetting the crossarms. The middle arm extends 6 feet–6 inches beyond the top arm and 5 feet beyond the bottom arm. The offset is to provide protection against conductor

contacts under conditions of dancing conductors or sleet unloading.

The basic tower height is 148 feet overall although the tower can be shortened 20 feet to take advantage of favorable topographical conditions in hilly country. An outline of the two circuit suspension tower is shown in Figure 6(A), and a similar tower now in use on the 132-kv American Gas and Electric Company system in Figure 6(B).

In order to reduce the weight of the towers it was decided to utilize silicon steel for the leg members. Silicon steel has a minimum yield point of 45,000 pounds per square inch as against 33,000 for carbon steel and consequent weight reduction more than offsets the higher cost of the material. The suspension tower is designed for a normal span of 1,100 feet with a 5-degree angle in the line or a tangent span of 1,700 feet. The angle tower is designed for a normal span of 1,100 feet with an angle in the line of 11 degrees. The strain tower is designed for a normal span of 1,100 feet with an angle in the line of 30 degrees.

Line Hardware

As cable diameters increase the tendency of vibration troubles increase. On the first line of the high-voltage system both armor rods and vibration dampers will be used. Although our experience with Stockbridge dampers on some 5,000 circuit miles of 132-kv line has shown that dampers are effective in preventing conductor breaks, the added precaution is taken of installing armor rods. This is partly due to the desire to prevent conductor damage from flashovers of the insulator strings. In Figure 7 it will be noted that the armor rods after installation are 18 feet–6 inches in length. The dampers are installed at the ends of the armor rods, and, in addition to damping the vibration, are also designed to form corona shields for the clamps holding the ends of the armor rods. An unusual feature of the dampers is that they extend transversely from the conductors instead of longitudinally like the conventional Stockbridge dampers. The dampers are 29 inches long and weight 25 pounds. The weights themselves are made of aluminum.

Insulator shields will be installed at the line end of the insulator strings. They will serve to grade the voltage distribution on the insulators and also to shield the conductor clamps from corona.

Conventional-type suspension clamps will be used. The dead-end clamps will be of the hydraulically compressed type.

Table IV. Insulation Characteristics, Extra High Voltage Lines

	Hoover-Los Angeles	Sweden*	American Gas & Electric Company
Rated Line kv, phase to phase	287	380	300/315
No. 5⅞″ insulators	21§	23‡	18
60-cy. Dry Flashover, kv	1,100	940†	965
60-cy. Wet Flashover, kv	780	760†	690
Impulse Flashover, kv	1,825	1,560†	1,585
Cond. clearance to ground	9′		7′×9′
At Angle of, degrees	30		35
Impulse Flashover	1,655		1,430
At Angle of 0 degrees			13′
Max. shielding angle of ground wire—degrees	38		33.5
Phase to phase, feet	24.5/32.5**	39	21.5/35.6‡

* See reference 17.
† Withstand values.
** First figure vertical—second, horizontal between conductors.
‡ First figure vertical between conductors—second figure horizontal between circuits.
§ Equivalent 5¾″ units.

Insulation for Transformers

As large savings in transformer costs are possible in the high-voltage range if insulation can safely be reduced below present-day standards, an intensive study of this problem was made. Here, as in the line insulator determination, three types of voltage have to be considered: impulse or lightning, switching surge, and 60 cycle.

The impulse (or basic insulation level) requirements were studied first. As lightning arresters will be used close to the transformers to limit lightning and surge voltages, the 60-cycle rating of the lightning arrester which would seal against dynamic voltage was determined, based on the maximum line-to-ground overvoltage under fault conditions, and 10 per cent added as a factor of safety. The protective level of this lightning arrester (maximum voltage drop when discharging 5,000 amperes) was increased by 20 per cent. This was the required basic impulse insulation level of the transformer. For the 315-kv rated system, the basic impulse insulation level so arrived at was 1,110, based on present-day station-type valve lightning arresters. A reduction of about 5 per cent in this basic impulse insulation level would seem to be justified, if advantage were taken of the diversity factor in stacking a large number of separate lightning arrester units all of which would not have the maximum protective level. This would give a 1,050 basic impulse insulation level, the value now known as the 230-kv insulation class. However, this 1,050 basic impulse insulation level was not selected, as further study indicated that the 60-cycle voltage test requirements inherently produced a higher basic impulse insulation level, namely 1,125.

A transformer, as well as other insulation, must have a 60-cycle insulation strength suitable for continuous normal operation. On the basis of present-day transformer insulation characteristics, experience, and risks in setting the 60-cycle test at an impractical low figure, a 60-cycle 1-minute test of 500 kv was agreed upon as the lowest permissible. Since there is a pretty well defined ratio between 60 cycle test and impulse test in high-voltage transformers today, this 500-kv 60-cycle test resulted in an inherent transformer impulse strength of 1,125. Thus the required 60-cycle test, in effect, set the basic impulse insulation level at a value higher than required for protection by the lightning arrester. This in effect results in a protective margin of nearly 30 per cent instead of 20 per cent between the lightning arrester level and the transformer basic impulse insulation level. This is in the right direction, since the lightning arrester cannot be located at the terminals of the transformers on a high-voltage system of this type on account of physical dimensions of the lightning arrester and required electrical clearances, and the added impulse margin may well be partially consumed in this "distance factor."

The insulation for the transformers has, therefore, been set at 500-kv 60-cycle 1-minute test, and basic impulse insulation level of 1,125. These values were found to provide adequate insulation strength against switching surge voltages permitted by the arrester.

Table V. Ratio of Insulator Flashover to Rated Line to Ground Voltage

Line	Hoover-Los Angeles 287 Kv	Swedish 380 Kv	A.G.E. Co. 300/315 Kv
60-cycle dry	6.6	4.9	5.3*
60-cycle wet	4.5	4.0	3.8*
Impulse	10.5	8.1	8.7*

* Based on rated voltage of 315 kv.

Insulation of Station Equipment (Except Transformers)

The insulation requirements within the station (except the transformers) has not yet been definitely decided. However, some of the preliminary thinking may be of interest.

The philosophy of having the main bus insulated higher than other equipment in the station it is planned to continue. Clearances to ground and between phases will be influenced by studied electrical requirements, the expected use of grading or corona shields in many locations, and the provision for hot-line maintenance.

The stations will be well shielded against direct lightning strokes. The insulation requirements on the circuit breakers will depend to some degree on whether lightning arresters are used on the circuit breakers in addition to those on the transformers. Circuit breaker economics may well decide this point.

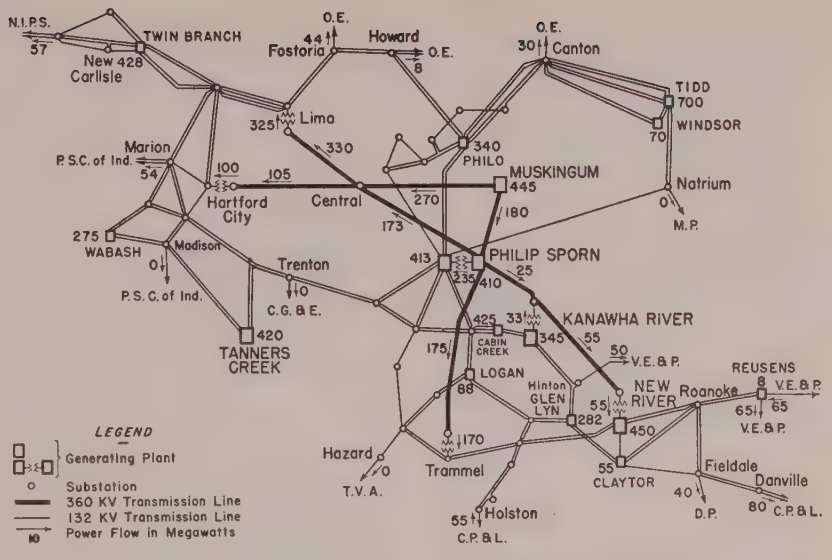

Figure 8. Power flow diagram on 4,500,000-kw 360-kv system

Relaying

Preliminary studies indicate that the electrical characteristics of the high-voltage system approach sufficiently close to those of systems now in operation that existing relaying methods and equipment can be applied with the same degree of success now being obtained on our lower voltage transmission systems. There will be some form of carrier relaying, which will probably be controlled by distance relays having phase angle discrimination, and by conventional ground directional relays. Some other possibilities of new types of relaying also are being considered, but these investigations have not yet been carried far enough to indicate their practical value.

The protective relaying equipment will be selected to meet the modern requirements of high-speed circuit interruption. Ability to carry maximum system loads and transient swings without false tripping, and adequate sensitivity to detect all line short circuits will be given special attention. Provision will be made for simultaneous tripping of circuit breakers at both ends of the line so as to permit high speed reclosing.

Switching

The circuit breaker problem on the 315-kv system as now projected does not appear to present any unusual difficulties. Calculated interrupting duties are well below 10,000,000 kva and circuit breakers have already been designed for high-speed 3-cycle interruption and 15- to 20-cycle reclosure. To take care of future expansion, it is believed that circuit breakers should be developed for not less than 15,000,000 kva and at this voltage there should be no serious difficulties of design or manufacture.

While switching arrangements for the ultimate system will be given considerably more study before final decisions are reached, the general trend of thinking, based upon studies of various switching schemes including ring-bus and modified ring-bus layouts, is that for major switching stations the present conventional double bus arrangement using one circuit breaker for each line circuit and two circuit breakers for each transformer circuit offers a high degree of flexibility and reliability at little greater cost than other less flexible schemes, such as modified ring-bus arrangements. A straight ring-bus for more than four circuit elements was not considered satisfactory in any event because of the certainty of having the system split apart if a line outage should occur during maintenance of any one line circuit breaker.

Projected Superposition of Extra High Voltage System on Present American Gas and Electric 138-Kv System

A description of the exemplification of all the ideas discussed heretofore in this paper in the form of the actual extra-high-voltage system planned to be built or being built is of natural interest. Some idea of the extent and scope of this system can be gathered from an examination and

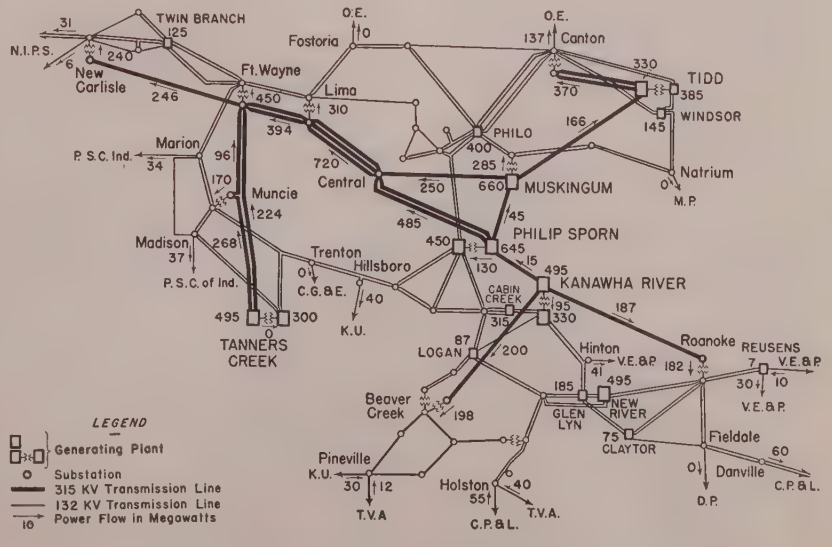

Figure 9. Power flow diagram on 6,000,000-kw 300-kv system

study of Figures 8 and 9. The latter of these 2, Figure 9, showing a study of a system load of 6,000,000 kw is of particular interest.

Of the extra-high-voltage links shown in Figure 9, the first authorized and under actual construction is the Sporn-Kanawha section. The other parts will come along as system loads further develop and plans for concomitant transmission additions are completed.

It is, of course, not to be supposed that present vision as to the future place and extent of growth is sufficiently clear to warrant a fixed transmission program being adopted. But, even with variations to be introduced due to unforeseen shifts in load density and capacity generation, the final plans adopted for construction can not differ materially in magnitude or essentials from those shown in Figure 9.

That being so, Figure 9 can be used as a test of the over-all economic soundness of the transmission program developed. Thus, a calculation on the basis of present costs indicates estimated costs of additional facilities called for in Figure 9 against those to be in service December 31, 1950, of $128,000,000. These increased transmission facilities will handle an additional 3,700,000 kw of capacity at a cost of $34.5 per kilowatt. In the final analysis, this is as rigid an economic test as is conceivable. The system here proposed seems to meet this test, to say the least, reasonably well.

References

1. Progress Report on 500 Kv Test Project of the American Gas and Electric Company—Corona, Radio Influence, and Other Factors, **Philip Sporn, A. C. Monteith.** *AIEE Transactions*, volume 69, part II, 1950, pages 891–99.

2. Transmission of Electric Power at Extra High Voltages, **Philip Sporn, A. C. Monteith.** *AIEE Transactions*, volume 66, 1947, pages 1571–82.

3. Corona Considerations on High-Voltage Lines and Design Features of Tidd 500 Kv Test Lines, **C. F. Wagner, Anthony Wagner, E. L. Peterson, I. W. Gross.** *AIEE Transactions*, volume 66, 1947, pages 1583–91.

4. Insulators and Line Hardware for Tidd 500 Kv Test Lines, **I. W. Gross, R. L. McCoy, J. M. Shadel.** *AIEE Transactions*, volume 66, 1947, pages 1592–1602.

5. Line Conductors—Tidd 500-Kv Test Lines, **E. L. Peterson, D. M. Simmons, L. F. Hickernell, M. E. Noyes.** *AIEE Transactions*, volume 66, 1947, pages 1603–12.

6. Transformers and Lightning Arresters—Tidd 500-Kv Test Lines, **F. A. Lane, J. K. Hodnette, P. L. Bellaschi, Edward Beck.** *AIEE Transactions*, volume 66, 1947, pages 1613–18.

7. Switchgear Equipment for Tidd High-Voltage Test Lines, **F. A. Lane, B. W. Wyman.** *AIEE Transactions*, volume 66, 1947, pages 1619–23.

8. Instrumentation and Measurement—Tidd 500-Kv Test Lines, **R. L. Tremaine, G. D. Lippert.** *AIEE Transactions*, volume 66, 1947, pages 1624–31.

9. Corona Investigation on Extra High Voltage Lines—500 Kv Test Project of the American Gas and Electric Company, **I. W. Gross, C. F. Wagner, O. Naef, R. L. Tremaine.** *AIEE Transactions*, volume 70, part I, 1951, pages 75–94.

10. Radio Influence Tests in Field and Laboratory—500 Kv Test Project of the American Gas and Electric Company, **G. D. Lippert, W. E. Pakala, C. D. Fahrnkopf, S. C. Bartlett.** *AIEE Transactions*, volume 70, part I, 1951, pages 251–69.

11. Co-ordination of Insulating and Spacing of Transmission Line Conductors, **W. W. Lewis.** *AIEE Transactions*, volume 65, 1946, pages 690–93.

12. Lightning Performance of 200-Kv Transmission Lines—II, **AIEE Committee Report.** *AIEE Transactions*, volume 65, 1946, pages 70–76.

13. Power Systems Overvoltages Produced by Faults and Switching Operations, **AIEE Committee Report.** *AIEE Transactions*, volume 67, 1948, pages 912–21.

14. Dielectric Strength of Station and Line Insulation to Switching Surges, **P. L. Bellaschi, L. B. Rodemacker.** *AIEE Transactions*, volume 65, 1946, pages 1047–53.

15. Insulator Surface Contamination, **H. A. Frey.** *AIEE Transactions*, volume 67, 1948, pages 1420–25.

16. Normal Voltage Short Circuiting Removes Conductor Glaze, **Philip Sporn.** *Electrical World* (New York, N. Y.), May 20, 1939.

17. The Swedish 380-Kv System, **Ake Rusch, B. G. Rathsman.** *Paper Number 410*, International Conference on Large High-Voltage Electric Systems (Paris, France), 1950.

Discussion

M. H. Knight (United States Bureau of Reclamation, Denver, Colo.): It is noted that in the design of the 315-kv system, it is planned to make provision for the melting of sleet on the new high-voltage circuits, by means of 138-kv sources applied directly to 315-kv lines, which will be short-circuited at the far ends of 60- to 75-mile sections. Over a line of such length, it is possible that sleet might be forming at a fast rate on, say, a 30-mile portion of such a section, with little or no sleet forming on the remaining portion of the line. If sleet has formed on one portion of the line to a radial thickness of about 1/2 inch before sleet-melting operations begin, will it be possible to melt such a coating of ice without overheating the conductors on the other portion of the line, which are not coated with sleet, to such an extent as to reduce their tensile strength? Are sleet-melting operations on the 138-kv lines generally started as soon as possible after sleet first begins to form, or after a coating of 1/4 inch or more of sleet has formed?

In connection with the evaluation of energy losses, is the value of the lost energy taken as the cost to produce the energy, or the average rate per kilowatt-hour at which the lost energy could be sold?

If the tower footing resistance of most of the towers is found to be about 20 ohms, is it proposed to lower such resistance as soon as feasible, or to wait until operating experience indicates whether lower footing resistance is necessary?

It is noted that only one circuit of the double-circuit line is to be installed at the present time. Is it proposed to string the second circuit with the first circuit energized, and, if so, what precautions will be taken to reduce the hazard to construction personnel (during stringing operations)?

Is it proposed to use special structures providing increased vertical and horizontal spacing of conductors for spans between 1,700 and 3,000 feet in length?

For the condition of galloping conductors were the clearance diagrams based on the movement of the conductors in one continuous loop, or in half-loops, between the points of support?

With the basic tower height of 148 feet and with the line located in an area over which there probably is considerable airplane traffic, is it proposed to install any lights at the top of the towers?

The broken conductor assumptions used for the suspension, angle, and strain towers, including the number, location, and tension of the broken conductors at the time of the break, would be of interest. Was any reduction made in the tension in the intact span, under broken-conductor conditions due to the insulator string on suspension towers swinging into the intact span? If such a reduction was made, was the resulting tension assumed to be a static or a dynamic (impact) load on the cross-arms?

The designers of this line appear to have taken a real step forward in the direction of reducing the cost of transmitting large blocks of power to load centers.

This paper is exceptionally interesting and should be of value to designers of high-voltage transmission systems.

P. L. Bellaschi (Consulting Engineer, Portland, Oreg.): The economic selection of higher transmission voltages is a fundamental problem in current system planning, the magnitude and complexities of which are amply illustrated in the paper under discussion, which pertains to one of the large systems—the American Gas and Electric system, an interconnected network preponderantly steam-generating.

Another extensive system is the Bonneville Power Administration system. This is one of the largest 230-kv networks. It comprehends the Columbia River basin, some 2½ million kw of hydro generation, and a potential generation that can well attain 10 million kw in the foreseeable future. During the past three years the writer has been engaged in studies directed to the development of this system. The problems associated in the selection of higher transmission voltages are many. Space will not permit but to touch upon certain ones of the major problems involved, and I shall confine myself to a few, to illustrate the approach.

In regard to type of conductor, these studies show that the standard aluminum cable steel-reinforced single-conductor line design is feasible up to 315 kv or 330 kv and possibly even as high as 345 kv. At these voltages conductor diameters in the order of 1.55 and 1.65 inch should be satisfactory. For still higher voltages (380 kv) the bundle conductor arrangement has advantages electrically, but it presents problems mechanically that need to be overcome.

Conductor clearances to tower, spacings between conductors, and insulation of the line are some of the factors in the line design. Inasmuch as switching overvoltages

are a consideration of prime importance in determining the electrical clearance requirements at the tower structure, this is one of the factors that should be considered in the first place. Extensive experience and studies on the Bonneville Power Administration 230-kv system definitely point to the conclusion that for a system of modern design operating with the neutral solidly grounded switching overvoltages to ground practically never attain 2.5 line-to-neutral crest voltage.

Since the spacing from conductor to tower depends on the probability of simultaneous occurrence of maximum swing of insulator assembly and maximum switching overvoltage, a further consideration in the selection of effective clearances rests upon a realistic evaluation of these two factors. For instance, in a survey of a 165-mile 287/302-kv line, the probability that maximum swing and maximum voltage might occur simultaneously was found to be less than once per year for the entire line. The degree of risk of a probable sparkover to tower becomes even more acceptable through the application of fast reclosing circuit breakers. From these and similar studies we found that actual design could be based conservatively on a 35-degree swing and that the permissible minimum clearances from insulator assembly to tower in Table I of this discussion will provide withstand strength in addition to a 25 per cent margin allowance.

As to the line insulation, the studies conducted show that 19 suspension insulators are adequate for 345 kv, 18 insulators for 315 kv, and 16 for 287 kv.

In regard to the transformer basic impulse levels, economic and practical advantages are found in proportioning the insulation to 75 per cent of the insulation level. For instance, for a 307/322-kv system operating with neutral solidly grounded, a 1,050-kv basic impulse level for the transformer insulation is considered adequate from the standpoint of lightning impulse protection, switching surge overvoltage, and 60-cycle continuous operation.

Line and station insulation based on these studies and compared with those in the paper are shown in Table II of this discussion.

In conclusion, we may point out that there are essentially three steps in the development of a high-voltage system: (1) a study and investigation phase, (2) design, and (3) the experience stage. In planning the system additional effectiveness and economies may be gained by a flexibility of design that recognizes that certain specific possibilities can further materialize through actual experience and operation of the system.

S. B. Crary (General Electric Company, Schenectady, N. Y.): The American Gas and Electric Service Corporation and their associates are to be congratulated for the excellent papers they have presented, which give in detail the basis of the selection of a higher voltage and their basic system design philosophy. Probably the most outstanding feature is the selection of as high a voltage as is considered practical for use with double-circuit towers. This is contrasted with the European selection of 380 kv using single-circuit towers and double conductors per phase. One cannot help but be convinced that the selection by the American Gas and Electric Service Corporation is correct for conditions prevailing in the United States, in view of the cost figures presented in a paper, "System Economics of Extra High Voltage Transmission," by Messrs. H. P. St. Clair and E. L. Peterson.[1] On the basis of the latter paper it is quite evident that the double-circuit tower for their conditions provides transmission at the lowest cost per kilowatt mile. This conclusion, which undoubtedly was one of the most determining factors in the selection of the voltage, is substantiated by single-circuit and double-circuit cost comparisons at lower voltage levels, particularly when right-of-way costs are an appreciable factor.

One of the many interesting results of these studies is the decrease in relative importance of line outages caused by lightning as compared with switching surges and normal frequency overvoltages in determining the insulation levels. This certainly appears most reasonable, particularly for interconnected systems of large capacities, where the reclosing procedure can be applied effectively for removal of temporary faults caused by lightning. It also is apparent that further increases in the operating voltage per disk of line insulation may be realized by giving additional attention to means of reducing the switching surge voltages. One of the most obvious and direct methods of accomplishing a further reduction is to use a circuit breaker which has a minimum tendency or no tendency to restrike.

These papers give added emphasis to the trend of high-voltage transmission system design in the United States by

1. The use of low-resistance conductors
2. The use of reactive kilovolt-ampere capacity for increasing the transmission line loading
3. Intermediate switching stations
4. Stepping up the new generation directly to the high-voltage system
5. Large capacity transformer ties to the lower voltage (138-kv system)
6. Full use of lightning arresters
7. Circuit breakers with higher interrupting capacity

Use of a double-circuit tower line which may carry as much as 800,000 kw in a tower head may present problems of developing operating procedures in case of a double-circuit tower outage. However, there are methods which may be applied to reduce the possibility of severe load interruptions when such an outage does occur. Also, for such a large interconnected system the loss of a fully loaded double-circuit tower line will become less important in the future as the system becomes more fully developed.

In considering this contribution to system design broadly, it will be recognized as giving a most excellent statement of modern American practice. At the same time this paper makes a significant contribution toward the use of double-circuit tower lines of high voltage and holds for the future the possibility of still further reductions in line insulation.

Table I. Electrical Clearances Required to Withstand Switching Overvoltages

Voltage Class	Switching Overvoltage, 2.5 Times 60-Cycle Crest, Kv	Impulse Voltage Equivalent to Switching Overvoltage, Kv	Equivalent Design Strength, 1½ — 40 Wave (25% Margin), Kv	Permissible Clearances, Conductor to Tower (25% Margin)
242 kv (230)	495	550	760	3 ft. 11 in.
302 kv (287)	620	690	950	5 ft.
362 kv (345)	740	825	1140	6 ft. 1 in.

Table II. Comparison of Line and Station Insulation Design

(Line Insulation)	According to Studies at Bonneville Power Admin. (307/322 Kv)	According to Studies at Bonneville Power Admin. (315/330 Kv)	According to Studies at American Gas & Electric (315/330 Kv)
Clearance from conductor to tower		5 ft. 6 in. based on 35-degree swing angle	7 ft. 9 in. based on 35-degree swing angle
Insulators (units in suspension string)	17	18	18
Conductor diameter, single-conductor ACSR	1.5 in.	1.55 in.	1.6 in.
Grading shield (at line end) (Station Insulation)	Recommended	Recommended	Recommended
Basic impulse level of transformers	1,050	1,075	1,125

Reference

1. System Economics of Extra High-Voltage Transmission, H. P. St. Clair, E. L. Peterson. *AIEE Transactions*, volume 70, part I, pages 841–851.

Philip Sporn, E. L. Peterson, I. W. Gross, and H. P. St. Clair: The authors are grateful for the discussions, both oral and written, which have been offered on this paper. These discussions have included a number of pertinent questions, which we shall attempt to answer.

In answer to questions by Mr. M. H. Knight, it is entirely true that sleet formation may be restricted to only a small portion of a given line section and the sleet-melting current then must be carried through the entire line, including perhaps the major portion of the line where no sleet has formed.

However, under the ambient temperature conditions existing and with the currents required to melt sleet in a period of, say, 20 minutes to one-half hour, we do not believe there is any danger of overheating on the conductors, certainly not to the extent of affecting their tensile strength. On our 132-kv system the sleet-melting routine has been worked out completely in advance so that the operation begins as near immediately as possible after the formation of any substantial amount of sleet has been established on any portion, even a few spans, of a given line. The method of detecting sleet formation by use of the carrier transmission channel was described in a paper by V. M. Marquis and G. G. Langdon.[1]

In all of our economic studies, both for I^2R losses, as well as corona losses, the value of energy losses has been taken as the production cost and not the selling price of the energy.

In regard to tower footing resistance it is not planned to carry out extensive or at least expensive measures for reducing the resistance in those cases where it is found to be above average low values. While the effect may be to increase slightly the frequency of flashovers, it is considered that the operating disadvantage of this increase in flashover frequency will be largely offset by high-speed reclosing.

With regard to stringing a future circuit on the double-circuit line, we propose to string this circuit with the initial circuit energized. We have carried out such construction at 132 kv with entire safety on a number of lines in the past. We do not believe, therefore, that any special problem will be involved but may on certain spans drop ropes to the ground suspended from the ground wire, which is located at the center of the tower.

On the line which we are constructing at present, the maximum span is 2,700 feet and we are using the standard outline of the tower as used on the normal spans. The tower, however, has been strengthened to take care of the larger mechanical loads.

The clearance diagram for the conductors is predicated mainly on the required clearance to ground under the assumed side swing and clearance requirements. We feel that we do, however, have sufficient clearances to protect against galloping conductors. Because of the severe conditions imposed on the line by galloping conductors, we will attempt to avoid such movements by means of sleet melting.

Table III. Comparison of Line Conductor-to-Ground Clearances

Rated Line-to-Line Kv	230*		315	
	287*	Maximum Minimum	BPA	AG&E
Clearance line to ground, feet	9.0	9.0 4.3	5.5	7.75
Line to ground Kv per foot	18.2	14.8 31.0	33.3	23.5
Average	21.3			

* See reference 2 of this discussion.

We do not propose to install any lights at the top of the towers.

With regard to the broken conductor assumptions used on suspension and angle towers, we have figured one broken ground wire at full load or one broken conductor at 60 per cent of the maximum assumed line tension. This load is assumed as a static load.

Mr. P. L. Bellaschi in his studies has arrived at a clearance from conductor to tower of 5 feet 6 inches against 7 feet 9 inches proposed on the American Gas and Electric 315/330-kv system. Our determination of clearance was checked in two ways. First, the conductor-to-tower clearance was balanced against the insulator string flashover and, second, the switching surge voltage on the system in question was determined, and factors of safety for "withstand" instead of "flashover" values and an over-all factor of safety of 15 per cent and an extra 12 inches for hot line maintenance requirements were added. The first method gave a clearance requirement of 7 feet 9 inches, and the second method, 7 feet 10 inches.

It is interesting to compare ground-to-conductor clearances on existing high-voltage lines with those proposed both by the Bonneville Power Administration and the American Gas and Electric Service Corporation. These are shown in Table III of this discussion.

It will be noted that the Boulder 287-kv line has a clearance of 9 feet, while existing 230-kv lines range from 9 feet to 4.3 feet. Also, the average kilovolts per foot of air on the 287- and 230-kv lines is 21.3 against 23.5 for the American Gas and Electric system and 3.33 proposed by Mr. Bellaschi.

In selecting conductor-to-ground clearance, other factors in spacing at the tower to prevent flashover must be kept in mind, for example, phase-to-phase separation of line conductors under wind and sleet conditions, and the all-important feature of line maintenance under safe working conditions. These were all considered in arriving at our conductor clearance of 7 feet 9 inches at the towers.

A basic impulse level (BIL) of 1,075 has been arrived at by Mr. Bellaschi as being sufficient for a 315/330-kv system, against 1,125 BIL selected by the authors. As pointed out in the paper, a 1,050 BIL could be justified on the basis of lightning protection alone, but this value was increased because the 60-cycle required strength of the transformers automatically provides 1,125 BIL. As a matter of fact, our studies indicated that the basic impulse level could have been reduced another 10 per cent to approximately 950 if a 10 per cent 60-cycle voltage margin had not been used in selecting the lightning arresters. It should be emphasized that in this high-voltage transmission range the required 60-cycle test of some apparatus may well determine the basic impulse level, and to attempt to push the basic impulse level too low may result in equipment not having the required strength to perform satisfactorily under long-time normal 60-cycle operation.

REFERENCES

1. CARRIER ATTENUATION DISCLOSES GLAZE FORMATION, **V. M. Marquis, G. G. Langdon.** *Electrical World* (New York, N. Y.), May 20, and August 12, 1939.

2. LIGHTNING PERFORMANCE OF 220-KV TRANSMISSION LINES—II, **AIEE Committee Report.** *Electrical Engineering* (*AIEE Transactions*), volume 65, February 1946, pages 70–75.

Corona Investigation on Extra-High-Voltage Lines—500-Kv Test Project of the American Gas and Electric Company

I. W. GROSS FELLOW AIEE
C. F. WAGNER FELLOW AIEE
O. NAEF MEMBER AIEE
R. L. TREMAINE ASSOCIATE AIEE

IN A group of papers[1–7] presented before the Institute in 1947, the subject of extra-high-voltage transmission lines was discussed and the need pointed out for additional information on corona and radio-influence effects before such lines could be built on a sound engineering and economical basis. One of these papers[2] outlines the field test research project which was being undertaken by the American Gas and Electric Company in co-operation with eight manufacturers of electric equipment to provide the much needed information on corona, radio influence, and other features.

The test site is located adjacent to the Tidd Power Plant. The project has been in operation for over three years and much valuable information has been obtained. It is the purpose of the present paper to present the high points and as much of the detail as possible of this investigation. This paper will be confined almost wholly to the effects of corona, particularly on conductors. Companion papers[8,9] cover the radio influence aspects and measurement technique and equipment in detail.

General Description of Test Facilities and Methods of Test

Although a general description of the testing equipment and facilities at the Tidd test site has been given previously,[2–7] a few of the high points of the facilities may be of interest here.

Three full size test lines, two 1.4 miles and one 800-feet long, were constructed in the field and energized through a 5,000-kva bank of three single-phase transformers. A test voltage range from about 150 to 500 kv phase-to-phase can be obtained by transformer taps and by connecting the low-voltage windings in either delta or Y. Provision was made for varying the conductor spacing and ground wire height. The conductors[4] tested ranged in size up to 2.0-inch outside diameter and were of steel-reinforced aluminum cable, copper HH, and copper I-beam types. Two-conductor bundles also were tested.

The towers are single circuit for flat configuration and liberally designed for flexibility in altering the test arrangements, and approximate the general dimensions which might be used if a 500-kv line were to be built.

The instrumentation includes supersensitive indicating and recording wattmeters for measuring corona loss, and indicating and graphic instruments for determining radio-influence effects. Other instruments consist of a photographic weather recording device, a ground gradient meter and conventional instruments to record temperature, barometric pressure and so forth. Special test setups were made to determine insulator losses and to simulate conductor temperature rise due to load current.

Corona loss is obtained both on indicating instruments by so-called "manual tests" and by graphic charts which are operated continuously. Manual tests are defined as those where observations are made on indicating instruments and recorded manually. For manual tests the voltage is varied over the range available in a relatively short time to obtain essentially constant weather conditions. For the graphic records the voltage is maintained constant for periods of several days.

The test lines have been energized practically continuously for the past three years except at such times as data were being obtained on single lines instead of all three lines simultaneously, or when single-phase measurements were being taken. During this 3-year period, supervising personnel have been in constant attendance at the station. It is worthy of note that during the entire test period no failure or defect of major equipment, or accident to operating personnel has occurred, although the test station was under eight feet of water during the spring flood of 1948.

A fuller description of the test instruments, methods of use and measurements, together with method of analyzing field records is given in a companion paper.[9] Unless otherwise stated here, all corona loss data were not corrected for air density.

To supplement the field tests, a laboratory setup, shown in Figure 1, was made at the Trafford Laboratory of the Westinghouse Electric Corporation. A vertical insulated screen 20 by 40 feet, shown in the background, was hung from the ceiling, and the test conductor was suspended either vertically or horizontally about ten feet from the screen. A wattmeter of the same kind as those used at Tidd was employed, and was connected between the screen and ground and to the primary winding of the test transformer used to supply the high voltage. By means of a phase-shifting device the phase position of the voltage was adjusted for each test to obtain essentially zero readings below the critical disruptive voltage. Correction was made for the stray loss of the circuit by obtaining the loss with the test conductor replaced by one having a diameter

Paper 51-12, recommended by the AIEE Transmission and Distribution Committee and approved by the AIEE Technical Program Committee for presentation at the AIEE Winter General Meeting, New York, N. Y., January 22–26, 1951. Manuscript submitted October 24, 1950; made available for printing November 16, 1950.

I. W. GROSS and O. NAEF both are with the American Gas and Electric Service Corporation, New York, N. Y.; C. F. WAGNER and R. L. TREMAINE both are with the Westinghouse Electric Corporation, East Pittsburgh, Pa.

Table I. Excessive Precipitation, Pittsburgh Airport—June 24, 1950

Period in minutes	5	10	15	20	60	120	180	24 hrs.
Precipitation in inches	0.50	0.76	1.00	1.23	2.00	2.07	2.18	2.38
Rate in inches per hour	6.00	4.56	4.00	3.69	2.00	1.04	0.73	0.10

Table II. Annual Precipitation in Inches

(Average of 40–50 Years)

Amarillo, Tex.	21.0
Atlanta, Ga.	48.8
Boston, Mass.	40.1
Chicago, Ill.	32.8
Denver, Colo.	14.0
Jacksonville, Fla.	49.7
Los Angeles, Calif.	15.4
Minneapolis, Minn.	27.2
New Orleans, La.	60.3
New York, N. Y.	43.0
Pittsburgh, Pa.	36.0
Portland, Oreg.	41.6
Salt Lake City, Utah	13.7
San Antonio, Tex.	27.1
San Francisco, Calif.	22.1
Washington, D. C.	41.9

of three inches. The ends of the test conductors were shielded with 2-inch grading rings 28 inches in diameter. Rain up to one inch per hour was simulated by means of the device shown in the upper part of the illustration.

General Considerations

The corona loss of a particular single (as contrasted with a bundle) conductor can be completely determined in terms of the "nominal gradient" at the surface for given weather and surface conditions. Nominal gradient as defined here is that gradient that would exist at the surface if there were no corona present and the conductor were a perfect cylinder. In practical configurations the charges on other conductors have a negligible effect upon the voltage gradient of the conductor under consideration, the gradient being determined almost entirely by the charge upon itself. The configuration does affect the charge upon the respective conductors. For a given configuration and voltage the charge and "nominal gradient" can be calculated by conventional means. For example, with a flat configuration the charge upon the center conductor is about 5 per cent higher than the charges on the outer conductors. For this reason the gradient at the center conductor is correspondingly larger. The fundamental corona data in this paper is, therefore, plotted in terms of the "nominal gradient" as the parameter. Since "nominal gradient" is proportional to the charge on the conductor and the charge in turn is proportional to the charging current, many of the curves have an additional scale showing this quantity. In many respects this is a more fundamental quantity than "nominal gradient" as it can be observed directly. To convert from current to "nominal gradient" the following formula can be used

$$G_n = 4404\ \frac{q}{r} = \frac{4404}{2\pi f}\ \frac{i}{r} = 11.7\ \frac{i}{r} \qquad (1)$$

where

G_n = nominal gradient in kilovolts per centimeter
q = charge in coulombs per mile
i = charging current in amperes per mile at 60 cycles
r = radius of conductor in inches
f = frequency in cycles per second

The authors make no apologies for the conglomeration of units. The English and metric units are interspersed because the critical value of G_n is usually expressed in kilovolts per centimeter. Peek[10] gives the crest value of the critical visual gradient as 40 kv per centimeter for conductors above one inch in diameter.

To orient the loss curves with practical line configurations the abscissae are sometimes plotted in terms of line-to-line voltage. Unless otherwise stated a 32-foot flat spacing is assumed. Since these scales cannot be exact for all curves they are marked "approximate."

For "bundle conductors" the presence of the other conductors comprising the bundle produces a nonuniform field around the periphery. For a 2-conductor bundle, Cahen[11] of France found that if a gradient equal to the mean of the maximum and average gradients were used the characteristics of a single conductor (multiplying by 2, of course) could be used to predetermine the characteristics of the bundle.

Unless the surface of a conductor is highly polished and the tests made under carefully controlled conditions considerable variation results in the values of corona loss measurements. For practical transmission lines these conditions do not prevail and it is essential that the loss be obtained on conductors as they are used in the field. Among the factors contributing to this variance and which were investigated are the following:

1. Normal variations in weather—fair, rain, fog, snow, and sleet.
2. Long time surface aging of the conductors.
3. Short time surface effects as the result of changes in the applied voltage.
4. Heating of conductors by load current.
5. Electrostatic ground gradient.

Definitions

"Fair weather" as defined in this paper is a condition of no visual abnormalities such as rain, fog, snow, sleet, or smoke in the vicinity of the conductor. "Foul weather" refers to all other conditions. Since rain plays such an important role in corona phenomena, to co-ordinate the data taken at Tidd with conditions elsewhere in the country the data is presented in such form that it can be converted to other weather conditions by means of information available from the United States Weather Bureau. The Weather Bureau records provide no means for differentiation between "fair" and "foul" weather except on the basis of precipitation. The graphic record data was, therefore, divided into "precipitation" and "apparent fair weather" periods, the former being defined as such times during which an indication of precipitation occurs on the rain gauge at Tidd. "Apparent fair weather" is then, conversely, those periods in which no indications of precipitation appear on the rain gauge. The more sensitive photographic recorder shows that there are times during which the precipitation is so light that it does not indicate on the rain gauge. The photographic recorder also indicates periods of fog and periods of moisture condensation on the conductors that would not be recorded as precipita-

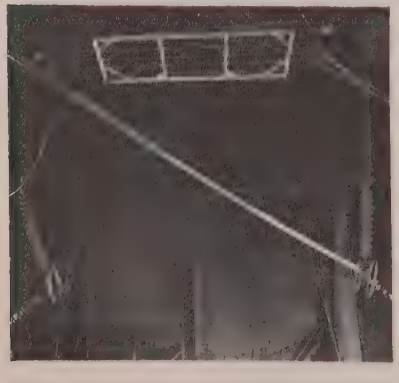

Figure 1. General view of test setup at Trafford Laboratory. For corona loss measurement, conductor under test is strung between grading shields

Figure 2 (A to F will be found on three succeeding pages). Corona loss on field test lines for six different conductors. Measurements made visually (manually). Unlabeled curves are fair weather data. All curves corrected to an air density factor = 1.0

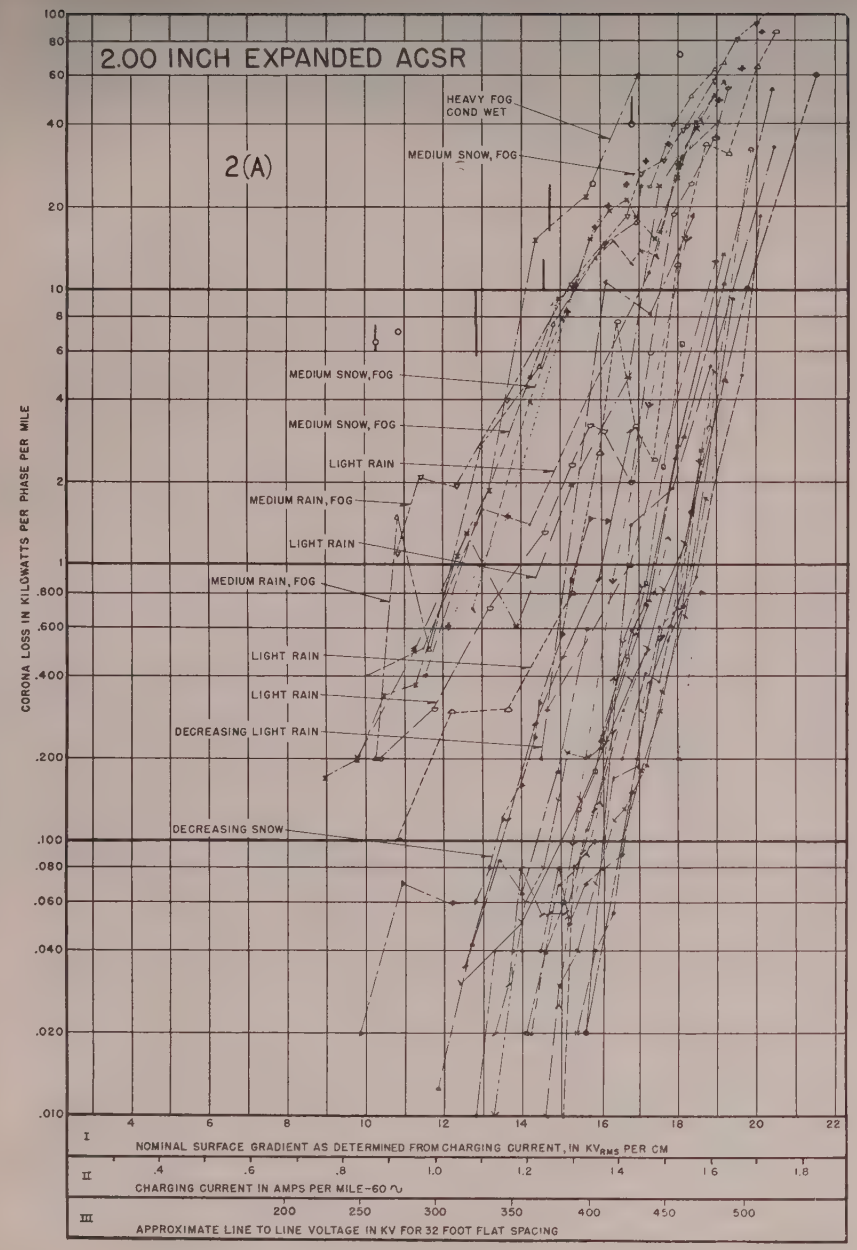
2.00 INCH EXPANDED ACSR
2(A)
HEAVY FOG COND WET
MEDIUM SNOW, FOG
MEDIUM SNOW, FOG
MEDIUM SNOW, FOG
LIGHT RAIN
MEDIUM RAIN, FOG
LIGHT RAIN
MEDIUM RAIN, FOG
LIGHT RAIN
LIGHT RAIN
DECREASING LIGHT RAIN
DECREASING SNOW
CORONA LOSS IN KILOWATTS PER PHASE PER MILE
I NOMINAL SURFACE GRADIENT AS DETERMINED FROM CHARGING CURRENT, IN KV RMS PER CM
II CHARGING CURRENT IN AMPS PER MILE-60 ∿
III APPROXIMATE LINE TO LINE VOLTAGE IN KV FOR 32 FOOT FLAT SPACING

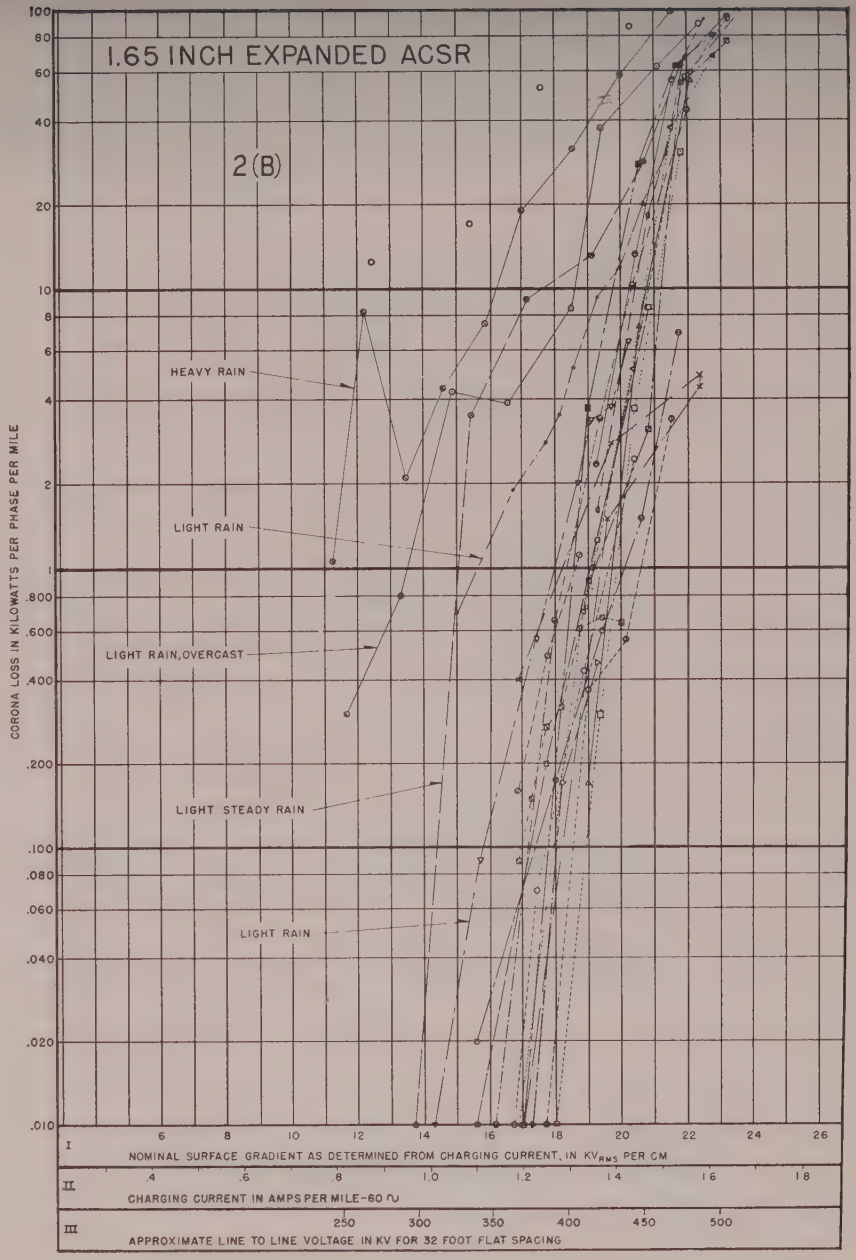
1.65 INCH EXPANDED ACSR
2(B)
HEAVY RAIN
LIGHT RAIN
LIGHT RAIN, OVERCAST
LIGHT STEADY RAIN
LIGHT RAIN
CORONA LOSS IN KILOWATTS PER PHASE PER MILE
I NOMINAL SURFACE GRADIENT AS DETERMINED FROM CHARGING CURRENT, IN KV RMS PER CM
II CHARGING CURRENT IN AMPS PER MILE-60 ∿
III APPROXIMATE LINE TO LINE VOLTAGE IN KV FOR 32 FOOT FLAT SPACING

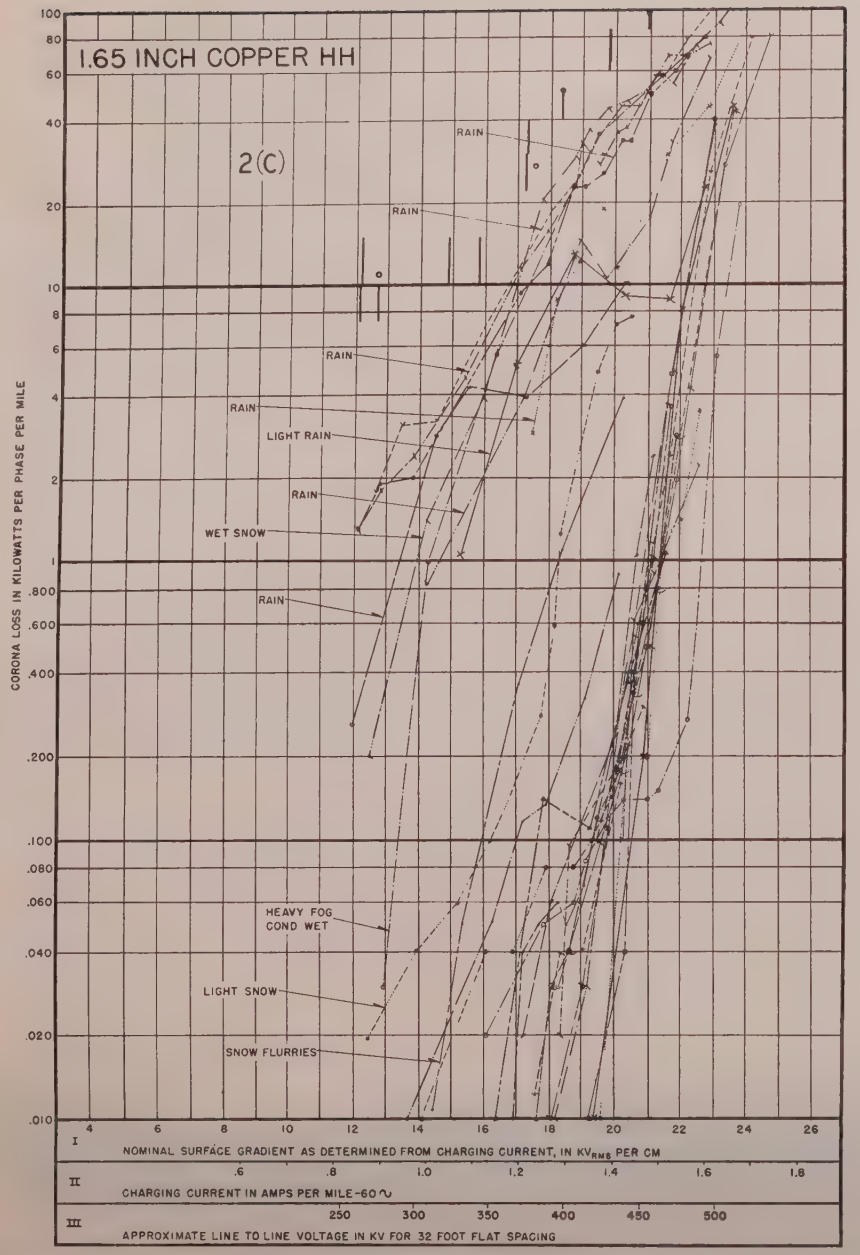
1.65 INCH COPPER HH
2(C)
RAIN
RAIN
RAIN
RAIN
LIGHT RAIN
RAIN
WET SNOW
RAIN
HEAVY FOG
COND WET
LIGHT SNOW
SNOW FLURRIES
CORONA LOSS IN KILOWATTS PER PHASE PER MILE
100
80
60
40
20
10
8
6
4
2
1
.800
.600
.400
.200
.100
.080
.060
.040
.020
.010
I
4 6 8 10 12 14 16 18 20 22 24 26
NOMINAL SURFACE GRADIENT AS DETERMINED FROM CHARGING CURRENT, IN KVRMS PER CM
II
.6 .8 1.0 1.2 1.4 1.6 1.8
CHARGING CURRENT IN AMPS PER MILE-60∿
III
250 300 350 400 450 500
APPROXIMATE LINE TO LINE VOLTAGE IN KV FOR 32 FOOT FLAT SPACING

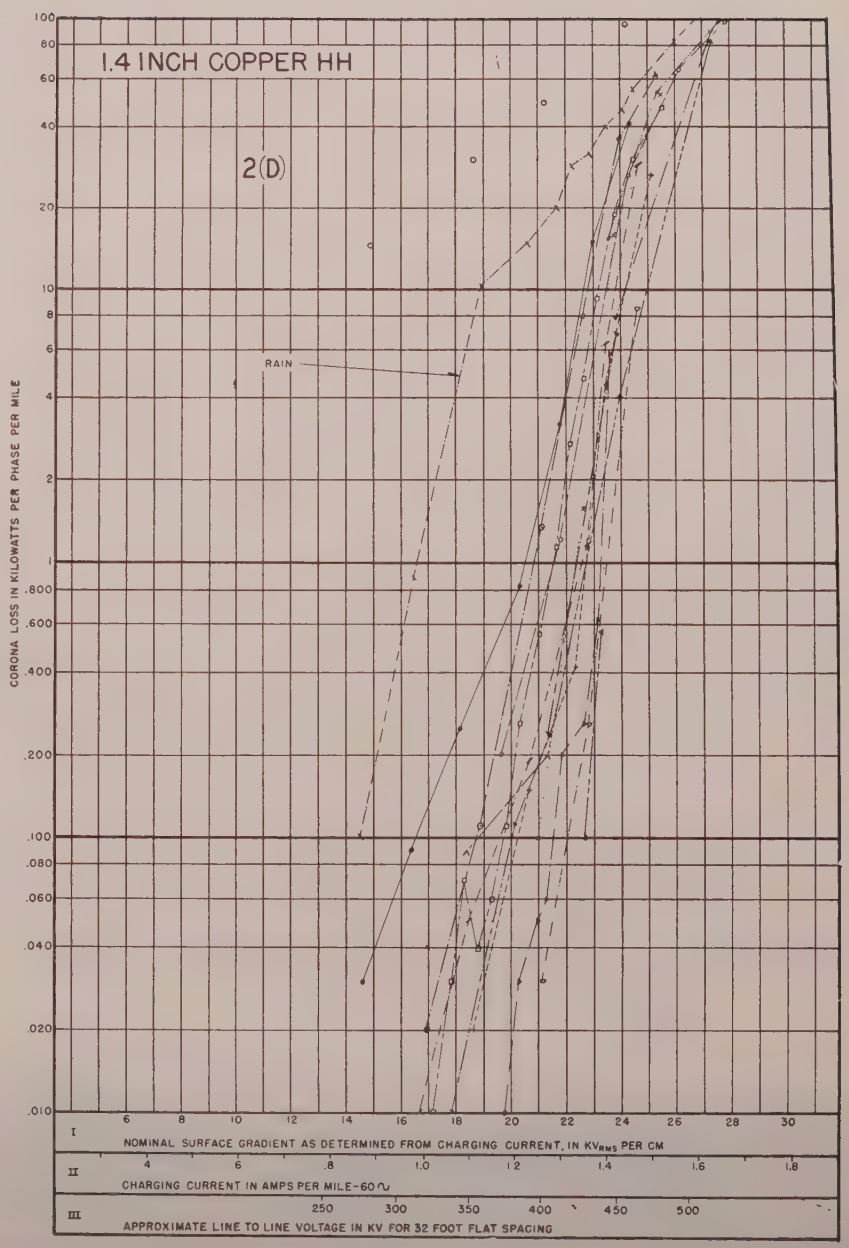
1.4 INCH COPPER HH
2(D)
RAIN
CORONA LOSS IN KILOWATTS PER PHASE PER MILE
100
80
60
40
20
10
8
6
4
2
1
.800
.600
.400
.200
.100
.080
.060
.040
.020
.010
I
6 8 10 12 14 16 18 20 22 24 26 28 30
NOMINAL SURFACE GRADIENT AS DETERMINED FROM CHARGING CURRENT, IN KVRMS PER CM
II
4 6 .8 1.0 1.2 1.4 1.6 1.8
CHARGING CURRENT IN AMPS PER MILE-60∿
III
250 300 350 400 450 500
APPROXIMATE LINE TO LINE VOLTAGE IN KV FOR 32 FOOT FLAT SPACING

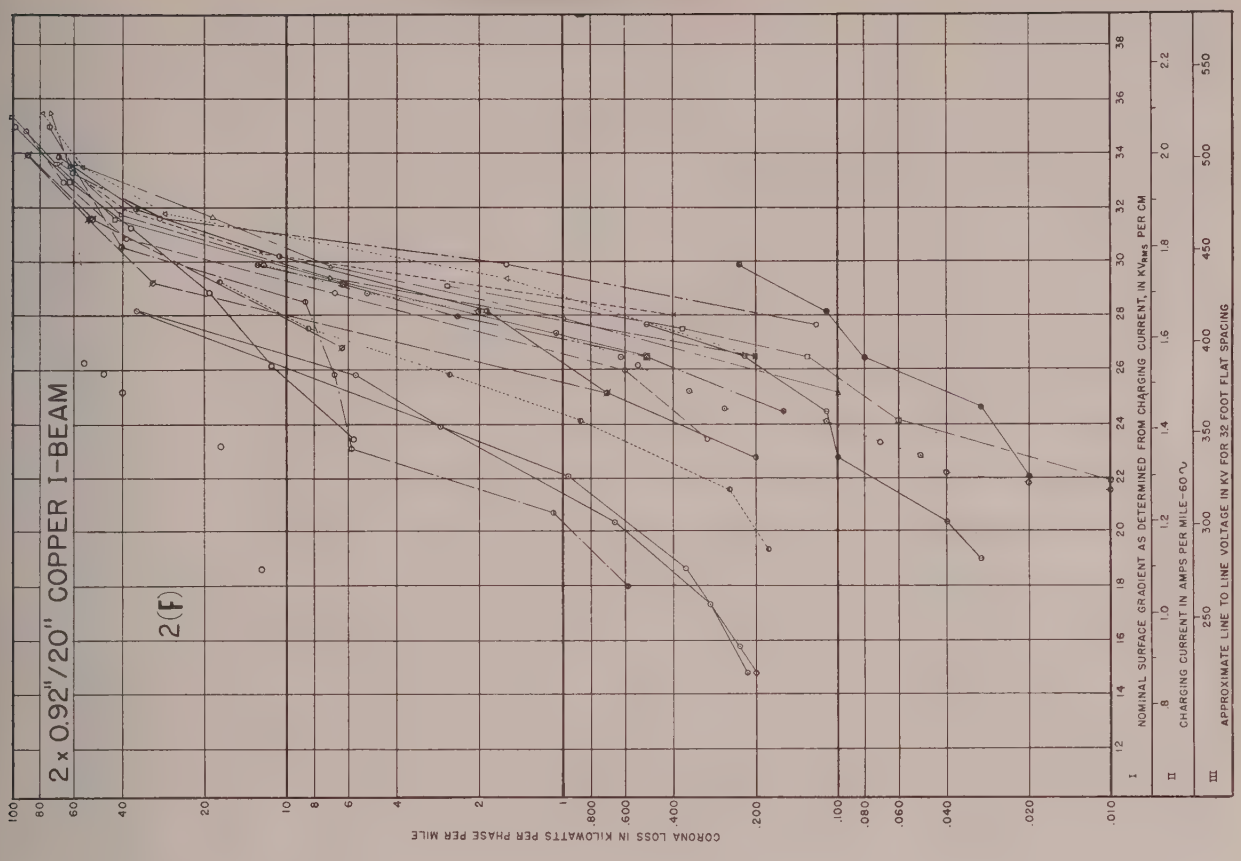
2 x 0.92"/20" COPPER I-BEAM
2(F)
CORONA LOSS IN KILOWATTS PER PHASE PER MILE
I NOMINAL SURFACE GRADIENT AS DETERMINED FROM CHARGING CURRENT, IN KV$_{rms}$ PER CM
II CHARGING CURRENT IN AMPS PER MILE-60 ∿
III APPROXIMATE LINE TO LINE VOLTAGE IN KV FOR 32 FOOT FLAT SPACING

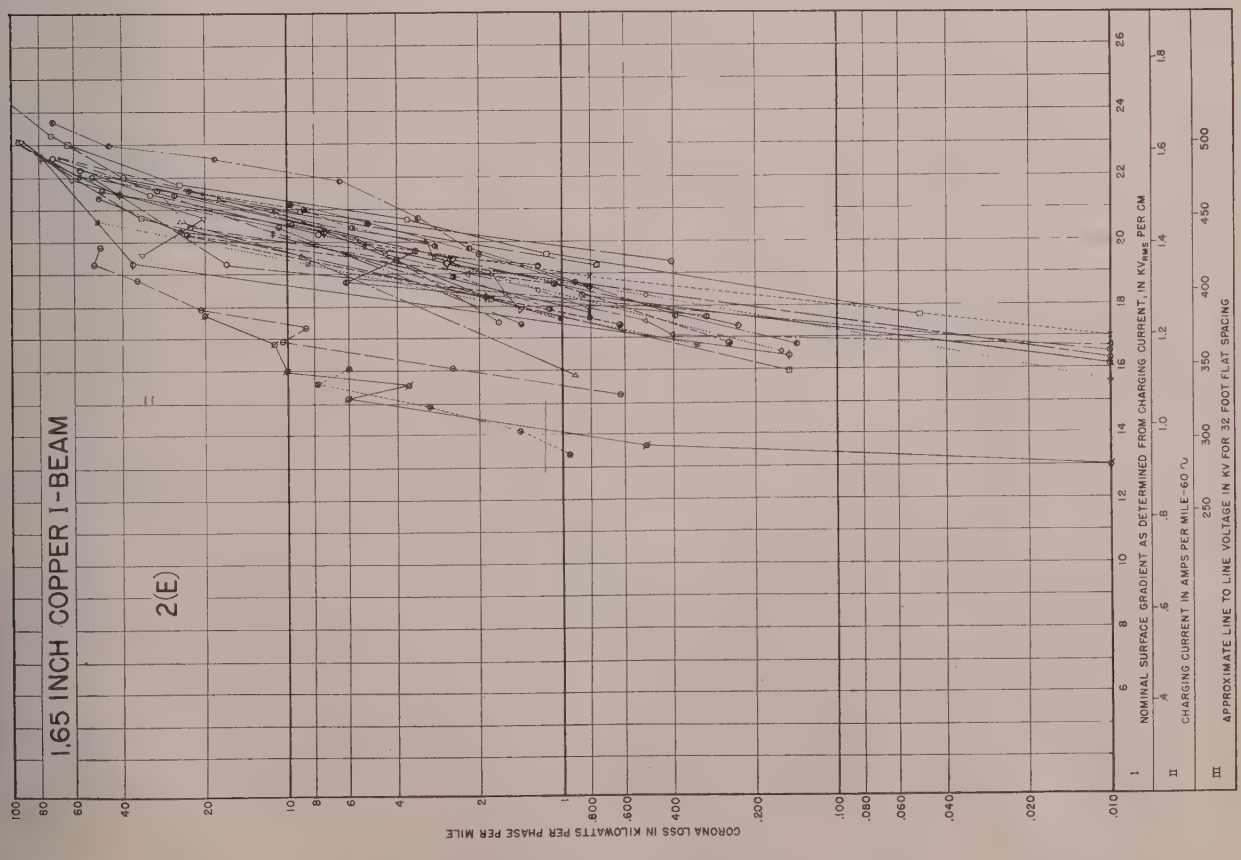
1.65 INCH COPPER I-BEAM
2(E)
CORONA LOSS IN KILOWATTS PER PHASE PER MILE
I NOMINAL SURFACE GRADIENT AS DETERMINED FROM CHARGING CURRENT, IN KV$_{rms}$ PER CM
II CHARGING CURRENT IN AMPS PER MILE-60 ∿
III APPROXIMATE LINE TO LINE VOLTAGE IN KV FOR 32 FOOT FLAT SPACING

tion periods. All of these just mentioned factors contribute to increased corona loss. It would be expected, then, that the loss during the "apparent fair weather" period from the graphic charts would be higher than the loss during fair-weather tests obtained by manual observations; and the field tests confirm this.

Fair-Weather Loss

Field Tests

Figures 2 (A) to (F) represent the corona loss as a function of voltage for short-time tests on the principal conductors tested during the investigation at Tidd. In each case the conductor was voltage seasoned just prior to testing in accordance with the technique described in a companion paper.[9] Those curves not specifically marked otherwise were made under fair-weather conditions. Some of these curves represent single-phase and others 3-phase tests. In the latter case it was found that the curves for the three individual phases superposed so closely that in general only one curve for each 3-phase test was plotted. All of these curves were corrected to standard atmospheric conditions, by dividing the test currents or voltages by the air density factor raised to the 2/3 power.

In spite of the seasoning process and the correction to standard conditions, great variation in day-to-day results still remains. Other investigators have obtained similar results. An attempt was made to determine the cause of these variations without very definite conclusions. Some of the explanations considered are:

1. Dust or foreign particles adhering to the surface. The number and size of such

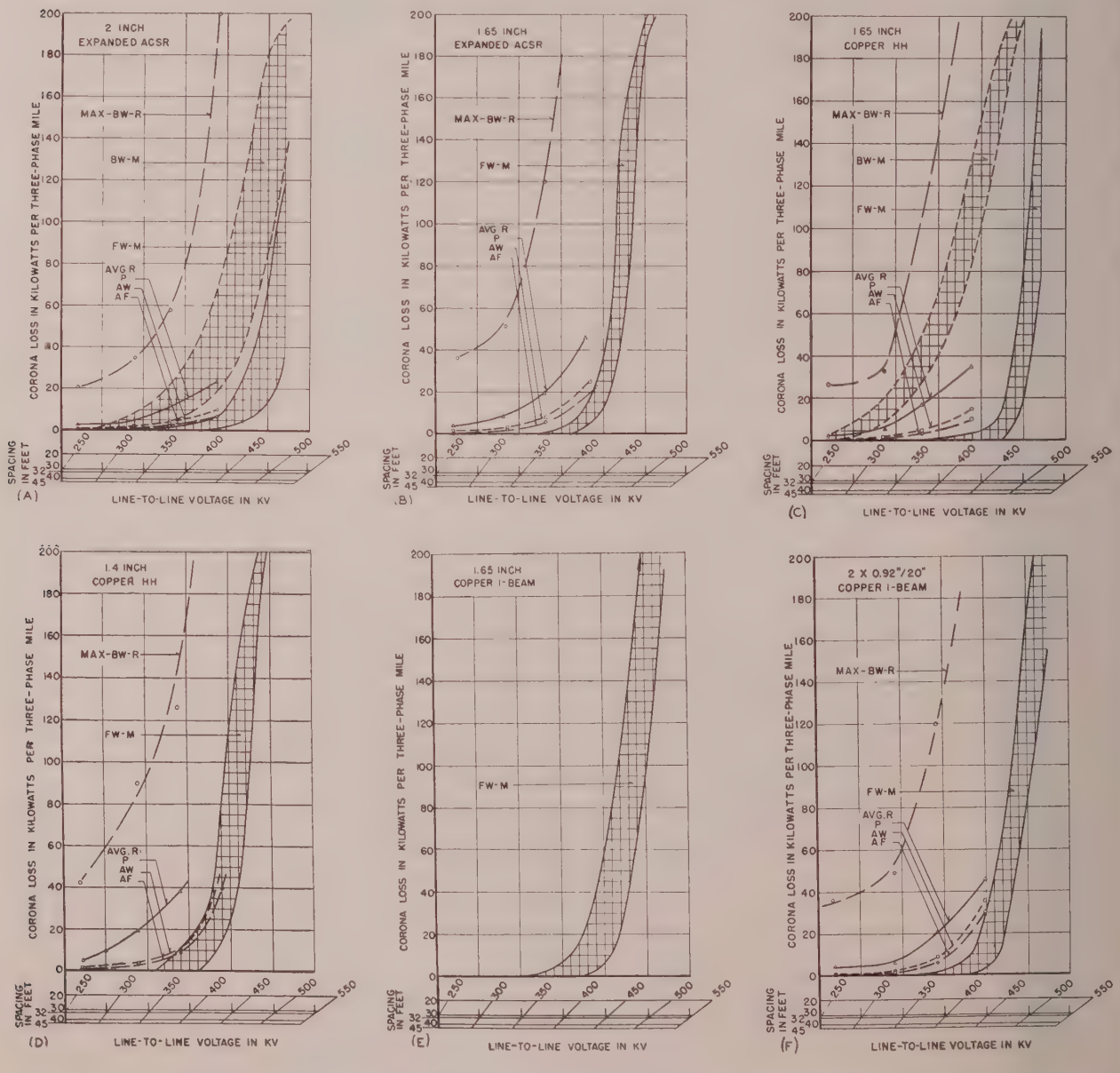

Figure 3 (A to F). Corona loss variation for different conductors—fair and foul weather. (Summary of data from Figures 2 and 4.) Manual data reduced to unity air density

M = manual data
R = recorded data
P = precipitation
BW = foul weather
FW = fair weather
AW = all weather
AF = apparent average fair weather

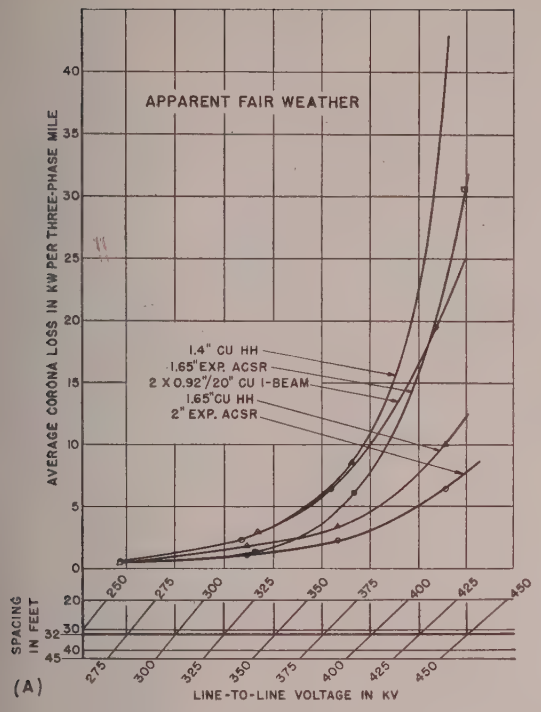

Figure 4 (A to C, left, lower left, and right). Corona loss for field test lines—long-time average from recorded data. Not all data taken simultaneously

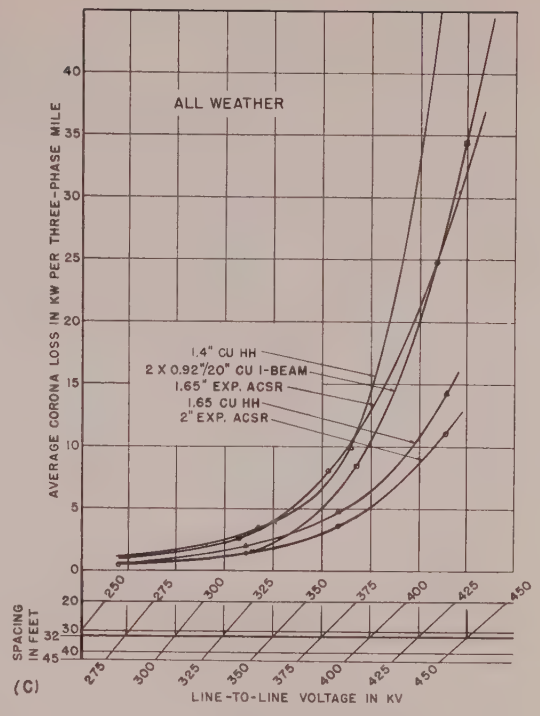

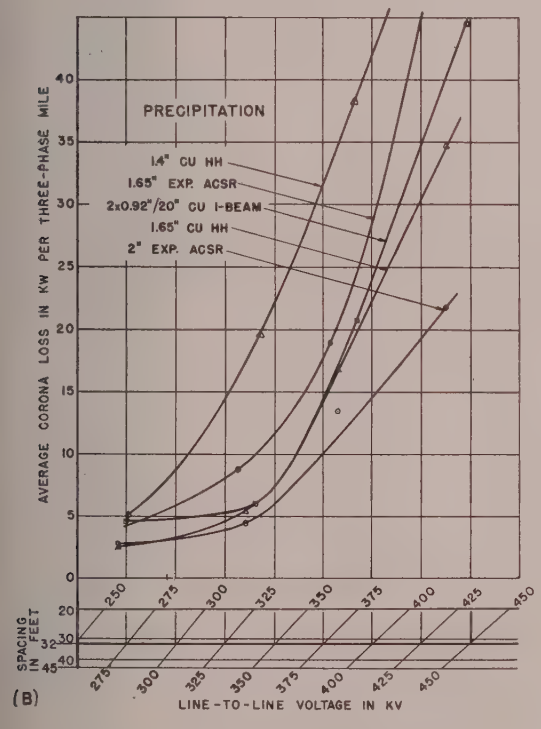

Figure 5 (right). Corona loss during fair weather on 2-conductor bundles of 0.92-inch copper I-beam conductors on field tests as a function of separation. Single-phase tests. Numbers on curves refer to test voltages and numbers in parentheses to equivalent line-to-line voltage for 32-foot flat spacing. Data reduced to unity air density

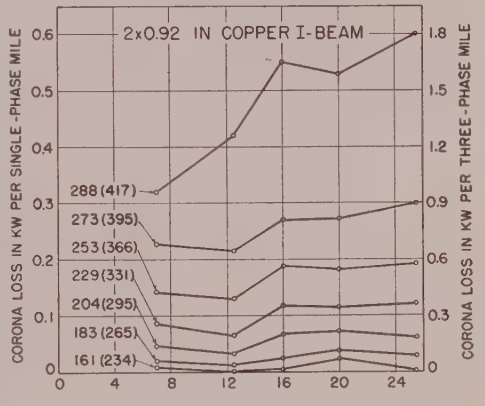

particles might vary with the adhesive character of the surface film and with the electrostatic forces present when the conductor is energized.

2. Changes in the surface condition occasioned by chemical action of the atmosphere.

3. Changes in moisture content of the surface film.

In plotting the points the measured, rather than the calculated charging current per mile in the respective phases, was used. The nominal surface voltage gradient was then computed by equation 1. The measured values of charging current do not agree with values calculated for particular configurations. The measured values while in the proper proportions in the respective phases are about 5 per cent higher. The increased charging current of the line due to the presence of the towers and the capacitance of the insulator strings probably accounts for most if not all of this increment. This factor must be borne in mind when comparing corona data that uses calculated values of current. The charging current in the region of intense corona increases faster than the first power of the applied voltage. This increment was intentionally not included. A current proportional to the applied voltage was used for plotting.

It can be shown that the charge on the outside conductors of a 3-conductor flat configuration is closely the same as the charge on a system of three conductors in triangular configuration remote from earth and having a phase spacing of $\sqrt[3]{2}$ times the flat spacing (the equivalent spacing). The center conductor will have a charge 5 per cent higher. These rela-

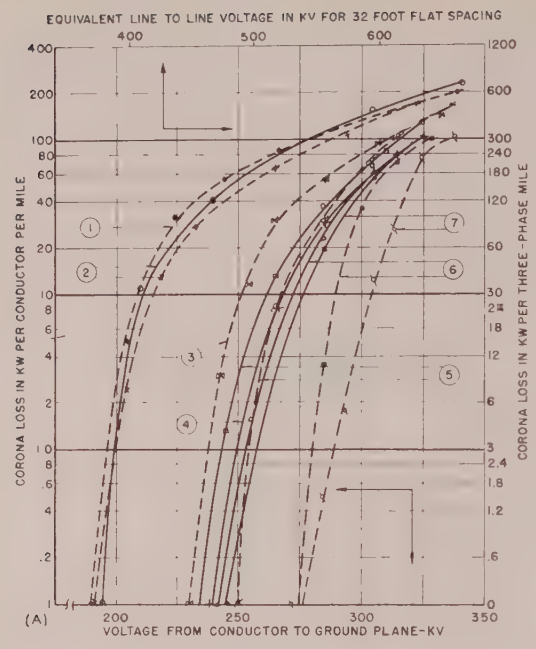
EQUIVALENT LINE TO LINE VOLTAGE IN KV FOR 32 FOOT FLAT SPACING
CORONA LOSS IN KW PER CONDUCTOR PER MILE
CORONA LOSS IN KW PER THREE-PHASE MILE
VOLTAGE FROM CONDUCTOR TO GROUND PLANE-KV
(A)

Figure 6. Corona loss on single conductors at Trafford Laboratory under (A) dry conductors and (B) under one inch of rain per hour. Full and broken lines refer to two different test setups

No.	Conductor
1	0.92″ cu. I-beam
2	1.1″ (795 mcm) ACSR
3	1.38″ ACSR
4	1.65″ expanded ACSR
5	1.4″ cu. HH
6	1.65″ cu. HH
7	2″ expanded ACSR (new)

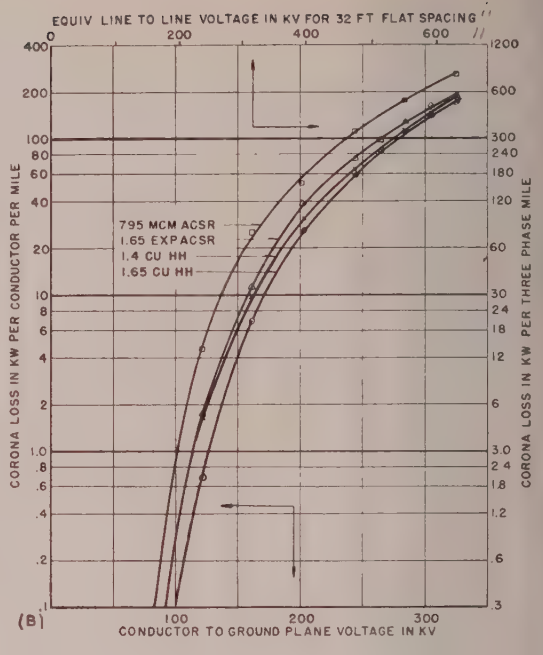
EQUIV LINE TO LINE VOLTAGE IN KV FOR 32 FT FLAT SPACING
795 MCM ACSR
1.65 EXP ACSR
1.4 CU HH
1.65 CU HH
CORONA LOSS IN KW PER CONDUCTOR PER MILE
CORONA LOSS IN KW PER THREE PHASE MILE
CONDUCTOR TO GROUND PLANE VOLTAGE IN KV
(B)

tions together with the 5 per cent difference between calculated and measured charging current were used to compute the 3-phase voltage scales.

The large number of curves and the irregularity in Figure 2 makes comparisons between conductors difficult. Figure 3 has, therefore, been prepared. The cross-hatched areas bounded by the full lines represent the zones in which the fair-weather curves fall. The abscissa on each curve is arranged so that the loss can be determined for any phase spacing. The other information on these curves is replotted from data that will be discussed subsequently.

As mentioned previously, loss data also were obtained with continuously recording charts. From indications on the rain gauge these records were divided into "apparent fair weather" and "precipitation" periods. With the lines operating at any given voltage, the loss for the "apparent fair weather" periods were averaged arithmetically. The results for these averages for different voltages and different conductors are plotted in Figure 4 (A). The test period for any given conductor and voltage varied between three and ten months. Comparing these curves which have been replotted in Figure 3 with the fair weather curves of Figure 3 it will be observed that the losses are greater. This results from the definitions of "fair" and "apparent fair" weather, the loss for the latter condition including loss during periods of fog, condensation of moisture on the conductors, and rain so light that it cannot be recorded on the rain gauge. As explained in a companion paper,[9] the manually observed values are further reduced by the test procedure, which was found necessary in order to obtain consistent results. This procedure enables accurate comparison between conductors, but caution should be exercized in applying these data to practical transmission lines.

Figure 5 shows the results of single-phase tests made at Tidd to determine the effect of subconductor separation of bundle conductors. These were made under fair-weather conditions. Each curve was made during about three or four hours so that weather conditions were as constant as possible for that curve.

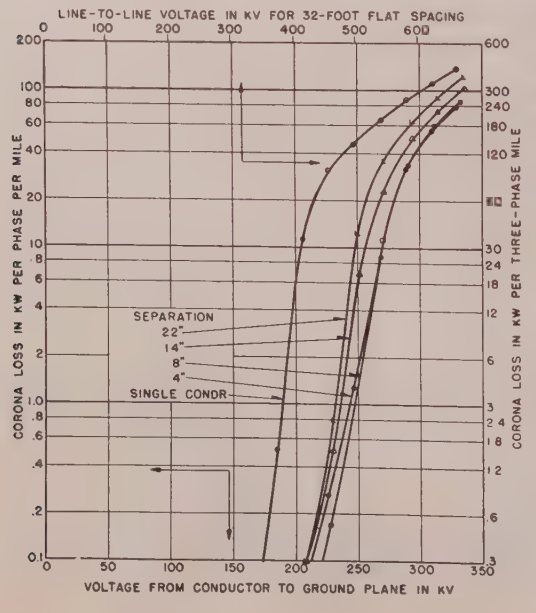

Figure 7 (left). Corona loss on dry 2-conductor bundles of 0.92-inch copper I-beam conductors at Trafford Laboratory for different subconductor separations

Figure 8 (right). Corona loss on dry 2-conductor bundles of 0.92-inch copper I-beam conductors as a function of separation. Numbers on curves are line-to-line voltages for flat 32-foot phase spacing. Replot of Figure 7

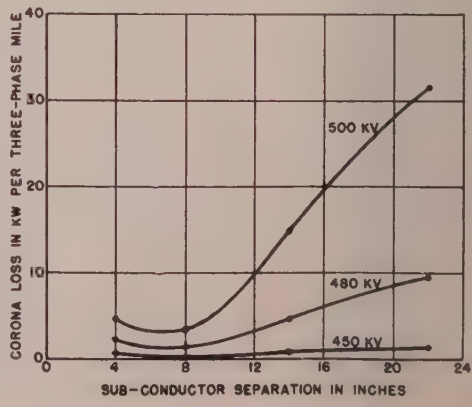

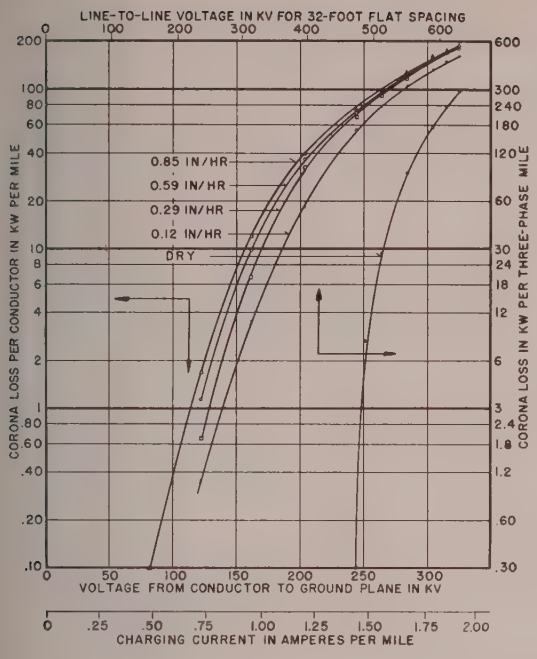
LINE-TO-LINE VOLTAGE IN KV FOR 32-FOOT FLAT SPACING
0 100 200 300 400 500 600
CORONA LOSS PER CONDUCTOR IN KW PER MILE
CORONA LOSS IN KW PER THREE-PHASE MILE
0.85 IN/HR
0.59 IN/HR
0.29 IN/HR
0.12 IN/HR
DRY
VOLTAGE FROM CONDUCTOR TO GROUND PLANE IN KV
CHARGING CURRENT IN AMPERES PER MILE

Figure 9. Corona loss of a single 1.65-inch expanded steel reinforced aluminum cable taken at Trafford Laboratory as a function of voltage for different rates of continuous precipitation

Figure 10 (A to D below). Effect of continuous uniform rainfall at Trafford Laboratory for different voltages. The voltage on each curve is the voltage from conductor to ground plane, and the number within the parentheses is the amperes per mile at 60 cycles. Broken line curves are replotted from Figure 13

All data were taken on the same day. As can be seen the results are not too conclusive. This point is discussed later in connection with the laboratory tests.

Laboratory Tests

The laboratory tests on single conductors for dry conditions are shown in Figure 6(A). The surfaces of the conductors were not specially treated by polishing or aging prior to testing but before taking a set of readings the conductor was seasoned for 20 minutes at 350 kv from conductor to ground plane. Two groups of tests were made at different times. While the various conductors retain, in general, the same position relative to each other in these two tests it will be observed that they are displaced horizontally with respect to the curves obtained at Tidd under fair-weather conditions. This result was not entirely unexpected. The laboratory tests were undertaken primarily to determine the effect of conductor radius upon the critical disruptive voltage and to supplement the field data. Therefore, it was necessary to remove any obvious imperfections in order to obtain consistent results. The laboratory test conductors were thus in better condition than those tested in the field. On the other hand the laboratory conductors had not been aged in service. In addition, a short length of cable such as used in the laboratory would not encompass as much variation in surface conditions as the longer lines at the test site. It would be quite fortuitous if the particular sample tested in the laboratory would correspond to the worst equal length of transmission line. For these reasons one would expect the laboratory curves to have a higher threshold corona voltage, which corresponds to the facts.

Bundle Conductors

Considerable interest has been exhibited by foreign countries in bundle-conductors, France[11] and Sweden[12] in a bundle of two and Germany[13] in a bundle of four. The tests at Tidd and at the Trafford Laboratory have to date covered only the 2-conductor bundle. The discussions will, therefore, be limited to this type.

The manner in which bundle conductors reduce corona can be visualized by considering two cylindrical conductors at equal distances above ground with unit charge on each. If the conductors are first separated by a great distance the voltage of each will be proportional to their individual capacitances to ground. Now if they be made to approach each

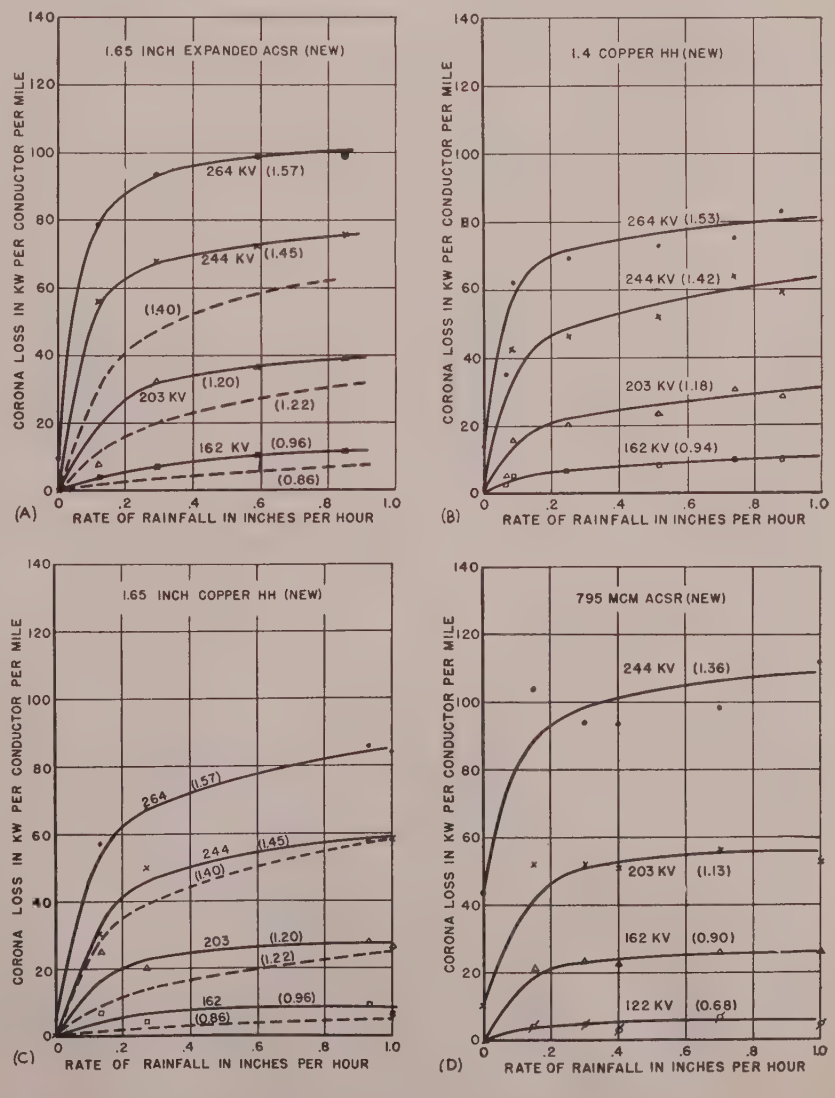

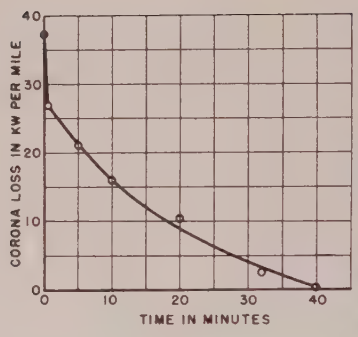

Figure 11 (left). Corona loss after stoppage of rain. Initial rain 0.75 inch per hour. Rain stopped at zero time. Single 1.65-inch expanded steel-reinforced aluminum cable, 203 kv-to-ground plane. The steady-state dry loss from a previous test at the same voltage was zero

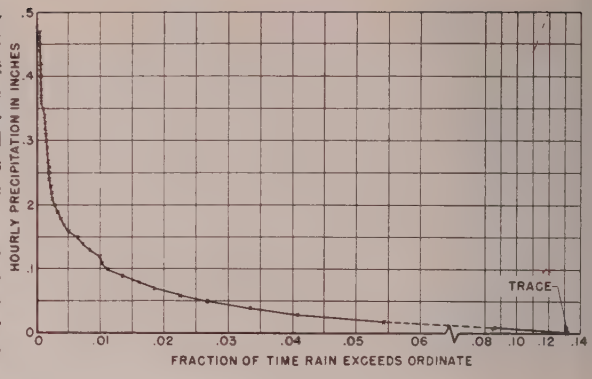

Figure 12 (right). Rainfall distribution compiled from data supplied by Weather Bureau for Pittsburgh, Pa., airport from December 1948 to September 1949, including 7,296 hours

other two effects occur. First, as they approach each other close enough their potentials increase, keeping of course their charges and, consequently their "nominal" surface voltage gradients, the same. Thus the voltage increases without any corresponding increase in gradient or corona loss. As the conductors approach still closer, however, a second effect occurs. The field gradient of the other conductor and the distortion effect of the conductor itself in this field add together to modify the voltage gradient at the surface of the conductor, keeping the average value the same.

Figure 7 shows a number of voltage runs made at the Trafford Laboratory on a double conductor having different subconductor spacings. For comparison with other curves the auxiliary scales have been added to convert to a typical 3-phase configuration. For this conversion it was assumed as with single conductors that the center phase had 5 per cent larger

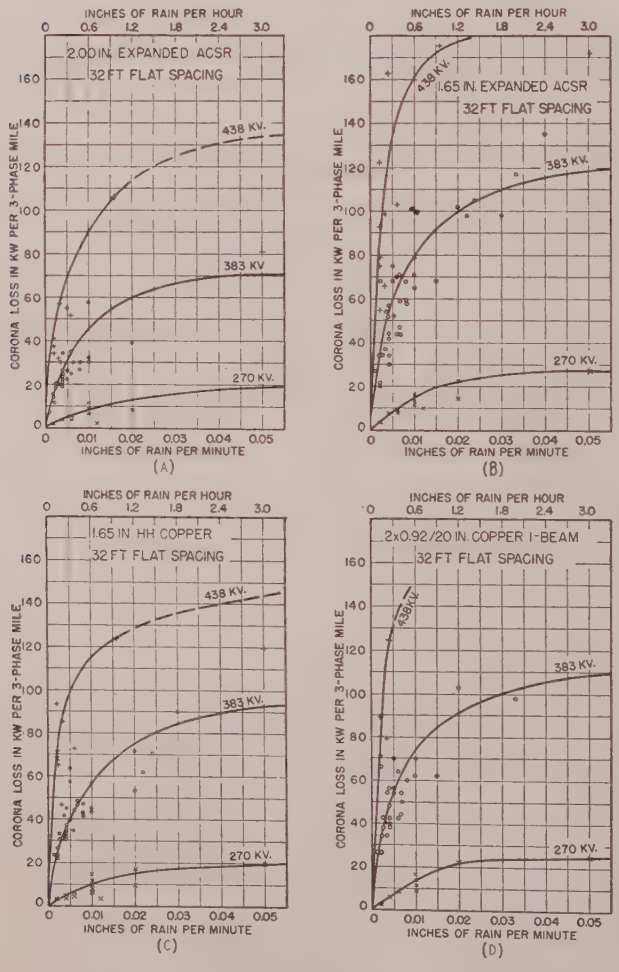

Figure 13 (A to D). Effect of rainfall for very short periods for the field test lines at different voltages. Both the loss and precipitation were averaged over very short periods (approximating instantaneous values). Graphic record data. The numbers on the curves are line-to-line voltages

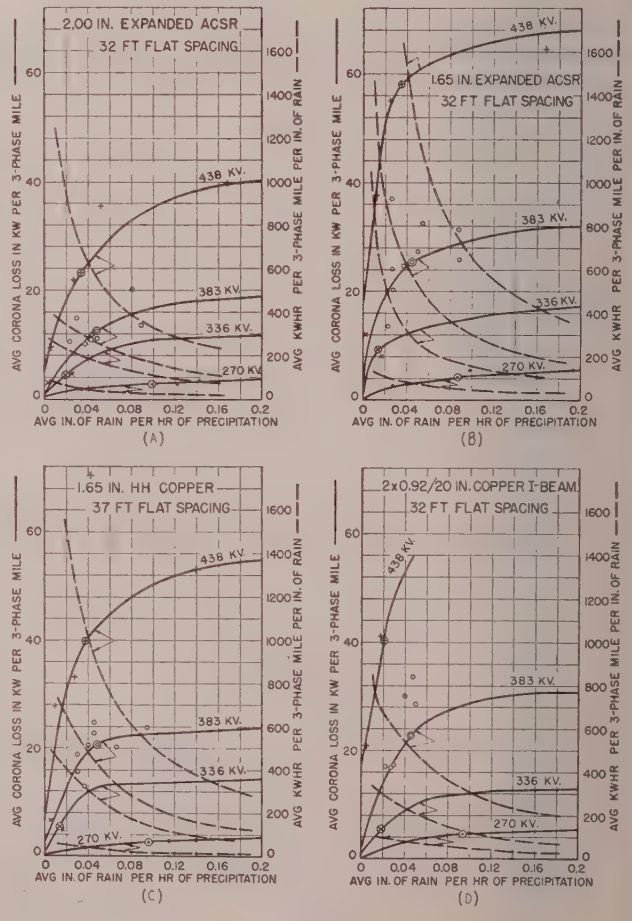

Figure 14 (A to D). Effect of rainfall during precipitation periods on the field test lines for different voltages. Both the loss and precipitation were averaged over storm periods only. Graphic record data. Small symbols are one month averages. Large circles are from one to nine month averages

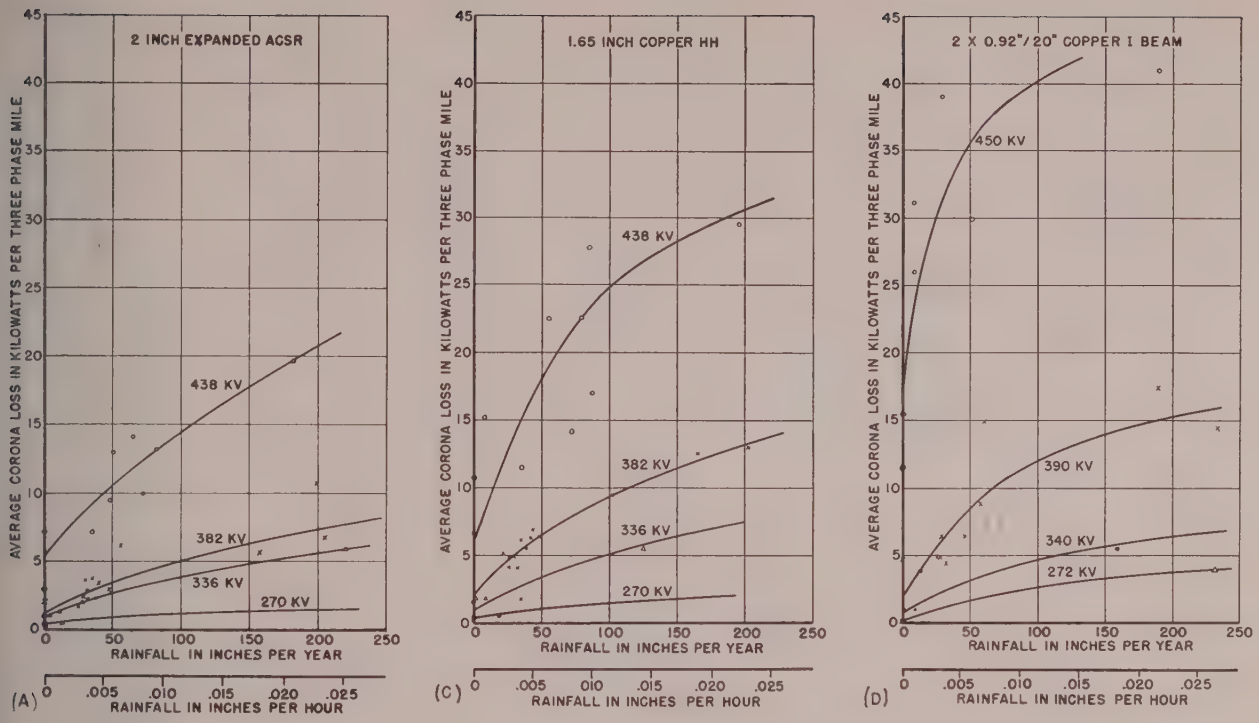

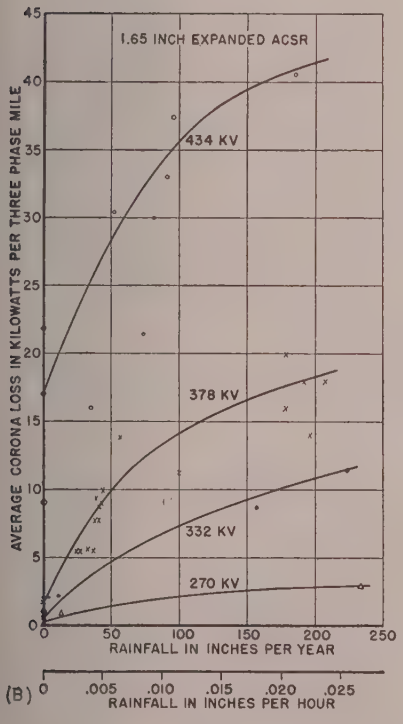

Figure 15 (A to D). Effect of rainfall for all weather on the field test lines for different voltages. Both the loss and precipitation were averaged over periods of several months including both precipitation and fair-weather periods. The numbers on the curves are line-to-line voltages for 32-foot flat spacing

charge than the outside conductors. The effect of subconductor separation is more clearly demonstrated in Figure 8. With Figure 8 in mind, a similar pattern can be discerned in the field tests of Figure 5, which pattern was obscured by minor variations in weather.

Foul-Weather Conditions

Before discussing the effects of foul weather it might be well to consider its importance and the means available for gauging and interpreting its magnitude in terms of conditions applying to practical systems. Corona losses under foul weather are so much greater than the fair weather values that recognition of them must be given in capitalizing the losses of transmission lines. Some form of average, taking all types of weather into consideration must be used to this end. Peak values also might be of importance in very special cases in determining whether extra generating capacity might be required to carry the additional load during storm conditions.

Foul weather encompasses all adverse weather conditions, such as, rain, fog, snow, sleet, and so forth. Of these the major contribution to foul weather loss occurs during rain. Furthermore, the records of foul weather available from the United States Weather Bureau are most complete for rain and contain a factor to include snow and sleet in terms of equivalent rain. Thus, rain appears to be the best single parameter to characterize the additional losses during foul weather.

Monthly bulletins which tabulate hourly precipitation are distributed by United States Weather Bureau stations throughout the country. In addition, some data also are tabulated concerning excessive precipitation for the maximum 5, 10, 15 and so forth, minute periods. For the day during which the record was established for the 1-2- and 24-hour periods at the Pittsburgh Airport the precipitations are given in Table I. It is interesting to note by way of comparison that the rate of precipitation for the standard wet test of insulators is 0.2 inch per minute or 12 inches per hour.

Figure 12, prepared from Weather Bureau data, helps to orient one with regard to the annual distribution of rain for 1-hour periods. Naturally the rain is not necessarily constant during these periods. It is difficult to determine the exact manner in which Figure 12 would be altered if the ordinate were changed from hourly precipitation to instantaneous precipitation expressed in inches per hour. The area under the curve would remain the same and certainly the high rates of precipitation would be increased.

The Weather Bureau also publishes data giving the total rainfall per year. In Table II are tabulated a few representative values for different parts of the country. With the foregoing data available it would be highly desirable if the corona loss could be interpreted in terms

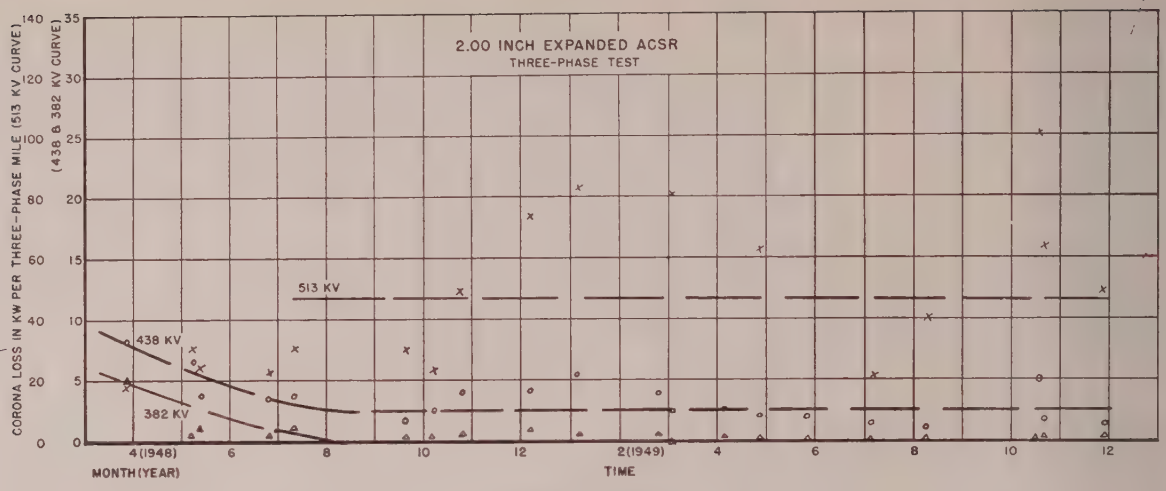

Figure 16 (A)

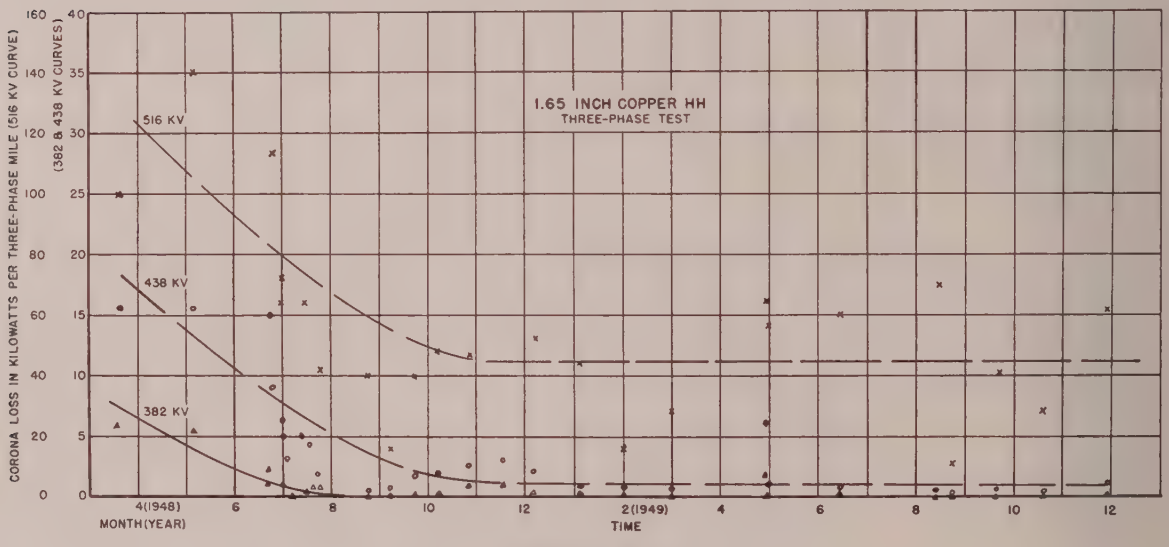

Figure 16 (B)

Figure 16 (A to E). Effect of weathering over long times. The numbers on the curves are line-to-line voltages for 3-phase tests, and line-to-ground voltages for single-phase tests

Figure 16 (C) (below)

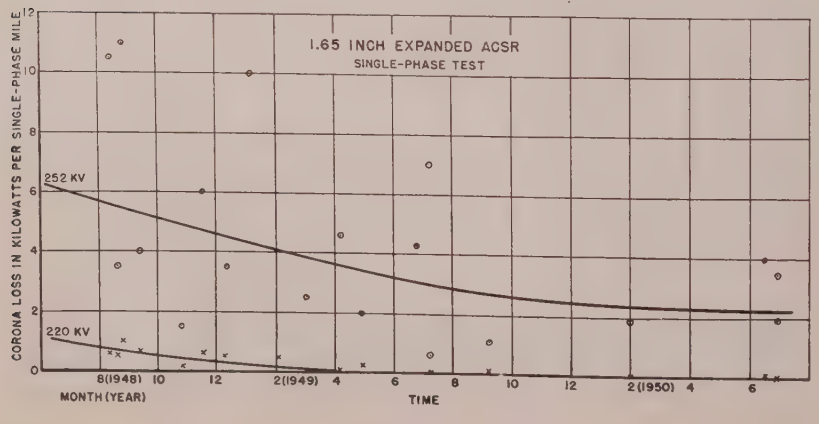

of this weather information so that the loss in any part of the country could be predicted.

Foul-Weather Loss

Laboratory Data

Field tests under foul weather conditions, such as, rain, snow, sleet, and fog offer innumerable difficulties, largely because the conditions do not remain constant. It was to obviate these limitations that laboratory tests were made. Artificial rain can be obtained in the laboratory at controlled rates. Because the ordinary rates of precipitation occurring in nature are so low in comparison with the standard insulator test rate, the conventional equipment could not be used and it was necessary to develop the special setup for producing rain mentioned previously. Figure 9 is typical of the tests and presents

Figure 16 (D) (right)

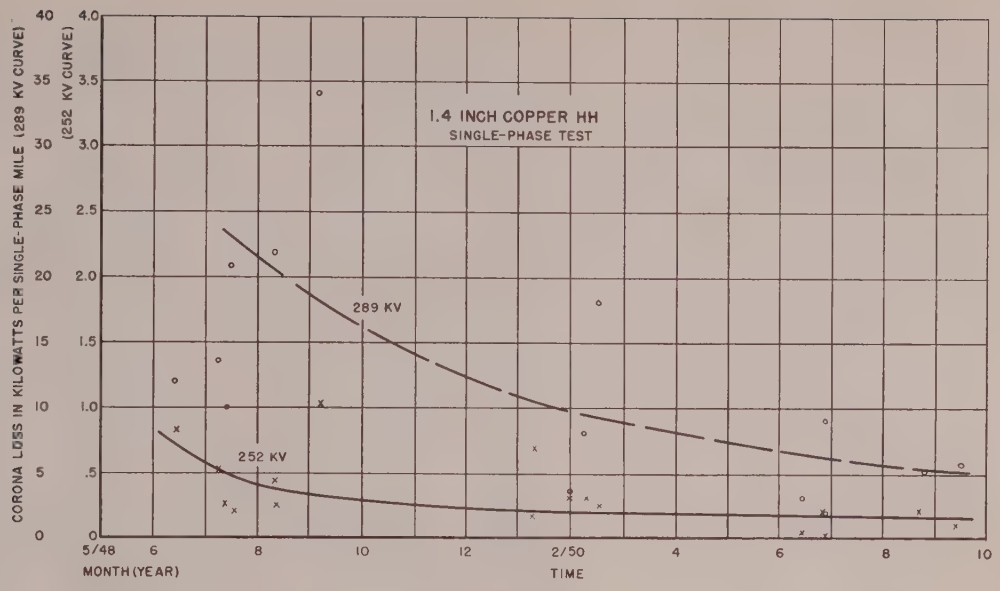

Figure 16 (E) (below)

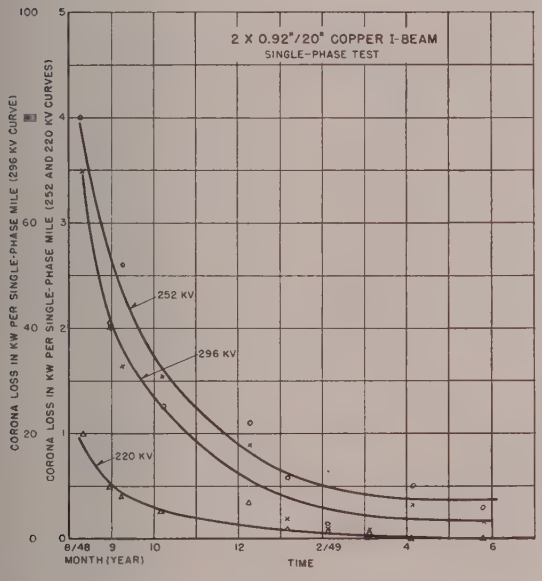

Figure 17 (below). Recorded average corona loss versus time in all-weather and precipitation periods at 383 kv line-to-line—32-foot flat spacing

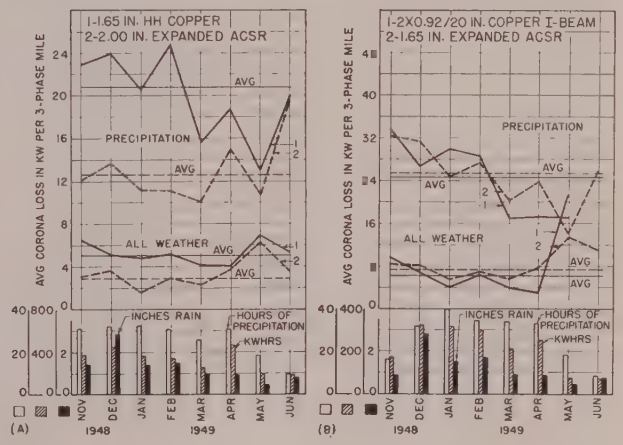

voltage runs on a new 1.65-inch steel-reinforced aluminum cable under both dry conditions and different intensities of constant rain. It will be noted that even a low rate of precipitation reduces greatly the threshold voltage of corona and causes tremendous increases in loss at the lower voltages. As appears to be typical, at the higher voltages, the dry and wet curves approach each other.

To illustrate the relative characteristics of conductors under wet conditions, Figure 6 (B) has been plotted for one inch of rain per hour. At the higher voltages it is interesting to note that diameter becomes of lesser importance.

Figure 10 shows the loss for a number of conductors at different voltages as a function of the intensity of rainfall. The data for these curves were obtained by setting the rain device for a given rate and then varying the voltage. The dry values of loss are plotted as zero rain fall. Again it will be observed that the range between dry and rain conditions is dependent upon the voltage. A characteristic of these curves is that above about 0.2 inch per hour a definite flattening occurs. Tests were made with tap water having a resistivity of 1,010 ohms per inch.[3] With distilled water (resistivity—38,800) only a minor difference in results was apparent.

To throw some light on the nature of the phenomena that occurs during rain conditions, a 1.65-inch new steel-reinforced aluminum cable was energized and the loss recorded just before the rain was stopped, and as a function of time thereafter. The result is shown in Figure 11. It can be seen that the loss decreased suddenly from 40 kw per mile to 30 kw per mile and thereafter gradually along a somewhat exponential curve to its final value. The sudden drop might be due to absence of drops of water falling near the surface but not striking it. These drops of water produce points of ionization and loss either because of their already small radius or because of the formation of small radii by distortion. Another possible explanation of the sudden change is the cessation of splashing of the drops as they hit the surface. Perhaps during rain some of the loss can be attributed to

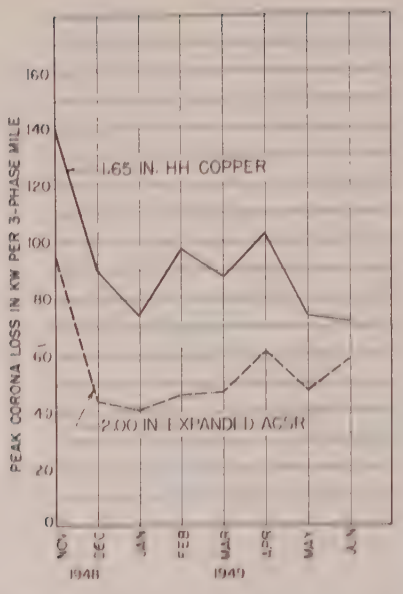

Figure 18. Recorded peak corona loss versus time at 383 kv line-to-line—32-foot flat spacing

the electrostatic repellent action of charged droplets leaving the conductor. The slow change is probably due to the evaporation of water from the surface.

Field Data

Atmospheric conditions fluctuate so greatly during foul weather that it is difficult to obtain a voltage run which will plot as a smooth curve. A large number of such tests were, however, made under a variety of conditions and are plotted in Figure 2. Each curve is marked in accordance with the prevailing weather. A large number of such tests are necessary to establish a relation between fair and foul characteristics. The general bands covered by foul weather conditions are plotted in Figure 3 for the 2-inch expanded steel-reinforced aluminum cable and the 1.65-inch HH conductors.

To illustrate the probable upper limit of corona loss under adverse conditions the curves marked "Max BW-R" have been plotted on Figure 3. These are instantaneous values which are the maximum values of the losses as recorded on the graphic charts for the entire period covered by these tests. It must be borne in mind, however, that these figures apply only to a line 1.4 miles long. Rain storms of the intensity that give rise to these peak values are limited in area and would not cover an entire transmission line at one time.

During rain storms both the instantaneous rate of precipitation and corona loss vary over such wide limits that it is difficult to establish a relation between

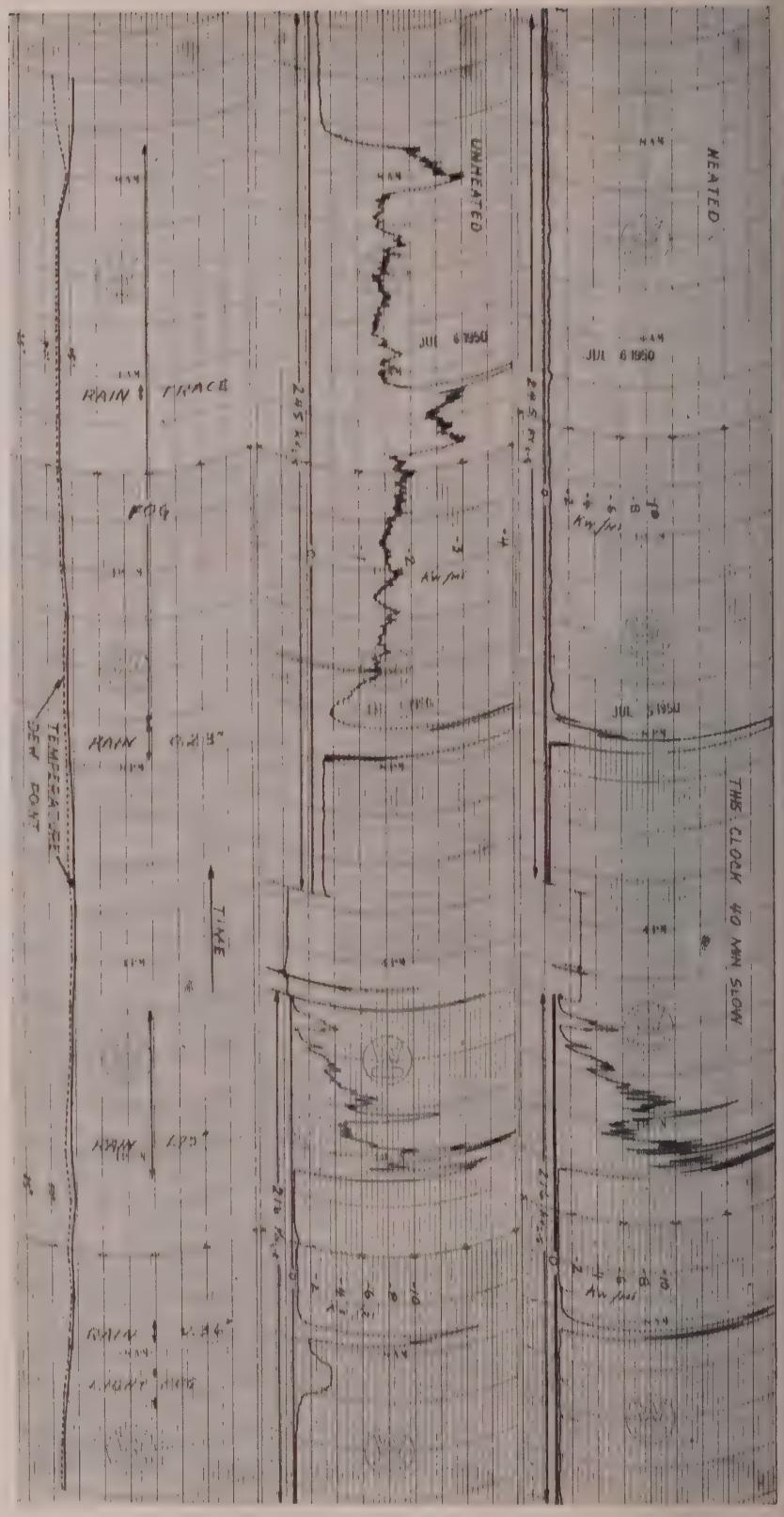

Figure 19. Comparison of loss in the heated and unheated conductor for two different voltages and pertinent weather information. Record from 5:00 a.m. July 5, 1950 to 11:00 a.m. July 6, 1950. Aged 2.00-inch steel-reinforced aluminum cable, single-phase tests. Approximate temperature rise 10 degrees Fahrenheit for 216 kv and 15 degrees Fahrenheit for 245-kv line-to-ground voltage

them. To study this relation periods from one to five minutes were chosen on the graphic charts in which the rain and loss were essentially constant. These data were then plotted in terms of loss per 3-phase mile as a function of intensity of rainfall as shown in Figure 13. For comparison with the laboratory data some of these are replotted in Figure 10, conversion being made on the basis of equal nominal gradient and expressed in charging current per mile. The laboratory curves show a tendency to saturate at lower rates of rainfall. This might be due to differences in aging characteristics or possibly to the effect of electrostatic ground gradient in the field tests.

To compare the conductors over longer periods, the storm periods were chosen from the charts and the average loss for these periods determined without regard to the intensity of the rain. The periods were selected in accordance with the definition of "precipitation" period. The results of this averaging cover precipitation periods for the entire period of the tests and are plotted in Figure 4 (B). In spite of the long time covered by the tests these curves are not strictly comparative as they do not always cover simultaneous periods.

A more detailed analysis was made during storm periods. The term "hours of precipitation" is used in the sense defined in the companion paper.[9] The results of this analysis are plotted in Figure 14. As was to be expected the average loss increases with the intensity of rain, but a degree of saturation is soon attained. This is in line with the results shown in Figures 10 and 13.

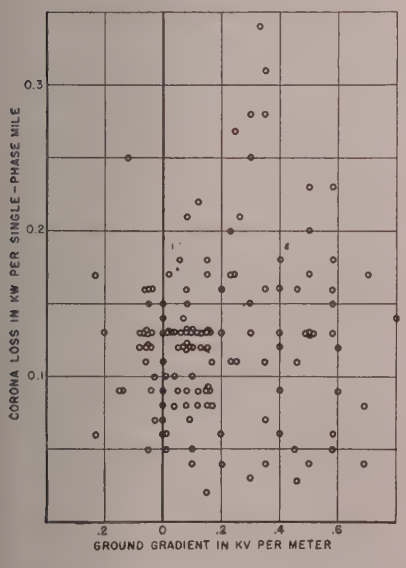

Figure 20. Relation between electrostatic ground gradient and corona loss from simultaneous graphic records. 2.00-inch steel-reinforced aluminum cable, single-phase, 245-kv-to-ground, fair weather, two ground wires

Figures 17 (A) and (B) are typical examples of the average corona loss over a period of seven to eight months on four conductors. Monthly peak losses recorded during the same period are shown on Figure 18. Though the test voltage was varied every few days, periods at the same voltage recurred at short intervals during a month. It is therefore believed that the average loss, Figures 17 (A) and (B), from these periods is a fair approximation of the average loss for a full month.

The sharp rise of the average all-weather loss in May, when recorded precipitation was at its lowest, calls for an explanation. During that month the station weather log at 6:00 a.m. lists medium-to-heavy fog on seven days, and misty rain on one day, no traces having been left on the rain gauge. For the month of April light fog was indicated on only two days. During fog, moisture condenses on the conductors, particularly at night when the conductors are cold. The losses caused thereby are of equal magnitude, and sometimes greater than those caused by precipitation. The greater number of foggy days during May therefore explains the higher all-weather losses during that month.

Of most significance is the effect of rain and all weather upon the average loss for the year. The curves in Figure 4 (C) are the averages over very long periods and include fair weather, rain, fog, snow, and sleet, in other words, all weather conditions experienced during the year. These values apply, of course, for the particular location in which they were obtained, Brilliant, Ohio. They might be different for other locations where the proportion of foul weather is different. In an effort to convert the data to a more useful form so that they can be more universally applied, the results were expressed in terms of inches of rain per year—a value that can be obtained for practically any location in the country. These results are plotted in Figure 15 for the four conductors tested that would most likely find application on systems of very high voltage. These curves were obtained by choosing operating periods varying in duration from two to ten days and averaging both the loss and the precipitation for each period. Extremes of adverse weather were avoided intentionally with the purpose of attaining a precipitation distribution that approximated actual annual distributions. For each curve two values are plotted for zero rainfall; the lower one (which might be zero) being the mean fair weather loss from Figure 3 and the upper one being the apparent fair weather loss from Figure 4 (A). The actual curve in each was drawn to an ordinate approximately midway between these values on the basis that the apparent fair weather period involves some precipitation and the fair weather values[9] are too low to be representative of the loss for sustained energization at constant voltage.

The data of Figure 15 is one of the important end products of this investigation. The authors believe that data in this form is the most practical in which to apply the information. By reference to the annual rainfall for the territory through which the line will be run, average annual corona loss can be predicted easily.

Loss Versus Weathering

Energized conductors undergo both a short and a long time aging. The former phenomenon is discussed in a companion paper[9] because it is vitally concerned with testing technique and is not important in the application of the conductor. The latter phenomenon is discussed here as it has an important bearing on the corona characteristics. Figure 16 shows the loss of five conductors as a function of time as observed from voltage runs from time to time. It will be observed that in all cases the loss starts at a particular value and decreases gradually with time requiring some six months or more to eventually stabilize. These curves are similar to the curves presented in the Sporn and Monteith[14] paper except that they have been corrected to unit air density factor which makes the aging pattern somewhat more apparent. The curves above 500 kv might not be representative of true aging because the lines were not energized continuously at this voltage. Upon the limited evidence available, copper appears to possess greater aging characteristics than aluminum.

Heating of Conductor

Continuous corona tests on short unloaded lines exposed to the weather differ in one respect which might have an important bearing on the results. Since only a very small current flows in the line, the rise in temperature above ambient is negligible. On a line in service the load current is usually sufficiently high so that the I^2R loss produces a temperature rise of 5 to 20 centigrade degrees above ambient.

Any object, particularly a good radiator, in the absence of radiation from the sun will acquire a temperature below ambient and will therefore condense moisture during periods of high humidity. Thus, condensation is more likely to occur in the case of the test conductor than on an actual line in service. To test this hypothesis a scheme was devised to raise the temperature of one conductor above ambient and compare its loss with that of a similar unheated conductor. One phase of the single-span line had been strung with a 2.00-inch steel-reinforced aluminum cable. The construction of this cable is such that the layers of aluminum are insulated from the steel core. At dead ends and connections, however, they are in electrical contact because of the nature of the connector that is normally used. For this test the far end was permitted to remain in contact, but at the near end the outer layers of aluminum were opened so that current could circulate down the aluminum and return in the steel core. The conductor current was approximately 125 amperes at 245 kv, sufficient to raise the conductor temperature about 8 centigrade degrees above ambient. A similar but unheated conductor on one of the long lines served as the reference conductor.

Figure 19 is a portion of the charts from simultaneous observations from about 5 a.m. July 5, 1950 to 11 a.m. the next day. Time proceeds from right to left. The upper chart gives the loss for the heated conductor and the middle chart for the unheated conductor. The lower chart gives the corresponding ambient temperatures obtained from the graphic chart and the dotted line is the dew point calculated from similar charts that gave the humidity. Other comments concerning the weather also are given.

Now examining the charts, it will be noted that a fog period occurred between 7:00 and 8:00 a.m. on July 5. The unheated conductor recorded an appreciable loss which was not present on the heated conductor. Fog was again recorded from 9:00 p.m. July 5 to 8:40 a.m. July 6 and again the unheated conductor recorded high loss which was not recorded on the heated conductor. On the other hand during three rain periods similar losses were produced on both the heated and unheated conductors. The explanation is quite obvious. Condensation of moisture occurred in the unheated conductor during fog periods which was prevented by the higher temperature of the heated conductor. This offers a partial explanation of why the "apparent fair weather" loss is higher than the "fair weather" loss. Sufficient data concerning this effect has not been obtained to date to justify positive conclusions, but it appears to be significant. No correction is made for this effect in Figure 4 and Figure 15.

Ground Gradient

It was suggested in one of the earlier papers[2] describing the Tidd test project, that electrostatic ground gradient due to charges in clouds might affect the corona loss as a result of the induced charge in the conductors. To test this hypothesis a special ground gradient instrument[16] was designed and built, which could record continuously the variation in ground gradient on a chart. The sensitivity is such that it can be set to measure at full scale, gradients of 60 to 60,000 volts per meter. This is well within the sensitivity requirement to test the validity of the hypothesis.

One conductor in each of the lines 2 and 3[2] was energized single phase and the corona loss compared with the ground gradient measurements. Extreme care was exercised to mitigate the effect of extraneous factors by not using data taken during the following periods:

1. Precipitation
2. Fog
3. 8 p.m. to 8 a.m.
4. Within 24 hours following a voltage change.

In Figure 20 the corona loss is plotted against simultaneously recorded values of gradient. As can be seen the result is a shot gun pattern without any apparent trend. The presence of the ground wires provides some shielding but calculations indicate that this is only of the order of 25 per cent.

Corona on Hardware and Fittings

In the design of the test setup, special consideration was given to eliminate corona and other effects from what might be called "accessories" to the conductor, that is, insulators, shielding line-hardware, and shielding points such as suspension or dead-end clamps, tap connections, and so forth. This was done so as to confine, as far as possible, the field study to the various effects of high voltage on the conductors themselves, independent of so-called accessories.

However, during the test, field observations were made on the corona effects on various features of construction, such as changing the number of insulators, modifying grading shield design, and adequacy

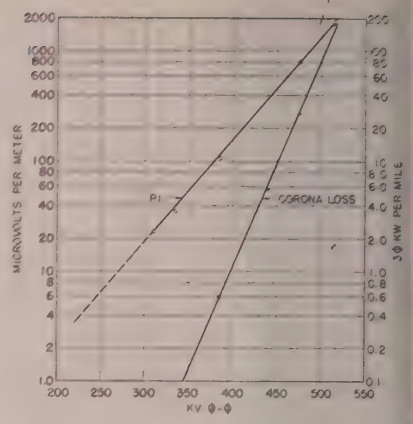

Figure 21. Relation between radio influence and corona loss for different voltages. Fair weather—quasi-peak radio influence at 1 megacycle, 100 feet from line—2-inch steel-reinforced aluminum cable—32-foot horizontal spacing

of shielding conductor fittings after use in the field. During such a staged test at night when corona could be visually observed, some insulator strings were reduced from the test standard 30, to 20, 22, and 24. Also grading shields were removed completely from one set of such insulators and the lines energized at three separate voltages of 374, 427, and 500 kv.

Without grading shields at 374 kv, no corona was observable on the insulator strings even down to 20 units. At 427 kv, slight corona appeared on insulators up to 30 units. At 500 kv and without shields, corona was observed up to 34 units.

Limited field visual observation when the lines were energized, indicated no corona problems would be encountered on conductor hardware such as dead-end conductor clamps, conductor splices, and tap connections, which would be of major concern if suitable grading shields were used on the line end of insulator strings.

Less extensive shielding at the line end of dead-end insulator assemblies on the line appears feasible, as evidenced by visual corona observations in the field with part of the existing grading shield of one type removed.

While shielding by insulator grading shields and special forming of line hardware was emphasized in the test layout, to limit corona loss measurements to conductor effects only, the above incidental observations may have some value when considering the design of extra-high-voltage lines for continued service.

The general conclusion drawn at the time of these tests was that for 374 kv and below, shields were not needed on insulator strings as low as 20 units if corona elimination only is essential. Other

eatures of line design, outside the scope of his paper, may warrant the use of grading shields at the line end at least.

Correlation of Corona and Radio Influence Data

An attempt to correlate radio influence data with corona loss failed to give conclusive results. The average of a few 3-phase manual tests in the field under fair weather conditions is shown for a 2.00 inch steel-reinforced aluminum cable in Figure 21. It will be noted that the radio influence increases less rapidly than the corona loss. It was hoped that a general relationship of ratio between radio influence and corona loss could be established which would be useful in transmission design work. The relation between radio influence and corona for all conditions has not been developed to date, but work is continuing on this phase of the investigation.

Conclusions

1. Great variations in conductor corona loss result from weather conditions, rain and fog raising the loss considerably above fair weather values. In the practical range of extra-high-voltage lines, conductor sizes, and conductor spacing now being considered, the maximum corona loss may be as high as 40 to 80 kw or more per 3-phase mile during rain, while the fair weather loss may be about 1 kw or less.

2. With increasing rates of rainfall the corona loss for a given conductor at any given voltage increases, but at a less rapid rate than the rain, tending to become constant at very high rates of rainfall.

3. Corona loss under wet and stormy conditions are of much greater importance economically than fair weather losses.

4. Determination of annual corona losses on a line can be made using the data presented in this paper when correlated with Weather Bureau records in the location where a transmission line is contemplated.

5. Corona loss during foul weather which blankets an extra high voltage system, may be sufficiently high as to require additional installed system generating capacity to supply the loss.

6. The aging or weathering of conductors requires from six months to a year to bring the initially high loss down to a comparatively stable lower value.

7. The surface potential gradient on the center conductor of a line of flat configuration exceeds by about 5 per cent that on either outside conductor.

8. The measured charging current (an index of the conductor surface gradient) is about 5 per cent higher than the calculated values determined from physical dimensions. This should be recognized when detailed calculations are made to predetermine corona performance of a conductor.

9. Ground voltage gradient appears to have a minor effect upon corona losses, although a study of this phenomena should be continued.

10. Radio influence begins when corona loss is still immeasurable, but increases at a lower rate than corona.

11. The presence of two ground wires on a line of flat configuration has no significant practical influence on the conductor corona loss.

12. The copper loss (I^2R) of a conductor in service raises the temperature sufficiently to prevent condensation of moisture during fog, with a resultant decrease in corona loss. Consequently, corona losses reported here for all weather and foggy weather are higher than will occur in service.

13. The corona loss performance of conductors should take into consideration not only the fair weather loss, but also the all-weather and storm-weather loss which are of more significance from an economic loss point of view.

14. The data presented in the paper, it is believed, provide the basic information for making a sound engineering choice of conductors for an extra-high-voltage system, if used in conjunction with other important considerations in regard to the conductor and its economic influence on a given line.

References

1. Transmission of Electric Power at Extra High Voltages, **Philip Sporn, A. C. Monteith.** *AIEE Transactions*, volume 66, 1947, pages 1571–82.

2. Corona Considerations on High-Voltage Lines and Design Features of Tidd 500-Kv Test Lines, **C. F. Wagner, Anthony Wagner, E. L. Peterson, I. W. Gross.** *AIEE Transactions*, volume 66, 1947, pages 1583–90.

3. Insulators and Line Hardware for Tidd 500-Kv Test Lines, **I. W. Gross, R. L. McCoy, J. M. Sheadel.** *AIEE Transactions*, volume 66, 1947, pages 1592–1602.

4. Line Conductors—Tidd 500-Kv Test Lines, **E. L. Peterson, D. M. Simmons, L. F. Hickernell, M. E. Noyes.** *AIEE Transactions*, volume 66, 1947, pages 1603–11.

5. Transformers and Lightning Arresters—Tidd 500-Kv Test Lines, **F. A. Lane, J. K. Hodnette, P. L. Bellaschi, Edward Beck.** *AIEE Transactions*, volume 66, 1947, pages 1613–18.

6. Switchgear Equipment for Tidd High-Voltage Test Lines, **F. A. Lane, B. W. Wyman.** *AIEE Transactions*, volume 66, 1947, pages 1619–21.

7. Instrumentation and Measurement—Tidd 500-Kv Test Lines, **R. L. Tremaine, G. D. Lippert.** *AIEE Transactions*, volume 66, 1947, pages 1624–30.

8. Radio Influence Test in Field and Laboratory—500-Kv Test Project, **G. D. Lippert, W. E. Pakala, S. C. Bartlett. C. D. Fahrnkopf.** *AIEE Transactions*, volume 70, part I, 1951, pages 251–69.

9. Techniques of Corona Loss Measurement and Analysis—500-Kv Test Project of the American Gas and Electric Company, **O. Naef, R. L. Tremaine, A. R. Jones.** *AIEE Transactions*, volume 70, part I, 1951, pages 496–506.

10. Dielectric Phenomena in High Voltage Engineering (book), **F. W. Peek, Jr.** McGraw-Hill Book Company, New York, N. Y., 1929.

11. Results of Tests Carried Out at the 500-Kv Experimental Station of Chevilly (France), Especially on Corona Behavior of Bundle Conductors, **Francois Cahen.** *AIEE Transactions*, volume 67, 1948, pages 1118–26.

12. The Swedish 380-Kv System, **W. Borquist, A. Vrethem.** *Paper number 412*, Conference on Large High Voltage Electric Systems (Paris, France). Appendices by B. Henning, S. Skagerland, S. Bylund, June 1948.

13. Bündelleitungen (group of papers), **W. V. Mangoldt, F. Busemann, A. Bürklin, G. Markt, F. J. Kromer.** Siemens-Schuckertwerke (Berlin, Germany), 1942.

14. Progress Report on 500-Kv Test Project of the American Gas and Electric Company—Corona, Radio Influence, and Other Factors, **Philip Sporn, A. C. Monteith.** *AIEE Transactions*, volume 69, part II, 1950, pages 891–99.

15. A Voltage Gradient Meter, **R. L. Tremaine, R. C. Cheek.** *AIEE Transactions*, volume 69, part I, 1950, pages 633–37.

Discussion

J. R. Robert (Electricite de France, Paris, France): This report confirms the results obtained from 1948 to 1950 at the Chevilly 500-kv experimental station. The conclusions of the paper, in particular those relating to conductor aging, to the five per cent difference between calculated and measured load current values, and to the importance of losses in the rain for the calculation of annual losses, are similar to those obtained from the Chevilly tests.

However, it seems opportune to consider again three important points.

First, Figure 2 of the paper shows that curves for the same conductor have a certain instability even after the corrections indicated in the paper have been made. Similar curves recorded at Chevilly show the same character in some respects, but it nevertheless has been possible to regroup them by means of the following additional corrections:

1. Elimination of points giving abnormally low losses which correspond to ill-defined conditions and certainly are abnormal because of their instability.

2. Additional correction taking into account space charge distortion in 3-phase operation. This space charge distortion increases the losses in the same proportion as an increase of about 2 per cent in the normal gradient. This correction is in addition to that necessitated by the difference observed at Chevilly between calculated and measured charge current values.

3. Additional corrections of records obtained in very hot weather, the correction proportional to air density factor to the two-thirds power having proved insufficient in these cases. The temperature to be used therefore is distinctly higher than the surrounding temperature.

Secondly, in order to predetermine losses in the rain for a given line, the paper proposes a method based on the curves of Figure 15 linking losses to the rate of rainfall. In

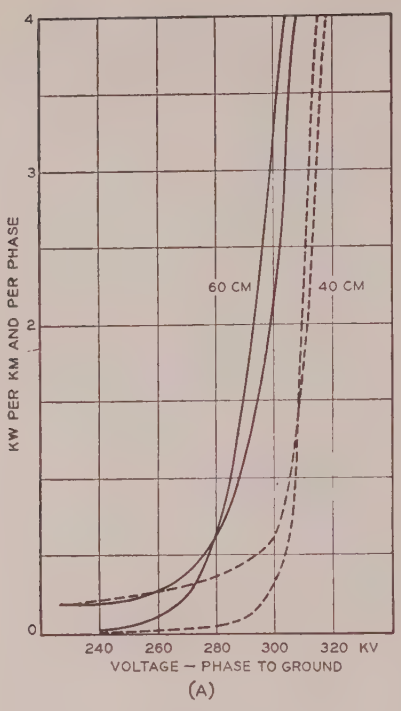

Figure 1(A)

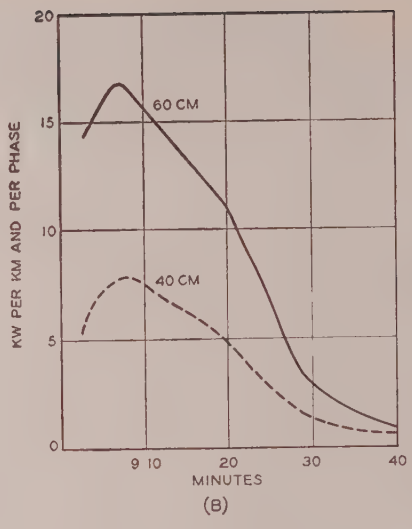

Figure 1(B)

1948 Mr. Francois Cahen indicated a slightly different method used in France.[1]

Finally, the tests carried out at Tidd on a bundle of two 0.92-inch conductors with a 20-inch spacing have yielded results comparable to those obtained on the 1.65-inch conductor, and this in fine weather as well as in the rain. This result does not seem to be in accordance with bundle tests that have been carried out up to the present in different countries. This may be explained by the fact that the bundle tested at Tidd is too far from its optimum spacing for corona. Figure 8 of the paper shows that the loss minimum, when this spacing varies, is obtained for a spacing $D_0 = 7$ inches between conductors. The 20-inch spacing used in line therefore is about threefold. The optimum spacing of the Chevilly bundles is $D_0 = 8$ inches (20 centimeters), and the spacing of bundles in line is only 2 D_0. Some tests in Chevilly were carried out with a spacing 3 D_0. When the spacing is changed over from 2 D_0 = 40 centimeters to 3 D_0 = 60 centimeters the critical voltage in fine weather is decreased by about 7 per cent, as shown in Figure 1(A) of this discussion, and losses in the rain are double, as shown in Figure 1(B) of this discussion. The influence of conductor spacing is small as long as this spacing does not exceed double the optimum values, but it becomes important henceforth. It therefore is advisable not to exceed about 2 D_0, that is, for the bundle of two 0.92-inch conductors a spacing of 14 inches. Bundles adopted in Sweden comply with this rule, that is, optimum spacing of $D_0 = 9.5$ inches has an actual spacing in the 380-kv line of 18 inches.

REFERENCE

1. See reference 11 of the paper.

A. R. Jones (Westinghouse Electric Corporation, East Pittsburgh, Pa.): When the paper was written, the analysis of the data on the effect of conductor temperature was hardly begun. It was thought that raising the temperature of the conductor above the ambient temperature of the air would reduce the average loss during apparent fair weather and during the all-weather period. The analysis completed at that time indicated that some effect was present during the precipitation periods. This was contrary to expectation, and it was felt that more of the data should be analyzed before conclusions were drawn. Since the paper was submitted, some additional data have been analyzed and the results obtained are presented here.

The data presented here were taken on a 2-inch expanded aluminum cable steel-reinforced conductor by recording graphically the loss on two similar conductors, one heated and one unheated, with the same voltage applied. These data were obtained during all types of weather from February through August 1950. The ratios given in Table I, column 4, of this discussion are the ratios of the average losses on the two conductors. The amount of data examined is indicated by the time in hours shown in column 5, and the voltage is indicated in column 2. This analysis was undertaken jointly by Mr. Naef of the American Gas and Electric Service Corporation and myself.

Since the normal I^2R loss of a conductor would not be expected to keep the conductor dry during rain, one would expect that heating a conductor would have a negligible effect during precipitation. It was very startling that the ratios during precipitation ranged from 0.58 to 1.1. The fact that some of the values exceed 1.0 by a small amount is due to the configuration. The difference in charging currents between the two conductors on a per-mile basis is about 2 per cent, which can explain the above discrepancy.

The effect of heating on precipitation losses can be explained by the method of analysis which is covered in detail in a companion paper.[1] By definition, all loss which can be reasonably attributed to rain, as indicated by the rain gauge, is classed as "precipitation" loss. Thus, loss occurring immediately before or after a period of known rain is included in the precipitation data. The loss occurring during these "end" periods can be reduced materially by conductor heating.

The authors show in Figure 11 that the drying-off time of an aluminum cable steel-reinforced conductor in the laboratory is 40 minutes, and undoubtedly it might be longer if the humidity were high. Figure 19 of the paper gives a comparison between the losses on heated and unheated conductors. It can be noted that the loss on the heated conductor during fog is practically zero and that its drying-off period is greatly reduced. Heating the conductor might prevent light traces of rain from increasing the loss at all.

Maximum values of loss are not reduced as they occur during very heavy rain on which normal heating has no effect.

It is important to note that the ratio is a function of voltage. The percentage of reduction in the average loss by heating the conductor is much higher at the higher voltages. This seems consistent, since an extremely small disturbance of the surface of the conductor, such as a fine drop of rain or a slight change in atmospheric conditions, can markedly increase the loss at the higher voltages. Conversely, the losses are only slightly increased by fog and drizzle and other minor disturbances when the applied voltage is relatively low.

A reasonable operating voltage for the

Table I

(1) Weather Condition	(2) Voltage, Kilovolts	(3) Configuration	(4) Ratio Heated / Unheated	(5) Time, Hours
Apparent fair weather	454*	3φ	0.49	144
	262†	1φ	0.4	559
	228	1φ	0.7	437
	194	1φ	0.7	157
All weather	454	3φ	0.64	209
	262	1φ	0.5	581
	228	1φ	0.8	463
	194	1φ	0.7	160
Precipitation	454	3φ	0.58	65
	262	1φ	0.7	22
	228	1φ	1.1	26
	194	1φ	1.1	3

* Line to line.
† Line to ground.

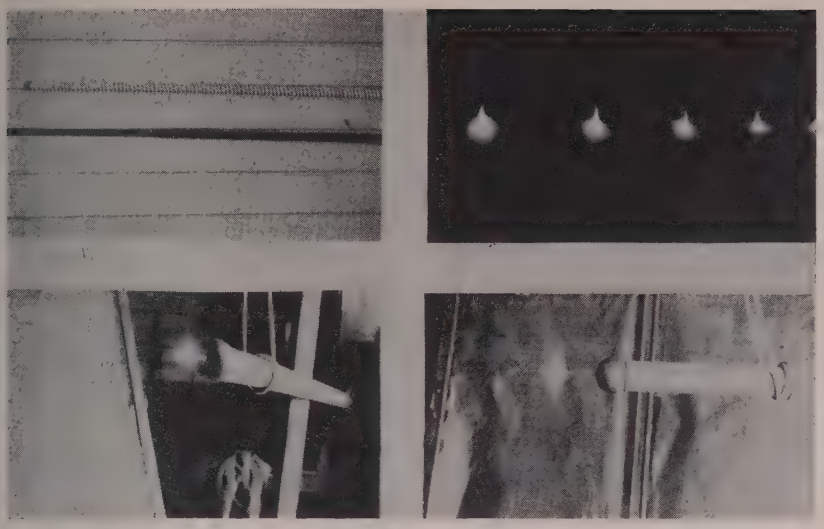

Figure 2. The results of tests when drops of water were used to create point discharges

Upper left—Rod with tacks on
Lower left—Single brush discharge
Upper right—Brushes on drops along rod
Lower right—Single brush discharge

particular conductor under test would be approximately 380-kv line-to-line, corresponding to a charge under single-phase conditions obtained at 262 kv line-to-ground. The heating used on the conductor under test at 262 kv was about 141 kw per 3-phase mile, which corresponds approximately to the I^2R loss to be expected on a practical line using this conductor.

An additional aspect of the problem of heating a conductor is the effect on radio influence. The percentage of time that high RI values exist is reduced as the "end" periods referred to previously are shortened by heating. If crest values of RI are the criterion of satisfactory service, conductor heating has no effect.

The heated conductor tests not only improve the accuracy of the results of this project, but also might be useful in evaluating data obtained by other investigators of corona.

REFERENCE

1. See reference 9 of the paper.

Joseph S. Carroll (Stanford University, Stanford, Calif.): Those who have read this paper carefully will realize at once the very great importance of the material that it presents so clearly. The process of working up the results given in this paper unquestionably has required an enormous amount of time and effort. The authors are to be complimented on their choice of methods of assembling such a large amount of data covering such a wide range.

Besides the regular corona loss data given in the paper the authors have made another valuable contribution, that is, the definition of weather as related to corona loss. In this connection the curves shown in Figure 3 of the paper are very valuable, in that they give the limits, both high and low, of the corona loss that might be expected for the different conductors.

The curves in Figure 10 of the paper show something very interesting. For a rate of rainfall above about 0.2-inch per hour the increase in corona loss with the rate of rainfall is rather small. This checks with some very limited tests made at the Ryan Laboratory on an outdoor 700-foot test line.

The minimum fair-weather curves shown in Figures 2(*A*) and 2(*D*) of the paper check very closely with published data taken at the Ryan Laboratory on a 700-foot test line using similar conductors having what was defined as a weathered condition.

This paper has taken care of a lot of very important, previously unanswered questions.

Thomas F. Peterson (Preformed Line Products Company, Cleveland, Ohio): Careful study of this excellent, thought-provoking paper—especially the sections relating to curves, Figures 10 through 15, prompts me to call to your attention the tremendous significance of a single drop of water. The case at hand seems not unlike those in which one must study the atomic or micro structure to gain an understanding of a galaxy or macro structure. Radio influence, corona loss, control of line design, as well as economic and physical feasibility of transmission at very high voltages, may be in large measure influenced by corona at drops of water.

Almost 30 years ago, after some of us at Stanford University had developed techniques and equipment for measuring corona loss accurately (even down to the rather small loss due to corona at a single point

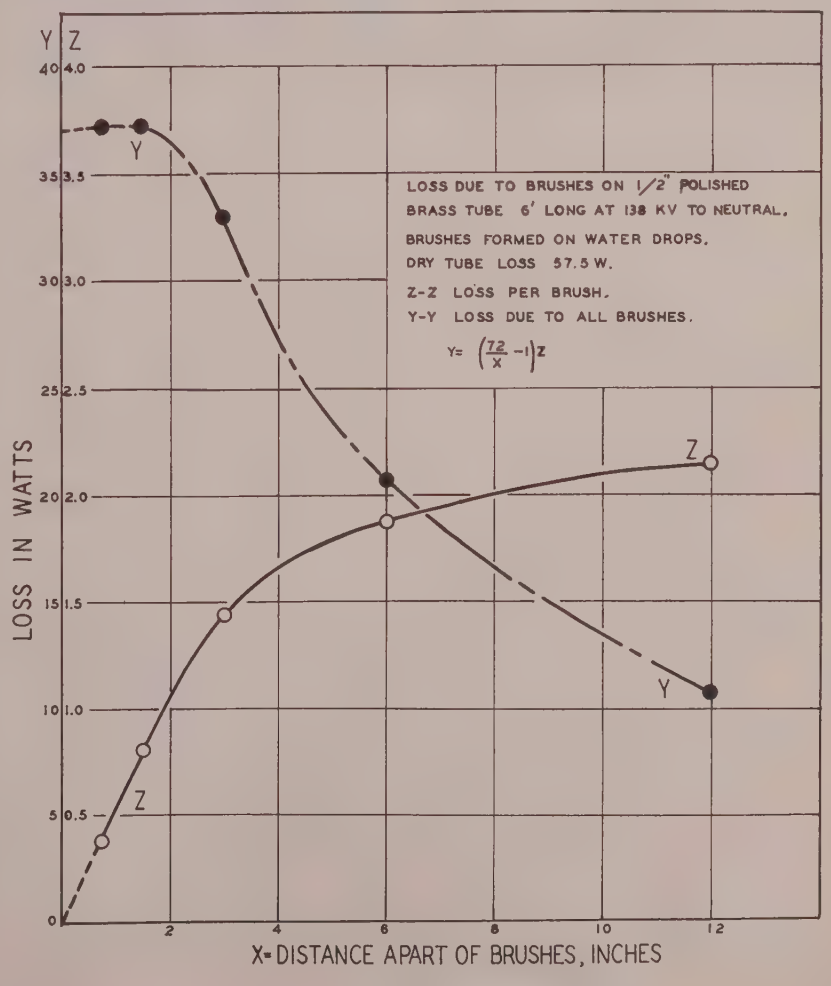

Figure 3 (right). Corona-loss tests—effect of mutual shielding

brush discharge), I set about observing the behavior of, and the losses encountered by, water drops on a smooth corona-free cylindrical conductor. The shielding effects of one drop on another and the integration of losses over a long length of conductor were most interesting. The results of test when drops of water were used to create point discharges are shown in Figures 2 and 3 of this discussion. It will be observed that, for a spacing of about 12 inches, the loss per drop, that is, per brush discharge, is a maximum, but the total loss for the full length of conductor is low. With decrease in spacing the loss per drop decreases—slowly at first, then rather rapidly—because of change in field and ultimately shielding which, as shown in Figure 2, may result in corona at alternate drops. The total loss reaches a maximum for spacings down around one inch and may drop back to zero for closer spacings.

The Y-Y curve as shown in Figure 3 of this discussion offers a possible explanation of the curves shown in Figures 10 to 15 of the paper, since increase in rate of rainfall would correspond to decreasing spacing of drops.

In view of the tremendous increase in total loss accompanying increase in rate of rainfall (decreasing the spacing of raindrop sources of corona discharge) with accompanying increase in radio influence, I have given thought to the economic feasibility of modifying the conductor surface by, for example, special stranding, treating and/or coating wire, and introduction of wetting agents, to preclude increasing drop formation with increasing precipitation. Periodic treatment of lines may be indicated in the case of very-high-voltage transmission lines.

I. W. Gross, C. F. Wagner, O. Naef, and **R. L. Tremaine:** Mr. Robert states that he and his associates in their investigations have obtained a somewhat smaller spread in their data by the elimination of "points giving abnormally low losses which correspond to ill-defined conditions." It appears to us that this action can be justified only on the basis of lack of stability in the instrumentation at low losses. We had made a very careful investigation of our instrumentation and found that, even in the low range of power, it was quite sensitive and stable. We, therefore, believe that the loss measured actually existed at the time and that these measurements should not be eliminated. Inspection of Figure 2 of the paper, particularly 2(*A*) and 2(*C*), which have a large number of individual tests, shows only a few points that one might consider in a range inconsistent with the other data. In converting the data from Figure 2 to Figure 3 of the paper, only these few extreme points were eliminated.

We presume that the "space load distortion" referred to by Mr. Robert is the space charge distribution of the kind investigated by Mr. Otto J. M. Smith in 1948.[1] From this paper, it is evident that a theoretical calculation of gradient, taking into account this factor as affected by single-phase or 3-phase configurations, would be extremely complicated. It can only be properly evaluated experimentally by determining conversion factors to apply to the conductors to convert readings taken under single-phase conditions to 3-phase values. Examinations of the variance of the single-phase tests as a group and the 3-phase tests as a group shows that the normal variance is so large as to mask completely a factor as small as two per cent. This is particularly true for the stranded conductors. The results in Figure 2(*C*) of the paper on a smooth conductor were taken under both single-phase and 3-phase conditions. There is no apparent difference in the average values for the single-phase and 3-phase conditions.

While one would expect a difference in loss because of the increased temperature of the conductor during hot weather, our tests under long-time conditions, involving two summers, do not indicate that a correction proportional to air density factor to the two-thirds power is not adequate.

We are sorry if the paper implied that we were recommending a space of 20 inches for the bundle conductor; such was not the intent. Short-time field tests had been made on bundle conductors at several spacings and a long-time test was made at a spacing of 20 inches. These tests are being continued. As a matter of fact, it was not intended that conclusions or recommendations for any conductor for any voltage would be included in the paper. The data only were presented.

Reference

1. The Space Charge Due to Corona, **Otto J. M. Smith.** *AIEE Transactions*, volume 67, part II, 1948, pages 1137–44.

Transient Response of Saturable Reactors with Resistive Load

H. F. STORM
MEMBER AIEE

THE object of this analysis is to determine the major factors which control the transient response of the saturable reactor with resistive load. Such response is analyzed with respect to changes of control voltage, supply voltage, and load resistance. Operating in the proportional region, the response of the load current to any of the previous changes is an exponential function, governed by a single time constant. This time constant is proportional to the load resistance and inversely proportional to the control-circuit resistance and the line frequency. Without forcing, the time constant of the parallel-connected saturable reactor is twice the time constant of the series-connected one. Within limits, speed of response and power gain of the series-connected saturable reactor are interchangeable. The power gain of a series-connected saturable reactor is in the vicinity of six, when based on a time constant of one cycle.

A rigorous analysis of saturable-reactor circuits becomes quite difficult because of the nonlinear and multivalued character of the magnetization curve. The following analysis relinquishes some rigor in return for a quicker and clearer understanding of the fundamentals. Good agreement between theoretical calculations and actual test results vindicates the introduction of certain simplifications.

One simplification consists in reducing the hysteresis loop to a single-valued function. The wide, present-day use of grain-oriented steels and other square-loop materials permits a further simplification of the magnetization line by representing it with three straight lines, Figure 1(A).[1] If the magnetic intensities in the core of the saturable reactor are very large with respect to H_s, a further simplification is possible by assuming $H_s = 0$. The result is the rectangular characteristic of Figure 1(B); this approximation becomes increasingly accurate with core materials of high differential permeability (50,000 gauss per oersted or more).

A further simplification consists in assuming the air-core reactance of the load windings negligibly small with respect to the load resistance R_L; the resistance of the load windings, instrument rectifier and ammeter are included in the load resistance R_L, Figure 2. The resistance of the control windings are lumped in the external resistance R_C.

The saturable reactor described in the following consists of two magnetic circuits (Figures 2 and 15), arranged in such a manner that voltages of fundamental frequency and odd harmonics are cancelling each other in the control circuit. The two magnetic circuits may consist of two separate units A and B as shown, or they may be embodied in a 3- or 4-legged construction without change of basic performance. Because of the connections of the load windings, the reactor circuit of Figure 2 is called series connected and the one of Figure 15 is called parallel connected. Each of the two units A and B is essentially a single-phase transformer consisting of an iron core, one winding $X1$-$X2$ called the load winding, and a second winding $Y1$-$Y2$ used as control winding. The rectifier instrument indicates the average value I_L of the load current.

The dots in Figures 2 and 15 signify winding polarities. A current is called positive when it enters the winding at the dot. The magnetomotive force F is called positive when derived from a positive current and positive direction is indicated by arrows F_A and F_B. The voltage across the winding is defined positive when the terminal with the dot is more positive than the other terminal. The a-c supply voltage e is counted positive when the a-c bus with the dot is the more positive one.

The Series-Connected Saturable Reactor

Control-Circuit Resistance Low

The control-circuit resistance is called low when its value, referred to the load

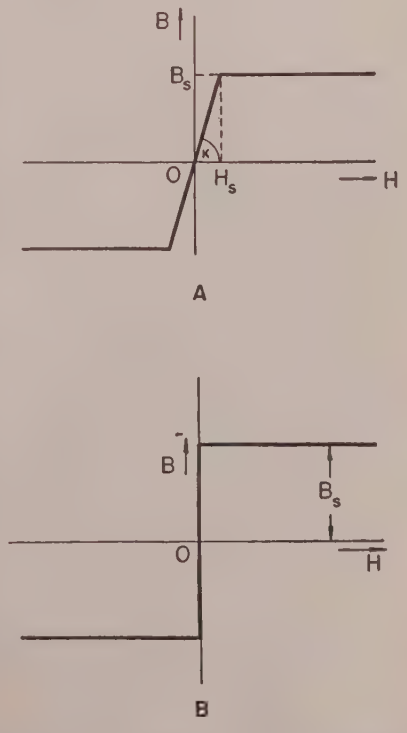

Figure 1. A. Magnetization line represented by three straight lines. B. Rectangular magnetization line

Paper 51-13, recommended by the AIEE Industrial Control Committee and approved by the AIEE Technical Program Committee for presentation at the AIEE Winter General Meeting, New York, N. Y., January 22–26, 1951. Manuscript submitted August 3, 1950; made available for printing November 16, 1950.

H. F. Storm is with the General Electric Company, Schenectady, N. Y.

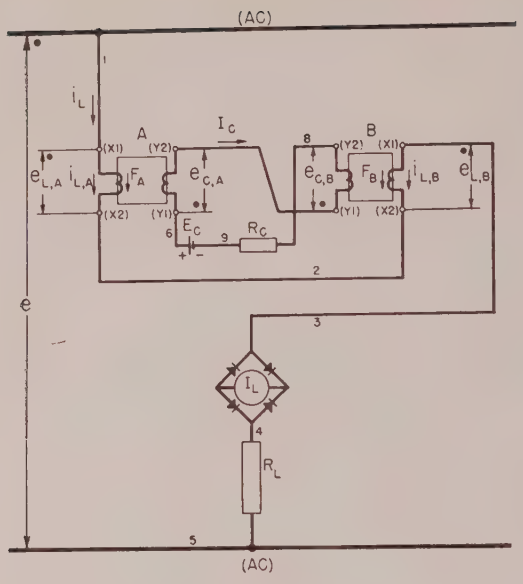

Figure 2 (left). Elementary circuit diagram of a series-connected saturable reactor

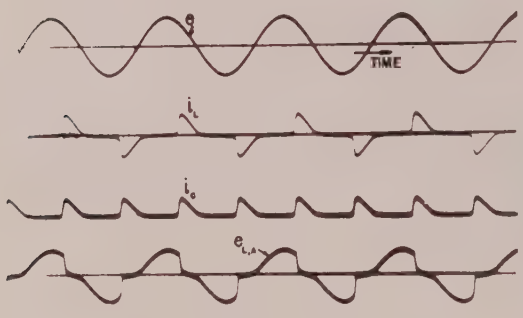

Figure 4 (left). Oscillogram showing the wave shapes of line voltage e, load current i_L, control current i_C, and voltage e_L, A across load winding of unit A

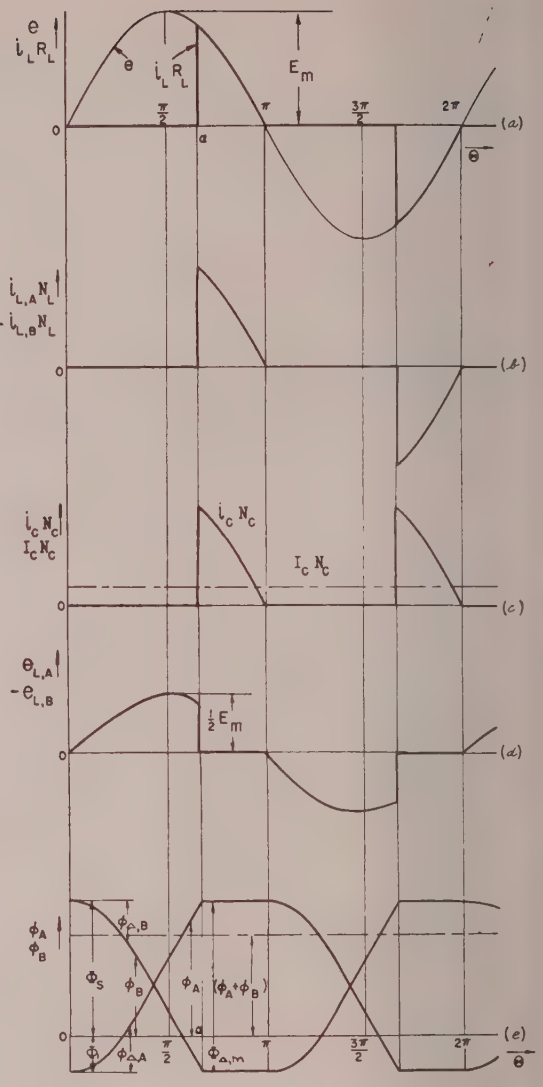

Figure 3 (right). Theoretical wave shapes of voltage, flux and current

winding, is small with respect to the load resistance R_L.

Voltage, Flux, and Current Wave Shapes

Consider the saturable reactor of Figure 2 operating in steady state. At $\theta=0$, Figure 3(E) the flux ϕ_A in core A equals Φ_1 (to be determined later) and the flux ϕ_B in core B equals the saturation flux Φ_s, the operating point being at this moment right at the knee of the magnetization line, Figure 1(B). The line voltage e will cause a magnetizing current to flow through the load windings $X1$, $X2$ of units A and B. With a rectangular magnetization line and operating on its vertical branch ($\mu=\infty$) during $0<\theta<\alpha$, such magnetizing current will be zero, and hence, no voltage drop occurs in the load resistor R_L. The voltage of point 3 is identical with the voltage of bus 5. Thus the line voltage is applied to the two units A and B in series, and because of the identity between units A and B during $0<\theta<\alpha$, one half will appear across $X1$, $X2$ of unit A and the other half will appear across $X1$, $X2$ of unit B, Figure 3(D).

As a result of the application of half the line voltage, a flux change $\phi_{\Delta,A}$ occurs in core A:

$$\frac{e}{2}=\frac{d\phi_{\Delta,A}}{dt}N_L 10^{-8} \tag{1}$$

The line voltage

$$e=E_m \sin\theta \tag{2}$$

where

$$\theta=\omega t=2\pi ft \tag{3}$$

Integrating equation 1 and substituting from equation 2, one obtains:

$$\phi_{\Delta,A}=\frac{1}{2}\frac{10^8}{\omega N_L}E_m\int_0^\theta \sin\theta d\theta=\frac{1}{2}\frac{10^8}{\omega N_L}E_m\times(1-\cos\theta) \tag{4}$$

The core flux ϕ_A is:

$$\phi_A=\Phi_1+\phi_{\Delta,A} \tag{5}$$

Because the load winding of unit B is connected into the same circuit, but with opposite polarity, the flux swing in core B has the opposite sign, hence:

$$\phi_{\Delta,B}=-\phi_{\Delta,A} \tag{6}$$

The flux ϕ_B in core B becomes:

$$\phi_A=\Phi_s-\phi_{\Delta,A} \tag{7}$$

Figure 3(E) illustrates how flux ϕ_A increases while ϕ_B decreases. Finally for $\theta=\alpha$, core A becomes saturated, and hence can no longer produce a voltage across terminals $X1$, $X2$ and $Y1$, $Y2$ of unit A. The terminals $Y1$, $Y2$ of unit B therefore see only R_C in the circuit. By premise R_C is small, and for the sake of simplicity let us temporarily assume $R_C=0$.

The external circuit as seen from the terminals $Y1$, $Y2$ of unit B is therefore a short circuit. The effective impedance across terminals $X1$, $X2$ of unit B becomes now zero and the line voltage e appears in full strength across the load resistance R_L. This is shown in Figure 3(D) where

at $\theta=\alpha$ the sinusoidal voltages across terminals *X1*, *X2* of units *A* and *B* collapse, and jointly reappear across R_L, Figure 3(A). For $\alpha<\theta<\pi$ the load current becomes:

$$i_L=e/R_L \tag{8}$$

Because the voltage $e_{L,B}$ across the load winding of unit *B* is zero for $\alpha<\theta<\pi$, no further flux change (equation 1) takes place and θ_B remains constant. However, the core flux ϕ_B can remain constant only if the sum of all magnetomotive forces acting on core *B* remains constant. This requires a current i_C in the control winding:

$$i_{L,B}N_L+i_CN_C=0 \tag{9A}$$

Remembering that $i_{L,B}\equiv-i_L$, it follows from equation 9A:

$$i_LN_L=i_CN_C \tag{9B}$$

as shown in Figures 3(B) and 3(C). The events during the next half cycle are analogous.

The control current i_C contains a d-c component I_C. This d-c component cannot be supplied by transformer action from the a-c system, but requires a discrete voltage E_C in the control circuit:

$$E_C=I_CR_C \tag{10}$$

The key position of E_C as a controlling agent now is evident.

The oscillogram of Figure 4 shows the close agreement between the theoretical wave shapes of Figure 3 and the actual observation.

The Law of Equal Ampere Turns

The equality of instantaneous ampere turns (equation 9) for the unsaturated core is an important, fundamental characteristic of saturable reactors. It follows that the average, rectified load ampere turns I_LN_L must equal the average control ampere turns I_CN_C:

$$I_CN_C=I_LN_L \tag{11}$$

The simplicity of equation 11 is striking: line voltage, line frequency, and load resistance are absent. The saturable reactor therefore can be visualized as a controllable, constant current device. Obviously, there are limits to the function as constant current device, which limits have been determined.[2]

As pointed out previously, the assumption of a rectangular magnetization curve is valid only if the magnetic intensities in the core are very large by comparison with H_s. Therefore, equation 11 and its ramifications should not be applied to the vicinity of $I_CN_C=0$. For instance, for zero control ampere turns, the load current cannot become zero because this would require an infinite reactance, which cannot be realized.

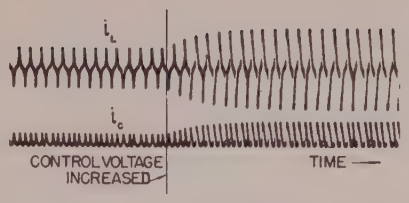

Figure 6. Oscillogram of load current i_L and control current i_C, when control voltage E_C is increased

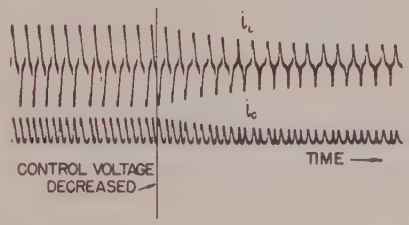

Figure 7. Oscillogram of load current i_L and control current i_C, when control voltage E_C is decreased

It also is evident that a continuous increase of control current cannot produce an unlimited increase of load current: the largest possible load current $I_{L,m}$ is limited by the load resistance R_L:

$$I_{L,m}=E/R_L \tag{12}$$

where E is the rectified average value of the line voltage with the crest value E_m:

$$E=\frac{2}{\pi}E_m \tag{13}$$

Actually, the maximum current does not quite reach the magnitude E/R_L because of air-core reactance of windings.

Figure 5 shows the results of the simplified theory by full lines, and the experimental results are indicated by dots. The section OA is called the proportional region. When using the same scale for both axes, the proportional region is a straight line with a slope of 45 degrees.

A reversal in the polarity of the control voltage E_C will produce a symmetrical characteristic OA′ C′. The load current depends only upon the absolute value of the control current.

In cases where the power loss in the resistance R_L becomes of interest, the effective value $I_{L,eff}$ can be expressed by the form factor k_f

$$k_f=I_{L,eff}/I_L \tag{14}$$

of which experimental values are plotted in Figure 5.

The rectified average current becomes

$$I_L=\frac{1}{\pi}\int_\alpha^\pi i_L d\theta=\frac{1}{\pi}\frac{E_m}{R_L}\int_\alpha^\pi \sin\theta d\theta$$
$$=\frac{1}{\pi}\frac{E_m}{R_L}(1+\cos\alpha) \tag{15}$$

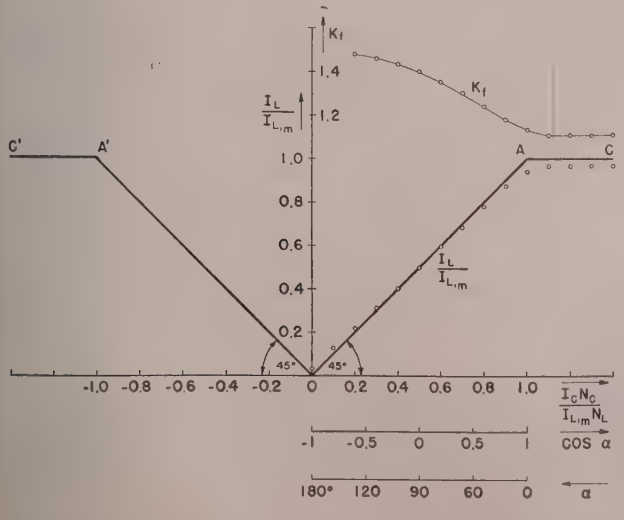

Figure 5 (left). Master graph

Figure 8 (below). Relative load current changes, obtained by averaging load current from Figures 6 and 7 over one half cycle. Solid line represents calculated values, dots and crosses denote measured values

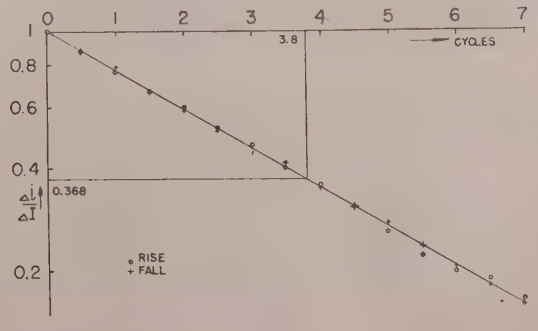

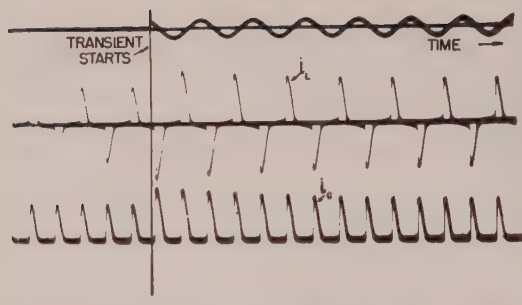

Figure 9. Effect of increase of supply a-c voltage. Upper trace: timing wave, middle trace: load current, lowest trace: control current

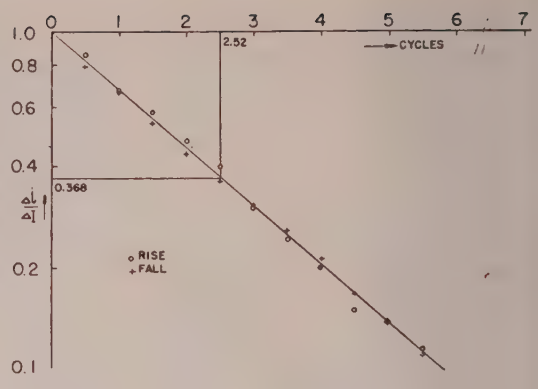

Figure 11 (right). Relative load current changes, obtained by averaging load current from Figures 9 and 10 over one half cycle. Solid line represents calculated values, dots and crosses denote measured values

where α is the angle of retard, Figure 3. From equation 13

$$I_L=\frac{E}{2R_L}(1+\cos\alpha) \tag{16}$$

and from equation 11

$$\cos\alpha=2\frac{I_C N_C}{I_{L,m}N_L}-1 \tag{17}$$

The angle of retard α and its cosine have been plotted on separate axes in Figure 5.

Apparent Inductance

The maximum flux swing $\Phi_{\Delta,m}$, Figure 3(E), is obtained from equation 4 by substituting $\theta=\alpha$ from equation 17 and further by equation 13:

$$\Phi_{\Delta,m}=\frac{10^8}{8fN_L}E(1-\cos\alpha)=\frac{10^8}{4fN_L}\times\left(E-\frac{E_C}{R_C}\frac{N_C}{N_L}R_L\right) \tag{18}$$

Let us define the rectified average no-load saturation voltage $E_{s,0}$ as the line voltage which will cause a flux swing of $2\Phi_s$ for $I_C=0$, then one obtains from equation 18

$$\Phi_{\Delta,m}=2\Phi_s=\frac{10^8}{4fN_L}E_{s,0} \tag{19}$$

$$E_{s,0}=8f\Phi_s N_L 10^{-8} \tag{20}$$

A reactor which is operated with a voltage equal to or smaller than $E_{s,0}$ is called normal excited and under excited, respectively. The preceding and following discussions deal exclusively with normal and under excitation.

The sum of the core fluxes follows from equations 5 and 7:

$$\phi_A+\phi_B=\Phi_1+\phi_{\Delta,A}+\Phi_s-\phi_{\Delta,A}=\Phi_1+\Phi_s \tag{21}$$

and is, quite interestingly, a constant quantity. Φ_1 is seen from Figure 3(E):

$$\Phi_1=\Phi_s-\Phi_{\Delta,m} \tag{22}$$

Substituting from equation 22 into equation 21

$$\phi_A+\phi_B=2\Phi_s-\Phi_{\Delta,m} \tag{23}$$

In order to express the sum of the core fluxes by the control current, substitution is made from equations 18 and 19:

$$\phi_A+\phi_B=\frac{10^8}{4fN_L}\left(E_{s,0}-E+\frac{E_C}{R_C}\frac{N_C}{N_L}R_L\right) \tag{24}$$

During steady-state operation, the flux linkages $(\phi_A+\phi_B)N_C$ of the control windings are constant throughout the cycle. The control windings of the saturable reactor therefore interlink a total flux which is similar to the flux of an ordinary, linear d-c reactor. It follows that any change in steady-state flux linkages, as may be caused by a sudden variation of E_C, E, R_L or f (equation 24) will be accompanied by an exponential transient or flux linkages with a time constant[3] $T=L/R$.

An exponential variation of the flux linkages will in turn cause a similar variation of $\Phi_{\Delta,m}$, equation 23, and hence an exponential variation of I_C and I_L, equations 18 and 11.

The next step is to determine L:

$$L=\frac{d\phi}{di}N10^{-8} \tag{25}$$

For small, finite changes of $\Delta\phi$ and Δi the inductance becomes

$$L\doteq\frac{\Delta\phi}{\Delta i}N10^{-8} \tag{26}$$

In our case, I_C and I_L are pulses, averaged over one half cycle, and hence equation 26 applies. The apparent inductance of the control circuit follows from equations 24 and 26:

$$L_C=\frac{\Delta(\phi_A+\phi_B)}{\Delta I_C}N_C10^{-8}=\frac{1}{4f}R_L\frac{N_C^2}{N_L^2} \tag{27}$$

One obtains the rather surprising result that the inductance of the control winding is proportional to the load resistance R_L and inversely proportional to the frequency, while the core permeability which is of paramount importance in linear reactors does not even appear in equation 27. For control ampere turns in the vicinity of

Figure 12 (below). Effect of increase of load resistance. Upper trace: timing wave, middle trace: load current, lowest trace: control current

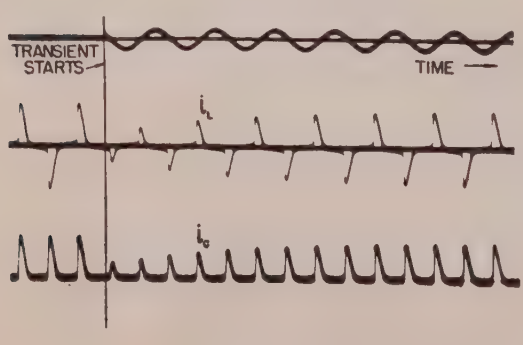

Figure 10 (left). Effect of decrease of supply a-c voltage. Upper trace: timing wave, middle trace: load current, lowest trace: control current

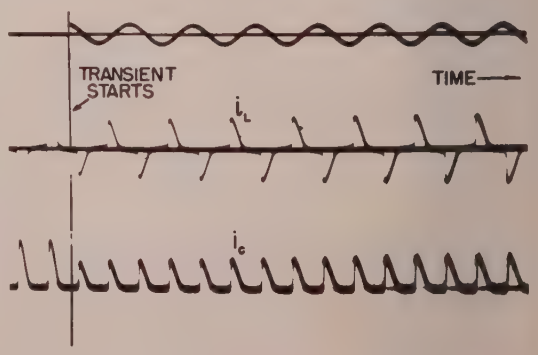

$I_C N_C = 0$, the operation of the saturable reactor is entirely different and equation 27 cannot be applied.

Time Constant

In the case of an ordinary, linear reactor L, connected to a resistor R, a sudden change in driving voltage ΔE will cause a steady-state change ΔI of the current.[3] Denoting by Δi the current change which is necessary to reach the final steady-state conditions:

$$\frac{\Delta i}{\Delta I} = \epsilon^{-\frac{t}{T}} \tag{28}$$

where the time constant

$$T = L/R \tag{29}$$

$$\log \frac{\Delta i}{\Delta I} = \log \epsilon^{-\frac{t}{T}} = -\frac{t}{T} \log \epsilon \tag{30}$$

which indicates, that an exponential function plotted on semilog paper becomes a straight line.

In order to enumerate the time constant T from an experimental response, let Δi_1 occur simultaneously with t_1. From equation 30:

$$T = \frac{-t_1}{\log \frac{\Delta i_1}{\Delta I}} \log \epsilon \tag{31}$$

For

$$\frac{\Delta i_1}{\Delta I} = \frac{1}{\epsilon} = 0.368 \tag{32}$$

$$\log \frac{\Delta i_1}{\Delta I} = -\log \epsilon \tag{33}$$

and from equation 31

$$T = t_1 \tag{34}$$

One obtains the time constant T by intersecting $\Delta i/\Delta I = 0.368$ with the response characteristic.

In a saturable reactor the load current changes with respect to time in a manner similar to equation 28. This is demonstrated in the oscillograms Figures 6 and 7. Figure 6 illustrates the case where the control voltage has been increased (rise) and Figure 7 where the control voltage has been decreased (fall). The upper traces indicate the load current, the lower traces the control current.

By plotting the average value of current for each half cycle (oscillograms of Figures 6 and 7) on semilog paper, a check is obtained with respect to the exponential character of the function. This has been done in Figure 8 and one recognizes that the points for rise and fall straddle very closely a straight line. The conclusion is that the current changes in an exponential fashion and therefore the change of load current with respect to time can be expressed by a time constant. This time constant is the same for rise and fall as proved by the single straight line of Figure 8. The experimental value of the time constant follows from equations 32 and 34 $T = 3.8$ cycles.

In analogy to the time constant of the linear reactor, equation 29, the time constant of the saturable reactor becomes:

$$T = \frac{L_C}{R_C} = \frac{1}{4f} \frac{R_L}{R_C} \frac{N_C^2}{N_L^2} \text{ seconds} \tag{35}$$

If we call R_C' the control-circuit resistance referred to the load circuit:

$$R_C' = R_C \frac{N_L^2}{N_C^2} \tag{36}$$

the time constant becomes:

$$T = \frac{1}{4f} \frac{R_L}{R_C'} \text{ seconds} \tag{37}$$

One recognizes that the load resistance and control-circuit resistance affect the time constant in an inverse manner: an increase in control circuit resistance speeds up the response, whereas an increase in load resistance slows down the response. The time constant also is inversely proportional to the frequency, becoming shorter with an increase of frequency. This fact also can be expressed by stating that the time constant, if measured in cycles, depends on the resistance ratio only:

$$T = \frac{1}{4} \frac{R_L}{R_C'} \text{cycles} \tag{38}$$

For the case shown in Figures 6 and 7 $R_L = 1{,}600$ ohms, $R_C = 5.2$ ohms, $N_L = 910$, $N_C = 200$, T follows from equation 38 as 3.7 cycles; the measured value of T from Figure 8 is 3.8 cycles.

It should be pointed out that for time constants of less than one cycle, equation 38 becomes inaccurate and indicates too small values for T. Furthermore, equation 38 will yield too small results if the cores are not well saturated during part of the cycle. Such lack of full saturation is encountered for control ampere turns in the vicinity of zero; under these circumstances the time constant may become many times larger than expressed by equation 38.

Reiterating equation 24, the average flux $\phi_A + \phi_B$ is affected by line voltage, line frequency, control current, and load resistance. The sudden change of any one of these parameters will cause an exponential transient with the time constant T. The following analysis deals with the effects of sudden changes of the above parameters, except for line frequency, which in most cases can be considered constant.

As in the preceding, the derivations involving the time constant hold only for the proportional region with the exception of the vicinity of $I_C N_C = 0$.

Load and Control Current as Function of Control Voltage

The steady-state value of the control current is:

$$I_C = E_C/R_C \tag{10}$$

If the control voltage changes suddenly by ΔE_C, the control current I_C will change exponentially as previously explained:

$$I_C = \frac{E_C}{R_C} + \frac{\Delta E_C}{R_C}(1 - \epsilon^{-\frac{t}{T}}) \tag{39}$$

where T is expressed by equation 37 in seconds, and by equation 38 in cycles.

Because of equations 9A and 11, the load current becomes:

$$I_L = \left[\frac{E_C}{R_C} + \frac{\Delta E_C}{R_C}(1 - \epsilon^{-\frac{t}{T}})\right] \frac{N_C}{N_L} \tag{40}$$

Voltage Gain. Defining the voltage gain by $\Delta I_L R_L / \Delta E_C$ and substituting from equations 36 and 40

$$\frac{\Delta I_L R_L}{\Delta E_C} = \frac{R_L}{R_C'} \frac{N_L}{N_C}(1 - \epsilon^{-\frac{t}{T}}) \tag{41}$$

The constant part of the gain is denoted by

$$K_e = \frac{R_L}{R_C'} \frac{N_L}{N_C} \tag{42}$$

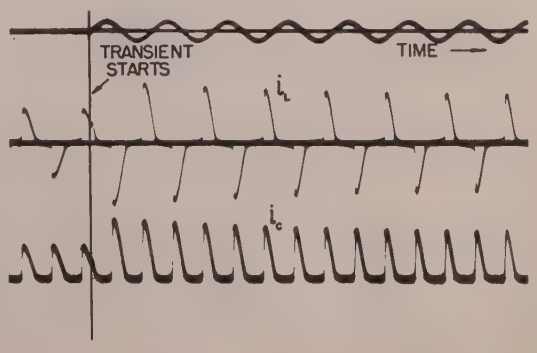

Figure 13. Effect of decrease of load resistance. Upper trace: timing wave, middle trace: load current, lowest trace: control current

K_e is proportional to the ratio of load resistance over control resistance when referred to the same side of the reactor, and also proportional to the transformation ratio N_L/N_C.

Power Gain. If the control voltage is varied by a small amount ΔE_C, the control current changes by $\Delta I_{C,m}$ and the change in control power ΔP_C is:

$$\Delta P_C = \Delta E_C I_C + E_C \Delta I_{C,m} + \Delta E_C \Delta I_{C,m} \qquad (43)$$

The power in the load will change by ΔP_L:

$$\Delta P_L = (2\Delta I_{L,m} I_L R_L + \Delta I_{L,m}{}^2 R_L) k_f{}^2 \qquad (44)$$

The constant part K_p of the power gain is defined by:

$$K_p = \frac{\Delta P_L}{\Delta P_C} \qquad (45)$$

Substituting equations 43 and 44 into equation 45, and neglecting terms of Δ^2 order, one obtains:

$$K_p = \frac{R_L}{R_C'} k_f{}^2 \qquad (46)$$

One recognizes that the power gain is equal to the quotient of load resistance over control-circuit resistance, when referred to the same side of the reactor, times the square of the form factor, see Figure 5.

Interrelation Between Power Gain and Time Constant (Relative Power Gain). A typical value for the time constant is 25 cycles. In some instances it is important to keep the time constant T below a certain value. In order to reduce T, additional resistance, called forcing resistance, is inserted into the control circuit. This measure increases R_C' and hence reduces T, equation 38. The increase of R_C', however, causes a proportional reduction in power gain K_p, equation 46, assuming the form factor k_f constant. Power gain therefore can be traded against speed of response.

There are some practical limits to this exchange: When sufficient forcing resistance is applied to reduce T to the order of one-half cycle, the control-circuit resistance can no longer be called small; therefore, the preceding conclusion should not be expected to hold accurately for such small time constants. There is, of course, an upper limit for the power gain, which is attained by eliminating the forcing resistor.

If one set of power gain K_p and its attendant time constant T is known, other sets can be easily deduced within the above limits. By relating the power gain to an arbitrary time constant of one cycle, the performance of the saturable reactor can be described by a single quantity K_p' instead of a set of two quantities K_p and T. This single quantity K_p' is called the relative power gain and follows by definition:

$$K_p' = \frac{K_p}{T} = 4k_f{}^2 \text{ per cycle} \qquad (47)$$

Except for the form k_f which varies from 1.11 to 1.5, see Figure 5, the relative power gain K_p' is a constant. This conclusion is of the utmost importance. It indicates that all series-connected saturable reactors with control source of low impedance have the same relative power gain, no matter what their size, core material, and other specifications. It follows that power gain and time constant can be calculated without knowledge of any details about the saturable reactor and its load.

Effect of Line Voltage Fluctuations

Suppose a saturable reactor is operating with constant control voltage E_C and constant load resistance R_L. Now the line voltage suddenly changes by an amount of ΔE volts average. The flux in the cores cannot jump to take care of the new voltage, equation 24, and therefore the change ΔE will be acting directly on the load resistance, producing a change of current $\Delta E/R_L$. With the passing of time the core fluxes will adjust themselves exponentially to the new voltage, and the changes in load current and control current will be wiped out with the time constant T:

$$I_L = \frac{E_C}{R_C}\frac{N_C}{N_L} + \frac{\Delta E}{R_L} \epsilon^{-\frac{t}{T}} \qquad (48)$$

and

$$I_C = \frac{E_C}{R_C} + \frac{\Delta E}{R_L}\frac{N_L}{N_C} \epsilon^{-\frac{t}{T}} \qquad (49)$$

One recognizes that the saturable reactor has lead-network properties.[4] It also is evident from equations 48 and 49 that line-voltage variations may cause large, although temporary changes in the currents. Such current peaks are especially severe when the saturable reactor is suddenly connected to the a-c supply, and may cause damage to instruments in those circuits.

The oscillograms, shown in Figures 9 and 10 show the effects of line-voltage change. The line voltage is $E = 43.6$ volts and has been suddenly increased in Figure 9 by $\Delta E = 6.8$ volts. The upper trace is a timing wave, the center trace is the load

Figure 14 (below). Relative load current changes, obtained by averaging load current from Figures 12 and 13 over one-half cycle. Solid lines represent calculated values, dots and crosses denote measured values

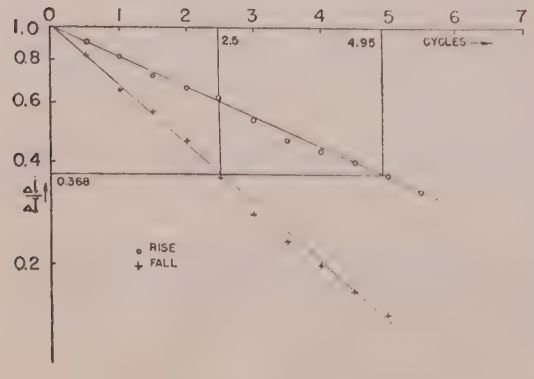

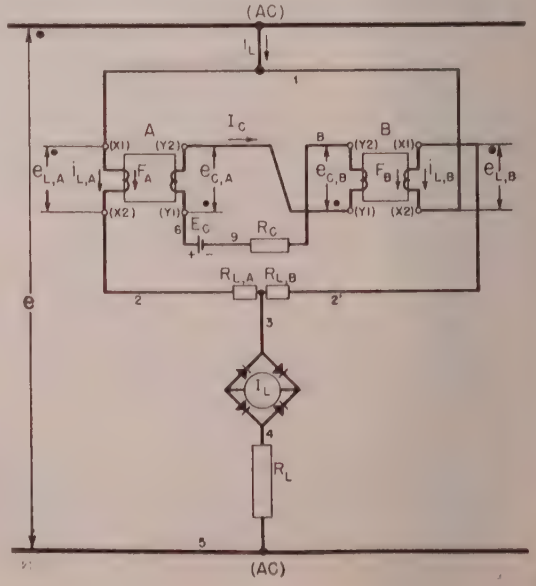

Figure 15 (right). Elementary circuit diagram of a parallel connected saturable reactor

current i_L and the lowest trace is the control current i_C. Conversely, Figure 10 shows an oscillogram where the line voltage is suddenly reduced by 6.8 volts. The average value (per half cycle) of the control current is determined experimentally and the ratio $\Delta i/\Delta I$ is plotted on semilog paper in Figure 11; ΔI is the maximum current change due to ΔE, and Δi is the current change which will occur until steady-state conditions are obtained. These current ratios are plotted in Figure 11 for rise (dots) and fall (crosses), and the time constant T is obtained as $T=2.52$ cycles. The calculated time constant follows from equation 40; for $N_C=400$, $R_C=15.6$ ohms, $N_L=592$, $R_L=350$ ohms, one obtained $T=2.56$ cycles which is in good agreement to the measured value.

Effect of Change of Load Resistance

The saturable reactor is connected to a constant line voltage and constant control voltage. Then the load resistance is suddenly increased by R_L. Because the core fluxes cannot suddenly jump to meet the new load resistance, equation 24, the voltage across the load resistance will remain the same at the instant of change and therefore the load current will suddenly change by its amount prior to the change times $-\Delta R_L/R_L+\Delta R_L$:

$$\Delta I_{L,m}=\frac{E_C}{R_C}\frac{N_C}{N_L}\left(-\frac{\Delta R_L}{R_L+\Delta R_L}\right) \tag{50}$$

This change will decline exponentially with the time constant T:

$$\Delta i_L=\Delta I_{L,m}e^{-\frac{t}{T}} \tag{51}$$

The load current becomes:

$$I_L=\frac{E_C}{R_C}\frac{N_C}{N_L}\left(1-\frac{\Delta R_L}{R_L+\Delta R_L}e^{-\frac{t}{T}}\right) \tag{52}$$

and

$$I_C=\frac{E_C}{R_C}\left(1-\frac{\Delta R_L}{R_L+\Delta R_L}e^{-\frac{t}{T}}\right) \tag{53}$$

The oscillograms in Figures 12 and 13 show the effect of resistance change. In Figure 12 the load resistance is increased from 350 ohms to 692 ohms, and in Figure 13 the load resistance is reduced from 692 ohms to 350 ohms. The time constants now are different for resistance rise and fall, because the amount of load resistance controls T according to equation 11. The current ratios are again plotted on semilog paper (Figure 14) and two lines are now the result. With $I_C=23$ milliamperes, $N_C=400$, $R_C=15.6$ ohms $N_L=592$ and $R_L=692$ ohms, the time constant becomes, equation 38, $T=5.1$ cycles; the measured value is 4.95 cycles. For reduction of load resistance from 692 ohms to 350 ohms, the calculated time constant is 2.52 cycles and the measured value 2.5 cycles.

It is important to note that the current-limiting function of the saturable reactor takes effect with a time delay, as expressed by the time constant T. While the saturable reactor is a current-limiting device for comparatively slow changes of load resistance, a sudden reduction of load resistance, for instance a short circuit, will cause high transient currents.

CONTROL CIRCUIT RESISTANCE HIGH

By increasing R_C' to the order of R_L the load-current wave shape becomes trapezoidal. Further increases of R_C' will cause the current wave shape to approach a rectangular form. The latter becomes quite pronounced for $R_C'=100\,R_L$ whence the control-circuit resistance is termed "comparatively high."

Obviously the mode of operation is different from the case with low control-circuit resistance and therefore the previous equations cannot be applied. Without going into the theory of the high resistance case,[5] high speed of response can be expected. In fact, load current and control current follow changes of the control voltage nearly instantaneously.

Saturable reactors used for the measurement of large direct currents fall in this category.

The Parallel-Connected Saturable Reactor

This circuit is shown in Figure 15. In contrast to the series-connected saturable reactor, only one half of the load current flows through each load winding of the parallel-connected reactor. Based on the same load current, the load ampere-turns of the parallel-connected saturable reactor are therefore only half as large. Denoting the number of turns of each load winding of the parallel-connected saturable reactor by $N_{L,p}$, all steady-state formulas in the section on The Series-Connected Saturable Reactor become applicable to the parallel-connected case when N_L is substituted by $N_{L,p}/2$.

$$N_L=N_{L,p}/2 \tag{54}$$

When dealing with transient response, attention must be given to the fact that any change of flux $\Delta(\phi_A+\phi_B)$ is not only interlinked with the control circuit as in the series-connected case, but also interlinked with a second loop, formed by the load windings. As seen from the cores, two parallel circuits now are interlinked with the changing flux $\Delta(\phi_A+\phi_B)$. The resistance R_C of the control circuit appears now in parallel with the resistance of the load windings $R_{L,A}$, $R_{L,B}$, when referred to the control winding. The equivalent resistance R_{eq} becomes:

$$\frac{1}{R_{eq}}=\frac{1}{R_C}+\frac{1}{R_{L,A}+R_{L,B}}\frac{N^2_{L,p}}{N_C^2} \tag{55}$$

Substituting into equation 35:

$$T=\frac{L_C}{R_{eq}}=\frac{1}{4f}R_L\left(\frac{1}{R_C}+\frac{1}{R_{L,A}+R_{L,B}}\frac{N_{L,p}^2}{N_C^2}\right)\frac{N_C^2}{N_L^2}\text{ seconds} \tag{56}$$

From equations (36) (54)

$$T=\frac{1}{4f}R_L\left(\frac{1}{R_C'}+\frac{4}{R_{L,A}+R_{L,B}}\right)\text{seconds} \tag{57}$$

or

$$T=\frac{1}{4}R_L\left(\frac{1}{R_C'}+\frac{4}{R_{L,A}+R_{L,B}}\right)\text{cycles} \tag{58}$$

Next the increase of the time constant over the series-connected case will be evaluated when no forcing resistor is used. For equal winding space, space factor, and wire material:

$$\frac{R_{L,A}}{R_C/2}=\frac{R_{L,B}}{R_C/2}=\frac{N_{L,p}^2}{N_C^2} \tag{59}$$

and

$$\frac{4}{R_{L,A}+R_{L,B}}=\frac{1}{R_C}\frac{N_C^2}{N_{L,p}^2}=\frac{1}{R_C'} \tag{60}$$

One arrives at the following important conclusion: When no forcing is applied, the time constant of the parallel-connected saturable reactor is twice the time constant of the series-connected saturable reactor. When forcing is applied, only the term $1/R_C'$ will decrease, equation 58. Even if R_C' is made infinity, the time constant is reduced by only 50 per cent. The series-connected saturable reactor without forcing has the same speed of response as the parallel-connected one with infinite forcing.

Even with $R_C'=\infty$, the equivalent control-circuit resistance referred to the load winding does not increase over $R_{L,A}+R_{L,B}$, equation 55. In practical applications $R_{L,A}+R_{L,B}$ is only a small fraction of the load resistance R_L. Therefore, no matter how large the actual control-circuit resistance is, the parallel-connected saturable reactor operates in steady state similarly to the series-connected saturable reactor with low control-circuit resistance.

Nomenclature

B = flux density, gauss
B_s = saturation flux density, gauss

e = line voltage, instantaneous value, volts
E = line voltage, rectified average, volts
E_m = line voltage, crest value, volts
$E_{s.o}$ = no-load saturation voltage, rectified average, volts
ΔE = step function change of E, rectified average, volts
E_C = control voltage, average, volts
$e_{L.A}$, $e_{L.B}$ = voltage across load winding A or B respectively, instantaneous value, volts
f = line frequency, cycles per second
F_A, F_B = magnetomotive force in core A or B respectively, gilberts
H = magnetic intensity, oersted
H_s = magnetic intensity at which saturation flux density occurs, oersted
i_C = control current, instantaneous value, amperes
I_C = control current, average, amperes
$\Delta I_{C.m}$ = maximum change of control current, average, amperes
i_L = load current, instantaneous value, amperes
I_L = load current, rectified average, amperes
$I_{L.m}$ = maximum load current, rectified average, amperes
$I_{L.eff}$ = load current, rms, amperes
ΔI_L = change of load current, rectified average, amperes
$\Delta I_{L.m}$ = maximum change of load current, rectified average, amperes
$i_{L.A}$, $i_{L.B}$ = current in load winding A or B respectively, instantaneous value, amperes
Δi = change of current necessary to reach final steady-state condition, rectified average, amperes
ΔI = change of current between start and end of transient, rectified average, amperes
K_e = voltage gain
k_f = form factor
K_p = power gain
K_p' = relative power gain, per cycle
L = inductance, henrys
L_C = apparent inductance of complete control circuit, henrys
N_C = number of turns of one control winding
N_L = number of turns of one load winding of the series-connected saturable reactor
$N_{L.p}$ = number of turns of one load winding of the parallel-connected saturable reactor
R_L = load circuit resistance, ohms
ΔR_L = sudden change in load-circuit resistance, ohms
R_C' = R_C referred to load winding, ohms
t = time, seconds or cycles
T = time constant, seconds or cycles
α = angle of retard, degrees or radians
ϵ = base of natural logarithm, 2.71828
θ = electrical angle, degrees or radians
μ = differential permeability of core material, gauss/oersted
π = 3.14159
ϕ_A, ϕ_B = core flux in core A or B respectively, instantaneous value, maxwells
$\phi_{\Delta.A}$, $\phi_{\Delta.B}$ = flux change in core A or B respectively, instantaneous value, maxwells
$\Phi_{\Delta.m}$ = maximum flux change, maxwells
Φ_s = saturation flux, maxwell
Φ_1 = core flux in core A at $\theta = 0$, maxwells
ω = angular velocity of θ, radians per second

References

1. Mathematical Analysis of Non-linear Circuits, **A. Boyajian.** *General Electric Review* (Schenectady, N. Y.), 1931, pages 531–37, 745–51.

2. Series-Connected Saturable Reactor With Control Source of Comparatively Low Impedance, **H. F. Storm.** *AIEE Transactions*, volume 69, part II, 1950, pages 756–65.

3. Electric Circuits, **Staff,** Massachusetts Institute of Technology. John Wiley and Sons, Inc., New York, N. Y., 1944, page 165.

4. Principles of Servomechanisms, **A. S. Brown, D. P. Campbell.** John Wiley and Sons, Inc., New York, N. Y., 1948, page 217.

5. Series-Connected Saturable Reactor With Control Source of Comparatively High Impedance, **H. F. Storm.** *AIEE Transactions*, volume 69, part II, 1950, pages 1299–1309.

6. Universal Curves for D-C Controllable Reactors, **W. C. Johnson, B. C. Merrell, R. E. Alley, Jr.** *AIEE Transactions*, volume 68, part I, 1949, pages 31–39.

7. An Analysis of Transients in Magnetic Amplifiers, **D. W. VerPlanck, L. A. Finzi, D. C. Beaumariage.** *AIEE Transactions*, volume 69, part I, 1950, pages 498–503.

8. Magnetic Amplifiers, **A. G. Milnes.** *Proceedings*, Institution of Electrical Engineers (London, England), June 1949, Vol. 96, part II, p. 329–338.

9. A Theoretical and Experimental Study of the Series-Connected Magnetic Amplifier, **H. M. Gale, P. D. Atkinson.** *Proceedings*, Institution of Electrical Engineers (London, England), volume 96, part II, June 1949, pages 349–54.

No Discussion

Neutral Inversion of a Single Potential Transformer Connected Line-to-Ground on an Isolated Delta System

LYLE L. GLEASON
ASSOCIATE AIEE

THIS paper deals with the voltage conditions and circuit characteristics accompanying the application of a single potential transformer connected line-to-ground on a 3-phase system that may become temporarily ungrounded.

The abnormal voltages of this circuit produced sustained voltages to ground in excess of field insulation test voltages. These voltages accompanied by the shift of the neutral completely outside the delta are limited only by the line-to-ground impedances. Circuits most subject to neutral inversion are those with the maximum capacitance impedance phase-to-ground. These maximum impedances, as determined by test for the circuits involved, range from 1.15 to 1.5 megohms. The combination of the normal impedance and excitation impedance of certain potential transformers produces an impedance which will cause these abnormal voltages. The potential transformer impedance is the element that may be controlled, and can be by specification for new transformers, and to some extent by capacitor secondary burden on existing potential transformers. The methods developed for predicting the probability and magnitude of neutral inversion indicate, that for the above normal capacitive impedance line-to-ground, the excitation impedance must be $+j3$ to 4 megohms at normal potential and not less than 1 megohm at 200 per cent of normal.

The specification of potential transformer excitation impedance is not generally practiced, but for this type of installation it will be essential to specify the excitation impedance limits.

Oscillograms of voltages and currents for actual circuits intentionally isolated from the grounded system for test purposes substantiate the results of the curves and calculations.

History

The circuit discussed here stems from a method of relaying for ground faults on the subtransmission at a primary network distribution substation. The distribution substation transformation is 26-kv delta to 4.3 kv Y. The subtransmission is a grounded system with the ground maintained and stabilized at the receiving substations. With certain circuit arrangements the distribution substation may become isolated from the grounded 26-kv system. The potential transformer is thereby connected line-to-ground on an isolated 26-kv delta system energized from the primary network.

The study and tests discussed in this paper followed an inadvertent isolation of the 26-kv delta primary of a distribution substation power transformer, while energized from the 4 kv, resulting in abnormal voltages and neutral shift. Under test conditions, sustained voltages as high as 56-kv line-to-ground occurred. The severity of the insulation stresses imposed on the power transformer insulation is indicated by the recommended American Standards Association 1-minute 60-cycle withstand voltage for field testing, (52-kv to ground).

The problem of neutral shift, or, in some instances, complete neutral inversion of the potential on the potential transformer of this circuit is not theoretically complicated, but since the excitation impedance of a transformer varies with applied voltage, a simple analytical approach is not available. The author has evolved a graphical method by which it is possible to predict potential transformer performance using simple circuit constants and the magnetization curve of the potential transformer. Preventive methods have been explored and tested for use on existing transformers with satisfactory results on some types.

Theory

A delta system is one of the common 3-phase systems used by electric utilities and differs from the Y system principally in not having a neutral as part of the system circuit. A delta system ungrounded by physical connection, has voltages from line-to-ground according to the impedances of line-to-ground capacitance coupling, leakage resistance, or other impedances as the potential transformer connection. Since the ground is the common point of the Y-connected impedances, it is taken as the neutral for the delta system. With normal equal impedances line-to-ground this neutral will have equal voltage to all three lines. This is considered the normal neutral position, and any change of the neutral from the normal is neutral shift.

The neutral shift has no limits other than the above requirements, and when it has shifted to a point such that the reference line to neutral voltage is approximately 180 degrees from its normal voltage, the neutral has inverted. (See Figure 3.)

Paper 51-14, recommended by the AIEE Transformers Committee and approved by the AIEE Technical Program Committee for presentation at the AIEE Winter General Meeting, New York, N. Y., January 22, 1951. Manuscript submitted September 11, 1950; made available for printing November 16, 1950.

LYLE L. GLEASON is with the City of Seattle Department of Lighting, Seattle, Wash.

Appreciation is extended to the Lighting Department of the City of Seattle for making all tests and study that seemed necessary for a solution of this problem. Some of the tests were conducted when there was some question of the ability of the equipment to stand the possible abnormal conditions. There was no apparent damage to any equipment in making the tests.

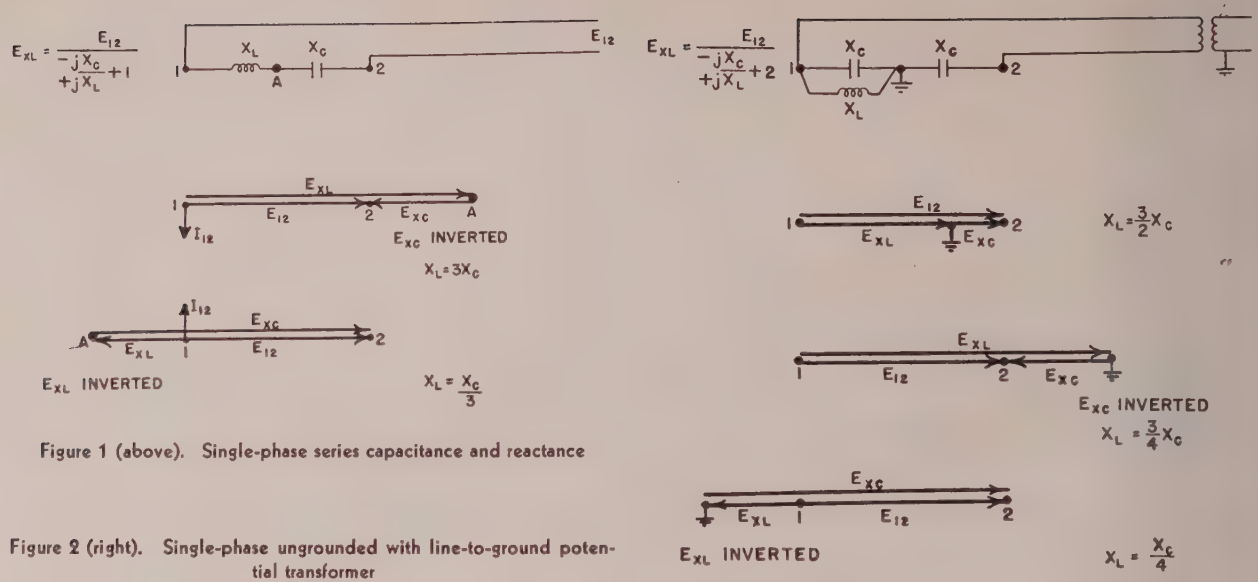

Figure 1 (above). Single-phase series capacitance and reactance

Figure 2 (right). Single-phase ungrounded with line-to-ground potential transformer

Circuit Analogy

In the 3-phase circuit (Figure 3), the capacitive reactance line-to-ground is the same for each phase, and the inductive reactance on one phase is that of the potential transformer primary excitation and equivalent secondary burden. An analogy to single phase (Figures 1 and 2) with the mathematical expression for the voltage drop across the inductive reactance or potential transformer impedance provides a simplified explanation of the problem of neutral inversion.

Figure 1 is a single-phase circuit with an inductive reactance in series with a capacitive reactance. The impedance of this circuit, neglecting all resistance, will be either capacitive or inductive except at series resonance. Consequently, junction "A" will always be shifted outside the applied voltage. The significance of this kind of a neutral shift is that the voltage across the larger impedance, or the one that controls the current, will always be greater than the applied voltage to the circuit, and that the voltage across the smaller impedance will always be inverted with respect to the line voltage.

Figure 2 is a single-phase circuit similar to Figure 1 except that a capacitive

Figure 3. Isolated 3-phase delta with a single line-to-ground potential transformer

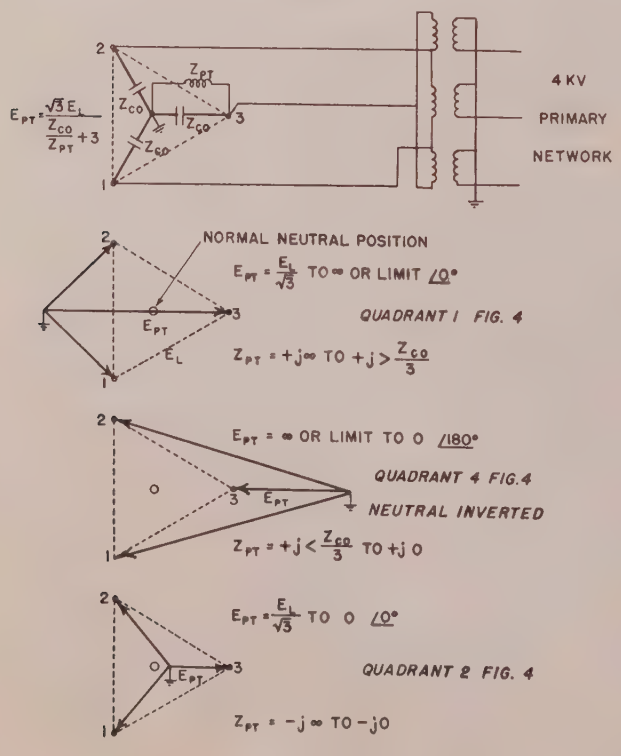
$E_{PT} = \frac{\sqrt{3}E_L}{\frac{Z_{CO}}{Z_{PT}}+3}$
Z_{PT}
Z_{CO}
4 KV
PRIMARY
NETWORK
NORMAL NEUTRAL POSITION
$E_{PT} = \frac{E_L}{\sqrt{3}}$ TO ∞ OR LIMIT ∠0°
QUADRANT 1 FIG. 4
$Z_{PT} = +j\infty$ TO $+j > \frac{Z_{CO}}{3}$
$E_{PT} = \infty$ OR LIMIT TO 0 ∠180°
QUADRANT 4 FIG. 4
NEUTRAL INVERTED
$Z_{PT} = +j < \frac{Z_{CO}}{3}$ TO +j 0
$E_{PT} = \frac{E_L}{\sqrt{3}}$ TO 0 ∠0°
QUADRANT 2 FIG. 4
$Z_{PT} = -j\infty$ TO $-j0$

Figure 4. Neutral voltage characteristic curves

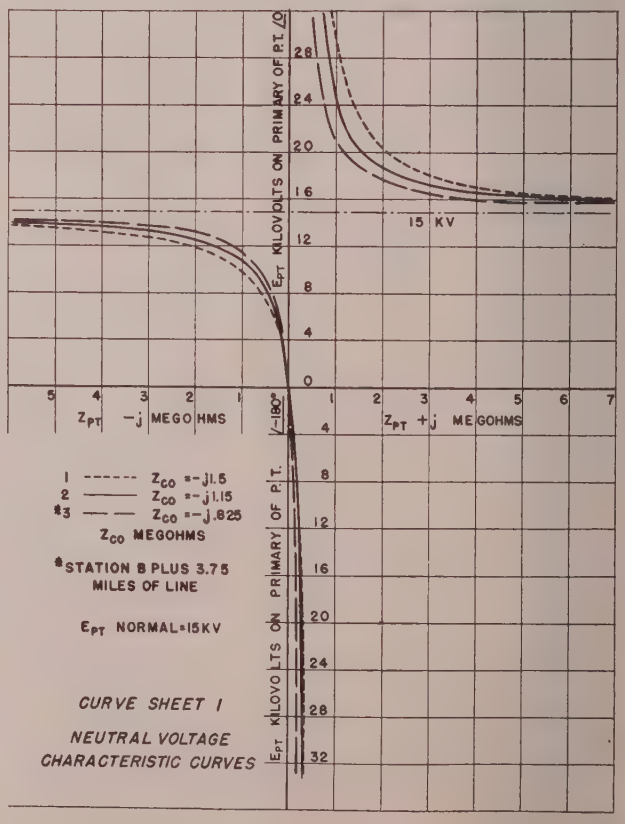
E_{PT} KILOVOLTS ON PRIMARY OF P.T. ∠0
15 KV
Z_{PT} −j MEGOHMS
Z_{PT} +j MEGOHMS
∠−180°
1 ------ Z_{CO} = −j1.5
2 ——— Z_{CO} = −j1.15
*3 — — Z_{CO} = −j.825
Z_{CO} MEGOHMS
*STATION B PLUS 3.75 MILES OF LINE
E_{PT} NORMAL=15KV
CURVE SHEET 1
NEUTRAL VOLTAGE CHARACTERISTIC CURVES
E_{PT} KILOVOLTS ON PRIMARY OF P.T.

reactance equal to the series capacitive reactance is in parallel with the inductive reactance. This is exactly the condition of a line-to-ground potential transformer on a ungrounded single-phase circuit where the inductive reactance is the potential transformer primary impedance, and the capacitive reactances are that of the line-to-ground capacitance. This circuit resolves into the simple series circuit when the parallel impedances are evaluated to an equivalent impedance. The equivalent impedance, characteristic of parallel inductive and capacitive reactances, will always be greater than the smaller of either individual reactance and will have the complex notation of the smaller element. Hence it is evident that when the inductive reactance is smaller than the capacitive reactance, the circuit will be equivalent to that of Figure 1. As the equivalent inductive reactance varies from infinity to a lesser value a condition of series resonance will occur, and there will be a complete inversion of the voltage across the inductance to ground in passing through this resonance point. This inversion occurs when the inductive reactance is less than one-half the capacitive reactance.

The equations for the voltage across the inductive element of Figures 1, 2, and 3 are as follows:

For Figure 1

$$\boldsymbol{E}_{XL} = \frac{\boldsymbol{E}_{1-2}}{\dfrac{-jX_C}{+jX_L}+1} \qquad (1)$$

For Figure 2

$$\boldsymbol{E}_{XL} = \frac{\boldsymbol{E}_{1-2}}{\dfrac{-jX_C}{+jX_L}+2} \qquad (2)$$

For Figure 3

$$\boldsymbol{E}_{PT} = \frac{1.732\boldsymbol{E}_{1-2}}{\dfrac{Z_{CO}}{Z_{PT}}+3} \qquad (3)$$

Delta Neutral Shift

A comparison of the three equations shows that they are all similar and for the condition that $Z_{CO} = 0 - jX$ and $Z_{PT} = 0 + jX$ $\boldsymbol{E}_{XL}$ or $\boldsymbol{E}_{PT}$ is easily evaluated. For the circuit of Figure 3 as Z_{PT} decreases from $+j$ infinity to a value equal to Z_{CO}, $\boldsymbol{E}_{PT}$ will have no phase shift and will change from normal to $1^1/_2$ times normal (see Figure 4). As Z_{PT} decreases further to a value of $^1/_3$ Z_{CO} $\boldsymbol{E}_{PT}$ will change from $1^1/_2$ times normal to infinity (quadrant 1). It is not possible to reach infinity in this phenomenon because of a limiting condition imposed by the variable inductive reactance of the potential transformer excitation impedance. Continuing on with a reduction of Z_{PT}, $\boldsymbol{E}_{PT}$ will decrease from infinity to zero, but, with pure reactances, will have a 180-degree phase shift or neutral inversion. Any further decrease of Z_{PT} results in a $-j$ value for which $\boldsymbol{E}_{PT}$ will be in phase and will vary from zero to normal as Z_{PT} varies from $-j0$ to $-j$ infinity. Figure 4 is plotted from equation 3 with Z_{CO} and $\boldsymbol{E}_L$ constant letting Z_{PT} vary from $-j$ infinity to $+j$ infinity. The $-j$ values are attained with a potential transformer by the addition of capacitor secondary burden.

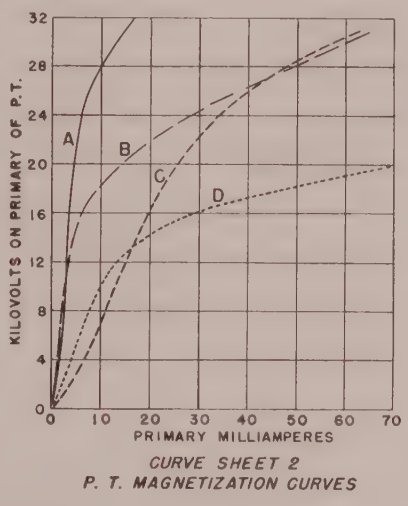

Figure 5. Potential transformer magnetization curves

It is possible to set up in a laboratory any or all of Figures 1, 2, and 3 with known values of circuit elements, but in actual practice the only values readily obtained are the line voltage and the indicated value of $\boldsymbol{E}_{PT}$ (voltage drop line-to-ground across the potential transformer). By having the two voltage values, the use of equation 3 readily permits the ratio of Z_{CO}/Z_{PT} to be determined. Since this ratio occurs in all of the equations, practically all of the previous articles about this subject have discussed the phenomenon on the basis of zones of instability as determined by the ratio X_{CO}/X_m, X_m being the magnetizing impedance of the potential transformer. Since an installation having neutral inversion in the zone where Z_{CO}/Z_m is greater than -3 has occurred, it has been necessary that the condition permitting such a phenomenon be determined and corrected.

Table I

Station	Transformer	Z_{co}
A	3,000 kva 3φ, design 1	$-j\ 1.5\times10^6$ ohms
B	3,000 kva 3φ, design 2	$-j\ 1.2\times10^6$ ohms
C	3,000 kva 3φ, design 1	$-j\ 1.5\times10^6$ ohms
D	6,000 kva 3φ, design 3	$-j\ 1.15\times10^6$ ohms

Note: The station code letter is chosen to conform to the curve designation on Figure 5.

Circuit Constants

The value of Z_{CO} is the line-to-ground coupling capacitive reactance of the isolated delta circuit. Z_{CO} is a maximum when the circuit consists of only the distribution substation transformer high-voltage winding. The values given in Table I are determined by test and have considerable difference between equivalent transformers of a different design and the same manufacturer.

The capacitance of the power transformers, which is distributed throughout the winding, was determined by test. Equation 3 was used to evaluate Z_{CO}. The procedure used is as follows:

1. Obtain magnetization curve of the potential transformer.
2. Plot the excitation impedance (X_m) from the magnetization curve (neglecting harmonics).
3. Select a capacitor rated for the potential transformer secondary voltage which will give an equivalent primary capacitive react-

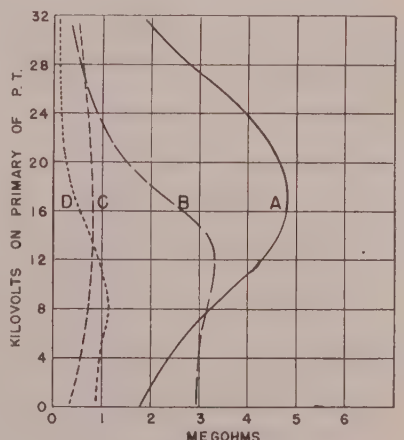

Figure 6. Potential transformer excitation impedance

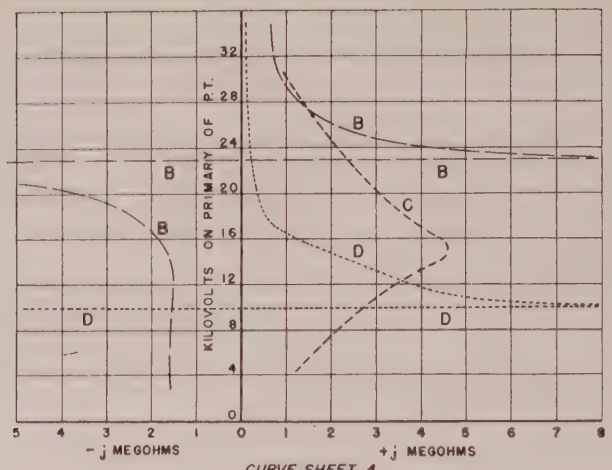
KILOVOLTS ON PRIMARY OF P.T.
B
C
D
- j MEGOHMS
+ j MEGOHMS
CURVE SHEET 4
COMBINED EXCITATION AND BURDEN OF P.T. ON PRIMARY
(40 MICROFARAD CAPACITOR SEC. BURDEN)
"A" P. T. 26000 - 118 V. MFG. 1
"B" P. T. 26000 220:1 & 127:1 MFG. 2
"C" P. T. 15000/26000Y - 63 - 118V. MFG. 3
"D" P. T. 15000 - 68 - 115V. MFG. 1

Figure 7 (above). Combined excitation and burden of potential transformer on primary (40-microfarad capacitor secondary burden)

Figure 9 (right). Graphical solution of neutral stability points with capacitor secondary burden

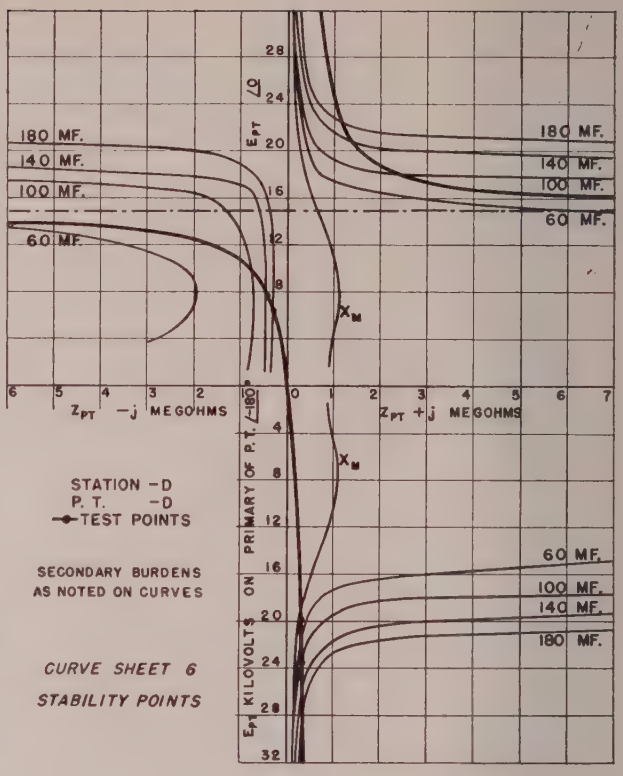

Figure 8 (below). Graphical solution of neutral stability points. No secondary burden

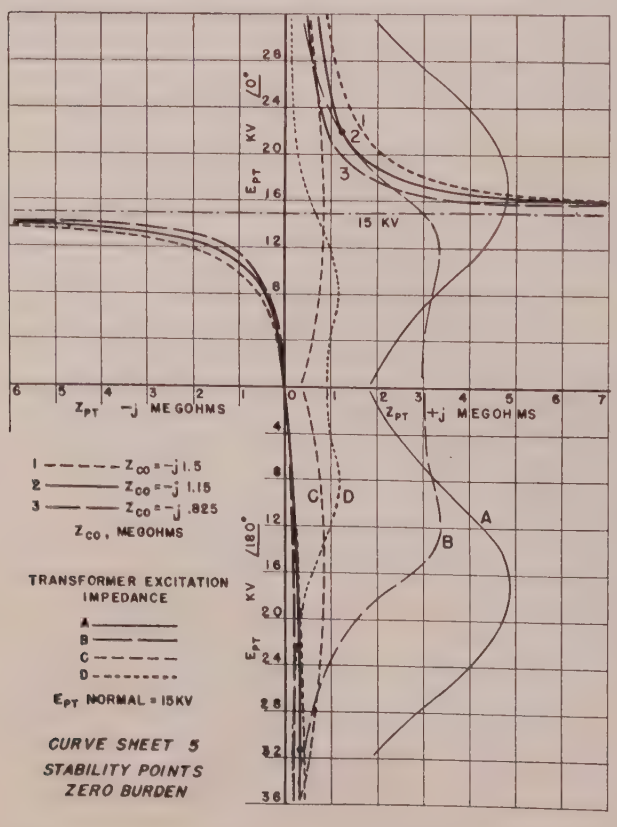

Figure 10 (below). Graphical solution of neutral stability points with resistance secondary burden

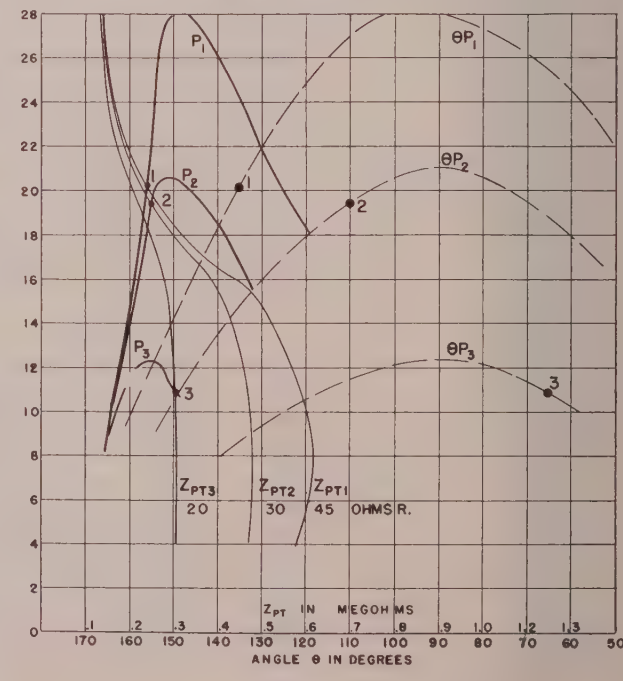

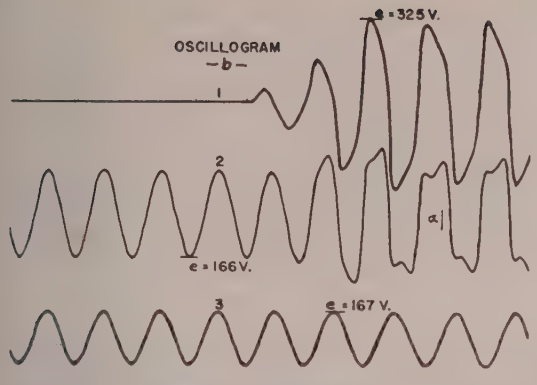

Figure 11(A). Oscillogram a of transformer *D* on an isolated delta at station D

Oscillogram a—no secondary burden. Trace 1—black light synchronizing connection of isolated neutral potential and normal potential. Trace 2—isolated neutral potential. Trace 3—normal neutral potential. "a"—isolated neutral potential phase shift. Potential transformer ratio 127:1

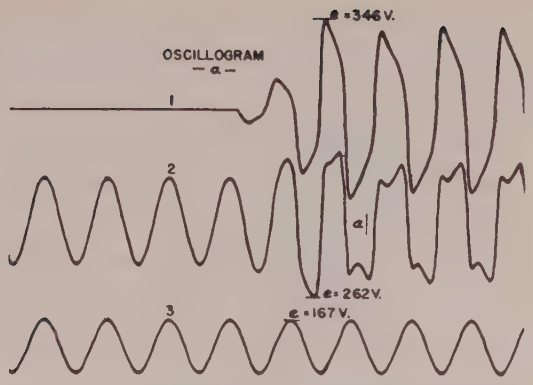

Figure 11(B). Oscillogram b of transformer *D* on an isolated delta at station D

Oscillogram b—260 watts of 125-volt lamps secondary burden. Trace 1—black light synchronizing connection of isolated neutral potential and normal potential. Trace 2—isolated neutral potential. Trace 3—normal neutral potential. "a"—isolated neutral potential phase shift. Potential transformer ratio 127:1

ance of about one-half the value of the maximum X_m.

4. Connect the potential transformer with its burden line-to-ground on the isolated delta which is being studied and read the delta line voltage $\boldsymbol{E}_L$ and the potential transformer voltage $\boldsymbol{E}_{PT}$.

5. Pick X_m from the excitation curve in accordance with $\boldsymbol{E}_{PT}$ and calculate Z_{PT}.

6. This supplies all the information necessary to calculate Z_{CO}.

In some of our tests several values of capacitor burdens were used, but 100 microfarads was suitable. The object of the capacitor burden is to obtain most accurate results by forcing the equivalent Z_{PT} to a capacitive value sufficiently low to hold $\boldsymbol{E}_{PT}$ well below the knee of the magnetization curve where the excitation impedance X_m is most nearly a linear inductive reactance.

A section of the 26-kv line was isolated with the transformer and tested in the same manner. The coupling capacitance to ground per mile per phase as determined by this method is 0.00085 microfarad.

Since the coupling capacitance to ground is dependent on the length of isolated circuit, there is little that can be done with it to prevent this phenomenon, except, of course, the possibility of installing 15-kva of Y-connected neutral grounded capacitors on the bank primary. Since the larger the Z_{CO} the more susceptible the circuit is to neutral inversion, it is considered sufficient to know the value of Z_{CO} for the minimum amount of circuit capable of being isolated. In most instances it consists of the power transformer only.

Therefore, since Z_{CO} cannot be modified, the remaining element of Figure 3 which can effect the phenomenon is Z_{PT}. Figure 5 shows a wide variation in the magnetization curves of potential transformers bought for the same service. Part of this variation is a result of seemingly minor changes in the specification for transformers. The principal factors which may have had considerable effect on these magnetization curves are as follows:

Transformer A. Specified and manufactured for full line-to-line 26,000-volt primary.

Figure 11(C) (below). Oscillogram c of transformer *D* on an isolated delta at station D

Oscillogram c—400 watts of 125-volt lamps secondary burden. Trace 1—black light synchronizing connection of isolated neutral potential and normal potential. Trace 2—isolated neutral potential. Trace 3—normal neutral potential. "a" — isolated neutral potential phase shift. Potential transformer ratio 127:1

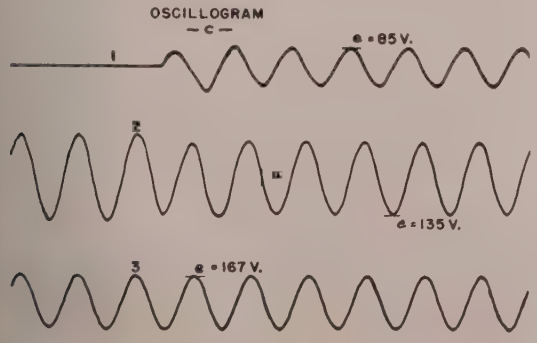

Figure 12 (below). Oscillogram of transformer *A* on an isolated delta at Station A

No potential transformer secondary burden. Trace 1—reference potential from 4.3-kv bus. (Equivalent ratio to 26-kv line to neutral 117.8:1.) Trace 2—isolated neutral potential (potential transformer ratio 220:1). Trace 3—isolated neutral potential transformer excitation current

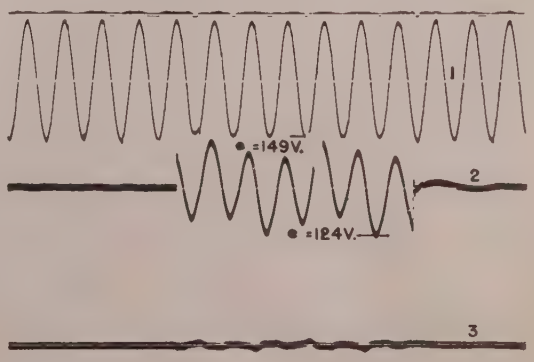

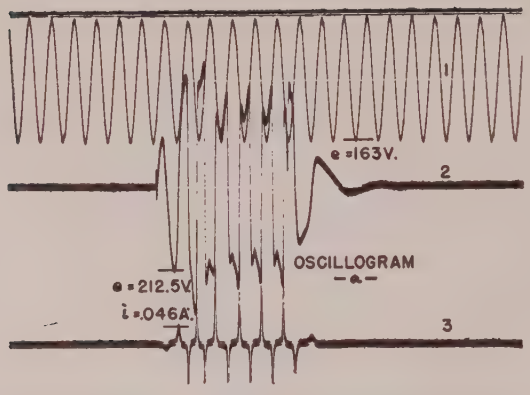

Figure 13(A) (above). Oscillogram a of transformer *B* on an isolated delta at station B

Oscillogram a—no secondary burden. Trace 1—reference potential from 4.3-kv bus. (Equivalent ratio to 26-kv line to neutral 115.6:1.) Trace 2—isolated neutral potential (potential transformer ratio 127:1.) Trace 3—isolated neutral potential transformer excitation current

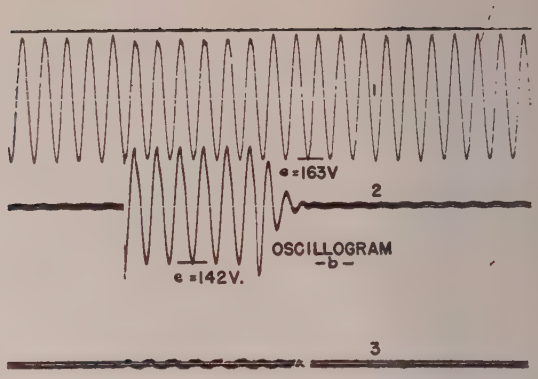

Figure 13(B) (above). Oscillogram b of transformer *B* on an isolated delta at station B

Oscillogram b—no secondary burden. Isolated delta bank plus 3.75 miles of 26-kv line. Trace 1—reference potential from 4.3-kv bus. (Equivalent ratio to 26-kv line to neutral 115.6:1.) Trace 2—isolated neutral potential (potential transformer ratio 127:1). Trace 3—isolated neutral potential transformer excitation current

Transformer B. Specified and manufactured for 15,000-volts primary and capable of standing 1.73 times normal voltage.

Transformer C. Specified for 26,000 volts but manufactured for 15,000 volts and to stand 1.73 times normal voltage.

Transformer D. Specified for 15,000 volts and manufactured for 15,000 volts.

Figure 6 excitation impedance shows that the impedance is variable with applied voltage. The impedance is used as all inductive reactance, but the inversion phase shift indicates that at about 30-kv the impedance of the C transformer is in the vicinity $(0.33 + j\ 0.358)\ 10^6$ ohms. Even with the assumption that all of the excitation impedance was reactance, an equation for the curve cannot be written. Since the curve of equation 3 and the excitation impedance curve have the same variables, a graphical solution can be made to determine the simultaneous value of $\boldsymbol{E}_{PT}$ and Z_{PT}. Figures 8, 9, and 10 consist of graphs of the two sets of curves. Curves 1, 2, and 3 are neutral voltage characteristic curves calculated from equation 3 and plotted with $\boldsymbol{E}_{PT}$, the dependent variable, and Z_{PT}, the independent variable. Curves A, B, C, D are plotted excitation impedance curves, with Z_{PT} the dependent variable and $\boldsymbol{E}_{PT}$ the independent variable. The intersection of these two curves constitute a particular solution and will be a stability point for the voltage phenomenon.

Neutral Shift Characteristics

Figure 8 is constructed to indicate the wide variation between potential transformers with respect to neutral inversion. Actual test points are indicated, but it must be pointed out that the curves are made for full 26-kv line voltage and the conditions for most of the tests were such that the actual line voltage was in the order of 23 kv. This drop in voltage has the effect of preventing inversion. The stability points on this sheet for transformers C and D have inverted neutral at all times. Transformer B has two stability points on curve 2 of Figure 8, one in the first quadrant in-phase with a higher than normal $\boldsymbol{E}_{PT}$ voltage and one inverted. Transformer A has only one stability point which is always in-phase and slightly higher than normal $\boldsymbol{E}_{PT}$ voltage. Magnetization curves have been checked for a 26-kv potential transformer that showed far better characteristics than A, but it was designed for a line-to-line 26-kv connection.

Transformer B indicates three stability points on curve number 3 of Figure 8 which consists of two in-phase in quadrant 1 greater than normal $\boldsymbol{E}_{PT}$ voltage, and one in quadrant 4 with inverted neutral. The point the neutral will stabilize is dependent on the degree of saturation of the potential transformer core at the time of isolation of the delta. That is, if the transformer has an excitation current due to a transient condition greater than that of any potential stability point on the curves of quadrant 1, neutral inversion will occur. Hence, Figure 8 provides sufficient information to permit the specification of the potential transformer excitation impedance such that neutral inversion will not occur. The first requirement of the specification is that the excitation impedance be large enough at normal line to neutral voltage such that the impedance curves "A," "B," "C," and so forth, intersect the neutral voltage characteristic curve 1 at not greater than 120 per cent of normal voltage. The second requirement is that the impedance curve will not recross the voltage characteristic curve below 200 per cent of nominal line-to-neutral voltage. The second requirement is predicted on the premise that 200 per cent is beyond the limit of the core saturation of the transient inrush excitation current. Transformer A satisfies both of these requirements.

Burden Application

The use of potential transformer secondary burdens has been recommended in previous articles on neutral instability. As pointed out, these articles discussed the Y-connection or 3-phase bank. For the Y connection a proper resistance burden on all 3-phases will stabilize the neutral. With the single potential transformer any burden applied will enter into Z_{PT} of equation 3 in combination with the excitation impedance to give the equivalent primary impedance Z_{PT}. Figure 7 shows the equivalent primary impedance Z_{PT} with a secondary burden of 40 microfarads for the three transformers of Figure 5 that had neutral inversion. Forty microfarads is not the best choice for each transformer but it is the best for transformer C. A comparison of the "C" curve on Figure 4 will show that transformer C with 40 microfarads satisfies

the requirements stated above for excitation characteristics. Curve "B" of Figure 7 is free of neutral inversion but has its stability point in the second quadrant of Figure 4 for which E_{PT} is in phase and about 80 per cent of normal. This under voltage can be had only by the application of a capacitor burden with equivalent primary reactance less than the excitation reactance at normal voltage.

Figure 9 shows a family of Z_{PT} impedance curves made for transformer D. These curves are for capacitor burdens ranging from 60 to 180 microfarads. It is obvious from these curves that equivalent impedance by the use of capacitor burden cannot be obtained for this transformer to satisfy the impedance requirements.

Figure 10 shows a family of Z_{PT} impedance curves made for transformer D with secondary resistance burden. This set of curves required a complete voltage curve and a phase angle curve for each resistance burden; therefore, they apply only for the transformer being studied. One important item shown by this set is that the resistance will limit the voltage but with considerable phase shift. It is also evident that the transformer loss has an effect to hold the inverted neutral voltage below what it would have been on a pure reactance basis.

Tests

Three series of tests were made on actual installations of single line-to-ground potential transformers. Each transformer discussed was tested in some manner for its inverting characteristics.

Test number 1. Test number 1 consisted of isolating transformer D at station D. Isolation in this station was obtained by opening a circuit breaker on the distribution substation transformer primary. With this manner of isolation, the circuit received very little disturbance and consequently there was very little transient excitation current, but the Z_{CO} factor would be about its maximum for this station. The instruments used on test number 1 were voltmeter, oscilloscope, and synchroscope. Inversion could be checked, but the transient of inversion could not be observed. Test number 1 made several isolations with combinations of capacitor burden applied varying from 40 to 180 microfarads. An interesting note on this test with secondary burden is that the burden was first applied to the secondary after inversion without any results except to change the voltage magnitude. During the procedure of applying the burden after inversion, one application was made with 140 microfarads that pulled the neutral out of inversion. The capacitors were then applied before isolation.

Test number 1 may be summarized as follows:

1. The neutral will not shift outside the delta if adequate capacitor secondary burden is applied before the delta is isolated.
2. With the stabilized neutral the synchroscope reads in-phase with the normal potential.
3. With the restrained position of the neutral the reference potential-to-ground will always be less than normal.
4. If the neutral does shift outside the delta, the magnitude will be greater with capacitor burden than without.

Test number 2. Test number 2 involved the making of several oscillograms of the same station and transformer as test number 1 with the application of resistance and inductive reactance burdens see Figures 11(A), 11(B), and 11(C).

There are several things of interest that were exposed by the oscillograms:

1. The voltage curve with neutral inversion has a very distorted wave. This distortion is explained as regulation in the primary leakage reactance from the high excitation currents, and the attempt of the circuit to shift to quadrant 1 as X_{CO} is reduced by the higher harmonic current.
2. The neutral shift does not occur instantly but requires about two cycles indicating that energy is involved. The transient of the shift is affected by the voltage at the time of isolation.
3. The phase shift of the line-to-neutral potential is shown to be about 120 degrees leading, which agrees with the calculated values.
4. The maximum instantaneous values are not as high as would be calculated from the rms voltmeter readings. This is because of the depressed top of the wave.
5. The inductive burden indicated, as calculated, that the inverted voltage would be reduced, see Figure 9, but inversion would occur, and could be forced to occur by the application of inductive burden.
6. The resistance burden, Figure 11(C), under one condition prevented the neutral from shifting outside the delta but had some phase shift (30 degrees). This could not be duplicated which indicated that it was dependent on the point on the cycle that the phenomenon was initiated. This condition can only be accounted for by our study on the basis that a lamp burden has a varying resistance. This resistance varies such that it has its lowest value at its coldest portion of the cycle. It is probable that since the phenomena was initiated at a declining voltage, the cold resistance could be in the vicinity of the resistance used on curve 3 of

Figure 14(A). Oscillogram a of transformer C on an isolated delta of station C

Oscillogram a—no secondary burden. Trace 1—reference potential from 4.3-kv bus. (Equivalent ratio to 26-kv line to neutral 117:1.) Trace 2—isolated neutral potential (potential transformer ratio 127:1). Trace 3—isolated neutral potential transformer excitation current

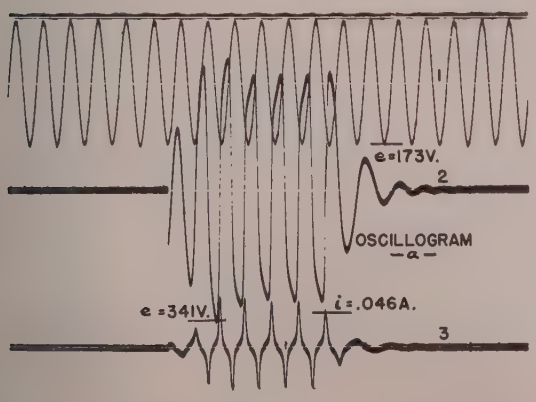

Figure 14(B). Oscillogram b of transformer C on an isolated delta of station C

Oscillogram b—106-microfarad capacitor secondary burden. Trace 1—reference potential from 4.3-kv bus. (Equivalent ratio to 26-kv line to neutral 117:1.) Trace 2—isolated neutral potential (potential transformer ratio 127:1). Trace 3—isolated neutral potential transformer excitation current

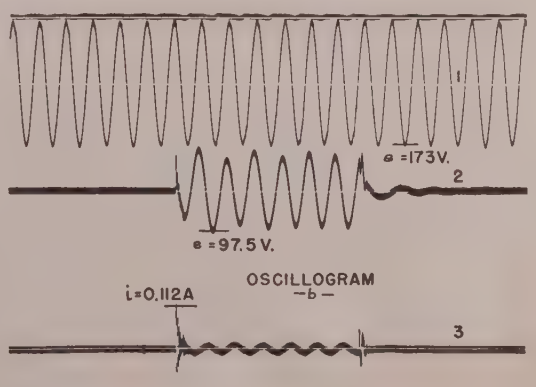

Figure 10 and consequently give the results obtained on the oscillogram, see Figure 11(C).

Test number 3. Test number 3 consisted of a series of tests on stations A, B, and C with their respective potential transformers *A*, *B*, and *C*.

These tests were made by isolation of the primary of the distribution substation power transformer with the potential transformer connected as Figure 3. The power transformer and the isolated delta were energized by closing the bank secondary circuit breaker. The circuit was set up so that the isolated circuit would be energized for 6 to 10 cycles. Thirty oscillograms were made, some without secondary burden, some with 106 microfarad secondary burden, and some with 26-kv line isolated with the transformer.

The results of these tests are as follows:

1. Station A potential transformer *A*, Figure 12, (15 oscillograms were taken of this station).

a. There were no inversions.

b. The potential shifted slightly in quadrant 1 of Figure 8 to a value 113 per cent of normal.

c. The excitation current showed very little transient.

d. There was a definite superimposed frequency on some of the shots which died out after a few cycles. This frequency is a natural frequency of the potential transformer excitation inductance and capacitance of the circuit.

2. Station B potential transformer *B*, Figures 13(A) and 13(B) (5 shots were made on this station).

a. According to Figure 8, characteristic curve 2, it would be possible to obtain two stability points. This was substantiated in the first two shots. Figure 13(A) has neutral inversion.

b. The excitation current maintained at about 20 times normal.

c. The E_{PT} stabilized at about 26-kv rms to ground with the characteristic 120 to 150 degrees phase shift leading.

d. This inversion gave approximately 52-kv line-to-ground voltage on phase 2. (See Figure 3.)

e. The superimposed frequency mentioned is evident on the energy oscillation after the isolated circuit was cleared by the opening of the secondary circuit breaker. The variation in the amplitude of the inversion transient is probably a result of the same natural frequency.

f. Station B stabilized on shot 1 at about 130 per cent of normal voltage in quadrant 1 of Figure 8. (Oscillogram is not included.)

g. Figure 13(B) has 3.75 miles of 26-kv line isolated with the transformer. The E_{PT} voltage stabilized on curve 3, quadrant 1, Figure 8.

h. With the 106-microfarad capacitor E_{PT} stabilized in quadrant 2 at 55 per cent of normal E_{PT}. (Oscillogram is not included.)

3. Station C potential transformer *C*, Figure 14(A) and 14(B). (Five oscillograms were taken of this station.)

a. Figure 14(A), oscillogram "a," has neutral inversion with E_{PT} equal to 30-kv rms sustained voltage.

b. The sustained voltage to ground of phase 2, Figure 3, is 56 kv.

c. The primary excitation current is 0.084 ampere, about three times normal but less than that of transformer *B* when inverted.

d. The inverted E_{PT} voltage was not as distorted as the inverted E_{PT} of transformers *B* and *D*.

e. Figure 14(B) is an oscillogram of an isolation with the 106-microfarad secondary burden. The transformer stabilized at 60 per cent of normal voltage. (See quadrant 2, Figure 8.)

f. A high-frequency transient oscillation of about 900 cycles was superimposed on the excitation current and E_{PT} of Figure 14(B). This is explained as a natural frequency within the circuit which has not been definitely identified. It was characteristic of all stations tested.

Conclusion

This study of neutral inversion is one of necessity because the phenomenon has occurred and with the extensive application of primary network distribution the probability of isolation of a 3-phase system from ground with the circuits described is increasing. The study and tests were made with the object of determining the nature of the phenomenon as well as a cure.

The results of the study with regards to the method of determining the inversion characteristics has been substantiated by tests. Three of the four transformers tested inverted their neutral under test.

It is evident that the industry has not been aware of the excitation impedance requirements for the single transformer. Transformers *B* and *C* are in accordance with the 1948 standards of the American Standards Association and other published information regarding Y primary grounded neutral application. Since the present design is not always satisfactory, potential transformers for the installation of this paper must have specification of minimum limits on the excitation impedance.

Secondary burden application to compensate existing transformers for low excitation impedance is a cure for neutral inversion if the impedance is 50 per cent or better of the required excitation minimum at 200 per cent of rated phase-to-ground voltage.

References

1. Theory of Abnormal Line-to-Neutral Transformer Voltages, **C. W. LaPierre.** *AIEE Transactions*, volume 50, March section, 1931, pages 328–42.

2. Physical Nature of Neutral Instability, **A. Boyajian, O. P. McCarty.** *AIEE Transactions*, volume 50, March section, 1931, pages 317–27.

3. Experiences with Grounded Neutral, Y-Connected Potential Transformers on Ungrounded Systems, **C. T. Weller.** *AIEE Transactions*, volume 50, March section, 1931, pages 299–316.

4. Abnormal Voltage Conditions in Three-Phase Systems Produced by Single-Phase Switching, **Edith Clarke, H. A. Peterson, P. H. Light.** *AIEE Transaction*, volume 60, 1941, pages 329–39.

5. Criteria for Neutral Stability of Wye-Grounded-Primary Broken-Delta Secondary Transformer Circuits, **H. S. Shott, H. A. Peterson.** *Electrical Engineering* (*AIEE Transactions*), volume 60, November 1941, pages 997–1002.

6. Grounding Principles and Practice, **A. A. Johnson.** *Electrical Engineering*, March 1945, page 94.

Discussion

Louis F. Ferri (Commonwealth Associates, Inc., Jackson, Mich.): Though the phenomenon of neutral inversion has been treated in the past by several authors and the theoretical basis has been expounded in great detail, it still represents a problem when it is faced by operating engineers. The author of this paper is to be commended for the clear presentation of the basic theory and its application to a specific case.

The use of three single-phase Y-connected potential transformers is quite common to provide polarizing potential for directional ground relays. It also is general practice to select transformers designed for full line-to-line voltage. The curves presented by the author indicate that the probability of complete neutral inversion is very remote when full line-to-line-rated potential transformers are used even with no resistance burden in the secondary winding.

The economy of the lower-voltage-rated potential transformer, however, points to its application particularly in the higher voltage classes. In most cases proper selection of the resistance burden in the secondary winding prevents neutral inversion when the reduced-voltage-rated potential transformers are used.

The application of single-phase potential transformer connected between phase and neutral is not as common as the 3-phase arrangement mentioned previously, except where voltage reclosing or synchronizing check relays are used. In such cases the economic advantage of the line-to-neutral-rated potential transformer over the full-voltage-rated transformer is not as great, as it involves only one transformer at each station. It is possible, however, that in the future this advantage may have to be considered, provided that the cost of preventive measures to protect against possible neutral inversion and subsequent failure of the potential transformer will not offset the possible saving. For instance, the cost of the 15-kva capacitor on the primary side, as suggested by the author, might be equal to

the saving in the potential transformer selected.

The use of capacity burden should be examined carefully, as it may have an effect opposite from that desired. If improperly selected, it will bring about neutral inversion rather than prevent it.

The use of resistance burden in the case of single-phase application, as the author pointed out, might cause the phase shift between the normal neutral potential and the isolated neutral potential, and this phase shift might make impossible the proper operation of the synchronizing check relays.

It would be of interest to know whether the author had any experience with the operation of synchronizing check relays using potential transformers connected between line and neutral on systems where the system ground may be removed temporarily.

E. C. Wentz (Westinghouse Electric Corporation, Sharon, Pa.): The demonstration and prediction of neutral inversion is of great interest. One thing it demonstrates in addition is that measurement of line-to-ground voltage on a system which is nearly isolated is quite meaningless, because the impedance of the measuring transformer determines what the voltage will be.

Clearly, some means will have to be taken to prevent neutral inversion of these cases, but the author's proposal that minimum exciting impedance be specified assumes that the transformers can be designed readily to have as much magnetizing impedance as may be desired; however, I believe the manufacturers of potential transformers will in general regard this as a tremendous problem.

It seems to me that the most straightforward solution of this problem is the loading of the secondary winding with resistance, the same as common practice for Y-grounded primary winding, broken-delta secondary winding banks, as discussed in reference 5 of the paper. The fact that the resistor produces a phase shift is of no consequence, because, as we have seen, we are not trying to measure anything when the system neutral has been lost—we are only trying to protect the transformer and connected equipment. The losing of the system neutral is an accident, and it seems that an associated accident could lose more of the system so that the line-to-ground capacitance might be different from the assumed value. In this event the impedance of the voltage transformer as determined for the normal system might not be low enough and inversion would still occur, but if the transformer were resistance-burden-loaded, inversion would be prevented. A number of circumstances can be imagined which would permit inversion if the magnetizing impedance were fixed, with no resistance load provided, but a resistance loading can be determined which will stabilize the neutral to a reasonable extent regardless of system connections. In addition resistors are cheap, reliable, and readily available.

Lyle L. Gleason: The discussions were very much appreciated, because the subject dealing with a single potential transformer did not have any substantiating reference material. The authors of the discussions obviously are familiar with the 3-phase Y-broken-delta or Y-Y potential transformer installation, but I do not believe they have taken into consideration the difference between the 3-phase installation and the single-phase potential transformer.

The 3-phase installation when producing abnormal voltages has an unstable neutral, but the single-phase installation produces principally a shifted neutral. In either condition a stabilized neutral at the normal neutral position is desired. With the 3-phase bank Y primary winding, the resistance burden is a means of reducing the zero-sequence impedance to stabilize the neutral at the normal. For the broken-delta secondary winding the stabilizing is accomplished by closing the delta partially in the same manner that a delta tertiary functions on a Y-Y power bank. For the broken-delta the resistance burden has current flow only when the neutral has shifted; therefore, a low resistance may be used with normally no watts dissipation. With the single-potential transformer the addition of resistance burden merely tends to shift the neutral to the phase of the potential transformer connection, which, of course, under certain conditions will restrain the abnormal voltage on the power bank to a reasonable value. The resistance used by the author, which gave reasonable results, was 500 watts burden dissipating heat at all times.

Since the means of reducing the zero-sequence impedance was not available for the single potential transformer, a means of reducing the neutral shifting admittance was attacked. The specifying of adequate excitation impedance does just that, and also the application of capacitor secondary winding burden functions to reduce the neutral shifting inductive admittance. An estimated cost for the capacitor secondary winding burden is about two per cent of the cost of a 34.5-kv insulated potential transformer. The capacitor must be purchased for twice the normal secondary winding voltage, giving it a long life.

The author does not share the fears that the capacitor may aggravate the neutral shift, because there are no continued abnormal frequency conditions with the single-phase, as there are with the 3-phase potential transformer. Also, with higher voltage potential transformers the charging current frequently is greater than the magnetizing current, making the excitation current leading rather than lagging.

It is quite common to hear the expression "buy transformers rated line-to-line voltage for use on line-to-neutral connection." The American Standards Association specifically states that single-bushing potential transformers shall stand line-to-line voltage continuously, but experience has shown that this does not necessarily provide adequate excitation impedance to prevent neutral inversion. The answer to the cost of specified minimum excitation impedance must come from the manufacturer.

Application of Shunt Capacitors at Transmission and Distribution Stations

F. M. PORTER
MEMBER AIEE

C. P. ZIMMERMAN
ASSOCIATE AIEE

IN THE period following World War II we were faced with unexpected load increases on the system of American Gas and Electric Company resulting in high loading of the transmission and distribution systems, including both lines and transformers. With the long-time delivery of equipment and material then existing, making it difficult to obtain facilities for maintaining adequate voltage conditions at many locations, we, like many other utilities, found it desirable and economical to obtain relief in many cases by installing shunt capacitors. While we found it practical to make quite a few low-voltage installations, ranging from 2.3 to 13.8 kv at distribution stations, advantages and savings also were found in providing at transmission stations, relatively large blocks of high-voltage capacitors, ranging in voltage from 22 to 44 kv. As a result of this program there now are approximately 225,000 reactive kilovolt-amperes of static capacitors in service at various substations on the system, and we are installing within the next year additional banks with capacity totalling approximately 50,000 rkva.

Paper **51-15,** recommended by the AIEE Transmission and Distribution Committee and approved by the AIEE Technical Program Committee for presentation at the AIEE Winter General Meeting, New York, N. Y., January 22–26, 1951. Manuscript submitted October 24, 1950; made available for printing November 17, 1950.

F. M. PORTER and C. P. ZIMMERMAN are both with the American Gas and Electric Service Corporation, New York, N. Y.

The authors wish to acknowledge the assistance of the engineering staffs of both the General Electric Company and the Westinghouse Electric Corporation. The authors also express their indebtedness to the organizations of the Appalachian Electric Power Company, Indiana and Michigan Electric Company, Kentucky and West Virginia Power Company, Inc., and The Ohio Power Company, who assisted in the tests described and who assembled most of the operating data used in the paper.

It is the purpose of this paper to review all of our capacitor installations at transmission and distribution stations and to describe several typical installations, particularly those of the high-voltage type. We will describe our experiences in the operation of all of these banks, including the switching problems involved. Special tests made on 44-kv and 33-kv installations at the time they were placed in service will be reviewed.

Description of Installations

Low-Voltage Banks

The first two station installations which were placed in service in 1947, are of small size on wood pole structures and each is arranged in three steps and switched under automatic voltage control. The first one, rated 2,025 reactive kilovolt-amperes, 13.8 kv, is switched by means of 15-kv relatively low-speed circuit breakers.

The second, rated 900 reactive kilovolt-amperes, 4 kv, utilizes as a main circuit breaker, a standard 15-kv 8-cycle outdoor circuit breaker, and for the second and third steps, capacitor-type switches which are, in effect, oil-insulated load-break devices suitable for interrupting charging current. In both of these cases the capacitors are not individually fused. These were followed by several 4-step banks installed in outdoor cabinets. Table I lists these and other low-voltage installations now in service on the system of American Gas and Electric Company.

It will be noted that all of the larger and more recent units are of the housed cabinet type, in which the circuit breaker for each step usually is included in the cabinet. These cabinets are found to be more economical and their installation could be completed more quickly than outdoor structures especially designed to hold the capacitors. It will be noted also that practically all of the banks purchased since 1948 utilize 25-rkva capacitors which cost less per rkva than the 15-rkva units furnished previously. Furthermore, additional economies result because of reduction in space requirements and in the number of connections.

Most of the installations are of two or more steps with banks switched on and off automatically under voltage control. A typical installation is shown in Figure 1 which covers the 13.8-kv 13,200-reactive kilovolt-ampere installation of the Spy Run Station of the Indiana and Michigan Electric Company in Fort Wayne, Indiana. This is a 4-step scheme utilizing a magne-blast circuit breaker for over-all bank protection and for switching the first step. The oil circuit breakers of steps 2, 3, and 4 are of much lower rupturing capacity and are used only for switching the respective steps on and off and not for short circuit protection. All of the 25-reactive kilovolt-ampere 7,620-volt capacitors are individually fused so that failure of one capacitor does not take the bank out of service and also it gives an indication of the faulted unit. Trouble on any bus or connections to the several steps is cleared by the main backup circuit breaker. An overvoltage relay is provided to de-energize the bank in case the bus voltage becomes high enough to be harmful to the capacitors.

High-Voltage Banks

The high cost per reactive kilovolt-ampere of providing switched capacitors at low voltage and the need for locating them at several locations in a given area, indicated the desirability of switching in large blocks at high voltage at transmission stations feeding that area. Also, heavy power interchanges on the 132-kv system were causing low-voltage conditions at several transmission stations and on the subtransmission systems. It was felt that the use of large capacitor banks during these periods would make it

Figure 1 (above). 13,200-reactive-kilovolt-ampere 13,800-volt, 4-step capacitor bank at the Spy Run Station of the Indiana and Michigan Electric Company

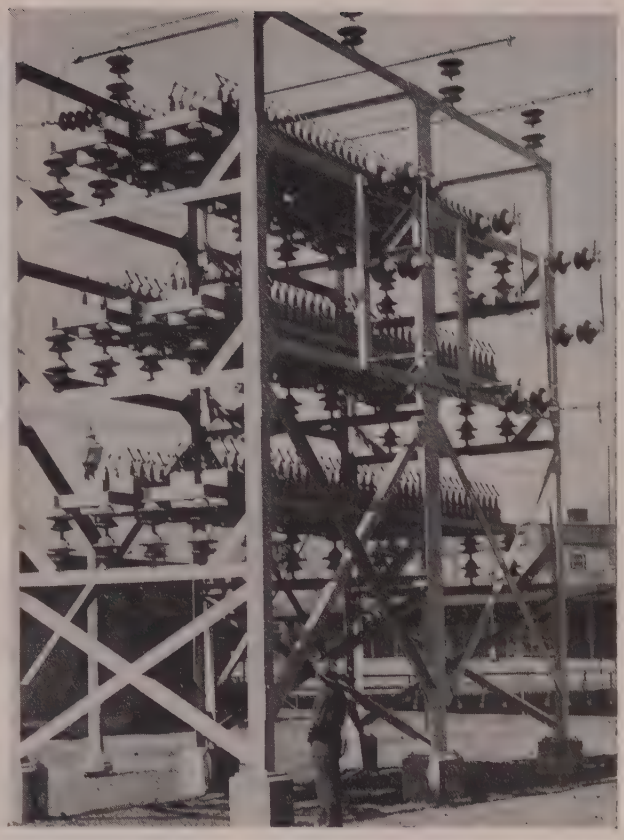

Figure 2 (right). 9,900 reactive-kilovolt-ampere 45,700-volt, capacitor bank at the Logan Station of the Appalachian Electric Power Company

possible to maintain reasonably satisfactory voltage levels.

There were several cases where existing synchronous condensers and regulating transformers had become incapable of maintaining proper voltage levels. It appeared that capacitors would provide the voltage increases necessary to permit these condensers and regulators to operate within their normal regulating range and thus make unnecessary the installation of additional or larger and more expensive equipment which, incidentally, would have taken longer to procure.

The possibilities of utilizing large blocks of high-voltage capacitors were, therefore, explored in 1948 and a number of banks rated 33,200 and 45,700 volts were ordered and placed in service in the early part of 1949. These banks, as well as ones placed in service later, are listed in Table II.

The first of these banks to be installed was the 9,900-reactive kilovolt-ampere 45.7-kv bank at Logan, West Virginia, placed in service in April 1949. Referring to Table II, Item 33, it will be noted that each phase is made up of four parallel groups in series utilizing 36 25-rkva 7,200-volt capacitors in each of the first, second and third groups, and 24 4,800-volt units in the fourth group.

Each capacitor is individually fused. With a Y-connected arrangement this results in a normal rating of 45.7 kv for the bank. One of the important considerations was whether to use available units of standard voltage ratings or to utilize 6,600- or 6,900-volt special units, which would have provided a simpler arrangement for 23-, 34.5-, and 46-kv bank ratings because all capacitors would have been of the same voltage rating. As Table II indicates, we decided to use standard rated units because there was a considerable saving in cost, there was greater availability for quick replacement and there was the possibility of using these capacitors later on distribution lines in case the high-voltage capacitor bank became unnecessary in the future because of system changes or developments.

Figure 2 shows a view of this capacitor bank at Logan, and Figure 3 is a simplified 1-line diagram showing method of connecting the bank to the 44-kv bus. Note that double-throw switches are provided for grounding the bank when out of service for maintenance purposes. The neutral of the bank is grounded solidly through a 1-to-1 ratio current transformer which is used for detecting unbalance phase current which may be caused by loss of one or more capacitors in any phase. For instance in case of loss of one or more capacitors in the 4.8-kv group of one phase it is calculated that the following overvoltages on the remaining capacitors of the group would result:

	Per Cent Overvoltage
Loss of one Capacitor	4.2
Loss of two Capacitors	7.1
Loss of three Capacitors	13

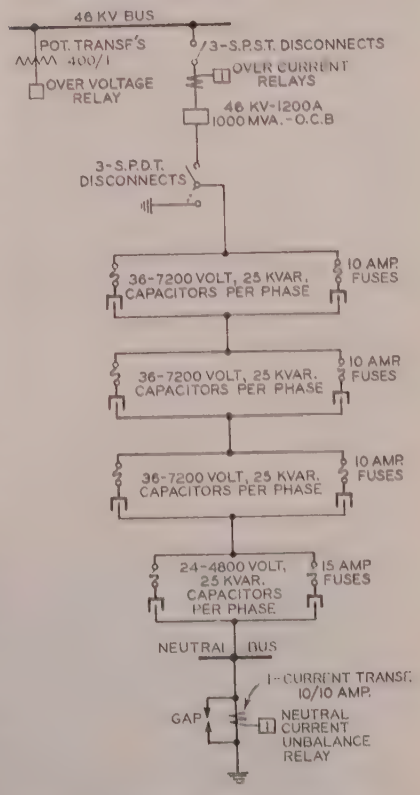

Figure 3. Simplified 1-line of 9,900-reactive-kilovolt-ampere 45.7-kv capacitor bank at Logan Station of the Appalachian Electric Power Company

Figure 4 (left). 9,900 - reactive-kilovolt - ampere 45,700-volt capacitor bank at Sprigg Station of the Appalachian Electric Power Company

Figure 6. 6,600-reactive-kilovolt-ampere, 45,700-volt capacitor bank at Mikegrady Station of the Kentucky and West Virginia Power Company, Inc.

From this it is seen that protection is required for failure of more than two capacitors in a group in order not to have excessive overvoltage on the other capacitors of the same group. The present industry standard on the application of capacitors gives an average 24-hour overvoltage limitation of 5 per cent and a maximum overvoltage of 10 per cent. This indicates that capacitors can stand 110 per cent of rated voltage for 12 hours during any 24-hour period. Therefore, we have been using 110 per cent as our voltage limit to be allowed on a capacitor in case of failure of one unit in a series group. It will be seen that loss of one or two 4.8-kv capacitors in the Logan bank will not put us in the danger zone, and therefore, it is intended to provide an alarm indication only for these cases. However, if a third unit fails in the same group before either of the first two have been replaced, it is intended to trip the bank automatically. The original plan at Logan was to switch the bank on only during daytime heavy load periods, but it has been found preferable to leave the bank energized at all times and to take the change of reactive requirements on the plant generators. The oil circuit breaker used for switching this bank is rated 46 kv, 1,200 ampere, 8 cycle and is equipped with special interrupters having two 300-ohm resistors which are momentarily shunted across the contacts at times of closing or opening the circuit breaker. When this installation was placed in service special tests were made on it, which are described later.

Another 9,900-rkva, 45.7-kv capacitor bank, listed as Item 34 in Table II and shown in Figure 4, was placed in service about the same time at Sprigg, West Virginia. It will be noted that this bank consists of 11 series groups in each phase of 12 2,400-volt units in parallel. While this results in a simple and economical arrangement, loss of one capacitor in a group gives approximately 9 per cent overvoltage and of two capacitors, 18 per cent overvoltage on the remaining capacitors of the group, thus making it undesirable to go to banks of this type in capacities below 9,000 reactive kilovolt-amperes at 44 kv and 6,000 reactive kilovolt-amperes at 33 kv. By utilizing capacitors with a minimum rating of 4,800 volts it is possible to go to minimum bank capacities of 2,400 reactive kilovolt-amperes at 33.2 kv and 3,825 reactive kilovolt-amperes at 45.7 kv, which sizes are incidentally about as small as can be justified on an economic basis considering the high cost of the circuit breaker installation.

Installation number 29 in Table II applies to a 12,000-reactive-kilovolt-ampere 33.2-kv capacitor bank at the Bellefonte Station of the Kentucky and West Virginia Power Company, Inc. Figure 5 gives a view of this installation. This bank is made up of two racks of 6,000 reactive kilovolt-amperes each and originally the neutral was solidly grounded. Early tests indicated excessive third harmonic current in the neutral and therefore the ground was removed and the current transformer connected between the neutrals of the two racks for protection against failure of individual capacitors. This bank as well as most of the others is switched on and off, by time-clock control so that reactive kilovolt-amperes are connected to the system during the heavy load periods.

As mentioned previously, all capacitors are designed for use on circuits whose average overvoltage does not exceed 5 per cent. In the case of the 33.2-kv bank at Bellefonte and elsewhere, this gave us a limit of 34.8 kv, which is too low for other parts of the system. Therefore, we have ordered recently several banks, such as the one covered by Item number 30 in Table II, having a rating of 5,925 reactive kilovolt-amperes at 34.7 kv. Also under Item 26 there was installed a 10,500-rkva capacitor bank rated 29 kv for a 27.6-kv system, which will later be changed to 33 kv, at which time the capacitor bank will be increased to a 12,000 reactive-kilovolt-ampere 33.2-kv arrangement by replacing the second group of 4.8-kv capacitors with 7.2-kv capacitors. Another view of a typical 45.7-kv installation connected to a 44-kv line in a remote location is shown in Figure 6.

Since the manufacturers' standard[1] indicates that capacitors can stand 10 per cent overvoltage it is inferred that even higher voltages can be withstood for short periods of time without unduly shortening their life. This will make it possible, in

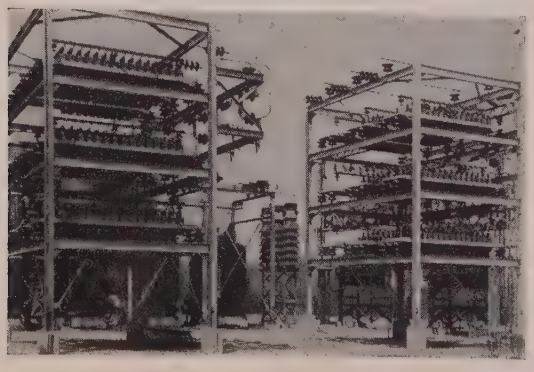

Figure 5 (left). 12,000 - reactive kilovolt - ampere 33,200 - volt capacitor bank at Bellefonte Station of the Kentucky and West Virginia Power Company, Inc.

Table I. Low-Voltage Capacitor Banks at Distribution Stations

Installation No.	Bank Rating Kvar	Bank Rating KV	No. Steps	Switching Main and 1st Step	Switching Other Steps	Type of Installation	Total No. Units	(Kvar) Size of Units	Method of Control	Service Date
1	1,620	2.4	1	OCB		S-STR	108	15	TC	9/48
2	720	4Y	1	Fuses		W-S-STR	48	15	Man	1/49
3	900	4Y	3	OCB	LBS	W-S-STR	60	15	Volt	6/47
4	2,160	4Y	4	OCB	OCB	C	144	15	Volt	2/49
5	2,700	4Y	5	OCB	OCB	C	180	15	Volt	12/48
6	3,060	4Y	4	OCB	OCB	C	204	15	Volt	12/48
7	4,860	4Y	3	OCB	OCB	C	324	15	Volt	2/49
8	4,950	4Y	1	OCB		S-STR	330	15	Man	1/49
9	5,040	4Y	1	OCB		C	336	15	Man	3/48
10	5,040	4Y	4	OCB	OCB	C	336	15	Volt	11/47
11	8,100	4Y	5	OCB	OCB	C	540	15	Volt	6/49
12	10,080	4Y	4	OCB	OCB	C	672	15	Volt	10/48
13	1,050	7.2	1	OCB		S-STR	42	25	TC	12/48
14	3,600	7.2	4	OCB	LBS	C	240	15	Volt	9/50
15	1,530	12.5Y	1	OCB		W-S-STR	102	15	TC	12/47
16	20,100	11.5Y	2	ABB	ABB	C	804	25	Man	7/50
17	2,025	13.2Y	1	OCB		C	81	25	TC	9/50
18	2,520	13.2Y	2	OCB	OCB	C	168	15	Volt	10/48
19	3,240	13.2Y	2	OCB	OCB	C	216	15	Volt	7/48
20	3,780	13.2Y	3	OCB	OCB	C	252	15	Volt	10/48
21	4,800	13.8Y	1	ABB		C	192	25	TC	9/50
22	2,025	13.8Y	3	OCB	OCB	W-S-STR	135	15	Volt	6/47
23	10,080	13.8Y	4	OCB	OCB	C	672	15	Volt	9/47
24	13,200	13.8Y	4	ABB	OCB	C	528	25	Volt	3/50
Total	117,180						6,714			

TC = time clock. Man = manual. LBS = load break switch. C = weatherproof cabinet. W-S-STR = wood steel structure. ABB = air blast circuit breaker.

Table II. High-Voltage Capacitor Banks at Transmission Stations

Installation No.	Bank Rating Kvar	Bank Rating Kv	No. of Racks	Capacitor Units Per Phase-Number and Voltage Rating of Series Groups: 1st Group	2nd Group	3rd Group	4th Group	Total No. of Units*	No. and Type of OCB**	Bank Neutral Grounded	Service Date
25	3,075	22.7Y	1	13-4.1	13-4.1	15-4.8		123	1-Std	Yes	4/49
26	10,500	29Y	2	30-7.2	20-4.8	20-4.8		420	1-R	No	11/49
27	6,000	33.2Y	1	30-7.2	30-7.2	20-4.8		240	1-R	Yes	2/49
28	6,000	33.2Y	1	30-7.2	30-7.2	20-4.8		240	1-R	Yes	4/49
29	12,000	33.2Y	2	30-7.2	30-7.2	20-4.8		480	1-R	No	4/49
30	5,925	34.7Y	1	30-7.6	30-7.6	19-4.8		237	1-R	Yes	12/50
31	6,600	45.7Y	1	24-7.2	24-7.2	24-7.2	16-4.8	264	1-R	Yes	8/49
32	6,600	45.7Y	1	24-7.2	24-7.2	24-7.2	16-4.8	264	1-R	Yes	8/49
33	9,900	45.7Y	1	36-7.2	36-7.2	36-7.2	24-4.8	396	1-R	Yes	4/49
34	9,900	45.7Y	1	11 Groups—Each 12-2.4				396	1-R	Yes	5/49
35	13,200	45.7Y	2	24-7.2	24-7.2	24-4.8	16-4.8	528	1-R	No	1/50
36	19,800	45.7Y	4	18-7.2	18-7.2	18-7.2	12-4.8	792	2-R	No	10/50
Total	109,500							4,380			

* All capacitors = rated 25 kva; individually fused and mounted on outdoor steel structures.

** Std = oil circuit breaker with standard interrupters.

R = oil circuit breaker with resistors on interrupters.

Table III. Experience with High-Voltage Capacitor Bank Installations

Installation No.	Bank Rating Kvar	Bank Rating Kv	Capacitors: Total Units in Bank	* Service Months	* Number of Failures	* Per Cent Number of Failures	Blown Fuses on Good Units	Circuit Breakers: Operations Total	Condition of: Oil	Contacts	Frequency of Bank Inspections
26	10,500	29	420	9	4	1.0	4	200	Fair	Good	Weekly
27	6,000	33.2	240	14	1	0.4	0	322			Daily
28	6,000	33.2	240	17	4	1.7	0	579	Good	Good	Weekly
29	12,000	33.2	480	17	6	1.2	0	454	Good	Good	Daily
31	6,600	45.7	264	13	1	0.4	0	141	Good	Good	Monthly
32	6,600	45.7	264	13	0	0.0	0	164	Good	Good	Monthly
33	9,900	45.7	396	17	1	0.3	0	103	Good	Good	Weekly
34	9,900	45.7	396	16	2	0.5	1	322			Daily
35	13,200	45.7	528	8	0	0.0	0	102	Good	Good	Biweekly
Total			3,228		19	0.6					

* As of September 1, 1950

some instances, to use smaller capacity series-parallel banks. It also will permit setting overvoltage protection to a higher value for both high-voltage and low-voltage installations.

Tests and Switching of High Voltage Capacitor Banks

When the Logan bank was first placed in service, tests were made to determine voltage and current surges at times of switching the bank. A modern 8-cycle oil circuit breaker with resistors was used. Tests also were made to determine the effect of losing 1, 2, or 3 4.8-kv capacitors in a group.

Magnetic oscillographs were used to obtain a record of the line currents, neutral current and line-to-neutral voltages on the 44-kv bus and on the capacitor bank. Since the number of 4,800-volt capacitors in parallel per phase is less than the number of 7,200-volt units, the loss of a 4,800-volt unit is more critical than the loss of a 7,200-volt unit. The voltage across the 4,800-volt group was therefore read with 1, 2, and 3 units disconnected. These overvoltages approximated the calculated values.

Figure 7 is a typical oscillogram taken during one of the tests and shows the conditions on energizing and de-energizing the Logan bank. The effect of the special resistors added to the interrupters on the circuit breaker, is quite noticeable during the first four or five cycles. The tests revealed the presence of a third harmonic current of 3 to 4 amperes flowing between the neutral of the bank and ground. Since this current is greater than the unbalance current that would be expected to flow if the capacitances on the three phases became unbalanced through the loss of one to three capacitors in the same group, it became impossible to use the neutral current as an indication of overvoltage. At present the bank is operating solidly grounded with these relays out of service. We have not, as yet, found an economical and practical solution to this problem, except to provide two similar banks and to use the neutral current flowing between the banks for protective relaying. The results of the tests may be summarized as follows:

1. Only one restrike was noted in the nine tests on which oscillograms were obtained and this did not result in any noticeable overvoltage.

2. Inrush line currents on energizing ranged from four to seven times normal.

3. Inrush or unbalance current in the neutral due to the three circuit breaker poles not making contact at the same instant, ranged from 65 to 104 amperes. The need of a gap to protect the neutral current transformer from a build-up of damaging overvoltage was indicated. The frequency of the inrush currents was in the order of 360 to 500 cycles.

Similar tests also were made on the 45.7-kv bank at Sprigg Station and the 33.2-kv bank at Bellefonte Station. Typical oscillograms of these tests are shown in Figures 8 and 9.

Table IV. Experience in Switching Low-Voltage Capacitor Banks

Installation No.	Bank Rating Kvar	Bank Rating Kv	Step No.	Circuit Breaker Trip Speed, Cycles	Total Operations	First Inspection: Operations before Inspection	First Inspection: Condition Contacts	First Inspection: Condition Oil	Last Inspection: Operations before Inspection	Last Inspection: Condition Contacts	Last Inspection: Condition Oil
2	720	4									
3	900	4	1	8*	1,082	712	Heavily pitted‡	Heavy carbon§			
			2	8**	2,785	1,471	Heavily pitted‡	Heavy carbon§			
			3	8**	2,426	1,303	Heavily pitted‡	Heavy carbon§			
5	2,700	4	1	8*		345	Slightly pitted	Slight carbon			
			2	8*		370	Heavily pitted	Heavy carbon			
			3	8*		216	Heavily pitted	Heavy carbon			
			4	8*		38	Slightly pitted	Slight carbon			
			5	8*		17	Slightly pitted	Slight carbon			
6	3,060	4	1	8*		417	Slightly pitted	Slight carbon			
			2	8*		406	Heavily pitted	Heavy carbon			
			3	8*		290	Heavily pitted	Heavy carbon			
			4	8*		73	Heavily pitted	Heavy carbon			
7	4,860	4	1	8*	1,144	83	Good	Slight carbon	3,894	Good	Slight carbon
			2	8*	1,097	103	Good	Slight carbon	828	Good	Slight carbon
			3	8*	472	91	Good	Slight carbon	307	Good	Slight carbon
8	4,950	4	1	8*	432						
11	8,100	4	1	8*	1,912	500†	Good	Good	1,800	Fair	Slight carbon§
			2	8*	2,178	500†	Good	Good	1,800	Fair	Slight carbon§
			3	8*	1,874	500†	Good	Good	1,800	Bad‡	Slight carbon§
			4	8*	1,455	500†	Good	Good	1,000	Fair	Slight carbon§
			5	8*	1,149	500†	Good	Good	1,000	Fair	Slight carbon§
12	10,080	4	1	8*			Good	Good		Fair	Slight carbon§
			2	8*	759	325	Good	Good	750	Fair	Slight carbon§
			3	8*	743	375	Good	Good	735	Fair	Slight carbon§
			4	8*	307	150	Good	Good	297	Fair	Slight carbon§
13	1,050	7.2	1	8*	571	474	Good	Good			
15	1,530	12.5	1	20*		300	Good	Good			
18	2,520	13.2	1	8*	321	58	Good	Good	239	Good	Good
			2	8*	324	92	Good	Good	277	Good	Good
19	3,240	13.2	1	8*	575	270	Good	Good			
			2	8*	577	394	Good				
20	3,780	13.2	1	8*	683	134	Good	Slight carbon	658	Good	Slight carbon
			2	8*	2,005	190	Good	Slight carbon	1,810	Good	Slight carbon
			3	8*	1,757	293	Good	Slight carbon	1,472	Good	Slight carbon
22	2,025	13.8	1	20*	1,479	537	Good¶	Heavy carbon§			
			2	20*	1,686	466	Good¶	Heavy carbon§			
			3	20*	2,457	311	Good¶	Heavy carbon§			

* Oil circuit breaker.

** Load break switches.

† Estimated.

‡ Contacts badly burned and replaced.

§ Oil replaced.

¶ Circuit breakers had thrown oil and excessive maintenance required.

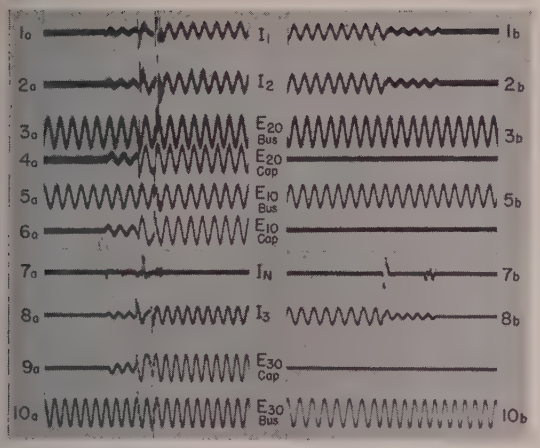

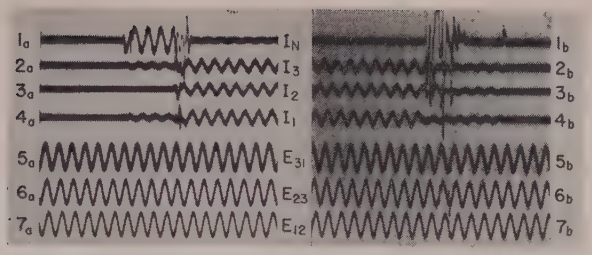

Figure 7 (left). Oscillogram of energizing and de-energizing 9,900-reactive-kilovolt-ampere 45,700-volt capacitor bank at Logan Plant of the Appalachian Electric Power Company

Figure 9 (above). Oscillogram of energizing and de-energizing 12,000-reactive-kilovolt-ampere 33,200-volt capacitor bank at Bellefonte Station of the Kentucky and West Virginia Power Company, Inc.

Operating Experience with High-Voltage Applications

Notwithstanding the problems that they have engendered, experience with high-voltage capacitor banks must be considered quite satisfactory. Only a few capacitors have failed, and usually only one at a time permitting replacement before failure of another unit. Recently we had a case of one capacitor failing and fuses blowing on two other capacitors of the same group, which caused the oil circuit breaker to trip off the bank. This is the only instance where the neutral current protection had a chance to function as planned and operated correctly. The blowing of the other fuses is attributed to the faulted capacitor not being cleared quickly enough by its fuse.

In Table III there have been assembled pertinent data regarding the performance of the capacitors and circuit breakers of high-voltage banks. It will be noted that the number of capacitor failures has been relatively small, amounting to only 0.6 per cent for the banks that have been in service approximately a year or more. Many of these failures occurred at the time of, or shortly after, initial energization, apparently due to poor workmanship during manufacture.

Inspection of the banks is necessary periodically to determine whether any fuses have blown or capacitors have failed. On the first three installations operators were available and daily checks were made. Satisfactory operating experience indicated less need for frequent inspection. Since later installations were at nonattended or somewhat isolated locations, it became desirable to increase the time between inspections for economy reasons, and it will be noted that monthly checks now are being made in several cases. It is entirely possible that this period can be increased still more, because of rare cases of capacitor failures.

Experience with circuit breakers having resistors has been satisfactory. It will be noted that several of the circuit breakers have been operated over 300 times without any noticeable deterioration of contacts, resistors, or oil. Circuit breakers are inspected after approximately 150 operations. In the case of one 6,000 rkva capacitor, 33.2-kv bank, a circuit breaker without resistors was inadvertently installed and for a period of approximately four months switched the bank on and off daily without causing any apparent difficulties due to the restrikes.

In most cases harmonic currents have been encountered in the neutral of the bank when the neutral was solidly grounded but, as pointed out, we have, wherever possible, gone to a double Y scheme, allowing the neutral to float.

Operating Experience with Low-Voltage Applications (Below 15 Kv)

Relatively few capacitors have failed and most of these failures occurred during the first few months of operation. The primary cause was defective workmanship of the capacitors during manufacture.

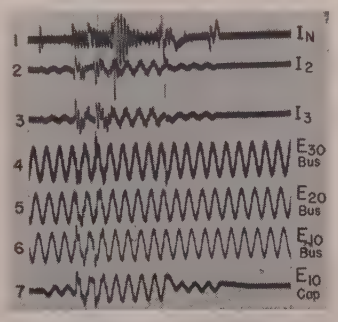

Figure 8. Oscillogram of energizing and immediate de-energizing of 9,900-reactive-kilovolt-ampere 45,700-volt capacitor bank at Sprigg Station of the Appalachian Electric Power Company

Initially there was some trouble with individual fuses which has been corrected. Also there was some difficulty with automatic control whereby there was insufficient time delay in connection with the switching, and pumping occurred, resulting in bus flashovers. There have been several cases where banks were re-energized too quickly, thus causing surges which damaged nearby lightning arresters. In general, experience with the operation of low-voltage capacitor banks has been satisfactory.

Pertinent data covering the switching of 14 low-voltage banks are given in Table IV. Generally old style 15-kv circuit breakers because of their relatively slow opening speeds and light contact structures were found to be unsatisfactory for switching capacitors. They have required frequent checks of the condition of the oil and contacts, usually at 2- to 4-month intervals, or every 200 operations. Some types of modern 8-cycle circuit breakers recommended by manufacturers for controlling capacitor banks have shown deterioration of contacts and heavy carbonization of oil after a relatively small number of operations. Other modern 8-cycle oil circuit breakers installed with banks listed in Table IV have performed properly with little maintenance required and with inspections about every six months. Our limited experience with capacitor load break switches has not been too satisfactory.

Conclusions

1. The use of low-voltage capacitor banks switched in one or more steps is an economical means for obtaining more kilowatt carrying capacity and for re-

ducing losses for all parts of the system involved including the generating units, transmission lines, and substation transformers.

2. The use of high-voltage capacitor banks in large blocks is another economical way to provide necessary kilovars, thus releasing more capacity and reducing losses for transmission stations, transmission lines, and generating units.

3. The performance of many low-voltage switched capacitor banks automatically controlled by voltage has demonstrated that with a reasonable amount of maintenance, excellent reliability and good results are obtained.

4. Similar excellent performance of high-voltage capacitor banks in voltages ranging from 22 to 44 kv and in sizes from 3,000 to 20,000 reactive kilovolt-amperes has shown that these installations are entirely reliable and suitable for transmission systems.

5. Several years experience and testing with high-voltage circuit breakers equipped with resistors indicate that satisfactory and reliable results can be obtained in the switching of large high-voltage capacitor banks.

6. Large savings result in utilizing static capacitor banks in conjunction with synchronous condensers and step-type regulating transformers to obtain necessary reactive kilovolt-amperes and voltage regulation required at a given location.

References

1. Standards for Shunt Capacitors. *Publication Number CAl-1949*, National Electrical Manufacturers Association (New York, N. Y.), 1949.

2. Tests and Analysis of Circuit-Breaker Performance When Switching Large Capacitor Banks, **T. W. Schroeder, E. W. Boehne, J. W. Butler.** *Electrical Engineering* (*AIEE Transactions*), volume 61, November 1942, pages 821–31.

3. Power Capacitors (book), **R. E. Marbury.** McGraw-Hill Book Company, New York, N. Y., 1949.

4. The Why of a 25-Kvar Capacitor, **M. E. Scoville.** *General Electric Review* (Schenectady, N. Y.), May 1949.

5. Report of the Operation and Maintenance of Shunt Capacitors, **AIEE Committee Report.** *AIEE Transactions*, volume 68, part II, 1949, pages 1208–19.

Discussion

C. R. Craig (General Electric Company, Pittsfield, Mass.): It is interesting to note that the authors of this paper have described another pioneering experience in the application of shunt capacitors. Until about 1949, capacitor applications were limited almost entirely to load areas at distribution voltages, and there is still plenty of room for power factor improvement at those voltages. Now, however, it has been shown that series-parallel groups of standard units can be safely connected directly to high-voltage transmission lines to give very economical voltage and power factor improvement. Information such as that reported by the authors is especially interesting and instructive to manufacturers, who are always interested in widening the application and improving the product.

I would like to point out some interesting information drawn from Table III of the paper. A relationship appears to exist between the per cent number of failures of the capacitors and the number of switching operations. A comparison of these two quantities, the seventh and ninth columns in Table III, shows that the highest per cent failure occurs in the bank having the most switching operations, while the lowest per cent failure occurs in banks switched less frequently. Installations numbered 28 and 33, both with 17 months of service, are good examples of this comparison.

While there are a great many things that may affect capacitor life, the proposed switching schedule for a bank may serve as a guide in setting up a schedule of bank inspections for blown fuses that indicate unit failures. For example, it appears that installation number 28 perhaps should be inspected more frequently than installation number 33, as it is switched more than five times as often. Actually, as pointed out by the authors of the paper, periods between inspections may very well be increased beyond a month or more because of the rare cases of capacitor failure.

H. E. Campbell (General Electric Company, Schenectady, N. Y.): Messrs. Porter and Zimmerman have done an outstanding job in using, testing, and reporting on high-voltage capacitor banks. Their records show that approximately 50 per cent of the reactive kilovolt-amperes installed at their stations have been of the high-voltage-bank type.

The authors pointed out in their paper that they found advantages and savings in installing large high-voltage capacitor banks. I do not believe they mean to imply that capacitors should be put on these higher-voltage lines instead of putting them in the distribution system if the reactive kilovolt-amperes are needed by loads in the distribution system. The difference in cost per reactive-kilovolt ampere at the two locations does not appear to be so great as to justify such a procedure. However, there might be cases where the distribution area is not available for capacitor installations, and the high-voltage banks would be a solution.

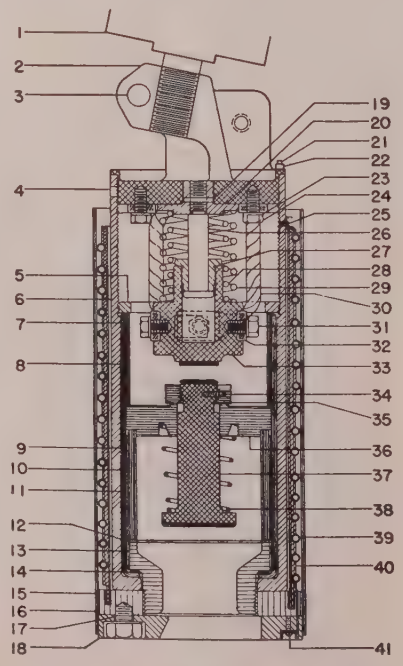

Figure 1

Since the authors installed their capacitors, a low-cost 15-kv switch has become available for switching small banks of capacitors. The lack of this switch a few years ago may have encouraged the authors to install a large percentage of their capacitors at the higher voltage. I believe that there will be little difference in the price of the low-voltage capacitor bank and the high-voltage capacitor bank when the low-voltage switch is used to its full capability. The reactive kilovolt-ampere of a lower-voltage capacitor will do everything the reactive kilovolt-ampere of a higher-voltage capacitor bank will do plus the releasing of capacity, reduction of losses, and/or improvement in voltage between the locations of a high-voltage capacitor and a lower-voltage capacitor. The value of these additional benefits of the lower-voltage capacitor should more than pay for the extra cost of a larger number of low-voltage installations.

Reactive kilovolt-amperes are needed in all parts of the system, and there is equipment available to supply the reactive kilovolt-amperes at any point of the system. As far as the high-voltage and low-voltage parts of the system are concerned, it appears that the reactive kilovolt-amperes should be supplied where they are needed, because of the small difference in the cost of supplying them at either place.

E. B. Rietz and **C. J. Balentine** (General Electric Company, Philadelphia, Pa.): We are happy to be able to supplement this paper with some of the design details of the high-voltage circuit breakers which are referred to as being equipped with resistors on interrupters. The development of these circuit breakers was at the request of the American Gas and Electric Service Corporation for the installations which are described in the paper. The function of the resistor unit is exactly the same as the resistors used on General Electric 115-to-230-kv circuit breakers to shunt the multibreak interrupter contacts so that they can interrupt line charging currents without the creation of abnormal overvoltages. Such resistors have been in service for the last seven or eight years and have given a very satisfactory account of themselves.

Resistor-equipped circuit breakers in the 15-kv class already had been developed and had been in service since 1943, and, therefore, it was entirely logical to extend this design to the 34.5- and 46-kv circuit breakers in question.

The general arrangement of such a resistor on a circuit breaker interrupter is shown in Figure 1 of this discussion. The resistor is a helically-wound nichrome wire assembled on a grooved insulating cylinder which with an outer insulation tube for mechanical protection makes up an assembly which can be readily mounted concentrically around a standard interrupter contact. Built into the lower throat opening of the enclosure is a metal electrode ring to which the lower end of the resistor is connected. Since the upper end of the resistor is attached permanently to the metal chamber, it is apparent that as the circuit breaker opens, a circuit is completed between the moving contact rod and the metal electrode ring either due to contact between the two parts or as a result of the breakdown of the small oil gap as voltage builds up.

During the develpment, many tests were made at the factory in addition to those field tests described in the paper using the criterion that overvoltages should not exceed two times normal. Successful performance up to equivalent 3-phase capacitor bank ratings of 30,000 kva were obtained with no indication that this was a necessary limit.

We are very much gratified at the operating record obtained with these special capacitor switching circuit breakers, which, according to Table III of the paper, have had over 2,500 operations with the condition of the oil and contacts reported as good. Therefore, it would seem that this approach to the problem makes it feasible to consider a wider use of high-voltage capacitor banks because circuit breakers are available which will have proper switching ability.

J. R. Robert (Electricite de France, Paris, France): During the last two years Electricite de France has put into operation numerous capacitor banks similar to those mentioned in this paper.

Electricite de France utilizes capacitors of five standardized types which may be assembled in various combinations in order to obtain Y- or delta-connected banks at the various voltages of the Electricite de France distribution network.

When these banks are Y connected the neutral is never grounded so as to avoid the circulation of currents of the 3, 6, 9, . . ., harmonics in the capacitors when the network neutral is grounded or also to exclude the possibility of ferroresonance when the network neutral is isolated.

The energizing or de-energizing of the banks is effected by means of load break switches which are able to cut the normal bank current but are not meant to eliminate short circuits when they occur.

The clearing of these short circuits is made either by fuses or by powerful air-blast circuit breakers for important banks only.

The banks utilized by Electricite de France often are divided into several partial banks controlled precisely by load break switches, the totality of the bank units being controlled by an air-blast circuit breaker.

The protection of the capacitor banks is designed in such a way that the bank is automatically de-energized as soon as an element in one unit is damaged; such a degree of protection sensitivity has been sought in order to eliminate as rapidly as possible the damaged capacitor and avoid the possibility of an explosion, always a danger for adjoining units, and also to avoid subjecting the capacitors to overvoltages when clearing off the fault. That is why the protection of the units by fuses has been given up as having too little sensitivity and a differential protection by voltage relay has been adopted: each bank, when Y connected, is divided into two half-banks and between the two neutral points of these half-banks is introduced a voltage relay directly connected with the high-voltage without a current transformer, which operates as soon as a coil in one of the half-bank units is damaged. Suitable precautions are taken when balancing the phases so as to group properly the capacities of each half-bank in such a way that there should not exist between the two neutral points a voltage higher than the operating voltage of the relay. The same relay is used in the protection of delta-connected banks, but in this case each phase has to be divided parallel and having a middle point (this necessitates having at least two units in series per phase). The relay is connected between the two mid-points of each half phase.

The advantage of the direct relay lies in the fact that it costs less than the price of the measurement transformer and low-voltage relay combination. It is now giving satisfactory results.

The location of the damaged units after relay action is detected easily by a swelling of the tank. In case this swelling should not occur, rapid capacity measurements by comparison between phases, half-phases, and so forth, permit quick detection of the damaged unit.

Charles I. Maust (The Barrett Division, Allied Chemical and Dye Corporation, New York, N. Y.): One General Electric Company engineer stated they now can build a circuit breaker to handle properly 10,000-reactive-kilovolt-ampere (kvar) banks of static capacitors, but I would like to know if the authors or the General Electric Company engineers have considered the "rocking" effect on the electrical system and interconnected systems when switching large blocks of static capacitors?

F. M. Porter and **C. P. Zimmerman:** Mr. Craig points out an apparent correlation between the percentage failures of individual capacitor units and the number of switching operations reported in Table III of the paper. He calls attention to the fact that installations numbers 28 and 33 have had the highest percentage failures and also the largest number of circuit breaker operations to date. We feel that because of the relatively short period of time that the capacitor banks have been in service, no definite conclusions can be drawn at this time, and that the relationship pointed out therefore must be attributed to coincidence only. It should be noted that on these two banks, a total of only five failures in 636 units was experienced, and a portion of these failures (perhaps all of them) might well have been caused by some manufacturing defects, such as poor workmanship or improper assembly, which might not show up until the capacitors have been in service for several months.

Mr. Craig also suggested that the number of switching operations be used as a guide for determining the frequency at which capacitor banks should be inspected for defective capacitor units. A schedule might well be set up on this basis for multistep banks which have a relatively large number of circuit breaker operations, and for the primary reason of checking on the condition of the circuit breakers, since experience has shown that some designs do not stand up as well as others on repetitive switching. As a matter of fact, some designs recommended by manufacturers require maintenance after

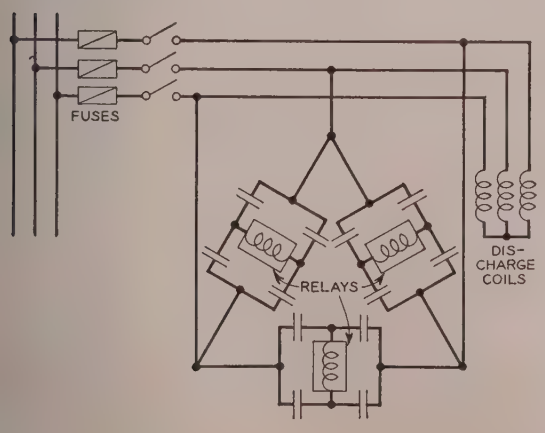

Figure 2 (left). Relay protection of delta-connected capacitors

Figure 3 (right). Protection of y-connected capacitors

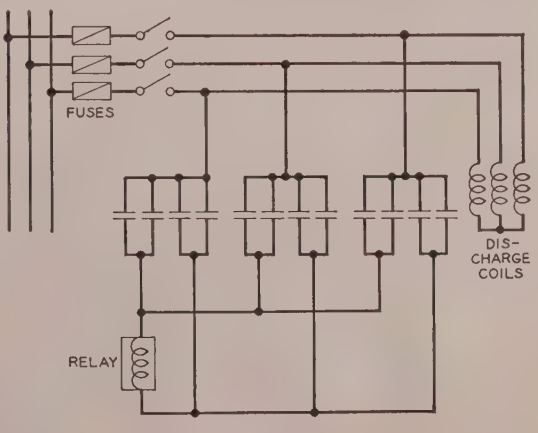

a relatively small number of operations. We believe, therefore, that for multistep banks, the circuit breakers should be inspected as frequently as experience indicates is necessary in each particular case. The capacitor units can be inspected at the same time as the circuit breakers at little or no additional expense. In the case of time-clock-controlled or single-step capacitor banks, such as those used on high-voltage installations, it is believed that the failure rate of the capacitor units taken over a period of several years will permit establishing a suitable frequency for bank inspection.

The authors did not intend to infer, as Mr. Campbell pointed out, that capacitors should be installed only in large high-voltage banks, in view of the fact that the installed cost per kilovolt-ampere of such banks is lower than the cost of capacitors installed at distribution stations or on distribution lines. We, of course, concur with him in that the farther down on the system (that is, from the generators) capacitors are installed, the more benefit will be derived in releasing transformer and circuit capacity. As pointed out in the paper, heavy power interchanges on a high-voltage system tend to cause low-voltage conditions primarily because of increase in reactive-kilovolt-ampere losses on the lines and the simplest, most direct, and most economical way to provide these reactive kilovolt-amperes is at high voltage at line terminals as we have done in numerous cases. Also, the use of static capacitors with existing synchronous condensers to increase capacity is an excellent arrangement. In either of the preceding cases it is not possible to accomplish the same results when the capacitors are located at numerous points and therefore are not capable of being switched on and off as desired. There are not only limits to the amount of unswitched capacitors that any system can stand without getting into difficulties in light load periods, but there are limitations on the number of switched capacitors that can be installed on the secondary buses of distribution stations for various reasons. Often one has a choice of putting in one or two large high-voltage capacitor banks as against a greater number of low-voltage multistep capacitor banks in several distribution stations. For a given number of reactive kilovolt-amperes to be provided, our experience indicates that the total installed cost per reactive kilovolt-ampere for the low-voltage banks amounts to $1^1/_2$ to 2 times the cost for high-voltage banks. The low-cost 15-kv capacitor switch will reduce this differential somewhat, but certainly will not eliminate it entirely.

Now that a low-cost 15-kv switch is available, we believe it advisable for manufacturers to investigate the possibility of developing automatic air break or load break switches that can be used for repetitive switching of high-voltage multistep capacitor banks.

The discussion of Messrs. Rietz and Balentine on the resistor-equipped circuit breakers is appreciated, since the description gives a detailed picture of the arrangement provided on these resistor-equipped interrupters of the circuit breakers such as used for switching the high-voltage capacitor banks mentioned in the authors' paper. It is particularly gratifying to learn that tests have been made indicating that capacitor banks up to 30,000 kvar can be switched successfully by modern circuit breakers with modified interrupters.

The authors considered the elimination of the individual capacitor fuses as reported by Mr. Robert in describing the experience with high-voltage banks in France. However, it was felt that these fuses were justified for at least two reasons—first, because they indicate which capacitor units have failed at the time of a subsequent inspection and, second, because they permit the capacitor bank to remain in service after one or more capacitors have failed. The large high-voltage capacitor banks that we have installed are depended upon to maintain voltage levels on our transmission system, and it is imperative to have as high a service factor on these banks as possible, and to have them connected to the system whenever required. Also, a good proportion of our banks are installed at remote locations so that if the unit fuses were omitted and the banks tripped out on the failure of the first capacitor, there would be delays of 12 to 24 hours or longer before the trip-out of the bank was ascertained and personnel dispatched to remove the defective capacitor and re-energize the bank.

Regarding Mr. Maust's question as to whether switching a 10,000-kvar bank will have any serious effect on system conditions, this refers to an isolated case of trouble which recently has come to our attention. We are investigating this matter thoroughly and expect to arrive at a solution to the problem satisfactory to all parties concerned. In general, the switching on and off of capacitor banks causes sudden small changes in voltage on adjacent buses and lines, but the result is very much the same as switching on and off of important lines between major stations. Therefore, in most cases no new problems have been introduced which would affect system conditions adversely.

The authors appreciate the many discussions and interest indicated in their paper and are grateful for the complimentary remarks received. We hope that the information presented will be of help to others considering the application of capacitor banks, particularly at the higher voltages.

Geometric Mean Distances of Angle-Shaped Conductors

P. C. MAGNUSSON
MEMBER AIEE

Synopsis: The self-geometric mean distance of a symmetrical angle-shaped conductor is approximately 0.393 times the width of the flange of the conductor, measured on the outer surface. The geometric mean distance between two symmetrical angular conductors, when arranged as shown in Figure 5, is very nearly equal to the distance between corresponding points on the two conductors, even for spacings approaching zero. Formulas are developed for the geometric self mean distance of an unsymmetrical angular conductor, and the geometric mean distance between two such conductors (equations 15 and 21 respectively).

GEOMETRIC mean distances of conductor cross-sections have been analyzed in considerable detail in the past, but one cross-section which apparently escaped attention was that of a right angle. Use of conductors with angular cross-section was recently proposed for the supply of the a-c powered cranes to be installed at McNary and Chief Joseph dams, and because of the length of travel from the feed point (in the order of 1,000 feet), reactance drop was considered important. This in turn required knowledge of the self-geometric mean distance and the geometric mean distance between two conductors of that type.

Concept of Geometric Mean Distance

The geometric mean of n quantities, where n is finite, is the nth root of the product obtained by multiplying all n quantities together. This also may be expressed by stating that the logarithm of the geometric mean of n quantities is $1/n$ times the sum of the logarithms of the quantities. This latter form may be extended to include the case of n approaching infinity by replacing the sum of the n logarithms, and the number n (by which that sum is divided), by integrals.

The application of the foregoing theory may be illustrated by the calculation of the self-geometric mean distance R of a straight-line segment, and of a rectangle. The latter of these results will be utilized in later derivations.

Self-Geometric Mean Distance of Line Segment

The co-ordinates for this problem are shown in Figure 1.

$$\log_\epsilon R = \int_0^a \left[\int_0^x \log_\epsilon u \, du + \int_0^{a-x} \log_\epsilon u \, du \right] dx \div \int_0^a \left[\int_0^x du + \int_0^{a-x} du \right] dx \qquad (1)$$

Figure 1. Co-ordinates for calculation of self-geometric mean distance of line segment

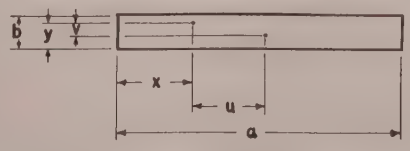

Figure 2. Co-ordinates for calculation of self-geometric mean distance of rectangle

Thus the logarithm of the distance u is integrated in both directions from a point x to the ends of the line segment, and the result integrated over all positions of x from one end of the line segment to the other. The mean value of the logarithmic function is obtained by dividing its integral by the integral of the independent variables over the same limits. Evaluation of the integrals indicated in equation 1 yields:

$$\log_\epsilon R = a^2(\log_\epsilon a - 1.5)/a^2 \qquad (2)$$

$$= \log_\epsilon a - 1.5$$

$$= \log_\epsilon 0.2235\, a \qquad (3)$$

$$R = 0.2235\, a \qquad (4)$$

Self-Geometric Mean Distance of a Rectangle

The self-geometric mean distance of a rectangle (Figure 2) is found by replacing each integral in equation 1 by a double integral.

$$\log_\epsilon R = \int_0^b \int_0^a \left\{ \int_0^y \left[\int_0^x \log_\epsilon \sqrt{u^2+v^2}\, du + \int_0^{a-x} \log_\epsilon \sqrt{u^2+v^2}\, du \right] dv + \int_0^{b-y} \left[\int_0^x \log_\epsilon \sqrt{u^2+v^2}\, du + \int_0^{a-x} \log_\epsilon \sqrt{u^2+v^2}\, du \right] dv \right\} dx\, dy \div (a^2b^2) \qquad (5)$$

$$\log_\epsilon R = \log_\epsilon \sqrt{a^2+b^2} - (1/6)(a^2/b^2) \times \log_\epsilon \sqrt{1+(b^2/a^2)} - (1/6)(b^2/a^2) \times \log_\epsilon \sqrt{1+(a^2/b^2)} + (2/3)(a/b) \times \tan^{-1}(b/a) + (2/3)(b/a) \tan^{-1}(a/b) - (25/12) \qquad (6)$$

This may be approximated to a good degree of accuracy (within 0.2 per cent

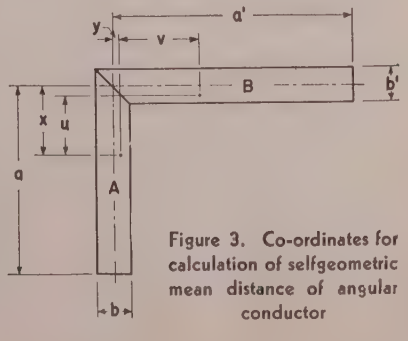

Figure 3. Co-ordinates for calculation of selfgeometric mean distance of angular conductor

Paper 51-16, recommended by the AIEE Transmission and Distribution Committee and approved by the AIEE Technical Program Committee for presentation at the AIEE Winter General Meeting, New York, N. Y., January 22–26, 1951. Manuscript submitted October 16, 1950; made available for printing November 17, 1950.

P. C. Magnusson is with the Oregon State College, Corvallis, Oreg.

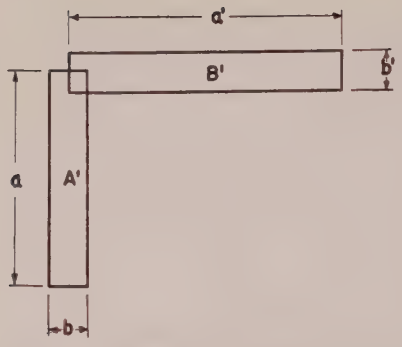

Figure 4. Simplifying approximation in cross-section of angular conductor

for all values of the ratio a/b) by the following:[1]

$$R=0.2235(a+b) \quad (7)$$

Self-Geometric Mean Distance of Angular Cross-Section

The integrals required to compute the self-geometric mean distance of the conductor shown in Figure 3 may be broken into separate parts as follows:

$$\log_\epsilon R = \left\{ \left[\begin{array}{c}\text{Integral of } \log_\epsilon\sqrt{u^2+v^2} \text{ with}\\ \text{respect to } u,\ v,\ x, \text{ and } y\\ \text{over area } A\end{array}\right] + \left[\begin{array}{c}\text{Integral of } \log_\epsilon\sqrt{u^2+v^2} \text{ with}\\ \text{respect to } u \text{ and } v \text{ over area}\\ B, \text{ and with respect to } x \text{ and}\\ y \text{ over area } A\end{array}\right] + \left[\begin{array}{c}\text{Integral of } \log_\epsilon\sqrt{u^2+v^2} \text{ with}\\ \text{respect to } u,\ v,\ x, \text{ and } y\\ \text{over area } B\end{array}\right] + \left[\begin{array}{c}\text{Integral of } \log_\epsilon\sqrt{u^2+v^2} \text{ with}\\ \text{respect to } u \text{ and } v \text{ over area}\\ A, \text{ and with respect to } x \text{ and}\\ y \text{ over area } B\end{array}\right] \right\} \div [(\text{area of } A)^2+(\text{area of } B)(\text{area of } A)+(\text{area of } B)^2+(\text{area of } A)(\text{area of } B)] \quad (8)$$

It will be assumed that the cross-sections A and B may be replaced by rectangles A' and B' (see Figure 4). The first and third integrals in equation 8 then have the same form as the numerator of the right-hand side of equation 5, and the approximate solution given in equation 7 may be adapted to this application.

$$\left[\begin{array}{c}\text{Integral of } \log_\epsilon\sqrt{u^2+v^2} \text{ with}\\ \text{respect to } u,\ v,\ x, \text{ and } y\\ \text{over area } A'\end{array}\right] = a'^2b'^2 \log_\epsilon 0.2235(a+b) \quad (9)$$

$$\left[\begin{array}{c}\text{Integral of } \log_\epsilon\sqrt{u^2+v^2} \text{ with}\\ \text{respect to } u,\ v,\ x, \text{ and } y\\ \text{over area } B'\end{array}\right] = a'^2b'^2 \log_\epsilon 0.2235(a'+b') \quad (10)$$

It will be further assumed that in evaluating those integrals which are with respect to u and v over one of the cross-sections, and with respect to x and y over the other cross-section, the average value of the integrand across each cross-section (with respect to v and y in A', and with respect to u and x in B') may be considered equal to the value at the center line of the cross section.

$$\left[\begin{array}{c}\text{Integral of } \log_\epsilon\sqrt{u^2+v^2} \text{ with}\\ \text{respect to } u \text{ and } v \text{ over area}\\ B', \text{ and with respect to } x\\ \text{and } y \text{ over area } A'\end{array}\right] = b'b\int_0^a\int_0^{a'} \log_\epsilon \sqrt{x^2+v^2}\, dv\, dx \quad (11)$$

$$= b'b[(a'a/2)\log_\epsilon(a'^2+a^2)-1.5\times a'a+(a'^2/2)\tan^{-1}(a/a')+(a^2/2)\times \cot^{-1}(a/a')] \quad (12)$$

$$\left[\begin{array}{c}\text{Integral of } \log_\epsilon\sqrt{u^2+v^2} \text{ with}\\ \text{respect to } u \text{ and } v \text{ over area}\\ A', \text{ and with respect to } x\\ \text{and } y \text{ over area } B'\end{array}\right] = b'b\int_0^{a'}\int_0^a \log_\epsilon \sqrt{y^2+u^2}\, du\, dy \quad (13)$$

$$= b'b[(a'a/2)\ \log_\epsilon\ (a'^2+a^2)-1.5\times a'a+(a^2/2)\tan^{-1}(a'/a)+(a'^2/2)\times \cot^{-1}(a'/a)] \quad (14)$$

Simplification of these expressions, and substitution into equation 8 yields:

$$\log_\epsilon R=[a^2b^2\log_\epsilon 0.2235(a+b)+a'^2b'^2\times \log_\epsilon 0.2235\ (a'+b')+2a'ab'b\ \log_\epsilon 0.2235\sqrt{a'^2+a^2}+b'ba^2\tan^{-1}(a'/a)+b'ba'^2\tan^{-1}(a/a')]\div(a^2b^2+2a'ab'b+a'^2b'^2) \quad (15)$$

In the special case of a symmetrical cross section, that is a equal to a' and b equal to b', this reduces to:

$$\log_\epsilon R=[2\ \log\ 0.2235(a+b)+2\ \log_\epsilon\ 0.2235\ a\sqrt{2}+(\pi/2)]/4$$

$$R=0.393\sqrt{a(a+b)} \quad (16)$$

If a is several times as large as b, the following approximation is valid:

$$\sqrt{a(a+b)}=a+(b/2) \quad (17)$$

Hence

$$R=0.393[a+(b/2)] \quad (18)$$

It may be noted from Figure 3 that $a+(b/2)$ is equal to the width of the angle flange, measured on the outside.

Geometric Mean Distance Between Angular Cross Sections

The calculation of geometric mean distance R' between two identical conductors of angular cross-section may be broken into the evaluation of separate integrals, just as was done in finding the self-geometric mean distance. The cross-sections and co-ordinates are shown in Figure 5.

$$\log_\epsilon R'=\left[\int_{A_1}\int\int_{A_2}\int \log_\epsilon\sqrt{u^2+v^2}\, du\, dv\times dx\, dy+\int_{A_1}\int\int_{B_2}\int \log_\epsilon\sqrt{u^2+v^2}\times du\, dv\, dx\, dy+\int_{B_1}\int\int_{B_2}\int\times \log_\epsilon\sqrt{u^2+v^2}\, du\, dv\, dx\, dy+\int_{B_1}\int\int_{A_2}\int \log_\epsilon\sqrt{u^2+v^2}\, du\, dv\, dx\, dy\right]\div [(\text{area of } A_1)(\text{area of } A_2)+(\text{area of } A_1)(\text{area of } B_2)+(\text{area of } B_1)(\text{area of } B_2)+(\text{area of } B_1)(\text{area of } A_2)] \quad (19)$$

Here all terms involve one integration over one cross-section and a second integration over a different cross-section, and the same simplifying assumptions will be made as were made in such terms in the preceding example.

$$\log_\epsilon R'=\left\{b^2\int_0^a\int_{c+a-x}^{c+2a-x}\log_\epsilon u\, du\, dx+b'b\int_0^a\int_0^{a'}\log_\epsilon\sqrt{(c+a-x)^2+v^2}\, dv\times dx+b'^2\int_0^{a'}\left[\int_0^y \log_\epsilon\sqrt{(a+c)^2+v^2}\times dv+\int_0^{a'-y}\log_\epsilon\sqrt{(c+a)^2+v^2}dv\right]dy+b'b\int_0^{a'}\int_{c+a}^{c+2a}\log_\epsilon\sqrt{u^2+y^2}\, du\, dy\right\}\div (a^2b^2+2aba'b'+a'^2b'^2) \quad (20)$$

Evaluation of these integrals yields equation 21.

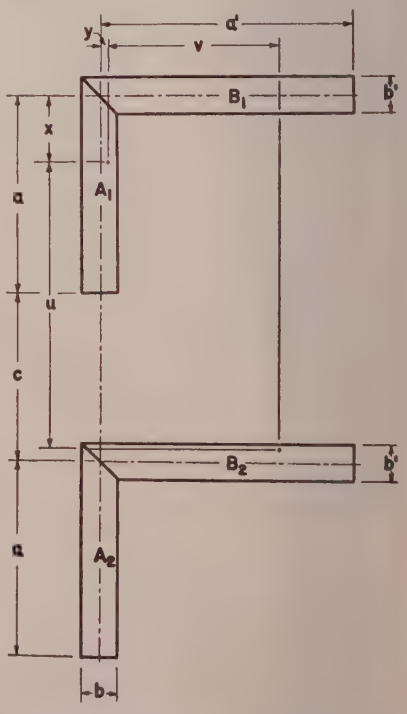

Figure 5. Co-ordinates for calculation of geometric mean distance between two angular conductors

$\log_e R' = ((b^2/2)[(c+2a)^2 \log_e (c+2a) - 2(c+a)^2 \log_e (c+a) + c^2 \log_e c - 3a^2] + (b'b/2)\{a'(c+2a) \log_e [(c+2a)^2+a'^2] - ca' \log_e (c^2+a'^2) + [(c+2a)^2-a'^2] \cot^{-1} [(c+2a)/a'] - (c^2-a'^2) \cot^{-1} (c/a') - 6a'a\} + (b'^2/2)\{(a+c)^2 \log (a+c)^2 + [a'^2-(a+c)^2] \log_e [(a+c)^2+a'^2] + 4a'(a+c) \tan^{-1}[a'/(a+c)] - 3a'^2\}) \div (a^2b^2+2aba'b'+a'^2b'^2)$ (21)

Substitution of the following values of the ratios c/a, a'/a and b'/b gives the corresponding values of R':

c/a	a'/a	b'/b	R'/a
0	1.0	1.0	1.012
0.5	1.0	1.0	1.501
1.0	1.0	1.0	2.000
2.0	1.0	1.0	3.000
1.0	1.5	1.0	2.000
1.0	1.0	2.0	2.023

The following empirical approximation to equation 21 would probably suffice in most practical applications:

$$R' = a + c \qquad (22)$$

Conclusions

General expressions for the self-geometric mean distance of angle-shaped conductors and the geometric mean distance between two identical conductors of that type are given in equations 15 and 21, and the symbols are defined in Figures 3 and 5. Simple empirical expressions which would probably yield sufficient accuracy for design calculations are given in equations 18 and 22 for symmetrical conductors. The validity of the latter approximation is not affected seriously by a reasonable amount of dissymmetry in the cross-section of the conductor, as is indicated in the table immediately preceding equation 22.

Reference

1. Formulas and Tables for the Calculation of Mutual and Self Inductance, **E. B. Rosa, F. W. Grover.** *Scientific Paper 169*, United States Bureau of Standards (Washington D. C.), volume 8, January 1912, page 167.

No Discussion

Protection of Transmission Lines Over Mountainous Region Where Lightning Incidence Is High

J. ELMER HOUSLEY
FELLOW AIEE

JOHN D. HARPER
FELLOW AIEE

Synopsis: This paper presents the application and beneficial results of protecting existing transmission lines which traverse mountainous country against direct lightning strokes by redesign of towers, alteration of overhead ground wires, installation of high speed relaying, and lowering of tower footing resistance by buried counterpoise wires.

Transmission System

THE Aluminum Company of America and subsidiaries own a double-circuit 154-kv transmission line extending from Alcoa, Tenn. to Santeetlah Power House in North Carolina, as shown in Figure 1, over a distance of 30 miles where lightning incidence is high. There are two 1.5 mile tap circuits from this line to the Calderwood Power House in Tennessee. The conductors are 500,000 circular-mil steel-reinforced aluminum cable. The overhead ground wires consist of 1/2-inch galvanized, high strength, stranded steel cable and there are a total of 231 steel towers. This line traverses very rugged country. The span lengths in the level country are fairly uniform and not over 800 feet, but in the mountains hardly any two spans are alike and several are over 2,000 feet; at one point, where the line crosses the gorge of the Little Tennessee River, the span length is 5,010 feet. The altitude of the line ranges from 700 feet at Alcoa to 2,600 feet in the mountainous sections. Part of the line, 16.72 miles, is on double-circuit towers and the remaining 13.57 miles is on single-circuit towers. The single-circuit towers are spaced on 70-foot centers on one right-of-way. The isokeraunic level in this area averages about 63 thunderstorm days per year and lightning is very severe. One of these lines was built in 1919 and the other in 1927, using the same tower design.

The lightning season extends from March 15 to October 1. Insulator flashovers occur mainly in the mountainous section of the line from tower number 81 to tower number 152. Prior to protective measures to this line beginning in 1944, line outages chargeable to lightning between 1927 and 1943 were 111, or an average of 6.53 per year, as shown in Figure 2.

Lightning Investigation 1928–1930

As a result of lightning research in the field and laboratory in the 1920's[2,3,4] by C. L. Fortescue, F. W. Peek, Jr., and others, valuable data were produced which encouraged Aluminum Company engineers to establish lightning protection techniques beneficial to this transmission line and its associated high-tension equipment.

Improvement to Lines Reduces Line Outages

Since 1944 continuous progress has been made in improving performance of these lines.

1. The relaying has been modernized as the art of relaying progressed. The lines and high-tension equipment now are protected by high-speed 4-terminal carrier relay system using Westinghouse type *HZ* relays and *JY* carrier equipment.

2. Towers have been redesigned and two ground wires have been installed on all single-circuit towers and ground wires have been raised on all double-circuit towers, thereby improving shielding of the lines as shown in Figures 3 and 4.

3. Lightning arresters of 161 kv rating have been installed on all terminals. Lightning arresters were not installed at the Calderwood terminals until October 1950.

4. Recognizing the progress made in the art of counterpoises[4] for protecting power transmission lines against damage from lightning surges where other methods do not reduce the tower footing surge impedance to the desired level, it was decided to install sufficient counterpoises to properly balance tower footing resistance, insulation, spacing, and so forth, in January 1946. Tower ground resistances were measured with the ground wires

Table I. Tower Footing Resistance—231 Towers Measured with Ground Wire Disconnected

Number of Towers	Range of Res. Ohms	Number of Towers	Range of Res. Ohms	Number of Towers	Range of Res. Ohms
19	0–5	8	46–50	2	91–95
19	6–10	5	51–55	8	96–100
20	11–15	9	56–60	0	101–105
30	16–20	4	61–65	1	106–110
26	21–25	6	66–70	0	111–115
18	26–30	6	71–75	0	116–120
17	31–35	4	76–80	0	121–125
10	36–40	5	81–85	1	126–130
11	41–45	2	86–90		

Paper 51-17, recommended by the AIEE Transmission and Distribution Committee and approved by the AIEE Technical Program Committee for presentation at the AIEE Winter General Meeting, New York, N. Y., January 22-26, 1951. Manuscript submitted October 11, 1950; made available for printing November 17, 1950.

J. ELMER HOUSLEY and JOHN D. HARPER are both with the Aluminum Company of America, Alcoa, Tenn.

The authors wish to acknowledge the assistance of associates and others in the preparation of this paper.

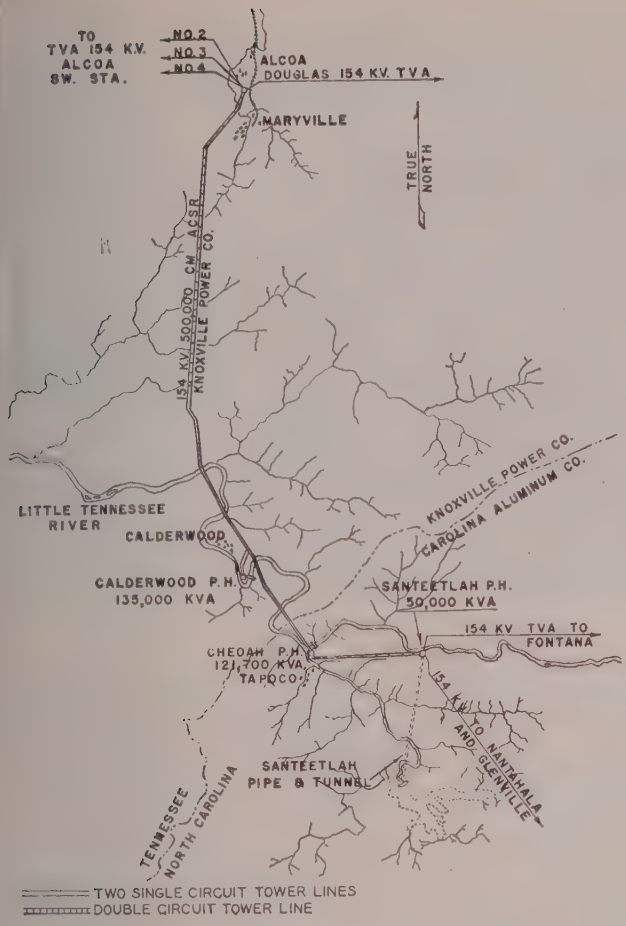

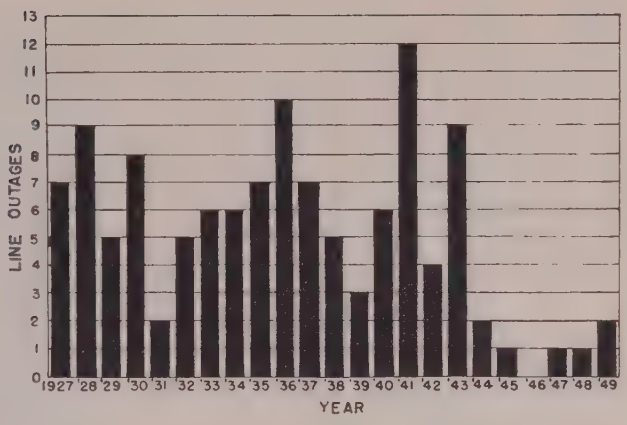

Figure 1 (left). Transmission system of Knoxville Power Company and Carolina Aluminum Company (western division), subsidiaries of Aluminum Company of America

Figure 2 (above). Number of outages per year due to lightning

disconnected from the towers and found to range from "zero" to 130 ohms. Table I shows a tabulation of the tower footing resistances with ground wire disconnected in the ranges of 0-5, 6-10, 11-15 ohms, and so forth, on 231 towers before the installation of counterpoises. Tower footing resistances have not been measured since the installation of the counterpoises, however, the calculated resistance is less than 20 ohms. The line insulation consists of 10 10-inch disks on suspension, and 12 10-inch disks on dead ends. After investigation, it was decided that tower footing resistance could be reduced to obtain an over-all protective level of 10,000,-

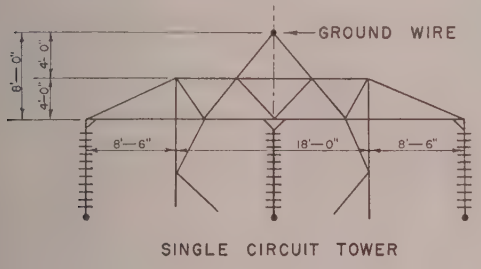

Figure 3 (left). Original arrangement of ground wires

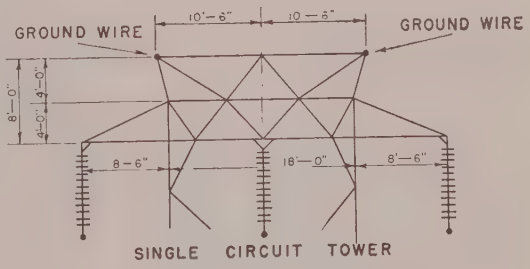

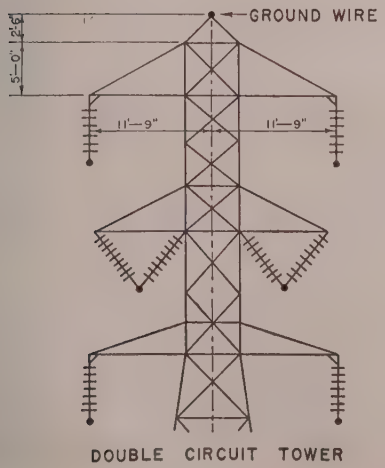

Figure 4 (right). Revised arrangement of ground wires

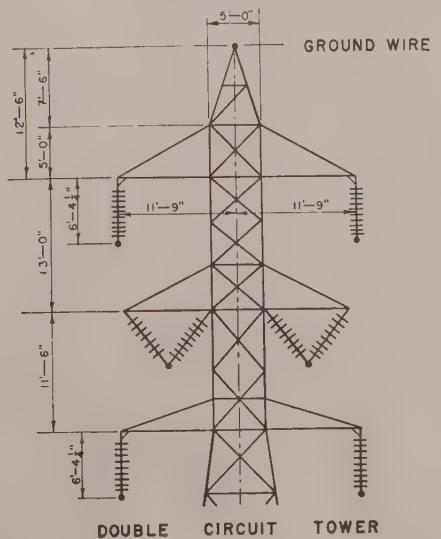

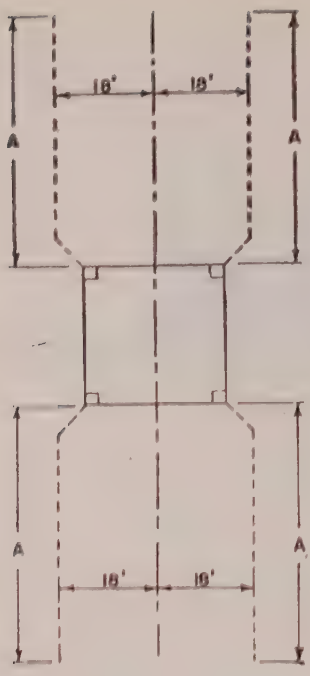

Figure 5 (left). Typical counterpoise installation

A—Depends on footing resistance of individual towers, 100-foot minimum

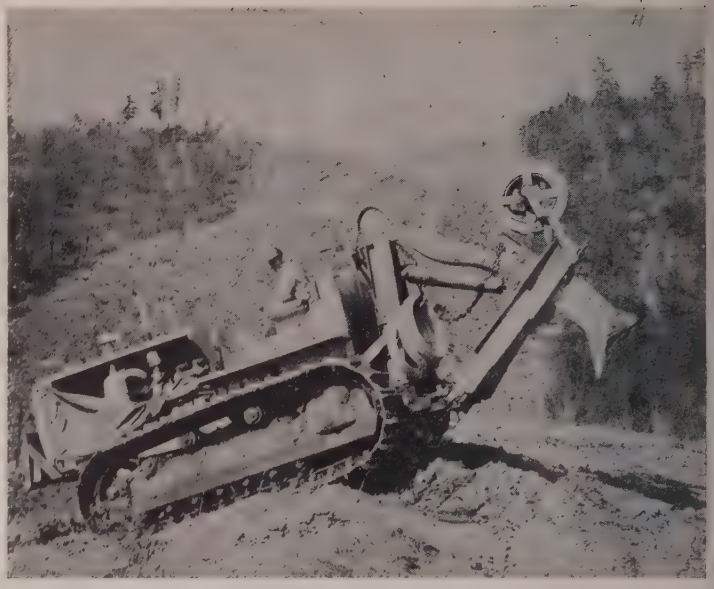

Figure 6 (right). Special cable plow

000 volts and theoretically reduce flashovers caused by lightning to 0.94 outages per 100 miles of line per year. It also was decided that protective gaps should be increased to 50 inches and this is in the process of being done at the present time.

Design and Installation of Counterpoises

The amount of counterpoise to reduce tower footing resistance to the desired level was computed. The detailed design called for 5/16-inch diameter, galvanized steel cable buried to a depth of 18 inches. Two counterpoise cables were used for each line approximately 26 feet apart, as shown in Figure 5. Clamp-type fittings were used for fastening cables to towers. Approximately 132,000 feet of counterpoise were required or extended about 20 per cent of the total circuit miles. This counterpoise is connected to 120 towers or about 52 per cent of the total. Requirements were such that continuous counterpoise was used between only 20 towers.

Unfortunately, most of the higher footing resistances were in very rugged terrain. This presented complications on installations. The first thought was that hand labor would be necessary since the conventional cable plow, as designed by American Telephone and Telegraph Company, or even more rugged designs used by some of the neighboring utilities could not be used. It was estimated that the cost of installation by hand labor would amount to approximately $0.30 per foot, because of the rugged terrain and the remote location of work requiring considerable travel time.

In view of this expected high installation cost, considerable study was given to mechanical methods of installation other than by the use of conventional plow previously described. After several methods were investigated and discarded, a special plow was designed for this job. This plow, shown in Figure 6, consists of a heavy duty pavement ripper tooth mounted on an adjustable frame actuated by a hydraulic hoist, is mounted on the rear of a *D-8* Caterpillar tractor by pin hinges. The reel was designed for a 500 linear foot coil of cable. A reel capable of holding one mile of cable can be substituted if required.

Work on the installation was started January 15, 1946 and was completed April 30, 1946. A total of 132,000 linear feet of 5/16-inch galvanized steel stranded cable was installed. A total of 47,455 linear feet of cable was installed by hand labor at a cost of $0.249 per foot. A total of 84,545 linear feet of cable was installed by plow at a cost of $0.099 per foot, or a saving of about 15 cents per linear foot by plow over hand labor. Unit cost against plowing cable includes back-fill, which was accomplished by running the *D-8* tractor back over the furrow.

Line Outages Due to Lightning from 1944–1949 Reduced

Referring to Figure 2, it will be noted that for a 17-year period, 1927-1944, the average line outages per year were 6.53 and since 1944 the outages have averaged 1.16 per year. This is a reduction of 82 per cent or a ratio of a little less than 6-to-1 improvement in line performance. Since the completion of the counterpoise installation in 1946, line outages chargeable to lightning through 1949 have averaged one per year. There have been no line outages on this line for the first ten months of 1950. The performance of the line since 1946 is in accordance with the expected outage rate of less than one per year. The decreased line outages have resulted in fewer interruptions to production and have contributed to smoother operation of the interconnected systems in the southeast.

References

1. The 150,000-Volt Transmission Line of the Knoxville Power Company, **Theodore Varney.** *AIEE Journal*, June 1920, page 563–70.

2. Theoretical and Field Investigation of Lightning, **C. L. Fortescue, A. L. Atherton, J. H. Cox.** *AIEE Transactions*, volume 48, April 1929, pages 449–79.

3. Lightning Investigation at Alcoa, Tenn., **J. Elmer Housley.** *AIEE Transactions*, volume 50, March 1931, pages 284–87.

4. Counterpoise for Transmission Lines, **Charles L. Fortescue.** AIEE Lightning Reference Book—1918–1935, page 1087.

Discussion

T. J. Allen (Georgia Power Company, Atlanta, Ga.): This paper is a report of the practicability of good transmission line shielding. Anyone familiar with the rugged terrain traversed by the line described will, I am sure, agree that the results as reported justify the work done.

Improved high-speed relays and oil circuit breakers have done much to reduce the

conductor damage and permanent faults caused by lightning flashovers, but basically they do not prevent the flashover. If, however, modern relays are used with high-speed circuit breaker reclosing, the service need not be interrupted because of a transient flashover.

The most improvement in the structure change was obtained on the single circuit towers, where the cone of protection was reduced from 51 degrees on the outside phases to 27 degrees. Assuming that the mid-span clearances are adequate, you might expect a few more outages on this line than on a similar one over level country, because in many spans, especially the long ones, the conductors at mid-span sometimes are 100 feet or more above the highest trees or other natural shield.

To plow in counterpoise in this mountainous country was quite an accomplishment. It would be interesting to know if erosion has uncovered any of the counterpoise since installation, or how erosion was prevented. When the authors calculated the ground resistance as being under 20 ohms, I wonder if they made the same error we did in assuming counterpoise ground resistance decreased after installation. We made this assumption because the resistance could be lowered by running the tractor over the recently installed counterpoise, thus packing the earth around it. Therefore, we reasoned that after the rain had thoroughly imbedded the counterpoise the resistance would be lower, or at least no higher than when installed. Check tests on the Georgia Power Company system made 12 months after installation indicated, however, that the ground resistance had increased from 15 ohms to 29 ohms at six out of eight structures tested. This fact has been confirmed in a report, by Grady L. Smith and R. C. Vickers[1] of counterpoise tests made at Meridian, Mississippi. This report compares the 9-year average of lightning interruptions of three double-circuit steel tower lines in Alabama, where the isokeraunic level is considered 70. The Alabama report shows 11.8 single-circuit and 17.3 double-circuit interruptions per 100 miles per year for a line with one overhead ground wire and no counterpoise, compared with 3.07 single-circuit and 0.55 double-circuit interruptions on a line with overhead ground wire and counterpoise.

This record almost parallels the improvement reported by Mr. Housley, which, calculated for 31.5 miles of exposure, shows 20.7 interruptions per 100 miles per year before and 3.68 miles per year after improvements were made. Therefore, it seems most of the improvement may be attributed to the addition of counterpoise.

REFERENCE

1. DESIGN, INSTALLATION AND OPERATING EXPERIENCES WITH COUNTERPOISE, **Grady L. Smith, R. C. Vickers.** Meeting of Southeastern Electric Exchange, March 1950.

I. B. Johnson and **L. E. Saline** (General Electric Company, Schenectady, N. Y.): Messrs. Housley and Harper have presented a report on the performance of a particular transmission line under severe lightning conditions. It is interesting to note the improvement that resulted from the lowering of the tower footing resistance by the addition of counterpoise and by decreasing the protective angle of the ground wires.

Similar results have been reported for other transmission lines and are summarized and discussed by Dr. W. W. Lewis in his book.[1] Some of these results are given in Table I of this discussion.

From this table it is seen that the outage rate for the Alcoa-Santeetlah Line is still quite high. This probably can be attributed to localized high isokeraunic level. Experience indicates that further improvement in line performance might be obtained by using two ground wires on the double-circuit towers, although it is appreciated that the protection obtained must be balanced against economic considerations.

Additional information concerning the effect of line design on line performance will be made available when the Joint AIEE-EEI Committee on Line Outages completes its report.

REFERENCE

1. PROTECTION OF TRANSMISSION SYSTEMS AGAINST LIGHTNING (book), **W. W. Lewis.** John Wiley & Sons, Inc., New York, N. Y., 1950

A. S. Runciman (The Shawinigan Water and Power Company, Montreal, Can.): For a 30-mile length of line, the lightning outage record appears high, in the order of 20-30 outages per 100 miles of line per year before counterpoising. This is reduced to about 3 or 4 outages per 100 miles of line per year.

If these results are compared with a system of considerably greater line mileage, it appears that still further improvement may be expected by measuring carefully, and reducing where high, the ground resistance.

As an example, the Shawinigan Water and Power Company operates two lines which have never opened on lightning. One is a 220-kv line 70 miles long and the other is a 110-kv line 35 miles long. Both lines were built in 1940. During construction ground-resistance measurements were made of all footings, and a maximum value of 50 ohms per tower was set before making the continuous 2-wire counterpoise connections. Where ground resistance was greater than 50 ohms two extra continuous wires were added, making four in all to one tower beyond the last 50-ohm footing.

This 220-kv line is insulated by 14 5 inch suspension discs and has the conventional two sky wires. Part of the right of way was quarry rock.

It also was noted that near rivers the footing resistances were high, requiring the four counterpoise wires.

From Table I of the paper it appears evident that enough data are available to make still further improvement in reducing lightning outages.

Fred C. DeWeese (Carolina Power and Light Company, Raleigh, N. C.): In this day and time most transmission lines are required to operate generally at or near their maximum capacity supplying loads, the continuity of service of which is of vital importance. Interruption to service may not only cause loss in production, but otherwise may be very costly.

Messrs. Housley and Harper have written a very clear and concise paper dealing with the protection from lightning of a given transmission line, and they are to be commended for the thorough manner in which they have carried out their study and the step-by-step procedure employed to transform a line which was previously a very bad actor to one now giving a very high standard of performance. When line outages caused by lightning for a length of line as described by the authors has been reduced from a little over 6.5 outages per year to a little over one per year, it indicates quite clearly that the methods employed have been very effective. The writer believes, however, that in many cases the installation or rearrangement of static wires and the installation of counterpoise are given more credit than they justly deserve, since, in most cases (as pointed out in this paper) faster relaying and circuit breaker operation also are obtained simultaneously. This certainly must account for at least a small part of the improvement in line performance.

Accessibility

In mountainous regions usually some one or more locations along a given line are quite inaccessible, and every method known to the designer should be employed to localize possible flashover and burn-downs to loca-

Table I

Line	Kilovolts	Physical Description	Years of Experience	Outages Per Hundred Miles Per Year
Wallenpaupack Siegfried	220	No ground wire No counterpoise	13	74
	220	2 ground wires and no counterpoise	4	20
	220	2 ground wires and short radial counterpoise (50 ft.)	9	1.5
	220	2 ground wires and continuous counterpoise	10	
Metropolitan Water District of Southern California	230	No ground wire	4	12
	230	2 ground wires	6	0.21
Alcoa-Santeetlah	154	1 ground wire on both single and double circuit towers No counterpoise	17	21.8
	154	1 ground wire on double circuit towers 2 ground wires on single circuit towers Counterpoise	5	3.85

tions which are accessible to vehicular traffic. For this reason, the writer has employed graded insulation, the idea being that the higher insulation value at or near the top of the mountain will have a tendency to prevent flashover until the lightning stroke or charge has, at least, reached a point well down the mountain side. For example, in this particular case the line is inaccessible except to pedestrians for a distance of some 6,000 feet on one side and is accessible by jeep only in good weather on the other side, and an outage on either side of this mountain, especially at night or when there is snow on the ground, would require an indefinite period of time to restore service.

This matter is mentioned in this discussion as a matter of interest, and the writer would be pleased to know if anyone has employed the method and what the results have been. This particular line is some 18 miles long and consists of 336,400-circular-unit steel-reinforced aluminum cable and two overhead 3/8" high-strength-steel static unbonded hardware, no counterpoise. It has been in operation at 110 kv for about 18 months, and there has been no interruption to service; however, I believe there have been two relay operations.

Mid-Span Clearance

Mid-span clearance between static wire and conductor is of importance especially in comparatively long spans; however, it is quite difficult without a considerable amount of calculations to determine the clearance except for the ruling span. To provide a simple method for finding the mid-span clearance to a close approximation for a given line and span length, the writer has developed the method illustrated here. A chart of this nature, however, must be prepared for each particular important line, the method of construction, of course, being very simple. It is necessary only to plot the sag at each given span for the static wire and also for the conductor, using the diagonal lines as a means for determining the mid-span clearance. It should be noted particularly that not only does the clearance increase with increased spans, but the shielding angle also is improved.

Counterpoise

The installation of counterpoise in mountainous regions is very difficult, and methods employed over the more level profiles, as the authors of this paper have discovered, are not readily applicable. The cost for counterpoise installation, exclusive of materials and the average over the more level profiles, usually runs from four to five cents per foot for plowing in and very probably in the order of 15 cents per foot for handwork. This is approximately half the cost for plowing in cable and approximately two-thirds of the cost for handwork as the figure given in the paper of about 10 and 25 cents per foot, respectively.

This paper is timely, comes from an authoritative source, and should certainly be well received by the engineering profession.

J. Elmer Housley and **John D. Harper:** The interest shown and the information given in the various discussions are appreciated. No doubt, some further improvement in performance might be obtained by reducing the tower footing resistances to still lower values; however, as a practical matter the law of diminishing returns takes effect here, and we doubt that further improvement is economically justifiable. The same consideration applies to the matter of adding a second ground wire on the double-circuit line. There were no outages in 1950, and thus far none in 1951, and we think that the average over a period of years will be less than one outage a year for the 60 miles of line and that the outage per 100 miles computed for comparison will be less than two per year.

In regard to Mr. Allen's comment on the change of counterpoise ground resistance, no measurements have been made; however, the computation did not take into account any changes after installation. The performance record does not indicate that the change, if any, in ground resistance has been material. The only action taken to prevent erosion was to dig cross-trenches on the slopes and hand-tamp the cross-trenches to break up any underground erosion around the counterpoise.

The method used by Mr. DeWeese for approximating the mid-span clearance between ground wires and conductors is of considerable interest. The 5,101-foot span on these lines is overinsulated in comparison to the remainder of the line in an attempt to prevent flashovers at this point, and this means has been quite successful, although there have been a few flashovers at the dead-end towers on this particular span. This is done for about the same reasons as Mr. DeWeese gives for similar overinsulation.

We wish to thank all the discussers for their contribution to this subject.

Switching High-Voltage Shunt Capacitor Banks

A. W. FUNKHOUSER
NONMEMBER AIEE

R. C. VAN SICKLE
FELLOW AIEE

D. F. SHANKLE
ASSOCIATE AIEE

THE Indianapolis Power and Light Company recently installed on its system one of the first 34.5-kv capacitor banks in this country. This capacitor bank, totaling 7,290 kva, was part of a program of locating reactive generation close to reactive load in the most economical and practical manner.

As there were very little test data available on the performance of circuit breakers in switching large capacitor banks at 34.5-kv, oscillographic records were made when the capacitor bank was placed in service. The overvoltages produced on the 34.5-kv system when the bank was switched, usually were less than 2.0 times the normal line-to-ground crest value but did reach a value of 2.4 times normal on one test. These overvoltages are within the range generally produced in the interruption of reactive currents. They caused no disturbance on the 34.5-kv system, but did cause lightning arrester failures on two connected 4-kv feeder circuits.

Investigation showed that a voltage surge at one voltage level produced by capacitor switching can set up relatively greater voltage oscillations at another voltage level under certain conditions of coupling and circuit constants.

The circuit breaker design was modified by auxiliary oil pistons after high power laboratory tests indicated this design change to be most effective in reducing both the magnitude and number of overvoltages produced in de-energizing the capacitor bank. This was borne out in final tests with the modified circuit breaker switching the 34.5-kv capacitor bank on the Indianapolis Power and Light Company system without any lightning arrester failures on the 4-kv feeders or other system disturbances.

Capacitor Bank Construction Details

The 34.5-kv 7,290-kva capacitor bank was installed at the Main Street general distribution substation along with a 34.5-kv oil circuit breaker to switch the bank. The Main Street substation, as shown in Figure 1, is very close geographically and electrically to three industrial substations totaling 18,750 kva in capacity. Here on the utility company's property were existing facilities for control from the load dispatcher's office.

The bank, shown in Figure 2, consisted of three housed 2,430-kva assemblies each made up of 162 15-kva capacitor units with individual fuses. The units, rated 6,600 volts, were connected to form a 3-phase ungrounded Y bank. Two 6,000/120-volt potential transformers with 34.5-kv class insulation were connected between the three neutrals of the housed banks with voltage relays on the secondary windings to detect failed units. The metal housings in which the capacitors are mounted were chosen to prevent personnel in the substation from contacting dangerous voltages when working on nearby equipment as well as to keep out wire, sticks, and so forth, which might be thrown into the capacitor units and possibly cause an outage. Each housed bank is a 3-phase unit with each phase and the neutral lead brought out to 34.5-kv bushings on the roof of the metal housing. Doors on each unit provide access to the individual capacitor units for inspection and maintenance.

Switching Tests and Results

A single line diagram of the various system components involved in this problem is shown in Figure 3. The Main Street substation has the 7,290-kva shunt capacitor bank connected to the bus by a 34.5-kv circuit breaker. Off the same bus are two 3,000-kva unit substations stepping down to 4 kv. Also shown is the Allison number 2 7,500-kva substation with its associated 4-kv feeder circuits. The locations of the lightning arrester failures on these 4-kv feeders also are indicated.

The energizing and de-energizing tests of the capacitor bank were made using a 9-element magnetic oscillograph to record the currents and phase-to-ground voltages on the bus side of the capacitor circuit breaker, and the phase-to-ground voltages on the capacitor side of the circuit breaker. The normal current to be interrupted was about 120 amperes, and restriking occurred during the tests. These restrikes produced voltages usually less than 2.0 times the normal line-to-ground crest value on the 34.5-kv system, but reached a value of 2.4 times normal on one test. These overvoltages are within the range produced in the interruption of reactive currents.

While no disturbances were produced on the 34.5-kv system by these overvoltages, lightning arrester failures did occur on two of the connected 4-kv feeder circuits. Therefore, additional tests were made to investigate the reasons for these failures and to find a solution of the problem.

The results of the tests on which oscillograms were made are given in Table I. The tests were made as a series of closing tests, followed after an interval of about five minutes by an opening of the capacitor circuit breaker. The tests were made with industrial load on the adjacent substations. The 34.5-kv system im-

Paper 51-18, recommended by the AIEE Switchgear and Transmission and Distribution Committees and approved by the AIEE Technical Program Committee for presentation at the AIEE Winter General Meeting, New York, N. Y., January 22-26, 1951. Manuscript submitted October 24, 1950; made available for printing November 17, 1950.

A. W. FUNKHOUSER is with the Indianapolis Power and Light Company, Indianapolis, Ind., and R. C. VAN SICKLE and D. F. SHANKLE both are with the Westinghouse Electric Corporation, East Pittsburgh, Pa.

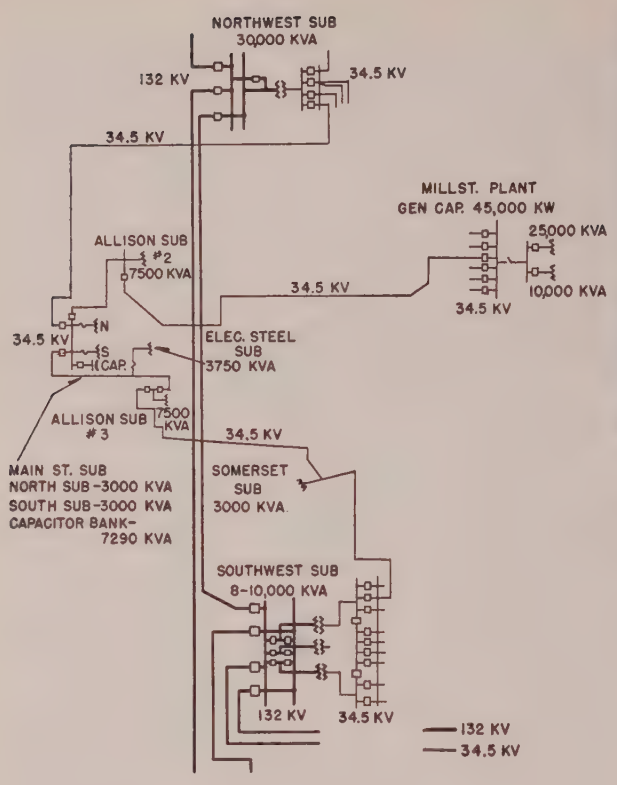

Figure 1 (left). Location of Main Street capacitor bank and industrial substations

Figure 2 (above). 7,290 kva capacitor bank installation at the Main Street 34.5-kv substation

pedance at the Main Street 34.5-kv bus was approximately 19 per cent on a 100,000-kva base. During the first nine tests no system disturbance involving damage to system equipment occurred. On the last opening (Test 10) a lightning arrester failed on phase "c" of a 4-kv feeder *F24* off the 4-kv bus of the Allison number 2 substation. For this test the oscillogram indicated a maximum overvoltage of 1.87 times the normal line-to-ground crest voltage on the Main Street 34.5-kv bus. This voltage was not considered excessive because it was within the range reached while opening inductive circuits, and equally high voltages had been reached on some of the preceeding tests. The oscillogram taken of the voltages on the 34.5-kv bus and capacitor bank during this test, Figure 4, shows two reignitions of one phase followed by a restrike between the two 34.5-kv phases "A" and "C" corresponding to the 4-kv phase-to-ground voltage, "c", on which the lightning arrester failed. (A reignition is defined as current flow resuming after a pause in the current of less than one-quarter of a cycle, and a restrike is defined as current flow resuming after a pause in the current of one-quarter of a cycle or more. A quarter-cycle is assumed to be the minimum which can cause overvoltages.)

There was no apparent reason for this lightning arrester failure on the 4-kv feeder from the Allison number 2 substation bus so testing was discontinued until the following week. A time was chosen when possible system disturbance would not affect service continuity to the industrial loads in the area. In this next series of five opening tests, lightning arresters again failed on the 4-kv feeders from the Allison number 2 substation bus. These occurred on the second, fourth, and fifth opening operations of the capacitor circuit breaker.

Table II shows the results taken from the oscillograms made on these five opening tests having the even test numbers 12, 14, 16, 18, and 20. On Test 14 a lightning arrester failed on feeder *F25*, "c" phase, about 1,100 feet from the Allison number 2 substation and about 60 cycles later short-circuited a 34.5-kv line located above it on the same pole. The oscillogram made on this test is shown in Figure 5. It produced four reignitions and one restrike that produced 2.2 times normal voltage on the 34.5-kv bus.

Test 16 was made after replacing the lightning arrester that had just failed on feeder *F25*. This opening of the capacitor circuit breaker resulted in one reignition with no transient overvoltage on the 34.5-kv bus and no system disturbance. Dur-

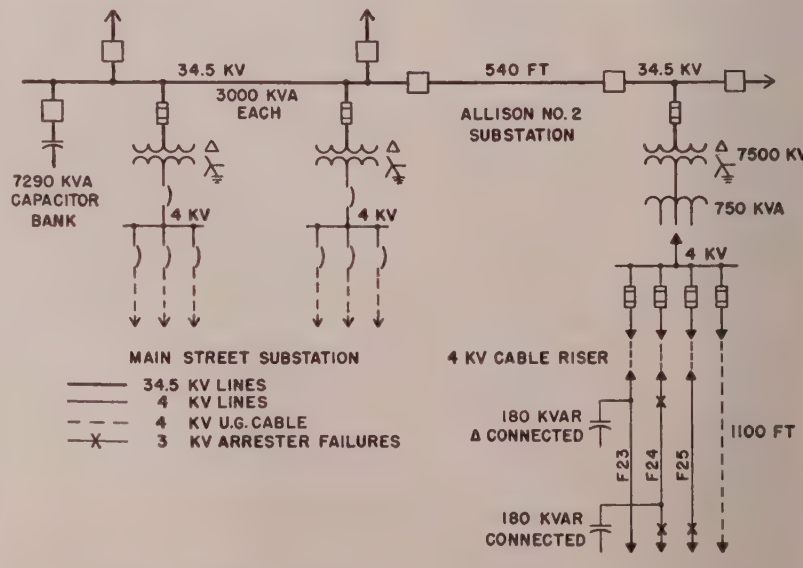

Figure 3. Main Street 7,290-kva capacitor bank and adjacent substations

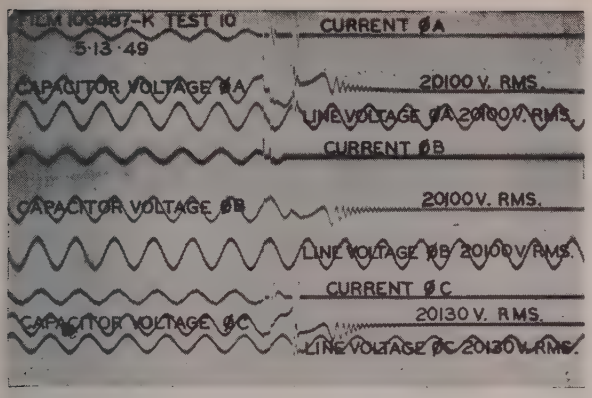

Figure 4. Main Street 34.5-kv bus voltages and capacitor voltages and currents during first lightning arrester failure on 4-kv feeder *F24* off Allison Number 2 substation bus

ing this test the oscillograph recorded the 4-kv bus phase-to-ground voltages at the Main Street substation where no lightning arrester failures were occurring. There was no apparent difference in oscillation frequency of the 34.5-kv and 4-kv bus voltages, and no transient overvoltage on the Main Street substation 4-kv bus.

Test 18 caused failure of the new lightning arrester which had replaced the one destroyed on "c" phase of *F24* during the first day of testing. There was no apparent difference in oscillation frequency of the 34.5-kv and 4-kv bus voltages at the Main Street substation. The maximum 4-kv voltage obtained was 1.5 times normal on "C" phase.

On Test 20 another 3-kv lightning arrester failed on the same feeder *F24*, this time approximately 1,100 feet away from the Allison number 2 substation. The oscillogram, Figure 6, showed that the maximum 4-kv bus voltage at Allison number 2 was 2.7 times normal on "c" phase and the maximum 34.5-kv bus voltage at Main Street was 1.8 times normal on "A" phase. It also showed that the voltage oscillations on the 4-kv bus at Allison number 2 were at a higher frequency and sustained for a longer time than on the 34.5-kv bus.

To study these oscillations a third series of de-energizing operations were made while the Allison plants were closed for vacations. The purpose of these tests was to obtain comparative magnitudes and frequencies of voltage oscillations on the 34.5-kv and 4-kv busses at Main Street, and the 4-kv bus and feeder *F24* at the Allison number 2 substation. Twenty-one oscillograms were obtained

Figure 5. Main Street 34.5-kv bus voltages and capacitor voltages and currents during lightning arrester failure on 4-kv feeder *F25* off Allison Number 2 substation bus

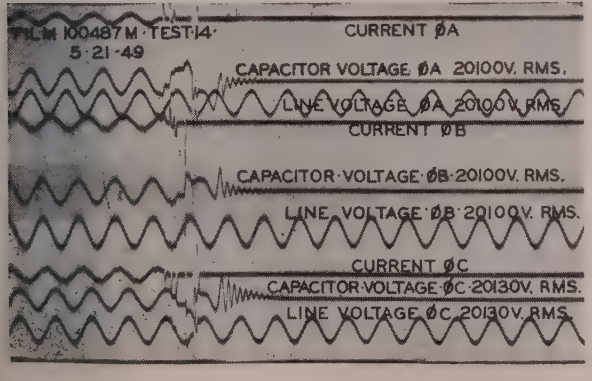

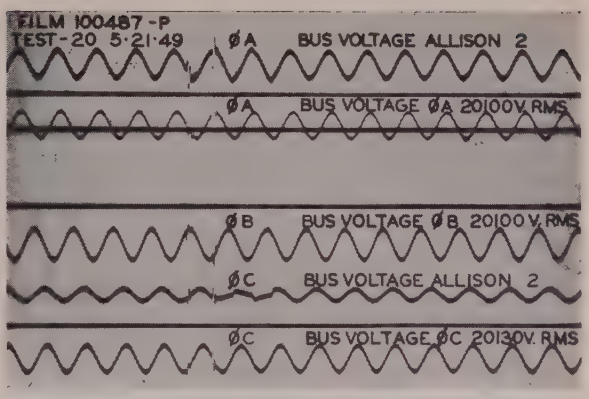
FILM 100487-P
TEST-20 5-21-49
ØA BUS VOLTAGE ALLISON 2
ØA BUS VOLTAGE ØA 20100V. RMS.
ØB BUS VOLTAGE ØB 20100 V. RMS.
ØC BUS VOLTAGE ALLISON 2
ØC BUS VOLTAGE ØC 20130V. RMS.

Figure 6. Main Street 34.5-kv bus voltages and Allison Number 2 4-kv bus voltages showing different transient oscillation frequencies. Lightning arrester failure on *F24* 1,100 feet from Allison Number 2 substation 4-kv bus

and no damage to system equipment occurred. On six tests no reignition or restrike occurred. The system impedance at the Main Street 34.5-kv bus was about 26 per cent on a 100,000-kva base for the first nine of these tests caused by a 34.5-kv line being open for maintenance. For the remaining tests the impedance was about 19 per cent as during earlier tests.

An oscillogram typical of these tests is

Figure 7 (right). Oscillograms showing different transient frequencies on Main Street substation 34.5-kv bus and Allison Number 2 substation 4-kv bus

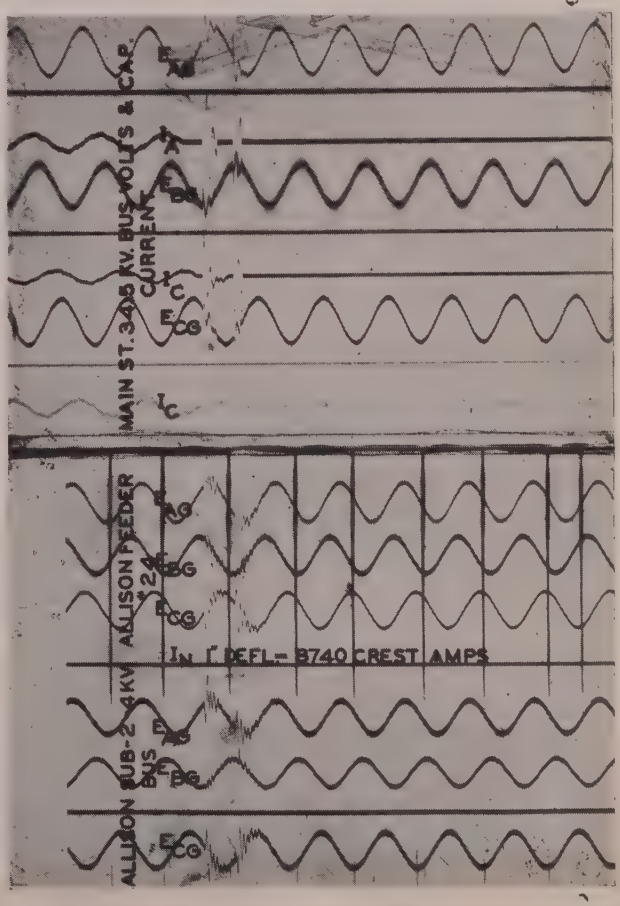

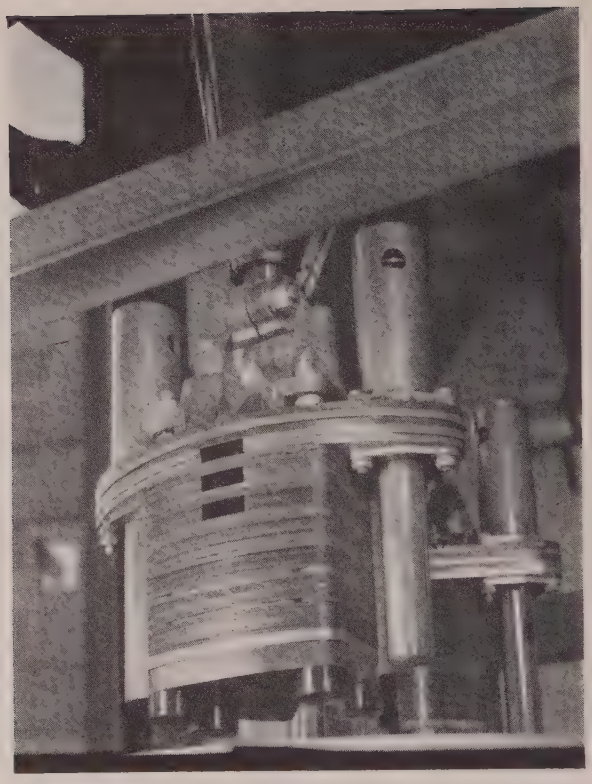

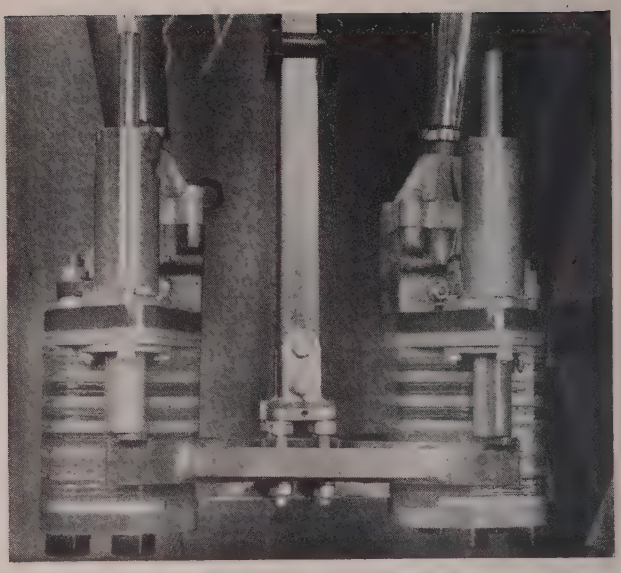

Figure 8 (left). Modified circuit breaker interrupter including oil pistons. Contacts in the open position. Experimental model

Figure 9 (above). Circuit breaker moving contacts showing arms for operating oil pistons. Contacts in the closed position. Experimental model

shown in Figure 7. Analysis of this oscillogram indicated that the 34.5-kv bus voltage oscillation frequency at Main Street was about 660 cycles per second as compared with the Allison number 2 4-kv bus voltage oscillation frequency of approximately 1,130 cycles per second. Other oscillograms indicated that the 34.5-kv bus and 4-kv busses at Main Street substation had voltage oscillations substantially of the same frequency, 480 cycles per second. While the phase-to-ground voltages at the Main Street 34.5-kv and 4-kv busses did not exceed 2.06 times normal, voltages at the Allison Number 2 substation went as high as 2.75 times normal.

This series of tests demonstrated the possibility of a driving voltage surge at one voltage level, such as produced by circuit breaker restriking during capacitor de-energization, setting up relatively greater voltage oscillations at another voltage level under certain conditions of coupling and circuit constants.

Modified Circuit Breaker Design

Since a number of the tests showed it was possible to de-energize the capacitor bank without restriking, the interrupters were studied to determine whether a modification could be made which would give this performance on all tests. The need was for an interrupter which at low currents deionized the arc path and established dielectric strength equal to 2.5 times the crest of the normal line-to-ground value in 0.5 cycle. Such performance already was given by high-voltage circuit breakers with interrupting times of three cycles. These circuit breakers have oil pumps which inject small quantities of oil between the contacts of the interrupter to effect low current interruption. The addition of this feature to the 34.5-kv deion grids was chosen after it and other alternatives were studied in a series of high power laboratory tests at East Pittsburgh.

The high power laboratory circuits were connected to give approximately the same results as obtained on the Indianapolis Power and Light Company system. Voltage was generated at 13.2 kv and stepped up by transformers to 34.5 kv. A circuit breaker switched a 3-phase ungrounded bank of capacitors at this voltage. Connected to the 34.5-kv bus was a bank of power transformers stepping down to 5.2 kv, the nearest step to 4.0 kv. Lightning arresters of the same type used on the 4.0-kv Indianapolis Power and Light Company system were connected to this circuit, the voltage still being within their rating.

To establish that the circuit gave approximately the same results as the circuit at Indianapolis, tests were made with the circuit breaker equipped with the same type of interrupter, and the re-

Table I. Initial 34.5-Kv Capacitor Switching Tests—Analysis of Oscillograms

Test	Type†	Arcing Cycles	Restrikes A	Restrikes B	Restrikes C	Maximum Voltage Capacitors to Gnd A	Maximum Voltage Capacitors to Gnd B	Maximum Voltage Capacitors to Gnd C	Maximum Voltage Bus to Gnd A	Maximum Voltage Bus to Gnd B	Maximum Voltage Bus to Gnd C	Peak Current Times Normal Crest A	Peak Current Times Normal Crest B	Peak Current Times Normal Crest C
1	C					1.0	1.49	1.32	1.0	1.43	1.32*			
2	O	1.64/0.66/1.64	3	0	2	2.86	2.16	2.9 & 3.5	2.35	1.20	1.0			
3	C					1.0	1.53	1.40	1.0	1.52	1.40*	3.4	5.9	8.1
4	O	1.05/0.98/1.05	2	1	1	1.58	1.48	1.86	1.58	1.32	1.46	11.0	8.2	8.6
5	C					1.00	1.40	1.40	1.00	1.34	1.40*	1.9	5.9	8.0
5A	C					1.58	1.00	1.12	1.59	1.00	1.12*	9.0	4.4	4.5
6	O	0.68/0.25/0.68	1	0	1	1.72	1.52	1.68	1.87	1.00	1.24*	14.0	1.0	14.0
7	C					1.38	1.00	1.35	1.30	1.00	1.35*	6.4	1.86	6.45
8	O	1.41/0.23/1.41	3	0	3	2.70	2.30	3.07	1.78	1.00	1.12*	14.2	1.0	14.0
9	O	1.03/0.68/1.03	2	0	1	1.62	1.12	1.80*	1.68	1.14	1.80	14.0	4.2	14.0
10	O	1.11/0.69/1.11	3	1	2	1.73	1.25	1.60	1.87	1.02	1.60	14.0	3.2	14.0

*From capacitor voltage record.

†C = closing capacitor circuit breaker; O = opening capacitor circuit breaker.

Table II. Second Series of 34.5-Kv Capacitor Switching Tests—Analysis of Oscillograms

Test	Type	Arcing Cycles	Restrikes A	B	C	Maximum Voltage Capacitors to Gnd A	B	C	Maximum Voltage Bus to Gnd A	B	C	Peak Current Times Normal Crest A	B	C
12	O	1.08/0.79/1.08	2	0	1	1.60	1.00	1.57	1.60	1.00	1.85	11.0	3.2	11.4
14*	O	1.09/0.74/1.09	3	2	4	1.6~ 2.3	1.79	1.85~ 2.00	2.20	1.23	2.10	11.5	6.4	12.2
												Main St. 4-Kv Voltage		
16	O	0/.25/0.25	0	0	0	1.43	1.63	1.75	1.00	1.00	1.00			
18**	O	1.44/1.12/1.44	4	1	2	2.27	1.32~ 1.37	1.66~ 2.42	2.27*	1.35	1.75	1.22	1.20	1.50
												Allison No. 2 4-Kv Voltage		
20†	O	0.85/0.85/0.85	2	1	2				1.80	1.44	1.57	2.36		2.70

*34.5-kv voltage collapsed "C" phase 59¾ cycles after circuit breaker cleared, "B" phase 62¾ cycles; voltage restored 64 cycles.

**No record of lightning arrester failure on this film.

†4-kv fault after second restrike, on phase "c", cleared in 1½ cycles. Not seen in 34.5-kv records.

sults were similar, even to the prompt destruction of the set of 3-kv lightning arresters. These lightning arresters were replaced with a different kind which did not fail when subjected to the same test. These lightning arresters remained on the 5.2-kv circuit for the remainder of the high power laboratory tests.

Various alternative interrupters were tried to establish their performance on this circuit. The one that gave the best performance was a modification of the deion grid which caused oil to be pumped into the space between contacts. The modified interrupter is shown in Figure 8. The device was prepared for operation by the moving contact charging the cylinders with oil by raising the pistons and compressing the piston driving springs during the closing stroke. On opening, the moving contacts draw the arcs and release the pistons which under action of the springs, force oil under pressure into the arc space to drive out the gases produced by arcing.

The moving contacts were fitted with arms which operated the pistons in the oil pumping devices as shown in Figure 9. The ends of the moving contacts were reduced in cross section so that the arc position was closely determined and the oil passages formed in the upper section of the grid could be brought close to the arc. In that manner only a small quantity of oil needed to be pumped.

The high power laboratory tests with these experimental grids showed that on 21 tests there was only one restrike producing a maximum voltage of 1.9 times normal on both the 34.5-kv bus and the 5.2-kv bus. On 21 tests at 33 kv the circuit breaker restruck once with a maximum 5.2-kv bus voltage of 1.4 times normal crest line-to-ground voltage. On 17 tests at 38 kv, it restruck once with a maximum voltage on the 5.2-kv bus of 2.3 times normal voltage. The circuit breaker also was tested to be sure that it was capable of closing against, and opening the short-circuit kilovolt-amperes it would encounter at 34.5 kv.

A set of interrupters was made to this design and installed on the circuit breaker at the Main Street substation for switching the 34.5-kv capacitor bank.

Final Tests

After installation of these interrupters a final series of 22 de-energizing tests were made with no damage to system equipment. Only one restrike and one reignition occurred in this series of tests. These are shown in the oscillograms of Figure 10 along with a de-energizing test showing no restrikes or reignitions as obtained on all the remaining tests. The maximum voltages produced were 2.1 times normal on the Main Street substation 34.5-kv bus and 1.9 times normal on the Allison Number 2 substation 4-kv bus.

After these tests, the capacitor bank was put into regular operation on the following schedule: Monday through Friday, on at 8:00 a.m. and off at 4:00 p.m.; Saturday, on at 8:00 a.m. and off at 12:00 noon; off on Sundays and holidays. During ten months of operation no damage to system or capacitor equipment has occurred.

Conclusions

This installation of a 34.5-kv 7,290-kva shunt capacitor bank on the Indianapolis Power and Light Company system demonstrated that high-voltage shunt capacitor banks can be switched without exceeding 2.5 times normal phase-to-ground voltage on the bus, a value in the range produced by interruption of short circuit currents.

There may be cases with certain conditions of coupling and circuit constants where restriking during capacitor switching produces surges which cause relatively higher voltages on other inductively coupled circuits.

In these special cases, circuit breakers can be equipped with special interrupters which reduce the overvoltages in both number and magnitude.

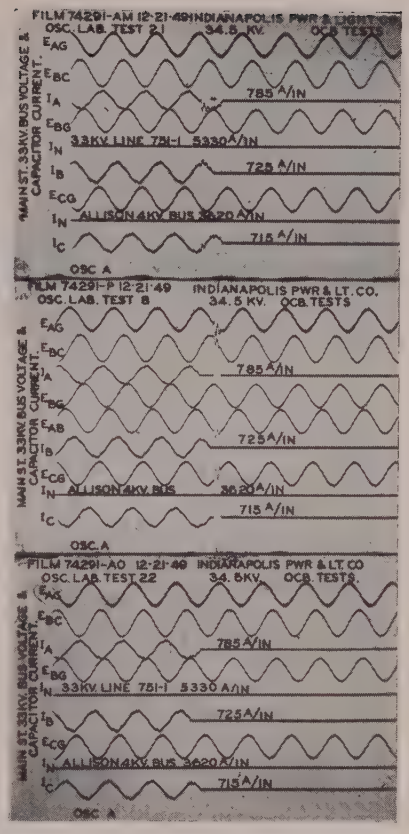
FILM 74291-AM 12-21-49 INDIANAPOLIS PWR & LIGHT CO.
OSC. LAB. TEST 21 34.5 KV. OCB TESTS
MAIN ST. 33KV BUS VOLTAGE & CAPACITOR CURRENT
785 A/IN
33KV LINE 751-I 5330 A/IN
725 A/IN
ALLISON 4KV BUS 3620 A/IN
715 A/IN
OSC A
FILM 74291-P 12-21-49 INDIANAPOLIS PWR & LT. CO.
OSC. LAB. TEST 8 34.5 KV. OCB. TESTS
785 A/IN
725 A/IN
ALLISON 4KV BUS 3620 A/IN
715 A/IN
OSC. A
FILM 74291-AO 12-21-49 INDIANAPOLIS PWR & LT. CO
OSC. LAB. TEST 22 34.5KV. OCB. TESTS.
785 A/IN
33KV LINE 751-I 5330 A/IN
725 A/IN
ALLISON 4KV BUS 3620 A/IN
715 A/IN
OSC A

Figure 10. Oscillograms of field tests made with final interrupter

Test 21, the one reignition
Test 9, the one restrike
Test 22, typical of remaining 20 interruptions

References

1. Capacitor Installation at Newport News. **V. R. Parrack, E. L. Harder.** *AIEE Transactions*, volume 63, 1944, pages 1165–73.

2. Tests and Analysis of Circuit-Breaker Performance When Switching Large Capacitor Banks, **T. W. Schroeder, E. W. Boehne, J. W. Butler.** *Electrical Engineering* (*AIEE Transactions*), volume 61, November 1942, pages 821–30.

3. Power System Overvoltages Produced By Faults and Switching Operations, **AIEE General Systems Committee.** *AIEE Transactions*, volume 67, part II, 1948, pages 912–22.

Discussion

H. A. P. Langstaff (West Penn Power Company, Pittsburgh, Pa.): Congratulations to the authors and others responsible for conducting these tests and presenting the conclusive results, which are of great value to the electrical industry. It would be of considerable interest to know more about the economics of the installation on the Indianapolis Power and Light Company System. I also would like to know what 3-kv lightning arresters were involved.

In November 1945, the West Penn Power Company connected to their 25-kv system one 3,240-reactive-kilovolt-ampere (kvar) bank of outdoor capacitors through an old 37-kv electrically operated manually controlled oil circuit breaker (see Figure 1 of this discussion). The capacitor installation is located on the property of one of our oldest power stations and is connected to one of two 25-kv lines between the power station and an adjacent substation. Restrikes within this circuit breaker when opening caused insulation failures in 1949, one failure being in an insulator on the power station 4-kv bus, the other at a remote point, namely, in the 100-watt lamp sockets in the Laurel Mountain Tunnel of the Pennsylvania Turnpike. After considerable study involving costs for new switching equipment, the problem was solved by eliminating the opening of the capacitor circuit breaker and in its place the 25-kv line is dropped by first opening the oil circuit breaker at the power station, followed by the opening of a 4-contact break Condit circuit breaker at the substation located 10 miles away. Oscillograph tests proved a limited number of restrikes went up to 1.33 times normal voltage after 1/2 of a cycle. This switching arrangement has caused no further disturbance—quite an economical solution to the problem.

In December 1949, two 4,500-kvar capacitor banks were connected to our 44-kv solidly grounded system by means of old-type *FO-40C* 37-kv Condit circuit breaker (see Figures 2 and 3 of this discussion). These are controlled automatically from a voltage relay and have been in service about one year with only one possible insulation failure on the terminal board of a 44-kv transformer. There have been several hundred operations on each circuit breaker.

In December 1950, we connected three 4,950-kvar capacitor banks to the 25-kv system at main substations, using the oil circuit breakers available on the system. A typical installation of these 25-kv capacitors is shown in Figures 4, 5, and 6 of this discussion. Two banks are provided with automatic voltage controls, but the switching is limited by means of a time clock to between 10:00 p.m. and 7:00 a.m. This prevents any tripping with possible restrikes during the day. This control arrangement is proving satisfactory.

Within a period of $2\frac{1}{2}$ months, 18,280 kvar in capacitors were purchased, installed, and placed in service at a cost of $6.44 to $7.72 per reactive kilovolt-ampere, or an average cost of $6.82 per reactive kilovolt-ampere.

Edward Beck (Westinghouse Electric Corporation, East Pittsburgh, Pa.): The paper mentions the transient voltages produced in the 4-kv system as a result of switching the capacitor bank on the 34.5-kv system. These voltages are of interest in the application of lightning arresters to the distribution circuit, as shown by the statement in the paper that lightning arresters on the 4-kv system were damaged. This occurred during the field tests and later during the laboratory tests. The results corroborate the wisdom in high 60-cycle sparkover values for distribution lightning arresters, a practice followed in the design of Autovalve and de-ion lightning arresters for which those lightning arresters sometimes have been criticized. The margin between distribution apparatus insulation and the impulse characteristics of distribution lightning arresters is large, and relatively high values of lightning arrester sparkover are permissible. Thereby the lightning arresters, as well as the apparatus, are safeguarded against damage, because with adequate 60-cycle sparkover the probability of lightning arrester operation on switching transients becomes small. The minimum 60-cycle sparkover of 3-kv Autovalve distribution lightning arresters as manufactured is 9 kv rms. Such lightning arresters rode through the laboratory tests described in the paper without damage.

F. M. Porter and **C. P. Zimmerman** (American Gas and Electric Service Corporation, New York, N. Y.): This paper, covering tests made in connection with one particular high-voltage capacitor bank, provides further data such as outlined in our recent paper.[1] It is hoped that additional data will be accumulated and reported in the future, since the application of capacitors, particularly in banks rated 22 kv and above, is relatively new and several problems in connection with such banks are in need of further solution.

It is noted that in the 7,290-kvar bank discussed in the paper the problem of overvoltage on individual capacitor units caused by the failure of one or more units in a given series group is taken care of by the use of a potential transformer between the neutrals of two Y-connected sections. This transformer energizes a voltage relay and measures the shift in the neutral voltage caused by an unbalance in the number of capacitors per phase. It would be interesting for the authors to give the sensitivity of this relaying scheme, particularly the magnitude of the unbalance voltage used for relaying. Were any tests made to verify the performance of this relaying scheme, such as deliberately disconnecting capacitor units?

It originally was decided to utilize on our capacitor banks a current transformer between the bank neutral and ground; however, in practically every case in which this was tried, third harmonic currents from 3.5 to 26 amperes were encountered, which prevented the use of standard overcurrent relays. Consequently, it is our practice now to split the banks wherever possible into two Y-connected sections, utilizing a current transformer between the two neutrals. Splitting the capacitor bank into two Y sections, however, doubles the minimum size of bank that can be protected satisfactorily against overvoltage on individual units. Since it appears, therefore, that it will be necessary to resort to single Y-connected banks in some cases, a practical relay scheme

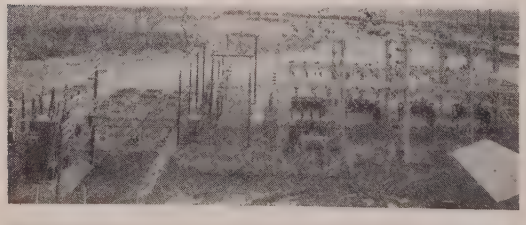

Figure 1 (left).

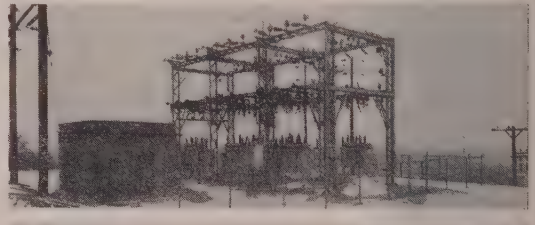

Figure 3 (right).

Figure 2 (left).

Figure 4 (right).

Figure 5 (left).

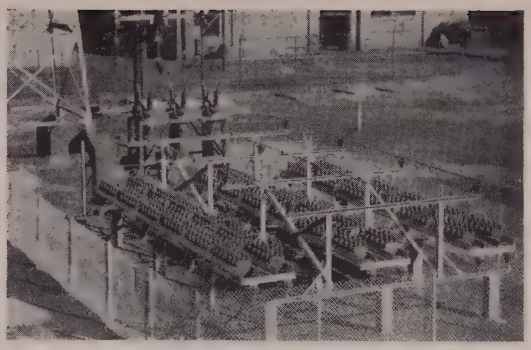

Figure 6 (right).

not affected by third harmonic currents will have to be developed. Several possible schemes are now being investigated.

The modification of the 33-kv circuit breaker mentioned in the paper was made necessary because 3-kv lightning arresters failed at several stations connected to the same system. It would be interesting to know the type of lightning arresters that failed and those which were finally installed. These failures could have been due either to excessive voltages beyond the lightning arrester rating, which were caused by restrikes permitted by the circuit breaker, or to discharge currents from the capacitor bank in excess of those which the lightning arresters were capable of dissipating. We wonder if the authors obtained any information which substantiates the actual cause of the lightning arrester failures. We presume that these failures were not caused by transient overvoltage conditions established by re-energizing the capacitors too soon after they were de-energized. We have experienced a few lightning arrester failures attributed to such switching, but after the operators were cautioned to take a minimum period of $1^1/_2$ minutes before re-energizing a capacitor bank or during circuit breaker tests to open the disconnect switches between the bus and the capacitor circuit breaker, no further lightning arrester failures have been reported.

All of the high-voltage capacitor banks on the American Gas and Electric Company System are mounted on steel racks using outdoor-type capacitors, because this appeared to be the most economical in cost and space required. It would be interesting to learn the cost per kilovolt ampere (including the circuit breaker) of the cabinet-type arrangement used by the authors and to learn the reason why they decided to use this type of arrangement in preference to a completely outdoor setup.

Apparently, in considering the modification of the circuit breaker to limit the overvoltages, the use of resistors also was taken into account, but was finally given up in favor of an oil piston. Was there any difference in the magnitude of overvoltages permitted by either type of modified interrupter, and for what particular reasons was the oil piston decided on? This point is quite interesting to us because 12 of the 13 34.5- and 46-kv oil circuit breakers which we have in service controlling 33- and 44-kv capacitor banks have resistors, and no difficulties with restrikes or overvoltages have been reported as yet after a year or more of operation. It might be mentioned, in passing, that we have had a standard 34.5-kv circuit breaker without resistors controlling a 3,075-kvar 22-kv capacitor bank for a period of 21 months to date with no troubles encountered.

One of the phases of switching high-voltage capacitor banks that we feel has not been ascertained too definitely is the frequency at which the oil circuit breakers must repetitively switch capacitor banks, particularly those under time-clock or voltage control and how often the circuit breakers must be inspected to determine the condition of their oil and contacts. Our 34.5-kv circuit breakers have averaged 500 operations to date and still appear to be in good condition. Just how far the inspection period can be extended is difficult to say at this time. Perhaps the authors can report on their experience in this regard.

REFERENCE

1. Application of Shunt Capacitors at Transmission and Distribution Stations, **F. M. Porter, C. P. Zimmerman.** *AIEE Transactions*, volume 70, part I, 1951, pages 112–20.

N. E. Dillow (General Electric Company, Schenectady, N. Y.): The authors are to be commended for reporting the investigation which showed that a voltage surge at one voltage level produced by capacitor switching can set up relatively greater voltage oscillations at another voltage level under certain conditions of coupling and circuit constants.

However, certain comments can be emphasized on the experience observed on this installation of a 34.5-kv, 7,290-kvar shunt capacitor bank. The experience indicates that a limitation does exist in the size of the capacitor bank which can be switched satisfactorily by a standard circuit breaker. It is of interest to note that the bank size is much smaller than is being considered by certain industry groups as within the reasonable capacitor-switching range for power circuit breakers.

Furthermore, the modified circuit breaker using an auxiliary device to pump oil into the space between the contacts did reduce the number of restrikes, but did not entirely eliminate restrikes and reignitions. It is not to be inferred that it is felt that the elimination of restrikes is a necessary criterion for satisfactory operation. A rational criterion for satisfactory circuit breaker operation is that the phase-to-ground voltage on circuit opening does not exceed the theoretical phase-to-ground voltage on circuit closing. Re-establishment of the arc may be permitted during circuit interruption provided this voltage limit is not exceeded. It should be noted that a limited number of restrikes and/or reignitions of the arc during circuit interruption are not of themselves detrimental unless excessive voltages accompany the phenomena. If it can be demonstrated that the voltage on circuit interruption can be held to a reasonable limit, such as established by the preceding criterion, then satisfactory performance can be obtained.

E. B. Rietz and **C. J. Balentine** (General Electric Company, Philadelphia, Pa.): This paper covers an application field similar to that described by Messrs. F. M. Porter and C. P. Zimmerman in their recent paper.[1] The solution used by the authors is similar to that of high-voltage impulse circuit breakers except that with these circuit breakers the mechanically driven oil piston moves enough oil to prevent restriking entirely. We know that an oil piston can be made to do a good job of interrupting capacitive currents.

However, it is interesting to call to your attention the results that can be obtained by providing a shunting resistor with practically standard interrupter units to do this job. As is well known, these resistor units have been used for a number of years on high-voltage circuit breakers to assist in the interruption of line-charging currents, and during the last several years wide use has been made of this same principle to provide proper circuit breakers in the 15 to 69 kv classes for switching of capacitor banks. Our criterion for the successful operation of these resistor units has been a voltage limit of not more than two times normal instead of the 2.5 times referred to in this paper. The many tests that have been made on resistor-equipped circuit breakers indicate that this is possible without hazarding any of the excellent interrupting performance characteristics of oil-blast interrupters. We feel that for the general run of tank-type circuit breakers, resistor units provide a rather inexpensive and effective means to obtain satisfactory switching ability.

In this connection, resistor-equipped circuit breakers are considered suitable for switching capacitor banks up to at least 30,000 kva in the voltage classes of 15 to 69 kv. The performance demonstrated on the equipment described in this paper certainly gives no indication of what could be expected on banks of such ratings.

REFERENCE

1. See reference 1 of F. M. Porter and C. P. Zimmerman's discussion of the present paper.

Alexander Dovjikov (Bonneville Power Administration, Portland, Oreg.): We were familiar with the overvoltages produced during interruption of line-charging currents

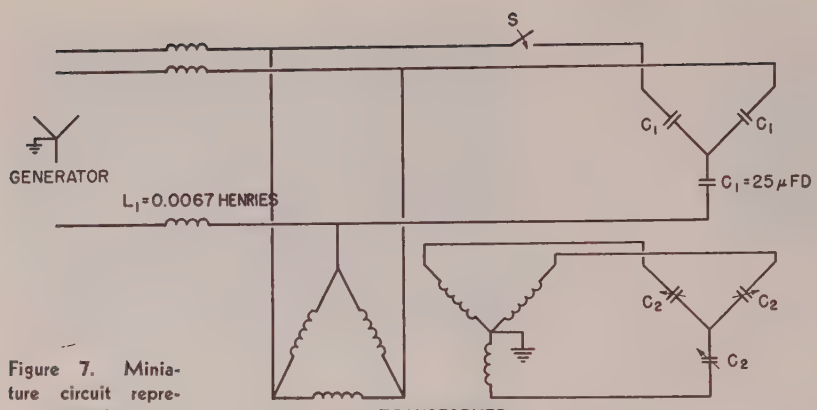

Figure 7. Miniature circuit representation

on our long 230-kv lines, and our specifications for the line circuit breaker permitted not more than one restrike. In preparing specifications for large shunt capacitor bank circuit breakers we were even more cognizant of the effects of overvoltages that may be produced by the restrikes in the circuit breakers, and the following is a paragraph of our specification for 115-kv circuit breakers for switching 15,000-kva 115-kv capacitor banks. Defining a restrike as "any current conduction between breaker contacts following an interval of zero current of 1/8 cycle or more in duration," the specification permits "not more than two restrikes per interruption and with no restrike between contacts following any interval of one-quarter cycle or more during which current is zero." A similar requirement is in our specification for circuit breakers switching 13.8-kv large capacitor banks.

In our previous staged field tests of switching lines and capacitor banks, we usually recorded oscillographically the voltage on the bus and on lines and capacitors during switching period, and our observed values of overvoltages correspond to those of the authors of this paper. As the values measured were below the insulation strength, either of the bus or of any switched equipment, we always had difficulty in proving to manufacturers of circuit breakers that the restrikes may be harmful to the system. Because of the lack of a sufficient amount of appropriate recording devices we could not prove by direct measurements the well-based suspicion (which was proved by the authors of the paper if not by measurements then by destruction of lightning arresters) that "a voltage surge at one voltage level produced by capacitor switching can set up relatively greater voltage oscillation at another voltage level under certain conditions of coupling and circuit constants." As these "conditions" are very difficult to precalculate and would change as fast as the system itself, we believe in elimination not of these conditions (which we could not discover and eliminate anyhow), but of the source of overvoltage, that is, elimination of restrikes in the circuit breakers opening capacitive currents—whether of static capacitors or of long high-voltage lines.

We hope that the experience of the authors may stimulate further development in the art of circuit breaker design—we hope in the direction of the compressed air circuit breaker—and for voltages not only of 13.8 kv, but higher.

I. B. Johnson and **J. R. Stevenson** (General Electric Company, Schenectady, N. Y.): Although perhaps dealing with rarities, the field experience and data presented in this paper on relatively greater voltage oscillations being produced at one voltage level compared with those at another voltage where a capacitor bank was being switched are of interest and significance in system design. That these phenomena are a function of certain circuit constant relationships and circuit configurations as stated by the authors also was demonstrated in a transient analyzer study on an idealized miniature system.[1,2]

In Figure 7 of this discussion is shown the miniature circuit studied. This circuit was considered to simulate approximately the essential circuit elements involved in the field system experience. The ungrounded Y capacitor bank, C_1, is being switched through same system reactance, L_1. Connected to the capacitor bank C_1 on the source side of the switch S is another capacitor bank, C_2 (possibly at another voltage level) through a delta-Y transformer bank. The delta-Y transformer bank is composed of miniature single-phase 1 to 1 transformers and the through 60-cycle reactance of one of the single-phase transformers is 18 ohms at 60 cycles. The values chosen for L_1 and C_1 in one series of tests are shown in Figure 7 of this discussion, while C_2 was varied.

Figure 8 of this discussion shows the voltages recorded as a function of the capacitance C_2 when one phase interrupts the charging current to one leg of the capacitor bank C_1 and then restrikes, keeping the other phases closed. The instant of restriking was adjusted to produce maximum transient voltage on the Y side of the transformer. The corresponding voltages are given in per unit of normal line-to-ground voltage on the delta side of the transformer and in per unit of normal line-to-neutral voltage on the Y side of the transformer. It is seen, then, that for a critical range of values of C_2 the line-to-ground voltages in per unit on the Y side of the transformer are appreciably greater than those on the delta side. For example, with $C_2 = 0.3$ microfarad, the per unit values are 3.7 and 2.3, respectively.

Other studies on the transient analyzer in which C_1 was varied and in which the switch S was closed to energize the open capacitor leg without restriking indicated:

1. Peak transient voltages across C_2 or from line to ground on the Y side of the transformer occurred for approximately the same ratios of C_1 to C_2 where C_1 is appreciably greater than C_2.

2. The peak transient voltages increased as C_1 was decreased, so that for $C_1 = 4$ microfarads the line-to-ground voltage on the Y side of the transformer was 3.75 as compared with 2.7 with $C_1 = 25$ microfarads.

It is to be mentioned that the possible damping effects of any load were not included in any of the studies.

Thus, for these special cases, there is an increased desirability in using circuit breakers equipped to reduce or keep to a minimum value the overvoltages that may result upon switching capacitors which are playing an ever-increasing part in power system design and operation.

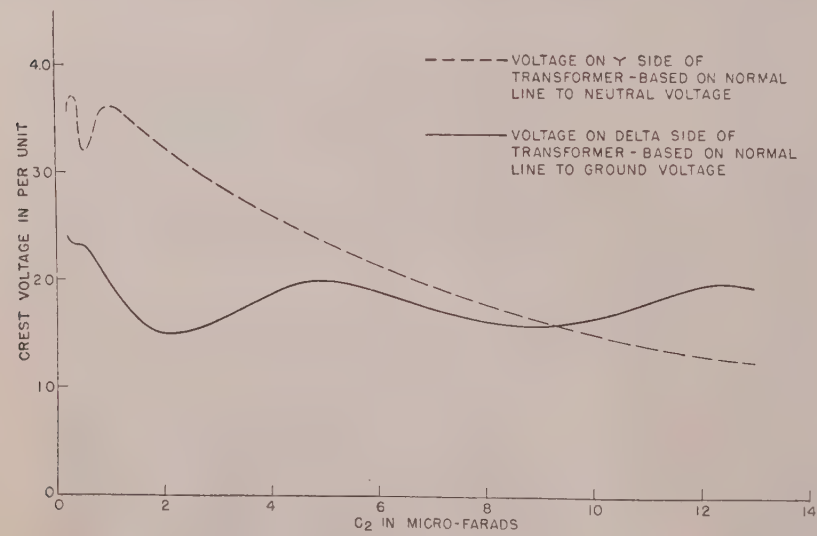

Figure 8. Maximum voltage across C_2 for one restrike versus magnitude of C_2

References

1. An Electric Circuit Transient Analyzer, **H. A. Peterson.** *General Electric Review* (Schenectady, N. Y.), volume 42, September 1939, pages 394–400.

2. Magnification of Switching Overvoltages in Coupled Oscillatory Circuits, **I. B. Johnson,**

John Berdy. *General Electric Review* (Schenectady, N. Y.), volume 53, December 1950, pages 22–24.

A. W. Funkhouser, R. C. Van Sickle, and **D. F. Shankle:** The authors are grateful to the discussers of this paper for their contributions of additional operating experience and opinions on the subject of switching high-voltage shunt capacitor banks. The discussions indicate some variation of opinion as to the type of switching equipment to use, as well as the magnitude of overvoltage to allow during switching.

Mr. H. A. P. Langstaff's discussion was most interesting and informative. By the use of circuit breakers of older design and proper sequence of system switching, he has been able to utilize circuit breakers available on his system. However, his experience does indicate the existence of some hazardous circuits, as shown by the 100-watt lamp failures in the Laurel Mountain Tunnel, the flashover of the terminal board of a 44-kv transformer, and the 4-kv insulator flashover at the power station. As to the economics of the Indianapolis Power and Light Company capacitor installation requested by Mr. Langstaff, the capacitors cost approximately $7.00 per reactive kilovolt-ampere, and the circuit breaker cost approximately $1.20 per reactive kilovolt ampere, or a total of $8.20 per reactive kilovolt-ampere for the circuit breaker and capacitors. Including supervisory, relaying, and installation charges, the total cost was $11.15 per reactive kilovolt-ampere. Using a larger bank with the circuit breaker would have reduced the circuit breaker cost per reactive kilovolt-ampere. The metal enclosures for the bank were used because of limited installation space and for safety to personnel working in the substation on other equipment.

Mr. Langstaff also requested the type of 3-kv lightning arresters involved in the failures associated with the switching of the Indianapolis capacitor bank. The lightning arresters were of the pellet type characterized by low 60-cycle sparkover voltage. The damaged lightning arresters were replaced by duplicate lightning arresters of the same manufacture and were not damaged when tests were made with the 34.5-kv oil circuit breaker modified by auxiliary oil pistons. It is of interest that lightning arresters made by three different manufacturers were located on the two 4-kv feeders and the 4-kv bus of the Allison number 2 substation. The pellet type was the only one failing. The discussion of Mr. Edward Beck indicates the possibility of forestalling some lightning arrester operations by the use of lightning arresters with higher 60-cycle sparkover voltages.

The discussion presented by Messrs. F. M. Porter and C. P. Zimmerman also is of interest because of the difficulties experienced with capacitor banks having their neutrals grounded. In order to eliminate the possibilities of third harmonic currents and possible telephone interference, the capacitor bank at Indianapolis was designed for ungrounded neutral operation. This also permitted the use of potential transformers between the neutrals of the bank for detecting neutral displacement and overvoltage on individual 15-kva capacitor units.

The magnitude of unbalance voltage used for relaying is as follows: 1 unit out, 2.0 volts; 2 units out, 5.2 volts; 3 units out, 9.2 volts; 4 units out, 12.0 volts. The relay was set to operate on 4 volts when 2 units were removed from a group of paralleled units to limit the overvoltage on the remaining 15-kva units to 9.5 per cent. The performance of the relaying scheme was determined by deliberately disconnecting capacitor units and measuring the voltage across the relays. These values checked calculated values very closely.

The manufacturing tolerance on the individual units permit a variation of -0 per cent to $+15$ per cent above their rated capacitances. In the case of the Indianapolis bank, a large number of the units with larger than average capacitance were installed in one phase of one of the 2,430-kva assemblies. This at first caused unbalanced voltages to appear between neutrals and resulted in relay operation when only one 15-kva unit was removed. The impedance of each parallel group in all phases of the three assemblies then was measured accurately, and by permanently removing one unit from a group having higher than average capacitance, the normal voltage unbalance between neutrals was corrected to approximately 0.2 volt. This difficulty should not occur on most installations because the units of highest capacitance normally will be well distributed among the other units in all three phases.

To answer the question of Messrs. Porter and Zimmerman as to why the oil piston instead of a resistor was chosen to modify the interrupter, the high-power laboratory tests showed the oil piston not only produced somewhat lower overvoltages than the resistor, but also reduced restriking to a negligible amount, such as one restrike in 21 opening operations at 34.5 kv. With the existence of a coupled 4-kv circuit that might magnify overvoltages produced by capacitor switching the authors believed a circuit breaker that would not only limit the overvoltage to the lowest value but also reduce the number of such overvoltages would reduce the possibility of lightning arrester failure to a minimum and would provide the best over-all performance for the Indianapolis installation. It is interesting to note that Messrs. Porter and Zimmerman have a standard 34.5-kv circuit breaker without a resistor controlling a 3,075-kva 22-kv capacitor bank and have had no trouble for a 21-month period of operation. Perhaps this has been possible because no coupled circuits of the proper constants exist on their system at the present time that magnify the transient overvoltages produced by capacitor switching.

Messrs. Porter and Zimmerman also requested our experience in connection with repetitive operation of the capacitor circuit breaker. Immediately after the final series of tests, the circuit breaker was opened and there was no sign of oil deterioration or contact pitting. As of March 2, 1951, the circuit breaker was still operating on the same schedule as given in the paper, with a total of 630 openings up to that time. However, the circuit breaker had not been opened for further inspection as of that date. On January 29, 1951, the first capacitor unit failure was discovered after a voltage balance reading indicated a change in balance. These voltage readings are taken daily. The capacitor fuse on the failed unit had functioned, but did not indicate; a swelling of the case gave visible indication of the unit in trouble.

The discussions presented by Mr. N. E. Dillow, and by Messrs. E. B. Rietz and C. J. Balentine suggested a criterion of 2.0 times normal voltage, which is met by applying special resistor-equipped circuit breakers for all applications. This is about 20 per cent lower than the maximum found with standard circuit breakers. Perhaps this small improvement is all that is required in most cases. The use of a resistor was not selected in this case because when resistors of suitable values were added to standard interrupters, the number of tests on which restriking occurred increased 60 per cent and because our first lightning arrester failure happened when the oscillograms indicated a maximum bus voltage of only 1.87 times normal (test 10, Table I of the paper).

Switching of Distribution Capacitors by Manual and Automatic Devices

R. J. HOPKINS
ASSOCIATE AIEE

N. R. SCHULTZ
MEMBER AIEE

ALL power factor capacitors are switched occasionally, even the so-called "permanently connected" units which are installed so that normal operation is continuous. Switching operations vary in nature from exceedingly rare switching of "permanently connected" capacitors for inspection or maintenance to frequent, often several times daily, switching of automatically controlled equipments.

It is well recognized that the major portion of base or unregulated system reactive kilovolt-amperes (kvars) can be most economically supplied by "unswitched" or "permanently connected" capacitors. In order to secure maximum benefits in terms of voltage improvement, loss reduction, and released power system capacity, such shunt capacitor banks are usually located on the distribution system as near to the load as practicable.

Typical of such installations are the small capacitor banks located on primary distribution feeders. In these cases, short-circuit protection in case of capacitor failure and a means of switching can be provided by the use of suitably rated fused cutouts. Use of fused cutouts for occasional manual switching of capacitor banks is discussed later in this paper.

Basically the requirement for switching of shunt capacitor banks arises when the kvar supply at time of peak system load exceeds the desirable supply at time of light load. Broadly the kvars of capacitors to be switched are the difference between peak and minimum load requirements.

The amount of unswitched capacitors which can be applied to a system is limited by the following general considerations:

1. Unswitched capacitors should not be applied to the extent that intolerably high voltage levels exist at time of minimum load.

2. The amount of unswitched capacitors should not be such that system generators will be operated with unduly low excitation from the viewpoint of stability at time of light load.

Since the peak-load kvar requirements of many systems may be two to three times the minimum kvar requirement, use of switched capacitors to follow the system kvar load pattern has become a common practice.

In addition to the foregoing broad classification, switched capacitors are also often employed in specific applications for the purpose of regulating voltage or kvars, and as such are often controlled automatically where manual switching may be inconvenient or unreliable. Automatic switching also is used occasionally to prevent overvoltage or undue losses during periods of light system load, or when load is suddenly lost, or to provide a voltage boost during time of low voltage caused by a system disturbance.

Application and Technical Aspects

De-energizing Problem

The problem of interruption of capacitive current has been the subject of several technical papers.[1] A brief description of the phenomena associated with interruption of capacitive current is included herewith for the sake of completeness.

A simplified single-phase circuit, Figure 1(A), can be used to illustrate the basic problem of interruption. It is ordinarily assumed that current interruption will take place at the first normal "current zero" following separation of the switch contacts. In a capacitive circuit this corresponds to a maximum or crest value of system voltage as shown in Figure 1(B). At the instant of interruption, the voltage across the switch is zero since the capacitor on one side of the switch holds the same crest voltage that existed just prior to interrupting. Since no initial voltage appears across the switch any circuit breaker or switch will interrupt quite easily at the first current zero following contact separation. However, as shown in Figure 1(B), following interruption, voltage begins to appear across the switch due to the alternating system voltage until it reaches a value of twice normal crest voltage just one-half cycle following interruption.

If the switch successfully withstands this double voltage without restriking, the interruption can be termed successful. If, however, the switch restrikes at or near the time of double voltage, the capacitor voltage can reach a value of approximately three times normal crest value. It is theoretically possible to compound successive clearings and restrikes in such a manner as to yield circuit voltages of many times normal value. However, extensive field tests by other investigators have shown that overvoltages due to restriking seldom, if ever, exceed three times normal voltage. For further detailed analysis of this phenomenon, refer to reference 1.

The preceding brief description of capacitive current interruption should be adequate to illustrate the point that the interrupting capacity of circuit breakers and other switches on capacitive circuits may be limited in comparison to the rating assigned for "normal" load or short-circuit current interruption. It should be emphasized that capacitive current interrupting limitations are usually assigned on the basis of limiting

Paper 51-19, recommended by the AIEE Transmission and Distribution Committee and approved by the AIEE Technical Program Committee for presentation at the AIEE Winter General Meeting, New York, N. Y., January 22–26, 1951. Manuscript submitted October 23, 1950; made available for printing November 17, 1950.

R. J. Hopkins is with the General Electric Company at Pittsfield, Mass., and N. R. Schultz is with General Electric Company at Schenectady, N. Y.

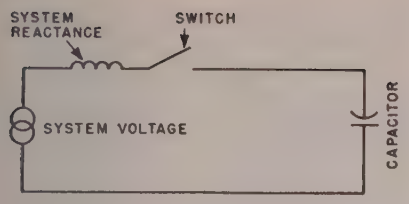

Figure 1(A) (left). Simplified single-phase circuit

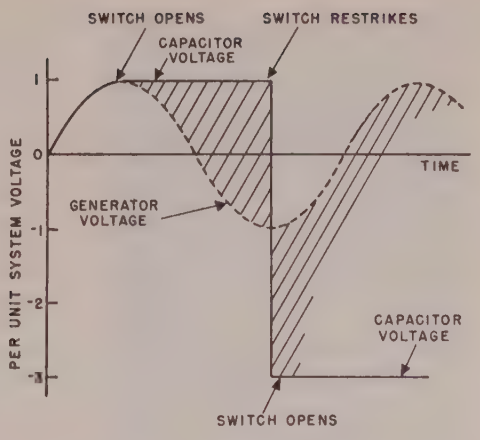

Figure 1(B) (right). Voltage appearing across switch contacts during opening of circuit to a capacitor bank

Height of shaded area at any time represents switch voltage

transient overvoltages to approximately twice normal voltage. Such limitations are not usually indicative of the ability of the switch or circuit breaker to eventually clear the capacitive circuit.

Practically speaking, many types of circuit breakers and switches are commercially available for switching capacitive current. Their ratings and suitability for this type of service have been determined by experience and comprehensive tests.

Energizing Problem

It has been shown that the inrush current to a capacitor bank is a function of the bank rating and available system short-circuit current.[2] Generally this transient inrush current is of very short duration being highly damped by inherent circuit resistance, and has a frequency many times greater than normal system frequency. Experience on nearly every type of capacitor switch has indicated that inrush currents associated with capacitor banks are not harmful to the switches and do not constitute a problem.

Proper Switch Selection

In selecting switches for capacitor banks, the subsequent requirements should be met.

Voltage Rating

The voltage rating of the switching device must be equal to or greater than the normal voltage of the circuit to which the equipment is to be connected. Both the 60-cycle potential test and impulse voltage test levels of the switch should be consistent with those of other apparatus in the same voltage class.

Continuous Current Rating

The continuous current rating of the switching device should be at least 135 per cent of rated capacitor bank current in accordance with section 4.12 of NEMA Standard CA1-1949[3] for shunt capacitors. Capacitor bank currents may exceed rated or nameplate values because of the plus manufacturing tolerance on the capacity of individual units and because of the possibility of overvoltage and harmonic current flow. The 35 per cent allowance factors in these considerations.

Interrupting Rating

If the switching device is used as a means of short-circuit protection in addition to its duty as a capacitor switch, it must, of course, have an interrupting rating adequate to handle short-circuits occurring in the equipment on the capacitor side of the switch.

In any event, whether the switching device is used for short-circuit protection or not, it must be able to interrupt the normal capacitor current without excessive transient overvoltages due to restriking.

If the switching device has no short-circuit interrupting rating of its own, protection against short circuits in the capacitor bank must be provided by other means. Capacitor units may be fused individually, or in groups. Or the entire capacitor bank and bus work may be protected by line fuses, cutouts, or circuit breakers of adequate interrupting rating.

When applying fuses, it is necessary to limit the fuse link size so that should failure of an individual capacitor unit occur, that unit will be promptly removed from the circuit. The fuses used should have total clearing times no greater than those of curve 2, Figure 2. Figure 2[4,5] shows the characteristic of current versus time for an internally short-circuited capacitor unit to rupture due to gas pressure after an internal failure occurs. Attention also should be given, of course, to the co-ordination of these individual fuses with any sectionalizing fuses which may be present on the circuit.

Momentary Current Rating

The switching device must have sufficient momentary current rating to adequately withstand system short-circuit currents for faults at its terminals. This consideration must be met even though the device is not used as a means of short-circuit protection.

Frequency of Operation

The mechanical and electrical design of the switching device should be such that it will withstand a reasonable number of operations without undue maintenance. This may require special con-

Figure 2. Current versus timefor a short-circuited capacitor unit to rupture due to gas pressure after an internal short-circuit occurs

Area below curve 1 is safe with no damage other than slight swelling expected. Area above curve 2 is unsafe. Rupture will occur frequently with possible damage to adjacent capacitors. Area between curves is region of doubtful operation. Slight case rupture and cracked bushings may occur

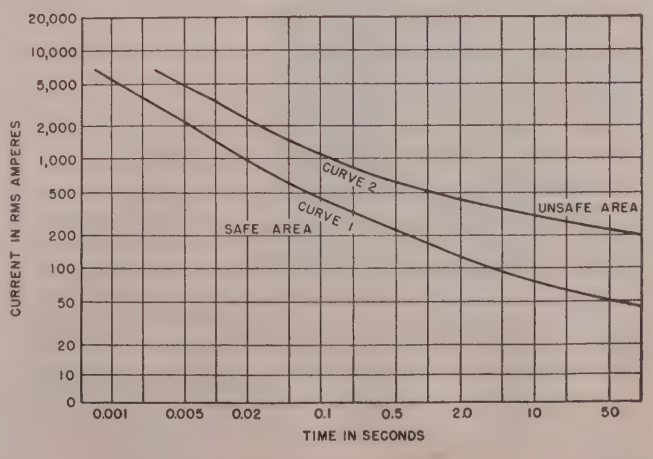

Figure 3. A typical application of three 5,200-volt 100-ampere cutouts on a 300-kvar 4,160-volt capacitor bank

sideration in some cases involving a number of switching operations each day.

Switching devices fall into several distinct types depending on whether they are to be manually operated or are to be actuated by automatic control devices.

Manual switching devices are usually used where switching is infrequent and the cost of electrically operated devices cannot be justified.

Electrically operated and/or automatically controlled switches are used where frequent operation, up to several times a day is required. These devices fall into further subdivisions depending on the short-circuit capacity of the system, the length of life required without

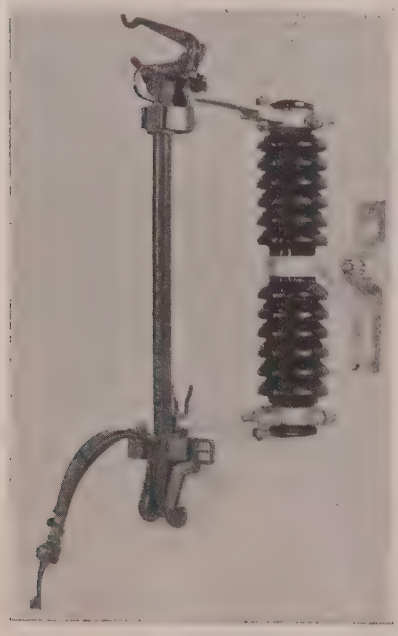

Figure 4. Fused disconnect switch rated 100 amperes, 15,000 volts

maintenance, and the capacitor bank sizes to be switched.

All of these classes of switches will be discussed in more detail in following sections.

Manual Switching of Capacitors

The device most commonly used for manual switching of capacitors is the fused cutout. This device also provides short-circuit protection for the capacitor installation within the limits of the relatively low interrupting ratings of these devices.

The successful switching of capacitors with air break devices such as fused cutouts depends to a considerable extent on the experience and technique of the operator, and the speed of opening. Until recently, published tables of capacitor bank sizes that could be switched by various cutouts were extremely conservative, judged by information from various utilities

In order to obtain more factual data on switching of capacitors with cutouts, a series of tests was recently made by the company with which the authors are associated to determine the actual limiting current that the various cutouts can open successfully. Tests were made on all of the various types of open and enclosed nonrepeating cutouts manufactured by this company.

All tests were made on a single-phase circuit, indoors in still air. Cutouts were opened manually. As criteria for successful switching it was decided that the particular current must be opened on ten out of ten trials, with the resulting arc rising not more than one foot above the cutout. Capacitor bank sizes were increased 25 kvar at a time until a current was reached which could not be successfully switched.

From results of these tests, Table I was compiled. This table gives the 3-phase capacitor kvar which can be switched under the conditions stated, for all the common types of nonrepeating cutouts. Operating experience may indicate that experienced operators can successfully switch larger bank sizes. During the tests, open-type cutouts successfully switched larger capacitor banks but with a considerably greater rise of the arc above the cutout. Thus, in locations where there are no circuits or other limiting structures above the cutouts, open-type cutouts could be used to switch larger banks of capacitors than shown in the table.

All of the cutouts listed have current carrying capacities double those listed under "rating" if a disconnect blade is

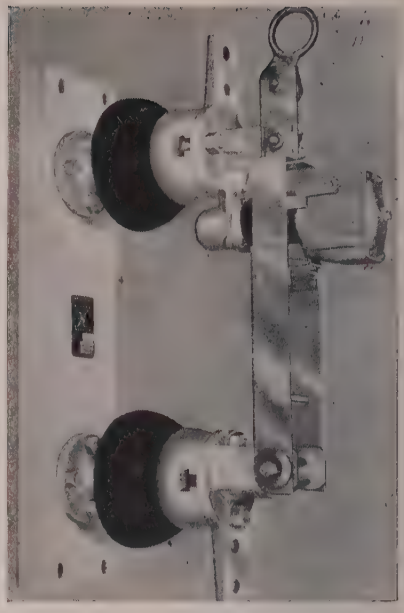

Figure 5. Disconnect switch rated 400 amperes, 15,000 volts, with special arc interrupting chamber

substituted for the fuse holder. With disconnect blades, larger banks than those given in Table I can be switched at 2,400-volts delta and 4,160-volts grounded Y by enclosed cutouts only as tabulated below. In these cases individual capacitors should be fused to protect against shortcircuits that might occur at the instant of switching and cause a hazard to the operator.

Voltage	3-Phase Kvar
2,400 volts delta	375
4,160 volts grd. Y	650

In compiling Table 1, certain rules were observed which are indicated below.

1. Fuse link sizes are limited to 50 amperes (N) for 50 ampere cutouts. For the 100- and 200-ampere cutouts, the fuse link rating is limited to 75 amperes (N) to avoid bursting a capacitor container in case of failure of a capacitor. These fuse link ratings are at least 165 per cent of the normal rated capacitor current as recommended by the NEMA standards for shunt capacitors.[3]

2. Where the maximum current switching ability is less than the maximum fuse sizes as determined in (1) above, the capacitor bank size was determined by making an allowance for overloads due to voltage, harmonics and over capacity encountered under average operating conditions.

A typical installation of pole mounted

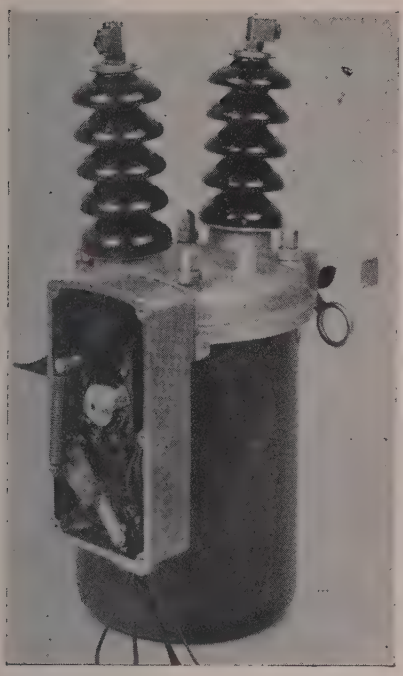

Figure 6. Type *GR* single-phase oil switch rated 100 amperes, 15,000 volts. View showing operating mechanism

capacitors, protected by enclosed cutouts is shown in Figure 3.

Also available from various manufacturers are a number of types of air break switches which may be used for manual switching of capacitors. Typical of these devices are those shown in Figures 4 and 5.

Figure 4 shows a fused disconnect switch, available in ratings of 100 amperes at either 7,500 or 15,000 volts. The upper end of the fuse link is held by a trip mechanism at the upper end of the fuse tube. When it is desired to disconnect the capacitor bank the trip lever at the upper end of the fuse tube is tripped by means of a switch stick. This releases the fuse link which is pulled out of the fuse tube by spring tension. The resulting arc is extinguished inside the expulsion tube. To return the bank to service, the entire expulsion tube is removed, refused with the same link, and the circuit closed by replacing the expulsion tube.

Tests have shown this device to be capable of interrupting 100 amperes at 15,000 volts without restrikes. As stated before, the maximum fuse link size should be no greater than the equivalent of curve 2 of Figure 2. This corresponds to the characteristics of a 75-ampere (*N*) cable-type, fast-blowing fuse link manufactured by the General Electric Company. Otherwise protection from case bursting in the event of a capacitor failure must be provided by other fuses.

Figure 5 shows a disconnect switch with a special arc interrupting chamber. The manufacturer's tests indicate that this device will interrupt 400 amperes capacitor current at 15,000 volts without restrikes.

The expulsion tube in the arc interrupter must be replaced after the number of operations given below.

Amperes Switched	Operations
400	25
200	50
100	100

With this device also, short-circuit protection must be provided by other means.

A mechanism can be added to improve the switching ability of open-type cutouts manufactured by the General Electric Company. With this device in place, it is possible to break the fuse link inside the expulsion tube by means of a switch stick. Interruption of current takes place inside the expulsion tube. With this device, capacitor banks of sizes up to

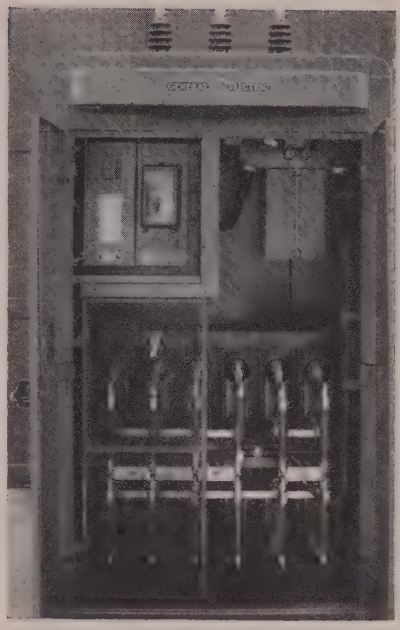

Figure 7. Typical installation of a type *CP*-3 oil switch on capacitor bank rated 180 kvar, 4,800 volts, 3-phase

the maximum that can be carried on a 75-ampere link can be successfully switched without restrikes. Each switching operation, of course, expends three fuse links for a 3-phase capacitor bank.

In certain locations, such as indoors, the open arc obtained when switching with ordinary cutouts may be undesirable for safety reasons. In these cases oil fuse cutouts may be used. These cutouts are subject to the same maximum fuse link size to prevent case bursting in the event of capacitor failure as are open and porcelain-clad cutouts. In general, oil fuse cutouts are capable of successfully switching the same bank sizes as corresponding ratings of porcelain-clad cutouts.

For applications where more frequent manual switching is required but where

Table I. Guide for the Application of Fuse Cutouts with Capacitor Banks

Type of Cutout	Cutout Ratings: Volts	Amperes	Interrupting Rms Amperes	Rated Capacitor Kvar, 3-Phase, 60 Cycles, That Can Be Switched: At 2,400 V Delta	At 4,160 V Delta	At 4,160 V Grd. Y	At 4,800 V Delta	At 7,200 V Delta	At 12,470 V Grd.
Enclosed-Type Expulsion Cutouts (with Fuses)									
Nonindicating	5,200	50	1,200	125	225	225	160		
Indicating and Dropout	5,200	50	1,200	125	225	225	200		
Nonindicating	5,200	100	3,000	190	275	330	160		
Indicating and Dropout	5,200	100	3,000	190	300	330	200		
Nonindicating	7,800	50	1,200	125	225	225	160	80	140
Indicating and Dropout	7,800	50	1,200	125	225	225	200	120	200
Nonindicating	7,800	100	3,000	190	275	330	160	65	115
Indicating and Dropout	7,800	100	3,000	190	300	330	200	160	280
Heavy Duty Indicating	5,200	100	5,000 @ 5.2 KV.	190	240	330	100		
Heavy Duty Indicating	5,200	200	8,000 @ 2.5 KV.	190	275	330	160		
Open-Type Expulsion Cutouts (with Fuses or Disconnecting Blades)									
Dropout	5,200	100	2,000	190	240	375	100		
Dropout	7,800	100	2,000	190	240	375	100	55	95
Dropout	15,000	100	2,000					40	65

Table II. Comparison of Oil Switch Characteristics

Type	Rated Volts	Rated Amperes	Phase	Momentary Amperes	Basic Impulse Insulation Level	Contact Life
CP-3	7,500	See Table III	3	5,000	75	10,000 operations—180 kvar or less 5,000 operations—225 or 300 kvar
G and *GR*	15,000	100	1	5,000	95	6,000 operations at rating
B-1	15,000	150	3	40,000	95	45,000 operations at 100 amperes 20,000 operations at rating

Table III. Allowable Size of Capacitor Banks, Kvar

Switch	2,400 Volts	4,160 Volts Delta	4,160 Volts Grd. Y	4,800 Volts	7,200 Volts	12,470 Volts	13,800 Volts
CP-3	225	225	300	225	225		
G and *GR*	300	530	530	600	920	1,600	1,760
B-1	450	800	800	900	1,350	2,400	2,700

automatic or remote control is not necessary, the type *G* oil switch is available. The type *G* is similar to the type *GR* shown in Figure 6 except that the motor operating mechanism is omitted. This switch is rated 100 amperes at 15,000 volts, single pole.

The rating, momentary and contact life of this switch are given in Table II. The 3-phase capacitor bank sizes that can be switched with a set of three switches are given in Table III. This switch, also, has the advantage over most air break devices that the arc is completely enclosed. This is a decided advantage where adjacent apparatus or circuits, or possible hazard to the operator make an open arc inadvisable.

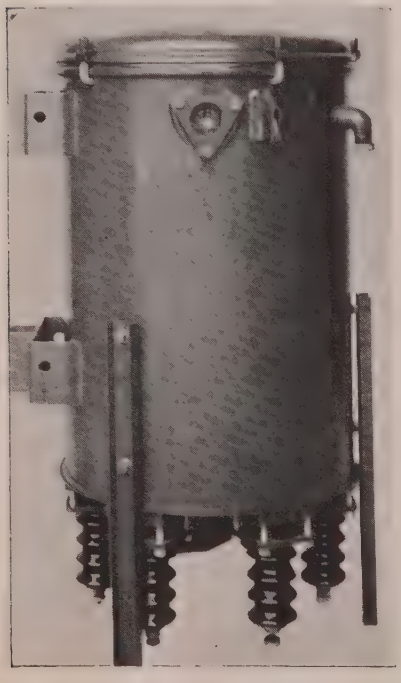

Figure 8. Type B-1, three-phase oil switch rated 150 amperes, 15,000 volts

Automatic Switching of Capacitors

For those locations where automatic switching of capacitors is required, switching devices are available for low cost switching of distribution capacitors in response to changes in current, voltage, or other load characteristics. These switches fall into two distinct classes:

1. Switches for use on circuits where low short-circuit currents are available.
2. Switches for use on circuits where high short-circuit currents are available.

In the first class are the type *CP-3* switch shown (installed in a capacitor housing) in Figure 7 and the type *GR* switch shown in Figure 6.

The type *CP-3* switch is a 3-phase 3-pole oil switch, rated 7,500 volts maximum. It is capable of switching bank sizes up to 225 kvar, 3 phase, at delta voltages up to 7200 volts; 300 kvar can be switched at 4,160 volts grounded Y. This switch has a basic impulse level of 75 kv and can carry currents up to 5,000 amperes for 6 cycles without excessive burning of contact tips or other damage.

Contact life is about 10,000 operations, close and open, at 180 kvar and about 5,000 operations at 225 or 300 kvar. Oil should be changed at the same time as the contacts. Mechanical life is in excess of 40,000 operations.

The *CP* switch is solenoid operated with the solenoid energized in the closed position. With a 110-volt coil, the coil holding current is about 1.9 amperes with an inrush of about 13.5 amperes.

A typical application of the *CP* switch to a 180-kvar bank of capacitors is shown in Figure 7.

The type *GR* switch is a single-phase, one pole, oil switch, rated 100 amperes, 15,000 volts. Three of these switches are required to switch a 3-phase capacitor bank. This switch has a basic impulse level of 95 kv and can carry currents up to 5,000 amperes for 15 cycles without excessive burning of contacts or other damage. Contact life is about 6,000 operations at full rating. Because of the small oil volume, oil should be changed at about half the contact life to maintain the full insulation level across the open contacts and between poles. Mechanical life is in the order of 10,000 operations.

The *GR* switch is operated by a motor

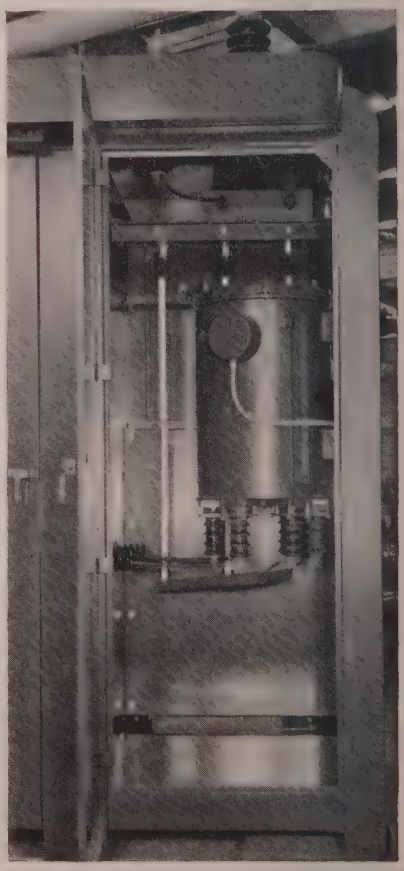

Figure 9. Typical installation of a type *B-1* switch in switch compartment of a 900-kvar 12,470-volt 3-phase capacitor equipment

wound spring mechanism, providing snap action opening and closing. The motor is energized only during actual operation of the switch.

Capacitor bank sizes that can be switched with the type *GR* switch are given in Table III.

For circuits where high short-circuit currents are available, or where a more rugged, longer lived switch than the *CP-3* or *GR* is desired, the type *B-1* switch is available. This switch is shown in Figure 8. The type *B-1* is a 3 pole oil switch rated 150 amperes at 15,000 volts. The resulting bank sizes that can be switched at the various voltages are given in Table III. The type *B-1* is a rugged switch designed on the principles of the well-known load ratio control mechanism for on-load tap changing in transformers. Snap action open and closing of contacts is provided by a motor wound spring mechanism. The motor is energized only during actual switch operation. The *B-1* has a basic impulse level of 95 kv and has a standard momentary current rating of 40,000 amperes, including d-c component. Contact life is 45,000 operations, close and open, at 100 amperes, or 20,000 operations at 150 amperes. Oil should be changed with the contacts. Mechanical life is in excess of 100,000 operations.

Figure 9 shows a typical application of a *B-1* switch in a 900-kvar capacitor equipment.

Ratings and characteristics of the three oil switches described above are given in Table II. The capacitor bank sizes that can be switched by the various switches are given in Table III. This table was calculated taking into account the rule that the switch rating should be 135 per cent of the rated capacitor current as previously discussed.

All three of these oil switches have no short-circuit interrupting rating in excess of their nominal current rating. Protection against line or bus faults in the capacitor bank or against case bursting in the event of a capacitor failure should be provided as described previously. All of these switches will interrupt their rated capacitor current at their rated voltage without restrikes.

The automatically controlled switching devices discussed thus far were designed specifically for capacitor switching. The type *CP-3* and *GR* switches are intended to fill the need for a low cost switching device for comparatively light duty. The type *B-1* switch, while more expensive than either the *CP-3* or *GR* switches, is a heavy duty device and still has a lower cost than standard circuit breakers. In addition its long life before requiring maintenance is a decided advantage over circuit breakers. Circuit breakers are not designed for frequent operation and require more frequent maintenance than the *B-1* switch.

However, where bank sizes in excess of those listed in Table III must be switched, circuit breakers must be used. Standard 15-kv air circuit breakers are available which will switch up to 30,000 kvar of capacitors. Standard 15-kv oil circuit breakers are available which will switch up to 10,000 kvar of capacitors. Other models of 15-kv oil circuit breakers can be modified so as to be suitable for switching up to 30,000 kvar of capacitors. Since these devices are not designed specifically for capacitor switching, freedom from restrikes is not certain. However, within the reactive-kilovolt-ampere limits given, transient overvoltages on switching will not exceed twice normal and will cause no trouble.

Types of Control

Various types of control systems are available for operating motor or solenoid operated switches in response to changes in circuit conditions.

The most commonly used control is voltage sensitive, so that capacitors are switched on at times of low voltage and off when voltage is normal or above. This type of control cannot be used in locations on the source side of the control point for induction or step voltage regulators. In these locations, voltage tends to be highest at time of heaviest load so that the capacitors will be off when most needed. Current or current compensated voltage controls should be used in these locations.

A voltage sensitive control panel, to control a type *CP* switch is shown in Figure 7. Another common control is sensitive to line current. The capacitor will be switched on when line current exceeds a predetermined value.

A third type of control is voltage sensitive but current compensated. For all values of line current below the predetermined value, the control acts as a straight voltage control. When line current exceeds the predetermined value, a relay closes, changing the calibration of the voltage sensitive device by inserting a series resistor. In effect the voltage sensitive device "sees" a lower voltage, switching on the capacitors. For all values of current above the predetermined value the capacitors will be on unless the circuit voltage rises high enough to offset the change in calibration of the voltage sensitive device. An advantage of this control over the straight current control is that during periods of low voltage due to system disturbances, the capacitors will be switched on and will stay on, until the voltage is normal, regardless of current. Thus capacitor kilovars are always on the system when most needed.

Control is available which will switch capacitors in response to changes in the reactive kilovolt-amperes flowing in the circuit. This is commonly called kilovar control. This control is relatively expensive and has little advantage over current compensated voltage control.

Controls also can be supplied responsive to time, where a load cycle is well enough known to make switching at definite times each day feasible.

Time modification can be added to current, voltage, current compensated voltage or kilovar controls to allow omission of any part of the week from automatic operation.

All control systems except straight time and current controls can be supplied to switch capacitor banks in steps. One switching device is necessary for each step. Up to five steps are available in standard controls, and 6-step controls have been supplied. Step controls can be provided with sequencing devices which provide for approximately equal service on all switches and capacitors. That is, over a period of time, all switches operate for part of that period as step 1, then as step 2, and so forth.

In conclusion, we can state that switching devices are available for switching economically practically any type of distribution capacitor. These cover the range of switching frequency from the once a year switching for inspection purposes to the three or more switchings per day of automatically switched capacitors. Control systems are available for automatic control of switching in response to almost any load variable.

References

1. Tests and Analysis of Circuit-Breaker Performance When Switching Large Capacitor Banks, **T. W. Schroeder, E. W. Boehne, J. W. Butler.** *Electrical Engineering* (*AIEE Transactions*), volume 61, November 1942, pages 821–31.

2. Analysis of Factors Which Influence the Application, Operation, and Design of Shunt-Capacitor Equipments Switched in Large Banks, **J. W. Butler.** *AIEE Transactions*, volume 59, 1940, pages 795–800.

3. Standards for Shunt Capacitors. *CAI 1949*, National Electrical Manufacturers Association (New York, N. Y.), 1949.

4. Report on the Operation and Maintenance of Shunt Capacitors, **AIEE Committee Report.** *AIEE Transactions*, volume 68, part II, 1949, pages 1208–19.

5. Connection Arrangements and Protective Practices for Shunt Capacitor Banks, **N. R. Clark, S. B. Farnham.** *AIEE Transactions*, volume 68, part II, 1949, pages 1226–31.

No Discussion

The Application of a Series Capacitor to a Synchronous Condenser for Reducing Voltage Flicker

P. M. BLACK
MEMBER AIEE

L. F. LISCHER
MEMBER AIEE

LARGE electric arc furnace loads which are supplied from power systems over long transmission lines frequently introduce difficult voltage flicker problems. An arc furnace load fluctuates violently with instantaneous changes in demand which may be as high as the kilovolt ampere rating of the furnace and at low power factor. The load fluctuations are of a random nature and may occur in one cycle or may increase or decrease in a series of steps for 8 to 10 cycles. Such a load may cause a disturbing voltage flicker on the transmission system, which in many cases requires special corrective equipment.

This paper deals with an unusual solution to one such voltage flicker problem for an arc furnace load. The solution that was adopted consisted of a series capacitor installed in the leads of an existing synchronous condenser. This installation was much more economical than the other methods considered, and the equipment required was obtainable in a minimum of time. Accumulated data on furnace load swings and test data on the effectiveness of the series capacitor are presented. A description of the installation and its performance to date are included.

Description of Load and Method of Supply

A steel company has a wire and rod mill and a rolling mill which are quite steady loads at high power factor. The company produces steel for these mills by 3 phase electric arc furnaces. The raw material for the furnaces consists of a wide variety of scrap iron and steel and junked heavy equipment such as locomotives. The furnaces are first charged with cold metal, and when the initial charge is melted, additional charges of cold scrap are added until the desired amount of molten metal is obtained. During the times when the furnace is melting the cold scrap, the temperatures in the furnace are low and the arc length varies more or less continuously. This results in an unstable arc which causes violent load changes. The electrodes are automatically controlled to maintain an average power factor of 71 per cent on the low side of the furnace transformer, but during the meltdown period the power factor of the load varies widely. The heaviest kilovolt-ampere demand and the lowest power factor occur when the cold metal falls against the electrodes and causes either a single-phase of 3-phase short-circuit of the furnace transformer.

The first of these electric furnaces was installed by the steel company in 1936 and consisted of two 7,500-kva 3-phase arc furnaces. The half-hour demand of the original installation was approximately 17,000 kw at 85 per cent power factor, which included 3,000 kw of non-fluctuating mill load. Operation of the plant was gradually expanded, and by 1945 the furnace load consisted of one 10,000-kva unit and one 15,000-kva unit. The half-hour demand had increased to 39,000 kw at 85 per cent power factor, which included 8,000 kw of mill load. In 1948 the customer requested additional power to increase the size of the 10,000-kva furnace to 25,000 kva. Studies indicated that this increase in furnace size would result in an increase in voltage flicker beyond the tolerable limit.

The steel mill load is supplied from a 138-kv system through a bank of 132–13.8-kv transformers, as shown in Figures 1 and 2. The 138-kv ties at *A* and *F* to other parts of the system are not shown in detail because their support to the 138-kv bus at *E* is negligible. The local generation at *D* consists primarily of a 50,000-kw base load unit, which is small in comparison to the generation elsewhere on the system. Therefore, the supply to the furnace load is largely dependent on the transmission lines as shown in Figure 1.

Shortly after the original arc furnace installation, a 20,000-kva synchronous condenser with a buffer reactor between the transformer secondary and the 13.8-

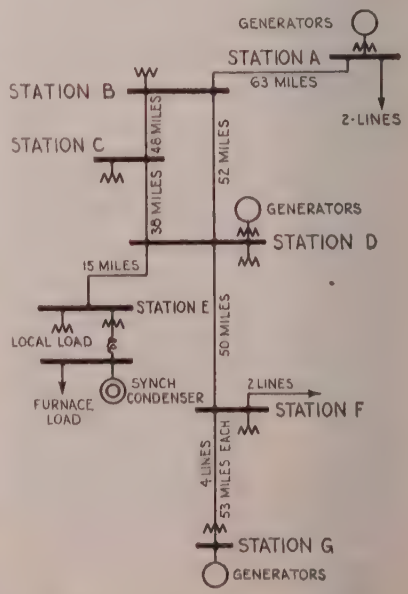

Figure 1. 138-kv transmission system

Paper 51-20, recommended by the AIEE Transmission and Distribution Committee and approved by the AIEE Technical Program Committee for presentation at the AIEE Winter General Meeting, New York, N. Y., January 22-26, 1951. Manuscript submitted October 23, 1950; made available for printing November 17, 1950.

P. M. Black is with the Illinois Northern Utilities Company, Dixon, Ill., and L. F. Lischer is with the Commonwealth Edison Company, Chicago, Ill.

The authors wish to express their appreciation to C. F. Andrews, H. C. Bartholomew, J. L. Neal, V. H. Kraybill, and C. F. DeSieno for their valuable assistance.

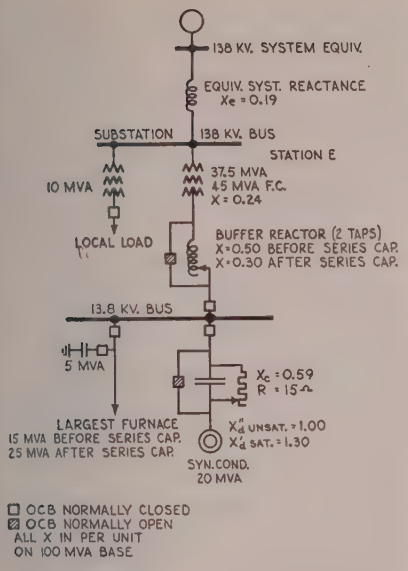

Figure 2. Schematic diagram of connections at station *E*

kv bus was installed to reduce the voltage flicker on the 138-kv system. In addition to correcting the voltage flicker, the condenser was equipped with automatic voltage control which was used to maintain the average voltage level constant on the 13.8-kv bus. This installation was described in an AIEE paper by T. G. LeClair.[1] This installation proved very satisfactory, and with system increases due to load growth, was able to maintain the voltage flicker within allowable limits through successive increases in the size of the steel mill arc furnaces.

From a system standpoint, the maximum load swing which can be supplied to the furnaces is determined by the permissible voltage fluctuation on the 138-kv busses at *D* and *E*. These busses serve 50 towns and communities and the surrounding rural areas. Experience had shown that the voltage flicker on these busses

Figure 5. Furnace megavolt-ampere rating versus furnace megavolt-ampere swing for two furnaces of same size operating simultaneously. (Swing for 1 furnace operating alone is 16.7 per cent less)

These swings (solid line) were used for calculation of voltage changes. The swings are not the maximum that may be obtained, but data show that these values are exceeded very infrequently. All points are at 0.5 power factor unless otherwise indicated.
⊗—test data by Jones and Stearns
⊙—test points based on oscillographic data for 1 furnace and increased by 20 per cent to permit comparison with other points. Points are maxima
+—test point based on average increase in current swings over 15-mva operation. Power factor of 0.5 is assumed
×—values used for calculations in this paper.

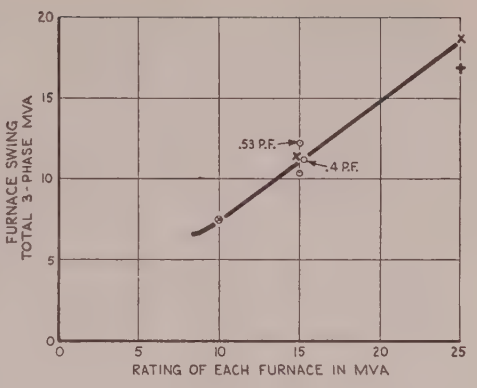

was at the tolerable limit at the time the customer planned to increase the 10,000-kva furnace to 25,000 kva. Therefore, additional system capacity or added local corrective equipment would be required to serve the larger furnace. Considera-

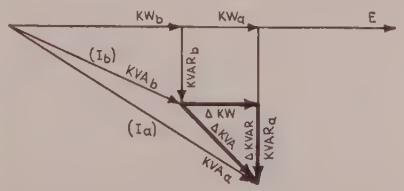

Figure 4. Basis for determination of instantaneous kilowatt and reactive-kilovolt-ampere change

Δ kw and Δkvar are determined from oscillographic data of kw_b, I_b, kwa, I_a. Subscript *b* represents quantity before change. Subscript *a* represents quantity after change. (Change may be instantaneous or take 3–4 cycles)

tion also was to be given to the possibility of increasing the second furnace to 25,000 kva at some future time.

Data on Furnace Load Swings

As the first approach to the problem of determining the amount of added capacity or local correction required, measurements were made of the present furnace load to determine its maximum instantaneous change and the corresponding change in 138-kv bus voltage. The voltage fluctuation thus determined was taken as the maximum permissible

The measurements were made with oscillographs which were operated during the initial meltdown periods when the flicker was most violent. This produced a record which gave a 1.5- to 2-minute sample of the furnace operation. Four such test runs were made. Three-phase readings of currents and watts for both the furnace and synchronous condenser were obtained. With the equipment available, it was practically impossible to measure accurately the changes in 138-kv bus voltage and evaluate them in terms of lamp flicker. Therefore, using the above-measured current and power quantities, the maximum voltage change was calculated, and this value was then established as the maximum permissible. Data of the furnace load swings were compiled so as to show the instantaneous kilovolt-ampere change as a function of power factor. Figure 3 shows some of these points for two of the test runs. The instantaneous kilowatt and kilovolt-ampere furnace load changes (Δkw and Δkvar) were determined in a manner as is shown in Figure 4. Maximum instantaneous kilowatt and kilovolt-ampere changes for the 10- and 15-megavolt-ampere (mva) furnace were compared with those shown by others[2] and fairly good agreement was found.

It was concluded that for voltage fluctuation studies the maximum instantaneous change of a 15-mva furnace operating

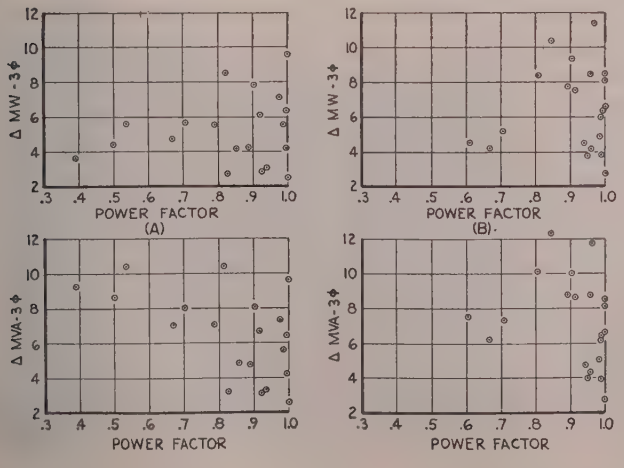

Figure 3. Magnitude and power factor of furnace load swings

A. 15-mva furnace alone during initial meltdown period
B. 10-mva furnace during initial meltdown period and 15-mva furnace during recharge period

alone could be taken as 9.35 mva at 50 per cent power factor. The maximum power swings of the 10- and 15-mva furnaces were increased by 20 per cent and plotted as in Figure 5. The 20 per cent increase allowed for simultaneous operation of two furnaces the same size and was based on the data of Jones and Stearns.[2] The curve was extrapolated to 25 mva. For two 25-mva furnaces, the maximum instantaneous power swing was taken to be 18.7 mva at 50 per cent power factor.

After the 25-mva furnace had been installed but was being operated at 15-mva maximum, another series of tests was made to verify this choice of increment mva. At this time the 15-mva furnace was operated at 15 mva and then at 25 mva. On a current basis only, operation at 25 mva showed 50 per cent greater furnace current fluctuation than at 15 mva, which checked reasonably well the assumed value shown in Figure 5.

Having established what the increased maximum instantaneous furnace load change would be with two furnaces operating at 25 mva, the problem then resolved itself into two possible solutions:

1. Reinforce the transmission system by the installation of an additional 138-kv line.

2. Increase the amount of local corrective equipment so that more of the load change is supplied locally.

Possible Methods of Supplying Increased Load

Additional Transmission Capacity

The construction of a new 138-kv transmission line, 43 miles in length, between stations E and F would have provided sufficient capacity at E to solve the flicker problem. However, this line would be an expensive method for providing the capacity and would require a long time for construction.

Additional Corrective Equipment

Synchronous Condenser

As indicated previously, the original flicker problem at station E was solved by the installation of a 20,000-kva synchronous condenser with a buffer reactor. In order to provide sufficient capacity to handle the larger furnace load, it would have been necessary to install 40,000-kva additional condenser capacity. The cost of such an installation would have been approximately 50 per cent of the cost of the new transmission line, but even this amount represented a substantial amount in relation to the size of the load that was being added to the system. Another disadvantage of this solution to the problem was the relatively long time required for the installation of a synchronous condenser.

Buffer Reactor

One possible method of forcing the existing synchronous condenser to supply a larger share of the fluctuating load would have been to increase the reactance of the buffer reactor. However, operating experience had shown that a higher value of buffer reactance would result in unstable operation of the condenser.

Use of Series Capacitor

In considering other possible methods for solving the flicker problem, it was suggested that the condenser could be forced to supply more of the fluctuating load by decreasing its sub-transient reactance through the installation of a series capacitor connected into its leads. So far as was known, such an application of series capacitors had not been attempted previously, and therefore no operating experience was available to serve as a guide. Previous studies indicated the possibility of various problems being encountered because of the transients that would be produced by a continuously changing load acting on a circuit consisting of the series capacitance and inductance of the condenser connected to the remainder of the system. A companion paper describes the mathematical studies that were made to determine the feasibility of this method of solving the flicker problem.[3]

It appeared from these studies that it would be practical to neutralize from 50 to 75 per cent of the subtransient reactance of the condenser. A study was made to determine the effects of a 75 per cent series capacitor on the 60-cycle operation of the system. The pertinent portion of the system as studied is shown in Figure 2. Based on two 25-mva furnaces, a furnace load of 49 megawatts (mw) and 38 reactive megavolt-amperes (mvar) was assumed with an initial condenser load of 10 mvar. 27 mvar of shunt capacitors were required in order to maintain a satisfactory voltage level on the 13.8-kv bus and keep the condenser loading down to 10 mvar. The system internal voltage and angle remaining constant, the furnace load was increased to 58.4 mw and 54.2 mvar, and the resultant voltages and currents were calculated. The synchronous condenser, with 75 per cent of its reactance neutralized, picked up 7 mw and 14 mvar, with the remainder of the mva furnished from the system. The shunt capacitors dropped 2 mvar owing to the decreased terminal voltage. The computed voltage on the 138-kv bus then showed a 1.5 per cent decrease. The stability of the synchronous condenser was checked for this condition of loading and was found to be stable with ample margin. Even several successive shocks of this magnitude would not result in instability. A similar study, but with the system as it was before the furnace load was increased (and before the series capacitor was added), showed a 1.8 per cent flicker on the 138-kv bus. This solution, therefore, indicated favorable

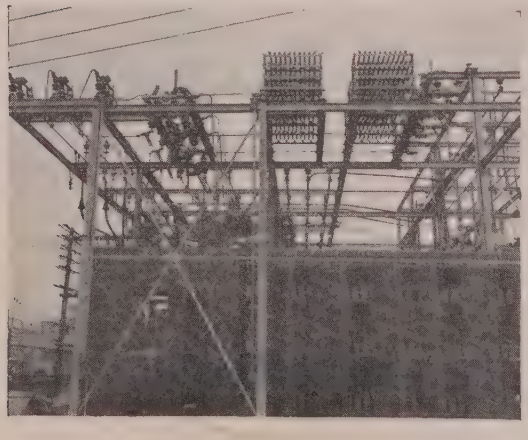

Figure 6 (left). General view of series capacitor installation. Shunt resistor units are at top

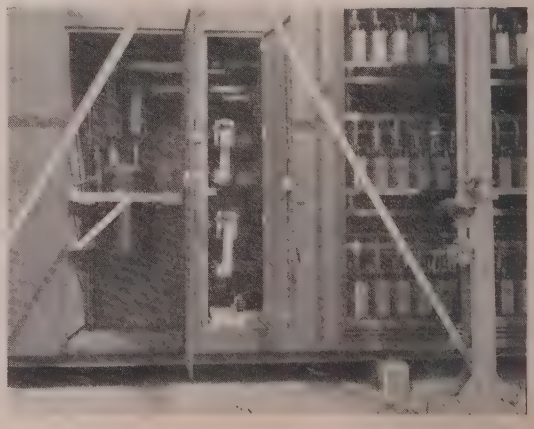

Figure 7 (right). Close-up view of series capacitor showing bypass circuit breaker at left, protective gaps in center, capacitor units at right

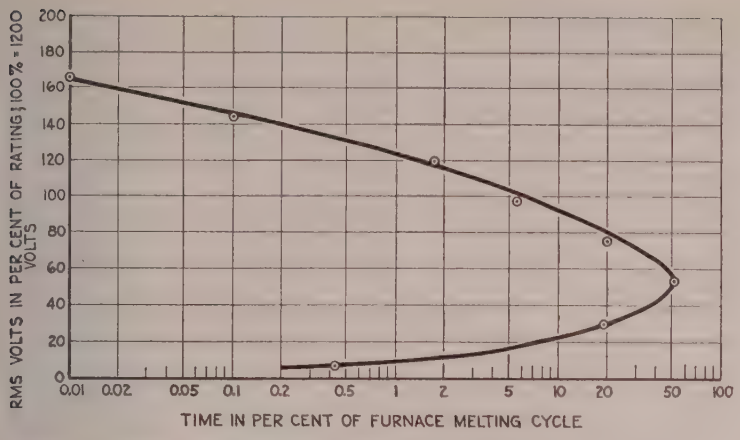

Figure 8. Series capacitor volts-time distribution curve one furnace meltdown cycle

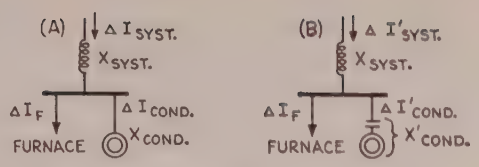

Figure 10 (above). Schematic diagram

A. Without capacitor

$$\Delta I_{syst} = \Delta I_F \left(\frac{X_{cond}}{X_{syst} + X_{cond}} \right)$$

B. With capacitor

$$\Delta I_{syst}' = \Delta I_F \left(\frac{X_{cond}'}{X_{syst} + X_{cond}'} \right)$$

results. This aspect of the problem is treated in greater detail in the companion paper.[3]

Method Selected for Solution of the Problem

In deciding the most favorable method of providing adequate capacity to serve the increased furnace load, two factors were of prime importance: cost, and length of time to complete the installation. For both of these considerations, the series capacitor offered the most desirable solution of the problem. In view of these advantages, it was decided to install a series capacitor, even though no operating experience was available on this type of application. The capacitor selected is rated at 3,600 kva and 1,200 volts. This resulted in a 59 per cent neutralization of the synchronous condenser direct-axis subtransient reactance. Although the calculations were based on neutralizing 75 per cent of the condenser reactance, the studies indicated that the 59 per cent neutralization would be adequate. The 59 per cent value was used because it permitted the use of standard 2,400-volt capacitor units utilizing a 1,200-volt center tap. In addition, 5,000 kva of shunt capacitors were installed to supply the heavier reactive load of the larger furnace. The cost of both capacitors was approximately 10 per cent of the cost of adding a transmission line.

Description of Installation

The series capacitor is rated:

3,600 kva, 3-phase 60 cycle
Line voltage: 13.8-kv
Capacitor working voltage: 1,200 volts
Continuous current: 1,000 amperes
Capacitor units: 80 15-kva units per phase
Ohms per phase: 1.2 based on nameplate rating: 1.12 based on average tolerance

All three phases of the series capacitor are contained in one outdoor housing approximately 10 feet high × 4 feet wide × 37 feet long. The first three compartments of this housing contain the control equipment, the 15-kv bypass oil circuit breaker, and the instrument transformers and protective gaps. The remaining eight sections contain the capacitor units, which are supported on racks, mounted on 15-kv insulators. The housing is grounded. A general view of the installation is shown in Figure 6.

The shunt resistor which is connected across the terminals of the series capacitor is composed of outdoor resistor units mounted on galvanized frames. Each frame consists of ten resistor units and is rated 15 ohms, 40 amperes. Each phase of the series capacitor is shunted with eight resistor frames in a series parallel combination with connections made so resistances of 30, 15, 10, or 7.5 ohms can be obtained with current ratings of 40, 80, 120, and 160 amperes, respectively. Owing to space limitations, outdoor resistor units were used and mounted on the steel substation structure on bus supports instead of mounting them in a steel housing similar to the capacitor units. These resistor unit assemblies appear in Figure 6.

The capacitor is connected in series with the phase leads of the synchronous condenser when the running circuit breaker is closed. The synchronous condenser normally is started at reduced voltage, and the starting circuit breaker is connected so that the series capacitor is not in the circuit during the starting period.

Overvoltage protection for the series capacitor is provided by a heavy cup-shaped graphite gap shunted across each phase of the capacitor. If the voltage across the capacitor exceeds the breakdown of the gap, it flashes over and automatically bypasses the capacitor. Whenever current flows in the gap circuit, an instantaneous overcurrent relay operates, which closes the circuit breaker that is shunted across both the capacitor and gap. Closing of the circuit breaker extinguishes the arc in the protective gap. The gaps and circuit breaker are shown in Figure 7.

Each phase of the series capacitor is protected from overload by an induction-type voltage relay which is supplied from a potential transformer connected across the series capacitor. The minimum pickup of the relays is set for a voltage which corresponds to 115 per cent of rated

Figure 9. Typical Brush oscillograph record

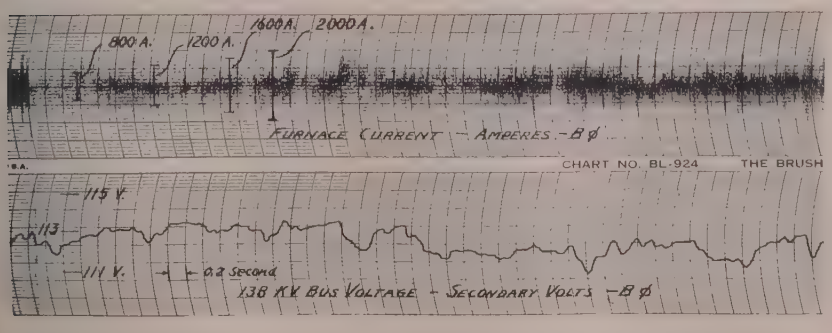

current. Differential protection is provided for each phase of the series capacitor by dividing the units on each phase into two equal groups. Each group is supplied through a separate current transformer and the two currents on each phase are differentially connected through an instantaneous current relay which closes the bypass oil circuit breaker whenever the unbalance in the circuit is more than three times the current rating of one capacitor unit. The bypass oil circuit breaker is controlled from either of two manual control stations. One is located at the switchboard and the other at the control panel of the series capacitor.

In addition to the bypass oil circuit breaker, the series capacitor is equipped with a gang-operated bypass air switch located on the structure above the capacitor. Also, gang-operated air break switches are located in both sets of leads to the capacitor for isolating it from the circuit. All switches are equipped with key interlocks to assure the proper sequence of operation. After the capacitor is removed from service, a grounding switch must be closed before the doors to the capacitor housing can be opened.

Test Results of the Series Capacitor Installation

At the time the series capacitor was placed in service, two extensive series of tests were made: the first to check the performance of the condenser with the series capacitor, varying such quantities as the value of the shunt resistor, amount of buffer reactance, and so forth; the second, to check the effect of the series capacitor on the 138-kv bus voltage flicker.

Condenser Performance

Oscillographic data were taken recording the following quantities:

Voltage across the series capacitor—$B\phi$
13.8-kv bus voltage—$B\phi$
Synchronous condenser current—$B\phi$
Synchronous condenser watts—I_B and E_{B-C} shifted 30°
Furnace current—$B\phi$
System transformer current—$B\phi$
138-kv bus voltage—$B\phi$

All tests were made on the 25-mva furnace, either during an initial meltdown period, or during a recharge period. See Figure 2 for symbols, and so forth. Test runs were made varying the following:

Furnace transformer on 15-mva tap

Furnace transformer on 22.5-mva tap

Buffer reactance set at 0.50 in per unit on 100 mva

Buffer reactance set at 0.30 in per unit on 100 mva

Buffer reactance short circuited

Series capacitor shunt resistance set at 7.5 ohms

Series capacitor shunt resistance set at 15 ohms

Series capacitor shunt resistance set at 30 ohms

Series capacitor shunt resistance open circuited

Series capacitor in and out of service

The tests showed that the optimum value of buffer reactance was 0.30. The original setting of 0.50 resulted in unnecessarily larger condenser swings of current; short circuiting the buffer reactance resulted in too much of the current being supplied from the system.

During the tests the series capacitor shunt resistance was found to be necessary, and 30 ohms was accepted as a tentative setting (to keep the losses as small as possible). An attempt to operate with the shunt resistance open resulted in large and repeated reactive kilovolt-ampere swings of the synchronous condenser, and it was necessary to close the capacitor bypass circuit breaker.

Figure 8 shows the voltage across the series capacitor as a function of time. This is based on one complete initial meltdown period. The record was obtained using a Brush oscillograph so that the voltage during the entire meltdown period could be recorded. These data indicate the voltage stresses and heating effects of the currents to be well within the capacitor capability. It must be borne in mind that the per-cent overvoltage on the capacitor is directly related to the average loading level of the condenser.

The oscillograms showed that when the series capacitor was in the circuit, the real power supplied by the condenser on furnace surges was approximately 50 per cent greater than when the series capacitor was not in service. These results agree with the anticipated behavior. A stroboscope (energized from the 138-kv bus) flashing on the end of the synchronous condenser shaft (with suitable angular markings) showed that the degrees of rotor swing were no greater when the series capacitor was in the circuit than when the capacitor was not in. The angular swings are no greater because, even though the real power now supplied on a swing by the rotor is greater, the effective reactance of the machine is less. The angular swing of the rotor is a function of the product of the in-phase component of current and the machine reactance, so the rotor swing is now no greater with respect to the 138-kv bus than it was when the series capacitor was not in the circuit. During the entire series of tests, by observation of the degrees of rotor swing with the stroboscope, it was never possible to tell whether the capacitor was in or out of the circuit, although it was evident that the swings were "snappier" when the capacitor was in the circuit.

Effect of the Series Capacitor on Voltage Changes

It was decided in measuring the voltage changes and the flicker voltage that the important point was not the absolute change in voltage on the 138-kv bus, but the change in voltage as it affected the output of an incandescent lamp. Accordingly, a lamp-photo tube type flicker meter was used. The input voltage is applied to a 10-watt incandescent bulb. The change in illumination is picked up by a phototube and the phototube output voltage is then suitably amplified and recorded on a Brush oscillograph. An instantaneous change in input voltage to the lamp shows up as a change in output, reaching 40 to 50 per cent of its change in one cycle and 90 per cent of its change in six cycles. Four quantities were recorded:

E_B = 138-kv B phase to neutral voltage (through lamp-phototube-type flicker meter).
I_A = A phase furnace current.
I_B = B phase furnace current.
I_C = C phase furnace current.

The four quantities were recorded on two Brush oscillographs running at synchronized chart speeds of five feet per minute. Figure 9 shows a typical sample of the record obtained.

The recorders were run for a total time of about one hour, not continually but only at times of observable flicker on the 13.8-kv bus at E. Two initial meltdown periods of the 25-mva furnace and one recharge period of this furnace were thus recorded. At various times the 15-mva furnace also was in operation. During refining periods, the recorders were shut off.

Basis for Analysis

From the recorded data, measurements of changes in the 138-kv bus voltage were taken for a total of 350 points; 200 points with the series capacitor in service; 150 points with the capacitor out. The rate of change of the voltage points considered varied from 0.1 second to 0.8 second with the average change taking place in 0.2 second. These voltage

changes were all noncyclic in nature and the larger of the changes were always over a longer period of time. In order to evaluate the voltage changes in terms of those which are perceptible, the changes were assumed to be recurrent (or cyclic), which is a pessimistic, but safe, assumption. The period or rate of recurrence of these voltage changes was found to be between 0.8 per second to 3.3 per second. The magnitude and period of such changes were then plotted on the generally accepted flicker perceptibility curves.[4] It is well known that if the change in voltage is made slowly enough, even a relatively large change will not be perceptible. The points thus plotted when the series capacitor was in the circuit fell well within the tolerable limits. When the series capacitor was not in the circuit, the points were at the top or slightly above the tolerable limit.

In order to evaluate quantitatively the effectiveness of the series capacitor, the voltage changes were computed on the basis of the furnace current change that produced the voltage change, in other words, $\Delta E/\Delta I$, where ΔE is the change in 138-kv B-phase bus voltage and ΔI the change in B-phase furnace current. Because of the importance of the power factor of the current change, a very large number of points must be considered before a comparison can be made. It also is important that the points considered be actually comparable. Because of the thermal delay of the lamp, there frequently are points where a large change in furnace current causes only a small change in lamp output, because the current changes in the reverse direction before the lamp can respond to the full effect of the first change. Therefore, for this analysis, only those points were considered where the current changed in value and was essentially constant for six cycles before and six cycles after the change.

Test Results

1. With series capacitor: $\Delta E/\Delta I=3$ (volts/1,000 amperes, average of 200 points)

2. Without series capacitor: $\Delta E/\Delta I=5.5$ (volts/1,000 amps. average of 150 points)

3. Voltage change without series capacitor (reference): 100 per cent

4. Voltage change with series capacitor: 55 per cent

5. Voltage change improvement with series capacitor: 80 per cent

Test Results Compared with Analytical Results

The improvement in voltage change was approximated by comparing the ratio of reactance of the condenser (with and without the series capacitor) to the reactance of the system in a manner as follows. Figure 10 shows schematically the system components and defines the symbols. Without the series capacitor:

$$\Delta I_{syst} = \Delta I_F \left(\frac{X_{cond}}{X_{syst}+X_{cond}} \right)$$

With the series capacitor:

$$\Delta I_{syst}' = \Delta I_F \left(\frac{X_{cond}'}{X_{syst}+X_{cond}'} \right)$$

Measure of improvement

$$\frac{\Delta I_{syst}}{\Delta I_{syst}'} = \frac{\dfrac{X_{cond}}{X_{syst}+X_{cond}}}{\dfrac{X_{cond}'}{X_{syst}+X_{cond}'}}$$

Results obtained will depend on the value of condenser reactance that is used. For rapid load changes, the subtransient reactance (unsaturated) should be used.[3] On a 100-mva base, this value is 1.0 per unit. For the slower changes, which includes most of those here considered, the transient reactance (saturated) should be used; this value on a 100-mva base is 1.3 per unit. Thus, using subtransient reactance, the measure of improvement is 60 per cent. Using the transient reactance, the calculated improvement is 30 per cent.

The test value of 80 per cent improvement compares favorably with the above-calculated values. The test value should be greater because the calculated improvement neglected transients, the stored energy in the capacitor, phase balancing effects, and so forth.

Cyclic Flicker

Cyclic flicker voltages were recorded at relatively infrequent intervals. There were not a sufficient number of these cyclic variations to permit a comparison of magnitudes to show the effect of the series capacitor. The cyclic variations that did occur were predominately at a rate of six cycles per second and lasted over a period of time from 0.3 second to 3.5 seconds, with the great majority lasting 0.5 second. Plotting these values on the flicker perceptibility curves[4] showed that these variations were within the tolerable limits. Observers' comments state that there is no objectionable flicker since the series capacitor is in operation, even with the increased furnace load (from 15 to 25 mva).

Operation

The series capacitor was placed in service in January 1950, and its operation has proved very satisfactory. With the series capacitor in service, the voltage flicker with the 25,000-kva furnace in operation is less than it formerly was with a 15,000-kva furnace. The average loading of the condenser was reduced approximately 8,000 kva to allow thermal capacity for the larger current swings in the machine. To compensate for this reduction, a 5,000-kva bank of automatically-switched capacitors was installed. The switching is controlled by the loading of the condenser.

The automatic voltage control of the synchronous condenser is equipped with a field limiting control which allows the 13.8-kv bus voltage to sag if the kvar required to hold it constant are more than the machine can supply without becoming overloaded. The field limiter control was readjusted and set not only for the thermal overload protection to the synchronous condenser, but also to prevent bypassing the series capacitor from overloads. This control is important in the successful operation of the series capacitor. After the correct setting had been obtained, by trial and error, operation of the series capacitor was much improved. A control for limiting the kvar taken by the condenser when the furnace load is off might also be desirable. Such a control should be actuated by the terminal voltage of the condenser.

After the initial tests were completed, the series capacitor was placed in service with the shunting resistor set at 30 ohms. During the first two weeks of operation the synchronous condenser tripped automatically ten times during periods when the condenser was lightly loaded. The value of the shunting resistor was decreased to 15 ohms and no further trouble has been encountered. No difficulties due to ferroresonance have been experienced.

Initially, the protective gaps were set to spark over at 2,700 volts, and they flashed over rather frequently at this setting. Very few overload operations occurred with the gaps set at this value. The setting of the gaps was increased to 3,100 volts sparkover, and the operation was much improved. At this value, about an equal number of overload and overvoltage operations occur.

The series capacitor is bypassed from overload or overvoltage approximately $2^1/_2$ times per day. This frequency of operation of the bypass protection is much higher than normally encountered in series capacitor applications; however, no adverse results have been noted. The number of operations could be reduced by decreasing the average reactive supplied by the synchronous condenser, which

would require additional power factor correction equipment. Further study is being given to this phase of the installation in order to determine the best compromise between the number of gap operations that should be permitted and the amount of equipment required to decrease the number of operations. Whenever the series capacitor is bypassed, the synchronous condenser remains on the line, although it may not be able to supply all of the corrective kilovolt-amperes needed.

This is not considered troublesome, as the installation is located at an attended station. Whenever the series capacitor is automatically bypassed, the operator does not restore the series capacitor to service until the synchronous condenser loading is less than 60 per cent of rated current.

After about eight months of operation with the series capacitor in service, the end bells of the synchronous condenser were removed and the windings inspected for evidence of mechanical stress or loosening of the coil bracing. This machine is very well braced at the coil ends and no evidence of any mechanical stress was observed.

From the operation to date, the series capacitor has proved to be a very satisfactory solution to a difficult voltage flicker problem.

References

1. Arc-Furnace Loads on Long Transmission Lines, **T. G. LeClair.** *Electrical Engineering* (*AIEE Transactions*), volume 59, April, 1940, pages 234–39.

2. Large Electric-Arc Furnaces—Performance and Power Supply, **B. M. Jones, C. M. Stearns.** *Electrical Engineering* (*AIEE Transactions*), volume 60, July 1941, pages 763–69.

3. Technical Problems Associated with the Application of a Capacitor in Series with a Synchronous Condenser, **R. L. Witzke, E. L. Michelson.** *AIEE Transactions*, volume 70, Part I, 1951, pages 519–25.

4. The Visual Perception and Tolerance of Flicker. Electrical Testing Laboratories (New York, N. Y.), 1937; Figure 11, page 49, and Figure 19, page 66. These figures also appear in the Electrical Transmission and Distribution Reference Book published by the Westinghouse Electric Corporation, second edition, 1943; Figure 1, page 477 and Figure 3, page 478.

No Discussion

Capacitor Switching Phenomena

R. C. VAN SICKLE
FELLOW AIEE

J. ZABORSZKY
MEMBER AIEE

THE capacitor switching performance of a circuit breaker has been found to depend on the power supply system as well as on the size of the capacitor bank switched. Experimental data show that the voltage drop produced by the capacitor current flowing through the source inductance determines the time when the arc first extinguishes and the corresponding contact separation. Restrike-free operation is obtained if the arc is extinguished only after a contact separation is reached which produces a dielectric strength always greater than the recovery voltage. This condition is not met by all breakers at all times, and the factors controlling capacitor switching phenomena reveal when and why restriking occurs.

These relations have been studied experimentally at voltages up to 14.4 kv and with capacitor banks up to 18,000 reactive kilovolt-amperes.

During the large number of tests, about 1,500 on oil circuit breakers and 600 on magnetic air circuit breakers, many of them with restrikes, the maximum voltages reached were 2.5 times the normal crest of phase-to-ground voltage for oil circuit breakers and 2.0 times for magnetic air circuit breakers. The compressed air circuit breakers tested up to 25,000 reactive kilovolt-amperes at 13.8 kv with and without a parallel bank operated restrike-free.

The increasing use of power capacitors and their application in larger sizes makes desirable a thorough knowledge of the phenomena which accompany their switching. The circuit breakers which are used for this service are subjected to conditions peculiar to these types of circuits. They must handle not only the normal current and short circuit currents but also the currents and voltages which appear during the closing and opening of circuits to capacitor banks.

To determine these phenomena and the performance of "De-ion" grid oil circuit breakers, plain-break oil circuit breakers, magnetic blast air circuit breakers, and compressed air circuit breakers, the extensive testing mentioned above has been conducted in the Westinghouse High Power Laboratory. These tests have established that for circuit breakers which may restrike the performance is determined by the circuits supplying the power and exerting their influence through the transient recovery voltage appearing across the contacts of the circuit breaker. The source impedance and the capacitances, including parallel capacitor banks if any, determine the amplitude and frequency of the initial part of the transient recovery voltage and thereby whether the circuit breaker will restrike.

At the outset of the investigation, unexpected results were obtained during a series of about 150 switching operations which were performed with an oil circuit breaker on a capacitor bank, the size of which was increased in steps while the voltage and the circuit which fed the capacitor were left unchanged. The number of restrikes and the magnitude of the overvoltage showed irregular fluctuations as a function of capacitor size up to a value above which the operation becomes completely restrike-free.

This result was not explained by the available literature and was actually contrary to the prevailing opinion which expected restrike-free operation below a certain critical capacitor size and restriking for capacitors in excess of this critical size. This inconsistency added interest to the experimental study.

About 2,100 oscillographically-recorded switching operations on capacitor banks, ranging in size from 1,300 to 18,000 reactive kilovolt-amperes were made. In some of the tests capacitor banks were connected to the source side of the circuit breaker. Oil circuit breakers, with contact speeds ranging from 3.7 feet per second up to 14.5 feet per second, magnetic blast air circuit breakers of the *DII* type and compressed air circuit breakers were used. The circuit for the 14.4-kv tests is shown in Figure 1. Both magnetic and cathode-ray oscillograms were taken. The voltage range from 14.4 kv down to 2.3 kv was tested.

Definitions

In the following discussion of the test results some terms will be used with the following specific meanings:

The term "restrike" is used to denote a

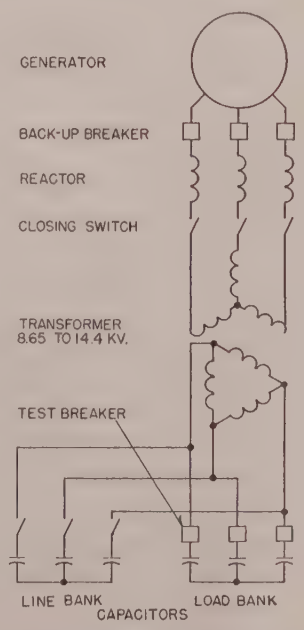

Figure 1. The test circuit provided for changing source impedance, line bank capacitance and load bank capacitance

Paper 51-21, recommended by the AIEE Switchgear Committee and approved by the AIEE Technical Program Committee for presentation at the AIEE Winter General Meeting, New York, N. Y., January 22–26, 1951. Manuscript submitted October 25, 1950; made available for printing, November 17, 1950.

R. C. VAN SICKLE is with Westinghouse Electric Corporation, East Pittsburgh, Pa., and J. ZABORSZKY is with the University of Missouri, Missouri School of Mines and Metallurgy, Rolla, Mo.

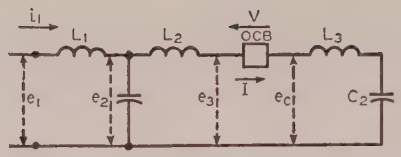

Figure 2. Equivalent circuit for capacitor switching

re-establishing of the current after a pause discernible on a magnetic oscillogram. Current pauses of less than 1/4-cycle duration can produce no significant overvoltages and frequently are referred to as either a reignition or a delayed reignition to identify them with the other unimportant reignitions of the arc which occur when the recovery voltage is able to restart the arc with no current pause discernible on a magnetic oscillogram. However, with the emphasis in this paper on the discernible pause, or arc extinction time and on whether the current flowed subsequently, it is simpler to group delayed reignitions with restrikes.

The term "arc extinction time" denotes the length of time from the separation of the circuit breaker contacts to the first extinction of the arc but does not include restrikes, if any. Therefore, it may be less than "arcing time" defined by standards of the American Standards Association.

Normal voltage denotes the crest of the phase-to-ground steady-state voltage with the capacitor bank energized.

Overvoltages are given in multiples of the normal voltage (1×normal voltage means no overvoltage.)

The number of restrikes is the percentage of 3-phase interruptions in which one or more restrikes occur.

Factors Controlling the Performance

In the experimental testing, as in actual service, the results of successive switching operations under the same main conditions vary. On almost all of the tests no attempt was made to part the contacts at a particular point on the current wave and several tests were made for each condition to determine the range of performance. With the contacts of all three poles parting simultaneously, the first current zero would occur anywhere within the first 1/6 cycle. At a contact speed of 5 feet per second, the contacts move 1 inch in 1 cycle so a slight variation in height or alignment of overlapping contacts can lengthen the time to the first current zero. Differences in arcing time cause differences in arc lengths, differences in the amount of gas produced,

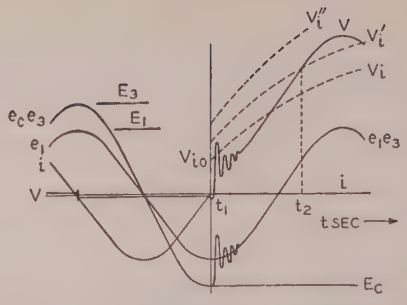

Figure 3. The inductive drop in the source impedance may produce a high frequency transient component in the recovery voltage across the circuit breaker

and differences in the recovery of dielectric strength, so slight variations in performance must be expected.

The performance of a circuit breaker, when switching capacitor banks, is determined jointly by the characteristics of the circuit breaker itself, the size of the capacitor bank and the characteristics of the system to which the capacitor is connected. All these factors exert their influences through only two quantities:

1. The recovery of the dielectric strength in the circuit breaker after the extinction of the arc. This quantity is mainly influenced by:

1. Characteristics of the interrupter of the circuit breaker.
2. Speed with which the contacts of the circuit breaker separate.
3. Special measures, like forced oil flow and so forth.
4. Size of the load bank (ionization of the arc space).

2. The first half-cycle of the recovery voltage. It has a system frequency component and a transient component with a magnitude and frequency which are independent of the characteristics of the circuit breaker itself (unless it inserts resistors) and are mainly influenced by:

1. Operating voltage (magnitude).
2. Size of load bank (magnitude).
3. Inductance and capacitance of the source (magnitude and frequency).
4. Inductance and capacitance of the line between source and capacitor (magnitude and frequency).
5. Size of the line bank (magnitude and frequency).

The influence of the initial transient component manifests itself in various ways. For instance, as will be shown, it alone accounts for the very marked difference in the performance of a circuit breaker on a certain load bank with and without a large line capacitor bank. On the other hand the dependence of the

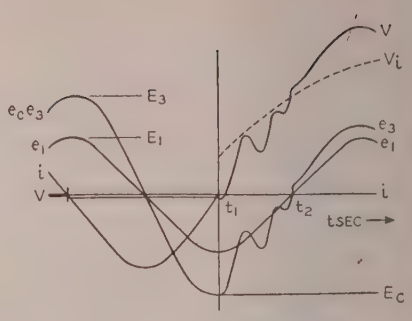

Figure 4. A parallel capacitor bank makes negligible the transient component of the recovery voltage across the circuit breaker

switching performance on the source reactance and the size of the load bank is determined jointly by the initial transient and the recovery of the insulation strength.

Capacitor Switching Circuit

Figure 2 shows the simplified, single-phase equivalent circuit of a source, capacitor bank, and circuit breaker. L_1 is the inductance of the source, C_2 the capacitance of the bank to be switched (the load bank), C_1 capacitance of the line or the line bank if any, and L_2 and L_3 are small line inductances in and between the two capacitor banks.

This equivalent circuit and consequently the mechanism of the interruption is qualitatively the same regardless of whether there is a parallel bank on the line. The difference is in the magnitude of C_1. The line capacitance is small but the capacitance of an actual line bank will be relatively very large. Consequently, the natural frequency of the L_1 and C_1 circuit with a major parallel bank on the line, $f_1 = 1/(2\pi\sqrt{L_1 C_1})$, will be low (usually much less than 1 kc), and high (in the order of 10 kc and above) with no parallel bank.

The Transient Recovery Voltage

That it is relatively easy to extinguish an arc in a capacitive circuit and that 1/2 cycle elapses before maximum recovery voltage is applied is well known. The nature of the transient recovery voltage has been recognized.[1] High-voltage circuit breakers interrupting the charging currents of transmission lines have been designed to take advantage of the sharp initial rise in transient recovery voltage. However, since it plays a big part in capacitor switching, its characteristics will be described.

The current will be interrupted at a current zero, t_1 (Figure 3). At this time

the terminal voltage on the capacitor e_c is maximum. Since the current through the circuit breaker is interrupted, the charge will be left on the capacitor and its voltage will remain constant E_c after the interruption. (The inductive drops in L_2 and L_3 are considered negligible except for transient currents between the two capacitor banks.)

Prior to the interruption, capacitive current is flowing in the inductance L_1 and consequently voltage e_3 is larger than e_1. When the current is interrupted at t_1, and if the current in C_1 is assumed to be very small, the induced voltage in the inductance L_1 disappears and consequently voltage e_3 has to become equal to e_1. Such a change in the oscillatory circuit L_1C_1 cannot happen instantly but is accomplished by a transient with a frequency equal to the natural frequency of the circuit f_1 and an initial amplitude equal to the disappearing induced voltage in L_1.

The voltage across the circuit breaker, the transient recovery voltage is approximately:

$$v = e_3 - e_c = -E_1 \cos 2\pi 60t - (E_c - E_1)\epsilon^{-kt} \cos 2\pi f_1 t + E_c$$

If no line bank is present the initial part of the transient is rapid and is determined almost entirely by the high frequency component because during this time $\cos 2\pi 60t$ remains practically constant.

$$v = (E_c - E_1)(1 - \epsilon^{-kt} \cos 2\pi f_1 t) \quad \text{(approximately)}$$

This transient voltage has a first crest of nearly twice the steady voltage drop in the source reactance and a frequency as determined by the circuit on the source side of the circuit breaker. Consequently this initial transient is completely determined by the size of the load bank (amplitude) and the characteristics of the system to which this bank is switched (amplitude and frequency) but is independent of the characteristics of the circuit breaker, assuming that for the load currents of capacitor banks the circuit breaker has negligible arc voltage and negligible post-arc conductivity.

If the transient is slow as shown on Figure 4, the insulation strength, v_t, at a short contact separation will exceed the recovery voltage up to time t_2. Consequently the arc is extinguished at t_1, a short arc extinction time, but restrikes at t_2.

A parallel bank connected to the system probably will make the natural frequency so low that the initial part of the recovery transient is determined by both the natural frequency and system frequency components. The rate of rise of voltage across the circuit breaker contacts is then so low that arc extinction occurs at the first current zero. Figures 5 and 6 show two cathode-ray oscillograms taken of the recovery voltage under identical circumstances except that in the case of Figure 6 a line bank was present. A low frequency of the transient component prevents any significant potential from appearing across the arc gap during the initial part of the transient recovery voltage. This shows that the importance of the transient component disappears when its frequency is reduced to only a few hundred cycles per second by the addition of a parallel bank.

The Recovery of Dielectric Strength

The recovery of the dielectric strength in the circuit breaker which is shown by dotted lines v_t, v_t', and v_t'' on Figure 3 will be determined by the characteristics of the circuit breaker and the current which is interrupted but is not influenced by the presence of a parallel bank. At any given current zero, an initial "dielectric strength" is available and depends on the contact separation and deionizing means. During the following half-cycle it increases as indicated, due to deionization and lengthening of the gaps.

If the current zero occurs with a contact separation which gives a recovery of dielectric strength corresponding to v_t the fast rising recovery voltage will cause the arc to reignite with no perceptible (on a magnetic oscillograph) pause in the current wave. The current will flow until a subsequent current zero at which time a greater contact separation may give a recovery of dielectric strength corresponding to v_t'. Since the dielectric strength now exceeds the high frequency component of the recovery voltage, the arc will extinguish but will restrike at t_2. If the dielectric strength has increased to curve v_t'' the recovery voltage never exceeds it and no restriking occurs. For other circuit breaker characteristics the slope of the curve may be greater and any gap which will cause extinction at t_1 will not restrike.

Recovery of Dielectric Strength and Restriking

To obtain restrike-free performance from a circuit breaker, the recovery of dielectric strength must exceed the recovery voltage at all times after the arc extinguishes. With an "infinite" source, $L_1 = 0$, the initial transient in the recovery voltage disappears and only a system frequency voltage appears across the circuit breaker contacts reaching a maximum in 1/2 cycle. By adequate speed, forced oil flow, blast of compressed air and so forth, a circuit breaker can be made to restore its dielectric strength at this rate or faster and it extinguishes the arc without restrikes at the first current zero, even if the contacts separate at that instant. Many circuit breakers do not meet this requirement and restrike.

The source inductance is, of course, never zero and the natural frequency component of the recovery voltage is always present. However, as already mentioned, the frequency may be so low when a load bank is connected that the natural frequency component is negligible in the comparison with the recovery of dielectric strength and consequently the performance is the same as with an infinite source.

When the source is not infinite and there is no parallel bank, the initial part of the transient may lengthen the arcing, causing the currents in one or more phases to pass through zeros without extinguishing. On these circuits, circuit breakers may operate restrike-free in one range of current and restrike in another as shown by the experimental data in this paper.

The Phenomena Discussed for Single-Phase Circuits is Basically the Same for 3-Phase Circuits and for a Resistance-Inserting Circuit Breaker

The discussion of restriking is on the basis of the single-phase diagram but the

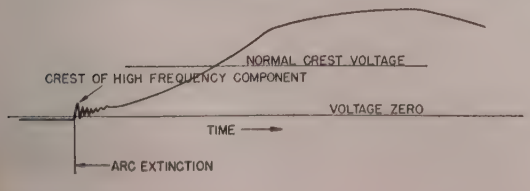

Figure 5 (below). Cathode ray oscillogram of recovery voltage across a circuit breaker with no parallel bank. Crest of high-frequency component caused reignition of arc at two previous current zeros

Figure 6 (right). Recovery voltage for condition identical to Figure 5 except a parallel bank was connected

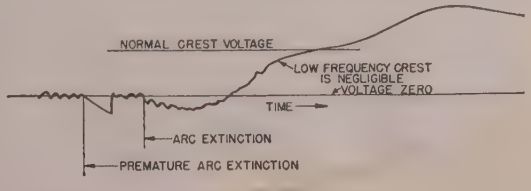

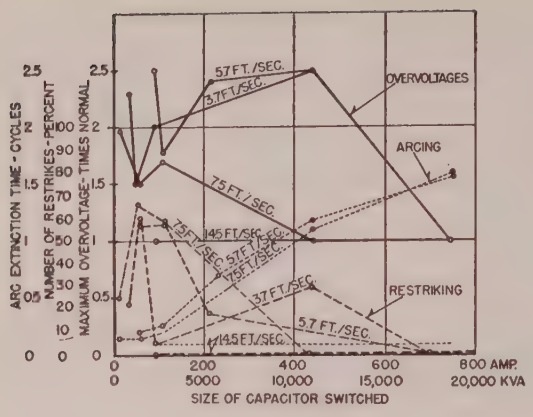

Figure 7 (left). Switching capacitors on a 14.4-kv circuit capable of producing a short circuit of 110 megavolt-amperes. Notice erratic performance at 3.7 feet per second

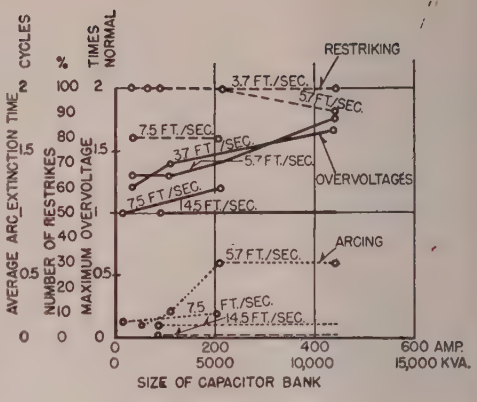

Figure 8 (right). A comparison with Figure 7 shows the effects of earlier arc extinction caused by an 8,000-kvar parallel capacitor bank

principles apply equally well to 3-phase switching and to the first step of capacitor switching by inserting resistance. In the case of 3-phase switching with ungrounded neutrals, the system frequency component of the transient recovery voltage reaches a value of approximately 2.5 times the normal phase-to-ground voltage due to a neutral shift after the first phase opens. The single-phase circuit would give about 2.0 times. If step-type interruption is used, the 2.5 times of the 3-phase circuit is reduced by an amount depending on the value of the resistor which is being inserted. The voltage on the source side is relatively independent of the resistor so the difference in recovery voltage on the circuit breaker will be caused by the voltage change on the capacitor as its charge is drained by the resistor.

The current flowing through the resistor is proportional to the voltage across it, so the initial draining of charge is small and a relatively low resistance must be used to make a significant reduction in the voltage at the end of the first half cycle.[2] At the time of current zero a resistor tends to keep the voltages equal on both sides of the circuit breaker and may prevent the initial voltage impulse from being able to reignite the arc. Thus early extinctions before adequate gaps are obtained may be produced.

This occurred on two series of tests when resistors were added to give 2-step interruption. Both sets of resistors increased the number of restrikes from about 60 to 100 per cent.

The Effect of the Size of the Capacitor Bank

The effects of varying the size of the capacitor bank at a given location and with no line bank, were determined by tests made at 14.4 kv on a circuit which could supply 110-megavolt-ampere short-circuit power. The results are shown in Figure 7. Except at the highest contact speed, arc extinction time increased almost linearly with the size of the capacitor bank. The number of restrikes were zero for large capacitor banks, but as the size of the bank was reduced the number of restrikes fluctuated widely, particularly with contact speeds of 3.7 feet per second as mentioned previously. Each of the points in Figure 7 is based on from 12 to 21 openings of the 3-phase bank and a larger number of tests should not have made a large shift in the location of a point.

The maximum overvoltages which are important criterions of the performance, fluctuated with the number of restrikes in general being lower when restrikes were more likely to occur. Restrikes usually occurred only in one of the three phases and repeated restrikes were exceptional. The largest overvoltage on the capacitor occurred in those exceptional cases when two of the phases restruck simultaneously while the third phase remained interrupted. The overvoltage above ground reached 2.5 times normal in both of the restriking phases with opposite polarity. For this voltage, the individual capacitors are subjected to voltages of 2.5 times their normal crest voltages if they are star-connected and $5/\sqrt{3}$ or 2.9 times if they are delta-connected.

The effect of speed in eliminating restriking is shown by the restrike-free performance at 14.5 feet per second. Although only one point is shown for this curve it is established because larger capacitor banks were switched without restriking on circuits of larger short-circuit power.

A Parallel Bank Increases the Tendency to Restrike

Striking differences in the switching performance are caused by the presence of a parallel bank. They are apparent from a comparison of Figures 7 and 8 which show corresponding data taken under identical circumstances except that in the case of Figure 8 a parallel bank of about 8,000 reactive kilovolt-amperes was connected on the source side of the circuit breaker.

Restrikes which usually had been limited to one in one of the phases and had occurred on some of the tests (from 0 to 80 per cent at a current setting) increased, when a parallel bank was added, to several in all of the phases and on all of the operations except for the tests at 14.5 feet per second which were restrike-free. At no other speed was statistically completely restrike-free operation observed with a parallel bank and even single restrike-free operations were quite exceptional. The restrikes in each phase were of short duration, high current intensity, high frequency, rapid attentuation and were usually repeated from one to six times at short intervals during a period of about 3/4 cycle.

Characteristic are the data given in Table I which refer to an 11,000-kva load bank at 14.4 kv and a contact parting speed of 5.7 feet per second:

Table I

Per Cent of Restrikes	Maximum Over-voltage Times Normal	Average Arc Extinction Time In Cycles
No parallel bank	9	2.5	1.2
30-kva parallel bank	33	2.5	0.8
8,000-kva parallel bank	90	1.8	0.5

Oscillograms in Figures 9 and 10 illustrate the differences in the phenomena. The origin of these differences is that the presence of a parallel bank reduces the initial rate of rise of recovery voltage across the circuit breaker and causes the arc to become extinguished at the first current zero, at which time the recovery of dielectric strength cannot prevent re-

striking except at very high contact speeds.

A Parallel Bank Reduces the Overvoltages

On the other hand, the overvoltage is bound to be relatively small with the presence of a line bank comparable in size to the load bank, since at the instant of the restrike i_2 the two banks are charged at different potentials (Figure 3) and are discharged against each other by the restrike. Consequently, their voltage tends to an intermediate value determined by their relative capacitances. The larger the line bank, the lower the amplitude of the voltage transient of the combined banks which oscillate with the inductance L_1.

The parallel banks, by increasing the tendency to extinguish the arc early, at small contact separations, also limit the voltage which can appear across the circuit breaker by the lower dielectric strength of the arc spaces. If the recovery voltage exceeds the dielectric strength, a restrike occurs and the transient equalizes the voltages on the two sides of the interrupter but the amplitude of the transient voltage is small and does not produce high overvoltages. The current of the restrike may leave the bank charged at less than a normal crest voltage and thereby reduce the voltage which can subsequently appear across the circuit breaker.

Both of these limiting actions have been discussed previously but another action of the parallel bank which was equally effective was observed in the oscillograms taken on these tests. Theoretical studies have assumed that the arc would extinguish at a normal current zero leaving the capacitor charged to the crest of its normal voltage. The arc in a capacitive circuit is no different than the arc in an inductive circuit and oscillograms on power circuit breakers have shown that such arcs may become unstable as they approach zero.[3] The instability is greater at relatively small currents and is observed throughout the range of currents encountered in capacitor switching. The instability of an arc is increased if a large capacitance is on the source side of the circuit breaker since a sudden decrease in the arc current is not accompanied by a large and rapid rise of voltage to sustain the arc. If in Figure 2 capacitances C_1 and C_2 are equal and the arc becomes unstable when $e_c = 0.8$ of E_c the arc interrupts the circuits and all of the current flowing through L_1 is forced to flow into C_1. This doubles the current flowing in C_1 and momentarily its voltage begins to rise at double its previous rate, $de/dt = i/C$. However, the voltage on C_1 reaches less than $0.8\,E_c + 2 \times 0.2\,E_c = 1.2E$ as higher voltage rise at C_1 reduces the current more rapidly to zero. Thus a parallel bank increases the instability of the arc and leaves the disconnected bank charged to less than crest voltage. This phenomena was so common on these tests that a cathode-ray oscillogram to illustrate the effect of the parallel bank on the transient recovery voltage could not be found with an interruption at a normal current zero. Consequently, Figure 6 also illustrates an interruption which left the capacitor charged to about 90 per cent of crest voltage.

In these three ways parallel banks so effectively facilitate interruption that even though several restrikes occur, the overvoltages are under 2.0 times normal.

A Parallel Bank Increases the Momentary Currents

When one capacitor bank is connected to another by the closing of a switch, or by a restrike, any difference of potential between the two banks is eliminated by a redistribution of charge. The equalizing current i_m flows through the switch and the small inductances of the connecting circuits L_2 and L_3 of Figure 2. The frequency and current of this equalizing transient are high:

$$f_2 = \frac{1}{2\pi \sqrt{(L_2+L_3)\,\dfrac{C_1 C_2}{C_1+C_2}}}$$

$$i_m = \frac{E_2 - E_c}{2\pi f_2 (L_2+L_3)} \sin 2\pi f_2 t$$

(approximately the maximum)

which reduces to:

$$I_m = (E_2 - E_c)\sqrt{\frac{C_1 C_2}{(C_1+C_2)(L_2+L_3)}} \times \sin \sqrt{\frac{C_1+C_2}{C_1 C_2 (L_2+L_3)}}\, t$$

The ratio of the maximum momentary current to the steady-state current (of a 3-phase capacitor) would be approximately:

$$\frac{I_m}{i_n} = 0.0066 \sqrt{\frac{C_1}{C_2} \times \frac{1}{(C_1+C_2)(L_2+L_3)}}$$

The inductances are not independent of the capacitances because an increase in the size of a capacitor bank causes an increase in physical dimensions and an increase in the inductance of the circuits.

For the various circuits used in the laboratory tests, the peak currents with parallel capacitors were up to 70 times the normal peak current and about four times larger than without parallel banks.

General Relationships are Disclosed by These Data

Knowing the performance of a circuit breaker switching various sized banks at a given location, with or without a parallel capacitor bank, leads to a general understanding of the phenomena and of what can be expected, but the possible combinations of power systems, circuit breakers, and capacitor banks are so

Figure 9. Switching an 11,000-kvar 14.4-kv bank of capacitors with no parallel capacitor bank

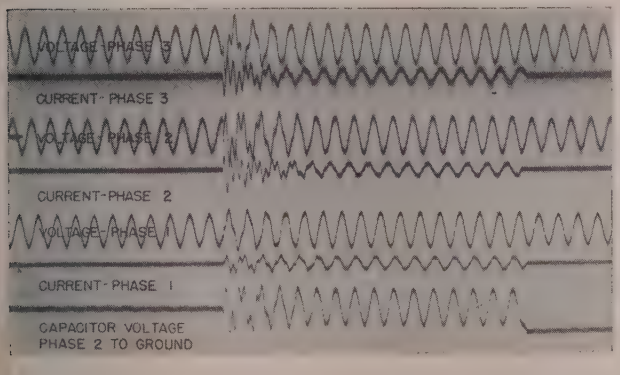

Figure 10. Switching a 11,000-kva 14.4-kv bank of capacitors with an 8,000-kvar 14.4-kv bank on the line

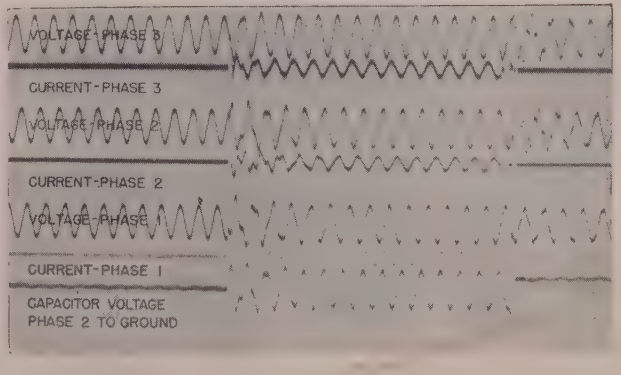

numerous that it is not always easy to estimate the performance for a new set of conditions from the known performance under another set. The tests show that the performance can be predicted if at a number of capacitor steps through the permissible current range, a determination is made of the value of the minimum source impedance L_1 (or inversely the short circuit current) which produces restrike-free operation.

Arc Extinction Time Proportional to Amplitude of High-Frequency Component of Recovery Voltage

The transient component of the recovery voltage determines when the arc is extinguished. The tests show that if this transient component has a frequency of over a few thousand cycles per second, its amplitude and the arc extinction time are directly proportional. Consequently, it determines the contact separation and dielectric strength of the arc gap at the time of arc extinction. At the time of current zero, this high frequency component imposes a recovery voltage on the circuit breaker similar to the recovery voltage of a lower voltage inductive circuit. Consequently, the initial value of dielectric strength V_{i_0} Figure 3 must be appreciable to accomplish an interruption and the minimum arc extinction time increases with the amplitude of this voltage.

This is demonstrated in Figure 11 by data taken with a contact speed of 7.5 feet per second and 14.4 kv with various values of load capacitor bank C_2 and source impedance L_1. The average arc extinction time varied almost linearly with the part of the voltage drop in L_1 caused by the current of the capacitor C_2. The deviation near zero might be accounted for by the nonlinear relation between arc extinction time and gap between contacts caused by the shapes of the moving contacts, stationary contacts and arcing horns, and by the acceleration of the contacts.

Table II

Size of Load Bank, Kva	Restrike-Free if Arc Extinction Time Exceeds Cycles
1,400	0.25
2,800	0.5
5,600	1.0
11,200	1.5
18,000	1.5

The data also indicates that the arc extinction time is independent of the size of the capacitor bank. The numbers at the plotted points give the size of the capacitor bank in megavolt-amperes and points for both 2.8 and 18 megavolt-amperes fall along a large part of the curve.

The results, therefore, indicate that the average extinction time is dependent only on the voltage drop in L_1 caused by the current of the capacitor C_2.

$$E_1 - E_2 = 2\pi f L_1 \times E_c 2\pi f C_2$$
$$= (2\pi f)^2 L_1 C_2 E_c$$

For a given product of L_1C_2 this voltage drop and the amplitude of the transient component of the recovery voltage was constant. Since the arc extinction times are equal, it follows that the initial dielectric strength at these times, or contact separations, must be equal and therefore is relatively independent of the current interrupted. This appears reasonable because these currents of less than 1,000 amperes produce no significant post-arc conductivity in the arc space of oil circuit breakers.[4] Any dependence that may exist is concealed by the inherent randomness of the phenomena and the inaccuracies of the measurements.

Arc Extinction Times Which Produce Restrike-Free Performance are a Function of Current

On Figure 11 black dots indicate the settings where restrikes occurred. Although the general trend is for the operation to become restrike-free at large per-unit voltage drops and corresponding longer arc extinction times, the minimum voltage drop or arc extinction time where the operation becomes restrike-free is a function of the interrupted current, or the size of the capacitor bank. For example as shown on Figure 11 with a bank of 18,000 kva restrikes occur as high as 0.09 per-unit voltage drop or 0.095 cycle average arc extinction time while on a bank of 2,800 kva the highest per-unit voltage drop where restrikes were measured is 0.058.

More specifically for every value of capacitor current the operation becomes restrike-free if the arc extinction time exceeds a critical value. This critical value can be determined easily from oscillograms. For example for the oil circuit breaker tested at 14.4 kv and 5.7 feet per second contact speed, the minimum restrike-free arc extinction time increases almost directly in proportion to the size of the smaller banks and less rapidly for larger banks. See Table II.

Although the initial recovery of dielectric strength is relatively independent of the current interrupted (in the range of capacitor bank currents), this indicates that the dielectric recovery which follows through the next half-cycle is dependent on the current which has been passing through the arc. Possibly the initial recovery is the recovery of an ionized arc path between contacts and the subse-

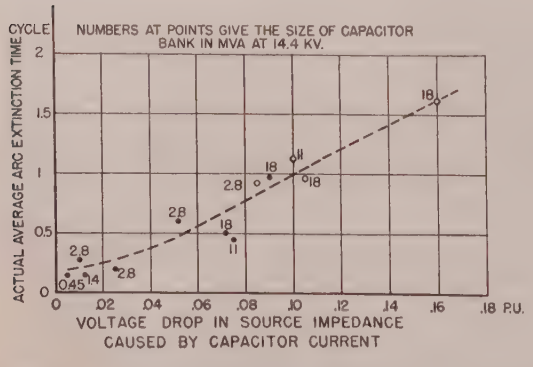

Figure 11. Arc extinction time varies almost linearly with the amplitude of the high frequency component of the recovery voltage

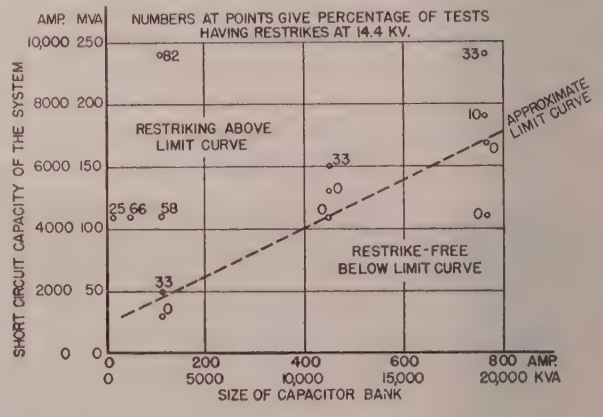

Figure 12. The operation is restrike-free if the maximum possible short circuit at the capacitor location is below a critical value indicated by the curve. This curve is for a "De-ion" grid oil circuit breaker switching a capacitor bank at 14.4 kv and having a 7.5-feet-per-second contact speed

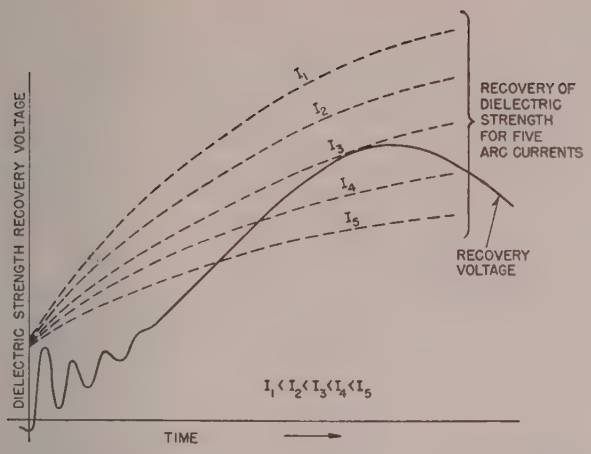

Figure 13. Interruption at the *nth* current zero. Dielectric strength a half cycle after arc extinction and at a given contact separation varies with current interrupted

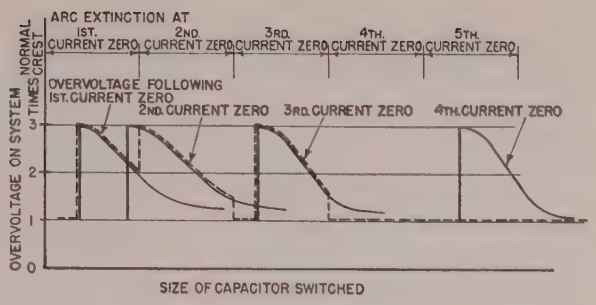

Figure 15. Overvoltages vary with the size of the capacitor bank which is being switched. If the contact movement is slow and several current zeros are passed to reach the arc extinction time of the largest banks, zones of high and low overvoltages alternate as the size of the capacitor is increased

quent recovery is the increase in dielectric strength of an increasing gap in a mixture of oil and gas. The larger the current and the longer the arc, the greater the amount of gas between contacts and the slower the recovery of dielectric strength.

It should be recognized clearly that the actual average arc extinction time is completely independent of the minimum arc extinction time at which the operation is restrike-free. The actual arc extinction time is determined solely by the high frequency component of the recovery voltage and may be either shorter or longer than the minimum restrike-free arc extinction time. It, in turn, is dependent only of the size of capacitor bank, and the voltage. If the actual arc extinction time is longer than the minimum restrike-free arc extinction time the operation will be restrike-free. If it is shorter the circuit breaker restrikes.

Restrike-Free Operation is Obtained when Short-Circuit Current is Below a Critical Value which is a Function of Capacitor Current

The voltage drop in the source inductance caused by load bank current was expressed as per-unit voltage, a value which is significant as representing the approximate voltage regulation caused by connecting or disconnecting the capacitor bank. Another related and significant quantity is the short-circuit power which can flow at the location of the bank. This is inversely proportional to the source inductance L_1 and therefore inversely proportional to the voltage drop through it caused by the capacitor bank. Consequently, the lower the short circuit current at a capacitor location, the higher will be the per-unit voltage drop caused by the capacitor, and the longer the average arc extinction time. At some value (called in the following "Critical short circuit current") the average arc extinction time exceeds the minimum time which produces restrike-free performance. For all lower values of short-circuit current the performance is restrike-free. For convenience, the critical value can be expressed as critical short-circuit power.

In a co-ordinate system of load-capacitor kilovolt-amperes versus system short-circuit kilovolt-amperes, these values of the critical short circuit power represent a limit curve which divides the plane into a restrike-free and a restriking region as shown in Figure 12. This figure illustrates the relations for 14.4 kv and 7.5 feet per second contact speed with no parallel bank on the line. It also contains points of actual measurement which serve as verification of this curve. Approximation of this limit curve is possible in the form of a straight line which has the equation:

$$\text{short circuit kva} = 25 + 0.0075 \times \text{capacitor mva}$$

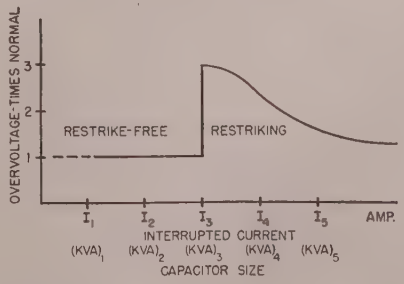

Figure 14. Interruption at the *nth* current zero. Overvoltages produced by a switching operation are highest when the currents are near the range of restrike-free operation

Similar relations can be established at other contact speeds and voltages.

Infrequent Restriking Produced the Highest Overvoltages

In general, overvoltages were higher when their occurrence was less frequent. To show the reason, it may be assumed that although current varies, the arc reaches a current zero and extinguishes always at the same arc extinction time and contact separation. This can be obtained by varying the inductance to keep the product of L_1C_2 constant. This also will keep the first crest of the recovery voltage at approximately the same value. The recovery voltage would vary with current as the frequency of one component depends on L_1C_1. However, as this frequency is many times 60 cycles the recovery voltage will be assumed identical for all currents and is shown in Figure 13. The recovery of dielectric strength is adequate for an initial arc extinction and if the current has been sufficiently low, I_1 or I_2, the arc will not restrike. With a larger current I_3 the recovery voltage equals the dielectric strength and the arc restrikes.

With system voltage close to crest at this time and the recovery voltage on the circuit breaker about 2 times normal, or 2.5 times normal voltage for 3-phase conditions, an undamped restrike would produce 3 or 3.5 times normal phase-to-ground voltage. (The tests on 3-phase ungrounded circuits, did not exceed 2.5 times normal because of inherent modifying influences.) For still larger currents I_4 and I_5, restrikes also occur but below peak voltage and the magnitude of the overvoltage decreases as shown qualitatively in Figure 14. This type of operation produces the highest voltages when the circuit breaker is operating close to the restrike-free range. This is in agreement with the test data providing one

other type of occasional restrike is recognized and excepted.

In series of tests which were otherwise restrike-free, occasional restrikes have occurred after a current pause of generally less than 1/4 cycle and after an arc extinction definitely earlier than those on the restrike-free operations. For these tests the current zero and arc extinction occurred practically simultaneously with contact parting. In one instance, the other tests in the series did not have any arc extinction occurring at a current zero which came within the first half-cycle. The oscillograph showed that the contacts separated at current zero and perhaps oil filled the gap to sustain low voltages. However, the moving contact had some overlap with the stationary contact and the gap increased rather slowly with respect to contact movement for the first quarter inch. The arc restruck after about 1/8 inch of contact travel or 1/12 cycle of current pause. A ripple occurred in both the current and voltage, but both were entirely negligible. Such restrikes, occurring with otherwise restrike-free operation, do not produce high overvoltages.

The Irregular Variation of Restriking and Overvoltages with Capacitor Size was Caused by Arc Extinction Time Varying Over Several Current Zeros

The variation of performance with size of bank is of direct interest when capacitors are to be added to an existing installation or for selecting an initial installation. As was mentioned earlier, irregular and unexplained performance, Figure 7, was obtained on early tests when the size of the 14.4-kv capacitor bank was varied, all other conditions remaining the same. The tests which followed and the relations discussed in this paper explain this performance.

The arcing time increased in proportion to the size of the capacitor bank and the corresponding voltage drop in the source impedance. The discussion of the relation of the initial peak of the transient recovery voltage to the arc extinction time and the size of capacitor being switched is in agreement with this.

If it is assumed, that the contacts always part at a particular point on the current wave, the first current zero in the arcs will always occur at time t and subsequent current zeros at intervals of 1/2 cycle for single-phase systems, or 1/6 cycle for 3-phase systems. Arc extinction time will lengthen in finite and equal steps with increase in capacitor size, because the arc can be extinguished only at or near a current zero.

At each current zero, the magnitude of the restrike generated overvoltage as a function of the capacitor size can be represented by a curve of the general nature of Figure 14.

If the curves for the overvoltages, produced after each current zero, are superimposed as shown in Figure 15, the performance over the whole range can be seen. As indicated at the top, it is assumed that arcs corresponding to capacitor sizes in the lowest 1/5 of the range shown are extinguished at the first current zero, that arcs for the next 1/5 are extinguished at the second current zero and so on. Overvoltages following the first current zero do not occur on the smallest sizes of capacitors as the recovery of dielectric strength prevents restriking. At a critical value, restriking starts and the overvoltages are a maximum. Further increase in size results in lower overvoltages until the size of capacitor is reached which does not extinguish at the first current zero. As shown by the curve, the recovery of dielectric strength is not rapid enough to withstand the recovery voltage and restriking always occurs after an arc extinction at this current zero but the peak voltage is slightly less than the maximum overvoltage.

The smaller of the currents which are not extinguished until the third current zero may stay extinguished but the larger ones are in the restriking range. Currents not extinguished until the fourth or fifth current zero will be restrike-free. This is the kind of performance shown in Figure 7 for a contact speed of 3.7 feet per second. The rate of dielectric recovery was low and the conditions paralleled those assumed for Figure 15.

Conclusion

Capacitor switching performance of a circuit breaker depends on the system supplying the power as well as on the size of the capacitor bank.

Restrike-free operation may be obtained at all system locations from circuit breakers which develop dielectric strength between contacts, at any initial contact spacing, faster than the system can apply voltage across its contacts.

Restrike-free operation also can be obtained from other circuit breakers used at locations where the initial part of the recovery voltage prevents the extinction of the arc until the contact spacing is large enough for the circuit breaker to develop dielectric strength faster than the system can apply voltage across its contacts.

A circuit breaker switching a capacitor bank with no parallel bank, operates restrike-free if the short-circuit capacity of the power source is below a critical value which is a function of capacitor size.

Parallel banks connected to the system increase the tendency to restrike and produce large momentary currents on closing and restriking, but reduce the magnitude of the overvoltages.

References

1. The Interruption of Charging Current at High Voltage, **W. M. Leeds, R. C. Van Sickle.** *AIEE Transactions*, volume 66, 1947, pages 373–82.

2. Resistors for 138 kv Cable Switching, **E. K. Sadler, T. M. Blakeslee.** *AIEE Transactions*, volume 66, 1947, pages 39–50.

3. Breaker Performance Studied by Cathode-Ray Oscillograms, **R. C. Van Sickle.** *Electrical Engineering* (*AIEE Transactions*), volume 54, February 1935, pages 178–84.

4. Transient Recovery Voltages and Circuit Breaker Performance, **R. C. Van Sickle.** *Electrical Engineering* (*AIEE Transactions*), volume 61, November 1942, pages 804–13.

Discussion

N. R. Schultz (General Electric Company, Schenectady, N. Y.): The authors of this paper have made an important contribution toward a better understanding of the capacitor switching problem. Their conclusion that the performance of a circuit breaker on capacitor switching depends on the characteristics of the power supply system as well as on the size of the capacitor bank switched is of particular interest.

The writer would like to call attention to Figure 12 of the paper, which illustrates an approximate limit curve for a particular circuit breaker. This curve is plotted with size of capacitor bank as the abscissa and short-circuit capacity of the supply system as the ordinate. The area above the limit curve is the zone in which restriking occurs, and the area below the curve is a restrike-free zone.

It is possible to plot on the same set of co-ordinates curves showing the voltage change caused by switching a given capacitor bank on a given system. These curves can be plotted from the relationship:

$$\text{Per cent voltage change} = \frac{100 \times \text{capacitor kilovolt amperes}}{\text{System short-circuit kilovolt amperes}}$$

In Figure 1 of the discussion the writer has replotted Figure 12 of the paper and curves for capacitor banks which would cause voltage changes of 1, 2, 5, and 10 per cent when switched. In most practical capacitor applications, the voltage change

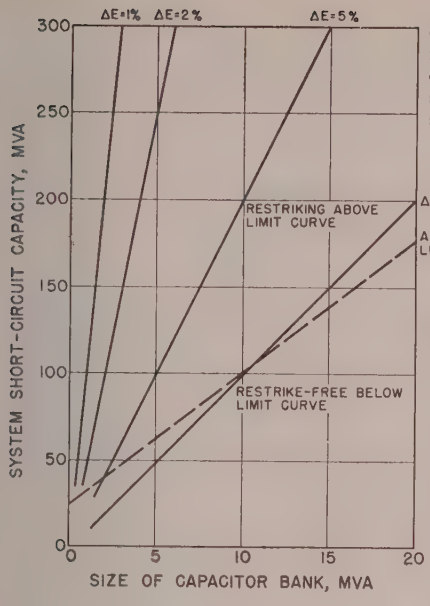

Figure 1

due to switching a bank is limited to the order of 2 or 3 per cent. It would, therefore, appear that most of the switched capacitor applications will fall in an area well above the limit curve, and consequently restriking of the circuit breaker could be anticipated.

E. B. Rietz and **C. J. Balentine** (General Electric Company, Philadelphia, Pa.): I think the electrical industry should be very appreciative of the investigation which is reported in this paper. Although the problems associated with the switching of capacitor banks and the de-energizing of long transmission lines have been known for a number of years, it is quite true that they have not been common knowledge. This paper makes some of this background available for general use, and I am quite sure will be welcome information to the users as they consider an increased use of capacitor banks for power factor correction and increased use of high-voltage cables and longer transmission lines.

The General Electric Company also has been working along similar lines. Our investigations cover many tests on capacitor switching phenomena on all the types of circuit breakers referred to in the paper. At the present time, we have a pretty complete knowledge of the capacitor switching ability of all types of outdoor oil circuit breakers, of indoor magnetic-type circuit breakers, and of indoor compressed air circuit breakers. A rough check indicates that the tests made to obtain this information would total almost 2,500, even more than enumerated by the authors.

Restrike-free operation, as stated, can be obtained by building up the dielectric strength between the contacts faster than the system can apply voltage across the contacts.

This is not easy to do with a circuit breaker having interrupters which use the current in the arc to build up pressure to move oil into the arc stream. Other types of circuit breakers, however, which make available at the moment of contact parting an insulating medium of high dielectric strength, can be expected to give this restrike-free operation. Examples of this are the low-oil-content impulse circuit breaker and compressed-air circuit breakers.

While the ideal situation undoubtedly is to utilize restrike-free circuit breakers, the essential criterion is whether the overvoltages developed during capacitor switching become dangerous to associated equipment. Therefore, there are other means of reaching this objective, such as resistors shunted across the interrupter breaks or auxiliary oil pistons; both of these, in effect, limit the voltage generated to a relatively safe value. In the case of resistors, the criterion has been established as twice normal. It would appear from published literature that a value of 2.5 is used with auxiliary oil pistons.

F. M. Porter and **C. P. Zimmerman** (American Gas And Electric Service Corporation, New York, N. Y.): It is gratifying to note that extensive tests are being made by manufacturers of switching equipment to determine the maximum amount of reactive kilovolt-amperes that can be switched safely and satisfactorily by various types of circuit breakers. Data derived from such tests will alleviate the apprehensions that many of us have had when considering the installation and switching of capacitor banks at substations.

It appears that the determination of the maximum size of capacitor banks that can be switched is based on the number of restrikes and the limitation of the maximum overvoltages that may be encountered during switching operations. It is believed that such a basis for determination is incomplete and may be misleading to prospective users of capacitors.

Tests and studies that have been made generally conclude that air-blast or magnetic-type blast circuit breakers, because of their faster opening speed, can do a better job of switching capacitors both in limiting the frequency and magnitude of restrike voltages and, on this basis, relatively larger banks can be switched with such circuit breakers than by standard oil circuit breakers. However, such circuit breakers cost somewhat more than oil circuit breakers, making it desirable on the part of those concerned with selecting circuit breakers for capacitor applications to take into account the relative merits of the two types from the standpoint of maintenance. With air-blast circuit breakers or magnetic-type blast circuit breakers, there is no problem of frequent check and replacement of the oil due to decontamination caused by repetitive switching, as is encountered with oil circuit breakers for multistep banks. Since the contact structures of air-blast and oil circuit breakers are quite different, and as a matter of fact they are different also in various types of oil circuit breakers, the number of operations of a circuit breaker before inspection or maintenance is required, is variable. It would, therefore, be desirable that the figures for maximum reactive kilovolt-amperes that can be switched without getting into overvoltage difficulties be tempered or supplemented with data showing the number of operations that each particular circuit breaker can be expected to experience in switching various sizes of capacitor banks without requiring inspection or maintenance of the contacts and oil. It has been our experience that some types of circuit breakers recommended by manufacturers for switching capacitors at 15 kv and below do not stand up as well as others, and therefore repetitive tests in the various types of circuit breakers should be undertaken by the several manufacturers. Also, tests should be made in switching of high-voltage banks and these data made available for the benefit of those interested in such installations.

Collection of data by utilities having capacitor banks of all voltage ratings also will help in determining which circuit breakers are more suitable for these applications.

R. C. Van Sickle: Mr. Schultz brought out a good point in calling attention to the system voltage change caused by capacitor switching in the restrike-free region of Figure 12 of the paper. It emphasizes the need for considering the impedance of the source when evaluating the significance of test data indicating restrike-free performance of circuit breakers. When I first noticed this relation, I used it to check such data in a paper already published[1] and found that the voltage change produced by switching was from 7.8 to 45.5 per cent, values well above the 2 or 3 per cent suggested as practical limits by Mr. Schultz.

Messrs. Rietz and Balentine included a remark that the sizes of resistors were chosen to limit overvoltages to 2.0 times and that published literature indicated an overvoltage limit of 2.5 with oil pistons. I would like to call your attention to the statement in the paper that during the tests on the oil circuit breakers no voltages in excess of 2.5 times normal were reached. Some of these tests were made with plain-break oil circuit breakers. Auxiliary oil pistons with adequate driving force to produce the extinction of charging currents not only reduce the magnitude but also the frequency of occurrence of overvoltages. Our tests, as reported in the paper, showed that conditions which had produced restrikes on about 60 per cent of the tests without resistors produced restrikes on all tests when resistors were added. A small reduction in overvoltage can be offset by the frequency with which overvoltages are produced.

Reference

1. Tests and Analysis of Circuit-Breaker Performance When Switching Large Capacitor Banks, T. W. Schroeder, E. W. Boehne, J. W. Butler. *Electrical Engineering* (*AIEE Transactions*), volume 61, November 1942, pages 821-31.

Thermal Expansion Effects in Power Cables

C. S. SCHIFREEN
MEMBER AIEE

DESIGN of underground plant to permit operation of paper and lead cables at maximum loadings consistent with reasonable life requires an intimate knowledge of conductor temperature, magnitude of cable movement during load cycles, and the effect of such move ment on life of the cable-sheathing. While much work has been done to develop a quantitative evaluation of many of these factors[1–9] little information has been published to make available a practical method of estimating the amount of cable movement to be provided for, and of evaluating the effects of cable construction upon cable movement and related sheath strains.

Data developed from laboratory investigations of the thermal expansion characteristics of duct-type 69-kv and 15-kv paper and lead cables are presented in this paper. These data permit computation of cable movement at duct mouths in manholes for various cable constructions, and offer a basis for practical comparative evaluation of such constructions.

Thermal Expansion Tests

Heat runs were conducted in the laboratory on 100-foot samples of the various cable constructions described in Table I. One end of each sample was successively unrestrained to allow "free" expansion; partially restrained to allow cable movement with increasing conductor temperature only after a predetermined value of compressive force was developed and then held constant; and totally restrained by applying the minimum forces required to prevent cable movement at the duct mouth with increasing temperatures. The other end of each 100-foot sample was permanently fixed so that the expansion measured at the moveable end was indicative of the amount of cable movement to be expected at either end of a flat and straight 200-foot stretch of cable for similar restraint at both duct mouths.

The ducts were installed with the aid of a transit to assure horizontal linearity. Split ducts were used to allow drawing a device along the duct structure on angle-iron rails to record the horizontal and vertical components of cable snaking. The top halves of the ducts were tied in place from time to time at the few points where needed to confine all cable snaking within the limits of the duct space.

Test Results

Longitudinal Thermal Expansion

The test results disclosed a rational influence of cable construction upon thermal expansion. Figure 1 shows a significant parallelism to the free thermal expansion rate of bar copper for the zero-, 750-pound and 1,500-pound restraint curves of a large single-conductor 69-kv cable (Sample 1). This linearity existed for conductor temperature rises in excess of that at which the entire cable developed the compressive reaction required to overcome the restraining force of friction and the force applied at the end of the sample.

Cable similar to Sample 1 also was tested in square terra cotta duct having $4^1/_4$-inch inside dimension and gave about 90 per cent of the movement observed in $4^1/_4$-inch round bore terra cotta duct. Similar heat runs on 69-kv single-conductor reinforced double-sheath high-pressure gas-filled cable (Sample 2) gave little less than those shown for Sample 1 construction, and were the same for tests in square and round bore ducts. Apparently, square duct has no merit as an expedient to minimize cable movement. All subsequent comparisons of the various cable constructions were therefore based upon tests on cable installed in the round ducts.

Three-conductor and triplex single-conductor cables are more compressible than large single-conductor cables, and consequently produce less cable move-

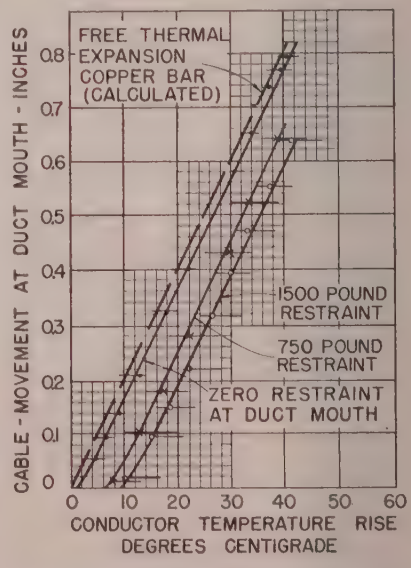

Figure 1. Longitudinal thermal expansion of 69-kv single-conductor oil-filled cable, sample 1

Dots, crosses, and open circles show rises (measured by change of resistance of test wire in conductor core) for zero, 750- and 1,500-pound restraint, respectively. Left and right ends of horizontal lines are temperatures measured by thermocouple in conductor core and by change of resistance of cable conductor, respectively

Paper 51-22, recommended by the AIEE Insulated Conductors Committee and approved by the AIEE Technical Program Committee for presentation at the AIEE Winter General Meeting, New York, N. Y., January 22–26, 1951. Manuscript submitted October 18, 1950; made available for printing November 17, 1950.

C. S. Schifreen is with the Philadelphia Electric Company, Philadelphia, Pa.

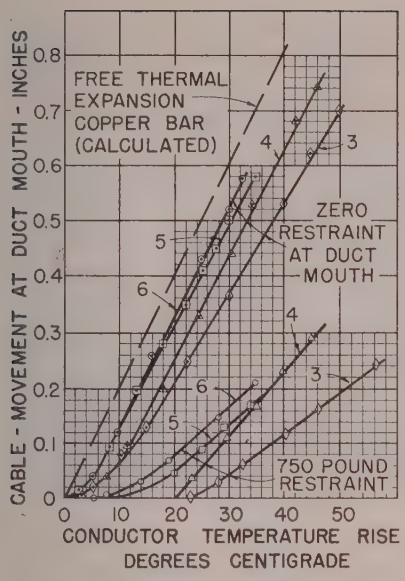
FREE THERMAL EXPANSION COPPER BAR (CALCULATED)
ZERO RESTRAINT AT DUCT MOUTH
750 POUND RESTRAINT
CABLE - MOVEMENT AT DUCT MOUTH - INCHES
CONDUCTOR TEMPERATURE RISE DEGREES CENTIGRADE

Figure 2. Longitudinal thermal expansion of 15-kv 3-conductor 350,000 circular mil cables

Sample 3 (belted, 60-inch lay); sample 4 (metal shielding tapes, 45-inch lay); samples 5 and 6 (carbon-black shielding tapes, 60-inch lay). Temperatures indicated as taken by thermocouples on conductors

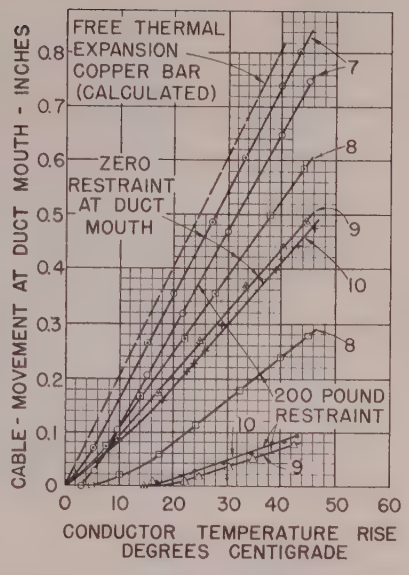
FREE THERMAL EXPANSION COPPER BAR (CALCULATED)
ZERO RESTRAINT AT DUCT MOUTH
200 POUND RESTRAINT
CABLE - MOVEMENT AT DUCT MOUTH - INCHES
CONDUCTOR TEMPERATURE RISE DEGREES CENTIGRADE

Figure 3. Longitudinal thermal expansion for 15-kv single-conductor cables

Sample 7 (parallel 500,000 circular-mils); Sample 8 (triplex 500,000 circular-mils, 48-inch lay); Sample 9 (triplex 350,000 circular-mils, 62.5-inch lay); Sample 10 (triplex 350,000 circular-mils, 37-inch lay). Temperatures indicated as taken by thermocouples on conductors of cables

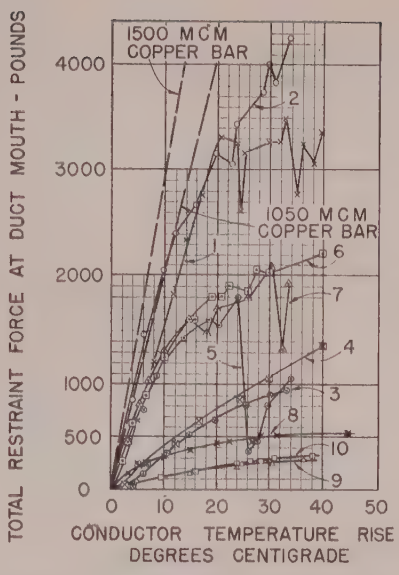
1500 MCM COPPER BAR
1050 MCM COPPER BAR
TOTAL RESTRAINT FORCE AT DUCT MOUTH - POUNDS
CONDUCTOR TEMPERATURE RISE DEGREES CENTIGRADE

Figure 4. Force required for total restraint

Sample 1 (69-kv single-conductor low-pressure oil-filled cable); Sample 2 (69-kv single-conductor high-pressure gas-filled cable). Other samples are described as given for Figures 2 and 3. The broken lines show calculated force required to restrain totally a copper bar

ment at the duct mouths. While the 15-kv 3-conductor cables at zero restraint are seen in Figure 2 to tend to parallel free bar-copper expansion, they give much lower rates of expansion under partial restraint. The triplex 350,000 circular-mil Samples 9 and 10, however, are seen in Figure 3 to have less expansion at 200-pound restraint than the 3-conductor samples are seen in Figure 2 to have at 750-pound restraint. In fact, the triplex cable partial restraint tests had to be rescheduled to 200 pounds because these cables were found to be totally restrained at values below 750 pounds. In contrast with this performance, the parallel lay Sample 7 (three straight single-conductor cables installed in the same duct) expanded at nearly the free copper rate for rises above 10 degrees, both at zero and 200 pounds restraint. It was interesting to observe that the weights of the triplex Samples 9 and 10 were sufficient to cause perceptible bird-caging of the cable adjacent to their fixed ends, even during the zero-restraint tests.

Forces Required for Total Restraint

Figure 4 shows considerable variations of forces required to restrain totally the various cable constructions tested. The 15-kv triplex 350,000 circular-mil cable Samples 9 and 10 required only about 200 pounds restraint to prevent movement at 20 degrees rise, while the 69-kv Sample 1 required about 3,300 pounds restraint at this rise, considerable snaking occurring at the higher conductor-temperature rises on this sample.

The forces required for total restraint on the various cables increased almost linearly up to about 15 degrees rise, indicating uniform compressibility within this range. At higher rises considerable snaking occurred, as seen, for example, in Figure 5(B). Considerable fluctuations in restraining forces were experienced once snaking existed with values of forces in excess of about 1,000 pounds on 15-kv 3-conductor cables and about 3,000 pounds on the 69-kv cables. These values are considerably in excess of those normally encountered in service so that cable snaking is not to be anticipated where such stiff cables are installed in straight conduit banks.

It was interesting nevertheless to observe from Figure 5(A) that snaking could be predicted to occur at locations where the cable column remained bent from a previous heat run. In contrast with such snaking, the short lay triplex sample to the left in Figure 5(D) bird-caged uniformly along its length during the totally restrained heat run. The longer lay sample in the duct to the right opened its convolutions in a rather haphazard manner. Figure 6 shows severe snaking under total restraint on the parallel lay single-conductor 500,000 circular-mil cables (Sample 7 in the right duct position). This is in marked contrast with the uniform bird-caging of the triplex 500,000 circular-mil cables (Sample 8 in left position in Figure 6).

Coefficient of Friction

Computation of cable movement for service conditions and the evaluation of the various test data required appropriate regard for the frictional forces imposed on the cable in restraint of cable movement by friction between the cable and the duct wall.

Table II shows the values of coefficient of friction determined for the various samples which had been lubricated with the same type of grease normally used in field installations. The lubricating compound used on Samples 3, 4, 7, 8, 9, and 10 was taken from a delivery in which a compound with increased tackiness was inadvertently supplied and whose use has been discontinued.

Analysis of Cable Movement

Rationalization of the test data resulted in the accomplishment of two objectives: (1) the evaluation of an "apparent modulus of compressibility" for

Table I. Description of Cable Samples

Sample Number§	Mfr	Conductor Size, Mcm	Voltage Rating, Kv	Outside Diameter, Inches	Weight Pounds, Per Foot	Ins. Wall, Mils	Sheath Wall, Mils	Stranding	Comments
1	X	1×1,500	69	2.48	10.85	315	125	Std. strand rd.	Low-pressure oil-filled cable, 0.5″ hollow core
2	Y	1×1,500	69	2.71* 2.38†	15.5	325	105* 130†	Comp. quad.-seg.	Self-contained high-pressure gas-filled cable‡
3	Y	3×350	15	2.25	9	156×78	125	Comp. strd. sect.	Belted cable; 60″ lay
4	W	3×350	15	2.38	9.25	175	120	Std. strand sect.	Metal shielding tapes; 3 paper binders; 45″ lay
5	Z	3×350	15	2.25	9.0	175	120	Std. strand sect.	Carbon black shielding tapes; 3 carbon black paper binders; 60″ lay; ordinary lead sheath
6	Z	3×350	15	2.25	9.0	175	120	Std. strand sect.	Carbon black shielding tapes; 3 carbon black paper binders; 60″ lay; *F3* alloy lead sheath
7	Y	3–1×500	15	1.40**	13.5	203	125	Comp. strand rd.	Three parallel cables (not twisted) Installed in one duct
8	Z	3–1×500	15	1.36**	13.3	175	125	Comp. strand rd.	Triplex cable—48″ lay
9	X	3–1×350	15	1.25**	9.5	175	95	Std. strand rd.	Triplex cable—62.5″ lay
10	X	3–1×350	15	1.25**	9.5	175	95	Std. strand rd.	Triplex cable—37″ lay

§Samples were tested in round 4¼-inch terra-cotta duct.

*Outer lead sheath.

†Inner lead sheath.

**Outside diameter of only one leg.

‡Reinforcement over inner lead sheath comprised: a bedding of two 18-mil cotton fabric tapes (intercalated, half-lap); six 8-mil brass tapes (2-inches wide, two wrapped reversed lay to first four); two 18-mil cotton fabric tapes (intercalated, half-lap) as bedding for outer lead sheath.

each cable construction (shown in Figures 7 and 8) for use in the computation of the maximum cable movement to be expected in service at the duct mouth; and (2) the determination of a basis for rating the various cable constructions (shown in Figure 9) to reflect their merit as an expedient to reduce cable-movement at the duct mouth.

Review of the test results indicated the possibility of pursuing several modes of analysis in order to determine the combined effects of conductor stranding, lay of insulated conductors, tightness of binders and of belt insulation, sheath tightness, triplexing, and other variables in cable construction together with the factors which introduce snaking, as influences tending to govern cable movement with conductor temperature rise over a wide range of restraining forces. Rather than adopt a ponderous empirical evaluation determinable graphically from the plotted data, the author developed cable parameters to correlate with the fundamental analysis followed in Mr. Bodicky's discussion of the author's earlier paper, reference 8. This mode of evaluation has the advantage of lumping all the cable-movement influences in one factor, referred to in that discussion as "compressibility", *c*. The author, however, prefers to evaluate these design features together with the phenomena of bird-caging and snaking in a factor to be referred to as the "apparent modulus of compressibility", C_c in inches per inch per pound per circular mil, which is equal to the product of compressibility (*c* in micro-inch per inch per pound of restraint) and area (*A* in circular mils) of the total copper in the core of the cable times ten to the minus sixth power.

The maximum amount of cable move-

Table II. Coefficient of Friction—Terra-Cotta Ducts

Sample No.*	Average† Starting Friction	Average† Moving Friction	Over-All Average
1	0.38	0.25	0.32
2	0.31	0.26	0.29
3	0.57	0.57	0.57
	0.41‡	0.45‡	0.43‡
4	0.56	0.56	0.56
	0.44‡	0.48‡	0.46‡
5	0.22	0.29	0.26
6	0.23	0.22	0.23
7	0.47	0.43	0.45
	0.39‡	0.40‡	0.40‡
8	0.41	0.37	0.39
	0.39‡	0.38‡	0.39‡
9	0.43	0.51	0.47
10	0.48	0.57	0.53
1S**	0.36	0.24	0.30
2S**	0.23	0.16	0.20

*All samples tested in round 4¼-inch bore terra-cotta duct, except *1S* and *2S* which were tested in square 4¼-inch terra cotta duct.

†Based on measurements taken to start movement both in tension and in compression; and for a movement in both cases of one inch at the remote end of the sample.

**Samples *1S* and *2S* were same construction as Samples 1 and 2 respectively.

‡These measurements taken at sheath temperatures ranging 53 to 56 degrees centigrade; all others at 18 to 22 degrees centigrade.

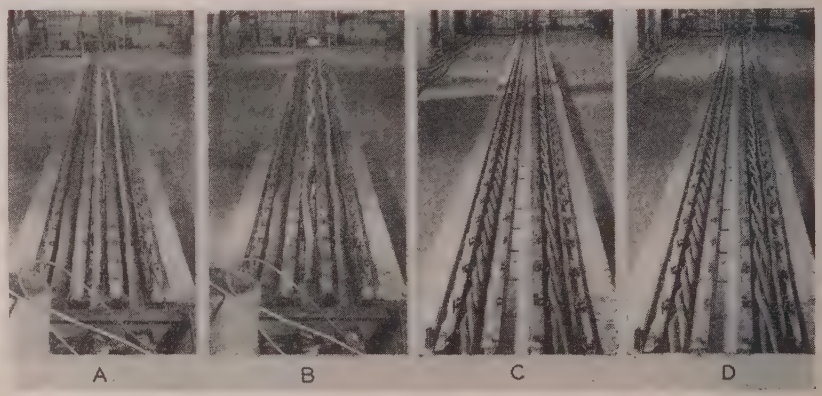

Figure 5. Snaking and bird-caging under total restraint

69-kv single-conductor oil-filled cables (Sample 1 in round duct at right and similar cable in square center duct) snake considerably in "B" at 3,400 pounds total restraint and 40 degree centigrade rise at locations evident in "A" (zero restraint and initial ambient temperature)

15-kv triplex single-conductor 350,000 circular-mil Sample 10 (left in "D") bird-cages uniformly along the duct at 390 pounds total restraint and 76 degree centigrade rise; but similar Sample 9 (except longer lay; right in "D") bird-cages nonuniformly along the duct at 360 pounds total restraint and 72 degree centigrade rise. "C" shows these cables at ambient temperature and zero restraint at the duct mouth

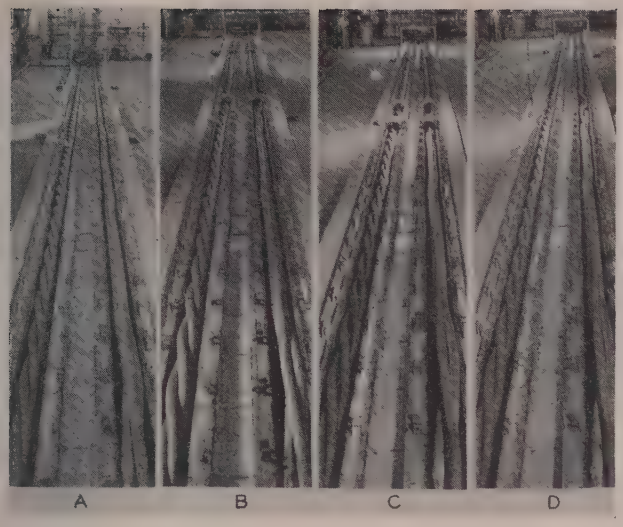

Figure 6. Bird-caging versus snaking under total restraint

15-kv single-conductor 500,000 circular-mil cables. Sample 7 (right, parallel) and Sample 8 (left, triplex, 48-inch lay), are shown in "A" for zero restraint and ambient temperature; in "B" for 530 pounds total restraint and 45 degree centigrade rise on Sample 8, and 1,845 pounds total restraint and 43 degree centigrade rise on Sample 7; in "C" for 675 pounds total restraint and 72 degree centigrade rise on Sample 8, and 1,557 pounds total restraint at 71 degree centigrade rise on Sample 7; and in "D" on following morning at ambient temperature and zero restraint before pulling cables back to their initial position comparable to overall length and position of cable in "A." The cables were permitted to cool over night without restraint so that the cable at the duct mouth contracted into the duct

ment (M in inches) to be anticipated at the duct mouths of a flat, straight stretch of cable may be computed from the appropriate use of the following two equations:

$$M = L(et - c(k + wfL/2))\ (10^{-6}) \qquad (1)$$

$$M = (et - kc)^2/2wfc\ (10^{-6}) \qquad (2)$$

where L is one-half of the manhole-to-manhole distance in inches; e, the thermal coefficient of expansion for copper (16.8 micro-inch per inch of length per degree centigrade rise in conductor temperature); t, the conductor temperature rise; c, the compressibility of the cable in micro-inch per inch per pound of restraining force acting upon the cable; k, the restraining force in pounds acting at the end of the cable; w, the weight of the cable in pounds per inch of length; f, the coefficient of friction.

Equations 1 and 2 are applicable during different periods of the heating cycle, depending upon two critical values of temperature rise for each cable construction. One is the threshold temperature rise (t_0) at which cable movement first occurs. This temperature rise is determined by the equation:

$$t_0 = kc/e \qquad (3)$$

The values of compressibility, c, were computed from equation 3 using various restraining forces at the end of the cable sample, k, and their respective threshold rises, (t_0) as taken for the various cable constructions from the curves shown in Figure 4. The corresponding values of "apparent modulus of compressibility", C_c, were then calculated and plotted as the cross points in Figures 7 and 8. Except for the large single-conductor 69-kv cables, the values of c and C_c so computed were found to vary considerably for the range of temperature rises at which the cables were tested at total restraint.

The second critical temperature is the minimum rise (t_1) at which every increment of cable length contributes to the longitudinal cable-movement at the duct-mouth, and is determined by equation:

$$t_1 = (k + wfL)c/e \qquad (4)$$

Equation 1 should be used in connection with cable-movement for temperature rises greater than the critical value, t_1; while equation 2 should be used for rises intermediate between t_0 and t_1.

The conventional derivation of the equations 1 to 4 refers to compressibility, c, as a constant parameter of cable construction. Evaluation of c and the corresponding determination of C_c were made using in these equations the respective values of movement, M, temperature rise, t, and restraining force, k, available from the curves in Figures 1, 2, and 3 for the various cable constructions.

These values of C_c also were found to vary considerably with temperature rises and restraining forces at the end of the 100-foot test samples. However, when plotted, as in Figure 7, each cable construction was found to possess a rationally correlated family of parameters for the various conductor temperature rises. Each temperature rise curve terminated at the value of total restraint beyond which the curves have no quantitative significance since no movement occurs beyond that point.

It is significant to observe in Figure 7 that the family of curves for the triplex 15-kv 350,000 circular-mil cable (Sample 9) turns upward with increasing restraining forces. It also has increasing compressibility with increasing conductor temperature rises. This is obviously the salutary influence of the ability of a triplex cable to bird-cage readily.

The 15-kv belted 350,000 circular-mil cable (Sample 3) performs somewhat differently. While the compressibility is found to increase with temperature rise, it diminishes as the cable at first goes into compression with increasing restraining forces and subsequently increases as the force approaches total restraint. The associated reduction in cable expansion near total restraint is apparently due to cable snaking, rather than an inherent increase in cable compressibility.

The 69-kv 1,500,000 circular-mil single-conductor cable (Sample 1) has only one curve in Figure 7 for all temperature rises. This follows from the fact that the movement curves in Figure 1 for zero-, 750-pound and 1,500-pound restraint

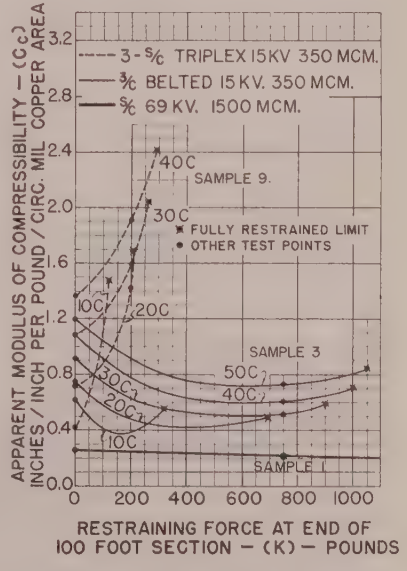

Figure 7. Apparent modulus of compressibility

Temperature rise curves for 15-kv triplex 350,000 circular-mil Sample 9 (broken line); 15-kv 3-conductor 350,000 circular-mil belted Sample 3 (light solid line); and 69-kv single-conductor 1,500,000 circular-mil Sample 1 (heavy solid line)

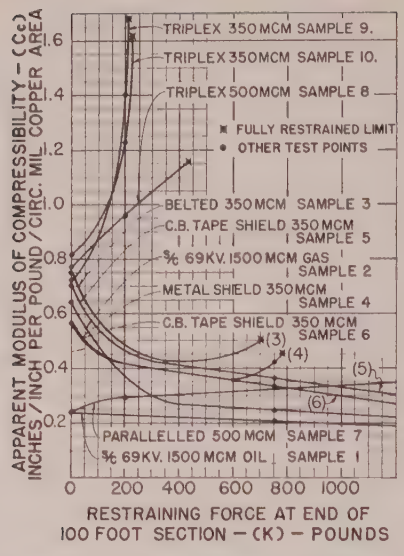

Figure 8. Apparent modulus of compressibility

20-degree conductor temperature rise curves for all cable constructions listed in Table I

parallel the slope for "free" bar copper (determined by the value of e). The linear portions of these plots are accordingly good point-by-point matches for the linear equation 1 by merely determining appropriate values of compressibility c, to produce adequate translation of the curves to the proper positions for the restraining forces, κ, applied during the tests.

Figure 8 shows the 20-degree rise curves for the three samples (1, 3, and 9) shown in Figure 7 together with the 20-degree similar curves for the other cable samples tested. The triplex cable Samples 8, 9, and 10 considerably differ from the other cable constructions because of their capability to bird-cage. The 69-kv 1,500,000 circular-mil single-conductor Samples 1 and 2 are least compressible, while the 3-conductor cable Samples 3, 4, 5, and 6 show little difference in performance with respect to each other. The 15-kv 500,000 circular-mil paralleled single-conductor construction showed a slight increase in compressibility which reflected cable-snaking.

Relative Stiffness of Cable Construction

Figure 9 illustrates a comparison of the various cable constructions as related to the stiffness of a rigid copper bar. The modulus of elasticity of soft-drawn copper (12,000,000 pounds per square inch) was chosen as the unit reference of stiffness. By inverting comparable values of "apparent modulus of compressibility" from Figure 8 into equivalent modulus of elasticity in compression ($E_c = 1/C_c$) with appropriate conversion of units, "relative stiffness" was readily determined at several values of restraining force selected to give similar stresses in the copper-conductors of the various cables with proper regard to conductor size. Comparisons were made at copper conductor stresses of 0.2-, 0.5-, and 1.0-pound per thousand circular mil of total conductor area, corresponding approximately to the range of restraining forces encountered by sections of cable in a long manhole-to-manhole stretch, whose positions in the duct vary from that adjacent to the duct mouth to that near the center of the stretch.

The particular merit of the triplex construction is clearly demonstrated in Figure 9 where the "relative stiffness" of the 15-kv triplex 350,000 circular-mil Samples 9 and 10 at 20 degrees rise and 0.2-pound per thousand circular-mil restraint is seen to be only one-third of that of the 15-kv 3-conductor constructions of the same conductor size. The outstanding advantage of the triplex construction, however, lies in the fact (shown for the 15-kv triplex Samples 8, 9, and 10 in Figure 9) that they are fully restrained at conductor stresses well below the higher values listed at which the other cable constructions (except Samples 3 and 4) have appreciable movement. Consequently, long lengths of triplex cable have no more cable movement than the short lengths. This can be observed in Table III which shows the same movement for 800 feet as for 200 feet. Triplex Sample 10 has only about 1/5 to 1/12 of the movements computed for the 3-conductor cables of the same conductor size at 20-degree centigrade rise.

Similarly, "relative stiffnesses" for the 69-kv Sample 1 range from 0.48 to 0.66; while in Table III, the cable-movements, likewise at 20-degree rise, are 0.35- and 1.11-inch for 200-foot and 800-foot stretches respectively—88 and 68 per cent respectively of the theoretical expansion of a free, rigid copper bar. The relative stiffness ratios are not exactly commensurate with these percentages because of the inherent differences between equations 3 and 1. These percentages are of the same order as the ratio between the 3,300-pound force indicated in Figure 4 for total restraint at 20-degree rise on Sample 1, and the 4,000-pound restraint

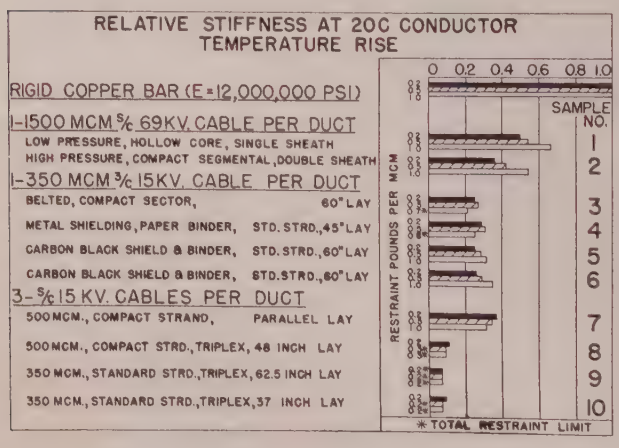
RELATIVE STIFFNESS AT 20C CONDUCTOR TEMPERATURE RISE
0 0.2 0.4 0.6 0.8 1.0
RIGID COPPER BAR (E=12,000,000 PSI)
SAMPLE NO.
1-1500 MCM ⅝ 69KV. CABLE PER DUCT
LOW PRESSURE, HOLLOW CORE, SINGLE SHEATH
HIGH PRESSURE, COMPACT SEGMENTAL, DOUBLE SHEATH
1-350 MCM ¾ 15KV. CABLE PER DUCT
BELTED, COMPACT SECTOR, 60° LAY
METAL SHIELDING, PAPER BINDER, STD. STRD., 45° LAY
CARBON BLACK SHIELD & BINDER, STD. STRD., 60° LAY
CARBON BLACK SHIELD & BINDER, STD. STRD., 60° LAY
3-⅝ 15 KV. CABLES PER DUCT
500 MCM., COMPACT STRAND, PARALLEL LAY
500 MCM., COMPACT STRD., TRIPLEX, 48 INCH LAY
350 MCM., STANDARD STRD., TRIPLEX, 62.5 INCH LAY
350 MCM., STANDARD STRD., TRIPLEX, 37 INCH LAY
RESTRAINT POUNDS PER MCM
1
2
3
4
5
6
7
8
9
10
* TOTAL RESTRAINT LIMIT

Figure 9. Relative stiffness of various cable constructions

Determined for a 20-degree rise in conductor temperature and for restraints of 0.2, 0.5, and 1.0 pound per thousand circular-mil of total copper conductor in cable core on a 100-foot section

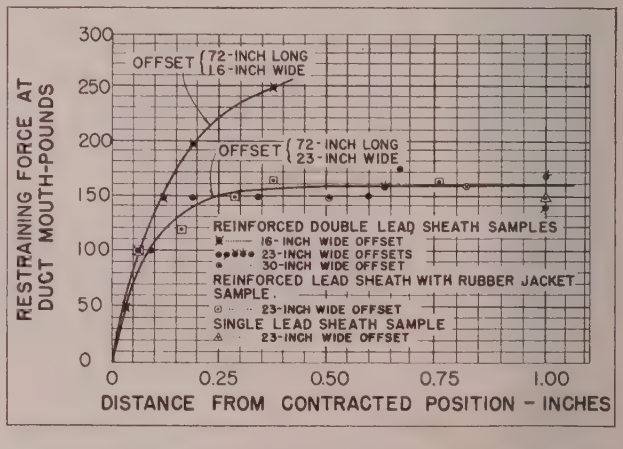

Figure 10. Restraining force at duct-mouth caused by cable training in manhole

The restraining force at the duct-mouth increases as the cable in the offset is flexed to accommodate the additional cable in the manhole as cable movement increases at the duct-mouth during the heating cycle

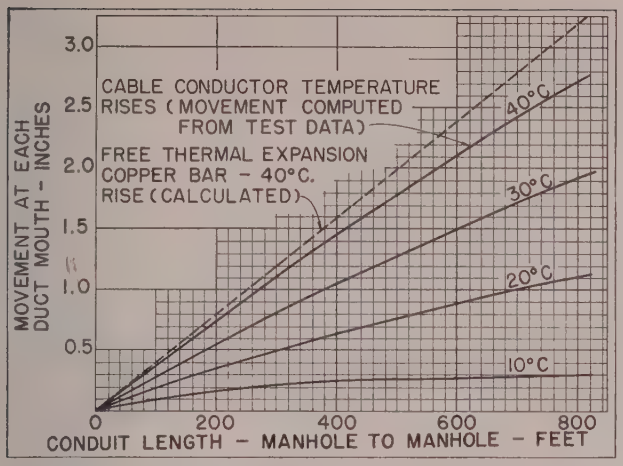

Figure 11. Maximum movement at duct mouth—straight flat conduit

69-kv single-conductor 1,500,000 circular mil oil-filled cable (Sample 1) maximum movement at each duct mouth of various conduit lengths of straight flat duct bank. The solid lines show computed values of cable movement. The broken line shows the theoretical expansion at 40 degree centigrade rise of an unrestrained copper bar

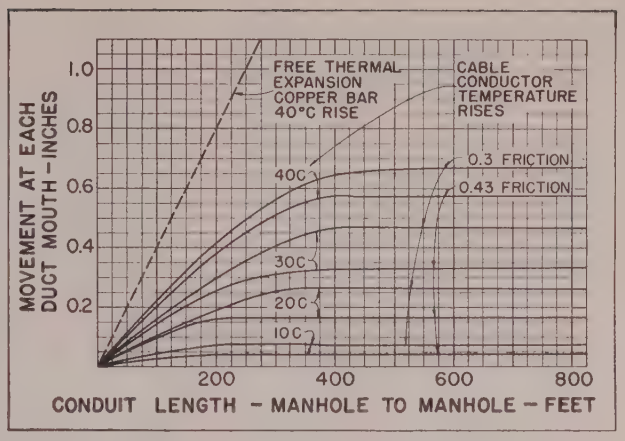

Figure 12. Maximum movement at duct mouth—straight flat conduit

15-kv 3-conductor belted 350,000 circular mil cable (Sample 3) maximum movement at the duct mouth of various conduit lengths of straight, flat duct bank

required to maintain unchanged the length of a rigid copper bar at a rise of 20 degrees on the basis of a modulus of elasticity of 12,000,000 pounds per square inch.

Computation of Maximum Cable Movement

All necessary tools now are available to compute the maximum range of cable movements for various cable lengths and conductor temperature rises. The solution of equations 1 and 2 for the calculation of movement, and of equations 3 and 4 for the determination of the threshold rise, t_0, and the critical rise, t_1, require only the information available in the family of curves for the particular cable construction involved, such as shown for Samples 1, 3, and 9 in Figure 7.

It is expedient to make cable movement calculations by dividing the manhole-to-manhole length into 100-foot sections, and determining the movement at each duct mouth of a flat, straight stretch by computing the increment of movement separately for each 100-foot section between the duct-mouth and the center of the stretch. An 800-foot stretch will accordingly involve four successive solutions of these equations, and the summation of the individual increments to get the total movement. The value of L in equations 1 and 4 should be 1,200 inches in each of these solutions. In addition, each 100-foot section will have its own restraining force at the end of the 100-foot section toward the duct mouth, analogous to the force, k, in Figure 7.

Accordingly, different values of "apparent modulus of compressibility" are indicated for each 100-foot section as well as for each temperature rise. The restraining force, k, at the duct-mouth end of the cable section adjacent to the manhole is a function of the dimensions of the cable training in the manhole, of the kind of arc-proofing on the cables, and of cable stiffness. The magnitude of this force for a cable similar to Sample 3 may be secured from the author's earlier paper (reference 8, Figure 18). Adjustment of the values secured from that source may be made for other cables on the basis of relative stiffness. These values become less critical for the longer cable lengths normally met in service. Values for 69-kv Samples 1 and 2 are given in Figure 10 based on tests in a full-size dummy manhole, increasing with amount of cable movement.

The restraining force for each 100-foot section, successively remote from the

Table III. Computed Cable Movement

Description	Sample Number	Maximum Movement at Each Duct Mouth—Inches: At 20C Conductor Temperature Rise For 200-Foot Length	For 800-Foot Length	At 30C Conductor Temperature Rise For 200-Foot Length	For 800-Foot Length
Free Copper Bar		0.40	1.61	0 61	2.42
1–1,500,000 Circular Mil Single-Conductor 69-Kv Cable Per Duct					
Low pressure, hollow core, single sheath	1	0.35	1.11	0.55	1.91
High pressure, compact seg., double sheath	2	0.28	0.71	0.48	1.52
1–350,000 Circular Mil 3-Conductor 15-Kv Cable Per Duct					
Belted; compact sectors; 60-inch lay	3	0.22	0.29	0.35	0.63
Metal shielding tapes, metallized paper binders; standard strand sectors; 45-inch lay	4	0.21	0.36	0.35	0.68
Carbon black shielding and binder tapes; standard strand sectors; 60-inch lay	5	0.23	0.39	0.34	0.65
Carbon black shielding and binder tapes; standard strand sectors; 60-inch lay	6	0.23	0.46	0.36	0.76
3-Single-Conductor 15-Kv Cables Per Duct					
500,000 circular mil compact strand round, Parallel lay	7	0.27	0.46	0.42	0.94
500,000 circular mil compact strand round, 48-inch lay	8	0.07	0.07	0.12	0.12
350,000 circular mil standard strand round, 62.5-inch lay	9	0.03	0.03	0.07	0.07
350,000 circular mil standard strand round, 37-inch lay	10	0.04	0.04	0.10	0.10

duct-mouth, is equal to the sum of the restraint at the duct-mouth and the frictional restraining force attributable to the weight of the cable between the given 100-foot section and the duct-mouth. For example, in the computations for a 20-degree rise on the 800-foot stretch of cable similar to Sample 1, the respective magnitudes of restraining forces were 150, 476, 802, and 1,128 pounds respectively (the friction of 100 feet of 10.85-pound per-foot cable being determined at a coefficient of 0.3). Figure 7 yielded values for C_e of 0.23-, 0.22-, 0.20-, and 0.18-inch per inch per pound per circular mil with corresponding values for compressibility of 0.153, 0.147, 0.133, and 0.12 microinch per inch per pound. Since the critical temperatures, t_1, for these sections were found to be 1.4, 4.2, 6.4, and 8.1 degrees from equation 4, the increments of movement for each section could be computed from equation 1 and were evaluated as 0.35, 0.29, 0.25, and 0.22 respectively, giving a total movement at each duct mouth of 1.11 inches for an 800-foot flat, straight stretch. Immediately evident from the foregoing are the values of 0.89-, 0.64-, and 0.35-inch at 20-degree rise for the total movement at each duct mouth on 600-foot, 400-foot, and 200-foot stretches, respectively. Similar computations at other temperature rises made available the information for the plotting of Figure 11.

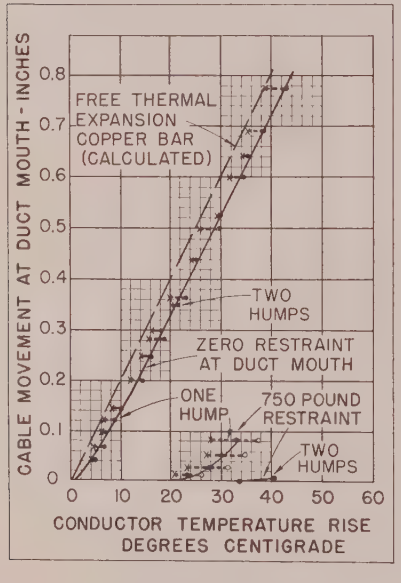

Figure 13. Longitudinal thermal expansion of "bent column" cable

69-kv single-conductor oil-filled cable, Sample 1. Expansion is approximately the same at zero restraint at duct mouth for tests with one hump (broken horizontal line) and with two humps (solid horizontal line). Crosses show conductor temperature rise measured by thermocouple in core of cable; dots show conductor temperature rise measured by resistance wire in core of cable; open circles show temperature rise measured by change of resistance of cable conductor

Figure 12 shows the cable movements calculated for cable similar to Sample 3. Computations were made for two values of coefficient of friction to show the influence of this factor on a cable as compressible as this 3-conductor construction.

Similar curves were plotted for all other constructions included in the test program. Table III was prepared by selecting four comparable values of cable movement for each sample. The equivalent expansions for free copper bar also were listed. These cable movements range for a 20-degree rise on an 800-foot stretch from 69 per cent of the bar copper value for Sample 1 to less than 3 per cent for triplex Sample 10.

It is significant to observe that the stiffness of the 69-kv cable in Figure 11 causes increases in cable movement for flat, straight lengths even beyond 800 feet, while the relatively more compressible 15-kv cable in Figure 12 shows no additional movement above the 400-foot length at 20-degree rise, and above 600-foot at rises up to 40 degrees.

The 15-kv cable movements were shown in Figure 12 for a small manhole with 11-inch wide offset, while Table III was prepared for a manhole training offset-width of 19 inches. The movements for the 69-kv cables were prepared for Table III and Figure 11 for a manhole restraint exerted by a 23-inch offset, a value somewhat smaller than would be considered good field practice. The influences of variations in offset widths or the consequent changes of duct mouth restraint upon the calculated values of cable movement for large stiff cables are not at all critical.

Effect of Changes in Conduit Profile

While the cable movement indicated in Figures 11 and 12 are in general agreement with the maxima values reported from field surveys on installations of similar cables, these maxima actually apply to only a small percentage of all the field measurements. This fact had been realized from the author's earlier work (reference 8, Figure 6).

Additional free expansion and 750-pound restraint tests were conducted on the 69-kv 1,500,000 circular mil oil-filled cable Sample 1 in an effort to approximate profile changes. The purpose of these special tests was to determine a design basis for reducing the magnitude of the cable movement indicated in Figure 11 to some average value which more appropriately reflected the influences of variations in conduit profile, and thereby attain more practical limits for the manhole design. In one setup, a "hump" was installed over a 24-foot portion of the laboratory conduit structure rising to a 12-inch high apex at its center point, 18 feet from the permanently fixed end of the structure. In a subsequent setup, a second hump was added extending over a 24-foot portion of the conduit and rising to an 8-inch high apex at its center point, 80 feet from the permanently fixed end of the structure.

It is of considerable interest to note that the data from the free expansion heat runs, plotted in Figure 13, showed practically no influence of either the one or the two humps. The movements measured in both heat runs were nearly equal to those shown in Figure 1.

The effect of the change in cable configuration due to these humps (bent column), however, is evident in Figure 13 where it is seen that only 0.05-inch movement was measured at 30-degree rise at 750-pounds restraint in the one hump heat run, and no movement with two humps.

The bent-column heat runs demonstrated the phenomenon which operates to reduce the cable movement in actual service below the maximum values suggested by the tests in a straight duct, Figures 11 and 12. It is of further interest to observe that the cable expansion, which was prevented from appearing at the duct-mouth as cable movement, appeared at the apex of the humps. Figure 14 shows that cable snaking at this location caused a 1.2-inch vertical rise of the cable in the duct at a conductor-temperature rise of 20 degrees, and caused

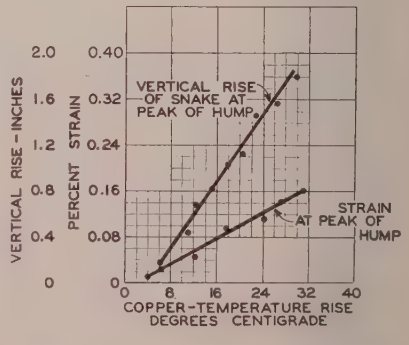

Figure 14. Cable snaking and sheath strains at fabricated hump in duct bank

69-kv single-conductor oil-filled cable, Sample 1. Measurements taken at apex of 12-inch hump on test with one hump in cable

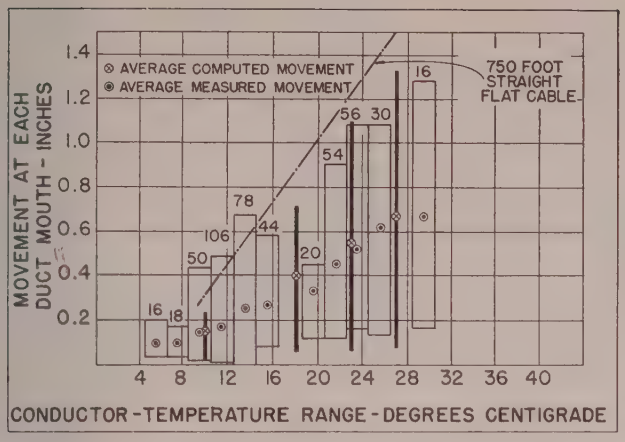
⊗ AVERAGE COMPUTED MOVEMENT
◉ AVERAGE MEASURED MOVEMENT
750 FOOT STRAIGHT FLAT CABLE
MOVEMENT AT EACH DUCT MOUTH - INCHES
CONDUCTOR - TEMPERATURE RANGE - DEGREES CENTIGRADE

Figure 15. Cable movement at duct mouth—estimated compared with measurements in field during operation of 69-kv cable

Commercial operation of 69-kv single-conductor 1,500,000 circular mil oil-filled cables. Vertical heavy solid lines represent ranges of cable movements estimated on bases of tests on Sample 1 (cross in circle shows the average value for a given range of conductor temperature). The vertical columns represent ranges of cable movements at the duct mouth measured in field for 2-degree blocks of measured conductor-temperature rise (dot in circle shows the average value for the number of measurements indicated at the top of the vertical column)

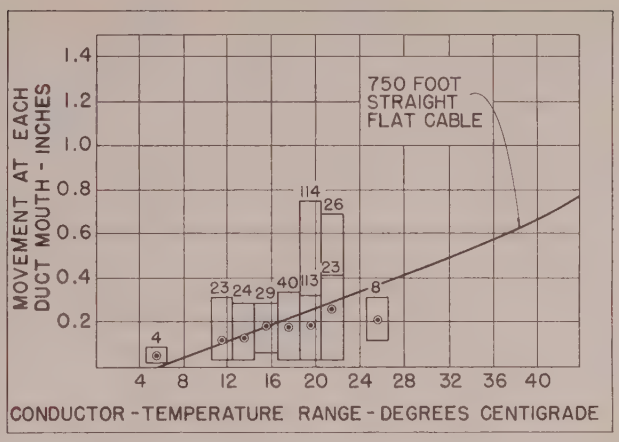

Figure 16. Cable movement at duct mouth—estimated maxima values compared with measurements in field during operation of 15-kv cables

Commercial operation of 15-kv 3-conductor belted 350,000 circular mil cables. The vertical columns represent ranges of cable movements at the duct mouths measured in field for 2-degree blocks of computed conductor-temperature rise (dot in circle shows the average value for the number of measurements indicated at the top of the vertical column). The solid line indicates the maximum movement estimated for a flat straight 750-foot cable stretch on basis on Figure 12

an increment of strain in the lead sheath of 0.1 per cent. It is evident that in actual operation such snaking takes place at changes in configuration in the duct bank, and consequently less movement appears at the duct-mouth.

A quantitative application of this information, however, in a practical design problem, requires analysis of the conduit profile. This was done by the author for a recent installation of two 69-kv lines, totalling 128 duct-bank terminations. Cable movements were computed at conductor-temperature rises of 10, 18, 23, and 27 degrees which were considered as most significant for the study, then being made. The method of analysis pursued to compute these movements was illustrated in the author's recent article on these lines (reference 9). The heavy vertical lines in Figure 15 show the ranges of values of cable movement computed.

The cable movement computations were made during preliminary engineering stages and were used to determine the appropriate dimensions of the manholes. Subsequently measurements of cable movement were made with the lines in normal operation. Conductor temperature ranges were determined from readings of temperature-rise indicators specifically designed to show conductor-temperature rise above ambient for cables, transformers, and similar electrical apparatus (reference 10). Each of the two 69-kv cable lines involved has one of these indicators installed on its switchboard as a means of monitoring cable loading. The actual temperature ranges and values of cable movements determined from the field measurements also are shown in Figure 15. It is particularly interesting to observe the splendid agreement of experience with the predicted movements.

Measurements of cable movement at the duct mouth also were taken on a group of 15-kv belted 3-conductor 350,000 circular-mil paper and lead cables, utilizing the same type of movement indicators used on the 69-kv cables involved in Figure 15. These devices were strapped to the cables adjacent to the duct mouth in the manholes as illustrated in Figure 5 of the author's earlier paper.[8] The ranges of conductor temperature were computed based upon the records of hourly load readings. The ranges of these movement data and the averages are shown in Figure 16 for 2-degree spreads of calculated temperature rises. The number at the head of each column represents the number of measurements included in the block below that number. While there is a fair correlation between field measurements and the estimates of movement in this figure, it naturally cannot be as close as noted on Figure 15 for the 69-kv cables where temperature ranges were based upon indicated rather than calculated values.

Manhole designers should always keep in mind that the service life of the lead sheath in a given line is determined by the average cable movement. The movement calculation should therefore be based upon the average daily copper temperature range. The corresponding cable movement and rate of sheath life loss will of course be much greater in some manholes than in others. It is generally impracticable to design all manholes with dimensions which would accommodate the maximum movement. Consequently, it is good business to select critical manhole dimensions[11] which will accommodate the average cable movement particularly because sheath reinforcement is practical and would be inexpensive in the few manholes where movement would otherwise cause excessive sheath life loss.

Conclusions

1. Properly accounting for effective compressibility is necessary in order to compute longitudinal cable movement with reasonable accuracy.

2. The effective compressibility has been evaluated from tests on several cable constructions. It is designated as "apparent modulus of compressibility" and equations are given for its use in determining the maximum longitudinal cable movement in any situation.

3. Triplexing of single-conductor cables without restraining their radial movement, results in a construction having far less longitudinal movement

than any other type of cable construction.

4. For the triplexed 1.25-inch diameter paper and lead cables tested, it was found that the 30-diameter (37-inch) lay of Sample 10 gave uniformly distributed bird-caging, whereas the 50-diameter (62.5-inch) lay of Sample 9 caused definitely nonuniform bird-caging. The 1.36-inch diameter paper and lead cable of Sample 8 was triplexed with a lay of 35 diameters (48 inches) and also had uniform bird-caging. It is therefore concluded that a lay in the order of 35 diameters should insure satisfactory performance of triplexed cables.

References

1. The Temperature Rise of Cables in a Duct Bank, **J. H. Neher.** *AIEE Transactions*, volume 68, part I, 1949, pages 540–46.

2. Load Ratings of Cable, **Herman Halperin.** *Electrical Engineering* (*AIEE Transactions*), volume 58, October 1939, pages 535–52.

3. Load Ratings of Cable, II, **Herman Halperin.** *AIEE Transactions*, volume 61, 1942, pages 930–41.

4. Maximum Safe Operating Temperature for 15-Kv Paper-Insulated Cable, **C. W. Franklin, E. R. Thomas.** *Electrical Engineering* (*AIEE Transactions*), volume 58, October 1939, pages 556–60.

5. Emergency Overloading of Insulated Power Cables. AIEE Special Publication 6, September 1943.

6. New 138-Kv Cable Lines in Los Angeles, **C. G. Mansfield.** *AIEE Transactions*, volume 63, 1944, pages 1240–49.

7. An Investigation of the Relationship Between Temperature and Movement of Cables in Ducts, **C. T. Nicholson, T. J. Brosnan.** *Electrical Engineering* (*AIEE Transactions*), volume 63, October 1944, pages 723–28.

8. Cyclic Movement of Cables—Its Causes and Effects on Cable Sheath Life, **C. S. Schifreen.** *AIEE Transactions*, volume 63, 1944, pages 1121–30 and pages 1388–98.

9. Oil-Filled Cable Forms Link in 66-Kv Philadelphia Loop, Part II, **C. S. Schifreen.** *Electric Light and Power* (Chicago, Ill.), August 1948, pages 64–69.

10. Thermal Circuit Gives Remote Hot-Spot Temperature, **A. H. Kidder.** *Electrical World* (New York, N. Y.), July 3, 1950, page 89.

11. Critical Inside Dimensions for Power Cable Manholes, **Edward S. Halfmann.** *AIEE Transactions*, volume 69, part II, 1950, pages 1576–81.

Discussion

R. W. Atkinson (General Cable Corporation, Bayonne, N. J.): Longitudinal movement of cables, with the resultant bending of the lead sheath, has come to be one of the outstanding considerations in connection with the design and operation of cable systems. Various authors have pointed out the reasons for this. When cable movement first came to be recognized as a significant matter, very little information was available as to its extent or, indeed, as to its significance. This was followed by extensive statistical information, together with increased recognition of the importance of cable movement. Then came correlations of movement with the characteristics of the system, particularly the recognition that the amount of movement was not a direct function of length between manholes. A further important contribution to this subject now is made by Mr. Schifreen in his very thorough additional experimental and analytical study of the constants affecting cable movement. It is gratifying to find how effectively this method has been found applicable to very practical system design.

G. J. Crowdes (Simplex Wire and Cable Company, Cambridge, Mass.): The latest contribution of this author to the subject thermal expansion effects in power cables is of a great deal of value both to the cable user and to the cable design engineer. The data seem to be in line with earlier work on this subject and bring out some pertinent facts concerning cable design worth commenting on. In particular, we would like to comment upon the relative stiffness of various cable conductors. The data shown in Mr. Schifreen's paper cover standard and compact stranded conductors, but do not seem to tend to separate them as well as might be desired. For example, one of the important cable characteristics which affects the restraining force and the starting force at which weaving or offset takes place is the stiffness of the conductor. There is a considerable difference with compact and regular stranding, as indicated by the tests described in the following paragraphs.

The tests were made with a 24-inch piece of conductor held horizontally, one end clamped in a vise, by hanging a weight on the free end and noting the deflection in inches from horizontal D_w with weight and D_0 after removal of weight. Weights of 1, 2, 4, and 8 pounds were used, but only the results with 8 pounds are given here. The tests were repeated with the ends of the conductors soldered to prevent slippage of the strands.

Table I. Test Results

Stranding	Position of Sector in Vise	D_w, Inches		D_0, Inches	
Noncompact	point down	8.00		3.25	
No solder	point up	8.00	Average = 8.00	2.75	Average = 3.00
	point at side	8.00		3.00	
Compact	point down	7.00		1.00	
No solder	point up	7.75	Average = 6.75	2.50	Average = 1.41
	point at side	5.50		0.75	
Noncompact	point down	5.00		1.50	
Solder	point up	6.00	Average = 4.83	2.00	Average = 1.58
	point at side	3.50		1.25	
Compact	point down	7.50		2.50	
Solder	point up	7.00	Average = 7.00	0.75	Average = 1.41
	point at side	6.50		1.00	

These tests seem to indicate that the compact stranding has a greater tendency to return to its original position after being bent and that this tendency is due to less slippage of the compact strands. There is no doubt from these tests that the compact conductor is stiffer and more springy. It does not stay in a bent position and tends to return to its original position, and considerably greater force is required to change it from a straight position. Some utilities have trouble in keeping the compact strand racked into position. This may be connected with the tendency for stiffness and unwillingness to change from any given shape. It may be that this different effect in stranding even shows up in the triplexed construction and may mask some of the other effects. We would like to see this subject pursued further with particular attention to correlation of the effects of various cable designs.

William A. Del Mar (Phelps Dodge Copper Products Corporation, Yonkers, N. Y.): This paper will remain a valuable one for many years for the wealth of experimental data it contains, as well as for the painstaking analysis of these data.

There are two minor points on which I should like to take Mr. Schifreen to task.

It is unfortunate that he uses the expression "triplex cable" to designate specifically three single-conductor cables twisted together, as the AIEE definition of a "triplex cable" covers, and originally was intended to cover, only the ordinary 3-conductor cable. A suitable term which has had some usage would be "triplexed cables," as we are dealing here with three cables, not one, each cable having a joint and a terminal of its own. Mr. Schifreen seems to have come around to this idea when he reached the conclusions at the end of his paper. Attention is called to this because it might cause confusion in applying equations 1 and 2 of the paper, as w is defined as weight of the cable in pounds per inch, and it is important to know what is meant by "the cable."

The other point relates to the accuracy of equation 3 of the paper, according to which the temperature rise, t_0, to start motion will be zero if there is no end restraint. I interpret this to mean that with $k = 0$, any temperature rise, however infinitesimal, will start cable movement. This, however, is not the case, as movement will not occur until the internal stress caused by expansion overcomes the static friction of the cable against the duct. It, therefore, seems to me that equation 3 of the paper should be of a form similar to equation 4 of the paper, but using the value of c for the copper conductor and a value of f corresponding to static friction.

L. H. Fink (Philadelphia Electric Company, Philadelphia, Pa.): Computation of cable movement in accordance with the formulas presented in Mr. Schifreen's paper is greatly facilitated by the reduction of these formulas to the graphical form shown in Figure 1 of this discussion. Evaluation of t_0 and t_1 is necessary in any case if equations 1 and 2 of the paper are to be employed properly. Once these values are known, the curves are read easily. The value of λ (equal to the ratio t_1/t_0) defines the curve applying to any given cable. The ordinate of the curve, when multiplied by δ (equal to $t_0 eL$), yields the maximum cable movement for any value of α (equal to the ratio t/t_0).

Figure 1 of this discussion is a plot of equations 1 and 2, which follow.

$$\frac{M}{\delta}=\frac{(\alpha-1)^2}{2(\lambda-1)} \quad (1\leqq\alpha\leqq\lambda) \tag{1}$$

$$\frac{M}{\delta}=(\alpha-1)-(1/2)(\lambda-1) \quad (\alpha\geqq\lambda) \tag{2}$$

As indicated, equation 1 of this discussion is applicable when the temperature lies between t_0 and t_1, while equation 2 is applicable when the temperature is greater than t_1. These equations are the dimensionless form of Mr. Schifreen's equations 1 and 2, and result from rewriting those equations, first in terms of the definitions of t_0 and t_1, as stated in his equations 3 and 4, and then in terms of the ratios of those temperatures, as defined in this discussion.

A curve for any value of λ not shown in Figure 1 of this discussion, and covering temperatures greater than $t_1(\alpha>\lambda)$, may be constructed easily by drawing a line parallel to those shown and intersecting the boundary ($\alpha=\lambda$) at the point where α equals the desired value of λ. Curves for temperatures less than t_1 may be similarly constructed if M/δ is plotted against (α—1) on standard log-log co-ordinates, since equation 1 of this discussion yields a straight line under these conditions.

C. S. Schifreen: The thoughtful discussions by Messrs. Atkinson, Crowdes, and Del Mar are gratefully acknowledged. Mr. Fink's proposed simplification of cable movement computations is likewise sincerely appreciated.

The data supplied by Mr. Crowdes substantially agreed with the results from bend tests in Philadelphia, on short samples of single-conductor 500,000-circular-mil cables, both standard strand and compact strand, and confirm the influence of compacting the strands upon the stiffness or springiness of the cable. The stiffness of large 3-conductor cables has been troublesome in splicing and manhole-racking operations, and there have been a few complaints relative to the smaller single-conductor cables. The extent to which the stiffness attributed to compacting may be charged with contributing to cable movement at the duct mouth appears to be slight and may be obscured readily by other factors such as length of lay, tightness of sheath and binders, belting, and binder materials. The cost of heat runs discouraged extension of the program, as would be necessary to include the large number of samples required to evaluate separately the influence of each factor on cable movement

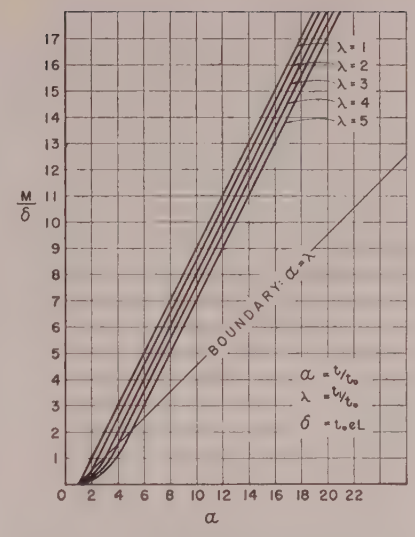

Figure 1. Universal curves to determine cable movement

at the duct mouth. It was, therefore, decided to evaluate composite effects only, on samples designed to represent maximum flexibility. For example, Sample 4 with standard strand sectors, 45-inch lay, and three paper binder tapes was found to be more flexible than the longer lay standard strand Samples 5 and 6, but all of these samples were stiffer than the Philadelphia Electric Company standard 3-conductor cable, tested as Sample 3, which had been regarded as a "stiff" cable with its compact-strand sector, 60-inch lay, and "tight" belt insulation. The great advantage of triplexing (evident from Table III and Figure 9 of the paper) for reducing cable movement, however, renders unimportant the effects related to compacting the strands. The little extra effort required by the splicer to train this slightly stiffer conductor in the manhole during the splicing and cable-racking operations can hardly justify the additional material which would be required if standard strand single-conductor paper and lead cables were specified.

Mr. Del Mar has quite appropriately emphasized the significance of the term "triplexed cables." Ambiguity, however, was thought to have been avoided in the paper by use of the cable descriptions given in Table I under the third column (headed "Conductor Size, Mcm").

Mr. Del Mar's difficulty in accepting the accuracy of equation 3 in the paper may be resolved by a review of the fundamental differential equation for cable expansion with rise in conductor temperature. The author had already referred to Mr. Bodicky's discussion of his earlier paper[1] for a general discussion of the appropriate equations, but some emphasis is in order. The fundamental relationship is

$$dm=etdx-wfc(L-x)dx-kcdx-wfc(dx)^2 \tag{3}$$

where dm is the increment of duct mouth movement caused by expansion in the differential length, dx, of cable at distance x from the center of the cable stretch. The component $etdx$ is the theoretical maximum expansion of a differential length of cable, dx, if there were no restraint. The component $wfc(L-x)dx$ is the reduction in expansion caused by compression produced by the frictional restraint of the moving cable ($L-x$) between the point x and the duct mouth, L being the distance from the center of the stretch to the duct mouth. The component $kcdx$ is the compression caused by the restraining force, k, at the duct mouth.

The component $wfc(dx)^2$ involves the point that Mr. Del Mar raised. This accounts for the static friction of the cable length dx against the duct and results in a restraining force, $fwdx$, on the cable increment, dx. This restraint produces a compression of the increment (dx) equal to the product of the force $fwdx$, the compressibility, c, and dx. This term, however, is a second-degree differential, which reduces to zero in equation 3 of this discussion, thus causing the static friction component to vanish. The subsequent integration required to evaluate the total duct mouth movement, M, therefore, need deal only with the following simplification of equation 3 of this discussion, as given by Mr. Bodicky:

$$dm=etdx-wfc(L-x)dx-kcdx \tag{4}$$

There apparently is no difficulty involved with equation 1 of the paper, which results from integrating equation 4 of this discussion between limits $x=0$ and $x=L$. For this case, the temperature rise is such that every increment (dx) of the entire stretch is contributing to the total movement, M.

The crux of the demonstration of the validity of equation 3 of the paper follows from an analysis of equation 4 of this discussion for the conditions that prevail for temperature rises between t_1 (equation 4 of the paper) and t_0 (equation 3 of the paper), during which every increment (dx) of cable in the stretch does not contribute to cable movement, M. For example, for every temperature rise t, there is a particular value of x, referred to as x_0, at which the cable expansion (dm) for the increment (dx) is zero, and equation 4 of this discussion reduces to

$$0=etdx-wfc(L-x_0)dx-kcdx$$

or

$$x_0=L+k/wf-et/wfc \tag{5}$$

Equation 5 of this discussion emphasizes that the length of cable, x_0, which does not contribute to cable movement depends on the length of the stretch, the restraining forces, and the temperature rise. There are two critical values of temperature rise. One value is t_1, at which $x_0=0$. This converts equation 5 of this discussion into the equation 4 of the paper. Any temperature rise above t_1 results in cable movement in accordance with equation 1 of the paper.

The other critical value is t_0 at which $x_0=L$. This converts equation 5 of this discussion into equation 3 of the paper and demonstrates its validity. At this temperature rise and below, there is no cable movement, since this condition represents a cable stretch that is totally restrained. Even the expansion (dm) for the last increment (dx) of cable adjacent to the duct mouth is zero.

The determination of the cable move-

ment M at the duct mouth for temperature rises intermediate in value between t_0 and t_1 is accomplished by integrating equation 4 of this discussion between the limits, $x = x_0 = L + k/wf - et/wfc$ (equation 5 of this discussion) and $x = L$. This results in equation 2 of the paper. It should be noted here again that equation 3 of the paper is consistent with equation 2 of the paper, since it is readily apparent that the term $(et-kc)$ must be equal to zero for the condition $M = 0$. Mr. Del Mar apparently has overlooked the full significance of the fact that at t_0 (when $M = 0$) we are dealing with only the last increment of cable (dx) adjacent to the duct mouth. Physically, this represents the fact that, since the coefficient of static friction is applicable only to that portion of cable which is on the verge of moving, it is at any instant applicable only to a differential length of cable, which is adjacent to the duct mouth for the limiting temperature rise t_0. At best, it can contribute only an infinitesimal force component which (since there is no finite length over which it can be integrated to yield a finite force) must be considered absolutely negligible at all times in relation to the other finite forces involved. Consequently, when $k = 0$, only an infinitesimal temperature rise will be required to start cable movement. The amount of this cable movement, however, also will be infinitesimal for such an infinitesimal temperature rise.

REFERENCE

1. See reference 8 of the paper.

Commutation in Universal-Type Motors

L. C. PACKER
MEMBER AIEE

Synopsis: The problem of commutation has always been one of the most important problems in the satisfactory operation of both d-c and a-c commutator motors. The universal motor has the problems of both a-c and d-c motors. The many factors influencing satisfactory commutation such as electrical and magnetic conditions, mechanical condition of the armature, carbon brush condition, and in some applications such as portable electrical tools, atmospheric conditions may be such as to influence commutations. In both the d-c and a-c motors, the armature conductors cutting across the magnetic field set up by the combined armature and field winding generate electromotive forces in the short-circuited coils which are proportional to the product of the speed of the armature, the flux which the armature conductors cut, and the number of turns in series. However, in the a-c motor, there is a voltage generated by the reversals of the main field flux just as the voltage is generated in the secondary of a transformer. In the noncompensated motor, commutation can be somewhat improved by using a strong main field and weak armature field and moving the brushes backward. However, this has no effect upon the transformer voltage. In the compensated universal motor there is a compensating winding distributed at 90 electrical degrees to the main field and opposing the armature field, or in the single field distributed winding the brushes are moved back a predetermined amount which compensates for the voltage due to the armature field.

THE universal-type motor is used principally in home appliances such as vacuum cleaners, food mixers, and drink mixers, office appliances of all types, and portable electrical tools and many miscellaneous applications. It is essential that the commutation be satisfactory in order to insure satisfactory life and performance. The conditions of operation cover a very broad field. In this country, the predominant voltage is 115 volts, 60 cycles alternating current with some direct current in the metropolitan districts and some shipboard use. However, for export the motors must operate on alternating current mostly 50 cycles, and a great deal of direct current. Many foreign countries have 200 to 250 volts alternating and direct current which makes it very difficult to obtain good commutation unless the motors are especially designed for these higher voltages which would mean adding more commutator bars and narrower brushes so that the brush span on the bars is no greater than for 115-volt motors. However, there are disadvantages to doing this for small high-speed motors because of the weaker mechanical construction.

Good commutation means more than satisfactory performance. It means increased life of the brushes, less burning and smutting of the commutator, and less heat in the commutator and armature and brush springs. There is then less heat carried to the bearings thus increasing the life of the lubrication in the bearings. In all, it means longer life to the motor and less service charges for the manufacturer and ultimate user.

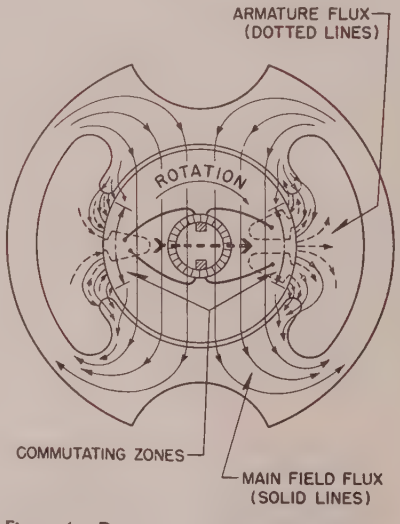

Figure 1. Diagram of main and armature flux in a noncompensated universal-type motor

Prior to 1923, the best brush life of noncompensated motors was under ideal conditions about 500 hours. The users accepted it then as satisfactory but improvements in appliances demanded greater life of the motor brushes.

The application of good design principles and proper manufacturing methods has made it possible to improve the commutation and increase the brush life considerably over this figure. However, the application still has considerable bearing upon the best commutation and brush life obtainable.

This paper endeavors to explain some of the theory of commutation as applied to universal-type motors and the principles of design and manufacture for good commutation.

Commutation Problems, Electrical and Magnetic Conditions

In commutator-type motors, the current is reversed in the armature coils as the commutator bars, to which they are connected, pass under the brushes. During the period of reversal the coils are short circuited due to the brush making contact with two bars to which the ends of the coils are connected. During the short-circuit period, the current in the short-circuited coil is determined by the voltage generated in that coil and the resistance of the coil, brush, and brush contact. The ideal condition would be when the voltage generated in the short-circuited coil would be such that the current in the coil would change at a uniform rate from full load

Paper 51-24, recommended by the AIEE Rotating Machinery Committee and approved by the Technical Program Committee for presentation at the AIEE Winter General Meeting, New York, N. Y., January 22–26, 1951. Manuscript submitted February 8, 1950; made available for printing November 20, 1950.

L. C. PACKER is with Westinghouse Electric Corporation, Springfield, Mass.

One cannot think of commutation problems without acknowledging the great contributions of the late B. G. Lamme and R. E. Hellmund. It was the privilege of the writer to receive their personal assistance and advice and also assistance and advice from G. H. Garcelon, R. Ehrenfeld, C. A. M. Weber, and the late B. H. Chatto, at the time when efforts were underway to improve the commutation of universal motors.

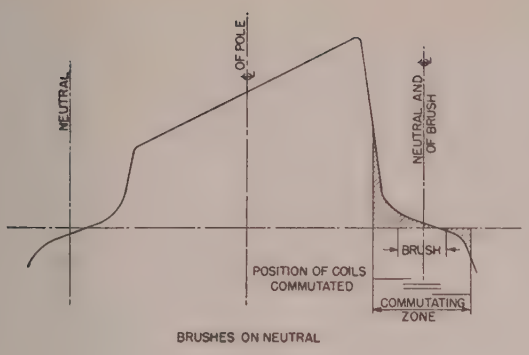

Figure 2 (left). Combined field form of a noncompensated universal - type motor with brushes on neutral. Counter-clockwise rotation

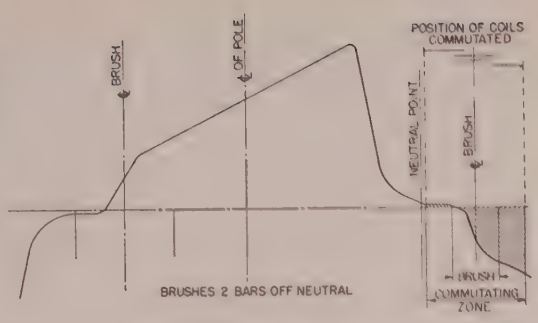

Figure 3. Combined field form of a noncompensated universal-type motor with brushes two bars off neutral. Counter-clockwise rotation

value in one direction to full load value in the opposite direction. This would mean that the short-circuit current would never be excessive and that the current would be flowing in the proper direction and would have the proper value when the commutator bar to which the coil is connected passes from under the brush.

In Figure 1, is shown for example the path of the main field flux and that of the armature flux of a noncompensated motor and also the location of the armature coils which are short circuited by the brushes. It can be seen that the whole main field flux (solid lines), passes through the coils while they are short circuited. Therefore with alternating current, the transformer voltage is then proportional to the number of turns in the armature coil, the total main field flux, and the frequency of the circuit. The transformer voltage is 90 degrees out of phase with the field flux and its value is independent of the speed of the armature.

The transformer voltage is usually of considerable value and it would be very desirable to generate a counter-voltage which would tend to reduce a short-circuit current due to the transformer voltage. So far there seems to be no means for providing such a counter-voltage since the ordinary means of correcting commutation trouble deals only with the rotational voltages.

The current in the armature conductors by its magnetic effect influences the magnetic field around the armature. This influence is known as armature reaction. The armature flux combined with the main field flux distorts the field form and sets up a field in the space between poles and in the commutating zone. Referring again to Figure 1, it will be noted that the short-circuited coils are moving through this field in the interpolar space. The commutating zone as indicated represents this space through which one or more short-circuited coils move. It is the flux within this space which concerns us in considering commutation. The value of the flux in the commutating zone is determined by the ampere-turns of the field, the ampere-turns of the armature, and the reluctance of the magnetic path. With the brushes on neutral, the reluctance of the magnetic path is high in the center of the commutating zone and decreases to a comparatively low value at the pole tips. The reluctance in the commutating zone is changed with the shifting of the brushes due to the fact that the relative position of the brushes and commutating zone remains constant.

In the d-c or the universal motor, assuming no compensation, there are three voltages generated in the short-circuited coil. One is due to the magnetic field in the interpolar space set up by the combined field and armature windings, another voltage due to the flux set up in the armature end winding in the zone of the short-circuited coil, and another voltage due to the armature flux which crosses from slot to slot. The short-circuited armature coils cutting across these three fluxes generate these short-circuited voltages, the values of which are proportional to the flux cut by the armature conductors, the speed of the armature in revolutions per second and the number of turns in series. These voltages are known as reactance or rotational voltages, and apply to both d-c and a-c operation.

The rotational or reactance voltages are in phase with the field flux and are 90 degrees out of phase with the transformer voltage in the short-circuited coil and for that reason cannot in any way affect the value of the transformer voltage. Unless there are conditions existing in an a-c series motor of which we do not have any knowledge, the transformer voltage in the short-circuited coil cannot in any way be affected by the shifting of the brushes or changing in any way the value of the flux surrounding the short-circuited coil.

Noncompensated Motors

Figures 2 and 3 are assumed field forms to show the effects of different field strengths in the commutating zone, upon commutation. By combining the fields produced by the armature and the main field and plotting these as shown in Figures 2 and 3 and then laying off the width of the commutating zone, we can determine the strength of the field surrounding the short-circuited coils. In Figures 2 and 3, the shaded portion below the horizontal base line is the field which generates the voltage tending to reverse the current in the short-circuited coil. It is evident that in Figure 2 the value of the field is very small and by noting the relation of the coils and the field, it will be seen that just

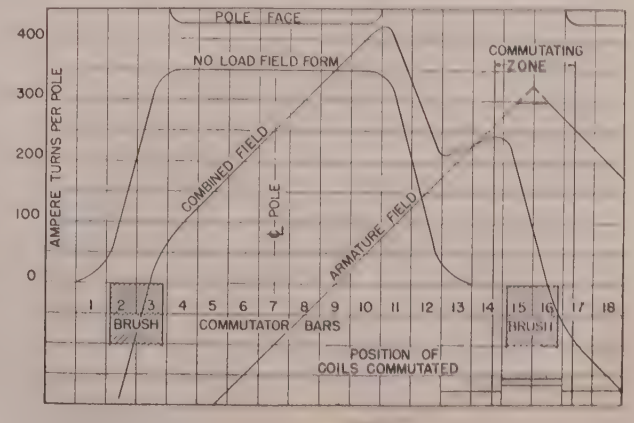

Figure 4. No load, armature and combined field forms in terms of ampere turns for a noncompensated universal-type motor. Commutator has 26 bars. Counter-clockwise rotation

the one side of the one coil is really affected by the field below the line. Figure 3 shows that all except one of the coil sides are in a strong field. This is the desired condition but the value of this field must be such as to give approximately the voltage required to reverse the current and bring it up to full load value while the coil is being commutated. Due to the high speed of these motors, a coil is short-circuited only a very short time, in the order of approximately 0.0005 second. It is probable that a higher voltage is required to build the current up in the short period of time than would be required in a slower speed motor. It is good practice to determine experimentally the proper value of field for the reversal of the current. Due to the small size of these motors this is practical because they are easier to handle.

In the noncompensated universal motors the ratio of armature and field strengths can be proportioned to reduce the field in the commutating zone and improve commutation. Shifting the brushes against rotation will further improve commutations. Further improvements can be made by the design of the magnetic circuit to reduce magnetic distortion and increase the reluctance of the armature. Deep slots in the armature are to be avoided as they decrease the reluctance and increase the reactance voltage.

A ratio of armature to field strengths in the order of 0.7 to 0.8, together with a brush shift of 20 to 26 electrical degrees, depending upon the field form, in a 2-pole motor will give good commutation and brush life. The brush shift necessary will depend somewhat upon the ratio of pole face to pole pitch and the chording of the armature winding and the ratio of the armature to field winding. If the brush shift is much more than indicated above, the main field flux is reduced to such an extent that the motor becomes very inefficient. It is the usual practice to get the equivalent of the brush shift by connecting the armature leads to the commutator bars off neutral an amount equal to the brush shift desired. If the motor is to be reversed, the brushes must be set on electrical neutral. These motors usually have two bars per armature slot.

The winding ratio mentioned previously is satisfactory for universal characteristics over a reasonable range of load or a lower range if a governor is used. Some applications that operate over the full range of speed from starting to no-load may require a weaker field than the above ratio to get desirable characteristics for operation on frequencies from 0 to 60 cycles. However, this means a sacrifice in commutating conditions and shorter brush life.

The rotational voltages due only to the interpolar flux can be determined approximately by laying out the field forms. All of the rotational voltages can be calculated by the methods following which, however, are only approximate but give reasonably good results. The transformer voltage is calculated directly from the full load main field flux. This flux is calculated from the no-load saturation curve correcting for brush shift and distortion caused by the armature flux.

The field forms shown in Figures 4, 5, and 6 are for an experimental motor. Figure 4 shows the no-load field form with no current in the armature, the armature field form, and the combined field, all in terms of ampere-turns per pole. The field ampere-turns are those in the air-gap.

A convenient method for laying out the no-load field form is to lay out the pole face, pole tips, armature surface, and air-gap to a large scale. Divide the surface of the pole face, tips and armature surface into equal divisions and connect the corresponding points with flux lines for a pole pitch. Measure these lines and plot the reciprocals of them as ordinates against the corresponding points on the armature as abscissa. These points should be so spaced as to be a multiple of 180 degrees, so that the abscissa can be converted to read from 0 to 180 degrees. Then assume the total height of this field form to be 100 per cent and let the calculated ampere-turns per pole in the main air-gap equal 100 per cent. Points on the side of field form are then proportional to the total height or maximum air-gap ampere-turns shown.

The armature ampere-turns per pole for a full pitch winding are equal to:

$$\frac{I_c Z}{2P} \qquad (1)$$

where

I_c = armature current per conductor
Z = total armature conductors
P = number of poles

This value represents the total height of the armature ampere-turn field form. This point is located 90 electrical degrees from the center of the no-load field form when the brushes are on neutral. Then draw a line from this point to the abscissa at the center of the main field no-load field forms of two adjacent poles. The north pole is above the line and the south pole is below the line. This triangle represents the armature ampere-turn field form for a full pitch winding when there is no current in the main field winding. Refer to Figure 4.

The curve will have a flat top for a

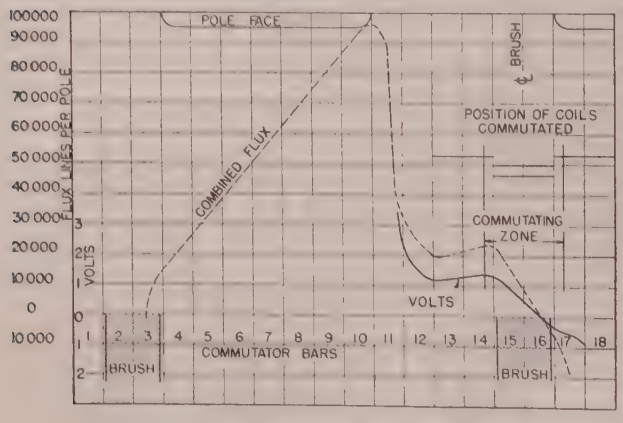

Figure 5. Combined field form in terms of flux, for a noncompensated universal-type motor. Counter-clockwise rotation

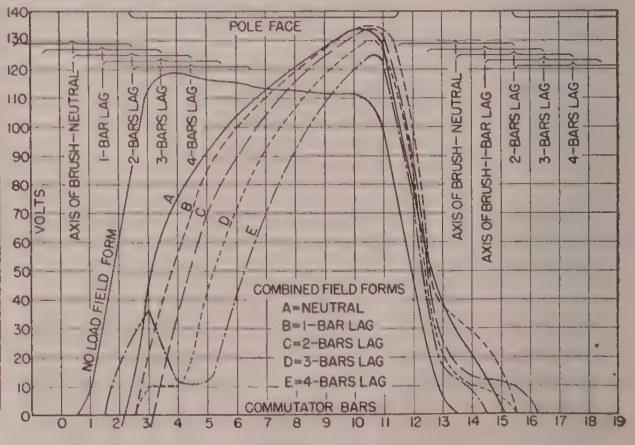

Figure 6. No load and load field forms of a noncompensated universal-type motor from tests with brushes moved back various number of bars. Commutator has 26 bars. Counter-clockwise rotation

chorded winding. Draw a horizontal line across the triangle near the peak at a height equal to equation 2 times a factor or:

$$\frac{I_cZ}{2P}\times\frac{S^1}{S} \qquad (2)$$

where

S = number of armature slots per pole
S^1 = number of slots spanned by the armature coils

The combined field form is obtained by adding the main field no-load field form and the armature field form. Figure 4 shows the layout of these field forms. In this case the abscissa is laid out in terms of commutator bars.

The flux field form, Figure 5, is calculated from the combined ampere-turn field form for the different air-gaps and the armature. This does not take into account armature teeth or pole tip saturation which may have an appreciable effect in some cases.

The voltages are calculated from the combined flux field form for the various points as shown in Figure 5. However, it is only necessary to calculate those voltages generated in the commutating zone. The following method from Lamme, may be used to calculate the width of the commutating zone in terms of slots.

$$\frac{C_s+B_s-1+(C_s\times\text{slots chorded})}{C_s} \qquad (3)$$

where

C_s = number of commutator bars per slot
B_s = number of commutator bars spanned by the brush

Figure 6 shows test field forms for the experimental motor for which the layouts in Figures 4 and 5 were made. The test was made with an exploring coil, on the armature, the coil having a sufficient number of turns so that the voltages would be sufficiently large to be readable on the voltmeter. The values in Figure 6 are for the no-load field and full load for all brush settings from 0 to 4 bars off electrical neutral. The voltage values should be multiplied by a factor of 0.09 to get the correct value of voltage generated in the armature coil. This represents the ratio of armature turns per coil to the exploring coil turns. The values in the commutating zone are reasonably close to the values calculated from the field form.

Figure 6 also shows how the combined field is weakened by increasing the brush shift from 0 to 4 bars. This motor was built with a brush shift of two bars. The armature was lap wound.

The three voltages, (1) that due to the flux in the interpolar space, (2) that due to the armature end winding, and (3) that which crosses from slot to slot may be calculated approximately by the following methods:

Voltage Due to the Flux in the Interpolar Space

The flux density B_i at the midpoint in the interpolar space is,

$$B_i=\frac{2\times3.19}{G}\times\text{armature ampere turns per pole (equation 1)}$$

$$=\frac{2\times3.19}{G}\times\frac{I_cZ}{2P} \qquad (4)$$

where

G = interpolar gap in inches between armature surface and the yoke

The voltage E_i in the coil due to its cutting the interpolar flux is calculated by the well known equation,

$$E=\frac{\text{Flux}\times\text{conductors}\times\text{rpm}}{60\times10^8} \qquad (5)$$

Then

$$E_i=\frac{(B_i\pi DL)\times2T_cR_s}{10^8} \qquad (6)$$

where

D = armature core diameter in inches
L = armature core length in inches
T_c = armature turns per coil
R_s = revolutions per second

Equation 6 further developed and multiplied by the factor C_1 which takes into account the chording and brush width, may be written

$$E_i=\frac{2\times3.19\times I_cZ\pi DLT_cR_s\times C_1}{GP\times10^8} \qquad (7)$$

C_1 = 1.0 to 1.5

Voltage Due to the End Flux

This voltage E_e is due to the flux in the armature end winding set up by the armature as a whole and may be calculated approximately by the following method from Lamme.

$$E_e=\frac{I_cZT_cR_s}{10^8}\times\frac{4\pi D}{P}(0.9+0.035S)C_2 \qquad (8)$$

where

S = number of slots per pole
C_2 = a constant depending upon the chording and equals S^1/S
S^1 = number of slots spanned by the armature coils

Voltage E_s Due to Flux From Slot to Slot

This voltage is due to slot flux which enters at the bottom of the tooth and spreads across the coil space, the space above the top coil and from the tooth top across the slot opening.

The total voltage E_s may be expressed by an equation derived from Lamme's equation as follows:

$$E_s=\frac{4\times3.19\times I_cZT_cR_sL}{10^8}\times\{C_s(K_s''+0.54\sqrt{n})\} \qquad (9)$$

where

K_s'' = slot constant
$n=\frac{\text{tooth width}}{\text{slot opening}}$ at the circumference

$$C_s=\frac{C_s}{C_s+B_s-1+(C_s\times\text{slots chorded})} \qquad (10)$$

where

C_s = number of commutator bars per slot
B_s = number of commutator bars spanned by the brush

The total voltage E_c per coil is,

$$E_c=E_i+E_e+E_s \qquad (11)$$

The total voltage E_b due to the brush span B_s is,

$$E_b=E_c\times B_s \qquad (12)$$

All of these voltages are on the basis of no brush shift. Brush shift does not alter the calculations for the end and slot voltages, but a correction must be made for the interpolar flux which can be obtained from the field forms.

The transformer voltage E_T in the short-circuited armature coil can be calculated by the well known equation

$$E_{Tc}=\frac{4.44\times\phi T_cf}{0.707\times10^8} \qquad (13)$$

where

ϕ = full load flux in lines (from the saturation curve) = 0.707 maximum value main field flux
T_c = armature turns per coil
f = frequency of the circuit

The voltage E_{Tb} per brush is, $E_{Tb}=E_{Tc}\times$ the bars spanned by the brush or,

$$E_{Tb}=E_{Tc}\times B_s \qquad (14)$$

The rotational voltages are spaced 90 degrees to the transformer voltage, and therefore, the resultant voltage E_{Rc} per coil is equal to,

$$E_{Rc}=\sqrt{E_{Tc}^2+E_c^2}\text{ volts per coil} \qquad (15)$$

The resultant voltage E_{Rb} per brush is equal to,

$$E_{Rb}=\sqrt{E_{Tb}^2+E_b^2} \qquad (16)$$

The short-circuit current in the coils being commutated depends upon the resistance of the coils, the contact resistance and resistance of the brush and the total voltage. The short-circuit current may

Figure 7. Field forms of a 2-field compensated motor

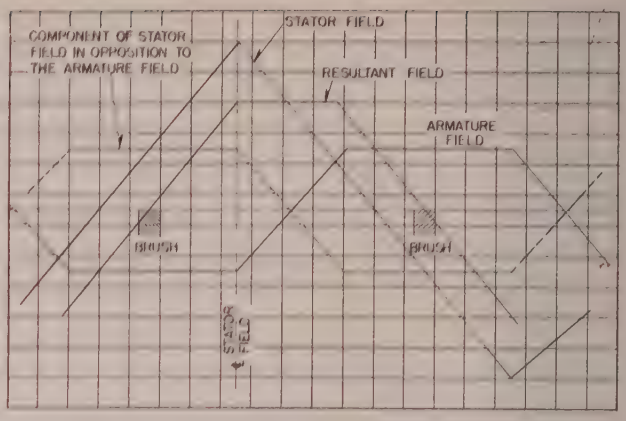

Figure 8. Field forms of a single-field compensated motor

be calculated from the short circuit voltages, armature coil resistance, brush drop, (approximately one volt per brush) and load current. Frequently this current is greater than the load current.

Calculations of the rotational and transformer voltages for the motor for which the field forms were made are shown in the Appendix. The results as well as general experience show that the greater portion of the short circuit voltage is due to the transformer voltage. In many cases it may not be worthwhile to plot the field forms just to estimate the voltage in the interpolar space. However, it is necessary to plot the no load field form in order to obtain the mean polar angle of the pole face and the combined flux field form should be made to show the distortion and maximum densities.

It requires only a little more time to figure the voltage in the interpolar space. It also may be necessary to do it anyway for low speed motors.

The noncompensated motors are usually so small that it is not practical to have more than two bars per armature slot or to have interpoles. It is generally possible to satisfy the application without interpoles and with two bars per slot.

Compensated Motors; 2-Field Type

Compensated universal motors have slotted primaries in which the main field is usually a single coil. The armature field is compensated by a distributed field in series with the armature but opposing the armature field and is at 90 degrees to the main field. The compensating magnetomotive force practically neutralizes the flux in the interpolar space, the armature end flux, and the flux from slot to slot. However, since the primary and armature do not have the same number of slots, it is not possible to match the armature field exactly but the match can be fairly close. It is better to over compensate slightly. This compensation leaves only the transformer voltage in the short circuited coil when operated on alternating current. This voltage can be kept to a safe value as this type of motor is usually large enough to make it practical to use three or more bars per armature slot thus reducing the turns and voltage per coil. However, the brush span must not be any more than for the two bars per slot. Figure 7 shows representative fields of the 2-field type. The brushes are on neutral and the motor may be reversed.

Compensated Motors; Single Field Type

The single field motor is similar to the 2 field motor except that the main field is a fully distributed winding and the compensation of the armature field is obtained by moving the brushes thereby moving the armature field with them as shown in Figure 8. The ratio of the armature ampere turns to the field ampere turns is usually less than 1, whereas the 2-field type may have a ratio over 1. In this case, like the 2-field type, we have only the transformer voltage to deal with. The motor cannot be reversed.

It is desirable to keep down the value of the short circuit voltage to 5 to 7 volts per brush and the short circuit current to a minimum at the full load point. The brushes should have sufficient resistance to assist materially in holding down the short circuit current and still not to increase the voltage drop at the brushes to an excessive value. The armature coil resistance and the contact resistance between the brush and commutator also help to hold down this current. If steps are not taken to hold down this current, it may exceed the load current. The short circuit voltage and current increase with increase in load. Changing the width of the brush may help commutation, but not always. If too narrow, the brush may not follow the commutator. It also may be mechanically weak and break easily.

Commutator and Brushes

The commutator performs a very important part in maintaining good commutation. It would be desirable to have as many bars as practical which means more coils in the armature with fewer turns per short circuited coil, thus reducing both the rotational and transformer voltages. However, the commutator diameter and brush span more or less limit the number of bars. If the bar is too thin, there is more of a tendency to loosen at high speeds, especially in small commutators. The brush span should be $1^3/_4$ to 2 bars. The minimum thickness of the insulation between bars is about 0.018 to 0.020 inch for this type of motor. If the insulation is undercut a narrow brush will not follow the commutator surface very well and will cause chattering and increased sparking and heat.

The commutator must be designed and manufactured so that at high speeds and at running temperatures it will not distort its surface or cause high bars. A difference of 0.0001 inch between adjacent bars will cause poor commutation. Out of-roundness due to all of the bars moving is also not desirable. The surface of the commutator should be diamond-turned concentric with the bearing surface. The bar surface will be more nearly a true arc conforming to the commutator diameter than if ground. Commutators can be built to withstand a surface speed of 5,000 feet per minute under normal load conditions and 15,000 feet per minute at no-load.

Commutators with mica bar insulation

for instance are usually undercut. If not undercut, the brush, even though having good cutting qualities, is liable to cut the copper bars below the mica or reduce the copper below the mica by the so-called electrolytic action, and thus cause the brush to hop from mica bar to mica bar and to chatter. Poor commutation, blackening of the bar surface, and increased temperature in the commutator and brush springs are the results. When undercutting the commutator mica bars, the depth should not be made greater than about 1/32 inch. In most cases this will permit less dirt to accumulate and that which does will be more easily thrown out, thus reducing the chances of short-circuiting the bars. All slivers of mica along the sides of the bar in the slot should be cleaned out, otherwise the brush will strike them and bounce, and cause poor commutation.

Commutators also now are being made with paper bar insulation but are limited in application as to speed and current. The paper may be left flush with the surface but care must be exercised in machining the commutator surface. Special grades of brushes are available that perform as well on these as on many undercut designs. In the small commutators of all types, it is practically impossible to build up the commutator without skewing the bars. This means that the undercutting will require wider slots in order to remove all mica. This wider slot causes more chattering of the brush. Many tests on both undercut mica commutators and flush paper bar insulation type commutators on the same design of motor have shown better commutation, and two to three times longer brush life with the flush paper bar insulation.

In general, the brush should be of such quality that the resistance helps materially in reducing the short-circuit current but does not cause excessive voltage drop at the brushes, cut the mica or paper bar insulation when not undercut without damaging the oxide film on the commutator surface, and under either the condition of undercut or flush mica or paper have minimum friction on the commutator surface, shall not chatter, and keep the commutator clean without injuring the oxide film and be of good mechanical strength.

In some motors the current may be high enough to require shunts, or so-called pig tails, in the brushes to divert the current from the springs, because excessive current through the springs will anneal them and cause them to "set" and become ineffective. In some applications, beryllium springs may be used without shunts because they will carry more current safely than a bronze spring. However, the loss in the spring should be calculated and checked with the characteristics of the wire.

The brush pressure should be approximately 5 pounds, (initial pressure) per square inch of brush surface and maintained as near that pressure as possible in order to maintain good contact with the commutator surface. It is desirable to maintain the brush friction loss below 6 watts per square inch of net commutator bar surface, (top surface) in order to prevent excessive heating of the commutator, winding, brushes, and springs. Difficulty also may be experienced with the soldered connections if the brush friction is above that value.

The clearance between the brush and brush holder box should be such that the brush will not chatter due to too much clearance, or have a tendency to stick in the box, due to small clearance plus an accumulation of carbon dust. It is advisable to refer to the tolerances established on brushes when setting up tolerances for the brush holder box.

Armature Winding and Running Balance

It is a well known fact that a good running balance improves commutation because it permits the brushes to follow the commutator surface, reduces the sparking. In order to maintain a good running balance the armature winding must be anchored so that the wires cannot move from their original positions. The shaft must also be straight and maintained in that position when running.

Atmospheric Conditions

An atmosphere that contains acid, and possibly alkali fumes may be detrimental to the oxide film on the commutator and may cause poor commutation and short brush life. Applications under this condition are confined mostly to electric portable tools and are probably very limited. Dust from the air also can cause poor commutating conditions.

Effect of Bearings and Lubrication Upon Commutation

If sleeve-type bearings have too much clearance at the start or later because of wear, the brushes will not follow the commutator properly, and poor commutation will result.

Ball bearings with dirt in them cause a roughness in running that produces increased sparking. This condition can be the result of dirt in the bearing when installed or due to the grease becoming deteriorated and carbonized.

Conclusions

It has been proved by experience that acceptable commutation in universal motors can be obtained by the proper application of the principles explained herein. A great deal can be seen if layouts of the field forms are made and used to check calculations. Tests show reasonable agreements with calculations and field forms as shown in the Appendix.

The transformer voltage is generally the major portion of the total short-circuit voltage in the noncompensated motors and is the only voltage to contend with in the compensated motors. It is essential that good design be supplemented with good quality of manufacture to produce good commutation.

The quality of commutation and the brush life also depend a great deal upon the application. Some applications are definitely more detrimental to good commutation and brush life than others.

Appendix

The following calculations of the various voltages are for an experimental motor for which field form layouts, Figures 4 and 5, and test field forms, Figure 6, were made.

The interpolar voltage E_i is calculated at the center of the armature field with the brushes on electrical neutral. The constant C_1 will vary from 1 to approximately 1.55 and calculations are shown for both values and compared with the values of E_i from the field form layouts and test field form, Figures 4, 5, and 6, with the brushes given a 2-bar lag against rotation.

Maximum values of E_i are shown as taken from Figures 5 and 6. The total resultant voltage per brush is an average value. The following symbols are used in these calculations:

where $B_g = 1.7$, $C_1 = 1.0$–1.55, $C_2 = 0.92$, $C_3 = 0.74$, $D = 1.583$, $f = 60$, $G = 0.55$, $I_c = 1.125$, $K_s'' = 1.09$, $L = 1.625$, $n = 2.82$, $P = 2$, $R_g = 150$, $S = 6.5$, $S' = 6$, $T_c = 20$, $Z = 1040$

Interpolar voltage E_i from equation 8, with brushes on electrical neutral:

$$E_i = 2 \times 3.19 \times 1.125 \times 1040 \times \pi \times 1.583 \times \frac{1.625 \times 20 \times 150}{0.55 \times 2 \times 10^8} \times 1.55 \text{ where } C_1 = 1.55$$

$E_i = 2.55$ volts by calculation (where $C_1 = 1.55$)

$E_t = 1.65$ volts by calculation (where $C_1 = 1.0$)

Voltage E_e due to armature end flux from equation 9

$$E_e = \frac{1.125 \times 1040 \times 20 \times 150 \times 4 \times \pi \times 1.583 \times (0.9 + 0.035 \times 6.5) \times 0.92}{2 \times 10^8}$$

$E_e = 0.36$ volts

Voltage E_s due to slot flux from equation 10:

$$E_s = \frac{4 \times 3.19 \times 1.125 \times 1040 \times 20 \times 150 \times 1.625\{0.74(1.09) + 0.54\sqrt{2.82}\}}{10^8}$$

$E_s = 1.07$ volts

Total rotational voltage per coil from equation 12:

$E_c = 2.55 + 0.36 + 1.07 = 3.98$ volts (where $C_1 = 1.55$)
$E_c = 1.65 + 0.36 + 1.07 = 3.08$ volts (where $C_1 = 1.0$)
$E_b = 3.98 \times 1.7 = 6.76$ volts (where $C_1 = 1.55$)
$E_b = 3.08 \times 1.7 = 5.24$ volts (where $C_1 = 1.0$)

Transformer voltage per coil from equation 14:

$$E_{Tc} = \frac{4.44 \times 51500 \times 20 \times 60}{0.707 \times 10^8}$$

$E_{Tc} = 3.88$ volts

Transformer volts per brush:

$E_{Tb} = 3.88 \times 1.7 = 6.58$ volts

Total rotational and transformer voltage per coil from equation 16:

$E_{Rc} = \sqrt{(3.88)^2 + (3.98)^2} = 5.55$ volts (where $C_1 = 1.55$)

$E_{Rc} = \sqrt{(3.88)^2 + (3.08)^2} = 4.95$ volts (where $C_1 = 1.0$)

Total rotational and transformer voltage per brush from equation 17:

$E_{Rb} = \sqrt{(6.58)^2 + (6.76)^2} = 9.45$ volts (where $C_1 = 1.55$)

$E_{Rb} = \sqrt{(6.58)^2 + (5.24)^2} = 8.4$ volts (where $C_1 = 1.0$)

Table I shows a compilation of all values of the voltages based on the previously calculated values and based on values of E_t taken from the field form layouts and tests per Figures 4, 5, and 6 for two bars lag in which case the value or the constant $C_1 = 1.0$.

Table I

Column	1	2	3	4
C_1	1.55	1.0	1.0	1.0
E_t, volts	2.55	1.65	0.51	0.81
E_c, volts	0.36	0.36	0.36	0.36
E_s, volts	1.07	1.07	1.07	1.07
Total volts per coil, E_c	3.98	3.08	1.94	2.24
Total volts per brush, E_b	6.76	5.24	3.3	3.81
Transformer volts per coil, E_T	3.88	3.88	3.88	3.88
Transformer volts per brush, E_{Tb}	6.58	6.58	6.58	6.58
Total rotational and transformer volts per coil, E_{Rc}	5.55	4.95	4.35	4.50
Total rotational and transformer volts per brush, E_{Rb}	9.45	8.4	7.4	7.65
Estimated short-circuit current per brush	2.86	2.55	2.24	2.32
Full load current	2.25	2.25	2.25	2.25

Values are shown based on E_t at the center of the armature field.

Column 1 = calculated values with $C_1 = 1.55$
Column 2 = calculated values with $C_1 = 1.0$
Column 3 = calculated and values from Figures 4 and 5 with $C_1 = 1.0$
Column 4 = calculated and values from Figure 6 with $C_1 = 1.0$

At the end of Table I are shown estimated short-circuit currents based on voltages at the center of the armature field.

Results of the calculations when corrected to the layouts of the field forms agree about as close as can be expected, without making very accurate flux plots in the interpolar space, with the test voltage in the interpolar space.

The maximum voltage E_t at the left side of the commutating zone is 1.35 volts from the field form layouts and 1.17 volts approximately from the test curve. The calculated value with $C_1 = 1.0$ is 1.65 volts, which is the maximum at the center of the armature field.

Test values of the resultant voltages are difficult to get, because of the small size of commutator and brushes, and are not very reliable. However, the transformer voltage, which is the major portion of the resultant voltage, can be accurately computed from test saturation curves, for any load.

The short-circuit current was estimated for this design and is shown at the bottom of Table I. This current appears high but it is doubtful if it builds up to more than a small fraction of the estimated value because it only takes about 0.0004 second for a commutator bar of this motor to pass under the brush.

This motor represents about the average design of a universal motor, but is not as good as those motors with a lower ratio of armature to field ampere turns from a commutation and brush life standpoint, but it was relatively good and the brushes would probably outlast the equipment for which it was built. It is satisfactory for other applications requiring similar speed and torque characteristics.

References

1. A Theory of Commutation and Its Application to Commutating Pole Machines, **B. G. Lamme.** *AIEE Transactions*, volume 30, part II, 1911, pages 2359–2431.

2. Physical Limitations in D-C Commutating Machinery, **B. G. Lamme.** *AIEE Transactions*, volume 34, part II, 1915, pages 1739–1800.

3. Flashing of Railway Motors Caused by Brush Jumping, **R. E. Hellmund.** *Electrical Engineering* (*AIEE Transactions*), volume 54, November 1935, pages 1178–85.

4. Sparking Under Brushes of Commutator Machines, **R. E. Hellmund, L. R. Ludwig.** *Electrical Engineering* (*AIEE Transactions*), volume 54, March 1935, pages 315–21.

5. Universal Type Motors, **L. C. Packer.** *AIEE Journal*, volume 44, December 1925, pages 1319–23.

6. Universal Motors, **L. C. Packer, R. P. Percy, W. E. Wier.** *Electrical Manufacturing* (New York, N. Y.), September 1948.

7. Influence of Temperature on Large Commutator Operation, **F. T. Hague, G. W. Penney.** *AIEE Journal*, volume 48, June 1929, pages 473–76.

8. Effects of Temperature on Mechanical Parts of Rotating Electrical Machinery, **C. Lynn.** *Electrical Engineering* (*AIEE Transactions*), volume 58, October 1939, pages 514–18.

9. The Black Band Method of Commutation Observation, **T. W. Schroeder, John C. Aydelott.** *AIEE Transactions*, volume 60, 1941, pages 446–51.

10. Maintenance of Good Brush Performance, **W. C. Kalb.** *Electrical Engineering* (*AIEE Transactions*), volume 64, December 1945, pages 819–25.

11. Effects of Commutator Surface Film Conditions on Commutation, **H. M. Elsey, C. Lynn.** *AIEE Transactions*, volume 68, part I, 1949, pages 106–12.

Discussion

A. F. Puchstein (The Jeffrey Manufacturing Company, Columbus, Ohio): This paper is an excellent treatment—one of the few in American technical literature. The following comments will be made. More strictly, current in the short-circuited coils is determined by voltages generated in the coil; resistances of coil, coil leads, brush material, and brush contact; time of commutation, bars under a brush; self- and mutual-inductances; and possibly supply frequency. The paper assumes that main current, field flux, and terminal electromotive force are sine functions of time. Hysteresis, saturation, and commutation cause departures which, together with other factors, limit the accuracy attainable by calculations.

For direct current, mathematical approaches were attempted around the turn of the century by such men as E. Arnold, G. Mie, A. Press, Thorburn Reid, and more recently in a paper by F. D. Olney.[1] For alternating current, a comprehensive discussion was given by Marius La Tour about 1904,[2] for starting conditions. A discussion for running conditions was given by the present writer in 1943.[3] No others seem to have appeared.

Engineering approaches are much more numerous. Among them, for direct current,

we may cite the work of Hobart, Arnold, Punga, Kennedy, Poole, Bewlay, Lamme, Senstius, Dreyfus, and Shenfer. For alternating current (different single-phase and polyphase types), the names of Arnold, Punga, Ossanna, Iwan Döry, and others may be mentioned.

The speed electromotive force, E_i, may be negative under certain conditions, as when brushes are shifted from the neutral, or if the machine is overcompensated. In regard to pole flux distortion, the classical view is that reducing distortion improves commutation. This is not always true, particularly if brushes are on the geometrical neutral. Assuming that the main field is strong enough to maintain stability, the line current sets up the armature flux whose density is B_i, of value proportional to and in time phase with itself. Looked at in this way, the speed electromotive force, E_i, for a given armature running at a given speed with a given current is independent of whether the flux distortion under the main poles is small or great. Of course, if the brushes are shifted from the neutral, the magnetomotive force delivered to the commutation zone by the field poles combines with that of the armature to set up a resultant flux density there, which is favorable to commutation. It is this resultant which is sensitive to the relative values of (air gap + tooth) and armature ampere-turns.

The ratio of series-field to armature ampere-turns recommended, 1/0.7 to 0.8, is the same as for standard d-c practice, with larger values for 60 cycles (and for larger size 25-cycle motors) in order to keep up the power factor. To plot the flux distribution to be expected at any point in the air gap at any point in the cycle (neglecting effects of commutation, which, however, are not negligible for precise work although we do not know how to include them), it is convenient to calculate the saturation curve for (one tooth + air gap + pole face). The ampere-turns available at any point in the gap (arc) are equal to the ampere-turns delivered plus or minus the armature ampere-turns, both taken at the point considered. The gap flux distribution under load conditions will change with time as the cycle proceeds. An expression for width of commutation zone of greater generality is

$$\Big[\text{Bars covered by brush} - (1+\text{No. of brush pairs omitted})\times \frac{\text{Armature paths}}{\text{Poles}} + \text{Coils per bundle} + \text{Phase difference}\Big]\times\frac{\pi\times\text{Armature diameter}}{\text{Commutator bars}},$$

where Phase difference

$$= \frac{\text{No. of commutator bars}}{\text{Poles}} - \text{Coils per bundle}\times\text{Teeth embraced by a coil}$$

This applies to simplex and multiplex windings of either lap or wave type. For certain machine-wound coils this zone width will be greater. For example, if a 2-pole 19-slot armature with a diameter of 3.75 inches has 38 coils, of which coil 1 is in slots 1 and 11 and coil 2 is in slots 1 and 10, the zone will be wider by one tooth pitch.

In spite of the work done during these many years, we still do not know very accurately the values to which the factors which control the quality of commutation or life of parts must be restricted. Assuming that the mechanical conditions are correct, it would seem that brush and commutator life are affected only by such factors as contact current-density, potential difference between bars and brush, temperature, and kind of atmosphere. To calculate the first two of these accurately is something of a problem. The following expressions have been set up from ideas suggested by several writers for the transformer electromotive force between brush tips for simplex lap and simplex wave windings:

Marius La Tour $E_{Tb}=(B_s+1)\dfrac{\text{Poles}}{\text{Paths}}E_c$

Behn-Eschenburg $E_{Tb}=B_s\dfrac{\text{Poles}}{\text{Paths}}E_c$

Punga $E_{Tb}=\dfrac{2B^2S}{2B_S-1}\dfrac{\text{Poles}}{\text{Paths}}E_c$

Mr. Packer adopted the second of these with poles/paths = 1.

Adding E_c in quadrature to E_{Tb} then gives equation 16 of the paper,

$$E_{Rb}=\sqrt{E_{Tb}^2+E_c^2}$$

He suggests that this be kept below 5 to 7 volts per brush. This agrees with the following figures for larger railway traction motors, which were given many years ago:

Behn-Eschenburg, 7 volts.

Arnold, 5 to 7 volts when stationary, 3 volts at rated speed.

Ossanna, 2.5 to 5 volts for heavy work (2,000 horsepower).

Punga states that E_{Tc} = 1.84 volts per coil with full load torque, and full load flux at starting is low enough to permit starting with two or three times full load torque with complete sparklessness. In an example he uses 2.38 volts per coil with two times full load torque. For rated load and speed, he uses $\sqrt{1.78^2+1.84^2}=2.55$ per coil, all for a brush arc = 1.23 centimeters, segment width = 0.33 centimeters, mica thickness = 0.08 centimeters.

Iwan Döry, commutation is good when $E_{Tc}=2$ volts even in the largest sizes. He used values at starting up to about 4 volts. The highest permissible value when running is 5 to 8 volts, but such high values require commutating fields, to be regulated in several steps. He used reactance voltages up to 10.8 volts, neutralized by interpoles.

Experiments by Liska with direct current showed that when circuits free from inductance are opened, as by brush and commutator, sparks begin to form when the voltage across the contact reaches 10 to 11 volts. His results were lower for metal-to-metal and other combinations. Were it not for mathematical difficulties, these figures could be made the basis of an exact method. Attempts to solve the problem for direct current, when considering speed and rate-of-change induced electromotive forces, date from before 1905 (Punga). (See also article by C. L. Kennedy written in 1907.[4]) Contact loss increases with the electromotive forces which appear in the short-circuited coils. Punga gave a formula for calculating it. La Tour showed that with alternating current and motor at rest, a value of the contact resistance exists for which the contact loss due to the resultant main and short-circuit current is a minimum.

While probably given in the original papers, more complete definitions of the constants C_1, C_2, and C_3 would help. Also, it would be convenient to have a means to calculate the way in which the area under curves B, C, D, and E depends on the brush position, and a more complete examination of the way in which the transformer, speed, and induced electromotive forces (due to greater proximity of pole "shoe" iron) vary with current and brush position. The discussion of the nonmathematical aspects and problems is an excellent review.

References

1. Resistance Commutation, **Frank D. Olney.** *AIEE Transactions*, volume 69, 1950, part II, pages 1207–18.

2. Commutation in Single Phase Commutator Motors at Starting, **Marius La Tour.** *Electrical World* (New York, N. Y.), December 3, 1904; January 14, 1905; March 10, 1906; September 8, 1906.

3. Commutation in A-C Motors, **A. F. Puchstein.** *Electrical Engineering*, volume 62, July 1943, pages 325–26.

4. Calculation of Dynamo Sparking Constants, **C. L. Kennedy.** *Electrical World* (New York, N. Y.), February 16, 1907.

J. H. Karr (Robbins and Myers, Inc., Springfield, Ohio): I am particularly interested in the contents of Mr. Packer's paper relating to practical considerations such as commutator finishing, dynamic balance of armatures, bearing types and fits, and their effects on the performance of high-speed universal motors. The very best and most careful design considerations are to no avail if any of the little details which affect commutation are neglected in manufacturing. Unfortunately, some of the principal contributors to poor commutation and short brush life are factors which are not too easy to evaluate. I am thinking particularly of commutator finishing. I have seen some examples recently of commutators which appeared to be properly finished. An indicator reading showed no unreasonable out-of-round condition or high bars. Yet, for no apparent reason, commutation was very poor. A light cut taken from the commutator surface with a carboloy or diamond tool when the armature was rotated at high speed changed the commutation situation completely.

I spent a number of years in the teaching profession and as a part of our preliminary design instruction, we devoted some time to electric and magnetic field mapping. Consequently, I was interested in the determination of field forms in this paper. My comment here probably involves an interpretation of Mr. Packer's statements regarding field mapping, since he has not actually shown such a map. Flux lines are not properly located by joining points on the pole surface and on the armature surface, which are equally spaced except in regions of uniform flux density as, for example, directly under the pole face. The reluctance of the gap at any point along the armature surface will be proportional to the length of the

flux line at that point. Permeance and, therefore, flux or flux density, will be inversely proportional to this length. It seems, then, that plotting reciprocals of lengths of flux lines should give a plot of field flux and not ampere-turns as, for example, is shown in Figure 4 of the paper.

I accept Mr. Packer's expressions for rotational and transformer voltages per coil. The latter is quite straightforward, and I have used an empirical relation for rotational voltage which gives values which are somewhat lower but of the same order of magnitude as Mr. Packer obtains in his sample calculations. However, I would like to raise two questions in regard to the results. First, what is the significance of "voltage due to brush span" obtained by multiplying the volts per coil by the actual span of the brush measured in terms of commutator bars? In the example, the brush spans 1.7 bars. Actually, the brush short circuits one coil for an instant, then two coils.

Second, I would like Mr. Parker to comment on what he considers are maximum acceptable values of volts per coil or volts per brush span. Personally, I am a little surprised at the magnitude of these voltages. How much higher can we work and still expect reasonably good commutation and brush life, assuming the field-to-armature ampere-turn ratio is kept fairly high?

L. C. Packer: The author appreciates the comments and references presented by Mr. Puchstein.

It is quite true that the items mentioned by Mr. Puchstein limit the accuracy attainable. Experience with high-speed motors has shown that commutation can be affected more by mechanical considerations and faults than by the variation in the accuracy of methods of calculation. The author realizes this, and so stated that the methods given in the paper were approximate. Although familiar with the work of the various references cited by Mr. Puchstein, the author of this paper was trained by Mr. Lamme in his methods, which were proved by ten years or more of experience prior to the publication of his work on commutation problems. It is natural that the author should follow more closely his experiences.

While not perfect, the methods cited in this paper have been used successfully by the author for about 28 years and have solved adequately the commutation problems that have been encountered with universal motors for use on both alternating current and direct current. There may be better methods that are not known to the author.

What Mr. Puchstein has stated about the effect of distortion is quite true.

In Mr. Puchstein's formula for the commutating zone, the "number of brushes omitted" means zero in a 2-pole motor or two if two of the four brushes of a 4-pole motor were omitted, and so forth. The coils per bundle would be two in the case of two commutator bars per slot, in which case there would be two coils per slot or two coils per bundle.

Eliminating the mechanical, temperature, and atmospheric conditions, it appears to the author that limiting the short-circuit current to a reasonable value is the big problem. Limiting the voltage between the bars and brush is part of that problem. In larger apparatus, there is more space to add auxiliary means to help limit the short-circuit current, but in small noncompensated motors the space is limited, thus making the problem more difficult.

The constant C_1 depends upon the chording and brush span. On these small motors the author always has used $C_1 = 1$. This value may run to 1.5, but on other classes of apparatus $C_1 = 1.25$ sometimes is used. $C_1 = 1$ checks very well with tests.

The constant C_2 is dependent upon the chording. Its effect upon the end winding is to reduce slightly the flux density in the commutating zone, which results in a slight reduction in electromotive force in the commutating coil. A much greater gain is obtained by shortening the end turns, thus reducing the end flux, which varies by the term $\log 2S'/\log 2S$, plus another gain of S'/S, where S = slots per pole and S' = slots spanned by the coil. This paper uses only the term S'/S, as the other term represents a relatively small value in this type of motor.

The constant C_3 depends upon the chording, brush span, and bars per slot. Refer to equation 10 in the paper.

The author agrees with Mr. Puchstein that it would be desirable to be able to calculate the way in which the areas under the curves in Figure 6 of the paper vary with brush shift. A future treatise would be desirable on this problem. While it is not a simple problem, it is possible to calculate the way in which the transformer, speed, and induced electromotive forces (caused by greater proximity of the pole shoe iron) vary the current and brush position. Mr. Karr has brought out several items that are important in the design and manufacture of commutator-type motors in general. The author believes that all designers of commutator-type motors will agree with Mr. Karr that poor commutation and brush life are all too often attributed to factors not easily evaluated.

Commutator finishing is one of these items. Prior to the time when diamond turning was started, the commutators were machined by an ordinary steel tool or ground. Turning by a steel tool left tool marks which wore down the brush until the tool marks were worn down. On large commutators the surface sometimes was stoned to eliminate the tool marks. Grinding the commutator crowned the bars so that the brush hit only the tops of the crowns, resulting in poor commutation.

Diamond turning the commutator surface at the proper speed and feed results in a smooth surface with a true radius. It also is important to finish the commutator surface from the same reference as the bearing surface and armature iron core, so that these parts all run concentric with each other.

It also is essential that the commutator bars be tight, so that there will be no movement of the bars under running conditions. One ten-thousandth of an inch between adjacent bars will cause excessive sparking. Sometimes the commutation may be poor on a motor, and indicator checks as mentioned by Mr. Karr will show no unreasonable out-of-round condition or high bars, then after a light cut was taken over the surface with a diamond or carboloy tool the commutation was improved. Small burrs on the edge of the bars projecting into the undercutting often bridge two bars when up to speed and cause running short circuits between bars or throw out enough to be picked up by the brush and cause the brush to lift up and cause excessive sparking. A light cut over the surface often cuts off these burrs. Often there is a condition where the bar is high at the outer end and low at the rear end. An indicator reading at the center of the bar may not show any appreciable rise. There have been cases where the bar has settled in that position and a light cut over the surface would correct the condition.

If the armature shaft is held in a 3-jaw collet, for instance, enough pressure may be exerted by the tool to spring the jaws slightly, causing a surface composed of three intersecting arcs instead of a true circular surface. This sometimes happens in grinding shaft surfaces. The difference is slight, but can cause trouble at high speeds. Slight slivers of mica in an undercut slot can cause excessive sparking. A light cut may break off the offending slivers.

Mr. Karr is correct in his idea about plotting the no-load field form. Since there is no saturation at no load, we are dealing only with the air-gap ampere-turns required to drive the flux across the air gap, therefore the author chose to measure the path of the flux and convert to ampere-turns. The armature ampere-turns then are plotted in the proper ratio to the field ampere-turns. This method always has seemed to be a good starting point.

When converted to flux, the field forms have had very close agreement to test field forms. As mentioned in the paper in the discussion of Table I, it would be more accurate to make a flux plot in the interpolar space, in which case the field form should be made on a flux basis.

In regard to the voltage caused by brush span, this is the voltage per coil times the brush span in terms of bars times poles/paths, and gives the average voltage of all the coils while moving through the commutating zone.

It is desirable to have 5 to 7 short-circuit volts maximum per brush to be sure of getting good commutation and brush life under average conditions, but the author has known of a case, as previously published, where the short-circuit voltage on 60 cycles was about 10 volts per brush and the motor was stopped after a run of 5,000 hours with an ultimate indicated life of 10,000 hours. However, the motor was built very carefully with an exceptionally well-balanced armature.

All conditions were ideal. This condition would be very expensive to maintain on a commercial basis. Designing for 5 to 7 volts per brush allows sufficient leeway in manufacturing to meet most commercial applications. High-torque motors for portable tools and the like pose another problem requiring higher ratio of armature to field ampere-turns. The voltage per brush will be higher than desired, causing shorter brush life than in other types of applications.

The type of application really limits the design as far as the short-circuit voltage and brush life are concerned.

Determination of Generator Stand-by Reserve Requirements

H. T. STRANDRUD
ASSOCIATE AIEE

Synopsis: During the past few years there has been a trend toward the use of statistics of forced (unscheduled) generator outages as a basis for calculating the proper amount of stand-by reserve generation for a given power system. This paper presents a method of analysis which was developed to fit the needs of a system having a large number of generators, but which, it is believed, can be used to advantage for small systems also. The method is based partially on previously published results.[1,2,3] This method lends itself readily to calculations, involves few approximations, and has sufficient flexibility to take account of several types of machines having different outage factors. Although the discussion is confined to generator outages, the method of analysis here presented may be used for calculation of simultaneous overlap of events of other types for which corresponding assumptions can be made. Examples are random outages of transmission lines and other types of equipment, random use of parallel communication channels, and supply of current to a number of items of equipment, each having a random duty cycle. The method is applicable to any situation which can be represented on a graph similar to Figure 1(A), provided that necessary statistical data are available.

DETERMINATION of the proper amount of generator stand-by reserve is an important problem in any power system. Too small a reserve would reduce system reliability below acceptable standards, while an excessively large amount of reserve means unnecessary plant investment. One suggested criterion[1] is that no more reserve should be maintained than probably will be needed at reasonably frequent intervals. It would be unwise, for example, to keep reserves which would be needed on the average only once in 75 years. On the other hand, reserves hardly could be considered adequate if generator outages could be expected once every two years to exceed the stand-by reserve capacity.

Selection of generator stand-by reserve capacity on the basis outlined above requires a prediction of how often the capacity of generators forced out of service can be expected to exceed a specified amount. A reserve equal to the megawatt capacity of the largest machine (sometimes assumed to be adequate) is not necessarily sufficient, because simultaneous outage of two or more machines usually can be expected often enough to be of importance. The most direct approach to this problem would be to assume that future multiple outages will occur with the same average frequency as in the past. However, this approach is not satisfactory because: available records of multiple outages are, in general, not extensive enough to give reliable averages; and growth of the power system concerned would make obsolete any statistics regarding multiple outages. For these reasons it appears that the most reliable predictions regarding multiple outages can be obtained from probability calculations based on statistics of single machine outages, a sufficient number of which have occurred to be a more reliable starting point.

This paper presents a method of calculating probable frequency of occurrence of forced (unscheduled) outages involving any given generator capacity or more and probable duration of these outages. Calculations are made for a given megawatt capacity rather than a given number of machines because several sizes of generators usually are involved. Data used for the calculations are statistics of average frequency of occurrence and average duration of forced outages of individual machines.

Paper 51-23, recommended by the AIEE Power Generation Committee and System Engineering Committee and approved by the AIEE Technical Program Committee for presentation at the AIEE Winter General Meeting, New York, N. Y., January 22–26, 1951. Manuscript submitted October 30, 1950; made available for printing November 20, 1950.

H. T. STRANDRUD is with the Bonneville Power Administration, Portland, Oreg.

The author acknowledges helpful suggestions from G. W. BILLS and B. V. HOARD on the preparation of this paper, and valuable assistance from L. J. BRADY, D. J. COCKERAM, and M. SONDHI in making calculations.

Assumptions

Outages occurring at any time of year are assumed to be equally important. This assumption is at least partially justified by the probable condition that, during off-peak seasons, some unused generators will be taken out of service for scheduled maintenance. It also is assumed that enough transmission line capacity is available to allow supplying any particular load from whatever generators are available.

Graphical Outage Records

Figure 1 is an example of a graphical record of outages for a hypothetical system, with the amount of forced outage time exaggerated for convenience.

The system of Figure 1 has eight generators. Machine number 1 is rated 5 megawatts, numbers 2 and 3 are 20 megawatts each, and numbers 4 through 8 are each 50 megawatts. In Figure 1(A) the history of each machine is shown in a separate horizontal space with forced outage time shown shaded. Outages of Figure 1(A) are totaled in Figures 1(B) and 1(C). Figure 1(B) is a graphical outage record showing the number of generators on forced outage at any given time. More important from an operating standpoint is the total rating of machines out at a given time, Figure 1(C). Note that the greatest megawatt outage does not necessarily occur at the time when most machines are out. This paper gives a method of predicting, for a given power system, how often and for how long a time (on the average) a graph such as Figure 1(C) may be expected to rise to a given value or to exceed that value.

Table I. Calculation of Generator Outage Expectancies for a System in Which All Machines Have the Same Outage Factor

1	2	3	4	5	6	7	8	9	10	11	12	13	14	15	16	17	18	19	20	21
r	r_1	r_2	r_3	s	s_1	s_2	s_3	$\frac{r}{t}$	$\frac{s}{T-t}$	$\frac{r}{t}-\frac{s}{T-t}$	$P_{r_1r_2r_3}$	$D_{r_1r_2r_3}$	m	m	$D_{r_1r_2r_3}$	E_{m+}	$\frac{1}{E_{m+}}$	$P_{r_1r_2r_3}$	P_{m+}	t_{m+}
0	0	0		18	10	8		0	4.37	−4.37	0.9102	−3.98	0	0	−3.98	0	∞	0.9102	1.0001	∞
1	1	0		17	9	8		46.3	4.13	42.2	0.0478	2.015	57	57	2.015	3.981	0.25	0.0478	0.0899	0.0226
	0	1		10	7						0.0382	1.611	125	114	0.1001	1.966	0.51	0.001128	0.0421	0.0214
2	2	0		16	8	8		92.6	3.89	88.7	0.001128	0.1001	114	125	1.611	1.866	0.54	0.0382	0.0410	0.0220
	1	1		9	7						0.002005	0.1779	182	171	0.00214	0.2551	3.92	0.00001579	0.002816	0.0110
	0	2		10	6						0.000702	0.0623	250	182	0.1779	0.2530	3.95	0.002005	0.02801	0.0111
3	3	0		15	7	8		138.9	3.64	135.3	0.00001579	0.00214	171	228	0.0000264	0.0751	13.3	0.000000145	0.000796	0.0106
	2	1		8	7						0.0000474	0.00641	239	239	0.00641	0.0750	13.3	0.0000474	0.000795	0.0106
	1	2		9	6						0.0000368	0.00498	307	250	0.0623	0.0686	14.6	0.000702	0.000748	0.0109
	0	3		10	5						0.00000737	0.000997	375	296	0.0001204	0.00633	158	0.000000663	0.0000461	0.0073
4	4	0		14	6	8		185.2	3.40	181.8	0.000000145	0.0000264	228	307	0.00498	0 00621	161	0.0000368	0.0000455	0.0073
	3	1		7	7						0.000000663	0 0001204	296	364	0.0001581	0.001234	811	0.000000870	0.00000868	0.0075
	2	2		8	6						0.000000870	0.0001581	364	375	0.000997	0.001076	930	0.00000737	0.00000781	0.0070
	1	3		9	5						0.000000387	0.0000703	432	432	0.0000703	0.0000790	12,650	0.000000387	0.000000435	0.0053
	0	4		10	4						0.000000048	0.0000087	500	500	0.0000087	0.0000087	115,000	0.000000048	0.000000048	0.0055

The following symbols are defined in the nomenclature:

$n_1 = 10$
$n_2 = 8$
$n_3 = 0$
$n = 18$

$m_1 = 57$
$m_2 = 125$
$m_3 = -$

$t = 0.0216$
$T = 4.1370$
$(T-t) = 4.1154$

$p = 0.00522$
$q = 0.99478$
$p/q = 0.00525$

Table II. Calculation of Generator Outage Expectancies for a System Having More than One Outage Factor

1	2	3	4	5	6	7	8	9A	9B	9C	10A	10B	10C	11	12	13	14	15	16	17	18	19	20	21
r	r_1	r_2	r_3	s	s_1	s_2	s_3	$\frac{r_1}{t_1}$	$\frac{r_2}{t_2}$	$\frac{r_3}{t_3}$	$\frac{s_1}{T_1-t_1}$	$\frac{s_2}{T_2-t_2}$	$\frac{s_3}{T_3-t_3}$	$9A+9B+9C$ $-10A-10B-10C$	$P_{r_1r_2r_3}$	$D_{r_1r_2r_3}$	m	m	$D_{r_1r_2r_3}$	E_{m+}	$\frac{1}{E_{m+}}$	$P_{r_1r_2r_3}$	P_{m+}	t_{m+}
0	0	0		25	20	5		0	0		4.86	0.83		−5.69	0.8891	−5.06	0	0	−5.06	0	∞	0.8891	1.0001	∞
1	1	0		24	19	5		46.3	0		4.62	0.83		40.8	0.0933	3.81	11.15	11.15	3.81	5.06	0.20	0.0933	0.1110	0.0219
	0	1		20	4			0	64.1		4.86	0.67		58.6	0.01158	0.678	20.2	20.2	0.678	1.251	0.80	0.01158	0.01772	0.0142
2	2	0		23	18	5		92.6	0		4.37	0.83		87.4	0.00465	0.407	22.3	22.3	0.407	0.573	1.75	0.00465	0.00614	0.0107
	1	1		19	4			46.3	64 1		4.62	0.67		105.1	0.001215	0.1277	31.35	31.35	0.1277	0.1661	6.02	0.001215	0.001494	0.0090
	0	2		20	3			0	128.2		4.86	0.50		122.8	0.0000603	0.00741	40.4	33.45	0.01962	0.03836	26.1	0.0001465	0.0002794	0.0073
3	3	0		22	17	5		138.9	0		4.13	0.83		133.9	0.0001465	0.01962	33.45	40.4	0.00741	0.01874	53.3	0.0000603	0.0001329	0.0071
	2	1		18	4			92.6	64.1		4.37	0.67		151.7	0.0000606	0.00919	42.5	42.5	0.00919	0.01133	88.3	0.0000606	0.0000726	0.0064
	1	2		19	3			46.3	128.2		4.62	0.50		169.4	0.00000633	0.001072	51.55	44.6	0.000590	0.002137	468	0.00000327	0.00001198	0.0056
	0	3		20	2			0	192.3		4.86	0.33		187.1	0.000000157	0.000029	60.6	51.55	0.001072	0.001547	646	0.00000633	0.00000871	0.0056
4	4	0		21	16	5		185.2	0		3.89	0.83		180.5	0.00000327	0.000590	44.6	53.65	0.000378	0.000475	2100	0.00001908	0.000002381	0.0050
	3	1		17	4			138.9	64.1		4.13	0.67		198.2	0.000001908	0.000378	53.65	60.6	0.000029	0.000097	10,300	0.000000157	0.000000473	0.0049
	2	2		18	3			92.6	128.2		4.37	0.50		215.9	0.000000316	0.000068	62.7	62.7	0.000068	0.000068	14,700	0.000000316	0.000000316	0.0046

The following symbols are defined in the nomenclature:

$n_1 = 20$
$n_2 = 5$
$n_3 = 0$
$n = 25$

$m_1 = 11.15$
$m_2 = 20.2$
$m_3 = -$

$t_1 = 0.0216$
$t_2 = 0.0156$
$t_3 = -$

$T_1 = 4.1370$
$T_2 = 6.0055$
$T_3 = -$

$(T_1-t_1) = 4.1154$
$(T_2-t_2) = 5.9899$
$(T_3-t_3) = -$

$p_1 = 0.00522$
$p_2 = 0.002598$
$p_3 = -$

$q_1 = 0.99478$
$q_2 = 0.99740$
$q_3 = -$

$p_1/q_1 = 0.00525$
$p_2/q_2 = 0.002604$
$p_3/q_3 = -$

Table III. Calculation of Generator Outage Expectancies for a System Having a Large Number of Machines

1	2	3	4	5	6	7	8	9	10	11	12	13	14	15	16	17	18	19	20	21
r	r_1	r_2	r_3	s	s_1	s_2	s_3	$\frac{r}{t}$	$\frac{s}{T-t}$	$\frac{r}{t}-\frac{s}{T-t}$	$P_{r_1r_2r_3}$	$D_{r_1r_2r_3}$	m	m	$D_{r_1r_2r_3}$	E_{m+}	$\frac{1}{E_{m+}}$	$P_{r_1r_2r_3}$	P_{m+}	t_{m+}
0	0	0	0	208	8	15	185	0	50.6	−50.6	0.3366	−17.04	0	0						
1	1	0	0	207	7	15	185	46.3	50.3	−4.0	0.01415	−0.566	125	125						
2	2	0	0	206	6	15	185	92.6	50.0	42.6	0.000260	0.01108	250	250	0.01108	0.0738	13.6	0.000260	0.000776	0.0105
3	3	0	0	205	5	15	185	138.9	49.8	89.1	0.00000273	0.0002435	375	252.8	0.00350	0.0627	16.0	0.00001920	0.0005156	0.0082
	2	1	0		6	14	185				0.00002045	0.001825	306.3	257.6	0.0225	0.0592	16.9	0.0002525	0.0004964	0.0084
	2	0	1		6	15	184				0.0002525	0.0225	257.6	260.4	0.001407	0.03670	27.2	0.00000615	0.0002439	0.0066
	2	0	0		6	15	184				0.0001220	0.01653	382.6	265.2	0.01653	0.03529	28.4	0.0001220	0.0002377	0.0067
4	3	0	1	204	5	15	184	185.2	49.6	135.6	0.00000265	0.000359	382.6	268.0	0.000404	0.01876	53.3	0.00001470	0.0001157	0.0062
	2	2	0		6	13	185				0.00000751	0.0001018	362.6	272.8	0.00711	0.01836	54.5	0.00003905	0.0001143	0.0062
	2	1	1		6	14	184				0.00001985	0.00269	313.9	280.4	0.002135	0.01125	88.9	0.00000933	0.0000752	0.0067
	2	0	2		6	15	183				0.0001220	0.01653	293.9	288.0	0.000488			0.0000001772		
	1	3	0		7	12	185				0.00000931	0.0001263	390.2	293.9	0.0001263			0.00000931		
5	3	0	2	203	5	15	183	231.5	49.3	182.2	0.00001280	0.0002335	390.2	301.5	0.0001647			0.00000904		
	2	2	1		6	13	184				0.00000729	0.0001327	370.2	306.3	0.001825			0.00002045		
	2	1	2		6	14	183				0.00000959	0.001744	321.5	309.1	0.0000997			0.00000436		
	2	0	3		6	15	182				0.00003905	0.00711	272.8	313.9	0.00269			0.00001985		
	1	3	1		7	12	184				0.00000904	0.0001647	301.5	321.5	0.001744			0.00000959		
	1	2	2		7	13	183				0.00001920	0.00350	252.8	329.1	0.000703			0.00003075		
6	2	1	3	202	6	14	182	277.5	49.1	228.4	0.00003075	0.000703	329.1	336.7	0.000202			0.00000735		
	2	0	4		6	15	181				0.0000933	0.002135	280.4	362.6	0.0001018			0.00000751		
	1	3	2		7	12	183				0.00000436	0.0000997	309.1	370.2	0.0001327			0.00000729		
	1	2	3		7	13	182				0.0000615	0.001407	260.4	375	0.0002435			0.00000273		
7	2	1	4	201	6	14	181	324	48.8	275	0.00000735	0.000202	336.7	382.6	0.000359			0.00000265		
	2	0	5		6	15	180				0.00001772	0.000488	288.0	390.2	0.0002335			0.00001280		
	1	2	4		7	13	181				0.00001470	0.000404	268.0							

The following symbols are defined in the nomenclature:

$n_1 = 8$
$n_2 = 15$
$n_3 = 185$
$n = 208$

$m_1 = 125$
$m_2 = 56.3$
$m_3 = 7.601$

$t = 0.0216$
$T = 4.1370$
$(T-t) = 4.1154$

$p = 0.00522$
$q = 0.99478$
$p/q = 0.00525$

Figure 2 is a portion of a graphical outage record similar to Figure 1(B) except that Figure 2 is for a system of n generators. This outage record shows four time intervals (A, B, C, and D) when r machines are out. The average number per year of such intervals (types A, B, C, and D) can be calculated by formulas of Adler and Miller.[2] Of more importance in selection of generator reserves is the average number per year of occasions when number of outages increases to r machines or more, as shown at E in Figure 2. This average can be calculated by the methods of Seelye[1] as discussed below. A simple relation (equation 24) between these two averages provides a check between the two methods.

Tabular Calculations

Calculations are simplified through use of a tabular method such as that described in this section. Samples are given in Tables I, II, and III. Slide-rule accuracy is sufficient for all calculations except the first value in column 12 (see discussion of column 12 in the following section).

All generators in the power system in question will be divided into three groups having average megawatt ratings per generator of m_1, m_2, and m_3. It is important that the generators having the highest megawatt rating be put in a separate group and not averaged in with small machines. Failure to observe this precaution will result in too small a calculated value of reserve capacity.

Outage Data Same for All Generators (Table I)

Table I shows a convenient arrangement of calculations for a system in which the same statistical outage data (values of T and t) are used for all machines.

Let T be the average interval in calendar years between starts of successive forced outages for individual machines, and t the average duration in years of such forced outages (see Figure 6). The probability that any specified generator is out at a given time (the "outage factor") is $p=t/T$ and the probability that the generator is not out of service is $q=1-p$.

Nonforced outage time must be considered in fixing the value of T. Statistical values of T usually are given for the condition of 100 per cent running time (machines operating 100 per cent of the time when not on forced outage). Values of T given on this basis must be divided

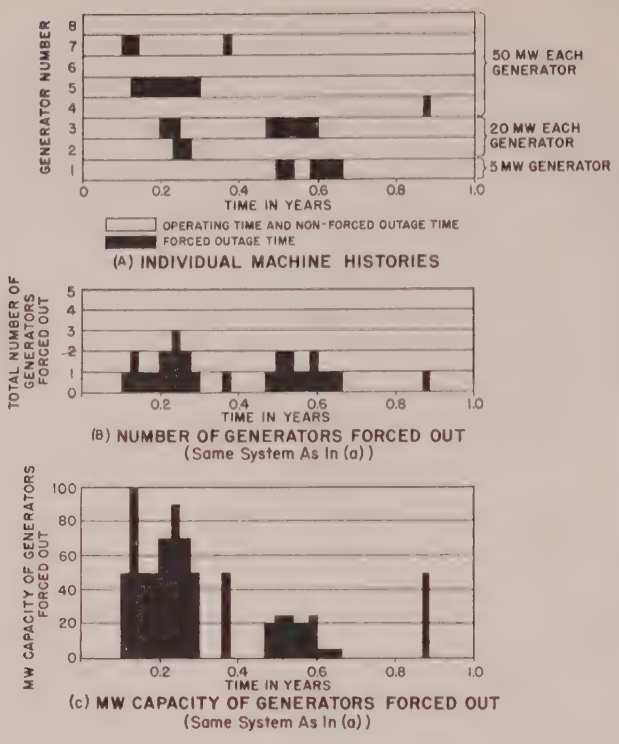
GENERATOR NUMBER
50 MW EACH GENERATOR
20 MW EACH GENERATOR
5 MW GENERATOR
TIME IN YEARS
OPERATING TIME AND NON-FORCED OUTAGE TIME
FORCED OUTAGE TIME
(A) INDIVIDUAL MACHINE HISTORIES
TOTAL NUMBER OF GENERATORS FORCED OUT
TIME IN YEARS
(B) NUMBER OF GENERATORS FORCED OUT
(Same System As In (a))
MW CAPACITY OF GENERATORS FORCED OUT
TIME IN YEARS
(c) MW CAPACITY OF GENERATORS FORCED OUT
(Same System As In (a))

Figure 1. Graphical outage records for a power system having eight generators

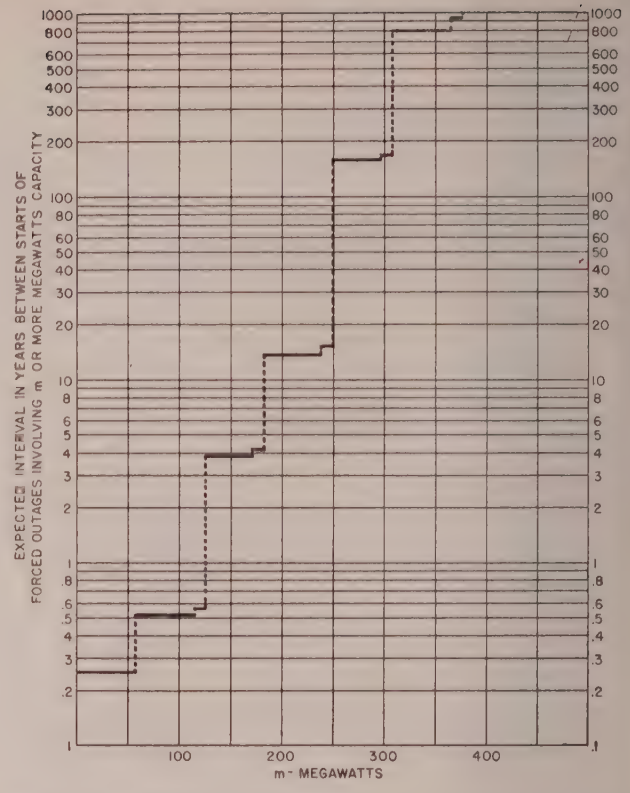

Figure 3. Generator outage expectancies for a system having all hydro generators (preliminary results for Bonneville and Grand Coulee plants)

by (per cent running time/100) to obtain T in calendar years.

Note that the method of calculations shown in Table II must be used if different values of T are used for the various sizes of machines.

In Table I a line is included for each combination of values of r_1, r_2, and r_3 up to the desired value of r. Explanation of the various columns follows:

Column 1: Assumed values of r. Use consecutive values from zero up to a value for which $D_{r_1r_2r_3}$ (column 13) becomes negligible.

Columns 2, 3, and 4: Assumed values. Include all combinations of r_1, r_2, and r_3 for which $D_{r_1r_2r_3}$ is not negligible.

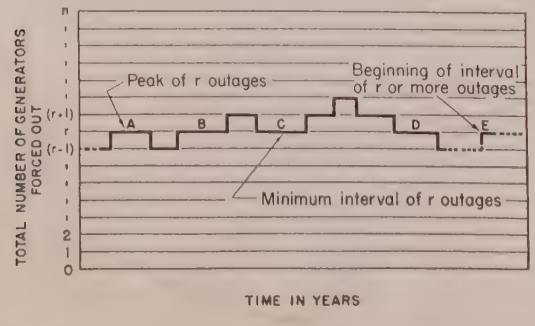

Figure 2. Graphical outage record for a power system having n generators

Column 5: Calculated from column 1:

$$s = n - r \tag{1}$$

Columns 6, 7, and 8: Calculated from columns 2, 3, and 4:

$$s_1 = n_1 - r_1 \tag{2}$$

$$s_2 = n_2 - r_2 \tag{3}$$

$$s_3 = n_3 - r_3 \tag{4}$$

Column 9: Divide each entry in column 1 by t.

Column 10. Divide each entry in column 5 by $(T-t)$.

Column 11: Subtract each value in column 10 from the value on the same line in column 9.

Column 12: $P_{r_1r_2r_3}$ is the probability that the number of machines out at a given time is r_1 of size m_1, r_2 of size m_2 and r_3 of size m_3. The first value in column 12 is

$$P_{000} = q^n \tag{5}$$

It usually is necessary to calculate P_{000} by means of logarithms to obtain sufficient accuracy. Find other values by using the recurrence formulas

$$P_{(r_1+1)r_2r_3} = \frac{s_1}{(r_1+1)} \frac{p}{q} P_{r_1r_2r_3} \tag{6}$$

$$P_{r_1(r_2+1)r_3} = \frac{s_2}{(r_2+1)} \frac{p}{q} P_{r_1r_2r_3} \tag{7}$$

and

$$P_{r_1r_2(r_3+1)} = \frac{s_3}{(r_3+1)} \frac{p}{q} P_{r_1r_2r_3} \tag{8}$$

For examples, value of r_1, r_2, and r_3 in the fifth line of Table I are 1, 1, and 0, respectively. P_{110} in line 5 could be calculated either from the value of P_{100} in line 2, using equation 7, or from the value of P_{010} in line 3, using equation 6.

Column 13: $D_{r_1r_2r_3}$ is the amount contributed to E_{m+} (see column 17) by outages of r_1, r_2, and r_3, respectively, of the three sizes of machines. Multiply values

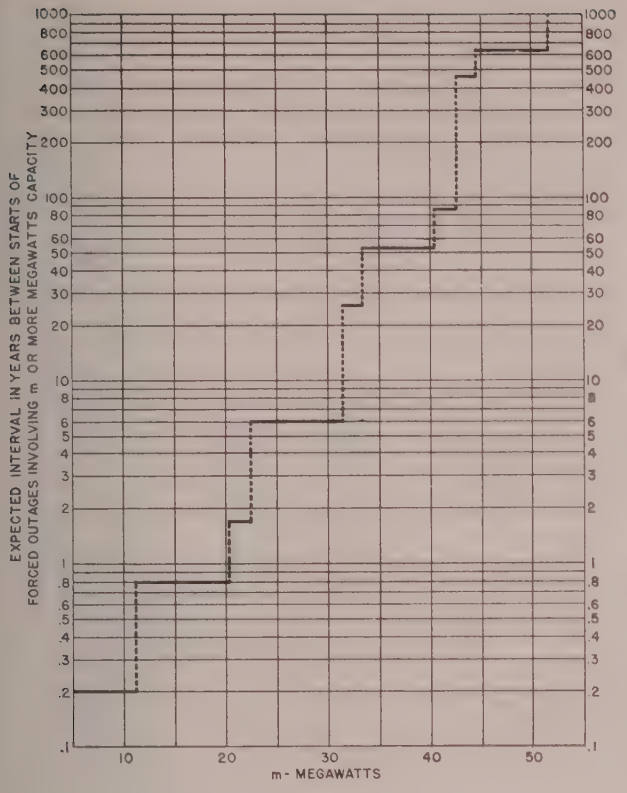

Figure 4. Generator outage expectancies for a system having both hydro and steam generators

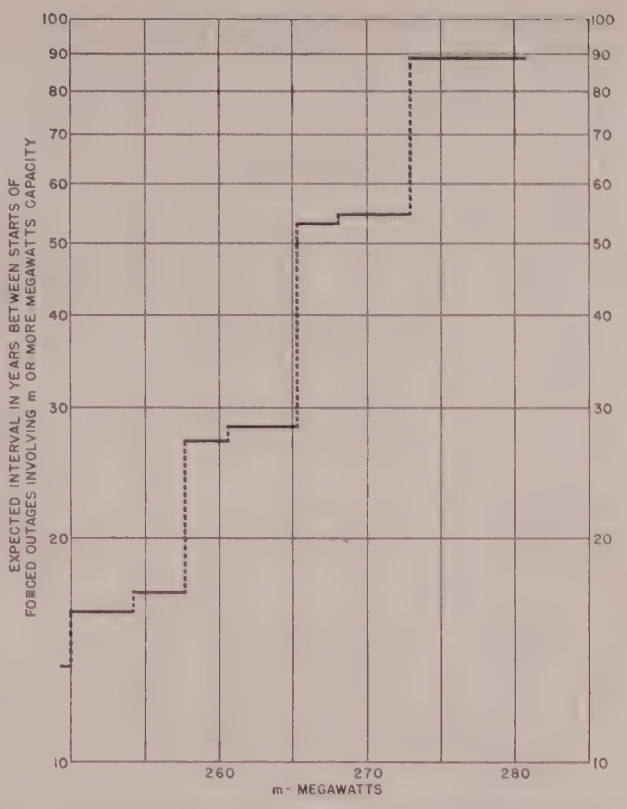

Figure 5. Generator outage expectancies for northwest power pool (preliminary results)

from the same line in columns 11 and 12:

$$D_{r_1r_2r_3}=\left(\frac{r}{t}-\frac{s}{T-t}\right)P_{r_1r_2r_3} \tag{9}$$

Column 14: m is the total megawatt capacity of machines out in each case, given by

$$m=r_1m_1+r_2m_2+r_3m_3 \tag{10}$$

Column 15: Rearrange values of m in order of size.

Column 16: Copy values of $D_{r_1r_2r_3}$ in order corresponding to the order of column 15.

Column 17: E_{m+} is the average number of times per year that megawatt capacity of simultaneous outages increases to a value of m or more. To obtain each value of E_{m+}, add values of $D_{r_1r_2r_3}$ corresponding to all values of megawatts equal to or greater than m. A check on calculations is provided by the fact that E_{m+} should be zero for $m=0$.

Column 18: $1/E_{m+}$ is the average interval in years between starts of occasions when megawatt capacity of machines out of service increases to m megawatts or more. Calculate each value of $1/E_{m+}$ from the value on the same line in column 17.

Column 19: Copy values of $P_{r_1r_2r_3}$ in order corresponding to the order of column 15.

Column 20: P_{m+} is the probability that total megawatt capacity of machines out at any given time is equal to or greater than m. To find each value of P_{m+}, add values of $P_{r_1r_2r_3}$ corresponding to all values of megawatts equal to or greater than m. A check on calculations is provided by the fact that P_{m+} should be 1.00 for $m=0$.

Column 21: t_{m+} is the average duration of occasions when machine capacity out of service is m megawatts or more. Find from values on the same line in columns

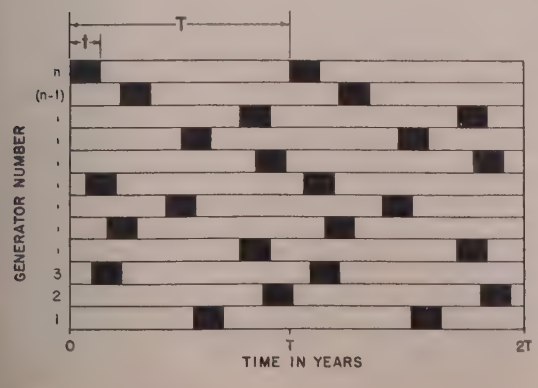

Figure 6 (left). Example of average machine histories

Figure 7 (right). Example of outage record to illustrate equation 24

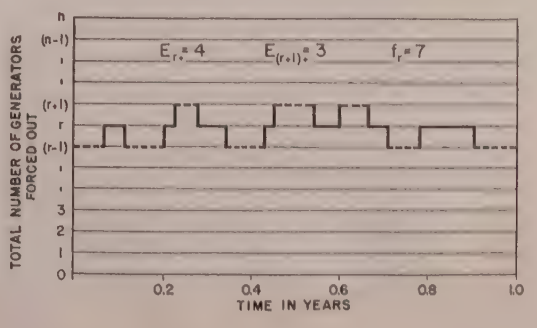

TYPE OF INTERVAL	EXAMPLE IN FIGURE 2	AVERAGE NUMBER PER YEAR		
⌐¬	A	$E_r=\left(\frac{E_{r+}}{f_r}\right)E_{r+}$	E_{r+}	f_r
⌐_	B	$E'_r=\left(\frac{E_{(r+1)+}}{f_r}\right)E_{r+}$		
⌐_¬	C	$E''_r=\left(\frac{E_{(r+1)+}}{f_r}\right)E_{(r+1)+}$	$E_{(r+1)+}$	
⌐¬	D	$E'_r=\left(\frac{E_{r+}}{f_r}\right)E_{(r+1)+}$		

Figure 8 (left). Types of outages of order r

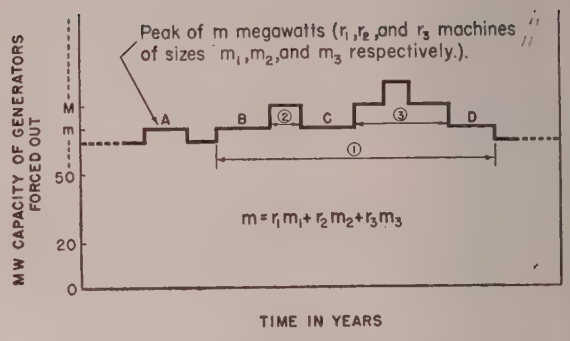

Figure 9 (above). Graphical outage record showing megawatt capacity of generators out for a system of n generators

17 and 20:

$$t_{m+} = \frac{P_{m+}}{E_{m+}} \tag{11}$$

Calculations can be simplified for certain special cases as follows:

1. If all machines are of the same size (and have the same outage factor), omit columns 15, 16, and 19. Use values of $P_{r_1r_2r_3}$ and $D_{r_1r_2r_3}$ without rearranging.

2. If duration of multiple outages is not required, omit columns 19, 20, and 21.

3. If one average size and one outage factor can be used for all machines, columns 19, 20, and 21 can be omitted and values of t_{m+} found from the approximation

$$t_{m+} = \frac{t}{r} \tag{12}$$

where r machines have a total capacity of m megawatts. This approximation is accurate only if

$$\frac{s}{r+1}\frac{p}{q} \tag{13}$$

can be neglected in comparison with 1.0.

Outage Data Not Same for All Generators (Table II)

Table II shows an arrangement of calculations for a system in which one value of T and one value of t are used for all machines in any one group, but different values are used for the three groups. Calculations in Table II are the same as those in Table I with the following exceptions:

1. Columns 9 and 10 in Table I are each replaced in Table II by three columns with self-explanatory headings.

2. Each value in column 11 of Table II is found by subtracting the sum of values on the same line in columns 10A, 10B, and 10C from the sum of values on the same line in columns 9A, 9B, and 9C.

3. The first value in column 12 is calculated from the formula

$$P_{000} = q_1^{n_1}q_2^{n_2}q_3^{n_3} \tag{14}$$

and succeeding values by using one of the recurrence formulas

$$P_{(r_1+1)r_2r_3} = \frac{s_1}{r_1+1}\frac{p_1}{q_1}P_{r_1r_2r_3} \tag{15}$$

$$P_{r_1r_1(r_2+1)r_3} = \frac{s_2}{r_2+1}\frac{p_2}{q_2}P_{r_1r_2r_3} \tag{16}$$

$$P_{r_1r_2(r_3+1)} = \frac{s_3}{r_3+1}\frac{p_3}{q_3}P_{r_1r_2r_3} \tag{17}$$

As in Table I, each value in column 13 is found by multiplying values on the same line in columns 11 and 12:

$$D_{r_1r_2r_3} = \left(\frac{r_1}{t_1}+\frac{r_2}{t_2}+\frac{r_3}{t_3}-\frac{s_1}{T_1-t_1}-\frac{s_2}{T_2-t_2}-\frac{s_3}{T_3-t_3}\right)\times P_{r_1r_2r_3} \tag{18}$$

Short-Cut Calculations for Large Systems (Table III)

Table III shows an abbreviated set of calculations for the Northwest Power Pool, a large system having 208 generators. A complete set of calculations for such a large system would be lengthy and, usually, unnecessary. Table I indicates that about 250 megawatts of reserve (see below) would be needed for a system which is a component part of the pool and which has about 40 per cent of the total generation of the pool. Since the entire pool would need a larger reserve, all machine combinations having a total rating of less than 250 megawatts were omitted from Table III. In other respects, calculations are the same as in Table I or Table II.

Graphs of Results

Results of the preceding calculations which are useful as guides in determining the proper amount of reserve for a system are:

1. $(1/E_{m+})$, the average interval in years between starts of forced outages involving m or more megawatts of machine capacity.

2. t_{m+}, the average length in years of outages involving m or more megawatts of machine capacity.

Figures 3, 4, and 5 show plots of $(1/E_{m+})$ for two power systems which are members of the Northwest Power Pool and for the entire pool. In Figure 3 the capacity of machines out would be 250 megawatts or more once every 14.6 years, on the average, indicating that a reserve of 250 megawatts would be needed every 14.6 years on the average. Each time it is needed, a 250-megawatt reserve would be in use for an average of 0.0109 year or four days, as indicated by column 21 of Table I. A reserve greater than 250 megawatts would be needed, on the average, not oftener than once in 158 years. On the basis of these figures, 250 megawatts would be a reasonable amount of reserve capacity for the system of Figure 3.

For the system of Figure 4, 31.3 megawatts would be a reasonable amount of reserve, since it would be used once every six years, on the average, while a larger reserve would be needed only once in 26 years. Table II shows that a reserve of 31.3 megawatts would be needed an average of 0.009 year or about three days on the occasions when the entire reserve is needed.

For the system of Figure 5, 258 megawatts would be a reasonable reserve capacity, since any larger amount would be needed only once in 27.2 years.

Decision regarding how often expected outages should be allowed to exceed reserves is a matter that must be decided for each system by considering such factors as the cost of reserves and the possible consequences of dropping load. The probable length of outages is of importance and should be considered in the light of how long an interruption of power can be tolerated without serious results. For some loads an outage of even a few minutes would be intolerable, while others might be interrupted several hours without serious results. If the system in question is carrying interruptible loads, an outage of several days might not be serious.

Appendix

Derivation of formulas is briefly outlined here. For a more complete discussion, see reference 7.

Outages of r or More Generators (E_{r+})

An adaptation of Seelye's[1] method is used here to derive an expression for E_{r+}, the average (expected) number of occasions per year when number of generators out will reach r or more on a system in which all machines have the same outage factor. Referring to Figure 2, E_{r+} is the average number per year of occurrences of the type shown at E.

Outage statistics of single machines are the basis for calculating E_{r+}. Necessary items of information are t, the average length in years of forced outages, and T, the average interval between starts of forced outages for any given machine. Figure 6 illustrates the meaning of T and t on a graph showing average outage records for a system of n machines. Although the outages for each machine are spaced at exactly T years, relative spacing between the various machines is random.

The probability that r generators out of n total are out at a specified instant is

$$P_r = C_r^n p^r q^s \tag{19}$$

and the probability that $(r-1)$ generators are out from a group of $(n-1)$ generators is

$$C_{r-1}^{n-1} p^{r-1} q^s \tag{20}$$

Consider a particular individual generator outage. The probability that this outage causes an outage of order r is equal to the probability that the other $(n-1)$ machines have outages combined to make an outage of order $(r-1)$ at the time of occurrence of the individual outage in question. But the probability that the outage in question causes an outage of order r is also equal to the fraction

$$\frac{\text{average number per year outages } r \text{ or more}}{\text{average number per year single outages}} = \frac{E_{r+}}{(n/T)} \tag{21}$$

Here the average number per year of individual forced machine outages is (n/T) since each of n machines goes out, on the average, once in T years.

Equating the above two expressions, 20 and 21, for the same probability and simplifying,

$$E_{r+} = \frac{r}{T} C_r^n p^{r-1} q^s = \frac{r}{t} C_r^n p^r q^s = \frac{r}{t} P_r \tag{22}$$

This is equivalent to a formula given by Doane.[3]

Equation 22 tells how often the number of machines on forced outage can be expected to reach any given number or more. This equation can be used directly for calculations only in the rare case when all machines on the system are the same size. It is used below in the derivation of formulas for average number of outages involving a given machine capacity rather than a given number of machines.

Outages of Exactly r Generators (f_r)

Adler and Miller[2] have given an expression for f_r, the average number of times per year when number of generators out is exactly r on a system in which all machines have the same outage factor. Their result can be written in the form

$$f_r = \frac{P_r}{t_r} = \left(\frac{r}{t} + \frac{s}{T-t}\right) P_r \tag{23}$$

Equation 23 gives the average number of times per year that number of outages is exactly r; or, in other words, the average number per year of intervals of the types marked A, B, C, and D on Figure 2.

Relation between E_{r+} and f_r

The preceding expressions for f_r and for E_{r+} have been derived by independent methods of reasoning. A check is provided by the following simple relation between the two quantities.

Figure 7 shows an example of a year's outage record. Dotted lines indicate intervals when number of outages increases to more than $(r+1)$ or decreases to less than $(r-1)$. For the case shown, $E_{r+}=4$, $E_{(r+1)+}=3$, and $f_r=7$. This illustrates the general relation

$$f_r = E_{r+} + E_{(r+1)+} \tag{24}$$

whose correctness can be verified by considering the geometry of graphical records such as Figure 7. Substitution of equations 22 and 23 into 24 reduces 24 to an identity, showing that these expressions for E_{r+} and f_r are consistent.

Separation of f_r into Four Types of Interval

Time intervals when r machines are out may be classified into four types, A, B, C, and D, as shown in Figures 2 and 8. The average number per year of each type is as follows:

1. Total of types A, B, C, and D is f_r by definition.

2. Total of types A and B is E_{r+}, since all occasions when r or more machines are out will start with an interval of type A or type B.

3. Total of types C and D is $E_{(r+1)+}$, since all occasions when $(r+1)$ or more machines are out will end with an interval of type C or type D.

4. To find number of outages of type A, note that the number of outages of order r ending thus (⌝) is E_{r+} (since all occasions when r or more machines are out will end with an interval of either type A or type D); while the number ending (_|) is $E_{(r+1)+}$ (since all occasions when $(r+1)$ or more machines are out will start with an interval of either type B or type C). Hence, a fraction (E_{r+}/f_r) of all outages of order r will end thus (⌝), and a fraction $(E_{(r+1)+}/f_r)$ of all outages of order r will end thus (_|). Since outages occur at random, the way an interval ends is independent of the way it began. The above fractions can then be used to divide the total of E_{r+} outages starting thus (⌜) into types A and B. Number of outages of type A is then

$$E_r = \left(\frac{E_{r+}}{f_r}\right) E_{r+} = \left(\frac{E_{r+}}{f_r}\right)^2 f_r \tag{25}$$

5. Similarly, number of outages of type C is

$$E_r'' = \left(\frac{E_{(r+1)+}}{f_r}\right) E_{(r+1)+} = \left(\frac{E_{(r+1)+}}{f_r}\right)^2 f_r \tag{26}$$

Results are summarized in Figure 8. Note that equation 24 is satisfied by the breakdown in Figure 8. Also, types B and D occur in equal numbers, as they obviously must.

The foregoing expressions give the average number per year of occasions when total number of machines out (all sizes) will reach a peak of r machines (equation 25) or a minimum interval of r machines (equation 26). Similar expressions are derived below for the number of peaks and minimum intervals involving a specified number, r_1, r_2, and r_3, respectively, of the three machine sizes.

Simultaneous Outages of Generators of Different Sizes

Part of the outages of r generators will involve a specified combination r_1, r_2, and r_3 machines, respectively, of the three sizes. Since occurrence of outages is assumed here to be independent of generator size, the average duration of these outages (of r_1, r_2, and r_3 machines, respectively, of the three sizes) is the same as the duration found previously for the average length of all intervals with outages of order r. Hence, the average number of times per year that

r_1, r_2, and r_3 machines of the three sizes are out is

$$f_{r_1r_2r_3} = \left(\frac{1}{t_r}\right) P_{r_1r_2r_3} \tag{27}$$

where

$$P_{r_1r_2r_3} = C_{r_1}^{n_1} C_{r_2}^{n_2} C_{r_3}^{n_3} p^r q^s \tag{28}$$

Since outages do not depend on machine size, the outages of r_1, r_2, and r_3 machines ($f_{r_1r_2r_3}$ in number) are divided into types A, B, C, and D (see Figure 8) in the same proportion that the outages of r machines (f_r in number) are divided into these types. Hence, comparing with equations 25 and 26, the number of outages of type A involving r_1, r_2, and r_3 generators, respectively, of the three sizes is

$$f_{r_1r_2r_3}' = \left(\frac{E_{r+}}{f_r}\right)^2 f_{r_1r_2r_3} \tag{29}$$

and the number of outages of type C involving r_1, r_2, and r_3 generators, respectively, is

$$f_{r_1r_2r_3}'' = \left(\frac{E_{(r+1)+}}{f_r}\right)^2 f_{r_1r_2r_3} \tag{30}$$

These expressions are used below in an analysis of total megawatt capacity of outages.

Outages of m or More Megawatt Capacity (E_{m+})

The problem considered in this section is that of calculating E_{m+}, the average number per year of occasions when total megawatt rating of generators out equals or exceeds any given number of megawatts, m. Figure 9 shows a portion of a graphical record of total megawatt capacity of generators out. This figure is similar to Figure 1(C), except that Figure 9 is for a system of n generators.

Total megawatt capacity corresponding to any combination r_1, r_2, and r_3 of the three sizes of generators is

$$m = r_1m_1 + r_2m_2 + r_3m_3 \tag{31}$$

Only those values of m corresponding to integral values of r_1, r_2, and r_3 will be considered. Assume that these values have been calculated for the system under consideration and tabulated in numerical order. In this tabulation, M will denote the number next higher than any selected number, m.

Assume that E_{M+} is known. E_{M+} will include all occasions included in E_{m+}, except peaks of m megawatts (intervals of type A in Figure 9). The number of these peaks is $E_{r_1r_2r_3}$ (equation 29).

On the other hand, whenever a minimum of m megawatts (such as C in Figure 9) occurs, there are two intervals, ② and ⑧, when outages increase to M or more megawatts corresponding to only one interval ①, when outages increase to m or more megawatts. The number of intervals of type C is $E_{r_1r_2r_3}''$ (equation 30).

To find E_{m+} it is thus necessary to add $E_{r_1r_2r_3}$ to, and subtract $E_{r_1r_2r_3}''$ from E_{M+}, or

$$E_{m+} = E_{M+} + E_{r_1r_2r_3} - E_{r_1r_2r_3}'' \tag{32}$$

Define

$$D_{r_1r_2r_3} = E_{r_1r_2r_3} - E_{r_1r_2r_3}'' \tag{33}$$

Then

$$E_{m+} = E_{M+} + D_{r_1r_2r_3} \tag{34}$$

An expression for $D_{r_1r_2r_3}$ that is convenient for making calculations is obtained by combining equations 29, 30, 24, 27, 23, and 22 in that order with equation 33 and simplifying. The result is

$$D_{r_1r_2r_3} = \left(\frac{r}{t} - \frac{s}{T-t}\right) P_{r_1r_2r_3} \tag{35}$$

Equations 34 and 35 make it possible to find any value of E_{m+} if the following value is known. Since $D_{r_1r_2r_3}$ is negligibly small for large values of m, all values of E_{m+} can be found by successive additions of $D_{r_1r_2r_3}$, starting with the value corresponding to the highest value of m for which $D_{r_1r_2r_3}$ is not negligible. It should be remembered that equation 35 applies only if all machines have the same outage factor. Equation 18 is used for systems in which the various groups of machines have different outage factors.

Duration of Outages of m or More Megawatt Capacity (t_{m+})

To find P_{m+}, the probability that outages of m or more megawatts of machine capacity exists at any given time, add values of $P_{r_1r_2r_3}$ corresponding to all values of megawatt capacity equal to or greater than m.

To find t_{m+}, the average length of intervals when total megawatt capacity of outages is m or more, note that

$$\text{Probability that } m \text{ or more megawatts are out} = \frac{\text{Average length of intervals with } m \text{ or more megawatts out}}{\text{Average interval between starts of outages of } m \text{ or more megawatts}} \tag{36}$$

or

$$P_{m+} = \frac{t_{m+}}{(1/E_{m+})} \tag{37}$$

Hence

$$t_{m+} = \frac{P_{m+}}{E_{m+}} \tag{38}$$

Here t_{m+} is the average length of time that a reserve of m megawatts would be in use on occasions when the entire m megawatts is called into service. Equation 38 applies to any system, whether or not all machines have the same outage factor.

Systems Having Two or More Outage Factors

In some cases considerable inaccuracy would result from assuming that all groups of machines have the same outage factor. Hydro and steam generators, for example, ordinarily have outage factors that differ considerably. For such cases, equation 18 is used instead of equation 9. Derivation[7] of equation 18 is a generalization of that given above for Equation 9.

Nomenclature

f_r = average number of times per year that exactly r forced generator outages exist simultaneously

$f_{r_1r_2r_3}$ = average number of times per year that forced machine outages exist consisting of r_1 machines of capacity m_1, r_2 machines of capacity m_2, and r_3 machines of capacity m_3

m = total megawatt capacity of machines that are on forced outage at a given time

m_1, m_2, m_3 are megawatt capacities of three average sizes of machines

n = total number of machines of all sizes in system

n_1, n_2, n_3 are numbers of machines of average capacities m_1, m_2, and m_3, respectively

$p = t/T$ = probability that any particular machine is out of service at a specified time (when same outage data are used for all generators) where t and T are defined below

$p_1 = \frac{t_1}{T_1}$, $p_2 = \frac{t_2}{T_2}$, and $p_3 = \frac{t_3}{T_3}$ are probabilities that any particular generator of size m_1, m_2, or m_3, respectively, is out of service at a specified time

$q = 1 - p$ = probability that any particular machine is not out of service at a specified time (when same outage data are used for all generators)

$q_1 = 1 - p_1$, $q_2 = 1 - p_2$, and $q_3 = 1 - p_3$ are probabilities that any particular generator of size m_1, m_2, or m_3, respectively, is not out of service at a specified time

r = total number of forced generator outages existing at any given time

r_1, r_2, r_3 are numbers of machines of sizes m_1, m_2, and m_3, respectively, on forced outage

$s = n - r$ = total number of machines not on forced outage at a given time

$s_1 = n_1 - r_1$ = number of machines of size m_1 not on forced outage

$s_2 = n_2 - r_2$ = number of machines of size m_2 not on forced outage

$s_3 = n_3 - r_3$ = number of machines of size m_3 not on forced outage

t = average length in years of forced outages of individual generators (when same outage data are used for all generators)

t_1, t_2, and t_3 = average length in years of forced outages of machines of megawatt capacities m_1, m_2, and m_3, respectively

t_{m+} = average length in years of intervals when capacity of generators on forced outage totals m or more megawatts

t_r = average length in years of intervals when exactly r forced generator outages exist simultaneously

$C_r^n = \frac{n!}{r!(n-r)!}$ = number of possible ways that combinations of r items can be selected from a total of n items

$D_{r_1r_2r_3} = E_{r_1r_2r_3} - E_{r_1r_2r_3}''$ = amount contributed to E_{m+} by outages of r_1 machines of size m_1, r_2 machines of size m_2, and r_3 machines of size m_3

E_{m+} = average number of times per year that total capacity of machines on forced outage equals or exceeds m megawatts.

E_{M+} = average number of times per year that total capacity of machines on forced outage equals or exceeds M megawatts.

E_r = average number per year of intervals of type A, Figure 2, when r machines are out (or, average number per year of peaks of order r)

E_r' = average number per year of intervals of type B or D, Figure 2, when r machines are out

E_r'' = average number per year of intervals of type C, Figure 2, when r machines are out (or, average number per year of minimum intervals of order r)

E_{r+} = average number of times per year that total number of machines out is r or more

$E_{r_1r_2r_3}$ = average number of times per year that number of forced outages reaches a peak composed of r_1 machines of capacity m_1, r_2 machines of capacity m_2, and r_3 machines of capacity m_3

$E_{r_1r_2r_3}''$ = average number of times per year that number of forced outages reaches a minimum composed of r_1 machines of capacity m_1, r_2 machines of capacity m_2, and r_3 machines of capacity m_3

M = value next larger than m on a tabulation of possible values of megawatt capacities for all possible combinations of machines

P_{m+} = probability that total capacity of machines on forced outage is m or more megawatts

P_r = probability that total number of machines on forced outage at a given time is exactly r

$P_{r_1r_2r_3}$ = probability that machines on forced outage at a given time consist of r_1 of capacity m_1, r_2 of capacity m_2, and r_3 of capacity m_3

T = average interval in calendar years between starts of forced outages of individual machines (when same outage data are used for all generators)

T_1, T_2, and T_3 = average length in calendar years between starts of forced outages of individual generators of sizes m_1, m_2, and m_3, respectively

References

1. Outage Expectancy as a Basis for Generator Reserve, **Howard P. Seelye.** *AIEE Transactions*, volume 66, 1947, pages 1483–88.

2. A New Approach to Probability Problems in Electrical Engineering, **H. A. Adler, K. W. Miller.** *Electrical Engineering* (*AIEE Transactions*), volume 65, October 1946, pages 630–32.

3. Discussion of reference 2, **Philip Doane.** *AIEE Transactions*, volume 65, 1946, page 1118.

4. Probability Methods Applied to Generating Capacity Problems of a Combined Hydro and Steam System, **E. S. Loane, C. W. Watchorn.** *AIEE Transactions*, volume 66, 1947, pages 1645–57.

5. Calculating Probability of Generating Capacity Outages, **W. J. Lyman.** *AIEE Transactions*, volume 66, 1947, pages 1471–77.

6. A Convenient Method for Determining Generator Reserve, **Howard P. Seelye.** *AIEE Transactions*, volume 68, part II, 1949, pages 1317–20.

7. Determination of Generator Stand-by Reserve Requirements, **H. T. Strandrud.** *Technical Report*, Bonneville Power Administration (Portland, Oreg.), March 1950.

Discussion

C. W. Watchorn (Pennsylvania Water & Power Company, Baltimore, Md.): The author has made a valuable contribution to the techniques of applying probability methods to various types of generating capacity problems, particularly certain phases of problems involving combined hydro- and steam-generating capacity. In the event that both the storage capacity and the physical capacity available at the hydro plants are in excess of the requirements for normal operating conditions, such excesses are available for use to avert what otherwise might be an emergency as the result of forced outages of steam-generating capacity. The extent to which the latter type of operation can be utilized depends largely on the magnitude, duration, and frequency of occurrence of forced outages of the steam-generating capacity, the amount of available storage, the amount of available physical hydro capacity, and the duration and frequency of low river flows. The techniques described by the author are generally useful in the determination of the duration and frequency of occurrence of forced outages of various magnitudes of steam-generating capacity as a factor in the determination of the extent to which excess physical hydro capacity can be utilized to avert emergency conditions coincident with forced outages of steam-generating capacity. Such operation and use is appropriately compared to the formerly well-established use of electric storage batteries for emergency use on d-c systems.

However, it is not sufficient in capacity problems, particularly those involving the use of limited hydro storage, to consider only the average outage duration such as would be obtained from an exact application of the specific techniques described in the paper. The vast majority of forced outages, particularly for the larger magnitudes of capacity on forced outage, for which the use of hydro storage to avert emergency conditions is the most effective, are for short durations, the major portion of which are shorter than the average duration. Table I of this discussion, which is based on the data given in Figure 1 of the closure of an earlier paper by Loane and Watchorn,[1] illustrates these characteristics very clearly.

However, critical capacity conditions may arise when the forced outage durations are longer than the average. The determination of the probabilities of occurrence of such long outages is essential to the correct evaluation of the risk of failure to carry the load in any appraisal of system capacity requirements or in any appraisal of the correct evaluation of the useful hydro capacity. The general methods developed by Mr. Strandrud would be very helpful in an analytical determination of the various probable lengths of time for use of the hydro storage, rather than using a conservative (longer than average) length of time for hydro storage, as was done in the Loane-Watchorn paper[1] for the conditions considered there. Such calculations provide the basis for determining the potential increases in the load-carrying capabilities of the hydro-generating capacity in averting emergencies, over such capabilities under normal operation for various load and river flow or water conditions as a factor to be used in the evaluation of the risk of failure to carry the load. Except for this previously indicated use of the techniques described by the author, it is not believed that the determination of either the average frequency or the average duration of forced outages is necessary in the determination of system installed capacity requirements; all that is required for this purpose, in so far as forced outages are concerned, is the much simpler and more significant determination of the probability of availability of physical capacity. One method of determining this quantity is as indicated for the determination of column 12 of Table I of the paper. The basis for the determination of the risk of failure to carry the load[1-3] is provided by such data,

Table I. Frequency and Duration of Large Capacity Outages (Boilers and Turbines) Based on 100-Years' Synthetic Forced Outage Experience for an Actual Steam Electric Generating System of about 1,000,000 Kw Capacity in 35 Turbine Units

	Forced Outages of Steam Generating Capacity Equal to and Larger than			
	75 megawatts	100 megawatts	125 megawatts	150 megawatts
Forced outages of all durations				
Number	510	220	62	11
Outage-days	1,487	565	120	14
Average interval between occurrences, years	0.196	0.454	1.61	9.09
Average duration, days	2.92	2.56	1.94	1.27
Forced outages of one-day's duration				
Number	298	132	40	9
Average interval between occurrences, years	0.336	0.757	2.50	11.1
Percentage of forced outages	58.4	60.0	64.5	81.8
Forced outages of two-days' duration				
Number	87	41	10	1
Average interval between occurrences, years	1.15	2.44	10	100
Percentage of forced outages	17.1	18.6	16.1	9.1
Forced outages of three-days' duration and longer				
Number	125	47	12	1
Outage-days	1,015	351	60	3
Average interval between occurrences, years	0.80	2.17	8.33	100
Average duration, days	8.12	7.46	5.00	3.00
Percentage of forced outages	24.5	21.4	19.4	9.1

in the form shown in either column 19 or column 20 of that table and also of Table II, in conjunction with data for the load adjusted for maintenance requirements and other capacity reductions, including the effect of reduced capacity with high river flows and low reservoir elevations and, also, with reduced load-carrying capability that may be the result of decreased energy availability during low water periods (after adjustment for the emergency load-carrying capability, if any, of the hydro capacity during such low water periods, as generally discussed in the preceding paragraphs). It is especially important that provision be made in such computations to include in the evaluation the effect of reduced load-carrying capability of the hydro plants with low water conditions. Otherwise, the results may be very misleading and may cause at least very embarrassing situations, particularly where the available hydro capacity is a substantial portion of the total installed capacity, and where the hydro energy available from time to time may vary over a wide range. In addition, provision also should be made in the computations to include the effect on the capacity requirements of the load variations that result from changes in the general load level with variations in business conditions and, also, for load variations that result from changes in weather and other conditions of a short time duration.[4]

References

1. Probability Methods Applied to Generating Capacity Problems of a Combined Hydro and Steam System, **E. S. Loane, C. W. Watchorn.** *AIEE Transactions*, volume 66, 1947, pages 1645–57.

2. Generating Reserve Capacity Determined by the Probability Method, **Guiseppe Calabrese.** *AIEE Transactions*, volume 66, 1947, pages 1439–50.

3. Determination of Reserve Capacity by the Probability Method, **Guiseppe Calabrese,** and discussion thereof by **C. W. Watchorn.** *AIEE Transactions*, volume 69, part II, 1950, pages 1681–89.

4. Elements of System Capacity Requirements, **C. W. Watchorn.** *AIEE Special Publication S-38*, August 1950, pages 5–42.

A Spring Mechanism for Hand Closing of Magnetic Power Air Circuit Breakers

R. C. DICKINSON
FELLOW AIEE

J. D FINDLEY
ASSOCIATE AIEE

Synopsis: Power air circuit breakers cannot be closed safely on energized circuits by direct manual operation because the force and speed required may, in the case of fault current, exceed the strength of the operator. But in some small installations, manual operation is very desirable. A device is here described, which stores manual work in a spring in easy increments and, when released, closes the circuit breaker with proper speed and power.

WHEN circuit power breakers are applied, the choice of closing method is determined ordinarily by the following considerations:

1. The importance of continuity of service on the lines fed through the circuit breaker.
2. Frequency of circuit breaker operation.
3. Necessity of closing and tripping from remote position.
4. The number of circuit breakers at one location.
5. Power requirements of equipment other than circuit breakers in which a common supply can be used.
6. Availability of skilled personnel for maintenance of switching equipment and closing power source.

These considerations usually lead to a d-c solenoid mechanism supplied by a storage battery, or by a dry metallic rectifier, or by a general supply from d-c rotating machines.

However, for many small installations, using only one circuit breaker, such as the primary circuit breaker for a transformer supplying a small factory or office building, a storage battery is usually undesirable because of initial cost, maintenance, deterioration, and sometimes because of space required. In such an installation, a dry metallic rectifier would ordinarily be supplied by a small auxiliary transformer which would have to be connected to the incoming line ahead of the circuit breaker to be closed. Therefore the rectifier and auxiliary transformer method involves difficulty in metering the continuous losses of the transformer and additional complication in providing fault protection. If no other source of electric power is available, the problem then arises of how best to close a circuit breaker without electric power.

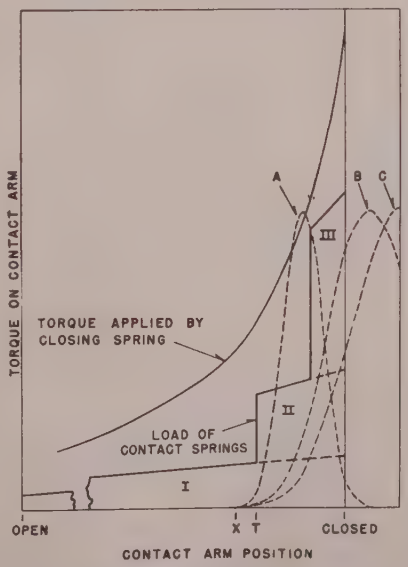

Figure 1. Variation of torque required to force contact arm closed, and torque actually applied by spring mechanism

Methods considered and investigated include:

1. Explosive gases driving a piston.
2. Manually compressed air.
3. Bottled compressed air or other gas acting directly on a piston.
4. Highly compressed gas acting against a liquid which in turn drives a small piston.
5. A falling weight.

These methods are undesirable for various reasons including possible unavailability when needed, mechanical complexity, cost, and lack of simplicity in what is required of the operator. By contrast with these methods, the method of storing energy in a spring is very desirable because it gives reliable availability, because it will repeat with uniformity, and because it may be designed so that its operation is simple. A man of moderate intelligence and strength may operate it safely.

Required Characteristics

The force, time, and travel characteristics of any power circuit breaker closing mechanism must be visualized in terms of the sequence of events that occur in closing against a fault current. Figure 1 illustrates that the closing mechanism must supply power first to lift the weight of the circuit breaker parts and load the accelerating springs, area I. The load of the arcing contact springs, area II, then appears suddenly when contacts touch at T followed a short space further by the load of the main current carrying contacts, area III. These areas represent the energy that must be supplied by the closing mechanism when the circuit breaker does not close against any fault current.

When the character of the load caused by the magnetic forces of the fault current is visualized, the time as well as the space relationship of events must be considered. Regardless of closing speed, fault current may begin before the arcing contacts touch at T. The maximum contact separation at which this can occur depends on the crest voltage and the

Paper 51-25, recommended by the AIEE Switchgear Committee and approved by the AIEE Technical Program Committee for presentation at the AIEE Winter General Meeting, New York, N. Y., January 22–26, 1951. Manuscript submitted October 27, 1950; made available for printing November 20, 1950.

R. C. Dickinson and J. D. Findley are both with the Westinghouse Electric Corporation, East Pittsburgh, Pa.

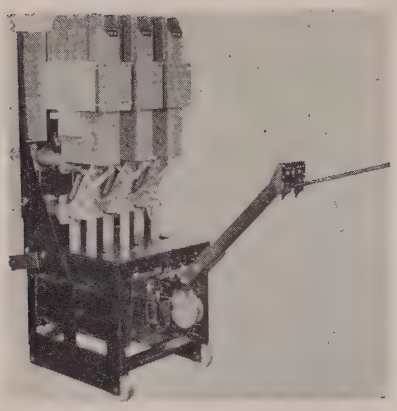

Figure 2 (left). 250 mva 4.16-kv circuit breaker equipped with manually loaded spring closer

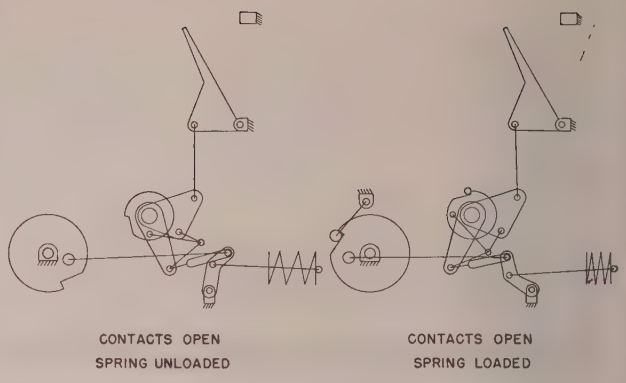

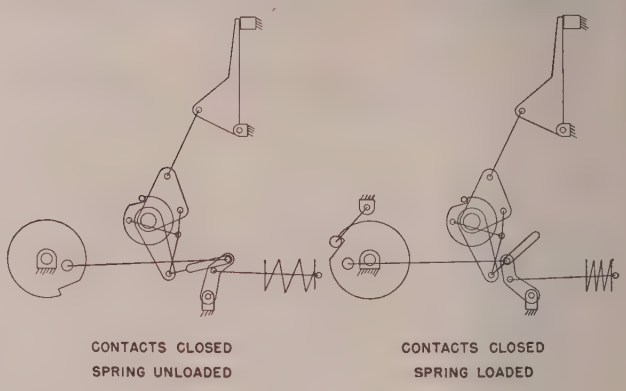

Figure 4 (right). Linkage positions

fluid between the contacts. The separation will, of course, be larger in air circuit breakers than in oil circuit breakers. In Figure 1, this point is indicated at X. The magnetic blowout forces caused by the fault current will rise approximately as the expression, $[\sin(\omega t-90°)+1]^2$, always reaching peak in approximately one-half cycle. Curves A, B, C are drawn to show the space-time relationship of the contact position and blowout torque that might exist for three different closing speeds. In A, contacts are moving slowly relative to the rise of fault current and the first crest of the fault current occurs after the arcing contacts touch but shortly before the main contacts touch. This means that contacts must make a current near maximum for the circuit. Also the large, and early peak force at A means relatively large decelleration of the contact arm. In B, the contacts are traveling faster relative to the rise of fault current. The crest occurs after main contacts touch and the contacts touch at a much lower value of current. In C, contact speed is still higher and current when touching is smaller than in A or B. Note that in B and C, peak forces occur after latching.

In general, the higher the contact speed from the beginning of fault current to latching, the smaller will be the closing force required to counteract magnetic blowout force and the smaller will be the current when contacts touch. Equally important, the shorter the time during which the arcing contacts must carry the rising current before the main contacts engage, the smaller will be the amount of burning, and the tendency to weld. Similarly the shorter the time from initial touch to full pressure on the main contacts, the smaller will be the damage to them. In actual practice, optimum speed must be a compromise between burning effects and mechanical impact effects.

The necessary contact speed can easily be obtained with closing springs because spring force acts almost instantly and the ratio of force to mass is high. There is no delaying factor such as fluid friction, or magnetic lag caused by eddy currents. However, if a simple straight line spring characteristic were applied direct to a contact arm with ordinary mass, the spring force at end of travel would have to be large enough to push to the latched position against the final loads. This

Figure 3. Side view of mechanism

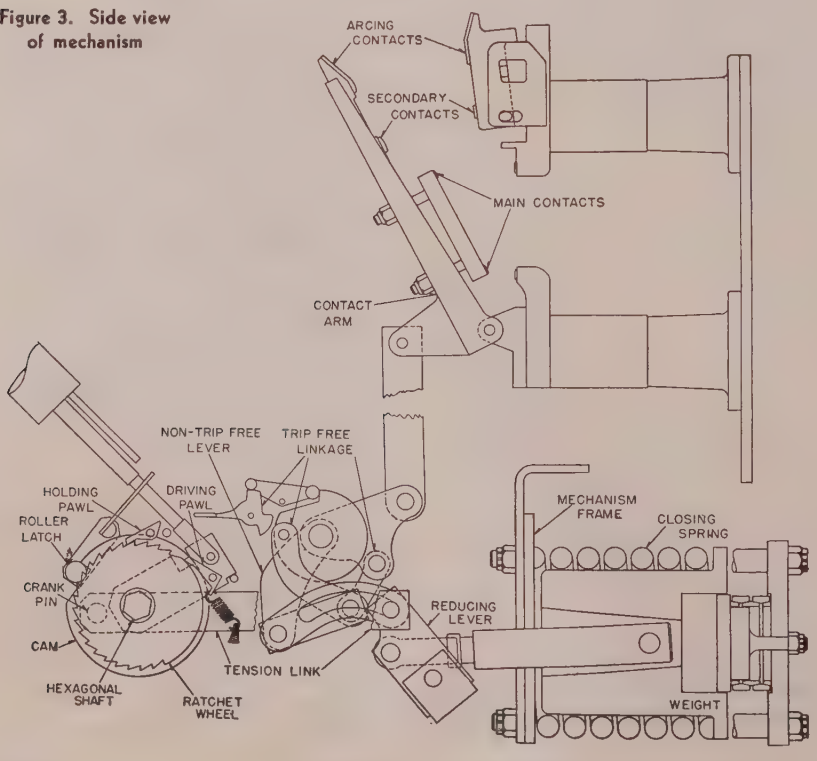

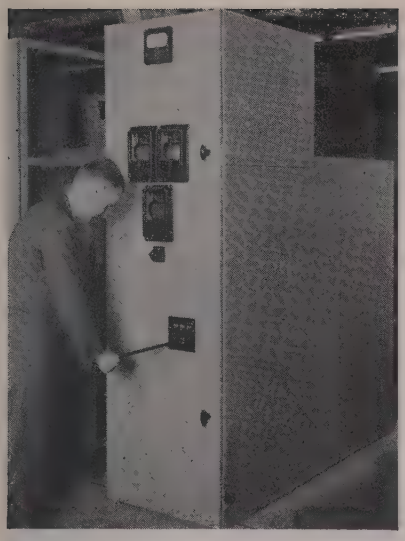

Figure 5. Typical 4.16-kv metalclad equipment arranged for hand closing. Operator loading the spring

would lead to a beginning spring force much too high, and excessive mechanical speed and shock. In the actual design of a spring mechanism, the linkage between the closing spring and the contact arm may be arranged so that a relatively low force is delivered to the contacts at the beginning of the motion and a relatively high force at the end of the closing motion. Resulting torque curve is shown in Figure 1.

New Manual Spring Mechanism

Since magnetic power air circuit breakers are practically universally applied in this country as part of metalclad switching equipment, a manual closing mechanism should be especially adapted to such equipment. In the development of a new manual closing mechanism by the Westinghouse Electric Corporation, it was decided that such a mechanism should have the following features of adaptation:

1. It should have safety features to prevent false operation, jamming, and so forth so that little special skill is required to operate it.

2. It should be possible to load the closing spring, close the circuit breaker and trip the circuit breaker from outside the cell door, with the door closed normally, as in the case of electrically operated circuit breakers.

3. There should be visual indication as to whether the closing spring is loaded or unloaded, and visual indication of the position of the circuit breaker contacts with the cell door normally closed.

4. It should be possible to close and open the circuit breaker contacts slowly under the control of the operator at all times, for inspection and maintenance purposes.

5. It should not interfere with the standardized method of inserting and withdrawing the circuit breaker from the metalclad cell.

6. It should be installed in the same location in the circuit breaker as is the solenoid mechanism in electrically operated circuit breakers.

7. It should be suitable for tripping by any of the standard methods, such as d-c or a-c shunt trip, capacitor trip, current transformer trip, undervoltage release, and manual trip.

Figure 2 shows a 4.16-kv 250 megavolt-ampere (mva) magnetic deion power air circuit breaker equipped with a new manual closing spring mechanism having all of the foregoing listed features. The closing spring in effect replaces the closing coil of the solenoid closing mechanism. This spring is compressed by a ratchet wheel by means of a lever inserted at the top of the control post. The control post contains an escutcheon on which are the socket for the removable loading lever, push plates for releasing the spring to close the circuit breaker and for tripping the circuit breaker, an indicating flag to show whether the spring is loaded or unloaded, an indicating flag to show the circuit breaker contact position, and an operation counter.

Figure 3 shows a side view section of the mechanism with the major parts labeled. The closing spring pushes against the frame of the mechanism on the left and against the weight on the right. This weight is connected to the nontrip free lever through the link and reducing lever system, which increases the ratio of contact arm force to spring force as the system moves toward the closed position. The tension link attached to the reducing lever connects the spring-weight system to the control mechanism on the left containing the cam, with a crank pin to which the tension link is attached, and the ratchet wheel all attached to the same hexagonal shaft. The ratchet wheel contains teeth for somewhat more than 180 degrees of travel and is driven step by step by the driving pawl and held between steps by the holding pawl. When the tension link and crank pin are turned thus slightly beyond dead center, corresponding to maximum spring compression, the cam is stopped and held against the spring force by the roller latch. To close the circuit breaker, this latch is released by movement of the push plate on the control post, not shown. Thus, in closing, the cam and ratchet wheel rotate in the same direction as when the spring is compressed.

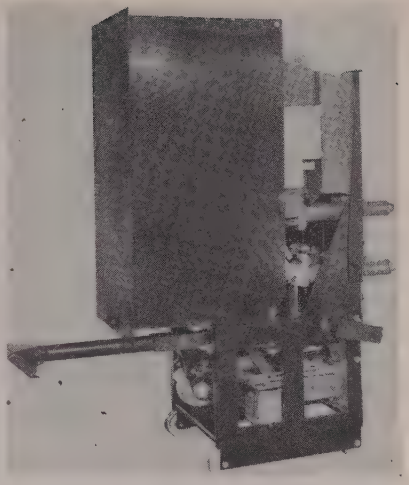

Figure 6. Control post lowered to horizontal to facilitate installation or removal of main barrier assembly

Since the energy stored in the closing spring exceeds the minimum closing requirements, the surplus energy is absorbed by a spring ring bumper, which operates in a short stroke by direct mechanical friction. This absorbs the mechanical shock without the use of dashpot, valve or other device.

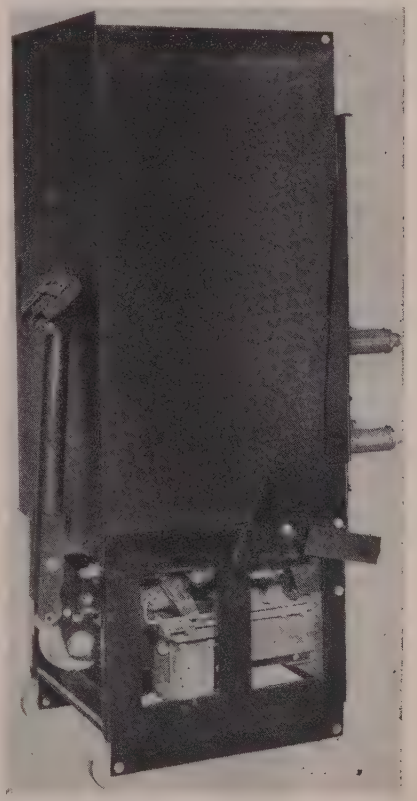

Figure 7. Control post raised to vertical so that cell door may be closed while drawout unit is in test or disconnected position

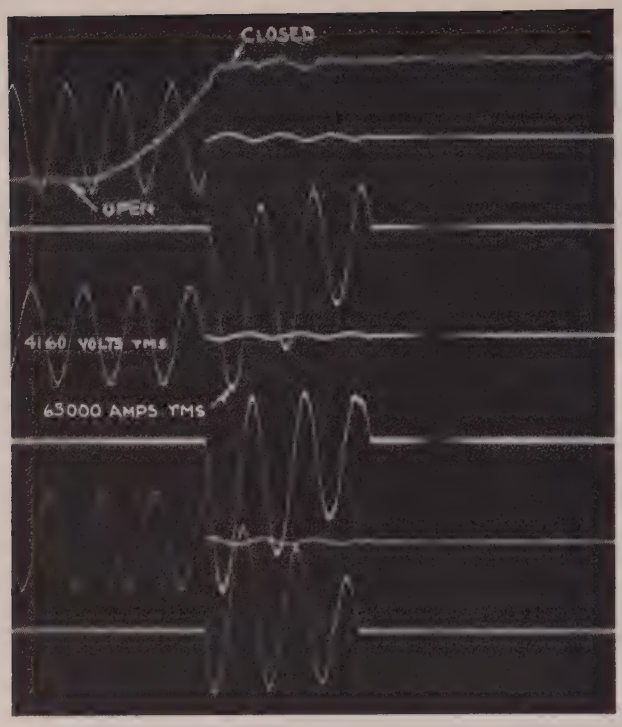

Figure 8. Oscillogram of closing and latching momentary current

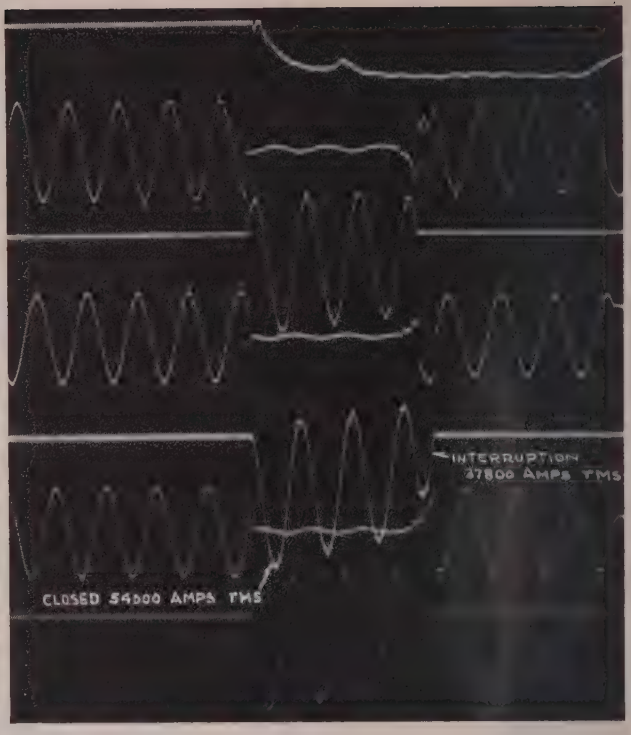

Figure 9. Oscillogram of a close open operation. Top trace is current through a shunt trip coil

In the spring compressing operation, the operator inserts the removable handle and "pumps" it 16 strokes. At this point the roller latch can be heard to snap into place and further operation of the handle accomplishes nothing. Thus he knows that the circuit breaker is ready to be closed. After closing, the spring may be reloaded for another closing operation.

Three safety features are provided in this device. One prevents the circuit breaker from starting to close when the spring is only partly compressed. This feature results because the angular motion of the ratchet wheel and cam is in the same direction for compressing the spring as it is when the circuit breaker is closing. If the "push to close" plate is pushed when compression is only partly completed, nothing happens because the cam has not yet completed its motion and the roller latch has not dropped into position.

It is possible to compress the closing spring while the circuit breaker is in the closed position, at any time after the circuit breaker is closed. If the "push to close" plate were pushed to release the roller latch under this condition, the closing spring would be released under full power with no load. To prevent this condition, a mechanical interlock is provided which prevents release of the roller latch unless the circuit breaker is in the open position

Drawout units provided with this manual closing mechanism are provided with standard mechanical interlocking to prevent insertion to, or removal from, the connected position unless the circuit breaker contacts are in the open position, or to prevent closing unless the circuit breaker is in one or the other extreme positions. The latter feature consists of a mechanical blocking arrangement that prevents movement of the solenoid core and attempted closing stops when the closing current is cut off. If this occurs with the spring closing device, the spring is jammed because the spring cannot be "cut off" as in the case of closing current. Consequently a simple mechanical interlock is provided that prevents movement of the "push to close" control when the mechanical block would prevent complete operation.

Figure 5 shows a typical 4.16-kv metal-clad equipment assembly with an operator loading the spring. The maximum force on the loading handle is approximately 20 pounds.

As shown in Figure 6, the control post may be lowered to the horizontal position to facilitate installation and removal of the circuit breaker main barrier assembly. It also can be raised to the vertical position as shown in Figure 7, to permit the drawout unit to be left in the test or disconnected position with the cell door closed.

Application and Test

This device is designed for application on circuit breakers rated 150 mva at 2.3 kv, 150, and 250 mva at 4.16 kv, 150, 250, and 500 mva at 13.8 kv. The highest momentary current rating involved in these circuit breaker sizes is 60,000 amperes, in the case of the 4.16-kv 250-mva circuit breaker. High power laboratory tests have been made using this circuit breaker size. Both close and close-open tests were made at various currents throughout the range. Sample oscillograms are shown in Figures 8 and 9. After five operations at currents in excess of rating, the contacts and interrupter were in good condition for further use.

Discussion

R. L. Webb (Consolidated Edison Company, New York, N.Y.): It will be interesting to some to know that the development of manually charged closing mechanisms was initiated several years ago in the EEI-AEIC-NEMA Joint Committee on Power Circuit Breakers.

At that time the NEMA members advised that for reasons of safety, small oil circuit breakers applied on circuits where the short-circuit current is 12,500 amperes or more should not be closed by hand and that magnetic power air circuit breakers should

never be closed manually on a live circuit.

The needs of the industry came in for considerable discussion, and out of this discussion came the committee recommendation that the manufacturers should develop manually charged closing devices for magnetic power air circuit breakers, without delay, since it was expected that the use of this type of circuit breaker soon would predominate. It was felt that there would undoubtedly be a number of installations where such circuit breakers are closed infrequently and where maintenance of some conventional closing power source would be too costly and therefore undesirable.

It is interesting to see this design of a manually charged spring-closing device described by Messrs. Dickinson and Findley. It is understood that other manufacturers of power air circuit breakers either have completed or have under development a device which will do the same job with their circuit breakers.

It is believed that these developments fill a definite need in the industry for certain types of circuit breaker installations.

O. B. Vikoren (Philadelphia Electric Company, Philadelphia, Pa.): The authors are to be congratulated on their success in having developed a spring mechanism which in certain applications not only takes the place of a solenoid mechanism but does so without increasing the over-all dimensions of the equipment with which it is associated, or presumably without sacrificing any of the safety features particularly required in metal-clad switchgear.

While the basic principle of the mechanism is covered clearly in the paper, it is unfortunate that the authors have not gone into a little more detail on some of the points which make the device rather intriguing. We have in mind particularly the steps which must be taken to raise the control post to the vertical position or lower it to the horizontal position. When we realize that this post carries all the control, including an operation counter, the following questions logically arise:

1. Can the control post be raised and lowered without any major disconnecting operation of the controls?

2. Will the moving of the control post in any way prevent the mechanical interlock, which the authors described in the section on the "New Manual Spring Operation," from functioning, whereby a loaded mechanism would release its full power with no load?

3. Assuming that the metal-clad circuit breaker is closed in the operating position and the spring mechanism has been reloaded subsequent to the last closing operation, is it possible to move the circuit breaker to the test position without unloading the mechanism? If not, it appears to be necessary to trip, reclose, and again trip the circuit breaker before it can be moved to the test position.

The paragraph which precedes the discussion of Figure 5 refers to a standard interlocking device used in metal-clad switchgear. It is believed that in the beginning of this paragraph the authors have in mind the interlock used on a solenoid-operated circuit breaker and later on they want to emphasize the difference between the interlock used on a solenoid mechanism and that used on a spring mechanism. This point could bear some clarification.

No doubt the authors have taken into account the items discussed herein, and perhaps the brevity of the paper is responsible for the raising of these points. Based on the assumption that the device meets all safety requirements, the paper covers a development which the industry has been looking forward to for a long time.

K. G. Darrow (General Electric Company, Philadelphia, Pa.): The authors are to be congratulated on their contribution to the fulfillment of the limited but very real need for stored-energy closing devices for medium-voltage oilless circuit breakers. It was just two years ago that a paper describing "A Manually-Operated Spring Mechanism for Medium Voltage Oilless Circuit Breakers" was presented before the Institute by B. W. Wyman and E. J. Casey.[1] Several of the mechanisms described therein are already in service. These authors, too, investigated and compared various stored-energy mechanisms, such as a piston driven by gunpowder or high-pressure bottled gas and spring drives. It is interesting to note that this subsequent investigation by Messrs. Dickinson and Findley compared these stored-energy mechanisms, as well as some additional ones, and reached the same basic conclusion, that of employing a spring as the energy-storage medium. In addition, both have recognized the desirability of using a mass with the spring in order to obtain the desired operating characteristics. The importance of the manner in which the mass is employed cannot be overemphasized for this reason. Closing devices for circuit breakers must deliver sufficient energy to close against the high magnetic forces of the momentary-rating current. However, the majority of circuit breaker closings are not against faults. Therefore, the problem of absorbing the excess energy delivered in order to prevent mechanical shock is an important factor in the design. This apparently has been recognized by the authors, who have employed a ring-spring buffer to absorb the excess energy, a device generally used where relatively large amounts of energy must be absorbed within a short stroke. It implies that considerable energy must be absorbed in this device at the end of the closing motion, with the resulting possibility of mechanical shock. This, of course, is not a problem where a rotating mass is used, since no matter how high a force is delivered at the end of the closing stroke the excess energy is restored in the spring by the rotating mass without mechanical shock.

The authors appear to have made a particular point of analyzing the effects of velocity and momentary forces. There is some indication that they are depending primarily on velocity for the closing force. Is the circuit breaker closing speed higher with the spring mechanism than it is with the standard solenoid operator?

REFERENCE

1. A MANUALLY-OPERATED SPRING MECHANISM FOR MEDIUM VOLTAGE OILLESS CIRCUIT BREAKERS, **B. W. Wyman, E. J. Casey.** *AIEE Transactions*, volume 68, part I, 1949, pages 357–63.

R. C. Dickinson and **J. D. Findley**: The authors are grateful for the ideas contributed by the discussers. Mr. Darrow asks about closing speed. On the closing tests for which oscillograms were shown, moving contact velocity at instant arcing contacts touch was approximately 20 per cent higher than certain solenoid-operated circuit breakers which are operated more frequently. The higher speed was chosen because circuit breakers on which this mechanism is used will be operated very infrequently. Mr. Vikoren asks about the control post. To move the control post from the normal 45-degree position to vertical or horizontal, two clamp screws are removed. The controls are not operative in the vertical or horizontal position, but they are not disconnected. When the post is returned to 45-degree position, the controls again are immediately operative. The main pump handle tension link has a flexible knuckle between the split pivots of the control post. The trip-and-close controls operate through compression rods guided within the post. When the post moves away from 45 degree position, the lower ends of these rods simply move away from the tabs they normally push. The indicators and operation counter are moved with flexible wires. Hence, the answer to Mr. Vikoren's question 1 is yes. In reply to his question 2, the interlock remains in effect against any accidental operation of the control tab. It would, of course, be possible to poke a rod deliberately into the mechanism and knock off the latch. In reply to Mr. Vikoren's question 3, it would be necessary to trip the circuit breaker only once before moving the circuit breaker out from operating to test position. The closing spring may remain charged while moving the circuit breaker. Further answering Mr. Vikoren, the authors meant to explain that the spring mechanism has an additional mechanical interlock which stops motion of the "Push to Close" control whenever the standard interlock (with which all drawout circuit breakers are equipped) is blocking the contact linkage from closing.

A Per-Unit Interpretation of Transmission Line Constants

D. J. POVEJSIL
ASSOCIATE AIEE

A. A. JOHNSON
FELLOW AIEE

THIS paper covers a powerful concept in the application of the per-unit method to transmission line constants. It results in a completely general set of constants which can be applied to any practical overhead electric power transmission line with great accuracy. This is brought about by the fact that the ratio of series inductive reactance per mile (x) to the shunt capacitive reactance per mile (x') is, for all practical purposes, a constant. The generalized line constants are presented in the form of a group of curves from which the impedances of any overhead transmission line can be found with a minimum of effort and opportunity for error.

The power engineer finds himself increasingly confronted with the problem of obtaining accurate constants for long transmission lines for the following reasons:

1. The number of long, high-voltage transmission lines continue to increase.
2. For economic reasons, transmission lines are operated at the highest possible loadings with the resultant narrowing of stability margins.
3. In the case of many interconnections between large systems, terminal impedances are small with respect to line impedances.
4. As a result of (2) and (3), the constants of the transmission line have become a major factor in the determination of system performance.

The calculation of line constants by hyperbolic functions is a task which is time consuming and easily subject to mechanical error. In 1926, Clarke[1] presented a group of curves which eliminated much of the drudgery entailed in the calculation of those constants. This paper presents a different approach to this problem which results in defining transmission line constants in per-unit terms. Thus, the per-unit method which has proved so useful in the definition of the constants of such terminal equipment as generators and transformers is extended to the constants of transmission lines.

Representation of the Transmission Line

The four most common methods of representing a transmission line for single frequency calculations are as follows:

1. $ABCD$ constants
2. Equivalent π
3. Equivalent T
4. Driving point and transfer impedances

Although any of the four systems could have been used in this paper, the use of $ABCD$ constants is most suitable for the following reasons:

1. The analytical expressions for these constants can be easily generalized and plotted in curve form.
2. The simplicity of obtaining the constants from the generalized curves.
3. The ease with which these constants can be combined with terminal impedances to form the overall system constants.
4. The check resulting from the fact that $AD-BC=1$.

The $ABCD$ constants of a transmission line are expressed in terms of the line parameters as shown in equations 1, 2, 3, and 4.

$$A=\cosh\left[S\sqrt{\frac{x}{x'}}\sqrt{-1+j\frac{r}{x}}\right] \quad \text{volts per volt} \quad (1)$$

$$B=\sqrt{(r+jx)(-jx')}\times \sinh\left[S\sqrt{\frac{x}{x'}}\sqrt{-1+j\frac{r}{x}}\right] \text{ ohm} \quad (2)$$

$$C=\frac{1}{\sqrt{(r+jx)(-jx')}}\times \sinh\left[S\sqrt{\frac{x}{x'}}\sqrt{-1+j\frac{r}{x}}\right] \text{ mhos} \quad (3)$$

$$D=A \quad (4)$$

where

r = series resistance in ohms per mile
x = series inductive reactance in ohms per mile
x' = shunt capacitive reactance in ohms per mile
S = line length in miles

Each of these constants is a complex quantity which can be expressed in the following form:

$$A=A_1+jA_2 \text{ volts per volt} \quad (5)$$

$$B=B_1+jB_2 \text{ ohms} \quad (6)$$

$$C=C_1+jC_2 \text{ mhos} \quad (7)$$

$$D=A \quad (8)$$

Shunt and Series Reactances of a Transmission Line

The primary part of the basic equations for consideration is the quantity, $\sqrt{x/x'}$. To illustrate the fundamental nature of this quotient, it can be rewritten as follows:

$$\sqrt{\frac{x}{x'}}=\omega\sqrt{LC}=\frac{\omega}{v} \quad (9)$$

where

$\omega=2\pi f$
v = velocity of propagation $=\frac{1}{\sqrt{LC}}$

Since the velocity of propagation is approximately equal to the speed of light for all overhead transmission lines, it follows that the quantity, $\sqrt{x/x'}$, will be very nearly constant for all overhead transmission lines.

In order to determine the precise nature of the variation of the parameter, $\sqrt{x/x'}$,

Paper 51-26, recommended by the AIEE Transmission and Distribution Committee and approved by the AIEE Technical Program Committee for presentation at the AIEE Winter General Meeting, New York, N. Y., January 22-26, 1951. Manuscript submitted October 25, 1950; made available for printing November 21, 1950.

D. J. Povejsil and A. A. Johnson both are with the Westinghouse Electric Corporation, East Pittsburgh, Pa.

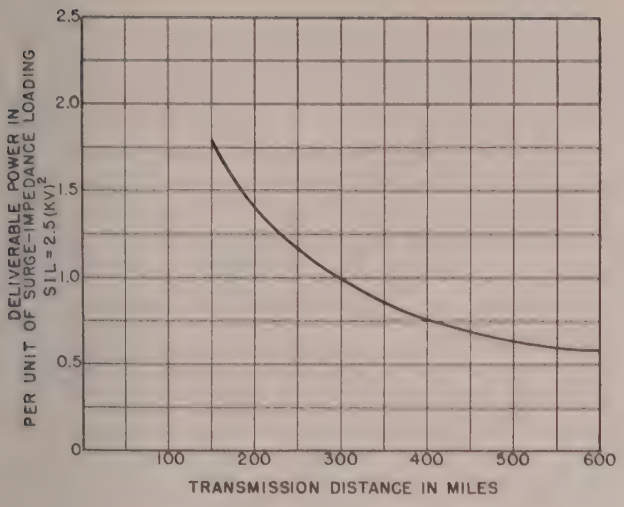

Figure 1 (left). Permissible loading of straight-away transmission lines as a function of line length in miles for voltages from 69 kv to 500 kv

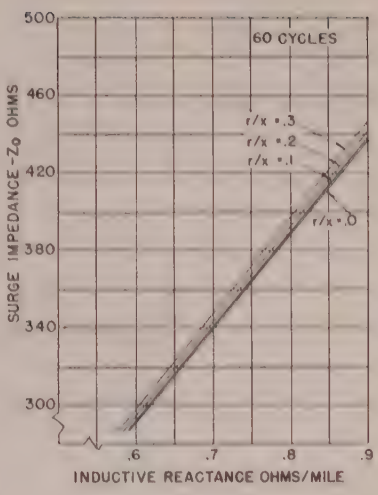

Figure 2 (right). Surge impedance of overhead transmission lines as a function of line inductive reactance per mile

Figure 3. The transmission line A_1 constant as a function of line length in miles

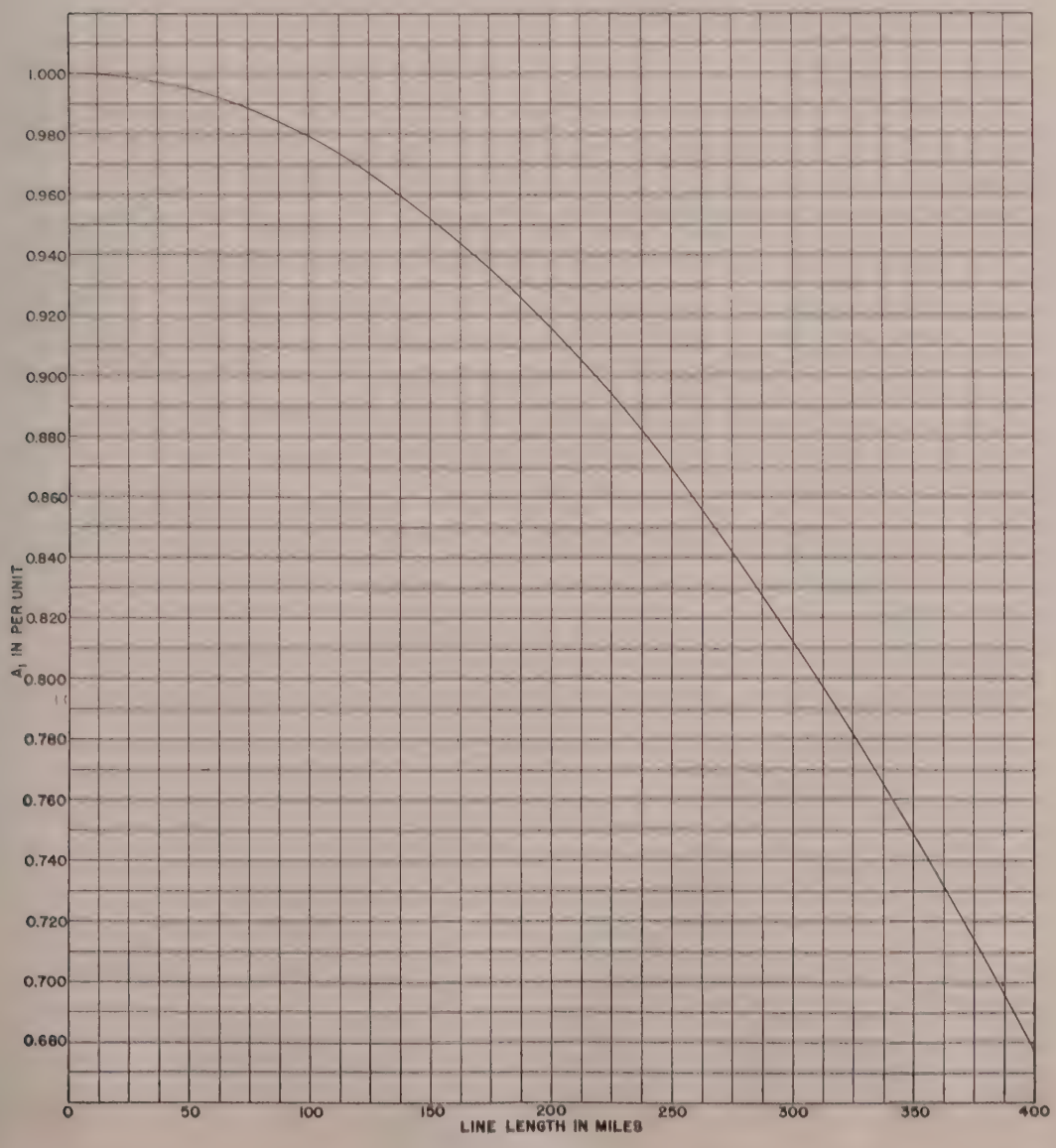

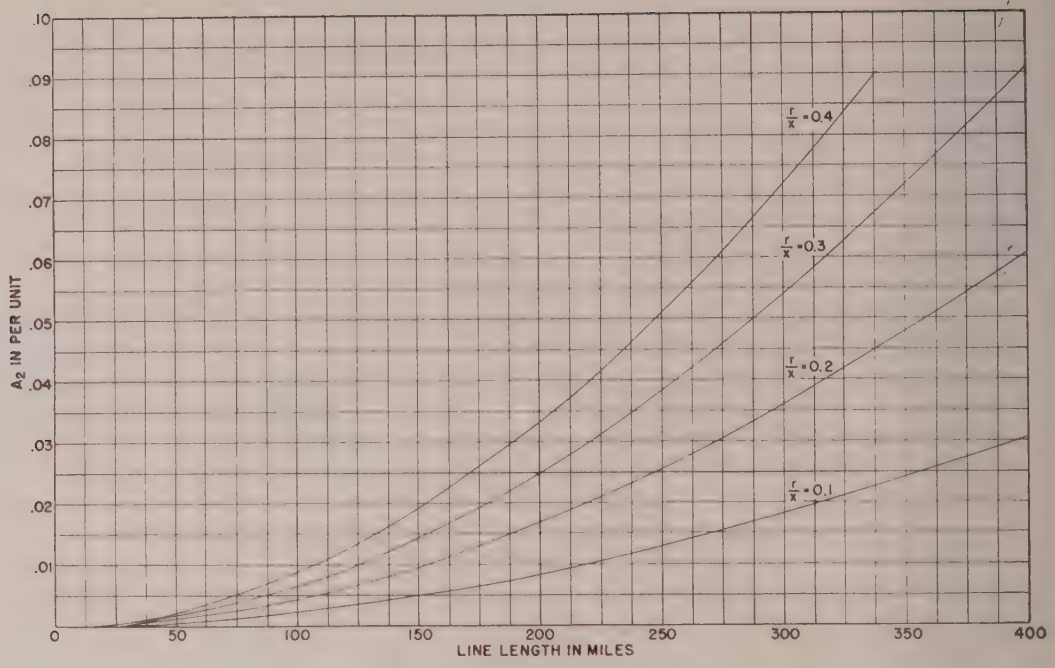

Figure 4. The transmission line A_2 constant as a function of line length in miles

with respect to conductor size, type, and spacing, this factor was calculated for a considerable number of existing lines, in voltage classes from 69 kv to 230 kv, using stranded copper or steel-reinforced aluminum cables. The maximum value of this quantity was found to be 2.07×10^{-3} and the minimum value 2.05×10^{-3}. (The maximum value is associated with 7-strand copper conductor on a 69-kv line and the minimum value with a large steel-reinforced aluminum cable on a 230-kv line.) Therefore, on the basis of this study, a value of 2.06×10^{-3} was assigned to this quantity with a resultant error of less than 1/2 of 1 per cent for stranded copper and steel-reinforced aluminum cables. This conclusion is verified analytically in Appendix I.

The importance of this fact cannot be over-emphasized because it establishes a basic point of similarity between all overhead transmission lines regardless of voltage, spacing, and conductor size. To a large extent, this ratio is also independent of the type of conductor. Therefore, the line constants, $ABCD$, are reduced to functions of length, r/x ratio, and surge impedance.

Surge Impedance and Surge Impedance Loading

By classical definition, the surge impedance of a transmission line is

$$Z_0/\underline{\zeta} = \sqrt{(r+jx)(-jx')} \text{ ohms} \qquad (10)$$

where

Z_0 = magnitude of surge impedance

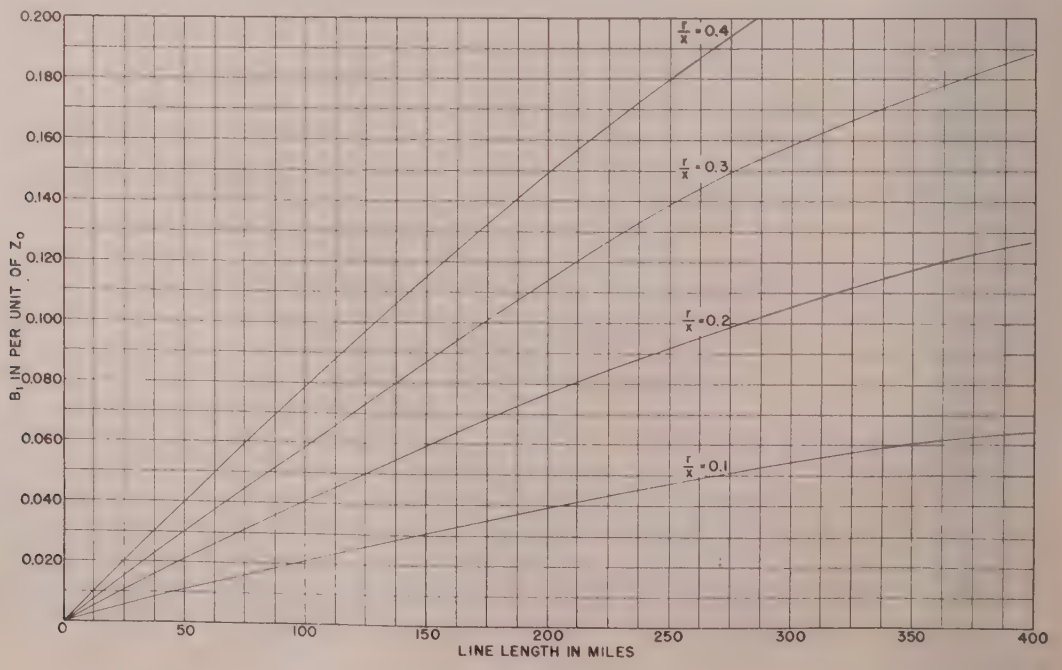

of Z_0 as a function of line length in miles

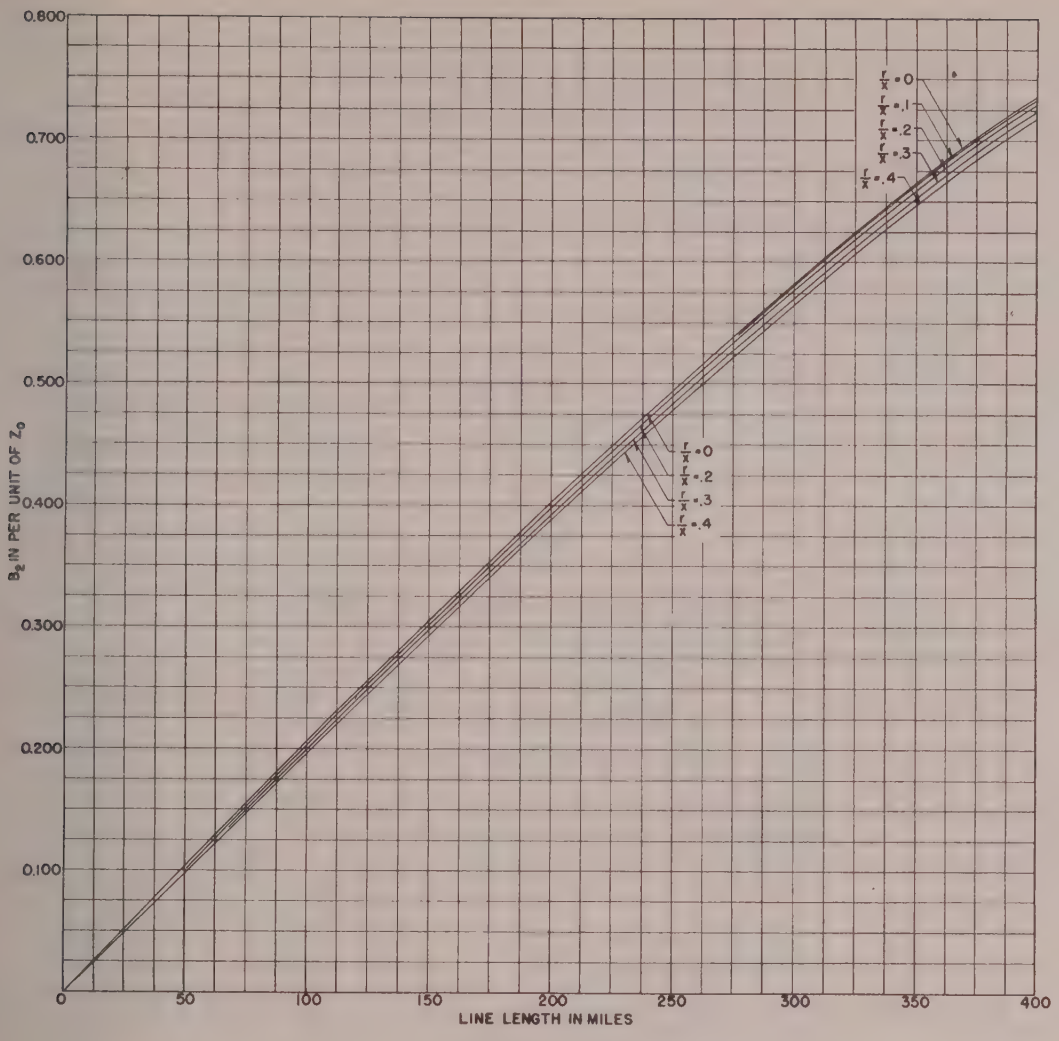

Figure 6. The transmission line B_2 constant in per unit of Z_0 as a function of line length in miles

$$\zeta = -\frac{1}{2}\tan^{-1}\frac{r}{x}$$

Neglecting the effect of resistance, this relation becomes

$$Z_0\underline{/0^\circ} = \sqrt{\frac{L}{C}} \text{ ohms} \qquad (11)$$

From equation 11, it can be seen that the surge impedance is independent of frequency and line length.

A physical interpretation of surge impedance which is of use to the power engineer is as follows: Neglecting line resistance, if a line of any length is terminated in a resistance equal to its surge impedance, the magnitudes of the voltages at the sending and receiving ends are the same and the sending and receiving end power factors are unity. By this definition, the surge impedance loading (*SIL*) of a line can be written

$$SIL = \frac{kv^2}{Z_0} \text{ megawatts} \qquad (12)$$

Based on voltage conditions at each end of the line, surge impedance loading is a very desirable type of loading. However, it does not take into account the factors of line length, terminal impedances, and stability. The results of an investigation by S. B. Griscom[2] of the effect of these factors on allowable line loadings is reproduced in Figure 1. This curve shows allowable line loadings as a function of line length For the case of a long interconnection between two large systems where terminal impedances can be neglected and losses rather than stability become the limiting factor, the values shown on Figure 1 are conservative.

An examination of Figure 1 shows that for long lines, permissible loadings are in the general neighborhood of one times the *SIL* of the line. This fact suggests that the surge impedance loading (in kw) of a line can be used as the base kilovolt-amperes of the line in the same sense that the nameplate rating of a transformer is used as the base kilovolt-amperes of the transformer. Likewise, the surge impedance Z_0 can be considered to be the base ohmic impedance of the line from which the *SIL* kilovolt-ampere base is established once the line voltage is known, equation 11.

The advantages of such a per-unit system are manifold. Of primary importance is the resulting generalization of the *ABCD* constants. When these constants are expressed in per unit of surge impedance, they become

$$A = A \text{ per unit} = \cosh\left[(2.06\times10^{-3})S\sqrt{-1+j\frac{r}{x}}\right] \qquad (13)$$

$$\frac{B}{Z_0} = B \text{ per unit} = \left\{\sinh\left[(2.06\times10^{-3})S\sqrt{-1+j\frac{r}{x}}\right]\right\}\underline{/\zeta} \qquad (14)$$

$$CZ_0 = C \text{ per unit} = \left\{\sinh\left[(2.06\times10^{-3})S\sqrt{-1+j\frac{r}{x}}\right]\right\}\underline{/-\zeta} \qquad (15)$$

$$D = D \text{ per unit} = A \qquad (16)$$

Thus, a set of constants is produced

which is dependent upon line length and r/x ratio. Curves can be plotted with r/x as a parameter showing the variation of the line constants with line length. These curves (Figures 3 to 8) can be used to determine the 60-cycle characteristics of any practical copper, stranded copper, or steel-reinforced aluminum cable line regardless of conductor size, spacing, operating voltage, or surge impedance. As will be explained later, the use of these curves can be extended to other frequencies and other types of conductors by the use of the proper conversion factors.

A second advantage of this per-unit system becomes apparent in the solution of problems of power flow over long lines. The constants of the line often represent the major impedances in problems of this sort. Therefore, it can be seen that a per-unit system based upon line capability represents a more realistic approach since the results may be interpreted immediately in terms of total line capability by means of Figure 1.

Application of Curves

The per-unit $ABCD$ constants of a 60-cycle line can be found from the curves shown in Figures 2 to 8 in the following manner:

1. Obtain r and x for line from conventional tables.
2. Calculate r/x.
3. Obtain the value of surge impedance from Figure 2.
4. Enter Figures 3 to 8 with line length and r/x ratio and read the per-unit constants A_1, A_2, B_1, B_2, C_1, and C_2.

Thus, a set of constants which are expressed in per unit of surge impedance is obtained. If desired, these constants can be put on an ohmic basis by multiplying B_1 (per unit) and B_2 (per unit) by Z_0 and dividing C_1 (per unit) and C_2 (per unit) by Z_0. The A and D constants can be used as read from the curves since they are the same on either per-unit or ohmic bases. An example showing the manner in which these curves can be used to solve a typical power transfer problem is given in Appendix II.

Correction Factor for Frequency

The curves of Figures 3 to 8 can be applied to a frequency other than 60 cycles by using the following relationship to obtain an effective 60-cycle length with which to enter the curves.

$$S' = \frac{Sf}{60} \tag{17}$$

where

S = actual line length in miles
f = frequency in cycles per second
S' = effective line length in miles referred to 60 cycles for use on Figures 3 to 8.

However, in calculating the r/x ratio, the line resistance and reactance based on the actual frequency must be used. The resistances and reactances based on actual frequency also should be used to calculate the surge impedance, Z_0, by means of equation (10).

Correction Factor for Type of Conductor

In order to apply these curves to other than stranded copper and steel-reinforced aluminum cables, the following procedure should be followed for a 60-cycle line:

1. Calculate $\sqrt{x/x'}$.
2. Calculate

$$S' = \frac{\sqrt{\frac{x}{x'}}}{2.06 \times 10^{-3}} S$$

where

S = actual line length in miles
S' = effective line length in miles for use on Figures 3 to 8.

3. Enter curves with S' to obtain line constants.

For a frequency other than 60 cycles, the correction for frequency must be applied, as indicated in the previous section, in order to use the curves in this paper.

For the case of hollow copper conductors, accuracies within 1/2 of 1 per cent can be achieved by multiplying the actual line length by 0.985 to obtain an effective line length with which to enter the curves.

Summary and Conclusions

The following conclusions can be drawn from this work:

1. The square root of the ratio of inductive to capacitive reactance ($\sqrt{x/x'}$) is essentially constant for practical transmission lines.
2. There is considerable justification for a per-unit system based upon surge impedance loading (SIL). First of all, the use of this per-unit system results in making the line constants of any practical transmission line virtually independent of voltage, spacing, and type of conductor except insofar as these factors affect the r/x ratio. Secondly, in the case of long lines, the surge impedance loading is approximately equal to the maximum capability of the line, Figure 1.
3. Because of conclusions 1 and 2, the $ABCD$ constants of any practical transmission line can be determined easily and accurately from a relatively small number of curves. These constants are especially useful for calculations involving the determination of real and reactive power flow over a long transmission line

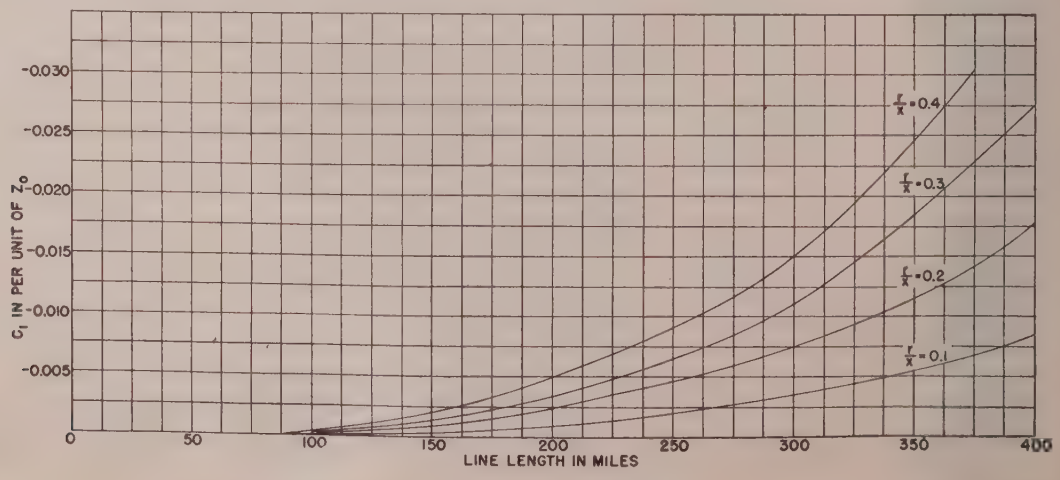

Figure 7. The transmission line C_1 constant in per unit of Z_0 as a function of line length in miles

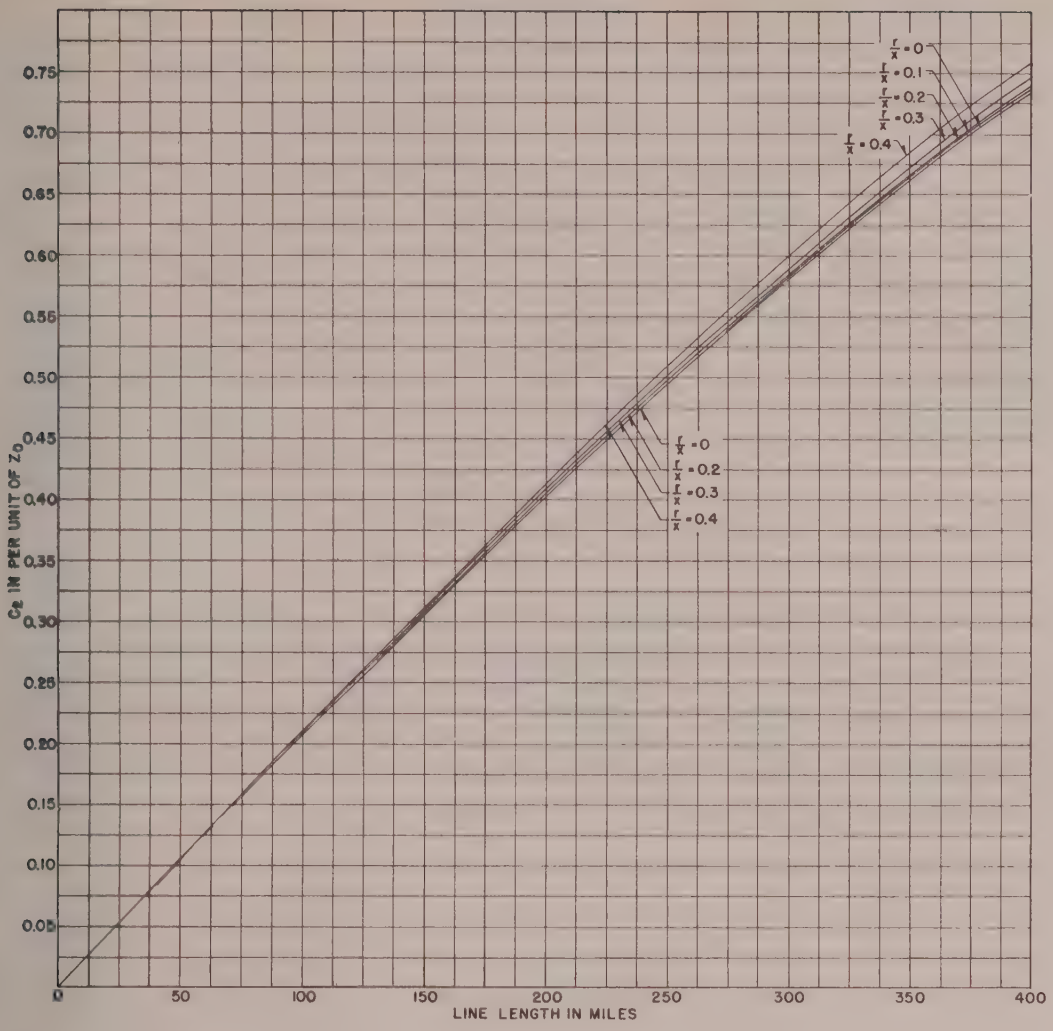

Figure 8. The transmission line C_2 constant in per unit of Z_0 as a function of line length in miles

by formulae or circle diagrams. In addition, these constants can be used in the positive and negative sequence diagrams for calculations involving unbalanced conditions.

Appendix I. Dependence of $\sqrt{x/x'}$ on Conductor Type and Spacing

The expression for the series reactance of a transmission line consisting of solid circular non-magnetic conductors is

$$x = 0.0303 + 0.2794 \log_{10} D/r \text{ ohm per mile} \qquad (18)$$

where

0.0303 is the reactance associated with flux internal to the conductor

0.2794 $\log_{10} D/r$ is the reactance associated with flux external to the conductor

Using the same nomenclature, the expression for the shunt reactance of an overhead line is

$$x' = 0.0683 \log_{10} D/r \text{ ohm-miles} \qquad (19)$$

The square root of the quotient of equations 18 and 19 is then

$$\sqrt{\frac{x}{x'}} = \sqrt{\frac{0.444}{\log_{10} D/r} + 4.09} \text{ per mile} \qquad (20)$$

An examination of this expression shows that the only term which can be affected by the type of conductor is the quantity, 0.444, which is based on a solid, circular, non-magnetic conductor. An examination of the geometry of conductor types shows that this factor will be slightly higher than 0.444 for a stranded copper conductor, slightly lower for steel-reinforced aluminum conductors, and considerably lower for hollow copper conductors.

However, since $\log_{10} D/r$ has a value of greater than two in practical transmission circuits, the effect of changes of internal inductance upon the magnitude of $\sqrt{x/x'}$ is negligible except in the case of hollow copper conductors. For this case, the value of $\sqrt{x/x'}$ may be from 1 to 2 per cent below the value obtained for copper, stranded copper, and steel-reinforced aluminum cable.

The other factor which can affect this ratio is conductor spacing. However, since $\log_{10} D/r$ is essentially constant for overhead lines and since this factor acts upon the smaller term of $\sqrt{x/x'}$, the effect of spacing is negligible.

Appendix II

Problem: Find the radii and centers of the sending and receiving end circles for the system of Figure 9.

1. From conventional tables, $r = 0.1288$ at 50 degrees centigrade, and $x = 0.8117$.
2. $r/x = 0.158$.
3. From Figure 2 $Z_0 = 395$ ohms.
4. From Figures 3 to 8, the per-unit

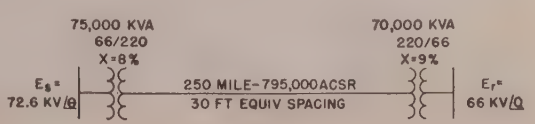

Figure 9. Single-line diagram for example in Appendix II

values of the line constants are:

$A_1 = 0.871 = D_1$
$A_2 = 0.0195 = D_2$
$B_1 = 0.074$
$B_2 = 0.490$
$C_1 = -0.0031$
$C_2 = 0.495$

5. $SIL = \frac{(220)^2}{395} = 122.5$ megawatts

Sending end transformer impedance on per unit of $SIL = X_{ts} = \frac{122.5}{75}(0.08) = j\,0.1305$

Receiving end transformer impedance on per unit of $SIL = X_{tr} = \frac{122.5}{70}(0.09) = j\,0.1575$

(For simplicity, transformer resistances were neglected.) The over-all $ABCD$ constants are:

$A_1' = (A_1 - X_{ts}C_2) = 0.806$
$A_2' = (A_2 + X_{ts}C_1) = 0.0199$
$B_1' = B_1 - A_2(X_{ts} + X_{tr}) - C_1(X_{ts}X_{tr}) = 0.069$
$B_2 = B_2 + A_1(X_{ts} + X_{tr}) - C_2(X_{ts}X_{tr}) = 0.731$
$C_1' = -0.0031$
$C_2 = 0.495$
$D_1' = D_1 - X_{tr}C_2 = 0.792$
$D_2' = D_2 + X_{tr}C_1 = 0.0199$

$A/\alpha = 0.806 + j\,0.0199 = 0.806/1.4°$ per unit
$B/\beta = 0.069 + j\,0.731 = 0.736/84.8°$ per unit
$D/\Delta = 0.792 + j\,0.0199 = 0.792/1.4°$ per unit
E_s(per unit) = 1.1; E_r(per unit) = 1.0

Center of sending circle $= \frac{DE_s^2}{B}/\beta - \Delta$
$= 1.30\ /83.4°$ per unit

Center of receiving circle $= \frac{AE_r^2}{B}/180 + \beta - \alpha$
$= 1.09/-96.6°$ per unit

Sending end radius (for $\theta = 0$)
$= \frac{E_sE_r}{B}/180 + \beta = 1.49/-95.2°$

Receiving end radius (for $\theta = 0$)
$= \frac{E_sE_r}{B}/\beta = 1.49/84.8°$

References

1. Simplified Transmission Line Calculations, **Edith Clarke.** *General Electric Review* (Schenectady, N. Y.), volume 29, May 1926, pages 321–29.

2. Electrical Transmission and Distribution Reference Book. Westinghouse Electric Corporation (East Pittsburgh, Pa.), fourth edition, 1950

3. Power System Stability (book), **S. B. Crary.** John Wiley and Sons, New York, N. Y., volume 1, 1945.

Discussion

R. M. Butler (General Electric Company, Schenectady, N. Y.): Although the application of the per-unit concept is not new in the solution of transmission line problems, this paper presents a valuable new approach which further reduces the effort required in solving long distance transmission power flow problems.

One approach to the per-unit system, used by many engineers has been to resolve a transmission line into an equivalent π or T using a constant value of 0.8 ohm per mile series reactance and 5.2 micromhos per mile shunt admittance. These values are approximately correct for lines of 69 kv and above. The equivalent π or T is then resolved into per-unit form by letting base ohms equal an approximate value of the surge impedance (Z_0). This approximate value is generally assumed to be a pure resistance of 400 ohms. Hyperbolic correction factors are then applied to correct for distance. Base kilovolt-amperes would then be equal to 1000 kv^2/Z_0 or 2.5 kv^2. In this way, voltage has been eliminated as a variable in the expression for per unit Z and Y. However, this method still tends to be laborious and does not have the inherent accuracy and complete independence of voltage as the method proposed by the authors. As stated in the paper, an assumption that the $\sqrt{ZY}$ is a constant is much more correct than assuming that the Z and Y of the line individually are constant values. This fact was actually recognized by Clarke in 1926, see reference 1 of the paper. However, further simplification is possible, as suggested by the authors, by letting base ohms always equal the exact surge impedance of the line, then the per unit line parameters are simply hyperbolic functions of $\sqrt{ZY}$ and may be plotted in convenient form.

The authors state that the best way to present these hyperbolic functions of $\sqrt{ZY}$ is in the form of the $ABCD$ constants. Although the $ABCD$ constant method is a perfectly acceptable and widely used method, it can be shown, however, that the use of the per unit $ABCD$ constants method is not necessarily the most suitable. The per-unit driving point and transfer impedances could have been plotted just as conveniently as the $ABCD$ constants using the per-unit system suggested in the paper. For instance, for a transmission line:

The per-unit driving point impedances

$$Z_{11}/\theta_{11} \text{ or } Z_{22}/\theta_{22} = \tanh\sqrt{ZY} = \frac{B\text{ constant}}{A\text{ constant}}$$

The per-unit transfer impedances

$$Z_{12}/\theta_{12} \text{ or } Z_{21}/\theta_{21} = \sinh\sqrt{ZY} = B\text{ constant}$$

By plotting the driving point and transfer impedances against distance, only four graphs would have been necessary, one each for Z_{11}, Z_{12}, θ_{11} and θ_{12}. These impedances may then be used directly in the power and reactive flow equations or to obtain the circle diagram coordinates.

The over-all driving point and transfer impedances of a line including terminal transformers can be determined using the same per-unit system as suggested in the paper with no more effort than that displayed in the sample problem solved in the paper.

Regardless of the method used ($ABCD$ constants or driving point and transfer impedances) the per-unit system suggested by the authors should prove to be very useful and should help to further increase the speed and accuracy in the solution of transmission problems.

R. D. Goodrich, Jr. (United States Bureau of Reclamation, Denver, Colo.): We have used $ABCD$ constants for a number of years, and agree with the authors that they have distinct advantages over other methods for representing long lines. We found per-unit notation was considerably simpler than the conventional ohms-volts-amperes, and so have made up curves of constants for our most common conductor sizes, spacings, and voltages, in per unit, usually on a 100-megavolt-ampere base.

However, this new approach will make it possible to reduce the number of our curves to a minimum. In fact it may be possible to use one set of curves for A and D, and another set for both B and C. The curves would in effect be graphs of $\cosh \gamma S$ and $\sinh \gamma S$ plotted against S, where $\gamma = 2.06 \times 10^{-3}\sqrt{-1 + jr/x}$.

The $\sinh \gamma S$ curves could be used for both B and C because:

$$B = \sinh \gamma S/+\zeta \qquad (1)$$

$$C = \sinh \gamma S/-\zeta \qquad (2)$$

when Z_0 equals unity.

Since $\zeta = -1/2 \tan^{-1} r/x$ it can easily be obtained, and the complex products indicated in equations 1 and 2 can be computed.

Perhaps the authors should have pointed out that it is often desirable to convert the constants to standard bases such as 20, 50, or 100 megavolt-amperes, particularly when constants for a-c network analyzer studies are to be computed. For these conversions:

$A_B = A_1$
$B_B = (\text{mva}_B/\text{Mva}_1)B_1$
$C_B = (\text{mva}_1/\text{Mva}_B)C_1$
$D_B = A_1$

where the subscript B refers to the new base, and subscript 1 refers to the values on surge impedance base. It will probably be sufficiently accurate to assume

$\text{mva}_B = 2.5\ \text{kv}^2$

for this conversion, although the better value

$\text{mva}_B = \text{kv}^2/Z_0$

where

$Z_0 = (\sqrt{x\,x'})\ \sqrt{1 - jr/x}$

can be used.

The surge impedance curves were checked against our curves for the following point: 115 kv, 100 megavolt-ampere base, 336,400 circular mil steel reinforced aluminum cable 150 miles, $r/x = 0.392$, $x = 0.780$ ohm, $x' = 184{,}500$ ohms.

From the surge impedance curves:

$A = 0.952 + j0.019$

$B = 0.114 + j0.293$
$C = -0.0004 + j0.308$
$A^2 - BC = 0.996 + j0.001$
$\text{mva}_B = \text{kv}^2/Z_0 = 32.5$

When converted to a 100 megavolt-ampere base these constants become:

$A = 0.952 + j0.019$
$B = 0.351 + j0.902$
$C = -0.0001 + j0.100$

From our curves:

$A = 0.952 + j0.019$
$B = 0.337 + j0.872 \quad |B| = 0.934$
$C = -0.0007 + j0.106$
$A^2 - BC = 0.999 + j0.001$

The authors indicate that per-unit constants based on line capabilities are to be preferred to constants referred to other bases. It is our opinion that consideration should be given to the recognized fact that capability varies with line length, and this factor should be taken into account. If the base is selected so that the absolute value of the line constant B is made unity then the constants will at least be based on the steady-state stability capabilities of the line. Moreover it will be found that the circle diagram formulas are very much simplified by the conversion. For the line described above B equals 1.00 when the constants are converted to a 107.1 megavolt-ampere base. Whence:

$A = 0.952 + j0.019$
$B = 0.361 + j0.933 = 1.000$
$C = 0.0007 + j0.099$

Constants of this order of magnitude will be obtained regardless of voltage, line length, and so forth.

D. J. Povejsil and **A. A. Johnson:** Mr. Goodrich and Mr. Butler have indicated a number of interesting and useful extensions of the data and concepts presented in the text of the paper.

It is interesting to note that each discussion demonstrates a method for reducing the required number of curves from six to four. Mr. Butler has taken advantage of the fact that three of the four $ABCD$ constants can be used to define the characteristics of the line in terms of driving point and transfer impedances. The justification for such a simplification is the fact that only three of the four $ABCD$ constants are independent functions. This is shown by the familiar functional relationship, $AD - BC = 1$ (for a static, linear, bilateral, 4-terminal network with no phase shifting transformers). However, it should be noted that the elimination of the dependent variable from the set of constants also eliminates the convenient verification of results afforded by the foregoing relationship. This is an important point to be remembered in the resolution of complicated networks where the likelihood of error is great.

Mr. Goodrich has pointed out that the number of curves can be reduced from six to four if the angle associated with the surge impedance is not included in the plots of the per unit B and C constants. This is very true, but it means that two complex multiplications must be performed after the B and C constants are read from the curves. However, if the curves in the paper are used, no complex multiplications are necessary.

Mr. Goodrich also mentioned that the per-unit constants can be based upon steady-state line capabilities if the kilovolt-ampere base is selected so that the absolute value of the B constant is made equal to unity. Such a concept would be especially useful in steady-state load flow studies of lines with fixed or predetermined high side voltages at the sending and receiving ends. For cases where transient stability and terminal impedances must be considered, a suitable kilovolt-ampere base may be chosen from Figure 1 of the paper, in which line capability is plotted as a function of line length and transient stability considerations for a system with typical terminal impedances.

In recent years, considerable interest has been shown in the use of bundle conductors for certain high-voltage lines. Therefore, a study was made of the reactances of such conductors to determine whether the curves in this paper could be used to determine the constants of transmission lines composed of bundle conductors. The investigation showed that for typical 60-cycle bundle conductor lines the value of $\sqrt{x/x'}$ is equal to 2.06×10^{-3} per mile. Since the curves in the paper are based on this value, it is obvious that they can be applied to bundle conductors in 60-cycle lines without using any correction factors.

A New 69-Kv Air Blast Circuit Breaker

R. B. SHORES
MEMBER AIEE

J. W. BEATTY
ASSOCIATE AIEE

Synopsis: A new air-blast circuit breaker rated at 69 kv, 2,000 amperes, 3,500 megavolt-amperes (mva) has been developed for outdoor service on the lines of a large metropolitan utility. Designed as individual roll-out circuit breaker poles in dust-tight, phase-isolated, outdoor metal enclosures with current transformers on the roof entrance bushings, the circuit breaker has its isolators enclosed within the air blast columns for more reliable operation under icing conditions for future application of the circuit breaker as outdoor porcelain-clad units. Recovery voltage control resistors are used to insure satisfactory performance of the circuit breaker at any circuit recovery rate which may arise on any system in this country.

THERE are several outdoor installations in this country of porcelain-clad air blast circuit breakers with ratings as high as 138 kv 3,500 mva. A description of the design and performance on field tests of such a circuit breaker was presented to the AIEE in 1945,[1,2] and the circuit breaker itself has continued to perform satisfactorily in service. Description and field tests of an earlier 138-kv 1,500-mva circuit breaker were presented in 1942,[3,4] and there are installations in this country of outdoor air-blast circuit breakers at lower voltages; both 69 kv 1,500 mva and 34.5 kv 1,000 mva are in operation on the lines of a metropolitan utility. All of these circuit breakers have porcelain-clad interrupter elements plus associated interlocked isolating switches.

Although selection of air-blast circuit breakers for these installations was based to a great extent on the elimination of the hazard of oil fires, the elimination of the large tanks of oil in an interrupter design usually results in a design permitting simpler and faster inspection of the interrupter elements. Furthermore, the use of an air interrupter eliminates oil maintenance and handling facilities, and permits longer intervals between maintenance outages.

As experience with outdoor installations of air-blast circuit breakers has confirmed the confidence placed in their reliability, the elimination of oil and low outage time for inspection makes them very attractive for many locations. They were therefore selected for installation at a generating station of a large metropolitan system where studies of the economical transmission and distribution of the power concentration had shown the need for circuit breakers rated 69 kv 2,000 amperes and capable of interrupting 3,500 mva under fault conditions. Since the initial installation of the new 69-kv circuit breaker is to form part of an outdoor, metal-enclosed switchgear equipment, it was desired that the circuit breaker be supplied with an outdoor, metal enclosure.

Major Design Features of New Circuit Breaker

In order to establish specifications for the new 69-kv air-blast circuit breaker, existing designs of outdoor, porcelain-clad 34.5-kv, 69-, and 138-kv air circuit breakers in this country and of high-voltage air circuit breakers abroad were reviewed, together with designs of 15-kv air-blast circuit breakers in metal-enclosed equipments. From these studies, the design features of the new circuit breaker were determined as follows:

1. The new air-blast circuit breaker should be designed to meet the AIEE and American Standards Association standards for the performance of a 69-kv 2,000-ampere 3,500-mva 5-cycle circuit breaker. Since, as is well known, the interrupting performance of an air-blast interrupter depends on both the voltage recovery rate and short circuit current, it would be desirable to design the new circuit breaker in such a manner that it would be capable of handling any circuit recovery rate which may be encountered and thereby permit application of the circuit breaker on a fault current basis only. It was therefore decided to determine the maximum voltage recovery rate which may be encountered in this country on an application requiring a 69-kv 3,500 mva circuit breaker and to design the circuit breaker to handle this recovery rate at its full interrupting rating.

2. In the initial installation proposed for the new circuit breaker, it was desired that the circuit breaker be designed as a unit of an outdoor, metal-enclosed switchgear equipment of dust-tight, phase-isolated construction. Although a metal-enclosed design may be desirable at other future metropolitan locations, 69-kv circuit breakers have been more commonly applied as porcelain-clad outdoor units. For general application, it therefore appeared important to consider all circuit breaker unit design features from both outdoor and enclosed service conditions. Although the initial installation would be metal-enclosed, future extension of the design to a porcelain-clad unit without a metal enclosure should be planned.

3. For outdoor service, an air-blast circuit breaker would have more reliable operation under icing conditions if the open-type isolating switch commonly associated with existing styles of outdoor air-blast circuit breakers was changed to an enclosed isolator. It was therefore decided to house the isolator within the air-blast column for the resistor current interrupter and to make the isolator a functional part of that interrupter.

4. Electrical clearances around 69-kv circuit breaker provide sufficient space within a metal enclosure for the performance of both inspection and maintenance without moving the circuit breaker out of the enclosure; it would, however, be advantageous to be able to readily remove a circuit breaker pole for interchange with a spare element or for maintenance at a more convenient point. Furthermore, the metal-enclosed, phase-isolated equipment at the first installation point of the new circuit

Paper 51-27, recommended by the AIEE Switchgear Committee and approved by the AIEE Technical Program Committee for presentation at the AIEE Winter General Meeting, New York, N. Y., January 22-26, 1951. Manuscript submitted October 25, 1950; made available for printing November 21, 1950.

R. B. SHORES and J. W. BEATTY both are with the General Electric Company, Philadelphia, Pa.

This development has profited materially by the continuing interest in oilless circuit breakers of A. M. de Bellis, of the Consolidated Edison Company of New York, who has, for many years, steadily furthered the progress of isolated-phase metal-enclosed equipments. The many new design features of the circuit breaker and its enclosure presented frequent problems, which have been solved largely by our associate H. N. Schneider.

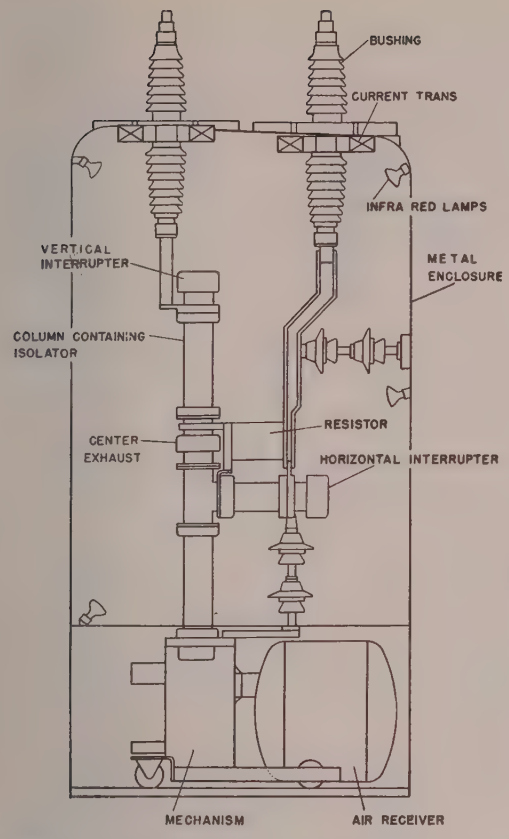

Figure 1 (above). Sectional view of 69-kv 2,000-ampere 3,500-mva air-blast circuit breaker in outdoor, dust-tight, metal enclosure

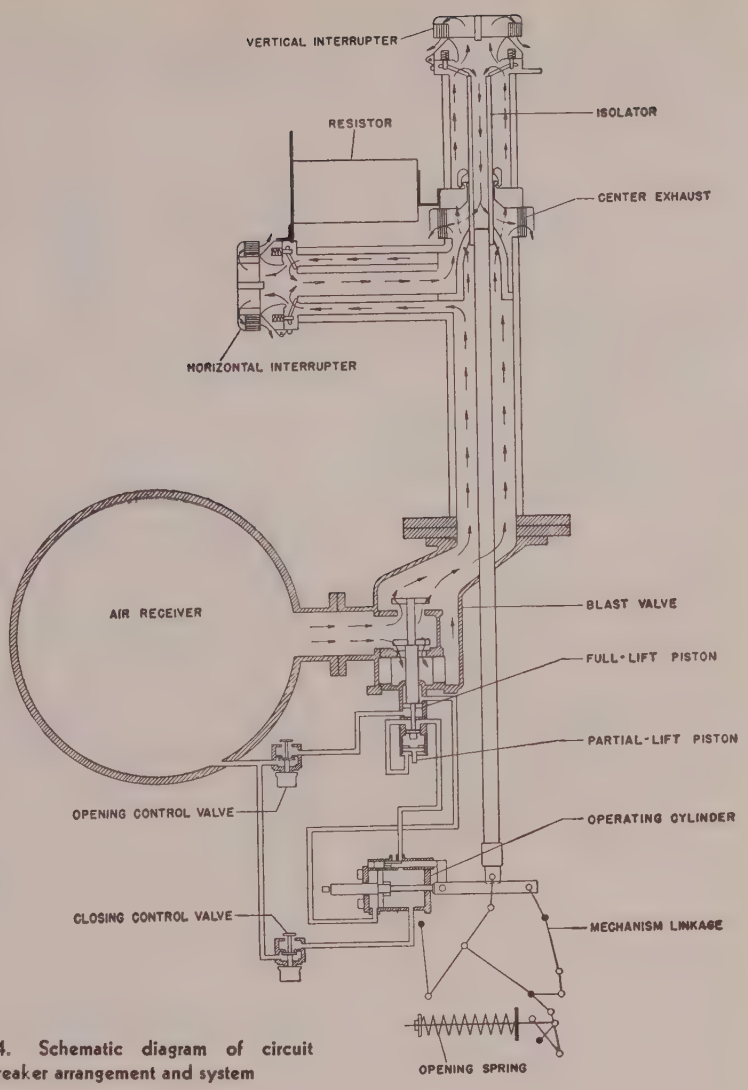

Figure 4. Schematic diagram of circuit breaker arrangement and system

breaker provides a complete metallic housing for each phase conductor with an air space between individual phase housings. It would be desirable to provide similar complete phase isolation throughout the circuit breaker unit. It was decided that the basic circuit breaker design would consist of three single-pole roll-out type units with each pole in an individual dust-tight, steel enclosure. Each circuit breaker pole and its enclosure was to be arranged to permit normal inspection and maintenance being readily accomplished inside the enclosure without removing any weathertight metal covers.

Figure 2. Scale model of isolated-phase, outdoor metal enclosures

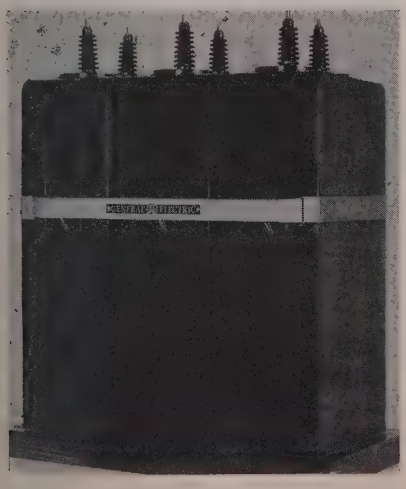

Figure 3. Single-pole roll-out unit of 69-kv 2000-ampere 3,500-mva air-blast circuit breaker in front of its outdoor, dust-tight, metal enclosure

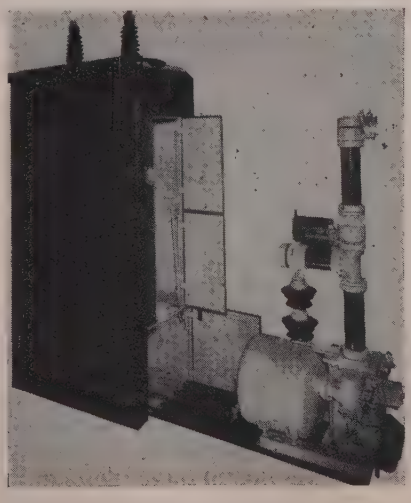

General Arrangement

Sectional view, Figure 1, and scale model, Figure 2, show the equipment arrangement and design appearance which were developed to meet the specifications for the new 69-kv air-blast circuit breaker. Three similar outdoor metal enclosures are used to provide a dust-tight, phase-isolated equipment.

Figure 3 shows a single-pole roll-out circuit breaker unit in front of its enclosure. The lower Herkolite blast tube and porcelain insulator stack support the interrupter and isolator elements of the breaker; this load is imposed directly on the main mechanism frame and not on the air receiver. The design for an outdoor

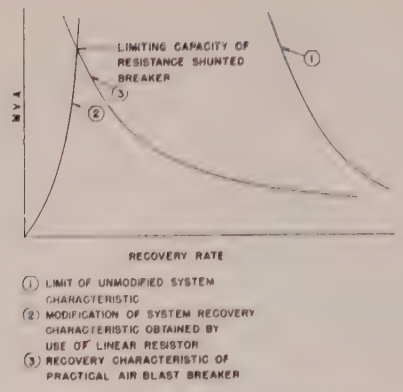
LIMITING CAPACITY OF RESISTANCE SHUNTED BREAKER
MVA
RECOVERY RATE
① LIMIT OF UNMODIFIED SYSTEM CHARACTERISTIC
② MODIFICATION OF SYSTEM RECOVERY CHARACTERISTIC OBTAINED BY USE OF LINEAR RESISTOR
③ RECOVERY CHARACTERISTIC OF PRACTICAL AIR BLAST BREAKER

Figure 5. Relationship between the performance of a practical interrupter without a shunting resistor and a possible 69-kv system requirement

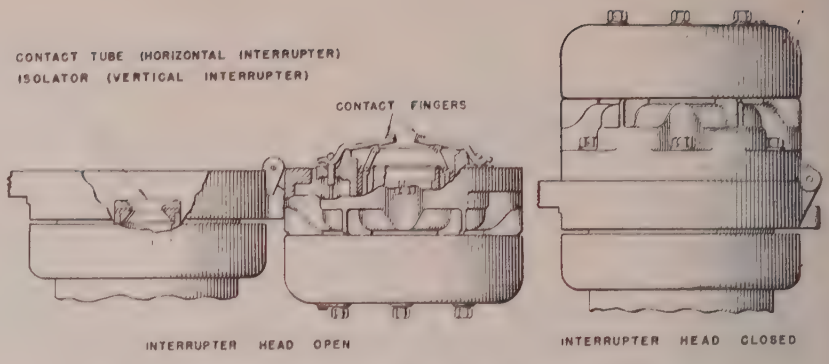

Figure 7. Interrupter unit. Hinge permits ready inspection of all contacts

installation of this circuit breaker without the metal enclosures will consist of the addition of porcelain around the vertical and horizontal insulating blast tubes, plus a metal housing for the mechanism.

The schematic diagram, Figure 4, indicates the arrangement of the interrupters, resistor, and isolator as well as the pneumatic system of the mechanism.

The Interrupters and Resistor

By reference to a report[5] of recovery rates existing at various points of several utility systems and by an analysis of system connections conceived possible in large metropolitan areas within the next ten years, a recovery rate of 6,000 volts per microsecond was determined as the maximum natural recovery rate which would be encountered at 3,500 mva duty.

There are many combinations of interrupter orifice diameters and pressure ranges in combination with single- or double-exhaust which will produce any particular rating of air-blast circuit breaker; the proper combination depends largely on the economics of construction, space limitations, and desirable pressure ranges. Fortunately, the performance of radial-flow interrupters can be predetermined mathematically; these calculations revealed that the air pressure, tank size and orifice diameter to handle 3,500 mva at a recovery rate of 6,000 volts per microsecond was impractical without the use of a shunting resistor of low ohmic value to control the recovery rate which would be imposed on the fault current interruption contacts. Figure 5 illustrates the relationship between the performance ability of an economical interrupter with a shunting resistor and the possible 69-kv system requirements. A double-interrupter style of circuit breaker was therefore developed to insure freedom in circuit-breaker application. One interrupter is used to insert a resistor limiting the recovery rate on the fault interruption contacts to a predetermined value regardless of the fault magnitude, but not exceeding the circuit breaker megavolt-ampere rating of course; a second interrupter is used to break the resistor current prior to opening of the isolator. Following interruption of the resistor current, the isolator is opened while the fingers of both interrupters are held open by air pressure.

Radial flow interrupter designs are simple and can be greatly increased in current handling ability by utilizing a double-exhaust instead of single exhaust if other factors remain the same. The arrangement of Figure 4 using radial flow double-exhaust units in a simple configuration allowing the use of two interrupters in series was therefore evolved. The interrupter heads are similar and utilize a common center exhaust port in addition to their own exhaust ports. The horizontal interrupter is shunted by a resistor and its contact fingers bear on the end of the fixed contact tube. The fingers of the vertical interrupter bear on the upper end of the isolator tube which is operated by the mechanism linkage. The contact fingers of the interrupters, arranged in a circular pattern as shown by Figure 6, are normally biased to bear on the ends of the tubes; when forced open by air pressure the fingers form one exhaust passage and each tube another. In each interrupter, the fingers are linked to a ring which, while allowing individual wipe on each finger, insures that all contact fingers operate together. The contact finger tips and contact tubes are faced with arc-resistant material. Arc transfer from the face of the finger tips to an arcing electrode at the top of the interrupter is so rapid when the contact fingers are opened by air pressure that only the one set of main current carrying fingers is required; this transfer actually takes place in a fraction of a cycle and, as proved by hundreds of fault interruption tests on a single set of fingers, burning is negligible. The interrupter is designed to separate the contact line between fingers and tubes, and is readily swung open for contact inspection as shown by Figure 7.

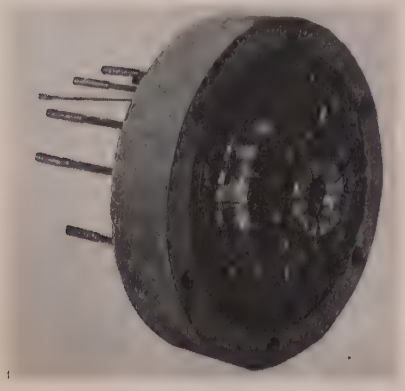

Figure 6. Contact finger assembly of interrupter unit

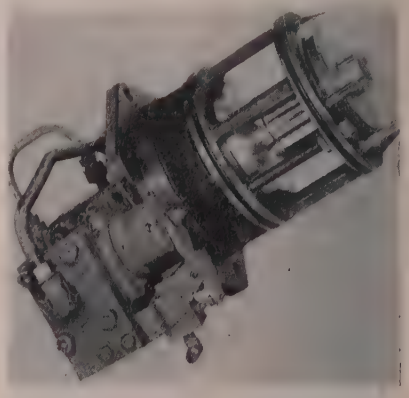

Figure 8. Assembled air-blast valve, pneumatic operator, and control valve ready for insertion into its housing. Seats for air-blast valve piston form part of removable assembly

Suitable coolers in the exhaust ports of each interrupter and of the center tee-casting prevent flame emission and reduce noise with a minimum increase in back pressure. Inspection of the wiping finger contacts on the isolator need only be performed at considerably longer intervals than inspection of the interrupter contacts; these wiping finger contacts, however, can be inspected by simple unbolting of their retainer housing without the use of special tools.

The Mechanism

As shown by Figure 4, the main operating mechanism for the isolator consists of a pneumatic operator, set of opening springs, and a straight line linkage of the type used for many years to operate lift rods of oil circuit breakers. In the fully raised position of the isolator, the linkage goes into an over-center position to hold the isolator closed. The air cylinder and piston is primarily designed for raising the isolator; on an opening operation, the piston is only required to pull the linkage from its over-center position as the opening springs provide the major effort. Hydraulic dashpots slow the movement of the isolator and mechanism linkage in the latter portion of their travel in both closing and opening directions to reduce the shock of operation.

The blast valve housing is located in front of the air tank and at the base of the Herkolite air blast tube. The design is unique in that it permits removal of the blast valve piston and piston seats together with the valve operating cylinders and opening control valve as one assembled package as shown by Figure 8. This blast valve assembly includes a main actuating cylinder to give complete opening of the blast valve on an opening operation of the circuit breaker, plus a partial lift operator for partial opening of the blast valve on a closing operation of the circuit breaker. The blast valve itself is a double-piston type; a slight difference in area between the two pistons provides a small unbalanced seating force holding the valve normally closed.

The air receiver volume is based on maintaining the air pressure for the interrupters at a sufficiently high level to insure satisfactory performance at 3,500-mva interruption on the second opening operation of a close-open 15-second close-open duty cycle without supplying additional air over the initial 250-pound-per-square-inch charge.

Metal Enclosure

The metal enclosure shown in Figure 9 is of steel and provides a completely phase isolated, dust-tight, weathertight housing for each pole of the roll-out type circuit breaker. Separate doors are provided for the primary circuit and mechanism compartments which are separated by a metal barrier to provide maximum safety to personnel. All doors are sealed against dust and rain by means of rubber gaskets and the ventilating louvres are backed by dust filters. Current transformers are located around the porcelain roof entrance bushings and are completely steel enclosed. Lights are provided in each compartment for illumination and in addition convenience outlets are located in the mechanism compartment. Secondary wiring connections between each roll-out circuit breaker and its enclosure side are made through plug-type disconnecting devices. A circuit-breaker position semaphore is provided for each pole and is shaped to be visible from the front or side. A control panel is located in the right-hand unit only. The air pressure gauge and a large veeder counter are located directly behind a section of thermopane glass inset in one of the mechanism compartment doors.

The use of air circulation and strip heaters is the usual approach to the problem of preventing condensation of moisture on the mechanism and insulation of electric equipment installed in otherwise unheated areas, whether within steel enclosures or masonry buildings. However, infrared lamps have been utilized in the metal enclosures for the new circuit breaker to warm organic insulations of the interrupter air columns to a temperature slightly above the air in contact with

Figure 9. Single pole of outdoor, dust-tight, metal enclosure with marquee removed for shipment

Table I. Typical Single-Phase Interrupting Tests

Test No.	Tank Pressure, Psig	Kv Rms Recov.	Kiloamperes, Rms	Equiv. 3-Phase Mva	Inter. Time† Main Current	Inter. Time† Resd. Current	Film No.
276	200	60	0.04		2.5	3.0	88384
279	200	60	0.06		3.2	3.2	88387
282	200	60	0.13		2.9	2.9	88390
285	200	60	0.19		3.5	3.5	88393
288	200	60	0.52		3.3	3.3	88396
291	200	60	1.06		2.7	2.7	88399
294	200	60	2.09		2.7	2.7	88402
35	200	60	3.44		2.2	2.4	87564
38	200	60	6.22		2.6	2.9	87567
42	200	60	9.14		2.6	2.9	87571
45	200	60	11.0		2.6	2.85	87574*
49	200	53	13.3		2.4	2.7	87578
371	250	65	21.2		2.3	3.0	91303*
374	200	64	22.1		2.55	2.9	91306
4	200	45	3.0		2.05	2.4	87531
7	200	45	6.1		2.4	2.8	87534
10	200	45	9.4		2.4	2.75	87537
14	200	45	12.0		2.1	2.35	87541
17	200	45	15.5		2.2	2.5	87544
22	250	45	30.5	3,650	2.2	2.4	87549
23	200	45	25.8	3,100	2.1	2.4	87550
207	250	45	18.0	2,160	2.2	2.5	88031
209	200	40	17.6	2,110	2.2	2.5	88033*
361	250	40	29.3	3,520	1.9	2.15	91293
362	225	40	31.4	3,740	1.85	2.1	91294
366	200	40	32.4	3,880	2.2	2.4	91298*

†50 cycle per second. *Oscillograms included in this paper.

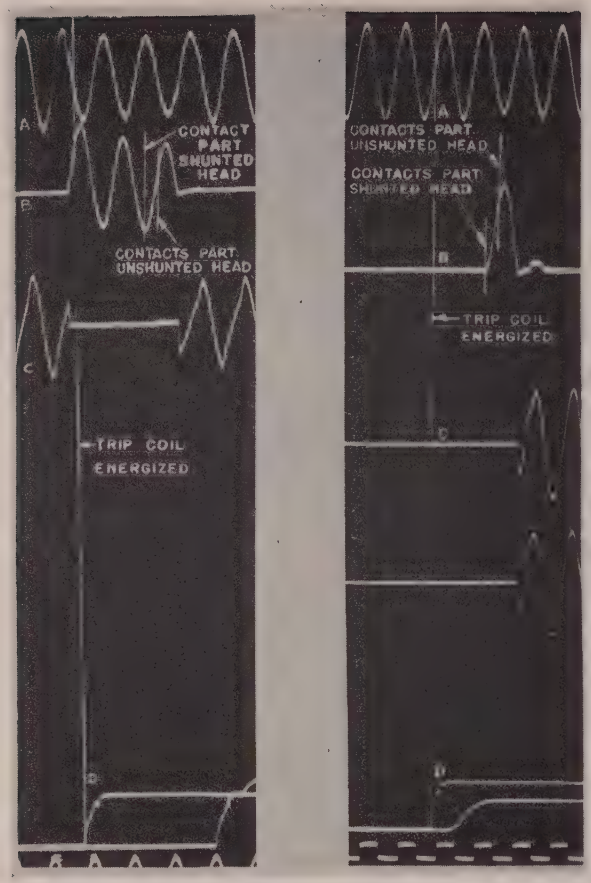

Figure 10. Magnetic oscillograms showing single-phase current interruption of 11.0 and 21.2 kiloamperes at 60-kv and 65-kv respectively in 2.85 and 3.0 cycles. Refer to Table I

Traces A—Line voltage
B—Short-circuit current
C—Recovery voltage
D—Trip-coil current

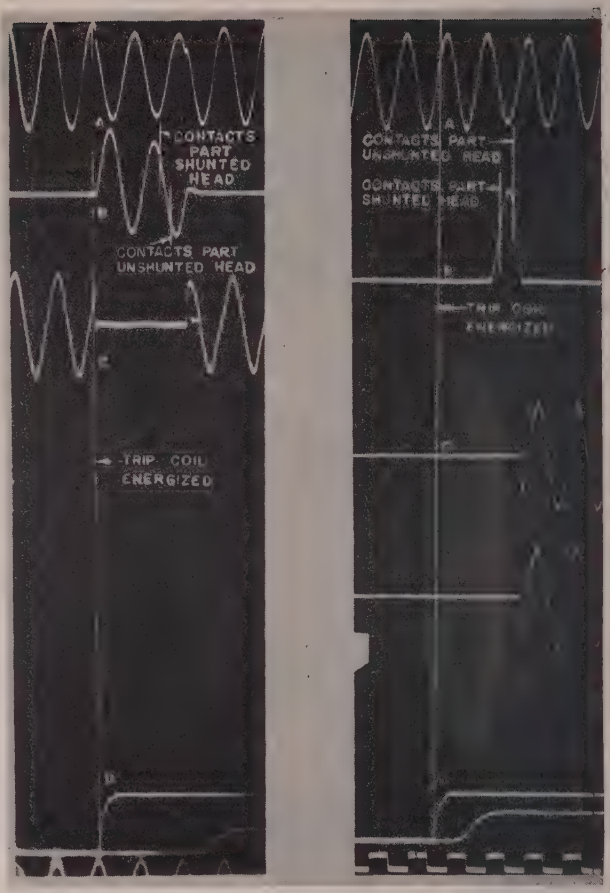

Figure 11. Magnetic oscillograms showing single-phase current interruption of 17.6 and 32.4 kiloamperes at 40 kv in 2.5 and 2.4 cycle respectively. Refer to Table I

Traces A—Line voltage
B—Short-circuit current
C—Recovery voltage
D—Trip-coil current

them; these infrared lamps are used at half-voltage to give almost unlimited life yet provide sufficient warmth exactly where desired to prevent condensation.

Operation of Circuit Breaker

Figure 4 is a schematic diagram of a single pole of a 3-phase circuit breaker; the isolator and interrupter contacts are shown in the closed position and the blast valve in the open position after the initiation of an opening operation. If the air pressure in the receiver is above the minimum operating pressure as determined by a pressure switch, the opening control valve can be energized, which admits compressed air into the main actuating cylinder for the blast valve, causing it to open to its full blast position as shown. Compressed air from the air receiver is thereby admitted into the lower end of the vertical Herkolite tube housing the isolator operating rod. This high pressure air is diverted by the restriction through the center tee-casting into the horizontal interrupter unit.

As a result of the pressure build-up in the horizontal interrupter, the contact fingers are lifted from the contact tube and this circuit interrupted; residual current of course continues to flow through the resistor and vertical interrupter head. The contact fingers of the vertical interrupter head open after the opening of the horizontal contacts as a result of the throttling action of the flow restriction through the center tee-casting. Interruption of the resistor current by the vertical interrupter head occurs after interruption of the main fault current by the horizontal interrupter. Interruption of the resistor current is followed by retraction of the isolator prior to closing of the blast valve and return to normal position of the contact fingers.

Complete lift of the main actuating piston of the blast valve uncovers a port in the actuating cylinder from which air is bled for subsequent admission into the "opening" end of the main operating cylinder for the isolator. Thus, movement of the isolator cannot be initiated until after the blast valve has been completely opened; this sequential arrangement avoids the use of an additional pneumatic interlock since the original operation could not have been initiated unless the air receiver pressure were sufficiently high. Retraction of the isolator results in de-energizing the opening control valve, which allows this valve to close; this shuts off the high-pressure air supply to the main actuating cylinder of the blast valve and exhausts the air from the actuating cylinder allowing the blast valve to close.

The closing control valve can be energized if the air pressure in the receiver

is above the minimum tank pressure required for satisfactory performance of the circuit breaker on an opening operation immediately following the closing operation; this condition is determined by a pressure switch with its contact in the closing control valve coil circuit. Opening of the closing control valve admits air into the main operating cylinder for the isolating disconnect. After a predetermined movement of the main operating piston, a direct-connected slide valve uncovers a port to provide air for partial lift of the blast valve, in order to minimize prestrike. At the end of movement of the main operating piston actuating the isolator, the slide valve cuts off the air supply for the partial opening blast valve operator, dumps this air, and thereby allows the blast valve to reclose. Since even partial opening of the blast valve lifts the contact fingers, actual closing of the circuit is performed by the closing of the contact fingers on the ends of the contact tubes after the air blast is shut-off. An auxiliary switch on the isolator operator permits an opening operation to be initiated during the closing movement of the isolator slightly before it has reached its maximum raised position. The air-blast valve simply opens completely since the diameter of the main actuating piston for the blast valve is larger than the diameter of the retarding piston for holding the blast valve at a partially open position. The circuit breaker is therefore pneumatically trip free.

Electrical interlocking insures that failure of any circuit breaker pole to close with the other two poles would result in an immediate trip-out of the poles which did close; this trip impulse is given to the closed poles prior to closing of their contact fingers on the ends of their contact tubes.

The three opening control valve coils are series-connected, as are the three closing control valve coils. No valves are used in the air connections between air receivers of the three poles to insure their functioning as a single unit; this of course permits the use of a single-pressure gauge and single-pressure interlock.

Test Results

Table I is a set of typical interruption tests for the new 69-kv circuit breaker. These tests range from 40 amperes at 60 kv through 32,400 amperes at 40 kv. All tests shown are on a single-pole basis with full voltage across the interrupters and were made on a complete interrupter column. Tests made at 200 pounds per square inch were checks on the interruption ability under air receiver pressure conditions corresponding to the second close-open operation of a duty cycle with the air receiver not being recharged from the station air system. Typical oscillograms for these tests are shown in Figures 10 and 11.

A complete sample pole of the circuit breaker and enclosures have satisfactorily passed the required impulse and 60-cycle high-potential tests, as well as a temperature rise test. A life test also has been successfully completed.

Conclusions

This new 69-kv air-blast air circuit breaker incorporates many new design features which should improve its ease of inspection and maintenance, and decrease its outage time. Its performance on test has indicated that the design can be extended to 5,000 mva when such an increase is required. The enclosed isolator is a feature which should result in ready acceptance of the circuit breaker as an outdoor porcelain-clad unit. The unit pole construction allows the use of individual steel enclosures for complete phase isolation and permits interchange with a spare element.

References

1. A 3-CYCLE 3500-MVA AIR-BLAST CIRCUIT BREAKER FOR 138,000-VOLT SERVICE, **H. L. Byrd, B. S. Beall III.** *Electrical Engineering* (*AIEE Transactions*), volume 64, May 1945, pages 229–32.

2. FIELD TESTS AND PERFORMANCE OF HEAVY-DUTY HIGH-SPEED 138-KV CIRCUIT BREAKERS—OIL AND AIR-BLAST, **Philip Sporn, Harry P. St. Clair.** *AIEE Transactions*, volume 64, 1945, pages 401–10.

3. A CONSERVED-PRESSURE AIR-BLAST CIRCUIT BREAKER FOR HIGH-VOLTAGE SERVICE, **W. R. Rankin, R. M. Bennett.** *Electrical Engineering* (*AIEE Transactions*), volume 60, May, 1941, pages 193–96.

4. FIELD TESTS AND PERFORMANCE OF A HIGH-SPEED 138-KV AIR-BLAST CIRCUIT BREAKER, **Philip Sporn, H. E. Strang.** *Electrical Engineering* (*AIEE Transactions*), volume 61, January 1942, pages 1–6.

5. TRANSIENT RECOVERY-VOLTAGE CHARACTERISTICS OF ELECTRIC-POWER SYSTEMS, **H. P. St. Clair, J. A. Adams.** *Electrical Engineering* (*AIEE Transactions*), volume 61, September 1942, pages 666–69.

Discussion

A. M. de Bellis (Consolidated Edison Company of New York, Inc., New York, N. Y.): I want to congratulate Messrs. Shores and Beatty for their excellent paper on this new 69-kv air blast circuit breaker.

At the same time, if I may, I would like to congratulate the several General Electric engineers who, to my knowledge, have worked in the development and testing of this circuit breaker. Three years ago, when we first began planning our East River generating station extension, we concluded that a new line of 69-kv outdoor metal-clad equipment would have to be developed if we were to meet certain requirements of service reliability, space limitations, and over-all station costs. It was also our desire to avoid the use of oil filled switching equipment.

The problem of developing a metal-clad 69-kv air blast circuit breaker was taken up with the circuit breaker designers and we were pleased to find them receptive to the idea.

This paper describes the results of one such development.

Our requirements of phase isolation and co-ordination with other station equipment have been met very satisfactorily. The designers also have introduced a number of design features which should prove attractive from the standpoint of maintenance and operation. Although operating experience alone will provide the final test on the adequacy of this new design, we are fully confident that its performance will be as expected. Naturally, our confidence in this new design is due, in no small measure, to the fact that the new interrupter has been amply tested in a high-power laboratory.

Reference is made in the paper to outdoor porcelain-clad air blast circuit breakers at present installed in this country. We were under the impression that these circuit breakers are few in number, and that in the higher voltages their performance has not been in general, shall we say, satisfactory. Two or three years ago, the circuit breaker designers were not prepared to develop a porcelain-clad outdoor circuit breaker of the 3,500 megavolt-ampere 69-kv class.

The paper seems to indicate that this new design can be offered as an outdoor porcelain-clad unit. It would be of interest to know how some of the design limitations which have caused failures in previous porcelain clad designs have been overcome.

The authors, in giving their reasons for the use of a shunting resistor, may leave the reader with the impression that the use of such a resistor was dictated by economical reasons when dealing with recovery voltages of the order of 6,000 volts per micro-second and short circuit currents of the order of 30,000 amperes.

There are at present in service air blast circuit breakers in the 15-kv class where shunting resistors are not deemed necessary, and yet the values of recovery voltage and short circuit current are considerably higher than those given for the 69-kv circuit breaker. We are not questioning the wisdom of using shunting resistors, but it seems that some additional explanation would be helpful. It would also be helpful if the authors were to specify the voltage values which apply to the tests given at the bottom of Table I.

The data given in Table I and in the text indicate that the tests on the single-pole circuit breaker were made at 40 kv. We generally think of the first pole to open in a circuit breaker interrupting 87 per cent of its phase-to-phase voltage, which for a 69-kv system would be 60 kv for a 3-phase ungrounded fault. It may be questioned, therefore, whether the 40-kv tests are indicative of what the circuit breaker will interrupt under 3-phase ungrounded fault conditions.

P. L. Taylor (Allis-Chalmers Manufacturing Company, Boston, Mass.): The authors are to be especially complimented for having achieved a very ingenious integration of components employing the more sound of the available principles.

The questions of fibrous insulating tubes under moisture conditions, and of the enclosed disconnecting device have already been discussed, leaving one principal question, upon which I want to place particular stress.

I am concerned with the method employed to close in against fault currents. As the method is described by the authors, the insulating switch is closed under partial air blast conditions, and a faulted circuit would be subsequently closed against by the return of the stationary finger contacts as they drift back on decaying air pressure. In our experience this would result in extreme contact burning at making currents of the order of 53,000 amperes, for which this circuit breaker is rated.

The test data given in Table I of the paper do not identify any "close-open" interrupting operations, but no doubt such tests have been made. Perhaps there is incorporated in the contact finger assembly design, some arrangement for producing a "snap" closing action of the fingers to reduce the prestruck arc time, thus reducing the contact deterioration.

If it would not be too time-consuming, I believe it would be of general interest for the authors to explain briefly the operation of the mechanical linkage shown in Figure 4 of the paper, which is described only as "of the type used . . . to operate . . . oil circuit breakers."

R. B. Shores and **J. W. Beatty:** The number of outdoor porcelain-clad circuit breakers installed in this country at present are still relatively few as pointed out by Mr. de Bellis. Their interrupting performance to the best of our knowledge has been very satisfactory. Some difficulties have been encountered in some of the designs in obtaining satisfactory mechanical performance, especially in obtaining reliable operation of the air mechanism and its associated auxiliary devices. However, the design of air mechanisms and their associated devices has now improved to the point that they are in common use for outdoor power circuit breakers, air or oil. A particular mechanical problem associated with one of our early outdoor air blast circuit breakers was breakage of a rotating porcelain column operating the isolating disconnect; the problem was eventually solved by reduction of the impact to which the porcelain column was subjected. Insofar as this specific problem is concerned, porcelain is not utilized in the new 69-kv circuit breaker for any part of the linkage operating the isolator. We also understand that failures have occurred in porcelain-clad outdoor air blast circuit breakers as the result of condensation in the space between organic insulation and its enclosing porcelain. Probably the best approach which could be used to solve the problem of a porcelain-clad air blast circuit breaker is the direct substitution of porcelain for organic insulation if the required strength can be designed into the porcelain.

The use of a resistor to control the recovery voltage rate was more economical in the design of the new 69-kv circuit breaker than utilizing additional interrupter units in series or higher air pressure to handle full recovery rate at full current rating. At 15 kv there are in service air blast circuit breakers without resistors on circuits where the values of recovery voltage and short circuit current may be even higher than those given for the 69-kv circuit breaker. There are likewise in service 15-kv circuit breakers on similar circuits which do utilize resistors to control the recovery rate; in general, these latter 15-kv circuit breakers also have arc chutes of very much smaller physical size in contrast to those without resistors. However, 15-kv circuit breakers have been of cross-blast design, which is very suitable for a low voltage and high current interrupter structure but has not proved very practical for high voltage interrupters due to the difficulty of obtaining sufficient insulation strength.

On the other hand, the radial blast design, of which the new 69-kv circuit breaker is an example, very readily provides long creepage paths and a short high-voltage withstand arcing gap. The voltage rating of the circuit breaker was therefore the prime factor in the selection of a radial-blast interrupter design; acceptable air pressure, reasonable air consumption and minimum number of interrupter units were other factors leading to the use of a resistor to control the voltage recovery rate the new circuit breaker might encounter.

The voltage values for the tests at the bottom of Table I were accidentally omitted from the preliminary draft of this table. They have since been added.

Only typical single-phase interrupting tests are included in Table I although tests have actually been satisfactorily carried out from 12-kv through 88 kv at various tank air pressures; tests have also been conducted successfully at voltages up to 120 kv although tank pressures above rating were admittedly used for these excessively high-voltage tests. We therefore have every reason to feel that the new 69-kv air blast circuit breaker will perform satisfactorily under all voltage conditions within its rating.

With reference to the question of adequate protection against moisture for the organic insulations of the new circuit breaker, dry air is bled continuously, but very slowly, into the base of each column from the high air pressure system; this bleed is taken from the station air system ahead of the check valve for the circuit breaker air receiver in order to avoid bleeding down the air receiver if the station air system failed for any reason. This use of dry air over the operating rod and over the inner surfaces of the insulating tubes and of infra-red lamps directed on the outer surfaces, together with the housing ventilation, very effectively prevent condensation of moisture on organic insulation.

In regard to the question of contact burning on circuit closing duty, the wide open exhaust on the downstream side of the contacts results in a very high rate of pressure decay after the blast valve closes. As a result, the contact closing speed and contact opening speed are relatively the same, approximately 12–14 feet per second. Therefore, contact deterioration, even on circuit closing duty at rated making current, is not excessive. Although no tables are included, "close-open" tests have been completely satisfactory.

The mechanism linkage indicated in schematic form only in Figure 4, is a combination of cranks to transform the $4^1/_4$-inch motion of the operating piston into the 24-inch straight line motion of the isolator. Except for its over-center feature, it is the same type of linkage as used in tank-type oil circuit breakers to convert the short stroke of the circuit breaker closing solenoid, cam, piston, or other power source to the considerably longer stroke required for the oil circuit breaker lift rod.

Output Analysis and Alignment Techniques for Phase-Rotation Single Side-Band Transmitters

OLIVER WHITBY
NONMEMBER AIEE

DONALD R. SCHEUCH
NONMEMBER AIEE

IT HAS long been recognized that the carrier radiated by a conventional amplitude-modulated transmitter yields no intelligence at the receiver and so wastes this power. In a single side-band transmitter such waste can be sharply reduced, and, in addition, there is a 2-to-1 saving in the use of the radio spectrum. Finally, single side-band systems seem to lend themselves better to the use of exalted carrier detection than do double side-band transmitters: this is a help in combating fading.

There are two main methods of single side-band generation. The system which has been employed in practice for many years is that using filters and linear amplifiers. As is shown in Figure 1, a balanced modulator operates with a fairly low carrier frequency to provide an output of two side bands with suppressed carrier. By means of a filter one of these side bands is picked out to be used as modulation in a succeeding balanced modulator with a still higher carrier frequency. After the original band of modulation frequencies has been translated high enough in frequency, its power level is increased by means of linear amplifiers.

The second system for generating a single side band at radio frequencies is the one with which this paper is concerned. The method has been known in principle since the mid-twenties,[1] but has only recently come into practical use through the work of a number of men among them Dr. Villard[2] at Stanford University. The second system is chiefly distinguished from the first one described by the fact that in it the single side band is generated at high level in the final stage of the transmitter. This is done in two balanced modulators, a circuit of which is shown in Figure 2. Tubes 1 and 2 form one balanced modulator, while tubes 3 and 4 constitute the other. These two modulators are driven by radio frequency voltages in quadrature with one another. Audio-modulating voltages are applied in push-pull to the grids of the tubes in each modulator, the audio voltages to the modulators also being in quadrature. These quadrature audio voltages are obtained from two wide-band 90-degree phase-difference networks having constant amplitude response from 300 to 20,000 cycles per second and the phase difference correct within 0.3 degree over that band. The plate current pulses of all four tubes develop power in a common plate tank circuit. When the equipment is operated properly only one side band is present in the output. The four Eimac *4-250A*'s used in this circuit were operated so that they drew neither screen nor grid current.

Misalignments and the Outputs to Which They Give Rise

The output of such a transmitter when properly adjusted and subject to modulation of a single tone is itself a sine wave of constant amplitude. If there are any unbalances in the voltages fed to the balanced modulators, if the tube characteristics differ from one another, or if these characteristics are nonlinear with audio level, the output will be other than a single sinusoid. In a detected or rectified version of the transmitter output there will appear a frequency equal to that of the modulating tone if either or both of the modulators are operating in an unbalanced fashion. The output will then contain carrier as well as the wanted side band. The size of the detected component in-phase with the modulating tone indicates the degree of unbalance of the modulator fed with in-phase audio signal. That of the quadrature component is a measure of the unbalance of the other modulator. This unbalance can come about in two main ways in the system under consideration. The first is by virtue of an unbalance in the audio-modulating voltage, while the second is through unequal transconductances in the two tubes, here controlled by their screen potentials. An inequality between the output of the two balanced modulators results in the appearance of unwanted side band. The inequality can arise in any of four ways: (1) unequal radio frequency drive, (2) unequal audio modulating voltages, (3) inequality of

Paper 51-28, recommended by the AIEE Instruments and Measurements Committee and approved by the AIEE Technical Program Committee for presentation at the AIEE Winter General Meeting, New York, N. Y., January 22–26, 1951. Manuscript submitted June 28, 1950; made available for printing November 21, 1950.

OLIVER WHITBY and DONALD R. SCHEUCH both are with Stanford Research Institute, Stanford, Calif.

This paper is based on work done at the Stanford Research Institute on Signal Corps Contract Number *W36-039sc-38199*.

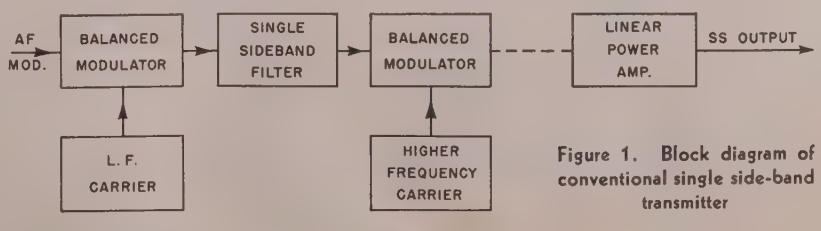

Figure 1. Block diagram of conventional single side-band transmitter

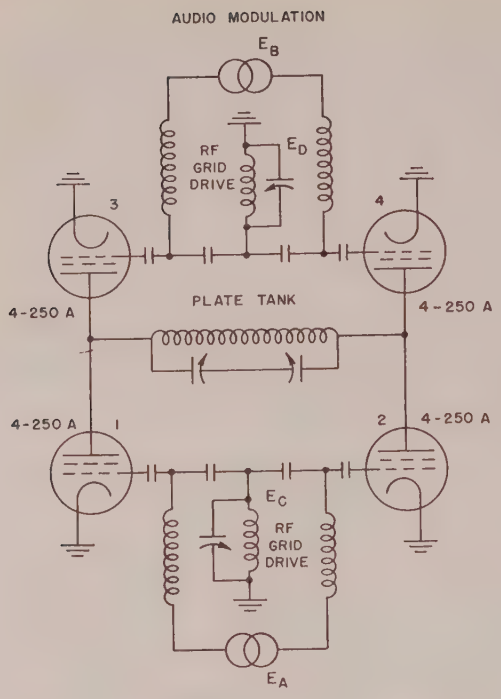

Figure 2 (above). Simplified diagram of high level single side-band balanced modulator

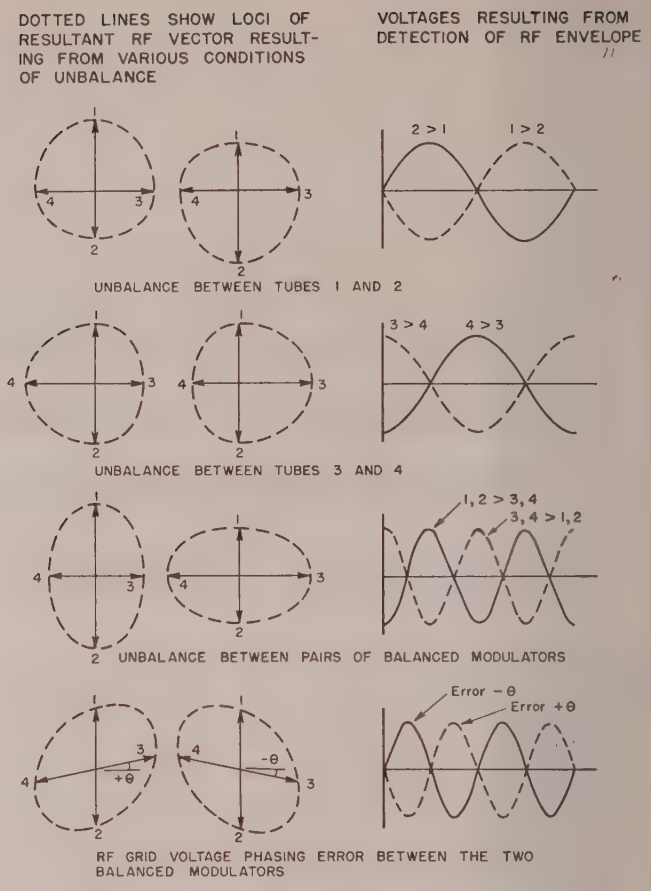
DOTTED LINES SHOW LOCI OF RESULTANT RF VECTOR RESULTING FROM VARIOUS CONDITIONS OF UNBALANCE
VOLTAGES RESULTING FROM DETECTION OF RF ENVELOPE
2 > 1
1 > 2
UNBALANCE BETWEEN TUBES 1 AND 2
3 > 4
4 > 3
UNBALANCE BETWEEN TUBES 3 AND 4
1, 2 > 3, 4
3, 4 > 1, 2
UNBALANCE BETWEEN PAIRS OF BALANCED MODULATORS
Error − θ
Error + θ
+θ
-θ
RF GRID VOLTAGE PHASING ERROR BETWEEN THE TWO BALANCED MODULATORS

Figure 3 (right). Vector diagrams of principal misalignments of balanced modulator

pairs of tube transconductances, and (4) departure from proper (quadrature) phase of the radio frequency drive. The first three misalignments will be noted to give rise in the detected output of the transmitter to a sinusoid of twice the frequency of the modulating tone. Lack of proper radio frequency phase will result in a similar double-frequency sinusoid, but in quadrature with the first. In Figure 3 are shown vector diagrams of the contributions of each tube to the output in each of the cases outlined. It is seen, therefore, that with each of a given set of misalignments there may be associated specific signals in the detected output.

The transmitter is in fact provided with means of unbalancing both modulators in a symmetrical manner so that carrier may be inserted in any amount up to −6 decibels of the power of the wanted side band.

Lack of perfect linearity in the transconductance of the tubes with audio level will cause the appearance of a sinusoidal component in the detected output having a frequency four times that of the modulating tone. This is due to the cyclical operation of the four tubes throughout the audio period.

Method of Aligning the Transmitter

It has been observed that the presence of certain components in the detected output of the transmitter may be associated with certain classes of misalignment in the balanced modulators. As there is not a one-to-one correspondence between each specific misalignment and each type of component in the output, some of the parameters must be left fixed while others are altered during the alignment procedure. If such an arbitrary association is made between certain misalignments and certain output components, a device which will indicate the magnitude and sign of these maladjustments may be constructed.

In discussing the device, let us consider that the incorrectly adjusted transmitter is modulated by a sinusoidal tone

Figure 4. Transmitter alignment indicator

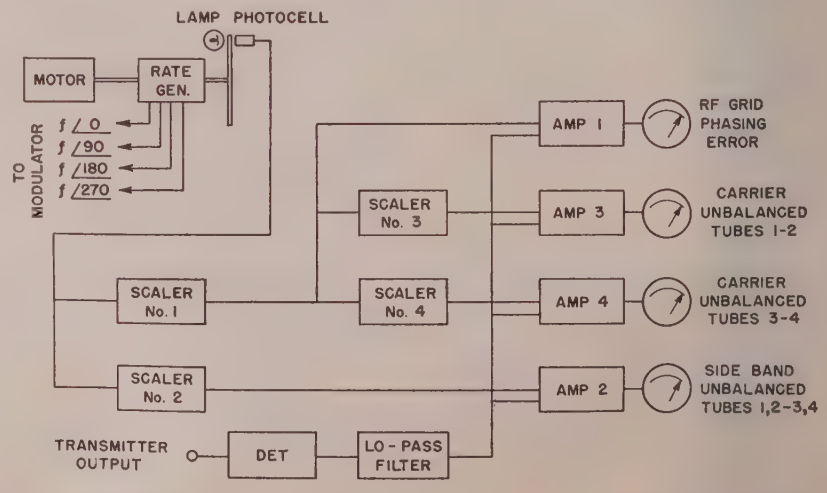

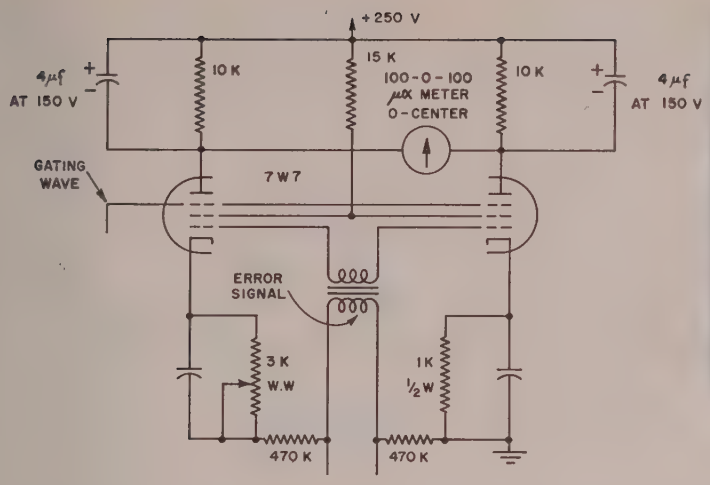

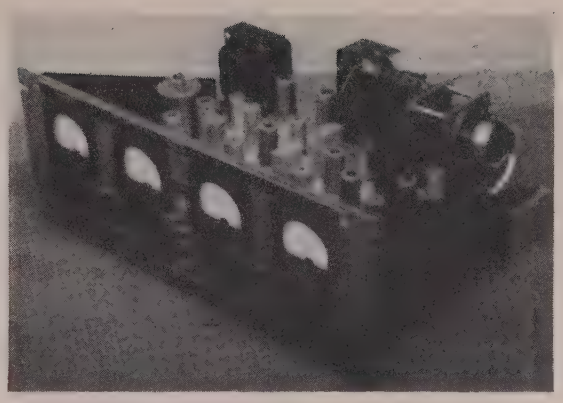

Figure 5 (left). Alignment indicator detector

Figure 6 (above). Alignment indicator

of frequency f. The detected output of the transmitter will then contain signals having frequencies and phases as follows: f, f plus 90 degrees, $2f$, and $2f$ plus 90 degrees.

The alignment indicator is basically a single-frequency test source of four quadrature audio modulating voltages and 4-gated phase sensitive detectors, each one of which is assigned to the exclusive examination of one of the components in the detected output of the transmitter. Figure 4 shows a block diagram of the indicator. A motor-driven 4-phase a-c generator in the alignment indicator provides four equal quadrature audio modulating voltages to the transmitter. On the same motor shaft there is a notched disk which generates square waves by interrupting a beam of light shining on a photocell. The disk is shaped so that the period of this square wave is one quarter of that of the voltage supplied by the 4-phase generator. This $4f$ square wave is amplified and used to trigger two bi-stable multivibrator scalers, one operating on the negative discontinuities, the other on the positive ones of the square wave. These multivibrators thus produce square waves in quadrature with one another which have periods equal to one-half that of the generator voltage. These new $2f$ square waves gate the detectors sensitive to $2f$ and also trigger two more bi-stable multivibrators, which in turn generate two square waves in quadrature, having periods equal to that of the 4-phase generator output. These last-derived square waves are used to gate the detectors sensitive to the f components.

Each of the four phase-sensitive detectors consists of two pentodes (*7W7*) in a balanced circuit, shown in Figure 5. The rectified output of the transmitter, hereafter called the error signal, is applied in push-pull to the control grids of each pair of tubes forming a detector. The suppressor grids of the tubes in each unit are connected in parallel and are fed with square waves from one of the multivibrators. Thus the detectors are gated through their suppressor grids respectively at frequencies of f, f plus 90 degrees, $2f$, and $2f$ plus 90 degrees. The plate of each tube contains a circuit having a time constant long with respect to the period of the modulating signal. With this arrangement each detector looks at the error signal only during the positive portion of its gating wave. The action is such that, if a sinusoidal signal is being examined by a phase-sensitive detector, the gating square wave of which is exactly in phase with the sine wave, the plate currents in the two tubes will change by equal amounts but in opposite directions. The effects of this change may easily be shown on a zero center meter. If, however, the gating square wave is in quadrature with the applied sine wave then during the on-portion of the gating cycle the average value of the plate current experiences no change. This principle also permits the two detectors which are gated at the frequency f to be insensitive to all signals of twice this frequency, for during any period equal to twice that of the $2f$ wave the average value of the $2f$ sinusoid is zero. Similarly, during a complete period of $1/f$ the detectors gated at $2f$ are insensitive to signals of the frequency of the modulating tone.

Figure 7. Equipment for output spectrum analysis

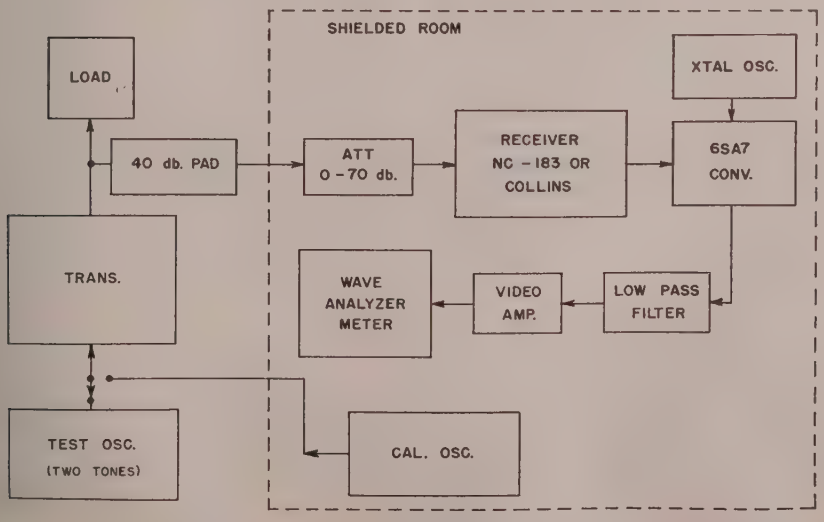

The error signal fed to the alignment indicator is passed through a bridged-tee filter arranged to take out the $4f$ component which arises from the tube nonlinearity in the balanced modulators.

Referring to Figure 2, we note the following procedure which has been found best in aligning a phase-rotation transmitter with the aid of the alignment indicator just described:

1. All screen voltages are set equal.

2. The quadrature audio voltages applied to the grids are all set equal.

3. The tuned coupled circuits supplying radio frequency grid drive are tuned to resonance and are coupled to give equal grid driving voltages to the two balanced modulators.

4. With all radio frequency and direct voltages applied, enough audio modulation is introduced to enable the plate tank circuit to be tuned to resonance.

5. With this modulation removed the screen voltages of the pair of tubes forming one balanced modulator are adjusted so that the radio frequency plate voltage falls to a minimum. The procedure is repeated for the tubes in the second modulator.

6. The alignment indicator is then used to modulate the transmitter

7. The final balance for minimum carrier in the modulator with tubes 1 and 2 is made by adjusting in opposite directions the audio voltages to these tubes. The alignment indicator meter labelled Carrier Unbalance Tube 1–2 is the one which must be zeroed to indicate by the presence of no f-error signal that this modulator is balanced. Note that the balanced condition could have been arrived at by adjustment of the screen potentials except for the fact that they were employed to secure balance with no audio modulation. The preceding method is repeated for the second modulator with the help of the other Carrier Unbalance meter on the indicator.

8. The correct phase relation is brought about between the radio frequency grid drives by changing slightly the tuning of the secondary of the coupled grid circuits. The correct setting is indicated on the appropriate meter of the indicator, at which point it shows the absence of a $2f$ plus 90 degrees component in the error signal

9. The screen voltages of one of the modulators are adjusted together in the same direction so as not to unbalance the modulator until the output of unwanted side band is just enough to completely cancel that from the other modulator. This condition shows as a zero reading on the meter of the alignment indicator marked Side Band Unbalance.

A repetition of the last four numbered steps should then be made to insure best alignment.

Method of Output Analysis

In order to check both the performance of the transmitter under a wide range of operating conditions and the accuracy of the alignment indicator, a method of accurately measuring the output spectrum of the transmitter was devised. Figure 7 shows in block diagram form the arrangement of the apparatus used for this task. Through an attenuator a small amount of the transmitter output was fed to a standard communication receiver in a shielded cage. The normal intermediate frequency signals of this set were fed into a second converter, and, with the aid of a crystal controlled local oscillator, were then translated downward in frequency until they stood within the range of a good audio wave analyzer. The practice adopted was that of tuning across the frequency range occupied by the two side bands and the carrier. As each component of the signal registered on the wave analyzer final tuning was accomplished with it. Accurate identification of the frequency of the component being investigated was made by switching the transmitter modulation tones from those under study to one from an audio oscillator under the control of the operator in the cage. In the case where components of the unwanted side band were being examined the side-band output of the transmitter had to be reversed for easy identification of the frequency component by the method just described. This reversal of side-band output can be arranged simply by reversing the audio modulating voltages in one of the modulators.

Because a measurement of the intermodulation products $2f_1-f_2$, $2f_2-f_1$, $2f_1+f_2$, and $2f_2+f_1$, resulting from the simultaneous application of two tones having frequencies f_1 and f_2, is one of the best ways to gauge the nonlinearity of a system, analyses of the transmitter output were carried out for various operating conditions with modulation tones of 1,000 and 1,700 cycles per second.

The following summary of the results of the analyses of the transmitter output by the apparatus in the shielded cage is given to show that the performance of the alignment indicator is satisfactory.

With a single modulation tone, for the full 500 watts output from the transmitter, and with -20 decibels of carrier, the unwanted side band was down more than 38 decibels and the wanted one varied in level by only 1.5 decibels for all modulating tones from 300 to 20,000 cycles per second.

For the 2-tone test with -20 decibels of carrier, and a total of 200 watts output, the intermodulation products were better than 42 decibels below the level of one of the wanted tones when searched for on the side of wanted side band. On the side of the unwanted side band they were down better than 36 decibels, a figure considered good for single side-band transmitters. Further, these figures varied less than 1 decibel for carrier levels from -30 to -10 decibels.

Similarly, the $2f_1-f_2$ intermodulation product never rose above -35 decibels for audio levels giving from zero to 500 watts of output. Finally, tests were made to see whether or not a general improvement could be obtained over that yielded with the alignment indicator by having the operator of the wave analyzer talk down the operator of the transmitter while he was carrying out his adjustments. It was found possible to achieve an improvement of approximately 10 decibels but at one given level and audio frequency, no marked over-all betterment resulting from talk down procedure.

Conclusions

It is concluded, due to the residual nonlinearities in the tubes and the lack of perfect matching of their characteristics at all levels, that the best alignment obtainable at one frequency and level can not be had at all levels and frequencies when the alignment is carried out with the alignment indicator. This is clearly not the fault of the indicator but rather of the transmitter. The alignment indicator does, however, enable the analysis equipment in the shielded room, usually associated with single side-band transmitters, to be done away with for routine alignments.

Perhaps the most promising future of the alignment indicator, or of devices of this sort, lies in the possibility that it can be adapted to permit automatic alignment of phase-rotation single side-band transmitters.

References

1. Phase Rotation for Single Sideband, **R. V. L. Hartley.** United States Patent Number 1,666,206, 1928.

2. A High Level Single-Sideband Transmitter, **O. G. Villard, Jr.** *Proceedings*, Institute of Radio Engineers (New York, N. Y.), volume 36, November 1948, pages 1419–25.

No Discussion

An Electromechanical Transducer

J. F. ENGELBERGER
NONMEMBER AIEE

H. W. KRETSCH
NONMEMBER AIEE

ANY telemetering system which accomplishes the indication or recording of a physical quantity at a remote point is usually considered to consist of three major components: the measuring and transducing device; the transmission system; and the end device.

The main transmission systems that are being used today can be divided into five general groups: the current, voltage, frequency, position, and pulse time systems. Their names indicate the type of electric signal which is used to transmit information about the magnitude of a physical quantity from the point where it is measured to the remote station where it is converted into an indicating or recording signal. For the sake of completeness, it should be mentioned that transmission also could be in other than electrical forms, such as pneumatic or hydraulic, but these will not be considered here.

The task of the measuring and transducing device is, then, one of changing the measured variable into the particular electric signal selected for the transmission system. Except for the special cases where current or frequency themselves in the proper range are to be measured or where the change-over to current or frequency could be accomplished by electric network only, a transducing device is necessary. This includes not only the obvious cases of measuring displacements or forces but also many electrical quantities which require an intermediate transducing device to express them in terms of the electric signal chosen for transmission.

Mechanical Design

The electromechanical transducer described in this paper changes mechanical and certain electrical quantities into corresponding electric current, mainly for purposes of remote transmission. Operating on the principle of a continuous torque balance, the "Microsen Balance" actually is a small servomechanism which, by virtue of using an external power supply for its operation, also is capable of raising the power level of the input signal. For electrical inputs, therefore, it becomes an electromechanical amplifier whose characteristics have already briefly been described and which will be discussed here in greater detail.[2]

First, with reference to Figure 1, a qualitative description of the transducer shall be presented. The Microsen Balance is a compact torque balance device which was designed to have the sensitivity of a galvanometer while being rugged enough to withstand stringent field conditions.

As shown, the torque measurements are made on a balanced beam structure wherein mechanical torques are applied through a hairspring at the fulcrum of the beam and wherein electric currents produce torque in the coil suspended in the efficient pot type magnet. The beam floats whenever the applied torques completely balance to zero. Input to the electromechanical balance is either mechanical rotation of the hair-spring or direct current running through one of the coils on the end of the beam. In any case, the beam is brought to balance by a current in the feedback coil, this current being proportional to the output electrical signal. Accordingly, whenever the beam is floating, the transducer is putting out an electric signal proportional to the input signal, whether the input be electrical or mechanical.

Paper 51-29, recommended by the AIEE Instruments and Measurements Committee and approved by the Technical Program Committee for presentation at the AIEE Winter General Meeting, New York, N. Y., January 22-26, 1951. Manuscript submitted June 19, 1950; made available for printing November 21, 1950.

J. F. Engelberger and H. W. Kretsch both are with Manning, Maxwell, and Moore, Incorporated, Bridgeport, Conn.

Electronic Circuit

The associated electronic circuitry is relatively simple. Assuming a d-c power supply, the circuit of Figure 1 employs only one tube in a bridge circuit. Bridge unbalance is the output as well as the feedback signal.

The tube is operated as a 40-megacycle tuned plate, tuned-grid oscillator which is self-biasing. Control of the intensity of oscillation is effected by the flag on the end of the electromechanical beam structure. This flag, moving over a total distance of approximately 0.010 inch, has complete control of the oscillator output. When the flag is nearest the pancake type grid coil, the oscillator is out of oscillation; as the flag moves away from the grid coil, oscillation begins and becomes proportionally stronger. The d-c impedance of the tube in the bridge circuit varies with the intensity of oscillation, since the grid leak on the tube supplies negative bias in proportion to the oscillator output.

Thus, what is effectively being done is that the flag is varying a resistor in a bridge circuit over the range of 3,000 to 20,000 ohms with no significant force being required in the accomplishment.

It becomes evident that one possible means of transducing would be merely to have the input motion position a flag with respect to a pancake coil and then consider the bridge output as the transduced signal. The frailty of such a setup lies in the fact that other factors besides the flag motion can affect the output; namely, such things as supply voltage and ambient temperature changes may cause appreciable shifts in the output.

This last point constitutes the main reason for including the feedback link and an electromechanical transducer which continuously measures both input and output signals and arrives at a null balance between them by controlling the output signal. This null detection principle eliminates dependence upon variations in the electronic circuit, the accuracy of transducing being a function merely of the sensitivity of the torque-balance device.

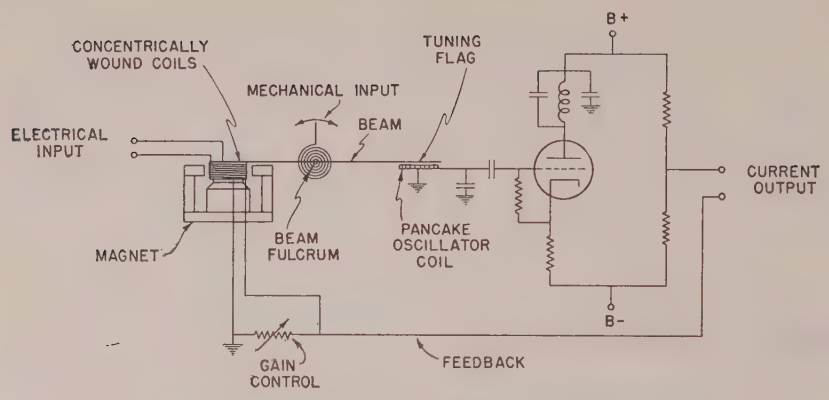

Figure 1. Schematic wiring diagram of transducer

Transducing Applications

Before going into a more rigorous analysis of the characteristics of this transducer with regard to its servo-stability criteria and ultimate accuracy, a brief description of some typical applications will be presented.

In Figure 2 the transducer is shown as a pressure transducer with a Bourdon tube supplying the input signal. Since the torque applied to the beam through the hairspring is proportional to the pressure being measured, when a torque balance is obtained, the output current is proportional to pressure. This scheme is typical wherever the signal being transduced may be translated into rotary motion.

When the transducer has an electrical input, strictly speaking it is not a transducer at all, but a d-c amplifier. Low level direct currents, such as from thermocouples and strain gauge bridges, may be amplified very accurately to a useful telemetering level. Zero drift characteristics of a wholly electronic d-c amplifier are not present since the feedback link goes back to the balance where output and input current are continuously compared in the same magnetic field.

One feature of this electromechanical d-c amplifying principle is that part of the input range may be suppressed by means of the hairspring at the beam fulcrum. For example, if the temperature band of interest for a telemetering channel were from 1,000 to 1,500 degrees Fahrenheit, the first 1,000 degrees Fahrenheit could be suppressed, with the entire output being available for the desired temperature band. Another point, sometimes valuable, is that the input circuit is completely isolated from the rest of the amplifier.

It should be noted, however, that this unit does require current in order to develop a measurable torque; therefore, it is not useful with high impedance input devices such as piezoelectric crystals.

The transducer also can be used as a computer. It is possible to add and subtract both electric and mechanical signals. Because the coil in the magnetic field is wound round, as is a loudspeaker voice coil, it becomes convenient to wind a number of concentric coils on the same form and thereby allow simultaneous additive or subtractive electrical inputs which are isolated from each other. Mechanical inputs at the fulcrum can obviously also be additive or subtractive. With any combination the feedback torque balances out the net resultant torque of all the inputs, and the output is proportional to this resultant.

Accuracy

Now, an attempt shall be made to set up the fundamental relationships governing the over-all accuracy of this transducing means and to present an analysis of the unit's stability criteria and frequency response characteristics. The symbols used in this analysis will be those established in Figure 3 and shown in the section entitled Nomenclature.

In considering the steady-state accuracy of the transducer, the Microsen beam is assumed to be an approximation to a null detector that compares the input with the feedbag torque. Since the beam is not a perfect null detector, the current must be expressed as

$$I_o = K_2(\theta)\theta_o + K_3$$

In this expression $K_2(\theta)\theta_o$ represents the characteristic curve of output current versus beam angle, while the constant term, K_3, represents extraneous shifting influences such as line voltage variations or tube characteristic changes. In Figure 4, an I_o versus θ_o curve is shown. As a typical example of the magnitude which may be taken by the extraneous shifting influences, curves are plotted showing the shift in the characteristic with normal line voltage variations.

It is evident that the approximation to a null detector becomes better as the total θ_t used becomes larger with respect to the total θ_o necessary to swing through the entire output current range. Based on the total input angle the percentage error

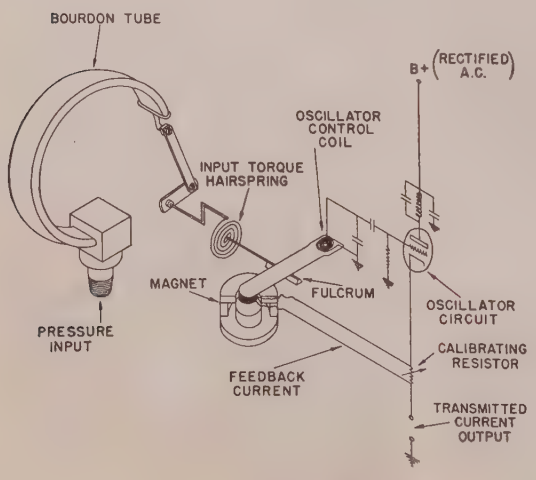

Figure 2 (left). Transducer used as pressure transmitter

Figure 3 (below). Operational schematic

There are three possible torque inputs: (1) direct torque application to beam; (2) direct current producing torque in coils; and (3) angular displacement of hairspring

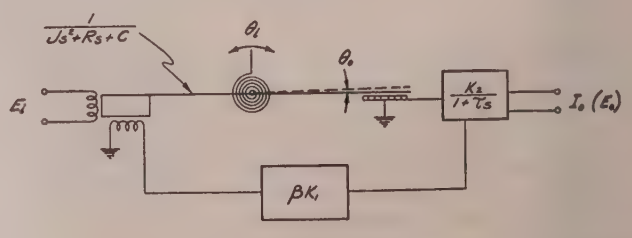

resulting from shifts in the output characteristic may be expressed as

$$\% \text{ error} = 100 \frac{\Delta\theta_o}{\theta_i}$$

where $\Delta\theta_o$ is the change in beam angle required to return output to the same level that existed before the shift occurred. Thus, noting in Figure 4 that the maximum shift resulting from line voltage variation is 0.15 angular degree and assuming a total input angle of 30 degrees, the percentage error would be 0.5 per cent.

Frequency Response

To investigate stability and frequency response, the transfer functions of the system are written as

$$\frac{I_o}{T_i - T_o} = H(s) = \frac{K_2}{(Js^2 + Rs + C)(1+\tau s)}$$

$$\frac{T_o}{I_o} = G(s) = \beta K_1 \qquad (1)$$

It should be noted that in the foregoing transfer functions K_3 has been neglected, since the long time shifts are not significant in analyzing system stability. Further for the sake of simplicity, K_2 is assumed to be a constant. This is essentially true for small deflections.

Because input is torque and output is current, $H(s)$ and $G(s)$ are not dimensionless quantities. To investigate stability, we can write the loop transfer function as

$$H(s)G(s) = \frac{\beta K_1 K_2}{J} \frac{1}{\left(s^2 + \frac{R}{J}s + \frac{C}{J}\right)(1+\tau s)} \qquad (2)$$

Examination of equation 2 shows that without the time constant τ of the electric amplifier, the transducer would always be stable. However, due to this delay, $\beta K_1 K_2 / J$ has to be limited to obtain a safe margin of stability.

As an example, the case of a voltage amplifier will be treated. The input voltage E_i is being introduced into the transducer in the form of current producing torque (case "B", Figure 3). Part of the output voltage is being fed back into another coil in the same magnetic field producing the restoring torque.

Neglecting C, which is the torque of a small zero adjusting spring and the current carrying leads, we can see in Figure 5 $H(s)G(s)$ both with and without the delay of the electronic amplifier. β is adjusted so as to give a voltage gain of 100.

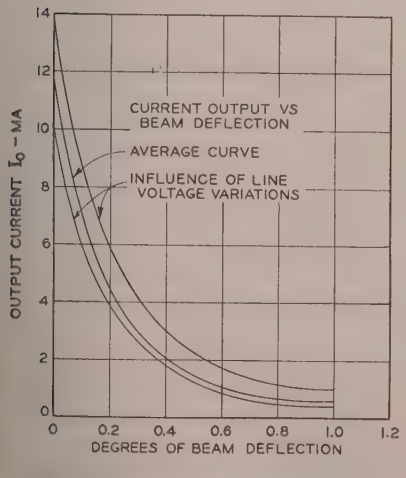

Figure 4. Characteristics of null detector

Nomenclature

J = inertia of beam, gram centimeters²
R = velocity damping, dyne centimeters per radian per second
C = spring rate, dyne centimeters per radian
θ_i = input angle to hairspring, radians
θ_o = deflection of beam, radians
T_i = input torque to beam, dyne centimeters
T_o = feedback torque to beam, dyne centimeters
I_o = current output of amplifier, milliamperes
E_o = voltage output of amplifier, millivolts
I_i = current input to amplifier, milliamperes
E_i = voltage input to amplifier, millivolts
K_i = feedback torque per unit of current, dyne centimeter per milliampere
β = ratio of feedback to output current
$K_2(\theta) \cong K_2$ = output current versus beam deflection
τ = time constant, seconds
$H(s)G(s)$ = transfer functions per equation 1

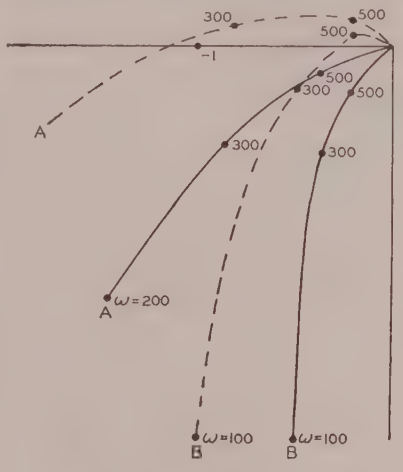

Figure 5. Stability of d-c amplifier

H(s)G(s) for gain = 100
——— without delay
– – – with delay
A—underdamped
B—critically damped

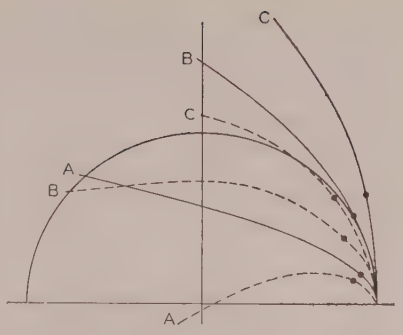

Figure 6. Frequency response of d-c amplifier

$\frac{1}{H(s)} + G(s)$ for gain = 100
——— without delay
– – – with delay
• $\omega = 100$
A—underdamped
B—critically damped
C—overdamped

A delay of 0.0025 second in the oscillator circuit and amplifier will make this system unstable if the damping reduces below the critical value. The value of the loop gain and the damping is of equal importance in determining the frequency response of the transducer. Using the inverse plane method from equation 1

$$\frac{T_i}{I_o} = \frac{1}{H(s)} + G(s)$$

$$\frac{T_i}{I_o} = \beta K_1 + \frac{J}{K_2}\left(s^2 + \frac{R}{J}s + \frac{C}{J}\right)(1+\tau s) \qquad (3)$$

Neglecting τs for first approximation and setting $C = 0$ as before

$$\left|\frac{T_i}{I_o}\right|^2 = \frac{\omega^2}{K_2}(R^2 - 2JK_1K_2\beta + \omega^2 J^2) + K_1^2\beta^2$$

Let R be chosen so that $R^2 - 2JK_1K_2\beta$ becomes zero, which is equivalent to critical damping.

$$\left|\frac{T_i}{I_o}\right|^2 = \frac{J^2}{K_2^2}\left(\omega^4 + \frac{K_1^2K_2^2\beta^2}{J^2}\right) \qquad (4)$$

This condition cannot be realized for all values of $2JK_1K_2\beta$ because R is obtained directly only through electrodynamic damping.

Interpreting equation 4, we see that the frequency response will be flat as long as

$$\omega^4 \ll \frac{K_1^2K_2^2\beta^2}{J^2} \qquad (5)$$

$K_1K_2\beta$ is the feedback torque produced per radians deflection of the Microsen beam and $K_1K_2\beta/J$ can be called the torque to inertia ratio of the system which, in turn, determines the frequency response.

However, because of the delay τ, this torque-to-inertia ratio must be kept below

a value which will cause instability. Moreover, the frequency response curve is altered slightly by the addition of $(1+\tau s)$ in the equation which is illustrated in the following.

Using the same example of a voltage amplifier with a gain of 100, we see in Figure 6 the frequency response curve on the inverse plane with and without the delay. Curve "B" shows the values for critical damping, curve "A" for slight underdamping, which is on the borderline of stability, and curve "C" for overdamping.

This frequency response is adequate for the d-c amplifier and transducer applications for which this instrument was developed. However, this analysis suggests various methods of improving this response by introducing corrective networks in either the $H(s)$ or $G(s)$ functions. In order not to impair the steady-state accuracy, only passive networks must be introduced into $G(s)$.

Current Transmission System

At the outset it was mentioned that there are basically five established approaches to electrical telemetering: the current, voltage, frequency, position, and pulse-time systems. Up to this point, we have considered the Microsen Balance only as a transducer supplying a signal at a level useful as an input to a telemetering channel. A signal of 5 volts direct current can readily be converted into a frequency shift in a frequency modulation channel, for example.

However, it should be recognized that this transducer also represents a transmitter for the least complicated of the five transmission techniques, the current transmission system. In closing our discussion, we shall consider the particular characteristics of d-c transmission.

Because the direct current is transmitted directly, a telemetering system of this type requires two wires between transmitter and receiver for each variable. Although several transmitters could use a common ground return, it is apparent that this system of telemetering is restricted to those applications of moderate distances where wiring does not constitute a great expenditure.

Wherever a number of signals must be simultaneously transmitted over some distance, a multichannel system becomes imperative. However, where it is applicable, current transmission offers compensation in its great simplicity, especially at the receiving end.

Next to the domestic watthour meter, the d'Arsonval type d-c milliammeter is the most widely used electric instrument. It exists in a great variety of types ranging from inexpensive, small size meters to precision laboratory instruments. During the last few years a number of instruments with 250-degree dial arcs have contributed towards increased readability and thereby greater usefulness in industrial installations. All these instruments are directly usable as receivers in this current system, it only being necessary to select a range to match that of the transducer.

For recording, any of the various self-balancing potentiometer recorders may be used with a d-c signal. This points up one significant advantage of current transmission. Standard multipoint recorders may be used for surveying a number of variables. This reduces end device costs and permits more compact controlhouse layouts.

As the telemetering art progresses under the impetus of both aircraft and industrial needs, the requirement for accurate transducing becomes more and more important. At the present time, transmission techniques have achieved levels of precision not attainable by the common proportional output transducer. It has been the purpose of this paper to describe a null-balance type of transducer inherently capable of achieving an accuracy comparable to that of present-day transmission links.

References

1. Telemetering, Supervisory Control, and Associated Circuits. *Special Publication S-12*, AIEE, 1948.

2. Electromechanical D-C Amplifier, **C. G. Roper, J. F. Engelberger.** *Electronics* (New York, N. Y.), November 1947.

3. Parallel Circuits in Servomechanisms, **H. Tyler Marcy.** *AIEE Transactions*, volume 65, 1946, pages 521–29.

4. The Frequency Response of Automatic Control Systems, **Herbert Harris.** *AIEE Transactions*, volume 65, 1946, pages 539–45.

5. Telemetering Guided-Missile Performance, **James C. Coe.** *Proceedings*, Institute of Radio Engineers (New York, N. Y.), November 1948, pages 1404–14.

6. A Universal Telemetering System, **L. Dale Harris.** *AIEE Transactions*, volume 67, part II, 1948, pages 1151–54.

7. A Versatile Power Line Carrier System, **H. W. Lensner, J. B. Singel.** *Electrical Engineering* (*AIEE Transactions*), volume 63, March 1944, pages 129–33.

8. Obtaining Attenuation-Frequency Characteristics for Servomechanisms, **H. Chestnut.** *General Electric Review* (Schenectady, N. Y.), December 1947.

9. The Frequency Response Method of Control Analysis, **William C. Moog.** *Instruments* (Pittsburgh, Pa.), volume 20, 1947, pages 811–16.

10. The Inverse Nyquist Plane in Servomechanism Theory, **George B. Criss.** *Proceedings*, Institute of Radio Engineers (New York, N. Y.), December 1947, pages 1503–04.

11. Considerations in Servomechanism Design, **J. W. Herwald.** *Electrical Engineering* (*AIEE Transactions*), volume 63, December 1944, pages 871–76.

12. Dynamic Behavior and Design of Servomechanisms, **G. S. Brown, A. C. Hall.** *Transactions*, American Society of Mechanical Engineers (New York, N. Y.), pages 503–24.

No Discussion

Frequency Compensation of A-C Instruments

JOHN H. MILLER
FELLOW AIEE

ALTHOUGH numerous papers and references[1-5] are available on the subject of frequency compensation of a-c instruments in the higher power frequencies, or up to 5,000 cycles, most of these appear to be limited to the study of a given design, or range in voltage or frequency. A general solution for one type of voltmeter compensation is presented here.

Voltmeters of both the electrodynamometer and iron-vane type are fundamentally milliammeters and measure current. When in series with a suitable resistance they respond to the applied voltage. However, they also have an inherent inductance as well so that as the frequency is increased the impedance rises and the instrument reads low. If the inductance is reduced by using fewer turns on the actuating coil or coils, the instrument takes more current for normal torque to the point where the power which must be dissipated is limiting.

The effect of the inductance on the instrument accuracy may be compensated by a capacitor shunted across a portion of the series resistance. This is discussed by C. V. Drysdale and A. C. Jolley[1] who give the fundamental equations. However, instead of obtaining a rigorous solution, an approximation is indicated which is of little use because it does not take into account any particular frequency range, and certain instruments may be much overcompensated if the approximation is used, and large errors may result.

The Circuit

The circuit given by C. V. Drysdale and A. C. Jolley is shown in Figure 1. The impedance of this circuit is given by,

$$Z=(R-r)+\frac{r}{1+C^2r^2\omega^2}+j\omega\left[L-\frac{Cr^2}{1+C^2r^2\omega^2}\right] \quad (1)$$

Note that if the absolute value of this impedance is made the same as the resistance R, the current through the instrument will be the same as at a low frequency approaching direct current and the error at the higher frequency will be zero, disregarding for the moment the effect of Foucault currents in the iron vanes, and incremental inductance as the pointer moves.

Since our attempt usually is to compensate the instrument for a specific frequency, it will simplify matters somewhat to substitute X_c for $1/\omega C$ and X_L for ωL. Equation 1 reduces to,

$$Z=R-r+\frac{X_c^2r}{r^2+X_c^2}+j\left[X_L-\frac{r^2X_c}{r^2+X_c^2}\right] \quad (2)$$

Taking the absolute value by the square root of the sum of the squares of the in-phase and j values, we have,

$$Z=\sqrt{\left[R-\frac{r^2}{r^2+X_c^2}\right]^2+\left[X_L-\frac{r^2X_c}{r^2+X_c^2}\right]^2} \quad (3)$$

Squaring and rearranging,

$$Z=\sqrt{R^2+X_L^2+\frac{r^2(r^2-2Rr-2X_LX_c)}{r^2+X_c^2}} \quad (4)$$

Condition for Compensation

It is obvious that if the sum of the factors to the right of R^2 equals zero, then $Z=R$ and the instrument reads correctly. Our criterion for exact compensation is, therefore, that in the foregoing circuit the several constants be so chosen that,

$$X_L^2+\frac{r^2(r^2-2Rr-2X_LX_c)}{r^2+X_c^2}=0 \quad (5)$$

This may be expanded to

$$X_c^2X_L^2-X_c(2X_Lr^2)+X_L^2r^2-2Rr^3+r^4=0 \quad (6)$$

Solving equation 6 for X_c, we arrive at that value of capacity reactance which gives the entire network the same value of impedance as its resistance, at the frequency in question. There is a considerable phase angle which is not a factor in a voltmeter; our concern is to obtain the same current in the actuating coil to give the same deflection.

$$X_c=\frac{r^2+r\sqrt{2Rr-X_L^2}}{X_L} \quad (7)$$

Use of Values in Terms of R

Equation 7 gives the value of capacity reactance for the indicated factors, and these, r, R, and X_L may be used with their actual values. However, in this analysis and in the actual use of the equations and curves it is found much simpler to express r, X_L and X_c in terms of R. This allows for general solutions for different instrument mechanisms, and conversion back to exact quantities is relatively simple when the final result has been obtained.

An Example

As an example of such compensation, a typical uncompensated Weston model 433 instrument for 150 volts may be considered, with values rounded off for discussion. In this instrument the total resistance, $R=5{,}000$ ohms. The coil resistance is 1,000 ohms so that r may be a maximum of 4,000 ohms or 0.8 in terms of R. The inductance associated with this instrument is 0.4 henry.

Paper 51-30, recommended by the AIEE Instruments and Measurements Committee and approved by the AIEE Technical Program Committee for presentation at the AIEE Winter General Meeting, New York, N. Y., January 22-26, 1951. Manuscript submitted August 23, 1950; made available for printing November 21, 1950.

JOHN H. MILLER is with Weston Electrical Instrument Corporation, Newark, N. J.

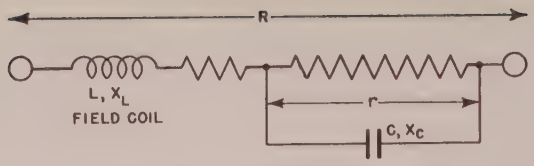

Figure 1 (above). Circuit diagram of a compensated voltmeter

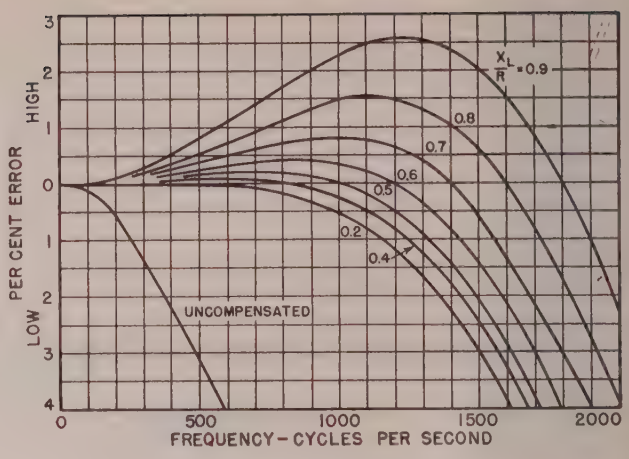

Figure 2 (right). Showing frequency errors in a 5,000-ohm voltmeter having 0.4-henry inductance and compensated at various frequencies; the curves are marked with the parameter X_L/R for the compensated frequency

This instrument is fundamentally designed to be satisfactory from 25 to 125 cycles and to have a frequency error under the worst condition, at 125 cycles, of the order of 0.2 per cent. Using the foregoing method of compensation we may analyze what can be accomplished up to 1,000 cycles using this same mechanism.

The reactance of 0.4 henry at 1,000 cycles is 2,500 ohms and, in terms of R, $X_L=0.5$. Solving equation 7 where $R=1$, $r=0.8$ and $X_L=0.5$, we get $X_c=3.14$, again in terms of R. Or, $X_c=15{,}700$ ohms and this value at 1,000 cycles is represented by a capacity of 0.01015 microfarad, which will exactly compensate the inductance at 1,000 cycles.

Practical Application

It is obvious, however, that it would be difficult to obtain a capacitor of some odd exact value, and accordingly, a slightly larger capacitor may be used connected across a slightly smaller portion of the series resistance, since C can be increased a little as r is lower. It can be shown, however, that the smallest available capacitor which will meet the requirements should be used across the largest value of r since this produces the flattest characteristic at lower frequencies.

In production, the required capacitor is solved as in the foregoing paragraphs from available data on inductance and resistance of a given design. The instrument then is assembled, placed in circuit with two dial boxes in series to serve as calibrating resistance, calibrated on low frequency—60 cycles for example—by adjusting one or both boxes, and the scale drawn. A stock capacitor of the next higher value than indicated by the calculation is shunted across one dial box. The instrument now is standardized on a source of the higher frequency by varying the resistance of the box shunted by the capacitor, while varying the other box to maintain their sum resistance the same as at low frequency. The final values of resistance are recorded, and spools or resistance sheets are adjusted to those values and connected in place within the instrument.

Errors at Other Frequencies

Since, in equation 4 the several factors to the right of R^2 represent the error introduced, and are small with respect to R, we can use the approximation that the error is half the sum of the terms to the right of R^2, or,

$$\text{Error} = \frac{X_L^2}{2} - \frac{r^2(X_L X_c + Rr - r^2/2)}{r^2 + X_c^2} \qquad (8)$$

When $R=1$ and other factors are in terms of R, this gives the error directly in terms of the reading. When the compensation is perfect, this value, of course, reduces to zero. Note that in this equation for other frequencies the term $X_L X_c$ is constant with frequency. Accordingly, in an analysis of the frequency errors in a compensated instrument, the numerator of the second term in equation 8 is constant and the only terms that vary are X_L^2 in the first term and X_c^2 in the denominator of the second term.

As an example of the frequency errors involved in a 150-volt instrument as described, without compensation, and as so compensated, the errors in per cent of the reading are given in Table I. While these are calculated values, no difference could be discerned in actual tests of the final instrument.

Up to 1,100 cycles the compensated instrument has a frequency error of less than 0.2 per cent whereas the standard instrument is within 0.2 per cent only up to 125 cycles. This gives a net gain of a nearly tenfold expansion of frequency coverage at the expense of a small capacitor. Similarly, the same instrument can be compensated at other frequencies to determine the extent to which the method may be used. In the example, if compensated at 400 cycles, $X_L/R=0.2$ and at 1,800 cycles $X_L/R=0.9$. The resulting instrument errors are shown in Figure 2. From these curves it will be noted that the error at 10 per cent above the compensated frequency is approximately equal to the greatest error at lower frequencies; hence it is customary to compensate at 90 per cent of the highest frequency to be covered in the interest of least error.

This general approach also allows for the use of curves to obtain the capacity values. Figure 3 shows the relationship between the required capacity reactance at the compensated frequency and the actual capacity for the example cited, both for $r/R=0.8$. For other resistance ratios a family of such curves can be developed giving X_c/R for various values of X_L/R.

Other Errors

If the higher frequency adjustment is made at about 80 per cent of full scale, it will balance well at other points where the inductance is slightly different owing to the position of the moving system. Only in the case of very high accuracy requirements—0.25 per cent instruments,

Table I. Frequency Errors of Standard and Compensated Instrument, in Per Cent

Frequency, cycles per second	60	100	200	400	600	800	1,000	1,200	1,400
Standard instrument	−0.05	−0.13	−0.50	−2.00	−4.50	−8.00	−12.50	−18.00	−24.50
Compensated instrument	+0.003	+0.01	+0.03	+0.12	+0.20	+0.19	0.0	−0.50	−1.49

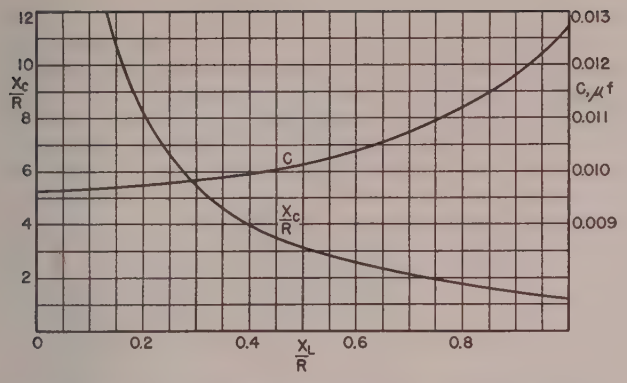

Figure 3 (above). The relation between X_c and X_L in terms of R, is indicated for $r/R=0.8$; C also is given for the cited example

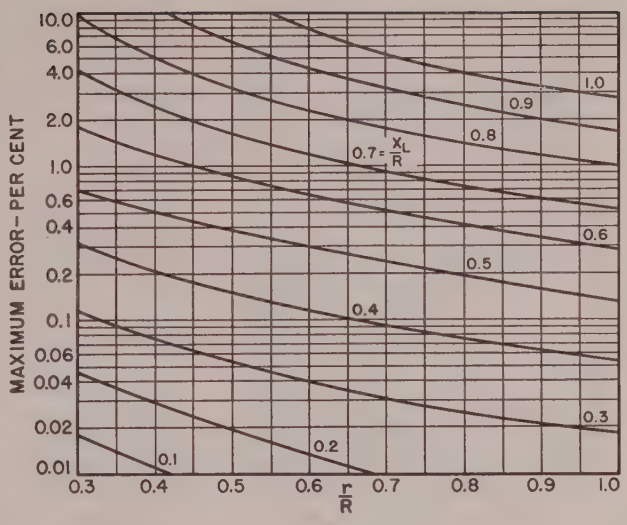

Figure 4 (right). The maximum error up to the compensated frequency is shown in general terms

does a scale error become a factor. Further, although the foregoing analysis is based upon maintaining $Z=R$, a high-frequency error exists in a current meter (something less than 0.8 per cent per 1,000 cycles for iron-vane instruments, much less for electrodynamometers). But by actually calibrating as shown, the impedance is slightly overcompensated to give the same end result.

Multiple Range Instruments

Adding a series resistance multiplier to an instrument compensated as described will give an overcompensated result; hence unless the compensation has been small, it appears necessary to use individual series resistors, each with its appropriate capacitor, for multiple range instruments.

Further Analysis

It can be seen from Figure 1, and can be proved by analysis, that the maximum frequency error in such a compensated voltmeter, below the compensation frequency, occurs at 70 per cent of that frequency. A formula for this error has been derived from equation 8, but expressed in terms of r and X_L. This allows for a rapid calculation of the maximum frequency error up to the compensated point, in terms of r and X_L, each in terms of R.

$$\text{Error at } 0.7f = \frac{X_L^4}{8r^2+16r+16r\sqrt{2r-X_L^2-4X_L^2}} \qquad (9)$$

Where f is the compensated frequency.

Since the ratio of series resistance to total resistance is usually over 0.8 as required for temperature compensation, we can assume $r=0.8$ in equation 9, and note the resulting errors for various values of the reactance in terms of the total resistance in Table II. Errors of the uncompensated instrument also are shown.

Table II. Maximum Frequency Errors in Per Cent, up to the Compensated Frequency, for $r/R=0.8$

X_L/R	1.0	0.9	0.8	0.7	0.6	0.5	0.4	0.3	0.2	0.1
Uncompensated instrument	41.4	34.6	28.1	22.1	16.6	11.9	7.8	4.5	2.0	0.5
Compensated instrument	4.2	2.5	1.5	0.78	0.42	0.20	0.08	0.024	0.005	0.0003

The errors resulting from various values of both X_L and r in terms of R, are plotted in Figure 4. Knowing the series resistance in terms of the total, and the reactance at the desired frequency in terms of the total resistance, an immediate indication of the maximum frequency error up to some 10 per cent above the compensated frequency can be had by inspection.

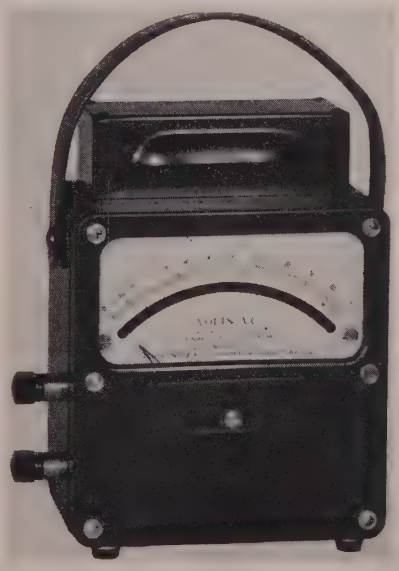

Figure 5. A compensated voltmeter, 25 to 2,500 cycles

The importance of shunting the correcting capacity across the maximum amount of series resistance also can be noted from these curves. For example, when $X_L/R=0.5$, if the capacity is across 80 per cent of the total resistance the maximum frequency error is about one-third as great as it would be if shunted across only 30 per cent, assuming in both cases perfect correction at the compensated frequency.

It should be noted that this analysis is entirely in relative values, hence is applicable to all voltmeter ranges. As a matter of interest, a 150-volt instrument compensated to 1,000 cycles, iron vane or electrodynamometer, takes just about 0.01 microfarad. A 15-volt range takes 1.0 microfarad, and a 1.5-volt range can be compensated with 100 microfarads. And all ranges, if of the same proportions, that is, the same mass of coil copper and turns inversely proportional to the voltage range, will have the same frequency errors in per cent.

Limits of the Method

In the foregoing example a standard mechanism was used, with moderate loss and normal torque. However, the inductance can be decreased materially through the use of fewer turns on the actuating coils, although this requires more current for a given voltage. To some extent this can be balanced by a reduction in torque to the point where a single range electrodynamometer instru-

ment, for example, only slightly subnormal in torque, and taking power somewhat in excess of normal, can be designed to be within 0.5 per cent of full scale on direct current and at all frequencies from 25 to 4,000 cycles.

Wattmeter Compensation

In a wattmeter or varmeter we are concerned with both magnitude and phase angle of the current in the potential system.

However, the moving coil of a wattmeter usually has a very small inductance and the current magnitude changes very little; the phase angle may shift considerably, however, at the higher frequencies, and is particularly important at low power factor. Phase angle correction in the moving coil circuit is obtained when, in equation 2, the j factor becomes zero, or when,

$$X_L = \frac{r^2 X_c}{r^2 + X_c} \tag{10}$$

This cannot be done and at the same time maintain the correct magnitude, but the fact is that the inductance in the moving coil of a wattmeter is so small that the magnitude error may be disregarded and correction made only for phase angle even though this does change the magnitude a very small amount. In the practical sense this is when X_L is less than $R/30$ and, when this is so, equation 10 may be further reduced to the approximate though adequate equation,

$$c = \frac{L}{r^2} \tag{11}$$

This is the equation given in the literature for wattmeter phase angle correction.

Conclusions

Through the use of a rigorous solution of the network of a voltmeter, frequency compensated by a capacitor in shunt to its series resistance, it has been possible to easily evaluate the resulting errors at other frequencies for any given instrument. Placement of the data in curve form allows for immediate estimate of the error limits for any design and indicates those parameters which are controlling to any end requirement.

Fortunately this analysis was made in 1941 and allowed for the practical manufacture of many types of relatively precise voltmeters for the higher frequencies as required by the Armed Forces. One such type of portable instrument made in large quantity is shown in Figure 5. With a range of 150 volts, and a loss of 9 watts at full scale, the over-all error from 25 to 2,500 cycles was guaranteed not over $1^1/_4$ per cent of full scale and ran much less in production.

It also might be pointed out that instruments compensated to 1,000 cycles, for example, are excellent for measurement of bad wave forms at lower frequencies, since they properly evaluate the higher harmonics.

With the approach described an increase in frequency coverage of nearly ten is obtained with a given mechanism and with the original error limits. This is had at the cost of a suitable capacitor, a practical manufacturing procedure, and the necessary simplified engineering analysis of each design combination.

References

1. Electrical Measuring Instruments (book), **C. V. Drysdale, A. C. Jolley.** D. Van Nostrand Company, New York, N. Y., 1924, part I, page 288.

2. Frequency Compensated A-C Ammeters and Voltmeters, **J. M. Whittenton, C. A. Wilkenson.** *AIEE Transactions*, volume 65, 1946, pages 761–64.

3. Performance of Conventional Indicating Instruments on Frequencies up to 3,000 Cycles, **S. C. Richardson.** *General Electric Review* (Schenectady, N. Y.), volume 46, October 1943.

4. Alternating Current Circuits (book), **R. M. Kerchner, G. F. Corcoran.** John Wiley and Sons, Inc., New York, N. Y., 1938.

5. Electrical Measurements and Measuring Instruments (book), **E. W. Golding.** Sir Isaac Pitman and Sons, Ltd., London, England, 1942.

Discussion

B. E. Lenehan (Westinghouse Electric Corporation, Newark, N. J.): We applied this method of compensation several years ago to recording instruments by using experimental methods. Later, an analysis was made which gave the same result as equation 7 of this paper, in a slightly different form. From this point, our analysis followed a different path leading to some results in addition to those given by Mr. Miller.

Equation 7 becomes imaginary when X_L^2 is greater than $2Rr$. This gives an upper limit of frequency for which an instrument can be compensated. For the instrument in the example, this is 2,536 cycles.

It is possible to expand the expression in equation 7 into a series whose terms can be represented by circuit elements

$$X_c = \frac{r^2 + r\sqrt{2Rr}}{X_L} - \frac{rX_L}{2\sqrt{2Rr}} - \frac{X_L^3}{16R\sqrt{2Rr}} \quad \ldots$$

The first term of this series can be represented by a capacitor

$$C = \frac{L}{r^2 + r\sqrt{2Rr}}$$

The second term is an inductance

$$L' = \frac{Lr}{2\sqrt{2Rr}} = \frac{L\sqrt{r/R}}{2\sqrt{2}}$$

The third term can be approximated by adding a capacitor

$$C' = \frac{L}{2r\sqrt{2Rr}}$$

in parallel with L', the resultant parallel impedance of L' and C' supplying the second and third terms of the series. Perhaps still closer approximations are possible with more circuit elements, but there are practical reasons for stopping with two terms and not using the third term. For one thing, the inductance, L, of the instrument is not a constant for all pointer positions.

These values give results with errors all on the negative side. The error equations are:

Uncompensated instrument

$$e_0 = {}^1/_2\left(\frac{X_L}{R}\right)^2$$

First approximation (adding C)

$$e_1 = \frac{\left(\frac{X_L}{R}\right)^4}{2\left(\frac{X_L}{R}\right)^2 + 2\left(\frac{r}{R} + \sqrt{\frac{2r}{R}}\right)^2}$$

Second approximation (adding C and L')

$$e_2 = \frac{\left(\frac{X_L}{R}\right)^6}{2\left(\frac{X_L}{R}\right)^4 - 8\sqrt{2}\left(\frac{r}{R}\right)^{3/2}\left(\frac{X_L}{R}\right)^2 + 16\frac{r}{R}\left(\frac{r}{R} + \sqrt{\frac{2r}{R}}\right)^2}$$

The equation for the third approximation error has not been worked out. Using the example given, the errors for these circuits are given in a form corresponding to Table I in this discussion.

Table I. Frequency Errors in Per Cent

Frequency, cycles per second	600	800	1,000	1,200	1,400	1,600	1,800	2,000	2,200	2,400	2,600
First approx.	−0.09	−0.29	−0 63	−1.41	−2.52	−4.17	−6.46	−9.48	−13.38	−18.15	−23.9
Second approx.	−0.03	−0.09	−0.226	−0.52	−1.08	−2.05	− 3.7	− 6.33	−10.25		
Third approx.						−0 07	−0.46	− 0 63	− 3 18	− 6.53	

The variation of inductance with pointer position will cause errors of about the same size as the second approximation errors given, making the third approximation of no practical value except for zero-reading instruments. The second approximation is useful, since it only requires a fixed coil in series with the capacitor used in the method given.

Ralph M. Rowell (General Electric Company, West Lynn, Mass.): This paper covers a very logical approach to the problem of compensating a-c instruments for use over a frequency range and is particularly timely considering the increased use of higher frequency systems. It presents much useful data for obtaining best average values of compensation and simplifies the calculation of proper compensating values.

We feel, however, that the simplicity of the problem has been unduly stressed. While some standard instruments undoubtedly could be compensated to give errors as shown in Table I of the paper, many instruments using standard windings would have excessive errors at intermediate points when compensated for 1,000 cycles. This is particularly true when the inductance/resistance ratio is relatively high. While a brief reference is made to the fact that inductance can be decreased materially by the use of fewer turns on the actuating coil at the expense of higher input, the importance of this has been minimized. From a study of a large number of instruments it appears that such a reduction in inductance and corresponding increase in burden is necessary in a majority of cases to secure compensation which is sufficiently flat over a wide frequency range. As an example, one sample of the compensated voltmeter shown in the paper (Figure 5), which was recently tested, requires 8 volt-amperes, compared with 2.5 volt-amperes for a standard instrument of the same voltage.

The statement also is made that "only in the case of very high accuracy requirements—0.25 per cent instruments, does a scale error become a factor." Our experience has indicated that with normally high values of inductance which vary considerably with pointer position, compensation will vary materially at different parts on the scale. It should be pointed out that special low-inductance high-burden instruments are very generally employed to reduce the effect of these variations to a minimum and to secure satisfactory accuracy over the usable scale range.

Since this paper is designed to be of a general nature and not to apply to any specific design, it is desirable that all major effects be evaluated. Compensation for a single particular frequency or a single scale point is indeed a simple matter, but complete compensation over a wide frequency range and over the entire usable portion of an instrument scale often requires considerable change in the instrument constants associated with obtaining lower circuit inductance and consequently higher volt-ampere burdens. This assumes, of course, that no sacrifice of torque or torque-to-weight ratios is permitted.

R. F. Estoppey (Weston Electrical Instrument Corporation, Newark, N. J.): Brief mention is made in the paper of errors such as scale error, caused by the change in inductance, and the error in multiple-range instruments using series resistance multipliers. Further discussion of these errors may be of interest and to show how convenient it is to use the error equation (equation 8 of the paper) for estimating these errors.

On 0.25 per cent instruments of the electrodynamometer type it is considered good practice to hold the frequency error to less than 0.1 per cent of full scale. Assuming that r/R will be 0.9, Figure 4 shows that the maximum X_L/R allowable for a maximum error of 0.1 per cent up to the compensated frequency will be approximately 0.45. A typical 150-volt instrument has an inductance at the 130-volt mark of 0.108 henry and a total resistance of 4,000 ohms. If it is assumed that the compensated frequency is 2,650 cycles, then X_L/R equals 0.45, and the maximum error at the 130-volt mark will be 0.1 per cent. At the 150-volt mark the inductance increases 5.5 per cent to 0.114 henry and X_L/R becomes 0.475. If this value of X_L/R is used in the error equation (8) along with the assumed value of 0.9 for r/R and a value of $X_c/R = 4.3278$ computed by equation 7 where X_L/R is 0.45, then the error equation shows an error of 0.75 per cent. This means that the indication will be low by 0.75 per cent at full scale if adjusted at the 130-volt mark. The same calculation can be made at other scale voltages below 130 volts, and it can be shown that the error in per cent of full scale also will reach a maximum of approximately 0.75, this error being in the opposite direction.

Lower values of X_L/R will decrease the scale error and for values of X_L/R of 0.3, 0.2, and 0.15, the error for this instrument becomes 0.31, 0.14, and 0.08 per cent, respectively. At 1,000 cycles the value of X_L/R becomes 0.17, which is a scale error of approximately 0.1 per cent, and therefore 1,000 cycles is the top frequency to which the instrument can be compensated accurately.

Iron-vane instruments usually have a smaller change in inductance with a change in position of the moving element, and in most cases the maximum value of X_L/R is limited by the error at 70 per cent of the compensated frequency as given in Figure 4. Each type of instrument must be considered for both of these errors, and the proper balance between total inductance, inductance change, and frequency must be evaluated to arrive at an optimum design.

The error caused by doubling the range by using a series multiplier can be evaluated by using the error equation (8). For the previous example, where the instrument was compensated at 2,650 cycles, adding series resistance will double the total resistance, and the values of r/R, X_L/R, and X_c/R obtained for the low range will be halved. By using these new values in the error equation, an error of 0.93 per cent (high) is computed. Using the values of r/R, X_L/R, and X_c/R obtained at 1,000 cycles in the error equation in the same manner gives a value of 0.12 per cent (high) for the error. This shows that it is possible to add series resistance to the low range to obtain the higher range if the instrument is compensated to 1,000 cycles, which will be the case, otherwise the scale error would be excessive.

The calculation of the high-range error assumes that there is no error as a current meter due to eddy currents. When the instrument is compensated it is slightly overcompensated as a voltmeter in order to compensate for both errors, and in actual practice it is found that the error for the higher range in series will be less than the calculated value. This can be proved by assuming that an infinite range is added. For this condition, the resistance is so high that X_L and X_c are negligible, and the error as a current meter is no longer compensated, resulting in a low indication equal to the eddy-current error. This same reasoning applies at lower resistances, and in some cases it is possible to obtain compensation on the high-series range by means of the eddy-current error.

It should be noted that the values used in this discussion are in relative values, and while the typical example uses a specific range and frequency, the errors obtained will be the same for other ranges and frequencies for the same values of X_L/R and r/R. These errors change very little for other values of r/R from 0.8 to 1.0, which makes it very convenient to work with only X_L/R in design analysis.

A New Lightweight Rapid Transit Motor

R. A. PETTERSEN
ASSOCIATE AIEE

Synopsis: A broadening application field for the Presidents' Conference Committee (PCC)-type electric car has introduced new and more severe requirements in the design of its propulsion equipment. This has resulted in a new traction motor embodying the latest progress in design and manufacture and particularly suited to dynamic braking at the high operating speeds currently coming into vogue

New Service Requirements

THE application of the PCC car to high-speed suburban service and the utilization of the same propulsion equipment for lightweight rapid transit service have set the stage for a redesign of this equipment to meet the new performance demands. Whereas a speed of 35 miles per hour (mph) rarely was exceeded in city service, speeds of 50 mph and above may be expected in rapid transit and suburban operation. Coincident with the increase in top speed is the requirement that dynamic braking be made available from these speeds without injury to the motor from overvoltage.

Design Improvements

In designing to meet the above conditions, other improvements have been incorporated in the new motor to obtain more performance per pound of weight. In general, these improvements include:

1. Better commutators.
2. Better utilization of space.
3. Wedged armature slots.
4. Better insulation materials.
5. Simplified bearing assemblies

Paper 51-31, recommended by the AIEE Land Transportation Committee and approved by the AIEE Technical Program Committee for presentation at the AIEE Winter General Meeting, New York, N. Y., January 22-26, 1951. Manuscript submitted October 16, 1950; made available for printing November 22, 1950

R. A. PETTERSEN is with the General Electric Company, Erie, Pa.

The net result is a motor differing both electrically and mechanically from its predecessor. An increase in the number of commutator segments and a shortening of the core allow an increase in the dynamic braking voltage. Refinements in the mechanical construction render the new motor better able to withstand the centrifugal forces experienced in high-speed operation.

Motor Description

The new motor, illustrated in Figure 1, is rated 55 horsepower at 300 volts. The frame is designed so as to be suitable for the same truck mounting as the earlier motors. It has the same outline dimensions in spite of the fact that the armature core diameter has been increased substantially. The characteristics shown in Figure 2 are such that cars equipped with these motors will have the same operating characteristics as present cars equipped with the earlier motors.

Construction details of the new motor are shown in the longitudinal section, Figure 3. The commutator is of the arch-bound design instead of the Vee-bound previously employed. In the arch-bound commutator, the cap and shell exert pressure only on the bottom side of the Vee in the segments, thereby retracting the bars toward the center of the commutator and building up the desirable high "arch" pressure between adjacent bars. This change is in accord with the modern trend in motor design and is a highly desirable improvement. In addition, the segments and steel parts have been strengthened to increase their ability to withstand high-speed operation. The commutators are seasoned by repeated cycles of heating and cooling while revolving at high speeds, followed by tightening.

Figure 1. New 55-horsepower, 300-volt, d-c lightweight rapid transit motor

The use of wedges has replaced the core binding wire for holding the windings in the slot. This eliminates the banding losses and also provides greater mechanical strength. Skewed slots are employed to minimize magnetic noise, an especially desirable feature on truck-mounted motors connected through metal-to-metal contacts all the way to the car body. The armature shaft, which can be replaced without disturbing the windings or the commutator, has been increased in diameter to add stiffness for high-speed service. Hot-stacking of the core on the shaft has dispensed with the shaft keys. The omission of the commutator key permits a more accurate line-up of commutator segments with the core slots.

Bearing assemblies have been simplified to facilitate maintenance without

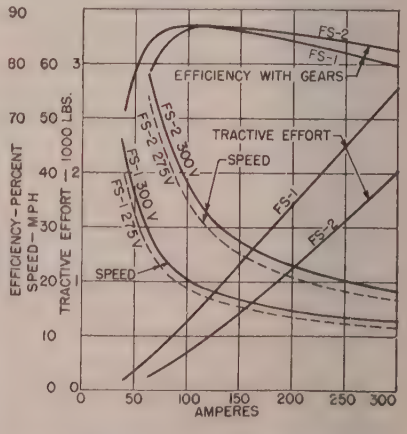

Figure 2. Motor characteristic curves on 300 volts, gear ratio 7.17 to 1, wheel diameter 28 inches

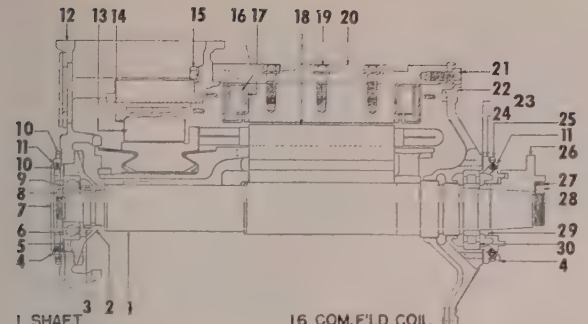

1 SHAFT
2 BEARING HOUSING
3 FLINGER
4 GREASE FITTING
5 GASKET
6 BALL BEARING
7 BEARING CAP
8 NUT
9 LOCKWASHER
10 CAPSCREW & LOCKWASHER
11 PIPE PLUG
12 FRAME HEAD
13 CARBON BRUSH
14 BRUSH HOLDER
15 CAPSCREW & LOCKWASHER
16 COM. F'LD COIL
17 EXC. F'LD COIL
18 ARMATURE
19 POLE PIECE BOLT & LOCKWASHER
20 MAGNET FRAME
21 CAPSCREW & LOCKWASHER
22 FRAME HEAD
23 GASKET
24 BEARING CAP
25 CAPSCREW & LOCKWASHER
26 COUPLING HUB
27 LOCKWASHER
28 NUT
29 COLLAR
30 ROLLER BEARING

Figure 3 (left). Longitudinal section through motor

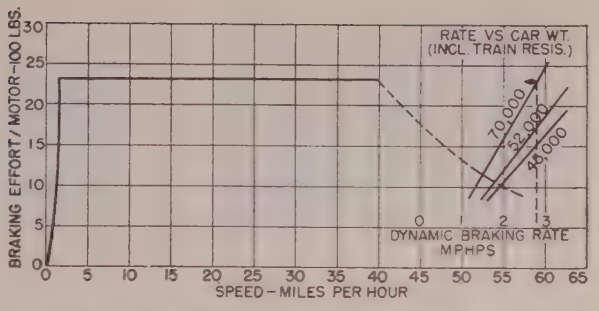

Figure 4 (above). Dynamic braking curve for rapid transit train of two cars each equipped with four motors, gear ratio, 7.17 to 1, wheel diameter 28 inches

sacrificing performance. The commutator end ball bearing, which locates the armature longitudinally, is carried in a cartridge-type assembly that fits into the bore of the framehead. The pinion end is fitted with a roller bearing to take up longitudinal movement of the armature. When the armature is removed, the complete bearing assemblies are removed with it—a feature that prevents the bearings themselves from being exposed to dirt. The armature conductors themselves are insulated with permafil-treated glass, and the ground insulation is mica and glass.

Dynamic Braking

The most significant contribution offered by the new motor is in the extended range of dynamic braking. The braking characteristic for a particular lightweight rapid transit application is given in Figure 4. This curve shows the range of braking effort available per motor for a 7.17 gear reduction and 28-inch diameter wheels. Also shown are the dynamic-braking rates available for a car weighing 45,000 pounds empty, 52,000 pounds with average passenger load, and 70,000 pounds with maximum load.

Below 40 mph, and down to approximately $1\frac{1}{2}$ mph where dynamic braking begins to fade, the maximum braking effort is obtained with full field strength on the motor. The armature current is held constant over this range by reducing the resistance load across the motor, which is operating as a series generator. Since the generated voltage on full field is directly proportional to speed, some means must be employed to hold the value within practical limits as speed is increased. The determining factor in arriving at the maximum desirable braking voltage is the volts developed between commutator bars. The "volts per bar" will not be uniform around the commutator, but will vary because of flux distortion due to armature reaction.

Experience has shown a value of 40 peak volts per bar to be the practical operating limit for .045-inch commutator side mica. In order not to exceed these limits when operating at speeds from 40 mph to the maximum of 58 mph, field shunting is employed to reduce the generated voltage while holding a constant value of load resistance across the motors.

Conclusion

A test car equipped with the new motors has been operating for some months in high-speed suburban service on the City of Shaker Heights, Ohio, transit system. The performance of this equipment over the maximum speed range in both motoring and dynamic braking has given conclusive proof of the success of the design and has established the significant contribution which the new motor will make toward the development of modern transit systems.

No Discussion

A New Lightweight Rapid Transit Control Equipment

I. W. LICHTENFELS
ASSOCIATE AIEE

H. G. MOORE
MEMBER AIEE

Synopsis: The application of the Presidents' Conference Committee (PCC) car in rapid transit service led to the development of a new control known as type *MCM*. This is primarily an all-cam control system comprising two motor-operated controllers. One controller, called the circuit controller, establishes various main and control circuits for power, braking cushioning, field shunting, and reversing. A second similar controller, called the resistance controller, varies the main motor circuit resistance to hold rate of accelerating or braking as desired.

Why a New Control System

SINCE its inception more than 15 years ago, dynamic braking, for example, has been speeded up and refined to the point where it is now used at full rate until the vehicle is practically at a standstill. As maintenance information is accumulated it is distributed regularly, to assure the best maintenance and reliability. We then may naturally ask, Why a new control system? The impelling reasons for the new control are two: increased weight and higher speed of the new cars. The original 32,000-pound PCC car has grown to weigh as much as 45,000 pounds. Part of this additional weight is in the couplers, draft gear, and stronger frame members necessary with multiple-unit operation. Maximum operating speed has been increased from 40 to 55 miles per hour. This is advantageous in rapid transit service with less frequent stops, as it provides higher schedule speed.

Design Considerations

In designing a control system certain fundamentals must be remembered. First, the purpose of a control system is primarily to translate the wishes of the car operator into car movement so as to transport people quickly but comfortably and safely. Putting this another way, electric circuits, timing, and rate of acceleration and deceleration must be controlled.

Second, mechanical design must provide maximum life with low maintenance cost. With this objective in view, cam operation was chosen since it greatly reduces impact stresses. Another source of maintenance expense, contact erosion, has been reduced by using cam action to force contact opening. Besides providing positive interlocking, cam operation permits the use of a large number of switches without great increase of cost or complication. Except for the main line circuit breaker equipped with overload protection, all magnetic power switches have been eliminated and only five main units are equipped with blowouts.

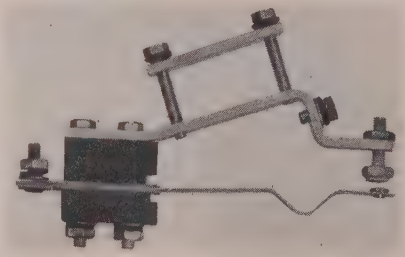

Figure 1. Cam-operated control contact

Assembling a System

Manufacturers and operators have a common and impelling interest in reducing the number and complexity of the different parts which enter into the construction of electric equipment. An ideal system is one which can be assembled from identical and simple components of a relatively few types, much like the building of a structural toy. The system described here takes fullest possible advantage of such techniques. It is principally constructed of the following parts:

36 cam-operated control contacts, illustrated in Figure 1.

47 main contact units, illustrated in Figure 2.

2 identical drive units, illustrated in Figure 3.

6 relays with identical frame and contact components, illustrated in Figure 4.

9 resistor units, illustrated in Figure 5.

These parts, assembled on a framework with the addition of a current-regulating relay and a separate protecting line circuit breaker with overload, comprise the main propulsion control equipment of a PCC car. Figure 6 is a schematic connection diagram including cam development. The sequence of switch operation is determined by the contour of the cams which open and close the switch units. Train line signals operate low-energy relays to translate the operator's wishes into controller movement.

Heat Dissipation

Full dynamic brake application at 40 miles per hour requires an output of approximately 250 horsepower from each

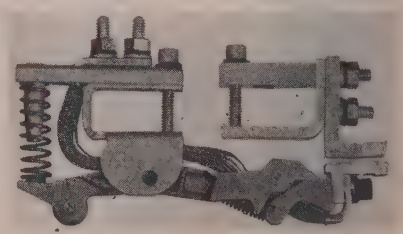

Figure 2. Cam-operated main contact

Paper 51-32, recommended by the AIEE Land Transportation Committee and approved by the AIEE Technical Program Committee for presentation at the AIEE Winter General Meeting, New York, N. Y., January 22–26, 1951. Manuscript submitted October 18, 1950; made available for printing November 22, 1950.

I. W. LICHTENFELS and H. G. MOORE both are with the General Electric Company, Erie, Pa.

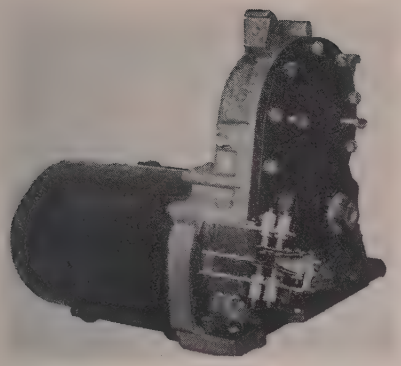

Figure 3. Controller drive unit

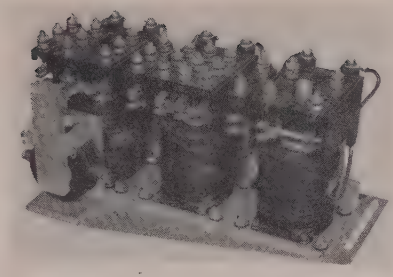

Figure 4. Auxiliary relay group

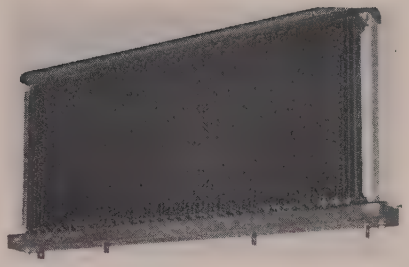

Figure 5. Honeycomb-type resistor unit

55-horsepower motor, or 1,000 horsepower for one car. A 10-car train represents a peak of 10,000 horsepower at the operator's command, to be dissipated as heat in the main motor resistors. Figure 5 shows one of the nine units of the resistor package assembly. This is an adaptation of the design used on locomotives with dynamic braking. All units are series blown and the individual units are shaped for most efficient utilization of cooling air.

Built-in Features

Simplicity was achieved primarily by building in certain features as inherent parts of the system. For example, with cam operation no crossinterlocking between power and brake circuits is necessary, simply because the cam contour makes simultaneous closing of conflicting switches impossible. Control of the motor field strength is built into the controller. Probably the greatest simplification for train operation was achieved by including the reverser as part of the circuit controller. For forward motion, the controller moves in one 180- degree sector and for reverse in the other. To accomplish this, it was necessary merely to use cams cut on both sides.

"All-Electric" Cars

The majority of PCC cars built in the last ten years have been "all-electric." Reliability of all-electric operation in performing primary car deceleration with dynamic braking supplemented by magnetic rail and solenoid-actuated drum brakes is a matter of record. Now a further step has been taken by the use of an all-electric notching control. An outstanding advantage of this new notching system is fast operation, such as is necessary with high-rate operation, but without destructive shock loading of parts. All shocks incident to stopping and starting the controller are absorbed in the magnetic circuit of the small driving motor. Magnetic cushioning of shock loads is a fact of great importance when we consider that the controller may stop and start millions of times a year.

Package Unit

To simplify resistor cooling, wiring, installation, and maintenance, all main propulsion-control equipment is factory assembled in a package unit, as shown in Figure 7. All contact tips, relay contacts, and lubrication points are accessible from the outside of a rectangular box formed by the resistor assembly. Resistors are in the form of individual honeycomb units held in place by two bolts, and a unit can be slid out readily and replaced in about ten minutes. The entire assembly is supported by four mounting bolts. It can be removed readily since most wiring is internal, and connections for external wiring are brought to convenient terminal points.

Resistor Proportioning

Prior types of control for PCC cars were generally of the multistep variety, in which the magnitude of individual accelerating and braking steps was limited by considerations other than the permissible increment of current or motor torque as each section of resistance was cut out.

As a consequence, the actual number of steps was not significant as a factor in the smoothness of acceleration or of dynamic braking. With the cam-operated contact units of this new con-

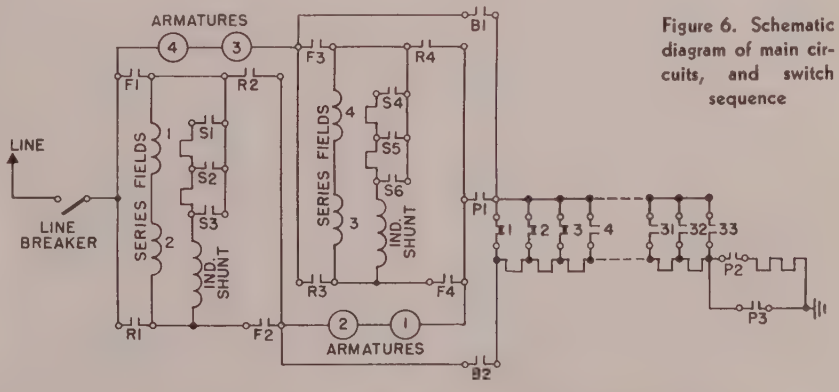

Figure 6. Schematic diagram of main circuits, and switch sequence

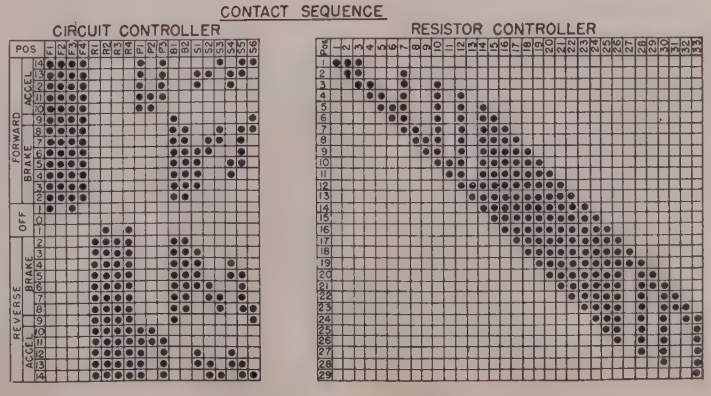

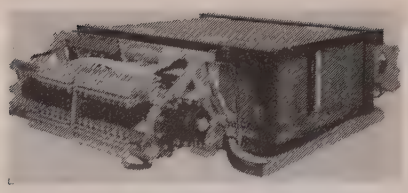

Figure 7. Assembled control group for type-MCM control

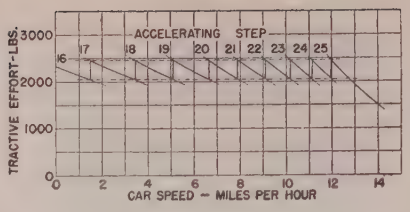

Figure 8. Acceleration curves with resistance steps proportioned for equal tractive effort increments

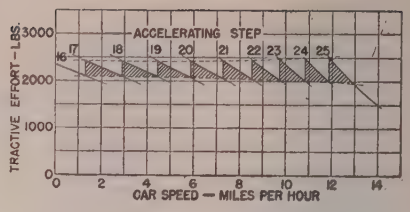

Figure 9. Acceleration curves with resistance steps proportioned for equal incremental impulses

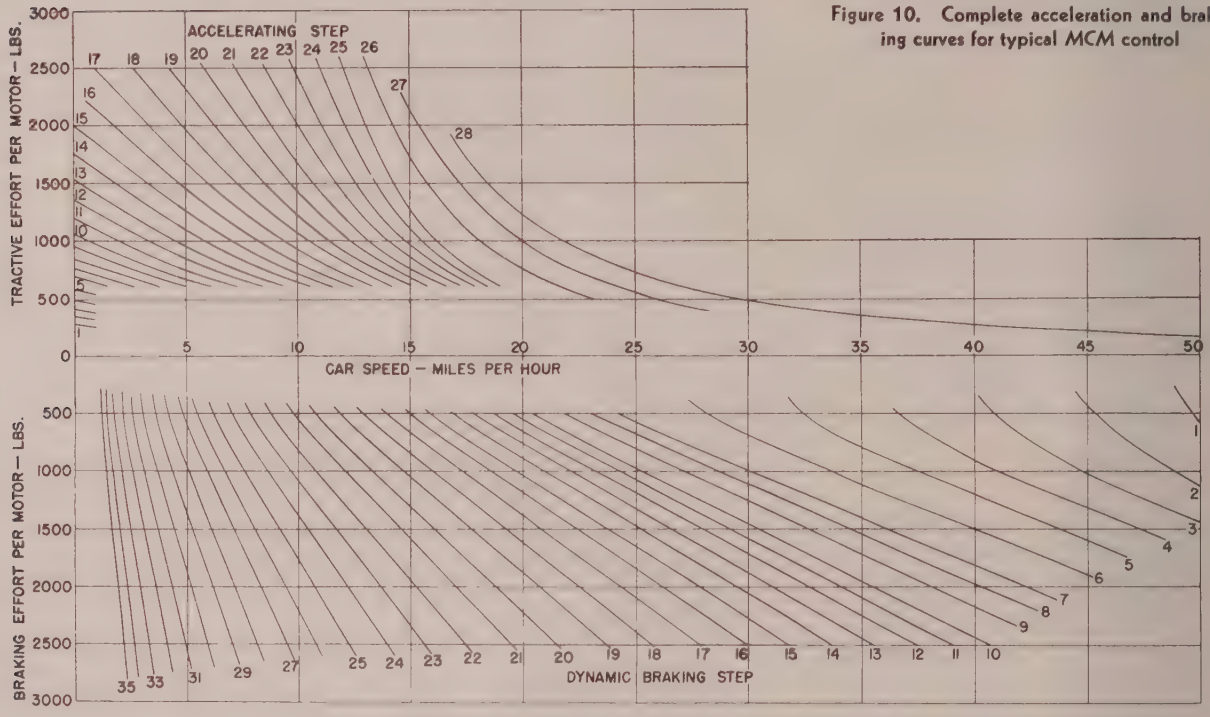

Figure 10. Complete acceleration and braking curves for typical MCM control

trol system, however, the ohmic value of each step is limited only by (*a*) the responsiveness of the current-regulating components of the system, relative to the timing and rate of change of motor current, to "sense" each step, and (*b*) by passenger consciousness of the pulsating forces in acceleration and braking. The latter limitation has led to a new concept and principle regarding the proportioning of a proper number of steps in both accelerating and braking.

Heretofore, it has been considered generally that an ideal acceleration was one in which the current (or torque) varied between constant maxima and minima, as illustrated by Figure 8. The art is well versed in the theoretical calculation of resistors on this basis, where the ohmic values of successive resistor sections are related by a geometric progression. It is well known, however, that where such steps come in rapid succession, a sensation of jerkiness can be felt under certain conditions.

A study of this problem and an analysis of recording accelerometer charts quickly led to the conclusion that the *duration* of each step was as great a factor in sensing steps as the magnitude of tractive effort increment. Accordingly, it was determined that the resistor sections should be proportioned for uniform maximum "incremental impulses" (products of tractive effort increment and step duration) of such magnitude that the steps normally are perceptible only by a sensitive accelerometer. Figure 9 illustrates this principle, the crosshatched areas of each step being equal.

This new concept was applied to the proportioning of resistance steps for dynamic braking as well as for acceleration. The resulting complete set of accelerating and braking curves is shown in Figure 10. Because nearly all the resistance sections are used in both acceleration and braking, and because of the wide range required in tractive and braking efforts, the actual "incremental impulses" are far from uniform, but in no case do they exceed the permissible value determined by service tests. Application of the principle, however, permits attaining a high standard of passenger comfort notwithstanding the use of a relatively few accelerating and braking steps.

No Discussion

Electric Equipment and Performance of Lightweight Rapid Transit Cars

W. R. ELLIS
ASSOCIATE AIEE

M. L. SLOMAN
NONMEMBER AIEE

Synopsis: The success of the Presidents' Conference Committee (PCC) car in city service has led to the development of a standard lightweight rapid transit car through the collaboration of the American Transit Association, the Transit Research Corporation, and interested manufacturers. The basic features and equipment of the PCC streetcar have been retained except where conditions peculiar to rapid transit service dictated modifications.

History

SINCE 1936, when the first production model PCC car went into operation in Brooklyn, all street railway equipment purchased for city transit service has been of the PCC type except for a few cars which had modifications of the PCC electric equipment. As of September 1, 1950, there were 4,899 cars in service or on order on 26 properties in the United States and Canada. This growth is recorded in Figure 1. During this 16-year period, the PCC car equipment has undergone many changes in component parts to reduce operating and maintenance expense and at the same time to increase the rider appeal of the car.

In 1940 a definite step was taken in the direction of rapid transit service when the first cars equipped for multiple-unit operation were placed in service by the Pacific Electric Railway Company. About the same time cars consisting of three articulated units mounted on four trucks were placed in operation by the Brooklyn Manhattan Transit Corporation, now a part of the New York Board of Transportation. Each car was equipped with two sets of PCC car electric equipment, each set consisting of a complete control unit and four 55-horsepower traction motors. This, then, was the first application of PCC-type electric equipment to rapid transit service. The car bodies were of a special articulated design involving the liberal use of aluminum.

Paper 51-33, recommended by the AIEE Land Transportation Committee and approved by the AIEE Technical Program Committee for presentation at the AIEE Winter General Meeting, New York, N. Y., January 22–26, 1951. Manuscript submitted October 24, 1950; made available for printing November 22, 1950.

W. R. ELLIS and M. L. SLOMAN are both with the Westinghouse Electric Corporation, East Pittsburgh, Pa.

Rapid Transit Requirements and Operating Conditions

A double-track rapid transit line may handle rush-hour loads of from 20,000 to 40,000 passengers per hour in one direction. Private right-of-way operation is required in the form of subway or depressed open-cut type of construction, elevated structure or roadway, or private right of way on the surface with grade crossing protection. Trains may vary from six to ten cars, depending upon the load, but in any case headways in the order of two to three minutes are involved, which means that stop time must be held to a minimum if schedules are to be maintained.

The rapid transit version of the PCC car has been designed for high-level platform loading with two or three large doors on each side of the car to hold the loading and unloading time to a minimum. The passenger capacity of the car has been increased to a maximum, consistent with weight and length limitations, by the use of special seating arrangements. The maximum capacity of the car has been increased to 180 passengers, or 44 per cent more than the standard car, while the number of seats has been decreased to 46, or only 15 per cent, with the longitudinal seating plan.

Operating conditions in rapid transit service are quite different from those encountered in normal street railway service, making it desirable to change some of the electric apparatus with respect to size, assembly, and method of operation. Rapid transit means definite stops at fixed locations spaced from one-quarter to three miles apart, whereas city service varies from 5 to 12 stops per mile plus innumerable slowdowns in congested areas dependent upon automotive traffic conditions.

Electric Equipment

Accelerations in rapid transit service are made against either a caution signal or a proceed signal, therefore two or three accelerating rates are provided on the new car rather than a continuous range of rates as on the surface car. The three accelerating rates—low, medium, and high—are ample for the service and keep the number of train line wires to a minimum, since the rates must be changed electrically through this medium in multiple-unit operation. On the Chicago all-

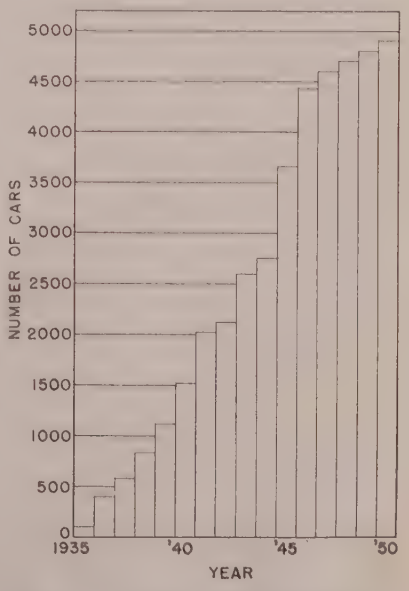

Figure 1. Cumulative annual purchases of PCC cars for surface operation

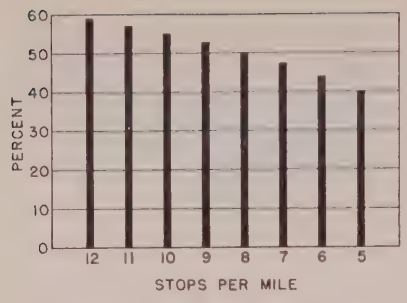

Figure 2. PCC surface car with average load—per cent of running time used for acceleration to shunted field position and for braking

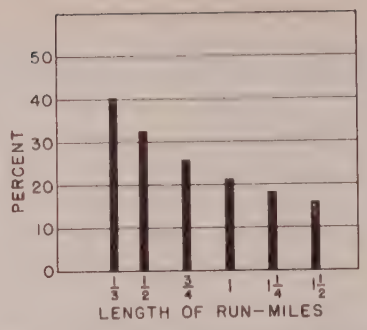

Figure 3. Lightweight rapid transit car—per cent of running time used for acceleration to shunted field position and for braking, 2-car train with average load

electric car, three dynamic braking rates are provided for normal service braking. For emergency braking, the maximum dynamic braking rate is augmented by the drum brake, which normally is used to stop and hold the car after the service dynamic brake fades out at a very low speed. The magnetic track brake, used for emergency braking and furnished as standard equipment on all PCC surface cars, may be applied on the rapid transit car. However, this type of brake has been omitted on the cars purchased to date because the presence of a properly signalled private right of way reduces the frequency of emergency conditions.

On cars equipped with air brakes, 15 steps of normal service braking are provided dependent on straight air-pipe pressure as determined by the position of the controller handle. The change in air pressure is transmitted through an actuator to a rheostat in series with a loading coil on the limit relay, thus changing the calibration of the relay to the desired dynamic braking rate. The air-brake application is held off by a lockout relay until the dynamic brake fades out, at which time the air brake is applied to complete the stop and hold the car while standing. The tread brakes also supplement the dynamic brake in such a manner that a smooth blending is obtained when the dynamic braking rate alone is insufficient for the load and grade conditions. In an emergency application, the air brakes alone provide a deceleration rate of 4.0 miles per hour per second (mphps).

Foot-pedal operation of the surface car has been replaced on the rapid transit car by hand-operated controls because the motorman is free of the fare collection duties. The car is controlled by a combined master and brake controller operated by a single handle.

Because of the longer runs in rapid transit service, the speed at which braking is applied is much higher than in surface operation. The application of both power and brake must be as smooth as possible to provide a comfortable ride for the passenger. To accomplish this result with the higher braking speeds, the resistance in the motor brake circuits must be approximately 50 per cent greater than that normally used on the standard PCC surface car. This added resistance is provided by the use of a larger accelerator, which has 135 resistance steps instead of 99. The dynamic brake builds up to full rate smoothly without jolting in approximately one second at all speeds up to 50 miles per hour (mph). Another feature of the larger accelerator is that an almost free coast is obtained up to 45 mph, with a slightly increased braking effort at higher speeds. To obtain prompt braking in the desired amount, the resistance in the main motor circuit must be adjusted to correspond to car speed. This is known as "spotting" the accelerator, and in effect is dynamic braking at a very low current. The additional resistance in the larger accelerator holds this current to a minimum value, which is important in rapid transit service where a considerable amount of coasting at high speeds may be desirable.

Most rapid transit systems are operated from a third-rail system which necessarily must have frequent gaps. A special line relay was developed for the new car to give adequate protection and smooth operation at all times. This device has a very fast opening and a delayed pickup which gives the control apparatus time so to readjust itself that the reapplication of power is smooth and normal.

Rapid transit trains may be made up of two to ten cars. In a long train the operator may be unaware that one car is dead or defective, therefore some protection must be provided to prevent "bucking" or build-up of braking currents on a car which is not functioning properly. A "loop" contactor has been added to the standard PCC car equipment and is placed in series with one pair of motors to break up the dynamic braking loop which comes into play when a reverser fails to operate correctly. The "loop" contactor closes when the line breaker closes and remains closed through the accelerating and braking cycle until the car comes to a stop. Thus on each run, beginning with the first application of power, the functioning is checked for proper operation of the reverser and other equipment. A failure automatically will eliminate power from that unit and allow the car to be pulled freely.

The specification that these cars be operated in a maximum train of ten cars required that the control load in the various train line wires be kept to a minimum. Therefore, the control load is supplied by the motor generator set on each car as far as practicable. Special operating coils were designed for all contactors, and relays were applied to the reverser and line breaker so that the full operating coil current was not required to be carried by the train line wires. In addition, the generator operates at 45 volts, which gives an added margin of safety for the operation of the equipment.

At the time the PCC electric equipment first was applied to rapid transit service, all the PCC surface cars in multiple-unit operation were equipped with air brakes and other air-operated devices. Pneumatically operated reversers also were used on these cars. However, because the first PCC cars built for rapid transit service were of the all-electric type, it was necessary to design a new all-electric power-operated reverser. It is powered by magnets of liberal design to obtain maximum reliability with minimum maintenance. Compensated fingers rest on cast drum segments which are fastened to an insulating shaft. Two relays are supplied to relieve the train line of the load required for operation. Most of the postwar standard PCC cars have been the all-electric type, but they are equipped with the standard manually operated reverser applicable to single-unit operation.

Basic-Unit Car Considerations

In 1947 the Chicago Transit Authority placed in service on its Rapid Transit Division a new design of car with PCC electric equipment. After several years of successful operating experience with its PCC surface cars, the management de-

Table I. Comparison of Lightweight Rapid Transit Cars

	Semi-permanently Connected 2-Car Unit	3-Body 4-Truck Articulated Unit
Total weight, lbs	79,600	93,000
Over-all length	96′-0″	88′-7½″
Over-all width	9′-4″	9′-4″
Seated passengers	96	96
Total passengers	320	250
No. doors each side	4	3
Weight of electric equipment, lbs	9,790	10,537
Motors (8), hp	55	55
Total motor hp	440	440
Total weight with max. passengers, lbs	124,400	128,000
Weight of empty car per max. passengers, lbs	249	372
Weight of empty car per seat, lbs	830	970
Weight of empty car per foot, lbs	830	1,050
No. passengers max. per foot	3.34	2.82
Max. passengers per side door	80	83
Length per side door	24′-0″	29′-6½″
Hp per ton, empty car	11.07	9.46
Hp per ton, max. loaded car	7.07	6.88

cided to design and test a new type of rapid transit car utilizing as much of the standard PCC car equipment as possible. Each car consists of three bodies articulated on four PCC-type trucks and has a passenger capacity equivalent to a base service train of two cars. The car weighs 93,000 pounds, which is within the capacity of the standard PCC-type motor in Chicago service. Two sets of PCC car equipment, modified as described previously, are applied to each car. After an intensive series of tests, the cars were placed in service. The performance of these cars met all the desired operating characteristics with a minimum of maintenance. In September 1948, after the sample equipment had been in operation for ten months, the Chicago Transit Authority placed an order for 130 rapid transit PCC cars. These cars differ from the sample cars in that each consists of a single body mounted on two trucks with one set of modified PCC-type electric equipment.

When the single-body car was selected, the decision was made to operate two cars as a semipermanently connected unit for economic reasons. One unit provides the passenger capacity required during the base traffic periods. Units may be combined in multiple-unit operation to form trains of four, six, eight, or ten cars, providing flexibility for the system under all load conditions. All cars are identical. However, only one end of the car is equipped with a control station, automatic coupler, and other apparatus necessary to operate as the head-end of a train. Two cars are connected back-to-back, so that a unit may be operated from either end. This operating procedure reduces the amount of equipment per car and results in substantial savings in first cost and maintenance expense.

Both types of car offer advantages for particular operating conditions, but many operators believe that the single-body car mounted on two trucks is more suitable for rapid transit service. Only one body section is required, hence the initial cost is lower as well as the investment required for spare equipment. One car of a 2-car unit may be taken out of service and replaced with an identical car. In the case of an articulated unit, either the entire unit must be withdrawn from service or else dummy trucks must be used in conjunction with body jacks in order to replace one body section. A 2-car unit can be built with less weight than the articulated car, as shown in Table I. Passenger capacity is sacrificed at the two articulation joints, whereas the 2-car unit has only one connection restricting standing passengers. On the other hand, the articulated unit permits easier and safer movement of passengers between cars. However, studies have shown that the daily rider boards the train at the approximate location where he wishes to get off, and there generally is very little movement between cars in rapid transit service. The 2-car unit also provides more flexibility in the door and seating arrangements with a consequent increase in passenger capacity. A truck derailment and broken axle or wheel on a single-body car necessarily poses a difficult operating problem in rapid transit service where the right of way is very restricted, but such a failure on an articulated unit, especially when the truck is at an articulated joint, is one of major proportion. These advantages, which vitally affect investment, fixed charges, operating and maintenance costs, are responsible for the fact that operators prefer the 2-car unit in spite of the improved riding qualities and other advantages of the articulated 3-body unit.

Performance Characteristics

The first units of the 130-car order were received by the Chicago Transit Authority in September 1950. The scale weight of the car is 39,800 pounds, slightly under the estimated 40,000-pound weight. The total weights with seated load and maximum load are 46,500 and 62,200 pounds, respectively. The corresponding figures for the average PCC surface car are 36,000, 43,500, and 52,800 pounds.

Accelerating and braking rates of 1, 2, and 3 mphps were selected, based on the 39,800-pound car weight with no load. Since the limit relay settings are at some fixed value of current, the tractive effort available for acceleration also remains constant and the accelerating rates decrease as the load increases. In dynamic braking, the rate also is controlled by the limit relay, consequently the rate decreases as the load increases.

A pneumatically operated variable load mechanism, commonly referred to as a load-weighing device, has been used on rapid transit cars equipped with an air-brake system. It automatically maintains a constant accelerating rate between fixed minimum and maximum total car weights by changing the limit relay setting by means of a rheostat with a mechanical linkage actuated by the deflection of the car springs. A lockout magnet valve is used to obtain smooth blending of air and dynamic brake when the braking

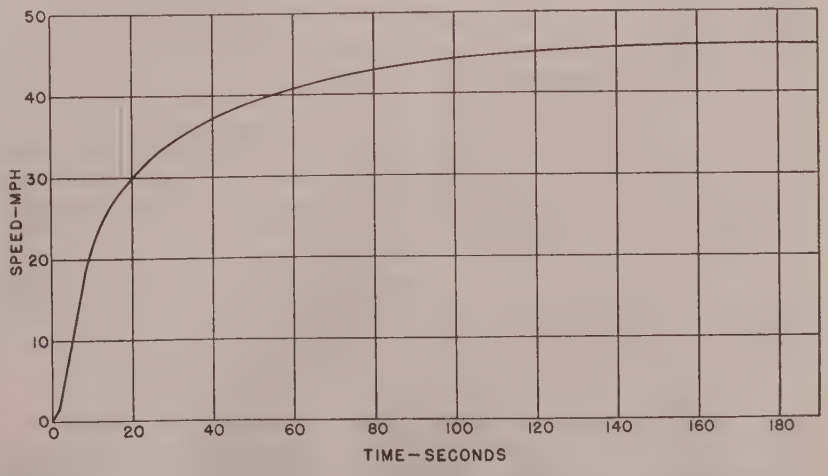

Figure 4. Speed-time performance curve—lightweight rapid transit car, 2-car train with average load, level track

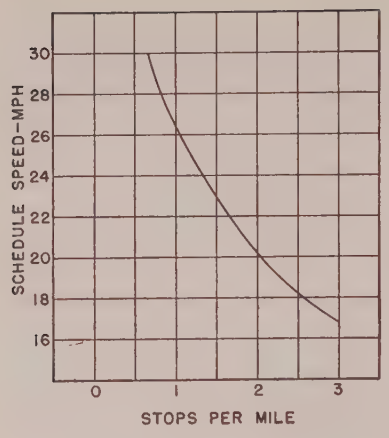

Figure 5 (left). Schedule speed performance — lightweight rapid transit car, 2-car train with average load, level track

Figure 6 (right). Chicago Transit Authority lightweight rapid transit car

rate selected by the operator exceeds the maximum dynamic braking rate obtainable.

For city transit service, the standard PCC car is capable of operating at maximum accelerating and dynamic braking rates of 4.75 mphps, although the average accelerating rate in service approximates 3.5 mphps. These high rates were necessary to maintain the car's position with respect to other street traffic in congested areas and to increase schedule speeds with respect to the old streetcars which the PCC car was designed to replace. On heavy traffic lines where streetcars are the most economical vehicle to operate, the number of stops per mile may vary from 5 to 12. Hence, the length of run is so short that much of the running time is consumed in accelerating and braking. This is shown graphically in Figure 2. Thus, the only way schedule speed could be increased was to provide motor capacity sufficient to obtain the highest practicable accelerating and braking rates.

Rapid transit service normally averages from one to three stops per mile. The longer runs permit much high-speed operation with the result that the accelerating and braking rates may be lower than in surface operation since a small percentage of time is consumed in these operations (see Figure 3). These two conditions, lower accelerating and braking rates and longer runs, have made it possible to apply the standard PCC car motor to the heavier cars and loads encountered in rapid transit service without exceeding its margin of safety.

The PCC-type of rapid transit car, equipped with four 55-horsepower traction motors, has a very high ratio of horsepower per ton weight on both an empty and a maximum load basis. With the standard PCC-type gear unit of 7.17-to-1 ratio and wheels with a diameter of 26 inches, the car with average load will attain a free running speed of 46 mph on level tangent track, as shown in Figure 4. A true measure of car performance is the ability to maintain high schedule speeds. This is doubly important in rapid transit service, for with proper headways and signal systems the car is on its own, unhampered by the traffic jams and traffic lights in surface operation. The performance of these cars permits high schedule speeds, as shown in Figure 5, which are a requisite of rapid transit service.

Advantages of the Lightweight Rapid Transit Car

In addition to its exceptional performance characteristics, the rapid transit PCC car has even more to offer. It is the lightest weight rapid transit car ever built and has the lowest first cost because of the mass production of the various components as well as the car body, which utilizes many of the basic structures of the standard car. From the experience of city transit operation of PCC cars for 16 years, it may be expected that these cars will produce real savings in operating and maintenance costs. After delivery of the first cars to Chicago, some of the most favorable comments were made by the maintenance department regarding the accessibility of all equipment in general and the traction motors and gear units in particular. This is caused by the fact that the basic truck design and small diameter wheel size of the standard car have been retained in the rapid transit design, which has a floor level approximately 13 inches higher.

To managements operating large fleets of PCC cars in surface transportation, the rapid transit PCC car offers other obvious advantages. Spare-parts inventory may be kept to a minimum since many of the parts are interchangeable. Maintenance practices already are established and maintenance tools and equipment are available. Skilled mechanics and electricians trained in the maintenance of PCC equipment need not be retrained, for the new car is equipped with identical traction motors and many mechanical features, as well as the same general control scheme and equipment as the standard car.

Conclusions

On September 1, 1950 the Chicago Transit Authority had 200 cars on order, and the Metropolitan Transit Authority of Boston had 40 cars on order. These cars are being built according to a specification drawn up by the PCC Rapid Transit Equipment Subcommittee of the Advisory Committee on PCC cars, Mechanical Division, American Transit Association. The design of a PCC car for rapid transit service has provided the transit industry with a new tool to supply fast, comfortable, efficient service with a minimum investment in new rolling stock.

This car has been designed especially for rapid transit service by men who must operate and maintain this type of equipment. It is believed that this lightweight car will be applied to many rapid transit systems on all but the heaviest lines. The consideration being given to this type of car in cities planning their initial rapid transit installations is evidence that its use will be extended to new systems.

Reference

1. Three-Compartment Articulated Cars for Test on Rapid Transit Division, Chicago Transit Authority, H. A. Otis. *AIEE Transactions*, volume 67, part 1, 1948, pages 416–18.

Discussion

H. G. Moore (General Electric Company, Erie, Pa.): This paper presents in an excellent manner the present status of certain improvements and expanding applications of the electrical equipment originally designed for the Presidents' Conference Committee (PCC) car. One very significant improvement was made in 1944. It was the provision of so-called "extended" dynamic

braking—the extension of the range of effective dynamic braking downward in speed nearly to standstill. This accomplishment permitted the abandonment of air-operated tread brakes in favor of propeller-shaft brakes actuated by electric magnets and the general adoption of the all-electric streetcar. This improvement imposed slightly more duty on the traction motors and load resistors, but necessitated no fundamental changes in ratings or design features.

In the application of this type of equipment to lightweight rapid transit cars, the authors recognize essentially different operating conditions and the necessity of again extending the range of dynamic braking this time appreciably upward in speed. The nominal rating of the equipment in terms of line voltage and rms load current is not increased, because the longer runs with less frequent starts and stops compensate for the increased car weights and higher speeds.

These increased weights and higher speeds, however, do require that the equipment now be capable of regularly absorbing materially increased peak loads in dynamic braking of approximately 450 per cent of the 1-hour rating. This capacity cannot be increased by higher values of load resistance and motor current without proportionally increasing the peak voltages to which the motors and power circuits may be subjected. It is, therefore, of particular interest that the authors state that the resistance in the motor-brake circuits must be approximately 50 per cent greater than that normally used in the standard PCC car.

An alternate method of increasing the range of dynamic braking to higher speeds is to shunt the motor fields. This method even permits reducing the maximum load resistance and provides a number of distinct advantages, such as

1. The motor voltages are limited to lower and more conservative values under conditions of high-speed braking.

2. The load resistance remains fixed at its maximum value until the speed drops to the full-field braking step, resulting in better utilization of available resistor capacity.

3. For a given amount of active material, a lower resistance results in a greater cross-section with corresponding greater strength and increased short-time current capacity.

W. R. Ellis and **M. L. Sloman:** The authors appreciate the comments by Mr. Moore. The Westinghouse Electric Corporation designed its original PCC-car motor to meet the Transit Research Corporation's specification, which included a very severe operating cycle. Although this cycle has never been approached in city transit service, the motor was designed with the capacity to brake at relatively high speeds without exceeding the commutating limit set by voltage. Since that time, a number of electrical and mechanical modifications have been made in the motor to increase this capacity as better insulation and materials have become available. This plus feature in surface car operation has made possible the application of this motor in rapid transit service, where peak dynamic braking loads may reach values approximating 400 per cent of the 1-hour motor rating.

We do not agree with Mr. Moore that these peak loads occur regularly. Three conditions, namely, maximum load, maximum dynamic brake, and car speeds well in excess of 40 miles per hour, must occur simultaneously in order to produce these peaks. Only on rare occasions will these conditions be encountered, for maximum speeds on many rapid transit lines are limited to values under 45 miles per hour by speed restrictions, signal spacing, and more often by station spacing, except in express service.

The method of increasing the range of dynamic braking to higher speeds by shunting the motor fields is a practice used in many applications of electrically propelled vehicles for all types of transportation service. We have tried this method on PCC cars, but on the lightweight rapid transit car it has been discarded in favor of the method described in the paper. The additional resistance provided in the braking circuit by the larger accelerator limits the current to the values required for the desired braking rates and also maintains the motor voltage within the permissible range. This method has advantages in that almost a free coast is obtained at the high operating speeds because the spotting current is low, and a smooth dynamic brake build-up is provided since the motor, operating as a series generator, is more stable in full field than in a shunted field connection. Thus, there is much less chance of an initial peak rate with its resulting jerk and discomfort to passengers.

The operation of approximately 100 of these cars in service on the Rapid Transit Division of the Chicago Transit Authority has furnished ample proof of the success of both the device and the method.

A Modern Cab Signaling and Train Control System for Railroads

L. R. ALLISON
ASSOCIATE AIEE

Synopsis: Increased safety of train operation is effected by the continuously controlled cab signal which may be augmented by means for applying the brakes automatically in case cab signal changes calling for a reduction in speed are ignored or predetermined speed limits are exceeded. The engine-carried apparatus is inductively linked and selectively responsive to coded alternating current in the running rails, the frequency of coding determining the cab signal indication displayed and being dependent upon traffic conditions ahead. Absence of rail current or the presence of uncoded current establishes the most restrictive speed conditions.

THE outstanding feature of modern systems of automatic train control is the signal in the cab. It provides in the cab, in full view of the enginemen, a miniature counterpart of the familiar wayside block signal.

The control of the cab signal indications is transmitted from the wayside to the locomotive through inductive coupling between alternating current flowing in the rails and a pair of iron-cored receiving coils on the locomotive. Changes in the character of the rail current, produced by changes in traffic conditions ahead, cause corresponding changes in the cab signal aspect.

Thus, the cab signal gives a continuous indication of conditions that are ahead and any change in these conditions affecting the safety of the train is reflected instantly in the cab signal indication regardless of the position of the train with respect to the wayside signals. This not only promotes increased safety of train operation, but reduces delays by permitting the engineman to increase speed when the cab signal changes to a more favorable indication without waiting until the next wayside signal is in view.

The controls on the locomotive which govern the cab signal indications are used in conjunction with other apparatus to enforce obedience to changes in these indications that require a reduction in speed. On some railroads, the control of the train speed is left entirely in the hands of the engineman, but any change in the cab signal to a more restrictive indication is accompanied by the continuous sounding of an audible warning device in the cab. The engineman may silence this audible indication, and thereby acknowledge his awareness of the changed conditions, by actuating a lever within his convenient reach. Should the engineer for any reason fail to acknowledge, the continued sounding of the warning device directs the fireman's attention to the need for action.

The controls may be arranged to apply the train brakes automatically if the engineman fails to heed the audible warning and to acknowledge within a specified number of seconds after the cab signal changes to a more restrictive indication. Once the automatic brake application has begun, it cannot be released until the train has been brought to a full stop or the cab signal has changed to a less restrictive aspect.

The cab signal also may form the foundation of a speed control system in which a governor fixes certain speed limits in accordance with the information given by the cab signal. A number of speed limits may be imposed up to but not exceeding the number of cab signal indications provided.

An automatic brake application caused by running above authorized speed may be suppressed by applying the brakes manually until the pressure in the brake cylinders reaches a predetermined value or the speed has been brought below the limit.

There also is a selection in the rate and gradation of the automatic brake application. The brakes may be applied at an emergency rate or at the manual service rate. If the latter, the brake pipe reduction may be unlimited or it may be limited to a value that will insure stoppage of the train within the allotted distance. The limited reduction can be made in two steps, the first of which serves to bunch the slack in the train before the second, or heavier, reduction begins.

It thus can be seen that there are available many different combinations of train control apparatus arranged to meet the varied operating needs and requirements of the different railroads. It is the purpose of this paper to describe one such combination; that comprising a 4-indication cab signal system with 4-speed control. This combination has been selected as the example because it is so extensive in its scope that it includes all of the main features that may enter into a train control system.

Early History and Development

The era of continuous inductive cab signaling and train control began on July 11, 1923, when an installation of 3-indication 3-speed automatic train control was placed in service between Lewistown Junction, Pa., and Sunbury, Pa., on the Pennsylvania Railroad. Its use has been extended until today more than 5,600 motive power units and 9,700 miles of track are equipped with cab signaling or continuous train control.[1]

The early train control systems were based upon the use of steady (uncoded) alternating current in the rails. For a 2-indication system, current of opposite in-

Paper 51-34, recommended by the AIEE Land Transportation Committee and approved by the AIEE Technical Program Committee for presentation at the AIEE Winter General Meeting, New York, N. Y., January 22-26, 1951. Manuscript submitted July 24, 1950; made available for printing November 22, 1950.

L. R. ALLISON is with the Union Switch and Signal Company, Swissvale, Pa.

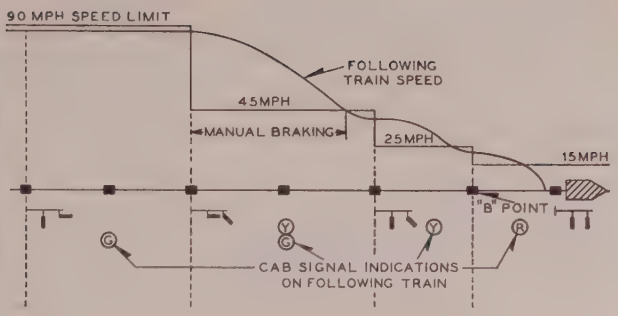

Figure 1 (left). Four-indication cab signal mounted in cowl center post of diesel-electric locomotive

Figure 2 (above). Changes in speed limits and cab signal indications as train approaches rear of train ahead

stantaneous polarity flowed in the two rails from the low-voltage winding of a transformer connected across the rails at the leaving end of the track circuit. Presence of this current in the rails under the receiver produced a clear signal in the cab. Absence of current, as when shunted away by the wheels and axles of a train ahead, produced a restricting cab signal. To obtain three cab signal indications, it was necessary to superimpose a second rail current upon the first and to provide on the locomotive a second receiver which would be responsive to it. This second current, called the loop current as distinguished from the first, called the track current, was caused to flow through a bridge circuit in which the rails and a midtapped resistor connected across the rails at each end of the track circuit formed the balanced arms. The loop and track currents were in quadrature-phase relationship.

The steady current systems possessed two important disadvantages which limited their usefulness. These were:

1. No more than three cab signal indications or controls could be obtained without using alternating current of more than one frequency.

2. Difficulty in confining the loop current of the 3-indication system to its designated track circuit, particularly in electric propulsion territory where cross-bonding and supplementary negative conductors provide diverting paths.

In these early systems, the train control relay was an a-c vane-type energized from a 2-stage 2-phase amplifier. The amplifier contained four triode vacuum tubes which required a 350-volt d-c plate supply. It is of historical interest that, so far as is known, this was the first industrial application of electron tubes, that is, in a field outside of radio, telephone, or telegraph communication.

The Code System

The disadvantages inherent in the use of steady energy led to the introduction of the code system in 1926. In this system, the train-carried apparatus is responsive to coded alternating current applied to the track circuit at its exit end and functions to maintain a continuous cab signal indication reflecting traffic conditions ahead of the train. To effect this response, the current in the rails is coded by interrupting it at certain rates, the number of interruptions per minute being determined by traffic conditions ahead. The absence of this track current or the presence of steady or uncoded current produces the most restrictive signal in the cab. The codes now used generally are 180, 120, and 75 interruptions or cycles per minute. The code pattern is uniform, the on-and-off periods being of approximately equal length.

Voltages of the same frequency and code rate as the rail current are induced in the engine-carried receiver and these voltages are amplified to operate the code-following relay which governs the decoding units that are responsive selectively to the code rate at which the master relay is operated. The decoding relays associated with the decoding units in turn control the cab signals, the audible warning devices, and the electropneumatic valve.

Coding of the rail current produces a number of important advantages not obtainable with the noncode system. These are:

1. The equipment operates safely in the presence of extraneous currents or magnetic fields. It responds only to coded alternating current of the proper frequency.

2. No line wires are required for control of signal indications because the controls are transmitted by codes through the rails.

3. More than three indications can be obtained. In fact, additional indications could be obtained by the use of other codes, but four indications generally have been found sufficient.

4. Increased track-shunting sensitivity and increased broken-rail protection are obtained because code operation is determined by the pick-up rather than by the release value of the code-following relay.

5. It is universally applicable to any class of motive power: steam, diesel, or electric locomotives and multiple-unit cars.

Figure 2 shows how the cab signal indication and speed control limits change on the modern 4-indication 4-speed control system, selected as an example, as a train overtakes a train ahead. Assume that the train is about to enter the first of four blocks, the fourth being occupied. The cab signal is displaying the "clear" (green) indication and the maximum speed limit of 90 miles per hour (mph) is in effect. As the engine passes the "clear" wayside signal, there is no change in the cab signal or in the speed limit.

When the next wayside signal, at "approach-medium," is passed, the cab signal changes to "approach-medium" (yellow over green) and the speed limit is reduced to 45 mph. The restrictive condition is made known to the engineer by the sounding of a buzzer, and unless he initiates a manual brake application within six seconds, the brakes will apply automatically. As long as he is applying the regular train brakes at the service rate, an automatic application of the brakes is suppressed. He must continue to maintain a service brake application until the speed of the train has been reduced below 45 mph, when he can release the brakes and continue at a speed below 45 mph until the next signal is passed. The buzzer will sound as long as the speed of the train is above the limit. The instant the buzzer stops, the engine-

man may initiate release of the brakes.

The speed limits of 90, 45, 25, and 15 mph have been chosen arbitrarily for the sake of illustration. While these may be considered typical, other speed limits may be selected by different railroads to suit their particular operating conditions.

When the next wayside signal, at "approach," is passed, the cab signal changes to "approach" (yellow), the speed limit is reduced to 25 mph, and the speed warning buzzer sounds and continues to sound as long as the speed is above this value. As before, an automatic brake application will be initiated within six seconds after the overspeed warning buzzer sounds unless it is suppressed by a manual application sufficient to reduce speed below the new limit.

Any time the speed limit is exceeded, the warning buzzer will sound and continue to sound until the speed is reduced below the limit.

The next wayside signal will be at "stop," and perhaps the rear of the train ahead is just beyond the signal location, as shown in Figure 2. It may be desired, therefore, to effect the next cab signal change, not at the signal itself, but at a point, called the "B" point, sufficiently in advance of the signal to insure that the train will be stopped automatically from the maximum speed of 25 mph before the signal is passed. As this point is passed, the cab signal changes from "approach" to "restricting" (red), and the speed limit is reduced from 25 to 15 mph. Again the buzzer will sound and will continue to sound until the speed is reduced below 15 mph, and again an automatic brake application will ensue if the engineman does not suppress it by applying the brakes manually.

As an additional safety measure, any time the cab signal changes to "restricting," a bell also will sound and, even though the speed already is below the 15 mph limit, an automatic application of the brakes will be initiated six seconds after the bell starts to sound unless the engineman operates an acknowledging switch. This switch may be either the foot-actuated or the hand-actuated type. The purpose of enforcing an acknowledgment of the "restricting" indication is to remind the engineman that he is approaching a "stop" wayside signal.

After first coming to a full stop, in accordance with standard railroad operating rules, the train may proceed into the occupied block not exceeding 15 mph, being prepared to stop within range of vision.

When the cab signal changes to a more restrictive indication, but the speed of the train is below the new limit, the buzzer will not sound. Likewise, cab signal changes to less restrictive indications are unaccompanied by sounding of audible warning devices because block conditions have changed to permit operation of the train safely at higher speed.

The Rail Current Control Equipment on the Wayside

The apparatus used for operation of the continuous cab signal and train control

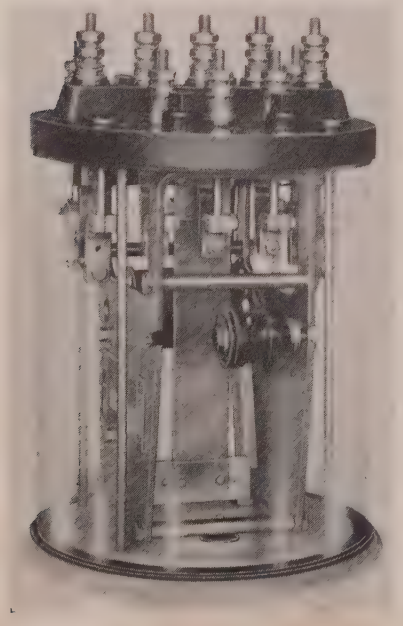

Figure 3 (left). Pendulum-type 180-code transmitter

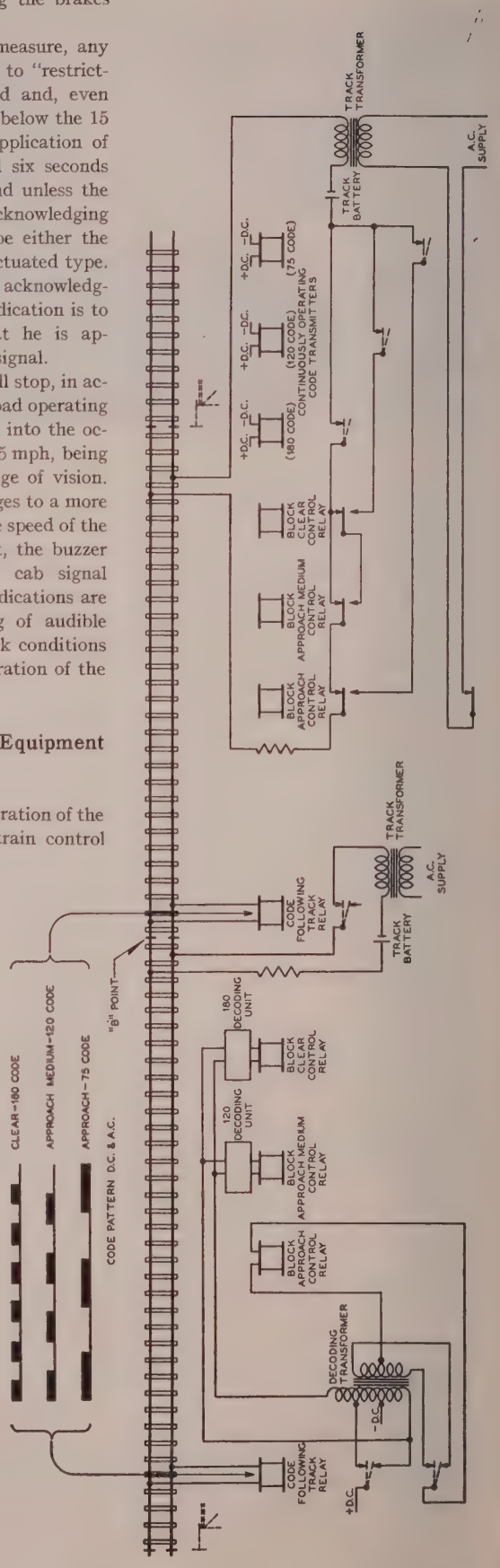

Figure 4 (right). Typical coded track-circuit control of cab signal indications

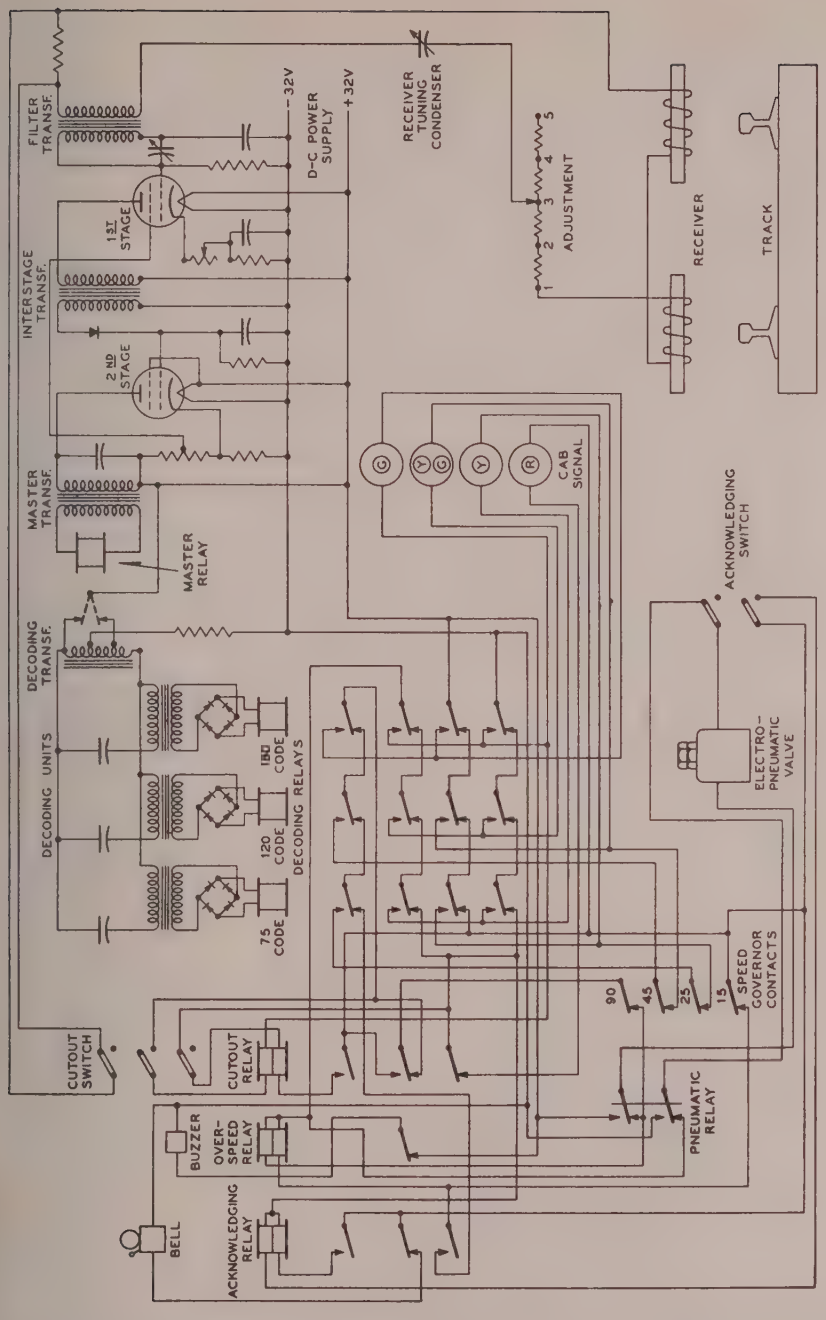

Figure 5. Circuit of electric equipment on the locomotive

system consists essentially of two main parts: that on the locomotive and that on the wayside.

The continuous indication in the cab is maintained by the track-circuit alternating current introduced into the running rails at the exit end of the track section and interrupted a definite number of times per minute according to the conditions ahead. This current induces a voltage in apparatus carried on the engine and so causes other engine-carried apparatus to function to establish the cab signal aspect and speed limit corresponding to the frequency of interruption of the track current.

In the wayside system the mechanism which interrupts the alternating current as it is fed to the rails is called a code transmitter. One type consists of contacts actuated by an electrically driven pendulum mechanically tuned to the code frequency. A separate code transmitter is used for each code frequency. A view of a pendulum-type 180-code transmitter is shown in Figure 3.

The advantages of code control of cab signals apply equally to the control of wayside circuits and signals. For that reason, the use of steady-energy track circuits for wayside signal control is being supplanted rapidly by coded track-circuit control. In 1932 the first coded track-circuit control installation was placed in service between Zoo Tower and Arsenal Tower on the Philadelphia Terminal Division of the Pennsylvania Railroad. Now more than 15,000 miles of track in the United States and Canada are equipped with coded track circuits.

The foundation of all successful railway signaling is the track circuit. Invented in 1872, it remains today the best means yet devised of detecting automatically that a defined section of railroad track is occupied or otherwise unsafe for the passage of another train. The rails themselves serve as the conductors of electric energy supplied by a low-voltage power source connected to the rails at one end of the circuit and delivered to the coils of the track relay connected to the rails at the opposite end of the circuit. Current is confined to the desired section of track by placing insulation in rail joints at the boundary points of the section. All other rail joints are bonded with flexible connectors to insure uniformly low resistance.

As long as the track circuit is unoccupied, with all rails intact and switches properly positioned, the track relay will receive energy, thus indicating the fact of nonoccupancy. The entrance of a train into the circuit, however, will shunt so much current from the coils of the track relay through the much lower resistance path of the wheels and axles of the train that the track relay will release and will remain in its released position. This will cause the wayside signal to assume the "stop" position.

In considering the track circuit, it is important to note that a failure such as may be caused by loss of power, a broken wire, a broken rail, a misaligned switch, or a short circuit will deprive the track relay of current, thus causing it to stay released and setting the controlled signal at its most restrictive indication. Not only the track circuit, but all vital circuits in railway signaling are designed to operate on this "fail-safe" or closed circuit principle. A circuit is said to be designed on the closed circuit principle when the integrity of its vital elements is being checked constantly.

A typical form of coded track-circuit control is shown in Figure 4. Both direct current from the track battery for operation of the code-following track relay and alternating current from the low-voltage

winding of the track transformer for cab signal operation are coded over the same contact of the continuously operating code transmitter at the signal location. The code transmitted to the rear from the signal location is determined by the position of the block-control relays which, in turn, are dependent upon the code being followed by the track relay at that signal.

The block-control relays receive energy from the decoding transformer. One contact of the code-following track relay reverses the direction of direct current in the primary winding of the decoding transformer with each operation of the code-following track relay. The code frequency alternating current induced in the secondary winding of the decoding transformer is rectified by a pole-changing contact on the track relay to cause unidirectional current to flow in the winding of the block-approach control relay. Only when the code-following track relay is operating continuously will energy be induced in the secondary winding of the decoding transformer. If the code-following relay stops with either its upper contacts or its lower contacts closed, the supply of direct current to the block-approach control relay is discontinued and consequently this relay opens its upper contacts and closes its lower contacts. Under this condition, only 75-code direct current can be transmitted to the circuit in the rear. Because the circuit controlling the block-approach control relay is not tuned or otherwise selective as to frequency, the block-approach control relay will be energized when the code-following track relay responds to 180-, 120-, or 75-code.

Where more than one code is used, it is essential to select among them. This is done by relays controlled from code-frequency selective decoding units connected to an auto-winding on the decoding transformer. Thus, the block-clear control relay responds only when its associated decoding unit is receiving 180-code energy, and the block-approach medium control relay responds only when its associated decoding unit is receiving 120-code energy.

These decoding units are similar to those used on the locomotive and will be treated in greater detail under a description of the equipment on the locomotive.

Frequencies commonly used for the a-c supply are 60, 80, and 100 cycles per second. The level of minimum alternating current under the receivers when the train is at the entering end of the track circuit usually is of the order of 2.0 amperes where electric propulsion territory is involved and 0.7 ampere elsewhere.

The Equipment on the Locomotive

In Figure 5 is shown a schematic circuit plan of the locomotive electric apparatus for a 4-indication 4-speed system, and Figure 6 shows in diagrammatic form the pneumatic equipment which controls the initiation or suppression of an automatic brake application.

The track receiver, shown in Figure 7, is the means by which the control is transmitted inductively from the rails to the apparatus on the locomotive. It comprises a pair of laminated iron cores and rubber-covered coils, one for each rail, mounted ahead of the leading truck at an elevation of about eight inches above the top of the rails. The coils are connected so that the voltages induced in each are additive.

One type of equipment box designed for application to diesel locomotives is shown in Figure 8. It houses the amplifier, decoding units, control relays, main terminal board, and test panel. All components of the apparatus are rack-mounted and the rack is suspended from the sides of the box on shear-type bonded rubber mountings designed to afford maximum protection from shock and vibration. The equipment case is of welded steel construction and is dustproof and watertight when closed.

All the functional elements, which are segregated into six control relays, three decoding units, and an amplifier, are detachable individually by means of plug-connector terminal boards. Locating the source of trouble is facilitated in this way, and the amount of equipment unnecessarily out of service because of one defective part is reduced to a minimum. Each unit is enclosed in a dustproof case equipped with a convenient handle for removal and carrying of the unit. The amplifier unit and each decoding unit are locked in place on the rack.

Each relay is mounted on a base permanently attached to the rack in the equipment box and is held securely in position by hexagonal nuts applied to the threaded ends of the two guide rods on the mounting base. These guide rods also serve to align the relay so that its plug connectors will engage the receptacles in the mounting base properly when the relay is plugged into position.

In series with the receiver is a condenser for tuning the circuit to the rail-current frequency, a tapped resistor for sensitivity adjustment, and the input winding of the filter transformer. The output winding of the filter transformer

Figure 6. Pneumatic equipment piping diagram

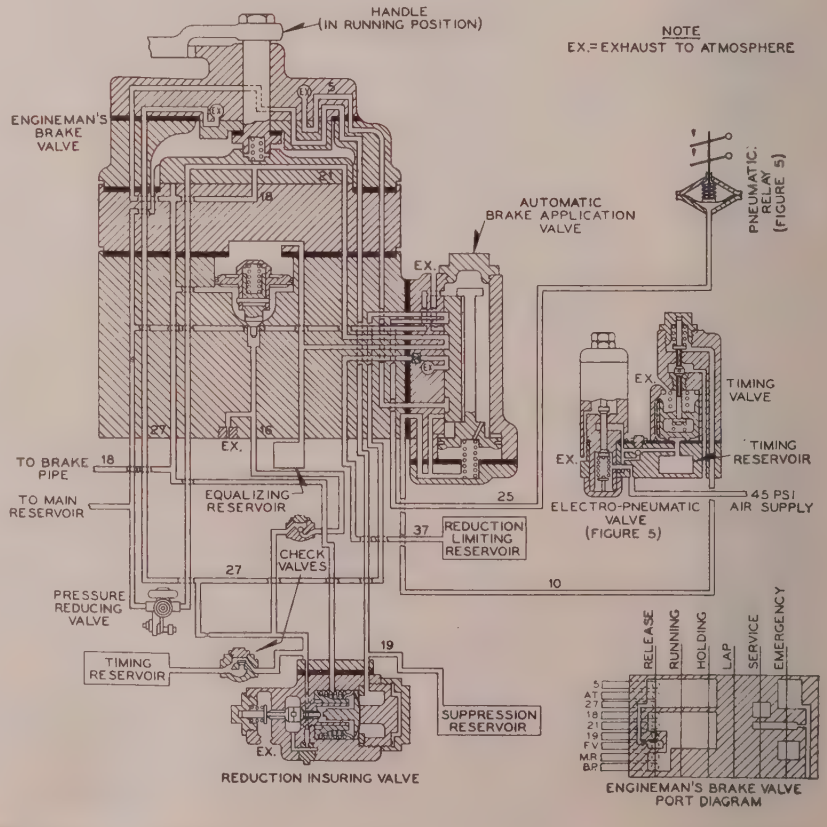

Figure 7 (above). 2-Piece receiver. Cable connects to coil through 2-way plug coupler

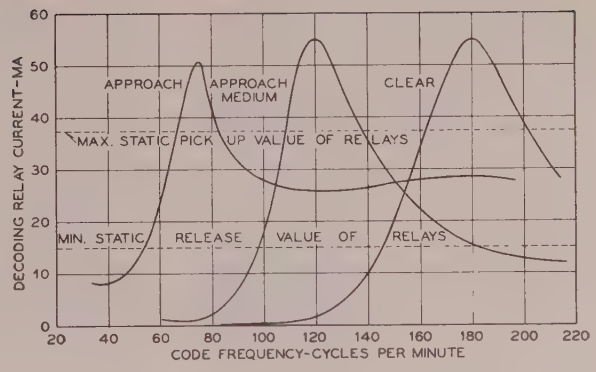

Figure 9 (right). Variation of decoding relay current with code frequency

also is tuned to resonance at the rail-current frequency to provide sharp discrimination against frequencies outside the desired band width.

The amplifier contains two identical beam-power tetrode vacuum tubes with indirectly heated oxide-coated cathodes. These tubes were designed especially for locomotive service and to operate from the regular 32-volt d-c supply. No dynamotor or other high-voltage plate supply is required. The tubes have a maximum rated transconductance of 6,800 micromhos.

Two stages of amplification are shown in Figure 5. In the first stage, the voltage output of the filter is increased by class-*A* amplification and the interstage coupling transformer. The second-stage tube action is that of a d-c amplifier. The copper-oxide rectifier causes only the positive half-cycles of voltage from the interstage transformer to be applied to the control grid of the second-stage tube. The capacitor between grid and −32 is charged to substantially the peak value of the positive half-cycles of voltage. A resistor in parallel with the capacitor allows the charge to leak off during the off periods of code, but not during the negative half-cycles of alternating current. The second-stage tube is biased to the cutoff point.

Thus, during the off period of the code cycle, no current flows in the plate circuit of the second-stage tube. During the on period of the code cycle, when current is flowing in the rails, the plate current rises to a value determined by the potential difference between the positive charge on the grid capacitor and the fixed negative grid bias. The result is that plate current flows in the primary winding of the master transformer when alternating current is flowing in the rails and ceases to flow when the rail current is interrupted by the code transmitter.

The rise and fall of plate current in the high-voltage winding of the master transformer causes alternating current of code frequency to flow through the low-voltage winding and the master relay connected to it.

The master relay is of the d-c polarized-stick type, that is, its armature will be held by the permanent magnet in whichever position it occupied when last de-energized. With alternating current of code frequency in its coil, the relay is energized periodically in opposite directions and, therefore, the contacts move from one position to the other at the code frequency. The relay thus responds to code frequency current only when this has a value greater than a predetermined minimum, and its contacts thus are held firmly closed by the permanent magnet in one position or the other except during reversals of current.

When the master relay is operating, it causes direct current from the 32-volt supply to flow alternately through one half or the other half of the primary section of the decoding transformer, causing the magnetic flux of this transformer to alternate in direction at the code frequency and thereby to deliver alternating current to the decoding circuits.

The output of the decoding transformer is applied to three tuned decoding units in parallel. Each decoding unit is a low-frequency filter tuned to resonance at one of the three code frequencies. Each consists of a condenser in series with the primary winding of an adjustable air-gap reactive transformer having its low-voltage winding connected through a double-wave copper-oxide rectifier to its associated decoding relay. The 180-code decoding relay thus will respond only when the voltage applied to its associated decoding unit has a frequency of 180 cycles per minute or three cycles per second. Likewise, the 120-code decoding relay is responsive to 2-cycle energy from the decoding transformer and the 75-code decoding relay, to $1\frac{1}{4}$-cycle energy.

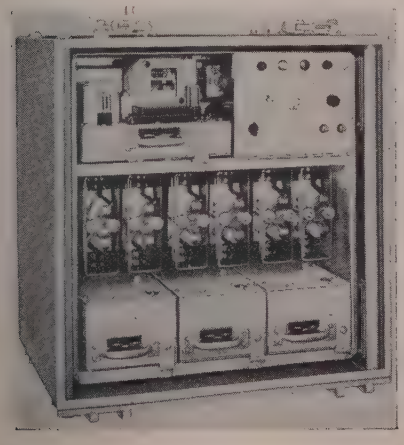

Figure 8 (left). Equipment box with door removed to show amplifier, decoding units, and relays

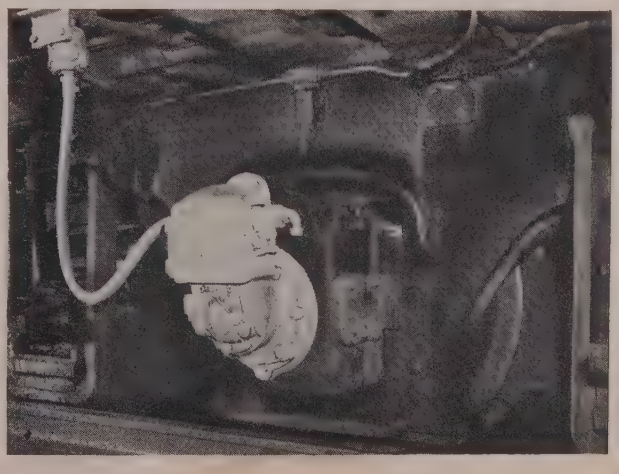

Figure 10 (right). Journal box mounted speed governor for diesel-electric locomotives. Governor is driven from end of axle through universal joint and electric connections are brought out through hose to plug coupler

The tuning of circuits to resonance at such low frequencies is uncommon in the field of electrical engineering. Typical curves showing the variation of decoding relay current with code frequency appear in Figure 9. These curves show that the "clear" decoding relay will not receive enough current to hold its armature closed on 120- or 75-code and that the "approach-medium" decoding relay will not receive enough current to hold its armature in the energized position on 75-code. A part of the selectivity obtained in the decoding circuits is attributable to the nonlinear voltage-current characteristic of the copper-oxide rectifier. Since each decoding circuit is series resonant, selectivity on the upper side of resonance is less than on the lower side. This is not important here, however, because the contacts of decoding relays responsive to one code frequency are not involved in the control of circuits associated with a higher code frequency.

The train control circuits are carried through relay contacts in both the positive and the negative sides of the d-c paths to prevent, as far as possible, improper operations caused by grounded wiring or short-circuited terminals.

Through the use of the cutout switch and its associated cutout relay, the train may move out of train-control-equipped territory without reducing speed, and the equipment will be conditioned for automatic restoration of the controls upon re-entering train control territory at any point. To accomplish this, a short stretch of track at certain designated points of departure from equipped territory is energized with 180-coded alternating current of several times the normal value. While the receiver is traversing this track section, the engineman reverses the cutout switch and holds it reversed until passage of the end of the cutout circuit is indicated by loss of cab signal illumination. Reversal of the cutout switch energizes one coil of the cutout relay over a normally open contact of the switch and the upper contacts of the 180-decoding relay. At the same time, enough resistance is added to the receiver circuit to prevent master relay operation except at the high level of alternating current used in these cutout circuits. This prevents a cutout from being effected at any but an authorized location. As soon as the receiver passes the end of the cutout circuit and the "clear" cab indication is extinguished, the engineman must restore the cutout switch to its normal position quickly in order to establish the holding circuit to the other coil of the cutout relay through the lower contacts of all decoding relays, an upper contact of the cutout relay, and a normally closed contact of the cutout switch.

As long as the cutout relay remains energized, the 15 mph speed limit, normally in force with all decoding relays down, is raised to 90 mph. As the train again enters train control territory and any one of the three decoding relays is energized, the circuit to the cutout relay will be opened and all control circuits will be restored to normal.

On some train control installations, the cutout function is performed automatically by coding the current in the cutout circuit at another code frequency and energizing the cutout relay from an additional decoding unit tuned to this frequency.

When the cab signal changes to "restricting" and the bell rings, the acknowledging relay is energized by the reversal of the acknowledging switch in much the same manner as that described previously for the cutout circuit.

Figure 6 is a schematic diagram of a typical set of pneumatic equipment and shows only that portion directly involved in the initiation or suppression of an automatic train control brake application. The position of the various valves is shown at the instant just after the timing valve has reversed, because of de-energization of the electropneumatic valve six seconds before, and just before reversal of the brake application valve. As its name implies, the timing valve with its reservoir measures a time interval of six seconds within which the engineman may take the action required to prevent an automatic application.

If this action is not taken, the air chamber below the brake application valve piston will be exhausted through pipe 10 and the upper timing poppet valve. This causes the brake application valve to shift downward and in so doing to produce the same result as if the engineman's brake valve handle had been moved to the service position for a definite period of time. Reduction of brake pipe pressure will continue until equalization of pressure occurs in the brake pipe, the equalizing reservoir, and the reduction limiting reservoir.

Upon re-energization of the electropneumatic valve and movement of the engineman's brake valve handle to "lap" position for a short time, the brake application valve will return to normal, after which the brakes may be released in the usual manner.

It should be noted that the control of the air brakes on a railway train also is on the closed circuit principle. The brakes are held released by maintaining air pressure in the brake pipe, which runs throughout the train and is coupled between cars by flexible hose. To apply the brakes, the engineman moves his brake valve handle to service position and allows air to escape from the brake pipe. The reduction of pressure in the brake pipe actuates valves on each car to admit air from a reservoir to the brake cylinders. Thus, any loss of air pressure in the brake pipe, such as by a broken air hose, will cause the brakes to be applied immediately throughout the train.

Any time the engineman moves his brake valve handle to service position prior to an automatic application, air pressure is applied to the pneumatic relay through pipes 18, 27, and 25. Operation of the pneumatic relay applies energy directly to the electropneumatic valve. After brake pipe pressure has been reduced a predetermined amount, the reduction-insuring valve will move to the left and stop the exhaust of air from pipe 27. This will permit the engineman to move his brake valve handle to "lap" position without loss of air pressure in pipe 25. In this manner, automatic control of the train brakes is suspended as long as the engineman is handling the braking system properly himself.

References

1. Interstate Commerce Commission Tabulation of Statistics (Washington, D. C.), January 1, 1950.

2. The Signal in the Cab. *Bulletin 144*, Union Switch and Signal Company, (Swissvale, Pa.), 1930.

3. Coded Cab Signals. *Bulletin 171*, General Railway Signal Company (Rochester, N. Y.), October 1937.

4. Description of Continuous Inductive Train Control Systems of the Union Switch and Signal Company. *Bulletin 8*, Committee on Automatic Train Control, American Association of Railroads (Washington, D. C.), January 1931.

5. Cab Signaling and Train Control on the San Francisco-Oakland Bay Bridge. *Railway Signaling* (Chicago, Ill.), May 1939, pages 274–79.

Discussion

W. G. Salmonson (Pennsylvania Railroad, Philadelphia, Pa.): Throughout his paper Mr. Allison has described how the cab signal aspects change in conformity with the position of the wayside block signals as they are passed, and in his Figure 2 he shows the relationship between the cab signal indication on the locomotive and the wayside signal as the locomotive overtakes a train ahead. Also in his Figure 4 showing a typical coded track-circuit control of the cab signal indications, the presence of wayside signals is indicated by dotted lines. Since it is the practice on some railroads to omit the wayside signals and operate by cab sig-

nal indication only, I think it would be helpful if Mr. Allison would enlarge upon this phase of the subject, citing instances where this is done.

With further reference to Figure 4 of the paper, a transformer is shown at each signal and cut-section location as the source of alternating current for cab signal operation. A reliable source of alternating current is not always available at such points, and I should like to ask what provision is made to obtain alternating current of the desired frequency in such cases.

L. R. Allison: In answer to Mr. Salmonson's question relative to operation on cab signals only without wayside signals, it is indeed true that this is feasible and is being done on a number of cab-signaling and train-control installations. It should be pointed out that the elimination of the wayside signals themselves does not result in as much cost saving as might at first appear, since most of the control circuits and apparatus would still be required. Furthermore, the presence of wayside signals is of considerable benefit in reducing train delays if there should be a failure of the locomotive cab signal equipment.

For those who are interested in existing examples of this type of signaling we refer to the Interstate Commerce Commission Tabulation of Statistics pertaining to signals, interlocking, automatic train control, and so forth, given as Reference 1 in the paper. Two important examples not included in the Interstate Commerce Commission tabulation are: the 4-indication 4-speed control system on the San Francisco-Oakland Bay Bridge and the 3-indication 2-speed control system on the Stockholm (Sweden) Tramways.

In answer to Mr. Salmonson's question as to what provision can be made to obtain alternating current energy for the track circuit where a reliable source of alternating current is not available, there are several installations where alternating current of the proper frequency is obtained from what is commonly referred to as a "tuned alternator." This is a direct current to alternating current inverter, similar in principle of operation to the vibrator used in automobile radios except that it is of more rugged and reliable construction and the armature is mechanically tuned to the frequency of the rail current. It is normally de-energized, being started in operation automatically by the entrance of a train into the block. Power for operation of the tuned alternator is supplied by a storage battery which is trickle-charged through a rectifier from any convenient source of alternating current. Thus, in the event of an alternating current power-line failure, cab signal operation will not be affected as long as sufficient energy remains in the storage battery to supply the tuned alternator.

Another advantage of the use of the tuned alternator is that the alternating current frequency may be converted from whatever is available for charging the storage batteries to whatever is desired for cab signal operation.

The absence of line wires for signal control, which is a feature of the coded track-circuit control system, together with the use of the tuned alternator for alternating current supply to the rails provides a combination that makes cab-signal control independent of the continuity of alternating current power for any reasonable period of interruption.

An example of the use of tuned alternators for cab signaling rail-current supply is on the Conemaugh Division of the Pennsylvania Railroad. Another example is the cab signaling installation on the Seaboard Air Line Railroad.

Why 4-Motor Multiple-Unit Car Equipments?

R. A. WILLIAMSON
ASSOCIATE AIEE

Synopsis: The amount and quality of railroad suburban commuter service will probably increase, rather than decrease, in the future. On electrified roads, multiple-unit trains with all axles motored are coming into use. In contrast with conventional equipment, having about one-half the weight on drivers, these new trains have design and operating features which especially suit them to fill present needs and anticipate future requirements. These qualities are enumerated, and the resulting benefits discussed in their relation to both the passenger and the railroad.

IN 1949 steam railroad commuter traffic was crowding the 6.6 billion passenger mile record of 1926 in spite of the inroads of private automobiles. There is an increasing urge for the large city breadwinner to live further and further from his work, yet experience has demonstrated the utter impossibility of ever providing enough parking and highway facilities for his private automobile. Obviously then, the business of transporting him by means of large, efficient units off the public highways is bound to become more and more rather than less and less important. This type of facility is best provided by our large railroads through their suburban service in metropolitan areas. The fact that they recognize their opportunity and responsibility and intend to meet them is shown by increasing activity all along the line. The Reading, Pennsylvania and New York Central railroads whose commuter territory is electrified have recently added to or commenced modernizing their fleets of electric multiple-unit cars. Non-electrified roads are experimenting with lightweight, high-capacity coaches handled by diesel-electric locomotives.

Acquisition of such new equipment—which, at least in the case of the New York Central multiple-unit cars, will not even train with hundreds of older units—is one more indication of the willingness of the railroads to cut loose from the past and face the future with the recognition that 1960 times cannot be served with 1906 machinery.

Various studies[1] have shown that electric multiple-unit cars are the best means for handling suburban passengers on those roads where volume of traffic justifies electrification. They also have tended to show that, where technically possible, all-motor-car trains are preferable to motor car-trailer car combinations. Railroads currently concerned with modernizing their multiple-unit car services are apparently confirming this view by their interest in trains consisting of motor cars only. The purpose of this paper is to go further and show particularly how trains having not only all cars motored but all axles motored, readily dispose of today's problems and anticipate tomorrow's needs as well.

Nature of Requirements

Passengers want fast, comfortable, dependable low cost service. The railroads need equipment which will:

1. Improve public relations through more attractive facilities and better service.
2. Increase return on investment through greater usefulness and availability of equipment.
3. Save money by reduced wear and tear on parts, by less need for attention, and by increased convenience of maintenance operations.
4. Stay young and up-to-date.

Fast schedules in frequent-stop service require high accelerating and braking rates. At the same time reasonably high top speeds are needed for express and semiexpress runs, since a large suburban operation is a composite of both. Fortunately, as the commuting radius expands, it is more convenient to supply semiexpress or skip-stop service. This tends to favor one design of equipment geared for all services.

Figure 1. Train of new 650-volt d-c multiple-unit cars, each equipped with four truck-mounted motors, New York Central Railroad

Paper **51-35,** recommended by the AIEE Land Transportation Committee and approved by the Technical Program Committee for presentation at the AIEE Winter General Meeting, New York, N. Y., January 22–26, 1951. Manuscript submitted October 16, 1950; made available for printing November 21, 1950.

R. A. WILLIAMSON is with the General Electric Company, Erie, Pa.

Figure 2. 11,000-volt, 25-cycle, single-phase a-c multiple-unit car equipped with four truck-mounted motors, Pennsylvania Railroad

The maximum practical accelerating rate for a train having two motors per car with 55 per cent weight on drivers is 1.5 miles per hour per second. At this rate the maximum adhesion on the driving axle which unloads because of weight transfer, reaches about 18.4 per cent. With every axle motored, 2.0 miles per hour per second can be obtained with a peak adhesion of only 12.9 per cent. Even digher rates are practical; 2.5 being a modern subway standard, and three or four miles per hour per second being obtained by Presidents' Conference Committee (PCC) cars every day on city streets, where rail conditions are by no means favorable.

High braking rates can be obtained by conventional methods without exceeding practical adhesion values, but the added wheel and shoe duty plus the complicated mechanisms required to protect against excessive damage in case of wheel sliding become very burdensome. Trains with every axle motored are ideally suited for the use of dynamic braking, with a 2.0 mile-per-hour-per-second decelerating rate producing a peak adhesion of about 11.1 per cent and a 2.5 mile rate 14.3 per cent.

Dynamic braking with only 55 per cent of the train weight on drivers (that is, with two motors per car) is not very attractive or practical, even the low rate of 1.5 miles per hour per second producing an adhesion of nearly 16 per cent.

Table I. Weights of Equipment

	New York Central (650 volt d-c 75-ton car. 1.5 mphps acceleration, no dynamic brake, 70 mph maximum)		Pennsylvania Railroad (11,000-volt 25-cycle a-c 68-ton car. 1.0 mphps acceleration, no dynamic brake, 80 mph maximum)	
	Motors Per Car		Motors Per Car	
	Four	Two	Four	Two
Motor weight	10,700	10,400	11,584	12,240
Control weight	4,500	4,500	12,716	15,060
	15,200*	14,900	24,300†	27,300

*Motors good for 2.0 mphps dynamic braking with some reduction in car weight.

†Motors good for 2.0 mphps dynamic braking.

Table II. Effect of Dynamic Braking on Brake Shoe Life

	Per Cent Without	Per Cent With
Trolley coach	100	300
Rapid transit train	100	500–1,300
Diesel-electric freight locomotives and train*	100	170–310
Diesel-electric passenger locomotives and train†	100	300–340

*3 1,350-horsepower unit hauling 80 car trains.

†3 2,000-horsepower units hauling 13 car trains.

Adaptability of 4-Motor Equipment

Only modern equipment with every axle motored serves all the foregoing needs best. Furthermore, better advantage can be taken of technical progress in reducing the weight of cars and equipment. Such weight reductions release motor capacity for other than purely weight hauling purposes. Trains with all axles driving can use this released motor capacity to produce extra performance without exceeding workable adhesion limits. This would be impossible with 2-motor equipments, whose performance is already pretty definitely limited by adhesion.

Distributing motor capacity over all axles instead of concentrating it on half the number or less, permits using space which would otherwise be wasted to secure important high-quality design features as described in a companion paper by F. C. Kreitler.[2] Truck-mounted instead of axle-hung, motors greatly reduce unsprung axle loading. Better riding qualities and reduced wear and tear on both motor and truck parts result from the corresponding reduction in road shock. Self-contained gear units are semipermanently axle-mounted on roller bearings. This completely eliminates friction bearings and the annoyance of gearing trouble caused by misalignment. Oil bath lubrication of gearing insures long, quiet, dependable operation. Smaller and lighter parts, and the possibility of dismounting either motor or gear unit without disturbing the other, facilitate handling and mean reduced maintenance expense. For example, the motor armature of the new 4-motor a-c equipment for the Pennsylvania Railroad weighs only 680 pounds compared to 1,880 for a comparable armature for a 2-motor car, and the motor itself weighs only 1,875 pounds instead of 5,000. Imagine what this can mean personnel and facility-wise.

Equipment of this general type has demonstrated its ability to operate for years in difficult service with one-half to one-third the frequency of inspection required for older conventional equipment, and at two-thirds the direct inspection cost. No intermediate shopping for attention to equipment is required between overhauls; therefore, greater savings actually accrue because of fewer trips to the shop. Not only is less attention needed, but it is more conveniently given.

Weight and Cost

Formerly the extra weight and cost of conventional 4-motor equipments as compared to 2-motor equipments tipped the scales against them. Modern designs and production now have equalized and, in the a-c case, reversed this situation. Table I shows how the weights of new 4-motor equipments recently placed in service by the New York Central Railroad (100 cars) and the Pennsylvania Railroad (50 cars) compare with those of comparable 2-motor equipments.

If reasonable quantities are purchased, the price of 4-motor equipments is no higher than that of 2-motor equipments.

Other Factors

Many factors, aside from the operational advantages previously described favor the use of four small motors in place of two larger ones.

1 Commutation constants are usually better, for both a-c and d-c motors.

2. Windings of both field and armature are simple and the coils are short, minimizing the effects of contraction and expansion so that they stay in good condition longer.

3. Bearings and other parts for the smaller motor cost only about one-fourth to one-half as much as those for the larger one.

4. The 6-pole a-c design becomes sturdy and simple enough to encourage self-

Table III. Approximate Energy Consumption of Transportation Vehicles

	Input Watt Hours Per Ton Mile	Per Cent of Input Dissipated by Brakes
Passenger trains (streamliners, average to mountainous territory)	32	15*
Freight train (average profile)	17.2	18*
Freight train (mountainous territory)	20	44*
Trolley coach (level)	237	60
Rapid transit car	82–103	67
Suburban multiple-unit car	100–158	68–72

*Estimated for trains of reference 4.

ventilation. With the gear ratio available this is quite practical. It has the advantage of eliminating costly air ducts, flexible connections, external blowers, and the nuisance and expense of maintaining them.

5. In neither a-c nor d-c design can the motors exceed maximum safe speed, therefore, no overspeed or slip protection is necessary. This is a new self-protecting feature in a-c motors. Many of the conventional motors now in use will run faster on the road than the maximum safe motor speed. This protective feature, brought about partly by the new fan load, considerably simplifies control problems.

6. Existing 2-motor a-c equipments have been judged too slippery to operate except with motors permanently in parallel. This requires the main motor circuits to handle very heavy currents. With accelerating adhesion reduced to one-half and the self-protecting features described under (5), four motors can be run two in series–two groups in parallel, doubling the transformer secondary voltage and halving the current. Thus the low-voltage low-flux, series motor design can be retained and reasonable power circuit currents secured at the same time. This motor grouping has made possible a motor-driven cam-operated main controller, something new to the a-c car field and an improvement which has been sought for many years. W. S. O'Kelly has described this new control system in a companion paper.[3]

Dynamic Braking

Dynamic braking seems so inevitably a part of the future development of the suburban multiple-unit car that more should be said about it here. The problem of moving trains is simply a matter of pouring energy in and draining it out. Elaborate, expensive, and sturdy machinery has been developed for the "in" process—yet it is often idle 25 per cent of the time the train is in motion. Certainly logic dictates putting this investment to greater use by making it serve the "out" cycle as well. This is accomplished by the addition of only a fraction of the total cost of the propulsion machinery. Against this fraction can be credited direct and secondary gains from reduced maintenance on brake shoes, wheels, brake equipment, and so forth.

Every transit vehicle whose preformance and acceptance have shown notable improvement in the past 20 years has overcome the deceleration obstacle by adapting its propulsion machinery to braking. The modern streetcar adopted dynamic brakes in 1930, when it shucked off a 30-year old shell and stepped out as the Presidents' Conference Committee model. The trolley coach outgrew friction brakes in the middle 1930's and the rapid transit car a little later. After a slow start, primarily as a holding brake for diesel-electric locomotives descending grades alone, the dynamic brake has earned its place on railway locomotives to the extent that at least one large western railroad has applied it to all road locomotives, both freight and passenger, and makes its use mandatory everywhere possible, in level as well as mountainous territory.

One of the reasons for this state of affairs is clearly shown in Table II. Obviously such increases in life mean substantial direct dollar savings in material and labor of application, to say nothing of indirect savings due to less handling and better planning. Evidence is available from rapid transit operations showing that wheel life is increased up to 100 per cent, which further adds to direct and indirect savings. It is reasonable to expect that suburban multiple-unit cars would show results substantially in line with those for rapid transit trains.

Not so much is known about the effect of dynamic braking on increased life of wheels on locomotive-hauled trains, but assuming that over-all life and miles between turnings can be increased from 30 to 50 per cent, savings would be at least equal to those obtained from increased brake shoe life.

The need for dynamic braking is directly related to the amount of energy dissipated in the brakes. This depends upon the energy input to vehicles in various services and the percent of this input appearing at the brakes. Both assume formidable values in high-schedule-speed and/or frequent stop service. Table III shows approximate representative values for these two factors. Technically, among all these vehicles, the suburban multiple-unit car needs dynamic braking most, yet it is the only one not using it. Time will serve only to increasingly accentuate this need.

Conclusion

Suburban trains having all axles motored and equipped with dynamic braking can furnish smooth, quiet, fast, dependable service. They appear best suited to the future requirements of a public already accustomed to floating power and rubber tires.

Equally important, they offer the railroads just as much as they do their customers:

1. Reasonable first cost.
2. Better utilization and more intensive use of rolling stock through more versatile and dependable equipment.
3. Reduced maintenance expense through higher quality design.
4. Smaller, lighter, less expensive parts.
5. More convenient to handle.
6. Less attention required and more convenient maintenance.

References

1. Handling Suburban Traffic on Steam Railroads, **M. L. Sloman.** *AIEE Transactions*, volume 67, part II, 1948, pages 1670–74.

2. A-C Multiple-Unit Car Motor, **F. C. Kreitler.** *AIEE Transactions*, volume 70, part I, 1951, pages 648–51.

3. A-C Multiple-Unit Car Equipment, **W. S. O'Kelly.** *AIEE Transactions*, volume 70, part I, 1951, pages 652–56.

4. Advantages of Dynamic Braking, **J. P. Morris.** *Railway Age* (New York, N. Y.), volume 127, December 17, 1949, page 1087.

No Discussion

A New Multiple-Unit Car Motor for the Pennsylvania Railroad

H. G. JUNGK
MEMBER AIEE

A NEW multiple-unit car motor designed and built for the Pennsylvania Railroad electrification is the type *431-A* single-phase series motor with a shunted interpole, no compensating winding, and with resistance leads in the armature winding. This motor has a continuous rating of 225 horsepower at 328 volts and 760 amperes at 1,270 rpm. The top sustained running speed is 2,800 rpm. The corresponding car speeds are 41.3 and 91.1 miles per hour respectively with 36-inch wheels and a 17/56–two diametrical pitch gear ratio. The average accelerating tractive effort of the car (two motors) is 7,000 pounds at 1,050 amperes per armature.

This motor has eight poles and eight brushholders with three brushes each of of 3/8 by $2^3/_8$ by $2^1/_2$-inch long electrographitic carbon. The ventilating air enters the air-intake at the rear or pinion end of the frame and is forced through three parallel paths to the front or commutator end where all of the air is baffled to pass down over the commutator and brushholders and out through the front housing.

These new motors are smaller than the *412-D* and *426-A* types now in operation on Pennsylvania Railroad multiple-unit cars and have smaller pinions and gear center distance but the frames are designed to fit in the same trucks with the same size axle bearings and the same nose suspension details as on the present cars. As a result, the frames, housings, axle bearings, axle caps, and other stator parts weigh about as much as on the corresponding *426-A* motors with fabricated frames but less than those of the *412-D* motors with cast steel frames. The armatures operating at twice the speed of the *412-D* armatures are much lighter. The comparison of weights are given in Table I.

Table I

	412-D	426-A	431-A
Weight—motor complete with gear case, axle bearings, and axle caps	6,490	5,938	5,344
Weight—pinion	135	116	61
Total	6,625	6,054	5,405
Weight armature	2,350	2,230	1,615

The *431-A* motors are geared to give the same starting and accelerating tractive efforts per car as the *412-D* motors but will operate up to 90 miles per hour as a sustained running speed while the *412-D*'s are limited to 70 miles per hour and the *426-A*'s to 80 miles per hour top speed. Although intended for the lighter *MP-54* cars, the *431-A* motors have the capacity to accelerate the heavier *P-70* cars if applied on them.

The two motors on a car are connected in parallel to the transformer rather than in series as is generally done on both a-c and d-c motors. This minimizes the tendencies of wheels to spin when a wheel slip occurs.

After a careful study of the experiences over the past 40 years with a-c multiple-unit car motors of various combinations of resistance leads, interpole fields, compensating windings on doubly-fed, repulsion and series types with high, low, and medium flux per pole, the type *431-A* motor was designed with series fields and interpoles in the stator and resistance leads in the armature to give simplicity in both motor and control. The mechanical and the electrical parts are substantially built and with sufficient margin in rating to insure low maintenance cost.

A number of features, incorporated in the design to eliminate some of the troubles experienced in the past and to simplify maintenance, are applicable to any motor while others are possible only with the resistance lead design.

The features adaptable to any design and their importance in reduced cost and maintenance are briefly as follows:

Rear End Ventilation

Many of the insulation failures on commutator motors are developed by introducing ventilating air at the commutator end. Overheating of front end ventilated 426 motors has been caused by improperly fitted commutator covers and resultant air leakage. On the *431-A* motor, ventilating air is introduced at the rear or pinion end, so that carbon dust from brush wear is blown out of the motor instead of into the windings. This materially reduces the possibility of accumulation of dirt on exposed creepage surfaces. It also has the advantage that if the commutator covers do not fit tightly or if they fall open or drop off, ventilation will not be affected.

Preinsulated Armature Coils

To reduce grounds and short circuits which now occur with the threaded in

Figure 1. View from pinion end–type *431-A* motor

Paper 51-36, recommended by the AIEE Land Transportation Committee and approved by the AIEE Technical Program Committee for presentation at the AIEE Winter General Meeting, New York, N. Y., January 22–26, 1951. Manuscript submitted October 25, 1950; made available for printing November 21, 1950.

H. G. Jungk is with the Westinghouse Electric Corporation, East Pittsburgh, Pa.

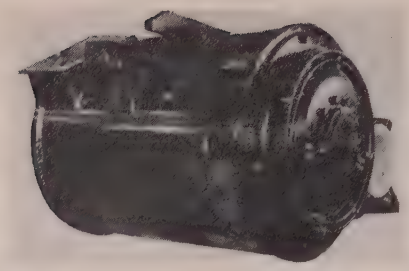

Figure 2. View from commutator end–type *431-A* motor

fold-over straps used on the more recent motors, open armature slots are used so that the coils may be preinsulated and baked before winding into the slots. The coils are still constructed from two half-coils connected at both ends after winding so as to retain the advantages of winding and ease of repairing such windings.

Preinsulated Stator Coils

To improve the insulation of stator coils, and to reduce coil lead breakage, the exciting field coils are formed, preinsulated and baked before winding into open slots. The coils are connected, all in series, to carry full line current and thus the conductors are of substantial cross section and strength. The interpole coils, like those on d-c motors, are completely wound, insulated, and baked before winding over the interpole. This makes the construction simple and rugged.

Brushholder Support

Commutator motors usually have brushholders mounted in the frame and any repairs, replacements or neutral adjustment tie up a complete motor. The *431-A* motor brushholder supporting arms are mounted on the housing thus providing for quick removal and replacement in case of trouble. This unit of housing and supports with brushholders can be repaired at the bench and location of holders checked and held on neutral.

Figure 3. Commutator end housing complete with brushholder supports and brushholders–type *431-A* motor

The features applicable only to a resistance lead design and their importance in reduced cost and maintenance follows:

Less Commutator Heating

Overheating of commutators, with resulting flat spots causing high commutator maintenance and brush breakage, has been one of the most elusive troubles with the commutator-type motors in locomotive service. The resistance lead design reduces commutator heating. The resistance leads carry current only when the corresponding commutator bars are under a brush. Since this occurs in any one lead only 10 to 12 per cent of the time, the resistance of the lead can be made high enough to substantially limit circulating current in the brush face and armature circuit at standstill, and at low speed and high tractive effort where the interpole has no effect because of zero or very low speed. Since the total brush loss and resistance loss in the windings is practically the same per horsepower regardless of poles and windings, part of this commutation loss can be absorbed in the resistance leads around the armature thus relieving local heating on the commutator surface and brushes.

Higher Flux Per Pole at Start

The circulating currents in the brush face are set up by voltage induced in the armature coils by the alternating flux per pole. Since the circulating currents can be held to safe values by resistance leads, the exciting flux per pole at start and for heavy currents on the *431-A* motor was increased to almost twice that permissible on a motor with no resistance leads. Hence it is not necessary to shunt the exciting field at start.

Higher Motor Voltage and Lower Current

Increasing the flux per pole increases the line voltage and lowers the line current and number of poles accordingly. Hence the required starting tractive effort of 7,000 pounds per car is obtained with only eight poles and at 1,050 amperes. A conventional motor without resistance leads geared for the same commutator peripheral speed would require 1,800 amperes and 12 poles for the same starting tractive effort.

Less Current in Cab Wiring

The lower current results in reduction in the size of the transformer low-voltage

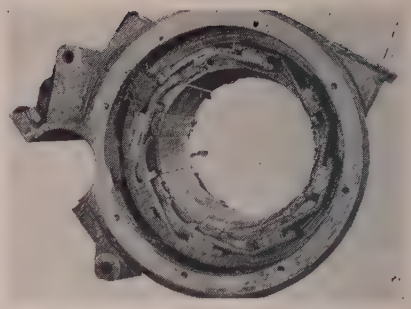

Figure 4. View of wound stator from pinion end–type *431-A* motor

terminals and the size of the car cable in the ratio of 720 to 1,120 or by 64 per cent, and in the current rating of the main circuit control apparatus.

Fewer Active Motor Parts

With a higher voltage and lower line current for eight poles, only 24 brushes are required and eight brushholders. Likewise, eight exciting field and interpole windings and only 204 commutator bars, reduce the weight, first cost, and maintenance cost.

Less Armature Weight

The 204 bar commutator is only $12^1/_4$ inches in diameter and can run at 2,800 rpm with 9,000 feet per minute peripheral speed to give a car speed of 90 miles per hour with 36-inch wheels. The lighter high-speed motor requires smaller shaft, roller bearings and pinion, all of which reduces weight and cost.

One Interpole Shunt Setting

Resistance leads absorb some of the higher frequency commutating currents and sparking. The interpole excited with 25-cycle current will only compensate for 25-cycle commutation but the resistance leads will compensate at any frequency. This means less sparking at the higher speeds and currents as well as at start

Figure 5. View of wound stator from commutator end–type *431-A* motor

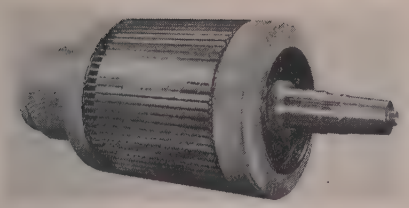

Figure 6. View of armature from pinion end–type *431-A* motor

where resistance leads are used. As a result only one interpole shunt setting is required and control is simplified.

Low Brush Current Density

High-voltage and low-line current make it possible to keep brush density at lower values, 67 amperes per square inch at continuous rating and 98 amperes per square inch at starting (7,000 pounds tractive effort per car).

No Breakage of Commutator Risers

Many failures have occurred in the past few years on armatures due to broken commutator risers. Armature coils are connected to the resistance leads and not to the commutator risers thus reducing the possibility of this breakage and also of burning behind necks, at the same time facilitating armature repairs if a failure should occur.

Equalization of Current to Brushholders

The introduction of resistance leads equalizes the division of load current between brushholders. On any full multiple wound armatures, there are as many parallel circuits as there are poles or brushholders. With armature cross connections, the impedance between brushholders is low especially for current surges and transients. The increase in resistance in paths due to resistance leads will tend to keep the current balanced in all the circuits and pairs of brushholders.

A view of the assembled motor from the pinion end, Figure 1, shows the pinion, axle bearings, motor-lead cables, and junction box, also the air intake just above the frame barrel. In Figure 2, the nose support, safety nose, commutator covers, air intake at the rear and air outlet openings in the commutator end housing are seen from the commutator end view.

The commutator end housing, Figure 3, complete with brushholders forms an assembly which is located on neutral by means of the half-hole in the flange. This half-hole fits around a dowel pin set on neutral and welded in place on the frame flange. The roller bearing cartridge mounts in the bored seat and is held in place by bolts through holes drilled in the housing.

Wiring and connections of the exciting field coils are made at the rear or pinion end of the stator as in Figure 4. Completely preinsulated and baked, these coils are wound under the main pole tips by a new and novel method of first expanding the coils to pass over the pole tips and then stretching again to bring the coil sides in place against the main pole body. The interpoles have no tips and the sides are parallel. Hence, after the exciting field coils are in place, the interpole coils, pre-insulated and baked, are dropped down over the poles in the usual manner.

Interpole field connections and leads to brushholders are at the commutator end of the wound stator, Figure 5. The air-baffle ring, also at this end, directs the air from back of the punchings down over the stator coil ends to the commutator surface. Above the frame at the terminal board the flexible straps from the stator wiring are shown bolted to terminal straps. These straps are mounted on insulators, two to a terminal, bolted to the frame plate. The dowel for locating neutral is not in this picture. The bolt hole by which the dowel is held in place before welding is between two of the housing bolt holes.

Armature coil ends are connected to re-

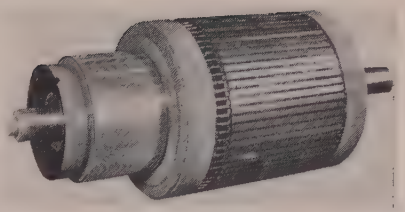

Figure 7. View of armature from commutator end–type *431-A* motor

sistance leads at the rear end of the armature as in Figure 6. The ventilating air, entering at the rear, blows down over these connectors and then under the coil support into axial holes through the armature punchings and out again at the front end between coils just ahead of the punchings. At the commutator end of the armature, Figure 7, the resistance leads pass from the bottom of the armature slots to the risers of the commutator bars thus connecting the armature coil ends at the rear to the commutator bars at the front end of the armature. The outside cylindrical surface of the risers is insulated with glass and mica and serves as a supporting surface upon which the armature coil ends are banded down in place.

This allows the armature coils to expand and contract independent of the commutator risers. The commutator is of the disk spring ring type designed for high-speed operation.

It is not the purpose of this paper to develop a treatise on the theory of design of motors but rather to point out new features of the *431-A* motor and to describe some of the advantages of this particular combination of design chosen to produce a multiple-unit car motor simple and rugged in structure in order to give reliable service. The new motor costs less and weighs less than previous designs and, at the same time, provides considerable margin in rating. With fewer working parts and simpler control, greater reliability in service and lower maintenance expense should be realized.

Discussion

R. Lamborn (General Electric Company, Erie, Pa.): We wish to thank the author of this paper for bringing the subject of resistance-lead motors once more before the public. If we take his paper at face value it indicates that the use of resistance leads alone has made possible numerous otherwise unattainable operating advantages.

I would like to point out that such is definitely not the case. Among the simplifications claimed for a multiple-unit car equipment using resistance-lead motors are listed absence of exciting field shunts for starting, and the need of but one interpole shunt setting. Multiple-unit cars operating on the Reading Railroad at Philadelphia have low-flux motors without resistance leads. They use no exciting field shunts for starting, and have but one interpole shunt setting. These motors have been operating on the Reading Railroad for almost 20 years.

A better comparison would be to choose two equipments designed at approximately the same date for the same service by two different groups of engineers. I refer to the Westinghouse 2-motor resistance-lead equipment versus the General Electric 4-motor low-flux motor equipment for the Pennsylvania Railroad multiple-unit cars covered in the paper by R. A. Williamson. The features shown in Table I of this discussion are all stated by Mr. Jungk to be definitely favorable to a resistance-lead design.

This comparison speaks for itself. The *GEA-630* low-flux motor equipment equals or excels the *431-A* resistance-lead design on every count.

Rather than providing advantages, the presence of resistance leads must be considered a disadvantage. In effect, they constitute an additional armature winding. This increase in the number of parts, the

Table I

Item	Resistance-Lead *W-431-A* Equipment	Low-Flux *GEA-630* Equipment
Exciting field shunt at start	None	None
"Lower" accelerating current	2,100 amp	1,630 amp
"Lower" continuous current	1,440 amp	1,140 amp
Number of soldered connections in armatures	2×204×6=2,448	4×171×2=1,368
"Less" armature weight	2×1,615=3,230 lb	4×680=2,720 lb.
Number of interpole shunt settings	One	One
Breakage of commutator risers	No problem	No problem
Equalization of current to brush holders	No problem	No problem

number of bare copper connections, and the greater area of insulation between live parts and ground must be considered a potential source of trouble and additional maintenance cost. When all the facts are weighed, we believe that resistance leads have no place in modern a-c railway motors.

REFERENCE

1. WHY 4-MOTOR MULTIPLE-UNIT CAR EQUIPMENT?, R. A. Williamson. *AIEE Transactions*, volume 70, part I, 1951, pages 240–42.

H. G. Jungk: The thoughts behind the choice of the Westinghouse *431-A* resistance-lead motor for multiple-unit service were:

1. A chief concern in multiple-unit car operation is to transport the maximum revenue passenger-miles with available equipment for the least expense in maintenance and operation.

2. Fewer working parts will require less attention and replacements and hence less maintenance expenditure.

3. Brushes, commutators, bearings, gearing, all require attention and replacement when worn. Windings, leads, and brushholders may be damaged in service and must be replaced occasionally.

Hence, the fewer there are of these parts and the easier it is to inspect and replace them, the lower should be the running expense and delays in service.

With the 2-motor equipment of type *431-A* resistance-lead motors we have reduced the number of working parts and have provided accessibility for inspection and replacements.

Mr. Lamborn refers to the Reading Railroad 12-pole motor, which has no resistance leads and operates with no exciting field shunts and with but one interpole shunt setting. We agree fully that this motor has a fine operating record on the Reading Railroad multiple-unit cars. Also, as applied, this motor has considerable margin in rating with the two motors per car and forced ventilation.

The *431-A* motor is designed to do all of this for less weight per motor, fewer working parts, and less current per motor, also with a generous margin of safety both in top operating speed and in emergency operation. We have gone a step further by connecting two armatures in parallel to minimize wheel slippage and, in case of failure of one motor, to provide for continued operation of the other motor on the car.

Mr. Lamborn has made a tabulation of figures to compare the four *GEA-630* motors with the two *431-A* motors. This should be amplified to include more of the working parts and also to include some of the Reading motor data.

As to the number of soldered joints, we have added the equalizer or cross-connection joints, which also are soldered. We always have considered the soldered joints in the commutator risers more vulnerable than those in the coil-end connectors at the rear of the armature, because the commutator bars are heated by commutation losses as well as by joint losses in the risers. This additional heat adds to the hazard of thrown solder. On the *431-A* motors, the commutator risers join to the resistance leads only, and thus these joints carry current but 10 to 12 per cent of the time, that is, when the corresponding commutator bars pass under the brushes. The resistance leads extend through the armature slots to the rear end, where they are then connected to the armature coil ends and equalizers.

The armature windings of both the *431-A* and the General Electric Reading motors are made up of half-coils with connections from bottom to top halves at both ends. This was done to simplify winding and repairs. The armature windings of the *GEA-630* motors are made up of full coils with continuous loops at the rear instead of connectors.

Table II of this discussion gives a comparison of all three types of motors. Since the General Electric Reading motor and the Westinghouse *426-A* motor are practically the same electrically except for the number of turns in the field windings, we have shown some and prorated other data from the *426-A* motor equipment in making up the tabulation for the General Electric Reading motor. On some of the earlier 12-pole armatures of this type, the equalizers were located at the rear end of the armature. On all of the later ones the equalizers were placed in the commutator risers.

This comparison of figures shows that the multiple-unit car equipment with two *431-A* resistance-lead motors per car has fewer poles, brushholders, brushes, exciting and interpole field coils, and no compensating field coils in the stator. In the two armatures on the car the *431-A* motor equipment has fewer commutator bars, fewer armature conductors, fewer equalizers, and fewer soldered joints, especially in the commutator risers. All of this should result in lower maintenance cost and lower operating expense.

Table II

Type Motor	*W-431-A*	G.E. Reading	*GEA-630*
Number of motors per car	2	2	4
Sets of gearing per car	2	2	4
Number of roller bearings per car	4	4	24
Weight of one armature	1,615	2,350	680
Weight of armatures per car	3,230	4,700	2,720
Ventilation	Forced	Forced	Self
Maximum speed, mph	91	72	92.5
Nominal continuous hp rating, one motor	225	212.5	125
Nominal continuous hp rating, per car	450	425	500
Continuous amperes per motor	720	1,100	570
Continuous amperes per car	1,440	1,100	1,140
Continuous tractive effort per car	4,100	4,160	4,100
Accel. amperes per motor	1,050	1,800	815
Accel. amperes per car	2,100	1,800	1,730
Accel. tractive effort per car	7,000	7,000	7,000
Poles per motor	8	12	6
Poles per car	16	24	24
Brush holders per car	16	24	24
Brushes per holder	3	4	3
Brushes per car	48	96	72
Exciting field coils per car	16	24	24
Compensating field coils per car	None	24	48
Interpole field coils per car	16	24	24
Stator coil end joints	64	144	192
Commutator bars per motor	204	306	171
Commutator bars per car	408	612	684
Armature conductors per car	816	1,224	1,368
Armature equalizers per car	136	612	684
Armature-half-coil ends per car	1,632	2,448	
Armature full-coil ends per car			1,368
Equalizer ends per car	272	1,224	1,368
Resistance lead ends per car	816		
Total ends	2,720	3,672	2,736
Armature coil ends in commutator risers per car		1,224	1,368
Equalizer ends in commutator risers per car		1,224	1,368
Resistance lead ends in commutator risers per car	408		
Total joints in commutator risers	408	2,448	2,736
Armature coil ends, front, not in risers	816		
Resistance lead ends, rear, per car	408		
Equalizer ends, rear, per car	272		
Armature coil ends, rear, per car	816	1,224	
Total joints, rear	1,496	1,224	
Total joints per car	2,720	3,672	2,736

Bibliography of Relay Literature 1947-1949

AIEE COMMITTEE REPORT

THIS interim report was prepared by the Project Committee on Relay Bibliography of the AIEE Relay Committee in order to make this information available to the entire industry as early as feasible. Again, as in 1948, when the last interim report was published, a 3-year period is covered.

Relay bibliographies have been published in the following reports:

1927–1939, *AIEE Transactions*, volume 60, 1941, pages 1435–47.

1940–1943, *AIEE Transactions*, volume 63, 1944, pages 705–09.

1944–1946, *AIEE Transactions*, volume 67, part I, 1948, pages 24–27.

The articles listed in this bibliography include all papers published in the United States in the field of relaying and in associated fields; it also contains articles published in foreign countries that are available through abstracts in *Engineering Index* or in *Science Abstracts, Section B*, if not directly in the journals concerned. The listing of the titles is subdivided into sections, depending upon the general substance of the article. In each section the entries are numbered consecutively and listed alphabetically by year, the name of the first author determining the alphabetical position. Each title is listed in one section only.

Section A. Line Protection—Distance

1. Fundamental Basis for Distance Relaying on 3-Phase Systems, **W. A. Lewis, L. S. Tippett.** *AIEE Transactions*, volume 66, 1947, pages 694–709.

2. A New Reactance Distance Relay, **C. G. Dewey, J. R. McGlynn.** *AIEE Transactions*, volume 67, part I, 1948, pages 743–46, and *Electrical Engineering*, volume 67, May 1948, page 445.

3. Graphical Method for Estimating the Performance of Distance Relays During Faults and Power Swings, **A. R. Van C. Warrington.** *AIEE Transactions*, volume 68, part I, 1949, pages 608–21.

Section B. Line Protection—Pilot Wire and Carrier Current

1. Ultra-High-Speed Relays in Fields of Protection and Measurement, **W. Casson, F. H. Last.** *Journal*, Institution of Electrical Engineers (London, England), volume 94, part II, 1947, pages 667–91.

2. Application of Pilot Wire Protection to Long 88-Kv Transmission Lines, **W. Fenwick, C. P. Marais.** *Transactions*, South African Institute of Electrical Engineers (Johannesburg, South Africa), volume 38, 1947, pages 128–30.

3. Protection by Phase-Comparison, I–III, **F. H. Brich.** *Electrical Times* (London, England), volume 113, 1948, pages 691–94; volume 114, 1948, pages 9–12.

4. Multiple Utilization of Power Line Carrier Links, **A. Goldstein.** *Brown Boveri Review* (Baden, Switzerland), volume 35, 1948, pages 120–24.

5. Coupling Capacitors and Traps for Rural Line Carrier, **AIEE Committee Report.** *AIEE Transactions*, volume 67, part II, 1948, pages 1426–28.

6. High-Frequency Protection Systems for High-Voltage Lines, **G. I. Atabekov, E. D. Sapir, I. I. Solovev.** *Elektrichestvo* (Moscow, U.S.S.R.), September 1949, pages 7–14.

7. Ultra-High-Speed Relays in Fields of Measurement and Protection, **W. Casson, F. H. Last.** *Proceedings*, Institution of Electrical Engineers (London, England), volume 96, part II, 1949, pages 50–56.

8. Sensitivity and Methods of Determining the Setting of a Longitudinal Differential Line Protective System, **G. T. Grek, I. N. Popov.** *Elektricheskie Stantsii* (Moscow, U.S.S.R.), volume 20, April 1949, pages 35–38.

9. Power Line Carrier for Relaying and Joint Usage—Part I, **G. W. Hampe, B. W. Storer.** *AIEE Transactions*, volume 68, part II, 1949, pages 864–72; *Electrical Engineering*, volume 68, November 1949, page 976.

10. A Proposal for Broad-Band Coupling of Power-Line Carrier Equipment, **R. H. Miller.** *AIEE Transactions*, volume 68, part II, 1949, pages 1028–31.

Section C. Line Protection—Ground Faults

1. A New Distance Ground Relay, **S. L. Goldsborough.** *AIEE Transactions*, volume 67, part II, 1948, pages 1442–47, and *Electrical Engineering*, volume 68, January 1949, page 27.

Section D. Line Protection—General

1. Desirable Features of Protective Relays. *Journal*, Institution of Electrical Engineers (London, England), volume 94, part II, 1947, pages 546–47, and *Engineering* (London, England), volume 163, number 4226, 1947, page 33.

2. Protective Relays, **W. Casson, F. H. Last.** *Electrical Times* (London, England), volume III, number 2895, 1947, pages 495–96, and *Electrician* (London, England), volume 138, number 3595, 1947, pages 1165–66

3. The Operation of Relays and Protective Systems in the Bewag System During Wartime, **W. Franke.** *Elektrotechnik* (Berlin, Germany), volume 1, 1947, pages 139–41.

4. Overload Protective Devices, **C. F. Hedlund.** *Electrical Contracting* (Chicago, Ill.), volume 45, November 1946, pages 119–21; volume 45, December 1946, pages 81–84; volume 46, January 1947, page 81–84.

5. Corrective Measures Improve Line Performance, **D. M. MacGregor.** *Electric Light and Power* (Chicago, Ill.), volume 25, February 1947, pages 76–78, 80; and March 1947, pages 52–54, 56–57.

6. Faulty Operation of Unbalance Protection of Parallel Lines During a Single-Pole Short-Circuit on the Adjacent Lines, **A. D. Bulitko, F. F. Deryugin.** *Elektricheskie Stanisii* (Moscow, U.S.S.R.), volume 19, October 1948, pages 27–28.

7. Double Earth Faults, **A. Salzmann.** *Electrician* (London, England), volume 140, number 3629, 1948, pages 29–32.

8. Concerning Selection by Interlocking Between Transformer and the Line Protective Devices, **J. Savatier.** *Revue Generale de l'Electricite* (Paris, France), volume 57, 1948, pages 102–04.

9. The Application of High-Speed Parallel Feeder Protective Gear, **G. L. Smith.** *BTH Activities* (Rugby, England), volume 19, 1948, pages 320–23.

10. Modern Approach to the Problem of Fault Clearance in High-Voltage Networks. *Brown Boveri Review* (Baden, Switzerland), volume 35, 1948, pages 131–34.

11. Relaying of Transmission Lines from the New Sunbury Generating System, **H. H. Green, J. A. G. Oewel, O. Ramsaur.** *AIEE Transactions*, volume 68, part II, 1949, pages 873–78, and *Electrical Engineering*, volume 68, December 1949, page 1031.

12. Protective Equipment of the Interconnected Austrian High-Voltage System, **W. Weller.** *Osterreichische Zeitschrift fur Elektrisitatswirtschaft* (Vienna, Austria), volume 2, 1949, pages 15–20.

Paper 51-38, recommended by the AIEE Relays Committee and approved by the AIEE Technical Program Committee for presentation at the AIEE Winter General Meeting, New York, N. Y., January 22–26, 1951. Manuscript submitted November 16, 1950; made available for printing November 24, 1950.

Personnel of the AIEE Project Committee on Relay Bibliography: Eric T. B. Gross, *Chairman*; S. Goldsmith; C. E. Parks; and C. L. Smith.

Section E. Bus Protection

1. Busbar Zone Protection. *Electrical Times* (London, England), volume 112, number 2907, 1947, pages 99–100.

2. Instantaneous Bus-Differential Protection Using Bushing Current Transformers, **H. T. Seeley, F. von Roeschlaub.** *AIEE Transactions*, volume 67, part II, 1948, pages 1707–19, and *Electrical Engineering*, volume 68, March 1949, page 236.

Section F. Apparatus Protection

1. Relay Protection of Power Transformers, **AIEE Committee Report.** *AIEE Transactions*, volume 66, 1947, pages 911–15; *Electrical Engineering*, volume 66, October 1947, pages 964–68.

2. Protection of Powerhouse Auxiliaries. *Power Plant Engineering* (Chicago, Ill.), volume 51, 1947, pages 118, 120, 122.

3. Transformer Protection (A) Protective Gear and Schemes, (B) The Selection of Transformer Protective Equipment, **G. Courvoisier, H. Meyer, J. Stoecklin, A. Matthey-Doret.** *Brown Boveri Review* (Baden, Switzerland), volume 34, 1947, pages 147–73.

4. Bank of Capacitors Reinforces 132-kv Grid, **L. F. Ferri, C. S. Dayton.** *Electrical World* (New York, N. Y.), volume 127, number 13, 1947, pages 66–69.

5. Simplicity in Transformer Protection, **Eric T. B. Gross.** *Electrical Engineering*, volume 66, June 1947, pages 564–69.

6. Typical Transformer Faults and Gas Detector Relay Protection, **J. T. Madill.** *AIEE Transactions*, volume 66, 1947, pages 1052–60.

7. Power Relay for the Automatic Connection and Disconnection of Condensers, **W. Aggestam.** *Ericsson Review* (Stockholm, Sweden), 1948, number 3, pages 105–08.

8. Thermal Protection of Power Transformers, **C. L. Denault.** *Westinghouse Engineer* (East Pittsburgh, Pa.), volume 8, 1948, pages 103–05.

9. Differential Current Protection Against Earthing of Generator Stator Windings, **V. L. Fabrikant, G. T. Grek.** *Elektrichestvo* (Moscow, U.S.S.R.), June 1948, pages 7–14.

10. Use of Relays Embodying Rapidly Saturating Transformers in Differential Protection, **M. I. Tsarev.** *Elektricheskie Stantsii* (Moscow, U.S.S.R.), volume 19, August 1948, pages 41–45.

11. Connection Arrangements and Protective Practices for Shunt Capacitor Banks, **N. R. Clark, S. B. Farnham.** *AIEE Transactions*, volume 68, part II, 1949, pages 1226–31.

12. Use of Current Transformers of Zero-Sequence with Annular Yoke for the Protection of Generators, **V. E. Kazanski.** *Elektricheskie Stantsii* (Moscow, U.S.S.R.), volume 20, March 1949, pages 39–41.

13. Practical Measures for Obtaining Differential Protection, **A. Muratori.** *Elettrotecnica* (Milan, Italy), volume 36, 1949, pages 32–37.

14. Rapid Field Suppression for Synchronous Generators (in German), **F. Moldenhauer.** *Zeitschrift fur Elektrotechnik* (Stuttgart, Germany), volume 2, 1949, pages 133–38.

15. Automatic Grounding and Air-Break Switches for Protection of Transformer Stations, **E. A. Ricker.** *AIEE Transactions*, volume 68, part II, 1949, pages 851–57; *Electrical Engineering*, volume 68, December 1949, page 1024.

16. Switchgear Differential Relaying, **H. T. Seeley.** *Distribution* (Schenectady, N. Y.), volume 11, number 3, 1949, pages 17–19.

17. Overload Current Protection of the Generators of Automatic Hydro-Electric Power Stations, **E. E. Sirotinskii.** *Elektricheskie Stantsii* (Moscow, U.S.S.R.), volume 20, November 1949, pages 46–47.

18. Current Protection of the Stator of a Generator Against Earth Faults, **I. I. Solovev, I. N. Popov.** *Elektricheskie Stantsii* (Moscow, U.S.S.R.), volume 20, June 1949, pages 17–23.

19. Improvement in the Differential Protection of Transformers with the KR-121 Relay, **M. I. Tsarev.** *Elektricheskie Stantsii* (Moscow, U.S.S.R.), volume 20, January 1949, pages 41–42.

20. Differential Protection of Generators with Auxiliary Transformers of Low Saturation Value, **M. I. Tsarev.** *Elektricheskie Stantsii* (Moscow, U.S.S.R.), volume 20. July 1949, pages 38–41.

Section G. Distribution and Network Protection

1. Considerations on the Behavior of Modern Distribution Networks Protected by Reclosing Circuit-Breakers, **F. Burlando.** *Energia Elettrica* (Milan, Italy), volume 24, 1947, pages 208–15.

2. Automatic Sectionalizing Applied to 4-kv, **H. C. Denison.** *Electrical World* (New York, N. Y.), volume 128, number 9, 1947, page 55.

3. Master Unit Sub-station Relay and Control Arrangements for Radial, Duplex, and Network Units, **E. M. Hunter, J. W. Yetter.** *General Electric Review* (Schenectady, N. Y.), volume 50, September 1947, pages 24–29.

4. Protection of Medium-Voltage Radial and Network Distribution Systems, **H. Petit.** *Bulletin*, Societe Francaise des Electriciens (Paris, France), series 6, volume 7, 1947, pages 315–22.

5. An Improved Overcurrent Tripping Device for Low-Voltage Circuit Breakers, **H. L. Rawlins, Jerome Sandin.** *AIEE Transactions*, volume 66, 1947, pages 1149–53, and *Electrical Engineering*, volume 66, December 1947, pages 1194–97.

6. Under-Voltage Tripping in Low-Voltage Networks, **J. E. Carlsson.** *ASEA Journal*, Allmanna Svenska Elektriska AB (Vasteras, Sweden), volume 21, 1948, pages 73–77.

7. Field Tests of Oil Circuit Recloser Substantiate Analytical Co-ordination Method, **G. G. Auer, R. A. Branflick, L. J. Woodward, W. C. McKinley.** *AIEE Transactions*, volume 68, part II, 1949, pages 801–10, and *Electrical Engineering*, volume 68, October 1949, page 864.

8. Protective Devices for Electrical Systems in Steelworks, **H. V. Benns, A. W. Tozer.** *Journal*, Iron and Steel Institute (London, England) volume 163, November 1949, page 331.

9. Selective Protection of Rural Supply Networks, **L. Bors.** *Elektrotechnika* (Budapest, Hungary), volume 41, 1949, pages 322–32.

10. Overcurrent Investigation on a Rural Distribution System, **G. F. Lincks, D. R. Edge, W. C. McKinley, J. H. Leh.** *AIEE Transactions*, volume 68, part II, 1949, pages 915–29.

11. Improving Low-Voltage Meshed Distribution Networks by the Use of Direct Acting Primary Directional Relays, **S. Matena.** *Elektrotechnicky Obsor* (Prague, Czechoslovakia), volume 38, 1949, pages 607–13.

12. Modern Concept of Sectionalizing and Over-Current Coordination of Distribution Lines, **R. F. Quinn.** *Proceedings*, Midwest Power Conference (Chicago, Ill.), volume 11, 1949, pages 238–51.

13. Selecting Distribution Line Sectionalizing Devices, **R. F. Quinn.** *Distribution* (Schenectady, N. Y.), volume 11, number 1, 1949, pages 3–5.

14. Network Relays, **A. Salzmann.** *Electrician* (London, England), volume 142, 1949, number 3691, pages 743–46, and number 3692, pages 811–14.

Section H. Service Restoration

1. Experience with Single-Pole Relaying and Reclosing on a Large 132-Kv System, **J. J. Trainor, C. E. Parks.** *AIEE Transactions*, volume 66, 1947, pages 405–12, and *Electrical Engineering*, volume 66, May 1947, pages 467–70.

2. Transient Shaft Torques in Turbine Generators Produced by Transmission Line Reclosing, **J. W. Batchelor, D. L. Whitehead, J. S. Williams.** *AIEE Transactions*, volume 67, part I, 1948, page 159–64.

3. Experience with High-Speed Reclosing, **G. E. Dana.** *Electrical Engineering*, volume 67, October 1948, pages 942–44.

4. Experience in Operation with Automatic Reclosing of Breakers after Line Faults, **G. Jancke.** *Report Number 306*, International Conference on Large High-Voltage Electric Systems (Paris, France), 1948.

5. Staged Tests and Operating Results on an 8-Kv Overhead Line System Using High-Speed Automatic Reclosing, **O. Naef, J. Wild.** *Report Number 331*, International Conference on High-Voltage Electric Systems (Paris, France), 1948.

6. Service Restoration with Automatic Air-Break Switches, **K. N. Reardon.** *AIEE Transactions*, volume 67, part I, 1948, pages 64–72.

7. High-Speed Reclosing Through the Years, **H. B. Ashenden.** *Allis-Chalmers Electrical Review* (Milwaukee, Wis.), volume 14, number 3, 1949, pages 4–11.

8. Insulator Flashover Deionization Times as a Factor in Applying High-Speed Reclosing Circuit Breakers, **A. C. Boisseau, B. W. Wyman, W. F. Skeats.** *AIEE Transactions*, volume 68, part II, 1949, pages 1058–67.

9. Deionization Time of High-Voltage Fault-Arc Paths, **E. J. Harrington, E. C. Starr.** *AIEE Transactions*, volume 68, 1949, pages 997–1004.

10. Thirty Years of Automatic Reclosing, **C. L. Headley.** *Allis-Chalmers Electrical Review* (Milwaukee, Wis.), volume 14, number 2, 1949, pages 16–17.

Section I. General and Miscellaneous Relaying

1. Schemes for Connecting a 3-Phase Power Direction Relay, **G. I. Atabekov.** *Elektrichestvo* (Moscow, U.S.S.R.), June 1948, pages 15–19.

2. Influence of Inverse-Time-Relay Characteristics on Discriminative Time, **E. W. Connon, E. Smith.** *Journal*, Institution of Electrical Engineers (London, England), volume 95, part II, 1948, pages 787–804.

3. Sensitive Relay Contact Protection Systems, **J. P. Dallas, T. H. McCully.** *AIEE Transactions*, volume 67, part II, 1948, pages 1204–07.

4. Voltage Surges in Relay Control Circuits, **T. R. Halman, L. K. Harris.** *AIEE Transactions*, volume 67, 1948, pages 1693–99, and *Electrical Engineering*, volume 68, April 1949, page 327.

5. Principles and Practices of Relaying in the United States, **E. L. Harder, W. E. Marter.** *AIEE Transactions*, volume 67, part II, 1948, pages 1005–23, and *Electrical Engineering*, volume 67, November 1948, pages 1075–81.

6. Electronic Protective Relays, **R. H. MacPherson, A. R. Van C. Warrington, A. J. McConnell.** *AIEE Transactions*, volume 67, part II, 1948, pages 1702–08.

7. Is Backup Protection Always Necessary?, **W. L. Ridenhour.** *Electrical World* (New York, N. Y.), volume 129, March 13, 1948, pages 104–05.

8. Electronic Selective Protection, **H. Touly.** *Report Number 316*, International Conference on High-Voltage Electric Systems (Paris, France), 1948.

9. Bibliography of Relay Literature, 1944–46 **AIEE Committee Report.** *AIEE Transactions*, volume 67, part I, 1948, pages 24–27.

10. Polarity of D-C Control, **AIEE Committee Report.** *Electrical Engineering*, volume 67, October 1948, page 985.

11. Protection of Stations Without High-Voltage Switching, **AIEE Committee Report.** *AIEE Transactions*, volume 68, part I, 1949, pages 226–32; *Electrical Engineering*, volume 68, June 1949, page 520.

12. Insulation Level of Relay and Control Circuits, **AIEE Committee Report.** *AIEE Transactions*, volume 68, part II, 1949, pages 1255–57; *Electrical Engineering*, volume 68, November 1949, page 1001.

13. New Relay Assures Feeder Resumption After Outage, **L. J. Audlin, M. H. Pratt, A. J. McConnell.** *Electrical World* (New York, N. Y.), volume 132, number 11, 1949, pages 99–103 and number 12, pages 95–98.

14. Electronic Relay for the Detection of Sudden Drops in Load of Electric Generators, **F. Cahen, A. Chevallier.** *Revue Generale de l'Electricite* (Paris, France), volume 58, 1949, pages 393–97.

15. The Electrical Protection of Large Hydro-Electric Power Stations. **L. Ferschl.** *Elektrotechnik und Maschinenbau* (Vienna, Austria), volume 66, 1949, pages 141–51.

16. Here's How Circuit Breakers Should Trip, **J. M. Geiger, L. L. Fountain.** *Power* (New York, N. Y.), volume 93, November 1949, pages 110–11.

17. Calculation of the Torques of an Induction Relay with Cylindrical Rotor, **L. A. Gelbukh.** *Avtomatika i Telemechanika* (Moscow, U.S.S.R.), volume 10, number 1, 1949, pages 8–12.

18. Preventing Corrosion in Relays, **A. E. Herman.** *Electrical Manufacturing* (New York, N. Y.), volume 42, May 1949, pages 116–18.

19. High-Speed Relaying Practice, **L. F. Kennedy.** *Distribution* (Schenectady, N. Y.), volume 11, number 3, 1949, pages 13–14.

20. A Review of British Practice in the Protection of Electric Power Systems, **C. H. Lackey.** *Transactions*, South African Institute of Electrical Engineers (Johannesburg, South Africa), volume 40, 1949, pages 215–46.

21. Electronic Relay Developments, **James J. Loving, Jr.** *AIEE Transactions*, volume 68, part I, 1949, pages 233–42, and *Electrical Engineering*, volume 68, June 1949, page 478.

22. Electronic Protective Relays, **R. H. MacPherson, A. R. Van C. Warrington, A. J. McConnell.** *AIEE Transactions*, volume 67, part II, 1948, pages 1702–08, and *Electrical Engineering*, volume 68, February 1949, pages 122–28.

23. Shipshaw Relay Protection, **J. T. Madill, F. H. Duffy.** *AIEE Transactions*, volume 68, part I, 1949, pages 50–58.

24. A New Loss-of-Excitation Relay for Synchronous Generators, **C. R. Mason.** *AIEE Transactions*, volume 68, part II, 1949, pages 1240–45.

25. Frequency Relays Disconnect Synchronous Motors Under High Speed Reclosure, **A. J. Meyers.** *Power Generation* (New York, N.Y.), volume 53, July 1949, pages 82–83.

26. One Slip Cycle Out-of-Step Relay Equipment, **W. C. Morris.** *AIEE Transactions*, volume 68, part II, 1949, pages 1246–48.

27. Single-Element 3-Phase Directional Power Relay, **V. K. Ponomarenko.** *Elektrichestvo* (Moscow, U.S.S.R.), July 1949, pages 25–29.

28. Operation of Inverse Time Relays, **A. Salzmann.** *Electrical Times* (London, England), volume 115, number 2989, 1949, pages 207–11.

29. Contribution to the Solution of Difficult Earthing Problems in Transformer Stations, **W. Schrank.** *Elektrotechnische Zeitschrift* (Berlin, Germany), volume 70, 1949, pages 199–202.

30. Protective Relaying, **H. P. Sleeper.** *Electrical World* (New York, N. Y.), volume 131, May 21, 1949, pages 295–99.

31. Modern Developments in Selective Protective Methods, **H. Titze.** *Elektrotechnik und Maschinenbau* (Vienna, Austria), volume 66, 1949, pages 301–06.

32. A-C Tripping and Reclosing of Line Sectionalizing Circuit Breakers, **C. E. Winegartner, H. E. Bonheimer.** *AIEE Transactions*, volume 68, part II, 1949, pages 1357–59.

Section J. Testing and Analyzing

1. Properties of High-Voltage Lines for High-Frequency Transmission and for Fault Locating with High-Frequency Carrier Devices, **H. Elger.** *Archiv der Elektrischen Uebertragung* (Wiesbaden, Germany), volume 1, 1947, pages 195–204.

2. Radar on New South Wales Railways, **A. H. Gray.** *Railway Signaling* (New York, N. Y.), volume 40, 1947, pages 237–38.

3. Testing Relays, **T. A. Ledward.** *Electrical Review* (London, England), volume 140, number 3621, 1949, pages 619–21.

4. New Method of Finding Fault Location by Shock Waves, **S. Margoulies, P. Fourmarier.** *Bulletin*, Association des Ingenieurs Electriciens Sortis de l'Institut Electrotechnique Montefiore (Liege, Belgium), volume 60, 1947, pages 123–59.

5. Over-Current Relays, **A. Salzmann.** *Electrical Times* (London, England), volume 111, number 2902, 1947, pages 700–03.

6. Is Your Relay Test Program Realistic?, **F. S. Fehr.** *Electrical World* (New York, N. Y.), volume 129, number 19, May 8, 1948, pages 88–89

7. Checking Electrical Protective Gear, **W. M. Gore.** *Power and Works Engineer* (London, England), volume 43, number 499, 1948, pages 18–19.

8. Fault Location on Hot Lines by Means of Impulse Waves, **E. Hueter.** *Zeitschrift fur Elektrotechnik* (Stuttgart, Germany), volume 1, 1948, pages 2–6.

9. Fault Location and Relay Protection, **E. W. Knapp, B. C. Hicks.** *Electrical News and Engineering* (Toronto, Canada), volume 57, number 12, 1948, pages 87–88.

10. The "Linascope"—An Echo-Ranging Type Fault Locator for High-Voltage Lines, **J. R. Leslie, K. H. Kidd.** *AIEE Transactions*, volume 67, part II, 1948, pages 1162–67.

11. The Localisation of Faults on Overhead Lines by Means of Impulse Waves, **S. Margoulies, P. Fourmarier.** *Report Number 307 and 307A*, International Conference on Large High-Voltage Electric Systems (Paris, France), 1948.

12. Relaying Difficulties Disclosed by Staged-Fault Tests, **W. A. Morgan, B. Evans.** *AIEE Transactions*, volume 67, part I, 1948, pages 73–82.

13. Pulse Radar Used to Locate Faults, **G. G. Mendenhall.** *Electrical World* (New York, N. Y.), volume 130, number 19, November 6, 1948, page 88.

14. Faults in Turbo-Generators, **A. Roggendorf.** *Elektrotechnik* (Berlin, Germany), volume 2, 1948, pages 209–14.

15. Directional Test of Directional Relays, **A. Salzmann.** *Electrician* (London, England), volume 140, number 3638, 1948, pages 709–13.

16. A Transmission Line Fault Locator Using Fault-Generated Surges, **R. F. Stevens, T. W. Stringfield.** *AIEE Transactions*, volume 67, part II, 1948, pages 1168–79, and *Electrical Engineering*, volume 67, November 1948, page 1060.

17. A Method for Detection of Sustained Earth Faults in Rural Overhead Lines Protected by Petersen Coils, **B. D. Zelikin.** *Journal*, Institution of Electrical Engineers (London, England), volume 95, part II, 1948, pages 617–19.

18. Report on Method of Measurements at Carrier-Current Frequencies, **AIEE Committee Report.** *AIEE Transactions*, volume 67, part II, 1948, pages 1429–32.

19. An Oscillograph for the Automatic Recording of Disturbances on Electric Supply Systems, **W. T. J. Atkins.** *Proceedings*, Institution of Electrical Engineers (London, England), volume 96, part II, 1949, pages 276–85.

20. Loss Measurements Made on Underground-Cable Overhead-Conductor 132-kv Transmission Line at Carrier Current Frequencies, **H. A. Cornelius, B. W. Storer.** *AIEE Transactions*, volume 68, part I, 1949, pages 597–601.

21. Testing of the Relay Protection of Generators and Power Transformers, **I. K. Erenkov.** *Elektricheskie Stantsii* (Moscow, U.S.S.R.), volume 20, March 1949, pages 36–38.

22. Spark Quenching at Relay Contacts Interrupting D-C Circuits, **A. Hamilton, R. W. Sillars.** *Proceedings*, Institution of Electrical Engineers (London, England). volume 96, part I, 1949, pages 64–76

23. Testing of the Protection of a Unit with Primary Current, The Generator Being Immobilized, **G. A. Kireev.** *Elektricheskie Stantsii* (Moscow, U.S.S.R.), volume 20, March 1949, page 34–36.

24. Fault Locating on High-Voltage Lines by Means of the Impulse Method, **C. L. Kober.** *Elektrotechnik und Maschinenbau* (Vienna, Austria), volume 66, 1949, pages 269–74.

25. Checking New Earth Fault Protection for Generators, **I. M. Sirota.** *Elektricheskie Stantsii* (Moscow, U.S.S.R.), volume 20, June 1949, pages 23–25.

26. Novel Test Circuits for Protective Relays, **W. K. Sonnemann.** *AIEE Transactions*, volume 68, part II, 1949, pages 1249–54.

27. A Transient Fault Locator for High-Voltage Transmission Lines, **L. R. Spaulding, C. E. Diemond.** *AIEE Transactions*, volume 68, part II, 1949, pages 1005–12.

28. Economical Method of Testing the Relay Protective System of Synchronous Generators and Transformers, **I. A. Syromyatnikov.** *Elektricheskie Stantsii* (Moscow, U.S.S.R.), volume 20, March 1949, pages 32–34.

29. Test Box for Protective Relays, **R. C. Yates.** *Electrical Engineer and Merchandiser* (Melbourne, Australia), volume 25, 1949, pages 386–87.

Section K. System Stability

1. Underexcited Operation of Turbogenerators, **C. G. Adams, J. B. McClure.** *AIEE Transactions*, volume 67, part I, 1948, pages 521–26

2. Circuit-Breaker Modernization and Faster Fault Clearing on Single-Phase Electrified Railroad, **H. F. Brown, H. A. Travers, C. A. Woods, Jr.** *AIEE Transactions*, volume 67, part I, 1948, pages 705–12.

3. Generator Stability at Low Excitation, **E. L. Michelson, L. F. Fischer.** *AIEE Transactions*, volume 67, part I, 1948, pages 1–6.

4. Power System Stability Requirements Determined by A-C Calculating Board Study and Operating Performance Proved by Staged Fault Tests, **W. A. Morgan, B. Evans.** *Report Number 319*, International Conference on Large High-Voltage Electric Systems (Paris, France), 1948.

5. Technical and Economic Aspects of the Transmission of Electrical Energy Over Long Distances, **W. Wanger.** *Journal*, Institution of Electrical Engineers (London, England), volume 95, part I, 1948, pages 340–51.

6. The Stability of Synchronous Generators, **C. Lavanchy.** *Brown Boveri Review* (Baden, Switzerland), volume 36, 1949, pages 264–70.

Section L. Methods of Calculation

1. Machine Computation of Power Network Performance, **L. A. Dunstan.** *AIEE Transactions*, volume 66, 1947, pages 610–23.

2. Calculating Fault Currents of Unsymmetrical Short Circuits, **E. Faessler.** *Schweizer Archiv* (Solothurn, Switzerland), volume 13, 1947, pages 70–82.

3. Calculation of Fault Currents in Electrical Networks, Circuit-Breaker Selection (book), **R. T. Lythall.** Sir Isaac Pitman and Sons, London, England, second edition, 1947, 77 pages.

4. The Evaluation of Simultaneous Faults on Three-Phase Systems, **J. R. Mortlock.** *Journal*, Institution of Electrical Engineers (London, England), volume 94, part II, 1947, pages 166–90.

5. Network Analyzers, **J. R. Mortlock.** *Electrical Times* (London, England), volume 111, number 2900, 1947, pages 635–39.

6. Practical Calculation Methods for Determining Short-Circuit Currents in 3-Phase Networks, **H. Wallgren.** *ASEA Journal*, Allmanna Svenska Elektriska AB (Vasteras, Sweden), volume 20, 1947, pages 179–87

7. Method of Calculation of Generator Protection from Earth Faults, **A. B. Barzam.** *Elektrichestvo* (Moscow, U.S.S.R.), February 1948, pages 58–63.

8. Use of A-C Network Calculator in Planning and Operating Electric Power Systems, **P. O. Bobo, H. A. Travers, E. E. George.** *Report Number 328*, International Conference on Large High-Voltage Electric Systems (Paris, France), 1948.

9. Short-Circuit Calculations for Circuit

BREAKERS, **R. E. Burlingame.** *Allis-Chalmers Electrical Review* (Milwaukee, Wis.), volume 13, 1948, pages 27–34.

10. A-C NETWORK ANALYZER, **I. S. Bruk, S. S. Chugunov, M. S. Libkind.** *Elektrichestvo* (Moscow, U.S.S.R.), January 1948, pages 34–44.

11. CALCULATION OF CURRENTS AND VOLTAGES FOR A COMPLETE ANALYSIS OF RELAY PROTECTION WITH SHORT CIRCUIT AND WITH SIMULTANEOUS OPEN CIRCUITS OF ONE PHASE, **A. B. Chernin.** *Elektrichestvo* (Moscow, U.S.S.R.), June 1948, pages 20–25.

12. THE GENERAL SOLUTION METHOD OF POWER NETWORK ANALYSIS, **L. A. Dunstan.** *AIEE Transactions*, volume 67, 1948, pages 631–38.

13. CALCULATION OF ERRORS IN THREE-WINDING VOLTAGE TRANSFORMERS, **T. Waterhouse.** *Journal*, Institution of Electrical Engineers (London, England), volume 95, part II, 1948, pages 71–78; Discussion, volume 96, part II, 1949, page 389.

14. SIMPLIFIED CALCULATION OF FAULT CURRENTS **AIEE Committee Report.** *AIEE Transactions*, volume 67, part II, 1948, pages 1433–35, and *Electrical Engineering*, volume 67, November 1948, pages 1085–87.

15. A NEW CALCULATING TABLE FOR ALTERNATING CURRENT. *Technique Moderne* (Paris, France), volume 41, 1949, pages 270–72.

16. CALCULATION OF THE CURRENT PROTECTION AGAINST EARTH FAULTS OF GENERATORS OPERATING ON BUSBARS, **A. B. Barzam.** *Elektricheskie Stantsii* (Moscow, U.S.S.R.), volume 20, April 1949, pages 29–34.

17. A NETWORK ANALYZER OPERATING AT 10,000 CYCLES, **W. B. Boast, J. D. Ryder.** *Proceedings*, Midwest Power Conference (Chicago, Ill.), volume 11, 1949, pages 72–78.

18. A NEW TABLE TO CALCULATE ALTERNATING CURRENTS, **F. Cahen.** *Revue Generale de l'Electricite* (Paris, France), volume 58, 1949, pages 49–61.

19. THE NEGATIVE-SEQUENCE REACTANCES OF AN IDEAL SYNCHRONOUS MACHINE, **W. C. Duesterhoeft.** *AIEE Transactions*, volume 68, part I, 1949, pages 510–14.

20. AN IMPROVED A-C NETWORK ANALYZER, **W. A. Morgan, F. S. Rothe, J. J. Winsness.** *AIEE Transactions*, volume 68, part II, 1949, pages 891–97

Section M. Instrument Transformers and Other Auxiliary Devices

1. SPECIAL METHOD OF EXPRESSING PROPERTIES OF MAGNETIC MATERIALS FOR SIMPLIFIED BUSHING CURRENT TRANSFORMER DESIGN, **P. Altmann.** *Journal*, Institution of Engineers (Sidney, Australia), volume 19, 1947, pages 197–203.

2. CURRENT AND VOLTAGE TRANSFORMERS FOR PROTECTIVE-GEAR PURPOSES. *Journal*, Institution of Electrical Engineers (London, England), volume 94, part II, 1947, pages 528–30.

3. GROUNDING OF INSTRUMENT TRANSFORMER SECONDARY CIRCUITS, **AIEE Committee Report.** *AIEE Transactions*, volume 66, 1947, pages 419–22, and *Electrical Engineering*, volume 66, April 1947, pages 335–37.

4. CAPACITOR VOLTAGE-TRANSFORMERS IN SWEDEN, **R. Nordell, L. Hogfeldt.** *Report Number 320*, International Conference on Large High-Voltage Electric Systems (Paris, France), 1948.

5. REVOLUTIONARY ADVANCE IN INSTRUMENT TRANSFORMER DESIGN, **I. F. Kinnard.** *General Electric Review* (Schenectady, N. Y.), volume 52, June 1949, pages 15–19.

6. MATERIALS PROBLEMS SOLVED TO DEVELOP NEW BUTYL-MOLDER TRANSFORMER, **I. F. Kinnard.** *Materials and Methods* (New York, N. Y.), volume 29, June 1949, page 47.

7. CURRENT TRANSFORMERS WITH CERAMIC INSULATION, **B. Olsson.** *ASEA Journal*, Allmanna Svenska Elektriska AB (Vasteras, Sweden), volume 22, 1949, pages 56–63.

8. OIL MINIMUM CURRENT TRANSFORMERS, **B. Olsson.** *ASEA Journal*, Allmanna Svenska Elektriska AB (Vasteras, Sweden), volume 22, 1949, pages 151–56.

Addenda to "Relay Bibliography—1940-1946"

Section A. Line Protection—Distance

1. BEHAVIOR OF REACTANCE RELAYS WITH SHORT CIRCUITS FED FROM TWO SIDES, **H. Gutmann.** *Elektrotechnische Zeitschrift* (Berlin, Germany), volume 61, 1940, pages 541–44.

2. A NEW RAPID DISTURBANCE PROTECTIVE DEVICE, **W. Kramer.** *Elektrotechnische Zeitschrift* (Berlin, Germany), volume 65, 1944, pages 193–95.

3. PRACTICAL EXPERIENCE WITH A RAPID DISTANCE RELAY ON THE 150-KV SYSTEM OF THE BERNISCHE KRAFTWERKE A. G. *Bulletin*, Association Suisse des Electriciens (Zurich, Switzerland), volume 36, 1945, pages 805–07.

4. DISTANCE RELAYS AND FREQUENCY-BIASED TIE-LINE CONTROL, **R. Keller, W. Streuli.** *Brown Boveri Review* (Baden, Switzerland), volume 33, 1946, pages 289–91.

Section B. Line Protection—Pilot Wire and Carrier Current

1. SELECTIVE PROTECTION BY CARRIER CURRENTS, **F. Cahen.** *Bulletin*, Societe Francaise des Electriciens (Paris, France), volume 6, 1946, pages 303–04.

2. PHASE-COMPARISON PROTECTION WITH CARRIER CURRENTS FOR HIGH-VOLTAGE LINES AND CABLES, **A. Chevallier.** *Bulletin*, Societe Francaise des Electriciens (Paris, France), volume 6, 1946, pages 305–20.

3. APPLICATION OF PILOT WIRE PROTECTION TO LONG 88-KV TRANSMISSION LINES, **W. Fenwich, C. P. Marais.** *Metropolitan-Vickers Gazette* (Manchester, England), volume 21, number 353, 1946, pages 229–40.

Section D. Line Protection—General

1. RAPID OPERATING DIRECTIONAL CROSS-COMPARISON PROTECTION FOR SHORT PARALLEL CABLES, **F. Frohlich.** *Elektrotechnische Zeitschrift* (Berlin, Germany), volume 62, 1941, pages 173–76.

2. DESIGN AND PROTECTION OF MODERN SYSTEMS, **E. Westerhoff.** *Elektrotechnische Zeitschrift* (Berlin, Germany), volume 63, 1942, pages 225–32.

Section F. Apparatus Protection

1. GENERATOR PROTECTION, **H. Schatzmayr.** *Brown Boveri Review* (Baden, Switzerland), volume 30, 1943, pages 25–38.

2. EARTH-LEAKAGE PROTECTION FOR ALTERNATORS, **H. Stadler.** *Brown Boveri Review*, (Baden, Switzerland), volume 31, 1944, pages 392–400.

3. ENHANCED TRANSFORMER PROTECTION THROUGH INRUSH-PROOF RATIO DIFFERENTIAL RELAYS, **G. Bertola.** *Brown Boveri Review* (Baden, Switzerland), volume 32, 1945, pages 129–33.

4. THE CHOICE OF GENERATOR PROTECTIVE GEAR, **L. Burckhardt.** *Brown Boveri Review* (Baden, Switzerland), volume 32, 1945, pages 178–91.

5. PROTECTION OF ELECTRICAL MACHINES AND TRANSFORMERS, **O. Hess.** *Brown Boveri Review* (Baden, Switzerland), volume 33, October 1946, pages 292–93.

6. A PERCENTAGE DIFFERENTIAL RELAY FOR TRANSFORMER PROTECTION DESIGNED TO REMAIN UNAFFECTED BY SWITCHING IMPULSES, **H. Hoel, J. Stoecklin.** *Bulletin*, Association Suisse des Electriciens (Zurich, Switzerland), volume 36, 1945, pages 160–63.

7. THE PROTECTIVE EQUIPMENT, **R. Keller.** *Brown Boveri Review* (Baden, Switzerland), volume 32, 1945, pages 159–77.

8. INSTANTANEOUS MAGNETIC BALANCE PROTECTION FOR POWER TRANSFORMERS, **J. G. Wellings, P. Mathews.** *Electrical Times* (London, England) volume 108, 1945, pages 556–58.

9. THE BUCHHOLZ PROTECTIVE RELAY, **F. Stumpf.** *Praktisches Wissen* (Graz, Austria), volume 8, 1946, pages 185–93.

10. INSTANTANEOUS MAGNETIC BALANCE PROTECTION FOR POWER TRANSFORMERS, **G. Wellings, P. Mathews.** *BTH Activities* (Rugby, England), volume 19, 1946, pages 30–32.

Section G. Distribution and Network Protection

1. THE PROTECTION OF LOW-VOLTAGE INDUSTRIAL SYSTEMS, **S. Hopperwieser.** *Brown Boveri Review* (Baden, Switzerland), volume 31, 1944, pages 192–95.

2. MODERN PROTECTIVE DEVICES FOR MEDIUM VOLTAGE NETWORKS, **A. Van Gastel.** *Brown Boveri Review* (Baden, Switzerland), volume 32, 1945, pages 123–28.

Section H. Service Restoration

1. ARC EXTINCTION IN THE ULTRA-RAPID SINGLE-PHASE RECLOSURE OF 220-KV LINES, **E. Maury.** *Revue Generale de l'Electricite* (Paris, France), volume 53, 1944, pages 79–90.

2. PROTECTION OF HIGH VOLTAGE NETWORKS, **L. Roche.** *Revue Generale de l'Electricite* (Paris, France), volume 54, 1945, pages 106–12.

3. HIGH SPEED RECLOSING OF CIRCUIT BREAKERS, **S. Margoulies, E. H. Hubert.** *Report Number 105*, International Conference on Large High-Voltage Electric Systems (Paris, France), 1946.

4. A PHASE SELECTOR FOR SELECTIVE PROTECTION OF LINES, **L. Roche.** *Bulletin*, Societe Francaise des Electriciens (Paris, France), volume 6, 1946, pages 329–32.

Section I. General and Miscellaneous Relaying

1. PROTECTIVE GEAR PERFORMANCE ON THE BRITISH GRID SYSTEM DURING THE WAR 1939–1945, **F. J. Lane.** *Report Number 343*, International Conference on Large High-Voltage Electric Systems (Paris, France), 1946.

2. NEW DEVICES FOR RAPID SELECTIVE PROTECTION OF HIGH TENSION TRANSFORMER STATIONS AND MAJOR DISTRIBUTING STATIONS AT MEDIUM VOLTAGE, **C. Ramelot.** *Report Number 309*, International Conference on Large High-Voltage Electric Systems (Paris, France), 1946.

3. DEVELOPMENT OF RELAY AND AUTOMATIC PROTECTIVE DEVICES IN POWER SYSTEMS, **I. I. Solovjev.** *Elektrichestvo* (Moscow, U.S.S.R.), October 1946, pages 16–27.

Section J. Testing and Analyzing

1. MORNING FAULTS ON EXTRA-HIGH-TENSION POWER TRANSMISSION LINES, **L. Cabanes.** *Revue Generale de l'Electricite* (Paris, France), volume 52, 1943, pages 197–203.

Section M. Instrument Transformers and Other Auxiliary Devices

1. SIZE OF TRANSFORMERS FOR RELAY CONTROL CIRCUITS, **O. Deissler.** *Elektrotechnische Zeitschrift* (Berlin, Germany), volume 62, 1941, pages 499–501.

2. CURRENT TRANSFORMERS FOR PROTECTIVE GEAR, **J. G. Wellings.** *Report Number 342*, International Conference on Large High Voltage Electric Systems (Paris, France), 1946.

No Discussion

Radio Influence Tests in Field and Laboratory—500-Kv Test Project of the American Gas and Electric Company

G. D. LIPPERT MEMBER AIEE W. E. PAKALA MEMBER AIEE S. C. BARTLETT MEMBER AIEE C. D. FAHRNKOPF ASSOCIATE AIEE

MEASUREMENTS of radio influence, designated as r.i. in this paper, have been made near the high-voltage line conductors at the 500-kv test project of the American Gas and Electric Company[1—7,17,18] to obtain data for use in the design of high-voltage lines. The test site includes one 3-phase line 800 feet long and two 3-phase lines 1.36 miles long all on steel towers with ground wires on the two longer lines. To supplement this work tests also were made at the Trafford Laboratory of the Westinghouse Electric Corporation and on operating 138- and 230-kv lines. It is believed that the data obtained as well as the instrumentation and test methods used will be useful in predicting radio influence characteristics of lines.

As test work progressed, it was necessary to change plans and procedures because the radio influence was affected by many unforeseen weather and circuit variables. Even progress during the last three years on instruments for measuring radio noise required repetition of some tests and revisions of others. There are several known factors which affect r.i. levels from a conductor. The most important factors from the standpoint of amount of change in r.i. on a conductor used for power transmission is the weather, or the conductor environment, and the conductor surface conditions such as water on the surface caused by condensation or rain. Smaller changes than those attributed to water occur on conductors left unenergized for some time. These changes probably are the result of loose dirt particles on the conductor since the r.i. value decreases in a few minutes after the conductor is energized to a relatively constant value.

As the work progressed tests disclosed several unexpected phenomena and additional tests were required to confirm results although reasons were not always apparent.

Paper 51-40, recommended by the AIEE Transmission and Distribution Committee and approved by the AIEE Technical Program Committee for presentation at the AIEE Winter General Meeting, New York, N. Y., January 22–26, 1951. Manuscript submitted October 24, 1950; made available for printing November 22, 1950.

G. D. Lippert and S. C. Bartlett both are with the American Gas and Electric Service Corporation, New York, N. Y., W. E. Pakala and C. D. Fahrnkopf both are with Westinghouse Electric Corporation, East Pittsburgh, Pa.

General

Corona is defined[8] as a "luminous discharge due to ionization of the air surrounding a conductor around which exists a voltage gradient exceeding a certain critical value."

Corona forms in a nonuniform electric field in air and the voltage at which this takes place will not increase greatly with conductor spacing for conductor diameters and spacings used for high-voltage lines, whereas the sparking voltage, which is a complete breakdown between electrodes, increases rapidly with spacing.

The threshold voltage for a-c corona occurs only at the peak of the negative half-cycle on dry conductors and as the voltage is increased corona begins to appear on the positive half-cycle. At what voltage it appears depends upon the surface of the conductor and this threshold voltage may vary over wide limits. If the conductor is wet, corona forms first on the positive half-cycle and at a much lower threshold voltage than on the negative half-cycle. This wet corona will gradually diminish as the conductor dries as shown by Figure 1. Radio influence has significant values at practical voltages on negative half-cycle on new and dry conductors and at positive half-cycle on wet conductors whether new or weathered.

Radio Influence Generation by Corona

It has been shown[9] that the corona current rise is very rapid and the resulting radio influence voltages and fields can be measured. When corona forms at a point on a transmission line conductor which is a circuit of pure resistance equal to the surge impedance, a pulse-type induction field is set up in the vicinity of the conductor and if a receiving system with tuned circuits is near the line, shock excitation of the receiver circuits occurs resulting in radio noise over a much greater time than the actual duration of the pulse field. The time duration of radio noise in a receiver output depends on the number of tuned circuits in the receiver and their damping coefficients.

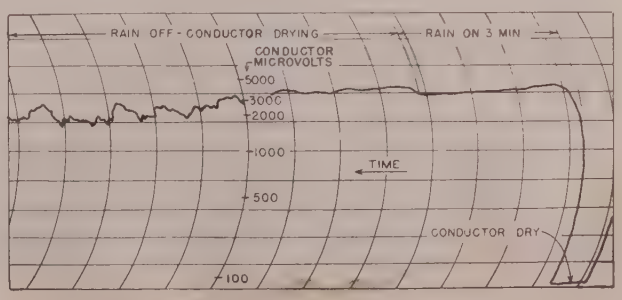

Figure 1. Radio influence chart record of laboratory rain test on 1.4-inch H-H conductor. 138-kv conductor to ground

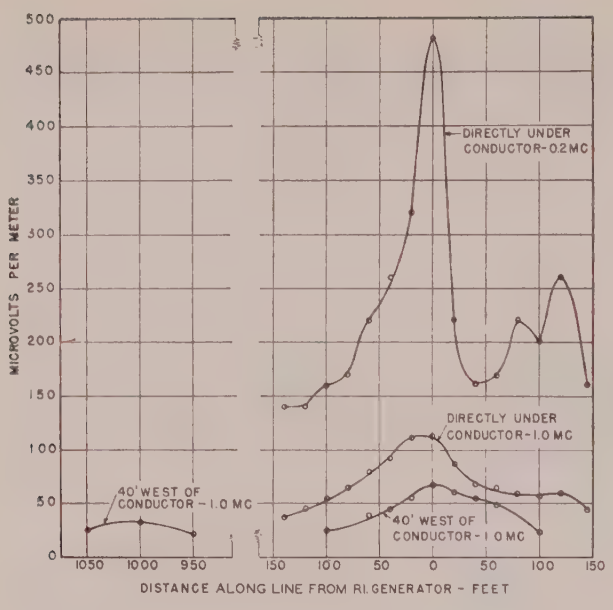
MICROVOLTS PER METER
DISTANCE ALONG LINE FROM R.I. GENERATOR - FEET
DIRECTLY UNDER CONDUCTOR-0.2 MC
DIRECTLY UNDER CONDUCTOR-1.0 MC
40' WEST OF CONDUCTOR - 1.0 MC
40' WEST OF CONDUCTOR - 1.0 MC

Figure 2. Field intensity near artificial r.i. generator attached to line conductor

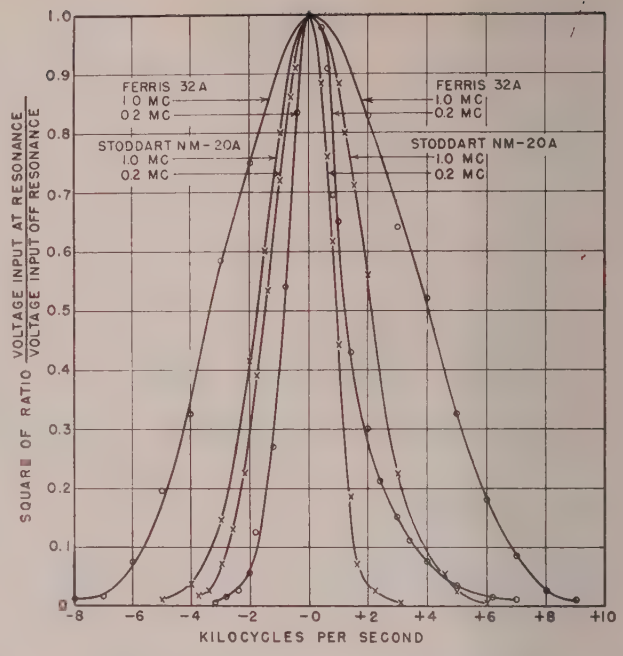
SQUARE OF RATIO VOLTAGE INPUT AT RESONANCE / VOLTAGE INPUT OFF RESONANCE
FERRIS 32A 1.0 MC 0.2 MC
STODDART NM-20A 1.0 MC 0.2 MC
FERRIS 32A 1.0 MC 0.2 MC
STODDART NM-20A 1.0 MC 0.2 MC
KILOCYCLES PER SECOND

Figure 4. Selectivity curves for radio noise meters

If the line is unterminated and short in length the field set up in the conductor vicinity will not be of the pulse type but will be a damped wave as obtained from any freely oscillating circuit. The result is to increase the average radio influence as compared to the peak value, and standing waves will exist along the conductor.

The conductor surface conditions and environment can change the r.i. magnitude by many times. The effect of rain is to increase greatly (individual tests showed increases up to 25 times) the r.i. voltage and field. After the conductor becomes wet the r.i. is independent of the amount of rainfall. Rain is the important weather factor, although other weather conditions approach it in importance.

Resultant of Several Radio Influence Sources and Propagation

There are many r.i. sources distributed at random along a conductor energized above the critical voltage. These sources are not in time phase because the regions where corona forms do not have exactly the same threshold voltage. The disturbances are random with time and it was shown by laboratory test that the resultant r.i. voltage from one to 15 generators varied as the square root of the number of r.i. generators (see Figure 21). On the other hand field intensity measurements at Tidd showed only a slight increase in r.i. from 1,900 feet to 7,160 feet of line. However, it was observed that r.i. values always were higher in the vicinity of a corona burst as located by

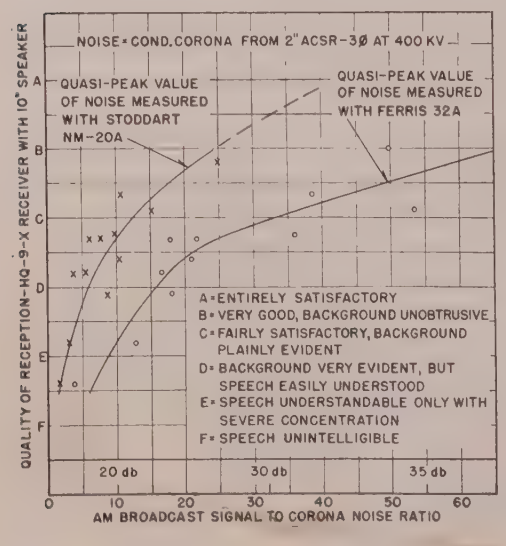
NOISE = COND. CORONA FROM 2" ACSR-3Ø AT 400 KV
QUASI-PEAK VALUE OF NOISE MEASURED WITH STODDART NM-20A
QUASI-PEAK VALUE OF NOISE MEASURED WITH FERRIS 32A
A = ENTIRELY SATISFACTORY
B = VERY GOOD, BACKGROUND UNOBTRUSIVE
C = FAIRLY SATISFACTORY, BACKGROUND PLAINLY EVIDENT
D = BACKGROUND VERY EVIDENT, BUT SPEECH EASILY UNDERSTOOD
E = SPEECH UNDERSTANDABLE ONLY WITH SEVERE CONCENTRATION
F = SPEECH UNINTELLIGIBLE
20 db
30 db
35 db
QUALITY OF RECEPTION-HQ-9-X RECEIVER WITH 10" SPEAKER
AM BROADCAST SIGNAL TO CORONA NOISE RATIO

Figure 3 (left). Signal-to-corona-noise ratios for various qualities of receptions

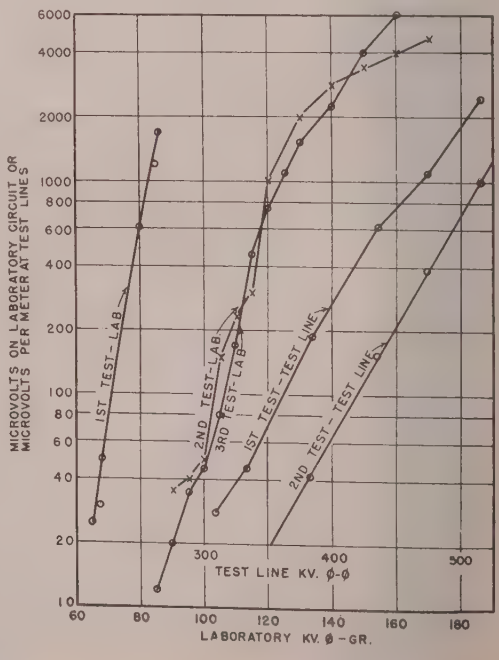
MICROVOLTS ON LABORATORY CIRCUIT OR MICROVOLTS PER METER AT TEST LINES
1ST TEST - LAB
2ND TEST - LAB
3RD TEST - LAB
1ST TEST - TEST LINE
2ND TEST - TEST LINE
TEST LINE KV. Ø-Ø
LABORATORY KV. Ø - GR.

Figure 5 (right). Radio influence from weathered conductors in laboratory and at Tidd showing variation from test to test

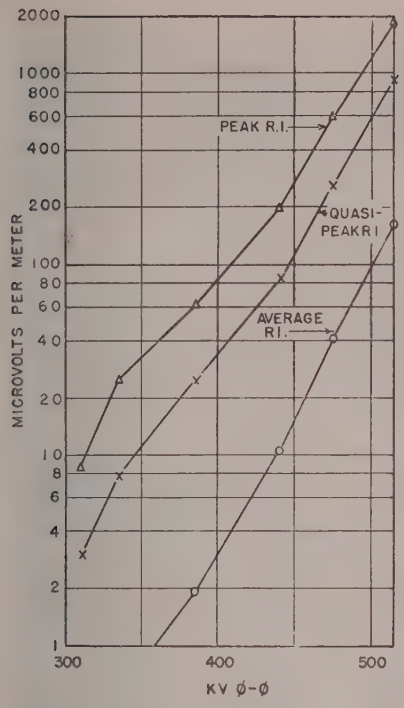

Figure 6. Typical voltage run at Tidd, 3-phase line, 2.0-inch diameter conductor. Average, quasi-peak, and peak values of r.i. at 1.0 megacycle

Figure 7 (below). Attenuation of r.i. field intensity with distance from transmission line

○ = average of 28 tests-138-kv lines
× = average of 22 tests-230-kv lines
△ = average of 42 tests-Tidd lines-280–450 kv
● = average of above 92 tests
□ = calculated attenuation
+ = typical test at 395 kv
All tests quasi-peak r.i. 0.2–1.5 megacycles. All weather—fair, rain, snow, and fog

ear. Therefore, a test using a single point artificial source of r.i. was made to obtain more information. It was found that for field intensity measurements a local burst will substantially raise the r.i. value measured from a corona generator as shown in Figure 2. Similar results have been reported by Pelissier and Renaudin.[14] It appears that the resultant field measured near the line consists of two parts: (1) that caused by many sources adding at random and (2) that resulting from a local source. It is believed that this increase noted at a local source is caused by a vertical current flow through ionized space and a local field superimposed on the field produced by the current in the horizontal conductor.

Effects on Various Communication Services

Radio interference can result from conductor corona unless conductor and line design is such as to limit the extent of corona. Because the r.i. level is highest at the lower frequencies, amplitude modulation (AM) broadcast, power line carrier, and low-frequency aircraft services require primary consideration. In the power line carrier frequency range, the wet weather r.i. voltage on a line conductor will be important. The AM broadcast band (0.54 to 1.6 megacycles) requires the most consideration because of home and automobile receivers in use in proximity to lines.

Television broadcasting uses amplitude modulation for the picture and frequency modulation for the sound in the TV bands 54—216 megacycles. It was determined by tests with a conventional TV receiver, with the antenna 50 feet above ground and 100 feet from the line and 45 miles from a transmitting station on channel 3, that no change in picture or sound quality was observed up to voltages above that which could be used, based upon other considerations.

Tests on lines indicate that no interference is expected from corona in the FM broadcast band (88 to 108 megacycles). The r.i. level is lower in this band than in the low end of the TV band, see Figures 18 and 19.

For estimating the effects on other communication services, application of average, quasi-peak, and peak values of r.i. can be made.

Instrumentation and Measurement

Need for Standardization

The measurement of radio noise with instruments constructed according to radio noise meter specifications[10,11,12] is necessary throughout a test program which is intended to give results applicable in the future. It is true that radio noise meters are far from ideal and have their limitations but they are nevertheless infinitely better for measurement of noise and for engineering comparison of data obtained by various observers than a commercial radio set which was primarily designed for entertainment. The latest specifications[11] for instruments require that meters read three characteristics of the noise; average, quasi-peak (weighted detector circuit) and the peak values after transmission through specified bandwidth circuits. Even with the advantage of these three types of measurement, the noise type is not entirely defined. It is useful to know whether pulses occur on positive or negative half-cycle and if so, where they occur, and what variation occurs in amplitude from cycle to cycle of the power frequency. Qualitative data on these can be obtained in the field without too much difficulty by using an oscilloscope in the noise meter output circuit.

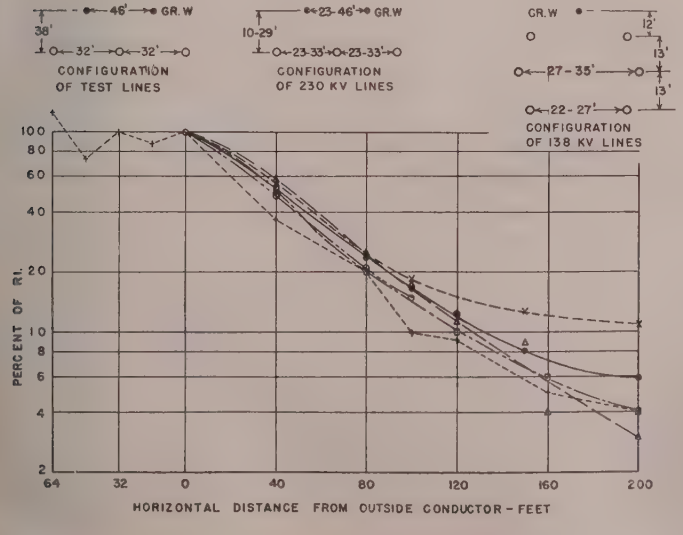
CONFIGURATION OF TEST LINES
CONFIGURATION OF 230 KV LINES
CONFIGURATION OF 138 KV LINES
PERCENT OF R.I.
HORIZONTAL DISTANCE FROM OUTSIDE CONDUCTOR - FEET

Figure 8. Radio influence analysis from test line chart records

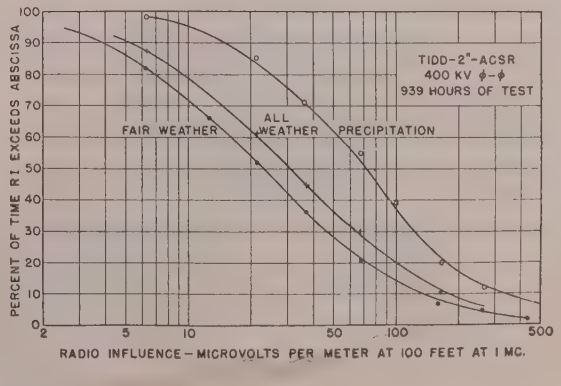
TIDD-2"-ACSR
400 KV ø-ø
939 HOURS OF TEST
FAIR WEATHER
ALL WEATHER PRECIPITATION
PERCENT OF TIME R.I. EXCEEDS ABSCISSA
RADIO INFLUENCE - MICROVOLTS PER METER AT 100 FEET AT 1 MC.

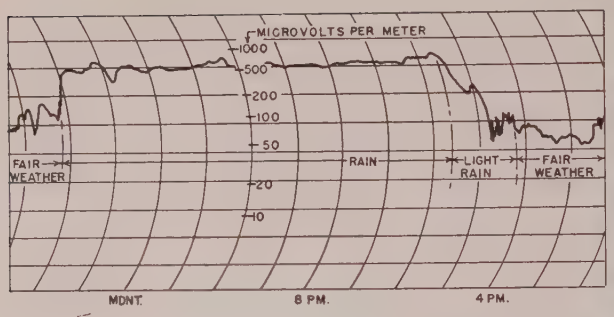

Figure 9 (above). Section of r.i. chart record for 2.0-inch diameter steel reinforced aluminum cable at 1.0 megacycle

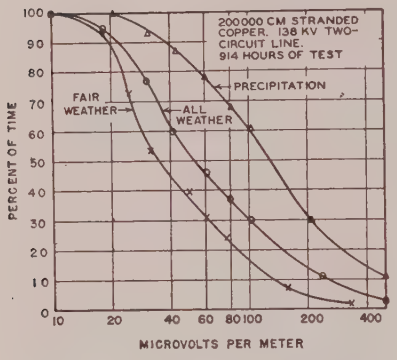

Figure 10. Radio influence analysis from Windsor-Canton 138-kv line chart records. Records obtained 100 feet from line at 1.0 megacycle

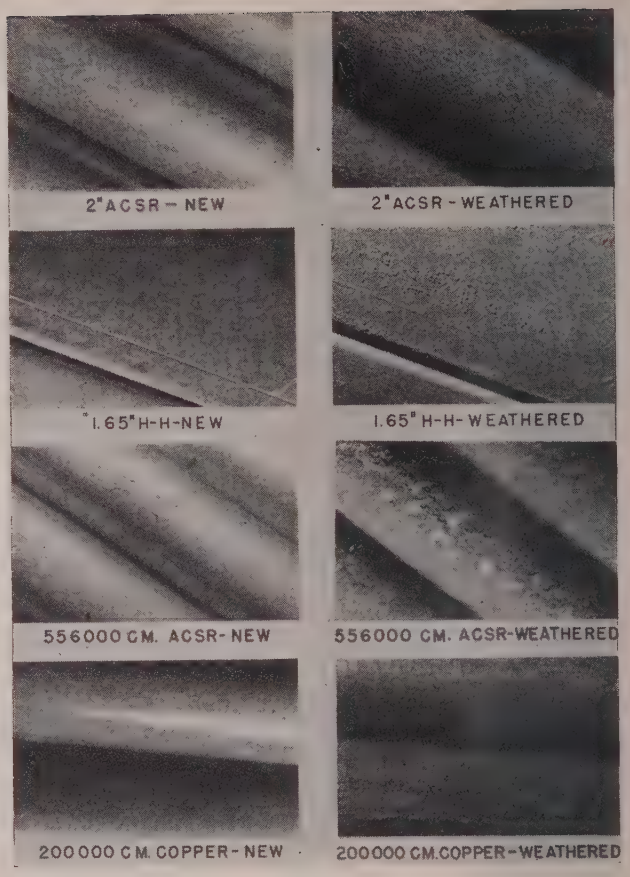

Figure 11 (right). Magnification (10 times) of new and weathered conductors

Difficulties of Measurement

A difficulty exists in obtaining a representative r.i. value, because r.i. is not always constant. Variations of greater than 2-to-1 are not uncommon within a space of a few seconds as local spots on the conductor are intermittently in corona. For effect of local r.i. generators, see Figure 2. As the distance from the line increases these local disturbances may become less noticeable, but even then values may not be repeated on different days although all conditions appear to be the same. (Precautions always are taken to have the meter properly calibrated.) Thus it is seen that a continuous graphic record of the noise meter output during an extended period of time would be more descriptive of changing noise level than a single instantaneous measurement.

Unattended graphic recording milliammeters driven by the noise meter were installed and have proved satisfactory. It was found that calibration and servicing of meters were required on the average only every two weeks.

It is, of course, necessary to protect the radio noise meter from the weather and it is preferable to do this without affecting the antenna input circuit. This can be done successfully by placing the meter with its antenna in a nonmetallic enclosure. Noise meters covering the ranges below 25 megacycles have vertical rod or loop antennas which fit directly into a socket in the meter and they should be used this way whenever possible. If the meter is enclosed and the antenna is mounted outside, necessitating a lead-in, there will be a mismatch between antenna and the meter input so that an over-all calibration of field strength readings is required. This can be done by setting up a known field by means of a signal generator and a radiating loop or by the more direct method of comparing the recording meter reading with that of a properly calibrated meter placed alongside on the ground and operating normally.

Radio influence measurements are subject at times to high ambient interference from atmospherics and, at frequencies above 30 megacycles, from man-made interference, even though the source may be many times farther from the antenna than the line from which r.i. is being measured. Since atmospherics are impulsive, and occur relatively infrequently, it is possible to obtain readings in the interval between atmospheric disturbances. On recording meters tuned to a frequency in the broadcast band care must be taken so that signals from distant stations are not picked up at night or during other periods when the meter is unattended.

Table I

	Ferris 32A	Stoddart NM-10A	Stoddart NM-20A	Stoddart NMA-5
Applicable spec.	Ref. 10	Ref. 11	Ref. 11	
Freq. range, mc/s	0.15–0.35, 0.55–20	0.014–0.25	0.15–25	15–400
Antenna type	rod	rod and loop	rod and loop	dipole
Bandwidth*	10 kc.	80–600 cycles	4 kc.	150–210 kc
Quasipeak charge time, ms	10	1	2.5–3	1
Quasipeak discharge time, ms	600	600	600	600
Peak measurement	None	Slideback	Slideback	Slideback
Avg. circuit	Conventional detector	600 ms. Avg.	600 ms. Avg.	

* See Figure 27.

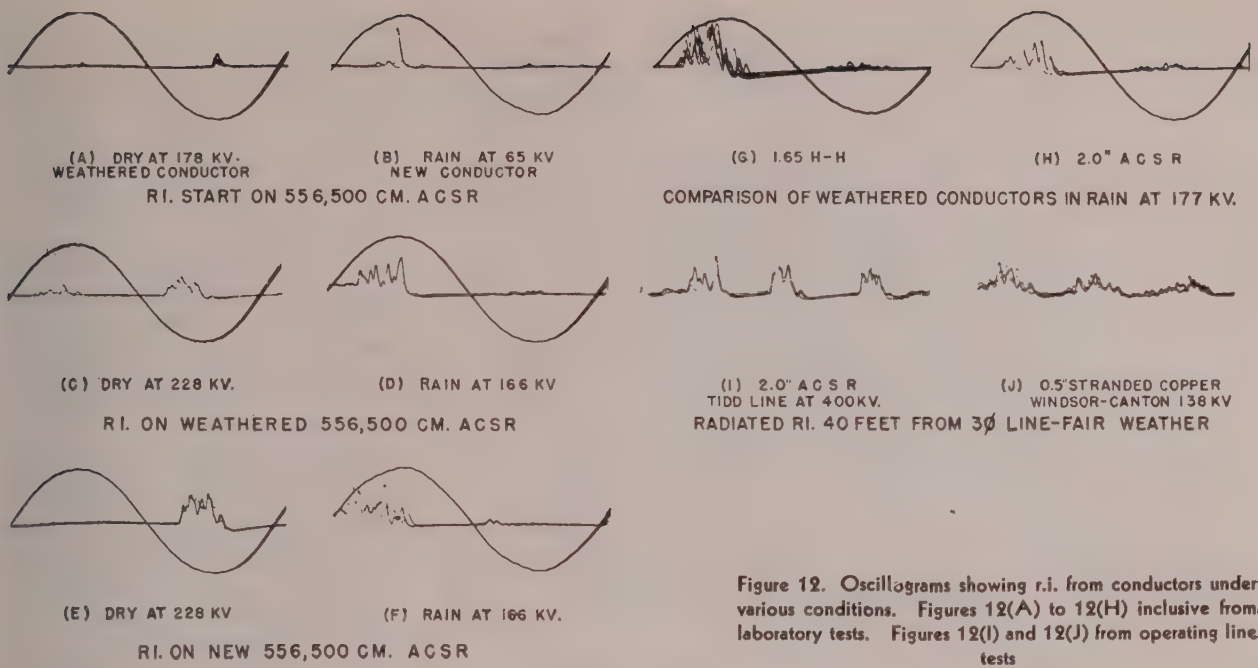
(A) DRY AT 178 KV. WEATHERED CONDUCTOR
(B) RAIN AT 65 KV NEW CONDUCTOR
RI. START ON 556,500 CM. ACSR
(G) 1.65 H-H
(H) 2.0" ACSR
COMPARISON OF WEATHERED CONDUCTORS IN RAIN AT 177 KV.
(C) DRY AT 228 KV.
(D) RAIN AT 166 KV
RI. ON WEATHERED 556,500 CM. ACSR
(I) 2.0" ACSR TIDD LINE AT 400KV.
(J) 0.5" STRANDED COPPER WINDSOR-CANTON 138 KV
RADIATED RI. 40 FEET FROM 3Ø LINE-FAIR WEATHER
(E) DRY AT 228 KV
(F) RAIN AT 166 KV.
RI. ON NEW 556,500 CM. ACSR

Figure 12. Oscillograms showing r.i. from conductors under various conditions. Figures 12(A) to 12(H) inclusive from laboratory tests. Figures 12(I) and 12(J) from operating line tests

Specifications for Radio Noise and Field Intensity Meters

The available American specifications and tentative specifications are given in the list of references.[10,11,12] The instruments used in tests up to the present time, and some of their important characteristics as to noise measurements, are given in Table I.

Complete data on instruments can be found in the applicable specification.

The quasi-peak values from conductor corona were found to be higher, as would be expected, with the 2.5 to 3 microsecond charge time than with the 10-microsecond charge time detector circuits. Peak values occurring at random and at very low repetition rates can be measured by use of headphones and the slideback control.

In order to have more complete data on the noise meters used, bandwidth response curves, at the frequencies where most tests were made were obtained by measurement (see Figure 4) and effective bandwidth curves over the frequency range of tests are given in Figure 27. The time constants and bandwidth of the radio noise meter, and the repetition rate and amplitude of the corona pulses determine what meter reading will be obtained at any one frequency setting of the meter. In the case of corona pulses from conductors of the size used for power transmission, the pulse amplitude varies from pulse to pulse at random, and the repetition rate can be obtained only by calculation. In Appendix I a method of obtaining the equivalent microvolts for each meter used is described.

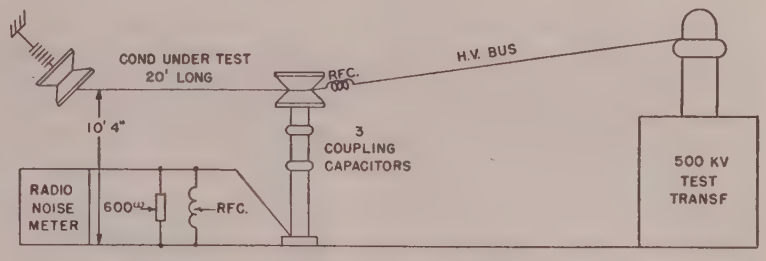

TRAFFORD H.V. LAB R.I. TEST SET-UP (REFERENCE 10)

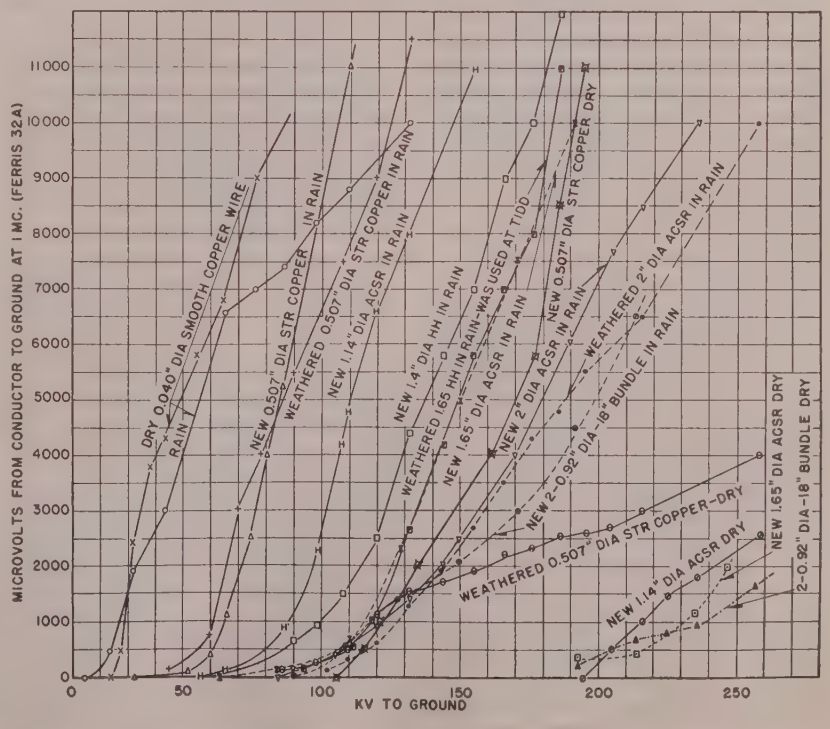
MICROVOLTS FROM CONDUCTOR TO GROUND AT 1 MC. (FERRIS 32A)
KV TO GROUND
DRY 0.040" DIA SMOOTH COPPER WIRE
RAIN
NEW 0.507" DIA STR COPPER IN RAIN
WEATHERED 0.507" DIA STR COPPER IN RAIN
NEW 1.14" DIA ACSR IN RAIN
NEW 1.4" DIA HH IN RAIN
WEATHERED 1.65 HH IN RAIN-WAS USED AT TIDD
NEW 1.65" DIA ACSR IN RAIN
NEW 2" DIA ACSR IN RAIN
NEW 0.507" DIA STR COPPER DRY
WEATHERED 2" DIA ACSR IN RAIN
NEW 2-0.92" DIA-18" BUNDLE IN RAIN
WEATHERED 0.507" DIA STR COPPER-DRY
NEW 1.14" DIA ACSR DRY
NEW 1.65" DIA ACSR DRY
2-0.92" DIA-18" BUNDLE DRY

Figure 13. Radio influence variation with voltage for conductors tested in the laboratory

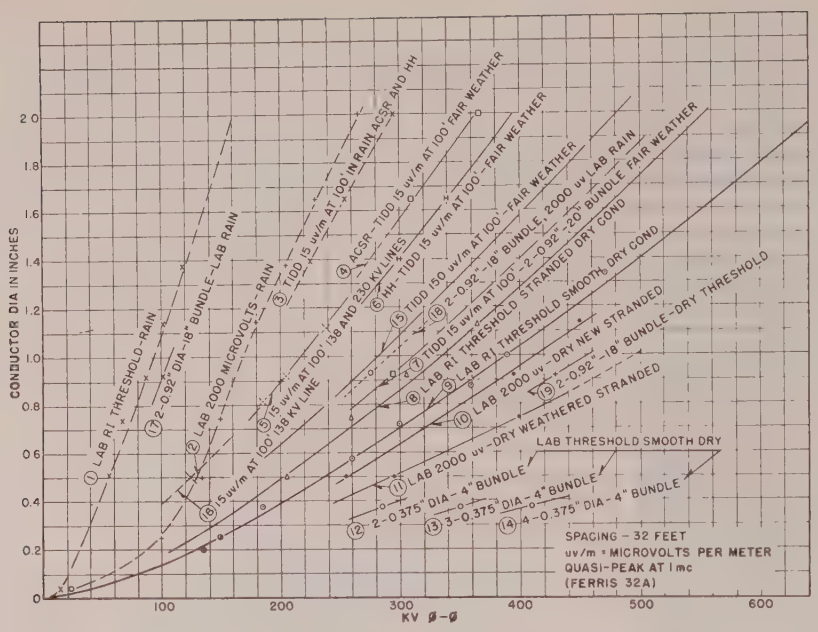
CONDUCTOR DIA IN INCHES
KV ø-ø
SPACING - 32 FEET
uv/m = MICROVOLTS PER METER
QUASI-PEAK AT 1 mc
(FERRIS 32A)
LAB THRESHOLD SMOOTH DRY
① LAB RI THRESHOLD - RAIN
② LAB 2000 MICROVOLTS - RAIN
③ TIDD 15 uv/m AT 100' 138 KV LINE
④ ACSR - TIDD 15 uv/m AT 100' IN RAIN ACSR AND HH
⑤ TIDD 15 uv/m AT 100' - FAIR WEATHER
⑥ HH - TIDD 15 uv/m AT 100' - FAIR WEATHER
⑦ TIDD 150 uv/m AT 100' - 2-0.92" - 18" BUNDLE, 2000 uv LAB RAIN
⑧ LAB RI THRESHOLD STRANDED DRY COND
⑨ LAB RI THRESHOLD SMOOTH DRY COND
⑩ LAB 2000 uv - DRY NEW STRANDED
⑪ LAB 2000 uv - DRY WEATHERED STRANDED
⑫ 2 - 0.375" DIA - 4" BUNDLE
⑬ 3 - 0.375" DIA - 4" BUNDLE
⑭ 4 - 0.375" DIA - 4" BUNDLE
⑮ 2-0.92" - 18" BUNDLE - DRY THRESHOLD
⑯ 15 uv/m AT 100' 138 KV LINE
⑰ 2-0.92" DIA - 18" BUNDLE - LAB RAIN
⑱ 2-0.92" - 18" BUNDLE, 2000 uv LAB RAIN
⑲ 2-0.92" - 18" BUNDLE - DRY THRESHOLD

Figure 14. Conductor diameter and phase-to-phase voltage relations from laboratory and field data

Application and Use of Instruments

Although graphic recording has many advantages, visual readings are necessary in order to make calibration tests and to compare readings at many different locations such as required in making lateral or longitudinal profiles, frequency runs, and voltage runs. The three values of r.i., average, quasi-peak, and peak always were measured within a few seconds of each other. Headphones were used to identify noise and to avoid taking readings which were affected by spurious signals. When taking readings, such as during a voltage run, it was found useful to use a graphic recorder for monitoring the r.i. prior to starting the tests and during the tests. Most of the tests had to be repeated in the field several times in order to obtain representative data. The principal reasons for this were changes in the noise level resulting from changes in the location of r.i. sources along the conductor and due to their variation in amplitude.

The first of the above reasons may seem unreal at first glance; however, tests such as described later proved that a corona discharge at some point will increase the r.i. field in the immediate vicinity without appreciably increasing the r.i. at points 300 to 400 feet away along the line. In the laboratory consistent day-to-day r.i. voltage values can be obtained on smooth conductors; whereas, on weathered conductors day-to-day variations similar to field results will be obtained, see Figure 5.

Test Procedure

Voltage Runs

To determine the change in r.i. with voltage, tests were made in the vicinity of the test lines from 265 kv to 530 kv phase to phase. The noise meter was usually located 40 feet from the outside line conductor at a point along the line where the standing wave of voltage was at a maximum value. In some instances, usually during single-phase conductor comparison tests, the noise meter was located directly under the line conductor. Tests were conducted at a minimum of five voltages and in some instances as high as 12 different phase-to-phase voltages were checked. Readings were usually obtained at two different frequencies (0.2 and 1 megacycle) but in some tests the radio influence was measured from 0.015 to 380 megacycles. A typical voltage run showing average, quasi-peak, and peak values is given in Figure 6. Voltage runs also were made in the laboratory on single conductors from 0.04 to 2 inch in diameter with and without rain and on 2-, 3-, and 4-conductor bundles.

Lateral Profiles

Measurements of r.i. were made at different distances from the lines in order to obtain a measure of the attenuation with distance from the sources. These tests were conducted for several voltages with constant line voltage for each test. Readings were taken at intervals of from 10 to 40 feet and generally were made from directly under the line conductor to a distance of 200 feet from the line. Some tests were made to 400 feet from the line, but usually in the voltage range below 300 kv and at frequencies above 2 megacycles the radio influence in fair weather was too low to be measured beyond 200 feet from the line. Data as to

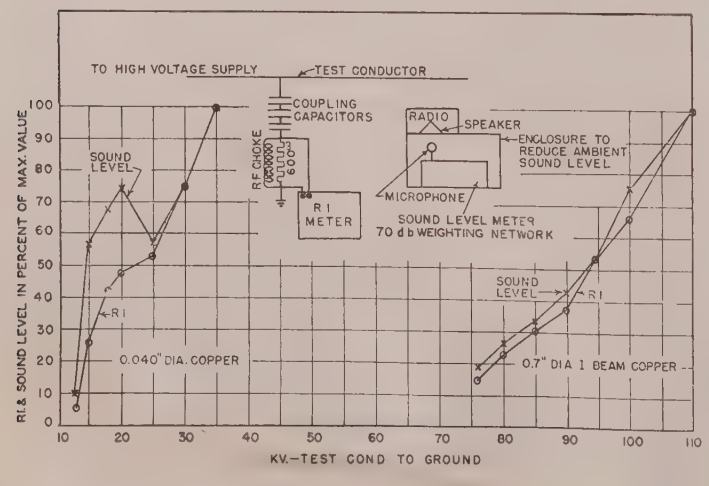

Figure 15 (left). Simultaneous r.i. and radio receiver sound level at different voltages

Figure 16 (below). Longitudinal tests on Tidd test line with and without line termination

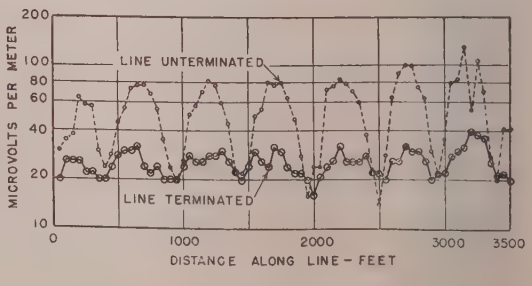

attenuation with lateral distance are given for several lines in Figure 7. The conductor configuration for each curve is shown on the curve sheet.

Longitudinal Profiles

Measurements were made parallel to the test lines and along operating transmission lines at intervals of 50 feet. The tests were made directly under the line conductor or parallel to it at 40 or 80 feet. On operating lines these tests indicated mainly the variation in r.i. along the line due to conductor surface irregularity, the conductor height, and the shielding effect of the line towers. On the test lines, when unterminated, these tests showed the magnitude and location of maximum and minimum points of the standing waves. From these tests it was possible to select a location along the line where average r.i. conditions existed and to avoid locations where unusual r.i. conditions existed due to conductor roughness or irregularities. For most voltage runs it was found that more representative results could be obtained by taking at least three readings 50 feet apart as measured along the line.

Frequency Runs

Measurements were made with standard instruments at different frequencies from 0.015 megacycle to 380 megacycles to determine the magnitude of r.i. with frequency. These tests were made with the meter at a fixed location, generally 40 feet from the outside line conductor, with the line energized at a constant voltage. Over the frequency range where standing wave effect was appreciable, readings were taken at successive maximum and minimum values.

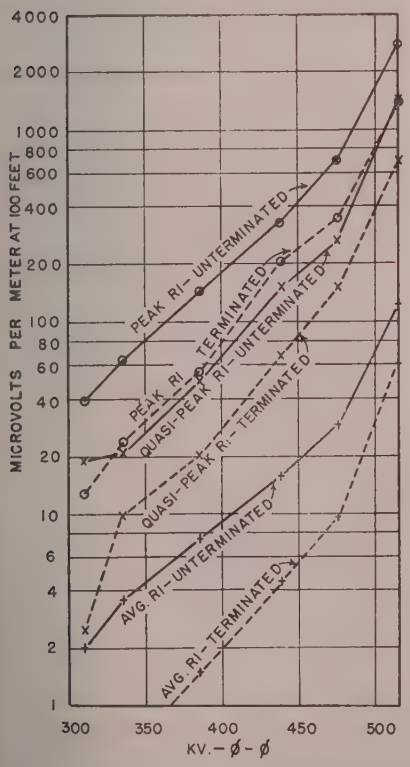

Figure 17. Radio influence variation with voltage for test line with and without termination. Stoddart *NM-20A* radio noise meter

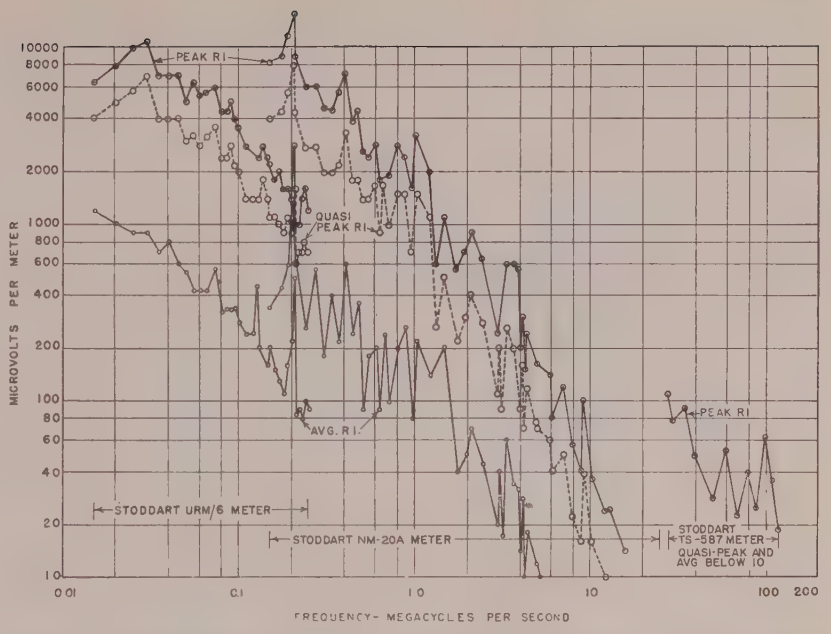

Figure 18. Radio influence variation with frequency at 400 kv, 3 phase on 2.0-inch diameter conductor. 7,160-foot test line

Single-Phase Termination Tests

In order to determine the r.i. field that would exist near a proposed long line from tests on a short line, it was necessary to terminate the short line in its own surge impedance to reduce the effect of standing waves. Termination tests were made on one phase of test line number 2. The terminating resistance value was obtained from measured values of the impedance with the conductor open circuited and short circuited to ground. The terminating resistance was connected to each end of the line through power line carrier current capacitors. The two line conductors that were disconnected from 60-cycle source during the tests also were terminated to ground in their surge impedance to simulate a 3-phase terminated line.

Voltage runs, lateral profiles, longitudinal profiles, and frequency runs were made with the line terminated and unterminated. To eliminate the effect of changing weather conditions during the tests the measurements were made with the line terminated and unterminated successively at one minute intervals.

Signal-to-Noise Ratio Tests

Listening tests were made at the test site and in the laboratory utilizing a radio receiver to grade reception quality and using the noise meter to measure broadcast signal and radio influence voltages at the receiver input. Listening tests were made with the lines energized at a voltage slightly higher than might be used for the conductor tested. The quality of reception was graded according to the definitions given in Figure 3, which gives signal-to-noise ratios for 3-phase corona.

Single-Phase Long-Line and Short-Line Tests

The r.i. at any location near a transmission line is the result of radio frequency currents and voltages due to corona on a considerable length of the line as well as the radiation from local corona. To determine the effect of line length on r.i., tests were made on a 1,900-foot section of line number 2 and compared with tests made with the entire line (7,160 feet) energized. In conducting these tests the line sections were terminated in their own respective surge impedance to reduce reflections. The tests consisted of taking readings every 50 feet along the line between line towers 1 and 2. Several tests were made on different days at 385 and 440 kv.

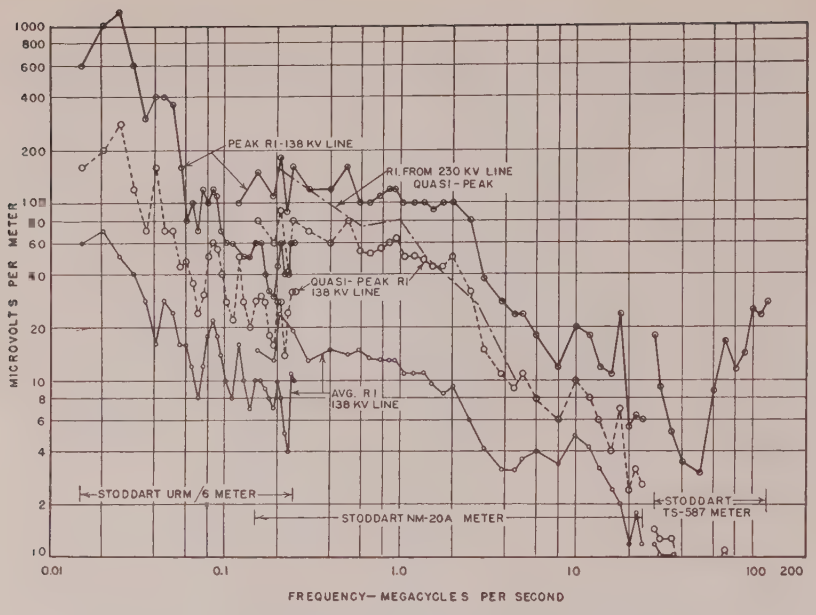

Figure 19. Radio influence variation with frequency on operating lines

Graphic Meter Operation

Two noise meters equipped for graphic recording have been in continuous operation for over two years. Initially the meters were installed 40 feet from the outside conductor of each of the two lines at a location between towers 2 and 3 where the standing wave of voltage was a maximum. Later one meter was moved from line 1 to a location 40 feet from line 2 where the standing wave of voltage was a minimum. These meters were operated continuously and during visual tests afforded a continuous check on the constancy of r.i.

Effect of Weather Changes During Tests–Graphic Records

Graphic instruments were in continuous operation for the purpose of recording weather data. These instruments recorded rainfall, humidity, barometric pressure, and temperature. In addition to the graphic meters, a photographic weather recorder which provided a measure of visibility, fog, and rain was in operation. The photographic recorder operated at 20-minute intervals. These recorded data were supplemented by the observations of personnel at the test site. From the weather data and the graphic records of r.i. the effect of weather on r.i. was obtained.

Effect of Atmospheric Disturbances

Radio influence due to atmospheric disturbances is usually of the impulse type and irregularly repetitive. The effect of these disturbances can usually be eliminated from the visual readings by reading r.i. between bursts of atmospheric disturbance. On the graphic records this disturbance appears as a sudden change in r.i. and can be discounted in the analysis of the chart data. During visual tests the ambient noise level was determined at frequent intervals by taking readings with the test lines de-energized.

Single-Phase and 3-Phase R.I.

Several types of conductors were installed in the 800-foot test line and the r.i. characteristics of these conductors were measured single phase. In order to convert these data to values that would be obtained from 3-phase tests, a number of comparative single-phase and 3-phase tests were made on line number 2. These tests were made at various distances from the line conductors, from directly under the line conductor to 150 feet from the conductor, and from 0.2 megacycle to 20 megacycles, and at voltages from 280 kv to 500 kv.

Visual Data from Operating Lines

For reference purposes and to determine what value of r.i. would be generally tolerable, tests were made along a number of operating transmission lines. Tests were made on 138-kv lines and 230-kv lines at seven locations. The tests consisted of longitudinal and lateral profiles and frequency runs.

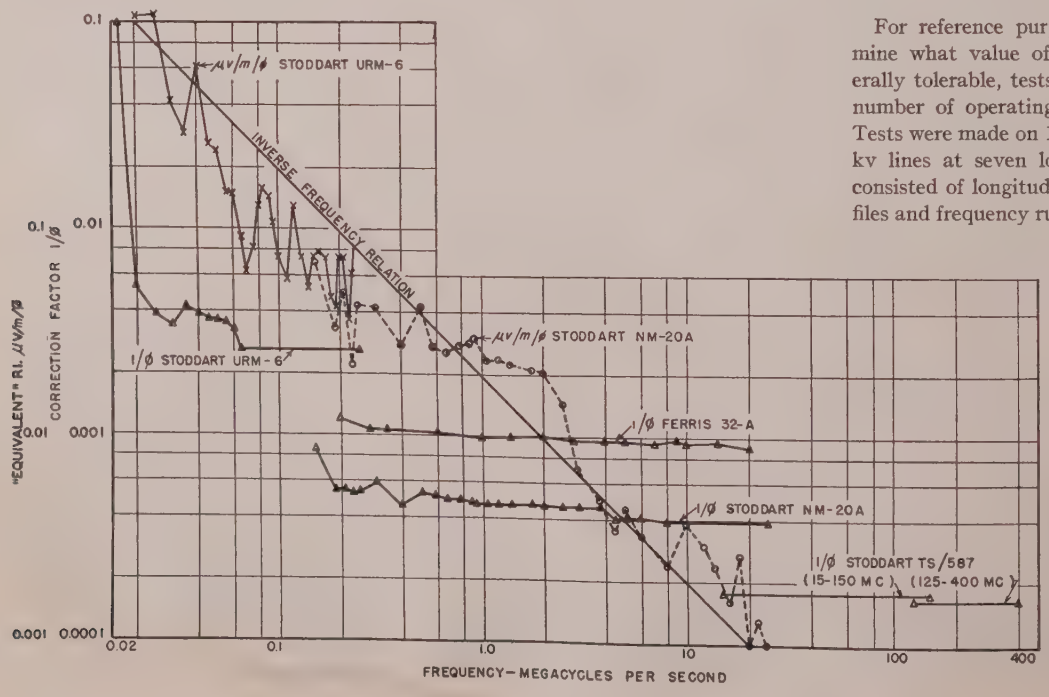

Figure 20. "Equivalent" microvolts per meter as a function of frequency, and bandwidth-time correction factors for radio noise meters used

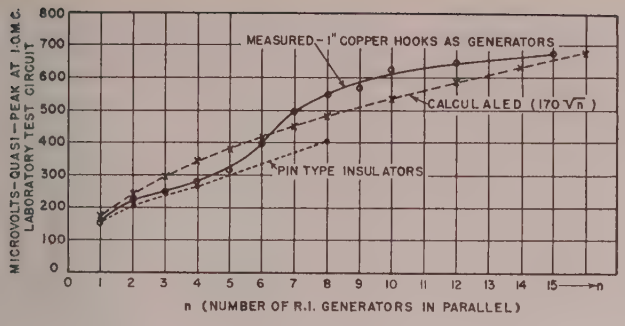
MICROVOLTS-QUASI-PEAK AT I.0 MC. LABORATORY TEST CIRCUIT
MEASURED-1" COPPER HOOKS AS GENERATORS
CALCULALED (170 √n)
PIN TYPE INSULATORS
n (NUMBER OF R.I. GENERATORS IN PARALLEL)

Figure 21 (left). Radio influence resulting from various numbers of corona generators

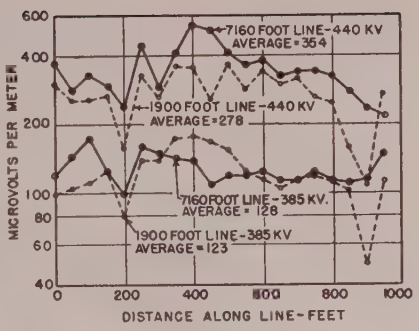
MICROVOLTS PER METER
7160 FOOT LINE-440 KV AVERAGE=354
1900 FOOT LINE-440 KV AVERAGE=278
7160 FOOT LINE-385 KV. AVERAGE=128
1900 FOOT LINE-385 KV AVERAGE=123
DISTANCE ALONG LINE-FEET

Figure 23 (right). Radio influence tests on long and short lines

Graphic Recorder Data on Operating Lines

At one of the 138-kv lines where the highest value of r.i. was measured a noise meter was installed at midspan 40 feet away from the line conductors. Records of r.i. were obtained during fair weather, rain, fog, and snow. Temperature, humidity, pressure, and rain in the vicinity of this meter were measured hourly.

Discussion of Test Results

Effects of Weather

Fair weather is considered to be any weather other than fog, rain, sleet, or snow environment around conductors and with conductor surfaces free of water, ice, or snow but includes the condition of dirt particles in the air or on the conductor. It was determined that r.i. at any test location will change even in fair weather from time to time, see Figures 8 and 10. This is believed to result from the r.i. contribution from local sources, and the change in location of these local sources which is equivalent to a change in distance to receiver antenna. The conductor environment preceding fair weather probably determines subsequent fair weather r.i. at any one point. A conductor when wet will show better r.i. consistency than when dry because the corona is more stable and there are more r.i. sources in the antenna vicinity all the time it rains. The local sources do not, therefore, show as pronounced an effect.

Rain will increase r.i. by several times for conductors of the size used for power transmission. Tests were made in fair weather and in rain on the same day or on consecutive days. These tests showed r.i. increases due to rain from four to 25 times for quasi-peak and peak values and three to six times for average values. Visual data and analysis of graphic records with results as shown in Figure 8 gave average increase of quasi-peak values of four times for Tidd conductors and an increase of four times for 138-kv lines in service, see Figure 10. Radio influence does not decrease immediately as rain ceases, rather it has no perceptible change immediately, but after a short time, depending on the voltage, begins to decrease gradually at a rate also depending on the voltage.

Fog may or may not produce a large increase in the r.i. value over the fair weather value. An increase will be obtained if sufficient condensation occurs to wet the conductor. Snow on the conductor increases r.i. but to a lesser extent than water. In one test with snow melting on the conductor, r.i. was 3.5 times greater than before the snow began to melt.

If the r.i. value for rain is established, it may be used as indicating the maximum which will exist, excluding conditions such as hoar frost and ice for which no data was obtained.

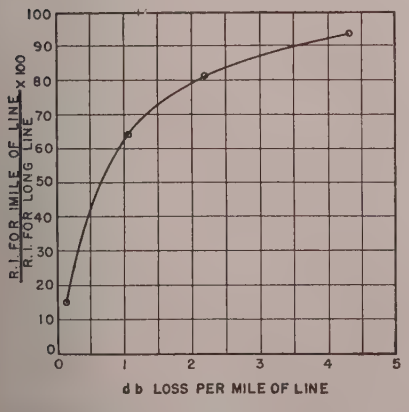

Figure 22. Effect of line length and attenuation on r.i. (See Appendix II)

Weathered Conductors

The conductor surface changes greatly in appearance when used outdoors while energized as can be seen by comparing new and used conductors, see Figure 11. The rough surface on used conductors contains no conductor material but rather deposits gathered from the atmosphere. Weathering can reduce r.i. at the higher voltages when the conductor is dry. However, the threshold voltage may be lower than for a new conductor and the test values from day to day are not as consistent as for a new conductor. In fact, the smoother and cleaner a conductor is the more consistent the test results.

With rain there is no significant difference between weathered and new conductors. It can be stated, therefore, that weathering of conductors will not result in any material increase in r.i. and can result in some reduction. What the amount of reduction can be depends on the condition of the conductor surface after installation. Fair weather visual data on Tidd conductors from December 1947 to September 1950 indicated large r.i. variations (7 to 1) on both HH and steel-reinforced aluminum cables at 373 kv with no significant trend. No data are available from October 1947, when line was first energized, to December 1947.

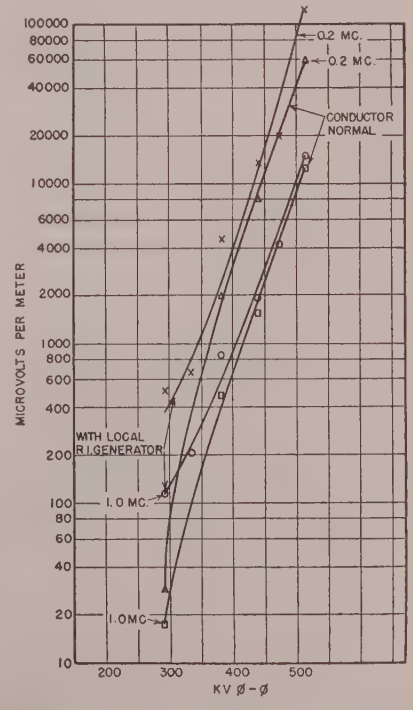

Figure 24. Radio influence variation with voltage, with and without artificial generator on 2.0-inch diameter conductors, measured 40 feet from the line

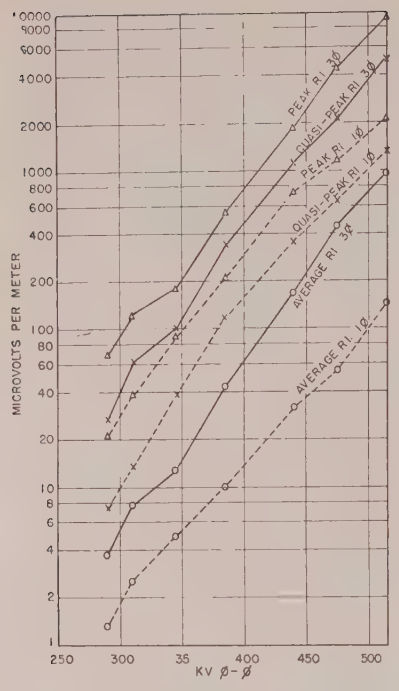

Figure 25. Radio influence correlation to single phase and three phase. Stoddart NM-20A radio noise meter

Effect of Conductor Voltage

As the voltage on a conductor is increased, the r.i. threshold voltage can be detected readily on new and dry conductors in the laboratory by radio noise meter headphones. On dry weathered conductors and on all conductors in rain the threshold voltage is not as clearly defined by listening. Radio influence occurs first on the negative half-cycle on new dry conductors and for usual operating voltages exists only on the negative half-cycle. With weathered conductors at usual operating voltages, r.i. exists on both half-cycles as can be seen by laboratory oscillogram Figure 12(C). For wet conductors r.i. is generated chiefly on the positive half-cycle for both the smooth and weathered conductors as can be seen from oscillograms Figure 12 obtained in the laboratory.

The films, Figures 12(A) and 12(B), obtained at the radio noise meter output, show r.i. occurring at the lower voltages at the crest of the negative half-cycle on a dry weathered conductor and near the crest of the positive half-cycle on a wet weathered conductor. As the voltage is increased, the time r.i. exists increases but only ahead of the voltage crest as shown by Figures 12(C) and 12(D). This effect was noted by F. O. McMillan[9] and is discussed by him.

It can be seen from Figure 12(C) that a weathered dry conductor has r.i. on both negative and positive half-cycles, whereas a new dry conductor at the same voltage shows no evidence of r.i. on the positive half-cycle. Similar pictures were obtained at Tidd on single phase. Oscillograms of 3-phase tests of r.i. at Tidd, 40 feet from a 2-inch steel-reinforced aluminum cable, are shown by Figure 12(I), and 40 feet from an existing 138-kv double-circuit line are shown by Figure 12(J).

With increase in conductor voltage beyond the threshold voltage, r.i. increases rapidly as shown by the Tidd curves of Figure 6 and laboratory curves Figure 13. It will be noted that the rate of increase of r.i. differs for smooth and weathered dry conductors, Figure 13; whereas in rain it is about the same for both. The average, quasi-peak, and peak values of r.i. increase with voltage at approximately the same rate as shown by Figure 6.

From the data obtained in the laboratory for the threshold voltage, the points near the calculated curves 8 and 9 of Figure 14 were obtained. The calculated threshold curve for stranded conductors is based on the relation:

$$V_0 = 21.1\left(1+\frac{0.3}{\sqrt{\sigma r}}\right) m\,\sigma r \log_e \frac{S}{r} \quad \text{Kv to ground} \quad (1)$$

where

21.1 = critical gradient for air in rms kilovolts per centimeter
σ = air density factor
r = radius of conductor, centimeters
S = spacing in centimeters (in this case $S=2h$ where h is height of conductor above ground plane used for laboratory tests)
m = surface factor

It can be seen that the test points fall well on the curve for equation 1 if the surface factor m of 0.846 for new stranded conductors is used. For smooth conductors the test points fall on a similar curve using surface factor $m=1$. The threshold curve with rain or wet stranded conductors, curve 1 of Figure 14, occurs at 28 per cent of the voltage for the same diameter dry conductor. This indicates that for rain on conductor the r.i. starting voltage can be obtained by using for the surface factor a value of 0.24 for conductors down to 0.25 inch in diameter.

A test was made in a laboratory to determine if the sound output level from a radio receiver speaker increased with conductor voltage in a manner similar to increase in r.i. with conductor voltage. The data obtained is plotted in Figure 15 for 0.04-inch diameter bare copper wire and for a 0.7-inch diameter copper I-beam conductor. Figure 15 indicates good correlation between r.i. as measured with a radio noise meter and the sound level measured in decibels from a radio receiver loudspeaker.

Effect of Conductor Diameter on R.I.

The effect of conductor diameter, as far as the starting voltage is concerned, is as given in equation 1 and is substantiated by the laboratory test data, see Figure 14. The voltage for a constant r.i. value for smooth dry conductors can be obtained by adjustment of the gradient constant in equation 1. Similar relations

Figure 26. Radio influence threshold voltages for bundles of smooth conductors from laboratory tests

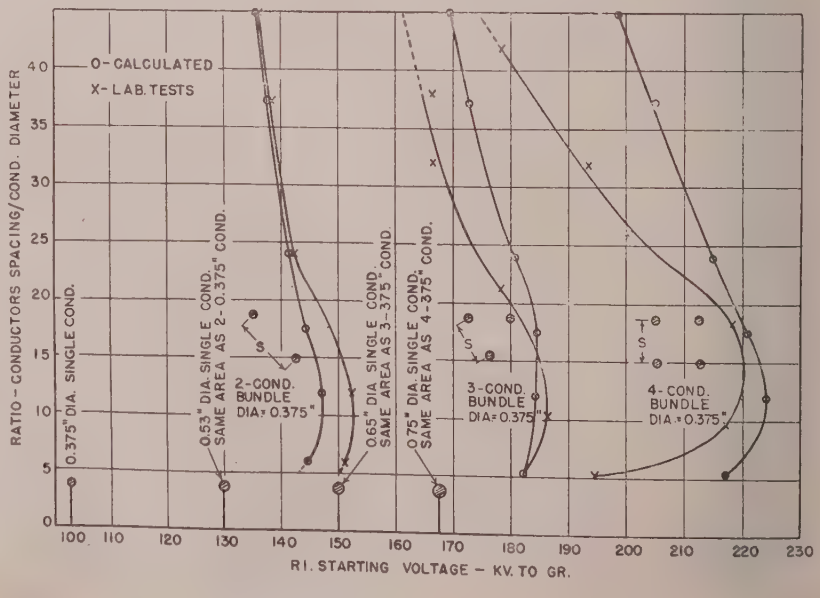
O-CALCULATED
X-LAB. TESTS
RATIO - CONDUCTORS SPACING/COND. DIAMETER
0.375" DIA. SINGLE COND.
0.53" DIA. SINGLE COND. SAME AREA AS 2-0.375" COND.
0.65" DIA. SINGLE COND. SAME AREA AS 3-.375" COND.
0.75" DIA. SINGLE COND. SAME AREA AS 4-.375" COND.
2-COND. BUNDLE DIA. 0.375"
3-COND. BUNDLE DIA. 0.375"
4-COND. BUNDLE DIA. 0.375"
RI. STARTING VOLTAGE - KV. TO GR.

of kilovolts to diameter apply with rain. It is of course necessary to use for rain a surface factor of 0.24 in conjunction with adjustment of the gradient constant. The constants for rain will give results agreeing within 10 per cent of test values, for conductor diameters between 0.25 inch and 1.65 inches. For instance, very fine wires such as 0.040-inch diameter will have values with rain less than when dry and the effect of water on conductors above 1.65 inch decreases at least up to 2-inch diameter. (No larger diameters were tested.) These effects appear reasonable since for small wires the effect of the water may be to tend to increase the effective conductor diameter, and for large conductors the water drops are better shielded, relatively, assuming water drop size independent of conductor size for the larger diameter conductors.

From the laboratory data on various conductors and the measured value of coupling factor (ratio of voltage V on one conductor to field $\mathcal{E}$ at 100 feet) referred to 100 feet from the line and by applying the single-phase to 3-phase correction, the relation for 32-foot spacing for line number 2 is

$$V = 132\,\mathcal{E} \qquad (2)$$

For instance, for 15 microvolts per meter at 100 feet from the outer conductor as measured with the Ferris *32-A* instrument,

$V = 15 \times 132 = 1{,}980$ (approximately 2,000 microvolts)

By the use of laboratory threshold and 2,000-microvolt values and Tidd and existing line data, curves of conductor diameter to kilovolt phase-to-phase for 32 foot spacing were obtained and are shown in Figure 14. It can be seen that the r.i. threshold test points agree quite well with the calculated values. The laboratory threshold curve number 1 with rain was drawn from the test values. The fair weather curve for Tidd conductors, curve number 4, for field intensity of 15 microvolts per meter at 100 feet is for stranded conductors. For HH copper conductors the corresponding curve number 6 is slightly to the right; however, for rain the stranded and HH conductor data fall on the same curve, number 3. A curve, number 15, for 150 microvolts per meter at 100 feet is shown in order to indicate what increase in voltages would be obtained if the field intensity were increased ten times. Limited laboratory data on new stranded dry, and weathered stranded dry, conductors for the 2,000-microvolt level are given in curves numbers 10 and 11. These curves indicate that the r.i. level is lower for weathered than for new dry conductors. Some of the data obtained on existing 138-kv and 230-kv lines are shown on curves numbers 5 and 16. The points for these lines were obtained from field measurements extrapolated to 15 microvolts per meter according to the r.i. to voltage curves at Tidd. The operating line data fall fairly well on a curve extended from the Tidd curve number 4.

Figure 28. Comparison of r.i. at 1.0 megacycle and corona loss on 1.65-inch diameter conductor

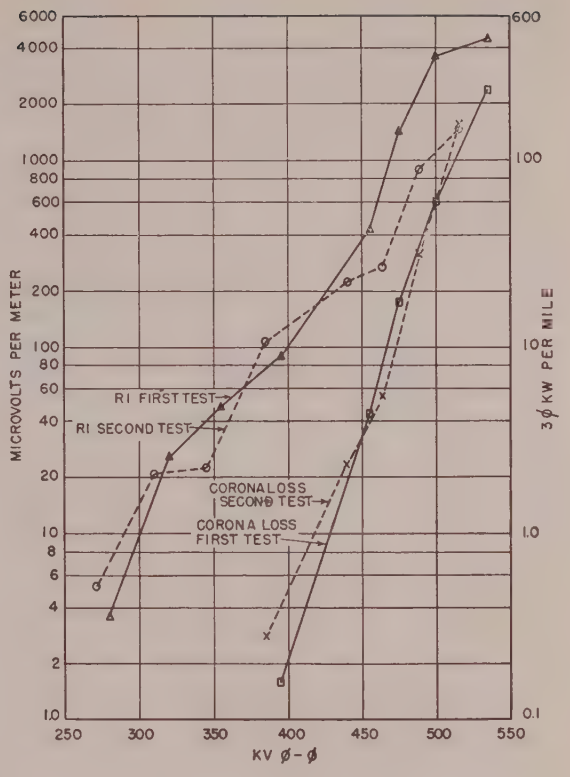

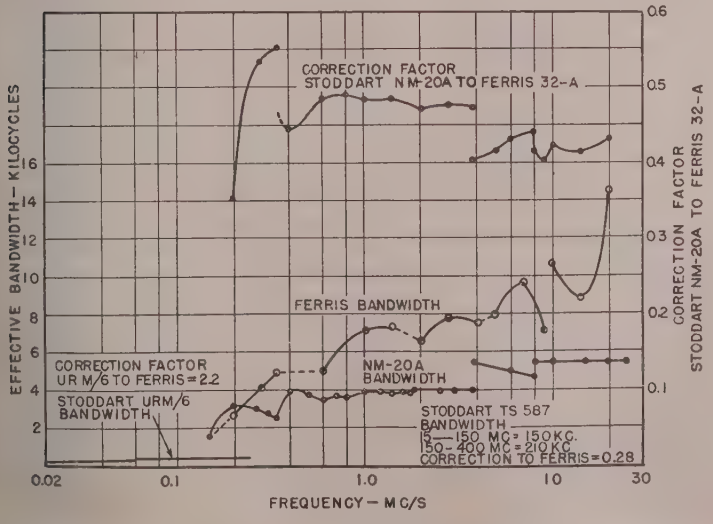
EFFECTIVE BANDWIDTH – KILOCYCLES
CORRECTION FACTOR STODDART NM-20A TO FERRIS 32-A
FERRIS BANDWIDTH
CORRECTION FACTOR UR M/6 TO FERRIS = 2.2
STODDART URM/6 BANDWIDTH
NM-20A BANDWIDTH
STODDART TS 587 BANDWIDTH
150 – 400 MC = 210 KC.
CORRECTION TO FERRIS = 0.28
FREQUENCY – MC/S

Figure 27. Effective bandwidths and noise meter conversion factors

Effect of Lateral Distance

As the distance from the line increases, the r.i. field intensity decreases rapidly as shown by Figure 7, which indicates the average values on several lines as well as the Tidd line, and a dashed curve calculated from the relation

$$P = \frac{100}{1 + \left(\frac{D}{H}\right)^2}$$

where P is percentage at lateral distance D from a point directly under the outside phase conductor, and H is the conductor height at Tidd at midspan. The values at 160 and 200 feet obtained from 138- and 230-kv line tests are believed to include ambient noise (noise other than that

from line) which could not be measured independently on these operating lines. A typical lateral run at Tidd including readings under each phase wire and between phase wires also is shown in Figure 7.

Radio Influence on Test Line with and Without Termination

Since the longest test lines are only 7,160 feet in length, the r.i. measured at the lower frequencies and with the lines unterminated depends on the point along the line where measurement is made. This effect is shown by the dashed curve of Figure 16. All the line conductors were terminated with a resistance which was equal to the surge impedance phase to ground. For the energized conductor, the resistance was connected in series with a 0.0006 microfarad coupling capacitor and sufficient inductance to cancel the capacitive reactance. For this condition, the solid line curve of Figure 16 was obtained. The standing wave ratio at one megacycle was changed by the termination of this type of line from 4.3 to 1.58. (These values are average of all waves shown in Figure 16). Measurements also were made at several voltages at a standing wave maximum by terminating and unterminating line conductors at one minute intervals so as to eliminate effects of weather or other effects which might change the r.i. level. From these data it was determined that the unterminated maximum measurement should be divided by 2.5 for 1 megacycle and by 4.5 for 0.2 megacycle to obtain a value more nearly representative of an operating line. Voltage runs with and without termination of the 3-phase conductors and with unenergized phases grounded also were made. The data at 1.0 megacycle are shown by curves of Figure 17. These results indicate that the r.i. field intensity in the vicinity of a short test line should be corrected for frequencies at which appreciable reflections exist.

Radio Influence Variation with Frequency

The value of r.i. field intensity over the portion of the frequency spectrum of significance, as far as high-voltage line conductors are concerned, was obtained on successive days and constant weather conditions on the Tidd test line (Figure 18), and on operating 138-kv lines. Figure 19 is for 138-kv lines in service with spacings as shown and for other lines as indicated. The effect on r.i. of an unterminated line can be seen over a large portion of the spectrum for the Tidd tests, where the frequency spacing between maximum values is essentially equal to twice 33 kc, where 33 kc is the frequency for a quarter-wave on the line. The data indicate that r.i. decreases quite rapidly as the frequency increases, and for line operating voltages at which reception in the broadcast band would be satisfactory, conductor r.i. may be ignored above 50 megacycles even for wideband communication such as television. Figure 27 shows Stoddart to Ferris correction factors and bandwidths of all meters used over the frequency range of tests. Figure 20 shows a curve for existing 138-kv line in terms of "equivalent" microvolts per meter and correction factors required to compensate for the varying bandwidths and time constants of the meters, see Appendix I. The method used for correction of readings is only approximate and is merely intended to indicate what factors affect meter readings.

Radio Influence Variation with Line Length

There were no test data available on the effect of line length on the r.i. field intensity. It was observed that corona was distributed along the test conductors and the problem therefore arose as to the effect of line length. It was determined in the laboratory that the r.i. voltage increased as the root sum square of the number of sources. Figure 21 shows results obtained by adding small wire hooks, each individual hook having approximately the same r.i. voltage, to a smooth brass conductor. From these data it appeared that a longer line than the Tidd test line might have a higher r.i. field especially at the lower frequencies since the correction for attenuation of far away sources would not be too large. Calculation (see Appendix II) indicated that if the loss were 1 decibel per mile, a 1-mile test line would give r.i. values of 62 per cent of an infinite line, Figure 22. This amount of reduction in r.i. at a relatively high attenuation value necessitated tests at Tidd to determine the effect of line length. The tests were made by terminating 1,900 feet of 2-inch diameter single-phase steel-reinforced aluminum cable and taking 20 readings along the line at intervals of 50 feet, and then adding the remainder of line for a total of 7,160 feet and repeating the previous test procedure. This procedure was repeated three times with results as depicted in Figure 23. The curves of Figure 23 indicate that the effect of line length depends on the line voltage. At 373-kv phase-to-phase the long line r.i. averaged only 4 per cent higher than for the short line, whereas at 425 kv the long line had 27 per cent higher average value. These tests along the line show appreciable variations due to local r.i. sources which could be detected aurally as tests were made. In order to find out what the relative contributions of local and distant sources might be, a test was made at Tidd using an artificial r.i. generator consisting of a 1-inch diameter brass sphere four inches from the line conductor and connected to it. In this way a definite local source was produced near the conductor surface. The field intensity was measured in the vicinity of this local source and at a point 1,000 feet away. As can be seen by the curves of Figure 2, the r.i. field near this local source was considerably greater than at 1,000 feet or even at 100 feet. It appears that because of the large contribution from a local r.i. source the effect of increasing the line length is not appreciable except at voltages considerably above what would be used for a given conductor diameter. This increase with line length at higher voltages is probably due to the increase in the number of sources along the conductor and their r.i. magnitudes, which by the root sum square addition add to the local source sufficiently to be measurable.

The field pattern obtained around the local generator indicates that a vertical r.i. current component through the ionized air space exists from conductor to ground and the resultant field is therefore dependent on this current as well as the horizontal current component in the line conductor.

A voltage run was made on line number 2 with and without the artificial r.i. generator and curves for this test are shown in Figure 24. It will be noted that the r.i. field at the test point was 3.5 times greater at 286 kv with this local source, and that at 530 kv the increase was only 1.15 times. This effect of voltage also was indicated by the data shown in Figure 23. The large effect of local sources especially at normal voltages means that if r.i. exists at a receiver location and if it decreases appreciably within 100 or 200 feet along the line it may be that the source on the conductor can be found and removed without too much difficulty. It is preferable, however, to inspect and clean the conductor surface during construction just before it is drawn into place, to reduce the possibility of having these high intensity local sources.

Single-Phase and 3-Phase Tests

Single-phase and 3-phase voltage runs were made on the same day to obtain the

correlation between r.i. for these two conditions. This was necessary because of the number of single-phase comparison tests made at Tidd. Typical fair weather voltage runs single-phase and 3-phase are shown in Figure 25. At a voltage which might be used for the conductor tested the 3-phase to single-phase ratios are: 3.5 for average meter reading, 2.4 for quasi-peak, and 2.3 for peak.

Correlation of Tidd and Laboratory Data

From Figure 14 we can see that laboratory data taken on dry conductors will indicate a conductor for r.i. which would be only one-third the diameter required. In fact, the dry threshold voltage in the laboratory is higher than the voltage at which considerable r.i. occurs on the Tidd line. For rain conditions, however, the laboratory data correlates quite well with field results. The results from laboratory and Tidd data for dry conditions, indicate the large effects of variations in the surface of weathered conductors. It was determined by oscilloscope studies, see Figure 12, that corona can exist on the positive half-cycle on dry weathered conductors, whereas on new conductors no corona appears on the positive half-cycle. It also was determined that during rain, r.i. appears mostly on the positive half-cycle. These results show that a dry weathered conductor is similar in some respects in r.i. characteristics to a conductor in rain or with water drops adhering to the surface. In the laboratory the test conductor was only 20 feet in length and one sample may not necessarily correlate with field data where much longer lengths of weathered conductors were tested. It was found on the test line that there were variations in fair weather data as shown by Figures 8 and 10. If many samples of weathered conductors had been tested in the laboratory similar variations and better correlation with field data might also have been obtained. In any case it appears that a test in the laboratory on a smooth dry conductor is necessary to establish that the test setup used will follow equation 1. Then tests on any conductor, dry and with rain, will establish its r.i. relationship to a smooth conductor or any conductor for which field and laboratory data are available.

Operating Line Data

It was determined that the r.i. level of lines of the 138-kv and 230-kv class have values quite consistent with other data presented in Figure 14. Experience also indicates that these lines are not the cause of radio noise complaints for AM or TV services and frequency runs made on these lines show that r.i. falls off rapidly with frequency, see Figure 19. Chart data from operating lines plotted as shown in Figure 10 are similar to those obtained at Tidd. The difference between fair weather and rain is well established for this type of line and checks with data of Figures 8 and 9. It is indicated by the field data that the r.i. effects for 138-kv double-circuit and single-circuit lines at distances 40 feet or more away from the line are about the same. It might be expected that the r.i. from a 2-circuit line would be equal to a single-circuit line times $\sqrt{2}$ if all conductors had the same r.i. However, because of the shielding effects of other conductors the over-all effect is about the same as for a single-circuit line. Close to the line values may be higher in some cases than under the line depending evidently on the relative magnitude of r.i. of each conductor at the point of measurement. Vertical 3-conductor configuration gave results about the same as for three conductors in horizontal configuration.

Bundle Conductors

Some tests were made at Tidd and in the laboratory on bundle conductors. Radio influence threshold and other values for bundles are given in Figure 14, curves 12, 13, 14, 17, 19, and 20. In the case of 2-, 3-, and 4-conductor bundles tested (see Figure 26) the r.i. threshold for 2-conductor bundle was within 5 per cent of the calculated value at the optimum spacing $S/d=10$ and less than this at greater spacings. The small amount of data obtained at Tidd on a 2-conductor bundle consisting of 0.92-inch diameter stranded copper conductors 20 inches apart was used to obtain the 15-microvolts-per-meter level at 100 feet from the line shown in curve number 7, Figure 14. From these data we see that the bundle conductor tested is equivalent in r.i. in fair weather to a single 1.53-inch diameter steel-reinforced aluminum conductor and to a 1.38-inch diameter HH conductor. From laboratory rain tests it is indicated that this 2-conductor bundle is equivalent to a 2.0-inch diameter steel-reinforced aluminum single conductor.

Correlation of Radio Influence and Corona Loss

Three-phase fair weather corona loss and r.i. were measured simultaneously at Tidd and the results of these measurements are plotted in Figure 28. It will be noted that corona loss increases more rapidly with voltage than r.i.; however, r.i. is measurable and has significant values at the lower voltages where corona loss would be considered negligible.

Present Radio Influence Situation on Operating Lines

The above presentation includes, principally, test procedures and test data. It also is necessary to evaluate the results in terms of the effect of r.i. on communication services.

The transmission lines of the American Gas and Electric Company system in the general voltage range of 69 kv to 138 kv have caused very little interference to radio reception under all weather conditions. The few cases of complaints that were definitely traced to the transmission system were found to be caused by defective insulators, and in some cases, defective line hardware, and replacement eliminated the interference.

With the increase in areas served by television broadcasting, complaints from television owners are increasing. These complaints are all investigated and almost without exception the cause of interference is traced to causes other than radio influence from transmission lines.

With the record of many years experience in the industry with existing transmission lines in the general voltage range of 69 kv to 230 kv and the relative freedom from radio interference in the vicinity of these lines, it is believed that the magnitude of radio influence generated by these lines is not sufficient to cause interference to AM radio or television, and that the existing r.i. levels can be considered as conservatively low for the design of new lines, see curve number 5, Figure 14.

Tolerable Radio Influence Level for Super-High-Voltage Lines

The effect of r.i. from high-voltage lines on communication services depends on factors such as:

1. Characteristics of r.i. due to corona.
2. Effect of this type of r.i. on communication services.
3. Communication signal intensities along line.
4. Signal-to-noise ratios tolerable to types of communication services which may be affected.
5. Distance of receivers from line.
6. Number of receivers per-unit length of line.
7. Transfer of r.i. to lower voltage circuits.
8. Effects of weather.

This paper will not attempt to make any evaluation of a tolerable limit based

on the foregoing factors. However, a reasonable approach can be made by the application of data presented in this paper and field experience with radio interference.

From Figure 14 we can see that curve 4 (Tidd tests) and curve 5, tests on operating 138- and 230-kv lines, fall very nearly along the same curve. This indicates that a proposed line using conductors based on curve 4 would be expected to have an r.i. level approximately the same as on the operating line, curve 5, and very little, if any, interference would be expected from conductors in the radio spectrum from 0.015 to 400 megacycles. Although no measurements were made above 400 megacycles, the frequency curves at 400 kv indicate that above 400 megacycles, conductor r.i. would be negligible.

The data of Figure 14 are believed to be conservative in predicting the r.i. effects for super-high-voltage lines. The principal reasons for this are:

1. Lines travel across country instead of paralleling roads and low-voltage distribution and other lines.

2. Fewer homes will be near these high-voltage lines.

3. The antenna coupling to lines is lower than for low-voltage lines because of greater conductor height and because of greater distances, on the average, from line to receiver antenna.

Conclusions

1. Instrumentation as used is satisfactory, and for the tests described gave very little trouble. Instruments for recording operated most of the time for periods of two weeks without any attention.

2. Tests on lines should include chart recording of r.i. and weather data as well as spot checks.

3. New conductors when dry have r.i. only during the negative half-cycle at practical operating voltages.

4. Weathered copper or aluminum conductors when dry have r.i. during both positive and negative half-cycles.

5. New or weathered conductors, in rain or when wet, have r.i. mostly in the positive half-cycle.

6. The r.i. threshold voltage for dry single or bundle conductors, as measured at 600-foot altitude checks the calculated corona threshold voltage. The correction (for air density factor) as used in equation 1 may or may not be accurate for r.i. threshold for lines at high altitudes.

7. The threshold voltage with rain on smooth or stranded conductors occurs at 24 per cent of the threshold voltage for a dry smooth conductor.

8. Under rain or wet conditions r.i. will increase, except for fine wires, by several times.

9. Under rain or wet conditions smooth and stranded conductors of the same diameter have the same r.i.

10. A wet conductor, either with a fine droplet surface or with larger water drops will have the same r.i. as when it is raining. The higher the voltage on the conductor, the more rapidly will r.i. decrease as it dries.

11. The relation between conductor diameter and voltage for radio frequency field intensities above the threshold values is of the same form as the threshold relation.

12. Radio influence as measured at any one location changes even in fair weather by several times. This is believed to be mainly due to the shifting along the conductor of the corona bursts.

13. Radio influence characteristics of line conductors under service conditions can now be predicted from laboratory tests.

14. It is believed that the r.i. characteristics of a conductor to be used on an operating line can be determined from the data presented here. These data together with field experience in the region proposed for a transmission line may be used as a basis for selecting the conductor.

15. The effects of changes in relative humidity, temperature, and pressure as encountered at Tidd are not significant.

16. The change from 45-foot to 32-foot conductor spacing at Tidd was to increase the r.i. by 14 per cent. This corresponds to an increase in voltage of 2 per cent whereas the calculated increase is 5 per cent.

17. Laboratory tests showed a bundle of two 0.92-inch diameter stranded copper conductors having the same r.i. as a 1.4-inch diameter steel reinforced aluminum conductor under dry conditions, and the same r.i. as a 2-inch diameter steel reinforced aluminum conductor when wet.

18. Radio influence variation along a transmission line at 100 feet from the outside conductor is not significant for line design.

19. Smooth, weathered conductors when dry have the same r.i. at 10 per cent higher voltage as stranded conductors of the same diameter. They have the same r.i. under wet conditions.

20. No appreciable difference in r.i. was observed between horizontal and vertical line conductor configuration or between single- and double-circuit lines.

21. At ground level, the r.i. field intensity readings were not affected by grounding or isolating the static wires.

22. Radio influence decreases inversely with frequency over the range of 0.015 to 400 megacycles covered by tests.

23. Although corona and r.i. start at the same voltage, corona loss, after it reaches a significant value, increases much more rapidly than r.i. with increase of voltage. Radio influence has significant values at the lower voltages where corona loss is negligible.

Appendix I. Procedure for Converting Noise Meter Readings to Equivalent Values

It has been shown[15] that the effect of a square wave on a radio noise meter is to produce an output voltage as shown by the following equation:

$$v=\frac{aE}{f_0}\quad \phi=\frac{aE}{f_0}\,\frac{(BNT_d)}{(BT_c+NT_d)} \tag{3}$$

where

v = indicated microvolts
a = constant depending on input waveshape
E = peak value of a-c component of input pulse in microvolts
f_0 = measurement frequency
B = bandwidth of radio noise meter
N = number of steep wave fronts or pulses per second
T_c = charging time, seconds, of detector weighting circuits
T_d = discharging time, seconds, of detector weighting circuits

The "equivalent value" of any noise measurement at f_0 is then

$$\frac{aE}{f_0}=\frac{v}{\phi} \tag{4}$$

This equivalent value is independent of the characteristics of the noise meter used, so that a plot of equivalent values over a frequency range involving several noise meters should show no discontinuities.

For conversion of readings on one meter (1) to a value equal to that read on another meter (2)

$$v_2=\frac{\phi_2}{\phi_1}\,v_1 \tag{5}$$

The value of N, pulses per second, depends upon the type of noise being measured, and for 3-phase line conductor corona has been found to be about 20. With corona bursts occurring only on the negative half-cycle of 60 cycles, the noise meter should receive at least 60 steep wave fronts per second, but because of the erratic nature of the corona bursts and the varying amplitudes of the pulses, the average value of N appears to the meters to be somewhat less.

Other constants used in the conversion equation are measurable constants of the individual meters. For this paper the published time constants were used for calculations at all frequencies. Values of effective bandwidth for all meters throughout their

ranges were derived from frequency response curves or checked at half power points.

The correction factors for converting Stoddart meter readings to Ferris meter readings are plotted in Figure 27 along with the bandwidths for all the instruments except for the 15- to 400-megacycle meter for which the bandwidth is 150 kc from 15 to 125 megacycles, and 210 kc from 125 to 400 megacycles.

The equivalent microvolt-per-meter readings as defined by equation 4 are plotted in Figure 20. This curve shows that meter response to corona-type r.i. varies approximately inversely as the frequency.

Appendix II. The Effect of Line Length

The r.i. field at a point near a transmission line with corona on the conductor depends on the resultant current of all the r.i. generators along the line. If it is assumed that the measurement point is at $X=0$, and that all the generators produce the same currents near their source, the effect of any generator n is to give a current equal to $I_n\epsilon^{-nx_1}$, where X_1 is some relatively short distance along the line. If we add all contributions from both directions from $X=0$, as the sum of the squared values, the resultant current is

$$2I_0^2(1+\epsilon^{-2\alpha x_1}+\epsilon^{-4\alpha x_1}+\epsilon^{-6\alpha x_1}) \qquad (6)$$

The radiated field we know to be proportional to the square root of this current and the resultant field is

$$\mathcal{E}_r=\mathcal{E}_0\sqrt{2(1+\epsilon^{-2\alpha x_1}+\epsilon^{-4\alpha x_1}+\epsilon^{-6\alpha x_1}\ldots)} \qquad (7)$$

As an example let us take $X_1=1$ mile and the loss per mile as 4.343 decibels. Then $\alpha=0.5$ and $\alpha X_1=0.5$.

Substituting in equation 7 for a long line,

$$\mathcal{E}_r=\mathcal{E}_0\sqrt{2(1+\epsilon^{-1}+\epsilon^{-2}+\epsilon^{-3})\ldots} \qquad (8)$$
$$=1.76\ \mathcal{E}_0 \text{ very nearly for a long line.}$$

For one mile of line each way:

$$\mathcal{E}_r=\mathcal{E}_0\sqrt{2(1+\epsilon^{-1})}=1.65\mathcal{E}_0 \qquad (9)$$

Hence a 2-mile test line should give 94 per cent of the r.i. value for a long line. Curve in Figure 22 shows how the ratio of r.i. for a 2-mile line to r.i. for a long line varies with the decibel loss per mile of line.

References

1. Transmission of Electric Power at Extra High Voltage, **Philip Sporn, A. C. Monteith.** *AIEE Transactions*, volume 66, 1947, pages 1571–82.

2. Corona Considerations on High Voltage Lines and Design Features of Tidd 500 Kv Test Lines, **C. F. Wagner, Anthony Wagner, E. L. Peterson, I. W. Gross.** *AIEE Transactions*, volume 66, 1947, pages 1583–9.

3. Transformers and Lightning Arresters—Tidd 500 Kv Test Lines, **F. A. Lane, J. K. Hodnette, P. L. Bellaschi, Edward Beck.** *AIEE Transactions*, volume 66, 1947, pages 1613–18.

4. Insulators and Line Hardware for Tidd 500 Kv Test Lines, **I. W. Gross, R. L. McCoy, J. M. Sheadel.** *AIEE Transactions*, volume 66, 1947, pages 1591–1602.

5. Line Conductors—Tidd 500 Kv Test Lines, **E. L. Peterson, D. M. Simmons, L. F. Hickernell, M. E. Boyes.** *AIEE Transactions*, volume 66, 1947, pages 1603–12.

6. Instrumentation and Measurement—Tidd 500 Kv Test Lines, **R. L. Tremaine, G. D. Lippert.** *AIEE Transactions*, volume 66, 1947, pages 1624–31.

7. Switchgear Equipment for Tidd High Voltage Test Lines, **F. A. Lane, B. W. Wyman.** *AIEE Transactions*, volume 66, 1947, pages 1916–23.

8. American Standard Definitions of Electrical Terms. AIEE, 1941.

9. Some Characteristics of A-C Conductor Corona, **F. O. McMillan.** *Electrical Engineering (AIEE Transactions)*, volume 54, March 1935, pages 282–92.

10. Methods of Measuring Radio Noise. Report of the Joint Coordination Committee on Radio Reception of EEI, NEMA, and RMA. Edison Electric Institute (New York, N. Y.), 1940.

11. Proposed American Standard Specification for a Radio Noise Meter—0.15 to 25 Megacycles. *C63.2*. American Standards Association (New York, N. Y.), October 1949. (Published for one year trial use.)

12. Specification for Ultra-High Frequency Radio Noise Meter. RMA Committee on Television Interference, Radio Manufacturers Association (Washington, D. C.), 1939.

13. The Swedish 380-Kv System, **W. Borquist, A. Vrethem.** *Paper 412*, Conference on Large High Voltage Electric Systems (Paris, France), appendixes by **B. Henning, S. Skagerlind, S. Bylund**, 1948.

14. Mechenism de L'Effet Couronne sur les Lignes de Transport D'Energie en Courant Alternatif, **R. Pelissier, D. Renaudin.** *Bulletin*, Societe Francaise des Electriciens (Paris, France), volume IX, series 6, number 89, February 1949.

15. A Study of Wave Shapes for Radio-Noise-Meter Calibrations, **C. W. Frick.** *AIEE Transactions*, volume 64, 1945, pages 890–901.

16. Factors Affecting the Accuracy of Radio Noise Meters, **Harold E. Dinger.** *Proceedings*, Institute of Radio Engineers (New York, N. Y.), January 1947.

17. The 300–315 Kv Extra-High-Voltage Transmission System of the American Gas and Electric Company, **Philip Sporn, E. L. Peterson, I. W. Gross, H. P. St. Clair.** *AIEE Transactions*, volume 70, part I, 1951, pages 64–74.

18. Corona Investigation on Extra-High-Voltage Lines—500 Kv Test Project of the American Gas and Electric Company, **I. W. Gross, C. F. Wagner, O. Naef, R. L. Tremaine.** *AIEE Transactions*, volume 70, part I, 1951, pages 75–94.

Discussion

C. W. Frick (General Electric Company, Schenectady, N. Y.): In a project such as the development of systems for power transmission at higher voltages, effort is apt to be concentrated on problems of equipment design and operating practice, and little attention given to related problems such as radio influence. On the other hand, the development stage is just the time when work on such problems can be done most effectively. The authors of this paper are to be commended for devoting time and effort to the study of radio influence during the development of the Tidd Project and coming forward with some practical answers at this time. This contribution and others that have been made in technical papers from time to time show that the electric power industry in America recognizes that there is a problem of radio influence and is trying to do something about it.

Subjects are included in the paper which are of broader interest than high-voltage transmission. The authors are among the first to report on the use of instruments with characteristics such as proposed for national adoption. Some of the results reported will be discussed. Another subject of general interest is the effect of weather. Previous experience has shown that radio influence is higher in wet weather. The paper gives a minimum ratio of 4-to-1 for this effect and shows that there are many factors involved. The question of the effect of weather comes up also in connection with some types of high-voltage outdoor apparatus, for instance those in which current-carrying members are exposed. When tested at the factory, such apparatus usually shows radio influence levels much lower than present commercial limits. One reason for allowing a fairly wide margin between limits and average test values has been the probable effect of weather. The present paper tends to substantiate this practice.

In the Conclusions, paragraph 14, it is implied that enough data have been obtained to provide at least a tentative basis for selecting the conductor for a proposed transmission line. The paper is not specific as to how a selection of conductor size could be made, thus leaving it to the judgment of the reader. Figure 14 of the paper might be used as a general guide. Curves are shown for a reference radio influence level of 2,000 microvolts on the conductor or 15 microvolts per meter at 100 feet, the two figures representing the same influence according to equation 2 in the paper. (This equation agrees quite well with the data in a paper presented in 1943 entitled, Measurements Pertaining to the Co-ordination of Radio Reception With Power Apparatus and Systems, by C. M. Foust and C. W. Frick.[1]) If this influence level is considered acceptable, a minimum conductor size might be estimated from curve 2. Such a size might be modified somewhat by considering other curves such as 3, 4, 5, and 16, in view of the particular conductor under consideration. Further modification would be necessary for conductor spacings other than 32 feet to which the curves apply.

No particular reason is given for the use of 15 microvolts per meter at 100 feet at 1.0 megacycle. Such a distance can be regarded only as an arbitrary value for reference since radio antennas would not be placed in such close proximity to a line operated at 220 kv or higher. If this level is representative of existing lines which are considered satisfactory from the radio standpoint, it would be reasonable to use it for such purposes as the selection of conductors in the absence of other information.

It should be remembered that the radio influence levels referred to in Figure 14

apply to a particular kind of measurement made at one frequency, 1.0 megacycle. According to data on chart the measurement is made with the type of radio noise meter which has been in use since 1940 by most groups although not actually adopted as an American Standard. A proposal is under consideration, to adopt as an American Standard, a specification for radio noise meter along similar lines but with some changes, particularly in the circuit for the quasi-peak measurement. The paper includes measurements with an instrument which approximates the proposed new characteristics for quasi-peak measurements. These measurements and others show a ratio of the order of 2-to-1 between the proposed standard instrument and the one used for Figure 14. From the practical standpoint, the difference can be taken care of by using a conversion factor.

The quasi-peak method has been found by experience to be the most useful means for evaluating radio influence or noise. It has been noted that "quasi-peak" is a term not very well known among engineers, and therefore a brief review of the principles may be of interest. The annoyance effect of noise consisting of a succession of short pulses is known to depend upon pulse amplitude and repetition rate. Early measurements of radio noise were made on an ammeter or a voltmeter in a conventional detector circuit. This arrangement worked on random noise or on pulses at several hundred per second, but did not properly evaluate pulse noise at rates as low as 10 or 20 per second. Therefore, a circuit was developed which gives meter indications dependent upon both amplitude and repetition rate.

The circuit used for this purpose consists of a capacitor which is charged from the detector at a moderately fast rate and is discharged between pulses at a slow rate. A single pulse charges the capacitor to only a fraction of the peak voltage. A succession of pulses builds up the capacitor voltage to a value dependent upon the time constants for charge and discharge, the repetition rate and the peak voltage in the detector output. The meter indication is a function of the capacitor voltage. Such an arrangement is called a "quasi-peak" voltmeter because of its similarity to a theoretical peak voltmeter consisting of an ideal capacitor which charges in zero time and holds the charge indefinitely and a voltmeter which draws no current. The quasi-peak voltmeter tends to approach the theoretical peak voltmeter at higher repetition rates. An ideal noise meter would give equal readings on two noises which are of equal annoyance effect or nuisance value. The 1940 instrument with 10-milliseconds charge time somewhat underrated noises characterized by repetition rates below 100 per second. In the proposed standard specification, the charge time constant has been reduced to one millisecond, with 600-milliseconds discharge time constant as before. The time constants of 1.0 and 600 milliseconds have been used for a number of years in radio noise meters for frequencies above 15 megacycles which were designed after experience had been gained with the 1940 instruments for the lower frequency range.

The proposed specification for radio noise meters provides for peak measurements by the slide back voltmeter method. This measurement is accomplished by manually adjusting a bias voltage until the sound or oscilloscope output is reduced to zero. The bias voltage is calibrated in terms of the microvolt input from a signal generator. The reading so obtained is independent of detector characteristics but does depend on the band width of the instrument. The effect of band width can be eliminated by reducing the reading to unit band width. This procedure has been used for some purposes such as the study of radio noise produced by automotive ignition systems.

The "equivalent value" of noise suggested in Appendix I of the paper is the same as the peak value per cycle bandwidth. It can be obtained from quasi-peak readings as in the paper, but a simpler method is to use the peak reading which is independent of pulse repetition rate. For example, in Figure 19 the peak value at 1.0 megacycle was 100 microvolts per meter. If the bandwidth is taken as 4,000 cycles, the microvolts per meter per cycle bandwidth would be 0.0025 which is close to the "equivalent value" of r.i. shown in Figure 20. It is, of course, necessary to know the value of bandwidth to use.

The stated bandwidth of 4 kc was evidently determined for random noise. Some tests we have made indicate that the bandwidth for pulse-type noise is not necessarily the same as for random noise, since the output is directly proportional to bandwidth for pulse-type noise and is proportional to the square root of bandwidth for random noise. Our tests indicate a bandwidth of about 6 kc on pulse noise for the type of instrument used.

The measurement of peak value per-unit bandwidth ("equivalent value") is a complex procedure. The quasi-peak method is much easier to use and to interpret in terms of nuisance value. The "equivalent value" is of interest for purposes of analyzing the characteristics of disturbances associated with radio noise. For example, Figure 20 of the paper shows a noise output which varies inversely with the frequency at which the measurement is made. An analysis of measurements on square waves in my paper, listed as reference 15 of the paper, shows such variation with frequency. The same variaton of noise with frequency is shown when a sudden change is followed by a gradual return to normal. Similar analysis made on short pulses, that is a sudden change and a sudden return to normal, show constant noise output up to a frequency which depends on pulse width. The data plotted in Figure 20 seem to indicate that the square-wave type predominates. This suggests some possibilities for future research.

The authors conclude that present instrumentation is satisfactory. They do not state whether the present basis or the proposed basis for quasi-peak measurements would be preferable. An early adoption of the proposed American Standard either in its present form or modified, if necessary, would help to meet the need for standardization pointed out in the paper. Some comparisons of signal-to-noise measurements with listening tests are reported in the paper but those shown in Figure 3 gave no indication as to which instrument would be preferable. If the pulse repetition rate is 20 per second or less, as stated in Appendix I, the instrument with the 1940 characteristics probably reads low. If so, the upper curve on Figure 3, which represents the newer instrument should give a better indication of the nuisance value. On this curve, 30-decibel signal-to-noise ratio corresponds to quality *B* reception which is defined as "very good". This would agree with the criterion of 30 decibels for acceptable reception which has been commonly used. The facilities used by the authors would give an excellent opportunity for further studies along these lines.

Reference

1. Measurements Pertaining to the Coordination of Radio Reception with Power Apparatus and Systems, C. M. Foust, C. W. Frick. *AIEE Transactions*, volume 62, June 1943, pages 284–91.

R. L. McCoy (Locke Incorporated, Baltimore, Md.): The authors and their associates who assisted in collecting, analyzing, and presenting the wealth of data contained in the paper are to be commended and congratulated on so fine a contribution.

Having had a little experience in making field measurements, and knowing the difficulties encountered in obtaining and interpreting the results, I can appreciate the work which was involved in making these tests, rechecking them, and interpreting the results to give a picture which is not full of inconsistencies and contradictions.

In connection with this paper there are two questions which I should like to ask the authors. These are:

1. I have been unable to find any reference in this paper to field tests measuring the radio influence voltage of the insulator assemblies at the various operating voltages which were tried. Insulator strings furnished by Locke Incorporated for the test project were investigated for corona formation voltage in the laboratory prior to being sent to the field for installation. Unfortunately the limit of testing equipment available prevented investigation of radio influence voltage of these units up in the range of higher voltages where interference might have been generated. Is any information available as a result of the investigation on the radio influence voltage of these insulator strings themselves?

2. It is apparent that considerable experience was obtained in these tests with two types of noise meters, namely those covered by specifications referred to in references 10 and 11 of the paper. We have had a great deal of experience with the meter specified in the specification under reference 10 in the laboratory, and a little experience with it in the field. For the most part it has proved to be a very satisfactory instrument. We have also had a small amount of experience in the laboratory in operating the meter to the new proposed specification now published for a one year trial use as referred to in reference 11. Based on this experience we felt that the meter was considerably more difficult to use because of the two decade logarithmic scale as against the 3-decade scale for the meter required under the specification reference 10. We found what we thought was considerably more difficulty in reading and interpreting the results, due to much more violent meter swings on rapidly varying

interference. I would be much interested in knowing the authors' reaction to the two types of noise meters. Which did they feel was the easiest to use, and did the meter referred to in reference 11 appear to give results which were more significant than those obtained with the meter per reference 10?

C. J. Miller, Jr. (Ohio Brass Company, Barberton, Ohio): The authors have done an excellent job in measuring and evaluating radio interference originating on the conductors of high-voltage transmission lines, both in the laboratory and in the field and are to be commended for the thoroughness of their work. The paper emphasizes the fact that it is the conductors themselves and not the supporting insulators and associated line hardware that are the primary sources of radio interference. Furthermore, the paper emphasizes the fact that the lines may have appreciable corona surrounding them without causing serious radio interference with radio and television reception. Conventional suspension insulators have inherently good corona and radio interference characteristics, yet the tendency has been to push specification requirements into regions where special treatments may be necessary to rid suspension insulators of the last vestige of corona and radio interference at 110 per cent of operating voltage. This procedure seems rather absurd when the conductors themselves can be in considerable corona without causing serious radio or television interference.

The authors indicate that r.i. voltage increases as the square root of the number of generators. In studies at the Ohio Brass Company's laboratory three series of tests were performed which indicate that radio noise voltages do not appear to add, but are controlled by the largest noise generator. In one test five 16-unit strings of insulators were tested first one at a time and then all five in parallel. The parallel test curve followed the upper envelope of the five individual curves, indicating no particular addition of radio noise level. In the second test, ten 3/8-inch carpet tacks were attached to a 1-inch diameter smooth conductor. A radio noise curve for the ten tacks practically coincided with the curve taken with one tack, nine having been removed, again showing no tendency to add. The third test consisted of running a curve with a 1-inch diameter smooth conductor sprayed with water from one end to the other. Then a second curve was run with the conductor wiped dry except for one drop of water. Again the single noise source gave just as much radio noise as several hundred points along a 12-foot conductor. All of these tests were made using the conventional EEI-NEMA-RMA recommended circuit and a Ferris *32A* radio noise meter tuned to 1,000 kv per second.

I would be interested in the author's comments on our observations that radio noise voltages do not appear to add in the above described tests.

R. M. Showers and **C. J. Fowler** (University of Pennsylvania, Philadelphia, Pa.): Present tendencies in electrical noise interference studies are in the direction of the determination of a common denominator for the measurement of noise so that such measurements will be as objective as possible and not depend on the particular meter or meters with which the measurements are obtained. It is ultimately desirable to be able to interpret such measurements in terms of interference to actual communications systems. One step toward this goal is the translation of the measured readings in terms of values independent of the noise meter bandwidth. In order to do this it is necessary to determine, to a certain extent, the characteristics of the noise being measured. One way of accomplishing this is by means of different detector circuits.

This paper is one of the first to present comparative readings obtained with the three circuits, peak, quasi-peak, and average. The differences between these three readings depend, of course, upon bandwidth and time constants of the meter, as well as the wave form of the noise signal being measured. For example, for a pure random type of noise, the ratio of quasi-peak to average will be relatively small on the order of 2-to-1 but be relatively independent of bandwidth and for impulsive noise the ratio of quasi-peak to average may vary from close to unity to values as high as 100-to-1, (in the latter case, it may not be possible to get a significant average reading because of overload characteristics of the noise meter) the ratio being highly dependent upon bandwidth and repetition rate. With regard to the application to the present results, an examination of the oscillograms in Figure 12 shows that the corona effects appear for only about 25 per cent of the time on single-phase lines, but that while corona is taking place the noise takes on a fairly random character. The present results on a single-phase line show a ratio of quasi-peak to average of about 10-to-1. This is explained by observing that the average reading should be reduced relatively more than the quasi-peak reading because of a low duty cycle over which the radio noise is produced. It is to be noted that on a 3-phase line, the duty cycle will be roughly three times as great as on a single-phase line with the result that the quasi-peak to average ratio would be expected to be less. On Figure 25, it is seen that the ratio is of the order of 6-to-1 for the 3-phase case. This is higher than would be expected for a 75 per cent duty cycle of random noise hence it might be concluded that the noise is intermediary between pulse and random types or that the duty cycle is actually lower than assumed. The exact amount of information obtainable with such detectors will depend on the outcome of further tests. The use of these ratios to distinguish between 1-phase and 3-phase corona noise might prove useful in locating the source of the noise in a complex transmission system.

The term "equivalent" used in connection with Figure 20 may cause some confusion among those less familiar with noise work. Actually, for the two meters, *PRM-1* (*NM-10A*), and *NM-20A* for which values have been plotted, the value of ϕ is closely equal to the bandwidth of the meter, the remaining correction being for time constants, so that this figure actually gives equivalent microvolts per meter per kilocycle bandwidth, provided the "equivalent" scale is multiplied by 500. To avoid the time constant difficulty with these meters the actual peak reading could be divided directly by the bandwidth for those meters employing a slideback voltmeter. This would also allow the extension of the range of Figure 20 to 120 megacycles. In the above it has been implicitly assumed that the response of the noise meter varies directly as the bandwidth which would be the case for pure square waves applied at the input. The discussion in the preceding paragraph, however, indicates that the noise is more nearly of the random type and for random noise the response of a noise meter would vary as the square root of the bandwidth. Therefore, equivalence should be obtained by dividing the average readings given on Figure 19 by the square root of the bandwidth of the meter used for the particular measurement. The ordinate would then read microvolts per meter per square root kilocycle bandwidth. Such a presentation might be more significant to the communications engineer who is trying to evaluate the interference effect of a particular case of corona on his communication system. It should be noted that equivalent readings in terms of microvolts per square root kilocycle show excellent agreement between different noise meters in ranges where their frequencies scales overlap.

J. R. Robert (Electricite de France, Paris, France): The principal conclusions given in the paper are in accordance with those obtained from the tests carried out at the 500-kv Chevilly Station. In particular, radio disturbances caused by the Chevilly 400-kv test line had already been observed to be no greater than those of the 220-kv lines in operation and the disturbing field became negligible as soon as a distance of 100 to 150 feet from the line had been reached.

Tests carried out at Chevilly have been

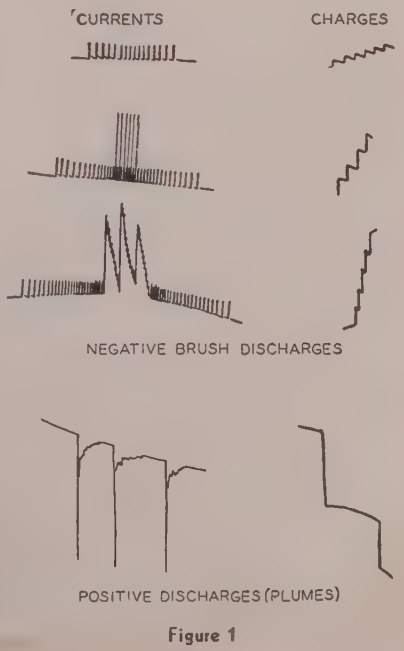

Figure 1

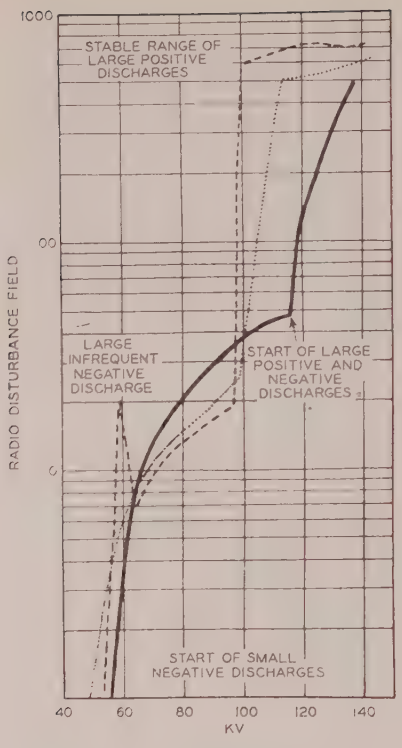

Figure 2

particularly directed towards a precise study of the relation between streamers and radio disturbances. The high increase of the radio disturbance field in the neighborhood of an important streamer had already been pointed out. A small test cage has been specially built, inside which the conductor remains at the earth potential while the test cage is at a high potential. It was thus possible to make oscillograph records of the current and load surge waves emanating from every streamer. These oscillograms are shown on Figure 1 of this discussion and have led to the following classification:

1. The first streamers to appear are negative and take on the appearance of one or several regular series so called: "Trichel waves".

2. When the voltage is quite close to the critical voltage, large irregular negative streamers appear. If the line is very dirty or wet, large irregular positive streamers also appear. The negative streamers which originate the Trichel waves create a low disturbance field which tends to become saturated for a value of this field which causes no perceptible radio disturbance. But as may be seen in Figure 2 of this discussion, the large irregular negative and positive streamers create a much higher disturbance field as soon as they appear. They are essentially responsible for the radio interference. In particular this has been confirmed by tests made on the Alpe d'Huez experimental line.[1]

In order to study high altitude influence on corona, two identical short lines have been built, one at Chevilly near Paris at an altitude of 100 metres, the other at the Alpe d'Huez in the Alps at 1,850 metres. When the two lines are subjected to the same normal gradient, losses are found to be three to four times higher at Alpe d'Huez than at Chevilly. But such is not the case with radio interference. As shown in Figure 3 of this discussion, the latter remains about six times lower. This is due to the surface conditions of the conductors. At Chevilly the atmosphere is polluted and dust deposits on the conductors provoke large irregular streamers. At Alpe d'Huez on the contrary, the atmosphere is pure, the conductor remains clean and there occur chiefly Trichel waves which produce severe losses but low radio interference. This phenomenon is important and it is advisable to take it into account for the study of lines laid across mountainous or uninhabited countries. Although far from radio transmitters, the disturbances due to the line have no chance of becoming annoying as they keep to a low level.

REFERENCE

1. Results of Tests Carried Out at the 500-Kv Experimental Station of Chevilly (France) Especially on Corona Behavior of Bundle Conductors, **Francois Cahen.** *AIEE Transactions*, volume 67, part II, 1948, pages 1118–27.

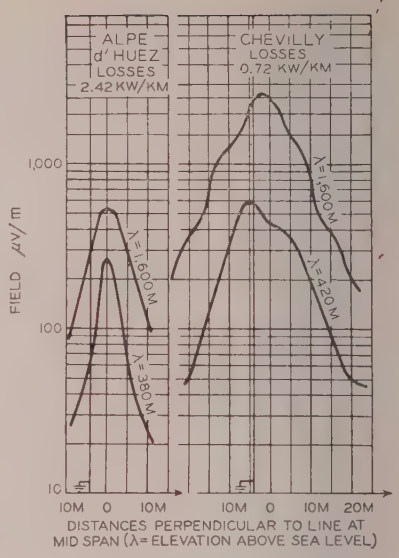

Figure 3

H. L. Rorden (Bonneville Power Administration, Portland, Oreg.): The data that have been obtained in the extensive undertaking contained in this as well as companion papers have contributed greatly to our information on this complicated and diversified subject. We are particularly impressed with the radio noise and loss measurements, since both are difficult to obtain with a fair degree of accuracy. It was well said in the presentation of a companion paper that one of the most conclusive observations during the investigation was the great variation and lack of uniformity of corona and radio noise characteristics.

The Bonneville Power Administration is conducting a rather extensive investigation leading toward the same objective as that reported in this and companion papers and it is of interest to compare results both where they agree and where some differences exist. Laboratory and field tests are being conducted in an effort to determine optimum conductor diameters for the higher voltages as well as to investigate the numerous other phases of radio noise and corona losses. The ultimate objective of radio noise investigations on transmission lines is elimination of interference in domestic radio reception, and the conversion factors between noise emanating from a line and tolerable limits for domestic radios are still to be established.

Of particular interest is the fact that generally results obtained in the laboratory or on a short length of transmission line are in general agreement with results reported in the Tidd investigation. Our laboratory data indicate, for example, that the intensity of rain on a conductor, insulators or hardware is of minor importance in establishing the noise level as long as they are dripping wet.

In order to be assured of the relation that exists between laboratory results and conditions in service, a radio noise measuring circuit of the so-called "NEMA" type was coupled to one conductor of a 230-kv line in service. At the test site, continuous chart measurements were obtained of the microvolts recorded by a Ferris meter coupled to the NEMA circuit, as well as by a record of the field strength obtained with an antenna pickup. In effect, the tests were made on a line of infinite length.

Data obtained on the line in service indicated that the intensity of rain plays an important part in the resultant radio noise. The noise level recorded by both direct coupling and the antenna pickup indicated during very severe rain a level two to four times that obtained during moderate and lighter rainfall. During the drying out period following the rain, the noise fell slowly to the fair weather level.

Other tests of a similar nature lead us to believe that noise generated on a transmission line over a considerable distance contributes to the level that might be recorded at any location. On this basis, it may be difficult to translate data obtained on a relatively short length of line into results that may be anticipated in service, even though the test span may be properly terminated in the equivalent surge impedance. This observation is further verified by data which indicate a considerable difference in the noise level obtained on the line in service with that obtained on a short length of conductor in the laboratory under as nearly as possible the same conditions of voltage, weather, rain, and so forth. Laboratory tests undoubtedly are useful in obtaining relative data, however, it is our belief that it is difficult to translate these data in terms of results that may be expected in service.

Arthur Bessey Smith (Automatic Electric Laboratories, Inc., Chicago, Ill.): My remarks are from the standpoint of a telephone engineer who is interested in suppressing such radio influence voltage as is produced by telephone switching apparatus. Our measurements are usually made on the apparatus itself and finally at the main distributing frame, where the telephone lines leave the central office. Incoming electric power lines also need suppressing for radio influence voltage knows no better than

to escape by all possible routes.

The present paper reveals aspects of the surfaces of electric power conductors which I believe are not commonly known. Experience with needle points formerly used in testing might have pointed to the effects of roughened surfaces of conductors, but radio was too new to be a factor. Now, with the much more sensitive radio the deposits on the power wires and the roughening of the surfaces have become important.

The authors mention "shock excitation." This strikes a responsive chord with us, for most of the radio influence due to telephone relay contacts is caused by abrupt changes in current. For many years most of the contacts which are rapidly made and broken have been protected against wearing out by the use of a capacitor and a resistor. This gave long life to the contact. But radio influence voltage continued to be generated, and we were forced to quench it by effective radio suppressors. From experience it seems that such a disturbance as we had to quench was about as near to a shock excitation or Heaviside unit function as we find in commercial machinery.

As to the radio frequency effects of power line corona being greatest in the low-frequency range, we found that telephone apparatus also acted just about the same. Above the broadcast band there was practically no complaint from the general public, though sometimes there might be an isolated measurable radio influence voltage of very narrow width.

On the whole this is an interesting and valuable paper and will be much consulted by engineers.

G. D. Lippert, W. E. Pakala, S. C. Bartlett, and C. D. Fahrnkopf: As pointed out by Mr. Frick, Figure 14 of the paper is intended as a general guide for the determination of r.i. characteristics of conductors. The selection of a conductor on the basis of its r.i. characteristics will require in addition to the exercise of judgment based on the data presented in the paper, a knowledge of field conditions along the proposed right-of-way such as: the number, location, and output power of broadcast stations in the general vicinity of a proposed line and the number of residents in close proximity to the line.

The 15 microvolts per meter, 100 feet from the line and 1.0 megacycle were offered as a basis of presentation because this r.i. value is representative of a large number of existing lines that have not caused any complaints of radio interference although a value considerably higher than 15 microvolts per meter may be entirely practical.

Messrs. Frick and McCoy have commented on the instruments designed in agreement with the 1940 recommendation and those meeting the present proposed standard. The authors found that the instruments designed to the 1940 recommendation were satisfactory for measuring quasi-peak r.i. and field intensity of broadcast signals, however the new proposed standard requires that the instrument be capable of measuring average field intensity, quasi-peak and peak r.i., and will provide considerably more information which may be of value.

Due to the constants of the detector circuit an instrument designed to meet the new proposed standards may be more responsive to sudden changes in r.i. and more difficult to read when the r.i. is changing rapidly but during the many days of testing the authors have experienced difficulty in reading only in a few instances with the Stoddart meter and then only when there were rapid changes in r.i.

Mr. McCoy asked if there were any data on r.i. contributions of the line insulators and hardware. The line insulator assemblies were equipped with corona control rings at the line end and these rings were effective in preventing visible corona on either the line hardware or the insulators. At 100 kv above the voltage where corona was visible on the conductors the insulators and hardware were free from visible corona. It was found that visible corona and measurable r.i. occurs at approximately the same voltage and the absence of visible corona led us to believe that the 30 insulator strings and hardware would not contribute any to the conductor r.i.

Mr. Miller's comments were most interesting as his tests did not indicate any increase in r.i. with an increase in the number of r.i. generators. The circuit and meter used by Mr. Miller was the same as that used by the authors. In our laboratory tests the r.i. very definitely increased as the square root of the number of r.i. generators. The generators used were tested individually and each produced approximately the same r.i. It is possible that by coincidence we selected an arrangement of r.i. generators that resulted in an increase in r.i. whereas other arrangements or other applied voltages may produce different results. It is known that if several similar r.i. generators are placed on a conductor in close proximity to each other the first one in corona will prevent the others from producing any r.i. As soon as a corona streamer starts to form there is a reduction in voltage gradient in the general vicinity of the corona streamer and the other r.i. generators will not produce corona, unless there is a considerable increase in applied voltage.

We agree with Messrs. Showers and Fowler as to their suggested three detector circuit method of measurement and appreciate their analysis of the ratio of quasi-peak to average r.i. for single-phase and 3-phase tests.

Their analysis of the data in Figure 20 with reference to the conversions of readings of the four different meters to the same base will reduce the confusion which might result in the interpretation of the test data in the paper and from other sources by those less familar with radio noise work.

The data presented by Mr. Robert on results obtained at Chevilly and Alpe d'Huez in France especially with reference to r.i. at high altitudes and the effect on r.i. of contaminated and clean atmosphere is most interesting. Their results indicate, as do ours, that the radio noise field is increased in the vicinity of a local streamer. The effect of dirty and weathered conductors is to increase radio noise due to positive streamers, as can be seen from the films of Figure 12(C) and 12(E) of the paper. It appears that the effect of dirt deposits is similar to that of rain in that these dirt deposits promote radio noise on the positive half cycle. At Chevilly the corona loss was less than at Alpe d'Huez (altitude 6,100 feet, but atmosphere very clean), whereas the radio noise was six times greater at Chevilly than at Alpe d'Huez. In most mountainous regions the conductor environment may be clean, however, there are regions where dust storms may produce dirty conductor surfaces and radio noise as high as in industrial and cultivated areas. Our 500-kv test site is subjected to considerable atmospheric contamination of a highly variable nature. In extreme cases the conductors were temporarily enveloped in smoke from passing coal burning locomotives or freight boats on the Ohio river. In these instances if testing was in progress the r.i. fluctuated violently and the tests were repeated as soon as clear atmospheric conditions were obtained. The tests on operating lines were all conducted at locations where comparatively clear atmospheric conditions existed.

It would be very useful if a correlation between radio influence readings made with French meters and those we used could be obtained so that data of both projects could be compared on the same basis.

Our test results with artificial rain in the laboratory agree with laboratory results obtained by Mr. Rorden. Also the average increase of r.i. with rain of three to four times agrees with the data shown in Figures 8 and 9 of our paper.

Mr. Rorden believes that noise generated at a distance from the point of measurement may contribute considerably to the r.i. measured. This will depend on the attenuation which in turn depends upon the frequency of the propagated wave. Tests were made at Tidd on 1,900 feet, and 7,160 feet sections of 2-inch steel-reinforced aluminum cable, and it was found that the increase from 1,900 feet to 7,160 feet was not appreciable at practical operating voltages, see Figure 23. In tests of this nature consideration must be given to the different resonant frequencies of the different line lengths or preferably, the lines should be terminated in their surge impedance to reduce the effects of reflections.

Mr. Rorden expressed his belief that there may be difficulty in translating the results of laboratory data in terms of results that may be experienced on long lines. In order to obtain the best possible correlation between tests on long lines in the field and short test specimens in the laboratory, the laboratory specimens were taken from the long lines where field tests were made. Specimens of all the different conductors tested at Tidd were also tested in the laboratory and it is believed that we now have a reliable correlation between conductors tested in the laboratory, on the 500-kv test site, and on existing long lines.

It is our opinion that the radio influence characteristics of conductor in the laboratory and in service are defined by curves such as given in Figure 14, all of which have the same form. The effects of tests of long lines in service are to shift the laboratory curve to the left, and that this shift is uniform for all conductor sizes used on lines. With rain the laboratory test curve number 2 as compared to Tidd in rain, curve number 3, are not very far apart. It is believed that with rain the test conductors used in the laboratory may be much shorter than for dry tests without introducing appreciable errors.

Detection of Turn-to-Turn Faults in Large High-Voltage Turbine Generators

ROBERT M. SEXTON
ASSOCIATE AIEE

ROGER J. ALKE
ASSOCIATE AIEE

Synopsis: A modification of the method of using the surge-comparison tester was investigated in regard to detecting and locating turn-to-turn faults in the stator windings of large high-voltage turbine generators. It was found that by using the method devised, the turn insulation can be stressed to as much as several times operating conditions, and both copper-to-copper faults and arcing faults can be detected easily. Limitations of the test method were explored, and recommendations for further improvement of the test, particularly as regards increasing the amount of stress on the insulation, are made.

IN THE design of turbine generators, to obtain operating voltages of 13,800 or more within a workable range of flux densities and stator slot sizes, the stator coils occasionally must be of the multiturn type. When the multiturn type of coil is decided upon, of necessity, an insulating barrier must be applied between turns as well as to ground. As a check on the quality of work done, it is highly desirable to test both of these barriers. There is little difficulty in doing this on individual coils and obtaining reliable indications of insulation condition. However, after the coils are tested they must be assembled in the stator, and in this process the possibility of damaging either or both of these barriers is ever present.

For many years the insulation to ground has been tested after assembly, and standards of acceptance have long been in effect. The insulation between turns, on the other hand, has not been tested after assembly principally because no means was known of making such a test on a turbine-generator winding. When the desirability of this additional test became apparent, efforts were made to develop a new testing technique which would indicate turn-to-turn faults or near-faults satisfactorily.

Paper 51-41, recommended by the AIEE Rotating Machinery Committee and approved by the AIEE Technical Program Committee for presentation at the AIEE Winter General Meeting, New York, N. Y., January 22–26, 1951. Manuscript submitted October 20, 1950; made available for printing November 24, 1950.

R. M. SEXTON and R. J. ALKE both are with the Westinghouse Electric Corporation, East Pittsburgh, Pa.

The authors gratefully acknowledge the assistance of J. S. Johnson, of the Westinghouse Electric Corporation, in developing this test method.

Early Trials

There are in general two widely used methods of testing between turns. First is the high-frequency test, wherein the damped oscillations of a capacitor discharge through the combination of resistance and inductance under test are picked up by a wavemeter tuned to the particular resonant frequency of the circuit. Secondly, there is the surge-comparison test, wherein a capacitor is charged to a given voltage and discharged through two windings, or portions of windings, which if free from faults are symmetrical. Faults are detected in the first system by changes in the resonant frequency and in the second by the dissymmetry of the discharge through the two windings as viewed on a cathode-ray oscilloscope tube.

The difficulty with the conventional method of using either of these tests on completed turbine-generator windings was that the impedance of the winding was so low, and the effect therefore was virtually to short circuit the terminals of the test set. With the high-frequency test under this condition a short circuit between turns did not produce a detectable change of frequency. With the surge-comparison test, the internal protective resistance was found to be of greater ohmic magnitude than the winding, with the result that the greater part of the capacitor voltage was dissipated before it reached the machine terminals.

The next attempt was made using external coils to induce voltage in the individual coils in a winding. The content of this paper is concerned mainly with this method.

Test Equipment

The surge-comparison tester consists of a repeating-type surge voltage generator, a cathode-ray oscilloscope, and synchronously driven switching equipment—all enclosed in one cabinet. The generator produces a rapid succession of voltage surges (60 per second when used with 60-cycle power) of controlled wave shape and easily adjusted magnitude. The voltage surges produced for the tests have a sufficiently high rate of rise (less than one microsecond) to put a high turn-to-turn stress on the insulation being tested.

The high voltage surge is produced by the discharge of a capacitor through a thyratron tube to the winding under test. The firing of this tube, as well as the initiating of the sweep pulse for the oscilloscope, are controlled by the same electronic circuit. The generated surge voltage goes through a synchronously driven reversing switch, which sends alternate surges through the two coils or windings under test, first through one, then the other on the next cycle, and so forth.

The surge-comparison tester is capable of putting out a relatively high voltage at a steep wave front (both required in turn-insulation testing) and in addition the equipment is portable and simple to operate. The usual method of using this tester is to introduce the surge through the machine terminals, thus putting the surge voltage through all the turns in series. With this method the voltage between turns will not exceed the operating voltage per turn on 13.8-kv machine windings, and so the surge-induction method of testing individual coils was devised.

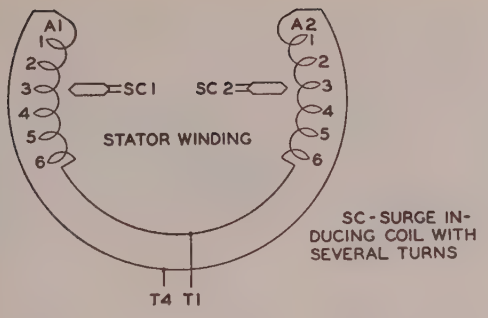

Figure 1 (left). A-c turbine generator 2-pole 2-parallel winding surge-induction test

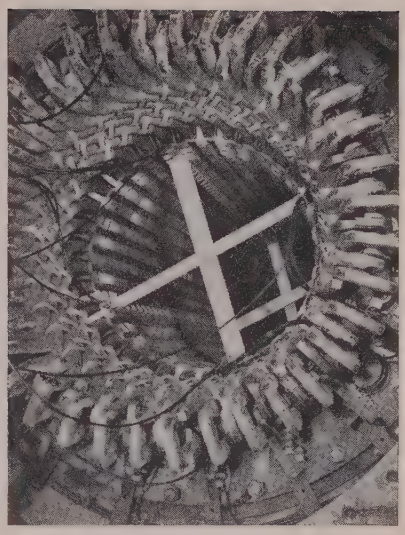

Figure 3 (right). Surge-induction test in shop

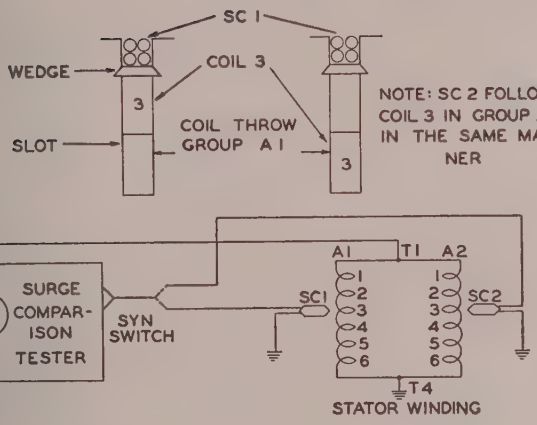

The surge-induction comparison test applies the surge voltage to multiturn coils in generator windings by inducing the voltages in the individual coils. Since the surges are applied (inductively) to individual coils it is possible to apply materially more voltage turn-to-turn than when the surge was applied directly to the winding terminals. The tester is designed to operate on the principle of balance and comparison; in this test it compares the voltage induced in two coils in the same electrical position in a phase at one time. If the winding is symmetrical, that is, if there are no faults, the waves induced in the winding across the phase to ground will be the same for either surge-inducing coil. However, if this symmetry is disturbed by anything, in this case a short-circuited turn, the voltage induced by the two surge-inducing coils across the phase will differ, and two dissimilar waves will appear on the oscilloscope screen. The persistence of the cathode-ray tube screen permits the two traces to be observed at the same time. The oscilloscope has the usual controls for adjusting the sweep, image clearness, and amplitude of the trace.

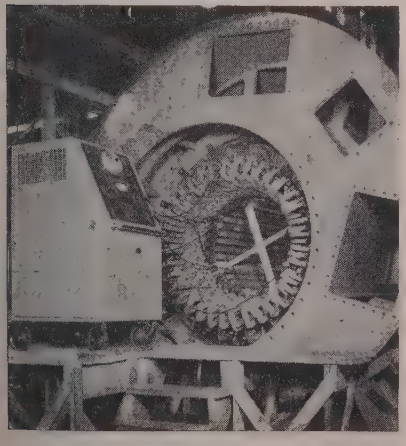

Figure 2. Surge-induction test in shop

To test a multiturn turbine-generator winding by the surge-induction test method, two surge-inducing coils are placed in the bore of the machine so that one surge coil couples one coil in the winding under test, and the other surge coil couples another coil in the winding in the same phase and electrical position. A channel (wood or metal) is used to contain the turns of the surge-inducing coils. This allows closer coupling throughout the bore of the machine between the surge-inducing coil and the coil under test and makes handling of the coils considerably easier.

The surge-inducing coils and channel are designed to fit the space in the slot above the wedges. Four leads (two from each surge coil) are brought out to the surge-comparison tester. One lead from each coil is grounded to the frame of the tester, the other lead from each coil being connected to separate terminals from the reversing switch. One side of the phase being tested is connected to ground, while the other lead is connected to the oscilloscope terminal of the tester for observing the trace of the voltage induced in that phase by each coil. Figure 1 is a schematic diagram of the complete connection, and an actual test setup is shown in Figures 2 and 3. It may be possible that the voltage traces are 180 degrees out of phase when voltage is applied to the surge-inducing coils. In this case it is only necessary to reverse the leads on one of the surge-inducing coils. A suitable voltage divider is used to reduce the trace voltage to a value that can be applied to the deflection plates of the oscilloscope.

There appear to be no critical limits on the surge-inducing coils. Generally, any insulated wire capable of withstanding the voltage and small enough to fit the required number of turns in the space available can be used. Surge-inducing coils of two, three, and four turns have been used successfully, the number of turns being determined by the number of turns in the coil being tested. Usually a one-to-one ratio of surge-inducing turns to winding-coil turns is the maximum desired because of the transformer action of the two coils. A step-up ratio could be used between surge-inducing coil and winding coil, but the internal impedance of the surge-comparison tester makes a 1-turn surge coil impractical, since most of the voltage is dissipated in the tester. Windings using a large number of turns per coil (five or more) are not commonly used in the larger turbine generators.

Types of Windings Tested

Tests were made on about 15 2-pole turbine generators with ratings from 10,000

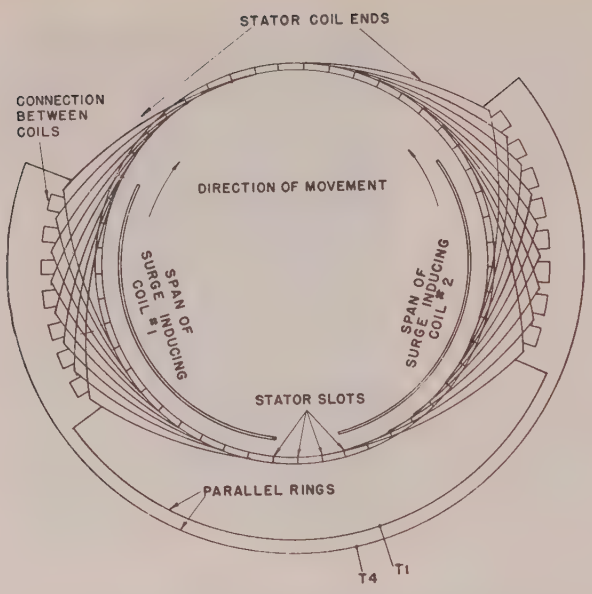

Figure 4 (above). Actual positions of the surge-inducing coils in testing a 2-pole 2-parallel winding using the machine terminals

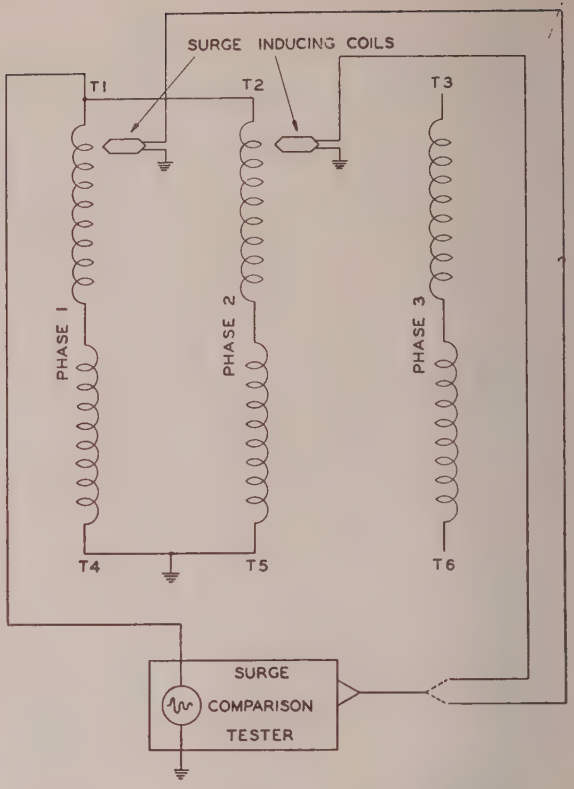

Figure 5 (right). Experimental surge-induction test on 2-pole series winding

to 30,000 kw, both in the manufacturer's plant and in the field. The tests made during manufacture took place after all the coils were wound and the turn taping of the connections was completed, but before the connections between groups were made. In tests made at this time a standardized procedure could be followed, since the type of connection, either series or parallel, was immaterial. On completed machines in the field the test must be made using the machine terminals, and in these cases either a slight modification is made for the parallel type of winding or the insulation on a connection is opened for the series type.

Figure 4 shows the connection for a field test on a parallel winding using only the terminals. Electrically this is the same as the connection shown in Figure 1, the only exception being that physically the surge-inducing coils are not diametrically opposite, as they are in the factory test. Figure 5 shows a typical series-type winding and the test connection from the terminals with which some experimental tests were made. It was found, however, that the series-type winding could not be tested in this manner because the testing of coils in two different phases was involved, and it was decided that when it was necessary to test these machines in the field, the insulation on the connection between the poles of any phase could be opened at some convenient location, thus permitting the connection shown in Figure 1.

Some of the field tests were made with the rotor in place. When this was done the surge-inducing coils were worked into position using the air-gap space. This method proved satisfactory, but two limitations were found: first, the severe space restrictions made it physically difficult to properly position the surge-inducing coils, and, second, the degree of electrical coupling was not consistent because the inducing coils sagged away from the stator in the upper half of the bore.

For other than 2-pole designs, additional connections between phase groups will have to be bared so that two coils of groups in the same phase can be compared. One machine of this type has been tested, but it is believed that only in rare instances will it be necessary to prove the turn insulation on other than 2-pole machines.

Results of Tests

Photographs were made of the oscilloscope traces observed during a typical test. The machine tested was of the 3-phase 2-pole design with 42 slots, giving seven coils per pole per phase. Figure 6 shows two superimposed traces when the surge-inducing coils were over the center coils of the two groups being compared with no faults in either group. The two traces are aligned closely, indicating that this condition (no faults) exists. Figure 7 shows the trace when the surge-inducing coils were in the position identical to that in Figure 6, but with an artificial turn-to-turn short circuit wired on the connection of the coil directly under the surge-inducing coil in one group. Comparison of Figures 6 and 7 indicates the degree of response the test has, and the corresponding reliability of indication. It has been found that even an arcing short circuit between turns produces the same noticeable difference between traces, although the difference exists only for the duration of the arc.

Figure 8 shows the trace observed when the surge-inducing coils are over the stator coils immediately adjacent to the coil with an artificial short circuit between

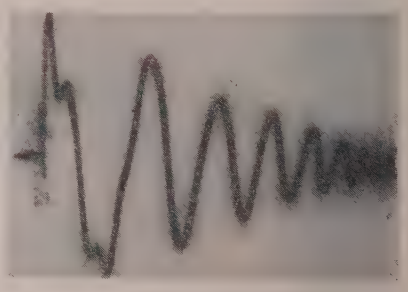

Figure 6. Oscilloscope trace of induced voltage across winding—no faults

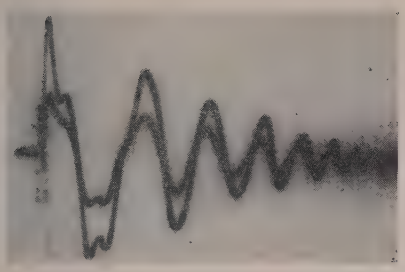

Figure 7. Oscilloscope trace of induced voltage across winding—1-turn fault—surge-inducing coil over short-circuited coil in winding

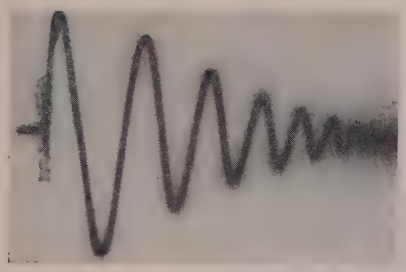

Figure 8. Oscilloscope trace of induced voltage across winding—1-turn fault—surge-inducing coil one slot away from short-circuited coil in winding

turns, in other words, the trace when a faulty coil is being approached but is still one slot away. Some slight dissymmetry can be noted, but it is of insufficient magnitude to be conclusive. To test a winding adequately, therefore, the surge-inducing coils must be placed over every stator coil and the traces observed.

A slight variation in traces also can be produced by minor differences in the degree of coupling between the two surge-inducing coils and their respective stator coils. When this occurs it frequently is found that the end turns of one of the surge-inducing coils has fallen away from the end turn of the stator coil under test. This indicates that even under the best conditions, the flux produced by the end turns of the surge-inducing coil contributes little to the voltage induced in the stator coil.

The amplitude of the trace on the oscilloscope screen is an indication of the total voltage induced in the group in which the stator coil being tested is located. This can be calculated if the voltage per-unit deflection of the oscilloscope tube is known. A variation in this voltage is noted as the test proceeds from one coil to another within the group. When the machine mentioned previously was tested, this voltage was between 1,860 and 2,360 volts, with an output of 10,000 volts from the tester. It is thought that this variation is caused by differences in coupling and the change in the impedance to ground as the progression from one coil to another is made within the group.

Studies were made of the distribution of voltage within the phase group. In all cases it was found that this distribution, if plotted for the various coils in the group, would produce a bell-shaped curve with a sharp peak for the stator coil under the surge-inducing coil and falling off rapidly on both sides. This indicates that by far the greatest proportion of the total voltage shown on the oscilloscope for the entire phase group is in the single coil of that group under test. A favorable condition therefore exists in which the available flux is concentrated sufficiently so that maximum stress can be placed on the insulation between turns of a single stator coil.

Limitations

The surge-comparison tester has several limitations which restrict the amount of voltage that can be induced in a coil in the winding. The first limitation is a series resistor in the load circuit, which is necessary to protect the main discharge tube. This resistance should be 100 ohms, and as the top voltage output is 10,000 volts, this only allows for a maximum current of 100 amperes. Using a one-turn surge coil the voltage drop across this resistance is a large portion of the voltage output of the test; however, with two or more turns the voltage drop is only a small proportion of the output voltage. A higher voltage output in conjunction with a tube capable of withstanding this higher voltage and passing larger amounts of current is definitely needed.

An inherent limit to the voltage which can be induced by a test of this kind is the coupling possible between surge-inducing coil and the coil under test. It is possible to couple closely only that half of the coil under test which lies in the top of the slot. Results indicate that only about 25 per cent of the voltage from the surge-inducing coil is induced in the coil under test. The effect of the loose coupling in the ends of the surge coils that extend beyond the core of the machine also reduces the voltage capable of being induced. From present indications, the ends of the surge coils induce very little voltage in the coil under test. Another limitation in the present equipment is the synchronous reversing switch. It is not capable of switching very large currents, so some other means would be needed successfully to reverse the larger currents needed to induce higher voltages and still keep the tester relatively portable.

The simplicity and the applicability of the surge-inducing test method leave little to be desired. However, to provide new test equipment capable of inducing the voltage desired in testing turn insulation, new discharge tubes and a novel method of reversing the discharge currents have been used in an "experimental" model. It is very possible that a high-power surge-comparison tester can be developed which will increase the amount of voltage capable of being induced by means of surge-inducing coils.

Conclusions

1. The surge-induction testing of turn insulation on completed half-coil-type windings is the only known method of stressing the turn insulation above operating stress and detecting and locating turn-insulation faults.
2. The test method used can be applied conveniently to test multiturn coils in wound stators of any type of winding without removing any coil insulation. The coil containing the short circuit can be located readily.
3. It is possible to test machines in the field with the rotor in place.
4. The desirability of test equipment which will produce even greater voltage stress on the turn insulation using the same method of testing has been recognized. Work on an experimental model of such a tester is under way and preliminary results are encouraging.

References

1. Insulation Testing of Electric Windings, C. M. Foust, N. Rohats. *Electrical Engineering* (*AIEE Transactions*), volume 62, April 1943, pages 203–06.

2. Winding-Fault Detection and Location by Surge-Comparison Testing, G. L. Moses, E. F. Harter. *Electrical Engineering* (*AIEE Transactions*), volume 64, July 1945, pages 499–503.

3. A High-Frequency Voltage Test for Insulation of Rotating Electrical Apparatus, J. L. Rylander. *AIEE Transactions*, volume 45, February 1926, pages 459–65.

Discussion

H. A. P. Langstaff (West Penn Power Company, Pittsburgh, Pa.): A turn-to-turn insulation failure occurred in a 27-year-old 35,300-kva, 12,000-volt, 1,800-rpm generator in the Springdale Station of the West Penn Power Company on December 27, 1950. See Figure 1 (left) of the discussion. This is a 1,700-ampere 85 per cent power factor generator with 250-volt, 460-ampere field. The unit had been operating most of the time at 97 per cent power factor and 2,250 amperes, an overload of 32 per cent.

Figure 1. Insulation failure in a 27-year-old 35,000-kva, 12,000-volt, 1,800-rpm generator

One stator coil failed beyond the slot and an arc flashed to the end finger plates on both sides of the coil. No iron was burned. The burning insulation and cording was extinguished with pyrene. This one coil blew out its insulation near both the extreme ends, as shown in Figure 1 of the discussion. Over-all differential protection functioned correctly, disconnecting the generator and its transformer from the 132-kv, 11-kv, and 2.3-kv buses and auxiliary system—dropping about 100,000 kva in capacity with no loss of load or system disturbance.

For about two years it had been known that the stator insulation was very brittle and all new facilities were ordered one year ago to rewind the stator completely with thermalastic insulated coils and other modern design features. All facilities were completed and partly shipped when the failure occurred. The unit is scheduled to be back in service in about 13 weeks, with an estimated total expenditure of $330,000.

When the pressure on the stator laminations was released by removing the through bolts, a serious unexpected condition was found. The 1936 flood caused the water level in the Springdale turbine room to rise to with 1/4 inch of the bottom of the stator slots.

Moisture penetrated the space between laminations and caused rusting and deterioration of the insulating varnish and paper. Numerous hot spots existed throughout the laminations. The steel was almost welded together in places adjacent to the coils and elsewhere. This necessitated removal and reconditioning of the entire stator core. The single coil failure occurred at about the 10:30 o'clock position on inboard end of stator. It is peculiar that the failure occurred well above any high water level and at a point beyond the stator core. In places, the laminations adjacent to the coils were almost welded together.

R. M. Sexton and **R. J. Alke:** Mr. Langstaff's discussion points out how critical turn-to-turn faults can be on an important unit of a power-generating system. In many respects, this type of fault is more serious than a failure to ground, because protective equipment does not isolate the fault and it usually must work its way to ground before the protective devices function. The subsequent burning in such cases can damage severely both the copper in the coil and the iron in the core. Fortunately, in this case the fault was sufficiently outside the slot so that the iron was not burned. It is thought that the surge-induction test, if applied at scheduled shutdowns, might detect and locate weak turn insulation, enabling repairs to be made at the time of the normal outage.

Relay Protection of A-C Generators

AIEE COMMITTEE REPORT

THE Project Committee on Generator Protection of the AIEE Relay Committee (Power Group) has reviewed a-c generator relay protection practices and presents its findings in this report. The latest developments in generator relay applications are discussed and preferred practices, based on information received from 25 operating organizations, are outlined.

A paper on "Protection of Electrical Apparatus, Recommended Practice"[1] contained a section on a-c generators in which those methods of protection considered good practice in the United States at that time were outlined. Since then developments in high-pressure steam turbine design have resulted in the manufacture of 3,600-rpm turbogenerators in very large sizes, hydrogen has come into general use as a cooling medium, and there is a greater tendency to operate generators and associated step-up transformers as units.

New problems in protection have arisen with the installation of the new machines; new protective devices have been developed; older protective relays have been improved; and opinions of relay engineers have been influenced by the need for providing adequate and reliable protection economically. It was felt that sufficient time has elapsed and enough progress has been made to warrant a review of those methods of generator protection which are in general favor and are considered good practice at the present time.

Copies of a questionnaire were sent to individuals representing public utility operating companies, engineering service organizations, and industries in the United States and Canada; answers were received from 25 operating organizations (see Table 1). The transmittal letter emphasized the distinction between existing practices and preferred practices and specifically requested that the questionnaire be answered from the viewpoint of protection that would be used in designing a new generating station today. It may be assumed therefore that the statements contained in this report reflect the opinions of those engineers engaged directly in the study of the protective problems associated with large a-c generators.

Unless otherwise noted, the discussion refers to 3-phase machines in the 11- to 15-kv voltage range, rated 10,000 kva and above. It must be recognized that the recommendations listed in the following paragraphs apply to general cases and that special conditions will arise where deviation is necessary. The protection recommended for machines rated 10,000 kva and above may be applied also to generators of lower rating where operating conditions or economic considerations warrant. On some of the protective problems opinion is quite diverse and general discussions of the surrounding factors are given rather than definite recommendations.

The problem of generator protection may be divided into a number of parts, each of which is discussed under its own heading.

Protection of Stator

Faults Involving Stator Winding

Faults involving the stator winding may be classified as phase-to-phase short circuits; phase-to-ground short circuits; short circuits between turns; and open circuits in windings.

Stator winding insulation failure may be caused by overvoltage, reduced dielectric strength, or a combination of both. Overvoltage may be caused by switching transients, lightning, or a combination of overspeed and sudden loss of load such as may occur in the case of hydro units when a transmission line tripping takes place. Reduced dielectric strength results from aging, baking of the insulation, accumulation of dirt, corona, moisture, rough treatment, or foreign material boring into the insulation. If a failure of the winding insulation can be cleared before the laminations are damaged, repairs can be confined to the replacement of the damaged coils, but if the iron is seriously burned, partial or complete restacking of the laminations is required. Winding faults should be cleared also before there is an opportunity for a general fire to develop in the stator assembly.

In general differential protection is recommended for a-c generators.

Phase-to-Phase Short Circuits. Differentially connected current relays are used to protect individually each phase winding of a generator. Current differential relays may be plain overcurrent relays with or without time delay, or they may be of the percentage type with either linear or variable restraint. To permit maximum sensitivity for differential relays, identical current transformers should be used at both ends of each phase, but even when this is done, the sensitivity of plain overcurrent relays is limited in order to prevent false tripping on heavy through-faults. For a number of years percentage differential relays with linear restraint have been used generally. Most of these relays pick up when the differential current in the secondary circuit exceeds 0.1 ampere without restraint and operate on a 10 per cent slope. The time delay for appreciable amounts of fault current is on the order of from three to five cycles on a 60-cycle basis. Where identical current transformers cannot be used, or where several sets of current transformers must be paralleled to give

Paper 51-42, recommended by the AIEE Relay Committee and approved by the AIEE Technical Program Committee for presentation at the AIEE Winter General Meeting, New York, N. Y., January 22-26, 1951. Manuscript submitted October 20, 1950; made available for printing December 4, 1950.

Personnel of the AIEE Project Committee on Generator Protection of the AIEE Relay Committee: H. R. Paxson, *Chairman;* L. L. Draper; L. L. Fountain; E. T. B. Gross; B. C. Hicks; L. F. Kennedy; S. C. Leyland; H. F. Lindemuth; W. E. Marter; J. B. McClure; A. J. McConnell; C. E. Parks; F. C. Poage; L. T. Rosenberg; H. P. Sleeper and C. L. Smith.

the total output of the generator, percentage differential relays working on a variable slope utilizing either summation or product restraint may be required. High-speed differential relays of the latter types, capable of operating in one cycle, have been developed in recent years, and because of their decreased sensitivity on severe external faults there is no danger of incorrect operation. It is advantageous to use these relays even when current transformers of the same type are involved. It is desirable to have no other burden except the differential relays on the current transformers supplying them; if it becomes necessary to include some additional burden in these circuits, the burden should be kept to a minimum. However, if the current transformers have other devices besides protective relays as a burden, the use of variable percentage relays is preferred, since the latter are less susceptible to misoperation due to burden than fixed percentage relays.

It is recommended that ground relays be used in addition to differential relays when a generator neutral is grounded through impedance that limits the fault current to a value below that to which differential relays can respond.

Phase-to-Ground Short Circuits. High-voltage generators usually are Y-connected and may have their neutrals solidly grounded, grounded through a low impedance, a high impedance, or may be isolated from ground. As a rule, some impedance is required in the generator neutral connection to ground so that the magnitude of a single phase-to-ground fault will not exceed the 3-phase short-circuit current; present standards do not require the generator windings to withstand fault currents greater than the 3-phase value. The effectiveness of differential relays in recognizing ground faults depends upon the available ground current. When the latter is high, as is the case when low impedance grounding is used, differential relays will respond to ground faults on all but a small percentage of the windings near the neutral. As the impedance in the neutral circuit is increased, differential relays protect a progressively smaller percentage of the windings until they are of no further use for recognizing ground faults. If full advantage of differential protection is to be obtained, it may be desirable to ground the neutral of the generator in question, to operate it in parallel with another machine whose neutral is grounded, or to establish the neutral by means of a separate grounding transformer so that ground current on the order of full load current will be available. In unit-type installations the generator neutral may be grounded through high resistance or the equivalent consisting of a distribution transformer with a resistor connected across its secondary terminals. As differential relays are not effective when the generator neutral is grounded through high impedance, an additional relay is needed to detect ground faults by responding to current flow through the neutral circuit. Y-connected generators which have only a single neutral connection brought out can be protected against ground faults by comparing the residual current in the phase leads with the current in the ground connection.

Short Circuits Between Turns. Although differential relays will recognize phase-to-phase faults at almost any place where they may occur, they will not recognize faults between turns of the same phase. Various schemes have been used or proposed in the past for protecting against this type of fault, but they usually have required bringing out additional terminals from the machine. Because of physical restrictions and the general use of hydrogen cooling on modern large high-voltage steam-driven generators, it is not practical to bring out additional terminals from the windings for the purpose of installing current balance schemes to detect faults between turns; furthermore, generators of this type usually have single-turn coils so that faults between turns cannot occur without involving ground, and on this basis protection against faults between turns generally is not provided. Split-phase protection, however, has been used extensively for large water-wheel generators.

Open Circuits in Windings. An open circuit in the windings of a modern generator is not likely because of the physical size of the conductors, and special protection against it is not provided as a rule on high-speed machines. Differential protection usually is installed on generators rated in excess of 5,000 kva and operating at 2,300 volts or above, but also may be used on machines as small as 1,000 kva.

It is recommended that the zone protected by differential relays include the generator leads and extend to the far side of the main circuit breaker.

Including within the zone of the differential relays the conductors which extend from the main terminals of the generator to the far side of the main circuit breaker furnishes a simple method of providing sensitive and fast protection for the generator leads without the need for providing additional relay equipment.

It is recommended that generator differential and ground relays trip simultaneously the main generator circuit breaker, the field circuit breaker, and the neutral circuit breaker.

When a fault occurs in the windings of a generator, the circuit breakers which connect it to the system, the main field circuit breaker and the circuit breaker in the neutral (if an adequate neutral circuit breaker is installed), should be tripped immediately. In the past, the field circuit breaker frequently was interlocked with the main circuit breaker so that the field circuit breaker did not open until the main circuit breaker first had opened. This practice seems to have developed when adequate hand-reset auxiliary relays were not available, and the intention was to avoid the possibility of the field circuit breaker tripping and the main circuit breaker remaining closed. Present-day practice trips the main circuit breaker and the field circuit breaker simultaneously. To minimize burning of the stator iron in

Table I. Individuals Submitting Replies to Questionnaire

M. J. Seale	Alabama Power Co.	Birmingham, Ala.
F. H. Duffy	Aluminum Company of Canada	Shipshaw, Que.
W. A. Morgan	Bureau of Reclamation	Denver, Colo.
S. Goldsmith	The Cincinnati Gas and Electric Co.	Cincinnati, Ohio
J. R. Linders	Cleveland Electric Illuminating Co.	Cleveland, Ohio
E. L. Michelson	Commonwealth Edison Co.	Chicago, Ill.
V. J. Hayes	Connecticut Light and Power Co.	Waterbury, Conn.
H. F. Lindemuth	Consolidated Edison Co.	New York, N. Y.
L. L. Draper	Department of Water and Power	Los Angeles, Calif.
T. R. Halman	The Detroit Edison Co.	Detroit, Mich.
W. E. Marter	Duquesne Light Co.	Pittsburgh, Pa.
R. J. Cooper	Georgia Power Co.	Atlanta, Ga.
W. A. Wolfe	Kansas Gas and Electric Co.	Wichita, Kan.
F. S. Fehr	Metropolitan Edison Co.	Reading, Pa.
R. C. Ericson	Northern Indiana Public Service Co.	Hammond, Ind.
L. F. Ferri	Ohio Public Service Co.	Elyria, Ohio
G. E. Dana	New York State Electric and Gas Corp.	Binghamton, N. Y.
W. B. Morton	Pennsylvania Power and Light Co.	Allentown, Pa.
G. W. McKenna	Philadelphia Electric Co.	Philadelphia, Pa.
M. A. Bostwick	Portland General Electric Co.	Portland, Oreg.
C. E. Parks	Public Service Company of Indiana	Indianapolis, Ind.
L. W. Marts	Public Service Electric and Gas Co.	Newark, N. J.
O. E. Charleton	Southern Services, Inc.	Birmingham, Ala.
K. N. Reardon	West Penn Power Co.	Pittsburgh, Pa.
G. W. Gerell	Union Electric Co.	St. Louis, Mo.

case of a ground fault, the neutral circuit breaker should be tripped in order to interrupt the fault current that would otherwise flow while the flux in the main field is decaying.

There is some difference of opinion as to whether the neutral circuit breaker should be tripped simultaneously with the main circuit breaker and the field circuit breaker or whether this tripping should be delayed until the other two have opened. If the generator is protected against switching surges, there appears to be little reason to require that the main circuit breaker be opened first. Even without such protection, many ungrounded generators are switched without apparent harm. From the standpoint of obtaining maximum over-all speed of clearing, all three circuit breakers should be tripped simultaneously, but there is a possibility of transient voltage stresses developing in the machine if the neutral circuit breaker should open a little before the others. In addition to tripping the generator circuit breakers, differential relays frequently are arranged to shut down the prime mover, operate fire-extinguishing equipment, and actuate various alarms and signals.

Overheating of the Stator

Overheating of the stator may be caused by overcurrent; short-circuited laminations; and failure in the cooling system. It is recommended that temperature indicators or recorders arranged to operate an alarm be used to recognize overheating of the stator.

Overcurrent. Overheating of the stator caused by the cumulative effects of overcurrent cannot be recognized by ordinary short time-delay overcurrent relays. Temperature indicators or recorders operated from embedded resistance detectors or thermocouples often are used to check stator temperatures; temperature recorders frequently are equipped to operate an alarm when the temperature exceeds a safe value. Large generators that are attended usually are not tripped automatically by temperature devices. A sufficient number of embedded temperature detectors is installed at representative points in the windings to obtain an adequate indication of temperature conditions in the stator. Where complete attendance is not provided, thermal or replica-type relays may be used for determining machine temperatures and may be arranged for automatic tripping where required.

Short-Circuited Laminations. Heating of the stator also may be caused by failure of core bolt insulation, where core bolts are used to assist in holding the laminations together, or by local heating in the core caused by uneven enameling of some of the punchings. Such localized heating may not cause sufficient rise in temperature in the area where the embedded temperature detectors are located as to be recognized, and consequently these detectors cannot be depended upon for an indication of this condition. If the lamination enamel should fail in the teeth near the detectors, considerably higher temperatures undoubtedly would be observed. There have been a number of cases where failure of insulation between laminations caused the generator iron to be melted away and resulted in complete failure of the generators.

Failure in the Cooling System. Overheating of a machine may result from some failure in the cooling system caused by accumulation of dirt or other obstructions in the ventilating passages, blocking of the air intake by closed louvers, blocked screens, or ice formation, or by failure of the cooling water supply in closed air or hydrogen systems. Any failure in the cooling system can be recognized by comparing the temperature of the air or hydrogen leaving the machine with the temperature which has been established as the maximum safe value. Thermometers or temperature-detecting devices should be located in both the intake and exhaust air (or hydrogen) streams. In some cases, these temperatures are recorded on the same chart with the temperatures indicated by the detectors embedded in the stator.

Protection of Rotor (Field)

Troubles in Generator Rotors

Troubles in generator rotors may be classified as short circuits in rotor windings; open circuits in rotor windings; grounds on the field circuit; and overheating. In general, tripping protection for the rotor is not recommended.

Short Circuits in Rotor Windings. Short circuits in rotor windings cannot be recognized by overcurrent relays in the field circuit if only a few turns are involved or if one pole of a slow-speed generator is short-circuited. Furthermore, it is highly desirable for field circuits not to be opened during system disturbances when high currents may be induced in the field circuit. For this reason, overcurrent protection usually is not considered for field circuits. If the windings on one pole of a generator should become short-circuited, the resulting unbalanced magnetic conditions would produce mechanical stresses and vibrations. If vibration is sufficient, the condition can be recognized by vibration-detecting equipment arranged to operate an alarm. The effects of short-circuited windings are more evident for generators with small numbers of poles.

Open Circuits in Rotor Windings. Open circuits in rotor windings may occur on any type of generator, but experience has shown that they are more likely to occur on the slower speed salient pole alternators. Aside from the possibility of high potential and burning at the point of fault, an open-circuited field causes loss of excitation, which is discussed in more detail under this heading.

Grounds on the Field Circuit. A ground on the field circuit is not serious in itself, but it indicates the presence of weakened insulation or mechanical failure, and serious damage may result if a second ground should occur. A simple form of ground indication consists of two lamps in series connected across the rotor winding with their mid-point grounded. This scheme of ground detection gives a positive indication only for faults near the terminals of the field winding. More sensitive ground indication can be obtained by replacing the lamps with resistors and connecting the mid-point to ground through a sensitive relay. Complete coverage can be obtained in all cases by the use of a separate a-c supply with a low-voltage transformer. One terminal of the transformer secondary winding is connected to the field winding, while the other terminal is connected to ground through a sensitive relay.

Overheating. Overheating of the rotor may be caused by excess rotor current; failure in the ventilating system; and single-phase or unbalanced current operation.

Although overheating of the rotor may be caused by excess field current such as might result from failure of a rheostat or voltage regulator, opinion favors the omission of overcurrent protection in field circuits in order to avoid any misoperation during system disturbances when high transient currents may be induced in the field. Although a slight rise in temperature might be detected in the ventilating medium, it is doubtful if this rise can be depended upon to call attention to overheating of the rotor.

Overheating of the rotor caused by failure of the ventilating system will be indicated by the temperature-detecting equipment associated with the stator and the cooling system.

Single-phase or unbalanced current operation will cause local heating in the pole faces of the rotor and severe vibration will be imparted to the machine foundation. Protection against unbalanced current operation normally is not provided for attended machines, dependence being placed upon the indications of the phase ammeters and the presence of vibration to disclose this condition.

Miscellaneous Protection

Motoring

Generators driven by steam turbines which do not have other provision against being operated from the electrical end with insufficient steam to prevent overheating of the turbine may be equipped with sensitive power directional relays. These may be arranged to give an alarm immediately when power flows from the bus back toward the generator and to trip if the power reversal persists long enough to cause damage to the turbine from overheating. Very sensitive power directional relays developing maximum torque at unity power factor have been used for this application. Generally a minimum time delay of one minute will be permissible between the time when the power reversal starts and tripping should occur. After an alarm is given, tripping may be left to the discretion of an operator. The time-delay feature prevents tripping of the generator circuit breaker on power surges caused by synchronizing or system disturbances.

Loss-of-Field or Weak Field

When the field excitation on a loaded generator is lost, the magnetic coupling between the rotor and the stator may be so weakened that the rotor advances and after a short period pulls out of synchronism with the system. Continued operation without excitation has harmful effects on both the generator and the system. An alternator running as an induction generator will have heavy currents circulating in the face of the rotor, particularly toward the ends, and these may cause injurious heating in local areas and arcing at metal wedges in the slots. Induced voltage or current will appear in the field winding, depending upon whether it is open-circuited or short-circuited. For complete loss-of-field on a large generator on most systems not equipped with automatic generator voltage regulators, seriously low system voltages may be reached in not more than 10 to 15 seconds and in some cases in as short a time as one second when the generator represents a relatively large part of the total system generation.

Loss-of-field protection has been developed for protecting generators against partial as well as complete loss-of-field. Time delay should be provided either inherently or by means of an auxiliary time-delay relay to prevent false tripping on momentary surges. If loss-of-field protection is intended primarily to protect the system rather than the generator, an undervoltage relay may be incorporated in the scheme to supervise tripping, but it may be difficult to select a setting that will safeguard the system and simultaneously protect the individual generator against damage. The need for loss-of-field protection applies to those systems where one or more of the following conditions exist: (1) most of the generators are not equipped with automatic voltage regulators, (2) one generator represents a fairly large portion of the total generation, and (3) the generators are loosely linked electrically. Every effort should be made to prevent loss-of-field by accidental opening of the field circuit breaker such as providing a control switch interlock to prevent the field circuit breaker from being opened while the main circuit breaker is closed. If an alert operator is in attendance at all times, loss-of-field protection may not be considered necessary.

Out-of-Step Operation

A generator when running out-of-step is subject to a succession of severe impacts whose cumulative effect may cause damage to the shaft, coupling, or stator mounting. Relays have been developed to recognize out-of-step conditions.

Overvoltage

Overvoltage protection is recommended for hydroelectric generators which are subject to overspeed and accompanying overvoltage upon loss of load.

Overvoltage also may result from trouble on automatic voltage regulators.

Overvoltage relays may be arranged to insert resistance in the exciter or generator field circuit, to operate an alarm, or to shut down the generator, depending upon local requirements.

Overspeed

Generators driven by prime movers which can reach dangerous overspeeds under abnormal operating conditions should be equipped with overspeed protection. This may be incorporated in the governing system of the prime mover, or centrifugal devices may be used. In the absence of mechanical overspeed devices frequency relays may be used. Large steam turbines have their safety overspeed governors adjusted to trip the throttle when the speed increases to ten per cent above normal. Water-wheel-driven generators may reach speeds of 220 per cent of their normal rating.

Single-Phase Operation

Single-phase operation of a polyphase machine will cause local heating in the pole faces of the rotor and the amortisseur windings, if used; also, severe vibration will be imparted to the stator and its foundation. Machines designed for single-phase operation are equipped with especially heavy amortisseur windings and spring mounting for the stator assembly. Protection against single-phase operation ordinarily is not provided for attended machines, dependence being placed upon the indications of the phase ammeters and the presence of vibration to reveal this condition. Single-phase operation can be recognized electrically by comparing the magnitude of the currents of each phase with current balance relays. Single-phase operation also can be recognized by relays responding to negative-phase sequence currents, but either type of relay must have time delay to prevent false operation on external phase-to-phase short-circuit currents or transient unbalanced loads.

Vibration

Vibration may be caused by single-phase or unbalanced current operation; magnetic unbalance in the rotor; and mechanical unbalance in the rotor.

Excessive vibration can be recognized by any one of several different types of vibration-detecting equipment, which may be associated with the generator assembly or may be incorporated in the prime mover.

Failure of the Cooling System

Heat losses in the generator stator and rotor are carried off by the circulation of cooling air or hydrogen through the machine, which in closed systems is cooled in turn by passing through a suitable heat exchanger. Provision may be made to detect the presence of water in such a cooling system. Where air is taken from the outside, it may be desirable or necessary under certain conditions to avoid changes in load that may result in condensation in the machine when humidity is high. Any failure of the cooling system will become manifest by a rise in stator temperature. Methods for detecting this are described under the heading "Protection of Stator." Heat developed in the bearings of large machines is carried from

the bearings by the lubricating oil, which in turn is cooled by a suitable heat exchanger. In attended installations bearing temperature is indicated by thermometers, but in unattended installations bearing temperature relays should be installed to shut down the machine if overheating should develop in any of the bearings.

Failure of Bearing Insulation

To avoid circulating induced currents through the bearings and damage which can be caused by them, insulation is provided between the bedplate and the main outboard bearing of large horizontal machines. Where failure of this insulation has occurred or has been short-circuited by protective guards or railings, serious bearing damage has resulted. Bearing-pedestal insulation failure can be detected by an overcurrent relay having one terminal connected to the bearing pedestal and the other to an insulated brush making contact with the generator shaft. The oil film in the bearing prevents the relay coil from being short-circuited.

Fire

Protection against generator fires has been provided by fire-extinguishing equipment arranged to release water or carbon dioxide into the windings. As the unintentional release of water into the machine presents considerable hazard, special precautions are taken when such a system is used. Carbon dioxide does not add to the damage caused by a fire, and its release may be under the control of the differential and ground relays. In hydrogen-cooled machines, combustion will not be supported by the hydrogen atmosphere, so that fire-extinguishing facilities may not be considered necessary. Hydrogen contaminated with air forms an explosive mixture, but the outside shells of hydrogen-cooled machines are designed to withstand an explosion of the maximum intensity that can occur. The hydrogen cooling system is arranged to detect the presence of contaminating air, water, or oil.

Backup Protection

In principle backup protection is recommended.

Backup relays may be considered as any relays which will clear a faulted piece of equipment in the event that the protective equipment which would normally clear the fault fails to operate. Backup protection associated with generators may operate to clear the various sources that would feed back into a generator fault if the primary generator protection is inoperative for any reason, or it may operate to trip the generator in case the first line of defense on an outgoing line, transformer, or bus fails to clear the faulted equipment. As a general principle, backup protection will be less sensitive, will take more time to operate, and may operate to disconnect more equipment than is involved in the original failure. Because of the big investment in large, modern generators, much thought has been given to the problem of providing backup protection.

Generators have been included within the backup protection of the busses to which they are connected or within the differential protection of associated transformers in unit designs. Time-delay overcurrent relays on transformers and tie lines also may be depended upon to act in a backup capacity for clearing severe faults. What is considered to be suitable backup protection is largely a matter of opinion, and the scheme that is used for a particular installation will be influenced by past experience, individual preferences, and what expenditures can be made. For these reasons no attempt can be made to make any specific recommendations on the use of backup protection for generators.

Recommendations

After analyzing the information collected, the project committee makes the following recommendations, which are intended to apply primarily to generators in the 11- to 15-kv voltage range, rated 10,000 kva and above. The recommended protection may be applied also to generators of lower rating where conditions warrant.

1. In general differential protection is recommended.
2. Ground relays are recommended to supplement differential phase relays when the current available in case of a ground fault is insufficient to operate the differential relays.
3. It is recommended that in so far as possible the zone protected by the differential relays include the generator leads and extend to the far side of the main circuit breaker.
4. It is recommended that generator differential and ground relays trip simultaneously the main generator circuit breaker, the field circuit breaker, and the neutral circuit breaker (if an adequate neutral circuit breaker is installed).
5. It is recommended that temperature indicators or recorders arranged to operate an alarm be used to recognize overheating of the stator.
6. In general tripping protection for the rotor is not recommended.
7. Overvoltage protection is recommended for hydroelectric generators which are subject to overspeed and accompanying overvoltage upon sudden loss of load.
8. Definite recommendations are not made regarding protection against miscellaneous troubles such as motoring, loss-of-field, out-of-step operation, single-phase operation, vibration, bearing-insulation failure, fire, and so forth, but these items should be considered for each installation and the extent of the protection determined by the specific requirements in each case.
9. In principle backup protection is recommended.

Summary of Replies to Questionnaires

GENERATOR CONNECTIONS

1. How many stator terminals should be brought out? Opinion was practically unanimous that six terminals should be brought out of generators rated 10,000 kva and above, with the qualification that 12 terminals may be necessary on the largest machines which have double windings or where there is a current limitation on the bushings. If multiturn coils are used, several felt that a mid-tap should be brought out from each phase, making a total of nine terminals. Opinion on the lowest kilovolt-ampere rating for which six terminals should be brought out was not sharply defined; one reply recommended 5,000 kva, two recommended 2,500 kva, and one recommended 1,000 kva as the lower limit. Hydrogen cooling has tended to keep the number of terminals down to the minimum consistent with adequate relay protection.
2. Should stator winding be split for application of current balance or similar protection? Sentiment generally was against this feature, particularly for generators in the lower ratings.
3. Which type of stator winding connection is preferred from the protective relay viewpoint? Preference for Y-connection was unanimous.
4. Which type of neutral ground connection is preferred for Y-connected generators? Solid grounding of the generator neutral was considered desirable by very few and in each case only for unit-type installations. It generally was recognized that sufficient impedance should be connected in the generator neutral circuit to limit single line-to-ground faults to a value not greater than the 3-line short-circuit current. A low value of resistance

was preferred where underground cable feeder circuits are supplied at generator voltage; low reactance grounding was considered acceptable where a nonextensive cable system was involved. High-resistance grounding was considered feasible in only two replies, one of which confined its use to unit-type installations. High reactance grounding was frowned upon unanimously. Distribution transformer grounding was preferred for unit-type installations in 70 per cent of the replies, whereas less than 10 per cent preferred potential transformers for this application. No one advocated ungrounded operation, although generators frequently are operated with their neutrals ungrounded when they are connected at generator voltage to a system whose neutral is grounded.

5. Would it be preferable to obtain a ground connection through a Y-delta or a zig-zag grounding transformer? With one exception all replies indicated a preference for grounding generator neutrals rather than establishing the ground connection by means of either a Y-delta or a zig-zag grounding transformer.

6. Should a neutral circuit breaker be used? It generally was agreed that a neutral circuit breaker should be used where generators use a common neutral resistor or reactor and connect to a common bus. It also was considered desirable to use a neutral circuit breaker to limit damage to the generator iron in case of ground faults when low impedance grounding is used. However, for unit installations using high-resistance grounding or the equivalent, generator neutral circuit breakers were not considered necessary. Although technical opinion favors neutral circuit breakers, cost considerations often have dictated their omission.

General Information

1. What is preferred generator terminal voltage? Eighty per cent of the replies indicated a preference for 13.8 kv. For very large generators in unit installations, several were of the opinion that higher generator voltages could be used to advantage, but felt that this should be determined by the generator designers.

2. Is automatic voltage regulation used? Over 90 per cent of the replies favored the use of automatic voltage regulation. One large utility does not use automatic voltage regulators except on generators having a low short-circuit ratio.

3. What is the primary consideration upon loss-of-field; (a) protection of system, or (b) protection of generator? Ideas varied on this question, with the majority feeling that protection of the generator was slightly more important. However, both objectives would be accomplished by the same protective equipment, and the comment in one reply declining to put either one subordinate to the other probably would summarize the general opinion.

Tripping Sequence of Generator Circuit Breakers

1. When protective relays clear a generator from the system, what is the relative sequence in which each generator circuit breaker and control device operate; (a) main circuit breaker, (b) field circuit breaker, (c) neutral circuit breaker, (d) main exciter field, (e) annunciator or bell alarm, (f) turbine throttle valve, (g) fire-extinguishing equipment, (h) field discharge resistor switch, (i) other? All the devices listed are not tripped by the generator protective relays in each case, but over 90 per cent of the replies stated that the devices designed to be tripped are operated simultaneously. The main circuit breaker, field circuit breaker, neutral circuit breaker (when provided), and annunciator or alarm are all tripped in each case. The main exciter field circuit breaker is tripped in about 60 per cent of the cases. It appears to have become general practice for generator relays to trip the throttle valves of steam turbines or the gate or governor shutdown solenoids of water-wheel generators; a few, however, depend on the overspeed governor to disconnect the prime mover. In one gas-fired unit installation the solenoid valve in the gas line to the boiler also was tripped. Fire-extinguishing equipment is operated automatically in about 30 per cent of the cases.

Stator Protection

1. Phase-to-phase or 3-phase fault. Differential protection was preferred by all for clearing phase-to-phase or 3-phase stator faults; 90 per cent preferred percentage differential relays to differentially connected relays without restraint. High-speed relays were preferred for generators rated at 50,000 kva and above and normal speed relays for those under 50,000 kva. Eighty-five per cent preferred percentage differential relays operating on a 10 per cent slope; 2.5 per cent slope was favored by one, 25 per cent by three, and 50 per cent by two. Several preferred relays operating on a nonlinear increasing slope or relays using current product restraint. Supervision of differential relays by fault detectors was considered unnecessary except for certain high-speed relays. Seventy-five per cent were of the opinion that current transformers used to supply differential relays should be matched and that there should be no other burden on them, particularly where current transformers of lower ratio are involved. Ninety per cent of the replies indicated that differential relays were considered adequate to protect the stator against phase-to-phase or 3-phase faults; one reply suggested the use of split-phase protection where applicable, and one reply preferred the substitution of split-phase protection for conventional differential protection.

2. Phase-to-ground fault. Agreement was general that phase differential relays could be depended upon to clear ground faults where generators were grounded through low impedance, but in unit installations where the generator neutrals are grounded through high resistance or the equivalent, sensitive relays responding to current in the generator neutrals also are required. Some of the latter relays are arranged to give an alarm and trip only after considerable time delay. Over 90 per cent saw no need for differential ground relays or directional overcurrent relays for supplementing phase differential protection.

3. Short-circuited turns in stator winding. Seventy per cent did not believe that any special relays should be used to detect short-circuited turns. The remainder thought that current balance or split-phase protection should be used on multiturn, multicircuit machines. In one reply current balance protection was considered only for generators in unattended plants.

4. Open circuit in stator winding. Answers to this question were almost identical with those for short-circuited turns.

5. Overload. Sixty per cent did not believe that overcurrent protection of any kind should be used on generators; 20 per cent did not believe that it should be used without voltage restraint; the remainder felt that it could be used with or without restraint. Because the settings of overcurrent relays are determined by their position in the system no conclusions regarding settings could be drawn from the replies. One reply indicated that frequency relays could be used to detect overloading of generators under 10,000 kva. One reply considered thermal relays arranged to operate only an alarm desirable for calling attention to generator overloading.

6. Load unbalance. Except for one hydroelectric installation using an instantaneous current balance relay, no one

favored the use of any special relays to detect load unbalance.

7. Overheating. Replies show that embedded resistance temperature detectors or thermocouples are used quite uniformly to record stator temperatures on strip charts. Recorders are arranged to give an alarm on high temperature, but do not trip. Thermal overcurrent relays of the replica type do not conform to present preferred practice for large generators.

8. Backup protection. In general it was considered good practice for transformer differential protection to overlap the generator differential protection where the generator and transformer are combined in a unit installation; only two replies disagreed with this principle. Seventy per cent saw no need to provide overcurrent backup protection either with or without voltage restraint. Of the remainder, opinion was about evenly divided between the use of plain overcurrent relays versus overcurrent relays with voltage restraint; one considered an impedance relay desirable; one uses a directional reactance relay; four preferred overcurrent relays on the transformers in unit-type installations. Approximately 30 per cent were of the opinion that bus differential protection should back up the generator protection by arranging the zone of the bus protection to overlap the zone covered by the generator differential relays. Two replies indicated that bus differential ground protection was extended to include generators, and one stated that a fault bus scheme was used for this purpose.

Rotor Protection (Field)

1. Faults not involving ground. With one exception overcurrent protection is not used for generator fields. Two companies use vibration-detector relays and one a vibration recorder to detect magnetic unbalance such as might be caused by a short circuit between turns of the field winding; in two companies field-winding temperatures are measured by rise of resistance; in one a temperature recorder equipped with a high-temperature alarm is used.

2. Ground fault protection. Thirty-five per cent provide no means for detecting a grounded field winding; 25 per cent depend on d-c ground lamps for indicating a grounded field; 15 per cent use some form of d-c voltmeter scheme; 13 per cent use both ground lamps and voltmeter; 12 per cent use an a-c relay with a transformer source.

3. Open-circuit protection. Sixty per cent provide no protection for an open-circuited field; 25 per cent use an undercurrent relay, and the remaining 15 per cent depend on special loss-of-field protection relays.

4. Overheating protection. Ninety per cent provide no protection against overheating of the field windings; two companies use thermal overcurrent relays; and one uses high-temperature alarm contacts on the field-temperature recorder. In each case the alarm is operated without tripping.

Miscellaneous Generator Protection

1. Loss-of-field. Fifty per cent of the replies indicated that no protection against loss-of-field was used; seven companies use directional reactive current relays for this purpose; two use undervoltage relays; three use undercurrent relays; one depends upon the turbine overspeed device and voltage-restrained overcurrent relays; one provides an interlock to trip the generator if the field circuit breaker opens.

2. Overvoltage protection. Replies indicated that in general overvoltage protection, except for that incorporated in automatic voltage regulators, is not used on steam-driven generators. Water-wheel generators are equipped with overvoltage relays which may be arranged to reduce the field excitation or to trip the field circuit breaker.

3. Protection against motoring. Seventy per cent provide no protection against generator motoring other than that which may be obtained incidentally from instruments on the steam turbine. Thirty per cent provide sensitive power directional relays which give an alarm and in several instances trip the generator after a time delay varying from 60 to 180 seconds.

4. Out-of-step protection. In general out-of-step protection is not used on steam turbine and water-wheel-driven generators. One reply, however, indicated that a reactance relay was used for this application on generators rated above 50,000 kva.

5. Overspeed protection. Steam-turbine-driven generators are protected against overspeed by overspeed safety governors on the steam turbine. Sixty-five per cent of the replies indicated that the safety governor was not arranged to trip the generator; five stated that the safety governor tripped the generator. Four replies, applying to water-wheel-driven generators, stated that a centrifugal switch on the generator shaft was used to trip the generator.

6. Cooling system supervision. Seventy-five per cent do not record relative humidity within generators. Five companies record relative humidity where generators are air cooled; moisture detectors are depended on in the case of hydrogen-cooled generators. Most large generators are equipped with automatic recorders for indicating and recording ingoing and outgoing cooling-medium temperatures. Bearing - temperature alarm relays are used by about 50 per cent.

7. Bearing - insulation protection. Only two companies use overcurrent relays to detect failure of bearing-pedestal insulation, and this feature is used only on machines rated above 50,000 kva.

8. Vibration protection. Approximately 50 per cent of the companies use vibration recorders on large generators but do not in general arrange them to give an alarm. The remainder indicated that no vibration-detection equipment is used.

9. Fire protection. Replies showed that in no instance was water released automatically for extinguishing generator fires. Thirty per cent have the stator protective relays arranged to release carbon dioxide into air-cooled generators. Sixty per cent using hydrogen as a cooling medium have provided contamination indication in the hydrogen cooling system.

References

1. Protection of Electrical Apparatus, Recommended Practice, **AIEE Committee Report.** *AIEE Transactions*, volume 52, June Section, 1933, pages 607–13.

2. Backup Protection for System Faults at the Generator, **D. C. Hoffman.** *General Electric Review* (Schenectady, N. Y.), volume 53, 1950, pages 38–41.

3. Present-Day Grounding Practices on Power Systems, **AIEE Committee Report.** *AIEE Transactions*, volume 66, 1947, part I, Grounding Practices at Generating Stations, pages 1525–37 and 1548–51.

4. Bibliography of Relay Literature 1927–1939, **AIEE Committee Report.** *AIEE Transactions*, volume 60, 1941, pages 1435–47.

5. Bibliography of Relay Literature 1940–1943, **AIEE Committee Report.** *Electrical Engineering* (*AIEE Transactions*), volume 63, October 1944, pages 705–09.

6. Bibliography of Relay Literature 1944–1946, **AIEE Committee Report.** *AIEE Transactions*, volume 67, part I, 1948, pages 24–27.

7. Bibliography of Relay Literature 1947–1949, **AIEE Committee Report.** *AIEE Transactions*, volume 70, part I, 1951, section F, pages 247–50.

Discussion

L. F. Lischer (Commonwealth Edison Company, Chicago, Ill.): This committee report is concise, yet comprehensive, and it lists definite recommendations where possible. Such a report is a welcome one to engineers concerned with generator protection. The practices of the Commonwealth Edison

Company agree, in general, with the recommendations of the committee. I should like to elaborate somewhat on the section dealing with loss-of-field protection, because of its importance, setting forth the practice of a utility having a large "solid" or low-reactance system.

Loss-of-field protection is provided for all generators rated 100 megawatts or greater (there are five such units on the "inner" system at present). This protection is primarily for the system and not the machine; automatic generator voltage regulators are, at present, not in general use. A study[1] had shown that during light load conditions, loss of field of a large unit could cause a reduction in system voltage to 65 per cent of normal, thus leading to instability of other units. Protection of the machine is secondary in that operators can be trained to recognize loss of field and to remove the generator manually before it is damaged. In certain cases (particularly on smaller, older machines) the operator may be able to restore the field.[2]

For this protection, a directional reactive current induction relay is used, and it is set to trip at 60 to 80 per cent of rated armature current. The trip circuit is supervised by an instantaneous phase-to-phase undervoltage relay set at 80 to 90 per cent normal voltage. An interesting application of the mho relay for this purpose may be found in the literature.[3]

Generators feeding into long high-voltage, overhead lines also are protected against loss of field. Transient analyses that were made in a manner similar to that described in the literature[4] showed that it would be possible for the loss-of-field relay to trip the generator on complete loss of field before impedance relays would trip intermediate lines due to low voltage and heavy reactive current, provided that the current setting on the directional reactive current relay were made sensitive enough. A setting of 35 to 40 per cent of rated armature current is used for this application, together with a 90 per cent voltage setting. This should not result in tripping on power swings caused by line faults.

Loss-of-field relays have operated three times in one and one-half years. In one instance, an attempt was made in error to close the generator to the system while the machine was still considerably below system frequency. The loss-of-field relay promptly tripped the machine. In another case, brushes were being changed on an exciter when the operator dropped the brush. The machine tripped with practically no burning at the point of short circuit. In the third case, exciters were being paralleled at low voltage when exciter instability developed, thus decreasing the generator field current to the point where the loss-of-field relay operated to trip the machine. In subsequent discussions these operations were all deemed to be proper, and the tripping of the machine was considered desirable under the circumstances.

REFERENCES

1. GENERATOR STABILITY AT LOW EXCITATION, **E. L. Michelson, L. F. Lischer**. *AIEE Transactions*, volume 67, part I, 1948, pages 1–9 (page 3).

2. REESTABLISHING EXCITATION OF A LOADED ALTERNATOR IN PARALLEL WITH OTHERS, **D. D. Higgins, E. Wild**. *AIEE Transactions*, volume 50, December Section, 1931, pages 1194–1200.

3. A NEW LOSS-OF-EXCITATION RELAY FOR SYNCHRONOUS GENERATORS, **C. R. Mason**. *AIEE Transactions*, volume 68, part II, 1949, pages 1240–45.

4. LOSS-OF-FIELD PROTECTION FOR GENERATORS, **G. C. Crossman, H. F. Lindemuth, R. L. Webb**. (*Electrical Engineering, AIEE Transactions*), volume 61, May 1942, May Section, pages 261–66.

J. H. Kinghorn and **H. C. Barnes** (American Gas and Electric Service Corporation, New York, N. Y.): It is surprising to find from the replies to the questionnaire that only three companies out of 25 make any attempt to protect against overheating of field windings, in spite of the fact that normal operating temperatures often approach closer to upper limits for rotor windings than for stator windings. When such is the case the rotor temperature may reach a dangerous value an appreciable time before the stator, either in the case of excess field current or failure in the ventilating system.

Field temperature recorders with contacts connected to give alarm on high temperature have been standard equipment on large generators on the American Gas and Electric Company System for 25 years. Approximately 37 generators, representing about 2,000,000-kva capacity, are provided with this type of protection. The instrument is of the field-resistance-measuring type, and any small error introduced by brush drop is negligible in such application. Pilot brushes are used in many cases and have given satisfactory performance with good temperature accuracy. In other cases where main brushes are used, the error is in the safe direction, indicating a temperature a few degrees higher than that which actually exists.

Aside from their direct protective value in detecting field overheating, the recorders have been helpful in indicating the existence of short-circuited field coils, and in at least one case they have furnished the first indication of a broken or arcing field connection which subsequently welded itself closed. They are, of course, also helpful, in the case of hydrogen-cooled machines, in determining when to increase gas pressure in order to keep field temperature below some maximum normal operating value. While a complete record of experience with these instruments is not immediately available, we are thoroughly convinced of their value as a guide to safe operation of generators. Despite the limitations imposed on committee work, it is suggested that an evaluation of the extent of usage of this device in terms of numbers of generators, installed kilovolt amperes, or recent trends might produce a somewhat different picture.

W. R. Brownlee (Southern Services, Inc., Birmingham, Ala.): The Project Committee is to be commended on their analysis of the survey material and on their application of engineering judgment in determining recommendations. Most types of protection have been discussed. However, careful consideration might well be given to an additional type, which might be termed "protection from protection."

Too much relay protection may jeopardize the reliability of the power-supply system. Adequate design usually will provide for a scheduled maintenance outage of a moderate-size generating unit plus the unscheduled outage of the largest generating unit. However, if any of the protective relays on other generators are even remotely susceptible to false operation during a system disturbance, then an intolerable capacity outage may result.

Adequate protection of generators is justifiable, in spite of the infrequency of faults, because of the substantial investment involved. However, each component of the protective scheme should be scrutinized thoroughly from the standpoint of risk of unnecessary disconnection of generating capacity. In terms of this risk, true costs of the last cycle of speed may be excessive.

H. R. Paxson: The members of the Project Committee wish to thank those who have contributed verbal or written discussions of this report. Mr. L. F. Lischer's discussion describing the practice and experience of the Commonwealth Edison Company with loss-of-field protection supplies valuable additional background to this part of the report.

Messrs. J. H. Kinghorn and H. C. Barnes have called attention to the practice of the American Gas and Electric Service Corporation with respect to the use of field-temperature recorders on large generators. Although there undoubtedly were good reasons for the widespread application described, it is surprising that with 25 years of experience only one instance was mentioned where a field-temperature recorder called attention to trouble. If it may be inferred that the recorders have seldom operated, it would appear that this discussion tends to confirm the conclusions of the committee.

Mr. W. R. Brownlee has added a warning against the danger of installing protective devices whose misoperation might cause more widespread service interruption than any of the hazards against which they are designed to protect. This is a worth-while note of caution from one who has had many years of protective relay experience.

Transmission Line Load Impedance for Maximum Efficiency

S. G. LUTZ
MEMBER AIEE

FOR maximum efficiency of transmission over a line of length, l, attenuation constant of α nepers per-unit length, phase constant of β radians per-unit length and characteristic impedance of $|Z_0|\epsilon^{j\theta}$, driven by a constant voltage (zero impedance) generator, the magnitude and angle of the load impedance should be:

$$|Z| = |Z_0| \sqrt{\frac{\sinh 2\alpha l \cos\theta - \sin 2\beta l \sin\theta}{\sinh 2\alpha l \cos\theta + \sin 2\beta l \sin\theta}}$$

and

$$\phi = \sin^{-1} \frac{\sin 2\theta (\cos 2\beta l - \cosh 2\alpha l)}{2\sqrt{(\sinh 2\alpha l \cos\theta)^2 - (\sin 2\beta l \sin\theta)^2}}$$

This best load impedance will be the characteristic impedance only if it is a pure resistance. For large attenuations the most efficient load approaches the conjugate of the characteristic impedance. The deviation from the characteristic impedance, and the consequent improvement of efficiency, becomes very substantial when the line length is less than a quarter wavelength, when the attenuation is low and when the angle of the characteristic impedance is large.

A reasonably careful search of textbooks and the periodical literature has failed to disclose any general analysis of the transmission line load impedance required for maximum efficiency of transmission. The problem may be stated more precisely as follows: "Given a transmission line of any specified characteristics, operating at a single frequency from a constant voltage generator, what load impedance will result in the maximum efficiency of power transmission?"

The reason why this problem seems to have been neglected probably is that its practical importance has been much lower than its theoretical importance. Power transmission engineers are concerned primarily with electrically short lines which can be studied with adequate accuracy by means of simple approximately equivalent circuits and, furthermore, they do not have complete control over a load which fluctuates at the whim of the customer.

On the other hand, communication engineers are concerned with transmission line performance throughout broad bands of frequencies and find it preferable to match their load to the characteristic impedance in order to minimize reflections. Certain new transmission line applications may increase the practical importance of this problem and, moreover, its solution should be of interest as a yardstick for evaluating the loss of efficiency resulting from any other load impedance, and for testing the accuracy of approximate methods of analysis.

A General Power Ratio Equation

For maximum efficiency of transmission the ratio of the real power input to output must be a minimum. If the load impedance is $|Z|\epsilon^{j\theta}$ and the output current is taken as the reference, the real power delivered to the load will be

$$W_r = I_r^2 |Z| \cos\phi \tag{1}$$

in which I_r is the rms magnitude of the received current. Designating the rms in-phase and quadrature components at the sending end as

$$\boldsymbol{E}_s = E_s + jE_s'$$

and (2)

$$\boldsymbol{I}_s = I_s + jI_s'$$

the real power supplied to the sending end is

$$W_s = E_s I_s + E_s' I_s' \tag{3}$$

The procedure for deriving an expression for the power ratio, W_s/W_r, will be to express I_s/I_r and E_s/I_r in terms of the long-line equations, split these into their real and imaginary parts and form the power ratio from equations 1 and 3. The long-line equations are:

$$\begin{aligned} (E_s/I_r) &= Z \cosh\gamma l + Z_0 \sinh\gamma l \\ (I_s/I_r) &= \cosh\gamma l + (Z/Z_0) \sinh\gamma l, \end{aligned} \tag{4}$$

in which the propagation parameter is

$$\gamma = \alpha + j\beta \tag{5}$$

α being the attenuation in nepers and β the phase parameter in radians, both per-unit length of line. The characteristic impedance has a magnitude, $|Z_0|$, and angle, θ. Breaking the terms in the long line equations into their real and imaginary parts,

$$\begin{aligned} \frac{E_s + jE_s'}{I_r} = {} & |Z|(\cos\phi + j\sin\phi) \times \\ & (\cosh\alpha l \cos\beta l + j \sinh\alpha l \sin\beta l) + \\ & |Z_0|(\cos\theta + \theta \sin\theta)(\sinh\alpha l \cos\beta l + \\ & j \cosh\alpha l \sin\beta l) \end{aligned} \tag{6}$$

$$\begin{aligned} \frac{I_s + jI_s'}{I_r} = {} & (\cosh\alpha l \cos\beta l + \\ & j \sinh\alpha l \sin\beta l) + \frac{|Z_1|}{|Z_0|}(\cos\phi + \\ & j \sin\phi)(\cos\theta - j\sin\theta)(\sinh\alpha l \times \\ & \cos\beta l + j \cosh\alpha l \sin\beta l) \end{aligned}$$

The expansion of these equations and the formation of the power ratio may be made less unwieldy by the introduction of the following abbreviations:

$$\begin{aligned} A &= \cosh\alpha l & E &= \cos\theta \\ B &= \sinh\alpha l & F &= \sin\theta \\ C &= \cos\beta l & G &= \tan\phi \\ D &= \sin\beta l & H &= (|Z|/|Z_0|)\cos\phi \end{aligned} \tag{7}$$

Paper 51-44, recommended by the AIEE Basic Sciences Committee and approved by the Technical Program Committee for presentation at the AIEE Winter General Meeting, New York, N. Y., January 22–26, 1951. Manuscript submitted October 23, 1950; made available for printing December 4, 1950.

S. G. LUTZ is Chairman of the Electrical Engineering Department of New York University, New York, N. Y.

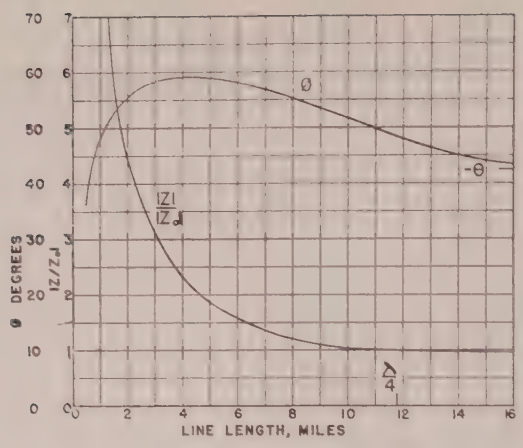

Figure 1 (left). Maximum efficiency load impedance ratio and load phase angle for 19-gauge cable

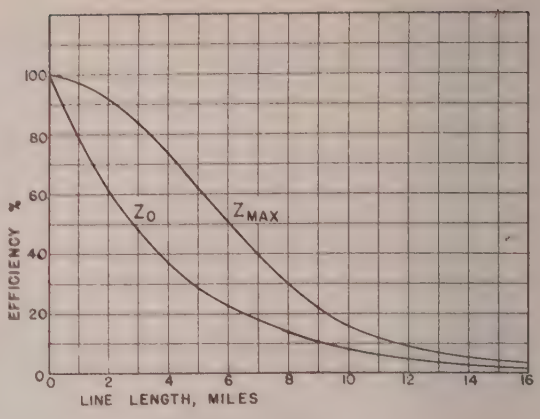

Figure 2 (right). Comparison of efficiencies with characteristic impedance and maximum efficiency loads for 19-gauge telephone cable

One thus eventually obtains

$$\frac{W_s}{W_r}=\frac{1}{H}(ABE-CDF)+(A^2C^2+B^2D^2)+(A^2D^2+B^2C^2)(E-F+2EFG)+H(ABE+CDF)(1+G^2) \quad (8)$$

After reinsertion of the functions and further reduction,

$$\frac{W_s}{W_r}=\frac{1}{2\cos\phi}\left[\frac{|Z_0|}{|Z|}(\sinh 2\alpha l\cos\theta-\sin 2\beta l\sin\theta)+\frac{|Z|}{|Z_0|}(\sinh 2\alpha l\cos\theta+\sin 2\beta l\sin\theta)\right]+\frac{1}{2}[\cosh 2\alpha l+\cos 2\beta l+(\cosh 2\alpha l-\cos 2\beta l)\times(\cos 2\theta+\sin 2\theta\tan\phi)] \quad (9)$$

This is a general expression for the power ratio, free from any restrictions on $|Z|$ or ϕ, and not restricted by short-line approximations.

Magnitude and Phase of Load Impedance for Maximum Efficiency

Equating the derivative of this power ratio with respect to the impedance ratio to zero leads to

$$\frac{|Z|}{|Z_0|}=\sqrt{\frac{\sinh 2\alpha l\cos\theta-\sin 2\beta l\sin\theta}{\sinh 2\alpha l\cos\theta+\sin 2\beta l\sin\theta}} \quad (10)$$

This result is independent of ϕ, the angle of the load impedance, indicating that this impedance magnitude ratio is best, irrespective of ϕ.

Next, differentiating the power ratio with respect to ϕ and equating to zero, one obtains

$$\phi=\sin^{-1}\frac{\sin 2\theta(\cos 2\beta l-\cosh 2\alpha l)}{\frac{|Z_0|}{|Z|}\sinh 2\alpha l\cos\theta-\sin 2\beta l\sin\theta)+\frac{|Z|}{|Z_0|}(\sinh 2\alpha l\cos\theta+\sin 2\beta l\sin\theta)} \quad (11)$$

Using the impedance magnitude ratio from equation 10, equations 9 and 11 reduce to

$$\left.\frac{W_s}{W_r}\right]_{|Z|_{max}}=\frac{1}{\cos\phi}\times\sqrt{(\sinh 2\alpha l\cos\theta)^2-(\sin 2\beta l\sin\theta)^2}+\frac{1}{2}[\cosh 2\alpha l+\cos 2\beta l+(\cosh 2\alpha l-\cos 2\beta l)(\cos 2\theta+\sin 2\theta\tan\phi)] \quad (12)$$

and

$$\left.\phi\right]_{|Z|_{max}}=\sin^{-1}\times\frac{\sin 2\theta(\cos 2\beta l-\cosh 2\alpha l)}{2\sqrt{(\sinh 2\alpha l\cos\theta)^2-(\sin 2\beta l\sin\theta)^2}} \quad (13)$$

Analysis of General Equations

Several conclusions are evident merely from inspection of the foregoing equations. Since equation 11 has a sin 2θ factor in its numerator, the best ϕ will be zero if θ is zero. That is, if the characteristic impedance is a pure resistance the best load impedance also must be a resistance. Furthermore, when $\theta=0$ the sin θ terms in equation 10 drop out, making unity the best impedance magnitude ratio. Consequently, the characteristic impedance will be the best load impedance whenever it is a pure resistance. Transmission texts show that the characteristic impedance of any line approaches a pure resistance as the frequency approaches either zero or infinity, while if the line satisfies the distortionless condition, $RC=LG$, its characteristic impedance will be a pure resistance at all frequencies.

Another obvious conclusion from equation 10 is that $|Z|=|Z_0|$ whenever the line length is a multiple of a quarter wavelength, making sin $2\beta l=0$. However, note that this does not make $\phi=0$.

As αl increases, sinh $2\alpha l$ soon will become so large as to mask the periodic fluctuations of sin $2\beta l$ in equation 10, so for very long lines the best magnitude of load impedance will not differ appreciably from that of the characteristic impedance. From equation 10 it might appear possible to have

$$\sinh 2\alpha l\cos\theta=\sin 2\beta l\sin\theta<0 \quad (14)$$

thus causing the quantity under the radical to become negative and indicating an impedance with an imaginary magnitude. If such an absurdity could occur it would be expected with a short line and large value of θ. The largest physically possible value of θ is $\pm 45°$, for which cos $\theta=\sin\theta=0.707$. As the line length approaches zero, sinh $2\alpha l$ approaches its hyperbolic angle, $2\alpha l$ nepers, but always is larger than it, while sin $2\beta l$ approaches its angle, $2\beta l$ radians, but is always smaller than it. Having a negative quantity under the radical under these conditions would require $2\beta l>2\alpha l$, but this is impossible when $\theta=\pm 45°$ for it can be shown that $\alpha=\beta$ in this limiting condition.

In practice, θ is almost always a negative angle and would approach $-45°$ in a cable having negligible inductance and leakage conductance. The above reasoning applied to such a cable indicates that its impedance magnitude ratio should approach infinity as the length approaches zero. Similar reasoning applied to the cos $2\beta l-\cosh 2\alpha l$ factor in equation 11 shows that under these conditions ϕ would approach zero. Therefore, the most efficient load impedance for such a cable would approach an infinite resistance as its length approached zero; in agreement with simple physical reasoning.

Some Special Cases

The $\theta=-45°$ case merits further analysis because it is so closely approxi-

mated by many nonloaded cables. Inserting the values of the functions of θ leads to the following simpler expressions.

$$\left.\frac{Z}{Z_0}\right]_{\theta=-45^\circ} = \sqrt{\frac{\sinh 2\alpha l + \sin 2\beta l}{\sinh 2\alpha l - \sin 2\beta l}} \quad (15)$$

$$\left.\phi\right]_{|Z|_{max}}^{\theta=-45^\circ} = \sin^{-1}\times \frac{\cosh 2\alpha l - \cos 2\beta l}{\sqrt{2}\sqrt{\sinh^2 2\alpha l - \sin^2 2\beta l}} \quad (16)$$

$$\left.\frac{W_s}{W_r}\right]_{|Z|_{max}}^{\theta=-45^\circ} = \frac{1}{2}\left[\sqrt{\sinh^2 2\alpha l - \sin^2 2\beta l + 2(\cosh 2\alpha l \times \cos 2\beta l - 1) + \cosh 2\alpha l + \cos 2\beta l}\right] \quad (17)$$

Another special case worthy of mention is that of the best load angle, ϕ, at line lengths which are multiples of a quarter wavelength, for which $\sin 2\beta l = 0$ and $\cos 2\beta l = \mp 1$. On making these substitutions, equation 13 becomes

$$\left.\phi\right]_{|Z|_{max}}^{l=n\lambda/4} = \sin^{-1}\left(-\sin\theta\,\frac{\cosh(2\alpha l)\mp 1}{\sinh 2\alpha l}\right) \quad (18)$$

Thus, while the best magnitude of load impedance is that of the characteristic impedance, for line lengths which are multiples of a quarter wavelength, there is not a correspondingly simple relation for the best load angle. The best load angle is proportional to $-\theta$, but becomes equal to it only as αl becomes infinite. This latter property is not peculiar to the quarter-wavelength points, however, as may be seen by letting the line length approach infinity in equation 13. Thus, for any line having very large attenuation, the load impedance for greatest efficiency will be the conjugate of the characteristic impedance. This, of course, is a well known relation.

Finally, setting $|Z| = |Z_0|$ and $\phi = \theta$ in equation 9 reduces the power ratio to

$$\left.\frac{W_s}{W_r}\right]_{Z=Z_0} = \epsilon^{2\alpha l} \quad (19)$$

This is in agreement with elementary transmission theory, since both current and voltage increase exponentially with distance back from this reflectionless load. The interesting aspect is that such a simple relation can be obtained from such a lengthy approach. Aside from serving as a partial check on equation 9, this power ratio for a characteristic impedance load serves as a useful reference for comparison with the power ratios obtainable with maximum efficiency loading.

Illustrative Example—19-Gauge Telephone Cable

A 19-gauge nonloaded telephone cable, operating at 1,000 cycles, serves as a good illustrative example because its characteristic impedance has such a large angle that the improvement of efficiency, over that obtainable with a characteristic impedance load, becomes very pronounced. The characteristics of such a cable are given in Table I.[1]

Figure 1 shows the impedance magnitude ratio and the load angle as calculated for maximum transmission efficiency. Figure 2 shows a comparison of the efficiencies obtainable with characteristic impedance loading and with the maximum efficiency load impedances from Figure 1.

Table I. Characteristics of 19-Gauge Nonloaded Telephone Cable

$R = 85.8$ ohms	per loop mile
$L = 0.001$ henrys	per loop mile
$C = 0.062$ microfarads	per loop mile
$G = 1.50$ micromhos	per loop mile
$\alpha = 0.1249$ nepers/mile	at 1,000 cycles
$\beta = 0.1338$ radians/mile	at 1,000 cycles
$\lvert Z_0\rvert = 470.1$ ohms	at 1,000 cycles
$\theta = -42.80$ degrees	at 1,000 cycles
$\lambda = 46.93$ miles	at 1,000 cycles

Conclusions

The preceding method for calculating maximum efficiency load impedances is reasonably direct and is not restricted with regard to line length. The method presented for calculating sending-to-receiving end power ratios is most suitable for lines of intermediate length, for which the better known approximate methods are inadequate. However, the calculating accuracy which is required becomes excessive for high-efficiency lines and a method for calculating the ratio of power lost to load power would be preferable.

It is hoped that other workers will develop a simpler and more teachable method for deriving the basic power ratio equation, 9, if indeed it does not already exist in some long-forgotten publication.

Reference

1. Principles of Electricity Applied to Telephone and Telegraph Work. American Telephone and Telegraph Company (New York, N. Y.), Table XIII, 1938, page 191.

No Discussion

Networks for which Magnitude or Phase Angle of Input Impedance or Transfer Admittance Remains Constant as Load Varies

RAYMOND S. BERKOWITZ
ASSOCIATE AIEE

CONSIDER a linear, constant parameter, passive network with two pairs of terminals across one pair of which is connected a passive load. If the impedance of the load is varied, the input impedance and the transfer admittance between the two pairs of terminals change. If the network is known, the changes in input impedance and transfer admittance can be computed. In this paper the converse problem is investigated, that is, the determination of conditions that must be satisfied by the network at constant frequency to obtain a particular variation of input impedance or transfer admittance when the load changes in a specified way.

The following special cases are treated, the results being summarized in Tables I-IV:

1. Input impedance constant as load impedance varies
2. Phase of input impedance constant as load magnitude varies
3. Magnitude of input impedance constant as load magnitude varies
4. Phase of input impedance constant as load phase varies
5. Magnitude of input impedance constant as load phase varies
6. Transfer admittance constant irrespective of load variation
7. Magnitude of transfer admittance constant as magnitude of load varies
8. Phase of transfer admittance constant as magnitude of load varies
9. Magnitude of transfer admittance constant as phase of load varies
10. Phase of transfer admittance constant as phase of load varies.

The basic theory of the steady-state behavior of two terminal-pair networks has been thoroughly developed.[1,2] The properties of a network can be specified practically in terms of complex numbers, such as impedances, admittances, transfer ratios, and general circuit parameters. The design or analysis of a network thus may be reduced to a study of the mathematical relationships between selected complex quantities under the different conditions of network operation.

In the expressions and formulas that follow a variety of symbols is used to designate the different quantities describing the networks studied. The meanings are explained as they occur, and in Appendix I can be found a summary of the most important ones. Standard notations are used wherever possible. Complex quantities are designated by boldface italic capital letters; $j=\sqrt{-1}$; $\underline{/\theta}=\exp j\theta$; $\boldsymbol{Z}^*$, $|\boldsymbol{Z}|$ are respectively the conjugate and the magnitude of the complex quantity $\boldsymbol{Z}$; $\mathrm{Re}(\boldsymbol{Z})$ and $\mathrm{Im}(\boldsymbol{Z})$ are, respectively, the real and the imaginary parts of $\boldsymbol{Z}$: $\boldsymbol{Z}=\mathrm{Re}(\boldsymbol{Z})+j\mathrm{Im}(\boldsymbol{Z})=R+jX$.

Paper 51-45, recommended by the AIEE Basic Sciences Committee and approved by the AIEE Technical Program Committee for presentation at the AIEE Winter General Meeting, New York, N. Y., January 22-26, 1951. Manuscript submitted August 1, 1950; made available for printing December 4, 1950.

RAYMOND S. BERKOWITZ is an Instructor at the Moore School of Electrical Engineering of the University of Pennsylvania, Philadelphia, Pa.

The work was done at the suggestion and with the assistance of Professor J. G. BRAINERD.

Theory and General Procedure

In Figure 1 is shown the typical 2-terminal-pair network. (The expressions "2-terminal-pair" and "network with two pairs of terminals" are used here interchangeably). $\boldsymbol{E}_1$, $\boldsymbol{I}_1$, $\boldsymbol{E}_2$, $\boldsymbol{I}_2$ are the voltage rises and currents at the input and output ends of the network as shown. $\boldsymbol{Z}_1$ is the impedance looking into the network when it is terminated by the load impedance $\boldsymbol{Z}_L$. It is well known[2] that the quantities $\boldsymbol{E}_1$, $\boldsymbol{I}_1$, $\boldsymbol{E}_2$, $\boldsymbol{I}_2$ are related by the following equivalent sets of equations

$$\begin{aligned} \boldsymbol{E}_1&=\boldsymbol{A}\boldsymbol{E}_2-\boldsymbol{B}\boldsymbol{I}_2, & \boldsymbol{E}_2&=\boldsymbol{D}\boldsymbol{E}_1-\boldsymbol{B}\boldsymbol{I}_1,\\ \boldsymbol{I}_1&=\boldsymbol{C}\boldsymbol{E}_2-\boldsymbol{D}\boldsymbol{I}_2, & \boldsymbol{I}_2&=\boldsymbol{C}\boldsymbol{E}_1-\boldsymbol{A}\boldsymbol{I}_1, \end{aligned} \qquad (1)$$

where $\boldsymbol{A}$, $\boldsymbol{B}$, $\boldsymbol{C}$, $\boldsymbol{D}$, are the general circuit parameters, complex constants for any 4-terminal network satisfying

$$\boldsymbol{A}\boldsymbol{D}-\boldsymbol{B}\boldsymbol{C}=1 \qquad (2)$$

With the network terminated by the load impedance $\boldsymbol{Z}_L$, the input impedance $\boldsymbol{Z}_i$ and the transfer admittance $\boldsymbol{Y}_t$ are given by

$$\boldsymbol{Z}_i=\frac{\boldsymbol{E}_1}{\boldsymbol{I}_1}=\frac{\boldsymbol{A}\boldsymbol{Z}_L+\boldsymbol{B}}{\boldsymbol{C}\boldsymbol{Z}_L+\boldsymbol{D}}, \qquad \boldsymbol{Y}_t=-\frac{\boldsymbol{I}_2}{\boldsymbol{E}_1}=\frac{1}{\boldsymbol{A}\boldsymbol{Z}_L+\boldsymbol{B}} \qquad (3)$$

If the two output (or two input) terminals of the network in Figure 1 are interchanged, the effect on the general circuit parameters is to multiply each by minus unity. As is well known, $\boldsymbol{Z}_i$ remains the same, but $\boldsymbol{Y}_t$ is the negative of its original value.

It is convenient to think of the above expressions as transformations in the complex plane, commonly known as bilinear transformations. The expression

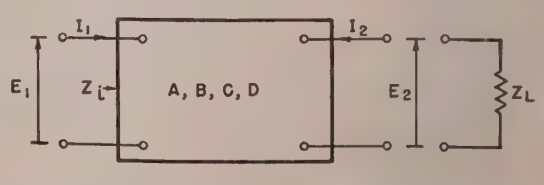

Figure 1. Network with two pairs of terminals

Table I. Networks Having Constant Input Impedance Characteristics with Varying Load Impedance: Basic General Conditions

Network Designation	2	3	4	5
1. Type of impedance variations	$Z_L = z_L/\theta_k$, $Z_i = z_i/\varphi_k$	$Z_L = z_L/\theta_k$ $Z_i = z_{ik}/\varphi$	$Z_L = z_{Lk}/\theta$, $Z_i = z_i/\varphi_k$	$Z_L = z_{Lk}/\theta$ $Z_i = z_{ik}/\varphi$
2. Basic definitions	$z_i = z_{i0}$ when $Z_L = 0$ $z_i = z_{i\infty}$ when $Z_L = \infty$ $Z_L = Z_{La} = z_{La}/\theta_k$ when $z_i = \frac{1}{2}(z_{i0} + z_{i\infty})$	$\varphi = \varphi_0$ when $Z_L = 0$ $\varphi = \varphi_\infty$ when $Z_L = \infty$ $Z_L = Z_{La} = z_{La}/\theta_k$ when $\varphi = \frac{1}{2}(\varphi_0 + \varphi_\infty)$	$z_i = z_{ia}$ when $\theta = 0$ $\beta_A, \beta_B, \beta_C, \beta_D$ = respective phases of A, B, C, D	$\beta_A, \beta_B, \beta_C, \beta_D$ = respective phases of A, B, C, D
3. Expressions determining values of A, B, C, D	$C^2 = \frac{/-\varphi_k - \varphi_k}{z_{La}(z_{i\infty} - z_{i0})}$ $A = Cz_{i\infty}/\varphi_k$ $D = Cz_{La}/\theta_k$ $B = Cz_{La}z_{i0}/\varphi_k + \theta_k$	$C^2 = \frac{/\frac{\pi}{2} - \theta_k - \varphi_\infty}{2z_{ik}z_{La}\sin\frac{1}{2}(\varphi_0 - \varphi_\infty)}$ $A = Cz_{ik}/\varphi_\infty$ $D = Cz_{La}/\theta_k + \frac{1}{2}(\varphi_\infty - \varphi_0)$ $B = Cz_{ik}z_{La}/\theta_k + \frac{1}{2}(\varphi_\infty + \varphi_0)$	$\left\|\frac{D}{C}\right\| = \left\|\frac{B}{A}\right\| = z_{Lk}$ $\beta_A + \beta_B + \beta_C + \beta_D = \pi$ $\cos(\beta_A + \beta_D) = \frac{1}{2z_{Lk}\lvert AC\rvert}$ $z_{ia} = \left\|\frac{A}{C}\right\| \frac{\cos\frac{1}{2}(\beta_A - \beta_B)}{\cos\frac{1}{2}(\beta_C - \beta_D)}$ $\varphi_k = \frac{\pi}{2} - (\beta_C + \beta_D) = \beta_A + \beta_B - \frac{\pi}{2}$	$z_{Lk}\lvert A\rvert = z_{ik}\lvert D\rvert$ $A(DD^* - z_{Lk}^2 CC^*) = D^*$ $BD^* = z_{Lk}^2 AC^*$
4. Conditions necessary and sufficient for realizability with a passive network. (Note: Use is made throughout of the fact that $R_L(Z_L) \geq 0$, $R_i(Z_i) \geq 0$)	for $z_{i\infty} > z_{i0}$ $1 > \frac{z_{i0}}{z_{i\infty}} \geq \frac{1 - \cos(\varphi_k - \theta_k)}{1 + \cos(\varphi_k + \theta_k)}$ and for $z_{i0} > z_{i\infty}$, $1 > \frac{z_{i\infty}}{z_{i0}} \geq \frac{1 - \cos(\varphi_k + \theta_k)}{1 + \cos(\varphi_k - \theta_k)}$	for $\varphi_\infty > \varphi_0$ $\frac{\cos\varphi_\infty \cos\theta_k}{1 - \cos\theta_k \sin\varphi_\infty} \geq \tan\frac{1}{2}(\varphi_\infty - \varphi_0)$ and for $\varphi_0 > \varphi_\infty$, $\frac{\cos\varphi_\infty \cos\theta_k}{1 + \cos\theta_k \sin\varphi_\infty} \geq \tan\frac{1}{2}(\varphi_0 - \varphi_\infty)$	$\cos(\beta_A - \beta_C)\cos(\beta_D - \beta_C) \geq$ $2\cos(\beta_A + \beta_D)\cos 2\beta_C$ $\cos(\beta_A - \beta_C) \geq 0$ $\cos(\beta_D - \beta_C) \geq 0$	$\frac{z_{ik}}{z_{Lk}} AA^* \cos(\beta_A - \beta_B) \cdot$ $\cdot \cos(\beta_D - \beta_C) \geq \cos^2\beta_C$ $\cos(\beta_A - \beta_C) \geq 0$ $\cos(\beta_D - \beta_C) \geq 0$

for Z_i is the most general example of such a transformation; that for Y_i is a special case. The significant property about such transformations is the fact that they transform circles into circles. (Both a straight line and a point are special cases of circles.) Thus, if A, B, C, D are given complex numbers, and Z_L traverses a circle in the complex plane, then Z_i also traverses a circle; a one-to-one, ordered, correspondence existing between every point on the Z_L circle and every point on the Z_i, "transformed," circle. Conversely, it is possible to specify originally two circles such that if Z_L traverses one, then Z_i traverses the other. This can be insured by proper selection of the parameters A, B, C, D. Use can be made of the fact that a circle is determined completely by three points on it. (For a straight line one of the three points must be the point at infinity.) Thus, specifying three points on the Z_i circle corresponding as in equation 3 to three given points on the Z_L circle, together with equation 2, completely determines A, B, C, and D. In the expression for transfer admittance there are only two parameters, A and B. This fact serves as a limitation on the number of circle transformations here available. To illustrate, for the Y_i circle to vary so that it passes through the origin, the Z_L circle must be a straight

Table II. Reactive Networks Having Constant Input Impedance Characteristics with Varying Load Impedance: Limitations and Passive T Representations*

Network Designation	2	3	4	5
1. Limitations caused by reactive network requirement	$\theta_k = \pm\frac{\pi}{2}$; $\varphi_k = \pm\frac{\pi}{2}$. Thus, only the trivial case of a reactive load with the resulting reactive Z_i satisfies this category.	$\theta_k = 0$ $\varphi_0 = \frac{\pi}{2}$, $\varphi_\infty = -\frac{\pi}{2}$ or $\varphi_\infty = \frac{\pi}{2}$, $\varphi_0 = -\frac{\pi}{2}$ $C^2 = -1/(2z_{ik}z_{La})$ $A/C = jz_{ik}$ } or { $A/C = -jz_{ik}$ $D/C = jz_{La}$ } or { $D/C = -jz_{La}$	$\beta_A + \beta_D = 0$ or 2π $\beta_C = \beta_B = \pm\frac{\pi}{2}$ $\varphi_k = 0$ $C^2 = -1/(2z_{ia}z_{Lk})$ $A/C = jz_{ia}$ } or { $A/C = -jz_{ia}$ $D/C = jz_{Lk}$ } or { $D/C = -jz_{Lk}$	for $\lvert D/C\rvert > z_{Lk}$, $\beta_A = \beta_D = 0$ or π $\therefore A = \frac{z_{ik}}{z_{Lk}} \cdot D$ $C = \pm j \cdot \frac{1}{z_{Lk}z_{ik}\sqrt{\lvert z_{ik}^2 D^2 - z_{ik}z_{Lk}\rvert}}$; for $\lvert D/C\rvert < z_{Lk}$ $\beta_A + \pi = \beta_D = 0$ or π $\therefore A = \frac{z_{ik}}{z_{Lk}} \cdot D$ $C = \pm j \cdot \frac{1}{z_{Lk}z_{ik}\sqrt{\lvert z_{ik}^2 D^2 + z_{ik}z_{Lk}\rvert}}$
2. T-section representations	$Z_1 = j\alpha$, $Z_2 = j\beta$, $Z_3 = j\gamma$; α, β, γ arbitrary real numbers	$Z_1 = jz_{ik} \pm j\sqrt{2z_{ik}z_{La}}$ $Z_2 = \mp j\sqrt{2z_{ik}z_{La}}$ $Z_3 = jz_{La} \pm j\sqrt{2z_{ik}z_{La}}$ or $Z_1 = -jz_{ik} \pm j\sqrt{2z_{ik}z_{La}}$ $Z_2 = \mp j\sqrt{2z_{ik}z_{ka}}$ $Z_3 = -jz_{ka} \pm j\sqrt{2z_{ik}z_{La}}$	$Z_1 = jz_{ia} \pm j\sqrt{2z_{ia}z_{Lk}}$ $Z_2 = \mp j\sqrt{2z_{ia}z_{Lk}}$ $Z_3 = jz_{Lk} \pm j\sqrt{2z_{ia}z_{Lk}}$ or $Z_1 = -jz_{ia} \pm j\sqrt{2z_{ia}z_{Lk}}$ $Z_2 = \mp j\sqrt{2z_{ia}z_{Lk}}$ $Z_3 = -jz_{Lk} \pm j\sqrt{2z_{ia}z_{Lk}}$	For given z_{Lk}, z_{Lk}, D can be specified arbitrarily, A and C readily determinable from the above expressions. For example, we can select $D = \frac{1}{z_{ik}}\sqrt{z_{ik}^2 + z_{ik}z_{Lk}}$. Thus, a typical representation is: $Z_1 = \mp jz_{Lk} \pm j\sqrt{z_{ik}z_{Lk} + z_{ik}^2}$ $Z_2 = \pm jz_{Lk}$ $Z_3 = \mp jz_{Lk} \pm j\frac{z_{Lk}}{z_{ik}}\sqrt{z_{ik}z_{Lk} + z_{ik}^2}$

* Refer to Table I and Figure 2 for definitions of the symbols used.

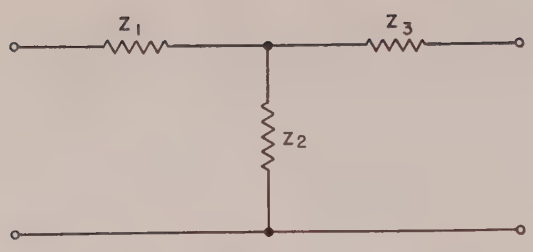

Figure 2. T-section

$A_T=(Z_1+Z_2)/Z_2$
$B_T=(Z_1Z_2+Z_1Z_3+Z_2Z_3)/Z_2$
$C_T=1/Z_2$
$D_T=(Z_2+Z_3)/Z_2$

$Z_1=(A_T-1)/C_T$
$Z_2=1/C_T$
$Z_3=(D_T-1)/C_T$

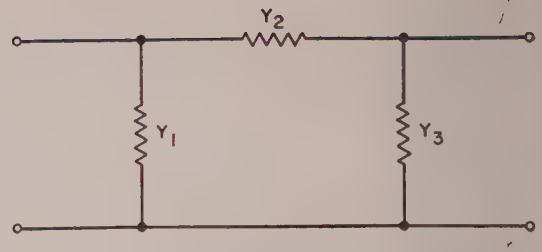

Figure 3. π-section

$A_\pi=(Y_2+Y_3)/Y_2$
$B_\pi=1/Y_2$
$C_\pi=(Y_1Y_2+Y_1Y_3+Y_2Y_3)/Y_2$
$D_\pi=(Y_1+Y_2)/Y_2$

$Y_1=(D_\pi-1)/B_\pi$
$Y_2=1/B_\pi$
$Y_3=(A_\pi-1)/B_\pi$

line, since Y_t will be zero only when $|Z_L|$ is infinite, unless A and B are both infinite, in which case the Y_t circle would consist entirely of the point at the origin of the complex plane.

For given values of A, B, C, D satisfying equation 2 a variety of network representations can be found. Such networks must have in general a minimum of three elements, each element being a self or mutual impedance or admittance representable by a complex number. In Figures 2, 3, and 4 are three such general networks. In each figure the values of A, B, C, D are given in terms of the element values, and the elements are given in terms of A, B, C, D.

Comparing Figures 2 and 3, a similarity is seen between the expressions relating A, B, C, D and the circuit elements. For given values of A, B, C, D, equivalent T and π networks can be constructed with the impedance elements of the T depending in a simple way on A, C, and D and the corresponding admittance elements of the π depending in exactly the same simple way on D, B, and A. This is an example of the principle of duality. In obtaining relationships leading to the construction of networks corresponding to given values of the general circuit parameters, it is sufficient to state those relationships in terms of A, C, and D, the implication being that similar relationships also can be expressed in terms of D, B, and A, leading to the construction of corresponding dual networks.

It is of interest to examine the properties of symmetrical networks, that is, 4-terminal networks whose behavior remains the same when input and output terminals are interchanged. For symmetrical networks $A=D$. Thus, the T and π sections in Figures 2 and 3 both can be symmetrical networks. In Figure 5 are given the relations connecting elements with A, B, C, D for the symmetrical lattice network. The network in Figure 4 is symmetrical only if $A_TD_T=n^2$.

Up to now, the only restriction on the values of A, B, C, D has been that $AD-BC=1$. In order that the single-frequency network be passive, however, certain other conditions must be satisfied. Passiveness requires that the input power never be less than the power leaving the network. As shown in Appendix II, this definition leads to the following two independent restrictions:

$$\mathrm{Re}(A/C)\geq 0;\ \mathrm{Re}(A/C)\mathrm{Re}(D/C)\geq [\mathrm{Re}(1/C)]^2 \quad (4)$$

The above inequalities are both necessary and sufficient for A, B, C, D to describe a passive network. Other necessary conditions that are useful in certain calculations are

$$\mathrm{Re}(D/C)\geq 0;\ [\mathrm{Im}(AD^*-BC^*)]^2\leq 4\mathrm{Re}(BD^*)\mathrm{Re}(AC^*) \quad (5)$$

Relations similar to equations 4 and 5 can be written at once from the principle of duality, by replacing A, C, D by D, B, A in the above expressions. The first inequality in equation 5 follows from equation 4. The second inequality is a direct result of the fact that with Z_L connected to the output of the network,

Table III. Symmetrical Networks Having Constant Input Impedance Characteristics with Varying Load Impedance: General Conditions Plus Typical Lattice Examples

Network Designation	2	3	4	5
1. Necessary and sufficient conditions for networks to be symmetrical	$z_{La}=z_{i\infty}$ $\varphi_k=\theta_k$ $C^2=\dfrac{/-2\theta_k}{z_{i\infty}(z_{i\infty}-z_{i0})}$ $A=D=C\underline{z_{i\infty}/\theta_k}$	$z_{La}=z_{ik}$ $\theta_k=\frac{1}{2}(\varphi_\infty+\varphi_0)$ $C^2=\dfrac{\underline{/\frac{\pi}{2}-\frac{1}{2}(3\varphi_\infty+\varphi_0)}}{2z_{ik}^2\sin\frac{1}{2}(\varphi_0-\varphi_\infty)}$ $A=D=C\ z_{ik}/\varphi_\infty$	$\cos 2\beta_A=\dfrac{1}{2z_{Lk}^2\lvert C\rvert^2}$ $\left\lvert\dfrac{A}{C}\right\rvert=z_{Lk}$ $\beta_C=\frac{\pi}{2}(\varphi_k+\beta_A)$ $\dfrac{z^2_{ia}}{z^2_{Lk}}=\dfrac{1+\sin(\varphi_k-2\beta_A)}{1+\sin(\varphi_k+2\beta_A)}$	$z_{Lk}+z_{ik}$ $\beta_A=0,\pi$ $AA^*-z_{ik}^2CC^*=1$ } or $\beta_A=\pm\frac{\pi}{2}$ $AA^*-z_{ik}^2CC^*=-1$
2. Conditions imposed by passive network requirement	for $z_{i\infty}>z_{i0}$, *no limitations.* for $z_{i0}>z_{i\infty}$, $\dfrac{z_{i\infty}}{z_{i0}}\geq\sin^2\theta_k$	for $\varphi_\infty\geq\theta_k\geq\varphi_0$, $\cos^2\theta_k\geq\sin(\varphi_\infty-\theta_k)$ for $\varphi_0\geq\theta_k\geq\varphi_\infty$ $\cos^2\theta_k\geq\sin(\theta_k-\varphi_\infty)$	$\cos^2(\beta_A-\beta_C)\geq 2\cos 2\beta_A\cos^2\beta_C$ which can be written: $\cos(^2\beta_A+^2\beta_C)\leq 1-\dfrac{1}{z_{Lk}^2\lvert C\rvert^2}$ also, $\cos(\beta_A-\beta_C)\geq 0$	$\cos(\beta_A-\beta_C)\geq 0$ for $\beta_A=0,\pi$: $\lvert A\rvert\geq 1$ for $\beta_A=\pm\frac{\pi}{2}$, $\lvert A\rvert\geq\lvert\cot\beta_C\rvert$
3. Typical passive network representations (symmetrical lattice, see Figure 5)	Let: $\begin{cases}z_{i\infty}=2z_{i0}=z_{La}=a\\ \varphi_k=\theta_k=\frac{\pi}{4}\end{cases}$ $Z_m=a-ja$ $Z_n=3a+ja$	Let: $\begin{cases}z_{La}=z_{ik}=a\\ \varphi_\infty=\frac{\pi}{4},\theta_k=0,\varphi_0=-\frac{\pi}{4}\end{cases}$ $Z_m=a(0.252-j0.391)$ $Z_n=a(1.162+j1.805)$	Let $z_{Lk}=a,\ \varphi_k=0,\ \beta_A=\frac{\pi}{6}$ $\therefore\lvert C\rvert=\dfrac{1}{a},\ \beta_C=\frac{\pi}{3},\ \lvert A\rvert=1$ $Z_m=a(0.366+j0.366)$ $Z_n=a(1.366-j1.366)$	Let $\begin{cases}z_{Lk}=z_{ik}=a\\ \lvert A\rvert=2,\ \beta_A=0,\ \beta_C=\frac{\pi}{4}\end{cases}$ $\therefore\lvert C\rvert=\dfrac{1}{a}$ $\therefore Z_m=a(0.707-j0.707)$ $Z_n=a(2.121-j2.121)$

$R_i(\boldsymbol{Z}_i)$ can never be negative as long as $\boldsymbol{Z}_L$ is passive; that is, $R_L(\boldsymbol{Z}_L) \geq 0$ (see Appendix II for details).

A *passive element* network is one in which the real part of the impedance of every element is not negative. Thus, from Figure 2, allowing for a possible reversal of the output terminals, the $\boldsymbol{A}$, $\boldsymbol{C}$, $\boldsymbol{D}$ for a passive-element T network must satisfy:

$$\mathrm{Re}(\boldsymbol{A}/\boldsymbol{C}) \geq |\mathrm{Re}(1/\boldsymbol{C})|; \quad \mathrm{Re}(\boldsymbol{D}/\boldsymbol{C}) \geq |\mathrm{Re}(1/\boldsymbol{C})| \quad (6)$$

As expected, equation 6 is a special case of equation 4. It is seen that passive networks are possible which *cannot* be represented by a passive-element T. However, if the use of an ideal transformer is permitted in cascade with the T network, as in Figure 4, it is always possible so to represent passive networks at a single frequency by selecting the transformer turns ratio n such that

$$\mathrm{Re}(\boldsymbol{A}/\boldsymbol{C}) \cdot \mathrm{Re}(\boldsymbol{D}/\boldsymbol{C}) \geq n\mathrm{Re}(1/\boldsymbol{C})\mathrm{Re}(\boldsymbol{A}/\boldsymbol{C}) \geq [\mathrm{Re}(1/\boldsymbol{C})]^2 \quad (7)$$

In the case of purely reactive networks all the terms in the above inequalities, equations 4, 5, 6, and 7, are zero, since for this type of network, $\boldsymbol{A}$ and $\boldsymbol{D}$ must be real numbers and $\boldsymbol{B}$ and $\boldsymbol{C}$ must be pure imaginary.

For symmetrical networks, where $\boldsymbol{A} = \boldsymbol{D}$, it is seen that the conditions in equations 6 and 4 become identical. Thus, it is always possible to represent a symmetrical passive network by a symmetrical T with the understanding that the output terminals may be reversed if necessary. An alternative representation is shown in Figure 5; it is seen that the conditions for the symmetrical lattice to be a passive element network are the same as equations 4 and 6.

Networks with Particular Types of Input Impedance Variation as Load Impedance Varies

The specific problem here is to start with circles in the complex plane, representing variations in load impedance and the corresponding variations in input impedance, determine the required ranges of values for the general circuit parameters, and show how passive networks can be constructed with the desired properties.

1. Input Impedance Constant as Load Impedance Varies

It is seen that this is a trivial limiting case, since both the voltage and the current at the load must vanish. Typical examples are the "short-circuited T" ($\boldsymbol{Z}_2 = 0$ in Figure 2 or 4) and the "balanced bridge" (as in Figure 5, with $\boldsymbol{Z}_m = \boldsymbol{Z}_n$). In this case, $\boldsymbol{A}$, $\boldsymbol{B}$, $\boldsymbol{C}$, and $\boldsymbol{D}$ are all infinite.

Such cases occur in general when the input and output branches of the network are what is known as conjugate to each other.

2. Phase of Input Impedance Constant as Load Magnitude Varies.

In this case both input and output can be represented by straight lines in the complex plane which, if extended, would pass through the origin. $\boldsymbol{A}$, $\boldsymbol{B}$, $\boldsymbol{C}$, $\boldsymbol{D}$ can be expressed in terms of the magnitudes of the three points on the $\boldsymbol{Z}_i$ line corresponding to $|\boldsymbol{Z}_L| = 0, \infty$, and an intermediate value. Other parameters are the respective constant phases of $\boldsymbol{Z}_i$ and $\boldsymbol{Z}_L$.

3. Magnitude of Input Impedance Constant as Load Magnitude Varies

Here the load is still represented by a straight line, as in 2, but the input representation now is the arc of a circle with center at the origin. $\boldsymbol{A}$, $\boldsymbol{B}$, $\boldsymbol{C}$, $\boldsymbol{D}$ now can be expressed in terms of the phases of the three points on the $\boldsymbol{Z}_i$ circle corresponding to $|\boldsymbol{Z}_L| = 0, \infty$, and an intermediate value, the other parameters being the magnitude of the input impedance and the phase of the load.

4. Phase of Input Constant as Load Phase Varies

In this case the input impedance is represented by a straight line passing through the origin and the load by a circle with the origin as a center. Here it is not found convenient to express $\boldsymbol{A}$, $\boldsymbol{B}$, $\boldsymbol{C}$, $\boldsymbol{D}$ explicitly in terms of corresponding points on the two circle diagrams. Instead, using the fact that if $\boldsymbol{Z}_L$ traverses a complete circle, $\boldsymbol{Z}_i$ must pass through both zero and infinity, necessary conditions for $\boldsymbol{A}$, $\boldsymbol{B}$, $\boldsymbol{C}$, $\boldsymbol{D}$ are obtained. The parameters of these expressions are the constant magnitude of the load, the constant phase of the input, and the particular value of the input magnitude when the load phase is zero.

5. Magnitude of Input Constant as Load Phase Varies

The representations of both input and load impedances are arcs of circles with the origin as center. Using the fact that both $\boldsymbol{Z}_i$ and $\boldsymbol{Z}_L$ vary with constant magnitude, necessary conditions which must be satisfied by $\boldsymbol{A}$, $\boldsymbol{B}$, $\boldsymbol{C}$, $\boldsymbol{D}$ are obtained, the parameters being the constant magnitudes of the input impedance and the load.

Table IV. Networks with Constant Transfer Admittance Characteristics with Variable Load Impedance

Network Designation	6	7	8	9	10
1. Type of impedance variations	$\boldsymbol{Z}_L = z_L/\theta$; $\boldsymbol{Z}_i = \frac{1}{\boldsymbol{Y}_i} = z_{ik}/\psi k$	$\boldsymbol{Z}_L = z_L/\theta_k$ $\boldsymbol{Z}_i = z_{ik}/\psi$	$\boldsymbol{Z}_L = z_L/\theta k$; $\boldsymbol{Z}_i = z_i/\psi k$	$\boldsymbol{Z}_L = z_{Lk}/\theta$, $\boldsymbol{Z}_i = z_{ik}/\psi$	$\boldsymbol{Z}_L = z_{Lk}/\theta$; $\boldsymbol{Z}_i = z_i/\psi k$
2. Basic conditions	$\boldsymbol{A} = 0$; $\boldsymbol{BC} = -1$ $\mathrm{Re}(1/\boldsymbol{C}) = 0$ $\boldsymbol{Z}_i = \boldsymbol{B} = -1/\boldsymbol{C}$ $\boldsymbol{D}$ arbitrary	Trivial case would require that $z_{ik} = \infty$ if $\boldsymbol{A} \neq 0$	Let $\begin{cases} z_i = z_{ia} \text{ when } z_L = 0 \\ z_i = z_{ib} \text{ when } z_L = \lvert z_{ia} \rvert \end{cases}$ $\boldsymbol{B} = z_{ia}/\psi k$ $\boldsymbol{A} = \frac{z_{ib} - z_{ia}}{\lvert z_{ia} \rvert} / \psi k - \theta k$ $\lvert D \rvert \frac{z_{ib} - z_{ia}}{\lvert z_{ia} \rvert} \cos\theta_k \cos(\beta_D - \psi_k) \geq \cos^2 \psi_k$ $\cos(\beta_D - \theta_k) \geq 0$	$\boldsymbol{B} = 0$, $\boldsymbol{AD} = 1$ $\beta_A = \beta_D = 0, \pi$ $\cos(\beta_A - \beta_C) \geq 0$ $\lvert z_{ik} \rvert = \lvert A \rvert z_{Lk}$ $\psi = \beta_A + \theta = \theta, \pi + \theta$ $\lvert C \rvert$ arbitrary	Trivial case: reduces to 6, since $\boldsymbol{A}$ must $= 0$
3. Typical network representations	Let $\frac{1}{\boldsymbol{C}} = ja$, a arbitrary real *T-section* $\boldsymbol{Z}_1 = -ja$ $\boldsymbol{Z}_2 = ja$ $\boldsymbol{Z}_3$ arbitrary		Let $\begin{cases} z_{ia} = a, \text{ arbitrary positive real} \\ z_{ib} = 3a,\ \psi_k = 0,\ \theta_k = \frac{\pi}{4} \end{cases}$ *Symmetrical lattice* $\boldsymbol{Y}_n = \frac{1}{\boldsymbol{Z}_n} = \frac{1}{a}(2.414 - j1.414)$ $\boldsymbol{Y}_m = \frac{1}{\boldsymbol{Z}_m} = \frac{1}{a}(0.414 - j1.414)$	Let $\boldsymbol{A} = \frac{1}{\boldsymbol{D}} = -2$, $\beta_C = \frac{3}{4}\pi$, $\lvert C \rvert = 1/a$, where a is arbitrary positive real $\therefore z_{ik} = -2z_{Lk}$, $\psi = \pi + \theta$ *T-section with transformer* $n = 1/2$ $\boldsymbol{Z}_1 = 0$, $\boldsymbol{Z}_2 = a(0.353 + j0.353)$, $\boldsymbol{Z}_3 = 0$	

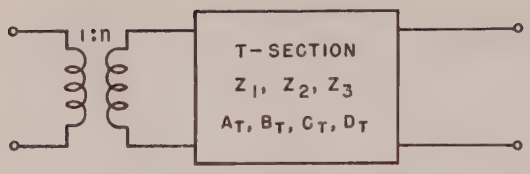

Figure 4. T-section with perfect transformer

$A_{TTR}=A_T/n$
$B_{TTR}=B_T/n$
$C_{TTR}=nC_T$
$D_{TTR}=nD_T$

$Z_1=(n^2A_{TTR}-n)/C_{TTR}$
$Z_2=n/C_{TTR}$
$Z_3=(D_{TTR}-n)/C_{TTR}$

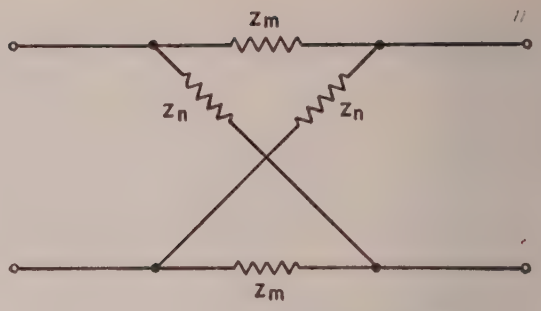

Figure 5. Symmetrical lattice

$A_L=D_L=(Z_n+Z_m)/(Z_n-Z_m)=(Y_m+Y_n)/(Y_m-Y_n)$
$B_L=2Z_mZ_n/(Z_n-Z_m)=2/(Y_m-Y_n)$
$C_L=2/Z_n-Z_m)=2Y_mY_n/(Y_m-Y_n)$
$Z_n=1/Y_n=(A_L+1)/C_L=[(A_L-1)/B_L]^{-1}$
$Z_m=1/Y_m=(A_L-1)/C_L=[(A_L+1)/B_L]^{-1}$

The necessary and sufficient conditions for networks of types 2, 3, 4, and 5 to be realizable by passive networks are shown in Table I. The first line of this chart shows the general types of variations that are considered in each case for Z_L and Z_i. The subscript k shows which, magnitude or phase, is kept constant in each instance. Line 2 defines the symbols in terms of which the required values of A, B, C, D are expressed in line 3. In line 4 are the added conditions that must be satisfied if the given networks are to be realizable with passive elements. To construct such networks, select suitable parameters that satisfy the conditions in line 4, then use line 3 to obtain the values of A, C, D or D, B, and A. The actual passive network construction follows. Thus, using the expressions in Figure 5, a T-transformer combination always can be found, the transformer turns-ratio satisfying equation 7.

In Table II is shown how the conditions of Table I are modified by the requirement that the 4-terminal network be reactive (that is, nondissipative). For type-2 networks it is seen that both the load and the input must vary along the imaginary axis. For type-3 networks, the load must vary only along the real axis, and in the case of type-4 networks the variation of the input impedance must be along the real axis when the load phase changes. In line 2 are shown T-section representations of these reactive networks. It can be noted that network types 2 and 5 each have three arbitrary parameters, whereas 3 and 4 have only two. Table III, lines 1 and 2, shows the limitations on the networks of Table I resulting from the requirement that the networks be symmetrical. In line 3, typical selections of network parameters are made and values of corresponding symmetrical lattice networks are shown.

Networks with Particular Types of Transfer Admittance Variation as Load Impedance Varies

In these calculations it has been found convenient to speak in terms of $Z_t=1/Y_t$, where Y_t is the transfer admittance defined as the ratio of load current to input voltage. The basic results for different combinations of impedance variations are shown in Table IV, together with some typical network representations. It should be noted that Z_t can be either positive or negative. A brief discussion of each type of network follows.

6. Transfer Admittance Constant Irrespective of Load Variation

This condition is satisfied provided $A=0$. For a passive network representation it is seen that C must be pure imaginary, in which case $Y_t=-C$ also must be pure imaginary. It is interesting to note that in the symmetrical case, where $D=A=0$, the input impedance is given by $Z_i=a^2/Z_L$, where $(1/C)=ja$. In other words, in this case the input impedance would be proportional to the reciprocal of the load impedance (a T-section representation of this type of network would be: $Z_1=Z_3=-ja$; $Z_2=ja$).

7. Magnitude of Transfer Admittance Constant as Magnitude of Load Varies

As noted in Table IV, it is impossible to obtain a network of this type that also is not of type 6.

8. Phase of Transfer Admittance Constant as Magnitude of Load Varies

This type of network is realizable for wide ranges of parameters. In line 2 of Table IV the necessary and sufficient values of A and B are specified in terms of θ_k and ψ_k, as well as two arbitrary real numbers, z_{ta} and z_{tb}. The inequalities necessary for the network to be passive always can be satisfied by proper selection of D. Knowing A, B, and D, admittance networks can be constructed at once. As an example, a selection of suitable parameters is made and the resultant symmetrical lattice representation is shown in line 3.

9. Magnitude of Transfer Admittance Constant as Phase of Load Varies

This type of network is possible provided $B=0$. For passive network realization it is necessary that A and D both be real; the magnitude and phase of C being for the most part arbitrary. Since the phase of Z_t can differ from that of the load only by θ or π, it is evident that the network representation can have no effective series impedance. Thus, in the example chosen in Table IV, the resulting network is simply a transformer with an impedance shunting its secondary winding.

10. Phase of Transfer Admittance Constant as Phase of Load Varies

As noted in Table IV, this type of network can be realized only by a network of type 6.

Appendix I

List of Main Symbols Used

E_1, I_1, E_2, I_2 = voltage rises and currents at the input and output ends of the 4-terminal network (see Figure 1)
Z_L = load impedance $=R_L+jX_L$
z_L = magnitude of load impedance $(z_L \geq 0)$
θ = phase of load impedance $\left(\frac{\pi}{2} \geq \theta \geq -\frac{\pi}{2}\right)$
Z_t = input impedance $=R_t+jX_t$
z_t = magnitude of input impedance $(z_t \geq 0)$
φ = phase of input impedance $\left(\frac{\pi}{2} \geq \varphi \geq -\frac{\pi}{2}\right)$
Y_t = transfer admittance
$Z_t=1/Y_t=R_t+jX_t$
ψ = "phase" of Z_t $\left(\text{taken such that } \frac{\pi}{2} \geq \psi \geq -\frac{\pi}{2}\right)$
z_t = "magnitude" of Z_t (allowed to take on negative values)

A,B,C,D = general circuit parameters
β_A, β_B, β_C, β_D = phases of A, B, C, D, respectively
a = real number
k = subscript denoting the constant part (magnitude or phase) of a varying impedance
a, b, 0, ∞ = subscripts denoting particular values of magnitude or phase of varying impedances
1, 2, 3, m, n = subscripts denoting elements of certain networks

Appendix II

Derivation of Limitations Imposed on A, B, C, D by the Condition That Network Be Passive

In equation 1, consider I_1 and I_2 as independent variables. The expressions for the voltages then become

$$E_1 = I_1(A/C) + I_2(1/C);$$
$$E_2 = I_1(1/C) + I_2(D/C) \quad (8)$$

For the network to be passive, the power going into it can never be negative, whatever the values of I_1 and I_2. In other words, $\mathrm{Re}(E_1I_1^* + E_2I_2^*) \geq 0$. From the above two expressions, this becomes:

$$|I_1|^2\mathrm{Re}(A/C) + 2\mathrm{Re}(I_1I_2^*)\cdot\mathrm{Re}(1/C) + |I_2|^2\mathrm{Re}(D/C) \geq 0 \quad (9)$$

Letting first I_1, then $I_2 = 0$, there results:

$$\mathrm{Re}(A/C) \geq 0;\ \mathrm{Re}(D/C) \geq 0 \quad (10)$$

Finally, to insure that expression 9 is never negative, the discriminant must not be greater than zero. Thus:

$$[\mathrm{Re}(1/C)]^2 - \mathrm{Re}(A/C)\mathrm{Re}(D/C) \leq 0 \quad (11)$$

Equations 10 and 11 are seen to constitute the necessary and sufficient conditions expressed in equation 4. Similar conditions were obtained for variable frequency networks in terms of open-circuit impedance parameters by Gewertz[3] in 1933.

Another necessary condition can be obtained from the fact that for $\mathrm{Re}(Z_L) \geq 0$, it also must be true that $\mathrm{Re}(Z_t) \geq 0$. Thus, suppose that $Z_L = jX_L = jx$. Thus, rationalizing the denominator of the expression for Z_t in the text, there results:

$$x^2\mathrm{Re}(AC^*) - x\mathrm{Re}j(BC^* - AD^*) + \mathrm{Re}(BD^*) \geq 0 \quad (12)$$

Thus, since $\mathrm{Re}(AC^*) \geq 0$, in order to insure that equation 12 holds for all values of x,

$$[\mathrm{Im}(AD^* - BC^*)]^2 \leq 4\mathrm{Re}(BD^*)\mathrm{Re}(AC^*) \quad (13)$$

References

1. Network Analysis and Feedback Amplifier Design (book), **H. W. Bode.** D. Van Nostrand Co., Inc., New York, N. Y., 1945.

2. Communication Networks (book), **E. A. Guillemin.** John Wiley and Sons, Inc., New York, N. Y., volume II, 1931.

3. Synthesis of a Finite Four-Terminal Network from Its Prescribed Driving Point Functions and Transfer Function, **C. M. Gewertz.** *Journal of Mathematics and Physics* (Cambridge, Mass.), volume 12, 1933, pages 1–257.

No Discussion

The Generalized Transmission Matrix Stability Criterion

PIERRE M. HONNELL
MEMBER AIEE

Synopsis: A generalized criterion for stability of a closed tandem connection of double-dinodes is given by the expression

$$A(\lambda) = a_{11} + a_{22} - |a| - 1 = 0$$

in which the a_{11} are the appropriate terms of the transmission matrix of the tandem network prior to closing the loop. If the λ-roots of $A(\lambda)$ have positive real parts, the network will oscillate spontaneously upon closing the transmission loop; that is, the network is unstable.

The generalized criterion is applicable to transmission loops incorporating bilateral amplifiers, and the transmission loop may be opened wherever desired without consideration of the impedances to the left and right of the cut.

The criterion is not limited to transmission networks employing amplifiers; likewise, it applies equally well to electromechanical networks or servomechanisms.

AMONG THE several methods for predetermining the stability of networks, that is, whether or not self-sustained oscillations or singing will exist, the Barkhausen and Nyquist criteria often are applied to those circuit configurations which employ electron-tube amplifiers. In these networks the concept of retroaction or feedback is useful, since this provides a mental picture of a voltage wave progressing unidirectionally through the electron tube, the passive feedback network, back to the tube input, and so on; it also leads to a simple scheme for computing the ratio of output to input voltage for the network, upon which the stability of the network apparently rests.

The Barkhausen[1] criterion, for example,

$$K \cdot V(i\omega) = 1 \qquad (1)$$

then expresses the intuitive reasoning that if the product of the loop gain K due to the amplifier, and the loss in the feedback network $V(i\omega)$ is just equal to unity, then spontaneous oscillations will occur in the network.

The criterion for oscillation given by equation 1 is known not to be entirely correct from the work of Black,[2] and as demonstrated experimentally by Peterson, Kreer, and Ware.[3] An exact formulation was given by Nyquist[4] as the following:

Rule: Plot plus and minus the imaginary parts of $AJ(i\omega)$ against the real part for all frequencies from 0 to ∞. If the point $1+i0$ lies completely outside this curve the system is stable; if not it is unstable.

In this rule, the complex quantity $AJ(i\omega)$ represents the ratio by which the amplifier and the feedback circuit modify the wave in one round trip; that is, the ratio of output to input voltage for the entire loop. The symbolism $\mu\beta$ now is commonly substituted for $AJ(i\omega)$. It should be understood that for amplifiers a nonoscillatory condition is classed as stable; for oscillators, however, a stable condition implies oscillations of unvarying envelope magnitude and is strictly not attainable solely with linear parameters.

There are certain restrictions to the criteria given above. One restriction has to do with the impedance in which the feedback loop is terminated. Although sometimes not explicitly stated, it is nevertheless necessary that the ratio $\mu\beta$ be unchanged upon closing the feedback loop. Since (or if) the grid-cathode impedance of an electron-tube amplifier may be assumed indefinitely large, this prerequisite is met directly when the loop is opened at the grid-cathode node pair. For some feedback loops, terminating impedances may be taken into consideration in the computation or measurement by appropriate circuit artifices. In any case, the electron-tube amplifier must be substantially a unilateral transmission device.

Another limitation depends upon the existence of subsidiary feedback loops within the μ-network itself, for example, a connection from plate to grid of the amplifier tube. In this case the $\mu\beta$ criterion is no longer directly applicable, as will be shown by an example, because of the bilateral character of the composite amplifier circuit.

Figure 1 shows a network for which the $\mu\beta$ criterion, as originally given by Nyquist, is not applicable. In this network, the ratio of output voltage V_2 to input voltage V_1, or $\mu\beta$, for the open feedback loop is given by the expression:

$$\frac{V_2}{V_1} = \mu\beta = \frac{g_m - g_c}{g_b + g_c + g_p + g_t + g_{LC} + j\omega C + 1/j\omega L} \qquad (2)$$

where the ideal transformer ratio is taken as $n = -1$.

It is instructive to consider the stability of this circuit for two sets of parameter magnitudes, tabulated in Table I. It will be noted that the only change between the parameter magnitudes listed under Condition I, Threshold Oscillations, and those under Condition II, Nonoscillatory, lies in a variation of the subsidiary feedback conductance g_c in the μ-network.

Substituting the parameter magnitudes for Condition II from Table I into equation 2 yields the following expression:

$$\mu\beta = \frac{1}{0.64 + j1.44(\omega/\omega_0 - \omega_0/\omega)} \qquad (3)$$

Paper 51-46, recommended by the AIEE Basic Sciences Committee and approved by the AIEE Technical Program Committee for presentation at the AIEE Winter General Meeting, New York, N. Y., January 22–26, 1951. Manuscript submitted August 14, 1950; made available for printing December 5, 1950.

PIERRE M. HONNELL is with Washington University, St. Louis, Mo.

The generalized transmission matrix stability criterion is a collateral result of an extended research program on seismographic instrumentation prosecuted under the guidance of the Reverend Dr. JAMES B. MACELWANE, S. J., Director of the Department of Geophysics, St. Louis University, St. Louis, Mo.

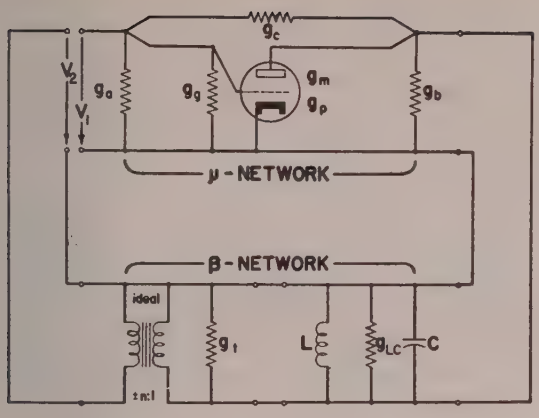

Figure 1 (left). Feedback circuit with subsidiary loop in the μ-network or amplifier

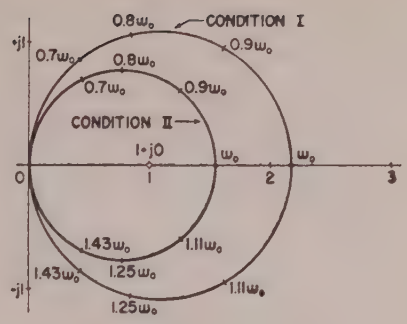

Figure 2 (right). Nyquist diagrams for the network shown in Figure 1, with parameter magnitudes for Condition I and II, as given in Table I

where $\omega_0=2\pi$ 1,006, the angular resonance frequency of the C and L alone. Plotting the Nyquist diagram of equation 3 yields the smaller circle shown in Figure 2, which encloses the critical point $1+j0$. The parameter magnitudes from Condition I listed in Table I when substituted into equation 2 also yield a similar Nyquist plot but of larger diameter, which is likewise plotted in Figure 2.

Clearly, according to the $\mu\beta$ rule, the network shown in Figure 1 with the feedback loop closed is fully oscillatory for either set of parameter magnitudes. Actually, the network is just barely oscillatory for the parameter magnitudes under Condition I, and completely nonoscillatory for parameter magnitudes in Condition II. The generalized transmission matrix stability criterion, on the other hand, correctly predicts the behavior of the network when the feedback loop is closed, as will be shown.

The principal objective of this paper is to derive the new generalized matrix criterion. The new matrix criterion is perfectly general and is not limited solely to networks incorporating electron-tube or other types of amplifiers. It can be applied only to those circuit configurations for which a principal transmission loop may be delineated in the network, and for which the transmission matrix is valid.

The Transmission Matrix

The computation of the ratio of output to input voltage for circuit configurations which include a recognizable transmission loop may be made by direct application of Kirchoff's Laws or rules deduced therefrom. However, the pre-eminent method of analysis for this type of network employs the algebra of matrices, because of its elegance, compactness, and ease of application.

For examples of the application of the transmission matrix to the study of stability, reference may be made to the papers by Jefferson,[5] Sulzer,[6] Hinton,[7] and Mathes,[8] all of which pertain to various phases of oscillator design. These authors limited their matrix approach merely to the derivation of the matrix network function corresponding to the Nyquist $\mu\beta$ criterion, while the present work extends these matrix methods.

The transmission matrix [a] of a double-dinode* relates the input and output voltages and currents in the following manner:

$$\begin{bmatrix} E_1 \\ I_1 \end{bmatrix} = \begin{bmatrix} a_{11} & a_{12} \\ a_{21} & a_{22} \end{bmatrix} \cdot \begin{bmatrix} E_2 \\ -I_2 \end{bmatrix} \tag{4}$$

with positive polarities for the variables taken as shown in Figure 3 for the $[a^1]$ network. The detailed methods of computing the transmission matrix of purely passive networks may be found in Guillemin[9] and Pipes,[10–12] while for active networks containing electron-tubes reference may be made to Feldtkeller[13] and Brown and Bennett.[14]

The over-all transmission matrix for n double-dinodes connected in tandem, as shown in Figure 3, is simply expressed as

$$\begin{bmatrix} E_1 \\ I_1 \end{bmatrix} = [a^1] \cdot [a^2] \cdots\cdots [a^n] \cdot \begin{bmatrix} E_n \\ -I_n \end{bmatrix} \tag{5}$$

or more concisely as

$$\begin{bmatrix} E_1 \\ I_1 \end{bmatrix} = [a^0] \cdot \begin{bmatrix} E_n \\ -I_n \end{bmatrix} \tag{6}$$

The over-all transmission matrix $[a^0]$ in equation 6 is obtained from the matrix product of the associated $[a^r]$ matrices for the individual double-dinodes, taken in the proper order.

*A network with but two accessible nodes is concisely called a dinode. A network with two pairs of accessible nodes may be called a double-dinode. This is the type of network considered herein, and to which the transmission matrix defined by equation 4 applies. A 4-terminal network constrained to function as a double-dinode should not be confused with the more general quadrinode.

The Two Special Transmission Matrix Stability Criteria

There are two special stability criteria, both of which pertain to certain networks exhibiting limiting conditions, as well as the generalized criterion, which are obtainable from the transmission matrix. The special criteria are considered first.

A tandem connection of double-dinodes, as shown in Figure 3, represents an open feedback loop which may be closed upon connecting nodes 1 and 1′ on nodes n and n' respectively. Now suppose that the electron-tube amplifier is within the network $[a^1]$, with the grid-cathode connected to terminals 1 and 1′, respectively, so that this node pair exhibits an indefinitely large impedance. If there is no subsidiary feedback loop within the network $[a^1]$, the impedance between 1 and 1′ remains indefinitely large and independent of the output load on the $[a^1]$ network. Upon closing the transmission loop (by connecting 1 and 1′ on n and n'), it is clear that the input and output voltages will be identical, and that the output and input currents will vanish. That is, the closing of the transmission loop introduces constraints on the variable such that

$$\begin{aligned} E_1 &= E_n \\ I_1 &= -I_n = 0 \end{aligned} \tag{7}$$

Equation 6 then yields the first special stability criterion:

$$\boxed{a^0_{11} - 1 = 0} \tag{8}$$

The second special stability criterion

Figure 3. The tandem connection of n double-dinodes

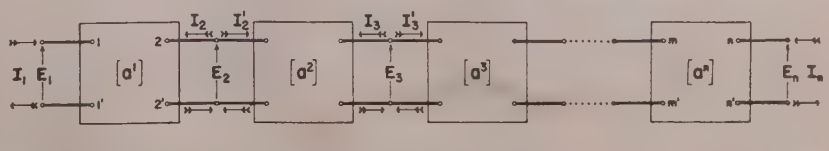

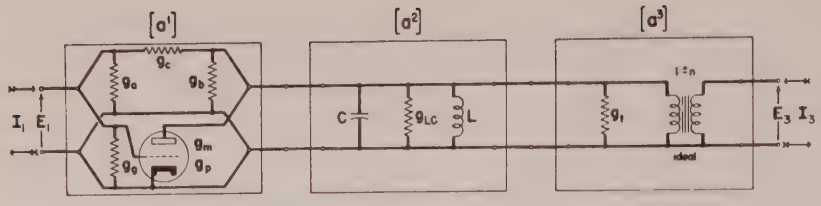

Figure 4. The feedback circuit shown in Figure 1 considered as a transmission network

would apply to amplifying devices which may be considered as purely current-actuated controls. It also is assumed that the indefinitely large input admittance of the amplifier is independent of the load admittance on its output terminals. Assume as before that the first network $[a^1]$ in Figure 3 contains the amplifying device with the input terminals on 1 and 1′. It is clear that in this case the terminal voltage will vanish when the transmission loop is closed (by connecting 1 and 1′ on n and n', respectively). The constraints on the variables are therefore given by

$$I_1 = -I_n$$
$$E_1 = E_n = 0 \tag{9}$$

Equation 6 then yields the second special stability criterion

$$\boxed{a^0_{22} - 1 = 0} \tag{10}$$

It is emphasized that the special criteria given by equations 8 and 10 are limited to those networks with unilateral transmitting properties having indefinitely large input impedance and admittance, respectively. Furthermore, it is interesting to note that the relation given by equation 8 is the matrix formulation equivalent to the Nyquist criterion $\mu\beta - 1 = 0$, since

$$\mu\beta \equiv E_2/E_1 = 1/a^0_{11}$$

This also is the matrix criterion employed by the authors to whose work previous reference has been made.[5–8]

The Generalized Transmission Matrix Stability Criterion

A generalization of the special transmission matrix criteria given by equations 8 and 10 is obtained in an analogous manner. In the general case, there can be no restriction as to the input impedance of the amplifying device, nor need the latter be unilateral. That is, the amplifier input impedance may be a function of the output load, as is the case, for example, in an electron-tube amplifier with a subsidiary feedback connection.

In the general case, therefore, the interrelation of the variables is set by specifying that the input and output voltages and currents of the transmission loop should be respectively equal. Accordingly, the constraints on the variables are given by

$$E_1 = E_n$$
$$I_1 = -I_n \tag{11}$$

From equation 6 there then follows

$$\boxed{A(\lambda) = a^0_{11} + a^0_{22} - |a^0| - 1 = 0} \tag{12}$$

Equation 12 may be called the generalized transmission matrix stability criterion. It represents the sum of the terms on the principal diagonal of the over-all transmission matrix $[a^0]$, minus the determinant $|a^0|$ of the transmission matrix, minus 1. In general, since $[a^0]$ is a function of λ, it follows that the generalized criterion A (λ) also is a function of λ, the complex frequency.

While the limited matrix stability criteria $a^0_{11} - 1 = 0$ and $a^0_{22} - 1 = 0$ require that the transmission loop be cut or opened at the zero admittance or zero impedance input terminals of the unilateral amplifying device, the generalized matrix criterion is not so limited. The transmission network may be cut wherever desired, and the generalized criterion automatically will take into account the impedances to the left and right of the cut.

But that is not all; if the amplifying device is bilateral, that is, if there is a subsidiary loop within the amplifying device, then a signal may be transmitted in either direction through the open loop. Because of the reciprocal properties of the direct and reverse transmission matrices for such networks, the generalized matrix stability criterion, equation 12, may be taken in either direction through the loop, and will still be valid. If the amplifier is unilateral, the transmission matrix may be taken only in the direction of propagation, for the reverse transmission matrix through the amplifier is (naturally) not defined.

Interpretation of the Matrix Criteria

First of all, it should be evident that the limited and generalized matrix criteria given in equations 8, 10, and 12 are artifices for predicting the stability of the closed transmission loop by means of matrix network coefficients obtained from the transmission loop before it is closed. This is useful because of the greater ease of computing the matrix coefficients (or $\mu\beta$, for that matter) for the tandem connection of double-dinodes for the open loop. (For simple networks, this advantage may not be important.) In the case of the closed transmission loop, the network stability is obtained most easily by computing the impedance matrix $[Z]$ or the admittance matrix $[Y]$ for the closed network, and determining the conditions for oscillation as given by either

$$|Z| = 0 \text{ or } |Y| = 0$$

which signifies the vanishing of the determinant of the circuit impedance or admittance matrices, as the case may be.

Furthermore, it should be clear that the network before the transmission loop is closed is not the same as the circuit obtained after the transmission loop is closed. That is, under open transmission loop conditions, the input and output voltages and currents E_1, E_n, and I_1, I_n may or may not be equal in magnitude and phase in the steady state. After the transmission loop is closed, this introduces constraints on the variables such that

E_1 must equal E_n, and

I_1 must equal $-I_n$

for all time, that is, for $-\infty < t < +\infty$. Obviously, there is then no longer any distinction between input and output of the transmission loop proper, and the closed loop circuit becomes a new network. This point of view clarifies somewhat the anomaly mentioned by Black[2] and investigated by Nyquist[4] and leading to the latter's $AJ(i\omega) = 1$ criterion. That is, a network may have $|E_n| > |E_1|$ with $\phi_n - \phi_1 = 2\pi k$ for more than one frequency on steady-state open transmission loop conditions, but nevertheless may not oscillate spontaneously when the transmission loop is closed; for, after all, the closed loop network becomes a new

Table I. Network Parameter Numerical Magnitudes

Network Parameter	Condition I Threshold Oscillations	Condition II Nonoscillatory
g_a, mhos	100×10^{-6}	100×10^{-6}
g_b, mhos	150×10^{-6}	150×10^{-6}
g_c, mhos	561×10^{-6}	833×10^{-6}
g_g, mhos	50×10^{-6}	50×10^{-6}
g_m, mhos	3030×10^{-6}	3030×10^{-6}
g_p, mhos	136×10^{-6}	136×10^{-6}
g_{LC}, mhos	76×10^{-6}	76×10^{-6}
g_t, mhos	210×10^{-6}	210×10^{-6}
C, farads	0.5×10^{-6}	0.5×10^{-6}
L, henrys	50×10^{-3}	50×10^{-3}

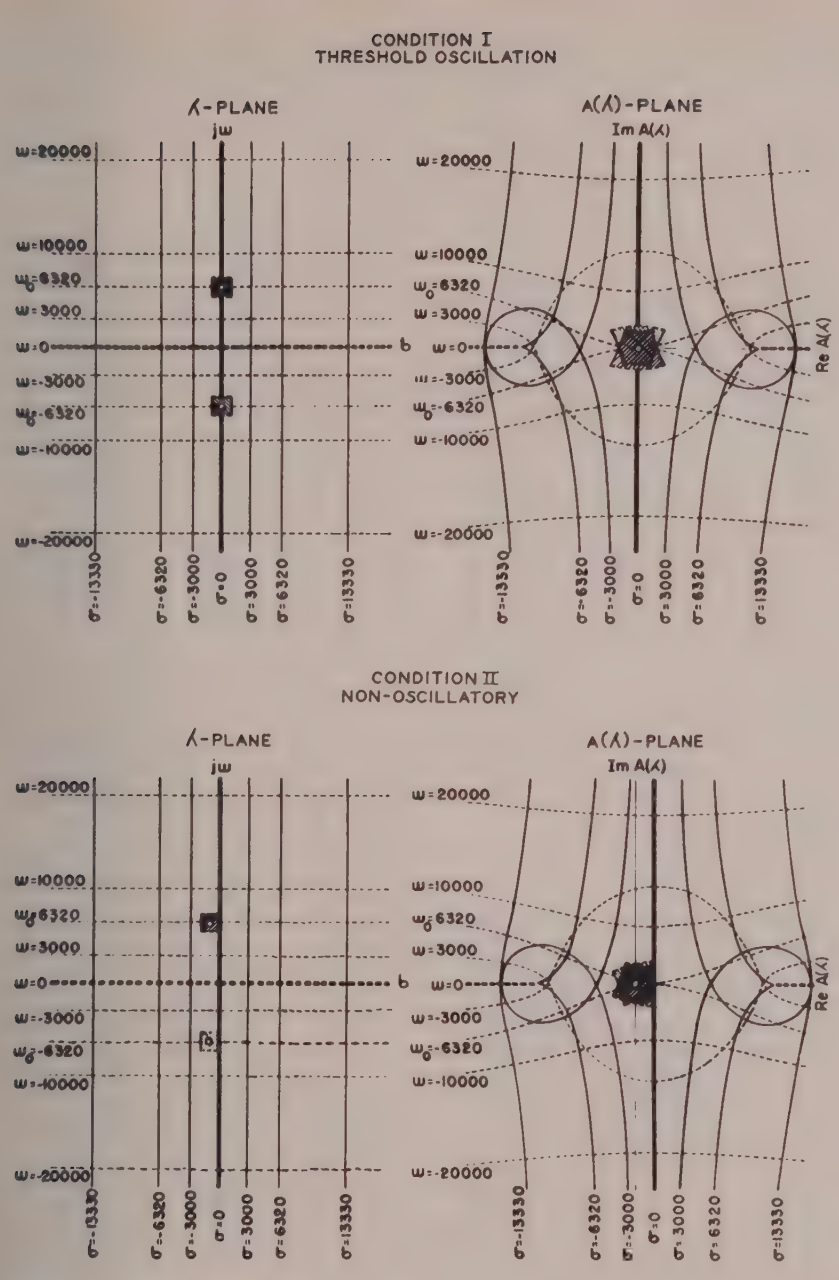

Figure 5. Mapping of the λ-plane onto the A(λ)-plane for the circuit shown in Figure 4 with parameter magnitudes for Condition I and II, Table I

and different circuit configuration.

In other words, the Nyquist $\mu\beta = 1$ rule, or the limited and the generalized transmission matrix criteria, are merely alternative expressions for obtaining the natural free response of networks which, for those comprising a finite number of lumped parameters, will be principally of the form $Ke^{\lambda t}$. The exponential term includes the parameter λ which is defined as

$$\lambda = \sigma + j\omega \tag{13}$$

and generally is called the complex frequency. Depending upon whether the real part of λ is negative, zero, or positive, the natural or transient response will decay, be stationary, or increase unendingly in magnitude with time. Of course, the latter condition is limited physically by nonlinearity or rupture of the network; while the case $\sigma = 0$ also requires special means for the continuation of constant amplitude oscillations.

The most illuminating, although not necessarily the most practicable, approach to the determination of whether any of the λ-roots of the criteria have positive real parts is that of mapping the λ-plane onto the $A(\lambda)$ plane.

Thus, if the λ-plane is mapped onto the plane defined by

$$A(\lambda) = a_{11}(\lambda) + a_{22}(\lambda) - |a(\lambda)| - 1 \tag{14}$$

then the values of λ corresponding to roots of $A(\lambda)$ will predict the natural responses of the network after the transmission loop is closed. This will be illustrated in the following section by application of the criterion to the circuit shown in Figure 1.

An additional point is, of course, that the criteria do not indicate the stability of the open-loop connection, but predict the conditions after the loop is closed. In networks employing bilateral networks, the oscillations present on open loop may well cease when the transmission loop is closed. The stability of open-loop conditions must be investigated independently in an identical manner.

Application of the Generalized Matrix Criterion

As an example of the application of the generalized transmission matrix stability criterion, consider Figure 4. This shows the feedback network of Figure 1, but now emphasizing the tandem connection of double-dinodes.

The over-all transmission matrix for the open loop shown in Figure 4 is given by:

$$[a^0] = [a^1] \cdot [a^2] \cdot [a^3] \tag{15}$$

in which

$$[a^1] = \frac{1}{g_m - g_c}\begin{bmatrix} -(g_b+g_c+g_p) & -1 \\ -(g_a+g_c+g_g)(g_b+g_c+g_p) - g_c(g_m-g_c) & -(g_a+g_c+g_g) \end{bmatrix} \tag{16}$$

$$[a^2] = \begin{bmatrix} 1 & 0 \\ \lambda C + g_{LC} + 1/\lambda L & 1 \end{bmatrix} \tag{17}$$

and

$$[a^3] = \begin{bmatrix} 1/\pm n & 0 \\ g_t/\pm n & \pm n \end{bmatrix} \tag{18}$$

Performing the operation indicated by equation 15 and substituting the results into the generalized criterion, equation 12

$$A(\lambda) = a_{11}{}^0 + a_{22}{}^0 - |a^0| - 1$$

then yields

$$A(\lambda) = \frac{g_a + g_b + 4g_c + g_g + g_p + g_{LC} + g_t - g_m + \lambda C + 1/\lambda L}{g_m - g_c} \tag{19}$$

in which the transformer turns ratio is taken as $n = -1$.

Equation 19 may be employed in several different ways. For example, the circuit conditions for the initiation of spontaneous oscillations are given by equating the real and imaginary parts of equation 19 to zero, which gives:

$$g_a+g_b+4g_c+g_g+g_p+g_{LC}+g_t=g_m \quad (20a)$$

$$\omega C+1/j\omega L=0 \quad (20b)$$

Another possibility — in view of the simplicity of equation 19 — is to solve for the complex roots $\lambda=\sigma\pm j\omega$ of $A(\lambda)=0$; these roots are the coefficients of the exponents of the exponential terms of the network transient response. It will be found that the parameter magnitudes tabulated in Table I lead to the following results when substituted into equation 19 and the roots of $A(\lambda)$ computed:

Condition I	Roots of $A(\lambda)$
Threshold of oscillations	$\lambda_1=64+j\ 0.995\omega_0$ $\lambda_2=64-j\ 0.995\omega_0$
Condition II	
Nonoscillatory ($\omega_0=2\pi 1{,}006$)	$\lambda_1=-1{,}018+j0.986\omega_0$ $\lambda_2=-1{,}018-j0.986\omega_0$

It is evident that Condition I parameters yield a pair of complex roots with a small positive real part and predict oscillations of the circuit shown in Figure 4 upon closing the loop. Condition II parameters lead to complex roots with negative real parts and thus predict that sustained oscillations will not result upon closing the loop. Both sets of computations agree with the physics of the problem.

Another presentation which situates the phenomena in a very clear light, as previously mentioned, is to map the λ-plane onto the $A(\lambda)$-plane for the two sets of numerical data given in Table I. This has been done in Figure 5, and provides a means for determining the type of oscillations which will ensue in the closed network. It will be noted that the $j\omega$ axis of the λ-plane mapped onto the $A(\lambda)$-plane separates the regions of positive σ from those of negative σ.

For Condition I parameters, the areas in the locality of $\lambda=0\pm j2\pi 1{,}000$ of the λ-plane map onto the region of zero of $A(\lambda)$. This indicates that oscillations just take place in the closed-loop network, for the points $A(\lambda)=0$, or the roots of $A(\lambda)$ correspond to $\lambda=\sigma\pm j\omega=64\times10^{-6}\pm j2\pi 995$ on the λ-plane.

For Condition II, the areas in the vicinity of $A(\lambda)=0$, or the roots of $A(\lambda)$, correspond to the areas in the vicinity of $\lambda=\sigma\pm j\omega=-1018\times10^{-6}\pm j2\pi 986$ on the λ-plane. In other words, all transient waves damp out in the closed feedback loop circuit, and sustained oscillations will not take place.

Additional nteresting deductions may be drawn from Figure 5. For example, if the network conductances shown in Figure 4 are adjusted progressively so that the real part of equation 19 becomes increasingly negative (L, C, and thus ω_0 being kept unchanged), it may be seen that the network would oscillate with increasingly positive exponential magnitudes and at slightly decreasing frequencies. For small changes of the circuit parameters, this is easily demonstrated experimentally. Further increase of the negative real part of equation 19 will result finally in λ-roots with positive real parts only. That is, when the net real part of equation 19 is made more negative by increasing g_m (C, L, and thus ω_0 remaining unchanged), then there are no longer oscillations with an imaginary $j\omega$ frequency. Rather, the oscillations must be interpreted as of zero frequency, but of exponential form increasing rapidly with time, in spite of the fact that the network incorporates a tuned inductance-capacitance network. This appears to substantiate qualitatively the well-known condition of the blocking oscillator, wherein such exponential oscillations are initiated but with amplitudes which immediately go beyond the linear portions of the tube characteristic (for which this linear analysis holds), and thereby gives rise to the well-known multivibrator actions. Quantitative data unfortunately are rather difficult to obtain in this region since it emphatically represents a run-away condition.

Conclusions

For circuits with clearly defined transmission loops, the elegant and powerful matrix methods of computing the circuit performance are well known. The usefulness of these methods has been enhanced by the derivation of the generalized transmission matrix stability criterion, which is particularly useful for feedback circuits. This criterion predicts the closed-loop behavior of networks from matrix coefficients derived from the open transmission loop. Unlike the similar (but more limited) $\mu\beta-1=0$ rule, the generalized matrix criterion applies to transmission networks with bilateral transmission properties, and the transmission loop for which the matrix coefficients are computed may be cut at any desired point at will.

The specific examples of the application of the $\mu\beta-1=0$ rule and the generalized matrix criterion to a definite network serve to illustrate the theoretical deductions and to emphasize that only the latter predicted stability in accordance with the physics of the problem.

Finally, it should be clear that the matrix criterion derived applies not only to purely electric networks. The matrix criterion applies equally well to electromechanical networks, or servomechanisms to use Hazen's term.[15] In fact, the matrix criterion was deduced during the course of an investigation of the stability of an electromechanical transducer (which employs feedback) for the testing of seismometers.[16]

References

1. Lehrbuch der Elektronen-Röhren, Band III [Textbook of Electron Tubes, volume III] (book, in German), **H. Barkhausen.** S. Hirzel, Leipzig, Germany, 1935.

2. Stabilized Feed-back Amplifiers, **H. S. Black.** *Electrical Engineering* (*AIEE Transactions*), volume 53, January 1934, pages 114–20.

3. Regeneration Theory and Experiment, **E. Peterson, J. G. Kreer, L. A. Ware.** *Proceedings*, Institute of Radio Engineers (New York, N. Y.), volume 22, 1934, pages 1191–1210.

4. Regeneration Theory, **H. Nyquist.** *Bell System Technical Journal* (New York, N. Y.), volume 11, 1932, pages 126–47.

5. Stabilization of Feedback Oscillators, **H. Jefferson.** *Wireless Engineer* (London, England), volume 22, 1945, pages 384–89.

6. The Tapered Phase-Shift Oscillator, **P. G. Sulzer.** *Proceedings*, Institute of Radio Engineers (New York, N. Y.), volume 36, 1948, pages 1302–05.

7. The Design of R. C. Oscillator Phase Shifting Networks, **W. R. Hinton.** *Electronic Engineering* (London, England), volume 22, 1950, pages 13–17.

8. Frequency-Constants and Spurious Oscillations of a Bridge-Stabilized Low-Frequency Oscillator (in German), **H. Mathes.** *Frequenz*, (Berlin, Germany), volume 4, 1950, pages 1–10.

9. Communication Networks (book), **E. A. Guillemin.** John Wiley and Sons, Inc., New York, N. Y., volume II, 1935.

10. Matrices in Engineering, **L. A. Pipes.** *Electrical Engineering* (*AIEE Transactions*), volume 56, September 1937, pages 1177–90.

11. Matrix Theory of Four-Terminal Networks, **L. A. Pipes.** *The Philosophical Magazine* (London, England), series 7, volume 30, 1942, pages 370–95.

12. The Transient Behaviour of Four Terminal Networks, **L. A. Pipes.** *The Philosophical Magazine* (London, England), series 7, volume 33, 1942, pages 174–214.

13. Einführung in die Vierpoletheorie [Introduction to Four-Pole Theory] (book, in German), **R. Feldtkeller.** S. Hirzel, Leipzig, Germany, 1943.

14. The Application of Matrices to Vacuum-Tube Circuits, **J. S. Brown, F. D. Bennett.** *Proceedings*, Institute of Radio Engineers (New York, N. Y.), volume 36, 1948, pages 844–52.

15. Theory of Servo-Mechanisms, **H. L. Hazen.** *Journal*, Franklin Institute (Philadelphia, Pa.), volume 218, 1934, pages 279–331.

16. The Application of Feedback to an Electromechanical Transducer for Seismograph Testing, **P. M. Honnell.** *Bulletin*, Seismological Society of America (Berkeley, Calif.), volume 40, number 3, July 1950, pages 217–31.

Discussion

Banesh Hoffmann (Queens College, Flushing, N. Y.): In his interesting paper on the criterion for stability, Professor Honnell expresses his results in terms of the components of the transmission matrix; and, as I understand it, the versatility of his criterion stems directly from the use of this matrix.

The following remarks may serve to amplify some aspects of his work and to point up the versatility of his criterion by showing how the same general ideas look when expressed in terms of impedance and admittance matrices.

Let us write Honnell's equation 6 in the form

$$\begin{bmatrix} E_1 \\ E_n \end{bmatrix}=\begin{bmatrix} Z_{11}Z_{1n} \\ Z_{n1}Z_{nn} \end{bmatrix}\begin{bmatrix} I_1 \\ I_n \end{bmatrix} \quad (1)$$

This is done by first writing his equation 6 in the expanded form

$$E_1 = a_{11}{}^o E_n - a_{1n}{}^o I_n$$
$$I_1 = a_{n1}{}^o E_n - a_{nn}{}^o I_n \qquad (2)$$

and then solving for E_1, E_n in terms of I_1, I_n.

The computation is quite straightforward, and yields the result

$$E_1 = \frac{a_{11}{}^o}{a_{n1}{}^o} I_1 + \frac{|a^o|}{a_{n1}{}^o} I_n$$

$$E_n = \frac{1}{a_{n1}{}^o} I_1 + \frac{a_{nn}{}^o}{a_{n1}{}^o} I_n \qquad (3)$$

From this we infer that

$$Z_{11} = \frac{a_{11}{}^o}{a_{n1}{}^o},\ Z_{1n} = \frac{|a^o|}{a_{n1}{}^o}$$

$$Z_{n1} = \frac{1}{a_{n1}{}^o},\quad Z_{nn} = \frac{a_{nn}{}^o}{a_{n1}{}^o} \qquad (4)$$

On solving these equations for the a's in terms of the Z's, we find that

$$a_{11}{}^o = \frac{Z_{11}}{Z_{n1}},\ a_{1n}{}^o = \frac{|Z|}{Z_{n1}}$$

$$a_{n1}{}^o = \frac{1}{Z_{n1}},\quad a_{nn}{}^o = \frac{Z_{nn}}{Z_{n1}} \qquad (5)$$

and also that

$$|a^o| = \frac{Z_{1n}}{Z_{n1}} \qquad (6)$$

Thus, using equations 5 and 6, we find that Honnell's expression $A(\lambda)$, defined in his equation 12, takes the form

$$A(\lambda) = a_{11}{}^o + a_{nn}{}^o - |a^o| - 1$$
$$= \frac{1}{Z_{n1}}\{Z_{11} + Z_{nn} - Z_{1n} - Z_{n1}\} \qquad (7)$$

The numerator of the expression on the right of equation 7 has a simple physical interpretation. For, consider the effect of closing the feedback loop on the double dinode network in Honnell's Figure 3. Before closing the loop, the network has an impedance matrix

$$[Z] = \begin{bmatrix} Z_{11} & Z_{1n} \\ Z_{n1} & Z_{nn} \end{bmatrix} \qquad (8)$$

After closing the loop, its impedance matrix reduces to a single element, the value of which may be found by inspection, or by applying a Kron transformation to the matrix in equation 8. Let us use the latter method.

Since we are dealing with impedances rather than admittances, we are concerned with the currents produced by impressed electromotive forces rather than with the electromotive forces produced by impressed currents. Thus, we interpret the closing of the feedback loop as imposing a constraint on the currents so that

$$I^n = -I^1 \qquad (9)$$

This may be written as the transformation

$$I^1 = \mathbf{I},\ I^n = -\mathbf{I} \qquad (10)$$

or

$$\mathbf{I} = [1 - 1]\begin{bmatrix} I^1 \\ I^n \end{bmatrix} \qquad (11)$$

Using the transformation matrix defined by equation 11, we now have for the new impedance

$$\mathbf{Z} = [1 - 1]\begin{bmatrix} Z_{11} & Z_{1n} \\ Z_{n1} & Z_{nn} \end{bmatrix}\begin{bmatrix} 1 \\ -1 \end{bmatrix}$$
$$= Z_{11} + Z_{nn} - Z_{1n} - Z_{n1} \qquad (12)$$

Thus the numerator in the expression on the right of equation 7 is just the impedance of the network that results when the feedback loop is closed. For the circuit to be oscillatory Honnell's criterion amounts to the familiar requirement that this impedance be zero.

If the impedance is zero, a zero impressed electromotive force can give rise to nonzero currents. The total impressed electromotive force is $E - E_n$. To reduce this to zero, we must have

$$E_1 = E_n \qquad (13)$$

Honnell applies the restraints, equations 9 and 13 simultaneously. If we do this on equation 1, we find

$$E_1 = (Z_{11} - Z_{n1})I_1$$

$$E_1 = -(Z_{n1} - Z_{nn})I_1 \qquad (14)$$

from which we at once obtain

$$Z_{11} + Z_{nn} - Z_{1n} - Z_{n1} = 0 \qquad (15)$$

From what we have written so far, there does not appear to be any marked advantage in the use of the transmission matrix. Indeed, the derivation of equation 15 by the imposition of the double restraint is infinitesimally quicker than the corresponding derivation of Honnell's criterion.

But let us now consider the case in which we are interested in the electromotive forces produced by impressed currents. Here we are concerned with admittances rather than impedances. We, therefore, wish to express Honnell's equation 6 in the form

$$\begin{bmatrix} I^1 \\ I^n \end{bmatrix} = \begin{bmatrix} Y^{11} & Y^{1n} \\ Y^{n1} & Y^{nn} \end{bmatrix}\begin{bmatrix} E_1 \\ E_n \end{bmatrix} \qquad (16)$$

The procedure is similar to that in the preceding case. We write Honnell's equation 6 in the form

$$I_1 = \frac{a_{nn}{}^o}{a_{1n}{}^o} E_1 - \frac{|a^o|}{a_{1n}{}^o} E_n$$

$$I_n = -\frac{1}{a_{1n}{}^o} E_1 + \frac{a_{11}{}^o}{a_{1n}{}^o} E_n \qquad (17)$$

from which we infer that

$$Y^{11} = \frac{a_{nn}{}^o}{a_{1n}{}^o},\quad Y^{1n} = -\frac{|a^o|}{a_{1n}{}^o}$$

$$Y^{n1} = -\frac{1}{a_{1n}{}^o},\quad Y^{nn} = \frac{a_{11}{}^o}{a_{1n}{}^o} \qquad (18)$$

Solving for the a's in terms of the Y's, we find

$$a_{11}{}^o = -\frac{Y^{nn}}{Y^{n1}},\ a_{1n}{}^o = -\frac{1}{Y^{n1}}$$

$$a_{n1}{}^o = -\frac{|Y|}{Y^{n1}},\ a_{nn}{}^o = -\frac{Y^{11}}{Y^{n1}} \qquad (19)$$

and

$$|a^o| = \frac{Y^{1n}}{Y^{n1}} \qquad (20)$$

Thus Honnell's expression $A(\lambda)$ now takes the form

$$A(\lambda) = a_{11}{}^o + a_{nn}{}^o - |a^o| - 1$$
$$= -\frac{1}{Y^{n1}}\{Y^{11} + Y^{nn} + Y^{n1} + Y^{1n}\} \qquad (21)$$

The numerator of the expression on the right of equation 21 turns out to be the admittance, $\mathbf{Y}$, of the network that results when the feedback loop is closed. Honnell's criterion here amounts to the familiar requirement that this admittance be zero. We may obtain this result directly by applying the simultaneous restraints, equations 9 and 13 to the basic equation 16, just as in the impedance case above.

The impedance and admittance cases are distinct. If they were not they would be contradictory, for setting $\mathbf{Z}$ equal to zero would imply that $\mathbf{Y}$ was infinite, and vice versa. The distinction apparently arises from the fact that when we are concerned with impedances, we regard the electromotive forces as impressed, and thus probe the closed-loop network at a mesh; while when we are concerned with admittances, we treat the currents as impressed, and therefore probe the network at a junction pair.

The interesting thing is that Honnell's single expression $A(\lambda)$ handles these two cases equally. This is in keeping with his remark that his method applies no matter where one cuts the transmission network.

Laurence G. Cowles (Bellaire, Tex.): Mr. Honnell's paper, according to the author's own conclusions, presumes to enhance the usefulness of the elegant and powerful matrix methods of computing circuit performance by the derivation of a generalized transmission matrix stability criterion.

In a brief critique of Nyquist's method the author first demonstrates that the Nyquist test is not applicable to a simple network, see Figure 1 of the paper. Since the author completely ignores the loading effect of the grid circuit upon the plate of the tube it is misleading to imply that even a first approximation of Nyquist's method has been attempted. I find that on making simple approximations to the input grid load, including feedback, one obtains a measure of stability in agreement with that secured by the author's elaborate matrix method. The real difficulties of Nyquist's method have been discussed in detail by Bode and need not be elaborated upon here but the source of the difficulty is not that obvious approximations cannot be used in such elementary examples.

The author's definition of the term double-dinode is inadequate, therefore a detailed description should be given of the constraints placed on a 4-terminal network functioning as a double-dinode. Is a special term really necessary?

Equations 8 and 10 arise because a network closed upon itself is subject to certain restrictions. These equalities are called by the author, "special stability criterions." Actually, equations 8, 10, and 12 exist regardless of whether or not the network is stable and therefore cannot be criterions (that is, a test) of stability. Moreover, con-

trary to the author's statement these relations cannot hold for all time because times prior to the closing of the transmission network must be excluded.

The succeeding section of the paper is, "a generalization of the special transmission matrix stability criterions . . . . obtained in an analogous manner." Since the problem of stability was treated over a half century ago by Routh, Hurwitz and others who have shown simply how stability could be determined from the characteristic equations (including very general systems), I would like to know how the author's equation 12, which is restricted to a special class of networks, is more convenient, simpler, or, in fact, different from the classical treatment of the problem when applied to closed systems as outlined, for example, in Section 7.4 of Bode's book.

A final section of the paper is an application of the matrix methods to an oscillator of the simplest type. Prior discussion in the paper has been concerned with the stability of feedback amplifiers presumably degenerative. However, connected degeneratively the example is obviously stable, whereas, the most elementary possible test of the stability criterion. is afforded by the in-phase connection. A much more illuminating example of the application of matrix algebra and of the generalized stability criterion would be afforded by a consideration of the stability of a servo-system of moderate complexity having at least three feedback paths with reactances at several points throughout the network.

The author's example is a bit unfortunate as it fails to demonstrate that the matrix methods effect some simplification. In fact, in more complex problems the solution for the roots of the characteristic equations soon become so difficult that it is unlikely matrix algebra could appreciably simplify any really practical problem. Further, on closing the loop in Figure 1, five of the six resistors are simply in parallel and the 1:1 transformer only changes sign so that both Figures 1 and 4 boil down to the simplest form of tuned plate oscillator. Matrix algebra was never intended as a substitute for simple arithmetic or for the carrying along of factors directly additive. Obvious trivialities must be stripped from problems long before we can afford to limit scientific literature to those who have been able to acquire an understanding of matrix notation and skill in the use of matrix algebra.

In closing, I would point out that Mr. Honnell has overlooked inclusion, in his extensive bibliography, of reference to several volumes treating with feedback systems. Introductions to advanced methods usually begin with a careful discussion of the difficulties in the classical approach. Everday problems have now reached such a state of complexity that their solution is usually handled by a specialist, consequently relatively few people know of and understand the tremendous progress represented by the work of present day pioneers in the theory of feedback systems.

Pierre M. Honnell: Dr. B. Hoffmann's discussion penetrates directly to the heart of the matter. He shows very clearly that the generalized transmission matrix stability criterion is an *alternative* method of expressing the stability condition given by the vanishing of the impedance and admittance of the closed transmission loop, corresponding to the two modes of probing the network. It is clear that the stability of a network, when stated in terms of electromotive forces and currents, must rest ultimately upon Kirchoff's Laws. The $[Z]$ and $[Y]$ matrices are direct expressions of these laws, and Dr. Hoffmann therefore quite accurately interprets the transmission matrix criterion in terms of these more familiar expressions.

Except for the concepts involved (which are fundamentally interesting and important in their own right) the question of which criterion is the most convenient for a specific example depends upon the network. This is analogous to the problem of whether the $[Z]$ or $[Y]$ matrix is the more useful in a given situation, which is decided principally by the network topology. Similarly, the transmission matrix is preferable for those networks for which the wave transmission properties are emphasized. That is, for topological configurations consisting of a transmission loop constructed of a number of double-dinodes connected in tandem. Here the advantages of the matrix analysis and of the transmission matrix stability criterion are pre-eminent.

Loci of Complex Impedance and Admittance Functions

EDWARD L. MICHAELS
ASSOCIATE AIEE

THE aim of this paper is to present a systematic and useful investigation of the loci of complex impedance and admittance functions of various combinations of 2-terminal, 3-element, linear, dissipative networks at all frequencies. The curves are extremely useful in the solution of many electrical engineering problems because of the direct, straightforward manner in which they show graphically the resistive and reactive components of complex impedance and admittance, the magnitude of impedance and admittance, and the phase shift at all frequencies between zero and infinity.

Curves of impedance and admittance in the complex plane not only give a large amount of useful information, but also reveal that the 16 possible combinations of 2-terminal 3-element networks fall into four main groups of four networks each. The important relationships which exist among the four networks of each group further enhance the usefulness of the curves. These relationships involve the concepts of inverse, reciprocal, and equivalent networks.

The first important concept is that of inverse networks. Two networks with impedances Z_1 and Z_2 are each the inverse of the other with respect to a real constant R if they satisfy the relation

$$Z_1 Z_2 = R^2 \tag{1}$$

or

$$Y_1 Y_2 = 1/R^2 \tag{2}$$

Paper 51-47, recommended by the AIEE Basic Sciences Committee and approved by the AIEE Technical Program Committee for presentation at the AIEE Winter General Meeting, New York, N. Y., January 22–26, 1951. Manuscript submitted March 14, 1950; made available for printing December 5, 1950.

EDWARD L. MICHAELS is with The Rauland Corporation, Chicago, Ill.

where Y_1 and Y_2 are the admittances of the two networks. Corresponding elements appearing in the inverse networks are related by

$$L/C = R^2 \tag{3}$$

where L is inductance in henrys, C is capacitance in farads, and R is resistance in ohms. Thus, the inverse of an inductance is a capacitance, and vice versa. Furthermore, elements appearing in series in a given network appear as inverse elements in parallel in the inverse network, as indicated in Figures 1 and 2. Conversely, elements appearing in parallel in a given network appear as inverse elements in series in the inverse network.

As an example of inverse networks, consider the two networks in the upper half of Figure 1. The impedance of the parallel resistance-capacitance combination is, in normalized form,

$$Z_1/R = 1/(1+j\omega RC) \tag{4}$$

To find the impedance of the inverse network, a series resistance-inductance network, equation 1 is used. The normalized impedance is, therefore,

$$Z_2/R = 1/(Z_1/R) \tag{5}$$

$$= 1+j\omega RC \tag{6}$$

However, equation 6 is not correct until C is replaced by its inverse, L, in accordance with equation 3. Thus,

$$Z_2/R = 1+j\omega R(L/R^2) \tag{7}$$

Equation 6 in correct form is then

$$Z_2/R = 1+j\omega L/R \tag{8}$$

The second important concept deals with reciprocal networks. Two networks are the reciprocal of each other if (1) the impedance of one is the conjugate of the impedance of the other, (2) the normalized frequency of one is the reciprocal of that of the other, and (3) corresponding elements are inverse in accordance with equation 3, but with the configuration of the network unchanged. An example of two reciprocal networks is shown in the right half of Figure 1. The normalized impedance of the series resistance-inductance network is given by

$$Z_2/R = 1+j(F/F_0) \tag{9}$$

where the ratio F/F_0 is defined as the normalized frequency. For this network it is

$$F/F_0 = \omega L/R \tag{10}$$

where

$$F_0 = R/2\pi L \tag{11}$$

is defined as the critical frequency and F is the frequency.

The reciprocal of the series resistance-inductance network is, as shown in Figure 1, a series resistance-capacitance network. To find its normalized impedance Z_3/R from equation 8, the first step is to take its conjugate, as follows:

$$Z_3/R = 1-j\omega L/R \tag{12}$$

The next step is to take the reciprocal of its normalized frequency:

$$Z_3/R = 1-jR/\omega L \tag{13}$$

The last step is to replace L by its inverse in accordance with equation 3. Then, the correct equation becomes

$$Z_3/R = 1-jl/\omega RC \tag{14}$$

Inspection of Figure 1 will confirm that elements appearing in series in a given network will appear as inverse elements also in series in the reciprocal network. Similarly, elements in parallel in a given network also appear as inverse elements in parallel in the reciprocal network.

The third important concept is that of equivalent networks. Two networks with impedances Z_1 and Z_2 are equivalent if

$$Z_1 = Z_2 \tag{15}$$

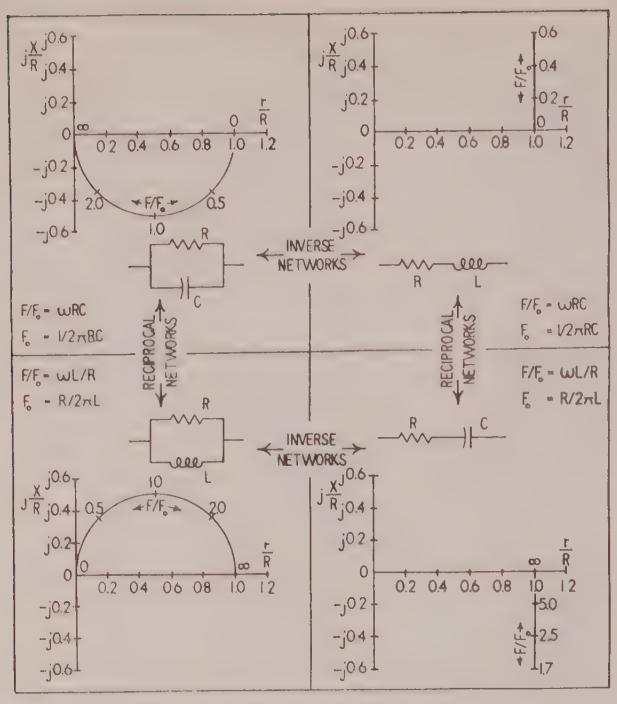

Figure 1. Normalized complex impedance curves for 2-element networks

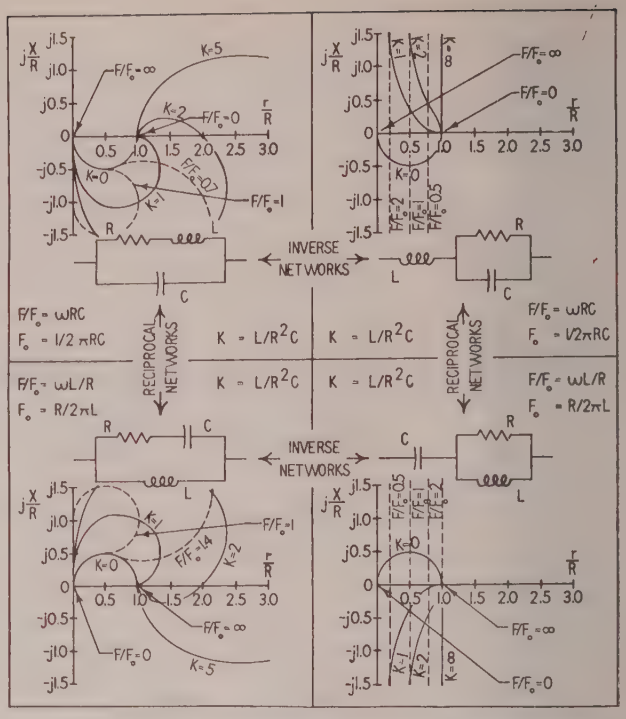

Figure 2. Normalized complex impedance curves for the four networks of group 1

at corresponding frequencies. Elements occurring in series in a given network appear not as inverse elements, but as elements of the same type in parallel in the equivalent network. Similarly, elements in parallel in a given network appear in series in the equivalent network. Examples of equivalent networks are shown in Figure 7.

The impedance curves for 2-element networks are given in Figure 1 as an introduction to the method used in plotting the impedance and admittance curves for the 3-element networks. In each of the four plots in Figure 1, the real and

Figure 3. Detailed plot of complex impedance and admittance for networks 1 and 2, respectively

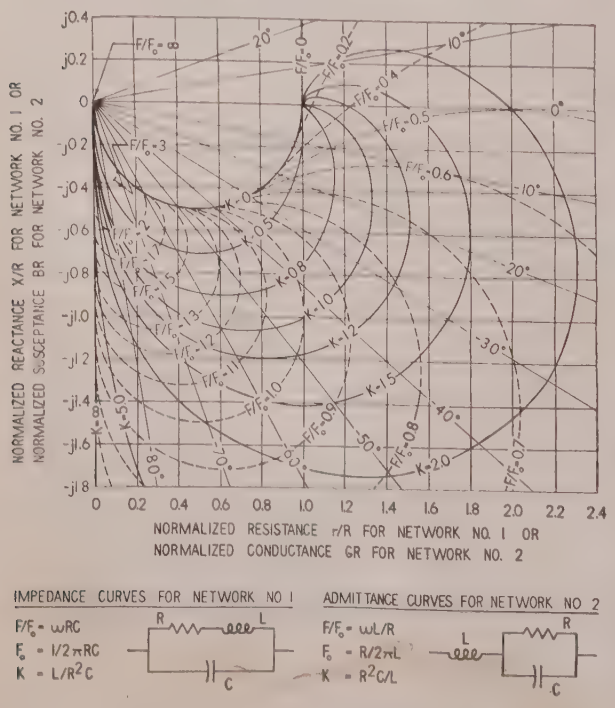
NORMALIZED REACTANCE X/R FOR NETWORK NO. 1 OR
NORMALIZED SUSCEPTANCE BR FOR NETWORK NO. 2
NORMALIZED RESISTANCE r/R FOR NETWORK NO. 1 OR
NORMALIZED CONDUCTANCE GR FOR NETWORK NO. 2
IMPEDANCE CURVES FOR NETWORK NO 1
F/F₀ = ωRC
F₀ = 1/2πRC
K = L/R²C
ADMITTANCE CURVES FOR NETWORK NO 2
F/F₀ = ωL/R
F₀ = R/2πL
K = R²C/L

Figure 4. Replot of Figure 3 with the normalized frequency parameter changed

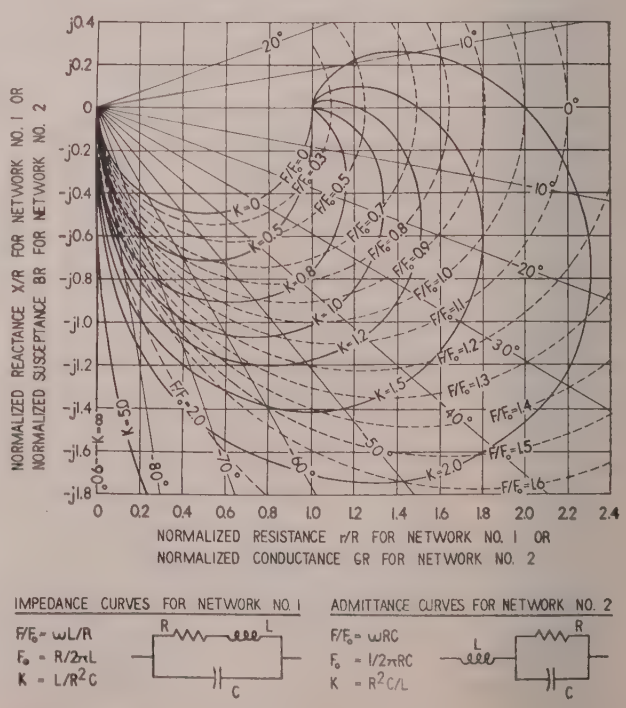
NORMALIZED REACTANCE X/R FOR NETWORK NO. 1 OR
NORMALIZED SUSCEPTANCE BR FOR NETWORK NO. 2
NORMALIZED RESISTANCE r/R FOR NETWORK NO. 1 OR
NORMALIZED CONDUCTANCE GR FOR NETWORK NO. 2
IMPEDANCE CURVES FOR NETWORK NO. 1
F/F₀ = ωL/R
F₀ = R/2πL
K = L/R²C
ADMITTANCE CURVES FOR NETWORK NO. 2
F/F₀ = ωRC
F₀ = 1/2πRC
K = R²C/L

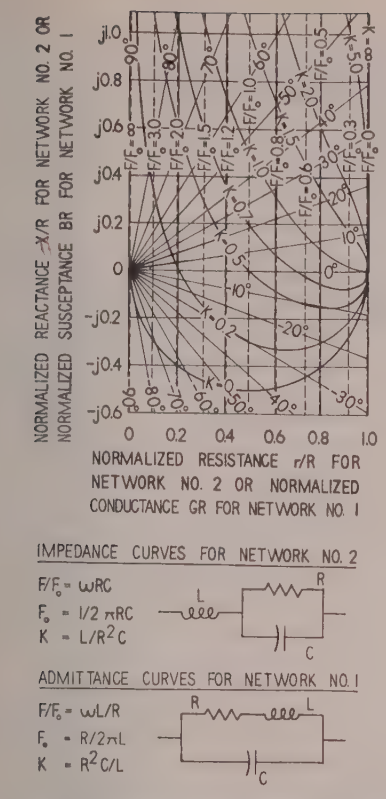
NORMALIZED REACTANCE ±X/R FOR NETWORK NO. 2 OR NORMALIZED SUSCEPTANCE BR FOR NETWORK NO. 1
NORMALIZED RESISTANCE r/R FOR NETWORK NO. 2 OR NORMALIZED CONDUCTANCE GR FOR NETWORK NO. 1
IMPEDANCE CURVES FOR NETWORK NO. 2
F/F₀ = ωRC
F₀ = 1/2πRC
K = L/R²C
ADMITTANCE CURVES FOR NETWORK NO. 1
F/F₀ = ωL/R
F₀ = R/2πL
K = R²C/L

Figure 5. Detailed plot of complex impedance and admittance for networks 2 and 1, respectively

imaginary components of normalized impedance are plotted along the real and imaginary axes of the complex impedance plane, respectively. A nonuniformly distributed scale of normalized frequencies, F/F_0, exists on each of the four plots. In the cases of the semicircles, the entire range of frequencies is covered, from zero to infinity. Knowing the values of the parameters in any of these networks, it is readily apparent that the impedance of the network may be found graphically at any frequency either in complex or in polar form.

The same type of plot shown in Figure 1 for 2-element networks is shown in Figure 3 for four 3-element networks. Since an additional variable is introduced by the extra element, a family of curves results. For example, the resistance-inductance-capacitance network of the upper left section of Figure 2 differs from the resistance-capacitance network of the upper left section of Figure 1 only by the addition of an inductance in series with the resistance. As the size of the inductance is increased, the original semicircle bulges out further and further. Each curve of the resulting family of curves corresponds to a certain value of K, which in this case is directly proportional to L for a given R and C:

$$K = L/R^2C \tag{16}$$

A more detailed plot for this network is

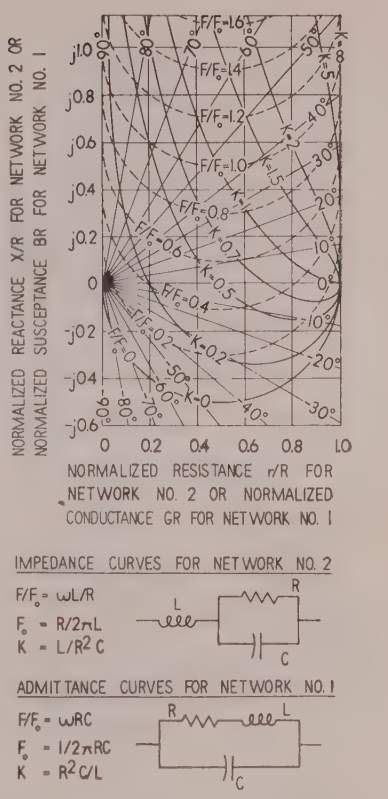
NORMALIZED REACTANCE X/R FOR NETWORK NO. 2 OR NORMALIZED SUSCEPTANCE BR FOR NETWORK NO. 1
NORMALIZED RESISTANCE r/R FOR NETWORK NO. 2 OR NORMALIZED CONDUCTANCE GR FOR NETWORK NO. 1
IMPEDANCE CURVES FOR NETWORK NO. 2
F/F₀ = ωL/R
F₀ = R/2πL
K = L/R²C
ADMITTANCE CURVES FOR NETWORK NO. 1
F/F₀ = ωRC
F₀ = 1/2πRC
K = R²C/L

Figure 6. Replot of Figure 5 with the normalized frequency parameter changed

Figure 7. Normalized complex impedance curves for the four networks of group 2

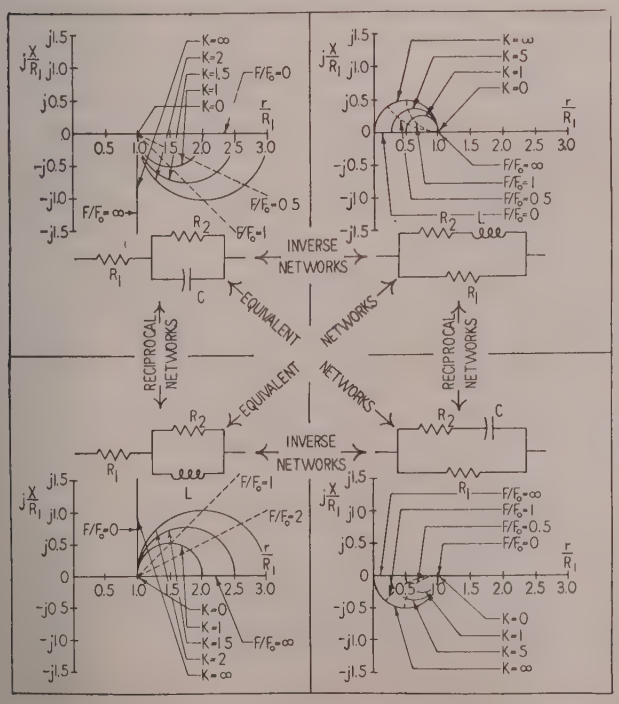

Figure 8. Detailed plot of complex impedance and admittance for networks 5 and 6, respectively

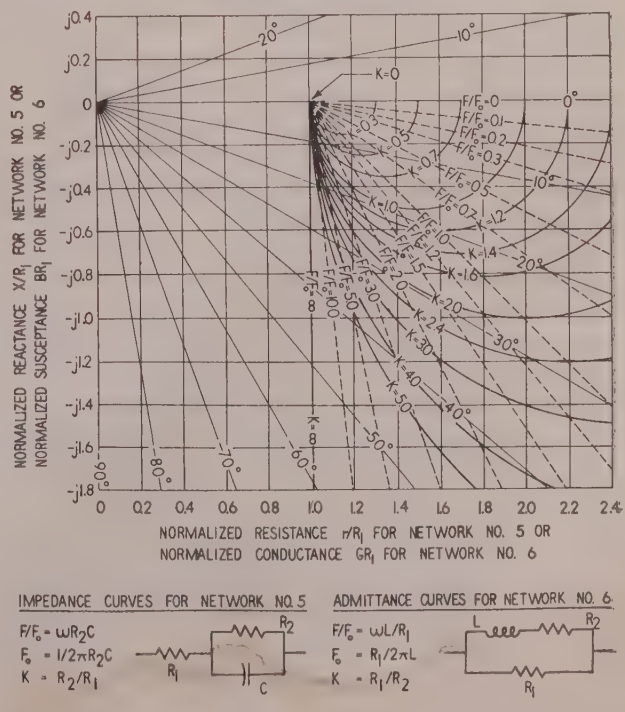
NORMALIZED REACTANCE X/R₁ FOR NETWORK NO. 5 OR NORMALIZED SUSCEPTANCE BR₁ FOR NETWORK NO. 6
NORMALIZED RESISTANCE r/R₁ FOR NETWORK NO. 5 OR NORMALIZED CONDUCTANCE GR₁ FOR NETWORK NO. 6
IMPEDANCE CURVES FOR NETWORK NO. 5
F/F₀ = ωR₂C
F₀ = 1/2πR₂C
K = R₂/R₁
ADMITTANCE CURVES FOR NETWORK NO. 6
F/F₀ = ωL/R₁
F₀ = R₁/2πL
K = R₁/R₂

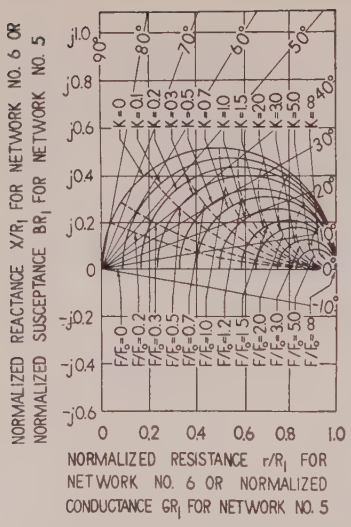
NORMALIZED REACTANCE X/R1 FOR NETWORK NO. 6 OR
NORMALIZED SUSCEPTANCE BR1 FOR NETWORK NO. 5
NORMALIZED RESISTANCE r/R1 FOR NETWORK NO. 6 OR NORMALIZED CONDUCTANCE GR1 FOR NETWORK NO. 5

Figure 9 (left). Detailed plot of complex impedance and admittance for networks 6 and 5, respectively

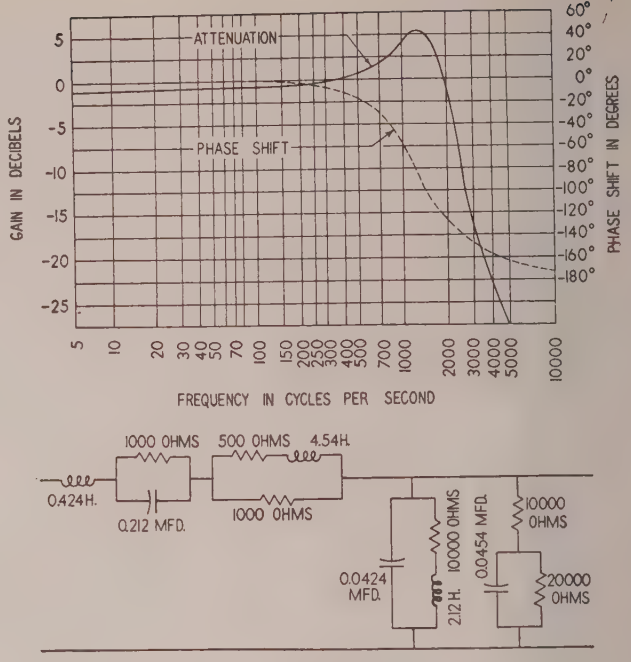

Figure 11 (right). Design of a low-pass filter with extremely low phase shift in the pass band

shown in Figure 3. Corresponding values of normalized frequency F/F_0 on each K curve are shown to lie on circles. For a fixed inductance and variable frequency a K curve becomes the impedance locus. For a fixed frequency and variable inductance an F/F_0 curve becomes the impedance locus. Impedance curves for the same network also are plotted in Figure 4. Here, however, F/F_0 was chosen as

Figure 10. Relationships among the various networks in each of the four basic groups

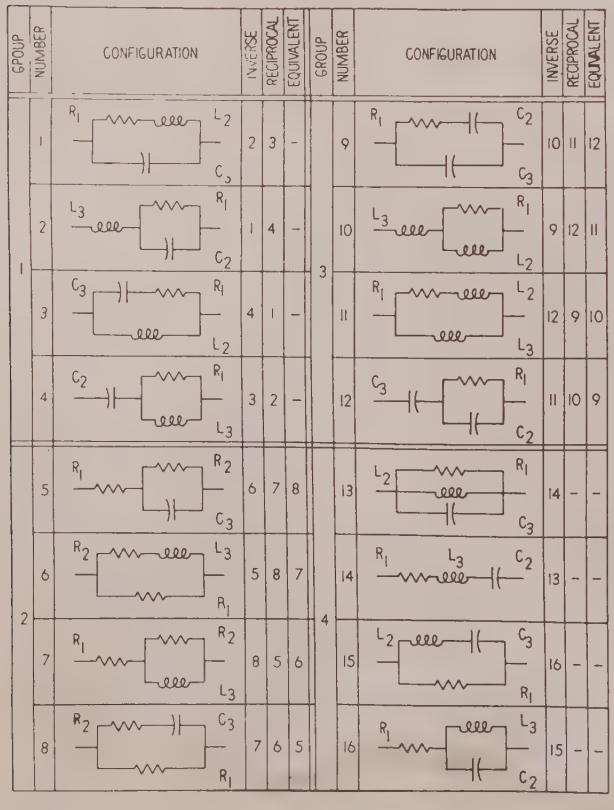

Figure 12. Design of a high- and low-frequency compensation network for a wide-band amplifier

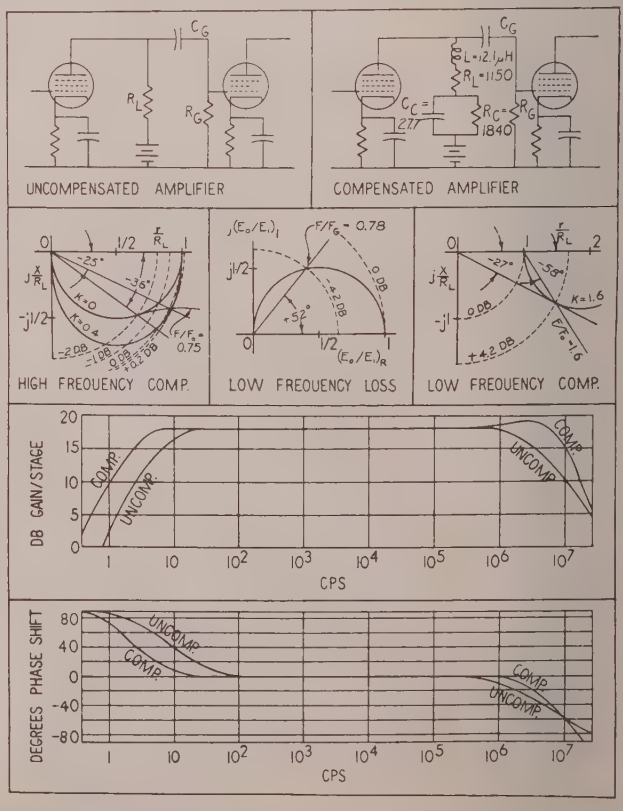

$\omega L/R$ instead of ωRC. Both Figures 3 and 4 represent the admittance curves for the corresponding inverse network.

The two plots shown in the upper half of Figure 2 are the inverse of each other with respect to R. A more detailed plot for the network in the upper right section of Figure 2 is shown in Figure 5. If the value of F/F_0 is changed from RC to L/R, the resulting curves will be those shown in Figure 6. The four networks of Figure 2, whose detailed curves are shown in Figures 3–6, constitute the first group of the four groups into which the 16 3-element networks have been classified. All four groups and 16 networks are tabulated in Figure 10.

The second group of networks is shown in Figure 7. The curves of the upper left and right sections are shown in more detail in Figures 8 and 9, respectively.

Applications

In one application a low-pass filter was designed to have very low phase shift from zero to 150 cycles per second. Use was made of the curves of Figures 5 and 9 for this design. The series arm of the filter, shown in Figure 11, consists of a combination of the network of Figure 5 for $K=0.2$ and of the network of Figure 9 for $K=0.5$. With these two networks in series, the phase shift of one canceled the phase shift of the other over the low-frequency range. The shunt arm of the filter consists of the inverses of these two networks. Thus, Figures 5 and 9 give the impedance curves for the networks in the series arm and the admittance curves for the networks in the shunt arm. The performance of this particular filter is shown in Figure 11.

In another application a wide-band amplifier was designed to have a variation in gain from the mid-band value of less than 0.2 decibels and a phase shift of less than 25 degrees between 5 cycles per second and 4.5 megacycles. A high- and low-frequency compensation network was designed, as summarized in Figure 12. The curves of Figure 3 were used for the high-frequency compensation, whereas the curves of Figure 8 were used for the low-frequency compensation.

Conclusions

Detailed impedance and admittance loci for several commonly used 2-terminal 3-element networks have been presented. The relationships existing among networks belonging to each of several groups were given.

Two applications were given to illustrate the usefulness of the curves. The number of possible applications is unlimited. As familiarity with the curves is gained, many specific applications suggest themselves. The curves are useful not only in communications, but also in connection with control circuits and other phases of electrical engineering.

The curves of normalized impedance and admittance presented here are particularly useful because of the wealth of information they contain. Network behavior is shown more completely and directly than by any other type of plot. The curves are especially useful in determining the most useful frequencies for accurate calculations and in showing readily the frequency ranges in which the effects of certain elements may be neglected.

Appendix

The impedance of network number 1, whose impedance curves are shown in Figure 3, is given by

$$\frac{Z_1}{R}=\frac{1+j\frac{\omega L}{R}}{1-\omega^2LC+j\omega RC} \tag{17}$$

or

$$\frac{Z_1}{R}=\frac{1+j(F/F_0)K}{1-(F/F_0)^2K+j(F/F_0)} \tag{18}$$

where

$$F/F_0=\omega RC \tag{19}$$

and

$$K=L/R^2C \tag{20}$$

By changing the normalized frequency as follows,

$$F/F_0=\omega L/R, \tag{21}$$

equation 17 becomes

$$\frac{Z_1}{R}=\frac{1+j(F/F_0)}{1-(F/F_0)^2K+j(F/F_0)K} \tag{22}$$

where

$$K=R^2C/L \tag{23}$$

A plot of equation 22 is shown in Figure 4. The curves of Figures 5 and 6 are the inverses of Figures 3 and 4, respectively.

The normalized impedance of network number 5, shown in Figure 8, is

$$\frac{Z_5}{R_1}=\frac{1+K+j(F/F_0)}{1+j(F/F_0)} \tag{24}$$

where

$$F/F_0=\omega R_2C \tag{25}$$

and

$$K=R_2/R_1 \tag{26}$$

The impedance of network number 8, the equivalent of network number 5, is

$$\frac{Z_8}{R_1}=\frac{1+K+j(F/F_0)\left(\frac{K+1}{K}\right)}{1+j(F/F_0)\left(\frac{K+1}{K}\right)} \tag{27}$$

where

$$F/F_0=\omega R_2C \tag{28}$$

and

$$K=R_2/R_1 \tag{29}$$

No Discussion

Contact Transients in Simple Electric Circuits

FRANK E. MARTIN
NONMEMBER AIEE

HENRY E. STAUSS
NONMEMBER AIEE

Synopsis: The proper functioning of electric contacts is of great importance. Much work has been done on contacts,[1,2] but comparatively little has been done on types of transient phenomena occurring at circuit break in inductive d-c circuits and their relation to contact erosion. Some work was done on transient types occurring at circuit break in telephone relay circuits by A. M. Curtis and his associates at the Bell Telephone Laboratories.[3] This study dealt with transients in d-c circuits, including the fixed inductance of a relay winding and the small distributed capacity of a line wire, and embodied a study of the effect on the transient phenomena of changing the length of the line wire. The present investigation covered the variation of transients occurring for a fixed contact pair over a range of lumped inductance and lumped capacity values in a contact circuit; in addition, effects on the transients of varying the steady-state current (by steady-state current is meant the current immediately preceding circuit break), the voltage impressed on the circuit, and the circuit resistance were studied.

Procedure

THE circuit shown in Figure 1 was used for this study. Capacity was introduced into the circuit at either of the positions indicated by the dotted lines. A single pair of silver alloy contacts in a telegraph key was employed throughout. The impressed electromotive force, always less than 100 volts, was provided by storage cells and a potential divider. Steady-state currents did not exceed 0.50 ampere.

Voltage transients were observed with an oscilloscope. Synchronized single sweeps were obtained by using a separate triggering circuit combined with a synchronizer employing delay circuits. With the voltage transients no amplifier was necessary. Leads from the contacts were short circuited through a 10-megohm potential divider and the voltage obtained from the divider was impressed directly on the deflecting plates of the oscilloscope. Another 10-megohm variable resistor was shunted across the line from the contacts and adjusted to eliminate 60-cycle ripple. The input circuit comprised of these two resistors provided the d-c return from the plates necessary for unbalanced signals. A high value in the recommended range of return resistance was chosen to minimize the effect of the measuring equipment on the phenomena being observed. Current transients were observed with a conventional oscilloscope. Timing oscillograms were interspersed between those of the transients. Measurements of the durations of transient components were restricted to regions of the oscillograms for which the sweep voltage was sufficiently linear for accurate relations to be established.

Experimental Results

Mr. Curtis identified two distinct types of transients, which he designated "A" and "B," and a mixed type. The classification was based on voltage characteristics. Transients corresponding to the "A" type are shown in Figures 2 and 3. These were characterized by a voltage plateau at about 300 volts, which was accompanied by a bluish-violet discharge at the contacts. Such plateaus frequently were preceded for short periods by the complex phenomena described in the following paragraphs, which for convenience we have designated as strikeovers. For steady-state currents above about 0.15 ampere, the plateaus frequently were preceded by arcs striking at about 12 volts. Such an arc is shown in Figure 8, and if both impressed voltage and steady-state current were high, as was the case here (90 volts and 0.5 ampere), voltage oscillations between arc and plateau levels frequently were observed. An arc-like discharge at about 70–130 volts, which was observed several times under similar conditions, also is shown in Figure 8.

"B" transients are shown in Figures 4 to 6. These consisted of a series of strikeovers or relaxation oscillations with high maximum voltages beginning at about 300 volts. In general the maximum voltages of successive strikeovers increased gradually, presumably because increased contact gap length led to increased breakdown voltage. Frequently a low-voltage arc occurred at the beginning of each strikeover. The rising and perforated lower base lines (zero contact voltage lines) in Figures 5 and 6 are evidences of these arcs (see Figure 8).

Paper 51-48, recommended by the AIEE Basic Sciences Committee and approved by the AIEE Technical Program Committee for presentation at the AIEE Winter General Meeting, New York, N. Y., January 22–26, 1951. Manuscript submitted August 17, 1950; made available for printing December 5, 1950.

FRANK E. MARTIN and HENRY E. STAUSS both are with the Naval Research Laboratory of the Office of Naval Research, Washington, D. C.

This paper is published with the permission of the United States Navy Department without endorsement of statements or opinions of the writers.

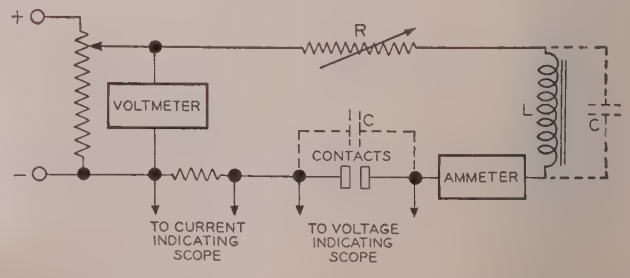

Figure 1. Contact circuit

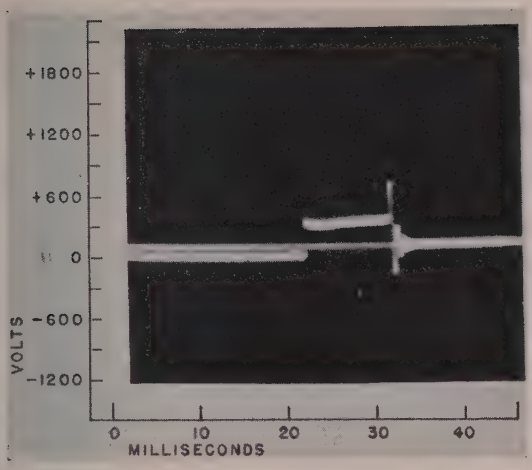

Figure 2 (left). Plateau transient, shunt capacity 160 micromicrofarads

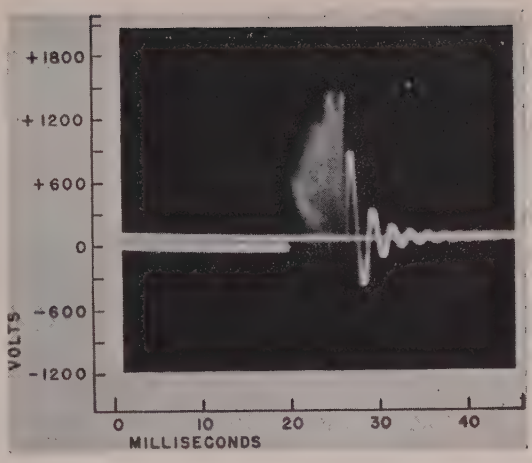

Figure 4 (right). Strikeover transient, shunt capacity 10,000 micromicrofarads

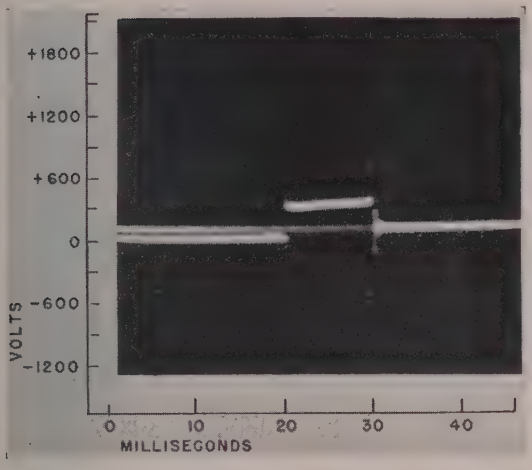

Figure 3 (left). Plateau transient, shunt capacity 1,000 micromicrofarads

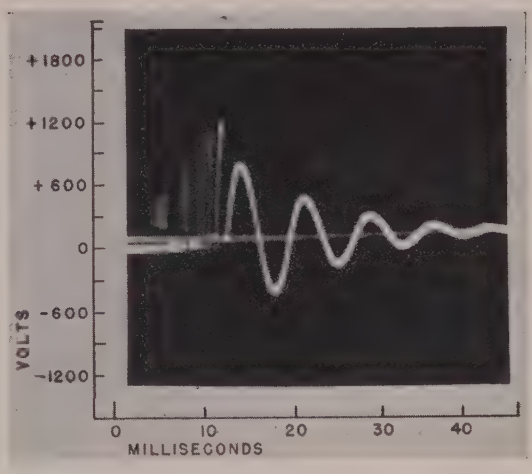

Figure 5 (right). Strikeover transient, shunt capacity 0.10 microfarad

Under these conditions, a greenish discharge was observed at the contacts. The "B" transient varied in frequency and maximum voltage with the capacity shunted across the contacts or the coil. Mixed plateau and strikeover transients were found, as in the earlier investigation.[3] In the present work plateau fragments were observed interspersed between strikeover series, and initial plateaus often gave way to strikeovers.

A comparison of Figures 2 to 7 with Figures 18 to 24 in Mr. Curtis' work shows that the sequence of transients obtained by shunting increased capacity across the coil was very similar to that obtained by lengthening the line wire. The greater transient duration in the present series is explained by the presence of greater inductance (nominal value 5 henrys) and capacities in the circuit. The transition series of Figures 2 to 7 was obtained for an impressed electromotive force of 90 volts and a steady-state current of 0.30 ampere. However, a similar transition sequence for increasing shunt capacities was observed for impressed voltages from 30 to 90 volts and steady currents from 0.05 to 0.50 ampere, and for an inductance as low as 520 millihenrys. Apparently the following relations are true for any values of impressed voltage, steady-state current, and inductance for which plateau transients may be observed:

1. For low shunt capacities plateau transients predominate.
2. As the shunt capacity is increased plateau transients give way to strikeover and mixed transients with the former predominating.
3. These in turn give way for high capacities to damped sinusoidal phenomena similar to those terminating the other transients.

Damped sinusoidal waves terminate all the voltage transients in the figures and, when the shunt capacity was sufficiently great, the transient phenomena consisted entirely of these waves, as in Figure 7. No discharge was seen at the gap under the conditions of Figure 7, nor was any distortion of wave form of the type accompanying gaseous discharge observed in any of the damped sinusoidal wave series. No contact current could be detected oscilloscopically during the terminal voltage waves, except for a very small damped sinusoidal current, flowing presumably by virtue of the capacity of the contacts and associated structures. Apparently the waves were initiated when, as the contact gap lengthened, the voltage was not adequate to induce or to sustain gap discharge.

Table I. Variation of Transient Characteristics with Current

Steady-State Current, Amperes	Initial Plateau Voltage, Trial 1	Initial Plateau Voltage, Trial 2	Plateau Duration, Milliseconds	Arc Duration, Milliseconds	Plateau Duration + Arc Duration, Milliseconds	Terminal Oscillation Duration, Milliseconds
0.05	270	290	2.5	0.00	2.5	2.3
0.10	280	290	4.7	0.00	4.7	2.4
0.20	280	300	7.3	0.34	7.6	2.9
0.30	290	310	9.3	1.1	10.4	3.4
0.40	290	310	9.3	3.9	13.2	3.4
0.50	320	330	9.6	4.9	14.5	3.4

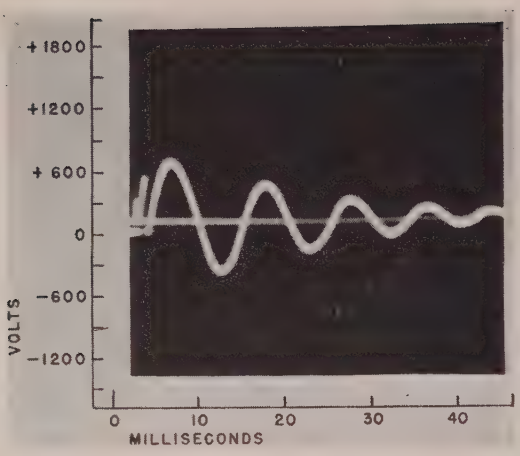

Figure 6 (left). Strikeover transient, shunt capacity 1.0 microfarad

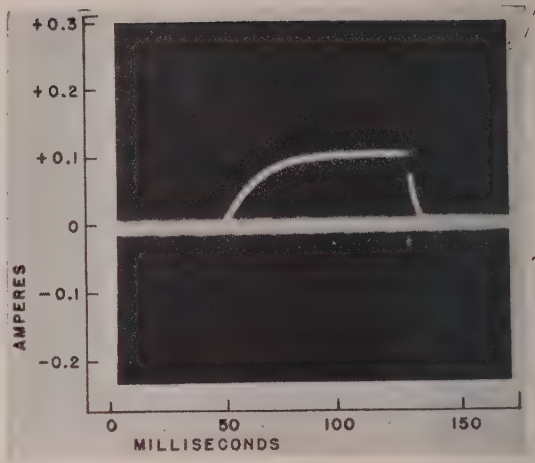

Figure 9 (right). Contact current for plateau transient

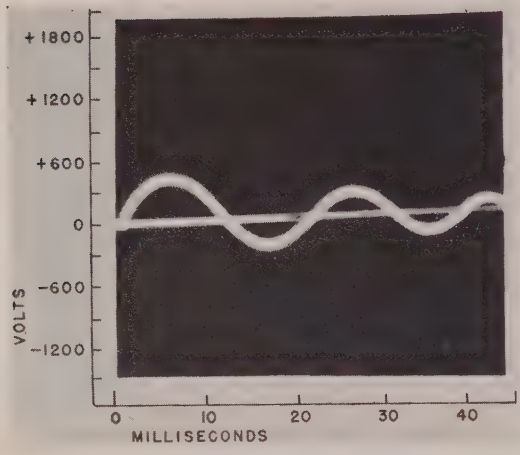

Figure 7 (left). Sinusoidal transient, shunt capacity 5.0 microfarads

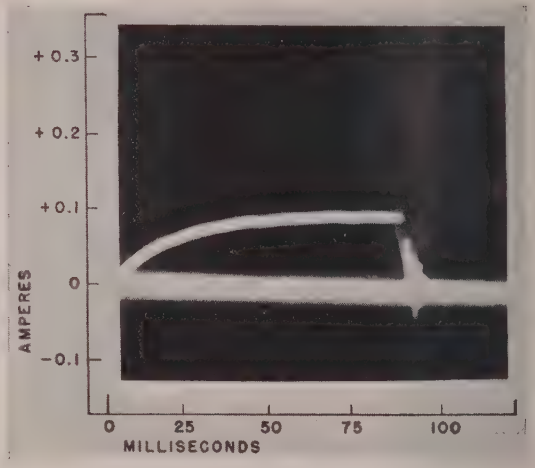

Figure 10 (right). Coil current for strikeover transient

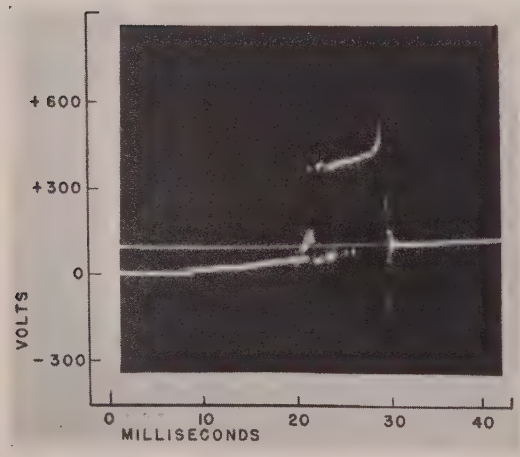

Figure 8 (left). Plateau interrupted by arcs

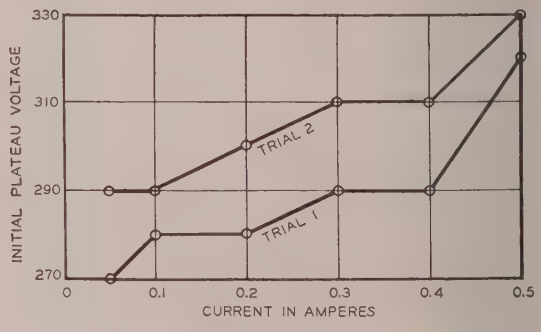

Figure 11 (right). Variation of initial plateau voltage with current

The sinusoidal voltage waves appeared to indicate merely an oscillatory transfer of energy between coil and capacitor of the type to be expected in resistance-inductance-capacitance circuits for certain ranges of the constants.[4] The analogous highly damped terminal phenomena of the earlier study[3] would be expected for other ranges of resistance-inductance-capacitance values, and these were found for low shunt capacities when a potential divider of lower resistance was used across the deflecting plates of the oscilloscope.

For low values of inductance, as the inductance was increased, an interesting sequence of voltage transients was observed. For very low values, low-voltage damped sinusoidal transients were obtained. As the inductance was increased, the initial voltage peak of the wave approached the plateau level (that is, a level

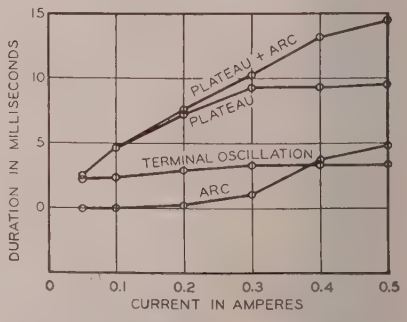

Figure 12. Variation of transient durations with current

of approximately 300 volts) and, when it reached this level, a dark spot formed on it. For still higher inductance values, the spot broadened into a typical plateau.

For the plateau transient the contact current is shown in Figure 9. This figure shows the slow rise in current following the make of the inductive circuit and indicates that the current had attained an almost steady state at the time of circuit break, as was true in all similar cases. At circuit break, as indicated by the discontinuity in the trace, initial current strikeovers of short duration occurred, evidences of which can be seen below the base line in Figure 9. The almost steady fall in current following the strikeover period corresponded with a similar fall in coil current and with the nearly steady plateau voltage, $e = -L(di/dt)$, across the contact gap. Terminal sinusoidal current waves, masked by the base line in the oscillogram, could be observed visually in similar cases.

For the strikeover transient the corresponding changes in coil current are shown in Figure 10. As in Figure 9, the slow rise of current in the inductive branch of the circuit is shown. Current strikeovers are shown after the current break. In this type of transient a sharp voltage drop followed each gap breakdown, and observation of transients consisting of a single strikeover showed that this drop was accompanied by a high surge current from the shunt condenser through the contacts. High surge currents also were observed for transients consisting of multiple strikeovers.

Circuit conditions which favored high surge currents at gap breakdown were the same as those that increased the probability that voltage strikeovers would occur to the exclusion of plateaus. Thus, increasing the shunt capacity was found to increase the surge current and the probability that voltage strikeovers would occur. Decreasing the circuit resistance or shunting a capacitor across the contacts instead of the coil (in which case the capacitor current did not flow through the circuit resistance), either of which should have heightened the surge current, was found to increase the strikeover probability. A curious effect of steady-state current on strikeover probability was noted. Increasing this current decreased the relative number of strikeovers for low shunt capacity, but increased it for high capacities.

Gap or contact conditions obviously influenced the probability that strikeovers would occur because, under identical circuit conditions, plateau discharges sometimes, but not always, were preceded by initial strikeovers. At times plateau discharges were found for very high shunt capacities when strikeovers were to be expected; at times strikeovers were found for low capacities (even for a capacity comprised only of that of the key, coaxial cable, and so forth, and of the distributed capacity of the coil) when plateaus were to be expected. Blowing the breath directly on the contacts increased the relative number of strikeovers (as noted by Mr. Curtis[3]); placing a drop of water between the contacts led to a long series of circuit breaks showing only strikeovers.

In some protective circuits, capacitors are shunted across contacts to minimize arcing. In the present study it was found that shunting a capacitor across the contacts instead of the coil resulted in somewhat better protection from initial arcing, in an increase in the number of strikeover transients and their duration, and in plateaus of longer duration when they occurred. With the capacitor across the coil, energy appeared to be dissipated in initial arcs that, in the other case, would have been expended in strikeovers or in plateau discharges of longer duration.

Data were obtained on the variation of some transient components with changes in steady-state current. For constant impressed voltage, initial plateau voltage increased slightly with increasing steady current. Two sets of data on this effect are given in Table I and are represented graphically in Figure 11. Oscillograms for Trial 1 were taken over a four-day period, those for Trial 2 over a period of a few hours. As a result of the method used in obtaining these data, the progressive changes in each trial are more significant than the differences between the trials.

Data also were obtained on the variation with steady-state current of plateau, arc, and terminal oscillation durations for an impressed electromotive force of 90 volts.

The graphs of Figure 12 bring out the relations observed. Arcing for the silver alloy contacts began at currents between 0.10 and 0.20 ampere. Arc duration increased slowly with currents less than 0.30 ampere and more rapidly for larger values. Plateau duration increased until a current of 0.30 ampere was attained and thereafter remained almost constant. These two increases complemented each other with the effect that the total duration (plateau plus arc) increased fairly uniformly throughout the entire range. Terminal oscillation durations showed a very gradual increase with currents below 0.30 ampere and remained constant for higher values.

Summary

Plateau, strikeover, and mixed transients observed over a range of lumped-constant values in a contact circuit were similar to those found by Mr. Curtis in telephone relay circuits. Increase in lumped shunt capacity across the coil was found equivalent to increase in line length in the earlier work.[3]

For all values of impressed voltage, steady-state current, and inductance which yielded clearly defined transients, the following transition sequence was observed:

1. Plateau transients (with the plateau at a level of about 300 volts) predominated for low shunt capacities across the contacts or the coil. Strikeovers of short duration frequently preceded plateaus.

2. With increase in shunt capacity plateau transients gave way to strikeover and mixed transients, with the former predominating.

3. A further increase in capacity led to transients consisting entirely of damped phenomena similar to those terminating the other transient types.

Arcs often preceded any type of transient, especially under conditions of high impressed voltage and steady-state current.

Circuit changes which resulted in an increase in the number of transients of the strikeover type were those which should have favored a high surge current at gap breakdown.

References

1. Bibliography and Abstracts on Electrical Contacts. American Society for Testing Materials (Philadelphia, Pa.), 1944.

2. 1944 Supplement to the Bibliography and Abstracts on Electrical Contacts. American Society for Testing Materials (Philadelphia, Pa.), 1945.

3. Contact Phenomena in Telephone Switching Circuits, **A. M. Curtis.** *Electrical Engineering* (*AIEE Transactions*), volume 59, June 1940, pages 360–68.

4. Electrical Contacts (book), **G. Windred.** Macmillan and Company, Ltd., London, England, 1940.

5. Introduction to Electric Transients (book), **E. B. Kurtz, G. F. Corcoran.** John Wiley and Sons, New York, N. Y., 1935.

6. Electric Contacts (book), **Ragnar Holm.** Almqvist and Wiksells, Stockholm, Sweden, 1946.

Discussion

Frank Spayth and **V. E. Heil** (P. R. Mallory and Company, Inc., Indianapolis, Ind.): The authors have presented an excellent picture of what occurs when the capacitance across the contacts or inductance is varied with a fixed inductance.

A similar type of phenomenon exists in an automobile ignition system. Our work has been concerned primarily with ignition sys-

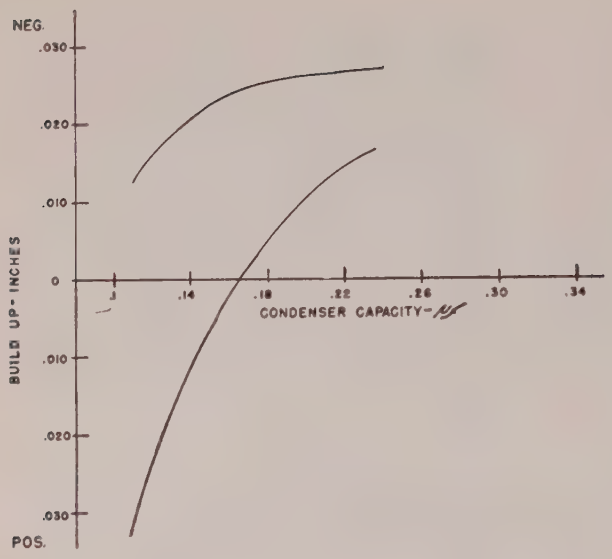

Figure 1 (left). Auto ignition contacts

550 rpm, 7.5 volts, 300 hours

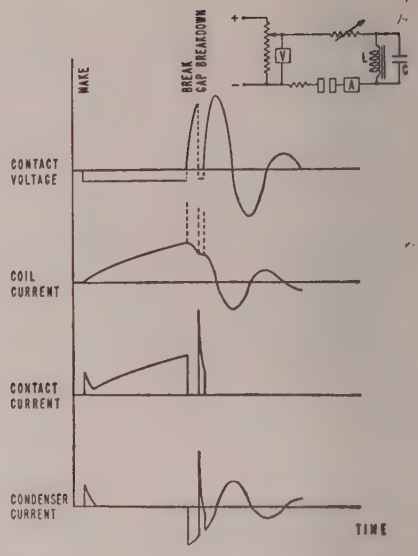

Figure 2 (right). Approximate contact voltage and branch current relations for a single-strikeover transient

tems using a 5- or 6-millihenry coil and capacitances varying between 0.01 to 0.5 microfarad. The break current in the system is approximately 5 amperes.

Results of these ignition studies are essentially similar to Messrs. Martin and Stauss's results.

It is interesting to note that by inserting a large enough capacitance across the contacts the sparking (or plateau) voltage is not reached, this capacitance is approximately 0.25 microfarad in the auto ignition circuit.

By lowering the capacitance to a point where the voltage rise across the contacts reaches the minimum sparking potential (that is, around 275–325 volts) we may expect an arc to form, as has been noted.

The length of time the arc will exist depends on the energy stored in the capacitance and the opening acceleration. When this energy is dissipated the voltage will rise again to the plateau. This process will continue or stop as a function of the opening acceleration and the energy across the contacts normally stored in the capacitance. By varying the steady-state current at a given inductance we may expect to obtain more arcing with the low capacitance than with the higher capacitance.

When contacts separate at voltages and currents above the critical arcing point, it is possible to form an arc without raising the voltage past the arc voltage. This phenomenon occurs as a result of the heating of the metal at the last point of contact and the subsequent formation of thermal electrons whose energies are sufficient to form an arc if the potential is high enough. At increased currents and low capacitances as compared to the same current and high capacitance we note that the total energy in the coil is the same in each case. If an arc strikes immediately when the contacts open, which we have noted to happen at a low capacitance, energy will be dissipated for that first instant. During this time, the separation of the contacts becomes greater and there is less chance of subsequent strikeovers to occur with the increased separation. This may be the explanation for the difference in the relative number of strikeovers at high and low capacitance.

It is interesting to note the material transferred in an inductive circuit with a varying capacitance. The inductance in this case is 6 millihenrys.

In Figure 1 of this discussion the lower curve represents a resistance of approximately 0.010 ohm and an inductance in the leads to the contacts from the condenser of 3×10^{-8} henrys. The upper curve represents a shortened lead with 0.0035 ohm and an estimated inductance of 10^{-8} — 10^{-9} henrys.

It is well to note that A. Hamilton and R. W. Sillars[1] have investigated carefully the effects of capacitance, inductance, resistance, opening acceleration, contact force, current, and voltage on the contacts.

The present paper covers a greater range of inductance and capacitance values and the authors are to be commended for their contribution to the literature.

Reference

1. Spark Quenching at Relay Contacts Interrupting D.C. Circuits, A. Hamilton, R. W. Sillars. *Proceedings*, Institution of Electrical Engineers (London, England), volume 96, part I, number 98, March 1949, pages 64–76.

F. E. Martin and H. E. Stauss: Our thanks are due to Mr. Frank Spayth and Mr. V. E. Heil for their interest in the work reported, and for calling to our attention the article of A. Hamilton and R. W. Sillars, which was published some while after experimental work for the present article had been completed.

While it appears possible that in some cases initial arcs dissipated energy that otherwise would have been expended in strikeover phenomena of longer duration, it should be noted that, if other conditions remained the same, the series of strikeovers observed for low shunt capacities comprised a larger number of individual strikeovers than similar series for high capacities.

The question raised by Mr. Spayth's discussion as to the relative numbers of relaxation oscillations in strikeover series, embracing as it does the question as to the factors determining the average frequency of the oscillations, is a complex one. Figure 2 of this discussion, showing approximate contact voltage and branch current relations for a single-strikeover transient, points up the complexity. If vertical lines are drawn in this figure, their intercepts on the lines representing transient phenomena will constitute points reached after equal intervals of elapsed time. Three imaginary vertical lines are identified as corresponding, respectively, with the times of make and break of the circuit and with the instant at which gap breakdown occurred.

Changes that accompanied an arc which took place immediately after gap breakdown are shown in the figure. If other conditions remain unchanged, the average frequency for a strikeover series would be expected to decrease if arcs are interspersed between individual strikeovers, and to decrease still more with increase in duration of the arcs, since in either case an increase in individual strikeover duration would be expected. Since the high current surge associated with the interspersed arc was confined to the circuit branch embracing the contacts and the capacitor, occurrence of the arc depended on the presence in this circuit of sufficient capacity for adequate energy storage. If, again, other conditions remain unchanged, the duration of the interspersed arc might be expected to increase with increase in capacity because of increased energy storage. Within limits, at any rate, the number of interspersed arcs was found to increase with increased capacity (not more than one arc was seen between a pair of strikeovers).

In the period between circuit break and gap breakdown contact current was found to be negligible. Consequently, the rise in contact voltage shown above the base line in Figure 2 of this discussion was very nearly equal to the increase in potential across the capacitor or the inductance in a simple series resistance-inductance-capacitance loop of low resistance. The time for this voltage to rise to any given value should depend on the circuit parameters for the loop. An increase in rise-time was noted for increased capacity. Thus, again, increased capacity led to increased duration for the individual strikeover and to decreased average frequency for the series.

As previously stated, in general the voltage maxima of successive strikeovers increased gradually, presumably because of increased contact gap length. For this reason, as pointed out by Mr. Spayth, the rate of contact opening would be expected to affect the average strikeover frequency. Thus, the slope of the envelope drawn through successive voltage maxima in a strikeover series (compare Figure 5 of the paper, in which the envelope is almost linear) would be expected to increase for increase in contact opening speeds; the consequent increase in voltage rise-time for each strikeover should decrease the frequency for the series.

This discussion (covering only cases for which relations between the inductance and the rates of current change in the resistance-inductance-capacitance loop after the break of the contact circuit are such, at proper times, that the products $-Ldi/dt$ exceed the gap breakdown voltages and a strikeover series may occur) does not imply that only the factors considered may influence the average frequency. Other factors, for example, ionization in the contact gap (through its effects on gap breakdown and arcing) may well influence strikeover frequency

Calculation of Flux Distributions with Saturation

H. PORITSKY
NONMEMBER AIEE

MAGNETIC fields often are computed by neglecting saturation phenomena, yet saturation is encountered often in physics and electrical engineering. Thus, in transformers, motors, and turbogenerators, flux distributions with saturation often occur. Again, in electric apparatus and devices utilizing permanent magnets the simplifying assumption of constant permeability certainly cannot be considered to be good enough. This neglect of saturation phenomena is due partly to the fact that the art of calculating flux distributions taking saturation into account is in a very rudimentary state.

In the following, several methods of determination of flux distribution in magnetic materials exhibiting saturation phenomena are reviewed. The main difficulty of the problem arises from its nonlinear character. It is of interest to point out that one of the four methods enumerated below converts the nonlinear problem into a linear one; this is done by passing from the physical plane to the plane in which the field components or flux density components are used as rectangular co-ordinates. This method is the analogue of the "hodograph-plane" method in the flow of compressible fluids, but does not appear to be sufficiently familiar to electrical engineers.

The analysis is based on the following assumptions:

1. There exists a definite relation between field intensity (H) and flux density (B) given by a single curve in the (H, B)-plane. This neglects the phenomena of hysteresis. To a certain extent, however, the method is applicable even if the latter is taken into account, as will be explained in the section on hysteresis.
2. The directions of H, B coincide. This neglects rotary hysteresis.
3. Eddy-current phenomena are neglected.
4. The fields are assumed to be 2-dimensional.

In regard to the first two assumptions, it is of interest to recall that in the linear case, for steady-state alternating fields, one can handle hysteresis phenomena and rotary hysteresis approximately by introducing complex permeability. It is not clear, however, how to extend this method of the nonlinear case.

The third assumption does not necessarily restrict the problems considered to static fields. Alternating fields are not excluded; however, it must then be assumed that the magnetic material is laminated and free from hysteresis, thus preventing eddy currents and time lag of flux penetration.

Four methods of field determination will be described: A numerical method based on the direct numerical integration of the nonlinear differential equations; a graphical of flux plotting method; the use of the d-c board; and an extension of the hodograph method.

As pointed out in the section on the d-c board method, all methods apply equally well to problems of current distribution in sheets of materials in which the resistivity is a function of the current magnitude.

Differential Equations

The differential equation for the magnetic 2-dimensional fields under consideration may be expressed either in terms of the magnetic scalar potential φ or in terms of tbe flux function ψ. The negative gradient of φ is the field:

$$H_x = -\varphi_x$$
$$H_y = -\varphi_y$$
$$\mathbf{H} = -\nabla\varphi \qquad (1)$$

Here subscripts on φ denote partial derivatives, but H_x, H_y denote components of $\mathbf{H}$. The curves ψ = constant are flux lines and

$$B_x = -\psi_y,\ B_y = \psi_x \qquad (2)$$

The condition of conservation of flux is

$$\frac{\partial B_x}{\partial x} + \frac{\partial B_y}{\partial y} = 0 \qquad (3)$$

and is satisfied automatically by expressing B_x, B_y in terms of ψ as in equation 2.

Since it is assumed that no angular hysteresis exists at any point, the magnetic flux density vector $\mathbf{B}$ points exactly in the same direction as the magnetic field vector $\mathbf{H}$:

$$\frac{B_x}{B_y} = \frac{H_x}{H_y} \qquad (4)$$

Between the magnitude of the flux vector and the field vector

$$B = (B_x^2 + B_y^2)^{1/2}$$
$$H = (H_x^2 + H_y^2)^{1/2} \qquad (5)$$

there exists a functional relation

$$B = B(H),\ H = H(B) \qquad (6)$$

displayed in Figure 1.

We introduce the permeability μ by means of

$$\mu = B/H$$
$$B = \mu H$$
$$\mu = \mu(H) \qquad (7)$$

Thus, at a point P of the curve of Figure 1, μ is the slope of the line joining P to the origin O. This definition is used consistently in the following, in spite of other well-known definitions (such as μ being the slope of the tangent to the (H, B)-curve). It follows from Figure 2 that between the field components and the flux components there exist the relations

Paper 51-50, recommended by the AIEE Basic Sciences Committee and approved by the AIEE Technical Program Committee for presentation at the AIEE Winter General Meeting, New York, N. Y., January 22–26, 1951. Manuscript submitted November 15, 1948; made available for printing December 5, 1950.

H. PORITSKY is with the General Electric Company, Schenectady, N. Y.

The author gratefully acknowledges the assistance of DRS. G. HORVAY and H. WEIL, and especially of Miss B. A. JENSEN.

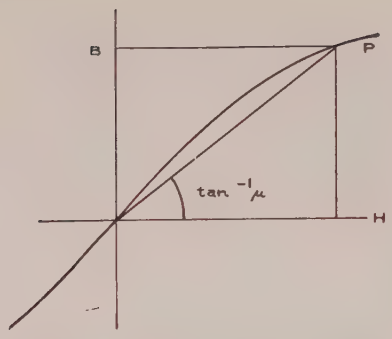

Figure 1. Permeability defined as the slope of a chord

$$\frac{B_x}{H_x}=\frac{B_y}{H_y}=\frac{B}{H}=\mu \tag{8}$$

where μ is defined by means of equation 7 and is a function either of H or of B. Replacing B_x, B_y by H_x, H_y in equation 1, equation 2 yields

$$H_x=\frac{B_x}{\mu}=-\frac{\partial\varphi}{\partial x}=-\frac{1}{\mu}\frac{\partial\psi}{\partial y}$$
$$H_y=\frac{B_y}{\mu}=-\frac{\partial\varphi}{\partial y}=\frac{1}{\mu}\frac{\partial\psi}{\partial x} \tag{9}$$

Elimination of ψ yields

$$\frac{\partial}{\partial x}\left(\mu\frac{\partial\varphi}{\partial x}\right)+\frac{\partial}{\partial y}\left(\mu\frac{\partial\varphi}{\partial y}\right)=0$$
$$\mu=\mu(H),\ H=|\nabla\varphi|=(\varphi_x^2+\varphi_x^2)^{1/2} \tag{10}$$

while elimination of φ leads to

$$\frac{\partial}{\partial x}\left(\frac{1}{\mu}\frac{\partial\psi}{\partial x}\right)+\frac{\partial}{\partial y}\left(\frac{1}{\mu}\frac{\partial\psi}{\partial y}\right)=0$$
$$\mu=\mu(B)$$
$$B=|\nabla\psi|=(\psi_x^2+\psi_y^2)^{1/2} \tag{11}$$

It will be noted that this is of the same type as equation 10 but with the μ replaced by its reciprocal. Either equation 10 or equation 11 may be considered as the field equation to be solved. Again, the mixed equations

$$\frac{\partial\varphi}{\partial x}=\frac{1}{\mu}\frac{\partial\psi}{\partial y},\quad \frac{\partial\varphi}{\partial y}=-\frac{1}{\mu}\frac{\partial\psi}{\partial x} \tag{12}$$

may be used (see equation 9). In fact, if equation 10 or equation 11 is solved for φ or ψ, the other function may be found from equation 12.

For constant μ, equation 12 reduces to the Cauchy-Riemann equations in $\mu\varphi$, ψ, and equations 10 and 11 reduce to the Laplace equation.

Numerical Methods

The numerical methods of integrating differential equations consist in approximating the derivatives by means of finite difference quotients. For this purpose a network, say a square network of constant spacing δ, is introduced over the region in question, and the derivatives at each point of the net are expressed in terms of the difference quotients of the values at this point and adjacent points of the network. Thus, for example

$$\frac{\partial\varphi}{\partial x}=\frac{\varphi(x+\delta,y)-\varphi(x-\delta,y)}{2\delta} \tag{13}$$

and similarly for second-order derivatives.

Writing equation 10 in the form

$$\varphi_{xx}+\varphi_{yy}+\frac{1}{\mu}(\mu_x\varphi_x+\mu_y\varphi_x)=0 \tag{14}$$

and introducing

$$M=\log\mu \tag{15}$$

one obtains

$$\varphi_{xx}+\varphi_{yy}+M_x\varphi_x+M_y\varphi_y=0$$
$$M=M(\sqrt{\varphi_x^2+\varphi_y^2})=M(H) \tag{16}$$

Introducing finite difference quotients (see Figure 3) one obtains

$$\frac{\varphi_A+\varphi_B+\varphi_C+\varphi_D-4\varphi_0}{\delta^2}+\frac{(M_A-M_C)(\varphi_A-\varphi_C)}{4\delta^2}+\frac{(M_B-M_D)(\varphi_B-\varphi_D)}{4\delta^2}=0 \tag{17}$$

This also can be written in the form

$$4\Sigma(\varphi_A-\varphi_0)+\Sigma M_A\varphi_A-\Sigma M_A\varphi_C=0 \tag{18}$$

where the sums are carried out over each of the four directions through 0.

A slightly different form for this equation is obtained by using equation 10 directly, evaluating $\partial\varphi/\partial x$ at a, the midpoint of $0A$ from φ_A, φ_0, then replacing $\partial/\partial x(\mu\partial\varphi/\partial x)$ by the difference quotient of $\mu\,\partial\varphi/\partial x$ at a and c. Replacing μ_a by $(\mu_A+\mu_0)/2$, and so forth, one obtains similarly

$$\Sigma(\varphi_A-\varphi_0)(\mu_A+\mu_0)=0 \tag{19}$$

The algebraic equations 17–19 are nonlinear. A method of solving them consists in assuming a set of values of φ, substituting them into equation 17, and calculating the values of the left-hand members. These values, known as the "residues," in general will not vanish, and will, therefore, form a measure of the inaccuracy of the assumed solution. One then "improves" the initial guess, recalculating the left-hand members of equation 17. This is repeated until the residues are sufficiently small.

As a way of calculating each next guess, one may use equation 17 to recalculate φ_0 in terms of the surrounding four values φ_A, φ_B, φ_C, φ_D. After the values of φ have been obtained, the corresponding values of μ and M have to be found by finding

$$H^2=(\nabla\varphi)^2=\varphi_x^2+\varphi_y^2 \tag{20}$$

and from the functional relation equation 7 (Figure 1), obtaining μ and M at each point.

Equation 11 can be handled similarly by writing it in the form

$$\psi_{xx}+\psi_{yy}-M_x\psi_x-M_y\psi_y=0$$
$$M=M(B)$$
$$B=\sqrt{\psi_x^2+\psi_y^2} \tag{21}$$

Graphical Method

The flux lines

$$\psi=\text{constant} \tag{22}$$

and the equipotentials

$$\varphi=\text{constant} \tag{23}$$

are perpendicular to each other. If drawn for values of the right-hand constants differing by constant $\Delta\psi$, $\Delta\varphi$, they divide the plane into curvilinear rectangles, as shown on Figure 4. Denote by Δn the rectangle sides along the flux lines, by Δs the sides along the equipotentials. Then the equations of the section on differential equations imply that the gradients of φ, ψ are normal and numerically equal to H, B. In equation form

$$H=\frac{\Delta\varphi}{\Delta n}$$
$$B=\frac{\Delta\psi}{\Delta s} \tag{24}$$

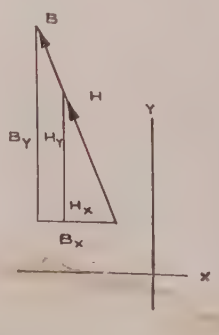

Figure 2 (left). An illustration of the colinearity of *B* and *H*

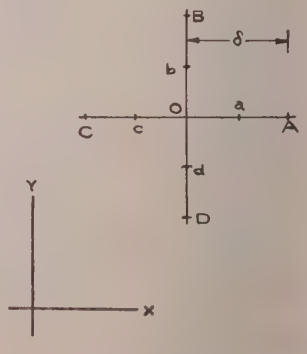

Figure 3 (right). Illustrating the numerical method of finite differences

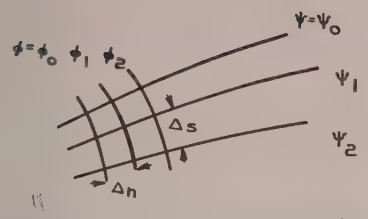

Figure 4. Flux lines in equipotentials

and, since $B=\mu H$

$$\frac{\Delta\psi}{\Delta s}=\mu\frac{\Delta\varphi}{\Delta n} \tag{25}$$

so that the ratio of the rectangle sides is

$$\frac{\Delta n}{\Delta s}=\mu\frac{\Delta\varphi}{\Delta\psi} \tag{26}$$

and varies as μ, the constant of proportionality being $\Delta\varphi/\Delta\psi$. Since one of the rectangle sides, say Δn, varies inversely as H, and μ is a function of H, it follows that the side ratio is a function of the length of one side, and hence that when one side length is given, the other side length is determined. Indeed, from Figure 1 the curve of Δn versus Δs also may be constructed by replotting the curve $1/B$ versus $1/H$ and noting the relations

$$\Delta n=\frac{\Delta\varphi}{H}$$
$$\Delta s=\frac{\Delta\psi}{B} \tag{27}$$

To summarize, the flux-plotting rule consists in drawing equipotentials and flux lines normally to each other and so as to form rectangles whose sides satisfy the relations in equations 26 and 27.

D-C Board Method

This method is based upon the observation that equations 10 and 11 also represent the equations for conduction of electric current in a plate of uniform thickness provided the conductivity of the material varies as μ, hence is dependent on the current density. In this analogy, the following replacements are implied

φ	μ	H_x,H_y,H	B_x,B_y,B
V	$\frac{1}{R}$	E_x,E_y,E	I_x,I_y,I

(28)

where

V = the electric potential (volts)
E_x, E_y, E = the electric field (volts per unit length)
I_x, I_y, I = the current across plate thickness (amperes per unit length)
R = the local plate resistance

To set up the problem on the d-c board one considers a network similar to the one in the section on numerical method and adjusts the resistance of each vertical side and each horizontal side to vary inversely as μ, the latter being determined as a function of the electric field E from Figure 1.

$$E=\sqrt{E_x^2+E_y^2} \tag{29}$$

The latter is calculated from the values of the potentials at adjacent points on Figure 3.

As a possible procedure one may first take constant resistance elements determined by an average value of μ. Reading of potentials V then are taken, the field computed from potential differences, the resultant field (equation 29) found, and the resistance adjusted to values proportional to $1/\mu$ for the local field E. With the new resistances, readings of potentials are taken once more, E_x, E_y, E found, and the resistances adjusted once more to correspond to these values. Both the vertical and the horizontal resistances at each point are changed simultaneously and so as to equal each other at the same point. Because of the finite size of the mesh, however, each resultant may be made to correspond to values of μ at the mid-point of its side.

The electrical analogy also may be set up in a different manner by noting that equation 11 may be identified with the equation for conduction currents in a plate of uniform thickness provided the conductance varies as $1/\mu$, hence the resistance varies as μ.

In place of (28) the following replacements now are made

ψ	μ	H_x,H_y,H
V	R	I_x,I_y,I

(30)

and a curve of μ versus B is used to adjust the resistances of the elements, which are proportional to μ, the flux density B being proportional to E.

Application of the Hodograph Method to the Solution of Field Problems with Saturation

As stated previously, the hodograph method is one of the most powerful methods in the theory of flow of compressible fluids. Its advantage lies in the fact that it renders the field equations linear; its disadvantage is its indirectness, since one never knows to what region in the hodograph plane the flow over a given region in the physical plane will correspond. For the sake of completeness, the derivation of the hodograph

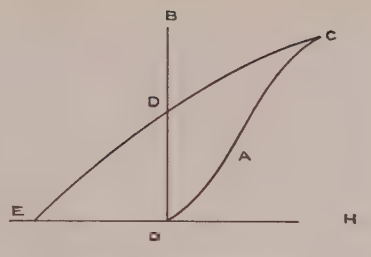

Figure 5. Hysteresis loop

fluid-flow equations is explained in the following paragraphs, before indicating how the method carries over to the magnetic problem.

The basic equations of 2-dimensional irrotational flow of a compressible fluid are

$$\varphi_x=u$$
$$\varphi_y=v \tag{31}$$

$$\psi_x=-\rho v$$
$$\psi_y=+\rho u \tag{32}$$

where

u, v = the velocity components
ρ = the density
φ = the velocity potential whose existence is equivalent to the assumption that flow is irrotational
ψ = the stream-line function whose existence follows from the condition of conservation of mass

Subscripts denote partial derivatives. The Bernoulli equation

$$\int\frac{dp}{\rho}+\frac{w^2}{2}=\text{constant} \tag{33}$$

furnishes a relation between the velocity magnitude $w=\sqrt{u^2+v^2}$ and the density ρ, provided that the pressure p is assumed to be a proper function of the density ρ

$$p=p(\rho) \tag{34}$$

In case of flow of a fluid this functional relation is derived from the adiabatic law.

Denoting the resulting integral in equation 33 by $P(\rho)$, one writes the Bernoulli equation in the form

$$P(\rho)+\frac{w^2}{2}=\text{constant} \tag{35}$$

From equation 35 one may solve for ρ in terms of w. Comparing equations 31 and 32 with equation 12, it will be seen that a complete analogy exists between the flow of a compressible fluid and the flux distribution with saturation, provided that μ is made to correspond to ρ and φ to $-\varphi$. This analogy is displayed in (36).

Fluid flow	w	φ	ψ	ρ	$\rho=\rho(w)$
Magnetic field	H	$-\varphi$	ψ	μ	$\mu=\mu(H)$

(36)

It will now be recalled how the fluid-flow equations are set up in the hodograph plane, that is, in the plane in which (u,v) form rectangular Cartesian co-ordinates.

Rewriting equations 31 and 32 in the form

$$d\varphi = udx + vdy$$
$$d\psi = -\rho v dx + \rho u dy \tag{37}$$

one may solve for dx, dy in terms of $d\varphi$, $d\psi$ and expressing $d\varphi$, $d\psi$ in terms of dw, $d\theta$, where w, $\theta(\theta=\tan^{-1}v/u)$ are the polar co-ordinates in the hodograph plane, one obtains

$$dx = x_w dw + x_\theta d\theta$$
$$dx = \left(\frac{\cos\theta}{w}\varphi_w - \frac{\sin\theta}{\rho w}\psi_w\right)dw + \left(\frac{\cos\theta}{w}\varphi_\theta - \frac{\sin\theta}{\rho w}\psi_\theta\right)d\theta$$
$$dy = y_w dw + y_\theta d\theta \tag{38}$$
$$dy = \left(\frac{\sin\theta}{w}\varphi_w + \frac{\cos\theta}{\rho w}\psi_w\right)dw + \left(\frac{\sin\theta}{w}\varphi_\theta + \frac{\cos\theta}{w\rho}\psi_\theta\right)d\theta$$

or, in complex form,

$$d(x+iy) = \frac{\epsilon^{i\theta}}{w}d\varphi + i\frac{\epsilon^{i\theta}}{\rho w}d\psi \tag{39}$$

Applying the conditions that the right-hand members are perfect differentials, namely $(x_w)_\theta=(x_\theta)_w$, $(y_w)_\theta=(y_\theta)_w$, we obtain

$$\frac{\sin\theta}{w}\varphi_w + \frac{\cos\theta}{\rho w}\psi_w = \frac{\cos\theta}{w^2}\varphi_\theta + \sin\theta\left(\frac{1}{\rho w}\right)'\psi_\theta$$
$$\frac{\cos\theta}{w}\varphi_w - \frac{\sin\theta}{\rho w}\psi_w = -\frac{\sin\theta}{w^2}\varphi_\theta + \cos\theta\left(\frac{1}{\rho w}\right)'\psi_\theta \tag{40}$$

where $'$ indicates differentiation with respect to w. Multiplying first by $\sin\theta$, $\cos\theta$, then by $\cos\theta$, $-\sin\theta$, and adding yields

$$\frac{\varphi_w}{w} = \left(\frac{1}{\rho w}\right)'\psi_\theta$$
$$\frac{\psi_w}{\rho w} = \frac{\varphi_\theta}{w^2} \tag{41}$$

By eliminating the function φ there results a second-order differential equation for ψ which is linear and whose coefficients are functions of w only. After this equation or the equations 41 are solved, a solution in the (x,y)-plane is obtained by integrating the equations 38.

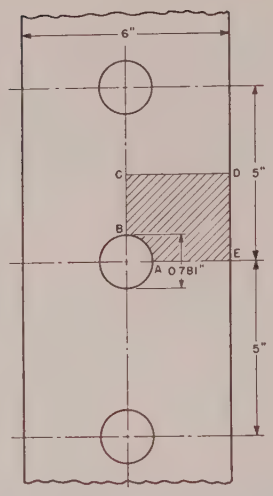

Figure 6. Schematic diagram of transformer lamination (not to scale)

The equations 41 or the equations obtained from them by eliminating φ or ψ are linear equations whose coefficients vary only with w. For the type of equations obtained from adiabatic flow of gases, these equations have been studied extensively.

By analogy to equations 41 one now obtains

$$\frac{\varphi_H}{H} = -\frac{d}{dH}\left(\frac{1}{\mu H}\right)\psi_\theta$$
$$\frac{\psi_H}{\mu H} = -\frac{\varphi_\theta}{H^2} \tag{42}$$

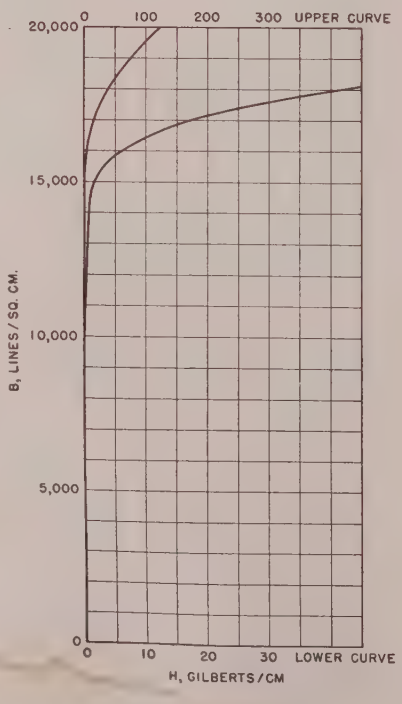

Figure 7. (B-H)-curve

Elimination of φ leads to the following equation in ψ

$$\frac{\partial}{\partial H}\left(\frac{H}{\mu}\frac{\partial\psi}{\partial H}\right) - \frac{Hd}{dH}\left(\frac{1}{\mu H}\right)\frac{\partial^2\psi}{\partial\theta^2} = 0 \tag{43}$$

Because the final equation is linear in ψ it follows that the sum of various solutions also is a solution and that a constant multiple of a solution also is a solution.

After a solution of equation 43 has been obtained, the function φ is found from equation 42 and x, y are determined from equation 39, which is now written in the form

$$d(x+iy) = \frac{\epsilon^{i\theta}d\varphi}{H} + i\frac{\epsilon^{i\theta}}{B}d\psi \tag{44}$$

Product solutions, that is, solutions which are a product of a function of θ by a function of H, exist, and it turns out that the function of θ is a trigonometric (or an exponential) function. On the other hand, the corresponding functions of H are not elementary functions, but have to be obtained from a solution of an ordinary differential equation. While this is to be regretted, the reduction constitutes quite an advance, since the art of solving ordinary differential equations is considerably more advanced both numerically and by means of proper devices such as the differential analyzer.

It has been shown by Chaplygin that the hodograph equations can be reduced to the Laplace equation provided that the (ρ,w)-relation is of a certain type. In the magnetic problem the analogue of this Chaplygin relation is given by

$$\mu = \frac{A}{\sqrt{H^2+C}} \tag{45}$$

where A, C are constants. While equation 45 will not do throughout the whole range of low and high saturations, the use of several such relations in different intervals is possible. For this method, and the conditions at the transition points, see the author's earlier paper on the polygonal approximation method.[1]

Equation 45 utilizes the notation of equation 2.34 of reference 1, but with A in place of B. The reduction of the Laplace equation is brought about by introducing as variables θ and W given by

$$W = K - 1n\frac{\sqrt{C}+\sqrt{H^2+C}}{H} \tag{46}$$

where K is a constant and C is as in equation 45.

It is of interest to point out that the analogy between the fluid flow and the magnetic phenomena may be carried out in an alternative way by replacing (36) by

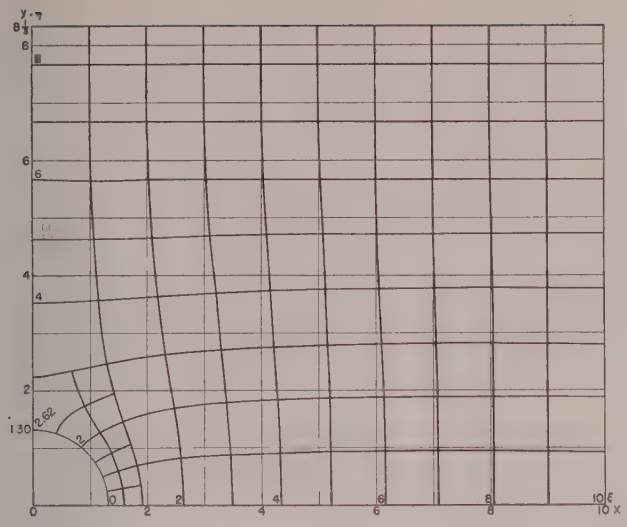

Figure 8. Small-square flux plot

Fluid flow	w	φ	ψ	$\rho=\rho(w)$
Magnetic field	B	ψ	φ	$\frac{1}{\mu}=f(B)$

(47)

In this analogy, the so-called "hodograph" plane is replaced by the (B_x,B_y)-plane. Equations 42 are replaced by

$$\frac{\psi_B}{B}=\left(\frac{\mu}{B}\right)'\varphi_\theta$$

$$\frac{\mu\varphi_B}{B}=\frac{\psi_\theta}{B^2} \tag{48}$$

and equation 43 by

$$\frac{d}{dB}\left[\frac{1}{\left(\frac{\mu}{B}\right)'}\frac{\psi_B}{B}\right]=\frac{1}{\mu B}\psi_{\theta\theta} \tag{49}$$

This suggests that, while it has not been customary, it is entirely possible to introduce the "hodograph" method in a mass-transport plane in which ρu, ρv are rectangular co-ordinates (rather than u, v).

Because of the relative newness of equations 43 and 49, no attempt at integrating them is made in this paper, nor is the illustrative example given in a following section treated by means of these.

Hysteresis

As stated previously, hysteresis phenomena can be accounted for to a certain extent. If one tries to take into consideration the complete hysteresis phenomena, including loops of various sizes depending upon the maximum field value before reversal occurs, the multiplicity of values μ would make things very difficult indeed. If, however, following an initial magnetization to saturation along a path OAC (see Figure 5) one attains various degrees of demagnetization along the path CDE, then treatment by means of the above methods is quite possible. It will be noted that if there is field reversal (along DE) the values of μ become infinite near D, the point at which this curve crosses the B-axis. To the right of

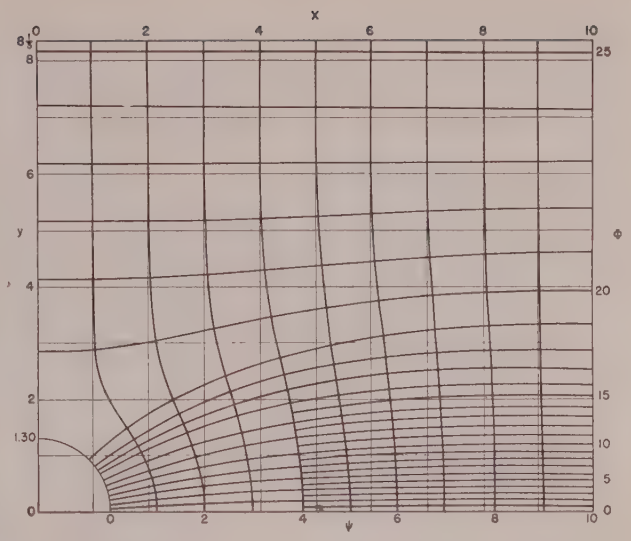

Figure 10. Flux plot with saturation

D the values μ are positive, to the left negative. Since μ had been assumed to be a single-value function in the numerical value of H, this will give rise to difficulties, and a double-valued solution in the hodograph plane may be required, one branch corresponding to DC, one to ED. This double-valuedness may be avoided by utilizing (B_x, B_y)- plane instead of the corresponding (H_x, H_y)-plane, as in the analogy in (47).

It will be recalled that for a constant permeability-alternating phenomena, hysteresis can be treated by assuming the permeability to be complex. Indeed, if the field and flux components are all assumed to be the real parts of

$$A\epsilon^{j\omega t} \tag{50}$$

where A is complex, independent of time, but varies from point to point for field distribution, then the calculations may be carried out on the complex expressions displayed in equation 50 without taking the real parts until the very end of the

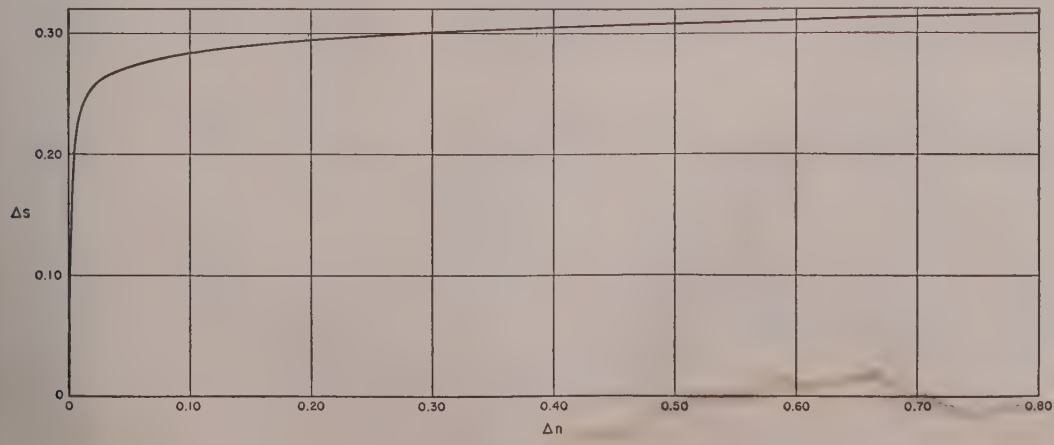

Figure 9. Δs versus Δn

calculation. On this basis, it is known that a complex value for the permeability μ in the equation

$$B=\mu H=|\mu|\epsilon^{j\varphi}H \qquad (51)$$

upon introducing the exponential factor (equation 50), and taking real parts, gives rise in the (H,B)-plane to (H,B)-curves for various $|A|$ which form similar ellipses and form a good enough approximation to hysteresis loops. It is not clear, however, whether introducing a general complex functional relation between B and H can be used similarly to handle the nonlinear saturation problem, since the simple expedients of introducing time as an exponential factor and taking real parts will no longer work because of the nonlinearity.

Illustrative Example

As a first example, we consider the distribution of magnetic flux in a transformer core with periodic circular bolt holes, for the dimensions indicated on the schematic Figure 6, for the (H, B)-relation shown in Table I and plotted on Figure 7, and for a total flux corresponding to an average flux density $B_0=15{,}500$ lines per centimeter,[2] across a 6-inch lamination width.

While in a transformer the flux is alternating, and the above value B_0 represents its time maximum, the thickness of the laminations is supposed to be fine enough so that the effect of eddy currents can be neglected, hence the flux distribution at any moment is the same as in the static problem corresponding to the same total flux at that instant. In particular, we shall consider the case where total flux is equal to 15,500 lines per square centimeter$\times$6 inches$\times$2.54 centimeters per inch lines per centimeter of lamination thickness. We denote by H_0, μ_0 the values of H, μ corresponding to $B_0(H_0=3.1,\ \mu_1=5{,}000)$.

Actually, the flux distributes itself both in the iron laminations, in the air space of the bolt holes, and also may cross the rectilinear boundaries of the laminations, though the holes are filled up with bolt bars, and except for a skin effect, the penetration of the flux into that space is prevented. This means that the flux distribution problem should really be solved both within the magnetic material and in the air spaces, proper attention being given to the boundary conditions at the common boundaries, namely, that the tangential magnetic-field component is continuous (leading to continuity in the magnetic potential φ), and the normal component of flux is continuous (leading to continuity in the flux function ψ). While the first three methods of solution certainly can be extended to cover problems involving flux distribution both within magnetic materials with saturation and in air spaces, the added complications which this would entail are considerable. To avoid these, and because the permeability within the magnetic lamination even under the conditions of maximum saturation still is considerably greater than that of air, we shall neglect the flux within the air space altogether, thus assuming that both the edges of the lamination and the boundaries of the circular holes are flux lines.

It will be sufficient to restrict the field determination to the shaded area of Figure 6, since by proper reflection across the rectilinear boundaries the rest of the field can be obtained from the field of this region.

Before attempting the graphical construction proper, a preliminary plot was made based upon the assumption of constant permeability, equal to μ_0. By proper choice of the increments in φ, ψ $\Delta\varphi=(\Delta\varphi)_0$, $\Delta\psi=(\Delta\psi)_0$, this plot becomes of the small-square type. The plot is shown on Figure 8, where, as will be noted, 10 flux spaces were used, leading to 8.6 potential spaces.

A plot utilizing the nonlinear (H, B)-relation of Table I and Figure 7 then was constructed and is shown on Figure 10. In making this plot, Figure 8 was used as a guide, but only for the flux lines, the completed plot being based on the relations between rectangle sides Δn, Δs indicated in equations 27, and shown on Figure 9. The same values of $\Delta\varphi$, $\Delta\psi$ were used in Figure 10 as in Figure 8, hence the same number (10) of flux spaces resulted; away from the circular hole (at the upper end of the figures) the plots resemble each other.

To render the relations of equations 27 dimensionless, these equations were rewritten in a form involving the ratios of φ, ψ, B, H to $(\Delta\varphi)_0$, $(\Delta\psi)_0$, B_0, H_0, and of Δn, Δs to the square side corresponding to the uniform flux distribution in absence of holes. Thus, the equations 27 were put in the form

$$(\Delta n)\text{ inches}/0.3\text{ inch}=H_0/H$$

$$(\Delta s)\text{ inches}/0.3\text{ inch}=B_0/B \qquad (52)$$

and Figure 9 was constructed from these equations.

Table I

B, Lines per Square Centimeter	H, Gilberts per Centimeter
500	0.0500
1,000	0.0645
2,000	0.0850
4,000	0.117
6,000	0.149
8,000	0.190
10,000	0.259
12,000	0.399
13,000	0.544
14,000	0.815
15,000	1.67
16,000	6.50
17,000	17.7
18,000	41.0

Figure 10 was drawn next by sketching the flux lines and equipotentials at right angles to each other, measuring the sides Δn, Δs for various rectangles, checking against the relation of Figure 9, erasing, redrawing, and checking the Δn, Δs relations, and repeating.

It will be noted from Figure 9 that a very small variation in the distance Δs makes the distance Δn change enormously. As a result, it was found necessary to make the Δs spaces between the flux lines nearly equal to each other along each equipotential. On the other hand, the variations in Δs on Figure 10 are very large indeed. Three plots of the above type were made by different individuals, and Figure 10 represents an averaged plot of the three. As in Figure 8, the boundary conditions on Figure 10, in addition to the conditions $\psi=0$ along ABC, $\psi=10(\Delta\psi)_0$, along DE, are $\varphi=0$ along AE and $\varphi=$constant along CD. However, the total difference of potential between AE and CD is unknown, and the values obtained in the three plots were 24.0, 25.1, and 26.2 potential spaces, respectively, leading to a tripling of the number of potential spaces relative to the number 8.3, which would be obtained in the absence of the hole.

The effect of saturation thus is very pronounced on the total value of magnetomotive force required to obtain the flux in question; even though the decrease in cross section along a line through the hole center is only 13 per cent, the effect on the magnetomotive force, as indicated, is to increase it by about 160 per cent. This is due entirely to the nature of the (H, B)-curve, and the fact that H_0, B_0 is just beyond the bend in this curve, a small increase in B leading to a very large change of H.

The same example also was worked by the numerical method described in preceding paragraphs. The equation of the type 19 was used in preference to equation 17. The initial set of values of the potential function φ was obtained from the flux plot of Figure 10. Going back to the derivation of equation 19 and Figure 3, but not replacing $\mu, \ldots$, by $(\mu_0+\mu_A)/2,\ldots$, one obtains

$$\Sigma\mu_a\varphi_a-\varphi_0\Sigma\mu_a=0 \qquad (53)$$

This equation will be replaced by

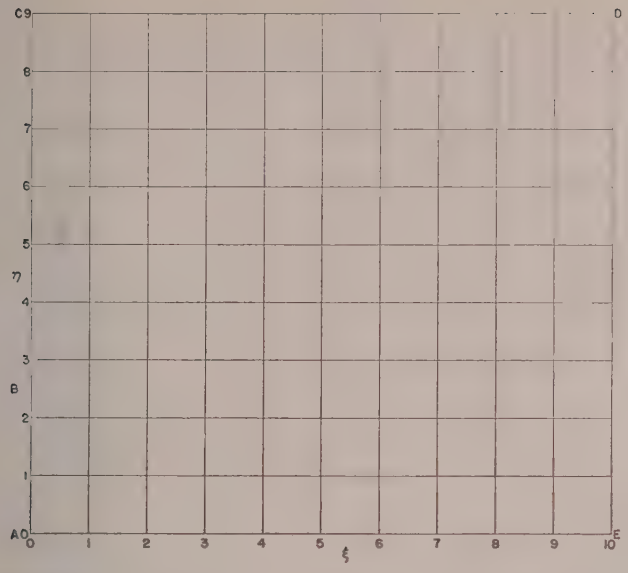

Figure 11. Conformal map of Figure 8 on a rectangle

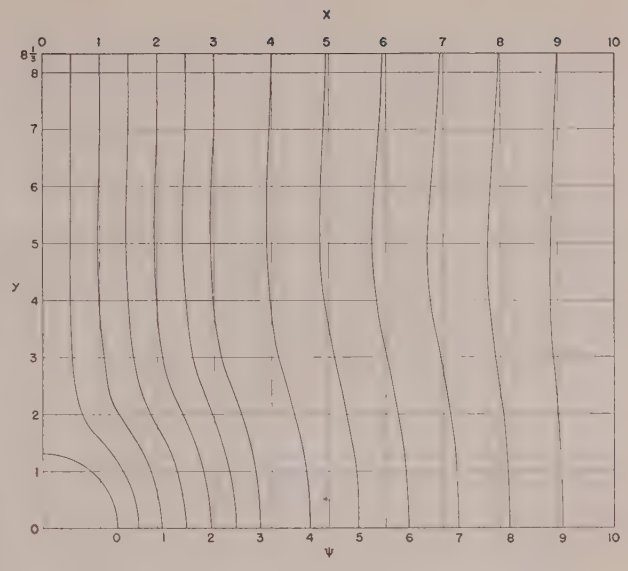

Figure 12. Result of relaxation calculations

$$\Sigma\mu_a\varphi_a-\varphi_0\Sigma\mu_a=R \tag{54}$$

where R is the "residue," which will vanish only when the "true" values of φ are used. The procedure consists in starting with the assumed values of φ at the proper lattice points of the shaded region of Figure 6, computing the residues R, then modifying the values of φ, recomputing the residues, and repeating the process until the residues are considered sufficiently small.

The initial φ values were taken from the plot of Figure 10, from which the μ-values also were obtained. First the μ-values were found at the center of each rectangle from the ratio of the sides and the relation

$$\frac{\mu}{\mu_0}=\frac{B/B_0}{H/H_0}=\frac{\Delta s}{\Delta n} \tag{55}$$

After the corrected values of φ were obtained, the μ-values were recalculated by plotting the curves $\varphi=$constant, measuring the spacing Δn, and finding μ from a curve of μ/μ_0 versus ($\Delta n/0.3$ inch), derived from equation 52 and Figure 7. An alternative procedure also was used, consisting in evaluating the derivatives $\partial\varphi/\partial x$, $\partial\varphi/\partial y$ at the lattice points, finding the gradient

$$|\nabla\varphi|=\left[\left(\frac{\partial\varphi}{\partial x}\right)^2+\left(\frac{\partial\varphi}{\partial y}\right)^2\right]^{1/2}=H \tag{56}$$

and H at the lattice points, then computing μ at the same points, and finding μ at the mid-points (a, b, c . . . on Figure 3) as proper means of μ at adjacent lattice points.

After the residues R were obtained by means of equation 54, the value of φ_0 (see Figure 3) was corrected by the addition of

$$\Delta_0=R/(\mu_a+\mu_b+\mu_c+\mu_d) \tag{57}$$

thus reducing the residue at 0 to zero and increasing the residues at A, B, C, D, by

$$\Delta_0\mu_a,\ \Delta_0\mu_b,\ \Delta_0\mu_c,\ \Delta_0\mu_d \tag{58}$$

respectively. This procedure distributes the residue at 0 to the residues at the adjacent lattice point A, B, C, D in the ratio of the permeabilities at a, b, c, d.

Because of the labor involved in the calculation of μ, the values of the latter were not changed each time the residues were reduced. Only after the residues were reduced all over were the values of μ recomputed.

At the boundary $y=0$ (AE in Figure 6), the boundary condition $\varphi=0$ enabled one to use negative reflection of the φ-values; along BC, DE positive reflection for φ was possible. Along CD, while φ is constant, its value is not known. To start with, this constant value of φ was determined from Figure 10, a check being made from the flux condition by evaluating the flux integral

$$\int\mu\frac{\partial\varphi}{\partial y}dx \tag{59}$$

for several values of y.

Along the circular boundary AB of Figure 6 the square mesh leads to irregular spacings δx, δy. After trying out generalizations of equations 18, 54, and of the other equations, to unequal δx, δy as well as of the methods of distributing the residues, a shift was made in the basic procedure.

To avoid the complications arising from the unequal δx, δy at the circular boundary, a conformal mapping was resorted to, based upon Figure 8. Indeed, if the potential lines and the flux lines of this figure be considered as ξ and η co-ordinates, then they map the region of Figure 10 upon a rectangle in the (ξ, η)-plane, shown in Figure 11. The flux line ABC, which consists of a quarter circle AB and the straight line BC, goes into the axis $\xi=0$ on Figure 11. The remaining rectilinear boundaries of Figure 8 go into $\xi=10$, $\eta=0$, $\eta=8.6$ on Figure 11. By moving the upper boundary to $\eta=9$ and dividing Figure 11 into 10 by 8 squares the difficulties of fractional δx, δy were eliminated.

To avoid the difficulty of the unknown boundary value of φ along $\eta=9$, a shift was made from φ to ψ, shifting at the same time from μ to $1/\mu$ (see equations 10 and 11). It may be shown that the basic differential equations 10 and 11 preserve their form in the new co-ordinates; thus, equation 11 transforms into

$$\frac{\partial}{\partial\xi}\left(\frac{1}{\mu}\frac{\partial\psi}{\partial\xi}\right)+\frac{\partial}{\partial\eta}\left(\frac{1}{\mu}\frac{\partial\psi}{\partial\eta}\right)=0 \tag{60}$$

Hence, exactly the same numerical methods of approximation are valid, for instance, in replacing equation 60 by an equation similar to equation 53 or 54:

$$\Sigma\frac{1}{\mu_a}\psi_a-\psi_0\Sigma\frac{1}{\mu_a}=R \tag{61}$$

There is, however, one complicating new feature, and that is that the permeability μ is no longer a function of the gradient of ψ in the new co-ordinates ξ, η. Indeed, the second half of equation 11 is transformed into

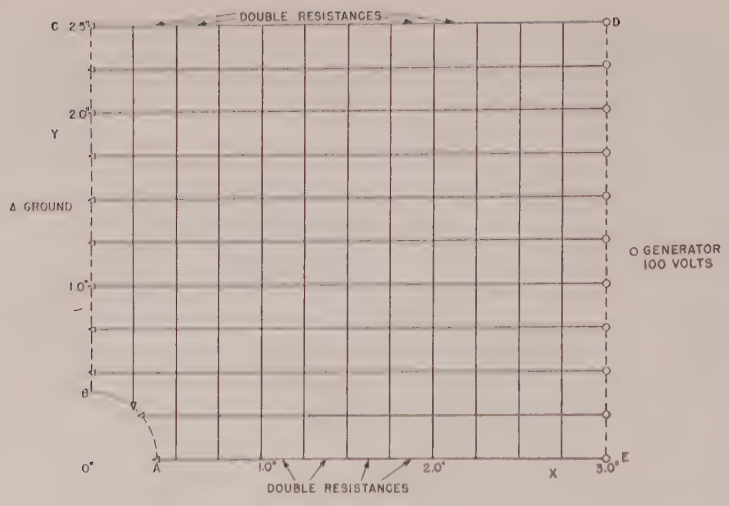

Figure 13. First d-c board setup

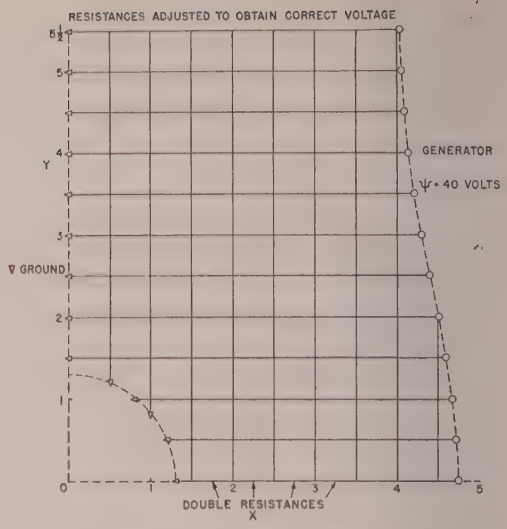

Figure 15. Network setup for lower left-hand corner of Figure 14

$$B=|\nabla_{x,y}\psi|=|\nabla_{\xi,\eta}\cdot\frac{d(\xi+i\eta)}{d(x+iy)}|=|\nabla_{\xi,\eta}\psi|r \tag{62}$$

where the factor r represents the ratio of the element of length in Figure 11 to the corresponding element of length in Figures 10 and 8.

To obtain the values of r which now were required before B and $1/\mu$ could be determined, the plot of Figure 8 was used. However, to insure greater accuracy near the left-hand corner, an analytical calculation was used there, based on the equation

$$w=\frac{10}{6}(\xi+i\eta)=z-\frac{a^2}{z},\ a=\text{radius of circle} \tag{63}$$

This is valid near the circular boundary, but not at an appreciable distance. The values of r were obtained by solving equation 63 for z, then differentiating. These values were joined smoothly to the values of r from the plot of Figure 8 and to $r=1$ at an appreciable distance.

Along the boundaries $\xi=0$, $\xi=10$ the values of ψ are known. Along $\eta=0$, $\eta=8$, positive reflections of the values of ψ could be used, and along $\xi=0$ negative reflection (and a similar procedure along $\xi=10$) to enable one to apply equation 59 in the same manner as at interval lattice points.

Reduction of the residues was repeated several times without changing the values of $1/\mu$ before a recalculation of the latter was carried out in the manner described in the preceding paragraphs.

After the final residues were judged to be small enough the ψ-values were carried over into the x, y-plane. The shape of the resulting flux lines is shown in Figure 12. The slight waviness in the area $y=4$ to 7 was very disappointing in view of the amount of labor spent in the calculations. Possibly its cause lies in the exceedingly high accuracy required for the Δs spacing, which now is affected by the inaccuracy in r. While every effort was made to obtain accurate values of r, apparently even greater accuracy is needed because of this high sensitivity variation of μ with Δs.

The same example also was set up twice on the d-c board, once before the flux plotting and numerical results had been obtained, once afterwards. The d-c board had 288 resistances, and to cover the whole area of Figure 10 a resistance network corresponding to a space interval $\delta x=\delta y=0.25$ inch first was chosen. This network, which is shown lightly on Figure 13, proved too coarse and insufficient to bring in correctly the effects of the circular boundary in its neighborhood; it will be noticed, in fact, from Figure 13 that this network cuts the quarter circle in only four points. Therefore, it was intended to cover the region nearest the circle by a closer mesh of half size, $\delta x=\delta y=0.125$ inch, using boundary conditions determined from the coarser network setup.

The analogy displayed in the array in equation 30, rather than in equation 28, was utilized in view of the greater ease of applying the condition of constant potential ψ, $\psi=0$, $\psi=10(\Delta\psi)_0$, by connecting the ground $V=0$ to ABC and the generator high-voltage terminal $V=100$ to DE.

At first the resistances were chosen to correspond to constant μ, that is, they were chosen all equal to each other, with the exception of the resistances at the boundary. There, the resistances corre-

Figure 14 (left). Second d-c board setup

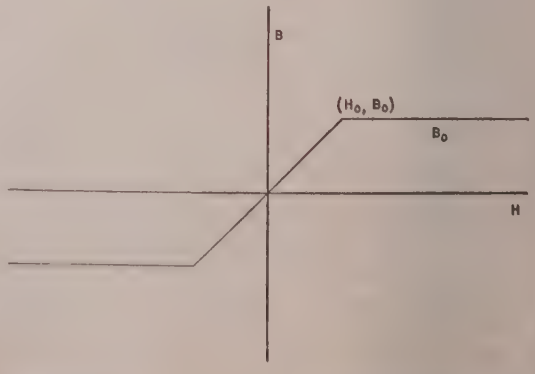

Figure 16 (right). Assumed straight line (B-H)-relation

sponding to the smaller δx or δy values were made proportionally smaller. Furthermore, along the lower and the upper boundaries $y=0$ inch, $y=2.5$ inches the resistances were doubled, and the points were left open-circuited. The reason for this procedure lies in the fact that, as on Figure 6, the field can be extended by reflection across the lower and upper boundaries. Hence, a similar reflected network can be imagined to extend below these horizontal boundaries, and each horizontal resistance, say along $y=0$, can be imagined to be made up of the resistances in parallel, of which only one is realized in the physical network setup.

The potentials V at the lattice points of the network were measured and the values of μ computed by determining the spacing Δs between the equipotentials and utilizing a curve giving μ/μ_0 as a function of $(\Delta s)/(\Delta s)_0=B_0/B$, obtained from Table I and Figure 7. To this end, curves of V versus x for fixed y and of V versus y for fixed x were drawn, smoothed out, and the points corresponding to $v=10$ volts, 20 volts, . . . 90 volts read off, and plotted in the (x,y)-plane. The distances Δs between the equipotentials then were measured, and the μ-values obtained at points corresponding to $y=0$, $y=\delta y$, $y=2\delta y$, . . . and mid-way between the equipotentials. These values of μ were plotted versus x, smooth curves were drawn between them, and the μ-values at the mid-points of the horizontal resistances obtained; similarly for the vertical resistances.

The resistances now were readjusted so as to be proportional to the values of μ obtained (in addition to the further adjustments at the boundary described above), readings of potential V were taken, and the above process was repeated several times. It was hoped that both the resistances and the potential values would converge; then the passage to the smaller mesh network was planned, utilizing boundary values along the new boundaries determined from the coarser network.

It soon became clear, however, that the potential V was not approaching any limiting value, but rather was undergoing violent fluctuations, causing the potential lines to crown in first to one side then to the other side. The process obviously was not a convergent one. It was decided that the difficulty lay with the extreme sensitivity of the method to small variations in Δs. The work on the d-c board was then stopped and effort was concentrated on the flux plotting method, as well as on the numerical calculations.

When work on the board was resumed, the results of the flux plot and of the numerical calculations were available, and the first setup on the board was based on the mean of these results. To avoid the fluctuations noted previously, the readjustment of the resistances was made only by an amount equal to 10 per cent of the change required by the μ-values calculated from the Δs values obtained in the preceding setup on the board.

It was discovered further that one cause of inaccuracies lay in the disturbances caused by the current drawn by the voltmeter when connected to measure the voltage at each mesh point. While the resistance of the voltmeter was quite high, it was not sufficiently high compared to the 100,000-ohm maximum resistance of the board elements along a constant y so that its connection did affect the mesh potentials and, therefore, also the voltage gradients. This point was checked on a uniform mesh corresponding to a 10×8 rectangle representing a potential varying linearly with x. Then the voltmeter was replaced by a galvanometer with a high resistance (30 megohms).

With the above changes, distinct improvements were obtained, but the results still were unsatisfactory. The procedure then was changed further by basing the determination of μ not upon the voltage V, and its gradient, but upon the currents in each branch. The currents I_x, I_y were read, the current resultant

$$I=\sqrt{I_x^2+I_y^2}$$

was computed, and the values of u were determined from a curve of μ/μ_0 versus $H/H_0=I/I_0$.

First the network shown on Figure 14 with the coarser mesh corresponding to δx, $\delta y=0.3$ inch was used. Based on considerations of Figures 8 and 10, it was decided that moving the boundary down from $y=8.6$ to $y=8$ produced very little disturbance in the field. It was estimated that in view of the rapid field gradients and large variations of μ near the circular boundary and the coarseness of the network, it would be more accurate to apply a boundary marked 1, 2, 3, 4, 5 on Figure 14; series resistances were adjusted to obtain these potentials. Both these potentials and the values of μ (required for the resistances) were obtained initially as means between the values determined from the flux plot and the numerical calculations, and the resistance was adjusted accordingly. The currents then were read in each resistance, the potentials also were determined, and the values of μ recalculated from the currents as well as from the potentials. Better results resulted from the values obtained from the currents; in fact, the μ values agreed with the initial values so that no further changes in resistances were deemed necessary.

The board was now connected to cover a smaller area near the circle, with a finer mesh and extending clear down to the circular boundary. As a right-hand boundary, the equipotential line corresponding to $V=40$ volts was used, the position of the right-hand boundary points being obtained from the flux plot as well as the preceding board connections. Along the upper boundary the horizontal and vertical resistances were adjusted until the values of potential obtained agreed with values obtained from the coarser network. The resulting mesh is shown on Figure 15, where as will be noted, a total of six points fall on the circular boundary. The procedure now was repeated in a very similar fashion, and again the values of μ calculated from the currents gave very close check with the values initially used in the board setup.

The hodograph method was not applied to this problem because a great deal of investigation would have been required to find out what solutions in the hodograph plane would correspond to the particular region of interest, namely, the region shown in Figures 6, 8, and 10.

Summarizing, it must be admitted that the graphical or flux-plotting method, though of limited accuracy, proved to be the most efficient one from point of view of the results obtained for the time spent. However, some of the difficulties encountered with the other methods now could be avoided in view of the experience gained.

Present day d-c boards were not built for the purpose of solving field problems, but rather for the analysis of short circuits in power systems. On the basis of experience gained in the above problem, one can readily suggest an improved design for a d-c board which would be more suited for solving field problems; this should have more units, the individual resistances should be calibrated to higher accuracy and one more decimal, and the board should possess a way of reading voltages and currents without producing any disturbance to the existing distributions.

The author cannot claim brilliant success for the numerical or so-called "relaxation" methods. It is true that greater success in the use of relaxation methods have been claimed by others.[2] While some of the difficulties indicated above could now be avoided, the fact re-

mains that these numerical methods of solving nonlinear field problems are exceedingly laborious and time-consuming, and require a great deal of patience as well as intuition on how to proceed in reducing a set of residues. It is to be hoped that high-speed computational machines can be adapted to these problems and speed up their solution.

Linear and Constant Flux Density

In this section, as a further alternative to the methods described previously, we shall approximate the saturation curve by means of an (H, B)-relation shown in Figure 16; this consists of a straight line through the corner points (H_0, B_0), $(-H_0, -B_0)$ joined to the two horizontal lines $B=B_0$, $B=-B_0$. While such a curve is never really encountered in practice, it is nevertheless true that some saturation curves can be approximated by means of such a curve to a fair degree of accuracy over a certain range. It will be shown now that such a saturation curve leads to certain simplifications.

Over the portion of constant flux density $B=B_0$ the flux function ψ has a constant gradient (see latter part of equation 11). This means that the curves $\psi=$constant, when drawn for values of the constant differing by the same amount $\Delta\psi$, are parallel curves; by parallel curves, it will be recalled, is meant a family of curves such that if one of them is given, the other members can be constructed from it by drawing normals to the given curve and plotting points at a constant distance along each normal. All parallel curves also have the property that they possess a common family of normals. These normals are all tangent to a given curve which is the evolute of all the curves of the parallel family. Thus, a parallel family of curves also may be described as the involutes of the same evolute curve (see Figure 17).

The curves perpendicular to the flux lines are, of course, the magnetic equipotentials $\varphi=$constant. Therefore, we arrive at a conclusion that over a portion of the plane where flux density is constant the magnetic equipotentials are straight lines.

In particular, let us turn to the examples discussed in the section on illustrative examples. Since the maximum saturation occurs near the point A of Figure 6, it follows that the flat portion of the curve of Figure 16 will cover part of the neighborhood of A along the x-axis. Over this portion one of the flux lines forms a circular boundary; hence, the other flux line must, therefore, be concentric circles, while the magnetic equipotentials are lines passing through the center of the circles. While the constant increments $\Delta\psi$ of the flux function corresponding to constant increments of radii of the flux lines, it is not true that constant increments of the magnetic potential function $\Delta\psi$ correspond to constant increments of the central angle θ. Indeed, from Figure 16 it will be seen that H can vary over the horizontal portion of the saturation curve through any values greater than H_0. The best that can be said for the present is, therefore, that the magnetic potential function is given by

$$\varphi=f(\theta) \tag{64}$$

Differentiation of this equation yields

$$H_\theta=-\frac{\partial\varphi}{r\partial\theta}=-\frac{f'(\theta)}{r} \tag{65}$$

Over the slanting line portion of Figure 16 the ratio of B to H is constant, μ is constant, and over the regions in the (x, y)-plane where the flux density is less than B_0 both φ and ψ satisfy Laplace's equation. By proper choice of $\Delta\varphi$, $\Delta\psi$ the equipotentials and the flux lines can be made to divide the plane into small squares. It is convenient to change the scales on the axes of Figure 16 so that the slanting line of the saturation curve becomes a 45 degree line, whereupon the sides of the squares may be considered to be inversely proportional to the co-ordinates of the sloping straight line. At the corner point, where the transition from the straight line to the constant density takes place, the squares have reached the minimum size, namely

$$\Delta n=\Delta s=\frac{\Delta\varphi}{H_0}=\frac{\Delta\psi}{B_0} \tag{66}$$

Thus, in the physical plane, at the transition from the parallel curve region to the small square region the squares are of a fixed size, given by equation 66.

If the transition curve is given, then by equating H_θ to H_0 one can determine from equations 65 and 66 the function $f'(\theta)$ and, therefore, by integration, function φ in equation 64. Stated physically, the condition in equation 66 amounts to the statement that the equipotentials be at a constant distance apart over the points of the transition curve. Actually the transition curve is not known, but must be determined from a small square plot which merges into the parallel-flux-line, rectilinear-equipotentials plot.

The approximation of the type shown in Figure 16 has been utilized by various people in various connections. An example is in the problem of torsion of a prism in which an ideal plasticity curve similar to Figure 16 is assumed between

Figure 17 (below). An illustration of the flux-plotting rules corresponding to constant flux density

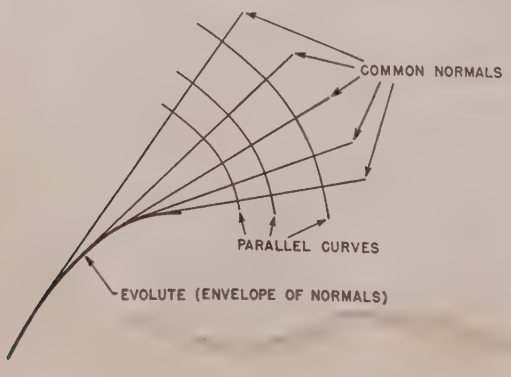

Figure 18 (right). Flux-plot corresponding to (B-H)-relation of Figure 16

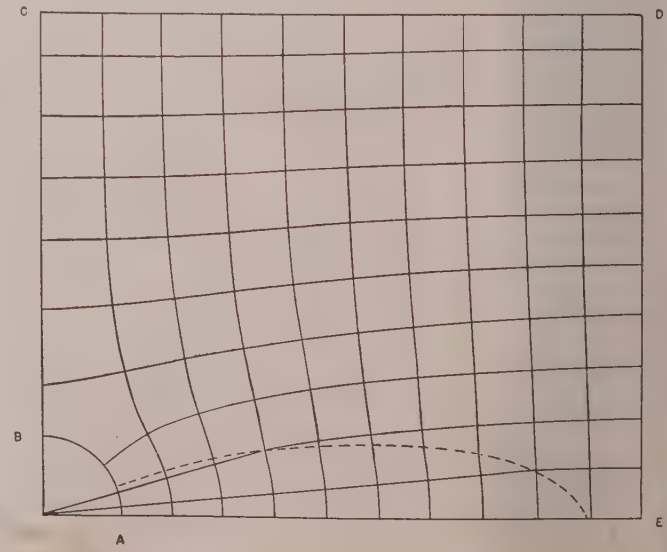

the shearing stress and the shearing strain, leading to Hooke's Law in the elastic part of the prism where the shearing stress is less than its limiting value, and to a constant shearing stress in the plastic region. A. Nadai[3] has described a sand-heap analogy for the stress function for the plastic region; when as much sand as possible is piled on a horizontal card, its free surface will have a constant slope corresponding to the angle of friction of the sand; the lines of constant level yield the direction of the shear (or of the magnetic flux lines). A further and more useful analogy to which attention has been called is that of a stretched membrane under a sloping roof. In the magnetic problem, the lines of constant level of the stretched membrane correspond to the flux lines. The sloping roof forms a restraint for the membrane over the saturated region where the membrane makes contact with the roof; in the nonsaturated region, the membrane is free. The membrane is stretched to a uniform tension, its edges are raised to proper levels over the parts of the boundary corresponding to flux lines, and the membrane takes up a shape which is partly free, and partly makes contact with the roof of constant slope. For the example of the preceding section where the saturated region stretches out horizontally from the point A on Figure 6, the restraining roof is a conical roof, with a center of the cone at the center of the boundary circle AB.

Figure 18 shows a freehand plot of the flux and potential lines for the example of the preceding section corresponding to the (H, B)-curve of Figure 16. This plot was obtained by freehand construction by starting with a plot of Figure 8 deleting the region inside the dotted curve, filling in the latter by means of circles concentric with the boundary circle and of constant difference in radii and with straight lines through the common center of the circles, and modifying the small square plot so as to obtain smooth transition at the dotted curve, at the same time assuring that the size of the squares along that curve is constant.

References

1. Polygonal Approximation Method in the Hodograph Plane, **H. Poritsky.** *Journal of Applied Mechanics* (New York, N. Y.), volume 16, number 2, June 1949 (paper number *48-APM-23*).

2. Relaxation Methods in Theoretical Physics (book), **R. V. Southwell.** Oxford Clarendon Press, London, England, 1946, chapter V, pages 144–92.

3. Plasticity (book), **A. Nadai.** McGraw-Hill, Book Company, New York, N. Y., 1931.

Discussion

T. D. Gordy (General Electric Company, Pittsfield, Mass.): Calculation of flux distributions when saturation is present is difficult and, as Dr. Poritsky points out, relatively little work has been done on developing methods that may be applied by the electrical engineer. A review of several methods that may be used is a worthwhile contribution to electrical engineering.

Flux obstructions such as bolt holes, key slots, and assembly guide slots are in magnetic circuits of most electric machinery using magnetic cores. The effects of these obstructions on the magnetic characteristics of the core are important and have been detected in the form of increased core losses and exciting currents. The example given in the paper demonstrates how saturation adds to the complexities of determining characteristics of the magnetic circuit.

To date, all methods of calculating flux distribution with saturation are time-consuming and laborious. Of the methods reviewed in the paper, the graphical one has been found to consume less time than the other methods when determining flux conditions in transformer cores. This method has given results which have been checked closely by tests. Although the method may lack in accuracy in some regions of the plot, it appears to be the best over-all method as measured by our experience. Assumptions made in the paper have been found to be justified in the problems solved thus far.

Numerical and graphical methods are the older methods; hence, they have a certain amount of past experience in them. As experience is gained with the d-c board and hodograph methods, it is very likely that application of these methods will increase.

H. Poritsky: Mr. Gordy has applied the graphical method successfully to even more complicated cases where not only is saturation involved, but where due to grain, μ depends both on B and on the directions of the flux.

In the field of compressible flow, the hodograph method has been attended with some success, though it cannot be said even at this date that it can be used to give desired answers to current flow problems. Anyone venturing on applying it to saturation flux problems will do well to review the fluid flow field first.

An Electronic Power Source for Large D-C Contact Testing

D. L. PETTIT
ASSOCIATE AIEE

A POWER source for a-c testing for currents up to 10,000 amperes is reasonably easy to obtain since it requires only a suitable transformer and a line supplying an adequate amount of power. No rotating equipment is necessary. If direct current is required, rotating equipment involving perhaps a 1,000-kw generator would be required to deliver 10,000 amperes at 250 volts. A larger set would be required for currents at 600 volts and 750 volts. Sometimes special motor-generator sets having a high inertia special windings, and an undersize driving motor are used to deliver the momentary power needed for contact testing. Such equipment is expensive, requires a large amount of space, and is not flexible so far as output voltage is concerned.

This paper describes a solution to this power requirement by using electronic tubes, showing its advantage from the standpoint of space and expense and pointing out some of the comparisons in characteristic.

Requirements

A first consideration is the service requirement. The primary requirement is to provide momentary power as required by the standard system of contact testing involving 50 repeated operations at 10-second intervals momentarily closing and opening the circuit, a test sometimes referred to as the 50 open-close-open test. A secondary requirement is the use of the power source for continuous loads. Major voltage requirements involve 250-volt systems with a lesser requirement at voltages near 600.

With these requirements in mind the welder ignitron tube in size *D* was considered particularly well adapted since it is designed for use on welding cycles usually more severe than those demanded in this application. It has a higher intermittent capacity and a lower cost than the corresponding rectifier tube. It is more susceptible to flashbacks than the rectifier tube because of the omission of the shielding in the tube.

This susceptibility to flashbacks led to the use of impedance in the feeder circuit, which limits the current to a value less than the published maximum instantaneous values for the size *D* ignitron tube. This value is approximately 14,000 amperes. In this particular installation this impedance is the combined transformer and feeder-line impedance without the use of any additional reactors or resistors.

Description

Figure 1 shows the rectifier. Figure 2 is a diagram of the manner in which the rectifier is connected to the power system and the test device. A schematic diagram of the internal connections of the rectifier appears in Figures 3 and 4.

Simplification of the firing circuit was obtained by using the load current to fire the ignitors. This arrangement also eliminated the problem of co-ordinating the phase shift of one voltage source with respect to the other when high currents were drawn from the transformer. In order to make this scheme successful, it is necessary to connect a load resistor to the rectifier so that it always draws sufficien current to cause the ignitrons to fire This resistor is reconnectable by a serie parallel switch loading the rectifier t about 100 amperes at 250 volts and 5 amperes at 600 volts.

For cooling, all six tubes were connecte in series to the city water supply, wit a flow switch at the outlet of the las tube arranged to interlock the circuit s that the rectifier could not be operate unless the water was turned on. N attempt was made to recirculate th water through the jackets.

A sequence control is provided (se Figure 4) to sequence the rectifier b establishing direct current through th load resistor just prior to the closing o the contacts of the device being teste A timer then opens the device, afte which the operator releases the pus button to de-energize the rectifier. Thi provides two desirable features in that i

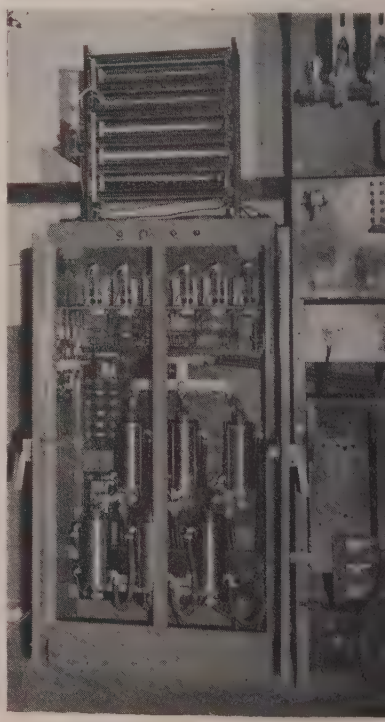

Figure 1. Rectifier installation

Paper 51-51, recommended by the AIEE Industrial Control Committee and approved by the AIEE Technical Program Committee for presentation at the AIEE Winter General Meeting, New York, N. Y., January 22-26, 1951. Manuscript submitted October 23, 1950; made available for printing December 6, 1950.

D. L. PETTIT is with the Square D Company, Milwaukee, Wis.

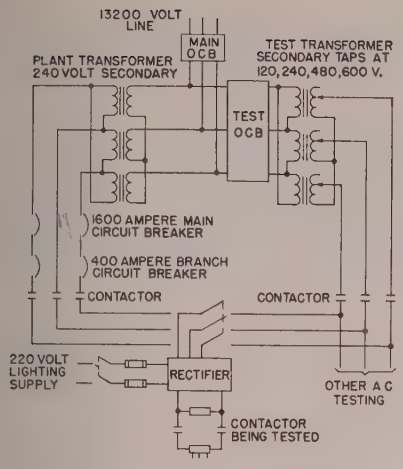

Figure 2. Connections to power supply

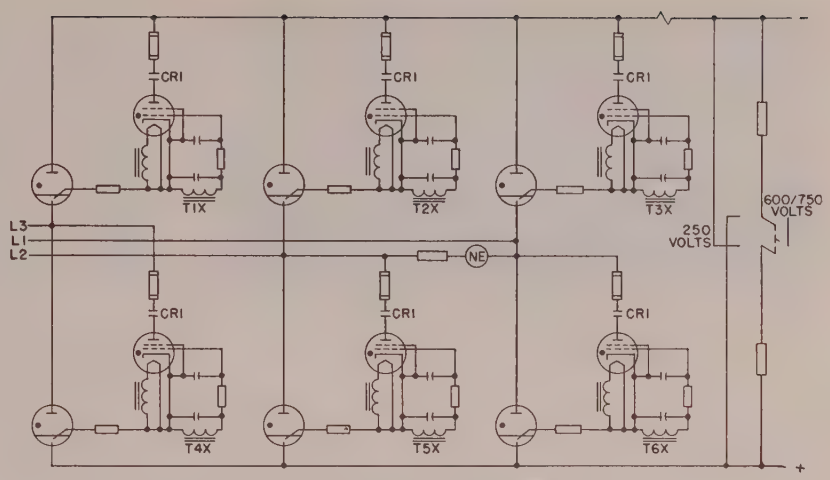

Figure 3. Rectifier power and ignitor circuits

saves power during the off period and gives the operator fingertip control of the current should the test contactor fail to open the circuit.

The use of the manual button to start each cycle of contactor operation has been chosen purposely to obtain random operation of the contactor with respect to the ripple voltage. Automatic timing in some cases has a tendency to cause the contactor being tested to be cycled closed at the same point of the cycle for each operation. Such an arrangement is considered an unfair test, although if zero phase back is used in the rectifier the ripple voltage is more or less insignificant. Reference to the oscillogram (Figure 5) will indicate the proportions of ripple voltage encountered.

It will be noted that six ignitron tubes are used, giving the equivalent of 6-phase operation, but that only three connections are brought out from the transformer. While this was a necessary part of this particular installation because the transformer was provided with only the three external connections for each set of voltages, it also provides additional limitations to the current in the case of flashbacks, because two tubes are always in series for conduction.

Voltage taps used on the transformer input are 240, 480, and 600. These taps give voltages on the d-c side of approximately 275, 600, and 750. Another tap available on the transformer at 120 volts could not be used because proper ignition of the ignitron does not occur at this low voltage. An attempt to use it caused the 3-ampere fuses to blow in the ignitor circuits. For voltages below 275 the phase-back control may be used. Phase-back control is not considered satisfactory for rupture tests since the ripple voltage becomes disproportionate and aids the device being tested in the interruption of the current. However, it is useful in supplying voltages for motors

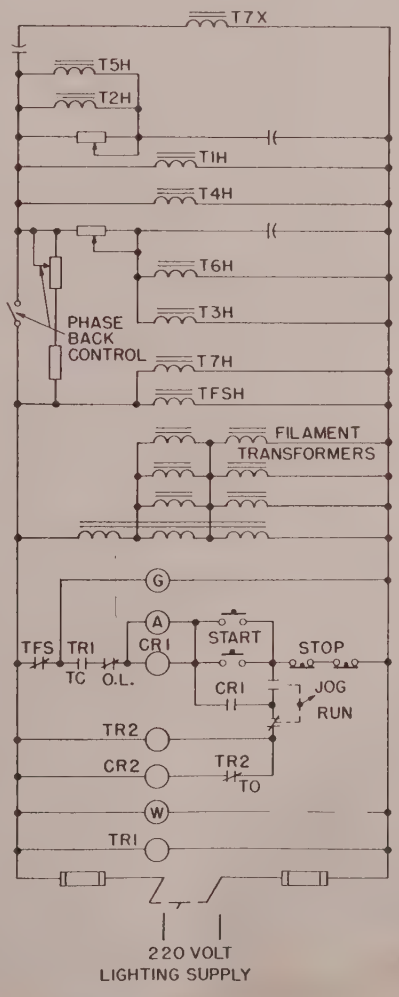

Figure 4. Rectifier control circuit

as the additional ripple voltage may be of little consequence.

It is realized that the rectifier is not identical to a generator because of the difference in the amount of inductance in the system. It will be noted from the oscillogram, however, that the recovery of voltage is fast in the case of the rectifier system. For test work a fast recovery of voltage usually leads to the earliest breakdown of the equipment being tested. However, a fast recovery voltage indicates a small amount of inductance in the circuit and may, therefore, fail to bring out a flashover which might be aggravated by some extra inductance. Up to about 30 amperes a blind spot-check was made on a special 100-ampere contactor. Failure by holding the arc occurred with the rectifier at 270 volts and with a 25-kw 250-volt d-c generator as the power source in such a way as to indicate that the results cross check.

This equipment is limited in capacity by the size of ignitron tube available, since one of the tubes must carry the entire current being drawn from the system at any one instant. Paralleling of tubes is not practical with this arrangement because the scheme does not provide assurance that both tubes in parallel would be fired and carrying current.

The rectifier terminal voltage plotted against current load is shown in Figure 6. It will be noted that this curve is not a straight line. Early effort indicated that this was traceable to errors in obtaining data. Refinement in data closely confirmed the shape of the curve as all data points touch the curve line. While firm conclusions were not reached, contributing factors may be capacitance effect at lower currents, internal resistance

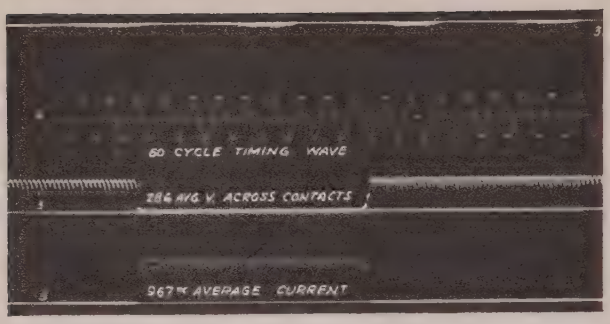

Figure 5. Oscillogram of ripple and recovery voltages

Figure 7. Contacts after testing

in the bus structure at higher currents.

Current and voltage readings are taken by using meters equipped with mechanical stops so that the hand may be preset to just below the anticipated value. The meter hand may then move through only a short distance to give a reasonably accurate reading on a current which flows less than one second. For voltage readings for the high currents an extra contact on control relay *CR*1 is used to connect the voltmeter at the same instant that the load is connected. This permits the use of a meter having a lower full-scale reading for the lower voltage readings.

The regulation of this rectifier together with the inductance and recovery voltage characteristics may or may not make it typical as a source of test power. Since there is a trend in the industry to use rectifiers as power supply, it may become increasingly important to use a rectifier as a source of power when testing devices which ultimately may be applied

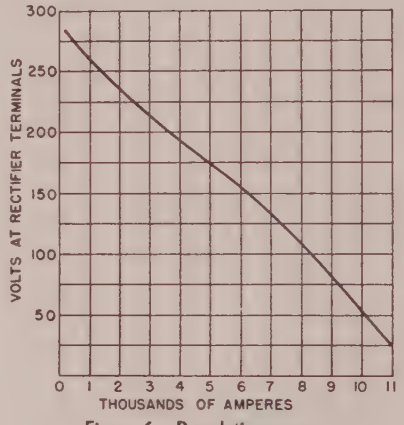

Figure 6. Regulation curve

where rectifiers are used as a source of direct current.

Figure 7 shows contacts that have undergone rupture tests using power from this unit. Note the separation of facing material on contacts in the upper left and lower right. Erosion of the backing material shows in the lower sets. Contacts at the upper right are a copper alloy enduring successfully over 10,000 amperes at 275 volts.

The floor space occupied by this equipment is 41 inches wide by 21 inches deep. The cabinet proper is 80 inches high. An additional 30 inches in height is used to mount the minimum load resistor. Water connections are brought in from the left and feeders from the right.

Conclusion

In summary we may say that this scheme of providing d-c power provides characteristics which are quite acceptable for testing up to 10,000 amperes at 250 volts, it has a greatly reduced cost when compared to rotating equipment, it is quite flexible as far as voltage output is concerned in the range of 250 to 750 volts, and it occupies a cubicle small by comparison with rotating equipment.

No Discussion

Transformer Magnetizing Inrush Current

T. R. SPECHT
MEMBER AIEE

THIS paper will develop formulas and curves for calculating approximately the magnetizing inrush curve of a transformer. Formulas have been given by others for calculating the peak of the first cycle of inrush current,[1] but no convenient method has been given for determining the shape of the inrush curve. This information is of interest for a number of reasons. Where a transformer is protected by fuses, the fuse must have characteristics such that it will carry the magnetizing inrush current. Overload and differential relays must have sufficient time delay so as not to operate falsely on magnetizing inrush. With the availability of a method for determining the shape of the inrush curve, it should be possible to precalculate to some degree the time delay it is necessary to include in any protective device and then determine how much protection the devices will give under steady loads.

Theory

The circuit that will be analyzed is shown in Figure 1. A source of alternating voltage, E, is applied to a series circuit consisting of the system reactance X_s, system resistance R_s, transformer winding resistance R_t, and transformer magnetizing reactance X_t. The transformer is assumed to be a single-phase transformer. Reference 1 describes how to use this data with a 3-phase transformer or bank of transformers. The winding of the transformer is assumed to have infinite reactance up to the saturation point and to have a finite reactance X_t above saturation. The eddy losses in the core are neglected. Essentially they represent a resistance load in parallel with the transformer, and if the system impedance is low, they should not materially affect the magnitude or rate of decay of the inrush transient. Experience factors will be used, which will help to take into account the effect of the iron.

Referring to Figure 2, the voltage is assumed applied to the transformer at −180 degrees at the voltage zero point. Also the residual flux is assumed to be in the same direction as the flux change due to the applied alternating voltage so that they will add. This combination will give the maximum inrush current. When the flux is below the saturation value, the current flowing is negligibly small. See Figure 3, a typical oscillogram of a magnetizing inrush. The system resistance and the transformer winding resistance are combined into one, R, for the purposes of calculation. Also, the system reactance and the transformer reactance are combined into one, X. For purposes of analysis, the transformer magnetic circuit will be divided into two parts, the core and the effective space between the coil and the core. For purposes of visualization, the system reactance is equivalent to an increase in the space between the coil and the core. The equation for the circuit is then

$$-\sqrt{2}E \sin \omega t = iR + \frac{Nd\phi}{dt}10^{-8} \quad (1)$$

The quantity ϕ is the flux linked by the winding excited. Integrating this equation from $-\pi/\omega$ to t:

$$\frac{\sqrt{2}E}{\omega}(1+\cos \omega t) = \int_{-\pi/\omega}^{t} iRdt + N(\phi-\phi_r)10^{-8} \quad (2)$$

Let ϕ_m be the maximum normal flux due to the applied voltage.

$$\phi_m = \frac{\sqrt{2}E10^8}{\omega N} \quad (3)$$

Then from equation 2 and 3,

$$\phi = \phi_r + \phi_m(1+\cos \omega t) - \frac{10^8}{N}\int_{-\pi/\omega}^{t} iRdt \quad (4)$$

The flux at the end of the cycle when $\omega t = +\pi$ is:

$$\phi = \phi_r - \frac{10^8}{N}\int_{-\pi/\omega}^{\pi/\omega} iRdt \quad (5)$$

From equation 5 it is seen that the integrated iR drop over a cycle has the effect of reducing the residual flux. As long as there is a d-c component in i, this term will continue to reduce the residual flux each cycle. The method used in this paper is as follows:

1. Use a simplified equation 4 for the first cycle assuming the integrated iR term is negligibly small. For most transformers supplied from normal sources of power this is true.
2. Using this simplified equation 4, determine the current for the first cycle.
3. From equation 5, determine the residual flux at the start of the second cycle. The evaluation of the integrated iR term for a cycle will subsequently be explained.
4. Use this new value of residual flux in simplified equation 4, and determine the current for the second cycle.
5. Continue this process to find the complete inrush curve.

Neglecting the last term of equation 4, this equation becomes:

$$\phi = \phi_r + \phi_m(1+\cos \omega t) \quad (6)$$

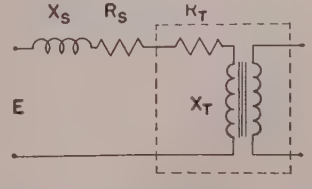

Figure 1. Circuit for transformer. The voltage applied is E. X_s and R_s are the supply reactance and resistance. R_t is the resistance of the transformer winding and X_t is the saturated reactance of the transformer

Paper 51-53, recommended by the AIEE Transformers Committee and approved by the AIEE Technical Program Committee for presentation at the AIEE Winter General Meeting, New York, N. Y., January 22–26, 1951. Manuscript submitted October 25, 1950; made available for printing December 5, 1950.

T. R. SPECHT is with Westinghouse Electric Corporation, Sharon, Pa.

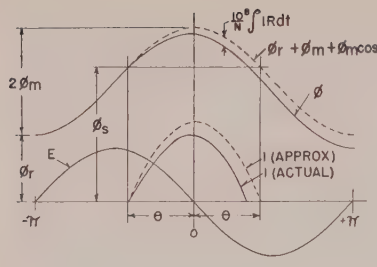

Figure 2. Instantaneous voltage, current, and flux in a transformer for one cycle of magnetizing inrush

and will apply for any particular cycle. Up to saturation there is no flux in the space between the core and coil. Above saturation the permeability of the core will be assumed to be constant, hence the coil will have an effective inductance L above saturation. The saturation flux in the core is ϕ_s. Above saturation the following equation applies,

$$N\frac{d\phi}{dt}10^{-8}=L\frac{di}{dt} \tag{7}$$

Integrating this from the instant at which the core saturates:

$$\int_{\phi s}^{\phi} N\frac{d\phi}{dt}\,10^{-8}dt=\int_0^i L\frac{di}{dt}\,dt \tag{8}$$

$$N(\phi-\phi_s)10^{-8}=Li \tag{9}$$

$$i=\frac{N10^{-8}}{L}(\phi-\phi_s) \tag{10}$$

Substituting into equation 10 the value of ϕ from equation 6,

$$i=\frac{N10^{-8}}{L}(\phi_r+\phi_m-\phi_s+\phi_m\cos\omega t) \tag{11}$$

Using equation 3,

$$i=\frac{\sqrt{2}E}{X}\left(\frac{\phi_r+\phi_m-\phi_s}{\phi_m}+\cos\omega t\right) \tag{12}$$

Let θ equal the angle at which $i=0$, that is, the angle at which saturation occurs:

$$\cos\theta=\frac{\phi_s-\phi_m-\phi_r}{\phi_m} \tag{13}$$

Substituting this in equation 12,

$$i=\frac{\sqrt{2}E}{X}(\cos\omega t-\cos\theta) \tag{14}$$

Next will be derived an expression for the saturation angle for any cycle. The saturation angle for the first cycle is from equation 13, where ϕ_R is the initial residual flux:

$$\cos\theta_1=\frac{\phi_s-\phi_m-\phi_R}{\phi_m} \tag{15}$$

Or,

$$\cos\theta_1=\frac{B_s-B_m-B_R}{B_m} \tag{16}$$

since these fluxes are all in the iron and are all referred to the same core area. The current flowing during the first cycle is,

$$i=\frac{\sqrt{2}E}{X}(\cos\omega t-\cos\theta_1) \tag{17}$$

The flux at the end of the first cycle is from equation 5,

$$\phi=\phi_R-\frac{10^8}{N}\cdot\frac{\sqrt{2}ER}{X}\times\int_{-\theta_1/\omega}^{\theta_1/\omega}(\cos\omega t-\cos\theta_1)dt \tag{18}$$

Let

$$\Delta(\theta)=\omega\cdot\int_{-\theta/\omega}^{\theta/\omega}(\cos\omega t-\cos\theta)dt=2(\sin\theta-\theta\cos\theta) \tag{19}$$

Figure 8 is a curve of $\Delta(\theta)$. Then,

$$\phi=\phi_R-\phi_m\frac{R}{X}\Delta(\theta_1) \tag{20}$$

The flux at the end of the $n'th$ cycle, which is the residual flux, is then by continuing the process,

$$\phi_r=\phi_R-\phi_m\frac{R}{X}\sum_1^n\Delta(\theta) \tag{21}$$

Substituting this in equation 13, the saturation angle θ for the $n'th$ cycle is:

$$\cos\theta=\frac{\phi_s-\phi_m-\phi_R}{\phi_m}+\frac{R}{X}\sum_1^{n-1}\Delta(\theta) \tag{22}$$

$$\cos\theta=\cos\theta_1+\frac{R}{X}\sum_1^{n-1}\Delta(\theta) \tag{23}$$

The maximum current for a particular cycle would be from equation 14,

$$i_M=\frac{\sqrt{2}E}{X}(1-\cos\theta) \tag{24}$$

The average current for the first n cycles will next be derived. For any particular cycle, for that cycle, from equation 14 and 19,

$$\int idt=\int_{-\theta/\omega}^{\theta/\omega}\frac{\sqrt{2}E}{X}(\cos\omega t-\cos\theta)dt \tag{25}$$

$$=\frac{\sqrt{2}E}{X}\frac{\Delta(\theta)}{\omega} \tag{26}$$

For the first n cycles, the average current would be,

$$i_{avg-n}=\frac{\int idt}{\frac{2\pi n}{\omega}}=\frac{\sqrt{2}E}{X}\frac{\sum_1^n\Delta(\theta)}{2\pi n} \tag{27}$$

The rms current for the first n cycles will next be derived. For any particular cycle, for that cycle, from equation 14,

$$\int i^2dt=\int_{-\theta/\omega}^{\theta/\omega}\left[\frac{\sqrt{2}E}{X}(\cos\omega t-\cos\theta)\right]^2dt \tag{28}$$

$$=\left(\frac{\sqrt{2}E}{X}\right)^2\cdot\frac{R(\theta)}{\omega} \tag{29}$$

where

$$R(\theta)=2\theta+\theta\cos 2\theta-\frac{3}{2}\sin 2\theta \tag{30}$$

Figure 9 is a curve for the $R(\theta)$. For the first n cycles, the rms current would be,

$$i_{rms-n}=\left[\frac{\int i^2dt}{\frac{2\pi n}{\omega}}\right]^{1/2}=\frac{\sqrt{2}E}{X}\left[\frac{\sum_1^n R(\theta)}{2\pi n}\right]^{1/2} \tag{31}$$

Practical Formulas

The formulas derived above should be modified by experience factors. These also will be affected by the formula chosen to calculate X_t. It was decided to calculate X_t in such a manner that it will give the same maximum current for the first cycle as in reference 1.

$$X_t=\frac{20fN^2A_s10^{-8}}{h}\text{ ohms} \tag{32}$$

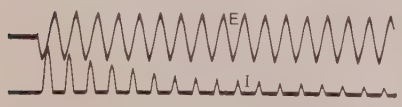

Figure 3. Oscillogram of magnetizing inrush for a 10-kva transformer. The peak of the first cycle of current, lower trace, is 663 amperes, and the rms value of the voltage is 450 volts

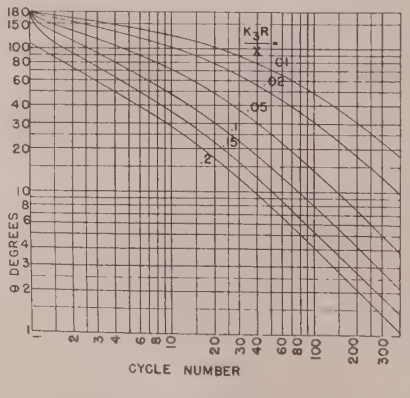

Figure 4. The saturation angle θ as a function of the number of cycles for various values of k_3 R/X. The curves are drawn for $\theta_1=180$ degrees except for the curve for k_3 $R/X=0.2$ where $\theta_1=110$ degrees

Three experience factors were decided on, the first is for the saturation angle for the first pulse:

$$\theta_1 = k_1 \cos^{-1} \frac{B_s - B_m - B_R}{B_m} \tag{33}$$

The second experience factor is for the maximum current for a cycle,

$$i_M = k_2 \frac{\sqrt{2}E}{X}(1 - \cos \theta) \tag{34}$$

The third experience factor affects the decay of the inrush.

$$\cos \theta = \cos \theta_1 + k_3 \frac{R}{X} \sum_{1}^{n-1} \Delta(\theta) \tag{35}$$

An analysis was made of seven units from 10 kva to 20,000 kva that had had their magnetizing inrush measured and the average values of these constants are as follows:

$k_1 = 0.90$
$k_2 = 1.15$
$k_3 = 2.26$

The value of k_3 was chosen so that the peak of the sixth cycle of current was matched.

A value of 20.2 kilogausses has been used for B_s, the saturation flux density, for both hot and cold rolled steels. The values for the residual flux density used are as follows:

$B_R = 60$ per cent B_m for hot rolled steel.
$B_R = 90$ per cent B_m for cold rolled steel.
$B_R = 50$ per cent B_m for type C cores.

The coefficient k_2 also will apply to equation 27 and 31 for the average and rms currents as follows:

$$i_{avg-n} = \frac{k_2\sqrt{2}E}{X}\left[\frac{\sum_{1}^{n}\Delta(\theta)}{2\pi n}\right] \tag{36}$$

$$i_{rms-n} = \frac{k_2\sqrt{2}E}{X}\left[\frac{\sum_{1}^{n}R(\theta)}{2\pi n}\right]^{1/2} \tag{37}$$

It is possible to draw curves of these various functions aud reduce the labor of calculations to a minimum. From equation 35 it is seen that θ is a function of θ_1, k_3R/X, and the number of the cycle, n. If, for example, the series of points for $\theta_1 = 180$ degrees and $k_3R/X = 0.1$ are plotted, it will be found $\theta_2 = 112$ degrees, $\theta_3 = 92$ degrees, and so forth. If the series of points corresponding to $\theta_1 = 112$ degrees and $k_3R/X = 0.1$ are plotted, the new $\theta_2 = 92$ degrees, the same as θ_3 above. It is rather evident from an inspection of equation 35 that all the points for the second series of points must coincide with the first series if the second series are all moved over one cycle number. This suggests the possibility of using one curve for all values of θ_1 for a given value of k_3R/X. Such a set of curves are shown in Figure 4 for various values of k_3R/X. To use this curve, calculate the value of θ_1 according to equation 33.

On the appropriate curve on Figure 4 find the cycle number where the angle is equal to θ_1. This number need not be an integer. Call this cycle number "p". θ_2 will then be read from the curve at $p+1$, θ_3 at $p+2$, and so forth. The portion of the curve between the first and second cycle number curves quite rapidly. This portion of the curve was determined indirectly. An intermediate value of θ_1 that lies between the first and second cycle number was assumed, and θ_2 calculated by equation 35. Then the cycle number for θ_2 is read from the curve and θ_1 marked on the curve at this cycle number less one. The curve for $k_3R/X = 0.2$ starts at $\theta_1 = 110$ degrees. This is necessary, for angles greater than 110 degrees cannot be considered by this method for $k_3R/X = 0.2$, for then the integrated iR term in equation 4 cannot be neglected. The value of 0.2 for k_3R/X is actually about as large as can be used. See the Appendix for further discussion of this point.

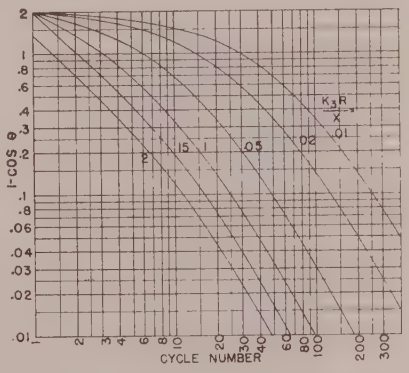

Figure 5. The value of 1 — cos θ as a function of the number of cycles for various values of k_3 R/X. The maximum current for a particular cycle is proportional to 1 — cos θ

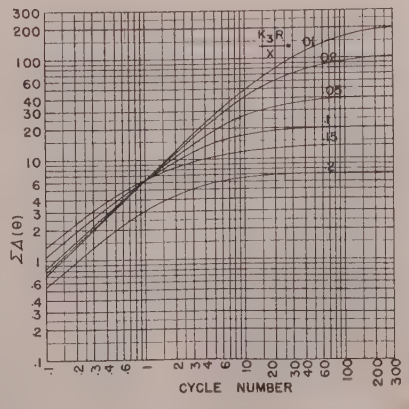

Figure 6. $\Sigma\Delta(\theta)$ as a function of the number of cycles for various values of k_3 R/X

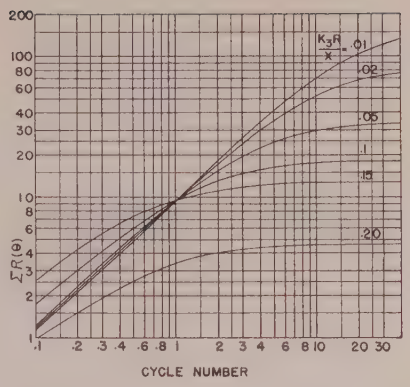

Figure 7. $\Sigma R(\theta)$ as a function of the number of cycles for various values of k_3 R/X

Figure 5 is a curve of $1 - \cos \theta$. The value of p is determined from Figure 4 as described previously. The value of $1 - \cos \theta$ for the first cycle is read at cycle number p, the value for the second cycle at cycle number $p+1$, and so forth. The maximum current for each cycle is then calculated by equation 34.

Figure 6 is a curve of $\Sigma\Delta(\theta)$ using the values of θ from Figure 4. To use this curve to find the value of $\Sigma\Delta(\theta)$ for n cycles proceed as follows. Find p as described from Figure 4. Read the value of $\Sigma\Delta(\theta)$ at $n+p-1$ and at $p-1$. The difference of these two quantities is the desired summation. The average current can then be calculated from equation 36. On Figure 6, the portions of the curve for cycle numbers less than one were deduced by an indirect process. The value of $\Sigma\Delta(\theta)$ at p, minus the value of $\Sigma\Delta(\theta)$ at $p-1$ must be equal to $\Delta(\theta_1)$ where θ_1 corresponds to p. Therefore the value of $\Sigma\Delta(\theta)$ at $p-1$ is equal to the value of $\Sigma\Delta(\theta)$ at p, minus $\Delta(\theta_1)$. For this, of course, p lies between 1 and 2.

Figure 7 is a curve similar to Figure 6 except for $\Sigma R(\theta)$. It is used in the same manner as Figure 6. With this, the rms current for the first n cycles can be calculated by equation 37.

Example

An example will be worked out for the transformer which has the magnetizing inrush curve shown in Figure 3. This transformer is rated 10 kva, 60 cycles. The value of θ_1 calculated by equation 33 was 95 degrees compared to 85 degrees measured. The value of k_3R/X was 0.154. Referring to Figure 4, for $\theta_1 = 95$ degrees and $k_3R/X = 0.154$, $p = 1.8$. To

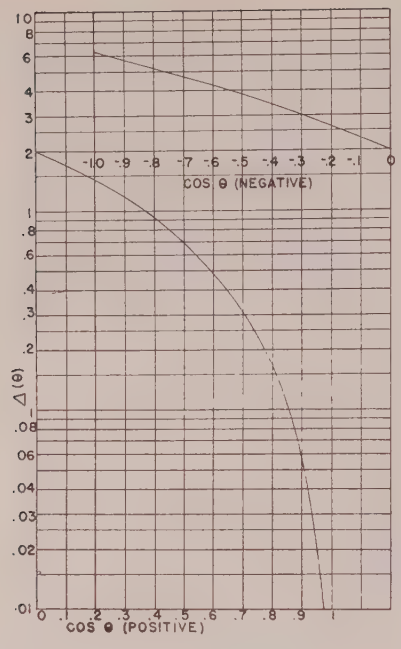

Figure 8. Δ (θ) as a function of cos θ. It is more convenient to have this plotted as a function of cos θ rather than θ for use with equation 23

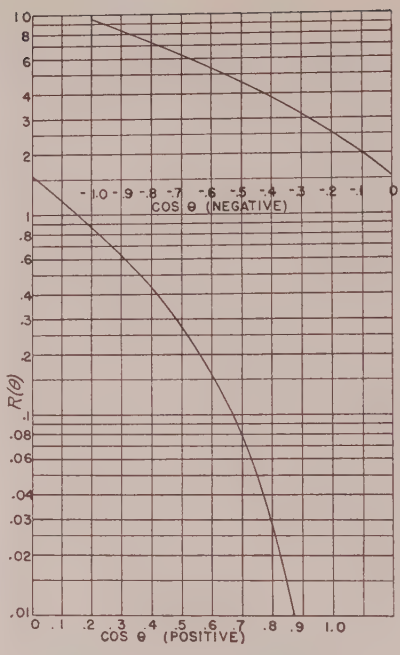

Figure 9. R (θ) as a function of cos θ

determine the maximum current for the first, sixth, and fifteenth cycles, read the value of $1-\cos\theta$ from Figure 5 at the following cycle numbers:

$1+1.8-1=1.8$: $1-\cos\theta=1.1$
$6+1.8-1=6.8$: $1-\cos\theta=0.29$
$15+1.8-1=15.8$: $1-\cos\theta=0.10$

The maximum current for the first cycle is from equation 34:

$$\frac{1.15\sqrt{2}\,(450)}{0.956}\times 1.1=841 \text{ amperes}$$

For the sixth and fifteenth cycles the currents are 222 and 77 amperes. The measured values are 663, 265, and 106 amperes.

To determine the average current for the first 15 cycles, read from Figure 6 the value of $\Sigma\Delta(\theta)$ at the following points.

$15+1.8-1=15.8$; $\Sigma(\theta)=12$
$1.8-1=1.8$; $\Sigma(\theta)=5.3$

The difference is 6.7. Then the average current for the first 15 cycles is:

$$i_{avg-15}=\frac{1.15\sqrt{2}(450)}{0.956}\cdot\frac{6.7}{15\times 2\pi}=54.5 \text{ amperes}$$

To determine the rms current for the first 15 cycles, read from Figure 7 the values of $\Sigma R(\theta)$ at the following points:

$15+1.8-1=15.8$; $\Sigma R(\theta)=11.2$
$1.8-1=0.8$; $\Sigma R(\theta)=7.8$

The difference is 3.4. Then the rms current for the first 15 cycles is:

$$i_{rms-15}=\frac{1.15\sqrt{2}(450)}{0.956}\left[\frac{3.4}{15\times 2\pi}\right]^{1/2}$$
$$=146 \text{ amperes}$$

Conclusions

This method of calculation will make it possible, by use of the curves, to readily calculate the maximum value of the magnetizing inrush current for any cycle of current, the average value of the current for the first n cycles, and the rms value of the current for the first n cycles. The accuracy is apparently as good as usual calculations for magnetizing inrush, ±40 per cent or so.

Symbols

A_s = area inside the mean turn of winding excited, square inches
B_m = maximum flux density in core due to the applied alternating voltage, E, steady state, in kilogauss
B_R = residual flux density in core at moment voltage is applied to winding, kilogauss
B_s = saturation flux density of core, kilogauss
E = supply alternating voltage, rms volts
f = frequency of supply voltage, cycles per second
h = height of winding excited, inches
i = instantaneous current in winding excited, amperes
i_{avg-n} = average current for the first n cycles, amperes
i_M = maximum current for a particular cycle, amperes
i_{rms-n} = rms value of the current for the first n cycles, amperes
k = cycle number where the saturation angle θ is $^3/_4$ radian
k_1 = correction factor for the saturation angle, about 0.90
k_2 = correction factor for the maximum current, about 1.15
k_3 = correction factor for the decay of the inrush, about 2.26
$L=X/\omega$, henrys
n = cycle number
N = turns in the winding excited
p = number of the cycle where θ is equal to θ_1 on Figure 4
R = sum of R_s+R_t, ohms
R_s = resistance of the supply circuit, ohms
R_t = resistance of the winding excited, ohms
$R(\theta)=R$ function of θ. See equation 30
t = time, in seconds
X = sum of X_s+X_t, ohms
X_s = reactance of the supply circuit, ohms
X_t = saturated reactance of the winding excited, ohms. See equation 32
$\Delta(\theta)$ = the Δ function of θ. See equation 19
θ = the angle before the voltage zero point where the core saturates, radians
θ_k = the value of θ for the k'th cycle about $^3/_4$ radian, radians
θ_1 = the value of θ for the first cycle, radians
ϕ = instantaneous flux linking the winding excited, lines
ϕ_m = maximum flux in core due to the applied alternating voltage, E, steady state, lines
ϕ_r = residual flux in core for a particular cycle, lines
ϕ_R = residual flux in core at moment voltage is applied to winding, lines
ϕ_s = saturation flux of core, lines
$\omega=2\pi f$, radians per second

Appendix

Maximum Values of $k_3\,R/X$

This value of $k_3\,R/X$ must not be too large. If R is too large compared to X, it will start to control the current. The formula was derived on the assumption that R is negligibly small in comparison to X. Substituting into equation 10 the exact value of ϕ from equation 4,

$$i=\frac{N10^{-8}}{L}\left(\phi_r+\phi_m-\phi_s+\phi_m\cos\omega t-\frac{10^8}{N}\int iRdt\right) \quad (38)$$

If the integrated iR term for a full cycle is held to less than $^1/_2$ of the maximum of the rest of the terms, it should not be too serious to neglect the last term.

$$\frac{10^8}{N}\int iRdt\leqq\frac{1}{2}(\phi_r+2\phi_m-\phi_s) \quad (39)$$

From equation 26,

$$\frac{10^8}{N}\,R\,\frac{\sqrt{2}E}{X}\,\frac{\Delta(\theta)}{\omega}\leqq\frac{1}{2}(\phi_r+2\phi_m-\phi_s) \quad (40)$$

And with equations 3 and 13, equation 40

can be rewritten,

$$\frac{R}{X}\Delta(\theta) \leqq \frac{\phi_r + 2\phi_m - \phi_s}{2\phi_m} = \frac{1 - \cos\theta}{2} \quad (41)$$

Introducing k_3,

$$k_3 R/X \leqq \frac{1 - \cos\theta}{2\Delta(\theta)} \quad (42)$$

For $\theta = 180$ degrees it is 0.16, for 120 degrees it is 0.20, and for 90 degrees it is 0.25. For smaller angles this increases indefinitely. Hence, if it is all right for the first cycle, it is all right for the rest of the inrush.

Relations for θ Less Than 3/4 Radian

It is possible to make certain simplifications when θ is less than $^3/_4$ radian that will be quite useful and reduce considerably the time required to draw the curves such as Figures 4, 5, 6, and 7.

$$\Delta(\theta) = 2(\sin\theta - \theta\cos\theta) \cong \frac{2\theta^3}{3}\left(1 - \frac{\theta^2}{10}\cdots\right) \cong \frac{2\theta^3}{3} \quad (43)$$

$$R(\theta) = 2\theta + \theta\cos 2\theta - \frac{3}{2}\sin 2\theta \cong \frac{4\theta^5}{15}\left(1 - \frac{4\theta^2}{21} \cong \frac{4\theta^5}{15}\right) \quad (44)$$

Let k be the cycle number where θ is $^3/_4$ radian or less. Then equation 35 can be written as follows:

$$\cos\theta = \cos\theta_1 + k_3\frac{R}{X}\sum_1^k \Delta(\theta) + k_3\frac{R}{X}\int_k^{n-1}\Delta(\theta)dn \quad (45)$$

Substitution of the integral for the summation is a good approximation for $\Delta(\theta)$ does not change appreciably in one cycle for θ less than $^3/_4$ radian. Differentiating this and substituting the value of $\Delta(\theta)$ from equation 43,

$$-\sin\theta\frac{d\theta}{dn} = k_3\frac{2R}{3X}\theta^3 \quad (46)$$

For angles less than $^3/_4$ radian, $\sin\theta$ is approximately equal to θ for the accuracy desired. Making that substitution and integrating the resulting equation from θ_k to θ and k to n,

$$\theta = \frac{1}{\frac{k_3 2R}{3X}(n-k) + \frac{1}{\theta_k}} \quad (47)$$

Where

$$\cos\theta_k = \cos\theta_1 + \frac{k_3 R}{X}\sum_1^{k-1}\Delta(\theta) \quad (48)$$

Also by appropriate substitutions and integrations,

$$\sum_k^n \Delta(\theta) = \int_k^n \Delta(\theta)dn = \int_k^n \frac{2}{3}\left[\frac{k_3 2R}{3X} \times (n-k) + \frac{1}{\theta_k}\right]^{-3} dn = -\frac{X}{2k_3 R}\left[\frac{k_3 2R}{3X}(n-k) + \frac{1}{\theta_k}\right]^{-2}\Bigg|_k^n = \frac{X}{2k_3 R}(\theta_k^2 - \theta^2) \quad (49)$$

By a similar process,

$$\sum_k^n R(\theta) = \frac{X}{10k_3 R}(\theta_k^4 - \theta^4) \quad (50)$$

References

1. Transformer Engineering (book), L. F. Blume. John Wiley and Sons, Inc., New York, N. Y., 1938, pages 23–36.

2. Electrical Transmission and Distribution Reference Book, (book). Westinghouse Electric and Manufacturing Company (East Pittsburgh, Pa.), 1942, pages 413–16.

Discussion

G. Camilli (General Electric Company, Pittsfield, Mass.): The author of this paper has developed an interesting method for the calculation of the magnetizing inrush current curve of a transformer. From the practical standpoint, however, it appears that the formulas have very limited applications. It is stated that the information will be useful in precalculating the values of any protective device, and for the selection of fuses. As far as the protective devices are concerned, the knowledge of the effective value and average value of the inrush current for the first few cycles may be of some value only when it is desirable to desensitize the differential relays or to make them entirely ineffective for a few seconds or until the inrush current has had an opportunity to decay. Unfortunately, this practice tends, in some measure, to defeat the purpose of the differential relays, since insulation failures in transformers have been known to occur at the instant of energizing.

The calculation of the wave shape of the inrush current has no practical consequence when harmonic restrained differential relays are used. In these relays the harmonic restraining forces are provided by harmonic components of current, and, since typical inrush current wave forms are rich in harmonic content, relay operation is prevented so long as the differential current is of this type.

In applying fuses in series with transformers, care should be taken to select fuses which are large enough so that they will not be damaged by the transformer inrush current. Essentially all the heat developed in a fuse during the transient inrush period goes into raising the temperature of the fusible element, very little being dissipated from the element during the short interval needed.

The following equation may be written applying to the heating during the inrush period:

$$I^2t = K$$

where I = current in the fuse in amperes
t = time in seconds
K = constant depending on the size and material of the fusing element

The I^2t of any fuse may be obtained from the manufacturer's published characteristics, usually given as a time-current curve plotted on logarithmic co-ordinates so that this portion is represented as a straight line. It is only necessary then to know the I^2t corresponding to the transformer magnetizing current, in order to select a fuse that will withstand it safely.

The I^2t representing the inrush for any specific transformer is, of course, a function of both the magnitude of the first current loop and the rate of decay, neither of which is usually known without a rather exhaustive study of the transformer and the system to which it is connected. A series of tests[1] has indicated that the total I^2t of the inrush may be approximated with sufficient accuracy for the purpose of fuse application. Although the maximum crest inrush current of the several sizes of transformers tested ranged from 11 to 20 times their normal full-load crest current, and the interval required for these transient currents to decay to normal values extended from 33 to 120 cycles, it was found that for each transformer tested the total I^2t in its magnetizing inrush was numerically almost the same as if 10 times normal full-load current had been flowing for 0.1 second.

This leads to a rather simple criterion for selecting fuses that will withstand magnetizing inrush currents safely. Allowing what appears to be a reasonable margin in excess of the total I^2t in the transformer inrush, it has been suggested that fuses be selected on the basis that at the 0.1-second point on the characteristic curve they be capable of carrying at least 12 times the transformer full-load current.

Mr. Specht's formulas apply only to a single-phase transformer with one wound (that is, active) leg.

In energizing a 3-phase transformer the inrush current generally will be quite different in all three phases. Furthermore, analysis may be complicated by the fact that all poles of the switch may not close simultaneously. Statistical studies, in these cases, similar to those made in reference 1 of this discussion are more useful than analytical studies based on uncertain conditions.

Reference

1. Transformer Magnetizing Inrush Currents and Influence on System Operation, L. F. Blume, G. Camilli, S. B. Farnham, H. A. Peterson. *AIEE Transactions*, volume 63, 1944, pages 366–75.

T. R. Specht: It is interesting that it has been concluded by Mr. Camilli that fuses can be applied by the rule that they be able to carry 12 times the transformer rated current for 0.1 second. I calculated the equivalent magnetizing inrush current for three transformers referred to 0.1-second basis. The values for 10-, 25-, and 6,000-kva transformers are 11, 7.5, and 9.2 times nor-

mal current With the number of variables that could affect the magnetizing inrush current, this is in good agreement

The formulas in the paper are applicable to single-phase transformers with more than one wound leg. The saturated reactance of each coil could be calculated and the sum used for the formulas. For 3-phase transformers an approximation to the current can be determined from the single-phase magnetizing inrush current by the methods given in reference 1 in the paper.

An Investigation of Audio Noise in Substation-Type Transformers

J. H. VIVIAN
FELLOW AIEE

R. R. PECK
MEMBER AIEE

UNTIL RECENT years, the audio noise emanating from substation transformers occasioned few complaints, but as substation installations in congested areas increased, utilities became aware of the necessity for limiting the intensity of transformer noise. Recognition of this developing noise problem a few years before World War II led to the collaboration of utilities and transformer manufacturers for adopting some sort of noise standards. This action resulted in the establishment of the National Electrical Manufacturers Association (NEMA) Standards* which consist primarily of tabulated ratings of the average noise levels of transformers then being produced, plus a margin of safety.

Attention is called to two developments relating to the application and manufacture of transformers that have taken place since the adoption of the present standards:

1. Economic studies have favored the utilization of the unit-type substation. This has resulted in a marked increase in the use of such substations located in well-developed residential and commercial areas. Often the transformers are immediately adjacent to homes and apartment buildings.

2. Manufacturers, in producing these unit-type substations, incorporated the latest type cold rolled steel which could be worked up to 100 kilo lines per square inch. This was done to make the use of such stations economically feasible, but in so doing, necessarily increased the noise level of the transformers.

The placing of noisier transformers close to residences has, of course, resulted in complaints. Utilities now face the following three questions:

1. Are the present NEMA standards adequate?

2. If the present standards are not adequate, what is acceptable?

3. What is the practical solution for correcting transformers with high noise levels which have already been installed or have already been purchased?

The Southern California Edison Company felt that the problem should be investigated by studying the conditions on its own system. This study would then give the company firm grounds for any change in standards it might request, and would also be of value to other utilities facing the same problem.

Southern California Edison Company Investigation

Noise Measurements. For the purpose of this study, the unit decibel is used throughout. In general, we may define the decibel as the smallest change in sound level which can be detected by the human ear. The zero decibel (db) level is at the threshold of hearing and is very seldom reached except under laboratory conditions.

Measurements were made with the General Radio Sound Level Meter and, whenever possible, were made in accordance with the NEMA Standard procedure. Three scales are available from this meter, namely, the A scale which is a weighted scale normally used for noise levels up to 60 db; the B scale for noise levels up to 90 db; and the C scale for levels above 90 db. All readings in this report were recorded on the A scale, since it is almost impossible to obtain average noise level readings in a given study by jumping from one scale to another, and since the majority of readings taken were below 70 db.

Noise Level of New Transformers. In order to verify or disprove the contention that the transformers now being received are close to NEMA Standards, a number of new transformers were checked in the Test Laboratory. Table I lists some of the typical transformers.

The noise levels of new transformers are generally close to the NEMA upper limit. It is interesting to note that although the NEMA Standards allow higher noise levels for larger transformers, the customer who hears the transformer noise makes no such distinction. Some noise complaints have been received when a small bank has been replaced with a bank of larger rating, even when the noise level of the new bank conformed to the NEMA Standard.

Determination of Ambient Noise Levels. One of the prime factors in deciding whether a transformer noise is objectionable or not depends on the ambient noise level and how much above or below this level a transformer noise can be identified. A typical residential, commercial, and industrial area was selected for a 24-hour test. Readings were made with a General

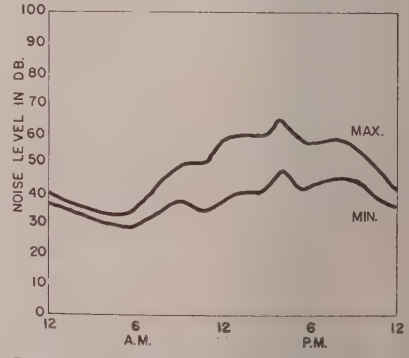

Figure 1. Noise levels encountered in a typical residential area

* NEMA Standards for Transformers. Publications Number 48-132, Section TR3-130, National Electrical Manufacturers Association (New York), September 1948.

Paper 51-55, recommended by the AIEE Transformers Committee and approved by the Technical Program Committee for presentation at the AIEE Winter General Meeting, New York, N. Y., January 22–26, 1951. Manuscript submitted October 18, 1950; made available for printing December 5, 1950.

J. H. VIVIAN is with the Southern California Edison Company, Los Angeles, Calif., and R. R. PECK is with the Line Material Company, Milwaukee, Wis.

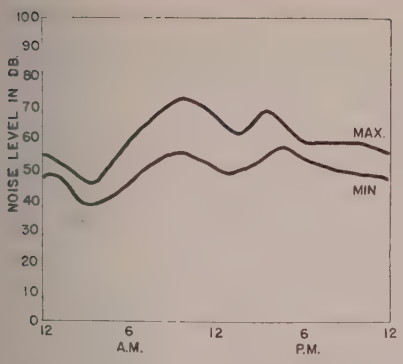

Figure 2. Noise levels encountered in a typical commercial area

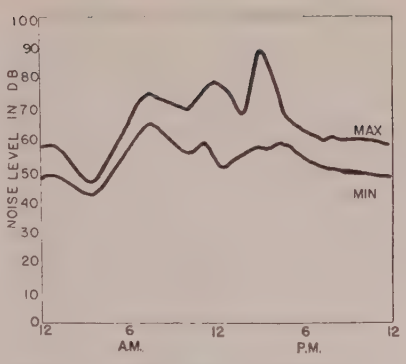

Figure 3. Noise levels encountered in a typical industrial area

Radio Noise Meter with sufficient regularity to permit the plotting of curves shown in Figures 1, 2, and 3. The locations of these tests were carefully selected in order to avoid the accentuation of any one given noise and to arrive at a true ambient noise level.

During the quiet part of the morning, a transformer noise was traced from the substation to the point at which it was no longer distinguishable. The results are plotted in Figure 4. This indicates that it is necessary to drop the transformer noise 8 db below ambient before it is lost. Apparently this is true because the majority of ambient noises are made up of numerous intermittent sounds of varying pitch, whereas, the transformer noise is a steady pitch.

In all cases, the minimum readings became the ambient level since it was necessary to lower the transformer noise 8 db below the minimum before it became inaudible, and since the quiescent periods were of relatively long duration.

Other utilities report that they have encountered minimum ambient noise levels of 25 db and that in some cases it was necessary to lower the transformer noise 10 db below ambient to lose it.

Effectiveness of Brick Wall Enclosures. Recently the Southern California Edison Company has built several substations with ornamental brick walls enclosing the station property. These walls have enhanced the appearance of the station considerably, but, nevertheless, noise from the transformers has been reported at various points away from the station. It was, therefore, thought advisable to investigate the manner in which the noise was leaving the substation.

One of the new brick wall substations was chosen in the residential area, and a number of noise measurements, both on the ground and in the air, inside and out of the station were made. These measurements were made with the assistance of a street lighting ladder truck and were made in sufficient number to establish the noise profiles as shown in Figure 5.

Numerous reflections were noted inside the station and in the air above the station, indicating that the walls and ground were good reflectors. Examination of Figure 5 indicates that the brick wall shields only a small area directly outside the substation.

Occasionally, reports of transformer noise have been received from a location relatively remote from a station, and a review of factors affecting the transmission of sound was made. The major factors may be briefly explained as follows:

Temperature Inversion. Whenever a relatively cold stratum of air is next to the ground with a warm stratum above it, sound may leave its source near the ground, travel upward until the air changes temperature and then bend to earth again. The path of the sound is the form of an inverted catenary. Cases have been reported where the ground acted as a reflector, causing the sound to make a second hop resulting in a series of diminishing concentric circles about the source. When warm air is next to the ground and cold air is above, the reverse path takes place and the sound is diverted upward and is lost.

Wind. Sound is known to travel great distances with the wind, but it also attenuates rapidly if it is against the wind.

Fog. A uniform stratum of fog transmits sound readily. Intermittent patches of fog tend to disperse the sound and attenuate it.

Applied Voltage. Each time the voltage applied to a transformer is increased, the flux density of the core is increased. A higher flux density will raise the noise level at the transformer.

It is, of course, possible for these effects to combine in a number of different ways, creating unusual noise patterns that make predictions difficult when wall-enclosed substations are involved.

Theoretical versus Experienced Attenuation of Noise. Theoretical formulas for sound attenuation indicate that the attenuation should be at the rate of 6 db each time the distance from the source is doubled. This curve is plotted in Figure 6 and is marked Theoretical Attenuation. The curve assumed a 65-db transformer as the source. Curves for other transformers may be visualized by simply raising or lowering the curve the required number of db.

The experience of our tests, as well as the experience of others, indicates that an attenuation of 4.5 db each time the distance is doubled, as plotted in the same Figure 6, is a much more realistic figure. This curve is marked Attenuation Experienced.

The 22-db line is also shown and represents the level to which transformer noise must be lowered in residential areas in order for it to become unidentifiable. This line is 8 db below the ambient noise recorded in the early hours of the morning. A similar line is shown at 30 db which is applicable in commercial areas.

From Figure 6 we may draw the conclusion that a 65-db transformer may be heard over an approximate mile radius during the early hours of the morning in a residential area, provided there are no obstructions such as houses, walls, trees, between the listener and the transformer.

From this same curve we may also deduct that a sound from a 40-db transformer would not be heard beyond a radius of 100 feet from the transformer.

Table I

Phase	Kva	Voltage	Actual Noise, decibels	NEMA Standard, decibels
1	3,333	39,800/69,000/12,000	70.4	66
1	3,333	39,800/69,000/12,000	68.0	66
1	3,333	39,800/69,000/12,000	65.0	66
1	3,333	38,800/69,000/12,000	66.7	66
3	1,500	15,000/460	63.1	63
3	1,500	15,000/460	61.5	63
3	1,500	15,000/460	65.6	63
3	2,000*	16,500/4,360/2,520	60.5	64

* Unit-type substation, switchgear, and housing were not attached to transformers at time of test.

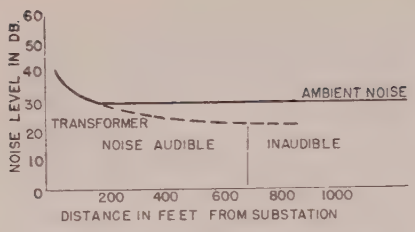

Figure 4. Attenuation of noise from residential substations. (Audible and inaudible points)

Figure 6 (right). Comparison of theoretical versus experienced attenuation from tests at substations

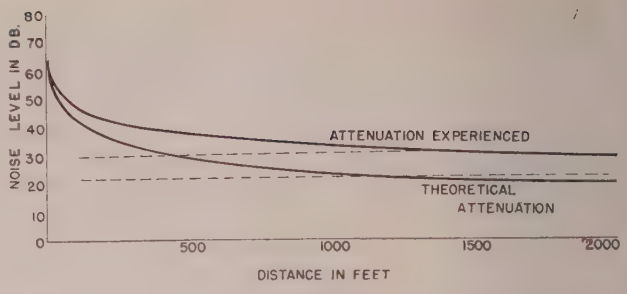

A few shrubs and incidental obstructions between the transformer and the adjoining residences would make the noise inaudible.

If the sound follows the path of the catenary caused by temperature inversion, the distance shown on the chart would represent the length of the catenary.

Objectionable Noises. A noise must be heard before it can be objectionable, but obviously all audible noises are not objectionable. It depends a great deal on the individual himself. Some of the major factors influencing the individual and his objections to a sound are listed as follows:

1. Like or dislike for the source of the noise.
2. Irritation by certain frequencies.
3. Nervous temperament and general health.
4. Working-sleeping schedule.

Utilities through good public relations and thoughtful consideration of substation enclosures can do a lot toward making people like the substations, but it may be a difficult task to satisfy a customer who is sensitive to certain sound frequencies, particularly if his sleeping schedule is disturbed. Also, a person who is awakened may find it difficult to return to sleep and any noise that he can identify at that time becomes objectionable and is immediately identified with his inability to sleep.

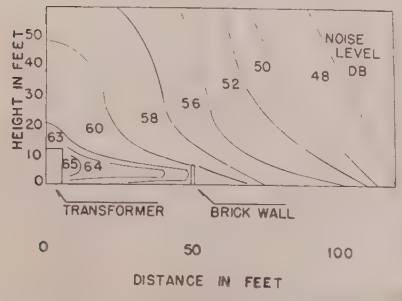

Figure 5. Results of noise profile tests at a substation showing effectiveness of brick wall

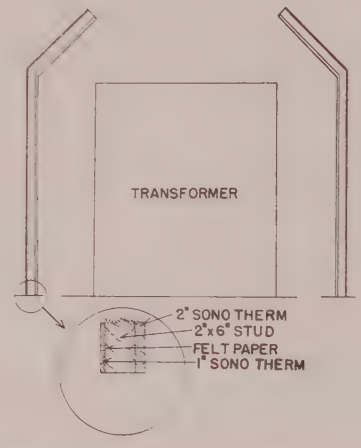

Figure 7. Cross section of proposed sound barrier and its relation to the transformers

Cost of Substations. Economic studies were made on a number of Southern California Edison Substations. These stations are of recent construction and vary from a chain link enclosure to a totally enclosed building. The cost per kva varies considerably, and is largely dependent on the kva capacity installed and the location. Zoning ordinances have in many cases required the installation of elaborate ornamental walls around substations. This is an expensive practice and lessens the economic advantage of unit type substations.

The Transformer Noise on a 60 Cycle System. The fundamental noise emitted by a transformer is 120 cycles per second and is caused by the expansion and contraction of the iron core, caused by magnetostriction. Various harmonics of 120 cycles are present in varying proportions. All parts connected to the iron core become radiators of sound, and if any of these parts are resonant to 120 cycles or one of its harmonics, the noise level will be increased. Tests were conducted to determine the method by which noise is transmitted from the core to the case of a transformer, and it was found that a large part of the noise was transmitted by the transformer oil. Attempts to control the transmission of sound in the oil proved to interfere with the transfer of heat and hence were abandoned. Loose and resonant components prove to be excellent radiators, but even they will not radiate sound unless actuated by the noisy core; therefore, it appears that the most effective results will eventually be obtained by the use of new and different transformer materials, or a new design of core stack which will have low magnetostriction noise.

Test on Sound Barriers. In order to provide a solution for noisy transformers already in service, a noise barrier was constructed in a substation on which considerable noise data were already available. This barrier was a frame structure covered on both sides with a weatherproof sound proofing material. The relation of the barrier to the transformer is shown in Figure 7. A direct comparison as to the effectiveness of this barrier may be made by examining Figures 5 and 8. The noise reduction obtained by this barrier is considerably greater than could be obtained by a like expenditure in purchasing transformers having low db levels. Other utilities have built heavy masonry barriers which depend on their mass to deaden the sound; however, any barrier, to be effective, must be located close to the transformer and high enough to prevent the sound bending downward over the top of the wall.

Operating clearances and proper venti-

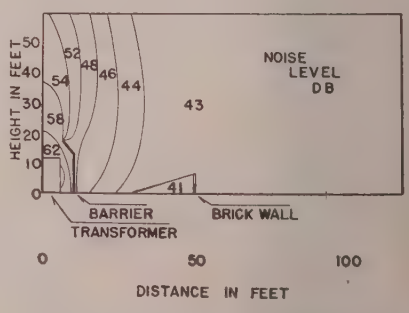

Figure 8. Noise profile at substation with sound barrier

NOTE: Brick wall acts as a shield from noise outside of station during the daytime

lation limit the practicability of any type barrier and, therefore, they should not be considered as a permanent solution for noisy transformers.

Conclusions

1. Our experience indicates that the noise levels tabulated in the NEMA Standards are too high for power transformers which are to be used in densely populated areas.
2. The noise level of transformers and associated apparatus must be such that average attenuation in air will bring the noise level at the nearest residence about 8 db below the ambient, if the installation is to be inaudible.
3. Sound barriers such as described in this paper may be used to control the sound, but these barriers have many disadvantages. The ultimate method of correction must be the elimination or control of noise generating sources in the apparatus. This can only be done by the manufacturers. Unless the designers can develop equipment with suitably low noise levels, the use of unit type substations will be greatly restricted. Low noise levels and pleasing appearance are vital to wide acceptance of this apparatus by the general public.

References

1. Transformer Audio Noise Problems on an Electric Power System, **C. S. Murray.** *AIEE Transactions*, volume 68, Part I, 1949, pages 740–52.
2. Transformer Sound Level Considerations, **A. J. Maslin.** *AIEE Transactions*, volume 69, Part II, 1950, pages 1142-47.
3. Quiet Transformer Installations—A Problem for Both Equipment and Substation Designers, **I. S. Mendenhall, F. L. Taylor.** *AIEE Transactions*, volume 69, Part II, 1950, pages 1148-53.
4. Audio Noise in Transformers in Residential and Commercial Areas, **C. E. Baugh.** *AIEE Transactions*, volume 69, Part I, 1950, pages 121–28.
5. Theory and Use of Architectural Acoustical Materials. **Paul E. Sabine.** Acoustical Materials Association, Chicago, Ill.
6. Acoustical Terminology. Pamphlet *Z24.1-1942*, American Standards Association, New York, N. Y., 1942.
7. Sound Level Meters for Measurement of Noise and Other Sounds. Pamphlet *Z24.3-1944*, American Standards Association, New York, N. Y., 1944.
8. Sound and the Human Ear, **S. Benton.** *Westinghouse Engineer* (East Pittsburgh, Pa.), March 1949, pages 60–64.
9. Magnetic Phenomena (book), **S. R. Williams.** McGraw-Hill Book Company, New York, N. Y., 1931.
10. Elements of Physics (book), **R. A. Millikan and H. G. Gale.** Ginn and Company, Boston, Mass., 1927.
11. Sound (book), **A. T. Jones.** D. Van Nostrand Co., Inc., New York, N. Y., 1937.
12. Textbook of Sound (book), **E. Catchpool and J. Satterly.** University Tutorial Press, Ltd., London, England, 1944.
13. Practical Acoustics (book), **Hope Bagenal.** Chemical Publishing Company, Brooklyn, N. Y., 1942.
14. Harmonic Index—A Tool for Transformer Audio Noise Investigation, **W. H. Mutschler, Jr., T. F. Madden.** *AIEE Transactions*, volume 69, Part I, 1950, pages 115–20.
15. Audible Noise of Power Transformers, **T. D. Gordy.** *AIEE Transactions*, volume 69, Part I, 1950, pages 45–53.

Discussion

T. R. Specht (Westinghouse Electric Corporation, Sharon, Pa.): In this paper the authors state that the standards of the National Electrical Manufacturers Association (NEMA) consist primarily of tabulated ratings of the average noise level of transformers then being produced, plus a margin of safety. This was more the case with the hot-rolled steels in use at the time the standards were recommended. With the newer cold-rolled steels, which can be worked at higher inductions, the limit on induction at present is determined by the NEMA sound levels in most of the ratings. The manufacturers are investigating the causes, reduction, and isolation of transformer noise, and are building the transformers as quiet as present skills and economic considerations permit. The largest percentage of transformer installations cannot justify the extra cost of very quiet transformers. It is most reasonable, then, that the standard line of transformers should have sound levels which are the minimum that can be attained without increasing the price of the transformer. This closely approximates the NEMA standards for noise level. There are locations where lower sound levels are necessary. Such cases should be investigated as to whether it is more economical to specify a special quiet transformer or to build a sound barrier around the transformer. It might be desirable to have two sets of sound level standards, one for specially quiet transformers and one for regular transformers.

The authors of this paper also state that the noise level of some new transformers varied as much as 10 decibels, but the transformers compared are of different size. The transformer with the highest sound level is 4.4 decibels above the NEMA level, and the lowest transformer is 3.5 decibels below its NEMA level. The range would be 7.9 decibels with respect to the NEMA levels. This would be a fairer basis of comparison for power transformers. The minimum NEMA level is 56 decibels, and small distribution transformers will be well below this figure when worked at higher inductions limited by efficiency and exciting current.

Considerable emphasis is placed in the paper on unit substations and their noise. Of course the unit substation is ideally suited to the small substation, but for a given load the unit substation incorporates the same size transformer parts that a separate transformer would require. The unit substation would have the same sound level as a separate transformer of similar construction and capacity.

The paper states that a transformer needs to be 8 decibels below the ambient sound level to be inaudible. It gives a minimum ambient of 30 decibels, and if there is an 8-decibel attenuation between the transformer and the listener, the transformer would have to be 30 decibels. Certainly a minimum ambient level is not encountered very often. At the present state of the art a 30-decibel level is attained in transformers less than one kilovolt ampere. It would require an extremely radical improvement of the core material in order to build, for instance, a 500-kva transformer this quiet. Others believe that a level of 40 decibels at the property line of the substation is adequate to prevent complaints.

The paper mentions the phenomenon of temperature inversion. Do the authors have any figures on the maximum variation in the sound level at a point about 150 feet out under various conditions?

T. D. Gordy (General Electric Company, Pittsfield, Mass.): The paper by Messrs. Vivian and Peck brings to our attention the importance of sound levels in substation-type transformers. This is one field of application in which quiet transformers are desirable and often necessary and an area in which much investigation has been made.

I do not feel that I can agree with the authors that cold-rolled steel was introduced in unit substations to make the use of such equipment economically feasible. Actually, the economics inherent in unit substations has fully justified their selection in a great many cases, and this was true both before and after the introduction of cold-rolled steel cores. Entirely aside from the question of substations, the utilization of an improved core material has been a major advance in the art. Such use has resulted in lower weights, smaller dimensions, improved core loss and exciting current characteristics, and a basic improvement in the over-all economy for the industry. Increases in flux density do have higher sound levels associated with them and thus present a specific problem. This is an important element, but I do not feel it should be allowed to outweight the many inherent advantages enumerated above.

Data on noise levels of new transformers indicate a variation of 5.4 decibels for the 3,333-kva transformers and 4.1 decibels for the 1,500-kva units. To obtain the 10-decibel variation between units, as stated in the paper, the kilovolt-ampere rating of the units must be disregarded. I do not feel this is logical, and it is not in accordance with the NEMA standard quoted in Table I of the paper.

The theoretical attenuation of sound from a source is dependent upon the type of source. Each time distance from the source is doubled, the following attenuations may be calculated for the particular source:

1. 6 decibels for a point source
2. 3 decibels for a cylindrical source
3. 0 decibel for a plane source

Obviously, a transformer is a combination of the above simple sources and should not follow either of the theoretical attenuation

laws. A 4.5-decibel rule falls between the attenuation from point and cylindrical sources, which is reasonable. The 4.5-db rule has been checked by other investigators.[1,2]

Assuming the diagram of Figure 5 of the paper is approximately to scale, it is not surprising that the brick wall was not effective in reducing sound levels away from the transformer. This wall was too low and too far away from the transformer to be effective at an appreciable distance from the wall. The effectiveness of a higher barrier close to the transformer is clearly shown by Figure 8 of the paper. Other data showing the effectiveness of such barriers have been given by Corbett McLean.[3]

Magnetostriction is an important source of sound in transformers, but other sources, such as joints, gaps, and flux wave shape, are very important.[2,4] It is the nonlinear characteristics of these other sources, as well as the nonlinearity of magnetostriction, that generates harmonics in emitted sound from transformers.

The authors' survey of ambient sound levels and their variations is very worth while in that the times at which minimums occur are clearly shown. It is these minimums that must be borne in mind when complaint investigations are made. Certainly, as the paper states, the individual himself is very important when sound at a particular site has been termed objectionable.

It is not necessary to have the transformer sound level inaudible at a site in order to have it unobjectionable. As the second conclusion in the paper states, transformer noise may have to be attenuated to 8 decibels below ambient for it to be inaudible, but this low a component of total sound at the site is not required in order to avoid a complaint. Factors such as frequencies present, relative intensities of the various frequencies, ambient variations, transmission medium variations, and many others must be considered when determining the sound level at which complaints are started.

The authors are to be commended on their contribution to experiences with transformer sound levels. Their data on ambient sound levels and sound level profiles around a transformer and its barrier are of particular interest. Obtaining such data is a difficult task and one demanding patience and good measurements technique.

References

1. Reference 1 of the paper.
2. Reference 15 of the paper.
3. Transformer Noise and Its Confinement, **Corbett McLean.** *AIEE Transactions*, volume 69, part II, 1950, pages 1409–16.
4. Transformer Sound Level Considerations, **A. J. Maslin.** *AIEE Transactions*, volume 69, part II, 1950, pages 1142–47.

R. R. Peck: The discussions by Mr. Gordy and Mr. Specht are apropos and are greatly appreciated by the authors of the paper.

Mr. Specht points out that a large percentage of the installations cannot permit the installation of a high-cost unit substation. This is very true, and we hope that as the art and science of metallurgy progress low noise level transformers will become available at nominal costs.

Both Mr. Gordy and Mr. Specht point out that Table I of the paper shows a less than 10-db variation between transformers of the same size. In this connection, I would like to offer the following comment: the size or voltage rating of a transformer is irrelevant to the customer complaining about the noise.

Mr. Gordy correctly states that a theoretical drop of 6 decibels is obtained each time the distance is doubled from a point source; we are of the opinion that a transformer becomes a point source at some distance. His explanation that a transformer falls some place between a plane source and a point source is very logical and doubtlessly accounts for the 4.5-db experienced.

Our field experience contradicts Mr. Gordy's statement that "It is not necessary to have the transformer sound level inaudible at a site in order to have it unobjectionable." We do not want to convey the idea that we think all noise levels must be lowered to this degree before a complaint can be settled. However, some people acquire such a dislike for a given noise that it remains objectionable as long as they can identify it.

Mr. Specht asks if test data for variance in sound attentuation have been measured at 150 feet from the source. We have not made any specific tests of this nature, but believe that wind might account for considerable difference. The distance of 150 feet probably would be too small for temperature inversion to affect the results.

Acoustic Models of Transformer Installations

BRIGGS GETTYS
ASSOCIATE AIEE

WILLIAM B. CONOVER
MEMBER AIEE

Synopsis: Noise problems caused by transformer installations in urban situations can be avoided, ameliorated, or corrected by several measures. The application of the least costly of these measures requires information which cannot be obtained easily by analytical methods. Measurements of an acoustic model of the transformer in its environment aids in the evaluation of the particular noise problem and gives design data for sound-reducing barriers.

THE continuing growth of system generating and distributing capacity has caused many power companies to consider most carefully the noise level of new transformer installations, or possible increases in the noise level at established stations and substations. The more critical transformer installations generally are recognized as such by power companies, and a survey will be made of the sound field at the location. This survey is difficult, lengthy, and does not provide sufficient information to determine the design of the most economical corrective measures. It is the purpose of this paper to demonstrate that additional helpful information can be obtained, particularly by the use of acoustic models. The model technique is the only feasible method of attack in certain acoustical problems. The instrumentation required for model testing is of comparative simplicity and availability. The measurements can be made successfully by many power companies with their sound specialists and their existing facilities.

Paper 51-56, recommended by the AIEE Transformers Committee and approved by the AIEE Technical Program Committee for presentation at the AIEE Winter General Meeting, New York, N. Y., January 22–26, 1951. Manuscript submitted October 26, 1950; made available for printing December 6, 1950.

BRIGGS GETTYS and WILLIAM B. CONOVER are both with the General Electric Company, Pittsfield, Mass.

Noise Control Measures

The following alternatives[1,2,3] are available to the power company and the choice depends upon cost, effectiveness, and the particular circumstance:

1. Purchase a transformer with a sound-level specification set below the NEMA (National Electrical Manufacturers Association) values.
2. Screen the station or substation with a planting of evergreen trees.
3. Construct a building completely enclosing the transformer or transformers.
4. Construct a barrier or a roofless enclosure.

The purchase of a low noise level transformer can entail a substantial premium in price. A screen of trees is psychologically valuable, but does not reduce the sound level appreciably.[4] Total enclosure by a building is effective, but cooling problems and interference with existing buswork renders the measure prohibitively expensive in many cases. A barrier is effective for a moderate reduction of level, is relatively inexpensive (though not a minor investment), does not complicate the transformer installation, and can be designed by the use of model technique.

Investigation of Particular Sound Fields

A survey of the sound field is used to evaluate the sound pressures existing over a certain environment, for one or more of these three purposes:

1. To attempt to establish what sound pressure level may be added to an existing ambient sound level without causing complaints from the public.
2. To investigate a complaint. This entails identification of the source of the noise added to the ambient sound level.
3. To ascertain how effective corrective measures have been in reducing the cause for complaint.

Briefly, a sound-field survey is an accumulation of total sound-level measurements and sound analyses made at selected significant locations, at significant times of day, over a period of time. The completeness of the survey is determined by judgment and the particular circumstance. The ambient sound level in an urban environment varies from moment to moment, with its lowest values usually existing from 10 p.m. through the early morning hours. It is the average of quiet moments, between the noise of passing trains, trucks, and so forth. At long distances from a sound source the sound received at the chosen measurement station will vary because of wind conditions, thermal gradients which cause refraction, and slight shifts in frequency of excitation which can result in a shift in the standing wave pattern at long distances. Moving objects near the source also can cause large changes.

A portable tape recorder, in addition to the sound-level meter, can reduce the effort required to make the survey. The ambient is available for later study as a function of time, and sound analyses for the identification of transformer sound components in the ambient can be made from the recorded material under more favorable conditions. The sound-field survey is costly in time and money, but usually is necessary.

Since the cheapest of corrective measures for a noise problem still represents a considerable investment, recourse to supplementary forms of investigation is indicated for design of the corrective measure. These investigations may consist of mathematical analyses, the simulation of transformer noise at the actual planned location, or acoustic model tests.

The prediction by mathematical analysis of a sound field in some urban loca-

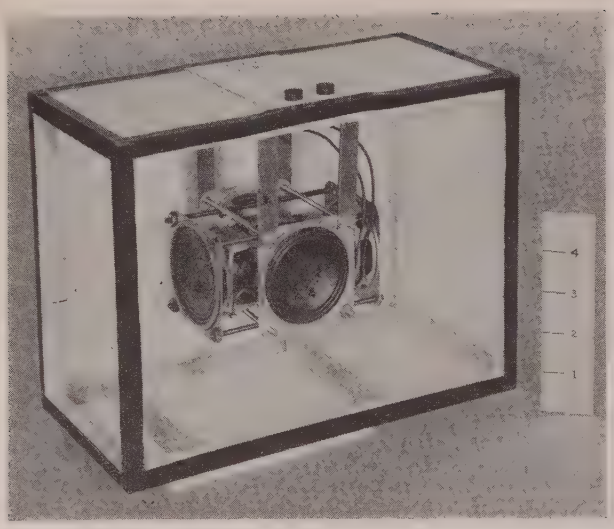

Figure 1. Acoustic model of power transformer with two paper panels removed to show loud-speaker arrangement

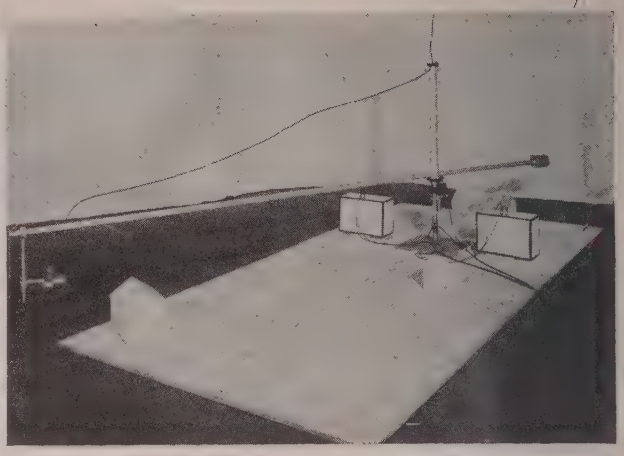

Figure 2. Typical acoustic model of transformer installation, showing transformers, buildings, and microphone transport mechanism

tions is of such complexity, even with the most radical simplifications, that little confidence can be placed in the quantitative results.

Of more promise is the use of a loud-speaker placed at the proposed location of the transformer. The sound field of a loud-speaker or loud-speakers may be made to approximate roughly that of a transformer in frequency composition, normal angular distribution, and intensity. The loud-speaker is functionally an acoustic model of the transformer. The effect upon the ambient sound level at distant critical areas then could be determined. Assuming that the equivalence between speaker and transformer level is proved, the information gained is the effect of the installation of a transformer with a certain sound level upon the ambient sound level. Experimentation with wall barriers would be on full scale, expensive, and difficult.

To our knowledge this potentially valuable procedure has not been put into practice because the amount of data needed is large and may not contain the points at which complaints arise, and because it is feared that the neighborhood will become sensitized to problems of noise.

The third procedure, that of acoustic model testing, has been and is being used. It does not establish absolute ambient sound levels as affected by the added transformer noise. But model testing does predict relative levels over areas of interest and supplies useful information which permits design of the barriers. An area of high concentration of sound energy, caused by reflections from buildings and topographical features, can be determined in advance by model technique, with the resulting possibility that slight changes in the installation can place these concentrations where the chance of complaints is small.

Acoustic Model Technique

The Acoustical Principle of Similarity[5] states that for any acoustical system involving diffraction and reflection phenomena it is possible to construct a new system on a different scale, which will exhibit similar performance, providing the wave length of the sound is altered in the same ratio as the linear dimensions of the new system.

This principle justifies the use of a model to predict the performance of an actual system. Theoretically an exact duplicate could be made to any scale whatsoever, but practical considerations impose limitations on the degree of similarity and on the scale which can be employed. It is impossible to duplicate exactly transformers or their environment to a small scale. Therefore, in place of transformers, comparatively simple sound sources are used; and in place of the complex array of buswork and other station equipment, only structures whose dimensions are large compared to the wave length of the sound under consideration are included. Since both structural and topographical features consist mainly of acoustically "hard" (that is, highly reflective) materials, wood is used for most of the model structures. Should it be necessary to duplicate the effect of partial acoustical absorbents, for example, a light layer of freshly fallen snow, the acoustical impedance of the corresponding model material would have to be chosen with some care.

The model scale must be small enough for the model to be accommodated in the available testing space; on the other hand, it must be sufficiently large to permit the use of a sound frequency which can be generated and measured readily. Since the velocity of sound in air at 20 degrees centigrade is 1,130 feet per second, the frequency of the model sound must be $f_m = 1{,}130/\lambda_m$ cycles per second, where λ_m is the wave length of the model sound in feet. To preserve similarity between model and prototype, $\lambda / \lambda_m = L/L_m$, where L and L_m are corresponding linear dimensions of the prototype and model, respectively. Tests to date have been concerned with the 360-cycle component of transformer noise. A scale of 30 to 1 gave a corresponding test frequency of 10,800 cycles, which is near the upper limit of measurement with generally available sound-level meters. (All instrumentation chosen for these particular model tests is of comparative simplicity and availability; similar measurements can be made successfully by many power companies with their sound specialists and existing facilities.)

The testing area should have an ambient noise level at least ten decibels below the minimum sound level to be measured. In addition, acoustic reflections from the walls and ceiling must be negligible. A hard floor usually is desirable, for it may be used to represent the ground, provided that the terrain is flat in the vicinity of the prototype. If a sound room meeting the requirements of low ambient noise level and nonreflective boundaries is not available, tests may be made out of doors, but this introduces the usual problems incident to testing in the field: dependence on weather, availability of

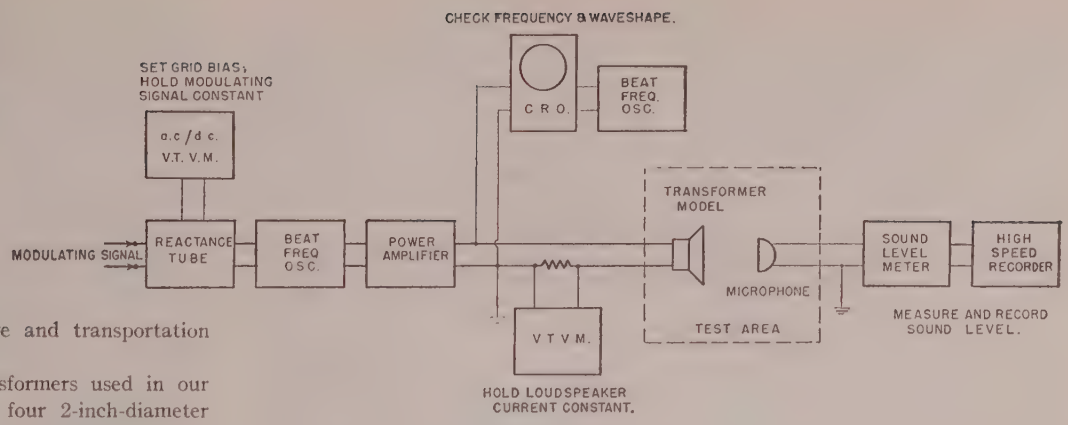

Figure 3. Block diagram of sound generation and measurement equipment for acoustic model tests

power, and storage and transportation difficulties.

The model transformers used in our tests consisted of four 2-inch-diameter loud-speakers mounted inside a rectangular wooden framework upon which a skin of bond paper was cemented and shrunk. The paper skin was used to simulate the complex vibrational pattern which exists in the tank walls of an actual transformer. Figure 1 illustrates a typical model transformer with two side walls removed to show the loud-speaker arrangement.

Because of wave interference, the sound field from any surface undergoing a complex mode of vibration, such as a transformer tank, exhibits a pattern with large abrupt changes in sound pressure as a function of location. These changes in sound pressure may be in the order of 10 or 20 decibels between two locations only a fraction of a wave length apart. The pattern of sound pressure from a transformer also may change as a function of time because of small changes in excitation frequency, variations in thermal gradients or wind velocity, or even the change in position of a reflecting or diffracting body such as an automobile parked in the vicinity. The variations in sound level resulting from such causes generally is more pronounced at points remote from the source. These variations mean that sound-level averages in space and time are required, rather than spot measurements, if meaningful data are to be obtained.

In model testing it is possible to accomplish this averaging automatically by using a warble tone as the test sound. In a typical test, a 10,800-cycle sound was frequency modulated between the limits of 9,700 and 11,900 cycles at a modulation frequency of 60 cycles. This procedure keeps the standing wave pattern varying at such a rapid rate that the sound level at a given location is averaged automatically by the measuring equipment.

In addition to averaging in a very short time the variations which occur over comparatively long periods in the field, the frequency modulation makes the data easier to interpret. If a constant frequency were used, curves of sound level versus position would be so ragged that accurate averaging, either arithmetically or by eye, would be almost impossible.

The sound from the transformer models was picked up by the microphone of a sound-level meter. In the majority of the tests the microphone was transported around the model at a fixed radius and height by a motor-driven rotating boom. A typical test setup is shown in Figure 2.

The microphone cable was connected to a sound-level meter in the next room. The output of the sound-level meter was in turn fed to a high-speed recorder. Since the recorder plotted a curve of sound level versus time and the microphone rotated at constant speed, the resulting charts showed sound level versus angular position of the microphone.

Figure 3 is a block diagram of the electroacoustic system used in this test. A reactance tube[6] driven by a 60-cycle modulating signal acted effectively as a sinusoidally varying capacitance. It was connected in parallel with one of the resonant circuits of a beat-frequency-oscillator, causing the output of the oscillator to vary from plus 10 per cent to minus 10 per cent about the center frequency, with virtually no amplitude modulation. This voltage was amplified and fed to the loud-speakers inside the transformer model. In addition to the instruments for measuring and recording the test sound, equipment for checking frequency, observing wave shape, measuring loud-speaker current, and so forth, are shown in the diagram.

Some typical recordings of sound level versus angular position for the setup illustrated in Figure 2 are reproduced in Figure 4. The microphone was 6 feet from the sound sources and 6.5 inches above the floor in these tests, corresponding to 180 feet and 16 feet, respectively, on the prototype. It should be pointed out that in these curves, the sound levels do not represent actual sound levels at the prototype, since the decibel *change* from one condition to another is what is desired. The model in Figure 1 is comparatively simple, with no large reflecting surfaces other than the ground. It is symmetrical about one axis, with the exception of the shed and the two cylinders representing potential transformers, whose effect on the sound pattern probably is negligible. This symmetry is shown in the sound-level recordings. The first recording is a curve of the sound level without walls around the transformers. The second one shows the sound level after a ⊏-shaped barrier 22

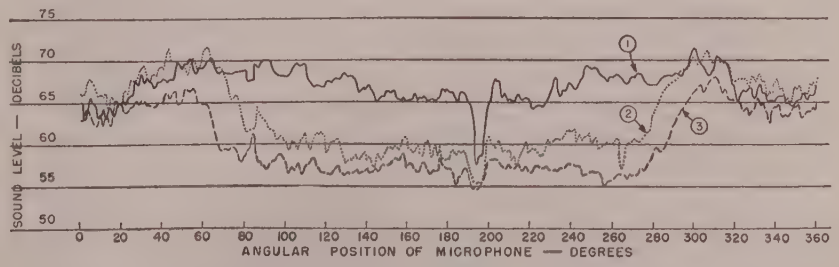

Figure 4. Recordings of sound level versus angular position for model illustrated in Figure 2

1. As illustrated, no barriers
2. ⊏-shaped barrier around each transformer, open sides facing 0-degree direction (toward background in Figure 2)
3. Same as 2, but barriers lined with acoustical absorbent

feet high was placed around each transformer with the open sides of the walls facing the 0 degree direction. An average reduction of about seven decibels may be observed in directions where a wall is between the microphone and the sound source. The diffraction of sound around the top of the wall prevents a sharp acoustical shadow where the wave length of the sound is an appreciable fraction of the dimensions of the obstacle. Near the wall the reduction in noise level is greater, but at long distances the reduction in noise level caused by the wall becomes independent of distance. There is a slight increase in sound level in the direction of the open end of the wall, as a result of the sound reflected from the inside of the wall. Lining the wall with a sound-absorbent material resulted in an average additional reduction of about four decibels, as shown in the third recording. Rather than merely redirecting the sound energy as in the case of hard walls, sound-absorbent walls dissipate some of it, thereby reducing the total energy radiating from the system. The dip in all three recordings at about 200 degrees is caused by the microphone passing partially through the acoustical shadow of the small house at this location.

Although the use of the motor-driven boom in conjunction with the high-speed recorder yields the most complete data for a minimum expenditure of time, it is apparent that point-by-point measurements also may be made with the microphone on a small standard.

The economy with which a great many wall designs may be tested on a model, as compared with the construction and test of even one design on the prototype, is apparent. The model just described is simple, for the purpose of illustration. Real situations usually are of greater physical and acoustical complexity. For example, a certain power company found that a new installation of transformers gave rise to unforeseen complaints of noise over an area a quarter-mile from the station. Field measurements made possible an estimate that a reduction of 10 to 15 decibels in sound pressure level would be necessary to end the noise complaints. Measurements were made of a model of the transformers set in their environment of reflecting buildings. More than 20 variations of sound barriers were tried, with measured attenuations ranging from 3 to 15 decibels. From these data the electric power company designed and built a barrier at the transformer installation, taking into account the factors of minimum cost for the requisite reduction in sound level, structural practicality, material availability, and so forth. The predicted attenuation for this barrier was 8 to 10 decibels, while in fact an attenuation of 9 decibels, on the average, was attained, and the complaints based on the transformer noise were alleviated. Such agreement between prediction and practice, together with the fact that acoustic models are sound in theory and that all phenomena observed so far are consistent with theory, establishes confidence in the results of model tests. Although this paper deals with the use of acoustic models for transformer noise problems, the technique is fully applicable to situations which involve the noise of other machinery.

Some General Observations Concerning the Effects of Walls

Although each transformer noise problem is unique, with its own particular acoustical, economic, and psychological factors, it is believed that some general data on the effects of walls will be of interest. Generalizations often serve as valuable guideposts in a field where the directions are not yet clearly marked.

The following material summarizes some of the results obtained from model tests made to date. It happens that these tests were concerned with the 360-cycle component of transformer noise, which frequently is the most pronounced. By diffraction theory, the same walls would have somewhat less effect on components of lower frequency and greater effect on those of higher frequency. The model walls represented real ones situated as close to the contours of the transformers as possible while still allowing convenient access to the unit and an adequate amount of cooling air, either by fan or by convection. They were 2 to 12 feet higher than the transformer tank cover. With these qualifications in mind, the following summary of general results is presented:

1. Roofless enclosures of acoustically non-absorbent material reduce the noise level at remote locations (more than 50 wave lengths from the source) near ground level by 7 to 10 decibels.

2. Lining a given enclosure with a good acoustical absorbent reduces the noise level by an additional 5 decibels approximately, giving a total reduction of 12 to 15 decibels.

3. An enclosure of the height of the transformer tank produces the major part of the sound reduction in remote areas near ground level, and further increases in height must be impractically large to result in substantial additional attenuation. For example, one series of tests showed only 2 decibels less noise when the wall height was increased from 20 feet to 40 feet.

4. In the absence of large reflecting surfaces in disadvantageous positions, a partial enclosure may be as effective as a complete roofless enclosure, if noise reduction in certain directions only is required.

5. The reduction in sound level effected by a wall diminishes as the angular height of the observer with respect to the source increases.

6. The shape of the curve of sound level versus angular position does not vary appreciably with radial distance, provided there are no large reflecting or diffracting structures near the path of the microphone. Each point on the curve tends to drop 6 decibels each time the distance from the source is doubled, in accordance with theory.

Conclusions

1. The prediction of the relative average values of sound pressure in the area around a transformer installation can be made effectively and rapidly by the use of an acoustic model.

2. The evaluation of many different designs for sound-reducing barriers is made economically feasible by tests on a model of the installation in question.

3. The cost of model testing usually is a small fraction of the investment savings obtainable by choosing the best sound control or corrective measures for the particular problem.

References

1. Audible Noise of Power Transformers, **T. D. Gordy.** *AIEE Transactions*, volume 69, part I, pages 45–53.

2. Audio Noise in Transformers in Residential and Commercial Areas, **C. E. Baugh.** *AIEE Transactions*, volume 69, part I, pages 121–28.

3. Transformer Audio Noise Problems on an Electric Power System, **C. S. Murray.** *AIEE Transactions*, volume 68, 1949, part I, pages 740–52.

4. Jungle Acoustics, **Carl F. Eyring.** *Journal*, Acoustical Society of America (New York, N. Y.), volume 18, 1946, page 257.

5. Elements of Acoustical Engineering (book), **H. F. Olson.** D. Van Nostrand, New York, N. Y., 1947, page 23.

6. Warbler for Beat-Frequency Oscillator, **J. L. Flanagan.** *Electronics* (New York, N. Y.), December 1949, page 93.

Discussion

T. R. Specht (Westinghouse Electric Corporation, Sharon, Pa.): The use of models has long been standard practice in other fields where full-scale experimentation has been costly. In the field of sound, calculation of the sound fields where radiation, diffraction, and reflection occur is very difficult for all but the simplest cases. Model methods should have considerable application, and it is gratifying to see this paper, which shows that simple apparatus and methods will yield answers to some standard problems that are in agreement with observations on actual installations.

The authors used a single-frequency modulated source, with a mean frequency of 360 cycles. Have they considered or tried using three oscillators of 120, 240, and 360 cycles to make a complex sound source with

the various components in the same relative proportions that are used in a transformer? This might lessen the effect of standing waves and make it unnecessary to frequency modulate the source. The possibility also exists of recording the sound of a transformer on a wire recorder, for instance, and playing it back at a higher rate to secure a higher multiple of the frequency. This actually may give a better representation of a transformer if the transformer sound were not predominately one frequency.

According to the photographs in the paper, a standard crystal microphone was used. At 10,000 cycles, the wave length is about one inch. Diffraction effects might enter in. Would it be desirable to use a microphone more suitable to higher frequency? Possibly, though, if the orientation of the microphone with respect to the direction of the propagation of the sound were kept constant, the error would be constant.

C. S. Murray (Consolidated Edison Company of New York, Inc., New York, N.Y.): As we all know, the transformer noise problem has become extremely important, and the operator welcomes any aid that may be given him toward solving the noise problems that may arise from either a proposed or an existing power transformer installation. Model testing shows promise of being such an aid, and the authors of this paper are to be commended for making the technique available to the industry.

Whether power companies can conduct such tests with a reasonable degree of accuracy is open to question. Technical personnel can learn the technique, and instruments are available at not too great a cost. However, the results of such tests depend a great deal on the ability to duplicate actual field conditions in the model. This means, among other things, that reflecting surfaces must not exist in the vicinity of the prototype that do not exist in the actual installation. To accomplish this might demand a soundproof room of a fair size, which many power companies do not have. The tests, of course, could be made out of doors, but here again further difficulties are encountered. The tests may have to be conducted by a sound laboratory having the proper facilities. In some cases the information gained from such tests may be necessary or of such value that it will be well worth the cost involved.

As far as noise control measures are concerned, it is felt that a combination of a reasonably quiet transformer and a sound barrier is worthy of mention for new installations. Provisions for such a barrier would be made in the layout but constructed only if found necessary after the transformer could be energized.

The authors mention the possibility of using a bank of loud-speakers placed at the proposed location of a transformer to simulate the noise that would be emitted by it. It would be very difficult to simulate such a noise so that the sound level would decrease with increasing distance similar to the noise emitted by the actual transformer. It is believed that, in the end, such a setup would be more expensive than a model test and less would be gained from it. Furthermore, it should be understood clearly by those interested in such tests that the noise at a remote point from the speakers would be subject to objective measurements only.

The model technique, as described, does of course have certain limitations for congested metropolitan areas. The buildings on the model would prevent the use of the microphone boom and would make it necessary to resort either to placing the microphone on a stand or suspending it at the location desired. Because of its physical size the normal microphone placed among the buildings on the model might change the sound pattern from that which would exist in the actual area. Further use of the technique may remove some of the limitations now existing.

The authors show that a reduction of as much as five decibels would result from the application of sound-absorbent materials on the sides of the walls facing the transformer. It should be kept in mind that the frequency of the noise used in model testing is considerably higher than the frequency of the transformer noise being studied. Since, in general, absorbent materials have a higher absorption coefficient at the higher frequencies, the model tests may show reductions in sound level values much higher than can be realized in actual practice.

The authors state that there is very little gained when the height of a roofless enclosure is increased much above transformer tank height. Nevertheless, it may be desirable, if practical, to extend the walls to a height above the line of sight between the top floor of the tallest residence in the area and the transformers in order to achieve the "out-of-sight, out-of-mind" effect.

In the conclusions of the paper it could have been pointed out that a study of an acoustic model not only indicates what the best sound control measure is for the particular problem, but also indicates what shouldn't be done which might result in more noise at a remote point. Model testing also removes much of the guesswork, which could prove costly.

T. D. Gordy (General Electric Company, Pittsfield, Mass.): It is generally agreed that model testing is desirable for experimental work, provided the model yields results which may be interpreted in terms of the full-size test piece. A common objection to model testing is that details cannot be built into the model; hence, its characteristics may not be the same as those of the prototype. In this paper, the authors have called attention to this shortcoming and have taken steps to overcome it.

Vibration of cooling radiators, junction boxes, control cabinets, and tap-changing compartments causes a very complex pattern of sound emission from the transformer. Slight changes in system frequency or variations in transmission medium cause shifts in standing wave patterns. At an appreciable distance from the transformer where sound level is being investigated, an averaged sound level is desired. Introduction of a warble tone does the desired averaging automatically and allows better interpretation of the data. Even with the warble tone, variations of sound level around the source are still present, as is shown by Figure 4 of the paper. It is not difficult to visualize how much larger variations would have been without the averaging warble tone.

The model testing technique and apparatus described are not complex, and those having field testing experience on actual installations should readily appreciate this simplicity. When tests are made in a quiet room, ambient is controlled. Lack of controlled ambient is one serious problem encountered in field testing.

The writer agrees with the authors that the models should not be used for absolute sound-level measurements, but do yield relative values that are significant. Usually, changes in sound level given by the model may be applied to the prototype by keying in several stations on the model and in the field.

Model tests as described by the authors are one more tool that can be used when studying complex sound fields, and they afford much flexibility for studying these fields. Application of such methods should be time-saving and worth while for operating companies confronted with sound level problems.

Briggs Gettys and **W. B. Conover:** The discussions of Messrs. Specht, Murray, and Gordy introduce points of technique which are of interest to others, who may apply acoustic models for the design of roofless barriers around transformer installations.

A single-frequency signal has been used to excite the model transformer, since (1) the frequency component with the largest (weighted) magnitude produced by the transformer is known or can be predicted with reasonable certainty and (2) diffraction effects, on which much of the attenuation of the barrier must depend, are a function of wave length. For understanding of the phenomena present in the model, it is not helpful to have measured the sum of several frequencies approximately equal in magnitude, which are diffracted more as their frequency is lowered. Unless the frequency components are approximately the same size, averaging will be poor. Thus, it would appear that a single frequency with ± 10 per cent f_0 frequency modulation, offers fair averaging and purity of test results.

In the prototype, the largest frequency component is found as the average of a number of sound analyses taken around the transformer. It is rare for a transformer to have, on the average, two frequency components of equal magnitude. It is true, however, that a different type of signal will give better averages and smoother curves. For example, a band of thermal noise 3,000–10,000 cycles per second corresponding roughly to 120, 240, and 360 cycles per second in the prototype, will give an ideally smooth curve—and less information.

Diffraction effects around the usual sound-level meter microphone result in directivity at high frequencies. Orientation of the axis of the microphone toward the sound source is necessary. If it is possible that reflected sound will arrive at the microphone from widely off-axis image sources, the use of certain of the miniature microphones is highly advisable. The polar pattern of such microphones is better by 6 to 12 decibels at 10,000 cycles per second, and the chance for significant error then is remote.

If the use of sound-absorbing material

were considered for lining the barrier, adjustment of the coefficient of absorption at the model frequency should be made, so that the coefficient is no higher than that attainable in a practical material at the transformer sound frequencies. The acoustic pulse technique[1] will be of service in the adjustment of the coefficient to the relatively low value needed. Repetitive reflected pulses of sound are used to compare the echoes from two reflectors, both normal to the pulse source and of the same size and distance. Various thicknesses of the unknown material are cemented to one of the reflectors until the desired ratio between the bare reflector and the covered reflector is obtained. The determination of the high-frequency sound-absorption coefficient by this method probably is no lower in accuracy than the realized value of coefficient of some material applied in the actual installation. Other parts of the model environment rarely need adjustment of absorption coefficients. Model surfaces which are more highly reflective than the corresponding ones on the prototype lead to conservative results.

It is a good practical rule to increase the barrier height to obscure the line of sight to the transformer, no matter what the model data indicate.

The line of sight "rule" is a reminder that the end product of acoustic model measurements is a reduction of the noise heard, or believed to be heard, by people. The model can give relative values of noise reduction, but the subjective factors are no less real, though unmeasurable. The application of the rule has a further advantage, since it forbids the unwise installation of a transformer in the courtyard of an apartment house. Roofless barriers to obscure view of the transformer from any height become impractical.

The use of model technique is not without pitfalls. The reproduction of a 3-dimensional sound field by the model, equivalent in configuration to that of the transformer, can be of importance in models of complex environments which contain many reflecting buildings. There have been few measurements, and less published, of the sound field of transformers except at ground level and at the standard heights. J. H. Vivian and R. R. Peck recently have given valuable information[2] concerning one unit. It is hoped that others in the field will be interested in the acquisition of such data.

References

1. Microphone Calibrator, **D. H. Bastin.** *Electronics* (New York, N. Y.), volume 21, November 1948, page 106.

2. An Investigation of Audio Noise in Substation-Type Transformers, **J. H. Vivian, R. R. Peck.** *AIEE Transactions*, volume 70, part I, 1951, pages 328 32.

Total Hemispherical Radiometers

J. T. GIER
NONMEMBER AIEE

R. V. DUNKLE
NONMEMBER AIEE

IN MANY fields of engineering it is convenient and many times necessary to use electric systems as an aid in the measurement of various physical phenomena. An exhaustive list could be culled as proof of this statement, but suffice it to say that in general electric systems are the rule rather than the exception.

The use of electric systems for the measurement of thermal quantities has been in effect for many years. Some important engineering applications have been as follows:

1. The thermocouple-galvanometer or the thermocouple-potentiometer system for the measurement of temperature above some datum which is frequently taken as the ice point (32 degrees Fahrenheit or 0 degree centigrade).

2. The thermopile-galvanometer or the thermopile-potentiometer system for the measurement of small temperature differences which would not be detectable with a single thermocouple; this system has considerable latitude in its utility and is particularly adaptable to the measurement of thermal radiation.

In the above cases the thermocouple and the thermopile are the transducers that actuate the electric instruments. If it is assumed that the electric instruments are properly calibrated and thus truly indicate the information supplied by the transducer, the valid performance of the system is dependent upon the judicious use of the transducer.

Heat transfer and radiometric research at the University of California has led to the development of several mensuration systems.[1,4,6]

For some time now there has been a need for an instrument, which is nonselective as a function of wave length, to measure the total hemispherical irradiation upon a plane surface, and for determining the net heat transfer by radiation from this surface to the surroundings. The lack of suitable radiometers has been particularly evident in connection with the problems of nocturnal and diurnal radiation and irradiation of the earth's surface.

A few of the important problems in which the total hemispherical irradiation is a major factor are:

1. Evaporation from exposed bodies of water.
2. Freezing of crops in winter.
3. Sterility or death of farm animals from overheating.
4. Cooling or heating loads in buildings.
5. Snow melting rates.
6. Soil temperatures and length of growing season.

In the past, measurements of total hemispherical irradiation generally have been made by the cumbersome method of traversing the sky with a directional radiometer[2,3] and graphically or numerically integrating the results to obtain the total irradiation. To obtain the net interchange between the sky and any surface, an additional calculation must be made which requires a knowledge of the surface temperature and emissivity. Such a procedure is time-consuming, and if conditions are varying rapidly, either with time or direction, the results are unreliable.

Another instrument which "sees" the whole hemisphere is the Eppley Pyrheliometer. However, the Eppley Pyrheli-

Figure 1. The components of a typical heat meter

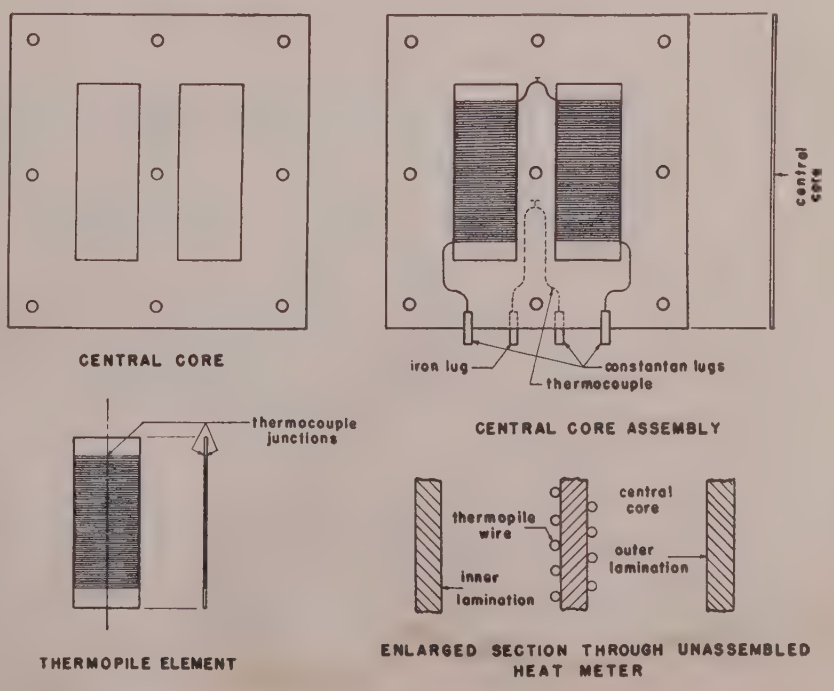

Paper 51-57, recommended by the AIEE Instruments and Measurements Committee and approved by the AIEE Technical Program Committee for presentation at the AIEE Winter General Meeting, New York, N. Y., January 22–26, 1951. Manuscript submitted March 14, 1950; made available for printing December 6, 1950.

J. T. GIER and R. V. DUNKLE are both with the University of California, Berkeley, Calif.

The development of these instruments was made possible through the Thermal Radiation Project, Number N7-onr-295, Task I, which is sponsored by the Office of Naval Research. Appreciation is expressed to Dr. F. A. BROOKS for his many helpful suggestions.

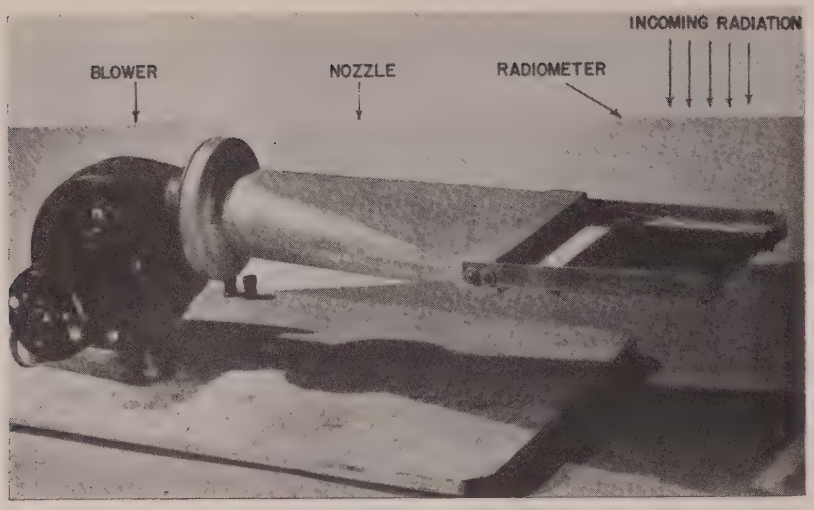

Figure 2. The total hemispherical radiometer showing the sensing element, nozzle, and blower

ometer is useful only for measurement of solar irradiation, as the spectral characteristics of the envelope and receiver are such that it responds only to short wave lengths.

Discussion

In consideration of the design criterion, instruments for measuring the total hemispherical irradiation or net interchange from the sky should have the following characteristics:

1. *Spectral characteristics:* The response of the instrument should be independent of the wave length of the incident energy. The instrument should have no windows, filters, or mirrors which would absorb radiation selectively. The blackening material on the radiation-absorbing surface should be nonselective, that is, the absorptivity should be independent of the wave length of the incident energy.

2. *Cosine law:* The blackening material should obey the cosine law. The absorptivity should be independent of the angle of incidence of the radiation.

3. *Shape factor:* The absorbing surface should be a plane surface and should be able to view the whole hemisphere.

4. *Transient response:* The instrument should respond rapidly to changes in irradiation or net interchange and should come to a steady state rapidly.

5. *Stability:* The instrument should give a stable, reproducible reading.

6. *Sensitivity:* The output of the instrument should be sufficient so that it can be fed into a conventional recording instrument or read upon a standard portable potentiometer.

7. *Weathering:* As the instrument is exposed to the weather, it should be constructed of materials which are subject to a minimum of deterioration.

8. *Portability:* The instrument should be rugged enough to withstand handling, and should be readily portable.

9. *Effect of surroundings:* The value obtained for the irradiation with the radiometer should be independent of the temperature difference between the radiometer and the ambient conditions, and of the irradiation falling upon the back side of the radiometer.

The instruments described herein have been developed in an attempt to satisfy the foregoing requirements; the devices have been developed primarily to measure the total irradiation, atmospheric plus solar, and can be used for both diurnal and nocturnal measurements. The instrument consists essentially of a heat flow meter, Figure 1, as a sensing element or transducer. The heat flow meter as usually constructed consists of three bakelite plates 1/64 inch by $4^1/_2$ inches by $4^1/_2$ inches, with the center plate slotted to hold thermopiles and the other two plates supplying mechanical strength and

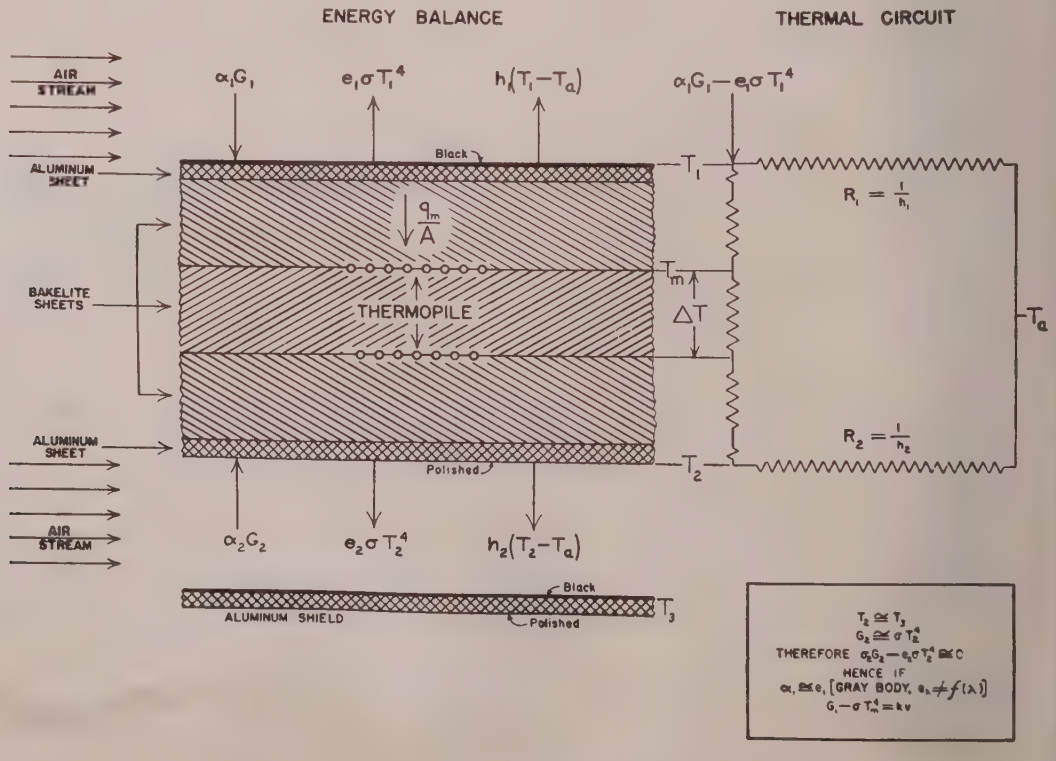

Figure 3. A schematic sketch showing the energy balance on the total hemispherical radiometer and the equivalent thermal circuit

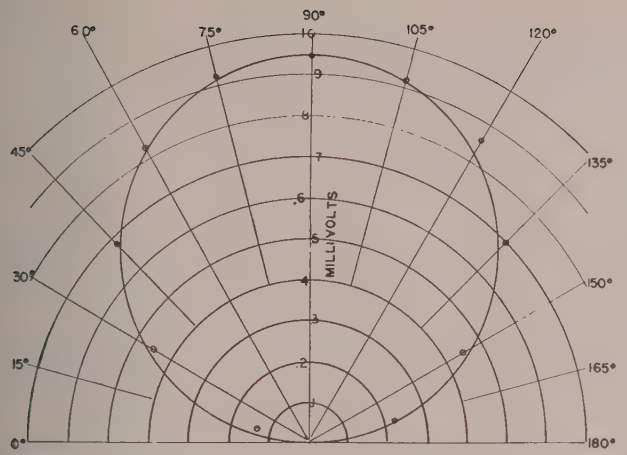

Figure 4. The response of the total hemispherical radiometer with respect to angle of incidence

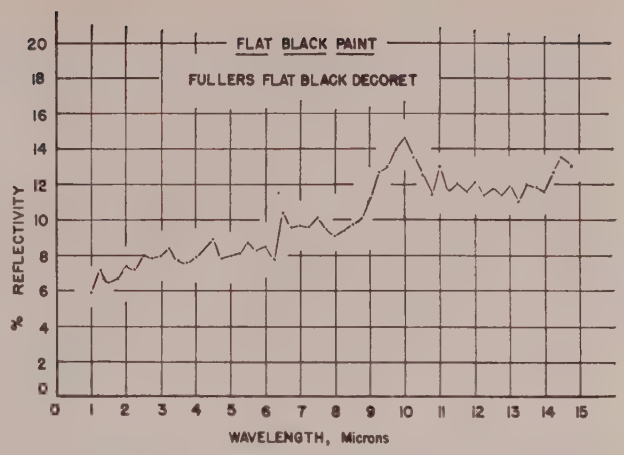

Figure 5. The spectral reflectivity as a function of wave length for the blackened surface of the total hemispherical radiometer

serving as protective covers for the thermopiles. Various other materials have been tried, but the bakelite has been found most satisfactory because of its stability and ease of fabrication.

The thermopiles are constructed by winding 40-gauge constantan wire onto a bakelite slab. Approximately 180 turns are wound on each slab by means of a small coil winder which is geared to wind 88 turns per inch. The wire is then silver plated over one-half the slab, giving in effect a series of thermocouple junctions on opposite sides of the slab. Although the thermal conductivity of the wire is appreciably higher than that of the plastic, the thermal short-circuit currents are small because the cross-sectional area of the wire is small relative to the area of the plastic. Electrically this type of plated thermopile is possible only because the electrical resistance of the constantan is much greater than that of the silver; consequently, the shunting effect of the constantan core is negligible and the silver sheath serves as the electric conductor. Heat meters may be built with these thermopiles connected in various series-parallel combinations depending upon the use and impedance matching requirements of the electric indicator or recorder. The thermopiles are inserted in the slots in the center plate and the whole ensemble is bonded together with a thermosetting cement, resulting in a compact and durable device. As the temperature drop between the hot and cold thermopile junctions is proportional to the rate of heat flow through the meter, the electromotive force of the thermopile is used as a measure of the heat flow through the meter. In the case of the irradiation meter, the electromotive force developed by the thermopile is proportional to the net exchange between the sensing element and whatever it "sees" in one-half space; in the case of the net exchange meter the electromotive force developed by the thermopile is proportional to the net radiant transfer across the plane of the sensing element, that is, the net radiant transfer between the upper one-half space and the lower one-half space.

When used for radiation measurements the sensing unit is mounted in the air stream from a small blower, Figure 2, so as to maintain uniform values of the unit thermal resistance from both meter surfaces. In this arrangement, any input thermal current (irradiation) is divided so that a portion flows to the upper air stream and the other portion flows through the sensing element, Figure 3, and out to the lower air stream. In flowing through the sensing element, a small temperature difference, ΔT, is developed; this temperature difference causes an electromotive force to be generated by the thermopile. As the convective losses on both the lower and the upper surfaces are maintained constant and the loss from the lower surface is by convection only, the heat flow through the sensing element is directly proportional to the net radiant transfer. This air stream also prevents the deposit of dust or dew on the meter surface. Wind tunnel tests made as to the effect of wind direction and velocity indicate that up to 15 miles per hour the maximum error is about 4 per cent. If the wind is blowing in the same direction as the blower discharge, the error is only about 2 per cent up to 30 miles per hour.

It will be noted that aluminum cover plates also are mounted on both sides of the thermopile. While these aluminum sheets give additional strength and weather resistance, their primary function is to increase the thermal capacity without appreciably increasing the thermal re-

Figure 6. Solar irradiation as a function of time of day at three locations in California

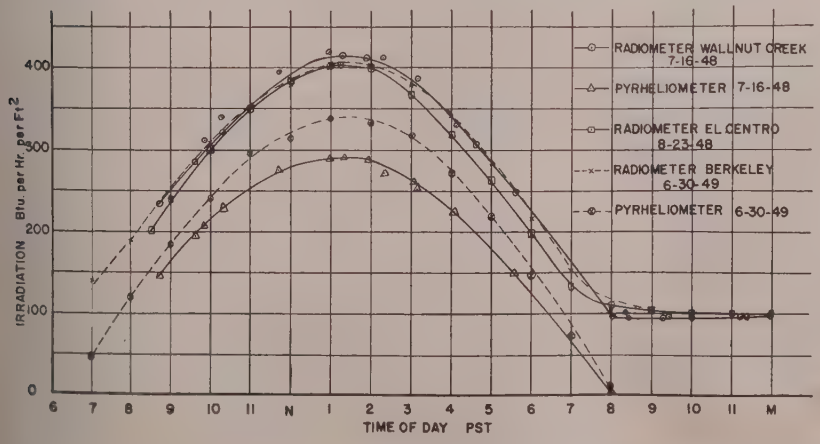

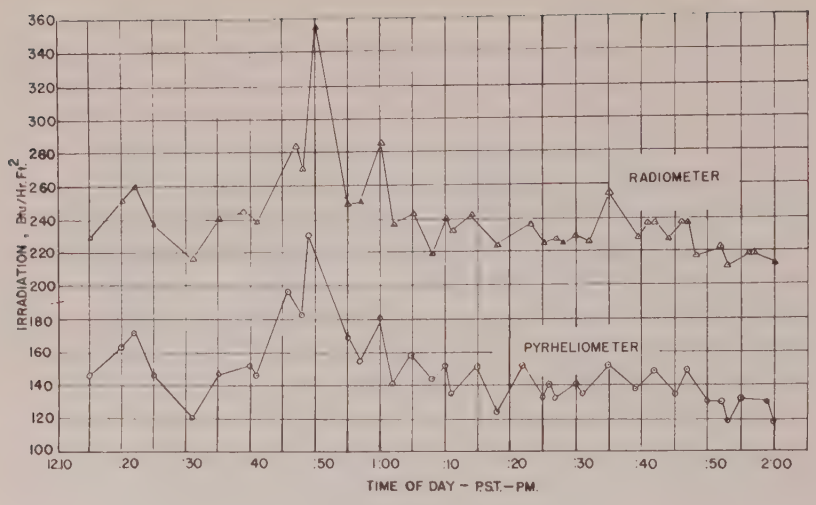

Figure 7. Comparison data for the total hemispherical radiometer and the pyrheliometer on a day with high fog

sistance, thus damping out minor variations in heat flow due to fluctuations in the air stream. Despite this increased thermal capacitance, the radiometer takes only about 12 seconds to reach 95 per cent of steady state response when suddenly irradiated.

The surface of the upper aluminum sheet is painted with Fuller Flat Black Decoret to absorb the incident radiation. In Figure 5 are shown the spectral characteristics of this paint. It is to be noted that the spectral absorptivity varies only slightly from 0.90, that is, the reflectivity is approximately 0.10. Since the radiometer is calibrated, the exact magnitude of the absorptivity is unimportant, but the receiving surface should act as a gray body, that is, the spectral absorptivity or emissivity should be independent of the wave length. Also, the instrument has no windows or mirrors to absorb radiation selectively.

Another important characteristic of the surface is that the absorptivity should be independent of the angle of incidence of the incident radiation; in other words, the surface should be perfectly diffuse. Figure 4 indicates that this is nearly true. The experimental points theoretically should fall on the circle if the cosine law holds.

The lower aluminum sheet is highly polished to reduce the emissivity and absorptivity to the lowest possible values. It has been found that a layer of evaporated gold will give lower initial absorptivity and will not deteriorate with time as rapidly as the aluminum. The net absorption of radiation by this lower surface of the meter should be made negligibly small.

In order to minimize the effect of the irradiation of the lower surface, a radiation shield is supplied. This is polished on the lower surface and blackened on the upper surface to prevent reflections onto the meter surface. As both the meter and the radiation shield approach air temperature, the temperature difference between the two is very small. Combining this small temperature differential with the low absorptivity of the lower heat meter surface results in a very small radiation exchange between the two surfaces. If this term is neglected, it is shown readily that the irradiation, G_1, upon the plane of the meter surface can be expressed in terms of the meter constant,

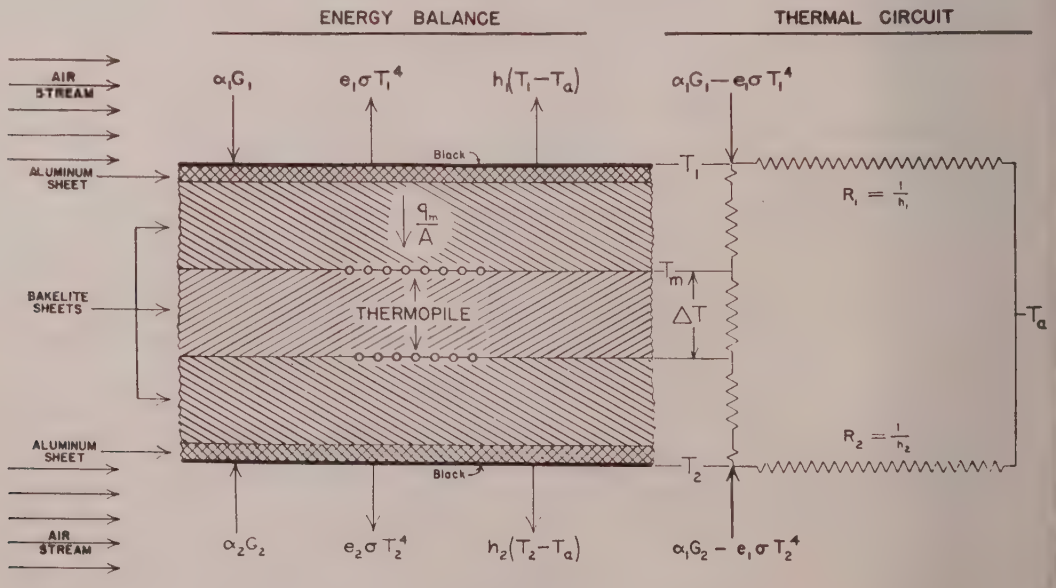

Figure 8. A schematic sketch showing the energy balance on the net exchange meter and the equivalent thermal circuit

$$\Delta T \cong C\left[\alpha_1 G_1 - e\sigma T_1^4 - \alpha_1 G_2 + e_1\sigma T_2^4\right]$$
$$\sigma T_1^4 - \sigma T_2^4 \cong \Delta T$$
$$G_1 - G_2 = kv$$

K, the millivolts produced by the thermopile, v, and the meter temperature, T_m in degrees Rankin (°R).

$$G_1 = Kv + \sigma T_m^4 \quad \frac{Btu}{hr ft^2}$$

where

σ = Stefan-Boltzmann radiation constant

$$= 1.72 \times 10^{-9} \frac{Btu}{hr ft^2 (°R)^4}$$

The calibration constant is obtained by exposing the meter to a standard radiation source which might be either a standard lamp or an ideal radiator.

Net Exchange Radiometer

For many applications the investigator is interested in the net heat transfer by radiation in addition to, or instead of, the irradiation upon the surface. If the flat plate radiometer, Figure 8, has both the upper and the lower surfaces blackened uniformly, it can be used to measure the net exchange instead of the irradiation, and hence is termed the net exchange radiometer.

The equation for this system is:

$$G_1 - G_2 = Kv$$

G_1 = irradiation of the upper surface of sensing element $Btu/hr ft^2$
G_2 = irradiation of the lower surface of sensing element $Btu/hr ft^2$
K = calibration constant of radiometer $Btu/hr ft^2 mv$
v = millivolts produced by the sensing element.

Measurements

The total hemispherical radiometer has been used to measure the nocturnal and diurnal irradiation of the earth's surface at several different locations at different seasons of the year. Some typical data are presented in Figures 6 and 7. In Figure 6 are shown typical curves for clear days in summer at Berkeley, Walnut Creek, and El Centro, Calif. As the altitude of the sun varied due to latitude and time of year, and atmospheric conditions were different, the curves do not coincide, but are very similar in shape and magnitude. It is interesting to note that the nocturnal irradiation was nearly the same in all three locations. The nocturnal irradiation drops to much lower values on clear cold nights in the winter and is much higher than the above values on warm, humid, and overcast nights in the summer.

For purposes of comparison pyrheliometer curves also are included for Walnut Creek and Berkeley. It will be noted that the pyrheliometer readings drop to zero at night, as the Eppley Pyrheliometer responds only to short wavelengths.

In Figure 7 are shown radiometer and pyrheliometer curves for a day with fairly thin high fog, characteristic of the San Francisco Bay region. It is interesting to note the correlation between the readings of the two instruments.

As yet, very few measurements have been made with the net exchange meter, as irradiation has been of greater interest. However, the net exchange meter was checked against two total hemispherical radiometers on a sunny afternoon in Berkeley. The procedure followed was to take readings on all three meters in their normal horizontal position. Then the two hemispherical radiometers were inverted and readings were made of the total radiation leaving the earth. The difference between the radiation falling upon the earth and that leaving the earth should check the reading of the net exchange radiometer. The comparison of the data from the three meters at 3:00 p.m. on August 23, 1949 is given in Table I.

Table I

Total Hemispherical Radiometers, Meter No.	G_1	G_2	$G_1 - G_2$	Net Exchange Meter $G_1 - G_2$	Per Cent Difference
7	365.5	210.4	155.2	149.5	3.6
8	361.7	206.8	154.9	149.5	3.5

It is seen that the agreement between the values for the net radiation exchange from the two types of radiometers is fairly good. Some of the discrepancy may be due to changes in conditions during the unavoidable delay between readings. Other sources of error are, of course, in the calibration constants of the radiometers, in the leveling and positioning of the radiometers, and in the voltage measurements made with the potentiometer.

The flat plate radiometer has been used extensively by the University of California College of Agriculture in studies of animal shelters and environment in the Imperial Valley and by the Cooperative Snow Investigations in making energy balances in connection with studies of snow melting rates in the Sierra Nevada Mountains of California. Both the total hemispherical radiometer and the net exchange radiometer should find further use in studies of evaporation, the problems of freezing of crops in winter, heating, ventilating, air conditioning, and refrigeration, and in micrometeorology studies.

References

1. The Silver Constantan Plated Thermopile, in Temperature, Its Measurement and Control in Science and Industry (book), **J. T. Gier, L. M. K. Boelter.** Reinhold Publishing Corporation, New York, N. Y., 1941, pages 1284–92.

2. Heat Transfer Notes, **L. M. K. Boelter, V. H. Cherry, H. A. Johnson, R. C. Martinelli.** University of California Press, Berkeley, Calif., July 1942, Chapter XVIII, page 45.

3. Observations of Nocturnal Winter Atmospheric Radiation in California, **F. A. Brooks, C. Lorenzen, Jr., L. M. K. Boelter.** *Bulletin*, American Meteorological Society, volume 20, December 1949, pages 433–39.

4. A Meter for the Evaluation of Heat Flow in The Operating Data Book (8th Edition), **J. T. Gier, R. V. Dunkle.** National Association of Practical Refrigerating Engineers, 1948, pages 3–7.

5. The Absolute Spectral Reflectivity of Certain Pigments and Metals in the Wavelength Range between 2 and 15 Microns, **J. T. Gier, L. Possner, A. J. Test, R. V. Dunkle, J. T. Bevans.** University of California, Engineering Research, Thermal Radiation Project, *Report Number 7*, NR-015-202, February 18, 1949.

6. The Two Radiometer Method for the Simultaneous Determination of Emissivity and Surface Temperature, **R. V. Dunkle, J. T. Gier.** University of California, Engineering Research, Thermal Radiation Project, *Report Number 6*, NR-015-202, December 14, 1948.

Discussion

George V. Parmelee (ASHVE Research Laboratory, Cleveland, Ohio): Messrs. Gier and Dunkle have developed a very useful instrument by a unique application of the well known heat flow meter. Its simplicity, compared with compensating instruments which have been used in the field of meteorology, is a highly commendable characteristic. The writer and his coworker, W. W. Aubele, have been greatly interested in this instrument because of their own experience in developing and using a hemispherical radiometer of the convection-compensated type. Their instrument is being used in research on heat flow through glass sheets and hollow glass block. The need for such an instrument became evident when it was found that the long-wave-length radiation received from the outdoor surroundings was a significant factor in heat flow and that it could not be readily evaluated by indirect means.

The writer has several specific comments regarding the radiometer and its use as follows:

1. The use of aluminum sheets on either side of the heat meter to dampen fluctua-

tions ties in with our experience that it is difficult to obtain a steady response. This appears to be due to rapid fluctuations in air temperature and in solar radiation intensity. Was it found that a single spot reading was satisfactory or would the average of a series of readings taken at regular intervals be a more accurate measure of the irradiation? Such an average could be obtained with a recording potentiometer.

2. Our experience in calibrating Eppley pyrheliometers, and data found in the literature, show that absorptance of surfaces is nearly constant up to about 60 degrees incidence but decreases rapidly at greater angles. Have the authors had any similar experience? Their radiometer surface does not appear to have this selective absorptance characteristic.

3. Figure 5 of the paper shows that the spectral reflectivity in the solar spectrum, between 0.3 and about 2.5 microns, is of the order of 6 to 7 per cent. The long-wavelength radiation from the sky for air temperatures of from about 30 to 125 degrees Fahrenheit is concentrated well to the right of 7 microns. Since the reflectivity in this region is of the order of 12 per cent, one would expect the instrument constant to vary for radiation from these two sources.

In conclusion the writer wishes to acknowledge the valuable contributions of Messrs. Gier and Dunkle in the field of thermal radiation. Their reports have been an invaluable source of data as well as techniques. This particular paper describes an interesting instrument and gives illustrative data regarding radiation phenomena that have been overlooked by many investigators.

L. J. Anderson and **E. R. Anderson** (United States Navy Electronics Laboratory, San Diego, Calif.): Referring to the paper by J. T. Gier and R. V. Dunkle it may be pertinent to comment briefly on a modified radiometer that they built for the evaporation studies being conducted at Lake Hefner, Oklahoma City, Okla. This instrument is being used as one component of a complete radiation station. The radiometer, together with an Eppley pyrheliometer, is employed to obtain the terrestrial radiation. Knowing the surface water temperature and the emissivity of water, the radiation of the lake to the atmosphere is obtained from the Stefan-Boltsman Law. The difference between the atmospheric radiation and lake radiation gives the net gain or loss to the lake of long wave radiation.

This particular application of the radiometer requires that the instrument be modified to utilize direct rather than alternating current. The flat plate employed is 2 inches square (standard version 4 inches square). The centrifugal blower is powered by a small 6-volt d-c Hanson motor drawing 250 milliamperes. Hence, it is well suited for portable field operations in locations remote from a-c power. The calibration constant in centimeter-gram-second units, is 0.341 calorie per square centimeter per minute per millivolt at 6 volts, with a maximum output for atmospheric radiation of approximately 6 millivolts. The output is recorded through a suitable amplifier on an Esterline-Angus recorder. A 15-point switch is used to record a reference, flat plate reading, flat plate temperature, upward looking Eppley, and a reflecting Eppley. In this way 4-minute records of each element are recorded every 20 minutes.

In addition to being used to determine terrestrial and effective back radiation, the temperature of the flat plate is being used successfully to determine the temperature of rain falling into the lake. This is an easy accurate method of determining this quantity.

The above described instrument has been in continuous use since March 1950. It has been subjected to temperatures of 30 to −12 degrees centigrade, rain, high winds, dust, and snow. The only maintenance has been an occasional cleaning of the flat plate and repainting of the upper black surface.

R. W. Gerdel (Snow, Ice, and Permafrost Research Establishment, St. Paul, Minn.): The development of the total hemispherical radiometer has provided a long needed tool for research in snow and ice. When used as a net exchange radiometer, the long wave radiation exchange between a snow pack and its environment may be measured with a precision not heretofore attainable.

The agricultural and industrial economy of that portion of the United States west of the 100th meridian is dependent upon the use of water supplies derived almost entirely from melting snow. Improvements in the forecasting of water supplies for these 17 western states requires that more precise information upon the diurnal heat balance be obtained. Radiation studies in the High Sierra, Cascades, and Rocky Mountains, using the Eppley pyrheliometer, limited to short wave radiation between 0.2 and 2.5 microns, emphasized the need for a more precise evaluation of the net long wave radiation exchange for wave lengths in excess of the maximum sensitivity of the Eppley instrument.

Both the total hemispherical and net exchange types of radiometers have been used in the Central Sierra Snow Laboratory near Donner Summit, Calif., to measure the incoming long wave radiation and the net exchange between the snow and clouds, trees, protruding rocks, and other effective portions of the environment.

In a preliminary report[1] of the Cooperative Snow Investigations the results of some of these experiments were summarized. It is concluded that the long wave component of radiation received by the snow pack is relatively constant throughout the entire 24-hour day and amounts to between 0.3 and 0.4 gram calorie per square centimeter per minute. Outgoing long wave radiation has a constant intensity of about 0.45 gram calorie per square centimeter per minute. In order to cause snow melt, the absorbed short wave radiation received during the day must overcome a radiation deficit of 0.05 to 0.15 gram calorie per square centimeter per minute. Under a dense forest canopy, the net exchange of long wave radiation between the vegetation and the snow pack appeared to be zero.

The tentative conclusions derived from the data collected with these unique instruments indicate that the snow melt-runoff equation may be improved by the inclusion of a net long wave radiation exchange function.

From the military standpoint, the trafficability of a snow surface is frequently dependent upon the production of a surface crust or a hardening of the snow to a considerable depth. The latter process is similar to sintering and may occur to a considerable depth even in very cold snow. Studies have been initiated at one of the Western Snow Laboratories by the Snow, Ice, and Permafrost Research Establishment of the Corps of Engineers, in which the total hemispherical and the net exchange radiometers are to be used to evaluate the relationship between long wave radiation exchange and the bearing capacity and tractionability of snow.

The authors are to be complimented on the development of such simple, precise, and reliable instruments. Without them, many of the thermodynamic and radiation problems associated with the civilian and military use of snow would be difficult if not impossible to solve.

REFERENCE

1. RADIATION HEAT EXCHANGE BETWEEN THE SNOWPACK AND ITS ENVIRONMENT, **J. M. Himmel.** *Technical Bulletin Number 12, CWI-171,* Cooperative Snow Investigation, Corps of Engineers (San Francisco, Calif.).

C. F. Kelly (University of California, Agricultural Experiment Station, Davis, Calif.): The total hemispherical radiometer described by Mr. Gier and Mr. Dunkle has been used since 1946 in studies of the effect of hot environments on livestock in the Imperial Valley and at Davis, Calif. This has been a co-operative project between the United States Department of Agriculture and the University of California.

A quick method of measuring the effectiveness of various shades in cutting off

Figure 1. Total hemispherical radiometer on tripod being used to measure total solar and sky radiation at Davis, Calif.

solar and sky radiation from livestock was needed. This need has been filled very well by the instrument described. Mounted on a tripod, as shown in Figure 1 of this discussion, and used with a good portable potentiometer, it makes a rugged field instrument. By the time it is leveled up in a new location, it comes to thermal balance with its new environment. In comparing two shades, a reading is made in the open, away from the shade, and then under each shade at the location where the irradiation is desired. The tripod is set so that the instrument is at the height of the animal's back. As a check an additional reading is made in the open. The percentage of total solar and sky radiation cut off can then be calculated and the shades evaluated. By turning the radiometer over, with the reflective side up, the same procedure can be used for measuring effect of shadow size, ground temperature, and so forth on lower hemisphere radiation.

The radiometer used in our first measurements did not have a forced air blast to even up the convection losses from the sides of the meter. The readings therefore were erratic except in very still air. The small blower has remedied this situation. We have also used the radiometer without the lower radiation shield. The lack of a shield did not affect the readings of the instrument when observations of upper hemisphere radiation were made. The same values for total solar and sky radiation were obtained at a given time when the reflective surface was "seeing" bare ground at 160 degrees Fahrenheit or green alfalfa at air temperature, about 110 degrees Fahrenheit. Shielding the reflective surface had no noticeable effect under these different conditions. However, when the radiometer was used to measure lower hemisphere radiation, and the reflective surface was pointed upward, thus receiving the full measure of sun energy, shading the instrument caused slight variations in response because the reflectivity of the polished surface is some value below 1.00. The radiation shield should correct this error to a large extent.

We found it necessary to calibrate the radiometer at fairly frequent intervals. The instrument with a polished aluminum reflecting surface (shown in the figure), originally had a meter constant, K, of 20 Btu per hour per square foot per millivolt. After being used for two summers under the dusty conditions of the Imperial Valley this constant had changed to 18.5. This change does not necessarily mean an error in direct proportion to the difference between the two calibration constants because the σT_m^4 fraction makes up a large part of the total irradiation G_1. For instance, a typical observation at noon in the Imperial Valley indicated a plate temperature of 118 degrees Fahrenheit and a meter response of 12.35 millivolts. The fraction σT_m^4 for 118 degrees Fahrenheit is 192.5 Btu per hour per square foot. The thermopile fraction when $K=$ 20 Btu per hour per square foot millivolts is 247 Btu per hour per square foot and when $K=18.5$ is 228.5 Btu per hour per square foot. The total irradiation of the plate is 439.5 Btu per hour per square foot in the first case and 421.0 Btu per hour per square foot in the second. A reduction of 7.5 per cent in the constant K reduced the observed solar and sky radiation only 4.2 per cent, neglecting any change in plate temperature which might occur through a lowering of the reflectivity of the polished surface. While a small change in calibration constant is not so important where differences between the effect of various structures on the microclimate are being measured, it is significant where absolute values are desired. To have a method of field calibration for the instrument would be valuable.

We have had no experience with the net exchange meter, but since it does not depend for its accuracy on a polished surface, it should be a more stable instrument than the hemispherical radiometer.

We wonder if the abscissa co-ordinates in Figure 6 of the paper have not been moved 1 hour too far to the left, since we have daylight saving time in California during the summer? It appears that the maximum irradiation of the plate should occur at 12:00 noon, solar time, if the sky is clear.

J. T. Gier and **R. V. Dunkle:** This is in reply to the discussion by George Parmelee.

Commenting on point number 1, it is thought that an average of a series of readings is preferable to a single spot reading. In most cases a recording potentiometer is used with the radiometer. On a clear day the fluctuations are small, but are appreciable on partially cloudy days.

With reference to point 2, the authors have not investigated the response of the Eppley pyrheliometer as a function of angle.

In comment number 3, Mr. Parmelee is correct in his statement that the variation in spectral absorptivity shown in Figure 5 should affect the response of the instrument. However, calibration with sources at difference temperature has shown good agreement on the calibration constants obtained, indicating that the surface actually obtained on the instruments may have a somewhat flatter reflectivity curve than shown in Figure 5.

Mr. Kelly is correct in that the time scale on Figure 6 is shifted by one hour and should read Pacific Daylight Time instead of Pacific Standard Time.

An Electromagnetic Induction Method of Measuring Oscillating Fluid Flow

ALBERT J. MORRIS
ASSOCIATE AIEE

JOSEPH H. CHADWICK
NONMEMBER AIEE

TO BE described is an electromagnetic induction method of measuring oscillating fluid flow which is linear, sensitive, instantaneous in response, and of good stability. The need for such an instrument arose during a study of a system of stabilizing ships against rolling by means of the controlled pumping of fluid between two tanks located on opposite sides of a ship. Located at Stanford University is a 5-ton dynamical model of a World War I destroyer which is being used for this study. For the purpose of orientation, Figure 1 shows the Stanford installation. The model system, shown on the left, is driven by a mechanism which simulates wave motion. A constant-speed propeller-type variable pitch blade pump located in one of the tanks provides the means for fluid transfer. The system is a closed loop servomechanism in which the waves act as an external disturbance which must be counteracted by the pumping of fluid. The difference in the rolling caused by the action of external wave forces and internal tank-water forces produces an "error" signal from the roll-sensing accelerometer which tends to, but of course can never be, zero. Figure 2 shows a block diagram of the servo loop. One of the important problems was to determine experimentally the transfer functions of the different components of the system in order that the system might be understood and its performance predicted. The flowmeter is used to study the dynamic transfer characteristic of the pump as a function of time and frequency. This portion of the loop is shown segregated between the vertical dashed lines on Figure 2.

Paper 51-58, recommended by the AIEE Instruments and Measurements Committee and approved by the Technical Program Committee for presentation at the AIEE Winter General Meeting, New York, N. Y., January 22-26, 1951. Manuscript submitted June 26, 1950; made available for printing December 6, 1950.

ALBERT J. MORRIS is with the Office of Naval Research, San Francisco, Calif., and JOSEPH H. CHADWICK is with Stanford University, Stanford, Calif.

The authors wish to acknowledge the support of the United States Navy Office of Naval Research and the United States Air Forces "Office of Air Research" which have, by a joint contract with Stanford University, supported this work. In addition, the co-operation of many persons at Stanford and Office of Naval Research, San Francisco branch is gratefully acknowledged.

Statement of the Problem

It is necessary to know, as a function of time, the instantaneous rate of transfer of fluid in the system. Requirements to be met are:

1. The instrument must measure fluid velocities linearly in the velocity range ±18 feet per second.
2. The data obtained should be recorded simultaneously with information on pump blade angle, tank position, and so forth to enable measurement of time and/or phase lag phenomena.
3. The measuring instrument should not appreciably disturb or distort the flow.
4. The instrument must respond only to fluid velocity and must not be sensitive to static or kinetic pressure forces.
5. The instrument must have an instantaneous response and not introduce any time lag of its own.

Careful study of these requirements indicates that they are indeed severe.

Methods of Measurement

The flow covers a very wide range of Reynolds numbers so that devices on which the fluid acts directly with a force such as paddles, pitot tubes, and current meters, are ruled out due to nonlinearity in their response over the flow range. In addition to the wide range of flow velocities involved, the fluid is usually accelerating in the tanks and the tanks themselves may be accelerating and at the same frequency. Therefore, any instruments sensitive to pressure are also affected by the change in pressure caused by two separate accelerating forces between which it is almost impossible to differentiate. This rules out any flowmeter on which the fluid acts directly. Photographic methods also have certain drawbacks. A photographic method was used by N. Minorsky[1] before the war for tank level metering but this proved unsatisfactory due to turbulence of the fluid level, the necessity for correcting for tilt of the tanks, and the great effort required in correlating the data with data taken simultaneously on other parts of the system.

There is however, an electromagnetic induction method of measuring fluid flow which appeared well suited to the purpose. It is simple in theory and elegant in practice. Its use is still relatively unknown although a good theoretical and experimental treatment by Thurlemann[2] and recent papers by Grossman,[3] et al are bringing it into well deserved prominence. Basic patents on electromagnetic velometry are held by Kolin,[4] Lehde,[5] Smith and Slepian.[6]

Theory of the Electromagnetic Flowmeter

The principle of the Electromagnetic Flowmeter is based on Faraday's[7] law of electromagnetic induction. Thus, if we establish a magnetic field in a region through which the conducting fluid flows, the fluid will act as a group of filamentary conductors in which will be induced a voltage proportional to the magnetic field strength and the fluid velocity. If u designates the permeability of the fluid, $\mathbf{v}$ the flow velocity and $\mathbf{H}$ the magnetic field strength, the electric field strength $\mathbf{E}$ is given by:

$$\mathbf{E} = u\mathbf{v} \times \mathbf{H} \qquad (1)$$

where $\mathbf{E}$ is induced in a direction mutu-

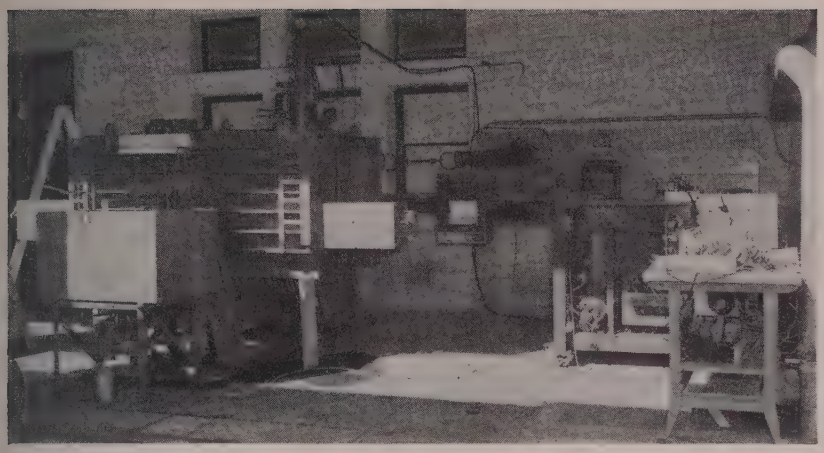

Figure 1. Five-ton ship stabilizer model

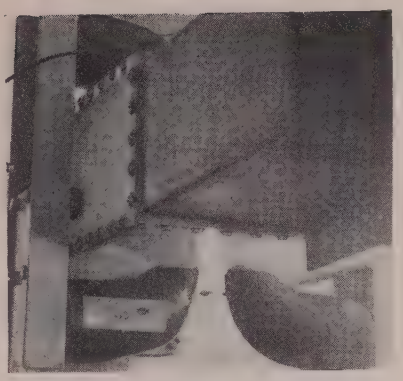

Figure 3. Electromagnetic induction-type flowmeter

ally perpendicular to the magnetic field and the direction of flow. Since **E** represents the gradient of potential in the fluid, two electrodes placed on opposite sides of the pipe or other medium through which the flow occurs will measure the induced potential which will be a measure of the average flow velocity. Inspection of equation 1 indicates that the only physical property of the fluid affecting the voltage generated is the magnetic permeability which is very nearly one for all nonferrous substances. The voltage generated is thus independent of such parameters as pressure, temperature, density, composition and electrical conductivity, which are so influential in more common methods of velocity measurements. Of greatest importance is the fact that, as Thurlemann[2] has shown, the induced voltage is directly proportional to mean flow velocity and is instantaneous in response.

Discussion of General Polarization Problem

In all measurements of this type polarization phenomena play an important role. The passage of a direct current through an electrolyte is accompanied by two effects: changes in composition of the solution which alter its conductance; and liberation of gas at the electrodes which sets up an electromotive force of polarization. The effects are minimized by low currents (our currents never exceed 3 micro-amperes) or nonpolarizable electrodes such as graphite or platinized platinum (we use graphite electrodes). The use of an alternating magnetic field to avoid this polarization problem was first proposed by Kohlrausch[3] in 1868. When an alternating field is used, the polarization potential produced by each symmetrical pulse is completely neutralized by the following reversed pulse. Grossman[3] and others used d-c magnets with no concern for polarization when they were interested in measuring fluctuation effects due to turbulence components instead of mean velocities.

Effect of Polarization Phenomena in This Application

It appeared possible that, since the flow was oscillating, one might be able to use a magnetic field constant with time. This possibility was particularly attractive in view of the availability of magnetron-type magnets of high field strength. The desirability of using compact permanent magnets if possible, rather than electro-magnets, is obvious. Of course, the frequencies are low, less than 1 cycle per second, so that the problem was not clean-cut; it was necessary to study the rates at which the troublesome polarization processes took place. If the reversals were fast compared to these proc-

Figure 2 (below). Block diagram of servo control loop

Figure 4 (right). Schematic diagram of electromagnetic flowmeter

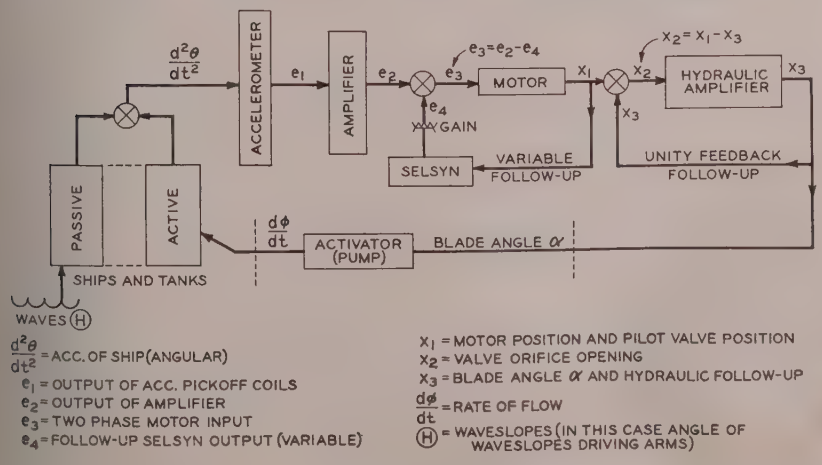

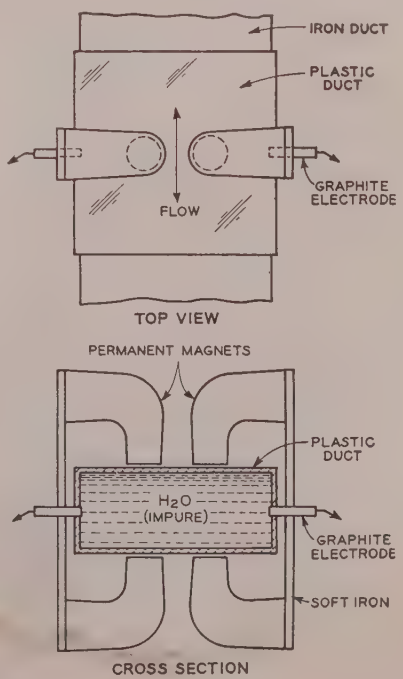

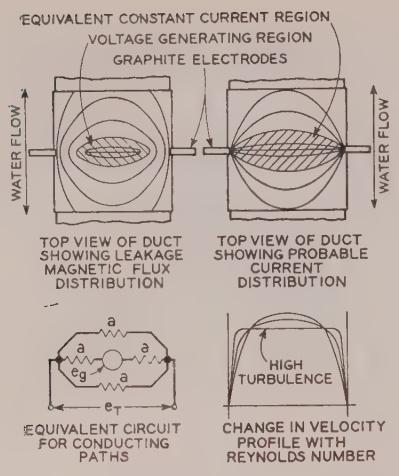

Figure 5 (left). Schematic diagrams of flowmeter characteristics

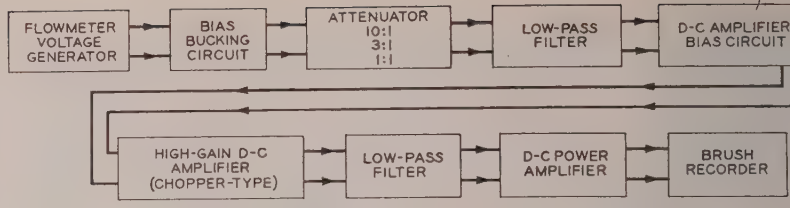

Figure 7 (above). Block diagram of associated flowmeter instrumentation

esses one need expect no difficulties. Glasstone[8] gives figures on ion mobility rates, electrophoretic mobility rates, and electrode dissociation rates. With a maximum gradient of about 500 microvolts per centimeter in our system, all of these processes appear to be slow compared to the flow reversal rate.

Actual Construction

As a result of the above considerations, a permanent magnet yoke was constructed utilizing two magnetron-type permanent magnets, each producing a field of 1,500 gauss across a 2-inch air gap. The gap was widened sufficiently to straddle the 5 inches thick, 12 inches wide rectangular duct where flow was to be measured. This installation is shown pictorially in Figure 3 and diagrammatically in Figure 4. A rough check of the resulting magnetic field strength distribution in the duct in the plane of the two electrodes shows an almost sinusoidal flux distribution with a maximum of 400 gauss in the center of the duct. A 1-foot section of the original iron duct was cut out and replaced by a lucite section in order to get a magnetic field through the water, to avoid attenuating the induced potentials, and to enable visualization of the flow.

Expected Performance

Rough calculations were made in order to estimate the probable level of the induced voltage to be expected. Assuming approximately constant velocity across the duct and sinusoidal flux distribution, and integrating the magnetic field over the width of the duct, one arrives at an expected order of magnitude of 2.81 millivolts per foot per second induced in the duct. Of the total voltage generated, only a fraction can be expected at the electrodes due to the internal impedance of the water. Figure 5 shows four diagrams which help explain what is taking place. The upper left diagram is a top view of the duct depicting the leakage magnetic flux distribution of the magnets. The upper right diagram shows the form of the probable current distribution in the water due to the induced voltage. Most of the current will take the path of least resistance between electrodes. There will, however, be some current taking longer paths since all of the water has conductivity. In view of the leakage flux and the diffusion of current, the system can be assumed to be equivalent in form to that shown in the lower left corner of Figure 5. The impedance of the direct path for current flow between electrodes was estimated to be about twice the impedance of the shunting water paths. On this basis, using simple Kirchoff's laws, the voltage at the electrodes comes out to be about 1/5 of the voltage generated or about 0.56 millivolt per foot per second in the duct. This then is the estimated measurable sensitivity. The impedance between electrodes was estimated at 10 kilohms by a similar approach.

Linearity

A meter of this type averages the flow velocity across the duct cross-section and gives a measure of the mean velocity. For the wide range of velocities covered the velocity profile will change during a cycle. Probable velocity profile types are shown in Figure 5 in the lower ri corner. Such a change in flow pro with a sinusoidal magnetic flux distri tion results in different "weighting" each flow element, and the possibility nonlinearity in voltage output versus f rate arises. However, the meter does record the change in the maximum of flow velocity but rather the change in "fundamental" of v_{max} since the magn flux distribution results in little volt contribution from flow elements near walls. Actually then, the interest is the expected change of the ratio v_{me} v_{max}. Rough calculations indicate tha 1 to 2 per cent deviation from linea can be expected to appear at the minals between the maximum range flow velocities. In the normal range operation only about 0.5 per cent need expected.

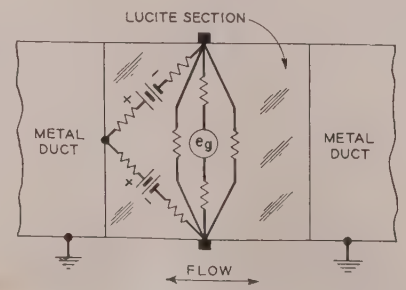

Figure 6. Equivalent circuit of flowmeter

Undesired Effects

Undesired voltages can be expected three forms: polarization drift, err disturbances, and noise pickup. polarization drift problem has been cussed. There always exists some voltage between electrodes which must cancelled out before applying the vary signal to the amplifier. This bias volt does not drift appreciably in operat and can be bucked out. There is trouble with erratic disturbances beca particular attention has been paid proper shielding of the equipment, pecially of the leads from the electrode the amplifier. Noise pickup can be eli nated entirely by establishing a c mon ground between the tank system the amplifier. This, however, leads other undesired effects. Reference Figure 6 will clarify this matter. T figure shows a more accurate equiva circuit of the flowmeter. From e electrode to the metal tank there is alw a bias voltage, usually exceeding millivolts. These voltages are ne equal, explaining the small residual voltage measured between electro Grounding one of the electrodes to el nate the noise shorts out half of

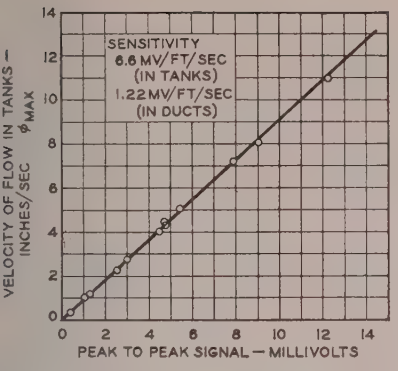

Figure 8. Flowmeter sensitivity calibration curve

voltage generating system and reduces the sensitivity by a factor of about two. In addition, the high bias voltage between the ungrounded electrode and the tanks proves to be erratic and drifts excessively. This of course could not be tolerated. Thus it was concluded that neither electrode should be grounded and that the signal must be derived from across both electrodes.

Associated Instrumentation

The problem then reduced itself to eliminating undesired voltages and amplifying and recording the desired voltage. The range of frequencies of interest of the desired voltage is primarily below 1/3 cycle per second. Therefore, up to 1/3 cycle per second, the amplifying, filtering, and recording apparatus must introduce only small and known phase shift so that the response can easily be corrected. The system should have fair response up to about 10 cycles per second however, in order to show the high frequency effects of closing of the pump blades, blade chatter, and possible other phenomena. The amplifying and recording system must be capable of handling flow signals between 1/4 to 15 millivolts. This, together with the frequencies of interest, dictated the use of a sensitive d-c amplifier. Since the signal required filtering anyway, a chopper-type d-c amplifier is used with its inherent high sensitivity and high stability. Figure 7 shows a block diagram of the final test setup. The bias signal from the electrodes is cancelled out by a "bias bucking" circuit. Immediately following the bias bucking circuit is a series of attenuators which are varied in steps to keep the signal input to the d-c amplifier below 1 millivolt to preserve linearity. Following the attenuators is a low-pass filter which eliminates all a-c noise voltages. Following the low-pass filter is another bias circuit which biases the chopper amplifier into a region of linear operation. The chopper frequency is 60 cycles. The output of this amplifier is filtered by a parallel-T notch-type filter which "kills" the 60-cycle carrier and is adjusted to effectively filter out the 120-cycle ripple as well. The output of this filter is fed to a straight-forward resistance-coupled direct power amplifier which drives a Brush oscillographic recorder. The phase lag introduced by this entire chain is essentially constant at 5 degrees up to 1/2 cycle per second. The amplitude is flat within 1 decibel over this range. The input impedance of the associated instrumentation loading the flowmeter is 25,000 ohms.

Flowmeter Tests

The impedance across the electrodes was checked and found to be 6,000 ohms. Repeated measurements have shown that the average bias level across the electrodes is less than 15 millivolts. In order to be sure that the only voltage measured was due to water flow and not due to motion of conductors in the stray magnetic field which exists around the system, the duct was completely blocked to prevent water flow and the tank system rolled at large amplitude. This and other tests indicated that the only measurable voltage generated in the system is due to flow of water past the electrodes in the presence of the field of the magnets. Tests of sensitivity and linearity were made by measuring the voltage directly at the electrodes. In these tests the servo-amplifier was excited by an artificial sine-wave generator causing sinusoidal oscillation of the pump blades and approximately sinusoidal flow in the duct. Both the frequency and amplitude of drive were varied. The measurements are plotted in Figure 8, maximum flow rate ($d\phi_{max}\ dt$) as the ordinate with corresponding maximum voltage induced as the abscissa. As can be seen, the linearity is excellent. From the curve, the measured sensitivity is 1.2 millivolts per foot per second in the duct which is about twice the estimated sensitivity.

The next step was to record the actual motion of the blades by means of a special pickoff and compare it with the flow voltage by presenting both signals on a twin channel Brush recorder. Sample records over a range of frequencies are shown in Figure 9. It is apparent that assumption of sinusoidal flow is a good one. Figure 9 also shows curves of flow rate versus blade angle where the blade is allowed to have a superimposed high-frequency oscillation due to removal of some damping in the servo system. These records are given to indicate the faithful response of the flowmeter to rapid changes in flow rate.

The drift of the zero level of the recorded flowmeter signal corresponding to zero flow was checked over a long period of time at various frequencies. At a frequency of 0.3 cycle per second the drift is about 0.044 millivolt per minute. At 0.03 cycle per second it is about 0.127 millivolt per minute. In neither case is the drift appreciable. For this purpose it is completely negligible. It has been confirmed experimentally that the response of the flowmeter is instantaneous by studying its response as a function of frequency, amplitude of water motion and blade angle.

It may be concluded that the electromagnetic method is well suited for measurements of this type. The system is linear, stable, instantaneous in response, and has high sensitivity. It responds only to fluid velocity and provides direct electrical signals which can easily be recorded. The associated equipment is fairly simple and easy to set up. The use of permanent magnets with oscillating flow has been shown to be feasible at very low frequencies. Such a system is highly useful in the study of the dynamic characteristics of variable-pitch blade pumps as it clearly indicates the effects of blade chatter, closing of the blades, change of blade angle, change of frequency, pump speed, and so forth. Adaptations of this

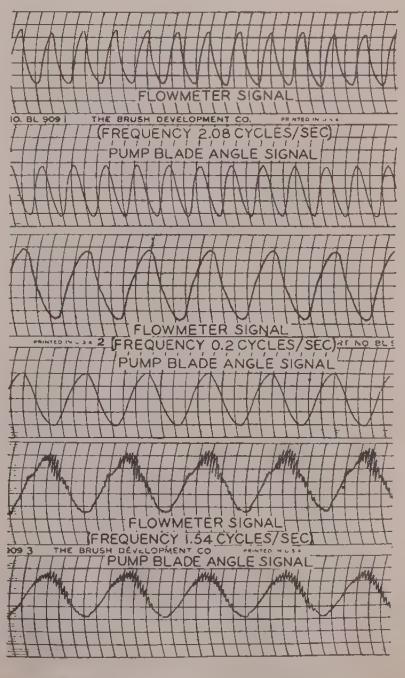

Figure 9. Flowmeter response curves

type of instrument to flow measurements of all kinds can be envisaged.

References

1. Experiments with Activated Tanks, N. Minorsky. *Transactions*. The American Society of Mechanical Engineers (New York, N. Y.), October 1947, pages 735–47.

2. Methode zur Elektrischen Geshwindig-Keitmessung von Flussigneiten, B. Thurlemann. *Helvetical Physica Acta* (Basle, Switzerland), number 383, 1941.

3. The Statistical Theory of Turbulence and the Measurement of Turbulence Velocity Components in Axi-Symmetric Fluid Flow, L. Grossman. *PhD Thesis*, University of California. 1949.

4. Apparatus for Measuring Fluid Flow, A. Kolin. United States Patent 2,149,847, March 7 1939.

5. Device for Measuring Rate of Fluid Flow. H. Lehde. United States Patent 2,435,043, January 27, 1948.

6. Electro-Magnetic Ships Log, G. L. Smith' J. Slepian. United States Patent 1,249,530, December 11, 1917.

7. "Diary," Michael Faraday. January 12–14, 1832.

8. Introduction to Electro-Chemistry, S. Glasstone. D. Van Nostrand and Company, New York, N. Y.

No Discussion

Three-Phase Measurements of Resistance

L. W. MATSCH
MEMBER AIEE

N. C. BASU
ASSOCIATE AIEE

G. R. HORCHER
ASSOCIATE AIEE

Synopsis: Unsymmetrical spacing of conductors produces errors in the values of a-c resistance measured on the individual conductors, of a 3-conductor system, with 3-phase current. The average of two sets of 3-phase measurements, one with positive sequence current and the other with negative sequence current gives the true value of conductor resistance. An analysis given in the Appendix evaluates the effect of unbalanced inductive reactance upon the measured resistance. Experimental data are shown which support the analysis.

THE purpose of this paper is to describe a method of measuring the true a-c resistance of the individual conductors of a 3-conductor system with 3-phase current. Large discrepancies between the measured values of three identical conductors with 3-phase current have been reported by observers.[1] It has been the practice to take the average of the values of resistance measured on the three conductors as being the true a-c resistance of each. This procedure is valid only if the resistances of the individual conductors are actually equal. Inequalities in conductor resistance can result from such causes as proximity effects and unsymmetrical location of the three conductors in one iron conduit. Unsymmetrical spacing of the three conductors produces unbalanced inductive reactances which in turn produce errors in resistance measurements. An analysis of the effect of unbalanced inductive reactances on the measured values of a-c resistance is shown in the Appendix. The method described in this paper is similar to that used by other investigators,[1,2] except that measurements are made first with 3-phase current of one phase sequence and then with three-phase current of opposite phase sequence. The average values of the resistance measured on any one conductor with the two-phase sequences is the true value of a-c resistance. The analysis in the Appendix and the test data show this to be true.

Test Methods

Figure 1 shows a diagram of the measuring circuit which is very similar to the one described by Summers.[2] The conductors on which resistance and reactance measurements were made are three copper tubes each 30 feet in length with an inside diameter of 0.375 and an outside diameter of 0.540 inch. Three-phase 60-cycle current was applied to the conductors by means of three inverted current transformers which were fed each by a variable autotransformer. Another set of three current transformers, each with a current ratio of 20-to-1 was used in the measuring circuit. A tuned 60-cycle vibration galvanometer with a sensitivity of 0.025 microampere per millimeter fed from battery powered amplifier with an amplification of 100 was used as a null detector.

Two sets of potential leads were connected to each conductor at the same two points 15 feet apart. One set of potential leads was connected inside each conductor and brought out through a small opening midway between the potential points. Once outside the conductor, the leads were twisted and brought away at right angles to the conductor for a distance of about 18 feet. The other set of potential leads was connected to the outside of the conductor and brought away at right angles to a distance of about 18 feet, then closed to form a rectangular loop. The leads were twisted from this loop to the measuring circuit. The inner potential leads formed negligibly small loops with their respective conductors

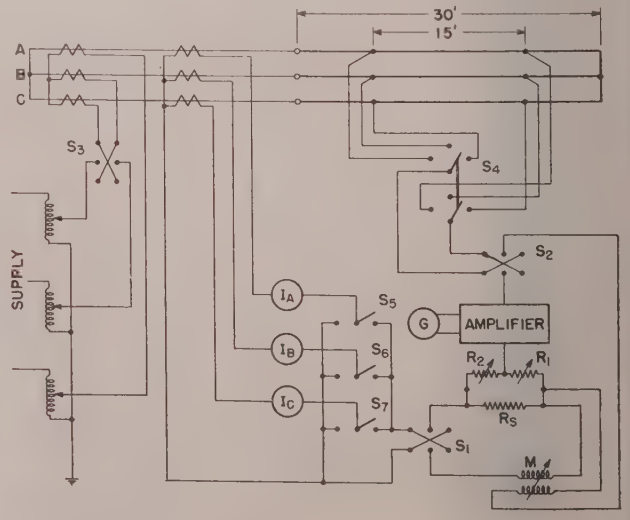

Figure 1. Diagram of circuit for 3-phase measurements of resistance and reactance

Paper 51-59, recommended by the AIEE Instruments and Measurements Committee and approved by the Technical Program Committee for presentation at the AIEE Winter General Meeting, New York, N. Y., January 22–26, 1951. Manuscript submitted November 1, 1949 and originally presented at the AIEE Winter Meeting, New York, N. Y., January 30-February 3, 1950 as paper 50-75. Made available for printing December 6, 1950.

L. W. Matsch and N. C. Basu both are with the Illinois Institute of Technology, Chicago, Ill., and G. R. Horcher is with the University of Kansas, Lawrence, Kan.

This paper is based on theses supervised by L. W. Matsch and submitted by N. C. Basu and G. R. Horcher to the Graduate School of Illinois Institute of Technology in 1949 in partial fulfillment of the requirements for the degree of M.S. in Electrical Engineering.

Acknowledgment is due to the Armour Research Foundation of Illinois Institute of Technology for the use of the facilities of the Ohmite Laboratory.

and were used for measurements to check those made with the external potential leads.

The measuring circuit is an a-c potentiometer. The voltage drop across a standard resistor, shunted by a voltage divider, in the secondary of a current transformer plus the voltage in the secondary of a mutual inductance is made equal to the drop between the potential points on the conductor. The conductor is in series with the primary of the current transformer and the primary of the mutual inductance is in series with the secondary of the current transformer.

In order to minimize the effect of stray fields, two measurements, with opposite polarities of potential and secondary current were made on each conductor for both phase sequences. The values of resistance and reactance are found as follows:

$R_s = 0.0338$ ohm fixed standard resistance
M = mutual inductance henrys
$T = 20$ current transformer ratio
$R = R_1 R_s/(R_1+R_2)T$ conductor resistance
$X = 377\ M/T$ conductor reactance at 60 cycles

The d-c resistance of the conductors was measured with a Kelvin bridge. The resistances of the three conductors were unequal probably because of a nonuniformity of material.

Test Results

External Potential Loops

The test data obtained, with the external potential loops, for conductor spacings of approximately 2, $2^1/_4$, and $2^3/_4$ inches are listed in Table I. Table I shows that the apparent resistance of A-phase conductor is 1.55×10^{-3} ohm when measured with positive-sequence current and 1.30×10^{-3} ohm when measured with negative-sequence current. Whereas the average of these two values is 1.43×10^{-3} ohm compared with a value of 1.406×10^{-3} ohm for the d-c resistance. The 60-cycle a-c resistance is substantially equal to the d-c resistance for copper conductors of the size and shape on which the preceding data were obtained.

Alternating current resistance values based on measurements with current of two phase-sequence check the d-c resistance values within 3 per cent for all three conductors, whereas values obtained with current of only phase sequence differ as much as 10 per cent (A-phase conductor positive-sequence measurement).

Measurements were repeated for different conductor spacings and the average values of a-c resistance for the individual conductors obtained with currents of opposite phase sequence were substantially the same as those shown in Table I.

Internal Potential Loop

With the internal potential loop arrangement, the discrepancies in measured a-c conductor resistance obtained with currents of opposite phase sequence were within 2 per cent. The setting of the mutual inductance, M, was practically zero, indicating that the magnetic flux linkages between the internal loop and the conductor were negligible.

Computed Positive-Sequence Resistance

It is shown in the Appendix that the error, with positive-sequence current in the measured value of a-c resistance of A-phase conductor (conductor 1) is

$$0.866(X_{d(12)} - X_{d(31)}) = \sqrt{3}(X_{bt} - X_{ct})$$

In Table I, $X_{bt} = 0.817 \times 10^{-3}$; $X_{ct} = 0.885 \times 10^{-3}$ and $X_{at} = 0.838 \times 10^{-3}$ ohm. Substituting these values into equations 10, 11, and 13 in the Appendix the error terms are $+0.118$, -0.081, -0.036 milliohms for A-, B-, and C-phase conductors respectively. If these terms are subtracted from the positive-sequence values of resistance shown in Table I we get

$R_a = 1.55 - 0.118 = 1.43$ milliohms for A-phase
$R_b = 1.08 + 0.081 = 1.16$ milliohms for B-phase
$R_c = 1.08 + 0.036 = 1.12$ milliohms for C-phase

These values are in good agreement with average values 1.43, 1.18, and 1.11 milliohms shown in Table I for A-, B-, and C-phase conductors respectively.

Table I. Three-Phase 60 Cycle—Resistance and Reactance Measurements

Phase Sequence	Ohms R_1	Ohms R_2	Conductor Resistance Milliohms Measured	Conductor Resistance Milliohms Average	Mutual Inductance, Microhenrys	Conductor Reactance Milliohms Measured	Conductor Reactance Milliohms Average
A-Phase Conductor $R_{dc} = 1.406\times10^{-3}$ ohm at 31°C							
Positive	Dir.	1,000	97	1.54	1.55	43.5	0.820
	Rev.	1,000	88	1.56		45.0	0.848
Negative	Dir.	1,000	307	1.29	1.30	44.7	0.841
	Rev.	1,000	296	1.31	1.43	44.7	0.841 0.838
B-Phase Conductor $R_{dc} = 1.152\times10^{-3}$ ohm at 31°C							
Positive	Dir.	1,000	562	1.08	1.08	43.7	0.824
	Rev.	1,000	562	1.08		43.7	0.824
Negative	Dir.	1,000	334	1.27	1.28	43.0	0.810
	Rev.	1,000	318	1.28	1.18	43.0	0.810 0.817
C-Phase Conductor $R_{dc} = 1.087\times10^{-3}$ ohm at 31°C							
Positive	Dir.	1,000	572	1.08	1.08	47.0	0.885
	Rev.	1,000	559	1.08		47.0	0.885
Negative	Dir.	1,000	480	1.14	1.14	47.0	0.885
	Rev.	1,000	493	1.13	1.11	47.0	0.885 0.885

Average conductor temperature = 31°C.
Current = 40 amperes per conductor.

Table II. Three-Phase Resistance Measurements Unbalanced Current

Phase Sequence	Conductor Resistance Milliohms Measured	Average
A-Phase Conductor $R_{dc} = 1.447\times10^{-3}$ ohm at 37°C		
Positive	1.51	
Negative	1.32	1.42
B-Phase Conductor $R_{dc} = 1.178\times10^{-3}$ ohm at 37°C		
Positive	1.07	
Negative	1.29	1.18
C-Phase Conductor $R_{dc} = 1.111\times10^{-3}$ ohm at 37°C		
Positive	1.08	
Negative	1.13	1.11

Average conductor temperature = 37°C.
Current in conductors $A = 49.0$ amperes $B = 40.0$ amperes $C = 37.0$ amperes.

Unbalanced Current

Unbalanced current in a 3-conductor system is comprised of positive- and negative-sequence components only, as there is no return path for zero-sequence current. It follows, therefore, that measurements with currents of opposite phase sequence will produce the true value of a-c conductor resistance even if the current is unbalanced. The effect of unbalanced currents on the measured value of a-c resistance is analyzed in the Appendix. Table II lists the results obtained with unbalanced current.

Conclusions

The analytical and test results, given previously, show that in a 3-phase measurement of resistance followed by one with currents of opposite phase sequence will yield data from which the true value of a-c resistance of each individual conductor can be obtained. This is true for conductors with unbalanced impedance and with balanced or unbalanced current. A definite quantitative correlation exists

between the errors in the measured values of resistance, using only one phase sequence, and the values of the unbalanced reactances. It is possible to compute the error in the measured value of resistance, using only one phase sequence, if precise measurements of reactance are made, thus making it unnecessary to repeat the measurement with current of opposite phase sequence.

Appendix

In a system of three conductors of the same size and shape, let the following be expressed in ohms:

R_a = a-c resistance of A-phase conductor
R_b = a-c resistance of B-phase conductor
R_c = a-c resistance of C-phase conductor
X_a = conductor component of inductive reactance[3] of each of the three conductors
$X_{d(12)}$ = separation component of inductive reactance between conductors 1 and 2 (A- and B-phases)
$X_{d(23)}$ = separation component of inductive reactance between conductors 2 and 3 (B- and C-phases)
$X_{d(31)}$ = separation component of inductive reactance between conductors 3 and 1 (C- and A-phases)
I_a, I_b, and I_c = currents expressed in amperes in A-, B-, and C-phases respectively.

All these quantities obtain for the length of conductor (15 feet) between the potential points.

The voltage between potential points, if the rectangular measuring loop is closed at a distance from the conductor which is great compared with the conductor spacings, is expressed by

$$E_a=(R_a+jX_a)I_a-jX_{d(12)}I_b-jX_{d(31)}I_c \quad (1)$$

If positive sequence current, only, is applied, then

$$I_a=I_{a1};\ I_b=a^2I_a\ ;\ I_c=aI_{a1} \quad (2)$$

where the coefficient a is an operator which advances a vector 120 degrees. Substituting equation 2 in equation 1

$$E_a=(R_a+jX_a-a^2jX_{d(12)}-jaX_{d(31)})I_{a1} \quad (3)$$

The positive-sequence impedance, expressed in ohms, is

$$Z_{a1}=\frac{E_a}{I_{a1}}=R_a-0.866(X_{d(12)}-X_{d(31)})+j\left(X_a+\frac{(X_{d(12)}+X_{d(31)})}{2}\right) \quad (4)$$

The real term, $R_a-0.866(X_{d(12)}-X_{d(31)})$, is the measured positive-sequence resistance and contains an error term, namely $-0.866(X_{d(12)}-X_{d(31)})$.

If negative-sequence current, only, is applied the operators a^2 and a in equation 3 are interchanged, and the negative-sequence impedance, expressed in ohms, is

$$Z_{a2}=\frac{E_a}{I_{a2}}=R_a+0.866(X_{d(12)}-X_{d(31)})+j\left(X_a+\frac{X_{d(12)}+X_{d(31)}}{2}\right) \quad (5)$$

The average value of equation 4 and equation 5 is

$$Z_a=\frac{Z_{a1}+Z_{a2}}{2}=R_a+j\left(X_a+\frac{X_{d(12)}+X_{d(31)}}{2}\right) \quad (6)$$

The error terms $0.866(X_{d(12)}-X_{d(31)})$ in equation 4 and equation 5 cancel, and the real term R_a in equation 6 is the a-c resistance of the conductor.

Determination of Error Term

The error term $0.866(X_{d(12)}-X_{d(31)})$ can be computed from the values of reactance measured with current of one phase sequence only.

$$X_{at}=X_a+\frac{X_{d(12)}+X_{d(31)}}{2} \quad (7)$$

$$X_{bt}=X_a+\frac{X_{d(23)}+X_{d(12)}}{2} \quad (8)$$

$$X_{ct}=X_a+\frac{X_{d(31)}+X_{d(23)}}{2} \quad (9)$$

In equations 7, 8, and 9, X_{at}, X_{bt} and X_{ct} are the total inductive reactances measured on A-, B-, and C-phase conductors respectively.

The error terms in the measured values of positive-sequence are:

$$-0.866(X_{d(12)}-X_{d(31)})=-\sqrt{3}(X_{bt}-X_{ct}) \text{ for } A\text{-phase} \quad (10)$$

$$-0.866(X_{d(23)}-X_{d(12)})=-\sqrt{3}(X_{ct}-X_{at}) \text{ for } B\text{-phase} \quad (11)$$

$$-0.866(X_{d(31)}-X_{d(23)})=-\sqrt{3}(X_{at}-X_{bt}) \text{ for } C\text{-phase} \quad (12)$$

Errors Due to Unbalanced Current

This analysis applies to 3-conductor systems only. In such systems no zero-sequence current can result from unbalance. The currents in the three conductors can therefore be expressed in terms of positive-sequence and negative-sequence components I_{a1} and I_{a2} respectively as follows:

$$I_a=I_{a1}+I_{a2} \quad (13)$$

$$I_b=a^2I_{a1}+aI_{a2} \quad (14)$$

$$I_c=aI_{a1}+a^2I_{a2} \quad (15)$$

Substituting equations 13, 14, and 15 in equation 1, we get

$$E_a=(R_a+jX_a)(I_{a1}+I_{a2})-jX_{d(12)}(a^2I_{a1}+aI_{a2})-jX_{d(31)}(aI_{a1}+a^2I_{a2})$$

which can be reduced to

$$E_a=(R_a+j)\left(X_a+\frac{X_{d(12)}+X_{d(31)}}{2}\right)I_a-0.866(X_{d(12)}-X_{d(31)})(I_{a1}-I_{a2}) \quad (16)$$

The measured impedance is therefore expressed by,

$$Z_{a1}=\frac{E_a}{I_a}=R_a+\text{real part of}\left(-0.866(X_{d(12)}-X_{d(31)})\frac{I_{a1}-I_{a2}}{I_a}\right)+j\left[\left(X+\frac{X_{d(12)}+X_{d(31)}}{2}-\text{imaginary part of}\left(-0.866(X_{d(12)}-X_{d(31)})\frac{I_{a1}-I_{a2}}{I_a}\right)\right]\right. \quad (17)$$

If the phase sequence is reversed the measured impedance is expressed by

$$Z_{a2}=R_a-\text{real part of}\left(-0.866(X_{d(12)}-X_{d(31)})\frac{I_{a1}-I_{a2}}{I_a}\right)+j\left[\left(X+\frac{X_{d(12)}+Xd_{(31)}}{2}\right)+\text{imaginary part of}\left(-0.866(X_{d(12)}-X_{d(31)})\frac{I_{a1}-I_{a2}}{I_a}\right)\right] \quad (18)$$

The average of equations 17 and 18 is

$$Z_a=\frac{Z_{a1}+Z_{a_2}}{2}=R_a+j\left(X_a+\frac{X_{d(12)}+X_{d(31)}}{2}\right) \quad (19)$$

where R_a is the true value of a-c conductor resistance.

References

1. Problems in the Measurement of A-C Resistance and Reactance of Large Conductors, **E. H. Salter.** *AIEE Transactions*, volume 68, 1948, pages 1390–96.

2. Effective Resistance and Inductance of 3-Conductor Shipboard Power Cables, **Samuel D. Summers.** *AIEE Transactions*, volume 68, 1948, pages 1345–50.

3. The Transmission of Electric Power, **W. A. Lewis.** Edwards Brothers Inc., Ann Arbor, Mich., 1948.

Discussion

E. H. Salter (Electrical Testing Laboratories, Inc., New York, N. Y.): The authors have presented an interesting attack on the problem which has at times caused some of us serious headaches. From a measurments point of view, some doubt originally was cast on accuracy of measurements when it was found that under certain operating conditions the individual conductors of the 3-phase system showed wide variations in measured apparent resistance, sometimes even exhibiting negative values. Investigation showed that such variations might be caused by mechanical dissymmetries in the cable arrangement or other similar factors which would shift the true neutral of the system. The average of the three individual phase measurements, however, was found to yield a value from which the true

I^2R losses could be computed. This was verified by wattmeter measurements.[1]

The authors present a theoretical analysis leading to a means of evaluating the "error term" or correction which they find would make it possible to determine true resistances of the individual conductors from measured values with only one phase sequence.

Recent calorimetric measurements with balanced 3-phase currents have shown the rate of temperature rise in each of the three conductors to be essentially the same, regardless of unbalance in measured a-c resistances. This would show the losses in the conductors themselves to be essentially equal in spite of wide variations in the apparent resistances of the individual conductors, a condition which has been verified even for the operation of a 3-phase system of conductors in a steel pipe, where pipe losses also are reflected in apparent conductor resistances. Under these circumstances, the average apparent conductor resistance, which is a measure of the over-all loss of the system, is the important characteristic of these conductors. The true effective resistance of the copper of the individual conductors then is of only academic interest.

The authors state, "it has been the practice to take the average of the values of resistance measured on the three conductors as being the true resistance of each." They then state that "this procedure is valid only if the resistances of the individual conductors are actually equal," though they fail to state whether this equality should be in d-c resistance or in effective a-c resistance. From their next sentence, however, it might be implied that they reason this to be true only when effective a-c resistances are equal, for they suggest that "inequalities in conductor resistance can result from such causes as proximity effects and unsymmetrical location of the three conductors in one iron conduit." They then further state that "the average values of the resistance measured on any one conductor with two phase sequences is the true value of resistance."

May I present the results of a-c resistance measurements of three 1,500,000-circular-mil paper-insulated conductors, pulled parallel in triangular spacing, 2.76 inches between centers, into $8^5/_8$-inch steel pipe. These measurements were made by the method shown in my papers on this subject, and the results are shown in Table I (below).

From these data you will note that measured a-c resistances show a range of almost 2:1, reactances, a range of about 1.3 to 1. By virtue of their arrangement in the steel pipe it would be expected that the true effective resistance of the three conductors would not be equal. Following the authors' method of analysis, the average of the measured values of any one conductor for the two phase sequences would be the true effective resistance of that conductor. This would mean that conductor A, which was at the apex of the triangle and farthest from the pipe, has an effective resistance lower than its d-c resistance, a condition not impossible, yet questionable in the light of calorimetric tests.

It will be noted further that the average effective resistance for the three conductors is the same for both phase sequences—this is most readily shown in the ratio of a-c to d-c resistances. This would appear to justify established practice of averaging these measurements.

An attempt to use here the suggested means of evaluating the "error term," in order to check the average values, leads to results which are obviously valueless, since the "error term" in most cases comes out larger than the measured a-c resistance. This suggests that the analysis is not applicable to the case of cables in pipe, probably because there then are at least seven components of inductive reactance rather than the four assumed in the authors' analyses. This makes for difficulties in the evaluation of the "error term."

REFERENCE

1. PROBLEMS IN THE MEASUREMENT OF A-C RESISTANCE AND REACTANCE OF LARGE CONDUCTORS, E. H. Salter. *AIEE Transactions*, volume 67, part II, 1948, pages 1390–97.

R. W. Atkinson (General Cable Corporation, Bayonne, N. J.): Messrs. Matsch, Basu, and Horcher have accomplished, by a very simple device, the isolation of the power consumed by the individual phases. A great deal of time has been given to the measurement of losses in cable circuits, and no one has previously come up with this answer, which is very definite evidence of the novelty of the present suggestion.

The experimental data should be considered illustrative rather than significant evidence of the accuracy of the method. For the experiments to constitute convincing proof of the theorem would require greater accuracy than is indicated by the test data and would require that the measurements be made on circuits in which the reactance considerably exceeds the resistance, instead of being considerably smaller. However, the authors' theorem does not require the evidence of experimental methods and can stand on purely analytical or theoretical considerations.

The significance of this determination of power from the individual phases may easily be confused. Thus, if "A" be determined as the power supplied by phase A, that is not necessarily the power converted into heat in conductor A. The measurement "A" includes all of the losses produced as a result of the current in A, that is, it includes the skin effect loss in conductor A and also includes proximity losses in conductors B and C as well as in neighboring conducting materials due to the current in A.

A further significant point brought out by the authors is that the losses in the individual phases are determinable by the method of reversing phase rotation even if the currents in the three conductors are unbalanced. We must add that the proportion of positive to negative sequence current must be the same in both measurements.

The method has theoretical possibilities in the measurement of 3-phase dielectric losses. It would be useful for someone to develop the practical possibilities of this.

L. W. Matsch, N. C. Basu, and **G. R. Horcher:** The interesting discussions by Mr. Salter and Mr. Atkinson are appreciated.

The purpose of the paper was to present an analysis of the effect of unsymmetrical spacing of conductors on the measured values of a-c resistance of the individual conductors in a 3-conductor system, using 3-phase current. As Mr. Salter suggests in his discussion, the method does not account for errors in the case of cables enclosed in pipe, the losses of which are reflected into the measured conductor resistance.

The paper enumerates several causes of inequality in conductor resistance, but treats only one of them, namely, unbalanced inductive reactance resulting from unsymmetrical spacing of conductors.

Mr. Salter's quotations from the paper regarding the validity of averaging the resistance of the three conductors deserves comment. Inequalities in conductor resistance may result from a number of factors: among them, conductors of different size or material, or identical conductors operating at different temperatures. In such cases, inequalities in resistance would exist in both the d-c and a-c values of resistance. However, identical conductors carrying equal currents at equal temperatures with the same current distribution in each will have equal heat losses regardless of inequalities in 3-phase resistance measurements. Under these conditions the average value is valid. Practical considerations warrant this procedure in the case of a system of three conductors in an iron pipe.

Mr. Salter's data are interesting. But the inequalities in measured resistance in those data include the effects of losses in the surrounding pipe and therefore are not

Table I. 3-Phase A-C Resistance Measurements 1,500,000 Circular Mil Conductors in Steel Pipe

Current Load	Measured Resistance, microhms, Phase A	Phase B	Phase C	Average	Measured Reactance,* microhms, Phase A	Phase B	Phase C	Average
D-c	260.1	260.4	260.1	260.2				
A-c	270.2	323.2	463.0	352.1	1,396	1,795	1,708	1,633
Average ratio $R_{AC}/R_{DC}=1.353$					(151)**	(450)**	(691)**	
Reversed Phase Rotation								
D-c	262.7	263.3	262.4	262.8				
A-c	244.9	474.0	350.9	356.6	1,414	1,664	1,827	1,635
Average ratio $R_{AC}/R_{DC}=1.357$					(279)**	(716)**	(433)**	
Average of Two Phase Rotations								
D-c	261.4	261.9	261.3	261.5				
A-c	257.6	398.6	407.0	354.4	1,405	1,726	1,768	1,634
Average ratio $R_{AC}/R_{DC}=1.355$								

* To neutral.

** Error terms computed on bases proposed by the authors of the paper.

solely due to unbalanced inductive reactance, although large unbalances in inductive reactance are shown in his table. Obviously, error terms, based solely on unbalanced inductive reactance, cannot correct for losses which occur in the surrounding pipe. Mr. Atkinson raises several interesting points. We do not agree with his comments regarding the significance of the experimental data. We consider the results shown in Table I of our paper significant evidence of the accuracy of the method. These results are supported by applying the error terms, computed from the values of reactance, to the values of resistance measured with currents of one phase sequence only.

We agree with Mr. Atkinson's comments regarding skin effect and proximity effects and with his comments on unbalanced current.

One of the authors, L. W. Matsch, has used this method in 3-phase dielectric power factor measurements of 3-conductor belted-type cable.

An Electronic Time Division Multiplex Telegraph Set

T. A. HANSEN
NONMEMBER AIEE

R. D. SLAYTON
NONMEMBER AIEE

Synopsis: The telegraph terminal set described forms an integral part of a time division multiplex system wherein two, three, or four channels are combined for transmission over a common communication circuit of minimum band width. Channel inputs and outputs are on a start-stop printing telegraph basis for flexibility in connecting to existing conventional start-stop systems. The equipment is packaged in such a manner that all components are readily accessible for maintenance during normal operation without interrupting the flow of traffic.

THE use of time division multiplex equipment in commercial telegraph service originated shortly after the turn of the century. One type of electromechanical multiplex equipment which first was manufactured about 30 years ago is shown in Figure 1. These and other types of early multiplexes were characterized by the use of motor-driven distributors in which the elements of the signal transmitted were initiated either through the motion of brushes across a segmented commutator or through the sequential closing of contacts. The detection of such signals at receiving terminals was accomplished by similar apparatus. Electrically driven tuning forks were used to control directly the speeds of both the sending and the receiving distributors. The perforated-tape sensing transmitters and the receiving printers which terminated the individual traffic channels usually were located close by the set because of the large number of interconnecting circuits required.

Converters or "extensors" later were developed which permitted the channels of the synchronous multiplex system to be connected directly to start-stop telegraph equipment which had come into general use, and around which extensive telegraph systems had been organized. Such start-stop equipment then could be located at the sources of traffic at more distant points, so that individual messages did not require manual handling or "relaying," or storage in perforated-tape form.

Electromechanical multiplex systems also were adapted to use on radio-telegraph circuits[2,3] where the multiplexing of channels served both to increase the traffic capacity of the individual circuits and to reduce the crowding of the radio spectrum through more efficient use of band space.[4] The success of these applications tended to stimulate interest in the use of multiplex techniques, particularly in view of the development of frequency shift keying for radio transmitters[5] and of improved radio receiving systems.

With this increased interest came the problem of the manufacture of additional multiplex equipments. Existing designs could have been used without changes, the equipment could have been redesigned utilizing the same basic principles, or an entirely new approach could be attempted. Since the electromechanical multiplex systems always had presented such problems as high maintenance expense, difficulty in phasing, low order of frequency stability, and susceptibility to loss of phase during adverse signaling conditions, it was concluded that the new approach should be undertaken to overcome these disadvantages. Also, advances made in the electronic art during World War II and the training of large numbers of personnel as technicians in the electronic field indicated that the application of electronic principles to the design of multiplex telegraph equipment should provide natural solutions to many of the old problems.

Information available had indicated that the tuning forks used in the mechanical system could be replaced with more accurate frequency standards, such as crystal-controlled oscillator driving sources, in order to obtain greater stability. Extensive laboratory studies also indicated that multiplex telegraph signals could be generated and detected readily by electronic commutating circuits, and that these circuits could be arranged so that the number of channels available could be changed at will. Need for such flexibility had been demonstrated many times on landline and radio circuits when signaling conditions became such as to reduce greatly the margins of operation. By cutting off one or two channels, the remaining channels could be operated

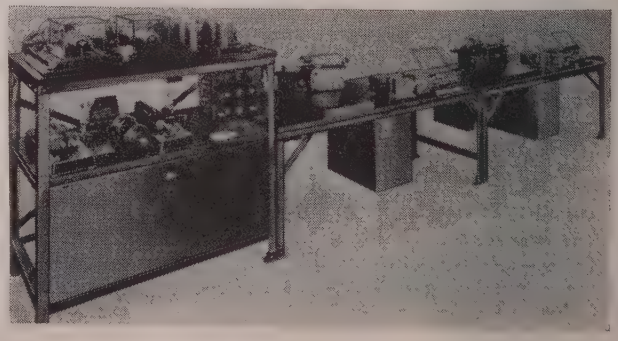

Figure 1. Electromechanical multiplex terminal set

Paper 51-60, recommended by the AIEE Telegraph Systems Committee and approved by the AIEE Technical Program Committee for presentation at the AIEE Winter General Meeting, New York, N. Y., January 22–26, 1951. Manuscript submitted October 23, 1950; made available for printing December 7, 1950.

T. A. HANSEN and R. D. SLAYTON are both with the Teletype Corporation, Chicago, Ill.

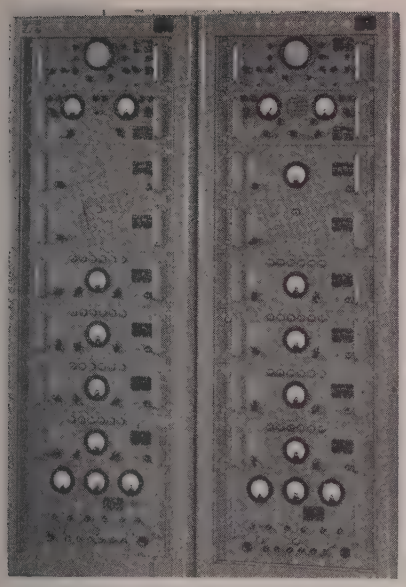

Figure 2 Electronic multiplex telegraph terminal set

successfully because the individual code elements were allowed a greater time duration and thus became less susceptible to distortion.

The Electronic Multiplex System

The newly developed electronic multiplex telegraph terminal set is shown in Figure 2. The cabinet on the left contains the transmitting equipment, while that on the right houses the receiving equipment. The terminal set, when provided with the appropriate start-stop printing telegraph transmitting and receiving apparatus and connected to similar multiplex and start-stop apparatus located at the distant end of a telegraph circuit, provides either two, three, or four 2-way start-stop channels of communication. The equipment may be used on either landline or radio circuits, the following description being based on the latter connection. Since conventional start-stop Teletype apparatus operates at either 60 or 75 words (consisting of five characters and one space) per minute, the multiplex set is readily adaptable to either speed at the time of installation.

Figure 3 is a block diagram showing the composition of an electronic multiplex set. The transmitting equipment group and the associated receiving equipment group at a typical terminal are shown. At the left, Teletype transmitters are shown which deliver start-stop signals to individual transmitting group telegraph code converters on the four channels designated "A," "B," "C," and "D." The start-stop transmitters are of the "free" type and may be either tape-sensing transmitters or printer keyboards. Their operation should be distinguished from that of the so-called "captive" type start-stop or multiwire transmitters, which require synchronization or "trip-off" from the multiplex distributor, as used in some earlier multiplex systems. Within the individual converters the signals are detected, the start-and-stop elements are deleted, and the remaining code combinations are stored for an instant. These code signals then are applied to the electronic transmitting signal distributor, which senses or sweeps over the outputs of the code converters in successive order, picking up a complete character signal in turn from each converter. The multiplex signal so generated then is amplified and applied to the control-monitor unit, where it is amplified further and coupled to the telegraph transmitting circuit. The path of progression through the set for "A" channel signals is indicated by the heavy lines in the figure. The signal distributor drive unit contains the crystal oscillator and other circuits which provide the signaling impulses for stepping the distributor unit. The control-monitor unit also acts as a switching center for various circuits which may be selected for attachment to an oscilloscope for monitoring purposes.

Multiplex telegraph signals received from a distant transmitter over the telegraph circuit are applied to the control-monitor unit in the receiving group at the right. There they are amplified and then passed to the receiving signal distributor, which samples the individual code elements, recognizes their character, and passes them on to the various receiving telegraph code converters. Within the converter the code elements are stored,

Figure 3. Simplified block diagram of electronic multiplex terminal set

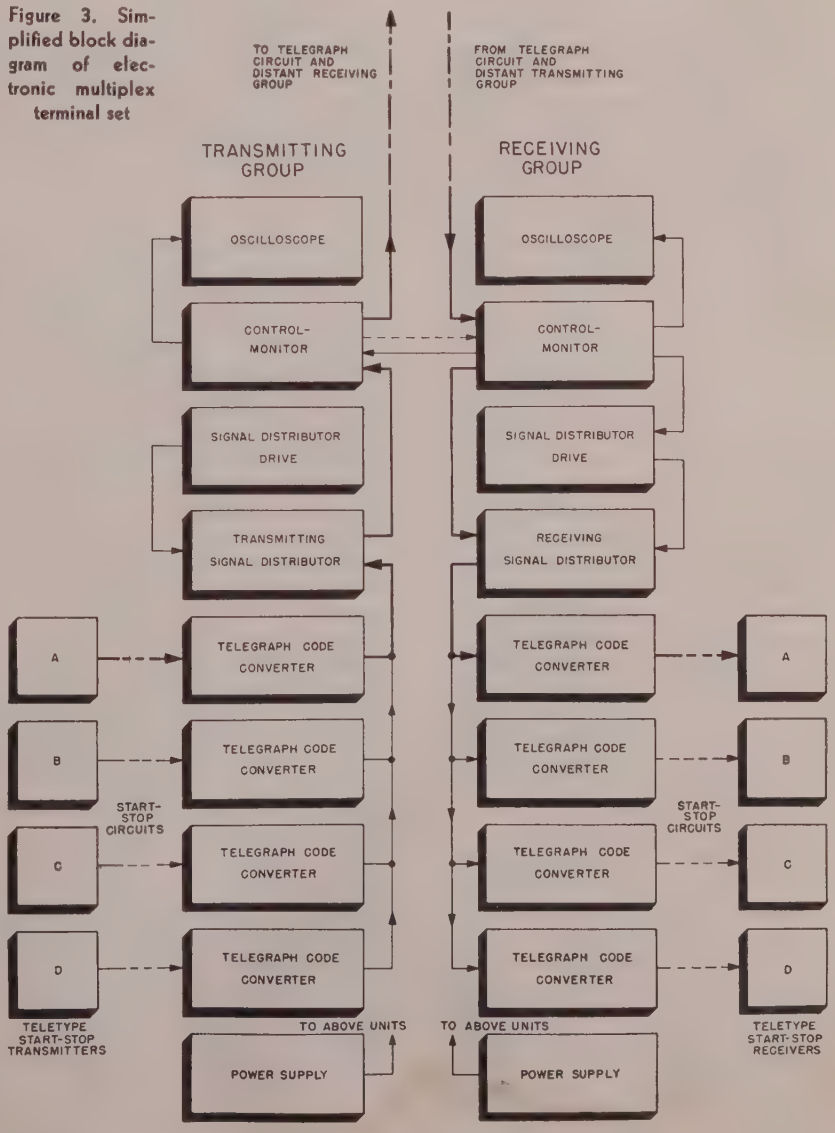

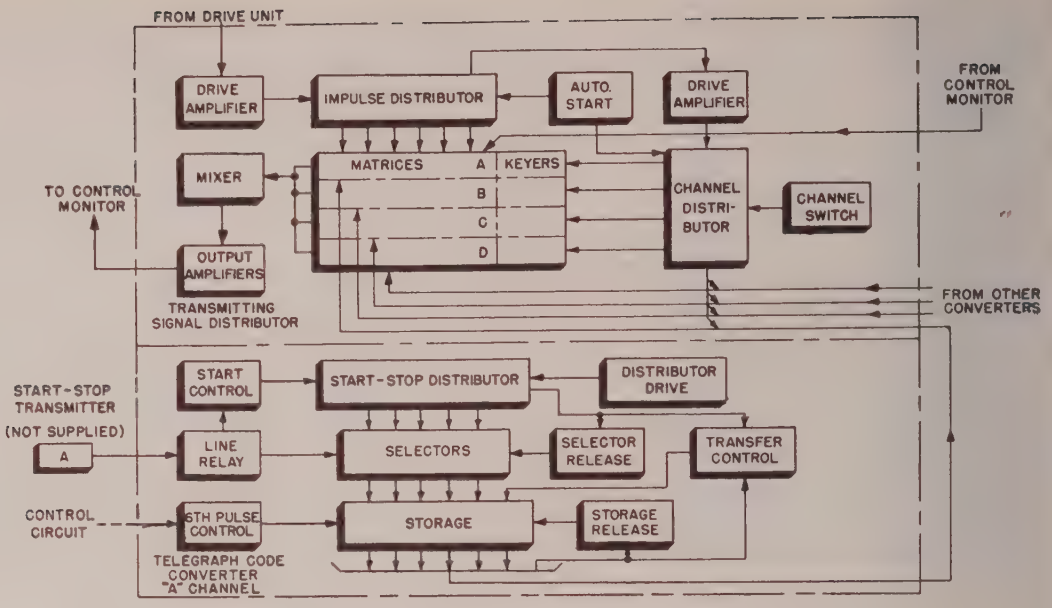

Figure 4. Block diagram of transmitting converter and distributor units

the start-and-stop elements are formed, and the regenerated start-stop signal thus developed is transmitted to the Teletype start-stop receivers. As in the sending group, the signal distributor drive unit energizes the receiving distributor. Since the distributor in this case must operate in synchronism with the signals received over the multiplex circuit, a connection which provides drive frequency correcting signals also is made from the control-monitor unit.

Two circuits also are shown interconnecting the transmitting and receiving groups at the terminal station. The dotted circuit indicates a temporary connection which may be made instantly at the will of the maintenance technician or supervisor. This connection causes the multiplex output signals from the transmitting group to be applied directly to the local receiving group, and thus permits the testing of the set on a local basis when making adjustments or in case of trouble. The solid circuit indicates the connection of a detection system which continuously retransmits a telegraph circuit continuity testing signal, which will be described more fully later.

The Multiplex Transmitting Group

The units of the transmitting group of the electronic multiplex occupy the same physical positions as in the block diagram discussed previously. A block diagram of the general circuits included in one channel converter and the multiplex distributor unit is shown in Figure 4. It should be understood that the converters on each of the other channels are duplicates of this one, and that the output signals of the other converters are applied to the distributor during those portions of the multiplex cycle wherein the converter shown is preparing to deliver a new signal to the distributor.

The Transmitting Code Converter

Signals received from the start-stop transmitter are applied to a line relay circuit consisting of a magnetically controlled diode tube (General Electric type *2B23*). Since this tube is the equivalent of a conventional neutral relay, it permits d-c isolation between the start-stop circuit and the multiplex equipment. Advantages of the magnetic diode are that it requires no maintenance, has very high operating speed, and introduces no bias in the output signal, such as might be caused by relay contacts in transit.

Each start-stop signal, in activating the line relay tube, causes a start control circuit to energize a start-stop distributor after a delay approximately equal to one-half of a basic signal element. The start control circuit is a conventional monostable (or "one-shot") multivibrator—a type of circuit extensively used in the electronic multiplex and herein designated a "univibrator" for brevity. The start-stop distributor itself consists of a series of hot cathode gas tubes connected in a chain-type counter circuit. It operates only while the start-stop signals are being received, coming to rest during the stop or "rest" intervals of such signals. Gas tubes are used because they operate in low impedance circuits, and output signals consisting of positive potentials may be taken directly from across grounded resistors in their cathode circuits.

Each time one of the gas distributor tubes fires it momentarily energizes one of the code element selector tubes (also of the gas type) to which the line relay circuit meanwhile has been applying a priming potential in accordance with the polarity of the received line signal. The sampling of each line signal code element is set to occur near the normal center of the element. This timing is adjustable for the entire start-stop signal sequence by controlling the amount of delay measured by the start control circuit, which thus in effect provides a "ranging" facility. The start-stop distributor itself is driven from a circuit which is energized by a resistance-capacitance oscillator which is turned off while the start-stop distributor is at rest. The oscillator starts and stops without transients and drives a triggering limiting amplifier[6] which provides precisely spaced impulses for the advancement of the start-stop distributor. It should be mentioned here that the various gas selector tubes are released during the "start" interval of each new code sequence through the action of a cathode-follower selector release circuit, which normally supplies steady plate potential to the selector tubes.

Since the incoming start-stop signals arrive at random intervals while the multiplex distributor is cycling continuously, means must be provided for holding the selected signals in storage until they have been retransmitted in multiplex signal form. Therefore a second group of gas storage tubes is provided, being jointly controlled by the selector

tubes and the multiplex distributor. A transfer control circuit, which is prepared for operation at the instant a new start-stop signal begins to arrive, is energized from the multiplex distributor and causes the storage tubes to be fired in the same code pattern as the selector tubes. This transfer must be completed before the selector release circuit extinguishes the selector tubes at the beginning of the next start-stop cycle, and must cause the storage tubes to be established in their new conditions before the multiplex distributor reads the combination in forming the multiplex signal. The code combination is applied directly to matrix tube circuits in the distributor unit, where the distributing circuits scan the elements in sequence. Immediately after the code signals have been used, the distributor furnishes a signal to a cathode-follower storage tube releasing circuit which causes the storage tubes to be extinguished, preparing the way for a new transfer to be made.

Earlier multiplex systems blocked the code signal "blank" or all-spacing signal condition from operating the receiving telegraph printers so that the latter could be allowed to rest when the channel was idle. The electronic multiplex provides a means for distinguishing between code blanks which occur when the channel is idle and code blanks which should be transmitted over the channel and delivered to the distant receiving circuit because they were among the start-stop signals received from the originating transmitters. The latter blanks now are being included as bona fide characters in the start-stop codes used with various types of Teletype apparatus. To take care of this situation, a sixth element has been added to the multiplex channel code. This element is made marking for each character combination received from the start-stop circuit and will be so detected at the receiving terminal. To supply the element, a sixth code storage tube in the converter is energized by the transfer control circuit. Thus, only when the channel is truly idle will an all-spacing combination be transmitted, and this will cause a steady marking "rest" pulse to be delivered to the receiving Teletype printer.

Should it not be necessary to reconstitute the start-stop code blank signal, the sixth code element may be used for an alternate purpose. For example, a control circuit may be energized from external means, causing the transmission of either a continuously marking or spacing sixth element. This signal then may be used for slow-speed supervisory signaling or for operating at the receiving station a relay which permits the regenerated start-stop signals to be delivered to either of two receiving circuits.

The Transmitting Signal Distributor Unit

As has been mentioned, the code signals received from the telegraph code converters are applied to the distributor matrix tube circuits. These matrices are gated or keyed as follows: (a) in channel order through individual keying circuits which are energized from a channel-switching distributor circuit and (b) in elemental order from an impulse distributor. Each distributor consists of a ring of gas tubes. The impulse distributor is driven by impulses received from the drive unit and provides a signal once per complete cycle of operation for advancing the channel distributor. The former thus marks off the individual bands or elements of the multiplex signal, while the latter controls the times of transmission from the individual channels. A channel control switch attached to the channel distributor permits the by-passing of one or two of the channel distributor tubes, thereby allowing the number of channels in use to be reduced to three, or even two, as traffic or radio signaling conditions warrant. Each distributor ring is provided with an automatic starting circuit which causes one gas tube to become fired at the time the unit first is energized.

The simultaneous application of signals from the impulse distributor, from the channel distributor via the keying circuits, and from the converters causes the generation of the multiplex signal. Some of the elements of this signal are reversed here, "mark" for "space" and vice versa, so that when all channels are idle, some marking elements or "reversals" will be transmitted. Such reversals control the maintenance of synchronism between the transmitting and receiving equipments during sustained no-traffic periods.

The gated output signals are combined and applied to a limiting amplifier mixing circuit which shapes the individual signal elements. The signals then are amplified further and applied to the control-monitor unit for coupling to radio circuit.

The Signal Distributor Drive Unit

The circuits contained in the drive unit and the control-monitor unit are shown in Figure 5. The basic frequency

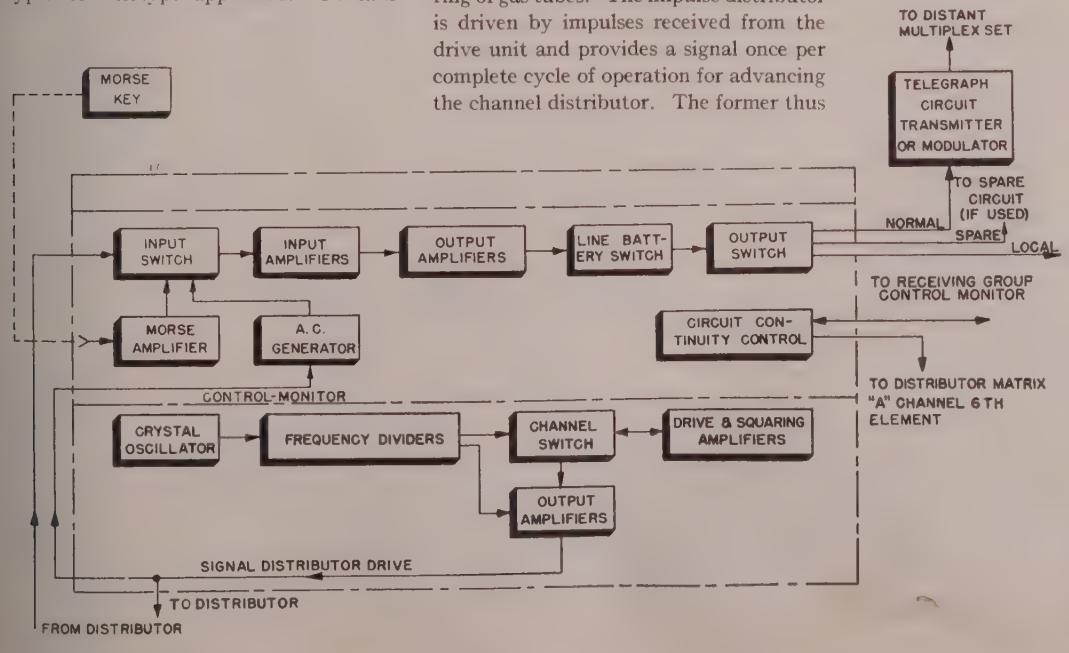

Figure 5. Block diagram of transmitting drive and control - monitor units

standard for the electronic multiplex is the crystal-controlled oscillator in the drive unit. This crystal operates at a frequency of 101.25 kc and is enclosed in a temperature-stabilized oven so that frequency drift is at a minimum. The high frequency is divided down through a number of controlled inductance-capacitance oscillator stages[7] to the fundamental frequencies required for 3- or 4-channel operation. The proper lower frequency is selected by a channel control switch which must be maintained in the same position as the corresponding switch in the transmitting distributor unit. The output frequency is amplified, squared, differentiated, and further amplified before application to the transmitting signal distributor circuits. The output signals for 2-channel operation are obtained from a conventional Eccles-Jordan binary divider following the squaring of the 4-channel frequency. The binary divider output signals then are applied to the differentiating stage, following which the further amplification is obtained.

The Transmitting Control-Monitor Unit

The multiplex telegraph signals generated in the transmitting signal distributor unit are passed through an input selector switch to the various amplifiers located in the control-monitor unit. The latter are designed to supply up to 0.060 ampere neutral telegraph signals at 120 volts to the output circuit. The input switch also permits connection to sources of other signals which may be required when lining up a telegraph circuit. For example, the "Morse" amplifier permits transmission of d-c impulses controlled by a Morse key which is externally connected to the set. Again, a connection may be made to a generator of alternate mark and space element signals. The resultant so-called "AC" signal then may be used in correcting for bias in the telegraph circuit.

Since some telegraph circuits may have their own battery source, provision is made either to supply battery from within the transmitting group or to accept that battery from the other source. An output switch permits connection to three different circuits at the choice of the operator. The normal connection is to the regular telegraph circuit, while an alternate connection may be made to a spare telegraph circuit which can be made ready and placed on stand-by until required. The third or local connection permits direct transmission from the transmitting group to the adjacent receiving group, as was mentioned previously.

The Multiplex Receiving Group

Comparable units of the receiving group in the electronic multiplex terminal set are located in levels similar to those in the transmitting group and as shown in Figure 3.

The Receiving Control-Monitor Unit

The circuits in the receiving control-monitor and drive units are shown in block form in Figure 6. An input switch which corresponds to the output switch of the transmitting group control-monitor unit allows attachment to the three circuits which correspond to those in the transmitting unit. Received electronic multiplex signals first are applied to a magnetic diode line relay in the control-monitor unit and then are amplified in several stages. Finally they are applied through an output selecting switch to the matrix tube circuits of the receiving signal distributor unit. The amplified signals also are differentiated and the pulses obtained therefrom then are amplified through a correction pulse generator circuit. These impulses energize crystal frequency-controlling circuits in the drive unit.

The output switch in the receiving control-monitor unit also permits reversal of the telegraph signals in case they have become "turned over" during transmission. The switch also may cut off the signals delivered to the distributor unit and instead cause them to drive a Morse amplifier circuit. The latter circuit energizes a loud-speaker (contained in the unit) with an on-off tone. This tone is derived from one of the intermediate frequency-dividing stages in the drive unit. The tone-modulated signals are available for emergency use during periods of radio circuit line-up or in the event of an equipment failure which could stop channel communication. It should be recognized that these Morse signals will be those generated at the transmitting terminal by the hand key mentioned in a preceding paragraph.

The Signal Distributor Drive Unit

The greater portion of the drive unit circuits are identical with those in the corresponding transmitting unit, includ-

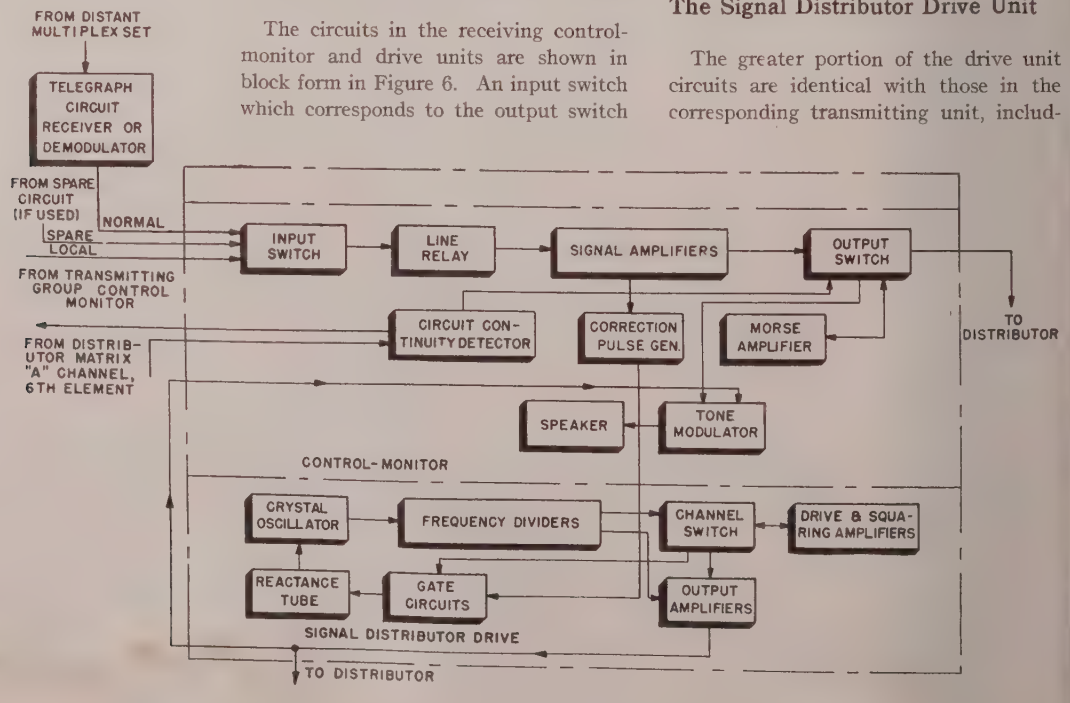

Figure 6. Block diagram of receiving control-monitor and drive units

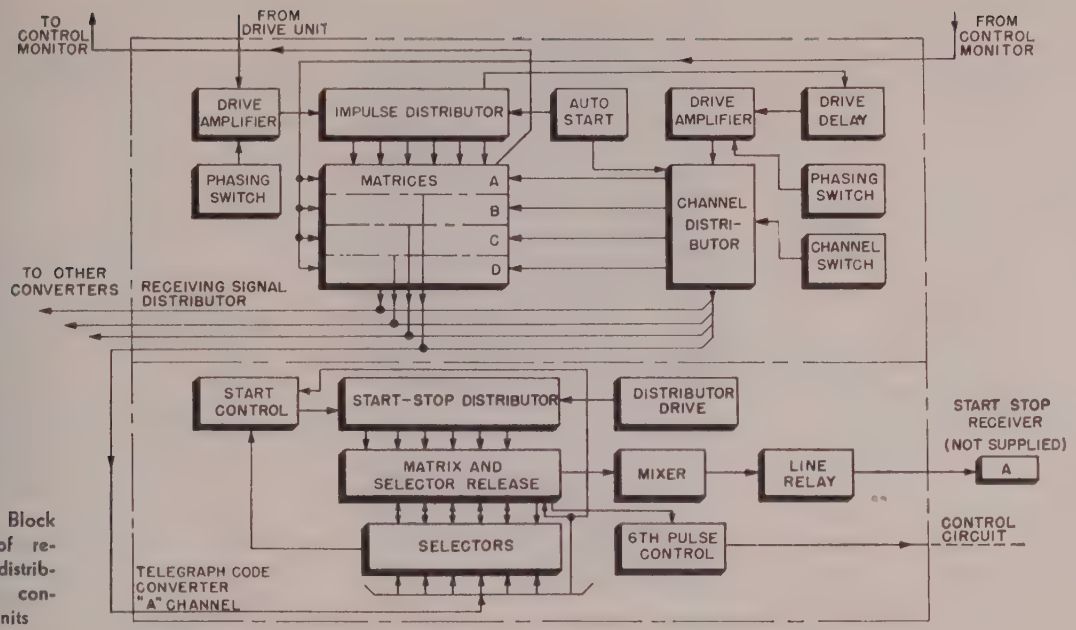

Figure 7. Block diagram of receiving distributor and converter units

ing the crystal oscillator, the frequency dividers, and the switching and amplifier circuits. The multiplex phase-correcting circuits have been added. These consist of gate circuits which compare the arrival time of the received multiplex signal transitions with their theoretically correct positions as determined by the locally generated signals which drive the receiving distributor. These circuits develop a bias potential across an integrating circuit in accordance with the signal displacement. The variations in bias then cause the reactance tube to change the crystal frequency slightly in a direction which tends to bring about the proper phase relationship. If no multiplex signal transitions are being received, the bias potential assumes a controlled average value which causes the frequency to be almost identical with that developed in the transmitting group drive unit at the distant terminal set.

The Receiving Signal Distributor Unit

Figure 7 is a block diagram of the circuits included in the receiving distributor and converter units. Many of the general circuits in the distributor are similar to those in the corresponding transmitting unit. Impulse and channel distributors, with their appropriate driving circuits are provided. A change is made in the manner in which the impulse distributor energizes the channel distributor, a slight delay being provided through the use of a univibrator, which operates at the instant the last received code element of a particular channel is being sampled. This causes the matrix tube circuits for the next channel to be prepared for operation well before the impulse distributor begins to detect the code elements belonging to that channel.

Phasing switches are provided in the driving circuits to the distributors, each switch supplying an additional untimed distributor-driving impulse whenever operated. Each such operation will cause the distributor timing to be advanced by an extra element or channel, such as may be required in order to establish the proper phase relationship with received signals. This action normally is required when starting up a multiplex circuit. It should be recalled that the corrector circuits in the receiving drive unit establish the proper time of sampling within the individual signal elements. It very rarely is necessary to operate the phasing switches once a circuit has been placed in operation, since the high stabilities of the crystal oscillators permit only a very slow drift in phase relationship to occur. It is possible for the radio-telegraph circuit to fail for a period as long as an hour and for the distributors still to be operating in phase synchronism when the circuit is restored.

The multiplex signal-detecting circuits are contained in the matrices which again are in channel groups. The individual matrix tubes are primed both by the channel distributor signals and by the amplified multiplex signals received from the control-monitor unit. As the impulse distributor operates, the matrix tubes are gated in sequential order, causing the marking or spacing selections to be made. Each marking selection is denoted by the production of a positive impulse, which is used to fire a corresponding gas selector tube in the receiving converter.

The Receiving Code Converter

As in the transmitting group, the receiving code converters are identical, only one being shown. In each, the gas selector tubes store the code signals while the start-stop signal is being regenerated. The first marking selection in any particular code group conditions a start control circuit. When all the selections in the group have been completed, the multiplex distributor unit supplies a signal which causes the start-stop distributor in the converter to begin cycling. The latter distributor and its driving circuits are identical with the same circuits in the transmitting group code converter. The start-stop distributor causes the gating of a group of matrix tubes which are also controlled from the selector tube circuits. Within the matrix, first the "start" and then the various "code" elements of the start-stop signal are formed. This signal is amplified by a mixer tube and applied to an isolating output line relay of the mercury contact type. This particular relay (Western Electric type *275B*) is used because it has high resistance to contact erosion, which always is a problem when driving inductive printer magnet circuits. Incidentally, the relay contacts are the only moving parts contained in the operating equipment of the electronic multiplex.

The function of the sixth pulse control circuit was discussed previously when the

transmitting converter unit was being described. In the receiving converter unit, a continuous sequence of received marking or spacing sixth code elements may be detected in an integrating circuit, causing a relay either to be operated or to be released. The relay then may be connected to an external circuit for supervisory signaling or switching of printer circuits.

Cabinet Arrangements

Some of the many features of the mechanical designs of the electronic multiplex cabinets may be seen in Figure 8. Each unit, except the very heavy power unit, is mounted within a sliding-drawer-type cradle assembly. In the closed position the drawers are fastened in place by quarter-turn-type fasteners. When released, they slide outward to an extreme position, where they may be latched in place.

When in the withdrawn position the cradles may be tilted upward until their bottom sides are exposed for maintenance purposes. Another latch fastens the cradle in either the tilted or the untilted position. A bottom plate, to one side of which a circuit diagram is attached, is provided for each individual chassis. This plate has been removed from the chassis shown in the tilted position. These plates also are attached with quarter-turn fasteners so that they may be removed quickly in case of trouble.

Figure 8. Cabinet arrangement of multiplex group

Flexible interconnecting cables are provided for each individual unit, so that the unit may continue in operation even when pulled out and tilted. The mercury contact output relay used with each receiving converter unit must not be tilted from its normal vertical position and therefore has been mounted on the nontilting portion of the slide assembly.

Since several hundred watts are dissipated by the electronic components in the multiplex, forced ventilation has been provided through the use of blowers. Two intake blowers, with filters, and one exhaust blower are used, giving a pressurized effect and preventing the infiltration of dirt through other small cabinet openings.

The Circuit Continuity Detection System

This system was mentioned previously, and the circuit continuity control blocks may have been noticed in Figures 5 and 6. This circuit is used in monitoring the operation of the radio-telegraph loop that interconnects the two terminals. When once set up, at the terminal being described, for example, it causes the continuous transmission of a particular signal condition on the sixth element of the "A" channel. At the distant receiving multiplex terminal the signal is detected in the receiving distributor matrix circuit and applied to an integrating circuit in the control-monitor unit. The continuation of a signal condition, whether marking or spacing, causes a relay to operate or re-

Figure 9. Typical electronic multiplex radio telegraph system

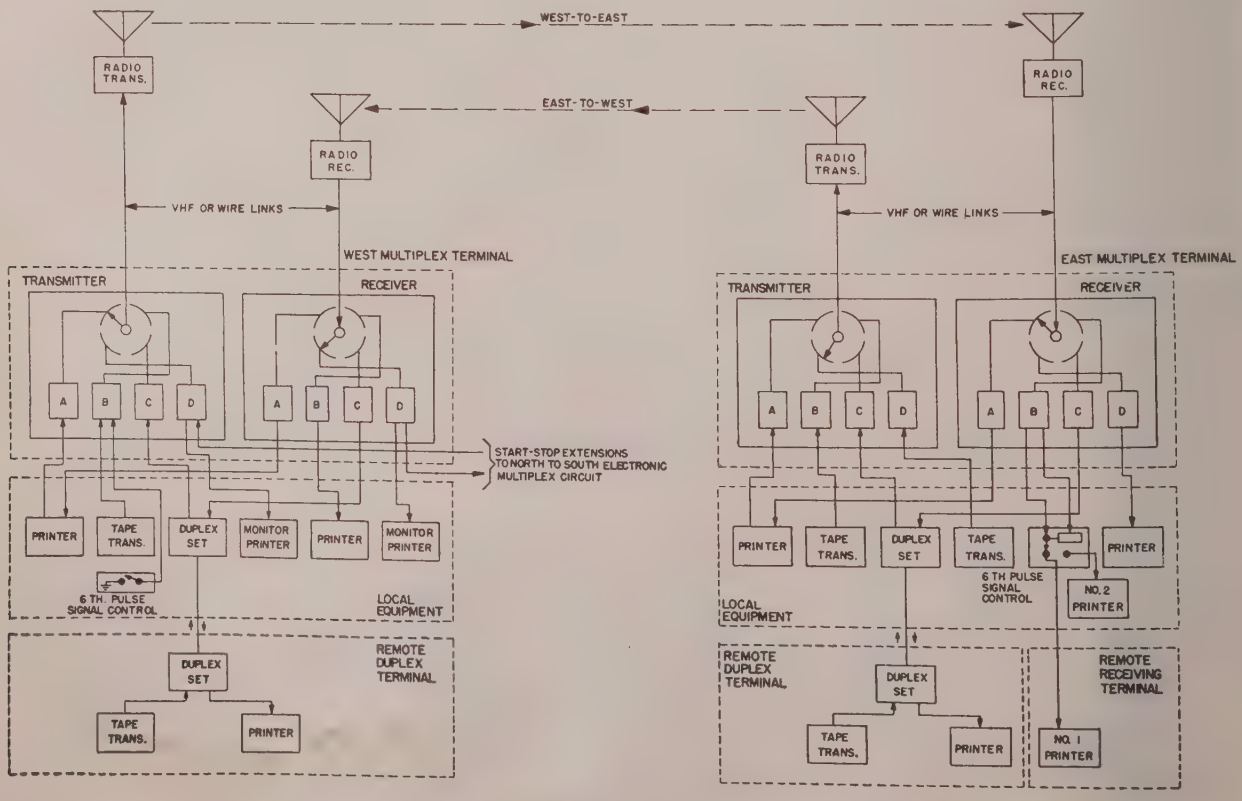

lease, sending a signal over a local connection to the adjacent telegraph transmitting group control-monitor unit. This causes the retransmission of the signal condition, again on the sixth element of the "A" channel. Back at the originating station the signal is detected and again retransmitted in a process that continues as long as both of the telegraph circuits are operating properly. The normal transmitted signal is a marking element. If a spacing element should be set up or either radio circuit should fail, the element will not be received. The circuit continuity detectors will note the change after a short time and will operate alarm signals at both stations, notifying maintenance and traffic personnel to take proper action.

Manual controls are used in establishing the original normal signaling condition of the alarm circuit. These switches also can be used to send slow-speed Morse or supervisory code signals when the radio circuits are intact. The alarm signal which is produced at each terminal consists of the on-off tone which energizes the loud-speaker.

System Applications

Figure 9 is a block diagram of a typical multiplex radio-telegraph system consisting of two send-receive multiplex terminal sets, associated radio transmitting and receiving equipments, and various methods of using start-stop telegraph circuit extensions.

On the "A" channel, the start-stop equipment at each terminal consists of a conventional send-receive printer, the keyboards being attached to the transmitting converters, while the printing units are connected to the receiving converters. This channel may be used for the transmission of general messages and miscellaneous routine traffic. It will not handle start-stop "blanks" since the facility for distinguishing between "blank" and "idle" is used for another purpose.

On the "B" channel, in the west to east direction a single-tape transmitter which sends traffic destined for two separate receiving circuits is used. The sixth pulse signal control circuit provides for the switching required at the receiving terminal. Again the sixth element has been diverted so that start-stop code blanks are not distinguishable from the idle channel condition. In the east to west direction a conventional tape-sensing transmitter-distributor sends traffic destined for a single receiving printer.

On the "C" channel, extensions to long duplex wire circuits are shown at both terminals, indicating how the multiplex equipment may be interconnected with existing start-stop systems. Long radio-Teletype extensions also may be used, as long as distortion due to transmission over such circuits remains within normal limits.

Interconnection to a channel of another electronic multiplex system designated the "north-south" circuit is indicated on the "D" channel at the west terminal. The placement of monitoring printers at this terminal on both the sending and the receiving sides also is indicated. At the east terminal, the conventional transmitting distributor and receiving printer terminate the circuits.

A number of sets have been carrying regular traffic in government service on high-frequency radio circuits for nearly a year on 24-hour schedules, with channels connected in various manners as described in the preceding paragraphs. Field reports indicate outstanding performance from an operating and maintenance standpoint. Operation on low-frequency radio circuits now is being considered.

In summarizing, it may be pointed out that the Teletype electronic multiplex described provides a compact, self-contained, packaged set, involving a minimum amount of equipment and practically no moving parts. It is exceedingly stable, flexible, and automatic in its operation and may be used with almost any type of communication circuit capable of handling the multiplex signaling frequencies. It may be set for operation at channel speeds of either 60 or 75 words per minute, providing up to four 2-way start-stop channels. The electronic multiplex fits readily into existing start-stop printing telegraph systems.

References

1. Printing Telegraph Systems and Mechanisms (book), **H. H. Harrison.** Longmans, Green and Company, London, England, 1923.

2. Time Division Multiplex in Radio Telegraphic Practice, **J. L. Callahan, R. E. Mathes, A. Kahn.** *Proceedings*, Institute of Radio Engineers (New York, N. Y.), volume 26, number 1, January 1938.

3. The Application of Western Union Multiplex to Navy Radio, **Ray Hoover.** *Western Union Technical Review* (New York, N. Y.), volume 2, number 1, January 1948.

4. Multi-Channel Radio-Telegraph System for High Frequency Circuits, **T. E. Jacobi.** *RCA Review* (Camden, N. J.), volume 9, number 4, December 1948.

5. Observations and Comparisons on Radio Telegraph Signaling by Frequency Shift and On-Off Keying, **Peterson.** *RCA Review* (Camden, N. J.), volume 7, number 1, March 1946.

6. Time Bases (book), **O. S. Puckle.** John Wiley and Sons, New York, N. Y., 1943, page 57.

7. The Inductance Capacitance Oscillator as a Frequency Divider, **E. Norman.** *Proceedings*, Institute of Radio Engineers (New York, N. Y.), volume 34, number 10, October 1946.

Discussion

Lloyd Espenschied (Bell Telephone Laboratories, New York, N. Y.): A historic touch and query may be pertinent.

The time-division multiplex originated in the 1850's in the fertile mind of a brilliant Yankee inventor whose name deserves to be known, Moses G. Farmer, born in Maine.

Frequency-division multiplex followed in the 1870's, having grown out of electro-acoustics, out of the electrically driven tuning-fork oscillators and resonators of Helmholtz, the same technological origin as the telephone.

Today we enjoy the greatly improved electronic versions of these two types of multiplex, and there arises all the more the question of which of the two types is preferable.

They are broadly equivalent, alternative methods. The difference between them is secondary and dependent upon the particular circumstauces of use, that is, the characteristics of the transmission system and signals conveyed.

Four- or Two-Channel Time-Division-Multiplex Telegraph System for Long-Distance Radio Circuits

W. C. PETERMAN
MEMBER AIEE

A. MINC
NONMEMBER AIEE

THE increased reliability of frequency shift transmission has made the use of time division multiplex systems feasible on long radio circuits. Time division multiplex provides a means, economical of the frequency spectrum, to handle traffic which is too great for one printer channel or that originates from or is destined to different places. A 4-channel multiplex system at a speed of 50 words per minute per channel, using the 5-unit Baudot code, has a unit pulse length of 0.010 second, which normally provides sufficient margin against signal shift due to radio multipath effects or other causes.

A combination electronic and electromechanical system was chosen for reliability and simplicity of maintenance. At the sending end, the electromechanical distributor provides a simple means of interleaving the signals for the various channels. It also provides a means for extending a channel on a start-stop-printer basis without the use of individual electromechanical translating devices, to a branch office so located that clutch pulses can be sent to it economically. Alternatively, a multiplex extensor may be used for more distant branch offices.

Any inaccuracies of signals from the sending distributor are eliminated by passing them through a simple electronic regenerator. Where the multiplex signals are passed over a keyed tone channel between the multiplex terminal and the radio transmitter, the sending-end regenerator makes possible the synchronization of the tone-channel carrier to the multiplex baud speed, which practically eliminates carrier distortion. The sending-end regenerator also makes it possible to send manual morse signals without disturbing the synchronism of the multiplex receiving regenerator, as all morse signals begin and end at the same time that multiplex signals would begin and end. The resultant distortion is too small to be noticeable to the ear.

At the receiving end, the signals are regenerated electronically with greater precision and reliability than by prior methods using electromechanical relays in conjunction with a rotary distributor. An automatic margin indicator provides one kind of indication if the margin falls below 40 per cent and another kind if below 20 per cent.

After regeneration, the signals are distributed very simply by an electromechanical distributor whose brushes do not require great contacting precision for this function. The use of an electromechanical distributor also provides a simple means of applying a modified Verdan scheme for error detection and permits monitoring of the channel signals just as they are leaving the distributor face plate.

The Verdan scheme of error detection is based on sending each character twice and comparing the received combinations. If they are the same, it is assumed that no error has occurred as the probability of an identical error occurring in two receptions of the same combination is very remote. If they differ, an error has occurred in one of the transmissions and an indication is made on the copy by printing a question mark. This scheme cuts the traffic capacity in half, which is equivalent to using a 10-unit code. However, as the error-indicating equipment can be cut in or out quickly, it need be used only when the automatic margin indicator shows that the margin of regeneration is low. Thus, if 40 per cent of the traffic is handled with error indication, the average length of the code would be seven units. If only 30 per cent is handled with error indication, the average length of code would be 6.5 units.

Apparatus

Sending End

The four channels are normally operated from standard sending operating tables equipped with multiplex perforators and multiplex transmitters. The distributing, translating, monitoring, regenerating, and general operating equipment is located on the sending distributor rack shown in Figure 1. The distributor has six pairs of rings and is driven by a phonic motor at a speed of 300 revolutions per minute from an electronically driven 200-cycle-per-second fork.

Receiving End

Reception is normally on four standard receiving operating tables equipped with start-stop printers and facilities for extending their respective channels through them to branch offices.

Regenerating and synchronizing equipment is mounted on the regenerator rack of Figure 2. It includes a 200-cycle-per-second fork, similar to the one in the sending distributor rack.

Distributing and monitoring equipment is located on the receiving distributor rack, which may be seen in Figure 3. The distributor is the same as the one used on the sending distributor rack and is driven from the fork on the regenerator rack.

Error-indicating equipment and chan-

Paper 51-61, recommended by the AIEE Committee on Telegraph Systems, and approved by the AIEE Technical Program Committee for presentation at the AIEE Winter General Meeting, New York, N. Y., January 22–26, 1951. Manuscript submitted October 24, 1950; made available for printing January 9, 1951.

W. C. Peterman (now retired) was with the All America Cables and Radio, Inc., New York, N. Y., and A. Minc is with the Mackay Radio and Telegraph Company, New York, N. Y.

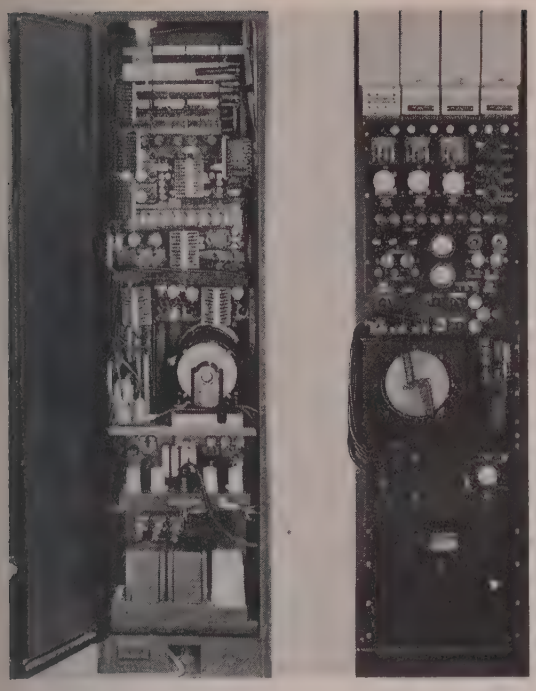

Figure 1 (left). Front and rear views of the sending distributor rack

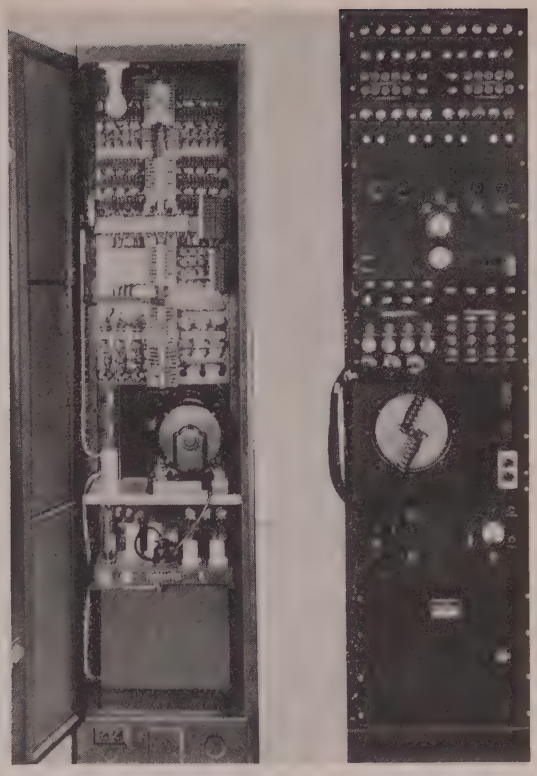

Figure 3 (right). Receiving distributor rack

nel-extension apparatus are mounted on the error-indicator rack displayed in Figure 4.

Sending-End Circuit

General

The sending-end circuits are shown in Figure 5. The various channel segments on the sending ring show that channels *A* and *C* are interleaved as are channels *B* and *D*, which follow. This was done for ease in changing from 4-channel operation to 2-channel operation, which can be accomplished by throwing switches. The marking polarity is positive on two of the channels, *A* and *D* in this case, and is negative on the other two channels (*B* and *C*), in accordance with the usual practice, to provide signal reversals for synchronizing even when all four channels are idle.

Channel *A* is always operated from a multiplex transmitter in the main office but channels *B*, *C*, and *D* can be extended

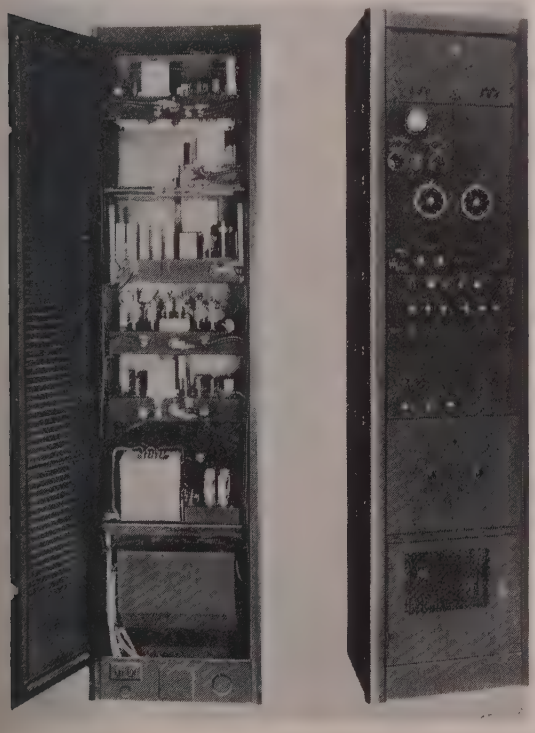

Figure 2 (left). Electronic regenerator rack

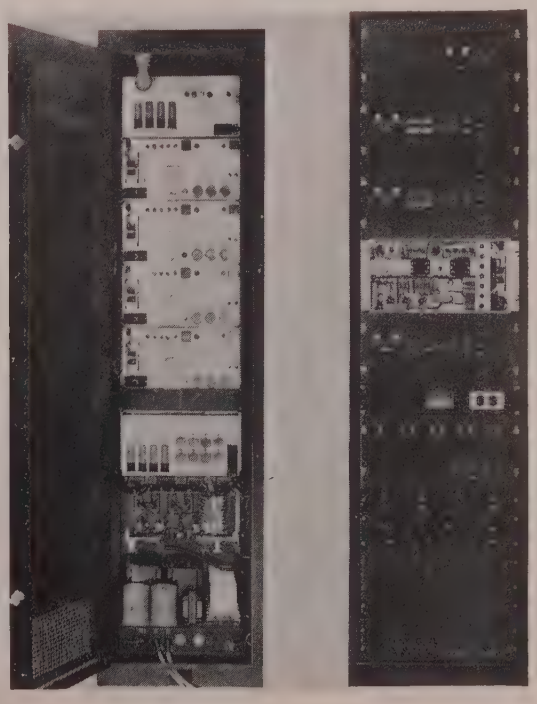

Figure 4 (right). Error - indicator rack. In the front view, the panel has been removed from one error-indicator chassis

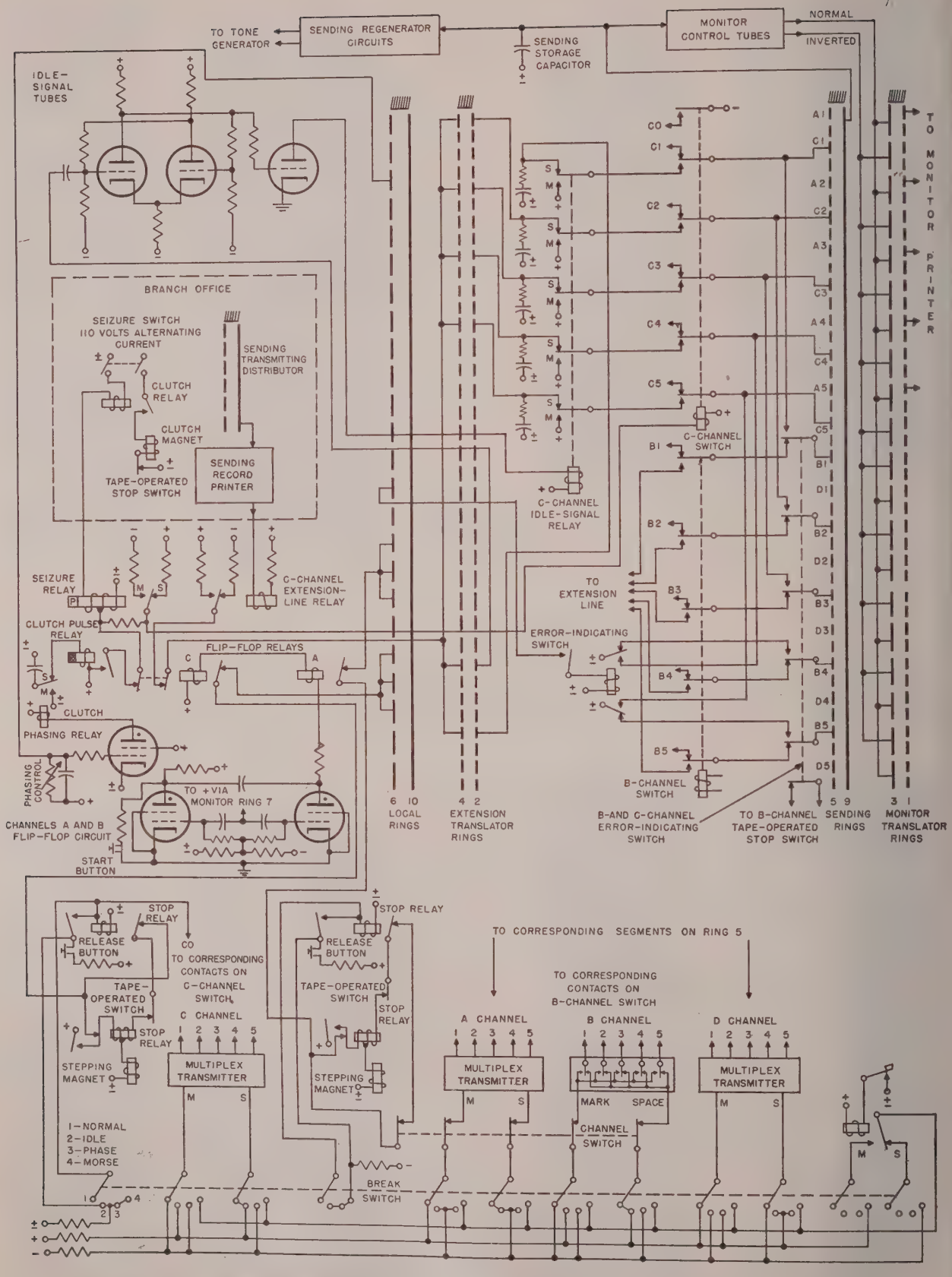

Figure 5. Sending-end circuits showing distributors, channel-switching system, and branch-office connections

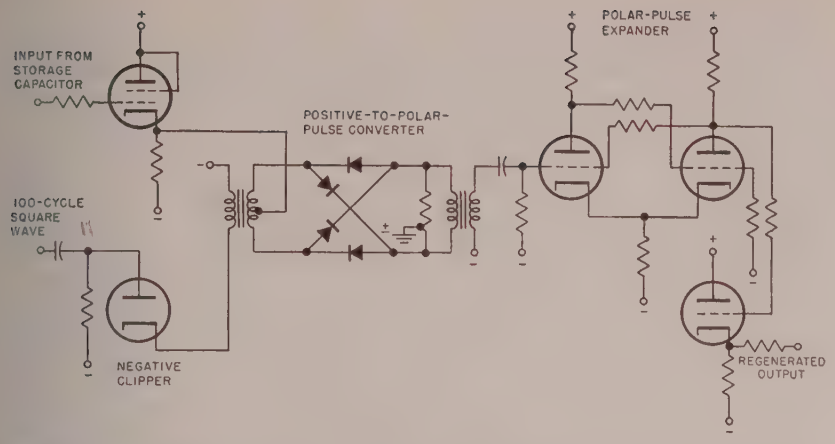

Figure 6. Sending-end regenerator circuits

to branch offices on a start-stop-printer basis.

Extension Circuits

Circuits are shown for extending only the *C* channel by closing the seizure switch in the branch office. The closing of this switch causes the clutch pulse to operate the seizure relay and the *C*-channel switch relay. The latter switches the *C*-channel sending segments from the multiplex transmitter to the extension storage capacitors through the *C*-channel idle-signal switch. Each clutch pulse releases the start-stop transmitter distributor clutch so that the signal combination for one character will be sent to the main office and the extension-line relay operated. From the tongue of this relay, polar signals are sent through the extension translator rings into the channel-extension storage capacitors from which they are sent through the proper segments of the sending ring. The clutch pulse, originating from a segment of the local ring, is phased by means of the phasing control rheostat so that the brush on the extension translator rings will be passing over each pulse segment when the signal for that pulse is arriving from the tongue of the extension-line relay. The segments on these rings are spaced so that the brush will pass from the beginning of one segment to the beginning of the next segment in 0.022 second, which is the duration of each selection pulse of the start-stop combination when operated at a 61-word-per-minute speed.

When the auto-stop contacts of the branch-office transmitter open due to a taut tape, the transmitter distributor clutch is not released by the clutch pulses and a solid marking current is sent to line which would cause the extension storage capacitors to be charged with marking potential and the "letter shift" combination would be set up. This would be a false combination and would result in errors if upper-case characters were being sent when the tape became taut. To prevent this, the idle-signal relay tongues transfer the sending segments from the storage capacitors to spacing potential, so that the "idle" signal is sent over the multiplex channel when a false "letter-shift" combination is received. The false "letter-shift" combination has no start pulse and this distinguishes it from the true one. This condition is detected by means of idle-signal tubes, which are controlled from a segment on the translator ring over which the brush passes when the start pulse is received. These tubes control the idle-signal relay.

Error-Indicator Circuits

For error indication, each character combination is sent twice. On a 4-channel basis, the same combination is sent on two successive revolutions of the distributor brushes and the traffic capacity is 25 words per minute per channel. When sending is from a multiplex transmitter, it is only necessary to open the transmitter step-pulse circuit on alternate revolutions of the brushes. This is done by flip-flop relays, operated at the proper time from a segment on one of the distributor rings. When sending is from a branch office, the clutch pulse is interrupted on alternate revolutions of the brushes and the extension relay is cut off from the translator rings on the same revolution by means of a flip-flop relay so that the same signal combination remains on the storage capacitors as on the previous revolution.

By using two channels for original transmission and the other two channels to repeat the combinations for comparison, a traffic-carrying capacity of 50 words per minute on each of two channels can be obtained. If two channels are used this way, the other two can be used with error indication at 25 words per minute per channel or either or both may be used at 50 words per minute per channel without error indication.

Error indication, on a 2-channel basis, is put into effect at the sending end by throwing a switch. The circuits for operation on *C* channel with repetition on *B* channel, by throwing *C*- and *B*-channel error-indicator switch, are shown in Figure 5. The first three pulses are repeated by a direct connection of the sending segments but the other two are repeated from overlap storage capacitors, as the tape on the *C*-channel transmitter is being stepped while they are being sent.

Monitor Circuits

Two multiplex 5-magnet tape printers are available for connection to any channel for monitoring the signals as they leave the sending ring. Since the signals from all channels are already aggregated on this ring, they must be separated again by channels on the monitor translator rings. The printer selections are controlled by monitor-control tubes, which reinvert the signals of the two inverted channels.

Sending Regenerator Circuits

Signals from the solid sending ring are regenerated before they are used to modulate the tone generator of the keyed tone channel between the telegraph office

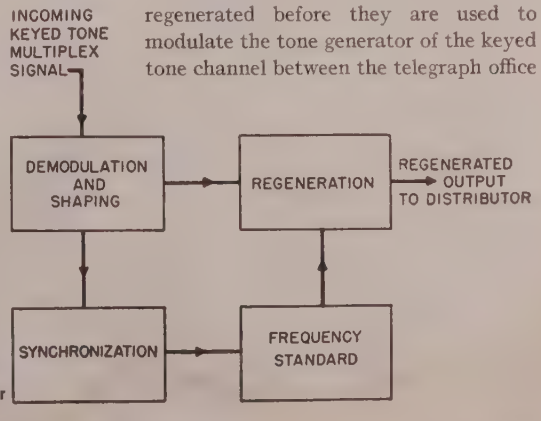

Figure 7. Receiving regenerator

and the radio station. As may be seen in Figure 6, they are passed by means of an isolation cathode-follower tube into the secondary of the input transformer of the positive-to-polar-pulse converter. Differentiated square waves, at baud speed, from a fork-driven counter are passed through a negative-pulse clipper and the positive pulses pass to the primary of the input transformer. These pulses constitute accurate time markers, adjusted to occur at the approximate center of the signals from the sending ring. They sample the signal for polarity and initiate with great accuracy of timing, a pulse of the polarity of the sampled signal. These polar pulses, brought out through the output transformer, are expanded into the regenerated polar signals in the polar-pulse expander. Due to the unbalanced ground connection across the primary of the output transformer, a small portion of the distributor signal as well as the polar pulses appear at the output of the converter, which facilitates monitoring.

Receiving-End Circuits

General

Three main functions are to be performed by the receiving multiplex terminal equipment.

Regeneration of the Received Signal

The received radio signals are subject to distortions by various types of transmission irregularities. Before the signal can be distributed to the respective automatic printing devices, it is necessary to remove such distortions by a regeneration process.

The regenerator unit retimes the signals and supplies to the rotating distributor a fully regenerated signal; a signal that maintains a fixed phase relationship to the respective distributor face-plate segments and that has rigorously equal mark and space elements.

Distribution of the Regenerated Signal

A rotary synchronous distributor distributes the regenerated signals to the proper channels and translates the 5-unit Baudot code into start-stop printer signals. The combination of gas and vacuum tubes provides the signal power for the receiving traffic and monitor printers, while both relay and vacuum tube outputs are available for channel-extension circuits.

Detection of Errors

When error detection is desired, the sending end is made to repeat the same character on two transmissions. The error indicator will compare the two transmissions and when a discrepancy is detected will switch the corresponding receiving printer from the multiplex signal to an internal signal source. A sequence of start-stop signals will then be supplied to the printer to print a question mark (?) right after the erroneous character; thereupon the printer is returned at the proper instant to the signal circuit.

Receiving Regenerator

General

The receiving regenerator logically subdivides into four functional sections, the interrelation of which is illustrated in Figure 7.

The radio receiving station normally relays the received signal in the form of a keyed tone over regional facilities (land line or very-high-frequency link) to the operating office where the regenerator and associated terminal equipment are located. This keyed tone, after demodulation and shaping into a d-c square-wave form passes to both the synchronization and regeneration chassis.

The frequency-standard unit generates two separate sets of timing pulses, each at signal-element speed, which are supplied to the synchronization and regeneration units, respectively.

Comparison of the phase of one set of timing pulses with the timing of the radio signal leading edges (cross-over from space to mark) is made in the synchronization unit. Departures from the correct phase will result in synchronizing impulses being applied to the vacuum-tube fork oscillator in the frequency-standard unit.

In the regenerator unit, the local timing pulses sample the polarity of every signal element of the received signal to produce an output pulse, which expanded to full signal-element duration is the regenerated signal.

In addition, an automatic margin indicator has been incorporated in the receiving-regenerator rack. This unit automatically indicates the degree of reliability of the regeneration process by lighting alarm pilot lamps should the signal be severely mutilated by transmission disturbances and it permits a range to be taken at any time without interfering with traffic.

Regeneration and Synchronization

The receiving-end regenerator rack has a precision vacuum-tube oscillator similar to the one used at the sending end. For proper synchronization, this receiving fork is adjusted to run faster than the sending-end fork by slightly more than the anticipated maximum speed difference between the two forks. With such an adjustment, the receiving end will always tend to run ahead of the sending end. A speed difference of about one part per hundred thousand was found adequate for an initial adjustment.

From the receiving-end fork, positive gating pulses are derived at signal-element speed which, of course, also tend to drift ahead of the received signal edges. By means of a manual phase-shifting device (synchronization phase shifter), these gating pulses are initially adjusted to lag slightly behind the signal edges. The gating pulses then will tend to drift into the edges of the radio signal. When the radio-signal leading edges (cross-over from space to mark) and the gating pulses coincide, a synchronization pulse of a fixed magnitude and duration is applied to the fork. For the duration of the synchronizing pulse, the fork is slowed down by approximately 30 parts per hundred thousand. The synchronization marker pulses are thereby effectively moved back to some position lagging the signal edges. Once the synchronization pulse is over, the receiving fork will tend to resume its original rate, drift again into the signal edges, and the cycle will repeat itself.

It is to be understood that the fork is to synchronize to a radio signal subject to random transmission disturbances. The time the signals require to travel from a transmitter to a distant receiver is likely to vary from instant to instant due to multipath and other effects. The receiving fork will keep in step with the signal by assuming a phase relation to the signal edges, such that only some leading signal edges will arrive late enough and produce synchronization impulses. The majority of signal edges will have no effect on the frequency of the receiving fork.

It is desirable to keep the speed difference between the sending and receiving forks small. Each rate correction can then also be made small, and the fork will not follow each random phase variation of the signal. The receiving-end fork then runs essentially at constant speed except for minute rate corrections that cancel the speed difference between sending and receiving forks. Each correction reduces the speed of the receiving-end fork by approximately 30 parts per hundred thousand and lasts 0.1 second. This is equivalent to a phase shift of approximately 30 microseconds. Considering that a 4-channel multiplex system

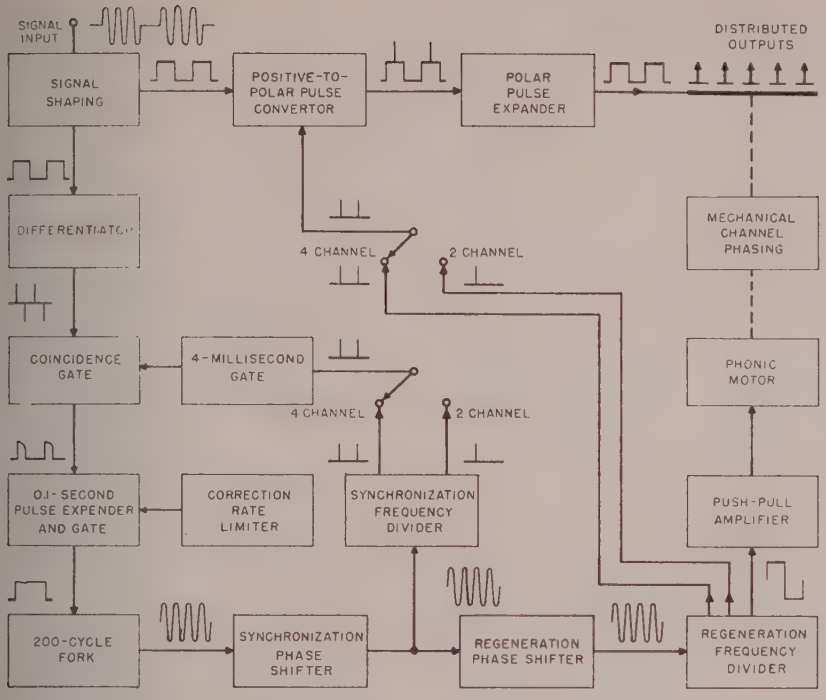

Figure 8. Details of receiving regenerator

operating at 50 words per minute per channel has a signal-element length of 10,000 microseconds, each individual correction represents indeed a minute phase shift.

The small effect of each individual correction also affords protection against over-synchronization. A signal may split due to severe multipath effect or noise. Such splits would simulate additional leading signal edges and might result in erroneous rate corrections. The effect of each correction being small, the receiving fork will not readily assume an incorrect phase with respect to the signal. In turn, should a few signals arrive exceptionally late, the phase of the receiving end will not be affected materially. As an additional protection against overcorrection, the maximum repetition rate of the synchronizing pulses has been limited to 120 per minute.

The receiving regenerator unit operates on the same signal-sampling principle as the sending-end regenerator. Sampling pulses are derived at signal-element speed from the receiving-end fork and are manually phased to coincide with the approximate center of the received signal elements.

The threshold of a regenerator is defined as the minimum signal margin that the regenerator will accept and still regenerate faultlessly. Even if a perfect signal is supplied to the regenerator, it is to be understood that the margin will be less than 100 per cent. Two main factors account for this: the width of the selection pulse and the synchronization-rate corrections.

Assuming that a perfect signal is received (4-channel operation), the range will be measured as 10 milliseconds minus the width of the sampling pulse. A further reduction of the margin reading results from the small retardations and accelerations to which the fork is subjected for synchronization.

At the sending end, where signals of only 3 to 4 per cent distortion have to be regenerated, a high regenerator threshold is quite adequate and allows for circuit simplicity. At the receiving end, where signal mutilation can be severe, the regenerator has to be designed for a very low threshold. This is done by using an effective sampling pulse width of approximately 50 microseconds (0.5 per cent of the signal element with 4-channel operation). Since the effect of the individual synchronization impulse is also small, the threshold of this regenerator is of the order of 1.5 per cent for 4-channel operation.

Theory of Operation

Figure 8 shows a block diagram of the receiving regenerator. At the lower left, a vacuum-tube-driven fork supplies a 200-cycle wave to the synchronization phase shifter. This is a magnetic-type phase-shifting device that allows continuous control of phase shifting by means of a knob on the front panel. The phase-shifter output is frequency divided in the synchronization frequency-division stages first to 100 and then to 50 cycles. Either 50- or 100-cycle outputs are available as pulses of about 50 microseconds width. These pulses initiate the synchronization timing pulses, which must occur at signal-element speed. Thus for 4-channel 50-word-per-minute operation, the 100-cycle output of the frequency-division stages will be chosen. For 2-channel 50-word-per-minute operation, the 50-cycle pulse output is used. A front-panel switch allows the selection of either output. Each pulse of the synchronization frequency divider will initiate a square-top positive pulse of 4 milliseconds duration through the gate.

The output of the input signal-shaping unit is a square-wave-type polar signal. This signal is differentiated by a short-time-constant resistance-capacitance network, the output of which will be a positive pulse for a leading signal edge and a negative pulse for a lagging signal edge. These signal edges and the 4-millisecond pulses are supplied to a coincidence gate. This stage is biased to cutoff so that neither the positive 4-millisecond pulses nor the positive signal edges alone will be sufficient to make the tube conduct. When the 4-millisecond pulses and the positive signal edges occur simultaneously, an output pulse will result from the coincidence gate. Obviously, the coincidence of a negative signal edge and a 4-millisecond pulse will not produce any output. Thus, a coincidence of the leading signal edges only with the 4-millisecond synchronization timing pulses is hereby achieved.

The coincidence of a positive signal and a 4-millisecond pulse will apply a synchronization pulse to the 200-cycle fork. The output of the coincidence gate is a pulse of too short a duration effectively to slow down the fork. This pulse is therefore first expanded to 0.1 second width. This is accomplished by applying the output of the coincidence gate to a pulse generator. On reception of a coincidence pulse, the 0.1-second gate will generate a square-top positive pulse of 0.1 second width. The energy of these 0.1-second pulses will slow down the fork electromagnetically. To insure against overcorrection, the maximum repetition rate of these 0.1-second rate corrections is limited to 120 per minute. A correction limiter renders the 0.1-second gate insensitive for an additional 0.4 second beyond the 0.1-second operation time of the gate. A front-panel neon lamp will flash every time correction pulses are applied to the fork.

The synchronization phase shifter feeds also a phase-shifting unit termed a re-

generation phase shifter. The regeneration frequency-divider following this phase shifter performs two functions: A) It supplies push-pull 50-cycle square-wave outputs, which after power amplification provide the driving energy for the phonic-wheel motor, and B) it provides scanning pulses at signal-element speed for regeneration.

Again, depending on whether 2- or 4-channel operation is desired, a switch allows the selection of either 100- or 50-cycle pulses from the regeneration frequency divider. These are positive pulses of 50-microsecond width and feed a converter stage simultaneously with the square-wave output from the signal-shaping unit.

Should a positive scanning pulse coincide with a positive signal element, the converter output will be a positive pulse. Coincidence of a positive scanning pulse with a negative signal element will result in a negative pulse output. The output of the converter will therefore consist of negative and positive pulses, the sequence of which will depend on the combination of positive and negative elements of the incoming signal. Since the polarity of these output pulses is determined by the signal polarity existing at the time at which scanning pulses are supplied to the converter, it is evident that the radio signal is hereby effectively sampled, signal element by signal element, by the scanning pulses.

The polar pulse output of the converter is expanded to full signal-element length by means of a flip-flop circuit. The output of the flip-flop is of square-wave type. The crossover from one polarity to the other of the flip-flop can only occur at 10-millisecond intervals, as timed by the scanning pulses. This flip-flop output will therefore have a unity mark-to-space ratio. It will also maintain a constant phase with respect to the regeneration frequency divider. This flip-flop output is now fed to the distributor face plate for distribution. Since the distributor is synchronously driven by the regeneration frequency divider, the flip-flop output will also maintain a constant phase relationship to the distributor face-plate segments. Therefore, a fully regenerated signal is supplied to the distributor.

In order to have signal reversals on the air even when all channels are idle, channels *A* and *D* have been made positive or direct channels. Channels *B* and *C* are negative or inverted channels. Thus, at the receiving end, another inversion of channels *B* and *C* must be performed before distribution to the printers. To accomplish this, the flip-flop stage has two (symmetrical) outputs; one direct and one inverted output.

Figure 9. Regeneration frequency divider

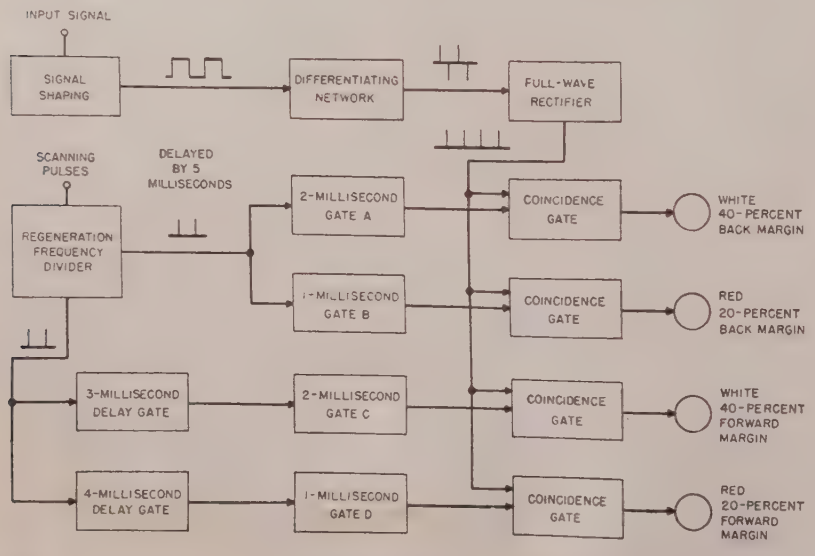

Figure 10. Timing of scanning and gating pulses in relation to the input signal from the radio receiver

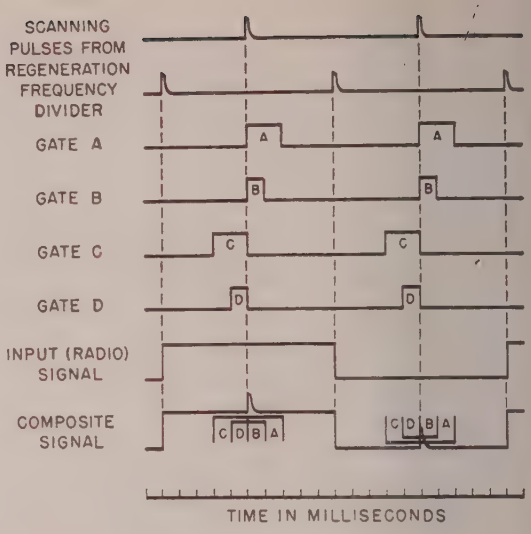

Automatic Margin Indicator

The automatic margin indicator provides an indication of the signal quality. The received radio signal is sampled by this unit into three classes.

1. Signals having more than 40 per cent margin. Such signals are to be considered as good signals, and no indication will be given by the automatic margin indicator.

2. Signals having less than 40 per cent margin but more than 20 per cent margin. For each such signal, a white neon lamp will flash on the front panel.

3. Signals having less than 20 per cent margin. Such signals are very poor, and the probability that error will occur is great. Should any one signal be received with less than 20 per cent margin, a red neon lamp on the front panel will light and remain on until it is manually extinguished.

The automatic margin indicator distinguishes between forward and backward signal margin. Four neon-lamp indicators are therefore provided on the front panel of the unit: two white lamps for 40 per cent backward and forward margin indications, respectively, and two red lamps for 20 per cent backward and forward margin indications, respectively.

The regeneration frequency divider, as shown in Figure 9, supplies to the automatic margin indicator: positive pulses at signal-element speed, which are identical with those used for regeneration and are termed "scanning pulses," and positive pulses at signal-element speed similar to the scanning pulses but delayed by 5 milliseconds with respect to them.

The "scanning pulses" initiate two gates at signal-element speed. A gate *A*, which generates positive square-top pulses of 2 milliseconds width, and a gate *H*,

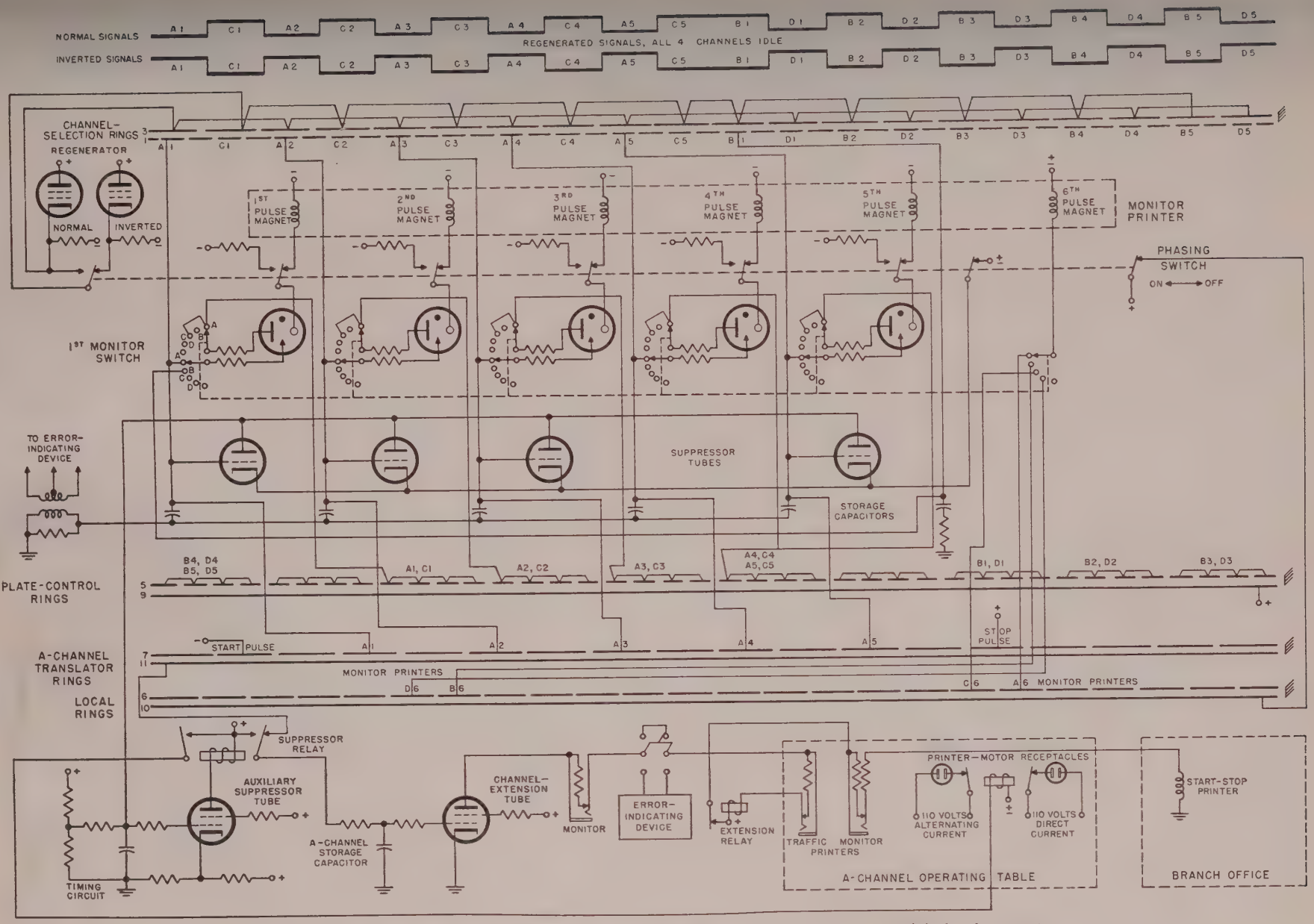

Figure 11. Receiving distribution, translation into start-stop signals, and error detection are accomplished in these circuits

which generates 1-millisecond square-top pulses. The scanning pulses that are delayed by 5 milliseconds initiate: a 2-millisecond gate *C* after an additional delay of 3 milliseconds, and a 1-millisecond gate *D* after a delay of 4 milliseconds. From Figure 11, it is seen that these four gates effectively surround the sampling pulse. Gates *A* and *B* are initiated at sampling time. Gates *C* and *D* are so timed that their lagging edges coincide with the sampling pulse.

The square-wave output of the radio signal-shaping unit is differentiated into positive and negative pulses. A full-wave rectifier converts all these polar pulses into positive pulses. Gates *A*, *B*, *C*, and *D* are fed into four coincidence stages, respectively. Each of these coincidence stages receives also the positive pulses derived from each radio signal edge. Coincidence of a signal edge with any of the four gates will result in an output from the corresponding coincidence stage. Thus, a coincidence output from gate *C* indicates that the forward margin is less than 40 per cent and a white neon lamp will flash for each coincidence pulse. In turn, coincidence of gate *D* and a signal edge indicates that the forward margin is less than 20 per cent and the red neon lamp will light and will remain lit until manually extinguished. Similarly, coincidence outputs corresponding to the gating time of *A* and *B* will indicate back margins of less than 40 per cent and 20 per cent, respectively. These lamp indicators therefore show the operator whether any adjustments of the circuit are required and indicate the reliability of the received signal.

The 40 per cent indicator lamps also allow the margin to be taken without interruption of traffic. Manual rotation of the regeneration phase shifter will change the scanning pulse phase with respect to the radio signal. Since the gates of the automatic margin indicator are initiated by the scanning pulses, they will move by the same amount as the scanning pulse. To take a margin with the automatic margin indicator, the regeneration phase shifter is manually advanced in phase until the forward 40 per cent light just starts to flash. The phase shifter is then backed up slightly to a position where no flashes occur for, say one minute. The regeneration phase shifter is then manually retarded in phase with respect to the signal and a similar reading is taken by observing the back 40 per cent light. The difference between the two dial readings of the regeneration phase shifter plus 40 per cent is equal to the signal margin. Since during this operation the scanning pulse stays clear of the signal edges, no interference with traffic will result.

The automatic margin indicator unit is provided with front-panel test jacks for cathode-ray-oscilloscope observation. For quick monitoring, a composite wave pattern, similar to that shown in Figure 10, is provided, showing on the oscilloscope the time position of: the radio signal edges, the scanning pulse, and the four gates of the automatic margin indicator. In addition, the 4-millisecond gate used for synchronization can be added to the cathode-ray pattern.

Receiving Distributor Circuits

General

The regenerated signals are supplied to the receiving distributor for channel distribution, for translation into start-stop signals, and for error detection as shown in Figure 11.

A- and *D*-channel signals are received from the normal regenerator output and those for *B* and *C* channels from the inverted output. These latter were sent inverted and must be "reinverted".

The brushes of the distributor are driven by a phonic motor that receives its power from the regenerator tuning fork and these brushes are adjusted so that they will be passing over one of the "live" segments of channel-selection ring 1 during approximately the center of the time interval for the reception of each signal pulse.

Channel phasing is accomplished by stepping the brushes backward on their drive shaft one line-segment interval at a time until the channels are properly phased. This is indicated by placing the phasing switch in the "ON" position and noting when a monitor printer on *D* channel receives the phasing-signal combination of all five marking pulses.

Translation Circuits

The signals are distributed through ring 1 to five storage capacitors for the signals of each channel. The monitor printers and the circuits that translate from multiplex to start-stop signals get their selection pulses from these storage capacitors. The start and selection pulses are of approximately 0.022-second duration.

For translation, the signals from the storage capacitors pass through a translator ring, the live segments of which are spaced so that the brush passes over successive segments at 0.022-second intervals, generating signal elements of this duration. Start and stop pulses are added through other segments at the proper intervals. Translation circuits are shown in Figure 11 for the *A* channel only; the signals of all channels are similarly translated.

The start and stop pulses being inserted independently of the signals, they would be present even when the circuit is idle. To prevent this, a suppressing means is made effective when the idle combination continues for more than 15 or 20 seconds.

In normal operation, the marking pulses of the multiplex signals, as they appear across the storage capacitors, are applied to the grids of suppressor tubes. A timing capacitor is charged through a high resistance and discharged through the relatively low resistance of the plate circuits of the suppressor tubes. When these marker pulses are not received, the timing capacitor charges and, through an auxiliary suppressor tube, operates the suppressor relay to put a solid marking signal in the start-stop circuit. This action is reversed on reception of the first marking pulse when the circuit resumes operation.

Monitor-Printer Circuits

The monitor printers can be switched to any channel. Their selection pulses are obtained from the storage capacitors through thyratron tubes whose plate circuits are controlled from the plate-control rings.

Error-Indicator Circuits

The equipment for error indication is mounted on a separate rack. When reception is on a 4-channel basis, the signal combination for each character is received twice, on successive revolutions of the distributor brushes, and one is compared with the other. If there is any difference, normal reception is interrupted and a question mark is printed after the questionable character. Normal reception is then resumed. The circuits for this operation are shown in Figure 12 for *C* channel only.

During the first reception of a character, the five signal-storage capacitors *SC1-SC5* are charged through *R1* in parallel with the primary winding of the input transformer. Pulses from the secondary winding are rectified and pass through the selector tube to the flip-flop circuit.

The path through the selector tube and *R2* is effectively a short-circuit as there is no plate current flowing through *R2*.

The flip-flop circuit is controlled by

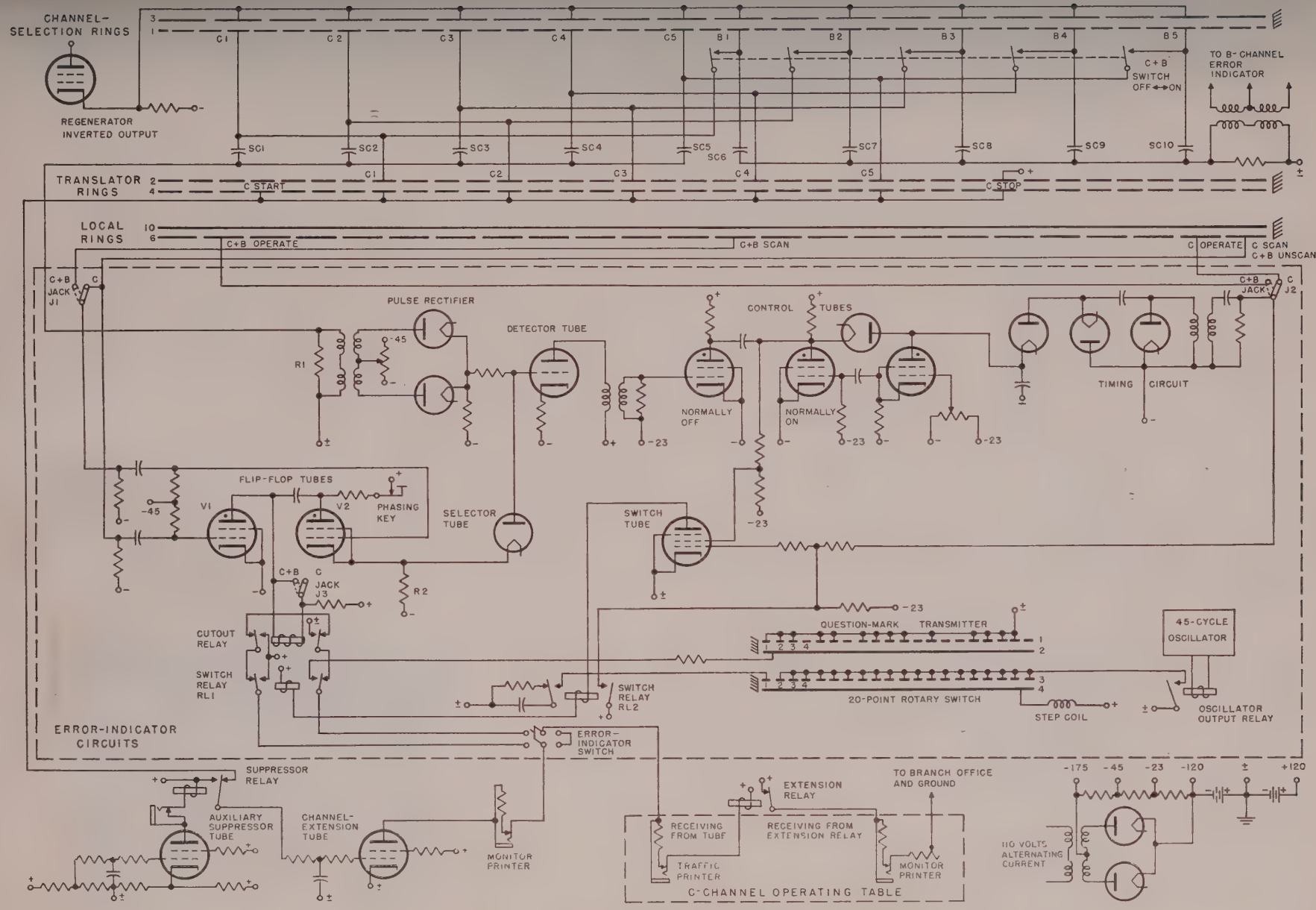

Figure 12. Error-indicator circuits

pulses from ring 6 of the distributor and is switched after each character is received. On this first character, *V1* of the flip-flop circuit is active and has energized the cutout relay, which disconnects the traffic printer from the channel extension tube, thus making it inoperative.

After the five channel pulses have been received, the flip-flop circuit is pulsed through ring 6 and *V2* becomes active. The voltage drop across *R2* from the plate current flowing through *V2* acts as a cutoff bias on the selector tube and any pulses through *R1* will be transmitted to the grid of the detector tube.

When the detector tube is pulsed, the traffic printer is switched from the normal receiving circuit to the question-mark transmitter through operation of switch relay *RL1*. The timing circuit is put into operation through *RL2* so that the traffic printer will be reconnected to the normal circuits after the question-mark transmitter has sent the start-stop combinations for "figure shift," "question mark," and "letter shift."

The question-mark transmitter is a 20-point rotary switch driven from a 45-cycle-per-second oscillator.

The switch relays *RL1* and *RL2* are in the plate circuit of the switch tube, which is operated from two control tubes. One of these is coupled to the detector tube and initiates the operation while the other determines the length of operation by means of a pulse from ring 6 through a timing circuit, thus preventing the traffic printer from being switched during the printing of a character.

Figure 12 also shows the circuits used when the original transmission is on *C* channel and *B* channel is used for comparison. The *C*+*B* switch is thrown to the "ON" position and *J1*, *J2*, and *J3* are plugged into the *C*+*B* jacks. The flip-flop tubes are now controlled from two segments on ring 6. Each character combination is set up on the combined *C*- and *B*-channel storage capacitors during reception over *C* channel.

Printing and scanning for errors are done when the character is being repeated on *B* channel. The timing of the switch from normal to the question-mark transmitter is changed to accord with the new comparison period.

No Discussion

A Nationwide Frequency-Modulation Telegraph Network

F. B. BRAMHALL
FELLOW AIEE

L. A. SMITH
MEMBER AIEE

Synopsis: With one exception, the carrier telegraph systems of the major record communication companies of the world are operated by the old familiar amplitude-modulated (AM) method. That exception is the huge trunk line and tributary network of the Western Union Telegraph Company which, while realizing excellent spectrum economy, employs frequency modulation. It is the object of this paper to report on the success achieved in operating that network. Years of experience with thousands of frequency-modulated (FM) telegraph channels have demonstrated they may be operated in long tandem chains with excellent continuity of service.

The Origin of FM Telegraphy

THE theoretical and technical aspects of recent advances in the carrier current telegraph art are well covered by the technical literature of record communication. Present-day AM carrier telegraphy is perhaps most comprehensively covered in an article written by A. L. Matte[1] which describes a 170-cycle-spaced channel system intended for single-printer working. A higher speed system with channels separated by 300 cycles, described by F. B. Bramhall[2] in 1940, was designed to provide transmission circuits for 4-printer multiplex working with a modulation speed of 132 bands. FM systems for these two classes of service are covered respectively in two other papers by Western Union authors.[3,4] An extensive network of narrow-band AM telegraph channels, after the design covered by Mr. Matte, provides trunk circuits for the private-wire lease services and the teletype timed-wire service (*TWX*) operated by the American Telephone and Telegraph Company. Now with d-c physical circuit telegraphy largely displaced for trunk-line services in Western Union's plant, there has come into being a nationwide network of narrow-band FM telegraph channels. During the past several years, considerable work has been done in an effort to establish the relative merits of the AM and FM methods for various conditions of operation. The results of this work also have been recorded by various authors, notably T. A. Jones and K. W. Pfleger,[5] by J. R. Davey and A. L. Matte,[6] and briefly in some of the articles already mentioned. For the most part, the comparisons recorded have been the result of laboratory work or short-term service trials. Now the operating results achieved on a narrow-band FM network can be reported as based on years of experience with nearly 2,000,000 miles of such circuits.

First Large-Scale Application

In 1946, Western Union undertook a modernization and mechanization program which resulted in a tremendous expansion of its existing carrier network. This involved a conversion of multiplex circuits previously employed for trunk-line service to single-printer operation and a replacement of the d-c physical circuits with carrier channels. The program covered practically all long-haul facilities and a large part of the shorter feeder circuits. A full appreciation of the conditions under which these circuits operate and the high performance standards demanded will be enhanced by an understanding of the routing and automatic switching methods by which separate telegraph circuits are interconnected in the modern telegraph plant. Manual relaying, the process of reproducing the telegraph message on paper and retransmitting it by a telegraph operator, has practically disappeared. A few relatively large reperforator switching offices have been established in heavily loaded traffic centers. Each such office serves a selected territory or area, all messages to and from that area being routed through the switching center and automatically or semiautomatically retransmitted to the offices of destination. A description of the reperforator switching system, which obviates manual handling and now serves the entire nation, is recorded in a paper by R. F. Blanchard and W. B. Blanton.[7] Fifteen switching centers are interconnected by a multiplicity of FM carrier telegraph channels as they also are connected to a great many smaller centers within each area. Only the very short circuit connections and those serving smaller towns remain on physical d-c telegraph wires.

Equipment

Present-day voice-frequency bands, either those derived from Western Union

Figure 1. Channel terminal equipment in large office

Paper 51-62, recommended by the AIEE Telegraph Systems Committee and approved by the AIEE Technical Program Committee for presentation at the AIEE Winter General Meeting, New York, N. Y., January 22–26, 1951. Manuscript submitted October 26, 1950; made available for printing December 1950.

F. B. BRAMHALL and L. A. SMITH both are with the Western Union Telegraph Company, New York, N. Y.

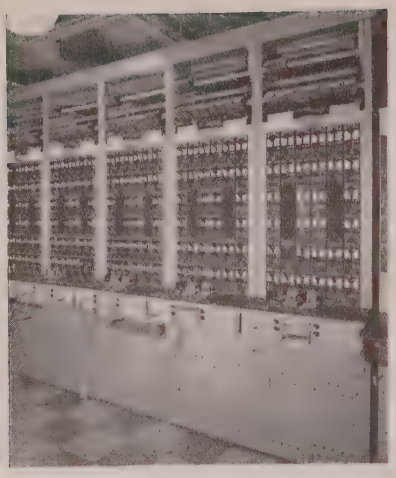

Figure 2. Centralized control and monitoring equipment for 160 channels

Table 1 Lost-Time Analysis, Second New York-Oakland 2-Channel Multiplex 24-Hour-a-Day Operation

Trouble	May 1946 All-Grounded Circuit 13 Repeater Sections: Number of Delays	Delay in Minutes	Trouble	August 1950 All-Carrier Circuit 2 Carrier Sections: Number of Delays	Delay in Minutes
Wire trouble			Carrier circuit failure	12	151
New York-Chicago	4	162	Loss of synchronism	25	25
Chicago-Denver	8	311	Fails and clears	4	9
Denver-Oakland	12	233	Total	41	3 hours 5 minutes
Circuit line-up					
Daily over-all	27	810			
Partial	40	1,021			
Other trouble					
Fails and clears	13	111			
Earth currents	6	135			
Equipment	5	63			
Loss of synchronism	71	84			
Miscellaneous	4	50			
Total	190	49 hours 30 minutes			

wire line or radio relay carrier systems or those leased from the American Telephone and Telegraph Company and associated companies, have a bandwidth of approximately 3,000 cycles. It has been found expedient to subdivide such bands into two subbands and to operate eight or nine telegraph channels in each subband. To provide maximum flexibility with minimum variety in the types of equipment required, the carrier equipment is built up of standard units arranged to meet various conditions. The telegraph channel terminals normally are assembled in groups of eight, completely wired on a 10-foot rack. These terminal sets, shown in Figure 1, are wholly electronic, the outgoing carrier being frequency modulated by the telegraph printer or other transmitting machine and the incoming carrier being detected and amplified to a power level sufficient to drive the reperforator or printer on the receiving side. Designed specifically for single-channel teleprinter service, they are capable of meeting the three most commonly required d-c leg conditions—full duplex, half duplex, and carrier terminals tandem connected back to back. The eight channels normally comprising one group of terminals have mid-frequencies spaced 150 cycles apart with the lowest channel centered at 525 cycles and the highest at 1,575 cycles.

The regulating equipment, such as rheostats for building out leg resistance, bias-adjusting potentiometers, common test equipment, and so forth, is divorced from the channel terminal bays and concentrated at a central location in the operating room. Several different arrangements are used for assembling the standard control items, each arrangement being designed for a given class of office. Figure 2 illustrates a typical method, employed at larger offices, with each of the five cabinets shown serving four groups of eight or nine channels per group. In this instance each group has been provided with only eight channels, the blank panels being left for future expansion.

Figure 3 shows schematically the subband separation and modulation equipment employed with this method of working. The method has two distinct advantages. First, manufacturing and warehousing economies are effected because the number of different types of oscillators, filters, and discriminators required is only half that needed under the older pattern, where all frequencies required to fill the voice band were directly generated, selected, and detected. Second, the smaller group of channels is found to be a more convenient unit from the standpoint of traffic routing and dispatching, since a large part of the total network is comprised of feeder cir-

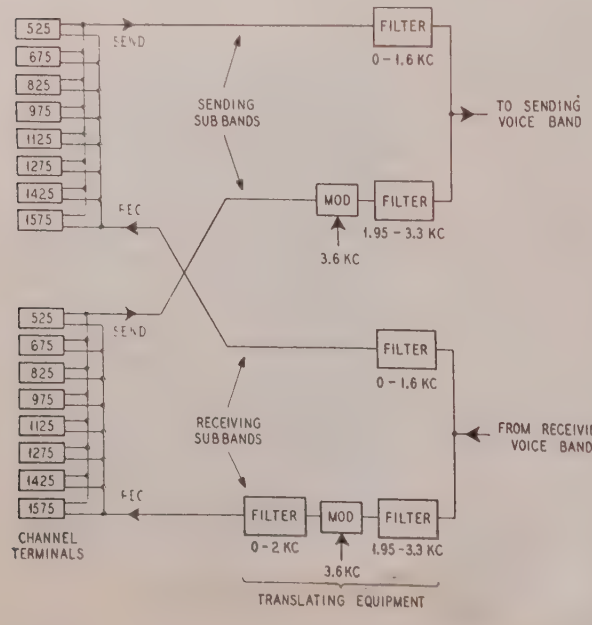

Figure 3 (left). Block diagram of subband grouping

Figure 4 (below). Typical subband interconnections

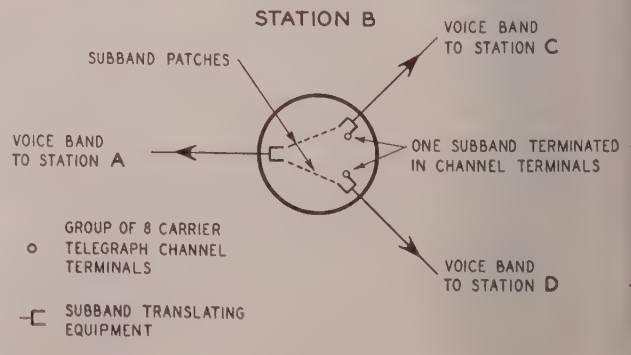
STATION B
SUBBAND PATCHES
VOICE BAND TO STATION C
VOICE BAND TO STATION A
ONE SUBBAND TERMINATED IN CHANNEL TERMINALS
VOICE BAND TO STATION D
GROUP OF 8 CARRIER TELEGRAPH CHANNEL TERMINALS
SUBBAND TRANSLATING EQUIPMENT

cuits to smaller communities which can be served by the small group of channels. This advantage results in the extension of subbands from one system to another by means of subband patches, as illustrated in Figure 4. Patches between complete bands, without separation into subbands, also are employed.

Voice bands over which the channels are operated are derived from a number of sources as dictated by circumstances. Still, to the telegraph channels all voice bands appear as two unidirectional paths (4-wire circuits), whether the ultimate transmission medium be a 2-wire or a 4-wire high-frequency carrier or a radio relay system. Commonly used transmission mediums are Western Union's own 2-wire and 4-wire carrier systems, which range in capacity from one subband in either direction using a top frequency of 3 kc to the 150-kc radio relay system which handles 64 subband groups.[8] In leased American Telephone and Telegraph Company facilities, channel groups, usually not less than two subbands, operate on C, J, K, and L carriers.[9,10,11,12]

The full capacity of the voice band is, of course, not realized when its load is only two groups of eight channels each. On many circuits where the traffic demands, a total of 20 channels is operated in the voice band by the expedient of assigning the frequency spectrum as depicted in Figure 5. Two additional channels are secured by adding the 375-cycle "J" channel to each group. If need be, the nineteenth and twentieth channels, the "K" and "L," are added, completely filling the space left as a guard band between the subband filters. These channel allocations are 1,725 and 1,875 cycles, respectively, maintaining the 150-cycle separation pattern.

Circuit Layouts

Figure 6 is a circuit map of the trunk carrier telegraph channels now operated between the reperforator switching centers. This circuit map does not show trunk connections to New York, Chicago, or Washington, three major traffic centers which originate a substantial proportion of the nation's telegraph traffic. The New York trunk carrier circuits, shown in the map in Figure 7, are typical of the three major offices which are not actually switching centers but involve large networks of carrier trunk circuits.

Circuits are considered direct carrier trunks if they are derived from two or more carrier bands with a patch between subbands or bands, the criterion being a continuous carrier frequency connection without intermediate conversion down to d-c signals. Where eight or nine channels suffice for trunk service between two traffic centers, a voice band between these centers is not utilized completely. The remaining capacity is, therefore, employed for establishing trunk service to some other distant center by a subband patch.

Referring to Figure 6, it will be seen

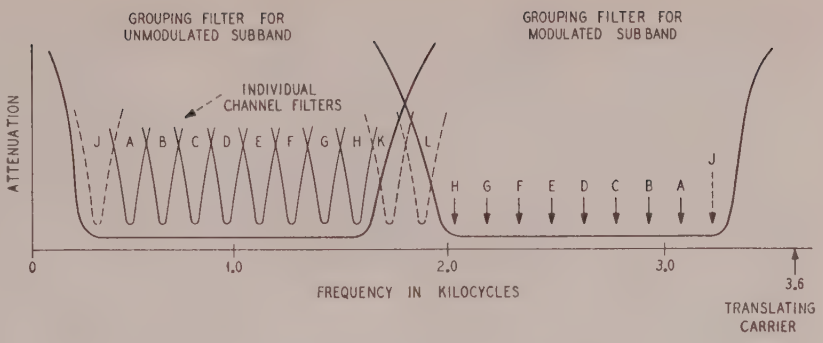

Figure 5. Channel allocation chart

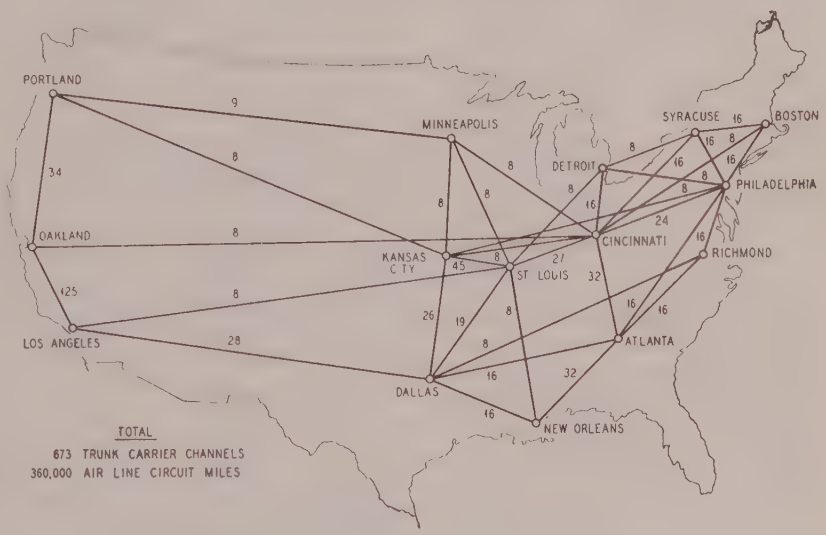

Figure 6. Direct carrier telegraph channels between switching centers

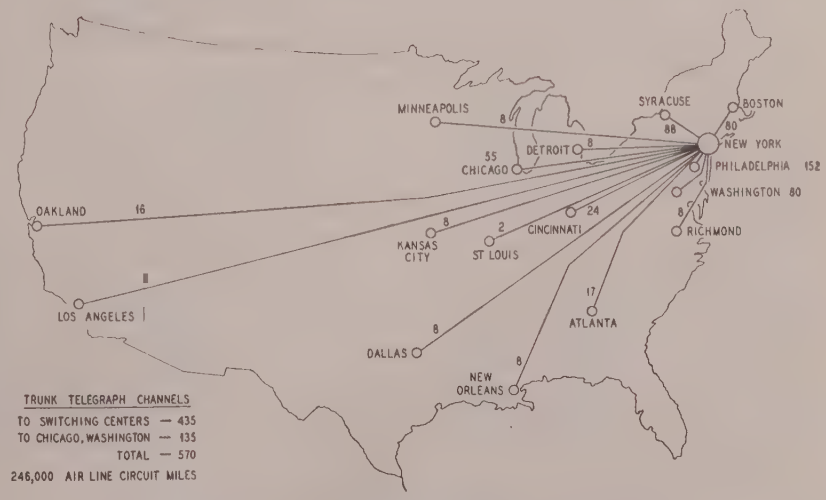

Figure 7. Direct carrier telegraph channels serving New York City

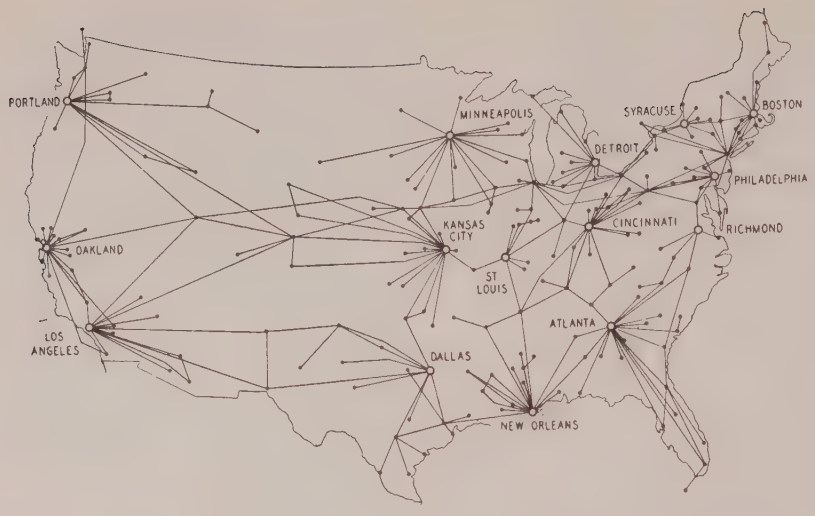

Figure 8. Tributary carrier circuits

that direct carrier trunks as defined above are not always provided between a given switching center and all other switching centers. Where a group of direct carrier trunks is not justifiable, carrier transmission is obtained by a d-c telegraph patch between two trunk carrier circuits. As an example, a Boston-Minneapolis connection is established easily by a d-c leg connection between a Boston-Cincinnati channel and a Cincinnati-Minneapolis channel.

The use of carrier circuits for all trunk services has proved an economical application of modern techniques. Still, the success of Western Union's switching system and carrier network can be credited in large measure to the so-called tributary carrier circuits which connect various points in each area to the switching centers. The term "tributary circuit" as used here also includes circuits operating to certain important telegraph offices, such as Buffalo, Cleveland, Denver, Pittsburgh, and so forth, since business from these points is routed via the automatic reperforating equipment at the established centers. Tributary circuits spread out radially from the switching centers, as illustrated in Figure 8.

The average switching center is equipped with 400 channel terminals, one-third of which operate in trunk-line service and two-thirds to scattered locations in the area. Figure 9 shows the assignments for the 318 channel terminals located in Minneapolis, a typical example. One hundred and three of these channels are assigned to trunk service and the remaining 215 channels provide carrier service to 16 towns and cities in the area. These tributary carrier circuits bring all the major cities, and the small towns as well, within direct reach of the reperforator switching mechanisms. Many of them are extended via d-c telegraph facilities, as illustrated in Figure 10. Here a small town, "A," operates via a relatively short d-c telegraph line into a carrier channel terminal in the tributary office, "B," and thence via a carrier channel direct to the switching center at office "C." Business originating at "A" is transmitted manually on a teleprinter circuit; but there is no handling of any kind at "B"; and at "C" the circuit terminates directly in the switching equipment which automatically handles the required retransmission.

All manner of direct telegraph connections, or the equivalent of direct connections without manual handling at intermediate points, are established by this arrangement. Nearly 6,000 channels now are in operation, totaling almost 2,000,000 circuit miles. Of this number, about 1,800 are employed for direct trunk connections, and around 4,000 for tributary circuits. The switching facilities provided at reperforator centers permit almost instantaneous connections between any two points in the network, regardless of the size of the offices involved or their locations.

Operating Performance

From the viewpoint of the traffic engineer, operating performance is measured in terms of teleprinter range and continuity of service provided. Distortion losses caused by filters and electronic equipment are extremely small. When a teleprinter circuit is operated through one carrier section the range obtained is practically a short-circuit range. Where two or more carrier sections are operated in tandem (with or without intervening relays at repeaters inserted for obtaining drops) the operating range decreases slightly with each added section. Figure 11 shows this effect. It is quite inevitable that any data such as recorded by this graph are gathered under more or less "controlled" conditions. Still, every effort was made, by continued repetition of measurements and by performing the tests on more than one set of tandem-connected channels, to get the best possible indication of the performance to be expected in traffic service. Whenever more than seven or eight tandem sections are involved in a given circuit, intermediate regenerative repeaters are provided

Figure 9. Carrier channel assignment of typical area center

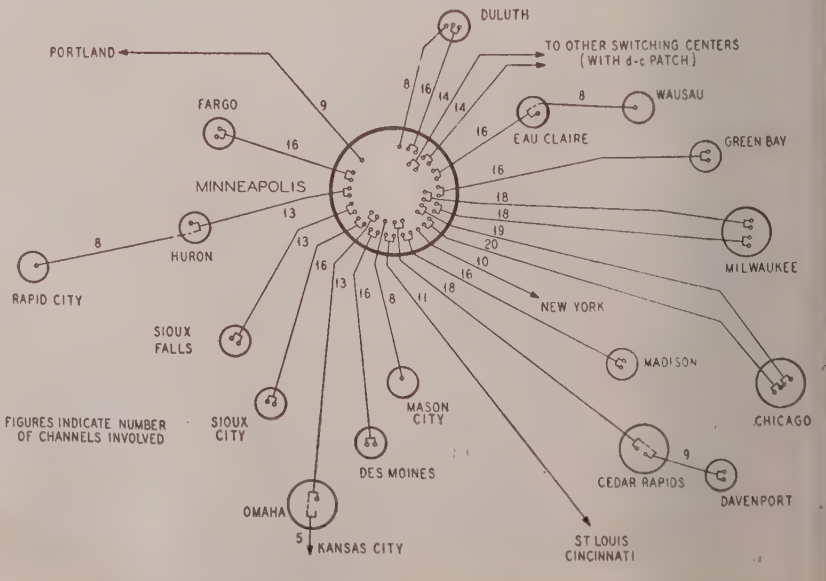

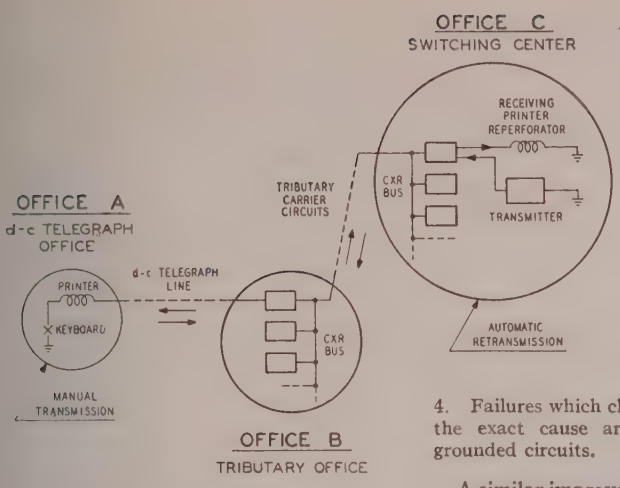

Figure 10 (left). Typical tributary circuit arrangement

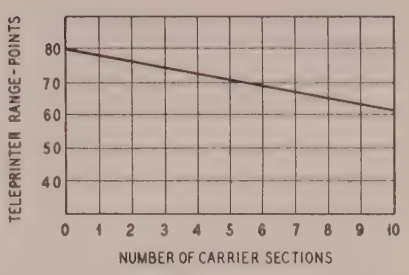

Figure 11 (right). Effect of tandem sections on teleprinter range

to reduce the net effect and to insure a minimum teleprinter range of at least 65 points.

Since any interruption requires transferring traffic to parallel facilities, or rerouting via other cities to maintain a telegraph connection, minimum lost time on each circuit is important. The improvement obtained in continuity of service through the use of the carrier network can be illustrated by examining the results of a lost-time study made on a transcontinental circuit. One of the few remaining multiplex circuits was used for this time study because it permitted a direct comparison of the same traffic circuit under an all-grounded condition (13 repeater sections) and an all-carrier condition (two carrier sections with d-c leg patch between). The all-grounded circuit employed two regenerative repeaters.

The tremendous decrease in lost time with carrier operation is attributable to several major factors:

1. Lost time caused by circuit failures decreases for two reasons. Present-day carrier circuits operate on all-cable leased facilities in many cases, and since cable circuits are less subject to failure than the open-wire lines formerly employed, the number of interruptions is decreased. When an interruption occurs, the time required for circuit restoration is comparable for grounded and carrier circuits but a circuit line-up is ordinarily not necessary for carrier, whereas eight to ten minutes usually were consumed by circuit realignment after a wire failure on a long-distance grounded circuit.

2. Routine or emergency circuit line-ups which required considerable time on the long grounded circuits are practically eliminated with carrier operation. The line-ups on grounded circuits were necessitated primarily by balance changes due to variable weather conditions.

3. Certain types of trouble, such as earth currents, affect grounded circuits, but have little or no effect on carrier circuits.

4. Failures which clear without location of the exact cause are more prevalent on grounded circuits.

A similar improvement in the operation of long-distance teleprinter circuits has been experienced, but comparative data cannot be presented because all long-distance circuits in the Western Union network were operated multiplex before the advent of carrier. However, studies of existing long-distance teleprinter circuits substantiate the excellent continuity of service obtained from carrier operation. Table II shows a few such circuits, selected at random, giving the total lost time for a 1-month period.

Table II

Circuit	Number of Carrier Sections	Total Lost Time (in Minutes)
New York-San Francisco	2	36
New York-Los Angeles	2	53
New York-Denver	2	106
New York-Houston	3	102
New York-San Antonio	5	100

Shorter circuits show considerably less lost time, many operating without interruptions of any kind for an entire month or longer.

A further example of operating performance, which clearly illustrates the reliability obtained, is the "round-robin" circuit of Figure 12. This circuit consists of a continuous loop with 23 individual carrier sections, totaling approximately 3,300 miles connected in tandem. Two independent message circuits, one operating clockwise and one counterclockwise, are established by this arrangement, with transmission originating at any one of 31 customers' stations scattered around the loop. Transmission from any given point is received at all other points. In spite of its complexity, the total lost time for all points in the circuit averages only 0.6 per cent.

Limited field installations during the 1930–1940 trial period convinced Western Union that FM operation was more desirable than AM operation for a carrier telegraph plant and also that carrier operation would be more advantageous than d-c physical operation. The results of a moderate increase in the carrier facilities a decade ago, followed by wholesale conversion in the past few years, have confirmed this conclusion. Installation, operation, and maintenance have been economical, and the continuity of service obtained has improved to a marked degree.

References

1. Advances in Carrier Telegraph Transmission, **A. L. Matte.** *Bell System Technical Journal* (New York, N. Y.), volume 19, 1940, page 161.

2. High-Speed Voice-Frequency Carrier Tele-

Figure 12. 3,300-mile circuit involving many carrier sections

graph System, **F. B. Bramhall.** *AIEE Transactions*, volume 59, 1940, pages 873–78.

3. A Frequency-Modulation Telegraph Terminal without Relays, **F. H. Cusack, A. E. Michon.** *AIEE Transactions*, volume 66, 1947, pages 1165–71.

4. Frequency-Modulated Carrier Telegraph System, **F. B. Bramhall, J. E. Boughtwood.** *Electrical Engineering* (*AIEE Transactions*), volume 61, January 1942, pages 36–39.

5. Performance Characteristics of Various Carrier Telegraph Methods, **T. A. Jones, K. W. Pfleger.** *Bell System Technical Journal* (New York, N. Y.), volume 25, 1946.

6. Frequency Shift Telegraphy—Radio and Wire Applications, **J. R. Davey, A. L. Matte.** *AIEE Transactions*, volume 66, 1947, pages 479–94.

7. Push Button Switching in Telegraph Systems, **R. F. Blanchard, W. B. Blanton.** *AIEE Transactions*, volume 67, part II, 1948, pages 1733–40.

8. A 150-Kc Carrier System for Radio Relay Application, **J. E. Boughtwood.** *AIEE Transactions*, volume 67, part I, 1948, pages 577–82.

9. A New 3-Channel Carrier Telephone System, **J. T. O'Leary, E. C. Blessing, J. W. Beyer.** *Bell System Technical Journal* (New York, N. Y.), volume 18, 1939.

10. A 12-Channel Carrier Telephone System for Open-Wire Lines, **B. W. Kendall, H. A. Affel.** *AIEE Transactions*, volume 58, 1939, pages 351–60.

11. An Improved Cable Carrier System, **H. S. Black, F. A. Brooks, A. J. Wier, I. G. Wilson.** *AIEE Transactions*, volume 66, 1947, pages 741–46.

12. Frequency Division Techniques for a Coaxial Cable Network, **R. E. Crane, J. T. Dixon, G. H. Huber.** *AIEE Transactions*, volume 66, 1947, pages 1451–59.

Discussion

R. B. Shanck (Bell Telephone Laboratories, Inc., New York, N. Y.): Some data are given in this interesting paper which show a large improvement, as regards lost time, for the FM telegraph system as compared to d-c grounded telegraph. A comparison of the FM with the AM voice-frequency telegraph would also be of considerable interest. Records kept in connection with Bell System private-line telegraph service, employing for the most part AM voice-frequency telegraph, show materially less lost time for comparable distances and periods than the figures quoted in this paper for the FM system. It is realized that differences in maintenance practices and the manner of keeping records are such that the data do not provide an accurate comparison. It would appear, however, that there is no outstanding difference between the two systems from the standpoint of performance in service, on wire lines of reasonably good quality.

I. S. Coggeshall (The Western Union Telegraph Company, New York, N. Y.): A systems paper like this one serves a useful purpose in enabling one who has only a passing acquaintance with the problems faced in designing a large communication system to get a bird's-eye view of the results achieved.

The filtered spectrum of Figure 5 of the paper, taken in connection with the FM features described in reference number 3 of the paper, accounts for an observed fact that 150-cycle center-spacing of adjacent channels in the subcarriers permits not only start-stop printer operation (which the authors describe in the first paragraph under the subhead "Equipment" as being basic to the design), but also permits equally satisfactory transmission of 2-channel time-division multiplexes at 66 words per minute per channel, coast to coast. Provided that regenerative repeaters are inserted, even 3-channel multiplexes can be employed with 150-cycle spacing. Yet the authors correctly refer to the second New York-Oakland 2-channel multiplex as one of the comparatively few multiplex circuits now remaining in Western Union landline service.

The design and installation of the enormous carrier program were quite understandably pointed to the adoption of the start-stop method of operation as optimum for simplicity and flexibility at a time when it was necessary to deal with other complexities. However, the facility with which bands and sub-bands are now patched, and start-stop d-c circuits are legged on, suggests to the operating man that, as a next step, there should be engineered a simple, reliable, standard-speed multiplex system incorporating enough intermediate pulse storage and sufficient frequency stability so that any of the 150-cycle-spaced carrier frequencies could be put into use in time-division multiplex. Thus, any individual multiplex channel could be directly corded into any other channel with the same degree of freedom, and with as little delay, as carrier channels now are patched.

To the usual economic challenge of such a development is now added the national emergency which will, in all probability, result in a heavy demand for additional facilities on trunk and tributary routes.

In the submarine cable system, frequency-division multiplex cannot be applied except on the shorter cables, and we are accustomed, perforce, to consider that since time-division multiplex always will be with us, it is worth while devoting a great deal of attention to perfecting it. The International Communications Department therefore is working out with the landline laboratories an improved multiplex system based upon the following objectives:

1. Precision, standard-speed master forks at each station.

2. Full use of the signaling capacity of each cable or landline section, including the use and recombining of fractional channels and provision for deriving various channel speeds.

3. Maintenance of synchronism through conditions of poor transmission and long periods of interruption.

4. Isolation of sections and complete regeneration, outward as well as inward.

5. Provision for stopping circuits for regulating or patching, with automatic, error-free restarting.

6. Direct patching of any inbound channel to any outbound channel without polarity- or speed-matching, including translation from multiplex to teleprinter, and vice versa.

7. Gauged construction; miniaturized, nonmarginal apparatus.

This development will lend itself to full realization of the additional capacity which will be obtained through the submerged repeaters, as discussed in the paper by J. J. Gilbert.[1]

Although the results of the projected program can only be assessed in prospect at the present time, it may be that results on the cables will be reflected ultimately in the landline system—a situation the reverse of that which hitherto has recurred so often.

Reference

1. A Submarine Telephone Cable with Submerged Repeaters, **J. J. Gilbert.** *AIEE Transactions*, volume 70, part I, 1951, pages 564–72.

F. B. Bramhall and **L. A. Smith:** Unfortunately, the authors can report only that universal use of FM voice-frequency carrier telegraph results in excellent long-term performance on a large network. A direct comparison of the FM and AM methods, as Mr. Shanck points out, would indeed be of great interest. The differences in operating practices and in methods of judging performance between two large operating companies, however, make such a comparison difficult, if not impossible. The authors have the highest regard for the FM-AM comparisons reported by J. R. Davey and A. L. Matte (see reference 6 in the paper), but take exception to the implication that voice-band media on which telegraph channels are operated are ever sufficiently stable and noise-free to vitiate the FM advantage

Some Effects of Lightning Arrester Protective Characteristics and Location upon Station Apparatus Protection

J. W. KALB
MEMBER AIEE

THE purpose of this investigation was to study the protection provided by lightning arresters of different protective ability located at various distances from the protected apparatus. Quantitative correlations of basic insulation levels and surge voltages are not considered.

Valve lightning arresters of 97-kv rating and various capacitors were connected to one end of a 1-mile test line. An impulse generator was discharged into the other end. This circuit was used to simulate 115-kv station equipment connected to a line with one mile of overhead ground-wire protection.

Relative protection afforded by lightning arresters of different discharge voltages singly and in combination was studied. The transformer was always represented by a 3,100-micromicrofarad capacitor.[1] Accessory equipment (circuit breakers, and so forth) was represented by 213- and 1,000-micromicrofarad capacitors. The test surge was a full wave of crest value slightly below that which would spark over representative 115-kv line insulation.

Table I summarizes tests performed and crest voltages at the "transformer."

The discharge voltage of a lightning arrester connected near apparatus such as a transformer may be higher than that based upon the lightning arrester characteristic and the magnitude and wave shape of the incoming surge alone. This is because the capacity of the apparatus adjacent to the lightning arrester is charged to lightning arrester sparkover voltage and then discharges through the lightning arrester at an initial rate of current rise which may exceed that of the incoming surge while concurrently the incoming surge front continues to arrive.

Care should be used when applying field data on rate of current rise through lightning arresters in stations. If the data were obtained from lightning arresters mounted directly adjacent to transformers, it would not be correct to use these rates of current rise in analytical or miniature system studies involving separation of the lightning arrester and the transformer.

Low lightning arrester impulse sparkover voltage is important because it controls the voltage to which the capacity of the connected apparatus is charged before lightning arrester discharge. This influences the maximum lightning arrester discharge voltage even though this may be higher than the initial sparkover voltage.

Two normal 97-kv lightning arresters in parallel were the equivalent of one lightning arrester of 87 per cent normal discharge voltage characteristic during these tests. See Table I, tests 1 and 4. Currents of the parallel lightning arresters divided about equally.

Two parallel lightning arresters at the transformer resulted in lower crest voltage at the transformer than with one at the transformer and one ahead of the transformer. See Table I, tests 1, 16, and 17.

As others have shown,[2,3,4,5,6] distance between the lightning arrester and protected apparatus adds to the crest surge voltage at the apparatus.

In protecting both transformer and accessory equipment an additional lightning arrester at the accessory equipment is of benefit in reducing the voltage at both, providing a lightning arrester is already located at the transformer. A lightning arrester at only the accessory equipment may be inadequate.

With a lightning arrester at both ac-

Figure 1 (below). 97-kv arrester connected for test with impulse generator in background

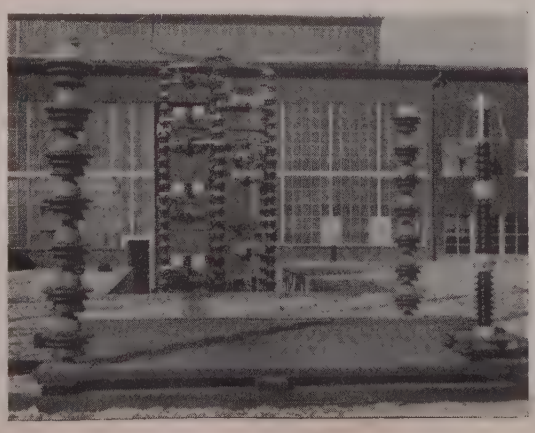

Figure 2. Surge of 590 kv at "station" end of 1-mile test line, with line terminated in 450-ohm characteristic impedance

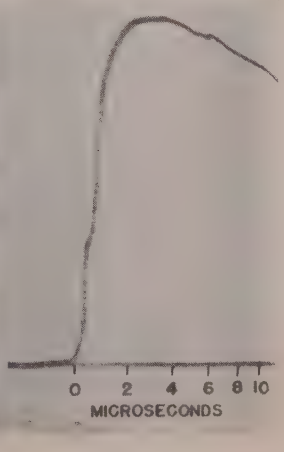

Paper 51-63, recommended by the AIEE Protective Devices Committee and Transmission and Distribution Committee, and approved by the AIEE Technical Program Committee for presentation at the AIEE Winter General Meeting, New York, N. Y., January 22-26, 1951. Manuscript submitted October 24, 1950; made available for printing December 8, 1950.

J. W. KALB is with The Ohio Brass Company, Barberton, Ohio.

Table I. Crest Voltage at "Transformer" for Various Test Conditions

Test	Lightning Arrester Location	Type of 97-kv Lightning Arrester	Accessory** Equipment Capacity, Micromicrofarads	Crest Transformer Voltage, Per Cent*
1	At "transformer"	Normal	0	123
2		93% normal discharge voltage	0	113
3		88% normal discharge voltage	0	107
4	2 at "transformer"	Both normal	0	107
5	At "transformer"	Normal	213	122
6		Normal	1,000	121
7	15-ft. separation, 10-ft. T connection	Normal	0	130
8		93% normal discharge voltage	0	122
9		88% normal discharge voltage	0	117
10	50-ft. separation, 30-ft. T connection	Normal	0	147
11		93% normal discharge voltage	0	138
12		88% normal discharge voltage	0	131
13	50-ft. separation, 30-ft. V connection	Normal	0	147
14		93% normal discharge voltage	0	135
15		88% normal discharge voltage	0	131
16	At "transformer" and 15-ft. separation, 10-ft. T-connection	Both normal	0	109
17	At "transformer" and 50-ft. separation, 30-ft. T-connection	Both normal	0	114
18	At accessory equipment capacity	Normal	213	144
19		93% normal discharge voltage	213	136
20		88% normal discharge voltage	213	132
21		Normal	1,000	147
22		93% normal discharge voltage	1,000	141
23		88% normal discharge voltage	1,000	139
24	Ahead of accessory equipment capacity, 30-ft. down lead	Normal	213	168
25		93% normal discharge voltage	213	154
26		88% normal discharge voltage	213	149
27		Normal	1,000	153
28		93% normal discharge voltage	1,000	146
29		88% normal discharge voltage	1,000	140
30	At "transformer"	Normal valve element alone	0	114
31		110% normal sparkover voltage	0	128
32		120% normal sparkover voltage	0	132
33	At "transformer" and accessory equipment capacity	Both normal	213	113
34		Both normal	1,000	111

* Per cent of 298-kv front-of-wave sparkover voltage of 97-kv lightning arrester.
** 50 feet ahead of "transformer" with 30-foot V-connection.

cessory equipment and transformer the surge current and voltage were higher at the transformer than at the accessory equipment.

Test Method

An impulse generator was discharged into a 1-mile test line of 4/0 aluminum cable steel-reinforced conductor. At the receiving end of the line, valve lightning arresters were used to protect various combinations of capacitors representing a transformer and accessory station equipment under surge conditions.[1] This test was used to represent a surge entering a 115-kv station over a line with one mile of overhead ground-wire protection. Figure 1 shows a 97-kv lightning arrester connected for test with the impulse generator in the background.

With the line terminated in its characteristic impedance of 450 ohms, the surge delivered into the line was negative 650 kv, 0.4 by 20 microseconds, representing a surge which would not flash over the 115-kv insulation at the end of ground-wire protection. At the receiving end the

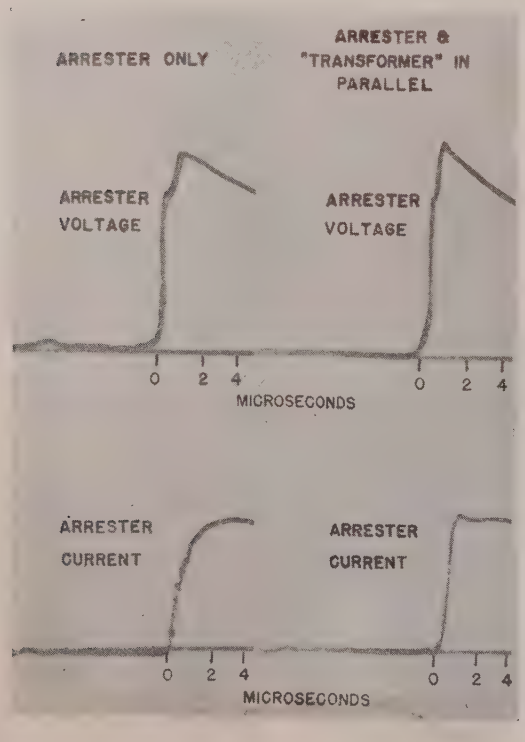

Figure 3 (left). Lightning arrester voltage and current with and without 3,100-micromicrofarad "transformer" in parallel

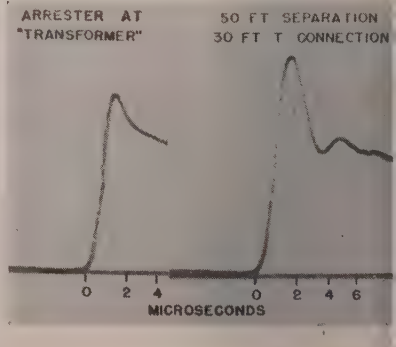

Figure 4 (right). "Transformer" voltage with lightning arrester at the "transformer" and with the lightning arrester 50 feet ahead of the "transformer" with 30 feet down leads

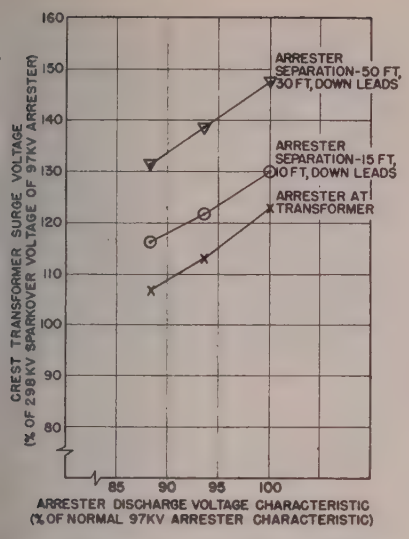
ARRESTER SEPARATION-50 FT, 30 FT, DOWN LEADS
ARRESTER SEPARATION-15 FT, 10 FT, DOWN LEADS
ARRESTER AT TRANSFORMER
CREST TRANSFORMER SURGE VOLTAGE (% OF 298 KV SPARKOVER VOLTAGE OF 97KV ARRESTER)
ARRESTER DISCHARGE VOLTAGE CHARACTERISTIC (% OF NORMAL 97KV ARRESTER CHARACTERISTIC)

Figure 5. Crest voltage at 3,100-micromicrofarad "transformer" as function of lightning arrester discharge voltage characteristic for various lightning arrester separations and lead lengths

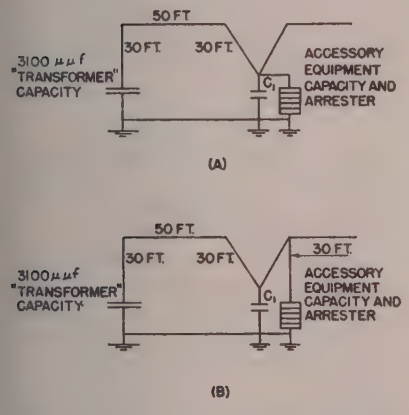

Figure 6. Test circuit representing transformer and accessory equipment with lightning arrester at accessory equipment

surge was attenuated and distorted to 590-kv, 3 by 27 microseconds. This represents the surge arriving at the station before being modified by line termination, lightning arrester, and various station capacities. Figure 2 shows the front of this wave.

For comparison, all voltage values are referred to front-of-wave sparkover at AIEE rate of the 97-kv Thorex, type *GP-97*, lightning arrester (298 kv) as 100 per cent. During the first few microseconds that an impulse wave is impressed across a transformer, the important electrical characteristic is the line-to-ground capacity of the transformer.[1] A 3,100 micromicrofarad capacitor was used to represent the transformer and will be re-

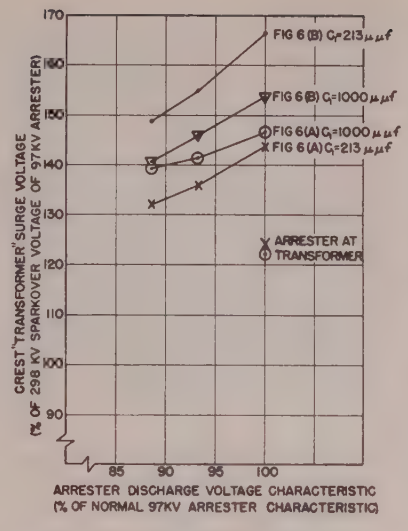
FIG 6 (B) C=213 μμf
FIG 6 (B) C=1000 μμf
FIG 6 (A) C=1000 μμf
FIG 6 (A) C=213 μμf
ARRESTER AT TRANSFORMER
CREST TRANSFORMER SURGE VOLTAGE (% OF 298 KV SPARKOVER VOLTAGE OF 97KV ARRESTER)
ARRESTER DISCHARGE VOLTAGE CHARACTERISTIC (% OF NORMAL 97KV ARRESTER CHARACTERISTIC)

Figure 7. Crest voltage at 3,100-micromicrofarad "transformer" as function of lightning arrester discharge voltage characteristic—lightning arrester at accessory equipment

ferred to as the "transformer." Representation of a transformer under surge conditions by a capacitor probably results in greater voltage oscillations than if a 115-kv transformer had been used.[4]

Effect of Transformer on Lightning Arrester Current

Although the transformer capacity tends to decrease the slope of an incoming voltage surge, its effect on lightning arrester discharge current may be the opposite. The transformer capacity is charged to lightning arrester sparkover voltage and then discharges through the lightning arrester at a rate of current rise which may exceed that obtained if the lightning arrester had been connected to the line by itself.

Figure 3 shows voltage and current oscillograms taken with the line terminated by a 97-kv lightning arrester alone and the same lightning arrester and a 3,100 micromicrofarad "transformer" in

Table II

	97-kv Lightning Arrester Alone	Lightning Arrester and Transformer in Parallel
Crest lightning arrester voltage, per cent*	115	123
Crest lightning arrester current, amperes	2,350	2,410
Effective rate of current rise, kiloamperes per microsecond (10%–90%)	1.8	4.4

* Per cent of 298-kv front-of-wave sparkover voltage of Thorex type *GP-97* lightning arrester.

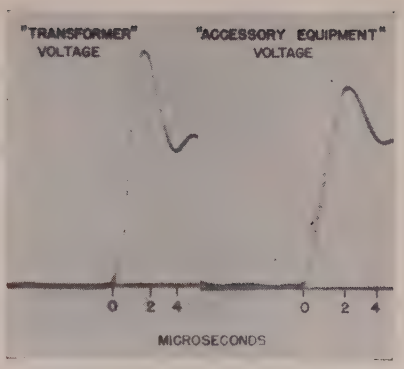

Figure 8. "Transformer" and accessory equipment capacity voltage with lightning arrester at accessory equipment capacity

parallel. The total lead length between the lightning arrester and the capacitor representing the transformer was five feet, the minimum possible length considering difference in height between the lightning arrester and the capacitor. The voltage divider was connected directly across the lightning arrester terminals. In Table II the voltage and current measurements from these oscillograms show quantitatively the effect of the "transformer" in increasing the rate of current rise through the lightning arrester and the lightning arrester voltage.

Effect of Lightning Arrester Sparkover Voltage

The margin of protection afforded by lightning arrester sparkover voltage often is greater than that of the discharge voltage. Therefore the discharge voltage frequently is considered more important when establishing lightning arrester protection practice. However, in the protection of station equipment against incoming surges, the sparkover voltage controls this discharge voltage to some degree by controlling the voltage to which the capacity of the protected apparatus is

Table III

	Crest Lightning Arrester Discharge Voltage, Per Cent*	Table I Test
97-kv lightning arrester valve element alone (no series gap)	114	30
Normal 97-kv lightning arrester	123	1
Impulse sparkover voltage 10% above normal	128	31
Impulse sparkover voltage 20% above normal	132	32

* Per cent of 298-kv front-of-wave sparkover voltage of Thorex type *GP-97* lightning arrester.

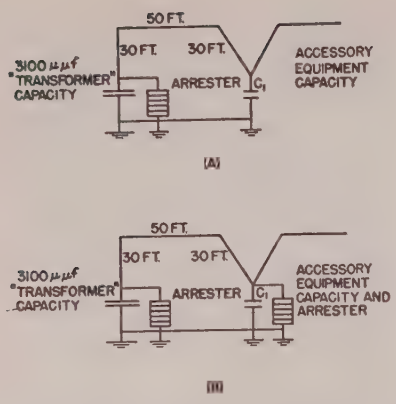

Figure 9. Test circuits representing transformer and accessory equipment with lightning arrester at transformer and at both transformer and accessory equipment

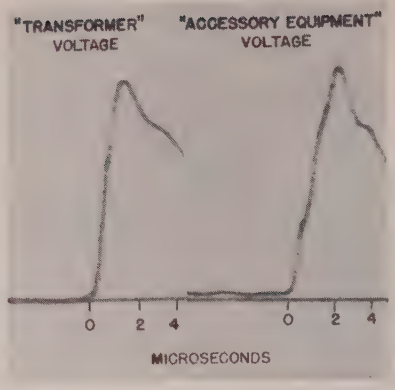

Figure 10. "Transformer" and accessory equipment capacity voltage with lightning arrester at transformer

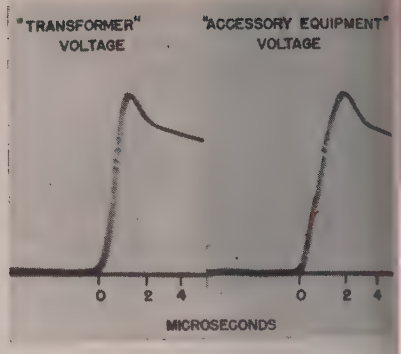

Figure 11. "Transformer" and accessory equipment capacity voltage with lightning arresters at "transformer" and accessory equipment

charged. To study this effect, tests were made with the line terminated by the 3,100-micromicrofarad "transformer" in parallel with different 97-kv lightning arresters. These were: a normal 97-kv lightning arrester, 97-kv lightning arresters with gap elements having 110 and 120 per cent normal sparkover voltage, and a 97-kv lightning arrester valve element with no gaps. As in the tests in the preceding paragraph the minimum possible lead length of five feet was used to connect the lightning arrester and the capacitor. Table III shows the effect of varying series-gap sparkover voltage upon crest lightning arrester discharge voltage.

Effect of Lightning Arrester Separation and Lead Length

The following test results confirm what others[4,5,6] have found in more detailed studies: lightning arrester lead length and separation should be kept to the minimum for best protection.

A normal 97-kv lightning arrester protecting the 3,100-micromicrofarad "transformer" allowed the crest voltages shown in Table IV.

Table IV

Lightning Arrester Connection	Crest Transformer Voltage, Per Cent*	Table I Test
At "transformer"	123	1
15-ft. separation	130	7
10-ft. T-connection		
50-ft. separation	147	10
30-ft. T-connection		
50-ft. separation	147	13
30-ft. V-connection		

* Per cent of 298-kv front-of-wave sparkover voltage of Thorex type *GP-97* lightning arrester.

Note that for these particular tests the V-connection showed no benefit over the T-connection.

Figure 4 shows oscillograms of "transformer" voltage with the lightning arrester at the "transformer" and with the same lightning arrester separated 50 feet, with 30-foot down leads. Voltage peaks of this type naturally are not as severe on all forms of transformer insulation as longer waves of the same crest value.[6,7] For major insulation, however, their severity is about as great as for longer waves.

Effect of Lower Lightning Arrester Discharge Voltage

In addition to the normal 97-kv lightning arrester, special lightning arresters with 7 and 12 per cent of the valve element removed also were tested. These represented 97-kv lightning arresters of 93 and 88 per cent normal discharge voltage characteristic.

When connected directly across the 3,100-micromicrofarad "transformer" their crest voltage was proportional to the valve element, as expected. That is, those with partial valve elements allowed crest discharge voltages of about 7 and 13 per cent less than the normal lightning arrester (see tests 1,2,3 of Table I).

When these special lightning arresters were separated from the transformer, the crest voltage at the "transformer" quickly exceeded that obtained with a normal lightning arrester connected directly at the "transformer." Figure 5 shows the crest voltages at the 3,100-micromicrofarad "transformer" as a function of lightning arrester discharge voltage characteristic for different arrester separations and lead lengths. These are tests 1–3 and 7–12 of Table I.

Table V

Second Lightning Arrester Location	Crest Transformer Voltage, Per Cent*	Table I Test
None	123	1
At "Transformer"	107	4
15-ft. separation	109	16
10-ft. T-connection		
50-ft. separation	114	17
30-ft. T-connection		

* Per cent of 298-kv front-of-wave sparkover voltage of Thorex type *GP-97* lightning arrester.

Protection With Two Lightning Arresters

With one lightning arrester at the "transformer" and a second lightning arrester ahead of them, the transformer surge voltage was reduced. However, with the second lightning arrester separations studied (15 and 50 feet), the transformer lightning arrester still discharged the heavier current.

The most effective use of the second lightning arrester in reducing transformer voltage was in parallel with the other lightning arrester at the transformer. This was equivalent to a single lightning arrester of about 13 per cent lower discharge voltage in protective ability. Currents through the two parallel lightning arresters were substantially equal in crest value and wave shape.

Table V lists crest "transformer" surge voltage when protected by normal 97-kv lightning arresters, one at the "transformer" and the second at the location shown.

Protection of Both Transformer and Accessory Equipment

Using the circuits of Figure 6, tests were made to study the effect of a lightning arrester at the accessory equipment on the protection of the transformer. In

Table VI

	Accessory Equipment Capacity, mmf	Crest Voltage, Per Cent*	Table I Test
"Transformer" voltage	213	122	5
Accessory equipment capacity voltage	213	125	5
"Transformer" voltage	1,000	121	6
Accessory equipment capacity voltage	1,000	128	6

* Per cent of 298-kv front-of-wave sparkover voltage of Thorex type *GP-97* lightning arrester.

Table VII

	Accessory Equipment Capacity, mmf	Crest Voltage, Per Cent*	Table VII Test
"Transformer" voltage	213	113	33
Accessory equipment capacity voltage	213	100	33
"Transformer" voltage	1,000	111	34
Accessory equipment capacity voltage	1,000	99	34

* Per cent of 298-kv front-of-wave sparkover voltage of Thorex type *GP-97* lightning arrester.

Figure 6(A) the lightning arrester was connected directly across the capacitor. In Figure 6(B) it was connected ahead of the capacitor by a 30-foot down lead. Figure 7 shows the crest voltages recorded at the "transformer" for values of 213 and 1,000 micromicrofarads for the accessory equipment and a 97-kv lightning arrester of 100, 93, and 88 per cent of normal discharge voltage characteristic. These are tests 18–29 of Table I. In no case, even with the lightning arrester of 88 per cent discharge voltage characteristic, was the crest "transformer" voltage as low as with a normal lightning arrester at the transformer. Figure 8 shows oscillograms of voltage at the station entrance and "transformer" with accessory equipment capacity of 1,000 micromicrofarads.

With the circuit configuration of Figure 9(A), and a normal 97-kv lightning arrester at the "transformer," the crest voltages shown in Table VI were recorded.

All these voltages, even at the accessory equipment, were below those shown on Figure 7 for the same capacity and circuit but with the lightning arresters at the station entrance. Voltages apparently are the same for either value of accessory equipment capacity. The crest "transformer" voltages from Table VI are shown on Figure 7 for comparison. Figure 10 shows oscillograms of voltage at the "accessory equipment" and "transformer" with accessory equipment capacity of 1,000 micromicrofarads.

With the circuit of Figure 9(B) and normal 97-kv lightning arresters at both the "transformer" and accessory equipment, the crest voltages shown in Table VII were recorded.

Figure 11 shows oscillograms of voltage at the "accessory equipment" capacity and "transformer," with accessory equipment capacity of 1,000 micromicrofarads.

Comparing these voltages with those of Table VII shows the benefit obtained in reduction of crest surge voltage by the addition of a lightning arrester at the accessory equipment. Voltages apparently are the same with 213 micromicrofarads as with 1,000 micromicrofarads.

These tests confirm that in the protection of station equipment against incoming surges, lightning arresters should be located near each transformer. Additional lightning arresters at the accessory equipment are of considerable benefit, but without lightning arresters at the transformers they may be inadequate.

The voltages considered in this study are crest voltages of relatively short duration, and their relative magnitude may not be an infallible indication of the relative severity of the various voltage surges with regard to all aspects of equipment insulation.[4,7] However, they should indicate the relative protection afforded major insulation by the different lightning arresters and connections studied.

References

1. Equivalent Circuits of Transformers and Reactors to Switching Surges, L. V. Bewley. *AIEE Transactions*, volume 58, 1939, pages 797–802.

2. Coordination and Protection of Station Insulation against Lightning, P. L. Bellaschi. International Conference on Large High-Voltage Electric Systems (Paris, France), volume III, 1939.

3. Field Investigation of Lightning Surges at Substations, I. W. Gross, G. D. McCann. *AIEE Transactions*, volume 66, 1947, pages 569–76

4. Evaluation of Lightning-Arrester Lead Length and Separation in Co-ordinated Protection of Apparatus against Lightning, T. J. Carpenter, I. B. Johnson, L. E. Saline. *AIEE Transactions*, volume 69, part II, 1950, pages 933–44.

5. Lightning Arresters as a Criterion for Insulation Levels, Harold L. Rorden. *AIEE Transactions*, volume 69, part I, 1950, pages 84–96.

6. Co-ordination of Lightning Arrester Location with Transformer Insulation Level, R. L. Witzke, T. J. Bliss. *AIEE Transactions*, volume 69, part II, 1950, pages 964–75.

7. Proposed Basic Impulse Insulation Levels for High-Voltage Systems, J. E. Clem, J. R. Meador, W. J. Rudge, A. H. Powell. *AIEE Transactions*, volume 69, part II, 1950, pages 953–63.

Discussion

A. M. Opsahl (Westinghouse Electric Corporation, East Pittsburgh, Pa.): Mr. Kalb describes a phenomenon wherein the addition of apparatus capacitance of about 3,000 micromicrofarads in parallel with the lightning arrester raises the lightning arrester discharge voltage above that which is normal for the wave shape of the incoming surge. He attributes this phenomenon to the rapid rate of discharge of the apparatus capacitance into the lightning arrester valve element after lightning arrester gap sparkover. This explanation is not borne out by the oscillograms of Figure 3 of the paper. The voltage continues to rise across the capacitance while it is said to be discharging into the lightning arrester. A capacitance absorbs energy while the voltage is rising. The voltage across a capacitance must fall when it discharges. The voltage across the capacitor (and lightning arrester) does not fall in Figure 3 of the paper, so that the capacitor can discharge some of its energy into the lightning arrester, until after it reaches the excess of voltage crest.

We made a test using a circuit in which the time to current crest and the current crest were reasonably independent of the load or termination, as was the case in Mr. Kalb's test. Apparatus capacitance which was large enough to absorb an appreciable amount of surge current energy slopes off the front of the voltage applied to the lightning arrester. This delays the build-up of voltage to lightning arrester gap sparkover while the capacitor is absorbing all of the incoming surge current. After the lightning arrester gap sparkover, the lightning arrester finally takes all of the incoming surge current in order to limit the voltage. Because of the delayed starting of the lightning arrester current, the time to crest lightning arrester current is decreased or, rather, the rate of rise of lightning arrester current is increased. The capacitor discharges its energy through the lightning arrester after the lightning arrester voltage begins to fall, that is, after any abnormal peak in the lightning arrester voltage, but not before. A small capacitance, such as an apparatus bushing, absorbs so little energy and delays

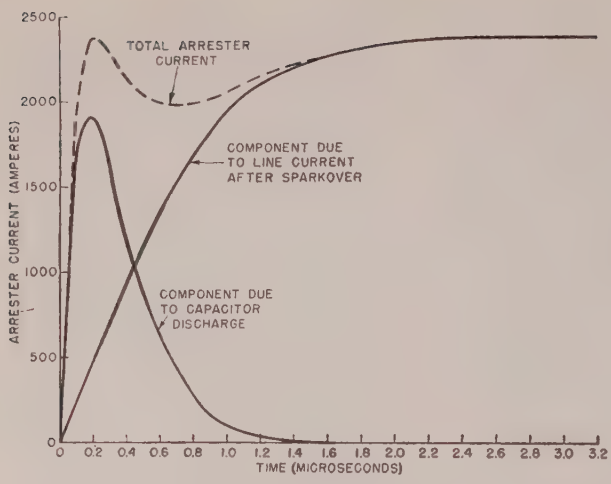

Figure 1. Calculated lightning arrester discharge currents

the build-up of lightning arrester current for so small a percentage of the total time to crest current that its effect is quite negligible.

The discharge voltage across a valve lightning arrester is somewhat dependent on the rate of rise of the surge current. The higher rate of rise of current through the lightning arrester with capacitor in parallel results in a short-time overvoltage across the lightning arrester. This overvoltage effect also is dependent on the diameter of the valve block. A lightning arrester known to the industry as "station type" had a small or negligible excess voltage rise in comparison to the smaller size lightning arresters known as "line type" when tested in this circuit.

I. B. Johnson and **L. E. Saline** (General Electric Company, Schenectady, N. Y.): The author presents interesting laboratory data on the effects of lightning arrester location and on the effects of connected apparatus and lightning arrester sparkover voltage on lightning arrester discharge currents caused by traveling wave voltages arriving over a 1-mile overhead line.

In this study one observation emphasized by the author is that the discharge voltage of a lightning arrester connected near protected apparatus may be higher than that resulting from the discharge of an incoming surge for which the effects of connected apparatus are not involved. And while this is demonstrated for a lightning arrester connected near apparatus—five feet of separation between the capacitor or "transformer" and the lightning arrester—the primary question is: What is the voltage on the capacitor or transformer being protected? Is it to be implied where data are given in the paper on crest lightning arrester discharge voltage for separations of five feet and on crest "transformer" voltage for separations of 15 and 50 feet that these were the crest voltages also measured at the "transformer" and the lightning arrester, respectively?

It is interesting to note that the current oscillogram of Figure 3 of the paper for the case of a lightning arrester and transformer in parallel can be approximated, using lumped circuit theory and the concept of superposition. That is, the total lightning arrester current is made up of two components: one due to the traveling wave line current after lightning arrester sparkover and the other due to initial capacitor ("transformer") charge. The first component may be assumed to be approximately that given in Figure 3 of the paper as "arrester current with arrester only." The second component can be calculated, assuming a simple series resistance-inductance-capacitance circuit. If the transformer capacitance C is charged to lightning arrester sparkover voltage (298 kv) and if R is the critical damping resistance (since the oscillograms in Figure 3 of the paper indicate at least critical damping of the oscillatory components), then, the lightning arrester current resulting from the discharge of C is

$$I = \frac{E}{L} t\epsilon^{-\frac{R}{2L}}$$

where

$$R = 2\sqrt{\frac{L}{C}}$$

Using $L = 10$ microhenrys for the total inductance of the capacitor-lightning arrester loop with $C = 3{,}100$ micromicrofarads and $R = 113.4$ ohms, the calculated discharge due to the charged capacitor is shown in Figure 1 of this discussion, which also shows that the calculated "total lightning arrester current" agrees very closely in magnitude with that shown in Figure 3 of the paper. The calculated effective rate or rise of current, however, is somewhat higher than that measured, indicating perhaps that the loop inductance in the paper was higher than the 10 microhenrys assumed in the calculation.

This simple analysis tends to lend a supporting argument to the observation that field measurements of lightning arrester discharge currents should involve an interpretation of the circuit configuration on the magnitude of its influence on the rates of rise and crest magnitude of the lightning arrester discharge currents.

In a previous study by the present writers[1] on the effects of lightning arrester lead length and separation, it was indicated, for separations of ten feet or more between the lightning arrester and the capacitor or transformer, that the voltage to which the capacity of connected apparatus is charged before lightning arrester discharge tends to decrease the oscillatory crest voltage at the transformer below that which would be obtained with no initial voltage on the capacitance of the connected apparatus. In this regard it would have been of interest for the author to have extended the study of the effect of lightning arrester sparkover voltage on crest lightning arrester discharge voltage and crest transformer voltage beyond the one reported for separations of five feet between lightning arrester and transformer to the other cases considered of 15- and 50-foot separations.

In connection with two parallel lightning arresters at the connected apparatus, the question is raised on the discharge ability of each lightning arrester to be used to handle currents of low magnitude but relatively long duration (several thousand microseconds) caused by lightning or switching surges, particularly where these surges are such that only one lightning arrester may spark over.

Finally, it is to be mentioned again that the paper is concerned only with lightning arrester discharge currents resulting from traveling waves arriving over one mile of overhead line. Other lightning arrester discharge currents that may be more severe result from strokes near or at the lightning arrester even on systems with overhead ground wires. An example of this in the literature[2] is a lightning arrester discharge current of 16,000 amperes in a 132-kv station. The stroke occurred within 400 feet of the station even though the station and line were shielded. It appears, therefore, that lightning arrester discharge currents from strokes near or at lightning arresters should be evaluated in their effects on lightning arrester protective characteristics and location with regard to the station apparatus being protected.

REFERENCES

1. See reference 1 of the paper.

2. LIGHTNING INVESTIGATION ON 132-KV SYSTEM OF AMERICAN GAS AND ELECTRIC COMPANY, **I. W. Gross, G. D. Lippert.** *Electrical Engineering* (*AIEE Transactions*), volume 64, February 1945, pages 76–84.

I. W. Gross (American Gas and Electric Service Corporation, New York, N. Y.): The study by Mr. Kalb is particularly interesting as it reports actual tests simulating what may be expected in practice. In this respect, it is somewhat more convincing than where theory alone is applied.

Some 15 years ago, when commercial impulse testing of transformers was first started, we initiated a test whereby an impulse voltage surge much in excess of the transformer strength was applied to the transformer with the lightning arrester directly connected at or near the transformer terminals. It was shown there that with steep front surges applied to the transformer and a separation of 25–50 feet between the lightning arrester and the transformer, the voltage at the transformer could be as much as 50 per cent higher than that measured at the lightning arrester. Also some rather surprising information was apparent on the lightning arrester performance which differed radically from data on lightning arresters published at that time. This

test, in a sense, somewhat simulates the test method employed by Mr. Kalb and gave comparable results.

It is shown clearly in Figures 4 and 8 of the paper that the voltage at the transformer, where the lightning arrester is some distance away, rises sharply for a short period of time and then drops to a value near the lightning arrester protective level (IR drop).

The steep front test on transformer insulation is important, to insure that a commercial transformer does have the relatively high voltage strength at short times which it is supposed to have. The chopped wave test alone now used is not sufficient for this purpose.

The better protection reported by multiple lightning arresters at a given location is most interesting. It does, however, raise two points. First, can commercial lightning arresters be relied upon to have sufficiently close tolerance so that if one lightning arrester functions the other also will come into action? It would seem that after one lightning arrester operated and limited the voltage, the other lightning arrester would not come into action at all. Perhaps the author has an excellent explanation why this did not occur in his tests. The other point is, why not increase the cross section of the active element in the lightning arrester and accomplish the same result as two lightning arresters in parallel?

It is brought out clearly in the author's tests that the "distance factor" has to be considered and evaluated in the over-all protection of a station. The idea that the impulse level for a given system voltage can be the same in all parts of the station and all the equipment can be equally well protected is fallacious unless a lightning arrester is placed at or close to every piece of equipment in the station. This, of course, is impractical. It seems preferable to place different classes of equipment at different impulse levels in a station if only one set of lightning arresters is used; or a different viewpoint can be taken: that the most expensive and important piece of equipment (such as the transformer) will be protected by the lightning arrester and a calculated risk will be taken on breakdown of insulation at other points in the station.

S. B. Howard (General Electric Company, Pittsfield, Mass.): Mr. Kalb's tests have demonstrated a phenomenon long familiar to those who have made laboratory impulse tests on transformers and lightning arresters in combination. Whether or not there will be an appreciable increase in lightning arrester discharge voltage produced by high-rate current discharge from adjacent apparatus capacitance is, however, somewhat dependent on the nature of the circuit supplying the impulse current to the apparatus-lightning arrester combination.

In the tests, an impulse generator of finite capacity was coupled to the apparatus under test by a 1-mile 115-kv class transmission line having a surge impedance of 450 ohms. Under these conditions, the current reaching the line termination was essentially a free traveling wave, limited by the line surge impedance and the line-insulation flashover level (about 650 kv). The lightning arrester current would have had a theoretical maximum of $2\times650/450=2{,}900$-ampere crest, which is a reasonably close check on the 2,350-ampere crest reported by Mr. Kalb through a 97-kv lightning arrester alone with a 650-kv surge impressed. The difference, of course, is accounted for primarily by the effect on the crest current of the lightning arrester impedance itself.

Similarly in Mr. Kalb's tests, when the lightning arrester is paralleled by the "transformer" capacitance, the 450-ohm surge impedance of the supply circuit confines the flow of current from the capacitance, after lightning arrester sparkover, to the local circuit consisting of lightning arrester, paralleling capacitance, and whatever small impedance exists between the two. It is not surprising, then, that the rate of rise of this local current would be high, and that it would produce the observed increase in lightning arrester discharge current and voltage.

Consider now the currents which have been measured in field investigations of discharges through lightning arresters in stations up to the 138-kv class. An average of the results of several of these investigations[1-3] will show that about 5 per cent of the lightning arrester discharge currents will exceed 5,000 amperes crest; about 1 per cent, 10,000 amperes. These currents are far in excess of the theoretical maxima which could result from free-traveling-wave currents over line surge impedance without flashover of line insulation, even allowing for the small increase resulting from the apparatus-capacitance discharge into the lightning arrester at sparkover.

It is obvious that Mr. Kalb's approach, based on a free traveling wave over line surge impedance, cannot take care of a substantial percentage of lightning arrester discharge currents measured in service. In fact, nearly 15 per cent of the measured lightning arrester discharge currents exceed the 2,410-ampere maximum reported by Mr. Kalb from his tests. Yet it is upon these higher currents that practical insulation co-ordination must be based. Therefore, his conclusions, generally speaking, are open to question, since they are based on assumptions incompatible with the more severe service conditions.

The higher lightning arrester discharge currents measured in service are explainable on the basis of the lightning stroke contacting the circuit close to the protected apparatus. Under this condition, the lightning arrester discharge current would not—as in the tests—be limited by line surge impedance, but would depend primarily on the characteristics of the stroke itself. Similarly, we are of the opinion that current discharged from apparatus capacitance into the lightning arrester at sparkover would have only a minor effect on lightning arrester discharge voltage at the higher levels of discharge current.

Mr. Kalb has claimed that two lightning arresters operating directly in parallel will provide a lower discharge voltage than one. In addition to the obvious disadvantages of higher cost and greater space requirement, the second lightning arrester in this arrangement can only spark over as the result of discharge voltage appearing across the first lightning arrester to operate. For any two individual lightning arresters in parallel, there will be some particular discharge current value below which the first lightning arrester would have to discharge the entire surge.

Assuming a lightning arrester of balanced design, wherein the impulse sparkover is set at approximately the discharge voltage level selected for insulation co-ordination, the second lightning arrester would operate only for currents in excess of the co-ordination current, say about 5,000 amperes crest. Hence, the required margin of protection must be obtained with only one lightning arrester operating. The latter condition is, of course, satisfied by the balanced protective levels available with the modern station-type lightning arresters, co-ordinated with modern apparatus insulation levels in all voltage classes.[4]

Assuming a lightning arrester having unusually low sparkover compared to its discharge voltage, there are possibilities of operating problems: first, from too low sparkover on 60-cycle voltage under certain service conditions; second, from unnecessary operations of the lightning arrester on switching surges.

For the latter case, the lightning arrester current associated with most switching surges will be so low that a parallel lightning arrester having a safe spark potential as related to system power voltage will not spark over on the discharge voltage of the first lightning arrester to operate. Therefore, the second lightning arrester can offer no reinforcement to any inadequacy of discharge capacity of the first lightning arrester. However, many switching surge currents, being of very long duration compared to the usual lightning currents, constitute the most severe type of duty on the one lightning arrester that operates.

This naturally raises the question of the lightning arrester's ability to discharge without damage repeated long-duration low-current switching and lightning surges and multiple-stroke currents. During the evolution of station-type lightning arresters in the United States, long-duration discharge capacity has been an important design criterion. The modern station-type lightning arrester has demonstrated by extensive service experience its ability to withstand successfully such discharge duty.

Regarding the use of a second lightning arrester located at accessory equipment and applied primarily for the protection of that equipment, we have long advocated this practice. Such an application is, of course, predicated on the improvement in protection to the accessory equipment obtained by minimizing the separation between the second lightning arrester and the accessory equipment.

Mr. Kalb has reported no benefit in his tests from the "V" connection of incoming line to the lightning arrester as compared with the "T" connection. This is contrary to the results obtained in earlier tests by other investigators. In particular, the value of the "V" connection in reducing total voltage at the apparatus terminals was first called to the attention of the industry in 1931 by K. B. McEachron and E. J. Wade,[5] and has received general acceptance in the industry for many years.

References

1. Lightning Currents in Arresters at Stations, I. W. Gross, W. A. McMorris. *Electrical*

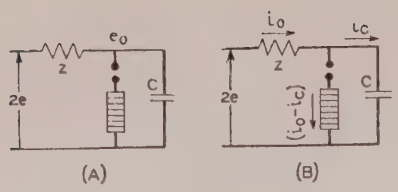

Figure 2

Engineering (*AIEE Transactions*), volume 59, August 1940, pages 417–22.

2. Field Research on Lightning Arrester Discharges, G. D. McCann, Edward Beck. *AIEE Transactions*, volume 66, 1947, pages 625–30.

3. See reference 3 of the paper.

4. See reference 7 of the paper.

5. Field Tests on Thyrite Lightning Arresters, K. B. McEachron, E. J. Wade. *AIEE Transactions*, volume 50, June Section, 1931, pages 479–89.

L. V. Bewley (Lehigh University, Bethlehem, Pa.): Mr. Kalb gives test data showing that the lightning arrester voltage is increased somewhat by the presence of terminal capacitance. He explains that this is because the capacitance becomes charged to the lightning arrester sparkover voltage, and thereafter consitutes an additional source of energy discharging into the lightning arrester. I should like to outline how this effect may be calculated, and to suggest that Mr. Kalb carry out such a numerical calculation corresponding to the characteristics and constants of the circuit which he tested. I cannot do so, as I do not have the lightning arrester characteristics. If Mr. Kalb will submit such a calculation I am sure that it will enhance the value of his paper, for once the matter has become predictable its engineering value will have reached a most satisfactory state.

The equivalent circuit for a traveling wave, e, on a line of surge impedance, z, terminating in a lightning arrester and capacitance in parallel is shown in Figure 2 of this discussion.

Before the lightning arrester gap sparkover the terminal voltage e_0 corresponding to a typical traveling wave $e=E(\epsilon^{-at}-\epsilon^{-bt})$ is, putting $\alpha=1/zC$,

$$e_0=\frac{1/pC}{1/pC+z}\,2e=\frac{2e}{zCp+1}=\frac{2E(\epsilon^{-at}-\epsilon^{-bt})}{zCp+1}$$
$$=2\alpha E\left[\frac{\epsilon^{-at}}{\alpha-a}-\frac{\epsilon^{-bt}}{\alpha-b}-\frac{(a-b)\epsilon^{-at}}{(\alpha-a)(\alpha-b)}\right] \quad (1)$$

Suppose the gap sparks over when this voltage reaches some value $e_0=E_0$ at time $t=t_0$. Thereafter the capacitance charged to voltage E_0 will discharge in parallel with the line into the lightning arrester. If the nonlinear lightning arrester characteristic is $i_a=f(e_0)$, then

$$i_c=C\frac{de_0}{dt}=\text{capacitor current} \quad (2)$$

$$i_0=(2e-e_0)/z=\text{line current} \quad (3)$$

$$i_0-i_c=f(e_0)=\text{lightning arrester current} \quad (4)$$

From equations 2, 3, and 4 of this discussion the ruling differential equation is

$$\frac{de_0}{dt}=\frac{2e-e_0-zf(e_0)}{zC} \quad (5)$$

Since the lightning arrester has a nonlinear characteristic, it is necessary to solve this equation by some step-by-step or numerical method. Substituting increments for differentials and rearranging

$$\Delta e_0=\frac{2e-e_0-zf(e_0)}{zC}\,\Delta t \quad (6)$$

and this is solved readily according to the tabular schedule in Table I:

Table I

t	Δt	$2e$	e_0	Δe_0	$f(e_0)$
(1)	(2)	(4)	(6)	(8)	(7)
(3)		(5)	(9)		(10)

The first entry (1) is the time of gap sparkover t_0. Adding to this a reasonable increment Δt, (2), we find the new time (3). Corresponding to times (1) and (3) are the traveling wave voltages $2e$, (4), and (5). As item (6) is the voltage E_0 at sparkover as computed from equation 1 of this discussion. The initial lightning arrester current corresponding to E_0 is entered as item (7). The increment Δe_0 in lightning arrester voltage is computed from equation 6 of this discussion and entered as item (8), which added to (6) gives (9). And corresponding to the new lightning arrester voltage (9) is the new lightning arrester current (10). The sequence of calculations is then continued.

If the lightning arrester were a pure resistance R, then we would have

$$f(e_0)=\frac{e_0}{R} \quad (7)$$

and equation 5 would become

$$\frac{de_0}{dt}=\frac{2e-e_0-e_0z/R}{zC} \quad (8)$$

$$\frac{de_0}{dt}+\frac{R+z}{zCR}\,e_0=\frac{2E}{zC}(\epsilon^{-at}-\epsilon^{-bt}) \quad (9)$$

The solution to this equation, subject to the initial condition that $e_0=E_0$ at $t=t_0$, is

$$e_0=\left[E_0-2E\left(\frac{\epsilon^{-at_0}}{\beta-a}-\frac{\epsilon^{-bt_0}}{\beta-b}\right)\right]\epsilon^{-\beta(t-t_0)}+$$
$$2E\left(\frac{\epsilon^{-at}}{\beta-a}-\frac{\epsilon^{-bt}}{\beta-b}\right) \quad (10)$$

in which $\beta=(R+z)/zCR$. If there were no capacitance, the voltage at the resistance would be

$$e_0=\frac{2RE}{R+z}(\epsilon^{-at}-\epsilon^{-bt}) \text{ for } C=0 \quad (11)$$

A numerical comparison of equations 10 and 11 would show the effect of the capacitance in increasing the voltage, depending, of course, on the voltage E_0.

A good approximation to the effect of a short length of line between the lightning arrester and the terminal capacitance is to replace the short length of line by its inductance L, as shown in Figure 3 of this discussion.

Then, if the lightning arrester voltage is taken as

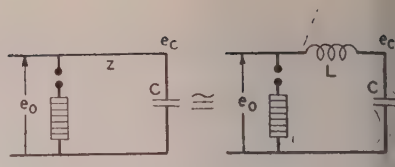

Figure 3

$$e_0=E(\epsilon^{-at}-\epsilon^{-bt}) \quad (12)$$

the differential equation for voltage at the capacitance is

$$LC\frac{d^2e_0}{dt^2}+e_0=e_0=E(\epsilon^{-at}-\epsilon^{-bt}) \quad (13)$$

and the solution to this is, putting $\omega=\sqrt{1/LC}$,

$$e_c=E\left[\left(\frac{\omega a}{a^2+\omega^2}-\frac{\omega b}{b^2+\omega^2}\right)\sin\omega t-\right.$$
$$\left(\frac{\omega^2}{a^2+\omega^2}-\frac{\omega^2}{b^2+\omega^2}\right)\cos\omega t+$$
$$\left.\left(\frac{\omega^2\epsilon^{-at}}{a^2+\omega^2}-\frac{\omega^2\epsilon^{-bt}}{b^2+\omega^2}\right)\right] \quad (14)$$

This equation includes oscillatory terms of the same nature as those shown in Figures 4 and 8 of the paper. It would be interesting and worth while if Mr. Kalb would undertake a numerical comparison; for if a good numerical check is obtained, and the approximation thereby justified, then design curves can be prepared of considerable use to operating engineers.

R. L. Witzke and **T. J. Bliss** (Westinghouse Electric Corporation, East Pittsburgh, Pa.): Mr. Kalb's paper is a valuable addition to the available literature on the general subject of insulation co-ordination and substation protection. Laboratory tests, as conducted by Mr. Kalb, give us results that are very useful in checking similar studies made on the transient analyzer or analogue computer. Broad studies can be made to best advantage on the analyzer or computer because of the inherent flexibility of the computing devices. However, our faith in the results obtained is improved considerably if the answers obtained compare favorably with laboratory and field tests.

Figure 4 of the paper shows the voltage at a transformer, represented by a 3,100-micromicrofarad capacitor, with the lightning arrester 50 feet ahead of the transformer and with a 30-foot downlead. In this test the author obtained a crest voltage of 438 kv at the transformer. As a matter of interest, we checked this case using the analogue computer data in our paper "Co-ordination of Lightning Arrester Location with Transformer Insulation Level".[1] Assuming an incoming surge having a rate-of-rise of 42 kv per microsecond and a crest of 590 kv which corresponds to the incoming surge used by Mr. Kalb, we obtain a crest transformer voltage of 475 kv. Our voltage is 8 per cent higher than Mr. Kalb's even though we used a maximum lightning arrester discharge voltage based on a 10×20 microsecond lightning arrester current. This comparison shows that the procedure outlined in our paper are sufficiently conservative for general application purposes.

Calculation of Transformer Voltage by Method of Reference 1

Incoming surge voltage from Figure 4 of the Kalb paper:

$e = 590$ kv

$\frac{de}{dt} = 421$ kv per microsecond

Lightning arrester and lead voltages: From Table VII of Reference 1:

$E_0 = 314$ kv
$R = 8.3$ ohms

$$I = \frac{2 \times 590 - 314}{450 + 8.3} = 1.89 \text{ ka}$$

$$\frac{di}{dt} = \frac{2 \times 421}{450} = 1.87 \text{ ka per microsecond}$$

$L = 30 \times 0.4 = 12$ microhenrys

Lead drop

$$L\frac{di}{dt} = 22.5 \text{ kv}$$

$IR = 15.7$
$E_0 = 314$
$E_s = 352.2$ kv

Transformer voltage:

$$F = \frac{352.2}{421} = 0.835 \text{ microsecond}$$

$s/v = 50/1{,}000 = 0.05$ microsecond

$$\frac{s/v}{F} = 0.06$$

$ZC = 450 \times 3{,}100 \times 10^{-6} = 1.4$ microseconds

$$\frac{ZC}{F} = 1.68$$

From Figure 6 of Reference 1:

$$\frac{E_r}{E_s} = 1.35$$

$E_r = 1.35 \times 352.2 = 475$ kv

REFERENCE

1. See reference 6 of the paper.

H. L. Rorden (Bonneville Power Administration, Portland, Oreg.): The rating of a lightning arrester is determined by the power frequency voltage which the lightning arrester is capable of sealing off. Once this level has been determined for a lightning arrester, it is desirable to maintain as narrow a margin as possible between this seal-off level and the discharge protective level. This margin, plus a factor of safety between the protective level of the lightning arrester and the basic insulation level of station equipment, determines the minimum insulation level to which station equipment may be designed. Both of these margins, therefore, contribute to the basic insulation level that can be adopted for any operating voltage level. These margins are responsible for a sizable fraction of the cost of high-voltage transmission equipment, such as transformers and circuit breakers. Ideally, a lightning arrester protective level could be the same as the lighting arrester rating or seal-off level (crest), which undoubtedly can never be achieved in a valve-type lightning arrester. It is desirable to have the protective level of a lightning arrester approach the ideal as closely as possible, since this will increase the protective margin according to present practice and may ultimately contribute to revising basic insulation levels downward. This, in turn, contributes to the economy and efficiency of transmission of power at high voltages.

In this respect, we are particularly interested in Mr. Kalb's contribution to the performance of lightning arresters for station protection. Mr. Kalb shows that by providing a low lightning arrester impulse sparkover voltage, the maximum lightning arrester discharge voltage is lower even though its crest may be higher than the initial sparkover voltage. It seems desirable to maintain gap flashover as low as possible commensurate with the magnitude of surges for which the lightning arrester should not discharge. By reducing gap flashover, the protective level of the lightning arrester described by Mr. Kalb is reduced accordingly, which is a desirable step in lightning arrester performance.

Mr. Kalb also has contributed further information on the timely question of lightning arrester separation from the protected equipment. It is our belief that considerably more work of this nature is desirable. Unquestionably, the lowest protective level is maintained when the lightning arrester is placed as near as possible to the protected equipment. However, present practice indicates that this close relationship is not always necessary, particularly in large stations containing considerable distributed capacitance as well as a multiplicity of lines terminating on the bus. For the case of a single line entering a station with perhaps only a single transformer bank, the overvoltages at the transformer terminal could readily become important if the lightning arrester were located some distance away, as Mr. Kalb has shown. The question is complicated because the peak of the initial oscillation, as shown in Figure 4 of the paper, occurs within the time at which transformer insulation has a withstand strength somewhat in excess of the critical level.

Little data are available on lightning arrester location for stations representing various combinations of impedances. Of particular importance in the question of lightning arrester location is that of protection for the circuit breaker if the lightning arrester is placed close to the transformer. Present practice indicates that it is not ordinarily necessary to provide separate lightning arrester protection for transformers and circuit breakers. However, when basic insulation levels are revised downward, this might prove to be a question of considerable importance.

J. W. Kalb: With regard to Mr. Opsahl's discussion, the paper does not attribute higher discharge voltage entirely to rapid rate of discharge of the apparatus capacitance into the lightning arrester valve element, but rather to the combined effect of the apparatus capacity which "discharges through the lightning arrester at an initial rate of current rise which may exceed that of the incoming surge, while concurrently the incoming surge front continues to arrive."

With this consideration it seems that the author and Mr. Opsahl are in basic agreement on the cause of these higher voltages. Calculations based on Figures 1 and 4 of this discussion show that there may be initial discharge of the apparatus capacity into the lightning arrester which contributes to the increase in discharge voltage. Whether the apparatus capacity voltage quickly increases or decreases seems to depend upon values assumed for L^* and the characteristics of I_1 of Figure 4 of this discussion.

It is reasonable that this time-voltage effect is dependent upon valve block diameter, as Mr. Opsahl says, because of the lower current densities in larger blocks. However, such an effect need only be true for blocks of the same basic composition. If valve elements of different diameters have the same discharge voltage, this is evidence that comparison of other performance aspects, on the basis of diameter alone, cannot always be employed.

Mr. Gross asks two questions regarding parallel operation of lightning arresters: (1) Is the tolerance of commercial lightning arresters adequate to guarantee operation of the second lightning arrester? (2) Why not increase the valve block cross section of one lightning arrester and achieve the same results?

Consider the 97-kv lightning arresters

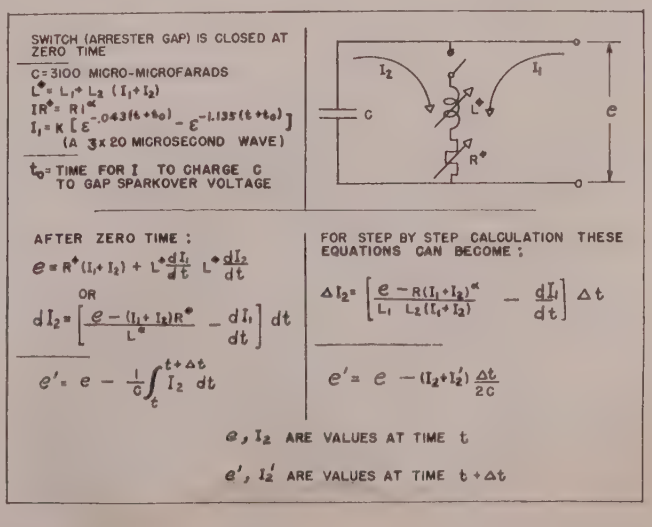
SWITCH (ARRESTER GAP) IS CLOSED AT ZERO TIME
C = 3100 MICRO-MICROFARADS
$L^* = L_1 + L_2\ (I_1 + I_2)$
$IR^* = RI^{\alpha}$
$I_1 = K\left[\varepsilon^{-.043(t+t_0)} - \varepsilon^{-1.135(t+t_0)}\right]$
(A 3 x 20 MICROSECOND WAVE)
t_0 = TIME FOR I TO CHARGE C TO GAP SPARKOVER VOLTAGE
I_2
I_1
C
L^*
R^*
e
AFTER ZERO TIME :
$e = R^*(I_1 + I_2) + L^*\frac{dI_1}{dt} L^*\frac{dI_2}{dt}$
OR
$dI_2 = \left[\frac{e - (I_1 + I_2)R^*}{L^*} - \frac{dI_1}{dt}\right] dt$
$e' = e - \frac{1}{C}\int_t^{t+\Delta t} I_2\ dt$
FOR STEP BY STEP CALCULATION THESE EQUATIONS CAN BECOME :
$\Delta I_2 = \left[\frac{e - R(I_1 + I_2)^{\alpha}}{L_1 L_2 (I_1 + I_2)} - \frac{dI_1}{dt}\right] \Delta t$
$e' = e - (I_2 + I_2')\frac{\Delta t}{2C}$
e, I_2 ARE VALUES AT TIME t
e', I_2' ARE VALUES AT TIME $t + \Delta t$

Figure 4. Circuit and basic equations for calculations of lightning arrester discharge voltage with apparatus capacitance in parallel

used during the tests. The maximum front of wave sparkover voltage of these lightning arresters is 328 kv, using 808 kv per microsecond rate of rise. The maximum critical 1.5×40 sparkover voltage is 265 kv. Assuming surge current fronts in the range of 3–10 microseconds, the second of two parallel lightning arresters should always operate on surges of 2,000 amperes or more, because of the discharge voltage of the first lightning arrester. Lightning arresters of higher maximum sparkover voltage will, of course, require higher discharge voltage to operate the second lightning arrester.

As suggested, the same result can be achieved by increasing the cross section of the active element, but this results in more severe interrupting duty on the gap element and increases the size and cost of other lightning arrester components. It then becomes a question of choosing the most satisfactory over-all design for general purpose apparatus protection.

Mr. Howard questions the conclusions regarding the effect of apparatus capacitance on lightning arrester discharge voltage because they are based on traveling waves. Since the conclusions were drawn only for free traveling waves, on a system with some ground wire protection, they are not concerned with conditions resulting from direct strokes to the station or to the line near the station. However, the calculations according to Figure 4 of this discussion are interesting because they show that the phenomenon explored in these tests takes place for the higher current direct-stroke type of surges mentioned by Messrs. Howard, Johnson, and Saline.

The assumed current waves for these calculations were 3×20 microseconds, 2,350 and 10,000 crest amperes, independent of circuit loading. The basic equivalent circuit of the lightning arrester valve element for positive rates of current change was obtained empirically by comparing discharge voltage oscillograms obtained with 10×20 microsecond current waves of 100 to 35,000 amperes. The constants were chosen to duplicate essentially the post-sparkover portion of the left-hand voltage oscillogram of Figure 3 in the paper, using a 2,350-ampere 3×20 microsecond current wave. Table II of this discussion shows calculated crest lightning arrester voltages for two current magnitudes, with and without the 3,100-micromicrofarad capacitor. Voltage (e) could be calculated directly for the case of no capacitor C. When the capacitor was considered, step-by-step calculation was necessary.

Table II. Calculated Crest Lightning Arrester Voltage Per Cent of 298-Kv Front-of-Wave Sparkover Voltage

	2,350-Ampere 3×20 Micro-seconds	10,000-Ampere 3×20 Micro-seconds
No capacitor	115	141
3,100-mmf capacitor	133	156

The actual test results in the paper show a crest lightning arrester voltage of 123 per cent rather than the calculated 133 per cent for the case of parallel capacitor and 2,350-ampere wave (as shown in Table II of this discussion), so the calculations are inaccurate to this extent. They show, however, that the same effect exists for the higher lightning arrester discharge currents.

Regarding parallel operation of lightning arresters, this was considered only from the standpoint of apparatus protection; and benefits, as demonstrated in the paper, are quite evident. The higher cost of operating lightning arresters in parallel also must be interpreted in terms of cost per lightning arrester.

I do not understand the concept of "balanced design" mentioned by Mr. Howard. The principal function of a lightning arrester is to protect. If the impulse sparkover voltage is lowered, without affecting the 60-cycle sparkover voltage, it would seem that the lightning arrester then is offering better protection. The possibility of more frequent operations on switching surges is of little interest, provided the lightning arrester can discharge such surges adequately.

It is gratifying to see the recent interest in long-duration discharge strength of lightning arresters, a long-neglected subject. However, the tests described in the paper were made to explore only the relative protection given by the different lightning arrester combinations. It is mentioned that station-type lightning arresters have demonstrated the ability to withstand sufficient service discharge duty. Does this mean that line-type lightning arresters have not demonstrated a similar practical ability to operate satisfactorily in service?

The paper did not report a general lack of benefit from using the V-connection. A footnote in Table IV of the paper called attention to a certain condition of lightning arrester location and surge: "Note that for these particular tests the V-connection showed no benefit over the T-connection." Of course, the V-connection often shows large benefits where lightning arrester separation is necessary.

The analytical methods shown in Professor Bewley's discussion, the comparative figures shown in the discussion by Messrs. Witzke and Bliss, as well as Figure 1 of the discussion by Messrs. Johnson and Saline, are most welcome. We are led, both by convenience and practical necessity, to rely on transient analyzer data or calculation for the broader studies of this sort.

Application of Resonant Grounding in Power Systems in the United States

ERIC T. B. GROSS
FELLOW AIEE

EDWARD W. ATHERTON
ASSOCIATE AIEE

Synopsis: Previous investigations indicated a trend toward increased application of resonant grounding in the United States. The application of resonant grounding in power systems operating at voltages from 2.4 kv to 230 kv has been analyzed on the basis of answers to a questionnaire received from all organizations using such grounding. Experience with resonant grounding has been very satisfactory. The equipment requires practically no maintenance and hardly any attention since detuning is permissible within reasonable margins. The major field of application of resonant grounding is at voltages of 69 kv and below. Operation on sustained faults has been successful in many systems for hours and even days. More equipment designed for extended time rating than for "10-minute" rating has been installed in the last few years. Many users of "10-minute" equipment feel that operation on sustained faults would have additional advantages.

THE latest general AIEE report on Grounding Practices[1] indicates that there is a trend toward greater use of resonant grounding[2] in this country. Figure 1, which is based on this report[3] shows this trend clearly. Amongst the many systems at and above 22 kv that were investigated, 6.8 per cent of the total mileage consisted of lines which belong to systems using resonant grounding.

The fact that resonant grounding is finding wider application in this country, especially at voltages below 115 kv, seems to be of particular significance and this investigation was undertaken in order to answer many pertinent questions with information from organizations with operating experience in this field. Questionnaires were sent to all operators who could provide answers on basis of at least one year's experience and this report covers all systems that had been so operated by the end of 1949. Figure 2 shows how the number of ground fault neutralizers (or Petersen coils, as these reactors are called frequently) increased from one in 1921 to 87 in 1949 and that resonant grounding had been applied in most systems for much longer periods than one year. Figure 2 shows further that there is a trend toward greater use of coils that have continuous rating (or extended time rating as defined in AIEE Standard number 32[4]). Whereas, in 1943, only 18 per cent of the ground fault neutralizers, then in service, were designed to permit operation with sustained ground faults, 40 per cent of nearly twice as many coils permitted such operation in 1949 (an increase in the number of such coils from 9 to 35). The number of "10-minute" coils decreased accordingly from 82 per cent in 1943 to 60 per cent in 1949 and there is reason to believe that the two curves "B" and "C" on Figure 2 will intersect again before long.

Questions and Answers

Grounding Practices

Considering that other grounding methods[1] are well established (74 per cent of all systems[3], corresponding to 78 per cent of the whole mileage under investigation, were solidly grounded), it would appear resonant grounding applications would be confined to new systems and to existing ungrounded (or delta) systems. An analysis of the distribution of grounding methods as indicated in Figure 1 shows, however, that many systems that now are resonant grounded were previously not ungrounded but grounded in some other manner. The answers to the question "what the grounding practices were before the installation of resonant grounding" are summarized in Figure 3. It is somewhat surprising to learn that only 48 per cent of systems at 22 kv and above now resonant grounded were previously delta systems (33 per cent) or new systems (15 per cent), whereas altogether 52 per cent were operated with some kind of neutral grounding before the change to resonant grounding was made. It is of particular interest that a large percentage of systems (35 per cent) had previously been solidly grounded.

This report covers all systems which were or had been in operation with resonant grounding at the end of 1949 and the breakdown of answers from 51 systems is given in the left section of Figure 3. It can be expected that changes from other grounding methods to resonant grounding also will be made in future years. However, it may be mentioned that 9 per cent of all systems[3] reporting in 1947 were then ungrounded, most of them at voltages below 115 kv.

There also were changes from resonant grounding to some other method, though in not many systems. Figure 4 contains a summary of all ground fault neutralizers (single-phase or 3-phase)[17,22] built for use in this country. The number of coils taken out of service is indicated in Figure 5 which contains a classification by voltage and by time rating. Most ground fault neutralizers taken out of service by 1949 were "10-minute" coils (9 of 61 or 14.8 per cent). The reason for discontinuation of resonant grounding was nearly always that interconnection with a large system grounded in a different

Paper 51-64, recommended by the AIEE Protective Devices Committee and approved by the Technical Program Committee for presentation at the AIEE Winter General Meeting, New York, N. Y., January 22-26, 1951. Manuscript submitted October 20, 1950; made available for printing December 7, 1950.

Eric T. B. Gross is Professor of Power Systems Engineering at the Illinois Institute of Technology, Chicago, Ill., and Edward W. Atherton is with the I-T-E Circuit Breaker Company, Philadelphia, Pa. Mr. Atherton was an Instructor in Electrical Engineering at the Illinois Institute of Technology when most of this investigation was made.

The authors want to express their thanks to Harold H. Brown, Cedar Rapids, Iowa, and Eugene Herzog, Dayton, Ohio, for valuable assistance and information in connection with the draft of the questionnaire, and to the administration of Illinois Institute of Technology, especially to E. R. Whitehead, for providing the secretarial help that made this study possible.

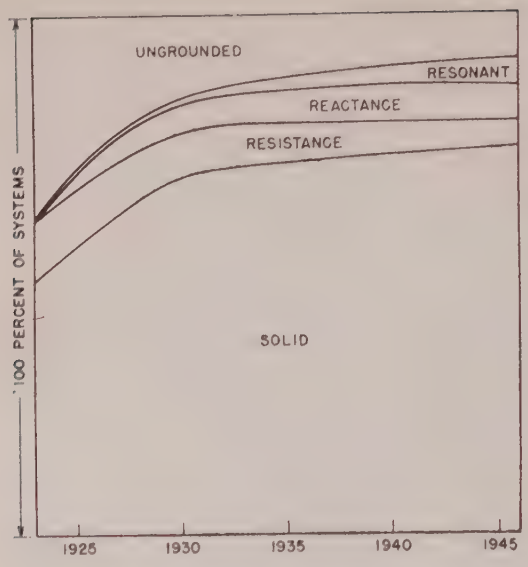

Figure 1 (left). Grounding of power systems in United States at and above 22 kv

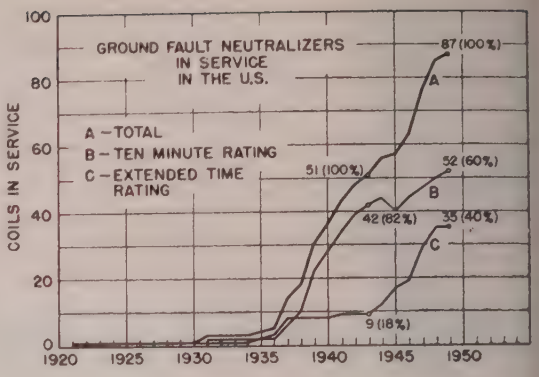

Figure 2 (right). Ground fault neutralizers in service, 1921–1949

manner would necessitate the purchase of a 1-to-1 isolating transformer. We now know that there are many technical and economic reasons to ground 230-kv systems solidly and resonant grounding of the 230-kv system, for example, was never intended to stay in operation after further system expansion.[14]

Figure 6 is a map of the United States showing how the resonant grounded power systems are distributed geographically. Since some of the systems extend into neighboring states, such systems are indicated in a different manner in the state which contains the smaller mileage of lines. Systems which are not resonant grounded any longer are omitted.

Rating of Ground Fault Neutralizer

Answers to the questionnaire were received from 56 systems; this response is quite good since this report now covers 26 more systems[5] than the general grounding report[1] of 1947. In these 56 systems, 23 had "extended time rating" coils installed permitting continuous operation on sustained faults, and 33 systems were operated with "10-minute" coils. However, these data include a few systems that at present (1951) are not operated with resonant grounding. The number of systems with resonant grounding in service is broken down in Figure 7 by voltage and by rating. It is noticeable that in one 140-kv system resonant grounding is still in use, though it now is recognized that the economical balance is at about 115 kv. Most ground fault neutralizers are in operation at system voltages of 69 kv and below.

Line Construction

As for the type of line construction, a number of questions were asked and the breakdown of the answers received is given in Table I.

The maximum and average mileage of the systems classified by voltage is given in Figure 8. One 34.5-kv system comprising 1,500 miles of lines is not only the largest system in operation with resonant grounding, but it also is the largest of all the many 34.5-kv systems in this country. A number of underground cable systems and also some mixed overhead-line and underground-cable systems at and below 13.8 kv are resonant grounded. The special symbol used in Figure 8 at 2.4 kv and 6.6 kv refers to underground cables. The larger number indicates the maximum mileage. The other symbol indicates overhead lines.

Tests

Answers to questions concerning tests indicated the following: Of 56 systems (100 per cent reporting), arcing ground tests at very nearly resonant tuning were made by 67 per cent. Such tests were not made by 33 per cent. Of 48

Table I

		Per Cent
Pole construction (54 systems = 100%)	Wood poles only	67
	Steel towers only	4
	Wood poles and steel towers, and wood poles only	96
	Wood poles and steel towers, and steel towers only	33
Ground wires (static wires) (54 systems = 100%)	Wood poles only	19
	Wood poles and steel towers	41
Insulators (53 systems = 100%)	Suspension-type only	23
	Pin and/or post type only	45
	Suspension-type and others	32
Grounding of hardware on wood poles (54 systems = 100%, wood poles only are in use on 67% of these systems)	Ungrounded hardware	53
	Grounded hardware (only at 35 and 69 kv)	14
Grounding of hardware (48 systems = 100%)	Totally ungrounded	69
	Totally grounded	12
	Partly grounded	19
New transpositions made, either in switching stations or on new structures (52 systems = 100%)	No changes	85
	Some transpositions	15

Table II. Number of Tap Changes Per Year

When Changes in the System Occur					
0	1 to 10	11 to 100	100 to 200	above 200	
27%	25%	29%	15%	0%	4%

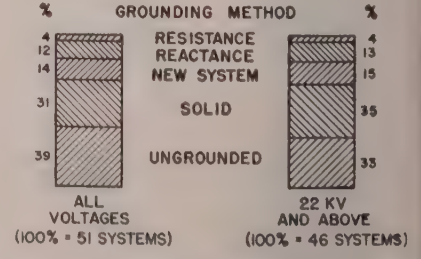

Figure 3. Grounding practices before using resonant grounding

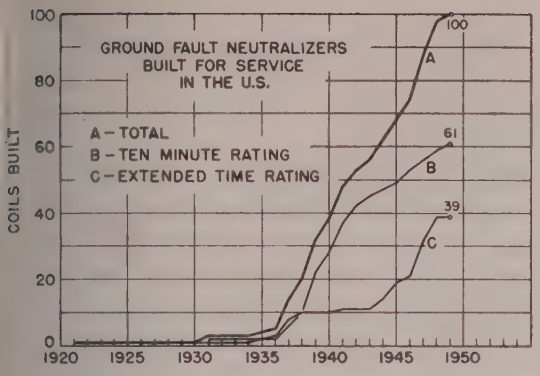

Figure 4 (left). Ground fault neutralizers built for service in the United States, 1921–1949

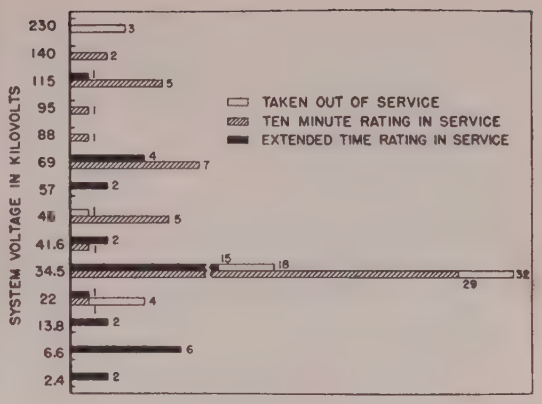

Figure 5 (right). Ground fault neutralizers classified by voltage

Table III. Results of Operation

Rating	Grading of Resonant Grounding as	Number of answers	Grading, Per Cent — Excellent	Good	Fair	Poor
Extended time	Protective device	21	33	53	14	0
Extended time	Economic investment	20	30	60	10	0
10-min. coil	Protective device	29	28	69	3	0
10-min. coil	Economic investment	29	17	69	14	0
All systems	Protective device	50	30	62	8	0
All systems	Economic investment	49	23	65	12	0

systems (100 per cent) reporting on arcing ground tests with large off-tune settings only 31 per cent made such tests; 69 per cent did not. In no case were limits for the maximum permissible out-of-tune ratio established.

Taps and Connection

Some very interesting data concerning taps and the changing of taps for the purpose of retuning were received. Of 45 systems (100 per cent) responding 40 per cent reported that more taps than necessary were available on the ground fault neutralizers that are installed. No one had insufficient taps available; but 60 per cent said the number of taps were just right. However, answers were received from 48 systems (100 per cent) about the number of tap changes per year and these data are broken down in Table II. The questions asked were: "How often are taps changed?" and "What is the average number of changes per year?"

In most cases power transformers are available for the connection of single-phase reactors; hence, of 53 systems (100 per cent) reporting, 70 per cent use power transformers with single-phase coils and only 30 per cent use 3-phase equipment. However, in a few systems when more than one coil is used in the system, and when a power transformer was not avail-

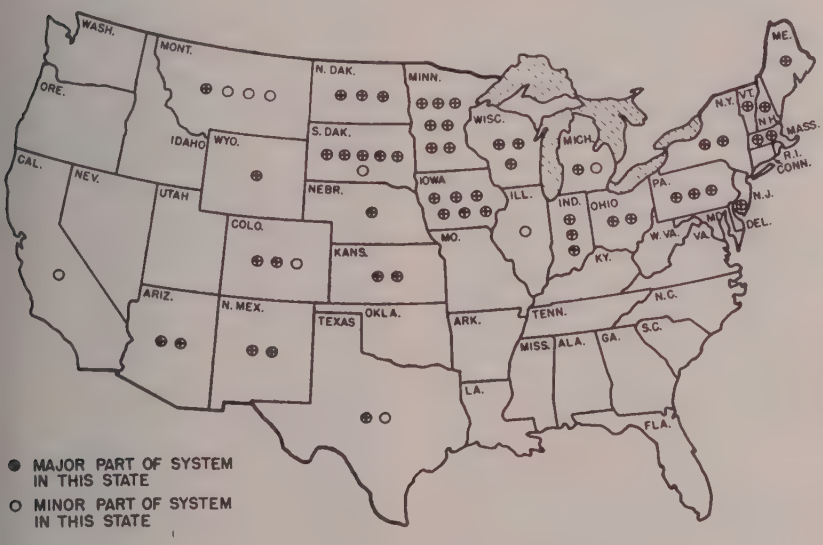

Figure 6 (above). Geographic distribution of resonant grounded systems, 1949

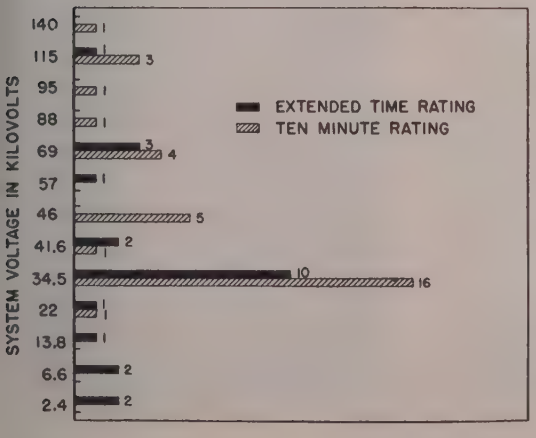

Figure 7 (left). Resonant grounded systems classified by voltage

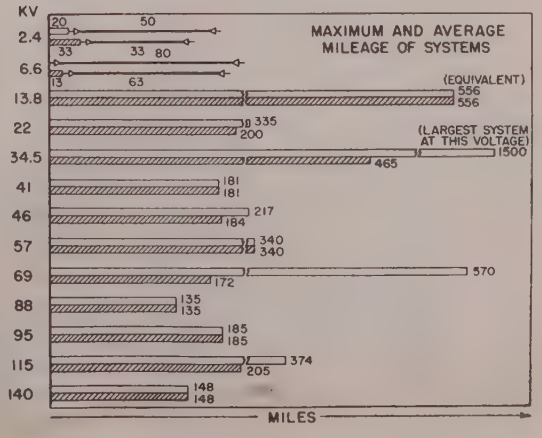

Figure 8 (right). Mileage of resonant grounded systems classified by voltage

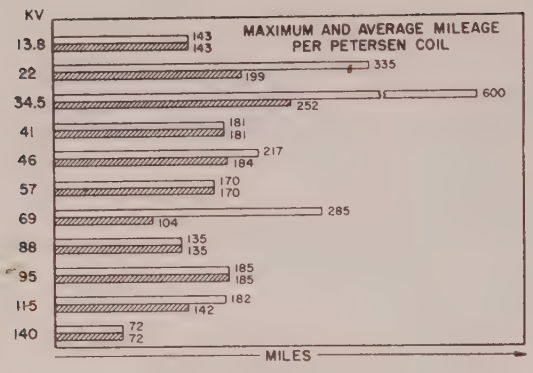

Figure 9 (left). Mileage of circuit per ground fault neutralizer classified by voltage

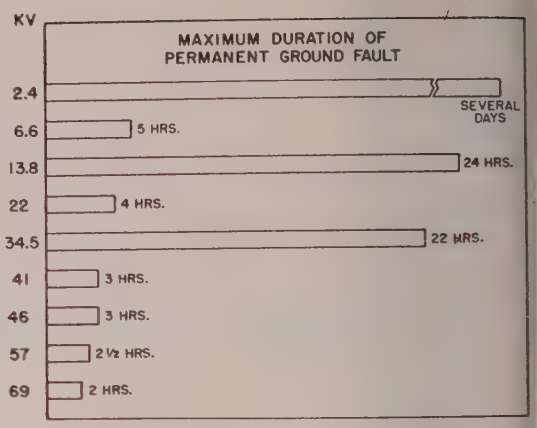

Figure 10 (right). Maximum duration of sustained ground faults classified by voltage

able everywhere, one or more of the coils were single-phase coils and the others were 3-phase equipment. Figure 9 shows the maximum and average mileage of circuit per coil at various voltages; the larger figure refers, of course, to the maximum mileage.

Permanent Faults

It is interesting that the advantages of extended time rating coils were utilized at all voltages up to 69 kv. Operation with permanent faults was continued for several days at 2.4 kv and the maximum duration of sustained ground faults became shorter at higher voltages, as Figure 10 shows. Though very satisfactory results have been achieved in all systems using coils with continuous rating (extended time rating), difficulties are sometimes experienced in finding the location of sustained faults. Of 22 systems (100 per cent) using such coils, 46 per cent have difficulties locating the fault; 54 per cent find it easy to detect the permanent fault. However, 17 answers (100 per cent) received to the question concerning the desirability of a sensitive relaying system for the determination of the fault[16] location, indicate that a very large number, 94 per cent, want such a relaying system developed and only 6 per cent do not think that relays are necessary.

Of 28 systems (100 per cent) using "10-minute" coils answering the question concerning their preference for the use of larger coils designed for continuous operation, 32 per cent said they would now install the larger coils in order to have the additional advantages of operation with sustained faults; 68 per cent are satisfied with what they have. Figures 11 and 12 show large ground fault neutralizers designed for extended time rating. The Petersen coil shown in Figure 11 is the largest coil of such design in operation in this country, its rating is 15,000 equivalent kilovolt-amperes.

Grading of Results

Answers to the questions for general grading based on observed operations are summarized in Table III. The average is between good and excellent especially on equipment with extended time rating.

Conclusions

1. Experience with resonant grounding has been very satisfactory.
2. There is a trend toward increased use of resonant grounding.
3. There is a trend toward the application of coils designed for extended time rating. (Operation with sustained ground faults.)
4. A sensitive ground relaying system for indication of the fault location would bring further improvements. The development of such relays is desirable.
5. In most cases, power transformers are available and the cheaper single-phase coils can be used.
6. The major field of application of resonant grounding is from 69 kv down to 2.4 kv.
7. Ground fault neutralizers require practically no maintenance. The tap changers are hardly ever operated. The systems may be operated off-tune without influence on the protective characteristics.
8. Operation on sustained faults has been successful for hours and even for days.
9. The increase of system mileage does not seem to limit the application of resonant grounding at voltages of 69 kv and below. The largest 34.5-kv system in the United States (1,500 miles total mileage) is resonant grounded.

Acknowledgment

The authors acknowledge the assistance of the following organizations which supplied pertinent data for this study:

Black Hills Power and Light Company, Rapid City, S. D.
Carnegie-Illinois Steel Corporation, Pittsburgh, Pa.
Central Maine Power Company, Augusta, Me.
Central Nebraska Public Power and Irrigation District, Hastings, Nebr.

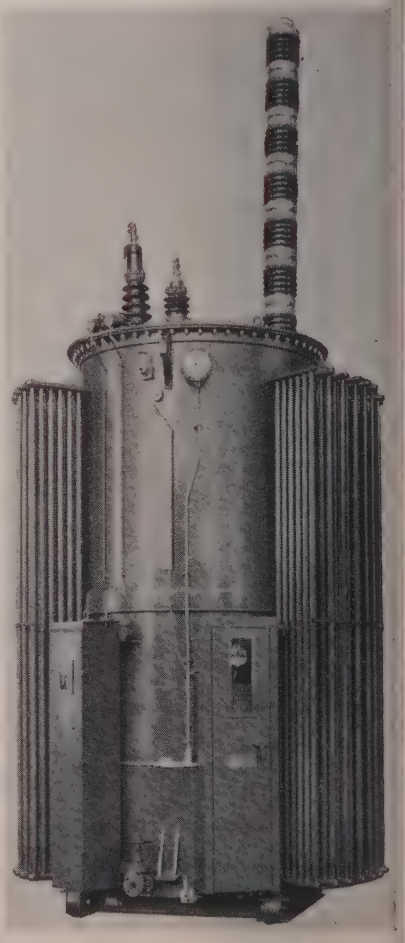

Figure 11 (right). Ground fault neutralizer for extended time rating for a 115-kv system, 180-amperes maximum current. Lightning arrester on cover, high-voltage bushing in rear. Courtesy General Electric Company

City Electric Department, Rochester, Minn.
Consumers Power Company, Jackson, Mich.
Dayton Power and Light Company, Dayton, Ohio
Dairyland Power Cooperative, LaCrosse, Wis.
Department of the Army, Corps of Engineers, Fort Peck District, Fort Peck, Mont.
Eastern Kansas Utilities, Inc., Fort Scott, Kan.
Georgia Power Company, Atlanta, Ga.
Indianapolis Power and Light Company, Indianapolis, Ind.
Interstate Power Company, Dubuque, Iowa
Iowa Electric Light and Power Company, Cedar Rapids, Iowa
Iowa Power and Light Company, Des Moines, Iowa
Iowa Public Service Company, Waterloo, Iowa
Kansas Gas and Electric Company, Wichita, Kan.
Lake Superior District Power Company, Ashland, Wis.

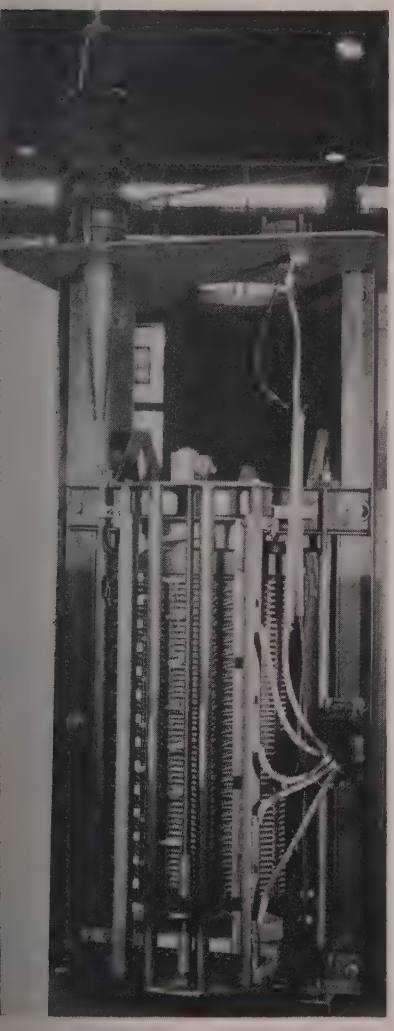

Figure 12. Ground fault neutralizer for extended time rating for a 69-kv system, 40-amperes maximum current. Core and coil assembly. Courtesy Westinghouse Electric Corporation

Metropolitan Edison Company, Reading, Pa.
Minnesota Power and Light Company, Duluth, Minn.
Minnkota Power Cooperative, Inc., Grand Forks, N. D.
Montana Dakota Utilities Company, Minneapolis, Minn.
New England Power Service Company, Boston, Mass.
New Jersey Power and Light Company, Dover, N. J.
New York State Gas and Electric Corporation, Binghamton, N. Y.
Northern Pennsylvania Power Company, Towanda, Pa.
Northern States Power Company, Minneapolis, Minn.
Northwestern Public Service Company, Huron, S. D.
Otter Tail Power Company, Fergus Falls, Minn.
Public Electric Light Company, St. Albans, Vt.
Public Service Company of Colorado, Denver, Colo.
Public Service Company of Indiana, Inc., Indianapolis, Ind.
Public Service Company of New Hampshire, Manchester, N. H.
Public Service Company of New Mexico, Albuquerque, N. M.
Rockland Light and Power Company, Boston, Mass.
Rural Cooperative Power Association, Maple Lake, Minn.
Sioux City Gas and Electric Company (Iowa Public Service Co.,) Sioux City, Iowa
Southern California Edison Company, Los Angeles, Calif.
Southern Indiana Gas and Electric Company, Evansville, Ind.
Southwestern Public Service Company, Amarillo, Tex.
U. S. Department of the Interior, Bureau of Reclamation, Denver, Colo.
Westinghouse Electric Corporation, East Pittsburgh, Pa.
Wisconsin Michigan Power Company, Appleton, Wis.

References

1. Present Day Grounding Practices on Power Systems, AIEE Committee Report. *AIEE Transactions*, volume 66, 1947, pages 1525–51.

2. The Why and How of Resonant Grounding, **Eric T. B. Gross.** *Electric Light and Power* (Chicago, Ill.), volume 25, July and August 1947.

3. Reference 1, page 1526.

4. Neutral Grounding Devices. AIEE Standard Number 32, 1947.

5. Reference 1, Table 25, page 1543.

6. The Relation of the Petersen System of Grounding Power Networks to Inductive Effects in Neighboring Communication Circuits, **H. M. Trueblood.** *Bell System Technical Journal* (New York, N. Y.), volume 1, 1922, page 39.

7. Operating Performance of a Petersen Earth Coil, **J. M. Oliver, W. W. Eberhardt.** *AIEE Transactions*, volume 42, 1923, page 435–45 and volume 45, 1926, page 165–68.

8. Petersen Coil Tests on 140 Kv System, **J. R. North, J. R. Eaton.** *Electrical Engineering* (*AIEE Transactions*), volume 53, January 1934, pages 63–74.

9. Test and Operation of Petersen Coil on 100-Kv System of Public Service Company of Colorado, **W. D. Hardaway, W. W. Lewis.** *Electrical Engineering* (*AIEE Transactions*), volume 57, June 1938, pages 295–302.

10. Petersen Coil Installed on 100-Kv Colorado Line, **W. D. Hardaway.** *Electrical World* (New York, N. Y.), volume 108, 1937, page 835.

11. Petersen Coils Protect Iowa System, **A. B. Hird, H. H. Brown.** *Electrical World* (New York, N. Y.), volume 112, 1939, page 587.

12. Application, Control and Record of 33 Kv Ground Fault Neutralizer, **A. MacDonald.** *Electric Light and Power* (Chicago, Ill.), volume 17, November, 1939, page 54.

13. Operating Experience with Petersen Coils on 66-Kv System of Metropolitan Edison Company, **H. M. Rankin, R. E. Neidig.** *Electrical Engineering* (*AIEE Transactions*), volume 58, November 1939, pages 568–75.

14. Engineering Features of the 230-Kv Boulder-Chino Transmission Line of the Southern California Edison Company, Ltd., **A. A. Kroneberg, E. M. Hunter.** *AIEE Transactions*, volume 59, 1940, pages 982–87 and 1176–77

15. Petersen Coil Protection Equals Lightning Proofing, **R. E. Neidig.** *Electrical World* (New York, N. Y.), volume 113, 1940, page 1211.

16. Sensitive Ground Protection for Transmission Lines and Distribution Feeders, **Eric T. B. Gross.** *Electrical Engineering* (*AIEE Transactions*), volume 60, November 1941, pages 968–71.

17. Bauch Transformer Damps Cable Faults, **L. M. Nelson, H. N. Muller.** *Electrical World* (New York, N. Y.), volume 122, 1944, page 86.

18. 100-Kv and 13-Kv Petersen Coils on the System of the Public Service Company of Colorado, **L. M. Robertson.** *General Electric Review* (Schenectady, N. Y.), volume 49, September 1946, page 14.

19. The Arc Quenching Effect of Petersen Coils, **W. Diesendorf.** *Journal*, Institution of Engineers (Sydney, Australia), volume 18, 1946, page 237.

20. Petersen Coil Tuning Determines Performance, **H. W. Hartzell, S. S. Cook, A. A. Johnson.** *Electrical World* (New York, N. Y.), volume 130, 1948, pages 62–65.

21. Resonant Grounding of Distribution Systems, **E. Herzog.** *Proceedings*, Midwest Power Conference (Chicago, Ill.), volume 11, 1949, pages 237–40.

22. Operation of a Ground-Fault Neutralizer on a Regulated Distribution System, **H. R. Tomlinson, F. B. Hunt.** *AIEE Transactions*, volume 68, part II, 1949, pages 1321–28.

23. Practical Experiences with Resonant Grounding in a Large 34.5-Kv System, **H. H. Brown, Eric T. B. Gross.** *AIEE Transactions* volume 69, part II, 1950, pages 1400–05.

Discussion

Byron Evans (United States Bureau of Reclamation, Denver, Colo.): The authors have presented data that will be of considerable interest to system designers and operators.

On a percentage basis, it appears that resonant and solid grounding are increasing while reactance, resistance, and ungrounded applications are decreasing. In general, resonant grounding has its best application on systems of about 69 kv and below, and I should like to see Figure 1 of this paper drawn to show the grounding methods used for systems in this voltage range.

Figure 6 of the paper seems to indicate the greatest application of resonant grounding to be in the mountain states and the more northern states extending from the Dakotas eastward to the Atlantic seaboard, with few if any applications in the southeastern

quarter and the Far West. It would be interesting to know what factors may have influenced this distribution of resonant grounded systems.

It is expected that location of permanent faults, in extensive systems with resonant grounding, would be difficult and would require considerable time if "cut-and-try" methods must be used. I understand that very sensitive ground relaying is feasible for resonant grounded systems, and I would appreciate the authors' comments on such relaying. Is this relaying reliable for tripping circuit breakers or would it be used only for alarm and indication, with the system operator considering information at several relay points before deciding on the faulted section? In general it appears that automatic tripping would be desirable for switching at isolated unattended stations on a system with neutralizers having short time ratings, while alarm and indication probably would be preferable if neutralizers have extended time ratings.

If a permanent fault is left on the system during a lightning storm, it seems quite possible that another fault could occur on another phase to cause a double-line-to-ground fault to trip out the circuit. This seems most likely for the lower voltage systems having triangular configuration of conductors, since the top conductor, likely to intercept lightning strokes, may be phase "A" at one point in the storm area and phase "B" or "C" at another point in this same storm area. The possibility of such multiphase faults would be increased if permanent faults were left on for some time, as would be expected with extended time rated neutralizers. I would appreciate the authors' comments on actual experience concerning this matter.

The paper did not give details on the current range or number of taps provided and used on the neutralizers now in operation. Coils with a current range of one to two, or even higher, are common, but it is understood that with such large current ranges it is difficult or even impractical to design for the desired saturation for all tap positions. If this is the case, the current range should be less than one to two if at all possible. This may, of course, be a difficult decision for the system designer when the extent of future system development is not definitely known, although the initial coil or coils are thought to be located to give satisfactory performance with the probable future system.

Considering satisfactory experience on out-of-tune operation, there is some question about providing numerous taps. When more than one coil is used, the system as a whole can be tuned accurately with fewer taps on each coil. It therefore appears that taps with steps of at least 10 per cent would be satisfactory in lieu of the commonly provided steps of 5 per cent. With regard to out-of-tune operation, four arcing fault tests on a 115-kv resonant grounded system resulted in a fault clearing at 21 and 51 cycles with the system in tune, and 1.5 and 8.5 cycles with some of the 115-kv line switched out to produce an out-of-tune condition with about 21.5 per cent excess of lagging current.

Lawrence M. Robertson (Public Service Company of Colorado, Denver, Colo.): The authors have collected some very valuable data on power systems, and these data are very helpful in system planning and operation. This represents a very large amount of work, and the authors are to be congratulated on their paper and the help which they have given the industry. Our experience with 100-kv and 13.8-kv Petersen coils has led us to concur in the authors' conclusions.

I feel that continuous review must be given of power systems and the changing conditions, economics, and all the various associated problems. What may have been the right procedure and solutions of the problems in the past may not be now or in the future. Sometimes practice with regard to engineering, design, and so forth, may be a matter of habit, therefore it is well to keep new ideas in mind.

The larger system capacity may make it very desirable to reduce the value of fault currents as much as possible, and maybe Petersen coils would be helpful. In any event, it is well to keep the various methods in mind. It might be that operating performance could be improved by adopting different measures than are now being used. It may be that the very-high-voltage systems cannot justify Petersen coils or impedance grounding of the neutral, but this should not be a firm conclusion.

T. W. Schroeder (Iowa Power and Light Company, Des Moines, Iowa): From this survey it appears that the use of resonant grounding for power systems is growing, which is somewhat the opposite of what this writer would have guessed in the absence of the record. There is no question but that, in general, the ground fault neutralizer gives a good account of itself in protecting the system to which it is applied, albeit this protection can be against ground faults only. The ground fault is, of course, the predominating type of fault experienced. In fact, the ground fault neutralizer appears to give a great deal of help even when grounding systems in which the lines have conductors closely spaced, relatively flat spacing, and the structures employ steel cross-arm braces and are apt to have high footing resistance. This help is evidenced by the indication on the neutralizer recording ammeter chart that numerous disturbances occur without resulting line outage. In fact, in some cases the number of disturbances as shown by the ammeter chart is considerably greater in a given period than actually obtained in a similar period before the installation of a neutralizer; therefore, it is felt that the neutralizer sometimes is given more credit than is really due it. This is no serious objection, however, since usual facts are that the number of outages is definitely decreased after a neutralizer is placed into service.

It is believed that the greatest use of the ground fault neutralizer type of protection is made on existing lines where the transmission line structure configuration and grounding conditions are inherently inimical to good lighting performance because here, even though theoretical considerations will show that the line cannot expect good neutralizer protection, it actually will experience considerable help. Of course, new construction connecting to existing neutralizer-protected systems logically can depend on protection from the existing neutralizer or neutralizers. However, where the opportunity exists to start a new section of a system which can be grounded separately, strong consideration should be given to the use of shield wire protection, which, unless the system becomes extensive, may be the most economical and at the same time afford protection against other types of faults in addition to the line-to-ground variety.

S. S. Cook (Westinghouse Electric Corporation, Sharon, Pa.): I have read with much interest this paper by Mr. Gross and Mr. Atherton. It represents a very valuable summary of a tremendous amount of data on the subject which has been collected by the authors. They deserve a great deal of credit, and I believe the paper is very timely.

It is interesting to note the comments on the number of taps and current ranges. The American Standard has been to have a current range of 4 to 1 with 25 positions or 2 to 1 with 15 positions. If these are unnecessary and the extremes are not used it, of course, would result in considerable saving to design for a smaller current range and fewer tap positions. It is interesting to note that we recently have received two orders for neutralizers for application in a foreign country. One order has a current range of 1.35 to 1 with a 5-position tap changer, while the other order has a current range of 2 to 1 with a 6-position tap changer. Perhaps this should be reconsidered by the AIEE Protective Devices Committee.

Another thing that seems interesting is the trend toward reactance or resonant grounding, as indicated in Figure 1 of the paper. I am wondering if it would be feasible in those cases where reactance grounding is changed to resonant grounding to put the neutralizer in series with the present reactor. It would seem that if the reactor were surplus it could be used to cut down the size of the neutralizer. By this means the system would not be dead grounded when the neutralizer is by-passed.

It is interesting to note the trend toward continuously rated neutralizers. The original idea, I believe, was for the neutralizer to clear swinging faults or others which would clear mechanically, but without quenching the arc. If a fault occurs that would not clear itself in 10 minutes, the relays are supposed to clear the system, resulting in an outage. For this purpose 10-minute neutralizers probably are satisfactory. Ten minutes, however, is an extremely short time to locate and clear a fault. It therefore would seem that longer rated coils would permit operation on most systems under fault conditions without opening the circuit. All this could be done with no more expense than the difference in price of a continuous rated coil over a 10-minute coil. We are glad that the trend is toward continuous rated coils, since that seems to be a logical development.

Howard K. Amchin (American Gas and Electric Service Corporation, New York, N. Y.): The authors and co-operating companies have provided a logical basis for re examining present-day resonant grounding practices. Based on the results of the questionnaire, it appears advantageous to mak

several changes in design and application of the ground fault neutralizer.

It would seem extremely difficult to justify the need for a 4-to-1 current range, or even a 2-to-1 range. Furthermore, the number of taps seems excessive.

It cannot be disputed that current range depends upon the particular system. However, how many systems, assuming that the coil is designed to operate in the middle of its tap range, operate regularly with from 25 to 50 per cent or more of their lines switched off? If this situation does happen regularly, the writer suspects that the system is split into two sections to be operated independently, thereby requiring two ground fault neutralizers to provide protection for each section. An arrangement of this sort would, of course, be independent of switching. As previously stated,[1] "The higher than normal range (4 to 1) of coil reactance has never been used, and large decreases in system capacity are unusual. It would have been a better design to put existing needs near the upper limit and use most of a smaller range for future expansion."

The paper states that "of 45 systems (100 per cent) reporting, 40 per cent indicated that more taps than necessary were available . . .," and the paper's Table II shows that of 48 systems (100 per cent) reporting, 27 per cent never change taps. Furthermore, an earlier paper[2] said that "taps 12 through 15 have never been used." On the other hand, it seems that current design practices produce Petersen coils with from 15 to 25 tap positions, or even with a continuously variable arrangement.[3]

The most satisfactory coil operation is obtained at about the knee of the saturation curve. Nevertheless, examination of saturation curves of several coils now in operation shows that these coils have from 25 per cent to 50 per cent of their taps below the knee of the curve.

Present practices which produce a coil with a current range of 2-to-1 (or higher) and 15 or more taps give, as a by-product, a coil which is too expensive and somewhat unsatisfactory from the technical viewpoint. A ground fault neutralizer with a lower current range, say 1.5 to 1, and fewer taps, say 5–7, should be quite satisfactory.

It might be said that the lesser number of taps, as suggested in the preceding sentence, would not permit proper tuning, and the writer is inclined to believe this idea to be one reason that 60 per cent of reporting companies stated that the present number of taps is "just right." However, as shown in Table I, which follows,[4] a relatively large degree of deviation from exact tuning will still permit the desired results to be obtained with the coil.

Table I

System Voltage	Deviation from Exact Tuning, Per Cent
20 kv and below	±30
30 kv–60 kv	±20
Above 60 kv	±10

This table would seem to offer further evidence that 15 or more tap positions are unnecessary. For example, if the taps are spaced within 10 per cent, it always will be possible to tune not more than ±5 per cent off resonance, which is satisfactory.

It is most unfortunate that no system reporting performed tests to determine the maximum permissible deviation from exact tuning, since the majority of them did make arrangements to perform arcing tests at nearly resonant tuning. Knowledge of this permissible deviation will reduce considerably the number of tap changes made each year (see Table II of the paper). That 4 per cent of the systems reporting make more than 200 changes each year is astonishing.

It is interesting to note the increased use of extended time rated coils, and that of 28 systems reporting that use "10-minute" coils, 32 per cent now would install coils for continuous operation. It would be helpful to learn the effects of continuous operations (Figure 10 of the paper) on adjacent telephone toll circuits, since it is believed that this type of operation leads to excessive noise in these circuits.

Of 17 companies reporting, 16 indicate the desirability of a sensitive relay system[5] to indicate the location of ground faults. We have high-sensitivity single-phase directional relays; the current transformer requirement is satisfied by three *identical* current transformers[6] (no special accuracy required); we may benefit from thousands of similar applications abroad. What else is required?

References

1. See reference 21 of the paper, page 177.
2. See reference 23 of the paper.
3. Tuning of Ground-Fault Neutralizers, **N. E. Dillow and J. R. Burkhart.** *General Electric Review*, vol. 52, December 1949, pages 31–37.
4. See reference 2 of the paper.
5. See reference 16 of the paper.
6. Sensitive Ground Protection, **AIEE Committee Report.** *AIEE Transactions*, volume 69, part 1, 1950, pages 473–76.

J. C. Russ (General Electric Company, Pittsfield, Mass.): Messrs. Gross and Atherton have performed a useful service in their survey of operators using resonant grounding equipment. From the point of view of the manufacturer it is encouraging to have this additional evidence of the successful performance of such devices.

The demonstrated trend toward greater use of extended time rated ground fault neutralizers is interesting. In this connection, it should be pointed out that there is very little difference in the over-all cost of 10-minute and extended time neutralizer equipments when they are compared complete with their auxiliaries. Thus, it may well be that an operator changing from an isolated neutral system to a resonant grounded system will install extended time neutralizers simply on the basis of saving himself the extra cost of the ground relay equipment which he would need with a 10-minute neutralizer installation. Ground relay equipment would involve, in some cases, the purchase of grounding transformers, which would add considerable expense to the application.

The survey shows that 35 per cent of the resonantly grounded systems previously were solidly grounded. An analysis of these installations to determine what proportion of them are 10-minute and what proportion are extended time might be significant. Since the basic cost of the two types of equipment is a stand-off and since the assumption is that the majority of the systems which previously were solidly grounded had ground relays available at the time of the change-over, the decision determining the choice of 10-minute or extended time neutralizer equipment, in these cases, must have been based on the operator's opinion of the relative operating advantages of the two types of equipment. In other words, the advantage of being able to operate for longer than 10 minutes with a ground fault on the system would be weighed against the advantage of being able to relay out a faulty section of the system by closing the grounding switch furnished with 10-minute neutralizer.

The question of safety could be a factor in some applications. For instance, an operator might consider operation with a broken conductor lying on the ground a hazard and might choose 10-minute neutralizer equipment on this account.

In the section on "Line Construction," it is pointed out in the paper that in 15 per cent of the installations it was necessary to make additional transpositions. The inference is that such transpositions were made to keep the residual unbalance current through the neutralizer below the 30 per cent value normally allowed in the neutralizer rating. There has been some agitation recently to reduce the 30 per cent unbalance current rating to, say, 15 per cent on the basis that most systems normally have less than 15 per cent unbalance current anyway. Studies have indicated that little or no saving in cost would result from such a reduction in rating, inasmuch as a 30 per cent continuous current capacity is inherent in most neutralizer designs.[1]

Most of the neutralizer applications in the 2.4 KV and 6.6 KV voltage classes have been on industrial power systems. Many of these systems require frequent retuning particularly where motors equipped with large protective capacitors are continually being switched on and off. For these applications there has been developed a tapless ground fault neutralizer capable of smooth, stepless reactance variation over the conventional 2:1 or 4:1 range. These neutralizers also have the advantage of being able to be tuned under load as contrasted to the tap type which must be by-passed or de-energized before taps are changed. All applications of this type have been extended time ratings.

Reference

1. Report on Survey of Unbalanced Charging Currents on Transmission Lines as Affecting Ground-Fault Neutralizers, **AIEE Committee Report.** *AIEE Transactions*, volume 68, part II, 1949, pages 1328–29.

George Dana (New York State Electric and Gas Corporation, Binghamton, N. Y.): I think the authors deserve our thanks for the preparation of a comprehensive questionnaire which shows us for the first time the extent of the trend toward the use of ground fault neutralizers and a nation-wide opinion of their value as a tool for improving continuity of power distribution.

For about 15 years the New York State Electric and Gas Corporation has been oper-

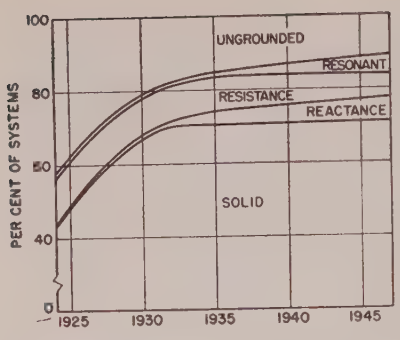

Figure 1. Grounding of power systems in the United States, 22 kv to 70 kv

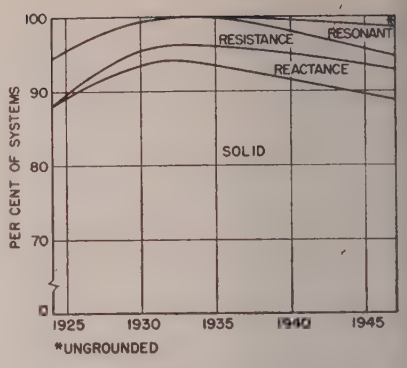

Figure 2. Grounding of power systems in the United States above 70 kv

ating a 46-kv system and a 33-kv system with 10-minute rated neutralizers. The 33-kv system is a joint system with Northern Pennsylvania Power Company and includes five grounding points, four of which are nonattended and two of which lack supervisory control facilities.

As pointed out in the authors' conclusions, ground fault neutralizers require a minimum of maintenance, but we believe the same cannot be said of the control and switching equipment associated with short time rated coils, especially in nonsupervised stations. The trend toward extended time rated coils and the desire for fault-locating relays substantiates our thoughts.

The number of taps furnished has been more than ample. ‹Over a period of years, system growth usually requires additional grounding points for relaying and stabilizing the neutral. This fact creates an ideal time and place for the installation of more neutralizer capacity and answers the question usually raised about "what will happen as the system outgrows the original coils."

Referring to Figure 3 of the paper, I notice with considerable interest that only 33 per cent of the systems of 22 kv and above have been ungrounded before installing neutralizers. This shows that the benefits claimed for resonant grounding are not due to any great extent to the mere fact that some kind of grounding was added.

I also believe that extended time rated coils would alleviate many inductive coordination problems with communication systems and that their value in this respect should be recognized.

E. Herzog (United States Army Air Forces, Wright Field, Dayton, Ohio): The authors are to be commended for their work in collecting the information presented. It is interesting to note that the method of resonant grounding had a rapid increase in the last few years, particularly on low-voltage systems.

The philosophy underlying the application of gound fault neutralizers by the Air Force has been that a well-built system will have faults only rarely. When a fault occurs the system should be operable until equipment and personnel is arranged for repairs, then repairs can be made when convenient and quickly; no unexpected interruptions can be tolerated. Accordingly, the neutralizer coil must have an extended time rating to permit arranging the outage. It also is important to have a good alarm system which permits location of the fault. An alarm system now is being installed which will indicate the faulted circuit. Much trouble has, however, been experienced in locating the exact point of the fault. The demonstration by the fault is so slight that operators have walked right by the fault without noticing, unless it was very quiet. To realize fully the advantage of the ground fault neutralizer, it will therefore be necessary to provide a fault-detection system that will indicate, not only the circuit, but the exact point of the fault. Then outages will be necessary only for the time necessary for repairs, and at the convenience of the operator.

Eric T. B. Gross (Illinois Institute of Technology, Chicago, Ill.): It is indeed gratifying that this paper has met with the interest which is indicated by these many discussions.

Some of the discussions deal with the same questions, and the answers, therefore, are given with reference to the various topics under consideration. It appears that there is general agreement as to the validity of the conclusions drawn in the paper.

A further breakdown[1] of the data collected for the latest general AIEE Report on Grounding Practices[2] leads to Figure 1 of this discussion concerning systems at voltages from 22 to 70 kv, and to Figure 2 of this discussion concerning systems at higher voltages. As pointed out by Mr. Evans, most of the Petersen coils are used in systems operated at 69 kv and below. It is not known completely why resonant grounding has not yet been applied in the southeastern and western parts of the United States. One reason may be that in the more northern states there are more isolated systems, which lend themselves readily to resonant grounding; other reasons may be that in the southeastern and western states less lines per unit area have been built or larger systems (such as the Tennessee Valley Authority and the Bonneville Power Administration) are operated at higher voltages with solidly grounded neutrals. This question deserves further study.

It seems that solid neutral grounding is more economical at 115 kv only if all possible advantages of this grounding method can be utilized. This voltage is sort of a borderline case. Mr. Robertson is quite correct in pointing out that it is necessary to investigate critically all phases of the problem and not to accept any practice as a matter of habit. In a number of resonant grounded systems which are operated at 115 kv, Petersen coils have established an excellent record.

Static wires, as emphasized by Mr. Schroeder, have their merits, though such ground wires are a means of preventing ground faults, whereas resonant grounding eliminates existing ground faults as a source of further difficulties. Static wires and Petersen coils act in very different manners and supplement rather than replace each other. A shield wire, if supplemented by low tower footing resistances, is helpful in the reduction of single and multiphase flashovers. However, it is obvious and has been shown by experience that resonant grounding will produce an additional outage reduction, and vice versa. Mr. Schroeder's reference to the discrepancy between ground

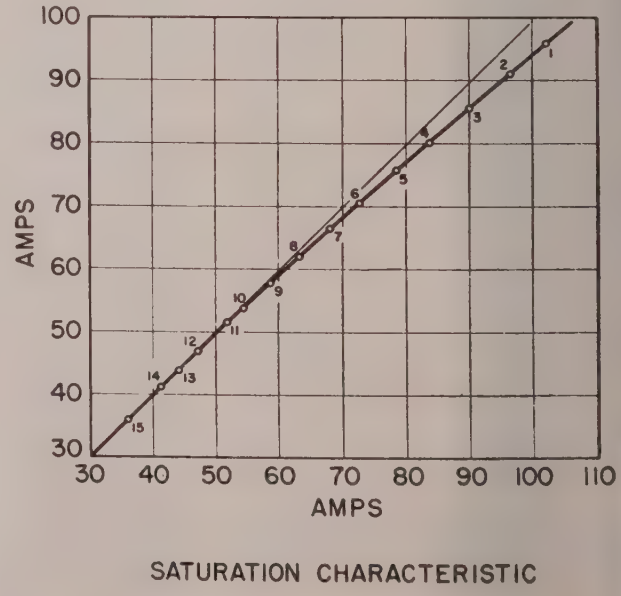

Figure 3. Ground fault neutralizer currents on 15 taps

fault neutralizer operation shown on the recording ammeter and apparent ground faults checks an observation made in many systems. A reason for this discrepancy is often found in the fact that switches and circuit breakers do not operate simultaneously on all three phases and the temporary electrostatic unbalance to ground of the three phases leads to a transient current through the ground fault neutralizer. Data check well if operation records are analyzed in the proper light.

A number of discussers seem to recommend a smaller current range and fewer taps, that is, a technically better design which also will result in a cheaper ground fault neutralizer. In Figure 3 of this discussion is drawn what may be called a saturation characteristic of a ground fault neutralizer with 15 taps. The ordinate for each point gives the current referred to rated voltage for the unsaturated reactance; the abscissa gives the saturated current values at rated voltage. The figure shows clearly that this coil does not saturate sufficiently on taps 9 through 15; eliminating these taps would result in a 63-to-102-ampere coil, that is, a range of about 1 to 1.6. I am in complete agreement with Mr. Cook's suggestions concerning the design of ground fault neutralizers. Mr. Amchin's conclusions are technically sound, since unusual conditions make it necessary to design the magnetic circuit so that saturation sets in when the zero sequence voltage approaches the value of the system phase voltage. It is possible to use an available short circuit limiting reactor in series with a Petersen coil, as suggested by Mr. Cook, if this arrangement is taken into account in the design of the ground fault neutralizer. Such a reactor acts like the zero sequence reactance of a power transformer or the grounding transformer used for the connection of the Petersen coil.

Ground fault neutralizers with a smooth variation of reactance may have limited advantages: they can be operated when on the system and are therefore always ready for operation, as pointed out by Mr. Russ. However, all the remarks relative to current range and saturation apply to them, and they also should not be designed for a larger current ratio than about 1 to 1.6. When tuning is done at smaller than full ground displacement, a correction for saturation must be applied. Such ground fault neutralizers have had a limited application for some 10 years.[3] However, the number of such installations in the United States is small, and at least one user concluded[4] that a smaller current ratio "would have been a better design." There was no indication that these users were among those who changed their taps very often; this is quite understandable, since the 6.6-kv and 2.4-kv industrial systems contain many underground cables so that the zero sequence capacitance of the whole system is not greatly changed by switching on or off motors with protective capacitors.

The noise-reducing effects of Petersen coil application have been pointed out by H. M. Trueblood[5] in an early investigation. I am familiar with cases in which the noise in an adjacent communication circuit decreased during a solid single line-to-ground fault on the high-voltage line of a resonant grounded system. Operation with sustained grounds seems to have been quite successful, and many systems have operated "10-minute" coils during cold winter periods for 30 minutes or longer. Of course, permanent faults can become a hazard, as Mr. Russ points out, but so can very large ground fault currents in effectively grounded systems, and it is difficult to decide which hazard is greater. Mr. Dana's comments about difficulties with the control and switching equipment of short-time-rated coils are confirmed by others with similar experience. The problems of synchronizing various by-pass and neutral grounding switches does not seem to have been solved satisfactorily.[2] Furthermore, the shock to the system produced by the operation of by-pass switches produces dips in the line-to-line voltages to which many users of power are quite sensitive.[6]

It is interesting to learn from Mr. Herzog that an alarm system to indicate the faulted circuit is being installed. It can be expected that the operation will be as successful as the application of resonant grounding. As apparently referred to by Mr. Amchin, the only new feature of such a relaying system is our frequency of 60 cycles, since numerous installations abroad have been in operation at 50 cycles for many years. These relays are in most cases indicating devices which help locate the fault. Switching off the line section is delayed until this can be done without interruption of service.[7] However, additional carrier or microwave channels between stations would provide a solution to the tripping problem mentioned by Mr. Evans. A fault detection system which seems to fulfill Mr. Herzog's requirement has been described recently in a paper by B. D. Zelikin.[8]

As for simultaneous faults (multiple ground faults), referred to by Mr. Evans, the records do not indicate that difficulties have been experienced. It is important to keep the insulators in good condition by making inspections and tests with full system voltage to ground (line-to-line). In order to eliminate damaged insulators or insulator elements, such tests should be made regularly in the spring before the lightning season.[9]

In these closing remarks, an attempt has been made to answer most of the questions raised in the discussions. The remaining questions require further studies for which not enough time is available now. The authors wish to thank all discussers for their valuable and very interesting contributions.

References

1. *Electrical World* (New York, N. Y.), volume 131, May 21, 1949, page 303.
2. See reference 1 of the paper.
3. The Brown Boveri Arc-Suppression Coil with Progressive Current Regulation, **A. van Gastel.** *Brown Boveri Review* (Baden, Switzerland), volume 30, 1943, pages 103-10
4. See reference 21 of the paper, page 177
5. See reference 6 of the paper.
6. See reference 23 of the paper
7. See reference 16 of the paper.
8. A Method for Detection of Sustained Earth-Faults in Rural Overhead Links Protected by Petersen Coils, **B. D. Zelikin.** *Journal* Institution of Electrical Engineers (London England), volume 95, part II, 1948, pages 617-19.
9. See reference 23 of the paper, authors' closure of the discussion.

A Study of Conduction Phenomena Near Current Zero for an A-C Arc Adjacent to Refractory Surfaces

T. E. BROWNE, JR.
MEMBER AIEE

A. P. STROM
MEMBER AIEE

Synopsis: As first steps in a general study of arc extinction in magnetic-type air circuit breakers, equipment has been developed for simultaneously measuring both arc voltage and arc current just before and after current zero, and studies have been made of arc path conductance and power input in this critical time region for small-scale tests with arcs of a few hundred amperes either magnetically pressed against or physically confined between refractory insulating plates. Analysis in terms of possible mathematical arc models has aided interpretation of the observations. The general nature of the arc reignition process under these conditions has been revealed clearly and the dynamic properties of the arc and surface leakage paths have been determined quantitatively for these tests in terms of the arc model values: conductance time constant and critical power input or critical applied voltage gradient. Some effects on these values of such controllable variables as plate composition and plate separation have been shown. The leakage conductance along the adjacent plate surfaces just after current zero was found to limit the interrupting ability of arcs under the small-sample test conditions, but the relative importance of this compared to the dielectric recovery of the gas space and other possible factors remains to be determined for very high current interruption in actual circuit breaker arc chutes.

CONFINING arcs between refractory insulating surfaces is one of many schemes used for aiding arc extinction in practical circuit-interrupting devices. This means of arc suppression has become increasingly important because of its wide use in the new magnetic-type air circuit breakers. Even in these relatively simple interrupters the processes involved in extinguishing an a-c arc are very incompletely understood, and much speculation[1] has taken place about the details involved and the role of the refractory arc-confining surfaces.

To be reported here are the first steps in a general investigation of the behavior of arcs being extinguished in magnetic-type circuit breakers. The results are still fragmentary, but they do shed new light on the phenomena attending the extinction or reignition of a-c arcs under such conditions of partial confinement, and so it is believed that they do constitute at least a significant beginning.

Special devices have been developed for making simultaneous measurements of arc voltage and current as functions of time during the important few microseconds just before and after current zero. From records of such measurements it has been possible in many cases to follow continuously the derived variables, arc power input and arc conductance, during this brief but critical period. Analyses of the behavior of the observed variables in terms of possible mathematical arc models[2] have helped to reveal the dynamic properties of the semiconfined arc near current zero and the function and behavior of the confining refractory surfaces.

Paper 51-65, recommended by the AIEE Protective Devices and Switchgear Committees and approved by the AIEE Technical Program Committee for presentation at the AIEE Winter General Meeting, New York, N. Y., January 22-26, 1951. Manuscript submitted March 15, 1950; made available for printing December 6, 1950.

T. E. BROWNE, JR., and A. P. STROM are both with the Westinghouse Electric Corporation, East Pittsburgh, Pa.

Measuring Equipment

In order to observe with accuracy the small values of current just before and the small leakage currents just after current zero, it was necessary to build a direct-coupled amplifier with high fidelity up to one megacycle and provided with cutoff devices so that only the portions of current below a few amperes could get through the final amplifier stage to the recording cathode-ray oscilloscope. Current input to this amplifier was taken from a specially constructed highly noninductive shunt of a few hundredths of an ohm in the ground lead of the test circuit. The amplifier and shunt were generally similar to those described by L. J. Lewis,[3] but the amplifier had a higher upper-frequency limit. Voltage from the current shunt was transmitted to the amplifier over a coaxial line with terminal impedances to prevent reflections.

Voltage across the arc terminals was transmitted to the oscilloscope over an open-wire line. The voltage was reduced, when necessary, by a resistance-capacitance divider. Particular care was taken to eliminate voltage pickup in the neighborhood of heavy currents by carrying the voltage leads inside of tubular current conductors.

In most of the tests, voltage was impressed on one axis of the oscilloscope while simultaneously the output of the current amplifier and limiter was impressed on the other. Thus, volt-ampere cyclograms such as that shown in Figure 2C were produced on the oscilloscope screen and photographed by an electrically tripped miniature camera. Volt-time and current-time records such as those shown in Figures 2A and 2B also could be taken. In any of these, time markers could be introduced by Z-axis blanking dots of known frequency.

Small-Sample Test Apparatus

The first test arrangement was devised to make use of single samples of refractory

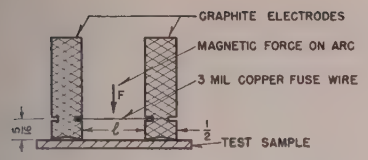

Figure 1. Single plate sample test arrangement

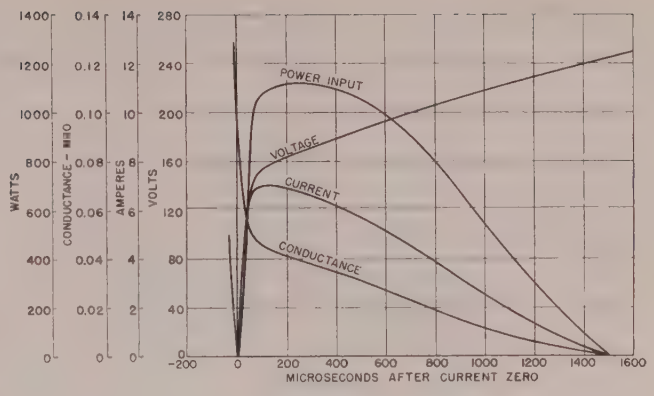

Figure 3 (right). Time variation of quantities from cyclogram of test number 30,720 (Figure 2C), also showing conductance and power input

plate material as small as two inches in diameter for the arc-adjacent surfaces. The sample was placed on a stand provided with terminals, adjustable electrode holders, and a series-excited iron core magnet located beneath the test stand. The magnet was arranged to produce a transverse field of about 1.25 peak gauss per rms ampere at the arc in a direction tending to hold it in contact with the sample surface. As shown in Figure 1, the arc electrodes consisted of half-inch-diameter graphite rods pressed against the surface. Arcs were started by 3-mil copper fuse wires stretched between the electrodes in deep grooves 5/16-inch above the sample surface. The electrode spacing was adjusted by trial to obtain an approximately critical distance for arc extinction at the current and voltage used in the test. Under these conditions the current-zero-period behavior of arc voltage and current was observed both at successful interruptions and at reignitions.

Results and Analysis of Single-Plate Sample Tests

Figures 2A and 2B show, respectively, current-time and volt-time cathode-ray oscillograms of early "failure" tests on zircon porcelain plates at 280 amperes, 192 volts, with $1^1/_4$-inch electrode separation. The timing blanks are 100 microseconds apart. The first passage of arc current and voltage through zero is displaced to the right of subsequent zeros. In Figure 2A, a marked partial pause in the current rise for about 500 microseconds after the first current zero is evident. In successful interruptions this pause of varying duration at a small reverse current is followed by a decay to zero instead of the accelerated rise observed here. The voltage record of Figure 2B is for a nearly identical test. The first transient voltage rise was followed by a much slower rise along the open-circuit voltage curve during the pause in rate of change of current. Subsequent voltage traces for zeros not marked by an extended current pause show that the arc voltage near current zero was almost as high as the open-circuit voltage under these near-critical conditions for arc extinction. It also is evident that the transient rate of voltage rise in these tests was determined largely by the shunting effect of the rather low resistance arc path rather than by the distributed capacitance of the circuit.

Test number 30,720, in which the volt-ampere cyclogram of Figure 2C was taken, was similar to those just described except that the arc failed to reignite at the end of the first half-cycle and so the test was "successful." The slope and curvature of the trace show that the arc path resistance was about 10 ohms at current zero and was rising rather rapidly. Slowing down of the voltage rise as open-circuit voltage was approached is indicated by thickening of the trace. The arc path resistance at this time was between 20 and 25 ohms.

An interpretation of the Figure 2C cyclogram on a time basis is shown in Figure 3. Time values near current zero were estimated by comparison with Figure 2B to obtain the steep part of the voltage-rise curve, and a section of the

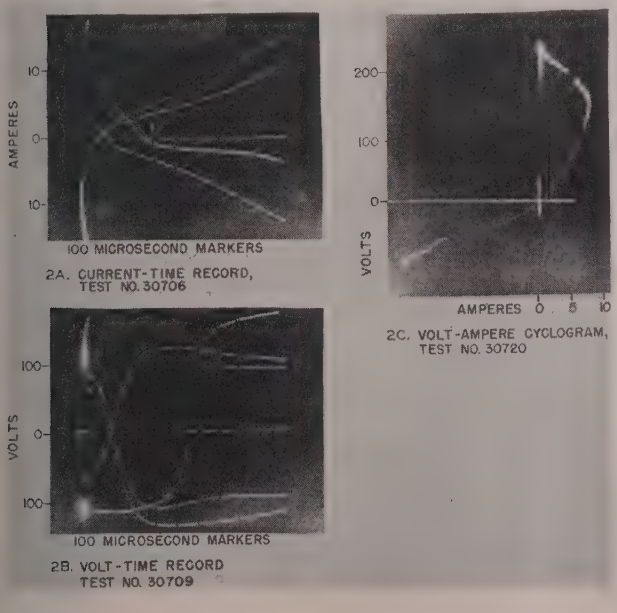

Figure 2 (left). Cathode-ray oscillograms and cyclogram of sample tests on single zircon disks at 280 amperes, 192 volts, $1^1/_4$-inch electrode spacing

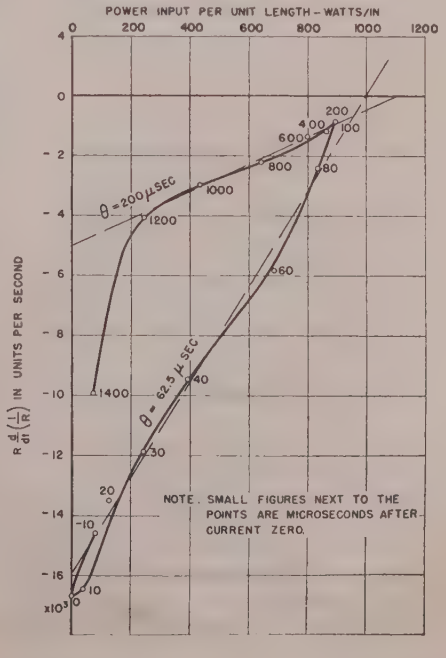
POWER INPUT PER UNIT LENGTH - WATTS/IN
θ = 200 μSEC
θ = 62.5 μSEC
NOTE. SMALL FIGURES NEXT TO THE POINTS ARE MICROSECONDS AFTER CURRENT ZERO.
x10³

Figure 4 (right). Plot of per-unit rate of change of conductance versus power input per inch of arc path for sample test number 30,720 (Figure 2C)

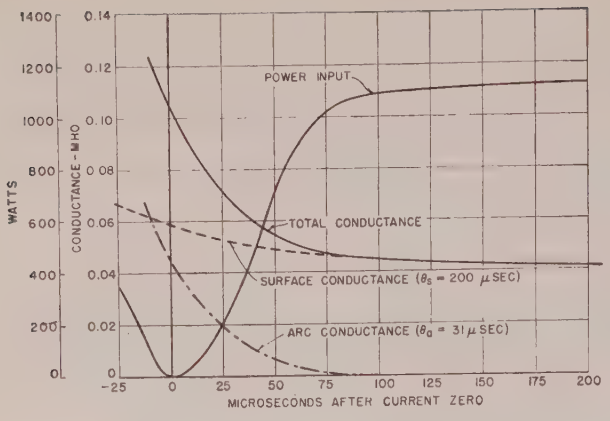

Figure 5. Analysis of apparent arc conductance near current zero for sample test number 30,720 (Figure 2C)

open-circuit sine-wave voltage curve was fitted to this as a means for estimating the time scale at longer times after current zero, when the rate of change of current had become so small as to have a negligible effect on the terminal voltage of the inductive test circuit. This procedure involves considerable possible absolute error in the time values, but the proportionate error becomes small at several hundred microseconds total time. From the estimated voltage-rise curve and the simultaneous current values of the cyclogram, the current-time curve also was plotted. From these, the ratio of current to voltage gave the curve of arc path conductance and the product gave the curve of power input to the arc path. The considerable errors of measurement, especially of small values because of uncertainty in locating the zero lines, undoubtedly explain the surprisingly abrupt apparent approach of the current and with it the conductance and power input to zero at 1,500 microseconds. Vagaries in these and later arc-conductance measurements very close to the current passage through zero are similarly explainable.

Analysis of Arc Path Conductance

Of particular interest from the standpoint of arc theory are the derived curves of arc path conductance and power input versus time. If it is assumed that the arc path conductance is associated in a simple way with the excess energy stored in the arc path by virtue of its elevated temperature, state of dissociation, excitation, and ionization, then there also should be a simple relation between rate of gain or loss of conductance and the difference between the power input to and the rate of energy loss from the arc path. In particular, the rate of change of conductance should pass through zero and change sign whenever the power input equals and then exceeds the rate of energy loss. A change from decreasing to increasing arc path conductance generally results in complete arc reignition, and the applied voltage required to accomplish this change may be defined as the dielectric strength[4] of a still conducting arc path. In mathematical terms, as explained earlier by one of the authors of this paper,[2] the general form of the differential equation for arc path conductance, assuming that there is a functional relation between conductance and excess energy content, can be written

$$R\frac{d}{dt}\left(\frac{1}{R}\right) = \frac{F'(Q)}{F(Q)}\,(W\text{-}N) \qquad (1)$$

where

Q = excess energy stored in arc path
W = electric power input to arc path
N = rate of energy loss from arc path
$F(Q) = \frac{1}{R}$ = arc path conductance

and $F'(Q)$ = derivative of $F(Q)$ with respect to Q (rate at which conductance changes with change in energy content). In one form, proposed by O. Mayr,[5] N is assumed constant and a simple exponential function is adopted for $F(Q)$, leading to the differential equation

$$R\frac{d}{dt}\left(\frac{1}{R}\right) = \frac{W-N_0}{Q_0} = \frac{\frac{W}{N_0}-1}{\theta} \qquad (2)$$

where

N_0 = assumed constant rate of energy loss
Q_0 = energy content increment necessary to change $1/R$ by the factor ϵ (2.718)
$\theta = \frac{Q_0}{N_0}$ = "time constant" of the arc path conductance, also assumed to be unvarying

With the variables arc conductance, power input, and time all experimentally determined, equation 2 makes possible a convenient check on the validity of this assumed law, and also a determination of the constants in the equation, if valid, by simply plotting $R\,d/dt(1/R)$ from a curve like that of Figure 3 against the power input, W, as has been done in Figure 4. (This procedure was employed first by J. V. Byrne, L. Dennie, W. O. Kelham, and R. G. Noble of the English Electric Company, Stafford, England, in an unpublished report dated Sept. 14, 1948.) In-

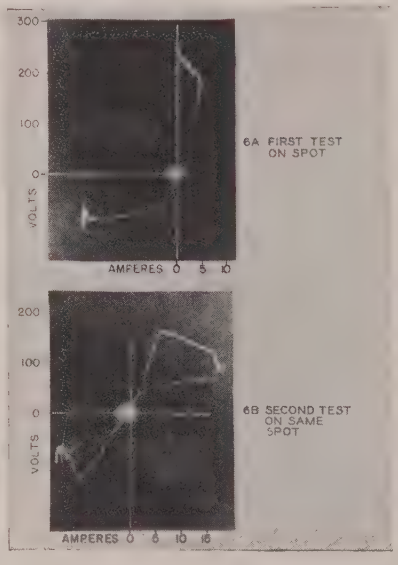

Figure 6 (above). Volt-ampere cyclograms of sample tests on gas-evolving plate at 300 amperes, 192 volts, 7/8-inch electrode spacing

Figure 7 (below). Time variation of quantities in Figure 6A

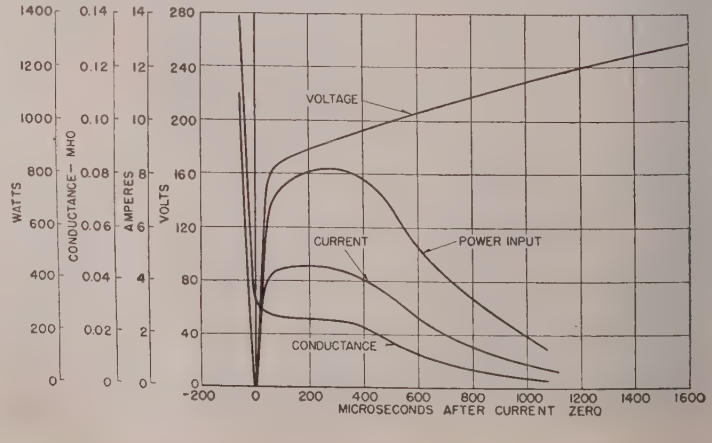

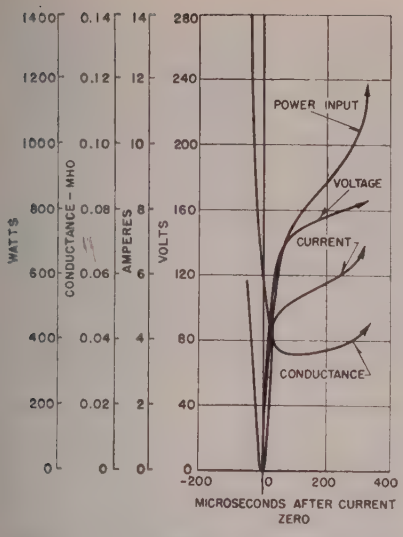

Figure 8. Time variation of quantities in Figure 6B

Figure 11 (right). Plot of per-unit rate of change of conductance versus power input per inch of arc path for sample of Figure 6B on gas-evolving plate

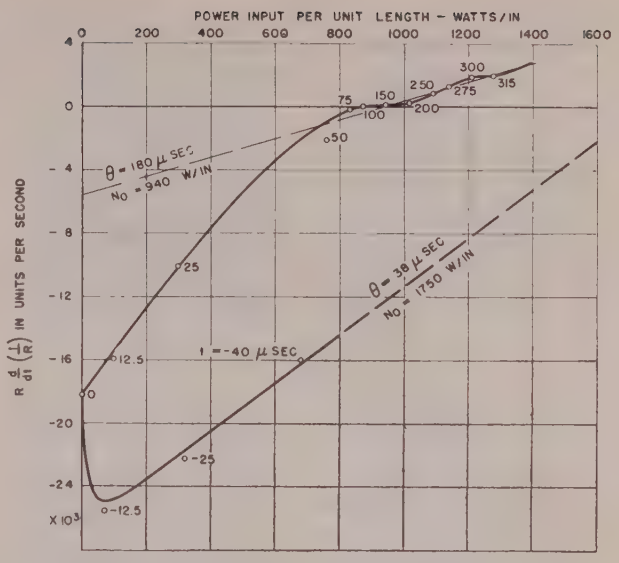

spection of equation 2 shows immediately that, for the law to be valid, such a plot should yield a straight line with intercepts

$$W = N_0 \text{ at } R\frac{d}{dt}\left(\frac{1}{R}\right) = 0 \text{ and } R\frac{d}{dt}\left(\frac{1}{R}\right) = -\frac{1}{\theta} \text{ at } W = 0$$

Figure 4 shows that this plot of the data from Figure 3 gives not one but two straight lines! The point at 1,400 microseconds may be ignored because of the likely inaccuracy in the conductance curve where the measured current was small. Between 20 microseconds before and 200 microseconds after current zero, the data strongly tend to follow a line with intercept values

$$N_0 = 1{,}000 \text{ watts per inch and } \theta = \frac{1}{16 \times 10^3} \text{ second} = 62.5 \text{ microseconds}$$

After 200 microseconds, however, the data tend to fit a line with intercepts at $N_0 = 1{,}100$ watts per inch and $\theta = 200$ microseconds. From this plot, as well as from the general appearance of the conductance curve in Figure 3 and of many similar experimental curves for ceramic sample tests, it has been concluded that the conducting arc path within 100 or 200 microseconds of current zero is effectively made up in these sample tests of two parallel paths with quite different time constants, namely, the gaseous arc column residue and the heated "arc trail" on the refractory surface adjacent to it. After 200 microseconds in the test of Figure 4, it is presumed that the conduction was almost entirely along the ceramic surface, which behaved much like the gaseous arc column except for the relatively long time constant of the sur-

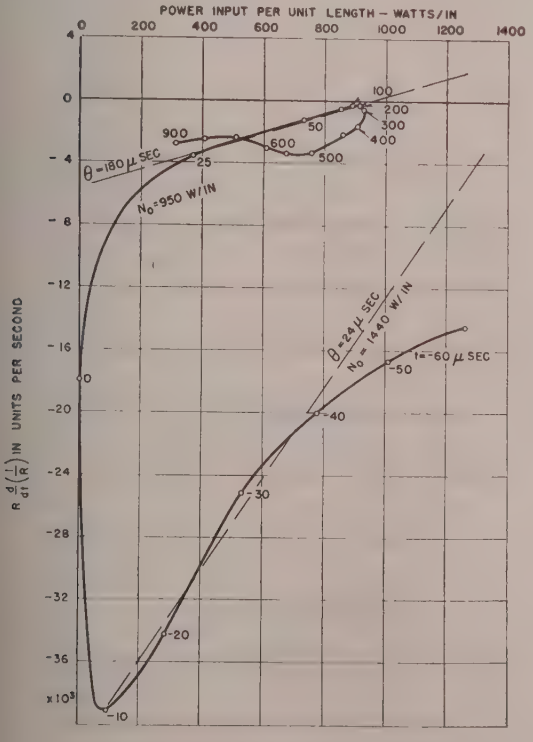

Figure 9 (left). Plot of per-unit rate of change of conductance versus power input per inch of arc path for sample test of Figure 6A on new gas-evolving plate

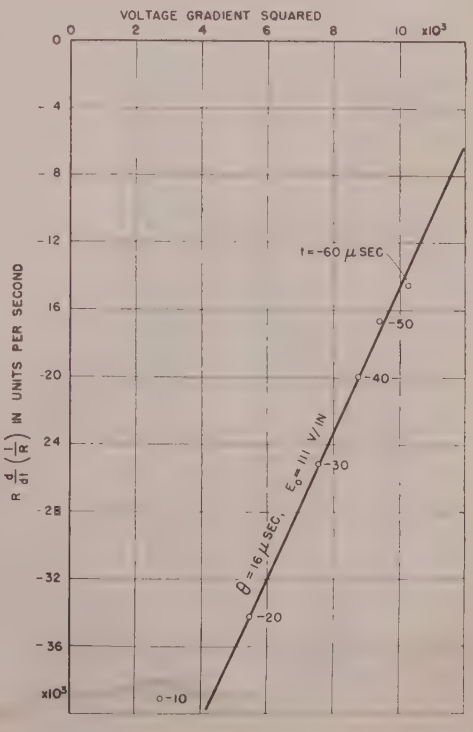

Figure 10 (right). Plot of per-unit rate of change of conductance versus square of the arc voltage gradient during the pre-current-zero period for sample test of Figure 6A on new gas-evolving plate

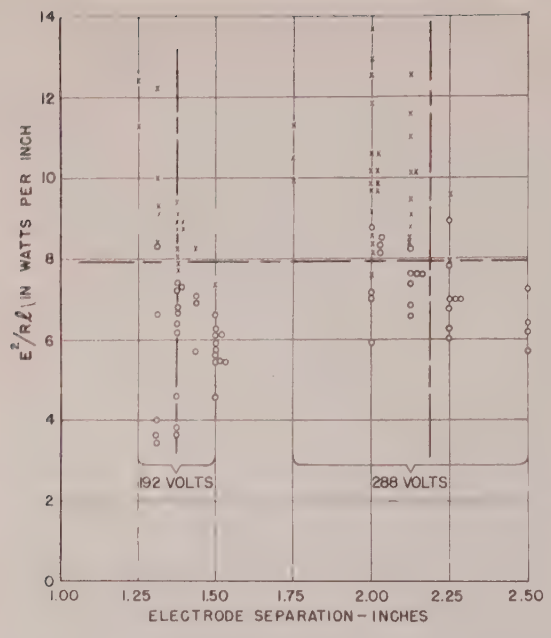

Figure 12. Plot indicating critical "watts per inch" and electrode spacings in sample tests with standard zircon at 300 amperes, 192 and 288 volts

Crosses denote arc reignition, circles, arc extinction

face path. This conducting surface path consisted of a thin layer only a few mils thick heated nearly to incandescence. Its energy loss was presumed to be mainly by thermal conduction into the body of the test sample. At times shorter than about 100 microseconds it is deduced that the remanent gaseous arc column still was carrying an appreciable part of the observed "leakage" current and, because of its much shorter time constant, gave a composite behavior with the apparent time constant of only 62.5 microseconds.

On the basis of this presumption, assuming equation 2 with the constants for the upper line in Figure 4 to hold at all times for the component of conductance along the ceramic sample and assuming also that all the measured power input went into the surface path (nearly true, since a considerable part of the loss from the gaseous path must be by conduction and convection to the closely adjacent solid surface), the surface conductance was extrapolated backward from 200 microseconds by numerical integration of equation 2 and was plotted as the dotted line in Figure 5. The difference between this extrapolated surface conductance and the observed total arc path conductance, the dot-and-dash line in Figure 5, is the deduced actual arc conductance. The latter is very nearly a simple exponential decay curve with a time constant of 31 microseconds, becoming virtually zero in about 100 microseconds. The power input to the gaseous portion of the arc path (not plotted) was comparatively small, reaching a maximum of 100 watts at 40 microseconds. From the near-exponential shape of the gaseous path conductance curve it may be surmised that the rate of energy loss from the gas was much greater than 100 watts, possibly being of the same order as N_0 for the ceramic surface path (estimated to be 1,375 watts).

It is clear from Figure 5 that, with the rate of voltage rise attained in these sample tests, the decay of gaseous arc conductance was little affected by the applied voltage and the gaseous arc was never in danger of being reignited directly by this voltage. When arc reignition did occur, it apparently was the result of breakdown of the much more slowly cooling ceramic surface leakage path some time after virtual disappearance of the gaseous arc conductance. However, had the rate of voltage rise been enough greater, the gaseous arc might have been reignited directly without the intervention of the surface leakage path.

As in all arc tests, apparently random variations in behavior from one test to the next make it difficult to pick out one particular sample test as typical. The test of Figure 2C was actually not quite

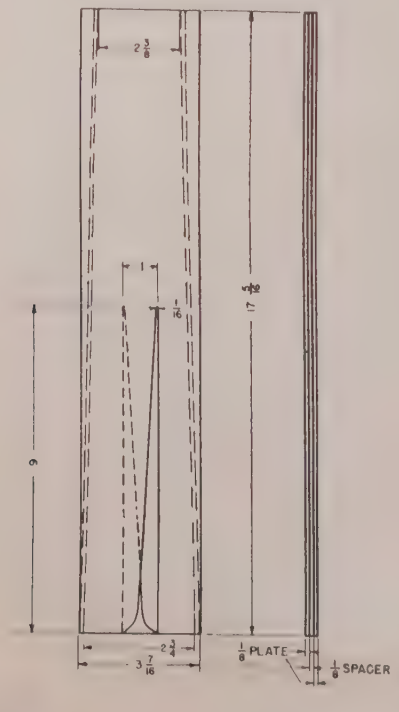

Figure 13 (left). Two standard plates assembled as in the arc chute of the circuit breaker

Figure 14 (right). Parallel plate sample test arrangement

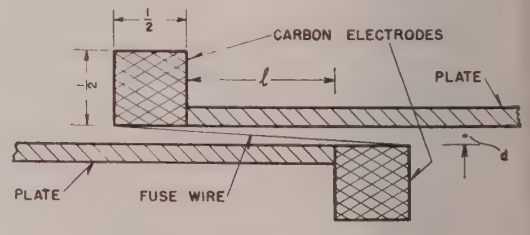

14A. PLACEMENT OF PLATES AND ELECTRODES FOR TEST.

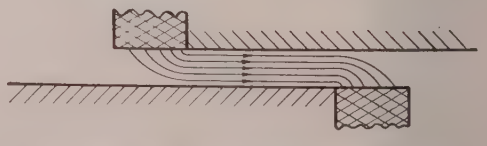

14B. CURRENT FLOW THROUGH HIGH CONDUCTIVITY GAS.

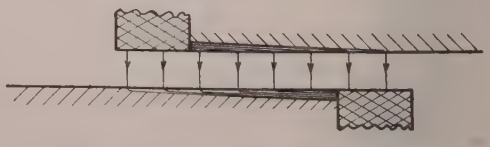

14C. CURRENT FLOW THROUGH LOW CONDUCTIVITY GAS.

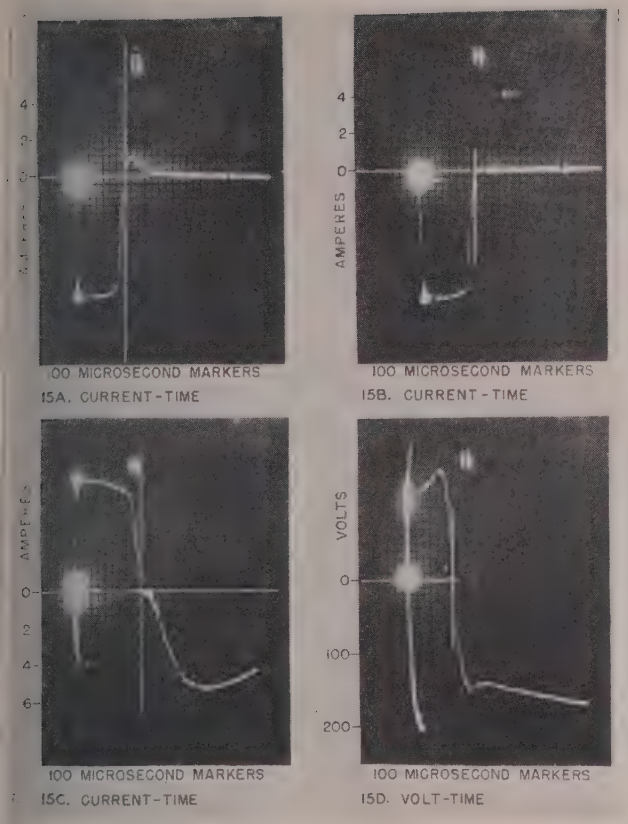

Figure 15. Cathode-ray oscillograms of parallel plate sample tests (zircon plates 1/8-inch apart with 7/8-inch electrode separation)

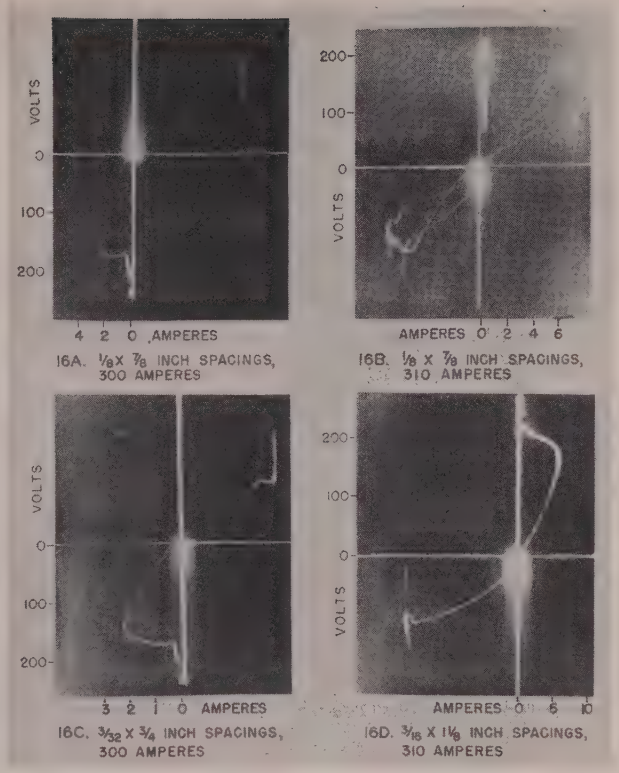
16A. 1/8 X 7/8 INCH SPACINGS, 300 AMPERES
16B. 1/8 X 7/8 INCH SPACINGS, 310 AMPERES
16C. 3/32 X 3/4 INCH SPACINGS, 300 AMPERES
16D. 3/16 X 1 1/8 INCH SPACINGS, 310 AMPERES

Figure 16. Volt-ampere cyclograms of near-critical parallel plate sample tests with zircon plates at various plate and electrode spacings, 192 volts, 300-ampere setting

typical in that its conditions were closer to critical than usual, resulting in a somewhat exceptionally long period of residual current flow. The marked pause in conductance change was more usually followed by an up- or down-turn soon after 200 microseconds, but longer pauses before eventual extinction or reignition of the arc were not uncommon.

Tests with Different Plate Materials

Tests on a number of other highly refractory ceramic materials gave results essentially similar to those on zircon. Tests on samples of less refractory materials like asbestos board gave noticeably different results in that the rate of fall of conductance just prior to current zero was higher and that just after zero was lower than with zircon. Such materials also successfully withstood higher restored voltage gradients on initial tests, but this ability rapidly disappeared with repeated arcing as the less refractory and presumably gas-generating components of the surfaces were baked out. It appeared that gas evolution from the fresh surfaces accelerated cooling and deionization of the gaseous arc, reducing its conductance practically to zero often by the time current zero was reached. The gas evolution also must have added significantly to the net rate of energy loss from the conducting surface layer and so made possible the higher observed dielectric strength.

The cyclograms of Figure 6 illustrate the behavior of semirefractory surfaces capable of a slight evolution of gas when heated by the arc. Figure 6A clearly differs from Figure 2C in the noticeably sharper curvature of the volt-ampere locus just before zero and the almost constant slope just after zero in Figure 6A. In Figure 6B, for the second test on the same spot, the gas-blast effect is less pronounced and the arc is reignited at the end of the first half-cycle. Time plots from these cyclograms are shown in Figures 7 and 8. The curves could be plotted with considerable accuracy during the 100 or so microseconds embracing the current zero because of the presence of clearly visible 10-microsecond time markers along the volt-ampere loci. The longer time values were obtained as before by fitting a section of the open-circuit voltage wave to the directly observed transient voltage rise. This method could not be applied, of course, beyond

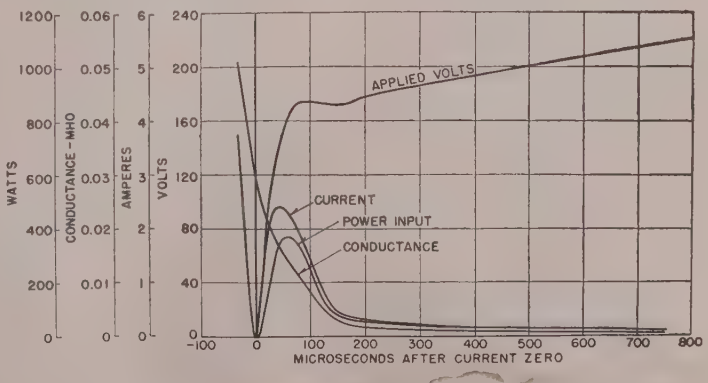

Figure 17. Time plot of quantities from Figure 16A, 1/8-inch plate spacing

the current upturn at 300 microseconds in Figure 8.

A plot of the variables of equation 2 taken from Figure 7 is shown in Figure 9. From 25 until 200 or 300 microseconds after current zero the locus follows very closely a straight line with the constants: $\theta = 180$ microseconds and $N_0 = 950$ watts per inch. At later times the rate of conductance decay was first much greater and then somewhat less than called for by the line. This wandering of the locus about a mean line seems to be a fairly characteristic pattern of behavior in these tests. It undoubtedly indicates long-time variation in the quantities assumed to be constant in equation 2, and it also may reflect inhomogeneity in the arc path. In particular, if the middle portion of the arc "bowed out" slightly, as it was often observed to do, striking a fresher and cooler surface, the middle portion of the surface leakage path might well have had a shorter time constant, θ, than the portions next to the electrodes. If this were true, the faster changing section of the path, being in series with the rest, might well have contributed a disproportionate share to the observed rate of conductance loss until voltage concentration across it tended to restore a balance.

Of special interest also in Figure 9 is the exceptionally long region before current zero in which the locus, though considerably curved, tends at its lower end to follow a line for $\theta = 24$ microseconds and $N_0 = 1{,}440$ watts per inch. By comparison with the results for plain zircon (Figures 4 and 5) these values suggest quantitatively a cooling and deionizing effect on the arc residue of a slight "blast" from the gas-evolving plate.

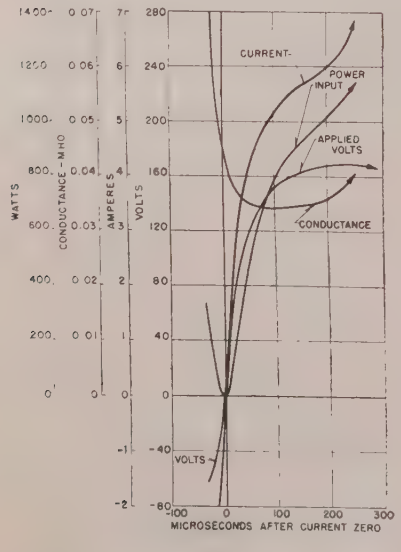

Figure 18. Time plot of quantities from Figure 16B, 1/8-inch plate spacing

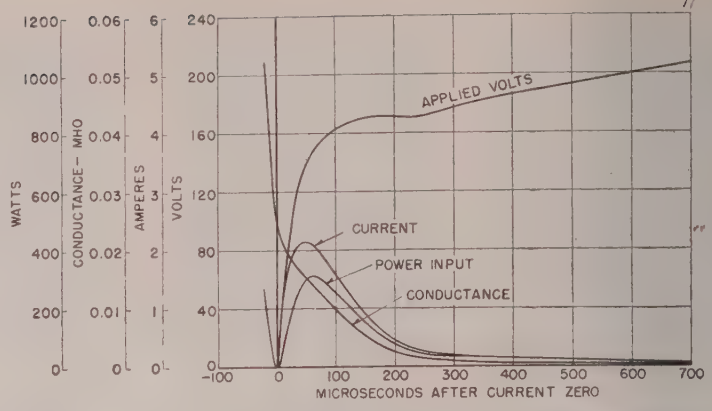

Figure 19. Time plot of quantities from Figure 16C, 3/32-inch plate spacing

It was shown by one of the present authors[2] that the arc during the highly conducting period before current zero could be represented better by a model equation of the type suggested by A. M. Cassie[6] than by equation 2. The Cassie-type equation, based on the concept of an arc of constant resistivity but varying cross section, leading to a characteristic arc voltage gradient in the steady state, can be written

$$R\frac{d}{dt}\left(\frac{1}{R}\right) = \frac{(e/E_0)^2 - 1}{\theta} \qquad (3)$$

where

e = applied voltage gradient
E_0 = steady-state arc voltage gradient
θ = time constant of arc conductance = ratio of energy storage per unit volume to rate of energy dissipation per unit volume

To test the applicability of this equation, the per-unit rate of conductance change before current zero in test of Figure 6A has been replotted in Figure 10 against the voltage gradient squared. It is evident that the values prior to 10 microseconds do fall in line according to equation 3 much better than they did according to equation 2. The line in Figure 10 has intercepts yielding the model values, $\theta = 16$ microseconds and $E_0 = 111$ volts per inch. It appears that the dynamic arc behavior in this test was of the Cassie type right up to current zero.

Figure 11 is a plot according to equation 2 of the data from Figure 8, showing the locus for an arc reignition. In this second test on the same spot, the pre-current-zero line indicates a somewhat longer arc time constant, 38 microseconds, than in the first test on the same spot, and the transition region appears to last longer than before—to about 50 microseconds instead of 25. After 50 microseconds, the values fall fairly close to a line with the same intercepts, $\theta = 180$ microseconds and $N_0 = 950$ watts per inch, as was drawn for this later region in Figure 9 for the first test. In this case, however, the power input exceeded N_0 and continued to rise with the rising voltage, leading to an upturn of conductance and eventually to complete arc reignition after 300 or so microseconds.

Critical Power Input to Plate Surface

A cursory study of a large number of volt-ampere cyclograms and of their time

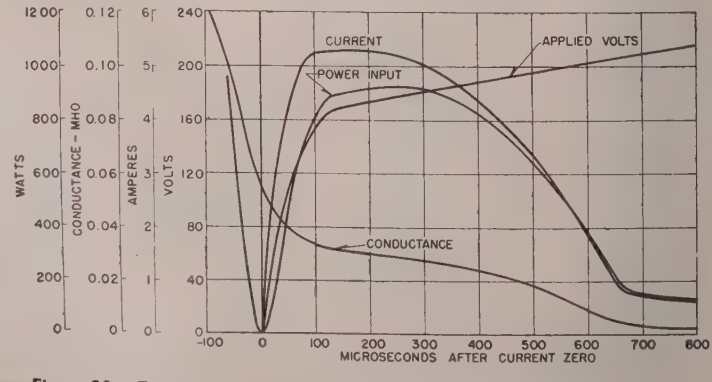

Figure 20. Time plot of quantities from Figure 16D, 3/16-inch plate spacing

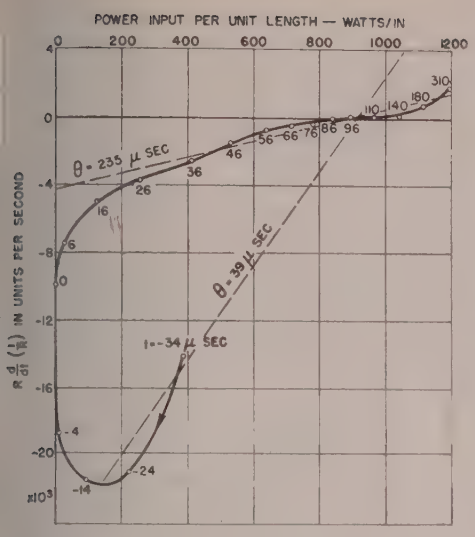

Figure 21 (left). Plot of per-unit rate of change of conductance versus power input per inch of arc path for parallel plate sample test of Figure 16B (1/8-inch plate spacing)

Figure 22 (right). Plot of per-unit rate of change of conductance versus power input per inch of arc path for parallel plate sample test of Figure 16C (3/32-inch plate spacing)

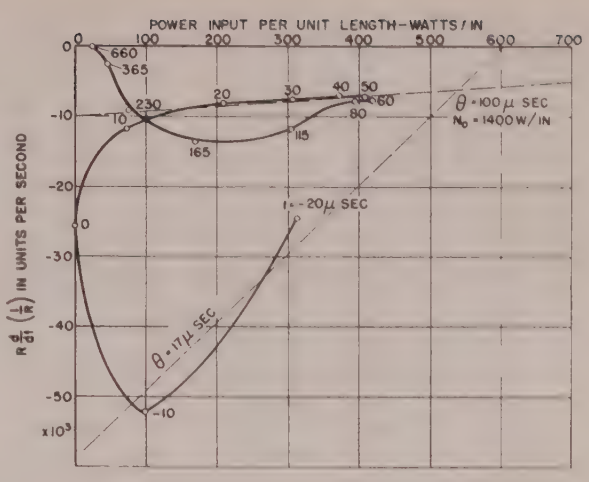

plots for the sample tests strongly suggested that the arc path resistances at the "knees" of the voltage-rise curves were critical in determining arc extinction or reignition. To test this suggestion and to aid in correlating the variable test results, a great many plots like that of Figure 12 were made. Against the experimentally adjusted variable, electrode separation, the "watts-per-inch" quantity, E^2/Rl, was plotted for each individual test with a given set of conditions. The value E was the rms circuit voltage, approximately equal to the restored voltage at the end of the transient rise. This voltage squared was divided by the arc path resistance, R, determined from the cyclogram by measuring the slope in volts per ampere of a line drawn from the origin to the point on the volt-ampere locus where thickening of the trace showed the beginning of the slower voltage rise along the sine wave of generated voltage. By dividing also by l, the electrode separation, the quantities were made comparable for all values of l. The plotted points in Figure 12 do fall into rather sharply defined regions, the "failure" points (crosses) lying mostly above and the "work" points (circles) lying mostly below a critical dividing line at 790 watts per inch. This was true at both 192 and 288 volts, the higher circuit voltage merely requiring a nearly proportionate increase in electrode spacing to equalize the chances of arc extinction or reignition. The vertical line at each voltage dividing the region of mostly circles from the region of mostly crosses indicates the critical electrode spacing at that voltage. Because of the method of calculation, actual applied volts not being used, the E^2/Rl values are not strictly equal to actual watts per inch, but it is interesting to note that the critical value, 790 watts per inch, is not far different from the N_0 values in watts per inch observed for the surface conductance lines in the equation 2 plots of Figures 4, 9, and 11.

Sample Tests with Arcs between Parallel Plates

The single-plate small-sample tests described previously fail to duplicate in several particulars the arc situation in the chute of a magnetic-type air circuit breaker. In one such circuit breaker, the Westinghouse *Type DH*, zircon porcelain plates with tapered offset slots as shown in Figure 13 are stacked alternately between the poles of the blowout magnet so that the arc is driven to the tops of the slots by the field and held there by the slot ends with most of the arc confined in the 1/8-inch spaces between the parallel plates, where the arc axis generally is parallel to the field flux. As a better approximation to this situation, the parallel plate arrangement shown in Figure 14A was devised for making further sample tests. In the circuit breaker chute, each elementary arc portion is joined to those in the adjacent interplate spaces by short sections of arc passing through the slots. In the test arrangement of Figure 14, the rectangular bar graphite electrodes take the place of the connecting arc portions in the plate slots. As in the circuit breaker, there is no direct continuous path along a plate surface immediately in parallel with the arc. There also is no transverse magnetic field driving the arc against one plate surface, as was the case for the single-plate sample tests.

Analysis of Conducting Paths with Parallel Plates

However, the differences with respect to arc extinction or reignition between the two sample test arrangements are less drastic than they may at first appear. When the arc-gas conductivity is relatively high, as it is during most of the current half-cycle, the current flow in the parallel plate sample test is something like that shown in Figure 14B, and there can be some current flow also through the heated conducting surface layers of the adjacent plates in parallel with most of the arc. As the arc-gas conductivity drops near current zero faster than the plate surface conductance, the current flow pattern will change through some transition period until it approaches that of Figure 14C for relatively low gas conductivity. In Figure 14C, the conductivity ratio is such that the plate leakage paths are practically equipotential surfaces and the applied voltage is essentially all across the gas space. Hence, in the final stages, the observed "leakage" currents are limited by the resistivity of the arc gas rather than by the surface resistance of the plates, a situation essentially different from that of the Figure 1 type (single plate) sample tests.

In the intermediate stages of conduction, between the extremes represented by B and C in Figure 14, the current flow lines must have some complex pattern which is difficult to analyze exactly but which is characterized by series-parallel connection of the gaseous and surface leakage paths with the flow and equipotential lines slanted so as to be neither parallel nor perpendicular to the plate surfaces. During this transition period the leakage current is limited jointly by the two elements: the conducting gas and the conducting surfaces. Because of the geometry of the situation, this period may be relatively long, since, when the extreme condition of Figure 14C is approached, the now relatively short and parallel paths through the gas may still be able to carry the residual current with

comparatively low voltage drop even though the gas conductivity in mhos per unit volume has reached small values. As an example, with 1/8-inch plate spacing and ten times as great ($1^1/_4$-inch) electrode separation, the gas space resistances would be essentially the same in Figures 14B and 14C if the gas conductivity in the latter case were only $1/(10)^2$, or 1 per cent of that in the former. (The gaseous conductor would now be one-tenth as long and ten times as wide as before.) Thus, there still may be a considerable period when the residual current is limited chiefly by the "leakage" resistance of the heated plate surfaces even though a gas space of diminishing conductivity is in series with the surfaces. This helps to explain the marked superficial resemblance between cathode-ray oscillograms of these parallel plate tests and those of the single-plate sample tests.

Oscillograms of Parallel Plate Tests

Figure 15 shows a series of four cathode-ray oscillograms of arc current and voltage near current zero for some of the early parallel plate tests, made as before at 192 volts and 300 amperes. Figure 15A is a fairly typical current-time record showing a test in which the residual current reached a peak of a little more than an ampere in 30 or 40 microseconds and decayed rather rapidly thereafter. In Figure 15B, there was no measurable residual current, apparently because of "rectification," or failure of the arc to develop a new cathode spot on the former anode terminal, indicating that the arc spot must have been in rapid motion. In Figure 15C there is a short "current-less" pause, followed apparently by breakdown along a path outside the confined space between the plates, since the subsequent larger and much more slowly varying residual current is characteristic of an unconfined arc of this magnitude in air. Figure 15D is a typical volt-time record showing the transition from the opposing arc voltage to the rising portion of the sine-wave line voltage with just a slight "overshoot." Timing-marker blanks in all the oscillograms are 100 microseconds apart.

In Figure 16 are shown volt-ampere cyclograms of four of a series of parallel zircon plate sample tests at three different plate spacings with electrode separations near the critical value for each. At a plate spacing of 1/8-inch, the critical electrode separation was only 3/4-inch, considerably less than the critical value for the single-plate sample tests. This difference seems to indicate considerable effectiveness of the series gaseous arc gap in reducing the power input to the ceramic leakage surfaces for the same average voltage gradient.

Figures 17 and 18 are replots, respectively, of cyclograms A and B in Figure 16, both for 1/8-inch plate spacing and 7/8-inch electrode separation. The curves in Figure 17 for the successful interruption are rather unlike those of Figure 3 for the single-plate sample test on standard zircon, but this difference seems to be mainly the result of difference in the nearness to critical conditions for arc reignition in the two cases. The much smaller current-zero arc path conductance in the test of Figure 17, where the electrode spacing was greater than critical, permitted a faster transient voltage rise than that in Figure 3 and also led to a much faster further decay of arc path conductance. In Figure 18 it may be seen that the arc path conductance at current zero was about 50 per cent greater than in the test of Figure 17. With this larger conductance, the power input increased enough faster, in spite of a somewhat reduced rate of voltage rise, to cause the conductance to level off and then increase again beyond 100 microseconds, leading finally to arc reignition. Figure 18 is generally similar to Figure 8 for the gas-evolving single-plate "failure" test, even having the same minimum value of conductance.

Effect of Plate Separation

With the parallel plate structure it was easily possible to try the effect of another variable, the distance between the adjacent plates. Values for the test of Figure 16C with a 25 per cent reduction in plate spacing to 3/32-inch are plotted in Figure 19, and values for the test of Figure 16D with a 50 per cent increase in spacing to 3/16-inch are plotted in Figure 20. The current-zero conductances in these two tests were nearly in the same ratio, 1 to 2, as the plate spacings and the rate of conductance decay was much slower, both before and after current zero, with the larger spacing than with the smaller.

Analysis in Terms of Model Equations

As was done before for the single-plate sample tests, an attempt has been made to interpret these data in terms of the simple arc model equations. This attempt has had more apparent success for the earlier parts of the conductance curves than for the later parts, where the interaction of the gaseous and solid surface resistance is far more complex than with the single-plate tests. In the model equation plots of Figures 21, 22, 23, and 24 for the parallel plate tests at 1/8, 3/32, and 3/16-inch plate spacing, the loci plotted before current zero show a very definite effect of plate separation on the time constants for this region of mainly gaseous conduction. As the plate spacing is made smaller one would expect the relative rate of power loss by gas cooling and deionization to increase, thus reducing the arc time constant, and conversely, since the power loss term, N_0, appears in the denominators of the fractions defining the time constant. In accordance with this expectation, the roughly indicated arc time constants with the different spacings are as follows: 17 microseconds at 3/32-inch (Figure 22), 39 microseconds at 1/8-inch (Figure 21), and 64 microseconds at 3/16-inch (Figure 23).

Figure 23. Plot of per-unit rate of change of conductance versus volts-per-inch squared for parallel plate sample test of Figure 16D (3/16-inch plate spacing)

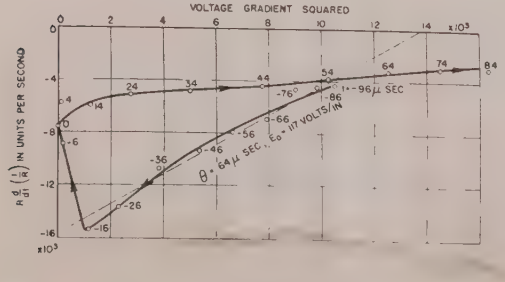

Figure 24. Plot of per-unit rate of change of conductance versus power input per inch of arc path for parallel plate sample test of Figure 16D (3/16-inch plate spacing)

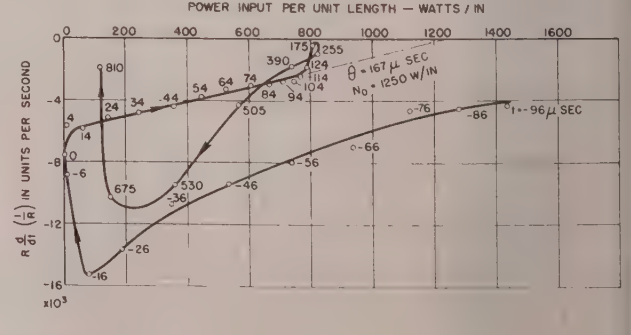

In the case of the test of Figure 16D at 3/16-inch plate spacing where values are available over an exceptionally long time before and after current zero, it again appears that the Cassie-type equation (Figure 23) gives a better linear fit with the data before current zero than does the Mayr-type equation (Figure 24). After current zero, however, when the conductance apparently was dominated by the more slowly responding solid surfaces, Figure 24 shows that a better and more reasonable fit is obtained with the power input plot for the Mayr-type equation.

The constants indicated for the latter region in Figure 24 are: $\theta = 167$ microseconds and $N_0 = 1{,}250$ watts per inch, values not far from those similarly obtained for the single-plate sample tests. In comparing the Mayr and Cassie arc model equations, 2 and 3, it can readily be seen that they are identical for small variations in arc power and conductance, the departure showing up only over an extended range of the variables.

Other Currents

As a basis for comparing the behavior of various plate materials, practically all the sample tests were made at the one current value, 300 amperes. A few tests have been made with the parallel plate arrangement at 1,100 amperes and similarly analyzed, but no essential difference in behavior at this higher current was revealed.

Conclusions from Sample Tests

This study of a-c arc extinction adjacent to refractory insulating plates has shown that:

1. The arc path conductance decays fairly slowly after a current zero, momentarily permitting appreciable residual currents to flow even when the circuit is finally interrupted.
2. Extinction or reignition of the arc after a current zero depends on the relative magnitudes of (a) the rate of energy loss from the arc path and (b) the power input resulting from the rising restored voltage applied to the arc path. Any sustained excess of power input over rate of energy loss generally results in arc reignition.
3. The residual conductance near current zero is made up of two essentially parallel parts: (a) the gaseous arc residue with a time constant for conductance change of some few tens of microseconds, and (b) the heated arc trail or trails on adjacent refractory surfaces with a time constant of the order of 200 microseconds.
4. The rate of decay of the gaseous arc conductance can be accelerated by (a) a gas blast through the arc such as may result from decomposition of the adjacent surface material, or (b) reducing the width of the space between arc-confining surfaces.
5. With comparatively slow rates of rise of restored voltage, such as characterizes sample tests at a few hundred amperes, the surface leakage path dominates the conductance and so largely determines the interrupting ability.

Application to Practical Circuit Breakers

Extrapolation of these results to the limiting conditions for interruption in magnetic circuit breakers with refractory arc chutes is difficult because of the much higher currents which must be interrupted by actual circuit breakers and also because of such additional influences as magnetically and thermally induced air flow in the circuit breaker chutes. Both these latter influences and the higher rates of current change near zero may alter essentially the relative importance of the limiting factors mentioned in the preceding section, but it is believed that the general conclusions 1, 2, 3, and 4 apply to the circuit breaker as well as to the sample tests.

Because of the possible differences, there clearly is need for extending studies of this type to actual circuit breaker arc chutes operating at currents up to their full interrupting limits. The authors are attempting to do this, and it is hoped that the very formidable experimental difficulties at these high currents may soon be overcome sufficiently to make accurate measurements and analyses of such larger scale tests also possible.

References

1. The Geometry of Arc Interruption—II; Current-Zero Phenomena, **E. W. Boehne.** *AIEE Transactions*, volume 63, 1944, pages 375–86.
2. A Study of A-C Arc Behavior Near Current Zero by Means of Mathematical Models, **T. E. Browne, Jr.** *AIEE Transactions*, volume 67, part I, 1948, pages 141–53.
3. Circuit-Breaker Current Measurements During Reignitions and Recovery, **Laurel J. Lewis.** *AIEE Transactions*, volume 66, 1947, pages 1253–57.
4. Extinction of a Long A-C Arc, **J. Slepian.** *AIEE Transactions*, volume 49, April Section, 1930, pages 421–30.
5. Beitrag Zur Theorie der Statischen und der Dynamischen Lichtbogens, **O. Mayr.** *Archiv Fuer Electrotechnik* (Berlin, Germany), volume 37, 1943, pages 588–608.
6. Arc Rupture and Circuit Severity: A New Theory, **A. M. Cassie.** International Conference on Large Electric High-Tension Systems (Paris, France), 1939, pages 1–14.

Discussion

R. C. Van Sickle (Westinghouse Electric Corporation, E. Pittsburgh, Pa.): As an engineer working on the development of power circuit breakers, I find these studies of arc characteristics near current zero of great interest. It is the conductivity of the arc space and its relative magnitude with respect to the capacitive impedance of the transient recovery voltage circuit that enables power circuit breakers to interrupt circuits having extremely high natural frequencies. The oscillographic records of voltage in this paper show almost no trace of the natural frequency of the circuit, indicating that the conductivity of the arc space was large enough to control the characteristics of the recovery voltage.

Such measurements as these on power circuit breakers will facilitate the application of circuit breakers at locations having high natural frequencies.

Is the apparatus which was used for these tests suitable for use at the larger currents encountered near the interrupting ratings of power circuit breakers?

Robert H. Nau (University of Illinois, Urbana, Ill.): The quantitative analysis of Browne and Strom agrees very closely with the qualitative observations I made of literally hundreds of interruption tests which accrued during the early development of the refractory arc chamber for both low and high voltages.

Arc chambers for the 750-volt magnetic circuit breaker were first developed. Spaced asbestos board plates with narrow V-slots were quite satisfactory for short-circuit currents from a few amperes to 100,000 amperes. When the development was extended to 2,500 volts with short-circuit currents above 10,000 amperes erratic behavior, as described in the section, "Tests With Different Plate Materials," began to hamper the development. The asbestos board possessed hygroscopic properties, contained fusible ingredients, and displayed erosion qualities which gave rather consistent patterns of test results on respective test chambers.

The discovery of the zircon refractory immediately raised the ceiling. By proper V-slot design, refractory plate spacing and co-ordination with the magnetic field, the several magnetic air circuit breaker ratings were obtained. The voltage which could be interrupted was found to be a function of the magnetic field strength and the number of refractory plates per arc chamber. The current that could be interrupted for a given voltage depended a lot upon the plate width, the spacing of the plates, and somewhat upon the slot shapes. The nature of the refractory plates fairly well eliminated any gaseous discharge or gas blast in the presence of the arc. It was found expedient to co-ordinate the several design features so that the arc would not slide up into the

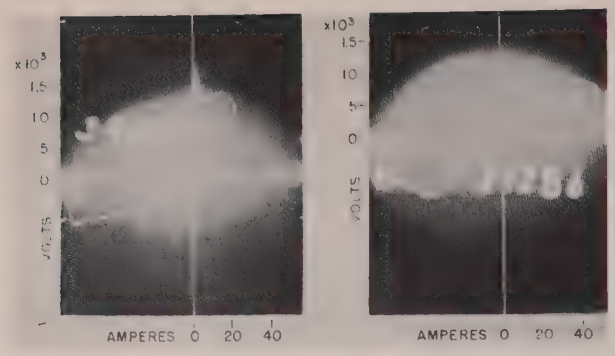

Figure 1. Volt-ampere cyclograms of model circuit breaker tests at 6,250 amperes, 1,150 volts, with four standard zircon plates in the chute, air-core field

(A) (left) Tests with $B_m/I = 0.15$, flux lagging the current by 20 degrees (B) (right) Test with $B_m/I = 0.125$, flux in phase with the current

narrow parts of the V-slots, under action of the magnetic field and the self-generated gas blast, until after the current had begun decreasing toward zero in cycle. Hence the arc was not permitted to play at any one spot, and, thus, to raise the surface conductance as much as might otherwise be expected.

It is evident that the space between the refractory plates provides a chimney or exhaust for the self-generated gas blast and arc by-products. The lateral space also provides deionization surfaces. Therefore, I wonder concerning the significance of the conclusion, part 4(b), which states that "reducing the width of the space between arc confining surfaces" accelerates the decay of the gaseous arc conductance.

It is gratifying that the quantitative analysis reported by Browne and Strom support almost completely the previously made qualitative observation.

W. O. Kelham (Liverpool University, Liverpool, England): The near zero current and voltage measurements presented in the paper give a good indication of the mode of operation of the interrupting device. Considerable residual conductivity after current zero is exhibited and the dynamic characteristic of the residual discharge under the influence of the factors stated by the author clearly determines whether or not the circuit is cleared at a particular current zero.

For near critical conditions the rate of rise of restriking voltage is independent of the circuit natural frequency and, following the knee in the recovery voltage waveform, the voltage across the interrupter is approximately constant. The "critical watts per inch" indicated by Figure 12, 790 watts per inch, for the period immediately following steadying out of the voltage wave, is noticeably close to the value of the product of voltage and current which would be obtained from a static arc characteristic for a carbon arc in air with the same applied voltage (160 volts) and electrode separation. Thus the criterion for failure or clearance at a particular current zero would appear to reduce to whether or not the current, immediately following steadying out of the voltage wave, exceeds that which would be obtained from a static arc characteristic under the same conditions.

If the power input (i.e., the current) at this time slightly exceeds the critical value $d/dt(1/R)$ is positive and the current increases. Conversely, if the power input is slightly less than critical $d/dt(1/R)$ is negative and the current decreases. For the case where the current has the critical value, power input equals power loss, the residual discharge is just stable under the influence of the applied voltage and $d/dt(1/R)$ is zero. Thus one would expect that the value of power input when $d/dt(1/R)=0$, obtained from such plots as Figures 4, 9, and 11 for near critical current zeros, would be the same as the "critical watts per inch."

It seems significant that the same value (800 watts per inch) of power input when $d/dt(1/R)=0$ is obtained in the plots of Figure 21 and Figure 24 even though the physical conditions of the interrupter and interrupting capability are somewhat different. If this is generally true, does it not mean that the factors which make one arrangement better than another are only effective in the near zero period at currents less than 5 amperes?

The plots of $Rd/dt(1/R)$ against the product of voltage and current and against voltage squared during the near zero period confirm that the dynamic characteristic of the discharge is of the general form $R\,d/dt(1/R)=F'(Q)/F(Q)/(W-N)$. There is a fair agreement to Cassie's form of the equation prior to current zero and to Mayr's form after current zero. However, the agreement is not exact even for this very simple interrupter and, together with the random variation, this means that the theories could not be used to predetermine accurately the performance of a particular arrangement.

The phenomenon of conductivity along the surface of the refractory plate would seem to merit a more thorough investigation, as it sets a limit to the performance of the interrupter. Is it possible that the conduction phenomena is related to the effect of the high temperature surface on adjacent layers of gas, rather than actual conduction through the refractory material?

In similar tests using a plain break in air between brass and steel electrodes, but with no adjacent refractory plates, it was my experience that the dynamic arc theories could not generally be applied. This was due to an effect at the new cathode after current reversal. The conditions at this electrode were such that no current flow (greater than 0.02 ampere) occurred until the restriking voltage exceeded 300 volts (approximately), a voltage of the order of the minimum breakdown voltage in air. Only at certain current zeros, particularly for high currents and low contact separation when no attempt was made to clear the circuit, was the new cathode at current reversal sufficiently heated to form a cathode spot immediately and permit current flow with a low arc voltage. Presumably the use of graphite electrodes eliminates this effect, graphite being a thermionic emitter of electrons, and this accounts for the absence of any marked zero pause in the author's tests.

Preliminary experiments using much more efficient blast types of interrupter under high current and high voltage test conditions have indicated that residual currents are not in general the determining factor governing whether or not the circuit is cleared at a particular current zero, although they may set an upper limit to the rate of rise of restriking voltage which can be dealt with. Failure at a near critical current zero normally occurs with a spark type breakdown some time after current zero. Continuous conductivity is apparent throughout the near zero period only for tests in which practically no attempt is made to clear the circuit. However, the near zero measurements of current and voltage give much useful information regarding the

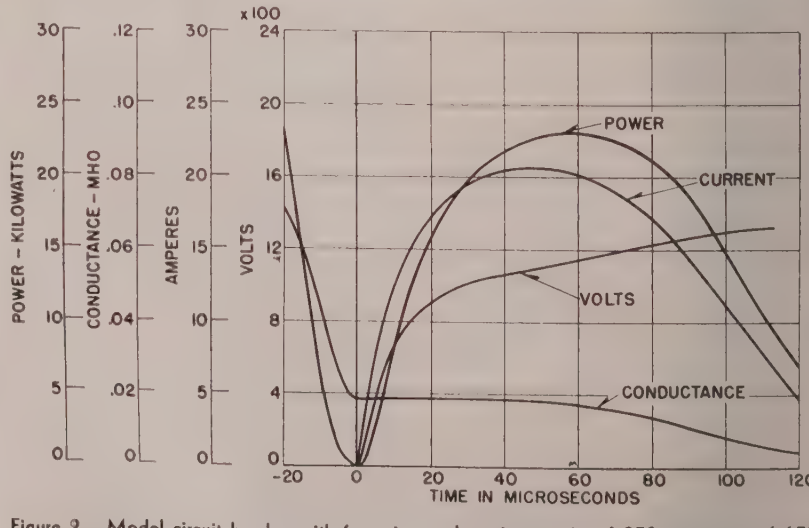

Figure 2. Model circuit breaker with four zircon plates interrupting 6,250 amperes at 1,150 volts, $B_m/I = 0.15$, flux lagging 20 degrees

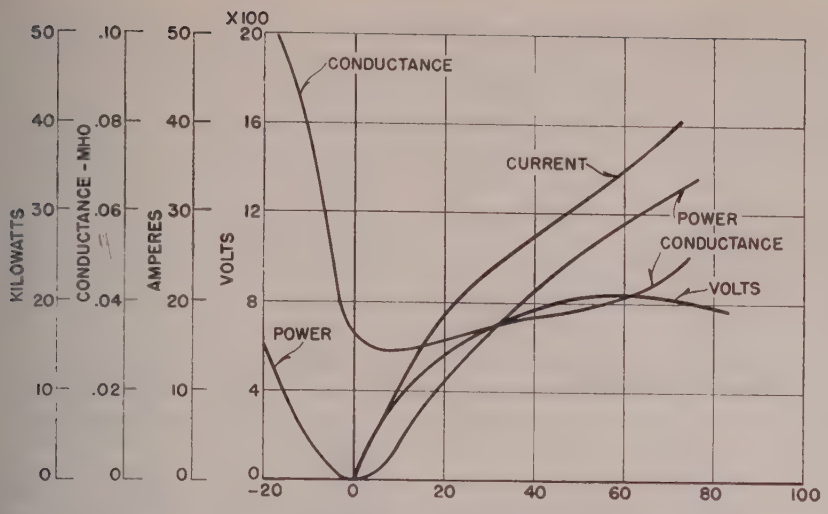

Figure 3. Model circuit breaker with four zircon plates failing at 6,250 amperes, 1,150 volts; $B_m/l = 0.125$, flux in phase with the current

mode of operation of the interrupters, and certainly they provide the only satisfactory method of checking the applicability of the dynamic arc theories.

T. E. Browne and **A. P. Strom:** In reply to Mr. Van Sickle's question regarding the application of these techniques to actual circuit breakers, we have attempted to apply this method of studying residual conductivity in the arc path following the last half cycle of power current in circuit breakers up to maximum currents of about 20,000 amperes. The present performance of the measuring devices does not permit us to make accurate measurements at the 20,000-ampere level, although approximate results can be obtained. However, up to about 10,000 amperes reasonably reliable measurements have been made.

Figure 1(A) of this discussion shows a volt-ampere cyclogram of a successful interruption at 6,250 amperes on a model circuit breaker consisting of four zircon plates like those shown in Figure 13 of the paper. Figure 1(B) of this discussion shows a similar volt-ampere cyclogram for a failure test at the same current.

Figures 2 and 3 of this discussion, respectively, show replots from the oscillograms 1(A) and 1(B) of volts, amperes, conductance, and power input to the arc space, plotted to a time base for a few microseconds just before and about a hundred microseconds just after the zero value of the arc current. In drawing these curves, some estimation was necessary in locating the zero current and zero voltage point, but this does not appreciably affect the curves except for a possible slight displacement along the time axis.

It may be observed in Figure 2 that the power input rose to 23 kw at approximately 60 microseconds after current zero. This large power input was absorbed by the arc space and the four ceramic plates of the interrupter without an increase in conductance. The conductance then dropped rapidly to zero. This test, however, was a near failure as indicated by the long period of nearly constant conductance. Figure 3 of this discussion, a replot from the failure test oscillogram Figure 1(A), shows about twice as much conductance at current zero as the successful operation. The arc space and ceramic surfaces were unable to withstand the resulting power input which reached almost 30 kw at 60 microseconds after current zero. This resulted in a rising conductance and failure.

It may be observed that the traces in the oscillograms of Figure 1 fail to pass directly through the origin of the axes. This, we believe, indicates a slight phase displacement in the current measuring equipment, since it is reasonably certain that the current and voltage in the arc space pass through zero simultaneously. Such deviations of the record can be accounted for by a remanent inductance in the current measuring shunt of as little as 10^{-8} henrys or by a small shift in the zero axis of the amplifier, or both.

The measuring difficulties naturally increase with increasing values of short circuit current, since the rate of change of current varies directly as the current, causing inductive voltages in shunts and higher effective frequencies to which the amplifier must respond. The maximum current that can be studied is thus mainly a problem of improvements in the measuring instruments and techniques. Such improvements are contemplated and it is hoped that these will eventually permit the methods described in this paper to be applied to the study of breakers operating at the highest short circuit currents.

We wish to thank R. H. Nau for his account of the background of our studies. Our tests were designed to approximate conditions in practical arc chutes near or just beyond the limits for current interruption where considerable heating of some plate areas does occur. Since all of the conditions could not be duplicated in our simplified sample tests, it is likely that our results with the samples indicate some but not necessarily all of the important factors. This applies especially to the relative importance of surface leakage and residual gas conductance. It is interesting to note, however, that our results with the parallel-plate sample tests agreed with previous design tests on breaker chutes in yielding a plate spacing of 1/8-inch for optimum volts-per-inch interrupted.

In reply to the very careful and appreciated discussion by W. O. Kelham, of Liverpool, England:

1. As mentioned in the paper, it *is* considered significant that the power input for $d/dt(1/R)=0$ in the plots of Figures 21 and 24 and the like agree so nearly with the "critical watts per inch" values of Figure 12, and incidentally of very many similar plots not published. These values should not be exactly the same, however, since as also mentioned, the "watts per inch" quantity was only approximately the same as true power input because rms circuit volts was used instead of actual instantaneous restored volts in computing the quantity in Figure 12.

2. It may very well be true, as Mr. Kelham suggests, that the deciding factors determining the advantage of one arrangement over another exist principally in the near-zero period where the currents are less than 5 amperes or so. This period can hardly be independent, though, of arc conditions just prior to the zero period, especially the rms magnitude and hence rate of fall of the arc current as zero is approached. Magnetic fields or thermally-induced gas flow in an arc chute may also be very important in "setting the stage" for the zero period.

3. The apparent fact of only approximate agreement between the plots and either Cassie's or Mayr's type of dynamic arc equation is freely admitted, but it is felt that these equations may still be useful even if they can serve only for very rough semi-quantitative computations or predictions, since more exact methods of approach are still unknown.

4. The conduction phenomenon along the heated surfaces of the refractory plates has received considerable thought and some experimental study not reported in the paper. It is considered doubtful that conductivity in the immediately adjacent gas layer can persist for the long times observed after the decay of the short-lived residual gas conductance associated with the main current flow, as illustrated in Figure 5. This surface conductance, though critical in the sample tests, may not always be a limiting factor in the more complex case of an actual breaker arc chute interrupting many thousands of amperes. On this point especially, more work does need to be done.

5. As pointed out by Mr. Kelham, the dynamic arc equations, which apply to the conductance of the positive column alone, do not work for comparatively short arcs between most metallic electrodes. He rightly presumes that we used graphite electrodes to eliminate this "new cathode" effect. The equations should apply to long arcs where restriking voltages can exceed several thousand volts, as in a full-size circuit breaker arc chute.

6. Mr. Kelham is probably correct in his impression that residual currents are not directly involved in the normal operation of air-blast circuit breakers employing high air pressures. It is felt, however, that they may be of dominant importance for such circuit breakers operating near their ultimate current interrupting limits in high-natural-frequency lower voltage circuits. The current limit for the importance of this effect will be much lower where low air pressures are used.

Power System Fault Control

AN AIEE COMMITTEE REPORT

Basic System Planning for Power System Fault Control

Outline of Problem

THE RAPID increase in the generating capacity of the electric power industry to meet its large postwar load demand has presented a serious problem in dealing with its increase in short-circuit concentrations.

To secure economical and adequate fault control* of both the present and future power system, the fault control function of the system should be as carefully planned as the other components of system design. The art of power system fault control has by now advanced to a point where it can usually be applied in clearly cut systematic plans that will not hamper system operation, become obsolete with system growth, or be unduly expensive.

Inquiries reveal a widely held opinion among power system engineers that the facilities which power systems have provided for short-circuit control have too often been haphazard, as though the result of afterthought, and without much regard for future system growth and change; rather than as fundamental parts of a master plan of system growth, to be included in the original designs of stations and system.

Since many of our power systems are making changes to handle their increased short circuits, this is an opportune time for the industry to establish the best practices in fault control. Certain broad and basic principles of fault limitation and removal should be chosen by each power system and be included in its philosophy of system development. These basic principles are emphasized in this report, while leaving the details of application to the system designers.

As a rule, the problem of fault control is one of balancing the cost of those facilities against the operating flexibility of the system. Most any system can, at a minimum cost, be split and divided at busses and between areas, or current limiting impedances can be inserted, so that the faults will be held within the interrupting capacities of most of its existing circuit breakers; and its relaying can be arranged so that any remaining heavy faults that do occur can be cleared by a few large back-up circuit breakers; but care is needed to see that these expedients are not carried too far. A power system, when so arranged, becomes a so-called soft or loosely-linked or loosely-knit system. If the system arrangement is too loosely-knit, the system becomes too unwieldy for good operation. At times of system disturbance, unnecessary and prolonged loss of loads or of whole areas can occur, spare tie line capacity may be unavailable to pickup loads, and dynamic instability can develop. During normal operation it may be difficult to maintain correct voltage levels in all areas, and nonuniform loading of tie lines can result in inefficient transmission capacity use.

A closely-knit system uses few or none of these fault limiting expedients and is generally free from such operating restrictions, but its circuit breakers must be large enough to handle its heavy short circuits, with an allowance for future growth, and hence, is costly. In fact, some of the larger power systems of both the metropolitan and high-tension transmission types cannot be given as closely knit an arrangement as their operators desire. Otherwise, their short-circuit concentrations will exceed the interrupting capacity of the largest circuit breakers the manufacturers are able to supply.

Thus, it is evident that many factors must be considered in planning for the control of short circuits as a system expands; and they must take into account both the present and future system arrangements. But in the main, the choice lies between cost and operating freedom.

This choice is greatly affected by the type of system being considered and may be illustrated by comparing the metropolitan and the high-tension transmission types of systems, as described later here.

As a rule, the larger power systems in the United States have adopted very definite basic principles of short-circuit control and their station and system additions are designed to fit in with those principles. Their very size makes such a policy necessary. They have gone through periods of large and rapid system growth and have been forced into extensive studies for system planning. They have gone through the period when it became necessary to adopt and include certain basic principles of short-circuit control as a major policy in their philosophy of development. We feel that as a result of their experience and studies they have, for the most part, achieved reasonable balances between the cost of fault control and flexibility of system operation; and we suggest that the principles of fault control which they have adopted be given careful consideration as a policy of system planning, by systems of lesser size which anticipate any considerable amount of system expansion.

Classification of the Methods of Power System Fault Control

A study of the various means of power system fault control shows that they can

* The term "fault control" refers to both the limitation of, and removal of, system faults. Limitation of faults refers to the limitation of fault currents, of overvoltages during faults and of recovery voltages.

Paper 51-66, recommended by the AIEE Protective Devices Committee and approved by the AIEE Technical Program Committee for presentation at the AIEE Winter General Meeting, New York, N. Y., January 22–26, 1951. Manuscript submitted August 21, 1950; made available for printing December 5, 1950.

This report was prepared by a Working Group on Power System Fault Limitation of the Fault Limiting Devices Subcommittee, AIEE Committee on Protective Devices, consisting of F. R. Longley, *chairman*, J. O'R. Coleman, E. M. Hunter, F. H. Kierstead, L. B. LeVesconte, H. F. Lindemuth, E. L. Michelson, and L. E. Sauer.

be classified into ten basic methods. These are:

1. Replacement of inadequate circuit breakers with circuit breakers of adequate interrupting capacity.

2. Use of current limiting devices in the phase wires. These include current limiting reactors, of both the simple and duplex types, split-winding transformers, and double-winding generators.

3. Use of current limiting impedances in the neutrals.

4. Use of ground fault neutralizers.

5. Isolated phase construction.

6. Sectionalization within stations. This divides a station into two or more parts connected only by synchronizing ties.

7. Sectionalization of system areas. This divides an entire power system into two or more areas with light synchronizing ties connecting the areas. The division into system areas might, and often does, include a split bus in one or more stations, with one side of a bus connected to one area and the other side connected to another area—and thus combines sectionalization within stations with sectionalization of areas.

8. Unit arrangements. Devices containing impedances are connected in series before their circuits are paralleled. Examples are: generating stations where each generator has its own transformer, the transformers being paralleled only on the sides away from the generators; and transmission lines, each with its own transformer, and the transformers paralleled only on the sides away from the major sources of fault current.

9. Pretripping. In case of heavy faults, one or more heavy duty backup circuit breakers reduce or clear the fault. The smaller breakers then isolate the faulted circuits. A backup circuit breaker may reduce the fault by splitting, or partly splitting, the system, or it may clear the fault by clearing a group of small circuit breakers between it and the fault.

10. Delayed tripping. Circuit breaker operation is delayed to allow time for the current decrement to reduce the fault current. This method is becoming obsolete.

The ten foregoing classifications could be reduced to three still broader classes. They would be: adequate circuit breakers, which would include number 1 only; fault limitation, which would include numbers 2, 3, 4, 5, 6, 7 and 8; and relay schemes, which would include numbers 9 and 10.

Classification of Power Systems, According to Their Methods of Fault Control

A study of different types of systems shows that distinctly different systems have evolved distinctly different philosophies of fault control. These systems may be divided in five categories as follows:

1. Large metropolitan systems which use a low ratio of X_0/X_1, that is the magnitude of ground fault current is comparable to the magnitude of fault current between phases, especially at station busses. (In practice, magnitudes of line-to-ground and 3-phase fault currents are usually held to about the same value at busses.)

2. Large metropolitan systems which use a large ratio of X_0/X_1, that is the ground fault current is small in comparison with the fault current between phases.

3. Metropolitan systems of medium size. These systems serve cities which have populations of about 100,000 to 500,000.

4. High-tension transmission systems.

5. Metropolitan-transmission systems.

Examples Illustrating the Philosophies of Power System Fault Control

As contrasted with transmission systems, the metropolitan system uses a large number of relatively short tie lines, and it uses many circuit breakers as compared with its miles of line. When the growing system's increasing fault duty exceeds the capacity of its circuit breakers, the replacement of all its under-rated circuit breakers with circuit breakers of adequate interrupting capacity becomes too costly, and in some cases impossible, for, as mentioned previously, there will be some locations where the unlimited fault will exceed the interrupting capacity of the largest circuit breaker manufactured. A compromise is the usual solution. The metropolitan type of system is so closely-knit inherently, that fault limiting devices and arrangements can be used rather freely without undue sacrifice of operating flexibility. Some circuit breakers have to be replaced, but for the most part the short-circuit currents are lowered by such expedients as a reduction in tie line connections, splitting of busses sectionalization both within stations and between areas, phase isolation, current-limiting reactors, double-winding generators, split-winding transformers, neutral impedances, synchronizing at the load, and pretripping.

The philosophies of fault control, as evolved by the power systems which supply the two largest cities in the United States, are described in the following paragraphs.

A Large Metropolitan System Which Uses a Low Ratio of X_0/X_1

This is a summary of methods used on the New York City system to reduce magnitude of fault current. In New York City the predominant amount of generation is 13,800 volts on the 60-cycle system and 11,000 volts on the 25-cycle system. The generating station busses are operated at generator voltage, with the exception of one generating station, which is operated at 27 kv. In this case the generators are connected to the busses through autotransformers. All high-tension distribution to the network system and substations is at generating station bus voltage. Tie feeders between generating stations are operated at 11 kv on the 25-cycle system and at 13.8 kv and 27 kv on the 60-cycle system.

High short-circuit currents are a problem on this system due to the close linkage between generating stations and the large amount of generation concentrated in each generating station (300–800 megawatts).

All generating stations built or revamped within the past 25 years are of the phase isolation type of construction. Those built within the last 12 years have the metal-clad type of construction. With this type of construction the number of faults that occur will be minimized and most faults that do occur will be line to ground. However, this does not help much in the limitation of fault currents, as the ratio of X_0/X_1 is three or less on the 60-cycle generating station busses.

The methods most commonly used on this system to limit the magnitude of fault currents are: (1) reactors; (2) sectionalization; and (3) pretripping.

Reactors are extensively used on this system to limit the magnitude of fault current. All distribution feeders, tie feeders, and generators are equipped with reactors at the generating station. These reactors not only limit the fault current, but also reduce the voltage disturbance on the system.

Most of the 60-cycle stations have a synchronizing bus to which the load busses are connected through reactor ties. The generators are connected to the load busses through reactors and the interstation tie feeders are usually connected to the synchronizing bus. The reactance of the reactor ties between the load busses and synchronizing bus is kept as low as possible, in order to keep the phase displacement between load busses at a minimum. This is necessary to limit the circulating current on the network feeders.

The 25-cycle generating stations use reactor ties between the load busses, but no synchronizing bus is used.

Sectionalization is employed in all generating stations to a greater or lesser extent, dependent upon the amount of generation in the station. Most generating stations are operated with four or more load bus sections, which are connected to

each other within the station only through the synchronizing bus, reactor ties, or three winding autotransformers used with the generators. In some cases the synchronizing bus is operated in two or more sections during peak load conditions.

Pretripping of circuit breakers is used in a few cases where the circuit breaker duty is excessive, and cannot be reduced by sectionalization and use of the reactors.

In regard to future trends, it is apparent now that as more generation and tie feeder capacity are added to the present system, sectionalization and the use of reactors will still be required to keep the magnitude of fault currents within reasonable limits.

Two 132-kv cable tie feeders, each having a capacity of approximately 200 megavolt amperes, will soon be installed between two of the larger generating stations. Initially, two substations will be connected to these ties, but ultimately a new generating station, having a capacity of 800 megawatts, will also be connected. These ties will normally be operated sectionalized.

Due to the low impedance of the cable and the large concentration of generation, the short-circuit currents on this interconnection will be high. In order to keep the circuit breaker duty within the limits of circuit breakers commercially available today, it will be necessary to install 132-kv reactors on these ties after installation of the new generating station.

A Large Metropolitan System Which Uses a Large Ratio of X_0/X_1

This is a review of the methods used on the Chicago system to minimize the possibility of faults and reduce the magnitude of fault currents. The high-voltage system in Chicago consists primarily of 66-kv underground cables between the various generating and distributing stations within the city. In order to reduce the number of lines and transformers in the system to a minimum, a close-linked system of connections is used. Because of the large concentration of generating capacity within the city, this type of system results in relatively high fault currents. Four principal methods have been used to control this situation. These methods are: (1) phase isolation; (2) sectionalization; (3) reactors; and (4) pretripping.

Phase Isolation

The use of phase isolation has been the principal method adopted in Chicago to combat the problem of excessive fault currents. All 66-kv terminals are constructed with the phases physically separated so that the possibility of phase-to-phase faults is practically eliminated. All lines between the principal terminals consist of single-conductor cables, so that again the possibility of phase-to-phase faults is extremely remote. While the possibility of simultaneous phase-to-ground faults on different phases does exist, actual experience with the Chicago system over a period of approximately 20 years has shown that there is small probability of such faults, none having been experienced on this system.

The magnitude of phase-to-ground fault currents is limited by the use of neutral resistors, the maximum ground fault current being limited to approximately 4,000 amperes.

As a result of the use of phase isolation and neutral resistors it has been possible to operate the system with circuit breakers whose ratings are below the calculated 3-phase short-circuit current, on the basis that these circuit breakers rarely will be called upon to interrupt a phase-to-phase fault.

System Sectionalization

As stated before, the principal generating and distributing stations in Chicago are tied together solidly by underground cables. However, in order to improve system reliability and at the same time reduce the phase-to-phase fault currents, the 66-kv system is separated into two parts, arbitrarily known as the red and blue systems. Each of the terminals on the system has a red bus and a blue bus and there are no direct connections between these busses, although they are tied together through the transformers connected to the lower voltage busses.

Reactors

In a few cases there are 3-conductor 66-kv cables supplied from one of the principal terminals to feed a radial load. In order to protect the system from possible phase-to-phase faults in these cables, 66-kv reactors of 3.5 ohms are used. These reactors are also used on a 66-kv overhead line supplied from a phase isolated terminal.

Pretripping

Recently, in considering the effect of additional generating units, the possibility of using reactors on the 66-kv system to reduce the short-circuit current was studied. Although these reactors would be effective in reducing fault currents and make it possible to postpone replacement of circuit breakers, they would introduce difficulties in the operation of the system and impose restrictions on future system changes and methods of connecting additional capacity to the system. As a result, it appeared more desirable to provide for the increase in fault current resulting from the new units by the use of a pretripping scheme which will reduce fault currents by splitting the faulted system.

12,000-Volt System

The methods previously described for controlling the occurrence of phase-to-phase faults and limiting their values are also applied to all the principal distributing centers in the city which operate at 12,000 volts. All the modern 12-kv switchhouses use the principle of phase isolation to limit the possibilities of phase-to-phase faults. Impedance grounding is used to limit the magnitude of ground fault currents to approximately 4,000 amperes.

System sectionalization also is used in the 12-kv switchhouses. In some cases the switchhouse is subdivided into the red and blue systems which are normally not tied together. In other cases, the red and blue systems are normally tied, but on the occurrence of a heavy fault the system sectionalizes automatically and is split into separate red and blue systems.

Reactors are used widely on the 12,000-volt system. They are used on each of the generators connected to the 12-kv bus and each of the transformers between the 66 and 12-kv busses. In one special case, bus reactors are used to separate the red and blue busses. In general, the use of bus reactors has not been too successful due to the difficulties they introduce in obtaining desirable division of power between cables on the distribution system. All 12-kv cables leaving the terminals to supply substations have a reactor at the generating station end. These reactors protect the phase isolated terminals from faults on the 3-conductor 12-kv cables and also aid in limiting the magnitude of 3-phase fault currents in the various substations.

Experience with the type of system described has been very successful from the standpoint of reducing the possibility of heavy faults at the major terminals on the system.

Metropolitan Systems of Medium Size

Discussions with engineers of the power systems in Minneapolis, Milwaukee, Indianapolis, Louisville, and Cincinnati, concerning the problem of controlling faults on their systems, may be summarized by the following eight conclusions:

1. The designs of these systems are deter-

mined by load flow and voltage regulation during normal and emergency conditions.

2. Fault currents and circuit breaker duty are secondary considerations.

3. The policy is to apply circuit breakers adequate for the duty and to rebuild present circuit breakers where necessary and feasible. Adequate circuit breakers are commercially available for all of these systems.

4. On some systems current limiting reactors have been used on busses at generator voltage to limit the fault current and reduce the voltage disturbance resulting from a fault.

5. A few companies operate with a split bus arrangement at main generating stations and with circuits paralleled at the load substations, as economic means to defer replacing the circuit breakers.

6. Most new stations avoid high concentrations at generator voltage by paralleling new generators only at transmission voltage.

7. Two companies report special problems of high ground fault currents. One uses neutral reactors to control them, but the other considers that the neutral reactors are not satisfactory.

8. All companies recognize that as the systems grow the fault currents will approach the limits that can be handled by available circuit breakers, but none of these systems have reached this point yet.

High-Tension Transmission Systems

As contrasted with the metropolitan system, the high-tension transmission system uses long lines, and has only a few circuit breakers as compared with its miles of line. The ratio of investment in circuit breakers to investment in lines is very much smaller than in a metropolitan system. It can generally afford to replace inadequate circuit breakers with circuit breakers of adequate interrupting capacity, and usually does. It is inherently a high impedance type of system, and, except for the few cases where circuit breakers of adequate interrupting capacity are not available, it is rarely necessary or advisable for a high-tension transmission system to sacrifice its operating flexibility for the sake of reducing its fault duty.

To determine the present-day operating practice in connection with fault control on high-voltage transmission systems, the committee canvassed 15 operators of major transmission systems. These systems were selected on the basis of obtaining diversified operating conditions.

Of the 13 companies that replied, 11 use closely-knit system designs. They make little or no effort to limit their 3-phase fault currents, but, as their systems expand, they meet the increasing short-circuit currents by replacing inadequate circuit breakers with circuit breakers of larger size. Two systems use loosely-knit system designs. They limit their short-circuit currents by means of sectionalization, system designs that insert transformer and line impedances at strategic points, and by use of fault current limiting devices.

There appears to be a tendency to rearrange loosely-knit transmission systems into the closely-knit design. However, one company which is doing this plans to go back to the loosely-knit type in the future if and when fault duties exceed the capacities of circuit breakers now being installed.

In a few instances, current limiting reactors in the phase wires, and system sectionalization are used, to limited extents, by closely-knit transmission systems, but only as temporary expedients.

Neutral impedance to limit phase-to-ground faults to 3-phase faults is used on several closely-knit systems. Ground fault neutralizers are used on one section of one system above 110 kv as a special application. Pretripping or delayed tripping is not used.

The replies received in response to a questionnaire covering systems 110 kv and above are summarized in the following paragraphs.

American Gas and Electric Service Corporation

Studies by this system of the problems of increased short-circuit concentrations have resulted generally in solutions calling for the replacing of inadequate circuit breakers with larger circuit breakers even to the extent of instigating the development of circuit breakers, in the voltage class required, of higher interrupting ratings than any previously available. In a few instances, bus sectionalizing reactors and feeder reactors in service lines have been used to keep down short-circuit currents. In most of these cases, however, the operating restrictions, or lack of complete flexibility introduced by such reactors, were a distinct disadvantage, and the present long-range plans contemplate the replacement of switchgear in most of these cases with sufficiently high capacity equipment to permit removal of such reactors as are now installed.

Bonneville Power Administration

The rated interrupting capacity of many of the existing 115- and 230-kv circuit breakers on this system now is or will be substantially exceeded. The policy has been, where possible, to rebuild the present circuit breakers for higher ratings or to replace them with new circuit breakers.

Staged tests have been conducted for the purpose of developing higher speed and higher interrupting capacity circuit breakers, particularly in the 230-kv class These tests have indicated that some of the circuit breakers are generously rated, particularly if a vigorous maintenance schedule is followed and further tests are planned with a view of rerating circuit breakers and thereby avoiding some of the replacements.

Buffalo Niagara Electric Corporation

This system is based on a soft system design. The 66-kv 25-cycle system is operated in two sections, paralleled only at the extreme ends, with part of the generating capacity in Buffalo connected to each half of the system and part of the generation at Niagara Falls similarly connected to each half of the system. By this method, the fault current does not much exceed 1,500,000 kva, even though the generating capacity is approximately 800,000 kw.

The 60-cycle system in the western division is similarly arranged.

Commonwealth Services, Incorporated

On all systems, circuit breakers are applied on the basis of expected future short-circuit duty within the limits of good economics. After some years of service, when circuit breakers become inadequate, they may be modernized or replaced by circuit breakers of higher rating with the lower rated circuit breakers used at other locations.

Two ground fault neutralizers were applied on a portion of a 138-kv system 17 years ago. These were the first installations of such devices in the United States at a potential of 110 kv or above.

System sectionalization, in order to reduce fault current, is used in so far as this is compatible with system operating requirements.

Current limiting reactors are not generally used in phase conductors or between busses. It is not our practice to use impedance in transformer neutrals on grounded neutral systems. We have not found it practicable to use pre-tripping or delayed tripping in order to reduce circuit breaker duty.

The Detroit Edison Company

The system, in general, comprises several subareas in each of which the generating capacity approximately equals the load. These areas are tied together by substantial transmission ties but their ties normally carry relatively little transfer power. The ties may, therefore, be of relatively high impedance in the form of medium voltage transmission with the intervening step-down transformers, re-

actors or regulating transformers. By this means, fault currents have been kept within values which are allowable on the available circuit breakers without resort to feeder reactors, neutral impedances, or other special provisions. Increasing system power has made it necessary to buy new circuit breakers with an interrupting capacity of 3,500 megavolt-amperes for locations with the highest fault currents. The existing circuit breakers of 2,500-megavolt ampere rating, or less, can still be used, however, for other locations where the duty is less.

Duke Power Company

In the past, this system has used neutral reactors, loose interdivisional ties and automatic bus splitting schemes for reducing circuit breaker duties. Today they are abandoning bus splitting schemes and tightening divisional ties in favor of full capacity circuit breakers.

Georgia Power Company

On this system circuit breakers of inadequate interrupting capacity are being replaced with circuit breakers of larger capacity. Some system sectionalizing is used as a temporary expedient.

The Hydro-Electric Power Commission of Ontario

The general practice on their main system is to replace circuit breakers having inadequate interrupting capacity. In normal times, this would be done without waiting for the existing circuit breakers to exhibit signs of distress. A continuing program of short-circuit studies is the method of determining the need for replacement to keep pace with system expansion.

The 230-kv transmission system is solidly grounded. The 115-kv subtransmission system is grounded through relatively high resistance at all generating stations and points of supply. However, it is planned, with the conversion of this system from 25 cycles to 60 cycles, to operate all transformers with solidly grounded neutrals at all points of supply and at all switching points. System sectionalizing is used to some extent, but synchronous operation is maintained.

New England Electric System

New power developments now contemplated by this system will increase the fault current from 1,500,000 kva up to 2,225,000 kva in certain sections. New 2,500,000-kva circuit breakers are being purchased for these locations and the existing 1,500,000-kva circuit breakers will be moved to locations where the duty is within their capabilities.

Northern States Power Company

This company replaces circuit breakers of inadequate interrupting capacity with larger circuit breakers. Current limiting impedances are being considered for use in the neutrals of certain 115-kv transformers to limit the phase-to-ground fault current to 3-phase values.

Southern California Edison Company

The problem of increased interrupting duty of circuit breakers on this company's 220-kv transmission system is being met through a program of modernization of older circuit breakers or their replacement with circuit breakers of larger capacity. Current limiting impedances, in transformer neutrals, are used at a number of locations to hold line-to-neutral fault current to approximately the 3-phase short-circuit current values.

Tennessee Valley Authority

The practice on this system has been to install circuit breakers of adequate interrupting capacity even where circuit breakers had to be developed for the purpose.

If, when, and where the short-circuit duty on the system increased to exceed the capacity of the existing oil circuit breakers, it has been the practice on this system to rebuild existing circuit breakers for greater capacity where possible; where impossible it has been the practice to replace the circuit breakers with adequate circuit breakers and use the existing circuit breakers at other locations where the capacity is not exceeded. Current limiting devices are used in transformer neutrals to limit ground fault current to values equal to the 3-phase fault current.

Union Electric Company of Missouri

In the past, fault currents have been limited to a great extent by terminating transmission circuits in transformers. In the new development under way at the present time, several new 138-kv busses are being established. Circuit breakers at these new substations will have an interrupting rating of 3,500,000 kva which is sufficient to take care of present requirements and a reasonable future expansion of the system.

The existing circuit breakers at locations remote from large generating stations are adequate for these new requirements.

As system capacity increases and greater duties are imposed, sectionalizing, pretripping, or other expedients to limit fault currents will be applied as required.

Metropolitan-Transmission Systems

A fifth type of system, of less frequent occurrence, is found in some densely settled areas. It is neither wholly metropolitan nor wholly transmission, but contains some of the features of each, and might be termed a metropolitan-transmission system. As a rule, it started out years ago as a high-tension transmission system but by the addition of paralleling lines and the insertion of generating, switching, and distributing stations, it has become more closely-knit than the usual transmission type. It is not as compact as the metropolitan system and it retains the high voltage necessary for transmission of large blocks of power. However, it is sufficiently compact to employ fault limiting arrangements and devices to some extent without excessive loss of flexibility; but it also needs rather large circuit breakers for future as well as present short-circuit duties. Its fault control is a combination of the metropolitan and transmission types, but tends to become more of the metropolitan type as more lines and stations are added.

Recent Commentaries on Current Limiting Reactors and Neutral Grounding Devices

Current Limiting Reactors

The Effect of the Magnetic Fields of Current Limiting Reactors on Installation Practice

A current limiting reactor is made without a ferromagnetic core. Hence there is, in general, no high permeability medium for confining the magnetic flux to a given path. An exception to this rule is the oil immersed current limiting reactor which usually has shields to confine the flux within its tank. The great majority of current limiting reactors, however, are of dry-type construction and all too frequently they are installed without consideration being given to the effect of their magnetic fields on surrounding metallic objects and, conversely, the effect of metallic objects on the magnetic field.

Loops with High Mutual Coupling

Any metallic loop which encloses flux from the coil becomes a short-circuited secondary, adding to the energy loss of the coil, exerting some force against the coil and increasing the field reluctance. One power company complained that a current limiting reactor was smoking even though it was not carrying its rated load, In-

vestigation disclosed that the cell designed by power company draftsmen was made of wide aluminum plates bolted at all corners to make a complete circuit about the reactor. In addition to strong eddy currents, a current of about 600 amperes would have circulated through the wall at normal load. Fortunately no short circuits occurred before this condition was corrected. While the short-circuited cell wall would have reduced the effective reactance only 5 per cent, the cell could have been completely ruined and anyone nearby could have been injured severely. There have been installations where metal cells have had properly insulated joints bridged by a ground bus, a control lead conduit, or a metal air duct. From the standpoint of personnel safety, it is advisable that more than one insulating joint be used about the reactor since what may be only 10 volts at normal current can become 200 to 300 volts or more in case of a short circuit.

Loops with Low Mutual Coupling

Metallic loops in structural members, station piping, and adjacent apparatus may not have sufficient mutual coupling to cause destruction of parts, but can contribute substantially to the over-all energy loss. For instance, a reactor cell wall may be made of nonmagnetic high resistance material and have relatively little loss in it—say 10 to 15 per cent of total coil loss. However, unless the adjoining switchgear is made of similar material, it may double the total loss and have some objectionable hot spots as well. Suitably placed shields of low loss magnetic material (laminated silicon steel) or of low resistance conducting material (aluminum or copper) can reduce this excess energy loss and attendant heating to very low values with no more than 1 per cent variation in coil reactance.

The idea seems to be quite prevalent that it is only magnetic material that needs to be kept away from reactors; that it is all right to have copper or aluminum near them as long as proper insulation strike is maintained. This is true provided that there is no broad side of these nonmagnetic metals presented to the flux. A 2 by 1/2-inch copper bar as much as 10 inches away from a coil no larger than 4 feet in diameter can attain a 60 degrees centigrade rise if the 2-inch side is perpendicular to the flux. A similarly located 1/8-inch thick, 10 inches wide, aluminum panel could reach 100 degrees centigrade rise, while such a panel of ordinary steel would have less than 70 degrees rise provided that it does not form a closed magnetic circuit.

The Effect of Current Limiting Reactors on Transient Overvoltages

When concentrated inductance in the form of a current limiting reactor is placed in series with a circuit, it introduces a reflection point for steep front voltages. This can cause an incoming surge to double in magnitude on the line side of the reactor. On the bus side the surge voltage will oscillate with station capacitance to ground and may reach nearly four times the magnitude of the incoming surge. Current limiting reactors also may generate overvoltages at various points in the system because of the forcing of current zero by circuit breaker openings or fuse clearings.

Various combinations of surge by-pass devices, depending on the application, are used as protection against damage from these overvoltages. Lightning arresters are commonly employed and are connected either from line or bus terminal to ground or from both line and bus terminal to ground. In addition, resistor shunts are often used across reactors. These are usually nonlinear resistors[1] or lightning arresters.

Reduced Insulation for Current Limiting Reactors

Substantial savings can be realized by specifying reduced internal insulation levels for oil-immersed current limiting reactors. Such reactors are insulated for full voltage from terminals to ground, but their internal or terminal-to-terminal insulation is reduced to co-ordinate with the maximum voltage allowed by a lightning arrester or nonlinear resistor connected in shunt across the winding.

The shunt for such application is chosen on the basis of the maximum dynamic voltage that can appear across the reactor under short-circuit conditions. This voltage will not exceed line-to-neutral voltage, and in practice most systems have enough reactance in them to limit the voltage to considerably lower values than this.

A reactor of this type is tested with the shunt disconnected. The test values correspond to those of the next higher insulation class above the rating of the lightning arrester shunt or equivalent resistor. A factor of safety in the reactor insulation is thereby demonstrated.

Duplex Reactors, Also Known as Spilt-Type, Differential, or Double-Flow Reactors

These current limiting devices are air core coils provided with a center tap. In operation, power normally flows into the tap and out each end of the coil into the separate circuits. Because the normal currents in the two halves oppose one another, the mutual reactance (which is of the order of 30 or 40 per cent of the self-reactance) subtracts from the self-reactance making the net reactance small if the currents in each feeder are of equal magnitude. However, when one circuit faults, the reactor currents become unbalanced, and an increased net reactance results. In effect, this type of reactor produces a substantially higher reactance under fault conditions than under normal conditions. Before applying such reactors, the characteristics of the particular system must be studied to determine whether the duplex reactor would offer advantages over two conventional reactors. For feeder application, the advantages of lower regulation and better division of load between parallel feeders must be weighed against these disadvantages:

1. For any given application, one duplex reactor usually costs more than two conventional reactors.

2. With certain circuit conditions found in practice, the voltage of the unfaulted feeder may rise to as high as 125 per cent of normal.

3. If circuit breakers are required between the reactor of each feeder and its bus, it may be necessary to make the duplex reactor liquid filled. This comes about from the fact that the two halves must be fully insulated from each other while maintaining, at the same time, a high mutual reactance between them.

Duplex reactors are often used advantageously for bus sectionalization. Many applications of this type result in lower regulation for a given short-circuit current than can be realized with conventional reactors.

In the past decade the advantages of duplex reactors have become more widely recognized and their use is increasing. The following are some of the utilities and industrials who are using duplex reactors in their system:

Public Service Electric and Gas Company
Public Service Company of Colorado
Consolidated Gas Electric Light and Power Company
Commonwealth Edison Company
Kansas City Power and Light Company
Hammerville Paper Company
Magnolia Petroleum Company
West Virginia Pulp and Paper Company
Republic Steel Company
Atlantic Refining Company

The Use of Neutral Grounding Impedance to Limit Currents

The determination of the proper impedance for grounding a system neutral

is not a matter of rule of thumb. The impedance should be selected after due consideration has been given to various technical and economic factors applying to the particular system. The following discussion reviews briefly the salient points determining the design and application of such impedance devices.

The trend in American power transmission practice 46 kv and above is towards operation with neutral solidly grounded or grounded through an impedance. This is done to reduce the high-voltage transients and to cause the flow of sufficient fault current to operate relays controlling the segregation of the faulty circuit. The trend in generator practice is towards reactance grounded or distribution transformer (secondary resistor) grounded neutrals.

Advantages of Neutral Impedances

The amount of zero sequence fault current which flows in any particular grounded neutral system is usually controlled by inserting impedance between the system neutral and ground. Placing the impedance in the neutral rather than in the line has several advantages:

1. It should be noted that for single phase-to-ground faults a single impedance in the neutral is the equivalent of three impedances, each of the neutral impedance ohmic value, one in series with each phase wire.

2. Savings can be realized by taking advantage of the fact that one end of the neutral is solidly grounded. This simplifies the insulation problem.

3. Because currents, when they do flow through a grounding device, are for short times only, the device does not have to be designed to dissipate continuous losses and can thus be built much more compactly an with less material and cost than a series device having the same ohmic value.

4. Since a grounding device carries no appreciable current except during ground faults, it has no effect on system regulation; in contrast to the series impedance device which has a continuous voltage drop.

5. On cable systems, the minimum series impedance necessary to protect cable sheaths from damage during faults would give rise to prohibitive system regulation. The neutral impedance on the other hand will protect very satisfactorily without disturbing the regulation.

6. The neutral impedance may be made to include a trap or traps which will suppress the flow of one or more harmonic components while at the same time limiting the flow of 60-cycle fault current to the desired value.

Time Ratings for Neutral Grounding Devices

AIEE Standard Number *32* for Neutral Grounding Devices[2] recognizes these operating conditions and has set up three short-time ratings and an extended time rating to meet them.

A *10-second rating* is given to grounding devices whose function is the protection of a given piece of equipment only. For example, an impedance in the neutral of a generator may be installed for the sole purpose of controlling ground currents through the windings of the generator.

One-minute rating. Where the grounding device is to control the flow of ground current in outgoing feeders, it is possible for it to have to handle several faults on different feeders in rapid succession. For such applications, a grounding device with a 1-minute rating is usually applied.

A *10-minute rating* has been set up to take care of the condition wherein the trouble is not cleared automatically by ground relays but where an operator is on hand to perform manually the necessary switching to remove the fault.

The *extended time rating* is given to grounding devices which operate in systems where faults are allowed to persist for longer than ten minutes. The continuous temperature rise of such apparatus is permitted to be greater than standard on the assumption that operation will be held to less than an average of 90 days per year.

This rating replaces the old continuous rating for apparatus (such as resonant neutral grounding devices) used on systems not provided with ground relays for fault segregation. In such cases the extended time rating permits the operator to allow a phase-to-ground fault to persist on the system until the faulted circuit can be conveniently removed from service.

Factors Determining the Choice of Reactance or Resistor for Neutral Grounding

The impedance used to limit ground fault current is normally a reactance, a resistance or more infrequently, a combination of reactance and resistance. In choosing between reactance or resistance, the following points should be kept in mind:

1. In general a reactor is less expensive than an equivalent resistor. The difference in cost is more pronounced the higher the voltage or the current rating.

2. A neutral reactor takes up less space than an equivalent neutral resistor.

3. If the ground fault current is to be limited to less than 25 per cent of the system 3-phase fault current a resistor should be used. Otherwise dangerously high transient

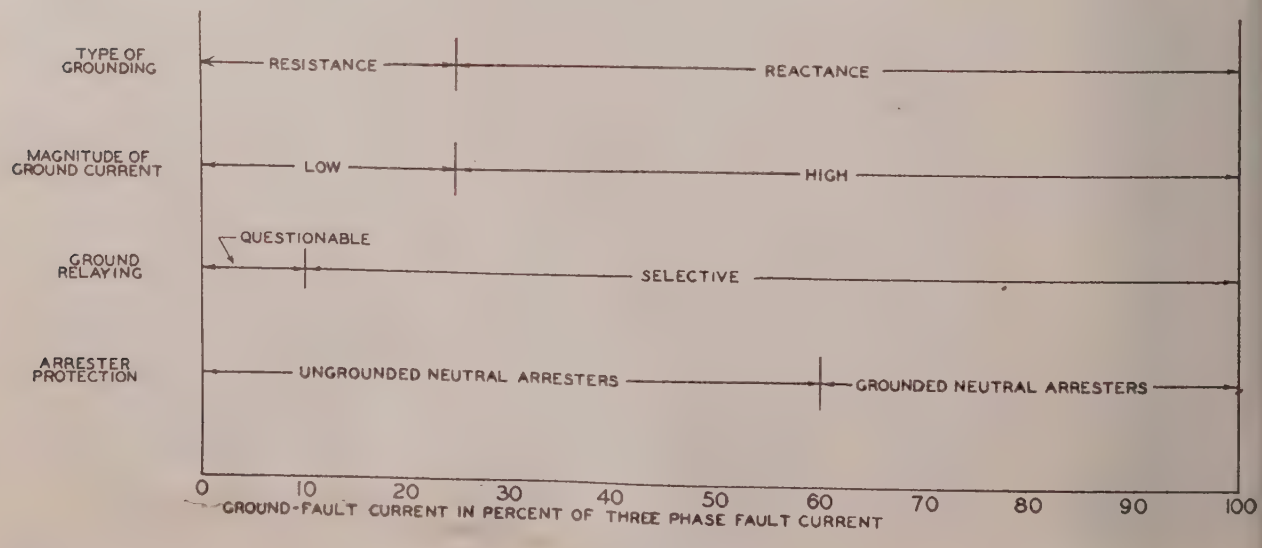

Figure 1. Major factors affecting choice of neutral ground impedance

voltages can occur on the system in conjunction with faults or switching operations.

In practice, the majority of the higher voltage systems in this country solidly ground the neutral or ground through a reactor. Lower voltage systems particularly in the industrial field use resistors quite extensively.

Factors Influencing the Value of Ground Current to Be Allowed

In choosing the optimum value of ground fault current for the system the following factors should be considered:

1. For most applications a minimum current of the order of 50 per cent of normal load current is required to operate zero sequence relays successfully.

2. If the ground fault current is limited to less than 60 per cent of the 3-phase fault current, the system neutral will be displaced, during a fault, to such an extent that arresters suitable for a nongrounded neutral system will have to be used. This will increase the protective level above that which could be obtained by using lightning arresters rated for grounded neutral operation.

3. The *higher* the ground fault current the *greater:* a. the danger of the fault spreading to include other phases, b. the danger of damage to equipment, c. the duty on circuit breakers, d. the disturbance to system stability, e. the undesirable effects of inductive coupling with adjacent circuits.

The ohmic value of the grounding impedance should be set only after a careful analysis of the system network has been made. Figure 1 summarizes in a general way the effect that magnitude of ground fault current has on the type of grounding, ground relaying, and lightning arrester protection.

Neutral Voltages

When an impedance is inserted between the system neutral and ground, the potential of the neutral will rise above ground whenever ground fault current flows and whenever voltage surges come into the transformer or generator from the line. The transformer or generator neutral and the neutral end of the impedance device must be insulated to withstand these voltages.

The magnitude of the 60-cycle voltage which will appear at the neutral under fault conditions is usually less than the line-to-neutral voltage. It depends on the vectorial relationship between the grounding device impedance and the total zero sequence impedance of the system.

The maximum crest transient voltage which can appear at the neutral is theoretically twice the transient crest voltage at the line. In practice the ohmic value of a neutral grounding resistor is usually small enough to hold the neutral transient voltages to reasonably low values. On the other hand, the use of a neutral reactor, unless it is of exceptionally low inductance, will allow high transient crest voltages to appear at the neutral. It is usually good practice with reactance grounding to shunt the reactor with a resistor (of the negative resistance type) or a lightning arrester. The maximum transient voltage is then predictable and the neutral can be insulated accordingly.

Ground Fault Neutralizer

If the reactance of a neutral reactor is increased until it just equals the system capacitance to ground, the system zero sequence network is in parallel resonance for ground faults. Under these conditions a fault current flows through the neutral reactor to ground. A current of approximately equal magnitude and about 180 degrees out-of-phase with the reactor current flows through the system capacitance to ground. These two currents neutralize each other, except for a small resistance component, as they flow through the fault.

The majority of these single phase-to-ground faults are self clearing within a few cycles. This is caused by three conditions: the low current passing through the fault; the fact that the current is nearly in phase with the voltage; and the very slow recovery rate of the voltage following arc extinction. The latter of these three conditions is of considerable importance and may not always be fully appreciated.

To take care of occasional persisting faults, American practice has developed along two directions. If this type of grounding reactor (ground fault neutralizer) has an extended time rating,* the need for extensive ground relays is eliminated because the fault can be allowed to persist on the system until the trouble can be located and corrected. On some circuits, such as underground primary feeders, a faulted circuit can be kept in service during heavy or important loads and the outage for repairs deferred until a period of minimum load or of less important load, occurs. The effect of such a persisting fault on communication circuits, and the possibility of it spreading to another phase should, of course, be kept in mind.

An alternative practice is to install a 10-minute rated ground fault neutralizer with a by-pass switch for solidly grounding the neutral. A persisting fault is then cleared by closing the switch and allowing the ground fault relays to operate.

Ground fault neutralizers are increasing in popularity as their advantages to system operation become more widely known. They offer greatly improved service for a relatively small investment, particularly when applied to existing isolated neutral systems.

* The extended time rating has been defined and discussed previously under the section entitled Time Ratings for Neutral Grounding Devices.

References

1. Shunt Resistors for Reactors—II, **F. H. Kierstead, L. V. Bewley.** *Electrical Engineering* (*AIEE Transactions*), volume 53, March 1934, pages 411–25.

2. Standard for Neutral Grounding Devices. *AIEE Standard Number 32*, May 1947.

No Discussion

69-Kv Medium-Pressure Gas-Filled Cable, Washington, D. C.

H. W. CLARK
FELLOW AIEE

Synopsis: The cable taken as the subject of this paper is the first medium-pressure gas-filled cable constructed for operation above 46 kv. It is believed to be the largest installation of this type of cable up to this time and its design includes several unique features. This discussion covers factors affecting its selection, details of the cable and accessories, special features of the conduit line, and salient facts in connection with its installation and operation.

THE decision of the Potomac Electric Power Company to locate its new Potomac River Generating Station on the west bank of the Potomac River within the northern limits of the city of Alexandria, Va., immediately brought up the problem of power transmission. This decision locating the plant approximately four miles outside the company's territory was predicated on the availability of water for condensing purposes, railroads for fuel supply, and the fact that on both sides of the river the intervening territory was occupied by property of the National Capital Parks or airfields. The ultimate capacity of the plant is 470,585 kva made up of five 80,000-kw 85 per cent power factor generators, each to be placed on the line at approximately 1-year intervals. Except for 90,000 kva which will be transmitted through submarine cables across the river, all this power has to be delivered by circuits on the west bank of the river. Because of airfields, park territory, populous area, and the fact that available routes are pre-empted by other utilities, overhead transmission was impractical and the problem became one of underground cable. Figure 1 shows the relation of the plant to the company's territory and the route of the conduit line to the Pentagon area. From economical considerations, sufficient cable capacity is to be installed as each generator is made available.

The submarine cables across the river will be of the low-pressure oil-filled type. Considering the length of the river crossing and the desirability of avoiding underwater joints, the weight of submarine medium-pressure gas-filled cable of the required capacity renders it impractical for this installation.

Selection of Type of Cable

In order to determine the type of cable to be employed, the initial requirement of 90,000 kva at 75 per cent load factor and 25 degrees centigrade earth ambient to be delivered to Substation 55, adjacent to the Pentagon Building, where it would serve the load at that point and tie into two existing 69-kv oil-filled cable circuits from the Buzzard Point Plant, a route length of 21,000 feet, was set up as basis for study. Transmission at both 115 kv and 69 kv was considered.

Comparison was made at 115 kv between a single-conductor 400,000-circular-mil oil-filled circuit and a pipe-type cable composed of 400,000-circular-mil compact round conductors utilizing oil as the pressure medium. The limited width of the available right of way immediately rendered the single-conductor cable impractical because of the lack of space to provide for the ultimate number of duct piles. For the initial installation, the pipe-type cable with its cost of $7.25 per kilovolt ampere was the most economical of all types of cable considered at either voltage. However, it was obvious that this saving would disappear as future circuits were added requiring additional excavation and pipe. Also, the right-of-way restrictions would prevent installation of the ultimate number of pipes properly separated for heat dissipation. Furthermore, the problem was not one of cable alone as transmission at 115 kv involved additional cost because of system considerations such as increased interrupting capacity and transformation to tie into the existing 69-kv system.

Detailed studies at 69 kv were reduced to the following types of 3-conductor cables, the over-all cost of material rendering unattractive both pipe-type and single-conductor duct cable. All kilovolt ampere costs are based on the installation of two cables, each having a capacity of 45,000 kva installed in a conduit structure providing for 180,000 kva. Also, the indicated costs, which include the entire duct structure, prevailed in the spring of 1947, at which time the study was made, and must be considered as relative only.

1. Low-pressure oil-filled cable, 500,000-circular-mil compact round, 315-mil insulation: cost per kilovolt ampere, $9.57.

This type of cable requires a complicated oil supply system involving reservoirs, relays, and stop joints. Installation requires a heavy labor outlay and operating costs are very high. Its sheath is subject to corrosion, and data from tests made on cables by the Philadelphia Electric Company indicates that its ultimate failure as the result of cable movement would occur in approximately one-third to one-fifth the time than would failure of the inner sheath of medium-pressure gas-filled cable.

2. Medium-pressure gas-filled cable, 600,000-circular-mil compact round, 400-mil insulation with double-reinforced lead sheath: cost per kilovolt ampere, $10.00.

This cable requires a relatively simple system for the maintenance of gas pressure, is self-supervising, and has low operating costs. Because of the con-

Paper 51-67, recommended by the AIEE Insulated Conductors Committee and approved by the AIEE Technical Program Committee for presentation at the AIEE Winter General Meeting, New York, N. Y., January 22-26, 1951. Manuscript submitted October 18, 1950; made available for printing December 7, 1950.

H. W. CLARK is with the Potomac Electric Power Company, Washington, D. C.

striction of the reinforcing, the inner sheath would have a life expectancy of three times that of oil-filled cable. However, the outer lead sheath would be subject to ultimate failure caused by corrosion, galvanic effects, and cable movement in the same manner as that of oil-filled cable, thus permitting the products of corrosion to affect the reinforcing tapes and inner sheath.

3. Medium-pressure gas-filled cable, 600,000-circular-mil compact round 400-mil insulation, inner sheath of lead, outer sheath of neoprene: cost per kilovolt ampere, $9.88.

In the tests cited above, neoprene sheaths developed no fatigue, with the result that the greater life expectancy of the inner sheath should be realized. Furthermore the cable can be trained on radii based on the diameter of the inner sheath, resulting in a saving in manhole widths. As it developed during the construction of the conduit line, protection against corrosion was of the utmost importance. In the event that moisture does pass through the outer jacket, it would be filtered and indications are that it would become a gas and therefore harmless. This cable also would have less weight, resulting in lower pulling stresses.

4. Medium-pressure gas-filled cable, 600,000-circular-mil compact sector, 400-mil insulation, inner sheath of lead, outer sheath of neoprene: cost per kilovolt ampere, $9.73.

This cable would have all the advantages of cable 3 and in addition would be of smaller diameter and less weight. The calculated maximum stress at the corners of the sector conductors is 191 volts per mil, which lies within allowable limits for medium-pressure gas-filled cable. While the cost of this cable exceeds that of oil-filled cable, it was adopted for this installation because of its greater life expectancy and its greatly reduced operating and maintenance costs.

Cable and Accessories

Medium-pressure gas-filled cable operates on the same basic principle as low-pressure gas-filled cable, that is, when the pressure in a gas is increased, the electrical stress required to initiate ionization also is increased. In medium-pressure gas-filled cable the nominal gas pressure is increased from 15 to 45 pounds per square inch, which allows the permissible average operating stress in the insulation to be raised from 66 to 100 volts per mil.

Figure 2 shows a cross section of the cable selected. Each of the three compact sector conductors is insulated with a 400-mil wall of paper, enclosed by one 3-mil perforated copper shielding tape intercalated with paper tape. Over the conductors as part of the insulation are included aluminum-backed tapes for the purpose of strand shielding. The impregnating oil has a Saybolt viscosity of approximately 100 at 100 degrees centigrade. In each of the filler spaces is a gas channel, two of these channels being open helical, steel or bronze, of 0.410-inch outside diameter, made up of 0.25-inch wide by 0.0271-inch thick metal, the third channel being a solid copper tube of 0.350-inch outside and 0.290-inch inside diameter. The three conductors and gas channels are enclosed by one bronze binder tape intercalated with paper tape. The dimensions of the spiral gas channels were selected as the nearest standard size that would support the binder tape and sheath midway between the conductors. Also, to provide further support for the sheath, the spaces between the channels, binder tape, and conductors are solidly packed with paper fillers. The cable core is enclosed in a copper-bearing lead sheath, 0.125-inch thick, reinforced by two 5-mil bronze tapes. As a second line of defense against the possibility of galvanic couples between the lead sheath and the reinforcing tapes, the Okonite Company on the initial order placed over the lead sheath a double-wrapped layer of asbestos-neoprene tape covered with an overlapped layer of neoprene-filled tape. This later was adopted as a requirement for all fabricators.

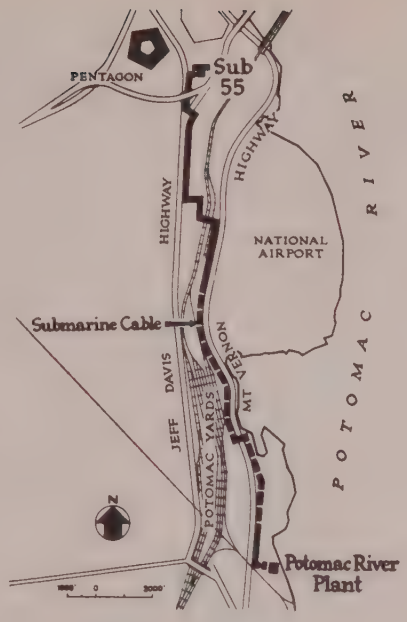

Figure 1. Route of cable from Potomac River Generating Station to Pentagon Area

The final element of the cable was the outer neoprene jacket, a substitution for the outer lead sheath normally specified for medium-pressure gas-filled cable. Two of the manufacturers, the General Electric Company and the Habirshaw Company, furnished a fabric-reinforced jacket made up as follows: One 0.0015-inch aluminum-backed acetate tape applied with approximately 10 per cent lap, three 0.030-inch neoprene hose jacket tapes with fabric face inside, applied close butt-wrapped, with joints staggered, one 0.030-inch hose jacket applied fabric outside with butt joints staggered, one 0.015-inch neoprene skin-coated tape, fabric side out with 10 per cent lap, all thoroughly vulcanized and bonded together with a coating of wax.

The jacket furnished by the Okonite Company is composed first of a fabric friction tape; over this is a solid wall of nonflammable neoprene without fibrous material; then a double wrap of fungicide-treated frictional fabric as a final protection. This entire covering is thoroughly vulcanized together to provide the best mechanical properties and is slushed with a wax and mica finish to ease pulling.

The above construction results in a cable with a calculated diameter of 3.86 inches and an estimated weight of 18.6 pounds per foot. Each length of cable is equipped with a gas-filled pulling eye and means of attaching gas cylinders at each end, the fitting on the trailing end being a Waterbury 1/2-inch number 108 nipple assembly complete with chain.

Figure 3 shows the principal features of the cable joint. Except for the added insulation the main body of the joint is of the same type as used for 3-conductor low-pressure gas-filled cable using a spun copper casing. The insulating medium is crepe paper tape. There is no external gas tubing, which is made unnecessary by a special fitting, to the center of which is brought the solid copper tube from the adjacent joint. Around this center orifice are smaller ports leading into the joint. Under normal operation a plug cap permits gas to pass from the tube to the joint. Replacement of this cap with a fitting which seals the ports into the joint permits the reading of the differential pressure at the next joint. An additional fitting facilitates the pressure reading in the joint itself. The sole remaining fitting is the plug on the bottom of the joint to permit the removal of excess compound.

The sealing of the neoprene cable jacket at the ends of the joint was a special problem. This is accomplished by

cutting back the jacket, fastening down the ends of the reinforcing tapes with piano wire, which then is covered by the lead wipe to the joint casing. A protective covering built up of rubber tape over which is vinylite tape and friction tape is the final seal from beyond the end of the neoprene jacket to the end cap of the joint casing.

The 3-conductor cable is terminated in a phasing spreader head round in shape and made up of spun copper to give strength and to avoid the porosity possible in cast types. The shielded conductors are carried through deoxidized copper pipe to the single-conductor terminals, which are rated 115 kv and are of the Herkolite barrier-type with gasket seals between the porcelain and metal of base and cap.

Nitrogen gas is supplied to the spreader heads at both terminations of each cable from a 200-cubic-foot gas tank through a manually operated pressure regulator and valve manifold. This equipment is installed in an adjacent metal cabinet. The relay actuating an alarm circuit in the event of either high pressure or low pressure is installed in the first manhole from the terminal and has a gas connection to the cable joint. This is done to prevent false alarms as the result of changes in outside ambient temperature.

The Conduit Line

Basically the conduit construction to the Pentagon area consists of two 4-way lines, each composed of 5-inch thin-wall Transite duct enveloped in concrete, one of which also includes a 3-inch auxiliary duct. The lines are spaced 6 feet $9\frac{1}{2}$ inches on centers with manholes so placed as to segregate two cables to each, neither of which would supply the same terminal station. The manholes are 4 feet wide by 15 feet long with 12-inch alcoves at the duct entrances. The two ducts enter and leave adjacent to one side wall, permitting the cables to be spliced on the opposite wall. Where space permits the manholes for each 4-way line have a common wall and the ducts are brought straight in. Where the width is restricted, single manholes were built in the space between the conduit lines. This required that either the top or the bottom two ducts be rolled into each alternate manhole, allowing the other two to pass by. This is accomplished by the use of 5-foot long 50-foot radius duct bends and short straight pieces. Because of lack of experience in pulling heavy neoprene-jacketed cables, it was felt that 600 feet between manholes was conservative. However, turns and cable segregation resulted in shorter runs and physical conditions required several longer stretches. The minimum radius of curves in the conduit line, either vertical or horizontal, was limited to 100 feet and the minimum cover is 36 inches.

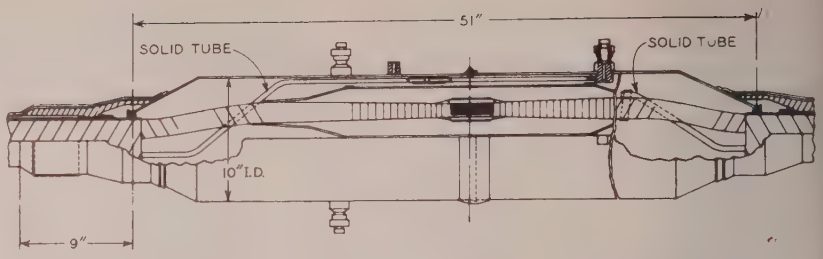

Figure 3. Principal features of joint

In crossing railroad property two embankments, one carrying heavy freight and the other high-speed passenger traffic, were encountered. At neither of these locations was an open cut permissible, nor was ordinary tunneling practicable. This problem was solved by pushing 5-foot sections of 42-inch inside diameter reinforced-concrete pipe, one for each 4-way line, below the base of the embankments, the distances being 120 and 30 feet. The four ducts were laid flat in each pipe and concreted in.

During the course of excavation for conduit construction, it became evident that soil conditions in some locations were unstable. As a result of extensive test borings, it was found that in a stretch of approximately 8,900 feet from the east side of the boulevard to opposite the airport, there was only a shallow crust of firm earth below which nothing was stable, evidently an ancient drainage basin area. A conduit line supported on piles was impractical both because of the depth of the instability and because the

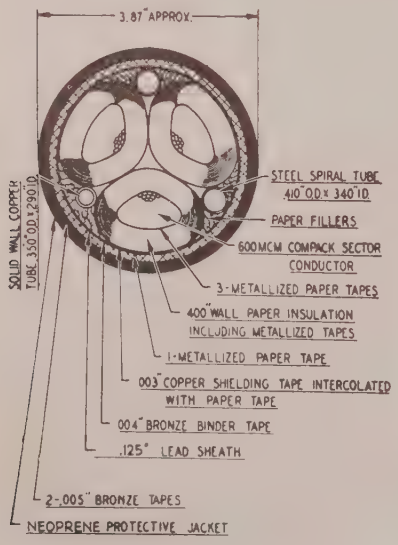
3.87" APPROX.
SOLID WALL COPPER TUBE 3.50" O.D. x .290" I.D.
STEEL SPIRAL TUBE 4.10" O.D. x 3.40" I.D.
PAPER FILLERS
600 MCM COMPACK SECTOR CONDUCTOR
3-METALLIZED PAPER TAPES
.400" WALL PAPER INSULATION INCLUDING METALLIZED TAPES
1-METALLIZED PAPER TAPE
.003" COPPER SHIELDING TAPE INTERCOLATED WITH PAPER TAPE
.004" BRONZE BINDER TAPE
.125" LEAD SHEATH
2-.005" BRONZE TAPES
NEOPRENE PROTECTIVE JACKET

Figure 2 (above). Cross section of cable

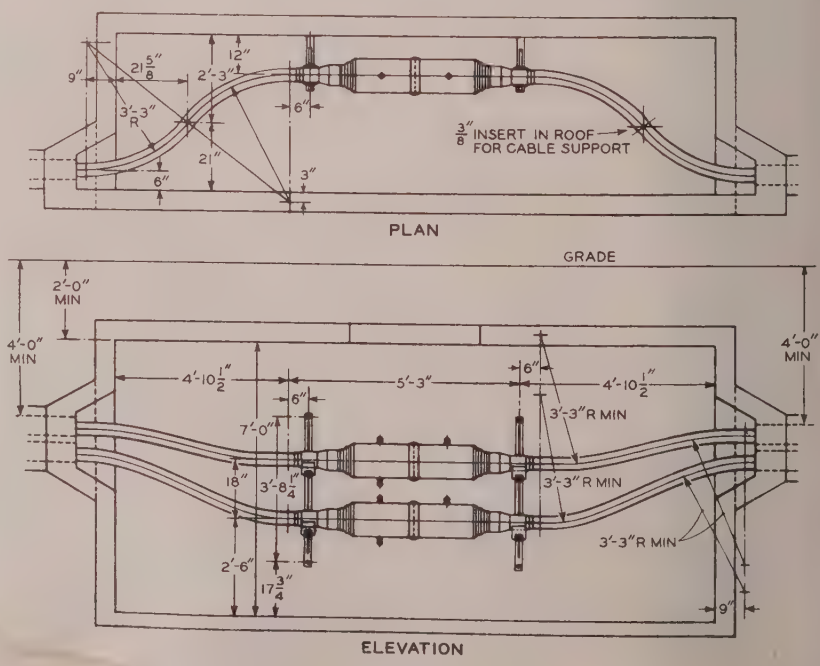

Figure 4 (right). Typical installation of cables and joints in manhole

pressure is upward as well as downward, as evidenced by ridges raised by past filling along the highway. Further future filling is proposed. An articulated conduit line was considered, consisting of a reinforced slab under the conduit with cross members as floats at the joints, at which point the ducts would telescope, but this was deemed uneconomical. Finally, it was decided to install submarine cable in lengths of approximately 1,100 feet anchored in manholes that would be permitted to float. Only four cables were installed, the remainder to be laid when required. An abandoned tunnel permitted the submarine cables to pass under the boulevard without excavation.

Installation and Operation

To insure against gas leaks, the cable on each reel as received is tested at a nitrogen gas pressure of 60 pounds per square inch over a 24-hour period with the requirement that there be no drop in pressure after making proper allowances for change in temperature. The fabricators are required to make similar tests at their plants before the cable is shipped.

No particular difficulty was encountered in pulling the cable into ducts. For lengths approximating 600 feet, the pulling tension varied from 3,700 to 4,700 pounds, resulting in coefficients of friction from 0.365 to 0.474. The pulling stress on the longest length of 809 feet was 5,600 pounds. These are well within the limit of 12,000 pounds at which pulling tension no stretching of the conductors or damage to the pulling eye is to be expected. Submarine cable was pulled in on rollers with the armor taking the strain.

Normally the cable joints are placed 30 and 48 inches above the manhole floor for convenience in splicing operations. The joint is supported at each end on porcelain insulators, the rubber tape seal of the neoprene jacket being flattened at the ends to reduce the span. The cable from the duct mouth is supported from the ceiling at its point of flexure. The minimum allowable bending radius for the cable is 39 inches, approximately 11.2 times the diameter of the lead sheath. This results in an offset of 30 inches. Figure 4 shows the training of the cable through manholes

The installation of cable in a gallery under the sidewalk of the Key Bridge connecting Virginia to the District of Columbia north of the Pentagon area is of an unusual character. This bridge is of cellular concrete construction and is free from vibration. The installation of joints on the bridge was undesirable both on account of space limitations and danger of tampering. Each of the three cables is installed in a transite tray, 12 inches wide and $2^3/_4$ inches in depth. Manholes were constructed as close as practicable to the bridge abutments. The cable was pulled in over rollers spaced at 5-foot intervals, and the maximum pulling tension for the 1,840-foot lengths was 6,600 pounds.

Four circuits, two of which have been energized for more than a year, are now in operation, the gas pressure ranging from 43 to 46 pounds per square inch. These cables, two of which are in each conduit line, have given no evidence of trouble or excessive movement. They have carried loads of 48,000 kva, which load will be reduced as future circuits are added. Observed temperatures are not excessive, the maximum empty duct temperature being 37 degrees centigrade.

Discussion

L. G. Brazier (British Insulated Callender's Cables, Limited, 38 Wood Lane, Shepherd's Bush, London, England): "Dealing first with the design features of the medium gas-pressure cable which is being used, it seems to us that at a pressure of only 45 pounds per square inch the maximum stress of 191 volts per mil is rather high, particularly when it is realized that after the cable has been in service for some time it will not be as fully impregnated as it is in its new state. The cable make-up shown in Figure 2 of the paper is such that compound migration is likely to take place quite readily, for example, along the steel spiral tubes, so that some parts of the cable may become deficient of compound in the course of time.

I am not able to comment on the joint design being used, as insufficient design data are given in the paper, but it does seem to me that certain hazards might well have been introduced by the difficulty of building up sound compact insulation over the sector-shaped conductors. Any weakness here would tend to make the design stresses too high. Our own experience shows that unless hand-applied and virgin dielectric are in firm contact with each other a definite source of weakness exists.

What I find to be the most surprising feature of the paper is the cost of the installation. If we were doing this job in England, we would not use a medium-pressure cable, but one operated at 200 pounds per square inch gauge, according to standard British practice. The cable would have the same size conductor as that described in the paper and would operate at a maximum conductor stress of 235 volts per mil. This stress is about 25 per cent greater than that which Mr. Clark used, but the factor of safety is higher because of the increased gas pressure. The cable would be 3-core with circular conductors, and the sheath would be provided with a steel reinforcement to withstand the internal gas pressure. This is all absolutely standard practice in Great Britain, and very many miles of such cable have been operating satisfactorily for a long time.

Figure 1 of this discussion shows the make-up of the cable which we would use. It is of interest to note that we are now producing our impregnated pressure cables with aluminum sheaths. These have the advantage that they are strong enough to withstand the internal gas pressure with a very comfortable safety margin, therefore no reinforcement is required. Further, they come out considerably cheaper than reinforced lead sheath cables. So far we are using them only at 33 kv, but the only thing which prevents us from using them at all voltages is the difficulty of obtaining large-diameter aluminum tubes of sufficient length.

There is just one final comment which I would like to make on this paper. This concerns the author's reference to "average stress" in the first paragraph of the section "Cables and Accessories." It is our experience that there is no direct connection between the performance of the cable and the average stress in its dielectric. All our test results show that the maximum stress is the important factor. For example, it is our opinion that the safety factor in a 220-kv cable working at an average stress of 140 volts per mil is about the same as that in a 66-kv cable working at an average stress of 200 volts per mil. Therefore, all of our designs for supertension cables are based on considerations of maximum stress.

L. I. Komives (The Detroit Edison Company, Detroit, Mich.): We think that requiring 500,000 circular mils for oil-filled cable and 600,000 circular mils for medium-pressure gas-filled cable is justifiable only in so far as we have had no field experiences with the latter. Our experience in Detroit indicates that high-pressure gas-filled cable may be operated at the same temperatures as oil-filled cable.

Commenting now on Mr. Brazier's discussion, in Detroit we use sector-shaped connectors on solid-type lower-voltage sector conductors, exclusively. We have had no difficulties with this construction; as a matter of fact, we think it is better to continue the sector shape rather than crushing the strands to a round shape in the connector.

It is interesting to note Mr. Brazier's statement that high-pressure cable having aluminum sheath would be considerably cheaper than reinforced lead sheath cables. The difference noted by Mr. Brazier between cable costs in the United States and in Great Britain may be questionable when based on rate of exchange only.

William A. Del Mar (Phelps Dodge Copper Products Company, Yonkers, N. Y.): There is one feature in the design of Mr. Clark's cables which is not mentioned in the paper. The cables furnished by Phelps Dodge have

four paper tapes between the bronze binder tape and the lead sheath. In the absence of these, there is danger that when the cable is bent, the lead on the outside of the bend will be pressed against and will slide on the bronze tape which is pressed outward rigidly by the hard underlying tubes. This may result in cutting of the lead sheath by the edges of bronze tape.

This construction is particularly desirable on wire-armored cable, as the armor puts additional pressure on the lead sheath at bends.

I would prefer to omit the bronze tape entirely, as its serves no useful purpose, but, as shown by H. Halperin and C. E. Betzer,[1] it gives a shorter life to the cable, under duct-mouth motion, than where a paper binder is used.

REFERENCE

1. LEAD-ALLOY SHEATHS FOR UNDERGROUND POWER CABLE, **Herman Halperin, C. E. Betzer.** *AIEE Transactions*, volume 70, part I, 1951, pages 423–35.

H. W. Clark: The answer to the questions raised by Dr. Brazier in regard to the maximum stress encountered in the cable described in the paper and the use of average stress rather than maximum stress in the design of low- and medium-pressure gas-filled cables rests entirely on the marked difference in characteristics of these two types of cables as compared to the high-pressure cable.

To obtain a clear picture of the differences between low-, medium- and high-pressure gas-filled cable from the standpoint of ionization voltage and maximum stresses, it is necessary to start with low-pressure gas-filled cable.

Refer to Figure 2 of this discussion, which shows the average of a large number of tests made by the General Electric Company on cable impregnated with medium viscosity compound at copper temperatures equal to or higher than normal operating temperature.

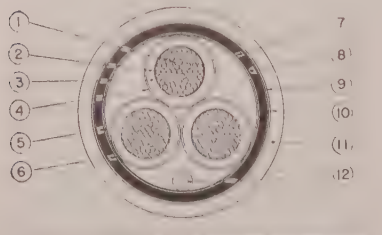

ITEM	MAKE-UP	CUM DIA INCHES
1.	CONDUCTOR TINNED COPPER 61/100"	0.900
2.	M.P. SCREEN	0.920
3	INSULATION	1.340
4	M.P. SCREEN	1.350
5	DIA. OVER LAID UP CORES	2.909
6	C.W.F. TAPE	2.939
7.	CLEARANCE	2.974
8.	LEAD ALLOY SHEATH	3.200
9.	BEDDING	3.220
10	STEEL REINFORCEMENT	3.300
11.	R.B.S. FINISH	3.820
12.	GAS CHANNEL PIPE INT. DIA. 0.25" EXT DIA. 0.375	

Figure 1. Design of cable
69-kv 3-core, screened conductor, impregnated pressure cable; 0.47-square-inch conductor

This type operates at an average voltage stress of 65 volts per mil, and the corresponding ionization voltage is approximately 80 volts per mil. This represents a relatively narrow margin between average operating stress and average ionization voltage. Also note that in this type of cable the gas pressure would have to drop to 5 pounds per square inch before ionization discharge starts. Here again there is a narrow margin of working gas pressure.

In spite of these narrow margins, there has not been an inherent service failure of low-pressure gas-filled cable since the first installation of such cable in 1938, there being between one million and two million feet of cable in service at the present time. In view of these narrow margins, it would be expected that occasionally incipient ionization tends to start at some critical or localized point, and that if this ionization were cumulative in its effects failures eventually would occur at such spots. That no such failures ever do develop is a result of the automatic grading and self-healing action, which has been fully discussed and demonstrated by C. B. Shanplin and H. T. Hatcher.[1-3] Refer particularly to Figure 7 of the paper. Note the marked self-healing effect when a medium viscosity impregnating compound is used, tending to extinguish incipient ionization without progressive damage. It is this self-healing effect that allows low-pressure gas-filled cable to work successfully very close to ionization margins. It explains why low-pressure gas-filled cable is always designed on the basis of average working voltage stress rather than maximum stress at the conductor surface. Automatic grading and self-healing action eliminates any problem of maximum stress at the conductor surface within the range of commercial design.

Referring to Figure 2 of this discussion, note that medium-pressure gas-filled cable is designed for an average working stress of 100 volts per mil and at 40 pounds per square inch has an ionization voltage of 130 volts per mil. Also note that the gas pressure must drop to 23 pounds per square inch before incipient ionization starts. While these margins are a little wider than those for low-pressure gas-filled cable, there still is the possibility of incipient ionization starting at localized spots in service. Here again it is necessary to have a marked self-healing effect to safeguard against this. It has been found that the self-healing effect in medium-pressure gas-filled cable impregnated with medium viscosity compound is practically as pronounced as in low-pressure cable. This is illustrated by Figure 8 in G. B. Shanklin's 1942 paper[2] and explains why there has been no service failure in medium-pressure gas-filled cable since the first installation a number of years ago.

The same degree of self-healing action does not hold for high-pressure gas-filled cable. The very slight amount of self-healing action at high pressure is not sufficiently marked to be counted on as a factor of safety. The relatively high energy in the ionization discharge at high pressure would render incipient ionization cumulative and probably would result in a failure. Therefore it is necessary to take maximum stress into account in the design of high-pressure gas-filled cable.

In regard to Dr. Brazier's comments on

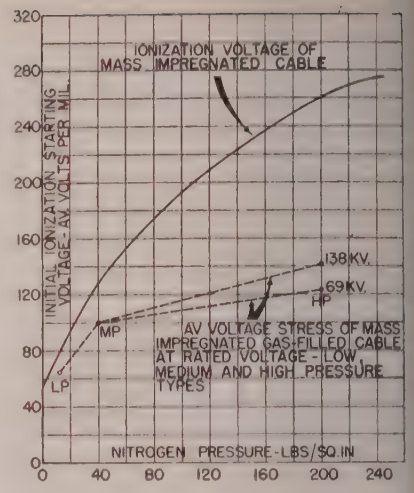

Figure 2. Comparison of ionization voltage and working voltage stresses in gas-filled cable

compound migration tending to create "dry spots" in the insulation cross section, the drainage channels provided in the American design eliminate the marked pressure differential found in solid-type cables. After the drainage of surplus impregnating compound, the remaining compound is held in the dense paper cross section entirely by capillary action and there is no pressure difference tending to cause it to migrate. This applies whether the cable is installed vertically or horizontally. This has been proved amply by the installation of gas-filled cables in shafts with no greater drainage being experienced than in horizontal installations.

Turning to Dr. Brazier's comments on costs, it is difficult to find an accurate basis for comparison between costs in England and in America. The costs given in the paper cover the complete investment, including such items as the restoration of roadway paving where required, the removal and replacement of shrubbery, and complete overhead charges. The relative costs of labor and materials in the two countries, as well as the monetary rate of exchange, also would have to be considered.

Years of experience with solid, oil-filled, and low-pressure gas-filled types of cable indicate that no difficulty is encountered in the application of hand-wrapped tape over sector-shaped conductors in the make-up of the cable joints.

In reply to Mr. Komives, the requirement of 600,000-circular-mil conductors in medium-pressure gas-filled cable to give equivalent ampere-carrying capacity to oil-filled cable with 500,000-circular-mil conductors arises from the fact that the transfer of heat through the thicker wall of insulation with its higher thermal resistance in the former is not balanced by the radiation from its greater outside diameter. The actual difference in outside diameter of the two cables is very small because of the necessity of using round conductors in the oil-filled cable in order to permit the installation of oil channels of adequate inside diameter in the interstices.

In reply to Mr. Del Mar, the inclusion of the four paper tapes between the bronze binder tape and the lead sheath furnished in the cable manufactured by Phelps Dodge

was not mentioned in the paper because it was not standard with all manufacturers.

This feature, as well as the omission of the bronze binder tape in shielded cables of all voltages, is under consideration at the present time.

REFERENCES

1. LOW-GAS-PRESSURE CABLE, G. B. Shanklin. *Electrical Engineering* (*AIEE Transactions*), volume 58, July 1939, pages 307–18.

2. LOW-, MEDIUM-, AND HIGH-PRESSURE GAS-FILLED CABLE, G. B. Shanklin. *Electrical Engineering* (*AIEE Transactions*), volume 61, October 1942, pages 719–26.

3. OPERATION OF LOW-PRESSURE GAS-FILLED CABLE, C. T. Hatcher. *Electrical Engineering* (*AIEE Transactions*), volume 63, November 1944, pages 788–92.

Lead-Alloy Sheaths for Underground Power Cable

HERMAN HALPERIN
FELLOW AIEE

C. E. BETZER
MEMBER AIEE

IN 1939 it was stated in a paper by Herman Halperin[1] that "for many cables the expected time of present-day commercial sheaths to cracking in manholes is only one-third to two-thirds of the life of the insulation" and that "better sheath materials are needed" to obtain a "balanced cable design." For over 20 years there has been an interest in the Commonwealth Edison Company in obtaining suitable lead-alloy sheathing that would have the desired improvements in properties over those of commercially pure lead sheaths.

This interest has been accentuated by the findings in recent years showing that the serviceability of insulation has been improved by changes that had been made in materials and in factory processes. The same procedures have been found necessary to obtain improved sheathing by developing lead alloys. For solid-type cables, as well as for oil-filled cable and low-pressure gas-filled cable, proof was obtained on the feasibility of safe operation of the insulation at conductor temperatures higher than previously thought safe; in 1942 supporting data were given, for example by Mr. Halperin[2] on the results obtained in accelerated-aging tests in the laboratories, experimental operation of field installations, and in occasional operation of commercial lines at high temperatures. Such data have been used as the basis for establishing permissible copper temperatures for emergency operation which are from 10 to 30 degrees centigrade higher than those permitted for normal operation for all three types of cable. Another result has been increases in the allowable temperatures for normal operation of oil-filled cable.

Until recent years, the rules for maximum allowable operating temperatures were applied generally to the maximum loading condition which usually occurred during emergencies when some of the lines in a group feeding a given load were out of service. Since the cable systems were built to avoid exceeding that limit, the normal daily loadings usually resulted in temperatures much below the allowable limits for normal operation. With the establishment of emergency load ratings in accord with the newly established increased temperatures for emergency operation, the permissible daily loadings of all types of lead-covered cables have increased considerably over those that previously obtained for normal operation. (Obviously, this practice has resulted in sizable savings in plant investment costs for taking care of growing loads.) Incidentally, there is evidence that temperatures higher than the standard values, especially for emergency operation, are feasible in some cases, all of which tends to accentuate the sheath problem.

With increased loads, the life of a given sheath to fracture decreases much faster than the rate of increase in amperes.[2] The fractures are due largely to breaks through the lead sheaths, which admit air and moisture into the insulation. A major cause of the sheath breaks is fatigue cracking resulting from the daily movement of the cables due to longitudinal expansion and contraction with changes during the day in load on the lines. Such cracking usually occurs in the manholes, where the cable movement causes slow bending, but sometimes it occurs in the ducts. It is especially troublesome on cables having sheaths larger than two inches in diameter.

Another cause of trouble is the expansion of the sheath as a result of internal pressure, since lead creeps slowly but surely at low tensile stresses. If substantial sheath expansion occurs, the electrical strength of the insulation may be affected seriously by, for example, excessive drainage of the impregnating compound into the newly created internal space. Also, the expansion may continue and may eventually cause sheath rupture. In either case, the result has been either cable failure in service or replacement of the faulty cable length before failure.

In solid-type cable, the internal pressure is produced during the heavy-load hours by thermal expansion of the oil in the cable, especially in those high-voltage cables having oil reservoirs connected at the joints or by hydrostatic head in riser cables or cables on slopes. In more recent years, cables with controlled continuous positive pressure on oil or gas in the cable have come into use. Thus, in order to withstand the internal pressure sufficiently throughout the life of the cable, the sheathing material must have both good resistance to creep (very low rate of expansion) and good elongation to fracture (ductility).

In these three types of cable, the use of increased conductor temperature causes increases in sheath temperatures and in daily ranges in temperature. The resistance of lead sheaths or lead-alloy sheaths both to fatigue cracking and to expansion by creep caused by internal pressure decreases rapidly with increases in temperature of the sheath. Therefore, in order to utilize the possibilities of higher loading, a need arose for a sheathing material which would withstand both the slow bending of small amplitude and the internal pressures better than commercially pure lead sheaths and would have other suitable properties. So far, such material has been found in the

Paper 51-68, recommended by the AIEE Insulated Conductors Committee and approved by the AIEE Technical Program Committee for presentation at the AIEE Winter General Meeting, New York, N. Y., January 22–26, 1951. Manuscript submitted October 20, 1950; made available for printing December 7, 1950.

HERMAN HALPERIN and C. E. BETZER are both with the Commonwealth Edison Company, Chicago, Ill

arsenical-lead alloys, of which several are now in use. One type, which was described by L. F. Hickernell and C. J. Snyder in 1946,[3] consists mainly of about 0.15 per cent arsenic, 0.10 per cent tin, and 0.10 per cent bismuth in lead. Other types contain much less bismuth and about 0.04 per cent copper.

The American cable manufacturers solved another lead-sheath problem very well 15 to 20 years ago. Prior to that time, sheath openings were developing rapidly in some solid-type cables, mainly those having heavy walls of insulation and oil-filled joints with reservoirs containing oil connected to them. High internal pressures were occurring during daily peaks in loading. These openings resulted mainly from local weaknesses in the sheath structures caused by oxides or dross in the metal and by lack of uniformity in thickness circumferentially. Both defects are rare in cable made recently.

In this discussion, commercially pure lead includes common desilverized lead *A*, chemical lead, and lead containing added copper. For the tests of strip specimens, the strips were obtained in all cases from sheathing which had been extruded on cable.

Life-to-Fracture in Bending

A dummy manhole simulating a full sized manhole in the streets was constructed in the laboratory. (A picture of this machine was shown in an earlier paper.[1]) Cable samples about 25 feet long with a joint in the middle were installed in the manhole and moved toward and away from the manhole in 70-second cycles, simulating the movement which occurs in service. Cycles of movement were counted to produce fracture of the sheath, which permitted air to leak out at a few pounds pressure. Most of the tests were made with 0.5-inch movement of the cable at the duct mouth at each end of the manhole, because this was found to be a typical daily movement on a well-loaded 500,000-circular-mil, 3-conductor, 12,000-volt line in Chicago. On such cable the average temperature of the sheath in the manholes is of the order of 110 degrees Fahrenheit (43 degrees centigrade) and in the ducts is somewhat higher.

The results of such tests have shown that the number of cycles to fracture for the arsenical-lead-alloy sheaths is about three times the number for lead sheaths under comparable conditions, and the ratio is sometimes greater. Data for one cable size are shown in Table I. In the tests recorded in this table the cable was moved 0.5 inch at each end of the manhole in 70-second cycles. Some bending tests also have been made for single-conductor and 3-conductor cables rated from 4 kv to 138 kv.

Table I. Bend Tests to Fracture of the Sheath on 500,000-Circular-Mil, 3-Conductor, 12-Kv Cable in Dummy Manhole

	Cycles to Fracture, 0.120-inch Lead Sheath	Cycles to Fracture, 0.120-inch Alloy Sheath
At Room Temperature:		
Belted cable	11,420 (2)*	35,471 (3)
Shielded cable with metal binder	5,081 (4)	17,943 (1)
Shielded cable with paper binder	9,720 (12)	22,564 (3)
At 43 degrees centigrade:		
Shielded cable with paper binder	2,755 (2)	14,468 (23)

* Figures in parentheses indicate number of tests.

The type of construction of the cable under the sheath exerts a considerable influence on the life-to-fracture of the sheath. If 3-conductor cable has a copper shielding tape over the insulation on each conductor and a copper or bronze tape with an intercalated-paper tape wrapped around all three insulated conductors to bind them together (the common construction of shielded cable), then the life-to-fracture of the lead sheath in bending is about half that of sheath on belted-type cable. The metal tape wrapped around the cable has some rigidity and tends to concentrate the working of the sheath over the edges of the metal tape. If the shielded cable has three or four paper tapes (total about 20 mils thick) instead of the metal and paper-tape binder, the life of the sheath in bending is appreciably better, but is still somewhat less than that of the sheath on belted cable. However, the alloy sheath on the shielded cable with paper binder has been found to have over twice the life-to-fracture of the lead sheath on belted cable.

Incidentally, proof has been presented by E. H. Salter, G. B. Shanklin, and R. J. Wiseman[4] that the paper binder affords adequate mechanical strength during short-circuit conditions. In the installation of cable with paper binder, the metal shielding around the conductor insulation is connected metallically to the lead sheath in each joint. Paper tapes in the binder, even though insulating, have caused no trouble because of transient potentials across them during fault conditions.

The shielded type of cable has some advantages in stability of the insulation under voltage and somewhat greater current-carrying capacity than belted cable with the same conductor size. For both normal and emergency operation, tests have shown that for solid-type cable, the shielded type can safely withstand higher loading than can the belted-type cable with the same 3-phase voltage rating. Higher temperature limits are, therefore, prescribed for the shielded type in the standard specifications. In general, there is a trend in usage for cables rated at more than 8 kv toward the shielded type; and some users specify that the binder consist of paper tapes.

Figure 1 shows the results of bend tests of one cable design with alloy sheath in which the number of cycles to fracture is related to the amount of repeated movement of the cable at each end of the manhole. The corresponding total strain produced in each cycle of bending of that particular cable for a given movement at the duct mouth also is shown. Most of the tests represented in these data were made on 25-foot samples in the dummy-manhole apparatus with an offset of 19 inches between the centers of the cable in the duct and in the joint. Some of them were made on 8-foot samples of cable bent into U-shape, held at one end and moved back and forth at the other end. With the motion adjusted to give the same maximum strain of the sheath in this test as in the dummy manhole, the resulting number of cycles to fracture of the sheath has been found to be about the same as in the dummy-manhole apparatus.

These results indicate that at 43 degrees centigrade with 0.32 per cent sheath strain (equivalent to 1/2-inch movement of the cable at each end of the manhole), the average life-to-fracture at a speed of about one cycle per minute is about 14,000 cycles for arsenical-alloy sheath. The 1/2-inch movement corresponds to a daily range in conductor temperature of about 25 degrees centigrade on sections of that cable longer than about 300 feet. Generally, cables operate with somewhat less temperature range during most of their service lives for which the test data show considerably increased lives for the sheath. These data relating movement to life-to-fracture of the sheath provide a

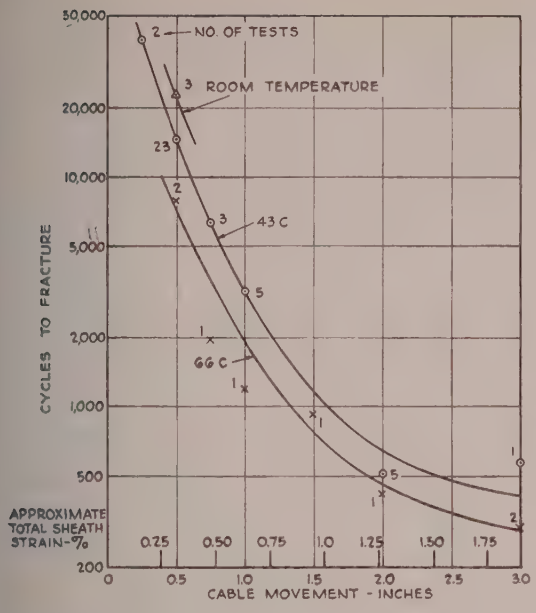

Figure 1 (left). Bend tests of 500,000-circular-mil, 3-conductor 12-kv shielded cable with lead-alloy sheath

Outside diameter of cable is about 2.37 inches

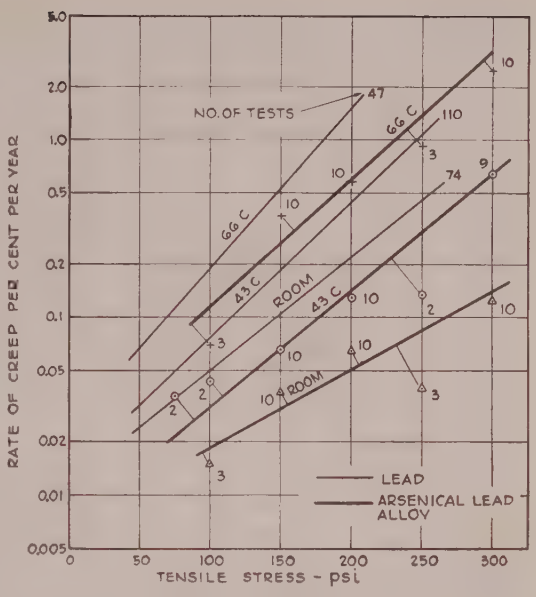

Figure 3 (right). Creep rate of strips Based on elongation from 1,000 to 2,000 hours under stress. Rates decreased slightly in most cases for longer periods of time

means of predicting the service life of the sheath for various current loadings of the line.

In commercial operation, the bending cycle generally is a 24-hour cycle corresponding to the daily-load cycle. In order to obtain an indication of the effect of slower movement than the 70-second cycles used in the dummy manholes on the number of cycles to produce fracture of the sheath, bend tests were made on strips cut from cable sheaths,[6] with 1-minute, 10-minute, and 60-minute cycles. The number of test results obtained to date is inadequate to establish definitely the relation between speed of bending and number of cycles to fracture, but they do give an indication which is of value in this presentation. As shown in Figure 2, extrapolation from the available test results indicates that the number of 1-day cycles to produce fracture is roughly one-third of the number with 1-minute cycles. Since the action within the structure of the metal is somewhat different in a strip of sheath when bent than it is in a sheath on a cable, the results of these tests cannot be applied directly to service conditions. However, it is believed that the relation between length of cycle and number of cycles to fracture can be applied on an approximate basis. The data indicate, then, that the life-to-fracture of the alloy sheath on a well-loaded 12-kv line is about one-third of 14,000 cycles, or about 5,000 cycles. If such load cycles are applied six days per week, the indicated life-to-fracture of the sheath in the manhole is about 16 years.

If the line is not regularly well-loaded, as is generally the case, so that the average daily cable movement is only 1/4 inch, for example, at the same temperature the sheath will fracture in about 40,000 cycles in the laboratory test, or more than 40 years in commercial service. Furthermore, with less load the sheath temperature in the manhole would be somewhat less than 110 degrees Fahrenheit (43 degrees centigrade) and the life-to-fracture would be even longer.

During emergencies, the cable occasionally might be more heavily loaded for a day or two, with the result that the cable movement might be as much as two inches at each end of the manhole. If the cable is in a well-loaded duct bank, the sheath temperature in the manhole may be about 150 degrees Fahrenheit (66 degrees centigrade). For such conditions the indicated life-to-fracture on test is only 500 cycles, and in service is, perhaps one-third of that, or 170 cycles. One or two load cycles under such conditions would, however, consume only about one per cent of the life of the sheath, which is a negligible part of the service life.

These bend tests have shown that the lead-alloy sheath has a life-to-fracture at 1-inch cable movement about equal to that of lead sheath at 0.50-inch movement. Data have been presented[2] relating cycles of movement to produce fracture to daily range in temperature. Based on those data, this increase in allowable movement corresponds to an increase in daily temperature range of about 50 per cent. Thus, for equal sheath life, the alloy permits about 22 per cent higher current loading of the cable.

Figure 2. Bend tests of strips at 0.3 per cent strain

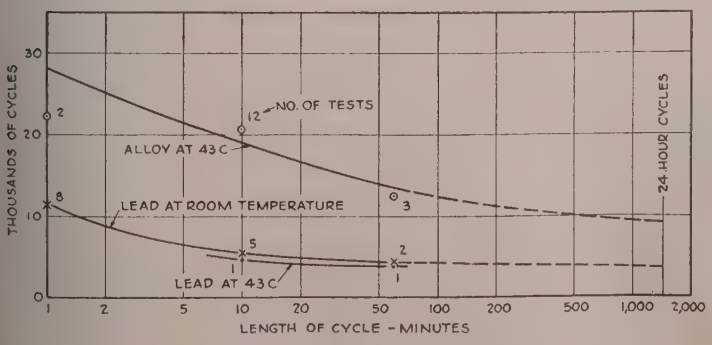

Resistance to Creep

Another important characteristic in which the arsenical-lead alloys are markedly superior to lead for cable sheathing is the ability to withstand stress, as indicated by rates of creep. The average results of a large number of tests of strip specimens under steady tensile stress[6] are shown in Figure 3. The results shown for lead alloy were obtained on the approved types. At temperatures between room temperature and 43 degrees centigrade, and at the stresses which are most common for cable sheaths in service, the alloys

take about 100 pounds per square inch (psi) higher stress than lead to produce a given rate of creep. At 66 degrees centigrade, the difference in stress is about 60 to 80 psi. Thus, though the advantage of the alloy is not so great at the higher temperatures which may be encountered at unusually warm locations or generally during emergency operation, the difference still is considerable.

These creep rates are based on the elongation of strip specimens under steady tensile stress between 1,000 and 2,000 hours after the load had been applied. Most of the tests on strips were run to 5,000 hours, but some were continued to as long as five years. Generally, after 2,000 hours the rate of creep under normal conditions of temperature and stress decreases slowly for a long period until finally a rising rate leading to failure develops. The decreasing trend occurs for both lead and the arsenical-lead alloys. Thus, the rates of creep shown in Figure 3 are a little higher than they would be for periods of years in service.

Toward the upper values of temperature and pressure that might be encountered in service, such as 300 psi and 66 degrees centigrade, the rate of creep for the alloys generally increases gradually with time. For example, an alloy that had a rate of 1.93 per cent creep per year at 300 psi and 66 degrees centigrade, based on the elongation between 1,000 and 2,000 hours, had a rate of 2.10 per cent based on the elongation between 4,000 and 5,000 hours. In service, however, such high sheath temperatures occur rarely, and then usually only for short periods during emergency operation. Such high hoop stresses sometimes occur in the sheaths of solid-type cable during the initial loading, but after the sheath has become expanded somewhat the stresses are much less.

The strip specimens used in these creep tests were 1/4-inch wide in the gauge section. An investigation was deemed necessary to determine whether the results could be applied directly to the sheath on cable with internal pressure. Six-foot samples of sheathing with sealed ends were filled with oil and were maintained with internal pressure at room temperature for some samples and at 66 degrees centigrade for others. The rates of radial expansion of these sheaths over long periods of time (one test ran 13 years until the sheath split) were compared with the rates of elongation of the strip specimens of the same materials. In most cases, the rates of creep for long periods of time were practically the same for both the strip and the cylindrical samples. In some cases, the rates for the sheaths with internal pressure were somewhat less than those for the strips. For purposes of determining suitable thicknesses of sheaths and allowable internal pressures, the rates of creep shown in Figure 3 are, therefore, considered to be conservatively on the high side.

Good creep resistance is especially important for cables which are maintained with internal pressure, such as oil-filled cable and gas-filled cable. For oil-filled cable, the ability of the sheath to withstand higher internal pressures makes possible savings in the provisions of oil reservoirs for the thermal expansion of the oil. For gas-filled cable, higher pressures make feasible the use of higher operating voltage by raising the ionization voltage of the insulation. For the arsenical-lead-alloy sheath, a limiting hoop stress of 175 psi has been established,[7] whereas the established limit for commercially pure lead sheath is 125 psi.

Generally, the sheath in the duct is somewhat warmer than that in the manholes, and for a well-loaded line may be about 50 degrees centigrade. Based on these data, a lead sheath at 50 degrees centigrade and 125 psi will expand by about 6.1 per cent in 40 years, while the alloy sheath at 175 psi will expand by about 5.5 per cent. These figures are slightly lower than those indicated in Figure 3 to allow for the decrease in rates of creep which occurs with time. Thus, the established limit of 175 psi for the arsenical-lead alloy is based on less ultimate expansion than is the limit of 125 psi for lead. In the following section the alloy is shown to be much better able than lead to withstand such expansion.

Long-Time Effects

Commercially pure lead does not harden with age. In fact, it will recrystallize quite readily under ordinary service conditions of temperature and stress. The tensile strength and hardness show little or no change with time, but lead is a relatively weak metal and its elongation to fracture decreases in a very long time under stress.

Small amounts of some alloying substances can make lead an age-hardening metal so that the tensile strength increases and the ductility decreases over a period of four or five years. The decrease in ductility might cause cracks to develop in cable sheathing in normal handling during installation or might cause early failure as a result of cable movement in service. Some alloys which were tried ten or twelve years ago were found to be age-hardening. Although the results of tests made shortly after the cable was manufactured were good, fractures developed within a few years in service. With age, the sheath lost in ductility and broke with very little elongation.

The arsenical-lead alloys that have been accepted for commercial use are not age-hardening materials. Their physical properties have been tested over a period of several years without showing any appreciable change in tensile strength or elongation. The hardness, as measured with a modified Rockwell tester, decreases somewhat in some cases.

In short-time, tensile-strength tests, strip specimens of commercially pure lead sheathing fracture at about 1,900 to 2,100 psi with elongation of about 50 or 60 per cent to fracture in a 2-inch gauge length. Metallurgical study of the specimen shows that the fractures in such tests usually go through the grains of the metal. If the specimen is subjected to a steady tensile stress of, say, 500 psi at 43 degrees centigrade, fracture might occur in about a year with much less elongation. Metallurgical study shows that the cracks in such tests generally follow the boundaries around the grains. Thus, the nature of fracture of sheaths in service appears to be somewhat different from that in short-time tests and depends more on the strength of the metal in the grain-boundary region.

Commercially pure lead cable sheaths in service with internal pressure have been found to burst open when the diameters have increased by as little as $3^1/_2$ or 4 per cent. These sheaths were fairly uniform in thickness around the circumference. The dependable life of such sheathing therefore can be considered to be ended when expansion of about that amount is reached.

The arsenical-lead-alloy sheaths have been found to have good ductility in long-time tests. Some typical test results are shown in Figure 4. In some cases, such as alloy *A*, the elongation to fracture remains almost unchanged in tests to over a year in duration. In other cases, such as alloy *B*, there appears to be a decline in ductility at first and then for tests of longer duration, higher values are shown. It is believed that over long periods of time in service these alloys can be depended upon to expand by at least 10 per cent before fracture occurs. This is more than enough for most practical purposes. The ability of the sheath to expand without bursting is of value for solid-type cable in which oil is fed to the cable from reservoirs connected to the joints or from terminals, or for cables installed vertically

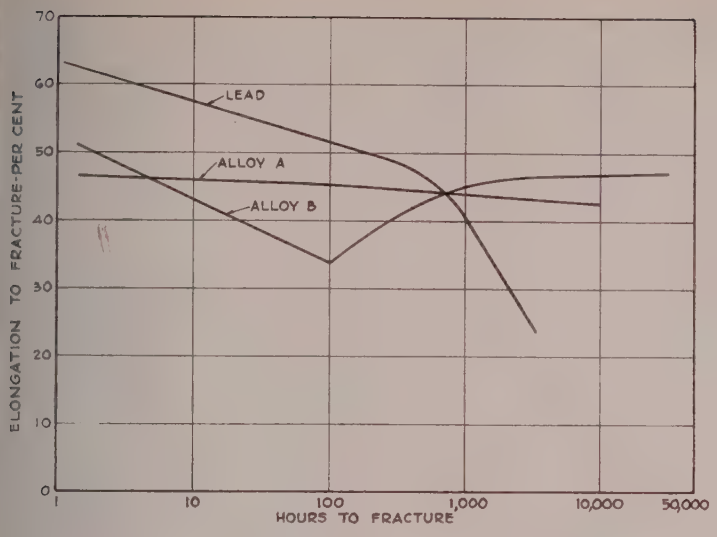

Figure 4 (above). Typical trends in ductility at 43 degrees centigrade

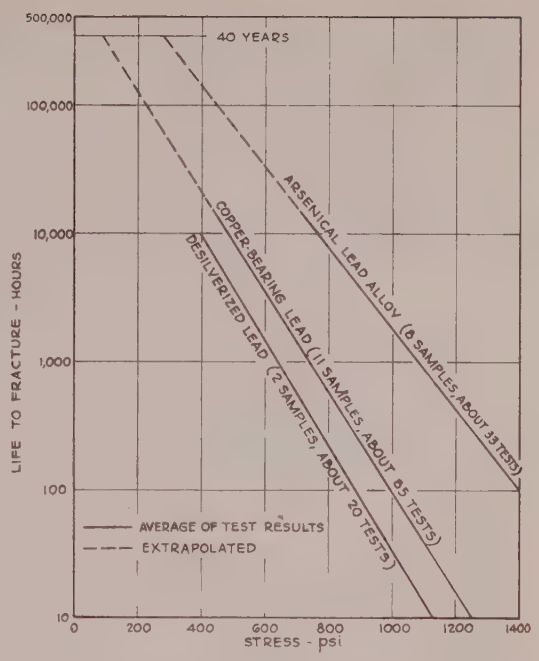

Figure 5 (right). Life-to-fracture of strips under steady tensile stress at 43 degrees centigrade

or on steep slopes where the hydrostatic head of oil creates internal pressure at the bottom. It is of value, also, for pressure-type cables such as low-pressure, oil-filled cable and gas-filled cable.

Figure 5 shows the relation between stress and time-to-fracture in tests of strip specimens at 43 degrees centigrade with steady tensile stress. In addition, a few tests on sheaths at stresses of 200 to 315 psi, some to fracture in as long as 13 years, have been made on cable samples with internal pressure, and the results generally have been in line with the relations shown on the figure. These data show that to produce fracture in 100 hours, for example, the alloy sheath requires about 400 psi greater stress than does copper-bearing lead sheath. The difference between alloy and lead decreases for longer tests at lower stresses. If these data may be extrapolated to 40-year life, the indication is that the average stress to produce fracture of the alloy sheath is about 280 psi, and that for copper-bearing lead sheath is about 90 psi. Such extrapolation from laboratory tests to obtain strength for 40 years is questionable, and the stresses derived might be changed considerably by further results of the very long-time tests. However, the data furnish definite evidence of the marked superiority of the arsenical-lead alloy.

Installation of Cable with Alloy Sheath

Since arsenical-lead-alloy sheath is somewhat harder and stronger than lead sheath, it is somewhat better able to resist scoring or abrasion when the cable is pulled into the duct. This feature is especially of value for the large and heavy cables that have been installed in recent years. Also, the higher tensile strength of the alloy sheath is of some slight advantage in withstanding the forces to pull the cable into the duct.

Slightly greater force is required to bend the cable to train it into position in the manholes. However, cables with large conductors having over-all diameters of 3.0, 3.3, and even 3.4 inches, have been installed in 4-inch precast-concrete ducts in 600- to 700-foot lengths of conduits without any substantial difficulty. For cables smaller than about 3.0 inches, the difference in this respect has not been noticeable.

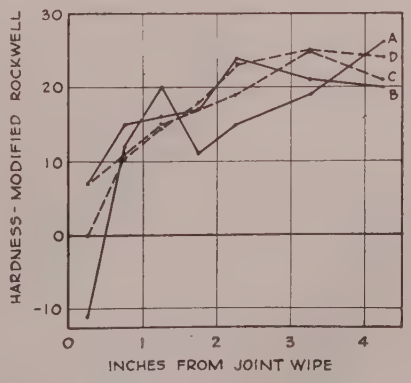

Figure 6. Effect of joint wipe on hardness of arsenical-lead-alloy sheath

A and B—Opposite sides of cable in one direction from joint

C and D—Opposite sides of cable in other direction from joint

In a few cases, cracks have developed during installation of some of the early alloy sheaths, mainly on cables having diameters about 3.3 inches. Those sheaths were found to be abnormally hard and low in ductility in the region of the fractures. This condition was the result of improper conditions of extrusion of the sheath at the factory. Investigations have shown that, in order to avoid such troubles and to obtain uniformly good properties of the alloy, close control of the treatment of the metal, both in the lead press and after it leaves the lead press, is necessary. The methods and control of the extrusion process have been improved greatly.

Some of the desirable properties of the alloy are lost adjacent to seals and wipes which are made with molten solder. Figure 6 shows the decrease that might occur in hardness of the alloy sheath within two inches of the solder wipe sealing the joint sleeve to the cable sheath. These hardness tests were made three weeks after the joint wipes were made. It would be desirable to eliminate this change in the properties. However, it should be noted that in the bend tests in the dummy manhole, as discussed previously, each sample contained a full-size joint made in the usual manner. Although the fracture in those tests usually occurred less than one inch from the joint wipe, the lives to fracture were much better than those for lead sheaths, as is discussed earlier.

The lead-alloy sheath withstands vi-

bration much better[3] than lead sheath. There have been a few cases where lead sheaths have been fractured with many cracks as a result of vibration at points of support caused by street or railway traffic. Vibration is especially troublesome to lead-covered cables on bridges. It also is a problem on lead-covered cables supported on aerial messenger wire.

Usage

Beginning in 1944, the Commonwealth Edison Company adopted the arsenical-lead alloys for sheathing on 4- and 12-kv, 3-conductor cables of the larger sizes (375,000 circular mil and larger) and on all 66- and 132-kv cables. Cable with these alloys has been furnished by six manufacturers. Some of the manufacturers are continuing their development work on various lead-alloy sheaths. Also, the tests described herein are continuing.

Possible Changes in Sheath Construction

Since the arsenical-lead alloy is considerably better than lead in the important characteristics for power-cable sheathing, could not the change from lead to alloy sheath be accompanied by a reduction in sheath thickness, with a corresponding reduction in the cost of the cable?

Some 500,000-circular-mil, 3-conductor, 12-kv cable was obtained with 100-mil alloy sheath, some with 85-mil alloy sheath, and some with 65-mil, in addition to cable with the standard 120-mil sheath. Bend tests were made in the dummy-manhole and in a U-bend machine for which the results are shown in Figure 7. While there is considerable scatter in some of the results, and alloys from three different companies are involved, there are enough data to give a fair indication of the trends. These data indicate that a reduction in sheath thickness from the present standard thicknesses would be accompanied by a percentage reduction in life-to-fracture in bending corresponding to, or a little more than, the accompanying percentage reduction in thickness. Where this property is not the controlling factor in the service life of the cable, the thickness might be reduced by about 10 per cent. With the corresponding reduction in life, the alloy sheath still would have an appreciable advantage in this respect compared with lead sheath.

Some bend tests were made of cable with 85-mil alloy sheath and 75-mil fabric-reinforced neoprene jacket and of cable with 65-mil alloy sheath and 90-mil

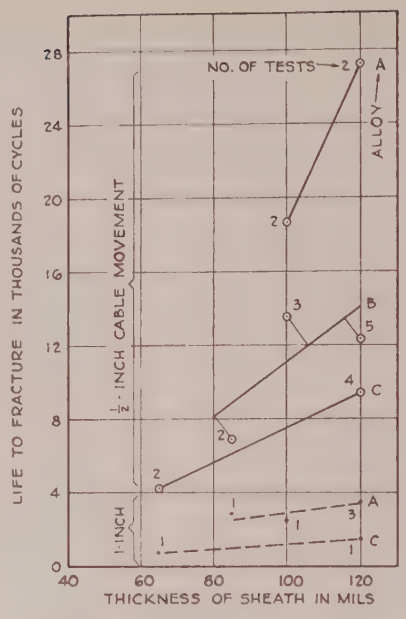

Figure 7. Bend tests of 12-kv cable with alloy sheath of various thicknesses at 43 degrees centigrade

Further developments have been made on these alloys since these samples were produced

extruded-polyethylene jacket. Difficulties were encountered in determining when the sheath under the jacket had cracked. However, the data are considered adequate to indicate that for these thin sheaths the life-to-fracture in bending is better with the jacket than without it. While the jacket is new and tight on the sheath, it is of benefit in lengthening the life-to-fracture, if the repeated bending strains are large enough to produce appreciable wrinkling or buckling of the sheath of reduced thickness without jacket. With age in service, however, the jacket might loosen on the cable and become of little or no help to the sheath. The use of a jacket, of course, practically eliminates the possibility of scoring of the sheath during installation. Such scoring might reduce its thickness at places by as much as 15 per cent. Based on this consideration mainly, the commonly used specifications[7] for oil-filled cable were revised recently to permit a one-sixth reduction in sheath thickness when jackets are applied over the sheaths.

Alloy sheath as thin as 65 mils on cable of this size is impractical for other reasons. It would be relatively weak to withstand the pulling forces involved in installing the cable in conduit. It would have a tendency to wrinkle when the cable was bent. Considerable care would be required to make solder wipes on such thin sheath for joints and potheads. With the addition of a jacket over the sheath, it would make little or no saving in the factory cost of the cable compared to 120-mil alloy-lead sheath.

Some consideration has been given to the possible use of materials other than lead or lead alloy for power cable sheaths. While some of the synthetic materials which are now commercially available have very good resistance to moisture, none of them will keep out water completely, which a lead sheath does. Most of the synthetics are relatively new and there is not adequate proof available that they can be depended upon under various service conditions for a 40-year life of the cable. With the recently increasing loads and higher ambient temperatures for power cables, sheath temperatures also are increasing. At least some of the available synthetics are not able to withstand the higher temperatures. In case of a failure to ground on the line, a conducting path must be available for the return fault current. The lead sheaths serve this purpose well. With nonconducting material, some other provisions would be needed. For these reasons, synthetic materials have not been adopted for paper-insulated, underground power cables.

Use of aluminum for cable sheaths has been considered from time to time, and some trials have been made in the United States to extrude it as cable sheathing. Recently, a method of drawing down an aluminum tube onto a cable has been developed in England. Aluminum is considerably stronger than the lead alloys, and this would be an advantage for many cable applications. With aluminum sheath an internal pressure of 200 psi could be used for self-contained, gas-filled, or oil-filled cable for extra-high voltages without additional metallic coverings to reinforce the sheath. Such cable could, in some cases, be used instead of cable installed in steel pipe. For aerial cable, the reduction in weight and in cost made possible by the use of aluminum instead of lead is especially attractive. However, for use underground, a covering over the aluminum to prevent corrosion would be required. This would make the cable unattractive from the standpoint of cost for most applications.

Since the conductivity of aluminum is about seven times that of lead, the losses in aluminum sheath of the same thickness would be about seven times those in lead sheath. Such losses are due both to circulating currents induced in the sheath by the flow of current through the conductors and to stray currents picked up from other sources. For example, for 500,000-circular-mil, 3-conductor, 12-kv cable with lead sheath, the induced sheath

losses are only 3 to 4 per cent of the conductor losses. If the sheath were aluminum and about 10 per cent thinner, the ratio would be about 22 per cent, which would cause an appreciable reduction in current-carrying capacity. These losses are based on 60-cycle current.

Conclusions

In order to carry safely the increased loads that correspond to the increases in temperatures that have been found feasible for the impregnated-paper insulation of underground power cables, a sheathing material better than commercially pure lead was needed to avoid considerable reductions in the life of the cable. Arsenical-lead alloys have been developed to meet this need. They are far superior to copper-bearing lead in ability to withstand repeated bending in manholes caused by thermal expansion and contraction of the cable, in resistance to creep caused by internal pressures, and in life-to-fracture under tensile stress. They also are somewhat better able to withstand the handling involved in installation of the cable. For some cables which operate continuously with internal pressure, arsenical-lead alloys permit use of a sheath without additional reinforcing coverings, with accompanying saving in the cost of the cable.

The improved ability to withstand bending makes feasible the use of less offset in the manholes between the center of the cable in the duct and in the joint. Thus, existing manholes can sometimes be used for the installation of an alloy-sheathed cable, where for the same cable having a commercially pure lead sheath enlargement of the manhole would be necessary to provide the necessary large offsets. For new manholes, a reduction in offset permits a reduction in the cost of the manhole.

The development work on arsenical-lead alloys is continuing and some of the cable manufacturers are searching for other suitable lead alloys.

References

1. Load Ratings of Cable, **Herman Halperin.** *Electrical Engineering* (*AIEE Transactions*), volume 58, October 1939, pages 535–56.

2. Load Ratings of Cable—II, **Herman Halperin.** *AIEE Transactions*, volume 61, 1942, pages 930–42.

3. F-3 Lead Alloy—An Improved Cable Sheathing, **L. F. Hickernell, C. J. Snyder.** *Electrical Engineering* (*AIEE Transactions*), volume 65, August-September 1946, pages 563–69.

4. Resistance and Reactance of 3-Conductor Cables, **E. H. Salter, G. B. Shanklin, R. J. Wiseman.** *Electrical Engineering* (*AIEE Transactions*), volume 53, December 1934, pages 1581–89.

5. An Investigation of Creep, Fracture, and Bending of Lead and Lead Alloys for Cable Sheathing, Series 1946, **C. W. Dollins.** *Bulletin Number 378* (University of Illinois Engineering Experiment Station, Urbana, Ill.).

6. An Investigation of Creep, Fracture, and Bending of Arsenical-Lead Alloys for Cable Sheathing, Series 1949, **C. W. Dollins.** *Bulletin Number 394* (University of Illinois Engineering Experiment Station, Urbana, Ill.).

7. Specifications for Impregnated-Paper-Insulated, Lead-Covered Cable, Oil-Filled Type. Association of Edison Illuminating Companies, New York, N. Y., fifth edition, January 1951.

Discussion

R. W. Atkinson (General Cable Corporation, Bayonne, N. J.): Utility engineers have contributed significantly toward the development of power cables in various ways, especially by studying and evaluating various service conditions and problems; and aiding the development and evaluation of practical test methods to measure the properties of a cable which control its ability to meet these service conditions.

In the case of equipment which is expected to serve for many decades, perhaps the most challenging problem, and one always present, is that of evaluating in a short time something which is subject in service to action over many decades. This is particularly pertinent to the lead sheath problem which the authors have studied and an important part of their work is the information which aids in the correlation of measurable characteristics with the service performance.

In the studies of fatigue of lead sheath it is significant that the emphasis is upon cycles of motion of from 1 minute to 24 hours in length. For many years, the discussion of fatigue of lead sheath was in terms of many hundreds of cycles per minute. While bending at such speeds, which may properly be called vibration, does characterize stresses which are sometimes imposed upon lead, it seems likely that speed of repetition of most of the fatigue stresses which lead sheaths have to meet is very low, very often one cycle per day. Because of this low rate, it becomes particularly important that correct criteria be determined for extrapolating to long time the results of tests of relatively short duration. Halperin and Betzer have given important data concerning this subject.

It is fortunate that, as mentioned by the authors, the arsenical alloys of lead, chosen primarily because of good creep resistance and good resistance to slow motion fatigue also have good resistance against vibration. Thus, the particular alloy which we have furnished has resistance to vibration fatigue that is quite comparable to that of the usual antimony-lead alloy which has long been used in locations where vibration is expected. It appears, moreover, that the arsenical alloy maintains its original properties better than does the antimony alloy.

The authors indicate finding a sheath life under fatigue conditions substantially in proportion to sheath thickness. Our considerable number of measurements also show this same general trend.

The authors refer to the testing of sheath protected by various nonmetallic coverings. We have overcome the difficulty of learning when sheath breaks occur by an electromagnetic exploring device which finds a break very soon after it has begun and long before any visual evidence occurs. We also have found that considerable increase in sheath life may be obtained in certain cases by the use of suitable sheath coverings. However, we urge caution on any who undertake these tests on protected sheath to exercise particular care to avoid erroneously favorable conclusions as a result of the difficulty which the authors mention of finding when a test sample has failed.

H. D. Short (Canada Wire and Cable Company, Toronto, Canada): I am going to confine my comments in particular to two aspects of the paper. But first, I should like to ask the authors what type of cable they have in mind when referring to "gas-filled cable". I surmise it to be the Shanklin-Hayman so-called low gas pressure cable, but should like this confirmed or have the authors' comments to the contrary.

The authors make the statement that the arsenical-alloy sheath is much superior to lead in respect of their relative resistance to fatigue under vibratory motion. This is distinctly opposed to the results we have obtained from accelerated vibration tests on several different types of lead alloys. Briefly, these tests were based upon attempts to simulate the actual conditions in service by making use of a calibrated vibration table. We could discern no apparent difference between the arsenical-alloy and plain lead in these tests. I should like to know if the authors have corroborative evidence other than the reference they have cited in this regard.

The authors also mention aluminum sheaths in their paper and I presume they have in mind my own paper on this subject before the Insulated Conductor Committee, and Mr. Hollingsworth's paper[1] before the International Conference on Large High-Voltage Electric Systems. I fail to grasp the force of their remarks in regard to a protective covering over an aluminum sheath as rendering it unattractive economically when used underground. Presumably by "underground" they refer to a buried duct bank. Nowadays, it seems to be not an uncommon practice to pull jacketed lead sheathed cables into ducts.

It is not reasonable to expect that it is less costly to jacket a lead sheath than an aluminum one.

I must also take some exception to the authors' categorical statements in the matter of sheath losses, reducing the current rating of aluminum sheath cables. The authors in their introduction have again emphasized the inability of lead sheaths to sustain the modern cable under contemporary loading practice. A chain is no stronger than its weakest link, and the mortality rate of lead sheath cables installed in duct banks is most frequently determined by the lead sheath. Aluminum sheaths have a fatigue resistance many times greater than lead; also they have no appreciable creep characteristics such as one finds in lead or in many other materials of a more or less plastic nature; again the crystal structure of aluminum sheaths is extremely stable. Hence, it obviously follows that the depreciating effect of the sheath losses may, in many instances, be readily offset by increas-

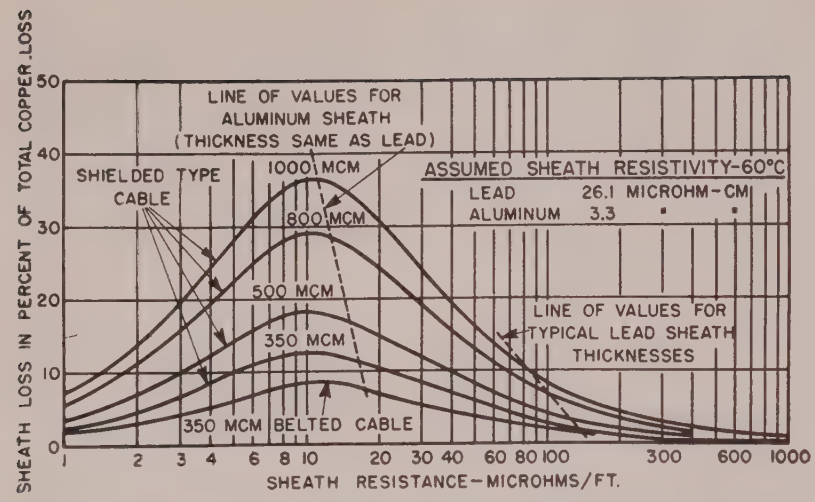

Figure 1. Sheath losses of 3-conductor cables with lead and aluminum sheaths (60-cycle values)

ing temperature of the conductor without impairing the life expectancy of the cable.

REFERENCES

1. CABLES SHEATHED WITH ALUMINUM—DEVELOPMENT IN GREAT BRITAIN, P. M. Hollingsworth. *Paper 203*, International Conference on Large High-Voltage Electric Systems (Paris, France), 1950.

R. W. Burrell (Consolidated Edison Company of New York, Inc., New York, N. Y.): Although commercially-pure lead has served the electrical industry well as a material for cable sheaths, its limitations are recognized. Through the years cable manufacturers have sought for improvement in lead sheath behaviour, carrying on an extensive research in the field of lead alloys. The sheath failure record reported in the annual Cable Operation Report[1] of the industry is sufficient evidence of the need for such research.

The relative advantages of arsenical-lead as a means of obtaining a better sheath performance and longer cable life have been thoroughly explored by the authors in this valuable paper. The authors have mentioned previously the possible use of aluminum as a substitute for lead and have brought out the fact that because of higher conductivity, sheath losses will be higher with aluminum than with lead sheaths. It is of interest to those who have considered the possible use of aluminum-sheath cables to compare the relative sheath loss of typical cables employing these two different sheath materials. It is with the subject of sheath losses in 3-conductor cables that this discussion is concerned.

The authors have quoted the conductivity of aluminum as about seven times that of lead. For the purpose of this discussion, the resistivity of lead has been taken as 26.1 microhm-centimeters at 60 degrees centigrade. This value, taken from the Smithsonian Physical Tables and quoted by Simmons[2] probably is high for actual lead sheath material. The resistivity of aluminum has been taken as 3.3 microhm-centimeters at 60 degrees centigrade. These values give a ratio of conductivity of nearly 8-to-1, which is probably somewhat high. However, this ratio was used in calculating relative sheath losses to produce an upper limit of probable increase in connection with a study of the possibilities of using aluminum-sheathed cable on the Consolidated Edison System.

The relative values of calculated sheath losses, for a range of 3-conductor cable sizes, are shown in Table I of this discussion. The cable sizes and types listed, with the exception of the 3 × 1,000,000 circular mil size are representative of the standard distribution feeder cables used on the Consolidated Edison System. As there is uncertainty as to the thickness of aluminum sheath which might be found desirable, comparative values are shown in Table I for the two materials, using standard lead thickness and 50 per cent reduced thickness. The calculated loss values are approximate, being based on a modification of Dwight's[3] formula for sheath losses of 3-conductor cables.

It will be noted that the ratio of sheath losses for aluminum versus lead sheath of equal thickness is in all cases less than the ratio of conductivities assumed. The behaviour characteristic of the resultant sheath loss is indicated more clearly, perhaps, by the curves of Figure 1 of this discussion which shows the variation of sheath loss ratio with sheath resistance for various 3-conductor cables.

In discussions of the effect on sheath loss of various metallic sheath constructions, the magnitude of the probable loss is sometimes taken, for approximate estimates, to be directly proportional to the conductivity of the sheath circuit. Actually, the resultant sheath current producing this loss is determined by the resultant sheath voltage acting on the sheath impedance which involves the reactance of the sheath as well as its resistance. For either zero or infinite resistance the sheath loss will be zero. For intermediate values of resistance the loss ratio curve has the well-known characteristic shape shown in Figure 1. The maximum value of sheath loss occurs when the sheath resistance and reactance are about equal. For practical purposes the sheath loss is a maximum when the sheath resistance is of the order of 10 to 12 microhms/foot. If the sheath resistance is appreciably above or below this value the sheath loss will be decreased. Above the critical value the sheath resistance is the controlling factor. Below the critical value, within practical limits, the sheath reactance is the controlling factor. Generally speaking, for all 3-conductor lead sheath cables the sheath resistance is of the order of 80 microhms/foot or more (at 60 cycles), and sheath reactance is of less concern. In this case the proportionality of sheath loss to sheath conductivity holds. However, when the lead sheath is replaced by aluminum or some other high conductivity material, this relation is no longer true and it is necessary to consider the characteristics shown in Figure 1 for a clear understanding.

In the case of multiconductor cables, the sheath currents are relatively small in comparison with those of single-phase cables inasmuch as the sheath surrounds all of the conductors and the inductive effects of one conductor current are to a considerable extent neutralized by the effect of the other conductor currents. With large conductors and large currents the degree of neutralization becomes less effective and the resultant sheath losses become appreciable in magnitude.

A formula for the open-circuit sheath loss of a 3-conductor cable was developed by Carter[4]. Arnold[5] bases his evaluation of the sheath loss of multiconductor cables on Carter's formula. Dwight's formula, mentioned previously, in connection with Figure 1, is also based on Carter's. Dwight's expression, which is in absolute units, can be put in the form

$$\lambda_s = 4\frac{R_s}{R_c}\sum_{N=1}^{N=\infty}(S/C)^{2N}\left[\frac{1}{1+\left(\frac{NR_s}{\omega}\right)^2}\right]\times \sin^2\frac{N\pi}{3} \quad (1$$

It is more convenient to express this equation in terms of more practical cable engi

Table I. Relative Sheath Loss on 3-Conductor Cables (60 Cycle Operation)

Size, Circular Mils	Type	Voltage Class-Kv	Sheath Loss* Per Cent of Total Copper Loss (D-C) Sheath Thickness			
			Standard		50 Per Cent	
			Lead	Aluminum	Lead	Aluminum
350,000	Belted	15	1.3	7.0	0.6	4.6
500,000	Shielded	27	3.8	18	2.0	13
800,000	Shielded	15	5.8	29	3.1	21
1,000,000	Shielded	15	10	38	5.3	33

* Based arbitrarily on conductor at 75°C and sheath at 60°C.

neering units as follows:

$$\lambda_s = 4\frac{R_s}{R_c}\sum_{N=1}^{N=\infty}(S/C)^{2N}\left[\frac{1}{1+\left(\frac{32.8NR_s}{\omega}\right)^2}\right]\times \sin^2\frac{N\pi}{3} \quad (2)$$

where λ_s = ratio of open-circuit sheath loss to total d-c copper loss
R_S = sheath resistance in microhms/-foot
R_C = conductor resistance in microhms/foot
S = distance from conductor center to cable center, in inches
C = mean sheath radius, in inches
$\omega = 2\pi \times$ frequency (in cycles per second)

As the value of S/C is generally close to 0.5 or less, the series is rapidly convergent and it is, therefore, unnecessary to use more than the first two terms in both of which $\sin^2 N\pi/3$ has the value 3/4. Equation 2, therefore, may be simplified to

$$\lambda_s = \frac{3R_s}{R_c}\left\{\left(\frac{S}{C}\right)^2\left[\frac{1}{1+\left(\frac{32.8R_s}{\omega}\right)^2}\right]+ (S/C)^4\left[\frac{1}{\left(1+\frac{65.6R_s}{\omega}\right)^2}\right]\right\} \quad (3)$$

For 60 cycle operation, equation 3 becomes

$$\lambda_s = 3\frac{R_s}{R_c}\left\{\left(\frac{S}{C}\right)^2\left[\frac{1}{1+0.00755R_s^2}\right]+ \left(\frac{S}{C}\right)^4\left[\frac{1}{1+0.0303R_s^2}\right]\right\} \quad (4)$$

For shielded types, S/C ranges from about 0.48 to 0.52 for typical distribution feeder cable constructions. Values for belted constructions will be somewhat lower.

These equations are by no means rigid. In the development of Carter's basic equation simplifying assumptions are made as to the uniformity of current density in the conductor cross-section and effect of sheath thickness. When the proximity effect in the conductors is large it is possible that the formulas given over-estimate the sheath loss, as the resultant external magnetic field is reduced by the crowding of the currents towards each other. Arnold[5] has introduced empirical correction factors for lead-sheathed cables, but test data on aluminum-sheathed cables are required to permit accurate evaluation for this type of construction.

It is believed that the data of Table I and Figure 1 represent approximate upper limits of possible sheath losses for aluminum-sheathed cables of the types listed. In the case of a 15-kv 3×800,000 circular mil cable, for which a lead sheath loss of approximately 6 per cent is calculated, the resultant value is 29 per cent with an aluminum sheath of the same thickness and 21 per cent for a sheath half as thick. For the same copper temperature limits, a resultant loss in current carrying capability of the order of 7 per cent is indicated. This loss in rating could be eliminated provided it is feasible to operate aluminum-sheathed cables at a copper temperature limit approximately 10 degrees higher than our present standard for lead-sheathed paper-insulated cables. Attained improvement in sheath performance would justify higher operating copper temperatures of the order required. For cables of smaller size the effect of aluminum sheath is of less concern.

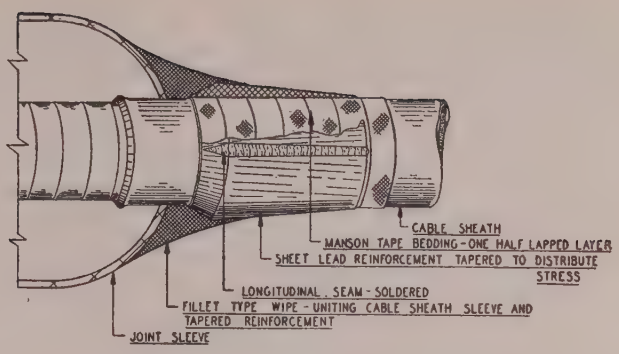
CABLE SHEATH
MANSON TAPE BEDDING - ONE HALF LAPPED LAYER
SHEET LEAD REINFORCEMENT TAPERED TO DISTRIBUTE STRESS
LONGITUDINAL SEAM - SOLDERED
FILLET TYPE WIPE - UNITING CABLE SHEATH SLEEVE AND TAPERED REINFORCEMENT
JOINT SLEEVE

Figure 2. Garrison joint

REFERENCES

1. CABLE OPERATION, 1947. *Publication 50-3*, Edison Electric Institute (New York, N.Y.), 1950.

2. CALCULATION OF THE ELECTRICAL PROBLEMS OF UNDERGROUND CABLES, **D. M. Simmons.** *Electric Journal* (East Pittsburgh, Pa.), May to November 1932.

3. PROXIMITY EFFECT IN CABLE SHEATHS, **Herbert Bristol Dwight.** *AIEE Transactions*, volume 50, September 1931, pages 993–98.

4. EDDY CURRENTS IN THIN CIRCULAR CYLINDERS, **F. W. Carter.** *Proceedings*, Cambridge Philosophical Society (London, England), volume 23, 1927, page 905.

5. EDDY CURRENT LOSSES IN MULTI-CORE PAPER-INSULATED LEAD-COVERED CABLES—ARMOURED AND UNARMOURED, CARRYING BALANCED THREE-PHASE CURRENT, **A. H. M. Arnold.** *Journal*, Institution of Electrical Engineers (London, England), 1940.

Robert J. Wiseman (The Okonite Company, Passaic, N. J.): Mr. Halperin and Mr. Betzer have written a very interesting paper on why lead sheaths have not given as long a life as expected and how the situation is being remedied by the use of lead-alloy sheaths with improved methods of installation and the replacing of a metal binder for a paper binder in shielded multi-conductor cables. Tests carried out under the guidance of his company show that arsenical alloyed lead sheaths have desirable properties of good tensile strength, a high creep resistance and very good resistance to bending. However, I am wondering how they intend to take advantage of the higher hoop stress and lower creep for oil-filled cables and low-pressure gas-filled cables. For oil-filled cables, do they intend to (a) keep the same lead thicknesses but raise the internal pressure; (b) lengthen out the section lengths between feed points, or (c) reduce the sheath thickness? I would prefer "a". For low-pressure gas-filled cable, do they intend to (a) raise the permissible internal pressure or (b) reduce the sheath thickness? I would prefer "a".

We have a dummy manhole set-up in which we have been carrying out bending fatigue tests. We heat the cable to give a sheath temperature of 110 degrees Fahrenheit, use a 4-minute cycle and a 1/2-inch cable movement on each side of the joint. We are getting results comparable to those which Mr. Halperin is reporting. Like him and others we find that the sheath fails close to the end of the sleeve wipe, say within 1 inch. Naturally, this raises a question as to how this can be overcome. It was recognized that actually the end of the sleeve acts as a fulcrum point for the flexing of the cable and, therefore, we should eliminate this concentration of bending. Several methods such as servings or binders were proposed, but we also appreciated that we should have a strengthening of the sheath at the wipe and then tapering off as we went away from the wipe. This resulted in the use of a tapered lead sleeve which we call the "Garrison joint sleeve". This is shown in Figure 2 of this discussion which describes parts of the joint. It can easily be put on when making the lead wipe. We like the fillet type of a wipe. Tests which we have made show the sleeve to function as expected. Where a set-up without it, with an alloyed lead, has given 10,000 cycles to failure, we have had 32,000 cycles without failure. Also we accentuated the stressing by using a 2-inch movement. In this case we obtained 2,927 cycles for a standard wipe and 7,717 cycles for the Garrison sleeve and failure occurred in the "S" bend of the cable. In both cases we have about three times the life when using the Garrison sleeve. We believe that this well pays for itself in the improved cable operation. It can help in meeting an unsatisfactory installation condition where it may not be possible to widen and lengthen a manhole to get better training of a cable.

John F. Eckel (General Electric Company, Schenectady, N. Y.): Strictly from a metallurgical point of view, I am keenly interested in some of the results obtained by the authors of this paper. It is from a desire to find satisfying answers to some of the troublesome questions in the general problem of lead sheath that I shall comment first on the repeated bending data of the authors and secondly upon an anomalous creep result that they report. I shall refrain from any comments concerning the merits of different types of cable construction except as they may affect the bending life of the lead sheath.

In any laboratory test to determine the bending life of lead (or any of its alloys) there are three fundamental variables that are operative provided the bending cycle is continuous with a simple harmonic type of motion. Of these, temperature and frequency are readily controlled. The third, maximum strain per cycle, is more elusive because of strain concentration factors resulting from the contour of the lead sample

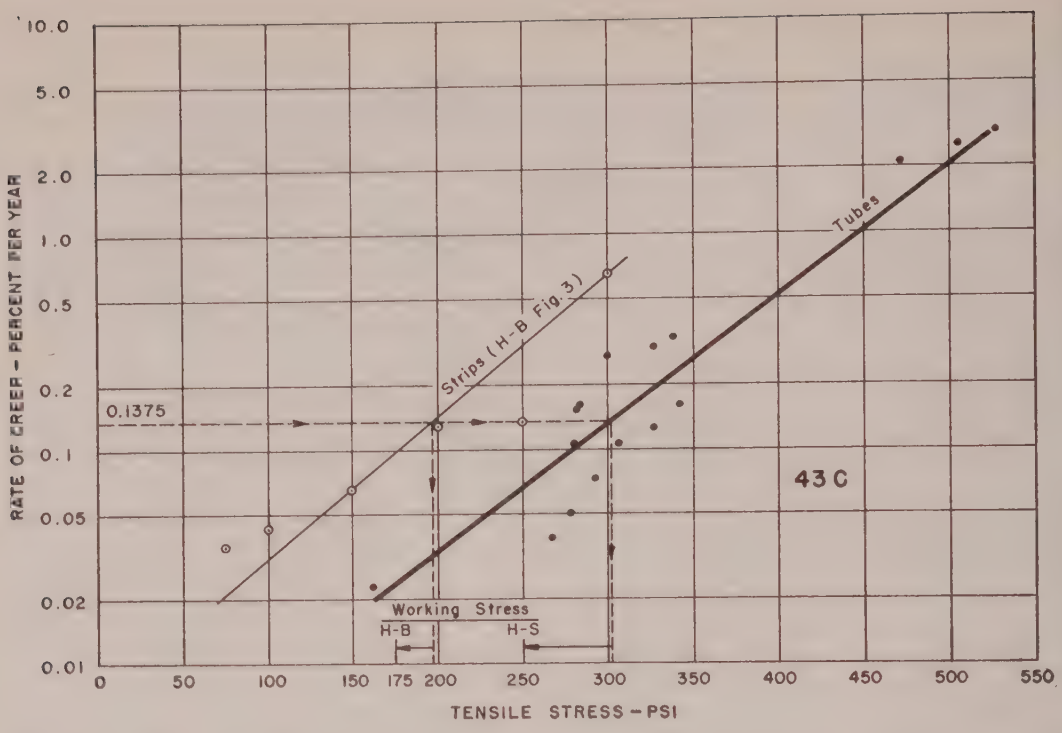

Figure 3. Creep rate of strips and tubes at 43 degrees centigrade

Strips—Elongation from 1,000 to 2,000 hours under stress
Tubes—Total elongation for 2 years under stress

under test. Perhaps bend tests on strips cut from sheath offer the best means for control of strain per cycle. Even this type of test may introduce uncertainties if there are irregularities in contour such as tape markings for example. Unless such strain concentrations are known and results expressed accordingly, it is difficult to obtain a clear picture of the bending life of any sheath material. The authors have shown the existence and magnitude of strain concentration at the joint wipe in their dummy manhole test by previous work.

It is shown by the results in Table 1 of the paper, that the construction of the core has a marked influence on the bending life of arsenical alloys, as well as commercially pure lead. Since temperature and frequency were both fixed at constant values in these tests, the large difference between the bending life of sheath on belted cable and shielded cable must be accounted for by a difference in the amount of strain per cycle. Or should we say that it should be accounted for by the effect of cable construction on strain concentration? It would be interesting to know if the authors have measurements that show how cable construction affects strain concentration in the dummy manhole test. If so, would not the bending life of sheath on belted cable fall on the same life versus strain curve as that of sheath on shielded cable?

Considerable spread in strip bend data is indicated by the results plotted in the upper curve of Figure 2. Although I believe that the general form of this curve is correct, as drawn, it does not appear to give enough weight to the results obtained at the 1-minute cycle. Furthermore, the difference between the bending life at one cycle per minute and that at one cycle per ten minutes appears to be too small. If we examine the nature of the testing equipment from which these results were obtained, we find that another variable may have been introduced. Adjustable nuts are used to produce the desired strain in each test by their position with respect to an actuating yoke. This results in some lost motion in each cycle so that two rest periods are introduced per cycle. The duration of each rest period decreases with increased strain per cycle and also increased frequency. These rest periods may be sufficiently long at the lower frequencies to permit some recovery before movement is again resumed thereby materially increasing the bending life. This, I admit is pure conjecture since we know very little about the role of recovery in such a bending cycle.

In discussing Figure 2 of the paper, the authors state that "the action within the structure of the metal is somewhat different in a strip of sheath when bent than it is in a sheath on a cable." This statement is difficult to comprehend. If all other variables are fixed at constant values, then strain per cycle is the common denominator of all laboratory tests. Perhaps reference is made to the possibility for recovery in the strip test I have just discussed. Or, the authors may have in mind the position of the neutral plane in each test with respect to the region of the lead sample subjected to maximum strain. One very real difference between bend tests on strip and cable samples is the tendency for wrinkles to form in the latter. This results in a gradual increase in the magnitude of strain per cycle during the test. Neither of these possibilities has anything to do with the behavior of the internal structure of the metal. Of course, if the alloy is in an unstable condition, straining may promote a reaction in the solid state and a change in internal structure would result. However, such a change would be controlled by the degree of unstability and the amount of strain necessary to promote the reaction, but not by the type of test. Perhaps the authors would like to elaborate on their statement I have quoted above.

There is another point I should like to emphasize in connection with repeated bending tests. What we measure as the bending life is actually the sum of two processes. The first is the time required to nucleate cracks and the second is the time required for crack propagation up to the point of failure. There has been little reported that would satisfactorily distinguish between these two processes. In the case of strip bend tests, the distance cracks must be propagated in one-half the thickness of the strip while in tests involving sheath on a cable, the crack must progress through the entire thickness of the lead. This difference in the fracturing mechanism may to some extent account for differences in test results. It may, however, be partially compensated for by the lower strain gradient through a sheath being tested on a cable. To separate these two processes and to evaluate each would materially increase our knowledge of the fracture of lead and its alloys. It is hoped that such information can be obtained.

The authors have pointed out that in the higher temperature and stress range of testing, the arsenical alloys show a gradual increase in creep rate. This anomaly can be explained by a tendency toward self annealing. However, there is another observation that should not be overlooked and which may be related. The authors state that over a period of time there is a decrease in hardness and in a previous paper (see reference 3 of the paper) it was shown that there was an initial decrease in tensile strength with time. In other words, there is some aging. Is this aging related to the increasing creep rate observed under certain conditions? This is entirely possible because it is a well known metallurgical fact that some solid state reactions are very sluggish and do not occur at all unless induced to do so by deformation of the alloy. This is another of the questions in the general problem of lead

sheath for which an answer would be welcome.

In conclusion, I should like to congratulate the authors on their paper, another step toward a fuller understanding of the fracture of lead and its alloys.

L. F. Hickernell and **C. J. Snyder** (Anaconda Wire and Cable Company, Hastings-on-Hudson, N. Y.): Naturally, we are very pleased to see these data published which, in general, confirm and extend our investigation (authors' reference 3). To discuss completely this paper would exceed the limitations placed upon discussion. Since we have a second paper in preparation, we will confine our discussion at this time to one characteristic; namely, creep. In doing so, perhaps we should point out that our data apply to *F-3* lead alloy as manufactured by us, whereas the authors' paper covers six arsenical alloys produced by as many manufacturers.

In 1946, we suggested a working stress of 200 pounds per square inch. This limitation was imposed due to the lower strength of the sheathing at lead-press stops. In the meantime, this condition has been improved by refinements in the extrusion process. Accordingly, we now recommend 250 pounds per square inch for *F-3* alloy as contrasted with 175 pounds per square inch for "arsenical lead" alloy as established by Association of Edison Illuminating Companies for oil-filled cable (authors' reference 7).

The limiting hoop stress of 175 pounds per square inch is based upon a total creep of 5.5 per cent in 40 years at 50 degrees centigrade; or 0.1375 per cent per year. Accepting these criteria for purposes of discussion, Figure 3 of this discussion shows a comparison of the creep data presented in Figure 3 of the paper with that obtained in our laboratories.

The authors' data were obtained on strips (American Society for Testing Materials dumbbell specimens) which to prepare require a certain amount of cold-working of the metal; that is, flattening the original round sheath, cutting to size, and machining a reduced section.

Our data were obtained on tubes prepared by removing the insulated core from the finished cable. These tubes, 15-inch long, were sealed on both ends with individually-fitted compression clamps. With this method of preparation, the metal was not subjected to cold-working. The tubes were filled with cable oil, enclosed in a constant-temperature cabinet at 110 degrees Fahrenheit (43 degrees centigrade), and connected to a reservoir maintained at 35 pounds gauge pressure. Creep was measured by *SR-4* (modified type *A*) strain gauges, $8^1/_2$-inches long by 1/8-inch wide, cemented around the circumference of the tube near the middle (see Figure 4 of this discussion).

We have conducted tests on strips removed from cable sheaths and found the results were more erratic than with tubes, especially during the first 1,000 hours or so. The more erratic results on strips are possibly caused by straightening of the strips when first placed under load together with a variable amount of strain hardening depending on the grain structure of the individual specimen. Possibly this accounts for the authors' preference to measure creep between 1,000 and 2,000 hours; that is, discounting the creep during the first 1,000 hours. Accordingly, we prefer to evaluate creep on a tube specimen because we believe the results are more indicative of the form in which the material is manufactured and used in service.

In Figure 3 of this discussion, the creep rate of tubes is based upon a test of 2 years (17,250 hours). The rate is determined by the total extension divided by the total time, without allowing for any initial extension (that is, including the first 1,000 hours). The stress is determined from the relation:

$$S = \frac{PD}{2t}$$

where

S = tensile stress, pounds per square inch
P = pressure, pounds gauge
D = inside diameter, inches
t = average wall thickness, inches

Referring to Figure 3 of this discussion: From strip tests, the authors' data show 197 pounds per square inch required to obtain 5.5 per cent total (0.1375 per cent per year) expansion at 43 degrees centigrade. This value is reduced to 175 pounds per square inch to convert to 50 degrees centigrade and "to allow for the decrease in rates of creep which occurs with time".

From tube tests, our data show 303 pounds per square inch is required for the same criteria. In reducing this test value to a recommended working stress of 250 pounds per square inch, we believe we are equally conservative.

In conclusion, we wish to point out that in over 7 years of test, no tubes of *F-3* alloy sheathing have burst at stresses below 1,000 pounds per square inch at room temperature, even though approaching 5 per cent expansion.

L. I. Komives (The Detroit Edison Company, Detroit, Mich.): Apparently, Chicago, New York, Boston, Philadelphia and others have had trouble with cable sheath breaking in manholes due to thermal expansion and contraction. For such conditions, arsenical lead sheath seems to be a better proposition than commercially pure lead.

In Detroit we have not had much trouble from this source. This may be because we had ample training space in our manholes, less loading on our cables, or both. About 20 years ago, we enlarged a number of our manholes and this may have helped conditions. Within the last ten years we reduced the width of our manholes somewhat. According to a chart presented in a recent AIEE Paper,[1] with the new dimensions we are on the borderline of being in trouble with our present manhole design. The chart indicates less than 20 years sheath life at the present loading and for this reason we are definitely interested in the development of higher strength lead sheath. At the present time we cannot justify premium on arsenical lead sheath on a more or less theoretical basis.

In Detroit we have always used asbestos tape fireproofing which is flexible and does not restrain the cable the way cement fireproofing does. We are wondering if the type of fireproofing has anything to do with our record. Flexible fireproofing does help to reduce the sheath strain, according to Clement S. Schifreen.[2]

With the present commercially pure lead cable sheath and joint sleeve, the joint seems to be the weak link in a cable line, its life around 20 years or so on our system. If we use the higher strength alloy sheath for cable, something must be done for the joint sleeve, otherwise its life will decrease. Logically, the same material used in the cable sheath is desirable in the joint sleeve.

REFERENCES

1. CRITICAL INSIDE DIMENSIONS FOR POWER CABLE MANHOLES. **Edward S. Halfmann.** *AIEE Transactions*, volume 69, part II, 1950, Figure 1, page 1577

2. CYCLIC MOVEMENT OF CABLE—ITS CAUSES AND EFFECTS ON CABLE SHEATH LIFE. **Clement S. Schifreen.** *AIEE Transactions*, volume 63, 1944, Table IV, page 1126

Edwin J. Merrell (Phelps Dodge Copper Products Corporation, Yonkers, N. Y.): The authors for many years have encouraged the development of improved lead sheath for power cables and in this paper have made an excellent summary of the status of alloy sheath. I would like to

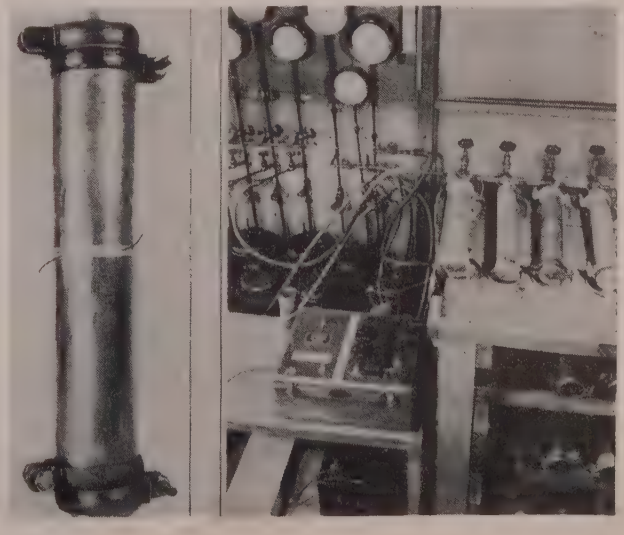

Figure 4. Tube specimen and apparatus for creep measurements

Left—Tube specimen with strain gauge attached
Right — Apparatus for creep measurement

highlight some points touched upon which seem quite pertinent to me, particularly with reference to the arsenic-alloy sheath.

The purpose of alloy sheath is two-fold: To increase flex-life, and to reduce creep.

As the authors have pointed out, the arsenic alloys double or treble flex-life per se. But there is another factor which they mentioned and which I think deserves equal consideration and should be made a standard construction; that is, the use of a paper tape bedding or binder directly under the sheath, instead of the metal binder tape usually employed on 3-conductor cable.

Creep characteristics of arsenic alloys are a function of the heat treatment at the lead press. In general, this factor has been brought under reasonably close control by accumulation of "know-how", together with improved techniques. However, the region of press stops probably will always remain a weak link with respect to creep for cable designs operating under high internal pressure. The only sure way to stabilize this region is to apply sheath reinforcement. We have found a polyethylene jacket very efficient in this respect in tests made at both room temperature and at 52 degrees centigrade. Thus creep tests on copper-bearing sheath which are still in progress up to 1,000 pounds per square inch hoop stress exhibit an increase in life-to-burst of at least 20 to 50 times, with comparable results on arsenic-alloy sheath in tests which have logged more than 20,000 hours.

We should all understand and fully appreciate the fact that the arsenic alloys have about half the elongation to fracture which is the characteristic of copper-bearing lead. Any thoughts along the line of reducing permissible manhole bending radii, such as voiced by the authors, should bear this fact in mind. Bending to a radius of ten times the cable diameter strains the sheath about 5 per cent, which is not critical. However, should the bend not be a uniform curve, but instead be a series of angles, a strain of as much as 40 per cent can be developed locally, which while undesirable for copper-bearing sheath, unfortunately is greater than that often characteristic of arsenic-alloy sheaths under rapid strain. The result can be a sheath crack in the field during initial training.

Incidentally, this matter of elongation necessarily will require consideration in the application of aluminum sheath, as even annealed aluminum sheath presently contemplated exhibits elongation of about 25 per cent to fracture. From the standpoint of manufacturing, the alloy leads, as presently constituted, require operation at the maximum design pressure of the lead presses. This entails considerably more maintenance; also, despite employing maximum pressures the extrusion rates are lower than that customarily obtained on copper-bearing lead.

Herman Halperin and **C. E. Betzer:** The authors appreciate the contributions of the discussers, most of whom have had an active part in the development of the arsenical-lead alloys for use as cable sheathing.

Mr. Atkinson has assisted in replying to Mr. Short's question about the advantages of these alloys in withstanding vibration. Also, Figure 12 of the paper by Hickernell and Snyder (reference 3 of the paper) showed a marked superiority of the *F-3* alloy in ability to withstand vibration. Mr. Short gives no details of the "accelerated vibration tests" that he uses as the basis for his report; if they were like some that have come to our attention, then they are open to question because the tests were so greatly different from service conditions that failures were obtained in about one day or less.

Mr. Burrell has very thoroughly shown the magnitude of the losses that would be present in aluminum sheath on various 3-conductor cables which helps to answer another question from Mr. Short. These losses could be reduced perhaps as low as the losses in lead sheath by the use of aluminum alloys that have high electrical resistance, but the methods that have been developed to produce aluminum sheath on cable have not been successfully demonstrated with such alloys. Mr. Short is correct that when a corrosion-protection jacket is required for lead-covered underground cable, then the necessity of such a jacket when using an aluminum-sheathed cable becomes no disadvantage; however, it should be noted that only a small fraction of the lead-sheathed cables in this country require jackets. Some other disadvantages of aluminum sheaths are its high coefficient of thermal expansion and the necessity to keep bending radii very large which would require large reels and extra large manholes for a conduit system. The further developments of aluminum sheaths will continue to be watched with interest.

In reply to another question by Mr. Short, the lead-alloy sheathing should prove advantageous in withstanding the pressures in low- and medium-pressure, gas-filled cable without covering over the sheath. The advantages would be to permit greater pressures without the added cost of reinforcing coverings. This applies to such cable which is installed in conduit.

Mr. Short emphasizes a point in the introduction of our paper, namely, that lead sheaths have some short-comings and an improved sheathing material is needed. The operating experiences with lead-covered cable plus the presented information on arsenical-lead-alloy sheaths show that such alloy sheaths can "sustain the modern cable under contemporary loading practice" for the expected life of about 40 years. Of course, some trouble due to mechanical injury, corrosion, and other external causes can be expected with any kind of sheath.

We agree with Dr. Wiseman in his preference for retaining about the same thicknesses for alloy sheath as for lead sheath on oil-filled and gas-filled cables and using the advantages of higher permissible internal pressures and better life in bending with higher-ampere loading.

Dr. Wiseman shows an interesting device to strengthen the sheath adjacent to the joint which the authors want to try. The cracking of the sheaths in the manholes in service is not, however, nearly so concentrated adjacent to the joints as it is in the dummy-manhole tests. In fact, a considerable number of cracks are developing far back in the ducts on long lengths of cable, as well as in the bends in the manholes. To decrease the bending adjacent to the joint wipe, by use of such reinforcing will increase the action at other locations and might necessitate larger manholes to accommodate the joints which are thus lengthened.

As suggested by Dr. Eckel, the relation between strain at the point at which the sheath fractures and life to fracture is probably the same for sheath on either belted or shielded cable. On cable containing metal shielding tapes, the strain for given cable movement is increased over the edges of such tapes so that the life of the sheath for given load cycles is less than that for sheath on belted cable.

In the bend tests of strips, the motion was in 70-second cycles which contained a brief pause at each end of the stroke. The effect of these pauses on the results of the tests is not known, but will be investigated.

In reply to Dr. Eckel's question, the difference in bending action on strips and on sheath on cable that is mentioned in the paper is the difference in neutral planes about which the action takes place. Tests have been made on the same material in strips and in cable sheath samples, and the results for equal strains by the two methods were found to be not directly comparable.

The phenomenon of the creep rates for the alloys to increase with the duration of the tests at the higher stresses and temperatures did not appear to be due to aging. The increasing rates occurred rather generally at 300 pounds per square inch and 150 degrees Fahrenheit and occasionally at 200 pounds per square inch and 150 degrees Fahrenheit. Decreasing creep rates in the later periods of a given test were generally indicated at 150 pounds per square inch and 150 degrees Fahrenheit, and at all three stresses at 110 degrees. The aging for these various conditions was the same.

Messrs. Hickernell and Snyder show considerably greater resistance to creep for their *F-3* lead alloy than is indicated in our average data. It does not appear probable to us that this difference in results is due primarily to the difference between strip specimens and tubes. In some cases, parallel tests have been made at the University of Illinois on the same material on 6-foot samples of cable with internal pressure producing about 300 pounds per square inch hoop stress and on strip specimens with the same tensile stress. As stated in the paper, the rates of creep for the cylindrical sheaths were in some cases slightly less than those for the strip specimens, but the difference was slight and in some cases the reverse was true in the tests at 150 degrees. (See Figures 10 and 11 of reference 7 of the paper.) Rates of creep measured at various locations along the 6-foot samples of cylindrical sheath were as variable as those for strips. Measurements made within six inches of sealed ends gave relatively low creep rates in many cases. We wonder whether their tests on 15-inch samples are partly due to the use of *SR-4* strain gauges which we consider rather unsuitable for this type of test. It is possible that later we will recommend a higher tensile limit than 175 pounds per square inch for arsenical-lead alloy, especially in view of the progress being made in controlling the uniformity of such sheaths.

As stated by Mr. Komives, stronger sheath on solid-type cable in which the pressures are not controlled will develop higher internal pressures when the cable is heated. Such pressures might require that the joint sleeves be strengthened. Two-piece lead sleeves with a solder wipe at the middle are

being used in Chicago on 12-kv joints. It is believed that arsenical-lead alloy sleeves would be better.

In reply to Mr. Komives, it does not appear to us that the difference in rates of sheath cracks in Chicago and in Detroit is due to a difference in fireproof covering on the cables in the manholes. For the last three years, the fireproofing used in Chicago has consisted of asbestos tape. Before that, a soft cement was used over a layer of asbestos tape. Tests have indicated that neither of these coverings has an appreciable effect on the life to fracture of the sheath.

Regarding Mr. Komives' remarks on not having much trouble with cracking of cable sheaths in manholes, a number of years of operation at increased loading is required before sheath cracking in manholes (and in ducts) appears. Studies made by various utilities have developed considerable background data to enable one to forecast the life of commercially-pure lead sheaths in manholes, and such studies frequently indicate a life to cracking with common operating conditions of only 10 to 20 years. (The authors know of one utility where numerous cracks recently occurred on one line, having copper-bearing lead sheaths and small offsets in the manhole, after only about five years of service.)

American manufacturers now have available lead alloys and well-developed means of applying them which at least triple the life of the sheath in service, thereby giving a balanced cable design for long service, and the additional cost of a few per cent for using these alloys is usually only a small fraction of the economic gain to the users. This is particularly true in order to obtain economic utilization of the larger underground cables through increased loading.

Aging of Class-B Insulating Material in Nitrogen

H. C. STEWART
MEMBER AIEE

L. C. WHITMAN
MEMBER AIEE

VERY little data have been published on thermal performance of class-*B* insulation since the creation of the definitions for such materials and the establishment of their permissible operating temperatures as set forth in the standards.[1,2] Definitions of such materials are very loose, and the long established rules for operating temperatures are vague.

By way of review, class-*B* insulation materials are defined as aggregates of inorganic materials, such as mica, glass, or asbestos bonded with organic resin. The resins used in class-*B* materials, although they are heat resisting, are class *A* by definition. Nevertheless, such resins are utilized to give both mechanical and electrical properties to composite class-*B* insulation. In contact with inorganic materials, they apparently withstand higher temperatures than when in contact with cellulose, but it is this essential organic bonding material which deteriorates with time and temperature.

Previous Work on Aging of Insulation

Many years of tedious study on class-*A* materials under oil have given answers as to life and laws of aging that are roughly confirmed by operating experience. The approach with class-*A* materials[3] was through measured degradation of some mechanical property, usually tensile strength. No such background existed on class-*B* materials. A method of determining the probable life of various materials of this class was described by the authors.[4] It was shown that the dielectric strength decreased progressively and consistently with time and temperature and, hence, results obtained at high temperatures in short time could be extrapolated to low temperatures, and the governing laws, life versus time, determined much as with class-*A* materials.[3] Since change in dielectric strength is even more important fundamentally than change in mechanical strength, this method has been employed for the further study of the aging of class-*B* material in nitrogen gas.

New Work on Aging of Class-B Insulation

Data are presented here on insulation, aged in nitrogen, subjected to temperatures in excess of presently established operating levels. From these data, extrapolation can be made to indicate anticipated life at any chosen operating temperature. The results shown here indicate the maximum life which can be expected from insulations when maintained continuously at a given temperature. In these tests, as with oil-sealed apparatus, there was no possibility of contamination by dirt or moisture absorption.

Materials Investigated

Commercial grade of asbestos sheets

Thickness—15 mils
Impregnant—Temperature resisting phenolic resin
Cooling medium—Nitrogen at 5 pounds gauge pressure.

Fiber Glass Yarn

Thickness—20 mils
Impregnant—Temperature resisting phenolic resin
Cooling medium—Nitrogen at 5 pounds gauge pressure.

These materials are representative of some of the class-*B* insulation used as winding material, insulating barriers, and cylinders in electric equipment. The curing time and temperature for test pieces are those recommended by the manufacturer for curing the heat-resisting phenolic resin used. The test pieces then were subjected to final life test.

Testing Technique

The samples were tested in a gas chamber as shown in Figures 1 and 2. Reference should be made to the previous paper[4] for details of sample preparation and complete testing procedure and measurement technique. Insulated electrodes leading from the gas chamber allow the application of current for supplying internal heat, and permit temperature measurements and dielectric test at operating temperatures. The gas pressure was maintained at 5 pounds gauge to insure the purity of the nitrogen gas by preventing the entrance of contaminants into the gas chamber.

Criterion of Life of Insulation Operated in a Gas

As formerly proposed,[4] the end of expected life of insulation when operated in a gas medium can be considered as reached when its final hot dielectric strength has decreased to 50 per cent of the initial value with a given temperature maintained. This is an entirely arbitrary selection but may well represent the end of life when the more severe operating conditions such as lightning, switching surges, and short circuit are considered in electric equipment.

Results

The solid-line graph shown in Figure 3 gives the life characteristics of impreg-

Paper 51-69, recommended by the AIEE Rotating Machinery, Standards, and Transformers Committees and approved by the Technical Program Committee for presentation at the AIEE Winter General Meeting, New York, N. Y., January 22–26, 1951. Manuscript submitted October 24, 1950; made available for printing December 5, 1950.

H. C. STEWART and L. C. WHITMAN are with the General Electric Company, Pittsfield, Mass.

Figure 1. Chamber for testing insulation pieces in nitrogen

Figure 2. Chamber for testing insulation pieces in nitrogen (cover removed)

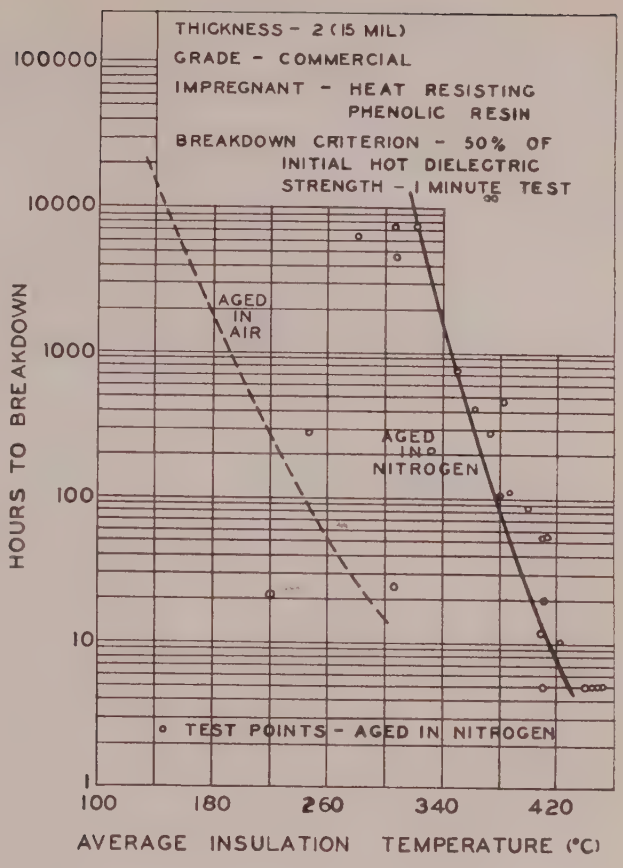

Figure 3 (right). Life characteristics—asbestos sheets

nated asbestos sheets aged in nitrogen gas. It is to be noted that this graph is plotted with the hours to breakdown on the logarithmic vertical axis, but that the average insulation temperature is plotted on the uniform horizontal axis with an evenly divided scale. For a convenient reference, the aging of samples of the same material in air is shown in Figure 3 as the dotted line at the left of the graph.[4] The results of these data are of great interest and show that class-*B* insulation operated in nitrogen gas can give comparable life at considerably higher temperature than is permissible for such material in air.

Tests are incomplete but life characteristics of impregnated glass yarn seem to follow the same pattern as the tests on asbestos. In other words, much longer life can be expected of glass yarn aged in nitrogen. As was to be expected where resin is the dominating factor, higher initial dielectric strengths were obtained in nitrogen. This is no doubt due to slower oxidation and the exclusion of moisture and other contaminants.

Conclusions

1. The method of evaluating the life characteristics of class-*B* material operating in nitrogen yields results consistent with the data formerly obtained on such materials in air.

2. The so-called "degree rule" (degrees increase in temperature to reduce life 50 per cent) for asbestos aged in nitrogen is approximately 10 degrees centigrade in the temperature range investigated.

3. The data indicate that class-*B* materials operated in nitrogen can be safely operated at the 180 degrees centigrade temperature now assigned to class-*H* materials. This is very important since it permits the building of completely sealed electrical equipment with the less expensive class-*B* material in place of class-*H* material.

4. These data would indicate a need for recognition in standards of the influence of the surrounding medium on the life of the present class-*B* insulations.

References

1. Standards for Transformers, Regulators, and Reactors. *C57.11—1948*, American Standards Association (New York, N. Y.), 1948.

2. Introduction to AIEE Standards, AIEE Standard Number 1, June 1947.

3. Preliminary Report on Laboratory Aging Tests on Class A Insulation. **AIEE Committee Report.** *AIEE Transactions*, volume 66, 1947, pages 879–83.

4. Aging of Dry-Type Transformer Insulation, **H. C. Stewart, L. C. Whitman.** *AIEE Transactions*, volume 67, 1948, pages 1600–07.

Discussion

T. R. Walters (General Electric Company, Pittsfield, Mass.): The authors again have added substantially to the available technical data on aging characteristics of class-*B* insulations. Their conclusion (3) that "The data indicate that class-*B* materials operated in nitrogen can be safely operated at the 180 degrees centigrade temperature now assigned to class-*H* materials" is a very important one, and one which opens up a new field of application for class-*B* insulation.

Life testing of class-*A* insulations has been admittedly very time-consuming and arduous, but data obtained in this series of tests points the way to much more rapid and accurate evaluation of the life of class-*B* materials. In view of the importance of this class of insulation to the whole electrical industry, it is essential that this type of study be intensified so that the full possibili-

ties of class-*B* insulation can be realized.

T. W. Dakin, in a 1948 paper,[1] implied the advantage of operation in an inert atmosphere when he pointed out that, along with other factors, the presence or absence of an oxidizing atmosphere would have an effect on the chemical changes which take place in an insulation, and then mentioned that the most common form of deterioration is slow oxidation. The authors of this paper have put some essential numbers on this factor.

REFERENCE

1. ELECTRICAL INSULATION DETERIORATION TREATED AS A CHEMICAL RATE PHENOMENON, **Thomas W. Dakin.** *AIEE Transactions*, volume 67, part I, 1948, pages 113–22.

E. L. Brancato (Naval Research Laboratory, Washington, D.C.): The authors have provided useful aging data for class-*B* insulation where the insulation is employed on equipment subject to lightning surges. However, the aging curves, Figure 3 of the paper, would not be applicable to electric equipment where failures result from physical disintegration of the insulation.

Class-*B* insulation consists of an inorganic material held in place by an organic binder. Because the ratio of the dielectric constants of the two materials vary from one-fifth to one-half (where the lower dielectric constant is associated with the organic binder) the dielectric test places the greater stress on the class-*A* binder. But even assuming equal distribution of stresses on the inorganic and organic components of the insulation, a finite reduction in the dielectric constant is an index of chemical change and not of the mechanical deterioration of the binder.

For electric equipment not subject to large electric surges, the ultimate criterion is mechanical failure. It is appreciated that class-*B* insulation does not lend itself to the direct measure of mechanical deterioration as for class-*A* insulation, because the inorganic components do not rupture at the aging temperatures employed. However, humidity can be used as a searching agent of rupture. The penetration of the aqueous film through the insulation can be sensed by the flow of current between the insulated conductor and ground resulting from the application of a moderate voltage between conductor and ground.

W. W. Satterlee (Westinghouse Electric Corporation, Sharon, Pa.): The authors are to be complimented on their presentation of a subject which is important, but not new, since it has been known for a long time that organic insulating materials may be operated at higher temperatures in an inert gas such as nitrogen with less deterioration than in air. For instance, the mechanical and the dielectric life of the materials used in liquid immersed transformers are greatly improved when protected with an atmosphere of nitrogen instead of air.

The paper makes reference to the use of class-*A* resins as bonds of class-*B* insulating materials and states that the resins are used to give both mechanical and electrical strength to the composite class-*B* insulation. This also is true of most composite class-*H* materials because few inorganic substances can be used satisfactorily as bonds. The apparent ability of class-*A* resins to withstand higher temperatures in contact with inorganic materials than when in contact with cellulose is likely due, at least in part, to the reduced amount of mechanical breakdown of the inorganic materials at the higher temperature.

While it may be true that relatively little information exists as to the life and laws of the aging of composite class-*B* materials, such information does exist on the binders, class-*A* substances, commonly used in class-*B* insulating materials. It seems questionable that an arbitrary change in the hot dielectric strength of class-*A* bonds as an end point of the expected life of the composite insulation is more important fundamentally than a change in mechanical strength. After all, class-*B* and even class-*H* insulating materials normally are used in electric apparatus whose major insulation is air and whose dielectric strength is largely, if not wholly, limited to the atmosphere in which it is expected to operate.

Much laboratory work on class-*B* and class-*H* insulating materials combined with the operation of hundreds of large dry-type transformers during the last 14 years, indicates that the criteria of long operating life may well be the mechanical strength of their insulating structures, with the dielectric strength depending on nothing more than the gas space separation in their winding structures.

Since the writer was responsible for the development of a line of large sealed dry-type transformers in 1942, and since nearly 100 of these transformers have been built with both class-*B* and class-*H* insulation structures and to operate filled with nitrogen, I can agree largely with the conclusions of the authors as to the value of excluding air.

However, it must be borne in mind that if the increased life of the insulation in the apparatus operating at the higher temperatures is dependent upon the nitrogen atmosphere, then this atmosphere must be maintained continuously. Also, if the data given in the paper would indicate a need for recognition in standards of the influence of the surrounding medium on the life of class-*B* insulations, so is there a need for similar recognition on the life of class-*H* insulating materials.

M. L. Manning (Pennsylvania Transformer Company, Canonsburg, Pa.): This paper presents data for tests made in nitrogen atmosphere on 15-mil commercial-grade asbestos sheets and on 20-mil fiber glass impregnated with phenolic resin. In the conclusions, the authors state that the data for tests indicate class-*B* materials operated in nitrogen can be operated safely at the 180 degrees centigrade temperature now assigned to class-*H* materials and that this is very important, since it permits the building of completely sealed electric equipment with the less expensive class-*B* material in place of class-*H* material. Three questions arise in reviewing the paper from the standpoint of applying these ideas concerning materials to transformers of sealed construction:

1. What percentage of phenolic resin was used compared with the base sheet thickness of asbestos and of fiber glass sheets? In other words, was the evaluation made mainly on phenolic resin or on fiber glass and asbestos materials?
2. Have the composite insulating materials of a transformer, such as wire covering, barriers, laminates, and impregnating varnish, been evaluated? The final evaluation of insulating materials comes about in the complete insulation structure of a transformer, where these materials are subjected to varied conditions for voltage creep and puncture and thermal requirements. It would be helpful to know if these conditions have been considered.
3. The third question concerns reliability. If nitrogen leakage occurs, the advantages outlined in the paper become questionable. We know that class-*H* insulation compared with class-*B* insulation has at least three outstanding advantages under different atmospheric conditions:

1. Moisture repellency
2. Heat stability at elevated temperatures
3. High thermal conductivity

In service, the possibility exists that nitrogen in some manner might escape subjecting the class-*B* insulation ultimately to atmospheric conditions. Has consideration been given to the problem of nitrogen leakage and its replacement by air?

H. C. Stewart and **L. C. Whitman:** Mr. M. L. Manning raises various questions concerning application of some of the ideas in this paper to transformers of sealed construction.

The amount of phenolic resin used in conjunction with the asbestos was approximately 40 per cent by weight of the total insulation. In the case of fiber glass, the percentage was approximately 20 per cent. Aging and temperature-resistance characteristics of an insulation are affected by the base material as well as the impregnant. This is obvious when it is realized that this is the basic difference between class-*A* and class-*B* materials. Thus, while the percentage of resin is a factor both in initial strength and life characteristics, the aging of a combination of base material and resin can be determined only by testing the combination, not by evaluation of the resin only, as Mr. Manning suggests.

The fiber glass-resin combination tested represents one generally used for wire covering. The asbestos-resin combination represents cylinders and some forms of barriers or laminations. The basic forms of dry-type insulation therefore were represented. The tests were made with dielectric puncture as the criterion. However, creepage also was present, and if there had been dangerous deterioration of this characteristic, it would have made itself known through failure by this means instead of by puncture.

Thermally, the temperatures considered were given as the average temperature of the insulation. The insulation tested was subjected to normal temperature gradients by virtue of heating the mandrel upon which the sample of insulation was wound. This gave the effect of normal temperature drop through the insulation as in a transformer, which is more representative than maintaining the entire insulation sample at the

same temperature, which would have been the case in oven tests.

Sealed dry-type transformers basically require a high quality of sealing. This is necessary not ony to maintain purity of filling medium, but also as regards the exclusion of moisture. In liquid-filled transformers, it is well known that either free breathing or complete sealing is required and that a middle ground is hazardous in that moisture will be accumulated with each temperature cycle and only a small percentage will be expelled. The basic reasons for sealing dry-type transformers are to eliminate the dirt and moisture problems associated with open dry-type units. Hence, any small differences in moisture-repellency characteristics, even if established, are unimportant.

It is believed that the really tremendous temperatures to which the class-*B* insulations were subjected establishes their heat stability when operated in nitrogen. The margin at 180 degrees centigrade appears to be very adequate.

In regard to thermal conductivity, we would point out that the base material in either class *H* or class *B* are the same. The thermal conductivities hence will be of the same order of magnitude. Also, in sealed dry-type transformers, the rise of the coils over the gas insulating medium is only about half that of open units, since in sealed dry-type transformers major thermal drops also exist between the gas and the tank, as well as between the tank and the outside ambient. Radial gradients in windings of natural draft transformers also are small compared to air film drop, so the net result is that even large differences in resin conductivity will result in very minor over-all improvement in thermal characteristics.

Mr. T. R. Walters is particularly qualified to speak on class-*B* materials, as he directed the development of the class-*B* material originally named Terratex, which was described by him in 1948,[1] and is now commercially available under the name Quinterra.

The reference to Mr. T. W. Dakin's paper (see Mr. Walters's discussion of the present paper) brings out the point that operating insulation in nitrogen practically eliminates the chemical deterioration caused by oxidation, which Mr. Dakin lists as the most common form of deterioration. The eventual decrease in electrical strength then must be chemically explained by evaporation of some of the constituents or else by purely thermal or internally catalyzed depolymerization of portions of the insulation. These chemical actions proceed at a slower rate than oxidation at any given temperature, which would logically explain the very considerable advantage of a nitrogen medium.

We are in full agreement that further intense study is needed to extend the understanding and economical application of class-*B* insulation to electric equipment.

Mr. E. L. Brancato points out that the criterion used in these tests was electrical rather than mechanical. It thus may be desirable to check the physical strength of the insulation for applications, such as motors, when there may be severe and continued vibrations of considerable magnitude. The authors would like to point out, however, that even in the case of the highest temperatures used, the insulations had a remarkable percentage of mechanical strength remaining as determined from visual examination and flexing.

The suggestion was made that a larger dielectric stress was placed on the class *A* binder than on the inorganic portions because of the lesser dielectric constant of the class *A* binder. This would be true if the binder were in layers with the inorganic material between, for example, in a surface coat only. However, in the given case, the materials were vacuum-impregnated, making the binder an integral part of the insulation. In effect, this places the binder in parallel with the inorganic base. Thus, all components are under essentially equal dielectric stress irrespective of dielectric constant. No measurements of dielectric constant were made during the tests; dielectric strength only was used as a criterion.

Mention is made of the use of humidification followed by a moderate voltage to search out cracks or regions of rupture. The authors believe that the application of a voltage large enough to break down the gas film remaining in any void is to be preferred. No reliance on capillary action or time delay is necessary when this method is used. The 50 per cent of initial breakdown voltage used insured that any crack would be searched out and a failure established. If the criterion had been reduced to 25 per cent of initial breakdown voltage, there might have been a question of voltage sufficient to break down the gap. However, even in this case, the situation has its own automatic warning, since no breakdowns would be obtained and tests would give no data. The requirement of humidification also has the drawback of requiring tests to be made at or near room temperature and not at operating temperature, where dielectric strength is almost invariably less.

Mr. W. W. Satterlee points out that it has been known for some time that organic insulating materials will deteriorate less in nitrogen than in air. The facts that the authors have brought out are that, first, this is true not only for organic materials, but for combinations of organic with inorganic, that is, class-*B* materials; and, secondly, some quantitative data have been presented allowing some practical application of this idea.

It is true that some portion of the dielectric strength of dry-type transformers is contributed by the gaseous medium they are in. However, a very considerable portion of the electrical strength can and should be built into the insulation structure of such apparatus. Turn insulation, phase barriers, and cylindrical coil barriers all contribute to the strength required for satisfactory operation to withstand not only normal operating voltages, but overvoltages occasioned by switching surges and impulse voltages. Even acceptance tests could not be made with reliance only on air insulation. Certainly, then, we must be sure we maintain the quality of these insulations so that the apparatus remains at a sufficiently high dielectric level to withstand these overvoltage conditions. Thus, a measure of this ability to withstand voltage is a necessary and valuable criterion of the life of such apparatus.

Mechanical strength is also, of course, required and its maintenance is of prime importance. Some correlation of mechanical and electrical deterioration has been made for operation of class-*B* insulations in air. No quantitative measurements of mechanical strengths were made as part of this study. We would expect, however, that electrical strength would be much more sensitive to deterioration to temperature than mechanical strength. Therefore, the electrical criterion would be the weaker link and would govern the expected life.

We are glad to have the independent confirmation that field experience gives favorable evidence to the value of excluding air from such apparatus.

The question of whether class-*H* insulations also benefit by operation in nitrogen would perhaps be given a rough answer by whether or not silicones react with oxygen. There seems to be evidence that there is such a reaction, but, of course, at higher temperatures and slower rates than with organic resins. A factual answer can be given only with tests similar to those already made using insulation both in air and in nitrogen with silicone impregnants. Recognition in the standards of improvement of class-*H* insulations operated in nitrogen cannot be given until sufficient data to show improvement have been published. In the case of class-*B* insulations, however, this paper does give data on improvement than can be expected when changing the medium from air to nitrogen. The large improvement, together with the considerable economic advantage, demonstrates the need for recognition in the standards of the influence of the surrounding medium on the insulation life and consequently on the allowable operating temperature of such a combination.

Reference

1. "Terratex"—A Thin Flexible Inorganic Insulation, **T. R. Walters.** *AIEE Transactions*, volume 67, part I, 1948, pages 123–27.

Economics of Power Transformer Application

J. E BARKLE
MEMBER AIEE

R. L. WITZKE
MEMBER AIEE

THE SELECTION of power transformers for generating stations and substations requires a detailed study of a large number of factors. Many economies can result from a correct choice of transformer type and characteristics; however, each application must be considered on its own merits. Conclusions reached regarding transformers for one location on a system may not apply on another system, or at another location on the same system.

The purpose of this paper is to review some of the factors that should be considered in making a power transformer application. The major factors discussed in this paper are as follows:

1. Comparison of single-phase and 3-phase transformers
2. Transformer insulation level
3. Types of cooling
4. Selection of method of cooling

Comparison of Single-Phase and 3-Phase Transformers

A 3-phase power transformation can be accomplished by a 3-phase transformer or by three single-phase units. The 3-phase unit has the advantages of greater efficiency, smaller size, and a lower installed cost when compared with a bank made up of single-phase units. The floor space required for a bank of single-phase transformers can approach twice the area required for a single 3-phase transformer. The increased bay size necessary for the single-phase units can result in a considerably higher installed cost when all factors are considered, particularly in locations where space is at a premium. This factor must be evaluated for each application because space limitations will vary between locations. The more involved connections to a bank of single-phase transformers complicate the bus structure, further increasing the installation costs chargeable to the transformers.

The choice between single-phase and 3-phase transformers is influenced to some extent by the need for spare capacity. When three single-phase units are used in a bank, it is possible to install a fourth unit at the same location as an emergency spare. However, transformers have a proved reliability higher than most other elements of a power system, and for this reason the need for immediately available complete spare capacity often is questionable. Three-phase units are used quite generally today with no on-the-spot spare transformer capacity. In these cases parallel or interconnected circuits of the system may provide emergency capacity or, for small and medium-size transformers, portable substations can provide spare capacity on short notice.

The ever-present demand for better service reliability and the consequent changes in system design have had a major influence on the selection of 3-phase transformers in distribution substations. In many applications, particularly in distribution substations serving radial subtransmission or distribution circuits, the use of a fourth single-phase transformer as a spare is not considered satisfactory unless several banks are used in the station. The time required to switch the spare into service manually often rules out this method of providing spare capacity. If the spare capacity must be in service, normally, the same spare capacity is required with either single- or 3-phase transformers.

Many factors in system design have decreased the dependence on any one transformer bank for maintaining service continuity. Examples are the unit system design in generating stations and the primary network system. These factors have contributed to the trend toward the general use of 3-phase transformers.

Handling and shipping limitations made it necessary to use single-phase transformers for many applications just a few years ago. Transformer developments, including improved steel, the form-fit construction, and forced cooling, have contributed to a radical reduction in weights and dimensions. Today, all but the very largest ratings can be built and shipped as 3-phase units.

Transformer Insulation Level

The basic insulation levels of power transformers having full insulation are given in column 2 of Table I. These levels should be used unless special study shows that a lower insulation level can be protected adequately against surge voltages. At locations where 75 or 80 per cent lightning arresters can be applied close to the transformer, important economies can be realized by reducing the transformer insulation level one class, as indicated by the basic insulation levels in column 3. These applications require a complete study of the transformer surge protection. First, it is necessary to estimate the maximum dynamic voltages to ground at the transformer location during normal and abnormal conditions. These voltages should never exceed the rating of the lightning arrester selected. If these studies show that the 75 or 80 per cent lightning arrester can be applied with safety, the second step is to determine the maximum permissible distance between the lightning arrester and the transformer. The data in

Paper 51-70, recommended by the AIEE Transformers Committee and approved by the AIEE Technical Program Committee for presentation at the AIEE Winter General Meeting, New York, N. Y., January 22–26, 1951. Manuscript submitted October 24, 1950; made available for printing December 18, 1950.

J. E. BARKLE and R. L. WITZKE are both with the Westinghouse Electric Corporation, East Pittsburgh, Pa.

Table I. Power Transformer Basic Insulation Levels

System Voltage, Kv	Transformer BIL, Kv Full Insulation	Insulation Reduced One Class
115	550	450
138	650	550
161	750	650
230	1,050	900
287	1,300	1,050
345	1,550	1,300

Table II illustrate the influence of the transformer basic impulse level (BIL) and the lightning arrester rating on the permissible distance between a 138-kv transformer and the lightning arresters. These data were taken from Tables II and III of a paper by R. L. Witzke and T. J. Bliss,[1] and are based on the following assumptions (see Figure 1):

1. The transformer is located at the end of a single overhead transmission line.
2. The lightning arrester is connected to the bus through a *T*-tap with a maximum of 35 feet of lead between the lightning arrester and the bus.
3. The overhead line is of steel-tower construction with a maximum of ten suspension insulators.
4. Protection is provided for a 500-kv per microsecond surge arriving at the station over the overhead line.
5. Station ground resistance is neglected.

The distances in Table II are measured between the transformer bushing and the lightning arrester connection to the bus (distance s in Figure 1). It will be noted that the permissible separation distance is approximately the same for the reduced-insulation transformer protected with a 117-kv lightning arrester as for the 650-kv transformer with a 145-kv ungrounded neutral lightning arrester, indicating that the protection for these two cases is comparable. Reducing the lightning arrester rating to 111 kv increases the permissible distance from 45 to 60 feet for the case involving reduced transformer insulation.

The relative distances of 133 and 45 feet, for the 650 BIL protected with a 121-kv lightning arrester and the 550 BIL protected with a 117-kv lightning arrester, illustrate in a definite manner the need for having the lightning arrester closer to the transformer when reduced insulation is used.

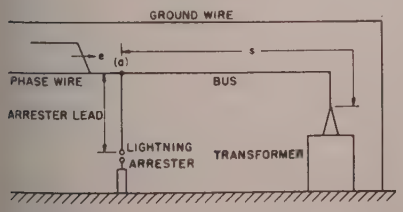

Figure 1. Circuit used in determining permissible distances between lightning arrester and transformer

The savings that result from decreasing the transformer insulation level one class on systems operating at 110 kv and above are very attractive and will more than justify the additional engineering time required to determine whether or not the reduced insulation can be protected adequately against surge voltages. Further savings may be possible at 230 kv and above by reducing the transformer insulation more than one step. For example, the industry is giving consideration to an intermediate basic impulse level of 825 kv, which is one and one-half steps below the 230-kv insulation-class basic impulse level of 1,050 kv. Some operating companies are satisfied that transformers having this basic level can be protected adequately with lightning arresters applicable to well-grounded 230-kv systems. The results of the investigation reported in the paper referred to previously[1] show that comparable protection is obtained with a 100 per cent lightning arrester and a 1,050-kv basic impulse level, and a 75 per cent lightning arrester and an 825 kv basic impulse level. The 75 per cent lightning arrester application, however, requires special study.

Types of Cooling

The basic types of cooling are designated as follows:

OA—Oil-Immersed Self-Cooled. In this type of transformer the insulating medium circulates by natural convection through external radiators.

OA/FA—Oil-Immersed Self-Cooled/-Forced-Air Cooled. This type is basically an OA unit with the addition of fans to increase the rate of heat transfer from the cooling surfaces, thereby increasing the transformer rating. The higher capacity attained by use of fans is dependent upon the self-cooled rating of the transformer and may be calculated as follows:

For 2,500 kva (OA) and below: kva (FA) $=1.15\times$kva (OA)

For 2,501 to 3,332 kva (OA): kva (FA)$=$ $1.55\times$kva (OA)$-1{,}000$

For 3,333 kva (OA) and above: kva (FA) $=1.25\times$kva (OA)

OA/FA/FOA — Oil-Immersed Self-Cooled/Forced - Air - Cooled/Forced-Oil Forced - Air Cooled. The rating of an oil-immersed transformer may be increased from its OA rating by the addition of both fans and oil pumps.

Table II. Influence of Transformer BIL and Lightning Arrester Rating on Permissible Distance between Transformers and Lightning Arresters that Might be Applied on a 138-Kv System*

Transformer BIL, Kv	Lightning Arrester Rating, Kv	Maximum Distance, Feet
650	145	44
	121	133
550	117	45
	111	60

* See text for conditions assumed in the preparation of this table. The distances given are based on adequate line and station shielding.

These triple-rated transformers usually are built only in ratings of 10,000 kva (OA) and above. The maximum kilovolt ampere rating, with both fans and pumps in operation, is 1.67 times the OA rating. If the transformer is operated at the intermediate rating, using fans but no pumps, the kilovolt ampere rating is 1.25 times the OA rating. Automatic controls responsive to oil temperature normally are used to start the fans and pumps in sequence as the transformer load goes up. In some applications part of the pumps and part of the fans are started when the load exceeds the transformer self-cooled capability. This operation decreases the hot spot to average winding temperature gradient over that obtained with fans and no forced circulation of the oil.

FOA — Oil - Immersed Forced - Oil-Cooled with Forced-Air Cooler. This type of transformer is intended for use only when both oil pumps and fans are operating, under which condition any load up to full-rated kilovolt ampere may be carried. Some designs are capable of carrying excitation current with no fans or pumps in operation, but this is not universally true. Heat transfer from oil to air is accomplished in external oil-to-air exchangers.

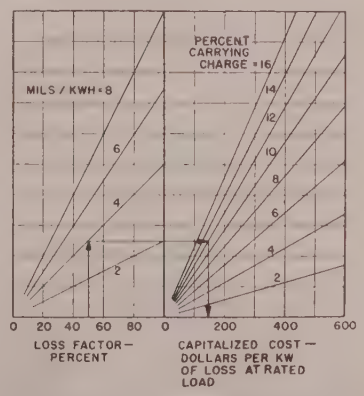

Figure 2. Chart for estimating capitalized cost of losses

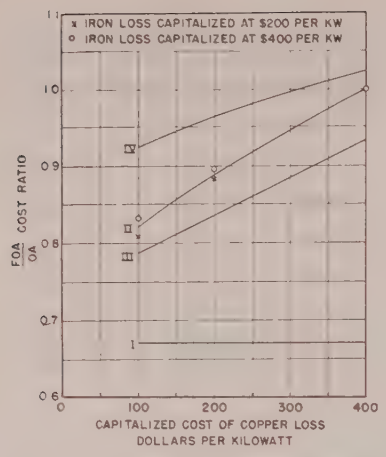
x IRON LOSS CAPITALIZED AT $200 PER KW
o IRON LOSS CAPITALIZED AT $400 PER KW
FOA/OA COST RATIO
CAPITALIZED COST OF COPPER LOSS
DOLLARS PER KILOWATT

Figure 3. Capitalized cost of 100,000-kva, 138-kv, 3-phase FOA transformer expressed in per unit of capitalized cost of corresponding OA transformer

I. Transformer selling price
II. Selling price and capitalized losses
III. Installed cost and capitalized losses
IV. Installed cost, and capitalized losses and reactive

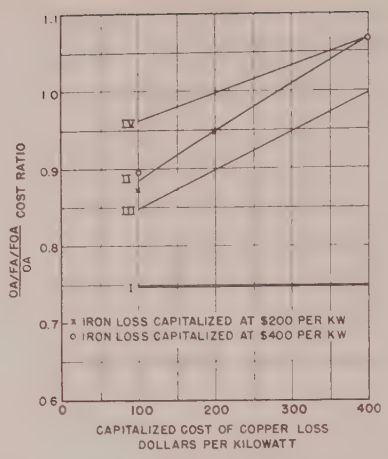
OA/FA/FOA/OA COST RATIO
x IRON LOSS CAPITALIZED AT $200 PER KW
o IRON LOSS CAPITALIZED AT $400 PER KW
CAPITALIZED COST OF COPPER LOSS
DOLLARS PER KILOWATT

Figure 4. Capitalized cost of 100,000-kva, 138-kv, 3-phase OA/FA/FOA transformer expressed in per unit of capitalized cost of corresponding OA transformer

I. Transformer selling price
II. Selling price and capitalized losses
III. Installed cost and capitalized losses
IV. Installed cost, and capitalized losses and reactive

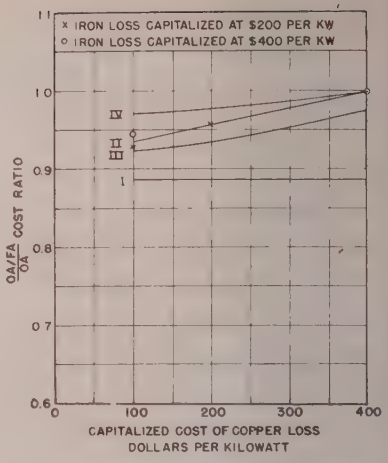
x IRON LOSS CAPITALIZED AT $200 PER KW
o IRON LOSS CAPITALIZED AT $400 PER KW
OA/FA/OA COST RATIO
CAPITALIZED COST OF COPPER LOSS
DOLLARS PER KILOWATT

Figure 5. Capitalized cost of 100,000-kva, 138-kv, 3-phase OA/FA transformer expressed in per unit of capitalized cost of corresponding OA transformer

I. Transformer selling price
II. Selling price and capitalized losses
III. Installed cost and capitalized losses
IV. Installed cost, and capitalized losses and reactive

OW—Oil-Immersed Water-Cooled. In this type of water-cooled transformer, the cooling water runs through coils of pipe which are in contact with the insulating oil of the transformer. The oil flows around the outside of these pipe coils by natural convection, thereby effecting the desired heat transfer to the cooling water. This type has no self-cooled rating.

FOW—Oil-Immersed Forced-Oil-Cooled with Forced-Water Cooler. External oil-to-water heat exchangers are used in this type of unit to transfer heat from oil to cooling water; otherwise the transformer is similar to the FOA type.

Selection of Method of Cooling

The selection of the method of cooling that should be used must be based on a complete engineering study, each application being considered on its own merits. The following factors may have an important influence on the choice of cooling: selling price, loss evaluation, installation costs, reactive evaluation, emergency capacity, and impedance.

Selling Price. The most important factor in the selection of the cooling method is the selling price of the transformer. Table III illustrates the relative costs of the six major types, based on approximate selling prices of 138-kv 3-phase transformers having 115-kv class insulation. The comparison is based on transformers having the same maximum continuous rating. In each case the selling price of a self-cooled transformer is used as the base price, with the cost of the other units expressed as a ratio to this base price. It will be noted that the OA is the most expensive and the FOW the least expensive for each rating given. It is evident that forced cooling will result in important savings and should be considered if the other transformer characteristics are suitable for a given application.

Loss Evaluation. One of the elusive items that must be studied in applying power transformers is loss evaluation. There still exists in the industry a wide difference of opinion in regard to how losses should be evaluated. As a complete discussion of this factor is beyond the scope of this paper, the authors have chosen to show the influence of loss evaluation on the cost of the different transformers by varying the capitalized cost of losses over a range that might be experienced in practice. In this analysis the losses are capitalized and added to the selling price of the transformer, rather than using the alternative procedure of calculating annual costs.

Table III. Approximate Relative Cost of 3-Phase, 138-Kv, 550-Kv BIL Transformers with Neutral Insulation Reduced to 15-Kv Class

Type	Transformer Rating, MVA 20	50	100
OA	1.00	1.00	1.00
OA/FA	0.90	0.89	0.89
OW	0.89	0.85	0.85
OA/FA/FOA	0.79	0.77	0.74
FOA	0.75	0.72	0.67
FOW	0.69	0.65	0.62

The capitalized cost of losses should include an energy charge as well as an equitable demand charge. The curves in Figure 2 may be used to determine the first component of the charge once the loss factor, energy charge, and carrying charge are known. For example, with a 50 per cent loss factor, an energy charge of four mils per kilowatt hour, and a 12 per cent carrying charge, the energy component of the loss is capitalized at $150 per kilowatt. The second component is a function of the additional system investment required to supply the losses during peak load periods. The total capitalized cost of a loss is taken as the sum of the two components. As used in this discussion loss factor is defined as follows:

$$\text{Loss factor} = \frac{\text{Average annual loss}}{\text{Loss at rated load}} \times 100 \text{ per cent}$$

A 100,000-kva, 3-phase, 138-kv transformer having a basic impulse level of 550 kv at the line terminals and 15-kv class insulation at the neutral will be used to illustrate the influence of loss evaluation on the capitalized cost of a power transformer. The essential data for this study are summarized in Table IV. The transformer losses can be obtained from the loss products and ratios as follows:

Per cent iron loss = $\sqrt{\text{Product/Ratio}}$

Per cent copper loss = Ratio times per cent iron loss, where

Product = product of per cent iron loss and per cent copper loss, and

Ratio = ratio of copper loss to iron loss

In using these products and ratios, it should be noted that the values are *not* expressed in terms of the maximum rating of the forced-cooled transformers. For example, the loss product and ratio for the FOA design are expressed on a base equal to 57 per cent of the maximum rating. To change the base, the loss ratio is multiplied by the square of the ratio of the new base over the old base, while the loss product remains the same. Fan losses for an OA/FA transformer are included at two per cent of the total loss, and pump and fan losses for the OA/FA/FOA and FOA transformers at seven per cent of the total loss. To permit generalization independent of the actual fan and pump duty cycles, these losses are capitalized the same as iron loss. In the following discussion, the capitalized cost of losses is the sum of the capitalized energy charge from Figure 2 and the appropriate demand charge.

Curve II in Figure 3 shows the influence of the capitalized cost of losses on the cost of an FOA transformer. The FOA cost is expressed as a ratio to the cost of an OA transformer. In each case the copper-to-iron loss ratio has been selected to give the lowest loss capitalization, giving due consideration to the limits in Table IV. Curves II, III, and IV in Figure 3 are calculated on the basis that the iron loss and copper loss are evaluated at the same rate for copper loss evaluations of $300 or more per kilowatt. For copper loss evaluations of less than $300 per kilowatt, the iron loss is capitalized at a constant value of $300 per kilowatt. This procedure was justified because variations in iron loss evaluation, compared with variations introduced by other factors, have a small influence on the cost ratio. The points shown on Figure 3 for iron loss capitalized at $200 and $400 per kilowatt illustrate the influence of this variation. Varying the copper loss evaluation between $100 and $400 influences the cost ratio by about 25 per cent, indicating the importance of having reasonably accurate data on this factor. Curve I, which is based on the selling price of the transformer, is included for comparison.

Table IV. Selling Prices, Loss Products, and Loss Ratios for 100,000-Kva, 3-Phase, 138-Kv, 550-Kv BIL Transformers with Neutral Insulation Reduced to 15-Kv Class

Type	Approximate Selling Price, Dollars Per Kva	Loss Product	Loss Ratio
OA	2.48	0.043	1.5–2.75
OA/FA	2.19	0.049*	1.5–2.75*
OA/FA/FOA	1.85	0.058*	1.5–2.75*
FOA	1.67	0.059†	1.2–2.0*

* Based on OA rating. † Based on 57,000 kva.

Installation Costs. Installation costs will have an important influence on the method of cooling that should be selected for a given application. As this factor varies through a wide range depending on local conditions, it is not possible to evaluate this factor accurately in any general comparison. Curve III is based on an installed cost equal to 150 per cent of the selling price of the transformer and is included to emphasize the importance of including installation costs in making comparisons. This is not intended to be any accurate comparison because installation costs vary considerably and may consist of different percentages for each type of cooling. Curve III also includes capitalized losses. It will be noted that installation costs decrease the spread in the cost ratio introduced by variations in the capitalized cost of copper losses.

Reactive Evaluation. As the reactance of an FOA transformer is higher than for an OA transformer, some evaluation should be placed on the reactive requirements of the transformers. Curve IV includes this factor as well as installed costs and capitalized losses. The reactances were taken as 7.5 per cent for the OA transformer and 11.25 per cent for the FOA transformer. Excitation requirements also are included at eight times the iron loss. Curve IV is based on an outside figure of $10 per kilovolt ampere of reactive. Direct interpolation between Curves III and IV is permissible if reactive is evaluated at less than $10 per kilovolt ampere. The spread between Curves III and IV shows that the reactive requirements of transformers have an important influence on the cost ratio.

Figures 4 and 5 illustrate a similar cost comparison for the OA/FA/FOA and OA/FA transformers.

Table V. Comparison of Capitalized Costs of 100,000-Kva, 138-Kv, 550-Kv BIL OA and FOA Transformers with Neutral Insulation Reduced to 15-Kv Class

	OA		FOA	
Losses, kw:				
Iron	146.6		126.3	
Fans and pumps			41.7	
Copper	293.2		467.3	
Reactive Losses, kva:				
Excitation kva	1,173		1,010	
I^2X	7,500		11,250	
Total reactive	8,673		12,260	
Evaluations:				
Iron loss	$400/kw		$400/kw	
Fans and pumps			$400/kw	
Copper loss	$200/kw		$200/kw	
Reactive	$7/kva		$7/kva	
Costs:				
Selling price	$247,618	45.0%	$167,480	33.6%
Iron loss	58,640	10.7	50,520	10.2
Fans and pumps			16,680	3.4
Copper loss	58,640	10.7	93,460	18.7
Reactive	60,711	11.1	85,820	17.3
Subtotal	$425,609		$413,960	
Installation*	123,809	22.5	83,740	16.8
Total	$549,418	100.0%	$497,700	100.0%

* Installation included at 50 per cent of transformer selling price.

Table V summarizes the costs included for one of the cases plotted in Figure 3. No-load losses are capitalized at $400 per kilowatt and load losses at $200 per kilowatt. Reactive is evaluated at $7 per kilovolt ampere instead of the outside figure of $10 per kilovolt ampere used in Figure 3. It will be noted that reactive charges account for 18.1 per cent of the total cost of the FOA transformer. Actually, if reactive were evaluated at as high as $7 per kilovolt ampere, consideration should be given to a more expensive, lower reactance transformer. Including installation costs at the same percentage for both transformers may not result in a fair comparison. The installation costs may be a higher percentage of the transformer selling price for FOA than for OA transformers.

Emergency Capacity. In stations where on-the-spot spare transformer capacity is to be provided, the OA/FA and OA/FA/FOA transformers have definite merit. In these cases these transformers could be operated within their self-cooled ratings normally, with the forced ratings reserved

for emergency conditions, or the triple-rated unit could be operated within its FA rating normally, with its maximum rating reserved for emergencies. In these applications the losses would be evaluated on the basis of the lower normal loading, which would be equivalent to using a lower copper loss evaluation in Figures 4 and 5. It also would seem reasonable to evaluate the cost of the transformer reactive at the normal fractional load, which decreases the forced-cooled/self-cooled transformer cost ratios. As an example, consider an 80,000/100,000-kva OA/FA transformer normally operated within its OA rating, with the FA rating reserved for emergencies. Also assume that copper losses are evaluated at $200 per kilowatt and reactive at $10 per kilovolt ampere at the transformer location. Following the above philosophy, the copper loss would be evaluated at 0.64×200, or $128 per kilowatt, in using Figure 4. Reactive would be evaluated at $6.40 per kilovolt ampere.

Impedance. The higher impedance of the forced-cooled transformers may have merit in locations where the short circuit kilovolt ampere approaches the rating of the installed circuit breakers. On the other hand, this higher impedance may influence unfavorably steady-state or transient stability limits in certain locations on a system. These factors should not be overlooked in selecting power transformers for specific applications.

Reference

1. Co-ordination of Lightning Arrester Location with Transformer Insulation Level, **R. L. Witzke, T. J. Bliss.** *AIEE Transactions*, volume 69, part II, 1950, pages 964–75.

Discussion

D. L. Beeman (General Electric Company, Schenectady, N. Y.): The points the authors have raised on 3-phase versus single-phase transformers are very timely and deserve the earnest consideration of users of transformers. The writer realizes that this comparison was not the main purpose of the paper and so would like to add some more points of comparison between 3-phase and single-phase transformers. These are made with particular reference to industrial users. In the industrial field the purchase of single-phase transformers has almost disappeared. This is a complete reversal of trend that has taken place in the last 10 years. One of the major factors for this trend has been the excellent reliability of transformers referred to in the paper. According to some figures which were made on Pyranol transformers in industrial plants, the failure record was of the order of one failure per 2,500 transformer-years. Putting this in another way, of all of the Pyranol transformers installed, less than 0.2 of one per cent had failed for any reason whatsoever.

The second major reason for this trend has been the unit substation. Three-phase transformers fit into unit construction easily from a mechanical standpoint, whereas three single-phase transformers are difficult to build into unit equipments. The unit equipment further multiplied the savings of the 3-phase transformer.

Open Delta

It used to be argued that one big advantage of three single-phase units is that open-delta operation can be maintained if one of the three single-phase units is out of service. The excellent operating record mentioned previously practically eliminated the necessity for ever going to open-delta operation. The present trend in industrial plants is to ground systems at all voltages. This means Y-connected secondary windings of transformer banks. A bank made of three single-phase transformers cannot very well be used to supply any polyphase power when one of the three single-phase units is out of service. Therefore, in the grounded system the single-phase transformers have lost that apparent advantage.

In a grounded-neutral system, somewhere in the neighborhood of 5 per cent to 10 per cent extra would be spent if the single-phase transformers had no advantage from this standpoint when compared with one 3-phase transformer.

If service reliability is important, then two half-size, 3-phase units can be used instead of one full-size 3-phase unit or three single-phase transformers. The two half-size transformers cost about 20 per cent more than the three single-phase units and provide substantially the same capacity with one unit out of service. The 3-phase bank, however, has many advantages. In the first place, should one unit be out of service, 3-phase loads can be served from the remaining transformer whether the system is grounded or ungrounded neutral. One transformer can be taken out of service for maintenance without dropping essential load in the plant. Automatic switching can be employed to isolate one of the units, should an internal failure develop, thus maintaining at least partial service without interruption. There are cases where it has taken as much as eight hours to locate trouble in one unit of a bank of three single-phase transformers.

If the single-phase transformers are considered on the basis of service reliability, that is only a partial answer to the over-all service reliability problem. There are far more outages due to circuit failures in cables and buses, and so forth, than there are in transformers. The most economical way to get over-all good service reliability is to provide the modern load-center system with double channels with an emergency tie between them as in the case of the secondary selective system. This provides alternate channels in the event of either transformer or cable outages. The 3-phase transformer fits this situation ideally.

Lester B. LeVesconte (Sargent and Lundy, Chicago, Ill.): If this paper had included a complete bibliography, it would probably have shown that in 1941 there was a paper by Philip Sporn and H. V. Putman discussing some transformer economics,[1] but for the following eight years, there was no AIEE paper on this subject. In 1949, the writer presented this subject to the Midwest Power Conference.[2] In 1950, the subject was covered quite thoroughly in three AIEE papers.[3–5]

The Midwest Power Conference paper indicated that the choice of the type of cooling to be selected on an economic basis actually depends upon the accounting procedure in the company and the theory of calculating the costs of losses. In this matter there seems to be a wide variation in the practices between the power companies and considerable work should be done to develop more uniformity, in the theory of the evaluation of costs of losses. This point is illustrated again by this paper.

Figures 3, 4, and 5 of the paper compare the cost of various types of forced cooling to the cost of a self-cooled transformer. Therefore, the different curves could be compared and the effect of the capitalized cost of the copper losses observed. If Curve II from Figures 4 and 5 are superimposed on Figure 3, the comparison is quite evident. Assuming that the transformers were to be compared on the basis of Curve II, which includes the selling price and the capitalized cost of losses, the lowest value of Curve II would indicate the most economical type to select. From this it is evident that the type FOA (oil-immersed forced-oil-cooled) would be the most economical for all values of copper loss up to $400 per kw. Above this the type OA/FA/FOA (oil-immersed self-cooled/forced-air-cooled/forced-oil forced-air cooled) is the least expensive up to $230, but between $230 and $400 the type OA/FA (oil-immersed self-cooled/forced-air cooled) is less expensive. The curve for type OA/FA/FOA crosses the ratio 1.0 line at $280, which indicates that beyond this point the type OA (oil-immersed self-cooled) would be less expensive.

Therefore, it is evident that the selection of the type of transformer for any application, if studied on an economic basis, depends on the theory of the evaluation of losses rather than on an engineering basis.

References

1. A New Transformer for Base-Load Stations, **Philip Sporn, H. V. Putman.** *Electrical Engineering* (*AIEE Transactions*), volume 60, October 1941, pages 916–18.

2. Economic Factors in Transformer Application, **L. B. LeVesconte.** Midwest Power Conference (Chicago, Ill.), 1949.

3. The Choice of Main Power Transformers for Generating Stations, **N. E. Dillow, J. W. Butler.** *AIEE Transactions*, volume 69, part II, 1950, pages 781–85.

4. Selection and Application of Power Transformers, **Howard P. Seelye.** *AIEE Transactions*, volume 69, part II, 1950, pages 830–33.

5. Selection, Design, and Operation of Power Transformers on American Gas and Electric Company System, **F. A. Lane, I. W. Gross, P. S. Pugh.** *AIEE Transactions*, volume 69, Part II, 1950, pages 786–95.

Progress Report of the AIEE Magnetic Amplifier Subcommittee

AIEE COMMITTEE REPORT

THE Magnetic Amplifier Subcommittee was formed in 1948 to provide a focal point in the Institute for a rapidly growing new activity of magnetic amplifiers. It was hoped that by tying together the scattered efforts a common meeting ground of terms and definitions and methods of expressing performance could be established at an early stage. The stimulation of technical meetings devoted exclusively to magnetic amplifiers also would be highly beneficial. The scope adopted was:

Fundamental developments, design, and application of magnetic amplifiers and of the materials and components as used. Standardization of definitions, nomenclature, symbols, and operating characteristics. Encouragement of the exchange of information, as by technical papers, conference sessions, and demonstrations.

This report combines the material developed to date by the three working groups of the subcommittee, together with some of the reasons. Comments and suggestions will be welcomed to assist the subcommittee in bringing this material to the status of formal standards.

I. Definitions

The following definitions have been approved by the subcommittee and will be recommended to the Standards Committee for adoption unless discussions of this report are received that seem to require further committee consideration.

Proposed Magnetic Amplifier Definitions

Reactor. A reactor is a device the primary purpose of which is to introduce reactance into an electric circuit.

Inductor. An inductor is a device the primary purpose of which is to introduce inductance into an electric circuit.

Saturating Reactor. A saturating reactor is an inductor operating in saturation without independent control means.

Saturable Reactor. A saturable reactor is an adjustable inductor in which the current versus voltage relationship is adjusted by control magnetomotive forces applied to the core.

Magnetic Amplifier. A magnetic amplifier is a device using saturable reactors either alone or in combination with other circuit elements to secure amplification or control.

Feedback. Feedback (in a magnetic amplifier) is a circuit connection by means of which an additional magnetomotive force, which is a function of the output quantity, is used to influence the operating condition.

Signal (Input, Control). A signal is an independent input variable. It is applied to the magnetic amplifier as an independent magnetomotive force.

Output Windings. The output windings of a saturable reactor are those windings other than feedback associated with the load and through which power is delivered to the load.

Power Windings. The power windings of a saturable reactor are those windings to which the power is supplied by a local source. Commonly the functions of the output windings and the power windings are accomplished by the same winding, which is then termed the output winding.

Control Windings. The control windings of a saturable reactor are those windings by means of which control magnetomotive forces are applied to the core.

Bias Windings. The bias windings of a saturable reactor are those control windings by means of which the operating condition is translated by an arbitrary amount.

Signal Windings. The signal (input) windings of a saturable reactor are those control windings to which the independent variables (signals) are applied.

Feedback Windings. The feedback windings of a saturable reactor are those control windings to which the feedback connections are made.

Self-Saturation. Self-saturation in a magnetic amplifier refers to the connection of half-wave rectifying circuit elements in series with the output windings of the saturable reactors.

Other terms which the definitions committee will undertake to define are: time constant or response time; power gain or amplification; figure of merit; control characteristic; output characteristic; and control characteristic linearity.

II. Ratings and Methods of Performance Expression

Magnetic Amplifiers

The general definition for a rating as given in American Standards Association, (ASA) publication C42 (1941, or the latest revision thereof approved by the ASA),[1] under section 05.50.040, clearly defines the requirements of a rating.

"A rating of a machine, apparatus, or device is a designated limit of operating characteristics based on definite conditions."

Paper 51-71, recommended by the AIEE Electronics Committee and approved by the AIEE Technical Program Committee for presentation at the AIEE Winter General Meeting, New York, N. Y., January 22–26, 1951. Manuscript submitted October 25, 1950; made available for printing December 7, 1950.

Personnel of the AIEE Magnetic Amplifier Subcommittee: E. L. Harder, *Chairman;* Edgar Weir, *Secretary;* W. J. Dornhoefer, sponsor, Group on Nomenclature and Definitions; E. B. McDowell, original sponsor, and R. W. Wolke, present sponsor, Group on Ratings and Methods of Performance Expression; L. A. Finzi, Group on Response Time Considerations; A. O. Black, L. W. Buechler, A. S. Fitzgerald, W. A. Geyger, A. B. Haines, J. E. Hart, A. D. Hitt, W. C. Johnson, R. E. Morgan, H. B. Rex, P. L. Schmidt, and D. W. Ver Planck.

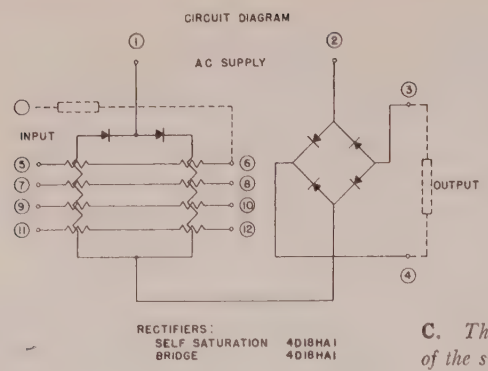

Figure 1. Circuit diagram

The following items are proposed by the subcommittee as necessary and sufficient for rating a magnetic amplifier. In each case the defining statement which will appear in the standards is italicized, and the explanation follows directly thereafter.

A. *The rating of a magnetic amplifier consists of the supply voltage, frequency, load resistance, output currents, control currents, and volt-ampere output assigned to it by the manufacturer. This rating shall be given for a specified connection of all components between the input and output terminals.*

The rating is intended to be an exceedingly brief specification of the amplifier, containing only such essential information as could logically be included on the nameplate. It is by no means intended to convey all of the necessary application information regarding the amplifier.

Recommended standard application data which should normally be available additionally from the manufacturer are listed in a subsequent section.

B. *The rated supply voltage is the supply voltage assigned in the rating. The magnetic amplifier shall be capable of operating continuously at this supply voltage at rated frequency and with rated load resistance for any values of output and control currents within its rating, without exceeding the established rating of any of its components.*

As noted in the definition, the magnetic amplifier may include, in addition to the saturable reactor, rectifiers, resistors, transformers, and other elements. It is not the intent here to establish ratings for these additional elements, which are all standardized elsewhere, but simply to state that the rating given to the complete amplifier involves operation of the additional elements within the already established limits. Multiple-voltage ratings are contemplated where external connections are provided therefor.

C. *The rated frequency is the frequency of the supply voltage assigned in the rating.*

As the saturation is a function of volts per cycle, operation at other frequencies is similar only if the applied alternating voltage is changed proportionately. Thus, the frequency is as necessary a part of the rating as the voltage.

D. *The rated load resistance is the resistance specified as a basis of the rating.*

This resistance is a value specified by the manufacturer, usually on the basis of maximum controlled power, although it may be based on some other criterion, depending on the purpose of the particular amplifier. It is needed in the rating to specify the output (**G**, in this section) and as a basis for response-time data, as well as simply to indicate the order of magnitude of resistance load with which the amplifier is intended to operate.

Information regarding performance at other load resistances is given in the application data.

While operation with inductive loads is common, the work of the committee has not reached a point where helpful information regarding this application can be incorporated in either the rating or the application data. Work is continuing on this feature, and suggestions will be welcomed.

E. *The rated output current is the greatest value of current that can be carried continuously, with all control windings carrying rated current simultaneously, without exceeding established ratings of any of the components. The rms value of current shall be specified for a magnetic amplifier with an a-c output. The average value of current shall be specified for a magnetic amplifier with a rectified output.*

For amplifiers with rectified output the rated (average) value of current can be carried continuously only if the ratio of rms to average currents is not greater than with rated resistance load.

Current ratings of amplifier output and of control windings are given on the basis that all windings carry rated current simultaneously. If there are two or more control windings it is generally possible to pass approximately rated current through each with a small differential net control current establishing rated output current at the same time. While this is an outside limiting condition, it does not appear to distort greatly the true capabilities of the amplifier, and it does provide a very simple basic application figure or rating. Refined applications may take advantage of the somewhat greater currents permissible in certain windings if others do not carry rated load simultaneously. There would, however, be too many combinations to consider under rating.

When but one control winding exists the test could be made at reduced supply voltage to obtain rated control and output currents simultaneously. The test code, not yet prepared, must be depended upon to fix uniform conditions for this test.

In settling on the "average current" for rating of amplifiers with rectified output the committee balanced the greater utility of this current for application purposes against the objection that it does not define the heating. Applications may exist in which the ratio of rms to average current is higher than for the test condition with rated resistance load. Application data must be relied upon for these cases.

The final sentence in the proposed section of the standard calls attention to this limitation.

F. *Each rated control current is the greatest current (alternating current or direct current, as specified by the manufacturer) that can be carried continuously, with all other currents simultaneously at their rated value, without exceeding the established rating of any of the components. (See note under* **E** *in this section.)*

G. *The rated volt-ampere output is the product of the rated load resistance (defined in* **D** *in this section) and the square of the rated output current.*

This is needed in the rating for quick indication of the ability of the amplifier to supply a particular load power if a suitable impedance match can be arranged. Actually, it is simply a combination of two other rating items, the rated output current and the rated load resistance. However, note that the volt amperes as defined are not the watts effective in heating a d-c load, but are the d-c component of power only.

H. *Temperature*

Although the treatment of temperatures has not been fully worked out, the following represents the committee's views at this time. The magnetic am-

plifier is an assembly of components which have been individually standardized, such as saturable reactors, rectifiers, and so forth. The temperature rise limitations and maximum temperature limitations will, in general, be different for each such component. Presumably the components have been applied properly, so that the complete assembly is suitable for operation at a given ambient temperature. Thus, the temperature rating given to the complete amplifier will be an ambient temperature rather than a rise or a maximum temperature. The standard ambients may very properly be 40 degrees centigrade, and 55 degrees centigrade, depending on whether the application is open or in an enclosure. This would agree with control device standards.

Thus, the temperature rise information given in Figure 2, to be discussed in a following section, applies only to the saturable reactor and is so marked. Where the amplifier consists only of a saturable reactor, or if the rectifiers are mounted separately, this information would show the change in reactor rating to allow for different ambients.

Application Data

Since the characteristics of magnetic amplifiers can be presented in many forms, the committee thought it wise to review the several methods in use and to agree, if possible, on a few preferred forms. Adherence to these will assist the users in achieving a familiarity with the presentation and will avert a hodgepodge of slightly varying forms of presenting essentially the same information. The following application information appeared most generally useful. Again, the statement intended to appear in the standards is italicized, and the committee's comments follow directly thereafter.

A. *The d-c resistance at a specified temperature and number of turns of each of the control windings*

These are needed in applying the amplifier in order to have desired input and feedback circuit characteristics and to predetermine the response time from the general response-time curves proposed. (See **C**, in this section.) This is illustrated in the example.

B. *A circuit diagram*

The circuit diagram, or supplementary information, should contain identification of the circuit elements, particularly if these are separately mounted, such as rectifiers.

C. *Curves describing the operating characteristics*

1. *Control characteristic. Plot of load current as a function of control ampere-turns for various loads and at the rated supply voltage and frequency*

2. *Plot of load current as a function of control ampere-turns for various values of supply voltage and at the rated load resistance and rated frequency*

3. *Plot of load voltage as a function of load current for various values of control*

4. *Plot of 63 per cent and 95 per cent response times as a function of control circuit turns squared per ohm, at rated supply voltage and frequency and rated load resistance. Alternatively, the response times may be plotted versus control circuit ohms per turn squared.*

The control circuit turns squared per ohms at which curves 1 to 3 are taken should be stated.

Curve 1 is a "control characteristic" of output versus input for various load resistances, whereas curve 3 is a set of "regulation curves" showing the output voltage versus load for various control currents. Both contain essentially the same information, the three variables related being control current, load current, and load resistance. Each presentation has peculiar advantages in particular applications, and the committee did not feel it wise to eliminate either one at this time.

Curve 2 is a control characteristic for various supply voltages in the neighborhood of normal.

Commutation alters the control characteristic and regulation curves when various control circuit impedances are used. Hence, curves 1 to 3 are to be taken with resistance only in the control circuits and the control circuit turns squared per ohm are to be stated.

Curve 4 is the recommended form of response-time data. It consists of curves giving the 63 per cent and 95 per cent response times as ordinate versus the accessible control-winding turns squared per ohm (or alternatively, ohms per turns squared) as abscissa. The accessible control-winding turns squared per ohm is the sum of the turns squared per ohm of each of the accessible control windings, which forms a closed circuit.

Use of Ratings and Application Data References

Self-Saturating Magnetic Amplifier with D-C Output

For a particular amplifier selected as an example the ratings and application data are as given in Tables I and II.

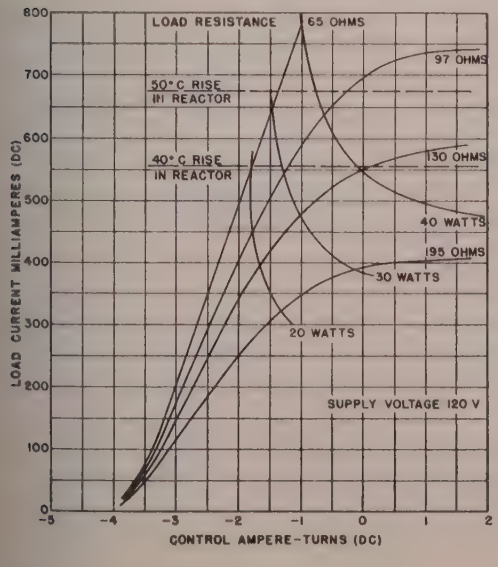

Figure 2 (left). Control characteristic at rated supply voltage and frequency, load resistance varied

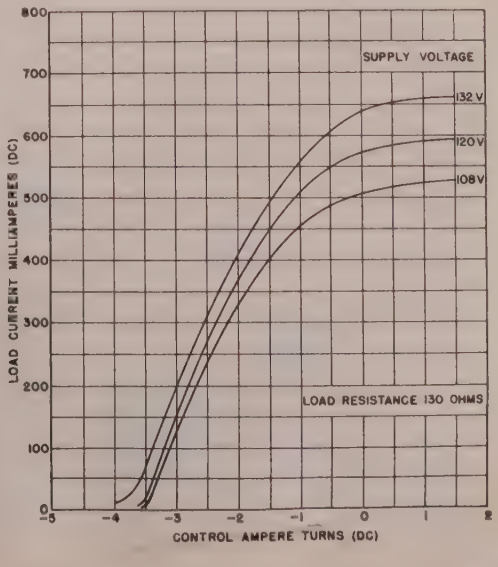

Figure 3 (right). Control characteristic at rated load resistance and frequency, supply voltage varied

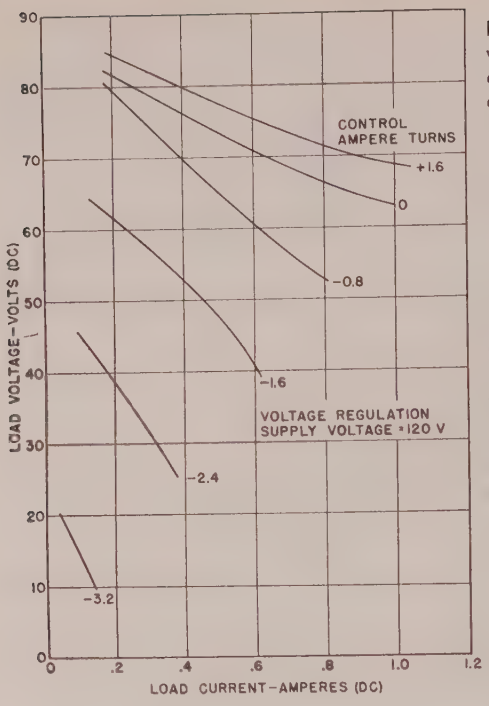

Figure 4 (left). Output voltage as a function of load current for various values of control ("regulation curves")

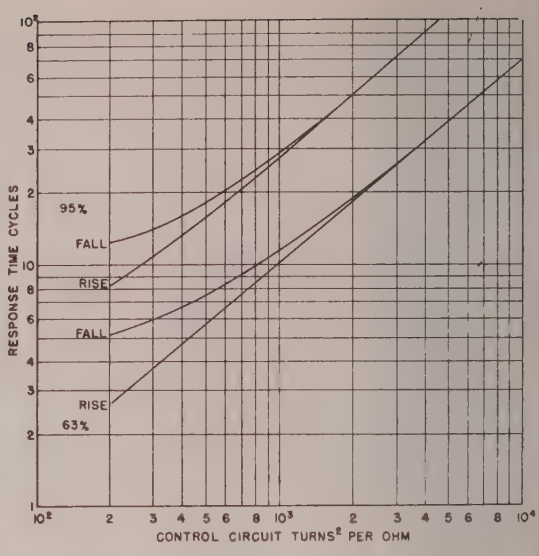

Figure 5 (right). Plot of 63 per cent and 95 per cent response times as a function of control circuit turns squared per ohm, at rated supply voltage and frequency and rated load resistance

Circuit Diagram

The circuit diagram, given in Figure 1, shows the connections upon which the performance is based, and the rectifiers used. Input is shown to a particular control winding simply by way of illustration. However, since the control characteristic is plotted against ampere-turns, that is, amperes in a given number of turns, the ampere-turns can be interpreted for the use of any of the accessible control windings as signal or input windings. They also can be interpreted for any of the accessible control windings used as bias or feedback windings, since they give the output for a given total control ampere-turns regardless of how obtained. The accessible terminals are indicated by circles.

Table I. Ratings Based on Operation with D-C Output According to Figure 1

Supply voltage	120 volts rms, 60 cycles, single phase
Load resistance	130 ohms
Output current	0.555 ampere
Volt-ampere output	40 volt-amperes
Ambient temperature	55 degrees centigrade
Control-winding rated currents, amperes	1. 0.041 2. 0.12 3. 0.54 4. 1.00

Table II. Application Data on Control Windings

Windings	Turns Per Core	D-c Resistance between Designated Terminals at 25 degrees centigrade, ohms
5–6	4,000	1,200
7–8	400	140
9–10	80	7.0
11–12	20	2.0

Curves Describing the Operating Characteristics

The control characteristic for various load resistances is given in Figure 2, the control characteristic for various supply voltages in Figure 3, and the regulation curves in Figure 4. The 63 per cent and 95 per cent response times are plotted against the turns squared per ohm in Figure 5.

Use of Ratings and Application Data

Suppose that a magnetic amplifier is required to control a 40-volt-ampere d-c resistive load from a 120-volt single-phase 60-cycle supply. What useful information is conveyed by the ratings and application data regarding the application?

The rating confirms the basic possibility that this amplifier might be suitable, since it is 40 volt amperes, 120 volts, 60 cycle, 1 phase.

The rated load resistance shows the ohms to which the 40-volt-ampere load should be built to be suitable for operation with the amplifier, although, as will be shown in a following paragraph, some variation from this value can be tolerated. In case the load already exists, the watt rating indicates the probability that an amplifier of similar size and characteristics could be built for other load resistances involving the same power, but here attention must be paid to two factors. With fewer turns of larger wire the supply voltage must be changed proportionately, and this may require a transformer. Rectifier changes are in discrete steps, and an equally advantageous match will not be obtainable at all load resistances.

The rated current, 0.555 amperes at 40 degrees centigrade rise in the reactor, and the corresponding control-winding current ratings are a set of currents that can be carried simultaneously without exceeding the 40 degrees centigrade rise. Ordinarily, applications will be made keeping each current within these thermal limits. In critical cases further information will be required to determine other permissible current combinations.

The application data consists of three parts, control-winding turns and resistance, the circuit diagram, and the characteristic curves. The control characteristic, Figure 2, show that, with a 130-ohm load, a variation of 4 ampere-turns will be ample to control from the continuous 40 degrees centigrade rise rating to a low value. For example, a variation from 0 to 10 mils negative in the 400-turns control winding, with the others open, will control over the full range. The corresponding control power would be 0 to 0.014 watts to control the output from approximately 40 watts to 0, a gain of

$$\frac{40}{0.014}=2{,}850$$

A bias winding might be used to center the control for operation between the 20 per cent and 80 per cent points, the approximate limits of high-gain linear operation. Taking the maximum output as 585 mils, the 20 per cent- to-80 per cent range will be from 117 mils to 468 mils output, with a center at 292 mils corresponding to −2.2 ampere-turns per core.

Such a bias might be secured with 0.55 mils in the 4,000-turn winding, for example. The control-winding variation to cover the 20 per cent to 80 per cent range then will be ±2.75 mils, or a total of 5.5 mils. The power gain in this region is

$$(351)^2 \times 130/(5.5)^2 \times 140 = 3{,}800$$

Let us now consider the response time. The bias-winding voltage is $0.00055 \times 1{,}200 = 0.660$ volts. Suppose this is obtained from a 100-volt d-c source. The total resistance in the bias circuit will be 181,000 ohms, and the turns squared per ohm $= 4{,}000^2/181{,}000 = 88.5$. If the signal winding has no external resistance its turns squared per ohm $= 400^2/140 = 1{,}140$. The total turns squared per ohm $= 1{,}228$. Note that the bias winding contributed a negligible part of this. From the response curve, Figure 5, the 63 per cent and 95 per cent response times are, respectively, 13 cycles and 33 cycles. If it is desired to reduce the 63 per cent response time to 5 cycles (for both rise and fall), the turns squared per ohm must be reduced to 200. Allowing 88.5 in the bias winding, the control turns squared per ohm must be reduced to 111.5. This necessitates a signal circuit resistance of $400^2/111.5 = 1{,}430$ ohms, of which 140 is in the winding and 1,290 ohms must be external. The power gain under this condition is:

$$\frac{(351)^2 \times 130}{(5.5)^2 \times 1{,}430} = 372$$

Returning to the control characteristic, Figure 2, note that the load resistance could be as high as 160 ohms at the expense of somewhat higher control current. The temperature rise would be lower. However, with a load resistance as high as 195 ohms, the load could not be controlled up to 40 watts at any control current. The linearity and gain are obviously better with the 130-ohm load resistance. In the other direction of decreasing load resistance the 40 degrees centigrade temperature rise would be exceeded at 40 watts. However, at 50 degrees centigrade rise the load resistance could be lowered to about 85 ohms. The gain and linearity are improved.

Refer to Figure 3, the control characteristic for various supply voltages up to ±10 per cent from normal. Note that moderate changes in the supply voltage result in a change in the output current for the same control current. This variation must be allowed for in controls.

A change in frequency has approximately the inverse effect of a change in voltage on the minimum, or "cutoff," output current. A change in frequency has little effect on the maximum, or "saturation," output.

In case the load resistance is to be varied, the regulation curves of Figure 5 will be particularly useful, showing the variation of load voltage with current for various settings of the control and fixed supply voltage. Note that unlike a d-c machine the regulation curves are not parallel, the regulation increasing as the no-load voltage is lowered.

Saturable Reactors

Since the saturable reactor was one of the major components of a magnetic amplifier for which no ratings had been established as yet, it was decided to begin with this component. However, the work of the committee has not progressed as far as with the magnetic amplifier. Nevertheless, to obtain the benefit of comments which might guide the further work of the committee, it was felt best to include these saturable reactor sections in the report in their present form.

Ratings

The following items are proposed as necessary and sufficient for rating a saturable reactor. In designating these the committee recognizes that the saturable reactor usually operates between two limits. In one limit it is saturated, carries full current, and has a low voltage across it. In the other the control current is minimum (usually zero), the absorbed voltage a maximum, and the output-winding current is minimum.

Full-range reactors operate to zero control current, but also employed are limited-range reactors which provide a smaller control range and absorb their maximum voltage while still partially saturated and having a definite value of control current. The ratings and application data take into account the possibility of saturable reactors designed for any control range whatever.

A. *The rating* of a saturable reactor consists of the output-winding voltage, current, volt amperes and frequency, and the control-winding currents and the temperature rise assigned to it by the manufacturer.

B. *Rated output-winding voltage* is the voltage assigned in the rating. The saturable reactor should be capable of absorbing this voltage continuously at appropriate values of control-winding currents (usually minimum) without exceeding rated temperature rise. This voltage is average 1.11 or equivalent sine-wave rms value of the voltage read with an average reading meter.

C. *Rated output-winding current* is the maximum rms current that can be carried continuously without exceeding rated temperature rise, while carrying rated control-winding current simultaneously.

D. *Rated volt amperes* is the product of rated output-winding voltage and rated output-winding current.

E. *Rated control-winding currents* are the maximum currents that can be carried continuously without exceeding rated temperature rise, while carrying rated output-winding current simultaneously.

F. *Rated frequency* is the frequency of the output-winding voltage assigned in the rating.

G. *Rated temperature rise* is the temperature rise which will produce normal life expectancy, and shall be in accordance with established standards as given in ASA publication C57.11 (1948, or the latest revision thereof approved by the ASA),[2] sections 11.020 and 11.121.

Application Data

To define adequately the operating characteristics of a saturable reactor the following data should be provided.

A. The d-c resistance at a specified temperature and number of turns of each of the windings.

B. The control ampere-turns and output-winding voltage corresponding to rated output-winding current.

C. The permissible output-winding current at rated output-winding voltage and the corresponding control ampere-turns.

D. Family of curves of output-winding voltage (average 1.11) versus output-winding current for various values of control ampere-turns, at rated frequency.

E. Typical operating conditions as a simple magnetic amplifier.

References

1. Definitions of Electrical Terms. Publication C42, American Standards Association, New York, N. Y., 1941.

2. General Requirements for Transformers, Regulators, and Reactors. Publication C57.11, American Standards Association, New York, N. Y., 1948.

Discussion

Ulrik Krabbe (Thomas B. Thrige, Odense, Denmark): I find the report most interesting, especially the discussion of the rating which is a rather difficult problem.

As a representative for Europe, I should like to propose the values of international standards instead of United States standards. If the United States standards have

to be decided on now I should find it valuable if the terminology used in Europe (especially in England) were taken into account.

I am sorry that the word "transductor" is not found in the report. The word transductor is a proper word; compared with magnetic amplifier it is one word instead of two. It covers a little more, arrangements for measuring large direct currents where it is not the amplification property which is utilized. It corresponds well to the new amplifier name, transistor. The word transductor is used in England, France, Holland, Belgium, Norway, Sweden, Denmark, and Finland, as well as being used in literature in the United States.[1-3]

As a compromise I recommend the word transductors for circuits with and without feedback, and the word magnetic amplifiers for self-saturated circuits. In this way, we should also be able to avoid new unnecessary words as amplistats, and so forth. The circuits with self feedback in separate windings will probably get less emphasis in the future.

The curve of Figure 5 in the report showing the transient response is a good way of defining the properties when specifications for the rating of the signal are known. This question is, however, rather difficult and I find, therefore, that it is a little dangerous to standardize curves like Figure 5 before this problem is solved, as otherwise such curves can be misused and misunderstood easily.

References

1. Use of the Current Transductor in the Aluminum Industry, **T. R. Specht, R. N. Wagner.** *Electrical Engineering*, volume 69, September 1950, pages 828–32, and *AIEE Transactions*, volume 69, part I, pages 441–52.

2. Some Fundamentals of a Theory of the Transductor or Magnetic Amplifier, **A. Uno Lamm.** *AIEE Transactions*, volume 66, 1947, pages 1078–85.

3. Bibliography on Transductors and Magnetic Amplifiers, **H. B. Rex.** *Instruments* (Pittsburgh, Pa.), volume 21, number 4, 1948.

E. L. Harder: Mr. Krabbe's recommendations regarding the terminology are being referred to the Definitions Subcommittee for consideration. The curves of Figure 5 are not standards but are application curves for a particular amplifier. The standard application data merely state that such should be available.

Steady-State Analysis of Self-Saturating Magnetic Amplifiers Based on Linear Approximations of the Magnetization Curve

WALTER H. ESSELMAN
ASSOCIATE AIEE

THIS PAPER introduces a method for predicting the output currents of self-saturating magnetic amplifiers. The initial work illustrates how the load currents may be computed by assuming a 3-straight-line representation of the hysteresis loop. A simplified procedure is then developed and applied to two half-wave amplifiers. The factors influencing the output of the full-wave and doubler circuits are then discussed and illustrated. The computed values of the points on the transfer curve agree closely with experimental results.

In recent years considerable interest has been revived in saturating reactor devices for controlling relatively large power with small control currents. This interest was stimulated by new magnetic materials and circuits which resulted in greatly increased ratio of controlled power to input power. Therefore the term "magnetic amplifiers" was devised to signify many of the varied circuits which utilized the saturation properties of ferromagnetic materials to secure amplification.

A large group of these amplifiers fall into a class called self-saturating circuits. The basic circuit of this type is the half-wave circuit shown in Figure 1. Variation of the control current I_0 changes the d-c magnetomotive force of the reactor called premagnetization, thereby varying the output current. The rectifier in the load circuit causes a d-c component to flow which contributes to the core premagnetization thereby increasing the amplifier output. These half-wave units are combined to give the more practical full-wave and doubler circuits shown in Figures 2 and 3. In the full-wave circuit the current flows through one reactor during the first half cycle and the other reactor during the second half, these currents being added in the load resistor. The output of the doubler circuit is alternating; each reactor carries the output during alternate half-cycles of current flow. A d-c load current is obtained by inserting a rectifier in the circuit as shown in Figure 4.

The scope of this paper will be to present an approach to computing the load currents of a half-wave amplifier, and to discuss the various factors which affect these computed values. The general shape of the transfer curves (output current versus control current) of the full-wave and doubler circuits will be also briefly considered.

The prediction of the output currents of a magnetic amplifier involves the solution of a nonlinear differential equation similar to that of a simple series circuit consisting of a resistance and nonlinear inductance. Such an equation can always be solved by means of numerical integrations,[1] but the computations are extremely lengthy. Another approach to the problem is to neglect the series resistance of the a-c circuit, thereby reducing the nonlinear equations to a simpler form[2,3] which are more readily solved.[2,3] The results of this solution are necessarily restricted to amplifiers with low load resistances. Other solutions to the problem which have led to reasonable results for the more sensitive magnetic materials are one based on an ideal magnetization curve,[5] and one based on a measured hysteresis loop of material.[4]

The analysis to be presented in the paper is not limited to a particular type of magnetic material nor size of load resistance.

Straight-Line Approximation

The basic method which is to be used in this paper was probably first introduced by A. Boyajian.[6] It consists in approximating the magnetization curve by a series of straight lines such as shown in Figure 5. Over each region of the magnetization curve, represented by one straight line, the reactor behaves like a constant inductance whose magnitude is proportional to the slope of this line. As the reactor magnetization varies from one region into an adjoining region, the equivalent fixed inductances changes abruptly from one value to another.

Application of this "straight-line" method converts the original set of nonlinear differential equations for the particular amplifier into several sets of linear equations; each set applying to one region of the magnetization curve. These differential equations are readily solvable, and the equation constants can be obtained by numerically satisfying the

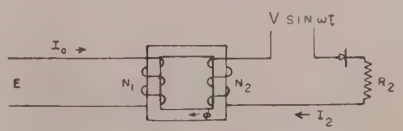

Figure 1. Half-wave circuit

Paper 51-72, recommended by the AIEE Electronics Committee and approved by the AIEE Technical Program Committee for presentation at the AIEE Winter General Meeting, New York, N. Y., January 22–26, 1951. Manuscript submitted August 30, 1950; made available for printing December 7, 1950.

WALTER H. ESSELMAN is with the Westinghouse Electric Corporation, Pittsburgh, Pa.

The work presented was performed in conjunction with a thesis program at the Polytechnic Institute of Brooklyn, N. Y. Acknowledgment is made for the helpful assistance of M. LIWSCHITZ and E. J. SMITH of this institution.

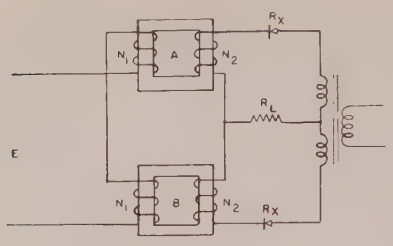

Figure 2. Full-wave circuit

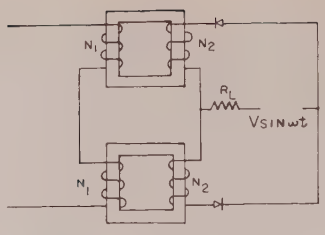

Figure 3. Full-wave doubler circuit a-c output

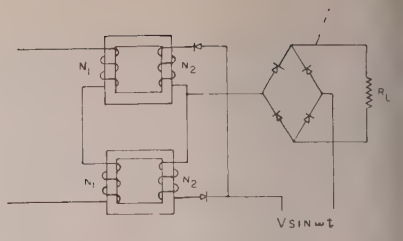

Figure 4. Full-wave doubler circuit d-c output

initial conditions and the boundary conditions at the juncture of the various regions.

Basic Assumptions in Analysis

The following assumptions were made in this analysis:

1. The magnetization characteristic of the core material can be represented by its normal d-c magnetization curve or if data is available and greater accuracy is desirable by a curve based on values of H midway between the rising and falling curves of the d-c hysteresis curve.

2. Hysteresis and eddy-current losses in the core are negligible.

3. The rectifier can be represented as a switch having a very large constant resistance to reverse current and a small constant resistance to forward current flow. The reverse current of the rectifier actually consists of resistive leakage and capacitive current, the latter of which is neglected.

4. A large choke is inserted in the control circuit to eliminate induced alternating current.

Tests show that the first assumption to be reasonable as the computed values agree closely with experimental data. (It might be noted that the straight-line method could be applied to a hysteresis loop without too serious complication provided sufficient data were available for asymmetrical magnetization conditions.) The second assumption appears reasonable when low-loss magnetic materials and thin core laminations are considered.

The third assumption deserves much attention and its effect on the full-wave and doubler circuits will be discussed briefly later in the paper. However, in order to simplify the solution of the problem this assumption is made.

The last condition of inserting a large choke in the control circuit is not essential. It is made only in order to eliminate the effect of induced currents and thus to facilitate the presentation. The case of finite control circuit impedance is treated in reference 7. The case analyzed in this paper is approached in many practical amplifiers since in combined circuits the control winding is in series with the windings of one or more other reactors which limit the induced currents.

Analysis

The fundamental equations for the amplifier shown in Figure 1 are

$$V \sin \omega t = I_2 R_2 + N_2 10^{-8} \frac{d\phi}{dt} \tag{1}$$

$$E = I_0 R_1 \tag{2}$$

where ϕ is the total flux passing through the power winding of N_2 turns and can be represented as follows

$$\phi = AB$$

But from Figure 5

$$B = B_n + \mu H$$

where μ is the slope of the straight line of the region being considered, and

$$H = H_0 + H_2$$

Differentiating ϕ, and since H_0 is constant

$$\frac{d\phi}{dt} = A\mu \frac{dH_2}{dt} \tag{3}$$

Also

$$I_2 = \frac{H_2 l}{N_2} \tag{4}$$

Now substituting equation 3 and 4 in equation 1 and solving the linear differential equation, one obtains

$$H_2 = \frac{V}{Z} \sin (\omega t - \theta) + C\epsilon^{-\frac{K_1 R_2}{\omega \mu} \omega t} \tag{5}$$

where

$$K_1 = \frac{10^8 l}{A N_2^2} \tag{6}$$

$$Z = \frac{\sqrt{(K_1 R_2)^2 + (\omega \mu)^2}}{K} \tag{7}$$

$$\theta = \tan^{-1} \frac{\omega \mu}{K_1 R_2} \tag{8}$$

$$K = \frac{10^8}{A N_2} \tag{9}$$

Equation 5 is the desired analytic result which gives a-c magnetization H_2 as a function of time over the particular region of magnetization having constant slope μ. The constant C is determined from initial and boundary conditions of the circuit and will be considered later. Reference 7 includes an analysis in which the effect of flux leakage of the reactor is also included.

Initial Conditions

At present, our interest lies in finding a steady-state solution for the amplifier. As noted before, the rectifier is assumed to act as a switch which possesses a high constant resistance to reverse current flow and a small constant resistance to forward current flow. During the negative half of the voltage cycle, the load (reverse rectifier) current is very small and, since capacitive currents are neglected, is in phase with the applied voltage. Hence, the reverse current goes to zero with the applied voltage. The action is illustrated in Figures 6*A* and 6*B* for a constant inductance in series with an "ideal switch" rectifier. The rectifier resistance decreases suddenly from R_r to R_f as the applied voltage goes positive, and remains constant at this value until the forward current decreases to zero at some time t_2, whereupon, the "switch" opens and the rectifier resistance increases once again to R_r.

Since the load current is zero at the start of each positive half cycle of voltage, it is necessary only to compute the current over a single cycle to determine the steady-state response.

Determination of the Constants of Integration

The solution of the differential equation contains an easily obtainable constant of integration for each region of the magnetization curve. Assuming the premagnetization H_0 lies in region I as shown in Figure 5 and applying conditions that $H_2 = 0$ at $t = 0$ to equation 5 one obtains

$$C_I = \frac{V}{Z_I} \sin \theta_I \tag{10}$$

where I subscript denotes the constant for region I. It is now possible to compute H_2 or load current in the first region as a function of ωt from equation

$$H_2=\frac{V}{Z_I}\sin(\omega t-\theta_I)+C_I\epsilon^{-\frac{K_1R_2}{\omega\mu_I}\omega t} \qquad (11)$$

At some later time $\omega t=\psi_1$, $H_2=h_1-H_0$ and the slope of the magnetization curve changes from μ_I to μ_{II}. Equation 5 for this region will then be

$$H_2=\frac{V}{Z_{II}}\sin(\omega t-\theta_{II})+C_{II}\epsilon^{-\frac{K_1R_2}{\omega\mu_{II}}(\omega t-\psi_1)} \qquad (12)$$

Now substituting boundary condition at $\omega t=\psi_1$ equation 12 can be solved for C_{II}

$$C_{II}=h_1-H_0-\frac{V}{Z_{II}}\sin(\psi_1-\theta_{II}) \qquad (13)$$

This process is repeated until H_2 has passed through each region, as shown in Figure 5.

Experimental Verification of Straight-Line Method

This procedure was tried on a Mumetal cored reactor in a half-wave circuit with various values of load resistance and control current.[7] The correspondence between the shape of the experimental and computed curves was very good. A typical result is shown in Figure 7.

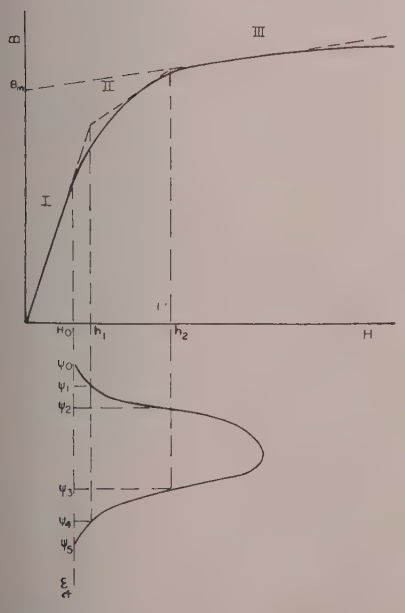

Figure 5. Typical representation of magnetization curve by three linear regions

I. Region I with slope μ_I
II. Region II with slope μ_{II}
III. Region III with slope μ_{III}

Simplification of Procedure

While the detailed analysis just presented is useful for computing a particular output wave shape, it is rather tedious, especially if an entire transfer curve is to be calculated by this procedure. Therefore, a simplified approach based on the same representation of the magnetization curve by linear regions was studied.

The first attempts at reducing the computations of this procedure were based upon a 2-straight-line representation of the magnetization curve. The results obtained were not too encouraging, but it became evident that if the proper slopes for each of the two regions were chosen, accurate values of load current could be computed. The problem of what slope to select was analyzed, and it was decided to utilize the average value of the slopes of the magnetization curve between the value of premagnetization H_0 and maximum magnetic intensity H_{max}, for all positive values of premagnetization. Subsequent computations and the analysis shown in Appendix I indicated that this value of slope can be used to compute accurate values of load current of the amplifier. For example the average value of H_2 in Figure 8*A* would be computed on the basis that the reactor presented a constant inductance determined by the value of the slope μ_{av}. Appendix I shows that this procedure while approximate contains only a small error, and the comparison of computed values with test results indicated that this procedure is satisfactory for any case of positive d-c control current.

It is then possible to compute the average value of output current for any case of positive premagnetization by means of a single straight-line region with a slope of appropriate value.

However, it has been found that for negative premagnetization more accurate results are obtained by two regions of operation as shown in Figure 8*B*. In this

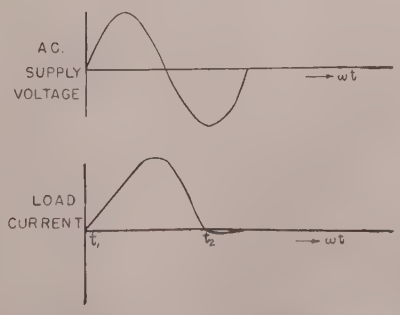

Figure 6A. Current flow in half-wave amplifier

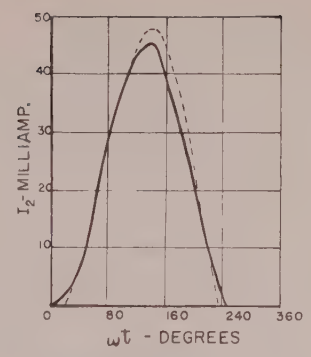

Figure 7. Output current wave of half-wave amplifier with Mumetal reactor

I. Control = 16 milliamperes
R_L = 100 ohms
– – – computed curve
——— experimental curve

case the slope of Region I is determined by the average value between H_0 and $H=0$, while the slope of Region II is the average value from $H=0$ and H_{max}. The case of negative premagnetization will be later described in detail.

In order to exploit this method for cases of positive premagnetization it is now possible to draw a curve of slope μ versus H of a material. This is shown in Figures 9*A* and 9*B* for data taken on a Hypersil reactor. The curve of μ versus H is not an incremental permeability or differential permeability curve, but is rather a curve of the slopes one would choose for consecutive regions of the magnetization curve. For example, referring to Figure 9*A*, the initial slope chosen is located half-way between the two curves of the d-c hysteresis loop and is shown as 120×10^3 on the slope curve. From this initial maximum value of μ the curve is made to approach, by the use of a straight line, the differential permeability curve of the material. It is now possible to represent the slope μ by the function

$$\mu=\mu_{max}\epsilon^{-\alpha H}+\mu_{min} \qquad (14)$$

For the materials and reactors tested this equation becomes

$$\mu=(120\epsilon^{-0.7H}+0.11)\times10^3 \text{ for hypersil reactor}$$
$$\mu=(136\epsilon^{-3.8H}+0.046)\times10^3 \text{ for orthonik reactor} \qquad (15)$$

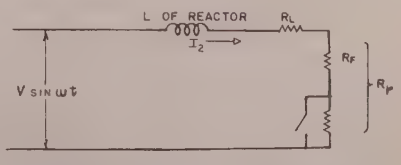

Figure 6B. Equivalent circuit of half-wave amplifier illustrating rectifier resistances

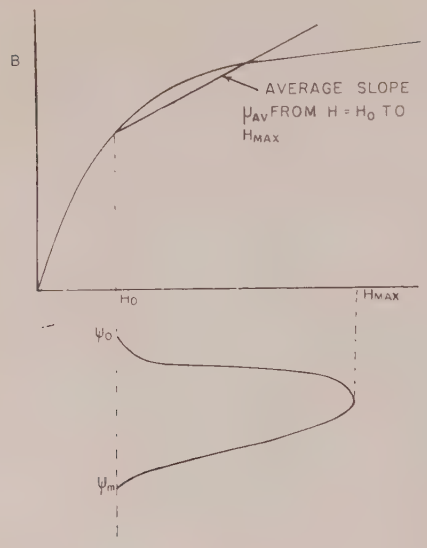

Figure 8A (left). Operation on a single region with average slope

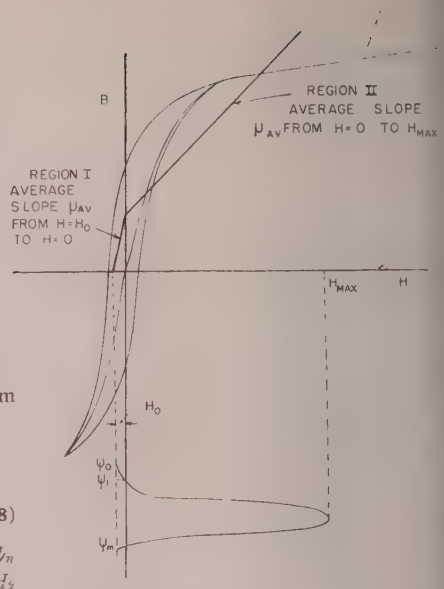

Figure 8B (right). Operation on two slopes for negative premagnetization

It must be understood that these equations were determined from magnetization curves of the actual reactors and may differ somewhat from manufacturers data. This procedure was followed to eliminate the introduction of extra errors in the computations of transfer curves. Nevertheless, these equations should be satisfactory for cores about the size of those tested. By proper considerations of the cores it should be possible to utilize the manufacturers data. In general the value of μ_{max} and exponential term will vary with the geometry of the core and μ_{min} is dependent upon the leakage fluxes which increase the saturated slopes of the magnetization curve.

The average value of μ over a cycle will then be

$$\mu_{av}=\frac{1}{H_{max}-H_0}\int_{H_0}^{H_{max}}(\mu_{max}\epsilon^{-\alpha H}+\mu_{min})dH=\frac{\mu_{max}}{(H_{max}-H_0)\alpha}[\epsilon^{-\alpha H_0}-\epsilon^{-\alpha H_{max}}]+\mu_{min} \quad (16)$$

Average Value of Load Current

In order to exploit the proposed method it is necessary to obtain an expression of $H_{2_{av}}$ for a single region of operation. It can be obtained from equation 5 by substituting $\mu=\mu_{av}$.

$$H_{2_{av}}=\frac{1}{\psi_2-\psi_1}\int_{\psi_1}^{\psi_n}\frac{V}{Z}\sin(\omega t-\theta)+C\epsilon^{-\omega t/\tan\theta}\,d\omega t \quad (17)$$

Also from equation 10 for a single region of operation and with

$H_2=0$ at $\omega t=0$

$$C=\frac{V}{Z}\sin\theta$$

Substituting for C and integrating from $\psi_1=0$ to ψ_n

$$H_{2_{av}}=\frac{V}{2\pi Z}[\cos\theta-\cos(\psi_n-\theta)+\sin\theta\tan\theta(1-\epsilon^{-\psi_n/\tan\theta})] \quad (18)$$

It can be seen that if the value of ψ_n which is the value of ωt at the time H_2 becomes zero is known, it is possible to compute the average value of H_2. Fortunately the exponential term in equation 5 in a practical case is very close to zero by the time $\omega t=\psi_n$; therefore.

$$H_2=\frac{V}{Z}\sin(\omega t-\theta)$$

as ωt becomes large, and

$$\sin(\psi_n-\theta)=0$$

at $H_2=0$, or

$$\psi_n=180+\theta \quad (19)$$

Substituting equation 19 into equation 18

$$H_{2_{av}}=\frac{V}{2\pi Z}\left[1+\cos\theta-\sin\theta\tan\theta\left(1-\epsilon^{-\frac{\pi+\theta}{\tan\theta}}\right)\right]$$

Following a similar procedure for the case of $H_2=0$ when $\omega t=\psi_1$, then

$$H_{2_{av}}=\frac{V}{2\pi Z}\left[1+\cos\theta-\sin(\psi_1-\theta)\times\tan\theta\left(1-\epsilon^{-\frac{\pi+\theta-\psi_1}{\tan\theta}}\right)\right] \quad (20)$$

Equation 20 can be rewritten as below

$$\frac{2\pi Z H_{2_{av}}}{V}=1+\cos\theta-\sin(\psi_1-\theta)\times\tan\theta\left(1-\epsilon^{-\frac{\pi+\theta-\psi_1}{\tan\theta}}\right) \quad (21)$$

which function is shown plotted for various values of θ in Figure 10. The usefulness of this set of curves will become obvious as one proceeds.

Application to a Half-Wave Amplifier

The preceding relations are applied to the computations of the output current of a half-wave circuit for all values of positive excitation in the following manner:

1. Utilizing equation 16 calculate μ_{av} between the value of d-c premagnetization H_0 and H_{max}. The value of H_{max} may be computed by assuming that the maximum current is determined by V/R_2, or if greater accuracy is desired, by $H_{max}=V/Z$ where Z is the value obtained from equation 7 when μ_{min} is substituted for μ.

2. With value of μ_{av} just determined, calculate Z and θ by means of equations 7 and 8. Knowing θ, the value of $2\pi Z H_{2_{av}}/V$ is found from curve of Figure 10 for case of $\psi_1=0$.

3. The value of $H_{2_{av}}$ can then be computed, and hence current I_2 by means of $I_2=\frac{H_{2_{av}}l}{n_2}$.

This process is comparatively simple, but for accurate results the determination of R_2 must be given further consideration, as it includes the nonlinear resistance R_x. The method used to compute the value of R_x is outlined in reference 5. In general, this procedure consists of drawing a load line on the rectifier forward a-c volt-ampere characteristic. This curve is a plot of the average alternating volts over the forward half cycle versus the average current in the forward cycle. The intersection of the load line and the characteristic curve gives a point of operation of the rectifier. The value of resistance computed by this manner corresponds to that which exists while the magnetic intensity passes through the saturated region of the magnetization curve.

Negative Premagnetization

For negative premagnetization (negative values of H_0) the computation of the

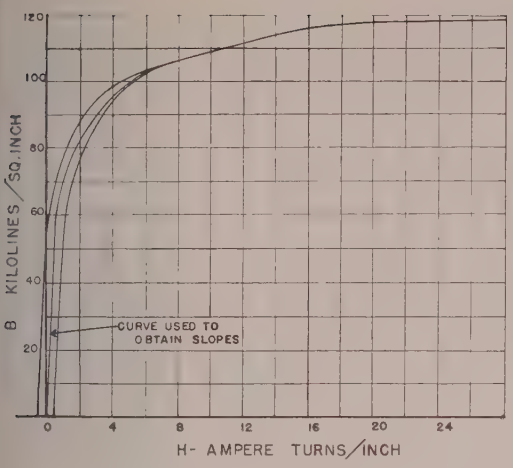

Figure 9A (left) D-c magnetization loop for Hypersil and curve used to obtain slopes

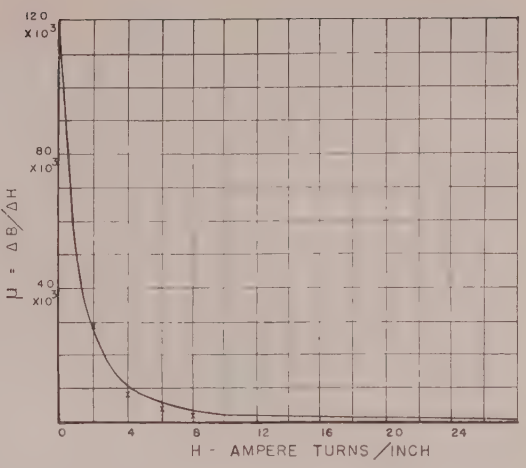

Figure 9B (right) Curve of slopes

x—point on $\mu = (120\epsilon^{-0.7H} + 011)10^3$

output curve is not quite as straightforward, because the two regions of the magnetization curves shown in Figure 8*B* must be considered. For simplification it can be assumed that the output current that flows before $\omega t = \psi_1$, at which time $H = H_0 + H_2 = 0$ does not contribute appreciably to the average value. A representative curve of H_2 versus ωt for this case will then be as shown in Figure 11. Actually current starts flowing at $\omega t = 0$, but its magnitude is very small; therefore, the operation below $H = 0$ can be considered as operating on a steep sloped region. The value of ψ_1 can be determined by substituting in equation 5 as follows

$$H_2 = H_0 = \frac{V}{Z_1} \sin(\psi_1 - \theta_1) + \frac{V}{Z_1} \sin \theta_1 \epsilon^{-\frac{\psi_1}{\tan \theta_1}}$$

But since for a steeply sloped region the value of θ_1 is very close to 90 degrees, this can be substituted for θ_1 and then solving for ψ_1

$$\psi_1 = \cos^{-1}\left(1 - \frac{Z_1 H_2}{V}\right) \qquad (22)$$

The problem remaining is to determine an adequate value of slope μ_1 for the negative region of operation.

In Figure 12 a curve of the variation of μ with excitation which was found to give good results is shown. This shape was obtained from d-c hysteresis loop illustrated in Figure 9*A*. The value of μ_{max} is determined by the maximum slope which is constant to $H = -h'$, and then decays as exponential curve which approximates the differential permeability curve as did curve of Figure 9*B*. Value h' is chosen as the point at which the magnetization begins to deviate rapidly from linearity.

The procedure for computing the output current for negative control excitations then proceeds as follows:

1. From equation of curve of Figure 12 compute average value of μ_1 from $H = H_0$ to $H = 0$.

2. Use equation 7 to determine Z_1 for this region.

3. Solve for angle ψ_1 by means of equation 22.

4. With average value of μ between $H = 0$ and H_{max} compute value of Z_{II} and θ_{II} by equations 7 and 8.

5. Determine value of $2\pi Z H_{2av}/V$ from curve of Figure 10 and values of θ_{II} and ψ_1 just computed. Using the value of Z_{II} found in the preceding step determine H_{2av} and I_2.

Experimental Verification of Simplified System

The transfer curves for two reactors computed by this method are shown in Figures 13 and 14. One of these reactors was constructed of Hypersil and the other of Orthonik, and it can be seen that the accuracy of the computations was satisfactory in either case. The curves shown are for two values of alternating supply voltage.

Full-Wave and Doubler Circuits

The half-wave circuit which has been analyzed to this point has limited application because of the high induced currents in the control circuit, and its comparatively low amplification; nevertheless, the formulas and the theory developed can be utilized for the full-wave-type circuits shown in Figures 2, 3, and 4. These full-wave and doubler circuits have the advantage of higher amplification and low induced currents in the control circuit, and are in general more "practical" circuits.

A brief study of these circuits reveals that they basically consist of two half-wave magnetic amplifiers coupled through a common load. With this knowledge one would consider adding the average output currents of the two half-wave amplifiers to obtain the load current of the doubler and full-wave amplifier circuits. Fortunately this procedure is approximately correct. However, detailed analysis of the functioning of these circuits also reveals two predictable effects which alter their output. A computation including these effects will give more accurate current values for these amplifiers.

Figures 15 and 16 show output of full-wave and doubler circuits compared to double the output of a half-wave amplifier for both Hypersil- and Orthonik-cored reactors. It is seen that the output of the doubler is greater than the full-wave and double of the half-wave circuit.

The curves for the amplifier with Orthonik cores show that the difference in load current of the full-wave and doubler circuits is small. Therefore, when reasonably good rectifiers are used double the output of two half-wave amplifiers should give an accurate indication of the output of either of these amplifiers. The curves for the Hypersil-cored amplifiers show a greater variation between the full-wave and doubler circuits; therefore, the relations which affect these amplifiers must be considered. There are apparently two factors which influence their operation:

1. Reverse current through rectifiers.

2. Overlap of the conduction period of each reactor, which results in simultaneous conduction of both reactors.

Each of these effects will be discussed separately.

Effect of Rectifier Leakage

This problem has been analyzed thoroughly by E. Smith in reference 9. Briefly, the rectifier leakage current has a demagnetization effect upon the cores. The listed reference develops three equations which relate the average value of

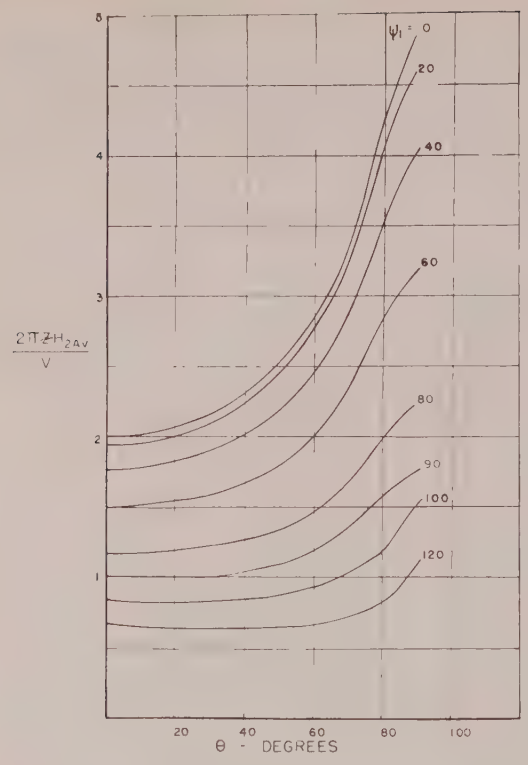

Figure 10 (left). Curves for obtaining average load current

Figure 11 (right). Variation of H_2 for case of negative premagnetization

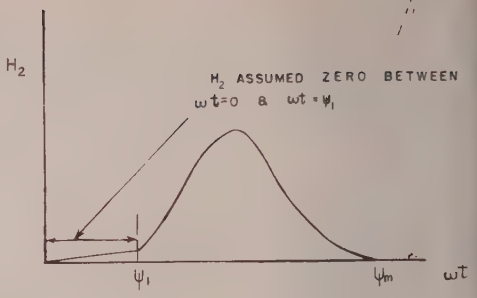

Figure 12 (right). Curve of slopes for negative premagnetization

Curve I equation.
$\mu=\mu_{max}\epsilon^{-\alpha H}+\mu_{min}$
Curve II equation.
$\mu=\mu_{max}\epsilon^{-\alpha(H-h')}+\mu_{min}$

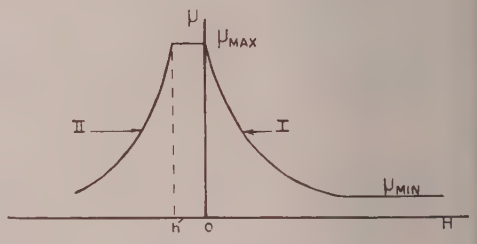

rectifier voltage during the inverse cycle to the amplifier output current. These formula are:

Half-Wave Amplifier
$$V_{zh}=2I_f(R_L+r+R_f)$$
Full-Wave Amplifier
$$V_{zh}=2I_f(2R_L+r+R_f)$$
Doubler Amplifier $V_{zh}=2I_f(r+R_f)$ (23)

where

V_{zh} = average value of rectifier voltage during the reverse cycle
I_f = average value of forward current flow in the rectifiers
r = resistance of the reactor windings
R_f = forward resistance of the rectifiers
R_L = load resistance

By means of suitable curves which data may be taken on the rectifiers, the average value of reverse current I_{LD} may be found. The magnitude of this demagnetizing current I_{CD} referred to the control circuit may be computed by

$$I_{CD}=\frac{N_2}{N_1}I_{LD} \qquad (24)$$

It is then assumed that the entire effect of the leakage current is to demagnetize the core, and therefore a higher value of control current I_0' is required to maintain the same output. Hence

$$I_0'=I_0+I_{CD} \qquad (25)$$

In order to correct for rectifier leakage it is therefore only necessary to determine I_{CD} by means of equations 23 and 24 for a particular value of output current corresponding to a control current I_0. This point is then shifted to a value of control current I_0' computed by equation 25.

It can be seen from equation 23 that the value of V_{zh}, and hence the effect of leakage, is greatest for the full-wave amplifier. It is less on the half-wave, and is a minimum on the doubler circuit.

Effect of Overlap or Dual Conduction

Overlap in a magnetic amplifier is illustrated in Figure 17; current flows in reactor B until $\omega t=\psi_n$ so that both reactors are conducting simultaneously. Reference 8 contains a detailed analysis of the effect of overlap in a full-wave amplifier based on three straight-line regions.

In the half-wave amplifier, current starts flowing essentially in phase with the beginning of the positive half cycle of the applied voltage. Referring to Figure 17 it is seen that this does not hold true for the full-wave amplifier, but rather in each reactor the current lags the voltage by angle β. This lag is caused by the dual conduction of both reactors, since the current flowing in reactor B causes a drop in the common load resistance. This drop subtracts from the applied voltage in the loop of reactor A.

The magnitude of angle β can be determined by considering the conditions at $\omega t=\beta$. Since current flow in reactor A is imminent, the voltage across rectifier R_x is zero. Therefore the following equation may be written concerning the mesh of reactor A

$$V\sin\beta-I_{22}R_L=0 \qquad (26)$$

where I_{22} is current in reactor B at $\omega t=\beta$ Rearranging and introducing

$$I_{22}=\frac{H_{22}l}{N_2}$$

equation 26 becomes

$$V\sin\beta=\frac{H_{22}lR_L}{N_2} \qquad (27)$$

The problem is now resolved into determining the value of H_{22} at $\omega t=\beta$, which problem is somewhat tedious if an exact solution is attempted. Since the value of β is usually of the order 0 to 30 degrees, only a small error will be introduced if H_{22} is computed for $\omega t=0$ (180 degrees of cycle of Reactor B). The procedure for calculating the value of β and its effect, then reduces to the following:

1 Compute H_{22} by means of equation 5 for a single region of operation and substitute the value of C shown in equation 10 in order to obtain

$$H_{22}=\frac{V}{Z}\left[\sin(\pi-\theta)+\epsilon^{-\frac{K_1R_2}{\omega\mu_{av}}\pi}\right]$$

where μ_{av} is the average slope as computed for half-wave amplifier.

2. Using this value of H_{22} calculate β by means of equation 27.

3. Now proceeding as in half-wave amplifier find the value of $2\pi ZH_{2av}/V$ from curves on Figure 10 considering β as a delay in conduction similar to angle ψ_1. It is now possible to compute H_{2av} and I_2 as previously outlined.

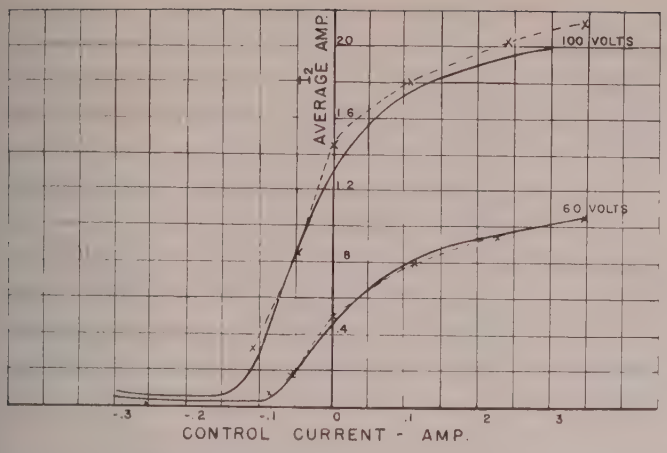

Figure 13. Transfer curves for half-wave amplifier with Hypersil core-load resistance $R_L = 15$ ohms

——— experimental curve
x - - - x computed curve

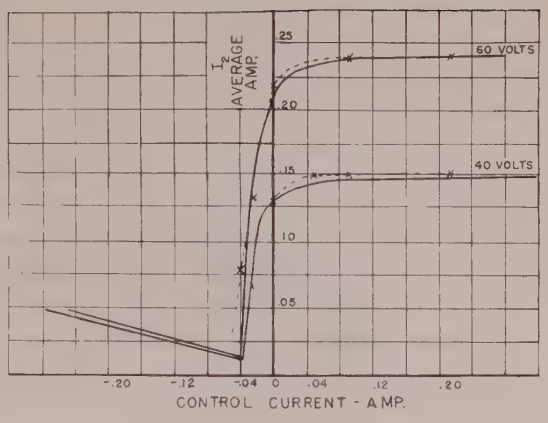

Figure 14. Transfer curves for half-wave amplifier with Orthonik core-load resistance $R_L = 80$ ohms

——— experimental curve
x - - x computed curve

These corrections were applied to a full-wave amplifier with the results shown on Figure 16. The complete procedure for calculating two points on the transfer curve is outlined in Appendix II.

Conclusions

The analysis proposed in this paper offers a rapid means of computing the transfer curves of self-saturating magnetic amplifiers. The accuracy of the results in comparison with tests is satisfactory. The method developed promises to offer a straightforward design procedure for self-saturating magnetic amplifiers.

A problem which was not discussed but which can be analyzed by this method is the inclusion of inductance in the load circuit. If this load inductance is constant, its effect can be predicted by merely increasing the slopes of each region of the magnetization curve. A possible exception to this is the full-wave circuit which may have trigger action with inductive loads.

Figure 15. Transfer curves for full-wave amplifiers with Orthonik cores

Load resistance = 80 ohms
rms a-c supply voltage = 60 volts
x = two times computed half-wave amplifier output
Curve I—Experimental curve of doubler circuit
Curve II—Experimental curve of two times half-wave circuit
Curve III—Experimental curve of full-wave circuit

Appendix I

The basis of the simplified straight-line method lies in the fact that an average value of the slopes of the regions of operation may be used to compute points over a large range of the transfer curve. The justification that the method gives an approximate solution to the problem will now be shown. Consider the curve of a-c ampere-turns per inch versus ωt as shown in Figure 18, where operation over four regions is illustrated.

If it is now proven that the value of H_{2av} may be computed by an average value of μ for two regions of the magnetization curve, then the operation over a number of regions can be thought of as consisting of combinations of two regions. For example, if this is true for regions I and II, they may be combined into single region with slope μ_{av},

Figure 16. Transfer curves for full-wave amplifiers with Hypersil cores

Load resistance $R_L = 15$ ohms
rms a-c supply voltage = 100 volts
Curve I. Experimental curve of doubler circuit
Curve II. Experimental curve of two times half-wave circuit
Curve III. Experimental curve of full-wave circuit
0 = Computed value of two times half-wave amplifier output
● = Computed value of two times half-wave amplifier output corrected for overlap
* = Computed value of two times half-wave amplifier output corrected for overlap and rectifier leakage

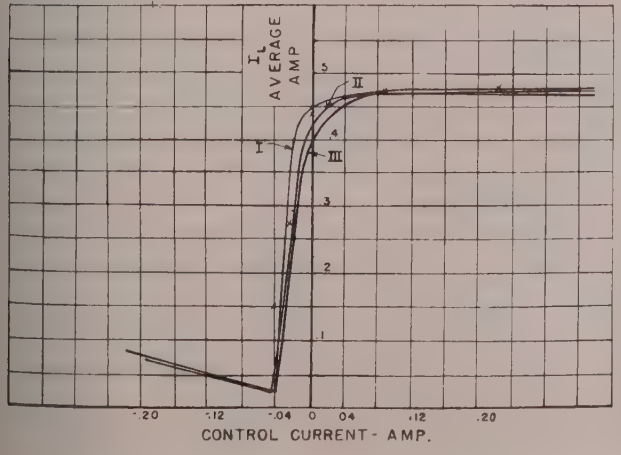

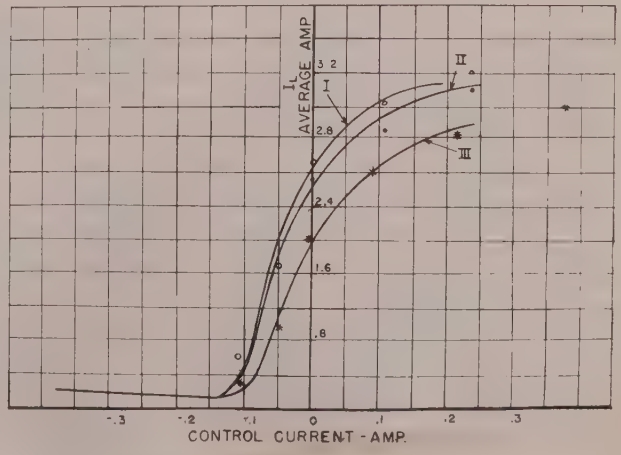

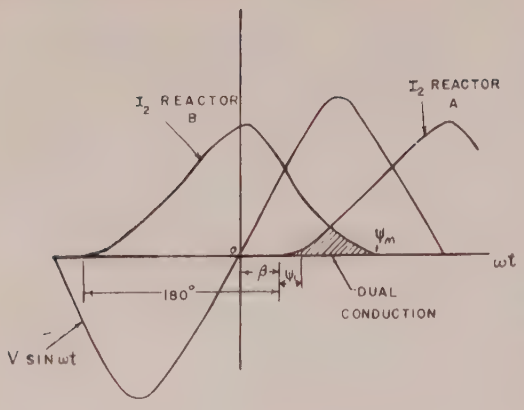

Figure 17 (left). Output current of full-wave amplifier illustrating overlap or dual conduction

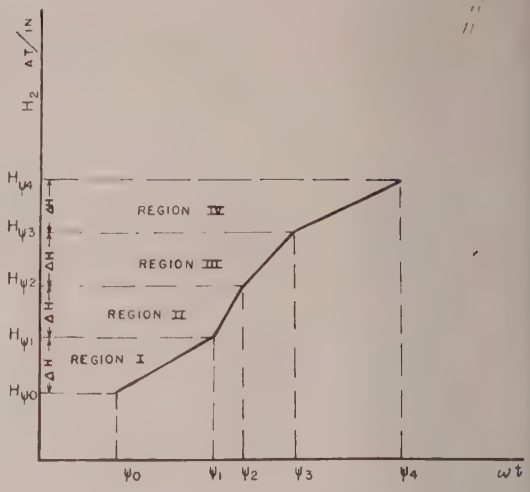

Figure 18 (right). General variation of output magnetic intensity H_2 through several regions of magnetization curve (utilized in analysis of Appendix 1)

which in turn may be combined with a region with average μ_{av} of region III and IV. In a similar manner the regions may be combined until the complete cycle of variation of H_2 is considered.

Proceeding by substituting equations 3 and 4 in equation 1, and then rearranging, the differential equations for each region

$$H_{1I}=\frac{VK}{K_1R_2}\sin\omega t-\frac{\mu_I}{R_2K_1}\frac{dH_{2I}}{dt} \qquad (28a)$$

$$H_{2II}=\frac{VK}{K_1R_2}\sin\omega t-\frac{\mu_{II}}{R_2K_1}\frac{dH_{2II}}{dt} \qquad (28b)$$

where the constants K and K_1, are given in equations 6 and 9, and the subscripts I and II indicate region of operation.

The average value of H_2 for operation through the regions I and II can then be

$$H_{2av}=\frac{1}{t_2-t_0}\left\{\int_{t_0}^{t_1}\left(\frac{VK}{K_1R_2}\times\sin\omega t-\frac{\mu_I}{K_1R_2}\frac{dH_{2I}}{dt}\right)dt+\int_{t_1}^{t_2}\left(\frac{VK}{K_1R_2}\sin\omega t-\frac{\mu_{II}}{K_1R_2}\frac{dH_{2II}}{dt}\right)dt\right\} \qquad (29)$$

Now

$$\frac{dH_{2I}}{dt}\,dt=dH_{2I}$$

and

$$\frac{dH_{2II}}{dt}\,dt=dH_{2II} \qquad (30)$$

which can be substituted in equation 29 with the result that

$$H_{2av}=\frac{1}{\psi_2-\psi_0}\left\{\frac{VK}{K_1R_2}(\cos\psi_0-\cos\psi_2)-\frac{\mu_I}{K_1R_2}[H_{\psi_1}-H_{\psi_0}]-\frac{\mu_{II}}{K_1R_2}[H_{\psi_2}-H_{\psi_1}]\right\} \qquad (31)$$

Referring to Figure 18 it is seen that by choosing the increments of H_2 equal to ΔH, the analysis is not restricted since the time in each region varies to conform to the actual curve. Then substituting this fact in equation 31 and allowing

$$\frac{\mu_I+\mu_{II}}{2}=\mu_{av}$$

it becomes

$$H_{2av}=\frac{1}{\psi_2-\psi_0}\left[\frac{VK}{K_1R_2}(\cos\psi_0-\cos\psi_2)-\frac{\mu_{av}}{K_1R_2}(H_{\psi_2}-H_{\psi_0})\right] \qquad (32a)$$

Using the average value of μ and computing the average value of H_2, considering as a single region, a similar equation is obtained. This equation can be written

$$H_{2av}=\frac{1}{\psi_2-\psi_0}\left[\frac{VK}{K_1R_2}(\cos\psi_0-\cos\psi_2')-\frac{\mu_{av}}{K_1R_2}(H_{\psi_2}-H_{\psi_0})\right] \qquad (32b)$$

Equations 32*a* and 32*b* would be exactly equivalent if the value of ψ_2 computed by the two region calculation equaled the value of ψ_2' computed by means of one region. It now remains to be shown that ψ_2 computed by both methods are very nearly alike.

If we assume the values of ΔH are taken of such magnitude that the variation of H versus ωt is nearly linear in each region then

$$\frac{dH_{2I}}{dt}=\frac{\omega\,\Delta H}{\psi_1-\psi_0}\text{ and }\frac{dH_{2II}}{dt}=\frac{\omega\,\Delta H}{\psi_2-\psi_1}$$

This value for dH_{2II}/dt can be substituted into equation 28*b* which can be written for $\omega t=\psi_2$ as

$$H_{\psi_2}=H_{\psi_0}+2\,\Delta H=\frac{VK}{K_1R_2}\times\sin\psi_2-\frac{\omega\mu_{II}}{K_1R_2}\frac{\Delta H}{\psi_2-\psi_1}$$

Solving for $\sin\psi_2$, and writing as follows:

$$\sin\psi_2=\frac{K_1R_2}{VK}\left[H_{\psi_0}+2\,\Delta H+\frac{\omega(\mu_I+\mu_{II})\,\Delta H-\omega\mu_I\,\Delta H\left(\frac{\psi_2-\psi_0}{\psi_2-\psi_0}\right)}{K_1R_2\quad(\psi_2-\psi_1)}\right] \qquad (33)$$

Now letting

$$\psi_2-\psi_0=(\psi_2-\psi_1)+(\psi_1-\psi_0)$$

and

$$\mu_{av}=\frac{\mu_I+\mu_{II}}{2}$$

and substituting

$$\sin\psi_2=\frac{K_1R_2}{VK}\left[H_{\psi_0}+2\,\Delta H+\frac{2\omega\mu_{av}\,\Delta H}{\psi_2-\psi_0}\right]+\frac{K_1R_2}{VK}\left[\frac{2\omega\mu_{av}\,\Delta H}{\psi_2-\psi_0}\left(\frac{\psi_1-\psi_0}{\psi_2-\psi_1}\right)-\frac{\omega\mu_I\,\Delta H}{\psi_2-\psi_1}\right] \qquad (34)$$

Computing $\sin\psi_2'$ by means of the average value of μ over both regions one obtains

$$\sin\psi_2'=\frac{K_1R_2}{VK}\left[H_{\psi_0}+2\,\Delta H+\frac{2\omega\mu_{av}\,\Delta H}{\psi_2-\psi_0}\right] \qquad (35)$$

Comparison with equation 34 shows that $\sin\psi_2$ may now be written as

$$\sin\psi_2=\sin\psi_2'+\text{Error} \qquad (36)$$

Analyzing and rearranging the equation for the error

$$\text{Error}=\frac{K_1R_2}{VK}\left[\frac{\omega\mu_{II}(\psi_1-\psi_0)-\omega\mu_I(\psi_2-\psi_1)}{(\psi_2-\psi_0)(\psi_2-\psi_1)}\right]\times\Delta H \qquad (37)$$

This error is self-compensating in that when μ_{II} is large $\psi_2-\psi_1$ is large, and similarly when μ_I is large $\psi_1-\psi_0$ is large. The magnitude of the error is dependent upon two values which tend to be equal, and hence H_{2av} as computed by equations 32*a* and 32*b* are nearly equal.

Thus, it has been shown that the average value of the slope of the magnetization curve may be used to compute an approximate value of H_{2av}. This method was tried and it was found to be accurate for all values of positive premagnetization.

Appendix II

Calculation of Sample Points on Transfer Curve Reactor Data

Material = Hypersil
l = 11.5 inches
A = 1.64 square inches
N_2 = 276 turns
N_1 = 100 turns
r = 1.4 ohms

Computing parameters K and K_1 by equations 6 and 9

$K_1 = 9.21 \times 10^3$
$K = 2.21 \times 10^5$

TEST 1. HALF-WAVE CIRCUIT

$R_L = 15$ ohms
$H_0 = 0$
$V = 100$ volts rms

By method of reference 10 the forward resistance of rectifier is 3.6 ohms; therefore,

$R_2 = 15 + 3.6 + 1.4 = 20$ ohms

and $H_{max} = V/Z$. Assuming $\mu = 0$ in equation 7 this reduces to

$$H_{max} = \frac{VK}{K_1 R_2} = \frac{141(2.21)10^5}{9.21 \times 10^3(20)} = 169 \text{ ampere-turns per inch}$$

By equations 15 and 16 for Hypersil

$$\mu_{av} = \left[\frac{120}{(169)0.7}\left[\epsilon^{-0} - \epsilon^{0.7(169)}\right] + 0.11\right] \times 10^3 = 1.11 \times 10^3$$

Computing Z and θ by equations 7 and 8

$Z = 2.07$
$\theta = 66$ degrees 10 minutes

Determining point corresponding to $\theta = 66$ degrees 10 minutes on the $\psi_1 = 0$ curve on Figure 10

$$\frac{2\pi H_{2av} Z}{V} = 3.25$$

Solving for H_{2av} and I_2

$H_{2av} = 35.4 \quad I_2 = 1.47$ amperes

TEST 2

Same as Test 1 except $H_0 = -0.5$ ampere turns per inch.

For Hypersil h' of Figure 12 corresponding to -0.5 ampere-turns per inch; therefore, μ_{av} of negative region is 120×10^3.

By equation 7 solve for Z but since

$\omega m >> K_1 R_2$

$$Z = \frac{\omega m}{K} = \frac{377(120 \times 10^3)}{2.21 \times 10^5} = 205$$

Solving for ψ_1 by equation 22

$$\psi_1 = \cos^{-1}\left(1 - \frac{205(0.5)}{141}\right)$$

$= 74$ degrees 10 minutes

Locating point on Figure 10 corresponding to this value of ψ_1 and the θ of case of $H_0 = 0$

$$\frac{2\pi H_{2av} Z}{V} = 1.85$$

which when solved for H_{2av} and I_2 results in $I_2 = 0.833$ amperes.

TEST 3. FULL-WAVE CIRCUIT

$H_0 = 0$
$R_L = 15$ ohms
$V = 100$ volts

Correction for Overlap

Compute H_{22} for $\omega t = 180$ degrees by means of equation 5

$$H_{22} = \frac{141}{2.07}\left[\sin(\pi - \theta) + \epsilon^{-\frac{\psi}{2.27}}\right] = 79 \text{ ampere-turns per inch}$$

Solving for β by equation 27

$$\sin \beta = \frac{79(11.5)(15)}{141(276)} = 0.00447\ H_{22}$$

where

$\beta = 20$ degrees 40 minutes

From Figure 10

$$\frac{2\pi H_{2av} Z}{V} = 3.05$$

and hence $I_2 = 1.38$ amperes; I_L for full-wave circuit will then be 2.76 amperes. Correction for rectifier leakage is computed for this same amplifier in reference 9.

Appendix III

List of Symbols

A . . . . Cross-section of core, square inches
B . . . . Flux density, kilolines per square inch
B_n . . . . Flux density at intersection of slope line of a region and B axis, kilolines per square inch
C . . . . Constant of integration, ampere-turns per inch
E . . . . Direct voltage on control windings, volts
H . . . . Total magnetic field intensity, ampere-turns per inch
H_2 . . . . Magnetic field intensity due to load winding, ampere-turns per inch
H_{2av} . . . Average value of magnetic field intensity due to load windings, ampere-turns per inch
H_0 . . . . Magnetic field intensity produced by direct current in control winding, ampere-turns per inch
H_{max} . . . Maximum value of H, ampere-turns per inch
h_n . . . . . Magnetic field intensity at juncture of the n and $n-1$ regions; $n = 1, 2, \ldots n$, ampere-turns per inch
I_{CD} . . . Equivalent demagnetizing control current due to rectifier leakage, amperes
I_f . . . . Average value of forward rectifier current, amperes
I_{LD} . . . Average value of reverse rectifier current, amperes
I_2 . . . . . Current in load circuit, amperes
I_0 . . . . . D-c value of current in control circuit, amperes
I_0' . . . . D-c value of current in control circuit corrected for rectifier leakage, amperes
K . . . . Composite parameters, square-inches $\times$ seconds-squared
K_1 . . . . Composite parameters, square-inches $\times$ seconds-squared
l . . . . . Length of magnetic flux path in core, inches
N_1 . . . . Turns on control winding, turns
N_2 . . . . Turns on load winding, turns
r . . . . . Resistance of reactor load winding, ohms
R_f . . . . Forward resistance of rectifiers, ohms
R_L . . . . Load resistance, ohms
R_r . . . . Reverse resistance of rectifiers, ohms
R_x . . . . Rectifier resistance, ohms
R_1 . . . . Series resistance of control circuit, ohms
R_2 . . . . Total series resistance of load circuit, ohms
V . . . . . Maximum value of applied alternating voltage, volts
V_{xh} . . Average value of rectifier voltage during reverse cycle, volts
Z . . . . . Composite parameter, ohm-inches per turn
β . . . . . Apparent current lag caused by dual conduction, degrees
α . . . . . Constant used to match μ curve
θ_n . . . . Phase angle of inductive lag in region n, degrees
ψ_n . . . . Angle at which transition from region n to region $n-1$ occurs; $n = 1, 2, \ldots n$, degrees
ϕ . . . . . Total flux linking the load winding, kilolines
$d\phi/dt$ . . Time derivative of flux, kilolines per second
μ_n . . . . Slope of magnetization curve in region n, kilolines per ampere-turn per inch
μ_{av} . . . Average slope of magnetization curve over number of regions, kilolines per ampere-turn per inch
μ_{max} . . . Maximum slope of magnetization curve, kilolines per ampere-turn per inch
μ_{min} . . . Minimum slope of magnetization curve, kilolines per ampere-turn per inch

References

1. NUMERICAL MATHEMATICAL ANALYSIS (book), **J. B. Scarborough.** Johns Hopkins Press, Baltimore, Md., 1930.

2. AN ANALYSIS OF INTERLINKED ELECTRIC AND MAGNETIC NETWORKS WITH APPLICATION TO MAGNETIC AMPLIFIERS, **D. W. VerPlank, M. Fishman.** *Proceedings,* Institute of Radio Engineers (New York, N. Y.), volume 37, September 1949.

3. AN ANALYSIS OF MAGNETIC AMPLIFIERS WITH FEEDBACK, **D. W. VerPlank, M. Fishman, D. C. Beaumariage.** *Proceedings,* Institute of Radio Engineers (New York, N. Y.), volume 37, August 1949.

4. SELF-SATURATION IN MAGNETIC AMPLIFIERS, **W. J. Dornhoefer.** *AIEE Transactions,* volume 68, part II, 1949, pages 835–50.

5. STEADY STATE RESPONSE OF HALF WAVE CIRCUIT, **E. J. Smith.** *Report R-229-49, PIB-174,* Microwave Research Institute, Polytechnic Institute of Brooklyn (Brooklyn, N. Y.), 1949.

6. MATHEMATICAL ANALYSIS OF NON-LINEAR CIRCUITS, **A. Boyajian.** *General Electric Review* (Schenectady, N. Y.), volume 34, 1931.

7. STEADY STATE ANALYSIS OF A MAGNETIC AMPLIFIER, **W. Esselman, E. J. Smith.** *Report R-196-49, PIB-140,* Microwave Research Institute, Polytechnic Institute of Brooklyn (Brooklyn, N. Y.), 1949.

8. STRAIGHT LINE ANALYSIS OF FULL-WAVE MAGNETIC AMPLIFIER, **W. Esselman.** *Report R-223-49, PIB-168,* Microwave Research Institute, Polytechnic Institute of Brooklyn (Brooklyn, N. Y.), 1949.

9. INVESTIGATION OF RECTIFIER REVERSE CURRENT FLOW AND STEADY-STATE ANALYSIS OF FULL-WAVE AND DOUBLER CIRCUITS, **E. J. Smith.** *Report R-230-50, PIB-175,* Microwave Research Institute, Polytechnic Institute of Brooklyn (Brooklyn, N. Y.), 1950.

No Discussion

The Effects of Loads and Disturbances upon Feedback Controllers

R. W. JONES
MEMBER AIEE

THE FUNCTION of many industrial regulating systems is to hold some process quantity (current, speed, voltage) at a reasonably constant value in the face of a diversity of disturbances which otherwise would cause that quantity to vary with time in an unacceptable manner. As usually conceived, such a feedback controller of the proportional type appears as in Figure 1, in which the regulated quantity, x_4, is compared with a standard or reference quantity, x^*, and the "error," x_1, is used to produce a correction of such a sign as to reduce the error.

However, it will be found that in many systems of the type under discussion the standard used to set the level of the regulated quantity frequently is not observable, and in many cases is even inaccessible. The criterion of good performance is that the regulated quantity remain within certain bounds in the presence of all disturbances to which the components of the system may be exposed. In this light, the actual error existing at any time is of no consequence. This situation is in contrast with that in a servomechanism, or position regulator, in which it is desired that the difference between the standard (now the input quantity) and the output position be kept at a minimum.

Paper 51-73, recommended by the AIEE Feedback Control Systems Committee and approved by the AIEE Technical Program Committee for presentation at the AIEE Winter General Meeting, New York, N. Y., January 22–26, 1951. Manuscript submitted October 20, 1950; made available for printing December 13, 1950.

R. W. JONES is with Northwestern University, Evanston, Ill.

The author wishes to thank H. W. COXY and A. C. HALTER of the Allis-Chalmers Manufacturing Company for their helpful discussion of this problem, and for their permission to use the example discussed in the section on nonlinear cases.

The above comparison should indicate that in a so-called industrial regulator the principal problem is that of minimizing any change in error, whereas with a servomechanism the problem generally is one of minimizing the error itself.

Furthermore, many industrial regulators are applied to situations in which the system gain is determined principally by limitations on the change in the steady-state value of the regulated quantity (frequently expressed as percentage accuracy), and the system must be suitably compensated to give satisfactory transient performance with this value of gain. With servomechanisms in which the steady-state positional error is theoretically zero, the question of gain is largely (but not exclusively) one of satisfactory transient characteristics or of minimum error with certain types of inputs. Although the subject of system disturbances and loads, and their effect upon controller design, has been touched upon in the literature,[1,2] it does not appear to have been covered adequately. It is the purpose of this paper to develop the necessary concepts for the determination of gain in a feedback controller.

Discussion of Typical Loads and Disturbances

It is the object of this section to describe certain typical disturbances such as are encountered in systems of the type under discussion, and to point out in particular that a qualitative description of such disturbances does not give an adequate picture of the quantitative aspects as they arise in system design. Consider, first, a number of disturbances classified for convenience as regards their location within the system.

Input disturbances are defined as those which affect the magnitude of the standard or reference which is used to set the level of the regulated quantity. In the systems under discussion, this standard is held constant, but random variations in its value will be reflected directly in the regulated quantity.

Load disturbances are defined as those demands upon the system which change the power level of the output, and as a consequence change the magnitude of the regulated quantity. An impedance connected across the terminals of a generator or a resisting torque impressed upon the shaft of a motor are obvious examples. These are sometimes referred to as demand disturbances.

Internal disturbances are defined as those changes in the several components of the system which effectively alter the magnitude of certain parameters. In the usual analysis these parameters would be considered as constants. The heating of a field winding and the change in speed of a generator may be cited as examples.

In order to see more precisely the effect of these disturbances it will be desirable to examine a few cases in some detail. Most of the following discussion will be directed toward the calculation of system gain required to maintain the regulated quantity within some percentage of its set value. With this an objective we shall be concerned primarily with the steady-state relations, although it will be of interest to point out certain aspects of the corresponding transient relations.

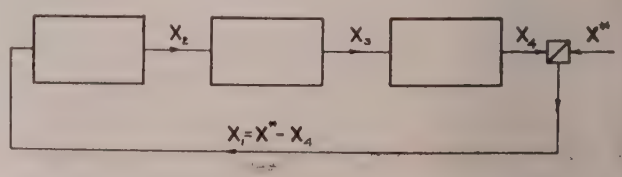

Figure 1. Block diagram of a feedback control system, proportional type

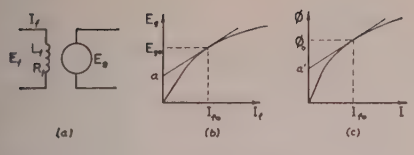

Figure 2. Separately excited d-c generator

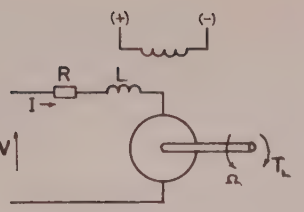

Figure 3. D-c shunt motor

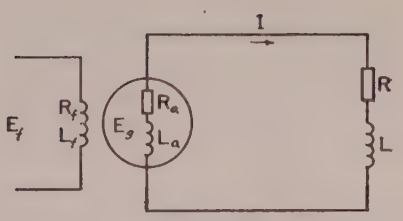

Figure 4. D-c generator with constant impedance load

Case 1. Field Heating of a D-C Shunt Generator

Figure 2 shows a separately excited generator assumed to be operating at a constant speed, together with two representations of its magnetization curve. Using the quantities defined in this figure one may write

$$E_f = R_f I_f + L_f p I_f \tag{1}$$

$$E_g = a + b I_f \tag{2}$$

and upon eliminating I_f

$$E_g = a + b\frac{E_f}{R_f + L_f p} \tag{3}$$

It will be seen that equation 2 makes use of a straight-line approximation to the magnetization curve, at the point I_{fo}, E_{go}.

In order to make a transient study of this machine one would assume small changes about this operating point. This would be done by expressing each of the variables as the sum of its equilibrium and incremental values. Thus

$$E_f = E_{fo} + e_f \tag{4}$$

$$E_g = E_{go} + e_g \tag{5}$$

$$I_f = I_{fo} + i_f \tag{6}$$

in which the subscripts o denote the equilibrium values and the lower case letters the incremental values. The relations between the equilibrium values, found by setting all derivatives and incremental terms equal to zero are

$$E_{fo} = R_f I_{fo} \tag{7}$$

$$E_{go} = a + b I_{fo} \tag{8}$$

$$E_{go} = a + \frac{b}{R_f} E_{fo} \tag{9}$$

Furthermore, if equations 4, 5, and 6 are substituted into equations 1 and 2, and the equilibrium relations (equations 7 and 8) subtracted therefrom, one obtains the incremental relations

$$e_g = b i_f \tag{10}$$

$$e_f = R_f i_f + L_f p i_f \tag{11}$$

It thus is seen that in terms of the equilibrium or "quiescent" values the relation between the generated and field voltages is that given by equation 9, whereas for the incremental values the relation is

$$e_g = \frac{b/R_f}{1 + \frac{L_f}{R_f} p} e_f \tag{12}$$

It is apparent that equation 12 is the one normally used as the transfer function for a d-c generator, and that equation 9 is quite different from it. It should be mentioned that the value of L_f to be used in equations 11 and 12 is the incremental inductance at the operating point.

The effect of field heating and a consequent increase in the field resistance may be seen from the above relations. A change in R_f will change the slope of equation 9, but not the intercept. In equation 12 a change in R_f will affect both the magnitude of this relation and the time constant.

Case 2. Change in Speed of a D-C Generator

The prime mover driving the generator in Figure 2 may exhibit a change in speed, either from the effect of loading or from some other cause. The relation between the machine flux and the field current (Figure 2C) will be approximated by a straight line as before; that is,

$$\phi = a' + b' I_f \tag{13}$$

and therefore

$$E_g = a' K\Omega + b' K\Omega I_f \tag{14}$$

Proceeding as before, the following equilibrium and incremental relations may be found

$$E_{go} = a' K\Omega + \frac{b' K\Omega}{R_f} E_{fo} \tag{15}$$

$$e_g = \frac{b' K\Omega}{1 + \frac{L_f}{R_f} p} e_f \tag{16}$$

It is concluded from the above relations that a change in speed appears as a change in both the intercept and the slope in the equilibrium relation, and as a change in the magnitude only in the incremental relation.

Case 3. D-C Shunt Motor with Constant Torque Loading

The motor of Figure 3 is assumed to have a constant field excitation. The voltage and torque equations for this machine are

$$V = RI + LpI + K\Omega \tag{17}$$

$$K_T I = T_L + Jp\Omega \tag{18}$$

in which K is the counter electromotive force constant, K_T is the torque constant, and J is the polar moment of inertia of the motor. The resulting equation of motion is

$$p^2\Omega + \frac{R}{L} p\Omega + \frac{KK_T}{JL}\Omega = \frac{VK_T}{JL} - \frac{RT_L}{JL} \tag{19}$$

Writing each of the variables as the sum of an equilibrium and an incremental value as before, the following two expressions may be obtained.

$$KK_T\Omega_o = K_T V - RT_L \tag{20}$$

$$p^2\omega + \frac{R}{L} p\omega + \frac{KK_T}{JL}\omega = \frac{K_T}{JL} v \tag{21}$$

Examination of the above equations shows that the constant torque loading does not affect the incremental relation and contributes a constant term to the

Nomenclature

a, a', b, b' = constants
E, e = voltage
I, i = current
J = polar moment of inertia of motor and load
K = motor counter electromotive force constant
K_T = motor torque constant
k = system gain
L = inductance
$m = k'/k$
N = number of turns
$p = \frac{d}{dt}$
R = resistance
T_L = load torque
V, v = voltage
x = process variable
x^* = reference quantity
ϕ = flux
Ω, ω = angular velocity

equilibrium relation. In addition it will be seen that a change in excitation of the motor will alter the value of both K and K_T. This would change both the slope and the intercept of equation 20 and the magnitude of two terms in equation 21.

CASE 4. D-C GENERATOR UNDER LOAD

In Figure 4 is shown a d-c generator feeding a constant impedance load. The following three expressions are self-evident.

$$E_g = a + b\frac{E_f}{R_f + L_f p} \tag{22}$$

$$V = E_g - R_a I - L_a pI \tag{23}$$

$$E_g = (R_a + R)I + (L_a + L)pI \tag{24}$$

The equilibrium and incremental relations are

$$V_o = \frac{R}{R_a + R}\left(a + \frac{b}{R_f}E_{fo}\right) \tag{25}$$

$$v = \left(\frac{\dfrac{R}{R_a+R} - \dfrac{L}{R_a+R}p}{1 + \dfrac{L_a+L}{R_a+R}p}\right)\left(\frac{b/R_f}{1+\dfrac{L_f}{R_f}}\right)e_f \tag{26}$$

If the above two equations are compared with equations 9 and 12 for the unloaded machine, the effect of the load may be clearly seen. In particular, the incremental relation will be seen to be of an entirely different form from that derived for the unloaded generator.

The preceding examples should indicate that any qualitative discussion of disturbances such as that which introduced this section is of little practical value. Rather, a classification of these disturbances on the basis of their analytical implications would appear to be more to the point. This is done in the following section.

Analysis of the Effect of Disturbances on the Steady-State Values

It is now evident that disturbances to the system result in such modification of the equilibrium relations that one is, in effect, concerned with two different sets of equations. The problem at hand, then, has to do with the variation in the solution of a system of equations, when that system is modified in some particular manner. For concreteness, consider the 3-component system of Figure 1, for which the following equilibrium relations may be written.

$$x_2 = a_1 + b_1 x_1 \tag{27}$$

$$x_3 = a_2 + b_2 x_2 \tag{28}$$

$$x_4 = a_3 + b_3 x_3 \tag{29}$$

$$x_1 = x^* - x_4 \tag{30}$$

The preceding equations assume that for each component a linear approximation is used to represent the relation between the input and output variables. A study of this system of equations in the light of the examples discussed previously reveals that one might expect any of the following changes to occur as the result of some disturbance.

1. A change in the value of one or more coefficients.
2. The addition of, or change in, the constant terms in the several equations.
3. The addition of one or more equations to the existing system of equations.

The preceding system of equations may be solved for x_4.

$$x_4 = \frac{b_1 b_2 b_3 x^* + a_1 b_2 b_3 + a_2 b_3 + a_3}{1 + b_1 b_2 b_3} \tag{31}$$

Equation 31 reveals that the intercepts (a_1, a_2, and so forth) contribute to the magnitude of the regulated quantity (x_4) in the same general manner as does x^*, except that the contribution of any one intercept depends upon the gain between that component and the regulated variable. Furthermore, x_4 will have a value other than zero even though $x^* = 0$, in which case the several intercepts act as reference quantities to set the level of x_4. However, in this case it still is necessary to include within the system a means for reversing the sign of the error (equation 30), which is, of course, required to provide regulatory action.

The application of equation 31 to study the effects of disturbances is not quite so straightforward as it may appear. This is because a change in any one of the a's or b's in this expression will, in general, change the operating point and thus bring about a change in all the other terms. There is one special case which is of some interest. Let

$$a_1 = a_2 = a_3 = 0$$

then

$$x_4 = \frac{b_1 b_2 b_3 x^*}{1 + b_1 b_2 b_3} \tag{32}$$

This obviously is the case of a linear system for which the linear approximations used previously are not necessary. Equation 32 will be recognized as the usual feedback expression, in which $b_1 b_2 b_3 = k$ is the over-all system gain. Consider the effect of a change in the gain from k to k'. Then

$$x_4 = \frac{kx^*}{1+k} \tag{33}$$

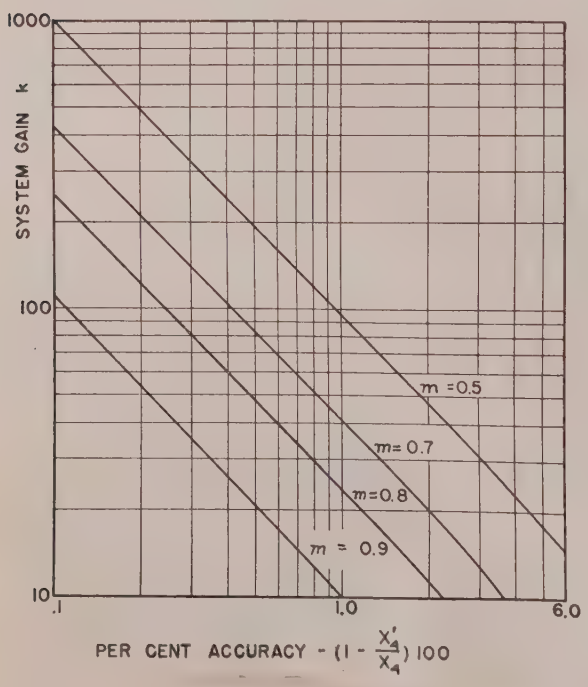

Figure 5 (left). Gain required in a proportional regulating system

Figure 6 (below). Current-regulating system using a buck-boost generator

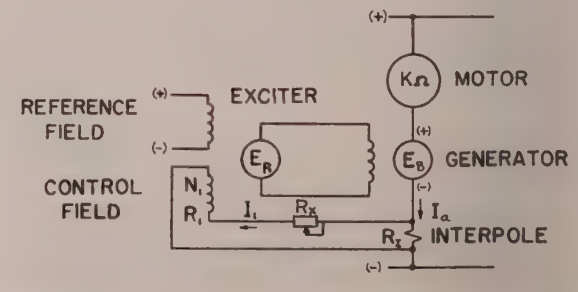

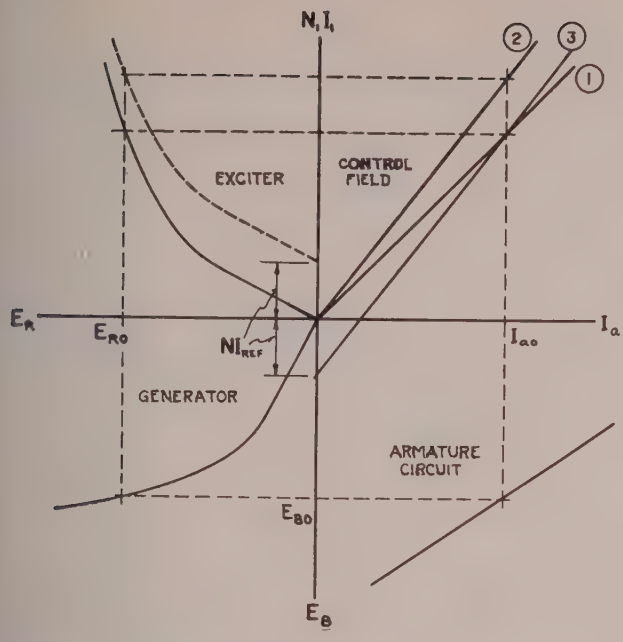

Figure 7. Graphical construction for finding equilibrium values in a nonlinear system

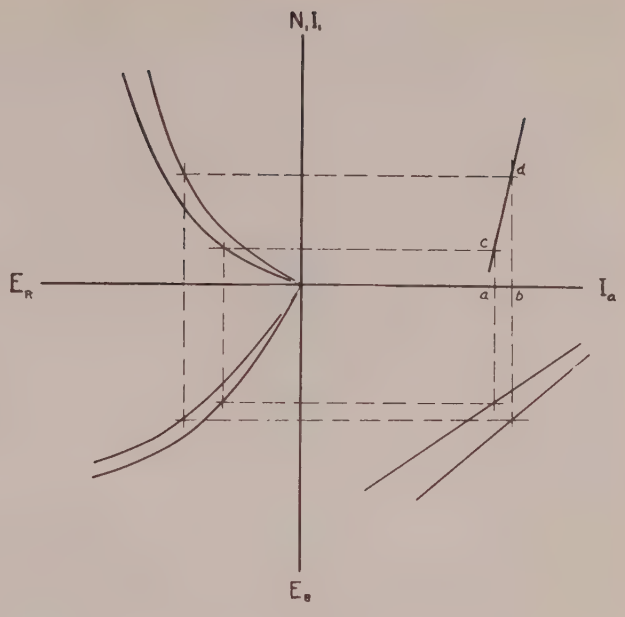

Figure 8. Graphical construction for finding the gain in a nonlinear system

$$x_4' = \frac{k'x^*}{1+k'} \tag{34}$$

The ratio of the two values of x_4 is

$$\frac{x_4'}{x_4} = m\frac{1+k}{1+mk} \tag{35}$$

Where $m = k'/k$. Solving for k,

$$k = \frac{(x_4'/x_4) - m}{m\left(1 - \frac{x_4'}{x_4}\right)} \tag{36}$$

Equation 36 is plotted in Figure 5.

Graphical Solution for Nonlinear Cases

It has been seen that the linearized equations discussed in the previous section are not applicable to the study of equilibrium conditions. This results from the fact that the solution to the system of equations depends upon the coefficients (a's and b's) and conversely. These remarks must not be taken as applying to the incremental relations. The use of linearized equations for the study of stability (the incremental relations) is a very powerful tool as described by F. E. Bothwell.[3] Since systems with one or more nonlinear elements are of considerable practical significance, a graphical method of calculating steady-state gain will be described.

Figure 6 shows a current regulator which used a buck-boost generator connected in series with the motor whose current is to be regulated. The motor armature circuit is connected across a constant potential bus. The potential drop across the generator interpole is used to energize the control field of a pilot exciter, which in turn feeds the field of the buck-boost generator.

Examination of this circuit will show that the reference field is not required for regulatory action, because the necessary reversal of signs is inherent in the circuit as shown. The purpose of the "reference" field will become clear from the following discussion.

A graphical solution for the equilibrium values of the several currents and voltages is readily secured by the construction shown in Figure 7. The steady-state characteristics of the four components are shown in the four quadrants, and the equilibrium relations are obviously those given by the dashed lines. Initially, this dotted-line construction must be found by trial and error, a process which is readily carried out on this diagram.

If the means for gain adjustment is assumed to be R_x, then an increase in gain would result in line 2 in the first quadrant. It is seen immediately that such a change would move the operating points out on each of the magnetization curves and upset the equilibrium value of $I_a(I_{ao})$. However, the reference field previously mentioned may be used to bring the operating point on each of the two magnetization curves back to its original value. This is accomplished in Figure 7 by constructing line 3 (parallel to line 2 for increased gain), and the reference field ampere turns may then be read directly from the diagram.

The effect of disturbances now can be analyzed by using this diagram as shown in Figure 8. Field heating, change of generator speed, and other factors will produce a band of characteristics in each quadrant. If one starts by assuming certain limits on I_o (points a and b) and then works clockwise through the four quadrants, points c and d will be found. These two points determine the slope of the line in the first quadrant and, therefore, the system gain (that is, value of R_x). The construction shown in Figure 8 is overly pessimistic in that it assumes a cumulative effect of all disturbances. A detailed analysis undoubtedly would show that this is highly improbable, and a more realistic study would show some compensating effects among the several possible disturbances.

In some instances the exciter and the generator are operated in an unsaturated condition and either equation 31 (or a simplified form of it) or the graphical construction previously described may be used. Self-excitation of the exciter (not shown in Figure 6) frequently is used to increase system gain. If the machine is unsaturated, this self-excitation is simply equivalent to a change in slope of the line in the first quadrant. Using the construction of Figure 8 one may calculate the required gain and then determine the values of separate and self-excitation required. The use of self-excitation with a saturated machine requires that one

compute a new magnetization curve for the second quadrant which would include the effect of this self-exciting field.

Conclusions

The previous discussion has shown that the calculation of gain required in a proportional feedback controller involves a detailed study of all system disturbances. This calculation cannot be performed with the usual transfer functions or incremental relations, but requires that one use the equilibrium or steady-state expressions. In a system containing nonlinear elements these nonlinearities must be used in the calculation of gain, and a graphical procedure is suggested. While the subject of transient analysis was not discussed, it is clear that since disturbances may alter the value of many parameters, it may be necessary to study the behavior for a range of values for each "constant."

References

1. Principles of Servomechanisms (book), **Gordon S. Brown, Donald P. Campbell.** John Wiley and Sons, Inc., New York, N. Y., 1948.

2. Instrument Inaccuracies in Feed-Back Control Systems with Particular Reference to Backlash, **H. Tyler Marcy, Morris Yachter, Jerome Zauderer.** *AIEE Transactions*, volume 68, part I, 1949, pages 778–88.

3. Stability of Voltage Regulators, **F. E. Bothwell.** *AIEE Transactions*, volume 69, part II, 1950, pages 1430–33.

No Discussion

Winding Insulation Tester for D-C Armatures

F. H. CATLIN
NONMEMBER AIEE

N. ROHATS
MEMBER AIEE

THE quality of the insulation system of electric apparatus is an important factor in the life and performance of that apparatus. To assure the required quality of insulation adequate and practical means of testing must be provided. These testing methods must meet several requirements. The test voltage stresses must be applied to the major insulation between the electric circuit and ground and also to the minor insulation between coils and turns. The test voltage applied must simulate service stresses. The test voltage levels must be sufficiently high to assure that all insulation defects and incipient faults will be discovered. The test must be simple in application and safe. The test equipment must be low in first cost and have reasonably long life.

Commonly Used Test Methods

By far the greatest amount of high-potential testing is done at power supply frequencies at voltage levels determined by experience in field operation. Generally these tests are made on major insulation only by applying voltage to all terminals with the framework grounded. This method of testing does not test coil-to-coil or turn-to-turn insulation.

Induced-voltage testing sometimes is used, generally at 120, 420, or 960 cycles, with the applied voltage across the winding under test.[1,2] The higher reactance at these frequencies permits higher applied voltages without overloading. Voltages and currents at these frequencies are not typical of operating conditions.

Surge testing has been adopted widely for transformers and switchgear. The advent of the Marx circuit and cathode ray oscillograph has permitted the application of test surges at any peak voltage required, as well as accurate measurements of applied wave shapes. These tests are made on the single-surge basis, using wave shapes regarded as simulating power line surges from lightning and other disturbances.

Surge testing of rotating machinery windings using repeating-type surge generators at 60 surges per second now is in extensive use on production lines.

Repeated-Surge Testing

The repeated-surge method of high-potential testing was developed and incorporated in a winding insulation tester for production line use in 1942.[3] Early applications were on 3-phase motors between 1 and 15 horsepower. A short time later a tester was built for larger machines up to 6,000 horsepower with 2,700-volt windings. Still later the method was adapted to single-phase motors, and now it is used for testing a large percentage of motors used on refrigerators, washing machines, and so forth. The wide acceptance of the winding insulation tester of Figure 1 is based on the economy and convenience of repeated-surge testing in providing the required insulation stresses from conductor to ground, between coils, and between turns. Figure 2 shows typical test waves on single-phase motors. "*A*" is with a good winding, "*B*" is with several short-circuited turns in one coil.

Experience with this tester has been that all insulation faults are detected and located, providing designers with information necessary for changes in design and manufacturing methods, which result in reducing rejections to well under one per cent.

Winding Insulation Tester for D-C Armatures

The success of repeated-surge testing on stators immediately suggested a possible application to d-c armatures, where similar problems of turn stresses due to surges must be met. Here the problem becomes more difficult because of the low impedance of the armatures to be tested and the correspondingly greater surge current required for a given turn-to-turn surge voltage.

This problem first arose during World War II, when the United States Army required a number of special d-c traction motors. The design of these motors was such that stringent insulation space limitations were imposed. Because of this, and also as a result of the rigid service specifications, it was necessary to make a severe turn-to-turn insulation test on the armatures.

These armatures were lap-wound and had the usual equalizer connections. The resistance between adjacent commutator segments was less than 0.01 ohm. From

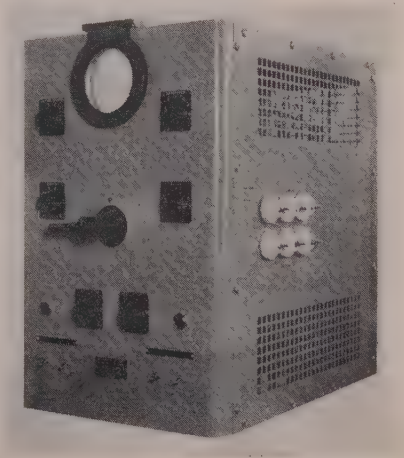

Figure 1. 10-kv winding insulation tester

Paper 51-74, recommended by the AIEE Instruments and Measurements Committee and approved by the AIEE Technical Program Committee for presentation at the AIEE Winter General Meeting, New York, N. Y., January 22–26, 1951. Manuscript submitted October 23, 1950; made available for printing December 7, 1950.

F. H. CATLIN is with the General Electric Company, Erie, Pa., and N. ROHATS is with the General Electric Company, Schenectady, N. Y.

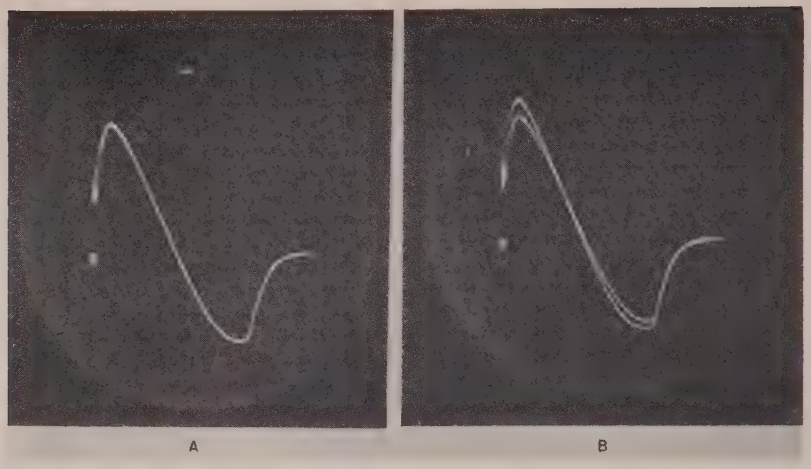

Figure 2. Test waves, single-phase motors, (a) good winding; (b) several short-circuited turns in one coil

previous experience with the type of insulation in this armature it was decided that a surge test giving 500 volts peak bar-to-bar would show up substandard insulation, but would not damage good insulation. Tests also indicated that at 500 volts peak the surge current would be in excess of 300 amperes. This power requirement was greater than could be obtained from any existing surge test equipment. To meet these power requirements a new surge tester was designed and built.

The main circuits of this tester are shown in Figure 3. The surge-generator capacitance, C, of one microfarad was charged in one half-cycle and discharged on the next half-cycle. The discharge was through a pair of thyratrons connected back to back to permit oscillatory and complete discharge of surge generator.

To minimize reactance drop the surges were led to the motor under test through coaxial cables. A well-insulated contact mechanism held by the operator applied the surges to adjacent commutator bars. A separate pair of contacts picked off coil potential, and another coaxial cable took it back to the oscilloscope for observation and measurement.

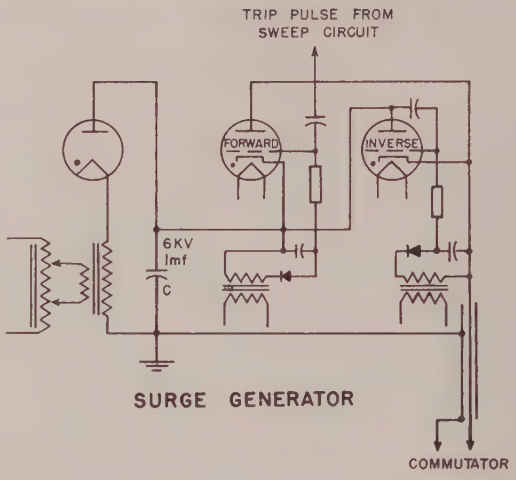

Figure 3. Main circuits of 10-kv winding insulation tester

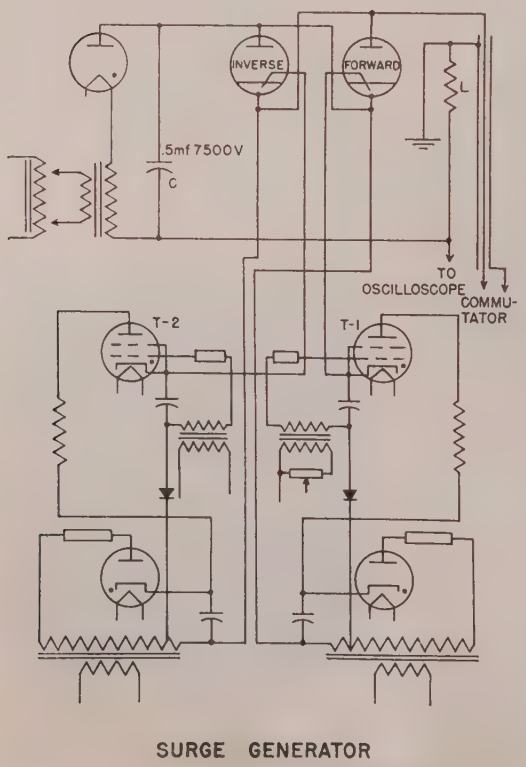

Figure 4 (left). High - current winding insulation tester, final design

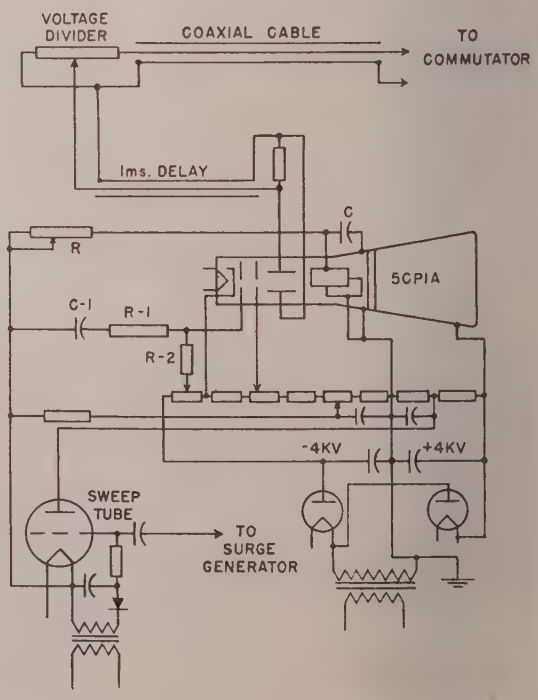

Figure 5 (right). Oscilloscope circuits

The armatures were checked at certain stages of manufacture when defects could be corrected at minimum expense. The performance of this special winding-insulation tester on this lot of motors proved the value of surge testing for incipient fault detection and insulation system evaluation.

The use of this tester was continued after the war to test armatures of various sizes and types of winding. From this background of experience it was decided in 1949 to extend the program of surge testing. This program included armatures of very low impedance. Tests showed that to provide bar-to-bar test potentials of 500 volts peak, crest currents of several thousand amperes would be required. The use of thyratrons to obtain these current values was impractical, so a new surge tester using small ignitrons was designed and built.

Description of the New Tester

The surge generator of the new high-current winding insulation tester as finally developed around the ignitrons is shown in Figure 4. The capacitor, *C*, is charged on one half-cycle and discharged on the next half-cycle of opposite polarity. The discharge tends to be oscillatory so a second ignitron is provided to carry the inverse current. Each ignitron has its own firing circuit, which sends a current pulse of 500 microseconds' duration through the ignitor. As the time required to fire the ignitor varies between 20 and 40 microseconds, and as the first half-cycle of the surge may be shorter, it is necessary to fire the inverse tube first. This insures that the inverse tube will always be ready when the inverse surge current comes along.

The inverse firing circuit thyratron *T-2* grid has a negative bias of about 30 volts, which is modulated by about 250 volts at 60 cycles, so that firing occurs very soon after the zero of the charging half-cycle. The forward firing circuit thyratron, *T-1* is controlled in the same way, but has its grid bias modulated by a lower 60-cycle voltage, so that firing is delayed a little longer.

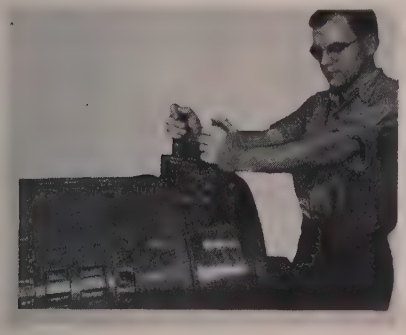

Figure 6. Contact mechanism for applying tester output to commutator

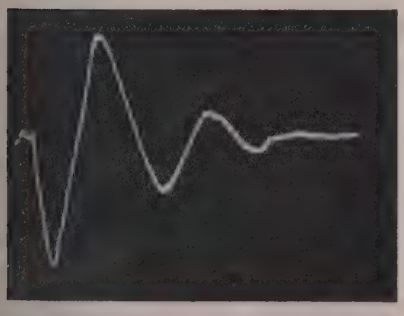

Figure 7. Oscillograph of voltage wave between adjacent bars of very low impedance armature

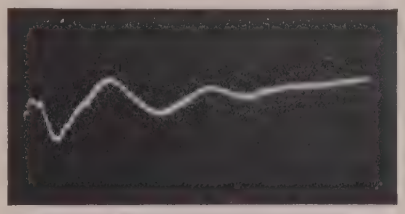

Figure 8. Oscillograph of voltage wave with deliberate insulation defect in armature circuit

The positive side of the surge generator is connected to ground through a small coil, *L*, of several turns. The positive drop across this coil is used for firing the sweep circuit of the oscilloscope, thereby giving a perfectly steady picture in spite of the variations of ignitron firing point.

The oscilloscope circuits are shown in Figure 5. A 5-inch fast-writing oscilloscope tube with ±4-kv acceleration, or a total of 8 kv, is used to give enough intensity for convenient observation. The time axis is produced by the discharge of a small thyratron into a resistance-capacitance circuit. The thyratron also drives the cathode-ray tube grid to establish the beam through a coupling capacitor, *C-1* and a resistance voltage divider, *R-1*, *R-2*. Power is supplied by taps in the main 8-kv power supply bleeder.

To avoid including the contact drop of the main contacts, the surge voltage to be measured is picked up by separate contacts and is conducted to the oscilloscope deflection circuit through a coaxial cable. The voltage divider is made up of noninductive resistors on a tap switch. The output of the divider is passed through a one-microsecond delay cable to the deflection plates. This delay makes up for the time lost in initiating the time axis circuit.

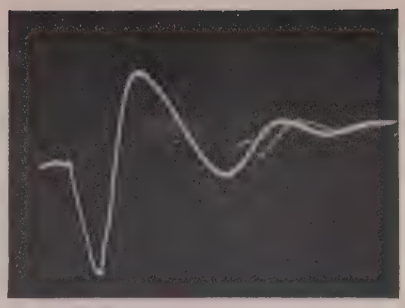

Figure 9. Oscillograph of voltage wave without insulation defect, on medium impedance armature

Several other elements which were omitted from the diagram for simplicity are a deflection selector switch, a d-c calibration supply, and a 500-kc damped-wave timing wave oscillator.

The contact mechanism for applying the tester output to a commutator is shown in use in Figure 6. It consists of a well-insulated body with two handles in which there are interlock switches. The operator is safeguarded in this way, as he must press both handles to complete the surge-generator primary circuit. The contacts are adjustable for commutators having bars of various widths, and they may be used on commutators up to 31 inches in diameter. For commutators of larger diameters another mechanism of similar design will be required.

Application Performance

The surge-generator capacitance of 0.5 microfarad and a maximum of 7.5 kv are capable of applying potentials of 500 to 1,000 volts between adjacent segments of any d-c armature now in production. An oscillograph record of voltage between adjacent bars of a very low impedance armature is shown in Figure 7. This voltage wave is of highly damped nature at a frequency of approximately 160 kc. The voltage amplitude of 500 volts between bars is only a portion of the total surge-generator voltage, the remainder being lost in the stray inductance of the leads. This wave shape is typical of an armature circuit with no insulation defects. In Figure 8 is shown the wave shape obtained when an insulation defect is present in the armature circuit. This particular defect was a short circuit between bars in a coil 120 degrees or one equalizer space from the point of surge application.

A typical wave shape on a medium impedance armature without insulation

defects is shown in Figure 9. The increased inductance of this armature reduces the oscillation frequency to approximately 130 kc. The general wave shape, however, remains quite typical of those for large armatures.

This new instrument extends the application of the winding insulation tester to very low impedance windings, such as large d-c armatures. It is expected that it will do an equally good job in this area in finding weak insulation and thereby pointing the way to improved design and manufacturing techniques.

References

1. Transformers, Regulators, and Reactors. *C57*, American Standards Association, New York, N. Y., 1948.

2. Measurement of Test Voltage in Dielectric Tests. *C68.1*, American Standards Association, New York, N. Y., 1942.

3. Insulation Testing of Electric Windings, C. M. Foust, N. Rohats. *Electrical Engineering (AIEE Transactions)*, volume 62, April 1943, pages 203–06.

No Discussion

A Hook-On Power Factor Meter

A. J. CORSON
MEMBER AIEE

A. L. NYLANDER
ASSOCIATE AIEE

HOOK-ON INSTRUMENTS for current measurement have been widely used for more than a decade. The small size, lightweight, and in particular, the absence of service interruption, have made such instruments invaluable for wide-range current measurements of moderate accuracy. Some of these instruments were adapted to potential measurement and in 1949, the present authors treated the problem of hook-on power measurement.[1] Further study has shown the practicality of wide-range power factor measurement by this method. The resultant instrument (Figure 1) has a measurement range of 0 lead to 0 lag power factor, 15 to 600 amperes, 100 to 600 volts on balanced 3-phase circuits. It has a calibration accuracy of 0.02 power factor, and weighs 4.1 pounds. Its principle of operation, as well as the solution to several interesting development problems, is set forth here.

Principle of Operation

Power factor usually is measured by a phase-sensitive deflecting instrument of the crossed-coil or moving-iron type. Such instruments are inherently suitable for accurate power factor measurement, but are limited to a narrow measurement range. They also require separate current connections involving either service interruption or a separate clamp-on transformer. The crossed-coil phase meter principle can be combined with hook-on operation directly, but calculations showed that the measurement range of this system was relatively limited.

These limitations were removed effectively by the adoption of a null principle of operation. As shown in Figure 2, the arrangement consists of a null reading watt-galvanometer and a calibrated cross-phase variable resistor. Power factor is measured by simply snapping the magnetic hook around one conductor, connecting the potential leads, turning the variable resistor until the wattmeter reads zero, then reading the power factor on the calibrated variable resistor dial.

The power factor range and calibration are established as follows. Assuming a balanced 3-wire 3-phase circuit completely energized, the only condition of null balance of the watt-galvanometer is quadrature relationship of moving coil current and field flux or line current. The calibrated variable resistor is connected to lines B, C, with the moving arm connected in series with the potential transformer primary which, in turn, completes the circuit to line A. The moving coil is connected across the secondary winding of this potential transformer.

It is apparent in all of the Figures 3 through 6 that the moving-coil current phase angle is adjustable over a 60-degree range, whose mid-point is 180 degrees displaced from the reference vector, I_A. If, now, the current vector, I_C is within a 60-degree range from the j axis, specifically, $+90 \pm 30$ degrees, its position can be established by adjustment of the potential circuit current, I_V, for the required quadrature relationship and null reading. Since the $+90+30$-degree position corresponds to unity power factor of current vector, I_C, the measurement range is 0 to -60 degrees or 1.0 to 0.5 lagging power factor. Similarly, the measurement range of vector, I_B, is 0 to $+60$ degrees or 1.0 to 0.5 leading power factor. The vector, I_A, is outside the measurement range of the potential circuit network for the power factor range of 0.5 lead to unity to 0.5 lag, but enters the measurement sector at 0.5 leading power factor and covers the range of 0.5 lead to 0 to 0.5 lag. Thus, the power factor of any balanced system can be measured by (1) finding out which of the lines A, B, or C will produce a null reading, and (2) reading the power factor on the correspondingly lettered scale (Figure 7).

The Watt-Galvanometer

The watt-galvanometer consists of the magnetic circuit and spring-restrained moving coil mechanism, illustrated in Figure 2.

The sensitivity is derived from fundamental electrodynamic wattmeter principles and the vector relations of Figures 3 through 6 as follows (see equation 32).

$$S = \frac{\sqrt{1-k+k^2}}{\sin\theta[\text{Req.}+(k-k^2)R_P]}$$

where

S = galvanometer deflection in radians per unit power factor per volt-ampere, divided by the galvanometer constant (equation 20)

Req. = equivalent transformer impedance in ohms with the galvanometer burden

R_P = total variable resistor ohms

k = ratio of variable resistor ohms in line B to total variable resistor ohms (Figure 3)

θ = power factor angle

Figure 1. Hook-on power factor meter

Paper 51-75, recommended by the AIEE Instruments and Measurements Committee and approved by the AIEE Technical Program Committee for presentation at the AIEE Winter General Meeting, New York, N. Y., January 22–26, 1951. Manuscript submitted October 27, 1950; made available for printing December 7, 1950.

A. J. Corson and A. L. Nylander are both with the General Electric Company, West Lynn, Mass.

The authors gratefully acknowledge the assistance of several associates, particularly S. C. Haley, R. M. Rowell, and N. P. Millar.

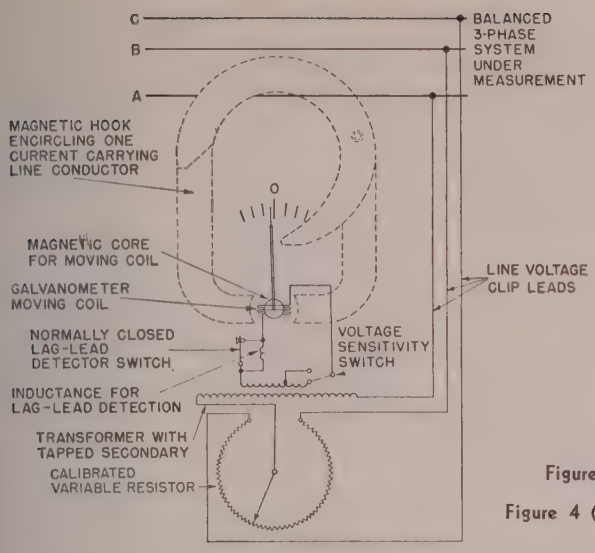

Figure 2 (left). Schematic connection diagram of hook-on power factor meter

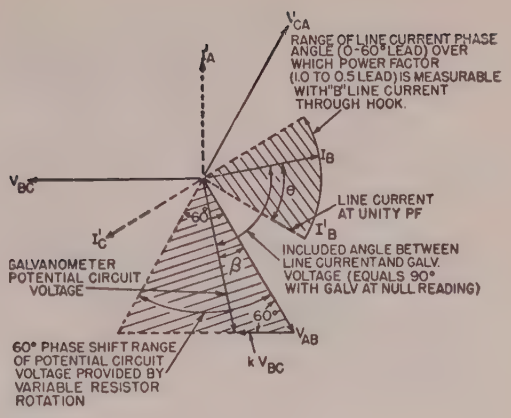
RANGE OF LINE CURRENT PHASE ANGLE (0-60° LEAD) OVER WHICH POWER FACTOR (1.0 TO 0.5 LEAD) IS MEASURABLE WITH "B" LINE CURRENT THROUGH HOOK.
LINE CURRENT AT UNITY PF
INCLUDED ANGLE BETWEEN LINE CURRENT AND GALV. VOLTAGE (EQUALS 90° WITH GALV AT NULL READING)
GALVANOMETER POTENTIAL CIRCUIT VOLTAGE
60° PHASE SHIFT RANGE OF POTENTIAL CIRCUIT VOLTAGE PROVIDED BY VARIABLE RESISTOR ROTATION

Figure 4 (above). Vector relations in hook-on power factor meter with "B" line current through hook

This function is plotted against power factor in Figure 8. It is apparent that the sensitivity increases somewhat between 0 and 0.8 power factor and becomes progressively higher between 0.8 and unity.

Potential Circuit Transformer

The potential circuit includes a small transformer which supplies an appropriate value of current to the moving coil. This arrangement results in high sensitivity over a wide measurement range without excessive heating. Other advantages are:

1. A simple moving coil winding, consisting of relatively few turns of large conductor.

2. Self-compensation for the phase angle error of the hook. Potential and current circuit phase angles are approximately equal and cancel each other.

3. Choice of sensitivities by a tapped secondary winding and potential switch. The full winding is designed for a range of 100 to 300 volts, and a suitable tap is provided for 300- to 600-volt operation.

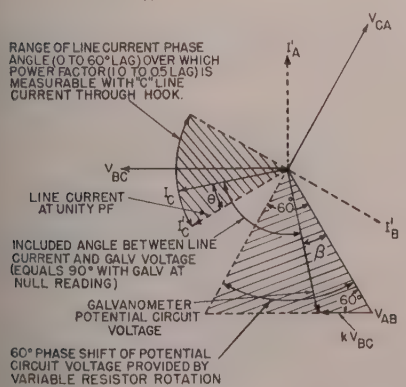
RANGE OF LINE CURRENT PHASE ANGLE (0 TO 60° LAG) OVER WHICH POWER FACTOR (1.0 TO 0.5 LAG) IS MEASURABLE WITH "C" LINE CURRENT THROUGH HOOK.
LINE CURRENT AT UNITY PF
INCLUDED ANGLE BETWEEN LINE CURRENT AND GALV VOLTAGE (EQUALS 90° WITH GALV AT NULL READING)
GALVANOMETER POTENTIAL CIRCUIT VOLTAGE
60° PHASE SHIFT OF POTENTIAL CIRCUIT VOLTAGE PROVIDED BY VARIABLE RESISTOR ROTATION

Figure 3. Vector relations in hook-on power factor meter with "C" line current through hook

Calibration of Variable Resistor

The calibration of the variable resistor dial is derived trigonometrically from the vector relations in Figures 3 through 6 (see Appendix I). For the four power factor ranges, the power factor angle, θ, is related to the fraction, k, of the full resistor rotation as follows:

For 0.5 to 1.0 lag power factor (C scale)

$$k = \frac{\sin \theta}{\sin (120 - \theta)} \qquad (5)$$

For 0.5 to 1.0 lead power factor (B scale)

$$k = \frac{\sin (60 - \theta)}{\sin (60 + \theta)} \qquad (8)$$

For 0 to 0.5 lag power factor (A scale)

$$k = \frac{\sin (\theta - 60)}{\sin \theta} \qquad (11)$$

For 0 to 0.5 lead power factor (A scale)

$$k = \frac{\sin (120 - \theta)}{\sin \theta} \qquad (14)$$

The resistance-rotation characteristic of the variable resistor is a straight line. This relationship is controlled to insure good measurement accuracy. The several distributions are plotted in Figure 9, showing that all scales are approximately uniform with power factor from 0 up to 0.8. In the interval 0.8 to 1.0, the scale becomes progressively expanded.

Operation

Power Factor Measurement

The power factor dial shown in Figure 7 has three scales, A, B, and C, each extending over an angle of approximately 300 degrees, providing total scale length of $13\frac{1}{2}$ inches. These scales cover the specific power factor ranges previously described and, in addition, are color coded. When the potential leads, marked A, B, and C, are connected to the lines in direct phase rotation, the red scales indicate leading power factor and the black scales indicate lagging power factor. If the phase sequence is not known, the power factor reading is obtained from the scale identified by the letter corresponding to that of the hooked line. This arrangement allows the user the convenience of connecting the voltage leads to the lines without regard to phase sequence.

Lead—Lag Determination

Provision is made for identification of leading and lagging power factors. In Figure 2, a series inductance is shown in the moving coil circuit. This normally is short-circuited by the single-throw push button switch. When this switch is opened, the series inductance is introduced into the potential circuit. This displaces the current slightly in the lag direction, causing the galvanometer to deflect. To restore galvanometer balance,

Table I. Performance

	Power Factor
Calibration accuracy	0.020
Error due to opening hook 0.050 inches	±0.002
Frequency error from 60 cycles	
(a) Maximum at 70 cycles	−0.002
(b) Maximum at 50 cycles	−0.006
Temperature error from 25 degrees centigrade	
(a) Maximum at +85 degrees centigrade	+0.002
(b) Maximum at −20 degrees centigrade	+0.002
Maximum sustained operation influence 600 amperes, 600 volts	+0.003
Maximum voltage error	−0.010
Maximum current error	−0.014
Wave form error	+0.017 with 10% 3rd and 10% 5th harmonics

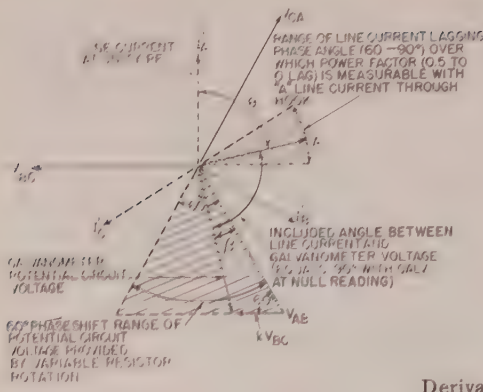
RANGE OF LINE CURRENT LAGGING PHASE ANGLE (60 −90°) OVER WHICH POWER FACTOR (0.5 TO 0 LAG) IS MEASURABLE WITH "A" LINE CURRENT THROUGH HOOK
INCLUDED ANGLE BETWEEN LINE CURRENT AND GALVANOMETER VOLTAGE (EQUALS 90° WITH GALV AT NULL READING)
60° PHASE SHIFT RANGE OF POTENTIAL CIRCUIT VOLTAGE PROVIDED BY VARIABLE RESISTOR ROTATION

Figure 5 (left). Vector relations in hook-on power factor meter with "A" line current through hook at lagging power factor

Figure 6 (right). Vector relations in hook-on power factor meter with "A" line current through hook at leading power factor

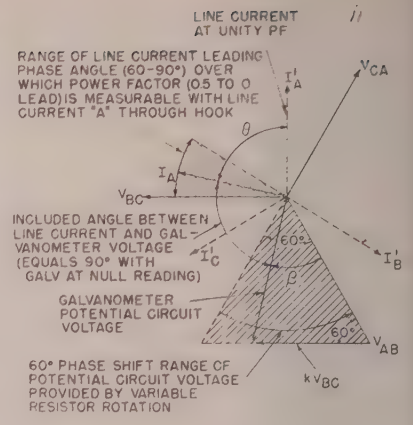
LINE CURRENT AT UNITY PF
RANGE OF LINE CURRENT LEADING PHASE ANGLE (60-90°) OVER WHICH POWER FACTOR (0.5 TO 0 LEAD) IS MEASURABLE WITH LINE CURRENT "A" THROUGH HOOK
INCLUDED ANGLE BETWEEN LINE CURRENT AND GALVANOMETER VOLTAGE (EQUALS 90° WITH GALV AT NULL READING)
GALVANOMETER POTENTIAL CIRCUIT VOLTAGE
60° PHASE SHIFT RANGE OF POTENTIAL CIRCUIT VOLTAGE PROVIDED BY VARIABLE RESISTOR ROTATION

the potential circuit current must be displaced in phase in the lead direction by turning the power factor dial. The effect is to increase the power factor dial reading in the case of lagging power factor and to decrease the reading in the case of leading power factor. This arrangement provides a lead lag detector simply by opening the switch, rebalancing the galvanometer, and noting whether the power factor reading decreases or increases.

Phase Sequence Determination

A coincidental, but important, feature of the lead lag identification circuit is that it provides for determination of phase sequence. This is accomplished by (1) making a power factor measurement, (2) determining whether the power factor is leading or lagging, and (3) noting the color of the scale on which the power factor is read. It follows from the foregoing discussion that the phase sequence is direct, if lagging power factor is noted on a black scale or leading power factor is noted on a red scale. Similarly, the phase sequence is reverse, if lagging power factor is noted on a red scale or leading power factor is noted on a black scale.

Performance and Summary

The use of the null principle in the watt galvanometer results in good over-all performance over the measurement range shown in Figure 10. As shown in Table I, only minor errors result from such factors as voltage and current variations, incomplete hook closure, also frequency and temperature change. This instrument is sufficiently sturdy to withstand the shock and abuse expected for this type of portable service instrument.

Reference

1. Power Measurement by the Hook On Method, A. J. Corson, A. L. Nylander. *AIEE Transactions*, volume 69, part II, 1950, pages 699-702.

Appendix I

Derivation of Power Factor Meter Dial Distributions for Balanced 3-Phase Conditions, and Straight-Line Resistance-Rotation Characteristic of the Variable Resistor

Referring to Figures 3 through 6, by the Law of Sines,

$$kV_{BC} = \frac{V_{AB} \sin \beta}{\sin (180 - 60 - \beta)} \qquad (1)$$

where

V_{BC}, V_{AB} = balanced 3-phase line voltages
k = ratio of variable resistor ohms in line B to total resistor ohms (Figure 3)
β = angle between V_{AB} and the galvanometer potential circuit voltage

From equation 1,

$$k = \frac{\sin \beta}{\sin (120 - \beta)} \qquad (2)$$

Case I. Lagging power factor range from unity to 0.5. From Figure 3, the included angle between the galvanometer current (line current, I_C) and galvanometer voltage is,

$$60 \text{ degrees} - \beta + 30 \text{ degrees} + \theta \qquad (3)$$

where

θ = power factor angle

Angle (3) equals 90 degrees at null galvanometer reading, from which,

$$\beta = \theta \qquad (4)$$

Substituting equation 4 in equation 2,

$$k = \frac{\sin \theta}{\sin (120 - \theta)} \qquad (5)$$

This establishes the C-scale distribution of Figure 9.

Case II. Leading power factor range from unity to 0.5. From Figure 4, the included angle between the galvanometer voltage and current (line current, I_B) is,

$$\beta + 30 + \theta \qquad (6)$$

from which, when equated to 90 degrees for null galvanometer reading,

$$\beta = 60 - \theta \qquad (7)$$

Substituting equation 7 in equation 2,

$$k = \frac{\sin (60 - \theta)}{\sin (60 + \theta)} \qquad (8)$$

This establishes the B-scale distribution of Figure 9.

Case III. Lagging power factor range from 0.5 to zero. From Figure 5, the included angle between the galvanometer voltage and current (line current, I_A) is shown to be

$$\beta + 60 + 90 - \theta \qquad (9)$$

from which, when equated to 90 degrees for null galvanometer reading,

$$\beta = \theta - 60 \text{ degrees} \qquad (10)$$

Substituting equation 10 in equation 2,

$$k = \frac{\sin (\theta - 60)}{\sin \theta} \qquad (11)$$

This establishes the lagging power factor A-scale distribution of Figure 9.

Case IV. Leading power factor range from zero to 0.5. From Figure 6, the included angle between the galvanometer voltage and current (line current, I_A) is shown to be

$$60 - \beta + 60 + 90 - \theta \qquad (12)$$

from which, when equated to 90 degrees for null galvanometer reading,

$$\beta = 120 - \theta \qquad (13)$$

Substituting equation 13 in equation 2

$$k = \frac{\sin (120 - \theta)}{\sin \theta} \qquad (14)$$

This establishes the leading power factor A-scale distribution of Figure 9.

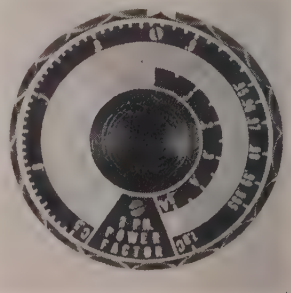

Figure 7. Hook-on power factor meter dial

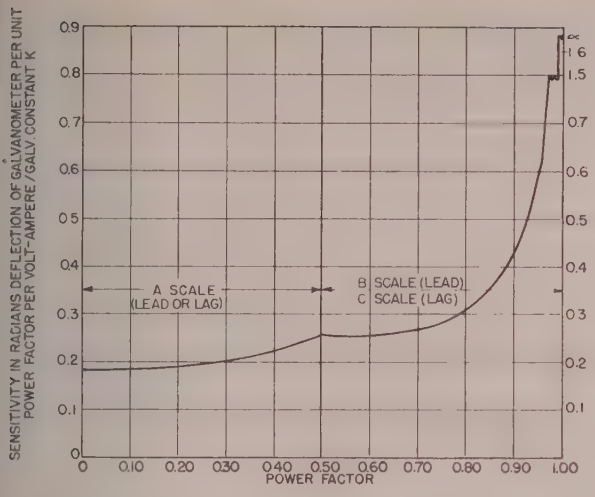
SENSITIVITY IN RADIANS DEFLECTION OF GALVANOMETER PER UNIT POWER FACTOR PER VOLT-AMPERE / GALV CONSTANT K
POWER FACTOR
A SCALE (LEAD OR LAG)
B SCALE (LEAD)
C SCALE (LAG)

Figure 8. Variation of hook-on power factor meter sensitivity with power factor

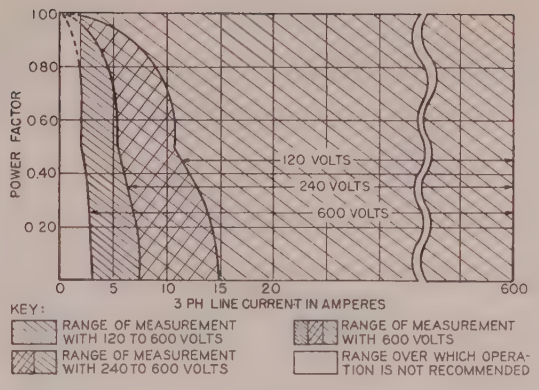
POWER FACTOR
120 VOLTS
240 VOLTS
600 VOLTS
3 PH LINE CURRENT IN AMPERES
KEY:
RANGE OF MEASUREMENT WITH 120 TO 600 VOLTS
RANGE OF MEASUREMENT WITH 600 VOLTS
RANGE OF MEASUREMENT WITH 240 TO 600 VOLTS
RANGE OVER WHICH OPERATION IS NOT RECOMMENDED

Figure 10. Voltage and current range of power factor measurement (based on minimum pointer deflection 0.012 inch per 0.01 power factor)

Appendix II

Derivation of Power Factor Meter Sensitivity for Balanced 3-Phase Conditions and Straight-Line Resistance-Rotation Characteristic of the Variable Resistor

For a ferrodynamic wattmeter,[1] whose magnetic circuit is designed to provide the following conditions:

(a) a constant space rate of change of mutual flux as the moving system is deflected,

(b) a negligible phase displacement of this mutual flux from the exciting current (line current through the magnetic hook), and,

(c) a linear relationship between this mutual flux and its exciting current,

the torque developed in a spring-controlled moving system at unity power factor is,

$$T = K_1 \boldsymbol{I}_V \Phi \tag{15}$$

where

T = torque in gram-millimeters
K_1 = coil turns, N, divided by 981
$\boldsymbol{I}_V$ = rms amperes through moving coil
Φ = mutual flux in rms maxwells

From condition (c),

$$\Phi = K_2 \boldsymbol{I} \tag{16}$$

where

K_2 = rms maxwells mutual flux per rms ampere through the magnetic hook
$\boldsymbol{I}$ = rms amperes line current through the magnetic hook

With the moving system, spring-controlled, the torque is proportional to deflection,

$$T = K_3 D \tag{17}$$

where

K_3 = spring constant, gram-millimeters per radian deflection
D = deflection in radians

Substituting equations 16 and 17 in equation 15, for any power factor,

$$D = K_4 \boldsymbol{I}_V \boldsymbol{I} \cos \angle^{\boldsymbol{I}_V}_{\boldsymbol{I}} \tag{18}$$

where

$K_4 = K_1 K_2 / K_3$ = constant

This ferrodynamic wattmeter may be used as a watt-galvanometer to obtain a null reading when the included angle between $\boldsymbol{I}_V$ and $\boldsymbol{I}$ is 90 degrees.

The electric circuit of one such instrument arrangement is shown in Figures 2, 11, and 12, and the vector relations in Figures 3 through 6.

Equation 18 may be used for this instrument, except that K_4 must be multiplied by the secondary to primary transformer current ratio, $1/a$, and equation 18 becomes,

$$D = K \boldsymbol{I}_V \boldsymbol{I} \cos \angle^{\boldsymbol{I}_V}_{\boldsymbol{I}} \tag{19}$$

where the "galvanometer constant"

$$K = \frac{K_1 K_2}{a K_3} \tag{20}$$

In equations 5, 8, 11, and 14 are the included angles between $\boldsymbol{I}_V$ and $\boldsymbol{I}$ (line current) for each power factor range. In these, β is independent of any change in the power factor angle, θ. It is dependent only upon the variable resistor setting.

In the general equation 18, $\boldsymbol{I}_V$ is independent of θ. It is dependent only upon the variable resistor setting for any given line voltage and circuit impedance.

Therefore, for any given line current, line voltage, and variable resistor setting, the change in deflection, D, in equation 18, with respect to θ, becomes a function of the change in the included angle, with respect to θ or,

$$\frac{\partial D}{\partial \theta} = K \boldsymbol{I}_V \boldsymbol{I} \frac{\partial}{\partial \theta} \left(\cos \angle^{\boldsymbol{I}_V}_{\boldsymbol{I}} \right) \tag{21}$$

But, it is seen by observation from Figures 3 through 6 that for each power factor range at given line voltage, current, and variable resistor setting, the included angle becomes the sum of a constant angle, represented by α, plus θ,

$$\angle^{\boldsymbol{I}_V}_{\boldsymbol{I}} = (\alpha + \theta) \tag{22}$$

from which,

$$\frac{\partial}{\partial \theta} \left(\cos \angle^{\boldsymbol{I}_V}_{\boldsymbol{I}} \right) = \frac{\partial}{\partial \theta} \cos (\alpha + \theta) =$$

$$-\sin (\alpha + \theta) \tag{23}$$

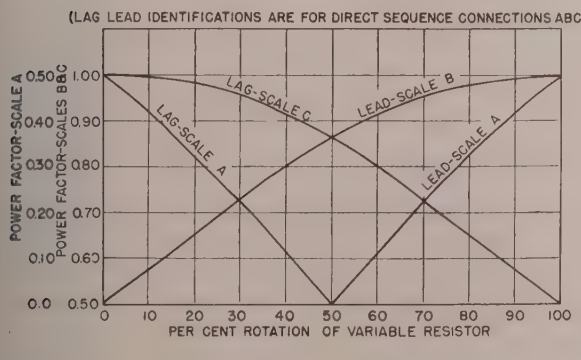

Figure 9 (left). Power factor dial calibration

Figure 11 (below). Equivalent potential circuit of power factor meter (Schematic—tap on transformer secondary winding not shown)

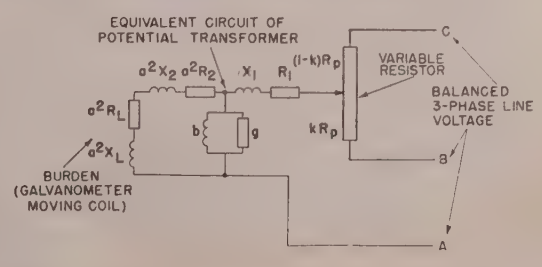

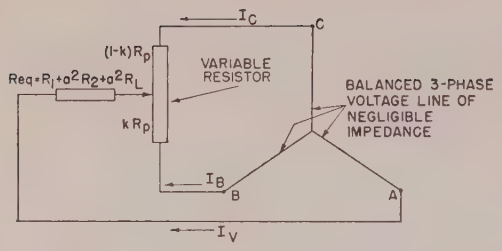

Figure 12. Simplified equivalent potential circuit of power factor meter (schematic—tap on transformer secondary winding not shown)

Substituting equation 23 in equation 21 we have

$$\frac{\partial D}{\partial \theta} = -KI_V I \sin(\alpha+\theta) \quad (24)$$

and

$$\frac{\partial D}{\partial(\cos\theta)} = \frac{\partial D}{\partial \theta}\frac{\partial \theta}{\partial(\cos\theta)} = [-KI_V I \sin(\alpha+\theta)]-\left[\frac{1}{\sin\theta}\right] = KI_V I \sin\frac{(\alpha+\theta)}{\sin\theta} \quad (25)$$

For the condition of no galvanometer deflection $(\alpha+\theta)=90$ degrees so that equation 25 becomes

$$\frac{\partial D}{\partial(\cos\theta)} = \frac{KI_V I}{\sin\theta} \quad (26)$$

To determine I_V, refer to Figure 12.

For a balanced 3-phase system,

$$I_V + I_B + I_C = 0 \quad (27)$$

Use V_{AB} as reference vector and neglect generator impedance, then,

$$V_{AB} = V\underline{/0} = -I_B kR_p + I_V \text{ Req.} \quad (28)$$

$$V_{BC} = V\underline{/-120} = I_B kR_p - I_C(1-k)R_p \quad (29)$$

$$V_{CA} = V\underline{/-240} = I_C(1-k)R_p - I_V \text{ Req.} \quad (30)$$

where

R_p = total variable resistor ohms

Req. = equivalent transformer impedance with the galvanometer burden

Solving equations 27 through 30 simultaneously gives the scalar galvanometer potential circuit current as

$$I_V = \frac{V\sqrt{1-k+k^2}}{\text{Req.}+(k-k^2)R_p} \quad (31)$$

Substituting equation 31 in equation 26,

$$\frac{\partial D}{\partial(\cos\theta)} = \frac{KIV\sqrt{1-k+k^2}}{\sin\theta[\text{Req.}+(k-k^2)R_p]}$$

or

$$S = \frac{1}{KIV}\frac{\partial D}{\partial\cos(\theta)} = \frac{\sqrt{1=k+k^2}}{\sin\theta[\text{Req.}+(k-k^2)R_p]} \quad (32)$$

where

S = galvanometer deflection in radians per unit power factor per volt-ampere, divided by the "galvanometer constant," K

The value of k, the variable resistance ratio, in terms of θ is given in equations 5, 8, 11, and 14 for each range of power factor, and when substituted in equation 32 provides the sensitivity curve of Figure 8.

No Discussion

A Full Automatic Private-Line Teletypewriter Switching System

W. M. BACON
NONMEMBER AIEE

G. A. LOCKE
ASSOCIATE AIEE

Synopsis: This paper describes a full automatic teletypewriter message switching system for use in private-line networks involving one or more switching centers and a multiplicity of local or long-distance lines, each of which may have one or more stations. This system provides fast teletypewriter communication from any station to any other station or group of stations in the network. At its point of origin a message first is perforated in tape accompanied by suitable directing and end-of-message characters, thereafter it is transmitted automatically, stored temporarily in perforated tape at a switching office, and then routed at high speed to its point or points of destination. Important features are the arrangements provided to permit efficient use of long full duplex transmission lines, the full automatic handling of multiple-address messages with only a single originating transmission, and the various guards and alarms which are provided to protect against loss of messages in case of trouble.

IN THE years before World War II a number of private-wire teletypewriter systems had grown to considerable size, some of them spanning many states or even the entire country. About 1940 it was felt that a faster more economical service could be secured by the use of automatic switching of teletypewriter messages, and the Bell System undertook the development of full automatic arrangements. In October 1941 a full automatic teletypewriter switching system was placed in service for the Republic Steel Corporation, just in time to handle the rush of war business.

Paper 51-76, recommended by the AIEE Communication Switching Systems Committee and approved by the AIEE Technical Program Committee, for presentation at the AIEE Winter General Meeting, New York, N. Y., January 22–26, 1951. Manuscript submitted October 25, 1950; made available for printing December 8, 1950.

W. M. Bacon and G. A. Locke are both with the Bell Telephone Laboratories, Inc., New York, N. Y.

World War II prevented the installation of additional systems of this type and interrupted the development program. Experience with the Republic Steel system during the war proved not only its many advantages, but the soundness of its basic features. Following the war, a wide interest in teletypewriter switching systems of this general type resulted in further studies and the renewal of the development program.

The studies indicated the need for even greater scope and versatility, with such new features as the use of more than one switching office in a system and the full automatic handling of multiple-address messages, which are messages originating as a single transmission to be delivered to more than one receiving station. As a result of the development program the present system, known as the *81C1* teletypewriter system, was produced and placed in service for five large customers with nationwide networks.

The *81C1* system provides efficient, accurate, and rapid handling of a continuous flow of messages between the various stations on extensive private-line teletypewriter networks involving a multiplicity of lines and stations. It functions in such a manner that a message may be sent from any sending teletypewriter and recorded on any desired receiving teletypewriter or group of teletypewriters in a network without requiring manual handling or operating attention other than the original perforation of tape at the sending station and the removal of the typed message from the receiving machine or machines to which it was directed. The switching operations are entirely automatic and are under the control of directing characters punched at the head of each message in the original transmitting tape and end-of-message characters punched at the end of each message.

Individual line circuits are full duplex and may be operated at either 60 or 75 words per minute, thus permitting maximum economies for any line loading.

The general objectives considered and met by the design include efficient usage of line circuits, rapid delivery of messages, and accurate handling of traffic, as well as many other requirements dictated by the customers' individual traffic patterns and problems. Different sizes of switching offices, the number of switching offices in a system, the number of trunks between switching offices, the number of stations in a system, the amount of traffic for local delivery in the vicinity of a switching office, the quantity of multiple-address traffic, and a number of other variations all must be considered when a system is engineered. Traffic which systems provided for industry must handle consists in general of relatively long messages which must be transmitted over the systems with speed and accuracy. On the other hand, traffic for transportation companies, particularly airlines, consists in general of much shorter messages, a high percentage of which must be transmitted over the systems within very short intervals. The design of the *81C1* system anticipated these variable factors and permits the installation of systems which provide for them without special engineering for each case.

Figures 1 and 2 show five examples of *81C1* networks now in service. Each of these systems presents different customer's problems handled by the standardized switching system.

The Pan American Airways layout shown in Figure 1 illustrates a system in which there are three widely separated areas, each with its own community of interest. Each area is served by a switching office with lines radiating to stations in the area. Single trunks between the switching offices at San Francisco and New York and between New York and Miami are sufficient to carry the traffic between the areas.

The Eastern Airlines layout, also shown in Figure 1, is an example of a system in

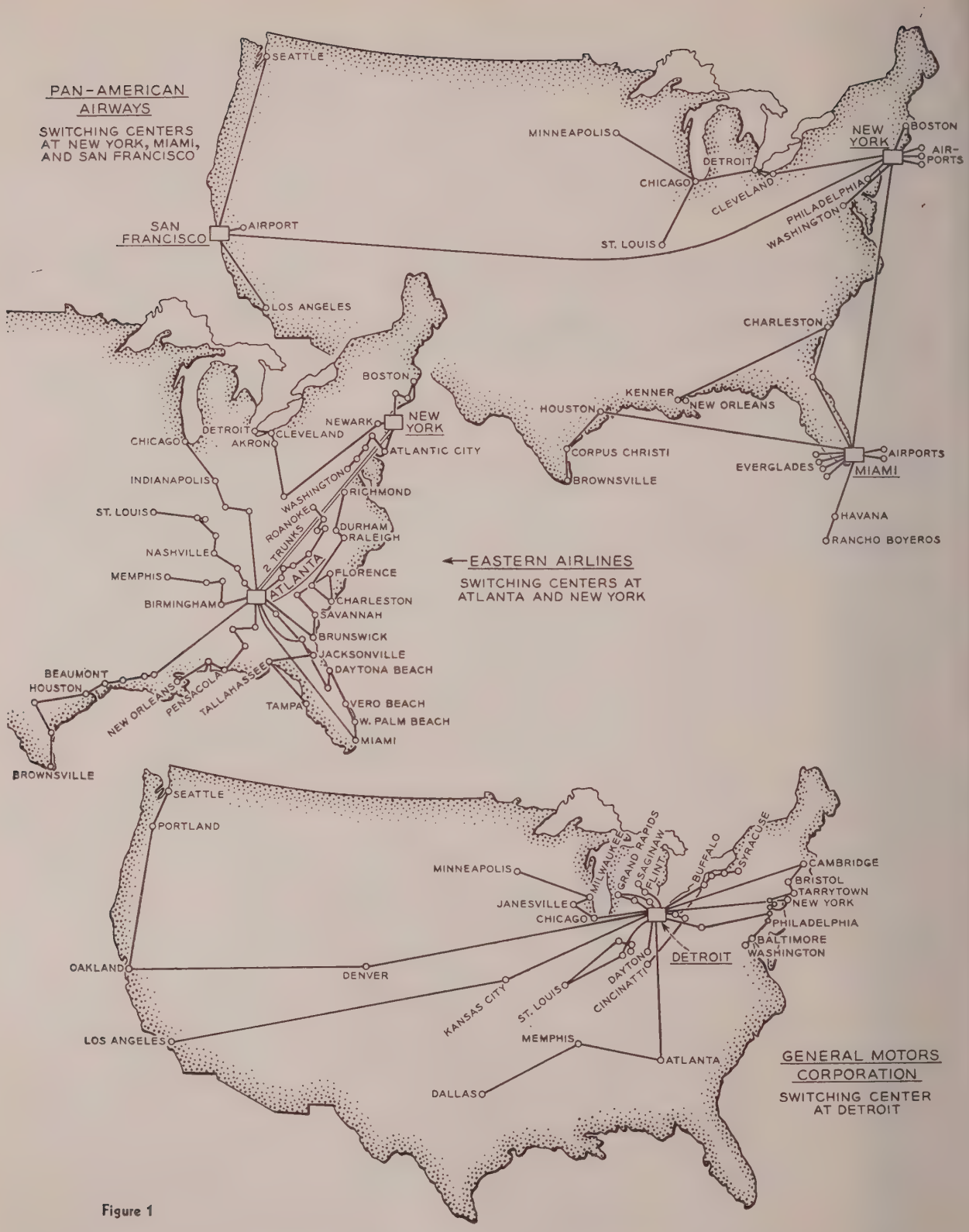

Figure 1

which there are two centers with a community of interest, each served by a switching office. In this case there is sufficient traffic between the switching offices at Atlanta and New York to warrant two trunks between them.

The General Motors Corporation layout shown in Figure 1 is an example of a system where one large switching office located at Detroit is best adapted to handle the traffic. In this case, the heavy volume of business for the headquarters office is delivered at the switching center and distributed principally by telephone, messenger, and pony wire.

Figure 2

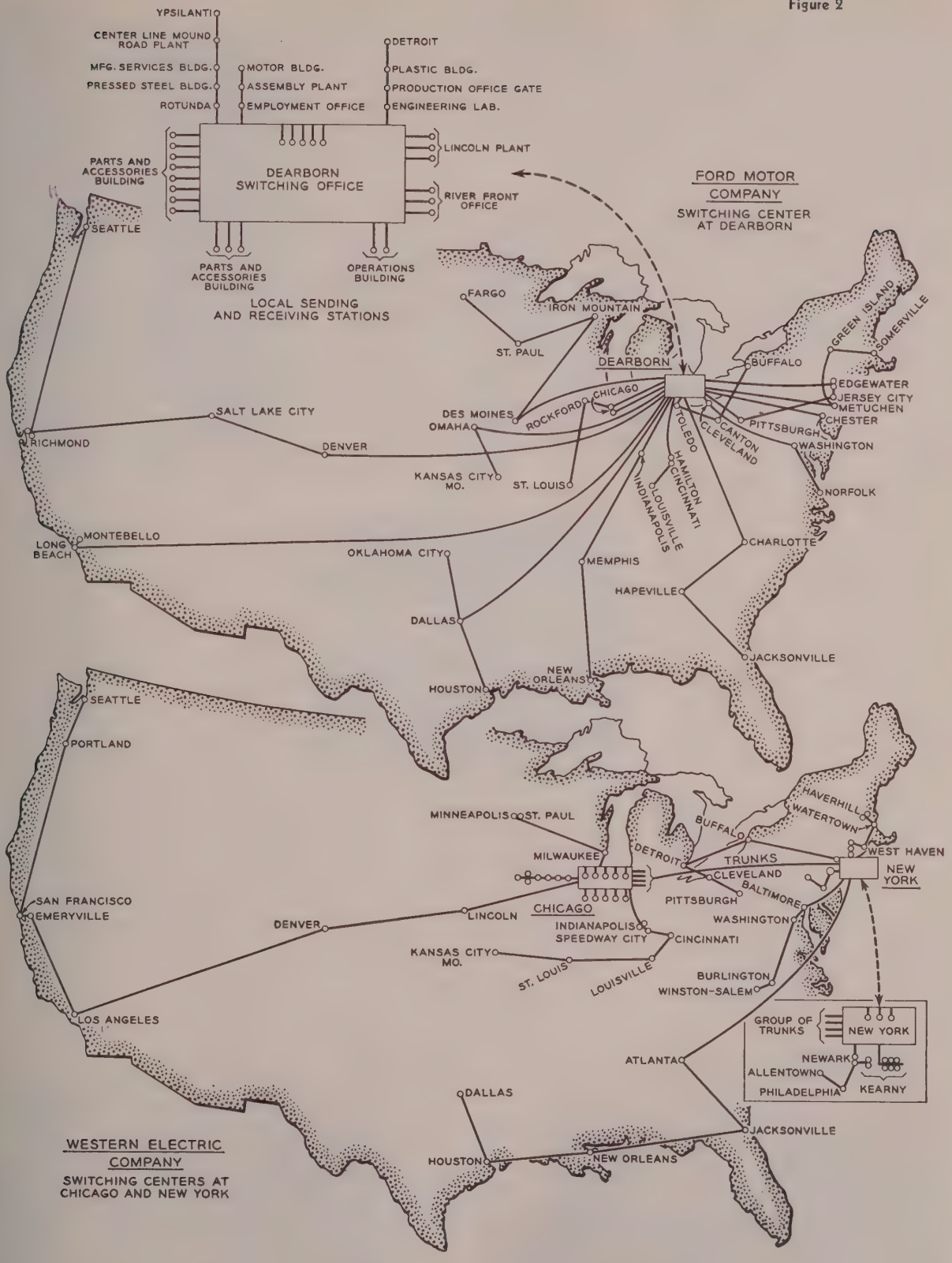

The Western Electric Company layout shown in Figure 2 illustrates a large industrial system in which there are two major centers of traffic served by two switching offices, but with a large amount of traffic between these offices necessitating a group of interoffice trunks.

The Ford Motor Company layout shown in Figure 2 is an example of a system where one very large switching office at Dearborn handles the traffic. In this case (see inset in Figure 2) there is a large

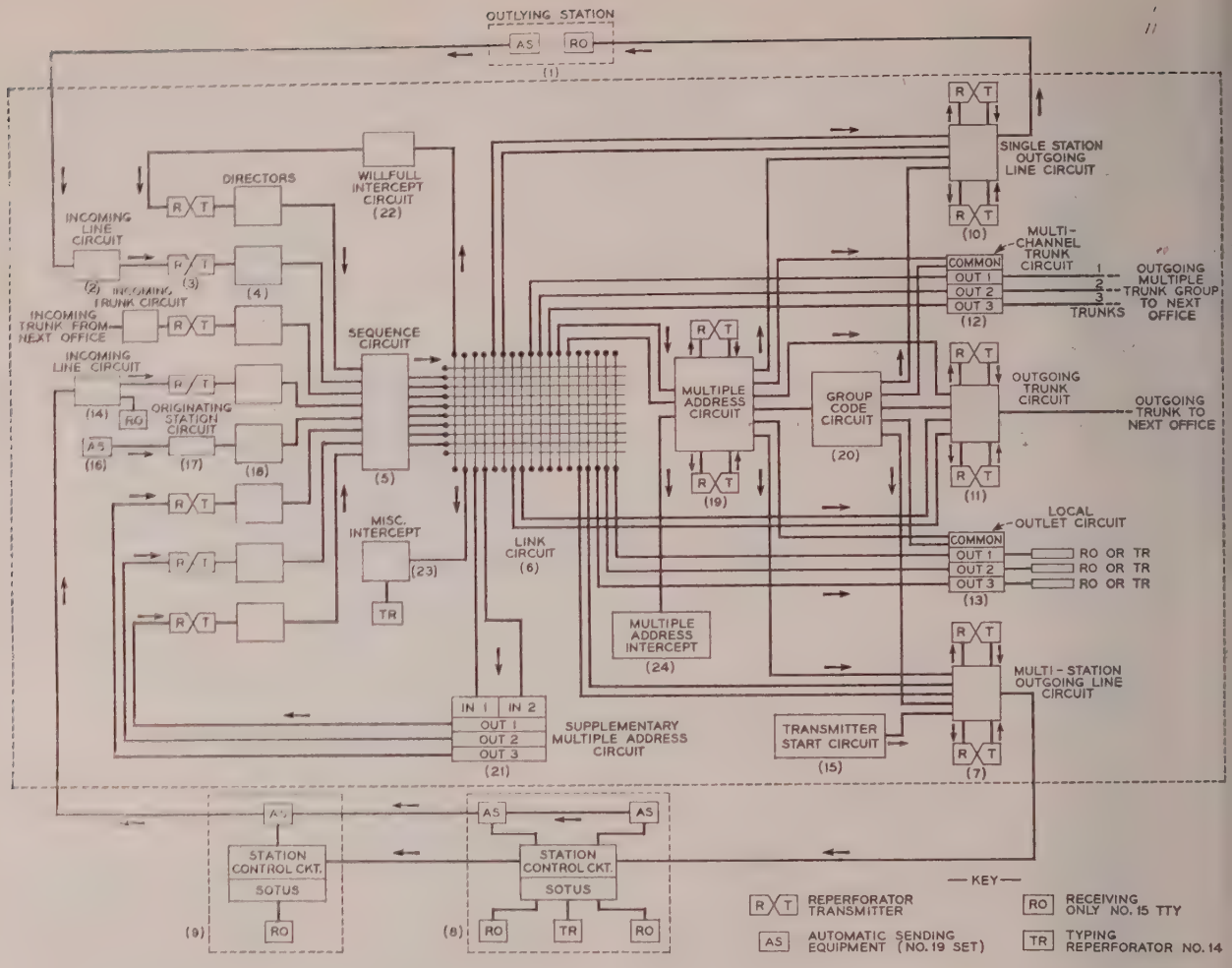

Figure 3. 81C1 system, block diagram

volume of local traffic to be distributed to stations within a short distance of the switching center.

General Method of Operation

Each station in the system is assigned a 2-letter code, and in order to direct a message from any sending station in the system to any receiving station, the operator perforates in the sending tape the 2-character code of the desired station, followed by a "Letters" signal. Twenty of the 26 letters of the alphabet are used for station code purposes, thus permitting up to 400 station codes. For various reasons the letters T, O, M, V, H, and Z are not used. The first four are apt to be produced in case of an accidental interruption or hit on an idle line, while H and Z are used for other switching functions which will be explained.

Referring to the block diagram Figure 3, the path of a message will first be traced from a sending station which has exclusive use of a line (1).* The message

* Numbers in parenthesis indicate location of circuits in Figure 3.

Figure 4 (left). Typical station on a multistation line

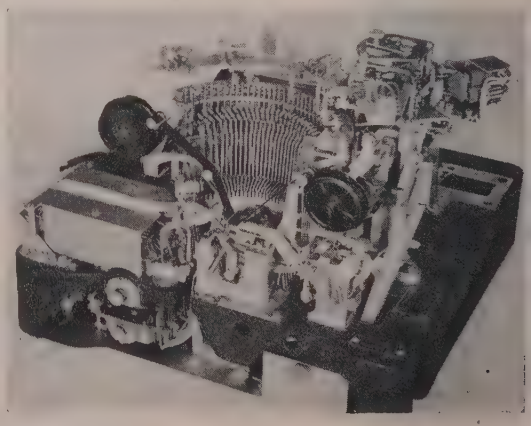

Figure 5 (right). Reperforator-transmitter

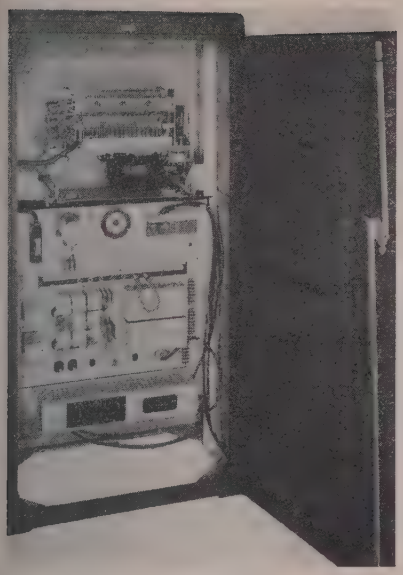

Figure 6. Station control cabinet

is perforated in a tape at the station, the text of the message being preceded by the 2-character code of the station of destination and followed by the characters "Figures," H, "Letters," which indicate the end of a message. This tape is sent from the transmitter-distributor which may be seen in Figure 4. No further action regarding this message is required on the part of the station operator.

The incoming line circuit (2) at the switching point associated with the line serving this station perforates the message in a tape on the receiving side of a reperforator-transmitter (3).

The reperforator-transmitter shown in Figure 5 is a machine which forms the heart of the switching system and warrants at least short description. This machine consists essentially of two parts, a receiver which perforates and prints tape identical with the tape made at the station and a transmitter which transmits the signals represented by the perforations in the tape and is arranged so as to transmit the last character perforated, thus eliminating the need for special tape feed-out arrangements to clear messages from the transmitter. The transmitting portion of the machine is arranged so that the reading of the perforated holes and the actual transmission can be controlled independently from external circuits when desired.

The presence of tape perforated with characters in the receiving side of a reperforator-transmitter brings into action an associated director circuit (4). The director circuit causes the reperforator-transmitter to read the first two characters, which are the code of the station of destination. These two characters taken together are decoded by the director circuit to indicate the outlet of the switching office over which the desired station may be reached. The five types of outlets which may be reached are described below.

Figure 8. Testing unit

Outgoing Multistation Lines

It first will be assumed that the station of destination is located on a multistation line. A multistation line may have connected to it up to ten receiving stations. The outgoing line circuit (7) is equipped with two reperforator-transmitters, on the receiving sides of which messages switched to this outlet are perforated for delivery to that line. The use of two machines in connection with an outgoing line materially cuts down the time this outlet will appear busy to incoming messages and also permits loading the line itself very close to its full capacity.

When the director determines that this outlet is the one on which the desired station is located, it tests the outgoing line circuit for the availability of the receiving side of one of its reperforator-transmitters.

If both machines are busy, the director circuit waits, maintaining its test until one of the machines becomes idle. As soon as one of the machines becomes idle, the sending side of the reperforator-transmitter of the incoming line is connected to the receiving side of the outgoing line machine by means of the sequence circuit (5) and the crossbar switches of the link circuit (6). The use of the sequence circuit prevents more than one connection from being made through the crossbar switches during the brief period while the connection is being established, but simultaneous connections up to the capacity of the switches may exist at one time.

When connection is made from an incoming line circuit to an outgoing line circuit, this connection being known as a cross-office connection, the directing code and the message are reperforated in the machine of the outgoing line, and when the director reads the "Figures," H, "Letters" characters at the end of the message, the cross-office connection is released.

The outgoing line circuit is arranged to deliver the traffic perforated in its two machines to the line on an alternate basis, so that traffic delivered to one machine will not receive preference in transmission over that in the other. The stations (Figure 4) connected to a multistation line are equipped with a station control circuit (Figure 6), including a selector unit, which is a motor-driven mechanical device for closing and locking a contact upon the reception of a number

Figure 9. Switching office, general view

Figure 7. Control board

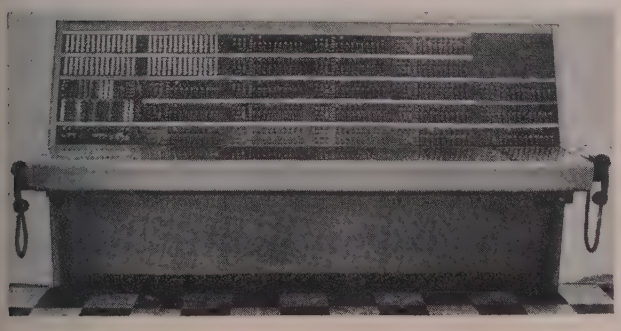

of characters received in a given sequential order. For example, a station is coded on a 2-character basis and to connect station (9) the characters *EF* must be received in that order.

When, therefore, the coding characters are sent to the line by the outgoing line circuit, the proper station is connected and the "Carriage Return," "Line Feed" signals, which precede the text of the message, will deactivate the selector units so that they will not respond to 2-character combinations in the message text that might connect other stations. The "Figures," H, "Letters" characters at the end of the message will disconnect the station and reactivate the selector units.

A station control circuit may control up to three receivers as at (8).

Outgoing Single-Station Lines

If the traffic to a receiving station is very heavy, the same type of outgoing line circuit (10) is used, but the line is equipped with only one receiving station, and this station, shown at (1), does not require a station control circuit.

Outgoing Single Trunk

The system is not limited to one switching office, but may have as many as desired. The number of switching offices is determined by a proper balance between the cost of switching equipment and the cost of lines. Messages received at a switching office are delivered to another switching office over trunks. The single outgoing trunk circuit (11) is arranged to deliver its traffic over a trunk to another switching point.

Outgoing Multichannel Trunks

The traffic between switching offices may be heavy enough so that one trunk does not provide adequate capacity. In this case a multichannel trunk circuit, which may have connected to it a minimum of two and a maximum of ten trunks as at (12), is used. Reperforator-transmitters are not used in this case as the trunks themselves provide the required multiple-switching paths. The speed of transmission over the trunk must be the same as the cross-office speed, which is 75 words a minute. Connection from an incoming line to an outgoing trunk is made on a "first idle trunk" basis.

Local Outlets

In some installations conditions arise where large volumes of traffic for the same destination must be delivered to points in the general locality of the switching office. The local outlet circuit is used for this purpose (13). These points may be equipped with ten receiving machines, which operate at cross-office speed directly from the inputs without reperforator-transmitters on the outlet side. These receivers are connected on a "first idle receiver" basis.

Traffic for Switching Office

Some traffic received on incoming lines is destined for the switching office itself. The incoming line circuits can be equipped with a receiving-only teletypewriter in addition to the reperforator-transmitter (14). This traffic then can be switched directly to the receiving-only teletypewriter without burdening the switching mechanism of the office, thus increasing its over-all efficiency. Two specific codes are assigned for this use: a first character followed by Z, which cuts on the receiving-only teletypewriter alone, or a first character followed by H, which cuts on both the reperforator-transmitter and the receiving-only machine for reception of the message both at the switching office and at some other station. When the volume of terminal traffic is not great enough to justify a receiving-only teletypewriter per incoming line, local outlet machines, as described previously, may be used.

Sending from Multistation Lines

In the previous discussion traffic was introduced into the system from a line equipped with only one station. It will be noted that all lines are full duplex, permitting simultaneous transmission both to and from stations on a line.

Multistation lines may be equipped with up to ten sending stations, as well as the ten receiving stations heretofore mentioned. Inasmuch as only one sending station may send at a given time, sending is controlled by a transmitter-start circuit (15), which is associated with the outgoing line. Each transmitter on the line is assigned a single-character transmitter-start code which, when sent over the line preceded by a specific pattern, causes the transmitter at a given station, if there is tape in it, to start sending.

Upon termination of sending from any station on a multistation line, the transmitter-start circuit (15) takes control of the outgoing line circuit and stops outgoing transmission. This stoppage may take place at any time during which the text of a message is being sent or between outgoing messages. A pattern is then sent out ("Blank," a pause, "Space") which cuts off the receivers connected to the line without mutilating the copy being received and conditions the station control circuits to control their transmitters. The transmitter-start circuit then sends the start character for the transmitter next in sequence. If this next station has traffic, transmission will begin and the receivers that were cut off will be restored. If it has no traffic, the next transmitter in sequence will be tried, and so on either until traffic has been found at some station or until all have been tested without finding traffic. In the latter case the circuit waits for a predetermined interval, which may be chosen to suit requirements, before it again starts to test stations for traffic.

Each message in the tape at the sending station is terminated by "Figures," H, "Letters," which indicates the end of a message, but it may not be economical of line time to limit a transmission from a station to one message. The station operators therefore are instructed by the customer regarding the maximum number of messages that may be included in a transmission. This number may be different for different stations, depending on traffic needs. Following the "Figures," H, "Letters" characters of the last message, two additional characters, H and "Letters," are perforated in the tape. These characters, when registered in the incoming line circuit, cause the transmitter-start circuit to test other sending stations on the line.

Originating Station

For traffic originating at the switching office an automatic sending teletypewriter set is used (16), which is connected to an originating station circuit (17) and a director (18). The action of this director is the same as (4), except that it controls the sending set instead of a reperforator transmitter.

Multiple Address

Traffic consisting of messages introduced at a sending point to be delivered to a multiplicity of receiving stations in the system is handled by the multiple address circuit.

When a sending operator prepares a message for delivery to a number of stations, a 2-character multiple-address code first is perforated in the tape. The operator then follows this specific multiple-address code by the codes of the stations of destination. There is no limita-

tion upon the number of station codes that may be inserted. The multiple-address code instructs the director at the switching office involved to deliver the message to one of two reperforator-transmitters associated with the multiple-address circuit (19). The whole message, including addresses and text, is perforated in one of the machines of the multiple-address circuit.

The multiple-address circuit is equipped with a special type of director which discards the multiple-address code and then starts reading the individual codes.

Assume the first code is for a station on the outgoing line (7). When the reading of the address by the multiple-address director indicates that this particular outlet is required, a bid is made to the outlet. If one of the outgoing line machines is idle, it is connected to the multiple-address circuit.

Connection of the outgoing line circuit to the multiple-address circuit causes the multiple-address director to send the code to the connected machine of the outlet and then without disconnecting from it to blind the transmission path. The second address is then read and connection to another outlet made in the same manner. If another address is for an outlet already connected, the transmission path is unblinded, the new address is transmitted, and the transmission path again is blinded. In like manner, all the addresses are read and the required outlets connected by means of multiple transmission paths.

If an address calls for transmission to another switching office, a trunk is connected. In connecting to a trunk, however, it is necessary to indicate to that trunk that this is a multiple-address message, so that it can be handled via the multiple-address message circuit in the next office. When, therefore, connection is made to a trunk for the first time, the multiple-address director inserts a multiple-address code ahead of the first address.

When all the addresses have been read and sent to the various outlets, the "Carriage Return," "Line Feed" signals preceding the text are read, which causes all the connected outlets to be unblinded and the text of the message to be sent to all outlets simultaneously. The "Figures," H, "Letters" characters following the message text release the connections.

Group Code

Part of the multiple-address traffic of many customers includes many messages which are sent to the same group of stations as a matter of routine. Considerable saving in operating time and better accuracy is obtained by assigning each of these groups a single 2-character code. When such a code is encountered by the multiple-address director a group code circuit (20) is called into action and makes a simultaneous bid to all the outlets concerned. When all the outlets involved have been connected, the multiple-address director sends the group code and the message to all these outlets.

Supplementary Multiple Address

When the volume of multiple-address traffic is large, the capacity of the multiple-address circuit may be augmented by using the supplementary multiple-address circuit (21), which handles 2-, 3-, and 4-address messages.

When using the supplementary multiple-address circuit, specific multiple-address codes are assigned to 2-, 3-, and 4-address messages, and the regular directors connect the incoming sources to one of a maximum of five input levels of this supplementary circuit. A maximum of ten outputs, each equipped with a regular director and a reperforator-transmitter, may be provided.

If an input level is called into action by the 2-address code, it is informed that two outputs are required. When two outputs are connected, the first address is placed on the machine of the first and the second address on the machine of the second. The text of the message then is transmitted to both machines and the connection is released. Thus, the 2-address message has been broken into two single-address messages, which are handled by the directors connected to the outputs in the same manner as does a director connected to an incoming line.

Similarly, the 3- and 4-address messages are reproduced as three single- and four single-address messages.

Interception

Different opening and closing times of stations because of time-zone differences or shutdown of stations for holidays or maintenance make it desirable to have a means of intercepting messages bound for such a station or stations for later delivery. Such a device, the willful intercept circuit (22) which may have one or two receiving paths, is provided for the interception of single-address messages. The operation of keys diverts the traffic to be intercepted to this circuit. At a later time, this traffic which is stored in a reperforator-transmitter can be re-entered into the system automatically by means of its associated director.

Multiple-address messages which use individual station codes are intercepted on typing reperforators by the multiple-address intercept circuit (24).

Another type of interception is necessary to take care of unassigned codes which may occur from errors on the part of the operators or troubles in transmission.

When an unassigned or mutilated code is encountered by either a regular director or a multiple-address director, a miscellaneous intercept circuit is called in (23) or (24), which records the addresses and text on a typing reperforator. Any traffic recorded in this circuit has its addresses corrected by the switching office attendants and is re-entered into the system at an originating station.

Guards Against Message Loss and Delay

Message-numbering methods such as point-to-point and channel numbering have been used on teletypewriter systems for many years to discover system failures or troubles which have resulted in lost or delayed messages. Messages are not considered lost if they are delivered to a wrong point, as they can be rerouted. Neither numbering method provides for quick discovery of the loss or delay of a message, and in high-speed systems a message may be worthless if delayed more than a few minutes. Extra clerical work, with its added opportunity for human errors, and the consumption of valuable line time for number transmission are additional weaknesses of number-checking methods.

If proper precautions are taken to guard against message loss and delay, the use of message-numbering may be curtailed or entirely eliminated except as it may be needed for message identification. With this in mind the *81C1* system was designed to include many safeguards against message loss, as well as alarms which quickly and forcibly call the attention of operating personnel to trouble conditions. Some of these safeguards and alarms are discussed briefly in the following paragraphs.

The substitution of one valid code for another at the head of a message due to operator error or trouble will result in delivery to the wrong station, from which point the message can be rerouted.

The appearance of an invalid code at the head of a message, due to operator error or failure of machines or lines, when received at a switching office will direct the message to miscellaneous intercept

with both an audible alarm and a visual alarm. If the invalid code appears on a multistation outgoing line, provision can be made so that the message will be typed on all receivers or on any master receiver selected for this purpose. An audible and visual alarm at the receivers then calls the operators' attention to the message.

If no end-of-transmission combination is received at the switching office from a multistation incoming line, an automatic end-of-transmission is registered after 45 seconds of idle line time.

An open line or trunk to the switching office is alarmed both audibly and visually at the switching office. An open outgoing multistation line is alarmed visually at each receiving station or at specific stations chosen for the purpose. Open single-station lines and loops to local outlets cause the receiving machine to run open.

The failure of an incoming line reperforator-transmitter or receiving-only machine to respond to signals, tape failing to feed through the punch blocks, torn tape, and low tape supply are all audibly and visually alarmed at the switching office. Similar conditions on other teletypewriter apparatus at the switching office not only are alarmed, but the machines also are automatically made busy to further messages until the condition is cleared.

Failure of the switching circuits to complete their functions, as well as certain other improper functioning of these circuits, is alarmed.

Maintenance of Service

All circuits and machines utilized in this system are wired through plug connectors in order to allow the immediate replacement of a defective circuit or machine by a spare. A system of keys and lamps is provided at a control board (Figure 7). At this board lamps indicate traffic flow and stations sending on all circuits, keys provide for controlling the traffic flow as desired, and other lamps identify alarm conditions in individual circuits so that the quick diagnosis of trouble is greatly facilitated.

Each office is equipped with a testing unit (Figure 8) to which nearly all circuits can be patched for test and at which all machines can be tested and repaired.

Equipment Arrangements

Figure 9 shows the switching office at the General Motors Corporation in Detroit, Michigan. The machine cabinets, each of which mounts two reperforator-transmitters, are shown at the right and in the rear of the middle row. These cabinets are of the unit type which allows for ready installation and additions. At the extreme right behind the reperforator-transmitter cabinets are the cabinets which house the relay circuits for the various functions that have been described. These relay cabinets are manufactured as packages containing combinations of circuit units, so that great flexibility as to the initial size of systems, as well as their expansion or contraction after they have been installed, is obtained.

At the left of the office are shown the originating stations, while in the front center appear the terminal traffic receiving-only teletypewriters which are associated with the incoming lines and the typing reperforators associated with the miscellaneous intercepts.

Continued Development

Active development is being continued to provide new and improved features for this type of system. This development is based on engineering studies of the needs of potential users, as well as the experience gained with the six large systems now in service. Increased speed of message delivery, greater line capacities, more rigid message security, greater switching office capacity, simpler operating procedures, and simplified circuit arrangements to reduce maintenance effort are among the items being covered in the present development program.

No Discussion

Automatic Trunk Selection in Reperforator Switching

W. B. BLANTON
NONMEMBER AIEE

A MAJOR phase of Western Union's mechanization program was greatly accelerated after World War II and was completed in 1950. This phase consisted of installing large reperforator switching centers to replace manual offices in 15 cities selected to serve as area centers for the various sections of the country. A concurrent phase of the program was the enlargement and improvement of the trunk and tributary circuit network, principally through the use of carrier current techniques, to provide a modern nation-wide transmission system for the 15 switching centers and their tributary offices. The result is a nation-wide telegraph system of greatly increased efficiency and capacity, with improved accuracy and speed of service.

Prior to 1948, 7 of the 15 reperforator switching centers had been installed. The methods and equipments employed in those installations have been described in previous AIEE papers. Plug and jack switching[1,2] (Plan 2) is used in the first 5 centers, while push-button switching[3] (Plan 20) is used in the next 2 centers. Since 1947, 8 reperforator switching centers that employ both push-button and automatic switching (Plan 21) have been installed. In addition, most of the older switching centers have been increased in size to permit enlargement and realignment of their areas, so that the 15 centers serve the entire country. It is the purpose of this paper to give a general description of the present network of interconnected switching centers and to describe the new developments in reperforator switching employed in the latest installations.

Paper 51-78, recommended by the AIEE Communication Switching Systems Committee and approved by the AIEE Technical Program Committee for presentation at the AIEE Winter General Meeting, New York, N. Y., January 22–26, 1951. Manuscript submitted October 25, 1950; made available for printing December 14, 1950.

W. B. BLANTON is with The Western Union Telegraph Company, New York, N. Y.

The Telegraph System Prior to Reperforator Switching

Prior to the installation of reperforator switching centers and the inauguration of the 15-area plan, the main office in each of the larger cities throughout the nation was in effect an area center or "relay" office. The term "relay" is used here to denote the physical operation of receiving a telegram into an office over one circuit and then, in accordance with its address of destination, "relaying" it or sending it out of the office over another circuit. Each of those relay offices, totaling more than 100, served the smaller cities, towns, and villages in its immediate vicinity over direct telegraph lines. Trunk connections were established between many relay offices, but it was not economically feasible to connect each of them with all the others. Each office relayed telegrams from its tributary offices to other relay offices, where they were relayed again either to point of destination or to still other relay offices until they were transmitted to point of destination. Each relay operation required a receiving operator to gum on a blank the incoming message produced by the tape printer, a pickup and distributing system to move it to the desired sending position, and an operator to retransmit it.

Block State Routing Areas

In determining the limits of the area that each reperforator switching center would serve, primary consideration was given to arranging the areas so that the address on a telegram would indicate readily the area to which it should be routed. This was achieved by dividing the country into areas along state lines. Each area comprises one or more entire states in which the telegraph offices in all cities, towns, and practically all the smaller communities have a direct connection to the reperforator switching center serving that area. Figure 1 illustrates the block state routing area plan and shows the area center for each of the 15 areas.

Each area center has direct trunk circuits to each of the 14 other area centers. Where the traffic load warrants, trunk circuits are provided between an area center and large tributary offices located in other areas. In addition, many of the large tributary offices located in the same area or in different areas are connected by trunk circuits. The tributary offices that have trunk connections to cities other than their own area center also are known as "terminal" offices. Many telegrams now receive a city-to-city service, and with but few exceptions the remainder of the telegrams are relayed through only one or two intermediate offices. Most of the relaying operations occur in the 15 area centers, where the relaying is accomplished by a switching operation and the automatic retransmission of the message.

Area Switching Centers

Each of the area switching centers also is the distribution point for the city in which it is located and, therefore, has connections to the public branch offices in that city. The connections to each of the tributary and branch offices, and to the centers and terminal offices in other areas, consist of one or more automatic printing telegraph circuits. Besides the telegrams handled over those circuits, an area center receives and sends telegrams over such facilities as patrons' teleprinter and facsimile tie lines, telephones, pneumatic tubes, and Morse. For technical or operating reasons, it is not practicable to connect these facilities directly into the re-

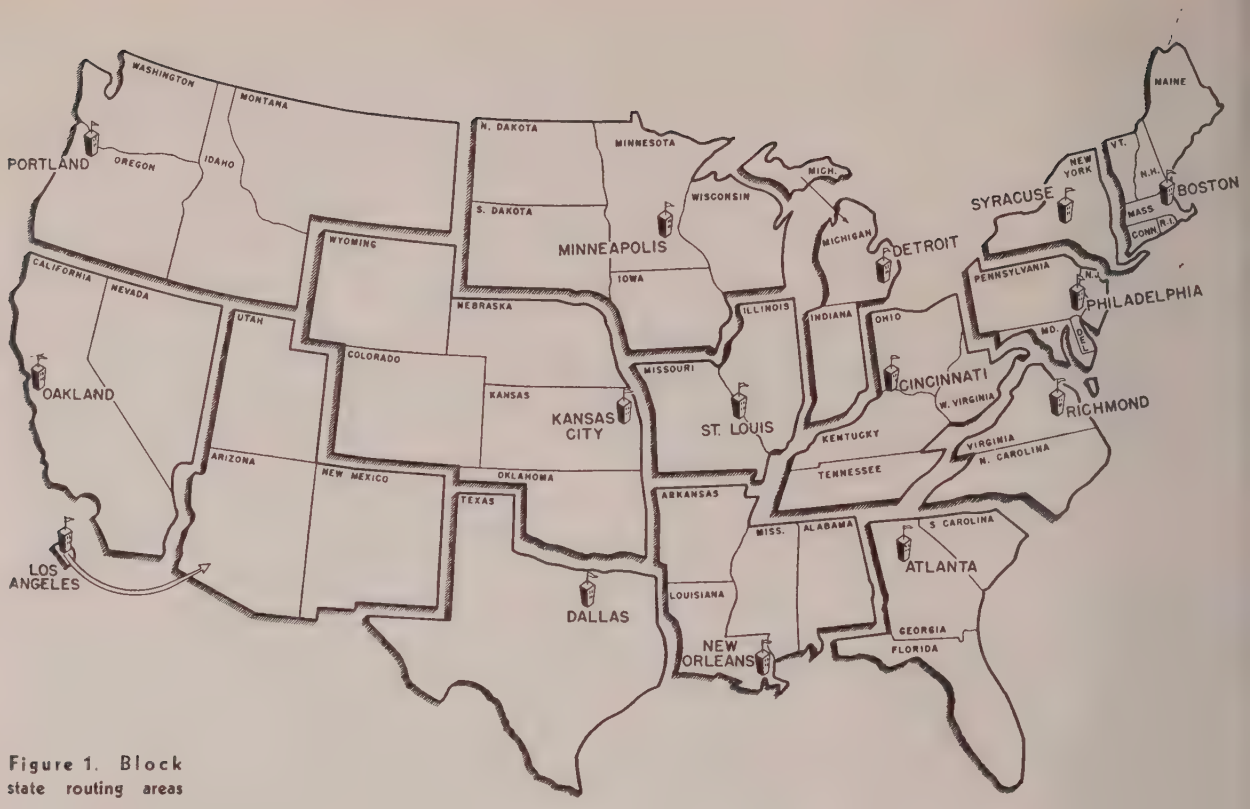

Figure 1. Block state routing areas

perforator switching system. Local sending and receiving positions therefore are provided in an area center for handling the interchange of telegrams between such facilities and the switching system.

The reperforator switching system installed in the last eight area centers is the Plan 21 system. In a Plan 21 area center, telegrams received from points within the area are switched automatically by means of selection characters prefixed to each message, while telegrams received over incoming trunks from other areas are switched manually by means of push buttons.

Provision is made for switching automatically from incoming tributary and branch office circuits and from local operators' sending positions to a maximum of 73 destinations. In a particular area center, these destinations comprise the other 14 area centers; the terminal cities in other areas to which the center has trunks; the large tributary cities within the same area; and various positions within the switching office which are used for segregating certain traffic. Table I lists the destinations to which messages may be switched automatically through the area center at Boston.

Provision is made for push-button switching from the interarea trunks to a maximum of 270 destinations. The destinations reached by push-button switching include all the interarea, intra-area, and intraoffice points to which the switching center has connections.

Since, for economic reasons, the automatic switching facilities do not reach directly all of the destinations included in push-button switching, "crossover" facilities are provided. Telegrams originating within the area and destined for points within the area that are not included in the automatic switching are prefixed with the call letters of the "home" area center. This causes them to be switched automatically and transmitted via the crossover facilities into printer-perforators at push-button switching positions, from whence they are switched to their destination.

The decision to switch messages automatically through the area center of origin and to switch them by push-button means through the area center of destination in the Plan 21 system was based primarily on the routing problems involved in a public telegraph system. With the block state routing plan, it is a relatively simple process for sending operators, either from memory or by reference to a brief and simple route chart, to route and prefix each telegram with selection characters to switch it through the area center of origin. The vast majority of these telegrams are switched automatically directly to outgoing trunks, while only a small portion pass through the crossover facilities and require a push-button switch. However, about one-half of the telegrams received at an area center from other area centers are destined to tie lines, branch offices, and so forth, in the area center city, and to small communities served by telegraph offices in towns adjacent to them. It is necessary to maintain elaborate route charts for the guidance of the switching clerks in directing these messages. For the present, it was deemed inadvisable to disseminate this routing information to all the telegraph offices throughout the country in order to permit automatic switching through the area center of destination.

Equipment and Circuit Arrangements at a Plan 21 Area Center

Figure 2 is a block diagram of the principal equipment and circuit arrangements employed in a Plan 21 area center. The receiving channels of typical circuits are terminated on the right-hand side of the diagram. The associated sending channels are terminated on the left-hand side. The intraoffice switching facilities serve to switch and transmit messages on a

selective basis from receiving equipments to sending positions.

Each line sending position (*S1* to *S8*) comprises an intraoffice reperforator for producing in perforated tape form the messages switched over the intraoffice facilities, one automatic numbering machine for each destination that the position serves, and a tape transmitter for repeating into the sending channel or channels the messages received by the intraoffice reperforator. The "SS" sending positions (*S-2*) and the "SS" push-button switching positions (*R-2*) represent the crossover facilities. Figure 3 shows the type of sending positions (*S-1* to *S-3*) used in the interarea trunk and heavy tributary sending section. The other sending positions (*S-4* to *S-8*) have the same general appearance.

The intraoffice connections between line receiving positions and line sending positions are established on a 9-conductor basis through multicontact, multiposition, electromagnet-operated rotary switches, termed "connector switches." In push-button switching, these switches are actuated by switching clerks depressing destination push buttons in a turret, while in automatic switching they are actuated by automatic switching units that "read" the two selection characters prefixed to each message.

Push-Button Switching

The receiving channels of interarea trunks (*R1* of Figure 2) are terminated in printer-perforators at line receiving positions. Associated with each printer-perforator is an intraoffice transmitter through which the tape, produced by the

Figure 2. Principal equipment and circuit arrangements of a Plan 21 reperforator office

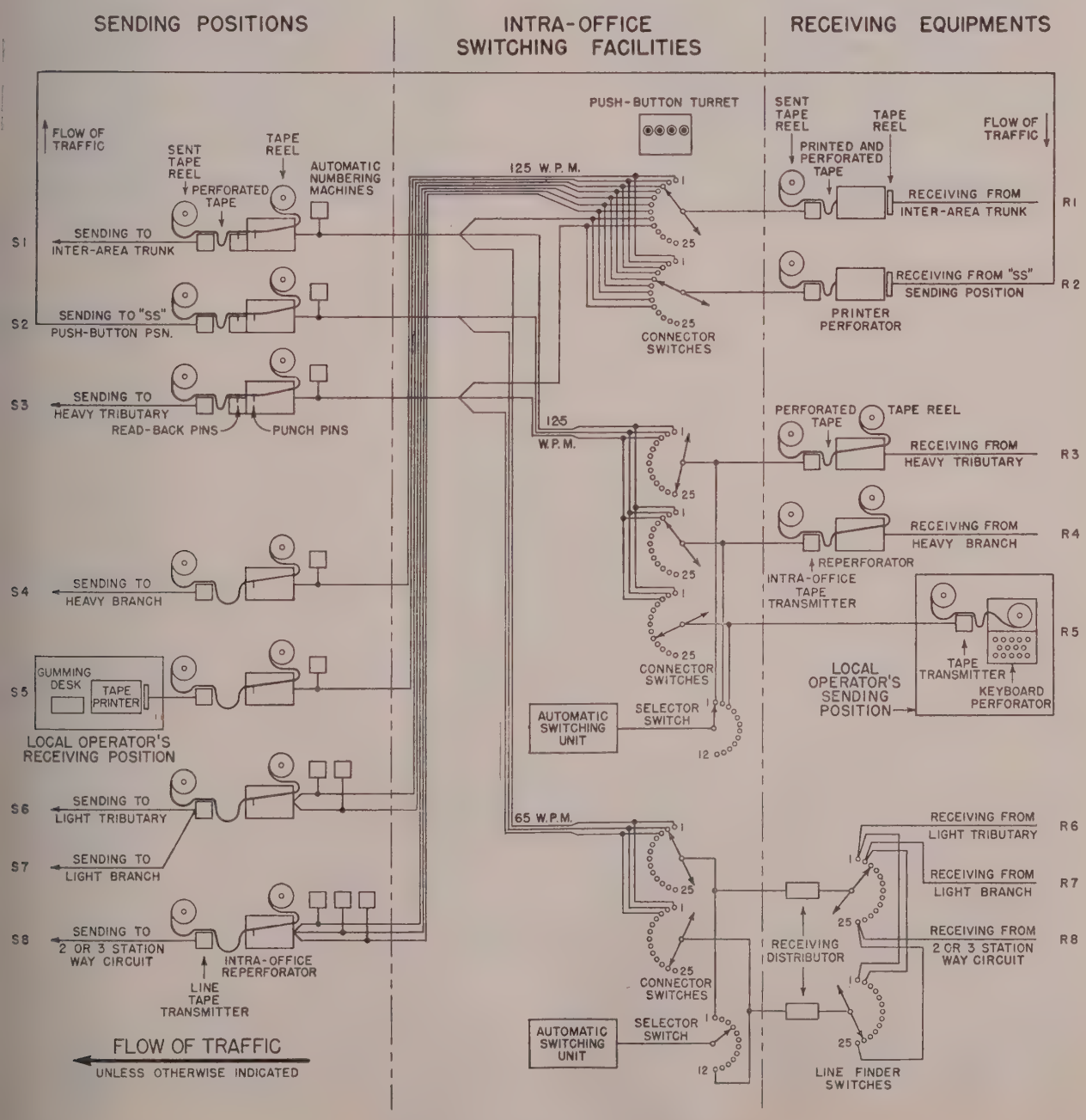

Table I. Automatic Switching Destinations in Boston Reperforator Office

Interarea Destinations

Area Centers	Selection Characters	No. of Sending Channels
Atlanta, Ga.	=A	3
Dallas, Tex.	=D	2
Kansas City, Mo.	=K	1
Los Angeles, Calif.	=L	2
Minneapolis, Minn.	=M	2
Oakland, Calif.	=O	3
Philadelphia, Pa.	=P	6
Richmond, Va.	=R	2
St. Louis, Mo.	=S	2
Cincinnati, Ohio	CT	4
Detroit, Mich.	DE	3
New Orleans, La.	NS	2
Portland, Ore.	PR	1
Syracuse, N. Y.	SY	5
Terminal Cities		
Chicago, Ill.	=C	4
New York, N. Y.	=N	7
Washington, D. C.	=W	3
Albany, N. Y.	AB	1
Baltimore, Md.	BR	1
Buffalo, N. Y.	BU	1
Cable Office, N. Y.	CD	2
Cleveland, Ohio	CL	2
Milwaukee, Wis.	MW	1
Miami, Fla.	MZ	1
Pittsburgh, Pa.	PG	1
Rochester, N. Y.	RH	1
San Francisco, Calif.	SF	1

Intra-area Destinations

Selectable Destinations	Selection Characters	No. of Sending Channels
Bangor, Me.	BG	2
Burlington, Vt.	BI	2
Bridgeport, Conn.	BP	3
Cambridge, Mass.	CA	3
Hartford, Conn.	HK	4
Lynn, Mass.	LY	2
New Britain, Conn.	NB	2
New London, Conn.	NP	1
New Bedford, Mass.	NX	2
New Haven, Conn.	NV	3
Portland, Me.	PD	3
Providence, R. I.	PV	3
Springfield, Mass.	SG	3
Stamford, Conn.	ST	2
Waterbury, Conn.	WY	2
Nonselectable Destinations		
"SS" positions	=B	17

Intraoffice Positions

Special Handling	Selection Characters	No. of Sending Channels
Canadian messages	CP	4
Book messages	B	2
Spill-over "A"	II	2
Spill-over "C"	OO	1
Fall-Back		
Fall-back "A"	AA	2
Fall-back "C"	CC	1
Fall-back "D"	DD	1
Supervisory and Testing		
T&R notes	TR	1
Test purposes	TT	1
Supervisor "A"	SA	1
Supervisor "B"	SB	1
Supervisor "C"	SC	1
Supervisor "D"	SD	1

printer-perforator, flows one message at a time for each switching operation. A push-button switching turret is provided for each three line receiving positions. Figure 4 shows the latest type of 3-position turret. The three printer-perforators are located on a lower shelf, while their associated intraoffice transmitters are located in line on the upper shelf, thus making the reading platform for all three printed perforated tapes at the same level. Since the push-button and automatic switching are integrated into one common system within a center, many of the basic circuit arrangements are the same.

In push-button switching, a switching clerk reads the address and destination of each message, determines the routing either from memory or by consulting a route chart, and then depresses an "initiate" push button located near the transmitter and the appropriate "destination" push button in the switching turret. This causes the connector switches to set up a potential connection to the selected intraoffice circuit. An intraoffice circuit may serve a destination that has one or several sending channels. In either case, potential connections are converted to actual connections by automatic allotting equipment only when one of the sending positions of the desired destination is idle.

When an actual connection is established between an intraoffice transmitter and an intraoffice reperforator at a sending position, the automatic numbering machine at the sending position sends to the intraoffice reperforator the call letter or letters of the area center, the channel designation, and the message sequence number for that channel, after which the intraoffice transmitter transmits the message. When the end-of-message signal, consisting of two periods, is detected by relays in the intraoffice circuit, the transmitter is stopped and disconnected. Thereby the sending position is cleared for another connection. At the same time, the intraoffice transmitter at the switching position is cleared so that the switching clerk may proceed to switch the next message.

Automatic Switching from Heavily Loaded Tributary and Branch Office Circuits

Tributary circuits and branch office circuits are divided into three classifications: heavily loaded circuits (more than 250 telegrams per day), lightly loaded circuits, and way circuits (two or three very lightly loaded tributary offices on one circuit). The out-office end of each of these circuits terminates in an operating position, Figure 5, on which is located a keyboard perforator and tape transmitter for sending telegrams and a tape printer for receiving them.

At the switching center, the receiving channels of heavily loaded tributary and branch office circuits are terminated in "start-stop" reperforators located at line receiving positions shown in Figure 6. Once such a circuit is opened for traffic for the day, the out-office sends at will. Each message is prefixed with two selection characters and an identifying preamble, and is terminated with two periods.

Assume that Quincy, Mass., a tributary of the Boston switching center, has a telegram to be transmitted to Scranton, Pa. The Quincy operator prepares the message in perforated tape form, preceding it with the following characters:

=*P* space *B.QYA* figure-shift 236

The first two characters are the selection characters for Philadelphia, the area center that serves Scranton. The following characters identify it as originating in the *B* (Boston) area from the *QY* (Quincy) office over the *A* (first) channel and being

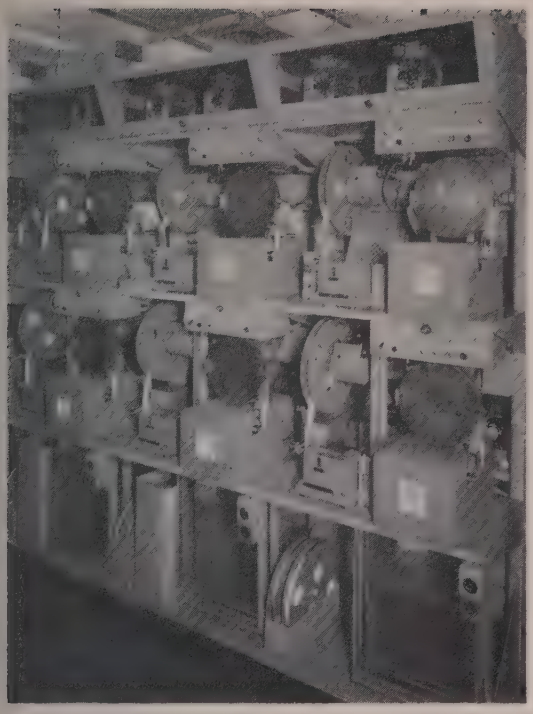

Figure 3 (left). Trunk sending positions

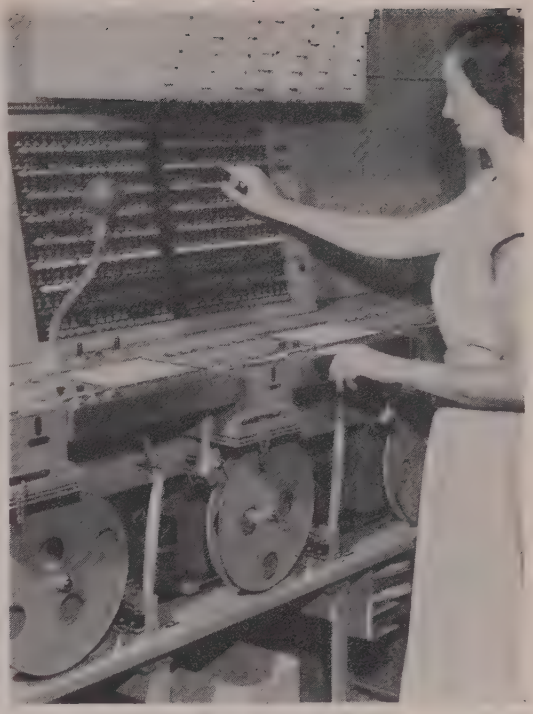

Figure 4 (right). 3-position push-button switching turret

the 236th telegram sent on the channel that day.

At Boston, incoming messages from Quincy are reproduced in perforated tape (no printing), which feeds into the intraoffice transmitter located adjacent to the receiving reperforator. Any "blank" characters between messages are stepped through the transmitter automatically until the first selection character of a message is over the feeler pins. A "message waiting" indicator, an electromechanical device that adds "one" each time the 2-period termination of a message is received and subtracts "one" each time a message is switched, is provided at each receiving position to indicate to the automatic switching equipment that there are one or more messages to be switched.

When there is at least one complete message on hand, an automatic switching unit, common to 12 positions, connects to that position. The intraoffice transmitter then sends the two selection characters and the following space character into the switching unit, which immediately functions to set up a potential connection to the intraoffice circuit of the desired destination, in this case Philadelphia. The automatic switching unit then is free to serve any of the 11 other positions with which it is associated.

If a Philadelphia sending position is idle, or when one becomes idle, the potential connection is converted automatically to an actual connection. The automatic numbering machine at the selected sending position functions, after which the intraoffice transmitter transmits the message into the intraoffice reperforator. During the transmission of the preamble, a call letters and sequence number comparison takes place as described later. The two periods at the end of the message cause the intraoffice transmitter to stop and be disconnected. If the "message waiting" indicator indicates that another complete message is on hand, that message then is switched in a similar manner. When the last message at a position is switched, the receiving reperforator feeds out sufficient blank tape to permit the last character of the message to pass through the intraoffice transmitter.

Local Operators' Sending Positions

Figure 7 shows a local operator's sending position. Local operators prepare messages in perforated tape form, prefixing each message with selection characters and an identifying preamble, and terminating each one with two periods. At each position the tape flows, one message at a time for each switching operation, through the intraoffice transmitter and the messages are switched automatically in the same manner as at heavily loaded tributary and branch office line receiving positions.

Sequence Numbering of Messages

One of the important features of Plan 21 switching centers is the automatic checking of sequence numbers of all incoming messages that are switched automatically. In handling commercial telegrams over a telegraph circuit, unrelated messages are transmitted, one after the other. It has long been telegraph practice to protect each message against possible failure or duplication resulting from equipment, circuit, or operators' errors, by the use of sequence numbers. At the sending end of each circuit, a sequence number is prefixed to each message. At the receiving end of each circuit, the sequence number of each message is checked, thus giving an immediate indication of the omission or duplication of a message. At reperforator offices, automatic numbering machines prefix sequence numbers to outgoing messages, while the sequence numbers on incoming messages that are switched manually are checked by the switching clerks on a number sheet individual to the circuit.

In Plan 21 automatic switching, whereby messages are switched through the office without human attention, electromechanical facilities check the sequence number of each incoming message. Not only do these facilities insure that each message is received at the switching center, but the protection is extended to checking, character by character, to assure that the entire identifying preamble of each message actually is perforated correctly in the tape of the intraoffice reperforator at the selected line sending position. Messages having a

Figure 5 (left). Out-station operating table

Figure 6 (right). Line receiving position for heavily loaded tributary and branch office circuits

correct preamble are accepted by a sending position, those with an incorrect preamble are rejected and routine measures are taken to have those messages retransmitted correctly from the sending offices or positions.

Call Letters and Sequence Number Equipment

The checking of the identifying preamble of each message automatically switched from an intratransmitter position takes place while the preamble and first few characters of the message are being transmitted into the intraoffice reperforator at the selected line sending position. These intraoffice reperforators, Figure 8, are equipped with read-back feeler pins much like the feeler pins on a tape transmitter. While a reperforator is punching into its tape a code combination received over five conductors from an intraoffice transmitter, the feeler pins "read" the fifth preceding code combination that was punched in the tape. The feeler pins actuate contacts that transmit this code combination back over the same five conductors to the intraoffice transmitter position, where it is compared electrically with a code combination as set up in a sequence number indicator.

A sequence number indicator, Figure 9, includes three rotary switches termed "call letters," "tens," and "units" switches. The call letters switch is wired for the fixed characters in a preamble. For example, at the Quincy *A*-channel receiving position it is wired for *B.QYA* figure-shift. Each of the tens and units switches are wired for the digits 1 to 0, inclusive. These two switches always indicate the tens and units digits of the sequence number of the next message to be checked at that position. Sequence numbers consist of three digits, for example, 001, 002, and so forth, to 999. The checking functions require that there be a hundreds digit, but a check is not made to determine if it is correct.

Call Letter and Sequence Number Comparison

In the description previously given of switching a message to Philadelphia from the Quincy receiving position, the intraoffice transmitter starts its transmission with the character *B* of the preamble *B.QYA* figure-shift 236. After each character transmitted, a read-back code

Figure 8 (right). Intraoffice reperforator equipped with read-back pins

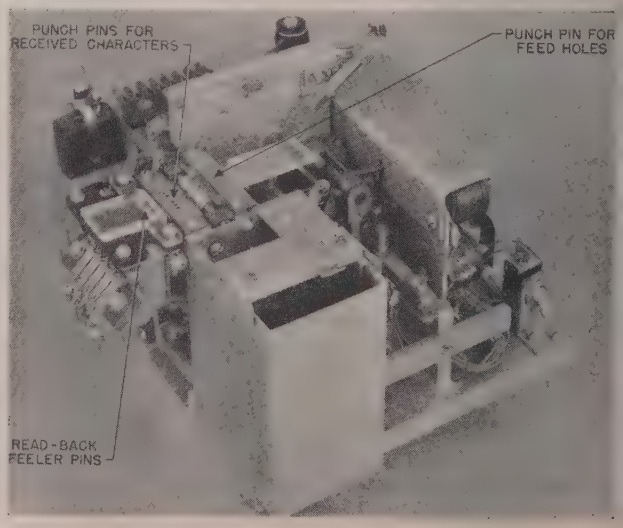

Figure 7 (below). Local operators' sending position

Figure 9 (left). Sequence number indicator

Figure 10 (right). Sequence number indicator rack for line finder circuits

combination is received at the Quincy receiving position from the Philadelphia sending position. Since the read-back characters are displaced five characters from the transmitted characters, the sequence number indicator merely counts the first five read-back characters and then compares each of the nine preamble read-back characters with the code combinations for these characters as set up in the indicator. If each character compares correctly, the intraoffice transmitter continues to transmit the remainder of the message, and the sequence number indicator advances to the next higher number in readiness to compare the sequence number of the following message.

When a read-back code combination differs from the code combination set up in the sequence number indicator, a wrong comparison results. Immediately the intraoffice transmitter is stopped and an electrical request is made for a "bust-this" unit that serves as many as 24 transmitter positions. The bust-this unit, an arrangement of rotary switches and relays that functions to transmit a series of fixed characters, connects to the intraoffice circuit and sends into the connected intraoffice reperforator the following characters:

letter-shift space *BUST* space *THIS* . .

The characters *BUST THIS* serve to cancel to the next office the trunk channel sequence number and that portion of the message received there. The two periods cause the intraoffice circuit to be disconnected, thereby freeing the line sending position for another intraoffice connection. A "wrong comparison" signal is operated at the intraoffice transmitter position to attract the attention of a supervisor, who takes routine steps to protect against loss or duplication of messages and to restore the position to operation.

Occasionally, wrong comparisons may occur because of tape or equipment trouble at a line sending position even though correct preamble characters are transmitted into that position. In order to detect such conditions, a check is made on the operativeness of each sending position when the bust-this unit sends into it. In the same manner as when the intraoffice transmitter was sending, the intraoffice reperforator transmits read-back code combinations to the bust-this unit. This unit compares the read-back characters for the first six characters it sent into the intraoffice reperforator. If a wrong comparison takes place on any of these characters, it indicates trouble at the sending position. Signals are operated at that position to call an attendant to restore the position to service.

Automatic Switching from Lightly Loaded Circuits

More economical facilities are provided at the switching center for lightly loaded tributary and branch office circuits than are provided for heavily loaded circuits. Each time an out-office on a lightly loaded circuit has a message for transmission, its receiving channel at the switching center, in effect, is switched automatically in accordance with the two selection characters that precede the message, to a sending position of the desired destination. Transmission of the message takes place from the tape transmitter at the out-office directly into the intraoffice reperforator of the selected line sending position at the rate of 65 words per minute. Thus, the intermediate reperforation that takes place at the line receiving positions of heavily loaded circuits is eliminated.

In the operation of a lightly loaded circuit, the tape transmitter at the out-office is controlled by the switching center for the transmission of each message. Control signals, consisting of long spacing signals of definite length, that is, several times longer than spacing signals that occur in regular transmission, are transmitted from the switching center over the sending channel to the out-office. When it is necessary to send a control signal, a stop-sending condition is applied to the switching center sending position for that circuit. This stops or prevents message transmission until the control signal is sent, after which the stop-sending condition is removed. The control signals are generated and read by electronic timers.

In connecting a 1-wire receiving channel of a lightly loaded circuit to an intraoffice reperforator, it is necessary to interpose a start-stop receiving distributor

to convert the 7-unit teleprinter code into the 5-unit code for simultaneous transmission into the 5-wire intraoffice circuit. Also, associated with each receiving distributor are other apparatus and circuit arrangements that assist in performing such functions as establishing connections and checking message preambles. The receiving channels are terminated in line finders, consisting of primary and secondary units, to permit a large number of receiving channels to be served by a smaller number of distributors, generally in the ratio of approximately three receiving channels to one distributor. A sequence number indicator quite similar to the one used at line receiving positions for heavily loaded circuits is associated with each receiving channel. These indicators are mounted on racks, as shown in Figure 10.

Out-office operators prepare each message in perforated tape form, prefixing it with selection characters and an identifying preamble and terminating it with two periods. For example, if the eighty-sixth message for the day from Concord, N.H., which terminates in the line finder at Boston, is destined for Detroit, the operator precedes the message with the following characters:

DE space *B.COA* figure-shift 086

When the Concord operator has perforated the complete message in tape form, she depresses a push button. Automatically, a spacing signal is sent over the circuit to Boston, thus placing a call in the line finder. The line finder responds and connects the Concord receiving channel and associated sequence number indicator to a receiving distributor, which in turn makes an electrical request for an automatic switching unit. When it connects, a 0.65-second spacing signal is sent to the Concord office, which causes the transmitter to send the two selection characters, *DE*, and the following space and stop with the character *B* over its feeler pins. In response to these selection characters, the automatic switching unit sets up a potential connection to the Detroit intraoffice circuit. When this connection is converted to an actual connection to a Detroit sending position, the numbering machine functions, after which another 0.65-second spacing signal is sent to the Concord office. This causes the Concord transmitter to restart and send the message. While the first few characters are being received by the intraoffice reperforator, a preamble comparison takes place between it and the Concord sequence number indicator. If the comparison is correct, the Concord sequence number indicator advances one digit and the message continues to its 2-period termination, at which time all equipments involved are disconnected.

If a wrong comparison occurs, the message is not accepted at the switching center and the sequence number indicator is not advanced to the next number. A 2-second spacing signal is transmitted immediately to the Concord office, which stops the transmitter and operates a "resend" signal which necessitates the operator taking routine action to correct and resend the message. At the switching center, a bust-this unit connects to the receiving distributor and functions in the manner previously described.

Automatic Switching from Way Circuits

Very lightly loaded tributary offices generally are combined on 2-station or 3-station way circuits which terminate in single line repeaters at the reperforator office. Separate sending and receiving channels extend from these repeaters to the switching center, but the circuit arrangements are such that transmission can be in only one direction at a time.

In automatic operation, it is essential that there be no clash between the transmissions of the way offices themselves or between those of the way offices and the sending position at the switching center. This is accomplished by an automatic arrangement at the switching center, which constantly assigns, in a regular sequence, the line to each of the way stations for incoming messages and to the switching center for outgoing messages.

Way circuits are terminated in the line finder in the same manner as other lightly loaded circuits, except that a separate sequence indicator is provided for each station on the circuit. When a way station operator has prepared a complete message in perforated tape form, she depresses the initiate push button. As soon as her station receives a signal that the line circuit is assigned to it, the automatic switching and transmission of the messages takes place as it does on any other line finder circuit.

Automatic Switching Units

Automatic switching units that serve 12 intraoffice transmitters and those that serve 12 receiving distributors are essentially the same in operation and appearance, their differences being primarily in the circuit arrangements that originally receive the two selection characters. In each type of unit, three 10-level, 25-point rotary switches, termed "A", "B" and "C" connector switches, are provided for each transmitter or distributor. Each transmitter or distributor is connected to the rotor (wipers) of its "A" connector. The first 23 points of the stator of this switch are connected to intraoffice circuits for 23 destinations, the twenty-fourth point is connected to the rotor of the "B" switch, and the twenty-fifth point to the rotor of the "C" switch. The stators of each of the "B" and "C" switches are connected to the intraoffice circuits of 25 destinations.

Except for a few necessary and desirable changes, the original call letters of offices are used as selection characters. In order that all selection character combinations may consist of two characters, an "equals sign" character is placed ahead of single letter office calls. Each automatic switching unit is provided with an "office call selector" consisting of a group of relays that serve to translate the series of unrelated selection characters into a uniform pattern for controlling the stepping of the connector switches. The office call selectors must be custom wired for each switching center, but the selectors in any one center are all alike.

Occasionally, because of the temporary loss of trunk circuits to a distant office or for other reasons, it is necessary to route messages at a switching center to outgoing circuits other than those to which the messages normally would be switched. It is impracticable to notify all out-offices of temporary routing changes Therefore a "traffic routing board," consisting of a group of jacks for each switching unit, is provided to permit a supervisor to control the switching units by inserting patching cords so that messages for any one or more destinations automatically will take the desired new routings.

Trouble Detecting and Protective Features

The automatic switching equipments are provided with trouble detecting and protective facilities to assure efficient operation. Generally, these facilities consist of electronic timers that are included in each step of the chain of operations. These timers start to function at the beginning of each event, and, if that particular operation is not completed within a predetermined length of time, some disposition of the connection is made that is compatible with safeguarding the message.

The merits of both manual and automatic reperforator switching methods in the area switching centers have been proved in actual day-to-day operation. Development studies still are under way for the further improvement of reperforator switching for use in the public telegraph system, with particular emphasis being placed on obtaining efficient systems for use in the terminal offices having a large city distribution.

References

1. Recent Developments in Telegraph Switching, F. E. d'Humy, H. L. Browne. *Electrical Engineering* (*AIEE Transactions*), volume 59, February 1940, pages 71–78.

2. American Telegraphy After 100 Years, F. E. d'Humy, P. J. Howe. *AIEE Transactions*, volume 63, 1944, pages 1014–32.

3. Push Button Switching in Telegraph Systems, R. F. Blanchard, W. B. Blanton. *AIEE Transactions*, volume 67, part II, 1948, pages 1733–40.

No Discussion

Single-Frequency Signaling System for Supervision and Dialing over Long-Distance Telephone Trunks

N. A. NEWELL
MEMBER AIEE

A. WEAVER
ASSOCIATE AIEE

Synopsis: The single-frequency signaling system for long-distance telephone trunks frees dial calls from the range and other limitations imposed by d-c signaling methods. It uses alternating currents in the voice range as the signaling medium and so can be used with any trunk of any length or type of line facility which meets voice-transmission requirements. The signaling requirements, design problems, main features of the circuit and equipment arrangements, and the operation of this system are outlined in this paper. The system described is the first practical arrangement of its type satisfactorily to meet all the conditions of telephone service in the Bell Telephone System.

IN PLANNING for nation-wide dialing of long-distance telephone calls, the desirability of providing an a-c signaling system for dial telephone trunks soon became apparent. In the past long-distance calls were completed manually or by dialing over limited distances. For these dial calls d-c signaling was adequate and was the most economical and reliable method. The extensive growth in carrier line facilities which do not have associated d-c paths and the planned expansion in dialing ranges for long-distance calls make it necessary to supplement the existing d-c signaling arrangements with an a-c signaling system. The single-frequency signaling system is designed for this service. It employs alternating currents in the voice frequency range to pass supervisory and dialing signals over the voice path of long-distance telephone trunks.

A telephone trunk is a complete communication channel between manual or mechanical switches. These trunks are the major links in most telephone calls and provide 2-way speech transmission and 2-way signaling to facilitate build-up and breakdown of the temporary connections commonly required. Dial system trunks which terminate in mechanical switches have more exacting signaling requirements than any other type of trunk.

Basic Plan

The single-frequency signaling system, although fairly complex in detail, is very simple in principle. It uses a distinctive frequency within the voice band which passes as readily as speech over the trunk transmission line. Normally, speech and the signal frequency are not on the line simultaneously. The signal frequency is applied and removed at each trunk terminal to operate and release a relay at the other end. The operation is similar to that obtained by closing and opening a d-c loop circuit for each of the two directions of signaling. Independent operation is obtained in each direction with one signal frequency on 4-wire lines which have separate 1-way transmission paths from terminal to terminal and with two different signal frequencies, one for each direction of transmission, on 2-wire lines.

The signaling system is provided as a separate entity. It is connected at each end of a trunk to the relay equipment by two 1-way signaling leads and is put in series with the line circuit on a 4-wire basis; that is, through separate transmitting and receiving branches. A typical arrangement for a 4-wire line having 2-wire switching at the West terminal and 4-wire switching at the East terminal is shown in Figure 1.

In the case of 2-wire lines, the signaling equipment is applied to the E-W and W-E transmission paths of the terminal repeaters, using a different frequency for signaling in opposite directions. This is done to avoid difficulties which would otherwise be caused by echoes introduced by unbalances in the 2-wire repeaters.

Table I

Trunk Condition Calling to Called End	Signaling Frequency
Idle (disconnect)	On
Seizure and hold (connect)	Off
Dial pulsing*	On, then off; on pulses corresponding with dial break intervals
Re-ring (ring forward)	On, then off, one pulse
Disconnect (idle)	On

* Multifrequency pulsing[1] is a faster means of transmitting number information often used instead of dial pulsing. Its use eliminates only the dial-pulsing signals.

Trunk Signals

Before going into the details of the signaling system itself it seems appropriate

Table II

Trunk Condition Called to Calling End	Signaling Frequency
Idle (on hook supervision)	On
Stop pulsing*	Off
Start pulsing	On
Flashing**	Off, then on; off pulses corresponding with off hook supervision
Answer (off hook supervision)	Off
Ring back	On, then off; on for duration of ring
Hang up (on hook supervision)	On

* Stop-and-start pulsing-control signals are required only in connection with common control switching equipment.

** Flashing signals appear on a supervisory lamp in the cord circuit of the originating operator and are used to inform her of the condition of a call.

Paper 51-79, recommended by the AIEE Communication Switching Systems Committee and approved by the AIEE Technical Program Committee for presentation at the AIEE Winter General Meeting, New York, N. Y., January 22–26, 1951. Manuscript submitted October 25, 1950; made available for printing December 8, 1950.

N. A. Newell and A. Weaver are both with the Bell Telephone Laboratories, Inc., New York, N. Y.

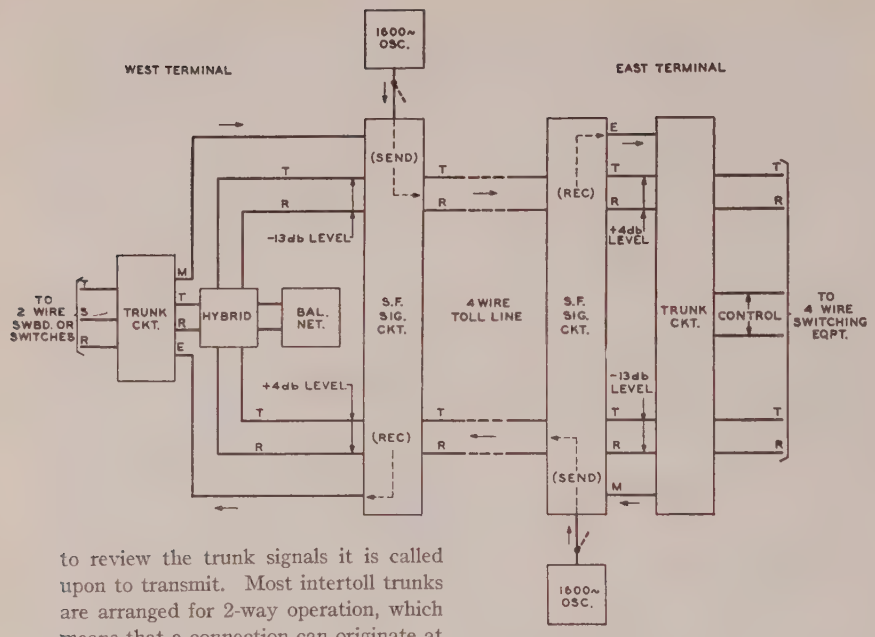

Figure 1. Trunk plan with 4-wire line and single-frequency signaling

to review the trunk signals it is called upon to transmit. Most intertoll trunks are arranged for 2-way operation, which means that a connection can originate at either end. To permit this operation, the signaling in each direction must be symmetrical and the trunk must allow the direction in which the connection is established to determine the signaling use. The latter is conveniently identified by different names for the trunk signals in the two directions. Only two signal conditions, that is, tone on or tone off, in each direction are required for all dial trunk signals. Tables I and II show the required dial intertoll trunk signals, together with the action taken in regard to the signaling frequency.

The signaling system must be able to handle the fastest signals needed. These are the dial-pulsing signals where the shortest signal element may be as low as 30 milliseconds. All other signals have longer durations.

The maximum permissible transmission time for signals between trunk terminals is determined by the allowable unguarded interval on 2-way trunks, during which double connections may occur, and also by the stop-pulsing signal recognition interval. This time is limited to 175 milliseconds.

The distortion permitted in the transmission of signals is proportional to the time duration of each signal. In general, variations in signal time should be within ±5 per cent. All effects of the trunk signal medium should be confined within the trunk terminals or be of such character as to have no adverse reaction in connected circuits. This is necessary for proper operation of switched connections.

General Design Factors

The single-frequency signaling system is an effective continuous (as contrasted to a "spurt") signaling scheme. Use of the voice path for this type of signaling is obtained only by compromise of a number of conflicting factors. The main problems in design are presented in this section in order to facilitate an understanding of this development, which has features that are quite different from those used for signaling in the past. These design problems are: Choice of signal frequency; interference to voice by signal frequency; impairment of voice by signaling equipment; imitation of signal by voice or other tone; interference to signal by voice, noise, or plant tone; impairment of signal by voice transmission equipment; and audibility of signal to operators and subscribers.

Choice of Signal Frequency

Although most lines transmit higher frequencies, the choice of a frequency for universal application is limited to the 300 to 1,700 cycles per second (cps) band, and in order to avoid signaling at the edges of the band, is restricted to a 400–1,600 cps range.

The frequency most favorable to trunk-signaling circuit design and operation is thought to be the highest frequency that can be used. Primarily, this is because the energy in speech, which may interfere with signaling, in general decreases with ascent in frequency above 1,000 cps. Accordingly, 1,600 cps is used for all 4-wire applications.

Two-wire voice channels require different frequencies for signaling in opposite directions. The use of 2,000 cps for the second signal frequency permits application of this system on practically all 2-wire lines.

Interference to Voice by Signal Frequency

The signal frequency is applied during the trunk idle condition and is removed for the connect and off-hook signals. This

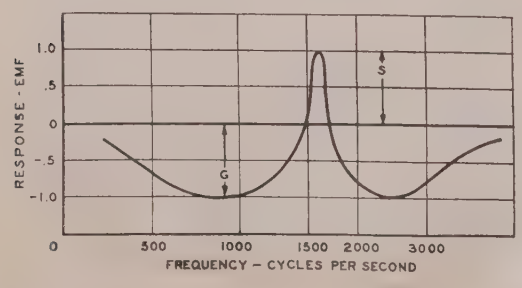

Figure 2 (left). Frequency response characteristic of signal, guard circuit

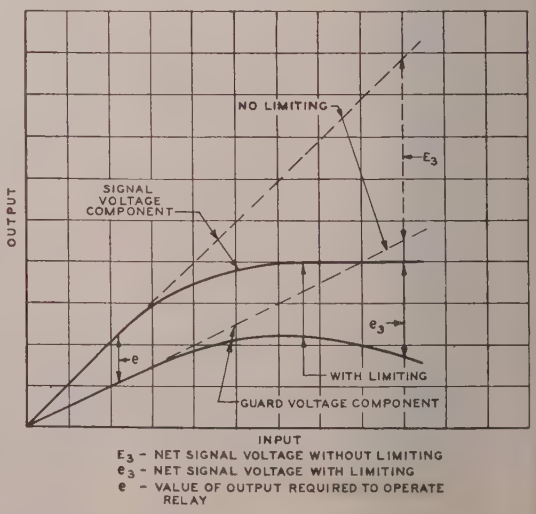

Figure 3 (right). Limiter characteristics

Figure 4. Elements of supply circuit

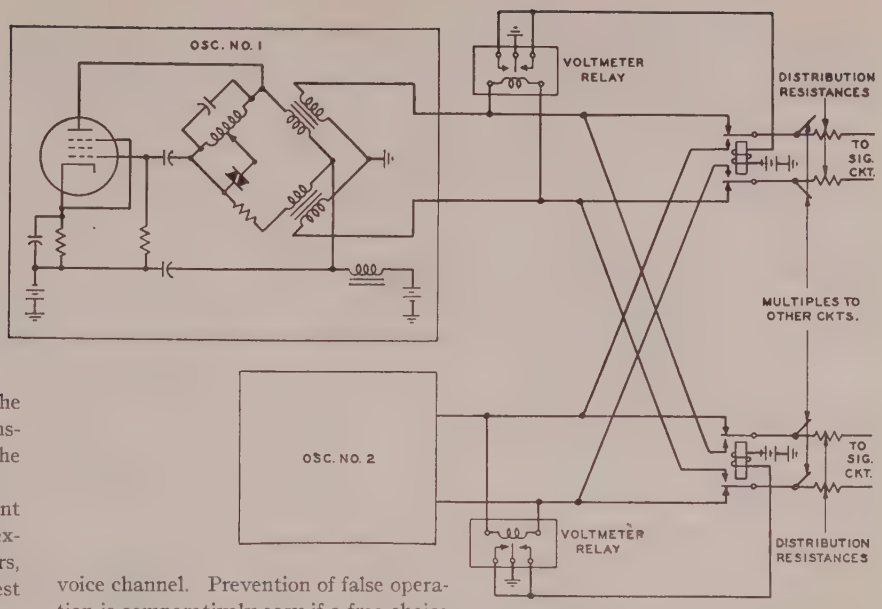

arrangement allows alternate usage of the voice channel for signal and voice transmission in most cases and normally the two are not on the line simultaneously.

In order to limit crosstalk into adjacent voice channels and to avoid adding excessive signal power to the repeaters, it is desirable to use the lowest practicable signal power on the voice channel. A power of −20 decibels below 1 milliwatt (dbm) at zero transmission level, which is just above the low quarter of the average voice power range, is satisfactory for steady application of the signal frequency. In order to obtain an over-all margin of 8 decibels (db) the operate sensitivity of the receiver is set at −28 dbm. A 14-db higher power is used for short intervals to overcome line noise and attenuation variations, as explained later.

Impairment of Voice by Signaling Equipment

Normally, no reduction in the frequency band width of the voice channel is permitted for signaling. An exception to this rule is necessary for single-frequency signaling on connections to intercept operators because off-hook supervision is not provided when speech occurs on these connections. Under this condition, the tone is cut off from the subscriber by a narrow 1,600 (or 2,000)-cycle filter. This filter also takes a "slice" out of the voice band, which results in an effective transmission loss of about 0.5 db.

The transmission loss to speech occasioned by the required continuous connection of the signal transmitter is about 0.1 db, and there is no loss for the signal receiver.

Imitation of Signal by Voice or Other Tone

Since the signal receiver must be connected at all times to the voice channel, precautions are necessary to prevent its false operation by any occurrence of the signal frequency in speech, music, plant tones, noise, and other energies on the voice channel. Prevention of false operation is comparatively easy if a free choice is permitted for any one of three design factors. These are (1) the signal frequency, (2) the operate sensitivity, and (3) the operate time of the signal receiver. The protection inherent in these items, however, is limited, the first two by the line requirements and the third by the trunk-signaling requirements. Additional protective devices therefore are provided through circuit design. These consist in (1) the use of "guard action," (2) the employment of as narrow a band width as practicable for the signal selection network, (3) the use of limiting, and (4) by means of relays the reduction of the operate sensitivity, the increase of the operate time, and the increase of guard action when the usual talking condition is established.

The "guard action" is the principal factor in protecting the receiver against operation on speech. Guard action consists of the use of all frequencies other than those in a narrow band on each side of the signaling frequency to generate a direct voltage and in the application of this voltage to oppose the direct voltage resulting from the signal frequency which is used to operate the receiver. The combination of these two voltages plotted against frequency is shown in Figure 2. A term which is used to specify the effectiveness of the guard action is "guard-signal ratio" (G/S in Figure 2) or just "guard ratio," a term also used by the British.[2] This is the ratio of the absolute value of the direct voltages at the grid of the d-c amplifier produced respectively by equal amounts of guard frequency (at maximum guard sensitivity) and signal frequency when separately applied. The provision of guard requires that more than the just operate power of signal frequency be available to operate a receiver when it is exposed to noise or other than signal frequency. Also, the provision of guard increases the operate time of a signal receiver. The amount of guard permitted is limited by the signal-to-noise relation when operation of the receiver is required and by the operate time requirement.

Protection is added by narrowing the frequency band accepted for operation of the receiver, since this reduces the effective operating power of voice and noise frequencies. However, the amount of this narrowing is limited, as the operating band width must be sufficient to allow for frequency variation in the signal supply, for carrier shift in the line, for variations in elements of the tuned circuit in the receiver, and for the proper relation of the minimum signal time duration and

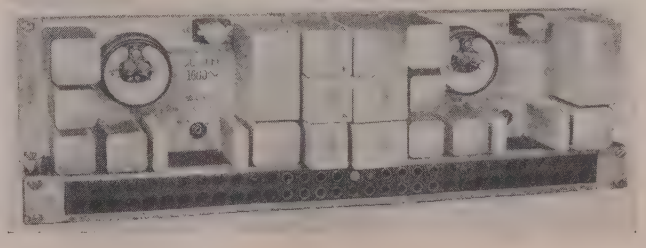

Figure 5. Supply unit

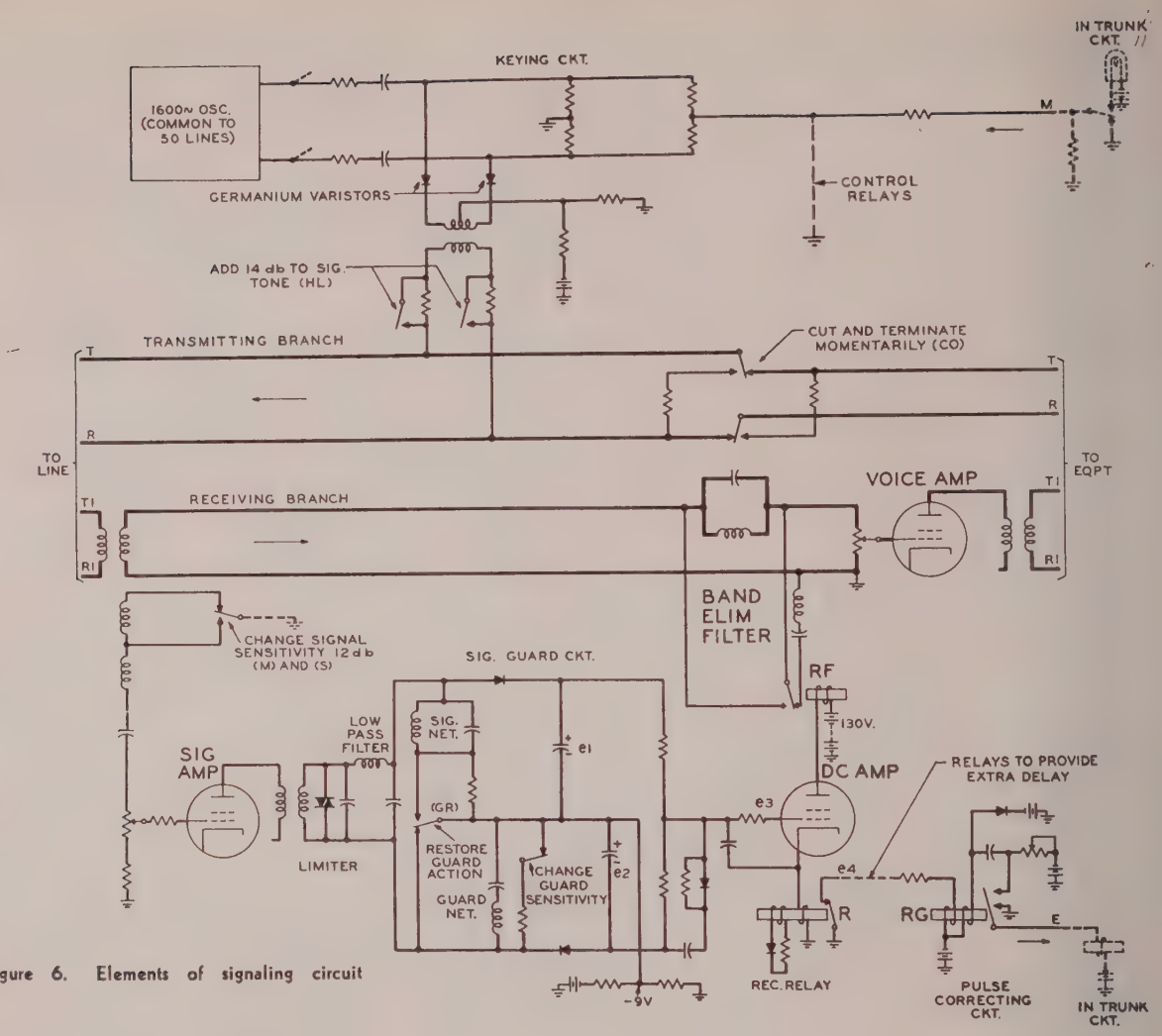

Figure 6. Elements of signaling circuit

the time required by the tuned circuit to reach a steady-state condition.

Volume limiting helps prevent false operation on high levels of speech. The theory of this action is illustrated in Figure 3. It is assumed that a burst of speech sounds contains a signal component, upper lines in Figure 3, and a guard component of one-half this value, lower lines. The dotted lines show a characteristic for a receiver with no limiting, while the solid lines are for one having limiting. As shown, a given large input will produce an output of E_s, the difference between the signal voltage component and the guard voltage component, in the former case and of e_s in the latter, which is about one-half as much. This will be less likely to operate the receiver (operate value e) when applied for a short interval of time. Either one will, of course, produce an operation if applied long enough.

The change in the sensitivity and operate time of the receiver are practicable by reason of the higher signal power permitted for short intervals of time and the longer time durations of supervisory signals. The lengthened-operate time also requires that the re-ring signal transmitted from the sending end be lengthened by a corresponding amount.

Interference to Signal by Voice, Noise, or Plant Tone

The use of guard action to prevent false operation of the receiver introduces the liability that voice, noise, or tones may prevent the operation of the receiver by signal frequency or may cause it to release falsely once it is operated. By design this last effect is confined to the operate time of the receiver. After the receiver is operated the guard action is disabled and all voice frequencies hold the receiver operated. This shift is delayed for a short time in order to avoid increasing the hazards of false operation and does not occur during dial pulsing. To permit release of the receiver after the shift takes place, the voice and noise power going into it must be about 3 db less than its operate sensitivity.

The frequencies that might interfere with receiver operation come from sources outside the trunk terminals either through connected circuits or by induction into the line. Ordinarily the power from connected circuits is much higher than that of line noise. This interference coming through the trunk terminals is eliminated effectively on 4-wire lines and its occurrence greatly reduced on 2-wire lines by use of a cutoff relay in the signal transmitter and a blocking amplifier in the signal receiver to isolate the signal path in the trunk. The cutoff relay is operated just long enough when the signal frequency is applied or removed to prevent noise at the transmitter terminal from interfering with the operation or release of the far-end signal receiver. The 1-way path of the blocking amplifier, which is the sole reason for its use as it is arranged for zero gain, is between the signal path of the receiver and its trunk terminal to shut out noise from that direction. Interference by line noise is overcome during operation by an increase of 14 db in the

Table III

Factor	Idle, Dialing, and Intercept Condition	Talking Condition
Signal frequency, cps	1,600 or 2,000	1,600 or 2,000
Receiver sensitivity (0 level), dbm	−28	−16
Receiver signal band width, cps	60	60
Guard-signal ratio, db	0	10
Start of limiting above just operate, db	5	5
Minimum signal duration for operate, ms	35	100
Minimum signal duration for release, ms	7	

signal power for a short initial period when it is applied to the line by the signal transmitter.

Impairment of Signal by Voice Transmission Equipment

Echo suppressors are examples of voice transmission equipment which may interfere with signaling arrangements using the voice channel. Only terminal echo suppressors can be used with single-frequency signaling and these must be located on the equipment side of the signaling equipment.

Single side-band carrier channels are subject to frequency shift, and this must be held within reasonable limits to avoid too much impairment of the signal frequency.

Audibility of Signal

The addition of signal frequency to the voice channel must not annoy subscribers or operators. When the call is established, the tone is cut off, except on calls to intercept operators. In this case, low-level signal frequency is transmitted over the line, but is reduced by a band-elimination filter, with the result that the power at the calling subscriber's telephone does not exceed about −60 dbm. At this time the power at the intercept operator's telephone does not exceed about −45 dbm. These levels are considered low enough to be inoffensive.

Summary

The values of the design factors used for the equipment described in this paper are given in Table III.

The design based on these factors is so nearly free from false operations caused by speech that these average fewer than one per 1,000 conversations.

General Description

The components of the single-frequency signaling system (Figure 1) consist of the following: The signal frequency supply; the signal transmitter and receiver; the auxiliary 1-way transmission path and filter; and associated test arrangements.

Signal Frequency Supply

The signal supply includes a pair of single vacuum tube oscillators, a trouble alarm and transfer circuit, test and patching jacks, and distribution resistances. The signal frequency is distributed on a 2-wire metallic basis. The basic elements of the oscillator supply and transfer circuit are shown in Figure 4, and the equipment unit, which is the same for either 1,600 or 2,000 cps, is shown in Figure 5. The output capacity of one supply unit is sufficient to provide signal frequency for 100 signaling circuits. The two oscillators operate continuously and normally share the load equally. In case of trouble in one oscillator its load is transferred automatically to the other. The oscillator circuit is basically the same as that used in multifrequency pulsing[1] and so is not described here in detail.

Signal Transmitter and Receiver

This is the main unit of the signaling system and one is required for each trunk terminal. The essential elements of this circuit are shown in Figure 6, and the equipment panel is shown in Figure 7. It connects with the trunk relays over two leads, *E* and *M*, and into the line circuit with eight leads, *T*, *R*, *T1* and *R1*, on both the line and equipment sides. The signal transmitter uses d-c biased germanium varistors to control the application of signal current through a low transmission loss bridge on the line and has four relays designated *M*, *CO*, *HL*, and *RR*. The principal functions performed by the first three of these relays are shown in Figure 6. The *RR* relay (not shown) in conjunction with the *M* relay lengthens the sent pulse for the re-ring signal because the far-end receiver at this time has a long operate time. The signal receiver, which is connected through a low transmission loss shunt path on the line, operates the signal relay in response to the appearance of signal frequency. In addition it introduces blocking between the terminal equipment noises and the signal

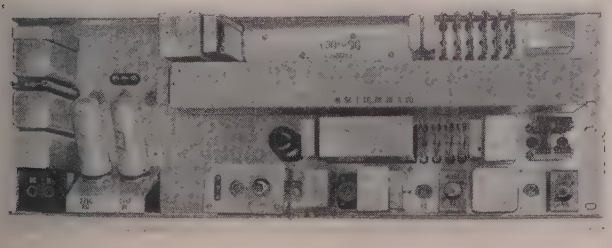

Figure 7 (below). Signaling panel

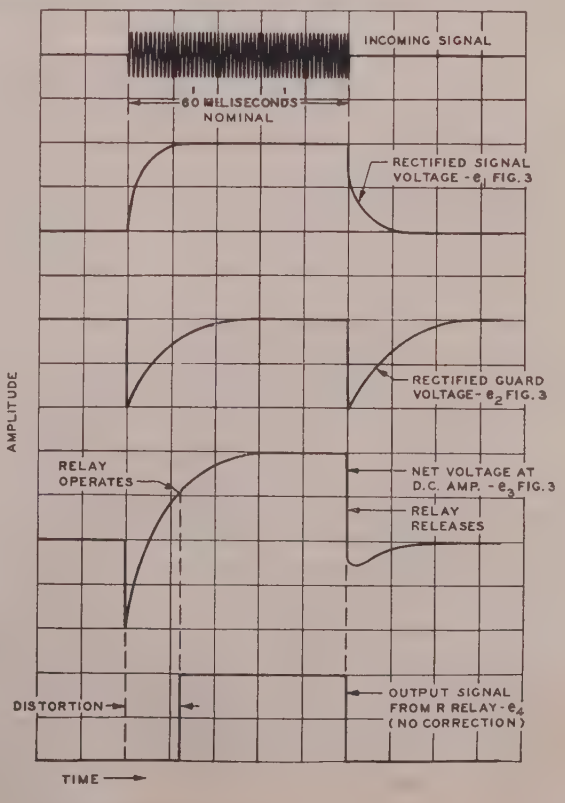
INCOMING SIGNAL
60 MILISECONDS NOMINAL
RECTIFIED SIGNAL VOLTAGE - e_1 FIG. 3
RECTIFIED GUARD VOLTAGE - e_2 FIG. 3
AMPLITUDE
RELAY OPERATES
NET VOLTAGE AT D.C. AMP. - e_3 FIG. 3
RELAY RELEASES
DISTORTION
OUTPUT SIGNAL FROM R RELAY - e_4 (NO CORRECTION)
TIME

Figure 8 (right). Typical wave forms

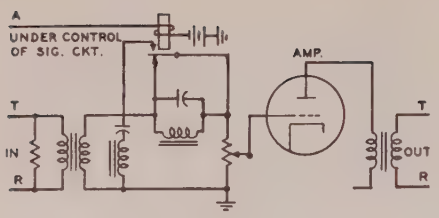

Figure 9. 1-way path and filter circuit

Figure 10. 1-way path and filter unit

path. Also, the level of signal frequency going past the signal receiver is reduced by a band-elimination filter.

The receiving portion of the circuit is shown in the central and lower portions of Figure 6. It is wired in series with the receiving branch of the line and translates signals coming in from the line to ground on the *E* lead, which in turn connects to the trunk circuit. The idle condition of the trunk is shown, tone is being received, and all relays shown are operated. The band-elimination filter is inserted to prevent the signal frequency from getting into a connected trunk and interfering with signaling there. The voice amplifier has zero gain and is used to prevent noise and other voice frequency currents, originating in switching equipment or connected circuits, from interfering with the operation of the receiver.

The signal currents, received from the line, are amplified by the signal amplifier, passed through a limiter and low pass filter, and applied to the signal-guard network, from which signal voltage is applied to the d-c amplifier to operate the *RF*, *R*, and *RG* relays and thus control the *E* lead, which extends into the trunk terminal equipment. Typical wave forms at several points in the circuit are shown in Figure 8. The extra operate time provided during the talking condition is obtained from a slow release relay, which is inserted at this time, in the path from the *R* to the *RG* relay. Relays *M* and *S* are provided, but not shown, to cut in and out as required, the lesser sensitivity, the increased guard sensitivity, and the extra delay in operation.

The *R* relay, because of guard action and the effect of its secondary winding being closed through a varistor and resistance, is relatively slow to operate and fast to release. For this reason some sort of pulse correction is necessary to get good dial operation. This is obtained with the *RG* relay and an associated condenser-resistance timing network, which results in an output pulse within the needed limits, even though the signal on the *R* relay is shortened considerably. To convert the receiver from operation on 1,600 cps to operation on 2,000 cps, it is necessary only to substitute networks.

Auxiliary 1-Way Path and Filter

This circuit is shown in Figure 9 and the equipment unit which provides two circuits is shown in Figure 10. The circuit consists of a simple zero-gain vacuum tube amplifier with optional arrangements for the addition of a signal frequency band-elimination filter and control relay. The circuit is connected into the voice-transmitting branch of the line on the equipment side of the single-frequency signaling main unit under two conditions: (1) on trunks equipped with terminal echo suppressors to prevent their false operation on signal current (the control relay and the filter are not provided for this application); (2) on trunks terminated in switchboards which are not arranged to disconnect the voice-transmission path while the operator is dialing. This is done to prevent false operation of the signal receiver when it is in the dialing condition, as at this time it is more susceptible to speech. This same circuit also is connected into the voice-receiving branch of 2-wire lines on the line side of the main signaling unit to prevent interference from the transmitted frequency at the same end.

It connects into the voice branch with four leads, *T* and *R* on its line and equipment sides and, when the filter is provided, to the main unit over lead *A*. The band-elimination feature of the filter in all cases is tuned for the transmitting signal frequency of the signaling circuit. This filter normally is switched out during conversation. The 1-way path feature prevents interference with the operation of echo suppressors by signal frequency. The amplifier circuit provides a convenient way to place the filter, which is of the same design as that used in the signaling circuit, in a transmission path without changing its impedance relations.

Associated Test Arrangements

Test jacks are provided in eight of the ten leads connecting the main signaling unit. These provide direct access for checking the performance of the operating features of this circuit. Two other test jacks are provided in the unit for checking internal portions of the circuit.

A fixed testing assembly is provided for each full or partial group of 100 signaling circuits. These facilities are supplemented by portable test sets. A full discussion of all the testing arrangements for this system is outside the scope of this paper.

Operation

It is assumed in the following brief outline of a typical operation that 4-wire lines are used and that the echo suppressor and blocking amplifier are not required.

Normal Idle Trunk Condition

The trunk circuits have ground on the *M* leads to the 1,600-cps signaling transmitters, which apply the signal frequency to the transmitting branch of the line circuit at each end. The signal frequency is received in the receiving branches and holds the relays in the signaling receivers. This keeps an open on the *E* leads to the trunk circuits.

Call Originating at West End

When a connection is made to the intertoll trunk, say at the left or West end, through the switchboard or switches, the West trunk circuit takes ground off and puts battery on the *M* lead there. The new signal to the West signaling transmitter causes it to remove 1,600-cps signal frequency from the West to the East branch of the line. The absence of signal frequency in the East receiving branch releases the signal relay in the East signaling receiver and this puts ground on the *E* lead to the East trunk circuit. This ground is the connect signal, which prepares the East terminal for an incoming call.

Pulsing

Pulsing now takes place. This may be either multifrequency pulsing[1] or dial pulsing, which consists in applying tone to the line for each break interval of the dial.

Called Subscriber Answers

When the connection is completed at the East end, the called subscriber answers and an off-hook signal is received

Table IV

	Rate Interruptions Per Minute	Duration Time in Seconds On Hook	Off Hook	On Hook	Off Hook
Subscriber line busy	60	0.5	0.5	Repeat	Repeat
Trunks busy, reorder	120	0.3	0.2	Repeat	Repeat
Trunks busy, hold (overflow)	30	1.7	0.3	Repeat	Repeat
Master busy	Uneven 60	1.3	0.2	0.3	0.2
Recall by subscriber	Irregular	Not less than		0.3	0.2

at the East intertoll trunk circuit, which takes ground off and puts battery on the *M* lead there. This signal to the East signaling transmitter causes it to remove 1,600-cps signal frequency from the East to the West branch of the line. The absence of signal frequency in the West receiving branch releases the signal relay in the West signaling receiver, and this puts ground on the *E* lead to the West trunk circuit. Since the call originated at the West end, ground on the *E* lead here is an off-hook or subscriber answer signal.

Conversation Takes Place

At this time there is no signal frequency on the line and no impairment to the voice transmission.

Called Subscriber Hangs Up

On normal calls when conversation is completed, the called subscriber hangs up his receiver and an on-hook signal is received through the switches at the East intertoll trunk circuit. This changes the condition on the *M* lead there, from battery to ground. Ground on the *M* lead causes the East signaling transmitter to apply 1,600-cps signal frequency on the East to West branch of the line. Presence of signal frequency in the West receiving branch operates the signal relay in the West signaling receiver and opens the *E* lead to the West trunk circuit, giving it the called subscriber's on-hook signal.

Disconnect

Release of the intertoll trunk at the calling end causes a disconnect signal at the called end in a similar manner to that just described for the passing of the on-hook signal. Trunk, signaling, and line circuits return to the normal idle condition.

Flashing

On some calls flashing signals from the called end may occur. Typical signals of this type are shown in Table IV.

References

1. Application of Multifrequency Pulsing in Switching, **C. A. Dahlbom, A. W. Horton, Jr., D. L. Moody.** *AIEE Transactions*, volume 68, part I, 1949, pages 392–96, and *Electrical Engineering*, volume 68, June 1949, pages 505–10.

2. The Influence of Signal Imitation on the Reception of Voice Frequency Signals, **G. T. Flowers, D. A. Weir.** *Proceedings*, Institution of Electrical Engineers (London, England), volume 96, part III, 1949, pages 223–35.

No Discussion

Techniques of Corona Loss Measurement and Analysis—500-Kv Test Project of the American Gas and Electric Company

O. NAEF
MEMBER AIEE

R. L. TREMAINE
ASSOCIATE AIEE

A. R. JONES
ASSOCIATE AIEE

THE TECHNIQUE of measuring corona loss on the 500-kv corona test lines has undergone successive refinements and expansion since the lines were first energized in October 1947. An earlier paper[1] describes the equipment for measuring corona loss and radio influence which was available at the beginning of the tests. This paper discusses the experience gained during two years of testing, the methods used in checking the instruments and in analyzing the data, new equipment supplied, and the accuracy which has been attained in this work. As a result of this work data have been obtained which are consistent to ±15 watts per single phase mile, which compares quite favorably with the initially hoped-for accuracy of ±150 watts per phase at 500 kv.

Test Equipment

The test equipment which was available at the beginning of these tests, as well as that which has been added, will be discussed. This section covers the corona loss and the weather instrumentation; the radio-influence equipment is discussed in a companion paper.[2]

Equipment Available at Start of Tests

Three 3-phase test lines, two 1.4 miles and one 800 feet, were available for experimentation. The corona-loss instrumentation is contained in aluminum housings mounted on top of the high-voltage bushings of the three 1,667-kva single-phase 500/66-kv transformers which supply voltage to the lines. Three-phase test voltages from 265 to 532 kv were available in 25 steps. Lower voltages, down to 152 kv, can be obtained by connecting the primary windings in wye.

An individual wattmeter is provided for each conductor on the three lines so that single-phase losses, and the loss on each phase under 3-phase conditions, can be measured. The wattmeters are highly sensitive null-type wattmeters developed especially for this project and so designed that readings can be taken visually or recorded graphically.

The circuit of the corona-loss instrumentation is shown schematically in Figure 1. Line current is passed directly through the current coil of the wattmeter and potential for the wattmeters is obtained from an extension of the main high-voltage winding, referred to as the metering winding, thus eliminating the use of current and potential transformers. The circuits at A and B provide automatic compensation for the variation in phase and magnitude between the terminal voltage of the metering winding and the actual voltage applied to the lines. The reactor at C adjusts the phase of the voltage-coil current so that it has the correct phase angle relative to the current-coil field. The circuit at D is used on the outside phases to compensate for the interchange of power caused by the flat configuration of the test lines, so that the wattmeter indications are actual corona loss.

The corona-loss meters are read by a telescope from an elevated observation booth about 50 feet away. Remote control of the instrumentation for changing scales of the wattmeters and performing various other functions is obtained by sending coded light pulses to operate a "phototroller" (light-sensitive device), which in turn operates a supervisory relay control circuit.

In addition to the corona-loss instrumentation, graphic weather instruments—barometer, thermometer, rain gauge, and hygrometer—and a number of radio-influence instruments[2] are provided.

Equipment Added

As the tests progressed, a number of special instruments were added to the test facilities. These instruments will be discussed individually.

Photographic Weather Recorder. This device is an automatic camera which takes a picture of visual weather every 20 minutes. Two sample conductors to determine condensation of moisture on the test conductors, a piece of slate to show presence of light rain, sleet, and snow, which are not recorded by the rain gauge, a sample insulator, and a clock are mounted so that they are photographed in the foreground of the picture. These objects are illuminated by eight 500-watt photospot lamps, which provide illumination brighter than daylight, so that the same lens opening can be used both day and night. In the background are two fog-indicating lamps located 1,000 feet and 2,500 feet away, respectively.

A timing relay is used to initiate the following sequence every 20 minutes: the lamps are turned on, a second relay is energized, which introduces a time delay of 1/2 second to insure that the lamps are at full brightness, the camera shutter then is tripped, the lights are turned off, and the first timing relay is reset. The camera

Paper 51-80, recommended by the AIEE Transmission and Distribution Committee and approved by the AIEE Technical Program Committee for presentation at the AIEE Winter General Meeting, New York, N. Y., January 22–26, 1951. Manuscript submitted October 24, 1950; made available for printing December 8, 1950.

O. Naef is with the American Gas and Electric Service Corporation, New York, N. Y. R. L. Tremaine and A. R. Jones are both with the Westinghouse Electric Corporation, East Pittsburgh, Pa.

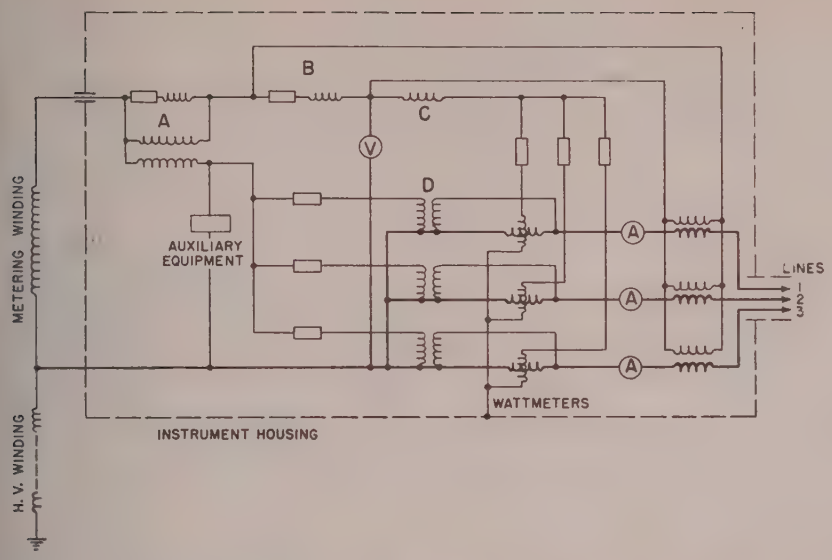

Figure 1. Schematic of corona-loss measuring circuit

is a standard 16-millimeter movie camera which is equipped with a single-exposure release and a telephoto lens.

Samples of the record obtained with this instrument are shown in Figure 2. This information has been extremely valuable in interpreting corona loss and radio-influence records, particularly with respect to light rains and fog. This record is supplemented by a station log of visual weather.

Voltage Gradient Meter. A detailed description of this instrument is presented in a paper by R. L. Tremaine and R. C. Cheek.[3] Briefly, it is a generator-type gradient meter having a rotor which alternately shields and exposes a stator to the earth's electric field. The change in the charge on the stator is a function of the voltage gradient at the surface of the earth. This instrument can be used either as a graphic meter or as an indicating meter and is protected suitably from weather for continuous recording. Graphic records of voltage gradient have been obtained since July 1949 and are correlated with records of corona loss and radio influence taken simultaneously.

Insulator Loss Setup. The insulator loss measurement setup is shown in Figure 3. The cap of the second insulator from ground is connected to ground through the wattmeter. The insulated ground plane is arranged so that it can be grounded through the wattmeter or connected directly to ground. Insulator current flows to ground either through the distributed capacitance of the insulator string or over the surface leakage. Thus, substantially all of the insulator current goes to ground through the wattmeter when the ground plane is connected. The ground plane is used primarily for determining insulator loss under dry conditions. For measurements under bad weather conditions, better accuracy can be obtained by disconnecting the ground plane. Six-inch stovepipe has been placed over the bus to minimize the possibility of corona near the string. A deflection of 2 per cent on the most sensitive scale is 0.5 watt.

The insulator loss setup normally is used to obtain graphic records of loss on a vertical string and then on a horizontal string alternately for periods of 20 minutes each. Provision also is made for making manual tests on either string.

Provision for Heating One Conductor. A question presented in the application of the data obtained in this program to

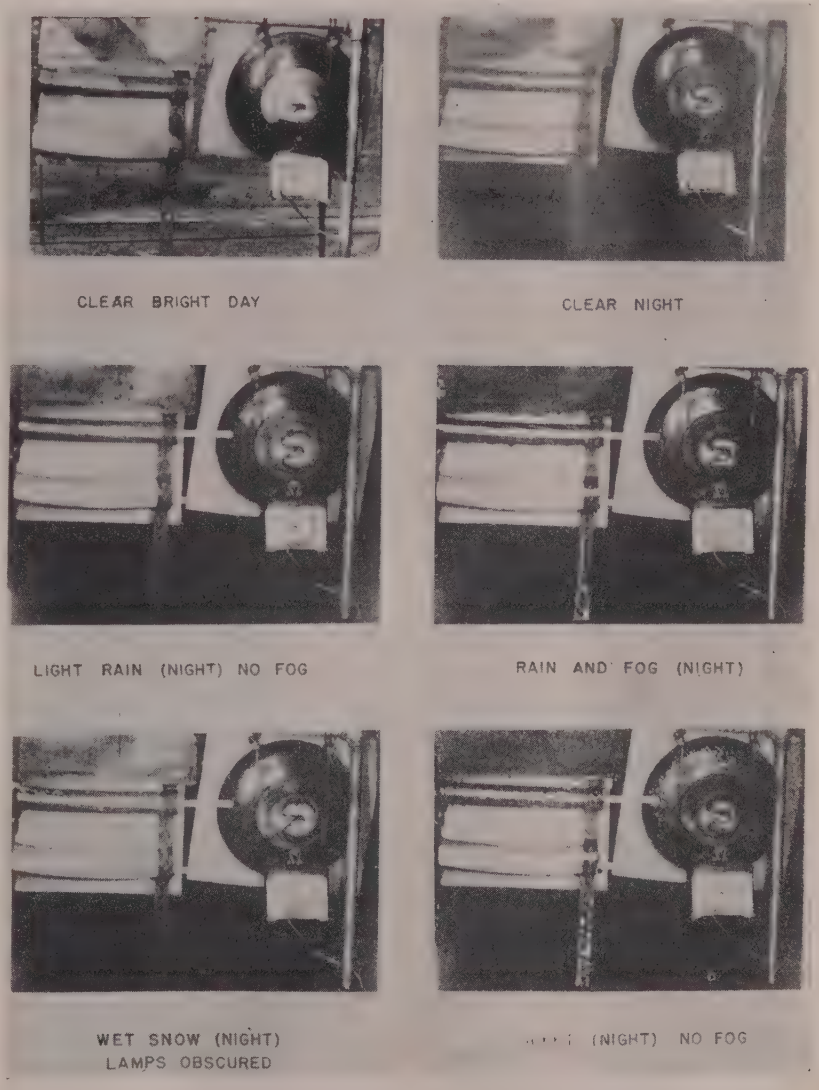

Figure 2. Sample pictures from the photographic weather recorder for various weather conditions. Fog-indicating lamps are not visible in these reproductions

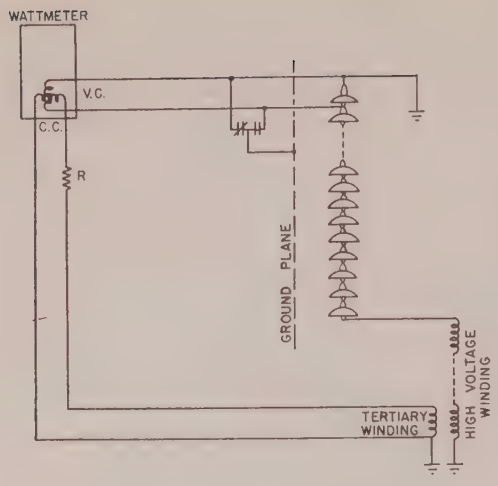

Figure 3 (left). Schematic of insulator-loss measuring circuit. C.C., current coil; V.C., voltage coil; R, ballast resistor

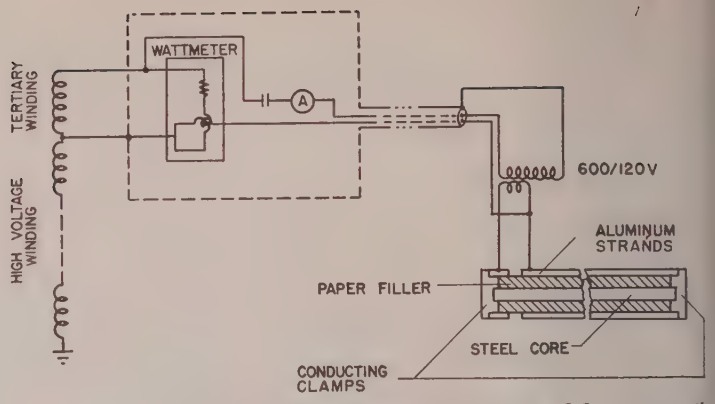

Figure 4 (above). Schematic of conductor heating circuit

future transmission lines is the effect of conductor temperature. This question is important because the conductors on an operating line normally are above ambient temperature and hence are not subject to condensation, whereas conductors on the experimental test lines, which carry only a small current, are subject to condensation. Moisture condensed on the surface of a conductor can increase corona loss and radio influence.

To answer this question, provision has been made to heat the 2.00-inch expanded aluminum cable steel-reinforced conductor on the 800-foot line. As shown in Figure 4, power is supplied from the metering winding, and current is circulated down the steel core and back through the aluminum sheath. With 454 kv applied to the lines, a current of 125 amperes is circulated in the conductor, which, in a light breeze, will raise its temperature approximately 14 degrees Fahrenheit above that of an unheated conductor. The heating transformer can be energized without interruption of the tests.

Because of the extremely low impedance of the metering winding, operation of the heating circuit does not affect the wattmeter indications appreciably.

Verification of Accuracy of Instrumentation

To appreciate the problem of obtaining accurate measurements of corona loss, it is necessary to understand the nature of corona itself and the special requirements of corona instrumentation. This section covers measurement problems peculiar to corona-loss investigations, the early tests, and the final verification of the circuit accuracy.

Corona-Loss Characteristics Which Make Loss Measurements Difficult

During the early days of testing, large variations in wattmeter indications under seemingly identical conditions were observed. These variations existed between recurrent readings on individual tests and between readings taken hours or days apart. At the onset, it was not possible to say whether these variations were caused by corona or by instability in the instrumentation.

By systematic testing, a large part of this variability was proved to be a consequence of the so-called "short-time" aging of conductors, a characteristic of corona. At the time this program was commenced, the authors knew of no discussions of this problem. (F. Cahen and R. Pelissier, in a paper published since the start of these tests,[4] mention this characteristic).

A typical test, made to show short-time aging, is shown in Figure 5. For some time prior to this test, the conductors had been energized at 370 kv, and immediately preceding the test they were de-energized for 24 hours. This phenomenon is most pronounced with increase in voltage as shown by Curves A and B, which give initial value of the corona loss and the loss after 20 minutes, respectively. Curves C and D give the corresponding information when the voltage was reduced, after energization at maximum voltage. It will be noted that Curve D shows a tendency to be slightly higher than Curve C.

Because of the short-time aging characteristic it was found necessary to precondition conductors for 15 or 20 minutes at maximum voltage prior to testing and to take readings only on decreasing voltage. This procedure results in loss indications at maximum voltage which will be too high because it is not feasible to wait sufficient time for the loss to stabilize. It also can be concluded that at lower voltages the loss indicated in a normal voltage run will be somewhat lower than would exist if the conductor had been energized continuously at each particular voltage. Since all conductors are tested with the same procedure the relations are valid, although caution should be exercised in using this type of data to predict fair-weather corona loss on operating lines.

After the effect of short-time aging had been minimized by preconditioning the conductors, successive measurements on the same conductor still varied considerably in fair weather, even after known corrections were made. Variations as large as 10 to 1 under ostensibly the same weather conditions were sometimes observed. This variability later could be proved to be also a characteristic of corona, caused chiefly by subtle changes in surface conditions which preconditioning failed to reduce to a common state.

The next phenomenon to cause considerable concern was the "long-time" aging characteristic of corona which is generally recognized, but the fact that it varies over a wide range and with the type and material of the conductor is not generally appreciated. This effect made the 1.65-inch *HH* conductor appear to have many times the loss of the 2.00-inch expanded aluminum cable steel-reinforced conductor and to be in corona at the lowest voltage initially available. This is contrary to the relative loss position of these conductors which would be expected from generally accepted formulas. The accuracy of the early measurements therefore was doubted, but subse-

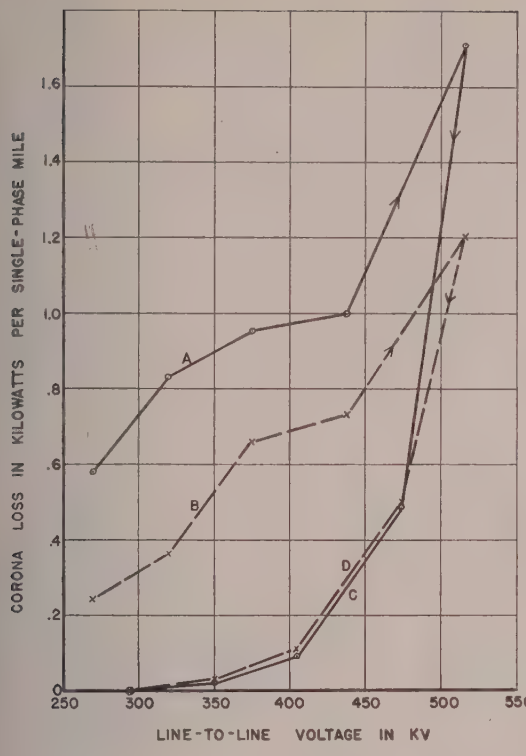

Figure 5 (left). Effect of "short-time" aging

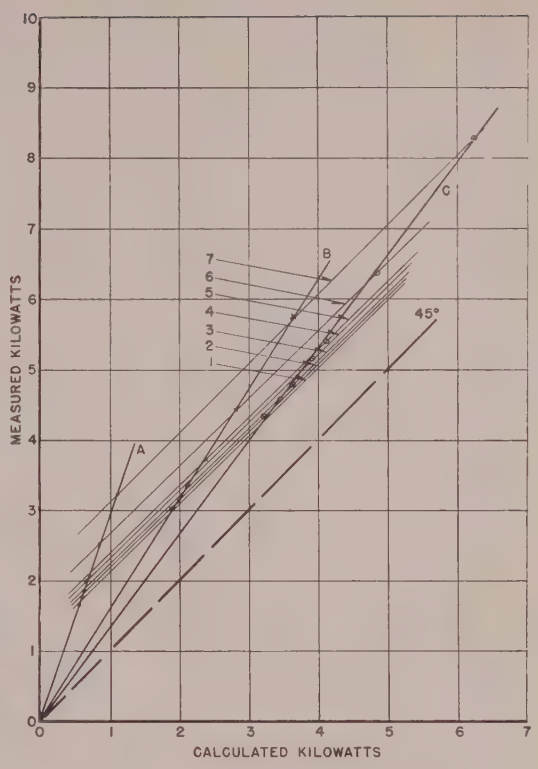

Figure 7 (right). Data from typical test made to verify phase-angle error in instrumentation

quent analysis of the data showed that the measured loss was correct.

Initial Tests of Accuracy

The variations discussed in the previous section finally were shown to be characteristics of corona, and not caused by the instrumentation. However, the work done up to this time did not prove that correct loss values were being obtained.

Circuits designed to measure corona loss must be able to operate at very much lower power factors than are encountered normally. To appreciate this problem one must reorient his thinking regarding the effect of minor factors which normally can be disregarded. At low values of corona loss, the current leads the voltage by an angle very close to 90 degrees. At 500 kv, a phase-angle error of one minute (0.000292 radians) will cause an error of about 1/2 kw per 3-phase mile. Thus, extreme care must be taken to insure that the exact phase relation between current and voltage is known. On the other hand, a given percentage of error in magnitude of current or voltage can result only in the same percentage of error in the loss indication, hence it is relatively unimportant.

Extensive laboratory tests had been made on the wattmeters alone and on the completed circuit prior to the tests. This work eliminated a number of sources of trouble; but tests at really low power factors can best be made in the field as the minimum practical laboratory power factor is about two per cent.

Analysis of the early results indicated that the corona loss on the 2.00-inch expanded aluminum cable steel-reinforced conductor was essentially zero over the lower portion of voltage range. In this range, the wattmeter readings varied as the square of the applied voltage and, therefore, could not be corona loss.

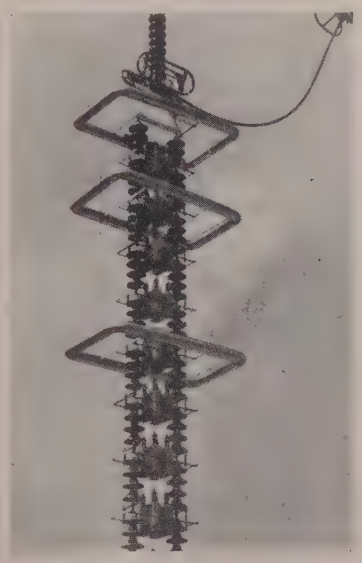

Figure 6. The top 16 units of high-voltage capacitor

Readings which vary as the square of the applied voltage can only be caused either by insulator loss or by an error in the phase of the current in the potential coil of the wattmeter. The latter was more probable, so much effort was devoted to finding the cause of this phase-angle error, which appeared to be of the order of 20 minutes.

Practically all conceivable sources of error result in deviations which vary as the square of applied voltage. The problem of tracking down each suspected error involved devising a special test, modifying the circuit, then analyzing the results. Some 20 special tests were made to find errors in the instrumentation. The results of most of these tests were negative, but a few warrant mention here to show that the more common causes of errors in corona-loss instrumentation have been checked.

1. Mutual coupling between wattmeters was found to be negligible.

2. Cathode-ray oscillograms proved that there were no harmonics in the voltage supplied to the test lines and to the metering circuit.

3. There was no effect due to the voltage between the bus and the shielded metering leads inside the bus.

4. Voltage-coil ballast resistors were replaced with noninductive resistors.

5. Test values of the leakage reactance of the metering winding were verified.

6. The power transfer circuit (circuit D,

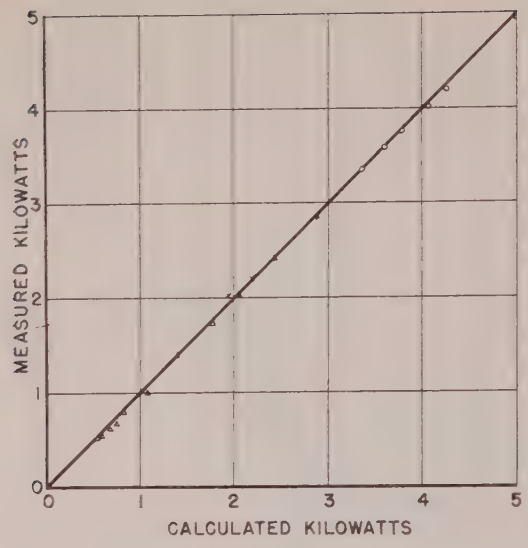

Figure 8 (left). Effect of adding reactance to the voltage-coil circuit

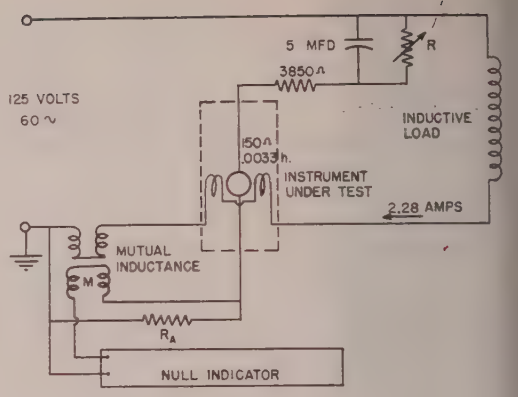

Figure 9 (right). Schematic of special test performed to determine angle between current—and voltage-coil currents for zero torque in the wattmeter

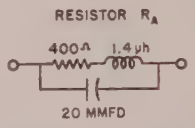

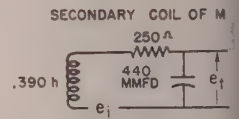

Figure 1), which is in shunt with the current coils, was checked and shown not to introduce an error.

The circuit which corrects for the impedance drop in the high-voltage winding (circuit B, Figure 1) was checked. A number of tests were made in which only the short line was energized. Under this condition the current in the high-voltage winding is approximately six per cent of the 3-line value, hence only a very small phase shift is introduced. Substantially the same readings are obtained on the short line whether the long lines are connected or not, indicating that the proper correction is being made.

A few minor errors were found. These were:

1. The drop in the ground lead to the wattmeters caused by line charging current introduced a voltage of $j0.15$ volts into the voltage-coil circuit, which was sufficient to cause a phase-angle error of 1.5 minutes. It was corrected by grounding the voltage-coil circuit separately.

2. The capacitance across certain contacts when they were open was in parallel with the voltage-coil ballast resistors. The circuit was changed to eliminate the effect of this capacity.

3. The voltage-coil leads from the ground end of the resistors to the wattmeters were shielded.

Direct Measurement of Phase-Angle Error

The minor corrections to the measuring circuit described in the preceding paragraph reduced the phase-angle error only slightly. To determine its magnitude with the desired precision a direct method of testing was used. For this purpose a known load was connected to the wattmeters, consisting of a high-voltage single-phase capacitor in series with an adjustable ohmic resistance. The capacitance of 0.0024 microfarads about equaled the line-to-ground capacitance of a long-line conductor. Figure 6 shows the upper half of the high-voltage capacitor, which was shielded by several large rings to prevent the formation of corona.

By taking wattmeter readings with several values of resistance in series with the capacitor, an error in calibration of the wattmeter could be distinguished from a phase-angle error. The wattmeters had been calibrated at unity power factor before they were installed at the test site, but it was considered desirable to prove that the calibrations were independent of power factor. The resistors in series with the capacitor were operated considerably in excess of their capacity and were known to introduce certain errors.

The results of a typical test are shown in Figure 7. Curves A, B, and C are the readings actually obtained with two, one, and zero resistors connected in series with the capacitor. Lines 1 to 7 are common voltage lines, that is, all points on each line were obtained at the same voltage. These lines are parallel to the 45-degree line, showing that regardless of the actual reading, the error was constant

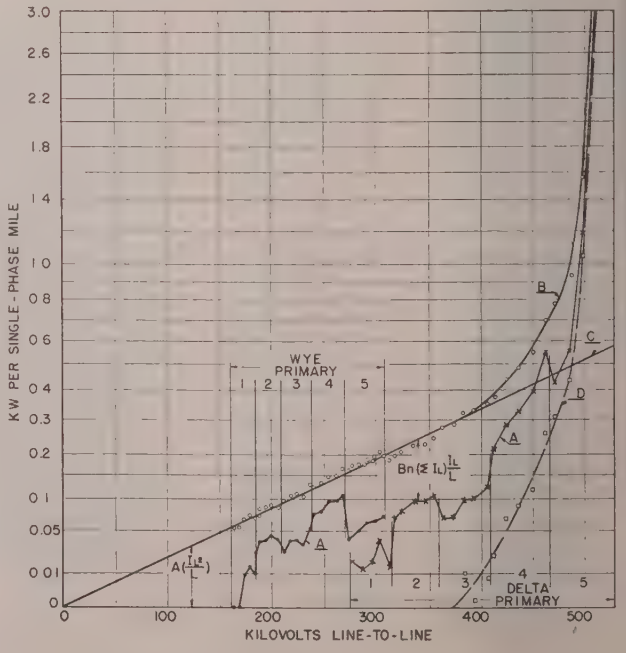

Figure 10. Reduction of manual data to conductor corona loss

A. Actual readings from 50-point single-phase voltage run on 1.65-inch *HH* conductor
B. Curve A corrected for transformer - tap variations
C. Residual square-law correction
D. Corona loss of conductor
1–5. Low-voltage winding tap positions

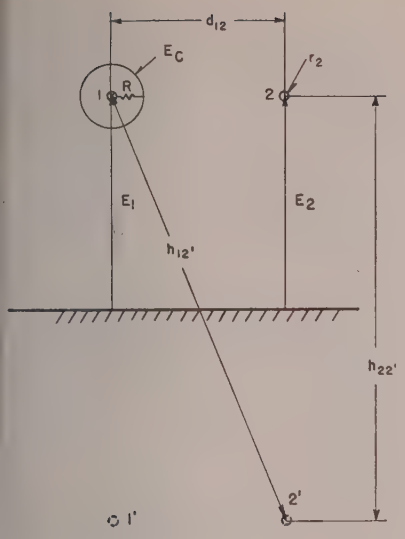

Figure 11 (left). Sketch for theoretical consideration of resistance coupling

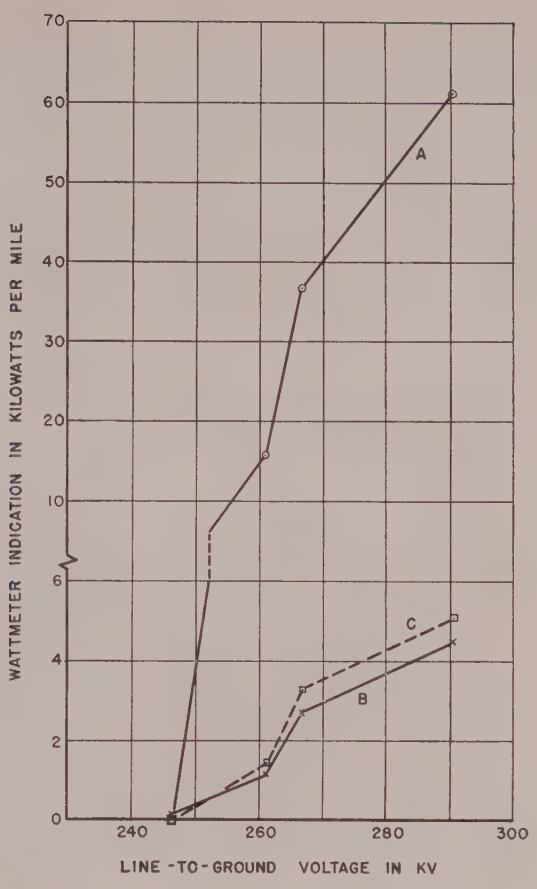

Figure 12 (right). "Resistance" coupling test

Curve A. Wattmeter reading on conductor in corona
Curve B. Wattmeter reading on corona-free conductor
Curve C. Anticipated wattmeter reading on corona-free conductor based on the equation presented in text

in magnitude. Since the kilovolt ampere rating was constant for each voltage, regardless of the resistance in the circuit, this fact shows that the calibration of the wattmeters was correct, and that a constant phase-angle error was present. The magnitude of the phase-angle error thus determined was 0.0053 radian (18.2 minutes).

An inductance of 21.1 millihenrys was inserted in the potential circuit, causing the voltage-coil current to lag its previous position by 0.0053 radian, and a check showed that the measured values were equal to the calculated values as shown in Figure 8.

A special test was made to detect errors caused by this inductance if harmonics were present in the metering circuit. The current coils of two wattmeters were connected in series and an inductance of 257 millihenrys was inserted in the voltage-coil circuit of one of them. The indications of the latter wattmeter were corrected for the phase shift caused by the inductance, on a 60-cycle basis. After this was done the readings of both meters essentially agreed, showing that adding inductance in the voltage-coil circuit had not made the circuit sensitive to harmonics.

At this time, since the phase-angle error had been shown to be constant and a means for correcting it had been obtained, it was not considered desirable to make further tests to determine the cause. Later a very sensitive test was made on the wattmeters to determine the phase angle between current and voltage-coil currents which gave zero torque. This test, which was made using the circuit shown in Figure 9, showed an error of about 14 minutes in the wattmeters. Mutual coupling between the current and voltage coils had been suspected previously as a possible source of error, but attempts to measure it had not been successful. The phase-angle error is a result of eddy currents in the magnetic shields around the individual wattmeters. Since three wattmeters are operated in a very limited space and adjacent to each other, it was necessary to design a very compact instrument and to use heavy shielding.

Using the Test Lines as a Zero Power Factor Reference

In the original design of the metering circuit it was thought that if a small phase-angle error were present, it could be detected by using the test lines as a standard of zero power factor. This procedure would have been followed if the error had not been so large. The direct measurement of a phase-angle error within a few minutes of the error, which had been deduced from previous observations, confirmed the original hypothesis that the line itself, below corona voltages, was the best available standard of zero power factor. It was most desirable to use the line for this purpose because capacitors have a high power factor compared to the range in which low corona-loss measurements are made. This assumption implies that insulator loss is zero. Other measurements[5] showed that fair-weather insulator loss can be neglected.

Effect of Transformer Taps

As the technique of analyzing the data was improved, inconsistencies became apparent when plotting data to greatly enlarged scales as used in Figure 10. The variations are small, the maximum deviation being ±0.000352 radians (±1.2 minutes) or ±80 watts per phase per mile at 357 kv.

These variations were found to be a function of low-voltage tap position and to a lesser extent of high-voltage tap position (±0.000054 radians or ±12 watts per mile at 357 kv). They are caused by changes in eddy and stray losses when the taps are changed. As the taps are changed, the distribution of the leakage fluxes changes, which in turn changes the losses. This is manifested to the metering circuit as a change in the resistance of the high-voltage winding. The error thus introduced is a function of the reactive component of the line current.

In order to determine the magnitude

of these errors, as distinguished from a residual, that is, not fully compensated, constant phase-angle error, careful 50-point, single-phase voltage runs (25 points wye connection and 25 points delta connection on the primary) were made. The wattmeter indications from one of these tests are plotted in Figure 10, Curve A. They can be expressed by the following equation:

$$P_n = A\frac{I_L^2}{L} + B_n(\Sigma I_L)\frac{I_L}{L} + P_i + P_c \qquad (1)$$

where

P_n = wattmeter indication in kilowatts per mile on tap combination n
P_c = corona loss in kilowatts per mile on tap combination n
P_i = power interchange in kilowatts per mile on tap combination n
I_L = charging current of the conductor
L = length of the conductor in miles
ΣI_L = total charging current in high-voltage winding (sum of charging currents of all energized conductors)
A = constant, independent of position of tap combination and current
B_n = constant for tap combination n, independent of current

AI_L^2/L is the correction for residual constant phase-angle error. $B_n(\Sigma I_L)I_L/L$ is the correction for the variable shift caused by the effect of the transformer taps. P_i is zero for single-phase tests and P_c is zero below the corona starting voltage. From 50-point voltage runs with various numbers of lines energized, and knowing the charging currents, the constant B_n has been determined for all tap combinations. With the aid of B_n the required corrections could be calculated for all test setups. When these corrections are applied, the data give extremely smooth curves, as shown in Figure 10.

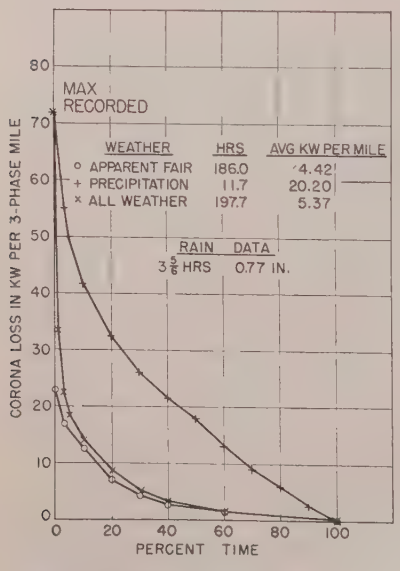

Figure 13. Per cent time that corona loss of 1.65-inch *HH* conductor at 397 kv exceeds the ordinate. 45-foot flat spacing; period of recording, May 26 to June 27, 1949

Effect of Resistance Coupling

If two conductors of markedly different corona-loss characteristics are energized at a voltage such that one conductor is in profuse corona and the other is corona-free, it is theoretically possible to obtain a loss indication on the conductor which is not in corona. The polarity and magnitude of this indication depend on the phase and magnitude of the voltage applied to the second conductor.

An exact calculation is not feasible in view of the nonlinearity of the circuit. However, the magnitude of this effect can be estimated knowing the dimensions of the setup and assuming that corona loss can be represented by a constant resistance during a cycle. The circuit shown in Figure 11 then can be used. E_1 is the voltage applied to the smaller conductor, number 1, and E_2 is the voltage applied to the larger conductor, number 2. The spacings are very large in comparison with the diameters. R is a resistance representing the corona loss and is connected in series with the corona cylinder whose voltage is given by $E_c = E_1 - Ri_1$. (The authors do not wish to imply that the average capacitance to ground of a conductor over one cycle is increased by moderate amounts of corona, or that corona forms a smooth cylinder of ionized gas.) It should be noted that the voltage on the surface of the corona cylinder is not in phase with the applied voltage. For the single-phase case the readings on the wattmeter connected to conductor 2 is

$$W_2 = -W_1\frac{E_2}{E_1}\frac{A_{12}}{A_{22}} \qquad (2)$$

where

W_1, W_2 = readings on wattmeters of conductors 1 and 2, respectively

E_1, E_2 = applied voltages

$$A_{22} = 2\log_e\frac{h_{22}'}{r_2}$$

$$A_{12} = 2\log_e\frac{h_{12}'}{d_{12}}$$

The actual loss on conductor 1 is the algebraic sum of the two wattmeter readings.

To measure this effect experimentally a test was made in which single-phase voltages were applied to the 1.4-inch *HH* and the 2.00-inch expanded aluminum cable steel-reinforced conductors on the 800-foot line. The voltage on the 2.00-inch expanded aluminum cable steel-reinforced conductor was kept constant at 152 kv, while the voltage on the 1.4-inch *HH* conductor was raised to 290 kv. Surprising agreement between the results expected from equation 2 and the actual effect was found, as shown in Figure 12.

This effect does not cause difficulty except when the 800-foot line is operated three phase. It has been found necessary to disregard or to correct data taken on the 2.00-inch expanded aluminum cable steel-reinforced conductor under this condition.

Technique of Corona Loss Analysis

The measurement techniques and data reduction methods which have been developed in the course of this investigation are discussed in this section. The tests fall into two classifications, manual data—information obtained from indicating instruments, generally voltage runs, and recorded data—information obtained from the records of graphic instruments, voltage generally held constant for long periods.

Reduction of Manual Data to Obtain Corona Loss

Most data of this type were obtained by varying the voltage through the range of 265 to 532 kv. At each voltage point, voltage, charging current, and

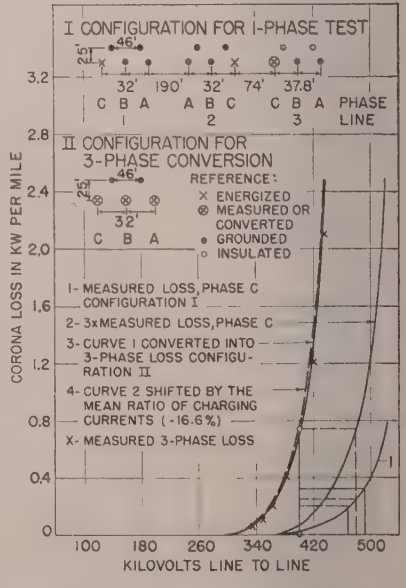

Figure 14. Conversion of single-phase data to 3-phase values

wattmeter indications are read.

The ammeters measure line current directly. As explained later, current readings provide a means of converting corona-loss information taken on any line configuration to a common base. Because the voltage varies with the number of conductors connected and between single- and 3-phase tests, it was found convenient to reduce all currents to nameplate voltage for comparison purposes. To minimize the influence of calibration errors, current ratios obtained on the same instrument are used wherever possible.

Square Law Method. If the square root of the readings of a wattmeter connected to a constant impedance load are plotted against applied voltage, a straight line through zero will be obtained Similarly, if a wattmeter having a residual phase-angle error is connected to a zero power factor load a straight line will be obtained. With increasing voltage the presence of corona loss is indicated by an increasingly rapid decrease in the shunt resistance of the conductor. This is the basis for the method used to determine corona loss in the presence of a phase-angle error and power interchange. For convenience in plotting, semiquadratic paper, similar to semilogarithmic paper, has been printed in which the ordinate is a square-root scale. Figure 10 is an example. Curve B shows the wattmeter indications corrected for transformer tap variations as explained previously. Through its lower straight portion line C is drawn, which follows a square function.

The presence of a straight line on semiquadratic paper does not in itself conclusively prove the absence of corona loss, since it is not inconceivable that corona could present a constant resistance for a voltage change of 50 or even 100 kv. Visual and aural tests, together with radio-influence tests, have shown that on certain fair-weather tests, voltages as high as 400 kv can be applied without the occurrence of corona. Line C, Figure 10, therefore does not indicate corona loss, but represents the phase-angle error which was present during this test.

Insulator loss could upset the previous discussion in so far as insulators do not present a constant resistance with voltage. Independent measurement[5] of insulator loss indicates that under fair-weather conditions it is less than one or two watts per string, hence the deviation of this loss from a square function is below the reading accuracy of the corona-loss meters.

It is possible to select a value for the reactor at C, Figure 1, such that the indications on the wattmeters would be actual corona loss, and it then would not be necessary to use the square-law method of analysis. However, the studies are made under a large variety of circuit conditions ranging from one conductor single phase to all three lines three phase. The power interchange between conductors and lines varies with different circuit connections. To take care of this situation it has been found desirable to set the reactor at C to such a value that the wattmeter indications always will be positive under any test setup.

Reduction of Recorded Data To Obtain Corona Loss

All nine conductors of the 500-kv test lines are equipped with recording wattmeters. Charts are replaced at intervals of approximately one month and inspected once every week. As a rule all three test lines are energized three phase. The voltage is changed periodically.

Determination of Wattmeter Zero. The deflection for zero loss on the charts is established by noting the minimum deflection during periods of fair weather, when the corona loss is known from voltage runs. The apparent losses caused by the residual phase shift, the transformer-tap variations, and any uncompensated amount of power interchange are thereby eliminated because they are constant as long as the voltage remains constant.

Accuracy of the Readings. The indicating and recording wattmeters have a common measuring element. However, the same degree of accuracy cannot be expected from the recording meters, nor is it required. Apart from the lower sensitivity of graphic meters, when they are set on a scale of sufficient range to record storm loss, the determination of the zero loss line is subject to certain errors, except in case of the larger conductors at voltages below 400 kv, when fair-weather corona loss is zero. At higher voltages the fair-weather loss is never absolutely constant, even under apparently constant atmospheric conditions. Air-density factor and voltage are subject to small variations. These variations are recorded and it is possible to correct for them; however, the advantage gained would not be commensurate with the effort spent. For voltages above 400 kv an average loss value from voltage runs in fair weather is therefore assigned to the minimum wattmeter deflection. While the error caused thereby might be not inconsiderable in the measured fair-weather loss, it is negligible in precipitation and comparatively small in the all-weather loss.

Method for Analyzing Graphic Charts. The graphic records of corona loss are analyzed by determining the time during which the loss exceeds certain values. These values are selected to cover the range of loss expected. The day is split into four 6-hour periods so that the variation of loss with time of day can be determined. The data obtained during periods of precipitation, as evidenced by the records of the graphic rain gauge, are separated. Then the data can be plotted as a distribution curve showing the loss in such weather categories as "Apparent Fair Weather," "Precipitation," and "All-Weather." An illustration of this type of data is shown in Figure 13.

The average loss during given periods can be obtained from such curves as shown in Figure 13, but is computed with greater accuracy from the calculated kilowatt hours and the number of hours. Correlating these records with the records of the rain gauge during the same periods, the relation between average corona loss and average rate of precipitation can be obtained. Peak losses also are recorded. From the analysis of short periods of substantially constant rainfall, curves giving corona loss versus rate of rainfall can be plotted. Since all these data are available from operation at different voltage levels, the results can be replotted as a function of voltage.

The 3-phase losses on lines 1 and 2 are the sum of the losses on the individual phases. Losses measured on the individual conductors of line 3 are converted into 3-phase values.

In order to distinguish between "Apparent Fair Weather" and "Precipitation" losses, the term "Hours of Precipitation" must be defined. It has been decided to designate as "Hours of Precipitation" the periods of increased losses caused by the precipitation of rain as registered by the rain gauge. This definition makes it possible to establish a relation between the losses and precipitation that can be applied to future lines on the basis of rain data obtained from the United States Weather Bureau.

The number of hours of precipitation is always greater than the number of hours registered by the rain gauge because the losses continue when the rain ceases until the conductor is dry again. Losses due to fog, smog, snow flurries, or drizzling rains, which leave no trace on the rain gauge, are of necessity classified as

"Apparent Fair-Weather" losses and are, of course, included in the "All-Weather" loss. The term "Apparent Fair Weather" is used to distinguish it from the term "Fair Weather," which is applied to voltage runs, and to indicate that some of the data are obtained during periods which ordinarily would not be considered fair weather.

Plotting of Corona-Loss Curves

Semilogarithmic paper is of value where a wide range of loss must be shown upon a single sheet and where it is desired to lend greater emphasis to the low values. The wide range of wattmeter scales justifies the expansion of the lower values. The use of rectangular co-ordinates and equal scales is indicated whenever it is desired to convey quickly and readily an impression of the relative magnitude of the data. The sharp upward bend in the corona-loss curves, which is accentuated on rectangular co-ordinates, facilitates the choice of conductors for a particular operating voltage.

Corona loss is plotted against voltage, charging current, surface gradient, rate of precipitation, and time (depending upon the information desired). Plotting the loss against charging current or surface gradient reduces the work necessary in applying this data to any specific configuration. Plots of loss against rate of precipitation have been used in an attempt to establish the relationship between rain and corona loss.

Conversion of Corona Loss for Line Configuration and Atmospheric Conditions

At the 500-kv Test Project, conductors are tested both single- and 3-phase, on lines of different lengths and configurations, and subjected to variable atmospheric conditions. In order to compare the corona losses of the different conductors, all data are converted to unity air density and to a common configuration. This configuration is a 3-phase line, 32-foot flat spacing, 56-foot average height, 2 ground wires spaced 48 feet apart, and 25 feet above the conductors. The methods of conversion discussed here can be extended to any specific set of conditions.

Principle of Conversion

The corona loss of a conductor is identical in different configurations if the surface gradient is the same and there is no change in atmospheric conditions. The gradient necessary to produce the proper amount of ionization for maintaining a particular value of corona loss is a function of temperature and barometric pressure. There is some disagreement in the literature as to what correction should be made to corona-loss data. In this investigation the corrections for deviations from unity air density are made by dividing the nominal surface gradient by the air density factor raised to the two-thirds power. "Nominal Gradient" as defined here is the gradient that would exist at the surface if there were no corona present and the conductor were a perfect cylinder.

The surface gradient of a smooth, round, bare conductor not in corona is a linear function of the charging current. Contamination on the surface, rough spots, deposits of moisture, and the like, locally increase the surface gradient. In the literature certain factors have been proposed to correct for some of these influences.

For constant values of corona loss the following equation can be written:

$$\frac{\text{Nominal Surface Gradient}}{\delta^{2/3}m} = k\,\frac{\text{Charging Current}}{\delta^{2/3}m} = \text{Constant} \qquad (3)$$

where

$\delta = \dfrac{17.9b}{459+T}$ = air density factor

b = barometric pressure in inches of mercury

T = temperature of the conductor in degrees Fahrenheit

m = surface factor

k = constant

It follows that, if the corona loss of a conductor is plotted versus charging current corrected for air density, the values of fair-weather loss from different tests all should lie on the same curve, regardless of the line configurations in which the conductor was tested, and the temperatures and barometric pressures prevailing during the tests. This supposes, of course, that the surface factor is constant and no other variables are present.

This method of plotting is useful for determining the dispersion between corona-loss curves from different tests. Voltage scales can be added for specific single-phase configurations and for 3-phase operation with conductors symmetrically spaced and removed from ground. For 3-phase transmission lines with flat configuration, only approximate voltage scales can be indicated because the three conductors carry unequal charging currents.

If corona-loss curves are plotted versus operating voltage in the conventional way, a change in line configuration, air density factor, or surface conditions produces a change in the voltage at which the same loss occurs. This is expressed by the equation:

$$E_2 = E_1 \frac{I_1}{I_2}\left(\frac{\delta_2}{\delta_1}\right)^{2/3}\frac{m_2}{m_1} \qquad (4)$$

which is derived from equation 3. E_1 and E_2 are the voltages corresponding to the original and new conditions, respectively, $(\delta_2)/(\delta_1)$ and m_2/m_1 are the ratios of the air density and surface factors, and I_1/I_2 is the ratio of the charging currents at a constant voltage. This conversion, if made for every point of the corona-loss curve, results in a horizontal shift accompanied by a slight change in slope. The shift $E_2 - E_1$ can be expressed conveniently in per cent of the original voltage E_1 and is the summation of the configurational shift, the atmospheric shift, and the shift for surface conditions.

Shifts for Surface Conditions

Published values of surface factors cover general design, roughness, and contamination, but not the effect of rain, snow, or condensation. When comparing corona-loss curves obtained on the same or on different conductors no use of these factors has been made.

Effect of Precipitation. The voltage shifts caused by precipitation far exceed those required for configuration and air-density factor, but no factors for converting fair-weather data into foul-weather data have been established yet. It appears that no constant percentage could be applied to every point of a corona-loss curve. Some information on corona loss versus rate of rainfall is available from field and laboratory tests. It is hoped that eventually some correlation can be established which takes into account both intensity and the size of the raindrops.

The comparison of foul-weather corona-loss curves obtained on different conductors is extremely difficult, because the character and intensity of precipitation varies over a wide range. The existence of three test lines with at least six different conductors tested simultaneously under what can be assumed to be the same meteorological conditions mitigates this difficulty. The data obtained on the individual conductors have been converted to unity air density and one standard configuration by applying the method outlined in this paper.

Atmospheric Shifts

Temperature and Barometric Pressure. These quantities are combined in the formula of the air-density factor. The influence of this factor on corona loss is given by equation 4, which is applied to both fair- and foul-weather corona-loss curves. If conversion is made to unity air density and no change in line configuration and surface conditions occurs, equation 4 assumes the simplified form

$$E_2 = E_1/\delta^{2/3} \qquad (5)$$

The temperature to be inserted into the formula of the air-density factor should be that of the area in which corona occurs.

No facilities exist at the test site for measuring the temperature of the conductors continuously, and ambient temperature therefore is used for all conversions. The variations caused by other weather effects greatly exceed that caused by any error in air-density correction, so that it is relatively unimportant whether conductor or ambient temperature is used.

Humidity. The relative humidity of the air is recorded continuously. Its influence on corona loss, so long as no moisture condenses on a conductor, has not been determined yet, but it seems to be very small. No correction for humidity is applied to fair-weather data.

If the moisture content of the air causes condensation on the conductor, its effect is similar to that produced by precipitation, that is, the losses increase sharply.

Atmospheric Voltage Gradient. No correction has been made because no correlation is apparent from field data so far obtained.

Precipitation. Its effect is a change in surface conditions and is considered elsewhere.

Configurational Shifts

The surface gradient for a given voltage on a test conductor is determined by the dimensions of the test setup and the charges on the other conductors. Configurational shifts are applied to correct for changes in these factors with various test setups. From tests, the ratios of the current with each test configuration to the current with the standard configuration were determined, and these values are applied as configurational shifts. Some typical values might be of interest here.

Under single-phase conditions, the charging current on the middle phase is increased 3.15 per cent by the addition of ground wires. If, in addition, the two outer conductors are grounded, the total increase is 6.1 per cent. Under 3-phase conditions, ground wires cause almost no change in the charging currents. For 3-phase operation, the middle conductor takes 118.6 per cent and the outer conductors 112.5 per cent of the single-phase charging current with the same line-to-neutral voltage.

A considerable amount of capacitive coupling exists between phase C of the short line and phase C of the adjacent longer line, the average distance between conductors being 74 feet. The effect on the shorter line is a 6 per cent decrease in charging current. The longer line is proportionately less affected. Smaller coupling effects exist between more distant conductors.

Single-Phase to 3-Phase Conversion. The basis for conversion from single-phase to 3-phase corona loss is indicated in the preceding section. In Figure 14 is shown a conversion from single-phase data taken with a particular test configuration, I, to 3-phase loss in the standard configuration, II. The measured charging current is 96.3 per cent of the single-phase value (reduced below 100 per cent by capacity coupling between phases C, lines 2 and 3). The charging currents for 3-phase operation are 112.5 and 118.6 per cent for the outside and middle phases, respectively.

Hence, for the same voltages the charging currents for the 3-phase configuration are 116.9 and 123.1 per cent of the test values. For this conversion 3-phase loss at any voltage is the sum of twice the test loss at 116.9 per cent plus the test loss at 123.1 per cent of the given voltage. Curve 3, Figure 14, was obtained from curve 1 in this manner. Generally it is sufficiently accurate to use the mean voltage shift (120.0 per cent in this case) for this conversion. In practice this can be done by multiplying the test loss by three and plotting it at a voltage reduced by the mean ratio of charging currents (−16.6 per cent in this case, curve 4).

For a comparison between converted and measured 3-phase losses on the 2.00-inch aluminum cable steel-reinforced conductor, the loss points from a 3-phase test in the standard configuration are indicated. The agreement is very satisfactory.

Conclusions

The adequacy of the method adopted for measuring corona loss has been confirmed. Every effort has been made to obtain accurate data and to account for all possible causes of the variations in corona loss.

The photographic weather recorder has been of great aid in explaining the increases in corona loss as recorded by graphic instruments which were not explained by standard weather instruments.

Artificially heating one test conductor has made possible the study of the effect of conductor temperatures.

The authors believe that the techniques and the instrumentation used at the test project provide one of the most accurate means which has been used in the measurement of corona. Data are obtained rapidly and with a high degree of accuracy in all weather conditions, and are reduced to a form applicable in the design of future extra-high-voltage lines.

References

1. Instrumentation and Measurement—Tidd 500-Kv Test Lines, **R. L. Tremaine, G. D. Lippert.** *AIEE Transactions*, volume 66, 1947, pages 1624–31.

2. Radio Influence in Field and Laboratory—500-Kv Test Project of the American Gas and Electric Company, **G. D. Lippert, W. E. Pakala, S. C. Bartlett, C. D. Fahrnkopf.** *AIEE Transactions*, volume 70, part I, 1951, pages 251–269.

3. A Voltage Gradient Meter, **R. L. Tremaine, R. C. Cheek.** *AIEE Transactions*, volume 69, 1950, pages 633–37.

4. Use of Bundle Conductors on Extra-High-Voltage Lines (in French), **F. Cahen, R. Pelissier.** *Bulletin*, Societe Francaise des Electriciens (Paris, France), Sixth series, volume VIII, number 79, 1948.

5. Corona Investigation on Extra High-Voltage Lines—500-Kv Test Project of the American Gas and Electric Company, **I. W. Gross, C. F. Wagner, O. Naef, R. L. Tremaine.** *AIEE Transactions*, volume 70, part I, 1951, pages 75–94.

6. Transmission of Electric Power at Extra High Voltages, **Philip Sporn, A. C. Monteith.** *AIEE Transactions*, volume 66, 1947, pages 1571–82.

7. Corona Considerations on High-Voltage Lines and Design Features of Tidd 500-Kv Test Lines, **C. F. Wagner, Anthony Wagner, E. L. Peterson, I. W. Gross.** *AIEE Transactions*, volume 66, 1947, pages 1583–91.

8. Insulators and Line Hardware for Tidd 500-Kv Test Lines, **I. W. Gross, R. L. McCoy, J. M. Sheadel.** *AIEE Transactions*, volume 66, 1947, pages 1592–1602.

9. Line Conductors—Tidd 500-Kv Test Lines, **E. L. Peterson, D. M. Simmons, L. F. Hickernell, M. E. Noyes.** *AIEE Transactions*, volume 66, 1947, pages 1603–12.

10. Transformers and Lightning Arresters—Tidd 500-Kv Test Lines, **F. A. Lane, J. K. Hodnette, P. L. Bellaschi, Edward Beck.** *AIEE Transactions*, volume 66, 1947, pages 1613–18.

11. Switchgear Equipment for Tidd High-Voltage Test Lines, **F. A. Lane, B. W. Wyman.** *AIEE Transactions*, volume 66, 1947, pages 1619–23.

Discussion

J. R. Robert (Electricité de France, Paris, France): The precision in measurement of very slight losses at the Tidd 500-kv station is superior to that obtained on the French Chevilly 500-kv experimental line. How-

ever for the complete range of measurements, the accuracy of results in the two stations seems comparable.

The systematic tests at Chevilly, have shown the necessity of a supplementary correction to be brought to the nominal gradient when comparing single and 3-phase losses. This correction, in fact, is small (of the order of 2 per cent), and Figure 14 of the paper is not on a sufficiently extended scale to show it off. The formula which is based on equality of nominal gradients supposes the corona phenomenon to be purely superficial. But the space charges, whose motions create the chief part of losses, have a non-negligible value at points at a distance of more than a foot from the conductors. They then may undergo an appreciable distortion because of the presence of the other phases. The calculation of this distortion and measurements shows that this influence is equivalent to an increase of about 2 per cent of the nominal gradient in the Chevilly line. This influence may be more important if, as on the Tidd experimental line, phases are set closer together. It therefore seems necessary to take this correction into account when comparing the losses of two lines in which phase spacings are distinctly different, as well as for the change-over from single-phase to 3-phase tests.

Joseph S. Carroll (Stanford University, Stanford, Calif.): The authors of this paper are to be complimented on their thoroughness and clarity in the presentation of the material in the paper. The frankness in the discussion of the errors found in the measurement of corona loss and details given of the methods of correcting these errors give a feeling of confidence in the final values of corona loss obtained. The errors seem to fall into two general classes: (1) those of the metering circuit, including the phase angle of the wattmeter instrument, the phase angle of the metering winding of the transformer, and troubles caused by power exchange in the two outer phases of the 3-phase circuit; (2) errors introduced because more than one circuit is energized at a time, in which there is a certain amount of power exchange between phases of the various circuits. The latter errors would be present even though the metering circuit itself were perfect.

Of all the errors, the most serious one seems to be the one introduced by the phase angle of the wattmeter instrument. It is my opinion that it should be possible by further refinements of design to reduce this error to a negligible quantity. This might be helpful for future corona-loss studies.

The null method used in this metering setup not only reduces to a minimum the effect of the mutual inductance of the two wattmeter coils, but makes possible the use of the indispensable graphic meter for continuous operation.

It is fortunate that all the errors of any importance, except those introduced by changing transformer taps, which can be evaluated, produce a wattmeter reading that is proportional to the square of the line voltage and that the part of the wattmeter reading caused by corona loss does not have this same relation to voltage. This makes it possible to obtain valuable corona-loss data under conditions where corona loss cannot be measured directly with a high degree of accuracy.

The most important external variable affecting corona loss is the weather. The weather-recording instruments described in this paper make possible some sort of correlation between the weather and corona loss. This is a valuable contribution.

O. Naef, R. L. Tremaine, and **A. R. Jones:** The authors agree with Dr. Carroll that the phase-angle error in the wattmeters could be reduced. This would require either more distance to the surrounding magnetic shields, which for space limitations was undesirable, or compensating the effect of the eddy currents induced in the shields, which would make the meters unfit for use in a different kind of mounting.

The space limitations in the instrumentation cabinet made it necessary to place the three wattmeters side by side, physically almost in contact. It also was necessary to design the wattmeters for minimum physical size. Because of the high sensitivity of these instruments, heavy shielding was required. These facts combined to make it extremely difficult to eliminate completely any residual phase-angle error. It should be remembered that this error is so small that it was necessary to devise a special technique in order to measure it. Thus, although it was comparatively large when compared to the phase angles present in corona-loss measurements, it still was a very small angle, being on the order of 15 minutes.

The most important consideration regarding any error present in any corona-loss instrumentation is whether or not it remains constant. Since the error was proved to be absolutely constant, it could be corrected with a minimum of complications by inserting an external reactance in the voltage coil circuit.

Mr. Robert refers to the effect of the space charge surrounding the conductor, which modifies the nominal surface gradient after corona has started. Both the nominal gradient and the effect of the space charge vary with the type of the configuration used in the test. However, whereas the gradient can be determined accurately by measuring the charging currents or by calculation, the effect of the space charge must be computed from a comparison of loss measurements. Of necessity, these measurements can only be made on different conductors or at different times, and changes in losses caused by these variable conditions require the averaging of a great many tests.

Mr. Robert states that the effect of the space charges on the single-phase-3–phase conversion of losses is about 2 per cent. Figure 2 of the companion paper on corona-loss results[1] shows that the normal dispersion of corona-loss data plotted versus nominal gradients is in excess of 2 per cent for stranded conductors tested under seemingly identical conditions. The curves in this figure are from tests taken under different configurations, but if they are segregated into groups no distinction between single-phase and 3-phase results is apparent. This point is discussed in further detail in the closing discussion of the companion paper on corona loss.

If any effect caused by space charges exists, it is certainly very small in comparison to that resulting from the application of the nominal gradient law, which for normal single-phase-3-phase conversions is of the order of 16 per cent. Considering the large number of different configurations, both single-phase and 3-phase, used at the test site, it would have been utterly impractical to attempt to determine these small effects with any degree of accuracy. It is firmly believed that neglecting them in no way impairs the accuracy of the corona-loss measurements or the single-phase-3-phase conversion.

REFERENCE

1. CORONA INVESTIGATION ON EXTRA-HIGH-VOLTAGE LINES—500-KV TEST PROJECT OF THE AMERICAN GAS AND ELECTRIC COMPANY, **I. W. Gross, C. F. Wagner, O. Naef, R. L. Tremaine.** *AIEE Transactions*, volume 70 part I, 1951, pages 75–94.

The Input-Output System of the EDVAC

R. L. SNYDER, JR.
MEMBER AIEE

A SHIFT-REGISTER TYPE of reader-recorder which appears to be sufficiently versatile so that every known type of input-output equipment and auxiliary memory can be conveniently adapted to serve with it has been developed. In many cases such mechanisms, if fully exploited, can be made to work at such high speeds that electronic computing systems can operate with relatively slight delay. In this particular system it is anticipated that in addition to a photoelectric tape reader now operating, several other large-volume devices will be added, notably a new type of high-speed printer which can print faster than binary information can be converted to binary coded decimal numbers by the computer, a magnetic drum which can store very large quantities of information and still provide relatively short access time, and card handling equipment which manipulates information at medium speeds but in very convenient ways.

The shift-register reader-recorder described here has replaced the original magnetized-wire input-output system of the EDVAC (Appendix I gives some pertinent details concerning the EDVAC).

The system uses the shift-register to act as the link between the computer, a synchronous machine, and the several asynchronous mechanisms which provide input data, record results, or act as external memory. Each of the auxiliary devices has been designed to maximize the performance of some specialized function. The shift-register is intended to serve these independent auxiliary devices and, in fact, has been so arranged that it can accommodate equipment which may become available in the future without requiring modification of the logic used in designing existing equipment.

The specifications for the reader-recorder required not only that it work with the internal system of the EDVAC (see Appendix I), but that it be capable of accepting information from perforated tapes punched cards, magnetic drums, and similar equipment, and that it be capable of producing information in the form that could be utilized by tape perforators, printers, card punches, magnetic drums, and similar devices.

The EDVAC proper is a synchronous device. Few, if any, of the input and output devices are synchronous in their operation, and none of them operates at the same speed as the EDVAC. Furthermore, as mentioned previously, all the information in the EDVAC is handled in a serial fashion in which the sign and the least significant digits of numbers precede the more significant digits, whereas most of the input and output information is presented in parallel or with the most significant digits at the beginning.

Input Tape

As an example of the type of input information to be handled, the illustration shown in Figure 1 represents a section of teletype tape with the four possible types of characters which can be presented by the keyboard and which must be accepted and transposed by the reader-recorder before transfer to the memory system. There are five digit positions across the tape which may be perforated or not to represent 1 or 0 to designate one of four types of characters. (For convenience, the order of arrangement of the digits is shown to progress from left to right, which is not the case in actual practice.) Near the top of the strip is a row of five information-carrying holes, together with a sprocket hole, to show all of the possible positions. Further down is shown a binary coded decimal character. The presence of a hole in the first position indicates this type of character. The next character presents an octanary number, that is, one in which the character can have any value from zero to seven and can be coded with three binary digits. This character is identified by no perforation in the first position and a hole in the second position, with the three remaining positions occupied by ones or zeros. A binary character is designated by no perforations in the first three positions, with a hole in the fourth position followed by a one or a zero. Finally, the end-of-word character is represented by no holes in the first four positions and a perforation in the fifth position. In all words, this character must be placed after 44 binary digits have been presented. The 44 binary digits may have been derived from any combination of the other three types of characters.

This is probably the most complex of the input-output media, and it is discussed here to demonstrate the versatility required of the reader-recorder.

Reader-Recorder

Figure 2 is a simplified block diagram of the reader-recorder. In this drawing, the arrows on the solid lines show the paths of information, whereas the broken lines indicate control lines. The principal element of this device is a shift-register,* which consists of 45 flip-flops, or electric toggles, each of which is capable of retaining binary information. These elements are so arranged that the information contained in one can be shifted to its right-hand neighbor in one microsecond. The output of the forty-fifth position is connected through a gate to the input of the first position. It thus is possible to store a 44-digit word in the register in a stationary condition or to move the word

Paper 51-82, recommended by the AIEE Computing Devices Committee and approved by the AIEE Technical Program Committee for presentation at the AIEE Winter General Meeting, New York, N. Y., January 22–26, 1951. Manuscript submitted November 9, 1950; made available for printing December 26, 1950.

R. L. Snyder, Jr., is with the Ballistic Research Laboratories, Aberdeen Proving Ground, Md.

* A similar device is used in the computing machine concurrently developed by the National Bureau of Standards.

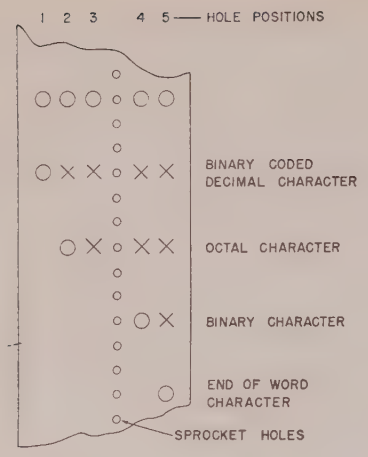

Figure 1. Teletype tape perforated to show permissible types of characters

through the register any number of steps at a speed which is synchronous with the rest of the EDVAC system. There is an extra space in this register. It is provided to accommodate a marker for keeping track of the progress of asynchronously inserted information. A large coincidence gate indicates when the first 44 positions are cleared.

The operation of this device in conjunction with the tape-reading or tape-punching equipment and the EDVAC memory may be described as follows: When the dispatcher receives any order, the order is automatically read into the shift-register one minor cycle after its entrance into the dispatcher. This word remains in the register until it is displaced by a new order. When the dispatcher receives a word having the order type indicating read-in or read-out, the word stored in the shift-register is moved out and the fourth address is picked off, returned to the dispatcher, and added to one to provide the fourth address necessary for selecting the order following the read or write operation. In this particular instance, the order in the dispatcher does not enter the register; instead, in the case of the read order, the register is cleared and a one signal is placed artificially in position 44 of the register. Following this, a character is scanned from the tape by the tape reader and is made available to the input of the fourth position of the register. If the character happens to be a binary coded decimal, the shifter is started and the first digit enters position four, the marker which had been in position 44 is advanced to 45; in the next shift (one microsecond later) the marker moves to position one and the second character is read into position four; another shift brings the marker to position two when the third character enters four; when the marker moves to position three, the fourth character is moved into position four. The register then is shifted until the first digit of the character arrives at position 44. It is noted that the marker now is in position 40: the system then waits until the next character is presented. Should the next character be a binary, the register will be shifted three spaces with no read-in, and then the single digit of the binary character will read into position four, just ahead of the preceding character. Following the transfer, the shift will continue until the binary character is in position 44. This operation will be repeated until 44 binary digits will have been accumulated in the register and the marker brought to rest in position 45. At this time, the tape reader should emit an end-of-word character whose coincidence with the marker in position 45 will cause the register to shift the word into the EDVAC memory. It is to be noted that between all shifting operations but the last, position 45 remains vacant. Should any irregularity develop in this arrangement, an error signal will be generated and the EDVAC will halt.

A somewhat similar procedure is involved in punching the output tape. In this operation the results of the computations are converted from the binary numbers used in the computer to binary coded decimal numbers and are stored in the memory to be read into the shift-register.

The shift-register is cleared, the circulation gate opened, and the number is read into position 44 with a marker impulse at the end. The most significant binary coded decimal character then occupies positions 45, 1, 2, and 3, which are connected to the appropriate punch elements. The operating impulse then trips the punch mechanism. After the punch is actuated, the four register positions concerned are cleared, and the register then is shifted 41 steps so that the next most significant character occupies positions 45, 1, 2, and 3. After this operation has occurred 11 times, the first 44 positions are clear, and the marker is in position 45. This condition causes the punch to record an end-of-word character.

The least significant binary coded decimal character is used only to provide the sign of the number. The end-of-word character actuates the carriage return on the automatic typewriter.

If the tape is to be used for long-term storage of information for reuse in the EDVAC, conversion of the information to binary coded decimal characters is not necessary. Such a tape will have all of the characteristics of an input tape, including the end-of-word character, so that no special provisions need be made.

Appendix I

The EDVAC System

In order to describe the logic employed in the design of the input-output equipment of the EDVAC, it is necessary to discuss the arrangement of the system as a whole. Figure 3 is a simplified diagram of the arrangement of the major elements of the EDVAC as they now exist and one element, the auxiliary memory, which is to be added. In this diagram, connections shown by solid lines carry information; those shown by broken lines act as controls.

The dispatcher controls all of the other units of the calculator during automatic operation. At the start of a problem, the operator initiates the program from the manual control by causing the dispatcher to order the reader-recorder to take information in the form of 44 binary digit words, which may be either numbers or orders, from the input apparatus and place it in the memory. The dispatcher then withdraws orders from the memory and causes their execution in the computer, the extract sys-

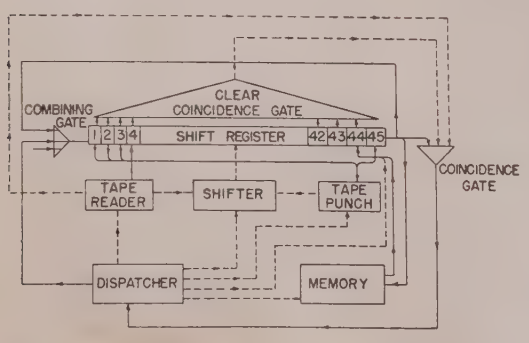

Figure 2 (left). Reader-recorder with perforated tape input-output system

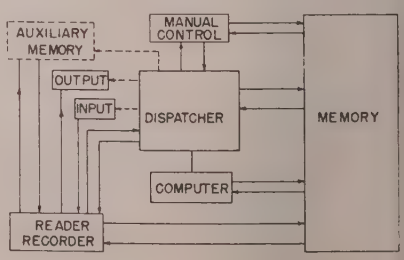

Figure 3 (right). Block diagram of EDVAC system

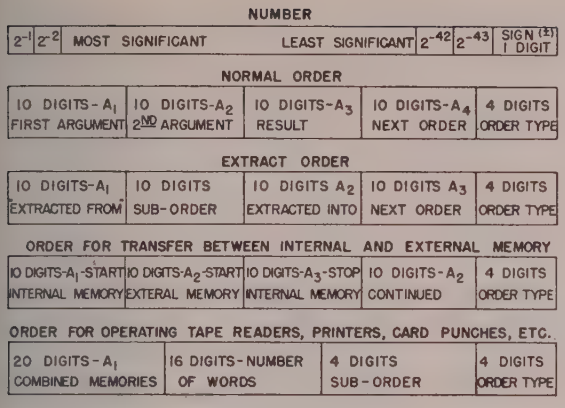
NUMBER
2^{-1} 2^{-2} MOST SIGNIFICANT LEAST SIGNIFICANT 2^{-42} 2^{-43} SIGN (±) 1 DIGIT
NORMAL ORDER
10 DIGITS-A_1 FIRST ARGUMENT
10 DIGITS-A_2 2ND ARGUMENT
10 DIGITS-A_3 RESULT
10 DIGITS-A_4 NEXT ORDER
4 DIGITS ORDER TYPE
EXTRACT ORDER
10 DIGITS-A_1 EXTRACTED FROM
10 DIGITS SUB-ORDER
10 DIGITS A_2 EXTRACTED INTO
10 DIGITS A_3 NEXT ORDER
4 DIGITS ORDER TYPE
ORDER FOR TRANSFER BETWEEN INTERNAL AND EXTERNAL MEMORY
10 DIGITS-A_1-START INTERNAL MEMORY
10 DIGITS-A_2-START EXTERAL MEMORY
10 DIGITS-A_3-STOP INTERNAL MEMORY
10 DIGITS-A_2 CONTINUED
4 DIGITS ORDER TYPE
ORDER FOR OPERATING TAPE READERS, PRINTERS, CARD PUNCHES, ETC.
20 DIGITS-A_1 COMBINED MEMORIES
16 DIGITS-NUMBER OF WORDS
4 DIGITS SUB-ORDER
4 DIGITS ORDER TYPE

Figure 4. Words used in EDVAC

tem in the dispatcher itself, and in the reader-recorder and the input and output devices. The memory has capacity to store simultaneously 1,024 words, each in a position which can be specifically designated by a 10-digit binary number. Such a number may be part of a word and is called an address. It can be decoded by the dispatcher and used to designate a memory position into which a word may be placed or from which one may be withdrawn. The computer consists of two identical arithmetic organs, one checking the operation of the other. The results of computations may be stored in the memory or sent through the reader-recorder to either the output mechanism or the auxiliary magnetic-drum-type memory.

An idea of the modus operandi of the system can best be had from Figure 4, which shows the various types of words used in manipulating the information which must be handled during computation. All of the words consist of 44 binary (that is, two-valued) digits. These words traverse the various channels in the EDVAC serially, that is, the digits following one another at one microsecond intervals. Each word, however, is allocated a 48-microsecond interval called a minor cycle, in which a 4-microsecond period at the end of the information is provided to allow time for switching. Any word may be interpreted by the dispatcher as a number or an order.

At the top of Figure 4 is shown a number word. It consists of 43 binary digits representing numerical information and a forty-fourth sign digit. The sign and less significant digits precede the most significant digit whose greatest absolute value is, for convenience, usually considered to be 2^{-1}.

The next line shows the normal order. This consists of four addresses identified by A_1, A_2, A_3, and A_4 and an order type. The order type has four binary digits, which can be arranged in 16 combinations. This element of the word is decoded by the dispatcher for the purpose of directing the machine to execute a desired operation, for example, add, subtract, multiply, and divide. Each of the addresses is made up of ten digits, from which 1,024 combinations can be formed, and these are used to select words from the memory to be used in the operation indicated by the order type. The first two addresses, when decoded in the dispatcher, select from the memory the two arguments of the computation to be performed; the third address provides the dispatcher with the information concerning the destination in the memory of the result of the computation. The fourth address enables the dispatcher to designate the next order to be taken from the memory when the operation is finished.

The third word shown in Figure 4 is used when the order type calls for the operation termed "extract." In this operation, certain elements of one word may be inserted in various ways into another word. The first address designates the word from which information is to be extracted; and the second address designates the word into which the information is to be inserted. The digits, which in the normal order would be the second address, form a suborder which designates what digits are to be removed from the first word and where they are to be placed in the second word. Both words retain their original positions in the memory. The third address defines the position of the next order.

The fourth word in Figure 4 is used to transfer information between the rather limited high-speed internal memory and the very extensive low-speed external memory. The first address indicates the location in the internal memory where the transfer is to start, the second address consisting of 20 digits split into two 10-digit groups defines the starting point in the external memory and the third address shows where in the internal memory the transfer is to cease. The order type indicates the operation. In this type of word, there is no space for a fourth address. For this reason, the next order is selected by adding one to the fourth address of the order which preceded the transfer order. (At the time of writing, the magnetic-drum memory is yet to be installed.)

The fifth word shown in Figure 4 is used to operate the input-output equipment. It consists of an order type designating the operation input-output, a 20-digit address for selecting the starting point in the combined memories, a 16-digit binary number designating the number of words to be transferred, and a 4-digit suborder which directs the machine to operate the input and output apparatus of various types as, for example, tape readers, tape punches, printers, card readers, and card punches. This order also has no fourth address and must depend on the preceding order for the information designating the next order.

No Discussion

A Method of Gating for Parallel Computers

A. G. RATZ
NONMEMBER AIEE

V. G. SMITH
MEMBER AIEE

Synopsis: A method of gating between two flip-flop circuits is described. The circuit uses two diodes and is particularly suited to parallel computers. The theory of the gating action and the necessary design information are given.

IN MODERN electronic digital computers, information is stored in electronic devices called registers. The information may be coded instructions for the machine or true arithmetic numbers. From time to time the action of the machine requires that the information be transferred from one register to another and the apparatus which sets the second register in accord with the first is called a gate.

Registers usually are compounded out of the circuit known as the Eccles-Jordan trigger circuit or, as it is almost invariably called, the flip-flop. This device has two stable states and is used because it is simple, can be made very reliable, and can change its state very rapidly. The registers are made up of banks of flip-flops, each recording by its state a segment of the information stored in the register.

In parallel computers, information is transferred simultaneously along parallel routes. To set one register according to another therefore requires that each flip-flop of the slave be set according to the state of the corresponding flip-flop of the master. The process is illustrated in Figure 1.

Paper 51-83, recommended by the AIEE Computing Devices Committee and approved by the AIEE Technical Program Committee for presentation at the AIEE Winter General Meeting, New York, N. Y., January 22–26, 1951. Manuscript submitted August 9, 1950; made available for printing January 3, 1951.

A. G. Ratz and V. G. Smith are both with the University of Toronto, Toronto, Canada.

The Flip-Flop Circuit

The basic flip-flop circuit is shown in Figure 2. It is essentially a 2-stage d-c amplifier coupled back on itself. To understand its properties, suppose that T_1 is conducting and that T_2 is not. This will cause the points a and b to be lower in potential than the corresponding points c and d. If r, R_1, and R_2 are chosen properly, the potential of b will be sufficiently negative to cut off T_2 and at the same time the potential of d will be sufficiently positive to allow T_1 to conduct. Hence, the circuit is stable with T_1 conducting, and by symmetry it also is stable if T_2 is conducting and T_1 is not. The circuit therefore has two stable states and remains in either state indefinitely unless compelled by some external force to change.

Gating

In parallel digital computers, registers may consist of 40 or more flip-flops. The total equipment required to set one register to another is that required to set one flip-flop to its mate times the number of flip-flops per register. Unless the gating circuits between individual flip-flops are made very simple, the over-all gating apparatus is likely to become extremely bulky. Any unnecessary apparatus not only increases the cost but adds to the probability of failure in the machine. For the greatest reliability it is essential that the gating device be sensitive only to the magnitude of voltage changes and quite independent of wave shapes. For this reason capacitor coupling cannot be used.

This paper proposes a new method of gating, particularly suitable for parallel machines. It uses what is probably the smallest possible amount of gating equipment, namely, two diodes per flip-flop plus one tube per register to provide the voltage pulse.

The Gate and Its Operation

Figure 3 shows the gating circuit. The two registers are the master, (1), and the slave, (2), consisting of an equal number of identical flip-flops, designated A, B, C . . . . The gate between the flip-flops is formed by the diodes D_1 and D_2, connecting the plates of the master flip-flop to the grids of the slave. E_1 and E_2 represent the plate supply voltages of the master and slave registers, respectively.

Except when transfer is desired, the two supply voltages are equal and the flip-flops are isolated, since they are identical and both plate voltages are positive with respect to both grid potentials. The cathodes of both diodes are therefore positive with respect to their plates and neither conducts. To understand the gating operation, consider a particular situation in which the tubes T_1 and T_4 are conducting. It is desired to change the state of the slave flip-flop to agree with the master, that is, T_3 is to conduct and T_4 is to be cut off. Note that the point a_1 is lower in potential than c_1 and that the point d_2 is lower in potential than b_2. Let E_1 decrease. When the plate potential (a_1) of tube T_1 falls below the grid potential (b_2) of tube T_4, the diode D_1 conducts, lowering the grid potential of T_4 accordingly. This decreases the plate current of T_4, thereby increasing

Figure 1. Gating in a parallel computer

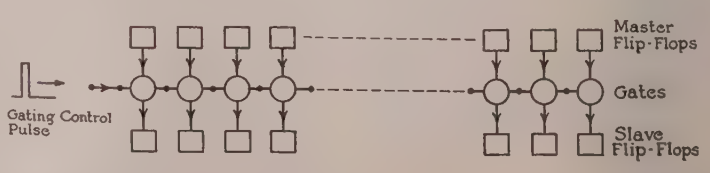

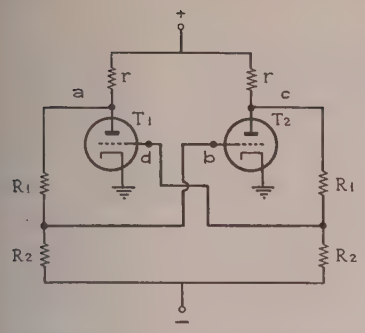

Figure 2. The basic flip-flop circuit

the grid potential (d_2) and decreasing the cathode potential of T_3. If these are sufficient to cause T_3 to conduct while the diode D_2 still is not conducting (a matter of design), the slave flip-flop changes its state and agrees with the master.

If, on the other hand, T_3 had been the conducting tube from the first, neither diode would have conducted, because of the proper choice of the voltage levels, and hence no change would have taken place. Further, if E_1 be reduced so far that both diodes conduct, then the slave flip-flop will be reversed as E_1 falls. As E_1 rises again, the diode D_2 will cease to conduct before the diode D_1 if

$$\frac{R}{r} > \frac{R_k - r_p}{2(r + r_p - R_k)} \qquad (1)$$

a condition easily realized in design. Hence, if this condition is satisfied, there is no tendency whatever for the slave to reset during the rise of E_1.

In this way, each flip-flop in the slave register is made to agree with its corresponding master flip-flop. A very simple device depresses E_1, and this serves to transfer the entire register. The more flip-flops there are in the registers, the more important this simplicity of control becomes and the greater the advantage of the new method in the saving of gating components.

In the circuit of Figure 2, the cathodes are at ground potential, whereas cathode resistors R_k are shown in Figure 3. These are necessary to make the flip-flops stable under wide fluctuations in supply voltage. In general, a flip-flop with a grounded cathode is stable over only a small range of supply voltages.

By reconnecting the diodes, the roles of master and slave are interchanged, and by using two pairs of diodes, the operation becomes bilateral, either register can be read into the other. Furthermore, it is possible to couple A_1 to A_2 and A_2 to B_1, or, indeed, to any other flip-flop in register number 1. In this way, information may be shifted a predetermined number of steps, either right or left. This arrangement makes, therefore, a fast, simple shifting mechanism.

Analysis of the Circuit

For stability reasons, the design of the circuit is such that the grid voltage of the conducting tube is positive with respect to the cathode, but is restrained by grid current to a value which is approximately zero. The tube resistance can, therefore, be represented quite accurately by the reciprocal of the slope of the plate characteristic for zero grid voltage. In Figure 4, the equivalent resistance of the tube is

$$r_p = \Delta e / \Delta i$$

By substituting a resistor, r_p, for the tube, a linear resistance network is obtained in which all currents and voltage drops are proportional to the applied voltage and the circuit behavior may be analyzed.

In Figure 5 are plotted the potentials at the points a, b, c, d for any pair of flip-flops in Figure 3 as the applied voltage is varied. In this diagram, the curves are interchangeable, as indicated, depending upon which tubes are conducting.

Suppose again that T_1 and T_4 are conducting, then the potentials of c_1, a_1, b_2 d_2 are as indicated. When E_1 is decreased to E_1', c_1 has moved to c_1' and a_1 to a_1', where it is at the same potential as b_2, which has not changed since E_2 has not changed. As E_1 decreases further, however, the diode D_1 conducts and a_1 decreases along a new line, $a_1' a_1''$, because of support from E_2. If the diode impedance is negligible in comparison with the network resistors, the potential of the point b_2 is essentially the same as that of a_1 for E_1 less than E_1'. Since the whole object is to depress the potential of b_2, it is undesirable for too much support to come from E_2, hence the impedance of the slave network as seen from b_2 should be very much greater than that of the master network as seen from a_1. Denoting the ratio of these two impedances by n, which should be not less than 5, then, as is shown in Appendix IV,

$$\frac{R}{r} = \frac{(2n-1/2)}{1 + \dfrac{r}{r_p + R_k}} \qquad (2)$$

where r_p is the tube resistance, and r and R_k are shown in Figure 3.

The maximum value of the impedance of the slave as seen from b_2 would be obtained if b_2 (and b_1, d_1, d_2) were at the midpoint of the $(r+2R)$ resistor group. The maximum is broad, however, and since $2R$ should be 10 or 20 times r the difference is quite negligible. The grid resistor has therefore been assumed evenly divided, though there may be some advantages in moving the grids a little closer to the plates. For one thing, the magnitude of the switching pulse would be reduced. The analysis of such a circuit would not be essentially different from that given here.

The potential of the common point (a_1, b_2) will, therefore, follow a curve such as a_1', a_1'', which can be computed accurately by an application of Thévenin's

Figure 3. The diode gate

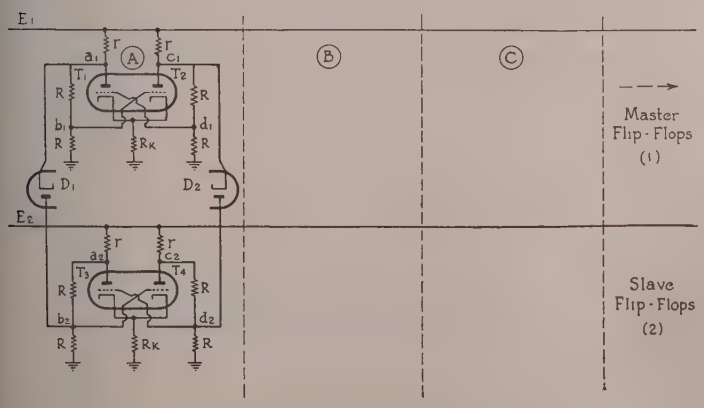

Figure 4. Tube characteristic

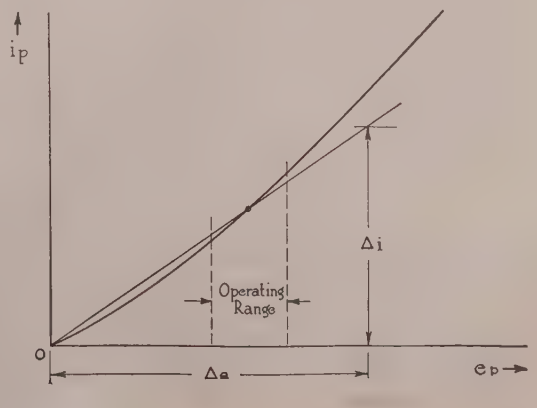

theorem, treating a_1 and b_2 as sources with internal resistances r_1 and r_2, respectively.

As the potential of b_2 falls, the cathode of T_4 must fall with it, and this requires that the current through T_4 and R_k decrease. Hence, the potential of d_2 rises and at some stage, before a_1'' is reached, the rising grid potential and the falling cathode potential of T_3 will cause this tube to conduct. This raises the cathode potential of T_4 and depresses its grid potential still more, thus resulting in a quick reversal of the slave flip-flop. The potentials involved in this course of events are readily computed.

Transition Time

While an exact analysis is difficult because of the presence of nonlinear elements, it is possible to discuss with fair approximation the transition of the slave flip-flop from one state to the other when a negative pulse is applied to E_1.

If E_1 is made to fall rapidly, the potentials of the various circuit points will not follow the curves of Figure 5 because of the unavoidable stray capacitances.

The first important point is to find assurance that the stray capacitances of the master flip-flops will not in some way cause a reversal when a fast pulse is applied to E_1. Fortunately, when triodes are used, the Miller effect creates a large effective capacitance from the grid to the cathode of the conducting tube, which assures that the tube will be kept in its conducting state by maintaining the grid potential during the pulse.

As the potential of b_2 falls, the cathode potential of T_4 falls accordingly, but only as fast as the cathode-ground capacitance can discharge. The maximum rate of discharge is when both tubes T_3 and T_4 are cut off, since they can only increase the charge. The time constant is then

Figure 6. The fall of E_1 during a gating pulse

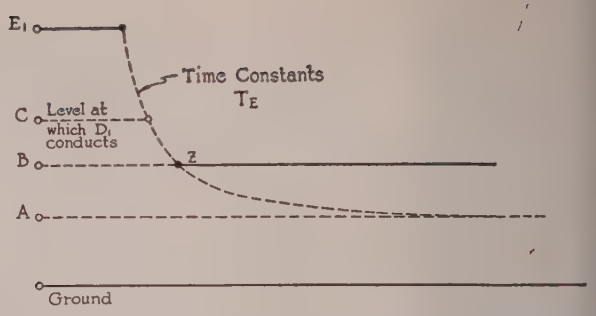

$$T_k = R_k C_k \qquad (3)$$

where C_k is the cathode-ground stray capacitance. During pulsing, E_1 also will have a rate of fall and a time constant, T_E, associated with it, where

$$T_E = RC \qquad (4)$$

and R is the equivalent resistance of all the master flip-flops in parallel and C is the total stray capacitance from the E_1 bus to ground.

Experience shows that T_E usually is several times T_k; this being the case, it is clear that the potential of the slave cathodes will follow the fall of b_2 very closely, the current through T_4 being reduced just enough to cause this to happen.

Figure 6 shows the application of the negative pulse to E_1, with the rate of fall determined by T_E. By making the pulse greater than required and using a diode to limit the potential fall to the correct value as at B, for example, the time of fall is greatly reduced.

Figure 7 shows the potential of the point b_2, where it is assumed for simplicity that the transition occurs when the cathode and grid potentials of T_3 are equal. (Actually, the transition starts as soon as T_3 begins to conduct.)

When the falling cathode potential and the rising grid potential, d_2, meet, or even a little before, the tube T_3 conducts and the cathode potential then will follow the rising potential of d_2. The combined effect of the further depression of b_2 and the rising cathode potential completes the cutoff of T_4 very rapidly. The subsequent rise in the potential of d_2 will be very rapid, since stray capacitances only are involved. Since grid and cathode remain at essentially the same potential, the grid-cathode capacitance does not have to be charged, hence only the cathode-plate capacitance is involved.

The points c_2 and d_2 rise in potential according to a time constant

$$T_R = \frac{1}{2} r C_{pk} \qquad (5)$$

where C_{pk} is the plate-to-cathode capacitance.

With little trouble, it is possible to make T_E as short as 0.25 microsecond and, using miniature triodes, T_R about 0.04 microsecond. A 1-microsecond pulse is more than sufficient, and at the end of the pulse the slave register has reached equilibrium. There is no need to use cross-coupling capacitors from the grid of one tube of a flip-flop to the plate of the other, as is the usual practice. Indeed, this would be disastrous, since it would provide support for b_2 from E_2, which is exactly what is not wanted and could result in reversing master flip-flop.

Figure 5. Showing the potentials of various points during gating

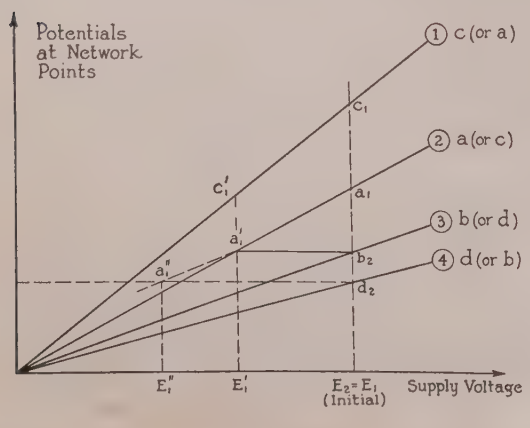

Figure 7. Transition potentials

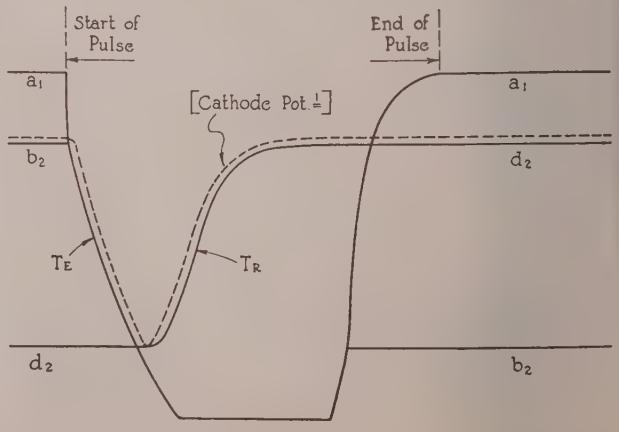

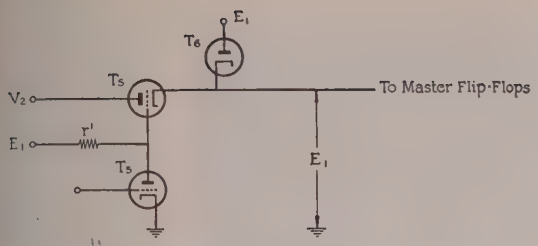

Figure 8. The series pulsing circuit

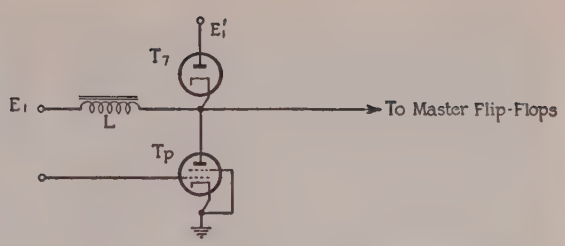

Figure 9. The parallel pulsing circuit

Experimental Results

An experimental register pair was constructed and tested. The circuit parameters were not the optimum but were deliberately chosen near the limits of possible values. The resistors were taken as purchased and had a 10 per cent tolerance. The circuit values were:

Plate resistors, $r = 10$k
Grid resistors, $R = 47$k
Cathode resistors, $R_k = 15$k
Supply voltages, E_1, $E_2 = 150$ volts
Pulsed down to $E_1' = 75$ volts
Pulse width $= 0.5 \times 10^{-6}$ seconds
Tubes used $= 6J6$, $6AL5$

This register proved to be very reliable. Another using better resistance parameters, greater supply voltages, and more flip-flops per register was built and tested; oscillograms illustrating its action are shown in Figure 11.

Conclusions

The circuit described in this paper meets all the basic requirements of a satisfactory gating device for parallel computers. It can be made reasonably fast (0.5 microsecond), the gating is by direct coupling, it is economical of components and requires only diodes, the most reliable type of tube.

Experiment confirms the reliability expected.

The basic idea underlying this method can be given other applications. It has been used successfully in quite complicated circuits with great saving in equipment.

It is possible in some cases to replace the $6AL5$ tubes by germanium diodes which require no filament supply, are of low capacitance, and are small in size.

Appendix I. Flip-Flop Design

In the present application, the flip-flops must meet the following requirements:

1. They must be stable over a wide range of applied voltage.

2. They must be stable despite the influence of the conducting diode, which increases the plate potential of the conducting tube of the master flip-flop.

3. The drop across the conducting tube must be reasonably small to limit the magnitude of the gating pulse.

4. The impedance looking in at the plate must be small compared with that looking in at the grid. This helps requirement 2 above.

5. The resistances must be small enough so that stray-capacitance time constants are satisfactorily short.

To meet requirement 1, the cathode resistor R_k is used.

To meet requirement 2, the conducting tube is made to draw grid current so that when the point a_1 is raised in potential, the cathodes also are raised, thus cancelling the effect of the increase in the potential of b_1 on T_2.

To keep the grid positive when the diode conducts, the potential to which the grid would rise if there were no grid current must be higher than the greatest master cathode potential during the switching operation. This requires, as shown in Appendix VI, that

$$\frac{R_k}{r_p} < \frac{R(R+3r)}{R(R+3r)+4r^2}\left[1+\frac{2R(R+r)}{(2R+r)(R+3r)}\frac{r}{r_p}\right] \quad (6)$$

To meet requirement 3, all resistors are made greater than the tube resistance, r_p. With equal grid resistors, it is necessary that $R_k > r_p$ to keep the nonconducting tube cut off.

To meet requirement 5, the desired switching speed and the choice of tube have to be considered. Miniature tubes and careful wiring will keep stray capacitances to a minimum and will raise the acceptable resistance values. Large resistors give more reliable operation by making the effect of the tube proportionally smaller.

In designing a flip-flop, the type of tube must first be chosen. In this application, triodes are ideal for the following reasons:

1. A double triode gives one flip-flop per envelope.

2. No screen voltages are required.

3. The Miller effect in the master flip-flop assists in giving stability.

For high speed, use triodes with a high transconductance ($6J6$, $2C51$).

A plate resistor, r, of from one to three times the d-c plate resistance gives satisfactory results. It is small enough to assure that equations 1 and 2 are easily satisfied without excessive values of R and large enough so that changes in the tube characteristics will have little effect on the circuit. The value of R should be at least five times that of r and preferably ten times it. Only the time constants T_E and T_R limit its value.

A value of $R_k = 1.5r_p$ usually permits a satisfactory design. The value of R_k must be larger than r_p, but small enough so that equation 6 is satisfied.

Appendix II. The Pulsing Circuit

The Series Pulsing Circuit

The first type of pulsing circuit is illustrated in Figure 8. It is capable of very high speed and high repetition rates, but requires a large tube, T_s, which has the entire master register as a cathode load. The tube T_5 is cut off except during the pulse, when it lowers the potential of the grid of T_s and the cathode follows the grid. The diode, T_6, limits the cathode fall to a predetermined value, E_1'.

The big disadvantage of the circuit is that the supply voltage must be increased by the normal drop across T_s, which has to be capable of passing the entire plate supply of the master register.

The Parallel Pulsing Circuit

The second type of pulsing circuit is illustrated in Figure 9. It eliminates the need for large power tubes and extra voltage supplies. The tube T_p is cut off except during the pulse. It is a beam power pentode and during gating only it must handle a substantial fraction of the total plate current to the master register so as to reduce the bus voltage to the required level. Since both the tube and the inductor are essentially constant current devices, the pentode robs the register of plate current and E_1 falls by I_pR volts, where I_p = the pentode current, and R = the equivalent resistance of the master register. By making the pentode current too great and limiting the fall of the bus voltage by the diode, T_7, greater speed is obtained.

Analysis of Parallel Pulsing

Figure 10 shows an equivalent circuit, obtained by using the transient form of Norton's theorem. In this $I(t)$ is the short-circuit current from the (E_1, L) source,

$$I(t) = I(0) + E_1 t/L$$

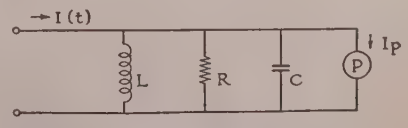

Figure 10. An equivalent circuit for the parallel pulsing circuit

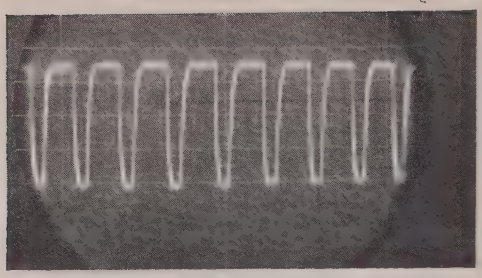

A. Gating pulses at the plate supply of the Master Register. Each negative pulse is 150 volts in magnitude and 2 microseconds in duration

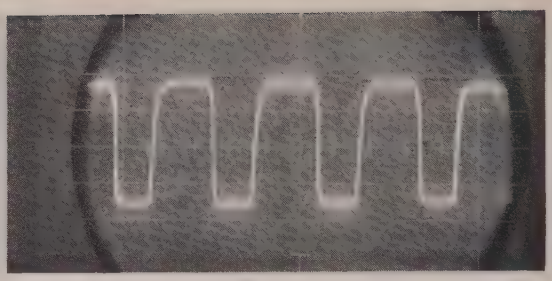

B. Plate voltage of a slave flip-flop under action of the pulses shown in (A). The master flip-flop is reversed by a separate mechanism between each gating pulse to give a repetitive trace

Figure 11. Waveforms

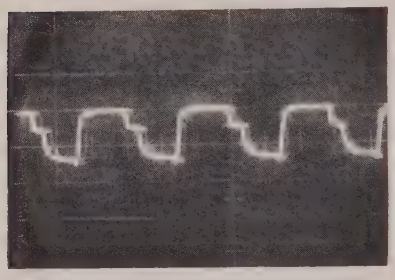

C. Waveforms at one grid of a slave flip-flop under the conditions for (B)

where

$I(0)$ = the initial current

R is the equivalent resistance of the whole master register and C is the entire capacitances to ground, including the stray capacitance of the inductor L. The pentode, P, demands a constant current $I(p)$. Let e_1 be the bus voltage during switching, then

$$I(0)+\frac{E_1}{L}t=\frac{1}{L}\int^{t} e_1 dt+\frac{e_1}{R}+C\frac{de_1}{dt}+I(p) \quad (7)$$

The solution of this is,

$$e_1=E_1-A(\epsilon^{m_1 t}-\epsilon^{m_2 t}) \quad (8)$$

where

$$m_1,\ m_2=-\frac{1}{2RC}\pm\sqrt{\left(\frac{1}{2RC}\right)^2-\frac{1}{LC}} \quad (9)$$

and

$$A=\frac{E_1-R\,[I(0)-I(p)]}{\sqrt{1-\dfrac{4R^2C}{L}}} \quad (10)$$

The minimum value of e_1 occurs at

$$t=2RC\frac{\cosh^{-1}\dfrac{1}{2R}\sqrt{\dfrac{L}{C}}}{\sqrt{1-\dfrac{4R^2C}{L}}}\ \text{seconds} \quad (11)$$

and its value is computed easily from equations 8, 9, and 10. In this application $L/C>>4R^2$.

Let

$$y=\frac{1}{2R}\sqrt{\frac{L}{C}}>>1 \quad (12)$$

then the following approximations hold,

$$\left.\begin{aligned} m_1&=-R/L,\\ m_2&=-1/RC,\\ A&=E_1-R[I(0)-I(p)]\\ t&=2RC\log\ (2y) \end{aligned}\right] \quad (13)$$

While it is easy to write a formula for the minimum value of e_1, the best method of computing is to use equations 8 and 11.

With flip-flops of the type discussed herein, it is possible to gate a register of 40 flip-flops with a single *6AQ5* miniature pentode and a 5-henry inductance. Either an ordinary power supply choke coil may be used, or, if greater speed is required, a special coil with low capacitance across its terminals and to ground may be designed.

From equations 13, it is apparent that E_1 drops initially with a time constant RC. To reduce the time of fall $I(p)$ is made larger than necessary and E_1 is prevented from falling below some chosen limit, E_1', by means of a limiting diode (see Figures 6 and 9).

Appendix III. Recovery from Double-Diode Conduction

When E_1 is depressed so severely that both diodes conduct, the slave flip-flop is set, if necessary, as E_1 is decreasing. It is very important that it shall not again be switched when E_1 is rising. This is assured if the diode D_2 ceases to conduct before the diode D_1, assuming that T_1 and T_3 are the conducting tubes.

Since we are concerned only with the instant of zero diode current we can let the diode currents be zero and examine the potentials. Diode current will change them, but will not reverse their relative sign.

Using the symbols as on Figure 3, let Z be the impedance from a_1 to ground:

$$Z=\frac{2R(r_p+R_k)}{2R+r_p+R_k} \quad (14)$$

The grid potential of a conducting tube is taken to be equal to the cathode potential, hence,

$$V_{d_2}=\frac{R_k}{R_k+r_p}V_{a_2}=\frac{R_k}{R_k+r_p}\,\frac{Z}{Z+r}E_2 \quad (15)$$

and

$$V_{c_1}=V_{d_1}+\frac{R}{R+r}(E_1'-V_{d_1})$$
$$=\frac{r}{R+r}\,V_{d_1}+\frac{R}{R+r}E_1' \quad (16)$$

where E_1' is the reduced value of E_1. But

$$V_{d_1}=\frac{R_k}{R_k+r_p}V_{a_1}=\frac{R_k}{R_k+r_p}\,\frac{Z}{Z+r}E_1' \quad (17)$$

Therefore,

$$V_{c_1}=\left[\frac{R}{R+r}+\frac{r}{R+r}\,\frac{R_k}{R_k+r_p}\,\frac{Z}{Z+r}\right]E_1' \quad (18)$$

The diode D_2 will cease to conduct when $V_{c_1}=V_{b_2}$, which is when

$$E_1'=\frac{\dfrac{R_k}{R_k+r_p}\,\dfrac{Z}{Z+r}}{\dfrac{R}{R+r}+\dfrac{r}{R+r}\,\dfrac{R_k}{R_k+r_p}\,\dfrac{Z}{Z+r}}E_2 \quad (19)$$

Again

$$V_{b_2}=\frac{1}{2}\qquad V_{a_2}=\frac{1}{2}\,\frac{Z}{Z+r}E_2 \quad (20)$$

and

$$V_{a_1}=\frac{Z}{Z+r}E_1' \quad (21)$$

The diode D_1 will cease to conduct when $V_{a_1}=V_{b_2}$, which is when

$$E_1'=\frac{1}{2}E_2 \quad (22)$$

The diode D_2 will cease to conduct at a lower value of E_1', therefore, if

$$\frac{\dfrac{R_k}{R_k+r_p}\,\dfrac{Z}{Z+r}}{\dfrac{R}{R+r}+\dfrac{r}{R+r}\,\dfrac{R_k}{R_k+r_p}\,\dfrac{Z}{Z+r}}<\frac{1}{2} \quad (23)$$

It is only a matter of algebra to reduce this to equation 1.

Appendix IV. On the Relative Internal Impedances

The impedance of the slave flip-flop as seen from b_2, r_2, say, should be at least five times that of the master flip-flop as seen from a_1. Call the latter r_1. We need to know the ratio of R/r to assure this. We have

$$\frac{1}{r_1}=\frac{1}{r}+\frac{1}{2R}+\frac{1}{R_k+r_p}$$

$$\frac{1}{r_2}=\frac{1}{R}+\frac{1}{R+r} \tag{24}$$

Suppose that $r_2=nr_1$, then

$$1+\frac{r}{R_k+r_p}=\left(n-\frac{1}{2}\right)\frac{r}{R}+\frac{n}{\frac{R}{r}+1} \tag{25}$$

Letting $k=1+r/(R_k+r_p)$ and $x=R/r$, we find that

$$x=\frac{\left(2n-\frac{1}{2}-k\right)+\sqrt{\left(2n-\frac{1}{2}+k\right)^2-4nk}}{2k} \tag{26}$$

For fairly large values of n this reduces to

$$\frac{R}{r}=\frac{2n-\frac{1}{2}}{1+\frac{r}{R_k+r_p}} \tag{2}$$

Taking $R/r=n$ is satisfactory for most design work.

Appendix V. On the Recovery of the Slave After Switching

Suppose that the tube T_3 has just switched on (Figure 3). The points c_2 and d_2 are depressed in potential. Tube T_3 would increase its current rapidly, but its cathode cannot rise much above the grid potential V_{d_2}. We assume, as usual, that the T_3 cathode and grid are at the same potential.

Let $V_{c_2}=v$ for brevity. The rate of rise of V_{c_2} is $dv/2dt$. This is also the rate of rise of the cathodes. Hence the rate of rise of the potential across the plate-cathode capacitance, which is effective in keeping c_2 and d_2 depressed, is also $dv/2dt$.

Therefore, where C_{pk} is the capacitance mentioned,

$$v=E_2-r\left(\frac{v}{2R}+\frac{1}{2}C_{pk}\frac{dv}{dt}\right) \tag{27}$$

which has the solution

$$v=V_{c_2}=\frac{2RE_2}{2R+r}\left(1-\epsilon^{-\frac{2}{rC_{pk}}\frac{2R+r}{2R}t}\right) \tag{28}$$

For large values of R/r the time constant is

$$\frac{1}{2}rC_{pk} \tag{5}$$

as noted in the text. The main point is its extremely small value.

Appendix VI. On Keeping the Master Grid Positive During Switching

It was noted that to avoid any chance that the master flip-flop might be reversed during the gating operation, it is desirable that the grid of the conducting tube shall not become negative with respect to the cathode at any time. The critical instant is just as T_3 is about to conduct and T_4 to cease conducting. At this instant, the plate of T_1 receives its maximum support from E_2 via the point b_2.

We assume, as an approximation, that T_3 starts to conduct when its grid and cathode reach the same potential. We first find the cathode potential.

Let I_4 be the current through T_4 at the instant preceding the switch-over, then

$$V_{c_2}=E_2-r\left(I_4+\frac{1}{2R}V_{c_2}\right) \tag{29}$$

whence

$$V_{c_2}=\frac{E_2-rI_4}{1+\frac{r}{2R}} \tag{30}$$

and

$$V_{d_2}=\frac{1}{2}\ V_{c_2}=\frac{E_2-rI_4}{2\left(1+\frac{r}{2R}\right)}=R_kI_4 \tag{31}$$

Therefore I_4 is found and hence

$$V_k=\frac{R_kE_2}{r+2R_k\left(1+\frac{r}{2R}\right)} \tag{32}$$

We further assume that the grid of T_4 is at the cathode potential. (Actually, both grids are negative with respect to the cathodes and the errors in the two assumptions tend to cancel.) Then we may write

$$V_{b_2}=\frac{R_kE_2}{r+2R_k\left(1+\frac{r}{2R}\right)} \tag{33}$$

also

$$V_{a_1}=\frac{r_p+R_k}{r+r_p+R_k}E_1 \tag{34}$$

At switch-over, these are equal if we neglect the diode resistance, and therefore

$$E_2=\frac{r+2R_k\left(1+\frac{r}{2R}\right)}{R_k}\ \frac{(r_p+R_k)}{r+r_p+R_k}E_1 \tag{35}$$

Just before switch-over, two sources support the point a_1. Their equivalent electromotive forces and resistances are

$$E_2'=\frac{R}{2R+r}E_2$$

$$r_2'=\frac{R(R+r)}{2R+r} \tag{36}$$

$$E_1'=\frac{2R}{2R+1}E_1$$

$$r_1'=\frac{2Rr}{2R+r} \tag{37}$$

Combined into a single equivalent source we have,

$$E'=\frac{2R(R+r)+2Rr\times\dfrac{r+2R_k\left(1+\frac{r}{2R}\right)}{R_k}\ \dfrac{r_p+R_k}{r+r_p+R_k}}{(2R+r)(R+3r)}E_1 \tag{38}$$

$$r'=\frac{2rR(R+r)}{(2R+r)(R+3r)} \tag{39}$$

The cathodes of the master flip-flop are therefore at the potential

$$\frac{R_kE'}{r'+r_p+R_k}=$$

$$\frac{2R(R+r)R_k+2R^2r\times\left(r+2R_k+\dfrac{2R_k}{R}\right)\dfrac{r_p+R_k}{r+r_p+R_k}}{(r_p+R_k)(2R+r)(R+3r)+2rR^2(R+r)}E_1 \tag{40}$$

The potential of the point d_1, if it were not depressed by the grid current of T_1, would be

$$V_{d_1}=\frac{R}{2R+r}E_1 \tag{41}$$

To assure a positive T_1 grid, we must have

$$\frac{R}{2R+r}>$$

$$\frac{2R(R+r)R_k+2Rr\times\left(r+2R_k+\dfrac{rR_k}{R}\right)\dfrac{r_p+R_k}{r+r_p+R_k}}{(r_p+R_k)(2R+r)(R+3r)+2rR(R+r)} \tag{42}$$

which is better written as

$$\frac{R+3r}{R+r}>\frac{2R_k}{r_p+R_k}\times\frac{1+\dfrac{r}{R}\left(\dfrac{R}{R+r}\ \dfrac{r+2R_k+\frac{r}{R}R_k}{r+r_p+R_k}\ \dfrac{r_p+R_k}{R_k}\right)}{1+\dfrac{2R(R+r)r}{(2R+r)(R+3r)(r_p+R_k)}} \tag{43}$$

Now

$$\left(\frac{R}{R+r}\ \frac{r+2R_k+\frac{r}{R}R_k}{r+r_p+R_k}\ \frac{r_p+R_k}{R_k}\right)$$

varies little and has a value from 1.67 to 2. Using the maximum value gives a safe approximation.

Solving the resulting simplified equation, we arrive at equation 44.

$$\frac{R_k}{r_p} < \frac{R(R+3r)}{R(R+3r)+4r^2} \left[1+\frac{2R(R+r)}{(2R+r)(R+3r)}\,\frac{r}{r_p}\right] \quad (44)$$

A further approximation, which is good if $R \gg r$, but not on the safe side, is:

$$R_k < r + r_p \quad (45)$$

The value of R_k should, however, always be checked by equation 44.

No Discussion

Systematization of Tube Surveillance in Large-Scale Computers

HOMER W. SPENCE
NONMEMBER AIEE

Synopsis: Operation of the ENIAC (electronic numerical integrator and calculator), a high-speed electronic computing machine, at the Ballistic Research Laboratories of Aberdeen Proving Ground, has shown that 90 per cent of the service interruptions are caused by vacuum-tube failures. At the beginning of 1950 a tube surveillance program was initiated in which all pertinent data concerning each tube in the system are recorded on punched cards. This paper describes the manner in which faulty vacuum tubes are detected and replaced, and gives the specifications used in testing the tubes and the manner in which the tube history is gathered. Preliminary results, using data collected during the first five months of 1950, are given.

THE ENIAC was designed in the most conservative possible manner known at the time. However, operating experience at the Computing Laboratory of the Ballistic Research Laboratories has shown that a more thorough knowledge of the behavior of systems involving large numbers of vacuum tubes would have led to different design procedures.

To correct certain unforeseen defects in the ENIAC and to accumulate data for guiding the designing of new equipment and tube-testing procedures, a program of detailed tube surveillance was inaugurated at the beginning of 1950. Systematic records are kept by recording on punched cards all the information relating to the service life of each tube. One card is used per tube. Items recorded on the card are: the tube type, kind of use, hours of life, manufacturer, panel location, type of failure, previous service, preheating schedule, date, and test readings. This system permits great flexibility in processing the information by means of standard International Business Machines equipment, and by the ENIAC itself.

In general, certain unusual conditions are present in this program which should be noted before applying the results of this study to other operations. First, both the filament and the plate voltages are applied at all times and the system is in operation 144 hours per week. This procedure has been established because it provides the most economical utilization of the equipment. Second, all the tubes in a faulty circuit are replaced at once and those removed from the system are rechecked. Bad and marginal units are discarded. In other types of service wherein only failures are removed from service and marginal elements are not, longer service life would be achieved.

Tube Replacement and Tests

There are approximately 18,000 tubes in the ENIAC. They are divided according to types, as follows: 35 per cent are *6SN7*'s; 22 per cent, *6L6*'s; 14.1 per cent, *6SA7*'s; 8 per cent, *6SJ7*'s; 6.5 per cent, *6L7*'s; 1.6 per cent, *6J5*'s; 7 per cent, *6V6*'s; 1.6 per cent, *6Y6*'s; 2.5 per cent, *6AC7*'s; and 1.8 per cent, *807*'s. Blanket changes in such a large number of tubes are impractical because the incidence of failures during the first 1,000 hours of life greatly exceeds the failure rate that exists after this period. On the other hand, replacing one tube at a time is undesirable because isolation of a single faulty tube requires expensive time-consuming tests. A compromise between these two extremes is most economical. When a malfunction is discovered, it is traced to a particular circuit. Then all the tubes in the circuit are replaced; there may be from one to eleven tubes in this group. This procedure eliminates bad combinations of marginals as well as complete failures. Satisfactory elements also are removed, making it necessary to test all removals. Good units are placed in storage, marginal and bad elements are discarded.

Faulty circuits are detected by means of two types of control tests. Operational tests, utilizing a check problem, detect malfunctions by comparing the result to a known correct answer. These tests are used for two purposes: first, for marginal checking, that is, the detection of weak tubes; second, as a guide to machine condition during long periods of problem operation. Marginal checking is achieved by increasing the speed of machine operations. This is accomplished easily in the ENIAC because of the synchronization of operations by a central pulse system. A pulse rate of 125 kc is used for this type of checking. Operational tests, used as an indication of machine condition, consist of sample calculations of the problem being solved and are made periodically under normal operating conditions. Normal operation involves the transfer of information pulses at rates ranging between 60 and 100 kc per second.

Oscilloscope tests are used to inspect and measure pulses. Corrective action is taken when these pulses do not conform to the prescribed shape or amplitude. The acceptance limits are set above the operational level necessary for correct circuit performance. Oscilloscope tests are more satisfactory than the operational tests for preventive maintenance. However, they are difficult to devise so that machine time is conserved. All tests are run at least once a week or as the need is indicated by the operational tests.

When oscilloscope tests are used for detection, defective tubes are removed sooner than with operational tests.

Paper 51-84, recommended by the AIEE Computing Devices Committee and approved by the AIEE Technical Program Committee for presentation at the AIEE Winter General Meeting, New York, N. Y., January 22–26, 1951. Manuscript submitted November 9, 1950; made available for printing January 3, 1951.

HOMER W. SPENCE is with the Ballistic Research Laboratories, Aberdeen Proving Ground, Md.

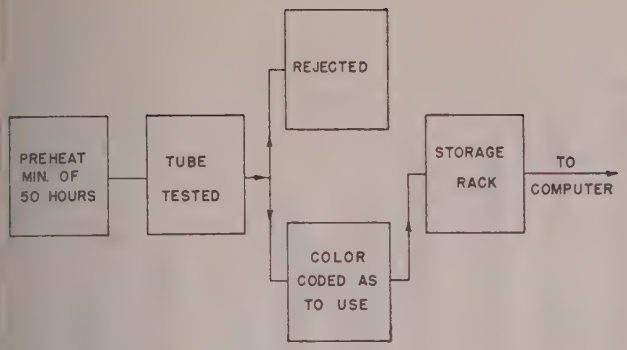

Figure 1A (left). Tube path to computer

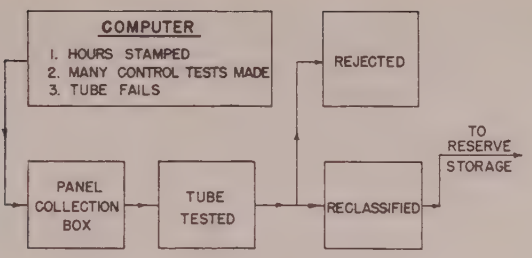

Figure 1B (above). Tube path from computer

Tube Standards

The routine which has been established for handling tubes from the time they are received until they are discarded is shown in Figure 1. Voltage is applied to the filament of a new tube for a minimum of 50 hours. The tube is then tested and may be rejected or passed. Good tubes are color-coded to designate the type of service in which they will serve and are stored until used in the machine.

When a tube is placed in service in the computer the reading of an hour counter, incorporated in the equipment, is stamped on the envelope. The tube stays in service until it is removed because of circuit failure and placed in a panel collection box. The tube is then tested and either discarded or reclassified and sent to the reserve storage. There are three general classes of tests. They disclose the condition of emission and cutoff and the presence or absence of short circuits.

The emission tests measure the current flow to the plate and screen with the control grid or grids at cathode potential. The voltages and currents specified in the standards have been established by experience and are shown in Table I.

Tests to determine tube performance when grids are operated at certain prescribed potentials are performed, as follows:

1. Measure the plate current at cutoff voltage of the first grid, the third grid being at cathode potential.
2. Measure the plate current at cutoff voltage of the third grid, the first grid being at cathode potential.
3. Measure the plate current with both the first and the third grids at cutoff voltage.
4. Measure the screen current at the cutoff voltage of the first grid.
5. Measure the ion and leakage current of the first grid with it at cutoff voltage.
6. Measure the ion and leakage current of the third grid with it at cutoff voltage.

Table II shows the cutoff voltages and maximum currents used. The plate and screen voltages for these tests are identical with those used in the emission tests shown in Table I.

The short-circuit tests measure the current flow with −100 volts between each element and all other elements connected together. The cathode-to-filament tests are made by impressing ±100 volts between them. The permissible leakage current for the *6L6*, *6SJ7*, *6SA7*, *6SN7*, *6AC7*, and *6J5* is 17 microamperes. The test for the *6L6*, *6V6*, *6Y6*, and *807* is the same except for the heater cathode leakage, where the maximum permissible current is 36 microamperes.

Tube History

After a tube has been discarded, its history is noted in a logbook, and is transferred later to punched cards. The tube type, kind of service, manufacturer, type of failure, test readings, and date are recorded. The color-coding system, mentioned previously as designating the type of service, divides the tubes into seven classes, four being specific circuits and three being types of circuits. The color code and the panel position identify the exact circuit in which the tube functioned in 80 per cent of the cases. The remaining 20 per cent can be identified as having functioned under certain maximum and minimum conditions. Collection boxes, placed at the rear of each panel, keep the removals separated according to their panel position.

The reading from the hour counter at the beginning of each week is stamped on the envelope of new tubes placed in service. At the end of each week, the collection boxes are emptied and the meter reading noted, thus establishing the service life of the tube. The greatest error in the number of hours of service life assigned to a tube is 218, which occurs when the tube is placed in operation just after all the new tubes have been marked and then removed just before the tubes are gathered. Very seldom is the error this great, since a preventive testing procedure is followed every Monday morning, making fewer tube failures occur during the early part of the week.

Preliminary Results

Some 5,000 tubes were removed and discarded from the ENIAC during the first five months of 1950. This is an average of 250 tubes per week, 70 per cent greater than the 1949 average. The increase is caused by an extensive overhaul of the machine that was conducted during this period and improved testing procedures. The average service life for tubes discarded during the period is shown in Figure 2.

The types *6Y6*, *6J5*, *6SN7*, and *6SJ7* had the highest average service life, ranging from 10,600 to 12,400 hours, while the *6AC7* and the *6L6* ranged from 5,800 to 6,600 hours. This average service life of the tubes should be weighted by the

Table I. Standard Voltages and Currents Used To Determine Emission Characteristics

Tube Type	Plate, Volts	Screen, Volts	Minimum Plate, Milliamperes	Minimum Screen, Milliamperes
6Y6	150	40	15	0.485
6L6	150	75	28	1.0
6V6	150	75	19.5	0.9
6L7	150	75	5	6.0
6SA7	150	75	5	7.5
6SJ7	150	75	5	1.25
6AC7	150	21	0.3	0.05
807	190	190–20 k	50	3.0
6J5	75		5	
6SN7	75		5	

following considerations: the kind of service, the type of test used to detect the faulty tube, and the degree of safety factor in the circuit where it is used.

It is known that some circuits in the ENIAC will function satisfactorily even though their tubes have a reduction in plate current as great as 40 to 50 per cent of the test standards. These tubes will have a longer service life principally because of the circuit design. Other circuits, unfortunately, do not allow as great a reduction in the plate current and therefore tubes are removed much sooner, making service life shorter.

The *6J5* and *6SN7*'s are used with a maximum plate potential of 150 volts. When the tube is used in the OFF condition, the grid voltage is three times the cutoff voltage, but when used in the ON condition, the grid is sufficiently positive to draw some emission current. The average service life for the *6J5*'s was 11,900 hours and for the *6SN7*'s was 11,000 hours. The *6J5* is used only in the OFF position, but the *6SN7* is used in three different ways; both halves of the tube conducting, both halves nonconducting, and one half conducting and the other half nonconducting.

Eighty per cent of the *6SN7* ring tubes rejected in the last five months failed because of low emission. When *6SN7* tubes are used in ring circuits where one side of the tube is normally conducting and the other side is not conducting, the conducting side has a much higher average test-plate current than the nonconducting side. The *6SN7*'s also are used in the same manner in a pulse-shaping circuit where the same results were obtained.

Eighty-five per cent of all other tube types used in the OFF condition, except the *807*'s, were discarded because of low emission. The number of tubes used in the ON condition and discarded for low emission ranges from 1 per cent to 66 per cent for any one type of tube. The life of the tubes used in the ON condition as compared with the same type used in the OFF condition is better by a factor of 50 per cent or more when only the low-emission type failures are considered.

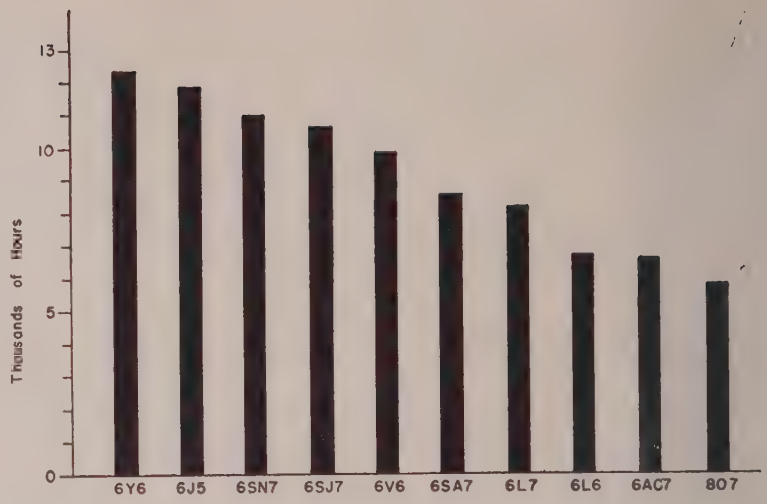

Figure 2. Average tube life

The *6SJ7*, *6L7*, and *6SA7* are all used as normally OFF tubes and all have low emission as the predominant type of failure. Their average lives are 10,600, 8,100, and 8,500 hours, respectively. The *6SA7*'s are used in two ways. One which has a duty cycle ten times that of the other has a longer average life by 1,600 hours.

For all tubes in the ENIAC, except the *6SA7* and the *807*, the tube lives terminated by low-emission failure averaged more than twice as long as those terminated by failure caused by poor cutoff, short-circuited elements, and burned-out filaments combined. The *6SA7* showed the same trend as the others, but to a lesser degree.

The *807* showed the reverse of this condition to be true, with low emission being 38 per cent less than all others. This behavior may be explained by the fact that these tubes operate with excessively high plate potentials.

The *6Y6* tube, having an over-all life average of 12,300 hours, is used only as a triode. In one circuit nine such tubes are connected in parallel. This makes it difficult to determine when one tube is faulty, because the safety factor in the circuit will allow it to function when one or two tubes are well below standard. Detection being difficult, a longer service life results. The type of malfunction most prevalent is short-circuited elements, the heater cathode short circuit being the most common. It is interesting to note that this failure does not cause the computer to malfunction because the heaters are at cathode potential.

The *6AC7* and the *807* have life averages of 6,500 hours and 5,800 hours, respectively. These tubes are used in a type of circuit in which the safety factor is small. The circuits are given extensive marginal tests every three or four months. Tubes are removed which are not causing circuit failures but indicate they will in the near future. The two conditions, low safety factor and extensive testing, cause lower service averages for these two tube types.

The *6AC7*'s which are used in the ON condition with a plate, screen, and grid of +80, +20, and +1 volt, respectively, fail 99 per cent of the time because of short-circuited elements or unsatisfactory cutoff conditions.

The *807*, which is used mainly in the OFF condition, with 600 volts applied to the plate and both grids at below the cutoff point specified in the test standards, has 40 per cent of its failures caused by short-circuited elements. A reason for this may be that the duty cycle of this *807*, even though it is classified as a normally OFF tube, is high because of the manner in which its circuit is used. It is ON for 300 microseconds at a time and is used many more times than any other normally OFF circuit in the ENIAC.

The *6L6* is used in both the OFF and

Table II. Standard Voltages and Currents Used To Determine Cutoff Characteristics

Tube Type	Cutoff Voltages, Grid 1	Cutoff Voltages, Grid 3	Maximum Plate Current, Milliamperes	Maximum Screen Current, Milliamperes
6Y6	−9.5		2.0	0.000070
6L6	−11.0		4.0	0.14
6V6	−10.0		3.0	0.13
6L7	−12.0	−8	0.7	0.85
6SA7	−7.0	−14	0.7	1.00
6SJ7	−5.5	−50	0.7	0.000170
6AC7	−2.0		0.04	0.000007
807	−100.0		0.000020	
6J5	−4.5		0.7	
6SN7	−4.5		0.7	

the ON condition with a low service life average of around 6,300 hours. For the OFF-type of service, the low emission was the predominant type of failure, while for the ON use failure was caused about 50 per cent by low emission and 50 per cent by cutoff, short-circuited elements, and burned-out filaments combined. The average life for an ON tube with a low-emission failure ran 10,200 hours, which is 70 per cent better than the life average for a low-emission failure in an OFF tube.

No Discussion

Technical Problems Associated with the Application of a Capacitor in Series with a Synchronous Condenser

R. L. WITZKE
MEMBER AIEE

E. L. MICHELSON
MEMBER AIEE

Synopsis: In January 1950, a 3,600-kva series capacitor was put into operation for the purpose of minimizing lamp flicker produced by large arc furnaces. This installation is unique in that the capacitor is located in series with the terminals of a 20,000-kva 13.8-kv synchronous condenser, rather than in series with the supply system. The capacitor has been operating successfully for over ten months and has produced the desired decrease in lamp flicker. This paper presents a summary of the studies made prior to the installation of the series capacitor, as well as a general discussion of the factors that should be considered in similar applications. Economic factors, which dictated the selection of a series capacitor for decreasing the lamp flicker in this case, and the results of field tests made since the installation was completed are covered in a companion paper.[1]

POWER to the steel company plant is supplied from a 138-kv system as shown in Figure 1. The 13.8-kv furnace bus is supplied from a 37.5/45 megavolt-amperes (mva), oil-immersed self-cooled forced-air cooled (OA/FA) transformer bank having a nominal ratio of 132/13.8 kv. In series with the 13.8-kv side of the transformer is a buffer reactor installed to limit the load fluctuations on the 138-kv system. The application of this reactor and the 20,000-kva synchronous condenser was reported by Mr. T. G. Le Clair.[2] The present plant load consists of two arc furnaces, rated at 15,000 and 25,000 kva, and a rolling mill with a demand of 8,000 kw at unity power factor. Future plans call for replacing the 15,000-kva furnace with a second 25,000-kva furnace.

The 138-kv bus at Station E in Figure 1 also is used to supply general industrial, commercial, and residential load in the area. Prior to the installation of the series capacitor reported in this paper, the operation of the arc furnaces produced borderline flicker in the area served by Station E. It was, therefore, evident that system changes had to be made before two 25,000-kva furnaces could be operated at the plant. As discussed in the companion paper,[1] a number of system changes were studied before a decision was made to install a series capacitor.

Since the series capacitor was placed in service in January 1950, the furnace transformer supplying the large furnace has been operated on the 25,000-kva tap. This furnace, operating alone or in combination with the 15,000-kva furnace, has caused no objectionable flicker.

Summary and Conclusions

1. A capacitor can be installed in series with a synchronous condenser to decrease the effective reactance of the machine, and thereby increase its ability to absorb a larger share of the power and reactive variations produced by rapid load changes, such as produced by arc-furnace operation.

2. The addition of a series capacitor to a circuit will cause low-frequency transient currents to flow in the system following load changes. These currents can, however, be neglected in lamp-flicker problems if the system has positive damping. It usually is sufficient to consider only fundamental frequency currents in calculating the improvements obtained with a series capacitor.

3. In evaluating the losses associated with the low-frequency transients in a circuit containing a series capacitor, it is necessary to treat the synchronous condenser as a negative resistance because it acts as an induction generator when the frequency of the stator currents is less than the system dynamic frequency.

4. The negative resistance of the synchronous condenser can be estimated as follows:

$$r = r_1 + \frac{2(r_2 - r_1)\sqrt{x_c/(x_2+x_a)}}{\sqrt{x_c/(x_2+x_a)} - 1.0}$$

where

r_1 = positive sequence resistance of the condenser
r_2 = negative sequence resistance of the condenser
x_c = 60-cycle reactance of series capacitor
x_2 = negative sequence reactance of the condenser
x_a = system reactance

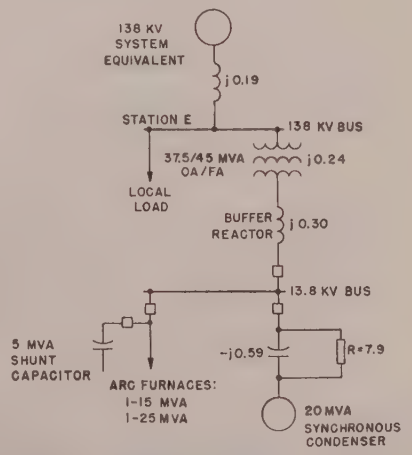

Figure 1. Simplified schematic diagram of presnet system

All impedances are in per unit on a 100-mva base

Paper 51-88, recommended by the AIEE Transmission and Distribution Committee and approved by the AIEE Technical Program Committee for presentation at the AIEE Winter General Meeting, New York, N. Y., January 22–26, 1951. Manuscript submitted October 23, 1950; made available for printing December 11, 1950.

R. L. WITZKE is with the Westinghouse Electric Corporation, East Pittsburgh, Pa. E. L. MICHELSON is with the Commonwealth Edison Company, Chicago, Ill.

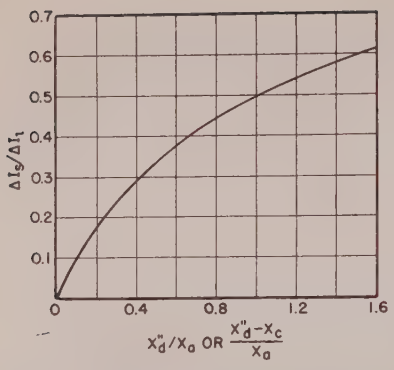

Figure 2. Change in system current as influenced by ratio of machine to system reactance

I_l = change in load current
I_s = change in system current
x_d'' = machine subtransient reactance
x_a = system reactance
x_c = series capacitor reactance

Note: All impedances should be on a common base.

5. If the system does not have sufficient loss to provide adequate positive damping of the low-frequency transients, additional damping can be obtained by installing a resistor in parallel with the series capacitor. Positive damping always can be obtained by selecting a resistor that just compensates for the negative resistance of the synchronous condenser, in which case the system losses provide all the damping. In this case the parallel resistor has a resistance estimated as follows:

$$R_{sh}=\frac{x_c(x_2+x_a)}{r}$$

where r, x_c, x_2, and x_a are defined as above.

6. The other technical problems considered in connection with this series capacitor application are as follows:

a. Self-excitation of the synchronous condenser

b. Ferroresonance

c. Hunting of synchronous condenser

d. Condenser heating

e. Excessive voltage at condenser terminals during underexcited operation

Self-excitation usually is associated with the starting of a machine through a series capacitor.[3] No trouble was expected in the present application due to this cause, since the series capacitor could be by-passed whenever the synchronous condenser was started. Actually the capacitor is installed in series with the condenser running circuit breaker and so cannot be connected in the starting circuit.

Ferroresonance may be experienced when a transformer is energized through a series capacitor,[4] in which case the transformer may continue to draw a large exciting current during steady-state conditions. Although this problem was not analyzed in detail, trouble was not anticipated because in this case transformers would be energized from two sources in parallel, only one of which would contain a series capacitor. Experience has indicated this conclusion to be correct.

Synchronous machines connected to a power supply through a circuit having a high ratio of resistance-to-reactance may have a tendency to hunt.[4,5,6] The addition of a series capacitor increases this ratio, thereby increasing the tendency to hunt. Data were not available to permit an accurate evaluation of the tendency for the condenser in this application to hunt after the series capacitor was installed; however, it was known that resistance could be used in parallel with the capacitor to prevent objectionable hunting. Experience has shown that the resistance required to provide positive damping of the low-frequency transient currents will prevent hunting in the installation discussed in this paper.

Machine heating was viewed as an important problem because of the large load swings to be imposed on the synchronous condenser. Margin for these swings could be provided in both the stator and the field circuits by limiting the average loading of the machine. As shown in Figure 4A, the capacitor application was based on limiting the initial loading of the machine to 10,000 kva or to one-half its rating. It was the authors' opinion that the damper windings would have capacity for the anticipated loadings, but that field experience was required definitely to establish their adequacy for the service. Experience to date has indicated no excessive temperature at any location in the machine; however, observations are to be made at intervals to be sure the machine is operated within its capabilities.

When a synchronous condenser is connected to a bus through a series capacitor, the bus voltage is higher than the condenser terminal voltage whenever the machine is delivering reactive kilovolt amperes. Conversely, when the condenser is absorbing reactive kilovolt amperes, its terminal voltage is higher than the bus voltage. As the condenser absorbs reactive kilovolt amperes only when the bus voltage is high, excessive voltages can be experienced at the machine if its underexcited loading is not limited.

It can be seen from the above that both the overexcited and the underexcited loadings of a synchronous condenser should be limited if a series capacitor is

Figure 3. Simple schematic diagram of 1948 system

Impedances are in per unit on a 100-mva base. Power and reactive flows indicated by the arrows are in megawatts and megavolt amperes, the figure in brackets being the reactive flow

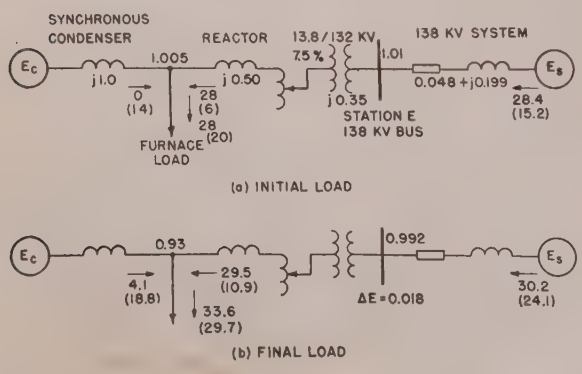

Figure 4. Simple schematic diagram of future system

Impedances are in per unit on a 100-mva base. Power and reactive flows indicated by the arrows are in megawatts and megavolt amperes, the figure in brackets being the reactive flow

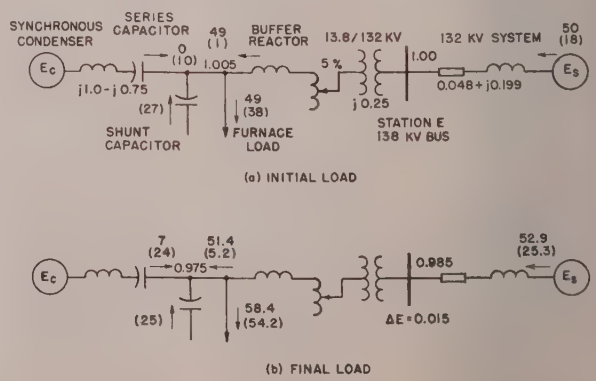

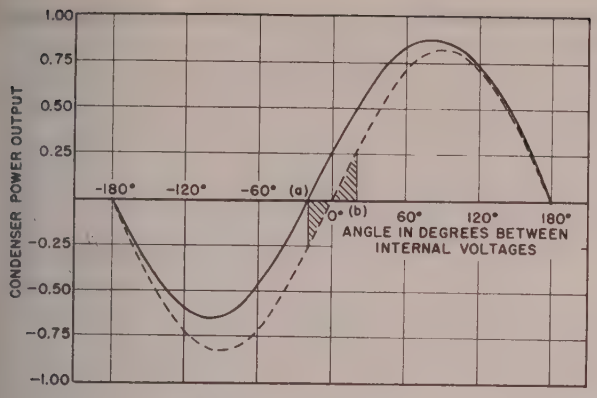

Figure 5. Power angle diagrams for future system

Solid curve = loads as in Figure 4A
Dashed curve = same system with all load removed

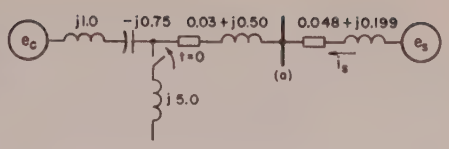

Figure 6 (right). Circuit used to calculate influence of transient current on flicker voltage

installed to force the machine to carry large load swings. This factor must be evaluated in economic studies relative to these applications.

The overvoltage and overcurrent protection of the series capacitor installation is described in the companion paper.[1]

Theory

An arc furnace is started by filling the furnace with scrap metal, then drawing arcs between the metal and the 3-phase electrodes. Additional scrap is added as the initial charge melts. During the "melt-down" period the furnace operation is very erratic, with violent swings in the power and reactive kilovolt amperes drawn from the system. If these swings in power and reactive kilovolt amperes are beyond the capabilities of the system, objectionable variation in system voltage will result. Lamps supplied from the system will flicker, resulting in complaints from customers in the area.

If the furnace load is supplied from two sources, the rapid changes in furnace current will divide between the two sources inversely as their impedances. In most installations involving large furnaces, the source resistances are small, and practical engineering accuracy can be obtained by assuming that rapid variations in furnace current divide inversely as the reactance of the sources. Figure 2 illustrates this division for a system such as the one in Figure 1. The curve shows the change in system current, expressed as a ratio to the change in load current, for a range of condenser-reactance to system-reactance ratios. The use of subtransient reactance, rather than transient reactance, for the synchronous condenser is discussed subsequently.

Adding a capacitor in series with the synchronous condenser decreases the effective subtransient reactance of the synchronous-condenser circuit by compensating for part of the machine reactance. The difference between the synchronous-condenser and series-capacitor reactances then is effective in fixing the division of the load-current changes between the condenser and the system. In this case the $(X_d''-X_c)/X_a$ ratio is used in Figure 2 to find the change in system current.

To illustrate the use of the data in Figure 2, assume a system having a reactance equal to the synchronous-condenser reactance. In this case the variations in system current are equal to 50 per cent of the rapid variations in load current. If a series capacitor having a reactance equal to one-half the machine reactance were installed in series with the synchronous condenser, the variations in system current would be only 33.3 per cent of the variations in load current.

It should be noted that the data in Figure 2 apply only for rapid and short-time duration changes in furnace current. Changes lasting longer than five or six cycles will depend on the transient, rather than the subtransient, reactances of the condenser and the system. Under steady-state conditions, that is, after transient effects can be neglected, all power must be supplied from the system, and the load reactive requirements will be influenced by the condenser voltage-regulator setting.

Load Changes and Permissible Flicker

The available data on the permissible amount of flicker voltage usually are expressed as a function of the frequency of cyclic pulsations. In the case of arc furnaces, the load changes are very erratic and cannot be classified as cyclic pulsations of a definite frequency. This situation makes it difficult to determine the magnitude of load changes and the limits of voltage variations to use in system design calculations. In making this series-capacitor application, all load variations were based on data obtained by Messrs. C. M. Stearns and B. M. Jones.[7] Field tests reported by Stearns and Jones showed a maximum change of 10,580 kva for two 10,000-kva furnaces operating in parallel, this change occurring only once during the series of tests. The second largest change was about 7,500 kva, all other variations being materially below this figure. The power factor of the large changes was on the order of 50 per cent. Stearns and Jones expressed the opinion that calculations probably should not be based on the largest load variations because of the infrequency of their occurrence. With this in mind, it was decided to use a load change of 18,700 kva at 50 per cent power factor for two 25,000-kva furnaces, this figure being $2^1/_2$ times the 7,500-kva change obtained with two 10,000-kva furnaces. This procedure was considered reasonably conservative because the load changes usually do not increase directly with the furnace rating.

The permissible flicker voltage was estimated by calculating the probable

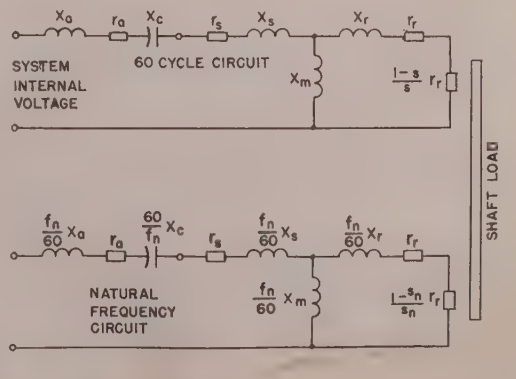

Figure 7. Schematic diagram of induction motor with series capacitor

r_a, X_a = system resistance and reactance
X_c = series capacitor reactance
r_s, X_s = stator resistance and reactance
r_r, X_r = rotor resistance and reactance
X_m = reactance of magnetizing branch
f_n = circuit natural frequency

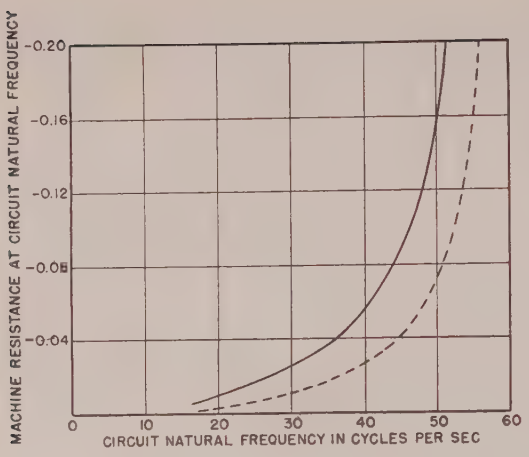

Figure 8. Negative resistance of a representative synchronous condenser

Solid curve = stator and rotor resistances equal to 0.005 and 0.03 per unit, respectively
Dashed curve = stator and rotor resistances equal to 0.005 and 0.015 per unit, respectively

flicker caused by the two furnaces in operation in 1948. A load change of 11,200 kva at 50 per cent power factor was assumed for the 10,000- and the 15,000-kva furnaces in operation at the time. This load variation is 50 per cent higher than the Stearns and Jones figure of 7,500 kva for two 10,000-kva furnaces. This procedure appears reasonable because field experience has indicated that the load variations are more closely related to the size of the largest furnace, rather than to the total furnace capacity.

As borderline flicker was experienced in 1948, it was decided that the calculated flicker with the two 25,000-kva furnaces had to be smaller than the calculated flicker for the 1948 operation.

Synchronous-Condenser Reactance

Preliminary tests showed that load changes as large as 11,200 kva, as estimated previously for the furnaces in operation in 1948, did not last over five or six cycles, which raised the question of using the transient or subtransient reactance of the synchronous condenser. One authority[8] states that "for load durations less than five cycles, it is likely that the regulation as calculated from the subtransient reactance determines the permissible flicker. While the voltage drop at the end of five cycles is greater than initially, the transition is gradual and it is doubtful if the eye can discern so small a difference." The condenser in this case has a subtransient time constant of three cycles, as compared to a thermal time constant of two cycles for a 10-watt lamp and somewhat longer time constants for the larger lamps. It therefore seemed reasonable to use subtransient reactance in estimating the flicker produced by the large load changes assumed. It is possible that some of the large load changes may persist for longer than five or six cycles, in which case the effective flicker will be greater than calculated on the basis of subtransient reactance. However, if the frequency of occurrence of these larger flicker voltages is small, they would not be expected to cause complaints.

On the basis of the preceding data, it was decided that the use of the synchronous-condenser unsaturated subtransient reactance of 20 per cent would be satisfactory. It should be emphasized, however, that the machine reactance to be used in any specific application depends upon the load changes assumed. If the large, short-time load changes are neglected, then it may be necessary to use transient rather than subtransient reactance. Considerable judgment is required in view of the complexity of the flicker problem in applications involving arc furnaces.

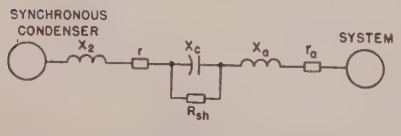

Figure 9. Application of parallel resistor to control damping of natural frequency currents

x_2 = condenser negative-sequence reactance
r = condenser negative resistance
x_c = series capacitor reactance
R_{sh} = shunt resistor
x_a = system reactance
r_a = system resistance

Flicker Calculations

Figure 3 shows, in simplified form, the system in operation in 1948. This system, as well as the loads given, is used as a basis for determining the permissible flicker voltage on the 138-kv bus at Station E. Figure 3A shows the power and the reactive-kilovolt-ampere flows and the voltage levels for an assumed initial furnace load. In Figure 3B the furnace load has been increased by 11,200 kva at 50 per cent power factor. The voltages and flows in this figure were calculated by assuming that the condenser and the system internal voltages did not change when the furnace load was increased. It will be noted that the Station E 138-kv bus voltage decreased from 101 to 99.2 per cent, a change of 1.8 per cent, when the furnace load was increased. As borderline flicker was observed in 1948, this calculated voltage change of 1.8 per cent is classified as borderline.

Figure 4A illustrates the system design considered for the future load of two 25,000-kva furnaces. A capacitor is used in series with the synchronous condenser to compensate for 75 per cent of the machine subtransient reactance, resulting in an effective subtransient reactance of 25 per cent on a 100,000-kva base. In order to permit margin for the load changes imposed on the synchronous condenser, the initial loading of this machine is limited to 10,000 kva, or to one-half the machine rating. Shunt capacitors on the 13.8-kv bus supply a major share of the reactive load requirements, very little reactive kilovolt amperes being supplied from the 138-kv system because of the large regulation of the transformer and the buffer reactor.

The furnace load in Figure 4B is approximately 18,700 kva higher than the load in Figure 4A, this being the assumed load change for two 25,000-kva furnaces. It will be noted that the Station E 138-kv bus voltage changes 1.5 per cent for the assumed load change. This compares to a change of 1.8 per cent illustrated in Figure 3 for the 1948 operation. These results indicated that the two 25,000-kva furnaces could be operated in the steel company plant with somewhat lower flicker voltages than those experienced in 1948. The present system, (Figure 1) is supplying load to one 15,000- and one 25,000-kva furnace without objectionable flicker, even though the series-capacitor compensation is only 59 per cent, as compared to 75 per cent assumed in Figure 4. The load fluctuations with two 25,000-kva furnaces are not expected to be materially above those now being experienced, indicating that only minor system changes will be required to handle the anticipated future loads.

System Stability

Mr. Le Clair reported[2] that the synchronous condenser pulled out of step with the 138-kv system on several occasions when the maximum buffer reactance

was in the circuit. This instability probably was caused by a succession of large, properly spaced load swings, because it is doubtful that one load swing could have caused the condenser to pull out of step. This early experience indicated the desirability of investigating the system stability with the contemplated operation with two 25,000-kva furnaces.

The power angle diagrams in Figure 5 were obtained for the system in Figure 4A excepting that the synchronous condenser was represented by unsaturated transient reactance. The solid curve applies for the system with the furnace load assumed in Figure 4A. The dashed curve is for the same system with all furnace load removed. If full furnace load is rejected from the system, the condenser momentarily absorbs approximately 25,000 kw from the system. The condenser internal voltage then swings forward in phase angle, the maximum swing being from point (a) to point (b), a change of approximately 35 degrees. After all oscillations are damped out, the condenser internal voltage is approximately in phase with the system internal voltage. This study shows that the system is very stable, and that even a succession of large load changes should not cause the condenser to pull out of step with the system.

Transient Currents

The flicker voltages in Figures 3 and 4 are based on a consideration of fundamental-frequency currents only. Low-frequency transient currents also will be present in a circuit containing a series capacitor, their frequency being determined by the inductances and the capacitance of the circuit. A special study was made to determine the influence of these transient currents on the flicker voltages, and it was concluded that their effect is negligible if the system has sufficient positive damping at the natural frequency.

The circuit selected for this study is shown in Figure 6, and is essentially the same as the one in Figure 4, except that the shunt capacitors and all initial loads are neglected. Point (a) in this circuit represents the 138-kv bus at Station E. A 5.0 per unit load reactance suddenly is applied at the instant the system voltage was equal to zero, this instant being chosen because switching at this time produces the maximum transient current. The current in the source for this switching operation is represented by the following approximate expression:

$$i_s = 0.072 \cos 377t + 0.177\epsilon^{-7.02t} \times \cos 257t - 0.249\epsilon^{-5.18t}$$

Figure 10. Influence of x_c/x_2 ratio on circuit natural frequency and per unit slip, s_n

Curves were calculated for $x_2 = 0.20$, $r_s = 0.005$, and $r_r = 0.03$ per unit. x_c, x_2, and x_a are defined in Figure 9

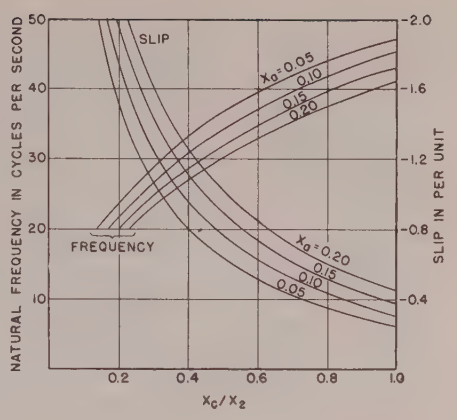

In this expression, the first term is the 60-cycle current, the second term a low-frequency, 41-cycle current, and the last term a d-c component. It will be noted that the low-frequency current actually is larger in magnitude than the 60-cycle current.

With the above current in the source circuit, the voltage at point (a) in Figure 6 is approximately as follows:

$$e = 0.99 \sin 377t - 0.0169\epsilon^{-7.02t} \times \sin 257t - 0.008\epsilon^{-5.18t}$$

This expression represents the voltage on the 138-kv bus at Station E following the assumed load change. In order to evaluate the influence of the assumed load change on lamps supplied from this bus, the rms value of the above voltage was calculated over a period of time equal to three cycles of the 60-cycle component. This time interval was chosen because it represents approximately one cycle of the heat introduced by the low-frequency component, and because voltage changes of shorter duration were not considered significant. The rms value of the voltage over three cycles is 0.99 per unit, the same as would have been calculated by neglecting the low-frequency and d-c components.

In evaluating the losses associated with the low-frequency transients in a circuit containing a series capacitor, it is necessary to consider the characteristics of synchronous and induction machines with low-frequency currents flowing in their stator circuits. Mr. C. F. Wagner[3] analyzes this problem by treating the induction machine as a reactance and a negative resistance when the frequency of the stator current is appreciably below dynamic frequency. The same approach is applicable to synchronous machines.

The upper circuit in Figure 7 is the conventional diagram of an induction motor, and applies for 60-cycle currents in the stator circuit. The lower circuit is the same as the upper one, except that it applies for natural-frequency stator currents of frequency f_n. In these circuits, s is the slip of the motor referred to 60-cycle stator currents, and s_n is the slip referred to stator currents of frequency f_n. If S is the 60-cycle synchronous speed of the motor, $f_n S/60$ is the synchronous speed referred to stator currents having a frequency f_n. Letting N be the actual speed of the motor,

$$s = \frac{S-N}{S}, \text{ and}$$

$$s_n = \frac{(f_n/60)S - N}{(f_n/60)S} = \frac{f_n S - 60N}{f_n S}$$

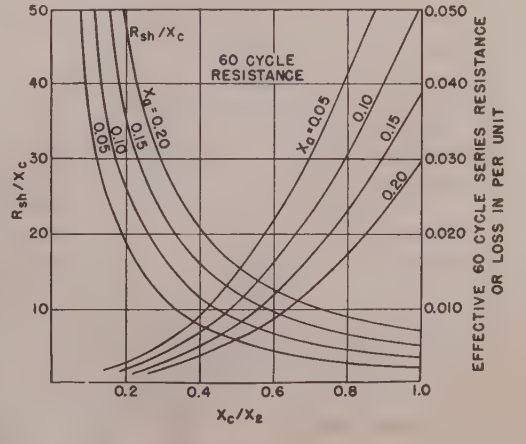

Figure 11. Influence of x_c/x_2 ratio on parallel resistance required and on 60-cycle loss

Curves were calculated for $x_2 = 0.20$, $r_s = 0.005$, and $r_r = 0.03$ per unit. x_c, x_2, and x_a are defined in Figure 9

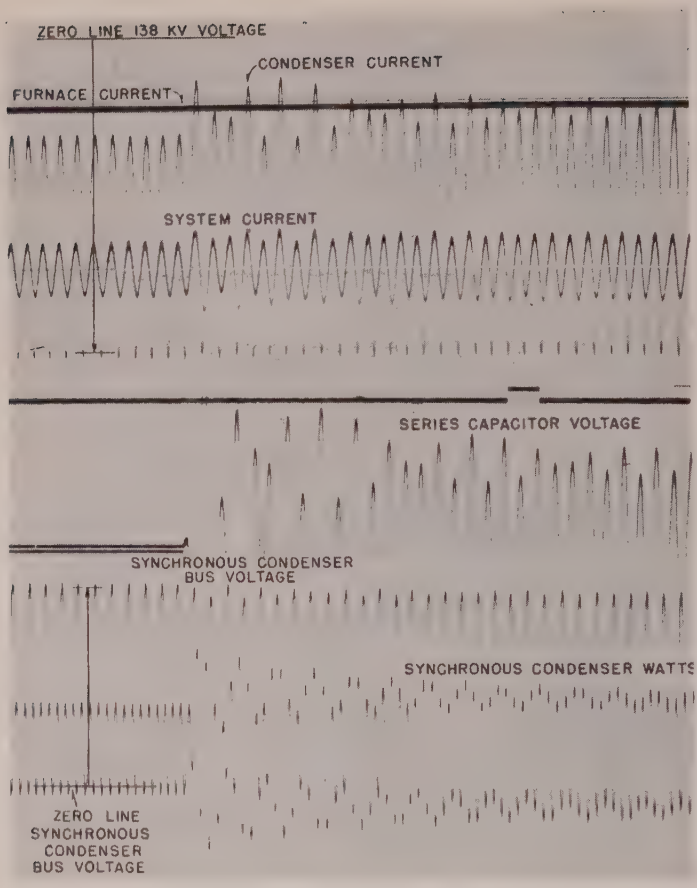

Figure 12 (left). Oscillographic records obtained in field tests

Transients initiated by opening series capacitor by-pass circuit breaker

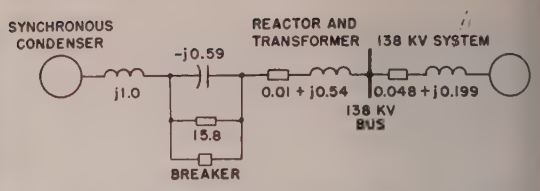

Figure 13 (above). System conditions during tests discussed in connection with Figure 12

All impedances are in per unit on a 100-mva base

It will be noted that s_n can be negative if the motor is running at some speed near its 60-cycle synchronous speed and the circuit natural frequency is appreciably less than 60 cycles. Under these conditions the resistance $r_r(1-s_n)/s_n$ in Figure 7 also is negative, which is interpreted to mean that this circuit element delivers power to the natural-frequency circuit. Natural-frequency currents established in this circuit by circuit changes either will increase or decrease in magnitude, depending upon the value of this negative resistance in comparison with other resistances in the circuit. In order to have positive damping this resistance must be less than the sum of the other circuit resistances. If this condition is not satisfied, the magnitude of the low-frequency current will be limited only by the ability of the 60-cycle circuit to deliver power to the natural-frequency circuit, the transfer of power between circuits taking place in the motor.

The above analysis also can be applied to synchronous machines, the only difference being that the 60-cycle circuit in Figure 7 is not used. In the case of synchronous motors, condensers, or generators, the machine does not slow down, but drops back in phase position, to deliver shaft power. The natural-frequency circuit in Figure 7 applies equally well to induction and synchronous machines.

In the case of a synchronous machine running at its 60-cycle synchronous speed, s_n can be expressed in terms of the circuit natural and dynamic frequencies, as follows:

$$s_n = \frac{f_n - 60}{f_n}$$

The net resistance of a synchronous machine is a function of the rotor and stator resistances, and can be expressed as follows:

$$r = r_s + r_r/s_n,$$

where s_n is defined as above.

This relation neglects the magnetizing branch in the machine equivalent circuit. The rotor and stator resistances can be calculated by a machine designer, or can be estimated from the machine positive and negative sequence resistances. In the latter case the stator resistance is assumed equal to the positive sequence resistance. The negative sequence resistance of a machine is equal to the stator resistance plus one-half the rotor resistance.[9] The rotor resistance then is estimated as follows:

$$r_r = 2(r_2 - r_s) = 2(r_2 - r_1)$$

The net machine resistance now can be expressed in terms of the sequence quantities.

$$r = r_1 + \frac{2(r_2 - r_1)}{s_n}$$

As estimated in this manner, the negative resistance of a machine will be on the high side because of skin effects in the rotor circuits. With 60-cycle negative sequence currents in the stator, 120-cycle currents are present in the rotor circuits, whereas, with low-frequency positive sequence currents in the stator, the frequency of the rotor currents is the difference between 60 and the frequency of the stator currents. In large machines, the low-frequency rotor resistance may be as low as one-half the value estimated from the positive and negative sequence resistances, the actual ratio depending upon the rotor dimensions and resistivity and the frequency of the rotor current.

Figure 8 is a plot of the negative resistance of a synchronous machine having a stator resistance of 0.005 and rotor resistances of 0.015 and 0.03 per unit. This calculated curve is included to show the variation of resistance with the circuit natural frequency, and particularly the rapid increase in resistance as the natural frequency approaches the system dynamic frequency. Theoretically the resistance is infinite at 60 cycles, that is, when the circuit inductance is fully compensated. These results are based on the assumption that the rotor and stator resistances remain constant, independent of frequency.

Parallel Resistor

In system problems involving lamp flicker, the natural-frequency currents can be neglected providing the circuit has some reasonable positive damping, as is discussed in the section on transient cur-

rents. It is expected that system losses will provide adequate damping in some, but not all, cases. Where additional damping is required, it can be obtained by paralleling a resistor with the series capacitor, as indicated in Figure 9. The ohmic value of the parallel resistor will depend upon the machine and system resistances and reactances, as well as the degree of compensation employed. Positive damping always can be obtained by selecting a resistor that just compensates for the negative resistance of the machine, in which case the system losses provide all the damping. This is accomplished by making the effective series resistance of the parallel resistor and capacitor, at the circuit natural frequency, equal to the negative resistance of the machine. In this case,

$$R_{sh}=\frac{X_c^2\left(\frac{60}{f_n}\right)^2}{r}$$

where R_{sh}, r, and X_c are expressed on the same base, and X_c is the 60-cycle reactance of the series capacitor.

When R_{sh} is larger than ten times X_c, which generally will be the case in practical applications, the circuit natural frequency is approximately equal to $60\sqrt{X_c/(x_2+x_a)}$. Using this relation, the negative and shunt resistances can be estimated as follows:

$$r=r_1+\frac{2(r_2-r_1)\sqrt{x_c/(x_2+x_a)}}{\sqrt{x_c(x_2+x_a)}-1.0}$$

$$R_{sh}=\frac{x_c(x_2+x_a)}{r}$$

The negative sequence reactance of the machine, x_2, is used in these calculations because the negative-sequence inductance of the circuit determines the natural frequency of the system.

Figure 10 shows the influence of the x_c/x_2 ratio on the natural frequency of the circuit in Figure 9. The curves in this figure were calculated for the machine constants indicated in the caption. It was assumed that the ohmic value of the parallel resistor was such as to make the effective resistance of the capacitor-resistor combination equal to the negative resistance of the machine at the circuit natural frequency. A range of system reactances, from 25 to 100 per cent of the machine reactance, is included to show the influence of this variable. The second set of curves gives the per unit slip, s_n, for the same range of constants.

Figure 11 gives the ohmic value of the parallel resistor, expressed as a ratio to the 60-cycle reactance of the series capacitor, for the same conditions as discussed previously. It will be seen that the ratio of the parallel resistance to the capacitor reactance decreases when the x_c/x_2 ratio is increased or when the system reactance is decreased. This, of course, increases the 60-cycle losses in the circuit, which is shown by the second set of curves in Figure 11. These results indicate that there is a practical upper limit to the machine compensation that should be used, particularly when the system reactance is small by comparison to the machine reactance.

The oscillograms in Figure 12 were obtained in field tests at Station E and are included to show the positive damping in the circuit. The circuit conditions for this test are shown in the simplified circuit in Figure 13. All furnace load was disconnected at the time the oscillograms were obtained.

The transient was initiated by opening the series capacitor by-pass circuit breaker with approximately 450 amperes in the synchronous condenser circuit prior to the switching operation. The calculated natural frequency of this circuit is 34.5 cycles per second, as compared to 33.4 as obtained from the data in Figure 12. The beat frequency of 26.6 cycles per second may be seen on the oscillograms.

The circuit time constant, as determined from the decrement in Figure 12, is approximately 15 cycles on a 60-cycle basis. This time constant and the total circuit inductive reactance of 1.74 per unit give a net resistance of 0.037 per unit on a 100-mva base. The 15.8 per unit parallel resistor introduces an equivalent series resistance of 0.071 per unit at 33.4 cycles per second. This value, in conjunction with the other series losses, gives a total series resistance of 0.129 per unit, excluding the synchronous condenser. From these values the condenser resistance is estimated at -0.092 per unit. This resistance was estimated at -0.145 per unit based on the machine positive and negative sequence resistances of 0.03 and 0.10 per unit on a 100-mva base. The major part of the difference between the two values is attributed to skin effects in the condenser rotor.

References

1. The Application of a Series Capacitor to a Synchronous Condenser for Reducing Voltage Flicker, **P. M. Black, L. F. Lischer.** *AIEE Transactions*, volume 70, part I, 1951, pages 144–50.

2. Arc-Furnace Loads on Long Transmission Lines, **T. G. Le Clair.** *Electrical Engineering (AIEE Transactions)*, volume 59, April 1940, pages 234–42.

3. Self-Excitation of Induction Motors With Series Capacitors, **C. F. Wagner.** *AIEE Transactions*, volume 60, 1941, pages 1241–47.

4. Analysis of Series Capacitor Application Problems, **J. W. Butler, C. Concordia.** *Electrical Engineering (AIEE Transactions)*, volume 56, August 1937, pages 975–88.

5. Effect of Armature Resistance Upon Hunting of Synchronous Machines, **C. F. Wagner.** *AIEE Transactions*, volume 49, July Section, 1930, pages 1011–26.

6. Negative Damping of Electrical Machinery, **C. Concordia, G. K. Carter.** *Electrical Engineering (AIEE Transactions)*, volume 60, March 1941, pages 116–19.

7. Large Electric-Arc Furnaces—Performance and Power Supply, **B. M. Jones, C. M. Stearns.** *Electrical Engineering (AIEE Transactions)*, volume 60, July 1941, pages 763–69.

8. Electrical Transmission and Distribution Reference Book, Westinghouse Electric Corporation, East Pittsburgh, Pa., fourth edition, September 1940, page 722.

9. Symmetrical Components (book), **C. F. Wagner, R. D. Evans.** McGraw-Hill Book Company, Inc., New York, N. Y., 1933, page 91.

No Discussion

Fundamental Effects of Series Capacitors in High-Voltage Transmission Lines

A. A. JOHNSON
FELLOW AIEE

J. E. BARKLE
MEMBER AIEE

D. J. POVEJSIL
ASSOCIATE AIEE

THE load capability and performance of many existing and future high-voltage transmission lines can be improved by the installation of series capacitors. However, the proper application of series capacitors depends upon an understanding of their fundamental effects on transmission. It is the purpose of this paper to outline and interpret these effects in order that the merits and limitations of series compensation can be evaluated for any particular circuit or system. Curves are presented showing the effects of series compensation on power transfer, power factor, and efficiency for lines of varying length, voltage, and impedance.

The application of series capacitors to high-voltage transmission lines has received considerable attention during the past decade.[1,2,3,4] This widespread interest can be attributed to the following factors:

1. Rapidly increasing load demands.
2. Increasing construction costs of new transmission lines.
3. Low capacitor cost per kilovolt-ampere.
4. Conservation of critical defense materials.

In spite of these factors, however, the application of series capacitors to high-voltage transmission lines did not become a reality until the recent development of adequate protective equipment. Under the impetus of this advance in the art, it seems probable that a number of series capacitor installations will be placed in high-voltage lines in the future. Some possible applications of series capacitors to transmission circuits are:

1. To effect the desired load division between parallel circuits.
2. To increase the load capacity of a transmission line by a nominal amount (0–50 per cent). The series capacitor is very useful for this type of system expansion because such an increase does not justify changing the system voltage or building another parallel circuit.
3. To provide increased line capacity so that the system can handle short-time emergency loads. In such applications, the line efficiency at peak loads for compensations over 50 per cent will be decreased materially.
4. To increase the transient stability limits of a system.
5. To improve voltage regulation and power factor for a given load condition by reducing the operating angle of the line.

During the past few years, the primary use of the series capacitor has been to raise voltage and decrease lamp flicker on a distribution bus or radial feeder. One of the most notable of such applications is the 10,000-kva series capacitor in a Duquesne Light Company 69-kv radial feeder which supplies an arc furnace.[5,6] This installation has been in successful operation since 1947. More recently the Bonneville Power Administration has purchased series capacitors for three separate installations on their 220-kv tie lines. The largest of the three units has a rating of about 80,000 reactive kilovolt-amperes.

Basic Principle of Series Compensation

Fundamentally, the series capacitor is used to compensate for the inductive reactance of a transmission or distribution circuit. In the case of the distribution circuit this is done to reduce voltage regulation or lamp flicker. For transmission circuits, the object is more likely to be an increase in the power transfer and stability limits.

In a normal transmission line without series capacitors (neglecting line resistance), the maximum power which may be sent over the line is

$$P_{\max} = \frac{E_s E_r}{X} \tag{1}$$

where E_s and E_r are the sending and receiving voltages respectively.

If a series capacitor is inserted in the line, the maximum power becomes

$$P_{\max} = \frac{E_s E_r}{X - X_c} \tag{2}$$

Thus, it can be demonstrated by Figure 1 that as the reactance between the sending and receiving end is decreased, the power limit of the system is increased. When line resistance and the line shunt capacitance are included, the power equation is modified, but the fundamental effect of a series capacitor is still the same.

Effect of Series Compensation on Line Constants

The circuit used to represent the transmission line is shown in Figure 2. The series capacitor is placed at the center of the line for reasons explained later. The transmission lines on either side of the series capacitor are represented by $ABCD$ constants as defined by the relations

$$E_s = AE_r + BI_r \tag{3}$$

$$I_s = CE_r + DI_r \tag{4}$$

The $ABCD$ constants are used because it is desired to take into account the effects of line resistance and line shunt capacitance and this method offers the easiest analytical approach.

Terminal impedances are not included

Paper 51-89, recommended by the AIEE Transmission and Distribution Committee and approved by the AIEE Technical Program Committee for presentation at the AIEE Winter General Meeting, New York, N. Y., January 22–26, 1951. Manuscript submitted October 23, 1950; made available for printing December 11, 1950.

A. A. JOHNSON, J. E. BARKLE, and D. J. POVEJSIL are with the Westinghouse Electric Corporation, East Pittsburgh, Pa.

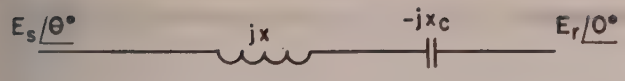

Figure 1. Single-line diagram

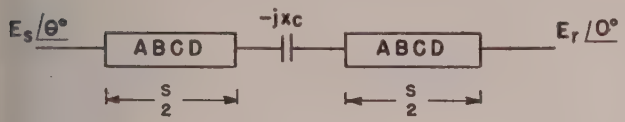

Figure 2. Equivalent circuit used in study

because it is desired to point out the effects of series capacitors on the performance of transmission lines without the masking effects resulting from consideration of various terminal impedances.

It is possible to obtain a great deal of information from the variation of these constants with line length and percent compensation. Accordingly, the *ABCD* constants are plotted against line length with per cent compensation as a parameter as shown in Figures 3 to 5. Resistance is neglected and a value of 400 ohms was chosen for the surge impedance of the transmission line. Per cent compensation of the line is defined as

$$\text{Per cent compensation} = \frac{X_c}{Sx} \times 100 \qquad (5)$$

where

x = line reactance—ohms per mile
S = line length in miles
X_c = series capacitive reactance—ohms

An examination of equations 3 and 4 reveals the following information concerning the nature of the *ABCD* constants.

(1) The *A* constant relates the sending and receiving end voltages for an unloaded line ($I_r = 0$). Therefore, the voltage at the end of an unloaded line is

$$E_r = \frac{E_s}{A} \qquad (6)$$

(2) The *B* constant represents the series impedance between the sending and receiving ends. As such it is the factor which largely determines the power which may be transferred over the line since, neglecting line resistance

$$P = \frac{E_s E_r}{B} \sin \theta \qquad (7)$$

The curves of Figure 3 show that the addition of series capacitance reduces the rise in voltage at the end of an unloaded or lightly-loaded line. This fact is extremely important for very long lines because the rise in voltage at the end of an unloaded line often causes problems with protective equipment.

The curves of Figure 4 show that the addition of series capacitors reduces the *B* constant, thereby increasing the amount of power which can be transferred over the line. It will be observed that a given per cent compensation as defined by equation 5 does not result in the same per cent reduction of the *B* constant. For instance, in a line 400 miles long, 75 per cent compensation causes a reduction of the *B* constant of 70 per cent.

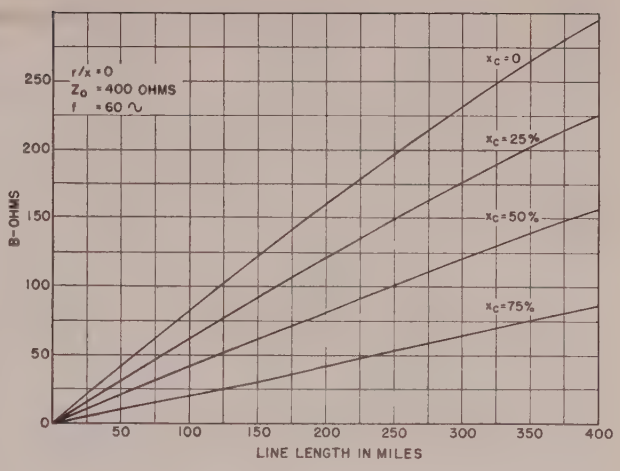

Figure 4. The *B* constant in ohms versus line length in miles for various values of compensation at center of line

Effects of Series Capacitor on Power Transfer Ability

Series capacitors have long been recognized as a means of increasing the power transfer ability of a transmission line. Therefore, they must compete both economically and performancewise with other established methods of accomplishing this objective. To summarize briefly, these other methods are:

1. Higher voltages.
2. Multiple lines.
3. Lower frequency.
4. D-c transmission.
5. Intermediate synchronous condensers.
6. Cable and shunt reactors.

Of these six methods, the last four are of little consequence at the present time for a multitude of economic and technical

Figure 3. The *A* constant versus line length in miles for various values of compensation at center of line

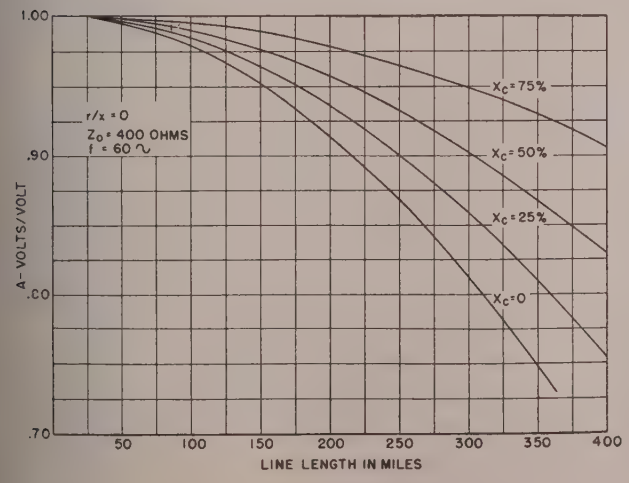

Figure 5. The C constant in mhos $\times 10^{-3}$ versus line length in miles for various values of compensation at center of line

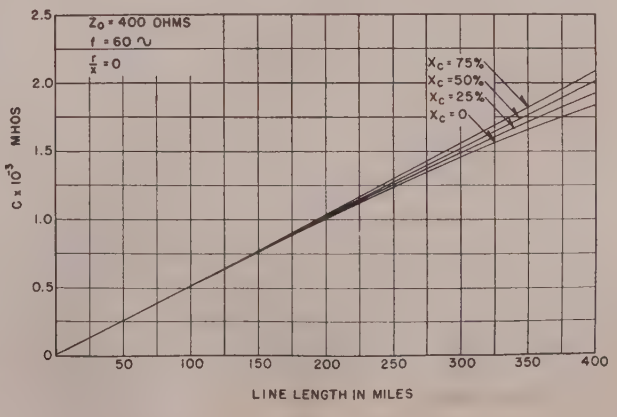

reasons. Therefore, series capacitors will be compared with the first two methods only.

There are several ways to analyze the effects of series capacitors on power transfer ability. One method is to assume typical values for terminal impedances in order to calculate the stability limit for various line lengths and percentage compensations. When this method is used, the terminal impedances are decreased as the transmitted power is increased to simulate an increase in generator and transformer capacity. Such an approach yields complete information about the assumed system[3] and if the values of the terminal impedances are chosen judiciously, the information gained from the assumed system can be applied to a number of practical cases. However, there are certain cases where data obtained by this means are not applicable. Examples of such applications are systems where terminal impedances are significantly different than the assumed impedances and systems where series capacitors are used to effect load division between two parallel lines.

In order to analyze such cases, a second approach to the problem is presented in this paper. The assumption is made that most long lines are operated with fixed or predetermined high side voltages at the sending and receiving ends. Therefore, the performance of the line and the series capacitor can be considered separately from the terminal equipment. Accordingly, the performance of the line and the series capacitor is analyzed with respect to line voltage, voltage gradient, line operating angle, and r/x ratio.

Towards this end, the power transfer ability of lines of varying length, voltage, and per cent compensation was plotted for fixed angles between sending and receiving ends as shown in Figures 6 and 7. The curves can be used to determine receiving end power for any value of compensation since most high-voltage lines have an r/x ratio in the neighborhood of 0.2. For instance, in a 220-kv line, 200 miles long, with 35 per cent compensation; the receiving end power at a line operating angle of 30 degrees is 230 megawatts.

These curves illustrate the following facts:

1. The power transfer ability of a line with 50 per cent compensation is approximately equal to the power transfer ability of two parallel lines of the same length and voltage.

2. The power transfer ability of a 138-kv line with 75 per cent compensation is approximately equal to that of a 220-kv line without compensation.

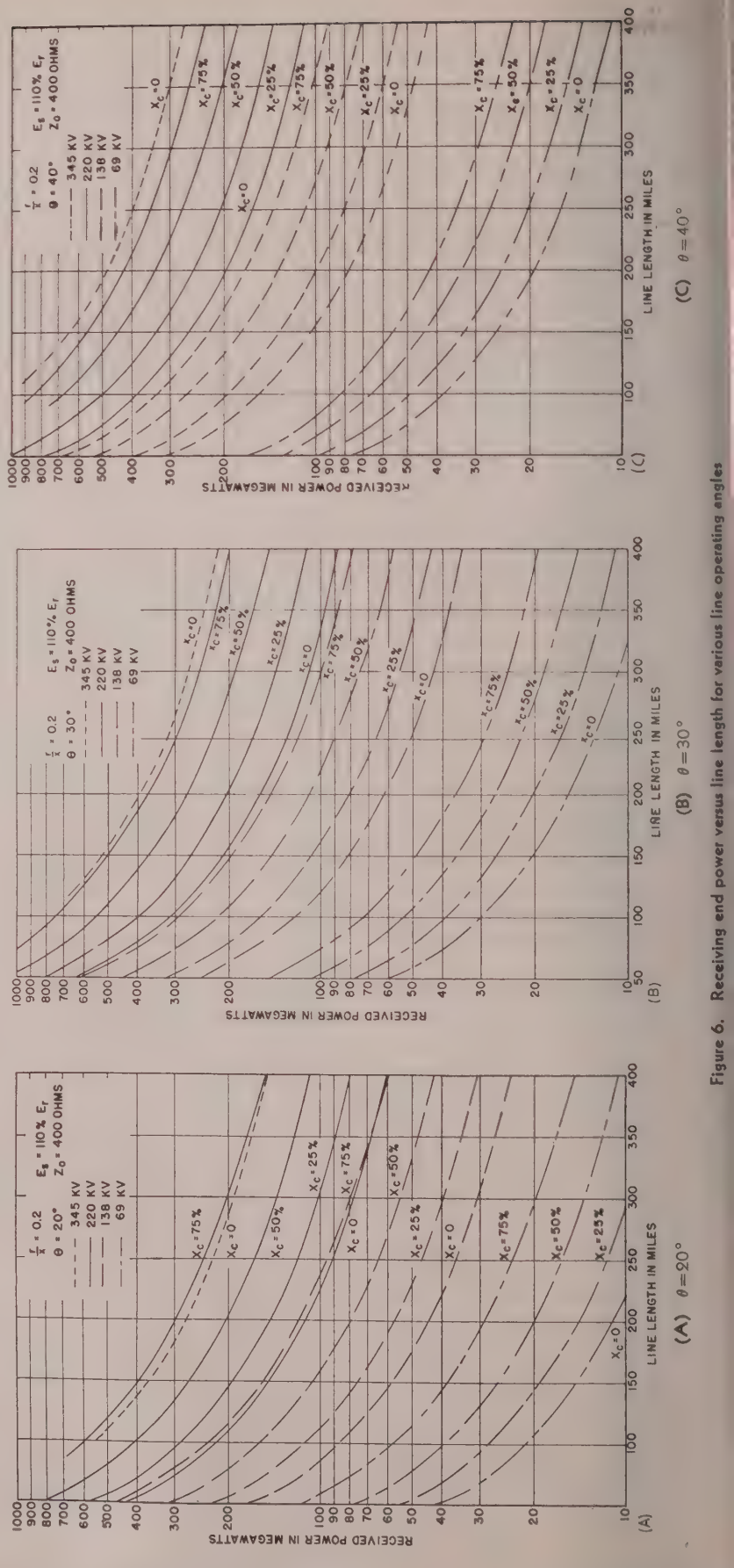

Figure 6. Receiving end power versus line length for various line operating angles

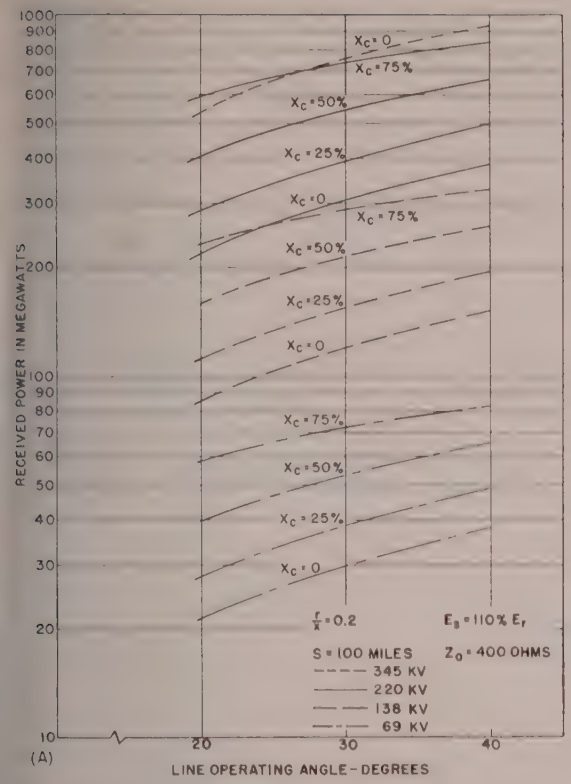

(A) S = 100 miles

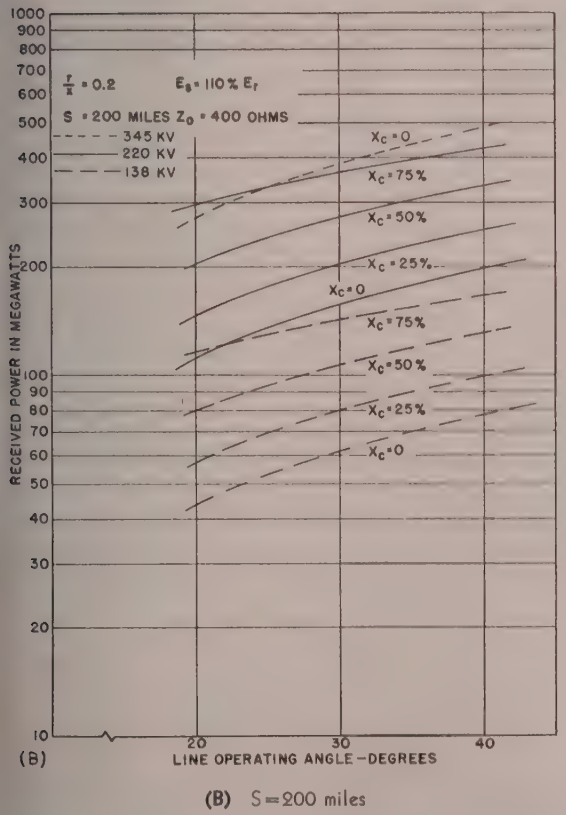

(B) S = 200 miles

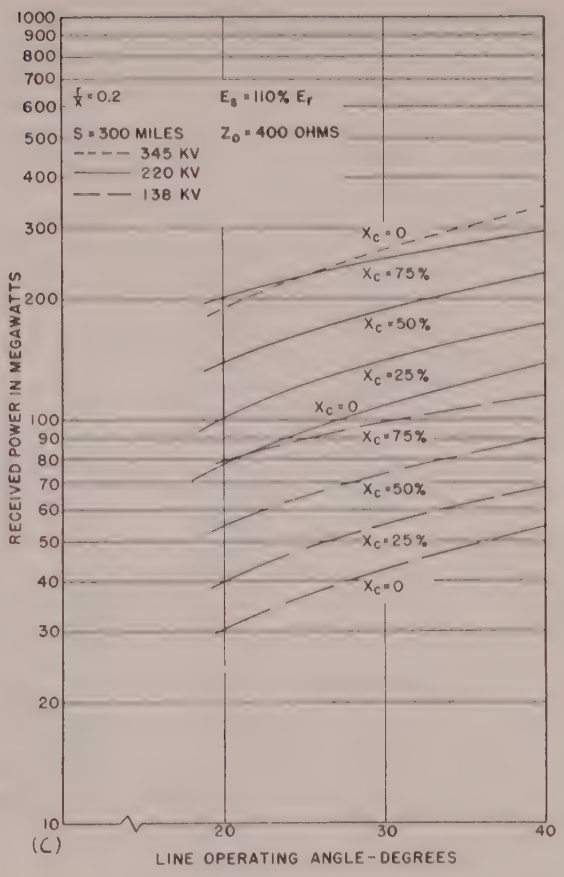

(C) S = 300 miles

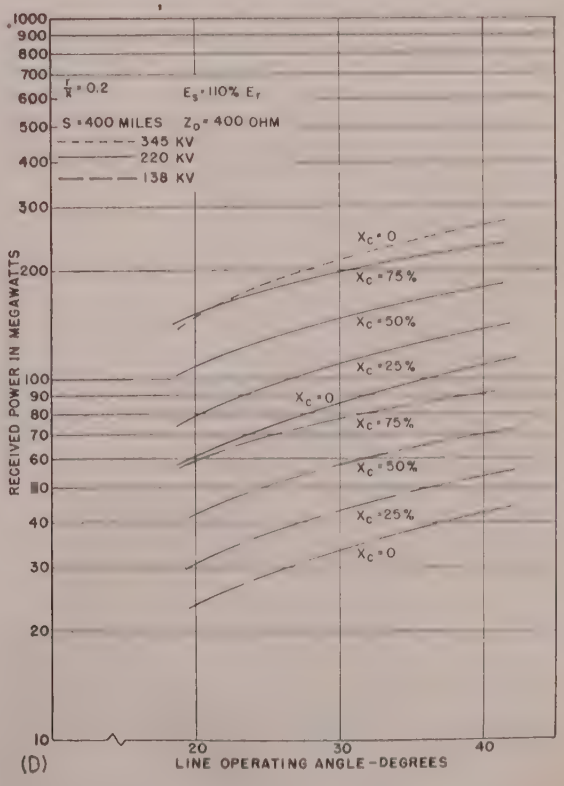

(D) S = 400 miles

Figure 7. Receiving end power versus line operating angle for various line lengths

3. The power transfer ability of a 220-kv line with about 75 per cent compensation is approximately equal to that of a 345-kv line without compensation.

Effects on Power Factor

The effects of series capacitors are not confined to increases in the power transfer ability of a transmission line. The curves of Figure 8 illustrate the variation of the sending and receiving end power factors with line length, per cent compensation, and angle. These curves are plotted for a ratio of 0.2 between line series resistance per mile and line inductive reactance per mile. However, the general trends which are shown apply to other r/x ratios.

Some of the general principles shown by the curves of Figure 8 are presented more concisely in the circle diagrams of Figure 9. The effect of series compensation on reactive power flow can best be illustrated with an example. If the received power is assumed as 2.0 per unit, the reactive power without compensation is -1.15 per unit. As compensation is added, the receiving-end reactive power becomes less negative, but when the compensation is greater than 50 per cent the receiving-end reactive power becomes more negative. Thus, there is a particular value of compensation that yields a minimum negative reactive power for the assumed received power and voltage gradient. For an assumed sending-end power of 2.0 per unit, the reactive power changes from $+0.4$ per unit for zero compensation to -0.5 per unit for 75 per cent compensation. Zero reactive power is indicated for a compensation of approximately 37 per cent. It is interesting to note that for small values of sending-end power the addition of series compensation causes a reverse effect; that is, the reactive power becomes more positive with increased compensation. The effect of series compensation on reactive power flow for other values of loading can be found in Figure 9.

A general explanation of the effects of series capacitors on power factor is somewhat involved because these effects are the cumulative result of two factors:

1. The effect of increased resistance-to-reactance ratio caused by series compensation.

2. The effects of line shunt capacitance as series compensation is increased.

An analytical discussion of the manner in which these two factors affect power factor is given in Appendix I.

In order to present a clearer view of the effect of series capacitors on power factor, two specific cases are considered. The

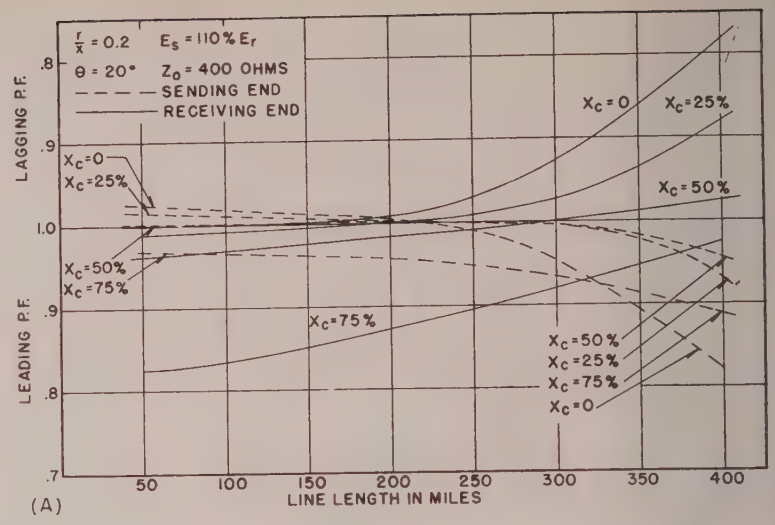

(A) $\theta = 20°$

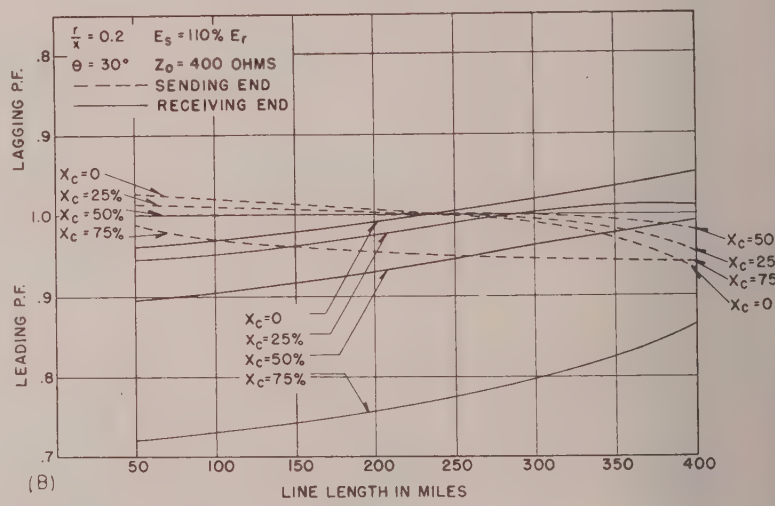

(B) $\theta = 30°$

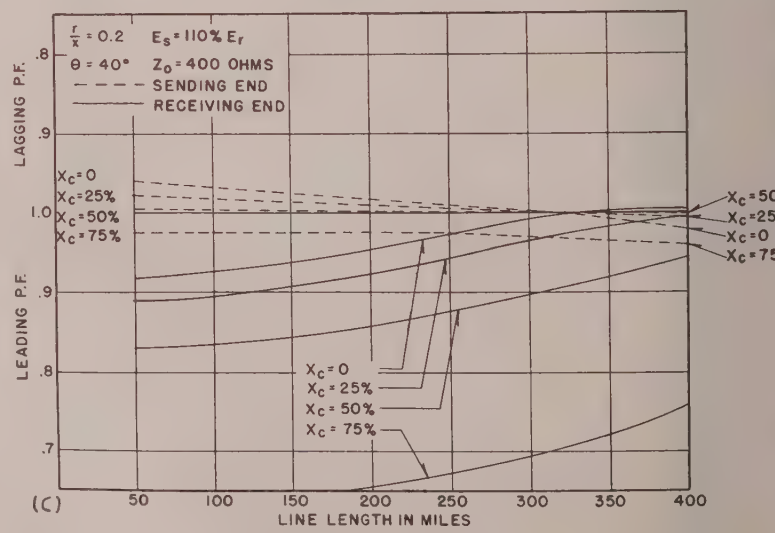

(C) $\theta = 40°$

Figure 8. Sending and receiving end power factors versus line length for various line operating angles

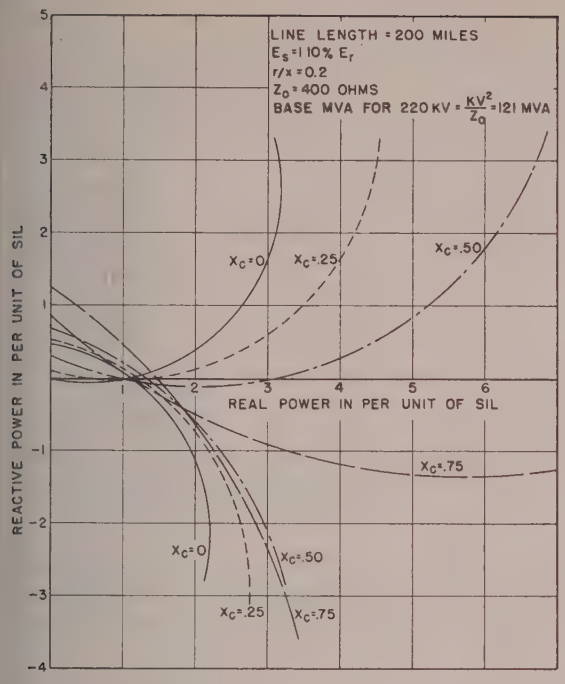

Figure 9 (left). Circle diagrams for 220-kv 200-mile line

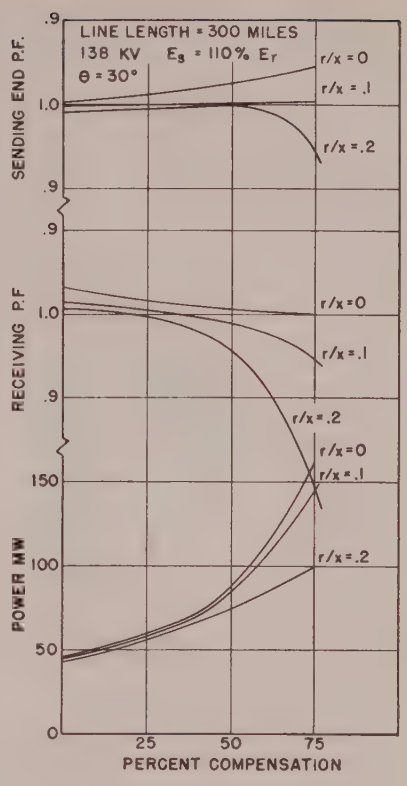

Figure 10. The effects of line resistance on power transfer and sending and receiving end power factors

first case is a comparison between two parallel uncompensated lines and one line compensated so that its power transfer capability is the same as that of the two uncompensated lines. The length, voltages, conductor size, and operating angle of each line are the same. The results of this comparison are shown in Table I. The values in Table I are obtained from Figures 6 and 8.

An examination of Table I shows that a greater amount of positive reactive power flows into the line at the sending-end for the two uncompensated lines than for the one compensated line. Likewise, less negative reactive power flows out of the receiving end for the two uncompensated lines than for the one compensated line. This is an important point because most loads require positive reactive power. Therefore, in order to maintain receiving end voltage and supply the reactive requirements of ordinary loads, more corrective capacity in the form of shunt capacitors or overexcited synchronous condenser capacity is required at the receiving end for one compensated line than for two uncompensated lines. There are three fundamental reasons for this phenomena.

1. The compensated line has only one-half the shunt capacitance of the two uncompensated lines. Thus, less corrective mvar is obtained from the line itself.

2. The resistance-to-reactance ratio of the compensated line is greater than that of the two uncompensated lines. This condition causes the sending end equipment to put less positive reactive power into the line for a given real power load.

3. Although a portion of the mvar required by the line series inductive reactance is supplied by the series capacitor, the remaining mvar which must be supplied for this purpose is greater than the total reactive megavolt-amperes required by the line inductive reactance of the two parallel uncompensated lines.

The foregoing statements assume that the compensated line and the two parallel uncompensated lines are transmitting the same amounts of power and are operated at the same voltage gradient from sending to receiving end. If the compensated line is operated at a higher gradient than the uncompensated lines as shown in the third row of Table I, its receiving end reactive power will approach that of the uncompensated lines.

The second case which is considered is a comparison between a compensated line and an uncompensated line of the same length. Both lines are operated at the same voltage gradient and the receiving end powers are equal. The results of this comparison are shown in Table II.

The tabulated values show that the insertion of series capacitance causes the sending end power factor to change slightly in the leading direction. However, the series capacitance causes an increase in the positive reactive power at the receiving end. This is a result of the fact that part of the positive reactive mva required by the line inductive reactance is supplied by the series capacitor.

A common fallacy in the application of capacitors is that a given amount of capacitive megavolt-amperes will effect the same power factor correction whether the capacitance is placed in series or shunt. The last three columns of Table II show that this is not true. The criterion used in the table is the total amount of capacitive megavolt-amperes in series and shunt needed to correct the receiving end power factor to unity. The tabulated results show that a total of 104 megavolt-amperes is necessary for the compensated line while only 61 megavolt-amperes are needed for the uncompensated line.

The primary reason for the disparity in the amount of capacitive megavolt-amperes required for each case is the increase in the total resistance-to-reactance ratio

Table I

	Received Power, Mw	E_s	E_r	Per Cent Comp.	Sending End, Mvar	Receiving End, Mvar
2 Parallel lines	315	242	220	0	30	−40
1 Compensated line	315	242	220	62	−70	−204
1 Compensated line	315	253	220	62	−41	−186

Note: Conditions of tests were: length = 200 miles; angle = 30 degrees; Z_0 = 400 ohms.

Table II

	Received Power, Mw	Line Angle Degrees	Per Cent Comp.	Sending End Power Factor	Receiving End Power Factor (Without Shunt Cap.)	Series Cap., Mva	Shunt Cap., Mva	Total
1 Uncompensated line	198	40	0	0.987 lag	0.956 lead	0	61	61
1 Compensated line	198	20	48	0.998 lead	0.987 lead	72	32	104

Note: Conditions during tests were: $E_s = 242$ kv; $E_r = 220$ kv; length = 200 miles; $Z_0 = 400$ ohms. Receiving end power factor corrected to unity by shunt capacitance.

of a transmission line when series capacitors are used. This forces the sending end machines to put more negative reactive power into the line than is required when the same power is transmitted over the same line without series capacitors. Therefore, a greater amount of capacitive megavolt-amperes are required to absorb this increase so that unity power factor may be maintained at the receiving end.

The Effects of Line Resistance as Series Compensation Is Increased

Line resistance is an extremely important consideration in the application of series capacitors to transmission circuits. It is one of the principal factors which determines the maximum practical per cent compensation in a given transmission circuit. In order to illustrate the effects of line resistance, a line length of 300 miles is considered. Then the sending and receiving end powers and power factors are calculated for an operating angle of 30 degrees and a nominal voltage of 138 kv with r/x as a parameter. The results are shown in Figure 10.

Of special interest is the variation of power transfer with percentage compensation. The power transfer ability of the line falls off very rapidly with r/x ratio for high values of compensation. This is because power transfer becomes more of a function of voltage difference between the ends of the line than angular difference.

Figure 10 also illustrates the effect of increasing r/x on the sending and receiving end power factors. As r/x is increased, both the sending and receiving end power factors become more leading. The explanation of this phenomena is given in the first part of Appendix I.

In addition to the aforementioned effects, the r/x ratio directly determines the line efficiency. Accordingly, a study was made of line efficiency for various combinations of series compensation, operating angle, line length, voltage gradient, and r/x ratio. The study showed that the efficiency of the line is relatively independent of line length and voltage gradient for a fixed line operating angle. Therefore, efficiency was plotted versus operating angle for various values of compensation and r/x ratio as shown in Figure 11. The values shown on these curves are accurate to within 1 per cent for line lengths up to 400 miles and voltage gradients up to 15 per cent.

This family of curves points out a number of interesting facts.

1. Line efficiency is a function of only two variables, r/x and operating angle, for purposes of estimation.

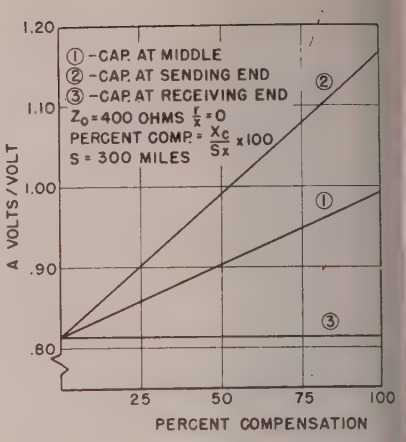

Figure 12. The A constant versus per cent compensation for a 300-mile line for various positions of series capacitor

2. Line efficiency is approximately a linear function of line operating angle between 20 and 40 degrees.

3. Series compensations in excess of 50 per cent cause prohibitive line losses unless r/x and the operating angle are small.

Position of Series Capacitor in Transmission Line

The position of the series capacitor is an important consideration in the case of long transmission lines where shunt capacitance cannot be neglected. To some extent, the capacitor location will also affect fault currents and relay operation.

A study was made of capacitor location considering the center of the line, the sending end and the receiving end. In order to illustrate the results of this analysis, a line length of 300 miles is chosen and line resistance is neglected. Since the three locations of series capacitance can be compared most easily by means of relative $ABCD$ constants, these constants are plotted versus per cent compensation as shown in Figures 12 and 13. The analytical expressions upon which these

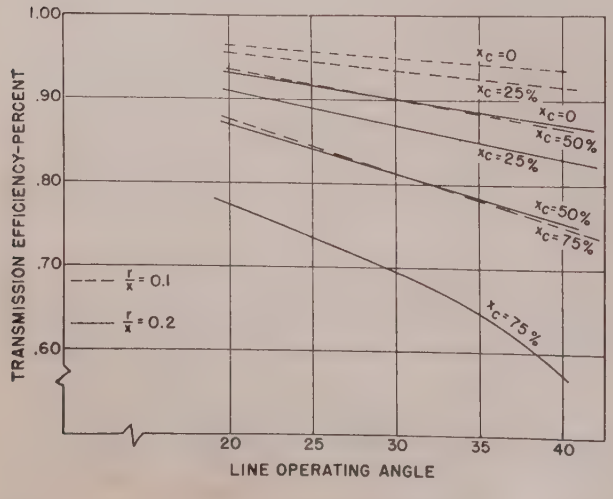

Figure 11 (left). Line efficiency versus line operating angle for various values of compensation

Figure 13 (right). The B constant in ohms versus per cent compensation for a 300-mile line for various positions of the series capacitor

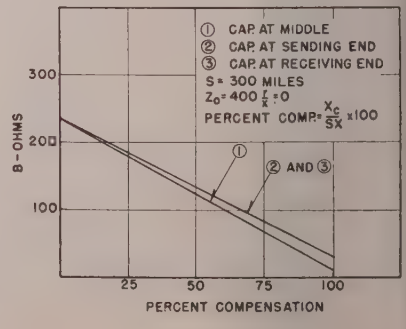

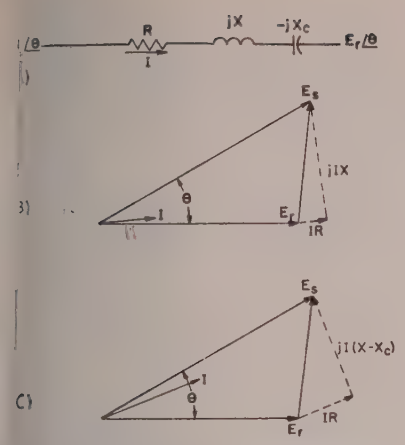

igure 14. Circuit and vector diagrams used for discussion in Appendix I

A) Single-line diagram
B) Vector diagram for zero compensation
C) Vector diagram for about 50 per cent compensation

:onstants are based are shown in Ap-)endix II.

The curves illustrate the following:

1. When the series capacitor is at the send-ng end, the voltage at the receiving end at no load is less than if the same amount of capacitance were placed anywhere else in the circuit.

2. When the series capacitor is placed at the receiving end, the receiving end voltage at no load is unaffected by the series capacitance.

3. More compensation per ohm of capacitance is obtained when the capacitor is at the center of the line.

The effect that these differences in the *ABCD* constants have upon the flow of real and reactive power is shown by the following example:

Example 1

Line length = 300 miles, $x = 0.825$ ohm/mile
220 kv—60 cycles
Line operating angle = 30 degrees
$r/x = 0$
Load = 253 megavolt-amperes
$E_s = 230$ kv
$E_r = 220$ kv

From this data, the required series capacitor megavolt-amperes and the reactive powers at the sending and receiving ends are calculated. The results are shown in Table III.

From the tabulated results it can be seen that the series capacitor megavolt-amperes required to effect a given reduction in the *B* constant is a minimum when the series capacitor is placed at the middle of the line, and a maximum when the capacitor is placed at the receiving end. However, this is not the sole determining factor in the placement of the capacitor.

Examination of the reactive powers at the sending and receiving ends shows the following:

1. When the capacitor is placed at the sending end, leading sending and receiving end power factors result.

2. When the capacitor is placed at the receiving end, lagging sending and receiving end power factors result.

3. When the capacitor is placed at the center of the line, the sending and receiving end power factors lie somewhere between the values for (1) and (2).

In evaluating these effects, the tacit assumption is made that leading power factors at the sending and receiving ends are undesirable. The reasons for this are the facts that leading power factor operation reduces the capability and steady-state stability of synchronous generators and most loads are lagging. On this basis, placement of the capacitor at the sending end is undesirable, because too high a voltage gradient would be required to cause lagging power factor operation. However, a good case can be made for placing the capacitor at the receiving end, because the line can be operated at lagging power factor with a low gradient. Obviously if the line is used for power transfer in either direction, the series capacitor should be placed in the middle.

The question of the capacitor position upon relaying and fault currents is one which must be decided for the particular line or system under consideration. Generally speaking, however, the impedance center of the line is the most advantageous location from this standpoint.

The general conclusions which can be drawn from the study of series capacitor position are as follows:

1. The series capacitor should not be placed at the sending end.

2. In general, the best place for the capacitor is at the middle of the line.

3. Satisfactory operation will result if the capacitor is placed at the receiving end. This statement implies that power is to be transferred in one direction only.

Effect of Series Capacitors on System Stability

The effect of series capacitors on steady-state stability has already been mentioned in this paper. However, transient stability is often of greater importance than steady-state stability. Since transient stability has received considerable coverage in the literature on series capacitors[1,2,3,4] and since it is a problem which must be solved for a

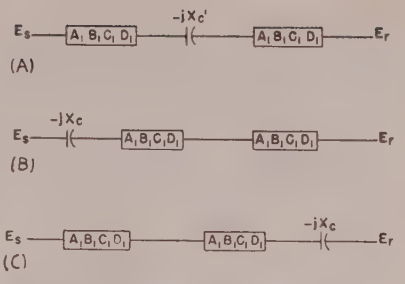

Figure 15. Equivalent circuits used for analysis in Appendix II

(A) Capacitance at center of line
(B) Capacitance at sending end
(C) Capacitance at receiving end

specific system, only general statements will be made in this paper.

Series capacitor installations as proposed for present-day systems are protected against abnormal power voltages by self-clearing gaps in parallel with the capacitor bank. These gaps are designed to flashover when the voltage across the capacitor bank exceeds $2^1/_2$ times normal voltage. Therefore, two types of fault operation are possible, depending upon the location and severity of the fault.

1. Faults which cause the gaps on one or more phases to flashover.

2. Remote or high impedance faults which allow the capacitor bank to remain in service.

The second type of fault is ordinarily not too severe from a stability standpoint. However, for the first type of fault, the capacitor may be partially or entirely ineffective during the fault condition because one or more phases of the capacitor will be shorted. After the fault is cleared, the capacitor is reinserted by special fast clearing gaps. Therefore, the series capacitor will help maintain stability under the new operating condition provided that the swing currents do not become large enough to cause the capacitor to flashover again.

From this discussion it can be seen that some increase in the stability limits will result from the use of series capacitors. However, the exact magnitude of this

Table III

	Capacitor Position		
	Middle	Sending End	Receiving End
ohms X_c	147	164	164
% X_c	59.5	66.5	66.5
I^2X_c—Mva	185	199	225
Q_s—Mva	47	−8	124
Q_r—Mva	−5	−68	45

increase is dependent upon many factors such as relaying and breaker times, gap operation, terminal impedances, and system inertia so that it must be evaluated for each particular case. Reinsertion time is an especially critical factor in determining the aid received from series capacitors in maintaining stability.[1,2,3]

Summary and Conclusions

Results of analytical studies illustrated in the figures of this paper show the following facts:

1. The power transfer ability of a transmission line can be increased considerably by the use of series compensation.

2. The receiving end power factor becomes more leading for the same line operating angle as the percent series compensation is increased.

3. Except for long lines with low values of compensation, the sending end power factor is made less lagging for the same line operating angle as the percent series compensation is increased.

4. For estimating purposes, the efficiency of the transmission line can be considered to depend upon only the r/x ratio of the line and the percent series compensation for a given line operating angle.

5. Reduced efficiency and the tendency towards leading power factor as series compensation is increased are functions of the r/x ratio of the line.

6. In general, the best location for the series capacitor is at the middle of the line.

7. If power is to be transferred in one direction only, it is feasible to place the capacitor at the receiving end.

These facts lead to the following conclusions concerning the application of series capacitors:

1. For lines with an r/x ratio in the vicinity of 0.2 or more, series compensations of more than 50 per cent are impractical for reasons of low efficiency and power factor, unless the line is to be operated at an angle of considerably less than 20 degrees. The importance of this conclusion cannot be over-emphasized since most existing transmission lines fall into the above stated r/x ratio category.

2. Series compensations above 50 per cent are practical if the purpose of the extra compensation is to increase the short-time overload capacity of the line or the transient stability of the system.

3. Due to the limiting effects of line resistance in the application of series capacitors, serious consideration should be given extra large conductor size in proposed lines. Oversize conductors would allow a greater future increase in the power transfer ability of the line.

4. Series capacitors should be considered for long high-voltage lines. An economic study may show that the addition of series capacitors will actually reduce the transmission cost per kilowatt transmitted.

Appendix I

Effect of Line Resistance on Sending and Receiving End Power Factors as Series Compensation is Increased

Neglecting shunt capacitance, the effect of line resistance on sending and receiving end power factors can be shown by the vector diagrams Figures 14(B) and 14(C) for the circuit in Figure 14(A). Figure 14(B) represents the vector diagram for zero compensation, while Figure 14(C) represents the vector diagram for 50 per cent series capacitor compensation and the same angular difference between E_s and E_r. From these diagrams, it can be seen that since the addition of series compensation reduces the net r/x ratio of the line, both the sending and receiving end power factors are made more leading by the addition of series capacitance.

Effect of Distributed Line Capacitance on Sending and Receiving End Power Factor as Series Compensation is Increased

Neglecting resistance, the real and reactive powers at the sending and receiving ends can be expressed as follows:

$$P_r = P_s = \frac{E_s E_r}{B} \sin\theta \tag{8}$$

$$Q_s = \frac{AE_s^2}{B} - \frac{E_s E_r}{B} \cos\theta \tag{9}$$

$$Q_r = -\frac{AE_r^2}{B} + \frac{E_s E_r}{B} \cos\theta \tag{10}$$

where θ is the angular difference between the sending and receiving end.

Using these expressions, the sending and receiving end power factor angles can be expressed as:

$$\phi_s = \tan^{-1}\left(\frac{AE_s}{E_r} - \cos\theta\right)\frac{1}{\sin\theta} \tag{11}$$

$$\phi_r = \tan^{-1}\left(-\frac{AE_r}{E_s} + \cos\theta\right)\frac{1}{\sin\theta} \tag{12}$$

From the curves shown in Figure 3, it can be seen that the A constant is increased by the addition of series capacitance. Thus the effect of distributed capacitance is to make the sending end power factor more lagging, for a constant value of θ, as series capacitance is increased since the positive term of ϕ_s is increased. Conversely, the receiving end power factor is made more leading or less lagging as the series capacitance is increased since the negative term or ϕ_r is increased.

This analysis offers an explanation of the curves shown in Figure 8 of the text. Both resistance and distributed shunt capacitance tend to make the receiving end power factor more leading as the amount of series compensation is increased. However, in the case of the sending end power factor these effects are opposed. Therefore, for short lines where distributed capacitance is small, the resistance effect will cause the power factor to be less lagging as series compensation is increased. In the case of long lines, the effects of distributed capacitance may outweigh the resistance effect and the power factor will become less leading as series compensation is increased from zero. At high values of series compensation, the resistance effect will again become the determining factor causing the power factor to become more leading. This effect is shown in Figure 8.

Appendix II. Comparison of Capacitor Locations

Capacitor in center of line—Figure 15(A)

$$A = (2A_1^2 - 1) + C_1 A_1 X_c' \tag{13}$$

$$B = j(2B_1 A_1 - A_1^2 X_c') \tag{14}$$

$$\text{Capacitor current } I_c = \frac{E_s - E_r}{j(2B_1 - jA_1 X_c')} \tag{15}$$

where

E_s = sending end vector voltage
E_r = receiving end vector voltage
Line resistance = 0
A_1, B_1, C_1, D_1 represent magnitudes of the constants of one-half of line
A, B, C, D represent over-all line constants including both line sections and series capacitor

X_c' = ohmic reactance of series capacitor

Capacitor at sending end—Figure 15(B)

$$A = (2A_1^2 - 1) + 2C_1 A_1 X_c'') \tag{16}$$

$$B = j[2B_1 A_1 - (2A_1^2 - 1)X_c''] \tag{17}$$

$$\text{Capacitor current } I_c = \frac{(2A_1^2 - 1)E_s - E_r}{j[2A_1 B_1 - (2A_1^2 - 1)Xc]} \tag{18}$$

where

X_c'' = ohmic reactance of series capacitor

Capacitor at receiving end—Figure 15(C)

$$A = (2A_1^2 - 1) \tag{19}$$

$$B = j[2B_1 A_1 - (2A_1^2 - 1)X_c''] \tag{20}$$

$$\text{Capacitor current } X_c = \frac{E_s - (2A_1^2 - 1)E_r}{j[2A_1 B_1 - (2A_1^2 - 1)Xc]} \tag{21}$$

In order for power transfer of the line to be the same for each capacitor position, the B constants must be equal.

$$2B_1 A_1 - A_1^2 X_c = 2B_1 A_1 - (2A_1^2 - 1)X_c'' \tag{22}$$

or

$$X_c'' = \frac{A_1^2}{(2A_1^2 - 1)} X_c' \tag{23}$$

References

1. Series Capacitors for Transmission Circuits, E. C. Starr, R. D. Evans. *AIEE Transactions*, volume 61, 1942, pages 963–73.

2. Characteristics of 400-Mile 230-Kv Series Capacitors, B. V. Hoard. *AIEE Transactions*, volume 65, 1946, pages 1102–14.

3. Steady-State and Transient Stability Analysis of Series Capacitors in Long Transmission Lines, J. W. Butler, J. E. Paul, T. W. Schroeder. *AIEE Transactions*, volume 62, 1943, pages 58–65.

4. Electrical Transmission and Distribution Reference Book. Fourth edition, Westinghouse Electric Corporation (East Pittsburgh, Pa.), 1950.

5. Design and Protection of 10,000-Kva Series Capacitor for 66-Kv Transmission Line, A. A. Johnson, R. E. Marbury, J. M. Arthur. *AIEE Transactions*, volume 67, 1948, pages 363–67.

6. 10,000-Kva Series Capacitor Improves Voltage in 66-Kv Line Supplying Large Electric Furnace Load, B. M. Jones, J. M. Arthur, C. M. Stearns, A. A. Johnson. *AIEE Transactions*, volume 67, 1948, pages 345–51.

Discussion

R. M. Butler (General Electric Company, Schenectady, N. Y.): The authors have made a comprehensive study of the effects series capacitor compensation have on the power and reactive flow over transmission lines of various length.

As emphasized by the authors, the effects on power and reactive flow caused by series capacitors are somewhat different from those caused by shunt capacitors. These effects of series capacitors are illustrated in the many curves shown in the paper. The authors have chosen to plot many of the curves (Figures 6, 7, 8, and 11) in terms of various values of line operating angles. This is a convenient way to show the effects of series compensation but it would seem that a clearer picture of the many effects of series compensation would be had if no reference had been made to line operating angle. This term is not normally used by the power system's engineer since it has little physical significance. It is possible to be completely familiar with the reactive and power flow conditions in a transmission system without knowing anything about the angular differences between station busses in the system. Therefore, a clearer grasp of the effects of series compensation could be had if Figures 6, 7, and 8 had been eliminated and replaced with curves similar to those of Figure 9 for different distances and values of compensation.

Several important facts should be mentioned concerning Figure 11.

Figure 11, although perfectly correct, may be misleading. It is seen in this figure that increasing compensation will cause reduced efficiency for a given operating angle. If Figure 11 had been plotted the way a power system's engineer would more likely comprehend, in terms of various receiver powers, it would be apparent that increasing the compensation would have very little effect on the losses for loadings up to the surge impedance loading (2.5 kv²) and at higher loadings the losses would actually decrease slightly with increasing compensation except at greater than 50 per cent compensation. At compensations greater than 50 per cent and these higher loadings, the losses would increase with increasing compensation. This may be seen in Table I of this discussion.

Table I

P_2	$\%C$	P_E
4.00	0	0.476
	25	0.412
	50	0.383
	75	0.431
3.08	0	0.232
	25	0.221
	50	0.220
	75	0.254
2.00	0	0.089
	25	0.0882
	50	0.0882
	75	0.1000
1.00	0	0.0204
	25	0.0205
	50	0.0206
	75	0.0208

Note: Conditions during test:
50 miles
$E_1 = E_2 = 1.0$ per unit
Base kva = 5.0 kv²
$r/x = 0.10$, $x = 0.8$ ohms per mile
Surge impedance loading = 2.5 kv² = 0.5 per unit
P_2 = receiver power in per unit
P_E = line losses in per unit
$\%C$ = per cent series compensation

Conclusions (2) and (3) under Summary and Conclusions in the paper would have been worded differently if based upon comparisons made for fixed receiver powers rather than fixed line operating angles.

The paper, however, does show very clearly the gain made in power transfer capability by increasing the line compensation. This is especially important when a line cannot be loaded up to its most economic loading point because of steady state stability considerations. This is a field of application most favorable to series compensation.

The authors might have stressed the fact that location of series capacitors at the center of the line would also be most desirable from the standpoint of having to withstand lower maximum and average fault currents at the center than at either end. The worst fault condition as seen by a capacitor bank located at the center of the line would be a fault right at the terminals of the bank. This would generally be less severe than a fault condition near the bank when the bank was located at either end of the line.

W. A. Morgan (Bureau of Reclamation, Denver, Colo.): The authors are to be congratulated upon a very worthwhile presentation of the fundamental effects of series capacitors in high-voltage transmission lines. This subject is of particular interest to the Bureau of Reclamation at this time because we are studying the development of a new large high-voltage power system. In addition to the determination of the nominal voltage for this system, we naturally are considering the effects of series capacitors. The series capacitor installations in Sweden have had satisfactory operating experience, and, with the installations presently being made in United States, it is necessary to carefully consider the economies of series capacitors in the design of any new transmission system.

The examples that were given in the paper will be of value to us in explaining to others about series capacitors. I have reference here to the following sections in the paper: "Effect of Series Compensation on Line Constants," "Effects on Power Factor," and "Position of Series Capacitor in Transmission Lines." While these relations and cases could be developed by the power system engineer, the availability of this analysis makes it necessary only to refer to this paper.

We have not completed our studies, as yet. However, we can confirm at this time the importance of large conductor sizes for series capacitor installations which was brought out in the paper. In the design of a new system, it is possible to select the proper size of conductor. However, where series capacitors are applied to an existing transmission system, it is quite possible that the conductors may be too small for the increased current flow the series capacitors make possible. It is suggested that this obstacle may be overcome by the installation of a second conductor per phase to make a "duplex-conductor" arrangement. It is understood that this remedy has been utilized by Swedish engineers on their 230-kv system where increased power flows have revealed the inadequacy of some of the single conductor sizes previously in use.

In our study, we have found difficulty with series capacitors in trying to keep the swing currents from causing the series capacitor gaps to flash-over right when the series capacitor is desired most from a stability standpoint. To increase the size of the capacitors to overcome this difficulty increases the cost. In view of other complications with series capacitors such as relaying, we would be interested in other means of improving stability. Would the authors give us an example showing that intermediate synchronous condensers are not worth comparing with series capacitors in their effect on power transfer ability?

A. A. Johnson, J. E. Barkle, and **D. J. Povejsil:** The method of plotting receiver power and sending and receiving end power factors was chosen by the authors after considerable deliberation. The authors agree with Mr. Butler that line operating angle is a term seldom used in general conversation by operating engineers, but the term is nevertheless generally appreciated and understood. Line operating angle is not a quantity which can be measured easily; however, in a basic discussion of the philosophy of long distance power transmission, line operating angle takes its place as the most important single factor—neglecting relaying and circuit breaker operating times—in the determination and improvement of power system stability.

To illustrate this point, consider what generally happens when more power is transferred over a line. First, the generator and transformer capacities are increased in about direct proportion to the desired increase in transferred power. Furthermore, the per-unit reactance of the added equipment will probably be comparable to the reactance of the existing equipment because the general practice in high-voltage transmission has been to install generators and transformers with the lowest reactance which could be justified economically. Therefore, the voltage drop and the angular displacement of voltage across these elements remains essentially constant as transferred power increases. However, the line impedance remains the same if the same lines at the same voltage are used, which is customary. Therefore, the voltage drop and angular displacement across the line is increased as the transferred power is increased. Stated briefly, it may be said that the increase in the total operating angle between sending and receiving ends as transferred power is increased is almost entirely due to the increased line operating angle. Therefore, if the effect of series capacitors on the line

operating angle is known, their effect on the over-all system operating angle is also known. By plotting power versus line angle as was done in this paper, the results are made independent of terminal equipment.

A second advantage of this method shows up in the application of series capacitors to divide load between lines which are bussed together. For this case, the two lines will obviously have the same operating angle. As an example, assume that it is desired to divide 300 megawatts between two 220 kilovolt, 200-mile lines so that 66 per cent of the power flows over one line. Examination of Figure 7(B) shows that a compensation of about 55 per cent will be required and that the line operating angle will be 18 degrees.

As a matter of general interest, the allowable line operating angle for a system with typical terminal impedances is about 30 degrees. This is based on transient and steady-state stability considerations.

Mr. Morgan has mentioned that some of the benefits of series capacitors are minimized on certain systems by the fact that calculated swing currents may cause the capacitor gaps to flashover when they are needed most. This problem has been recognized and more data are needed to select gap settings which will protect the capacito units as well as allow swing currents t flow without flashing over the gap.

In regard to the matter of an intermediat synchronous condenser, space does not pe mit a complete explanation. However, may be said that such a device cannot b justified economically for power increase of more than about 10 per cent.

On the basis of field tests and preliminar analog computer studies, no serious diff culty is anticipated in the relaying of line with series capacitors. However, mor complete information on this subject wi appear in the near future.

D-C Power Supplies and Isolation of Faults on Electric Transit Systems—Part I

D-C Power Supply

S. S. WATKINS
FELLOW AIEE

M. E. REAGAN
FELLOW AIEE

IN THE discussion of electric traction distribution systems, it is necessary to consider the power flow from the source, through the a-c supply lines, the substation with its current-limiting transformers and conversion equipment, and the d-c feeders to the load. Each segment of these circuits has some elements of resistance, capacitance, and inductance which, added together determine the magnitude and rate of rise of direct short-circuit currents (see Figure 1).

While a companion paper,[1] Part II, is primarily on the isolation of d-c faults through the operation of the d-c reclosing feeder circuit interrupters and their associated relays, this present paper, Part I, considers the conversion apparatus and its operating characteristics. Such conversion equipment may consist of motor-generator sets, synchronous converters, or rectifiers. The rectifier is being applied on practically all new installations because of its higher operating efficiency and lower maintenance costs. The d-c regulation curves of these three types are different, and this factor has a bearing on the magnitude and rate of rise of feeder short-circuit currents. Rectifiers have a no-load voltage rise which might affect the reclosing calibration of feeder circuit breakers. A "no-load" resistor, of a value to take about 0.5 per cent of the rectifier full-load rating, keeps the voltage from going too high, and a voltage regulator is used to maintain a desired voltage characteristic above this load value.

General Operating Conditions

Feeder circuit breakers must be operative even when the conversion units in a substation are out of service. This means that the bus voltage is determined by the feeder regulation from other substations. During heavy load conditions, when the feed through the d-c bus is most important, the voltage may be too low for proper feeder control operation. Such conditions make it desirable to employ a storage battery in the station for tripping and reclosing service. The feeder circuit breakers should be able to reclose successfully even under conditions when the station bus is completely de-energized.

Where more than one conversion unit is in a single substation, service continuity demands that troubles occurring on one unit do not take other units out of service. When rectifiers are used, arc-backs occasionally occur. With two rectifiers in parallel, it is practically impossible to distinguish which rectifier has arc-backed by instantaneous relays located in the transformer primary-current transformer circuits, since they have about equal currents. With more than two units operating in parallel, current differentiation is practical but, since only two of the units may be used for certain load periods, it should never be applied. (With three units, there is about 20 per cent difference in primary current; 60 per cent with four units; 90 per cent with five units; and 130 per cent for six units.)

Therefore, when applying rectifiers for multiunit electric traction service, the overcurrent relays are set for faults within the transformer and not beyond. With two or more units operating in multiple, there always is an adequate, reliable source of reverse current to trip the cathode circuit breaker, which also electrically trips the a-c circuit breaker. When an arc-back fault occurs, both the a-c primary circuit breaker and the cathode circuit breaker must trip, as the arc-back represents a fault on both the a-c and the d-c systems. When an anode circuit breaker is used, opening only the faulted anode pole will clear the fault from both systems. Adequate speed of clearing arc-backs, and still not jeopardizing tube life too much, calls for a maximum of 0.133 second (8 cycles on a 60-cycle base) for the a-c circuit breaker-opening and 0.05 second (3 cycles) for the cathode circuit breaker. In large-unit installations (2,000 kw and above) high-speed anode circuit breakers should be used to insure clearing the arc-back within one cycle for adequate tube and transformer protection.

Even with multiunit substations, there are times when a single unit will be in operation with no assurance that an adequate value of reverse current is available for cathode circuit breaker tripping. Should an arc-back occur under this condition, the tripping of the a-c and d-c circuit breakers would be delayed several cycles waiting for the time-delay overcurrent element to operate. Two methods of protection for this condition are being used. The first one is the use of the anode circuit breaker. The second is the application of a differential protective circuit which balances the incoming alternating current with the direct output current. Under normal conditions, the two values are balanced and no protective relay operation results. As the arc-back occurs, the alternating current rises

Paper 51-90, recommended by the AIEE Substations Committee and approved by the Technical Program Committee for presentation at the AIEE Winter General Meeting, New York, N. Y., January 22–26, 1951. Manuscript submitted October 25, 1950; made available for printing December 8, 1950.

S. S. WATKINS is with Gibbs and Hill, Inc., New York, N. Y., and M. E. REAGAN is with Westinghouse Electric Corporation, East Pittsburgh, Pa.

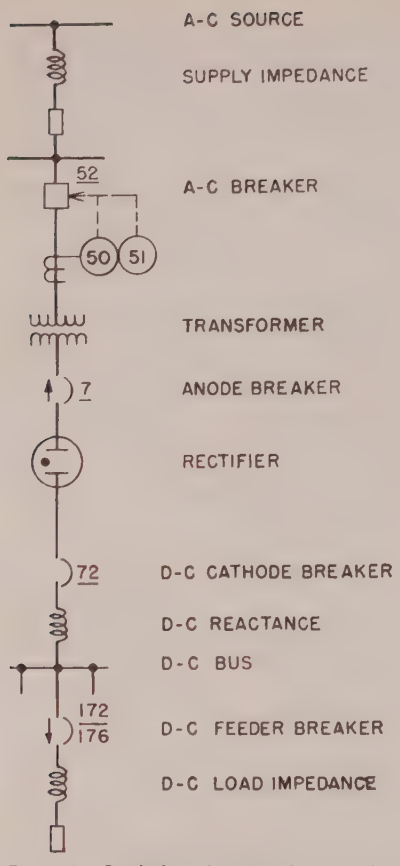

Figure 1. Single-line diagram of a-c to d-c distribution system

to some high level, such as eight times full-load current, while the direct current either goes to zero or reverses in the circuit. This results in destroying the circuit balance completely and operating a relay which trips both circuit breakers.

As d-c feeders are used in practically every electric traction substation, it is imperative that no instantaneous trip be applied to the cathode circuit breaker. Otherwise, the cathode circuit breakers would trip on a near-by feeder short circuit and woul dnot maintain normal service to the unaffected feeders. Backup protection in the form of a time-delay trip is at times used but, for the most part, the overcurrent trip is eliminated entirely from the cathode circuit breaker, leaving the backup function to the time-delay alternating overcurrent relays. Therefore, the cathode circuit breaker usually has its reverse current trip and a shunt trip for normal tripping.

Mechanical Structures

The d-c cathode and feeder circuit breaker physical structures have changed greatly in recent years. The open-type structures using insulated panel materials such as marble, slate, and ebony-asbestos mounted on pipe or angle-iron supports have been superseded by all-steel structures with drawout trucks carrying the circuit breakers.

Not too many years ago, design and operating engineers demanded as much separation between the positive and negative connections as it was physically possible to get. This was because of experience with ionized gas, from faults and circuit breaker operations, spreading to remote points of opposite potentials and causing other short-circuits and spreading the damage. The techniques of handling ionized gas, whereby the arcing time (which enormously affects the volume of gas) has been reduced greatly and the gases controlled to the point where they can be directed to safe areas, have been developed to the point where the new constructions are much safer to personnel and equipment than the old.

Most operating engineers of electric traction substations have learned to respect the damage that can be caused by d-c arcs and ionized gases. D-c arcs are much more prolific in gas production than a-c arcs. The a-c arc goes through zero twice per cycle and also has its potential reversed every half-cycle. The energy in the d-c arc also is much higher than in an a-c arc of equal current as the arc voltage of the alternating current is quite low while the direct current requires a higher arc voltage than service voltage in order to interrupt the circuit.

As a circuit interrupter opens its contacts, the resulting arc should be interrupted quickly to reduce the volume of ionized gases. Within the arc stream space, the transition from high conductivity to high resistivity is very fast for an a-c arc as it goes through zero. With the d-c arc, time is taken for the arc voltage to increase to a greater value than the supply voltage and it must remain higher until the current goes to zero. In general, the higher the inductance of the circuit, the longer the arcing time. As long as the arc exists, high temperatures cause the contact materials, such as carbon and copper vapors, to combine with the arc stream, and these conducting vapor gases take an appreciable time to cool. In the older type of air circuit breaker, the hot gases cause restriking after extinguishing several times as the contacts separate. The deionizing of the arc space would be much more rapid were these hot materials not present.

In air, there is a minimum breakdown voltage of about 300 volts, regardless of contact separation, but this does not hold when conductive vapors are present. Under such conditions, the breakdown voltage varies inversely with the density of such ionization and is independent of contact separation.

Open Structure

With open-type circuit interrupters which have been used in d-c traction systems for years, the gases were not controlled to any great extent. Insulating barriers sometimes were used to protect against direct contact. The rapidity of the dielectric recovery was slowed down by the inductance of the circuit and by the chemical composition of the gases. With the contact materials vaporizing, oxygen was diffused into the vapor, which caused a flame. Such flames can be observed rising in the air after the circuit is broken. They have a very low dielectric strength and can bridge any nearby points of opposite potential (see Figure 2).

During recent years, a great deal of development work has been done not only to speed up the interruption, which greatly reduces the volume of gases, but to direct the flow of the gases to areas where they can do no harm to personnel or equipment (see Figure 3).

A very successful method of speeding up the deionization process is the use of plates, which splits the arc into pieces of relatively short sections. By this process, many of the ions disappear by discharging into the plates, and the space charges adjacent to the plates consume some of the impressed voltage, making each plate act somewhat like a cathode. With a large number of plates, but not enough materially to limit the area of the passage the dielectric recovery time is reduced.

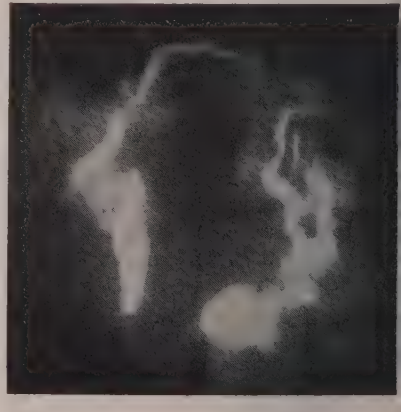

Figure 2. An uncontrolled 20,000-ampere 750-volt 12.5 millihenry arc

Metal-Enclosed Structure

Although the volume of ionized gas is lessened by the use of this method, there still is the problem of handling the gases which are formed so that no damage will result. One method is to direct the gases through an insulated stack or chimney which carries them to the outside atmosphere. Thus, the conducting vapor is isolated from any live parts within the structure and is permitted to cool before it can reach any point of opposite polarity (see Figures 4–6).

Grounding D-C Structures

Experience gained many years ago on 600-volt traction systems, in which one side of the electric circuit was grounded, caused design engineers to install all surrounding structures so that they are insulated from ground. On open panels, the boards were set on wood sills and the wall braces insulated from the wall. Where modern structures completely surround the d-c circuit breakers, bus, and associated equipment, it is of even more importance that this structure be insulated from ground such as is provided by the floor with its imbedded building steel. This is conveniently done by the use of a suitable floor covering of high dielectric linoleum.

Safety codes provide that the metal structures be grounded to drain off any static charges. This is accomplished by means of a ground protective relay with its coil connected between the steel structure and the station ground. Only one relay per station is required, as the circuit breaker structures are all tied together with a "ground bus."

There is a diversity of opinion on the application of the ground relay. Some believe it should have a series coil of very low resistance, while others believe that it should have a high-resistance operating coil. The authors of this paper belong to the latter school of thought for reasons expressed here.

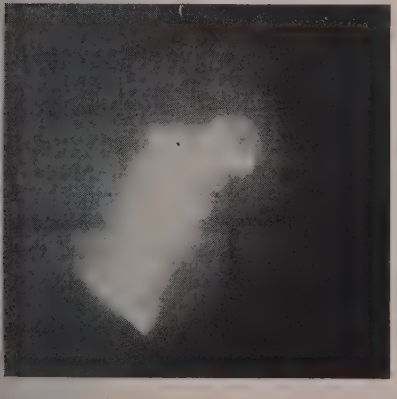

Figure 3. A controlled arc under same condition as Figure 2

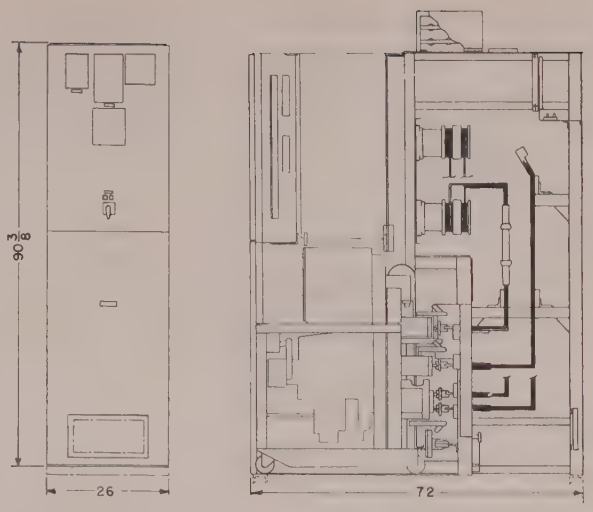

Figure 4. Front and section view of modern drawout-type d-c interrupter showing insulated stack for guiding ionized gases through the roof of structure

Practically all faults within modern cubicles will be caused accidentally and may be caused by maintenance men working on equipment while it is energized. Should an accidental short circuit occur, the low-resistance ground relay coil would permit large currents to flow. This would form ionized gases, which would spread quickly to all points within the structure. The maintenance man is exposed to two dangerous elements. The first is the flame, which may blind him temporarily and possibly set his clothes afire. The other is the voltage to which his body is exposed should he bridge the structure to a grounded part such as a steel conduit. With a heavy current flowing, the system regulation will drop the d-c bus voltage—possibly to the order of 350-400 volts on a 600-volt traction system—but practically all of this drop would be on the ground bus between the structure and ground resulting in the structure being raised almost that amount above ground. The resistance of a d-c arc varies with the current and the length of the arc. For currents of large magnitude (above 20,000 amperes), the voltage drop is approximately 30 volts per inch in the arc. When a high-resistance relay is used, the fault current is limited to milliamperes where very little or no arc will result. There will be practically no hot gases formed to spread damage, no blinding flash, and no arc damage to the maintenance man who may have caused the fault. He would be subjected to a higher value of direct voltage if he happened to be bridging the gap between the structure and ground. There would be but small difference in the effect of the electric shock on the man in being exposed to 350 volts in one case or 600 volts in the other for the three to eight cycles taken to trip the circuit breakers and de-energize the fault circuit. Therefore, taking all factors into consideration, it is our firm belief that a high-resistance ground fault protective relay should be used rather than one of low resistance.

With trolley coach operation, the practice of grounding varies throughout the country. Some systems operate ungrounded, some with but a single system ground, and others with many grounds. Even on ungrounded systems, it is recommended that the foregoing structure insulation and high-resistance relay grounding be used, as grounds can occur on such a widespread system without sounding an alarm. Ground detection schemes covering the whole d-c distribution systems are difficult to apply.

A ground relay alarm system is advisable constantly to supervise the continuity and workability of the scheme. One method now in use utilizes a separate alternating current source through an insulating transformer and rectified to direct current. The direct current operates through a Wheatstone bridge circuit to measure the resistance of the ground relay circuit. The alarm relay is set so that the normal current of the measuring circuit keeps the moving contact between two stationary contacts. Should the ground relay coil be accidentally short-circuited, the current in the measuring circuit increases to sound the alarm. Should the ground relay coil become open-circuited or the source of alternating current disappear, the measuring relay would get less current, which also sounds the alarm. This is shown schematically in Figure 7.

Synchronous Converters

The synchronous converter is somewhat similar to the rectifier in that it electrically connects the alternating current to the d-c system. Should the alternating supply voltage vary, the direct voltage would follow unless a regulator were used. The converter employs a series field winding with adjustable shunting resistor to obtain a desired voltage characteristic. With a rectifier, a compensated voltage regulator is used for this purpose. Converters and rectifiers can be and have been operated successfully in parallel where identical voltage characteristics apply.

The operating hazards of synchronous converters are connected chiefly with "flashovers." Flashovers are caused mainly by d-c feeder short circuits unless the a-c supply becomes unstable. The converter being a synchronous machine, the rotor drops back in phase position as the load increases—say about eight electrical degrees at full load. Short-circuit currents make the armature drop back in phase position in proportion to its magnitude. Because of the ratio of inductance to resistance (the time constant) of the circuit, the rate of rise on traction system current is relatively slow. The magnetic fields of the converter have time to be controlled by the commutating and compensating field windings, so that if the voltage between commutator bars is short-circuited by the brushes, the current which is circulated is not too large to be commutated successfully. The feeder circuit breaker detects the fault and opens, but, being relatively slow, opens after the fault current has reached its maximum value. The sudden interruption of the fault current releases the armature of the great proportion of its load and it quickly changes its phase position to correspond. This action is so fast that there is considerable field flux displacement, which creates a high voltage between the commutator bars being short-circuited by the brushes. Large circulating currents in this path cause the brushes to leave the commutator and draw an arc. Again, this arc creates ionized gases which can be swept by windage to reach the opposite polarity brush arm or the frame of the converter, causing a short circuit of "flashover." Flash barriers between the brush arms, if properly designed, can aid in directing the hot gases away from the next adjacent brush arm. Here again, if a ground detecting relay is used with its coil connected between the machine frame and ground, a high-resistance coil is recommended.

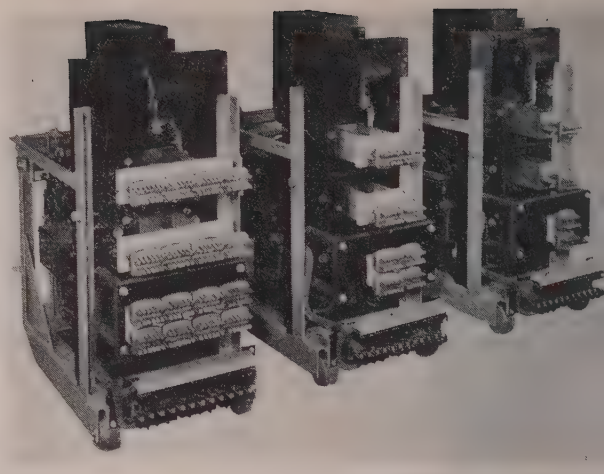

Figure 5. 8,000-, 4,000-, and 2,000-ampere truck-mounted d-c interrupters withdrawn from cells

It is important that the first feeder tap to the trolley be made at a distance sufficient to limit the short-circuit currents to a value which will not cause flashing or possibly permit the converter to "slip a pole."

One method of eliminating flashover caused by d-c feeder short circuits is the use of a high-speed circuit breaker with a shunting resistance which has a value sufficient to limit the converter output to approximately three times full-load current. The high-speed circuit breaker, which can limit the current rise in approximately one-half cycle, is fast enough on traction applications to keep the current within the commutating capacity of the machine. The feeder circuit breaker then may open and the three-times-normal load may be dropped without "flashing the commutator." As soon as the current drops to a normal value, the high-speed circuit breaker recloses to restore normal voltage on the bus and the unfaulted feeder circuits. The use of the high-speed circuit breaker reduces the duty on the feeder circuit breakers.

Another method which has been used on traction systems, but not to as great an extent, is the use of high-speed circuit breakers as feeder circuit breakers. The circuit breaker limits the current rise and opens the circuit so rapidly that the armature does not have time to assume a bad phase-angle position. High-speed circuit breakers have, inherently, a rate-of-rise tripping characteristic which may be valuable in discriminating between normal loads and short circuits. Other flash-eliminating schemes have been used, but have proved too expensive for popular application.

Motor-Generator Sets

Because of their lower efficiency, motor-generator sets are not widely used in traction substations. They do no readily operate successfully in parall with converters or rectifiers, since the a and d-c systems are electrically separate Power is transmitted mechanicall through the shaft. If the alternatin voltage varies up or down, the direct ou put voltage of the generator remains u changed. On the other hand, should th system frequency change, the moto speed would follow and would result in change of direct voltage. It is therefo important to recognize that regulatin equipment again is necessary to perm the parallel operation of motor-generat sets, synchronous converters, and rect fiers within the same substation. D generators are much less likely to flash over than converters. However, if th current gets high enough, the brushes wi leave the commutator and will start a arc with similar disastrous effects.

Types of Feeders—Definitions

The d-c distribution system starts wit the substation bus and extends to the r mote ends of the feeders. In general, th ideal feeder circuit breaker will remai closed under all conditions of legitima load and trip when a fault occurs even a the most remote point.

Two general types of feeders must b considered, although the methods tripping and reclosing may be identica The simpler type, known as a stub (radia feeder, is defined as one which connects load with its only source of power. Th other type, known as a multiple feeder, defined as one which is connected to common load in multiple with one more feeders from independent source The combination of these two is the usu type applied in transportation servic since operating setups may require th circuit breaker to operate under bot conditions. Tie-feeders, which tie tw

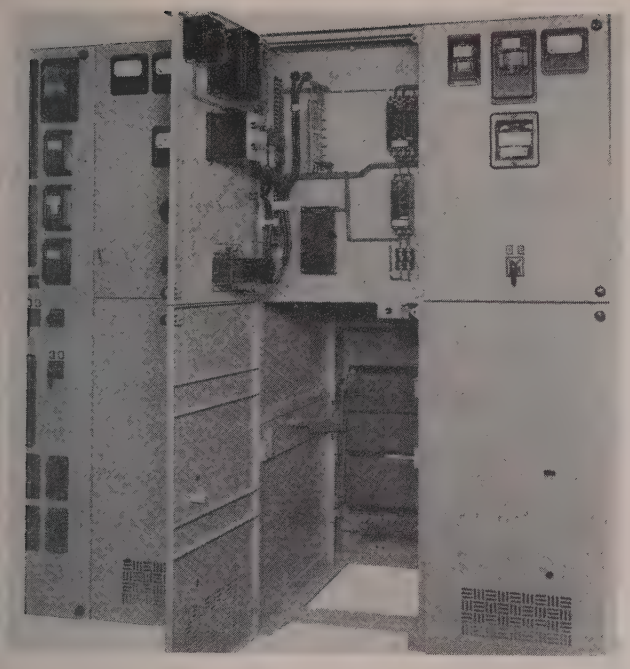

Figure 6. View of cell with truck removed showing automatic shutters covering main contacts

substations together with no trolley connection, and parallel feeders, which parallel circuit breakers from the same source, are rarely used in transportation service. Sectionalizing circuit breakers, while part of the distribution system, are not considered feeder circuit breakers.

Feeder Circuit-Breaker Tripping

Two general types of feeder circuit-breaker tripping systems are used in traction service; the overcurrent system and the rate-of-rise system.

A device designed to trip as rapidly as possible on a set value of current is termed "instantaneous" overcurrent. Limitations of the instantaneous device are overcome to some extent by inclusion of a time delay that is an inverse function of current magnitude, whereby the device is termed "inverse overcurrent." Either or both of these devices may be built into the circuit breaker, the oldest and simplest circuit breakers having used instantaneous devices in this manner. Or the same functions may be provided by overcurrent relays arranged to trip the circuit breaker through a shunt-trip coil.

Current-rate-of-rise tripping devices, either built into the circuit breakers or employing relays and shunt-trip coils, have had increasing use on d-c feeders during the past thirty years.

In addition to the two foregoing types, a limited use has been made of undervoltage tripping, which uses excessively low voltage as a criterion of short circuit. Because operation may require that circuit breakers remain closed under low voltage conditions, such as might occur on a d-c bus with all conversion apparatus out of service, the use of undervoltage release is not recommended for tripping feeder circuit breakers.

Evaluation of the fields of application and the limitations of the various tripping devices requires a review of the desired performance of such devices and the manner in which this performance is affected by characteristics of the feeder systems and the load.

Sectionalizing Circuit Breakers

Sectionalizing circuit breakers are used to improve traction service. They serve two general purposes. First, they may be used to sectionalize long feeders where the overcurrent tripping relay may be set down to a value below the short-circuit current at the end of the feeder. This feature reduces the need for discriminating tripping at the substations in locations where it may be applied. The second use is to isolate branch lines so that troubles there may be disconnected, permitting normal service on the rest of the system.

Sectionalizers are of the automatic reclosing type which reclose after the short circuit clears.

Reclosing the Feeder

After the feeder circuit breaker has been opened to free the system of a fault, the next problem is to reclose it safely as soon as the fault disappears. With manual operation, the old trial-and-error method of testing the circuit by reclosing the circuit manually after a definite time is still used in many places. This practice puts unnecessary strain on the equipment and should be avoided. In unattended stations, the circuit is tested by a relatively small test current which, operating through relays, recloses the circuit breaker only after the fault has cleared. The value of test current is too low to cause annealing of copper in the contact wire circuit.

To give a reliable indication of the load which will be picked up as a feeder circuit breaker recloses, the normal relaying scheme in use today is quite adequate. As it is a collection of devices simply to measure the resistance or voltage of the individual feeder, it can perform its duties quite accurately. There is one hazard that must not be overlooked. That concerns a feeder such as is used to feed a storage yard circuit when a large percentage of the load is streetcar and coach lighting. Modern lamps, when cold, reduce their resistivity to about 10 per cent of their hot value. The reclosing value must be set for a lower value or some time-delay must be used to delay tripping for the few cycles it takes to heat the lamp filaments and raise their resistance to their normal value.

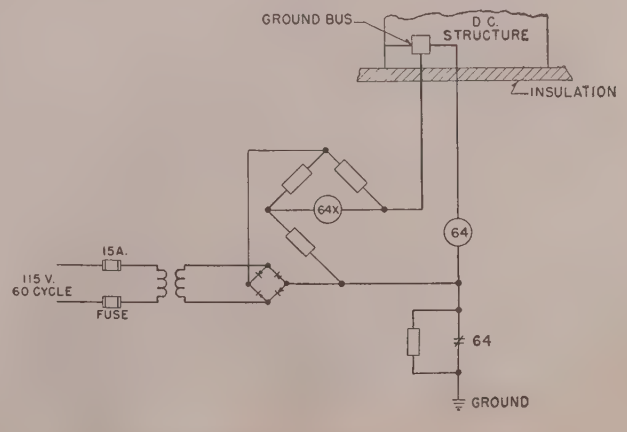

Figure 7. Diagram of ground protective scheme with supervision circuit

For a stub feeder, the reclosing scheme could be much simpler than for a multiple type. In fact, the first reclosing equipment devised was applied to a stub feeder and was a simple divided circuit. The safe resistance of a feeder circuit for reclosing should be slightly more than will permit full load to be picked up. Thus, for a 2,000-ampere feeder, the reclosing equipment might be safely set for 1,800 amperes or less. In a substation with a normal bus voltage of 600 volts, the feeder circuit would have a resistance value of 0.33 ohm. With the feeder circuit breaker open and a solid short circuit on the feeder, the resistance of the feeder circuit would be low compared with 0.33 ohm. Should a relatively high resistance, say 100 ohms, be so connected that one end of the resistor is attached to the bus while the other end divides—one portion leading to the load side of the circuit breaker and the other going through a low-resistance relay coil to the negative bus—a very simple reclosing scheme could be provided. The coil and feeder resistances are so low that, regardless of the feeder resistance value, the current through the resistor would be six amperes. This measuring current would divide into the two branches in inverse proportion to the resistance of the two branches. Under the short-circuit condition, most of the six amperes would feed the fault and very little would traverse the relay coil. When the feeder circuit increases its resistance to 0.33 ohm half of the current would be in each leg of the divided circuit. Should the relay be calibrated to operate on three amperes, its contacts could reclose the circuit breaker, which could pick up 1,800 amperes as it closes.

This simple circuit cannot be used on traction systems where voltage may be applied from the load side. Should 600 volts be applied to a coil of such small resistance, damaging currents would ruin the relay.

For multiple feeders, the reclosing circuitry is more complicated and is arranged so that the relays cannot be damaged if the remote feeder circuit breaker should close. In one form, a Wheatstone bridge circuit is used to indicate when it is safe to reclose the feeder circuit breaker. Also, the equipments usually are arranged so that proper reclosing conditions can be measured in either direction. The sequence of operation after the circuit breaker is tripped is usually

1. A timing relay set for about ten seconds is operated to prevent regenerated voltages from any rolling stock giving false indications of circuit conditions.

2. At the end of the timing period, the voltage relays have determined in which direction (toward or from the bus) the measuring circuit will be connected, and other relays connect it in the circuit.

3. The reclosing relay makes contact to reclose the circuit breaker as soon as the feeder short circuit clears.

Lightning Arresters for Overhead Feeders

Since the aerial feeders and trolley systems are exposed to lightning, some form of lightning protection is advisable. Suitable d-c lightning arresters should be installed at the point where the feeder leaves the building. If underground, they should be installed where the cables emerge from the conduits. Voltage ratings of the lightning arresters must not be too low as, particularly with third-rail circuits, a great deal of energy can be stored in them. Voltages as high as 2,400 volts have been measured on 600-volt circuits. When lightning arresters are mounted in the substation, they should not be housed within the d-c cubicles. High alternating voltage service wires sometimes come in contact with the 600-volt distribution cables and wires, causing the d-c lightning arresters to fail. Here again, this type of failure can cause large volumes of ionized gas to form. Therefore, the lightning arresters should be mounted with a great deal of open space around them.

Supervisory Control of Feeders

When supervisory control is used to superintend the operation of traction substations, the control of the feeder circuit breakers usually is such that the automatic features of tripping and reclosing are retained. When the operator trips a feeder circuit breaker from the dispatching office, the circuit breaker not only is opened by the operation of the shunt-trip mechanism, but the reclosing circuitry is also de-energized so that it will make no attempt to reclose. When the dispatcher sends the closing code through to the substation, the circuit breaker usually is not closed directly, but simply unlocks the reclosing circuits which take over to close the breaker only if the line characteristics are satisfactory.

Reference

1. D-C Power Supplies and Isolation of Faults on Electric Transit Systems—Isolation of D-C Faults, Part II, S. S. Watkins, M. E. Reagan. *AIEE Transactions*, volume 70, part I, 1951, pages 543–50.

Discussion

H. F. Brown (New York, New Haven and Hartford Railroad, New Haven, Conn.): The 2-part paper by Messrs. Watkins and Reagan is a valuable addition to the technical literature associated with railway electrification.

As electric train loads have increased, especially on the older low-voltage electrified systems, it has become increasingly difficult to distinguish between train loads and short circuits. The simple overcurrent relays or tripping devices used in the early days of electric traction now no longer apply to this type of service. Even on the higher voltage systems (3,000 volts direct current) the greater distance between substations permitted by the higher voltage, together with the increased resistance of the feeder circuits, presents the same problem in distinguishing between train loads and faults.

On the 11-kv a-c traction systems, especially those systems which consist of multitrack networks with a large number of circuits in parallel, it is still possible to use the simple overcurrent relays to clear faults in many cases, although here again the longer distance between sectionalizing and switching stations may cause the same difficulty in discriminating between heavy train loads and short circuits on long feeders.

The first part of this paper is an excellent outline of the latest thoughts in substation design, especially in connection with switching and protective equipment for traction power supply on grounded systems. The second part of the paper is an equally valuable analysis of the modern methods for discriminating between heavy loads and faults, together with the methods of clearing, with minimum interruption to service, faults from the system. The authors are to be congratulated on their valuable contribution to technical literature on this subject.

D-C Power Supplies and Isolation of Faults on Electric Transit Systems—Part II

Isolation of D-C Faults

S. S. WATKINS
FELLOW AIEE

M. E. REAGAN
FELLOW AIEE

THIS paper, Part II, is a continuation of Part I, "D-C Power Supply,"[1] which covered conversion apparatus and circuit breakers. The present paper, Part II, deals with the problems of selective isolation of faults on the d-c distribution systems and with automatic devices for selective tripping.

Fundamentals of Selective Tripping

Tripping devices for d-c feeder circuit breakers must satisfy the following fundamental requirements:

1. Prompt isolation of the faulted section on occurrence of each short circuit.
2. Nontripping on load current.
3. Noninterruption of current in unfaulted sections.

Critical short-circuit cases for tripping-device performance are illustrated in Figure 1, which is a 1-line diagram of a typical section of contact system supplied by a substation at each end. Each line between substations represents the positive trolley or third rail in the case of rail transit system, or the positive and negative trolleys in the case of a trolley coach system.

If a short circuit occurs on any trolley close to Substation 2, the fault currents through circuit breakers *A* and *D* at Substation 1 are equal, and no discrimination is possible at Substation 1 until the Substation 2 circuit breaker feeding the fault has opened. To avoid interruption of current on unfaulted sections, the tripping action must be sequential, with the tripping devices of circuit breakers distant from the fault delayed sufficiently to permit prior tripping of the near-by circuit breaker, such as circuit breaker *C* in Figure 1.

Instantaneous Overcurrent Tripping

For near-by faults instantaneous overcurrent tripping is the ideal protection. Short circuits may be interrupted by various available devices within the following approximate times:

High-speed circuit breaker with built-in overcurrent device, seconds	0.02
Medium-speed circuit breaker with built-in overcurrent device, seconds	0.07
High-speed relay energizing shunt-trip coil on circuit breaker, seconds	0.08

Limitation of damage to apparatus and circuits and avoidance of hazard to persons dictate that maximum possible use be made of instantaneous overcurrent tripping. A short circuit at the substation d-c bus can have values ranging from twice to ten times the maximum load swing, depending on the characteristics of the system of power supply and distribution. But as the position of the short circuit is moved away from the substation, the resistance of the contact and feeder system rapidly reduces magnitude of the fault current. The following figures for a particular substation and feeder circuit are taken from a recent study on a system using multiple-unit trains on heavy suburban traffic:

D-c bus voltage, approx.	700
Distance to next substation, miles	2.1
Instantaneous overcurrent setting of feeder circuit breaker, amperes	10,000
Short circuit at d-c bus, amperes	45,000
Short circuit distant about $1^1/_2$ miles, amperes	10,000
Short circuit at end of 2.1-mile section, amperes	7,350

These figures show that in the sample case used for illustration, the advantages of instantaneous overcurrent protection extend a mile and a half from the substation, or about 70 per cent of the section length. Similar figures should be calculated for every d-c transit or railway feeder. The extent of the zone of instantaneous overcurrent tripping is an important criterion of the protection afforded.

Minimum Short Circuit and Maximum Load Currents

The critical test of any system of selective tripping is its ability to trip on short-circuit currents of minimum value and also to avoid tripping on maximum load swings. This critical requirement may be illustrated by considering circuit breaker *A* in Figure 1 when a minimum short circuit occurs at the far end of the section at *C*. The value of the minimum short-circuit current is determined mainly by the resistance of the circuit from *A* to the end of the section at *C* and return by running rails or by negative trolley. Satisfaction of the dual requirements of isolation of all short circuits and nontripping on load depends upon the ratio of minimum short-circuit current to maximum load current, a ratio that is related closely to the voltage drop for which the feeder and contact system is designed. This relation may be expressed mathematically for an idealized case in which, for purposes of voltage-

Paper 51-91, recommended by the AIEE Substations Committee and approved by the AIEE Technical Program Committee for presentation at the AIEE Winter General Meeting, New York, N. Y., January 22-26, 1951. Manuscript submitted October 25, 1950; made available for printing December 11, 1950.

S. S. WATKINS is with Gibbs and Hill, Inc., New York, N. Y., and M. E. REAGAN is with Westinghouse Electric Corporation, East Pittsburgh, Pa.

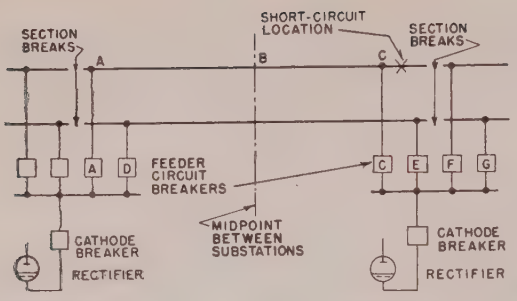

Figure 1 (left). Typical feeder circuit layout between two substations

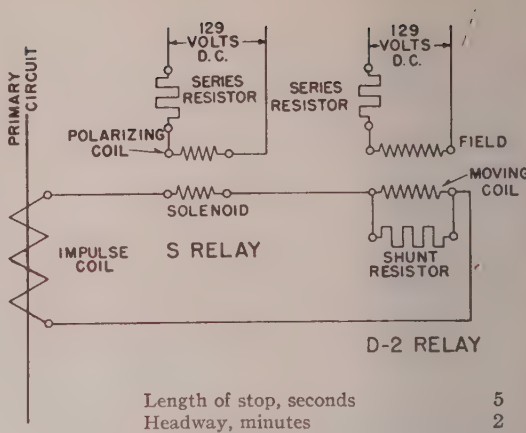

Figure 3 (right). Diagram of connections for the *S*- and *D*-type short-circuit-detecting relays

drop design, the average load of a rush-hour period is taken as uniformly distributed over a trolley section between two substations with equal d-c bus voltages. The relation is as follows:

$$I_{SC} = I_L \div (4D) \qquad (1)$$

Again referring to Figure 1, the symbols have meanings as follows:

I_{SC} = short-circuit amperes through circuit breaker A for short circuit at end of section at C, neglecting any parallel load current at time of short circuit

I_L = load amperes through circuit breaker A under assumption of average load uniformly distributed between A and C

D = per cent voltage drop expressed as a decimal, from d-c bus at A to section midpoint at B, while carrying load I_L

R = resistance in ohms of one loop circuit, substation to midpoint and return

E = direct volts at substation bus

Equation 1 is expressed graphically in Figure 2, where an average drop of 8 per cent is seen to permit a ratio of minimum short circuit to average load of 3-to-1. However, the actual margins available for satisfactory performance of tripping devices are considerably less than indicated by Figure 2, for the following reasons:

1. Tripping devices must be set to carry maximum loads, not average loads.

2. Tripping devices must have some margin under calculated minimum short circuits to allow for resistance in the fault, error in performance of device, and error in calculated data.

The equation and graph are given to emphasize the effect of excessive voltage drop. They have value as a starting point in preliminary feeder design.

However, each specific application must be studied carefully and the short-circuit currents and loads calculated for the actual operating conditions. Concentration of load in large units such as trains of multiple-unit cars in interurban service will cause load swings that are several times the average load. A transit system using a large number of small units, such as trolley coaches on close headway, may approach the uniformly distributed load which was a basis of idealized mathematical treatment. But even here the tripping devices must carry maximum loads in excess of the average loads.

Trolley Coach Systems

A hypothetical trolley coach system has been studied for the relation between maximum load and minimum short-circuit values. The assumed data are as follows:

Schedule speed, miles per hour (0.28 mile per minute)	16.8
Stops per mile	6
Length of stop, seconds	5
Headway, minutes	2
Average distance between coaches, miles	0.56
Distance between substations, miles	3.36
Average number of coaches on section	6
Duration of cycle, including acceleration, running, braking, and 5-second stop, seconds	35
Average current during cycle, amperes	140
Highest 5-second average during cycle of one coach, amperes	260
Substation d-c bus voltage	600

If the foregoing system were designed to permit a drop of 8 per cent from substation bus to midpoint between substations for the average load, the following values would result:

Loop resistance from circuit breaker A to end of section at C, ohms	0.456
Current through circuit breaker A to short circuit at C, amperes	1,315
Average load current through circuit breaker A, amperes	420
Ratio of minimum short-circuit current to average load current	3.13

Although the average load current through circuit breaker A (Figure 1) is 420 amperes during the rush-hour period, the circuit breaker must carry considerably higher currents for several seconds at least. Change of traffic lights would

Figure 2. Curve showing ratio of minimum short circuit to average load current for various voltage drops

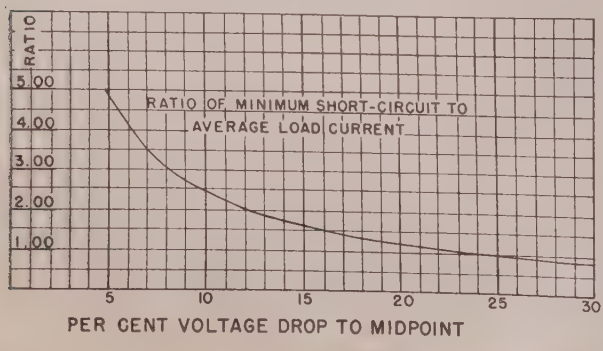

Figure 4. Curves showing rise of primary current and both measured and calculated secondary current

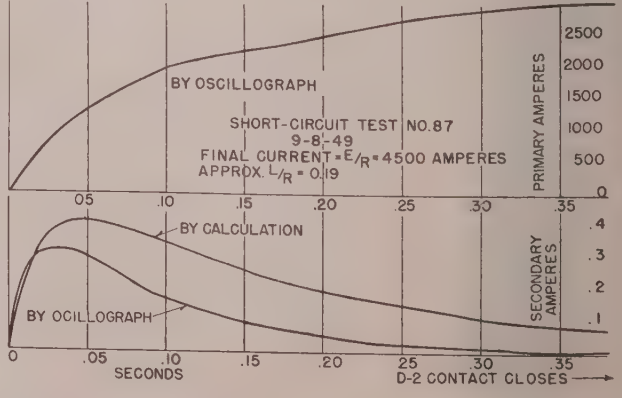

cause most or all of the six coaches on the section to start within a few seconds. Bunching in traffic could increase the number of coaches to more than the average six per section. Current swings of 1,000 amperes lasting several seconds might be expected frequently, with occasional swings to 1,300 amperes, approximately equal to minimum short-circuit current.

Under these conditions, any tripping device depending on current magnitude alone would cause undesirable tripping on load swings if it were adjusted to protect the section against short circuits. If the system were designed for greater voltage drop than the assumed 8 per cent, the short-circuit protection would become still more unsatisfactory if based on current magnitude alone.

Heavy Third-Rail Service

Multiple-unit trains greatly increase the problem of feeder protection, especially on interurban systems with great concentration of load in single trains. This is illustrated strikingly on the electrified zone of the Long Island Rail Road, a third-rail system now operating at about 700 volts on substation busses.

Since the original operation in 1905, the increase of load has been great, from time to time requiring the installation of additional substations to carry the increased load and to keep voltage drops within limits. A recent program of improvements added a considerable number of rectifier substations, generally at intermediate locations, so as to reduce the spacing between substations. During this program the problems of feeder protection received intensive study. Trains consist of as many as eight motor cars and four trailers. Feeder circuit breakers, in use before the improvements, had overcurrent tripping devices generally set to trip at 10,000 amperes. Operating experience had shown these settings to be necessary for carrying the load without frequent tripping on load swings. The necessity of these high settings resulted largely from the high values of acceleration currents of single trains. Figures on a test train showed an initial current rush of 4,300 amperes on the first notch and a rise to 9,000 amperes during the accelerating period.

Weights of rail vary, with 150-pound third rail and 112-pound and 100-pound running rail predominating. Section lengths from substation to substation range from less than one mile to more than four miles. Minimum short circuits were calculated over a considerable part of the electrified zone. The difficulty of feeder protection is illustrated by the representative values shown in Table 1. Of the selected sections, only the Hillside-St. Albans section could be protected to the end of the section by an overcurrent tripping device set for 10,000 amperes. Even this one might fail occasionally, as 15 per cent margin is quite inadequate to cover inaccuracies of tripping devices and allow for resistance in the fault. The other sections, which are representative of the greater part of the zone that was studied, definitely could not be protected to the ends of the sections by the 10,000-ampere overcurrent setting.

Thus it is apparent that no system d-c traction feeders, either for the light coach service or for heavy multiple-car, interurban trains, may be certainly and completely protected by d-c overcurrent relay devices alone.

Application Field of Overcurrent Tripping

Instantaneous overcurrent tripping is the ideal protection against short circuits close to the substation and as far away as load and selectivity permit. For the short circuits of smaller value near the next substation, selectivity on parallel sections requires sequential tripping, and overcurrent devices must be supplemented with time delay. A combination of instantaneous and time-delay overcurrent tripping may give satisfactory protection where the ratio of minimum short circuit to maximum load current is high. The time delay must be co-ordinated carefully with the duration of the load swings. As the ratio of short circuit to load falls toward unity and below, overcurrent tripping entails one or more of the following compromises:

1. Occasional trippings on load must be accepted.
2. Time-delay settings must be so great as to permit damage from prolonged arcing on distant short circuits.
3. Current settings must be made so high that automatic tripping on distant short circuits is abandoned.

Tripping Devices Utilizing Current Rate-of-Rise

The limitations of overcurrent devices under the load and short-circuit conditions described in previous paragraphs have led to the development of a number of tripping devices that utilize current rate-of-rise as the criterion for distinguishing between short circuits and loads. Before proceeding to the particular device to be described in this paper, the following characteristics and limitations common to all current rate-of-rise devices should be noted.

1. Short circuits on the contact and feeder circuits of d-c transit systems rise to nearly the sustained value in a fraction of a second. Therefore rate-of-rise devices readily distinguish between short circuits and loads which may be greater than the minimum short circuits, so long as the loads are constant or change at relatively low rates.
2. A rate-of-rise tripping device protects against short circuits, but not against sustained overloads. The latter must be protected against by other devices, such as thermal devices on the cables or long-time direct overcurrent relays set on an operating value below the minimum short-circuit current.
3. Since rate-of-rise devices fundamentally depend on voltage generated by change of current, they will respond to sudden decrease of current such as occurs on opening of a circuit breaker under heavy load or fault, unless the device is suitably polarized. Tripping should occur only on *increase* of *outgoing* current.
4. Acceleration of transit equipment also causes sudden increase of current, tending to cause operation of rate-of-rise tripping devices. Each application must be examined for co-ordination between short-circuit protection and acceleration-current inrushes.

Table I

From	To	Distance in Miles	Amperes	Minimum Short Circuit Per Cent of Overcurrent Setting of 10,000 Amperes, Per Cent
Hillside	St. Albans	1.4	11,500	115
Hillside (express)	Bellaire	2.42	5,470	55
Lindenhurst	Babylon	2.1	7,350	74
Cedar Manor	Laurelton	2.66	4,780	48

The D-C Short-Circuit Detector

About 28 years ago, the principle of current rate-of-rise was applied to the tripping device that is shown in wiring diagram form in Figure 3. This device, called the "short-circuit detector" for the purposes of this paper, consists of an im-

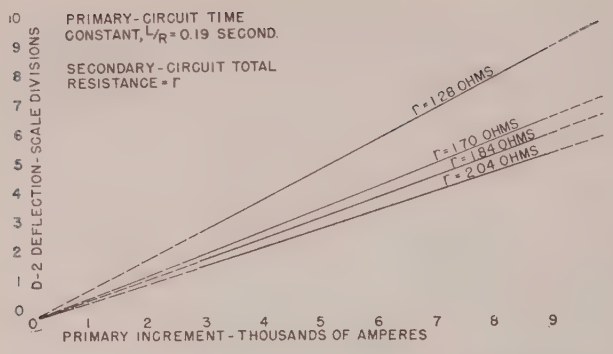
PRIMARY-CIRCUIT TIME CONSTANT, L/R = 0.19 SECOND.
SECONDARY-CIRCUIT TOTAL RESISTANCE = Γ
Γ = 1.28 OHMS
Γ = 1.70 OHMS
Γ = 1.84 OHMS
Γ = 2.04 OHMS
D-2 DEFLECTION-SCALE DIVISIONS
PRIMARY INCREMENT-THOUSANDS OF AMPERES

Figure 5. Curves of *D*-relay deflections with various values of secondary circuit resistance

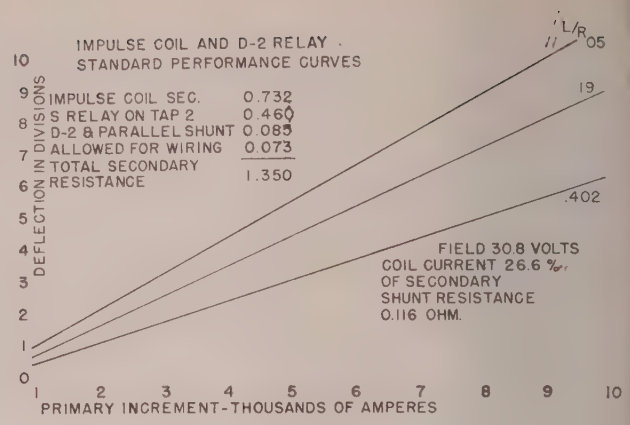

Figure 8. Standard performance curves of *D* relay (shunt resistance = 0.116 ohm)

pulse coil in the primary circuit, with two d-c relays, the type *D* and the type *S* connected in series in the impulse coil secondary circuit. Relay contacts are connected to energize a shunt-trip coil on the feeder circuit breaker. The construction of the impulse coil is similar to that of a window-type a-c transformer with air gaps. The feeder circuit that is to be protected is carried through the window, so that it constitutes the 1-turn primary circuit of the impulse coil.

While primary current through the impulse coil is increasing or decreasing, direct current is induced in the secondary circuit through the relays. The relays are polarized and are connected so as to close contacts when the secondary current is in the direction caused by increase of outgoing primary current. So long as the primary current is constant, no matter how large, no current is induced in the secondary circuit.

Prediction of Performance

D-c short-circuit detectors, operating on the principles just described, have been applied to the protection of d-c railway and transit feeder circuits over a period of 28 years. Superiority of this protection over devices depending on overcurrent alone has been demonstrated by staged short-circuit and load tests and has been proved by operating experience.

However, both the application and adjustment of the detectors to specific situations had been dependent largely on field tests, observations, and trial-and-error adjustment. When more than 100 feeders on the Long Island Rail Road were to be equipped with improved protection, it became evident that quantitative prediction of performance and predetermination of desired settings would be a necessity.

To this end several series of tests on a sample detector were run during 1949 in the high-power d-c laboratory in East Pittsburgh. These tests resulted in some redesign and improvement of components, in quantitative performance data and a clearer understanding of the operating principles, and, finally, in the development of techniques for calibration, routine testing, application to specific load and fault conditions, and settings for predetermined performance.

The components of the detectors used in this recent application and the performance data are described in succeeding paragraphs.

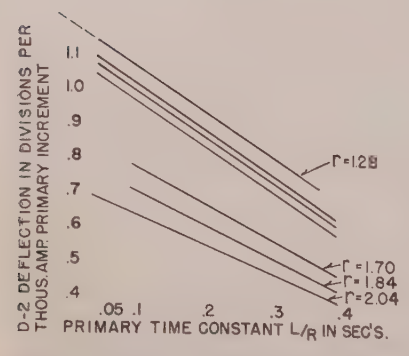

Figure 6. Curves of *D*-relay deflections with various secondary circuit resistance and time constants

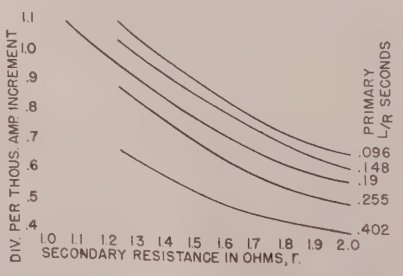

Figure 7. Curves of *D*-relay deflections with various secondary circuit resistance and primary time constants

The Impulse Coil

The impulse coil is an adaptation of a window-type, 4,000-to-5 current transformer. It has the following characteristics:

Number of secondary turns	798
Secondary-coil resistance, ohms	0.732
Mutual inductance, henrys	0.000028
Self-inductance of secondary coil, henrys	0.0228

The inductance figures apply for flux densities below saturation. The core is constructed with 12 air gaps of 3/32-inch each, increasing the magnetic reluctance so that the flux density remains below the saturation point up to a magnetomotive force of 17,000 ampere turns.

The Type-*D* Relay

Type-*D* relays have been used for many years as reverse current relays and temperature relays in addition to use as elements of the d-c short-circuit detectors. This relay is a d'Arsonval-type d-c contact-making milliammeter. The new design, recently adopted as standard, employs permanent magnets for the fixed field. The relays applied as short-circuit detectors up to the present time have used field coils to produce the fixed field.

The type-*D* relay recently applied as a short-circuit detector on the Long Island Rail Road has the following characteristics:

Resistance of moving coil, ohms	0.32
Resistance of field winding (with two coils in parallel), ohms	700
Resistance of field series resistor, ohms	2,232
Total, ohms	2,932
With control bus, volts	129
Drop across series resistor, volts	98.2
Voltage across field winding	30.8

With a field strength produced by 30.8

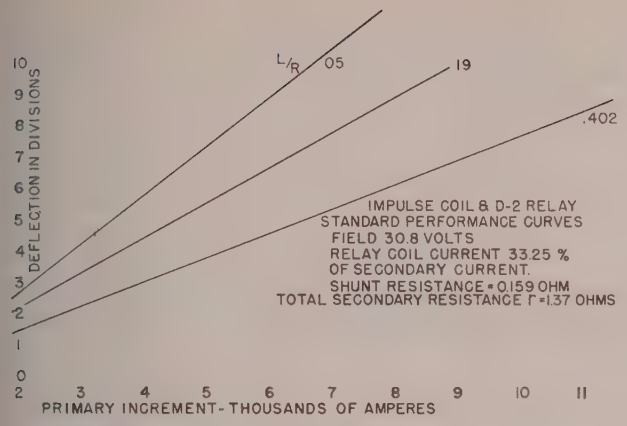

Figure 9. Standard performance curves of *D* relay (shunt resistance = 0.159 ohm)

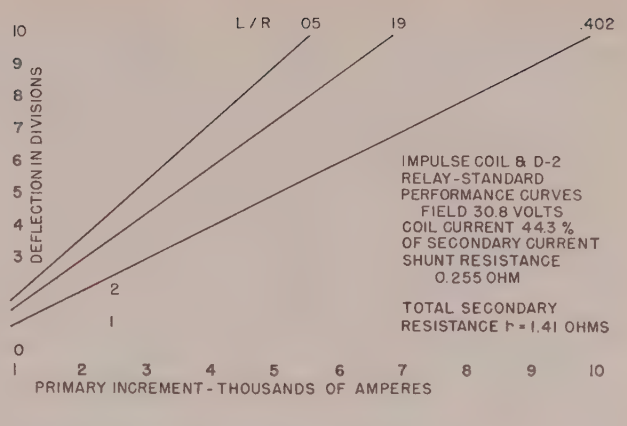

Figure 10. Standard performance curves of *D* relay (shunt resistance = 0.255 ohm)

volts at the field terminals a test relay of this application gave a fixed deflection of 0.3 division per millivolt applied to the terminals of the moving coil, or nine-tenths of the full scale of ten divisions when 30 millivolts were applied.

This relay has mechanical characteristics similar to those of a ballistic galvanometer and has little damping. As a mechanical system of mass and spring it had a natural oscillating period of about 1.6 seconds, or about 0.8 second for a full swing in one direction. When a constant potential suddenly is applied to the moving coil, the initial full swing is about double the value of the steady deflection that is produced by the same potential when the moving coil has come to rest.

The Type-*S* Relay

The type-*S* relay is a high speed, solenoid type, d-c relay. The relay is designed to pick up at high speed when the instantaneous value of secondary current equals the value of the adjustment tap that is being used. A polarizing coil is provided to prevent pickup of the relay on secondary current in the reverse direction. If reverse secondary current reaches a value three times that of the tap being used, the polarizing coil is overcome and the relay functions as a nondirectional current relay with pickup at three times the tap value.

The type-*S* relays used on the application here described have seven taps, ranging from two to six amperes, with solenoid resistances ranging from 0.46 to 0.122 ohm.

Theory of the Short-Circuit Detector Performance

Although the impulse coil is an adaptation of a 4,000-to-5 ampere, a-c transformer, any conception of this coil as a current transformer, having a current ratio, is not applicable to its use in the short-circuit detector. The 4,000-to-5 ratio applies only on alternating current after the energizing transient has subsided.

But as the impulse coil is used in d-c circuits, its entire performance is transient and alternating current does not exist. The impulse coil should be considered fundamentally as a transformer wherein change of primary current generates secondary voltage. The transformer constants of mutual inductance and secondary self-inductance include the effect of turn ratio.

The following symbols are used in analysis of the performance of circuits:

Instantaneous values:

t = time in seconds
i_p = primary current in amperes
i_s = secondary current in amperes

Constants:

R = resistance of entire primary circuit, in ohms
L = inductance of entire primary circuit, in henrys
E = constant direct voltage on primary circuit
N = turn ratio of impulse coil
M = mutual inductance of impulse coil, henrys
l = inductance of entire secondary circuits, henrys
$\epsilon = 2.7183$—Base of Naperian logarithms
$1-\epsilon^{-1} = 63.2$ per cent

The primary and secondary circuits are shown in Figure 3. On application of the voltage E to the primary circuit, the primary current rises to its sustained or E/R value exponentially as expressed by the following equation:

$$i_p = \frac{E}{R}\left(1-\epsilon^{-\frac{Rt}{L}}\right) \qquad (2)$$

Its rate of rise at any instant is:

$$\frac{di_p}{dt} = \frac{E}{L}\left(\epsilon^{-\frac{Rt}{L}}\right) \qquad (3)$$

The ratio L/R is the time constant of the primary circuit and may be determined by measuring time on an oscillograph record to the point where the primary current has reached 63.2 per cent of its sustained value.

The changing primary current produces a secondary voltage which instantaneously is the product of the mutual inductance and the rate of change of primary current. This changing secondary voltage is applied to the secondary circuit, which in turn consists of a resistance r and an inductance l, and has a time constant, l/r. The resultant secondary current is defined by the following equations:

Instantaneous value:

$$i_s = \frac{M\frac{E}{R}}{\frac{Lr}{R}-l}\left(\epsilon^{-\frac{Rt}{L}}-\epsilon^{-\frac{rt}{l}}\right) \qquad (4)$$

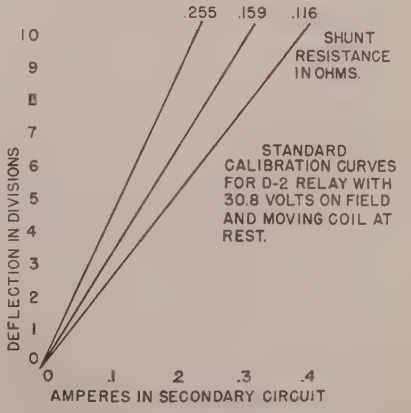

Figure 11. Standard calibration curves of *D* relay with 30.8-volt field excitation

Maximum secondary current:

$$I_s = \frac{ME}{Lr}\,\epsilon^{-\frac{Rr}{L}} \quad (5)$$

Time to occurrence of maximum secondary current:

$$T = \frac{\log r/l - \log R/L}{r/l - R/L} \quad (6)$$

Calculated values of secondary current are compared in Figure 4 with oscillograph values from a short-circuit test on the sample short-circuit detector. While the numerical values are not close, the similarity of shapes indicates a satisfactory agreement between theory and test performance.

The inductances of secondary leads and relays were found to be negligible, therefore the self-inductance of the impulse-coil secondary was taken as the secondary inductance, l. In determining the secondary circuit resistance, r, all relays, adjusting shunts, and leads must be included.

Examination of the graphs and of equation 4 shows that the secondary current is the resultant of two exponential quantities. It may be considered as the effect of applying to a secondary circuit of resistance r and inductance l, a voltage which starts at the value $E_M = ME/L$, but decreases exponentially as determined by the primary circuit time constant.

The deflection of the D relay depends upon duration as well as magnitude of secondary current, being proportional to the area under the current-time curve, but with a varying ratio of deflection per ampere-second. Because of the ballistic characteristic of the D relay, momentum acquired during the impulse of secondary current continues to move the contact after the secondary current has diminished to negligible value. In the test from which the oscillographic record on Figure 4 was taken, the secondary current had diminished to 18 per cent of maximum value in 0.2 second, but the contact swing to 4.1 divisions and closed at 0.4 second after the start of the primary current impulse.

Test Data and Performance Prediction

Preliminary tests were made on the D relay as a separate device. At different values of voltage applied to the fixed-field coils, measured millivolts were applied to the terminals of the moving coil, and the steady deflections in scale divisions were noted. Deflection per millivolt on the moving coil increases directly as field strength, and with a fixed field, deflection increases directly as millivolts applied to the moving coil. These same tests emphasized the fact that a fairly strong field is necessary to minimize variations in residual magnetism and to permit consistent performance of the relay as a measuring instrument. A field strength of 30.8 volts was used throughout the final series of tests and was adopted for the application of the short-circuit detectors on the Long Island Rail Road.

The shunt resistor that is shown in Figure 3 is used for adjusting the trip setting by controlling the percentage of total secondary current that passes through the moving coil of the D relay. By comparing deflections on steady and sudden applications of measured millivolts it was proved that the percentage calculated for a given value of shunting resistor with steady current remains the same under transient conditions. Throughout the final series of tests from which the performance data were derived, the moving coil was shunted by a resistor of 0.116 ohm, which fixed the percentage of secondary current passing through the moving coil at 26.6 per cent.

For purposes of the test, a primary winding of 150 turns was wound through the impulse-coil window. This produced 150 ampere turns for each primary ampere, so that a primary current of 60 amperes, the limit of the test facilities, produced the effect of 9,000 amperes as the short-circuit detector is used in actual service. For the purposes of this paper, primary currents have been converted to actual service values.

Primary current was controlled by a fixed inductance, consisting of an available motor winding and a resistor variable in steps. The fixed inductance had a measured value of approximately 1.5 henrys. For each test, primary voltage and sustained primary current were measured, and primary resistance was calculated from these readings. From this resistance and the value of fixed inductance, the approximate primary time constant L/R was calculated.

For measuring the D-relay deflection, several successive applications were made at the same setting of primary voltage and resistance, with adjustment of the D-relay contact until the deflection was just sufficient to light a pilot lamp in the contact circuit. Oscillographic records were taken of primary and secondary currents and of time at which maximum deflection occurred.

The first series of primary impulse tests showed that the impulse coil as then designed was adversely affected by saturation at values within the range of service load conditions, since short circuits may occur while the impulse coil is magnetized by full-load current. The secondary current and the relay deflection were materially less on addition of an increment to an existing primary current than on application of the same primary current increment from zero. The oscillograms of secondary current, when compared with a calculated curve such as in Figure 4, failed to show the long concave-upward tail of the calculated curve, but dropped off rapidly after passing maximum value. These observations were explained as results of a decreasing mutual inductance as the core became saturated with increasing primary current.

The impulse coil then was redesigned to avoid saturation up to 17,000 ampere turns, by providing 12 $^3/_{32}$-inch air gaps in the core. Tests on the redesigned impulse coil showed nearly the same values of relay deflection for increments of zero to 4,500 amperes and of 4,500 to 9,000 amperes.

Test results, as plotted in Figures 5, 6, and 7, show the increase of D-relay deflection with increase of primary current increment, and show the inverse effect of primary-circuit time constant and secondary circuit resistance. From these test curves of the sample short-circuit detector, standard performance curves as shown in 8, 9 and 10 were derived for use in applying the detectors to service conditions and predicting performance.

Figure 8 first was derived for the same value of shunt resistance, 0.116 ohm, as was used in the tests. Figure 7 was used to interpolate for values of secondary circuit resistance that were expected to be average values for installations in service. Although the shunt resistor previously had been an adjustable device, it was decided that interchangeable shunt resistors of three different fixed values would give sufficient flexibility of adjustment in a more reliable manner. Therefore, standard performance curves for a 0.159-ohm shunt and for a 0.255-ohm shunt were derived from Figure 8 and are shown on Figures 9 and 10.

Each of the performance curves on Figures 8, 9, and 10 shows expected deflection as a function of primary current increment. In the case of a short circuit from no load, the primary current increment is equal to the final value of the short-circuit current. Each figure includes a family of curves, with time constants (L/R ratio) ranging from 0.05 to 0.40 second. All the curves on any one figure are calculated for the same value of shunt resistance and secondary circuit resistance.

In Figure 11 standard calibration

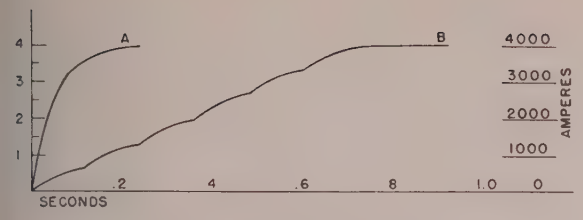

ACCELERATION OF 12-MOTOR-CAR TRAIN.
CALCULATED PRIMARY CURRENT ON FIRST NOTCH.
ASSUMPTIONS: E/R = 4000 AMPERES.
TIME CONSTANT = L/R = .05 SECOND.
CURVE A: ALL MOTORS STARTING SIMULTANEOUSLY.
CURVE B: CONTACTORS OF TWO CARS CLOSING SIMULTANEOUSLY AND THOSE OF SUCCESSIVE PAIRS AT INTERVALS OF 0.12 SECOND.

Figure 12 (above). Primary current of 12-motor-car train acceleration

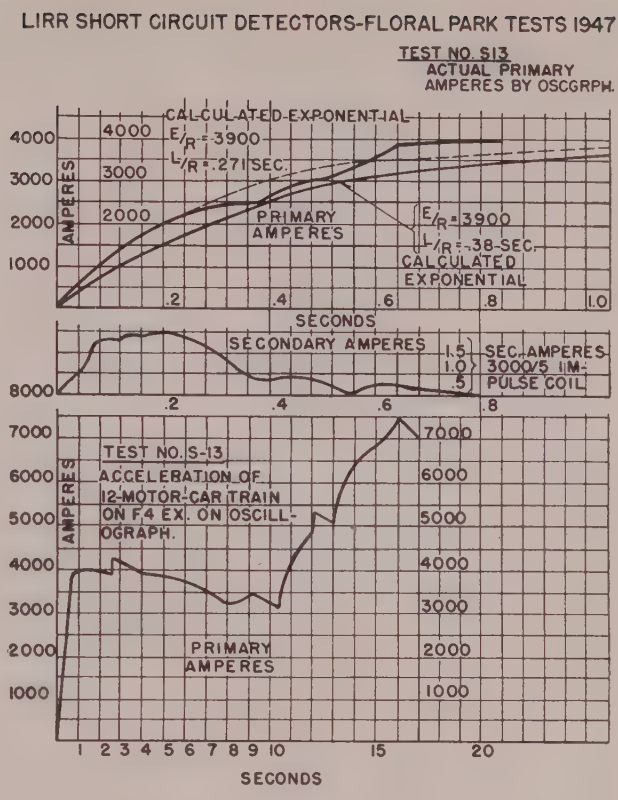

Figure 13 (right). Test curves on Long Island Rail Road by oscillograph

curves of the sample relay are given in terms of steady-state deflection plotted against amperes in the secondary circuit, for each of the values of shunt resistance that appears on Figures 8, 9, and 10. By the use of these curves, a suitable correction factor may be calculated for any specific relay that departs materially from the calibration curves of the sample relay. Where the secondary circuit resistance departs materially from the values given on Figures 8, 9, and 10, a correction factor may be calculated by use of Figure 7.

Application of the Short-Circuit Detector to Heavy Interurban Service

Salient characteristics of the loads and feeder circuits of the Long Island Rail Road have been described in earlier sections of this paper. In the protection of these third-rail circuits, some of the problems encountered are typical of heavy d-c railway service. The heavy inrush of current on acceleration is a critical factor, as this current also produces current in the secondary circuit of the impulse coil.

The secondary current and the relay deflection are affected directly by the magnitude of the primary current increment and inversely by primary-circuit time constant, the L/R ratio. Some efforts have been made to use primary-circuit time constant as a means of discriminating between acceleration and short circuit as causes of primary current increment. It was concluded that this was not practicable for the Long Island Rail Road application, in the light of the available data.

During staged short-circuit and acceleration tests at Floral Park in 1947, oscillographic records were obtained which yielded an average time constant of 0.15 second for the third-rail and return circuit of four or more tracks. Test trains produced initial-current swings of 3,000 to 4,300 amperes, rising to as high as 9,000 amperes during the accelerating period. Study of these and other test data shows that secondary current sufficient to operate relays occurs only during the first second of acceleration, although the primary current continues to rise as the controller is moved over successive positions. Oscillographic records of current during the first second of acceleration were so irregular as to make rather unsatisfactory the calculation of time constant on the exponential curve basis. By taking the horizontal portion of highest value in the first second as the E/R value, a time constant of 0.38 second was calculated.

Tests on the Staten Island Rapid Transit System in 1926 gave time constants of 0.36 second for a third-rail and track return circuit and of about 0.05 second for an 8-car train on the first notch. From an oscillographic record of acceleration taken at Bellaire on the Long Island Rail Road in 1949, a time constant of about 0.04 second on the first impulse was calculated, the scale of the film being too small for much accuracy.

The great variation in the figures for acceleration time constants may be explained by lack of synchronism in the closing of contactors on the several motor cars on a long train. Taking the data on one of the Floral Park acceleration tests, a composite current curve for the 12-motor-car train has been calculated on the assumption of 0.05-second time constant for each car and an arbitrary interval of 0.12 second between closings of successive pairs of contactors. The composite curve is shown in Figure 12 and the oscillographic record in Figure 13. By different adjustments of the time of closing successive contactors the apparent time constant, not a true L/R value, may be made to vary from 0.05 to 0.40 or the curve may be made to approximate the oscillographic record.

From the foregoing considerations and with the very limited test data available on time constants of acceleration and of short circuits, it is seen that time constant does not provide a means of discrimination, but actually may increase the difficulty of securing selectivity between accelerating current and short circuit, because the combination of small time constant on accelerating current and large time constant on distant short circuit may occur, with consequent decrease in the margin for selectivity.

Therefore, in establishing initial settings for the short-circuit detectors on the Long Island Rail Road, the following procedure was used. Minimum "bolted" short circuits to the end of each third-rail sections were calculated. Using the *D*-relay performance curves of Figures 8, 9, and 10, settings have been made to give nontripping for 4,300 amperes accelerat-

ing current at 0.05-second time constant and to give tripping at the calculated minimum short-circuit current with 0.40-second time constant. Some compromise with this very conservative basis was necessary in a few cases where sections were exceptionally long or contained lighter than usual rail. In making settings the shunt resistors have been selected in each case so as to place the adjustable fixed contact as high as possible on the scale.

It is recognized that actual operation is the best check on assumptions. Accordingly, the relays were equipped with instrument pointers so that the deflections may be read accurately during operation. Recommendations were made to observe relays during rush-hour periods, especially at locations where selective settings were difficult. After several months of service it was reported that the relays were clearing faults and avoiding load trippings.

Application to Trolley Coach Service

While heavy traction service of the third-rail distribution type represents the maximum as far a sinductance and long time constant is concerned, trolley coach distribution probably represents the minimum with the shortest time constant. The inductance for third-rail distribution may run about 13 millihenrys per mile, while two to three is representative of the average streetcar system, depending on the rail size. With trackless trolley coaches, the inductance will run less, since there is no iron in the circuit and the loops are small.

Assuming a maximum inrush of 200 amperes on acceleration of two coaches starting at the same instant, a minimum short circuit of 1,000 amperes at the most remote point of the feeder, and maximum load swings of 1,000 amperes, it again is apparent that overcurrent tripping of feeder circuit breakers cannot be used.

Here, the discrimination between fault and load currents can be distinguished by the *D* relay only, although the higher speed of the *S* relay also may make it desirable for use. Should the *S* relay be omitted and the *D*-3 relay (with three times the field strength of the *D*-2) be used, the deflection for a given moving coil current would be tripled. Should the moving coil be shunted by a 1-ohm resistor, the percentage of secondary current passing through the moving coil would be about tripled, from 26.5 to 75 per cent. The combined effect would be to multiply the deflection by nine, making a 1,000-ampere short circuit on the trolley-bus system equivalent to a 9,000-ampere fault on the Long Island Rail Road system.

Reference

1. D-C Power Supplies and Isolation of Faults on Electric Transit Systems—D-C Power Supply, Part I, S. S. Watkins, M. E. Reagan. *AIEE Transactions*, volume 70, part I, 1951, pages 537–42.

Discussion

H. F. Brown (New York, New Haven and Hartford Railroad, New Haven, Conn.): The 2-part paper by Messrs. Watkins and Reagan is a valuable addition to the technical literature associated with railway electrification.

As electric train loads have increased, especially on the older low-voltage electrified systems, it has become increasingly difficult to distinguish between train loads and short circuits. The simple overcurrent relays or tripping devices used in the early days of electric traction now no longer apply to this type of service. Even on the higher voltage systems (3,000 volts direct current) the greater distance between substations permitted by the higher voltage, together with the increased resistance of the feeder circuits, presents the same problem in distinguishing between train loads and faults.

On the 11-kv a-c traction systems, especially those systems which consist of multitrack networks with a large number of circuits in parallel, it is still possible to use the simple overcurrent relays to clear faults in many cases, although here again the longer distance between sectionalizing and switching stations may cause the same difficulty in discriminating between heavy train loads and short circuits on long feeders.

The first part of this paper is an excellent outline of the latest thoughts in substation design, especially in connection with switching and protective equipment for traction power supply on grounded systems. The second part of the paper is an equally valuable analysis of the modern methods for discriminating between heavy loads and faults, together with the methods of clearing, with minimum interruption to service, faults from the system. The authors are to be congratulated on their valuable contribution to technical literature on this subject.

Group Regulation of Urban 4-Kv Feeders

C. L. GRIM
ASSOCIATE AIEE

H. B. PECK
MEMBER AIEE

A COMBINATION of system development and compelling conditions involving outmoded equipment resulted in changing some of the Consolidated Gas, Electric Light, and Power Company's old urban substations from individual feeder regulation to group feeder regulation. For economic reasons, a type of group feeder regulation also was adopted at new urban substations. The purpose of this paper is to describe, for both old and new substations, conditions warranting this program; to outline the method followed; and briefly to describe some operating conditions and planning guides. The treatment is confined to urban feeders which are underground from the station to the feeder point.

The successful operation of 3-phase group regulation requires investigation and supervision of load and voltage conditions, as well as a flexible distribution system. With feeders whose heavy-load voltage drops from the substation to the feeder point are in the order of 5 to 7 per cent, it is essential that the feeders "match," so that the condition of satisfactory voltage on some feeders and low or high voltage on others does not exist. When feeders with maximum voltage drops in the order of 2 per cent are regulated together, dissimilar load patterns and unequal feeder drops are unimportant, since the variation from a mean is small.

Conditions Warranting the Program

Old Substations

Excepting the downtown network, Baltimore City is served by a 60-cycle 4-kv radial distribution system which is supplied by prewar and postwar substations. Until about five years ago, all 4-kv feeders were regulated by single-phase induction regulators, many of which were 30 or more years old. Fault currents exceeded ratings of the smaller regulators and the oldest oil circuit breakers. This equipment was indoor and some buildings had become congested. These factors constituted potential serious service hazards.

Improvements were begun at the end of World War II and, considering several factors, four stations were selected for replacement of oil circuit breakers and open-type bus arrangements with metal-clad switchgear. The regulator aisles were very seriously congested. There have been several regulator failures, but no serious fires of the type that could occur. Space segregation and replacement or removal of the more vulnerable regulators were vital to the improvement program.

New Substations

After extensive studies, which were carried out during the wartime curtailment of construction work, it was decided to continue the 4-kv radial system and relieve overloaded substations by new substations utilizing factory-assembled switchgear. A new economical design was adopted and designated "multiplex" by engineers of the Consolidated Gas, Electric Light, and Power Company of Baltimore.[1]

Each transformer at these new substations normally supplies and regulates two 4-kv feeders. This example of group regulation is economical because it simplifies substation design and reduces equipment and space requirements. It is partially responsible for elimination of an auxiliary bus and partially facilitates automatic operation of the new substations.

Description of the Program

Old Substations

Monument Street Substation. The only way to permit segregation at the first substation modified was to eliminate some of the regulators.

The Monument Street substation has no outdoor yard, all equipment including transformers being inside. It is a multi-service substation, and floor space is completely occupied. A 20,000-kva synchronous condenser was connected to the 13-kv bus in 1942, and there are two old 6,875-kva frequency changers which are connected on the 60-cycle end to two of the three 4-kv bus sections and operated at reduced rating as condensers. The synchronous condenser was installed to improve the voltage of the 13-kv bus supplying unregulated high-tension customer feeders and to reduce the wartime-kilovolt-ampere peak on the 13-kv supply cables.

Having had no previous experience with group regulation of urban feeders, the company decided in 1943 to obtain experimental data. As a result of preliminary investigations, 11 feeders were selected for an extended period of trial operation. Feeder-point voltage charts were obtained with the regulators both normal and blocked in the neutral position and also with the condenser on and off. The condenser operation was adjusted to follow the voltage requirements of the group. As a result of the trial operation, six feeders and later a seventh were selected for group regulation. Regulators were retained on the remaining four feeders tested.

Coincident with the trial operation period, 4-kv metal-clad switchgear was

Paper 51-92, recommended by the AIEE Substations Committee and approved by the AIEE Technical Program Committee for presentation at the AIEE Winter General Meeting, New York, N. Y., January 22–26, 1951. Manuscript submitted October 23, 1950; made available for printing December 11, 1950.

This paper was originally presented as a District paper at the Middle Eastern District Meeting in Baltimore, Md., October 3–5, 1950.

C. L. Grim and H. B. Peck are both with Consolidated Gas, Electric Light, and Power Company of Baltimore, Md.

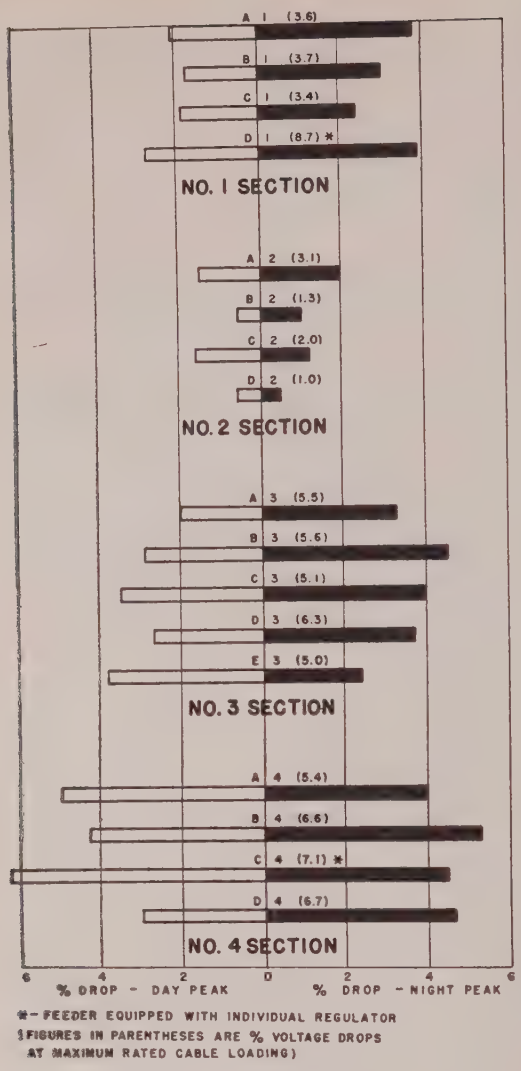

Figure 1 (left). Estimated 1950 peak load feeder voltage drops, by section, Philadelphia Road Substation

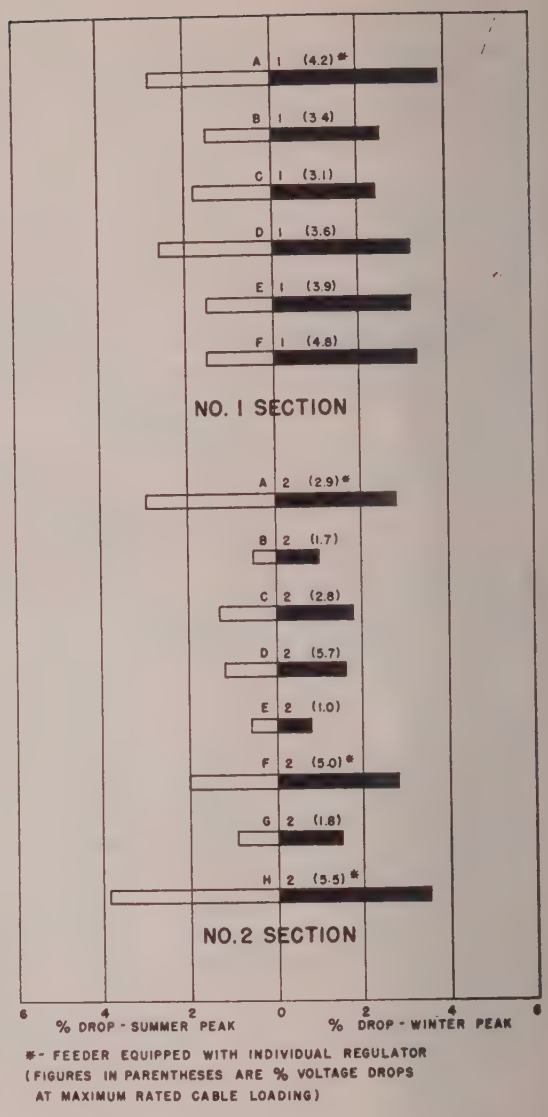
A 1 (4.2) *
B 1 (3.4)
C 1 (3.1)
D 1 (3.6)
E 1 (3.9)
F 1 (4.8)
NO. 1 SECTION
A 2 (2.9) *
B 2 (1.7)
C 2 (2.8)
D 2 (5.7)
E 2 (1.0)
F 2 (5.0) *
G 2 (1.8)
H 2 (5.5) *
NO. 2 SECTION
6 4 2 0 2 4 6
% DROP - SUMMER PEAK
% DROP - WINTER PEAK
*- FEEDER EQUIPPED WITH INDIVIDUAL REGULATOR
(FIGURES IN PARENTHESES ARE % VOLTAGE DROPS
AT MAXIMUM RATED CABLE LOADING)

Figure 3 (right). Preliminary estimate of 1949 peak load voltage drops, by section, Woodbrook Substation

ordered and plans were made to respace the regulators utilizing, for maximum obtainable clearance, the space occupied by the sets to be released. The feeders to be group-regulated were allocated to the sections of the new gear to which the small frequency changers were connected; the frequency changers would serve for voltage control of these sections when the condenser is out of service. Only individually regulated feeders were to be supplied from the remaining section.

As a result of the group operation, regulator spacing was considerably improved in Monument Street substation. Furthermore, additional regulators will be released by transfer of some feeders to a new substation now in service.

Philadelphia Road Substation. Philadelphia Road substation has four 7,500-kva, 110/4-kv 3-phase outdoor transformers supplying four indoor bus sections. Each transformer has a + or − 10 per cent tap changer in 5/8-per cent steps and, to reduce fault currents, normally supplies the load of its section only. Group regulation of a few feeders was introduced by trial operation in 1945 and will have been extended to include, by the end of 1950, all but two of the 17 4-kv feeders. The remaining regulators will be outdoor and the oil circuit breakers will be replaced with air circuit breakers, resulting in a completely oil-free indoor installation.

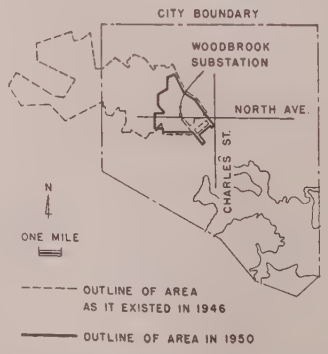

Figure 2. Outline map of Baltimore City showing area supplied by Woodbrook Substation in 1946 and in 1950

Figure 1 shows estimated voltage drops by section for 1950 peak conditions. It is evident that the spread between unregulated feeders on each section is in general about 1 per cent, with extremes approximating 2 per cent. The hypothetical percent voltage drop at maximum rated cable loading is shown in parenthesis opposite each feeder designation.

During the 5-year period that modifications have been in progress at Philadelphia Road, the marked postwar load growth has resulted in an acceleration of normal feeder changes, such as replacement of old cable with larger cable, in-

stallation of new feeders, transfer of load between feeders, and addition or removal of 4-kv industrial loads. Finally, in 1950, two regulated feeders not included in Figure 1 are to be transferred to a new substation. The relative loading of the four separate 4-kv busses thus has been in a constant state of flux, necessitating some transfers of feeders between busses to avoid transformer overload. It has been possible to co-ordinate these many changes and still meet voltage requirements during this period of intense activity without returning any regulators that have been removed.

Woodbrook Substation. The third and latest of the large stations at which group regulation has been introduced is Woodbrook, which, like Philadelphia Road, is a single-purpose substation for supplying 4-kv radial feeders. There are two indoor 4-kv bus sections, each carried by two outdoor 6,000-kva, 13/4-kv autotransformers, which are in turn supplied by 13-kv underground cables from a generating station. Coincident with the provision of major relief by the transfer of area to two new substations, air circuit breakers and metal-clad switchgear are being substituted for oil circuit breakers and typical open-gallery construction.

Figure 2 shows, in dotted outline, the territory in Baltimore served by Woodbrook in 1946, while the solid outline represents the territory as it will be at the end of 1950. The average length of the 4-kv feeders supplying the latter territory is approximately 4,400 feet. The station is now much better centered with relation to its load and the area is greatly reduced. Load density is in the order of 5,000 kva per square mile. Furthermore, the Woodbrook territory is more nearly homogeneous in character than either the Philadelphia Road or the Monument Street territories. Nearly all of the load is residential and commercial, there being very little 4-kv industrial load. The station peak traditionally occurs in December and has followed a uniform pattern for many years. The diversity factor of the sum of the feeder peaks versus the station peak is in the order of 1.05 to 1.10.

These physical conditions and load characteristics indicated the feasibility of considering group regulation in connection with installation of the new switchgear. Since the existing induction regulators interfered with locating the new switchgear and because they constituted the only remaining indoor oil-filled equipment, adoption of a plan which would eliminate regulators seemed desirable. As a matter of fact, the design based on retaining the regulators would have required converting a gallery to a second floor at an added cost of $19,000.

Whereas the adoption of group regulation at both Philadelphia Road and Monument Street was decided finally on the results of trial operating periods, the nature of the modifications at Woodbrook required that the decision be made during the design stage. To determine feasibility of group regulation a tabulation was made of coincident ampere loads of all feeders to remain supplied from Woodbrook. Because there are two bus sections, the feeders first were listed in two groups, according to impedance. Simultaneous loads were tabulated for several significant hours during a heavy load day and a light load day chosen from each of the four seasons of the previous year. By inspection of these data, it was apparent that the critical conditions to be satisfied were the heavy load days in the winter and summer (maximum and minimum load seasons, respectively). Accordingly, the estimated voltage drop was calculated for each of the aforementioned hours for estimated 1949 winter and summer conditions.

Peak-hour conditions as first estimated for 1949 operation are given in Figure 3. The small difference in voltage drop between feeders showed conclusively that group regulation was practical, and it was adopted. The final modification designs were then based on regulating the two bus sections by outdoor step regulators connected in the low-voltage leads of each of the four transformer circuits.

The installation of metal-clad switchgear and the elimination of regulators as planned in 1948 will be completed in 1950 when final load transfers are made to relieve Woodbrook. In the meantime, numerous feeder changes have occurred since the data in Figure 3 were first accumulated. For example, some cable sizes have been increased and some feeder layouts and feeder loads have been adjusted. The net effect of these changes on estimated 1950 operation has been to reduce the spread between feeder voltage drops, as shown by Figure 4. In order to rebalance bus loading, regulated feeder *H-2* is now to be on number 1 section. Regulator assignments are unchanged except that regulators are scheduled for feeder *F-1* instead of feeder *A-1*. As before, feeders *A-2*, *F-2*, and *H-2* require regulators because of diversity.

Table I

Individual Feeder Regulation		
15 sets of regulators	$100,000	
Cost of installation	3,500	
Construction work to accommodate new switchgear	19,000	
	$122,500	
Overhead charges	12,200	
Total costs		$134,700
Group Feeder Regulation		
4 bus regulators	$ 32,000	
Cost of installation	7,500	
5 sets of regulators	33,000	
Cost of installation	2,500	
Construction work to accommodate new switchgear	5,700	
	$ 80,700	
Overhead charges	8,100	
Total costs		$ 88,800

The relative station costs in the case of Woodbrook show a considerable advantage favoring group regulation. As most old feeders are being changed to 350,000 circular mils, the costs of individual feeder regulators in the comparison in Table I are for new units sized for the larger cable.

In addition, there is a difference in capitalized value of regulator losses favoring group regulation by approximately $3,500.

New Substations

The multiplex substation, described in detail in an earlier publication,[1] was designed to meet the following requirements:

1. Failure of a transformer or high-tension supply line should not impair continuity of service.
2. Adequate voltage regulation should be provided on distribution feeders.
3. Ordinary maintenance and inspection work on substation equipment should be feasible at any time without interference to operation.
4. Addition of new capacity may be made when necessary without increasing the interrupting duty of circuit breakers.
5. Reliable service should be provided on an unattended basis.

The substation connections are illustrated by Figure 5, while its operation can be visualized through reference to Figure 6. Each 3,750-kva transformer is connected to and regulates a short 4-kv bus section which can serve two feeders normally.

Automatic transfer of each feeder to its adjacent transformer on loss of normal potential is the essential operating feature of this type of substation.

One of the two feeders of each pair is termed "pilot feeder." Bus voltage is controlled by one phase of the pilot feeder, which has compensation added in such amount as to give required feeder-

point voltage under varying load conditions. Although multiplex design provides 3-phase voltage regulation in groups of two feeders, yard space is allocated at each station for future installation of a limited number of feeder regulators. Six multiplex substations have been placed in service within the city limits since 1948, and a seventh is scheduled for operation early in 1951. To date, no feeder regulators have been required on entirely underground feeders. Single-phase regulators were initially installed on two feeders having appreciable overhead portions, and a similar feeder from the seventh multiplex substation is scheduled to be individually regulated by a 3-phase regulator.

Operation

In March and April 1950 extensive load and voltage tests were made on practically all of the feeders supplied from the three old substations previously discussed and Calverton multiplex substation. Arrangements were made to obtain bus voltage and feeder loads at the station at the same time voltage at the feeder points was being recorded. With only a few exceptions, so-called feeder-point voltage readings were taken on the low-voltage side of distribution transformers closest to the feeder points. The tests disclosed no appreciable difference in voltage spread between feeders or phases which can be charged to a particular method of regulation. Should excessive voltage differences develop because of appreciable inequalities in load growth of feeders or between phases of one feeder, corrective action may simply consist of a load transfer or rebalancing of phase loading. The installation of new feeders to relieve thermally overloaded feeders and mains also serves to maintain minimum differences in feeder-point voltage levels. If the substation load is carried on a split-bus basis to limit fault currents, the individual bus loading is limited by transformer capacity. Transfer of a feeder or feeders between buses to improve load balance also can often be accomplished in such a manner as to improve voltage conditions on feeders requiring improvement. In

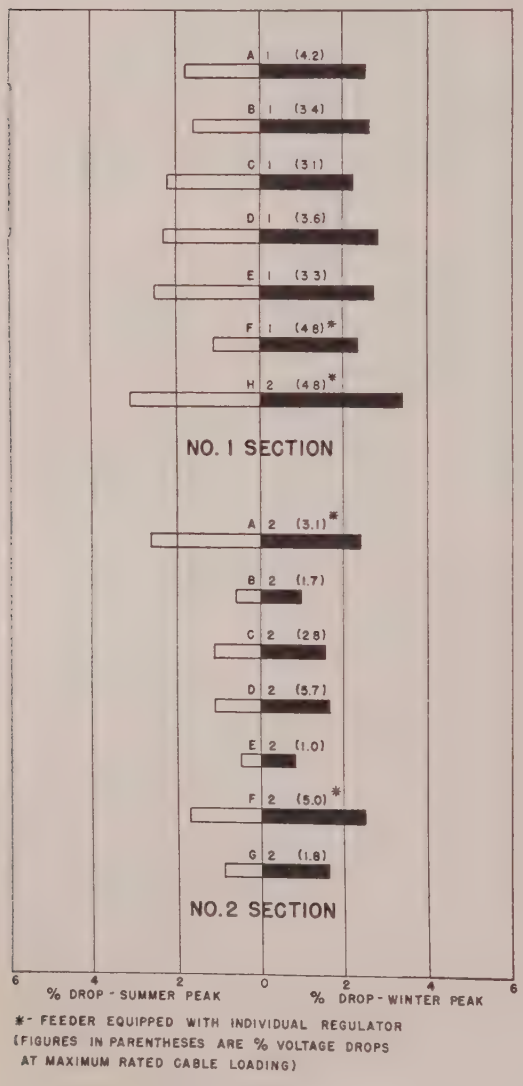
A 1 (4.2)
B 1 (3.4)
C 1 (3.1)
D 1 (3.6)
E 1 (3.3)
F 1 (4.8)*
H 2 (4.8)*
NO. 1 SECTION
A 2 (3.1)*
B 2 (1.7)
C 2 (2.8)
D 2 (5.7)
E 2 (1.0)
F 2 (5.0)*
G 2 (1.8)
NO. 2 SECTION
6 4 2 0 2 4 6
% DROP - SUMMER PEAK
% DROP - WINTER PEAK
*- FEEDER EQUIPPED WITH INDIVIDUAL REGULATOR
(FIGURES IN PARENTHESES ARE % VOLTAGE DROPS AT MAXIMUM RATED CABLE LOADING)

Figure 4. Current estimate of 1950 peak load voltage drops, by section, Woodbrook Substation

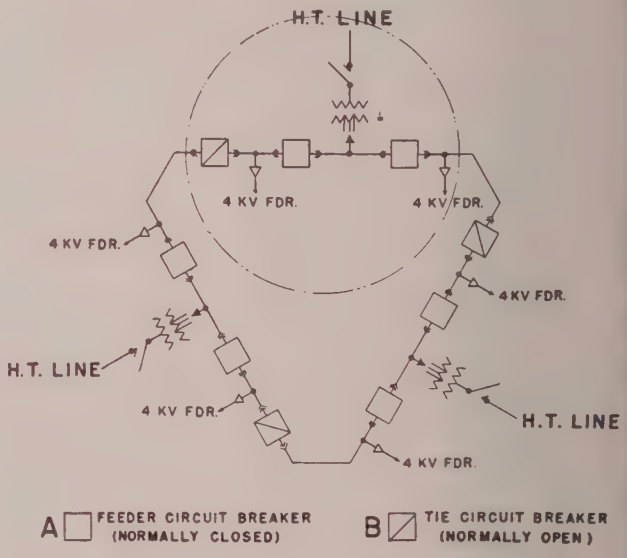

Figure 5. Principle of the "multiplex" scheme

Identical "units," of which one is circled by broken line, are connected as a ring with tie circuit breakers B normally open

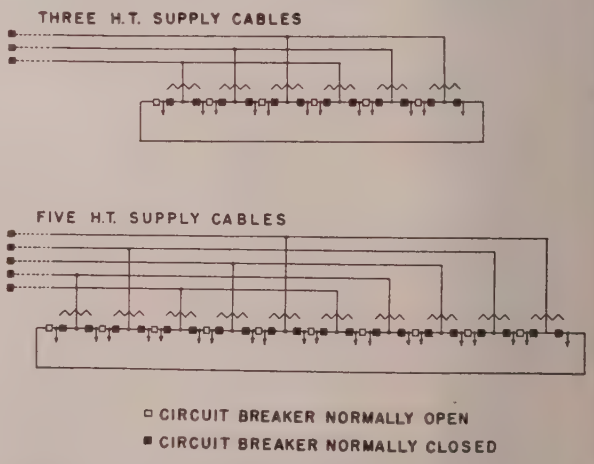

Figure 6. Staggered connection of transformers at a "multiplex" substation

Three or five subtransmission circuits are used to avoid simultaneous de-energizing of adjacent transformers in case of failure of one circuit

any event, increasing the size of secondary transformers and low-voltage mains to remove customers from the complaint area because of low feeder-point voltage would be expensive and undesirable.

The extreme limits of permissible voltage cover a band of 12 volts between 114 and 126, the nominal voltage being 120 volts. This 10 per cent spread between the first and last customer's voltage is established by the Public Service Commission and is an accepted standard of design in the industry.[2] By way of comparison, the voltage profile of an average distribution feeder in Baltimore is shown in Figure 7. Average values of drop for the various components applicable to urban feeders have been indicated for heavy and light load conditions. It will be noted that the first customer is connected to a lightly loaded transformer during both heavy and light load conditions. At heavy load the voltage spread between the first and last customers is about 7 volts; at light load, 0.5 volt. Lower voltages than those shown on Figure 7, which are caused by overloaded transformers and secondary mains, are corrected on an individual basis. Somewhat higher voltages than shown can be tolerated, for high-voltage problems have been infrequent on urban feeders.

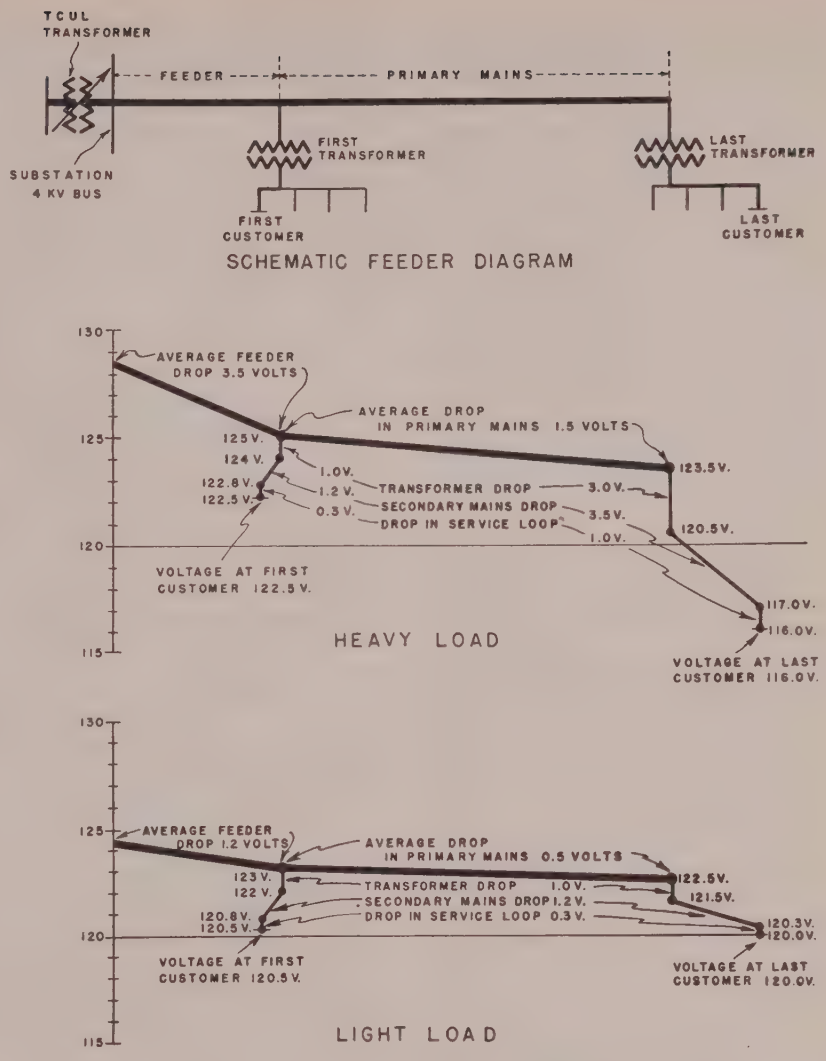

Figure 7. Voltage profiles of an average underground 4-kv feeder

Discussion

All feeders in any group obviously do not have exactly the same load shapes and voltage drops. The usual difference in simultaneous voltage drops ranges anywhere from 0.5 to 2.5 per cent under heavy load conditions. Since all grouped feeders receive the same bus voltage, it is desirable to provide a voltage base which will satisfy average requirements.

In the case of two feeders with voltage drops of 0.5 per cent and 2.5 per cent, respectively, a compromise setting would be chosen which would provide for 1.5 per cent drop over peak. If the nominal feeder-point voltage were 125 volts, one feeder then would receive approximately 126 volts and the other 124 volts. Had no compromise been made, feeder-point voltages would have been approximately 125 and 123 volts, respectively, if the compensation were adjusted to give nominal voltage to the feeder with the least drop.

With individual single-phase regulation the control equipment would be set to furnish 125 volts at peak load to each feeder point. Even so, there may be complaints from the most distant customers because normal load growth on the system tends to overload distribution transformers and secondary mains, creating low-voltage conditions. With group regulation it is logical to assume that on the feeder receiving the higher feeder-point voltage those customers who were in the fringe area would now have slightly improved voltage and would not register complaints. On the feeder receiving the slightly lower voltage, however, it is also logical to assume that there are additional customers who could enter voltage complaints. Thus, the total number of low-voltage complaints received should be approximately equal for these two feeders, whether group regulated or individually regulated, provided the difference between feeder-point voltages is not excessive.

The preceding analysis can be extended from two feeders to cover a group of more than two feeders. Furthermore, experience has shown that any number of feeders can be successfully regulated in one group if the voltage drop at maximum rated cable loading of all feeders in the group ranges from nominally zero to approximately 2 per cent. With such a group there need not be any investigation made of load shape or diversity, because the maximum range, or difference that can exist between feeders, matches the permissible range.

Obviously, if a permissible difference of 2 per cent is established between the minimum and maximum *simultaneous* drops, then group regulation of feeders for drops at *maximum rated cable loading* exceeding 2 per cent should be based on an analysis of daily and seasonal load shape of each feeder. For example, if the range of drops at maximum rated cable loading is from 5 to 7 per cent, the analysis is necessary to determine the simultaneous range. Should one of the 5 per cent feeders have only 1 per cent drop at a time when the entire group ranges from 3 to 5

per cent, it would receive 3 per cent high voltage and either should not be included in that group or should be equipped with a regulator.

Voltage drops at maximum rated cable loading range anywhere from nominally zero to a maximum of approximately 7 per cent for practically all underground feeders at the substations which have group regulation. There is some value of voltage drop at maximum rated cable loading which constitutes a limit beyond which it is not generally feasible to attempt to group-regulate. Beyond that point the feeders involved would have such high impedance that normal increments of load would produce intolerable voltage differences. The system would be sensitive to such normal occurrences as (1) a feeder in the group growing faster or slower than the average; (2) a necessary load transfer between feeders; and (3) addition or removal of 4-kv industrial loads.

The foregoing normal occurrences also will change the voltage spread between feeders of very low impedance, but to a degree that will not violate the design standard of a maximum simultaneous spread of 2 per cent. The stations described have successfully operating groups such as numbers 3 and 4 sections at the Philadelphia Road substation, Figure 1, where the feeder drops at maximum rated cable loading range in the order of 5 to 7 per cent. It is believed that this range approaches the practical limit for application of group regulation to urban feeders.

Special circumstances may justify deviations from the limits outlined. For example, feeder *D-2* of Figures 3 and 4 supplies one industrial customer with a fairly constant demand. Although this feeder is grouped, without supplemental regulation, with feeders having approximately 2 per cent voltage drop, the fact that its drop at maximum rated cable loading is in the order of 5.5 per cent has no significance because it is expected that the customer will be transferred to high-tension service prior to increasing present demand. As another example, some of the multiplex stations supply one or two fairly long feeders whose drop at maximum rated cable loading will be in the order of 10 per cent. These feeders now are lightly loaded and are group-operating satisfactorily. As load grows, it may be necessary to equip some of them with regulators. Eventually, however, these would be the feeders to be transferred to future new stations, at which time any regulators involved could be used elsewhere.

Summary

The best way, theoretically, to maintain ideal voltage conditions on a given feeder is to equip each of its phases with a regulator. However, other factors in addition to voltage regulation must be considered in a practical co-ordinated design. The engineering approach toward accomplishing a purpose with the minimum physical facilities must be adhered to both in improving an old substation and in designing a new one. A very strong incentive to streamline and simplify substations as an outgrowth of congested conditions in old stations and as a means of reducing time and money requirements in building new ones, finds an ally in the closely coupled and densely loaded condition of today's distribution system. The availability of economical and reliable tap-changing equipment and the existence of short distribution feeders together permit, by group regulation, realization of very significant simplifications of substation design, construction, and operation.

The preceding examples of conversion to group regulation have three important points in common:

1. The underlying reasons for the changes have been to make space and/or eliminate indoor oil-filled equipment.

2. The work to regroup the feeders by bus section voltage has been an engineering problem only, inasmuch as the change from open-type bus work to metal-enclosed switchgear required moving the feeders physically within the three stations regardless of voltage requirements.

3. Voltage conditions have improved thus far as normal development and changes of the distribution system have occurred during group operation.

Whereas the old stations are attended, the multiplex is an unattended station, a feature contributing to its economy and justification. The old stations, being located closer to the center of the city, have short feeders and small areas, as illustrated previously in the case of the Woodbrook substation. It is thus feasible to regulate the feeders in groups of four or more. The new stations, being nearer the perimeter of the city, have somewhat longer feeders. The inherent feature of one regulating voltage per pair of feeders thus facilitates successful group operation at the new stations.

Finally, as applied to underground urban distribution feeders:

1. Group regulation permits economies in substation construction and operation, and no significant offsetting sacrifice of revenue or distribution economy should result if the maximum simultaneous deviation of feeder voltage drops is in the order of + or − 1 per cent from the mean.

2. Feeders can be grouped indiscriminately when the voltage drops at maximum rated cable loading are in the order of 2 per cent.

3. Operating experience indicates that when two or more regulating voltages are available, feeders can be grouped in such a way as to meet the restriction in statement 1 in this section when the voltage drops at maximum rated cable loading do not exceed approximately 7 per cent, provided care is taken to choose feeders with similar load and impedance characteristics for each group.

4. In regulated groups, any feeders which do not meet these conditions either should be placed in other groups or should be equipped with individual regulators.

References

1. "Multiplex" Substations for Urban Distribution, M. Mortara. *Electric Light and Power* (Chicago, Ill.), volume 27, January 1949, pages 80–82, 87–89, 93.

2. Basic Concepts of Voltage Regulation, C. J. Lake. *Electrical World* (New York, N. Y.), volume 131, February 26, 1949, pages 72–76, 149.

No Discussion

Analogue Computing Techniques Applied to Economics

R. H. STROTZ
NONMEMBER AIEE

J. F. CALVERT
FELLOW AIEE

N. F. MOREHOUSE
NONMEMBER AIEE

Electrical Analogues and Economics

IF A single group of equations can be written which defines the assumed performance for two separate systems (each of which within itself represents an orderly or definable behavior), one system may be called the complete analogue of the other. Since many electric systems are much more easily constructed and varied than those in other media, they afford a ready means for the study of a variety of other systems which have electrical analogies. Economic phenomena may often be found to be representable by analogous electrical circuits. Electrical analogue computing techniques may therefore have broad applications in the study of economic problems. This paper also presents a brief survey of suitable problems in theoretical economics, and discusses electrical representations in terms of present and imminent developments in analogue computing techniques. Throughout the paper economic terms will appear in italics where first introduced.

"Models" in Theoretical Economics

Economic Models

Over the past 15 years the word "*model*" has become as prominent in the writings of economists as is the word "circuit" in the works of electrical engineers. Both "models" and "circuits" may be described by mathematical relationships, although the economist's term refers not to a strictly physical prototype, as might be the case in engineering, but rather to an idealization of human behavior.

Perhaps the simplest of all economic models is also the most familiar. This model explains the determination of market price in terms of demand and supply relationships:

$$q = D_1(p) \tag{1}$$

$$q = S_1(p) \tag{2}$$

This model is *static*, *exact*, and *microeconomic* in nature. The antonyms of these terms are *dynamic*, *stochastic*, and *macroeconomic*.

Static and dynamic have the usual engineering connotations. Exact means that the equations uniquely define the quantities involved, while stochastic implies that a term representing random disturbances, or, in engineering terms, "noise", is present in the system. Microeconomic models deal with specific sections of an economy such as a firm, while macroeconomic models deal with aggregate quantities such as national income or a price index. The terms micro- and macroeconomic represent only general classifications, and are not so concisely defined as are the former. Clearer concepts of each will be gained from the examples to follow.

Consider as a second model the equations (also see Figure 1):

$$p_d = D_2(q) \tag{3}$$

$$p_s = S_2(q) \tag{4}$$

$$dq/dt = F_2(p_d - p_s) \tag{5}$$

Here p_d is demand price, or the highest price at which consumers will be willing to purchase a given quantity of product per-unit of time; p_s is supply price, or the lowest price at which sellers will be willing to continue selling a given quantity of product per-unit of time; q is quantity sold per-unit of time; and dq/dt is the rate of change in sales per unit of time, t. The inclusion of the adjustment equation (5) makes this a dynamic model even though initial or boundary conditions are not specified. We may note furthermore that economists often employ difference rather than differential equations, for example,

$$q(t) - q(t-T) = F_3[p_d(t-T) - p_s(t-T)] \tag{6}$$

where T is a fixed period of time.

A dynamic model may include historically given functions of time as well as those functions which are specified by the model. The former are called *exogenous* variables; the latter *endogenous* variables. For example, suppose that equation 4 were replaced by

$$p_s = S_3(q, w) \tag{7}$$

where w, a wage rate, is regarded as a known function of time. In this example, w is an exogenous variable, while p and q are endogenous variables. If difference equations appear in the model, some endogenous variables may be *lagged*, for example, $q(t-T)$ of equation 6 is a lagged endogenous variable at time t. Lagged endogenous variables as well as all exogenous variables are called, collectively, predetermined variables.

All of the foregoing examples have been exact in nature, but nonexact or stochastic models also are employed in theoretical economics. For example, suppose that the demand and supply functions of the previous example were written as follows:

$$p_d = D_4(q, u_d) \tag{8}$$

$$p_s = S_4(q, u_s) \tag{9}$$

$$dq/dt = F_4(p_d - p_s) \tag{10}$$

where u_d and u_s are called stochastic variables which may or may not be statistically related. Stochastic or random variables represent the disturbing effects

Paper 51-93, recommended by the AIEE Computing Devices Committee and approved by the Technical Program Committee for presentation at the AIEE Winter General Meeting, New York, N. Y., January 22-26, 1951. Manuscript submitted October 24, 1950; made available for printing December 13, 1950.

R. H. Strotz, J. F. Calvert, and N. F. Morehouse all are with Northwestern University, Evanston, Ill.

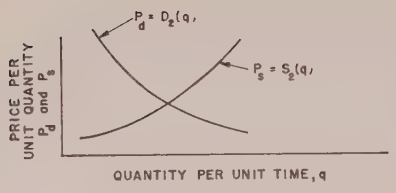

Figure 1. Demand and supply curves

of many other factors that have not been introduced explicitly into these equations. These random disturbances mean that for any given value of q, the functions of equations 8 and 9 may take on any value in accord with some probability distribution. For example, u_d and u_s at any point in time may be regarded as a drawing from a joint normal (Gaussian) distribution which is specified by mean values of zero, standard deviations of σ_d and σ_s (these are rms measures of dispersion), and the covariance (the expected or mean value of $u_d u_s$). Furthermore, it may be supposed that these random disturbances, which are values assumed by u_d and u_s at different points in time, are serially (or temporally) correlated for a given time interval, for example, $u_d(t)$ and $u_s(t)$ may depend statistically upon $u_d(t-T)$ and $u_s(t-T)$. In general, models containing stochastic variables are formulated with an eye towards subsequent statistical investigation. Suitable electrical representations for random disturbances will be discussed later.

The preceding examples have all been microeconomic in character in that they purport to explain the behavior of a single market, or an industry. These stand as a general class of models in contrast to macroeconomic models which relate major economic magnitudes at the national level, such as national income, net foreign trade balance, total expenditure by consumers, rates of interest, and a price index for consumer goods. Thus the macroeconomic models are concerned with broad aggregates and index numbers. A very simple example of the latter class is the national income model expressed by equations 11 through 13. This specific model is also stochastic and dynamic in nature.

$$C(t) = \alpha_1 + \beta_1 Y(t) + u_1(t) \tag{11}$$

$$I_p(t) = \alpha_2 + \beta_2 Y(t-T) + u_2(t) \tag{12}$$

$$Y(t) = C(t) + I_p(t) + I_g(t) \tag{13}$$

In these three equations all terms may be expressed in billions of dollars per annum. Specifically, $C(t)$ is consumer expenditure; $Y(t)$ is national income; $I_p(t)$ is net private investment; $I_g(t)$ is exogenous, government investment; and $u_1(t)$ and $u_2(t)$ are stochastic variables. The parameters are real numbers.

The Investigation of an Economic Model

There are three distinct interests an economist may have in the study of a particular economic model which will be stated and later illustrated.

1. It may be desired to discover only the general topological features of a model. Is the model stable or explosive? Does it give rise to a limit cycle, thus is it finite and periodic? How will variation in certain parameters alter the dynamic response of the model? To study the general topological features, it is unnecessary to have estimates of the actual values of the parameters, although the possible range of the parameters may be restricted by given inequalities.

2. For a given model it may be desired to solve its system of simultaneous equations, and in so doing to employ those values for the parameters which have been obtained from independent statistical estimates.

Table I. Notation for Inventory Oscillation Model

Economic Symbol	Definition of Economic Term	Electrical Analogue
P_d	Demand price. The highest price consumers are willing to pay for a given quantity of product per-unit of time	V_1
P_s	Supply price. The lowest price at which producers will be willing to continue producing a given quantity of product per-unit of time	V_2
Q_c	Quantity solid per-unit of time	i_1
Q_p	Quantity produced per-unit of time	i_2
t	Time, as employed in the economic model and in the electrical analogue even though it must be kept in mind that the time scales differ	t
α_1, α_2	Intercept constants with the dimension of price	E_1, E_2
β_1, β_2	Slope coefficients with the dimension of price divided by quantity	R_1, R_2
λ_1	Coefficient of marketing inertia	L_1
λ_2	Coefficient of production inertia	L_2
γ	Coefficient of inventory inflexibility	C
μ	A time constant, which is a measure of the promptness of re-establishing equilibrium inventories	R_3/L_3
ϵ	2.71828	ϵ
0	A superscript denoting a value in the initial equilibrium position	0
1	A superscript denoting a value in the final equilibrium position	1

Table II. Values Employed in Obtaining Solution Shown in Figure 4

Electrical Element	Numerical Value
L_1	3.0 henrys
L_2	3.0 henrys
L_3	1.5 henrys
R_1	550 ohms
R_2	550 ohms
R_3	50 ohms
C	1.0 microfarad
E_1	Changed from 12 to 18 volts
E_2	0
E_3	6 volts
E_4	90 volts

3. For a given model such as equations 11 through 13 it may be desired to estimate the numerical values of the parameters which are shown as Greek letters, when the functions of time, with the exception of the stochastic variables, are assumed known over some historical period.

The Electrical Representation of Illustrative Economic Models

Three economic models will be presented, each formulated for a different kind of investigation. It will be shown how each model may be solved by use of an analogue computer.

A Model of Inventory Oscillations

This is an illustration of a dynamic microeconomic model which is to be examined on an analogue computer only for the purpose of observing its topological features.[1] Consider an idealized industry which produces and markets a single product. Consumer behavior is assumed to be described by a linear demand function, that is, a linear relation between price and quantity. The industry is assumed to determine its production in accordance with a linear output function, that is, another linear relation between price and quantity. The industry is furthermore assumed to maintain inventories and to follow a long-run policy of keeping inventories at a constant level, although short-run deviations from this policy result from market disturbances. In particular, it is desired to study the effect of an increase in market demand. The flow diagram of this model is described by Figure 2. Goods flow along the solid lines from factories to consumers and to inventory warehouses, and from inventory warehouses to consumers. It is further assumed that inertias resulting from either psychological or technological factors appear whenever there is a change in the flow of goods to consumers or in the flow of goods off the production lines. Marketing inertia reflects the difficulties of altering the rate at which goods may be

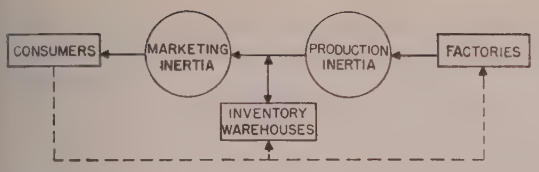

Figure 2 (above). Economic flow pattern

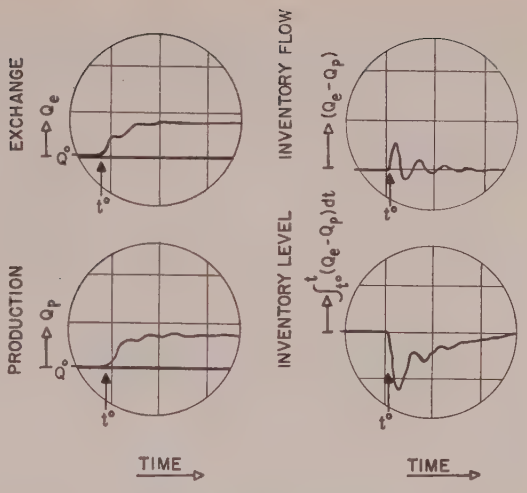

Figure 4 (right). Dynamic response as observed on analogue computer

made available at retail outlets; production inertia reflects the difficulty of promptly changing the rate at which goods are produced in the factories. The inertias are assumed to be linear. This model is represented by the equations:

$$P_d = \alpha_1 - \beta_1 Q_e \tag{14}$$

$$P_s = \alpha_2 + \beta_2 Q_p \tag{15}$$

$$P_d - P_s = \lambda_1 \frac{dQ_e}{dt} + \lambda_2 \frac{dQ_p}{dt} \tag{16}$$

$$P_d - P^0 = \lambda_1 \frac{dQ_e}{dt} + \frac{1}{\gamma}\int_{t^0}^{t}(Q_e - Q_p)dt + (P^1 - P^0)[1 - \epsilon^{-\mu(t-t^0)}] \tag{17}$$

Equation 14 is the demand function; equation 15 is the output function; equations 16 and 17 are the dynamic adjustment relationships.

Refer now to Table I. The concept of price is of particular interest. Economically, price may be interpreted as a measure of the incentive to purchase or to produce. Electrically, price is represented by a potential difference. The circuit shown in Figure 3 is constructed to represent the economic model. The mathematical description of this circuit is given in equations 18 through 21, which correspond term for term with equations 14 through 17, respectively.

$$V_1 = E_1 - R_1 i_1 \tag{18}$$

$$V_2 = E_2 + R_2 i_2 \tag{19}$$

$$V_1 - V_2 = L_1 \frac{di_1}{dt} + L_2 \frac{di_2}{dt} \tag{20}$$

$$V_1 - V^0 \cong L_1 \frac{di_1}{dt} + \frac{1}{C}\int_{t^0}^{t}(i_1 - i_2)dt + (V^1 - V^0)\left[1 - \epsilon^{-\frac{R_3}{L_3}(t-t^0)}\right] \tag{21}$$

In the electrical circuit, diodes are introduced to prevent a reverse current flow, because that would imply economically that consumers sold goods back to the firms and that finished goods were converted back into raw materials and productive services.

The purpose in introducing the L, R, C loop beneath the capacitor is to describe the industry as following a long-run policy of maintaining inventories at a fixed level. Otherwise, a change in equilibrium prices and quantities would cause the industry to alter its equilibrium level of inventories, or, in terms of the electrical circuit, to alter the charge on the capacitor. E_4 is set equal to $V^0 - q^0/c$ where q^0 is the initial charge on the capacitor. The equation for the subsidiary loop is

$$R_3(i_1 - i_2) + R_3 i_3 + L_3 \frac{di_3}{dt} = E_3 \tag{22}$$

Neglecting the mutual impedance term $R_3(i_1 - i_2)$, which may be made negligibly small, we obtain

$$R_3 i_3 \cong E_3\left[1 - \epsilon^{-\frac{R_3}{L_3}(t-t^0)}\right] \tag{23}$$

E_3 is then set equal to $(V^1 - V^0)$ to obtain the required function.

E_1 is always greater than E_2. This requirement, which is given by economic considerations, states that the equilibrium quantity produced and sold is greater than zero. It is assumed moreover, that Q_e, Q_p, and $\int_{t^0}^{t}(Q_e - Q_p)\,dt$ + (initial inventories) are always greater than zero, even during the period of disequilibrium.

In the electrical circuit it is unnecessary to introduce the battery E_2, as the entire voltage level of the circuit may be lowered.

Our interest is in observing the transient response of the system resulting from a sudden increase in demand (increase in α_1 or E_1). One series of oscillographic data for the behavior of the magnitudes Q_e, Q_p, $(Q_e - Q_p)$, and $\int_{t^0}(Q_e - Q_p)dt$ for a given set of parameter values is shown in Figure 4. The particular values for which these solutions are obtained are given in Table II. Similar sets of data have been taken to observe the effects of various alterations in the parameter values.[1]

A Nonlinear National Income Model

This model has been presented by Dr. R. M. Goodwin[2] in an effort to describe the general pattern of the business cycle in terms of a very few but very basic relationships. It is intended to show next how an analog computer might be employed in the solution of this dynamic

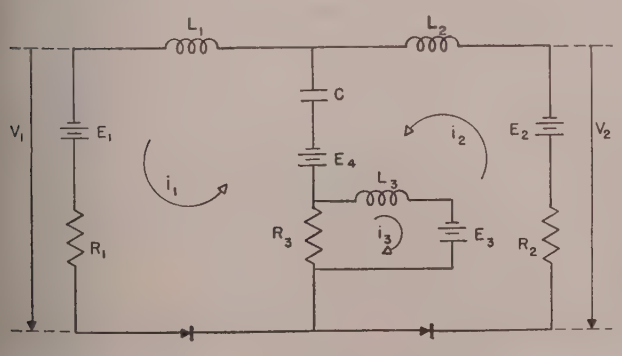

Figure 3 (left). Electrical circuit analogue

Figure 5 (below). The adjusted endogenous component of real investment shown as a function of the rate of change of the real national income, lagged

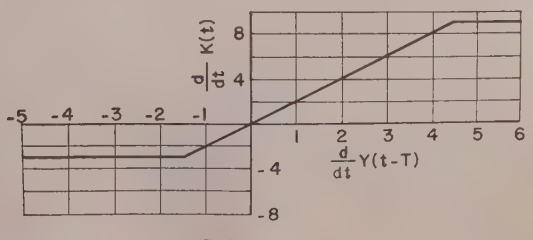

economic model for which independent statistical estimates of the parameters are available. The terms are defined in Table III, and the equations for this model are as follows:

$$C(t)=\alpha Y(t)+\beta-\gamma\frac{d}{dt}Y(t) \tag{24}$$

$$Y(t)=C(t)+\frac{d}{dt}K(t)+D(t) \tag{25}$$

$$\frac{d}{dt}K(t)=F_s\left[\frac{d}{dt}Y(t-T)\right] \tag{26}$$

where the function in equation 26 is of the form shown in Figure 5. These equations reduce to

$$\gamma\frac{d}{dt}Y(t)+(1-\alpha)Y(t)-F_s\left[\frac{d}{dt}Y(t-T)\right]=\beta+D(t)=G(t) \tag{27}$$

Goodwin has suggested that, on the basis of available statistical evidence, the following magnitudes may be assigned to the parameters of the economic model.

t = time in years
γ = 0.5 year
T = one year
α = 0.6, a dimensionless number

$$\frac{d\left\{F_s\left[\frac{dY(t-T)}{dt}\right]\right\}}{d\left\{\frac{d}{dt}Y(t-T)\right\}}=2.0 \text{ years}$$

where $-\$3$ billion $< F_s\ [d(Y(t-T)/dt] < +\$9$ billion, adjusted to the general level of prices for the period of the great boom and depression.

Equation 24 states that current consumption depends upon current national income and upon the current rate of change in national income. (Note that consumption, income, and investment are rates, that is, so much per annum.) The rate of change in income appears in order to allow for the fact that consumer expenditures depend in part upon whether incomes are rising or falling. Equation 25 is an accounting identity, national income being by definition equal to the sum of consumer expenditure plus both endogenous and exogenous investment. It is useful to write endogenous investment expenditure as the rate of change in that portion of the stock of capital which becomes altered as a consequence of other changes in the system. Exogenous investment may be regarded as the real value of the rate of government expenditures minus receipts. One may also wish to include as part of exogenous investment residential construction and important innovations such as the development of atomic energy. Equation 26 describes how endogenous investment depends upon the rate of change in national income.

Table III. Notation for a Nonlinear National Income Model

Economic Symbol	Definition of Economic Term	Electrical Analogue
t	Time, as in Table 1	t
T	A finite period of time	T
$C(t)$	Real consumption, that is, consumption expenditure in billions of dollars per annum adjusted by multiplying by 100 and dividing by a price index	$i_C(t)$
$Y(t)$	Real national income, that is, money national income similarly adjusted	$i_y(t)$
$\frac{dK(t)}{dt}$	The endogenous component of the rate of change in the real stock of capital, that is, endogenous real investment adjusted by the same price index	
$F_s\left[\frac{d}{dt}Y(t-T)\right]$	An acceleration function having the dimension of $Y(t)$	
$D(t)$	Exogenous real investment adjusted by the same price index	
α	A dimensionless constant	α
β	A constant having the dimension of $C(t)$, $Y(t)$, and so forth	i_β
γ	A coefficient having the dimension of time	L/R
$G(t)$	$\beta+D(t)$	$i_g(t)$

It is an original feature of Goodwin's model to introduce this nonlinear relationship. Goodwin argues that the desired stock of capital, such as factory equipment, is proportional to national income, and that if national income rises the desired stock of such real capital rises. This causes a positive rate of endogenous investment, but it is well to assume that this rate has a practical upper limit. The positive rate of investment must therefore persist over a sufficient period of time if existing real capital must be brought up to the desired level. Similarly, if there occurs a drop in national income, the desired stock of capital will decline. This may necessitate negative investment (or disinvestment) in order to reduce the existing stock of capital to the lower level which is now desired. This process of disinvestment will also require time, for there is a lower (negative) limit on investment given by the maximum rate of depreciation. Referring to equation 26 and to Figure 5, the slope of this function with respect to the argument is the coefficient of acceleration where acceleration refers to the fact that investment depends upon the rate of change in the national income of an earlier period. The reason for the time delay is that a finite length of time is generally required before decisions to invest can be carried out.

A possible electrical analogue will now be indicated in both equation and diagram form. From equation 27 and Table III, the electrical equation may be written

$$L\frac{d}{dt}i_y(t)+(1-\alpha)Ri_y(t)-RF_s\left[\frac{d}{dt}i_y(t-T)\right]=Ri_g(t)=e_g(t) \tag{28}$$

The circuit requirements are indicated in Figure 6.

A Stochastic National Income Model

The third model to be presented is an elementary macroeconomic model concerned with the determination of national income. This model is a severe oversimplification from the economist's point of view, but it will serve to illustrate the possibility of estimating unknown parameters by the use of an analogue computer. This particular model has been chosen because it involves features which occur in many of the more complicated econometric models, solutions to which may involve a nearly prohibitive amount

Table IV. Notation for Stochastic National Income Model

Economic Symbol	Definition of Economic Term	Electrical Analogue
t	Time, as in Table 1	t
T	A finite period of time	T
$C(t)$	Total consumer expenditures in billions of dollars per year	$e_C(t)$
$Y(t)$	National income in billions of dollars per year	$e_y(t)$
$I(t)$	Sum of private investment plus government deficit plus net foreign trade balance, each in billions of dollars per year	$e_I(t)$
$u(t)$	A normally distributed stochastic variable with a mean value of zero, a standard deviation of σ, and a coefficient of serial correlation of ρ. Its dimension is billions of dollars per year	$e_u(t)$
α	A constant having the dimension of billions of dollars per year	e_α
β	A dimensionless constant	β
γ	A dimensionless constant	γ

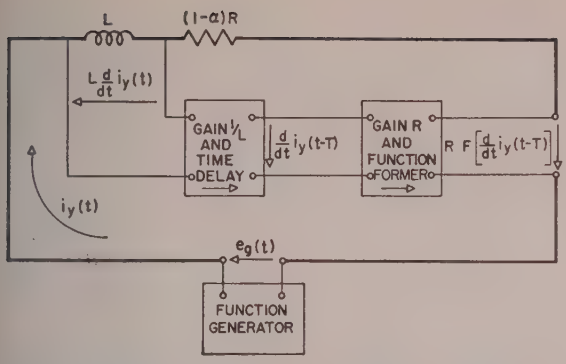

Figure 6. Electrical analogue for a nonlinear national income model. With each block is associated high input and low output impedance

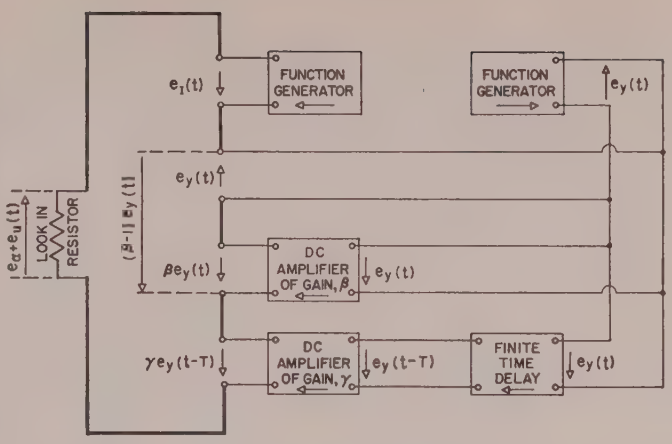

Figure 8. Electrical analogue for stochastic national income model arranged for statistical inference. With each block is associated high input and low output impedance

of computational work. The model chosen for study contains two equations:

$$C(t)=\alpha+\beta Y(t)+\gamma Y(t-T)+u(t) \qquad (29)$$

$$Y(t)=C(t)+I(t) \qquad (30)$$

Equation 29 is a behavior relationship called a "consumption function". Equation 30 is an accounting identity. The symbols are defined in Table IV.

From equations 29 and 30

$$u(t)+I(t)+\alpha+(\beta-1)Y(t)+\gamma Y(t-T)=0 \qquad (31)$$

This is the economic relationship which we wish to study. The problem is to find numerical estimates for the parameters α, β, γ, and T such that for the known function $I(t)$ and a selected function $u(t)$, the resulting function $Y(t)$ will best approximate its observed behavior over a chosen period of years past. $I(t)$ is obtained directly from relation 30 and from statistical records of functions $Y(t)$ and $C(t)$ over the same period. The stochastic term $u(t)$ is introduced to account for random disturbances. It is assumed to be normally distributed about a mean value of zero. Figure 7 illustrates approximately what is meant. One may imagine a very rapidly changing function with both positive and negative peaks with an average height of zero. A random distribution of this type is specified by the standard deviation σ, which is a measure of its dispersion. The dispersion increases as the number of peaks which are very different from zero increases. One may also suppose that there is serial correlation (expressed by the coefficient of serial correlation ρ), that is, that the height of the function at one point in time depends upon its height at some previous point in time. The value of ρ depends upon the time lag between successive values of the function considered in its computation. One may consider that a good set of values for α, β, γ, and T has been found only if σ can be kept small. Otherwise, $u(t)$ may be large relative to the other functions of time, and considerable doubt will be cast upon the usefulness of the model.

Equation 31 now is rewritten utilizing equivalent electrical terms as listed in Table IV.

$$e_u(t)+e_I(t)+e\alpha+(\beta-1)e_y(t)+\gamma e_y(t-T)=0 \qquad (32)$$

An electrical circuit to which equation 32 applies is presented in Figure 8. An alternative way of representing the same equation is by the circuit shown in Figure 9. The circuits of Figures 8 and 9 are different with respect to what is assumed known. In Figure 8, $Y(t)$, $Y(t-T)$, and $I(t)$ are introduced as historically given functions; β, γ, and T are treated as parameters; and $[\alpha+u(t)]$ is the dependent variable. In Figure 9, $I(t)$ and $u(t)$ are introduced as known functions, although $u(t)$ can be regarded only as a sample of successive observations drawn from the probability space defining $u(t)$; α, β, γ, and T are regarded as parameters; and $Y(t)$ as well as $Y(t-T)$ appear as dependent variables.

For purposes of statistical estimation, the circuit of Figure 8 is the relevant one. The solution for $[\alpha+u(t)]$ may be observed on the oscilloscope screen as a time function, and the mean value of this function will be α because it is specified that the mean value of $u(t)=0$. The procedure is to vary the parameters β, γ, and T until the standard deviation σ of the observed solution for $[\alpha+u(t)]$ is at

Figure 7 (below). A sample of random disturbances

Figure 9 (right). Electrical analogue for stochastic national income model arranged for parameter study. With each block is associated high input and low output impedance

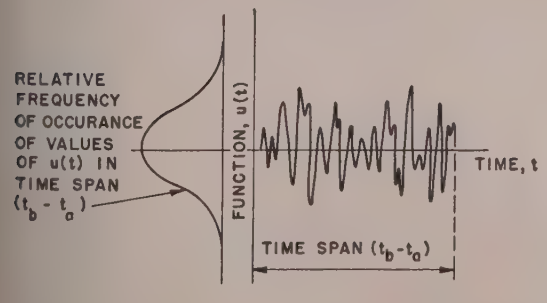

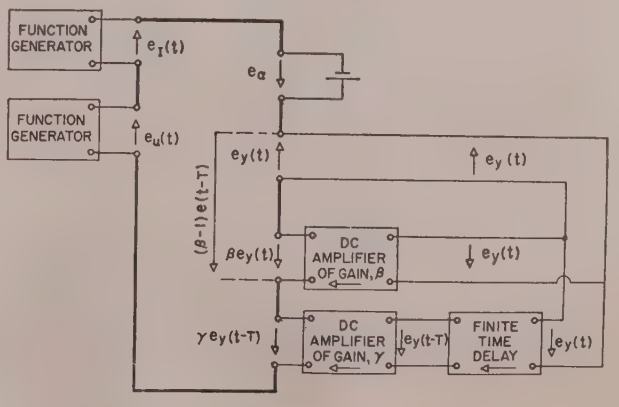

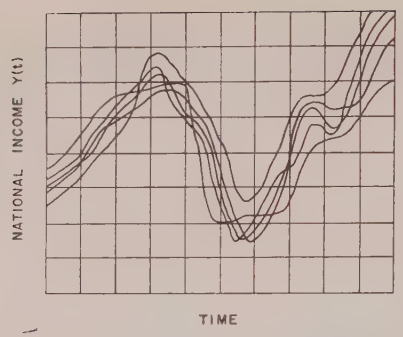

Figure 10. Representative of behavior of national income for various samples of disturbances

a minimum. The values of these parameters which minimize σ may then be regarded as statistical estimates of the true values, granted the correctness of the specifications of the model.

It should be understood that the process of deciding which of all possible sets of parameters is the "best" depends upon visual determination and not upon formal methods of statistical inference. It may be that electrical techniques can be developed that will indicate a "best" fit when certain statistical inference formulas are satisfied; but no such methods are at present suggested.

One problem that remains is that of how one may examine the parameter space so that the "best" parameters will be found. We believe that in general this may be done by an iteration process, a process of adjusting each parameter in turn. Once the best set of parameters has been selected, the standard deviation and coefficient of serial correlation of the random disturbances may be measured from a photograph of the time function $[\alpha+u(t)]$ as displayed on the oscilloscope.

After estimates of the parameters have been made, it may be desirable to examine the model with respect to its sensitivity to variations in the random disturbances. We may like to know what the behavior of the model would have been over the past period of time (on the basis of which the estimates were made) had there been a different sample of random disturbances drawn from the probability space whose constants have been found. To do this, the circuit for the particular model used here as an example should be that of Figure 9. In this circuit the endogenous variables appear as dependent variables, and the random disturbances are treated as known. The procedure would be to examine the response of the circuit for each of a series of different samples of the random disturbances. By a sample of disturbances $u(t)$ we refer to a selection of the time function $u(t)$ drawn from the probability space that defines $u(t)$. $u(t)$ may be introduced by playing into the circuit a sample of atmospheric noise recorded on a magnetic tape, provided that $u(t)$ has an approximately normal distribution. One may adjust the standard deviation of a sample of noise by altering the amplitude with which it enters the circuit. Similarly, the coefficient of serial correlation for a given (finite) time lag may be altered by varying the speed with which the recording is played into the circuit. By playing repeatedly different samples of noise, a series of solutions for $Y(t)$ may be observed. If recorded on a single photograph this set of solutions will appear as suggested by Figure 10. One may then observe the extent to which the inclusion of the random disturbances affects the theoretical response of the model. If the various solutions for $Y(t)$ are very different, that is, if the past history of national income could have been greatly altered had there occurred some other probable set of random disturbances, the model may be said to place very great emphasis on the random disturbances, and may therefore be regarded as of dubious value. Otherwise, the model may be regarded as specifying the behavior of the economy within narrow bounds. The same method suggested here may be used to examine the system for other arbitrary movements of the exogenous variables which may be of interest.

Summary

A wide variety of models of interest to economists may be represented by electrical circuits. These models therefore lend themselves to investigation by use of an electrical analogue computer. The economist may study a model with any of three questions in mind: What are its topological features? What is its quantitative behavior for given parameters? What are good estimates of the parameters? This paper shows that analog computing techniques may be useful in helping economists answer all three of these questions.

References

1. An Electro-Analog Method for Investigating Problems in Economic Dynamics: Inventory Oscillations, **N. F. Morehouse, R. H. Strotz, S. J. Horwitz.** *Econometrica* (Chicago, Ill.), volume 18, number 4, April 1950, pages 313–28.

2. The Nonlinear Accelerator and the Persistence of Business Cycles, **R. M. Goodwin.** *Econometrica* (Chicago, Ill.), volume 19, number 1, January 1951, pages 1–17.

Discussion

Otto J. M. Smith and **R. M. Saunders** (University of California, Berkeley, Calif.): Analogue computing techniques have been applied to a dynamic study of Kalecki's equations relating consumption and the production of capital goods. The effect of time delays in production and the depreciation rate on the frequency of oscillation and degree of stability of national income were investigated at the University of California.

Five basic equations were instrumented.

The first states that deliveries of capital goods lag behind the investment orders by the production time delay θ in years:

$$L(t)=I(t-\theta) \tag{1}$$

The total volume of existing industrial equipment is equal to the running integral of deliveries minus replacements of depreciated items:

$$K=\int_0^\tau (L-U)dt \tag{2}$$

The production rate at any instant is the average of the delivery rate for the following time interval θ, or the average of the investment rate for the preceeding time interval θ.

$$A_\tau=\frac{1}{\theta}\int_\tau^{\tau+\theta} Ldt \tag{3}$$

or

$$A=\frac{1}{\theta}\int_{\tau-\theta}^{\tau} Idt \tag{4}$$

This is equivalent to the running integral

$$A=\frac{1}{\theta}\int_0^{\tau} (I-L)dt \tag{5}$$

The personal consumption of noncapital goods is assumed to be an irreducible minimum plus an increment proportional to the total national income.

$$C=C_{\min}+\lambda B \tag{6}$$

$$B=A+C \tag{7}$$

The rate of investment orders to produce capital goods is proportional to total national income less a pessimism factor times the total capital goods on hand.

$$I=\alpha B-nK=\alpha(A+C)-nK \tag{8}$$

$$I=\frac{\alpha(A+C_{\min})}{(1-\lambda)}-nK \tag{9}$$

where

C = personal consumption rate of capital include milliards per year
U = demanded rate of restoration of industrial equipment

I = rate of investment orders
A = rate of production of capital goods
L = rate of deliveries of investment orders
B = total national income
$n = -\partial I/\partial K$, decrease of investment order rate with increase in total volume of existing equipment (positive parameter, units, reciprocal years)
$\alpha = \partial I/\partial B$, increase of investment order rate with increase in national income. (dimensionless)
$\lambda = \partial C/\partial B$, increase in consumption with increase in national income
$m = \alpha/(1-\lambda)$, Kalecki's optimism parameter

Equations 1, 2, 5, and 9 can be combined in the block diagram shown in Figure 1 of this discussion. The two integrators were actually replaced by one in the feedback path for simplicity of construction.

The analogue was constructed with a time base of 200 microseconds equal to one year. The time delay θ was made in two forms: (1) A 4-element-distortionless inductance-capacitance delay line, and (2) a 3-time-constant resistance-capacitance nonloading ladder network with appreciable high-frequency attenuation. The former represents equation 1 but the latter is closer to economic reality, because not all manufactured goods have the same delay in production.

The analogue has a double-triode integrator, two tubes in the I-L subtractor, two phase inverters, and three adding tubes. Germanium diodes were used for a nonlinear characteristic for α. A switch was provided for comparison with linear operation. In the former case, the wave shape was the familiar boom-bust triangular wave.

Credit time constants in the positive-feedback consumption loop, and changes in depreciation proportional to the rate of change of production can be easily added.

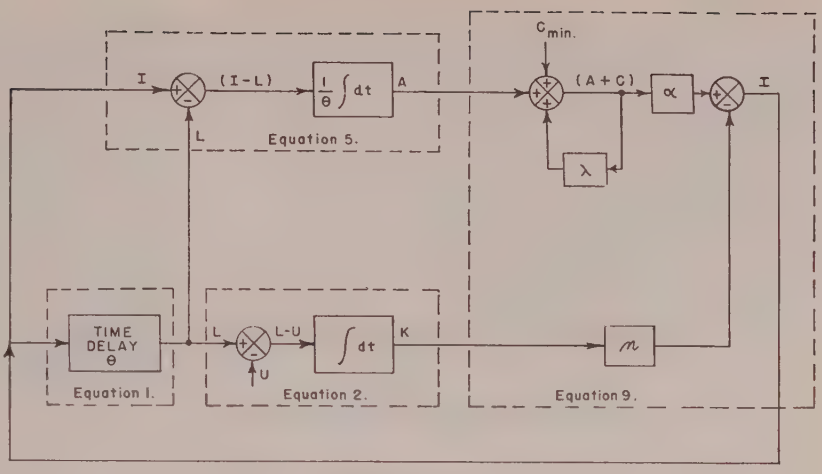

Figure 1. Analogue of Kalecki's economic system

This relatively simple analogue has proved to be a very valuable tool for determining the implications and conclusions to be drawn from different economic hypotheses. It is far superior to digital or analytical methods because of the rapidity of solutions and the visual presentations of results.

The parameters α, λ, and n were linear potentiometers. In operation, their values for critical stability, and the corresponding frequency, were determined quickly with a frequency meter. The damping factors for nonoscillatory operation were obtained from oscilloscope observations using square wave inputs on U or C.

R. H. Strotz, J. F. Calvert and **N. F. Morehouse:** The authors sincerely appreciate the comprehensive discussion presented by Messrs. Smith and Saunders. We have read their description of a dynamic study of Kalecki's equations with much interest. It is our opinion that this is a very considerable contribution to the art of analogue computing in relation to economic models and hope that there may be a further exchange of information concerning such work.

A Submarine Telephone Cable with Submerged Repeaters

J. J. GILBERT
MEMBER AIEE

THIS paper describes the recently installed Key West-Havana submarine cable telephone system in which repeaters designed for long life are incorporated in the cable structure and are laid as part of the cable.

In April 1949 there was installed between Key West, Florida and Havana, Cuba a submarine telephone cable system involving a radical departure from the conventional art of long-distance submarine telephony. This departure consisted of the inclusion within the armor of the submarine cable of electron tube repeaters which are designed to pass through the cable-laying machinery and sink to the ocean bottom like a length of cable, and which, over an extended period of perhaps 20 years, should not require servicing for the purpose of changing electron tubes or defective circuit elements. The repeater has the appearance of a bulge in the cable about three inches in diameter and tapering off in both directions to the cable diameter of a little over an inch. The total length of the bulge including the taper at each end is about 35 feet. The bulge is flexible enough so that it can conform to the curvature of the brake drum and of the various sheaves in the laying gear on the cable ship. A repeater, with stub cables, is shown in Figure 1.

Historical

The new cable system, comprising cables numbers 5 and 6 of the Cuban-American Telephone and Telegraph Company, represents another step in the development of telephonic communication between the United States and Cuba, which has presented many interesting problems. Natural conditions make it difficult, if not impossible, to employ some of the usual methods of communication. One such condition is the absence of high ground in Florida that would permit the use of economic radio systems. Another is the stretch of water between Florida and Cuba, which, in places, is as much as 6,000 feet in depth and restricts the type of cable that can be used. The practical solution has been to go from the point of contact with the Bell System toll lines at Miami, over the Keys to Key West by land line (with some water crossings), thence to Havana, an air-line distance of about 100 nautical miles (n.m.), by submarine cable of the deep-sea type of construction, having a single coaxial circuit, insulated with water-resistant material. There are problems involved in building and maintaining the Miami-Key West connections, but these are outside the scope of this paper.

Telephone communication between the United States and Cuba was initiated in 1921, when three submarine cables were laid between Key West and Havana.[1] Each cable provided a telephone circuit operated on a 2-wire basis and two or more telegraph circuits, direct and alternating current. The cables were continuously loaded with iron wire, insulated with gutta-percha, and had return conductors consisting of copper tapes laid on the insulated core and exposed electrically to the sea water. These cables were the first ones to employ the copper return conductor, which also has been used in subsequent cables. The copper return was employed after a theoretical study had indicated that the armor and sea water, which for the low frequencies then involved in cable telegraphy furnished a low-resistance return conductor, would not be satisfactory at voice and higher frequencies. At these frequencies skin effect causes the return current to concentrate in the armor wires, which are naturally poor conductors for alternating currents, and this makes the resistance of the return path rise to undesirable values. The copper return effectively removes the armor wire and sea water from the transmission circuit at all but very low frequencies. This has the further advantage of reducing the exposure of the circuit to static noise.

Although the iron-wire loading was very effective in reducing attenuation in the voice range, the eddy current resistance due to the loading wire made itself felt to a rapidly increasing degree for frequencies above the voice band. Consequently, when additional circuits were required some years later and it was decided to extend the frequency range in order to make use of newly developed carrier frequency equipment, it was necessary to dispense with magnetic loading. In 1930 the Key West-Havana Number 4 cable was laid embodying new materials and novel principles of design.[2] The insulating material in this case was paragutta, which had been developed recently by the Bell Telephone Laboratories and which possessed electrical characteristics and stability much superior to gutta-percha. An intensive study had been made of the design of coaxial cables for carrier frequencies with the aim of obtaining optimum electrical performance by proper proportioning and construction of the conductors, and these principles were employed in the new cable. Initially, 3-carrier telephone circuits were obtained on the Number 4 cable using the equivalent 4-wire method, with separate frequency bands for transmission in opposite

Paper 51-94, recommended by the AIEE Wire Communication Systems Committee and approved by the AIEE Technical Program Committee for presentation at the AIEE Winter General Meeting, New York, N. Y., January 22-26, 1951. Manuscript submitted October 23, 1950; made available for printing December 19, 1950.

J. J. GILBERT is with the Bell Telephone Laboratories, Inc., Murray Hill, N. J.

The author wishes to acknowledge the assistance of the engineers of the Bell Telephone Laboratories who were involved in the success of this undertaking.

Figure 1 (left). Submarine cable repeater

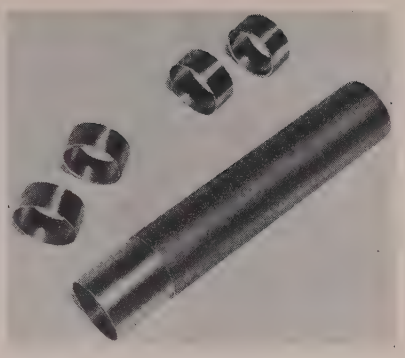

Figure 2 (right). Steel rings and copper tube of container

directions. The cable had been designed with considerable transmission margin and in 1940 the need for additional circuits to Cuba resulted in the installation of new terminal equipment which enabled it to provide seven 2-way high-quality circuits on an equivalent 4-wire basis.

The Key West-Havana Number 4 cable design has proved very popular in other parts of the world. Several such cables have been laid between England and the Continent, between England and Ireland, and between Australia and Tasmania, and others were used in connection with the war effort. A cable of this design also has been laid between two of the Japanese islands.

Submerged Repeaters

The demands for circuits to Havana continued to grow, and, after the close of World War II, the time appeared ripe for making use of a new development which had just come to a head in the Bell Telephone Laboratories after a period of experimentation. This development was the submerged repeater. The need for periodic strengthening of signals transmitted over considerable distances is about the same in submarine cables as it is in land lines and, as in land lines, the permissible spacing between repeaters usually diminishes as the desired frequency increases. The great difficulty in the case of submarine cable routes is that there usually are no land sites on which repeaters can be located. Artificial islands consisting of floating platforms or buoys have been proposed as a solution, but ocean currents and storms have disastrous effects on such structures. Interruptions as the result of such causes would make it difficult to meet the requirement on continuity of service which is necessary in the case of important telephone circuits. Thus it seemed that the safest place for a submarine cable repeater is on the ocean bottom.

Requirements on Repeater

The decision to place the repeater on the ocean bottom resulted in special requirements on the structure, the first of which is that it should be capable of resisting the considerable hydrostatic pressure that is encountered in deep water. It also seemed desirable that the operation of getting the repeater overboard from the cable ship should not impede the smooth functioning of the laying process. The best way of meeting this requirement appeared to be to make the repeater structure flexible, within practicable limits, and as small as possible in diameter so that it could pass around the drum and sheaves of the laying gear like any length of cable.

In order to make such a repeater attractive from operating and commercial points of view another requirement was necessary, namely, that the electric circuit elements of the repeater, including electron tubes, resistances, condensers, and coils, be designed for long life under operating conditions, so that there would be assurance of freedom from trouble or need of replacement of parts over a long period, perhaps 20 years or more. Servicing of the repeater would be in the nature of a cable repair, and the repair of a submarine cable is something not to be sought. The procedure is apt to be expensive and time-consuming, because of circumstances beyond control, such as bad weather or unavailability of a repair ship, and the disturbance of the cable involved in lifting it to the surface and dropping it again, possibly in something of a heap, is not desirable. It is obvious that the requirement on long life of circuit elements presents a difficult problem, especially since the space available for these elements is minimized in order to keep the repeater diameter small.

There was still another requirement on circuit elements, that of ruggedness. The stresses involved in laying cables in deep waters are quite considerable. The cable is under a tension of several thousand pounds, and incidents might occur which would have no effect on an ordinary cable but might result in dangerous shocks to the delicate elements of the repeater.

Also, as a consequence of the cable tension, the armor unlays somewhat, and this imposes twist and elongation on the interior structure, either coaxial circuit or repeater housing. The cable circuit can be designed to withstand this distortion, but the repeater housing is much more susceptible to damage from this cause.

The Repeater Housing

The requirements on flexibility and watertightness under ocean-bottom pressures were the factors of outstanding influence in the design of the repeater housing and of the end seals by means of which the cable enters and leaves the housing. In the present form the housing consists of a long tube of soft copper, $1^3/_4$ inches in diameter and 0.03-inch thick, supported internally against collapse under sea-bottom pressure by an assemblage of abutting steel rings, each 3/4-inch wide, and given a degree of rigidity by means of thinner steel rings of the same width overlaying and staggered relative to the thicker rings. When this structure is sealed at the ends it is capable of withstanding pressures as high as 10,000 pounds per square inch, and it can be bent to a radius as small as three feet without undue distortion of the copper envelope. Details of the structure are shown in Figure 2.

Into each end of the housing is led the insulated conductor of the cable by means of a series of seals. The inner or vapor seal is of the glass-metal type especially developed for this particular purpose and capable of withstanding considerable hydrostatic pressures. Next in line is a seal comprising a central brass tube and an external brass member, both vulcanized to rubber, which is joined to the insulating material of the cable. These

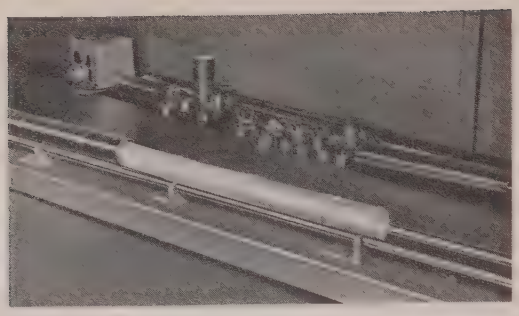

Figure 3 (left). Repeater with portion of rings in place

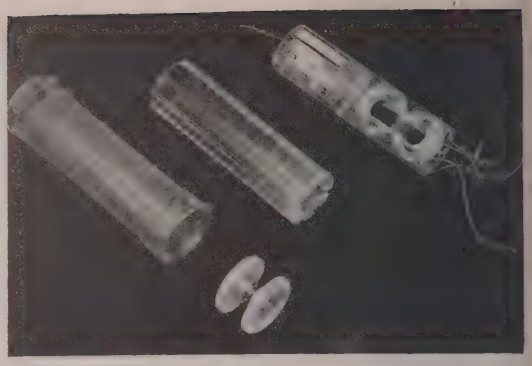

Figure 4 (right). Typical section of repeater

seals are coaxial in form, the outer member in each case being brazed to the copper tube of the housing or an extension thereof. Finally, a closely fitting core tube of copper, extending over the cable insulation for a distance of about seven feet, is brazed to an extension of the copper envelope of the housing, filled with vistac, and sealed at the distant end by means of a neoprene sleeve firmly joined to the core tube and to the cable insulation.

The repeater housing and the core tube are provided with corrosion-protection layers and a bedding for the armor wires, the bedding over the core tube being built up in the form of a taper. The armor is a continuation of the cable armor wires with additional wires interspersed because of the larger diameter of the repeater. To prevent twisting of the container as a result of the unlaying of the armor wires under tension, a second layer of wires with a direction of lay opposite to that of the main armor is employed. The repeater may be armored as part of the cable or it may be armored separately, with a stub on each end, and spliced into the cable.

The components of the housings and seals, as well as the complete armored housing, have been subjected to exhaustive tests of various sorts. The rubber-brass seal, for instance, was tested for penetration of moisture vapor over long periods of time. Methods of making this seal were checked by tension tests until a uniformly high degree of adhesion was obtained. Armored housings were tested on a laboratory setup in which laying conditions could be simulated by bending the structure under tension and in motion around a six-foot-diameter drum.

The Repeater Circuit

The diameter of the housing had been chosen originally on the assumption that the bulge caused by the repeater should not be more than two or three times the diameter of the cable proper in order to reduce the possibility of overriding turns on the brake drum during laying. Mechanical tests indicated that this diameter also was safe from the standpoint of deformation of the copper envelope during bending. Accordingly, it was required that the repeater structure be restricted in cross section so as to fit inside this tube, with as much length as would be needed.

The problem then became one of packaging the elements involved in a high-gain electron tube amplifier in the restricted space available. The method finally adopted is shown in Figure 3. The completed amplifier consists of an articulated assemblage of composite lucite cylinders, each about five inches long, successive units being held together by a spring assembly. Each lucite cylinder contains the related electric elements of a particular part of the repeater circuit. The groups of smaller elements are mounted rigidly in a lucite form which slides into an insulating envelope consisting of two closely fitting lucite shells and is held in place by end pieces of lucite. Eight copper tapes laid in axial slots between the shells and extending over several sections, where necessary, permit electric interconnection of the various parts. A representative assemblage is shown in Figure 4. In the case of the Key West-Havana repeater the complete assemblage is 84 inches long and comprises 15 sections.

Circuit Elements

Early in the development general principles were developed regarding the type of circuit best suited for underwater repeaters, and on this basis requirements were established on the characteristics necessary for the circuit elements, including electron tubes, and on their arrangement in the repeater. Decisions in such matters could not be arbitrary, of course, but had to be carefully worked out in order to freeze designs as early as possible so as to facilitate the start of significant life tests.

The electron tube is the most important of the elements. Work had been begun on a tube suitable for this use as long ago as 1933. Thus, when a decision was made to lay the new cables, a long background of experience was drawn on in the manufacture of the tubes. Early models of the type had been operated on continuous life test for as long as ten years. Designed primarily for long life, the tube is a suppressor grid pentode with an indirectly heated cathode. Of rugged design to withstand the shocks of cable laying, the spacings between electrodes are relatively large. Unusual care was taken in manufacture to insure solid welds and to avoid the presence of loose particles. During various stages of assembly, rigorous inspections were made on all tubes by engineering personnel. Selection of tubes for use in the cable was based on a thorough examination of all details in the history of each tube, as well as the history of the group in which it was manufactured. All tubes which were candidates for the cable were aged several thousand hours before preliminary selection was made. Also, other tubes from the same production group were life-tested several thousand additional hours to establish the quality of the group. One early decision was to power repeaters by direct current fed from land over the cable conductor. The tube heaters connected in series would furnish plate and grid potentials. This was an important factor in setting the nominal power requirements for the tube, which are about

Figure 5. Assembling the repeater

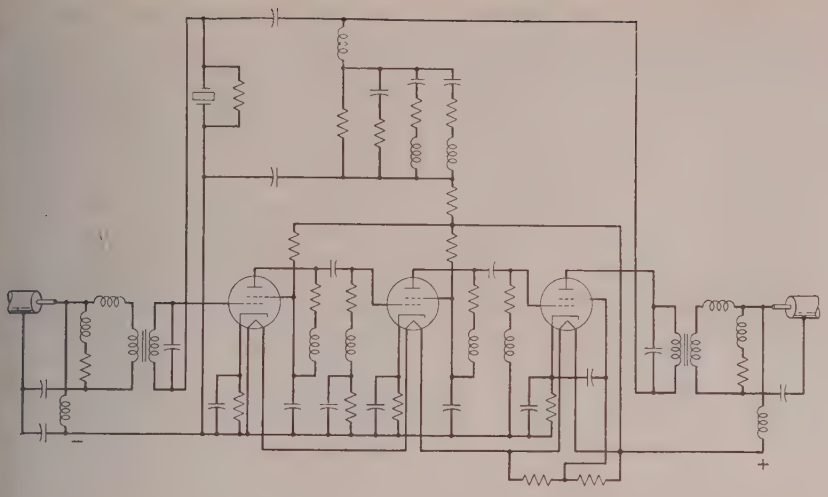

Figure 6. Repeater circuit

1/4 ampere at 20 volts for heater supply and plate potentials of 40 to 60 volts.

While the electron tube usually is the most vulnerable element in electric circuits from the standpoint of life, attention must be given to other elements—condensers, resistances, and coils—especially where they are subject to long-continued application of electric potentials as in the case of power separation filters. The factors that determine the life and performance of these elements are not completely under control. It was felt, however, that the best assurance on dependability could be obtained by careful, conservative design and by manufacturing and assembling the elements into repeaters under the best possible conditions of cleanliness. An air-conditioned space was provided for this purpose at the Murray Hill Laboratory. In addition to cleaning the air in this space, precautions were taken against the entrance of dirt by other means, for example, on the clothing or persons of operators. The humidity of the air was controlled carefully to prevent contamination from perspiration during handling of the parts. Manufacture was carried out by selected workmen, and the product was inspected at various stages by engineers. A view of one of the operations is given in Figure 5.

Field Trials

Simulated laying tests in the laboratory covered a period of several years. Special pains had been taken to include as far as possible all aspects of the laying operation, even those which were judged to be free of hazard to the repeater. Tests also were made to determine the effect, if any, of the laying operation upon the electric transmission characteristics of the cable. Likewise, comprehensive electrical tests had been made to insure that no unexpected effects would be encountered because of the immersion of the repeater in water.

A large-scale test was needed, however, to establish the practicability of the repeatered cable. This is because the suspended length of cable trailing the ship may be as great as 10 n.m. or more during the laying operation, and in this length there occur complex mechanical phenomena which cannot be simulated in the laboratory with a great degree of assurance. After preliminary trials from a barge in Long Island Sound, a deep-water test of the repeatered cable was made in 1948 in the Bahamas. The cable ship *Lord Kelvin* of the Western Union Telegraph Company was chartered for the purpose. Lengths of cable up to 15 n.m. were paid out along with repeaters in depths of water up to 2 n.m. Several repeaters were laid, measured while on the ocean bottom, and then hauled back to the ship, a procedure that involves much more severe treatment than a mere laying operation. The repeater shown in Figure 1 experienced this treatment. Tests also were made with repeater housings containing specially designed accelerometers to determine the shocks resulting from possible abuse during laying. The results indicated that the repeaters as well as the cable could take the punishment with considerable margin of safety.

The Transmission System

Designing the electric circuit of the repeater was largely a matter of getting the most out of the long-life electron tube in the way of stability of repeater gain and low modulation while obtaining as much gain as the system permits. For most efficient use of tubes and to simplify the structure a unidirectional repeater design was decided upon.

The repeater employed in the Key West-Havana cables has three stages with negative feedback, the circuit being as shown in Figure 6. The gain frequency characteristic is shown in Figure 7. The transmission band is from 12 kc to 120 kc. The insertion gain at 108 kc, the top frequency employed in traffic, is 65 decibels. The repeater gain equalizes the loss of about 36 n.m. of cable, the attenuation frequency characteristic of which is shown in Figure 8. The characteristics of the earlier cables are also shown here.

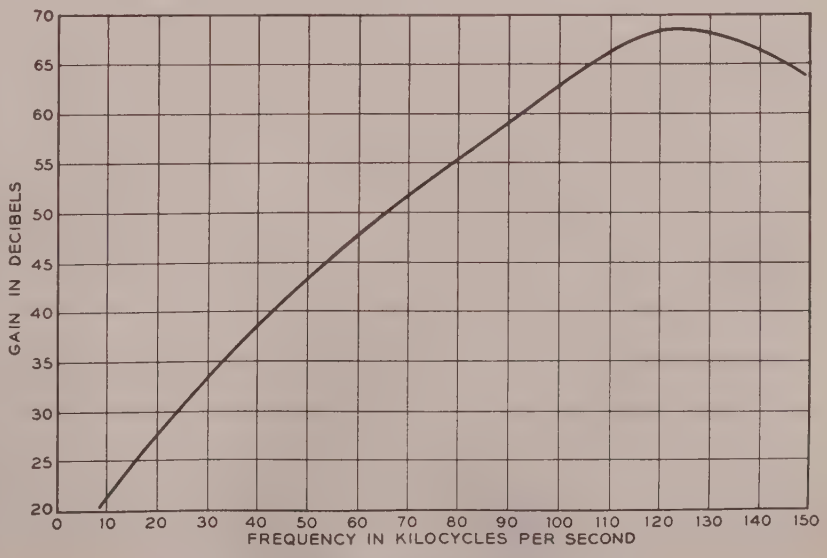

Figure 7. Gain versus frequency characteristic of repeater

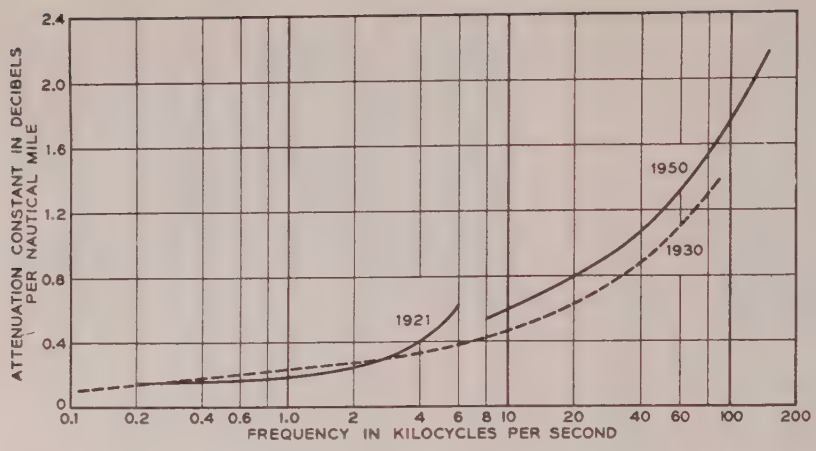

Figure 8. Attenuation versus frequency characteristic of cable

The layout of the new repeatered cable installation is shown in Figure 9. There are two cables, one for each direction of transmission. The East or Number 5 cable, transmitting south, is 114.55 n.m. in length. The West or Number 6 cable transmits north and is 124.97 n.m. in length. Each cable has three repeaters spaced approximately 36 n.m. apart. Two of the six repeaters are in a depth of 0.9 n.m. and two in about 0.35 n.m. The last repeater in each cable is located as close as possible to deep water so as to strengthen the signal before it enters shallow water and land sections of cable where static noise and crosstalk might be picked up. In Havana the last repeater is located in a large vault on the beach. At Key West the last repeater is located close to Sand Key Light, where the water begins to deepen.

At manholes near the shore at both ends the cables are spliced directly to underground cables running in ducts to the terminal equipment at the offices, a distance of three miles at Havana and one mile at Key West. The underground cables have the same coaxial circuit as the submarine cables, but in place of the mechanical protection of jute and armor they are provided with electrical protection of helical steel tapes, layers of paper, and over all a lead sheath.

The 12 kc to 108 kc pass band yields 24 channels in each cable, each channel occupying a band of 4 kc. The signal to noise ratio for these channels is about the same as for the same length of high-grade carrier-frequency circuit on land.

The Cable

The cable has a copper return, as in the case of the earlier installations, but differs from them in being insulated with polyethylene. It also involves some new principles of design that render the cable circuit less subject to change of electrical characteristics caused by laying stresses. This is a matter of considerable importance in the case of a system with submerged repeaters, since after the cable has reached the bottom it is impossible to adjust the repeater to compensate for changes in cable attenuation during laying, a matter that in ordinary cables is taken care of by adjusting the equipment on shore.

In order to avoid undesirable irregularities in transmission characteristics, special precautions were taken during manufacture to obtain a higher than usual degree of uniformity of the cable impedance as seen by a repeater. Because of the wide transmission band, schemes heretofore employed for reducing the effect of the variation of impedance among the core lengths constituting the cable would have called for core lengths so short as to increase seriously the number of joints. The irregularities were, therefore, minimized by careful control of conductor and insulation diameters and by continuously insulating lengths of the order of 12 n.m., cutting them only as was necessary for handling, and reassembling the shorter lengths as far as possible in insulating order to assure random addition of reflections caused by impedance irregularities. The success of this technique is evidenced by the impedance deviation curves shown in Figure 10.

The structure of the cable is shown in Figures 11 and 12. The central conductor consists of a solid wire 0.131 inch in diameter, on which are laid three copper tape surrounds, each 0.0145-inch thick and

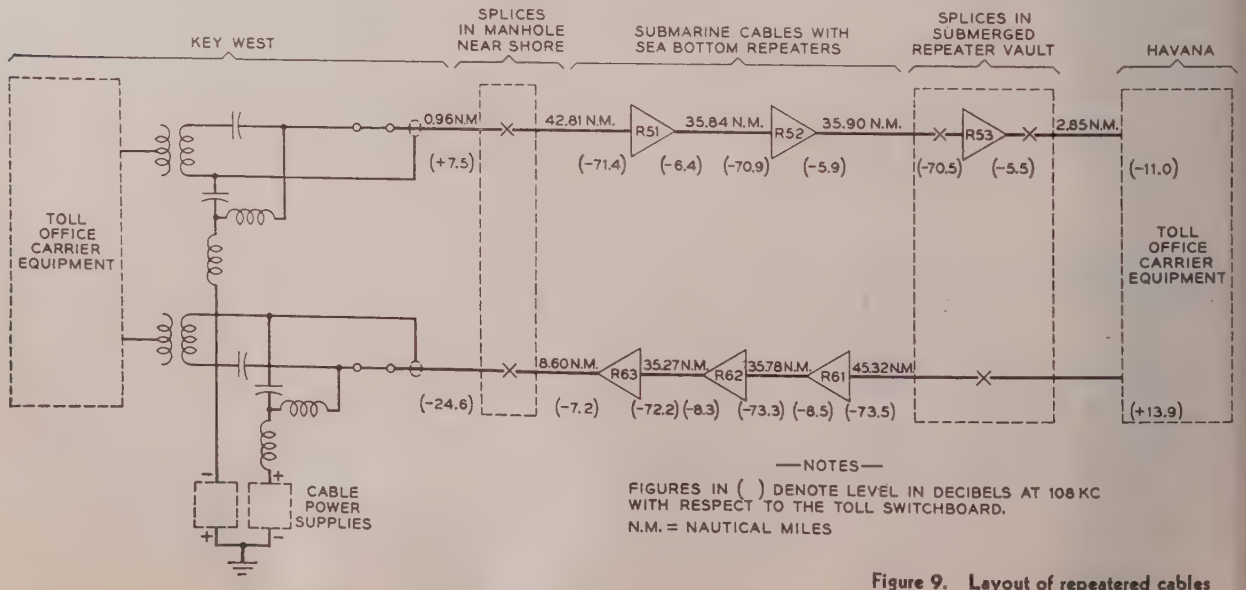

Figure 9. Layout of repeatered cables

0.148-inch wide, closely conforming to the solid wire. The interstices of the conductor are filled with polyethylene. The stranded conductor, 0.160 inch in diameter, is insulated with polyethylene to a diameter of 0.460 inch. Directly on the polyethylene insulation is laid the return conductor comprising six copper tapes, each approximately 0.016-inch thick by 0.241-inch wide, preshaped so that when in place they conform to the surface of the insulation. Both the return tapes and the tape surrounds of the central conductor have left-hand lay. Over the return conductor is wound a teredo tape approximately 0.003-inch thick with overlap. Over all is the cutched jute, the armor, and the outer jute serving to which are applied the usual cable compounds. Four types of armor are employed in the cable for use in various depths of water or for special shore conditions.

The lengths of the various types of armor, in nautical miles, as they appear in the two cables, starting at Key West are shown in Table I.

Figure 10. Impedance deviation of cable sections

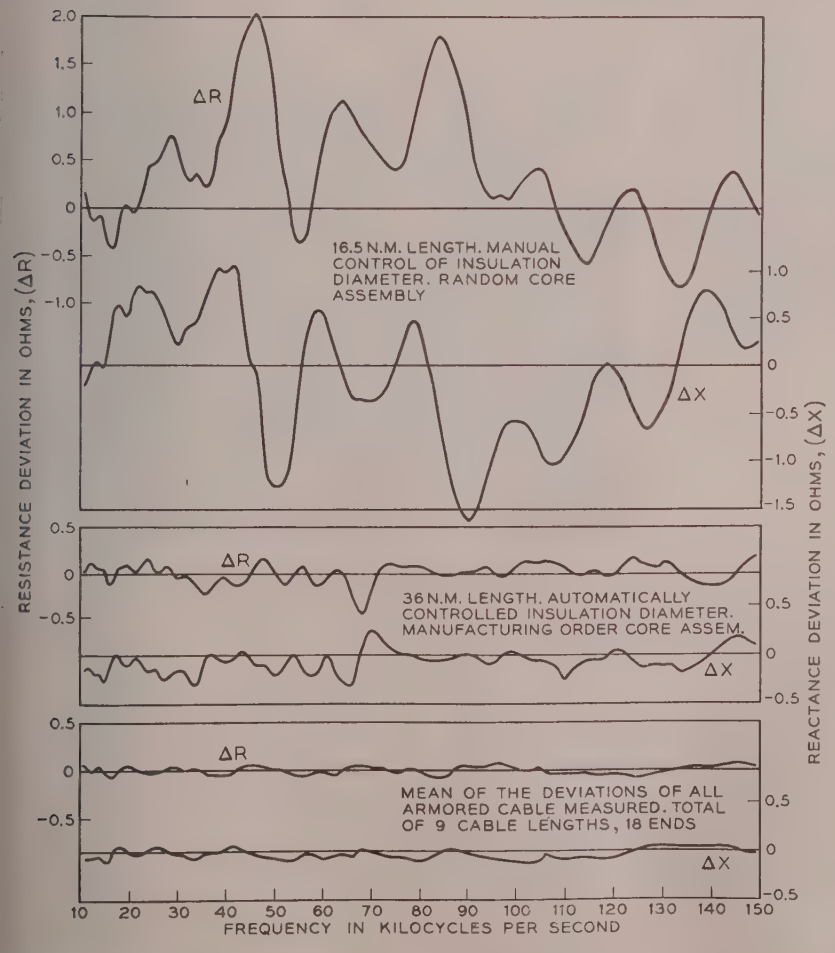
ΔR
16.5 N.M. LENGTH. MANUAL CONTROL OF INSULATION DIAMETER. RANDOM CORE ASSEMBLY
ΔX
ΔR
36 N.M. LENGTH. AUTOMATICALLY CONTROLLED INSULATION DIAMETER. MANUFACTURING ORDER CORE ASSEM.
ΔX
ΔR
MEAN OF THE DEVIATIONS OF ALL ARMORED CABLE MEASURED. TOTAL OF 9 CABLE LENGTHS, 18 ENDS
ΔX
RESISTANCE DEVIATION IN OHMS, (ΔR)
REACTANCE DEVIATION IN OHMS, (ΔX)
FREQUENCY IN KILOCYCLES PER SECOND

During the course of manufacture and in splicing on board ship, joints in the copper conductors were silver soldered. For joining the polyethylene insulation a special molding machine was designed and built by means of which polyethylene under high pressure and an elevated temperature was applied to the surfaces to be joined.

The cable was manufactured by the Simplex Wire and Cable Company of Cambridge, Mass., and incorporated the results of a co-operative development program conducted by this company and the Bell Telephone Laboratories. The excellent quality of the cable is a tribute to the manufacturer in this very difficult and exacting field.

Terminal Equipment

The transmission apparatus at Key West and Havana is mostly standard equipment employed in land-line carrier systems, and the operations involved in combining the 24 voice circuits into one band and separating them again are largely conventional. Special equalizers, power separation filters, and an auxiliary amplifier had to be designed, and the standard transmitting amplifier used in the *J* system was modified to accommodate the lower frequency band. A feature of particular interest is the equipment for testing the electrical condition of the repeaters from measurements at Key West. Each repeater contains a sharply tuned circuit by means of which the gain of the repeater is increased above normal at a distinctive frequency outside the transmission band of the repeater. With the aid of a loop circuit at Havana the gain with reduced feedback of the individual repeaters can be measured by scanning the test frequency region with an oscillator and detector at Key West. An indication of incipient decay of gain of any repeater thus is given.

Table I. Lengths (in Nautical Miles) of Various Types of Armor Used in Cables

Type	Number 5 Cable	Number 6 Cable
A	14.31	12.65
B	25.60	31.22
D	72.73	76.17
B	1.44	4.39
A	0.16	0.18
AA	0.31	0.36

The power for the repeaters is supplied over the cable conductor from Key West. A positive potential of about 250 volts is applied to one cable and −250 volts to the other, with a loop connection between the two cables at Havana to complete the d-c circuit. This neutral point also is connected to ground. The current in the cable conductors is at present maintained at 0.23 ampere. A view of the rectifying and control equipment for one of the polarities is given in Figure 13. Precautions are taken against interruption of the power supply to the cable and sensitive controls are provided to maintain the current constant in spite of earth currents and to guard against excessive currents or potentials in the cable system in case of trouble in the power supply or in the cable itself.

Laying the Cables

The laying of the cables was completed without undue incident by the cable ship *Lord Kelvin*. The task was one of unusual difficulty, since modifications had to be made in the cable-laying gear, some of them untried, and it was particularly desirable that the prescribed lengths and courses be realized.

Modifications were made in the cable-laying gear in order to obtain an additional margin of safety in laying repeaters. As indicated previously, the re-

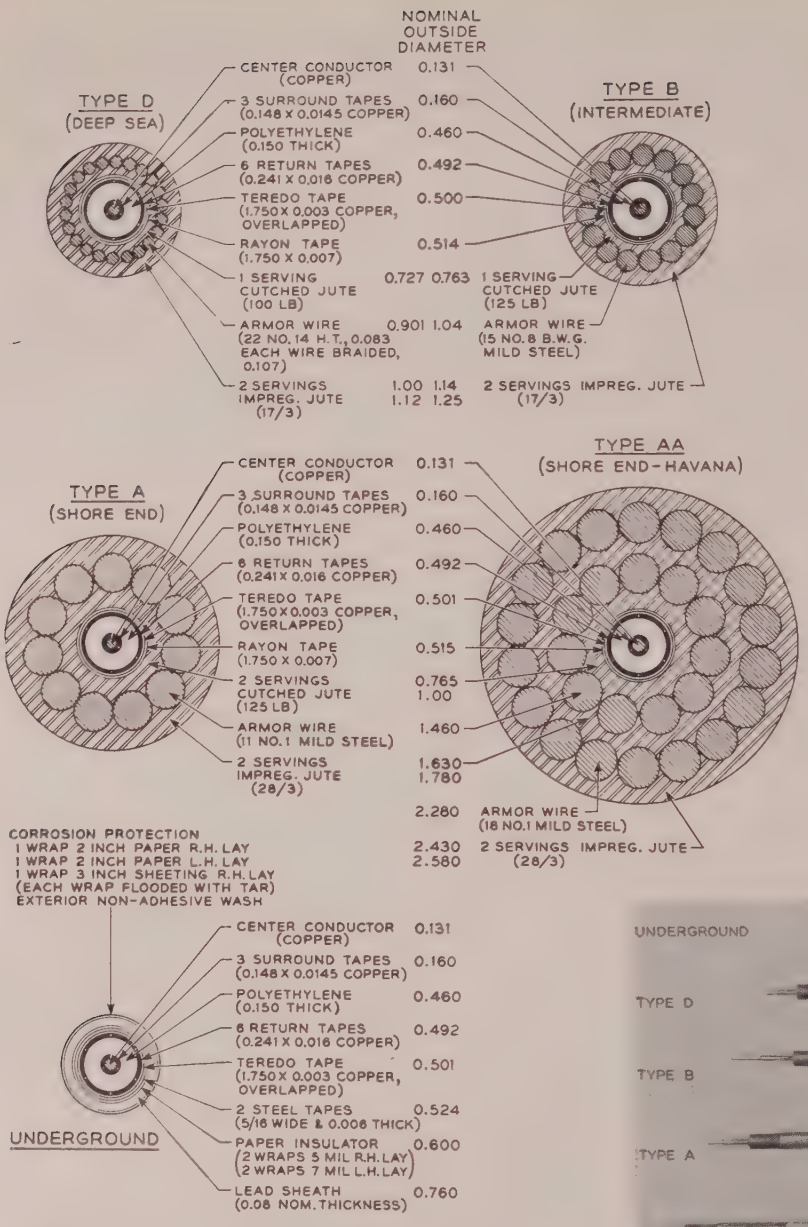
NOMINAL OUTSIDE DIAMETER
TYPE D (DEEP SEA)
CENTER CONDUCTOR (COPPER) 0.131
3 SURROUND TAPES (0.148 X 0.0145 COPPER) 0.160
POLYETHYLENE (0.150 THICK) 0.460
6 RETURN TAPES (0.241 X 0.016 COPPER) 0.492
TEREDO TAPE (1.750 X 0.003 COPPER, OVERLAPPED) 0.500
RAYON TAPE (1.750 X 0.007) 0.514
1 SERVING CUTCHED JUTE (100 LB) 0.727 0.763
ARMOR WIRE (22 NO. 14 H.T., 0.083 EACH WIRE BRAIDED, 0.107) 0.901 1.04
2 SERVINGS IMPREG. JUTE (17/3) 1.00 1.14 1.12 1.25
TYPE B (INTERMEDIATE)
1 SERVING CUTCHED JUTE (125 LB)
ARMOR WIRE (15 NO. 8 B.W.G. MILD STEEL)
2 SERVINGS IMPREG. JUTE (17/3)
TYPE A (SHORE END)
CENTER CONDUCTOR (COPPER) 0.131
3 SURROUND TAPES (0.148 X 0.0145 COPPER) 0.160
POLYETHYLENE (0.150 THICK) 0.460
6 RETURN TAPES (0.241 X 0.016 COPPER) 0.492
TEREDO TAPE (1.750 X 0.003 COPPER, OVERLAPPED) 0.501
RAYON TAPE (1.750 X 0.007) 0.515
2 SERVINGS CUTCHED JUTE (125 LB) 0.765 1.00
ARMOR WIRE (11 NO. 1 MILD STEEL) 1.460
2 SERVINGS IMPREG. JUTE (28/3) 1.630 1.780
TYPE AA (SHORE END - HAVANA)
ARMOR WIRE (18 NO. 1 MILD STEEL) 2.280
2 SERVINGS IMPREG. JUTE (28/3) 2.430 2.580
CORROSION PROTECTION
1 WRAP 2 INCH PAPER R.H. LAY
1 WRAP 2 INCH PAPER L.H. LAY
1 WRAP 3 INCH SHEETING R.H. LAY
(EACH WRAP FLOODED WITH TAR)
EXTERIOR NON-ADHESIVE WASH
UNDERGROUND
CENTER CONDUCTOR (COPPER) 0.131
3 SURROUND TAPES (0.148 X 0.0145 COPPER) 0.160
POLYETHYLENE (0.150 THICK) 0.460
6 RETURN TAPES (0.241 X 0.016 COPPER) 0.492
TEREDO TAPE (1.750 X 0.003 COPPER, OVERLAPPED) 0.501
2 STEEL TAPES (5/16 WIDE & 0.006 THICK) 0.524
PAPER INSULATOR (2 WRAPS 5 MIL R.H. LAY, 2 WRAPS 7 MIL L.H. LAY) 0.600
LEAD SHEATH (0.08 NOM. THICKNESS) 0.760

Figure 11 (above). Cable structures

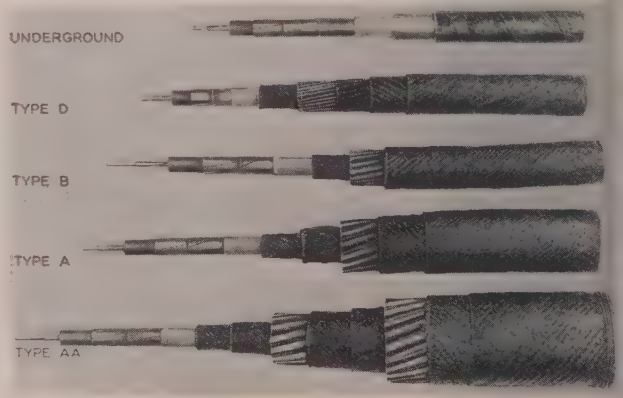

Figure 12 (right). Cable types

It was important to measure the transmission characteristics of the repeatered cable before, during, and after laying, and the special equipment needed for this purpose was more than could be contained in the electrician's room usually provided on cable ships. The jointers' store room accordingly was taken over and converted into an electrical laboratory, shown in Figure 15.

The cable, loaded on board the *Lord Kelvin*, with the deep-sea repeaters spliced in and stowed away in the tanks, arrived off Key West on April 21, 1950. Courses had been laid out for the two cables with the idea of keeping a 5-mile separation between the two most of the way and a 5-mile separation from the nearest of the cables that constitute the rather complicated network between Key West and Havana. It is hoped thereby to avoid having the new cables picked up by mistake in connection with the repair of other cables and to avoid confusing the two cables in case either one of them is in need of repairs.

The stretch of water between Key West and Sand Key Light, a distance of about 8 n.m., is too shallow for the operation of a ship of the size of the *Lord Kelvin*, so the sections of the two cables in this area had been laid from barges by the Long Lines

peater is capable of bending without harm on a diameter of approximately 72 inches, and the existing cable drum, approximately 68 inches in diameter, would have been adequate. It was felt desirable however, to build the drum on the *Lord Kelvin* out to an 85-inch diameter to match the diameter of the bow sheaves. The dynamometer sheaves and the sheave leading the cable off from the brake drum presented more of a problem. The lead-off sheave was replaced by a ring sheave, 85 inches in diameter, supported on wheel bearings. The frame supporting these bearings was hinged at one end and the pressure on the other end of the frame, caused by the tension of the cable passing over the sheave, offered a ready means for measuring this tension. For this purpose a resistance pressure cell was employed with a recorder, which not only gave a continuous record of tension, but also relayed the signals to a vertical indicator on deck for the guidance of the brake operator and to a smaller indicator on the bridge. This arrangement is shown in Figure 14. It is felt that it has much to recommend it over the conventional dynamometer from the standpoints of sensitivity and quickness of response.

Department of the American Telephone and Telegraph Company. At Havana a new landing place had been selected. Experience with existing cables which land in Havana Harbor indicates that considerable deterioration of armor takes place in this locality, and there also is the anchor menace. In addition, closeness to an existing carrier frequency cable might have given rise to undesirable crosstalk. The new landing place at the foot of B Street in Havana is about three miles from the harbor. Figure 16 shows the landing site as viewed from the cable ship during the laying operation. A view of

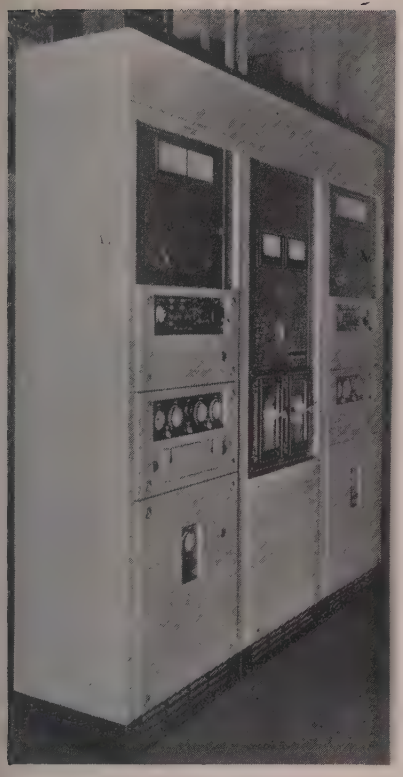

Figure 13 (above). Terminal power supply

splice. The ship then proceeded to Havana and landed the manhole repeater, which was spliced to the underground cable to the office. The ship then floated the end of the cable ashore on barrels with the aid of a line operated by a winch manned by Cuban Telephone Company personnel. As soon as the end reached shore it was spliced to the repeater, the barrels were cut off, the cable was dropped to the bottom, and the cable on shipboard was paid out until the point of final splice was reached, where the end on board was spliced to the previously buoyed end to complete the connection between Key West and Havana.

The ship then returned to Havana, landed the end of Number 6 cable by means of barrels and winch line, and paid out cable to the point of final splice, which in this case was about four miles from Sand Key. The end of Number 6 at Sand Key was then picked up, a repeater was spliced to it and to the end of the cable in the tank, and the latter was paid out to the point of final splice. Within a short time after completing this splice, insulation measurements had been completed on the two cables, the power supply was connected in to activate the

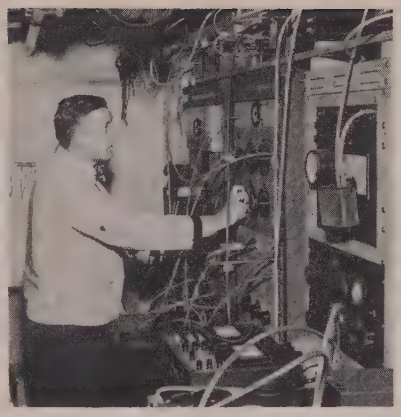

Figure 15. Electrical laboratory on board ship

position of the ship and gave satisfactory information on slack. The conditions for cable laying between Key West and Havana are far from good. The Gulf Stream is swift and erratic. The velocity of the current at any particular point as indicated by the stream at the buoys was found to vary considerably over a fairly short period of time. As an indication of the degree of precision obtained by careful navigation of the ship, the final results

Figure 14 (above). Ring sheave and dynamometer scale

Figure 16 (above). Havana landing site

Figure 17 (below). Repeater vault, showing splices and covered trough containing repeater

the interior of the vault on the Havana shore is given in Figure 17.

After mark buoys had been put out at strategic points and at intervals of about 12 n.m. along the course of the cable, the Key West shore end of Number 5 cable was picked up at Sand Key and spliced on to the cable in the tanks. Then 32 n.m. of this cable were paid out, and the end was buoyed at the point of final

repeaters, and conversation over the cable system took place.

Careful attention was given to the amount of slack paid out, that is, the excess of cable length over the actual distance traversed. The latter distance usually is determined by observing the length of a taut wire paid out continuously during the laying. In the absence of taut wire gear other methods had to be devised. Observations on buoys by radar and range finder provided almost continuous information regarding the

show that in each of the cables the specified length was missed by only 0.2 n.m., which is quite an unusual achievement.

Acknowledgment is made to the Western Union Telegraph Company, the owners of the *Lord Kelvin*, for their cooperation in providing the special equipment for the ship, and to the captain of the *Lord Kelvin*, his staff, and crew, for the very satisfactory performance of the laying operation.

Since the installation of the new system it has been subjected to comprehensive tests involving measurement of noise and intermodulation between channels, as well as precise measurements at numerous frequencies of net loss of the repeatered cables at intervals of time. The system has proved to be very stable and has met the requirements laid down for it. This was as expected. Nothing unfavorable to the submerged repeater has made itself felt, but in accordance with conservative submarine cable tradition, its performance will be observed critically over a period of time.

References

1. Key West-Havana Submarine Telephone Cable System, **W. H. Martin, G. A. Anderegg, B. W. Kendall.** *AIEE Transactions*, volume 41, 1922, pages 1–19.

2. New Key West-Havana Carrier Telephone Cable, **H. A. Affel, W. S. Gorton, R. W. Chesnut.** *Bell System Technical Journal* (New York, N. Y.), volume 11, April 1932, pages 197–212.

3. The Future of Transoceanic Telephony, **O. E. Buckley.** *Bell System Technical Journal* (New York, N. Y.), volume 21, July 1942 pages 1–19.

No Discussion

Noise Evaluation of Fluorescent Lamp Ballasts

C. P. HAYES
ASSOCIATE AIEE

H. R. GOULD
NONMEMBER AIEE

Synopsis: Noise testing of fluorescent lamp ballasts has been studied from a number of approaches and found unsatisfactory. A system has evolved which, if acceptable to the industry, may provide a basis for industry specifications and standards regarding this type of measurement. Study and comment by industry is encouraged.

THE fluorescent lamp is a gaseous discharge device, and therefore, if connected to a constant voltage source, it will draw more and more current until the lamp is destroyed. A ballast, or impedance, must be connected in series with the lamp to limit the current to the value for which the lamp was designed. Usually, since these lamps require various voltages to start them, the ballast also includes a means for transforming the available circuit voltage to the proper voltage for starting the particular lamp. For 60-cycle alternating current systems, the most efficient means of limiting the current is by a reactor, and the usual device for voltage transformation is the transformer or autotransformer. Although many combinations now are in use for various lamps and for multilamp operation, nearly all such devices are made up of laminated core structures of magnetic steel and copper windings.

These assemblies, like other electromagnetic devices, are a source of audible radiation. Noise may be defined as undesired audible radiations as contrasted to pleasing sounds, such as music. However, under certain conditions any of these audible radiations may be undesired and, hence, become noise. Although many devices make noise of relatively high levels, such as the automobile, the vacuum cleaner, and the adding machine, to name a few, light sources through the ages have been relatively quiet. The early campfire was accompanied by a characteristic crackle, but more recent light sources such as the oil lamp, the candle, and the incandescent electric lamps are almost devoid of noise. The past two decades have seen tremendous strides toward quieting of nearly all types of equipment, such as the automobile, the clock, and the electric refrigerator. However, the introduction of the fluorescent lamp brought an appreciable *increase* in noise to lighting of this type while the whole environment of modern man was enjoying a great reduction of distracting noise from other devices. This made the job of the ballast designer a very difficult one because, compared to other electromagnetic devices, the ballast was relatively quiet, but in low noise level locations, the ballast was an irritating source of noise.

The human ear varies greatly from individual to individual and from time to time, but many exhaustive tests by hundreds of observers have established that the ear can detect frequencies as low as 20 or 30 cycles and it increases in sensitivity to a maximum in the vicinity of 4,000 cycles. Sensitivity tapers off again and the ear can detect no noise at some point between 10,000 cycles and 16,000 cycles, see Figure 1. (Figure 1 was taken from Z 24.2-1942.)[1]

The fluorescent lamp, because of its nonlinear impedance characteristics, draws current of high harmonic content through the ballast. As a result the ballast has a frequency spectrum very similar to the ear response curve. Typical frequency spectra of ballast noise are shown in Figure 2. The elimination of these harmonics of the 120-cycle fundamental would help to reduce noise and reduce its objectionable qualities, but little progress has been made along this line of attack.

Noise generated by the ballast usually is greatly amplified by the lighting fixture in which it is used. The relationship between the ballast as the generator of noise and the fixture as the amplifier of noise is shown in Figure 3.

The noise generated by the energy source within the ballast is transmitted to the fixture by mechanical vibration of the ballast surfaces in contact with the fixture and by air-borne noise which impinges on the fixture surfaces. To evaluate completely the noise characteristics of a fluorescent ballast, both components which contribute to fixture noise must be considered. If any great progress in noise reduction is to be made, a method of measurement which will evaluate these components certainly is indispensable.

Early Work

Early noise evaluation was made by listening to the ballast alone in a low noise level area. The ballast was placed on a

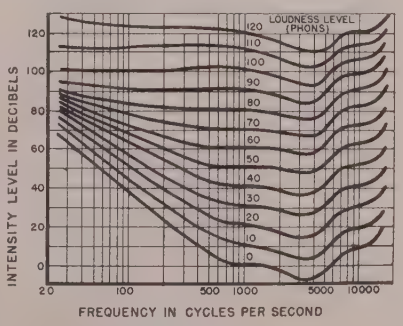

Figure 1. Loudness level contours for response of the human ear with variations in the frequency of sound

Paper 51-95, recommended by the AIEE Production and Application of Light Committee and approved by the AIEE Technical Program Committee for presentation at the AIEE Winter General Meeting, New York, N. Y., January 22–26, 1951. Manuscript submitted June 30, 1950; made available for printing December 11, 1950.

C. P. HAYES is with the General Electric Company, Lynn, Mass., and H. R. GOULD is with the General Electric Company, Fort Wayne, Ind.

The authors wish to acknowledge the assistance of Dr. R. O. FEHR, C. M. SUMMERS, and S. A. ZIMMERMAN of the General Electric Company, and the Armour Research Foundation of Illinois Institute of Technology, Chicago, Ill.

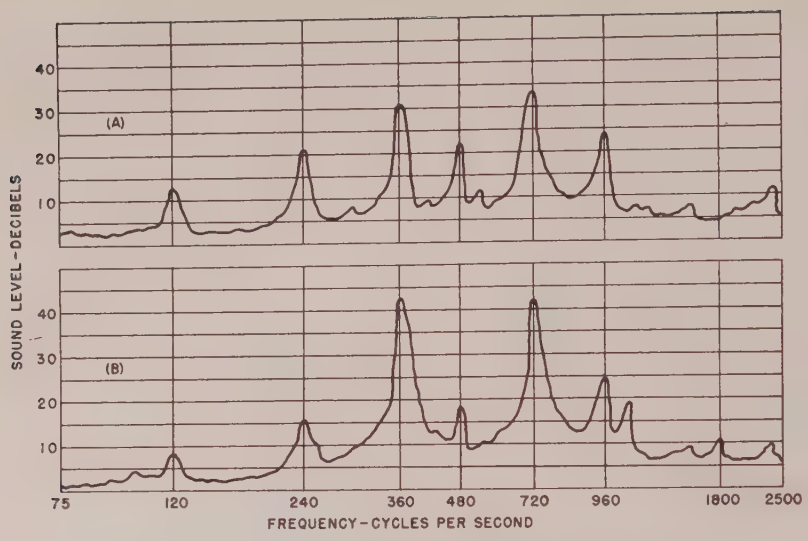

Figure 2. Typical frequency spectra of fluorescent lamp ballasts

(A) Measured noise level = 37.0 decibels
(B) Measured noise level = 46.0 decibels

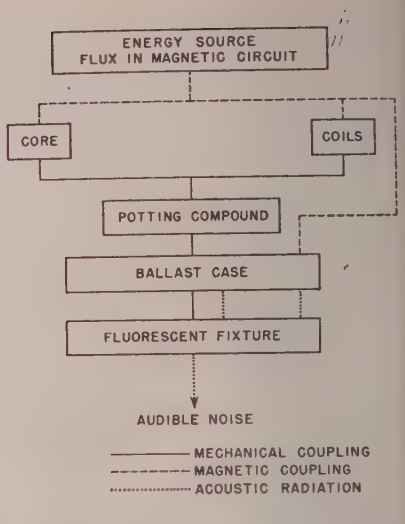

Figure 3. Block diagram of the paths for transmission of ballast noise to the fluorescent lamp fixture

felt pad in a very quiet room, see Figure 4. A quick-acting switch later was incorporated so that two ballasts could be operated on the same lamps, one at a time. By means of the switch, the lamps could be transferred from one ballast to the other. In this way, comparison was much easier. However, this method only evaluated the air-borne noise, and correlation with actual performance in a fixture was poor. Some work was done by listening with a stethoscope, which enabled the observer to place the probe of the stethoscope at various points on the ballast and then compare the vibration of one ballast against vibration of another. Experience has shown that the vibration of the ballast surface varies considerably from one point in the surface as compared with another point. The location and severity of vibration varies considerably from ballast to ballast, even of the same design. Therefore, a systematic and laborious comparison of many points on two ballasts under study would be required. The observer then would be forced to make an over-all guess as to comparable quality after reviewing those comparisons and making some sort of mental integration of the over-all results for each ballast. This proved unsatisfactory, since the only way to evaluate an unknown unit was to compare it for audible noise and surface vibration, as described above, with some standard. With nothing better available, this system was used to evaluate development samples, results of design changes to reduce noise, and as a spot check on production. It was subject to numerous disadvantages:

1. The system was subject to the frailties of one pair of human ears per observer. For practical purposes, this meant one pair of ears for many tests, although on important comparisons more observers were used.

2. An observer is influenced by fatigue. After studying a few ballasts intently, he becomes nervous and doubtful of his own ears. He can rarely do consistent work for more than five or ten units at one period. If more units are tried, he will not be able to repeat results unless differences are very great.

3. The system still had no numerical basis which could be repeated with any degree of accuracy.

4. The method was laborious, slow, and expensive.

5. As mentioned previously, it did not correlate particularly well with field experience.

Measurement by Sound Meter

The next approach to this problem was to measure the noise of the ballast with a sound-level meter. A standard sound meter was used, with the standard 40-decibel weighted network, which discounts the high and low frequencies by about the same amount as the human ear for this level. The sound meter pickup was placed at various distances from the ballast in an attempt to get a reading that would represent ballast noise. With extremely low noise level surroundings, 18–20 decibels, it was necessary to bring

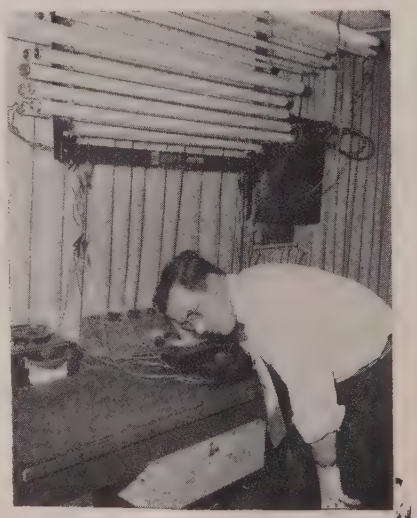

Figure 4(A). Ear listening test employed to evaluate fluorescent ballast noise

Figure 4(B). Listening test incorporating the use of stethoscope

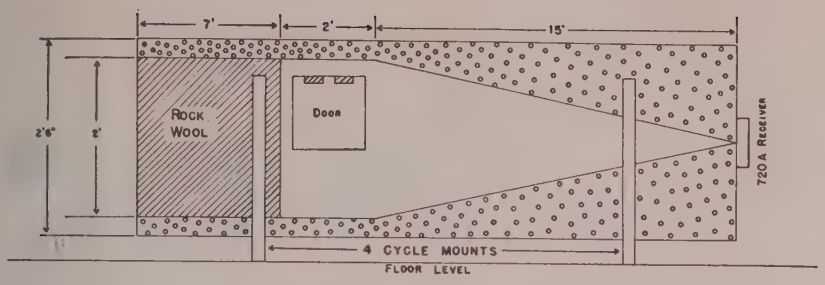

Figure 5(A) (above). Cross section of concrete noise tunnel

Figure 5(B) (below). Concrete noise tunnel

the pickup within one inch of the ballast to get readings high enough above the prevailing noise level of the room to provide reliable readings, about 22 decibels. This is far less noise than that normally generated by many other electromagnetic devices which have become more or less accepted. There is some indication that the ballast noise acceptance level for most users is increasing, but it is far below that of most other electromagnetic equipment for the reasons outlined earlier—light sources have been essentially noiseless for many years.

The method of direct noise measurement was not entirely satisfactory, but, for the first time, numerical values of noise could be determined. For these measurements to be of any value, the noise had to be measured at numerous points over the ballast surface and a weighted average had to be used. That is, it was recognized that noise emanating from the mounting areas and those surfaces likely to be in contact with fixture surfaces would result more readily in a noisy fixture than the noise originating from other surfaces of the ballast. In the early work, four readings on the side opposite the mounting surface and four readings on the mounting surface were used to describe the unit. No definite weighting scheme for the various readings was developed, because the system had other shortcomings which resulted in its discontinuance before such refinements could be made. These shortcomings were:

1. Very quiet ballast could not be measured reliably even in an 18-decibel room with the pickup at one inch.

2. There were many indications that results of this method could not correlate reliably with actual listening tests on the ballasts when installed in representative fixtures.

3. Considerable error could be introduced from small variations in setup, since the distance from ballast surface to noise meter pickup was small.

Concrete Horn

A device for amplification of readings was made by building a long concrete tunnel, which is shown in Figure 5. The length allows flat frequency response down to about 60 cycles. The ballast is inserted through the door near the large end of the horn. The rock wool absorbs all sound emanating in that direction, and the pickup at the small diameter collects noise emanating from the surface of the ballast facing the pickup. The entire structure is isolated by flexible mounts from the supporting floor. The heavy concrete walls greatly reduce the noise inside the tunnel caused by outside noise level. A very high gain amplifier was used, and this device is still useful for certain engineering studies, but is subject to the same lack of correlation with fixture performance as the listening tests and the air-borne sound meter tests.

Parabolic Sound Reflectors

Another method which has been used is to place the ballast at the focal point of a parabolic reflector several feet in diameter. Another identical reflector is placed some distance away, and the noise meter pickup is placed at the focal point of the second parabolic reflector (see Figure 6). This method probably was fairly successful in integrating the noise emanating from one area on the ballast. However, it had to be used in a very quiet location. Results were not very satisfactory.

It became increasingly evident that some method of test was necessary that would:

1. Amplify the ballast air-borne noise and its surface vibration in a manner similar to an actual fixture, dealing in both of these components.

2. Produce repeatable readings to as high a degree of accuracy as possible.

3. Evaluate a ballast with a single number which would be a fair representation of its performance in an actual fixture, in other words, place various ballasts in proper quality order as corroborated by listening tests in various commercially available fixtures.

Present Measurement System

Dummy Fixture

The present measurement system used by the authors appears to be a fairly good answer to the above requirements. It has been in use for about two years, and has had quite a few modifications and refinements during the early part of that period. It is described here in the hope that others interested in this problem may use it, evaluate it, criticize it, improve it, and perhaps it may form the basis for an industry-wide method of noise evaluation.

The system consists of a special dummy fixture *A*, Figure 7, approximately 4 feet

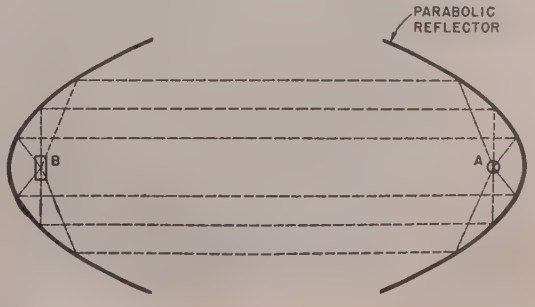

Figure 6. Parabolic reflector scheme of ballast noise measurement

A—Noise meter pick-up at focal point of parabolic reflector

B—Ballast at focal point of the other parabolic reflector

long and suspended by isolating mountings, *B*. A collecting horn, *C*, is placed below the fixture by other independent isolating mounts, *D*. The horn collects noise emanating in a downward direction from the fixture and carries it to a standard sound meter pickup. The ballast to be tested is placed on the horizontal surface by special mounts, *E*. These mounts may be adjusted for a particular ballast size, and subsequent mounting of these ballasts is a rapid and consistent operation.

The primary purpose of developing a ballast noise measurement system was to obtain a realistic noise quality number which would define the noise characteristic of any ballast. This test was designed to be a standard noise test for all fluorescent ballasts. In order that readings for today, tomorrow, next week, and next year could be compared, all variables except the ballast itself had to be investigated and carefully controlled.

The first variable to be controlled or to be defined was the noise test fixture on which the ballast was to be mounted. Commercial fixtures vary greatly in design and mechanical construction so that it seemed almost impossible to select a representative, "standard" fixture for this test. Since the ballast would be mounted in the fixture for the noise test, an open-type fixture appeared to be the most suitable for this application. Most commercial fixtures completely enclose the ballast in a channel, so that the louvers or glass, lamps, and reflector must be removed to remove or mount the ballast. The time required for such a procedure was considered prohibitive in a noise test fixture to be used for evaluating the noise characteristics of fluorescent ballast.

Commercial fixtures vary in length from approximately 20 inches for the 15-watt lamp to 100 inches for the 96-inch slimline lamps, so that some compromise in length also was necessary. Ballasts vary in length from about 2 inches to 20 inches, so that it was decided to use a 48-inch fixture, since this length of fixture is widely used in 40-watt fluorescent lighting.

Mounting

Fluorescent ballasts normally are either mounted flush to the surface of the fixture or on embossed sections at the mountings. The flush mounting was subject to additional variables because of the irregularities both in the mounting surfaces of the ballast and in the fixture. Thus, it was necessary to select a method of mounting which would couple the ballast to the fixture without introducing variables in the mounting. Extensive testing with the fluorescent ballast mounted flush to the fixture with spring clamps indicated that large variations in ballast noise resulted from the irregularities in mounting surface and the spring clamps. To eliminate these variables, the fluorescent ballast was spaced up 3/16-inch off the fixture surface on a square lock nut with a circular mounting surface one inch in diameter. This assembly is shown in Figure 8, with the ballast mounted in position for noise test.

Test Lamps

The fluorescent lamp, which is the load for the ballast, was subject to variations which also affected ballast noise. Noise tests conducted with new (seasoned for 200 hours) and old lamps (near end of life) indicated that the noise level of the 40-watt ballast would be approximately two decibels higher with lamps which were near end of life. The fluorescent lamps used in this aging study were taken from the same lot of lamps. It also has been observed that as a fluorescent lamp warms up to its operating temperature and lamp watts become stable, the ballast noise level also becomes stabilized. The relationship between the warm up of various lamps and ballast noise is plotted in Figure 9. The curves plotted in Figure 9 were taken with three lamps of different size and rating, to show the change in ballast noise level as the fluorescent lamp warms up. The errors encountered due to the age and temperature of the fluorescent lamps are not excessive, but these variations were particularly undesirable whenever ballasts were tested during this warm-up period or after a change in lamps. To avoid these variables, the lamps are replaced periodically, and a 30-minute, minimum lamp warm-up period is required before starting any ballast noise test.

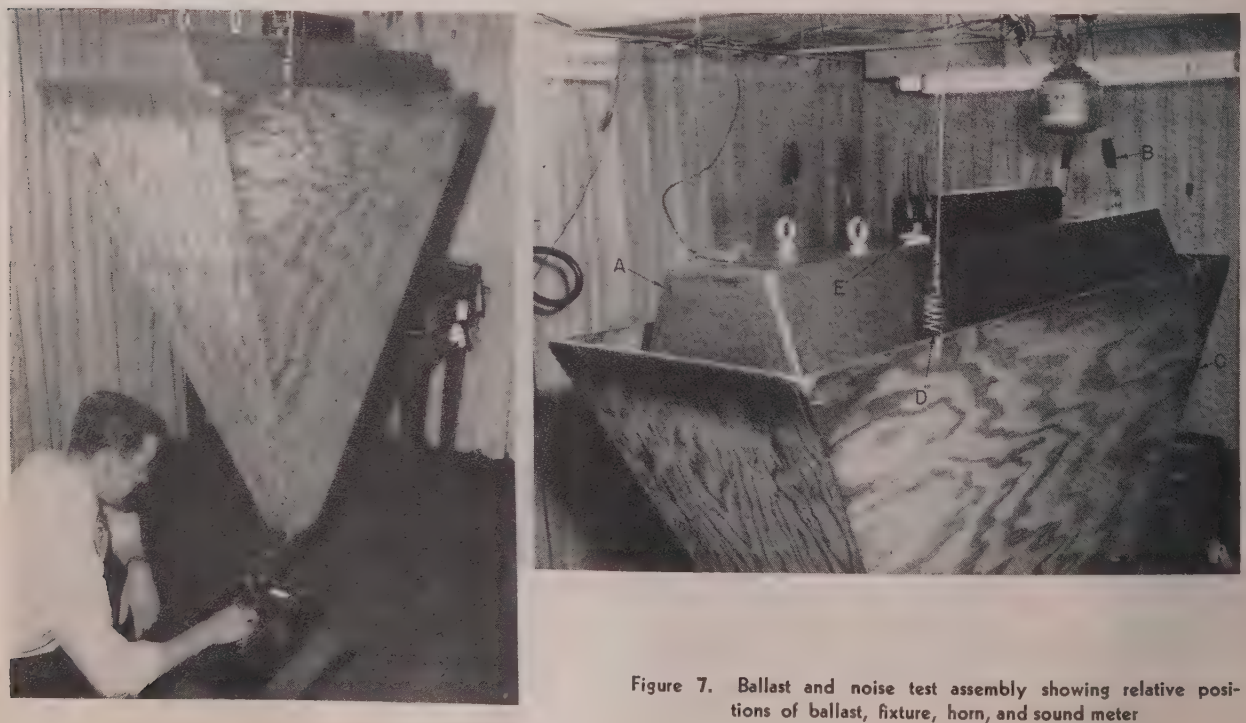

Figure 7. Ballast and noise test assembly showing relative positions of ballast, fixture, horn, and sound meter

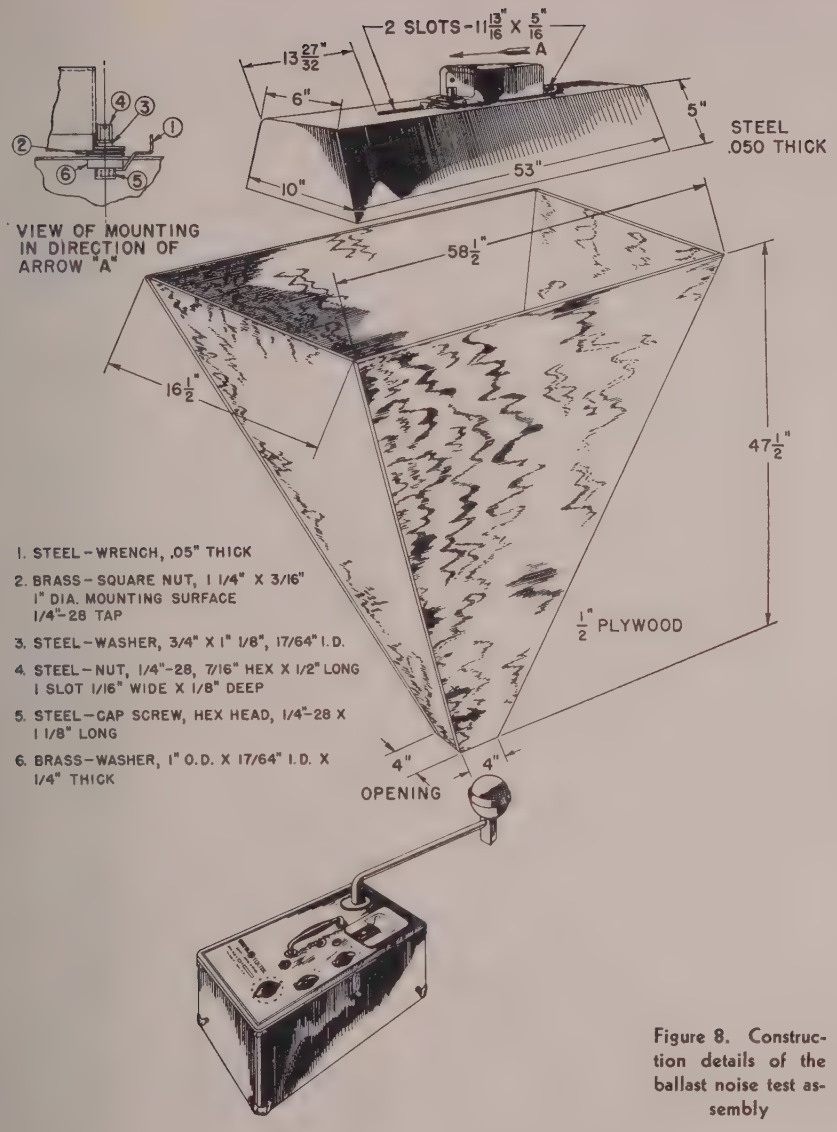
2 SLOTS - 11 13/16" X 5/16"
A
13 27/32"
6"
5"
STEEL .050 THICK
53"
10"
VIEW OF MOUNTING IN DIRECTION OF ARROW "A"
58 1/2"
16 1/2"
47 1/2"
1. STEEL - WRENCH, .05" THICK
2. BRASS - SQUARE NUT, 1 1/4" X 3/16" 1" DIA. MOUNTING SURFACE 1/4"-28 TAP
3. STEEL - WASHER, 3/4" X 1" 1/8", 17/64" I.D.
4. STEEL - NUT, 1/4"-28, 7/16" HEX X 1/2" LONG 1 SLOT 1/16" WIDE X 1/8" DEEP
5. STEEL - CAP SCREW, HEX HEAD, 1/4"-28 X 1 1/8" LONG
6. BRASS - WASHER, 1" O.D. X 17/64" I.D. X 1/4" THICK
1/2" PLYWOOD
4"
4"
OPENING

Figure 8. Construction details of the ballast noise test assembly

The mounting of the fluorescent test lamps also presented a problem, since it was impractical to design a separate ballast noise test fixture for each length of lamp. To simplify the test setup, the fluorescent lamps were removed physically from the test fixture with circuits available for selecting any desired fluorescent lamp and ballast combination. The test circuit is wired so that the test lamps are operated continuously by a "stand-by" or auxiliary ballast, except during the actual time when the lamp load is switched to the ballast on the noise test fixture. This circuit is described in detail in Figure 10. With this arrangement it is possible to keep the lamps at a normal burning temperature during the intervals between individual test readings. The test lamps are mounted horizontally in the sound room, but the auxiliary ballasts are mounted outside, so that they will not contribute to any increase in room noise.

Temperature Conditioning

In testing ballasts for developmental and production quality studies, it was realized very early that the temperature of the ballast also affected the recorded ballast noise level. Fluorescent ballasts in general do not generate the same amplitude of noise at room temperature as they do at elevated temperatures, so that the ballasts must be compared at the same temperature to obtain repeatable noise data. The most consistent results have been obtained with the ballast conditioned in a 65 degrees centigrade ambient for a minimum period of four hours and a maximum of approximately 24 hours. The ballasts are conditioned in their normal operating position during this period, with the base of the ballast up. It is noted that in some installations the ballast may possibly be mounted base down, but the base-up conditioning eliminated most of the shifting of the core and coil in the warm potting compound during the conditioning period. It also is admitted that the user of the fluorescent ballast will hear the ballast first at room temperature, but as the ballast temperature rises because of core and copper losses, the ballast will attain a "hot" condition. This variation of ballast noise with temperature is illustrated in Figure 11. The fluorescent ballast, to have an acceptable noise characteristic, must be quiet both hot and cold. But, for the study of the effect of treatments, potting materials, core designs, and manufacturing technique on ballast noise, the "hot" condition generally is the most critical and most suitable for these evaluations.

General Factors

The purpose of controlling the variables described is to make possible a reliable, repeatable ballast noise test. The variables described in the measurement of ballast noise do not produce noisy ballasts, but, if uncontrolled in this test, individual ballast noise levels would be almost without value. These controls are extremely important in making decisions in ballast design which will insure a quieter fluorescent lamp ballast.

In the adoption of a noise test fixture, it was realized that this fixture definitely would have a resonant frequency in the audio range near the fundamental or one of the many harmonics of the noise generated by the ballast.

The noise test fixture shown in Figure 8 has a resonant frequency of approximately 100 cycles per second. This resonant frequency has proved low enough to prevent errors as a result of fixture resonance. The gain of the combination of fixture and horn is approximately 12 decibels. This is the gain in ballast noise level above the intensity of noise detected at one inch from the mounting surface of the ballast. Frequency spectra of ballast noise as measured at one inch in air may be compared with the noise amplified in the test fixture (see Figure 2). Such a comparison indicates that the dummy fixture produces a faithful amplification of the ballast noise. The ballast noise test assembly responds to both the air-borne and vibration-borne (mechanical coupling) components of ballast noise. As discussed previously, this type of test is more desirable than a measurement of only the air-borne component of ballast noise. This noise test

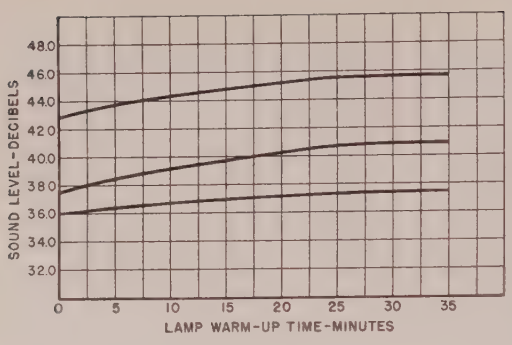

Figure 9 (left). Lamp warm-up time versus ballast noise level

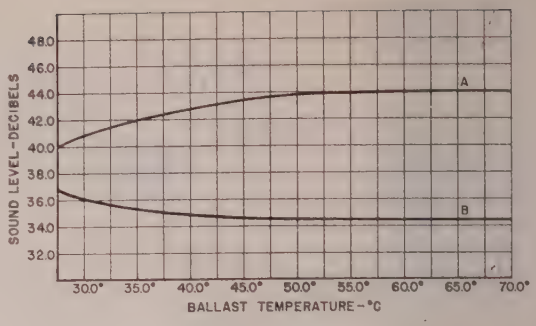

Figure 11 (right). Curves of ballast temperature versus ballast noise level. Curves A and B are typical for ballasts with increasing and decreasing characteristics

fixture has been proved more critical of ballast noise than any available commercial fluorescent fixture.

Calibration

Several methods have been investigated for calibration of this ballast noise measurement system, such as magnetic standards, standard ballasts, and air jets. The magnetic sources have not proved stable enough for calibrating the fixture, and the air jet does not generate sufficient fixture vibration for calibration. The air-borne noise generated by the rush of air through the air jet can be used for calibrating the sound meter in the test assembly, but a nonpitched acoustic calibrator is much more suitable for this purpose. The sound-level meter is calibrated before each test period with the General Electric Company acoustic calibrator, catalogue number 9,146,262-*G*1. The day-to-day variation in the sound meter has never exceeded more than 0.5 decibel, so that errors in the sound meter are at a minimum. The fixture setup, including horn, sound meter, and ballast mounting are checked carefully before each test period. Specially prepared ballasts are used to check the gain of the equipment, so that a very close control is maintained on the entire ballast noise test.

The control of the variables in fluorescent test lamps, ballasts, and noise test assembly has made possible a comparison of ballast noise data on designs built today

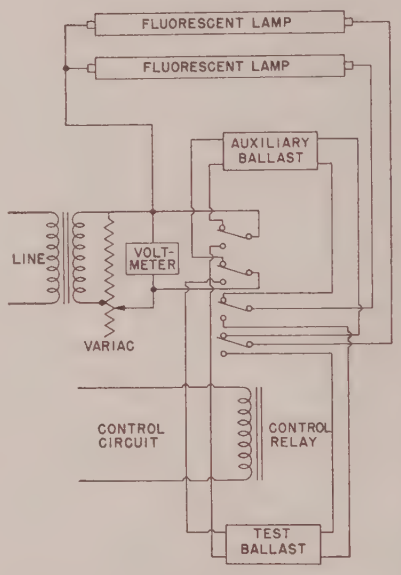

Figure 10. Circuit diagram of connections for ballast noise test with an auxiliary ballast

with those assembled in the past or those to be assembled in the future. Listening tests are not employed for objective measurement of noise, but they do aid in correlating noise data with the response of the human ear. Data received from the many installations in the field provide a very important and helpful evaluation of the customers' response to the ballast noise measured in the laboratory and the factory.

Applications

The ballast noise test described in this report has had several important applications. One of the most valuable has been as a tool for evaluating possible methods for reducing ballast noise. This has included evaluations of various ballast cements, treatments, potting methods, core designs, and production assembly methods. To make a change in process or design without knowing its effect on noise would result in expensive factory trials and possible complaints if the change should be unsuccessful. Noise-study trials on a small sample basis are possible with this noise test, to evaluate the effect of the proposed change in methods or design. After any change has proved successful on a sample basis, it can be placed in production with confidence that a noise reduction will be realized. Some changes may result in only small reductions in noise level, but an accumulation of such changes may result in noise reductions which are very significant. The noise test has made possible a complete noise evaluation of many ballast designs before the ballast ever reached the regular production floor.

This noise test also can be used in maintaining a close watch on the noise quality of the ballast shipped to the customer. It is not, however, suitable for a 100 per cent check on all ballasts shipped to the customer. As stated previously, this test is too lengthy and would be too expensive for such a purpose. A quality sam-

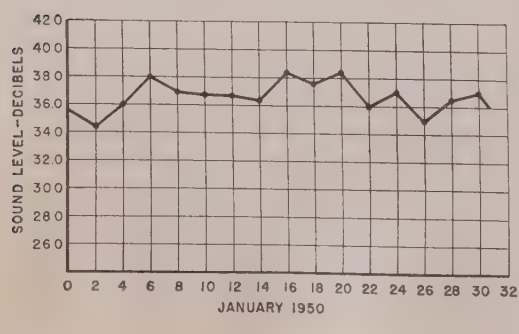

Figure 12 (left). Variation in ballast noise level as indicated by quality noise tests

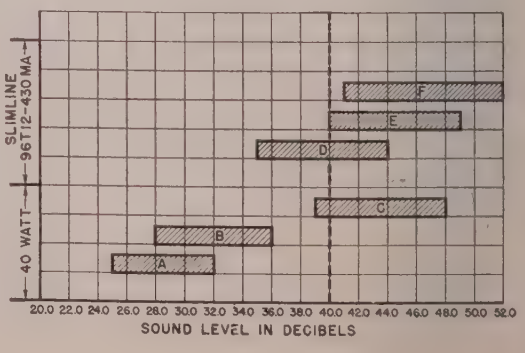

Figure 13 (right). Typical noise rating of various fluorescent lamp ballasts

pling of ballasts from the production line is possible, however, and has proved very useful in detecting and correcting any tendency toward increase in noise level of production units (see Figure 12).

Production Testing

Noise ambients on the production line range from 70 to 80 decibels, so that it is not practical to attempt to obtain the 20-decibel noise ambient, recorded in the sound room. Such ambients can not be obtained easily on the production floor, so that some other system must be employed for the production noise test. The 100 per cent production noise test is not impossible, and two promising methods are available. The primary requirement of any method for testing production noise is that it must reject all ballasts above an established, acceptable limit for ballast noise. This limit may be established either to control the over-all noise level of ballast installations or merely to reject only the ballasts with extremely high noise levels (buzzers).

Testing experience has proved that a ballast which is considered objectionable in a fluorescent fixture also will have a very high component of air-borne noise. Construction of a sound box for detecting extremely high noise levels is possible even for use on the factory floor with a 70–80-decibel ambient. This sound box is assembled by placing one box or more within another, acoustically isolated, so as to obtain about a 50-decibel ambient. A measurement then is made of the air-borne component of ballast noise, with "buzzers" producing readings as high as 70 decibels.

Another system which is even more suited for production testing is a measurement of ballast vibration. Close correlation has been found not only between objectionable ballast noise and the air-borne component, but also between ballast noise and case vibration. Early tests indicated that very little correlation exists between the over-all ballast noise level and ballast vibration measured over very small areas, so that a single-point measurement of vibration is not satisfactory for noise testing. Measurement of vibration over a relatively large area of the ballast mounting surface does, however, correlate with ballast noise. This test can be simply accomplished by the use of several (crystal) vibration pickups or by using a single-contact microphone attached to a special mounting plate. Thus, with the ballast excited while in contact with the vibration pickups or mounting plate, the relative amplitude of the measured vibration correlates with fixture noise levels. By properly isolating the crystal pickups from external vibration, it is possible to obtain relatively low ambients, so that this test is quite suitable for production noise testing.

It is to be noted that whatever system may be employed on the production line, that system must separate the "good" from the "bad." This means that, first of all, some absolute system of noise measurement is needed to determine acceptable noise levels and to maintain a continuous check on the production noise test. Without a standard ballast noise test, no correlation can be expected among the many systems employed to determine acceptable noise levels or to define a "quiet" ballast.

Conclusions

The system for the measurement of ballast noise described in this paper has been proved very reliable in comparing the noise levels of the many fluorescent ballasts manufactured today. Experience with this test equipment indicates that with the variables of mounting, heating, and fluorescent lamps closely controlled, it is possible to obtain reproducible noise data. The data obtained are not only reproducible, but also correlate with actual noise tests on commercial fluorescent fixtures.

The noise levels recorded with test equipment can be used to advantage in rating ballasts from the various ballast manufacturers. Such a rating is illustrated in Figure 13. The limit for acceptable ballast noise level shown at 40 decibels will not hold true for all installations; but it is representative of what generally will be acceptable for most users of fluorescent lighting. These readings were recorded with the General Electric sound-level meter using the 40-decibel weighting network. It is recognized that some ballasts have different frequency characteristics, but field experience has indicated that these noise ratings generally are true. With the rapid changes in ballast design and manufacturing technique it is hoped that a much lower limit may be established in the near future.

The noise-measuring system as presented in this paper is by no means complete, and it is hoped that others will try this system so that further improvements may be possible. It is felt that this measuring system has been developed far enough to be considered by others who are concerned with the problems of ballast noise and its measurement. During the past few years the user of fluorescent lighting has become very conscious of the existence of ballast noise. He does not accept noise willingly as a necesary part of fluorescent lighting. This undesirable characteristic must be eliminated as soon as possible, if the fluorescent lamp is to be completely acceptable for all lighting applications.

Reference

1. Noise Measurement. *Z24.2-1942*, American Standards Association (New York, N. Y.), 1942.

No Discussion

Progress in the Development of Large Turbine Generators

E. D. HUNTLEY
MEMBER AIEE

H. D. TAYLOR
FELLOW AIEE

MORE THAN 20 years have elapsed since the presentation of the last general descriptive papers[1,2] on this subject by writers connected with the General Electric Company, and the whole complexion of turbine generator designs has changed radically since that time. It might even be said that today's designs are the products of a new generation, with some of the progress resulting from improvement and extension of principles given to us by previous generations and proof by experience of their courageous pioneering, while other departures are much more radical. It therefore seems appropriate to review the progress which has been made. This progress has touched practically all aspects of turbine generators. In 1929, 60-cycle generators larger than about 15,625 kva rating were designed for a speed of 1,800 rpm; and 62,500 kva was considered quite a large rating. All turbine generators were air-cooled, practically all being designed for closed-circuit cooling, with finned-tube coolers located beneath the generator. Since then, hydrogen cooling has superseded air-cooling in practically all new machines for central-station service; and a tremendous growth of about ten to one has taken place in the size of 2-pole 3,600 rpm generators. This paper is intended to give a general survey of these changes, with a description of some of the more interesting and important design features which contribute to the reliability, efficiency, and good operation of present-day machines; and a final section deals with the continuing increase in size of 3,600 rpm generators.

Paper 51-96, recommended by the AIEE Power Generation Committee and approved by the AIEE Technical Program Committee for presentation at the AIEE Winter General Meeting, New York, N. Y., January 22–26, 1951. Manuscript submitted October 23, 1950; made available for printing December 12, 1950.

E. D. HUNTLEY and H. D. TAYLOR are both with the General Electric Company, Schenectady, N. Y.

The authors gratefully acknowledge the helpful advice and suggestions of C. E. KILBOURNE, D. S. SNELL, L. P. GROBEL, B. M. CAIN, J. H. CARTER, and W. J. GILSON in the preparation of this paper.

Hydrogen Features

The use of hydrogen as a cooling medium for rotating electrical machines has been so well covered by previous papers,[3–9] that little space can be justified for the general subject here. Nevertheless, the advantages of using hydrogen are greatest in large high-speed generators such as the turbine driven type, and have been so well recognized that air cooled machines are now seldom built for 60 cycle ratings larger than about 15,625 kva for use in the United States. This did not come about all at once. The first hydrogen cooled generator was ordered in 1935, and put in operation in 1937. However, even before this pioneer machine was built, many operating companies were convinced of the value of hydrogen cooling, probably because of the earlier success achieved with synchronous condensers. About 20 per cent of the orders received by the General Electric Company in 1936 for turbine generators of 12,500 kva rating, and larger, were for hydrogen cooled machines. This percentage has continually increased; amounting to 35 per cent in 1937, 50 per cent in 1940, and about 90 per cent in 1946. Not including 15,625 kva and smaller ratings, the present percentage is practically 100 per cent. Since 1935, the authors' company has received orders for 450 hydrogen cooled generators totalling approximately 28,000,000 kva rating; and 264 of these are in service (as of October 1, 1950).

The first ten years of operating experience with hydrogen cooled generators established an extremely good record for reliability of these new type machines. Those built by General Electric Company all employed auxiliary equipment for vacuum treatment of the shaft sealing oil, with pumps, tanks, float valves, regulating valves, and various provisions for emergency operation in case of failure of any of these auxiliaries. This vacuum system appeared rather complex to the uninitiated, but was so well thought out and built that in 10-years' operation of all the 132 generators in service there was not a single major service interruption chargeable to the hydrogen features. This does not mean that all the auxiliaries performed perfectly all the time, but, that such troubles as did occur were of a relatively minor nature, and had been backed up in such a way as to avoid the necessity for taking the generator out of service. In the 11th year, this record was broken, and a service outage occurred on one machine because of a succession of events, starting with leakage of air into the main seal oil pump caused by loose bolts on the pump suction flange, and including failure of some alarm devices to function properly, and misoperation by the station personnel. Such combinations of circumstances are quite rare, which serves to emphasize the reliability of the vacuum system of hydrogen auxiliaries when properly installed and operated.

A new simplified hydrogen system was developed several years ago by the General Electric Company, and has been used on a considerable number of machines. This is known as the Continuous Scavenging System, which has been described in a recent paper.[10] It does away with the use of vacuum treated oil, and materially cuts down the number and size of the auxiliaries, so that the operation is greatly simplified, and the floor space required for the auxiliary equipment is materially reduced. A comparison of the sealing oil auxiliaries for the older vacuum treating system and the

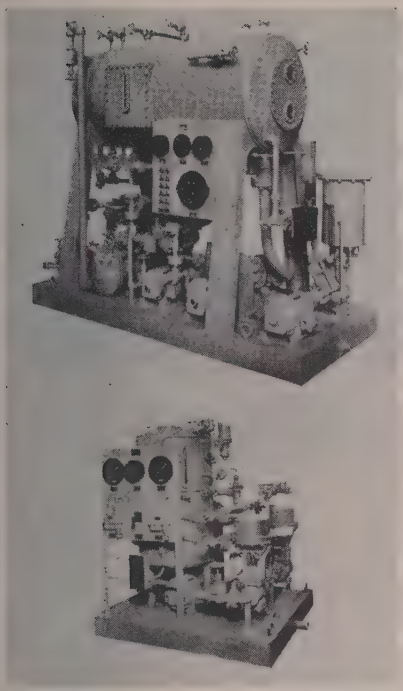

Figure 1. Comparison of auxiliary seal oil supply units for vacuum system (above) and continuous scavenging system (below, to same scale)

newer continuous scavenging system is shown in Figure 1. Operating experience has thoroughly proved the reliability of the new system. It is now a standard feature on all but the largest sizes of new hydrogen cooled turbine-generators, and will probably be used also on the larger sizes within another year or two.

Improvements in Ventilation

Internal ventilation of turbine generator fields was a major improvement of the 1920's. In those days, this ventilation was arranged to flow axially inward from the ends of the rotor through subslots or tunnels just underneath the field coil slots, and was discharged radially through holes drilled in the teeth between the field coils. In the 1930's, an improved type of ventilation was applied to the larger two-pole rotors then being developed, wherein the tunnels or subslots were superseded by narrow ventilating slots cut directly in the teeth and closed by small wedges through which discharge holes were drilled in the central portion of the rotor. These tooth ventilation ducts had a double advantage over the tunnels, in that they provided a more direct path for the flow of heat from the field coils into the ventilating ducts. These ducts also relieved the mechanical duty on the roots of the teeth caused by centrifugal force, so that more copper could be carried in the field slots for the same limiting tooth root stress. This construction was particularly adapted for use in 2-pole designs on account of the more pronounced taper of the teeth as compared with 4-pole machines. A more recent improvement in rotor ventilation employs both sub slots and tooth ventilation ducts as in Figure 2, which shows a full-size model of a section of a generator field structure. This arrangement practically surrounds the field coil with active ventilation so as to achieve a minimum temperature rise, together with improved uniformity in the radial distribution of the temperature in the various turns of the field winding. The advantages of this construction are fairly obvious, so much so, that it was suggested repeatedly by many different designers. It was not adopted, however, until a suitable means was devised for discharging the ventilating gas from the tunnel without unduly impairing the strength of the tooth root structure. This has been accomplished by drilling a number of radial holes in the central part of the rotor down from the ventilating slot in each tooth deep enough to be alongside of the sub-slot, from which a matching hole is drilled circumferentially to meet it. One of these circumferential holes can be seen in the near corner of the model in Figure 2. It will also be observed that the sub slot has been widened at this spot by means of a radial drill of the same diameter as the width of the main coil slot. Many visitors at the General Electric factory become highly curious as to how this circumferential hole is drilled near the bottom of a fairly deep slot. It is really quite simple, as the drilling device consists of a train of spur gears carried between two steel plates, and driven by a motor. This assembly fits down into the slot with a considerable clearance. The bottom member of the gear train carries a small end mill projecting from the side of one of the supporting plates. The whole device is arranged to swing on a set of pivots located in a framework which clamps to the surface of the rotor, and the hole is drilled simply by starting the driving motor and swinging the assembly so that the end mill cuts through at the proper place near the bottom of the slot. Anticipated difficulties with this operation did not materialize, and this construction has now been used for several years. It is particularly adapted to the larger size 3,600 rpm 2-pole generators, where the radial depth of the copper field coils is somewhat limited by mechanical considerations.

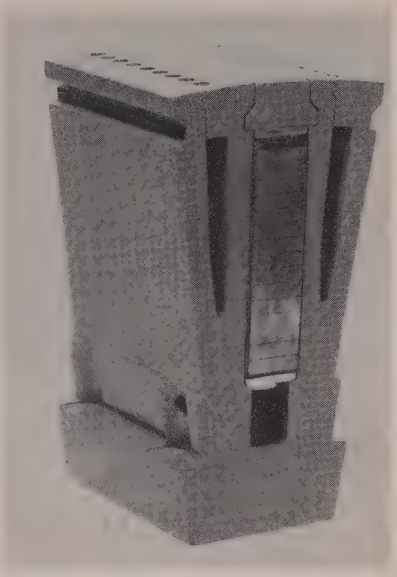

Figure 2. Model of generator field structure showing combined tooth duct and tunnel ventilating system

Propeller type fans have long ago been found to be better adapted to the ventilation of 3,600 rpm generators than the older centrifugal fans, partly because they are more efficient, but also because the inlet conditions are more favorable and a more compact design can be arranged. The centrifugal fans require that the inlet gas must flow through an annular opening between the shroud ring and the shaft, which is a very serious limitation in the case of large high-speed generators. With propeller type fans, however, there is no such limitation. For these reasons, propeller fans have been standard now for quite a number of years on the larger 3,600 rpm generators. One difficulty, however, was observed and corrected when they were first applied. This is the matter of the distribution of the total ventilating flow among the various parallel circuits of the multiple radial ventilating system, which has long been standard. The axial discharge from the propeller fans quite naturally favored the circuits through the ends of the machine (directly into the air gap) at the expense of the circuits employing inlet sections in the central part of core structure. This is in contrast to the tendency of the centrifugal fans, with radial discharge, which favored the core inlet sections. This shift in distribution of flow of ventilating gas caused by changing over to propeller type fans was readily corrected by the use of baffles, and as this was provided for on the first hydrogen cooled generators employing propeller fans, no difficulties have resulted. As a matter of fact, very com-

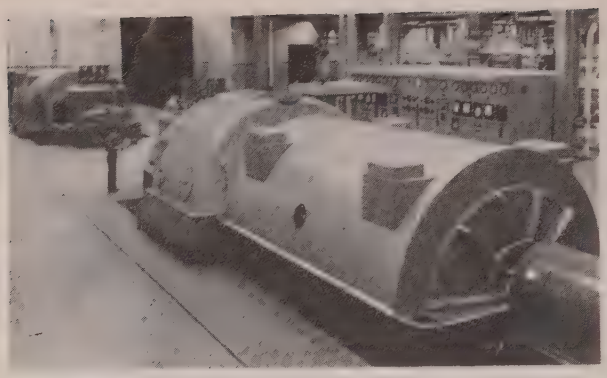

Figure 3. Hydrogen-cooled turbine generator with welded steel plate end shields having removable bearing caps and access ports; also showing vertical cooler arrangement

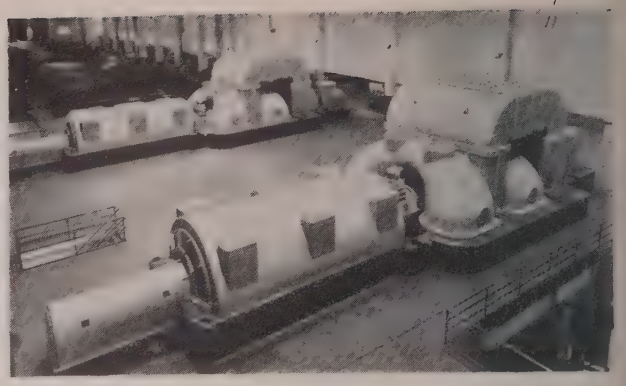

Figure 4. Two 125,000 kva 1,800 rpm hydrogen-cooled turbine generators, each with six vertical coolers

plete tests on this point were carried out in a special half-scale model set-up, which was operated with propeller fans over a period of a year or more with various combinations of duct and fan and baffle arrangements. The results of these tests are quite detailed and are beyond the scope of the present paper. However, the work may be summarized by the statement that optimum arrangements were determined and have been used to advantage in the design of ever larger 3,600 rpm generators.

These developments in the ventilation of both stator and rotor have been most fruitful, as the temperature rises of the windings in new generators which have been designed to take advantage of these improvements have proved to be very conservative. This will be touched upon somewhat further in the last section of this paper.

Mechanical Improvements

Most of the earliest hydrogen-cooled turbine generators employed heavy split cast steel end shields, designed both to withstand possible explosion pressures safely, and to support the main bearings. Such castings proved to be rather expensive and were often porous. Much trouble was experienced in their manufacture, since defects frequently were not discovered until the parts were nearly finished, so that extra costs and annoying delays were caused by the necessity of major repairs. In addition, it was a tedious and fussy job to fit the top and bottom half-shields together in such a way as to make a gas- and oil-tight joint, and at the same time to clamp the bearing properly. A major improvement was made several years ago by changing the end shields over to fabricated construction, using welded steel plates. This eliminated the casting troubles completely. At the same time, the basic design was changed in several ways. Inspection holes with readily removable cover plates were provided in the top half shields for convenient access to the inside of the machine at each end. Separate bearing caps were made, apart from the top half shields, so that the fitting of the shields and bearings was greatly facilitated. Also, the hydrogen seals were divorced from the bearings and mounted on the shields, so that with this construction it was possible to roll out the bearings for inspection without removing the top half end shields, and without purging the generator casing of hydrogen. This type of shield construction is illustrated in Figure 3

An annoying characteristic of many of the large early 3,600 rpm generators, was the magnetic double-frequency vibration caused by elliptical distortion of the stator core and frame by the magnetic pull of the 2-pole rotor on the inside of the core. This vibration appeared and disappeared as voltage was built up or reduced on the armature winding. It was usually communicated to the machine foundation and adjacent parts of the power station, such as beams, floor plates, instrument panels, and gauges. The resulting vibration and noise were often disagreeable and occasionally destructive—especially if there happened to be a condition of vibrational resonance which resulted in magnification of the rather small amplitudes transmitted from the machine. This magnetic core vibration is isolated from the frame in modern machines by an elastic core suspension, as has been described in previous papers,[11,12] so that it is ordinarily impossible to tell by touch or by ear when excitation is applied. Another type of double-frequency vibration, independent both of excitation and mechanical balance, has occasionally shown up on the machine bearings or on overhung portions of the shaft such as the collector. This is associated with the slight difference in the bending stiffness of the 2-pole rotor between the polar axis and the axis through the slotted region of the field body, which may give the rotor a tendency to rise and fall ever so slightly twice per revolution.[11,13] In the authors' experience, this mechanical double-frequency vibration of the rotor has been much less serious than the magnetic vibration of the stator core, and has never caused any serious operating trouble. In fact, it has seldom been large enough to be noticeable, and then only in cases involving mechanical resonance of the whole machine and foundation structure. Since these cases of resonance are practically impossible to predict, it has become standard practice on large machines to reduce the stimulation by partial compensation of the inequality of the field body stiffness so as to insure smooth operation within fine limits in all cases.

An improved arrangement of the hydrogen gas coolers, mounted inside the generator frame, gives a number of advantages, as compared with older designs usually employing four coolers running lengthwise of the generator. Vertical coolers mounted at the four corners of the machine (Figure 3), permit a simpler, stronger, lighter frame design, and facilitate manufacture; especially with respect to cleaning out chips, etc. But, more important, this arrangement makes it easy to keep the cooler water-boxes, gaskets, and all piping outside of the gas space, thus eliminating several possible sources of troublesome water leaks inside the generator. Also the piping is arranged below the operating floor, out of the way. And the coolers can be as-

sembled or removed much more readily by simply using light crane facilities. Very large machines may employ six or eight vertical coolers, as in Figure 4.

Improvements in Insulation

There are three major insulating functions in large turbine generators: (1) insulation of the relatively low voltage d-c field windings, which must stand up under severe centrifugal loading and thermal expansion; (2) insulation of the high voltage a-c armature coils, which have no centrifugal forces but are subject to thermal expansion stresses and must withstand severe mechanical shocks and occasionally voltage surges at times of system disturbances; and (3) insulation of the segmental core laminations against eddy current losses and heating. Significant improvements in all three of these insulations have been made in recent years.

Mica tape made with a copal type varnish and applied with shellac was the standard turn insulation for turbine generator field windings for many years prior to the rapid increase in size of 3,600 rpm machines, beginning in 1935. This tape proved to be inadequate to withstand the increased centrifugal pressures in the large 3,600 rpm fields designed with copper windings (although it was quite satisfactory with aluminum windings), and it was superseded between 1935 and 1940 by two improved insulations: (1) hard-pressed sheet mica of high quality containing very little binder, used as a separator between turns; and (2) a glass cloth-backed mica tape made with a synthetic resin base varnish. These were both used for a period of years, the separators on the larger machines, and the tape on the smaller ones. It was recognized that the separators were advantageous in the slot region, giving a better space factor. The tape was advantageous for the end portions, as it would stay in place better, although both had been found quite satisfactory in service in both regions. Present practice on all of the larger machines employs the logical combination of double separators in the slots and tape around the ends, the tape being applied to alternate turns and enclosing single separators. This turn insulation has been proven to be completely reliable both by severe laboratory tests and by many years of service. Less drastic changes have been made in the ground insulation for field windings, consisting of molded U-shaped armors for the slot region made of sheet mica protected by asbestos cloth, all impregnated with suitable varnishes to give the desired strength and toughness. The varnishes have been changed to synthetic types; and a thin protective layer of glasbestos cloth (made of a combination of glass and asbestos fibers) has been added on the inside of the U, so that the mica is now sandwiched between protective coverings. The previous slot armors have been virtually free of trouble for many years, and the new ones are even better. At the ends of the coils, where the entire coil sections were previously taped with half-lapped layers of mica and asbestos tapes, the coils are now left bare for improved ventilation, and the ground insulation consists of a cylindrical ring between the coils and the retaining ring, molded of mica and asbestos cloth like the slot armors. The coil ends are separated from each other and blocked securely in place both axially and circumferentially by accurately fitted insulating blocks, made of asbestos cloth base Textolite. This construction is illustrated in Figure 5, which also shows the large radius corners of the field coils, which permit thermal expansion to take place without excessive bending stresses in the coil material.

Reliability in service has been an outstanding characteristic of the high-voltage insulation used for large turbine generator armature coils. The annual Edison Electric Institute reports showing the outage hours credited to various causes, reveals that over the years 1940 to 1947 (the last year reported), machines were available for operation, as far as armature insulation is concerned, 99.871 per cent of the demand time. Expressed in another way, armature insulation has been available for service 799 out of every 800 machine operating years. No failures connected with girth cracks or tape separation have been experienced in any hydrogen-cooled machines. It is believed that this record has been achieved by virtue of a program of continual improvements in the methods of applying this insulation. Such changes as better asphaltic type varnishes and compounds, more exacting manufacturing techniques, more searching methods of inspection, and the application of quality control methods have continually raised the mechanical and dielectric characteristics of the finished coils. With regard to manufacturing, the sequence of the compounding operation has been changed in such a way as to produce a denser, more completely filled coil. Moulding operations have been modified, obtaining a marked increase in dielectric strength. Handling operations in the shop have been safeguarded in many ways, eliminating accidental damage during manufacture. New inspection routines have been established and increased testing facilities provided to continually check and control earlier operations. New materials include an improved vertical separator, serving as an insulating bond between the two tiers of strands in the Roebel type transposed bars or half coils, the separator being made of glasbestos cloth (glass and asbestos) treated with a synthetic varnish which is excellent both as insulation and as a binder. On the surface of the slot portion of the coils, a coat of moderately high resistance varnish is applied for corona protection, supplemented at the ends outside the core by a much higher resistance coating which serves to taper off the potential gradient and minimize any concentration which might cause discharges. Perhaps the most important change in materials has been the elimination of Class A insulating materials formerly used, such as cotton tape, fiber fillers, linen cord, cambric tape (on loops, connections, terminals). These have been replaced by Class B materials: glass tape, asbestos fillers, glass cord, and glass-backed mica tape; so that the winding can realistically be called Class B throughout, from terminal to terminal. With these new features, the reliability of high-voltage insulation on the stator coils of large turbine generators can be counted upon to be even greater than would be indicated by the excellent records set in the past years.

Simultaneously with these improvements, extensive laboratory work on the use of new insulating materials has been carried on. In spite of all this work, mica remains the backbone of high-voltage insulation. However, new stickers and compounds and new forms of mica give

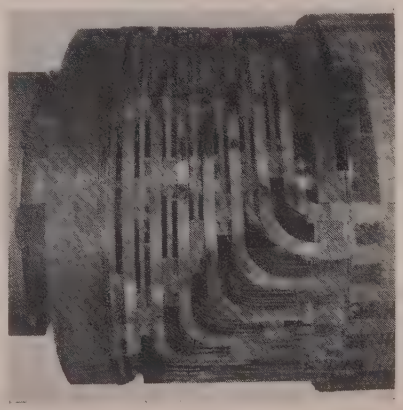

Figure 5. Close up view of end portion of revolving field of turbine generator with retaining ring removed to show ends of field coils

considerable promise for the future. A number of the most promising combinations are now undergoing severe tests. In view of the excellent performance of presently used insulation, and the very small percentage increase in machine availability obtainable even with a perfect insulating system, it is felt that new insulations must undergo the most rigorous testing procedures, and even more important, must prove themselves in actual service on suitable machines before risking the reliability of many major units. In short, an insulation change should be an evolutionary process, not a revolutionary one.

Major improvements have been made in core plate enamel within the last decade, and the flash process of applying it to the punchings of turbine generators has been superseded. In the first place, the somewhat rough pickled surface of the sheet steel punchings themselves has been made comparatively smooth by a special cold rolling operation which is carefully controlled to avoid increase of magnetic losses. This is a basic improvement, as it is next to impossible to put a good thin insulating film on a rough pickled surface. Secondly, a new type of enamel is used, made of a thermo-setting synthetic resin, mixed with a considerable percentage of inorganic material—finely divided silica particles. When properly baked, the enamel "sets up" and thereafter cannot be softened by any amount of heat, even to the extent of burning it off. And even if it should be deliberately burned off (as is done regularly for test purposes on sample punchings) there is a residue of silica which forms a very effective insulating barrier or firewall. Thirdly, new baking type ovens have been provided for applying the new enamel, with adequate controls to insure proper baking to produce a hard, tough film. Finally, inspection techniques have been greatly improved, and the quality of the finished punchings is controlled by insulation tests on frequent samples of the actual punchings, under heat and pressure conditions more severe than exist in service. This enamel does not absorb moisture, as do straight inorganic films such as water glass, and organic ones made of cellulose paper; and it has such excellent insulating properties that no supplementary insulation is needed in the core. Its heat resistant properties are so good that it has been used successfully in special high-temperature cores for small motors and generators in which silicone insulated coils have been capitalized for reduction in dimensions and weight.

Improved Field Coil Materials

The need for improvement of the mechanical strength of field coils in large turbine generators was recognized by different generator designers in the United States and in Europe at different times, depending upon their experience with and observations of difficulties arising from the thermal expansion of field coils in large machines, particularly machines which were frequently stopped and started. There have long since been enough such difficulties, resulting from distorted coils, grounds and short circuited turns, so that the problem has been well recognized, and quite well covered by previous papers.[14–17] However, for greater clarity, a brief statement of the problem is included. It was universal practice for many years to employ ordinary soft annealed copper for the field coils of turbine generators. Large machines require rotating fields of great length and considerable diameter, subject to high centrifugal forces. The centrifugal forces tend to clamp the field coils against wedges carried in the solid steel field body, in such a way as to restrain them at least partially against thermal expansion relative to the body. In normal operation a machine is brought up to speed after a shut down with the field winding and the field body at about equal temperature, possibly room temperature if the shut down has been of considerable duration. When carrying load, the coils tend to expand considerably more than the field body, partly because of the difference in temperature between the copper and steel corresponding to the thermal drop through the insulation, and partly because of the higher coefficient of expansion of the copper as compared with the steel. As a result of this differential expansion being largely restrained by the friction imposed by centrifugal force, a considerable compressive stress is built up in the coil material, which might easily exceed the elastic limit of the copper, or possibly the coil might tend to buckle in some way. Generally, the coil does not buckle, but instead the material may be upset in compression, in such a way that when the machine is shut down and allowed to cool off, the entire coil or warmer turns of the coil contract slightly, suffering a permanent plastic deformation. With successive cycles of service (starting, carrying load, and stopping) the coil or some of its turns would start each time from a new position, and would suffer progressive contraction, which in time may be enough to cause serious trouble.

Two fairly obvious solutions to this problem were apparent: (1) to change the operating procedure in such a way as to expand the coils prior to their being clamped by centrifugal force; and (2) to produce field coils of sufficiently high mechanical strength to stand up under the compression stresses resulting from the restrained thermal expansion, without being upset, or suffering from creep or relaxation effects. Both of these proposed solutions have been studied at length, and have been proved to be effective. The first one which involves preheating of the field coils before the machine is brought to speed was the subject of a previous AIEE paper,[15] presented in 1944. Later experience with one of the very large generators referred to in that paper, which has been regularly preheated, has been very good. This machine had the largest two-pole rotor in the world, and was wound with coils made of soft copper. It has carried heavy loads and has been shut down frequently over a period of six or seven years but has been preheated regularly on starting without suffering appreciable deformation of the coils. Previous experience with this machine with similar operation over a period of only two or three years without preheating resulted in severe deformation. It seems clear from this experience that preheating, properly carried out, is definitely beneficial. Preheating has been recommended on quite a number of other machines on which experience is being accumulated. Also, much analytical work has been carried out to interpret observations on these machines, and to help determine the best procedures. A paper on this particular subject is planned and it is hoped that it can be presented before long.

Improved mechanical strength of field coil material without appreciable sacrifice of electrical conductivity appeared to be a more generally acceptable solution to the expansion problem. For this reason, a broad research program was initiated in 1944 to explore the possibilities of adding various alloying elements to copper or to aluminum. Aluminum had been used to some extent in large 3,600 rpm generators, but had proved to be more plastic than the soft annealed copper. With regard to copper, the beneficial effects of small fractional percentages of silver had been recognized by 1940, and silver bearing copper, so called, was in regular use on large turbine generators. The silver helped the copper in two ways: first, by a marked increase in the rupture strength, as a function of sustained stress at a moderate temperature over extended periods of time; also the silver made a

marked increase in the recrystallization or annealing temperature of the copper, so that the effect of moderate cold work in raising the yield strength of the copper would not be lost over a period of years at operating temperature. The research program was intended to search out other alloying elements which might be even better for copper base field coils; and also to find some way to improve aluminum correspondingly.

The work in the Research Laboratory was supplemented by evaluation tests conducted by the Works Laboratory with the active cooperation of Professor Sayre of Union College. The apparatus used for these evaluation tests (Figure 6) includes a series of cylindrical ovens arranged to be heated automatically to temperatures in the range of 100 to 150 degrees centigrade, with automatic control for maintaining constant temperature as desired. The tests were run in compression, because the basic problem in the generator field was one of compression rather than tension, and we had reason to believe that the compression properties were not necessarily the same as the tension properties. The technique of compression testing was distinctly novel, and was developed especially for this research program. A forthcoming paper is planned which will describe both the equipment and the results in greater detail than can be reported here. Little emphasis has been given to the matter of creep or relaxation effects in previous papers on this subject. However, it seemed fairly clear that if alloyed conductor materials could be developed to have the required yield strength on a short time basis, even though measured at operating temperature, nevertheless the compression stress resulting from the restrained expansion in service at full load would be considerably higher than would be the case with soft conductor materials; so that over long periods of time creep or relaxation would surely be an important item. The tests as actually carried out, therefore, included room temperature stress strain curves in compression, operating temperature stress strain curves, and compression creep tests. Altogether a great mass of data have been obtained, which have been most valuable and informative.

As to the new materials which have come out of this research and development work, the evaluation of the silver bearing copper which was in use when the program started has shown that it is an excellent and highly satisfactory material for use in even the largest machines under construction at present. Among the other alloying elements which might be added to copper to improve its properties no others were found as good as the silver, except cadmium which our tests indicate would be somewhat better. It may be recalled that cadmium was used years ago as a hardening alloy for use in trolley wires. The project for an improved aluminum material appeared much more venturesome at the outset, but has been richly rewarded. The metallurgical story has been told in a paper presented to the American Society for Metals.[18] In brief, 11 different elements were tried out as additions to pure aluminum, and their effects measured as to conductivity and mechanical strength in the annealed and work-hardened conditions. None of these singly gave the answer. However, several gave marked advantages in some particular property. A combination of two elements chosen produced a triple alloy, which turned out to give the results desired. In fact, its properties are almost unbelievably good. This alloy has been given the name Cond-Al, meaning conductor aluminum. It contains small fractional percentages of iron and magnesium. This material has been used for the rewinding of several old fields originally wound with soft aluminum, and one of these has been in service since December 1949. The use of this material is expected to contribute significantly to the development of much larger 3,600 rpm generators than have been ordered so far.

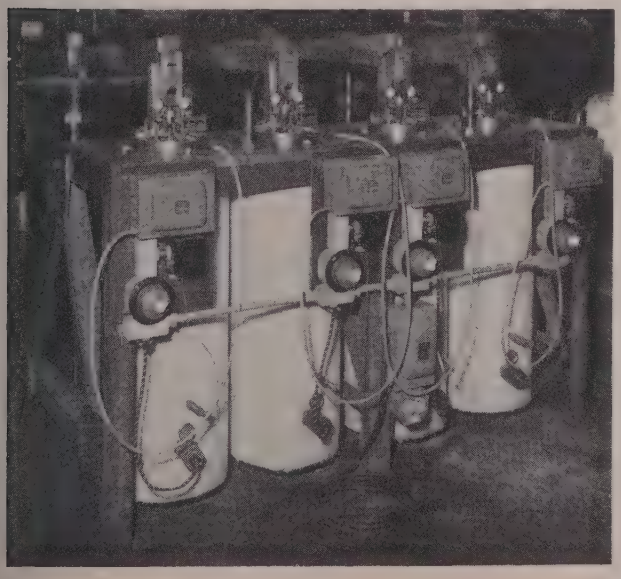

Figure 6. Apparatus for compression testing of field coil conductor materials at operating temperatures

Improved Magnetic Materials

The rotors of large turbine generators are now almost universally made of solid steel forgings. Other types such as those consisting of plates bolted together or with laminations mounted on a through shaft have practically disappeared. The development of these large forgings is quite a story in itself, the emphasis having been on obtaining the required high mechanical strength in all parts and throughout very heavy sections. This is done by employing an alloy steel containing about 2.5 to 3.0 per cent nickel and usually a fractional percentage of molybdenum, often with some vanadium; and the forging is given an elaborate heat treatment. In general, only the physical properties have been included in the forging specifications, and neither the chemical constituents nor the magnetic properties have been specified. By actual analysis, the chemistry of these large shaft forgings has been remarkably uniform among the several suppliers. The magnetic properties for the most part also have been quite good and reasonably uniform, although some exceptions have occurred in the past. About ten years ago, two generator fields had to be replaced on account of excessive excitation caused by poor magnetic properties. A long-term investigation has been carried out since that time, with the twin purposes of obtaining more consistent magnetic properties and of improving the average level as much as possible. The steel suppliers, the Works Laboratory, and the Research Laboratory have cooperated in this investigation, which has progressed rather slowly but surely in the right direction. Some of the findings are that the carbon and chromium content of the forgings should be kept to a minimum, and that the heat treatment should be controlled within certain limits. The results have been excellent. No more cases of excessive excitation have occurred, and the average magnetic

properties have improved appreciably, without sacrifice of mechanical strength. This permits some increase in the magnetic loading of the electrical design, since it usually is the saturation of the rotor steel which limits the amount of useful flux corresponding to the rated voltage of the generator. Ultrasonic testing of the rotor forgings has been in general use for three years, and has proved to be an exceedingly valuable means for detecting internal flaws, as described in a recent paper.[7]

Another recent development is the application of oriented-grain strip steel to the stator cores of turbine generators. This might seem a misapplication, on account of the fact that the principal direction of the flux path in the teeth is at right angles to that in the outer portion of the core. This outer portion, however, is quite massive in turbine generators, and accounts for a large majority of the core loss. Also, the cross grain properties of good oriented-grain strip steel are comparable with the properties of the previous standard hot-rolled sheet steel, both in losses and in excitation requirements. Consequently, a major gain can be made by arranging the grain in the circumferential direction to favor the larger loss in the outer portion of the core, without prejudice to the tooth region. This arrangement was tried out on a 1,250 kva shop generator in 1945, and thorough tests indicated a marked advantage. Since that time, oriented-grain strip steel has been applied to progressively larger generators, of which about a dozen have been tested and put into service. Factory facilities have been provided for the higher temperature annealing process required for realization of the improved magnetic properties, and the application of this new material is rapidly being extended to the largest sizes of turbine generators.

There are two ways to use this strip steel to advantage. Working it at previous magnetic densities brings about a handsome reduction in core loss, which has usually been the largest loss in hydrogen-cooled turbine generators. Or, by cutting down the radial depth of the outer part of the core, and working at higher magnetic densities, the weight and dimensions of the machine may be reduced appreciably. This is of especial importance in very large machines in which the weight and dimensions of the stator are such as to crowd shipping limitations. Very large generators of both 4-pole and 2-pole design are on order which would require a double frame with separate shipment of the inner frame with core and coils assembled, and the outer frame in two or three pieces, except for the advent of the new oriented-grain steel which makes it possible for them to be designed with a single stator frame arranged for complete assembly and test in the factory and shipment in one piece. It is anticipated that the use of oriented-grain strip steel will become general in turbine generators in the near future.

Increasingly Large 3,600 Rpm Generators

The phenomenal growth in capacity of 3,600 rpm generators in the past 20 years has not come about because of any inherent advantages over the well-established 4-pole 1,800 rpm machines. Actually, the higher speed generators are somewhat bulkier, heavier, and less efficient, and are subject to quite a number of distinctive problems and limitations. The advantages of the 3,600 rpm design are all to be found in the turbine end of the set, where the quest for ever higher thermal efficiency and over-all economy of power production has led to continual increases in steam temperatures and pressures. To meet these modern steam conditions, it has been found both technically and economically necessary to use the highest feasible speed of rotation, which permits minimum diameters of turbine shells and minimum numbers of stages. The production of increasingly large high-speed generators to go with these turbines has been an intensely interesting development.

In extending the rated capacity of 3,600 rpm generators from about 12,500 kva in 1929 to over 125,000 kva in 1950, with much further progress in sight, a great many problems have had to be solved, some of which have been touched upon in the previous sections of this paper. Hydrogen cooling was a basic innovation; without it and the other improvements in ventilation, modern generators of large output would hardly be feasible. Various mechanical improvements, particularly the means for elimination of double-frequency vibration, have also been a practical necessity. Other basic improvements have been made in field coil materials which resist thermal distortion, and in the magnetic materials of both rotor and stator, as well as in insulations. All of these are essential for the large machines now being built, and the larger ones to come. However, the old and long-familiar limitations of dimensions are still present. These are: the limitation of rotor diameter by centrifugal stresses, of rotor length by vibrational considerations (critical speed), of stator diameter by shipping clearances, and of weight of stator by railroad car capacity. Means have been found to overcome these limitations somewhat, or to increase generator capacity in spite of them, in many ways.

Rotor diameters for 3,600 rpm have been increased greatly, taking advantage of increased strength and uniformity of the forgings, and of improved field coil conductor materials and insulation; and also keeping within established safe limits for the principal stresses in the bore hole and tooth roots, and particularly in the crushing pressure of the coils on the insulation, and in the hoop stresses in the retaining rings or cylindrical caps which carry the end portions of the field coils. The retaining rings are a major limitation, as in a modern large machine using alloy steel rings, the hoop stress may be 65 per cent to 75 per cent due to the weight of the rings themselves, and only 25 per cent to 35 per cent due to the useful coil load they carry. In such a case, a surprisingly small increase in diameter would require the coil load to be reduced to zero, as the limiting stress would be

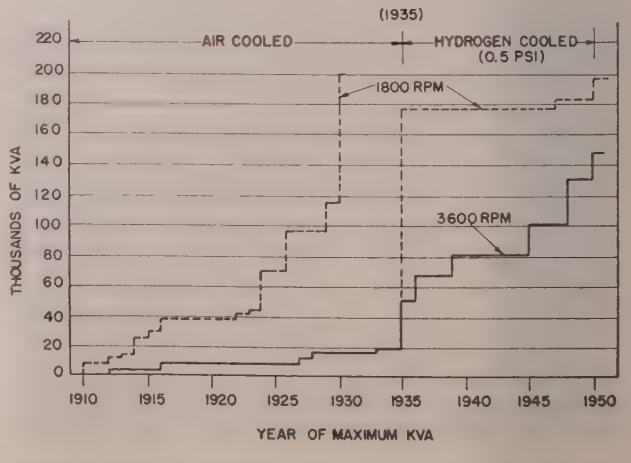

Figure 7. Chart showing increase in rating of 3,600 and 1,800 rpm turbine generators since 1910

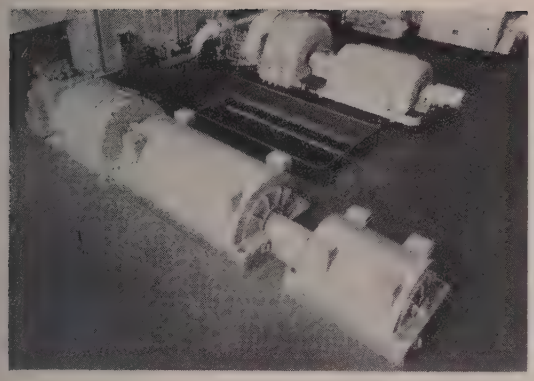

Figure 8 (left). Turbine generator rated 111,765 kva, 3,600 rpm, 15 pounds per square inch gauge H pressure, in service since December 1947

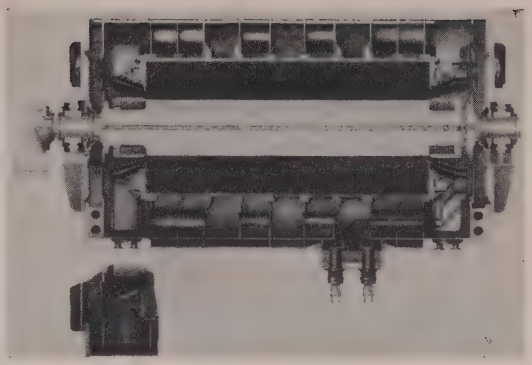

Figure 9 (right). Longitudinal section of 111,765 kva generator shown in Figure 8

reached in the component due to the ring itself. In this connection, a major gain is made possible by the development of Cond-Al, which is the aluminum alloy previously referred to, having both good electrical conductivity and excellent mechanical strength and creep resistance.

Rotor lengths have also increased greatly, even in relation to the larger diameters now found possible, and this has come about by a whole series of developments, including ventilation, conductor materials, and research on vibration and balancing technique. Exhaustive studies have been made on the critical, or more properly resonance, speeds of generator shafts, including observations on many machines in service, tests on dozens of scale models, and the development of improved analytical methods. This work might well be the subject of a very interesting and valuable paper. Suffice it to say here that a much better understanding has been obtained of the vibrational characteristics of long high-speed rotors, and techniques have been developed to insure that they can be well balanced and will run smoothly, even better than the standards of operation which were acceptable on the smaller machines of the past.

The diameter and weight limitations on the stator are fixed by shipping clearances and weight limits. In the 1920's, these were overcome, in the case of very large 1,500 and 1,800 rpm air-cooled generators, by double frame designs; the inner frame, carrying the core and coils, being shipped in one piece; while the outer frame was subdivided for shipment. So far, this double frame construction has not been found necessary for generators designed for hydrogen cooling, even up to 183,333 kva 1,800 rpm, although it may be used soon for very large machines. Its use has been contemplated recently, but has been postponed by the introduction of oriented-grain strip steel for the stator core, as mentioned previously.

Figure 7 shows the increase in the basic kva rating of 3,600 rpm generators, both air-cooled and hydrogen cooled, over the years since 1910. For comparison, data are also included on 1,800 rpm generators. The time scale shows the year in which these machines were ordered; and the rating scale indicates the nameplate kva rating, which in the case of hydrogen cooled machines is based on 0.5 pounds per square inch hydrogen pressure. Starting about 1939 advantage was taken of the improved cooling effect obtained by increasing hydrogen pressure to 15 pounds per square inch gauge, for which a 15 per cent increase in capacity was obtained. And in 1945, a further increase was recognized for pressures up to 25 or 30 pounds per square inch. This subject of increased capacity of hydrogen cooled generators as a function of gas pressure was discussed at length in a recent AIEE paper.[20] It will be observed that a tremendous jump in the capacity of 3,600 rpm generators took place in 1935 and 1936, with the advent of high pressure, high-temperature turbines, and hydrogen cooling for the generators. The largest air-cooled generator for 3,600 rpm was a 50,000 kva machine ordered in 1936. In the past five years, another series of large steps has been taken and the end is not nearly in sight, as design studies and even tentative quotations have been made on 3,600 rpm machines of 180,000 kva base rating.

The first 100,000 kva 3,600 rpm generator, which is shown on the graph as ordered in 1945, actually went into service in December 1947, at the Essex Station of the Public Service Electric and Gas Company of New Jersey near Newark. This machine (Figure 8) was actually given a special nameplate rating at 15 pounds per square inch gas pressure (111,765 kva, 0.85 power factor, 95,000 kw, 13,800 volts with a special short circuit ratio) which is equivalent to the 100,000 kva 0.8 power factor standard rating at 0.5 pound per square inch and the same design has been used for this rating. The operation of this machine has been eminently satisfactory, as it runs smoothly and both armature and field windings are remarkably cool. This pioneer machine has been followed by many others of the same or equivalent rating, and 9 of these are now in service, with 12 more on order. Figure 9 shows a longitudinal section through this machine. A similar generator of somewhat greater length was designed for 112,500 kva and orders have been received for nine of these machines. The first of these was for the new Yates Station of the Georgia Power Company near Newnan, Ga., and went into service in September 1950. Its rating is 111,111 kva, 100,000 kw, 0.9 power factor. The others of this size are in process of manufacture, shipment, or erection. In 1948, a still larger generator of similar design was ordered by the Public Service Company of Northern Illinois for their Waukegan Station, being rated 129,412 kva, 110,000 kw, 0.85 power factor. This machine is now nearing completion in the factory, and is expected to be installed in 1951. Six others of equivalent rating are on order. All of these machines rated 100,000 kva and above have been designed with one-piece stator construction, and have been or will be completely assembled and tested at the factory. The dimensions and weight of the finished stators have been such as to tax the limitations of railway shipment facilities, and there are spots in this country where great difficulty would be encountered in delivering so large a machine. Figure 10 shows one of these machines being hauled over the highway at the end of its transcontinental train trip for installation near San Francisco in Station "P" of the Pacific Gas and Electric Company.

The largest 3,600 rpm generator on order at present (October 1, 1950) is a 147,000 kva, 125,000 kw, 0.85 power factor rating for the Philadelphia Electric Company, the order for which was placed

in the spring of 1950. At the time this machine was quoted the preliminary design was based on double frame construction with shipment to be made disassembled. However, further design studies capitalizing the advantages of oriented-grain strip steel have resulted in the abandonment of the double frame feature for this machine, as it has been found possible to build it closely within the weight and dimensional limits of the Waukegan generator. Another feature of this Philadelphia machine is of special interest, as its output is to be transmitted at the generator voltage 13,800 volts. So large a kva rating at this voltage runs the current capacity up to an unprecedentedly high value—6,150 amperes per phase at base rating. In view of the inherent limitation of armature windings for 2-pole generators to not more than two parallel circuits per phase, and in view of the fact that delta connected armature windings have been generally unacceptable, the current to be carried by each coil is required to be 3,075 amperes at nameplate rating, and proportionately more with increased hydrogen pressure. This is about 20 per cent above past experience. An armature coil for such heavy current must be of distinctly special design. It necessarily requires wide, deep slots in the stator core, so wide that the conventional 2-wire wide Roebel transposition bar is not practical on account of the extreme width of the conductors; particularly as the depth required is so great as to require unusually fine stranding of the conductors. A practical solution has been found by employing a special 4-wire wide Roebel transposed bar. This bar is unusually heavy, and may prove to be rather expensive, but should be entirely practical. The two parallel circuits of the armature winding are brought out through separate sets of bushings at opposite ends of the stator, and are to be permanently paralleled externally.

For optimum generator design as well as for best economy for handling the output current in the power station, it seems that generator voltages for 3,600 rpm machines larger than 112,500 kva should be increased above the long-established standard voltage of 13,800 volts. (Also there are advantages in raising the excitation voltage from 250 to 375 volts.) The actual armature voltage to be chosen is subject to some adjustment, but in general should be higher as the kva rating is increased. In case of special requirements as at Philadelphia, special designs can be developed; but it is felt that, in general, over-all economy can best be served by employing higher voltages up to as high as 20 or 22 kv for the largest ratings. In this connection it might be well to point out that 8 large generators in the Chicago area have been in service for about 20 years running at 22 kv, and have given a good account for themselves. In view of this experience and the considerable advance in insulation practices since these machines were built, there should be no doubt about the reliability of generators designed for the higher voltages suggested.

There is much more progress to be made in future years in the development of large high-speed generators, and many projects for improvements yet to be realized have been under way for years. Not only will still larger machines be built, as they are found to be economically and technically feasible; but the present high levels of general quality, reliability, and smoothness of operation in all sizes will be raised even higher.

References

1. Large Steam Turbine Generators, **W. J. Foster, E. H. Freiburghouse, M. A. Savage.** *AIEE Transactions*, volume 43, 1924, pages 1249–58

2. Design Features That Make Large Turbine Generators Possible, **W. J. Foster, M. A. Savage.** *AIEE Transactions*, volume 49, January 1930, pages 60–67

3. Hydrogen as a Cooling Medium for Electrical Machinery, **E. Knowlton, C. W. Rice, E. H. Freiburghouse.** *AIEE Transactions*, volume 44, 1925, pages 922–34.

4. Outdoor Hydrogen Ventilated Synchronous Condensers, **R. W. Wieseman.** *AIEE Transactions*, volume 48, October 1929, pages 1221–29.

5. The Application of Hydrogen Cooling to Turbine Generators, **M. D. Ross.** *AIEE Transactions*, volume 50, March 1931, pages 381–86.

6. Hydrogen Cooled Turbine Generators, **M. D. Ross, C. C. Sterrett.** *Electrical Engineering* (*AIEE Transactions*), volume 59, January 1940, pages 11–17.

7. The Hydrogen Cooled Turbine Generator, **D. S. Snell.** *Electrical Engineering* (*AIEE Transactions*), volume 59, January 1940, pages 35–50.

8. Application of and Operating Experience with Hydrogen Cooled Synchronous Condensers and Alternators, **P. Sporn, F. M. Porter.** *AIEE Transactions*, volume 59, 1940, pages 890–907.

9. Nine Years' Operating Experience with Hydrogen Cooled Generators, **D. S. Snell, L. P. Grobel.** *Power Plant Engineering* (New York, N. Y.), volume 51, May–June 1940, pages 68–72, 78–82.

10. Continuous Scavenging System for Hydrogen Cooled Generators, **D. S. Snell, L. P. Grobel.** *AIEE Transactions*, volume 69, part II, 1950, pages 1625–36.

11. Special Problems of Two-Pole Turbine Generators, **C. M. Laffoon, B. A. Rose.** *Electrical Engineering* (*AIEE Transactions*), volume 59, January 1940, pages 30–34.

12. Suppression of Magnetic Vibration and Noise of Two-Pole Turbine Generators, **A. L. Penniman Jr., H. D. Taylor.** *Electrical Engineering* (*AIEE Transactions*), volume 60, June 1941, pages 283–88.

13. Critical Speed Behavior of Unsymmetrical Shafts, **H. D. Taylor.** *Journal of Applied Mechanics* (New York, N. Y.), volume 7, number 2, June 1940, pages A-71–79.

14. Deformation of Turbo-Alternator Rotor Windings, Due to Temperature Rise, **G. A.**

Figure 10. 180 ton stator of 111,765 kva generator in transit near San Francisco

Juhlin. *Journal of the Institution of Electrical Engineers* (London, England), volume 85, October 1939, pages 544–52.

15. Prevention of Rotor-Winding Deformation on Turbogenerators, **J. G. Noest.** *Electrical Engineering* (*AIEE Transactions*), volume 63, July 1944, pages 514–19.

16. The Operation of Large Turbo-Alternators to Reduce Rotor Winding Deformation, **R. H. Coates, B. C. Pyle.** *Journal of the Institution of Electrical Engineers* (London, England), volume 93, 1946, pages 192–204

17. Turbo Alternator Rotor Coil Shrinkage, **W. D. Horsley, R. H. Coates.** *Proceedings*, International Conference on Large Electric High-Tension Systems (Paris, France), paper number 118, 1946.

18. The Effect of Single Addition Metals on the Recrystallization, Electrical Conductivity, and Rupture Strength of Pure Aluminum, **R. H. Harrington.** *Transactions of the American Society for Metals*, volume 41, 1949, pages 443–59.

19. Thermal Cracks in Turbine and Generator Rotor Forgings, **A. W. Rankin, C. J. Boyle, C. D. Moriarty, B. R. Seguin.** *Paper number 50-S-16*, The American Society of Mechanical Engineers, New York, N. Y., April 1950.

20. Loading of Hydrogen-Cooled Generators at Elevated Gas Pressures, **D. S. Snell.** *AIEE Transactions*, volume 69, part I, 1950, pages 186–204.

Discussion

Frederic A. Lane (American Gas and Electric Service Corporation, New York, N. Y.): The authors have cited numerous interesting developments which have taken place in recent years in the design of large turbine generators. The following comments may be pertinent.

The vacuum systems for generator seal oil as initiated 12 years or so ago are rather complex but the performance of this equipment as we have experienced it has been quite satisfactory. The more recent and very much simplified continuous scavenging system is being used on all of the new machines, both large and small, and, of course, offers very definite advantages.

An important advantage of using hydrogen which the authors did not mention is that the insulation may be expected to last many times longer than it does in air-cooled machines. Stator insulation in the Logan generator after 13 years of operation is in excellent condition, as is also the insulation in the 20,000-kva synchronous condenser at the Turner Transmission Station after 22 years of operation.

About 1940 the use of aluminum armor on generator rotors for holding end turns in place was discontinued and insulating blocks used instead. This left the side of the conductor bare for better cooling. At Cabin Creek we had two similar generators installed within a short time of each other and one of these had one type of end turn insulation and ventilating arrangement, and the other had the improved arrangement. In the case of the machine having the improved ventilating set-up, the temperature rise of the rotor was approximately 15 degrees less at full load than in the case of the other machine, and this furthermore reduced the heating of the end turns which previously had been running hotter than the rest of the winding.

With respect to improvements that have been made in insulation, the authors make the point that development along this line should be evolutionary in nature and not revolutionary. I agree heartily with this. I think that improvements in insulation must necessarily come the hard way and that the gain at any one time may be rather small. It is decidedly beneficial, however, that all the gain that may be obtained be striven for on the basis that better insulation will give us longer lived machines and I think we must all realize that with economics as they are today, anything we can do to lengthen the life of insulation in major equipment will go a long way towards easing the burden of maintenance.

We have been quite interested in the matter of preheating which the authors touch upon. We have taken definite steps with respect to preheating in some of the generators where the type of winding was such that we had experienced or could anticipate trouble of a kind which preheating might alleviate. We believe that it is beneficial. Quantitatively we are not yet in a position to state to what degree it is beneficial.

There is no doubt but that as the size of generators increases, we need to consider higher voltage. This is not solely a matter of generator design as far as necessity is concerned. It enters into the switching and the connections to the generator very decidedly. The handling of the heavy currents that go along with low voltage becomes more burdensome and can result in extremely expensive construction. We need to get a better balance between the voltage for which the generator is designed and the equipment which will get the output of the generator into the system for the best economic relationship. It may be of interest to note here that there has been in service a large synchronous condenser with a 24,000-volt winding for something over 20 years with complete success.

With regard to higher gas pressures, we have made full use of the operation of machines at higher gas pressures and with all of the later units the design of the entire installation is based on utilizing the capacity of the generator which will be available at 25 pounds gas pressure. The number 5 compound unit at Twin Branch has been operating at 25 pounds gas pressure almost continuously since August 1949. Initially there was some difficulty with excess gas leakage but this now has been reduced to a moderate amount.

W. J. Carfrae (The British Thomson-Houston Company, Ltd., Rugby, England): The authors are to be congratulated on a masterly summary of turbogenerator history during the past 25 years.

It may not be altogether irrelevant to contribute one or two items regarding European practice and experience in the same field.

In view of the basic frequency in Europe being 50 cycles, the point at which hydrogen cooling of alternators becomes an economic proposition is quite different and at the present time is probably not well defined. Indications are that an output greater than 50,000 or 60,000 kva at 3,000 rpm is necessary to justify hydrogen cooling. Largely in consequence of this increased rating the application of hydrogen cooling in Europe has lagged behind that in the United States.

The first hydrogen cooled machine in Great Britain was designed before World War II but its construction was delayed until after the War. A fair number of machines rated at 75,000 kva, 3,000 rpm are now on order utilizing hydrogen cooling and two or three machines are now in successful commercial service.

Propeller fans have been used to a limited extent in Great Britain but the lower rotational speed reduces the advantages and the application of propeller fans is, at the present time, not universal.

Some trouble due to double frequency vibration of stator cores has been experienced in Great Britain, particularly with machines wound for a high operating voltage which have unusually deep stator slots. At the present time, special precautions are taken in the design of these machines as regards both core and frame to ensure that excessive vibration is avoided.

Acoustic resonance also has been observed on one or two occasions in offices adjacent to the engine room and it has proved necessary to alter the dimensions of these offices by the erection of partitions or by other means.

I can support the author's experience that mechanical double frequency vibration on the rotor has not proved a serious difficulty. The company with which I am associated has had two isolated instances, both on shaft overhangs, due to the milling of slots for the rotor leads and this difficulty has been overcome by the milling of two further dummy slots at right angles to the lead position.

I can endorse the writer's remarks about the question of field coil insulation and material, and can say that our experience in Great Britain with silver bearing copper has been uniformly satisfactory. I was particularly interested to read of the new aluminum alloy "Cond-Al" though it would not seem that any output at present contemplated in Europe would necessitate a rotor winding using this material.

Regarding shaft forgings we have had uniformly satisfactory results with a nickel-chrome-molybdenum alloy steel and have been using ultrasonic testing for the past five or six years with very satisfactory results. Contrary to the author's experience we have never found that the presence of chromium in our forgings has any bad effect.

It is hoped that it will be possible to make some experiment with oriented grain material when such material becomes more readily available in Great Britain. At the present time this trip is produced only in limited quantities suitable for transformers.

I can support the author's contention that higher generating voltages are desirable for very large outputs. The company with which I am associated has, in service, 1,112,588 kva of plant operating at 33,000 volts with a further 75,000 kva of plant on order. These machines (some built 17 years ago), have given entirely satisfactory operation and outages due to armature faults have been negligible and were confined to two very early machines having a graded type of winding which was aban-

doned a good many years ago. These very high voltage machines are probably not suited for general application being somewhat more bulky and less efficient than those wound for conventional voltages but it would seem well worthwhile going to voltages of the order of 22,000 for very large outputs. Any output current involving more than about 3,000 amperes per armature path tends to introduce excessive complication into the design.

John G. Noest (Consolidated Edison Company of New York, Inc., New York, N. Y.): A paper, such as the one by Huntley and Taylor, is in my opinion very valuable for two principal reasons: The first is that it acquaints a large number of us, who would not otherwise be in a position to acquire such information, with the progress which is steadily being made in this field and brings about an appreciation of the constant research which must go on to solve the problems associated with the construction of ever larger turbo-generators.

The second reason is that such a paper exposes the limitations and the compromises the designers must necessarily make as the ratings of generators are increased. As a direct result of this, the operators of such units are made more keenly aware of the designers' problems so that the better understanding brought about may well be expected to benefit both the operators and the designers.

The problem of deformation of rotor windings, discussed in this paper, is of intense interest to me since, I believe, the Consolidated Edison, with which I am associated, was the first to apply preheating on their machines as a practical solution of this problem.

Preheating has proved itself as a satisfactory method in securing an acceptable life for the rotor windings of the older turbo-generators, where, because of loading conditions and frequent shutdowns, the field winding life would not otherwise be satisfactory.

This method, however, would not be readily accepted for new units. Therefore, the problem of rotor winding deformation must be solved by the designers.

In their paper, Huntley and Taylor describe the methods by which the rotor winding deformation phenomena is being attacked. New conductor materials have been developed which possess improved physical properties, so that they can withstand greater stresses at acceptable creep rates. This, together with improved ventilation of the winding, which means lower, and what is most important, more uniform temperature throughout the field coils is, in my opinion, all in the right direction toward the solution of the problem from the design standpoint. I wish to particularly emphasize the necessity for greater uniformity in the temperature of field coils because I believe that a considerable amount of shortening of rotor coils can be tolerated if the coils were to shorten uniformly so that the separation of some of the turns from the remainder, which occurs in the winding heads, is avoided. If this were accomplished, the excessive unit pressures on the insulation, caused by eccentric loading when turns separate, which usually is the immediate cause of failure, would also be avoided.

In relation to the problem of field winding deformation (and this applies also to the problem of insulation migration on stator coils) there is one other factor that I must call attention to. It has to do with the frequency of starting and stopping of main units.

On the Consolidated Edison Company System, the ratio of off-peak to peak load is in the order of 1 to 4 or 5. Probably other systems are in similar situations in this respect. Since 1938 there have been added to the Consolidated Edison Company System 11 new generating units with a total capacity of 620 megawatts. At the present time, there are under construction or in project six additional units with a capacity of 860 megawatts. Therefore, 23 per cent of existing capacity is now high efficiency equipment and this percentage will rise to 40 per cent within a few years. This is now in excess of the requirements for off-peak operation and this excess will probably increase.

The point being made is that fewer units can be operated as base load units, or conversely, that more and more of these high efficiency units must be shut down daily. The base load unit of yesterday has within the span of a few years become the peak load unit of today. The design of generators must recognize this situation. Generators must be designed so that they will operate satisfactorily with frequent shutdown.

Recognizing that increasing frequency of shutdowns must be accepted, a question also arises in respect to the method of operation of the units. Since field winding distortion as well as insulation migration of the stator coils is caused primarily by temperature change which in turn is the result of load change, shutdowns included, is there not something worth while to be gained in life expectancy of generators by the operation of the cooling system in a manner so as to minimize temperature changes? If, after consideration of all of the factors involved, the answer to this question should be in the affirmative, then the developments of convenient means for accomplishing such cooling system regulation appear justified.

M. D. Ross (Westinghouse Electric Corporation, East Pittsburgh, Pa.): The authors have presented a summary of the development of turbine generators over a very interesting period when large high speed machines and hydrogen cooling have come into the picture. Many of these developments have been paralleled in the company with which I am associated. It might be of interest to indicate here some of the differences in design practice which have developed over the years. Taking them in the order in which they appear in the paper:

1. So far, we have found it desirable to continue the use of vacuum treatment of the gland seal oil except in the very smallest units. We believe this method insures low hydrogen gas consumption with high gas purity and low windage losses. Some years ago we simplified our gland oil auxiliaries and the size and complexity of this equipment would not seem to be materially different from that shown in the lower part of Figure 1 of the paper.

2. We have used propeller-type blowers on large turbine generators since 1928. The earlier blowers were of formed steel plate welded to a steel hub. Later blowers were of the air foil type. The most recent designs involve new blade shapes which give much higher pressure and volume than were formerly obtained.

3. With reference to access to the generator for inspection purposes, large hydrogen-cooled machines of our manufacture produced during the past four years have access manholes between the two axial coolers which permit examining a large part of the interior of the machine after the gas is removed, but without removing the generator bearing brackets. It is possible to inspect the stator and rotor coil ends quite thoroughly by the use of lights and suitable mirrors while standing in the air intake passage to the blowers.

4. The flexible mounting of the stator core of large two pole machines has been achieved in the author's case by connecting the vibrating core to the outer frame by certain spring devices. These springs inherently transmit a certain portion of the core magnetic forces to the outer frame and introduce certain problems in maintaining the core in position during a short circuit. Our solution of this problem consists of mounting the stator core in a suitable inner structure which vibrates with the core. The inner structure is then attached to the outer frame by a series of flexible links which are anchored to the core member at a point of practically zero tangential motion. These links are quite rigid in regard to short circuit or other torque forces and maintain the core concentric with the rotor. They transmit very small radial vibration forces to the outer frame as the forces required to deflect the links radially a distance of one mil or less, are very small.

5. In the case of double frequency vibrations of the rotor, it has been our practice for about 12 years to put part circular saw cuts in the pole centers of the larger rotors to practically equalize the rigidity of the rotor in the two axes and thus remove this source of vibration excitation.

6. For some years we used a transverse gas cooler arrangement which, in many respects was similar to the vertical gas cooler design except the coolers were horizontal rather than vertical. We later adopted our present practice of using two axial coolers located in the upper part of the frame with each cooler split into two parts on the water side in order that only one quarter of the surface might be out at any one time for cleaning, if that is done with the machine in operation. With this design, shutting off water to part of the coolers will not unbalance the gas temperatures in the machine. With the transverse or vertical coolers, shutting off the coolers at one end might produce high temperatures while the other end indicated quite cool.

7. It has been our practice since about 1930 to tape the top turns of the rotor end winding only with glass and mica tape leaving the inner turns bare for better ventilation. This taping of the top turns is provided in addition to the insulated lining in the retaining ring so that, in effect, a double insulation is provided.

8. Referring to the matter of preheating rotors we have had no experience with this procedure on our older units but our analysis indicates it should be quite effective in reducing field copper shortening on air

cooled units with separate driven fans, but that it would be very difficult to attain suitable differentials in field copper and rotor forging temperatures with internal fan designs. We have therefore not advocated preheating of internal fan machines.

9. Referring to the characteristics of rotor winding materials, the authors do not indicate the amount of cold working of the materials provided in addition to the alloying elements. Our experience has been that cold working the copper to obtain appreciable yield point values is very beneficial to good rotor performance and our large rotors built from 1932 to date have such cold working. Since 1944 silver has been added to improve the creep strength of the material. The earlier rotors without the silver alloy material but with cold working have given uniformly good performance over as much as 18 years of operation.

10. With reference to oriented armature steel experiments on 6,250-kva machines indicate some reduction in core loss but not as much as would be assumed from the paper. We have used the highest grade of hot rolled transformer iron for many years in our turbine generator stators. The amount of gain due to oriented iron would then depend upon the grade of "standard" hot rolled sheet steel.

11. With reference to stator windings for turbine generators above 100,000-kw rating we have not yet run into a condition where we require anything other than the standard Roebel transposed design with two wires wide in the slot. For the same type of stator winding (single or double) we believe the lowest cost unit will be obtained with the lowest stator voltage consistent with limitations of stator slots and winding combinations and current carrying capacity of bushings. We do not therefore see the particular advantages of 20 kv to 22 kv stator voltages as many of these units could be built with lower voltages.

The authors have presented a very interesting paper which is a valuable contribution to the literature on turbine generator design.

Sterling Beckwith (Allis-Chalmers Manufacturing Company, Milwaukee, Wis.): Mr. Huntley and Mr. Taylor have presented a very interesting and useful description of turbo-generator design. It might be of interest, however, to emphasize a slightly different aspect than that of maximum size.

Figure 1 of this discussion shows the rating which has been placed upon two given 3,600-rpm turbine generator frames. The one which dates back 38 years has a 24-inch diameter rotor. The other is not a single frame, but is typical of the largest hydrogen cooled machines. On the same scale is shown the average hourly labor index and an index of material cost. These are important design factors to the extent that one varies more rapidly than the other. Both frames shown are plotted in units proportioned to kva/D^2L. The smaller diameter is air cooled, and the larger is hydrogen cooled.

It is well known, in connection with the Allis-Chalmers hydrogen seal that no auxiliaries are required except a U-tube in the hydrogen drain. It is, however, not generally known that the first of our machines had

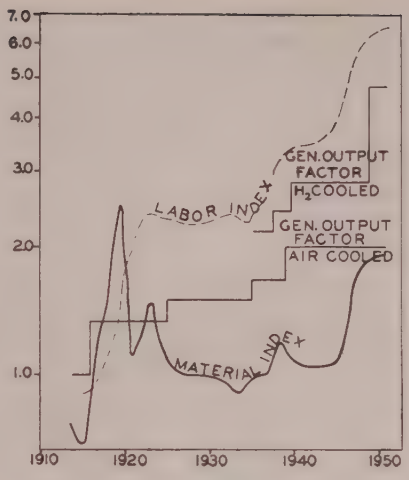

Figure 1

provision for ready addition of continuous scavenging. It has not been necessary, however, to resort to its use, and it has not been provided for since the first machines.

Double frequency vibration effects are described on both the rotor and stator. My experience leads me to question the adequacy of the explanations given in this or in other articles. The double frequency rotor vibration can be avoided, and has been avoided in all our machines, by proper avoiding of operation at half the third critical speed and by avoiding operation at half of any combined critical speed where the double flexibility of the rotor can introduce a self-sustaining disturbance. On the other hand, the double frequency stator vibration cannot be avoided (although it can be minimized), but mention is seldom made of the fact that magnetostriction will produce a vibration almost equal to that produced by air gap forces. Our routine testing of large completely assembled stator cores by setting up 100 per cent flux circumferentially in the core has demonstrated this. The test is primarily used to set up full voltage between adjacent laminations thereby checking core plate varnish, core loss and possible core damage during winding. The magnetostriction tests have been obtained simultaneously.

L. T. Rosenberg (Allis-Chalmers Manufacturing Company, Milwaukee, Wis.): The authors speak of the 4-strand-wide Roebel transposition as an aid to utilization of the wide slots of large machines. This adaptation of the completely transposed conductor has been found useful when the current exceeds 5,000 or 6,000 amperes. It was employed as early as 1926 on a turbine generator rated at 7,530 amperes. We also found the cost somewhat high as it involves twice as many strands as the normal Roebel transposition with two strands in width.

More recently, a 3-strand-wide completely transposed conductor has been developed offering an intermediate step, and promising an appreciable cost advantage over the 4-strand-wide conductor.

The splendid operating record of high voltage generators is borne out also by Allis-Chalmers experience with 16.5-, 18-, and 22-kv machines over the past 20 years. The longest generator built has a core length of 282 inches and is rated 18,000 volts. This unit will soon complete its nineteenth year of satisfactory service. Five 22,000-volt generators have been built dating back to 1930. The original coils of all high-voltage machines above 14.4 kv are still in service.

E. D. Huntley and **H. D. Taylor:** The several discussions have brought out quite a number of interesting aspects of our subject which could not well be included in the paper within a reasonable length. Many of these points do not seem to need further comment; however, there are several to which we would like to reply.

Messrs. Lane, Noest, and Ross appear to differ somewhat on the rather controversial subject of "preheating" of very large turbine generator field windings for prevention of distortion caused by expansion and contraction effects with repeated stops and starts in regular service. So far as new machines are concerned, this should not be an issue, as the windings are made of materials of sufficient mechanical strength to withstand expansion stresses without suffering distortion. On older machines wound with soft annealed coils, additional experience is being obtained which should soon demonstrate whether preheating is worthwhile or not. We believe that it is worthwhile, and have some evidence to that effect already on machines with integral fans (in addition to compelling evidence on a large machine with separate blowers). It has been our practice, therefore, to recommend preheating on all very large machines, new or old, to ease the wear on the insulation due to expansion under centrifugal pressure, as well as to reduce the conductor stresses caused by expansion against centrifugal restraint. It is, however, an extremely complicated problem to analyze in detail. And there are apt to be some operating limitations, which should be recognized, such as the absence of a suitable separate excitation source, or the heating limitations of permanently connected transformers at low frequencies and abnormal flux densities. We have checked transformers in several cases and found them satisfactory for the preheating program recommended for the generators. It is our conviction that, in many cases, preheating will be found both feasible and advantageous.

Mr. Noest raises a very interesting question regarding the possibility of operation of generator cooling systems in such a way as to minimize temperature changes resulting from load changes, including shutdowns, in order to reduce field winding distortion and insulation migration of the stator coils, and thereby increase the life expectancy of generators. Since field winding distortion seems to be primarily the result of restrained differential expansion of the field coils, relative to the solid steel field body, and only indirectly the result of temperature changes, it would seem that the quantity to try to minimize would be the amount of restrained differential expansion. The really critical quantity then is the temperature difference between winding and field body (that is, the temperature drop through the insulation) which accounts for by far the greater part of

the differential expansion. It hardly seems practical to maintain this temperature difference during a shutdown, or even during load changes. However, it can be restored at the end of a shutdown period, by suitable preheating, so that the differential expansion is also restored, to a considerable extent, before the coils are restrained by the full centrifugal pressure. Maintenance of full load winding temperatures during shutdowns would surely help a little, as the differential expansion on starting up would be reduced slightly. It is our conviction, however, that preheating would be much more effective. Our experience with migration of stator coil insulation has been so limited (zero on machines built since 1935) that we are not so well prepared to answer for this phenomenon. However, as we understand it, this also seems to be a problem of differential expansion, which might be helped somewhat by keeping the machine warm during shutdowns, though this would probably not be a complete solution.

Mr. Ross mentions the possibility of local high temperatures resulting from "shutting off the coolers at one end" of a generator having transverse or vertical coolers. We have always furnished at least four vertical coolers, and have never contemplated shutting off more than one at a time for cleaning while the generator is in service. Also we have made provision for equalizing gas temperatures between the two ends of machines with four coolers, by an arrangement of the internal gas passages which gives "cross-flow", with cool gas from the fans at each end flowing past the centerline of the generator to help cool the other end. With this arrangement, a cooler can be cut out of service at either end, without a large change in temperature at any point on coils or core. Tests at full load on a 30,000-kw machine with a cooler cut out resulted in a moderate increase in operating temperature on some of the resistance temperature detectors, such as would be compensated for by a small reduction in load.

The application and test results of oriented-grain strip steel briefly mentioned in the paper will be more fully covered in a paper The Use of Preferred Orientation Strip Steel in Turbine Generator Stators by J. W. Apperson and C. B. Fontaine to be presented to the Institute in the near future.[1]

Mr. Beckwith points out that mechanical double-frequency vibration of 2-pole rotors can be avoided by avoiding operation at half of the third critical speed, or any critical speed of the combined turbine and generator set susceptible to stimulation from the double flexibility of the generator rotor. We agree most heartily, as this has been our understanding of the matter for many years. However, our experience has been that while these higher critical speeds can be calculated quite accurately for the usual assumed conditions of rigidly supported bearings, the actual critical speeds are likely to come very much lower on account of unavoidable slight flexibility of bearing supports and machine foundations. Much interesting and valuable work, as yet unpublished, has been done on the calculation of such critical speeds with allowance for flexibility in the bearing supports; and many tests have been carried out on models and full-sized machines, and have proved the accuracy of the new methods of calculation. But in most practical cases, the degree of flexibility of bearing supports is an indefinite quantity, not subject to the control of the generator designer, as it is usually dependent to a large extent on the foundation design, and has widely different values in the vertical and horizontal directions, so that there are two sets of critical speeds to avoid, both unknown over rather wide ranges. For these reasons, it has seemed wise to us to reduce the double-frequency stimulation, so that the rotor will run quite smoothly on any foundation, regardless of the higher critical speeds.

Messrs. Lane, Rosenberg, and Ross seem to agree that higher voltages than 13.8 kv are needed for 3,600-rpm generators larger than 112,500-kva rating at 0.5 pound per square inch hydrogen pressure, although Mr. Ross questions the need for 20 to 22 kv, and states further that the most economical generator design corresponds to the lowest voltage consistent with the limitations of stator slots and winding combinations, and so forth.

So far as this last statement is concerned, we are in hearty agreement. It is our conviction, however, that these very limitations themselves will lead to optimum voltages of 20 to 22 kv in very large generators in the range of 150 to 200 megavolt-ampere rating.

The continuing startling growth in the size of 3,600-rpm generators, even since this paper was written, is illustrated by recent orders for still larger machines. The present record for the largest on order was set by a generator rated 176,470 kva, 150,000 kw at 0.85 power factor and 0.8 short circuit ratio, at 20,000 volts, at 0.5 pound per square inch hydrogen pressure, for the Philadelphia Electric Company. This voltage was chosen as an optimum value for the rating. The data given in Figure 7 of the paper are out of date already.

Reference

1. The Use of Preferred Orientation Strip Steel in Turbine-Generator Stators, J. W. Apperson, C. B. Fontaine. *AIEE Transactions*, volume 70, part I, 1951, pages 836–840.

Modern Practice in the Balancing of Large Turbine-Generator Rotors

C. M. LAFFOON FELLOW AIEE
A. C. HAGG NONMEMBER AIEE
C. H. JANTHEY NONMEMBER AIEE
P. R. HELLER NONMEMBER AIEE

Synopsis: In the manufacture of large high-speed turbine-generator rotors, balancing is instrumental in contributing to the over-all performance characteristics of the entire unit. Balancing equipment and instrumentation must be adequate to meet the rigorous demands imposed by shop production requirements. In addition, procedures and techniques must be capable of coping with the various problems that may arise in production balancing. This paper presents a review of the equipment and procedures introduced in shop and field balancing by the Westinghouse Electric Corporation as part of a continuing program of design and manufacturing development. It is hoped that the discussion may be of service in furthering an understanding of vibration control as reflected in the primary goal of improving machine performance.

THE design and manufacture of modern high-speed electric machines requires careful attention to the problems of rotor balancing in the control of mechanical vibration. Two- and 4-pole generator rotors are highly stressed structures combining materials of widely varying properties.

Unbalance thus may be caused by geometrical errors, nonhomogeneity of materials, or distortion under operating conditions of speed and temperature. It is the purpose of balancing to offset these imperfections by adjustment of the rotor mass distribution so as to secure a rotor which will run smoothly enough that only acceptably small periodic forces will be transmitted to the supporting bearings and foundation.

In most cases unbalance is caused primarily by geometrical errors and nonhomogeneous materials and adjustment is accomplished by addition or subtraction of material in selected planes along the rotor. Final adjustment is dependent, of course, on adequate rotor seasoning under operating conditions of load and temperature so that any shifts or adjustments of the rotor parts, such as the coils, are complete.

Distortion causes a variable unbalance and although it usually is small, in certain cases special treatment is required. Two types of distortion can be distinguished: (1) dynamic distortion, that occurring in flexible rotors and caused by dynamic stresses, and (2) static distortion, that due to nonrotational effects such as thermal or pressure stresses. Adjustment of the location and number of balance planes is the primary consideration where control of dynamic distortion is necessary.[1] Static distortion often can be compromised satisfactorily by correction to the mean distortion unbalance. In certain cases of excessive thermal distortion that exhibit fixed patterns of vibration as a function of temperature rise, reduction or elimination of this distortion can be secured by selective adjustments in rotor ventilation. Correction of thermal distortion by this means is called thermal balancing and may be required occasionally on rotors where small temperature variations across the rotor diameter can lead to appreciable unbalance vibration.

The technique of balancing has progressed steadily during the past two and one-half decades from an art of trial and error to a fundamentally sound concept based on precision measurement. No longer are the operating characteristics of high-speed rotors shrouded in mystery where large shaft vibrations must be considered normal. Today, with scientifically developed instruments and a thorough grounding in available methods, it is possible to reduce shaft vibrations to satisfactorily low levels.

With the ever-increasing requirement of larger units to meet power demands, however, the balancing problems have become accentuated. In order to maintain the high degree of rotor quality required for continuous reliable service, without introducing serious production delays, modern practice in balancing must be appropriate to deal effectively with all the various unbalance conditions.

Balancing Equipment

To insure that the rotor will operate satisfactorily in the field, balancing and seasoning is performed in a rig that approximates as closely as feasible the characteristics of the assembled unit on the customer's foundation.

Westinghouse currently has in operation a number of such balancing rigs capable of balancing, seasoning, and overspeeding all large 3,600-rpm rotors. Several similar rigs are used for commercial and engineering tests and final balance checks of the rotors assembled in their frames. The drives consist of either geared d-c motors, electronic speed-control drives, or direct-driven 2-pole motors, and are capable of close speed regulation from zero to 4,400 rpm. The method of coupling to the rotors is through either a flexible drive shaft or flexible coupling depending on the size of the unit.

A large 3,600-rpm balance rig, as operated by an electronic speed-control drive, is shown in Figure 1. The same rig with a seasoning heater box encasing the rotor is shown in Figure 2. The heater box is capable of maintaining the rotor tem-

Paper 51-97, recommended by the AIEE Power Generation and Rotating Machinery Committees and approved by the AIEE Technical Program Committee for presentation at the AIEE Winter General Meeting, New York, N. Y., January 22-26, 1951. Manuscript submitted October 16, 1950; made available for printing December 20, 1950.

C. M. LAFFOON, A. C. HAGG, C. H. JANTHEY, and P. R. HELLER are all with the Westinghouse Electric Corporation, East Pittsburgh, Pa.

The authors wish to express appreciation to their associates who contributed to the successful introduction of the procedures and equipment discussed in this paper, in particular R. A. BAUDRY and F. STOTHART.

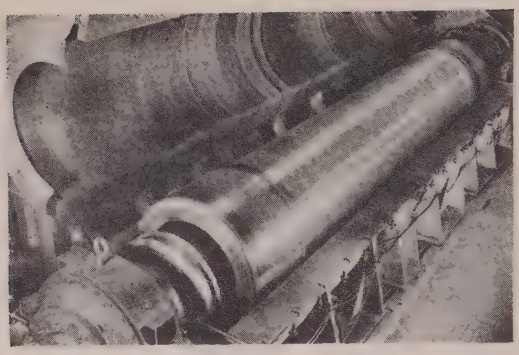

Figure 1 (left). A high-speed balancing and seasoning rig with heater box open

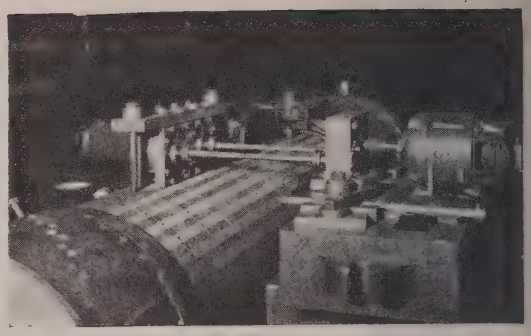

Figure 3 (right). Oscillator mounted on a turbine - generator rotor

perature at 130 degrees centigrade by means of automatic thermal controls. The box consists of an insulated and heavily ribbed outer shell, space heaters, and a thin inner baffle shell which directs the air through the heaters and rotor body. Intake and discharge baffles control the amount of make-up air to the rotor. At full speed the windage loss of large rotors often is sufficient to maintain the required rotor temperature. The top of the box is hinged to facilitate assembly of the rotor in the rig or application of weights during balancing at temperature (see Figure 1).

As an additional aid in determining the vibration characteristics of the rotor, an oscillator or shaker has been constructed capable of operating up to 10,000 cycles per minute and producing measurable vibrations in rotors weighing more than 100,000 pounds. When the oscillator is mounted on a rotor, as shown in Figure 3, it is possible to determine the flexibilities of the rotor and its modes of vibration. While such a static test does not fully take into account oil-film flexibilities and gyroscopic effects, it does provide a valuable adjutant in substantiating design characteristics beyond the safe overspeed limit of the rotor and in interpreting balance data. It further aids on new designs by indicating the probable optimum balancing speeds for the greatest balancing efficiency. A typical record of the modes of vibration is shown in Figure 4. In actual operation, oil-film flexibility will lower the first critical speed, while at the higher speeds the combination of oil-film flexibilities and damping coupled with the gyroscopic effects of the rotor tends to raise the second critical speed.

Instrumentation

The most accurate and reliable instrumentation for unbalance determinations is the wattmeter-type vibration-measuring equipment.[1,2,3] In operation, a small 2-pole sine-wave generator is coupled directly to the rotor to be balanced and its output is connected to the current coil of the wattmeter. An electromagnetic pickup unit is applied to the rotor journals and the pickup output voltage is connected to the potential coil of the wattmeter. The phase angle of the generator current relative to the pickup voltage can be varied by simple rotation of the generator stator, and the wattmeter indication thus depends on the angular setting of the generator. The zero reading requires an accurate adjustment of the stator position so that this angular position for zero wattmeter reading is an indication of the phase angle of the vibration. Shifting the phase of the generator 90 degrees from this zero position gives a maximum reading which indicates the amplitude of the vibration. Since the voltage across the current coil of the wattmeter is a high purity sine wave of running frequency, harmonics other than running frequency are effectively filtered out.

The electromagnetic pickups are applied directly to the shafts through suitable carbon followers and lightweight pushrods. The pickups are supported seismically on readily positioned stands. This arrangement, which can be seen in Figure 1, enhances the accuracy of measurement and also permits a single operator to conveniently follow the vibration of a rotor through testing cycles of speed and temperature.

The sine-wave generator for production balancing usually is mounted permanently on the end of the driving jack shaft of the balancing rig, as shown in Figure 2. The rotatable stator has an angular position scale with the smallest division being 1 de-

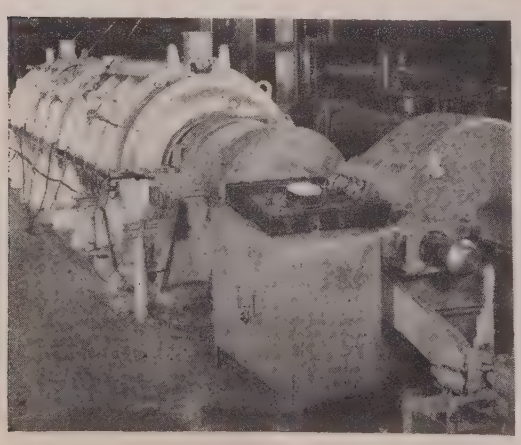

Figure 2 (left). High-speed balancing rig viewed from driving end, showing the vibration-recording equipment

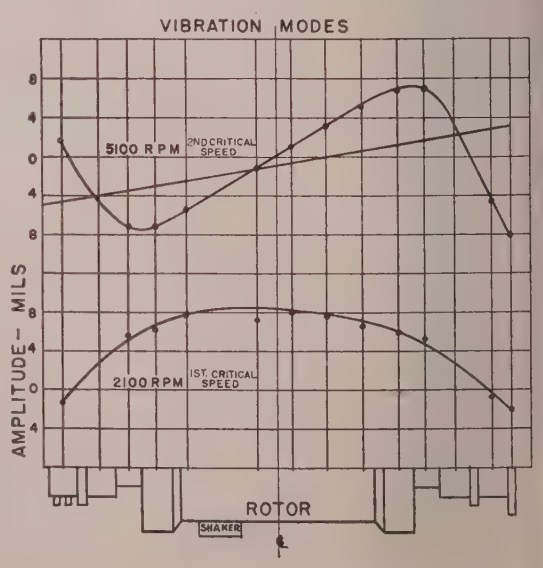

Figure 4 (right). Axial survey of rotor vibration as excited by oscillator

Figure 5 (left). Hand-held sine wave generator prior to engagement with clutch plate

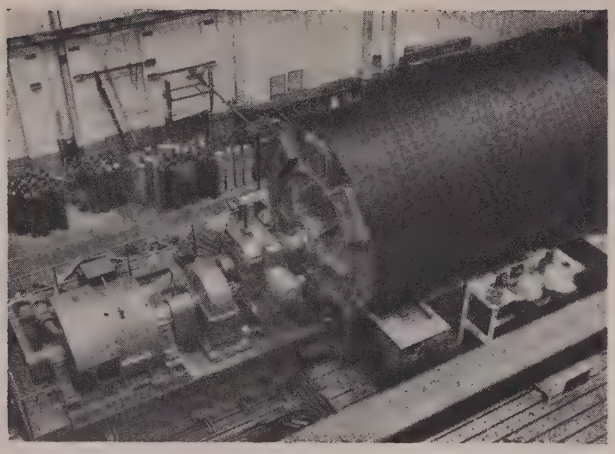

Figure 7 (right). Assembled turbine - generator on test

gree. A rotating scale or protractor fastened to the generator rotor can be used for locating angular positions of unbalance corrections. The normal speed range for this generator is 300–10,000 rpm.

Two other generator designs are used for special purposes. One is a small high-speed unit for application to rotors running up to 20,000 rpm. Another is a hand-held generator, shown in Figure 5, which can be clutched to rotating shafts, thus avoiding shutdowns. This generator, intended primarily for periodic checking of equipment in the field, utilizes a tachometer-type drive through a small clutch plate on the shaft end for preliminary engagement and centering. The final positive drive is through an axially resilient pin on the generator, which engages a matching hole in the clutch plate.

Although the wattmeter-type vibration-measuring apparatus is particularly rugged and reliable, it is obviously desirable, nevertheless, to maintain a close check on the sensitivity and calibration of the various units. For this purpose a small laboratory is maintained with equipment to check the instrumentation periodically and to make minor repairs when necessary. A calibrated mechanical oscillator and generator current supply is useful in giving an over-all calibration check of the wattmeter circuit and pickups. A d-c meter-type polarity indicator is used to insure proper phase relations on repair of pickups and cable extensions. Magnetizing means also are available to restore pickup and generator outputs to normal strength. Maintenance of the many duplicate instrumentation units in uniform calibration permits the convenience of free interchange of these elements and enhances the confidence in measurements and the accuracy of the over-all balancing operation.

Another useful instrument for shop and field measurement of total vibration is the Westinghouse direct-recording vibrograph, which scribes the vibration form directly on a recording tape.[4] By means of a low-power microscope, the amplitude can be determined from 0.0001 to 0.060-inch for frequencies of 10 to 250 cycles per second. This instrument may be used to determine the existence of multiple or submultiple vibrations, as well as running-speed vibrations.

Production Balancing

In production balancing, 3,600 rpm turbine-generator rotor body sizes range from 16 inches in diameter, weighing 2,700 pounds, to over 40 inches in diameter and weighing over 100,000 pounds. For the smaller sizes the first critical speed is well above the normal operating speed, so that excellent results are obtained from low-speed balancing in a conventional balancing machine[5] where the rigid rotors are supported in flexible pedestals and corrections are made in only two planes. A check of the balance is made at full speed in a test rig and at operating temperature in the generator frame.

In the larger sizes, however, the operating speed normally lies between the first and second critical speeds. The shaft then may be considered to be flexible and recourse must be made to several additional balance planes. As shown in Figure 6, seven balance planes are pro-

Figure 6 (below). Position of balance and reference planes on a turbine-generator rotor

Planes 1, 3, 4, 5, 7, A, B, C, D, E, F used in shop balance
Planes 1, 2, 6, 7, A, B, E, F used in field balance

Figure 8 (right). Method of installing thermal balance plugs in rotor vent ducts

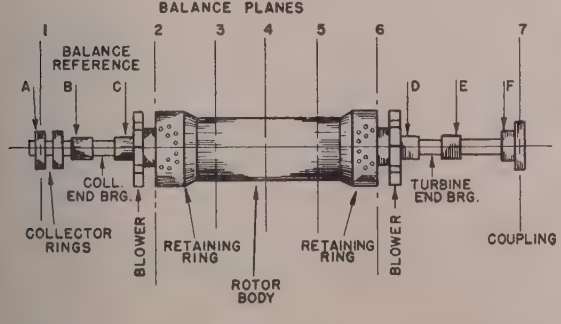

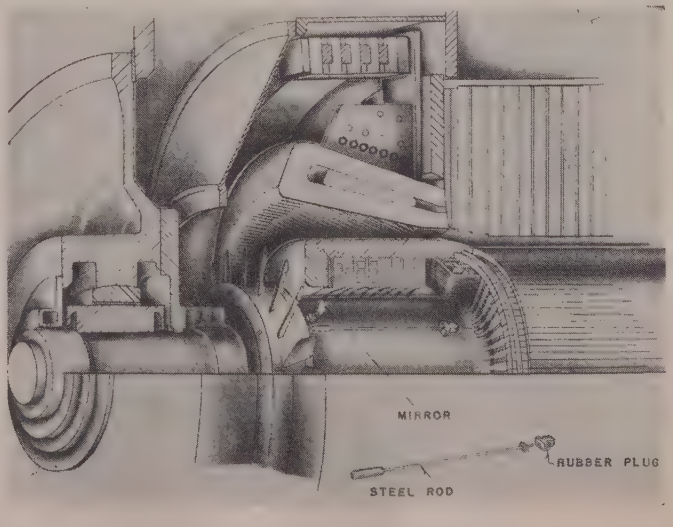

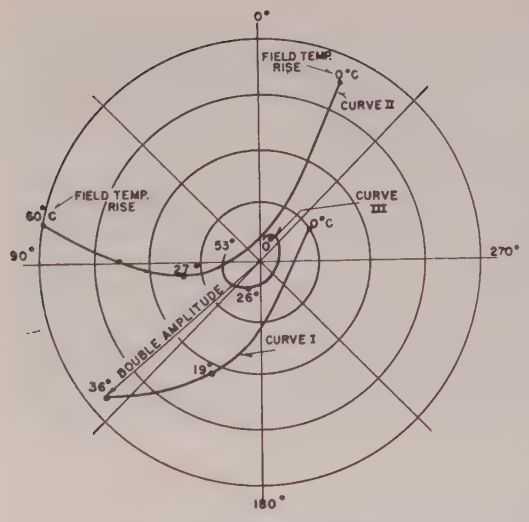

LOCI OF VIBRATION VECTORS

Figure 9 (left). Vibrationchanges with respect to rotor temperature rise

Curve I—initial balance; Curve II — compromise mechanical balance; Curve III—final balance after thermal balancing

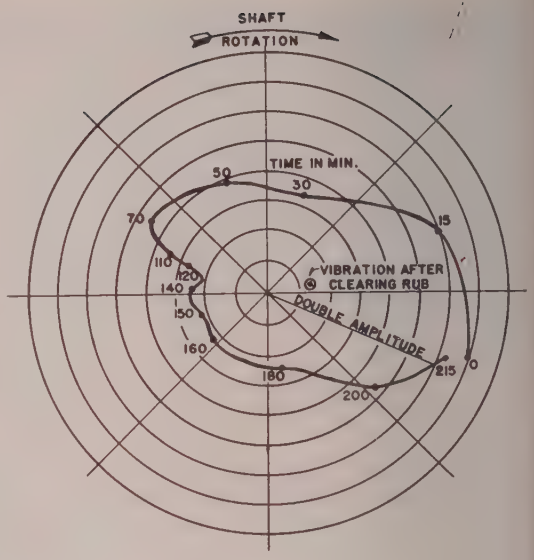

Figure 10 (right). Vibration drift with respect to time produced by a shaft rub

vided, of which five are used in the manufacturer's plant. The two planes located in the retaining rings (Planes 2 and 6) are left open for those occasional cases where a touch-up balance may be required in the frame during test or at the installation. Vibration readings are taken at the six lettered positions indicated in Figure 6.

To insure geometrically true rotors, the rotors are given five periodic truth checks during the course of manufacture from the rough forging to the finally wound and machined rotor. These checks are recorded on a chart accompanying the rotor through its various phases, thus providing direct control over the geometry of the rotor. This procedure has been effective in reducing the residual unbalance as well as in improving the quality of machining. In addition to the usual hollow-drill test and magnetic particle testing of the rotor ends, the rotor body also is borescoped and ultrasonically inspected to insure sound material.

Since there is always some unbalance in the rotor which must be corrected, the rotor is provided with tapped holes in the teeth between coil slots and in the poles to facilitate mass adjustment during balancing by means of steel screw plugs. In those occasional cases where the amount of unbalance in any one plane exceeds that correctable with the steel plugs, current practice is to utilize lead-filled or special alloy plugs. The lead-filled plugs permit an increase of 1.5 in weight, while the alloy plugs are over two times heavier than steel. While such plugs are more expensive than the steel plugs, their availability permits the elimination of an additional drilling sequence, thus accomplishing a desirable reduction in the balancing time.

Normal Shop Procedure

As part of the normal shop balancing procedure the rotor is heated to a uniform temperature of 130 degrees centigrade and balanced to its full operating speed of 3,600 rpm. To insure that complete adjustment of the various components and the organic insulation has taken place, the rotor is seasoned for eight hours at full speed and temperature and is given a shakedown run at 110 per cent of normal speed.

Experience has demonstrated the effectiveness of this procedure in producing a rotor which will remain stable during normal operation.

After a final touch-up balance the rotor vibrations are checked in both the hot and cold conditions to uncover any tendency for thermal variations. With the present-day equipment and techniques, the normal balancing and seasoning period for large rotors averages approximately five days, which represents a considerable reduction from the three to five weeks required in the early history of turbine generators.

All rotors are rechecked in the frame during routine shop tests and are given overspeed tests of 120 per cent to demonstrate their stability and reliability. A typical test setup utilizing a geared d-c drive is shown in Figure 7.

The manufacturer's limits of vibration on the rotor journals and collector rings have been set at a sufficiently low value that touch-up balance in the field normally is not required. Under these conditions the frame and bracket or bearing vibrations are well within acceptable limits.

Thermal Balancing

With the advent of the longer and larger diameter rotors associated with modern high-capacity 3,600-rpm generators, occasional cases are experienced where a change in balance occurs with rotor temperature. Normally, these isolated cases arise from a slight bowing of the shaft such as might be produced by minor temperature variations across the diameter of the rotor or by differential expansion of the several dissimilar materials.

In any case, the initiating factor is small as demonstrated by the minor diametral temperature gradient of approximately one-fourtieth of a degree centigrade per inch required to produce an appreciable effect in a rotor. While careful control is exercised over all components, commercial tolerances in insulation, slot and copper dimensions, and vent ducts could in combination produce variations of this order. Nonuniform paint thickness or accumulation of dirt in air-cooled machines also may be a factor.

Sensitivity to such variations increases with rotor size so that this effect was not evident on smaller units. In addition, it was more difficult to recognize in the past since reliable checking apparatus was not readily available and users, consequently, were not as vibration-conscious as at present. If the observed change is small, it is possible to make a compromise mechanical balance such that the shift passes through zero while maintaining the maxi-

mum amplitudes of vibration within acceptable limits. If the change is considered to be excessive, however, it is possible to balance the rotor thermally by a method that is both inexpensive and highly satisfactory. Thermal balancing,[6] as employed in this case, consists essentially of neutralizing troublesome temperature distortion of the rotor by effectively introducing a counterbowing by means of an artificial temperature gradient across the diameter of the rotor. This may be accomplished simply by partially obstructing the axial ventilation ducts with special silicone rubber plugs. The plugs are 1/2 inch in thickness and are inserted under the overhanging end turns by means of the tools shown in Figure 8, which also illustrates the method of inserting the plugs in a rotor.

The procedure consists of determining the vibration characteristics of the rotor versus the rotor temperature rise throughout its normal operating range, first without plugs and secondly with a trial set of plugs. It is possible initially to estimate the approximate required location of the plugs so that the final step consists of making a simple corrective move both in number and phase location of the plugs. Since these trials normally are performed with air as the cooling medium to facilitate the work, a slight overcorrection is employed to allow for the greater cooling efficacy of hydrogen. If required, a mechanical compromise also is incorporated to yield the best possible operating balance.

All large units currently are checked for this condition during shop tests and corrections are made if necessary. The same procedure can, of course, easily be employed in the field if such occasion should arise. The normal incidence of troublesome cases is small as only five units have been involved out of all the large generators constructed during the past five years.

To illustrate the effectiveness of the thermal balancing procedure, an extreme case, as experienced on a large rotor having a weight of the order of 45 tons, will be presented.

During initial operation, the rotor vibration amplitude was observed to change as shown in Curve I of Figure 9 for one characteristic point on the shaft. It was not possible to operate at high loads, or high rotor temperature rise, without exceeding a safe vibration limit, so that a mechanical balance was made to favor the vibration level at the higher load condition. The subsequent vibration characteristics are shown in Curve II of Figure 9.

By the introduction of six plugs on each end of the rotor plus a mechanical compromise balance, the vibration characteristics were reduced as shown in Curve III of Figure 9. The maximum thermal change then was only 20 per cent of that originally observed, while the maximum vibration of the shaft at any load was well within normal tolerances.

The increase in field temperature resulting from the introduction of the plugs was less than one degree centigrade, and since the normal field temperature rise was low, this slight increase was acceptable.

Other Problems in Vibration Control

Control of unbalance vibration has been of primary concern in this discussion. However, other vibration phenomena that may be encountered in rotating machines should be mentioned. Of interest is the forced vibration caused by oval, 3-sided or 4-sided journals which excite frequencies of two, three, and four times running speed. The errors in journal roundness usually are extremely small and often are difficult or impossible to detect by standard micrometer measurements. Nevertheless, if a natural frequency coincides with the impulses of the out-of-round journal, the high magnification at resonance results in serious vibration, particularly when involving overhung masses from the out-of-round journal. Out-of-round journals sometimes are traceable to errors in shaft centers caused by improper use of reamers or nonuniformity of reamer cutting action produced by local hard spots in the material, the error pattern of the center being duplicated in subsequent journal machining.[7] Correction may involve detuning the vibrating system, but in some cases this may not be wholly practical. Instead it may be more desirable to eliminate the journal errors by careful lapping.

Double-frequency vibrations also may occur on large 2-pole rotors because of the difference in mechanical rigidity of the two major axes. This problem can be avoided by proper provision of transverse slots in the pole face to produce uniform deflection of the rotor in all planes.

Sometimes rubs occur under certain operating conditions because of lack of clearance between rotating and stationary parts. The rub, usually at the most eccentric point, causes heating and distortion, and the original unbalance complemented by the distortion unbalance leads to a new eccentricity at some angle of lag to the original eccentricity. The rotor now is rubbed at the new high spot, with the result that such a process may continue indefinitely. The vibration also may continue to increase so that the machine will have to be shut down, or the rotor may rub itself free. Measurements of rotor vibration reveal a phase wandering in a direction, for the most part, opposite to the direction of rotation, Figure 10. This wandering or drift of the phase of the vibration affords a means for detecting a rub and indicates that inspection for adequate running clearances is in order. The cycling time depends largely on the type and location of the rub and on the relation of the operating speed to the critical speed.

Where rubs are severe and impacting occurs, a self-excited vibration subharmonic resonance may occur.[8] The motion is nonlinear with a fundamental frequency of 1/2, 1/3 ... of running speed. Of the higher harmonics that exist in the motion one thus corresponds to running speed. Hence, unbalance forces can do work on this harmonic and sustain the complete nonlinear motion. This type of vibration is not uncommon where couplings or bearings are out of alignment, particularly when appreciable unbalance exists. It appears that subharmonic resonance sometimes is mistaken for oil whip, another self-excited vibration phenomenon. Oil-whip frequencies invariably are less than 1/2 running speed[9] and bear no simple numerical relationship to running speed, whereas subharmonic frequencies are exactly 1/2, 1/3, 1/4 ... running speed. Typical records of oil-whip and subharmonic resonance are shown in Figure 11 and show clearly the differences in the two types of vibration phenomena. (It is only incidental that the oil-whip record was taken from an 1,800-rpm machine, whereas the subharmonic vibration occurred on a 3,600-rpm machine.)

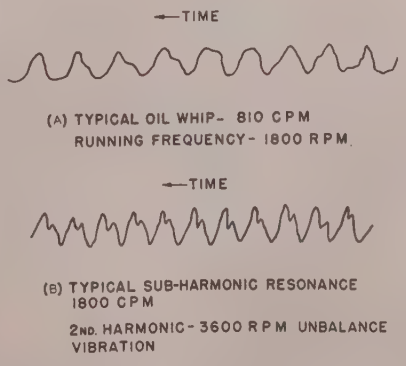

Figure 11. Typical records of oil whip and subharmonic resonance

Conclusions

The equipment and methods utilized in the current balancing practice for high-speed electric rotors have been described. Coupling the generator rotor to the turbine rotor will alter, in general, the critical speeds of the combined unit somewhat, but the amplification factors at the operating speed will be essentially the same. Consequently, if each component is properly machined and balanced, the assembly also will be in balance. The effectiveness of this practice is demonstrated by the unusually low number of cases where additional balancing is required in the field.

The usefulness of thermal balancing in those few cases where temperature distortion is appreciable has been described. Other problems in vibration control, such as out-of-round journals, distortion due to rubs, and self-excited vibration phenomena, have been discussed and corrections indicated.

While control of unbalance vibration of electric machines is particularly effective, we should not overlook the rapid increases in sizes and speeds of rotors, which place increasing emphasis on improved balancing instrumentation and techniques and on the complementary aspects in the design and manufacture of rotors.

References

1. Balancing Rotating Machines in the Field, **F. C. Rushing, B. A. Rose.** *Electric Journal* (East Pittsburgh, Pa.), November 1937.

2. Balancing Rotating Machinery, **F. C. Rushing.** *American Machinist* (New York, N. Y.), April 1941.

3. Westinghouse Type HQ Portable Balancer, *Instruction Book IB 85-921-1*, Westinghouse Electric Corporation, Baltimore, Md.

4. New Method of Measuring Mechanical Vibration, **H. C. Werner.** *Instruments* (Pittsburgh, Pa.), volume 15, number 3, March 1942.

5. Vibration Problems in Engineering (book), **S. Timoshenko,** D. Van Nostrand Co., Inc., New York, N. Y., second edition, 1944, page 68.

6. Thermal Balancing of Large Rotors, **W. F. King.** *Allis-Chalmers Electrical Review* (Milwaukee, Wis.), Second Quarter 1947.

7. The Geometry of Quasi-Circular Shapes and the Behavior of Drills and Reamers, **E. V. Wait.** *Engineering* (London, England), March 17, 1950.

8. Self-Induced Vibrations, **J. G. Baker.** *Paper APM-55-2*, section 13, American Society of Mechanical Engineers (New York, N. Y.), volume 55, 1933.

9. The Influence of Oil-Film Journal Bearings on the Stability of Rotating Machines, **A. C. Hagg.** *Journal of Applied Mechanics* (New York, N. Y.), September 1946, page A211.

Discussion

L. P. Grobel (General Electric Company, Schenectady, N. Y.): The authors have written a worth-while paper which shows the rather elaborate equipment necessary to obtain the accurately balanced generator rotors desired for modern high-speed machines. Our experience has shown that such equipment is extremely valuable, since effective corrections for unbalance forces can be made more quickly and accurately than by running large high-speed rotors in their armatures. It is interesting to note that the balancing rigs, the instrumentation, and the methods of compensating for unbalance described in the paper are similar to those employed by the General Electric Company. Probably this is natural, as it seems likely that there is just one general solution to the problem of precision balancing these rotors.

The authors describe the method of heating the rotors in the balancing rigs in which the heating units are inside the balancing rig enclosures, but external to the rotors. It appears, then, that current is not supplied to the rotor windings at this time. Does this mean that when thermal balancing is required on an occasional rotor the thermal balancing is done later, when the rotors are run in the armatures?

Referring to the shaker tests described in the paper, Figure 4 of the paper shows an observed second critical speed of 5,100 rpm. If this is obtained by vibrating a high-speed rotor weighing 50,000 pounds or more it indicates extremely stiff rotor supports. Equally stiff bearings and bearing supports in the balancing rigs would mean that the rotors are balanced on more rigid supports than the foundations on which the rotors run in the power stations.

Oil-film flexibility is described as being the cause of the depression of critical speeds of generator rotors below the infinitely stiff support condition assumed in calculating critical speeds. We have been interested in the effect of oil-film flexibility on lowering critical speeds; however, we have been unable to obtain any real evidence that it is an important factor on large rotors such as the authors describe. Our present data indicate rather that flexibility and mass of the foundation and other supporting members have the major effect.

The authors mention a case of oil whipping of an 1,800-rpm machine. We have not observed oil whipping of an 1,800-rpm turbine generator and consequently are interested in the circumstances responsible for this type of vibration. It might be assumed that depression of the rotor critical speeds caused by unusually flexible supports would be responsible. If the authors have the information it would be interesting to know if this was the cause of the oil whipping or, if not, what the contributing factors were.

C. M. Laffoon, A. C. Hagg, C. H. Janthey, and **P. R. Heller:** Mr. Grobel's comments relative to the parallel experience of his company are of interest. The equipment and methods developed by the industry for the precision balancing of large high-speed rotors represent many years of painstaking effort to provide the ultimate consumer with the most efficient and reliable generating units possible.

Referring to the question concerning the seasoning cycle, the rotors are heated by external heaters rather than by the rotor coils primarily to avoid heating and distortion of the balance rig and equipment by the rotating flux field. Since thermal balancing is required rarely and should be performed under the same ventilation characteristics experienced in the stator, the most natural sequence of operations is to include the thermal balancing procedure during commercial testing of the unit. No major disassembly of the generator is required, so that no serious production delay is involved.

In discussing the application of a mechanical shaker to the determination of natural frequencies and modes of rotor vibration, it was merely pointed out that the influences of oil films and gyroscopic effects are excluded because the rotor is stationary in the rig. The authors agree that the flexibility and mass of the foundation and other supporting members can have considerable effect; these, however, are included in a shaker test. In certain cases, reductions of 20–25 per cent in the actual critical speeds have been observed, which unquestionably were caused by oil-film flexibility as indicated, first, by large motions of the journals as compared to motions of the bearing supports and, secondly, by comparison to shaker tests. In addition, proper theoretical allowances for oil-film effects correlate well with actual performance.

The operating characteristics of the rotors in the balancing rigs are in satisfactory agreement with those observed on the assembled units. Consequently, it is believed that the rigs approximate, as closely as is feasible with single units, the flexibilities and masses encountered in most practical foundations.

The vibration record of oil whip (Figure 11 of the paper) was intended to be significant only in illustrating the difference between this vibration phenomenon and subharmonic resonance. The record actually was taken on a test machine, and to the authors' knowledge oil whip on an 1,800-rpm turbine generator has not been observed. This phenomenon is associated principally with higher speed units.

Pulse-Time Modulation Telemetering Systems for Rocket Application

JOHN T. MENGEL
NONMEMBER AIEE

Synopsis: The Naval Research Laboratory has designed and operated two long-range multichannel pulse-time modulation telemetering systems for over 55 V-2 and Viking rocket firings at the White Sands Proving Grounds. Design and operational data are given for a 23-channel, 1-kw peak pulse power system and for an improved 30-channel, 4-kw peak pulse power system, together with photographs of the equipment and sample records obtained.

THE USE of any rocket as a vehicle for upper-atmosphere research is premised on the ability of the research scientist to recover data originating within the rocket during flight. Actual recovery of a record either by ejection during flight or from the wreckage after impact presents problems of considerable magnitude that have as yet been solved only partially. At present, although physical recovery methods have been utilized, telemetering techniques appear to furnish the most satisfactory means of data recovery for high-altitude research in rockets.

Radio telemetering equipment designed by the Rocket Sonde Research Branch of the Naval Research Laboratory has been used at the White Sands Proving Grounds for recording data throughout the flights of 45 V-2 and Viking rockets. The service furnished to perform this function is basic both to the upper-atmosphere research program and to basic rocket performance studies. Typical of the basic research data telemetered by the system are temperatures and pressures in the upper atmosphere, cosmic radiation characteristics, ionosphere properties, solar radiation, and pulses from auxiliary equipment to indicate altitude of operation by reference to flight time included on the final telemetering record. For studies of rocket performance, data are telemetered on such quantities as speed, acceleration, altitude, engine pressure, pump pressure, skin temperature, and control fin operation.

The over-all telemetering problem includes the functions of measuring, of transmitting, of receiving, and of recording. This paper discusses only the last three of these functions, the first function being the responsibility of the experimental or rocket group for whom the telemetering is being performed. In order to permit a standardized telemeter transmitter to be used, a characteristic voltage range for data has been adopted of from 0 to +5 volts, which is to be provided by all experimental groups.

Up to the present time, the Naval Research Laboratory has provided and operated two types of telemetering systems at the White Sands Proving Grounds, each of which utilized pulse-time modulation of an r.f. (radio frequency) carrier to convey the channel data intelligence to a ground receiving station where a continuous record of all channels was made as a function of channel voltage versus time for the 300 or 400 seconds of flight. This paper discusses the operation of both systems in an attempt to explain the growth of the pulse-time modulation system in this application.

Sequential System

Telemeter Transmitter

The first telemetering system put in operation at White Sands was a sequential pulse-time modulation system. This system converts the data voltages into time intervals. These intervals, defined by voltage pulses, correspond in length to the data voltages. The data voltages are sampled in a specific order and are used to generate a series of pulses, the time intervals between which measure the sampled data voltages. These intervals maintain the same time sequence as the sampled voltages, the pulse marking the end of one interval serving as the initial pulse of the succeeding interval. A complete sampling of all data voltages is used to form such a group of time intervals periodically, at a rate determined by a master keyer. The distinction between different groups is made possible by a gap between groups of time intervals determined by the master keyer period.

Figure 1 is a block diagram of the telemeter transmitting unit for the sequential system. This unit converts the data voltages into time intervals between pulses and modulates an r.f. oscillator with these pulses for transmission to the

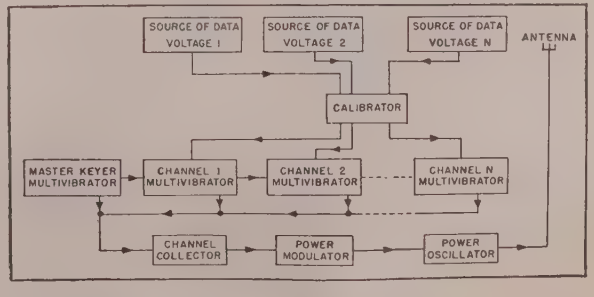

Figure 1. Block diagram of sequential telemeter transmitting unit

Paper 51-98, recommended by the AIEE Special Communication Systems Committee and approved by the AIEE Technical Program Committee for presentation at the AIEE Winter General Meeting, New York, N. Y., January 22–26, 1951. Manuscript submitted November 9, 1949; made available for printing January 8, 1951.

JOHN T. MENGEL is with the Naval Research Laboratory, Washington, D. C.

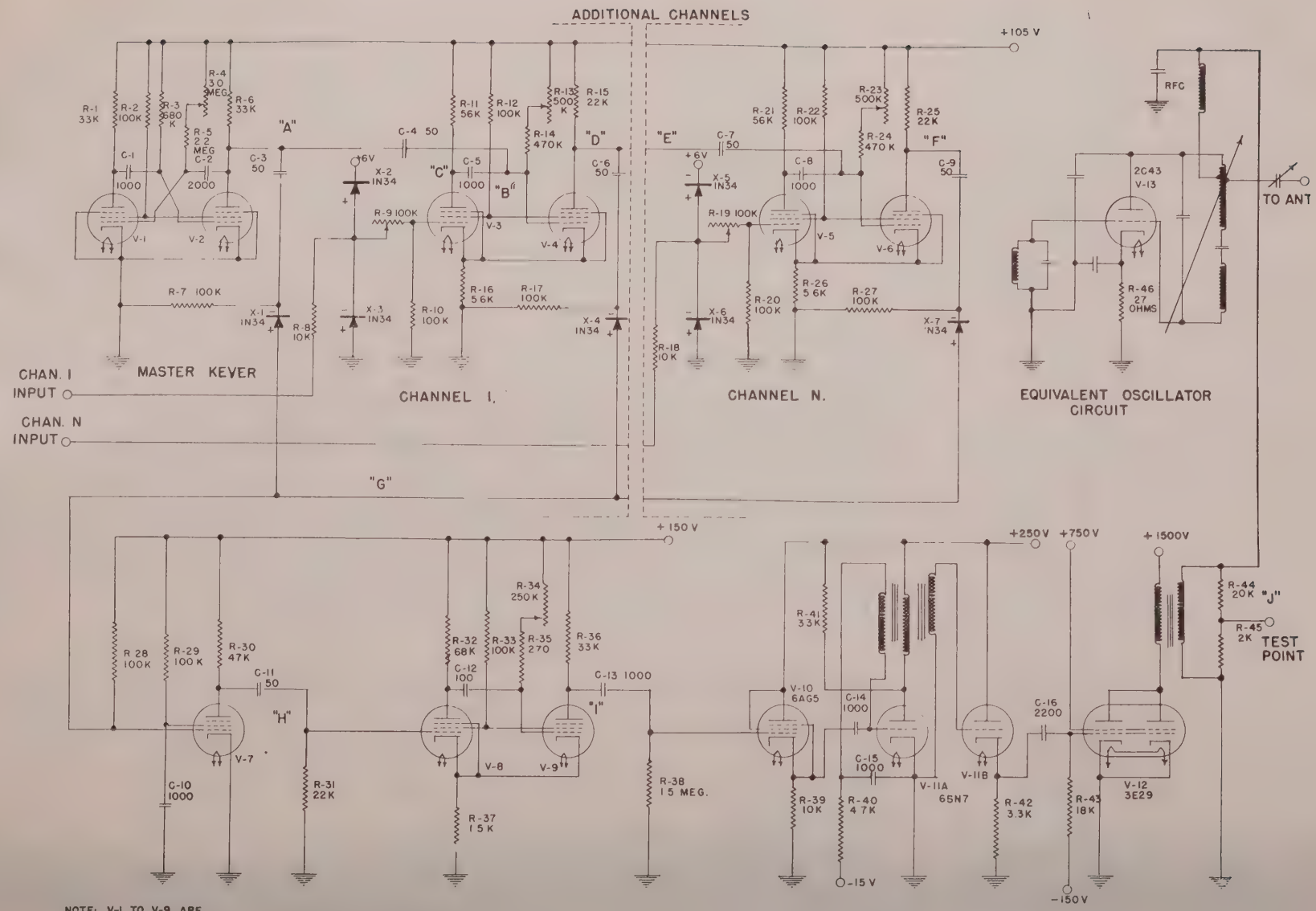

Figure 2. Schematic diagram of telemetering air-borne unit

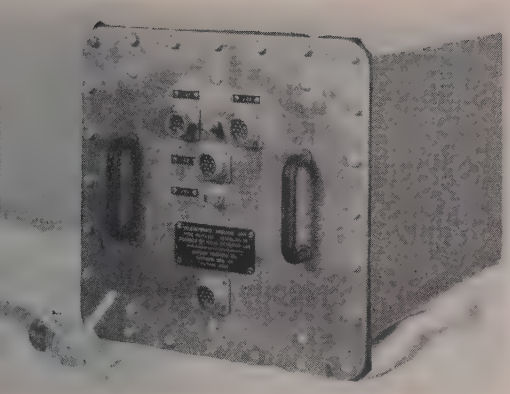

Figure 3 (left). Sequential telemeter transmitter set

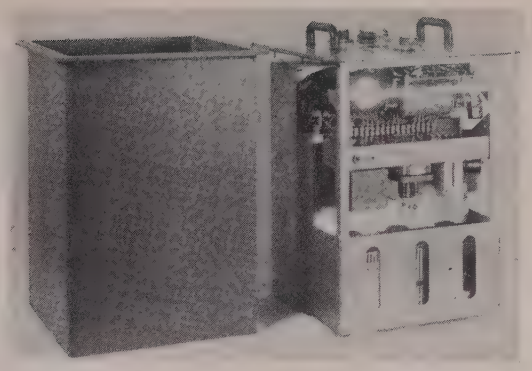

Figure 4 (right). Sequential transmitter showing modulator

ground station via a radio link. A master keyer multivibrator running with a constant period of about 5,800 microseconds generates the first pulse of each group. This pulse is fed to a channel collector, a circuit common to all channel outputs, and also to channel multivibrator number 1, as a trigger. All channel multivibrators are of the "single-kick," or self-returning, type, the recovery time of which is determined by the corresponding channel data voltage, which is fed into the control grid of the normally "off" tube. Upon recovery, channel multivibrator number 1 delivers a pulse to the channel collector, and also to channel multivibrator number 2. The multivibrator of channel number 2, in turn, triggers that of the next channel and delivers an output pulse to the collector. This process is repeated in sequence until all time channels have operated, after which the circuit is quiescent to transmit the gap necessary for ground station synchronization, after which the master keyer again initiates the sequence. The channel output pulses delivered to the channel collector by the various multivibrators are fed to a blocking oscillator to form 1.0-microsecond pulses of sufficient amplitude to key a normally off-power modulator which pulses a very high frequency power oscillator.

Figure 2 gives a circuit diagram of the telemeter transmitter unit. Tubes V-1 and V-2 form the master keyer multivibrator, with V-3, V-4, V-5, and V-6 forming typical channel multivibrators. Tube V-7 is the channel collector triggering the output multivibrator, tubes V-8 and V-9. Tube V-10 is a cathode follower which drives tubes V-11A and V-11B, the pulse former and buffer which key the power modulator tube, V-12. The r.f. oscillator tube, V-13, is a lighthouse tube mounted in an L-band inductance-band very high frequency resonant line cavity, which drives a 50-ohm output r.f. line by capacitative coupling.

Figure 3 shows the sequential telemeter transmitter set as installed in V-2 rockets, with inside views shown in Figure 4. Pertinent characteristics of this unit are the following:

1. 23 input data channels
2. 180 samples per second per channel
3. 0 to +5 volts channel input voltage
4. .110-megohm input resistance
5. Over-all accuracy of ±2 per cent
6. Average output power in the r.f. pulse of 1 kw
7. R. f. output frequency of 1,025 megacycles per second
8. Alternate 0- and 3.5-volt calibration of all input channels every 20 seconds
9. Dry battery high-voltage supplies, storage battery filament supply
10. Case size 14 inches by 14 inches by 20 inches, plus storage battery case 4 inches by 8 inches by 6 inches
11. Weight, less r. f. feed cable, 150 pounds

Ground Station

Figure 5 is a block diagram of the sequential system ground station. The antenna is trained by an optical director or by signal-maximizing techniques to follow the rocket in flight. The detected output of the receiver is fed through a video amplifier into the decoder unit, the purpose of which is to recover the original voltage forms from the time-modulated pulses.

The decoder input is fed to a pulse-width discriminator, which rejects pulses having appreciably different duration than 1.0 microsecond. The discriminator output is fed to both the synchronizing pulse generator and to the input of each channel separator after pulse inversion. The synchronizing generator output consists of one pulse at the start of every group of received pulses, which goes to channel separator number 1, triggering a multivibrator. This multivibrator is returned to its original state by the second pulse group now arriving from the inverter. When separator number 1 is returned, it delivers a pulse which triggers number 2 separator. The return of number 2 separator is effected by the third pulse of the incoming series relayed by the pulse inverter. This action con-

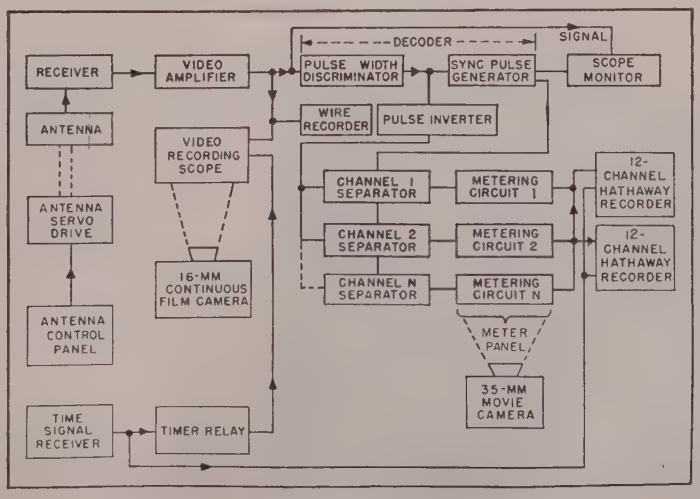

Figure 5. Block diagram of sequential ground station

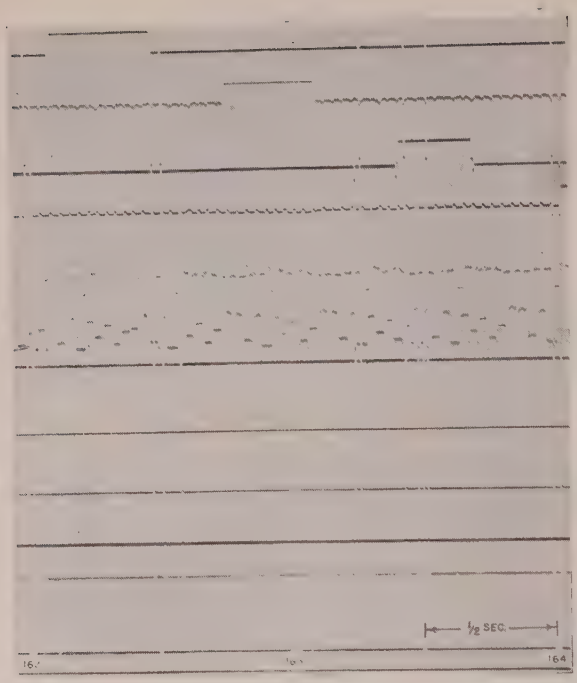

Figure 6 (left). Sequential system record section

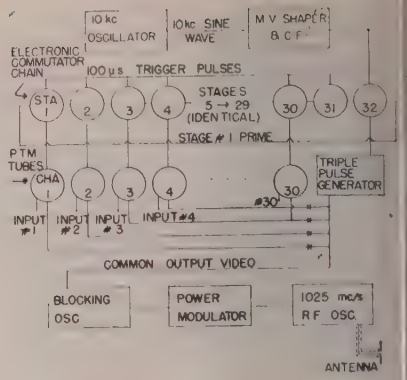

Figure 8 (right). *AN/DKT-2* telemeter transmitting set block diagram

tinues, each channel separator triggering the following channel while being itself returned by the incoming signal.

During the conduction period for any channel separator, the corresponding metering circuit is fed a constant voltage, the same for all channels, for a length of time equal to the interval representing the corresponding data voltage. A capacitor is charged thereby to a potential which depends upon the duration of the voltage applied. By a suitable circuit, this potential is measured by a vacuum tube voltmeter, the magnitude being a linear function of the original data voltage on that channel. This voltage is indicated on separate voltmeters for each channel and also is fed to a string galvanometer in a multichannel magnetic string oscillograph for recording on $9^1/_2$-inch film for the final record. Figure 6 shows a typical record obtained with the sequential telemetering system. Figure 7 shows one sequential system ground station as operated at White Sands, complete except for the Hathaway magnetic string oscillographs.

Matrix Telemetering System

As a result of an expanded V-2 firing schedule at White Sands, additional units beyond the 35 sequential telemeter transmitter unit originally ordered became necessary. The Naval Research Laboratory therefore designed a second pulse-time modulation telemetering system to include improvements found desirable as a result of field usage of the sequential system. The following improvements were considered basic in any new system:

1. Use of a definite coded pulse to indicate the start of a new sampling group, rather than a gap as was used in the sequential system.

2. Use of a "fly-wheel"-type synchronization generator at the ground station.

3. Use of storage batteries for all power supplies, with converters to obtain the high voltages required for the transmitter.

4. Use of a multistep calibration voltage operating at ten-second intervals.

5. Use of direct photographic recording of the received video signal on cathode ray tubes, thus eliminating all ground station channel metering units.

6. At least 3 kw of power in the r.f. output pulse.

7. An over-all system accuracy of ±1 per cent, with channel crosstalk minimized.

8. Quick-access-type case for ease of disassembly when required.

9. Increase of data input channels to 30.

The telemetering system developed to fulfill these requirements is called the Matrix Telemetering System, and the telemeter transmitter is designated the *AN/DKT-2*.

Matrix Telemeter Transmitter Unit

The matrix telemetering system utilizes pulse-time modulation to convey 30 channels of input information. Data in the form of varying direct voltages are supplied to the equipment from the various experiments. The data channels are sampled successively and the whole proc-

Figure 7 (left). Sequential system ground station

Figure 9 (right). Matrix system telemeter transmitter set

Figure 10. Interior, matrix system telemeter set showing r.f. and power converter

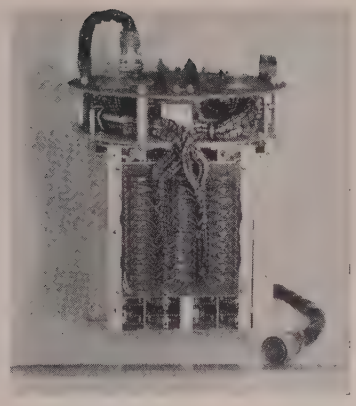

Figure 11. Matrix telemeter transmitting set showing premodulator

ess is repeated at a 312.5-cycle rate. A coded triple pulse identifies the start of each group and establishes a time reference framework, or matrix, of 32 intervals of 100-microseconds each. Within 30 of these intervals, single data pulses occur, the position of the pulse within its interval indicating the voltage being measured on the channel. This chain of pulses is used to modulate an r.f. transmitter operating at a frequency of 1,025 megacycles per second with an average power in the pulse of about 4 kw.

Figure 8 is a block diagram of the matrix telemeter transmitting unit. This diagram shows the 10-kc oscillator to be the independent initiating part of the circuit. The sine wave output of this oscillator is fed to a multivibrator which serves to shape it to derive a series of pulses 100 microseconds apart from it. These pulses are fed through a cathode follower to a bus feeding each of the 32 tubes of the electronic commutator. These tubes are arranged as a chain so connected that only one tube can conduct at a time. As any one of these thyratron tubes fires, it readies the next tube in the chain. Upon the appearance of the next pulse on the triggering bus, conduction shifts to the next succeeding tube, and so on down through the whole chain of 32 tubes, and the process is repeated when the last tube readies the first tube for conduction. As each of the first 30 of the chain tubes fires in turn, it generates a sawtooth wave form which is added electrically to the input voltages for the channels. When the sum of these two voltages reaches a predetermined level (as it will at some time during the 100-microsecond interval) it will cause its corresponding pick-off thyratron to fire, producing a time-modulated output pulse. The greater the input voltage, the sooner the sum of the input voltage and sawtooth will reach the firing voltage. The output pulses from the various channels are collected on a common bus.

For synchronization of the time base generators at the ground station, a coded pulse group consisting of three pulses each separated by 7.9 microseconds is generated in a multivibrator circuit triggered by channel 32. This multivibrator has an inductance-capacitance ringing circuit in the plate of the normally on tube having a 7.9 microsecond period, with associated limiting and differentiating circuits. This output is combined with the channel video pulses on the common bus.

The output of the common bus triggers a blocking oscillator to form a 0.9-microsecond pulse, which is used to key on a coaxial inductance-band very high frequency cavity by means of a pair of *3E29* modulators. The output of this cavity feeds a 50-ohm line with an average pulse power of 4 kw at a frequency of about 1,025 megacycles per second.

For calibration each input channel is connected to its data input via a single-pole double-throw micro switch operated by a synchronized motor-driven cam unit. For about 2 per cent of the time, data input is removed from the input channel and a calibrating voltage, consisting of 1-volt steps from 0 to ±5 volts, is substituted, derived from a voltage-regulated source. This step voltage is repeated on each channel in sequence every ten seconds during flight. For any channel requiring continuous input data recording, this calibration can be removed.

For ease of dissassembly of the unit from the rocket, aircraft-type quick-disconnect straps are used for mounting, with a vee-ring pressure seal using similar quick-disconnect toggle snaps to seal the pressurized transmitter case to its top bulkhead. Figure 9 shows the *AN/DKT-2(XN-1)* telemeter transmitter set as used in V-2 rockets, with Figures 10 and 11 showing internal views of the set.

The total weight of the telemeter transmitter set, with batteries suitable for 30 minutes' operation, is about 130 pounds. Two Willard-type-*ER-8-28*, 28-volt plastic-cased storage batteries are used in conjunction with a vibrator-type converter unit to provide the various plate voltage and bias supplies, and four type-*ERH-25-2*, 2-volt plastic-cased storage batteries are used for the filament supplies. Total power requirements for the system are 15 amperes at 28 volts and 20 amperes at 8 volts.

Matrix Ground Station

Each ground station comprises four racks of two main types of unit. The monitor rack contains receiving and decoding apparatus as well as a monitoring oscilloscope. Three recording racks, all identical, are used with each ground station.

The ground station receives the recurrent train of pulses from the remote transmitter in a suitable receiver. The triple pulse is recognized by a discriminator and is used to generate a 10-kc matrix in exact phase with the matrix in the transmitter. From this, signals are obtained at any particular time in the matrix which are used to generate the sweep voltages for the cathode ray tubes on which the data are presented as intensity modulation. Pulses generated at the beginning of each matrix interval also are applied to the display and the scopes are photographed on a continuous-film camera. There results a graph of the variation of the input voltage with time, with

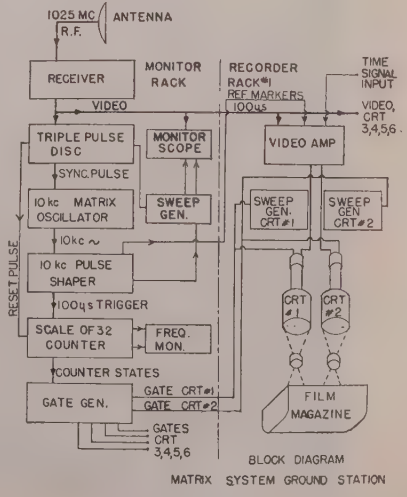

Figure 12. Block diagram matrix system ground station

reference lines (which do not vary in position) between each of the data lines.

Each ground display has six cathode ray tubes upon which the 30 data channels can be applied in any combination. Sweeps of appropriate duration and timing in respect to the triple pulse are so arranged that one tube after another is swept in succession until all channels are recorded. Additional information also is supplied on the record by the application of signals to the cathode ray tube to indicate time from a standard source.

Referring to the block diagram for the matrix-system ground station, Figure 12, main signal paths are indicated by heavy lines. The receiver delivers the video signal on two lines—to the recording racks and into the synchronizing pulse discriminator, where the triple pulse is recognized—and supplies a pulse which is used to phase- and frequency-lock the 10-kc matrix oscillator to the air-borne oscillator. The output of the oscillator is shaped and fed into the scale-of-32 binary counter. This counter operates in synchronism with the chain counter in the air-borne unit. It is reset by the synchronizing pulse, when necessary, so that particular states correspond in both units. By means of resistor networks from different stages of the counter, the state selector delivers a timed series of 100-microsecond long pulses to a patchboard on the panel of the unit. Suitable connections are made to the trigger and gate unit to form gates for controlling the sweep circuits in the recorder racks.

There are several auxiliary units in the monitor rack. The frequency monitor determines whether the matrix oscillator is operating on the proper harmonic of the 312.5-cycle synchronizing signal, and indicates the proper frequency by means of lights on the face of the unit. The monitor oscilloscope is used for adjustment of the units and for monitoring the signal during operation. It is swept from associated generators which are synchronized from 312.5-cycle and 10-kc pulse sources. Appropriate power supplies are included in the unit, as are switches to control the operation of the recording racks.

Each of the three recorder racks contains a double recording unit consisting of two type-*5RP11* cathode ray tubes and a continuous $9^1/_2$-inch film camera.

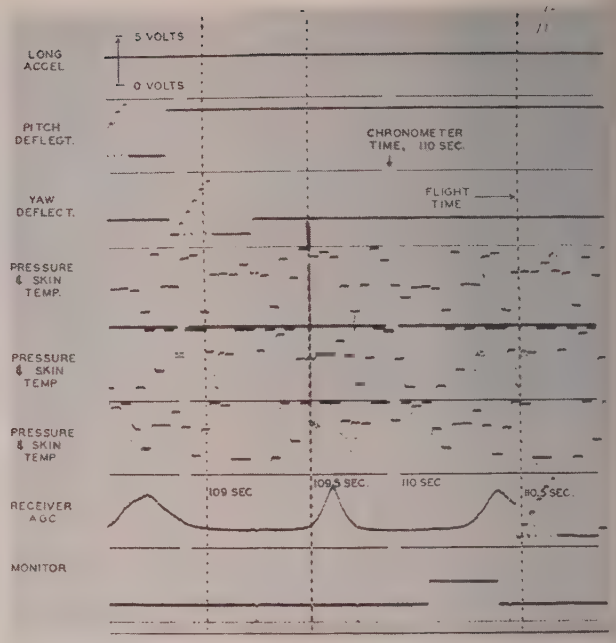

Figure 14. Typical record matrix telemetering system

Appropriately timed gates from the monitor rack allow sweep generators to operate one after another and, at the same time, unblank the cathode ray tube so that the video pulses from the receiver in the monitor rack can be presented as intensity modulation on the tube. Necessary video amplifiers are included in this unit, as are circuits for mixing the video with timing signals and with the reference pulses generated by the 10-kc matrix oscillator on the ground. There also are controls for positioning and focusing the cathode ray tubes, as well as necessary power supplies.

The image on the face of the cathode ray tubes is focused on a slit on the front plate of the unit by means of two lenses, placed side by side. A film magazine is placed so that the image from both tubes is recorded on it as the film is drawn continuously past.

The ground station operates on 110 volts, 60 cycles alternating current, with a power consumption of about 3,000 watts. Voltage regulation of the primary power for these units is obtained from Sola Constant Voltage transformers. All plate supplies under 600 volts are electronically regulated against load variations. The high voltage supolies required for the cathode ray tubes are $-2{,}000$ volts obtained from a conventional transformer-rectified unregulated circuit and $\pm 10{,}000$ volts obtained from an r.f. power supply operated from an electronically regulated 300-volt power supply.

Because of the complexity of the ground station circuits and the number of tubes involved, two complete and separate

Figure 13. Matrix system ground station at White Sands

ground stations are used for every flight.

In normal flights six $9^1/_2$-inch film records of about 120 feet in length are produced, corresponding to about 450 seconds of flight. These films give a complete graph of voltage versus time for all 30 channels and are reproduced in the form of black-line paper prints.

Figure 13 shows one of the two matrix-system ground stations as operated at White Sands, with a typical record section shown in Figure 14.

Telemeter transmitting units for both the sequential system and the matrix system were designed by the Naval Research Laboratory. The former was built by the Raytheon Manufacturing Company, the latter by the Hazeltine Electronics Corporation. All ground stations for both systems were designed and constructed at the Naval Research Laboratory. Present operation of the ground stations at White Sands is by a contract with personnel from the New Mexico College of Agriculture and Mechanic Arts, assisted by Naval and Marine technical personnel.

No Discussion

Some Design Criteria for Automatic Controls

PAUL T. NIMS
MEMBER AIEE

Synopsis: The design of automatic control systems to give "optimum" response is discussed in terms of the area between a step disturbance and the control response. It is shown that this "control area", and also a "weighted control area" may be calculated directly from the system parameters without finding the roots of an algebraic equation. Assumed optimum values of these areas permit direct synthesis of the necessary control sensitivities for an "optimum" control response. An example of an aircraft engine control is given and the connection with zero velocity error servos is shown.

IN RECENT years the analysis of automatic control systems has been discussed extensively from several standpoints. The earliest, and most direct, method is based on the solution of the differential equations of the system for some initial disturbance.[1,2] This transient analysis is perfectly general and, seemingly, may be applied to any problem which can be formulated in differential equations. However, even with the aid of the powerful methods of the Laplace transformation, synthesis of a complex control is a difficult process.

In synthesizing a control, the problem, after stability is achieved, usually is to choose the sensitivity factors, time lags, and inertias, which will give as rapid a response to disturbances as is consistent with reasonable deviations of the controlled variables. Obviously, the definition of reasonable varies with the application of the control, as will be discussed later. One author,[5] in order to facilitate calculations and permit the ready determination of constants of control systems, has calculated "standard forms" corresponding to linear differential equations up to the sixth order. These forms define a reasonable response for a special class of remote positioning controls.

Other authors have noticed the similarity between the equations of a particular class of automatic control systems and the equations of electrical amplifiers with a feedback connection. From this idea, the method of frequency response analysis has been developed into a useful tool for designing remote position controls.[3,4] The method considers the input to be a sinusoidal function of time and then determines the steady-state amplitude and phase relationships between the output and input over the important frequency range. The frequency response of an ideal system would have a flat amplitude response and a zero phase response over the entire frequency range. As this cannot be obtained, a general design rule used by A. C. Hall[6] is to limit the peaks of the amplitude response to from $1^1/_3$, to $1^1/_2$, and to place the predominant peak at a frequency at least three times the inverse of the period allowed for a transient to disappear. A more recent paper by H. Chestnut and R. W. Mayer[7] gives detailed design criteria of this type for certain classes of systems.

The frequency analyses method is widely used for the design of servomechanisms and is especially useful for single loop systems with feedback independent of frequency, as many graphical methods are available. However, some kinds of aircraft engine controls have two controlled quantities (speed and torque) and two variables available for control (propeller pitch and fuel flow). These quantities are interrelated within the powerplant in a complex way and are subject to step disturbances initiated by the pilot. For problems concerning this kind of regulators and governors, the transient analysis method is preferable; and it can be made to yield numerical information on the amount of overshoot of the controlled quantity.

Although, for many controls, a limit on this overshoot together with as rapid as possible a reduction in the magnitude of error is the criterion of design, these data cannot be entered directly into an equation which will give the needed control sensitivities. It has instead been necessary to analyze a series of designs for their transient behavior in order to find the sensitivities required.

For the case of controls analyzed by the transient method, it has been proposed that the "control area" be used as a design criterion.[8,15] That is, if the response is known to be overdamped, it is proposed to compute the area included between the curve of a step function disturbance and the response curve and attempt to minimize this quantity. Figure 1 shows the nature of this area for the

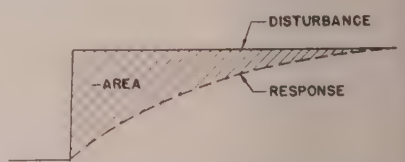

Figure 1. The control area for an over damped response to a step disturbance

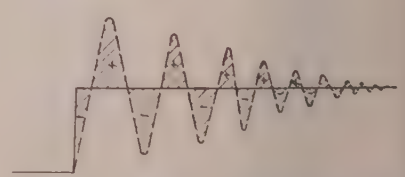

Figure 2. The effect of minimizing control area without regard to the degree of damping

Paper 51-99, recommended by the AIEE Feedback Control Systems Committee and approved by the AIEE Technical Program Committee for presentation at the AIEE Winter General Meeting, New York, N. Y., January 22–26, 1951. Manuscript submitted July 26, 1950; made available for printing December 14, 1950.

PAUL T. NIMS is with the Chrysler Corporation, Detroit, Mich.

This work was inspired by the lengthy and patient calculations carried on by the author's colleague, Alexander Chadwick. Discussions with Dr. A. W. Jacobson, of Wayne University, and with Dr. E. F. Trombly, of the University of Chicago, were also very helpful.

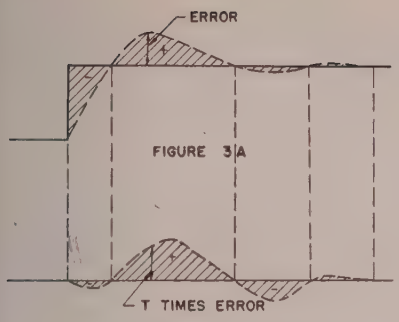

Figure 3(A). Control area for a typical underdamped response to a step disturbance Figure 3(B). Weighted control area for the above case

limiting case of a periodic response. However, many controls require a faster response, that is, slightly oscillatory, and further, the degree of damping obtained in a control is one of the unknown quantities in the problem. In fact, the criterion of minimum control area applied blindly is likely to give the result shown in Figure 2 where the response becomes more violently oscillatory as the net area approaches zero.

However, contemplation of the overshoot in this error curve suggests a more useful criterion than this control area. We can see that the initial error will always be present in many physical control systems, but the magnitude of the error at later times may be minimized by suitable selection of control sensitivities. Hence, study of an error curve weighted in accordance with some function of time would lead to a more useful criterion. One such weighted error curve would be simply t times the error, as shown in Figure 3. The criterion is then the "weighted control area." This quantity does not give any direct information about the magnitude of the overshoot following a step disturbance, nor about the response to sinusoidal disturbances, but the two control areas and a certain ratio of them (to be defined) give numerical measures of some of the properties of the response to step disturbances and are of use in the design of certain types of controls. This paper is concerned with the derivation and use of a simple formula for the weighted control area.

Formulation of a Typical Control Problem

Consider an automatic control system such as one that might be used to govern an aircraft engine. In Figure 4 the input quantities are the governor setting N^* and the engine torque Q_E and the output quantity is the engine speed N. In a more general problem there might be additional disturbing torques caused by variations in airspeed or even by an automatic control system for the engine torque; however, a simple problem will best show the method.

Figure 4 (left). Block diagram of a typical controlled system

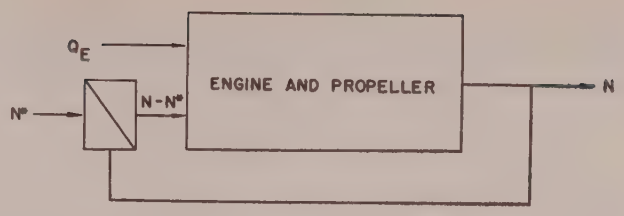

Inasmuch as the system is usually in balance before a change in operation takes place, it is convenient to write equations representing only the changes in the variables. That is, N^* is the change in governor setting and N is the change in speed. Under these conditions $N(0) = N'(0) = N''(0) = 0$ and the initial conditions of the differential equations are vastly simplified.

We may now write down the differential equations representing the accelerating torques on the engine, the behavior of the propeller governor chosen, the propeller load torque, and any time lags in the system. This gives a set of differential equations to be solved subject to an assumed disturbance to the controls or engine.

As mentioned above, the Laplace transformation is useful in solving the differential equations of control systems as it permits the substitution of a set of algebraic equations in a new variable S for the differential equations in t. It is treated in detail in several books[9,10] and only a few necessary theorems will be mentioned here. However, the definition of the transform is

$$L\{N(t)\} = n(S) = \int_0^\infty \epsilon^{-St} N(t)dt$$

provided the integral converges for some value of the complex variable S. And from this definition it may be shown that (for zero initial conditions)

$$L\{N'(t)\} = Sn(S)$$

$$L\{N''(t)\} = S^2 n(S)$$

and

$$L\left\{\int_0^t N(t)dt\right\} = \frac{n(S)}{S}$$

Thus the differential (or integral) equations representing the elements of our control system (initially in balance) may be replaced by algebraic equations by writing S^n for d^n/dt everywhere and $1/S$ for $\int_0^t$ where needed. The set of equations may then be solved by ordinary algebraic methods to give

$$n(S) = \frac{n^*(S)a(S) + q_E(S)c(S)}{b(S)}$$

where $a(S)$, $b(S)$, $c(S)$ are rational algebraic functions of the complex variable S. For a normal transient analysis, a step function change in governor setting would be made ($n^*(S) = 1/S$) or a step change in engine torque ($q_E(S) = 1/S$) and the inverse transformation of $n(S)$ computed by reference to a table of transform pairs. This requires factoring $b(S)$ into linear and quadratic factors, and is a laborious numerical procedure for complicated systems. Further, a numerical solution gives little information about the effect of various control parameters.

Without going through the inverse transformation, useful information still can be obtained. Stability can be examined by investigating the roots of $b(S) = 0$ by the Routh-Hurwitz criterion. Stable behavior will obtain if the real parts of the roots are negative.

Test Functions of Routh and Hurwitz

The real parts of the roots of $b(S) = b_n S^N + b_{n-1} S^{n-1} + \ldots . b_1 S + b_0 = 0$ will be negative provided:

1. All the terms have the same sign.
2. If b_n is positive, all the following are positive:

$$T_1 = b_{n-1}$$

$$T_2 = \begin{vmatrix} b_{n-1} & b_n \\ b_{n-3} & b_{n-2} \end{vmatrix}$$

$$T_3 = \begin{vmatrix} b_{n-1} & b_n & 0 \\ b_{n-3} & b_{n-2} & b_{n-1} \\ b_{n-5} & b_{n-4} & b_{n-3} \end{vmatrix}$$

and so forth, until a determinant identically zero is reached. The total number of test functions is usually equal to the degree of the equation.

For a third order system, we would have:

$$b_3 S^3 + b_2 S^2 + b_1 S + b_0 = 0$$

If all the coefficients are positive, T_1, is satisfied. T_2 will be positive if $b_2 b_1 > b_0 b_3$

and T_3 will be positive if $b_2b_1b_0 > b_0^2b_3$. If the coefficients are positive these last two criteria are identical. For higher order equations, more criteria of stability will have to be satisfied.

We may also examine the final value of $N(t)$, that is, its value as $t \to \infty$. The theorem of final value[10] states that:

$$\lim_{S \to 0} Sn(S) = \lim_{t \to \infty} N(t)$$

Provided that the real parts of the roots of $b(S)$ are not zero and negative, that is, provided that the system is stable.

For this case, if a unit step function change in governor setting and a unit step function change in engine torque are made ($n^*(S) = 1/S$ and $q_E(S) = 1/S$) we have:

$$n(S) = \frac{1}{S}\,\frac{a_mS^m + \ldots a_1S + a_0}{b_jS^j + \ldots b_1S + b_0} + \frac{1}{S}\,\frac{c_kS^k + \ldots c_1S + c_0}{b_jS^j + \ldots b_1S + b_0}$$

$$\lim_{S \to 0} Sn(S) = \frac{a_0}{b_0} + \frac{c_0}{b_0} = N(\infty)$$

The first term represents the response to a change in governor setting and should be equal to 1 for the kinds of governors commonly used for engine control. Hence, we choose $a_0 = b_0$. The second term is the final speed after a change in torque and should be zero with this type of governor. Hence, we choose $c_0 = 0$. Calculation of these two final values is usually merely a check on the formulation of the problem, as the control is chosen heuristically to achieve these results. With these proper final values the error at any time is $N(t) - 1$ for a unit step change in governor setting and no change in engine torque.

Computation of Control Areas

As was mentioned above

$$L\left\{\int_0^t N(\tau)d\tau\right\} = \frac{n(S)}{s}$$

Likewise

$$L\left\{\int_0^t [N(\tau) - 1]d\tau\right\} = \frac{n(S) - 1/S}{S}$$

Therefore the final value theorem gives

$$\lim_{t \to \infty} \int_0^t [N(\tau) - 1]d\tau = \lim_{S \to 0} S\left[\frac{n(S) - 1/S}{S}\right] = \lim_{S \to 0}\left[n(S) - \frac{1}{S}\right]$$

provided the integral exists. The integral will converge if $b(S) = 0$ has no roots with zero or positive real parts. This integral is the "control area" mentioned above, which we will call A_{10}.

$$A_{10} = \lim_{S \to 0}\left[\frac{1}{S}\,\frac{a(S)}{b(S)} - \frac{1}{S}\right] = \lim_{S \to 0}\left[\frac{a_mS^{m-1} + \ldots a_1 + \frac{a_0}{S} - b_jS^{j-1} - \ldots - b_1 - \frac{b_0}{S}}{b_jS^j + \ldots b_1S + b_0}\right]$$

If we remember that $a_0 = b_0$,

$$A_{10} = \frac{a_1 - b_1}{b_0}$$

In similar fashion, we may find the control area for a unit step change in torque, where the error is $N(t)$ as $c_0 = 0$

$$A_{00} = \lim_{S \to 0} L\left\{\int_0^t N(\tau)d\tau\right\} = \frac{c_1}{b_0}$$

provided the roots of $b(S) = 0$ are proper.

These control areas are easy to compute from the transform expression, but, as mentioned above, simply making them a minimum by adjusting the system parameters may give a wildly oscillating system.

Weighted Control Areas

Another theorem of Laplace transform theory[9] gives the transform of t times a time function:

$$L\{tN(t)\} = -\frac{d}{dS}n(S)$$

provided $n(S)$ exists. Therefore, for a step change in governor setting

$$L\{t[N(t) - 1]\} = -\frac{d}{dS}\left[n(S) - \frac{1}{S}\right]$$

and

$$L\left\{\int_0^t \tau[N(\tau) - 1]d\tau\right\} = -\frac{1}{S}\,\frac{d}{dS}\left[n(S) - \frac{1}{S}\right]$$

and

$$\lim_{t \to \infty} \int_0^t \tau[N'(\tau) - 1]d\tau = \lim_{S \to 0}\left\{-\frac{d}{dS}\left[n(S) - \frac{1}{S}\right]\right\}$$

provided the integral converges. This will be true if the roots of $b(S) = 0$ again have no zero or positive real parts. This is the Weighted Control Area A_{11}

$$A_{11} = \lim_{S \to 0}\left\{\frac{d}{dS}\left[\frac{a_mS^{m-1} + \ldots a_1S + \frac{a_0}{S} - b_jS^{j-1} - \ldots - b_1 - \frac{b_0}{S}}{b_jS^j \ldots b_1S + b_0}\right]\right\} = \frac{(a_1 - b_1)b_1 - (a_2 - b_2)b_0}{b_0^2}$$

In similar fashion we may find the Weighted Control Area for a step change in torque

$$A_{01} = \int_0^\infty tN(t)dt = \frac{c_1b_1 - c_2b_0}{b_0^2}$$

This now gives a choice of four "Areas" which we may compute readily from the transform, and which are related in some fashion to the "goodness" of the responses of the control.

Example of Use of Control Areas

As an example of the use of these quantities, let us consider a simple second order control system, comprising an aircraft engine and a propeller governor. Over a moderate range of engine speeds, the torque depends only on throttle setting and is independent of speed, that is, the change in engine torque Q_E is a constant for each change of throttle setting. However, the propeller torque is a function of both propeller blade angle and engine speed. For moderate changes, the following expression represents these effects well enough

$$Q_p = cN + dP$$

where N is the change in engine speed from an initial steady state, P is the change in propeller blade angle from an initial equilibrium position, and c and d are numerical coefficients. The difference in these two torques represents the torque available for acceleration

$$Q_E - Q_p = 2\pi I\frac{dN}{dt} = Q_E - cN - dP$$

Let us choose a simple governor, having what some servomechanism texts would call integral control.

$$P = K_1\int_0^t (N - N^*)dt$$

A more familiar form for the governor equation is

$$\frac{dP}{dt} = K_1(N - N^*)$$

In transform notation these equations are (remembering that all initial values are zero)

$$2\pi ISn(S) = q_E(S) - cn(S) - dp(S)$$

$$Sp(S) = K_1n(S) - K_1n^*(S)$$

These equations may be combined to give

$$n = \frac{n^*K_1d + Sq_E}{2\pi IS^2 + cS + K_1d}$$

We are now in a position to examine the response to a step function change in governor setting $n^* = 1/S$. The final value is 1, as was intended in choosing an

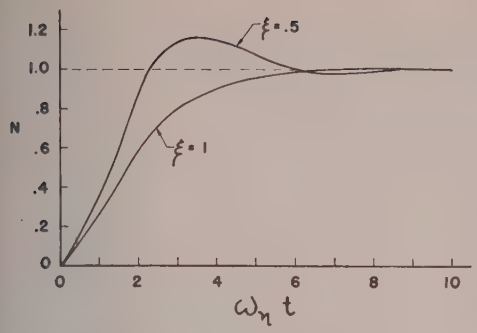

Figure 5 (left). Response of second order control system to step disturbance, showing two different damping ratios

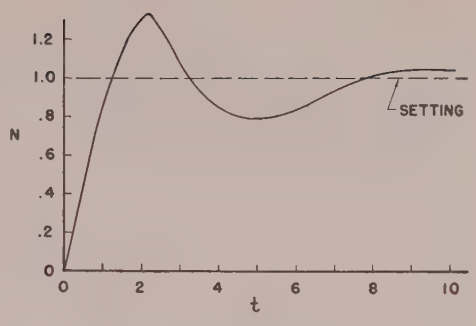

Figure 7 (right). Response to a unit step disturbance of a third order system with $A_{01}=0$ and $A_{11}=0$

integral control. The control area is

$$A_{10}=\frac{-c}{dK_1}$$

and the weighted control area is

$$A_{11}=\frac{2\pi I}{dK_1}-\left(\frac{c}{dK_1}\right)^2$$

We can change to a notation introduced by Draper[11] and used by Brown and Hall[12] by making the following substitutions

$$\xi=\frac{1}{2}\frac{c}{\sqrt{2\pi I dK_1}}$$

$$\omega_n=\sqrt{\frac{dK_1}{2\pi I}}$$

Here ξ is the damping ratio and equals unity for critical damping and ω_n is the undamped natural frequency. In this notation

$$n=\frac{n^*\omega_n^2}{S^2+2\xi\omega_n S+\omega_n^2}$$

and

$$A_{10}=\frac{-2\xi}{\omega_n}$$

$$A_{11}=\frac{1-4\xi^2}{\omega_n^2}$$

To see the effects of varying these we may write the inverse transformation for ξ less than unity.

$$N(t)=1-\epsilon^{-\xi\omega_n t}[\cos\omega_n\sqrt{1-\xi^2}t+\xi\sin\omega_n\sqrt{1-\xi^2}t]$$

This can be plotted in nondimensional form of amplitude versus ω_n for various values of ξ. For $\xi=1$ we have the case of critical damping

$$n=\frac{n^*\omega_n^2}{(S+\omega_n)^2}$$

$$N(t)=1-(1+\omega_n t)\epsilon^{-\omega_n t}$$

Figure 5 shows $N(t)$ for $\xi=1$ and $\xi=0.5$. The latter value corresponds to $A_{11}=0$ and represents a reasonable response for this engine control system. By accepting some overshoot we have obtained a more rapid response.

Example of a Third Order System

As an example of a more complicated system let us consider a governor with two orders of sensitivity and with a time lag in the response of the propeller pitch to the governor output. That is, let

$$dG/dt=K_1(N-N^*)+K_2dN/dt$$

and

$$\tau dP/dt+P=G$$

where G is the governor output signal and depends not only on the error in speed but also on engine acceleration, and τ is the time constant of propeller pitch response.

In transform notation the set of equations becomes

$$2\pi I Sn=q_E-cn-dp$$
$$Sg=K_1(n-n^*)+K_2Sn$$
$$p(\tau S+1)=g$$

This gives

$$n=\frac{S(\tau S+1)q_E+dK_1n^*}{2\pi I\tau S^3+(2\pi I+c\tau)S^2+(dK_2+c)S+dK_1}$$

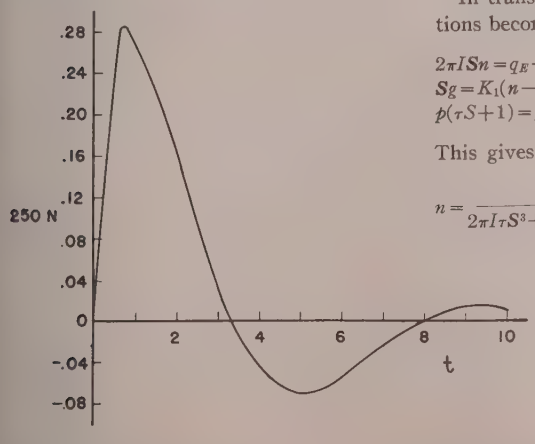

Figure 6. Response to a unit change in torque of a third order system with $A_{01}=0$ $A_{11}=0$

Consider a step change in governor setting and no change in throttle position.

$$n^*=1/S$$
$$q_E=0$$

$$A_{10}=\frac{-(dK_2+c)}{dK_1}$$

$$A_{11}=\frac{dK_1(2\pi I+c\tau)-(dK_2+c)^2}{d^2K_1^2}$$

If we choose $A_{11}=0$

$$(dK_2+c)^2=dK_1(2\pi I+c\tau)$$

$$K_1=\frac{(dK_2+c)^2}{d(2\pi I+c\tau)}$$

This gives one relationship connecting K_1 and K_2 with the fixed constants of the engine and another is needed. (Note that for $\tau=0$ the equation is still useful.)

In order to find a relationship between K_1 and K_2, other than the maximum permissible values set by the Routh-Hurwitz criterion, consider the effect of a step change in throttle setting. That is, let $q_E=1/S$ and $n^*=0$. For this case

$$n=\frac{1}{S}\frac{(\tau S^2+S)}{2\pi I\tau S^3+(2\pi I+c\tau)S^2+(dK_2+c)S+dK_1}$$

and the final value is zero, as it should be

$$A_{00}=\frac{1}{dK_2+c}$$

$$A_{01}=\frac{dK_2+c-\tau dK_1}{(dK_1)^2}$$

If we put $A_{01}=0$ then

$$dK_2+c=dK_1\tau$$

Combining this with the relationship from A_{11} we have

$$K_1=\frac{2\pi I+c\tau}{d\tau^2}$$

$$K_2=\frac{2\pi I}{d\tau}$$

To use these relationships it is convenient to have numerical values for the quantities and a convenient set of data were given by Weiss[13] in connection with a similar problem. These data are

listed in Table I. The values of velocity and altitude are given to indicate their effects on the "numerical constants" and the values of N and P are the steady-state values before initiation of the transient. Using data of Case I of Table I in the expressions for K_1 and K_2 we obtain

$K_1 = 1.09$
$K_2 = 0.289$

For a unit step change in torque and these values of K_1 and K_2

$$n = \frac{S+0.695}{250(S+3.125)[(S+0.327)^2+(0.689)^2]}$$

by inverse transformation

$$N = \frac{1}{250}[0.292\epsilon^{-0.327t}\cos 0.689t - 0.292\epsilon^{-3.125t} + 0.265\epsilon^{-0.327t}\sin 0.689t]$$

and this is plotted in Figure 6. Similarly for a step change in governor setting $n^* = 1/S$, we have:

$$n = \frac{1.82}{(S+3.125)[(S+0.327)^2+(0.689)^2]}$$

By inverse transformation

$$N = 1 - 0.07\epsilon^{-3.125t} - 0.93\epsilon^{-0.327t}\cos 0.689t - 0.76\epsilon^{-0.327t}\sin 0.689t$$

and this value is plotted in Figure 7. There is considerable overshoot here even though the weighted control area is zero. As a check on the method, several other values of K_1 and K_2 were tried with the same weighted area, but no substantial improvement in overshoot could be obtained.

It is interesting to compare the weighted area criterion with the Routh-Hurwitz criterion which requires:

1. All coefficients in the denominator positive
2. $b_1 b_2 > b_3 b_0$ or $(dK_2+c)(2\pi I+c\tau) > 2\pi I\tau dK_1$

When these two values are equal, we have a curve defining the stability limit.

In Figure 8, K_2 is plotted versus K_1 to show the relationship which must be maintained between the two orders of sensitivity. It may be seen that any value on the solid curve from $K_1 = 0$ up to K_1 maximum will give a "good" response, in the sense of weighted control area. The larger values of K_1 should give a faster response and possibly more overshoot, but values larger than that defined by the dotted curve will give sustained oscillation.

Another Example

As an example of a system which gives a transform expression of another type, consider the transient response of a special thermocouple circuit having three thermocouples connected in series, two aiding and the third bucking. This construction was proposed by Dahl and Fiock[14] to increase the initial rate of response of the system. If E is the reading of a thermocouple exposed to a hot gas stream of temperature T the following equation is obeyed

$$\frac{1}{a}\frac{dE}{dt} + E = T$$

where $1/a$ is related to the mass of the thermocouple and its heat transfer coefficient from the gas and is the time constant of the unit. If the gas temperature is zero initially and is suddenly changed one degree, then in transform notation we have

$$\left(\frac{1}{a}S+1\right)e = \frac{1}{S}$$

or

$$e = \frac{1}{S}\,\frac{a}{S+a}$$

Table I. Data for Example (adapted from Weiss)[13]

	Case I	Case II
Velocity, miles per hour	250	0
Altitude, feet	8,700	Sea level
N, revolutions per second	24.1	24.1
P, degrees	29	18
$c/2\pi I$	3.08	1.24
$d/2\pi I$	2.40	2.43
$2\pi I$	250	250
τ	1.44	1.44

NOTE: Engine is Wright *R-1820 G-3* geared 16:11 delivering 840 bhp at 2,100 rpm and 8,700 ft. Prop diam 12 ft. Inertia of combination referred to prop 40.4 lb. ft. sec.^{2}

If there are three couples in series, and the two aiding couples have time constant $1/a$ while the bucking couple has time constant $1/b$ then

$$e = \frac{1}{S}\,\frac{a}{S+a} + \frac{1}{S}\,\frac{a}{S+a} - \frac{1}{S}\,\frac{b}{S+b}$$

$$= \frac{1}{S}\,\frac{(2a-b)S+ab}{S^2+(a+b)S+ab}$$

Here

$$A_{10} = a - 2b/ab$$

and there is a possibility of making $A_{10} = 0$. This requires $a = 2b$ and gives the response curve shown in Figure 9. Also $A_{11} = (a^2-2b^2)/a^2b^2$, and when this is zero $a = \sqrt{2}b$ and the response curve for this is also shown, together with the curve for $a = b$ which corresponds to three identical couples. (This is the same as a curve for one couple alone, due to the bucking connection.)

Other Relationships

There are two other relationships among the four areas which are of occasional use. One is the ratio:

$$R = \frac{A_{11}}{(A_{10})^2} = \frac{(a_1-b_1)b_1-(a_2-b_2)b_0}{(a_1-b_1)^2}$$

This gives a number which is not too

Figure 8 (left). Comparison for a particular control of the weighted control area criterion with the Routh-Hurwitz criterion

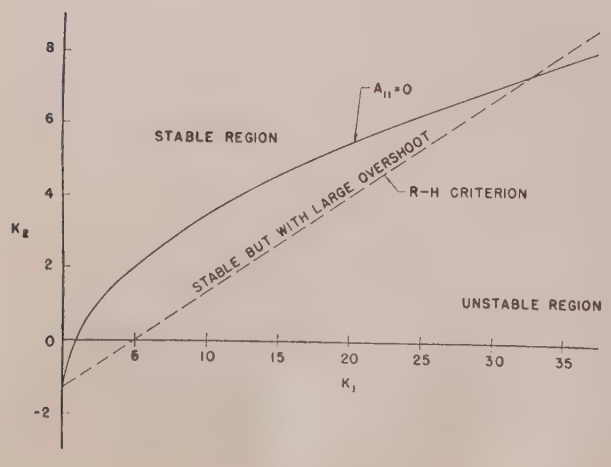

Figure 9 (below). Response curves of another type of control showing effect of different values of control areas

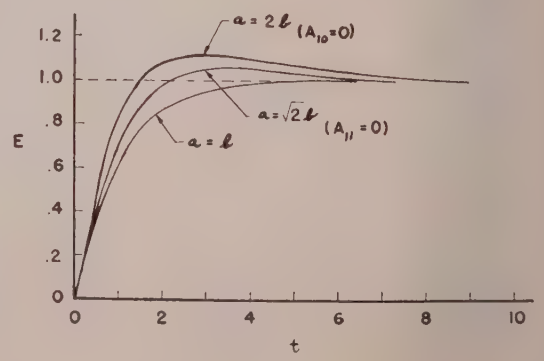

strongly dependent on b_0, the product of all the roots of $b(S)$, and may be used in those cases when it is not desirable to make $A_{11}=0$. A typical value for R is $-1/2$, and in the second order case mentioned above, this leads to a damping ratio $\xi=0.707$.

Sometimes we are not interested in the net area between a response and the step input to the control but rather the net area between the response and some "ideal" response. In such a case, it may be shown that the net area between the response and the ideal is equal to the difference of the net areas between the response and the step and between the ideal and the step. This is not surprising, as the equations are all linear. The result is also true for weighted areas, and permits rapid computation of any special control areas desired when the transform of the "ideal" response is known.

Remote Position Controls

Servomechanisms are often used to position an output shaft in accordance with the position of an input shaft. These devices, like the controls we have discussed, have inertia, time lags, damping, and control sensitivities. They may be characterized by differential equations and written in transform notation. When the transformed equations are simplified, expressions of the following type occur

$$\theta_0=\frac{a(S)}{b(S)}\theta_1$$

where θ_0 is the transform of the angular position of the output shaft and θ_1 is the transform of the angular position of the input shaft.

If the input shaft is given a unit step change in position

$$\theta_0=\frac{a(S)}{b(S)}\frac{1}{S}$$

and the final value of this expression is a_0/b_0. Hence $a_0=b_0$ for zero final error due to a constant displacement. Such a system is said to have zero displacement error.

If the input shaft is moved with constant velocity so that $\theta_1(t)=t$ and $\theta_1(S)=1/S^2$. Then

$$\theta_0=\frac{a(S)}{b(S)}\frac{1}{S^2}$$

and the error in displacement is

$$\theta_0-\theta_1=\frac{1}{S^2}\left(\frac{a(S)}{b(S)}-1\right)$$

The final value of this error is $(a_1-b_1)/b_0$ (provided that $a_0=b_0$) and hence, a system with $a_1=b_1$ and $a_0=b_0$ has a zero final error due to a constant velocity input. This is also exactly the condition for $A_{10}=0$. This is called a zero velocity error system in the literature.[5]

Similarly, it may be shown that, if the input shaft is given a constant acceleration, it will have a zero final position error if $a_2=b_2$ as well as $a_1=b_1$ and $a_0=b_0$. Such a system is called a zero acceleration error system. Note that such a system has

$$A_{11}=\frac{(a_1-b_1)b_1-(a_2-b_2)b_0}{{b_0}^2}=0$$

However, the converse is not true, A_{11} may be zero without the system having zero acceleration error.

Conclusion

Certain theorems have been developed relating in an especially simple manner the areas under control response curves to the Laplace transforms of these curves. The various "control areas" defined thereby are related, in a general way, to the "goodness" of the response curves of a control system. Hence, numerical values (usually zero) can be assigned to the areas in question and the resulting equations supply useful relationships between the parameters in a typical control design problem.

References

1. Directional Stability of Automatically Steered Bodies, **N. Minorsky.** *Journal*, American Society of Naval Engineers (Washington, D. C.), volume 34, number 2, May 1922, pages 280–309.

2. Theory of Servomechanisms, **H. L. Hazen.** *Journal*, Franklin Institute (Philadelphia, Pa.), volume 218, September 1934, pages 279–331; 543–80.

3. Principles of Servomechanisms (book), **Gordon S. Brown, Donald P. Campbell.** John Wiley and Sons, Inc., New York, N. Y., 1948.

4. Theory of Servomechanisms (book), edited by **Hubert M. James, Nathaniel B. Nichols,** and **Ralph S. Phillips,** under the supervision of the Office of Scientific Research and Development, National Defense Research Committee. McGraw-Hill Book Co., Inc., New York, N. Y., first edition, 1947.

5. Theory of Servo Systems, **A. L. Whitely.** *Journal*, Institution of Electrical Engineers (London, England), volume 93, part II, August 1946, pages 353–67.

6. Application of Circuit Theory to the Design of Servomechanisms, **Albert C. Hall.** *Journal*, Franklin Institute (Philadelphia, Pa.), volume 242, October 1946, pages 279–307.

7. Comparison of Steady-State and Transient Performance of Servomechanisms, **Harold Chestnut, Robert W. Mayer.** *AIEE Transactions*, volume 68, part I, 1949, pages 765–77.

8. The Dynamics of Automatic Controls, (book), **Rudolf Carl Oldenbourg, H. Sartorius** translated and edited by **H. L. Mason.** American Society of Mechanical Engineers, New York, N. Y., 1948.

9. Modern Operational Mathematics in Engineering (book), **Ruel V. Churchill.** McGraw-Hill Book Company, Inc., New York, N. Y., 1944.

10. Transients in Linear Systems Studied by the Laplace Transformation (book), **Murray Frank Gardner, John L. Barnes.** John Wiley and Sons, Inc., New York, N. Y., 1942.

11. Design Factors Controlling the Dynamic Performance of Instruments, **C. S. Draper, G. P. Bentley.** *Transactions*, American Society of Mechanical Engineers (New York, N. Y.), volume 62, July 1940, pages 421–32.

12. Dynamic Behavior and Design of Servomechanisms, **G. S. Brown, A. C. Hall.** *Transactions*, American Society of Mechanical Engineers (New York, N. Y.), volume 68, July 1946, pages 503–24.

13. Dynamics of Constant-Speed Propellers, **Herbert K. Weiss.** *Journal of the Aeronautical Sciences*, Institute of the Aeronautical Sciences (New York, N. Y.), volume 10, January-October 1943, pages 58–67, 70.

14. Shielded Thermocouples for Gas Turbines, **A. I. Dahl, E. F. Fiock.** *Transactions*, American Society of Mechanical Engineers (New York, N. Y.), volume 71, February 1949, pages 153–61.

15. A Note on Control Area, **Thomas M. Stout.** *Journal of Applied Physics* (New York, N. Y.), volume 21, November 1950, pages 1129–31.

No Discussion

Effects of Carrier Shifts on Derivative Networks for A-C Servomechanisms

GEORGE M. ATTURA
MEMBER AIEE

THE CARRIER frequency servo can be stabilized by shaping the frequency response of the servo amplifier. The networks more commonly used are the parallel T, the bridged T, and the series resonant resistance-inductance-capacitance circuit. The resultant frequency transmission has a minimum value at some frequency, ω_0, and rises sharply for values above and below it. The damping introduced by this shaped frequency response approximates that which would be obtained if the servo amplifier were to drive the motor with both the error voltage and its first derivative.

The ω_0 of these networks generally is designed to coincide with the carrier frequency, ω_c. The symmetry of this frequency response about ω_0, and the fact that the minimum transmission occurs at this frequency, may suggest that the damping introduced will be reduced if the carrier drifts away from ω_0. This problem is a very real one, since the servo loops in many air borne installations derive their power from inverters whose output frequency is not well regulated.

It is the purpose of this paper to discuss the effects of carrier shifts on the damping action of these a-c derivative networks, when they are followed by phase-sensitive actuators or motors. The network output, when the circuit is driven by sinusoidal modulation, will be resolved into its components, whose passage through the servo motor will then be studied. It will be shown that the damping introduced by the shaped frequency response in combination with the servo motor is not destroyed by relatively large carrier shifts. Experimental studies will be cited to confirm this conclusion.

Paper 51-100, recommended by the AIEE Feedback Control Systems Committee and approved by the AIEE Technical Program Committee for presentation at the AIEE Winter General Meeting, New York, N. Y., January 22-26, 1951. Manuscript submitted July 25, 1950; made available for printing December 13, 1950.

GEORGE M. ATTURA is with the Industrial Control Company, Long Island City, N. Y.

The author wishes to acknowledge the help extended by Mr. CHARLES REHBERG, Associate Professor of Electrical Engineering, New York University. This paper is an abstract of a thesis submitted in partial fulfillment of the requirements for the Degree of Master of Electrical Engineering, College of Engineering, New York University.

The Derivative Network with Centered Carrier Frequency

$H(j\omega)$ of Several Networks

In the vicinity of ω_0 the carrier frequency response, $H(j\omega)$, of the networks mentioned above, has the same approximate general form for each one. For the parallel T of Figure 1,[3] we have

$$H(j\omega) = j\frac{\delta}{2\omega_0} \tag{1}$$

For the bridged T[4] of Figure 2

$$H(j\omega) = \frac{2}{p^2+2} + j\frac{2p}{(p^2+2)^2}\cdot\frac{\delta}{\omega_0} \tag{2}$$

and for the series resonant circuit[5] of Figure 3

$$H(j\omega) = \frac{R_L}{R_1+R_L} + j\left[\frac{2\omega L}{R_1+2R_L}\right]\frac{\delta}{\omega_0} \tag{3}$$

where

$$\delta = \omega_c - \omega_0 \tag{4}$$

In all three cases there exists a reactive term that varies with frequency. In addition, the bridged T and the resistance-inductance-capacitance circuit have an invariant real term. It will be shown later that the reactive term generates the derivative component, while the real term provides the one proportional to the error itself. The symmetrical, full-rejection parallel T shown in Figure 1 does not give a proportional term. This must be obtained either with a by-pass path or through a modification of the circuit values of the T.[2]

When the carrier frequency, ω_c, is centered on ω_0, δ becomes zero, and the reactive term disappears. Hence, the real term is the transmission at ω_0, or the gain of the network with centered carrier.

The generalized form of the carrier frequency transfer function for the proportional plus derivative a-c network can be written as

$$H(j\omega) = R + jK\delta \tag{5}$$

This is shown in Figure 4.

Relation between $H(j\omega)$ and $G(j\omega_d)$

The $H(j\omega)$ of a network determines its carrier frequency response. However, to analyze the effect of the network on the performance of the servo, it is necessary to determine its data frequency transfer function, $G(j\omega_d)$. The latter concerns itself with the effect of the network on the servo error intelligence passing through it.

The $G(j\omega_d)$ can be derived from the $H(j\omega)$ by a method discussed by A. Sobczyk.[1] This is an important transformation, since the $H(j\omega)$ is the more easily determined network characteristic, while the $G(j\omega_d)$ is the one important in the servo stabilization problem. This transformation is reviewed in the following paragraphs.

If a network is driven by a suppressed carrier sinusoidal modulation of ω_c (the form in which error intelligence appears

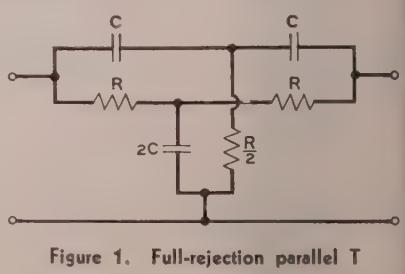

Figure 1. Full-rejection parallel T

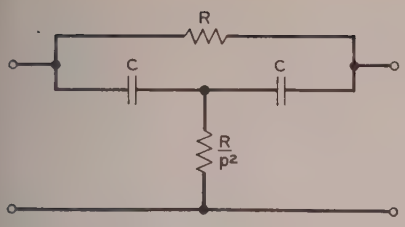

Figure 2. Bridged T

in an a-c servo), the output of the network will yield its $G(j\omega_d)$. The driving voltage has the form

$$e_i = E \cos \omega_d t \cos \omega_c t \quad (6)$$

which can be expressed as

$$e_i = \frac{E}{2}[\cos (\omega_c+\omega_d)t + \cos (\omega_c-\omega_d)t] \quad (7)$$

$$= \frac{E}{2}[\cos \omega_u t + \cos \omega_l t] \quad (8)$$

Here, ω_d is the data frequency; ω_u the upper sideband $(\omega_c+\omega_d)$; and ω_l the lower sideband $(\omega_c-\omega_d)$.

The output of a network driven by this modulation will be

$$e_o = \frac{E}{2}(A_l+A_u) \cos (\omega_d t+\phi_d) \cos (\omega_c t+\phi_c) + \frac{E}{2}(A_l-A_u) \sin (\omega_d t+\phi_d) \times \sin (\omega_c t+\phi_c) \quad (9)$$

where

$A_l = |H(j\omega_l)|$
$A_u = |H(j\omega_u)|$
$\phi_l = \angle H(j\omega_l)$
$\phi_u = \angle H(j\omega_u)$

ϕ_d = data phase shift $= \dfrac{\phi_u - \phi_l}{2}$

ϕ_c = carrier phase shift $= \dfrac{\phi_u + \phi_l}{2}$

Equation 9 consists of two distinct modulation terms, each identical in form to the driving voltage e_i. The various amplitudes and phase shifts are determined directly from the $H(j\omega)$ of the network. The two terms are in exact quadrature with each other. The first component Sobczyk[1] called the signal envelope, and the second, the quadrature term. The latter also has been called the distortion term, since it changes the waveshape of the network output from that of the driving voltage, equation 6.

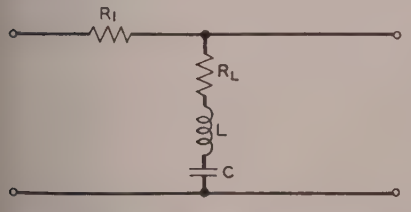

Figure 3. Series resonant resistance-inductance-capacitance circuit

The $G(j\omega_d)$ of a network concerns itself with the ϕ_d and the envelope amplitudes, expressed as functions of the data frequency, ω_d. The distortion term seemingly complicates the analysis, for there are two envelopes which could be demodulated in the motor and have torque components acting on the load.

However, the $G(j\omega_d)$ of the network alone has little importance. The amplified error voltages will drive some carrier frequency actuator, such as a 2-phase induction motor or a phase detector. The phase discrimination of these actuators must be considered here. These devices all exhibit an output torque or voltage which is either a sine or cosine function of the phase angle, θ, between the reference and error voltage. Thus,

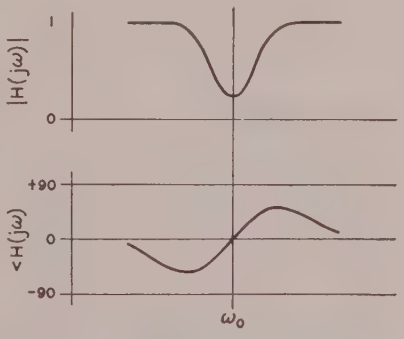

Figure 4. Carrier frequency transfer function of proportional plus derivative network

the stall torque of such a motor will be proportional to sin θ, and the d-c output of a phase detector to cos θ.

Because of this, the motor will develop no net torque for in-phase voltages across the control winding. Similarly, the phase detector will have no d-c component in its output for voltages in quadrature with the reference voltage.

The signal and distortion terms of equation 9 have carrier phases in exact quadrature with each other. If the reference voltage is adjusted to give a maximum torque for the signal envelope, then the distortion term will produce no net torque and will contribute nothing to the $G(j\omega_d)$ of the network.

It is for this reason that the resolution of equation 9 is chosen. The separation into signal and quadrature components allows ready recognition of the role of the servo motor and permits a fairly simple analysis of these networks.

$G(j\omega_d)$ of Derivative Networks with Centered Carrier Frequency

The generalized $H(j\omega)$ for the networks under discussion is given by equation 5.

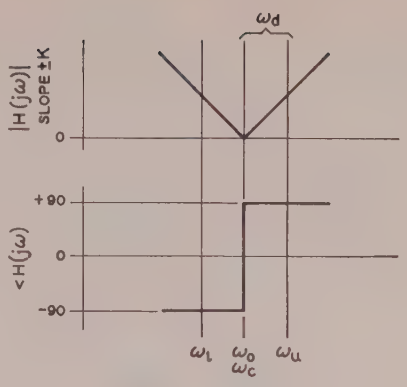

Figure 5. Plot of $jK\delta$

For this analysis, it will be assumed that this transfer function is generated by two parallel circuits. One will establish the real term R, and the other, the reactive term $jK\delta$. The path which establishes the real term must have a frequency characteristic in the vicinity of ω_0 of constant amplitude and zero phase shift. Because of this, it will contribute nothing to any effects which may be observed when the carrier shifts. Hence, we may neglect the real term of equation 5 and determine the damping action of these networks by studying the $G(j\omega_d)$ of the reactive path in combination with the motor or phase detector.

Figure 5 shows the $H(j\omega)$ of the reactive term, $jK\delta$. The disposition of the upper and lower sidebands is shown for the data frequency, ω_d, and with the carrier centered on ω_0. By inspection, the principal terms of the output of the reactive path may be tabulated.

$\phi_d = 90$ degrees
$\phi_c = 0$
$\dfrac{A_l+A_u}{2} = A_u = K\omega_d$
$\dfrac{A_l-A_u}{2} = 0$

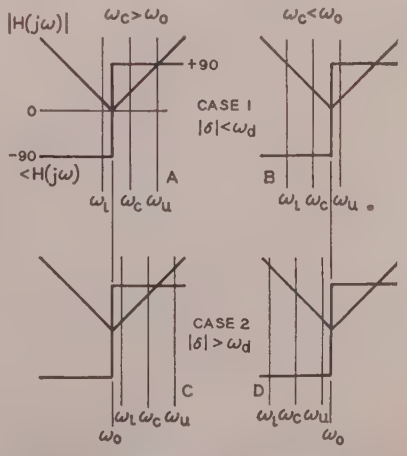

Figure 6. Disposition of sidebands on $jK\delta$ for all possible values of δ

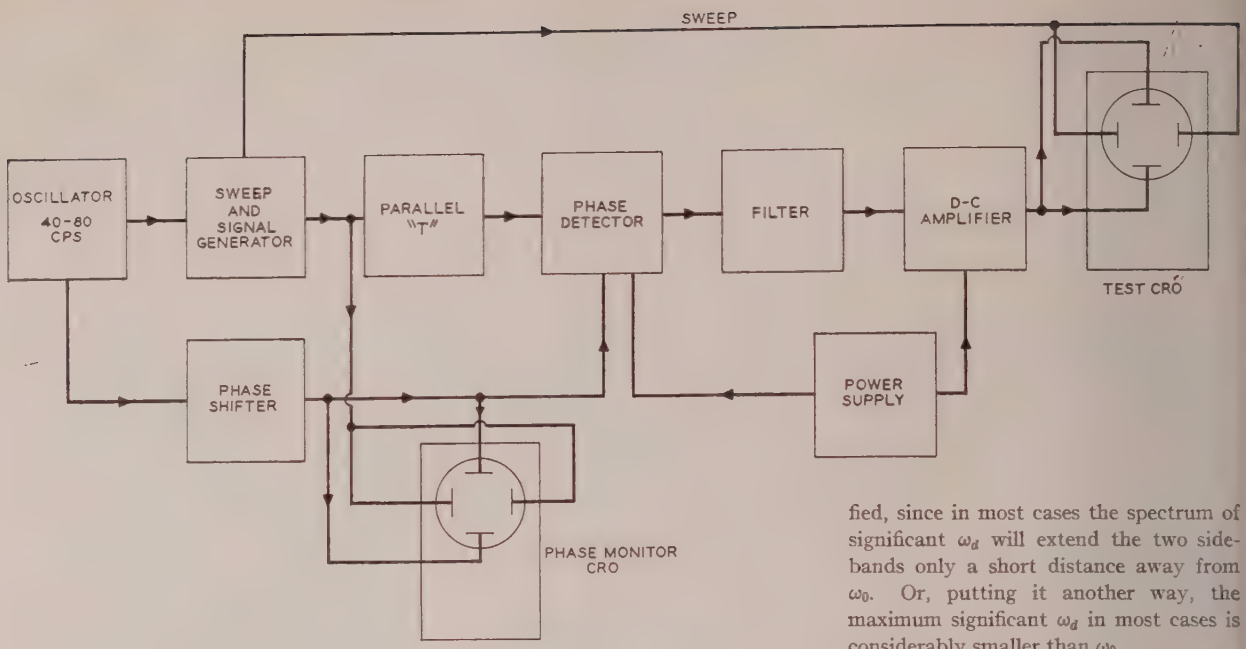

Figure 7. Experimental equipment

Since the amplitude of the quadrature envelope is zero, the analysis is simplified considerably. In this case, the phase discrimination of the phase detector is not needed. The $G(j\omega_d)$ may be written as

$$G(j\omega_d) = jK\omega_d \tag{10}$$

This is the transfer function of a true derivative device and accounts for the terminology used in this paper. The proportional plus derivative transfer function would be

$$G(j\omega_d) = R + jK\omega_d \tag{11}$$

This $G(j\omega_d)$, when used in the error path of a carrier frequency amplifier, would damp the loop with error rate control.

The preceding analysis holds only for frequencies near ω_0, since the $H(j\omega)$ of equation 5 does not apply outside of this region. The exact $H(j\omega)$ is sufficiently complex to make analysis of the $G(j\omega_d)$ difficult. This simplification is justified, since in most cases the spectrum of significant ω_d will extend the two sidebands only a short distance away from ω_0. Or, putting it another way, the maximum significant ω_d in most cases is considerably smaller than ω_0.

The Carrier Frequency Shift Problem

Effect of the Carrier Shift on the Derivatives $G(j\omega_d)$

It has been shown in the preceding section that the carrier frequency derivative damping is introduced by an

Figure 8. Schematic phase detector, filter and d-c amplifier

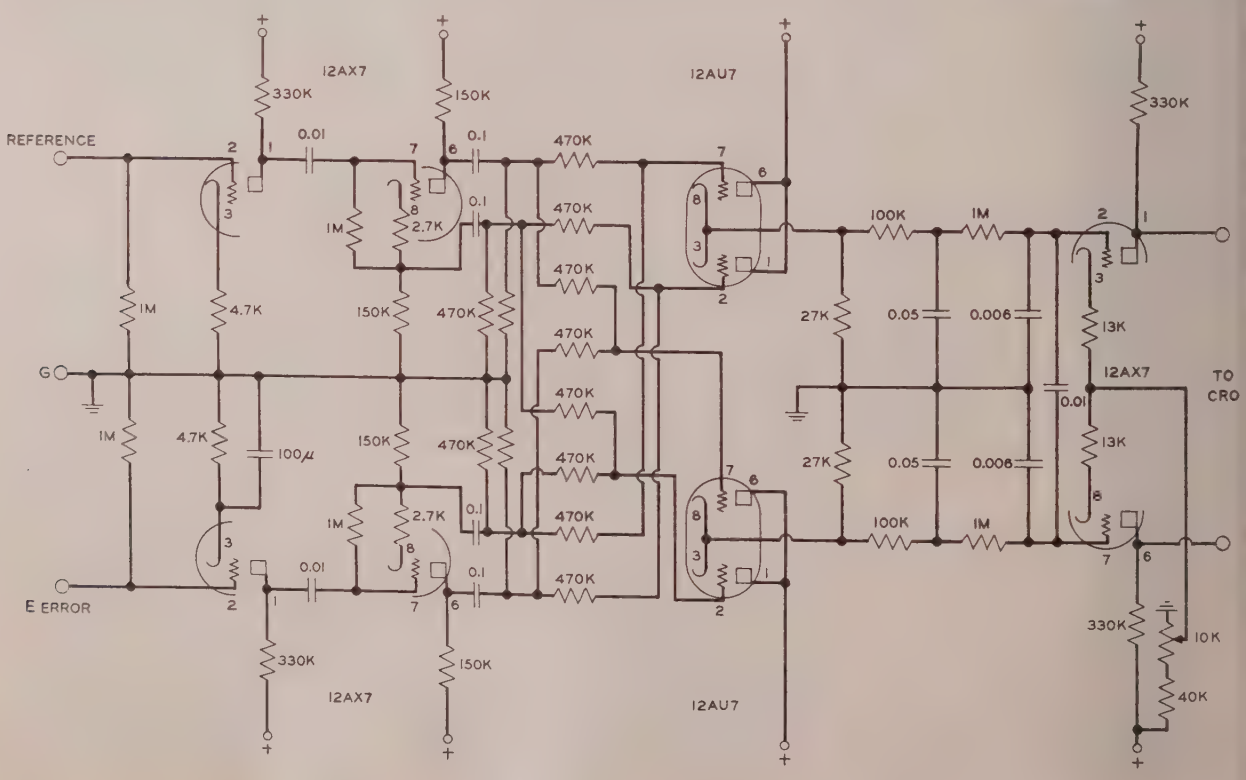

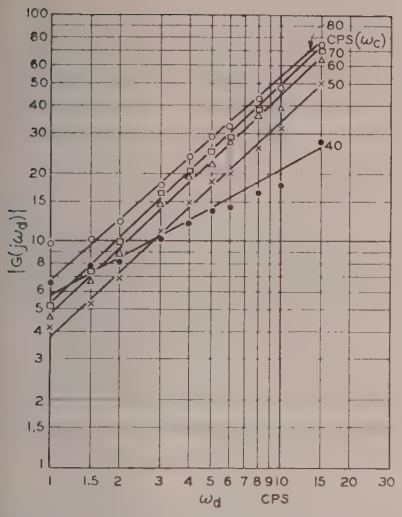

Figure 9. $|G(j\omega_d)|$ of a full-rejection parallel T tuned to 60.0 cycles per second

$H(j\omega)$ of the form of equation 1 when ω_c is centered, and that the addition of an invariant real term gave the necessary proportional plus derivative characteristic. We can study the effect of the carrier swing on the derivative $G(j\omega_d)$ alone and then extend our analysis to include the proportional plus derivative case.

Two general cases must be considered in this analysis: $|\delta|<\omega_d$ (case 1); and $|\delta|>\omega_d$ (case 2).

The disposition of the sidebands on the $H(j\omega)$ under consideration is shown in Figure 6 for both the above cases, and for both positive and negative δ.

With the aid of equation 9, the $G(j\omega_d)$ can be found for both cases shown. The procedure shall be to determine the principal terms of equation 9 in each of the two cases, tabulate them, and from this table write the $G(j\omega_d)$. This will be the actual transfer function between the input to the derivative network, and the motor torque.

In case 1 (Figure 6A and 6B) the sidebands ω_u and ω_l always fall on opposite sides of ω_0. Hence

$$\phi_d=\frac{90-(-90)}{2}=90°$$

$$\phi_l=0$$

$$\frac{A_l+A_u}{2}=K\omega_d$$

$$\frac{A_l-A_u}{2}=-K\delta$$

For case 2 (Figures 6C and 6D) both sidebands fall on the same side of ω_0. This gives

$$\phi_d=0$$

$$\phi_c=+90° \text{ for } \omega_c>\omega_0$$
$$\quad -90° \text{ for } \omega_c<\omega_0$$

$$\frac{A_l+A_u}{2}=K|\delta|$$

$$\frac{A_l-A_u}{2}=\begin{matrix}K\omega_d \text{ for } \omega_c>\omega_0\\ K\omega_d \text{ for } \omega_c<\omega_d\end{matrix}$$

This material is tabulated in Table I.

Now we can establish the $G(j\omega_d)$ for the motor or phase detector sensitive to one or the other of the two possible preferred phases. For sensitivity to $\cos\omega_c t$ the following is true:

1. When $|\delta|<\omega_d$, $\phi_c=0$, and the only component at the output of the motor will be that due to the signal envelope. The carrier phase of the distortion term will be $\sin\omega_c t$, and it will be suppressed. Taking the appropriate values from Table I, the complete expression for the signal envelope will be

$$K\omega_d\cos(\omega_d t+90)\cos\omega_c t \qquad (12)$$

and its demodulated torque output

$$K\omega_d\cos(\omega_d t+90) \qquad (13)$$

2. When $|\delta|>\omega_d$, $\phi_c=\pm 90°$, and now the distortion term will have the preferred phase, with the signal envelope producing no net torque output. Again taking the appropriate values from Table I, the distortion term will be

$$\mp K\omega_d\sin\omega_d t\sin(\omega_c t\pm 90)$$
$$=K\omega_d\cos(\omega_d t+90)\cos\omega_c t \qquad (14)$$

and its demodulated torque output

$$K\omega_d(\cos\omega_d t+90) \qquad (15)$$

Equations 13 and 15 are identical. They represent the demodulated output

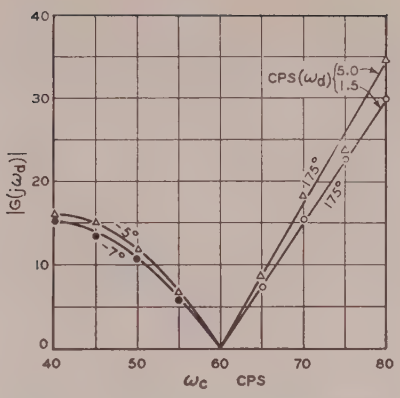

Figure 11. $G(\omega j_d)$ with sin $\omega_c t$ the preferred phase at the detector

of a device with a true derivative characteristic. As $|\delta|$ goes through ω_d, the burden of the output intelligence switches from the signal to the distortion envelope. But since the demodulated output is the same in both cases, the carrier shift does not reduce the derivative damping. The $G(j\omega_d)$ is $jK\omega_d$; and this is the same as when the carrier is centered (equation 10).

Thus, the shaped frequency response is inherently insensitive to carrier frequency shifts, with a reduction in damping observed only when the sidebands fall on a region of the $H(j\omega)$ when it no longer resembles that of a derivative device. It also suggests that this frequency characteristic, though convenient, is not at all necessary, with simpler networks available to provide derivative control and carrier frequency insensitivity even greater than that observed for the circuits under discussion.

The $G(j\omega_d)$ with the phase detector or motor sensitive to $\sin\omega_c t$ is of interest since it gives another set of equations similar to 13 and 15 which can be checked by experimental studies in later sections. However, this output intelligence is of no obvious use in the servo, for it represents the envelope that is suppressed when the derivative characteristic is required.

Again from Table I we may establish the following:

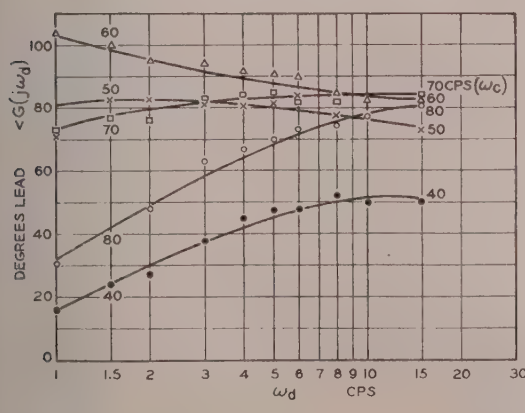

Figure 10. (left) $<G(j\omega_d)$ of a full-rejection parallel T tuned to 60.0 cycles per second

Figure 12. $<(Gj\omega_d)$ for a 60.0 cycles per second parallel T with 0.10 transmission at 60.0 cycles per second

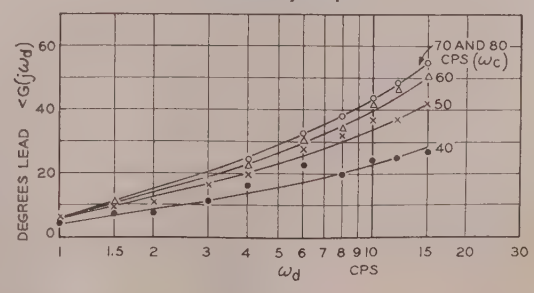

1. When $|\delta| < \omega_d$, $\phi_c = 0$. The motor output torque will be a demodulated distortion term. The distortion term is given by

$$-K\delta \sin (\omega_d t + 90) \sin \omega_c t \quad (16)$$

and its demodulated component

$$-K\delta \cos \omega_d t \quad (17)$$

2. When $|\delta| > \omega_d$, $\phi_c = \pm 90°$, and now the distortion term is suppressed, with the signal envelope carrying the intelligence. Again from Table I, this term is given by

$$K|\delta| \cos \omega_d t \cos (\omega_c t \pm 90) \quad (18)$$

and its demodulated component

$$-K\delta \cos \omega_d t \quad (19)$$

Again, equations 17 and 19 are identical, showing that the transfer function of this combination is unaffected by the carrier swing.

Effect of the Carrier Shift on the Proportional plus Derivative $G(j\omega_d)$

The preceding analysis can be used to evaluate the effect of the carrier shift on servos stabilized by a proportional plus derivative $H(j\omega)$ of the form shown in Figure 4.

Inspection of this phase characteristic shows that the carrier phase, ϕ_c, will be zero only when the carrier is centered on ω_0, for only at this point will the phase shifts of the two sidebands be equal and opposite in sign. Moreover, when ω_c shifts, ϕ_c becomes a function of δ. This presents some difficulty, since it was shown that to suppress the unwanted envelope over a range of ω_d and δ, it was necessary that the carrier phase be kept constant. If equation 9 is applied directly to the $H(j\omega)$ of Figure 4, its resolution would yield two terms, neither of which could be suppressed, since their carrier phases would be functions of ω_d and δ.

However, further consideration shows that this difficulty has been caused by an incomplete resolution of the output of the network. For the analysis three components must be considered: the proportional envelope similar in form to the driving voltage of equation 6 and transmitted by the proportional characteristic of the network; the signal envelope from the derivative transmission which results when the proportional term is subtracted from the over-all $H(j\omega)$; and the distortion envelope from the same derivative transmission. These three components are the following:

Proportional term =

$E \cos \omega_d t \cos \omega_c t$

Signal term transmitted by reactive path =

Table I

$\lvert\delta\rvert < \omega_d$		$\lvert\delta\rvert > \omega_d$	
ϕ_d	90°	0	
ϕ_c	0	+90°	$\omega_c > \omega_0$
		−90°	$\omega_c < \omega_0$
$\frac{A_l + A_u}{2}$	$K\omega_d$	$K\delta$	
$\frac{A_l - A_u}{2}$	$-K\delta$	$-K\omega_d$	$\omega_c > \omega_0$
		$+K\omega_d$	$\omega_c < \omega_0$

$$\frac{E}{2}(A_u + A_l) \cos (\omega_d t + \phi_d) \cos (\omega_c t + \phi_c)$$

Distortion term transmitted by reactive path =

$$\frac{E}{2}(A_l - A_u) \sin (\omega_d t + \phi_d) \sin (\omega_c t + \phi_c)$$

Now the proportional term is transmitted by a path whose $H(j\omega)$ is purely resistive. It will yield a demodulated term which will always be proportional to the error, and which will not be affected by carrier shifts. The other two terms are exactly those of the analysis of the previous section. It was shown that when a motor demodulated these terms, if the $\cos \omega_c t$ was the preferred phase, then a derivative $G(j\omega_d)$ would result, which was not affected by the carrier shift. Thus, the same insensitivity to δ found in the derivative network will be present in the proportional plus derivative one. The $G(j\omega_d)$ of the modified parallel T or the bridged T and resistance-inductance-capacitance network will still introduce damping in a servo whose carrier has shifted from ω_0, provided the sidebands still fall on a portion of the $H(j\omega)$ where equation 5 still holds.

Error Signal Saturation

The analysis of the preceding sections holds only if the system is linear. In practice, the instantaneous amplitude of the suppressed or unwanted term might overload the driving amplifier and drive the system into nonlinearity.

Equations 17 and 19 show that the magnitude of this unwanted term increases linearly with the carrier shift, with its value given as $K\delta$. The nature of this term is of interest. When the servo is at rest, its value will be zero and the system will remain linear regardless of the value of the carrier shift. When the servo is in motion, an error voltage will appear at the input to the damping network, giving rise to an unwanted term with value set by δ.

Thus, the effect of the carrier shift will be to introduce a voltage at the motor amplifier in quadrature with the error signal, whenever the servo is in motion. The effect of any saturation which may result will be progressively to restrict the linear range of the servo amplifier as the carrier shift becomes more severe, still retaining linearity at low error signal levels.

This presents the second limitation to the use of these networks for carrier frequency damping. At large carrier shifts some reduction in the maximum linear output of the servo amplifier must be expected.

Experimental Studies

The conclusions derived in the section on the carrier frequency shift problem have been checked by experiment. This work, given in this section, has shown that the phase discrimination of the carrier frequency actuator can be used to isolate the individual envelopes of equation 9. Specifically, there has been sought experimental confirmation of the relations arrived at in equations 13 and 15 as well as equations 17 and 19. Also, the $G(j\omega_d)$ for a proportional plus derivative parallel T has been obtained for various values of ω_c different from ω_0.

Experimental Equipment

The experimental equipment is of interest, since it allowed the observation of the individual component envelopes in a complex waveshape with a facility rivaling their mathematical resolution. The $H(j\omega)$ studied was that of a full rejection, symmetrical parallel T, made of precision components, and trimmed for an attenuation of over 2,000 at 60.0 cycles per second. This network was driven by a voltage of the form of equation 6, generated by a rotating autosyn driven by a variable speed control. The output of the T was resolved by a full-wave phase detector. This was followed by a 2-stage filter which reduced the ripple present,

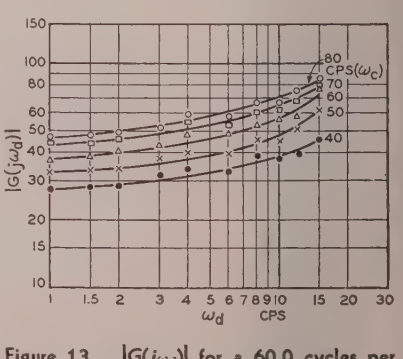

Figure 13. $|G(j\omega_d)|$ for a 60.0 cycles per second parallel T with 0.10 transmission at 60.0 cycles per second

and then drove a d-c amplifier whose output deflected the vertical plates of a long persistence cathode-ray oscilloscope.

The excitation for the rotating autosyn was obtained from a low-frequency oscillator. A portion of its output voltage, after passing through a phase shifter, served as the reference for the phase detector. This phase shifter allowed setting first cos $\omega_c t$ then sin $\omega_c t$ as the preferred phase at the detector. A linear sweep, synchronized with the driving voltage, deflected the horizontal plates of the oscilloscope. A regulated power supply furnished plate and filament voltages, and special care was taken to insure that the circuits were operating linearly.

Figure 7 is the block diagram of the equipment, while Figure 8 is the schematic of the phase detector and d-c amplifier.

Limitations of Experimental Method

In an effort to substantiate experimentally some theoretical work, many factors arise which are not present in the original analysis. It then becomes necessary to study their effect on the results obtained, and thus account for any departure from theory that may be observed. A number of these points must be considered in these experimental studies, since the problem of extracting the individual envelopes from some complex waveshape is a novel one. These factors are as follows:

1. The phase shifter employed was a bridge whose $H(j\omega)$ is

$$H(j\omega) = \epsilon^{-j2 \tan^{-1} \omega RC} \tag{20}$$

This has an amplitude invariant with frequency, but a phase shift dependent on it. This means that if the phase detector reference voltage is adjusted for optimum phase at 60.0 cycles per second, then at the extremes of 40 and 80 cycles per second these conditions will no longer prevail, and the $G(j\omega_d)$ observed will have a small component of the unwanted envelope. This condition is exactly that which may exist in a practical servo amplifier, and suggests the desirability of obtaining the carrier phase shift by networks which have no phase slope throughout the range of carrier drift.

2. There are two coupling time constants in each amplifier channel before the phase detector (Figure 8) and a cathode by-pass in the first stage of the error amplifier. The time constant of this by-pass is so large it can be neglected. The coupling time constants produce no differential phase shift at the grids of the phase detector, since they are the same for each channel. The output of the phase detector is independent of the reference voltage magnitude and is given by

$$e_{DC} = E_{error} \cos \theta \tag{21}$$

The attenuation of the coupling time constants in the reference channel will not affect the phase detector output. But the corresponding attenuation in the error channel will be superimposed on the $G(j\omega_d)$ measured.

3. Two factors will introduce inaccuracies in the measurement of the phase and amplitude of the $G(j\omega_d)$: the residual ripple reaching the vertical plates of the cathode-ray oscilloscope and the small amount of waveshape distortion present in the output of the phase detector.

However, it will be seen that the experimental work substantiates the theoretical analysis despite these limitations.

Analysis of Results

Equations 13 and 15 state that as long as the $H(j\omega)$ of the network is that of equation 1, no amount of carrier frequency shift can destroy the derivative action of the rejection network cascaded with the phase detector or motor. However, equation 1 represents a simplification of a more complex $H(j\omega)$ in the region of ω_0. Hence, the limit of carrier frequency shift is solely the distance away from ω_0 in which this simplification holds.

To check the accuracy of this conclusion, the $G(j\omega_d)$ of a full-rejection parallel T (Figure 1) cascaded with a phase detector was obtained, with the preferred phase fixed at cos $\omega_c t$. This data was taken for various values of ω_c, centered on ω_0, as well as a considerable distance away. The results are plotted in Figures 9 and 10, for values of ω_d between 1.0 and 15 cycles per second.

Figure 9 gives the $|G(j\omega_d)|$ measured, with the value of the carrier between 40 and 80 cycles per second. Between 50 and 80 cycles per second, the amplitude increases with frequency with a logarithmic slope of substantially plus 1. This is the correct slope for a derivative device. The plot for 40 cycles per second shows a smaller slope and indicates that the sidebands have reached a portion of the $H(j\omega)$ where the underlying simplification no longer holds.

The slight spacing between the curves of 50 and 80 cycles per second may be attributed to the coupling time constants in the phase detector preamplifiers. The scattering of the points is caused by the factors discussed in the previous section.

The phase plot for a derivative device is a fixed phase lead of 90 degrees regardless of frequency. Figure 10 plots the $\angle G(j\omega_d)$ again measured with ω_c set at values between 40 and 80 cycles per second. Between 50 and 70 cycles per second the ϕ_d was substantially 90 degrees leading. However, at 40 and 80 cycles per second it was considerably lower, suggesting again that the sidebands were outside the region where equation 1 holds.

The large scatter in the phase plots at low data frequencies is caused by the difficulty inherent in making accurate phase measurements of envelopes with small amplitudes. Since the network was operating as a derivative device, the output of the phase detector for low values of ω_d was small.

The above shows that the derivative action of the parallel T tuned to 60.0 cycles per second is unchanged for values of ω_c between 50 and 70 cycles per second, or for a carrier shift of 10/60 or 16 per cent.

The $G(j\omega_d)$ with the phase detector sensitive to sin $\omega_c t$ also was measured, to substantiate the identity of equations 17 and 19. The results are plotted in Figure 11. The insensitivity to ω_d should be noted, as well as the linear variation with δ in the upper frequency region, and the invariant ϕ_d of either zero or 180 degrees. This plot was taken especially to prove the practicality of this technique in separating and observing separately the constituent envelopes.

The last data taken were concerned with the insensitivity of a proportional plus derivative network to carrier frequency shifts. The same parallel T was used. To achieve a proportional transmission, a resistive divider was placed across the input to the T, with the point generally grounded, returned to the junction of the resistors in the attenuator. Both the phase (Figure 12) and the amplitude (Figure 13) plots are approximately those for the true proportional plus derivative network. The interesting observation here is that this network exhibits some degree of derivative damping for ω_c as far out as 40 and 80 cycles per second. This represents a carrier shift of 20/60, or 33 per cent.

Conclusions

1. The derivative damping introduced by the shaped frequency response is not destroyed if the carrier drifts away from ω_c, provided phase conditions at the motor are adjusted so that the unwanted terms of equation 9 will be suppressed.

2. The necessary phase condition is that quadrature exists between the reference voltage and the error voltage across the motor windings. This should be set with the carrier centered and should be maintained as much as possible as the carrier drifts

3. The maximum allowable theoretical shift is limited by the network $H(j\omega)$. As long as the sidebands generated fall on a portion of the network $H(j\omega)$ which still approximates equation 1, no reduction in the derivative action will be observed.

4. A second, but practical, limitation to the maximum allowable carrier shift is the saturation which the unwanted terms of equation 9 may cause in the servo amplifier. At large carrier shifts some reduction in the maximum linear output of the servo amplifier must be expected, which will become progressively more severe as the carrier shift becomes greater.

5. Experimental tests show that a carrier shift of 16 per cent causes no change in the derivative $G(j\omega_d)$ of a symmetrical full-rejection parallel T (Figure 1).

6. Experimental tests show that a carrier shift of 16 per cent causes no change in the $G(j\omega_d)$ of a proportional plus derivative parallel T adjusted for a transmission at ω_0 of 0.10.

7. An analytical method has been suggested to determine the significant $G(j\omega_d)$ of carrier frequency networks. The resolution into component envelopes,[1] when combined with the phase discrimination of the motor or actuator, permits evaluation of any $G(j\omega_d)$, regardless of carrier shift or asymmetry in the $H(j\omega)$ about ω_0.

References

1. Stabilization of Carrier Frequency Servomechanisms—I. Gain Phase Margin Diagrams of Controller Characteristics, **A. Sobczyk.** *Journal*, Franklin Institute (Philadelphia, Pa.), volume 246, July 1948.

2. Stabilization of Carrier Frequency Servomechanisms—II. Design Formulae for Proportional-Derivative Networks, **A. Sobczyk.** *Journal*, Franklin Institute (Philadelphia, Pa.), volume 246, August 1948.

3. Analysis of Resistance-Capacitance Parallel-T Network and Applications, **A. E. Hastings.** *Proceedings*, Institute of Radio Engineers (New York, N. Y.), volume 34, March 1946.

4. Servomechanism Fundamentals (book), **H. Lauer, R. Lesnick, L. E. Matson.** McGraw-Hill Book Co., New York, N. Y., 1947.

5. Envelope Transfer Functions in Carrier Frequency Servomechanisms (thesis), **G. M. Attura.** New York University, New York, N. Y., 1950.

No Discussion

Network Synthesis by Graphical Methods for A-C Servomechanisms

GEORGE A. BJORNSON
ASSOCIATE AIEE

IN ORDER to improve the performance of a servomechanism, one often employs compensation networks which offset its dynamic limitations. Designs of such networks when the intelligence appears as a d-c signal are described in the references.[1,2] However, in a-c servomechanisms the data appear as modulation on a carrier. Hence, for compensation, one should employ networks (termed "carrier-frequency networks") which will modify the modulation rather than the signal as a whole. If such a network produces the same effect upon the data as a d-c (or data-frequency) network, it may be said to "simulate" the data-frequency network.

The first section of this paper is a summary of the usual approach to this problem.[3,4,5] Expressions are given which describe the effect of a carrier-frequency network in terms of its transfer function. From these the standard procedure for synthesizing a carrier-frequency network, which approximately simulates the desired data-frequency network, is developed. Because this simulation is only approximate, this procedure of synthesis should be followed by a more exact evaluation of the effect of the network by the direct application of the mathematical expressions. If this effect is not adequate, the synthesis procedure might then be altered, and then a new analysis made.

Paper 51-101, recommended by the AIEE Feedback Control Systems Committee and approved by the AIEE Technical Program Committee for presentation at the AIEE Winter General Meeting, New York, N. Y., January 22–26, 1951. Manuscript submitted October 24, 1950; made available for printing December 19, 1950.

GEORGE A. BJORNSON is with the Massachusetts Institute of Technology, Cambridge, Mass.

The aid given by various members of the Massachusetts Institute of Technology Servomechanisms Laboratory in the preparation of this paper is gratefully acknowledged.

In order to simplify this process (which involves alternate synthesis and analysis), this paper proposes: (1) A quick graphical method of analysis; (2) A more general method of synthesis.

Usual Approach to Problem

Mathematical Analysis of Carrier-Frequency Network

Figure 1 illustrates the portion of the a-c servomechanism to be considered. The data signal enters the modulator, is combined with the modulator reference ($\cos \omega_o t$), to form the modulated signal e_i. The signal e_i is then altered by the carrier-frequency network, and emerges as the modulated signal e_o. This enters the demodulator (often a 2-phase motor), is compared with the demodulator reference, and is demodulated to form the data-frequency output.

The following discussion (presented in more detail in Appendix I) will show that the effect of the carrier-frequency network may be determined by the functions $\mathbf{G}_d$ and $\mathbf{G}_q$, which relate to the data signal, the modulations of the components of e_o in phase and in quadrature with respectively, the modulator reference. On first approximation, $\mathbf{G}_d$ is the data-frequency function simulated by the carrier-frequency network.

If the data signal is a sinusoid of frequency ω_m, and the carrier frequency is ω_o, the modulator output is $(\cos \omega_m t) \times (\cos \omega_o t)$. This amplitude-modulated signal may be considered as the sum of two components of frequencies $(\omega_o+\omega_m)$ and $(\omega_o-\omega_m)$. These components will be transmitted through the carrier-frequency network, and hence will be altered, respectively, by the values of the network transfer function at those frequencies. If we designate this transfer function as $\mathbf{D}(j\omega)$, we are interested in the values $\mathbf{D}[j(\omega_o+\omega_m)]$, $\mathbf{D}[j(\omega_o-\omega_m)]$, which we shall abbreviate as $\mathbf{D}^+$, $\mathbf{D}^-$. (The symbol $\mathbf{D}$ is used throughout this paper to represent carrier-frequency functions, while the symbol $\mathbf{G}$ will be reserved for data-frequency functions.)

Each of the functions $\mathbf{D}^+$ and $\mathbf{D}^-$ operates upon its respective frequency component, varying its magnitude and phase to produce the signal e_o. When these frequency components of e_o are recombined they may be expressed as two modulated waves of carrier frequency ω_o: one with the form $e_{md}(t)\cos\omega_o t$, which we shall designate as the direct component, since its carrier, $\cos\omega_o t$, is in phase with the modulator reference; and the other, designated as the quadrature component, with the form $e_{mq}(t)\sin\omega_o t$. The functions $e_{md}(t)$ and $e_{mq}(t)$, which represent the modulation of the components, are sinusoids of frequency ω_m.

Now, when the voltage applied to the reference winding of a 2-phase motor is in quadrature with the voltage applied to the control winding, the torque developed is approximately proportional to the modulation—that is, the magnitude—of the control-winding voltage. Hence, if the reference-winding voltage is in quadrature with the modulator reference, the torque will be proportional to the modulation of the component of e_o in phase with the modulator reference—which is the direct component. Thus, the 2-phase motor acts essentially as a demodulator, the output of which is the torque, and the input of which is the direct component of e_o.

Since the demodulator output is approximately proportional to the modulation of the direct component of e_o, the following transfer function $\mathbf{G}_d$, which relates this modulation to the data signal, is essentially the data-frequency function simulated by the carrier-frequency network:

$$\mathbf{G}_d = \mathbf{E}_{md}/\mathbf{X} = (1/2)(\mathbf{D}^{*-}+\mathbf{D}^+) \qquad (1)$$

$\mathbf{E}_{md}$ and $\mathbf{X}$ are, respectively, the transforms of $e_{md}(t)$ and the data signal $x(t)$

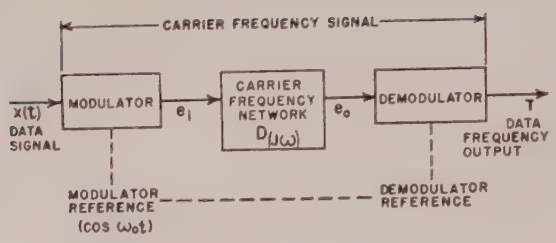

Figure 1 (left). Carrier-frequency portion of a-c servomechanism

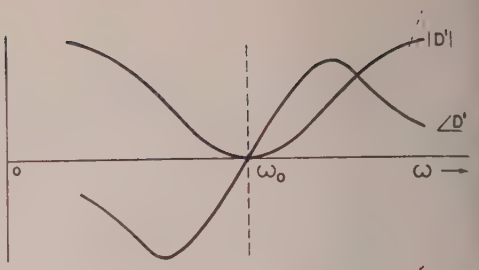

Figure 2 (right). Symmetric carrier-frequency function

while $\mathbf{D}^{*-}$ is the symbol for the conjugate of $\mathbf{D}^{-}$.

We are also interested in the quadrature component, because a more exact analysis of the 2-phase motor shows that there is a small component of torque proportional to the derivative of its modulation. The transfer function of the modulation of the quadrature component is

$$\mathbf{G}_q = \mathbf{E}_{mq}/\mathbf{X} = (1/2j)(\mathbf{D}^{*-} - \mathbf{D}^{+}) \qquad (2)$$

where $\mathbf{E}_{mq}$ is the transform of e_{mq}. Often the modulator itself produces a small component in quadrature with e_i, which in turn produces two more components of torque. A sample analysis, taking all these effects into account, is presented in Appendix III.

Standard Method of Synthesis

Now, let us determine a method of synthesizing a carrier-frequency compensation network. Essentially, such a network should produce (1) as small a quadrature component as possible and (2) a direct component, the modulation of which is related to the data signal by the desired data-frequency function.

Referring to equation 2, it is seen that for the quadrature component to be zero requires that

$$\mathbf{D}^{*-} = \mathbf{D}^{+} \qquad (3)$$

This means that the function should be symmetric about the carrier, its magnitude being an even function of deviations from the carrier frequency and its phase being an odd function. If this condition exists, the transfer function of the direct component reduces to

$$\mathbf{G}_d = \mathbf{D}^{+} = \mathbf{D}[j(\omega_o + \omega_m)] \qquad (4)$$

To illustrate this point, let us refer to Figure 2, a plot of a symmetric carrier-frequency function, which we shall designate as $\mathbf{D}'(j\omega)$. A plot of the transfer function of the modulation of its direct component, which we shall designate as $\mathbf{G}'(j\omega_m)$, may be obtained from this graph by shifting the curves to the left a distance ω_o, and considering the positive sideband, as shown in Figure 3.

One should also note that the negative sideband would also coincide with the plot of $\mathbf{G}'(j\omega_m)$, if it were folded about the 0-frequency axis and the sign of its phase reversed. That is, $\mathbf{G}'(j\omega_m)$ represents either the positive sideband or the conjugate of the negative sideband of the function $\mathbf{D}'(j\omega)$.

Now, let us reverse this process by defining $\mathbf{G}'(j\omega_m)$ as a data-frequency function (which we shall call the "desired data-frequency function") that we would like to simulate by a carrier-frequency network. If $\mathbf{G}'(j\omega_m)$ is itself realizable as a d-c network, it can be shown that its magnitude would be an even function and its phase an odd function of frequency, if the frequency variable (ω_m) were permitted negative as well as positive values. The dotted curves in Figure 3 show its form for negative values of (ω_m). Hence, if we replace each (ω_m) by the variable $(\omega - \omega_o)$ we would shift the curves to the right a distance ω_o thus producing the function $\mathbf{D}'(j\omega)$. Hence,

$$\mathbf{D}'(j\omega) = \mathbf{G}'(j\omega_m)\big|_{j\omega_m \to j(\omega - \omega_o)} \qquad (5)$$

$\mathbf{D}'(j\omega)$ thus simulates $\mathbf{G}'(j\omega_m)$, since the latter is the transfer function of the modulation of the direct component of $\mathbf{D}'(j\omega)$.

However, $\mathbf{D}'(j\omega)$ is unrealizable, since it must contain the factor $j\omega_o$. Nevertheless, an approximation which yields a realizable network is available by varying the substitution to

$$j\omega_m \to j(\omega - \omega_o)(\omega + \omega_o)/2\omega = (1/2j\omega)[(j\omega)^2 + \omega_o^2] \qquad (6)$$

The transfer function thus formed—which we designate as $\mathbf{D}(j\omega)$, the "realizable carrier-frequency function simulating (approximately) $\mathbf{G}'(j\omega_m)$"—is always theoretically realizable as long as $\mathbf{G}'(j\omega_m)$ is itself realizable. (One such network may be obtained by substituting for each capacitance C in the network of $\mathbf{G}'(j\omega_m)$ a parallel combination of capacitance $C/2$ and inductance $\omega_o^2/2C$; and for each inductance L a series combination of inductance $L/2$ and capacitance $\omega_o^2/2L$.)

For ω approximately equal to ω_o—that is, for small values of data frequency—the substitution of equation 6 reduces to that of 5; hence, $\mathbf{D}(j\omega)$ closely approximates $\mathbf{D}'(j\omega)$ and closely simulates $\mathbf{G}'(j\omega_m)$.

Letting $j\omega \to s$ in equation 6, the substitution becomes

$$s \to (1/2s)(s^2 + \omega_o^2) \qquad (7)$$

Thus, the procedure of synthesis is as follows. After picking a desired data-frequency function $\mathbf{G}'(s)$, replace each (s) in $\mathbf{G}'(s)$ as shown in equation 7. This produces a carrier-frequency function $\mathbf{D}(s)$ which is realizable, and which approximately simulates $\mathbf{G}'(s)$. Since this simulation is only approximate, however, the modulation functions $\mathbf{G}_d$ and $\mathbf{G}_q$ should then be calculated in order to determine the exact effect of $\mathbf{D}(s)$.

Graphical Analysis

This synthesis procedure may be facilitated greatly by graphical means of (1) determining a plot of the function $\mathbf{D}(j\omega)$ directly from a plot of $\mathbf{G}'(j\omega_m)$ and then (2) determining from $\mathbf{D}(j\omega)$ plots of the functions $\mathbf{G}_d$ and $\mathbf{G}_q$.

Determination of $\mathbf{D}(j\omega)$

In Figure 4 is a sketch of the functions $\mathbf{D}'(j\omega)$ (shown by the solid curves) and $\mathbf{D}(j\omega)$ (shown by the dotted curves). If these curves are shifted to the left a distance ω_o, and the lower sideband magnitude and phase are appropriately folded about the 0-frequency axis, one obtains the graphs of Figure 5. Since the function $\mathbf{D}'$ is symmetric, its sidebands will coincide on the curve of $\mathbf{G}'$, as pointed out previously. The realizable function $\mathbf{D}$, however, being unsymmetric, will produce two sideband curves. Let us designate the upper as $\mathbf{G}(+j\omega_m)$ and the conjugate of the lower as $\mathbf{G}^*(-j\omega_m)$ which

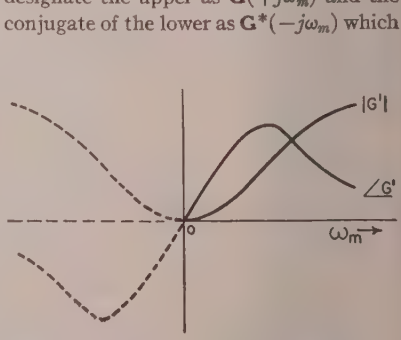

Figure 3. Transfer function of direct component of D'

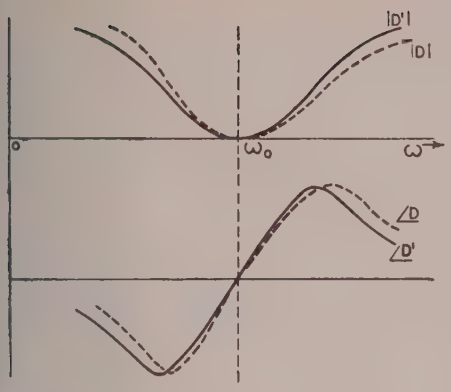

Figure 4 (left). Carrier-frequency functions simulating G'

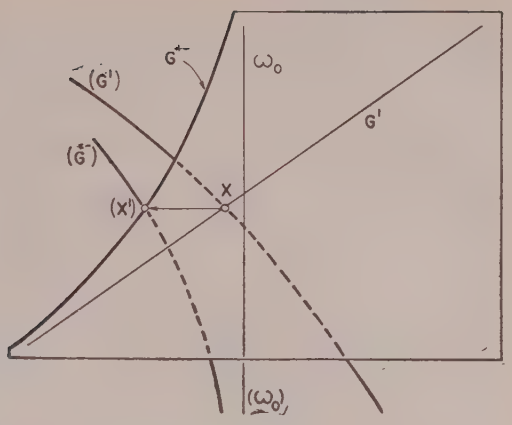

Figure 7 (right). Lower sideband template

we shall abbreviate, respectively, as $\mathbf{G}^+$, $\mathbf{G}^{*-}$.

For a given value of data frequency ω_m, the values of $\mathbf{G}^{*-}$ and $\mathbf{G}^+$ are equal respectively to the values of $\mathbf{D}^{*-}$ and $\mathbf{D}^+$. Hence, equations 1 and 2 may be expressed as follows

$$\mathbf{G}_d = (1/2)(\mathbf{G}^{*-} + \mathbf{G}^+) \tag{8}$$

$$\mathbf{G}_q = (1/2j)(\mathbf{G}^{*-} - \mathbf{G}^+) \tag{9}$$

It is far simpler to obtain $\mathbf{G}_d$ and $\mathbf{G}_q$ by employing equations 8 and 9, because the plots of $\mathbf{G}^{*-}$ and $\mathbf{G}^+$ need not be computed, but can be obtained directly from a plot of $\mathbf{G}'(j\omega_m)$.

The method of obtaining the plots of $\mathbf{G}^{*-}$ and $\mathbf{G}^+$ (proven in Appendix *B*) is illustrated by the curves of Figure 6, which may represent either magnitude or phase of the functions. From a given point A on the $\mathbf{G}'$ curve, points x and y on the $\mathbf{G}^{*-}$ and $\mathbf{G}^+$ curves may be determined by moving negatively and positively, respectively, the frequency interval $\Delta\omega_A$. In other words, the function $\mathbf{G}^+$ has the same value at the frequency $(\omega_A + \Delta\omega_A)$ that $\mathbf{G}'$ has at the frequency ω_A and that $\mathbf{G}^{*-}$ has at the frequency $(\omega_A - \Delta\omega_A)$. This frequency interval is related to the frequency at which the point occurs, by the relation:

$$\Delta\omega_A = \sqrt{\omega_0^2 + \omega_A^2} - \omega_0 \tag{10}$$

This procedure may be employed for any desired data-frequency function, as long as that function is realizable, and the carrier-frequency function $\mathbf{D}(j\omega)$ is obtained from it by the substitution of equation 6.

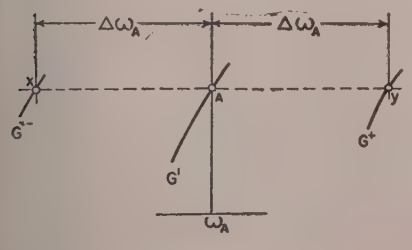

Figure 6 (left). Determination of sideband plots

The task of plotting $\mathbf{G}^{*-}$ can be greatly facilitated if one constructs a transparent template as shown in Figure 7. The line $\mathbf{G}'$ on the template is drawn at a convenient angle, and the curved edge, labeled $\mathbf{G}^{*-}$, obtained by moving negatively from it the frequency interval of equation 10. Placing the template so that the vertical carrier-frequency index line lies at the frequency ω_o, one locates the point x on the plot of $(\mathbf{G}')$, and from

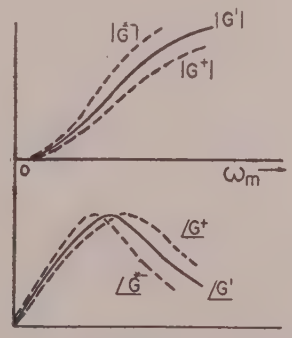

Figure 5. Sidebands of carrier-frequency functions

it obtains (x') on the plot of $(\mathbf{G}^{*-})$. A similar template may be constructed for obtaining $\mathbf{G}^+$.

Computation of $\mathbf{G}_d$ and $\mathbf{G}_q$

We should like to express the relations for $\mathbf{G}_d$ and $\mathbf{G}_q$ in such a manner that they may be calculated easily from the plots of the sideband functions $\mathbf{G}^{*-}$ and $\mathbf{G}^+$, which, being data-frequency functions, should each be represented by two curves (in the same manner as ordinary d-c compensation functions[6]):

1. The magnitude of the function in decibels versus the logarithm of frequency; that is, $20 \log_{10} |G|$ versus $\log_{10}(\omega)$.

2. Phase angle in degrees versus $\log_{10}(\omega)$.

(The reader may find, however, that it is more convenient to nondimensionalize the frequency scale in terms of the carrier frequency ω_o. That is, one plots these sidebands as functions of $\log_{10}(u)$, where $u = \omega/\omega_o$.)

Since, by equation 8, $\mathbf{G}_d$ is the vector average of the sideband functions, let us assume, as a first approximation, that it is equal to their graphical average—that is, its magnitude and phase plots would be graphical averages of the magnitude and phase plots of $\mathbf{G}^{*-}$, and $\mathbf{G}^+$. Let us designate this average—the first approximation of $\mathbf{G}_d$—as the mean function $\mathbf{G}_m$, defined as:

$$|G_m| = \sqrt{|G^{*-}| \times |G^+|} \tag{11}$$

$$/G_m = (1/2)(/G^{*-} + /G^+) \tag{12}$$

Let us define the incremental variables ϵ and δ

$$\epsilon = \sqrt{|G^{*-}|/|G^+|} = |G^{*-}|/|G_m| = |G_m|/|G^+| \tag{13}$$

$$\delta = (1/2)(/G^{*-} - /G^+) = /G^{*-} - /G_m = /G_m - /G^+ \tag{14}$$

Substituting these into equation 8, $\mathbf{G}_d$ becomes

$$\mathbf{G}_d = \mathbf{G}_m[(1/2)(\epsilon/+\delta + (1/\epsilon)/-\delta)] \tag{15}$$

Since the expression within the brackets represents the variation of $\mathbf{G}_d$ from its approximation $\mathbf{G}_m$, let us define it as the

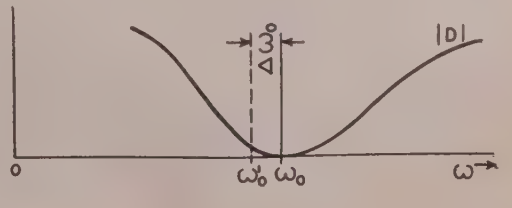

Figure 8 (right). Effect of carrier drift on D function

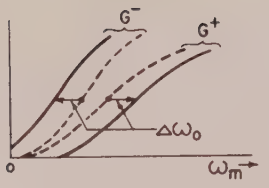

Figure 9. Effect of carrier drift on sideband plots

"direct component correction function $\mathbf{C}_d$." Since $\mathbf{C}_d$ is an incremental quantity, it is more easily computed than $\mathbf{G}_d$, because approximations are more easily made. The magnitude and phase of $\mathbf{C}_d$ are equal to:

$$|C_d| = (1/2)(\epsilon+(1/\epsilon)) \times \sqrt{1-[2(1-\cos 2\delta)/(\epsilon+(1/\epsilon))^2]} \quad (16)$$

$$/C_d = \tan^{-1}[(\tan\delta)(\epsilon^2-1)/(\epsilon^2+1)] \quad (17)$$

Similarly $\mathbf{G}_q$, from equation 9, may be expressed as

$$\mathbf{G}_q = (\mathbf{G}_m/2j)(\epsilon/\underline{+\delta} - (1/\epsilon)/\underline{-\delta}) \quad (18)$$

$$= \mathbf{G}_m \sin\delta[(1/2)(\epsilon+(1/\epsilon))(1-j(\epsilon^2-1)\times (\cot\delta)/(\epsilon^2+1))] \quad (19)$$

Since the expression within the brackets closely approximates unity for small values of $(\epsilon-1)$ and δ, as a first approximation, $\mathbf{G}_q$ becomes

$$\mathbf{G}_q \backsimeq \mathbf{G}_m \sin\delta \quad (20)$$

Let us define the expression within the brackets of equation 19 as the "quadrature component correction function $\mathbf{C}_q$," which represents the variation of $\mathbf{G}_q$ from the approximation of equation 20. The magnitude and phase of $\mathbf{C}_q$ are as follows:

$$|C_q| = (1/2)(\epsilon+(1/\epsilon)) \sqrt{1+((\epsilon^2-1)^2(\cot^2\delta)/(\epsilon^2+1)^2)} \quad (21)$$

$$/C_q = -\tan^{-1}[(\epsilon^2-1)(\cot\delta)/(\epsilon^2+1)] \quad (22)$$

By employing these expressions, plots of the functions $\mathbf{C}_d$ and $\mathbf{C}_q$ may be computed readily from the plots of $\mathbf{G}^{*-}$, $\mathbf{G}^+$. The functions $\mathbf{G}_d$ and $\mathbf{G}_q$ then may be obtained by combining these plots of $\mathbf{C}_d$ and $\mathbf{C}_q$ with the plots of $\mathbf{G}_m$ and $\mathbf{G}_m \sin\delta$, respectively. Since $\mathbf{C}_d$ and $\mathbf{C}_q$ are incremental quantities, it is not necessary to calculate them very accurately, because a fairly large variation in them has little effect upon the values of $\mathbf{G}_d$ and $\mathbf{G}_q$.

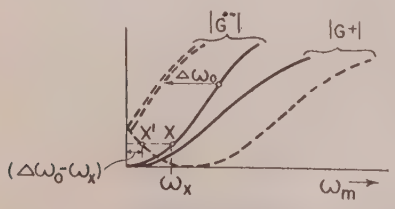

Figure 10. Magnitude plot illustrating effect of carrier drift

Generalization of Synthesis

In the standard method of synthesis, the network is designed to be balanced (that is, approximately symmetric) about the carrier frequency. A more general approach would be to design a network composed of factors balanced about frequencies greater than, and/or less than, the carrier frequency. Some advantages that such a network might have are as follows:

1. It might be more easily realized. For example, in Appendix IV is an inductance-capacitance lead network which is composed of two factors balanced about slightly different frequencies.

2. It might be less sensitive to a drift of the carrier frequency. Methods of designing such a network are discussed in a recent paper by A. P. Notthoff.[4]

Let us digress for a moment and examine a method of analyzing the effect of a drift of the carrier frequency which, in turn, will suggest a method of analyzing the effect of this more general network. The problem of carrier-frequency drift is also very important, in and of itself, because it often is a basic limitation of the use of carrier-frequency compensation networks.

Figure 8 is a magnitude plot of $(\mathbf{D}j\omega)$, balanced about ω_o. Let us investigate the effect of allowing the carrier to drift to the frequency $\omega_o' = \omega_o - \Delta\omega_o$. One could obtain the new sidebands corresponding to this condition by folding the graph about the (ω_o') axis, and shifting it to the left a distance ω_o', as shown in Figure 9. The dotted lines represent the sidebands when the network $\mathbf{D}(j\omega)$ is operated at the nominal carrier (ω_o), while the solid lines represent the new sidebands when the carrier is shifted to the frequency $(\omega_o - \Delta\omega_o)$. Thus, it is seen that a negative drift of the carrier frequency may be accounted for by a positive shift of the upper sideband and a negative shift of the lower sideband equal to the frequency interval of drift $\Delta\omega_o$. The reverse is, of course, true for a positive drift.

Now, to return to the problem of synthesis, let us balance the function $\mathbf{D}(j\omega)$ (or a factor of the function) about the frequency $(r\omega_o)$ rather than about the nominal carrier frequency (ω_o), simply by changing the usual substitution (of equation 7) to

$$s \rightarrow (1/2s)[s^2+(r\omega_o)^2] \quad (23)$$

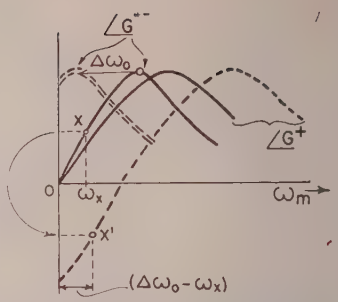

Figure 11. Phase plot illustrating effect of carrier drift

Plots of the sideband functions of $\mathbf{D}(j\omega)$ could be obtained as follows. If we assume that the carrier is temporarily shifted to the frequency $(r\omega_o)$, the network is now balanced about the new carrier frequency, and hence its sidebands can be plotted as before by using the templates, but indexing them at the frequency $(r\omega_o)$, rather than at the nominal carrier frequency (ω_o). Now, to complete the process, we can allow the carrier to return to its nominal value, accounting for this shift by shifting the sidebands by the same interval: $\Delta\omega_o = (\omega_o - r\omega_o)$.

To investigate the potentialities of this generalization, we note that every factor of $\mathbf{G}'$ of the form $(s+\omega_1)$ will produce a factor in the $\mathbf{D}$ function as follows:

$$(s+\omega_1) \rightarrow (1/2s)[s^2+2\omega_1 s+(r\omega_o)^2] \quad (24)$$

If the data-frequency function $\mathbf{G}'$ is a ratio of single-order factors, the same number of numerator and denominator (which is usually the case), the $2s$ terms in the carrier-frequency function $\mathbf{D}$ will cancel each other out.

The important thing to note about this substitution is that the quadratic factor of the $\mathbf{D}$ function thus formed is perfectly general. Now, any carrier-frequency transfer function can be expressed as a ratio of factors of s, single-order factors, and quadratics. The first two, if they are present, would have to be plotted by the usual means. That is, they would be plotted as functions of signal frequency ω, and the sidebands obtained by

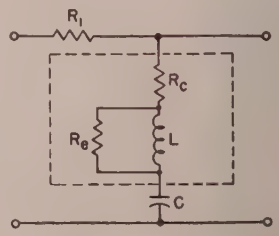

Figure 12. Inductance-capacitance carrier-frequency phase-lead network

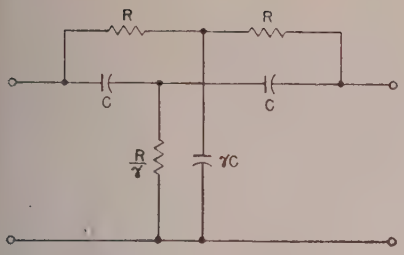

Figure 13. Symmetric parallel "T"

folding about the carrier frequency ω_o, as shown in Figures 4 and 5. (The factors of s need not be considered, however, if they are related to quadratics, as in equation 24.) The quadratics, however, which ordinarily are the most troublesome, need merely be plotted as single-order $\mathbf{G}'$ factors, which are then shifted by appropriate amounts to obtain the sideband plots.

Thus, in handling any carrier-frequency network, one expresses each quadratic in the form $[s^2+2\omega_1 s+(r\omega_o)^2]$, and then derives the sideband plots of this factor, by plotting the data-frequency function $(s+\omega_1)$ and shifting it by the proper amount. By combining the plots of these individual factors, the total sidebands of $\mathbf{D}$ may be formed.

Summary of New Approach

In order to summarize the approach that has been presented in this paper, let us consider various steps one might take in synthesizing a specific carrier-frequency network. First, one might determine a plot of the desired data-frequency function, and then plot the sideband functions obtained by the standard method of synthesis.

The functions $\mathbf{G}_d$ and $\mathbf{G}_q$ could then be determined by employing the correction functions in conjunction with the mean function $\mathbf{G}_m$. If carrier drift is likely to occur, these sideband plots should be shifted accordingly, and new values of $\mathbf{G}_d$ and $\mathbf{G}_q$ obtained. An exact expression for the over-all effect of the network might even be computed, by employing the plots of $\mathbf{G}_d$ and $\mathbf{G}_q$ in an analysis similar to that described in Appendix III.

One might find, however, that the transfer function $\mathbf{D}(j\omega)$ thus obtained is not adequate, either because the network is difficult to synthesize or because its over-all effect does not sufficiently approximate the desired response. Hence, a more general synthesis procedure might be employed, and by a trial-and-error process, an optimum design obtained.

Difficulties Met in Sideband Shifting

Before concluding, let us consider a problem met in shifting the sideband plots. If a point is shifted negatively an interval greater than the frequency at which it occurs, it will become a point on the other sideband curve. For example, in the magnitude plot of Figure 10, the sidebands corresponding to a negative drift of the carrier, $\Delta\omega_o$, are shown as dotted curves (the lower sideband being represented by a double dotted curve), while the original sidebands are shown as solid curves. It is seen that a point x, at the frequency ω_x, on the original lower sideband, becomes the point x' at the frequency $(\Delta\omega_o-\omega_x)$ on the upper sideband.

However, in the case of a phase plot, the sideband curves represent, respectively, the upper sideband and the conjugate of the lower sideband. For a negative drift of the carrier, a point on the original lower sideband curve becomes a point on a curve of the conjugate of the new upper sideband curve. Consequently it is the conjugate of this new point that occurs on the curve of the upper sideband. This is illustrated in Figure 11.

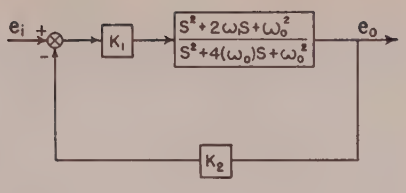

Figure 14. Feedback around parallel "T"

where

$$e_{md}=(1/2)\,[|D^-|\cos(\omega_m t-\underline{/D^-})+|D^+|\cos(\omega_m t+\underline{/D^+})] \quad (31)$$

$$e_{mq}=(1/2)\,[|D^-|\cos(\omega_m t-\underline{/D^-}-\pi/2)-|D^+|\cos(\omega_m t+\underline{/D^+}-\pi/2)] \quad (32)$$

Since the modulations e_{md}, e_{mq} are sinusoids they may be represented, respectively, by the vectors $\boldsymbol{E}_{md}$, $\boldsymbol{E}_{mq}$:

$$\boldsymbol{E}_{md}=(1/2)\,[|D^-|\exp(-j\underline{/D^-})+|D^+|\exp(j\underline{/D^+})]$$

$$=(1/2)(\mathbf{D}^{*-}+\mathbf{D}^+) \quad (33)$$

$$\boldsymbol{E}_{mq}=(1/2)\,[|D^-|\exp j(-\underline{/D^-}-\pi/2)-|D^+|\exp j(\underline{/D^+}-\pi/2)]$$

$$=(1/2j)(\mathbf{D}^{*-}-\mathbf{D}^+) \quad (34)$$

These expressions for $\boldsymbol{E}_{md}$ and $\boldsymbol{E}_{mq}$ are equal, respectively, to the transfer functions $\mathbf{G}_d$ and $\mathbf{G}_q$, because the vector representing the data signal is merely $\bar{\mathbf{X}}=1/\underline{0}$.

Appendix I

Derivation of Relations for $\mathbf{G}_d$ and $\mathbf{G}_q$

If the data signal $x(t)$ in Figure 1 is a sinusoid, and the modulator reference is $\cos\omega_o t$, the output from the modulator is

$$e_i=x(t)\cos\omega_o t=(\cos\omega_m t)(\cos\omega_o t) \quad (25)$$

For simplicity, the magnitude of the input and the constants of the various elements are taken as unity. Expanding, e_i becomes

$$e_i=(1/2)\cos(\omega_o+\omega_m)t+(1/2)\cos(\omega_o-\omega_m)t \quad (26)$$

It thus consists of two frequency components, designated as e_i^+ and e_i^- respectively, which are transmitted to the network $\mathbf{D}(j\omega)$.

By simple steady-state a-c analysis, the steady-state output from $\mathbf{D}(j\omega)$ corresponding to the component e_i^+ is

$$e_o^+=\mathrm{Re}\{(1/2)\mathbf{D}[j(\omega_o+\omega_m)]\times\exp[j(\omega_o+\omega_m)t]\} \quad (27)$$

$$=\mathrm{Re}\{(1/2)|D^+|\exp(j\underline{/D^+})\times\exp[j(\omega_o+\omega_m)t]\}$$

$$=(1/2)|D^+|\cos[\omega_o t+(\omega_m t+\underline{/D^+})] \quad (28)$$

Similarly, the output corresponding to e_i^- is

$$e_o^-=(1/2)|D^-|\cos[\omega_o t-(\omega_m t-\underline{/D^-})] \quad (29)$$

By trigonometric manipulation, the total output from the network, e_o, which is the sum of equations 28 and 29, may be put in the form

$$e_o=e_{md}(t)\cos\omega_o t+e_{mq}(t)\sin\omega_o t \quad (30)$$

Appendix II

Proof of Graphical Determination of $\mathbf{D}(j\omega)$

Since the desired data-frequency function is realizable, it will be composed of factors of the form

$$\mathbf{G}'(j\omega_m)=(j\omega_m+p_n) \quad (35)$$

where p_n may be real, zero, or complex $\mathbf{D}(j\omega)$ is obtained by employing the substitution of equation 6.

$$\mathbf{D}(j\omega)=([j(\omega-\omega_o)(\omega+\omega_o)/2\omega]+p_n) \quad (36)$$

Now, at the frequency $\omega=(\omega_o+\omega_m)$, this is equal to $\mathbf{D}^+$, which in turn is equal to $\mathbf{G}^+$:

$$\mathbf{G}^+(j\omega_m)=\mathbf{D}(j\omega)|_{\omega\to(\omega_o+\omega_m)}=([(j\omega_m)(2\omega_o+\omega_m)/2(\omega_o+\omega_m)]+p_n) \quad (37)$$

Comparing equations 37 and 35,

$$\mathbf{G}^+(j\omega^+)=\mathbf{G}'(j\omega_m)|_{\omega_m\to\omega^+(2\omega_o+\omega^+)/-2(\omega_o+\omega^+)} \quad (38)$$

where ω^+ is a specific data frequency at which we are to consider $\mathbf{G}^+$. Similarly, the function $\mathbf{G}^-$ is

$$\mathbf{G}^-(j\omega_m)=\mathbf{D}(j\omega)|_{\omega\to(\omega_o-\omega_m)}=([(-j\omega_m)(2\omega_o-\omega_m)/2(\omega_o-\omega_m)]+p_n) \quad (39)$$

Therefore, its conjugate is

$$\mathbf{G}^{*-}(j\omega_m)=([(+j\omega_m)(2\omega_o-\omega_m)/-2(\omega_o-\omega_m)]+p_n^*) \quad (40)$$

If p_n is not complex, then $p_n^* = p_n$, and hence

$$\mathbf{G}^{*-}(j\omega^-) = \mathbf{G}'(j\omega_m)|_{\omega_m \to \omega^-} \times (2\omega_0 - \omega^-)/2(\omega_0 - \omega^-) \quad (41)$$

If p_n is complex, $\mathbf{G}'(j\omega_m)$ must have a pair of factors:

$$\mathbf{G}'(j\omega_m) = (j\omega_m + p_n)(j\omega_m + p_n^*) \quad (35a)$$

Hence $\mathbf{G}^{*-}$ will also have a pair of factors, one with the form of equation 40 and a similar one containing the conjugate of p_n^*—that is, p_n. Consequently, equation 41 is still valid.

Thus, at the frequency $[\omega^+(2\omega_0+\omega^+)/2(\omega_0+\omega^+)]$—which we shall designate as ω_A^+—$\mathbf{G}'$ has the same value that $\mathbf{G}^+$ has at the frequency ω^+; while at the frequency $[\omega^-(2\omega_0-\omega^-)/2(\omega_0-\omega^-)]$—designated as ω_A^-—$\mathbf{G}'$ has the same value that $\mathbf{G}^{*-}$ has at the frequency ω^-. If we let ω_A^+ and ω_A^- be equal to the frequency ω_A, we may express ω^+ and ω^- in terms of ω_A as follows, by employing the quadratic formula:

$$\omega^+ = \omega_A - \omega_0 \pm \sqrt{\omega_A^2 + \omega_0^2} \quad (42)$$

$$\omega^- = \omega_A + \omega_0 \pm \sqrt{\omega_A^2 + \omega_0^2} \quad (43)$$

Since ω^+ must be greater than zero, and ω^- less than the carrier frequency ω_0, we choose a positive sign for the radical of ω^+, and a negative sign for that of ω^-. Hence, the frequency intervals $(\omega^+ - \omega_A)$, $(\omega_A - \omega^-)$ are both equal to

$$\Delta\omega_A = \sqrt{\omega_0^2 + \omega_A^2} - \omega_0 \quad (44)$$

Appendix III

Analysis of the Effects of Quadrature Components

An exact determination of the effect of quadrature components in a-c servomechanisms requires a detailed analysis of the specific modulator and demodulator. Primarily for the purpose of illustrating how such an analysis may be made, the writer will present an approximate analysis, involving a synchro-data system as modulator and 2-phase motor as demodulator, based upon assumptions which may or may not be justified in specific cases.

Let us assume that the synchro control transformer is attached to the output member, and the shaft of the synchro generator, attached to the input member, is held stationary (which is justified for the purposes of stability considerations). Ignoring hysteresis and eddy currents and considering small deviations, the complete output from the control transformer, for an error signal $x(t)$ and reference $\cos \omega_0 t$, is

$$e_t = x \cos \omega_0 t + \left(\frac{dx}{dt}/\omega_0\right) \sin \omega_0 t \quad (45)$$

Hence, the transfer functions relating the modulations of the direct and quadrature components of e_t to the data signal, are, respectively: $\mathbf{G}_{dt} = 1$; $\mathbf{G}_{qt} = s/\omega_0$.

The direct component of e_t, on being transmitted through the network $\mathbf{D}(j\omega)$, produces both a direct and a quadrature component, the modulations of which have, respectively, the transfer functions: $(\mathbf{G}_{dt})(\mathbf{G}_d) = \mathbf{G}_d$; $(\mathbf{G}_{dt})(\mathbf{G}_q) = \mathbf{G}_q$. The quadrature component of the signal e_t will produce a component in phase with it—another quadrature component—with the transfer function: $(\mathbf{G}_{qt})(\mathbf{G}_d) = (s/\omega_0)\mathbf{G}_d$. It will also produce a component in quadrature with it—and, hence, 180 degrees behind the modulator reference—which is a direct component subtracting from $\mathbf{G}_d$: $-(\mathbf{G}_{qt})(\mathbf{G}_q) = -(s/\omega_0)\mathbf{G}_q$.

Consequently, the transfer function of the modulation of the total direct component of e_o, is

$$\mathbf{G}_{dt} = \mathbf{G}_d - (s/\omega_0)\mathbf{G}_q \quad (46)$$

while that for the total quadrature component is

$$\mathbf{G}_{qt} = \mathbf{G}_q + (s/\omega_0)\mathbf{G}_d \quad (47)$$

In an analysis of the 2-phase motor by N. B. Nichols,[7] which made numerous simplifying assumptions, the equation for the torque, when the reference-winding voltage is $\sin \omega_0 t$, was derived.

$$T = e_o \cos \omega_0 t - \left(\frac{de_o}{dt}/\omega_0\right) \sin \omega_0 t \quad (48)$$

If e_o, the control-winding voltage, contains direct and quadrature components as shown in equation 30, equation 48 becomes (after employing the double-angle trigonometric formulas),

$$T = e_{md} - (1/2\omega_0)\frac{de_{mq}}{dt} + \left(\frac{de_{mq}}{dt}/2\omega_0\right) \times \cos 2\omega_0 t + \left[e_{mq} - \left(\frac{de_{md}}{dt}/2\omega_0\right)\right] \times \sin 2\omega_0 t \quad (49)$$

Neglecting the sinusoid terms, since, being of such high frequency, they do not produce real torque, the transfer function relating the torque to the data signal is

$$\mathbf{T}/\mathbf{X} = \mathbf{G}_{dt} - (1/2\omega_0)s\mathbf{G}_{qt} \quad (50)$$

$$= \mathbf{G}_d[1 - (s^2/2\omega_0^2)] - 3s\mathbf{G}_q/2\omega_0 \quad (51)$$

Appendix IV

Examples of Carrier-Frequency Lead Networks

Let us investigate two commonly used carrier-frequency lead networks. In the first, shown in Figure 12, the elements within the dotted lines represent the equivalent circuit of an inductor, where R_c and R_e account for the copper and eddy-current losses respectively. If we let the carrier frequency ω_0 be $1/\sqrt{LC}$, the transfer function of the network may be expressed in the form

$$\mathbf{D}(s) = \frac{s^2 + 2\omega_1 s + (r_1\omega_0)^2}{s^2 + 2\omega_2 s + (r_2\omega_0)^2} \quad (52)$$

where

$$r_1 = [1 + (R_c/R_e)]^{-1/2} \approx 1 \quad (53)$$

$$r_2 = [1 + (1/R_e)(R_1 + R_c)]^{-1/2} \approx 1 \quad (54)$$

$$\omega_1 = \frac{R_c + (L/R_eC)}{2L(1 + (R_c/R_e))} \approx \frac{R_c}{2L} + \frac{1}{2R_eC} \quad (55)$$

$$\omega_2 = \frac{(R_1 + R_c) + (L/R_eC)}{2L(1 + (1/R_e)(R_1 + R_c))} \approx \omega_1 + \frac{R_1}{2L} \quad (56)$$

Ordinarily, for most inductors employed, R_e is much greater than R_c, and, hence, the quantities r_1, r_2 are very close to unity, which means that the quadratics of $D(s)$ (equation 52) are essentially balanced about the carrier. If this were not so, it might be better to adjust the elements so that the carrier is equal to $(r_1\omega_0)$ or $(r_2\omega_0)$—preferably the former, since the numerator contains the lower break frequency.

It is obvious that $\mathbf{D}(s)$ will approximately simulate the data-frequency function:

$$\mathbf{G}'(s) = (s + \omega_1)/(s + \omega_2) \quad (57)$$

which is a lead network, since ω_1 is less than ω_2. The main limitation on this network, however, is that the lowest value one can obtain for ω_1 is given approximately by the equation: $\omega_1/\omega_0 = 1/2Q_o$, where Q_o is the quality of the coil at carrier frequency.

A circuit which behaves very much like the inductance-capacitance network described previously, but which is capable of a much higher effective Q, is the parallel T. A symmetric form of the parallel T which is quite useful is shown in Figure 13. It has the transfer function

$$\mathbf{D}(s) = \frac{[s^2(RC)^2 + s(RC)((2/\gamma) - 1) + 1][s(RC) + 1]}{[s^2(RC)^2 + s(RC)(1 + (2/\gamma) + \gamma) + 1][s(RC) + 1]} \quad (58)$$

If the carrier frequency ω_o is $1/RC$, this reduces to equation 53, where r_1 and r_2 are unity and

$$\omega_1 = [(1/\gamma) - (1/2)]\omega_o \quad (59)$$

$$\omega_2 = [(1/2) + (1/\gamma) + (\gamma/2)]\omega_o \quad (60)$$

Consequently, this network will also simulate equation 57. In this case, however, ω_1 can be reduced as low as desired—even to zero—but ω_2 cannot be reduced below the value $(1/2 + \sqrt{2})\omega_o$, or approximately $2\omega_o$. Hence, this requires an attenuation ratio of the lead network of at least $2\omega_o/\omega_1$, which for small values of ω_1 will be quite large; and, hence, the servo may be excessively bothered by noise.

Unsymmetric parallel-T networks may be employed;[5] but even for the general case, ω_2 cannot be reduced below the value ω_o. Besides, in order to avoid low input impedance, ω_2 should not be allowed to approach too closely to ω_o.

A more promising way of reducing the attenuation ratio is by the use of negative feedback, as illustrated in Figure 14. The over-all transfer function becomes

$$\mathbf{D}(s) = \frac{K_1}{1 + K_1K_2} \times \frac{s^2 + 2\omega_1 s + \omega_o^2}{s^2 + [(2s)(2\omega_o + K_1K_2\omega_1)/(1 + K_1K_2)] + \omega_o^2} \quad (61)$$

Thus, the upper break frequency ω_2 can be lowered to the value

$$\omega_2 = (2\omega_o + K_1K_2\omega_1)/(1 + K_1K_2) \approx 2\omega_o/(1 + K_1K_2) \quad (62)$$

Appendix V

Important Symbols

$\mathbf{C}_d = \mathbf{G}_d/\mathbf{G}_m$ = deviation of $\mathbf{G}_d$ from its approximation $\mathbf{G}_m$

$\mathbf{C}_q = \mathbf{G}_q/\mathbf{G}_m \sin\delta$ = deviation of $\mathbf{G}_q$ from its approximation $\mathbf{G}_m \sin\delta$

$\mathbf{D}$ = realizable carrier-frequency function approximately simulating $\mathbf{G}'$

$\mathbf{D}'$ = carrier-frequency function exactly simulating $\mathbf{G}'$

$\mathbf{D}^+$, $\mathbf{D}^-$ = the values of the function $\mathbf{D}$ at the frequencies $(\omega_o+\omega_m)$, $(\omega_o-\omega_m)$

e_i = input to network $\mathbf{D}(j\omega)$; output from modulator

e_o = output from network; input to demodulator

$e_{md}(t)$, $\mathbf{E}_{md}$ = modulation, and its transform, of direct component of e_o

$e_{mq}(t)$, $\mathbf{E}_{mq}$ = modulation, and its transform, of quadrature component of e_o

$\mathbf{G}'$ = desired data-frequency function

$\mathbf{G}^+$, $\mathbf{G}^{*-}$ = sideband plots of $\mathbf{D}$

$\mathbf{G}_d$, $\mathbf{G}_q$ = transfer functions relating respectively $\mathbf{E}_{md}$ and $\mathbf{E}_{mq}$ to $\mathbf{X}$

$\mathbf{G}_m$ = graphical average of the plots of magnitude (in decibels) and phase of $\mathbf{G}^+$, $\mathbf{G}^{*-}$; a first approximation of $\mathbf{G}_d$

$x(t)$, $\mathbf{X}$ = data signal and transform; the modulation of e_i, and its transform

$\delta = \underline{/G^{*-}} - \underline{/G_m} = \underline{/G_m} - \underline{/G^+}$

$\epsilon = \overline{|G^{*-}|/|G_m|} = |G_m|/|G^+|$

ω = general frequency variable

ω_m = frequency of data signal

ω_o = (nominal) carrier frequency

$\Delta\omega_A$ = interval of shift for determining sideband dissymmetry

$\Delta\omega_o$ = interval of carrier-frequency drift

References

1. Principles of Servomechanisms (book), **G. S. Brown, D. P. Campbell.** John Wiley and Sons, Inc., New York, N. Y., 1948.

2. Theory of Servomechanisms (book), **H. M. James, N. B. Nichols, R. S. Phillips.** Massachusetts Institute of Technology Radiation Laboratory Series, volume 25, McGraw-Hill Book Company, Inc., New York, N. Y., 1947.

3. Stabilization of Carrier Frequency Servomechanisms, **A. Sobczyk.** *Journal*, Franklin Institute (Philadelphia, Pa.), July, August, September, 1948.

4. Phase Lead for A-C Servo Systems with Compensation for Carrier Frequency Changes, **A. P. Notthoff, Jr.** *AIEE Transactions*, volume 69, part I, 1950, pages 285–92.

5. Reference 2, pages 117–24.

6. Reference 1, chapter 8.

7. Reference 3, July 1948, page 37.

No Discussion

A Note on the Design of Conditionally Stable Feedback Systems

PAUL TRAVERS
ASSOCIATE AIEE

IT IS THE PURPOSE of this paper to present, for a class of conditionally stable systems, equations which relate parameters of the loop transfer function to the relative stability of the system transfer function and to indicate the condition for which the system bandwidth is a minimum when the magnitude of the loop function is required to have a specified value at a specific frequency.

A conditionally stable system becomes unstable when the loop gain is reduced sufficiently from the normal value. The dependence of loop gain upon system bandwidth in the case of absolutely stable systems has been shown by H. W. Bode.[1] The advantage of the conditionally stable system lies in the fact that larger loop gains are permitted compared to absolutely stable systems of the same bandwidth, or, for the same loop gain, a smaller bandwidth is required.

The problem of determining the increase in loop gain which can be obtained in going from an absolutely to a conditionally stable system is one which naturally suggests itself. Inasmuch as there does not appear to be a unique function which defines the conditionally stable system, a function is selected to satisfy the requirements of mathematical simplicity and approximate correspondence to practical structures.

Some of the results of this analysis are compared to a related study[2] in order to indicate the difference in analytical procedure.

Paper 51-102, recommended by the AIEE Feedback Control Systems Committee and approved by the AIEE Technical Program Committee for presentation at the AIEE Winter General Meeting, New York, N. Y., January 22–26, 1951. Manuscript submitted March 14, 1950; made available for printing December 12, 1950.

PAUL TRAVERS is with the Massachusetts Institute of Technology, Cambridge, Mass.

This work was sponsored by the United States Air Force (Armament Laboratory, Air Materiel Command), under Contract number W-33-038ac-13969.

Formulation of the Problem

Figure 1 depicts the salient characteristics of the type of feedback system to be considered. Conditionally stable systems are to be analyzed for which the useful gain A is specified as a requirement over a useful band of frequencies, the upper limit of which is ω_a. For reasons which will be apparent later, the effective bandwidth of the system is characterized by ω_m. At this frequency the system function has a maximum magnitude M_{max} which is a measure of the degree of stability of the system.

The argument of D. Herr and I. Gerst[2] relative to the desirability of minimizing the system bandwidth is pertinent here. They point out that the two principal reasons for minimizing the system bandwidth are: (1) to minimize the transmission of noise by the system; and (2) to require the lowest frequency-response characteristic for the physical elements of the system.

The loop function class analyzed by Herr and Gerst is particularly appropriate to the problem at hand. This loop function is

$$KG(j\omega) = \frac{K\left(1+\frac{j\omega}{\omega_1}\right)^s}{(j\omega)^r\left(1+\frac{j\omega}{\omega_2}\right)^t} \qquad (1)$$

where $r \geq 2$ and $t \geq 1$. The parameters r, s, and t are variables which control the attenuation rate and ω_1 and ω_2 are the corner frequencies associated with the logarithmic representation of the loop-function magnitude which is shown in Figure 2.

The problem may be stated explicitly: given A, M_{max}, and the high-frequency attenuation rate, determine that attenuation rate r_0 which minimizes ω_m/ω_a, the bandwidth ratio.

Before proceeding with the solution, the relevant work of Mr. Herr and Mr. Gerst is reviewed.

The Analysis of Herr and Gerst

The significance of Herr and Gerst's organization of a systematic approach to the synthesis of feedback systems results mainly from their comprehension of the suitability of the class of functions studied. This review is necessarily brief and mentions only those aspects which are pertinent to this paper.

Herr and Gerst used for a normalizing frequency the intersection of the extension of the low-frequency asymptote with the 0-decibel ordinate (shown in Figure 2 as having the value $\sqrt[r]{K}$). With four combinations of r, s, and t to define the functions analyzed, they determined the useful loop and system function param-

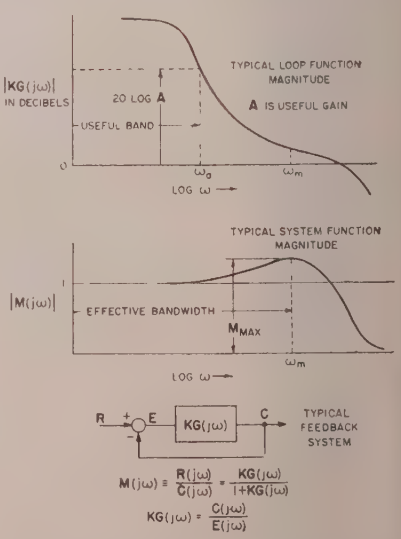

Figure 1. Loop function and system function versus frequency and schematic for typical feedback system

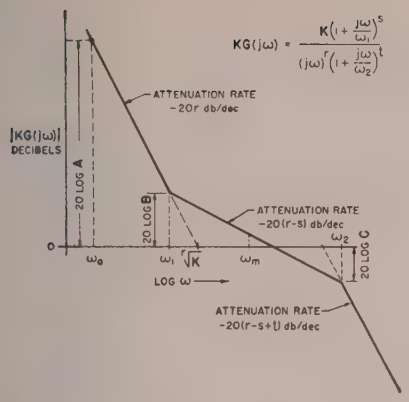

eters in the frequency domain and the system response in the time domain for the constraint that the ratio $\omega_2/\sqrt[r]{K}$ be a minimum for the specified M_{max}. They obtained the two corner frequencies $\omega_1/\sqrt[r]{K}$ and $\omega_2/\sqrt[r]{K}$ which completely determined the loop and system functions for each set of r, s, t, and M_{max}.

A straightforward approach to the problem of determining the optimum low-frequency attenuation rate would be to extend the analysis of Herr and Gerst by selecting other sets of r, s, and t and by trial-and-error noting when $\omega_2/\sqrt[r]{K}$ is a minimum. This is not a practical method because of the complexity of the algebra involved when large values of r and t are used. The complexity of the results based on minimizing $\omega_2/\sqrt[r]{K}$ may be observed by noting the polar co-ordinates

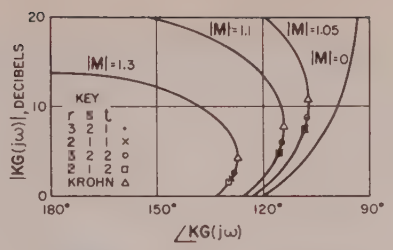

Figure 2 (left). Asymptote representation of the magnitude of the loop function

Figure 3 (above). The points of tangency of Herr and Gerst compared with those of Krohn

of the loop function at ω_m, that is, the point of tangency to the M-contour. Figure 3 shows that $KG(j\omega_m)$ varies with r, s, and t when M_{max} is fixed.

The reason for emphasizing the co-ordinates of $KG(j\omega_m)$ is to consider a criterion for which $KG(j\omega_m)$ has a single value for each M_{max}. This criterion, noted by Krohn,[3] states that from the standpoint of utilizing the maximum phase margin of a system, the loop transfer function should be tangent to the M-contour at the point of maximum phase margin, providing the curvature of the loop function does not exceed the curvature of the M-contour. The curvature requirement is satisfied by setting s equal to r-1 in equation 1. Phase margin is taken here to be the sum of the loop-function phase and π radians. The subsequent analysis shows that, starting with Krohn's criterion, the optimum low-frequency attenuation rate can be found. To the extent of using Krohn's criterion, this paper diverges from the approach of Herr and Gerst. The analysis also includes a comparison of the important frequencies obtained from each of the procedures and concludes that, except for the relative values for ω_m, the differences between the two methods for determining the tangent point are not significant.

Analysis Based on Krohn's Criterion

The polar co-ordinates of $KG(j\omega)$ at ω_m can be expressed as a function of M_{max},

$$|KG|(j\omega_m)| = M_{max}/\sqrt{M^2_{max}-1} \qquad (2)$$

$$/KG(j\omega_m) = (\sin^{-1}1/M_{max}) - \pi \qquad (3)$$

Since the phase of $KG(j\omega)$ is a maximum at ω_m, the differentiation of the expression for phase angle obtained from equation 1 and the use of equation 3 permits the corner frequencies and their ratios with ω_m to be obtained as functions of r, t, and M_{max}.

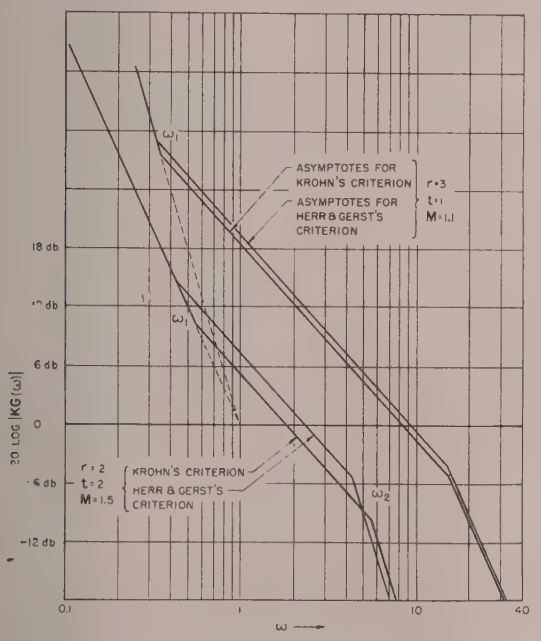

Figure 4 (above). Comparison of two sets of asymptotes

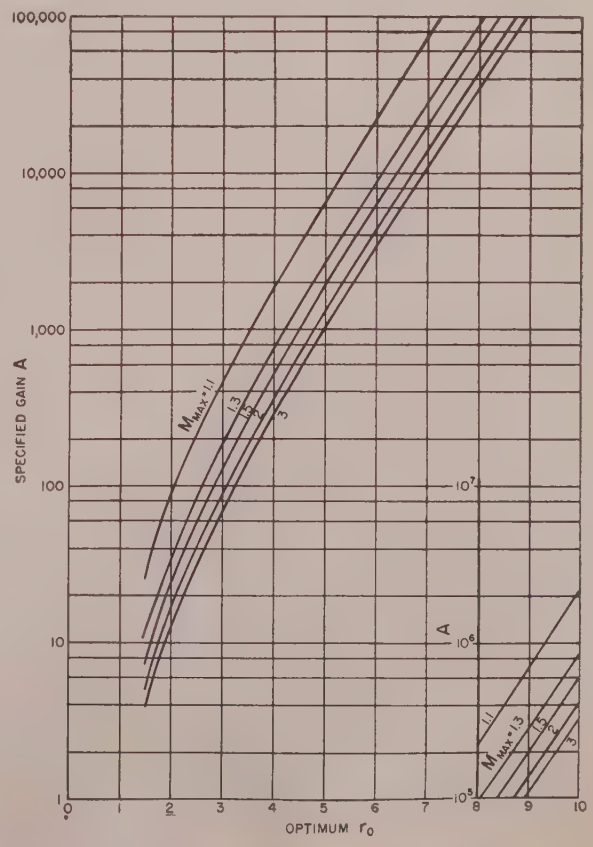

Figure 5 (right). The optimum r_0 for minimum ω_m/ω_a as a function of specified gain A and relative stability M

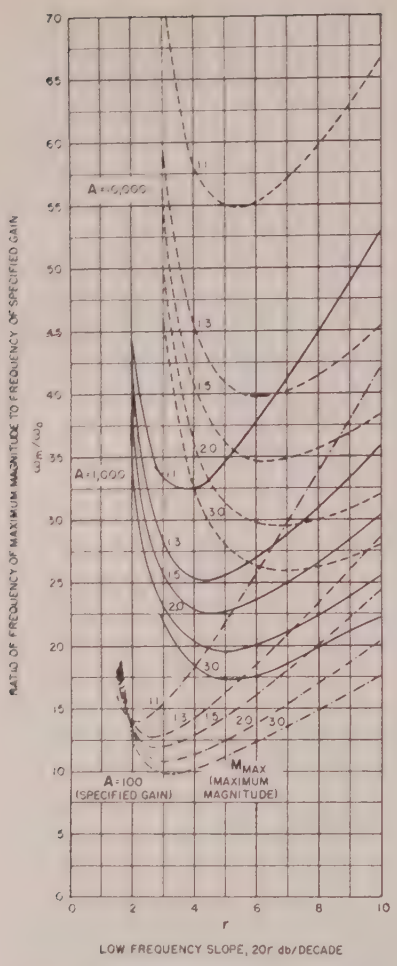

Figure 6. Bandwidth as a function of low-frequency slope

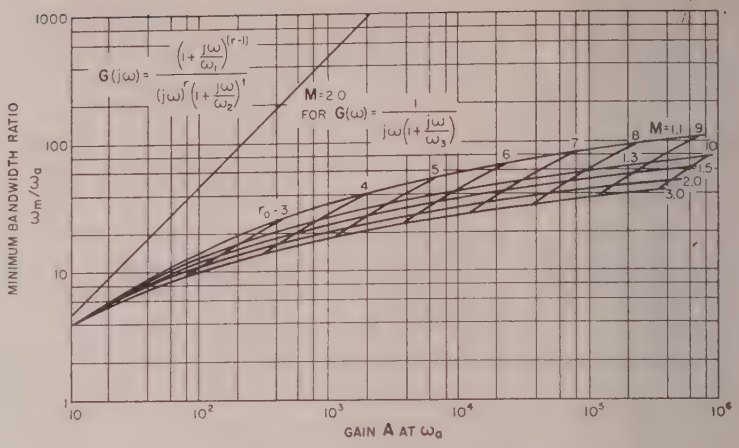

Figure 7. Minimum bandwidth ratio as a function of specified gain

$$\frac{\omega_2}{\sqrt[r]{K}}=2t[2(r-1)]^{\frac{r-1}{r}}\left(\cos^{-1}\frac{1}{M_{\max}}\right)^{\frac{1-2r}{r}}\times$$

$$(M_{\max}/\sqrt{M^2_{\max}-1})^{-\frac{1}{r}} \quad (7)$$

When $\sqrt[r]{K}$ is set equal to unity, ω_2 from equation 7 can be compared with the value b' given by Herr and Gerst to determine how much bandwidth is sacrificed when Krohn's criterion is used. Table I is a comparison for four combinations of r and t and for three values of $M_{\max}$. The values for b' are, with one exception, slightly lower than those for ω^2. However, the response of the system to noise at high frequencies is not simply a function of ω_2, but of the frequency of intersection of the extension of the high-frequency asymptote with the 0-decibel ordinate. This frequency is a function of ω_2, t, and the loop-function asymptote gain at ω_2.

To illustrate this point two pairs of asymptotes are plotted in Figure 4, using values for the frequencies which are normalized so that $\sqrt[r]{K}$ equals unity. In the case of $r=2$, $t=2$, $M=1.5$, the high-frequency asymptote determined by Herr and Gerst lies slightly below that obtained from equations 4 to 7. In the second case where $r=3$, $t=1$, $M=1.1$, the situation is reversed even though the value of ω_2 of Herr and Gerst is the lesser. The difference in each case is small, and one concludes that it is negligible as far as the noise response caused by the high-frequency asymptote is concerned.

Table II compares the values of $\omega_m/\sqrt[r]{K}$ with Herr and Gerst's x_m for four combinations of r and t and for three values of $M_{\max}$. The values for x_m are higher by 25 to 40 per cent. The comparison of the noise-transmission characteristics resulting from the differences in ω_m is outside the scope of this paper, but may well be the object of future work.

Table III compares two sets of corner-frequency ratios, ω_2/ω_1 and b'/a' and the values for b'/a' are higher but not significantly so.

$$\omega_2/\omega_1=4(r-1)t/\left(\cos^{-1}\frac{1}{M_{\max}}\right)^2 \quad (4)$$

$$\omega_m/\omega_1=2(r-1)/\cos^{-1}\frac{1}{M_{\max}} \quad (5)$$

$$\omega_2/\omega_m=2t/\cos^{-1}\frac{1}{M_{\max}} \quad (6)$$

The details leading to these results are given in the Appendix.

It is noted that ω_m/ω_1 is not dependent on t and ω_2/ω_m is not dependent on r. The use of Krohn's criterion with this class of loop functions permits the separation about ω_m of the effects of the low- and high-frequency attenuation rates. This separation is the justification for defining the effective bandwidth as ω_m. The effective bandwidth is independent of t, and t is used only to determine ω_2/ω_m.

Equations 2, 5, and 6 are used to determine the ratio of ω_2 and the intersection of the extension of the low-frequency asymptote with the 0-decibel ordinate in Figure 2, $\sqrt[r]{K}$.

Table I. Comparison of $\omega_2/\sqrt[r]{K}$ with b'

r	t	M = 1.1 $\omega_2/\sqrt[r]{K}$	M = 1.1 b'	M = 1.3 $\omega_2/\sqrt[r]{K}$	M = 1.3 b'	M = 1.5 $\omega_2/\sqrt[r]{K}$	M = 1.5 b'
3	1	15.29	14.96	8.040	7.402	6.09	5.338
2	1	6.455	6.094	3.925	3.310	3.16	2.431
3	2	30.58	30.70	16.08	15.90	12.18	12.11
2	2	12.91	12.61	7.85	7.402	6.32	5.76

Table II. Comparison of $\omega_m/\sqrt[r]{K}$ with x_m

r	t	M = 1.1 $\omega_m/\sqrt[r]{K}$	M = 1.1 x_m	M = 1.3 $\omega_m/\sqrt[r]{K}$	M = 1.3 x_m	M = 1.5 $\omega_m/\sqrt[r]{K}$	M = 1.5 x_m
3	1	3.279	4.213	2.789	3.681	2.565	3.569
2	1	1.385	1.965	1.362	1.914	1.331	1.878
3	2	3.279	4.114	2.789	3.554	2.565	3.372
2	2	1.385	1.949	1.362	1.884	1.331	1.825

Table III. Comparison of ω_2/ω_1 with b'/a'

		M = 1.1		M = 1.3		M = 1.5	
r	t	ω_2/ω_1	b'/a'	ω_2/ω_1	b'/a'	ω_2/ω_1	b'/a'
3	1	43.26	44.01	16.66	17.41	11.3	12.12
2	1	21.63	22.24	8.33	8.98	5.65	6.35
3	2	86.52	88.50	33.32	35.35	22.6	24.94
2	2	43.26	43.80	16.66	17.43	11.3	11.98

In summarizing the comparisons it may be said that, to the same frequency scale, the resonant frequencies of Herr and Gerst are consistently higher to a greater degree than the extent of the differences between the high-frequency asymptotes.

The bandwidth ratio ω_m/ω_a is derived in the Appendix from equations 2 and 5

$$\frac{\omega_m}{\omega_a} = [(A\sqrt{M_{\max}^2-1}/M_{\max})]^{\frac{1}{r}} \times \left[2(r-1)\cos^{-1}\frac{1}{M_{\max}}\right]^{\frac{r-1}{r}} \quad (8)$$

Differentiation of equation 8 with respect to r gives the optimum r_0 which minimizes ω_m/ω_a,

$$(r_0-1)\epsilon^{r_0} = [A\sqrt{M_{\max}^2-1}/2M_{\max}]\times \cos^{-1}\frac{1}{M_{\max}} \quad (9)$$

The optimum r_0 is plotted in Figure 5 as a function of A for five values of $M_{\max}$. The bandwidth ratio ω_m/ω_a as a function of r for specified values of A and $M_{\max}$ is depicted in Figure 6 to indicate the nature of the optimization. In Figure 7 the minimum bandwidth ratio is drawn as a function of the specified gain for the conditionally stable systems of equation 1 and for a simple absolutely stable system characterized by the loop function

$$KG(j\omega) = \frac{K}{j\omega\left(1+j\frac{\omega}{\omega_3}\right)}$$

The curve of bandwidth ratio as a function of r shows that the minimization is less critical when $M_{\max}$ is increased, and that the slope is greater for values of r less than r_1 than it is for values of r greater than r_0.

Conclusions

With the conditionally stable systems of Herr and Gerst as the basis for study, it has been shown that the loop function parameters can be explicitly related to the degree of stability when the loop-gain criterion of Krohn is used. Furthermore, it is demonstrated that the loop-gain setting of Herr and Gerst based on minimizing the upper-corner frequency leads to essentially the same high-frequency asymptote as does the loop-gain setting of Krohn based on tangency to the M-contour at the frequency of maximum phase-margin. The major difference between the two gain criteria lies in the frequency at which the system function is a maximum and the latter criterion results in the lower frequency. For the systems studied, the principal advantage of Krohn's criterion is that the polar coordinates of the loop function at the frequency of tangency to the M-contour is a function only of the degree of stability $M_{\max}$. This simplifying dependence upon $M_{\max}$ allows the effect of the loop parameter r upon the system bandwidth ratio to be analyzed, and it is found that an optimum r_0 exists which is a function of the useful gain A and the degree of stability $M_{\max}$ and for which the bandwidth ratio is a minimum.

This study complements the analysis of Herr and Gerst in that an alternative gain-setting criterion has been established and the effect of varying r has been investigated.

Appendix

From the loop function

$$KG(j\omega) = \frac{K\left(1+\frac{j\omega}{\omega_1}\right)^{(r-1)}}{(j\omega)^r\left(1+\frac{j\omega}{\omega_2}\right)^t} \quad (1)$$

the phase margin ϕ is obtained

$$\phi(\omega) \triangleq /KG(j\omega)+\pi = (r-1)\tan^{-1}\frac{\omega}{\omega_1} - t\tan^{-1}\frac{\omega}{\omega_2} - (r-1)\frac{\pi}{2}+\frac{\pi}{2} \quad (10)$$

Differentiating (10) and equating to zero

$$\frac{\partial\phi(\omega)}{\partial\omega} = \frac{(r-1)\omega_1}{\omega_1^2+\omega^2} - \frac{t\omega_2}{\omega_2^2+\omega^2} = 0 \quad (11)$$

the frequency ω_m at which ϕ is a maximum is obtained

$$\omega_m = \omega_2\sqrt{\frac{1}{\psi}\frac{\psi\rho-1}{\psi-\rho}} \quad (12)$$

where

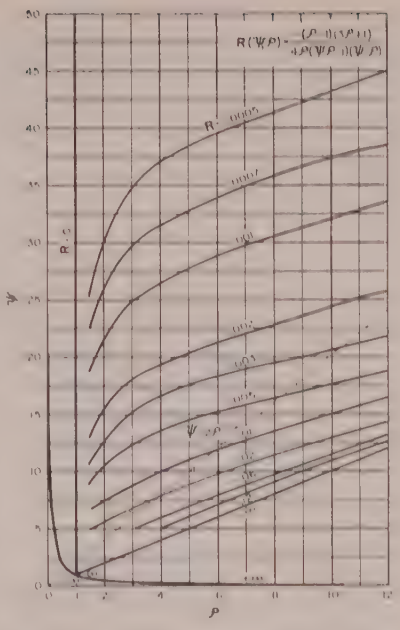

Figure 8. Loci of constant R in the ψ, ρ plane

$$\rho \triangleq \frac{\Delta r}{t} - 1$$

and

$$\psi \triangleq \frac{\omega_2}{\omega_1} \quad (13)$$

Equation 12 is substituted in equation 10

$$\psi_{\max} = t\left[\rho\tan^{-1}\sqrt{\psi\frac{\psi\rho-1}{\psi-\rho}} - \tan^{-1}\sqrt{\frac{1}{\psi}\frac{\psi\rho-1}{\psi-\rho}} - \rho\frac{\pi}{2}+\frac{\pi}{2t}\right] \quad (14)$$

The $\tan^{-1}$ functions are approximated

$$\phi_{\max} = t\left[\rho\left(\frac{\pi}{2}-\sqrt{\frac{1}{\psi}\frac{\psi-\rho}{\psi\rho-1}}\right) - \sqrt{\frac{1}{\psi}\frac{\psi\rho-1}{\psi-\rho}} - \rho\frac{\pi}{2}+\frac{\pi}{2t}\right] \quad (15)$$

ψ is obtained as

$$\psi = \frac{4t^2\rho}{\left(\frac{\pi}{2}-\phi_{\max}\right)^2}[1+R(\psi,\rho)] \quad (16)$$

where R is

$$R(\psi,\rho) = -\frac{(\rho-1)(3\rho+1)}{4\rho(\psi\rho-1)(\psi-\rho)} \quad (17)$$

Figure 8 shows the loci of constant R in the ψ, ρ plane. The range of parameters r, t, M likely to be encountered lie in the region above the line $\psi=2\rho$, and it can be seen that $R \ll 1$ so that R may be neglected in equation 16.

From equation 16 and 3

$$\psi \approx \frac{\omega_2}{\omega_1} = \frac{4(r-1)t}{\left(\cos^{-1}\frac{1}{M_{\max}}\right)^2} \quad (4)$$

It can be demonstrated that neglecting R in equation 16 is equivalent to approximating $(\psi\rho-1)/(\psi-\rho)$ by ρ in equation 12, then, when equation 4 is substituted in equation 12,

$$\frac{\omega_m}{\omega_1}=\frac{2(r-1)}{\cos^{-1}\frac{1}{M_{max}}} \tag{5}$$

and

$$\frac{\omega_2}{\omega_m}=\frac{2t}{\cos^{-1}\frac{1}{M_{max}}} \tag{6}$$

In Figure 2 the gain at ω_m is, from equation 2,

$$20\log\frac{M_{max}}{\sqrt{M_{max}^2-1}}$$

The gain at ω_1 is

$$20\log\left(\frac{2(r-1)}{\cos^{-1}\frac{1}{M_{max}}}\ \frac{M_{max}}{\sqrt{M_{max}^2-1}}\right)$$

The gain at ω_a is

$$20r\log\frac{\omega_1}{\omega_a}+20\log\times\left(\frac{2(r-1)}{\cos^{-1}\frac{1}{M_{max}}}\ \frac{M_{max}}{M_{max}^2-1}\right)=20\log A$$

The frequency ratio ω_1/ω_a is

$$\frac{\omega_1}{\omega_a}=\left(\frac{A\sqrt{M_{max}^2-1}}{M_{max}}\right)^{\frac{1}{r}}\left(\frac{2(r-1)}{\cos^{-1}\frac{1}{M_{max}}}\right)^{-\frac{1}{r}}$$

Using equations 4 and 5, ω_m/ω_a and ω_2/ω_a are

$$\frac{\omega_m}{\omega_a}=\left(\frac{A\sqrt{M_{max}^2-1}}{M_{max}}\right)^{\frac{1}{r}}\left(\frac{2(r-1)}{\cos^{-1}\frac{1}{M_{max}}}\right)^{-\frac{r-1}{r}} \tag{8}$$

$$\frac{\omega_2}{\omega_a}=\left(\frac{A\sqrt{M_{max}^2-1}}{M_{max}}\right)^{\frac{1}{r}}\left(\frac{2(r-1}{\cos^{-1}\frac{1}{M_{max}}}\right)^{\frac{r-1}{r}}\times\left(\frac{2t}{\cos^{-1}\frac{1}{M_{max}}}\right)$$

To find the optimum r_0 equation 8 is differentiated with respect to r and equated to zero, and the transcendental equation which is obtained is

$$(r_0-1)\epsilon^{r_0}=\frac{A\sqrt{M_{max}^2-1}}{2M_{max}}\left(\cos^{-1}\frac{1}{M_{max}}\right) \tag{9}$$

In Figure 2 $\sqrt[r]{K}$ is obtained from the equation

$$20\,r\log\frac{\sqrt[r]{K}}{\omega_1}=20\log\left(\frac{2(r-1)}{\cos^{-1}\frac{1}{M_{max}}}\ \frac{M_{max}}{\sqrt{M_{max}^2-1}}\right)$$

$$K=\omega_1{}^r\frac{2(r-1)}{\cos^{-1}\frac{1}{M_{max}}}\ \frac{M_{max}}{\sqrt{M_{max}^2-1}}$$

Using equation 5

$$K=\omega_m{}^r\left(\frac{2(r-1)}{\cos^{-1}\frac{1}{M_{max}}}\right)^{1-r}\ \frac{M_{max}}{\sqrt{M_{max}^2-1}}$$

References

1. Network Analysis and Feedback Amplifier Design (book), **H. W. Bode.** D. Van Nostrand Company, Inc., New York, N. Y., 1945, chapter 18.

2. The Analysis and an Optimum Synthesis of Linear Servomechanisms, **D. Herr, I. Gerst.** *AIEE Transactions*, volume 66, 1947, pages 959–70.

3. Theory of Servomechanisms (book), **H. M. James, N. B. Nichols, R. S. Phillips.** McGraw-Hill Book Company, Inc., New York, N. Y., 1947, page 182.

No Discussion

A Phase-Plane Approach to the Compensation of Saturating Servomechanisms

ARTHUR M. HOPKIN
ASSOCIATE AIEE

THE GENERAL approach to the analysis of servomechanisms is one which is based on the assumption that the dynamics of the system can be expressed to a reasonable degree of accuracy by linear differential equations.[1] It is then possible to use frequency response methods and Laplace transform type of analysis.

An idealized system represented by such a linear approximation is shown in the block diagram and equations of Figure 1. The particular ideal system represented would give an instantaneous following of all inputs with no error as a result of the first- and second-order derivative compensation paths. However, any actual physical system will depart from the idealized system when there is some large error, or a large output velocity, or large output acceleration, since there is a maximum limiting value of all physically generated quantities.

When this limiting or saturation occurs anywhere in the system the idealized linear representation is not valid and can no longer be used to describe the servomechanism performance. If the servomechanism is to be a high-performance device, then in all probability it must be designed to follow input signals whose velocity and acceleration are high enough to produce saturation in some part of the system. For this case the analysis based on linear approximation fails. There are then two alternatives: to eliminate the source of saturation from the servomechanism, or to use some other approach which will lead to improved performance in spite of the saturation effects. This paper is concerned with the latter alternative.

The phase-plane analysis[2,3,4] will be used to synthesize servomechanisms, taking saturation effects into consideration. The dynamic performance of a second-order system can be completely specified in terms of two variables. It is customary to delineate the response of a system in terms of a plot of output displacement versus time for some given input. However, the same information can be displayed by relating other pairs of variables. For the purpose of this paper the phase-plane plot used will consist of a rectangular-coordinate plot of system velocity versus the system displacement at the same time instant. The locus or trajectory of the points in the phase plane will be used to describe the system performance.

The use of the phase-plane concept as a basis for analysis imposes an immediate limitation. The analysis can be applied only to systems whose differential equations of motion are of second order. Later there will be developed the requirement that the general shape of all the system trajectories be the same. This requirement places the further restriction on the system that the equation of motion contain no terms which are functions of position.

These two restrictions can be stated more precisely by saying that the discussion is restricted to servomechanisms in which the relationship between the manipulated variable m and the controlled variable c can be expressed by a differential equation of the form

$$m = f\left(\frac{dc}{dt}, \frac{d^2c}{dt^2}\right) \qquad (1)$$

In order to specify optimum performance of a servomechanism there first must be established some criterion of performance. For the purpose of this paper the following criterion of performance is set up:

> The optimum performance of a servomechanism shall be that behavior in which the system returns to rest with zero or minimum error in the shortest time following a step input.

The expression zero or minimum error is used to take into account the effect of coulomb friction.

This criterion for performance is a dynamic one and does not specify the steady-state error. Because it is based on a step input it does not specify the response to a constant-velocity input. However, this criterion does give a measure of system performance under many conditions. Later in the paper the response to constant-velocity inputs is considered and an additional criterion is implied in terms of the following of a constant-velocity input with minimum steady-state (constant-velocity output condition) error.

The objective of this paper can now be set forth. The first and major objective is to describe a control means that will give optimum performance when the servomechanism motor and load have been previously specified, using the performance criterion already established. The second and minor objective is to consider methods of modifying the control means of the servomechanism so that it will not only fulfill the given performance criterion but also will follow a constant-velocity input with a minimum following error when constant-velocity output is attained.

Paper 51-103, recommended by the AIEE Feedback Control Systems Committee and approved by the AIEE Technical Program Committee for presentation at the AIEE Winter General Meeting, New York, N. Y., January 22–26, 1951. Manuscript submitted October 21, 1950; made available for printing December 20, 1950.

ARTHUR M. HOPKIN is with Northwestern University, Evanston, Ill.

The author wishes to acknowledge the advice and assistance of Professor RICHARD W. JONES in the work leading to the preparation of this paper.

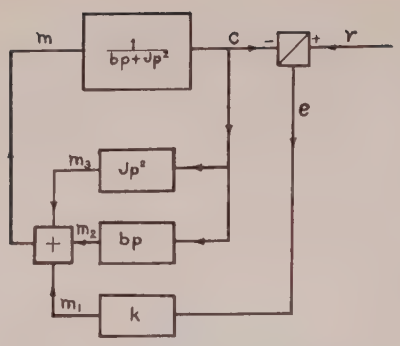

Figure 1. Ideal positioning control device with the following equations of motion

$(bp+Jp^2)c=m$

$r-c=e$

$m_1+m_2+m_3=kr-kc+bpc+Jp^2c=m$

$(bp+Jp^2)c=kr-kc+(bp+Jp^2)c$

$c=r$

This requires an error signal, a first derivative of the output, and a second derivative of the output

The Desired Performance of the Control Means

In order to make servomechanism output change from one position to another in a minimum time, the control means must be able to bring about the following operation:

1. The maximum safe forward value of manipulated variable must be applied from the instant of the step input until a specific later time. In response to this maximum safe value of manipulated variable, the servomechanism will be accelerated at a maximum rate for each value of output velocity.

2. At a specific time the manipulated variable must be reversed to a maximum safe reverse value so that the system will be decelerated at a maximum rate for each value of output velocity. The instant of reversal of the manipulated variable must be so selected that the system is decelerated to a stop precisely at the desired value of servomechanism output.

3. At the instant that the system stops at the desired value of output the manipulated variable must be returned to zero value so that the system will remain at rest at the desired value of output.

It must be shown that the above given performance of the control means results in the optimum performance for the system. Phase-plane relationships necessary to the proof first must be derived. Figure 2 shows a general phase-plane plot of the time derivative dx/dt of some response of a second-order system, plotted against the system displacement x. The slope M of the trajectory at some point P is

$$M=\frac{d}{dx}\frac{dx}{dt}$$

The product of the slope at point P and the value of dx/dt at point P is given by

$$\frac{dx}{dt}\cdot M=\frac{d}{dx}\frac{dx}{dt}\frac{dx}{dt}=\frac{d^2x}{dt^2}$$

Thus the expression for the acceleration at point P is

$$\frac{d^2x}{dt^2}=\frac{dx}{dt}M \qquad (2)$$

For a given value of dx/dt the acceleration of the system is proportional to the slope M of the phase-plane plot at that value of dx/dt. This relationship holds true for all points except where $dx/dt=0$. This property is used to give a comparison of acceleration at the same velocity in the phase plane.

The time required to go from one point to another in the phase plane can be determined from the following integral equation:

$$t_{a\to b}=t_b-t_a=\int_{t_a}^{t_b}dt=\int_{x_a}^{x_b}\frac{dt}{dx}dx=\int_{x_a}^{x_b}\frac{1}{\frac{dx}{dt}}dx \qquad (3)$$

A graphical interpretation of equation 3 shows that the time required to go from one point to another along a trajectory in the phase plane can be obtained by drawing an auxiliary graph of $1/dx/dt$ plotted versus x and measuring the area under this inverse plot between the x-co-ordinates of the two points involved; that is:

$$t_{a\to b}=\int_{x_a}^{x_b}\frac{1}{\frac{dx}{dt}}dx=\text{area under inverse curve from } x_a \text{ to } x_b \qquad (4)$$

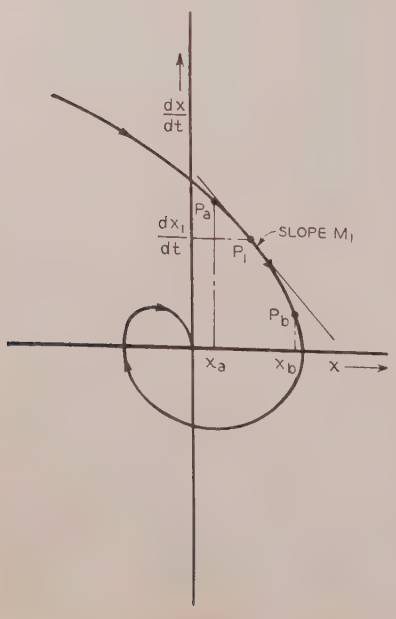

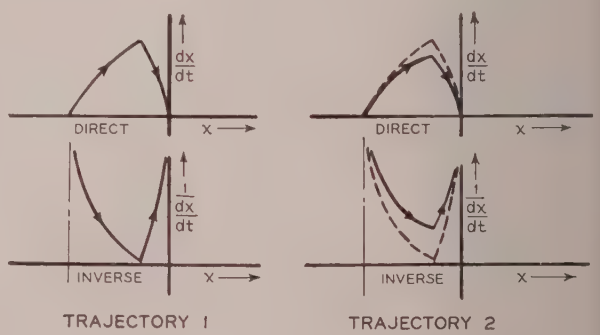

Figure 2 (left). A representative phase-plane plot

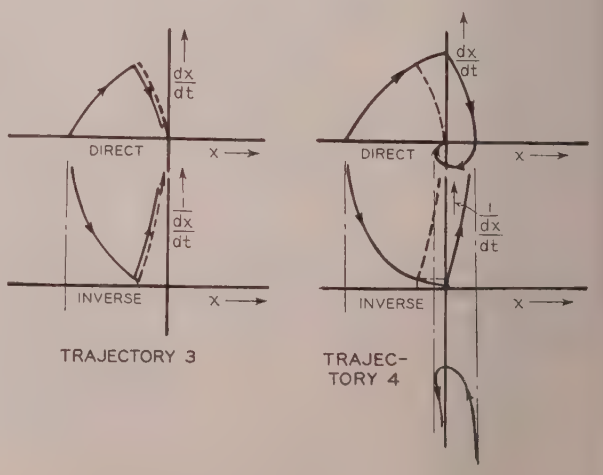

Figure 3 (right). Corresponding direct and inverse phase-plane plots for a second-order positioning system for four different cases

Trajectory 1 is dashed in on all plots for comparison

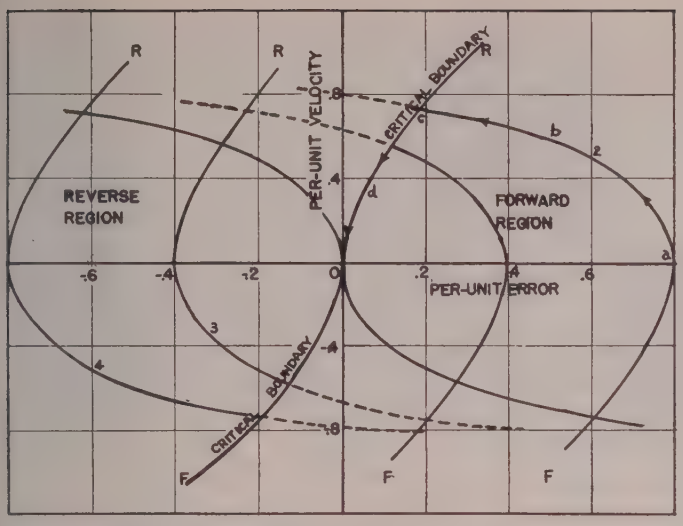

Figure 4. Phase-plane trajectories for a linear position controller

F represents trajectories for a forward value of manipulated variable. R represents trajectories for a reverse value of manipulated variable

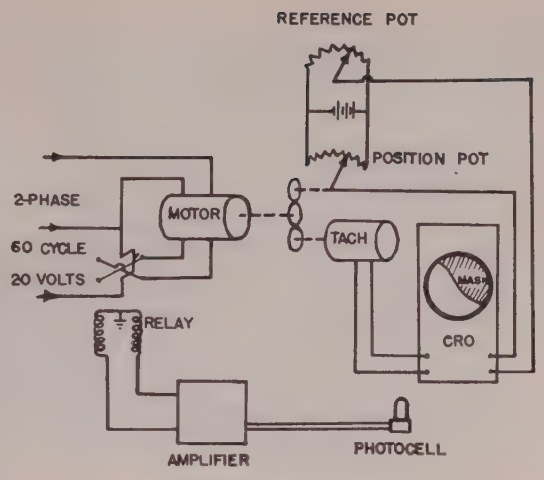

Figure 5. Schematic diagram of an oscilloscope-photocell anticipator servomechanism

Servomechanism system phase-plane trajectories representing the results of the application of different types of manipulated variable functions are shown in Figure 3. To facilitate discussions involving time, the plot of inverse velocity versus displacement was drawn directly below the direct plot for each type of manipulated variable function. Trajectory 1, in both direct and inverse plots, represents the performance with the optimum control means already described, and is dashed in on all of the plots for a comparison. It represents maximum acceleration for a specific time interval, and then maximum deceleration until the velocity becomes zero. The point of reversal of the manipulated variable is so selected that the system stops at the desired (zero) displacement. Trajectory 2 represents a similar performance except that both acceleration and deceleration are less than maximum for part of the trajectory. Trajectory 3 represents maximum acceleration and deceleration at all times but the point of reversal of the manipulated variable takes place too soon, with the result that the system tends to stop short of the desired displacement. This tendency is corrected by two more reversals of the manipulated variable. Trajectory 4 represents maximum acceleration and deceleration at all times but with the reversal of the manipulated variable too late, with resultant overshoot. Another reversal of the manipulated variable is required to bring the system to a stop at the desired displacement.

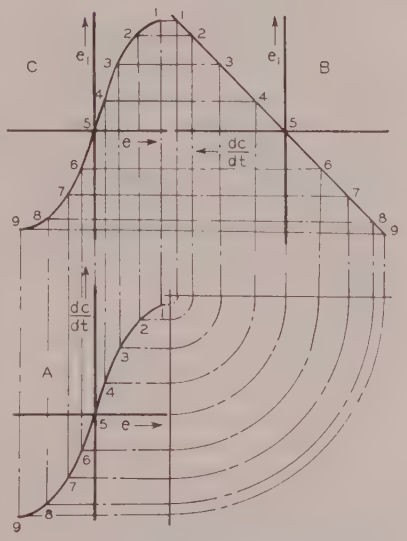

Figure 6. Graphical representation of linearization of the phase-plane critical boundary by use of a nonlinear network

Curve A is the boundary on the original phase-plane plot. Curve B is the desired linearized boundary. Curve C is the required nonlinear-network transfer function

Since the time required to go from one displacement to another is proportional to the total area bounded by the inverse curve, the x-axis, and the initial and final x-ordinates, examination of the trajectories of Figure 3 shows that the performance represented by Trajectory 1 involves the minimum time of any shown. Since all trajectories that differ from Trajectory 1 have less acceleration or deceleration, or have the initial reversal of the manipulated variable sooner or later than Trajectory 1, all trajectories differing from Trajectory 1 represent a longer time interval than does Trajectory 1. Hence Trajectory 1 represents optimum performance.

The Method of Obtaining the Desired Control Means Performance

In order to obtain the optimum performance, some type of switching device is required to apply the maximum safe value of manipulated variable in one

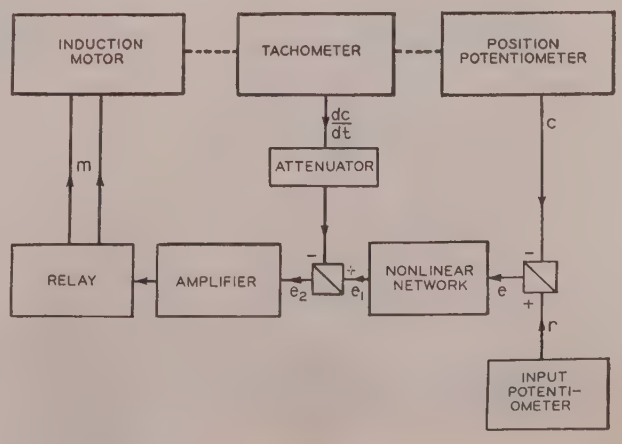

Figure 7. Block diagram for the shaded-pole induction motor servomechanism using a micropositioner relay and a nonlinear element type anticipator

direction, or the other, or not at all, as necessary. A device also is required to control the time of application, reversal, and removal of the manipulated variable so that the system output will traverse the minimum-time path in the phase plane. This device will be referred to as the anticipator. In order to set up the control means, a practical anticipator must be devised.

Figure 4 shows the phase-plane trajectories for a linear positioning system[b] with a constant maximum value of manipulated variable. The system is a closed loop system and the trajectories are plotted as output velocity versus error displacement. As a result the trajectories are a valid representation of the system dynamic performance only when the reference input is constant (as it is for a step input). In Figure 4 the error is considered positive when the output is less than the reference input. The velocity is considered positive when it is in such a direction as to correct for a positive error.

By referring to Figure 4, it can be seen that if the system is to come to zero velocity with zero error it must travel along one of the particular phase-plane trajectories which come into the origin in the first and third quadrants.

The locus made up of the combination

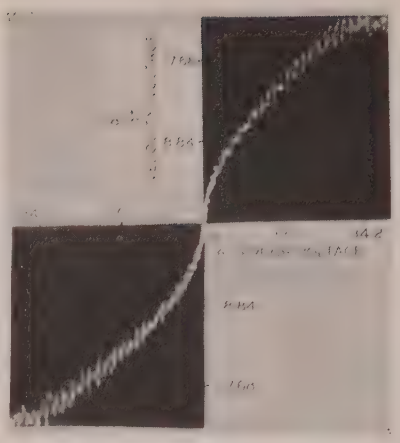

Figure 9. Phase-plane trajectories combined to make the critical boundary for the shaded-pole induction motor servomechanism

of these two particular trajectories which come into the origin shall be called the *critical boundary*. This critical boundary is the boundary in the phase plane at which the manipulated variable must be reversed in order to bring the system error to zero at zero velocity. For the control system to perform properly the relay which controls the manipulated variable must operate as follows:

1. It must be in a forward position whenever the system operating point is to the right of the critical boundary.
2. It must be in a reverse position whenever the system operating point is to the left of the critical boundary.
3. It must be open (giving zero-value manipulated variable) when the system operating point is at the origin.

For a system operating thus, consider the response when a step of 0.8 per unit displacement is put into the reference input. The initial operating point is point *a* (0.8,0) on Figure 4. Since this point is to the right of the critical boundary, the manipulated-variable relay must close in

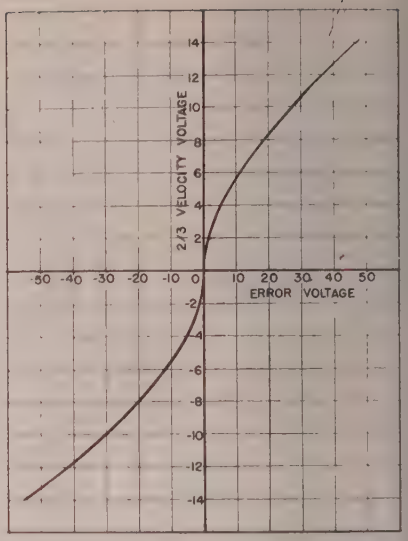

Figure 10. Critical boundary for the shaded-pole induction motor servomechanism

the forward direction, causing the operating point to move along forward Trajectory 1 past point *b* to intersect the critical boundary at point *c*. At this point the manipulated-variable relay must reverse, causing the operating point to move down along the reverse trajectory which forms the critical boundary in the first quadrant, past point *d* to the origin. At the origin the relay must open to bring the value of the manipulated variable to zero so that the system remains at rest with zero error.

Thus a practical anticipator can be made up as a device which at a given moment senses the region of the phase plane containing the system operating point and which operates the manipulated-variable relay accordingly.

Figure 5 shows a schematic diagram for a system whose anticipator is based on a straightforward application of this concept. An oscilloscope has its deflection

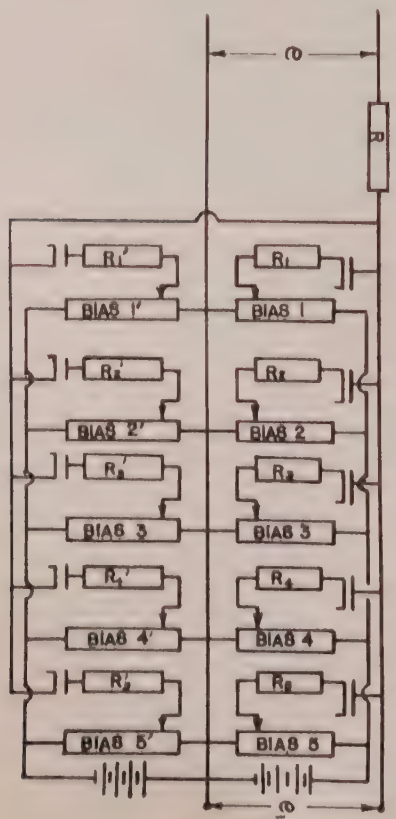

Figure 8 (left). Biased-diode type nonlinear element

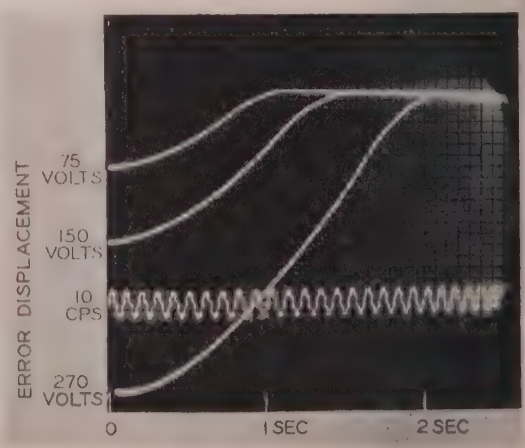

Figure 11 (right). Positioning system response to step-error inputs at various amplitudes. The timing signal is ten cycles per second

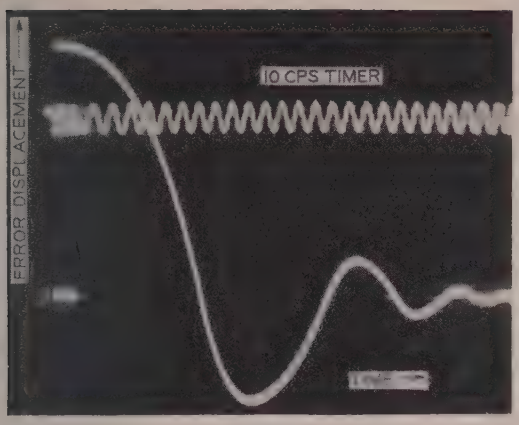

Figure 12 (left). Photograph of the response of a simple relay servomechanism for a step error

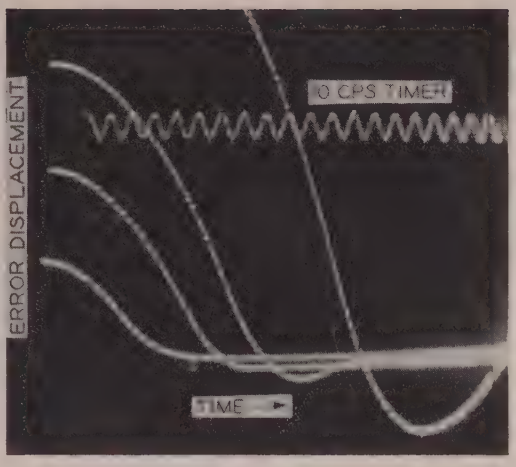

Figure 13 (right). Photograph of the response of a velocity - compensated relay servomechanism for a step input

plates supplied with velocity and displacement voltages in such a manner that the system phase-plane plot is displayed on the face of the tube. An opaque mask cut with one border the shape of the critical boundary is placed on the face of the tube so that it just covers the forward region of the phase plane. The tube face is viewed by a 931-A photocell with a balanced amplifier so arranged as to close the forward contacts of a balanced relay when the spot is behind the mask, to close the reverse contacts when the spot is visible, and to close neither set of contacts when the spot is split by the edge of the mask.

This system was set up and found workable. However, the bulk and electronic complexity of the oscilloscope-photocell combination was considered undesirable.

Another method of realizing the anticipator has proved more practical. This method consists of inserting a non-linear network in the error-voltage output to so modify the shape of the phase-plane trajectories that the critical-boundary curve becomes a straight line of 45 degree slope. This concept is shown graphically in Figure 6. The forward region of the phase plane is represented by the condition that the distorted error voltage be greater than the velocity voltage, the negative region by the condition that the error voltage be less than the velocity voltage.

The anticipator is set up by using the proper nonlinear network to distort the error voltage, and by adding this distorted error voltage to the negative of the velocity voltage. The sum voltage of these two signals operates a polarity-sensitive relay which controls the manipulated variable of the system.

A practical application of this method was set up in the form of the servomechanism shown in the block diagram of Figure 7. A Barber-Coleman reversing shaded-pole motor was used as the positioning device, with a Barber-Coleman micropositioner relay used to control the manipulated variable by short-circuiting one or the other of the two shading coils. The motor was connected to the line at all times. Ten-turn helical potentiometers were used to convert the reference-input position and the output position to voltages. An Elinco permanent-magnet generator was used to provide a velocity signal. A biased-diode non-linear element[6] as shown in Figure 8 was used to distort the error voltage, and a balanced differential amplifier was activated by the difference between distorted error voltage and velocity voltage to operate the micropositioner relay.

The shape of the critical-boundary curve was obtained by fluttering the micropositioner relay. The phase-plane trajectory was displayed on a cathode ray oscilloscope as a closed loop and was photographed. The photograph was cut along the error axis and the two halves of

Figure 14. Comparison of the response of the anticipator servomechanism with the responses of other types of relay servomechanisms

Solid lines represent the response of the anticipator servomechanism. Dotted lines represent the response of the simple relay servomechanism. Dot-dash lines represent the response of the relay servomechanism with velocity compensation

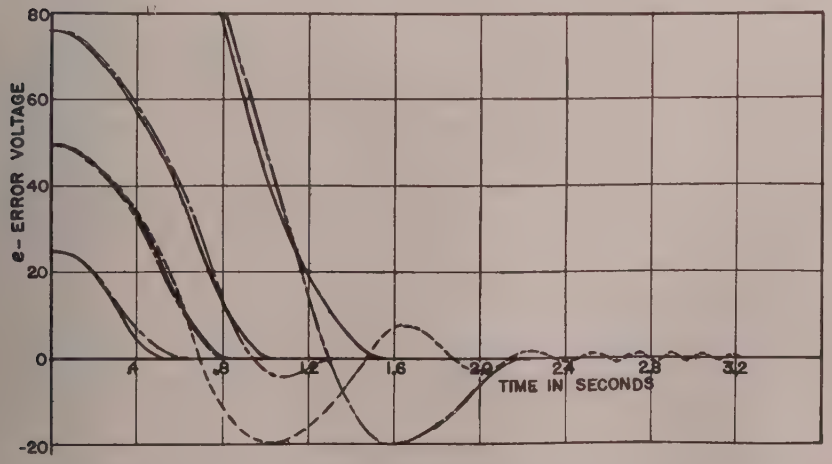

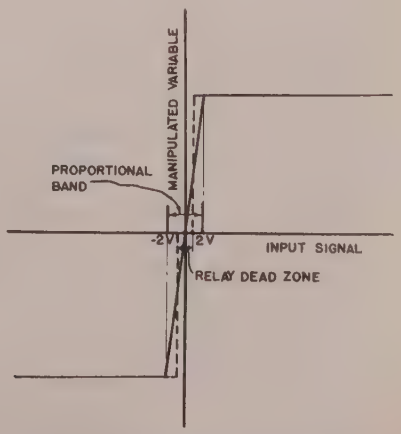

Figure 15. Comparison of characteristics of a narrow-proportional-band amplifier and a relay with dead zone

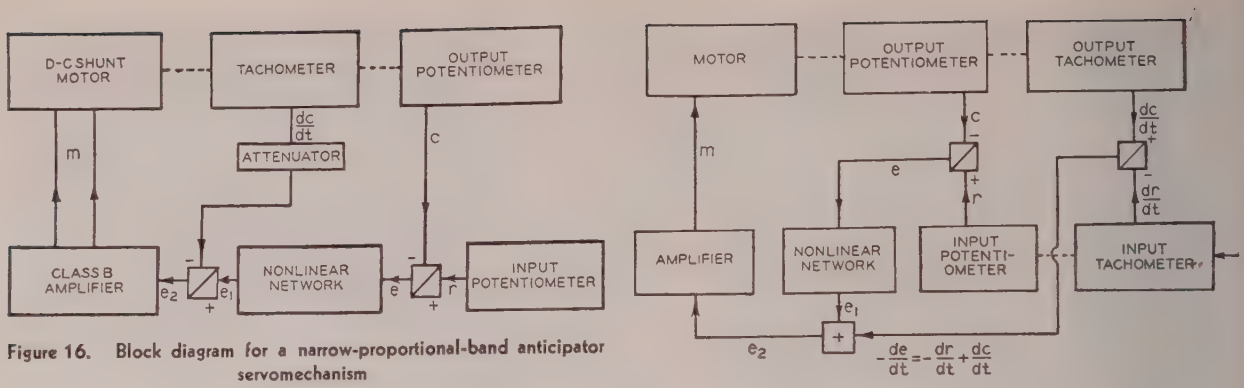

Figure 16. Block diagram for a narrow-proportional-band anticipator servomechanism

the photograph were shifted with respect to one another until the two decelerating portions of the curves lined up, as shown in Figure 9. Since the shape of all decelerating trajectories for the positioning system are the same, the trajectories of Figure 9 can be used to determine the critical boundary plotted in Figure 10.

The time response of this system to various values of step input is shown in Figure 11. Similar responses for systems using the same components but without the anticipator element are shown in Figures 12 and 13. A comparison of the different system responses is shown in Figure 14, indicating the improvement of response resulting from the use of the anticipator element.

When this induction-motor positioning system is used with constant-velocity inputs, the micropositioner relay chatters continuously with resultant wear. Therefore this system is not ideal for such use.

Methods of Obtaining Improved Response With Constant-Velocity Inputs

In order to obtain a system which will follow constant-velocity inputs smoothly it is necessary to replace the relay with some device which can give a wide range of values of manipulated variable. At the same time this device should have properties very close to the properties of a relay if the system is to approach optimum performance in response to a step input.

The device which fulfills these requirements is a narrow-proportional-band saturating amplifier. In Figure 15 the properties of such an amplifier are compared with those of a relay with dead zone. An anticipator servomechanism using a d-c shunt motor and a narrow-proportional-band amplifier is represented by the block diagram of Figure 16. A linearized phase-plane plot showing the linearized critical boundary as a function of velocity voltage and distorted error voltage is shown in Figure 17. The region close to the critical boundary in which the manipulated variable (output of the narrow-proportional-band saturating amplifier) is proportional to input signal is the region where the magnitude of the input signal ($e_1 - dc/dt$) is less than two volts This proportional region is

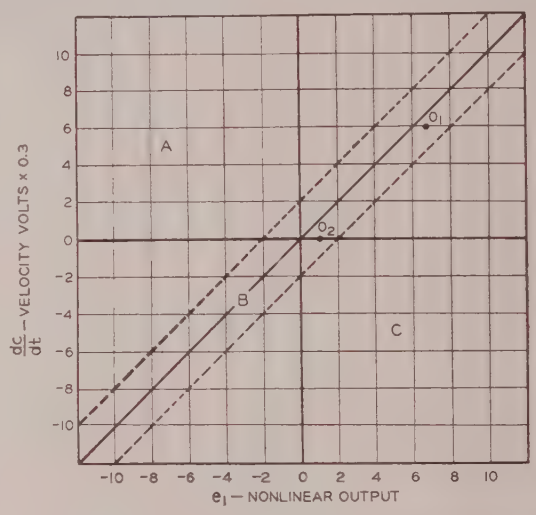

Figure 19 (above). Block diagram of a velocity-error narrow - proportional - band-anticipator type servomechanism

Figure 17(left). Plot of velocity voltage versus nonlinear network output voltage

The solid line is the critical boundary on the transformed phase plane. The two dashed lines are the forward and reverse saturation limits of the amplifier. Region A is the reverse-saturation region, region B is the proportional region, and region C is the forward-saturation region

Figure 18(below). Phase-plane plot showing the critical boundary as a solid line, and the forward and reverse saturation boundaries as dashed lines

A typical system trajectory is shown as the solid line with arrowheads. The maximum reverse region is indicated by the letter A; the proportional region is indicated by B; and the maximum forward region is indicated by C

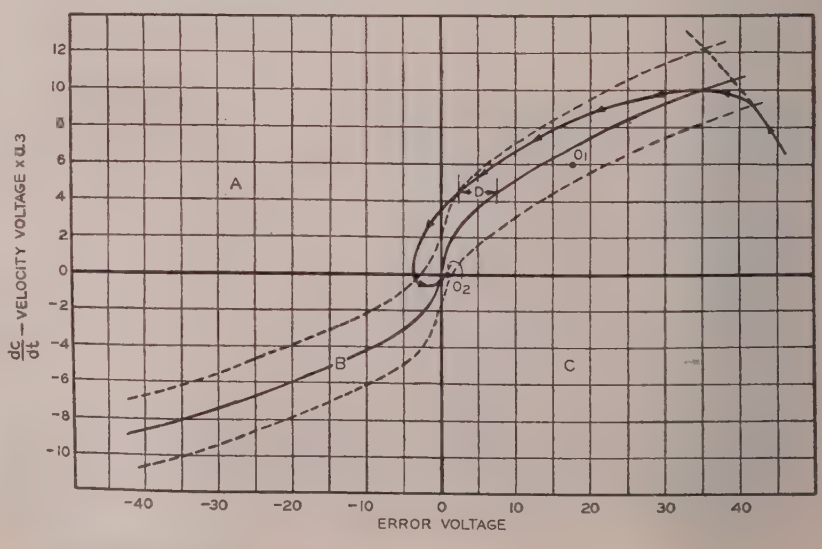

shown in Figure 18, enclosed by the forward- and reverse-saturation boundaries, which are the straight lines $e_1 - dc/dt = \pm 2$. The region to the right of the forward saturation boundary represents the region of maximum forward value of manipulated variable, while the region to the left represents the region of maximum reverse value of manipulated variable.

If the value of the input e to the nonlinear network corresponding to each output value e_1 is found, a phase-plane plot of system output velocity versus system error (dc/dt versus e_1) can be made up as shown in Figure 18. Here the same regions exist as shown in Figure 17, but the boundaries are no longer straight lines. In the region between the two saturation boundaries the value of the manipulated variable will change smoothly, but will not be a linear function of error voltage minus velocity voltage. The manipulated variable in this region will be some function of $(e_1 - dc/dt)$ depending on the transfer function of the nonlinear network.

The dynamic behavior of this system can be visualized by considering the response to a step input. In response to a step input producing an error displacement of 52 volts, the operating point of the system moves to point (52,0) on the phase plane, which is in the region in which the value of the manipulated variable is at the maximum. The system accelerates along a trajectory which has maximum magnitude of slope for each value of velocity (because with the maximum applied value of manipulated variable there will result a maximum magnitude of acceleration for each velocity). This trajectory continues until it crosses the forward saturation boundary and the amplitude of the manipulated variable decreases so that the magnitude of the slope of the trajectory becomes progressively less than the slope of the trajectory for maximum manipulated variable. At the point where the actual trajectory crosses the critical boundary the manipulated variable goes through zero and then builds up in the reverse direction.

As the trajectory comes closer and closer to the reverse saturation boundary the slope of the actual trajectory at a given velocity approaches the slope of the critical boundary at that same velocity. Once the trajectory crosses the reverse saturation boundary, the system trajectory will be parallel to the critical boundary. However, it will be displaced horizontally by the distance D, where D is the horizontal distance between the critical boundary and the point where the system trajectory crosses the reverse-saturation boundary. (See Figure 18.) Thus the system will come to zero velocity with an overshoot error of magnitude D and will oscillate before coming to steady state at some very small error. The nature of the oscillation can be approximately determined by linear theory, using the theory of small oscillations about the zero error point.

The simplest way to reduce the overshoot D is to make the proportional band width of the amplifier as narrow as possible. The overshoot can also be reduced by changing the nonlinear element so that its transfer curve has a shape slightly different from that of the critical boundary.

In response to a constant-velocity input this servomechanism has a stable operating point in the phase plane. For a one-volt input to the narrow-proportional-band amplifier there is obtained a steady-state velocity output of six volts. In order for the system to be in equilibrium, the error voltage must be sufficient to provide one-volt input to the narrow-proportional-band amplifier. Since the velocity voltage is six volts, the output of the nonlinear element must be seven volts, and the input must be eighteen volts of error voltage.

Thus there can be a constant-velocity operating point in the phase plane at $dc/dt = 6$, $e = 18$, as labeled O_1, in Figures 17 and 18. At a constant velocity the system acts as if it had a constant inserted error equal to the amount of the velocity voltage. An additional error is of course necessary to excite the amplifier in order to produce the required manipulated variable. The effect of the nonlinear network in the error channel is to increase the error voltage still more.

Thus the system proposed can be made to give a good response to a step function and to follow constant-velocity signals

Figure 21. The phase-plane trajectories obtained by putting various amplitudes of step input into an anticipator servomechanism with a narrow-proportional-band amplifier

Vertical scale 18.2 volts per inch, horizontal scale 150 volts per inch

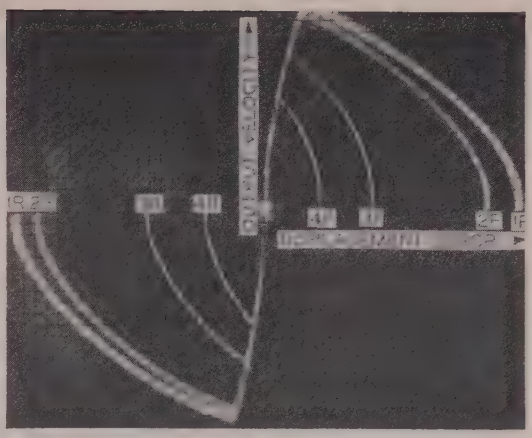

Figure 20. Critical boundary and saturation boundaries for the shunt motor servomechanism

The solid curve is the critical boundary and the two dashed curves are the forward and reverse saturation curves. The area between the two saturation boundaries represent the proportional region

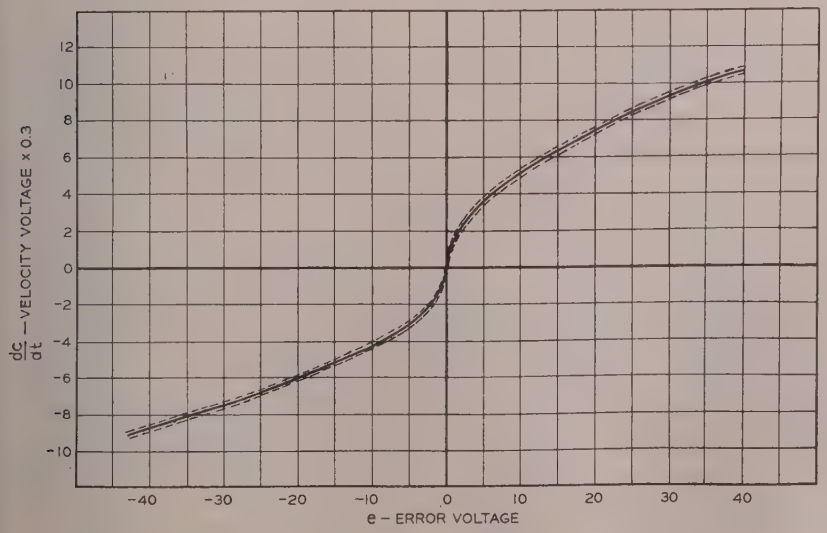

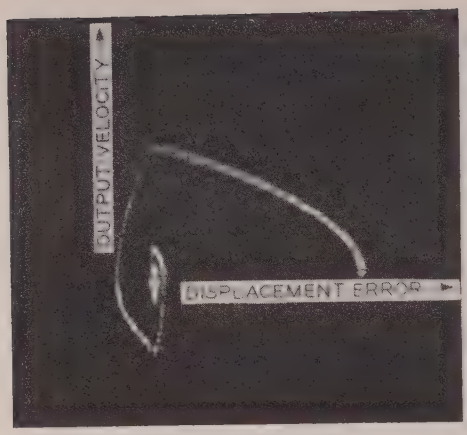

Figure 22 (left). The phase-plane trajectory obtained by putting a step input into a simple proportional servomechanism with a narrow-proportional - band amplifier

Figure 23 (right). The time reponse to an exponential input function for an anticipator servomechanism with a narrow-proportional - band amplifier

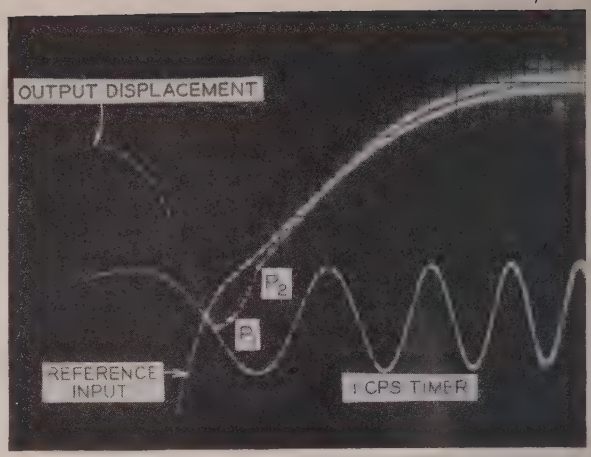

smoothly. However, the following error may be large.

A further modification will produce a servomechanism which will have the same properties in response to a step input but will follow a constant-velocity input with very small error. The difference between the input velocity and the output velocity may be used as the velocity-error signal in a system such as is shown in Figure 19. As the velocity error of the servomechanism approaches zero the point of error velocity versus error displacement moves down to the zero-velocity-error axis. As it does so, the required displacement-error voltage decreases until the steady-state operating error becomes equal to the amplifier input required to maintain the velocity: one volt for the example given. This error is small and could be made smaller by making the proportional band width of the amplifier less.

A narrow-proportional-band amplifier anticipator servomechanism of the type indicated in Figure 16 was made up using d-c shunt motors driven by a high-gain, narrow-band electronic amplifier. The velocity was converted to a voltage signal by a permanent-magnet tachometer, and helical potentiometers were used to obtain displacement voltages. The critical-boundary phase-plane trajectories were determined by oscillating the motors and photographing the closed-loop phase-plane plot on an oscilloscope screen. A biased-diode nonlinear network was then set up to give the corresponding transfer function. Figure 20 is a phase-plane plot showing the critical boundary and the saturation boundaries for the actual system. In the actual system the proportional band width was about 0.2 volt. It was found that the maximum steady-state error for the system was one-fourth degree in 3,600 degrees. The system hunted continuously at a frequency of about 40 cycles per second with an amplitude of about one-tenth degree.

The system response to various amplitudes of step inputs in each direction is shown in the phase-plane plot of Figure 21. For comparison the response of a similar system without the nonlinear network or the velocity input is shown in Figure 22. Note that the vertical scale is different for the two figures. Figure 22 represents overshoot with several cycles of oscillation, while in Figure 21 each trace represents maximum acceleration up to the critical boundary, and then sudden reversal of the manipulated variable to decelerate the output along a trajectory very close to the critical boundary so that the system comes smoothly to a stop without overshoot.

The response of the system to a varying input is shown in Figure 23. The input was actually the voltage obtained across a resistance-capacitance network with an applied step input and consisted of an initial jump followed by an exponential decay of voltage. The output-displacement curve is shifted on the vertical axis one small square above the input curve as a result of oscilloscope drift. This system first fails to follow fast enough, then overshoots, and finally reaches essentially a steady-state velocity.

Discussion of the System

The anticipator servomechanism has several advantages which make it worthy of consideration:

1. Since the anticipator system operates the motor with maximum value of manipulated variable most of the time, the utilization factor for the motor is excellent, and better performance can be obtained for given motor and load components. This improvement is obtained without the use of improved components.

2. It provides a means of stabilizing a servomechanism with high effective gain. As has been pointed out, when a narrow-proportional-band amplifier system is used, increasing the gain (narrowing the proportional band) decreases any overshoot and shortens the time required for the system to come to steady state following a step input. The actual compensation for a second-order system consists of the first-derivative signal and the nonlinear network.

3. Since the method of compensation is not dependent on any linear theory, nonlinear components such as split-field series motors and induction motors can be used in the systems without any increase in the difficulty of design of the servomechanism.

4. The anticipator system is readily applied to the compensation of relay servomechanisms. There are methods of compensation for relay dead zone and operating time.

At present this approach has the restriction that the physical system must have such dynamic properties that the relationship between manipulated variable and the system output can be expressed only by a second-order differential equation with no terms which are functions of the output position.

This requirement entails two disadvantages:

1. The restriction that the system equation be one of second order comes from the fact that the two-dimensional phase-plane trajectories are not meaningful expressions of the system dynamics for systems whose equations of motion are higher than second order.

2. The restriction that the system equation possess no terms which are functions of output position means that there can be no spring-type forces in the system. It also means that all system trajectories must have the same shape, with different initial conditions represented by the trajectories being shifted varying distances along the displacement axis. Therefore the critical boundary always has the same shape regardless of the value of the reference input. If the shape of the critical boundary changed with change of reference input, the design of the nonlinear network for the anticipator system would be much more difficult.

Conclusion

The purpose of this paper is to describe a new control device for use with positioning systems in order to produce the correction for a step error in minimum time, taking into consideration the saturation effects existing in any physical system.

By means of a phase-plane approach the optimum control device is shown to be one in which a maximum value of manipulated variable is applied first in one direction and then reversed at the critical time to a reverse-maximum value so as to bring the system to a stop at the desired position.

The device which controls the application and reversal of the manipulated variable has been given the name of anticipator. It senses the point where the actual system phase-plane trajectory crosses the particular trajectory making up the critical boundary, that is, one of the two which go into the phase-plane origin. It there reverses the manipulated variable to bring the system operating point along the critical boundary to zero velocity with zero error. The anticipator unit utilizes a nonlinear element.

A variation of this system, using a narrow-proportional-band amplifier to control the manipulated variable, is proposed to give a better response to a constant-velocity input.

This approach is limited to use with systems whose differential equations of motion are second order and possess no terms which are a function of position. However, it permits better performance to be obtained with the same components, and it is as easily applied to nonlinear systems as to linear ones. It is especially well adapted to use with relay servomechanisms.

Nomenclature

m = manipulated variable
$f(\ )$ = function of ( )
c = servomechanism controlled output variable
$\frac{dc}{dt}$ = servomechanism output velocity
$\frac{d^2c}{dt^2}$ = servomechanism output acceleration
x = general displacement of some system
$\frac{dx}{dt}$ = general velocity of some system
$\frac{d^2x}{dt^2}$ = general acceleration of some system
M = slope of a phase-plane trajectory
$t_{a\rightarrow b}$ = time to go from a to b in the phase plane
t_a, t_b = time at point a or point b
x_a, x_b = the x coordinate of point a or point b
e_1 = distorted error voltage output of the nonlinear network
D = horizontal distance between critical boundary and a saturation boundary at the point where the system trajectory crosses into the saturation region
e = servomechanism error $= r - c$
O_1, O_2 = anticipator servomechanism operating point for a constant velocity input
r = reference input quantity
m_1, m_2, m_3 = components of the manipulated variable
p = time derivative operator d/dt
p^2 = second order time derivative operator d^2/dt^2
b = damping coefficient
J = inertia coefficient
k = gain constant
e_2 = difference between nonlinear network output and velocity output $= e_1 - dc/dt$
R = resistance

References

1. Principles of Servomechanisms (book), **Gordon S. Brown, Donald P. Campbell.** John Wiley and Sons, Inc., New York, N. Y., 1948.

2. The Introduction to Non-Linear Mechanics (book), **N. Minorsky.** J. W. Edwards Bros., Ann Arbor, Mich., 1947.

3. Theory of Oscillation (book), **A. A. Andronow, C. E. Chaiken, translator.** Princeton University Press, Princeton, N. J., 1949.

4. Fundamental Theory of Servomechanisms (book), **LeRoy A. MacColl.** D. Van Nostrand Company, New York, N. Y., 1945.

5. Analysis of Relay Servomechanisms, **H. K. Weiss.** *Journal of Aeronautical Sciences* (New York, N. Y.), volume 13, number 7, July 1946.

6. Electronic Techniques in Analogue Computation, **G. D. McCann, C. H. Wilts, B. N. Locanthi.** *Proceedings*, Institute of Radio Engineers, volume 37, August 1949, page 954.

No Discussion

Selection of Equipment for Multiple-Unit Cars

W. M. HUTCHISON
MEMBER AIEE

Synopsis: Electric multiple-unit cars afford the most economical method of handling suburban passenger service, provided the volume of traffic warrants the high initial expense of electrification. Nevertheless, because of the low use factor of these cars in commuter traffic, fixed charges are a high percentage of the total cost of the service. It is important to reduce these fixed charges by finding means for lowering the initial cost of multiple-unit car equipment. It also is important to simplify such equipment in order to minimize maintenance costs.

One method which has proved to be effective in reducing costs in many other fields is that of standardization. The development of rectifier-type motive power for application on high-voltage a-c systems gives promise of effecting a degree of standardization for the majority of applications by the wider use of low-voltage d-c traction equipment. Further economies should be possible by careful selection of available alternatives in details of the equipment. Various choices are discussed with particular reference to low cost and low maintenance.

SUBURBAN commuter traffic has been a problem to the railroads of the country for a long time. The nature of the traffic is such that a heavy volume occurs for a limited period during morning and evening rush hours. For the rest of the day a large portion of the equipment is idle. As a result, the fixed charges are a relatively high percentage of the total cost of providing this service.

For this reason, it is important that the initial expenditure for such equipment be as low as possible consistent with the fundamental requirement of affording the public safe, comfortable, convenient service.

It has long been recognized that the electric multiple-unit car is an ideal means for handling suburban traffic. It has advantages in operating flexibility, in relatively high rates of acceleration as compared to locomotive-hauled trains, and in practically uniform accelerating rates regardless of the length of train, provided a constant ratio of motor cars to trail cars is maintained.

However, electrification is expensive and it is important that further progress be made in reducing costs not only if additional extension of electrification is to be considered, but to obtain a reasonable return from this service on those units now in operation.

For these reasons, three important objectives to be sought in new multiple-unit cars are low initial cost, simplicity, and low maintenance expense. Low initial cost is important to reduce the fixed-charge content of the total cost of operation. Simplicity of construction and circuits is necessary to assist in achieving low maintenance expense, without which no operation can be economical.

One of the most effective ways to reduce the first cost of multiple-unit car equipments is to employ standardization of systems and apparatus to a much greater degree than has been done in the past. There is a wide variation in equipment which has been selected for multiple-unit cars by various companies, both in power supply systems and also in the details of the traction apparatus. The effect of standardization in keeping costs low is well illustrated in the diesel-electric locomotive field. In the period from 1939 to 1948 the price per pound of a 2,000 horsepower diesel-electric road locomotive increased an average of only approximately 20 per cent as compared to an increase during the same period of approximately 150 per cent for a 4-8-4 type steam road locomotive. This relatively low increase for the diesel-electric locomotive in a period of rising labor and material costs may be attributed largely to mass production of standardized units.

Systems of Suburban Electrification

Suburban electrification in this country may be divided into three general systems as related to the power supply—11,000 volts 25 cycles alternating current, 600 volts direct current, and 1,500 volts or 3,000 volts direct current.

Each system has certain advantages. The high voltage of the a-c system makes it possible to supply economically large amounts of power over long distances. The low-voltage d-c system includes the advantage of the d-c traction motor in higher efficiency, better starting tractive effort characteristics and, relatively low maintenance expense. The high-voltage d-c system approaches the advantages of the a-c system in reducing transmission losses while retaining some of the advantages of the d-c traction motor.

It has been necessary until very recently to weigh the relative advantages of these systems and to select that which appeared to be the best compromise for the particular application, relinquishing the advantages of the others. Today, however, the excellent results which have been obtained with Ignitron rectifier-type motive power, as applied for trial in 1949 to a Pennsylvania Railroad multiple-unit car, give promise of a new system which embodies the advantages of high-voltage a-c transmission with the superior characteristics of low-voltage d-c motors.

The relative number of motor cars and trail cars in service on electrified main lines in each of the three power supply classes is indicated graphically in chart (a) of Figure 1. Sixty-three per cent of the total number of cars are operated at 600 volts direct current 22 per cent at 11,000 volts alternating current, and 15 per cent

Paper 51-104, recommended by the AIEE Land Transportation Committee and approved by the AIEE Technical Program Committee for presentation at the AIEE Winter General Meeting, New York, N. Y., January 22-26, 1951. Manuscript submitted October 23, 1950; made available for printing December 12, 1950.

W. M. HUTCHISON is with the Westinghouse Electric Corporation, East Pittsburgh, Pa.

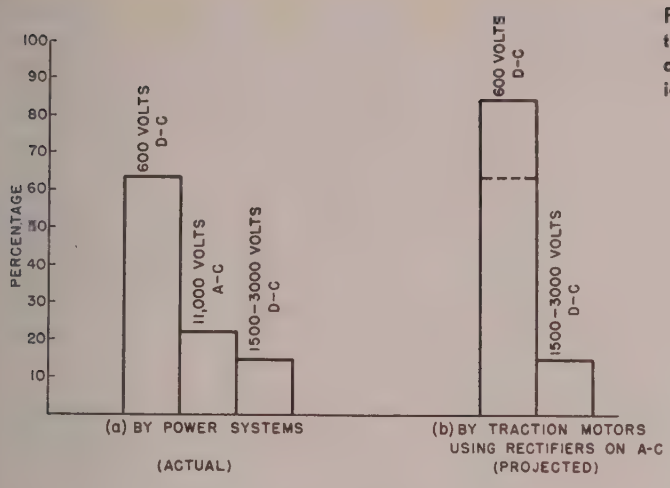

Figure 1. Distribution of multiple-unit cars in main-line service in the United States

at 1,500 or 3,000 volts direct-current.

The wide use of low-voltage d-c motors and control is one of the factors which stimulated the development of Ignitron rectifier equipment for a-c electrifications. The basic requirement for this type of service using modern cars of 60 to 70 tons is approximately 400 horsepower per car. In this range, 600 volt d-c equipments, using either two or four motors, have been produced in considerable quantities. The ease of extending the use of such equipment to a-c systems and hence obtaining the advantages of standardization in lowering costs is indicated in Figure 2. As shown, the essential elements of a rectifier-type a-c multiple-unit car equipment are a standard d-c package, including motors and control, and a conversion unit including transformer, Ignitron rectifier, and associated details.

Reference to chart (b), Figure 1, illustrates how application of 600-volt d-c motors and control to existing a-c systems would increase the preponderance of low-voltage d-c equipment to 85 per cent of the total.

Thus, rectifier motive power not only has advantages over a-c single-phase motive power of lower weight, less space, higher efficiency, and higher power factor, but it also advances the cause of standardization of multiple-unit car equipment. This is in addition to the possibility it affords of using commercial 60-cycle frequency power for new electrifications, thus further applying the principle of standardization to reduce costs.

It is realized that this possibility for standardization depends upon proof of satisfactory long-range operation of rectifiers and associated equipment in motive power service. At the present writing an a-c multiple-unit car equipped with Ignitron rectifiers and d-c motors has operated for a total of 36,000 revenue miles over a period of 12 months. During this period nothing has occurred to raise any doubts as to its satisfactory life. Further evidence will accumulate as service continues. Further trial applications are in progress. Two 6,000-horsepower rectifier locomotives will be delivered to the Pennsylvania Railroad early in 1951. Also, the French, who are interested in electrification at 50 cycles, 20,000 volts, have arranged to install an Ignitron equipment on a multiple-unit car for trial.

Coincident with the development of Ignitron rectifier equipments for traction applications, considerable progress has been made in the design of a-c motors and control recently applied in multiple-unit car service, with particular emphasis on the objectives of low cost, simplicity, and low maintenance. Since, obviously, whether the ultimate multiple-unit car equipment is to be alternating current, direct current, or a combination of the two, standardization in the details of the traction apparatus will be effective in reducing costs, several of the choices available are discussed from the standpoint of relative cost, simplicity, and maintenance.

Number of Motors Per Car

The relative advantage of 2-motor and 4-motor equipments for multiple-unit car service recently has received considerable attention. Four motors per car generally are necessary where trailer operation is employed and are used commonly on high-voltage d-c equipments to permit the application of two half-voltage motors in permanent series connection. Equipments with four 300-volt series wound, self-ventilated spring-borne motors and insulated for operation with two motors permanently connected in series on 600 volts are used widely in streetcar and rapid transit service. Recently application of four spring-supported motors has been made to suburban multiple-unit cars on both an a-c and a d-c system.

Under certain conditions, a 4-motor equipment has definite advantages over the 2-motor type. The division of the total car weight on the four driving axles permits exerting relatively high tractive effort without slipping the wheels. This makes possible higher accelerating rates than can be used effectively on 2-motor equipments. For the short runs common in local subway service, this feature is desirable to maintain schedule speeds.

An important advantage is spring suspension of the motor from the truck, instead of suspending it from the car axle. As a result, the motor is cushioned against road shocks. By subdividing the required motor capacity into four instead of two units, there usually is adequate space in the car trucks sufficient for the motors and the drive elements required with truck mounting. This is more

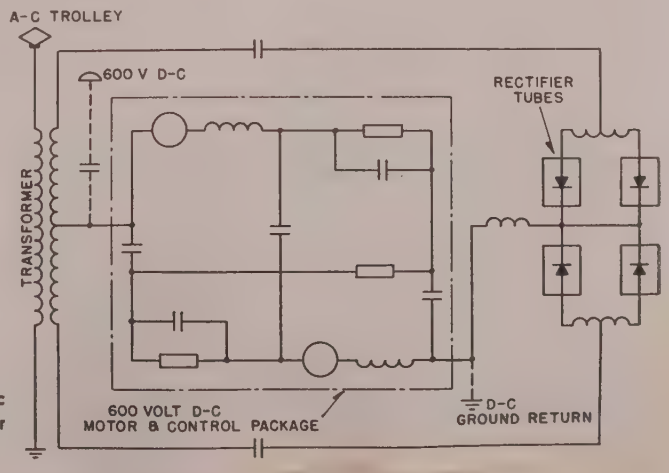

Figure 2. Schematic diagram of rectifier multiple-unit car

difficult where two larger motors are used per car.

Not all these advantages apply to cars for suburban service, particularly for operation in trains of all motor cars. As compared to average runs of less than one-half mile in local rapid transit service, runs in typical commuter service may range up to 10 miles or more, with averages for all runs from 1.25 to 2.0 miles. High accelerating rates under these conditions result in little improvement in schedule speed with a relatively large increase in power consumption. For example, a study made of multiple-unit car operation on a 1.3-mile run with various accelerating rates indicated that raising the rate from 1.0 to 1.5 miles per hour per second increased the schedule speed only 3.3 per cent, with an increase in power consumption of 4.7 per cent. The advantages of four motors in making higher accelerating rates practicable, therefore, cannot always be utilized economically in such service.

The particularly attractive feature of the 4-motor equipment is its adaptability to cushioned mounting of the motors on the truck, together with flexibility in the drive between the motor armature and the car wheel. There is no question of the desirability of this type of mounting and drive. It is important, however, to examine its benefits in the light of the over-all cost to obtain them.

The favorable results to be hoped for are improved life of motor parts, such as insulation, brush holders, bearings, and possibly shafts because of reduction of shock forces imposed; improved life of gears and pinions because of better alignment and lubrication; improved ride for passengers because of less noise and fewer shocks transmitted from motors to trucks to car body; and reduced stresses on the track because of the reduction in unsprung weight.

However, increased costs are to be expected with the spring-suspended truck-mounted arrangement. With the same margin in design and the same manufacturing conditions, smaller motors actually cost more per horsepower to manufacture than larger ones. The 4-gear drive units (gears, pinions, gear cases and bearings, couplings and suspension links) are substantially more than twice as expensive as the parts they replace in a 2-motor axle-mounted design (gear, pinion, and gear case). The assembly of truck-mounted motors and drive units in the car trucks is a considerably more complicated operation than with 2-axle hung motors. The closer tolerances which must be maintained with the gear unit and coupling require a higher grade of maintenance or, without it, more frequent attention. Car wiring is more expensive with both trucks motorized instead of only one. Maintenance of four smaller motors instead of two larger ones normally is more expensive. The motors and their principal parts are in either case too large to be handled without crane facilities. There are twice as many armatures, stators, commutators, brush holders, and many detailed parts.

The use of four motors rather than two motors for multiple-unit cars operating in all motor car trains in suburban service may, therefore, result in an increase of considerable magnitude both in first cost and in maintenance costs. For this reason, extreme care should be exercised in making a choice. There are, of course, some instances beyond the operator's control, such as passenger preferences, which influence the choice.

Trailer Operation

With electric multiple-unit cars, three methods of operation are possible—all motor cars, semipermanently connected 2-car units consisting of one motor car and one trailer, and motor car and trailer operation in varying make-up of trains limited to a minimum fixed ratio of motor cars and trailers. Each method has its advantages and all are in use successfully.

The most economical method of operation is the greatest possible use of trailers during the rush hours to reduce the investment for equipment which has a poor load factor, and the use of all motor cars during the non-rush hours to provide the fastest service to attract new patrons. However, motor car and trailer operation gives the least amount of flexibility. All-motor-car operation requires a minimum of terminal switching and affords the greatest protection of equipment and schedules in case of failure of one car in a train

In spite of the larger relative investment in motive power and higher fixed charges because of poor utilization, most postwar purchases of new equipment have been for all-motor-car operation.

A weighing of the relative economies of low fixed charges or of high operating flexibility has led to the conclusion that the maximum flexibility obtained with a consequent reduction in terminal facilities and costs justifies the additional investment required for all-motor-car operation. Moreover, fixed charges and operating expenses can be lowered by maximum utilization of the new equipment in both base and peak service and by augmenting the latter with existing cars.

Another reason for all-motor-car operation is the public demand for faster and more de-luxe commuter service in keeping with the latest trends of through service. Illustrating this trend are recent lightweight, semistreamlined commuter cars equipped with air conditioning, automatic heating and ventilating controls, fluorescent lighting, and better seats and washroom facilities.

Dynamic Braking

Dynamic braking has been used widely in city, rapid transit, and locomotive service, but no applications have been made in the United States in multiple-unit commuter service. There is no fundamental reason why it should not be used. It is again simply a question of whether the results obtained from its use justify the additional cost and complication.

The benefits to be expected are increased safety, lower wheel temperatures, and savings in brake shoes—the latter variously estimated at $50 to $250 per car per year.

Dynamic braking has the following disadvantages:

1. Machines designed primarily to perform the motor function do not have sufficient capacity for full service braking from maximum speeds. Its use may involve 15 per cent to 20 per cent more weight in the motor, with a corresponding increase in cost.
2. It adds to the complexity of the control equipment.
3. It involves increased complication of the air-brake equipment to secure blending of dynamic and air brakes.

None of these difficulties are insurmountable, and in fact dynamic braking has been applied satisfactorily in other fields. However, it usually has been applied primarily to obtain results peculiar to the specific application, such as holding locomotives on long grades, because of rubber insert wheels on Presidents' Conference Committee cars, or to reduce brake-shoe dust in the subways. The additional cost and complication have militated against its use on multiple-unit cars.

Conclusions

The development of the Ignitron rectifier for motive power, although still in the experimental stage, offers interesting possibilities in reduction of costs of electric multiple-unit car equipment, by standardization of both systems and

traction apparatus. Low-voltage d-c motors and control are available employing either two or four motors per car, and can be used directly from a 600-volt d-c trolley or third rail or from a high-voltage a-c trolley through rectifiers. The use of a common equipment for either 600-volt d-c systems or high-voltage a-c systems may extend the advantages of standardization and quantity production to this field.

Further advantages are to be gained from careful selection among the various alternatives in details of the traction apparatus available. The selection of equipment for multiple-unit cars is not an exact science, but rather an opportunity for the exercise of engineering judgment. Careful selection, based on the fundamental premises of low initial cost, simplicity, and expected low maintenance for each individual application, should result in the optimum service to the public and profit to the railroad.

Discussion

D. R. MacLeod (General Electric Company, Erie, Pa.): Since the object of his paper is to discuss various choices of multiple-unit car equipment with particular reference to low cost and low maintenance, it would be helpful if Mr. Hutchison were to give comparative data that would enable the reader to evaluate the various alternatives which he presents. We heartily concur with his emphasis on standardization as a means of achieving low first cost, and on simplicity of equipment as a means of reducing maintenance costs.

We note the paper states that "The use of four motors rather than two motors for multiple-unit cars operating in all-motor-car trains in suburban service may, therefore, result in an increase of considerable magnitude both in first cost and in maintenance costs." We do not agree with this statement. While the paper also makes a casual reference to "the considerable progress in the design of a-c motors and control," presumably of the type presented in the papers by Messrs. H. G. Jungk[1] and S. E. Newhouse,[2] it does not cite advantages or disadvantages of this type of equipment. Does this mean that they are no longer recommended? The paper devotes considerable attention to rectifier-type multiple-unit car equipment similar to that which has been in experimental operation on the Pennsylvania Railroad for more than a year, but it does not present any conclusions based on this experiment. After careful study we have reached the opinion that rectifier-type multiple-unit car equipment does not have enough merit to justify it as a new standard for application to 25-cycle electrifications in the United States; probably it can be justified for single-phase 60-cycle electrification, but as none of these are in prospect in the United States, any consideration of a standard 60-cycle multiple-unit car equipment at this time is academic.

If rectifier-type multiple-unit cars should be specified by the operators of 25-cycle electrified systems, consideration should be given to a design based on the d-c 4-motored equipment, 100 of which have been placed in operation recently on the 600-volt third-rail system of the New York Central Railroad.

Truck-mounted motors of the same type also are used on multiple-unit cars of the Illinois Terminal Railroad and on rapid-transit cars of the New York City subways, so that a relatively high production of these motors is assured. A truck-mounted 4-motored rectifier car would be superior to the axle-hung 2-motored type advocated by Mr. Hutchison.

During 1950 we made complete a-c 25-cycle single-phase rectifier tests on the General Electric type-*1240* motor as used on the New York Central Railroad cars except for a minor modification of the field structure.

These tests were made with various degrees of smoothing and at voltages within the operating commutating limit of the motors, and data have been accumulated from which design factors necessary for the precise design of the main power transformer and smoothing reactors have been derived.

These data have enabled us to make an accurate study of the weight and first cost of the rectifier-type multiple-unit car in comparison with the 4-motored a-c series-motor-type equipment described in Kreitler's paper.[3] As a result of these studies, we have no hesitation in recommending the simple 4-motored a-c series-type equipment that we have put into service recently on the Pennsylvania Railroad as the standard for a-c 25-cycle multiple-unit cars in the United States.

Four of the a-c motors, described in the paper by F. C. Kreitler, Jr., complete with gears, pinions, gear cases, and flexible coupling, weighed 11,584 pounds for one car. Four of the d-c motors used on the 100 new General Electric equipped New York Central Railroad cars, together with the gear units and the couplings, weigh a total of 9,720 pounds for one car. The corresponding power control items on the 600-volt d-c New York Central Railroad cars, which would be included in the "600-volt d-c package" for a rectifier-type car, are 865 pounds lighter than the comparable items on the 50 General Electric 11,000-volt 25-cycle 4-motored cars recently delivered to the Pennsylvania Railroad. The rectifiers, smoothing reactor, firing circuit, water-cooling equipment, and protective housing required for a 25-cycle a-c rectifier-type car therefore can weigh only 2,729 pounds without exceeding the weight of a straight a-c car.

Our estimates show that, for 25-cycle multiple-unit car application, there is no weight saving in changing to rectifier-type equipment; that rectifier-type multiple-unit car equipment takes up considerable more space under a car than corresponding straight a-c equipment; and that it is questionable whether there are any potential savings in cost. The comparison appears to be more favorable to the rectifier-type equipment for higher frequency system application such as those being seriously considered in Europe; however, even in these cases it should be evaluated carefully on a comparable basis with other types.

References

1. A New Multiple-Unit Motor for the Pennsylvania Railroad, **H. G. Jungk.** *AIEE Transactions*, volume 70, part I, 1951, pages 243–46.

2. New A-C Multiple-Car Control for the Pennsylvania Railroad, **S. E. Newhouse.** *AIEE Transactions*, volume 70, part I, 1951, pages 645–47.

3. A-C Multiple-Unit Car Motor, **F. C. Kreitler, Jr.** *AIEE Transactions*, volume 70, part I, 1951, pages 648–51.

H. F. Brown (New York, New Haven, and Hartford Railroad, New Haven, Conn.): This paper mentions the various systems currently being used in the United States for suburban electrifications, but it does not include the combination ac-dc system such as used on the New York, New Haven, and Hartford Railroad, where 11-kv alternating current is used on the longer part of each run and 600-volt direct current is used to enter the terminal. This type of equipment has been used for the past 40 years and is necessarily heavy and complicated.

The application of the ignitron rectifier to standard d-c equipment of this kind would seem to offer many advantages and possibilities in weight reduction and in further standardization of electric equipment for multiple-unit cars. It is conceivable that the more recently designed d-c suburban equipment might be used on the a-c system almost in its entirety, including lighting and air-conditioning, by the simple addition of the transformer and rectifier. In his discussion of this paper Mr. MacLeod has implied that the rectifier equipment is not so applicable to 25-cycle systems as to the 50- or 60-cycle systems. It is not clear why this limitation should be implied in view the excellent performance during 1950 of the experimental equipment of this type, which has been in commercial operation on the Pennsylvania Railroad 11-kv 25-cycle system. It would seem that any new device such as the rectifier, which will permit of further standardization of railway motors, and control, should be given the greatest amount of attention in these days of rapidly mounting costs of both labor and material.

W. M. Hutchison: We note that Mr. MacLeod is in complete agreement with the emphasis on standardization as a means of achieving low first cost and on simplicity of equipment as a means of reducing maintenance costs. As stated in our paper, the selection of equipment for a-c multiple-unit cars from the various alternatives available is not an exact science, but rather an opportunity for the exercise of engineering judgment. It appears probable that the divergence in conclusions reached by Mr. MacLeod from those expressed in our paper results either from his lack of comparative data, as he has implied, or from the interpretation of the information which he has available.

We believe that several of the questions raised would have been unnecessary if the paper had been read more carefully. For example, Mr. MacLeod asks if the "casual" reference to progress in a-c motors and control (which he presumes refers to the equipment discussed in the papers by H. G. Jungk and S. E. Newhouse) without citing the

advantages or disadvantages of this type of equipment means they are no longer recommended. In the latter portion of the paper we discuss the reasons for the selection of the type of equipment described by Mr. Jungk and Mr. Newhouse, the detailed advantages of which are outlined in their papers (see references 1 and 2 in Mr. MacLeod's discussion of this paper).

It also is suggested that consideration should be given to truck-mounted 4-motored equipment for application to rectifier multiple-unit cars. One of the advantages which we cited for the rectifier equipment is the availability of low-voltage d-c equipments "employing either two or four motors per car." We are thoroughly familiar with 4-motor truck-mounted equipment, since we pioneered in the development of high-speed spring-borne motors with self-contained gear units 25 years ago. We recommended this type to the New York City subways and recently have supplied them with 375 equipments. The choice between two and four motors per car with rectifier-type equipment may be made by each customer, weighing the relative advantages for his particular application.

Mr. MacLeod remarks that data have been accumulated during 1950 from which, after careful study, he has reached the opinion that rectifier-type multiple-unit car equipment does not have enough merit to justify it as a new standard for application to 25-cycle electrification in the United States. He also states that as a result of those studies, there is no hesitation in recommending the simple 4-motored a-c series-type equipment recently put in service on the Pennsylvania Railroad as the standard for a-c 25-cycle multiple-unit cars.

In our paper, we reviewed the advantages accruing to the railroads with rectifier-type equipments through the use of standard d-c motors and control, which have been built in considerable quantities. The trial equipment on the Pennsylvania Railroad was developed after several years of intensive study.

During the whole of 1950, in parallel with the successful operation of this car in revenue service, we have continued fundamental research studies in the laboratory. As a result of these years of study, it is our considered opinion that rectifier-type equipment for a-c multiple-unit cars does have great merit. We hope, however, we never reach the conclusion that any specific development has exhausted all the possibilities of further progress.

We agree with Mr. H. F. Brown's suggestion that rectifier-type equipment is peculiarly fitted for application to a combination ac-dc system, such as used on the New York, New Haven, and Hartford Railroad. In addition to the features cited by Mr. Brown, it has the advantage over a-c motors of providing series-parallel operation in the d-c zone.

New A-C Multiple-Car Control for the Pennsylvania Railroad

S. E. NEWHOUSE
NONMEMBER AIEE

THE CLASS *MP54E5* multiple-unit cars on the Pennsylvania Railroad possess certain features that are not provided on a-c multiple-unit cars previously placed in service on the Pennsylvania and other railroads. The Westinghouse Electric Corporation has furnished the motors, transformer, control, and auxiliary apparatus for the 50 cars on this order. A number of these cars have been in service for several months. Figure 1 shows the main circuit schematic diagram.

The two traction motors are the resistance-lead type. The motors are connected in parallel to minimize the amount of wheel slippage. With wet rail, it has been demonstrated on these cars that when one pair of wheels slips, the slippage is for only a small fraction of a revolution. On older multiple-unit cars, the two motors are connected in series. When one pair of wheels starts to slip, the voltage across the motor driving them increases and the wheel slippage becomes progressively worse until power finally is removed by the slip relay. No slip relays are required on *MP54E5* cars.

These new cars possess another advantage. The failure of one motor on an old car necessitates cutting both motors out of circuit because they are connected in series. On the new cars, the motor in trouble is disconnected by opening switch *M1* or *M2*. Only half of the tractive power is lost. This means less overload for the remaining cars in the train.

Paper 51-105, recommended by the AIEE Land Transportation Committee and approved by the AIEE Technical Program Committee for presentation at the AIEE Winter General Meeting, New York, N. Y., January 22–26, 1951. Manuscript submitted October 24, 1950; made available for printing December 12, 1950.

S. E. Newhouse is with the Westinghouse Electric Corporation, East Pittsburgh, Pa.

A feature of these cars is that separate blowers are provided for ventilating each of the traction motors and the main transformer. The two traction-motor blowers are provided with cleaning devices to remove dirt and snow by centrifugal action, thus reducing failures from these sources. If the traction-motor ventilating air pressure is too low, a diaphragm-type air relay opens the traction-motor switches.

The primary winding of the askarel-filled transformer is connected to the pantograph by a high-tension cable. A lightning arrester located on the roof is connected to the pantograph. The six low-voltage secondary taps are located at one end of the transformer. They are protected from dirt and water by a metal housing. The six insulated copper straps connected to the taps are brought out of this housing through a block of insulation. Short flexible cables connect them to the main control box terminals, which are all located at one corner of the control box.

On all multiple-unit cars built in the past, the terminals of the main control boxes have been brought out directly in back of the unit switches. While this simplified the construction of the box, it was necessary for the Pennsylvania Railroad to run a number of insulated straps between the transformer and the control box. The limited working space between apparatus under the car made this a difficult construction problem. The Pennsylvania Railroad specified that all terminals connecting to the transformer be brought out at one corner of the main control box. This required six insulated straps running lengthwise inside the box to the various switches. By careful layout work, this was accomplished without exceeding the cross section dimensions of the main control boxes on the old cars.

In addition to five tap switches, the main control box also contains two motor switches and one preventive coil switch. All eight of these electropneumatic switches are identical except for the interlocks. The interlocks are of the modern cam-type. A micarta cam attached to the movable portion of the switch bears against a steel contact finger which opens or closes the interlock contact.

Figure 2 shows the main control box as viewed from the side of the car with covers removed. The 2-motor reverser, mounted at the right-hand end of the control box, is the drum type. The straps emerging from the box above the reverser are connected to traction-motor cables on the car. Directly below these straps is the shield for the six terminals that connect to the transformer. At the opposite end of the box is a compartment containing the sequence switch, the limit relay, the sequence relay panel, and the ground detector relay panel. These devices are mounted so as to be inspected and maintained easily. Figure 3 shows this compartment.

The sequence switch is a positive notching electropneumatic device that opens and closes the five tap switches and the preventive coil switch in the desired order. It consists of an insulated drum driven by a rack and pinion under the action of two air cylinders. Control fingers ride on copper segments mounted on the drum. When the master controller is moved to one of its operating positions, the two motor switches and the *A1* switch close. The sequence switch "ON" magnet valve is energized. This admits air to the notching cylinder, which advances the sequence drum to Notch 1. Just as the drum reaches the first notch, the "ON" magnet valve is de-energized automatically. The notching cylinder then returns to its original position under the action of a spring. The sequence drum then is ready to take the second notch. It cannot advance until the contacts of the limit relay close. There are a a total of nine notches. When the master controller is moved to the "OFF" posi-

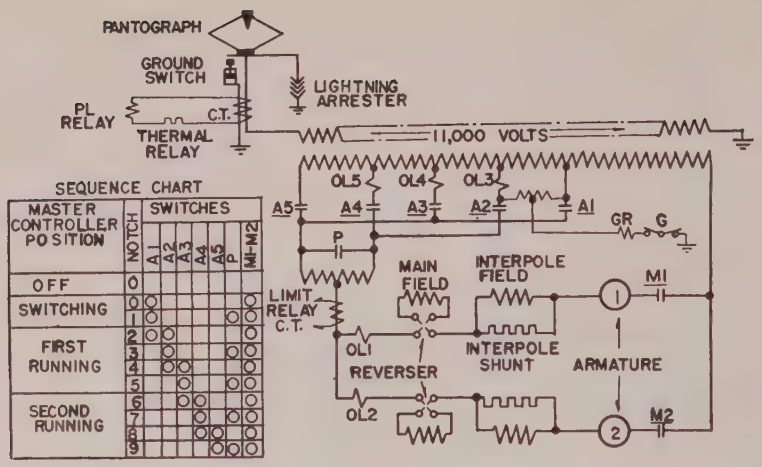

Figure 1. *MP54E5* multiple-unit car main circuit schematic diagram

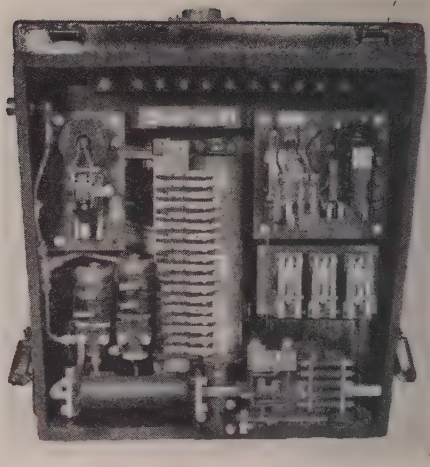

Figure 3. End view of *MP54E5* multiple-unit car main control box

tion, air is admitted to the return cylinder under the action of the "OFF" magnet valve. This causes the sequence drum to return to the "OFF" position.

The limit relay is a statically balanced quick-acting device. It is set to give the desired accelerating current. The setting is not affected by vibration or road shock. The current transformer for the limit relay carries 2-motor current. If one of the motor overload relays, *OL1* or *OL2*, operates, the corresponding motor switch, *M1* or *M2*, is opened. With one motor cut out of circuit, a resistor normally in parallel with the limit relay is disconnected automatically. Because the impedance of the relay and the resistor are equal the accelerating current for the motor in circuit remains the same as it was when both motors were operating. The accelerating tractive effort for the car is half the normal tractive effort. An overload-indicating light in the auxiliary and protective control box and another inside the car give a warning when one of the motor overload relays has operated.

The three relays on the sequence relay panel are the low-energy type. They require only one-third the operating current of a reverser or switch magnet valve. They are connected to the following train-line wires: forward, reverse, and the wire that feeds the tap switches and preventive coil switch. When energized by the train-line wire, the sequence relay connects the proper magnet valve to the car battery. Occasionally it has been found impossible to operate the rear cars on a long train of older multiple-unit cars because of excessive voltage drop in the above-mentioned train-line wires. This trouble will not occur on a long train of *MP54E5* cars. A mixed train of old and new cars will benefit from the reduced train-line load of the new cars.

The ground detector relay panel is another feature of the new cars. It consists of an a-c relay, *GR*, and a d-c relay, *G*. As shown in Figure 1, *GR* is connected to the midpoint of a small autotransformer and to ground through the "OUT" contacts of relay *G*. If a ground occurs in any of the secondary circuits, *GR* will operate. This causes *G* to close, which breaks the ground connection to *GR*. The intentional ground thus is removed and *GR* opens. *G* holds itself closed and lights a ground-indicating light in the auxiliary and protective control box and one inside of the car. The first ground does no harm. The car is permitted to continue in service. The Pennsylvania Railroad personnel are instructed to send the car to the repair shop as soon as possible so that the ground may be located and removed.

In addition to some auxiliary contactors, circuit breakers, and relays, the auxiliary and protective control box contains the transformer thermal auxiliary relay. A thermostat is immersed in the askarel in the main transformer. When the temperature reaches 90 degrees centigrade, the thermostat contacts close and energize the thermal auxiliary relay. The closing of this relay opens the traction-motor switches. A target attached to the relay shows through a small glass window in the box and indicates that the relay has operated.

Additional transformer protection is provided by three transformer tap-overload relays, *OL3*, *OL4*, and *OL5*, a pantograph lowering relay, *PL*, and a thermal relay in series with *PL*. All these are shown in Figure 1. If an overload of large magnitude occurs, the *PL* relay operates and energizes the magnet valve that admits air to the pantograph ground switch. The resulting high trolley current trips the substation circuit breaker and clears the line. When power is removed, the *PL* relay goes to the position that energizes the "Pantograph Down" magnet valve. This lowers the pantograph on the car that is in trouble. The *PL* relay latches itself in this position. The operator cannot raise the pantograph. An overload below the *PL*-relay setting, but high enough to damage the main trans-

Figure 2. Front view of *MP54E5* multiple-unit car main control box

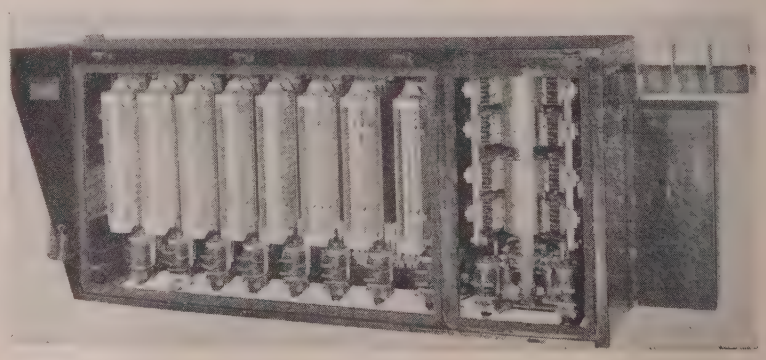

former if it persists too long, causes the thermal relay to operate. This energizes the magnet valve that admits air to the pantograph ground switch. As shown in Figure 1, the ground switch current passes through the current transformer supplying the *PL* relay. Being a very high-speed device, the *PL* relay operates before the substation circuit breaker clears the line. When power is removed, the pantograph is lowered by the *PL* relay.

If a short circuit occurs across half of the transformer secondary winding or the full secondary winding, the resulting primary current will cause the thermal relay to operate. If the short circuit occurs across certain low-voltage sections, the resulting primary current will not be high enough to operate the thermal relay. This is the reason for overload relays *OL3*, *OL4*, and *OL5*. They are located inside the transformer low-voltage terminal housing. The closing of one of these relays energizes the magnet valve that admits air to the pantograph ground switch. The sequence of operation is the same as described previously for the thermal relay.

The 9-notch control scheme utilizing transformer taps, a preventive coil, and a sequence switch is the same as that which has proved successful in 18 years of service on the Class-*MP54E3* cars. To this, the new *MP54E5* cars add the great advantage of parallel motors and the numerous protective features described in this paper.

Discussion

H. S. Ogden (General Electric Company, Erie, Pa.): The author is to be complimented on this paper which brings us up to date on the latest control schemes manufactured by the Westinghouse Electric Corporation for their standard a-c multiple-unit car equipments. It is appreciated that the development of the control system herewith described has been subordinated to the efforts which the Westinghouse Company has recently put into the development of their rectifier-equipped multiple-unit car.

The paper describes the use of parallel connected traction motors and the benefits to be derived from this connection are substantial when the cars are operated at or near the slipping point of the wheels. There are other more or less equivalent connections which will develop the beneficial features of the straight parallel connection without some of the complications. For instance, in a "4-motor equipment" where adhesion is a factor, the traction motors may be connected two in series and two groups in parallel and the mid-point of each of the two groups connected together by a power bus. Such a connection would provide the advantages of relatively low transformer currents at a higher voltage. The advantages of such a circuit are increased with the increase in number of the motor circuits.

Although the complications of running the power bus bars longitudinally through the main control group as described in the paper complicate the manufacturer's job in the design and construction of the group, the advantages of such an arrangement are considerable when it comes to putting in the power leads on the car. Such an arrangement is well worth the additional effort which it takes.

When reading the paper, a number of questions occur concerning the details of the equipment. For instance, there was mention of operating the car with traction motors cut out, presumably by means of the overload relay. Is this manual, in addition to the automatic means provided by the overload relay?

The paper also mentions the use of low energy relays for the purpose of insuring successful operation of long trains of these multiple-unit cars. It would be interesting to have the author's definition of "long" so that we might know how many cars it would be possible to operate together.

We notice the omission of car performance curves and feel that considerable benefit would be derived had such information been included in the paper; particularly a comparison between this equipment and that in service on the Class-*MP54E3* cars mentioned in the last paragraph of the paper. We believe that the resistance lead traction motor with which the control under discussion is operating would have a rather poor power factor due to the omission of the compensating winding and it would be interesting to see the effect this has on car characteristics, particularly operating power factors. This 2-motor equipment will be deficient if dynamic braking is ever added to these cars.

S. E. Newhouse: Mr. Ogden's interest in my paper is appreciated. In answer to his first question, either of the traction motors may be cut out of circuit by closing the corresponding motor overload relay by hand. This opens the motor switch. The motor overload relay will latch itself in the closed position. When the reset coil is energized, the latch is released and the overload relay returns to its open position.

The definition of "long" train, as applied to the Pennsylvania Railroad, is a multiple-unit train of 10 to 14 cars. The three low energy relays insure more reliable operation of long trains.

A car performance curve would have been a desirable addition to my paper. The first notch on the *MP54E5* car provides 3,200 pounds tractive effort at standstill. The next two notches are also "build-up" notches. The limit relay is set to give 7,000 pounds average accelerating tractive effort. The peak swing of tractive effort is 7,900 pounds.

This 2-motor equipment has not been designed for future conversion to dynamic braking.

A-C Multiple-Unit Car Motor

F. C. KREITLER, JR.
NONMEMBER AIEE

Synopsis: A major factor in the development of the 4-motor equipment for use on a-c multiple-unit cars was the design of a suitable truck-mounted traction motor. Numerous electrical and mechanical problems had to be solved. The resultant design differs radically from the conventional axle-hung motor employed in such applications for the past 20 years. Preliminary operating experience indicates advantages comparable to those being realized with similar d-c equipment.

AS SET forth in a companion paper by R. A. Williamson,[1] there is a marked trend toward motorizing all axles with flexibly mounted motors for multiple-unit car service. Heretofore, especially with single-phase power supply, only a fraction of the axles have been driven, and hence motor units have been of larger size. The new motor is a small, truck-mounted, low-cost design, of high quality, which should result in low maintenance costs and high reliability.

The motor is a 6-pole 25-cycle, single-phase, commutator, series-type with commutating poles and pole face windings.

The maximum operating speed is 3,900 rpm, corresponding to a road speed of 90 miles per hour. The weight complete with the mounting bracket is 2,000 pounds.

Design Features

The electrical constants are, in general, similar to those of modern a-c traction motors now in operation.[2] Chiefly because of the smaller size of this unit, there are numerous mechanical departures from existing designs.

The commutator is $9^{3}/_{4}$ inches in diameter, so that at the maximum operating speed its peripheral speed is 10,000 feet per minute. For the past two decades the practice for a-c series motors has been to use spring ring commutators with the copper segments V-bound. Recent developments have shown that arch-bound commutators are superior to the V-bound type.

This commutator is of the arch-bound type using the simple, inexpensive, yet effective ring-nut construction that has been employed in d-c motors of similar size for years. The commutator has been proportioned so that the stresses are lower than those in most existing a-c commutator motors.

The armature core is 14 inches in diameter and has open slots. This makes possible the single-piece coil construction using preinsulated wire and permitting complete insulation of the polycoil before assembly. The armature of this new a-c motor, shown in Figure 1, thus is very similar to those of d-c motors used with 4-motor equipments in service on 600-volt d-c subway cars and on railroad multiple-unit cars.[3]

The armature complete with fan weighs 680 pounds. It is mounted on a 60-millimeter ball bearing at the commutator end and a 70-millimeter roller bearing at the drive end. The commutator-end bearing is enclosed in a cartridge, as shown in Figure 1, so that the armature can be removed from the frame without disturbing the bearing. It should be noted that these bearings carry very little load other than the weight of the armature, since the gear reaction is taken by the bearings in the gear unit.

The stator windings are fairly conventional, as indicated by Figure 2. Preinsulated conductors are used throughout and, since the compensating slots have no overhanging tooth tips, the compensating coils are completely insulated before assembly. The fact that there is considerably more room around the stator-end windings than in larger machines makes the winding job easier.

One of the major problems with a-c traction motors has been brush accessibility.

Inspection is simplified in the case of this design, as the motor is small and has relatively few poles and brushes. Fixed brush-holder supports are used. The support blocks are mounted on three frame arms, as shown in Figure 2. The brush holders are accessible through the large openings between the frame arms, four from directly below the motor and two from above.

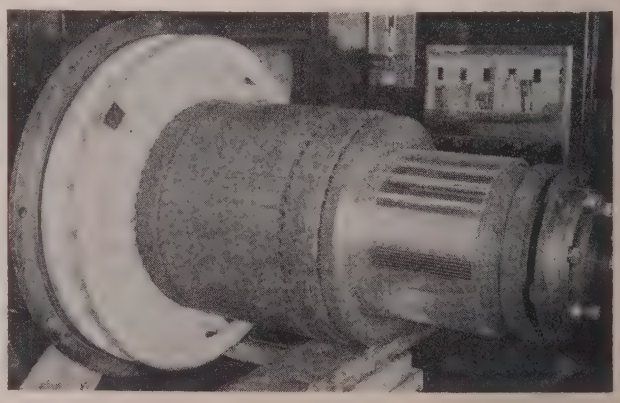

Figure 1. A-c traction-motor armature showing cartridge-type bearing assembly on commutator end and fan on drive end

Paper 51-106, recommended by the AIEE Land Transportation Committee and approved by the AIEE Technical Program Committee for presentation at the AIEE Winter General Meeting, New York, N. Y., January 22–26, 1951. Manuscript submitted October 16, 1950; made available for printing December 12, 1950.

F. C. KREITLER, JR., is with the General Electric Company, Erie, Pa.

Figure 2 (left). A-c traction-motor stator with brush holders in place

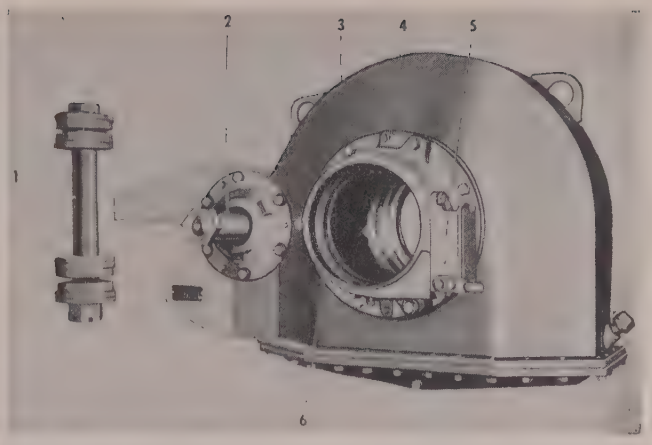

Figure 4. Gear reduction unit for use with a-c trunk-mounted motor

1, Suspension unit; 2, High-speed pinion; 3, Gear box; 4, Bearing housing; 5, Ground brush holder; 6, Axle housing

Ventilation

The motor is self-ventilated by means of a cast aluminum fan (see Figure 1) that is bolted to the drive-end armature head. Earlier a-c traction motors, principally because of space limitations, were blown from an external source through a system of ducts. This small, high-speed motor is adaptable to self-ventilation in the same manner as d-c motors of similar size in use on subway cars and small locomotives. The principal advantage of self-ventilation is the elimination of expensive blowers and ductwork, with greatly improved accessibility for brush and commutator inspection and maintenance.

The ventilating air is taken in through commutator covers, which are built as a series of baffles (see Figure 3). These baffles act to turn the air as it enters the motor and cause any included dirt to be deflected. The outer baffle prevents the direct entrance of water or snow into the motor and, on the bottom cover in particular, also acts as a plow to keep snow from packing into the commutator chamber. The inner baffle keeps anything that might get through the other baffles from striking the commutator. Dirt-separating tests show this cover to be very effective in keeping dirt out of the motor.

Air is discharged at the fan end. The arms over the air outlet are skewed and have rounded edges to keep noise at a minimum. A small-diameter rod is welded over the air outlet to prevent flying ballast from damaging the fan. The top portion of the air outlet is covered completely to prevent melting snow or water from running into the motor and freezing during long layovers.

Figure 3. Complete a-c traction motor showing air-intake baffles on commutator covers, mounting bracket, and rubber supports

Mounting

A major problem in 25-cycle single-phase traction-motor design has been the isolation of the 50-cycle torque pulsations generated in the motor from the axle, truck, and car body. One reason for this isolation is to keep shaft torsional stresses and gear-tooth pressures low. Another reason is to reduce noise in the car. The method of mounting and the rubber-supported members of the new motor have been effective in achieving this.

One of the advantages of the truck-mounted motor is the simplicity of the mounting. The motor is supported by, and overhung from, the truck transom with a key and five bolts. To remove a motor, with the truck out from under the car, it is necessary merely to unbolt the coupling, remove the five bolts holding the motor to the transom, and lift the motor out of the truck. This method was developed for d-c subway-car motors.[3] A similar mounting is used for the a-c motor, with the addition of rubber in certain locations in the system to obtain the necessary torsional isolation.

The first sample equipment was built with the motor mounted on cylindrical rubber bushings, which were clamped in a vertical position at the center line of the motor. Two bushings rested on the truck transom and a third was on an arm that reached over the axle and rested on a transverse truck member. This mounting was abandoned, however, because the transverse truck member complicated the truck and interfered with brush accessibility.

The next step was to try to duplicate more closely the d-c motor transom mounting. This was accomplished by building an intermediate bracket which fastened to the truck by means of a key. This bracket located the motor longitudinally from the axle and has three vertical bolts through the key to hold the motor down and two horizontal bolts at the bottom to keep the motor from swinging. Cylindrical rubber bushings are located between the motor and the mounting bracket, as shown in Figure 3. The

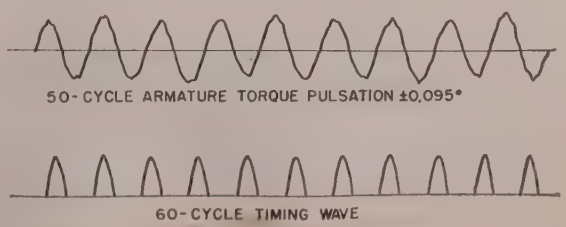

Figure 5 (right). Torsiograph showing 50-cycle pulsations at 1,320 rpm, full load

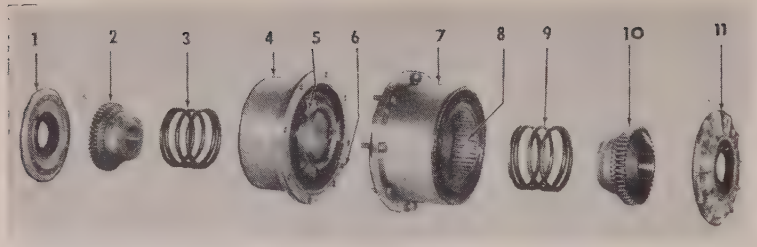

Figure 6 (left). Exploded view of flexible coupling

1, End cap assembly (gear unit end); 2, Pinion; 3, Centering spring; 4, Female sleeve assembly; 5, Mechanical jaws; 6, Alignment pin; 7, Male sleeve assembly; 8, Internal ring gear; 9, Centering spring; 10, Pinion; 11, End cap assembly (motor end)

bracket is attached to the motor on the bench, and the assembly is put in the trucks as a unit. Four bushings are used, placed so that their shear axis is tangential to the motor frame. Two bushings are approximately 45 degrees above the horizontal center line and two 45 degrees below. The upper pair of bushings is spaced as far apart as possible, while the lower pair is close together, thus effecting a 3-point mounting. This positioning of the rubber has the advantage of having the rubber soft in the tangential direction and stiff in the vertical direction. As a result, about 93 per cent torsional isolation is realized, and only 7 per cent of the 50-cycle torque pulsation is transmitted to the truck; yet the deflection at the center of the motor, caused by its weight, is less than 1/32 inch.

Gear Unit

The motor drives the axle through a separate gear reduction unit, shown in Figure 4, with a flexible coupling between the motor and gear unit. Helical gearing is used to reduce gear noise to a minimum. The pinion is carried on tapered roller bearings and the gear unit is mounted on the axle with tapered roller bearings to take the thrust of the helical gearing. The gear unit is oil-tight and the gears and bearings are lubricated with oil.

These gear units are practically identical with those now in service on d-c 4-motor car equipments.

Coupling

With the motor frame mounted flexibly, the armature still delivers 50-cycle pulsating torque. Figure 5 shows a torsiograph of the armature with the frame mounted on rubber. The 50-cycle torque pulsation is very pronounced. Past practice has been to try to isolate these torque pulsations from the axle by means of spring gears. The spring gear usually was designed so that the gear rim did not deflect until a fairly high torque was applied, so that there was no isolation at low loads. These gears had flat or coil springs and sliding metal surfaces to locate the gear rim, which made for high maintenance costs. The presence of high friction in the spring drive was undesirable because it helped to transmit the torque pulsations.

The truck-mounted motor requires a flexible coupling between the motor and gear unit to take care of truck spring deflections. This becomes a convenient place to include a torsionally flexible member, especially as the torque of the motor shaft is low compared to the axle. Because of this low torque, rubber can be used to provide the necessary torsional flexibility, with low stress in the rubber.

The rubber is put into the coupling as a cylindrical ring surrounding the internal gear of a spherical gear-type coupling and is attached to an outer sleeve. Figure 6 shows details of this coupling. A "fail-safe" device is built into the coupling by putting jaws on the internal gears at the center of the coupling. These will drive if the rubber should fail. The jaws are placed so they will make contact at about four times normal accelerating torque and prevent damage in case of accident.

A torsional isolation of 95 per cent is desirable. Torsiograph tests on the first coupling built showed that the rubber was too stiff to give the desired isolation. The rubber compound was made softer and the desired torsional isolation was obtained.

Conclusions

A small, high-speed, 25-cycle commutator motor has been developed for 4-motor a-c multiple-unit cars. The motor is much simpler and less costly than previous a-c traction motors. Its maintenance costs are expected to be low, on the basis of experience with similar d-c motors currently in service. The motor is truck-mounted and can be removed easily. Self-ventilation simplifies car construction by eliminating blowers and ducts.

Isolation of the motor from the truck and axle by rubber assures that the passengers will get a smoother, quieter ride than ever before experienced on an a-c multiple-unit car in the United States.

References

1. Why 4-Motor Multiple-Unit Car Equipment?, **R. A. Williamson.** *AIEE Transactions*, volume 70, part I, 1951, pages 240–42.

2. The Modern Single-Phase Motor for Railroad Electrification, **F. H. Pritchard, Felix Konn.** *AIEE Transactions*, volume 50, March Section, 1931, pages 263–68.

3. The Design of New York Subway Motors for Dynamic Braking, **B. A. Widell.** *AIEE Transactions*, volume 66, 1947, pages 808–10.

Discussion

W. S. H. Hamilton (New York Central System, New York, N.Y.): This discussion, while relating specifically to this paper, relates even more to the remarks made by Mr. D. R. MacLeod relative to the papers by W. M. Hutchison[1] and H. D. Jungk.[2] As I understand it, Mr. MacLeod still believes in recommending any and all designs of 25-cycle a-c commutator motors for use on 25-cycle a-c multiple-unit cars, although he admits that for a 60-cycle system the equipment would have to be d-c motors with ignitron rectifier equipment as now in operation on the Pennsylvania Railroad on a multiple-unit car, and soon to be supplied on some locomotives now being built for the Pennsylvania Railroad.

If there ever was a time when standardization of equipment for electrification was necessary, it is now, in these days of rising costs of materials, labor, and so forth. If the General Electric type-*1240* motor and its Westinghouse counterpart, which are already in use on 600-volt d-c systems, are anywhere near as good as is claimed for them, then in my opinion they should be adopted for these multiple-unit car equipments, together with the ignitron rectifier, for both 25- and 60-cycle multiple-unit car equipments. This will give us one standard form of traction motor and will enable us to benefit by the reduced cost obtainable by production in larger quantities. While I am not in possession of the costs covering the ignitron rectifier and its associated equipment for use on 25-cycle a-c multiple-unit cars, it seems to me that by using a standard d-c traction motor with its known lower maintenance and higher reliability, the cost of maintenance and the initial cost of the ignitron rectifier equipment will be more than offset.

Furthermore, and what is most important, railroad managements would not then be confronted with conflicting claims from the two major electrical manufacturing companies, each recommending a different solution for the problem. While railroads that

have long been electrified may understand thoroughly the problems and the reasoning behind these conflicting solutions, such an attitude is most discouraging to those of us who are trying to secure a standard system of electrification that can be recommended for future electrifications.

With all due respect for the various authors of the group of papers of which this is one, and for the ingenuity with which they have carried out their different motor designs, I still think that it would have been best in the broadest interest of all concerned, if d-c motors and ignitron rectifiers had been used instead. Furthermore, I believe that similar problems in the future should be solved in this manner for both 25-cycle and 60-cycle systems.

References

1. Selection of Equipment for Multiple-Unit Cars, **W. M. Hutchison.** *AIEE Transactions*, volume 70, part I, 1951, pages 640–44.

2. A New Multiple-Unit Motor for the Pennsylvania Railroad, **H. G. Jungk.** *AIEE Transactions*, volume 70, part I, 1951, pages 243–46.

F. C. Kreitler, Jr.: We are in complete agreement with the sentiments expressed by Mr. Hamilton regarding the desirability of having one standard equipment for all multiple-unit cars in the United States. Mr. MacLeod's discussion, to which Mr. Hamilton refers, is in agreement with his thought that the 4-motored equipment, consisting of General Electric type-1240 motors and cam-operated resistance control, should be used for a-c rectifier-type cars.

The New York Central Railroad cars do not have dynamic braking, but the cars of the Board of Transportation of the City of New York are equipped with General Electric type-1240 motors and have dynamic braking. Therefore, there is available a fully developed d-c system on which a single-phase rectifier and transformer may be superposed to produce a 25-cycle 11,000-volt equipment for motor cars with, and without, dynamic braking.

Mr. Hamilton assumes that the performance of a d-c traction motor operating on rectified single-phase alternating current is the same as a motor on direct current. It is not economical to put enough reactance in a traction motor circuit to reduce the ripple current to a negligible value. As a result, there is a pulsating component of current tending to cause sparking at the brushes. Also, the double frequency component of field flux will produce transformed volts at the brushes, as in an a-c motor.

Practical considerations determine that commutation of a d-c traction motor on a single-phase rectifier power supply will be approximately equal to that of an a-c series motor.

The modern a-c series motor is satisfactory in this respect, and the rectified d-c motor, adjusted to the same standard of commutation, should be equally satisfactory if the rms currents in the windings are kept within acceptable limits.

We are very interested in the single-phase rectifier for traction because of the possible opportunity for standardizing. This is a very attractive prospect. However, the manufacturer does not control this situation entirely, but must be influenced to the extent that his customers demand equipments that best serve their particular interests. Whether the single-phase rectifier is the answer for a-c electric multiple-unit cars, only time will tell.

A-C Multiple-Unit Car Control Equipment

W. S. O'KELLY
NONMEMBER AIEE

Synopsis: Recent years have witnessed a growing demand for improvements in a-c multiple-unit car equipments. This paper, together with three companion papers,[1,2,3] deals with principal objectives of the improvement program and shows how they were attained in new equipments now going into revenue service on a large eastern railroad. The principal improvements center in the use of four newly designed traction motors per car, instead of the usual two, and a resistance acceleration scheme containing a new motor-driven cam controller. Improvements also were made in protective schemes and in arrangement of apparatus. Dynamic braking, now being worked out as a next logical development step for a-c cars, also is discussed briefly.

FOR THE past 22 years the design of a-c multiple-unit cars has followed the general pattern that was established with the introduction of the axle-hung, low-flux series motor and preventive coil control. Recent years have witnessed a growing demand for improvements.

A new propulsion system of superior performance, increased reliability, and relatively low first cost, combined with low maintenance cost and great rider appeal, has been developed for a-c multiple-unit cars. Two new apparatus developments have made this possible. The first is a high-speed, self-ventilated, cushioned, truck-mounted traction motor driving the axle through flexible couplings. This is described in the companion paper by Mr. F. C. Kreitler, Jr.[2] The second is a motor-driven, cam-type controller used in conjunction with a 2-voltage resistance acceleration scheme described in this paper. In the companion paper by Mr. R. A. Williamson,[3] the principal objectives for which this new equipment was designed are discussed. In the present paper, these objectives are amplified from the point of view of the design engineer, and a description is given of the control system and some of the component apparatus devised to achieve them.

Paper 51-107, recommended by the AIEE Land Transportation Committee and approved by the AIEE Technical Program Committee for presentation at the AIEE Winter General Meeting, New York, N. Y., January 22–26, 1951. Manuscript submitted October 16, 1950; made available for printing December 12, 1950.

W. S. O'KELLY is with the General Electric Company, Erie, Pa.

The author wishes to acknowledge his indebtedness to I. W. LICHTENFELS for information on the notching mechanism described in this paper.

Background Problems

An examination of the existing 2-motor equipments serves to reveal four major features where experience has shown improvement to be desirable.

First, the fundamental difficulty with such equipments is that they operate at relatively high wheel-to-rail adhesion. This is particularly true when a trail car is also involved. Consequently, the equipment is liable to damage and delay resulting from slipping.

Second, in order to obtain sufficiently small increments of accelerating tractive effort for optimum performance, a relatively large number of transformer terminals and tap switches are needed. For a given number of acceleration steps, the tap switch and preventive coil scheme is inherently heavy, complex, because of elaborate electrical sequence interlocking, and relatively expensive, both in first cost and in maintenance cost.

Third, a scrutiny of the protection used revealed schemes ranging from practically no protection for the equipment to very elaborate systems and devices. An objective of the new control is to furnish the optimum practical degree of protection with the least complication.

Fourth, the arrangement of apparatus offered opportunities for providing increased accessibility, greater compactness, and improved appearance.

For future development, the problem of reduction of brake shoe and wheel wear is important. To date no domestic a-c multiple-unit car has been equipped with dynamic braking. Although dynamic braking is not included in the equipment described herein, an adaptation of this equipment to include it is currently under development.

Objectives

The principal objective of this development has been to answer the challenge to "Do something about" these difficulties. Analyzed in detail this meant: Design and build a-c multiple-unit car electric equipments which:

1. Will multiple with existing equipment.
2. Will operate at much lower maximum adhesion.
3. Have lower first cost and weight, lower maintenance cost, greater reliability, and smoother riding and accelerating qualities.
4. Offer optimum protection of persons and equipment with least complication.
5. Have improved arrangements of apparatus with emphasis on accessibility and appearance.
6. Will be adaptable for future dynamic braking with minimum of change.

Solutions

General. The prime requisite of the development, regardless of any improvements made in the design either of the motors or of the control equipment, is that new cars must be able to operate in multiple with existing ones. Hence, the traction-motor speed-tractive effort characteristics were preordained within limits. Likewise, the master controller and control train-wire circuits were not amenable to change. This requirement posed some interesting circuit problems in connection with the radically different acceleration scheme to be described in following paragraphs.

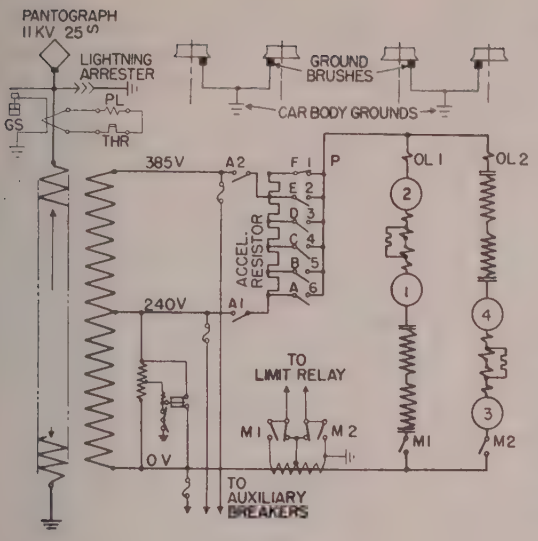

Figure 1 (left). Schematic diagram of main circuits

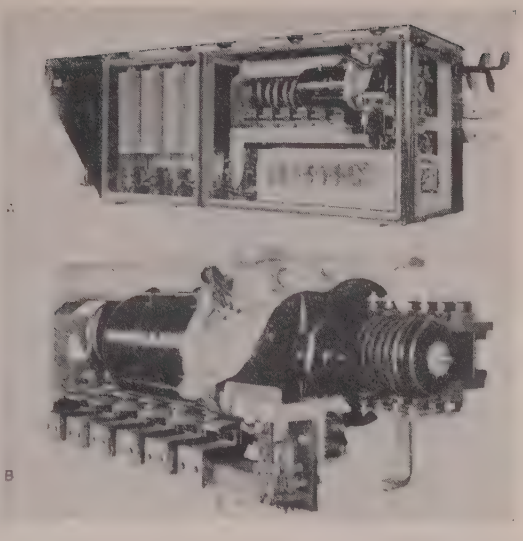

Figure 2 (right). A, Main control group arranged for undercar mounting; B, Cam controller showing current-carrying contacts on left and cam-operated interlock circuits on right

Adhesion. Obviously, the answer to operating a given weight of car at lower maximum adhesion per axle is to use more driven axles with the same total car tractive effort. The 4-motor equipment here described uses a permanent series-parallel connection as shown in Figure 1. This gives added insurance against slipping damage and also serves to hold total secondary voltage and current within practical limits. Moreover, it is well suited for the addition of dynamic braking at a future date.

Costs and Performance. In order to achieve lower costs and weight,[2] while providing improved reliability and smoother riding and accelerating qualities, it was apparent from the first that a bold departure from existing practice would be needed. The traction-motor and truck design described by Mr. Kreitler[2] play a most important role in achieving these ends. From a control standpoint, the accelerating schemes previously used were discarded and a fresh start was made. The scheme selected centers in a 2-voltage resistance acceleration system shown in Figure 1, modulated by a new motor-driven cam controller illustrated in Figure 2.

This system offers the following advantages:

1. A relatively small, compact unit replaces all but two of the electropneumatic tap switches.

2. Positive mechanical interlocking of the sequence improves reliability and reduces risk of damage from malfunctioning.

3. Two items of control maintenance are reduced because the controller contacts do not interrupt current, and there is no preventive coil (an item which requires periodic cleaning, dipping, and baking, and occasionally has been a source of damage when the cooling air supply failed). It should be noted that the accelerating resistor supplied on the new equipment is unblown.

Main Circuit Connections. Single-phase power at 11 kv 25 cycles is provided between an overhead contact wire and the rails. It is transformed to low voltage and utilized by the traction motors through a modulated accelerating resistor and one transformer tap change. Referring to Figure 1, the paths of current flow may be traced as follows:

A pantograph collects one side of the single-phase power from the overhead contact wire. Directly connected to the pantograph are a thyrite lightning arrester and a grounding switch contact plate, both mounted on the car roof. The feeder cable passes from the pantograph through the window of a roof-mounted outdoor-type current transformer, and thence to the high-voltage bushing of the askarel-filled main transformer, which is hung under the center sill of the car. The ground bushing of the primary winding is connected to the transformer tank, which in turn is grounded to the car body. Four sets of cables connected to axle ground brushes carry primary current from the car body to the axles, acting as shunts around the rubber motor mountings, the flexible couplings, and the roller bearings.

The secondary winding of the transformer has just three terminals (*M*, *A11*, and *A21*, in Figure 1) located in a housing at one end of the transformer case. Connected to each of these terminals are two bus leads, a main and an auxiliary. They emerge from the housing as bus-bar terminals to which, on one side, the main control group is connected by cables and, on the other side, the auxiliary equipment is connected. The auxiliary fuses shown in Figure 1 also are in the transformer terminal housing.

Lead *M* (0 volt), after entering the main control group, passes through a current transformer and connects to the blowout sides of two electropneumatic contactors, *M1* and *M2*, which are the motor line switches. Lead *A11* (240 volts), after entering the main control group, connects to tap switch *A1*. Similarly, lead *A21* (385 volts) connects to tap switch *A2*.

Car Operation. The equipment is arranged for double-end multiple-unit operation, with 36-volt nominal d-c control. The 2-voltage resistance scheme is arranged to produce automatic acceleration of the car from 0 to 30 miles per hour (mph) at an average rate of one mile per hour per second in 11 steps, total. From 30 to 85 mph, the car accelerates along the 385-volt motor characteristic curve as shown in Figure 5. The 240-volt tap provides a running step starting at a much lower speed: about 12 mph. This transformer tap-changing feature (a) halves the resistor losses, (b) reduces the number of controller contacts and resistor leads, (c) is accomplished with something less than the average accelerating tractive effort increment, and (d) limits the current surge at the tap switches to roughly one-eighth the amount handled in the preventive coil scheme. Provision is made to stop on any intermediate step. The control will not "back down," that is, under load, it can only advance.

The first running position of the master controller provides for short movements of the car with full resistance on the low-voltage tap. When the master controller is placed in this position, the sequence relays close *M1*, *M2*, and *A1* (Figure 1).

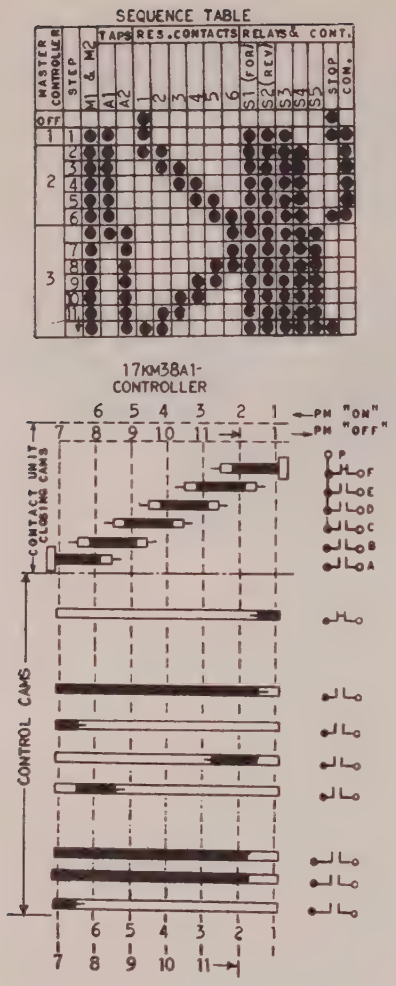

Figure 3. Development of master controller drum, and switch sequence table

Figure 4. Diagrammatic sketch of electric notching system for controller

A, CL relay dropped out, initiating a notch; B, Contacts closed, picking up CL relay; C, Completion of notch, pilot motor braking

Current flows from the 240-volt transformer tap through the entire accelerating resistor (*A* to *F*), thence through cam controller contact number 1, through the motor circuit overload relays, then to the motors, and returns through *M*. Note that the cam controller has not moved.

The second master controller position provides acceleration up to and including the 240-volt running step. The operator places the master controller in this position (Figure 3), and the cam controller advances one step at a time under control of the current limit relay until contact number 6 is closed, short-circuiting all the resistor sections. The car then will continue to accelerate along the 240-volt characteristic curve (number 6, Figure 5).

The third master controller position provides for acceleration up to and including the full voltage curve. When the master controller has been or is subsequently placed in this step (Figure 3), the cam controller will continue on to end position 7 which, in sequence: (a) opens contact 5 (Figure 1); (b) causes *A2* to close; (c) causes *A1* to open; (d) thus places sections *A* through *E* of the accelerating resistor again in series with the motors now connected to the 385-volt tap; and (e) reverses the direction of controller rotation so that it will take steps (still under control of the limit relay), until contacts 2 and 1 are closed in step number 11. The car then can accelerate along curve 11 (Figure 5) until a balancing speed of about 85 mph is reached.

Whenever the master controller is shut off, the tap switch (whichever is closed) and the two line switches open first. Only after this will the cam controller resume the first position, in which only contact number 1 is closed. Should the master controller be returned to its first run position while the cam controller is in process of advancing, the cam controller will stop immediately in whatever step position it is then in or moving toward and will remain there until the operator either advances or shuts off the master controller.

Once the line and tap switches are open, they cannot reclose until the cam controller has returned to the first position. Hence, sudden application or reapplication of excessive motor voltage is precluded, even in the event of a jammed controller, because the car automatically becomes inoperative following the first shut-off after such an occurrence, and remains so until the trouble is corrected. Along these same lines, the control relaying and electrical interlocking used in signaling the various operations of the power devices were designed to guard against or minimize damage resulting from every malfunction, either foreseeable in design or developed in test. As an example, assume that tap switch *A1* (Figure 1) welds or jams in the closed position. During the sequence *A2* would close in step 7, as shown in Figure 3. The controller then is constrained to stop and, after a short time-delay, *M1*, *M2*, and *A2* open before the resistor can overheat. The controller is held in this step and cannot return to the first position until *A1* is cleared. The car thus is rendered inoperative under this condition. Likewise, should *A2* become jammed closed, the controller cannot return to the first position, and the car becomes inoperative after the first shut-off by the operator.

Cam Controller. This controller, shown in Figure 2, is the heart of the new system. It is unique in that the cam-closing torque peaks of the mechanism are reduced to practical values by the use of both opening and closing cams and overlapped contacts. It represents the first time that a compact direct-operating power controller, with a capacity of 1,350 amperes, continuous and driven by a

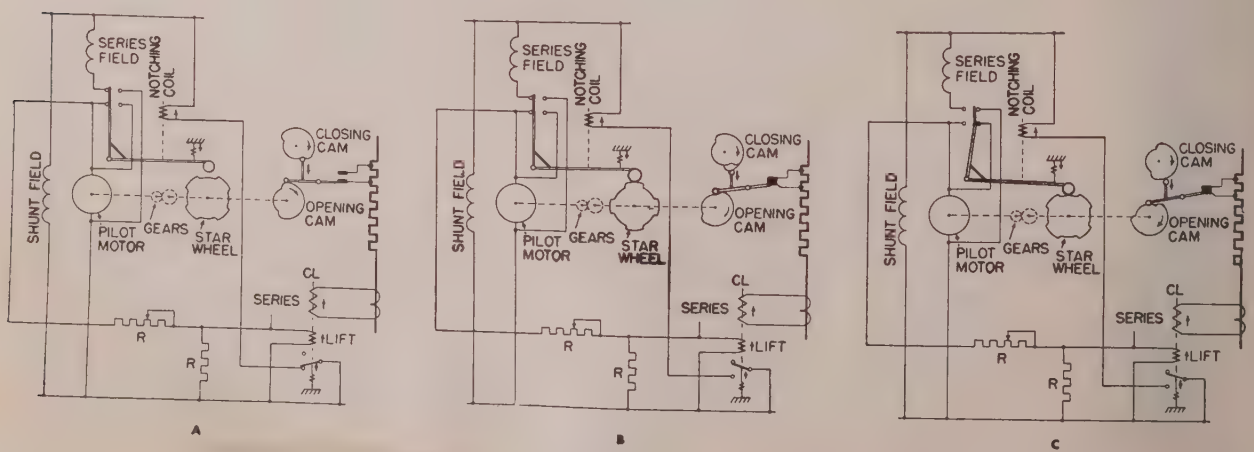

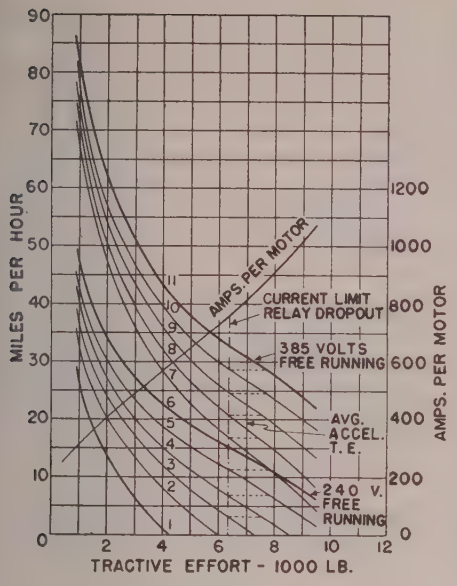

Figure 5 (left). Car characteristic curves with four traction motors (two series, two parallel) gear ratio 128/28, resistance acceleration

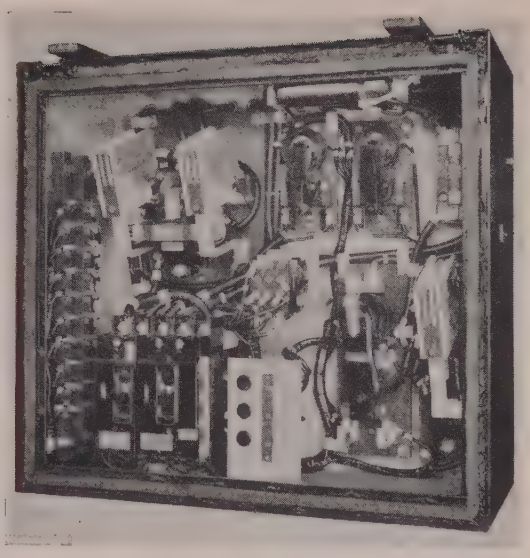

Figure 6 (right). Auxiliary control group

small d-c motor, has been developed for this type of application. Figure 4 illustrates the principle of its operation. The starwheel and follower shown do not constitute a mechanical stop, merely a signaling device. Short-circuiting of the motor armature stops the controller. Whenever the current limit relay drops out, the motor will run, unless specific pilot circuits are de-energized. When the limit relay picks up, either from driving motor or control circuit voltage appearing on the d-c lift coil, or from the presence of current in the a-c motor element, or both, the controller stops. Controller motor armature voltage appearing at the current limit relay lift coil through the adjustable series resistor causes the controller to take one step at a time regardless of the presence or absence of alternating current in the relay. This resistor prevents a control short circuit when the lift coil is separately energized to stop the controller. Also, it provides an adjustment with respect to interstep timing.

A combination flexible coupling and cushioned mechanical travel-limit device inhibits transmission of shocks to the gears and motor and provides positive backup prevention of overtravel at the rotation limits in either direction.

Protection. The protective schemes are divided into four mutually dependent categories. These are primary, ground detection, traction-motor overload, and auxiliary.

No slip relays are needed, since the maximum accelerating adhesion with empty car is only 6 per cent, a value that renders slipping very unlikely. Overspeed protection is not required because these cars will balance at a safe speed, and even if slipping occurs, the motor will not exceed its design speed limit.

The primary protective scheme consists of:

1. A pantograph grounding switch which may be energized either by a thermal relay (*THR*) in case of lower order sustained overloads or by an instantaneous relay (*PL*) in case of higher current faults. The operation of the grounding switch or a very high current fault will cause the track circuit breakers to trip. *PL* also serves to prevent lowering of the pantograph during fault conditions and to lower the pantograph after the track circuit breakers open. (A high-voltage primary fuse is under development which may, on future applications, replace the above devices.)
2. A thyrite lightning arrester.
3. A transformer thermostat which causes the line switches to open in case of overheating of the main transformer.

The ground detection relay (*GR*) located in the main control group, Figure 6, operates in case of a secondary ground. It energizes a normally closed relay (*G*) connected in series with the ground lead from *GR* coil, thus opening the normal ground. *G* has a self-latching circuit which can be reset remotely.

Traction-motor overload relays are of the bus-bar type, one for each pair of shift motors, and are designed for instantaneous overcurrent protection. The car will shift automatically to 2-motor operation if just one overload trips.

Auxiliaries, such as the transformer blower-generator set, compressor motor, car heat, and lights, are protected by means of thermal-magnetic circuit breakers, backed up by auxiliary bus fuses located in the transformer terminal housing.

Indicating lights are provided to notify operating and maintenance personnel of the existence and location of trouble, as follows:

1. Traction motor overload tripped.
2. Ground relay tripped.
3. Transformer thermostat tripped or primary fault (*PL* and *THR* tripped).

There are three lights on the saloon bulkhead and three duplicates which are visible through a window in the auxiliary control group, Figure 6, which is undercar mounted and therefore in view of car inspectors on the ground or in the pit.

Apparatus Arrangement

Considerable emphasis was placed on logical and accessible arrangement of apparatus within control groups and on the location of connections. All parts requiring inspection and routine maintenance are accessible without disassembly of control groups. Interconnection between the main control group and the transformer, accelerating resistor, and traction motors is accomplished without the crossing of cables.

Referring to Figure 2, it is apparent immediately that the contents of the main control group was arranged for maximum efficiency in space utilization. Tap and line switch magnet-valves, contacts, interlocks, and arc chutes are accessible through the front cover. The controller can be removed for major overhaul by disconnecting, removing three bolts, and sliding it out on the lower flange of the mounting channel. Routine maintenance can be performed without removal. The enclosed sequence relay panel can be re-

moved by disconnecting a single multipoint connector and removing four small bolts. Individual relays can be replaced quickly without removing the panel. Two static devices, the grounding autotransformer and the thyrite resistor, which require little or no maintenance, can be reached by removing the bottom cover. Most of the bus bars, the ground relay panel, and the air connections are accessible through the back cover. The reverser, one overload relay, and one terminal board are reached through the far-end cover, while the control cams of the controller, the current-limit relay, and two terminal boards are accessible through the near-end cover.

Dynamic Braking Developments

The continuous rating of the traction motors is nominally greater than the duty for the car as applied. This is because they were so designed that the same motors could be used should dynamic braking be employed in the future. Studies to date indicate the desirability and practicability of adding dynamic braking, and a development along these lines is in progress. Details of the circuits and equipment are in process of development.

Conclusions

The superior performance of the 4-motor a-c propulsion equipment has been demonstrated by the new cars, many of which are now in revenue service. Acceleration is smooth and riding qualities excellent. Noise is reduced to a minimum because of the motor mounting and because there is but one blower and only two tap switches, on which the switching duty is very low. It is apparent that when these cars have been "shaken down" and all details finally adjusted, they will prove to be an important forward step in the development of this type of transportation.

References

1. New A-C Multiple-Unit Car Control for the Pennsylvania Railroad, S. E. Newhouse. *AIEE Transactions*, volume 70, part I, 1951, pages 645–47.

2. A-C Multiple-Unit Car Motor, F. C. Kreitler, Jr. *AIEE Transactions*, volume 70, part I, 1951, pages 648–51.

3. Why 4-Motor Multiple-Unit Car Equipments?, R. A. Williamson. *AIEE Transactions*, volume 70, part I, 1951, pages 240–42.

No Discussion

A New Train Performance Calculator

S. V. SMITH
NONMEMBER AIEE

Synopsis: This paper describes a new train performance calculator recently placed in service by the Pennsylvania Railroad in Philadelphia. This calculator was developed to compute and record mechanically and quickly information required by a railroad to determine the economics, application, proper size, and tonnage ratings for new types of motive power, which information previously was assembled from a large number of tedious step-by-step mathematical calculations. The machine consists of three self-balancing, potentiometer-type, curve-drawing instruments, electrically interconnected, and a low-energy auxiliary circuit. The latter contains apparatus necessary to represent effective forces which influence the movement of a train and to represent certain types of motion which must be calculated to determine the performance of a theoretical train. The simplicity of its control and operation makes it suitable for continuous use in a quiet engineering office.

TO CALCULATE the performance of a given train over a given route, it is necessary to know the tractive effort at any speed of the motive power, the weight and resistance of each car or locomotive in the train, the profile, alignment, and speed restrictions, and the number and duration of station stops. These factors establish acceleration and braking for the train. Speed, distance, and time must be determined thereafter by applying the principles of mechanics.

The calculator described in this paper provides:

1. A means for representing known track resistances and restrictions
2. A means for representing known acceleration and braking forces as small voltages
3. A means for properly totalizing and applying acceleration and braking
4. A means for integrating acceleration or braking with respect to time, regulating a second voltage in proportion to speed in the process thereof
5. A means for integrating speed with respect to time to produce an indication of distance
6. A means for recording data relating to acceleration, braking, speed, distance, and time at any instant

It is composed largely of well-known instruments and apparatus which were developed for other applications and have been adapted to the solution of train performance problems with relatively few changes in basic design. The services of one operator are required to make adjustments for changes in grade and in types of motion. Completely automatic operation may be obtained when the present development of certain electronic devices for other purposes has progressed to the stage required for office use.

Apparatus

A front view of the new train performance calculator is shown in Figure 1. All of its operating components are mounted on two self-supporting steel panels, which are bolted to the floor for additional protection. The only external connections to the panels are three wires from the office lighting circuits, which supply 110-volt 60-cycle energy from two phases of a 3-phase distribution system. Two phases are required for operation of the instrument-balancing motors. Three-ampere fuses in each ungrounded wire indicate what a small amount of energy is required to operate the machine. No auxiliary voltage supplies of any nature are required.

On the left-hand panel there are two low-energy, self-balancing, potentiometer-type, curve-drawing instruments. The top instrument is designated the speed recorder; the bottom instrument, the distance-recorder. Both designations refer to the primary quantity measured by each. A similar instrument, designated the acceleration recorder, is mounted near the top of the right-hand panel. These three instruments contain all the apparatus which perform the calculations and assemble the required information. Measuring mechanisms in these instruments are balanced through a-c potentiometer circuits by small 2-phase induction motors, the control windings of which are energized through amplifiers. The use of a-c potentiometer circuits eliminates inaccuracies which might otherwise develop from resistances of interconnecting leads and from fluctuations in the alternating voltage supply. The time required for full-scale travel of the recording pens to a balance is approximately three seconds. The integrating mechanisms are operated through

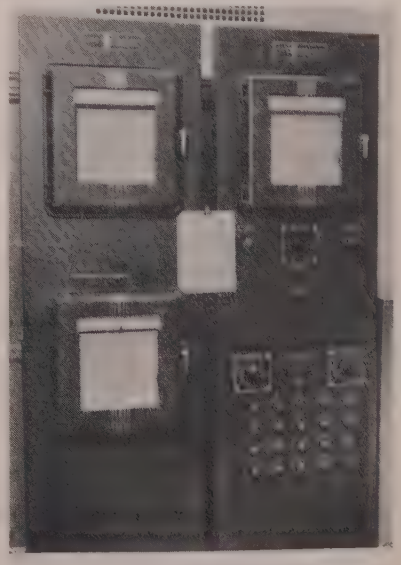

Figure 1. Front view of the new train performance calculator

Paper 51-108, recommended by the AIEE Land Transportation Committee and approved by the AIEE Technical Program Committee for presentation at the AIEE Winter General Meeting, New York, N. Y., January 22-26, 1951. Manuscript submitted October 25, 1950; made available for printing December 12, 1950.

S. V. SMITH is with the Pennsylvania Railroad, Philadelphia, Pa.

The author acknowledges contributions from W. E. PHILLIPS and other engineers of Leeds & Northrup Company in the design and assembly of the new train performance calculator.

gears driven by small synchronous motors and are controlled by notched disks positioned with the measuring slidewires. Each integrating mechanism performs 25 operations per minute. In the upper instruments, the synchronous motors also advance the charts at a rate of one inch each five minutes, which for a normal operation represents five minutes of train time. The chart in the distance meter is advanced by a special motor at a rate proportional to the calculated speed of the same train, which represents distance.

Below the acceleration recorder, reading from right to left, are a power ON-OFF switch, a grade and braking rheostat, and an operations switch. The power switch provides a means for energizing or de-energizing all apparatus on both panels. Each instrument is provided with an individual cutout switch for calibration purposes. The grade and braking rheostat, which is equipped with a dial calibrated from −2.0 miles per hour per second to +0.8 mile per hour per second, is adjusted as required to regulate a voltage proportional to the acceleration produced by profile and alignment of the track or proportional to the retardation needed for braking. The operations switch provides three positions which are used as required to simulate three conditions of train motion, namely: A, acceleration; FS, operation at fixed speed; and B, braking. In the A position, this switch connects to the measuring element of the acceleration recorder a totalized voltage proportional to the instantaneous algebraic sum of motive power and track-originated acceleration forces. In the FS position, no voltage is supplied. In the B position, a negative voltage proportional to braking retardation on a particular grade is connected from the grade and braking rheostat to the acceleration recorder.

An aperture below the grade and braking rheostat shows the scale and pointer of a galvanometer which is supported on a shelf attached to the rear of the right-hand panel. This galvanometer, normally disconnected from the operating circuits by a toggle switch, is provided to simplify the adjustment of rheostats, operating portions of which are shown on the lower half of the same panel. Each of the 20 rheostats shown in the lower four rows is connected between two taps on a retransmitting slidewire in the speed recorder. These taps correspond to speed positions, in even 5- or 10-mile steps, along the slidewire. Dials are marked to indicate the speed step around which each rheostat is connected. The entire lower assembly is calibrated initially to adjust the voltage gradient along the slidewire to the shape and proportions of the net acceleration curve for a given train; it remains fixed thereafter until the consist of the train is changed. The manner in which this is accomplished and the functions of the remaining rheostats, which are designated top speed tractive effort, air conditioning, and standardizing, will be explained later in this discussion.

Recording Instruments

Functions and special features of the recording instruments which adapt them to the train performance calculator are outlined as follows:

1. The acceleration recorder measures a voltage proportional to the totalized motive power and track acceleration forces, or to the braking force, and provides a permanent record of train acceleration at any time. A pointer attached to the recording-pen carriage indicates instantaneous acceleration along the lower instrument scale, which is calibrated from −2.4 to +2.4 miles per hour per second. A mechanical integrating device operates in conjunction with the acceleration-measuring mechanism and moves a contact over a straight section of slidewire located behind the upper instrument scale. This contact is attached to a pointer which indicates speed on the upper instrument scale calibrated from 0 to 120 miles per hour. The straight slidewire transmits to the speed recorder a voltage proportional to speed.

2. The speed recorder measures this voltage and provides a record of train speed at any time. A pointer associated with the pen indicates speed on a scale calibrated from 0 to 120 miles per hour. This instrument contains two retransmitting slidewires and a mechanical integrating device, which are positioned by the speed-measuring mechanism. One slidewire transmits to the acceleration recorder a voltage proportional to acceleration; the other transmits to the distance recorder a voltage proportional to speed. The integrating device through relays and cam-actuated contacts regulates the speed of the special chart-drive motor in the distance recorder.

3. The distance recorder measures speed and provides a permanent record of speed on a prepared chart which represents the track. The curve-drawing pen represents the train. A pointer moving with the pen indicates speed along the right-hand section of the instrument scale, calibrated from 0 to 120 miles per hour. A solenoid-operated pen, located under the left-hand section of the scale and actuated by a timing motor, provides a permanent record of time by drawing short horizontal lines at 5-minute intervals. The left-hand sections of the scale and the chart are ruled from 0 to 60 minutes. This portion of the chart is completed manually, to show time in hours and minutes at any location, following conclusion of the calculation. The special chart-drive motor advances the chart in steps of .02 inch for each 0.1 mile of calculated performance.

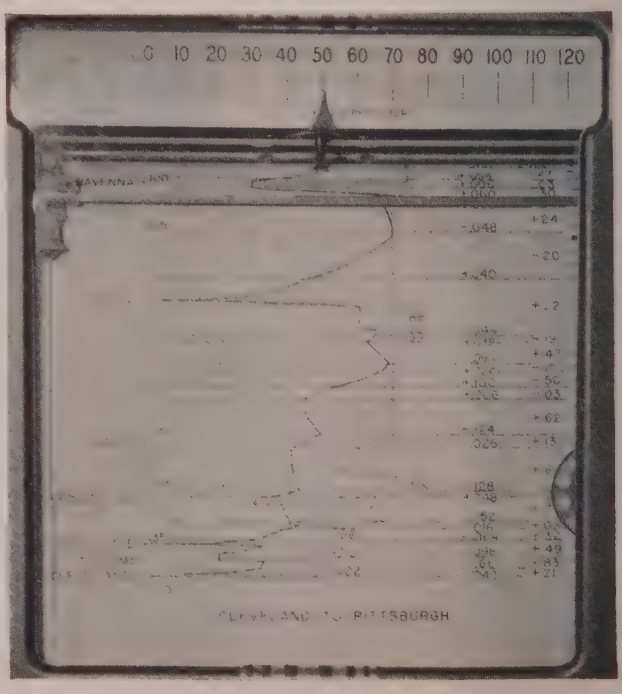

Figure 2. Speed-distance chart in the distance recorder

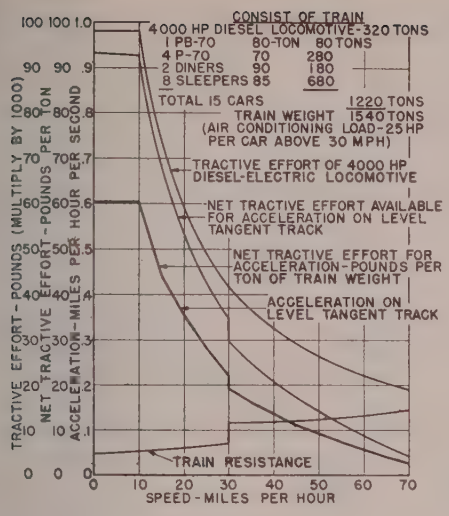
CONSIST OF TRAIN
4000 HP DIESEL LOCOMOTIVE-320 TONS
1 PB-70 80-TON 80 TONS
4 P-70 70 280
2 DINERS 90 180
8 SLEEPERS 85 680
TOTAL 15 CARS 1220 TONS
TRAIN WEIGHT 1540 TONS
(AIR CONDITIONING LOAD-25 HP PER CAR ABOVE 30 MPH)
TRACTIVE EFFORT OF 4000 HP DIESEL-ELECTRIC LOCOMOTIVE
NET TRACTIVE EFFORT AVAILABLE FOR ACCELERATION ON LEVEL TANGENT TRACK
NET TRACTIVE EFFORT FOR ACCELERATION-POUNDS PER TON OF TRAIN WEIGHT
ACCELERATION ON LEVEL TANGENT TRACK
TRAIN RESISTANCE
TRACTIVE EFFORT-POUNDS (MULTIPLY BY 1000)
NET TRACTIVE EFFORT-POUNDS PER TON
ACCELERATION-MILES PER HOUR PER SECOND
SPEED-MILES PER HOUR

Figure 3 (left). Steps in the reduction of train data

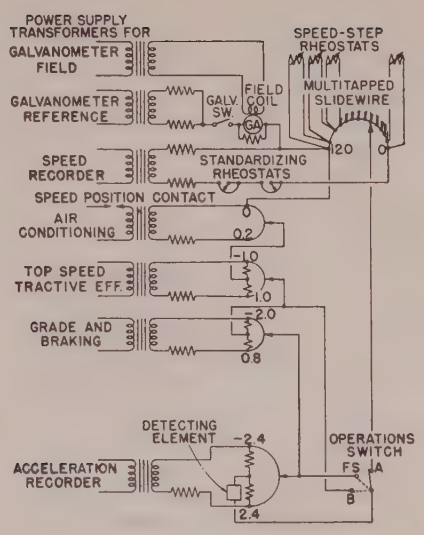

Figure 4 (right). Schematic diagram of the acceleration voltage circuit

Preparation of Data

Prior to making a calculation, the known data must be prepared and placed in the machine. The track information is represented on the speed-distance portion of the chart in the distance recorder, where it can be observed and followed by the operator. The train information is reduced to terms of net acceleration on level tangent track, then translated into proportional voltage, where it can thereafter be handled automatically.

The track information is shown on the speed-distance chart in the distance recorder in Figure 2. Horizontal lines are printed on this chart to indicate points one mile apart. Certain mileages and significant locations are indicated along the vertical zero speed line. Compensated grades, expressed in terms of per cent, are indicated along the maximum speed line. Points at which changes in grade occur are represented by dark horizontal lines drawn across the chart. At each of these lines, the value of acceleration corresponding to the approaching grade has been marked. (One per cent of compensated grade is considered capable of producing an acceleration of 0.2 mile per hour per second, the acceleration for down-grade being positive and for upgrade being negative.) Maximum permissible operating speeds are indicated by vertical lines to represent values and by horizontal lines to indicate location. Braking lines, drawn from templates, are placed at the approach to each speed reduction or station stop, with the rate of retardation, which is dependent upon grade, conveniently indicated in miles per hour per second.

Accumulating and plotting track data are time-consuming undertakings. Such data must, however, be accumulated and condensed before performance of a train can be calculated by any method. Once plotted on the chart, the information can be reproduced in a comparatively short time by tracing from the original over an illuminated table. One chart can and has been used as often as four times by changing the color of ink in the recorder pens. This practice is especially effective when comparing different types or sizes of motive power with the same consist of trailing cars.

Steps in the reduction of train data are illustrated in Figure 3. The top curve represents the tractive effort of a 4,000-horsepower Diesel-electric locomotive. The value in pounds is indicated on the first vertical scale from the left. Tractive effort up to a speed of 10 miles per hour has been limited to 25 per cent of the weight on drivers, which for this locomotive is 392,000 pounds. As speed is increased, tractive effort steadily decreases until at 80 miles per hour it has reduced to 16,100 pounds. The bottom curve represents resistance of 15 passenger train cars computed from well-known Davis formulae, to which has been added axle-driven, air-conditioning load. The latter becomes effective at 30 miles per hour and accounts for the abrupt increase at that speed. The second curve from the top is obtained by subtraction of the preceding two curves. It represents net tractive effort available for acceleration on level tangent track. The basic form of the third curve from the top is developed by dividing the second curve by train weight in tons. Its value is expressed in pounds per ton on the second scale from the left. It is common practice to assume that 100 pounds per ton of net tractive effort can produce an acceleration of one mile per hour per second on level tangent track. The third curve becomes an acceleration curve by referring to the third scale from the left. If now the even 5-mile speed values on the third curve, up to 80 miles per hour, are joined by a continuous series of straight lines as shown superimposed over the basic curve form in Figure 3, they can be translated into voltage values which the acceleration recorder can measure and integrate.

A schematic diagram of the acceleration voltage circuit, Figure 4, has been prepared to illustrate the calibration procedure. The circuit contains the multitapped slidewire positioned in the speed recorder, the air-conditioning rheostat, the top speed tractive effort rheostat, the grade and braking rheostat, and the measuring slidewire in the acceleration recorder, each of which is connected through small transformers to the main power supply. Also connected are the 20 speed-step rheostats, the two standardizing rheostats, the operations switch, and the standardizing galvanometer, the latter through a toggle switch which is closed only when held depressed to the right.

Calibration

The calibration procedure is outlined as follows:

1. Individual operating switches on the speed and distance recorders are moved to open position. The switch in the acceleration recorder is left closed.

2. The mechanism of the speed recorder is rotated until the pointer indicates the maximum speed which is desired for the calculation. To simplify this description, a maximum speed of 75 miles per hour will be assumed.

3. The operations switch is moved to the A (acceleration) position.

4. The grade and braking rheostat is adjusted to the negative value of accelera-

tion shown in Figure 3 for a speed of 75 miles per hour, or −0.012 mile per hour per second.

5. The power switch is moved to ON position.

6. The speed-step rheostats with dials marked 80–90, 90–100, 100–110, and 110–120, and top speed tractive effort rheostat are adjusted to zero.

7. The air-conditioning rheostat is adjusted for the difference of acceleration values indicated at 30 miles per hour. From Figure 3, these values are 0.224 and 0.194, the difference is 0.03 mile per hour per second. In Figure 4 is shown a position contact located in the speed recorder, which de-energizes the supply transformer for this rheostat at a speed of 30 miles per hour, thereby producing the straight vertical line at that speed.

8. The mileage rheostat marked 75–80 is adjusted until the acceleration recorder balances at zero.

9. If the recorder will not balance at zero, the top speed rheostat is adjusted until such a balance is obtained.

10. The galvanometer switch is depressed and the standardizing rheostats are adjusted until the galvanometer is returned to its zero position.

11. Steps 8, 9, and 10 are repeated until no further adjustments of the standardizing rheostats are required.

12. The speed recorder is rotated to the next tapped position, corresponding to a speed of 70 miles, and steps 8, 9, 10, and 11 are repeated with the grade and braking rheostat set to −0.027 mile per hour per second, the negative value of acceleration for a speed of 70 miles per hour, and adjusting speed step rheostat 70–75. This operation is repeated for each next lower tapped position until the entire range has been covered.

The calibration as outlined above can be completed for any train in less than 15 minutes. The standardizing rheostats, by maintaining constant current through the transformer supplying the multi-tapped slidewire, make it unnecessary to recheck any point which has once been set. The top speed tractive effort rheostat, with a range from −1.0 to +1.0 mile per hour per second, is used to extend the range of train acceleration above its balancing speed on level tangent track. The range of all rheostats has been designed to provide for all shapes of railroad motive-power acceleration curves which have been experienced. The only apparent limitation would be an acceleration curve with values which increase with speed. This appears unlikely at the present time.

Operation

When the calibration has been completed, all instruments are set to their zero positions, except the acceleration recorder, which is adjusted to maximum calibrated value. The prepared speed-distance chart is checked to make sure that the recorder pen rests at the proper starting position, the grade and braking rheostat is adjusted to the acceleration indicated for the initial grade, all instrument cutout switches are closed, and the operations switch is placed in the acceleration position. The power switch is operated to the ON position and the machine proceeds to calculate and record train performance in the actual time which the train would require to operate over the represented track. The operator observes the curve drawn by the pen in the distance meter and adjusts the grade and braking rheostat and the operations switch in accordance with the indications provided on the prepared chart, as the chart is advanced.

Maximum scales of 2.4 miles per hour per second for acceleration and 120 miles per hour for speed are in excess of maximum values produced from present-day railroad motive power. They were selected primarily to expand the distance and time scales for suburban trains, which make frequent stops at short intervals and rarely exceed a top speed of 60 miles per hour. For calculations on such trains, speed values on the acceleration curve are multiplied by two and the machine is calibrated accordingly. Top speed of 60 miles per hour appears on the chart as 120 miles per hour, and the speed-distance chart must be laid out for 1.25 miles to the inch, instead of 5.0 miles to the inch. With this arrangement, the calculator performs its work in twice the time which would be required for the train movement. However, a much better record of train operation is obtained for inspection and analysis. Similarly, a long freight run can be calculated in one-half train time by doubling the acceleration values, including braking and track values, and using actual speed scales. Distance scales thereby are changed from five miles to the inch to ten miles to the inch. Doubling both acceleration and speed values has been applied to some problems involving top speed below 60 miles per hour. This procedure provides a distance scale of 2.5 miles to the inch, but permits the performance to be calculated in train operating time.

Conclusions

This new train performance calculator was placed in service in the Office of the Electrical Engineer of The Pennsylvania Railroad in April 1950. It has been operated to determine performance of new types of motive power in passenger, freight, suburban, and helper service. It has been particularly useful in determining the extent to which short-time ratings of new Diesel-electric locomotives could be utilized in establishing tonnage ratings on ruling grades, and also in analyzing the amount of horsepower which should be applied to certain services. The records which have been produced adapt themselves to a compact filing system and are easy to analyze because of their graphic nature. There has been no indication of inaccuracy in the calculation process to date, despite numerous studies wherein different locomotives have been applied to the same train on the same prepared chart. The time saved in making these calculations and the records produced have provided opportunities for investigating other aspects of train performance which could not have been considered had it been necessary to make numerous step-by-step mathematical calculations. Maintenance routine, in accordance with the manufacturer's recommendations, has required less than one hour per month. There have been no apparatus failures or replacements.

No Discussion

Circuit Analysis Method for Determination of A-C Impedances of Machine Conductors

D. S. BABB
ASSOCIATE AIEE

J. E. WILLIAMS
ASSOCIATE AIEE

PRECISE CALCULATIONS of rotor bar impedances at several frequencies are essential if the induction motor designer is to achieve adequate accelerating torques while meeting present requirements of starting current, starting torque, pull-out torque, and efficiency. Calculation of a-c resistance of stator windings is important for large 60-cycle machines and for smaller machines operating at higher frequencies.

This paper presents a fundamental approach to the calculation of impedances of conductors and coils in motor slots on the basis of equivalent circuits. Equivalent circuits are developed for a single rectangular bar, T-shaped bar, idle bar, and a 2-turn coil. Extensions of the method can be made to include bars of any shape and coils with any number of turns. Experimental measurements of several conductor arrangements are made and compared with values calculated from the equivalent circuits.

The equivalent circuits used in this paper are similar to the distributed circuits representing transmission lines. In this paper, use is made of the following transmission line equations.

$$\boldsymbol{E}_S = \boldsymbol{E}_R \cosh \sqrt{\boldsymbol{YZ}} + \boldsymbol{I}_R \sqrt{\boldsymbol{Z}/\boldsymbol{Y}} \sinh \sqrt{\boldsymbol{YZ}} \quad (1)$$

$$\boldsymbol{I}_S = \boldsymbol{I}_R \cosh \sqrt{\boldsymbol{YZ}} + \boldsymbol{E}_R \sqrt{\boldsymbol{Y}/\boldsymbol{Z}} \sinh \sqrt{\boldsymbol{YZ}} \quad (2)$$

Paper 51-109, recommended by the AIEE Rotating Machinery Committee and approved by the AIEE Technical Program Committee for presentation at the AIEE Winter General Meeting, New York, N. Y., January 22–26, 1951. Manuscript submitted July 17, 1950; made available for printing December 12, 1950.

D. S. Babb and J. E. Williams are both with the University of Illinois, Urbana, Ill.

where $\boldsymbol{I}_S$ and $\boldsymbol{E}_S$ are sending-end current and voltage and $\boldsymbol{I}_R$ and $\boldsymbol{E}_R$ are values for the receiving end. $\boldsymbol{Z}$ and $\boldsymbol{Y}$ are, respectively, the series impedance and the shunt admittance of the line.

Equivalent Circuits

Three Small Bar Elements

Figure 1 illustrates the case for three small bar increments connected in parallel and located in a rectangular slot. The magnetic flux above bar A is proportional to the vector sum of the currents $\boldsymbol{I}_A+\boldsymbol{I}_B+\boldsymbol{I}_C$. This flux produces equal voltage drops of $j2\pi fL_0(\boldsymbol{I}_A+\boldsymbol{I}_B+\boldsymbol{I}_C)$ in all three bar elements. The magnetic flux between bars A and B is proportional to $\boldsymbol{I}_B+\boldsymbol{I}_C$ and induces voltages of $j2\pi fL_B(\boldsymbol{I}_B+\boldsymbol{I}_C)$ in bar elements B and C. The magnetic flux between bar elements B and C is proportional to $\boldsymbol{I}_C$ and induces a voltage of $j2\pi fL_C\boldsymbol{I}_C$ in bar element C. In the equivalent circuit of Figure 1 it is found that the sum of the self- and mutual-impedance drops for any bar element equals the voltage applied to the bar. The circuit is therefore adequate for calculation of the resistance and reactance of the three parallel elements at any desired frequency.

One Rectangular Bar

A solid rectangular bar may be considered as a large number of parallel elements. The circuit of Figure 2 is essentially the same as in Figure 1, but the number of elements has been greatly increased. L_1 of the circuit of Figure 2 corresponds to L_B+L_C of Figure 1 and is equal to $4\pi d_1/10^9 W_1 \times$length of bar in centimeters. L_0 is the same as in Figure 1 and is equal to $4\pi/10^9$ henrys times the permeance of the slot and air gap above the bar. This circuit is solved in the same manner as the distributed circuit involving an open-circuited transmission line

$$\boldsymbol{E}_{BAR} = j2\pi fL_0\boldsymbol{I}_{BAR} + \boldsymbol{E}_S \quad (3)$$

From equations 1, 2, and 3

$$\boldsymbol{E}_{BAR} = j2\pi fL_0\boldsymbol{I}_{BAR} + \boldsymbol{E}_R \cosh \sqrt{\boldsymbol{YZ}} \quad (4)$$

$$\boldsymbol{I}_{BAR} = \sqrt{\boldsymbol{Y}/\boldsymbol{Z}}\boldsymbol{E}_R \sinh \sqrt{\boldsymbol{YZ}} \quad (5)$$

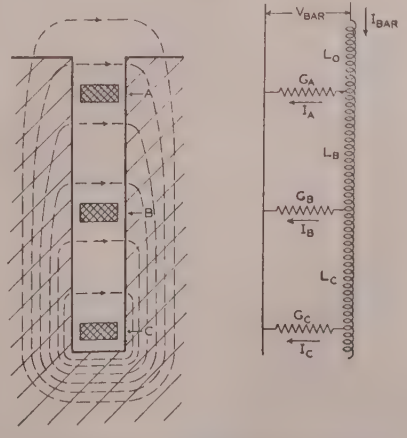

Figure 1. Three bar-elements in a rectangular slot

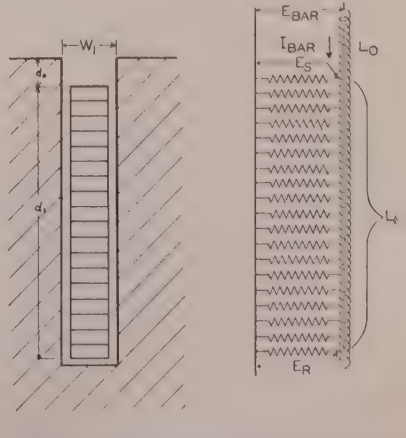

Figure 2. Equivalent circuit for a rectangular bar in a rectangular slot

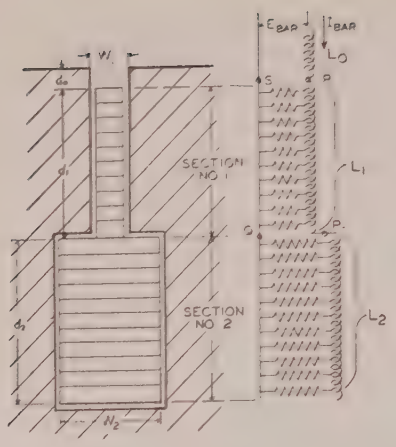

Figure 3. Equivalent circuit for a T-shaped bar

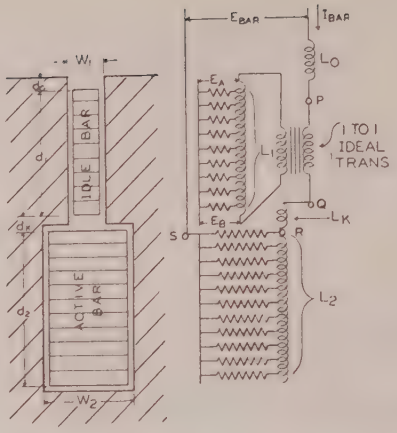

Figure 4. Equivalent circuit for one active bar plus one idle bar

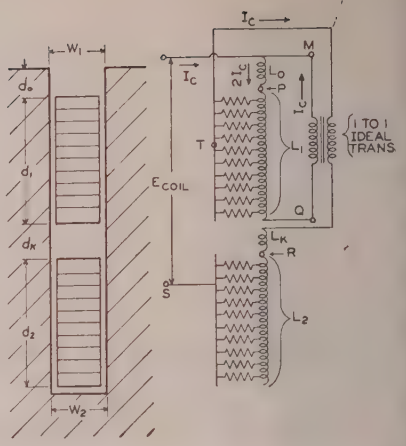

Figure 5. Equivalent circuit for a 2-turn coil

then

$$Z_{BAR} = j2\pi fL_0 + 1/Y\sqrt{YZ}\ \text{ctnh}\ \sqrt{YZ} \quad (6)$$

where $1/Y$ is the resistance of the bar in ohms. $Z = j2\pi fL_1$ ohms. Z_{BAR} then is specified in ohms.

T-Shaped Bar

The equivalent circuit of the T-bar, Figure 3, is obtained by combining the equivalent circuits of the two rectangular elements. The constants are as follows:

$L_1 = 4\pi 10^{-9} l d_1/w_1$ $\quad Z_1 = j2\pi fL_1$

Y_1 = conductance of Section 1

$L_2 = 4\pi 10^{-9} l d_2/w_2$ $\quad Z_2 = j2\pi fL_2$

Y_2 = conductance of Section 2

where l is length of the bar in centimeters and L_0 is defined as for the rectangular bar.

In calculating the equivalent circuit for the T-bar, the impedance of section 2 may be calculated using the method specified for the rectangular bar. This impedance is substituted for the distributed circuit of section 2 at terminals P and Q. The input impedance E_{BAR}/I_{BAR} then is conveniently calculated.

One Active and One Idle Bar

The case for a rotor slot containing one active and one idle bar is illustrated in Figure 4. The idle bar has no electrical connection with the end ring or with the active bar; therefore, it has a net current of zero. The voltage difference between the top and bottom elements of the idle bar is produced by flux through the idle bar. All constants are defined as for the T-bar. The reactance due to the flux above the slot is given by

$$X_0 = j2\pi fL_0 \quad (7)$$

The impedance reflected from the idle bar is given by E_{PQ}/I_{BAR}. In the solution of this reflected impedance it is noted that

$$E_A = -E_B = E_{PQ}/2 \quad (8)$$

From equation 2

$$I_{BAR} = I_{BAR}\cosh\sqrt{Y_1Z_1} + E_B\sqrt{Y_1/Z_1}\sinh\sqrt{Y_1Z_1} \quad (9)$$

$$E_{PQ}/I_{BAR} = 2/Y_1\sqrt{Y_1Z_1}\,(\text{ctnh}\ \sqrt{Y_1Z_1} - \text{csch}\ \sqrt{Y_1Z_1}) \quad (10)$$

The reactance due to flux between bars

$$X_K = j2\pi fL_K \quad (11)$$

where

$L_K = 4\pi 10^{-9} d_K/w_K \times$ (bar length in centimeters)

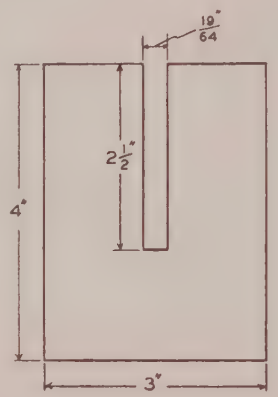

Figure 6 (left). Lamination and slot dimensions

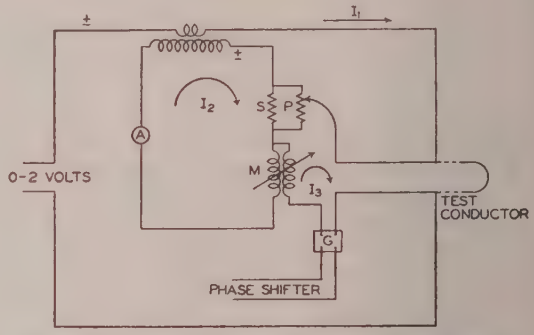

Figure 8 (above). Schematic diagram of test circuit

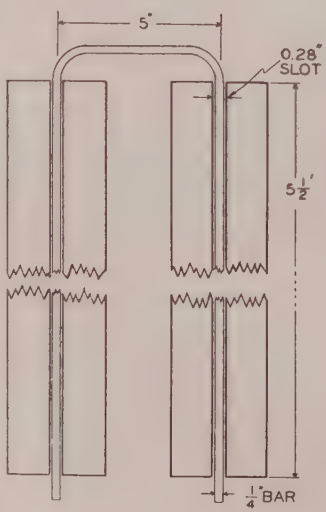

Figure 7 (left). Slot and conductor arrangement showing dimensions

Conductors insulated from slot sides with 10-mil paper. Slot width is 0.28 inch

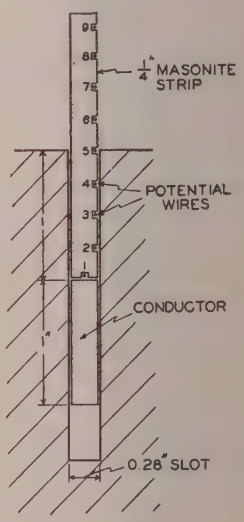

Figure 9 (right). Conductor arrangement for determining reactance as a function of slot depth (see Table II and Figure 14)

Table I. Measured and Calculated Values of Resistance, Reactance, and Inductance as a Function of Frequency

Frequency	Measured Values R Microohms	Measured Values X Microohms	Measured Values L Microhenrys	Calculated Values R Microohms	Calculated Values X Microohms	Calculated Values L Microhenrys
0.0				402	0	10.5
13.85	469	875	10.06	491	883	10.15
19.0	548	1,175	9.81	559	1,181	9.88
30.0	703	1,750	9.27	721	1,758	9.30
39.3	850	2,240	9.06	840	2,203	8.91
48.5	965	2,670	8.75	946	2,614	8.52
60.0	1,095	3,150	8.37	1,058	3,110	8.26
70.1	1,160	3,660	8.31	1,140	3,542	8.03
79.0	1,242	4,090	8.25	1,211	3,923	7.88

Test conditions: One rectangular conductor with top edge at top of slot. Conductor current of 320 amperes. 0.28-inch slot width. Assumed temperature is 30 degrees centigrade.

Table II. Measured and Calculated Values of Reactance as a Function of Distance Above Conductor

Potential Wire Number	Inches Above Conductor	Volts Measured	Reactance Measured, Microohms	Reactance Calculated, Microohms
1	0.007	6.42	7,650	7,382
2	0.25	5.46	6,520	6,357
3	0.50	4.22	5,030	4,932
4	0.75	3.00	3,580	3,507
5	1.00	1.98	2,365	2,080
6	1.25	1.25	1,492	
7	1.50	0.95	1,133	
8	1.75	0.76	907	
9	2.00	0.63	753	

Test conditions: Top of conductor 1 inch below top of slot. 0.28-inch slot width, conductor current 838 amperes, voltage 8.10 volts, 790 watts, and assumed temperature 30 degrees centigrade.
Conductor impedance: 1,058 + j8,810 microohms calculated 1,124 + j9,600 microohms measured.

The impedance of the active bar omitting effects of flux above the active bar is calculated in the same manner as the impedance of the rectangular bar (equation 6).

$$\boldsymbol{E}_{RS}/\boldsymbol{I}_{BAR} = 1/\boldsymbol{Y}_2\sqrt{\boldsymbol{Y}_2\boldsymbol{Z}_2}\ \text{ctnh}\ \sqrt{\boldsymbol{Y}_2\boldsymbol{Z}_2} \quad (12)$$

The total impedance of the active bar is given by the sum of equations 7, 10, 11, and 12.

Coil of Two Turns

Figure 5 gives the equivalent circuit for a 2-turn coil in a rectangular slot. The flux above the top conductor is proportional to coil current times turns, and induces a voltage of $j2\boldsymbol{I}_C(2\pi fL_0)$ in each of the two turns. L_0 is the same as for Figures 1, 2, 3, and 4, and is equal to $4\pi 10^{-9}$ henrys times the permeance of the slot and air gap above the bar. There is more flux across the conductor nearest the air gap; therefore, the skin effect is greatest in that conductor. The current distribution in each conductor can be determined from the equivalent circuit. The impedance of the top turn is given by

$$\boldsymbol{Z}_{TOP} = \boldsymbol{E}_{MT}/\boldsymbol{I}_C = j2(2\pi fL_0) + \boldsymbol{E}_{PT}/\boldsymbol{I}_C \quad (13)$$

The circuit between P and Q is similar to a transmission line with input voltage $\boldsymbol{E}_{PT}$, input current $2\boldsymbol{I}_C$, output voltage $\boldsymbol{E}_{QT}$, output current $\boldsymbol{I}_C$, series impedance $\boldsymbol{Z}_1$ (where $\boldsymbol{Z}_1 = 2\pi f 4\pi 10^{-9} d_1/w_1 \times$ length of bar in centimeters), and shunt admittance $\boldsymbol{Y}_1$ (where $\boldsymbol{Y}_1$ = conductance of the bar in mhos.) From the transmission line equations 1 and 2

$$\boldsymbol{E}_{PT} = \boldsymbol{E}_{QT}\cosh\sqrt{\boldsymbol{Y}_1\boldsymbol{Z}_1} + \boldsymbol{I}_C\sqrt{\boldsymbol{Z}_1/\boldsymbol{Y}_1}\sinh\sqrt{\boldsymbol{Y}_1\boldsymbol{Z}_1} \quad (14)$$

$$2\boldsymbol{I}_C = \boldsymbol{I}_C\cosh\sqrt{\boldsymbol{Y}_1\boldsymbol{Z}_1} + \boldsymbol{E}_{QT}\sqrt{\boldsymbol{Y}_1/\boldsymbol{Z}_1}\sinh\sqrt{\boldsymbol{Y}_1\boldsymbol{Z}_1} \quad (15)$$

From equation 15

$$\boldsymbol{E}_{QT} = \boldsymbol{I}_C 1/\boldsymbol{Y}_1\sqrt{\boldsymbol{Y}_1\boldsymbol{Z}_1}(2-\cosh\sqrt{\boldsymbol{Y}_1\boldsymbol{Z}_1})(\operatorname{csch}\sqrt{\boldsymbol{Y}_1\boldsymbol{Z}_1}) \quad (16)$$

Combining equations 14 and 16

$$\boldsymbol{E}_{PT}/\boldsymbol{I}_C = 1/\boldsymbol{Y}_1\sqrt{\boldsymbol{Y}_1\boldsymbol{Z}_1}\left[\frac{2-\cosh\sqrt{\boldsymbol{Y}_1\boldsymbol{Z}_1}}{\sinh\sqrt{\boldsymbol{Y}_1\boldsymbol{Z}_1}} \times \cosh\sqrt{\boldsymbol{Y}_1\boldsymbol{Z}_1} + \sinh\sqrt{\boldsymbol{Y}_1\boldsymbol{Z}_1}\right] \quad (17)$$

From 13 and 17

$$\boldsymbol{Z}_{TOP} = j4\pi fL_0 + 1/\boldsymbol{Y}_1\sqrt{\boldsymbol{Y}_1\boldsymbol{Z}_1}\left[\frac{2-\cosh\sqrt{\boldsymbol{Y}_1\boldsymbol{Z}_1}}{\sinh\sqrt{\boldsymbol{Y}_1\boldsymbol{Z}_1}}\cosh\sqrt{\boldsymbol{Y}_1\boldsymbol{Z}_1} + \sinh\sqrt{\boldsymbol{Y}_1\boldsymbol{Z}_1}\right] \quad (18)$$

The impedance of the bottom turn is given by

$$\boldsymbol{Z}_{BOTTOM} = \boldsymbol{E}_{TS}/\boldsymbol{I}_C = 4\pi fL_0 + \boldsymbol{E}_{PQ}/\boldsymbol{I}_C + 2\pi fL_K + \boldsymbol{E}_{RS}/\boldsymbol{I}_C \quad (19)$$

The impedance reflected from the top bar to the bottom bar is given by

$$\boldsymbol{E}_{PQ}/\boldsymbol{I}_C = \boldsymbol{E}_{PT}/\boldsymbol{I}_C - \boldsymbol{E}_{QT}/\boldsymbol{I}_C$$

from equations 17 and 16

$$\boldsymbol{E}_{PQ}/\boldsymbol{I}_C = 1/\boldsymbol{Y}_1\sqrt{\boldsymbol{Y}_1\boldsymbol{Z}_1} \times \left[\frac{(2-\cosh\sqrt{\boldsymbol{Y}_1\boldsymbol{Z}_1})(\cosh\sqrt{\boldsymbol{Y}_1\boldsymbol{Z}_1}-1)}{\sinh\sqrt{\boldsymbol{Y}_1\boldsymbol{Z}_1}} + \sinh\sqrt{\boldsymbol{Y}_1\boldsymbol{Z}_1}\right] \quad (20)$$

$\boldsymbol{E}_{RS}/\boldsymbol{I}_C$ is calculated in a manner similar to the impedance of a single rectangular bar (equation 6)

$$\boldsymbol{E}_{RS}/\boldsymbol{I}_C = 1/\boldsymbol{Y}_2\sqrt{\boldsymbol{Y}_2\boldsymbol{Z}_2}\ \text{ctnh}\ \sqrt{\boldsymbol{Y}_2\boldsymbol{Z}_2} \quad (21)$$

The impedance of the bottom turn may be calculated from equations 19, 20, and 21.

Specific Tests and Calculations

Test Conductors and Slot

Copper bars 12 feet long, 1/4 inch wide, and one-inch deep are used as test conductors. Laminations were cut from 14-mil stock with dimensions as given on Figure 6. Approximately 9,000 of these laminations, sprayed on one side with insulating paint, were stacked and compressed to give a slot 11 feet long. Test conductors are placed in this slot, insulated from the slot sides with 10-mil paper. The actual slot width will be some value between 0.27 inch and 0.291 inch. A slot width of 0.28 inch is assumed. See Figure 7 for conductor and slot arrangement.

Test Circuit

The schematic diagram of Figure 8 represents the testing circuit and equipment used to measure the effective a-c resistance and leakage reactance of the test conductor. The equipment used consists

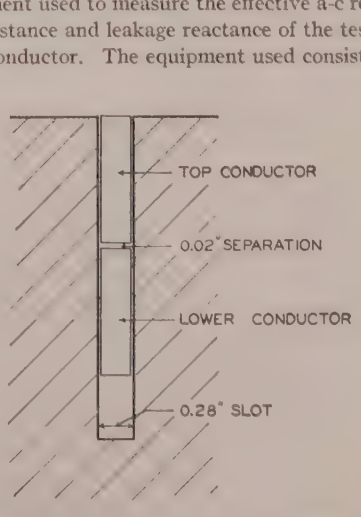

Figure 10. Arrangements of conductors for determining impedance of (1) one active bar and one idle bar or (2) a 2-turn coil

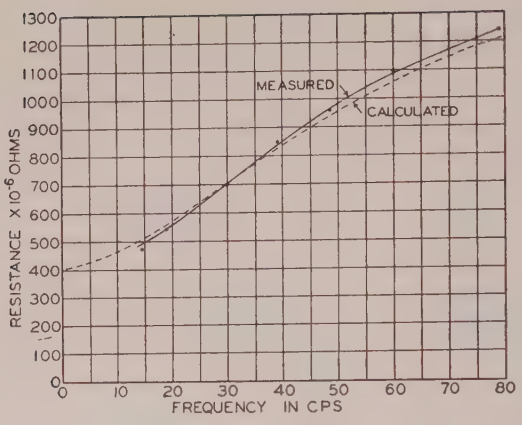

Figure 11 (left). Measured and calculated resistance as a function of frequency for one rectangular bar in a rectangular slot (see Table I)

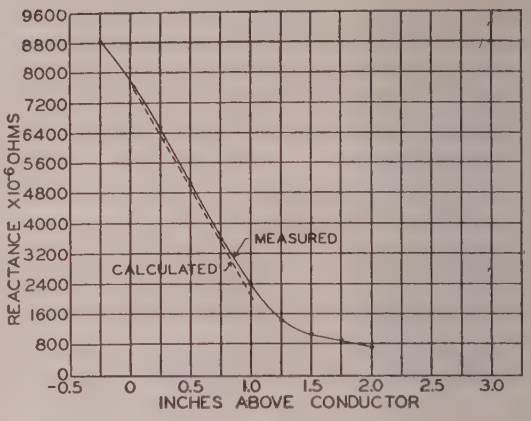

Figure 14 (right). Measured and calculated reactance as a function of slot depth (see Table II)

of a current transformer, standard resistance S, potentiometer P, variable mutual inductance M, electrodynamometer, phase shifter, and ammeter. By adjusting the potentiometer P and the variable mutual inductance M to give zero deflection of galvanometer regardless of setting of phase shifter, the current I_3 is made equal to zero.

For balanced conditions, the resistance and reactance of the test conductor may be determined.

$$R = r/T - x/T \sin \beta \qquad (22)$$

$$X = x/T + r/T \sin \beta \qquad (23)$$

where

β = phase angle error of current transformer
$r = Sp/(S+P)$
$x = 2\pi fM$
T = Corrected transformer ratio

The more precise experimental measurements were made using the circuit of Figure 8. Several additional tests were performed using voltmeter, ammeter, and wattmeter when the ranges of the instruments of Figure 8 were inadequate.

One Rectangular Bar Near Top of Slot

The following calculations and test results are for one rectangular conductor in a rectangular slot with the top edge of the conductor at the top edge of the slot. Conductor and slot dimensions are as given in the preceding paragraph. The flux above the slot is assumed to be double the leakage flux of the bar in air. On this basis the calculated value of L_0 is 5.52×10^{-6} henrys.

From Figure 2, $L_1 = 4\pi10^{-9}1.00/0.28$ henrys per centimeter length of conductor and for a slot 11 feet long, $Z_1 = j95f$ ohms. The ohmic resistance of the portion of the conductor in the slot (11 feet), assuming temperature of 30 degrees centigrade, is

$R_1 = 1/Y_1 = 374\times10^{-6}$ ohms

and at 60 cycles, $Z_1 = j5{,}700\times10^{-6}$ ohms. The impedance of the 11-foot section of conductor as calculated from equation 6 is $(j2{,}080+1{,}030+j1{,}030)\times10^{-6}$ ohms or $(1{,}030+j3{,}110)\times10^{-6}$ ohms, which, when corrected to include the resistance of that portion of the conductor not in the slot, becomes $(1{,}058+j3{,}110)\times10^{-6}$ ohms. The reactance correction has been considered previously in the reactance because of fringing.

The impedance measured at 60 cycles by the method of Figure 8 is $(1{,}095+j3{,}150)\times10^{-6}$ ohms. Measured and calculated values for other frequencies are listed in Table I. Graphs comparing measured and calculated values of resistance, reactance, and inductance are shown in Figures 11, 12, and 13.

One Rectangular Bar Located Deep in Slot

Figure 9 illustrates the conditions for this test. One rectangular conductor is located one inch below the top of the slot, with nine potential wires located at 1/4-inch intervals above the top edge of the conductor. The impedance of the conductor is determined as in the preceding case, but having an additional reactance of $j5{,}700\times10^{-6}$ ohms, which is caused by the leakage flux between the top of the conductor and the top of the slot. The total calculated impedance is $(1{,}058+j8{,}810)\times10^{-6}$ ohms at a frequency of 60 cycles.

The impedance as measured by ammeter, voltmeter, and wattmeter is $(1{,}124+j9{,}600)\times10^{-6}$ ohms.

Table II lists measured and calculated values of reactance due to leakage flux at various points above the conductor. The graphs of Figure 14 also give a comparison of these measured and calculated values of reactance.

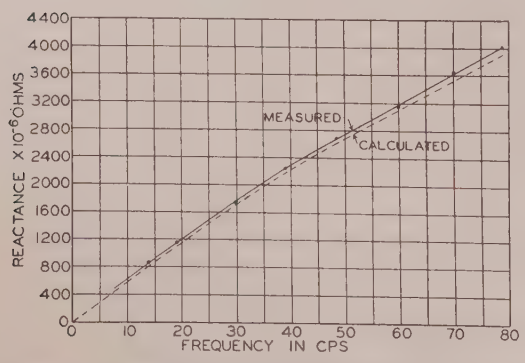

Figure 12. Measured and calculated reactance as a function of frequency for one rectangular bar in a rectangular slot (see Table I)

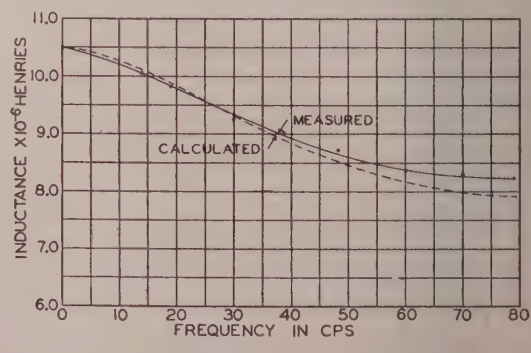

Figure 13. Measured and calculated inductance as a function of frequency for one rectangular bar in a rectangular slot (see Table I)

Two Rectangular Bars in Slot

Figure 10 illustrates the arrangement of conductors in the slot for this condition.

If the lower bar is excited and the top bar is idle, the calculated values of impedance in microohms are as in the following list. Equations 7 through 12 have been developed previously for these calculations. A temperature of 60 degrees centigrade is assumed for calculations.

Reactance (fringing)	$+j2{,}080$
Impedance (reflected from idle bar)	$2{,}310+j2{,}690$
Reactance (flux between bars)	$+j\ 119$
Impedance (flux across lower bar caused by current in lower bar)	$1{,}118+j1{,}090$
Total impedance of lower bar	$3{,}428+j5{,}979$
Measured impedance of lower bar (Voltmeter, ammeter, wattmeter)	$3{,}110+j5{,}950$

If the two bars are in series, the calculated values of impedance in microohms are as given in the following list. A temperature of 60 degrees centigrade is assumed. Equations 13 through 21 have been developed for these calculations.

Reactance of top bar because of flux above top bar	$+j\ 4{,}160$
Impedance of top bar because of flux across top bar	$2{,}208+j\ 2{,}180$
Total impedance of top bar	$2{,}208+j\ 6{,}340$
Reactance of lower bar because of flux above top bar	$+j\ 4{,}160$
Impedance reflected from top bar to lower bar	$3{,}470+j\ 3{,}800$
Reactance because of flux between bars	$+j\ 119$
Impedance of low bar neglecting current and flux above lower bar	$1{,}118+j\ 1{,}090$
Total impedance of lower bar	$4{,}588+j\ 9{,}169$
Total impedance of both bars in series	$6{,}796+j15{,}509$
The impedance measured by ammeter, voltmeter, and wattmeter are as follows:	
Impedance of top bar	$2{,}210+j\ 6{,}590$
Impedance of lower bar	$4{,}350+j\ 9{,}210$
Impedance of both bars in series	$6{,}560+j15{,}800$

Conclusions

The circuit analysis method for determination of a-c impedance of machine conductors may be applied to problems more complex than those considered in this paper. The method illustrated for a 2-turn coil may be expanded for a coil of any number of turns. A coil which shares a slot with a coil of another phase also can be handled conveniently. The method illustrated for the T-bar may be used for accurate determination of a-c impedance of rotor bars of any shape. Saturation of slot leakage paths is detected quickly in the equivalent circuit method and the circuits modified to yield saturated values of impedance.

The circuits used in this paper make it possible to determine the current density in each part of each conductor and the voltage across each turn of a multiturn coil. The impedances reflected from one conductor to other conductors in the same slot are determined easily. The calculations of impedance and comparative test data for the idle bar and the 2-turn coil are tabulated to illustrate the various components of impedance.

The measuring circuit as shown in Figure 8 and described briefly in the paper was very accurate and satisfactory for measuring low values of impedance. The authors would prefer to use this method for all the measurements given in this paper. The available inductometers and standard resistors had insufficient range, however, for the higher measured impedances. The ammeter, voltmeter, and wattmeter method was used for measurement of these higher impedances.

References

1. The Calculation of the Armature Reactance of Synchronous Machines, **P. L. Alger.** *AIEE Transactions*, volume 47, February 1928, pages 493–513.

2. Skin Effect in Tubular and Flat Conductors, **H. B. Dwight.** *AIEE Transactions*, volume 37, part II, 1918, pages 1379–1403.

3. Eddy Currents in Large Slot-Wound Conductors, **A. B. Field.** *AIEE Transactions*, volume 24, 1905, pages 761–88.

4. Electrical Measurements and Measuring Instruments (book), **E. W. Golding.** Sir Isaac Pitman & Sons, Ltd., London, England, 1933.

5. A-C Resistance of Rectangular Conductors, **S. J. Haefner.** *Proceedings*, Institute of Radio Engineers (New York, N. Y.), volume 25, April 1937, pages 434–47.

6. Alternating Current Bridge Methods (book), **B. Hague.** Sir Isaac Pitman & Sons, Ltd., London, England, 1945.

7. Experimental Researches on Skin Effect in Conductors, **A. C. Kennelly, F. A. Laws, P. H. Pierce.** *AIEE Transactions*, volume 34, part II, 1915, pages 1953–2021.

8. Chart Atlas of Complex Hyperbolic and Circular Functions (book), **A. E. Kennelly.** Harvard University Press, Cambridge, Mass., 1914.

9. Heat Losses in the Conductors of Alternating-Current Machines, **W. V. Lyon.** *AIEE Transactions*, volume 40, 1921, pages 1361–1409.

10. Electric Power Transmission and Distribution, **L. F. Woodruff.** John Wiley and Sons, Inc., New York, N. Y., 1938.

Discussion

P. L. Alger (General Electric Company, Schenectady, N. Y.): I commend the authors for a very interesting and useful contribution to the art of electrical motor design.

This problem of calculating the skin effect, or a-c impedance of slot embedded conductors, has been under development for more than 40 years. The AIEE paper by A. B. Field[1] in 1905, for which he received the Lamme Medal, gave the differential equations and their solutions for the case of multiturn form wound coils. Later papers by Gilman[2] in the AIEE and by Taylor[3] in the Journal of the Institution of Electrical Engineers gave more complete formulas. Taylor developed the solutions in the form of an infinite series, from which useful approximate formulas were derived.

Professor W. V. Lyon[4] made important contributions to the calculation of squirrel-cage bar impedances, employing vector equations.

The present authors, however, have used an equivalent circuit, instead of merely equations, so that solutions can be obtained by measurements on a network as well as by calculation.

The important feature of this new presentation is the use of equivalent transmission lines with distributed constants instead of lumped constants, to represent those parts of the conductors which have large skin effect. In this way, any element of the impedance can be examined in as much detail as desired; while the remainder of the circuit is treated in the usual simple way with lumped constants. This method of representing the impedances is in line with the modern trend of employing equivalent circuits, instead of equations wherever possible.

This method is also in line with the recent proposal of L. Bergeron[5] for analyzing equivalent circuits by graphic means, based on the transmission line theory of traveling waves. Bergeron has pointed out that any lumped impedance, when replaced by a distributed impedance, can be considered as a transmission line over which the current and voltage waves travel at a uniform speed. This enables the voltage and current distribution to be calculated either directly or graphically, by summing up the values of transmitted and reflected waves without the need of employing formal equations. The method is particularly useful for nonlinear impedances.

It seems likely that the Bergeron method will be helpful in determining squirrel-cage impedance values with the Babb-Williams circuits.

References

1. Eddy Currents in Large Slot-Wound Conductors, **A. B. Field,** *AIEE Transactions*, volume 24, 1905, pages 762–88.

2. Eddy Current Losses in Armature Conductors, **R. E. Gilman,** *AIEE Transactions*, volume 39, part I, 1920, pages 997–1056.

3. Heat Losses in the Conductors of Alternating-Current Machines, **W. V. Lyon,** *AIEE Transactions*, volume 40, 1921, pages 1361–1409.

4. Eddy Currents in Stator Windings, **H. W. Taylor,** *Journal*, Institution of Electrical Engineers (London, England), volume 58, Apr. 1920, pages 279–98.

5. Du Coup de Belier en Hydraulique au Coup de Foudre en Electricite, **L. Bergeron.** *Paper Number 128*, International Conference on Large High Voltage Electric Systems (Paris, France), 1950.

John F. H. Douglas (Marquette University, Milwaukee, Wis.): In this paper in equations 6, 12, and 21 a term occurs which can often be computed most easily by a series expansion such as Pierce's equation 793.[1] This formula, is

$$x \operatorname{ctnh}(x) = 1 + x^2/3 - x^4/45 + 2x^6/945 - x^8/4{,}725 \mp \ldots \quad (1)$$

It is rapidly convergent at 60 cycles, up to a depth of 0.5 inch in copper.

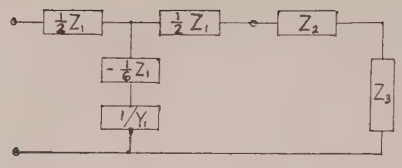

Figure 1. Circuit of double cage motor and based an 3-winding transformers

The authors discuss the T shaped bar, and in this connection the paper by H. V. Putnam published in 1927 should be cited.[2] The most convenient way of using Putnam's results, found in my notes, and expressed in the symbols in this paper is as follows:

$$Z_{BAR} - Z_2 = \left(\frac{Z_1 - Z_2^2 Y_1}{Y_1 Z_2 \pm (Y_1 Z_1)^{1/2} \operatorname{ctnh} (Y_1 Z_1)^{1/2}} \right) \quad (2)$$

In this form it can be easily applied to T-shaped bars with a lower part of any shape and to double cage motors.

The authors have used infinitestimal sections in their equivalent circuit in Figure 2. An investigation into the use of finite sections indicates that in copper at 60 cycles the elements in Figure 2 may not be greater than 0.05 inch if an error of over 1 per cent is to be avoided. The late Alfred Oklund proposed a slightly different circuit from Figure 2, based on the theory of a 3-winding transformer, and which was accurate up to 0.1 inch. Unfortunately this is not in print.

In Figure 1 of this discussion, Z_1 is the reactance of the top cage, Y_1 the conductance of the top cage, Z_2 the impedance of the slit, and Z_3 the impedance of the bottom cage. Mr. Oklund did not consider this circuit applicable to die-cast rotors. It is to be noted that according to the theory of the 3-winding transformer a negative reactance must be inserted the branch representing the conductance. This circuit checks equation 2 of this discussion when Z_2 is made the combined impedance of the slit and lower cage, provided the depth of the top cage is not over 0.1 inch.

References

1. A Short Table of Integrals, **Pierce.** Ginn and Company, Boston, Mass., third edition, equations 793, page 93, 1929.

2. Starting Performance of Synchronous Motors, **H. V. Putnam.** *AIEE Transactions*, volume 46, 1927, pages 39–59.

D. S. Babb and J. E. Williams: Impedances of machine conductors may be calculated from the circuits of this paper in a number of ways. Unless a network analyzer is available the authors believe the solutions based on the transmission line equations to be the easiest method as well as the most precise. If numerous calculations are to be made, curves of hyperbolic functions of $X/45°$ are very helpful. When these curves are not available they may be quickly calculated from the series expansion for these functions as Mr. Douglas illustrates in his equation 1.

If a network analyzer is to be used the circuit would be represented by a number of finite sections. Work along this line by the authors indicates that best results with a moderate number of sections occurs when the conductor is divided into unequal sections with the smallest sections near the top. For example, the 1 by 1/4 inch bar was represented by four T-sections equivalent to bars 0.1-, 0.2-, 0.3- and 0.4-inch deep. Solution of the resulting circuit gave answers within 6 per cent of true values from zero to 60 cycles per second.

The authors appreciate P. L. Alger's historical contribution to the paper.

A Simplified Method for Predicting Induction Motor Performance

HENRY E. WEBKING
ASSOCIATE AIEE

THIS paper offers a method for predicting the performance characteristics of polyphase induction motors which requires appreciably less time and effort than any of the present methods and yet gives results which are comparable in accuracy. The speed and simplicity which this method embodies arise from the use of a set of curves which eliminate the majority of the usual calculations.

Like most of the other methods, this one is based upon the equivalent circuit for an induction motor or actually upon its graphical representation, the circle diagram.[1] In order to make the curve system practical, the approximate circle diagram is used.[1] Theoretically, the accuracy is thus slightly reduced. Practically, however, the difference in accuracy can seldom be discerned except occasionally in the case of very small motors. In fact, due to unaccounted-for variables in the design, such as saturation and varying rotor frequency, more accurate results can often be obtained with the approximate circle diagram than with the exact circle diagram.[2]

Most of the common methods in use at the present time for predicting induction motor characteristics are analytical solutions of the equivalent circuit. The circle diagram is sometimes used but the unwieldiness of such a graphical solution greatly limits its use. Compared to the analytical methods of predicting induction motor performance, such as that proposed by Mr. Veinott,[3] the method offered here gives, in addition to greater speed and simplicity, two other very distinct advantages. Using the common analytical methods, the characteristics cannot be determined for a given load, such as rated load, without using a trial-and-error process. That is, it is necessary to assume some value for slip or primary current and then solve for the power output. Using these curves, the characteristics may be determined directly for any given output. In addition, these curves give a visual indication of the effects of changing the ratios between various design parameters. For example, the speed torque curves show very clearly that increasing the ratio of rotor to stator resistance increases the breakdown and starting torques and decreases the full-load speed.

In 1930, W. J. Branson[4] proposed a set of curves for predicting induction motor characteristics. However, since the curves were based upon the exact circle-diagram for an induction motor, the required number was large (approximately 100) and a comparatively complex calculation sheet was still required. As far as is known, these curves have never been published. The method offered here requires only one curve sheet each for efficiency, power factor, and current and about three curve sheets for the speed and current versus torque curves. The curves themselves are self-explanatory and no additional calculating form is required.

Paper 51-110, recommended by the AIEE Rotating Machinery Committee and approved by the Technical Program Committee for presentation at the AIEE Winter General Meeting, New York, N. Y., January 22–26, 1951. Manuscript submitted July 19, 1950; made available for printing December 11, 1950.

HENRY E. WEBKING is with General Motors Corporation, Dayton, Ohio.

Notation

E_p = impressed voltage per phase
r_1 = primary resistance per phase
r_2 = secondary resistance per phase in primary terms
$R = r_1 + r_2$ = short-circuit resistance per phase
X = short-circuit reactance per phase, neglecting the shunting effect of the magnetizing reactance
X_m = magnetizing reactance per phase
Q = 3-phase horsepower output $\times X \div E_p^2$

$$C = \frac{R}{X}$$

$$K_x = \frac{X}{X_m}$$

$$K_r = \frac{r_2}{r_1}$$

R_m = a resistance representing friction, windage, and core loss

Derivation of Curves

This method is based upon a new analytical solution of the approximate circle diagram by Professor C. F. Cameron of the Oklahoma Agricultural and Mechanical College. That solution is given in the Appendix. By substituting design values into the final equations of this solution, equations for the performance characteristics have been derived which depend upon the ratios: R/X, X/X_m, r_1/r_2, $(E/R_m) \div (EX/Z^2)$, and an independent variable, A.

To simplify the curves, $(E/R_m) \div (EX/Z^2)$ was taken as a constant of 0.006. This assumption seems justifiable because variations from this value produce relatively small differences in the predicted performance characteristics. A similar assumption was also used by Branson even in the solution of the exact circle diagram.

By assuming values for R/X, X/X_m, and r_1/r_2, and taking a range of values for A, a set of curves may be drawn giving horsepower output, efficiency, power factor, torque, and slip as a function of A; and speed and current as a function of torque. Since all characteristics are plotted as a function of a single independent variable, A, the characteristics may be determined for a given horsepower output without using a cut-and-try process such as is required by most solutions.

Use of the Curve Sheets

In order to use the curves, the following values must be known either from the de-

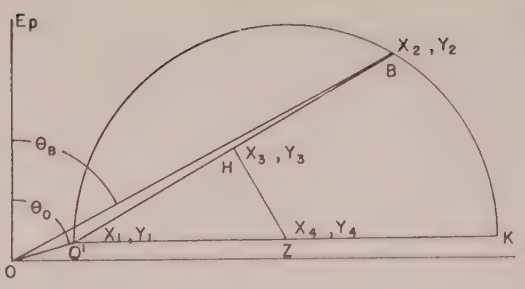

Figure 1 (left). Circle diagram for an induction motor

Figure 2 (right). Circle diagram as used for predicting induction motor performance

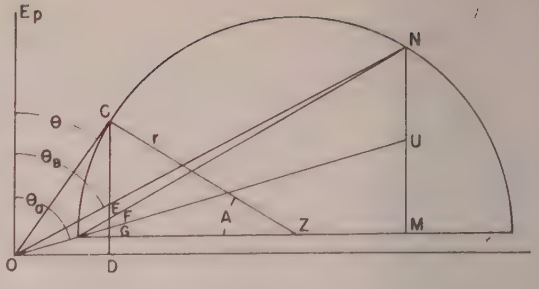

sign or test data: R, X, r_1, r_2, and X_m. The following constants are then calculated:

$$C = \frac{R}{X}$$

$$K_x = \frac{X}{X_m}$$

$$K_r = \frac{r_2}{r_1}$$

If the values for X and r_2 are taken as being different for running and starting, these constants may be calculated for both conditions. Next, the output constant is calculated for the desired 3-phase horsepower output:

$$Q = \frac{hp \times X}{E_p^2}$$

Using this value on the output curve sheet, the value for A at the given load is found. Having this value for A, the load characteristics may be quickly found from the curve sheets for efficiency, power-factor, and primary current. Curves may be drawn also for torque and slip versus A but they are not included in this paper.

It may be noticed from the curve sheets that the values for efficiency and power factor are read directly from the curves. For primary phase current, the value read from the curve must be multiplied by E_p/X.

The torque characteristics are taken from the speed-torque curves. To obtain the 3-phase torque in pound feet, the value read from the curve is multiplied by

$$\frac{E_p^2}{X \times \text{syn. rpm.}}$$

The current-torque curves are plotted to the same torque scale. The value obtained from the curve must be multiplied by E_p/X to obtain the phase current.

For this presentation, speed-torque curves have been plotted for two values of X/X_m. Since variations of this ratio have such a small effect upon the speed-torque curves, it is believed that a set of speed-torque curves for each of two or three values of X/X_m is sufficient.

The range of constants used for the curves presented here is sufficient for most design A (normal starting current-normal starting torque) motors. A larger range of constants should be used in plotting curves for general design use.

Example

The motor used in this example is the same one used as an example by Kuhlmann in his design book.[5] The rating of this motor is: 15 horsepower, 220 volts, 1,200 synchronous rmp Y-connected. The constants are, in per-phase values:

$X = 0.46$ ohm
$X_m = 8.20$ ohms
$r_1 = 0.114$ ohm
$r_2 = 0.113$ ohm
$R = 0.227$ ohm

Then

$$C = \frac{R}{X} = \frac{0.227}{0.46} = 0.494$$

$$K_x = \frac{X}{X_m} = \frac{0.46}{8.20} = 0.056$$

$$K_r = \frac{r_2}{r_1} = \frac{0.113}{0.114} = 0.99$$

$$Q = \frac{15 \times 0.46}{127^2} = 12.8 \times 10^{-3}$$

From the 3-phase output curves,

A = 13.6

From the efficiency and power-factor curves,

Efficiency = 89.5%
Power Factor = 86.5%

For the full-load phase current, the curve value = 0.136 so

$$I_p = \frac{0.136 \times 127}{0.46} = 37.6 \text{ amperes}$$

From the speed-torque curve, the values at breakdown and starting are 7.7 and 4.15 respectively so

$$\text{Breakdown torque} = \frac{127^2}{0.46 \times 1{,}200} \times 7.7 = 29.2 \times 7.7 = 225 \text{ lb. ft.}$$

at a slip of 26 per cent. The starting torque = $29.2 \times 4.2 = 122.8$ pound feet. The starting current factor, from the curve, is 0.89 so the starting current per phase

$$= 0.89 \times \frac{127}{0.46} = 246 \text{ amperes}$$

Appendix

In the diagram of Figure 1, E_p represents the applied voltage per phase and is taken as a reference. OO' represents the no-load current which lags the applied voltage by an angle θ_o. OB represents the blocked rotor current lagging the applied voltage by an angle θ_B. The equation of the line O'B is

$$y - y_1 = \frac{y_2 - y_1}{x_2 - x_1}(x - x_1) \qquad (1)$$

or

$$y - y_1 = m(x - x_1)$$

where m equals the slope of the line. Then

$$y = mx - mx_1 + y_1$$

Since the co-ordinates of H are

$$x_3 = \frac{x_1 + x_2}{2}$$

and

$$y_3 = \frac{y_1 + y_2}{2}$$

the equation for HZ is

$$y - y_3 = -\frac{1}{m}(x - x_3)$$

or

$$y = -\frac{x}{m} + \frac{x_3}{m} - y_3 \qquad (2)$$

When $y = y_4$, equation 2 may be solved for X or X_4. Since $y_1 = y_4$,

$$y_1 = -\frac{x_4}{m} + \frac{x_3}{m} + y_3$$

and

$$x_4 = x_3 + m(y_3 - y_1); \qquad (3)$$

but

$$x_3 = \frac{x_1 + x_2}{2}$$

and

$$y_3 = \frac{y_1 + y_2}{2}$$

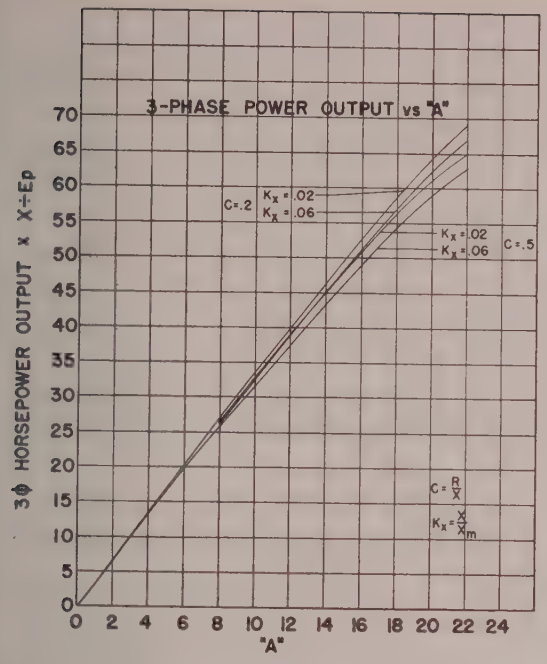

Figure 3 (left). Curves of 3-phase power output versus "A"

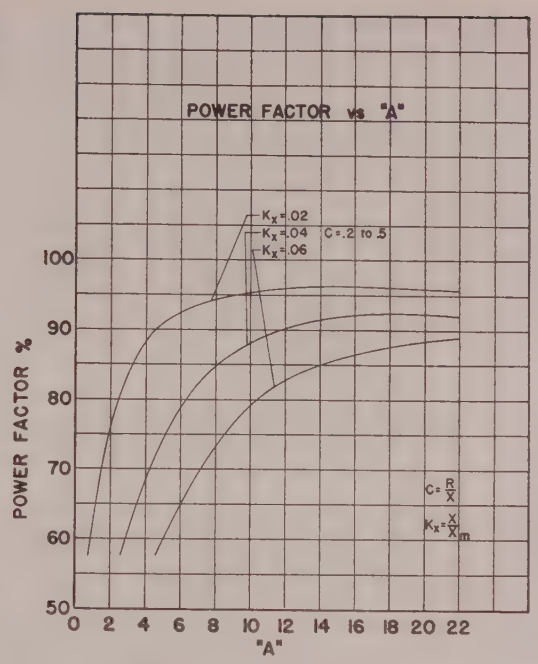

Figure 5 (right). Curves of power factor versus "A"

so

$$m=\frac{y_2-y_1}{x_2-x_1} \tag{4}$$

The co-ordinates of O′ and B may be found from the no-load and blocked rotor tests. These values are:

$x_1=I_O$ os θ_O
$y_1=I_O \sin \theta_O$
$x_2=I_B \cos \theta_B$

and

$y_2=I_B \sin \theta_B$

An equation which gives x_4 in terms of the co-ordinates of O′ and B may be determined by substituting values of x_3 and y_3 in equation 3. Then

$$x_4=\frac{x_1+x_2}{2}-m\left(\frac{y_1+y_2}{2}-y_1\right) \tag{5}$$

The co-ordinates of Z are x_4 and y_4 but $y_4=y_1$ and y_1 is known which locates Z. From the diagram,

$r=x_4-x_1$

so from equation 5,

$$r=\left(\frac{x_1+x_2}{2}-x_1\right)+m\left(\frac{y_1+y_2}{2}-y_1\right)$$

or

$$r=\frac{x_2-x_1}{2}+m\,\frac{y_2-y_1}{2} \tag{6}$$

The formulas for the analytical solution of the circle diagram are derived as follows:

$CG=r \sin A$ (7)

$O'Z=r$ (8)

$GZ=r \cos A$ (9)

$O'G=AZ-GZ=r-r \cos A$

$O'G=r(1-\cos A)$ (10)

$CD=CG+GD$

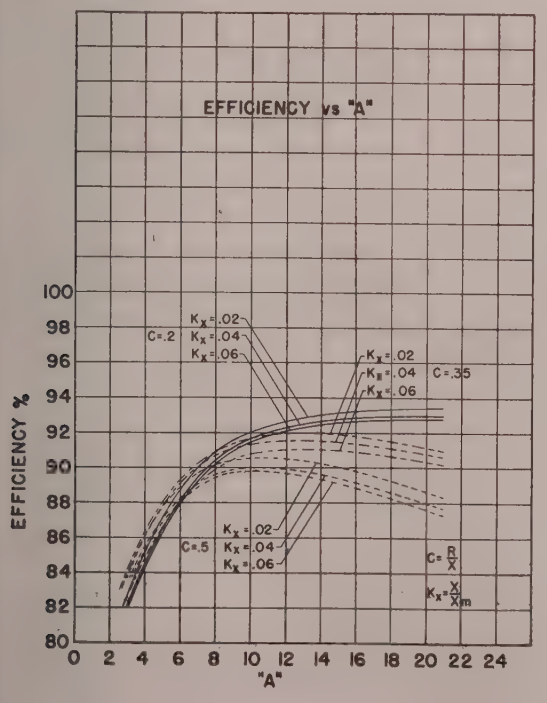

Figure 4 (left). Curves of efficiency versus "A"

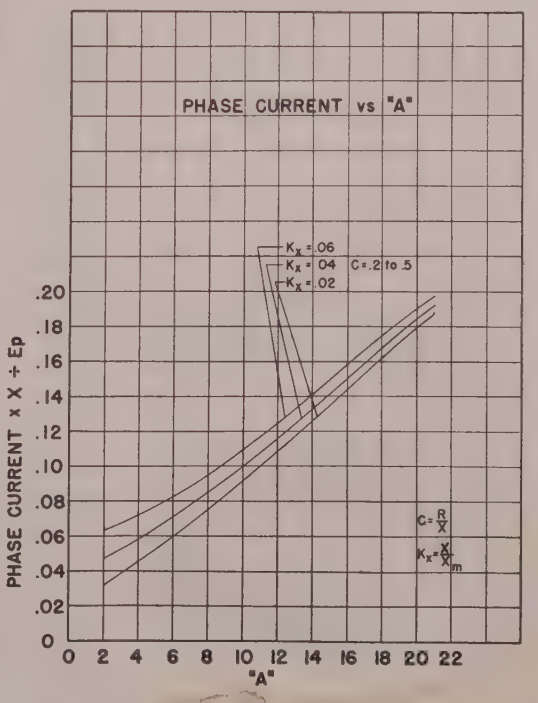

Figure 6 (right). Curves of current versus "A"

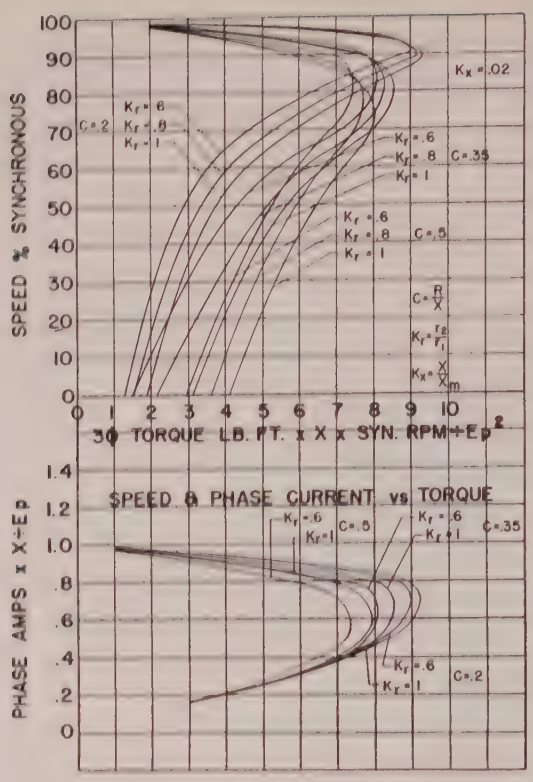

Figure 7 (left). Speed - torque and current-torque induction motor curves

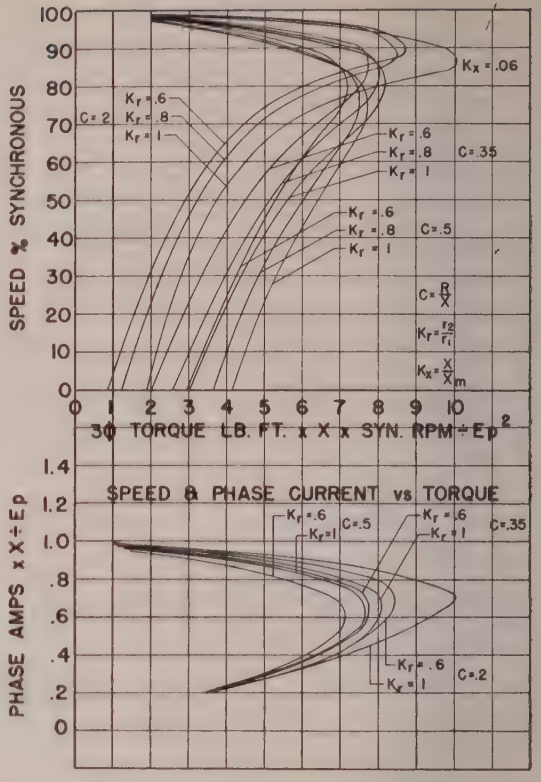

Figure 8 (right). Speed - torque and current-torque induction motor curves

$CD = y_1$

$$CD = (7) + y_1 \tag{11}$$

$$\frac{MN}{EG} = \frac{O'M}{O'G}$$

$$EG = O'G\frac{MN}{O'M} = r(1-\cos A)\frac{y_2 - y_1}{x_2 - x_1}$$

$$EG = mr(1-\cos A) \tag{12}$$

$$\frac{EF}{FG} = \frac{r_2}{r_1} \tag{13}$$

$$\text{and } FG = EG - EF \tag{14}$$

$$\text{so } EF = \frac{EGr_2}{r_1 + r_2} \tag{15}$$

$$CE = CG - EG \tag{16}$$

(16) = (7) − (12)

$$FC = EF + CE \tag{17}$$

(17) = (15) − (16)

$$OC = \text{Current/phase} \tag{18}$$

$$= \sqrt{[OO'\cos(90-\theta_0) + O'G]^2 + CD^2}$$

$OO'\cos(90-\theta_0) = x_1$

$O'G$ = (10)

CD = (11)

$$I_p = \sqrt{[x_1 + (10)]^2 + (11)^2}$$

Power input to stator/phase = $CD \times$ volts/phase

$$P_i = (11)E_p \tag{19}$$

Torque, synchronous watts/phase = $FC \times$ volts/phase = (17) × E_p (20)

$$\text{Slip, per cent} = \frac{EF}{FC} = \frac{(15)}{(17)} \tag{21}$$

$$\text{Efficiency, per cent} = \frac{CE}{CD} = \frac{(16)}{(11)} \tag{22}$$

$$\text{Power factor, per cent} = \frac{CD}{OC} = \frac{(11)}{(18)} \tag{23}$$

3-phase output = $3 \times CE \times$ volts/phase = $3 \times (16) \times E/ph.$ (24)

The foregoing equations may be put in terms of design constants by making the following substitutions.

$x_1 = E/X_m$
$y_1 = E/r_m$
$x_2 = EX/Z^2$
$y_2 = ER/Z^2$

By substituting these values in the equations and assuming that $(E/R_m) + (EX/Z_2) = T = 0.006$, the following equations are obtained.

$$m = \frac{C - T}{1 - K_x(C^2+1)} \quad \text{see equation (4)}$$

$$P = \left[\frac{1}{C^2+1} - K_x\right] + m\left[\frac{C}{C^2+1} - \frac{T}{C^2+1}\right]$$

where $P = \frac{2rX}{E}$ see equation (6)

$$\frac{I_p X}{E_p^2} = \frac{P}{2}\left|\sin A - m(1-\cos A)\right|$$

W = watts output per phase

$$\frac{I_p X}{E_p} = \sqrt{\left[K_x + \frac{P}{2}(1-\cos A)\right]^2 + \left[\frac{P}{2}\sin A + \frac{K_r}{C^2+1}\right]^2}$$

$$\text{Eff.} = \frac{\sin A - m\cos A}{\sin A + \frac{2T}{P(C^2+1)}}$$

$$\text{P.F.} = \frac{\sqrt{\left[K_x + \frac{P}{2}(1-\cos A)\right]^2 + \left[\frac{P}{2}\sin A + \frac{T}{C^2+1}\right]^2}}{\frac{P}{2}\sin A + \frac{T}{C^2+1}}$$

$$\frac{\text{Torque} \times X}{E_p^2} = \frac{P}{2}\left[\frac{(1+K_r)\sin A - m(1-\cos A)}{1+K_r}\right]$$

$$\text{Slip} = \frac{mK_r(1-\cos A)}{(1+K_r)\sin A - m(1-\cos A)}$$

Taking, then, various combinations of values for C, K_x, and K_r, and using a range of values for A in each case, a set of curves such as are given here may be plotted.

References

1. Alternating Current Machines, **A. F. Purchstein, T. C. Lloyd.** Second edition, page 266.

2. Induction Motor Characteristics, **C. F. Cameron, J. O. Grantham, H. E. Webking.** *Publication Number 65.* Oklahoma Engineering Experiment Station, page 20.

3. Performance Calculations on Induction Motors, **C. G. Veinott.** *AIEE Transactions*, volume 51, September 1932, pages 743–55.

4. Polyphase Induction Motors, **W. J. Branson.** *AIEE Transactions*, volume 49, January 1930, pages 319–32.

5. Design of Electrical Apparatus (book), **T. H. Kuhlmann.** John Wiley and Sons, Inc. New York, N. Y., second edition 1946, page 326.

Discussion

J. S. Gault (University of Michigan, Ann Arbor, Mich.): Mr. Webking has presented a great time-saving method for predicting the performance of induction motors, from constants obtained either from design calculations or from no-load and locked test readings.

I should like to bring up three minor questions.

1. The curves of Figures 3 to 6 are plotted against an arbitrary parameter "A." Apparently this is measured in degrees for the angle shown in Figure 2. Would it not be better to label the abscissa scale "angle A-degrees"?

2. It is not clearly stated in the paper whether the quantity X is the sum of primary and secondary reactance per phase or the quadrature component of the locked impedance, which is not quite the same.

3. The range of maximum efficiency and power factor values in Figures 4 and 5 imply a somewhat limited range of ratings for which the curves in the paper would be usable. I wonder if Mr. Webking would state for approximately what range of motor ratings these curves would be suitable?

An Experimental Study of Induction Machine End-Turn Leakage Reactance

E. C. BARNES
MEMBER AIEE

Synopsis: There are a number of empirical and rationally derived methods described in the technical literature for the predetermination of the end-turn leakage reactance of an induction machine stator winding. The use of these calculation methods will yield widely different results when applied to a particular machine winding. Since the isolation of the end-turn leakage reactance from test results requires extensive and tedious experimental work, the designer seldom, if ever, has the opportunity to verify the accuracy of the calculation method which he uses. It is the object of the subject study to determine experimentally the actual end-turn leakage reactance for a limited size range and variety of 3-phase squirrel-cage induction motor winding conditions. The experimental data are used to evaluate the relative accuracy of several published calculation methods, and to suggest refinements in one of these methods which will permit attainment of practical degrees of accuracy in design calculations. An empirical calculation method published by Alexander Gray is found to be more accurate in its predictions for the range of machine sizes involved than any of the other methods considered, however, it is limited to use with stator windings having only full pole pitch coils. Since modern design practice dictates, from several considerations, the use of fractional pitch coils, it is necessary to develop additional empirical data to enable calculation of end-turn leakage reactance for this condition. The findings of the experimental study reveal that the end-turn leakage reactance of small integral-horsepower induction motors can be determined more simply by empirical, or semiempirical methods than by any of the rigorously derived methods which are currently available. As a subsidiary revelation of the experimental study, it appeared that the presence of squirrel-cage rotor in the stator bore had no effect on the value of stator winding end-turn leakage reactance.

THE accuracy with which performance may be predetermined in the basic design of an induction machine is largely dependent on the ability of the designer to calculate the several components of leakage reactance of the machine. One of these components is the stator end-turn leakage reactance. The degree by which this particular component of reactance affects the accuracy of the performance calculation is dependent on its magnitude in relation to all the other reactive components. In many cases the end-turn leakage reactance may amount to as much as one-third to one-half of the total leakage reactance of the machine at standstill.

The writings of past designers and the expressed opinion of contemporary designers reflect the viewpoint that the least amount of certainty is attached to the end-turn leakage calculation when compared to the other reactive components in the machine. In September 1947, each member of a committee of seven experienced induction machine designers in the AIEE, employing their best efforts calculated the various reactive components of a particular machine for which dimensional data were supplied.[1] In the comparison of the results, the end-turn reactance calculation results among the seven designers were found to vary more widely than the results of any of the other significant reactive components in the design. The highest calculated value was approximately 170 per cent of the lowest. It was the informal conclusion of this committee that the need for more accurate methods for the determination of end-turn leakage reactance was foremost in the induction machine design art.

Because of the exceeding difficulty or impossibility of isolating the test value of end-turn reactance from the total value of test reactance in a particular design, the designer can seldom compare test values against calculated values of the individual reactive components of the machine. Rather, the sum of the calculated reactances is compared with the sum of experimentally determined reactances, leaving opportunity for wide variations among the individual components within the total. Therefore, improvement in the ability to predetermine accurately the end-turn reactance will permit detection of inaccuracies, and also refinement, of calculation methods for other components of reactance.

In view of the foregoing, the subject study was undertaken for the purpose of evaluating several end-turn leakage calculation methods available to the induction machine designer, and to develop empirical data for practical design purposes. Further, these data may be employed in conjunction with rigorously derived relationships to permit a clearer physical conception of the end-turn leakage phenomena.

The experimental study was made on stator cores of the size range ordinarily used for polyphase induction motors of from two to five horsepower rating as 4-pole 60-cycle machines. Three-phase, double layer, random wound stators with semienclosed slots were used throughout the study. The stators were wound, successively, with windings having three different values of pole pitch for each of the 2-, 4-, and 6-pole conditions.

Leakage Reactance Components in the Squirrel-Cage Induction Machine

The basic design process for an induction machine for the purpose of predetermination of performance, entails the calculation of several resistive and reactive circuit components which are gov-

Paper 51-111, recommended by the AIEE Rotating Machinery Committee and approved by the AIEE Technical Program Committee for presentation at the AIEE Winter General Meeting, New York, N. Y., January 22–26, 1951. Manuscript submitted October 20, 1950; made available for printing December 12, 1950.

E. C. BARNES is with The Reliance Electric and Engineering Company, Cleveland, Ohio.

This subject and portions of the experimental data included in this paper were the basis of a thesis submitted by the writer to the faculty of Case Institute of Technology, May 1949, in partial fulfillment of the requirements for the degree of Master of Science in Electrical Engineering.

erned by the winding and the detail physical dimensions of the active core material. Generally, these calculations are made on a per-phase basis, and include the constants identified in the approximate equivalent circuit shown in Figure 1(A). Precise treatment of the excitation path (X_e, R_e) requires that it be shunted across the secondary circuit composed of X_2 and R_2 in series, however, for most design purposes the error committed by placing the excitation admittance as shown in Figure 1(A) is not commensurate with the additional calculation required for precise treatment.

The elements of X_1, R_1, X_2, and R_2, composing the locked-rotor or stationary impedance are each calculated using particular electric and magnetic circuits in the machine. It is the stator reactance which embodies the stator end-turn reactance as a component, therefore, prior to a detailed consideration of the end-turn reactance, the reactive components of the stator will be enumerated.

The machine reactance is composed principally of the following components:

1. Stator slot leakage.
2. Rotor slot leakage.
3. Differential or airgap leakage. (a) Zigzag leakage. (b) Belt leakage.
4. End-turn leakage.

Each of these has been treated extensively from a theoretical point of view in the technical design literature, however, a review of the factors affecting the end-turn leakage reactance will assist in defining the current problem.

End-Turn Leakage

The end-turn leakage flux is composed of both fundamental frequency and higher order space harmonics which link the unembedded portion of the stator conductors extending from pole to pole beyond the ends of the active core material. These fluxes are caused by the magnetomotive force of the end-turn windings, acting principally on air paths. In linking the end-turn conductors, reactance voltages are generated which are reflected as ohmic reactance in the stator winding. Because the end-turn leakage flux paths are almost all, if not totally, in air, the flux bears a constant relationship to the current in the end-turn conductor: that is, it is unaffected by magnetic saturation, and the inductance of the end-turn is practically constant for wide ranges of machine excitation.

The length of the end conductor is dependent on the diameter of the stator bore, the number of poles of the winding, and the pitch of the winding with respect to full pole pitch. Increases in any of these necessitates the use of increased length of end conductors; and results in increased flux linkages, and consequently, increased reactances. Because the end conductors are not active in the production of torque in the machine, their length is held as short as practical in the interest of reducing reactance and losses.

The geometry of the coil cross-section, that is, the ratio of depth to width, will affect the flux linking the coil for a given current flowing in it. For random wound coils (as contrasted with form wound coils) the shape of the cross-section of the end portion of the coil is generally different than in the slot portion due to its tendency to "nest" with other end conductors.

The shape of the end portion of the coil will also affect its reactance. Random wound coil ends may depart materially from their original "V" shape when they are wound in the stator core and shaped to produce a flared bell-shaped coil head. On most windings the coil extends for a short distance straight out from the core before it is bent at an angle to proceed to the next pole. The flux linkages of this straight portion will be different from those elsewhere in the end connection.

Most wound cores are not mounted in nonmagnetic surroundings, but rather, are surrounded by the machine frame structure and air deflecting baffles of magnetic material. If these magnetic structures are close to the coil ends, the end-turn leakage flux will be greatly increased.

Background

A summary of the approaches of several writers warrant inclusion here from the standpoint that they provide the basis for most calculation procedures now in practical use.

C. A. Adams applied the work of several others toward the development of a practical end-turn reactance solution.[2,3] He viewed the two end portions of a stator coil as constituting a circular coil in air, and then applied rationally derived procedures to determine the inductance of the circular coils when they were arranged physically to simulate the coil end pattern of the double-layer wound induction machine stator. Because of the complexity introduced when all the physical factors of this arrangement were accounted for mathematically, and because the assumed circular coil end did not closely enough approach the actual shape of the coil end, Adams found it necessary to rely heavily on empirical data in the calculation of end-turn reactance by his method.

An entirely different approach to the problem was made by P. L. Alger in a paper[4] applying principally to synchronous machines, however, the basic thinking is also applicable to induction machines. In this approach, the currents flowing in the end-turns were resolved into axially and peripherally directed components with respect to an axis coincident with the shaft of the machine. The reactance attributed to each of these components of current was solved according to basic electromagnetic theory, and the sum of the two reactances was deemed to be the end-turn reactance. With the inclusion of several practical assumptions, a concise end-turn leakage formula resulted. The development probably constituted the most complete rational approach, and least cumbersome result up to that time (1928), and, when applied to synchronous machine with form wound coils, yielded a practical answer for several conditions for which experimental data on coil-end leakage were available.

Later, J. F. H. Douglas conceived and outlined a novel rational approach for the end-turn reactance development.[5] However, it was not his object to carry out the actual development, but rather to suggest the mathematical tools which could be used.

B. H. Caldwell, Jr., following Douglas' suggestions,[6] visualized the coil ends of

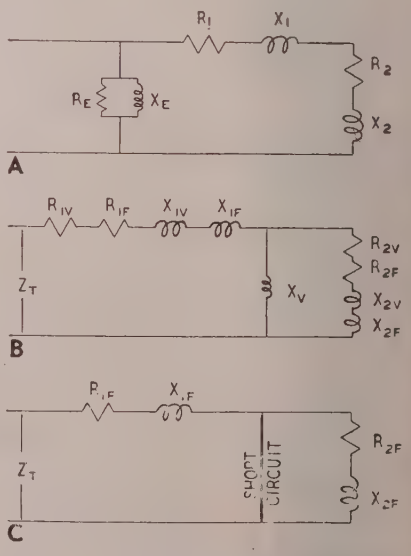

Figure 1. (A) Approximate equivalent circuit per phase for the induction machine

(B) Approximate equivalent circuit per phase for a finite core length induction machine

(C) Equivalent circuit for an induction machine having zero core length

the winding as developed in a plane. By the use of image conductors carrying reflected currents he was able to solve for the magnetomotive force and the flux existing in the region of this grid of end conductors. The solution for the reactive voltages induced in the end connections overcame the rather troublesome matter of limits and end conditions by employing Rayleigh flux conducting and flux insulating partitions. The partitions were established to permit integration of flux-ampere linkages only in the region of the current grid which was represented by real, rather than image conductors. Since the development was made principally for the synchronous machine, Caldwell carried the analysis further to include the effect of stray flux from the excited field structure.

Another approach by Gray qualitatively analyzes end-turn reactance in terms of the ampere-flux linkages per unit length of a belt of end conductors.[7] This method openly depends on empirical methods for calibration, however, the experimental results of the subject study indicate that Gray's empirical calibration applied only to coils having full pole pitch.

The foregoing examples represent several rational and empirical approaches to the end-turn leakage problem, however, it is not intended to represent them as being exhaustive of attempts or manner of approach covered in the technical literature. These examples are, however, sufficiently basic and unique to justify their mention over others.

Experimental Approach

After careful consideration of the objects and motivation of the current study, a method for the measurement and isolation of end-turn leakage reactance was selected which most closely approached actual conditions in a 3-phase induction stator winding intended for use with a squirrel-cage rotor. Fundamentally, it is desired to separate the end-turn component of leakage reactance from the other components of reactance in the core portion of winding which are directly proportional to core length; the end-turn reactance is constant and independent of core length. Therefore, if the test value of reactance for several machines differing only in core length is known, the reactance per-unit length of the embedded portion of the winding can be determined. The core portion of the total measured reactance for each condition can be subtracted from the total measured reactance to yield the end-turn reactance. Practically, the end-turn reactance is determined directly by plotting the total measured reactance against core length for several machines and extrapolating the curve to zero core length. The intercept on the reactance scale at zero core length is the end-turn reactance for the particular end winding condition applying to the test machines.

For this method to be applicable, the windings for all cores must have the same pitch, same placement in the slot, and the end-turns must be as nearly identical as possible in shape and location relative to the core boundaries. Special effort must be made to assure that the reactance per-unit length of core will be the same for the several core length machines. This requires the use of laminations having identical slotting with respect to quantity, location and dimensional detail, and the length of airgap on all machines must be held to very close limits in order that variations in magnetizing and differential leakage will not distort the extrapolated result. The windings for the different core length machines need not have the same number of turns per coil since this can be accounted for, however, it is essential that the shape and area of the coil cross-sections be the same. Because differences in the degree of saturation of magnetic paths in the laminated iron core will markedly affect the reactance per-unit length of embedded conductor, it is necessary that the total reactance for each of the several core lengths be determined at comparable values of core saturation. Further, this is necessary so that the value of magnetizing reactance will also be constant per-unit length of core, that is, will vary directly with core length.

Figure 1(B) represents one phase-to-neutral of the exact equivalent circuit diagram for a polyphase induction machine with a finite core length and having a short circuited squirrel-cage rotor. Resistance elements of the circuit are denoted by the letter R and inductive reactance elements by X. The subscript "1" denotes stator components, and "2" rotor components. The letters v and f embodied in the subscripts refer to whether the particular circuit element is variable or fixed, respectively, as the core length of the machine is varied.

The physical elements in the machine represented by the symbols in Figure 1(B) are:

R_{1v} = resistance of the portion of the stator winding embedded in the slots of the core

R_{1f} = resistance of the end-turn portion of the stator winding

X_{1v} = reactance of the portion of the stator winding embedded in the slots of the core

X_{1f} = reactance of the end-turn portion of the stator winding

X_v = magnetizing reactance

R_{2v} = resistance of the rotor bars embedded in the rotor core

R_{2f} = resistance of the rotor short-circuiting ring

X_{2v} = reactance of the rotor bars embedded in the rotor core

X_{2f} = reactance of rotor short-circuiting ring

Z_t = total impedance of the machine

$$= \sqrt{(R_{1v}+R_{1f})^2+(X_{1v}+X_{1f})^2}+\frac{X_v\sqrt{(R_{2v}+R_{2f})^2+(X_{2v}+X_{2f})^2}}{X_v+\sqrt{(R_{2v}+R_{2f})^2+(X_{2v}+X_{2f})^2}} \quad (1)$$

In Figure 1(B), the assumption is made that the conductance of the excitation path (generally shown in parallel with the magnetizing susceptance) is infinitely large and therefore is not shown in the circuit. For low values of excitation under the stationary rotor condition this is a practical assumption and the error introduced by such treatment is small. The conductance branch of the excitation path, when used, is inserted to account for core loss in the magnetic core.

As the length of the core approaches zero, all elements of the circuit, Figure 1(B), bearing the subscript "v" will approach zero and Figure 1(C) becomes true.

The physical significance of the short-circuit across the rotor impedance in Figure 1(C), as the magnetizing impedance becomes zero, is that the entire voltage impressed across the stator under this condition is consumed in the stator resistance and reactance drops. Only stator end-turn winding leakage flux is present in the machine; no magnetizing or rotor leakage flux exist by reason of the premise that the core and airgap section have become zero, theoretically.

The total impedance of the circuit in Figure 1(C) is:

$$Z_t = \sqrt{R_{1f}^2+X_{1f}^2} \quad (2)$$

which is, virtually, the impedance of the end-turn portion of the stator winding from which the reactance component is readily separable.

Experimental Equipment

Stator Cores

Throughout the experimental program four stator cores of 1/2, 1, 2, and 4 inches length respectively were successively wound, tested, stripped, and rewound with the various winding combinations. The cores were jig-stacked to desired lengths and welded axially at their outer periphery at eight points in order to maintain dimensional stability during the

Figure 2. Close-up view of coil head and airgap section of wound stator

testing operations. The laminations composing the core were punched from 26-gauge core-plated silicon steel by a multiple-slot die which inserted all slots in a lamination upon one stroke of the punch press. This assured that the laminations in all of the cores were identical for practical purposes. The outside diameter of the laminations was $8^5/_8$ inches, and the inner bore was $5^1/_2$ inches in diameter. The 36 equally spaced slots were of semi-enclosed type having an opening at the gap of 0.11 inch. The main body of the slot was parallel-sided 0.30-inch wide extending radially to a depth of 0.85 inch into the stator lamination from the gap diameter.

Considerable care was exercised in all steps of manufacture of the stator cores in order that they be as nearly identical as practicable except with respect to length of stacking.

Stator Windings

Twenty-eight sets of 36 coils were prepared in order to study seven different winding conditions on the four different core length stator cores. The winding conditions are shown in Table I.

Table I. Experimental Winding Conditions

Winding Condition	Stator Poles	Coil Pitch (Decimal of Full Pole Pitch)
A	2	0.66
B	2	0.50
C	4	1.00
D	4	0.66
E	4	0.44
F	6	1.00
G	6	0.66

The four sets of coils for each winding condition were wound having, as nearly as practicable, identical end-turn extension dimensions. The portions of the coils which were to be embedded in the stator cores had lengths corresponding to the four stator core stacking lengths. In preparing the stators for test, the coils were placed in the insulated stator slots and secured with maple wedges $^1/_4$-inch thick. For all pole and pitch combinations, the coils were connected 3-phase Y series circuit. After placing the coils in the slots and connecting them, the coil heads for all of the four different core length stators for a given winding condition were shaped to meet the same profile gauge. Figure 2 shows one of the wound stator cores.

Rotor Cores and Windings

Four rotors were constructed having the same core length, respectively, as the stator cores. The rotor laminations were punched from 26-gauge core-plated silicon steel with a multiple-slot die having 45 equally spaced slots and a centerhole for receiving the motor shaft. The slots were of the totally-enclosed type 0.370-inch deep and 0.165-inch wide and the centerhole diameter was $1^9/_{16}$ inches. The rotor windings (bars and end rings) were pressure die-cast from molten aluminum into rotor core stacking with the rotor bars skewed approximately 100 per cent of a rotor slot pitch.

The outside diameter of the rotors was machined to a diameter of 0.02 inch smaller than inside bore diameter of the stators in order to produce a single airgap of 0.01 inch when the rotors were placed in the stator bores. After the machining operation on the rotors the bars in the slots remained covered with a bridge of steel 0.005-inch thick. Because the stators and rotors were to be tested together without benefit of a shaft and bearing to locate the rotor centrally in the stator bore, a layer of 0.01-inch thick fiber was cemented to the outside surface of the rotor to serve as a spacer between the rotor and stator during testing.

Experimental Tests

Four stators, one of each core length, constituting a particular winding condition in number of poles and pitch were prepared for test at one time. Balanced 3-phase 60-cycle voltages were applied to the stator winding terminals and measurements of voltage, power, and current were made and recorded for the locked rotor condition. Measurements were made for 10 to 15 values of applied voltage ranging from approximately 5 per cent to 20 per cent of the excitation which would be applied to the core under normal operation as a motor. The ohmic resistance of each stator winding was measured from terminal to terminal and the winding temperature and resistance recorded.

Figure 3. Wound stator with rotor arranged for test

Each stator winding was tested first with a rotor of corresponding core length in place in the stator bore. The rotor was then removed and the test repeated on the stator winding for approximately the same range of applied voltages.

To facilitate testing and also to eliminate extraneous effects of the proximity of magnetic materials, the stators were mounted in a wooden fixture as shown in Figure 3 during the conduct of the stationary impedance tests.

Treatment of Experimental Data

For each of the 56 tests (with and without rotor in the stator bore), values of current and power input were plotted against voltage and smooth curves were drawn through the plotted points. Using equations 3, 4, and 5, values of phase-to-neutral reactance were calculated for the same range of voltage used in the ex-

Table II. Experimental Values of End-Turn Leakage Reactance

Winding Code	Poles	Coil Pitch	Length End-Cond.	Experimental End-Turn Leakage Reactance Ohms Per Phase
A	2	0.5	7.3	5.7
B	2	0.66	11.0	9.3
C	4	0.44	4.1	1.6
D	4	0.66	5.2	3.3
E	4	1.00	7.3	4.6
F	6	0.66	4.1	1.6
G	6	1.00	5.2	2.8

perimental tests. These values of reactance were also plotted against voltage impressed across the stator terminals. Figure 4 is an example of one of these curves.

$$Z = \frac{V}{\sqrt{3}I} \tag{3}$$

$$R = \frac{W}{3I^2} \tag{4}$$

$$X = \sqrt{Z^2 - R^2} \tag{5}$$

where

Z = total impedance per phase
R = total resistance per phase
X = total reactance per phase
V = line voltage
W = total watts input
I = line current

In Figure 4 it is noticed that the reactance determined by equation 5 varies quite widely with voltage because of saturation of leakage flux paths in the core. Comparison of the values of reactance from tests on the several lengths of cores for a particular winding condition must be made at comparable degrees of core saturation. This was accomplished by arbitrarily choosing a value of winding magnetomotive force and determining the reactance values of all four lengths of cores at this value of magnetomotive force. Because coils for the different winding conditions studied were not all wound with the same number of turns, it was necessary to refer all reactances to a common number of turns per coil before comparisons could be made. Throughout this study and data analysis 30 turns per coil were chosen as the common denominator. The reactances will vary as the square of the turns per coil. Accurate determination of the mean length of the conductors comprising the windings was accomplished by computations involving the measured resistance of the winding and the resistance per-unit length of the magnet wire with which the coils were wound.

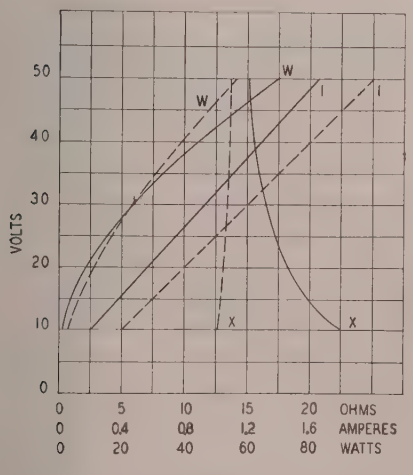

Figure 4. Experimental data and reactance curves

Dotted curves—without rotor
Solid curves—with rotor
W = total watts input
I = current per terminal
X = reactance, ohms per phase

Table III. Comparison of Calculated and Experimental End-turn Reactance

Winding Condition	Poles	Pitch	Experimental Value Ohms	Experimental Value Per Cent	Calculated Values (%) Method I*	Method II*	Method III*	Method IV*
A	2	0.5	5.7	100	110	68	116	113
B	2	0.66	9.3	100	133	83	105	103
C	4	0.44	1.6	100	70	40	119	90
D	4	0.66	3.3	100	94	58	105	73
E	4	1.00	4.6	100	169	84	100	70
F	6	0.66	1.6	100	88	53	114	67
G	6	1.00	2.8	100	118	61	88	51

* Method I—Caldwell,[6] Method II—Alger,[4] Method III—Gray,[7] Method IV—Kuhlmann.[8]

The end-turn leakage reactance for a given winding condition was determined by plotting test values of reactance for each of the four lengths of cores against the core lengths in inches. Figure 5 is an example of one of these curves. A summary of the experimentally determined end-turn reactances is shown in Table II. In each instance the reactance is referred to 30 turns per coil. It is significant to note that the end-turn reactance determined from test data taken with the rotor in place in the stator bore was indistinguishable from that determined from test data taken when the rotor was not in the stator bore. In other words, the presence or absence of the rotor in the stator bore did not affect the value of end-turn reactance. In future studies of end-turn reactance, knowledge of this fact will permit avoiding the troublesome element of leakage flux path saturation.

Comparison of Experimental Results with Calculated Results

The end-turn reactances of the winding conditions studied experimentally were calculated by each of four published calculation methods. A comparison of these calculated values with the corresponding experimentally determined values is shown in Table III. The experimental values are arbitrarily designated as 100 per cent in the tabulation and the calculated values are expressed as percentages of the experimental values.

A detailed analysis was made for each calculation method in an effort to determine a significant correlation of the departures between the calculated and experimental results. The conclusion is that Method III (Gray) most consistently accounts for the physical phenomena occurring in the generation of reactance voltages in the winding end-turn region for the variety of winding conditions studied.

Analysis of Gray's Method (III) for Calculation of End-Turn Leakage Reactance

Notwithstanding the relatively better over-all agreement of test and calculated values of end-turn reactance by Gray's method compared with others, it is significant that the departures from the experimental values are greater as the values of winding pitch depart from full pitch. In view of this further examination of Gray's method (equation 6) appears warranted. The derivation of this formula is included in Appendix I along with the identification of mathematical terms.

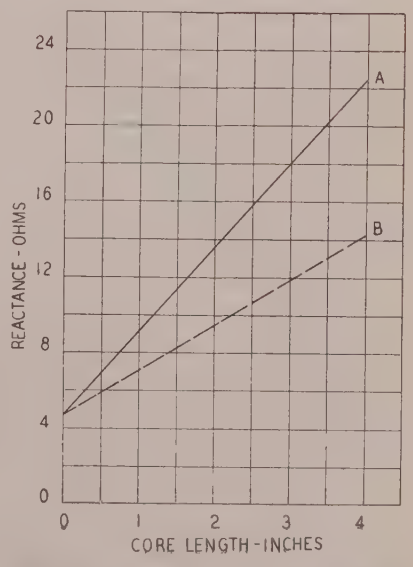

Figure 5. Curves of reactance versus core length

Curve A—with rotor
Curve B—without rotor

$$X_{end} = 2\pi f b^2 c^2 K_p^2 P n \left[\frac{\phi_e L_e}{2n}\right] \times 10^{-8} \text{ ohms per phase} \quad (6)$$

The value of $\phi_e L_e/2n$ must be determined from an empirical curve relating $\phi_e L_e/2n$ and the pole pitch in inches.

Study of Table III suggests these data were established for the case of full pitch winding only. This is not necessarily inferred from the discussion accompanying Gray's disclosure, however, it is strikingly evident when the results of the current study are analyzed. When values of $\phi_e L_e/2n$ determined from experimental results are plotted against pole pitch (in inches) not one, but rather a family of curves results wherein each curve corresponds to a particular value of winding pitch, Figure 6. In Gray's disclosure only the curve for the 100 per cent pole pitch condition is given. Since good design practice from the standpoint of airgap harmonic flux and, in the case of larger machines, ability to design the winding to secure proper values of pole flux require use of fractional pitch windings, the end turn reactance calculation should be adaptable to this condition.

Another limiting feature of Gray's method arises from the lumping of the term L_e with ϕ_e in the empirical curve. If it can be achieved simply, it is desirable that an end-turn calculation method permit evaluation of the effects of independent variations in L_e for a given pole pitch and coil span. Otherwise, it is necessary to produce a family of curves involving $\phi_e L_e/2n$ for which each curve of the family corresponds to a particular relationship between L_e and coil pitch. Figure 7 is a curve of the relationship between L_e and coil pitch for the experimental windings used in the subject study. Different manufacturers, or even different designs of a given manufacturer will not necessarily follow a particular curve relating L_e and coil pitch, therefore, flexibility in an end-turn calculation method to account for this is desirable for a uniform degree of calculation accuracy among a variety of winding conditions.

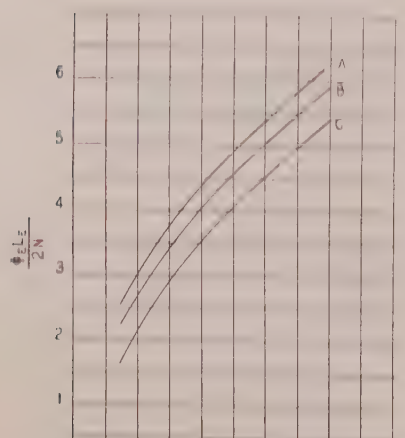

Figure 6. Empirical end-winding constant versus pole pitch

Curve A—Coils having 100 per cent pole pitch (also Gray's curve)
Curve B—Coils having 66 per cent pole pitch
Curve C—Coils having 50 per cent pole pitch

In an attempt to determine how coil pitch and L_e might be accounted for independently, equation 6 was solved for values of $\phi_e/2n$ using experimental values of X_{end} and L_e. When these values of $\phi_e/2n$ were plotted against pole pitch, no distinguishable relationship between $\phi_e/2n$ and coil pitch, for a given pole pitch, resulted. However, when $\phi_e L_e/2n$ was plotted against pole pitch, and the coil pitch for the particular points noted, Figure 6, an individual curve may be drawn through the points corresponding to each particular value of coil pitch.

This points out that, for the range of machines studied $\phi_e L_e/2n$ does not vary directly as L_e when all variables are held constant except L_e. The measure by which $\phi_e L_e/2n$ departs from a direct relationship with L_e appears to be greater for shorter values of coil and pole pitch. A study of Figure 7, the relationship of L_e and coil pitch, indicates that this result may be expected, since for the smaller values of coil pitch, L_e departs in increasing degree from being a direct function of coil pitch. This is occasioned by the necessity of permitting the coil conductors to extend axially some distance beyond the core before proceeding peripherally to the next pole of the winding; for still smaller values of coil pitch, the cross section of the coil itself becomes large relative to the coil pitch length and requires lengthened L_e with respect to coil pitch.

Toward further evaluating the variation of X_{end} with changes in L_e, attempts were made to correct the end-turn reactance of several stator windings having lengthened and shortened values of coil head length by the direct ratio of L_e. This treatment resulted in a much too great change in the value of X_{end} when compared with test values. Again this points out that, for the sizes of machines dealt with in the experimental study, X_{end} is not directly proportional to L_e when other conditions are held constant for a particular winding condition. When this manner of correcting for differences in L_e was applied to a machine having 15.5 inches pole pitch, the resulting X_{end} appeared very reasonable when compared with experimental results. For this machine the relationship of L_e and coil pitch is essentially a straight line.

These two instances suggest that X_{end} may vary directly with L_e when the machine is large enough to permit L_e to vary directly with coil pitch length. The experimental data taken for this paper do not encompass a wide enough range of machine sizes to verify this postulate or to define limits of its applicability.

Conclusions

In fulfillment of one of the stated objects of the study, that is, the recommendation of an improved method of end-turn reactance calculation for practical design purposes, the writer recommends use of equation 6 for which the term $\phi_e L_e/2n$ is determined from Figure 6. When applied to windings having random wound coils and with end-turn lengths comparable to those shown in Figure 7, this method of calculation will yield values of end-turn reactance which are of entirely adequate accuracy for practical design purposes. It is the opinion of the writer that values of end-turn reactance so calculated will be within ±5 per cent of experimentally determined values.

When end-turn lengths are encountered which are not comparable to those shown in Figure 7, it is recommended that the end-turn reactance be corrected directly as the first power of the ratio of the actual end-turn length to the end-turn length given in Figure 7. For stators having bore diameters of less than 8 inches the end turn reactance should be corrected

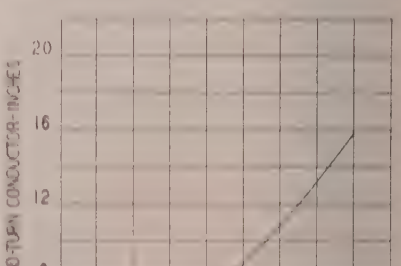

Figure 7. Length of end-conductor versus coil span for experimental stators

directly as the square-root of the ratio of actual end-turn length to the end-turn length shown in Figure 7.

From analysis of the experimental data several additional observations regarding the nature and treatment of end-turn reactance appear warranted. These are:

1. The effect of a squirrel-cage rotor in the stator bore is to produce very little, if any, change in the end-winding reactance of the stator from that which exists when the rotor is not in the stator bore.

2. There is some evidence that for very short core lengths, the end-turn reactance is greater than for longer core lengths, due to mutual linkages of the end-turn flux.

3. The end-turn reactance for a given core and winding condition does not vary directly as the end-turn length in machines having gap diameters less than approximately 8 inches.

4. Because of the relationship between end-turn length and coil pitch length, and because of the inexactness of the coil end shape, the predetermination of end-turn reactance for small machines is most easily accomplished by empirical methods.

Areas for future experimental study are, in their probable order of importance:

1. Effect of varying length of end-turn conductor when all other elements are held constant. This should be done for a wide range of machine sizes.

2. Effect of magnetic material, such as end shield and air-directing baffles, which are normally in close proximity with the end-windings in actual machines.

3. Detailed analysis of the several rationally developed formulas in light of the experimental data revealed in this study in order to determine if the theoretical approach should be modified to conform with physical fact.

More accurate and reliable methods for determination of end-turn reactance for all sizes of machines are necessary for progress in the induction machine design art, not only from the viewpoint of end-winding reactance alone. Objective study of slot and differential reactance components is contingent on reducing the relatively large and unknown variations which have been attributed to the end-winding reactance. Therefore, the end-leakage problem is not an isolated portion of the total design function, but rather an inter-related key element, without knowledge of which, the other elements cannot be determined for a wide number of design conditions.

Appendix I. Derivation of Gray's Formula for End-Turn Leakage Reactance[7]

In his consideration of end-turn leakage, basically Gray reasoned that,

$$X_{end} = K(\phi_e L_e) \tag{7}$$

where

X_{end} = end turn reactance
ϕ_e = lines of magnetic force linking one inch length of the belt of end connections per ampere conductor in the belt
L_e = length of one end-turn in inches, core to core
K = constant involving units, frequency, turns of winding, and so forth.

The term ϕ_e will vary inversely as the length of the path it traverses, that is, will vary inversely as the distance around a pole-phase belt of end connections. This length is directly proportional to the airgap periphery and inversely proportional to the number of poles and phases, therefore,

ϕ_e is proportional to $\frac{pn}{\pi D}$ and,

$\frac{\phi_e}{n}$ is proportional to $\frac{p}{\pi D}$ but,

$\frac{P}{\pi D} = \frac{1}{\text{pole pitch}}$ and, $\frac{\phi_e}{n}$ is proportional to $\frac{1}{\text{pole pitch}}$

where

n = phases
p = poles
D = gap diameter in inches

When ϕ_e/n is substituted into equation 7,

$$X_{end} = K\frac{(\phi_e L_e)}{n} \tag{8}$$

When the proper units and winding constants are inserted,

$$X_{end} = 2\pi f b^2 c^2 K_p^2 p n \left[\frac{\phi_e L_e}{2n}\right] \times 10^{-8} \text{ ohms per phase} \tag{9}$$

where

f = frequency
b = conductors per slot
c = slots per pole per phase
K_p = pitch factor = sin $(\theta/2)$
θ = coil pitch angle in electrical degrees
p = poles
n = phases
ϕ_e = lines of magnetic force linking one inch length of the belt of end connections per ampere conductor in the belt
L_e = length of end-turn conductor in inches, core to core

Gray frankly recognized that the foregoing qualitative analysis required quantitative calibration by empirical means, therefore, he determined from experimental data a curve relationship between $\phi_e L_e/2n$ and pole pitch.[7]

References

1. Induction Motor Leakage Reactance Calculations, **AIEE Committee Report.** *Electrical Engineering*, volume 67, May 1948, pages 430–34.

2. The Leakage Reactance of Induction Motors, **C. A. Adams.** *Transactions*, International Electric Congress (St. Louis, Mo.), 1904, pages 706–24.

3. The Design of Induction Motors—with Special Reference to Magnetic Leakage, **C. A. Adams.** *AIEE Transactions*, volume 24, 1905, pages 649–84.

4. The Calculation of Armature Reactance of Synchronous Machines, **P. L. Alger.** *AIEE Transactions*, volume 47, April 1928, pages 493–513.

5. Reactance of End Connections, **J. F. H. Douglas.** *Electrical Engineering* (*AIEE Transactions*), volume 56, February 1937, pages 257–60.

6. End-Winding Inductance of a Synchronous Machine, **B. H. Caldwell, Jr.** *Electrical Engineering* (*AIEE Transactions*), volume 56, April 1937, pages 455–61.

7. Electrical Machine Design, **Alexander Gray.** McGraw-Hill Book Company, New York, N. Y., 1926, pages 218 and 368.

8. Design of Electrical Apparatus, **J. H. Kuhlmann.** John Wiley and Sons, New York, N. Y., 1940, page 315.

Discussion

J. S. Gault (University of Michigan, Ann Arbor, Mich.): Since the 1947 meeting in Dayton, when this paper was promised, we have been awaiting its appearance with much interest. I wish to congratulate the author on a job well done and also express gratitude for the considerable amount of time and energy expended in carrying it through. I do not wish any of my further remarks to be taken as detracting from it in any way.

1. I wish one more column had been added to Table III of the paper to show the calculated value using the Barnes' formula.[6] This is not necessarily the same as the test value. For winding condition D, I computed 94 per cent which is the same value as shown by Method I, for example.

2. Formula 6 should be divided by the square of the number of parallel paths in the winding, otherwise it gives a value four times too large for a parallel winding. I tried it out on a certain motor with 48 slots, stator bore 7.135 inches, 14 turns per coil, 5/6 pitch, L_e = 8.3 inches, parallel-Y connection. From design data and locked test, the value of end-turn reactance appears to be 0.437 ohm, which will be called 100 per cent. By the corrected Barnes' formula, I compute 0.472 or 108 per cent; by Kuhlmann's formula, which is the same as Alger's formula in the Standard Handbook, 81 per cent; by Alger's 1928 formula as used in the paper, 83 per cent; by Gray's formula, 109 per cent. For this case at least, Barnes' formula comes closer than any of the others, and has the advantage of simplicity. Because the pitch is not very short, this formula does not give a value very different from the value given by Gray's formula.

3. From theoretical considerations, it appears that K_{sl} should be used in the formula rather than K_p^2. For the values of pitch used in the paper, the value is the same, but for 5/6 pitch, K_{sl} = 0.875 while K_p^2 = 0.933. Making this change the end reactance of the above motor comes out

0.442 ohm or 101 per cent. I should like to see the formula written:

$$X_{end}=\frac{2\pi f W^2 K_{s1} n}{P\times 10^8}\times\frac{\phi_e L_e}{2n}$$

where W = series conductors per phase and $\phi_e L_e/2n$ is obtained from Barnes' curves in Figure 6.

P. L. Alger (General Electric Company, Schenectady, N. Y.): The author has made a very worthwhile contribution to our knowledge of induction machine reactances, as he has provided us with accurate and well-documented test data of unique value. In my view, the best way to calculate reactance is, first, to derive a formula which is correct from a dimensional viewpoint, including all of the important parameters, and, second, to calibrate this formula by comparison with test results. In the process of calibration, it is, of course, desirable to simplify the formula, using approximations suited to the particular type of machine for which the formula is intended. The formulas given in my 1928 Institute paper,[1] which the author employed in calculating column II of Table III in the paper, were derived for large synchronous machines, and were adjusted for this purpose.

There is given a very simple formula for end reactance, intended for polyphase induction motors, in Section 7 of the Standard Handbook for Electrical Engineers.[2] This formula is:

$$X_e=\frac{4fqDN^2K_{s1}}{10^7P^2}\text{ ohms per phase}$$

where

f = frequency
q = number of phases
d = air gap diameter
N = turns in series per phase
P = poles

The values given by this formula for the seven tests in the paper are listed in column IV of Table I of this discussion. It will be noted that these values are a little too high for two poles and considerably too low for six poles. A much more complete and exact formula, which I have developed, gives results shown in column V of the table.

In applying this more complete formula to the motor described by Mr. Barnes, I have assumed that the end windings extend axially to an effective distance of 3/4 inch beyond the iron on each end, and that the angle at the bend of the coil is 60 degrees. These values check the end conductor length given in Table II of the paper. By dividing each of the given lengths by the pitch and multiplying them by the number of pairs of poles, the equivalent end conductor length of a 2-pole full pitch machine is found to be closely 11.5 inches for all of the windings except B. For the B winding, the corresponding figure is 14.2 inches, indicating that this particular winding was in some way out of line. (After the meeting Mr. Barnes told me that, observing this condition, he had a new B winding made, for which the end conductor length was found to be 9.2 inches, instead of 11.0 inches; and the end turn reactance 8.5 instead of 9.3 ohms.)

Table I

Winding Condition	Poles	Pitch	Handbook Formula	Reactance by Complete Formula	Test
A	2	0.5	6.8	5.9	5.7
B	2	0.66	10.2	9.4	9.3 (8.5)
C	4	0.44	1.4	1.6	1.6
D	4	0.66	2.6	3.1	3.3
E	4	1.0	3.4	4.6	4.6
F	6	0.66	1.1	1.7	1.6
G	6	1.0	1.5	2.5	2.8

The reactance due to the straight portion of the core is calculated from the relation that the radial flux in an air core is equal to Pg/D times the flux produced in a normal rotor, where P = number of poles, g = normal air gap, and D = air gap diameter. This gives an air core reactance value equal to

$$\frac{5.44LK_p^2}{P}\text{ ohms}$$

where L = core length, and P = number of poles.

In addition to this air core reactance, there must be added the slot reactance of the stator, which for this particular machine is $0.89\ LK_{s1}$ ohms per phase, for the dimensions given by the author. For the particular case of the 4-pole full pitch winding, shown in Figure 5 of the paper, this formula gives a reactance for the 4 inches of core length with rotor removed equal to

$$4\left(\frac{5.44}{4}+0.89\right)=9.0\text{ ohms}$$

which compares favorably with the test value derived from Figure 5 of the paper, of 9.5 ohms, approximately.

In the complete formula for the reactance due to the end connections, there are two terms, one for the reactance due to axial currents, and the other for that due to peripheral currents. Each of these terms has the form of a difference between the total flux produced by the currents and that portion of it which links the secondary. For small motors, and when the rotor is removed, the latter terms are small, but they are important in large machines. The values given above neglect these subtractive terms, and, therefore, apply specifically to the case when the rotor is removed.

References

1. See reference 4 of the paper.

2. Standard Handbook for Electrical Engineers, **A. E. Knowlton**. McGraw-Hill Book Company, Inc., New York, N. Y., 1949.

L. W. Buchanan (Westinghouse Electric Corporation, Lima, Ohio): It is gratifying to have an experimental study of induction machine leakage published particularly on end turn leakage which has apparently defied analytical derivation of a successful formula. It is only by calculating each component of leakage reactance carefully that we can hope to determine a total leakage which will hold for a large number of variations in motor design. Although this paper recommends an empirical method, which was published in 1926, for determining the end leakage, it adds further substantiation to this method. This empirical method then points the direction for modifying existing analytical studies to obtain closer results.

In order to arrive at a check of our calculating formula, an unpublished study was made of the total tested end leakage reactance of a line of motors by Messrs. J. C. Burdett, F. C. Bradshaw, and L. W. Buchanan. The motors studied used one punching which was smaller than that described by Mr. Barnes, and windings were concentric single-phase windings. However, since many single-phase formulas for reactance are merely those for one phase of a 2-phase motor, a comparison of these results should prove interesting.

In routine calculations, we ordinarily calculate a leakage permeance which when multiplied by $2\pi fCK_w^2 10^{-8}$ gives the leakage per phase where CK_w is total effective conductors per phase. In terms of Mr. Barnes' paper, this leakage permeance is

$$P_e=\frac{n}{p}\left[\frac{\phi_e L_e}{2n}\right]$$

On a 4-pole motor using a 6-inch diameter punching, it was necessary to extend Gray's curve. By this method, I calculate a leakage permeance of 1.25. The results of our studies of tests indicate a value between 1.2 and 1.4. Our present method of calculating end leakage permeance results is a value approximately 50 per cent of the tested value. Gray's method gives much better results.

This method, therefore, points the way to better calculation of end turn leakage on single-phase motors of the above description. Unfortunately, in order to use this formula, we must reduce some other leakage component so as to continue calculating the total leakage as closely as we have been.

E. C. Barnes: Professor Gault is correct in suggesting that formula 6 in the paper be divided by the square of the number of parallel paths in the winding. I do not concur, however, that $K_S{}^1$ should be used in the formula in lieu of the $K_P{}^2$ now shown. The conditions which are present in the core portion of the winding, and which require the use of the $K_S{}^1$ factor, do not obtain in the end conductor region. In the core portion, the upper and lower conductors in the slots are relatively closely coupled as a result of the surrounding core and teeth, and in the case of certain fractional pitch windings, the resultant leakage flux which links these two conductors is not in phase with the cur-

rent flowing in each of the conductors. As the pitch of the windings is changed, the K_S[1] factor changes by discrete amounts and it is not a continuous function with pitch over the regularly used range of pitch values. On the other hand, the end conductors of a given phase belt are carrying currents which are in phase with each other and these conductors are relatively loosely coupled by the leakage flux in air paths. The magnetic flux linking a phase belt of end conductors and inducing a reactive voltage in these conductors is essentially in phase with the current flowing in the conductors. Because of the configuration of the coil head, the leakage flux produced by the adjacent inner or outer layers of end conductors is relatively ineffective in producing reactive voltages in the adjacent outer or inner phase belt, respectively. For this reason, it is my opinion that the K_P[2] factor is correctly used in formula 6.

With respect to P. L. Alger's discussion, I recognize that the comparison in the paper is somewhat unfair in that Alger's formula which is used, is a simplification of his complete formula, employing assumptions which are legitimate only for larger machines having form-wound coils. In his discussion, Mr. Alger shows that quite good agreement exists between test values of this paper, and calculated values of end-turn leakage reactance using his complete formula. Also in his discussion he calculated a value of stator slot reactance for the condition without the rotor in the stator bore, which agrees relatively closely with test values.

Mr. Buchanan reported calculating a value of end-turn reactance for a concentric-coil single-phase winding using the principles given in the paper. This calculated value agreed reasonably with experimental data which he had developed for this winding.

It would be interesting and worthwhile to have further verification of the applicability of the method outlined in the paper to concentric-coil windings, since the method was intended primarily for double layer windings.

11-Year Operating Record—Rural Line Sectionalizing by Repeater Fuses

R. M. SCHAHFER
MEMBER AIEE

F. H. STROUT
ASSOCIATE AIEE

REPEATER fuses have been used on rural lines of the Northern Indiana Public Service Company for the last 15 years. During this period our methods of application have been improved to the point that the results obtained make us feel that this method of automatic sectionalizing of rural lines is quite satisfactory. Three-shot repeater fuses now are standard for sectionalizing rural lines for the entire company.

This paper is intended to give a comprehensive picture of the performance of repeater fuses as we have found it, so that other engineers may have the same information when studying alternative plans for sectionalizing on their own system.

It is self-evident that a large number of sectionalizing points in a line makes the location of trouble a localized problem, and the smaller the fuse size at the end of a line, the more sectionalizing points may be put in series without using fuses of excessive size at the start. Our transformer fusing table (see Figure 2) shows that we use the smallest possible fuse for each size transformer, which permits us to use the maximum number of sectionalizing points on our lines. By this method we have been able to use 113 sectionalizing points on 384 miles of line in one district, or an average of 3.3 miles per section.

In connection with minimum transformer fusing, we use a common ground on all of our distribution transformer installations, which interconnects the secondary neutral, the transformer case, and the lightning arrester ground. The lightning arrester is connected on the line side of the transformer fuse so that a lightning arrester operation cannot cause a transformer outage.

In assigning locations and sizes of sectionalizing fuses, consideration must be given to several factors. The location of hazards, such as bad tree conditions, exposure to heavy road traffic, or routes difficult to patrol, will determine the location of certain points for operating reasons. Grouping of customers and relative importance of certain loads on a circuit indicate other points which will give the best service to preferred sections or loads. Fuse link sizes are determined by the normal loading of the section to be isolated plus the added load which appears after a prolonged outage as a result of simultaneous starting of automatically controlled equipment.

About 13 years ago, this application of repeater fuses became common enough that studies were made to co-ordinate groups of fuses in certain locations. This work has been continued until we now have fusing maps, based on further studies for each district, which are simplified single-line drawings showing the locations and recommended fuse link for all present sectionalizing points. These maps also show proposed fuse locations for what is believed to be the ultimate development, and from time to time, as extensions or changes are made, they are revised and brought up to date.

Fusing maps are distributed to the Engineering and Operating Departments and serve not only to show present and future plans, but also to instruct the men in the field as to the proper size of link to be used when replacing blown fuses.

Proper co-ordination of sectionalizing points requires that the repeater fuse nearest a source of trouble shall blow all three fuses, in case of a permanent fault, before any fuse is blown in any sectionalizing point nearer the source of supply. Also, any repeater fuse should sectionalize trouble, either transient or permanent, before the main circuit is opened at the substation.

In a few cases, the advantage of an extra sectionalizing point in a circuit is great enough to warrant installing fuses in series having ratings which are too nearly the same to give proper selectivity. In such cases, the maximum deviation we permit is that a repeater should blow only one fuse, while all three of the fuses of the repeater nearer the source of trouble are blowing.

Co-ordination between fuses and oil circuit breakers at our substations is accomplished by equipping the circuit breakers with overcurrent relays having extremely inverse time characteristics. This, in effect, makes the tripping time of the circuit breaker similar to the time characteristics of fuse links.

The successful operation the Northern Indiana Public Service Company has experienced with repeater fuses has been the result of careful attention to the following details:

1. Choosing proper locations for sectionalizing points.
2. Recommending the correct size of fuse link for each location.
3. Using fuse links of the same time characteristics throughout the company to simplify the engineering problems of co-ordination.
4. Instructing the men in the field as to the size of fuse link to be installed at each location.

We have found that the replacement of blown fuses does not present a difficult problem. Each 3-shot repeater restores service in two cases of transient faults and, in most cases, some time will elapse before a third fault occurs. This time interval permits some employee, in the

Paper 51-112, recommended by the AIEE Protective Devices, Relays, and Transmission and Distribution Committees and approved by the AIEE Technical Program Committee for presentation at the AIEE Winter General Meeting, New York, N. Y., January 22-26, 1951. Manuscript submitted May 19, 1950; made available for printing December 22, 1950.

R. M. SCHAHFER and F. H. STROUT are both with the Northern Indiana Public Service Company, Hammond, Ind.

Figure 1. Fusing map, southern part of Lake County, Indiana, showing location, type, and size of all fuse locations other than those at individual transformers

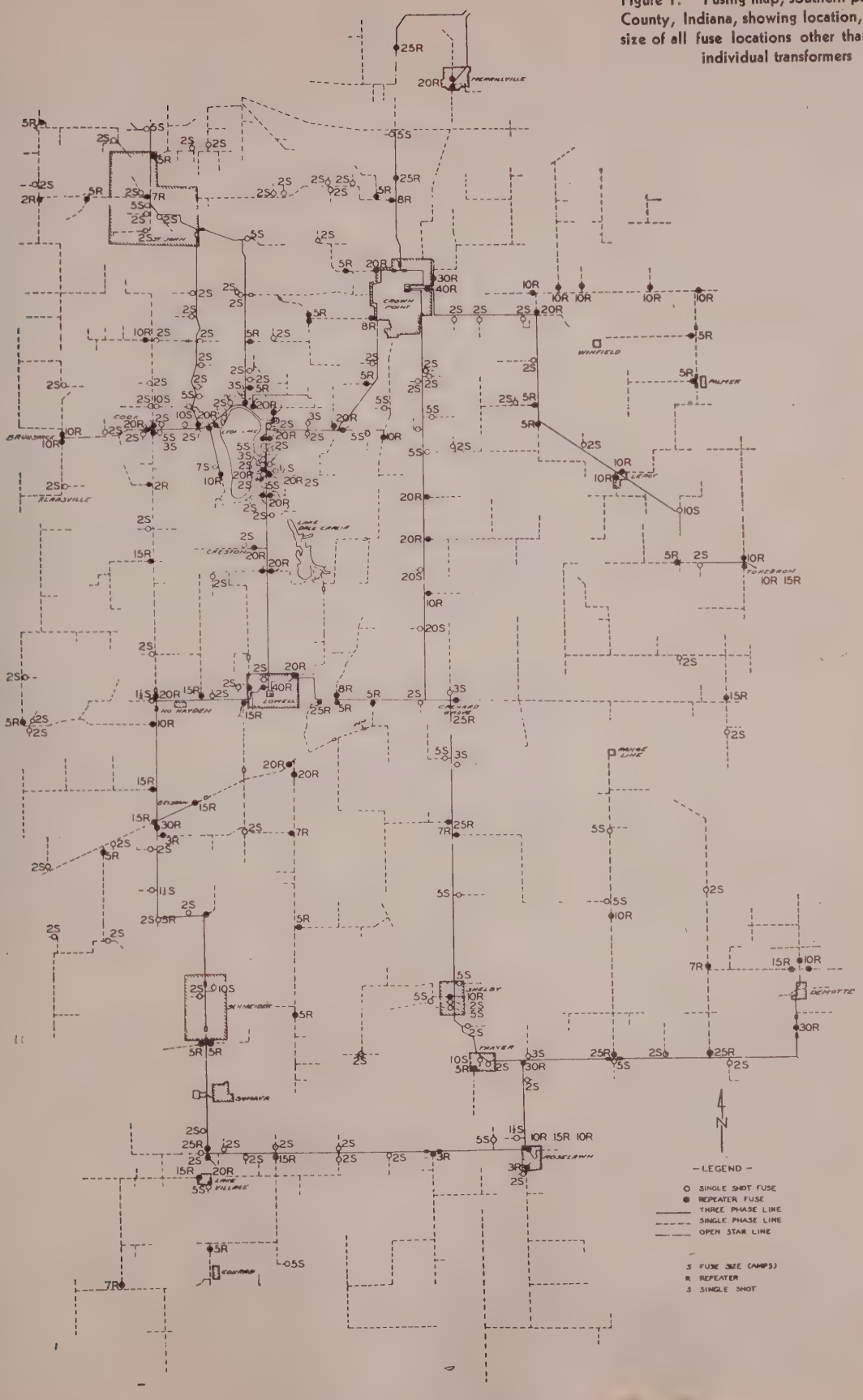

course of his regular work, either to replace the blown fuses or to report them to someone qualified to do so. Permanent faults are reported quickly by the customers out of service, and the blown fuses are replaced as soon as the cause of the fault is removed. Common practice is to make a patrol as soon as possible after each major storm to locate and replace blown fuses. Also, all employees whose routine work takes them through the district are instructed to observe the condition of all fuse locations as they pass. From our experience we believe no additional regular patrol is necessary.

Development of our sectionalizing plan could not proceed intelligently without a knowledge of the frequency and cause of the faults which occur, and therefore we began to accumulate these data by an analysis of our records soon after we started a general program of sectionalizing all our rural lines. One of our districts was chosen as a representative area of sufficient size and diversity of character to give accurate results from a detailed analysis of its operating records. This district is in the southern part of Lake County in the northwest corner of Indiana, is mainly rural, and has one large and a few small communities. Figure 1 is a single-line diagram of this district, showing the location, type, and sizes of all fuse locations other than those at individual transformers.

There are 144 individual 3-shot repeater-fuse units now in service at 113 locations. In addition there are 150 single-shot fuse units in service at 129 locations consisting of three 3-phase, one 2-phase, and 118 single-phase installations.

Single-shot fuses generally are located on minor branches and, since this is a report on repeater fuses, these single shots will be ignored in the remainder of this analysis and report.

The following data have been taken from the regular interruption reports of this district. Reports turned in by the serviceman state the cause and the number of fuses blown and are accepted as his best estimate as governed by the

Table I. Miles of Line Protected by Repeater Fuses

Line Voltage	Miles 1943	1947	1949
2,300 volt, 1 phase	16	17	3
2,300 volt, open Y			5
4,000 volt, 3 phase	6	6	6
7,200 volt, 1 phase	205	246	261
12,500 volt, 3 phase	100	100	101
Total	327	369	384

FUSE RATING - AMPERES

KVA Each Transformer or Capacitor	Single Phase or 3¢ Wye or 3¢ Open Wye or 3¢ Open Delta — KV Across Transformer 2.4	7.2	11.5 or 12.5	Capacitor 2.4	7.2	3¢ Closed Delta — KV Across Transformer 2.4	7.2	11.5 or 12.5	Capacitor 2.4	120V. 120/240V. 1¢ Banked Secondaries*
1	5	-	-	-	-	5	-	-	-	Not
1 1/2	5	2	-	-	-	5	2	-	-	To Be
2	5	2	-	-	-	5	2	-	-	Banked
2.5	5	2	1 1/2	-	-	5	2	1 1/2	-	25
3	5	2	1 1/2	-	-	5	2	1 1/2	-	25
5	5	2	1 1/2	-	-	7	2	1 1/2	-	25
7 1/2	7	2	1 1/2	-	-	10	3	2	-	40
10	7	3	1 1/2	-	-	10	5	2	-	40
15	10	3	2	10	3	15	5	3	15	50
20	15	5	3	-	-	20	7	5	-	50
25	15	5	3	15	5	25	10	5	25	75
30	20	7	5	20	7	30	10	7	30	75
37 1/2	25	7	5	-	-	40	15	7	-	75
40	25	7	5	-	-	40	15	10	-	75
45	-	-	-	30	10	-	-	-	40	-
50	30	10	7	30	10	50	20	10	50	100
60	-	-	-	40	15	-	-	-	50	
75	40	15	10			80	25	15	-	
100	50	20	10	-	-	100	40	20	-	
150	80	30	15	-	-		50	30	-	Not
200	100	40	20	-	-		65	40	-	To Be
250	See	50	25	-	-	See	80	50	-	Banked
300	Test	65	30	-	-	Test	100	65	-	
333	Dept.	65	40	-	-	Dept.		65	-	
400		80	40	-	-			80	-	
500		100	50	-	-			100	-	

The above fusing is based on the use of N. I. P. S. Co. Standard Primary and Secondary Links.

* For any banked secondary, the secondary fuse shall be that size specified for the smallest transformer immediately adjacent to that particular secondary fuse.

Figure 2. Fusing transformers, capacitors, and banked secondaries

Fuse Wire:

Increase the fuse size of the above table by 50 per cent whenever fuse wire must be used.

Single Rated Liquid Fuses:

Increase the fuse size of the above table by 50 per cent whenever a liquid fuse is used that has only one rating stamped on it.

Double Rated Liquid Fuses:

The above table applies to the smaller figure whenever a liquid fuse is used that has two ratings stamped on it. For example, if the table calls for a 20-ampere fuse, a fuse stamped 30/20E is the proper size.

Above 12.5 kv:

Follow Test Department recommendations on all fusing at voltages above 12,500.

Table II. Fuse Links Used for Line Sectionalizing 3-Shot Repeaters

Size Fuse	Number of Repeaters	Per Cent of Total	Cascaded Position in Line 1st	2nd	3rd	4th
40	6	4	6			
30	6	4	3	3		
25	14	10	11	3		
20	40	28	33	7		
15	14	10	13	1		
10	18	12	2	11	5	
7	14	10	10	2	1	1
5	27	19	7	9	11	
3	3	2		1	2	
2	2	1		1	1	
Total	144	100	72	50	21	1

Table III. Link Size of Fuses Used for Sectionalizing

Type of Cutout	Fuse Link Size Max.	Small	Number of Repeaters with Small Size Links 1943	1947	1949
Single shot	20	2	60	80	102
Three shot	40	2			2
		3		3	3
		5	35	17	27

Table IV. Summary of 11-Year Operations

Number of	1939 1940	1941 1942 1943	1944 1945	1946 1947	1948 1949	11-Year Total
Fuses blown	325	949	574	466	626	2,940
Cases of trouble*	123	345	260	216	322	1,266
Fuse locations involved	41	65	66	64	78	

* In this table, a case of trouble involving one or more cutouts of a multiphase installation is classified as one case of trouble.

Table V. Frequency at Which Trouble Occurs at a Given Location

Number of Cases of Trouble at a Given Location	1939 1940	1941 1942 1943	1944 1945	1946 1947	1948 1949
1	14	10	16	18	17
2	10	9	12	12	16
3	5	7	6	13	8
4	2	9	5	7	9
5	3	6	10	4	12
6	4	5	4	4	7
7	1	5	5	1	3
8	0	1	1	1	3
9	2	1	3	1	1
10	0	4	2	0	2
11	0	4	0	1	0
12	0	1	0	1	0
13	0	0	1	1	0
14	0	0	1	0	0
15	0	1	0	0	0
16 or more	0	2	0	0	0

conditions he finds when he replaces the fuses.

These data are accurate as to location, number of locations, and number of interruptions, and the causes assigned to cases of blown fuses, and the number of fuses blown for each cause, are reasonably accurate. For use in this analysis, the number of fuses found blown on any one inspection are attributed to the same case of trouble.

Tables I, II, and III are statistical records showing the types of line protected and the combinations of fuse sizes. As shown in Table I, there has been a regular growth in the number of miles of line installed, and some changes in voltage classifications have been made. Table II shows the range of fuse sizes and the groupings used. Table III is intended to show that we use a good percentage of small-size fuse links, and it will be brought out later that no excessive blowing results from this application.

In the 11 years shown in Tables IV and V we have blown 2,940 fuses on 1,266 cases of trouble. As shown in Table V, the majority of locations have had three or less cases of trouble in any period analyzed, indicating a widespread area of fuse blowing rather than a few aggravated cases of localized trouble. These tables, and some of those to follow, are set up by 2- and 3-year periods so that any change in trends can be identified.

Classification of blown fuses according to the cause as given by the serviceman's report shows that 62.7 per cent of our trouble results from lightning, tree limbs, and lightning arrester failure. These three causes will be analyzed further.

Lightning has been assigned as the cause of blowing 1,010 fuses in 595 repeaters during the 11-year period analyzed. In 76 per cent of the cases, service was restored by 3-shot repeaters, while two shots would have restored service in only 54 per cent of the cases. Table VII shows that the performance has been very consistent through all periods analyzed.

We have used the term "Lightning" as the cause of the blown fuses in Tables VI, VII, VIII, and IX because that is the term used in the interruption reports from which this analysis was made. Actually, few fuses are blown by lightning, but the serviceman recognizes that lightning is the initiating cause and attributes the operation to lightning. In substantially all cases, the cause of fuse blowing is the 60-cycle short-circuit current which follows the ionized path established by the lightning stroke. However, exceptions may occur where a high-current stroke hits a line in a span adjacent to a fuse and goes to ground through a lightning ar-

Table VI. Number of Cutouts with Blown Fuses Classified by Cause

Cause	1939 1940	1941 1942 1943	1944 1945	1946 1947	1948 1949	11-Year Total Number	11-Year Total Per Cent
Lightning	57	171	170	97	100	595	40.8
Tree limbs	62	98	30	22	28	240	16.5
Lightning arrester failure	10	38	17	10	3	78	5.4
Caused by public	9	12	13	21	23	78	5.4
Defective insulators	4	13	5	6	9	37	2.5
Rain and wind	3	11	7	5	5	31	2.1
Sleet, storm, and wind		22	1	2	10	35	2.4
Conductor failure		1	5	5	3	14	1.0
Slack spans	4	5				9	0.6
Broken poles	3	2	1	1	5	12	0.8
Under fused	2	2			1	5	0.3
Defective cutout		2				2	0.1
Other	2	5	3	10	4	24	1.6
Unknown	5	40	53	67	131	296	20.5
Total	161	422	305	247	322	1,456	100.0

Table VII. Repeater Fuse Operation Caused by Lightning

	1939 1940	1941 1942 1943	1944 1945	1946 1947	1948 1949	11-Year Total
No. of cutouts involved						
Single phase	34	95	134	62	74	399
Open Y	0	32	16	4	0	52
Three phase	23	44	20	31	26	144
Total	57	171	170	97	100	595
No. of fuses blown	90	304	280	169	167	1,010
No. of cases with 1 fuse blown	36	87	95	50	50	318
No. of cases with 2 fuses blown	9	35	40	22	24	130
No. of cases with 3 fuses blown	12	49	35	25	23	144
Per cent of cases in which service was restored	79	71	79	74	76	76

Table VIII. Number of Cases of Lightning Trouble Per Size of Fuse Link, 1939–1949 Inclusive

Size Fuse	Number of Cases of Trouble	Number of Installations of This Size	Cases of Trouble Per Installation
40	99	4	25.0
30	15	2	7.5
25	38	14	2.7
20	49	21	2.3
15	45	14	3.2
10	50	19	2.6
7	111	25	4.4
5	195	43	4.5
3	3	3	1.0
2	0	1	0.0

rester or some low-impulse gap on the opposite side of the fuse.

There is no need to avoid the use of small-size fuse links if such avoidance is based on the theory that lightning will result in excessive blowing of small links. Table VIII shows that there is no correlation between fuse size and the number of cases of trouble. There is, however, a better correlation between the number of outages and the number of miles of line protected by a fuse, as shown in Table IX. Assuming that in due time every mile of line will receive the same number of lightning strokes, then the number of cases of trouble caused by lightning should be a function of the number of miles of line sectionalized by a given fuse, and not a function of the fuse link size.

Reclosers Following Cases of Trouble Caused by Tree Limbs

As seen in Table X, service was successfully restored in 18 per cent of our cases of trouble caused by tree limbs, and the use of a 3-shot device instead of a 2-shot device increased the record of successful reclosures from 12 per cent to 18 per cent. Information from the field shows that the remaining cases of trouble generally are severe and tree limbs must be removed before service can be restored, indicating that the 18 per cent successful reclosures is as good as can be expected.

Most cases of swaying branches are not included in the above summary as they operate only one or two fuses, service is restored automatically, no report of outage is received, the fuse is replaced when found, and the cause listed as unknown.

Reclosures Following Cases of Trouble Caused by Lightning Arrester Failures

Lightning arrester failures have been isolated satisfactorily, but service has been restored in only a very low percentage of the cases of trouble. An analysis of the fuses blown on lightning arrester failures is shown in Tables XI and XII.

Our standard transformer installation places the lightning arrester on the line side of the transformer fuse, and therefore a faulty lightning arrester usually creates a permanent short circuit from line to ground. In some cases, large-size fuses will hold long enough to blow a lightning arrester clear, but the number of lightning arrester failures is small and there is little point in increasing fuse sizes for this purpose. We prefer the advantage of more sectionalizing points gained by using smaller transformer fuses. The big advantage we have gained is that we have installed so many sectionalizing points that this type of trouble, so difficult to locate, has been restricted to a minimum number of miles of line. There is little benefit in a 3-shot over a single-shot installation for clearing faulted lightning arresters.

It should be noted in Table XI that the number of cases of lightning arrester failure has shown a marked decrease in the 11-year period analyzed. This, we believe, is the result of patrolling our

Table IX. Cases of Lightning Trouble Per Mile of Line Beyond Each Size Fuse Link, 1939–1949 Inclusive

Size Fuse	Miles of Line Beyond Fuse of Tabulated Size Max.	Min.	Total	Number of Cases of Trouble	Cases of Trouble Per Mile
40	13.2	0.5	19.9	99	5.0
30	9.3	5.8	15.1	15	1.0
25	11.0	3.9	63.6	38	0.6
20	11.0	0.1	82.6	49	0.6
15	11.9	0.1	58.1	45	0.8
10	7.2	0.4	57.8	50	0.9
7	13.6	0.1	75.3	111	1.5
5	8.9	0.1	122.7	195	1.6
3	14.1	0.6	27.3	3	0.1
2		0.9	0.9	0	0.0

Note: Installations where fuse sizes have been changed appear in Tables VIII and IX under each size of fuse used.

Table X. Fuses Blown by Tree Limbs

	1939 1940	1941 1942 1943	1944 1945	1946 1947	1948 1949	11-Year Total
No. of cutouts involved	62	98	30	22	28	240
Total no. of fuses blown	153	273	83	62	77	648
No. of cases with 1 fuse blown	15	7	2	2	2	28
No. of cases with 2 fuses blown	3	7	3	0	3	16
No. of cases with 3 fuses blown	44	84	25	20	23	196
Per cent of cases in which service was restored	29	14	17	9	18	18

Table XI. Fuses Blown by Lightning Arrester Failures

	1939 1940	1941 1942 1943	1944 1945	1946 1947	1948 1949	11-Year Total
No. of cutouts involved	10	38	17	10	3	78
No. of fuses blown	26	114	47	25	9	221
No. of cases with 1 fuse blown	2	0	1	1	0	4
No. of cases with 2 fuses blown	0	0	2	3	0	5
No. of cases with 3 fuses blown	8	38	14	6	3	69
Per cent of cases in which service was restored	20	0	18	40	0	12

Table XII. Size of Fuse Link Blown by Lightning Arrester Failures, 11-Year Total

Size Fuse, Amperes	Number of Cases of Trouble
40	1
25	4
20	9
15	9
10	5
8	17
5	33

Note: This table is not weighted by number of installations.

Table XIII. Fuses Blown by Other Miscellaneous Causes

	1939 1940	1941 1942 1943	1944 1945	1946 1947	1948 1949	11-Year Total
No. of cutouts	32	115	88	117	191	543
No. of fuses blown	56	258	164	207	369	1,054
No. of cases with 1 fuse blown	11	36	45	62	97	251
No. of cases with 2 fuses blown	3	15	10	17	28	73
No. of cases with 3 fuses blown	18	64	33	38	72	225
Per cent of cases in which service was restored	44	44	63	68	64	59

Table XIV. Fuses Blown from All Causes

	1939 1940	1941 1942 1943	1944 1945	1946 1947	1948 1949	11-Year Total
No. of cutouts involved	161	422	305	246	322	1,456
No. of fuses blown	325	949	574	466	626	2,940
No. of cases with 1 fuse blown	64	130	143	115	153	605
No. of cases with 2 fuses blown	15	57	55	42	55	224
No. of cases with 3 fuses blown	77	235	107	89	121	629
Per cent of cases in which service was restored	51	44	65	63	63	57

rural lines with a portable radio set and locating lightning arresters which are beginning to break down before actual failure occurs. Leakage current across the gaps in the faulty lightning arrester sets up radio interference along a line, and the peak level of the noise points out the culprit.

Reclosures Following Cases of Trouble Caused by All Other Miscellaneous Causes

Previously we have analyzed the fuses blown by lightning, tree limbs, and lightning arrester failures, these causing the most interruptions and representing 57 per cent of the total number of blown fuses during the 11-year period.

An analysis of all other blown fuses, as made in Table XIII, shows that, over the 11-year period, 59 per cent of the cases of trouble were of a transient nature and service was restored by the use of 3-shot repeaters.

Summary of Reclosures—All Causes

Summarizing all cases of trouble for the 11-year period, we find the analysis shown in Table XIV.

Operation over the 11-year period analyzed has been quite consistent as to the percentage of successful reclosures. Summarizing all cases of trouble for the 11-year period, we find that service was restored in 57 per cent of the cases, as shown in Table XIV. This percentage of reclosures would have been 41 per cent if 2-shot fuses had been used, indicating that there is a decided advantage in the general use of 3-shot devices. We believe that this analysis is sufficiently complete to show that sectionalizing rural distribution lines by means of 3-shot repeating fuses is a satisfactory method of isolating permanent faults and restoring service to as many customers as possible after a fault occurs.

Improper Operations

Faulty operations have occurred from time to time during the 11 years of operations analyzed, and are to be expected when using a man-made device.

The following summation covers only those cases of trouble which are apparent on the daily interruption reports:

25 cases cleared the first fuse but failed to trip the second fuse
13 cases cleared the first and second fuses but failed to trip the third fuse
1 case, the 5-ampere link failed to blow even with the line lying in the trees
7 cases, the fuse wire bunched up and the tube did not drop out
1 case, failure caused by gunfire
1 case, defective fuse link
3 cases, improper adjustment of stop on the cutout
8 cases, cutouts failed to operate because of ice
1 case, fuse tube failed to drop because of carbonized condition of bore of fuse tube

It is probable that the above record is not a complete report because the first consideration on finding blown fuses is to restore service, and the time to make a careful investigation of the cause is not available. We know, of course, that severe ice conditions can prevent a fuse tube from falling out after the fuse link is blown, but the first and second groups of failures covering the majority of the cases listed are unexplained. We believe that these faults are not inherent in the equipment, but are the result of incorrect installation or adjustment.

Economics

The installed costs of fuse-sectionalizing devices, using 1947 prices, are estimated as follows:

	Number of Fuses Per Cutout		
	1	2	3
Installed, each	$ 64.72	$ 111.90	$ 125.92
Less cost of pole and line hardware	32.38	32.38	32.38
Increase in line costs	32.34	79.52	93.54
Total district costs, 115 units	3,719.00	9,145.00	10,757.00
Annual costs at 15 per cent	558.00	1,372.00	1,614.00

Referring to Table XIV, the average number of cases of trouble per year was 132. Of these cases, 55 blew one fuse, 20 blew two fuses, and the remaining 57 cases blew all three fuses. Therefore, if only single-shot fuses had been used, an annual fixed charge of $558.00 would have served to sectionalize 132 cases of trouble, or an average of $4.23 each.

If 2-shot fuses had been used instead of single-shot fuses, the fixed charges would be increased from $558.00 to $1,372.00, or an increase of $814.00 per year. This would have restored service automatically and made patrol work unnecessary in 55 cases of trouble, a cost of $14.80 per case of service restored.

Following this reasoning in the case of the 3-shot fuses in use, the fixed charges were $1,614.00, or a further increase of $242.00 per year to restore service to 20 additional cases of trouble, at an average cost of $12.10 each.

It is difficult to estimate what the average cost of replacing single fuses would be, since the number which would be taken care of at overtime rates is not known, but we believe that the expenditure in each successive step, as estimated above, is justified from a purely economic viewpoint.

An entirely different approach to the economics is to assume that all those outages which were reclosed by the second or third fuse operation would have been reclosed successfully by the automatic reclosing circuit breaker at the point of origin of each entire circuit. With such an assumption, credit can be given to line fuse devices only to act as fault sectionalizing devices; in other words, automatic trouble shooters. Of the 132 cases of trouble per year, 57 were permanent. Hence, the fixed charges of $1,614.00 per year computed for 3-shot fuses indicate that it cost us $28.31 to localize each case of permanent fault. If the five circuits in the district had protection only at the substation, it would be necessary to patrol an entire circuit to locate and clear each permanent fault. With 384 miles of line in service, this would mean an average of 77 miles of line to patrol in each case. We cannot estimate accurately the cost of such a patrol, but, again, we believe that the cost of sectionalizing fuses is well warranted.

There should be added to the economic value a factor for increased revenue, better customer relations because of less outages, and the fact that workmen perform better when it becomes easier for them to

do their work; that is, in this case, easier to locate trouble.

Conclusions

The foregoing analysis has made no reference to automatic reclosers other than the oil circuit breakers at the substation, which, as mentioned earlier, are equipped with extremely inverse time overcurrent relays to provide proper coordination with fuses. Pole-mounted automatic reclosers have been developed to a large extent since the time we started sectionalizing with fuses, and the early reclosers had neither the interrupting capacity nor the inverse time characteristics which were needed. Modern automatic reclosers undoubtedly can be applied to accomplish the same results as our repeater fuses, and in several special cases we are considering their use in place of fuses. However, an economic comparison between the use of fuses and automatic reclosers is not intended in this report.

The cost of using 3-shot repeaters is warranted over the cost of 2-shot repeaters on the basis of cost per case of trouble restored, because of better service to our customers due to more successful reclosures, and because expensive routine patrols and inspections are less necessary.

In addition to the economic justification, there is an additional almost inestimable value in service-restoring devices because they lessen the demand for workmen during the time of peak trouble, when few of us have sufficient help and manpower is at a premium.

Value must be given line sectionalizing devices, not only because they restore service, but also because they automatically restrict the faulted line to a small area and thus become automatic trouble shooters. It should be noted that we have 113 installation points in 384 miles of line. Repeater fuses should be inspected when fuse links are replaced to be sure that no burr or badly burned spot has been created which will prevent future correct operation.

Repeater fuses may be of little value in restoring service during certain sleet and ice conditions because the first tube may be frozen in place and fail to trip in the next fuse, but they will sectionalize the line trouble.

The repeater fuse clearly shows a lockout to the patrolman, except during sleet conditions, and so aids in speedy line patrolling.

We are well pleased with the performance of repeater fuses and plan to continue their use.

No Discussion

Economics of Trolley Coach Power Supply

G. R. McDONALD
ASSOCIATE AIEE

J. C. PRICE
ASSOCIATE AIEE

Synopsis: The total cost of power delivered to trolley coaches is influenced by system engineering as well as by prevailing power rates. In the case of a single-unit rectifier substation, the equipment cost per kilowatt decreases as substation rating increases. With increases in substation rating, however, proportionately more feeder copper is required to distribute the power from each station. Evaluation of these factors for various headways reveals substation ratings and spacings which result in minimum system investment. Cost of power delivered at the trolley coach is the sum of fixed charges and operating costs of the substations and overhead. Such factors as the number of points of power delivery, maintenance expense, and depreciation rates affect the over-all power cost. Their influence upon selection of substation rating is discussed. By careful investigation of all variables, the transit operator is able to minimize the cost of power delivered to his vehicles.

ELECTRIC power is a commodity which is purchased by transit companies at established rates. However, engineering decisions of the transit operator may affect appreciably the total cost of power delivered to the trolley coach.

The purpose of this paper is to show how the size and spacing of traction substations may affect the cost of power delivered to the trolley coach.

The study in this paper applies to the case where the transit company purchases a-c power from the power company at each conversion substation. It is based upon the use of fully automatic, single-unit, rectifier substations, which have demonstrated their reliability in transit service. Substation units are loaded to the extent of their rating during rush hours. Spare conversion capacity is not included, but suggestions are made concerning how to obtain spare capacity.

The total cost of providing power to trolley coaches consists of substation expense and distribution expense.

Substation expense includes:

1. Fixed expenses: Depreciation, interest, and taxes
2. Operating expenses: Cost of power purchased, and maintenance

Distribution expense includes:

1. Fixed expenses: Depreciation, interest, and taxes
2. Operating expenses: Maintenance

Fixed Charges

Fixed charges, particularly depreciation and interest charges, are dependent upon the total investment in the substations and distribution system. Taxes also are related to the total investment. In general, therefore, fixed charges may be reduced by keeping total investment in substations and distribution system at a minimum.

Two major factors are involved in determining the size and spacing of substations for a minimum system investment: (1) The cost per kilowatt of rectifier substation equipment decreases as the kilowatt rating of the equipment increases; (2) as the kilowatt rating of substation equipment increases, the substations are spaced farther apart, and proportionately more copper is required between adjacent substations to provide adequate voltage conditions and adequate short circuit protection.

The effect of these two factors upon system investment is analyzed, using the method described by one of the present authors in 1948.[1] Briefly, this method is:

1. Supplementary feeder cable is proportioned to assure tripping of feeder circuit breakers under short-circuit conditions on any part of the feeder it protects, and to provide adequate voltage at coaches.
2. Substation sizes are selected to handle rush-hour traffic on their 150 per cent 2-hour rating or on their short-time load swing rating, whichever is limiting.

Substation Capacity

Figure 2 shows the number of coaches which can be supplied by various sizes of rectifier unit. This curve is based upon an average power consumption of 55 kw per coach at the substation d-c bus, for 12 miles per hour schedule speed, and upon an instantaneous current demand of coaches as shown in the diversity curve, Figure 1. The 1-minute rating of typical rectifier units is 200 per cent for units rated 1,000 kw and below, or 300 per cent for units rated 1,500 kw and above. Actually, the load swings encountered in trolley coach service are of very short duration and, for the purpose of this paper, a 300 per cent commutating limit has been assumed for units rated less than 500 kw. The number of coaches per substation unit is based upon the 2-hour rating of the equipment, except in the case of the 200-kw rectifier, where the

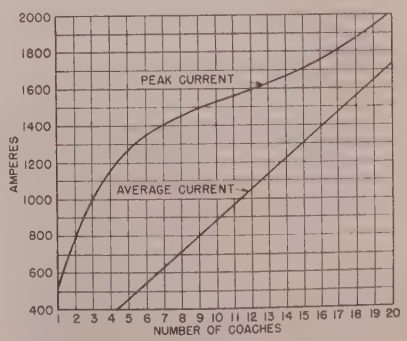

Figure 1. Trolley coach diversity curve

Paper 51-115, recommended by the AIEE Land Transportation Committee and approved by the AIEE Technical Program Committee for presentation at the AIEE Winter General Meeting, New York, N. Y., January 22–26, 1951. Manuscript submitted October 2, 1950; made available for printing December 13, 1950.

G. R. McDONALD is with the General Electric Company, Erie, Pa. J. C. PRICE is with the General Electric Company, Schenectady, N. Y.

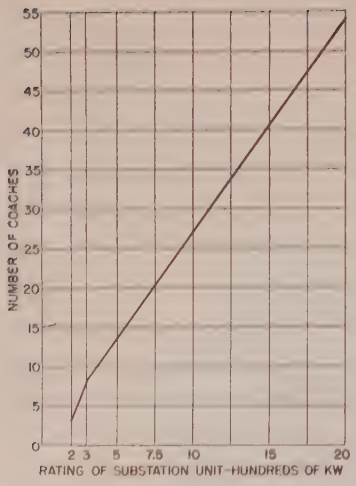

Figure 2. Number of coaches which can be supplied by the 150 per cent 2-hour rating of various sizes of substation units; schedule speed 12 miles per hour; 50 kw per coach plus 10 per cent line loss

number of coaches is limited by commutation rather than heating.

Figure 3 shows the length of 2-way route which may be supplied by the various standard sizes of substation unit, for a number of different conditions of headway.

Figures 4, 5, 6, and 7 show investment in substation plus supplementary feeder copper as a function of trolley coach headway for various feeder arrangements. The cost figures used in preparing these curves are detailed in the section on "System Costs."

System Costs

The assumed cost of single-unit rectifier substations includes electric apparatus, installation cost, and the cost of the building but not of the land. The figures given in Table I are based upon 1948 costs. Adjustments may be made to suit local conditions which affect building and installation costs.

Building cost is approximately 8 to 16 per cent of the total substation cost. Installation costs range from 2½ to 5 per cent of the total cost. Percentagewise, these costs are lower for large size stations.

The amount of feeder copper required in each case was calculated using the methods of the 1948 paper.[1] The cost of feeder copper installed was taken at 50 cents per pound.

Fractional values of trolley coach

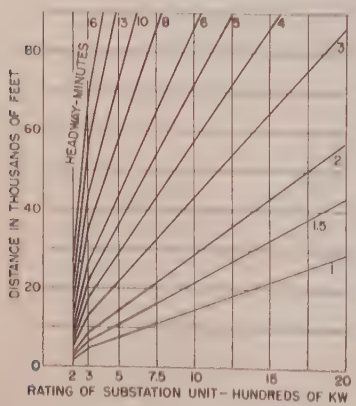

Figure 3. Length of 2-way trolley coach route that can be supplied by the 150 per cent 2-hour rating of various sizes of substation units with various operating headways; schedule speed 12 miles per hour; 50 kw per coach plus 10 per cent line loss

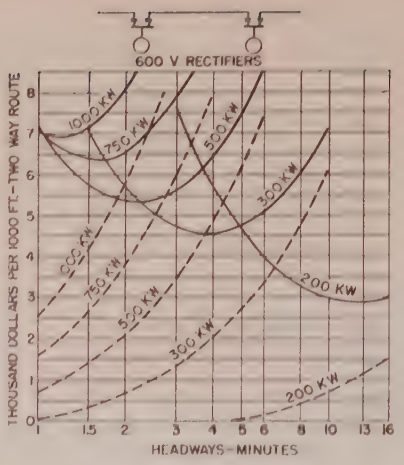

Figure 4. Cost of substation and feeder copper per 1,000 feet of 2-way trolley coach route

Various headways and sizes of single-unit substations; dotted lines, feeder copper only at 50 cents per pound; solid lines, substation cost plus feeder cost; schedule speed 12 miles per hour; trolleys 2/0–80 per cent conductivity; no sectionalizing between substations

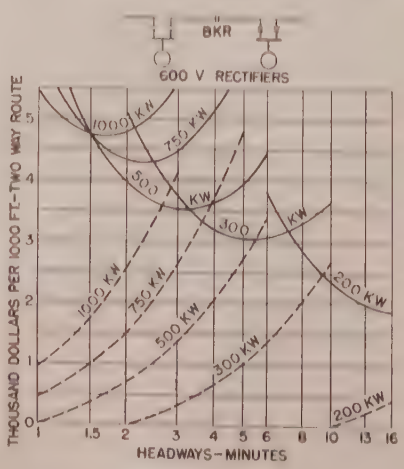

Figure 5. Same as Figure 4 with sectionalizing circuit breakers between substations

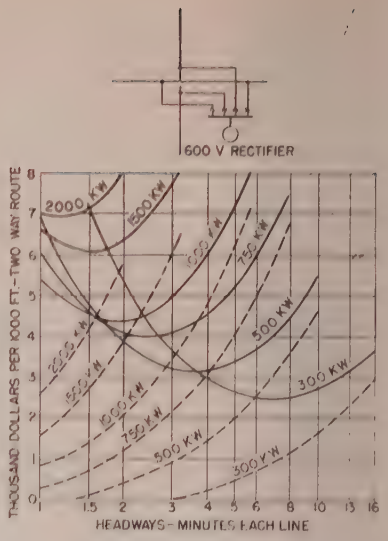

Figure 6. Cost of substation and feeder copper with substations located at the intersection of two routes

Various headways and sizes of single-unit substations; same headway for both routes; dotted lines, feeder copper only at 50 cents per pound; solid lines, substation cost plus feeder cost; schedule speed 12 miles per hour; trolleys 2/0–80 per cent conductivity; no sectionalizing between substations

loading were assumed, and the feeder copper was laid out to exact size. In all cases copper of uniform section along the feeder was assumed. As a result of this, in some instances the section of the copper leaving the substation is inadequate from a heating point of view. The over-all weight of copper considered for each of these cases, however, is such that rearrangement to use more copper adjacent to the substation is possible.

Figure 4 shows the cost of substation

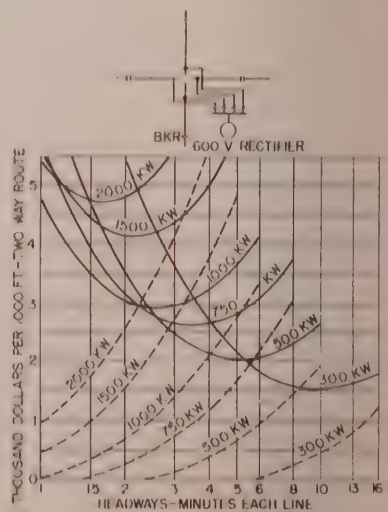

Figure 7. Same as Figure 6 with sectionalizing circuit breakers between substations

Table 1. Installed Cost of Single-Unit Substation, Less Land, Based on 1948 Costs

KW Rating	200	300	500	750	1,000	1,500	2,000
Single line	$36,500	$43,800	$47,100	$59,800	$65,000	$103,500	$121,900
Crossing lines	39,600	46,900	50,300	62,900	68,100	110,609	129,000

equipment and feeder copper for substations supplying a single trolley coach line of considerable length with feeder circuits continuous between substations. This figure indicates the size of substation unit required to give the least cost per thousand feet of route. For instance, for 4-minute headway, the total cost for substation plus feeder copper per 1,000 feet is $6,350 when 500-kw stations are used, $5,750 for 200-kw stations, and $4,550 for 300-kw stations. Hence, the selection of 300-kw stations for this traffic condition will result in lowest over-all investment in substations plus supplementary feeder copper. With 300-kw stations, $2,050 of the $4,550 cost per 1000 feet is for supplementary feeder copper.

As a second example, 500-kw units result in minimum investment when 2-minute headway is considered.

Figure 5 shows automatic reclosing sectionalizing circuit breakers installed at the mid-point between substations. This layout results in a reduced amount of copper and a lower first cost. The sectionalizing circuit breakers should have a trip current setting of one-half the value used for substation feeder circuit breakers. This imposes limitations on the application of this layout because it is not adapted to handling a block of power in event of the outage of a substation.

Figure 6 shows the cost with a substation located at the intersection of two lines, or where two lines can be supplied from the same substation. Equal headways are assumed on both lines. If headways are different, an average figure may be used without materially affecting the results. Figure 7 is practically the same as Figure 5 except that automatic reclosing sectionalizing circuit breakers are installed in each of the feeder circuits.

The significance of Figures 4–7 is that total system investment can be minimized by careful study of size and spacing of rectifier substations.

Spare Capacity

Spare capacity is a necessity on any system. Figures 4–7 are based upon use of the entire rating of a substation for normal service. Spare capacity may be provided by using single rectifier units of a rating larger than actual load requires, or by using a second unit in "key" substations. The final selection will be governed by the relative costs per kilowatt of providing extra capacity in each of these ways, and by local conditions which may affect the choice.

Other Factors

In deciding upon rating of substation equipment, the following factors which affect fixed costs should be considered in addition to total investment:

1. Annual depreciation charges. It will be noted that, with the larger substation capacities, investment in feeder copper is a greater part of the total than it is with smaller substation capacities. Overhead systems generally are depreciated at a lower rate than substation equipment. This, for example, would make 1,000-kw units relatively more attractive in comparison to 500-kw units than Figures 4–7 indicate.

2. Real estate taxes. Considering a specific example, the amount of land and building required for one 1,000-kw station usually is less than that required for two 500-kw stations. Depending upon local conditions, this factor also may make fewer substations attractive from the tax viewpoint.

3. Interest. This factor is assumed to depend only on the total investment.

Operating Expense

Operating expense of the substations and distribution system may be affected appreciably by the size of substation selected. Consideration of the various items which comprise operating expense will illustrate this point. For example, the cost of the power purchased and maintenance charges are two important components of operating expense in a fully automatic substation.

Maintenance expense can best be evaluated by operating companies which have wide experience in the operation of rectifier equipment. However, the general statement may be made that maintenance expense varies as a fractional power of substation size. Thus, a system with one 1,000-kw substation would be expected to show less substation maintenance expense than a system with two 500-kw substations. The same principle applies to maintenance of feeder copper: little variation would be expected in feeder maintenance cost over a wide variation in size of feeder.

Cost of power purchased may be affected by the number of points of power delivery. As an example, consider a route with 1-minute rush-hour headway. Reference to Figure 4 for a single route with no sectionalizing shows that 1,000-kw substations and 500-kw substations are about equally attractive from the standpoint of total investment.

However, the use of 1,000-kw stations in this case may reduce the cost of power purchased because of the benefits of buying power in large blocks. In typical situations, the use of 1,000-kw substations instead of 500-kw substations may save 5 per cent to 10 per cent in power cost. This factor has the effect of extending the economic application of a given rating of substation to longer headways than shown in Figures 4–7.

Conclusions

The first cost of providing equipment to convert power and deliver it to trolley coaches may be kept at a minimum by the method outlined in this paper. Selection of substation size can be made to result in minimum expenditure for substation equipment plus feeder copper.

The size of rectifier substation which will result in the lowest over-all cost of power delivered to trolley coaches is determined by a study of several variables. The effect of depreciation and taxes upon fixed charges must be evaluated. Also, the effect of the cost of power purchased and of maintenance charges upon operating cost must be determined.

By careful study of all factors involved, the transit operator will be able to minimize the over-all cost of providing power to electric vehicles.

Reference

1. Trolley Coach Distribution System, G. R. McDonald. *AIEE Transctions*, volume 67, part I, 1948, pages 393–402.

No Discussion

Equivalent Circuits and Their Application in Designing Shaded Pole Motors

S. S. L. CHANG
ASSOCIATE AIEE

THE shaded pole motor is well recognized as simple in construction, but complicated to analyze. Compared to other types of induction motors, it is complicated by two factors: the abundance of space harmonics, and the existence of the different groups of leakage reactances in the stator.

The first factor is well recognized. Pertaining to the first factor, the amount of harmonics is influenced somewhat by the shading coil pitch, and by the shape and extension of the magnetic bridge; the undesirable effects of the harmonics are reduced by rotor skew and other means. The second factor is generally known, but has not been definitely stated. The four different groups of stator leakage flux are those that links: the primary coil only; the shading coil only; one shading coil and one primary coil; and one shading coil and two primary coils.

The clarification of the four groups of stator leakage reactance is necessary for determining the phase shift of the shaded pole flux, as some groups increase the phase shift and others reduce it or do not affect it one way or the other.

In this paper, first, cross-field and revolving-field equivalent circuits are derived with all the above factors considered; second, the equations for the circuit constants are derived; and third, some desirable ranges of values for shading coil pitch, rotor skew, magnetic bridge, shading coil resistance, and so forth are deduced from the equivalent circuit.

The circuit can be solved by an a-c calculating board based on an equivalent circuit or by calculation. It is numerically more complicated than other types of single-phase motors. However, better understanding of the working relationships between the various factors of the shaded pole motor can be attained from studying the equivalent circuit without solving it.

Derivation of the Equivalent Circuits

Fundamental Concept

There are three possible sources of space harmonic flux in a shaded pole motor:

1. Stator harmonic magnetomotive force and fundamental air-gap permeance.
2. Fundamental magnetomotive force and harmonic air-gap permeance.
3. Harmonic magnetomotive force and harmonic air-gap permeance.

In this analysis, only the first source is treated because the harmonic magnetomotive force necessarily exists in a motor with concentrated windings. The other two sources of harmonic flux can be minimized by making the air gap approximately uniform, and are assumed to be minor effects in a properly designed shaded pole motor. A justification from experience for this assumption is that in most commercial motors, the gaps between adjacent poles are either nonexistent, very small, or are bridged over by a magnetic bridge. A large gap between adjacent poles gives rise to excessive magnetizing current and harmonic flux with bad accelerating characteristics and poor efficiency as a result.

To select a set of reference axes, the main axis is chosen as the center of the arc, along the air gap, which is under the influence of the unshaded portion of the primary; and the auxiliary axis is chosen as the center of the arc which is under the influence of the shaded portion of the primary. As a corollary of the previous assumption, the effective arc of the shaded pole and the effective arc of the unshaded pole add up to the complete pole pitch of 180 electrical degrees approximately, and the main and auxiliary axes are 90 electrical degrees apart.

The stator is assumed to have three sets of windings, two of which represent an imaginary division of an actual winding; the short circuited shading coil, a coil of N turns at the same position as the shading coil, connected in series with a coil of N turns around the unshaded pole. Since the inner coil sides of the two coils of N turns overlap and carry equal and opposite currents, the two coils are equivalent to the actual case of one single coil around the entire pole.

Along the auxiliary axis, the primary coil and the shading coil have coil sides in the same position. Their combined effect on the rotor circuit is equivalent to that of the primary coil alone carrying a current of $I_s = I_1 - I_h$, where I_1, I_h are the primary current, and the shading coil current in primary terms respectively.

From the above discussion, the actual shaded pole motor of Figure 1(A) is transformed to the equivalent shaded pole motor of Figure 1(B).

Derivation of Rotor Equivalent Circuit

By Fourier analysis, each of the two coils of Figure 1(B) can be resolved into a series of sinusoidally distributed windings of p, $3p$, $5p$.....poles. The effective numbers of conductors are, $n = 1,3,5\ldots$

$$C_n = C \sin (n\vartheta_m/2) \text{ for the main winding} \quad (1)$$

$$C_n' = (-1)^{(n-1)/2} C \sin (n\vartheta_s/2) \text{ for the auxiliary winding} \quad (2)$$

The magnitude of the n-th harmonic magnetomotive force, due to a current passing through a stator winding of Figure 1(B), is the same as that due to the same current passing through a sinu-

Paper 51-116, recommended by the AIEE Rotating Machinery Committee and approved by the AIEE Technical Program Committee for presentation at the AIEE Winter General Meeting, New York, N. Y., January 22–26, 1951. Manuscript submitted September 28, 1950; made available for printing December 13, 1950.

S. S. L. Chang is with Robbins and Myers, Incorporated, Springfield, Ohio.

Nomenclature

C = number of actual conductors
C_n = effective number of conductors of the main phase n-th harmonic. (Defined in (1))
C_n' = effective number of conductors of the auxiliary phase n-th harmonic. (Defined in (2))
D_r = rotor ring diameter at which conductors enter the ring
E_s = electromotive force induced in the primary winding by the total auxiliary phase flux
E_m = electromotive force induced in the primary winding by the total main phase flux
E_{sn} = electromotive force induced in the primary winding by the auxiliary phase, n-th harmonic mutual flux
E_{mn} = electromotive force induced in the primary winding by the main phase, n-th harmonic mutual flux
E_{n+}, E_{n-} = positive and negative sequence electromotive forces respectively of the n-th harmonic in main phase terms
f = line frequency
I_1 = line current
I_h = shading coil current in primary terms
$I_s = I_1 - I_h$
I_{n+}, I_{n-} = positive and negative sequences of the n-th harmonic primary current
I_{n+}'', I_{n-}'' = positive and negative sequences of the n-th harmonic rotor current
I_{xn}, I_{yn} = auxiliary and main phase (with 90-degree phase shift) n-th harmonic rotor current
K_s'' = rotor slot constant
K_{s1} = primary winding slot constant
K_{s2} = slot constant of the shading coil inside slot
l_g = effective length of air gap (in inches) accounting for slot openings and saturation of iron
l_a = length per turn of shading coil (in inches)
N = number of turns per pole of primary winding
n = order of harmonics, $n = 1, 3, 5, \ldots$
p = number of poles of the shaded pole motor
R = primary resistance
R_a = shading coil resistance
R_n = n-th harmonic rotor resistance
S_a = total section of shading coil conductors per coil, in square inches
S_c = section of rotor conductor in square inches
S_r = section of rotor end ring, in square inches
S_s = number of rotor conductors
S = ratio of actual speed to synchronous speed of the fundamental flux
SK = rotor skew in inches
T_f'' = rotor tooth face in inches
V = line voltage
W = length of stack in inches
ϕ_1' = stator leakage flux which links the primary coil only
ϕ_2' = stator leakage flux which links the shading coil only
ϕ_3' = stator leakage flux which links one shading coil and one primary coil
ϕ_4' = stator leakage flux which links one shading coil and two primary coils
X_1', X_2', X_3', X_4' = leakage reactances due to ϕ_1', ϕ_2', ϕ_3', ϕ_4', respectively
X_n'' = rotor leakage reactance in main terms for n-th harmonic current
X_{mn} = mutual reactance in main terms for n-th harmonic current
λ_p = pole pitch in inches
θ_m = angle of the unshaded portion of the pole arc in electrical radians
θ_s = angle of the shaded pole arc in electrical radians
θ_{sk} = angle of rotor skew in electrical radians
ϕ_b = magnetic bridge flux, total lines per pole
$\text{mmf} = \frac{C}{2p}(2I_1 - I_h)$
Span_1, span_2: coil spans in inches, of primary and shading coils respectively.

---

soidally distributed winding of np poles with C_n or C_n' effective conductors. Conversely, if a current passes through all the windings of p, $3p$, $5p$ poles with C_1, C_3, C_5 effective conductors in series, a magnetomotive force of rectangular wave form is obtained. These hypothetical windings, when connected in series, are equivalent to the concentrated windings of Figure 1(B).

The stator flux of np poles induces in the rotor cage a current distribution of the same number of poles. Since the interaction between current and flux of different numbers of poles vanishes by averaging over a full cycle of the fundamental flux, only the interactions between the stator and rotor flux and currents of the same number of poles need to be considered. The motor of Figure 1(B) is equivalent to a series of motors with common shaft and with their main and auxiliary windings connected in series as shown in Figure 1(C). The main difference between Figure 1(B) and Figure 1(C) is that in Figure 1(B) the two windings are concentrated windings, while in Figure 1(C) the windings of all the motors are sinusoidal and the results of machinery analysis can be readily applied to the individual motors.

In Figure 1(C), the effective number of turns per pole are indicated for each winding. The minus signs on the 3rd, 7th harmonics, and so forth, in equation 2 indicate a change in polarity of adjacent main and auxiliary poles if the polarity of the two axes for the fundamental flux are fixed. However, the signs of sin $n\theta_n/2$ and sin $n\theta_s/2$ may also be different. The sense of rotation of a certain harmonic flux depends on the final signs of the two effective numbers of conductors C_n and C_n'. If the signs are identical, the larger rotating component of the harmonic flux has the same sense of rotation as that of the main flux.

The next step is to replace each hypothetical harmonic motor of Figure 1(C) with an equivalent rotor circuit for that harmonic. In Appendix A of reference 4, a cross-field theory equivalent circuit is derived for the capacitor and other single-phase motors. As the differences between the capacitor motor and the hypothetical harmonic motor exist only in the stator circuit and not in the rotor circuit, the same steps leading to the rotor equivalent circuit Figure 1(A) and torque equation 1 of reference 4 lead to an equivalent circuit for the n-th harmonic and an equation for the torque due to the n-th harmonic. By replacing each hypothetical motor in Figure 1(C) with an equivalent circuit so derived, we obtain the equivalent rotor circuit of Figure 2. The torque equation 4 is derived by summing up the torques due to the fundamental and harmonic hypothetical motors.

Since the winding ratios C_n'/C_n are different for different harmonics, an ideal transformer of the ratio C_n'/C_n is provided in the auxiliary circuit so that the auxiliary phase circuits can be connected in series. The ratio S is defined as the ratio of the actual speed to the synchronous speed of the fundamental flux. Since the synchronous speed of the n-th harmonic is only one n-th that of the fundamental, that ratio is nS instead of S in the harmonic equivalent circuits. The torque equation 1 of reference 4 is expressed in terms of synchronous watts. The harmonic torque calculated from that equation is in units of synchronous watts of that harmonic. To convert it uniformly to synchronous watts in fundamental terms, each component in equation 4 is multiplied by its respective order of harmonic n.

The transformer ratio C_n'/C_n can be positive or negative, zero or infinity. The physical meanings of the last two cases are evident from the definition of this ratio:

1. $(C_n'/C_n) = 0$, the n-th harmonic flux does not exist in the auxiliary phase in which case, the n-th harmonic equivalent circuit can be disconnected from the auxiliary phase circuit.

2. $(C_n'/C_n) = \infty$, the n-th harmonic flux does not exist in the main phase. The n-th harmonic equivalent circuit should be rewritten in auxiliary phase terms instead of in main phase terms, and disconnected from the main phase circuit. The ideal transformer can be removed.

Stator Circuit Elements

The stator circuit elements are necessary for determining the currents I_1 and I_h from the line voltage. They include the primary resistance, the shading coil resistance, and the four groups of leakage reactances.

The effect of the shading coil is represented as a shunt across the auxiliary phase. X_1', the leakage reactance due to flux linking the primary coil only, includes the following components:

1. The stator slot leakage
2. The end leakage.
3. The skew leakage and the total reactance of the higher orders of harmonics of the unshaded pole which are not expressed in the equivalent circuit.

X_1' can be represented as a series reactance in either the main phase or the line side of the auxiliary phase. Since the two phases are in series except for a phase shift of 90 degrees, the presence of a reactance in either phase is the same as in the other.

X_2' the leakage reactance due to flux linking the shading coil only, includes the shading coil slot leakage reactance of the lone conductor, and the coil end leakage. It is represented as a reactance in series with the shading coil resistance.

X_3' the leakage reactance due to flux linking one shading coil and one primary coil, includes the skew, and high order harmonic leakage of the shaded pole. It is represented as a reactance in series with the motor side of the auxiliary phase.

X_4' the leakage reactance due to flux linking one shading coil and two primary coils, includes the flux by-passed by the magnetic bridge and the flux between adjacent pole tips. Since the winding ratio between the primary and the shading coil is normally N:1 instead of $2N$:1, this group of leakage reactance is represented as a reactance in series with X_1' perfectly coupled with an equal reactance in series with X_3'.

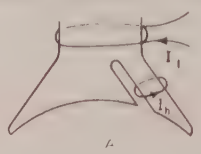

A

The four groups of leakage reactances are illustrated in Figure 3. By adding stator circuit elements to the equivalent circuit of Figure 2, the complete equivalent circuit of Figure 4 is obtained. The positions of the four groups of leakage reactance on the equivalent circuit of Figure 4 can be verified by checking the electromotive force equations derived from flux considerations against the mesh equations of the equivalent circuit. The same equations are obtained both ways.

The two phase currents on the equivalent circuit are equal but 90 degrees apart. They are necessarily equal as the same primary winding energizes both the main and the auxiliary phases. Corresponding to the 90-degree phase shift on the equivalent circuit, the actual currents in the motor coincide with each other. This relation between the cross-field equivalent circuit and the actual motor is derived and explained in reference 4.

The line voltage $\boldsymbol{V}$ is equal to the sum of $\boldsymbol{E}_s$ and $\boldsymbol{E}_m$ vectorially.

$$\boldsymbol{V}=\boldsymbol{E}_s+\boldsymbol{E}_m \tag{3}$$

The torque in synchronous watts is

$$T=\sum_{n=1,3,5}\left\{\frac{n^2SR_n}{1-n^2S^2}|I_{zn}+I_{yn}|^2+\frac{2nR_n}{1+nS}I_{zn}I_{yn}\cos\left(I_{zn},I_{yn}\right)\right\} \tag{4}$$

The mutual reactance jX_4' can be replaced by the T-circuit as shown in Figure 5. The two circuits are interchangeable for alternating current of the line frequency. This substitution is made in Figure 6. By substituting the T-circuit for the mutual reactance, the effect of the magnetic bridge flux can be made more apparent.

The Revolving Field Theory Equivalent Circuit

Figures 4 and 6 are the cross-field theory equivalent circuits. The revolving field theory equivalent circuit can be derived in a similar manner. For the n-th harmonic, the revolving field voltages and currents and the cross-field voltages and currents are related to each other according to the following equations:

$$2\boldsymbol{I}_{n+}=\left[(\boldsymbol{I}_1-\boldsymbol{I}_h)\frac{C_n'}{C_n}-j\boldsymbol{I}_1\right] \tag{5}$$

$$2\boldsymbol{I}_{n-}=\left[(\boldsymbol{I}_1-\boldsymbol{I}_h)\frac{C_n'}{C_n}+j\boldsymbol{I}_1\right] \tag{6}$$

$$2\boldsymbol{E}_{n+}=\left[\boldsymbol{E}_{zn}\frac{C_n}{C_n'}-j\boldsymbol{E}_{mn}\right] \tag{7}$$

$$2\boldsymbol{E}_{n-}=\left[\boldsymbol{E}_{zn}\frac{C_n}{C_n'}+j\boldsymbol{E}_{mn}\right] \tag{8}$$

Solving $\boldsymbol{E}_{zn}$ and $\boldsymbol{E}_{mn}$ in terms of $\boldsymbol{E}_{n+}$ and and $\boldsymbol{E}_{n-}$ from equations 7 and 8, we have

$$\boldsymbol{E}_{zn}=\frac{C_n'}{C_n}(\boldsymbol{E}_{n+}+\boldsymbol{E}_{n-}) \tag{9}$$

$$-j\boldsymbol{E}_{mn}=\boldsymbol{E}_{n+}-\boldsymbol{E}_{n-} \tag{10}$$

From equations 5, 6, 9, 10 and the individual revolving field theory harmonic equivalent circuits, the equivalent circuit of Figure 7 is obtained. Since the transformer ratio C_n'/C_n is different for different harmonics, the currents $\boldsymbol{I}_{n+}$ and $\boldsymbol{I}_{n-}$ are, in general, different for different harmonics. This is one of the essential differences between the equivalent circuits of this paper and that of reference 1.

The torque in synchronous watts is

$$T=\sum_{n=1,3,5\ldots.}2\left\{|I_{n+}''|^2\frac{nR_n}{1-nS}-|I_{n-}''|^2\frac{nR_n}{1+nS}\right\} \tag{11}$$

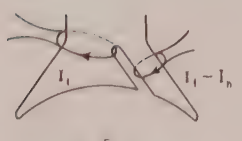

B

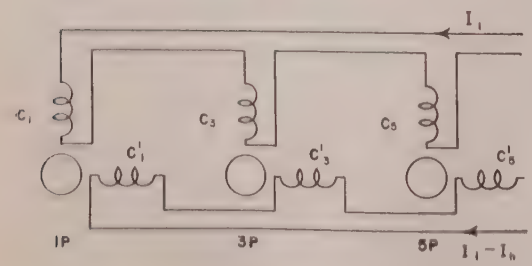

C

Figure 1 (left). Actual and equivalent shaded pole motor

Figure 2 (right). Rotor equivalent circuit

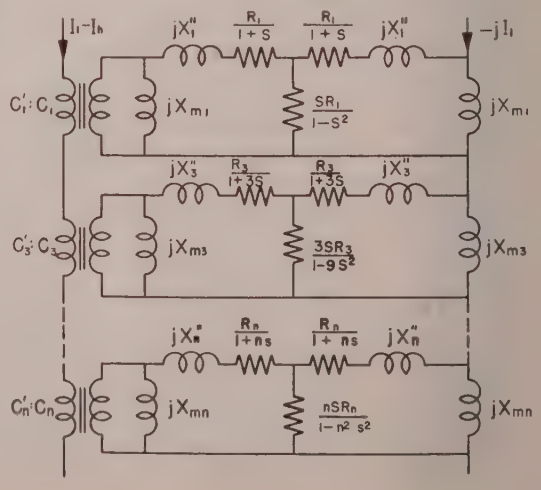

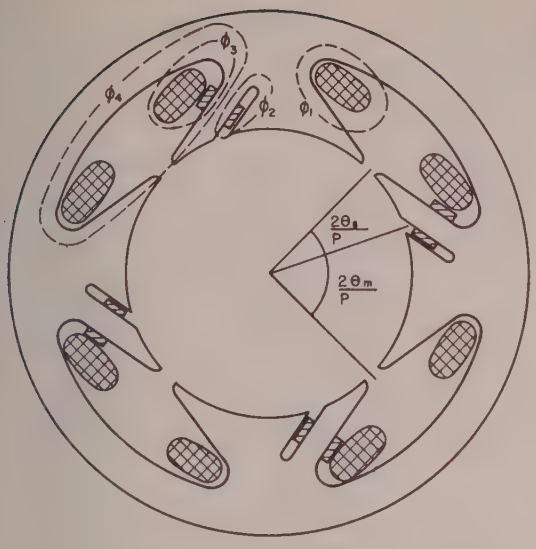

Figure 3 (left). Four groups of stator leakage flux

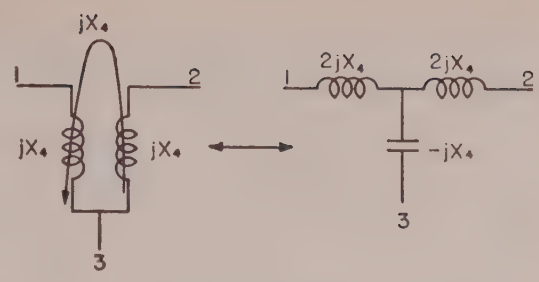

Figure 5 (right). Equivalent circuits for the magnetic bridge

The equivalence between equations 11 and 4 can be readily established by using the following equations:

$$I_{n+}{}'' = \frac{1}{2}(I_{zn} + I_{yn}) \tag{12}$$

$$I_{n-}{}'' = \frac{1}{2}(I_{zn} - I_{yn}) \tag{13}$$

Solution of the Equivalent Circuits by A-C Calculating Board

Theoretically, the equivalent circuit can be solved by solving the mesh equations. It can be done with less effort by calculating the open circuit and transfer impedances of the main and auxiliary circuits. However, considerable amount of time can be saved by actually laying out the circuit on an a-c calculating board.

Both the main and auxiliary phase currents can be supplied by a 2-phase alternator with very high synchronous impedance as compared to the impedances of the equivalent circuit. As the alternator operates at virtually short-circuited condition, the two phase currents are always equal and in quadrature. The sum of $\boldsymbol{E}_s$ and $\boldsymbol{E}_m$ can be measured directly by a phase sequence voltmeter as shown in Figure 8. Its value can be adjusted to equal the line voltage by adjusting the field current of the alternator. It is evident that the open circuit voltage of the alternator would be many times higher than the line voltage with this arrangement, and care must be taken to keep the circuits closed always.

The phase sequence voltmeter in Figure 8 can be made from an ordinary voltmeter by adding a capacitor of the same reactance as the resistance inside the meter. This would not introduce appreciable error if the impedance of the meter coil is sufficiently low.

The transformers in Figures 4, 6, and 7 are ideal transformers which have infinite magnetizing reactance and zero leakage reactance. The magnetizing reactance and leakage reactance of an actual transformer can be absorbed in the series and parallel reactances X_3', X_n'', and X_{mn}.

The iron-loss in a shaded pole motor is partly due to the fundamental flux and partly due to the harmonic flux. Its effect can be accounted for in the equivalent circuit by adding series or shunt resistors to the leakage and mutual reactances.

However, the main difficulty in constructing a calculating board for the shaded pole motors is the presence of negative resistances in both the cross-field and revolving field equivalent circuits. These negative resistances can be replaced by small generators, the adjustments of which are likely to be difficult.

The fundamental and the third harmonic are the only important circuits to be present in the calculating board. The other harmonics have little or no effect to the primary and shading coil currents and can be calculated as corrections to the torque and watts after the primary and shading coil currents have been determined.

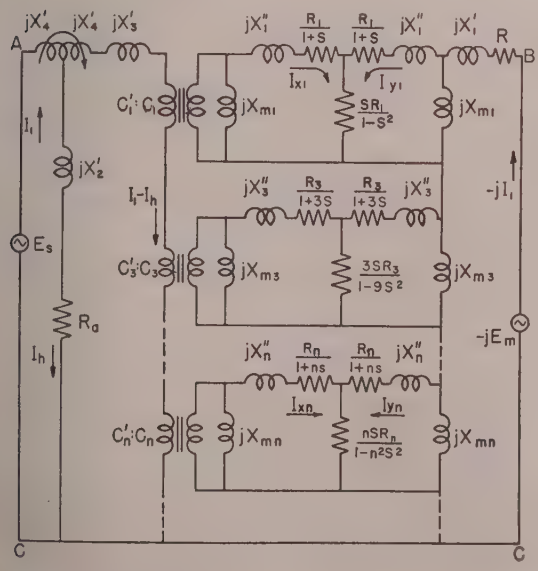

Figure 4 (left). Equivalent circuit of the shaded pole motor–cross-field theory

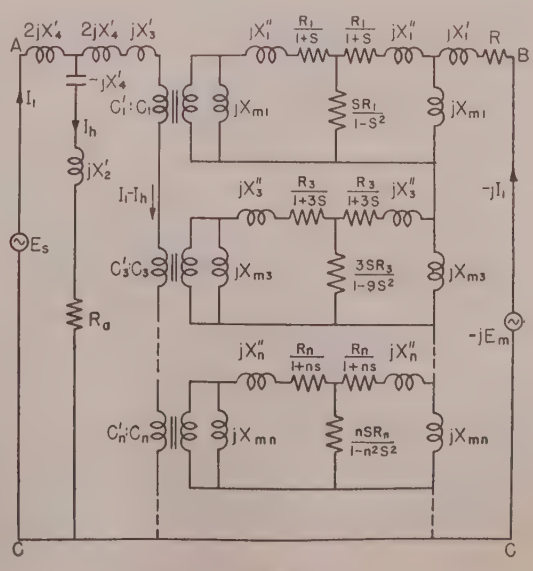

Figure 6 (right). An alternative form of the equivalent circuit

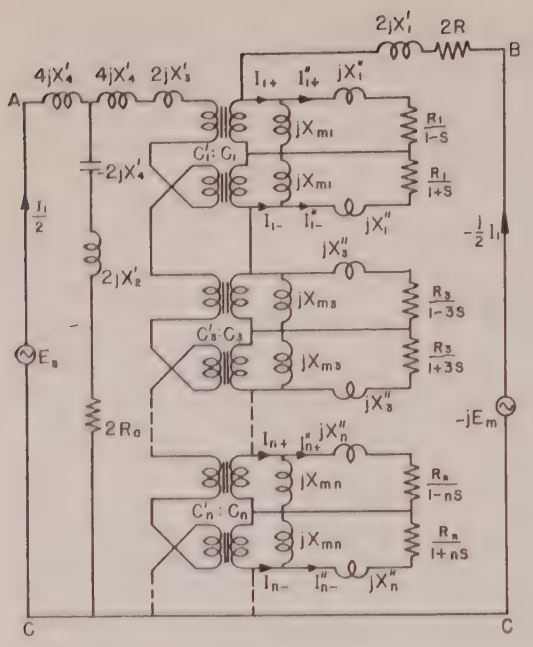

Figure 7 (left). Equivalent circuit of the shaded pole motor–revolving field theory

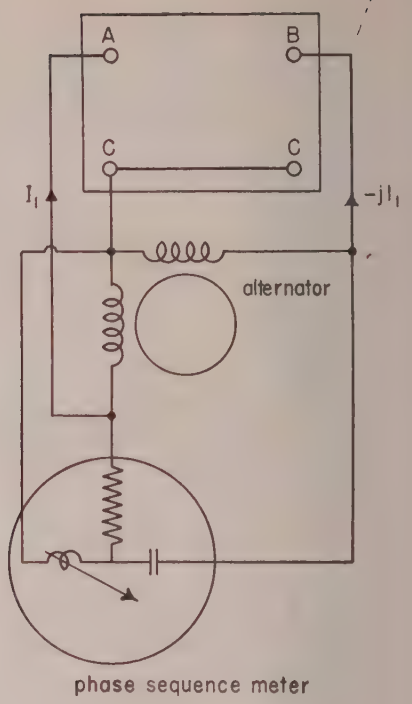

Figure 8 (right). An a-c board for the equivalent circuits

Calculation of Circuit Constants

The equations for circuit constants are based on Trickey's papers,[2,3] with necessary modifications for the harmonic circuits

Resistances

R, primary winding resistance: This is preferably measured or calculated from the wire table.

R_a, shading coil resistance:

$$R_a = 0.693 \frac{l_a}{S_a} \frac{C^2}{4p} \times 10^{-7} \qquad (14)$$

for copper shading coil at 25 degrees centigrade.

Equation 14 is mathematically equivalent to Trickey's equation of shading coil resistance. There is a difference in the definition of S_a. For motors with one shading coil per pole, the two definitions are the same. For motors with more than one shading coil per pole S_a is defined as the total section in this paper. Thus

$$[S_a] = S_a/N_a$$

The sign [ ] is used to denote the S_a in accordance with Trickey's definition. Also by definition

$$C_a = 2pN_a, \quad l_{mca} = \frac{1}{2} l_a$$

Substituting the above expressions in Trickey's equation, we have

$$r_a = 1.385 \frac{\frac{1}{2} l_a}{\frac{S_a}{N_a}} N^2 p \left(\frac{C}{2pN_a}\right)^2 \times 10^{-6}$$

$$r_a = 0.6925 \frac{l_a}{S_a} \frac{C^2}{4p} \times 10^{-6}$$

R_n, the n-th harmonic rotor resistance:

$$R_n = \left(\frac{\sqrt{W^2 + SK^2}}{S_c S_s} + \frac{0.637 D_r}{S_r p^2 n^2}\right) \times 1.385 C_n^2 \times 10^{-6} \qquad (15)$$

$n = 1, 3, 5 \ldots$, for copper bars and rings at 25 degrees centigrade. From equation 15, it is evident that while the resistance of the conductors affect the fundamental and harmonic currents equally, the resistance of the end ring is mainly in the fundamental circuit.

Mutual Reactances

X_{mn}, mutual reactance of the n-th harmonic:

$$X_{mn} = 2\pi f C_n^2 10^{-8} \left(\frac{0.647 W \lambda_p}{l_g p n^2}\right) \frac{\sin n\theta_{sk}/2}{n\theta_{sk}/2} \qquad (16)$$

for the n-th harmonic equivalent circuit, where $n = 1, 3, 5 \ldots$

In equation 16, the average effective value of the air gap l_g is used. Sometimes, it is found desirable to have a larger air gap along the unshaded portion of the pole arc. This is in effect a reactance shunted across the main phase to shift the main phase flux further in the lead. Its effect can be accounted for in the equivalent circuit by calculating the mutual reactance separately for the main and auxiliary phases, using two different values of l_g, but for the fundamental flux equivalent circuit only. For the harmonic flux, the main and auxiliary poles are well distributed along the pole face. Since some among each group are in the long air gap range and others in the short air gap range, the same weighted average value of the air gap is used for both the main and auxiliary in the harmonic flux equivalent circuits.

Stator Leakage Reactances

There are four types of leakage reactances:

1. Slot leakage
2. End leakage
3. Harmonic leakage
4. Skew leakage

The lower order harmonic flux of the stator windings are accounted for in the equivalent circuits while the higher harmonics appear as leakage reactances. This and the skew leakage can be calculated as the difference between the total air gap reactance and the sum of the mutual reactances of various harmonics.

The four groups of the stator leakage reactances can be calculated according to the equations below:

$$x_1' = 2\pi f c^2 10^{-8} \left(\frac{3.19 W}{2p} K_{s1} + \frac{\text{span}_1}{2p} + \frac{3.19 W \lambda_p}{4 l_g p} \frac{\theta_m}{\pi}\right) - (x_{m1} + x_{m3} + \ldots.) \qquad (17)$$

$$x_2' = 2\pi f c^2 10^{-8} \left(\frac{3.19 W}{4p} K_{s2} + \frac{\text{span}_2}{2p}\right) \qquad (18)$$

$$X_3' = 2\pi f C^2 10^{-8} \left(\frac{3.19 W \lambda_p}{4 p l_g} \frac{\theta_s}{\pi}\right) - \left[X_{m1} \left(\frac{C_1'}{C_1}\right)^2 + X_{m3} \left(\frac{C_3'}{C_3}\right)^2 + \ldots.\right] \qquad (19)$$

$$X_4' = 2\pi f c^2 10^{-8}\left(\frac{3.19W}{4p}\frac{\delta_1}{e_1}\right) + \frac{\phi_b f C^2}{45\times 10^6 2p(\text{mmf})} \quad (20)$$

Rotor Leakage Reactances

The rotor leakage reactances are different for rotor currents of different numbers of poles. The rotor leakage reactance for each stator harmonic has to be individually calculated. The n-th harmonic flux of the stator induces in the rotor a current distribution of np poles. Because of the finite number of rotor bars, the rotor current of np poles, produces rotor flux of $2S_s \pm np$ poles, $4S_s \pm np$ poles...in addition to rotor flux of np poles. If the stator current induced by the extra rotor flux is neglected, the effect of the extra rotor flux can be considered as part of the rotor leakage reactance to the rotor current of np poles.[5] The value of this leakage reactance is of the order:

$$2\pi f c_n^2 10^{-8}\left(\frac{0.647W\lambda_p}{l_g p n^2}\right)\left(\frac{np}{2S_s \pm np}\right)^2$$

For higher orders of space harmonics, for which $2S_s - np < np$, this leakage reactance is considerably higher than the mutual reactance X_{mn} and limits the rotor current in the harmonic equivalent circuit to a very low value. Consequently the effect of the stator harmonic flux of the order S_s/p or higher can be neglected.

For the fundamental current and lower harmonic current, the rotor harmonic leakage reactance can be approximately calculated from the "overlap" point of view with zigzag reactance formula.

$$X_n'' = X_{n_{slot}}'' + X_{n_{end}}'' + X_{n_{skew}}'' + X_{n_{zigzag}}'' \quad (21)$$

$$X_{n_{slot}}'' = 2\pi f C_n^2 \times 10^{-8}\frac{6.38W}{S_s} K_s \quad (22)$$

$$X_{n_{end}}'' = 2\pi f C_n^2 \times 10^{-8}\frac{\lambda_p}{2pn^2} \quad (23)$$

$$X_{n_{skew}}'' = 2\pi f C_n^2 \times 10^{-8}\left(\frac{0.647W\lambda_p}{l_g p n^2}\right)\times\left(1-\frac{\sin n\theta_{sk}/2}{n\theta_{sk}/2}\right) \quad (24)$$

$$X_{n_{zigzag}}'' = 2\pi f C_n^2 10^{-8}\frac{6.38W}{S_s}\frac{T_f''}{4l_g} \quad (25)$$

$n = 1, 3, 5....$

Useful Deductions from the Equivalent Circuits

Though the solution of the equivalent circuit is numerically complicated, some useful results can be obtained from the circuit without solving it. Besides problems common to other types of motors, the main concern in designing a shaded pole motor is:

1. To obtain sufficient phase shift of the shaded pole flux without having excessive shading coil copper loss.

2. To reduce the harmonic flux or to render it ineffective.

Phase Shift

The common effects of the four groups of stator leakage reactances are increased saturation of the stator lamination and reduced output due to the reactive voltage drop. Besides the undesirable effects, X_2' reduces the lagging angle of the shaded pole flux, X_3' increases the angle slightly, X_4' is most effective to increase the angle, while X_1' does not affect the angle in one way or the other. These effects can be seen from the equivalent circuit of Figure 6.

The following measures are helpful to increase the angle of phase shift:

Shading Coil Position. The inside conductor of the shading coil should be close to the air gap to reduce X_2'. The outside conductor of the shading coil should be close to the slot bottom to increase X_4' and to reduce X_1'.

Shading Coil Pitch. Between the harmonic leakage reactances, X_3' is less objectionable than X_1', as X_3' helps to increase

Table I. Performance Calculation

①	②	③	④	⑤	⑥	⑦	⑧	⑨	⑩	⑪	⑫	⑬	⑭
S	Z_{1+}	Z_{1-}	Z_{2+}	Z_{2-}	$Z_m+R+j(X_1'+2X_4')$	$Z_s+j(X_3'+2X_4')$	Z_t	Z_a	I_s/I_1	V/I_1	I_1	I_s	I_h
	(39)	(40)	(39)	(40)	(42)	(41)	(43)	(38)	(44)	(45)	115/⑪	⑩×⑫	I_1-I_s
	3.42 ..	3.42 ..	0.71 ...	0.71....	5.47	1.72	....	14.7	0.714	10.87	5.1	3.64 ...	2.82
0	...+j4.43..	+j4.43..	+j2.75...	+j2.75...	+j13.35.....	+j11.36....	0	....+j1.30....	/−32.6°...	+j19.52..	/−60.8°...	/−93.4°...	/−16.8°
	5.61 ..	2.45 ..	−0.92 ...	0.36 ...	6.08	0.91	0.16	14.7	0.715	11.60	4.90 ...	3.50...	2.68
0.4	...+j4.89..	+j4.30..	+j4.18...	+j2.57...	+j13.52.....	+j12.04....	−j0.86....	+j1.30....	/−32.1°....	+j20.3...	/−60.2°...	/−92.3°...	/−16.2°
	15.0 ..	1.90 ..	−0.55 ...	0.24 ...	10.50	2.35	1.56	14.7 ...	0.648 ...	15.62	4.27 ...	2.77 ...	1.84
0.8	...+j10.0..	+j4.25..	+j2.65...	+j2.50...	+j16.05.....	+j11.98....	−j3.56....	+j1.30...	/−17.6°....	+j21.96..	/−55.5°...	/−73.1°...	/−28.4°
	21.4 ..	1.80 ..	−0.46 ...	0.22 ...	13.65	3.31	4.48	14.7 ...	0.522 ...	18.66 ...	3.59 ...	1.87	1.74
0.9	...+j20.7..	+j4.24..	+j2.62...	+j2.50...	+j21.39.....	+j13.55....	−j5.33....	+j1.30...	/−6.5°	+j25.93..	/−54.3°...	/−60.8°...	/−47.2°
	20.2 ..	1.75 ..	−0.43 ...	0.21 ...	13.05	3.33	8.47	14.7....	0.36	19.37 ...	3.14 ...	1.13 ...	2.01
0.95	...+j35.4..	+j4.23..	+j2.60...	+j2.50...	+j28.72.....	+j15.71....	−j5.02....	+j1.30...	/1.7°	+j31.1...	/−58.1°...	/−56.4°	../−59.1

Table I. Performance Calculation (Continued)

⑮	⑯	⑰	⑱	⑲	⑳	㉑	㉒	㉓	㉔	㉕	㉖	㉗	㉘
I_{1+}	$\lvert I_{1-}\rvert$	$\lvert I_{1s}\rvert$	Fund.	3rd. H.	Torque (Oz. Ft.) Friction and Windage	Net	Watts Output	Theo-retical	Watts Input Iron Loss	Total	Efficiency, %	Power Factor, %	Rpm
(5) ...	(6) ...	⑬/2	(46)	(46)	−0.3	⑱+⑲	Real	㉓+㉔	㉒	㉕			1,800S
					−0.5S^2	+ ⑳	Part of VI_1					V_1I_1	
			2.32....	0	−0.3	2.02							0
3.06	2.11	1.75	5.20	−1.48	−0.38	3.34							720
2.47	2.04	1.39	10.4	−0.57	−0.62	9.2	118	286	35	321	36.8	65.5	1,440
1.92	1.81	0.94	9.1	−0.23	−0.7	8.17	117	240	35	275	42.5	66.6	1,620
1.59	1.61	0.57	5.84	−0.08	−0.75	5.01	76	192	35	227	33.5	62.8	1,710

Note: Z_{1+}, Z_{2-}, I_{1+}, I_{1-} are calculated in auxiliary phase terms. Equations 41, 42, and 43 are correspondingly modified.

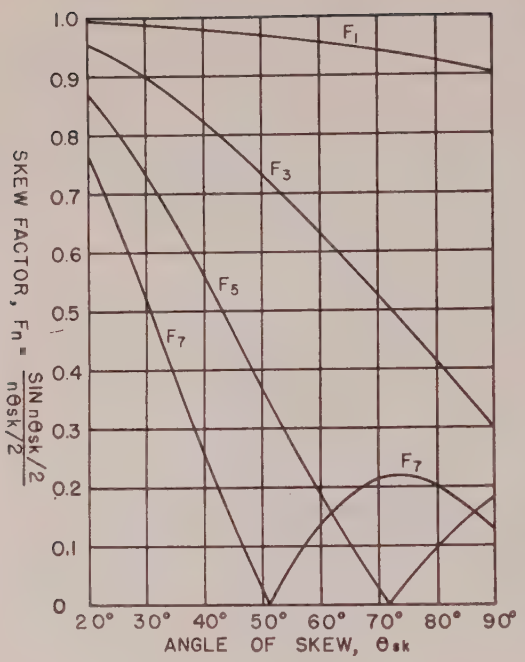

Figure 9 (left). The skew factor

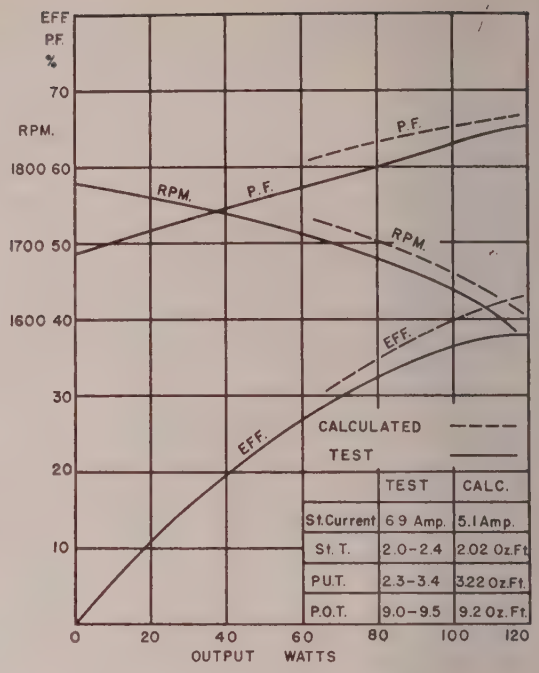

Figure 10 (right). The calculated and test performance of a 1/10-horsepower 4-pole shaded pole motor

the phase shift. The harmonic leakage flux of the unshaded pole should be kept at a minimum. The ratio of the harmonic leakage reactance, including lower order harmonics, to the reactance due to the fundamental flux is

$$\frac{X_{\text{harmonic}}}{X_{\text{fundamental}}} = \frac{1.232\,\frac{\theta_m}{\pi}}{\sin^2\frac{\theta_m}{2}} - 1$$

For this ratio to be a minimum, its derivative is equated to zero. The result is

$$\theta_m = 2.33 \text{ radians} = 133.5° \quad (26)$$

$$\theta_s = 180° - 133.5° = 46.5° \quad (27)$$

Since the ratio of X_h/X_f is fairly constant near the minimum value, a smaller value of θ_m and a larger value of θ_s can be used than that given in equations 26 and 27. But no possible advantage can be gained by making the shading coil pitch θ_s less than 46.5 degrees.

Shading Coil Resistance, and Magnetic Bridge Reactance. The auxiliary phase current can be readily calculated for the locked rotor condition. It is:

$$\frac{I_1 - I_h}{I_1} = \frac{-j(X_4' - X_2') + R_a}{j(x_2' + x_3' + x_4') + R_a + Z_s} \quad (28)$$

where Z_s is the auxiliary phase impedance at standstill.

$$Z_s = \sum_{n=1,3,5,\ldots} \left(\frac{C_n'}{C_n}\right)^2 \frac{jX_{mn}(jX_n'' + R_n)}{j(X_{mn} + X_n'') + R_n} \quad (29)$$

Equation 28 indicates that for satisfactory starting condition:

$$X_4' > X_2' \quad (30)$$

$$R_a \cong |j(x_2' + x_3' + x_4') + Z_s| \quad (31)$$

Reduction of Harmonic Flux

The harmonic flux causes low pull-in torque and excessive rotor copper loss. The rotor copper loss due to harmonic currents is the more undesirable as it acts as a brake or a mechanical friction. Since the frequencies of the rotor harmonic currents are very high, this loss is manifested by the skin effect which increases the rotor resistance and reduces its slot leakage reactance.

To nullify the harmonic flux, there are four factors at a designer's disposal:

Shading Coil Pitch

Equations 1 and 2 show the effect of coil pitch on the amount of harmonic flux. Since $\theta_m + \theta_s = \pi$, equation 2 can be written as

$$C_n' = C \cos(n\theta_m/2) \quad (32)$$

From equations 1 and 32, we have

$$C_n^2 + C_n'^2 = C^2 \quad (33)$$

Equation 33 shows that, though the harmonic flux of a certain order can be reduced in any one of the two phases, by changing the coil pitch, this necessarily increases the harmonic flux of the same order in the other phase. No complete elimination of a certain harmonic is possible.

Since the main phase current I_1 is considerably larger than the auxiliary phase current $I_1 - I_h$, the total amount of a certain harmonic flux can be reduced by eliminating it from the main phase. Among the various harmonics, the third harmonic is most difficult to nullify by other means. It can be eliminated from the main phase by making $\theta_m = 120°$. However, this angle is not critical.

From equations 1 and 2, C_3 and C_3' are both negative if $\theta_m > 120°$, one positive and one negative if $\theta_m < 120°$. When C_3 and C_3' are of the same sign, the third harmonic flux increases the starting torque.

The proper range of the shading coil pitch is, therefore:

$$46.5° < \theta_s < 60° \quad (34)$$

Rotor Skew

One effect of the rotor skew is to reduce the amount of rotor current induced by the stator harmonic flux. This reduction is shown on the equivalent circuit through a decrease in the mutual reactances X_{mn} and an increase in the leakage reactances X_n'' as given in equations 16 and 24.

In Figure 9, the skew factor is plotted as a function of the angle of skew. The third harmonic current in the rotor can be completely eliminated by a skew angle of 120 electrical degrees. This large skew angle is not only difficult to make, but also is undesirable as it causes excessive leakage reactance in the fundamental circuit. A good compromise for preserving the fundamental flux and reducing the various harmonic flux is a skew angle of 60 electrical degrees. At 60 degrees, the fundamental flux is reduced by 4.5 per cent, but the third, fifth, and seventh harmonics are reduced by 36 per cent, 81 per cent, and 86.5 per cent respectively.

Number of Rotor Conductors

As pointed out in a foregoing paragraph, when the rotor conductors are too few to follow the wave form of a high order harmonic flux, very little rotor current is induced by that flux. Its effect is the same as an additional leakage reactance in the rotor circuit for that harmonic. This leakage reactance, together with the skew leakage reactance, is sufficient to limit the rotor current to a negligible value for harmonics of the order S_s/p or higher. The optimum number of rotor conductors is about 11 to 13 per pair of pole, and the effect of the harmonic flux above the fifth or the seventh can be neglected. Too few conductors result in high zigzag leakage reactance which reduces the motor output.

Rotor Conductor and End Ring Resistance

It is apparent from the equivalent circuits that the rotor resistance is not a factor in limiting the harmonic currents. To reduce the rotor copper loss due to harmonic currents, the rotor resistance for harmonic currents is preferably as low as possible. But proper amount of rotor resistance is necessary for the fundamental current to give adequate starting torque. This can be done by making the rotor bar resistance as low as possible and increasing the rotor ring resistance to make up the required rotor resistance for the fundamental current. The end ring resistance is negligible for harmonic currents.

An Example of Performance Calculation

The performance of a 4-pole 60-cycle 115-volt shaded pole motor is calculated and the results are compared with test values. The motor constants, except the primary winding resistance R, are calculated from the dimensions and winding data. They are:

$\theta_s=57°$	$S_r=0.076$
	$S_s=34$
$\theta_m=123°$	$D_r=2.15$
$C=760$	$K_s=1.0$
$p=4$	$K_{s1}=0.60$
$W=2.5$	$K_{s2}=1.6$
$\lambda_p=1.96$	$T_f''=0.182$
$\theta_{sk}=58.2°(SK=0.63)$	$\text{span}_1=2.0$
$l_a=5.875$	$\text{span}_2=0.4$
$l_g=0.0264$	e_1 = slot opening between adjacent poles = 0.120
$S_a=0.010$	
$S_c=0.0346$	d_1 = depth of the slot opening = 0.060

Because the opening e_1 is comparatively small, magnetic bridge is not used. The motor constants are calculated from equations 1, 2, and 15 to 25 inclusive:

$C_1=668,\ C_3=-60,\ C_5=-603,\ C_7=716$ (1)

$C_1'=363,\ C_3'=-759,\ C_5'=463,\ C_7'=254$ (2)

$R=2.05$ (measured)

$R_a=14.7$ (14)

Mutual Reactances	In Main Terms	In Auxiliary Terms	
X_{m1}	48.4	14.3	
X_{m3}	0.03	4.66	(16)
X_{m5}	0.37	0.22	
X_{m7}	0.13	0.02	
Total	48.93	19.20	

$X_1'=7.82$ (17)

$X_2'=1.85$ (18)

$X_3'=6.20$ (19)

$X_4'=0.55$ (20)

Since C_3 and X_{m3} in main phase terms are very small, the third harmonic effect of the main phase is negligible; and the third harmonic rotor constants are calculated in auxiliary phase terms. C_3' instead of C_3 is used in the calculations.

$R_1=4.11,\ R_3=3.71,\ R_5=2.26,\ R_7=3.16$ (15)

Rotor leakage reactances:

	Fund.	3rd	5th	7th	
Slot plus zigzag	2.12	2.73	1.73	2.44	(22), (25)
End	0.41	0.06	0.02	0.01	(23)
Skew	2.02	2.55	1.27	1.05	(24)

Total $X_1''=4.55,\ X_3''=5.34,\ X_5''=3.02,\ X_7''=3.50$ (21)

Since the mutual reactances X_{m5}, X_{m7} are much smaller than the rotor leakage reactances X_5'' and X_7'' respectively, the effects of the 5th and 7th harmonics can be neglected. This will be verified numerically in calculating the pull-up torque.

The equivalent circuit of Figure 7 is referred to for the solution below:

$$\boldsymbol{E}_s-2jX_4'\boldsymbol{I}_1=(\boldsymbol{I}_1-\boldsymbol{I}_s)Z_a \tag{35}$$

$$\boldsymbol{E}_s-2jX_4'\boldsymbol{I}_1=[Z_s+j(X_3'+2X_4')]\boldsymbol{I}_s+Z_t\boldsymbol{I}_1 \tag{36}$$

$$\boldsymbol{E}_m=\boldsymbol{I}_1(Z_m+R+jX_1')-Z_t\boldsymbol{I}_s \tag{37}$$

where

$$Z_a=R_a+j(X_2'-X_4') \tag{38}$$

$$Z_{n+}=\frac{jX_{mn}\left(\frac{R_n}{1-ns}+jX_n''\right)}{\frac{R_n}{1-ns}+j(X_n''+X_{mn})} \tag{39}$$

$$Z_{n-}=\frac{jX_{mn}\left(\frac{R_n}{1+ns}+jX_n''\right)}{\frac{R_n}{1+ns}+j(X_n''+X_{mn})} \tag{40}$$

$$Z_s=\sum_{n=1,3,5}\frac{1}{2}\left(\frac{C_n'}{C_n}\right)^2(Z_{n+}+Z_{n-}) \tag{41}$$

$$Z_m=\sum_{n=1,3,5}\frac{1}{2}(Z_{n+}+Z_{n-}) \tag{42}$$

$$Z_t=\sum_{n=1,3,5}-\frac{j}{2}\left(\frac{C_n'}{C_n}\right)(Z_{n+}-Z_{n-}) \tag{43}$$

From equations 35 and 36, we obtain

$$\frac{\boldsymbol{I}_s}{\boldsymbol{I}_1}=\frac{Z_a-Z_t}{Z_s+Z_a+j(X_3'+2X_4')} \tag{44}$$

and

$$\boldsymbol{V}=\boldsymbol{E}_s+\boldsymbol{E}_m=\boldsymbol{I}_1[Z_m+Z_t+R+j(X_1'+2X_4')]=\boldsymbol{I}_s[Z_s-Z_t+j(X_3'+2X_4')] \tag{45}$$

The ratios $\boldsymbol{I}_s/\boldsymbol{I}_1$ and $\boldsymbol{V}/\boldsymbol{I}_1$ are calculated from equations 44 and 45. The currents $\boldsymbol{I}_r$ and $\boldsymbol{I}_s$ are then calculated from these ratios. From equations 5 and 6 the currents $\boldsymbol{I}_{n+}$ and $\boldsymbol{I}_{n-}$ can be calculated.

The torque can be readily calculated from the primary currents instead of the rotor currents as Z_{n+} and Z_{n-} have already been computed.

$$T=\frac{225.4}{1{,}800}\sum_{n=1,3,5}n\{|I_{n+}|^2R_{n+}-|I_{n-}|^2R_{n-}\} \tag{46}$$

where R_{n+} and R_{n-} are the resistive components of Z_{n+} and Z_{n-} respectively. The detailed calculations are given in Table I.

The effect of the fifth harmonic is calculated for the point $S=0.4$. From equations 5, 6, 39, and 40, we obtain the following:

$|I_{5+}|=2.07$

$|I_{5-}|=3.37$

$Z_{5+}=-0.019+j0.343$

$Z_{5-}=0.009+j0.33$

From equation 46, the torque due to the fifth harmonic is

$$T_5=\frac{225.4}{1{,}800}\times5\times[2.07^2\times(-0.019)-3.37^2\times0.009]=-0.12 \text{ ounce feet}$$

The fifth harmonic torque is smaller for higher speeds and is neglected in calculating the pull-out torque and running performance.

The foregoing calculations can be repeated for a motor without skew, but otherwise the same as the above example. At $S=0.4$, the third harmonic torque is

about −3.5 ounce feet and the fifth harmonic torque is about −2.4 ounce feet. With a negative net torque, the motor evidently would not pull up to speed. Not so disastrous but rather poor results are obtained with $\theta_s = \theta_m = 90$ degrees while keeping θ_{sk} at 58.2 degrees.

The comparison between calculated and test results are given in Figure 10. The calculation is based on strictly theoretical equations and equivalent circuits without the slightest modification of an empirical constant. It is evident that better agreement would be obtained if the effects of saturation on leakage reactance and the effects of temperature rise and skin effect on rotor resistance are considered in calculating the motor constants.

References

1. Equivalent Circuits of the Shaded-Pole Motor With Space Harmonics, **Gabriel Kron.** *AIEE Transactions*, volume 69, part II, 1950, pages 735–41.

2. An Analysis of the Shaded Pole Motor, **P. H. Trickey.** *Electrical Engineering* (*AIEE Transactions*), volume 45, September 1936, pages 1007–14.

3. Performance Calculations of the Shaded Pole Motor, **P. H. Trickey.** *AIEE Transactions*, volume 66, 1947, pages 1431–38.

4. The Equivalent Circuit of the Capacitor Motor, **S. S. L. Chang.** *AIEE Transactions*, volume 66, 1947, pages 631–40.

5. Differential Leakage with Respect to the Fundamental Wave and to the Harmonics, **M. M. Liwschitz.** *AIEE Transactions*, volume 63, 1944, pages 1139–50.

Discussion

L. C. Packer (Westinghouse Electric Corporation, Springfield, Mass.): The shaded pole motor is one of those small unglamorous but important types of simple construction, of which several millions are made every year to drive ventilating fans and other devices. However, the design of them has been a laborious task because they are complicated to analyze.

Experienced induction motor designers have been able to do a reasonably good job by following induction motor procedures as far as possible and then applying their experience with shaded pole motors to complete the job. Trickey's two papers[1] have helped considerably to expose some of the mysteries of shaded pole motors, followed by papers by Kimberly, Kron and others and then this paper by Chang, all of which have added considerably to the art of designing a type of motor which is probably the most difficult and laborious to design.

Chang has presented his analysis in a clear and concise manner and his method of calculating performance is in relatively close agreement with test results considering that he has not taken into account saturation and temperature. Trickey's method for calculating performance also agrees reasonably well with tests. These two methods together with Kron's analysis should prove valuable tools for shaded pole designers.

Figures 1 and 2 of this discussion may be of interest to shaded pole motor designers.

Figure 1 shows a flux study and phase relations (running) of a shaded pole motor. The search coils were connected to three elements of the oscillograph. The harmonics show very clearly. The speed was 87 per cent of synchronous speed.

Figure 2 shows the phase relations, with the rotor locked. The magnitude of the waves has no significance as the oscillograms were taken for phase sequence only.

Reference

1. See references 2 and 3 of the paper.

L. A. Doggett (Bucknell University, Lewisburg, Pa.): For many years I have been interested in the design of shading coils. Some ten years ago I ran a 2-year investigation of the design of shading coils for a-c contactors. I had hoped to continue this investigation to cover the design of shaded pole motors. Mr. Chang has now done much of this work for me. Although shading coils for contactors and motors have much the same physical appearance, the reason for their use is quite different in the two cases. For contactors, reduction of the pulsations in pull is sought, whereas in the case of the shaded pole motor we wish to achieve the best starting torque and as large a pull-out torque as possible.

One striking contrast between the two cases is brought out by the following table:

Contactors	Shaded Pole Motors
Shading Coil Spans 2/3 to 3/4 of Pole Face	Shading Coil Spans 1/3 to 1/4 of Pole Face

The curves of Figure 10 would be improved by extending them a little beyond the pull-out point. If this were done, the speed curves would take a sharp downward bend at the 120-watt edge of the figure and head towards the 720-rpm 21-watt point. Similarly the power factor curves would turn back on themselves and head for the 52 per cent, 21-watt point. A better picture of the performance can be obtained if rpm, power factor, efficiency, and current are plotted against torque. This suggestion has been partly carried out in Figure 3 of this discussion, where the test results are shown by broken lines and the calculated results by solid lines.

The motor tested had a 26.4-mil air gap. Is not that a rather long air gap for a 0.1-

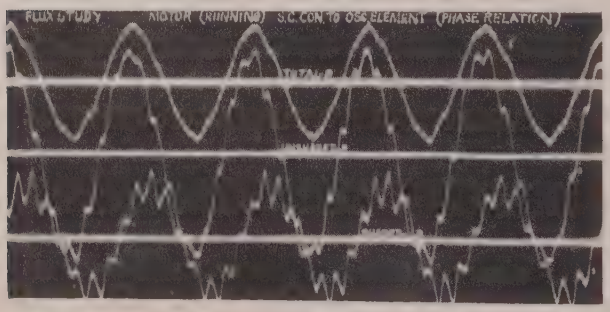

Figure 1 (left)

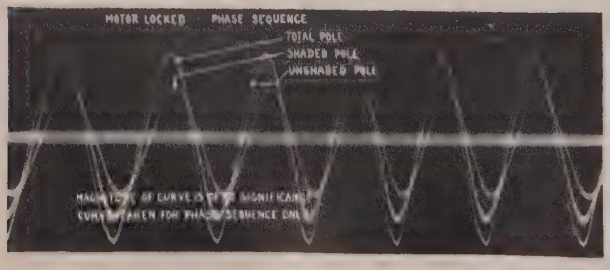

Figure 2 (left)

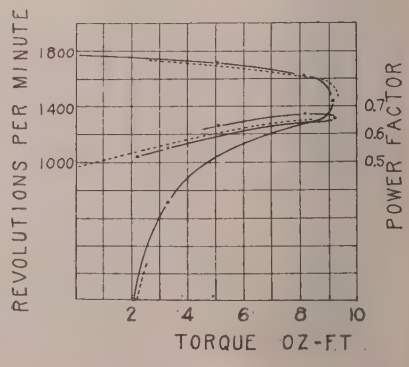

Figure 3 (right)

horsepower motor? A little further discussion by the author of the effect of air gap length on motor performance would be appreciated.

I would like to congratulate the author on the progress he has made in analyzing the extremely difficult problems associated with this extremely simple appearing motor.

S. S. L. Chang: The writer appreciates the kind remarks of Mr. Packer and Mr. Doggett. Figures 1 and 2 of Mr. Packer's discussion show the flux of the shaded pole and unshaded pole plotted against time. These illustrations clearly indicate an increase in the phase difference between the shaded pole flux and unshaded pole flux at running condition. This agrees with calculated results from the equivalent circuit and provides another link between theory and test.

Mr. Doggett asked about the effect of air gap on motor performance. In most induction motors, a smaller air gap usually gives better performance by reducing the magnetizing current, however, this is not always the case for shaded pole motors. Especially for 2-pole and 4-pole motors, we found that an adequately large air gap gives better torques and efficiency than a small air gap.

The effect of air gap can be well understood from the equivalent circuit. As the leakage reactances of 2-pole and 4-pole shaded pole motors consist largely of skew and harmonic components, which are almost inversely proportional to the air gap, a small air gap makes the leakage reactances too high for adequate output. The harmonic mutual reactances are also inversely proportional to the air gap. These reactances are preferably small to reduce the harmonic rotor currents. On the other hand, too large an air gap increases unduly the primary copper loss. In a well-designed shaded pole motor, the air gap is such that the primary copper loss is a small but substantial part of the total loss. The proper air gap for 2-pole and 4-pole motors are usually larger than the minimum feasible value from the mechanical and manufacturing standpoints. For motors of six poles and above the air gap is preferably small.

Sometimes the starting torque can be improved by making the air gap larger at the unshaded pole tip to assimilate the effect of reactive split phase. This was done in the motor cited in the example. The air gap was 0.017 inch except at the unshaded pole tip where it was 0.040 inch. The value 0.0264 inch used in the paper was the weighted harmonic average value with the effect of slot openings considered.

Measurement of D-C Machine Parameters

ROBERT M. SAUNDERS
MEMBER AIEE

Synopsis: An equivalent circuit is suggested to represent the d-c machine when operating under near normal current conditions. This equivalent circuit contains resistances, inductances, and speed-voltage constants. Certain d-c tests are suggested for obtaining the resistances and speed-voltage constants. Either the transient or a-c methods may be employed for ascertaining the inductances although the a-c method seems the simpler; circuits and techniques are described for both methods. Experimental verification of the equivalent circuit and methods of measurement take the form of application to a compound motor and to the amplidyne, a complex d-c machine with many diverse windings on the same magnetic circuit.

PARAMETER measurement methods for the d-c machine have been of considerable interest of late because of the necessity of predicting short circuit characteristics and applications to servomechanism circuits. A d-c machine short-circuit involves extremely large armature currents while servo circuits involve currents of a much smaller magnitude. It is with the latter problem that this paper is mainly concerned. While the currents are of more or less rated magnitudes in servo circuits, these currents may change sufficiently rapidly so that the inductive effects in the machine must be considered along with the resistances and other factors; in other cases the rates of change of currents may be sufficiently low so that the inductive effects can be ignored. The standards do not cover the inductance measurement problem, and further, the methods of determining the resistances prescribed by the standards are based on giving values accurate enough for efficiency data but do not result in accurate results in servo system calculations. The author has had some success in the use of a d-c machine equivalent circuit for servo system analysis and has developed a means of measuring the parameters of this equivalent circuit by means of certain d-c plus power-frequency a-c measurements. It is the purpose of this paper to present this equivalent circuit and to discuss the measurement of the parameters of the circuit by various means; experimental verification will be presented to illustrate the validity of the analysis.

In this approach, it is assumed that the observer has no knowledge of the machine design information and is more or less approaching the machine as a "black box" problem. In general, the usual d-c machine may be considered as a 6-terminal network in which there are resistances, self-inductances, mutual effects between the fields and armature circuits, and speed-induced voltages. Because the general features of the d-c machine are known, one may set down an equivalent circuit without resorting to the generalized 6-terminal network analysis.

Undoubtedly Miller's equivalent circuit[1] was formulated by others at an earlier date (1933), but his is the first notation that has come to the author's attention; others[2,3] have used this circuit. Figure 1 shows this equivalent circuit. The shunt field has a certain resistance and self-inductance, R_1 and L_1. The shunt field also will induce a transformer-type voltage in the armature circuit to which it is inductively coupled through brush shift, or demagnetizing effect of armature reaction, all these inductive effects being summarized as a mutual inductance, M_{1a}; in addition, there is also a transformer induced electromotive force present in the series field due to the mutual inductance, M_{1s}. The shunt field will induce a speed-generated voltage at the brushes due to the rotation of the armature; this speed induced voltage constant is designated by K_{1a} ohms per rpm (induced volts per ampere of field current per-unit speed). Similar constants, R_s, L_s, M_{sa}, M_{1s}, and K_{sa}, will be associated with the series field and be defined in the same fashion. Any other windings in the same magnetic circuit as the shunt field will have similar constants. Considering now the armature circuit, it will have a resistance, R_a, which represents the resistance of the armature conductors, brushes, and interpoles; and a total self inductance, L_a, corresponding to the same circuit elements. The armature circuit is loosely coupled to the shunt field through M_{1a} and to the series field through M_{sa}. It will also self-generate a speed-voltage at the brushes due to current in the armature alone, the constant describing this voltage defined as K_a.

It is with the determination of the constants R_1, R_s, R_a, L_1, L_a, L_s, M_{1a}, M_{sa}, M_{1s}, K_{sa}, K_{1a}, and K_a that this paper is concerned.

There are three approaches to the solution of this problem that have been reported to date, (1) the transient method basically presented by Bower[4] in his paper on amplidyne characteristics, (2) the bridge method presented by Koenig,[5] and (3) the a-c method discussed very briefly by the author in a previous paper,[3] and by Snively and Robinson.[7] The bridge method has been well expostulated, but neither the transient nor the a-c methods have been applied to the whole d-c machine. Thus, this paper will be confined

Paper 51-118, recommended by the AIEE Feedback Control Systems and Rotating Machinery Committees and approved by the Technical Program Committee for presentation at the AIEE Winter General Meeting, New York, N. Y., January 22–26, 1951. Manuscript submitted October 23, 1950; made available for printing December 26, 1950.

ROBERT M. SAUNDERS is with the Division of Electrical Engineering, University of California, Berkeley, Calif.

The author wishes to acknowledge the contributions made by former students in applying the methods suggested in this paper to their own problems; in particular, H. G. Wilson and W. P. Spehar, both of the Hughes Aircraft Company; J. D. Crevier, Lockheed Aircraft Company; and J. P. Lindley, University of California.

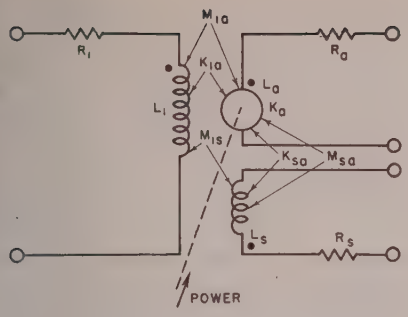

Figure 1. Equivalent circuit for the compound dynamo

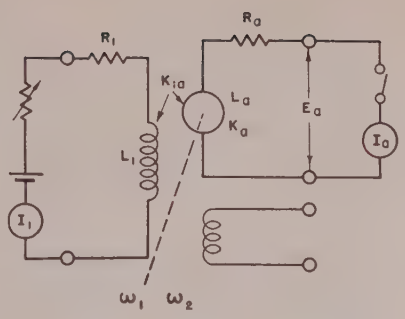

Figure 2(A). Test circuit for ascertaining the d-c constants of a machine. The current, I_1, is varied and corresponding values of E_a and I_a are read for two different speeds, ω_1, and ω_2

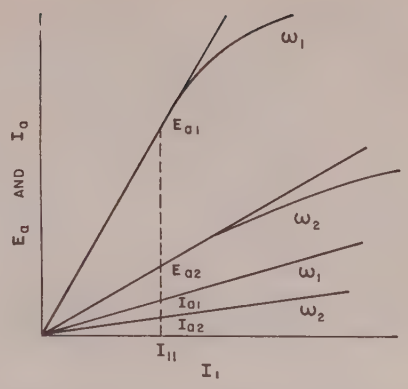

Figure 2(B). Curves resulting from the data collected from the circuit of Figure 2(A)

to the applications of Bower's work to all d-c machines and to an amplification of the a-c techniques which the author has employed and which Snively and Robinson have used to determine the armature self-inductance.

D-C Measurements

All quantities except the self- and mutual inductances may be measured by certain d-c tests. The field winding resistances may be measured by means of voltmeter-ammeter, Wheatstone, or Kelvin Bridge methods. The resistance of the armature and the other constants can be obtained by means of the open and short circuit tests as a d-c generator, a test somewhat synonomous to the synchronous impedance test for alternators. Figure 2(A) shows the manner of conducting the tests. Curves of open circuit voltage and short circuit current as a function of shunt field current for two different speeds, ω_1 and ω_2, are found and plotted as shown in Figure 2(B). This test should be confined to the lower portion of the saturation curve where the cross magnetization due to armature reaction does not introduce a net demagnetization of the poles. If this is done, the curves will be nearly straight lines over the lower portion. In Figure 2(B), at the field current, I_{11}, and at the speed ω_1,

$$\frac{E_{a1}}{I_{a1}} = R_a + K_a\omega_1$$

At the same field current but at a speed of ω_2:

$$\frac{E_{a2}}{I_{a2}} = R_a + K_a\omega_2$$

From which

$$R_a = \frac{1}{\omega_2 - \omega_1}\omega_2\left(\frac{E_{a1}}{I_{a1}} - \omega_1\frac{E_{a2}}{I_{a2}}\right)$$

$$K_a = \frac{1}{\omega_2 - \omega_1}\left(\frac{E_{a2}}{I_{a2}} - \frac{E_{a1}}{I_{a1}}\right)$$

The constants K_{1a} and K_{sa} are the slopes of the open-circuit saturation curves divided by the speed. For the shunt field:

$$K_{1a} = \frac{E_{a1}}{I_{11}\omega_1}$$

For the series field the use of a series field saturation curve in a similar manner will ascertain K_{sa}. The ratio of the series and shunt turns also is needed and this is obtained by generating a voltage with one field separately excited and then generating the same voltage with the other. When voltages are equal: $N_1I_1 = N_sI_s$. Since I_1 and I_s are known, N_1/N_s can be found; this assumes that the leakage paths for the two fields are the same. Thus, from resistance measurements and the open and short circuit tests R_1, R_s, R_a, K_a, K_{1a}, K_{sa} and N_1/N_s can be ascertained leaving only L_1, L_s, L_a, M_{1s}, M_{1a}, and M_{sa} to be found.

Transient Method

Briefly, this method, first enunciated by Bower,[4] calls for the measurement of the time constants by means of oscillograms when step values of voltage are applied to the various circuit elements.

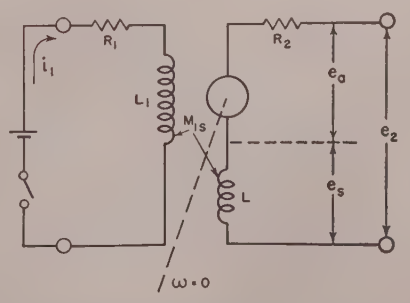

Figure 3(A). Transient method of measuring the shunt field self-inductance and mutual inductance to the series field

Figure 3(A) shows the circuit necessary to obtain L_1, M_{1s}, M_{1a}, and R_1 (it may be preferable to measure resistances as described in the last section). These values may be checked by taking the decay of current as well when a low value of resistance is connected suddenly across the field terminals. In Figure 3(B) the shunt field resistance is the ratio E_1/i_{10} and L_1/R_1 is t_1. The value of M_{1s} can be determined at any convenient point, t_1, by taking the slope of the shunt field current curve; from which

$$M_{1s} = \frac{e_s}{\left.\frac{di_1}{dt}\right|_{t_1}}$$

While the foregoing test for M_{1s} must be performed while the machine is standing still (to obtain e_s due to mutual induction only) the shunt field time constant may also be determined with the armature rotating. In this case, the time constant of e_a is the time constant of the shunt field. This method has the advantage that, if there are time delays due to hysteresis and eddy current effects, they are included as increases in the control field time constant.

To find the armature circuit parameters, it is best to ascertain the time

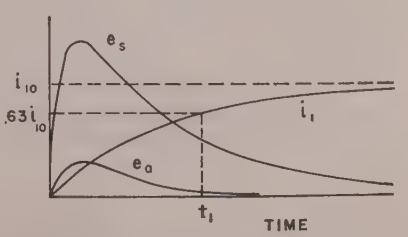

Figure 3(B). Oscillogram resulting from closing the switch in Figure 3(A)

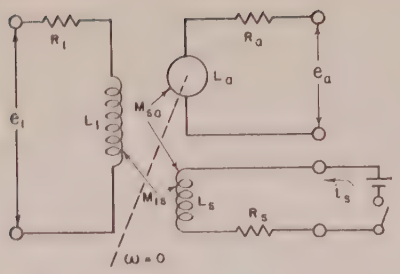

Figure 4(A). Transient method of measuring the series field self-inductance and mutual inductance to the armature

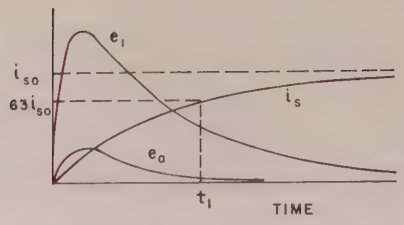

Figure 4(B). Oscillogram resulting from closing the switch in Figure 4(A)

constants of the armature and series field separately. The series field resistance and time constant may be found in a manner analogous to that for the shunt field; Figure 4(A) shows the circuit employed. From this circuit it is possible to obtain the self-inductance of the series field, L_s, and the coupling between the series field and the armature circuit, M_{sa}. In the usual d c machine with the brushes set on the neutral, M_{sa} is very small with respect to M_{1s}, so that M_{1s} approaches M_{12}, the total shunt field to armature circuit mutual inductance. As before, an alternative test is to measure the rise of e_a as the machine rotates, thus including the delay due to hysteresis and eddy currents

If the armature proper does not link the series or shunt fields, often the case when the brushes are on the neutral, a test may be made solely for the armature resistance and self-inductance. Even though the rotation of the armature may introduce some extraneous results, it is considered better to have it rotating slowly, say at ten per cent speed, while the resistance and self-inductance are being found by oscillograms. The slow rotation tends to reflect the proper commutation effects without introducing large ripple and residual voltages. Figure 5(A) shows the circuit diagram employed for this test. If the armature does link mutually the series or shunt field, this test should be performed at standstill, that is, with $\omega=0$ in Figure 5(A). The oscillogram of Figure 5(B) will permit the obtaining of M_{1a}, L_a, and M_{sa}. According to the development in Appendix I, the armature circuit inductance and mutual inductance to the shunt field when the armature and series field are cumulatively connected in the circuit are respectively:

$$L_2 = L_s + L_a + 2M_{sa}$$

$$M_{12} = M_{1s} - M_{1a}$$

As Snively and Robinson[7] point out, and the author concurs, the transient method of testing is not as convenient as the a-c method since a low impedance source of direct current is required as well as the difficulty of interpretating the oscillograms—always somewhat tedious. In addition, it is much more difficult to associate the inductances found by this test with the degree of saturation present in the machine.

A-C Methods

Briefly, the a-c method involves the use of alternating current of either low or power frequencies in place of the direct current employed by Bower, measuring the input conditions, and applying transformer theory to obtain the desired constants. Consider first the obtaining of self-inductances, L_1 and L_s, and the mutuals, M_{1s} and M_{1a}, of Figure 1. If the observer wishes to obtain values of inductance as a function of the degree of saturation within the machine, the circuit of Figure 6(A) may be employed. On the other hand, the circuit of Figure 6(B) may be used if an error of 25 per cent in inductance values can be tolerated.

The basic difference between the two experimental circuits is that the former permits the superposition of a direct current upon the alternating current employed for inductance measurement purposes, while the latter finds the inductances of an essentially unsaturated machine. In Figure 6(A), the reactor, X_x, serves to block the flow of alternating current through the battery, which usually has a much lower impedance than the field under test. If X_x can be made sufficiently large, then the a-c component of current flowing to the left into the battery circuit will be negligible with respect to the alternating current that flows into the machine under test. If X_c is very small with respect to R, then the circuit of Figure 6(A) may be replaced by that of Figure 6(B). Assuming that these conditions can be met or that the unsaturated values of inductance are sufficiently accurate, observations of the quantities V_g, V_R, V_1, V_s, V_a, and I_1 are made.

From these quantities the vector diagram may be constructed graphically as in Figure 7 utilizing the equivalent circuit of Figure 6(C). In Figure 7(A) the magnitudes of V_g, V_R, and V_1 are laid off to scale; this fixes the position of the current vector, with respect to the others. In Figure 7(B) the voltages aE_s ($a=N_1/N_s$), and I_1R_1 are laid off on the original diagram, the vertical projection of I_1R_1 on the radius line $|aE_s|$ represents the magnitude of the I_1X_{l1} drop. Since no current flows in the series field circuit, all the current I_1 flows in the parallel branch consisting of X_{1s} and R_c. Only the current flowing through X_{1s} is of interest; this current can be found by separating the current I_1 into its components as in Figure 7(C). The values of L_1, M_{1s}, and M_{1a} can be ascertained as shown in the inserts of Figure 7.

The series resistor is used to assist in the construction of the vector diagram of the circuit by providing a known phase relationship between one voltage drop and the current; it is not required if some other means may be employed for determining the phase angle between the current and voltage. Vacuum tube voltmeters or other types of infinite input impedance devices generally are required since the power levels are low. When the power levels are low, the wattmeter becomes unreliable; hence, the circuit of Figure 6(A) is recommended. Care

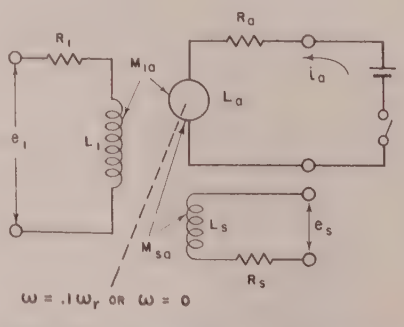

Figure 5(A). Transient method of measuring the armature self-inductance and mutual inductance to the shunt field

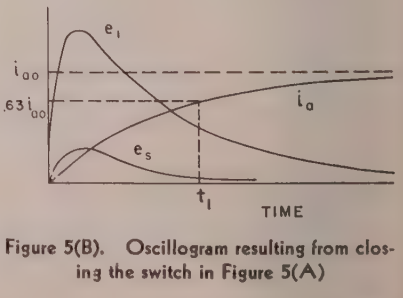

Figure 5(B). Oscillogram resulting from closing the switch in Figure 5(A)

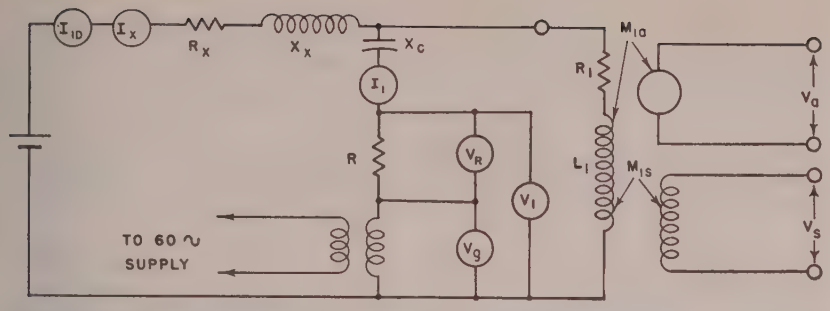

Figure 6(A). Circuit arrangement for measuring the machine parameters by a-c tests when provision is made to include the effects of superimposed d-c fields

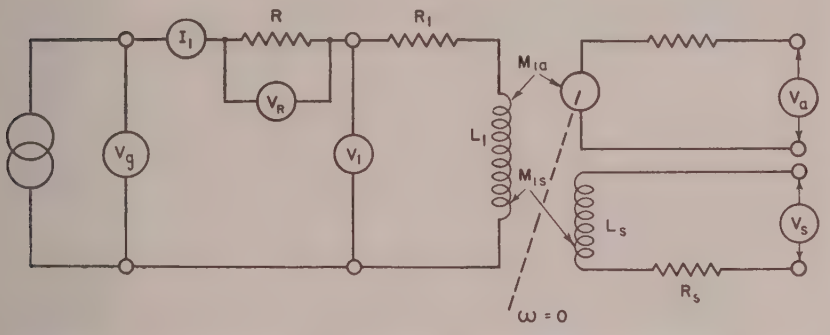

Figure 6(B). Circuit arrangement for measuring the same quantities as in Figure 6(A) when no direct current is to be superimposed or when the battery circuit a-c impedance is high compared to the d-c machine

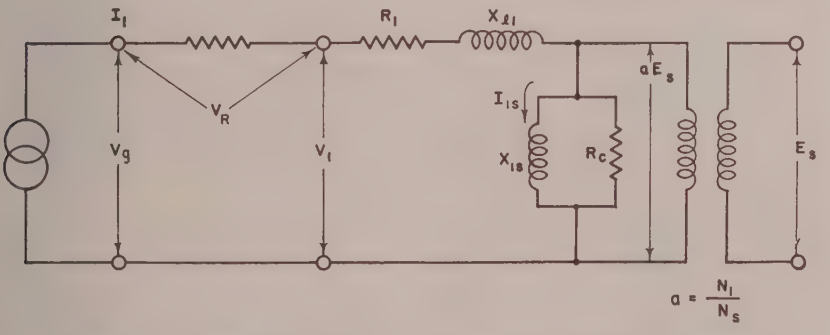

Figure 6(C). Equivalent circuit of the d-c machine while undergoing a-c tests

must be exercised to see that reasonably good sine waves are present at all times; this is not difficult in most machines since the air-gap is large.

For the series field, the same test yields L_s, M_{1s}, and M_{sa}. For the armature circuit, the same test made with the machine rotating slowly is considered better than a stationary test since the effects of commutation are included in the measurements and yet the ripple and residual voltages are not so large as to influence the results. Because the mutual inductance effects are small in this case, the self-inductance is composed almost entirely of leakage inductance. For that reason the armature self-inductance does not seem to vary greatly with armature current nor with field current.

The results of the test of a 25-horsepower 230-volt variable-speed compound motor with interpoles but no compensating winding are shown in Figure 8. The data for the sample test run are shown as circles and indicate the relative experimental error encountered.

Experience with the machines mentioned herein, which are admittedly small, seems to indicate that it is not correct to assume that the impedance of the armature or any other circuit in the machine is predominantly inductive in nature. Very grievous errors can result by making this assumption. In the author's opinion the presumption should be that the various circuits have resistive components until proved otherwise.

In working with normal armature

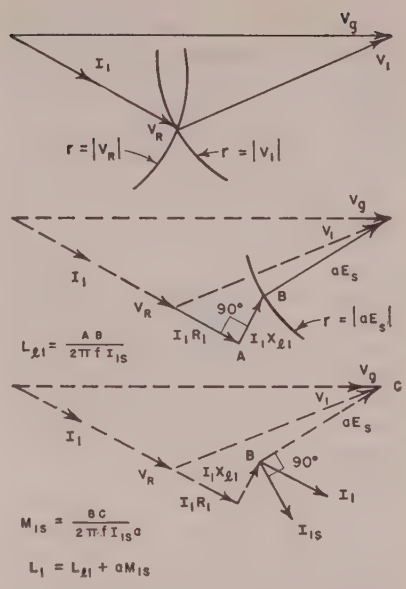

Figure 7. Evolution of vector diagram of the circuit of Figure 6(C) by triangulation methods. The dotted lines indicate the vectors found in the upper figure

currents it is recommended that the brushes be left seated in their usual in-service fashion. If this is done, the brush resistance and the inductive effects of the short-circuited coils will be reflected in the over-all parameters of the machine; this is quite desirable in predicting over-all characteristics.

Applications

Extensive use of the equivalent circuit and the a-c method of parameter determination has been made by the author and his associates, mainly in the realm of the dynamoelectric amplifier. The Amplidyne probably represents as rigorous a test of these methods as any d-c machine since it is essentially two machines in one magnetic circuit, thus resulting in unusual mutual and self-inductive effects. In the paper[3] on class-*A* operation of dynamoelectric amplifiers, there was very good correlation for an Amplidyne and a Rototrol between experimental and calculated frequency response curves for zero to 100 per cent negative feedback, even though the methods presented in this paper were not as well developed and certain approximations were made. Figure 9 is one set of such curves analytically and experimentally ascertained for a 3/4-kw 250-volt Amplidyne; the equivalent circuit employed for the analytical computations is shown in the inset. It will be noted that there is fairly good correlation between the analytical and experimental curves.

Howard G. Wilson[6] recently determined the frequency of oscillation of Amplidynes using a capacitively-coupled positive-feedback circuit. He predicted the frequency within 7.4 per cent in the region from 5 to 23 cycles per second from a fifth-degree operational equation of the loop response employing parameters obtained from a-c measurements.

W. P. Spehar (in a University of California thesis as yet unsubmitted) will show even better correlation between experimental and test results for the positive-feedback nonoscillating dynamoelectric-amplifier frequency-response curves than was the case for the negative-feedback instance mentioned in a preceding paragraph.

In operating over the region of Figure 8 of variable inductance, it would be expected that nonlinearities of response would result. Such is not the case in practice; for, even with large changes of field current, the response of the circuit usually turns out to be linear providing the speed-voltage constants, K_{1a}, K_{sa}, and K_a have not changed. In cases of this type it has been observed that the values of inductance chosen should be those associated with the maximum swing of current. For example, if, in Figure 8, it were desired to ascertain the correct circuit parameters for operation with a sine wave of shunt field current equal to 0.8 per unit, the proper inductances would be: $M_{1a}=3.8$mh (millihenrys), $M_{1s}=52$ mh, $M_{as}=0.05$mh, $L_1=38$ henrys, $L_a=11.1$mh. When operating with d-c values of shunt or control field current, the values used in the equivalent circuit should be chosen for the particular value of current employed.

Conclusions

As a result of these investigations it is concluded that:

1. The d-c machine may be represented by an equivalent circuit containing resistances, mutual and self-inductances, and speed-generated voltage constants.

2. The resistances and speed-generated voltage constants of the equivalent circuit can best be ascertained by certain d-c tests.

3. Either the transient or the a-c method is suitable for obtaining the mutual and self-inductances, but the a-c method is considered less laborious and more convenient and more adequately incorporates saturation data.

Nomenclature

K_a = armature self-induced speed-voltage constant, ohms/rpm
K_{sa} = series field to armature speed-voltage constant, ohms/rpm
K_{1a} = shunt field to armature speed-voltage constant, ohms/rpm
L_a = self-inductance of armature circuit, henrys
L_s = self-inductance of series field, henrys
L_1 = self-inductance of shunt field, henrys
L_2 = self-inductance of combined series field and armature circuit, henrys
M_{sa} = mutual inductance between series field and armature, henrys
M_{1a} = mutual inductance between shunt field and armature, henrys
M_{1s} = mutual inductance between shunt and series fields, henrys
M_{12} = mutual inductance between shunt and series fields and armature, henrys
N_1 = shunt field turns
N_s = series field turns
R_a = resistance of armature circuit, ohms
R_s = resistance of series field, ohms
R_1 = resistance of shunt field, ohms
ω = speed, rpm

Appendix I. Combination of Mutual Inductances for a Compound Machine

When the mutual inductance between the armature and the series and shunt fields is appreciable, the following analysis applies which shows how the mutual inductances combine to give one over-all mutual inductance for the coupling between the field and armature circuits. Ignoring the speed induced voltages, or considering the machine at standstill, the circuit equations in terms of the over-all mutual inductances for a cumulatively compounded machine are as follows:

$$e_1 = R_1 i_1 + L_1 \frac{di_1}{dt} + M_{12} \frac{di_2}{dt}$$

$$0 = R_2 i_2 + L_2 \frac{di_2}{dt} + M_{12} \frac{di_1}{dt} + V_L$$

In terms of the individual mutual and self-inductances:

$$e_1 = R_1 i_1 + L_1 \frac{di_1}{dt} - M_{1a} \frac{di_2}{dt} + M_{1s} \frac{di_2}{dt}$$

$$e_1 = R_1 i_1 + L_1 \frac{di_1}{dt} + (M_{1s} - M_{1a}) \frac{di_2}{dt}$$

$$0 = R_2 i_2 + L_s \frac{di_2}{dt} + L_a \frac{di_2}{dt} - 2M_{sa} \frac{di_2}{dt} - M_{1a} \frac{di_1}{dt} + M_{1s} \frac{di_1}{dt} + V_L$$

$$0 = R_2 i_2 + (L_s + L_a - 2M_{sa}) \frac{di_2}{dt} + (M_{1s} - M_{1a}) \frac{di_1}{dt} + V_L$$

Hence:

$$L_2 = L_s + L_a - 2M_{sa}$$

$$M_{12} = M_{1s} - M_{1a}$$

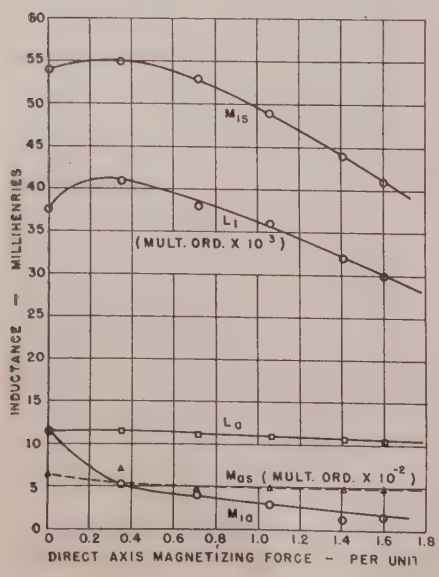

Figure 8 (left). Inductance curves for a 25-horsepower 230-volt 350–700 rpm variable-speed compound motor Experimentally determined points are shown by the circles, squares, and triangles

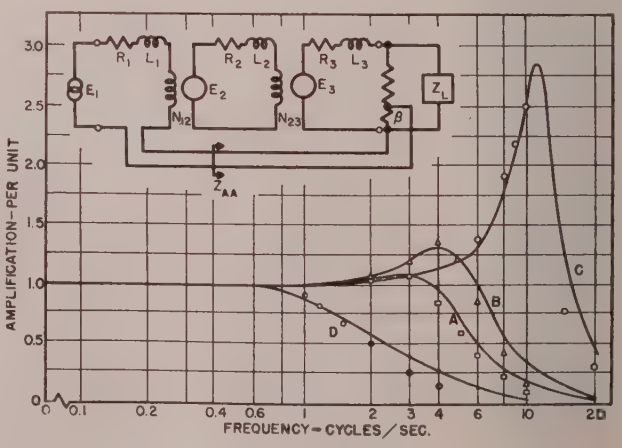

Figure 9 (right). Frequency response curves for a 3/4-kw 250-volt amplidyne as determined by using the equivalent circuit shown in the inset

Curves A, B, and C are for a β of 10, 20, and 100 per cent negative feedback respectively. Curve D is for zero feedback. The solid curves are test values; the calculated points are indicated by the circles, triangles, and so forth. In this figure $N_{12}=\omega K_{12}$ and $N_{23}=\omega K_{23}$

References

1. Transients in Arc Welding Generators, **A. R. Miller.** *AIEE Transactions*, volume 52, March 1933, pages 260–67.

2. Transient Characteristics of D-C Motors and Generators, **A. T. McClinton, E. L. Brancato, R. Panoff.** *AIEE Transactions*, volume 68, part II, 1949, pages 1100–06.

3. Dynamoelectric Amplifier—Class A Operation, **R. M. Saunders.** *AIEE Transactions*, volume 68, part II, 1949, pages 1368–73.

4. Fundamentals of the Amplidyne Generator, **J. L. Bower.** *AIEE Transactions*, volume 64, 1945, pages 873–81.

5. Transient Response of D-C Dynamos, **H. E. Koenig.** *AIEE Transactions*, volume 69, part I 1950, pages 139–45.

6. The Amplidyne as an Oscillator, (thesis) **Howard G. Wilson.** University of California, Berkeley, Calif., 1950.

7. Measurement and Calculation of D-C Armature Circuit Inductance, **H. D. Snively, P. B. Robinson.** *AIEE Transactions*, volume 69, part II, 1950, pages 1228–37.

Discussion

John O'Connor and **John Cybulski** (Naval Research Laboratory, Washington, D. C.): The author is commended for his investigation and simplification of measurements of parameters in an inductively coupled mesh network. We feel, however, that some unwarranted simplifications have been made which may result in considerable error in the determination of the quantities R_a and K_a.

The author determines the "constants" R_a and K_a from the simultaneous solutions of the following equations:

$$\frac{E_{a1}}{I_{a1}} = R_a + K_a\omega_1 \qquad (1)$$

$$\frac{E_{a2}}{I_{a2}} = R_a + K_a\omega_2 \qquad (2)$$

He has formulated these equations on the assumption that the short circuit current characteristics (I_a) are straight lines, which will result in giving a constant value for R_a at all speeds. It was stated that R_a represents the resistance of the armature conductors, brushes and interpole windings. It is well known, however, that the combined resistance of carbon brushes and brush contact is not independent of current. The effect of this variable resistance characteristic may be observed in Figure 1 of this discussion, where effective armature circuit resistance $(E_a - V_t)/I_a$ is plotted as a function of I_a for several speeds. (V_t in this expression is the voltage measured across the external short-circuiting resistance.) It may also be observed in Figure 1 that the effective armature circuit resistance is more a function of armature current than of speed. Data for Figure 1 of this discussion was obtained from Figure 2 where the open and short-circuit characteristics are given for a 90-horsepower motor which was used to obtain the experimental data.

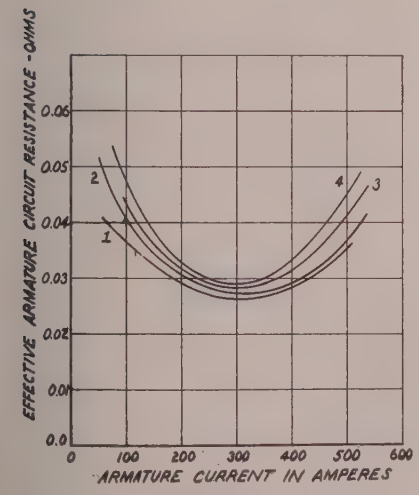

Figure 1. Variation of effective armature circuit resistance as a function of armature current with speed as a parameter

Curve	Rpm	Machine Data
1	300	90-hp 1750-rpm
2	600	250-v 300-amperes,
3	900	shunt connection
4	1,200	interpoles

From the open and short-circuit curves of Figure 2 values of R_a and K_a were obtained using the author's methods. The results are tabulated in Table I and indicate considerable variation of these quantities depending on the speeds used in their determination. It may be noticed that the value of field current selected also introduces variations. In the short circuit tests the armature was in series with a small external resistance. The author's equations were therefore modified so as to exclude this resistance in determining R_a by using $E_a - V_t$ instead of E_a. V_t is, as previously indicated, the voltage measured across the external short circuiting resistance.

If it is desired to obtain the variation of armature circuit resistance as a function of speed, only, it is suggested that the field and short circuit armature currents be kept fixed throughout the speed range investigated. The adjustment in short-circuit current at each speed would be made with a variable load resistance across the armature terminals and the magnitude of this external resistance can be found, at each speed, by reading the terminal voltage.

We join with the author and agree that a-c measurement methods outweigh the d-c transient methods as regards ease of measurement, interpretation and time involved. The value of inductance obtained is, dependent on whether:

1. Alternating current employed produces minor hysteresis loops superimposed on direct current.
2. Alternating current alone is employed with no direct current for saturation.
3. Direct current alone is used.

We have used circuits similar to those proposed by the author and found that in a-c measurements direct current should be used to simulate the degree of saturation.

Table I

I_f, Amperes	Speeds, Rpm	R_a, Ohms	K_a, Ohms/Rpm
0.2	300–600	0.0330	12.3×10^{-5}
0.2	600–900	0.0554	-25.0×10^{-5}
0.2	900–1,200	0.0428	-11.0×10^{-5}
0.4	300–600	0.0401	-18.3×10^{-5}
0.4	600–900	0.0281	1.6×10^{-5}
0.4	900–1,200	0.0116	20.0×10^{-5}

Robert M. Saunders: The author is indebted to Messrs. O'Connor and Cybulski for amplifying some of the problems associated with the application of techniques developed in this paper, and appreciates their contribution to the paper.

Concerning the nonlinearity of the armature circuit resistance introduced by the brushes, they are quite correct in their statement that this effect will tend to make the armature circuit resistance a function of the armature current as shown in Figure 1 of their discussion. However, this paper is primarily concerned with the servo motor and generator where the load resistance normally will be large compared with the armature circuit resistance so that a nonlinearity of the latter will have a small effect on the total circuit resistance. For the machine they use as an example, the armature resistance would be nearly 4 per cent of the load resistance at full load making the per-unit resistance of the circuit about 1.04. As the current is increased or decreased,

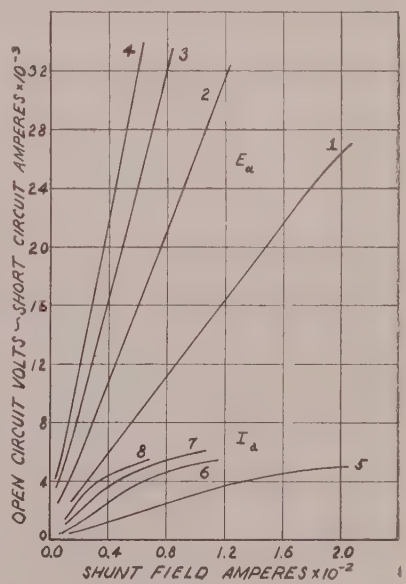

Figure 2. Open circuit and short-circuit characteristics of a d-c machine operated at several speeds

Curve	Connection	Rpm
1	Open circuit	300
2	Open circuit	600
3	Open circuit	900
4	Open circuit	1,200
5	Short circuit	300
6	Short circuit	600
7	Short circuit	900
8	Short circuit	1,200

Machine Data
90-hp 1750-rpm
250-v 300-amperes,
shunt connection
interpoles

they show the armature circuit resistance to increase by a factor of two, thus making the total resistance increase to 1.08, a 4 per cent change. On the other hand, if the external circuit resistance becomes small compared to the armature circuit resistance, the nonlinearity they mention certainly will become significant, and the armature circuit resistance can no longer be considered to remain constant.

Referring to their Figure 2, the decreasing slope of the short-circuit armature current (curves 5–8) is due mainly to the saturation of the pole tips by the armature flux. This results in a net demagnetizing effect in the direct axis, this effect increasing the apparent resistance. The use of the short-circuit curves must not be extended into this range since the whole paper is predicated upon the assumption that no such saturation of the pole tips exists. At the lower ends of all the curves of Figure 2 there are apt to be nonlinearities due to the residual effects. The problem, then, is to find a region outside the residual effect zone and short of the pole tip saturation zone. If, in Figure 2, a straight line is drawn along the curves and through the origin and if these lines are used for ascertaining K_a and R_a, there will result average values of $K_a = +3.44 \times 10^{-6}$ ohms/rpm and $R_a = 0.0422$ ohm, respectively. In this example the maximum deviation of the armature resistance is ± 10 per cent and the self-induced speed voltage constant ± 300 per cent. Returning now to the case of the previous paragraph, for an armature circuit resistance deviation of ± 10 per cent, the total resistance will now have only a 1 per cent deviation under full load conditions.

The total armature circuit resistance is $R_a + K_a\omega$. For this example, at 1,200 rpm the contribution of the latter term to the total circuit resistance is thus seen to be approximately 10 per cent. This is a somewhat larger component than the author has encountered in standard d-c machines with interpoles, for, with proper brush setting on the mechanical neutral, there should be no component of the armature magnetomotive force in the direct axis. In amplidynes, however, $K_a\omega$ is often equal to R_a, but, in such cases K_a has a deviation from the mean of similar magnitude to R_a rather than the magnitude of the example used here.

Finally, the justification for the assumptions used in the paper must rest upon the results obtained when these assumptions are employed. The author feels that the application section of the paper presents an adequate verification of the methods contained herein when applied to servo equipment.

The author is gratified to learn that Messrs. O'Connor and Cybulski agree that the a-c methods have proved to be the easiest to apply and that they concur in the manner of simulating degree of saturation,

Rules for Designing Frog-Leg Windings of D-C Machines

H. B. DWIGHT
FELLOW AIEE

R. G. HALTMAIER
NONMEMBER AIEE

FROG-LEG armature windings comprise a class important in the field of large d-c motors and generators. They were first installed in 1925 and were described in that year by W. H. Powell and G. M. Albrecht.[1] By 1940 the total ratings had passed 750,000 kw. Because of the importance of these windings, it is suitable that electrical engineers should study their principles of operation and the rules for designing them, with reasons for the rules.

Frog-leg machines have two complete windings on the armature, one lap and one wave. A coil of each is shown in Figure 4. The shape gives rise to the name frog-leg. In every slot there are two lap coil sides and two wave coil sides. Every commutator bar has four connections, two to the lap winding and two to the wave winding. This is somewhat similar to putting two windings on an induction motor to give two different speeds, except that the lap and wave windings are designed for the same voltage and operate together in parallel.

A simplex lap winding connects to all the commutator bars in order, 1, 2, 3,.... A duplex lap winding connects together all the odd-numbered bars, 1, 3, 5,.... and then all the even-numbered bars. This makes two windings in parallel, so that changing from simplex lap to duplex lap doubles the number of parallel paths through the armature from the plus terminal to the minus terminal of the machine. A triplex winding connects bars 3, 6, 9,.... Wave windings also may be duplex, triplex, or multiplex to 10, 12, or even higher degrees. Multiplex wave windings are used in all frog-leg wound armatures.

Very few practical machines, not of the frog-leg type, use multiplex windings. One special case is that of an 8-pole, duplex wave winding with diametral cross connections. It is a 4-circuit winding and so is intermediate between a 2-circuit wave winding and a simplex, 8-circuit, lap winding. It is quite practical but opportunities for using this special type seldom occur. The choice of one of the three types just mentioned depends principally on the width of commutator bar which each type requires.

All practical lap windings must have armature cross connections, or else excessive heating in the armature and sparking on the commutator will occur. It is usually considered too expensive and cumbersome to provide such a connection for every commutator bar. However, frog-leg windings are inherently cross-connected and do not need special copper connectors for this purpose. Their cross connection is for every commutator bar.

The cross connection inherent in a frog-leg winding is illustrated in Figure 1. The lap winding is made, as usual, so as to have points of equal potential such as *a* and *b*, which are exactly two poles apart in the winding. These can be, and in an ordinary lap winding should be, connected by a copper strap such as *acb*. However, in a frog-leg winding external connectors such as *acb* are not used since one can go from *a* to *b* through the copper path *aefghb*, which has no net voltage along it and so is equivalent to an ordinary cross connection. The path goes first down and then up through slot 11 and also twice through slot 22, and so induced voltages cancel out. The lap and wave windings have the same number of paths and the same size of conductors. The current in the conductors and the voltage drop is the same. In traversing the path *aefghb*, one goes with the current for one-half the distance and against the current the other half, so that voltage drops cancel out exactly. There is a cross-connecting path as in Figure 1 entering every commutator bar, and this makes all the cross connections that a winding can have, thus giving a completely internally cross-connected winding.

In order to have points of equal potential two poles apart in the lap winding, the usual requirement for all one turn per coil lap windings is to be met, namely, that b/q must be an integer, where b is the number of commutator bars and $q=p/2$ is the number of pairs of poles.

In a frog-leg winding the number of paths through the lap winding is pm_1, where m_1 is the degree of multiplicity of the lap winding, that is, $m_1=1$ for simplex lap, 2 for duplex, and so forth. The number of paths through the wave winding, which is the same as the number through the lap winding, is $2m_2$, that is, 2 for simplex wave, 4 for duplex, and so forth, where m_2 is the multiplicity of the wave winding. Then, $pm_1=2m_2$, and $m_2=qm_1$ (Rule 1). See the list of rules in Appendix I.

The commutator pitch of the lap wind-

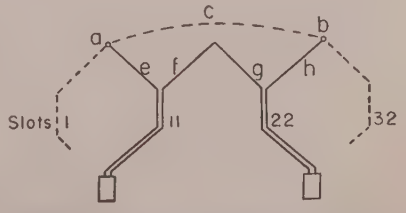

Figure 1. A portion of a simplex lap, duplex wave, frog-leg winding, 42 slots, 4 poles. See Appendix III

Paper 51-119, recommended by the AIEE Rotating Machinery Committee and approved by the AIEE Technical Program Committee for presentation at the AIEE Winter General Meeting, New York, N. Y., January 22–26, 1951. Manuscript submitted February 21, 1950; made available for printing December 13, 1950.

H. B. DWIGHT and R. G. HALTMAIER are both of the Massachusetts Institute of Technology, Cambridge, Mass.

The investigatory work described in this paper was done in connection with a thesis by R. G. Haltmaier, at Massachusetts Institute of Technology.

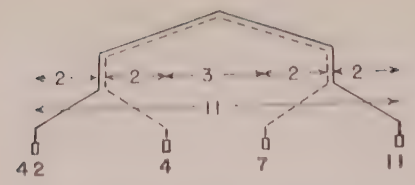

Figure 2. Coils for the winding in Appendix II. The position is that for the first line of the wave winding table

ing is m_1, and that of the wave winding is

$$\frac{b \pm m_2}{q} \quad \text{(Rule 2)}$$

Using the minus sign, making a retrogressive wave winding, saves a little in the length of the coil ends and in the over-all length of the armature.

The matter of re-entrancy is now to be considered. If a duplex lap winding has an odd number of commutator bars, the first and last are of course adjacent and are both odd-numbered. In connecting to the odd bars, 1, 3, 5..., one comes to the last bar and then to bar 2 and to all the even bars. The last even bar connects to bar 1, and the winding is said to re-enter itself. This winding is singly re-entrant. If a duplex lap winding has an even number of commutator bars, after connecting to all the odd bars the winding re-enters itself at bar 1. Then a start is made at bar 2 and all the even bars are connected. This part of the winding re-enters itself at bar 2. This duplex winding is doubly re-entrant.

In general, if the number of commutator bars and the commutator pitch are divisible by a common factor f, the winding is re-entrant at least f times.

It was found many years ago that if the two parts of a duplex, doubly re-entrant winding are connected in parallel only by their contact with the brushes, they are not likely to divide the current load equally. Heating and sparking will take place.

With frog-leg windings, if the lap and wave windings are both doubly re-entrant or both triply re-entrant, the parts are connected in parallel only at the brushes. To avoid overheating and bad commutation, either the lap or the wave winding should be singly re-entrant. Then all the paths which are in parallel will be thoroughly cross-connected. This gives rise to Rule 3, as follows:

$\frac{b}{m_2} = \frac{b}{qm_1}$ must not be an integer, when m_1 is greater than 1.

This rule was enunciated by Powel and Albrecht.[1]

If b were divisible by qm_1, then the lap winding, whose commutator pitch is m_1 would be re-entrant m_1 times. Let $b = cqm_1$ where c is an integer. Then the wave commutator pitch is

$$\frac{b - m_2}{q} = \frac{cqm_1}{q} - \frac{qm_1}{q}$$

which is divisible by m_1. Thus b and the pitch would both be divisible by m_1 and the wave winding would be re-entrant at least m_1 times. Evidently, if both windings are not to be re-entrant m_1 times when m_1 is greater than 1, b/m_2 must not be an integer.

Other rules deal with the number of slots, s. In any lap winding, whether frog-leg or not, s/q is to be an integer or there will be circulating currents in the winding. For instance, in a 6-pole, lap-wound armature with 40 slots, 120 commutator bars, bars per slot $= b/s = 3$, there are points on the winding that are all exactly 40 commutator bars apart. However, if they are connected by cross connections, three portions of the winding are put in parallel. Two of these portions will each have 40 bars and 13 teeth but the third portion will have 40 bars and 14 teeth. The teeth have alternating magnetism and it can be seen that the dividing points in the winding are not actually equipotential points. Therefore, there will be alternating voltage between the points and alternating circulatory currents will flow. Similarly, a 4-pole winding with 35 slots, 70 bars $b/s = 2$, is not suitable for a lap winding. Thus, the ratio s/q should be an integer as well as b/q. See Rule 4.

From this it follows directly that, since $q = p/2$, the number of teeth per pole must be either an integer or an integer plus 1/2.

If the multiplicity of the lap winding, m_1, is an even number, it can be shown that the number of teeth per pole cannot be an integer but must be an integer plus 1/2. If s/p were an integer then s would be even since p is always an even number. Let $b/s = n$, which, being the number of conductors across the top of the slot, is an integer. Therefore, $b = ns$ would be even and b/p would be an integer.

The commutator pitch, or throw, of the wave winding is

$$t_2 = \frac{b - m_1 q}{q} - \frac{2b}{p} - m_1$$

If m_1 is even and b/p is an integer, then t_2 is even. With both b and t_2 even, the wave winding would be at least doubly re-entrant, and with b and m_1 even, the lap winding would be at least doubly re-entrant. There would be two parts of the complete armature connected in parallel

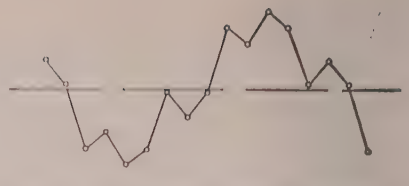

Figure 3. Commutator potential distribution, Appendix II

only at the brushes, which is impractical. Therefore, if m_1 is even, the number of teeth per pole must be an integer plus 1/2. See Rule 5.

If the number of slots per pole is an integer plus 1/2, the number of slots for a pair of poles, s/q, is an odd number. Then, for symmetrically shaped coils connected as in Figure 1, where a wave coil helps connect two points which are exactly two poles apart, the slot pitch of a wave coil is different from that of a lap coil since the two add together to make an odd number. It is seen that in Figure 1 the slot pitch of the lap coil is 10 and that of the wave coil is 11.

This means that a lap coil and a wave coil in such a case cannot lie together as completely as indicated in Figure 2, but they will have an appearance as indicated in Figure 4 and the lap coils and wave coils will have slot pitches which differ by one slot. Such coils are used in some frog-leg windings in practice, as is indicated in a photograph in a book on windings by C. S. Siskind.[3] This photograph was ascribed to the Allis-Chalmers Manufacturing Company, who are the manufacturers of large d-c machines with frog-leg windings.

An alternative to the use of two different slot pitches is theoretically available, as shown in Appendix IV. With this arrangement, the lap and wave coils have the same slot pitch, but the shape of the coils is unsymmetrical. Some of the coil ends, that is, the parts of the coils that go at an angle from the slots to the commutator, are about twice as long as for symmetrical coils. This would add several inches to the over-all length of the armature. Therefore, the coils which are of symmetrical shape but which have unequal slot pitches seem to be preferable and advisable where s/q is an odd number.

Rule 5 is therefore written that if m_1 is even, s/q is to be an odd number and the slot pitches of lap and wave coils are to differ by one slot.

Windings with two different slot pitches for the lap and wave coils may be used in other cases than where m_1 is even, if for any reason the number of slots is such that s/q is odd.

A final rule, Number 6, enunciated by Powell and Albrecht,[1] is that the number of bars per slot, $n=b/s$, is to be prime with regard to m_1.

From Rule 3, $b/(qm_1)$ is not to be an integer when m_1 is greater than 1, and from Rule 4, s/q is to be an integer. Now

$$\frac{b}{qm_1}=\frac{sn}{qm_1}$$

and since s/q is an integer, n/m_1 is not to be an integer when m_1 is greater than 1. That is, n is to be prime to m_1. Note that an integer is prime to another when they have no common factor except unity.

Accordingly, with a duplex lap winding in a frog-leg winding ($m_1=2$), the number of bars per slot, $n=b/s$, may be 1, 3, 5, . . .and so forth and with a triplex lap winding, $n=b/s$ may be 1, 2, 4, 5, ...

If a lap winding and a wave winding have the same number of paths in parallel and the same number of conductors per path, one at least of the windings being multiplex, and if they operate under the same poles, it is evident that they will develop the same average voltage between brushes. It has been shown in this paper that equipotential points should be suitably cross-connected through the winding and that rules should be followed so that the multiplex windings will not be reentrant too many times. It is of interest, and it is a useful check, to tabulate the potential developed at each commutator bar by the lap winding and the wave winding, and see that they agree exactly for every bar, assuming equal pole strengths. This is done for three sample cases of frog-leg windings in Appendixes II, III, and IV. The flux distribution was taken to be the same for all the poles.

In order to make this part of the investigation as strict as possible, the flux was taken to be crowded toward one pole horn, as occurs under load conditions. The windings shown have not necessarily been used on actual machines.

It is the purpose of this paper to derive the rules by which various types of frog-leg windings may be designed. While improvements in operation can scarcely be discussed without describing comparative tests, mention may be made of some features which would ordinarily be expected to give improved operation.

The omission of copper cross connectors removes a location of possible breakdowns. Since most machines do not have a cross connector for every commutator bar, the provision of thorough cross connection for every bar, as given by frog-leg windings, would be expected to reduce heating and improve commutation compared with present usual conditions.

In a paper published by W. V. Lyon, E. Wayne, and M. L. Henderson,[2] formulas were given for skin-effect loss in d-c armature coils and it was shown that this extra loss had a value that was a considerable percentage of the I^2R computed for direct current. This extra loss, as in a-c machines, increases rapidly with the vertical dimension of each copper conductor. As with a-c machines, the conductors could be laminated, but for best results the laminations should be twisted or transposed as is done in large a-c generators and transformers.

If the number of parallel paths in an a-c machine is multiplied by 2, the size of a conductor is decreased by one-half, and the heat from eddy-current loss is reduced. A similar reduction in armature heating, and an increase in efficiency, might be expected from the use of frog-leg windings, since they have twice as many paths as usual and one-half as large conductors. In addition to the paths in the lap winding, there is an equal number of paths in the wave winding.

It is known that if a d-c machine is redesigned so as to have more commutator bars, each of narrower width, an improvement in commutation is expected and is usually obtained. Such a change could be made by changing from a wave to a lap winding. Improvement is usually ascribed to the fact that a smaller current is broken when a brush leaves a bar and that the voltage between adjacent bars is less.

There are machines with simplex lap windings which ordinarily have commutator bars wider than 3/8 inch. Such ratings are those of several hundred kw or more at 250 volts, large 600-volt machines, and some plating generators. There is a theoretical possibility that such machines could be built with duplex or triplex lap windings and more commutator bars. This has not been done to any extent with ordinary windings. Possibly it might be successful with frog-leg windings, which have fewer amperes per path than the corresponding standard windings.

A machine of this type is shown in Appendix II. The smaller average voltage per bar might be expected to improve commutation and flashover conditions. However, this latter expectation might be diminished by the observation from Figure 3 that there are some pairs of adjacent bars with comparatively large voltage between them, perhaps the same as would have been obtained with a simplex lap winding.

Appendix I. List of Rules for Frog-leg Windings

Rule 1. $m_2=qm_1$

Rule 2. Commutator pitch of the lap winding $=m_1$ and commutator pitch of the wave winding $=\dfrac{b\pm m_2}{q}$

$\left(\text{usually } \dfrac{b-m_2}{q}\right)$

Rule 3. $\dfrac{b}{m_2}=\dfrac{b}{qm_1}$ is not to be an integer when $m_1>1$

Rule 4. s/q and b/q are to be integers

Rule 5. If m_1 is even, s/q is to be odd and the slot pitches of the lap and wave coils are to differ by one slot

Rule 6. $n=b/s$ is to be prime to m_1

where:

p = number of poles
$q=p/2$ = number of pairs of poles
s = number of slots
b = number of commutator bars
$n=b/s$ = number of commutator bars per slot
m_1 = multiplicity of the lap winding
m_2 = multiplicity of the wave winding

Appendix II

This machine has 42 slots, 42 bars and 6 poles with frog-leg winding, triplex lap, and 9-plex wave. The lap winding is triply reentrant, and the wave winding is singly reentrant. The configuration of the windings and voltages developed in this type of machine are given in Tables I, II, and III.

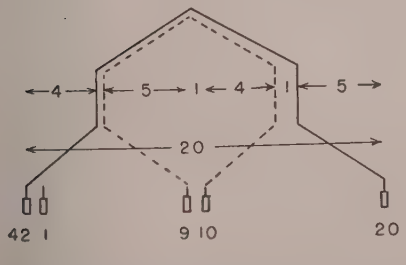

Figure 4. Coils for the winding in Appendix III. The position is for the first line of the wave winding table

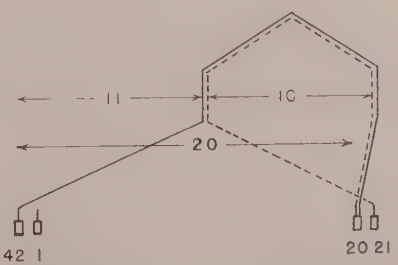

Figure 5. Coils for the winding in Appendix IV. The position is for the first line of the wave winding table

Table I

Volts Developed	0	5	6	7	8	9	10	0	−5	−6	−7	−8	−9	−10	0
Slots	42	1	2	3	4	5	6	7	8	9	10	11	12	13	14
	14	15	16	17	18	19	20	21	22	23	24	25	26	27	28
	28	29	30	31	32	33	34	35	36	37	38	39	40	41	42

Table II. Wave Winding

Bar No.	+Slot No.	−Slot No.	Pot. Diff. Volts	Pot., Volts
42	2	9		0
			12	
11	13	20		12
			−20	
22	24	31		−8
			−14	
33	35	42		−22
			0	
2	4	11		−22
			16	
13	15	22		−6
			10	
24	26	33		4
			−18	
35	37	44=2		−14
			−12	
4	6	13		−26
			20	
15	17	24		−6
			14	
26	28	35		8
			0	
37	39	46=4		8
			−16	
6	8	15		−8
			−10	
17	19	26		−18
			18	
28	30	37		0
			12	
39	41	48=6		12
			−20	
8				−8
19				−22
30				−22
41	Bar 28 is exactly 4 poles, 28			−6
10	slots from the start, bar 42.			4
21	The potentials after bar 28 re-			−14
32	peat.			−26
1				−6
12				8
23				8
34				−8
3				−18
14				0
25				12
36				−8
5				−22
16				−22
27				−6
38				4
7				−14
18				−26
29				−6
40				8
9				8
20				−8
31				−18
42 (Re-enters)				0

Take potential of Bar Number 1 from wave winding, since it is the singly re-entrant winding and the following data is obtained:

1	41	6		−6
			−20	
4	2	9		−26
			12	
7				−14
.				.
.				.
.				.

All potentials of lap winding agree with those of wave winding. A summary of this type of winding is shown in Table IV.

Table III. Lap Winding

Bar No.	+Slot No.	−Slot No.	Pot. Diff. Volts	Pot., Volts
42	40	47=5		0
			−18	
3	1	8		−18
			10	
6	4	11		−8
			16	
9	7	14		8
			0	
12	10	17		8
			−14	
15	13	20		−6
			−20	
18	16	23		−26
			12	
21	19	26		−14
			18	
24	22	29		4
			−10	
27	25	32		−6
			−16	
30	28	35		−22
			0	
33	31	38		−22
			14	
36	34	41		−8
			20	
39	37	2		12
			−12	
42 (Re-enters)				0

Table IV. Recapitulation

Bar No.	Pot.
42	0
1	−6
2	−22
3	−18
4	−26
5	−22
6	−8
7	−14
8	−8
9	8
10	4
11	12
12	8
13	−6
14	0
15	−6
16	−22
. . .	. .
. . .	. .
. . .	. .

Appendix III

This machine has 42 slots, 42 bars and 4 poles with frog-leg winding, simplex lap, and duplex wave. The wave winding is doubly re-entrant. The configuration of the windings and the voltages developed in this type of machine are given in Tables V, VI, and VII.

Table VI. Lap Winding

Bar No.	+Slot No.	−Slot No.	Pot. Diff., Volts	Pot., Volts
42	37	5		0
			−27	
1	38	6		−27
			−31	
2	39	7		−58
			−35	
3	40	8		−93
			−39	
4	41	9		−132
			−43	
5	42	10		−175
			−23	
6	1	11		−198
			9	
7	2	12		−189
			13	
8	3	13		−176
			17	
9	4	14		−159
			21	
10	5	15		−138
			25	
11	6	16		−113
			29	
12	7	17		−84
			33	
13	8	18		−51
			37	
14	9	19		−14
			41	
15	10	20		27
			45	
16	11	21		72
			−4	
17	12	22		68
			−11	
18	13	23		57
			−15	
19	14	24		42
			−19	
20	15	25		23
			−23	
21	16	26		0
			−27	
22	17	27		−27
			−31	
23	18	28		−58
			−35	
24				−93
25				−132
26	Bar 21 is exactly 2 poles, 21			−175
27	slots from the start, bar 42.			−198
28	The potentials after bar 21 re-			−189
29	peat.			−176
30				−159
31				−138
32				−113
33				−84
34				−51
35				−14
36				27
37				72
38				68
39				57
40				42
41				23
42				0

Take potential of Bar Number 1 from lap winding to obtain the following:

1	5	16		−27
			27	
21	25	36		0
			23	
41	3	14		23
			19	
19	23	34		42
			15	
39				57

All potentials of wave windings agree with those of lap winding.

Table V

0	5	7	9	11	13	15	17	19	21	23	−4	−6	−8	−10	−12	−14	−16	−18	−20	−22	0
																					Volts Developed
42	1	2	3	4	5	6	7	8	9	10	11	12	13	14	15	16	17	18	19	20	21
21	22	23	24	25	26	27	28	29	30	31	32	33	34	35	36	37	38	39	40	41	42
																					Slots

Table VII. Wave Winding

Bar No.	+Slot No.	−Slot No.	Pot. Diff., Volts	Pot., Volts
42	4	15		0
			23	
20	24	35		23
			19	
40	2	13		42
			15	
18	22	33		57
			11	
38	42	11		68
			4	
16	20	31		72
			−45	
36	40	9		27
			−41	
14	18	29		−14
			−37	
34	38	7		−51
			−33	
12	16	27		−84
			−29	
32	36	5		−113
			−25	
10	14	25		−138
			−21	
30	34	3		−159
			−17	
8	12	23		−176
			−13	
28	32	1		−189
			−9	
6	10	21		−198
			23	
26	30	41		−175
			43	
4	8	19		−132
			39	
24	28	39		−93
			35	
2	6	17		−58
			31	
22	26	37		−27
			27	
42 (Re-enters)				0

Table VIII

0..	5..	7..	9..	11..	13..	15..	17..	19..	21..	23..	−4..	−6..	−8..	−10..	−12..	−14..	−16..	−18..	−20..	−22..	0
Volts Developed																					
42..	1..	2..	3..	4..	5..	6..	7..	8..	9..	10..	11..	12..	13..	14..	15..	16..	17..	18..	19..	20..	21
21..	22..	23..	24..	25..	26..	27..	28..	29..	30..	31..	32..	33..	34..	35..	36..	37..	38..	39..	40..	41..	42
Slots																					

Table IX. Lap Winding

Bar No.	+Slot No.	−Slot No.	Pot. Diff., Volts	Pot., Volts
42	32	42		0
			−4	
41	31	41		−4
			45	
40	30	40		41
			41	
39	29	39		82
			37	
38	28	38		119
			33	
37				152
.				.
.				.
.				.

Table X. Wave Winding

Bar No.	+Slot No.	−Slot No.	Pot. Diff., Volts	Pot., Volts
42	11	21		0
			−4	
20	31	41		−4
			45	
40	9	19		41
			41	
18	29	39		82
			37	
38	7	17		119
			33	
16				152
.				.
.				.
.				.

All potentials of wave winding agree with those of lap winding.

Table XI

m_1	p	m_2	b	s	b/s	s/p	t_2	b/(qm_1)	
1	4	2	24	24	1	6	11	12	
1	4	2	42	42	1	10½	20	21	(Appendix III)
2	8	8	204	68	3	8½	49	25½	
2	6	6	171	57	3	9½	55	28½	
3	6	9	42	42	1	7	11	4⅜	(Appendix II)
4	8	16	420	140	3	17½	101	26¼	

Appendix IV

This machine has 42 slots, 42 bars, and 4 poles with frog-leg winding, simplex lap, and duplex wave. The wave winding is doubly re-entrant. Configuration of the windings and voltages developed in this type of machine are shown in Tables VIII, IX, and X.

Because of the long connections to the commutator, the arrangement shown in Tables IX and X is not recommended.

Appendix V

Examples of frog-leg windings are given in Table XI, although they have not necessarily been used in actual machines.

References

1. Frog-leg Windings, **W. H. Powell, G. M. Albrecht.** Iron and Steel Engineer (Pittsburgh, Pa.), September and November, 1925.

2. Heat Losses in D-C Armature Conductors, **W. V. Lyon, E. Wayne, M. L. Henderson.** *AIEE Transactions*, volume 47, April 1928, pages 589–98.

3. Direct-Current Armature Windings (book), **C. S. Siskind.** McGraw-Hill Book Company, New York, N. Y., chapters 16 and 17, 1949, page 118.

Discussion

G. W. Arnold (Canadian Westinghouse Company, Ltd., Hamilton, Ont.): The necessity of cross connecting every commutator bar is in some measure dependent on the mechanical stability of the commutator. By rigid quality control of commutator mica and building processes we feel that we have for many years produced commutators which are performing successfully without cross connections on every bar or even on every slot. It is common practice to cross connect bars 1-5-9. . . . where there are two bars per slot, or 1-7-13. . . . where there are three bars per slot.

Regarding circumferential face width of commutator bars, we have a 4,000-ampere 250-volt synchronous booster converter which did not perform successfully with bars having a pitch of 0.856 inch, but when the bar was split, and the commutator was built with mica between the split bars, the machine commutated successfully. As the commutator riser consists of two straps it was a simple matter to connect one strap into each commutator bar.

We have been using laminated armature conductors in large d-c machines for several years. Generally the conductor is divided into 3 or 4 laminations in depth. In a typical generator rated 1,000 kw, 600 volts, 750 rpm, having 6 poles, the calculated eddy loss in the armature conductors, with four laminations in depth per coil, is 0.80 watt per square inch of armature surface, and 1.88 watts with one deep conductor of equivalent cross section. This loss of course varies with the frequency and laminated armature conductors need not be considered in slow speed exciters.

E. R. Martin (University of Michigan, Ann Arbor, Mich.): The paper makes no mention of thickness of brushes. In the ordinary simplex winding, the brushes usually cover about as many bars as there are bars per slot. The lap winding requires as many brush sets as there are poles. If multiplex windings are employed, presumably the brushes should be wider, at any rate, they must be wide enough to feed all parallel paths simultaneously. In Appendix II, a 9-plex winding is used with a 6-pole 42-bar winding, and the minimum brush width possible, to allow commutation time equal to the time taken for a bar to move its width, would be three bars. With brushes three bars wide, each of the brush sets of one polarity would feed six paths of the wave winding in rotation, all brushes feeding different paths when only touching three bars. At the latter instant, no coils would be under commutation, and there would be 12 paths through two coils in series and six paths through three coils in series for a total of 42 coils. When the commutator

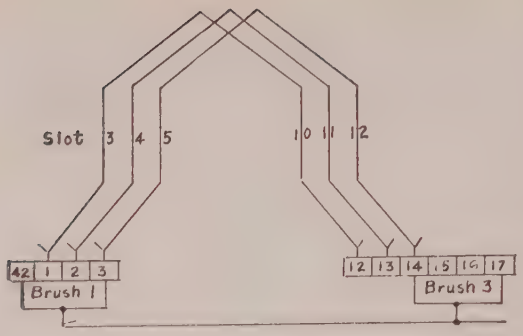

Figure 1 (left)

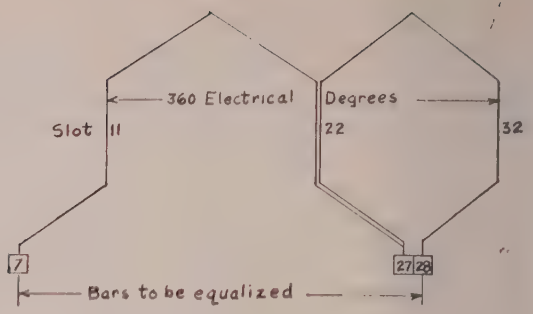

Figure 2 (right)

moves 1/2 bar, there are 18 paths with two coils in series in each path and the other six coils are short-circuited through the brush connections.

While the author's example has no doubt purposely used only a few bars for simplicity, and voltage per path calculations would not mean too much, they do show an unbalance in the ratio of 2-to-3 between the several paths. If this were so to a less degree in a winding of several times as many bars, and there is a strong probability that it would be in an eighteen path wave winding, the unequal voltages would cause circulating current at no-load with uniform conditions under all poles, as well as under load with shifted pole flux.

Commutation occurs in the wave winding by transferring a coil from one path under a brush to another path under an adjacent brush of the same polarity, see Figure 1 of this discussion. No coils are short circuited under any brush; while in the lap winding, the bar entering is connected to the bar leaving contact with each brush. Although the brushes cover three bars, the commutating zone is only one bar or one tooth pitch wide and commutation looks feasible.

This is a very unorthodox winding and should not be used without very careful checking on the volts per path. While frog-leg windings have been used successfully, it appears doubtful that they could have as many paths as 36 in a 6-pole machine.

Figure 1 of the paper shows the equalizing at the wrong end. The equalizing is done at the commutator end and should be shown as in Figure 2 of this discussion.

It is not necessary to use large conductors in large lap wound armatures. In fact it is common practice to use parallel conductors, when the copper section requires too deep a conductor.

There is a growing tendency to install the regular equalizer connections just back of the commutator. While they are very inaccessible, they can be installed and protected much better, and so are not vulnerable to failure. Designing engineers have usually preferred the standard equalized lap winding because of its simplicity, its better slot space factor, and better adaptability to different numbers of slots.

H. B. Dwight and **R. G. Haltmaier:** Cases are not common in which commutator bars are so wide that a d-c machine can be redesigned so as to use twice as many bars, and the description of a large machine of this type, given by G. W. Arnold, is very interesting.

The example he gives of the advantage of laminating a d-c armature winding is also interesting.

In the discussion by E. R. Martin it is stated that there are some paths with two coils in series and some with three, in Appendix II, and "voltage per path calculations. . .show an unbalance in the ratio of 2 to 3." It is the number of conductors in series which he seems to have found in unbalance and it does not appear that he has made any calculation of voltage per path. The developed voltage per path does not depend very directly on the number of conductors per path since there are conductors near the ends of a path which lie in the interpolar region and develop little or no voltage.

With a simplex lap winding, conditions are repeated exactly from pole to pole, when the pole strengths are equal. A path goes from a positive brush to a negative brush and there should be no complaint about inequality of voltage per path in a simplex lap winding. But the voltage developed between any two commutator bars is exactly the same, with equal pole strengths, for the multiplex wave winding of a frog-leg winding as for the lap winding, as has been shown in the paper, for windings with fewer bars and more irregularities in proportion than would be probable in practice.

The voltage per path is shown approximately in Figure 3 and is the difference in potential between the highest and lowest points in that figure. There are small irregularities with a multiplex lap winding, as mentioned in the paper, and the question whether duplex lap windings are advantageous in the few but important cases where the commutator bars would otherwise be unusually wide should be decided by practical trial.

Fault Transients in Aircraft D-C Systems

DONALD G. SCORGIE
ASSOCIATE AIEE

PROBLEMS such as system protection and circuit breaker design have made it desirable to understand more fully the transient behavior of d-c generator-regulator systems upon application or removal of a fault. Work along these lines has been accomplished,[1–4] but it has been recognized[2] that the results are in some instances not satisfactory. Particularly in dealing with aircraft problems one finds that these references will not provide solutions. T. M. Linville and H. C. Ward, Jr.,[1] for instance, have assumed that after a fault the shunt field flux linkages remain constant for a range of time up to the peak surge load current. This presupposes a larger time constant for the field circuit than appears justifiable with aircraft generators. Another element peculiar to aircraft systems is the quick-acting voltage regulator, which of course has not been considered in transient analyses of large generators.

In the analysis presented here simultaneous linear differential equations that describe the fault transients are set up and solved. Linearizing assumptions enormously simplify the mathematics permitting us to obtain equation 8, which is an expression in closed form for the entire fault current transient. By means of equation 8 fault currents have been predicted accurately without assuming constancy of field flux linkages. In effect, a less restrictive assumption has been substituted, namely, that the slope of the flux versus magnetizing force curve for the field pole remains constant. The peak fault current is expressed in equation 10 as the ratio of the driving voltage to a quantity R_t which is expressed in terms of the system parameters.

Calculations using equation 8 show the extreme importance of evaluating the slopes of the generator saturation curve and the external characteristic at the initial operating point prior to the fault in order to obtain good predictions of the fault transient. This represents a departure from many previous analyses, where the saturation curve has been approximated by a straight line through the origin and the point of rated voltage.

The solutions obtained have been calculated nearly to the steady state; however there is little hope of predicting steady-state values accurately. This is due both to the fact that the linearity assumptions become worse with time, and because the steady-state external characteristic of the machine exhibits poor reproducibility.

The analysis in this paper should be applicable to large generators. However, it must be remembered that in obtaining empirical verification of the theory certain experimental difficulties are not present with small low-voltage machines. There was, for instance, no evidence of flashing over on the commutator during the faults. Also, for initiating experimental faults a knife switch was used, thereby eliminating contactor bounce.

Fault currents of both separately excited and self-excited generators are considered in this paper, and a method is given for predicting the effect of a carbon-pile voltage regulator. The resistance value of a fault affects the resulting transient, and this is taken into account by introducing fault resistance in the boundary conditions and as a parameter of the circuit. Variations of transient load current with speed and initial load are automatically taken into account, since the parameters introduced in this paper are those measured at the condition existing prior to the application of the fault.

Through experimental observations H. J. Finison and R. H. Kaufman[3] have arrived at a definition of transient resistance in terms of incremental changes from the initial conditions. For zero fault resistance identical values are obtained using their definition and the definition derived analytically in the following paragraphs, but a difference exists which becomes greater with higher fault resistance.

The factors affecting the voltage transient upon removal of a fault will be discussed briefly toward the end of this paper.

Basic Equation for the Armature Circuit

The analysis which follows gives in closed form the load current as a function of time where a fault resistance R_L is

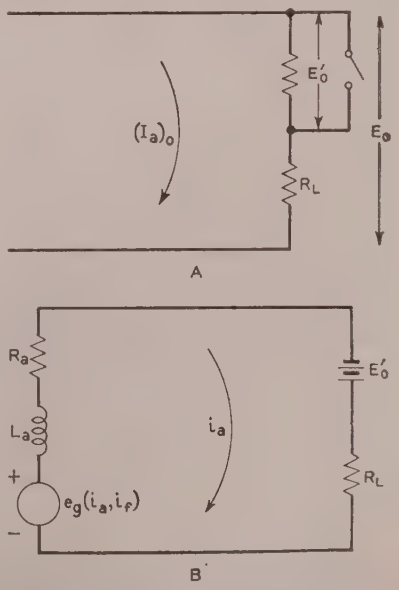

Figure 1. Equivalent circuit for armature equation

Paper 51-120, recommended by the AIEE Air Transportation and Rotating Machinery Committees and approved by the AIEE Technical Program Committee for presentation at the AIEE Winter General Meeting, New York, N. Y., January 22–26, 1951. Manuscript submitted October 24, 1950; made available for printing December 21, 1950.

DONALD G. SCORGIE is with the Naval Research Laboratory, Washington, D. C.

The author wishes to express his appreciation to D. H. SCHAEFER, who made the measurements contained in this paper, and whose criticisms have been most valuable.

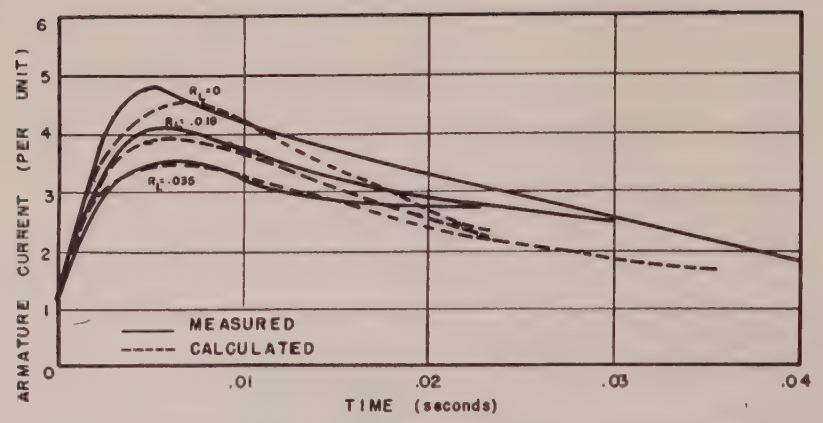

Figure 2. Shunt generator faults. No regulator, generator self-excited, full initial load

suddenly applied to the system. Results which have been obtained indicate that for this purpose two simultaneous linear differential equations can be written which describe the current surge satisfactorily for a simple shunt generator. We shall assume that our fault is initiated by closing a switch across a portion of the existing load at $t=0$, leaving some remaining fault resistance R_L, as shown in Figure 1(A). The armature circuit is then assumed to consist of a resistance (R_a+R_L), and inductance L_a, and two equivalent perfect generators all connected in series, as in Figure 1(B). R_a and L_a are the resistance and the incremental self-inductance, respectively, of the armature plus any compensating and commutating windings. The first of the equivalent generators is the driving input, which is a voltage step introduced at $t=0$ and equal to the voltage across the switch before closing. Since the circuit is not passive, a second equivalent generator must be inserted, the voltage of which is equal to the change of the machine's generated voltage as a function of the change of armature and field currents. The change from the initial generated voltage will be represented by $e_g=e_g(i_f,i_a)$, where i_a is the incremental change from the initial value of load current and i_f is an incremental change from the initial value of field current. The generated voltage e_g can be expanded in a Taylor's Series for a function of two variables, and if the partial derivatives of e_g with respect to i_a and i_f are constants, the expansion reduces simply to

$$e_g=D_a i_a+K_s i_f^* \tag{1}$$

where

$$D_a\equiv\frac{\partial e_g}{\partial i_a} \text{ and } K_s\equiv\frac{\partial e_g}{\partial i_f}$$

* Throughout this paper lower case i and e will be used to indicate increments from the initial currents and voltages.

The constant D_a represents the demagnetization caused by armature reaction and cross ampere turns, and usually will be a negative number. K_s is the slope of the saturation curve at the initial operating point and will be a positive constant.

Let E_0 and $(I_a)_0$ be the terminal voltage of the machine and its load current, respectively, prior to the application of a fault. By definition we let

$$E_0'=E_0-(I_a)_0R_L$$

so E_0' represents the step voltage introduced at $t=0$. The basic equation of the armature circuit during the transient is therefore

$$E_0'+e_g(t)=(R_a+R_L)i_a(t)+L_a\frac{di_a}{dt} \tag{2}$$

which, using equation 1, may be rewritten

$$E_0'=(R_a+R_L-D_a)i_a(t)+L_a\frac{di_a}{dt}-K_s i_f(t) \tag{2'}$$

Basic Equation for the Field Circuit

Equation 2', which pertains to the armature circuit, holds whether or not a voltage regulator is included in the system, and for both separately and self-excited generators. Each of these four cases must be considered individually, however, when writing the field circuit equation. In each case the symbol M is used to indicate an inductive coupling between armature circuit and the field winding. M is defined simply as $N_f\,\partial\phi_f/\partial i_a$, where ϕ_f is the flux linking the shunt field windings. M is not considered as a mutual coupling coefficient in the usual sense. Ordinarily M will be a negative number. The comparable term may be left out of equation 2' without appreciably affecting the solution, but this coupling must be included in the field equation.

The four field circuit equations are obtained as follows:

Case 1. No voltage regulator, self-excitation

Let the incremental self-inductance of the shunt field be L_f, and the field circuit resistance be R_f. The change of terminal voltage after the fault is applied is given by $-E_0'+R_L i_a(t)$, and the transient field circuit equation is

$$R_L i_a(t)-E_0'=L_f\frac{di_f}{dt}+M\frac{di_a}{dt}+R_f i_f(t) \tag{3}$$

Case 2. No voltage regulator, separate excitation

The transient field circuit equation is given by

$$0=L_f\frac{di_f}{dt}+M\frac{di_a}{dt}+R_f i_f(t) \tag{4}$$

Case 3. Carbon-pile voltage regulator operating self-excitation

Provided the fault resistance is small enough so that the generator terminal voltage drops more than a volt or two, the carbon-pile resistance can be assumed to change instantly to its minimum value

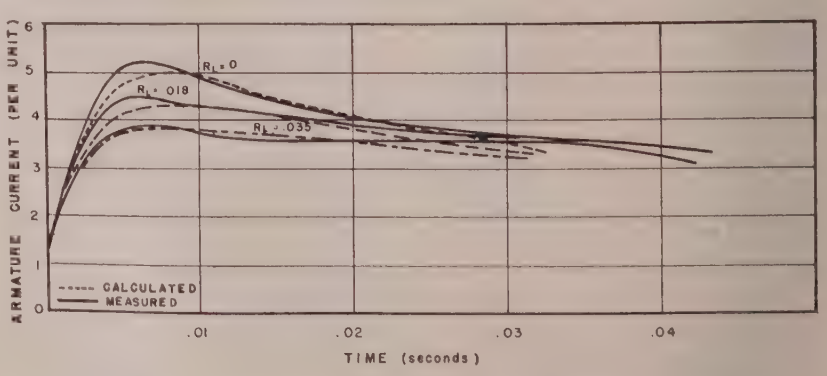

Figure 3. Shunt generator faults. No regulator, separate excitation, full initial load

The field circuit resistance changes instantly from its initial value $(R_f)_0$ to its minimum value R_s. This assumption appears valid both in theory[5] and in practice.

Calculations from reference 5 show that if, for instance, the change of terminal voltage at $t=0$ were 30 volts, then the rate of change of carbon-pile resistance would be approximately 15,000 ohms per second for a typical regulator. Oscillographic records have confirmed this, therefore the portion of the field circuit comprised of minimum resistance R_s and the field inductance experiences a change of voltage equal to $-E_0''+R_Li_a(t)$.

$$E_0'' = \frac{R_s}{(R_f)_0}E_0-(I_a)_0R_L$$

which is the difference between the voltages across this portion of the field the instant before and the instant after the fault.

The field circuit equation in this case is given by

$$R_Li_a(t)-E_0''=L_f\frac{di_f}{dt}+M\frac{di_a}{dt}+R_si_f(t) \qquad (5)$$

Case 4. Carbon-pile voltage regulator operating, separate excitation

Here again the same assumption can be made regarding the instantaneous change of carbon-pile resistance. The voltage change experienced by the remainder of the field is given by

$$-V=E\left(1-\frac{R_s}{(R_f)_0}\right)$$

where E is the constant excitation voltage. In this case the field circuit equation is given by

$$-V=L_f\frac{di_f}{dt}+M\frac{di_a}{dt}+R_si_f(t) \qquad (6)$$

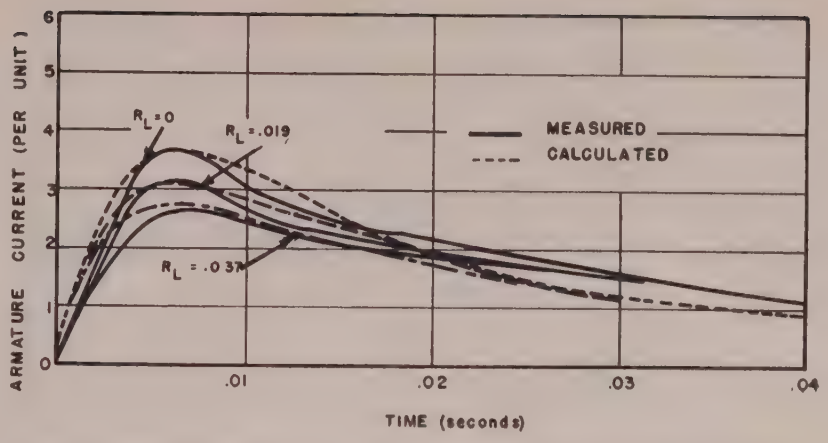

Figure 5. Shunt generator faults. No regulator, generator self-excited, initial load zero

Solution of Equations for Fault Current

Equation 2′ easily may be solved simultaneously with either equation 3, 4, 5, or 6. The LaPlace Transform of the total load current in all four cases will have the form:

$$I_a(s)=\frac{(I_a)_0}{s}+\frac{E_0'}{L_as}\left[\frac{S+\beta_j}{(S+A)^2+B_j^2}\right] \qquad (7)$$

where

$$A={}^1/_2(\alpha+\beta)$$

$$\alpha=\frac{R_a+R_L}{L_a}$$

$$\beta=\frac{R_f}{L_f}$$

B_j will be defined.

The subscript j equals 1, 2, 3, or 4 and refers to the four conditions under which the field circuit equation was written. The corresponding constants are defined as follows:

Case 1. No-regulator, self-excitation

$$\beta_1=\beta-\frac{K_s}{L_f}$$

$$B_1=\sqrt{\beta\alpha'-\frac{K_sR_L}{L_aL_f}-A^2}$$

where

$$\alpha'=\alpha-\frac{D_a}{L_a}$$

Case 2. No regulator, separate excitation

$$\beta_2=\beta$$

$$B_2=\sqrt{\beta\alpha'-A^2}$$

Case 3. Voltage regulator operating, self-excitation

$$\beta_3=\beta-\frac{K_s}{L_f}\frac{E_0''}{E_0'}$$

$$B_3=B_1$$

Case 4. Voltage regulator operating, separate excitation

$$\beta_4=\beta=\beta_2$$

$$B_4=B_2$$

It is shown[6] in Appendix 1 that

$$M=\frac{D_aL_f}{K_s}$$

Therefore, in deriving equation 7 from the differential equations the inductive coupling coefficient was eliminated by using the other more easily determined constants.

Transient load current as a function of time is given by the inverse transform of equation 7, namely

$$i_a(t)=E_0'[K_1+K_2\epsilon^{-At}\sin(B_jt+\psi)] \qquad (8)$$

or

$$I_a(t)=(I_a)_0+F_0']K_1+K_2\epsilon^{-At}\sin(B_jt+\psi)] \qquad (8')$$

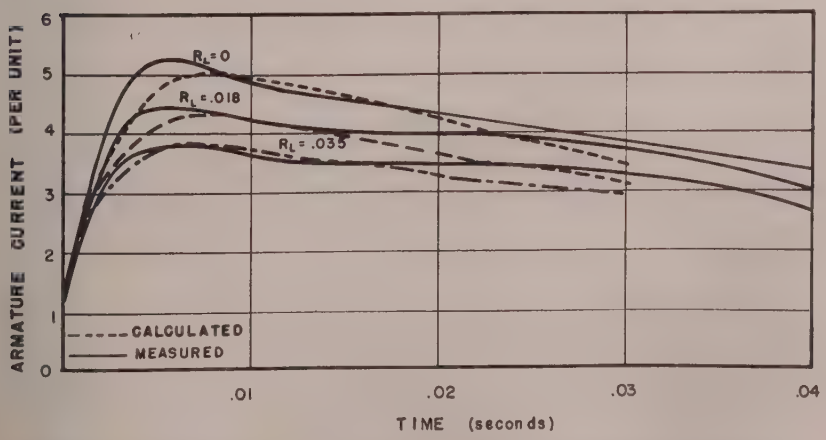

Figure 4. Shunt generator faults. Regulator operating, self excitation, full initial load

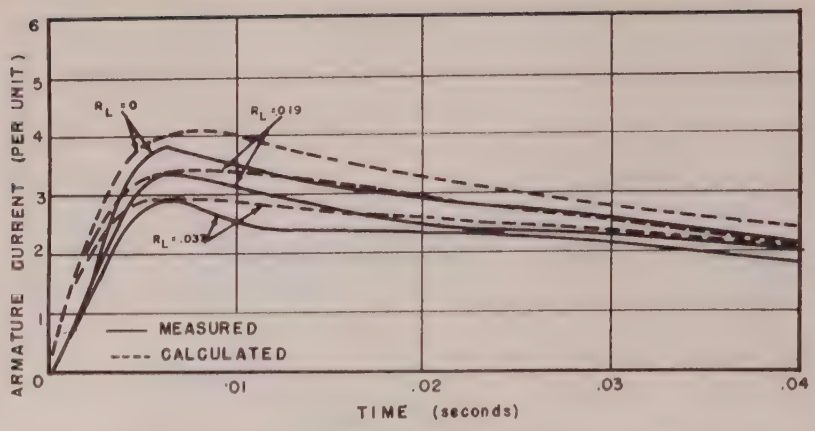

Figure 6. Shunt generator faults. No regulator, separate excitation, initial load zero

where

$$\psi = \tan^{-1}\left(\frac{B_j}{\beta_j - A}\right) + \tan^{-1}\left(\frac{B_j}{A}\right)$$

$$K_1 = \frac{\beta_j}{L_a(A^2 + B_j^2)}$$

$$K_2 = \frac{\sqrt{(\beta_j - A)^2 + B_j^2}}{L_a B_j \sqrt{A^2 + B_j^2}}$$

and $I_a(t)$ is the total armature current.

Differentiating equation 8 and setting it equal to 0, the time at which peak current occurs is given by

$$t_p = \frac{1}{B_j}\tan^{-1}\left(\frac{B_j}{A - \beta_j}\right) \qquad (9)$$

Combining equations 8 and 9 we obtain the peak incremental current in terms of the generator parameters and the fault resistance:

$$i_a(t_p) = E_0' \times \left[K_1 + K_2 \epsilon^{-\frac{A}{B_j}\tan^{-1}\frac{(B_j)}{A-\beta_j}} + \sin\left(\tan^{-1}\frac{B_j}{A}\right)\right] = \frac{E_0'}{R_T} \qquad (10)$$

The reciprocal of the term in the square brackets of equation 10 has the dimension of resistance and will be designated by R_T. Unfortunately, its form is not simple. The best we can do is to determine the relative importance of the parameters by calculating families of curves using a practical set of parameters and varying one of them. It is hoped in this way to be able to understand better what factors must be considered. Recently attempts have been made to find a correlation between transient resistance of a d-c generator and the product horsepower times speed.[7] The attempt in this paper has been to express the current transient in terms of factors which can be measured easily and which can be calculated from the physical structure of the machine.

Determination of Constants of Generator

Resistance Values

Six constants of the generator must be determined before solving equation 8. Of these, two are the resistances of the field and armature circuits, which in the main are measured by well-known methods. The resistance of the armature circuit is far from constant, but changes greatly as a function of load for small currents. The change is connected with commutator film and surface polish of the carbon brush.[8] At low-current densities the resistance of the carbon-copper contact is high and is a function of time. This portion of the resistance drops rapidly to a low value at high-current density. The value of R_a used in this paper is always measured at full load.

Demagnetization Constant

D_a was defined earlier in this paper as $\partial e_g/\partial i_a$. If the terminal voltage E_t is expressed as a function of the armature and the field currents,[9] the expression may be differentiated partially with respect to armature current giving

$$\frac{\partial E_t}{\partial i_a} = \frac{\partial e_g}{\partial i_a} - R_a$$

Adding armature resistance to both sides gives the constant D_a. These partial derivatives can be approximated by incremental measurements in the neighborhood of the initial operating point, and the transients calculated in this paper used values obtained in this manner. For simple shunt-wound generators this leads to no difficulty, but for compensated machines trouble is encountered in the region of small armature currents. In this region the changes of brush-contact resistance with current density are on the order of magnitude of D_a itself and thus introduce prohibitively large errors unless great care is taken.

Slope of Saturation Curve

K_s is the slope of the generator saturation curve at the initial operating point. Again, the value may be obtained either by differentiating an analytical expression for terminal voltage, this time with respect to field current, or by direct measurements holding load current constant if the machine is available. Good results were obtained only when D_a and K_s are evaluated in the neighborhood of the initial operating conditions.

Mutual Inductance between Field and Armature Circuits

M is a magnetic coupling coefficient expressing the effect upon the field circuit of changes in armature circuit current. No attempt has been made to argue whether it is a bilateral mutual inductance in the usual sense. The question is of no practical importance, because the voltage

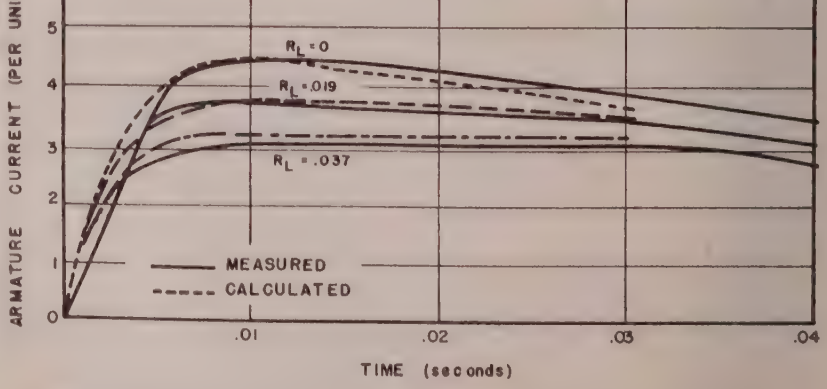

Figure 7. Shunt generator faults. Regulator operating, self-excitation, initial load zero

introduced into the armature circuit because of typical rates of change of field current is found to be negligible. As stated above, the relationship $M = D_a L_f / K_s$ justified in Appendix I was used in this paper to eliminate the need for evaluating M directly. The assumption necessary to derive this relationship is that there exists a proportionality between the flux responsible for generated voltage and the flux linking the field pole winding.

Field Self-Inductance (Incremental)

L_f is defined as

$$N_f(\partial\phi_f)/\partial i_f \times 10^{-8}$$

where N_f is the number of turns in the shunt field winding. The flux linking the field winding is related to the effective air-gap flux by a leakage coefficient which in aircraft generators is quite large and must be taken into account. If the generator is available L_f may be obtained by direct measurement in either of two ways. With no generator load an oscillographic record may be made of the response of the field current to a step change of resistance with constant excitation, or sinusoidal resistance change[6] can be introduced and voltage and current phase relationships observed as a Lissajou figure. The latter method is to be preferred, but a sinusoidally variable resistance generally is not available. To determine L_f with the generator loaded, the value of K_s was first determined in the vicinity of the loaded operating point. The loaded L_f can be calculated from the loaded K_s and the L_f and K_s for some no-load case, reducing L_f in proportion to the K_s's and making the proper adjustment for the change of leakage coefficient.

Armature Circuit Incremental Self-Inductance

Methods for calculating L_a from a knowledge of the physical characteristics of the generator have recently been published,[10] and it is not the purpose of this paper to attempt an improvement of these calculations. It is clearly recognized that L_a is variable and probably the treatment of it here as a constant is the weakest assumption which has been made. The approach here will be merely to define L_a and indicate the manner in which it was measured.

As previously stated, L_a is the incremental self-inductance of the entire armature circuit, including commutating and compensating windings, at the initial operating condition. In a previous paper[6] the terminal voltage transient was expressed as a function of time upon removal of load from a regulated generator. Two discontinuities occur in the voltage transient, one at $t=0$ and a second when the load current reaches zero. Both are primarily discontinuities in the $L_a di_a/dt$ voltages of the armature circuit. To a very good approximation L_a is given by dividing the step-function change of terminal voltage at the instant full load is initiated by the rate of change of load current. It is recognized that L_a is influenced by eddy-current paths in the field poles and rotor, and hence is a function of the speed of flux variations. However, the checks between empirical and calculated transients appear sufficiently close to substantiate the measurements of L_a made in this fashion.

Application to Existing Generators

The equations derived in the preceding paragraphs have been applied to two aircraft generators; generator number 1 has a simple shunt field and is rated at 75 amperes, 30 volts, while generator number 2 has compensating and commutating fields and is rated at 200 amperes, 30 volts.

Figures 2 through 7 show families of curves calculated for generator number 1 with various values of fault resistance. In Figure 2 it was assumed that there was no regulator, that the generator was self-excited, and that the initial load current was 75 amperes, corresponding to full load. Figure 3 assumes the same conditions, but with separate excitation. In Figure 4 it was assumed that a carbon-pile voltage regulator was connected, that the generator was self-excited, and the initial load was 75 amperes. Figures 5, 6, and 7 are the corresponding cases calculated assuming the initial load equaled zero. The constants in these calculations were as follows:

Initial Load	L_a	R_a	K_s	D_a	L_f	R_f	R_s
0	2.5×10^{-4}	0.08	15.5	−0.080	0.55	21.3	4.16
Full	2.5×10^{-4}	0.08	8.0	−0.113	0.25	10.1	4.16

Each figure also shows the corresponding measured transient load currents, and the agreement is fairly good in each case.

Figure 8 shows a typical comparison between measured and calculated transients with the compensated generator number 2. The constants, such as L_f and D_a, for this machine are much smaller (by a factor of 5 to 10) than with generator number 1, yet the absolute magnitude of the magnetic hysteresis in both generators is nearly the same. With the simple shunt machine hysteresis could account for a maximum error of ±8 per cent in the value of D_a, whereas with the compensated generator hysteresis causes changes in D_a up to ±30 per cent. It is reasonable, then to obtain the better fault current predictions assuming linearity with generator number 1. However, at least two additional factors should be investigated in connection with the problem, namely, the effects of interpole saturation and eddy currents upon effective armature inductance.

Factors Affecting Transient Response

The transient resistance, R_T, of d-c generators has been defined in various ways by different investigators.[1,3] In reference 1 it was defined as the ratio of the initial generated voltage to the total peak surge current. In reference 3 it was defined as the ratio of changes of load voltage and current taken at the instant of peak surge current. From equation 10 it can be seen that the ratio of peak i_a to E_0' is expressed in terms of the parameters of the generator and the fault resistance. Therefore this appears to be a fundamental relationship. E_0', it should be recalled, is the driving voltage which appeared across our switch before it was closed short-circuiting all or part of the initial load resistance. We are defining transient resistance as the ratio of this step function input voltage to the peak incremental armature current.

The fact that the peak change of load current rather than peak total current is fundamental explains in part why other investigators[2] have found transient resistance defined in the first manner to decrease with increased initial load current. The difficulty with specifying a unique transient resistance for a particular generator even by the use of equation 10 is that the generator parameters change as a function of initial conditions. With a compensated machine such as generator number 2 in this paper, the parameters vary relatively little with initial conditions. If, for instance, the parameters are measured at 30 volts, both no-load and full-load, the constants will remain about the same except for a decrease of R_f. This results in an increased time constant for the shunt field which in some cases decreases the transient resistance slightly.

Transient resistance, R_T, defined as above has repeatedly proved to contain a constant of the generator which is independent of fault resistance. If the fault resistance is subtracted from R_T one gets the zero-fault transient resistance $(R_T)_0$. Table I shows values calculated from the series of measured curves in Figures 1 through 6. Values of R_T calculated by equation 8 will differ from the values in Table I by less than 6 per cent.

The parameters affecting transient resistance depend a great deal upon which condition is being analyzed, and in particular which term of equation 10 dominates. If the transcendental term dominates as, for instance, with a self-excited generator with no regulator and a small fault resistance, the transient resistance is critically dependent upon the mutual inductance between the shunt field and the armature circuit. If the constant term of equation 10 dominates, such constants as the armature and fault resistances and the demagnetization coefficient are the determining factors, as no inductance terms appear in K_1. In this case, the field resistance and the slope of the saturation curves also are important, especially if the generator is self-excited. Experiments have been performed varying the field time constant when the generator was separately excited. The effect upon the fault current transients was virtually negligible.

Generator speed has been observed[2] to affect the transient resistance, always increasing it with increased speed. For cases when the transcendental term of equation 10 dominates this is due primarily to the increase of the mutual inductance coefficient and the decrease of the shunt field-circuit time constant with speed.

A most pronounced effect upon transient peaks and therefore upon transient resistance is caused by a change of the self-inductance of the armature circuit. Figure 9 shows a typical set of calculated curves in which reducing the self-inductance of the armature circuit by 50 per cent increases the transient peak current by 18 per cent. In the same figure the effect of decreasing the magnitude of K_s by 35 per cent and D_a by 25 per cent is illustrated. In general a decrease of the magnitude of either D_a or K_s raises the calculated steady-state fault current, and to a lesser extent raises the peak current surge.

It was stated earlier that the generated voltage and field flux decrease markedly by the time the peak fault current is reached. One quantitative example will suffice to illustrate this point. Consider the zero-fault transient plotted in Figure 2, in which the values of $D_a = 0.080$ and $K_s = 15.5$ were used. Solution of the equations show that at time of the peak fault current $i_a = 270$ amperes and $i_f = 0.82$ ampere. From equation 1 it follows that the generated voltage has decreased 9.0 volts, or 30 per cent of its original value. The fact that by use of a constant flux leakage coefficient correct fault currents were calculated is presented as proof that the shunt field flux decreased proportionally to the generated voltage.

Table I

Regulator	Excitation	Initial Load	R_L	Measured R_T	$(R_T)_0 + R_L$
No	Self	0	0	0.111 = $(R_T)_0$	0.111
No	Self	0	0.019	0.128	0.130
No	Self	0	0.037	0.151	0.148
No	Separate	0	0	0.105 = $(R_T)_0$	0.105
No	Separate	0	0.019	0.119	0.124
No	Separate	0	0.037	0.143	0.142
Yes	Self	0	0	0.091 = $(R_T)_0$	0.091
Yes	Self	0	0.019	0.109	0.110
Yes	Self	0	0.037	0.131	0.128
No	Self	Full	0	0.105 = $(R_T)_0$	0.105
No	Self	Full	0.018	0.122	0.123
No	Self	Full	0.035	0.144	0.140
No	Separate	Full	0	0.095 = $(R_T)_0$	0.095
No	Separate	Full	0.018	0.112	0.113
No	Separate	Full	0.035	0.129	0.130
Yes	Self	Full	0	0.095 = $(R_T)_0$	0.095
Yes	Self	Full	0.018	0.110	0.113
Yes	Self	Full	0.035	0.127	0.130

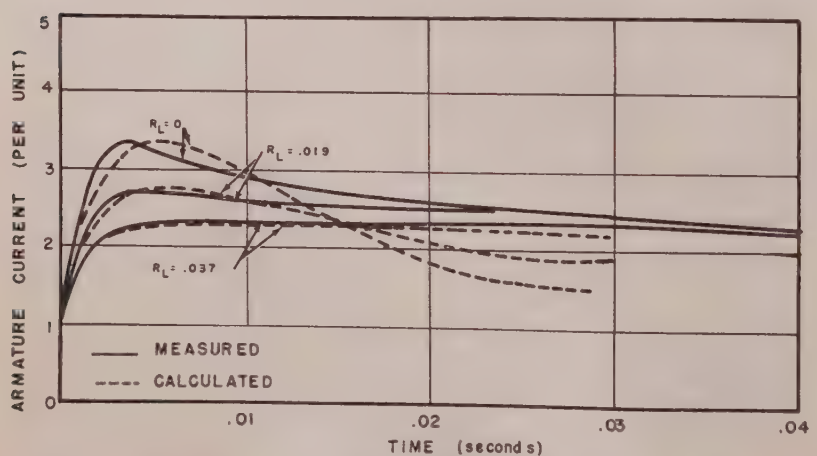

Figure 8. Compensated generator faults. No regulator, self-excitation, full initialload

Removal of Fault

This paper has dealt with problems of interest to the designers of circuit interrupter equipment. For the sake of completeness a word should be said about the terminal voltage transient resulting from the clearing of a fault. The author has included in a previous paper[6] two calculations of terminal voltage transients following the removal of a full normal load from a regulated generator.

The question has been raised as to what peak voltage the circuit breaker sees during the time a fault is being removed. From the available data it appears that the answer can be furnished using the previous work in conjunction with the present paper. However, no attempt will be made to discuss it in detail here. Only two tentative results will be mentioned, namely:

1. The peak terminal voltage during load removal is not a function of the generator alone, but is equally dependent upon the circuit breaker characteristics.

2. The incremental self-inductance, L_a, and ohmic resistance, R_a, of the generator armature circuit (including commutating and compensating windings) are the only generator parameters which affect this voltage peak.

If the fault current has come to a steady state I_1 before being cleared and the terminal voltage at that instant is E_1, then the peak voltage seen by the circuit breaker will be $E_1 + R_a I_1 + L_a di_a/dt$ where L_a and di_a/dt are evaluated the in-

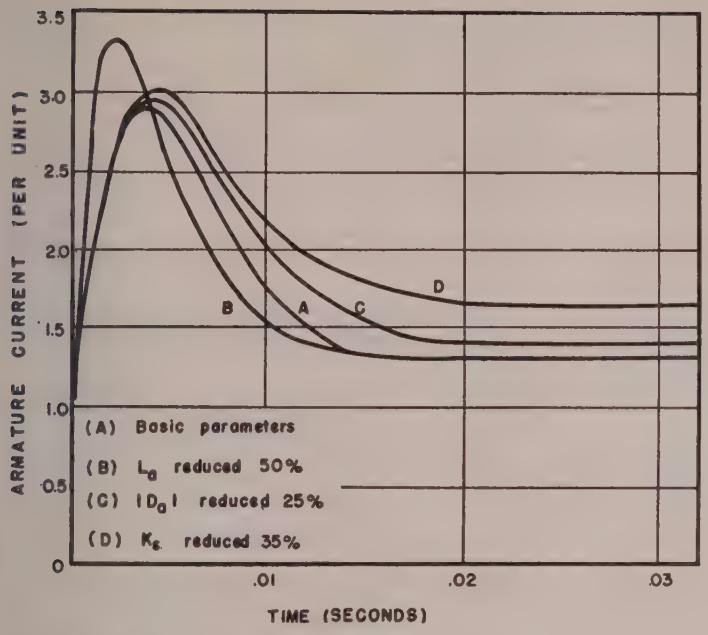

Figure 9. Calculated fault currents with various generator parameters

stant before the fault current reaches zero.

Summary

Expressions for the transient fault currents of both regulated and unregulated aircraft d-c generators have been derived. Linearity of incremental inductance coefficients, demagnetization caused by load current, and saturation curve slope were assumed, and two simultaneous linear differential equations were written which satisfactorily describe measured transient fault currents up to and past the peak surge. The solution to these equations indicates that a reasonable definition for transient fault resistance of a generator is the ratio of the step function driving voltage (or voltage short-circuited at the instant of fault) to the maximum incremental load current. Nevertheless, by this definition the effect of initial conditions, excitation, and the presence of a voltage regulator must be considered. The voltage regulator is found to decrease transient resistance, and this decrease is reasonably well accounted for by the differential equations which have been solved.

Solutions to the equations show that generated voltage has decreased about 16 per cent in typical cases at the peak current surge although decreases up to 30 per cent have been noted.

The values of mutual inductance used everywhere in this paper were derived assuming that the leakage flux coefficient remained constant throughout each transient. Results appear to justify this assumption in the case of the simple shunt generator. However, the presence of interpoles and compensating windings introduce some inaccuracy in the results. Further investigation will be necessary to determine whether the difference is caused by magnetic hysteresis, changing leakage flux coefficient, or the changing self- and mutual-inductance coefficients. It was stated previously that probably the worst assumption made in the paper is that L_a remains constant. Treatment of L_a in equation 2 as a function of i_a is possible, particularly if one has available the services of an analogue computer, such as the REAC. In this direction lies the best chance of improving the results of the paper.

Appendix I

Elimination of M

Throughout the paper it has been assumed that

$$M=\frac{D_aL_f}{K_s} \tag{11}$$

which follows from the assumption that ϕ_f is proportional to the flux ϕ_a responsible for generated voltage, that is:

$$\phi_a=k\phi_f \tag{12}$$

Definitions of D_a, L_f, K_s, and M have been given in the text. If one utilizes the fact that for a constant generator speed

$$e_g=K\phi_a \tag{13}$$

where ϕ_a is the flux responsible for generated voltage, the definitions take the form:

$$\left.\begin{aligned} K_s&=K\frac{\partial\phi_a}{\partial i_f}\\ D_a&=K\frac{\partial\phi_a}{\partial i_a}\\ L_f&=N_f\frac{\partial\phi_f}{\partial i_f}\times10^{-8}\end{aligned}\right\} \tag{14}$$

From equations 12 and 14:

$$\frac{D_aL_f}{K_s}=N_f\frac{\partial\phi_f}{\partial i_a}\times10^{-8} \tag{15}$$

Which by definition is equal to M.

Appendix II

Nomenclature

R_a = The d-c resistance of the armature circuit consisting of the armature winding and, if any, the compensating and commutating winding

R_L = The total external fault resistance

$(R_f)_0$ = The shunt field circuit resistance prior to the application of fault

R_s = The minimum field circuit resistance with carbon-pile resistor at its least value

R_f = The field circuit resistance after fault (R_s when a regulator is connected, and $(R_f)_0$ with none)

$(I_a)_0$ = Load current prior to fault

i_a = Incremental change of armature current

i_f = Incremental change of shunt field current

e_g = Incremental change of generated voltage from that existing prior to fault

E = Constant excitation voltage with separately excited field

$V=E\left(1-\frac{R_s}{(R_f)_0}\right)$

E_0 = Terminal voltage prior to fault

$E_0'=E_0-(I_a)_0R_L$

$E_0''=\frac{R_s}{(R_f)_0}E_0-(I_a)_0R_L$

L_a = Incremental self-inductance of the armature circuit

L_f = Incremental self-inductance of the shunt field circuit

$D_a=\frac{\partial e_g}{\partial i_a}$ with constant field current

$K_s=\frac{\partial e_g}{\partial i_f}$ with constant armature current

ϕ_f = Flux linking shunt field winding

$M=N_f\frac{\partial\phi_f}{\partial i_a}\times10^{-8}$ with constant field current

References

1. Solid Short Circuit of D-C Motors and Generators, **T. M. Linville, H. C. Ward, Jr.** *AIEE Transactions*, volume 68, part I, 1949, pages 119–24.

2. Transient Characteristics of D-C Motors and Generators, **A. T. McClinton, E. L. Brancato, Robert Panoff.** *AIEE Transactions*, volume 68, part II, 1949, pages 1100–06.

3. D-C Power Systems For Aircraft, **R. H. Kaufmann, H. J. Finison.** *General Electric Review* (Schenectady, N. Y.), volume 48, October 1945.

4. Short Circuits of D-C Generators, **H. P. Yermolin.** *Electrichestvo* (Moscow, U.S.S.R.), volume 7, July 1948, pages 26–32.

5. Dynamic Characteristics of Carbon Pile Voltage Regulators, **R. L. Mills.** *AIEE Transactions*, volume 69, part II, 1950, pages 1347–53.

6. Transient Analysis of a Voltage-Regulated Aircraft D-C System, **D. G. Scorgie.** *AIEE Transactions*, volume 69, Part II, 1950, pages 1318–23, equation 30.

7. Maximum Short-Circuit Current of D-C Motors and Generators, *AIEE Transactions*, volume 69, part I, 1950, pages 146–49.

8. Cause of Selective Action with Carbon Brushes, **P. F. Soper.** *BEAMA Journal* (London, England), August 1949.

9. Steady-State Analysis of Aircraft D-C Generators, **Ernest Van Valkenburg.** *AIEE Transactions*, volume 67, part II, 1948, pages 1351–58.

10. Measurement and Calculation of D-C Machine Armature Circuit Inductance, **H. D. Snively, P. B. Robinson.** *AIEE Transactions*, volume 69, part II, 1950, pages 1228–37.

Discussion

Donald G. Scorgie: Verbal discussions after the presentation of this paper, and subsequent exchanges of personal letters with members of the audience, have indicated that several points were in need of clarification.

At the time of writing the paper, we did not realize that our results represent an exact analytical justification for the empirical work on aircraft generators by R. H. Kaufmann and B. J. Finison (reference 3 of the paper). Simple algebra shows that transient resistance as defined by them always will differ from ours exactly by the value of the fault resistance, so that the results are intimately related. Transient resistance, as defined by Finison and Kaufmann, is given by

$$[E_0' - (i_a)_p R_L]/(i_a)_p$$

where $(i_a)_p$ is the peak change of armature current.

The important point is that Finison and Kaufmann, through a large number of observations, have in effect concluded with us that E_0' is the driving voltage which actuates the fault transient. Those who are attempting to establish procedures to explain these phenomena should not let themselves be restricted by the desire to carry over results from synchronous machine theory. Both the results of reference 3 of the paper and our own results have indicated that an attempt to relate transient response with generated voltage prior to the fault is physically unrealistic when there is large initial load or large fault resistance. Some of the resulting difficulties, clearly pointed out in reference 2, of the paper, are resolved here because this assumption was abandoned.

Much controversy centered upon equation 12 of the paper and upon what becomes of field current during the transient. The conflicting view of transient flux behavior, as stated in reference 1 of the paper, is that ϕ_f remains constant until the peak fault current; that ϕ_a decreases; and that the leakage flux increases sharply to counterbalance the change of ϕ_a. Such conflicting views can be resolved by direct measurement. With shunt-wound aircraft generators, equation 12 is confirmed, since the flux ϕ_f is found to decrease in proportion to ϕ_a. The leakage flux linking the field winding also decreases in spite of the field current rise, and the explanation rests on the saturation of the pole tips with armature current.

Another line of reasoning indicates that the view of transient flux distribution which sees ϕ_f as a constant ought to be re-examined. Consider for the moment a fault transient as viewed by the field winding in a separately excited machine. The only mechanism by which the field winding can detect the transient at all is through a change of ϕ_f with time. A high rate of change, $d\phi_f/dt$, continues for as long as 0.01 second in aircraft generator faults, and longer with large machines. At the end of this time, the total decrease in ϕ_f must be very considerable to explain the observed transient field current. For the reasons stated previously, the assumption that ϕ_f is a constant must not be made; and if insisted upon, leads to the rather peculiar situation in which the field current is not dependent upon the driving voltages induced in the field circuit, but acts as a sort of independent variable which ultimately determines the flux distribution.

Mr. Linville's assumption regarding ϕ_f was motivated by the desire to use the constant flux linkage theorem, which is an excellent theorem when it is applicable. The constant flux linkage theorem applies to instantaneous changes only, and is only moderately useful when flux linkages are assumed constant over the relatively long periods of time which elapse before peak fault current is reached.

The feeling was strong that an understanding of field current transients should be demonstrated using our approach. Field currents were calculated and measured for all transients in Figures 2 through 8 of the paper. Where armature current calculations were correct, the calculated field currents were correspondingly good, and where the predicted rate of rise of i_a was small, the calculated field current was low. Figure 1 of this discussion compares calculated and measured field currents for the transient with $R_L = 0.035$ ohm in Figure 3 of the paper. Note that the peak field current always occurs earlier than the peak armature current, which is in line with experience on all sizes of machines.

Discussions of the paper have stressed that the reactance voltage of commutation

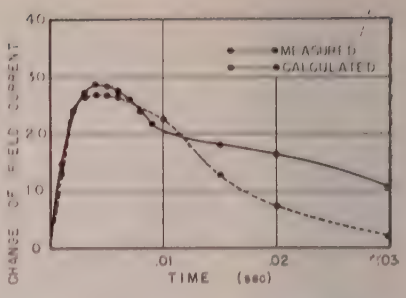

Figure 1. Calculated and measured field currents for the transient compared with R_L = 0.035 ohm

and the resulting brush drop should not be overlooked. The phenomenon is extremely complex and an oversimplified analysis tends to exaggerate its effect. The following points, for instance, should be considered:

1. The crowding of current to one edge of the brush leads to abrupt commutation and hence higher induced voltage for a shorter time. The time integral, however, is the important consideration, and this does not necessarily increase.

2. Two phenomena reduce the effective resistance of the brush contact at high current density; namely, the decrease in resistivity resulting from the breakdown of contact film, and the constant voltage characteristic of an arc.

3. It has been shown[1] that it is impossible to change the voltage instantaneously across a sliding carbon-copper contact. In this respect, the contact acts like a leaky condenser.

4. The sudden decrease in direct-axis armature flux during a fault transient induces, through transformer action with the short-circuited turns, an electromotive force in the proper direction to oppose the reactance voltage.[2]

Notwithstanding all these effects, the brush drop is known to be appreciable in large machines. In aircraft generators the effect is relatively small. Some very careful measurements by Loren Schroeder of this Laboratory indicate that the brush drop in a typical aircraft machine remains level near one volt and increases extremely slowly for higher currents. This relatively constant increase in brush drop with current does not invalidate the use of the equations in the paper, since it is absorbed automatically in the directly measured D_a. If the magnitude of the brush-drop-change with armature current becomes too large, it is necessary to make some slight adjustment of the value of M obtained through the use of equation 11 of the paper. This was not found to be necessary with the aircraft machines tested.

References

1. Carbon Brush Contact Phenomena, **T. F. Soper.** *Beama Journal* (London, England), volume 54, March 1947, pages 101–03.

2. The Commutation of D-C Generators under Momentary Overloads, **M. P. Yermolin.** *Elektrichestvo* (Moscow, U.S.S.R.), number 6, 1947, pages 28–34.

A New High-Voltage Insulation for Turbine-Generator Stator Windings

C. M. LAFFOON
FELLOW AIEE

C. F. HILL
FELLOW AIEE

GRAHAM LEE MOSES
FELLOW AIEE

L. J. BERBERICH
FELLOW AIEE

Synopsis: This paper reports the development of a new synthetic resin bonded mica tape insulation for high-voltage stator windings. It reviews the problems associated with earlier forms of high-voltage machine insulation. The general construction and processing of the insulation are described briefly. Comprehensive test data are presented on the characteristics of the materials employed and the resultant physical and electrical properties obtained on the composite insulation. This new insulation is now being applied to turbine generators for central station service.

EVER since the first central station generator started delivering power in New York City in 1882, insulation has presented a challenge to the designer. No other single component of the generator determines its reliability and continuity of service more than the insulation. While the earliest generators had treated fibrous insulation of cellulosic origin, mica was applied as early as 1892. Mica has a unique combination of electrical, mechanical, and thermal properties that have not been equalled by any of the many synthetic materials which have appeared in the last 50 years. Mica has been and still is the key material around which all high-voltage rotating machine insulations have evolved.

Mica, while having excellent properties, unfortunately is not available in continuous film form and therefore must be applied in the form of flakes of varying sizes. This necessitated the use of some organic materials such as paper, cotton cloth, and resinous binders such as shellac or asphaltic compounds to apply the insulation and fill the voids. Most of the advances made in the last 40 years in this type of insulation have involved either the development of better resinous binders for the mica flakes or improvements in the process of applying such binders to obtain a low loss and relatively void-free insulation. The presence of voids in insulation has a marked effect on the dielectric strength, and hence considerable effort has been expended on the development of insulation having a minimum of voids not only when new but also during the long period of service expected.

The first major advance in high-voltage machine insulation was made when the mica folium insulation was developed in Europe.[1] The Haefely process for applying this insulation was first brought to this country by Westinghouse in 1911. Mica folium originally consisted of wide sheets of fabricated mica backed with thin paper and bonded together with shellac. This insulation was applied to the straight parts of the coils by means of the Haefely machine which heated and rolled the folium onto the coils. The end turns were then insulated with multiple layers of varnished cambric tape. This insulation was excellent from the electrical standpoint, but as machines became longer some difficulty was experienced with the joint between the mica folium on the straight parts of the coil and the varnished cambric on the end turns. This difficulty was a result of differences in expansion and contraction of the copper conductors, the insulation, and the iron in the stator in going through temperature cycles. Also the organic end turn insulation possessed the disadvantage of having a somewhat limited life as machine operating temperatures were increased.

This mica folium insulation nevertheless served very well for about 15 years with only minor modifications. The first appreciable change was made in this country in the 1920's,[2,3] when the relatively hard and brittle shellac bond was replaced by a softer asphaltic type of bond; and mica tape was substituted for the varnished cambric end turn insulation formerly used. Similar improvements also were made in Europe.[4] These changes increased the flexibility, lowered the dielectric losses, reduced the swelling, and provided an end turn insulation with higher thermal stability. The joint between the mica folium insulation on the straight part of the coil and the mica tape still remained and caused occasional difficulties in the longer machines.

As machines became still larger and economic consideration dictated that turbine generators with very long stators be built, the joint had to be eliminated. The first asphalt-bonded, continuous, joint-free mica tape insulation was developed about 1920.[5,6] By the early 1930's most of industry in this country had adopted the continuous mica tape type of insulation for all types of high-voltage rotating machines. The bond widely used in this mica tape insulation is a somewhat flexible, thermoplastic asphaltic compound. This compound enables the insulation to adjust itself to a certain degree to the dimensional changes brought about by the differences in expansion of the metal parts and the insulation during normal operating temperature cycles. The insulation adjustment is generally distributed over the whole length of the coil instead of being concentrated at the joints used in the earlier insulation.[7] This insulation permitted a considerable increase in size of machine. It has had a rather successful period of application and is still being used.

Paper 51-121, recommended by the AIEE Rotating Machinery Committee for presentation at the AIEE Winter General Meeting, New York, N. Y., January 22–26, 1951. Manuscript submitted October 18, 1950; made available for printing December 7, 1950.

C. M. Laffoon, C. F. Hill, Graham Lee Moses, and L. J. Berberich all are with the Westinghouse Electric Corporation, East Pittsburgh, Pa.

A development of this magnitude involved contributions from many individuals. The authors gratefully acknowledge the contributions of N. C. Foster, W. W. Pendleton, H. M. Philofsky, J. Swiss, F. A. Yeoman, E. Bindschadler, L. R. Hill, L. A. Kilgore, J. S. Johnson, and J. C. Botts as well as the many other collaborators

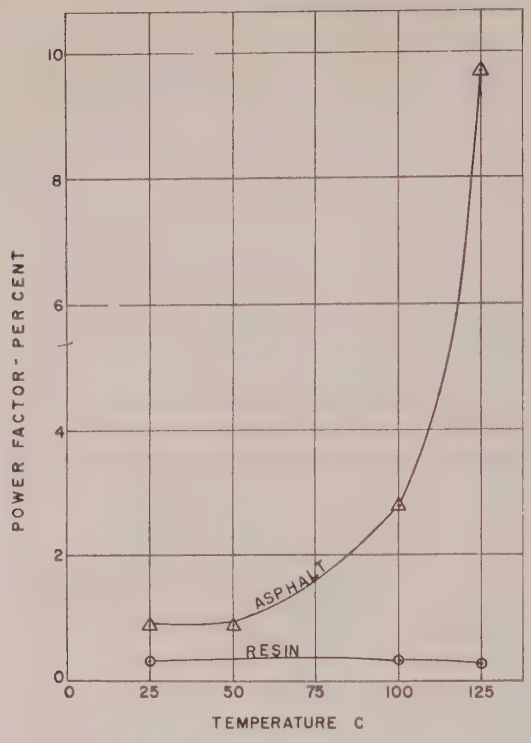

Figure 1 (left). Power factor temperature data on asphalt and synthetic resin

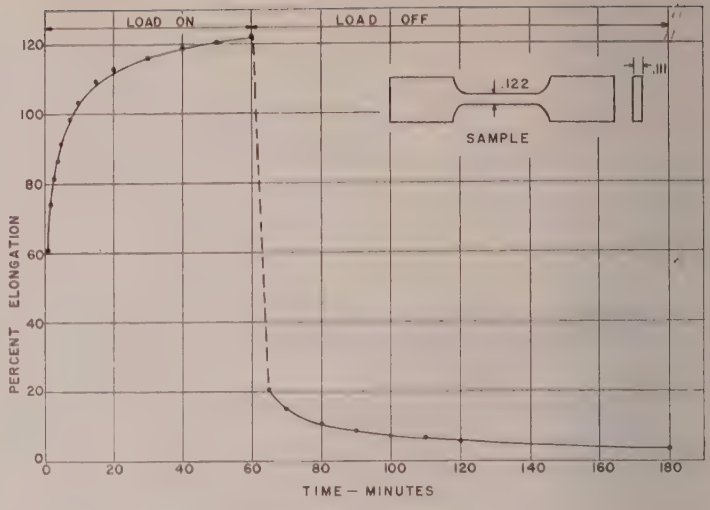

Figure 2 (above). Elastic behavior of synthetic resin at 100 degrees centigrade

It is of historical interest that in the late 1920's there was considerable discussion, first in England, and then in this country, about going to higher voltage generators. It was pointed out that a number of machines of relatively small kilovolt-ampere rating had been generating power in Italy at 30 kv since 1905, while in the United States generated voltages were largely in the range of 11 to 15 kv. This development resulted in the construction of the Parsons generator[9] in England with its circular and concentric coil construction designed for 33-kv operation. The construction of an appreciable number of machines having voltage ratings in the ranges from 16 to 22 kv soon followed in this country. These machines which were built by several manufacturers were largely of conventional design but involved a number of improvements in the insulation.[3,7] The radically different coil construction used in the Parsons generator in England was never adopted in this country largely for economic reasons.

The trend in this country has been to machines of larger and larger kilovolt-ampere rating rather than to higher voltage rating. This trend together with the practice of operating the machines at considerable overloads during the years of World War II has resulted in some difficulty in a few machines even with the asphalt bonded continuous mica tape insulation. This difficulty appeared in the form of a somewhat unpredictable migration of the insulation, generally just beyond the stator iron in the end turns. This phenomenon was reproduced in the laboratory and a subsequent study of the problem showed that the insulation movement occasionally observed could be attributed to the thermoplastic nature of the asphaltic bond. Thus, the results of this investigation indicated that further improvement in the mica bond was necessary for the completely successful operation of large machines at the higher temperatures. It is the purpose of this paper to describe the work that has been done in the last 10 years to achieve this end.

The work on which this paper is based was started in the Westinghouse Research Laboratories in 1940, where a new series of solventless polyester resins was under development. This start was made at a time when a strong trend was developing toward the use of synthetic resins in place of such natural resins as shellac, asphalt, copal, and so forth. Considerable time and effort was required to develop the best resin bond for this important application and to devise the radically new processes required for its production. This new insulation was made possible by progress in the development of synthetic materials through chemistry, an era which began primarily in the decade between 1930 and 1940. The application of this new insulation to turbine generator coils started in 1949. This paper will present (a) properties of the resin impregnant, (b) description of the mica tape, (c) discussion of construc-

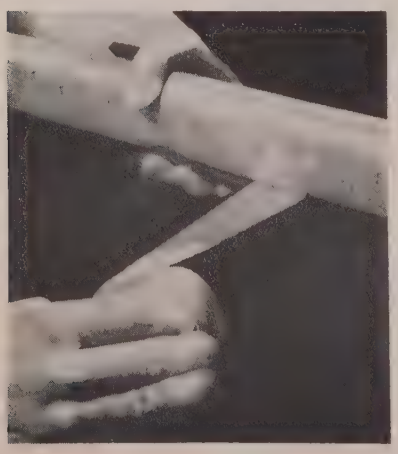

Figure 3. Close-up view of taper applying mica tape to a high-voltage generator half-coil

Figure 4. Close-up view of fiber glass finishing tape being applied to coil

Figure 5 (left). Pilot treating system where coils are impregnated with synthetic resin

Figure 7 (right). Coils with synthetic resin bonded mica insulation receiving finishing treatments

tion and processing together with (d) physical behavior, and (e) electrical properties of the new insulation.

Properties of the Impregnant

The impregnant plays a very important role for it serves as the mica bond and determines to a large extent the mechanical and electrical properties of the composite insulation. The asphaltic compounds, previously used, have given a good account of themselves but they have two shortcomings. These are (1) multiple impregnations at high temperatures and pressure are necessary to obtain adequate filling of the voids because they have very high viscosity at ordinary temperatures, and (2) they flow much like a viscous fluid at the higher machine operating temperatures because of their thermoplastic nature. Conventional synthetic varnishes of the thermosetting type which do not flow at any temperature have been investigated. These were, however, soon found to be unsatisfactory because they contain high percentages of nonreactive solvents which must be removed after the impregnating operation. The space occupied by the solvent in this type of impregnant must therefore finally appear as voids in the composite insulation. Much effort was therefore expended in developing a solventless thermosetting resin with the desired improvement in electrical and mechanical properties.

A considerable number of solventless resins now are available but most of them are unsatisfactory for this application because they lack some of the electrical or mechanical properties deemed essential. The impregnant finally developed consists of a resin belonging to a class of synthetic resins known as linear polyesters which is dissolved in a special heat reactive monomeric resin. This combination of resins can easily be impregnated into the mica tape insulation at ordinary temperatures because it is quite freely flowing before the co-polymerizing reaction takes place. After the composite resin is in place and heat is applied, the components react with each other to produce a cross-linked, thermosetting solid resin. This final reaction occurs without the formation of any gaseous or liquid by-products, thus making possible almost complete filling of the void spaces.

The impregnating resin has excellent electrical properties as can be seen from Figure 1. Not only is the power factor appreciably lower than for the asphaltic compound, but it also is almost independent of temperature up to 125 degrees centigrade. This obviously makes for a higher quality insulation.

The mechanical properties are as important as the electrical properties in this

Figure 6. Mobile press with coils in place showing how the new insulation is pressed and restrained during oven curing of resin

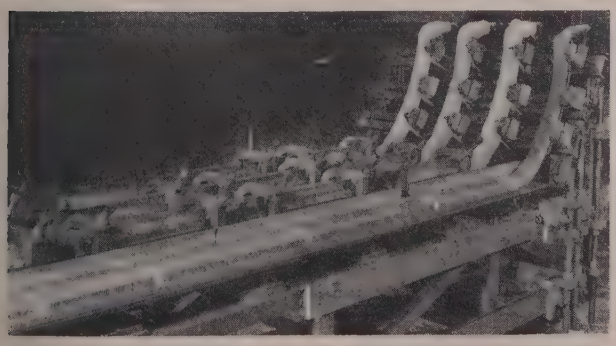

Figure 8. Thermal cycling test model with half-coils in a section of a turbine generator core

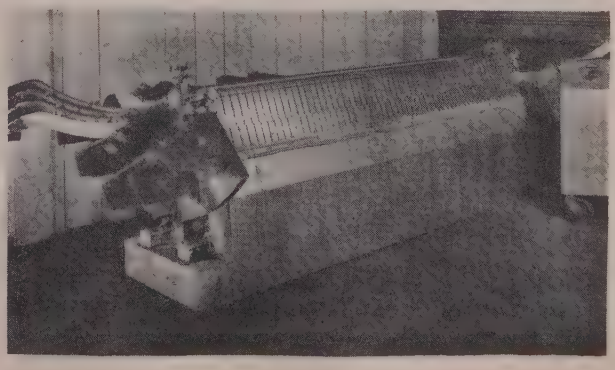

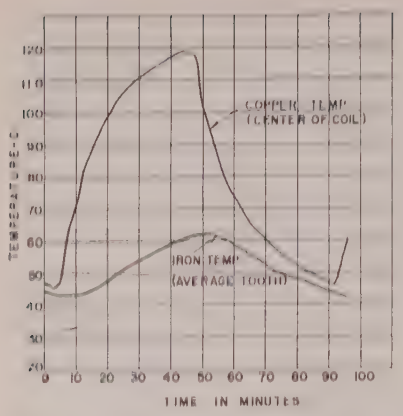

Figure 9. Typical heating and cooling cycle of coils and iron during thermal cycling model test

application and, therefore, the behavior of the resin under load was carefully investigated, particularly in the range of 75 to 125 degrees centigrade. It will be observed from Figure 2 that upon application of a load there is an instantaneous elastic elongation which is followed by a gradual further elongation requiring more than an hour to reach its final value. This behavior is almost completely reversed when the load is removed. Recovery is almost complete two hours after removal of the load as Figure 2 also shows. This elastic recovery even though delayed is sufficiently complete to provide an adequate restoring force when the insulation is displaced during temperature cycles.

Asphalt, surprisingly enough, shows a very similar behavior at temperatures of about 50 degrees centigrade and below.[10] The instantaneous elastic displacement is, however, a smaller fraction of the total displacement and the delayed elastic recovery is less complete than is the case for the new synthetic resin. This perhaps accounts for the acceptable performance that asphalt bonded insulation has experienced. At the higher temperatures, however, the elastic properties of asphalt completely vanish and at 100 degrees centigrade and higher it behaves like a very viscous fluid. The new resin bond, in striking contrast, exhibits elastic properties at the highest machine operating temperatures which explains its excellent performance in the wide range temperature cycles to be discussed later.

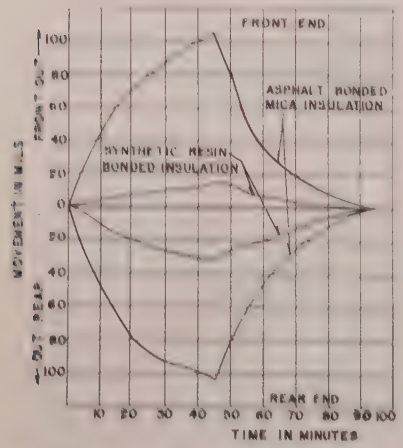

Figure 10. Typical cyclic movement of old and new insulation on coils with respect to end of core on coils during thermal cycling test

Mica Tape

The basic dielectric barrier for the ground insulation is provided by mica flakes applied in tape form. The mica tape is machine built with good quality muscovite mica splittings. The mica portion of the tape is built on a thin strong fibrous backing with a second layer of fibrous backing applied to the top side after the mica splittings are laid. The backing is coated and the mica flakes bonded to it with a synthetic resin which is compatible with the solventless heat reactive resin used for impregnating the finished coils. The bond has low electrical loss and contributes to the low power factor and high dielectric strength of the composite insulation. The finished mica tape is a strong, easily applied material which has no objectionable features insofar as its physical application is concerned. The higher tensile strength of this tape permits tighter application than was possible on asphalt bonded mica tape without breaking it.

Construction and Processing of Coil Insulation

Basically, the new insulation consists of a continuous mica tape impregnated with the synthetic resin just described. For turbine generator windings, conventional half-coil construction is employed with all strands of each conductor individually insulated by varnished fiber glass covering. Before the ground insulation is applied the assembled strands are bonded solidly together as a rigid structure in the slot portion. Up to this point the coils do not differ from those insulated with asphalt bonded tape.

The ground insulation consists of multiple layers of the continuous mica tape as illustrated in Figure 3. The mica tape is applied without brushing a bond between layers of tape, such as was necessary with asphalt bonded tape. The elimination of the brushing bond not only

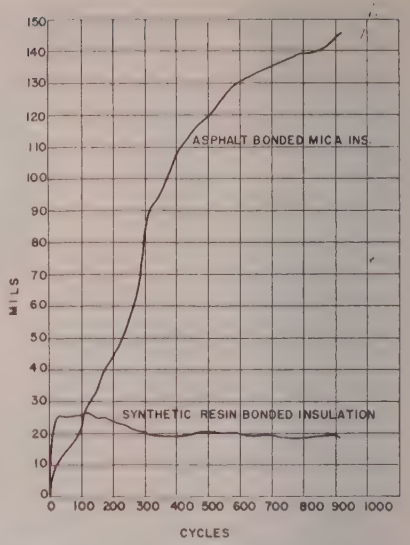

Figure 11. Permanent migration of old and new insulation as produced by thermal cycling test

makes the application of the tape a simpler, cleaner operation but also results in an increase in the physical strength of the tape. Moreover, it facilitates tight application without tape rupture resulting in better control of dielectric quality level. The process requires no multiple intermediate impregnations as all the tape is applied before impregnation. This differs from the asphalt bonded mica tape processing as the taped ground wall was applied in several steps with an intermediate impregnation after each group of tape layers was applied. After application of all layers of the synthetic resin bonded mica tape, the coil is finished by taping over-all with a fiber glass tape to provide a strong abrasion resistant surface as shown in Figure 4. This finishing tape is subsequently solidly bonded to the mica to eliminate slippage and its voids are completely filled to prevent corona within the tape interstices.

Table I. High Voltage Generator Insulation—Physical Properties

Tensile Strength	Asphalt Bonded Insulation	Thermalastic Insulation
Room temperature	2,000 psi	6,600 psi
100° C	90 psi	2,800 psi
Coefficient of Expansion Per Degree Centigrade		
Thickness	300×10^{-6}	72×10^{-6}
Length	6.85×10^{-6}	6.66×10^{-6}
References		
Steel	11.5×10^{-6}	
Copper	17×10^{-6}	

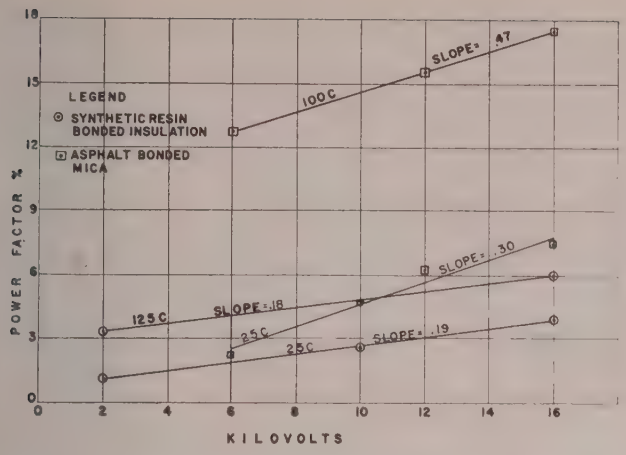

Figure 12. Power factor voltage test data on asphalt bonded and synthetic resin bonded insulations

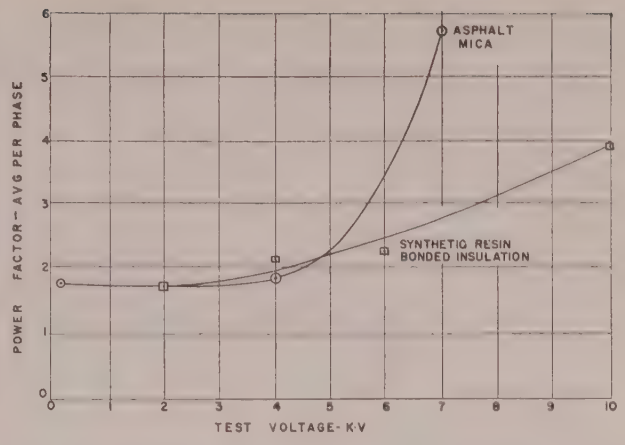

Figure 14. Power factor test data on complete phase groups of asphalt bonded and synthetic resin bonded insulations high-voltage windings

On asphalt bonded coils the outside binder tape was usually applied separately after all impregnation processes were complete.

Next, the coils are heated and evacuated at high vacuum to remove moisture and gases. They are then impregnated in the manner shown in Figure 5 by vacuum and pressure with the synthetic resin. The process used results in the unusually high degree of filling of the coil interstices shown by the electrical tests as well as physical examination.

After the vacuum and pressure impregnation special mobile presses shown in Figure 6 are employed to clamp and support coils during oven curing of the resin. These mobile presses place restraint on the slot portion ensuring that the proper finished slot size is obtained. Support blocks hold the coil ends during cure to ensure that all coils are the same and will fit the core and coil supports. The mobile presses with coils in place are moved into an oven and the impregnating resin is cured with the coil positively held in the desired size and shape. After completion of oven cure of the resin, the coils are given their usual conducting surface treatments on the slot and end winding portions as illustrated in Figure 7.

Physical Behavior

Some of the physical properties of the new insulation are compared to those of the older asphalt bonded mica insulation in Table I. This table shows that the increase in tensile strength of the new insulation is more than 3-to-1 at room temperature and is more than 30-to-1 at operating temperature (100 degrees centigrade). The reduction in coefficient of thermal expansion in the thickness dimension is an important characteristic of the new insulation as also indicated in Table I. The improvement in physical strength and reduction in thermal expansion of the new insulation when heated are favorable to its operation in large generators.

The tests on insulation samples have been supplemented by simulated shock tests on full size coils as well as short-circuit tests on complete windings. These tests confirm the greater strength of the new insulation and its ability, when properly supported, to withstand expected physical loads during normal operation and occasional short circuits.

An important part of this development consisted of studying the effect of differential expansion of iron, copper, and insulation. Early studies were conducted on small models and the final phase was carried out in a 108-inch long section of the core of a standard turbine generator. The test model and coil setup are shown in Figure 8. Standard coils were employed with various types of insulation. Coils were heated by passing current through them and cooled by blowing air through the core vent ducts. A typical heating and cooling cycle is shown in Figure 9. The cyclic movement

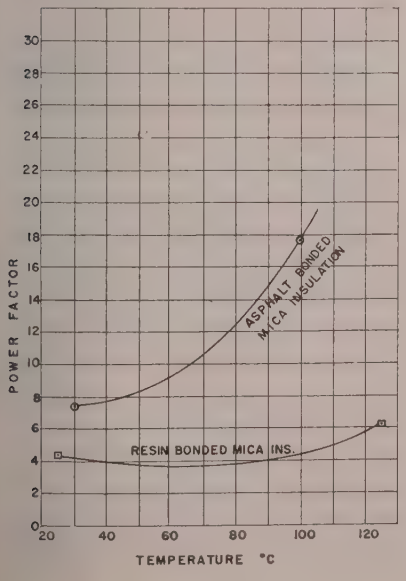

Figure 13 (left). Power factor versus temperature test data on asphalt bonded and synthetic resin bonded insulations

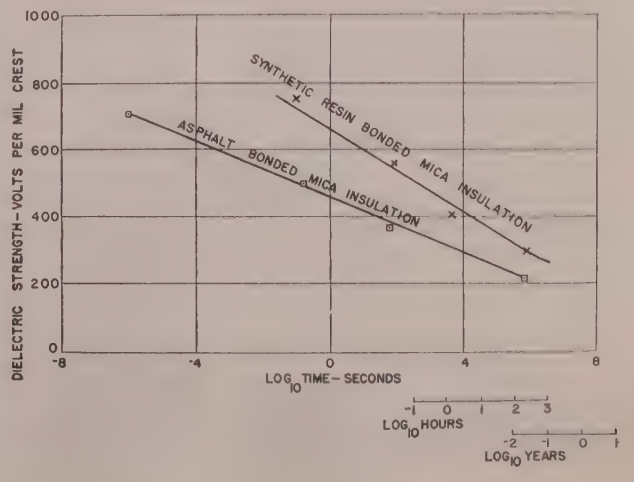
SYNTHETIC RESIN BONDED MICA INSULATION
ASPHALT BONDED MICA INSULATION
DIELECTRIC STRENGTH - VOLTS PER MIL CREST
LOG10 TIME - SECONDS
LOG10 HOURS
LOG10 YEARS

Figure 15 (right). Dielectric strength and voltage endurance data on old and new insulations

of the insulation out of the ends of the core was observed by dial gauges that can be seen in Figure 8. Typical cyclic movement for two types of insulation is shown in Figure 10. Permanent migration of the insulation is illustrated in Figure 11, which clearly indicates the continued creep of the asphalt bonded mica insulation and the inherent stability of the synthetic resin bonded mica. The actual test experience is more impressive than the comparison shown, as not all the creep of the asphalt bonded insulation was registered on the dial gauges. For example, a 0.250-inch observed movement was sometimes accompanied by a 1-inch or wider separation of the surface tape on asphalt bonded insulation as localized movement frequently exceeded the total net movement between gauges. The significant point is that in no case did any observable separation or crack occur in the synthetic resin bonded mica tape insulation during these tests, whereas various degrees of insulation migration and tape separation were produced on coils with asphalt bonded insulation under identical conditions. While these accelerated cyclic tests were more severe than normal operating conditions, they reproduced serious insulation migration effects such as had been observed on a relatively few machines.

Electrical Properties

The power factor voltage relations for asphalt bonded and resin bonded insulations are compared in Figure 12. In every condition tested the power factor of the synthetic resin impregnated mica insulation is lower than the power factor of the asphalt bonded mica. At operating voltage and temperature the power factor of the new insulation is approximately one third that of the older insulation as shown in the curve.

The temperature effect on insulation power factor at 60 cycles is presented in Figure 13. This shows the effect of temperature is negligible on the power factor of the new insulation but that the power factor of asphalt bonded mica rises sharply with temperature increase.

The power factor of complete windings is of interest and such data are presented in Figure 14. This shows relatively little difference in power factors of the two types of insulation at voltages below 5 kv but a significant difference thereafter in favor of synthetic resin bonded insulation.

The dielectric strength and voltage endurance of an insulation system are two very important criteria of insulation quality. These characteristics are presented in Figure 15 where time to breakdown is shown for various voltages for the synthetic resin bonded insulation in relation to asphalt bonded mica insulation. In examining these data it is well to realize that the wall thicknesses of the test samples are the same and that the same grade of mica splittings is employed on both. A significant improvement is shown in the data for the dielectric strength obtained at any time of voltage application on synthetic resin bonded mica as compared to asphalt bonded insulation. The increase in time to breakdown for the new insulation at any given voltage gradient is of the order of 1,000-to-1 which is indicative of the improved filling and reduction in size and quantities of internal voids in the new insulation.

This increased voltage endurance correlates with the small effect of voltage on power factor.

Conclusions

This new type of synthetic resin bonded insulation offers promise of even greater reliability for high-voltage machines. The basic insulation is mica which has been proved through more than half a century of successful service. The new insulation substitutes a solid yet elastic bond for the rigid brittle shellac bond and the plastic semiliquid asphalt bond used previously. It makes available the good intrinsic dielectric properties of mica to a greater degree than was heretofore obtainable. The insulation wall is built-up in a solid, well-filled structure which possesses the inherent ability of accommodating itself to the deformation resulting from differential thermal expansion of iron, copper, and insulation. The new insulation employs a bond between mica flakes that possesses greater physical strength than the inherent interlaminar strength of mica itself and permits cyclic elastic deformation of the composite insulation structure. The nature of the resin bond and processing technique result in a high degree of filling of the insulation voids with the consequent improvement in important dielectric characteristics such as power factor, dielectric strength, and voltage endurance.

The desirable characteristics of this new insulation have led to its adoption as the standard insulation for all Westinghouse turbine generator stator windings employing half-coil construction, which includes those rated at 12,500 kva and larger. Development work is now in progress to apply this new insulation to full coils. The voltage endurance, dielectric strength, and power factor characteristics of the new insulation should make possible an eventual increase in the operating stress and a reduction in wall thickness for a given voltage.

In conclusion, it should be emphasized that the older insulations were adequate electrically as built. Experience with these older insulations has indicated that in general, electrical failure is preceded by serious mechanical deterioration. While striking gains in initial electrical and physical properties are obtained with this new insulation, the mechanical endurance is the most significant characteristic as it should maintain the dielectric quality at a high level far better than was possible with the older insulations.

References

1. High Speed Turbo-Alternators—Designs and Limitations, **B. G. Lamme.** *AIEE Transactions*, volume 32, part I, 1913, pages 1–78.

2. Improvements in Insulation for High-Voltage A-C Generators, **C. F. Hill.** *AIEE Transactions*, volume 47, July section, 1928, pages 845–52.

3. Increased Voltages of Synchronous Machines, **C. M. Laffoon.** *AIEE Transactions*, volume 49, January section, 1930, pages 213–25.

4. Improving the Insulation of High-Voltage Machines, **F. Beldi.** *Brown Boveri Review*, (Baden, Switzerland), volume 17, 1930, page 304.

5. *Discussion* by **P. L. Alger** of reference 2, page 852.

6. *Discussion* by **R. W. Wieseman** of reference 7. *AIEE Transactions*, volume 55, 1936, page 178.

7. Insulation for High-Voltage Alternators, **C. M. Laffoon, J. F. Calvert.** *Electrical Engineering* (*AIEE Transactions*), volume 54, June 1935, pages 624–31.

8. Closure of reference 7. *Electrical Engineering* (*AIEE Transactions*), volume 55, February 1936, pages 180–81.

9. Direct Generation of Alternating Current at High Voltages, **C. A. Parsons, J. Rosen.** *Journal*, Institution of Electrical Engineers (London, England), volume 67, 1929, page 1065.

10. The Penetrometer Method for Determining the Flow Properties of High Viscosity Fluids, **W. W. Pendleton.** *Journal of Applied Physics* (New York, N. Y.), volume 14, 1943, page 170.

Discussion

C. E. Kilbourne (General Electric Company, Schenectady, N. Y.): The authors are to be congratulated on the presentation of a most interesting paper, and upon the announcement of a synthetic resin bonded mica tape for high-voltage turbine-generator stator windings. While synthetic resin mica tapes have been used in the windings of other kinds of machines for several years, this is the first publication of their use in such a large high-voltage application. The records of the AIEE show many examples of the employment of synthetics in the insulation field, and this and other papers at this meeting add to that record. This trend, because

of the great variety of new materials being made available by chemistry, can be expected to accelerate in the future.

The authors, in their introduction, state the important role that insulation plays in determining the reliability and continuity in service of the machines to which it is applied. A full appreciation of this fact has shaped insulation development in the General Electric Company since its early beginnings. In large rotating machines mica tape using shellac or copal as resinous binders was introduced over 50 years ago. The continuous application of tape without joints in the insulation, over the slot as well as the end portions of large coils and bars such as those used in turbine generators, is, and always has been, a characteristic of the windings made by the General Electric Company. When the Haefely process of slot-applied mica folium with its problems of a joint at the end of the slot portion and a different construction of insulation for the ends of coils and bars was developed in Europe, it was never adopted by General Electric for large high-voltage windings. Consequently, their windings did not encounter the problem of separation between the mica folium and the end insulation which the authors mention, nor did they require special end construction to care for the creepage problem of a high-voltage joint.

The continuous joint-free shellac- or copal-impregnated windings, with mica around the entire coil or bar, gave excellent service. However, as the authors have noted, shellac and copal resins are relatively hard and brittle, particularly when heat aged, and realization of this fact led in 1913 to an intensified search for better binding and impregnating materials. In 1916 asphaltic materials were substituted for earlier resins in the manufacture of mica tape, and before 1920 many machines were running with the new type coils. In fact, reference 5 of the paper, a discussion presented in 1928, notes that two 22,000-volt synchronous condensers insulated with mica tape and treated with black asphalt varnish around the entire coil had been operating in India for five years. This was a conservative statement. Two 12,500-kva, 22,000-volt condensers were built in 1919. These high-voltage machines were undertaken only after considerable practical experience with the new materials. As the authors note, it was several years after this 1928 presentation that continuous-tape asphaltic resin impregnated coils and bars came into general industry-wide use in the United States.

The advantages of increased flexibility, thermoplasticity, and longer life under operating temperatures, which the early asphaltic-type binder materials offered in contrast to shellac and copal, served only to emphasize the need for further work to find even better materials. This search has continued over the years since 1916, to result today in resins and compounds which have quite different characteristics from pure or even slightly modified asphalts. Concurrently with material improvements, constant attention to manufacturing processes and techniques and to the details of design have all contributed to the high level of performance obtained today.

This performance differs in may respects from the performance which the authors present as the characteristics of asphalt bonded insulation. To be truly descriptive, present General Electric turbine generator insulation should be more properly classified as a "Modified Bitumen Bonded Mica Insulation." It is believed that the performance record and over-all characteristics of this "Modified Bitumen" insulation will be of interest.

The annual reports of the Prime Movers Committee of the Edison Electric Institute afford a valuable record of the service reliability of insulation in the power generation industry. This record covers a large number of turbine generators, the great majority of which are of American manufacture and virtually all of which contain asphaltic or modified bitumen mica insulated armature bars or coils. Quite a large percentage of the machines have the modified bitumen insulation. The record reports the total percentage of outage time charged to power generation equipment from all causes, and then breaks down the total outage into several categories, one of which is credited to armature windings. Table I of this discussion presents that record covering all machines reported during the years 1940 through 1947, a total of about 2,000 machine years of operation. This table shows that the average outage time per year of a machine, due to armature insulations, was 0.150, or about 1/8 of 1 per cent of the available operating time. In other words, machines were available for service 99.850 per cent of the demand time in so far as the successful operation of armature insulation is concerned. An examination of all outage records on the modified bitumen insulated machines, which are available to this discusser, indicates over 99.9 per cent availability. However, it is recognized that the latter record may not be as complete as the former one, and since so many of the machines included in the former record have the modified bitumen insulation in them, that figure, that is, 99.850 per cent availability, is a good benchmark.

In discussing the performance of asphaltic insulations the authors state that the power industry trend to larger and larger machines, plus overload operation during Word War II, has resulted in some difficulties with asphalt-bonded insulations. This difficulty, consisting of an unpredictable migration of the insulation generally beyond the stator iron in the end turns, perhaps has received greater emphasis since the war and, therefore, may have exerted little influence on the data of Table I of this discussion. In an attempt to check the extent of tape migration troubles and any consequent winding failures on modified bitumen-insulated machines, this discusser has surveyed all the records available to him on machines built since 1916. This survey, covering many hundred machines, brings out a number of interesting points. On a few machines built prior to 1935, when a design change in coil construction was made to minimize end-winding differential expansion insulation stresses, such tape migration and separation has been observed. However, no service failures have been attributed to this cause. Repairs have been satisfactory and the machines are delivering power today. These cases fall into one or both of two categories. Either they occurred on unusually long or very-high-voltage machines, or on machines which have had many years of service, some at overloads, which because of integrated time-temperature deterioration, and often because of peak load operation, have put unusually severe service on their insulation. In several cases such units have been rewound since 1935 and no further similar difficulties have been reported. All remaining machines, including over 98 per cent of those in service today, and including 100 per cent of the modern hydrogen-cooled units, are completely free of any such reported troubles.

The physical properties of modified bitumen insulations, tested in the manner indicated in Table I of the paper, also are different from the published asphalt bonded data.

For example, the tensile strength of the modified bitumen product at room temperature is over 3,000 pounds per square inch as compared with 2,000 pounds per square inch for the asphaltic insulation described in the paper, and is correspondingly higher at elevated temperatures. The exact significance of these facts or of similar tests on other insulations is a bit obscure, as no figures for the mechanical strength of any insulations are sufficient to indicate that this strength plays an appreciable part in the thermal expansion of a coil or bar. In other words, moduli of insulation and copper are so far apart and the cross-sectional areas of the materials in high-voltage insulation sufficiently comparable, that the insulation necessarily is forced to conform with the movements of the copper. This raises a question on the interpretation of the data presented in Figures 9 and 10 of the paper. The model core setup shown in Figure 8 is 108 inches long, and presumably this is the distance over which the movements shown in Figure 10 took place. The copper temperatures indicated in Figure 9 vary from 46 degrees centigrade cold to 118 degrees centigrade hot, a rise of 72 degrees centigrade. If this may be assumed to be representative of the average temperature rise of the copper relative to the steel, then if the

Table I. Summary of Edison Electric Institute Operating Records for Armature Windings, 1940–1947

Year	No. of Machines Reported	Armature Outage as a Percentage of Total Outage	Total Outage as a Percentage of Operating Time	Armature Outage as a Percentage of Operating Time
1940	354	6.41	0.94	0.060
1941	366	23.24	0.85	0.198
1942	366	25.04	1.09	0.273
1943	366	9.06	0.84	0.076
1944	103	0.00	0.77	0.000
1945	118	2.53	1.08	0.027
1946	120	23.98	1.62	0.386
1947	128	2.91	1.05	0.031
Total	1921		Average	0.150

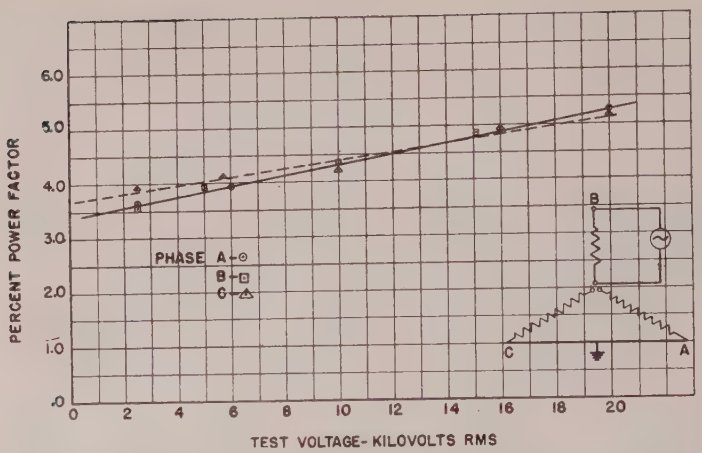

Figure 1. Power factor test data on the three phases of a modified bitumen insulated 75,000-kva 3,600-rpm 13,800-volt turbine generator

All tests were made using an a-c bridge, one phase under test at a time, with the other two phases grounded, winding temperature 27 degrees centigrade

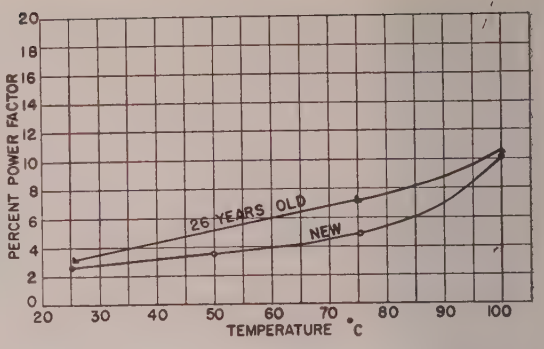

Figure 3. Test data on power factor versus temperature at 5-kv crest voltage on modified bitumen insulations, new and 26 years old

winding were a solid copper bar, its total expansion would be

$$108 \times 72 \times 0.0167 = 130 \text{ mils}$$

However, other tests on solid and stranded sections usually indicate that a stranded section will expand less under similar conditions than the corresponding solid one, hence the temperature rise of this test leads to the expectation that the total expansion should be less than 130 mils. However, from Figure 10, the total expansion indicated for the asphalt bonded insulation, adding together both the front and rear movements, is approximately 210 mils. As a second point, if one assumes that the asphalt bonded bar really increased its length 210 mils, while the synthetic resin bonded bar had a total expansion of only approximately 45 mils, then crediting no strength to the asphalt insulation, the synthetic resin insulation must have had sufficient strength to prevent an expansion of 210-45 = 165 mils, or an average of over 1.5 mils per inch over the 108-inch length. From an examination of Figure 8, it appears that the test bars have a copper cross section of about 1.0 square inch and an insulation cross section of about 1.7 square inches. It would require a force of 24,000 pounds to compress a 1.0-square-inch section of copper one inch long a distance of 1.5 mils, and if this force were restrained by the insulation, the stress in 1.7 square inches of insulation would be 14,100 pounds per square inch. However, since in Table I of the paper the tensile strength of Termalastic insulation is given as 2,800 pounds per square inch at 100 degrees centigrade, it is obvious that it could not have taken this stress without failure. These two puzzling situations probably have some simple explanation. Perhaps the clamps which transmitted bar movement to the gauges were tipped at an angle, by bending of the ends of the bars when warm, and this resulted in gauge readings containing other effects in addition to pure expansive movements of the bars.

The authors discuss two electrical characteristics of the compared insulations, power factor and dielectric strength. Modified bitumen insulation differs from both of the insulations discussed in the paper in each of these characteristics.

Power factor is not a very definite characteristic in determining the quality of an insulated winding. It is primarily a laboratory tool to investigate the material dielectric loss characteristic; the state of cure of the resinous components of the system, and, by the shape of the curve obtained from carefully controlled tests, to determine the presence or absence of voids. As a practical tool to weigh the merits of a finished product it possesses many weaknesses. In the first place insulation losses have little significance in the operation of a turbine generator. In a large machine, as pointed out in an unpublished paper by F. Brown, Jr., A. D. Coggeshall, A. Pletenik, and G. W. Young, entitled "The Development of Insulation Systems," the size of these losses is entirely

Figure 2 (below). Power factor versus voltage

Test data on high-voltage modified bitumen insulations, new and 26 years old

Figure 4 (right). Dielectric strength and voltage endurance data on modified bitumen insulations

60 cycle-60-second high-potential withstand voltages on windings 18 to 34 years old indicated by *X*

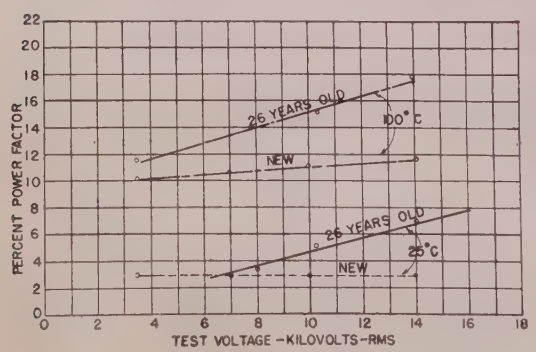

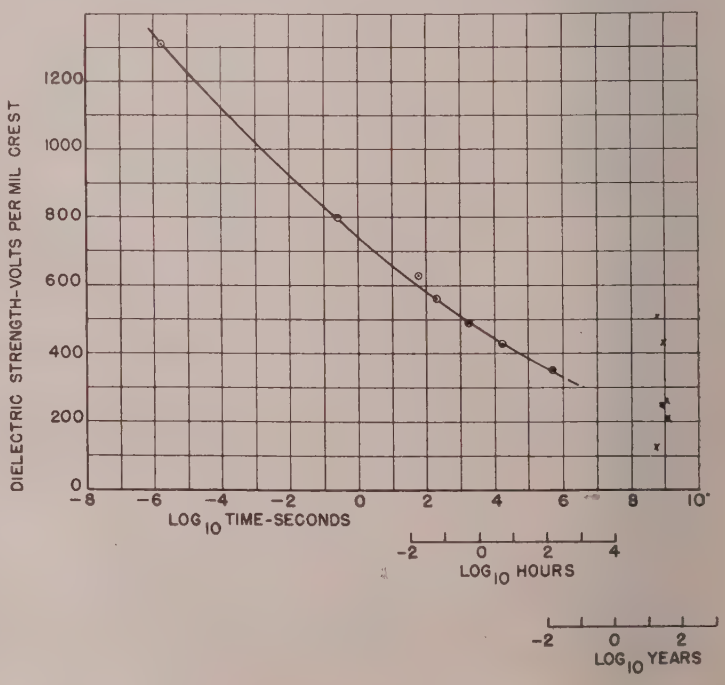

insignificant with respect to both efficiency and heating. In a machine, since the slot wall is used as one electrode and the copper of the winding as the other, the over-all power factor measured is not only that of the insulation, but also that of its surroundings. Consequently, conclusions drawn from such measurements must be subject to very careful interpretation. In this interpretation the age and past temperature-time history of the machine must be considered as well as its present state of freedom from moisture and its general cleanliness. Since such facts are seldom accurately known, analysis of tests is difficult. However, for what such information may be worth, test results on the power factor of a new large turbine-generator winding insulated with modified bitumen resin binders is presented in Figure 1 of this discussion. This may be compared with Figure 14 of the paper. The comparison will show higher power factors in the low-voltage range and lower power factors in the high-voltage range for modified bitumen insulation versus either of the insulations discussed in the paper.

Laboratory tests taken on new, and on a particular group of 26-year-old high-voltage modified bitumen insulated bars clamped in a slot to simulate their service conditions are shown in Figure 2 of this discussion. At both 25 degrees centigrade and 100 degrees centigrade the new bar characteristics differ substantially from the corresponding asphalt characteristics given in Figure 12 of the paper both in the magnitude of the readings and in the slopes of the power factor versus voltage curves. The characteristics of the 26-year-old bars, however, agree fairly well with those given by the authors.

Another interesting comparison of the characteristics of these old and new bars is shown in Figure 3 of this discussion. The higher power factor of the older bars shows either the effects of age or, if that is neglected, perhaps of changes in materials and techniques which have taken place in the interim. The greater slope of the new bar characteristics at higher temperatures indicates the probability of some curing yet to come. Under normal conditions the power factor of such bars should decrease somewhat with age and heating, then after a number of years, start a very gradual increase until, unless overheating is encountered, it stabilizes somewhat below its present new values.

The low power factors of thermalastic insulation as given in Figure 12 of the paper are to be expected from the resin characteristic given in the paper's Figure 1. However, it is puzzling to co-ordinate the power factors of the resins and the bars, as they differ particularly at the higher temperatures. The power factor of the resin at 125 degrees centigrade is in Figure 1 of the paper, about 0.3 per cent, while the lowest power factor of the synthetic bonded insulation at this temperature is more than ten times as great. The same kind of divergence exists at other temperatures and also with the asphalt insulation. Tests made in General Electric Laboratories indicate a relatively close agreement between the power factors of the modified bitumen impregnating resins and the finished insulating systems under similar conditions of temperature and voltage. This seems to be a logical situation and it has been duplicated using other resins and other compositions of insulations. A divergence from this agreement, particularly having the finished insulating system with a power factor several times greater than that of the impregnants, may indicate a condition of lack of cure of the resins, voids in the insulation, or some unknown condition.

As the authors have pointed out, the dielectric strength and the voltage endurance of an insulation system are important criteria of its quality. Again, in both these respects, modified bitumen insulations differ from the authors' data for the asphalt and synthetic resin systems. Figure 4 of this discussion shows test results on modified bitumen insulations on a similar plot to the data given in Figure 15 of the paper. The modified bitumen characteristic is not only somewhat higher than either of those given in the paper, but it also shows a distinct tendency to flatten out at the longer values of time. To substantiate somewhat this latter characteristic, data on a few high-potential breakdown tests on windings 18 to 34 years of age, which have recently been tested, have been added to the endurance characteristic.

These points are the 60-cycle-60-second withstand voltages, and are of interest in endurance principally as an indication of the relative withstand value on this test, on new insulations and on ones that that been aged. The great divergence between these values is associated with the operating history of the various machines as evidenced by the physical state of the insulation when these tests were made. The highest point represents an insulation 19 years old, which still possesses, because of conservative operation, about 80 per cent of its initial dielectric strength. The lowest point is from a machine 18 years old whose insulation was badly charred from heat.

In a companion paper by Mr. Graham Lee Moses,[1] one of the authors of this paper, data are presented which are of interest in connection with this paper. These data concern tests on a batch of 50 specimens of 13,800-volt insulated bars, presumably asphalt type, and presumably similar to those used for turbine-generator bars, since the data agree well with the endurance data of Figure 15 of this paper. Some similar data on 13,800-volt modified bitumen insulated bars are available and will further serve to illustrate the characteristics of this insulation.

1. 1.5/40 microsecond impulse wave	247-kv peak average held $\sigma = 21.2$
2. D-c rapid rise test to breakdown	291-kv maximum average held $\sigma = 21.2$
3. 1-Minute step-by-step a-c tests to breakdown	80.5-kv rms average held $\sigma = 4.21$
4. Samples stressed continuously at 57-kv a-c (rms) to failure	Hours to failure: 3.0–4.25–4.5 13.3

When the above data are studied there may be some question about the consistency of items (1) and (2), since the impulse and d-c rapid rise values usually are closer together. Item 1 is based on more test data than item 2, even though the latter data had a sufficient number of points to permit probability analysis. Perhaps the truth for item 2 may be found closer to item 1 when more data are available. Item 3 is based on a large amount of test data and there is no question as to its substantiation. In fact, if the annual records of tests for this type of information over the past years are inspected, the value has shown a moderate but steady increase with time.

In summary, it is believed that both the physical and electrical characteristics that an insulating system may possess are dependent, not only on the materials used to construct the system, but also upon the manufacturing methods and techniques used in its production. Thus there may exist a number of visually similar types of structures that possess quite different characteristics. The strength or weakness of such systems is inseparable from these characteristics, and it is difficult, if not impossible, precisely to predict these characteristics based on the composition of the system. Experience alone tells the whole story. Work on new insulations is going on in many places and experience is accumulating. However, as the advantages of new systems must be weighed against the benchmarks of performance and experience available with the existing systems, their introduction requires very careful consideration. The authors are to be congratulated upon the announcement of their realization of this goal.

REFERENCE

1. ALTERNATING AND DIRECT VOLTAGE ENDURANCE STUDIES ON MICA INSULATION, **Graham Lee Moses.** *AIEE Transactions*, volume 70, part I, 1951, pages 763–69.

Herman Halperin (Commonwealth Edison Company, Chicago, Ill.): Regarding this very interesting development of generator insulation, I have the following questions and points: Figures 9 and 10 of the paper give movement in connection with the steep temperature rise that obtained during the first 45 minutes of the heating and cooling cycle for the coils in a laboratory section of a generator core. It would be of interest to learn what indications the authors have for such movement after the temperature becomes more or less steady, as applies for a machine carrying a given heavy load for several hours in service. Some measurements made in the field on a somewhat similar situation, that is, underground cables in ducts, indicate an increase in movement may occur with time after reaching a given temperature rise for the cable conductors above ambient.

Figure 14 of the paper shows a smaller rise in power factor as the test voltage is increased for the resin-bonded insulation than for the asphalt-mica insulation. The rise for the former still seems to be about one per cent, however, between low voltage and operating voltage. Some ideas as to the physical significance of this increase and its effects in service would be of interest.

The data in Figure 15 of the paper show a considerable advantage in unit dielectric strength for the new insulation as far as the tests have gone, and similar data for tests of longer duration would be of interest. Have any data on dielectric strength been obtained at elevated temperatures? Perhaps the advantage indicated to date in unit dielectric strength for the new insulation will be utilized in the design of generator insulation, especially for the higher voltage machines and for machines of very large capacity at a later date after more background in operating and test experience has been accumulated. Of course, reductions in in-

sulation thicknesses have the advantage of reducing the thermal drop across the insulation as well as permitting a small decrease in dimensions throughout the stator.

C. M. Laffoon, C. F. Hill, Graham Lee Moses, and **L. J. Berberich:** The operating experience for high-voltage insulation on rotating machinery has been good but not perfect, as indicated by Mr. Kilbourne's discussion. Data which he presented apply to equipment made by all manufacturers. Recognizing that even a good record can be improved, the authors' efforts have been directed toward even greater reliability.

The development of this new insulation covering as it did within a period of 10 years, with four years in the pilot plant stage, has resulted in the accumulation of a great deal of test data. No attempt has been made to report all of these data. The data presented indicate some of the types of observations and are illustrative of the general characteristics of the insulation. The primary objective of the program has been to develop a composite coil structure in which the insulation expands and contracts elastically. This has been accomplished as has been clearly demonstrated by model tests and operation.

Discussions of the relative merits of competitive insulations are welcomed, as this will contribute to a better general understanding of insulation problems. The availability of such information will permit evaluation of competitive insulations on the basis of facts that can be discussed openly and frankly.

One point raised in discussion concerned the mechanical forces and differential expansion of the various structures. There is no simple answer, as the problem is very complicated because of the mechanical system which involves end winding structure as supports as well as the core, copper of the coil, and composite insulation. In connection with the criticism raised, it should be noted that the data presented do not refer to total movement of the insulation, but relative surface movement of the insulation as observed with respect to the ends of the core. It is important to recognize that the surface of the new insulation does not follow the cyclic movement of the copper completely. This is attributed to the fact that the resin bonds between mica flakes and resin tape are established while the copper is at an intermediate temperature (and length).

Power factor data are presented as an interesting sidelight which indicates degree of cure of the resin and filling of the voids for a particular resin. Differences between Figures 1 and 13 of the paper are that the first curve is for a pure void-free resin at relatively low voltage where power factor is largely a question of ionic conductivity. In Figure 13 of the paper the composite insulation is measured at high voltage and therefore power factor is determined by voids in the structure as well as ionic impurities introduced by the solid materials.

As indicated in the paper the new insulation has considerable margins of quality with respect to physical and dielectric strengths, which may ultimately lead to reduced wall thicknesses for a given operating voltage. However, this step lies ahead and is dependent upon further operating experience.

Synchronous Machine Damping and Synchronizing Torques

CHARLES CONCORDIA
FELLOW AIEE

THE object of this paper is to present the results of some calculations of the damping and synchronizing torque coefficients of synchronous machines over a range of system parameters. The torques were calculated by the formulas given by R. H. Park in an AIEE paper[1] published in 1933, and the calculations were themselves made some time ago. It is, however, considered worth while to publish them at this late date because of a continued interest in damping and synchronizing torques[2,3,4] and also in order to demonstrate that the more exact equation given by Park is practically as simple and convenient to use as any of the numerous approximations that have been proposed from time to time.

The general case considered is a machine tied to an infinite bus through an impedance and oscillating (hunting) with fixed excitation about its operating angle. The effects of various values of resistance and reactance in the tie line, of various types of rotor circuits, and of load and field excitation are shown.

The equations given by Park in reference 1 form a simple and convenient means of calculating the components of hunting torque with fixed excitation.

For a machine operating at no load and unit excitation:

1. For an external reactance greater than about 0.4 per unit, the damping torque coefficient is not affected greatly by armature circuit resistances less than 0.2 per unit.

2. The synchronizing torque coefficient is not significantly affected by armature circuit resistance r in the range $r < 0.2$, but is decreased somewhat for $r = 0.4$ per unit.

3. For any fixed value of armature circuit resistance and for a machine with an amortisseur, the damping torque coefficient never decreases (and usually increases) with decreasing external line reactance in the range of system parameters studied.

4. Practically all of the positive damping torque is produced by the quadrature-axis amortisseur circuits.

For a machine with an amortisseur equivalent to either of those treated in this paper, the damping torque remains positive for any of the values of armature circuit resistance considered and independent of load angle.

For a machine with an amortisseur, the concept that stability (as far as hunting is concerned) improves with load is not a valid one, as to the contrary the damping torque is in general smaller under load than at no load, except at extremely small hunting frequencies.

With the combination of extremely high field excitation and armature circuit resistance, and low bus voltage, it seems possible for the damping torque to become negative even with an effective amortisseur.

For a machine with an amortisseur, there is a considerable variation of synchronizing torque coefficient with hunting frequency in the range studied.

Machine Characteristics

The machines chosen for study had the following characteristics. (All quantities are expressed in per-unit on the machine base.)

x_d = direct-axis synchronous reactance or inductance = 1.10

$x_{afd} = x_{ald} = x_{fld}$ = common mutual inductance between direct-axis armature winding, field, and amortisseur (if present) = 0.90

x_{ffd} = field self inductance = 1.12

x_{lld} = direct-axis amortisseur self inductance (if present) = 1.05

x_d' = transient reactance = 0.377

x_d'' = direct-axis subtransient reactance (with amortisseur) = 0.281

r_{fd} = field resistance = 0.0005

r_{ld} = direct-axis amortisseur resistance (if present) = 0.02

x_q = quadrature-axis synchronous reactance = 0.74

x_{alq} = mutual inductance between quadrature-axis armature winding and amortisseur (if present) = 0.54

x_{llq} = quadrature-axis amortisseur self inductance
= 0.84 for amortisseur number 1
= 0.69 for amortisseur number 2

x_q'' = quadrature-axis substansient reactance (with amortisseur)
= 0.393 for amortisseur number 1
= 0.317 for amortisseur number 2

r_{lq} = quadrature-axis amortisseur resistance (if present)
= 0.04 for amortisseur number 1
= 0.02 for amortisseur number 2

These machine constants might be met in a large salient-pole generator. For small machines the per-unit field resistance might be as much as ten times, and the amortisseur resistances two or three times, the values shown here.

Hunting at No Load

For the case of a machine operating at no load ($\delta_o = 0$) and with equal excitations on both machine and bus, and oscillating with per-unit frequency s about its operating angle δ_o, equation 2 of reference 1 may be reduced to

$$\frac{1}{T} = x_q(js) + j\frac{sr}{1-s^2} + \frac{r^2}{(1-s^2)^2\left[x_d(js) + j\frac{sr}{1-s^2}\right]} \quad (1)$$

where T is the complex torque coefficient, so that

$$\Delta T = T\,\Delta\delta = (T_s + jsT_d)\,\Delta\delta \quad (2)$$

where

ΔT = oscillatory component of torque
$\Delta\delta$ = oscillator component of rotor angle

Paper 51-122, recommended by the AIEE Rotating Machinery Committee and approved by the AIEE Technical Program Committee for presentation at the AIEE Winter General Meeting, New York, N. Y., January 22-26, 1951. Manuscript submitted October 23, 1950; made available for printing December 8, 1950.

CHARLES CONCORDIA is with the General Electric Company, Schenectady, N. Y.

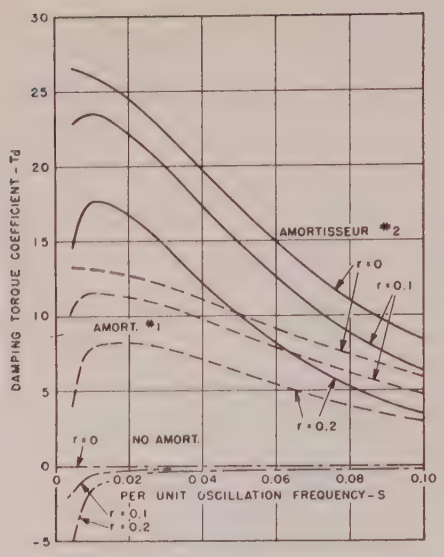

Figure 1 (left). Damping torque coefficient of a synchronous machine as a function of hunting frequency—for various line resistances and rotor circuits

No load ($\delta = 0$)
Excitation voltage $E = 1.0$
Bus voltage $e = 1.0$
Line reactance $x_e = 0$

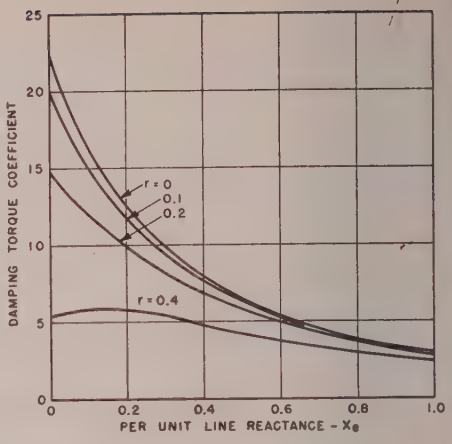

Figure 4 (right). Damping torque coefficient of a synchronous machine as a function of line reactance x_e—for various line resistances

No load ($\delta = 0$)
Excitation voltage $E = 1.0$
Bus voltage $e = 1.0$
Hunting frequency $s = 0.03$
Amortisseur number 2

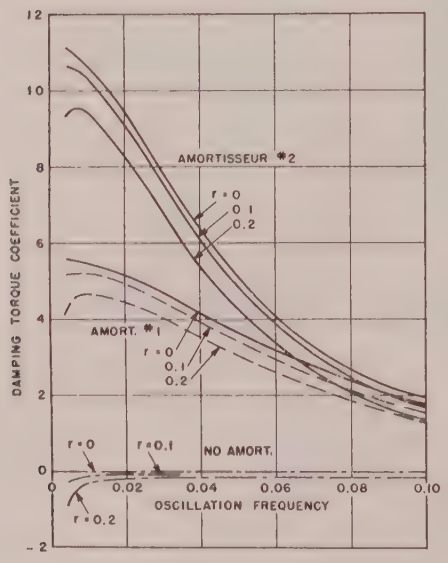

Figure 2 (left). Damping torque coefficient of a synchronous machine as a function of hunting frequency—for various line resistances and rotor circuits

No load ($\delta = 0$)
Excitation voltage $E = 1.0$
Bus voltage $e = 1.0$
Line reactance $x_e = 0.4$

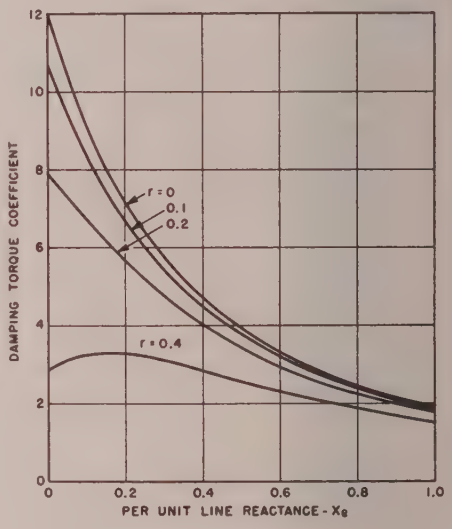

Figure 5 (right). Damping torque coefficient of a synchronous machine as a function of line reactance x_e—for various line resistances

No load ($\delta = 0$)
Excitation voltage $E = 1.0$
Bus voltage $e = 1.0$
Hunting frequency $s = 0.03$
Amortisseur number 1

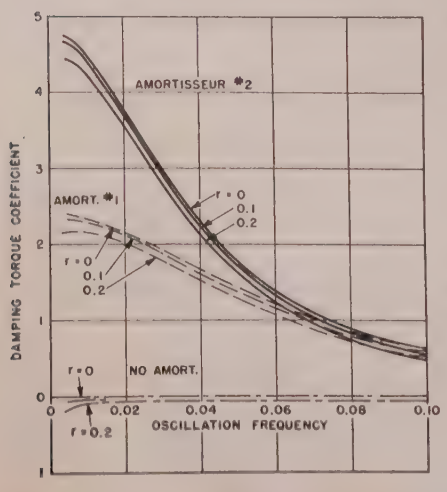

Figure 3 (left). Damping torque coefficient of a synchronous machine as a function of hunting frequency—for various line resistances and rotor circuits

No load ($\delta = 0$)
Excitation voltage $E = 1.0$
Bus voltage $e = 1.0$
Line reactance $x_e = 1.0$

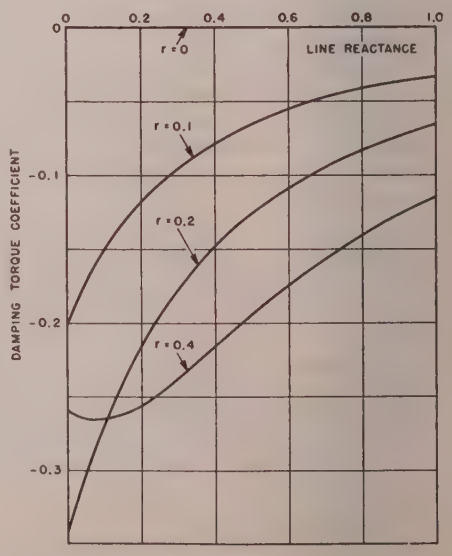

Figure 6 (right). Damping torque coefficient of a synchronous machine as a function of line reactance x_e—for various line resistances

No load ($\delta = 0$)
Excitation voltage $E = 1.0$
Bus voltage $e = 1.0$
Hunting frequency $s = 0.03$
No amortisseur

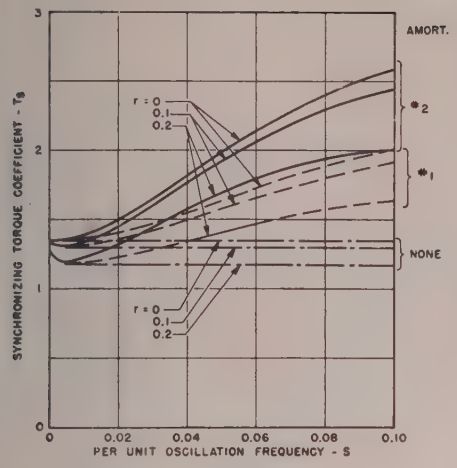

Figure 7 (left). Synchronizing torque coefficient of a synchronous machine as a function of hunting frequency—for various line resistances and rotor circuits

No load ($\delta=0$)
Excitation voltage $E=1.0$
Bus voltage $e=1.0$
Line reactance $x_e=0$

Figure 10 (right). Synchronizing torque coefficient of a synchronous machine as a function of line reactance x_e—for various line resistances

No load ($\delta=0$)
Excitation voltage $E=1.0$
Bus voltage $e=1.0$
Hunting frequency $s=0.03$
Amortisseur number 2

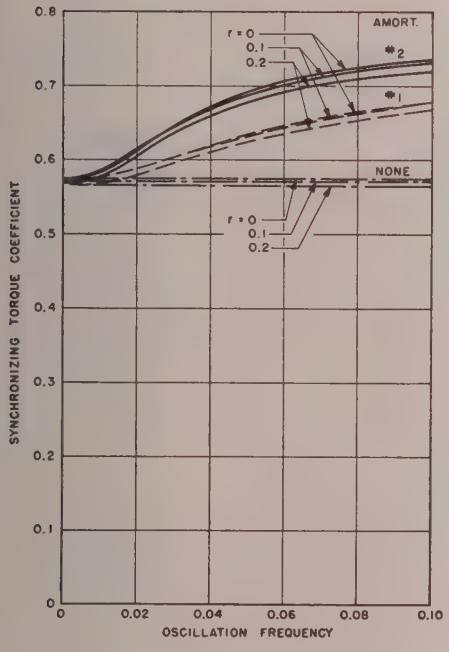

Figure 8 (left). Synchronizing torque coefficient of a synchronous machine as a function of hunting frequency—for various line resistances and rotor circuits

No load ($\delta=0$)
Excitation voltage $E=1.0$
Bus voltage $e=1.0$
Line reactance $x_e=0.4$

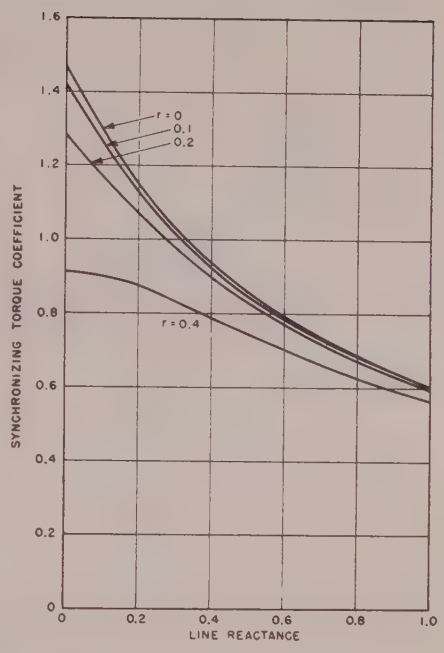

Figure 11 (right). Synchronizing torque coefficient of a synchronous machine as a function of line reactance x_e—for various line resistances

No load ($\delta=0$)
Excitation voltage $E=1.0$
Bus voltage $e=1.0$
Hunting frequency $s=0.03$
Amortisseur number 1

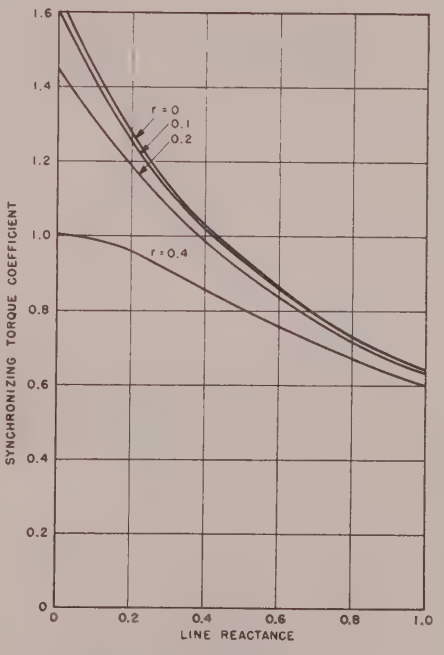

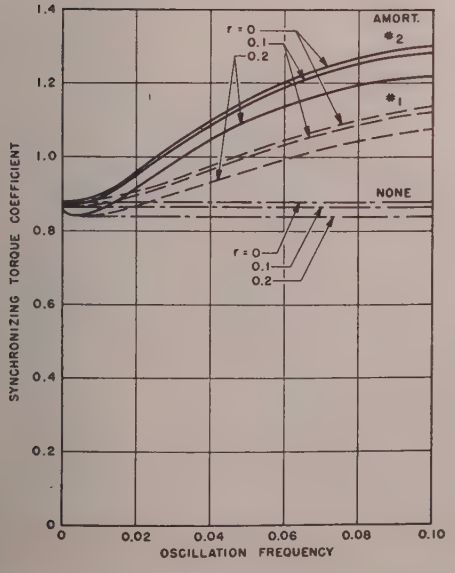

Figure 9 (left). Synchronizing torque coefficient of a synchronous machine as a function of hunting frequency—for various line resistances and rotor circuits

No load ($\delta=0$)
Excitation voltage $E=1.0$
Bus voltage $e=1.0$
Line reactance $x_e=1.0$

T_s = synchronizing torque coefficient
T_d = damping torque coefficient
r = total armature circuit resistance including the tie-line resistance $x_d(js)$ and $x_q(js)$ are the operational impedances[5,6] of the synchronous machine at the hunting frequency s and including the reactance x_e of the tie line

If the line resistance r is not very large, equation 1 shows directly that the principal positive damping arises from the quadrature-axis amortisseur circuit, the direct-axis circuit having very little effect, and that the line resistance produces

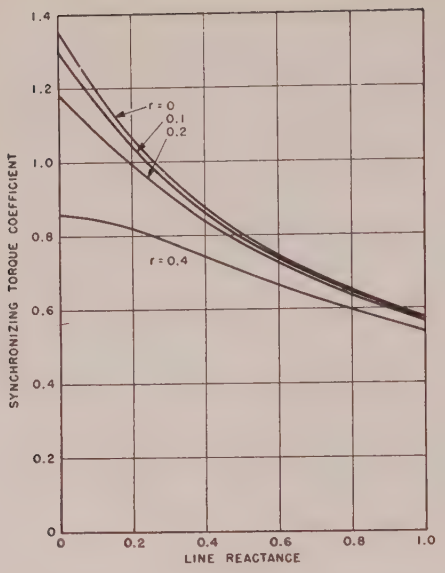

Figure 12 (left). Synchronizing torque coefficient of a synchronous machine as a function of line reactance x_e—for various line resistances

No load ($\delta = 0$)
Excitation voltage $E = 1.0$
Bus voltage $e = 1.0$
Hunting frequency $s = 0.03$
No amortisseur

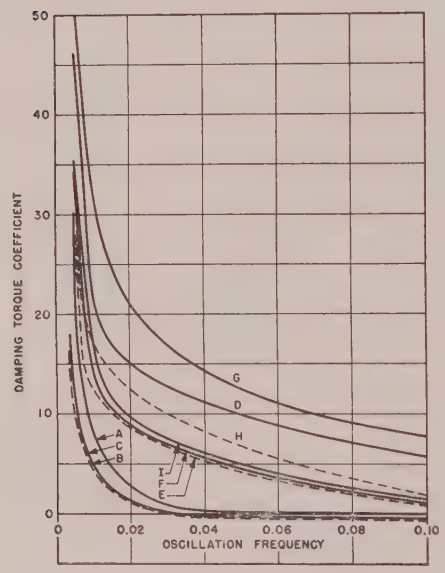

Figure 13 (left). Damping torque coefficient of a synchronous machine as a function of hunting frequency—for various line resistances and rotor circuits

Full load, unity power factor
Terminal voltage $= 1.0$
Line reactance $x_e = 0$

Curve	r	Amortisseur	Case
A	0	None	M and G
B	0.2	None	M
C	0.2	None	G
D	0	#1	M and G
E	0.2	#1	M
F	0.2	#1	G
G	0	#2	M and G
H	0.2	#2	M
I	0.2	#2	G

Note: M = Motor
G = Generator

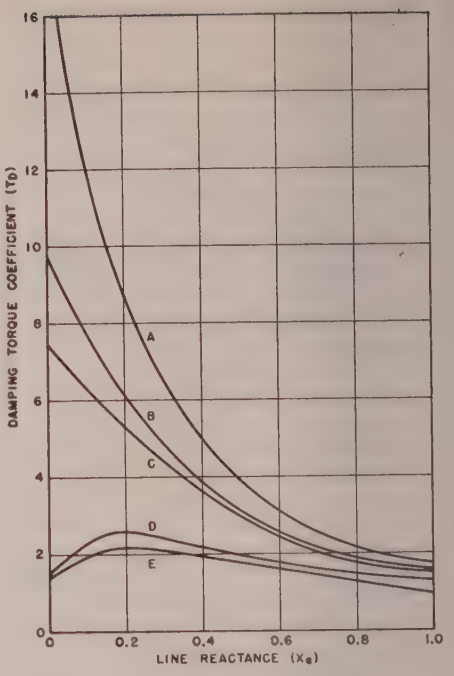

Figure 14 (right). Damping torque coefficient of a synchronous machine as a function of line reactance x_e—for various line resistances

Full load, unity power factor
Terminal voltage $= 1.0$
Hunting frequency $s = 0.03$
Amortisseur number 2

Curve	r	Case
A	0	M and G
B	0.2	M
C	0.2	G
D	0.4	M
E	0.4	G

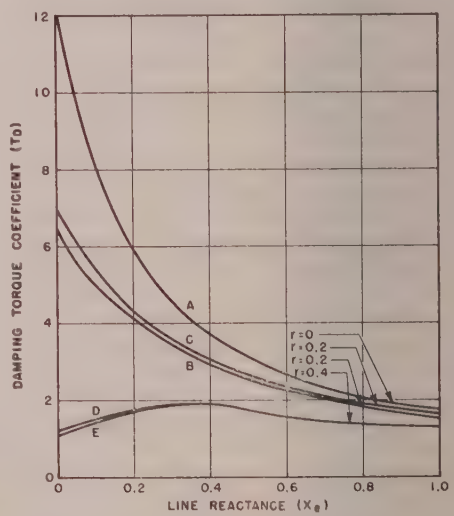

Figure 15 (right). Damping torque coefficient of a synchronous machine as a function of line reactance x_e—for various line resistances

Full load, unity power factor
Terminal voltage $= 1.0$
Hunting frequency $s = 0.03$
Amortisseur number 1

Curve	r	Case
A	0	M and G
B	0.2	M
C	0.2	G
D	0.4	M
E	0.4	G

negative damping. This is in accord with experience.

Calculations of damping and synchronizing torques have been made for tie line reactances x_e from 0 to 1.0, tie line resistances r from 0 to 0.4, and hunting frequencies s of 0.005 to 0.1. The damping torque coefficients are shown in Figures 1 to 6; the corresponding synchronizing torque coefficients are shown in Figures 7 to 12. In Figures 1 to 3 and 7 to 9, the torque coefficients are plotted against hunting frequency for various kinds of amortisseur and values of armature circuit resistance, while in Figures 4 to 6 and 10 to 12 they are plotted against the tie line reactance for a hunting frequency of $s = 0.03$.

It is evident that either type of amortisseur considered here is sufficient to produce a net positive damping. Figure 4 shows, for example, that at a line reactance of $x_e = 0.2$, a very high line resistance of $r = 0.4$ reduces the damping torque only to slightly less than half of its value at $r = 0$. This is a very extreme case that would not be expected to arise very often, if at all.

It is further evident that it is the magnitude of the armature resistance, rather than the ratio of resistance to reactance, that is the important factor in the practical case of a machine with an amortisseur, even though the ratio has been shown[7,8] to be significant in the case of a machine with no amortisseur. This is shown by the fact that for a given value of armature resistance the damping torque coefficient practically always increases with decreasing armature reactance, whereas the ratio of r/s is, of course, becoming greater.

It is of interest also from Figures 7 to 9 that for the machine with either type of amortisseur the synchronizing torque varies considerably with frequency in the range $s = 0$ to $s = 0.1$ considered.

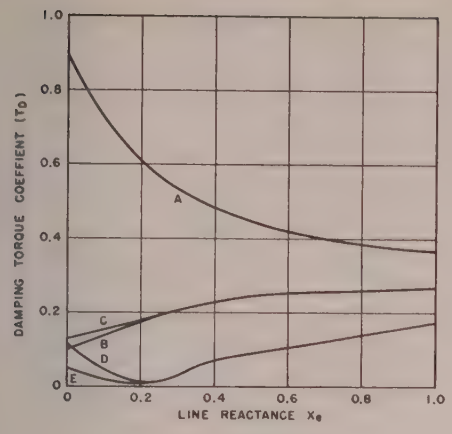

Figure 16 (left). Damping torque coefficient of a synchronous machine as a function of line reactance x_e—for various line resistances

Full load, unity power factor
Terminal voltage =1.0
Hunting frequency $s=0.03$
No amortisseur

Curve	r	Case
A	0	M and G
B	0.2	M
C	0.2	G
D	0.4	M
E	0.4	G

Note: M=Motor
G=Generator

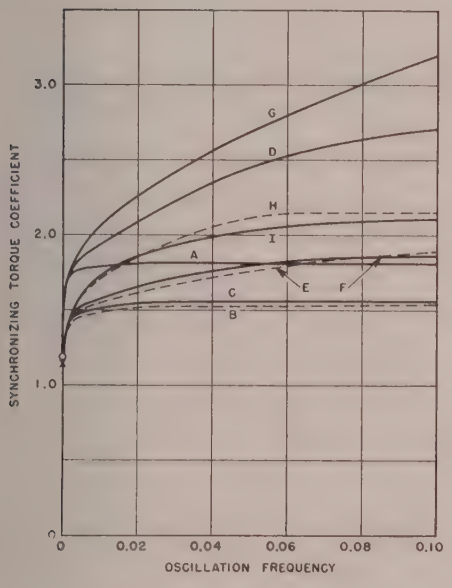

Figure 17 (left). Synchronizing torque coefficient of a synchronous machine as a function of hunting frequency—for various line resistances and rotor circuits

Full load, unity power factor
Terminal voltage =1.0
Line reactance $x_e=0$

Curve	r	Amortisseur	Case
A	0.0	None	M and G
B	0.2	None	M
C	0.2	None	G
D	0.0	#1	M and G
E	0.2	#1	M
F	0.2	#1	G
G	0.0	#2	M and G
H	0.2	#2	M
I	0.2	#2	G

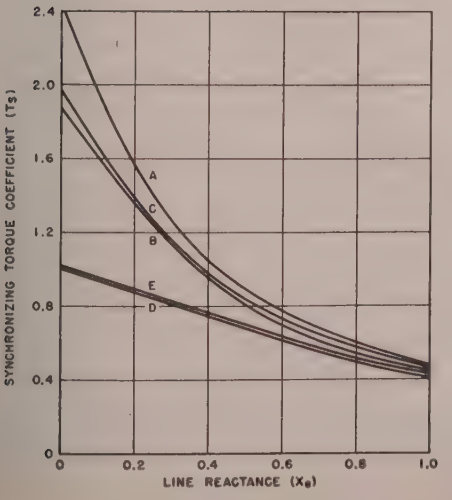

Figure 18 (left). Synchronizing torque coefficient of a synchronous machine as a function of line reactance x_e—for various line resistances

Full load, unity power factor
Terminal voltage =1.0
Hunting frequency $s=0.03$
Amortisseur number 2

Curve	r	Case
A	0	M and G
B	0.2	M
C	0.2	G
D	0.4	M
E	0.4	G

Hunting at Full Load

In order to show to some extent the effect of load angle, equation 2 of reference 1 has been applied directly to the calculation of the damping and synchronizing torque coefficients at full load for the same cases as were previously considered at no load. Figures 13 to 20 show the results of some of these calculations. In Figures 13 and 17 the torque coefficients are plotted against hunting frequency for zero external reactance only, while in Figures 14 to 16 and 18 to 20 they are plotted against external reactance for a fixed hunting frequency of $s=0.03$. For convenience, the equation used is repeated here, in a form adapted to hunting calculations.

$$T=T(js)=\{[\psi_{do}+i_{do}x_q(js)]\times[(e\sin\delta_o+js\psi_{do})z_d(js)+(e\cos\delta_o+js\psi_{qo})x_d(js)]+[\psi_{qo}+i_{qo}x_d(js)][(e\cos\delta_o+js\psi_{qq})z_o(js)-(e\sin\delta_o+js\psi_{do})x_q(js)]\}\div D(js) \quad (3)$$

where

$$D(js)=z_d(js)z_q(js+x_d(js)x_q(js) \quad (4)$$

s = hunting frequency
e = voltage at infinite bus
ψ_{do} and ψ_{qo} are the armature circuit flux linkages including the linkages of the tie line reactance
$z(js)=r+jsx(js)$

The machine has been taken as operating at full load (armature current = 1.0) both as a motor and as a generator with unity power factor and unit voltage at its terminals. All of the armature circuit resistance has been assumed to be in the tie line rather than in the machine, as the armature resistance of the machine armature winding itself is usually very small. Thus the infinite-bus voltage will vary with the tie line resistance and reactance, as well as with change from operation as a generator to operation as a motor.

Comparing Figure 13 with Figure 1 shows that over most of the range of hunting frequencies considered the damping under load is somewhat smaller than at no load, but that at very low frequencies the damping becomes very large. This large damping at very low frequencies is produced by the field winding resistance, which is very small compared to that of the amortisseur. The most striking effect is that under load positive damping is obtainable at low hunting frequencies without an amortisseur. It can also be seen that the effect of armature resistance is greater under load than at no load.

Figures 14 and 15 confirm the conclusion that the effect of armature resistance is greater under load than at no load.

Figure 16 shows that at full load (and

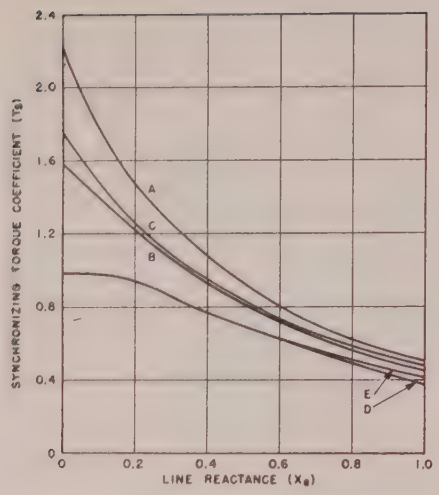

Figure 19 (left). Synchronizing torque coefficient of a synchronous machine as a function of line reactance x_e—for various line resistances

Full load, unity power factor
Terminal voltage $=1.0$
Hunting frequency $s=0.03$
Amortisseur number 1

Curve	r	Case
A	0	M and G
B	0.2	M
C	0.2	G
D	0.4	M
E	0.4	G

Note: M = Motor
G = Generator

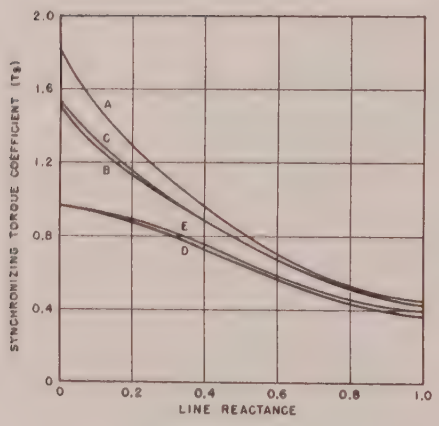

Figure 20 (left). Synchronizing torque coefficient of a synchronous machine as a function of line reactance x_e—for various line resistances

Full load, unity power factor
Terminal voltage $=1.0$
Hunting frequency $s=0.03$
No amortisseur

Curve	r	Case
A	0	M and G
B	0.2	M
C	0.2	G
D	0.4	M
E	0.4	G

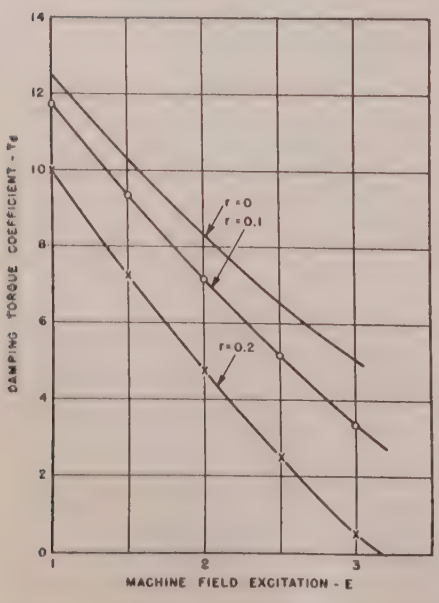

Figure 21 (left). Damping torque coefficient of a synchronous machine as a function of field excitation—for various line resistances

No load on machine
Terminal voltage $=1.0$
Hunting frequency $s=0.03$
Amortisseur number 2
Tie line reactance $x_e=0.2$

Armature current $i_d=\dfrac{E-e_t}{x_d}$

$=\dfrac{E-1}{1.1}$

Figure 22 (right). Synchronizing torque coefficient of a synchronous machine as a function of field excitation—for various line resistances

No load on machine
Terminal voltage $=1.0$
Hunting frequency $s=0.03$
Amortisseur number 2
Tie line reactance $x_e=0.2$

Armature current $i_d=\dfrac{E-e_t}{x_d}$

$=\dfrac{E-1}{1.1}$

for a hunting frequency of 0.03) the damping remains positive without an amortisseur even for a line resistance as high as 0.4.

Finally, Figure 17 confirms the conclusion that, for a machine with an amortisseur, the synchronizing torque varies considerably with hunting frequency.

Effect of High Field Excitation

Figures 21 and 22 show the effect of changing the field excitation with various armature circuit resistances. The machine has been assumed to be at no load (for example operating as a condenser) with the terminal voltage maintained at unity as the excitation is varied. The tie line reactance is $x_e=0.2$ and the resistance has been taken as $r=0$, 0.1, and 0.2 Thus the infinite bus voltage decreases as the machine excitation increases.

It is evident from Figure 21, or indeed from the equation for torque itself, that without armature resistance the damping torque is simply proportional to the square of the infinite-bus voltage. However, with armature resistance the reduction in torque from the zero-resistance case does not increase with field excitation as fast as even the first power of field excitation. The reduction is approximately proportional to the average of the machine and bus voltages. It may

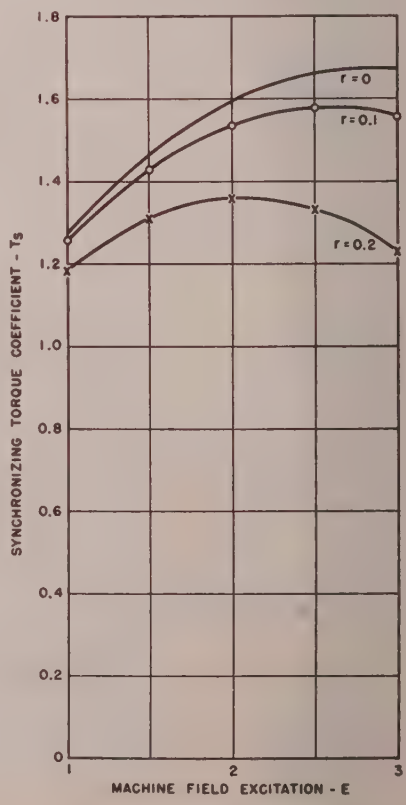

be recalled[9] that without rotor resistances the damping is proportional to the product of the machine excitation voltage and the average of the machine and bus voltages.

With the system parameters used in this study, it is only with extremely large values of excitation, corresponding to an armature current of almost 2 per unit, that it seems possible to reduce the damping to zero.

Finally it may be of interest to record the reduced form of equation 3 for the case of zero armature resistance and no load. In this case equation 3 becomes

$$T = T(js) = \frac{[e + i_{do}x_q(js)]e}{x_q(js)} = \frac{e^2}{x_q(js)} + ei_{do} \quad (5)$$

Effect of Higher Rotor Resistances

It should be emphasized that the magnitudes of the torque coefficients shown in this paper apply only to the synchronous machine specified in the table of machine characteristics. As this machine has rather low rotor resistance, it is of interest to consider what would be the nature of the curves for a machine having higher rotor resistances. This may be estimated without further calculation by noting first that the operational impedances $x_d(js)$ and $x_q(js)$ are functions of the ratio of rotor resistance to hunting frequency so that, if for example all of the rotor resistances are doubled and the hunting frequency is also doubled, the operational impedances will remain unchanged. Moreover, if in addition the armature circuit resistance is very small, it is evident from equations 1 or 3 that the torque coefficient, $T(js) = T_s + jsT_d$, is also practically unchanged. Thus the curves of T_s and T_d versus hunting frequency for the cases of small stator resistance will still be valid if the scale of hunting frequency is doubled, so that the abscissa runs from $s=0$ to 0.2 instead of from $s=0$ to 0.1, and if in addition the scale of T_d is halved so that in Figure 1, for example, the ordinate runs from -2.5 to $+15$ instead of from -5 to $+30$. These higher values of rotor resistance will in general be more nearly correct for the smaller machines, so that for these smaller machines the variation of damping and synchronizing torque coefficients will not, in general, be as great for a given range of hunting frequency in cycles per second, as for a machine having low rotor resistances.

In regard to the effect of variations in reactance, it is evident from the equation that, if all of the reactances and resistances are varied in proportion, the torque coefficients will simply vary in inverse proportion.

References

1. Two-Reaction Theory of Synchronous Machines—II, **R. H. Park.** *AIEE Transactions*, volume 52, 1933, pages 352–54.

2. Positive and Negative Damping in Synchronous Machines, **M. M. Liwschitz.** *AIEE Transactions*, volume 60, 1941, pages 210–13.

3. Oscillographic Study of Synchronous Motor Hunting, **E. B. Kurtz.** *AIEE Transactions*, volume 67, part II, 1948, pages 647–52.

4. Spring and Damping Coefficients of Synchronous Machines and Their Application, **L. A. Kilgore, E. C. Whitney.** *AIEE Transactions*, volume 69, part I, 1950, pages 226–29.

5. Two-Reaction Theory of Synchronous Machines—I, **R. H. Park.** *AIEE Transactions*, volume 48, 1929, pages 716–27.

6. Operational Impedance of a Synchronous Machine, **S. B. Crary, M. L. Waring.** *General Electric Review* (Schenectady, N. Y.), November 1932.

7. Stability of Synchronous Machines—Effect of Armature Circuit Resistance, **C. A. Nickle, C. A. Pierce.** *AIEE Transactions*, volume 49, 1930, pages 338–50.

8. Negative Damping of Electrical Machinery, **C. Concordia, G. K. Carter.** *AIEE Transactions*, volume 60, 1941, pages 116–19.

9. Synchronous Machine Damping Torque at Low Speeds, **C. Concordia.** *AIEE Transactions*, volume 69, part II, 1950, pages 1550–53.

No Discussion

Factors Affecting Minimum Surface Leakage Distances in D-C Power Systems

J. E. HART
ASSOCIATE AIEE

W. W. ROSENBERRY
NONMEMBER AIEE

A. T. McCLINTON
MEMBER AIEE

THE DESIRABILITY of providing more compact installations of electrical power equipment requires that studies be made of the dielectrics used to determine their properties and limitations. One important phase of this broad problem is the establishment of minimum safe leakage* distances for d-c power systems.

The present standards and knowledge of minimum leakage distances are inadequate.

The information that is now available does not recognize the full effect of environmental conditions nor does it represent the limitations of the insulating materials. In an effort to establish reliable values for leakage distances, the factors which effect them must be determined and evaluated. A knowledge of these factors will lead to the establishment of minimum safe leakage distances which is mandatory if complete freedom from insulation breakdown is to be obtained in a compact design.

Surface Leakage Current

An important factor in establishing the leakage distance for insulation is the magnitude and effect of surface leakage currents. The magnitude of these currents depends upon the characteristics of the surface, surface contamination, and the voltage gradient. Since the power loss due to the flow of the leakage currents is inconsequential in power systems concern need be given only to the damage that these currents may do to surface of the insulation.

It is quite well known that the application of voltage of sufficient magnitude can cause a surface breakdown of the insulation. The carbonization or other damage to the insulation resulting from this breakdown voltage is caused by the surface leakage currents. Contaminating the surface of the material with a conducting electrolyte will reduce the magnitude of voltage required to produce breakdown as illustrated by Figure 1.

The leakage current that flows across the insulation due to voltages of the order of breakdown voltage or higher, however, does not represent the minimum current required to damage the insulation. Assuming all other conditions constant, as the voltage gradient is reduced, the corresponding leakage current and resulting surface damage is reduced. In place of the deeply burned groove in the insulation, smaller charred islands or carbon tracks are formed. For any given material and environment the minimum voltage that will cause damaging leakage currents to flow is termed tracking voltage. The comparative magnitudes of this voltage and breakdown voltage are shown in Figure 1.

Although those voltages which are equal to or greater than tracking voltage but less than breakdown voltage cause only partial damage to insulation, the damage becomes cumulative. Repeated applications of the same voltage will cause ultimate failure; the higher the voltage is above tracking voltage, the fewer the number of applications required. This is illustrated in Figure 2. This curve was obtained by using the techniques and procedure outlined in the appendix, except that the contaminant was re-established after each application of the voltage. The normal tracking voltage for the material and conditions was 400 volts. The progression of damage resulting from repeated applications of a voltage above tracking voltage is shown in Figure 3.

It is important to note that the curve of Figure 2 represents the upper limit of failures. Certain uncontrollable factors such as the imperfection of the surface of the insulation can reduce this curve. A small scratch on the material was found to cause it to fail with two applications of a voltage 175 per cent of tracking voltage.

Before considering further the importance of this tracking voltage a brief discussion of the phenomena will be given. This may help to clarify the nature of results obtained showing the effect of environmental conditions, types and quantity of surface contamination, and type of insulating material.

When an insulating material between two electrodes has a continuous film of electrolyte on its surface and a voltage less than the tracking voltage is impressed, the resulting leakage current will have a magnitude proportional to the conductivity of the electrolytic film. However, the flow of current in this film will act to decrease the film area due to vaporization of the liquid by the Joule heat. Since the film is never of uniform thickness, this heating will cause random breaks in the continuity of the film and eventually its complete rupture. Figure 4A shows a typical current versus time curve for these conditions. The current rises abruptly to a peak when the voltage is applied and then decreases as the sur-

* Leakage distance is defined as the shortest path on the surface of an insulating material over which leakage currents may flow.

Paper 51-123, recommended by the AIEE Rotating Machinery Committee and approved by the AIEE Technical Program Committee for presentation at the AIEE Winter General Meeting, New York, N. Y., January 22–26, 1951. Manuscript submitted October 10, 1951; made available for printing December 12, 1951.

J. E. HART and A. T. McCLINTON are both with the Naval Research Laboratory, Washington, D. C. W. W. ROSENBERRY is with the Naval Engineering Experiment Station, Annapolis, Md.

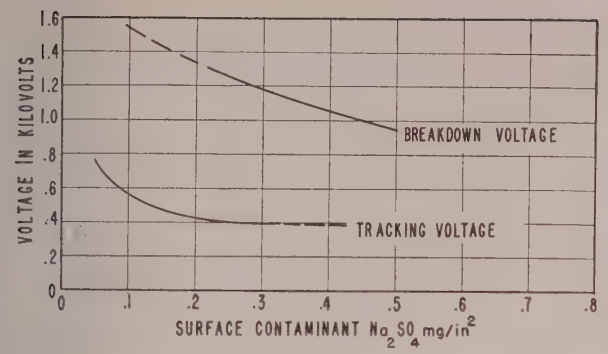

Figure 1. Effect of surface contamination on breakdown voltage and tracking voltage

Material: laminated glass phenolic
Electrode spacing: 0.5 inch
Surface moisture: 45 mg/in.^{2}

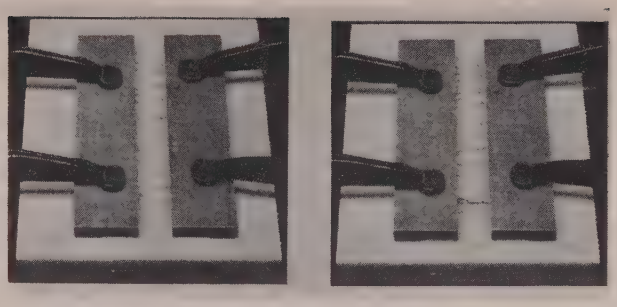

Figure 3. Accumulative damage to insulation resulting from application of a voltage 275 per cent of tracking voltage

Material: laminated glass silicone
Electrode spacing: 0.5 inch
Surface moisture: 45 mg/in.^{2}
Normal tracking voltage: 510 Volts

face moisture begins to vaporize. As the film thickness decreases, breaks occur in the film surface. The current thereby decreases further until it finally approaches a negligible quiescent value. However, at the time of separation of the film small arcs may form on the surface of the insulation. If the energy in these arcs is low, as in the case of this example, no damaging tracks occur on the insulation. If a greater amount of contamination were employed, the severity of arcing would increase and the insulation would be damaged. Figure 4B is a representative oscillogram of the leakage current for this condition. (The irregularities in this current curve indicate arcing.) In this case the arc resisting ability of the insulation is exceeded and the insulation surface is damaged. Figure 4C is for identical conditions as 4B except that a material with a higher arc resisting ability was employed and no damage resulted. Thus it is seen that the tracking voltage is related to the arc resisting property of the insulating material.

The above analysis of the effects of leakage currents on insulation and the relationships to environmental conditions indicates the following:

1. The minimum safe leakage distance is determined by the absence of damage to the insulation by leakage currents.

2. The magnitude of leakage currents is dependent upon the spacing of conductors on the insulation, that is, the leakage path, the voltage gradient, and the amount and nature of contamination.

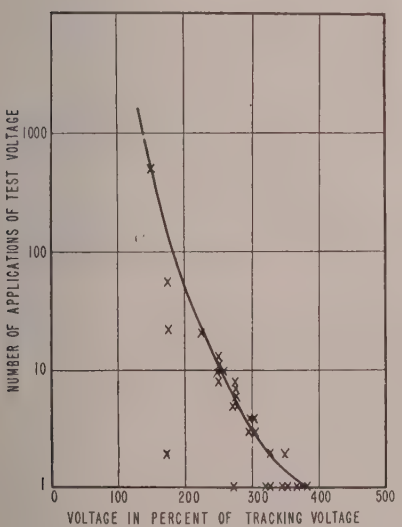

Figure 2. Insulation breakdown resulting from accumulated damage

Material: laminated glass phenolic
Electrode spacing: 0.5 inch
Surface moisture: 45 mg/in.^{2}
Surface contaminant: 0.2 mg/in., Na_2SO_4

Surface Contamination

The dependency of minimum leakage distances on surface contamination emphasizes the need of specifying these distances on the basis of the maximum amount of contamination found where the equipment is to be used. An analysis of the contaminants found on electrical panels which had been in service in marine applications provides such a basis for this paper. The results of these analyses are utilized as a range of concentrations of sodium sulfate. The leakage distances presented may therefore be extended to any application where the soluble contaminants can be represented as equivalent amounts of sodium sulfate. The relative effect of carbon or other insoluble contaminants on leakage distances will be indicated below.

An additional factor to consider is that of surface moisture. Under conditions of high humidity it was found that moisture condensed on the insulating panels. The combination of this moisture and the soluble contaminants provides the conditions most conducive to the production of damaging leakage currents.

Using the data from the chemical analysis and the techniques for measuring tracking voltage described in the appendix, studies were made to determine the minimum leakage distances for variations in parameters of contaminants, ambient conditions, and insulating material.

Minimum Leakage Distance

The variation in tracking voltage as a function of the number of milligrams per square inch of sodium sulfate for a laminated glass melamine insulation is presented in Figure 5. It can be seen that the tracking voltage for this material approaches a constant value as the concentration of contaminant is increased above 0.1 milligram per square inch.

The effect of the carbon which was found in the chemical analyses of the shipboard panels also is shown in Figure 5. A quantity of 0.5 milligram per square inch, which is greater than the maximum

Table I. Effect of Electrode Configuration on Insulation Breakdown

Configuration of Electrodes	Tracking Voltage	Number of Applications of 1,100 Volts to Cause Breakdown (Average of 3)
Stud to stud	550	2.5
Bus to bus	525	5.3
Positive bus to negative stud	575	3.3
Negative bus to positive stud	575	24.4

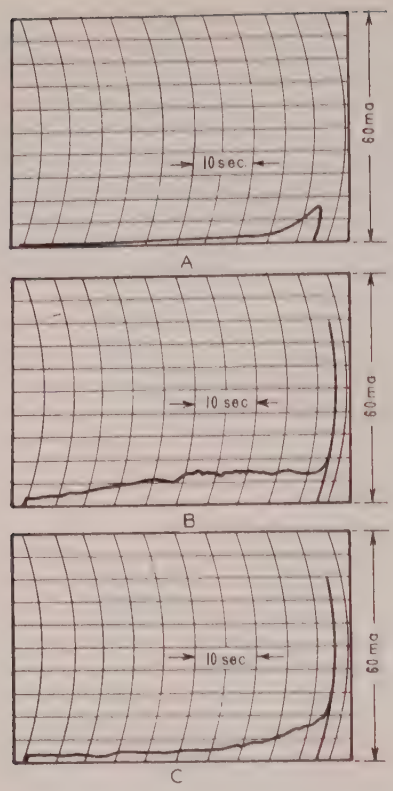

Figure 4. Transient leakage current

(A). Material: laminated glass phenolic
Electrode spacing: 0.5 inch
Surface moisture: 45 mg/in.²
Surface contaminant: 0.02 mg/in.² Na_2SO_4
Applied voltage: 500 Volts

(B). Material: laminated glass phenolic
Electrode spacing: 0.5 inch
Surface moisture: 45 mg/in.²
Surface contaminant: 0.15 mg/in.² Na_2SO_4
Applied voltage: 500 Volts

(C). Material: laminated glass melamine
Electrode spacing: 0.5 inch
Surface moisture: 45 mg/in.²
Surface contaminant: 0.15 mg/in.² Na_2SO_4
Applied voltage: 500 Volts

Table II. Minimum Permissible Leakage Distances in Inches for Various Values of Contamination and Voltage

Contaminant in Mg/in.² of Na_2SO_4	1,000 Volts				500 Volts				250 Volts			
	0.3	0.2	0.1	0.05	0.3	0.2	0.1	0.05	0.3	0.2	0.1	0.0
Materials:												
Laminated Glass Silicone	*	*	*	0.75	0.25	**	**	**				
Laminated Glass Melamine	*	*	1.3	0.0	0.35	0.25	**	**				
Laminated Glass Phenolic	*	*	*	2.0	1.5	1.3	0.25	**				
Asbestos Phenolic	*	*	*	2.0	0.75	**	**	**				
Cotton Phenolic	*	*	*	*	+	*	0.7	**				
Silicone Rubber	1.5	0.0	0.25	**	**	**	**	**				
Hard Rubber Selected Type	*	+	*	*	*	*	1.6	0.25				

* Greater than 2 inches.
** Less than 0.25 inch.

All less than 0.25

amount of the analyses, was added to the sodium sulfate solution. It will be noted that this had no measurable effect on the value of tracking voltage.

The effect of variations in the amount of surface moisture for a constant weight of sodium sulfate per square inch and several electrode spacings is indicated in Figure 6. The important consideration is that the tracking voltage has a minimum range for condensed moisture from approximately 20 to 40 milligrams per square inch. The amount of moisture which may be condensed on a panel under adverse conditions is also in this range. In view of this fact all basic tracking voltage tests were performed with a comparable moisture density.

A family of curves showing the variation of tracking voltage with electrode spacings for several values of contaminant is presented in Figure 7. The lack of any proportional relationship between the minimum leakage distance and the voltage is evident. Since the insulation is damaged by the arcs that form when the moisture film ruptures, it is the voltage gradient at the break in the film that is paramount in the production of damage. As the spacing between electrodes is increased the resistance of the surface film in series with the damage producing arcs is increased. However, this resistance is small compared to the resistance of the gaps, and therefore the increased leakage distance has only a small effect on the tracking voltage.

It is also evident from Figure 7 that for realizable shipboard contaminants there exist definite upper limits of voltage if the specified leakage distances are to be held to a reasonable maximum value. The value of these limiting voltages depends, however, on the type of insulation material employed. By employing materials with characteristics which are improved over those of existing insulation, reductions of the minimum leakage distance will be possible. A few test points obtained from a sample of laminated glass-teflon illustrates this. A comparison of these results with those for glass melamine, Figure 8, reveals not only the quality of this material, but, of greater importance, the desirability of recognizing the minimum permissible leakage distance for each insulating material. The use of superior insulating materials, thereby, permits the reduction in size and weight of electrical installations.

Variation of the ambient condition of temperature and relative humidity was

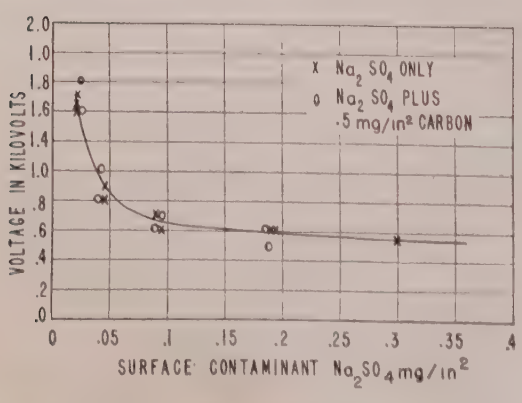

Figure 5 (left). Effect of surface contamination on tracking voltage
Material: laminated glass melamine
Electrode spacing: 0.5 inch
Surface moisture: 45 mg/in.²

Figure 6 (below). Effect of surface moisture on tracking voltage
Material: laminated glass melamine
Surface contaminant: 0.1 mg/in.² Na_2SO_4

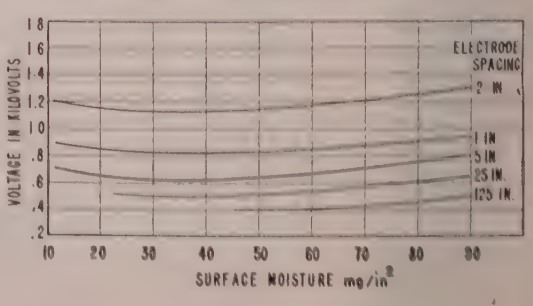

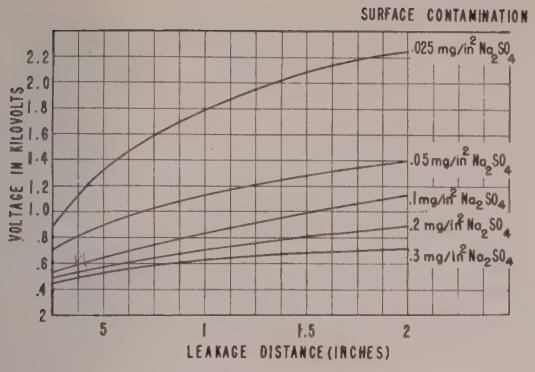

Figure 7 (left). Tracking voltage as related to electrode spacing

Materials: laminated glass melamine
Surface moisture: 45 mg/in.²

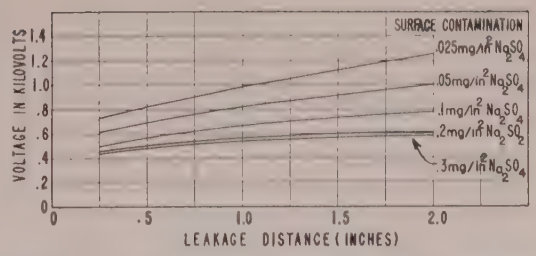

Figure 9 (above). Tracking voltage as related to electrode spacing

Material: machined laminated glass melamine
Surface moisture: 45 mg/in.²

found to produce no measurable effect on tracking voltage. The lack of any dependence is not surprising in view of the fact that tracking voltage is dependent to a large measure on the arc resistance of the material, conductivity of the electrolyte and the moisture, none of which will be materially changed by the ambient temperature or humidity.

Machining the surface of the insulation that is exposed to the leakage currents, on the other hand, had an influence on the minimum permissible leakage distance. Figure 9 shows the results for laminated glass melamine. It was noted also that machining or otherwise altering the surface of the glass-teflon reduced the permissible voltage level shown on Figure 8 to approximately the same value as shown for glass-melamine. In general, machining of the glass laminated structures increased the minimum leakage distance. This evidently results from the presence of the exposed fibers of glass that either (1) are more susceptible to the arc than to the basic insulation, or (2) change the voltage gradient.

In addition to studying the effects of contaminant and environmental condition on tracking voltage, an investigation was made of the influence of electrode configuration. The arrangements used were two bus bars, one bus bar and a 3/8-inch stud, and two 3/8-inch studs. It was found that the tracking voltage was not affected by the geometry of the electrodes, for those considered, but the number of applications of a selected voltage above tracking voltage to cause breakdown differed considerably for the several conditions. Table I shows these results.

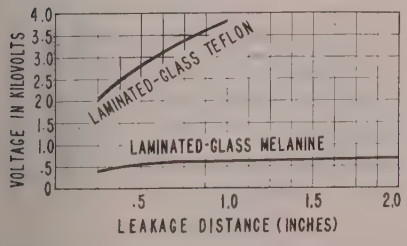

Figure 8. Comparison of tracking voltage for two materials

Surface moisture: 45 mg/in.²
Surface contaminant: 0.36 mg/in.² Na_2SO_4

Summary

A summary of the minimum leakage distances for the several insulating materials investigated is presented in Table II. These data were obtained for direct current applications using the measuring techniques described in the appendix.

The determination of safe minimum leakage distances for power installations is dependent upon the following considerations:

1. The minimum safe distance is dependent upon the leakage current across the surface of the insulation. The voltage associated with the minimum safe current, namely tracking voltage, serves as a criterion for establishing this minimum distance. Exceeding this criterion either by increased voltage or reduced distance will result in ultimate breakdown and complete destruction of the insulating properties of the insulation.

2. The establishment of minimum safe leakage distances requires an accurate knowledge of the environmental conditions where the insulation will be employed. The deposition of water and soluble conducting contaminants such as sodium chloride and sodium sulfate will affect the tracking voltage greatly.

3. The arc resisting qualities of an insulating material will, to a large extent, determine the safe minimum leakage distance.

Further investigation should be made to determine the factors affecting leakage distances in alternating current systems and the relationship to direct current values. Surge voltages and the benefits derived from barriers should also be analyzed to add further knowledge to the limitations of insulation and insulated structures.

Appendix

Measurement of Tracking Voltage

Tracking voltage is defined as the minimum voltage which will cause damage to

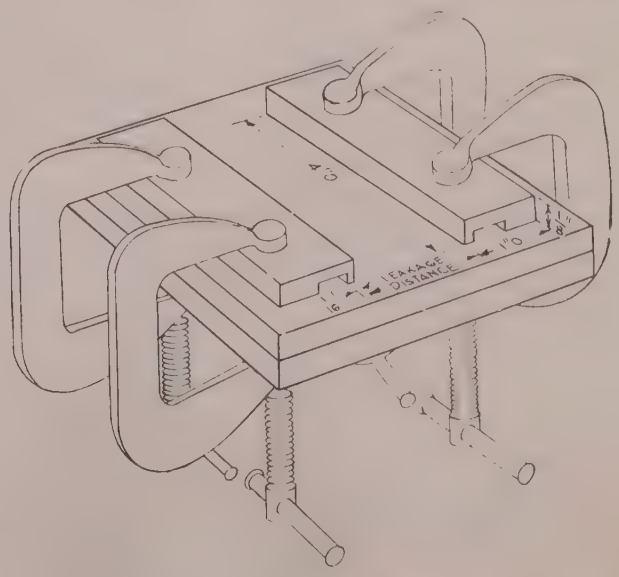

Figure 10. Insulation sample prepared for tracking voltage measurement

the surface of an insulating material for a given set of conditions. The procedure for determining a tracking voltage value is as follows: A sample of the insulation to be evaluated is prepared by clamping a set of copper electrodes (bus bars) on its surface a measured distance apart. The surface between the electrodes is washed with distilled water and allowed to dry. A specific amount of contaminant, either dissolved or mixed with a specific amount of water, is spread over the surface of the insulation between the electrodes. A step function direct current voltage is immediately applied to the electrodes and maintained until the leakage current reaches its quiescent value. This may be a period from 30 seconds to several minutes. After removal of the voltage the sample is lightly wiped with a sponge wet with distilled water and allowed to dry. It is then optically scanned under a 15 to 20 power binocular microscope for evidence of tracking.

This complete procedure is repeated at successively higher voltages with the tracking voltage recorded as the minimum voltage for which tracking is observed. The entire procedure is repeated as necessary to obtain representative data for each point on a curve.

Several important details that are necessary to assure consistent and accurate results are as follows: The under side of the bus bars are grooved (Figure 10) to prevent loss of the surface moisture by capillary action. The deposition of a specific amount of surface moisture is accomplished by the use of either a calibrated medicine dropper or a hypodermic syringe. A small camel's hair brush pre-wetted is employed to spread the contaminating solution over the leakage surface. To provide uniform spreading of the surface moisture a non-ionic wetting agent was added to the contaminating solution.

The power supply or voltage source used in these measurements should be well regulated and have a capacity of not less than 500 milliamperes. The transient response should allow a voltage variation of not more than about two per cent to eliminate errors which may otherwise be caused by the rectification in voltage gradient available when the leakage currents flow.

The resulting values of tracking voltage obtained on laboratory contaminated samples using the above techniques were compared with data obtained on panels removed from operating machinery. The results were in good agreement.

No Discussion

Telephone Influence Factor in Synchronous Machines

G. L. OSCARSON
MEMBER AIEE

IKEL C. BENSON
MEMBER AIEE

TO CONVEY speech with acceptable fidelity requires a telephone system which will transmit frequencies covering a large part of the audible range. Obviously a near-by power line inducing corresponding frequencies in the telephone system may set up continuous interference.

The growth of power transmission and distribution lines, particularly those paralleling telephone lines, has created a consciousness of telephone influence factor (commonly abbreviated TIF). This paper is a resume of analyses made of the effect of power system harmonics on telephone systems and of the measures taken by designers of synchronous equipment to avoid generation of these interfering frequencies.

Telephone Influence Factor Defined

There are two components of TIF, balanced and residual.

Balanced Component

Balanced-component TIF of a 3-phase synchronous machine is the ratio of the square root of the sums of the weighted rms values of the fundamental and nontriple series harmonics to the rms value of the normal no-load voltage wave.

Balanced TIF is measured terminal to terminal of the machine, usually open circuit, no load. The possible elements contributing to this component are the nontriple odd harmonics, such as the fifth, seventh, eleventh, and so forth. In any symmetrical rotating machine, the even-numbered harmonics cannot be present, as they cancel out. Within the machine itself, triple harmonics may circulate in a delta connection, but they do not appear external to the machine. The algebraic sum of the balanced-component voltages or currents is zero with respect to a point in space. Theoretically their effect on a telephone system can be neutralized by transposition of power or telephone conductors.

Present standards of the National Electrical Manufacturers Association (NEMA) on balanced component of low-speed synchronous generators are shown in Table I.

Residual Component

Residual-component TIF of a 3-phase synchronous machine is the ratio of the square root of the sum of the squares of the weighted values of one-third the rms fundamental and harmonic residual voltage to the rms value of the normal voltage from line to neutral.

If a machine is operated grounded neutral, the triple harmonics—third, ninth, fifteenth, and so forth, will flow through the load and return via the ground lead. As shown in Figure 1, these harmonics are themselves in phase. They, therefore, combine and return through the neutral. The direct inductive effect on telephone conductors cannot be modified by transposition. The ground return also may parallel telephone circuits, thus causing harmonic currents to flow.

NEMA standards on residual component for low-speed synchronous generators are shown in Table II.

Table I

Kilovolt Amperes	Balanced Component
62.5– 299	300
300– 699	200
700– 999	150
1,000–2,499	125
2,500–9,999	60
10,000 and above	50

Table II

Kilovolt Amperes	Residual Component
62.5 299	180
300– 699	120
700– 999	90
1,000–2,499	75
2,500–9,999	30

Determination of Weighting Factor

History

The definitions mention weighted values of the harmonics. The determination of weighting factors for various frequencies, the method of measurement, and the effect of grounded and ungrounded power systems on telephone interference are all of general interest in establishing a basic understanding of this problem.

The first quantitative measure of power system interference on telephone systems was established by an AIEE Subcommittee in 1919.[1] The standard proposed by this committee was known as Telephone Interference Factor. However, the problem is not primarily one of wave form. A nineteenth harmonic having an amplitude of 2 per cent of the fundamental will cause much more interference than a fifth harmonic with an amplitude of 20 per cent.

Accordingly, a second committee[2] attacked the problem from the standpoint of interference caused by individual harmonics. A new standard, known as Telephone Influence Factor, was adopted in 1935. This established the currently accepted weighting for telephone interference.

To determine the actual effect of various frequencies on a telephone system,

Paper 51-124, recommended by the AIEE Rotating Machinery Committee and approved by the AIEE Technical Program Committee for presentation at the AIEE Winter General Meeting, New York, N. Y., January 22–26, 1951. Manuscript submitted August 28, 1950; made available for printing December 8, 1950.

G. L. Oscarson and Ikel C. Benson are both with the Electric Machinery Manufacturing Company, Minneapolis, Minn.

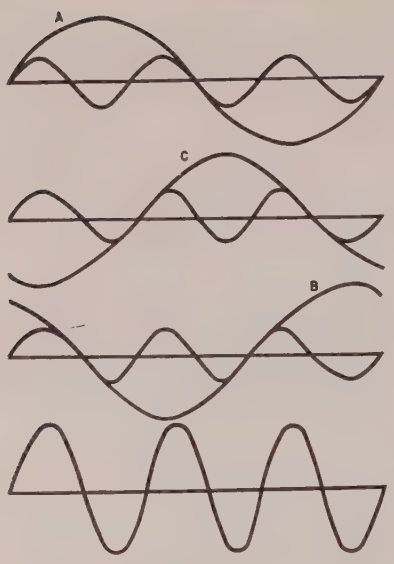

Figure 1. Three-phase fundamental and triple harmonics

tests were made by reading news items to various listeners and also by articulation of unrelated syllables while currents of equal amplitude, but of various frequencies, were superimposed on the circuit. The relative interfering effect, as determined by thousands of tests, is plotted in Figure 2. The interference is proportional to the amount of current. It varies widely with the frequency as shown.

It was desired to adjust the values in Figure 2 so they would represent the effect of the power system harmonics, taking into account the coupling effect on the telephone system as well as the telephone system itself. This new series of values was obtained by multiplying the values in Figure 2 by a factor proportional to the frequency itself. This resulted in the values shown in the curve and tabulation in Figure 3, weighted on the basis that TIF at 60 cycles is equal to one. The fundamental and all harmonics are assumed to be true sine waves; also, it is assumed that any 60-cycle wave with a TIF greater than one can be resolved into the 60-cycle fundamental with one or more harmonics superimposed on it.

Figure 4 illustrates a 60-cycle fundamental with a nineteenth harmonic having an amplitude of 10 per cent. As defined and in accordance with the table

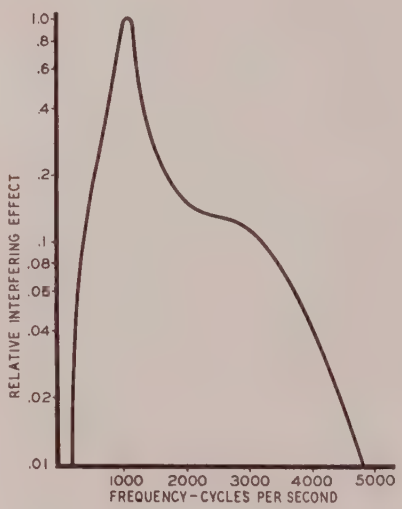

Figure 2. Relative interference at various frequencies

in Figure 3 we find:

$$\text{Balanced component} = \sqrt{1^2+(0.1\times 11{,}100)^2} = 1{,}110$$

Even if the amplitude of a nineteenth harmonic is reduced to one per cent of the fundamental the resultant TIF will be 111. Since many specifications call for balanced-component values as low as 15, it is obvious that there can then be substantially no contribution by the seventeenth or nineteenth harmonics.

The relative interfering effect of two machines is proportional to the product of current times TIF. A generator, or synchronous motor, with a current of 100 and a balanced component of 20 has twice as much relative interfering effect as a unit with a current of 25 and a component of 40.

Measuring Telephone Influence Factor

To measure TIF requires a circuit having an admittance characteristic as represented by the curve in Figure 2. One such circuit is shown in Figure 5. The meter is a thermocouple-type d-c milliammeter. To measure the balanced component the terminals of the meter are connected, usually through a potential transformer, as shown in Figure 6, to the machine or circuit under test. Readings are taken of the volt input and of current flowing through the network. Quantitatively:

$$\text{Balanced component} = (\text{micro-amperes})/(\text{volts})$$

A 60-cycle sine-wave generator im-

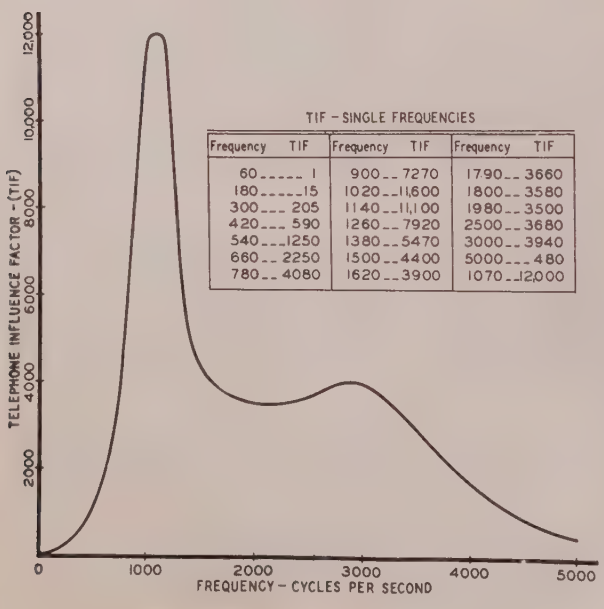

TIF – SINGLE FREQUENCIES

Frequency	TIF	Frequency	TIF	Frequency	TIF
60	1	900	7270	1790	3660
180	15	1020	11,600	1800	3580
300	205	1140	11,100	1980	3500
420	590	1260	7920	2500	3680
540	1250	1380	5470	3000	3940
660	2250	1500	4400	5000	480
780	4080	1620	3900	1070	12,000

Figure 3 (left). Frequency weighting for TIF measurements

Figure 4 (below). Fundamental and 10 per cent nineteenth harmonic

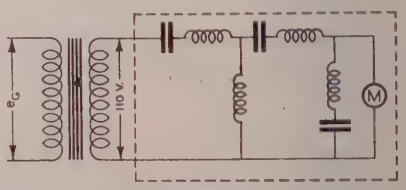

Figure 5 (above). Circuit for one type of meter

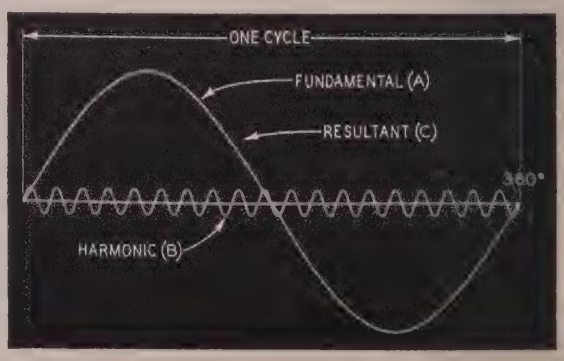

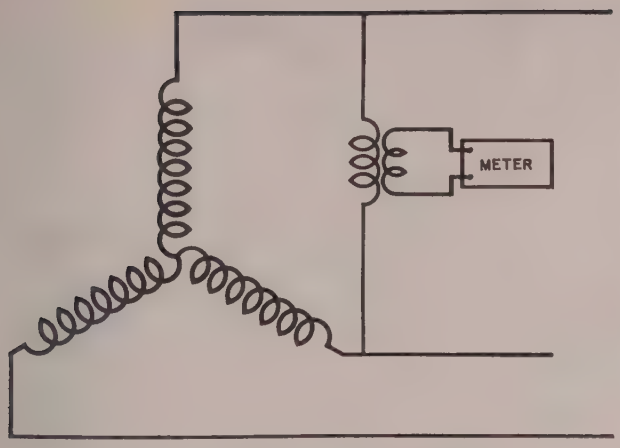

Figure 6. Connections to measure balanced TIF

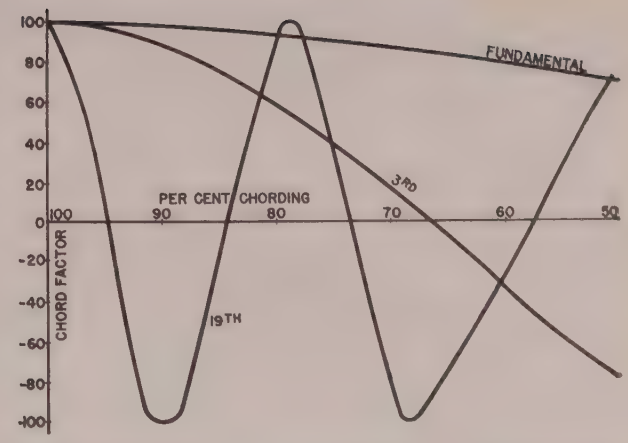

Figure 9. Chord factors for various chordings on fundamental, third, and nineteenth harmonics

pressing 100 volts on the meter terminals will cause 100 micro-amperes to flow through the milliammeter. The balanced component of any machine is a direct measure of its interfering effect on a telephone system, compared to interfering effect of an equivalent 60-cycle pure sine wave.

To measure the residual component the machine is delta connected with the meter connected across one corner, as shown in Figure 7. If triple harmonics are present in any substantial amount, a potential transformer or resistor may be necessary to limit the voltage at the meter terminals.

The presence of harmonic voltages as determined previously is primarily important in that it causes harmonic currents to flow, these harmonic currents by inductive action causing currents to flow in the telephone system, with subsequent interference. Current TIF which is a measure of harmonic currents, can be measured with a meter by using a current coupler.

If a harmonic filter is to be used to reduce interference of an existing installation, it is important to know the frequency and amplitude of the harmonics present. A harmonic analyzer is used with the meter to determine the contribution of each of the existing frequencies.

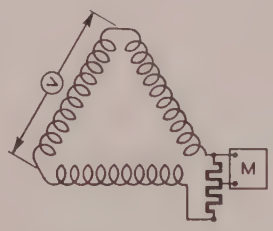

Figure 7. Connections to measure residual TIF

General

The balanced component generally is much lower under load than it is open circuit. However, this may not be true if capacitors are present, as they will accentuate higher harmonics.

The effect of the residual component may be more pronounced at higher loads, as higher line currents also will cause higher absolute values of triple harmonic current to flow. Generators to be operated grounded neutral should be designed for low values of residual component.

A series of voltage transformations generally will reduce harmonic content in a wave form and therefore reduce interference. However, highly saturated transformers will introduce triple harmonics and, if operated grounded neutral, may result in substantial residual currents.

Although this discussion covers only synchronous machines, it also is possible for induction motors to introduce harmonic currents. If the counter electromotive force of the induction motor has a high harmonic content, harmonic currents will flow in the feeder to this motor with possible subsequent telephone interference.

In any electric circuit, the first source of voltage-wave distortion is in the gener-

Figure 8. Under- and over-chording effects illustrated for fundamental and third harmonic waves

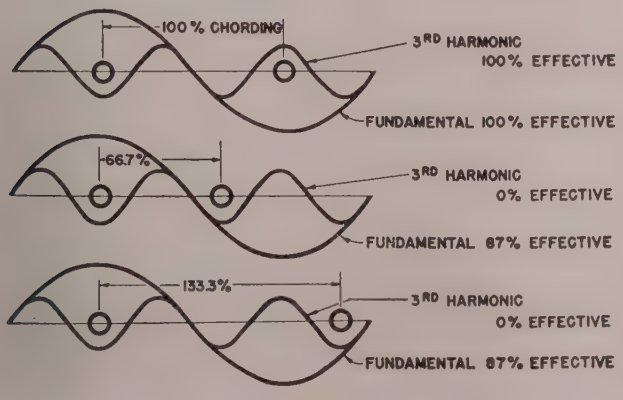

Figure 10. True-arc poles of various pole embraces and corresponding field flux plots

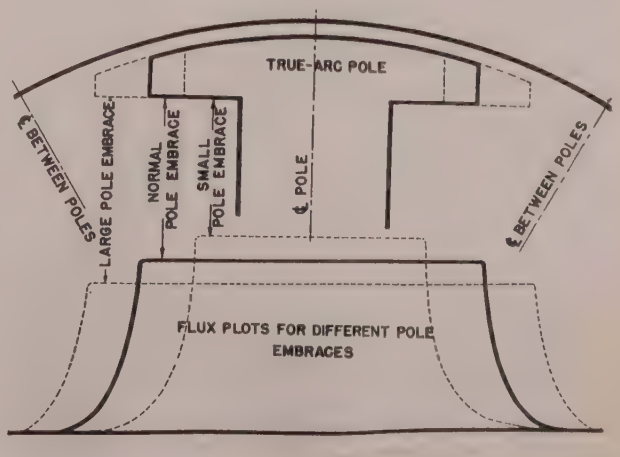

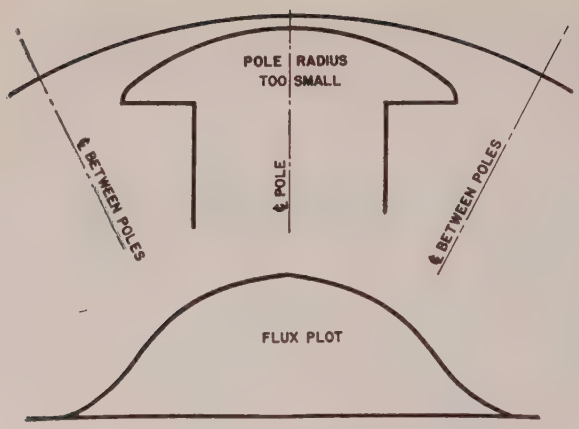

Figure 11 (left). True-arc pole having small radius and its field flux plot

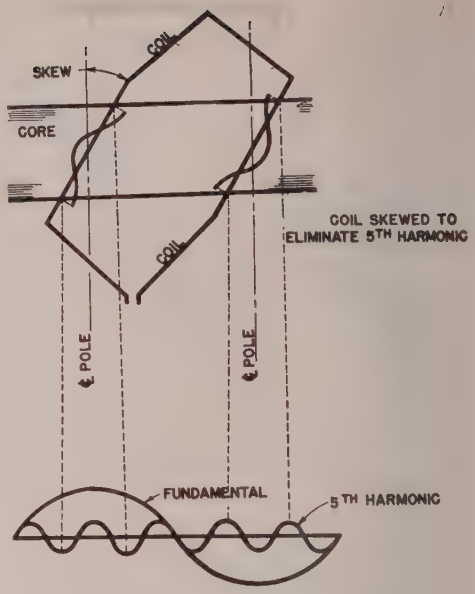

Figure 13 (right). Skewing effects illustrated for fundamental and fifth harmonic waves

ator. At no-load and normal voltage (generator armature being open-circuited), the generated instantaneous voltage is directly proportional to the instantaneous rate of cutting lines of magnetic force. A simple conductor revolving at constant speed in a uniform magnetic field generates a sine voltage wave. The generator voltage wave and TIF will be affected by:

1. The stator slotting—fractional slotting is desired
2. The coil pitch of the armature coils
3. The number of coils and turns per slot
4. The angular span of the phase belts
5. The skewing of stator slots, or rotor poles, or both
6. The pole arc and shape
7. The air gap and relation of slot width to slot pitch
8. The magnetic saturation in the magnetic circuits

Stator Slotting

The slotted armature affects the distribution of the magnetic flux and produces pulsations in the field that cause distortions in the voltage wave. The movement of the field poles in relation to the armature slots produces pulsations of the magnetic reluctance of the field circuit and hence, even with constant field excitation, a pulsation in the magnetic flux. Therefore, this pulsation caused by the armature slots is the source of two harmonics in the voltage wave having frequencies of twice the number of slots per pole plus one times the fundamental frequency and twice the number of slots per pole minus one times the fundamental frequency. Thus, nine slots per pole (three slots per pole per phase for a 3-phase generator) produces seventeenth and nineteenth harmonics which in a 60-cycle generator results in 1,020 and 1,140 cycles per second, respectively. By reference to any TIF curve, it can readily be seen that both these frequencies are in the resonance zone and therefore are very objectionable, so that they should be avoided. Integral slotting is known as A slots per pole per phase, wherein A is any integral number.

Fractional slotting is $A+(b/c)$ slots per pole per phase, where b/c is a fraction reduced to its lowest terms. Fractional slotting has a vernier effect from pole to pole, so that c poles are required before the relationship of slot to pole repeats. This is equivalent to many more slots per pole per phase and is electrically equivalent to $(Ac+b)$ slots per pole per phase. Thus, $2^5/_8$ slots per pole per phase is electrically equivalent to 21 slots per pole per phase. The order of the slot harmonic, m, becomes $2 \times$ phases $\times (Ac+b) \pm 1$, which in this example results in harmonics of the 125th and 127th order in a 3-phase generator. The corresponding frequencies are 7,500 or 7,620 cycles per second,

Figure 12. True-arc pole having large radius and its field flux plot

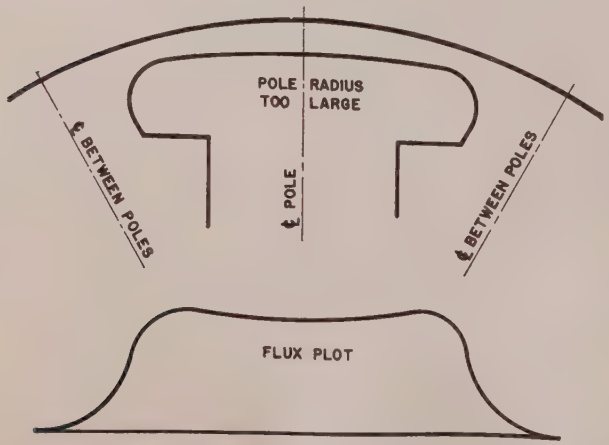

Figure 14. Skew factors for various skewings on fundamental, third, ninth, nineteenth, and twenty-third harmonics

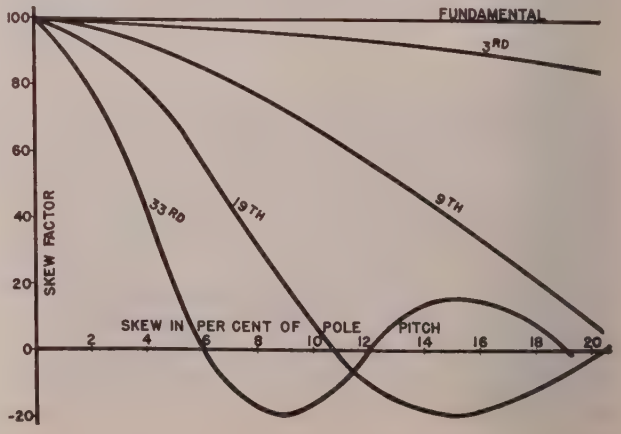

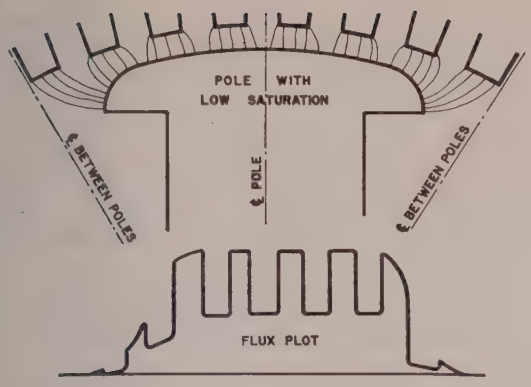

Low magnetic saturation effects and its flux plot

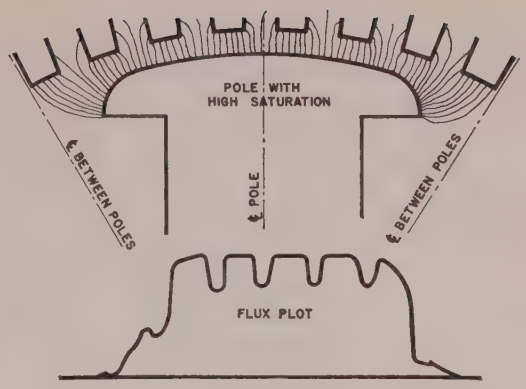

Figure 16 (right). High magnetic saturation effects and its flux plot

which are not objectionable from the standpoint of telephone interference. Thus, it becomes important to pick the proper fractional slotting in order to control the slot harmonic frequencies which have a direct effect on TIF.

The reduction factor for any harmonic of a fractional-slot winding due to the vernier slot effect is:

$$F_{fsm} = [\sin (ms+\delta/2)]/[y \sin (m\alpha/2)]$$

where

s = slots per pole per phase
m = order of harmonic
δ = angle in electrical degrees between slots
y = numerator of improper fraction (reduced) of s; thus, for an s of $2^2/_3$ slots per pole per phase or $^{21}/_8$ slots per pole per phase, y is equal to 21
α = phase belt degrees divided by y. There generally are 60 degrees in each phase belt for 3-phase generators and 90 degrees in each phase belt for 2-phase generators

Chorded Stator Coils

When the coil pitch differs from the pole pitch, the generated voltages developed in the two sides of a single coil will differ in phase by an angle B, which is the number of electrical degrees by which the coil pitch differs from the pole pitch. It is called the pitch differential factor, K_p, or K_{pm} when referred to harmonic m.

Long-pitched coils cover more than 100 per cent of the pole pitch and short-pitched coils cover less than 100 per cent of the pole pitch. Generally, for commercial generators, the coil pitch varies from 70 to 90 per cent, and this results in efficient use of the armature copper along with satisfactory operating characteristics, including telephone influence effects. Figure 8 shows the effects of 100 per cent, 66.7 per cent, and 133.3 per cent chording on both the fundamental and third harmonic frequencies. It should be noted that the third harmonic and multiples of the third harmonic are eliminated by utilizing 66.7 per cent or 133.3 per cent coil pitch. At these two coil pitches, the fundamental voltages are only 87 per cent (86.6) effective, so that 13 per cent of the maximum value of voltage (that at 100 per cent coil pitch) becomes ineffective. Thus, two-thirds pitch stator coils or two-thirds slotted rotor (on turbogenerators) eliminates all triple harmonics and multiples thereof.

The pitch differential factor, K_{pm}, also known as the chord factor $F_{chm} = \cos (MB/2)$, where B is the number of electrical degrees by which the coil pitch differs from the pole pitch and M is order of the harmonic. Figure 9 shows this relationship for the fundamental, third, and nineteenth harmonic frequencies. The resultant harmonic is proportional to the pitch differential factor for that harmonic and where it passes through zero, the harmonic is eliminated.

Pole Arc and Shape

The normal pole arc embraces from 65 to 75 per cent of the pole pitch. Then the pole constant varies from 0.68 to 0.70 and the winding constant varies from 0.42 to 0.43, so that the form factor of the voltage wave approaches 1.11, which is the value for a sine wave.

By utilizing true-arc poles, that is, pole arcs having only one value of radius, the preferred ratio of maximum air gap to minimum air gap is from 1.2 to 1.4. Figure 10 shows three true-arc poles and their corresponding field flux plots. Figure 11 shows the effects of too small a pole-arc radius on the field flux plot, resulting in a peaked voltage wave. Figure 12 shows the effects of too large a pole-arc radius on the field flux plot, resulting in a flat or hollow voltage wave, both of which are objectionable.

Skewing

Either the stator slots or the rotor poles or a combination of both may be skewed to reduce or even eliminate any specific harmonic frequency, as shown in Figure 13. To eliminate any specific harmonic, m, the amount of skew in inches equals twice the pole pitch inches divided by the order of the harmonic, m.

Any multiple of this amount of skew also may be utilized to eliminate the specific harmonic, but the more the skew, the more the losses, heating, and so forth. The skew factor,

$$F_{sm} = [\sin (m\lambda/2)]/[(m\lambda/2)]$$

where λ is the electrical angle in radians of the skew and m is again the order of the harmonic. Figure 14 shows the skew factors for several different harmonic frequencies with skewing up to 20 per cent of pole pitch. Note that the thirty-third harmonic is reduced to zero at three different values of skew within the 20 per cent of pole pitch.

By examining this formula, it will be noted that by skewing the slots exactly one slot pitch distance, all slot harmonics disappear. Also, if the slotting is $A+(b/c)$ slots per pole per phase, then $1/c$ of the slot pitch is the minimum distance to skew to eliminate the slot harmonics.

Air Gap and Carter's Coefficient

By increasing the air gap, the flux pulsations between rotor and stator become less, resulting in lesser amplitudes of the harmonic voltages and a lower TIF.

By lowering Carter's coefficient, which is the factor relating to the increased effective air gap due to the slotted gap surfaces, the ratio of slot width to slot pitch is reduced, so that the flux pulsation is lowered, resulting in a lower TIF. Naturally, by doing the opposite of the preceding statements, the resulting TIF will be increased.

Magnetic Saturation

Magnetic saturation in the teeth, core, poles, pole body, and rotor rim will all have their effect on the magnetic circuit which directly affects the voltage wave

and the resulting TIF. By comparing Figures 15 and 16, and especially the flux plots, it becomes evident that increased gamnetic densities in the teeth cause flattening of the field flux form to result in a more uniform flux distribution and a lower TIF. It is important to have similar magnetic circuits in the entire generator and thereby avoid any distortions resulting from unequal or dissimilar magnetic circuits. A cast-iron rotor rim having a flaw at a critical location may increase the TIF by 30 per cent.

Manufacturing Factors Affecting TIF

1. The pole-to-pole spacings on the rotor should be uniform. On one generator, more uniform spacing lowered the TIF from 106 to 28.
2. If the poles are skewed, make certain the skewing angle is correct and that all poles are skewed the same amount, so that the poles are parallel to each other.
3. If the pole-arc surfaces are turned, all poles should have the same shape and contour.
4. Every field coil should have the same number of turns per pole with no short-circuited or grounded turns thereon. One case on record showed a reduction of TIF from 42 to 8.5 by clearing all short-circuited turns.
5. The air gap should be equal at all locations, so that the rotor is concentric with respect to the gap bore. This helps to maintain similar magnetic circuits in the generator in so far as the air gaps are concerned.
6. Equal magnetic circuits throughout the generator require similar materials and dimensions. Thus, avoid flaws, defects, variations, or other dissimilarities.

Operating Factors Affecting Telephone Influence Factor

In commercial generators, distortions in the voltage wave may be caused by: (1) variation in the speed; (2) nonuniform or pulsating magnetic fields; or (3) distribution and connection of the armature conductors.

The electric load on the generator may change the TIF. The no-load TIF may be reduced from 20 to 50 per cent by applying full load, if balanced on all phases. The magnitude of the load current affects the magnetic saturation within the generator and thereby also affects the TIF. The power factor of the load which relates the load current to its voltage and in turn the rotor position with respect to the stator, will affect TIF. Generally, unity power factor loads, or even lagging power factor loads, will result in a lower TIF than on leading power factor loads.

References

1. Review of Work of Sub-Committee on Wave Shape Standards of the Standards Committee, **Harold S. Osborne.** *AIEE Transactions*, volume 38, January Section, 1919, pages 261–88.

2. Measurement of Telephonic Noise and Power Wave Shape, **J. M. Barstow, P. W. Blye, H. E. Kent.** *Electrical Engineering (AIEE Transactions)*, volume 54, December 1935, pages 1307–15.

3. Telephone Interference and Alternator Wave Shape, **L. T. Rosenberg.** *Allis-Chalmers Electrical Review* (Milwaukee, Wis.), volume VIII, June 1943, pages 5–11.

4. Induced Voltages of Electrical Machines, **L. V. Bewley.** *AIEE Transactions*, volume 49, April Section, 1930, pages 456–66.

No Discussion

A Maintenance Inspection Program for Large Rotating Machines

JOHN S. JOHNSON
MEMBER AIEE

Synopsis: A maintenance inspection program making available manufacturer's experience is described. General service experience with high-voltage machine insulation is reviewed. Several specific field problems are discussed. Likely failure causes are found to result from disturbance to the physical integrity of the insulation rather than a gradual deterioration caused by sustained electric stress. Inspection procedures, testing techniques, and equipment available in connection with the program are outlined.

THE insulation of large high-voltage rotating machines is of sufficient importance to justify planned maintenance with the objective of preventing failures in service. A successful program of this type may be expected to permit correction of many potential troubles in an orderly fashion before service interruptions occur with consequent damage which may result in prolonged outages at inconvenient times.

The nature and value of insulation tests is of great importance and has justifiably been the subject of a great deal of thought and study by many engineers in both manufacturing and operating organizations. The Electrical Equipment Committee of the Edison Electric Institute undertook a study of the problem in 1935, and in 1937 a special committee was assigned to the subject of "Generator Insulation and Testing." The report of this committee was presented in 1940.[1] Operating engineering and maintenance organizations have indicated active interest in this important problem. Illustrative of this interest is a paper presented to the Edison Electric Institute in 1949 by L. F. Hunt and J. H. Vivian, outlining an aggressive and comprehensive program of maintenance inspection and testing.[2] There undoubtedly is much more to be learned about the insulation problem relating even to this particular type of electric equipment than is known at present. Some phases of this problem particularly relating to testing and interpretation of test data are controversial.

Reputable manufacturers always have been interested (and have felt a responsibility in connection with) field performance and problems associated with proper preventive maintenance. The belief that the progress toward mutual objectives of the manufacturer and the operator in this respect could be aided materially to a more organized approach has led to the initiation of a maintenance inspection service for large high-voltage rotating machines.

Objectives

Accordingly, the maintenance inspection program has the following basic objectives:

1. To make available to the users of Westinghouse machines an integrated program designed to anticipate and correct difficulties which may arise before they become operating hazards and in general to promote the greatest possible usefulness of the machines.
2. To encourage consultation and to co-operate with operators in connection with the administration of operators' maintenance programs which are already in existence or which may be developed.
3. To bring to each user the experience and perspective gained from a knowledge of over-all service experience.
4. To provide for more systematic and efficient accumulation and evaluation of performance experience to be used as a guide in directing attention to the need for development or improved manufacturing control methods.
5. To use the experience thus obtained as a basis for studying the over-all maintenance problem with the objective of improving present techniques and developing improved inspection and testing techniques and test equipment.

Approach

In the administration of a sound inspection and maintenance program two questions naturally arise.

1. What parts of the machine insulation are apt to be in need of inspection and maintenance? What should be looked for and to what extent does the machine need to be disassembled to make an adequate inspection?
2. The second question relates to diagnostic methods. What techniques or test methods are available to assist in determining condition and possible need for maintenance or repair?

A knowledge of over-all field experience and performance, as well as design and construction of the machine, affords a very valuable background for answering the questions which relate to the need for maintenance inspection.

Insulation Design and Construction

The objective sought in the design of any machine insulation is the utilization of materials and application processes which assure the manufacture of reliable machine insulations capable of meeting service requirements and enjoying long service life. Basically, this involves the selection of chemically and thermally stable materials which have suitable

Paper 51-125, recommended by the AIEE Rotating Machinery Committee and approved by the AIEE Technical Program Committee for presentation at the AIEE Winter General Meeting, New York, N. Y., January 22–26, 1951. Manuscript submitted October 23, 1950; made available for printing December 7, 1950.

JOHN S. JOHNSON is with the Westinghouse Electric Corporation, East Pittsburgh, Pa.

The author gratefully acknowledges the guidance and collaboration of C. M. LAFFOON, L. A. KILGORE, G. L. MOSES, M. D. ROSS, W. SCHNEIDER, C. T. YARBROUGH, and C. C. BRINTON. The conception of this program and its development is the result of combined efforts of many of the author's colleagues.

Figure 1. Superficial and acute tape separation produced in laboratory tests

physical properties and are processed in such a manner as to secure adequate insulation properties and render them resistant to normal deteriorating and contaminating influences.

The problems which exist in fulfilling these basic requirements in the design of high-voltage machine insulation are associated with the following factors.

1. The machines involved usually are of large physical size.
2. The operating voltage stress on the insulation is relatively high.
3. The somewhat complicated shape of the end winding presents problems in connection with limiting excessive corona-producing voltage gradients on coil surfaces and in the surrounding gas.
4. The importance of the machines involved imposes the need for an unusually high level of service reliability.

In general, the best over-all design involves a compromise of several more or less conflicting requirements.

1. The insulation must provide an adequate dielectric barrier in a minimum wall thickness. The resulting high unit stress therefore requires the selection of low dielectric loss materials.
2. Substantially void-free insulations are considered desirable in the interests of minimizing internal ionization and obtaining good thermal conductivity.
3. The physical characteristics of the composite insulation are of great importance, particularly on larger machines, because of the very considerable differential expansion of the iron, copper, and insulation parts.
4. The insulation must be in form suitable to be applied by simple, controllable processes, so that required quality is obtainable readily in production.
5. Material constituents which provide dielectric strength must have suitable thermal endurance for operation at permissible temperatures without an excessive rate of degradation.
6. A combination of judicious selection of basic materials and the application of proper processing techniques is necessary to produce insulation with suitable voltage endurance characteristics so that many years of service at operating voltage with occasional overpotentials are realized.

The development of satisfactory high-voltage machine insulations has been an evolutionary process. While the basic insulation has been mica since the early years of this century, the form of the insulation, bonding resins, and supporting structure has changed. New materials and processing techniques have changed radically over the years. Accordingly, insulations on modern machines are distinctly different from the earlier units. Also, the physical size of machines has increased and will continue to increase. A knowledge of the particular type of insulation on a given machine and problems which may have arisen in connection with its use would be expected to have an important bearing on the maintenance of the unit.

Service Experience

The insulation of a large rotating machine is a rather complicated structure. Primarily an insulation barrier of adequate strength must be provided between conductors and grounded parts. The insulation itself and the mechanical supporting structure are subjected at times to severe mechanical shock and other physical forces incident with machine operation.

Figure 2. Acute tape separation produced in service

More effective maintenance inspection is possible when there is an understanding of some of the known potentialities for distress in a specific design and what means are available for properly diagnosing conditions in need of correction.

Tape Separation Problem

Stator winding insulation among other things is subjected to physical forces incident to thermal expansion and contraction of conductors during cyclic loading conditions. The extent to which insulation is stressed in this respect varies with machine type and size, and with machine loading. The degree to which insulations accommodate to conductor expansions and contractions is somewhat unpredictable for asphalt-bonded mica insulations. Particularly under conditions of severe stress (long conductors and cyclic loading) a phenomena called tape separation may occur. Basically, tape separation occurs where stator coil insulation is unable to follow the successive expansion and contraction of copper conductors. During a given load cycle, the insulation elongates longitudinally with the conductors during heating. Because the asphalt bonding material is essentially a high-viscosity liquid, the insulation lacks the elastic properties possessed by the conductors. Therefore, on cooling, the insulation may fail to return to the same position held prior to the heating cycles. The total permanent stretch for a given cycle is very small (being of the order of 0.001 to 0.002 inch). However, the effect sometimes is cumulative, so that after a relatively large number of thermal cycles appreciable separations may occur. This separation occurs quite consistently either just outside the end of the core or under the end wedge. Most of the separations which occur are just outside of the core.

Separations which may occur fall into two classifications. The most frequently occurring type is called a superficial or surface separation. It is so called because the insulation migration has occurred in a manner such that the dielectric strength of the coil insulation has not been reduced significantly. The other and relatively rare type is called acute separation. In this case the insulation migration has produced a serious fracture of the insulation at the point or in the vicinity of the observed separation. Under these conditions operation is hazardous and the coil insulation must be repaired or replaced.

Figure 1 shows the two types of tape separation which were produced by temperature cycling in the full-size core model described in a companion paper.[3] The upper coil section shows an acute separation and the lower coil section is illustrative of a superficial separation.

Figure 2 shows an acute separation which occurred in service on a relatively long turbine generator. In general superficial separations are characterized by relatively firm insulation in the vicinity of the surface separation. Acute separations are characterized by a "necking down" of the insulation wall in the vicinity of the visible separation. This more serious condition usually is detectable by inspection.

The first few years of operation appear to be critical with respect to the possible development, the extent, and the seriousness of tape separation. Most machines under average conditions of use do not have, or have only a negligibly small amount of, tape separation. The shorter machines generally do not have tape separation.

Acute tape separation has been observed on several relatively long hydrogen-cooled turbine generators. Many such machines have been inspected which show no evidence of separation. There are, however, a number of turbine generators which have superficial tape separation in varying amounts. It is important to watch for these conditions and to note trends. In the event that serious weakening of the insulation is detected, repairs may be made when the machine is down for normal inspections.

Tape separation phenomena as described in the foregoing paragraphs appear to be characteristic of asphalt-bonded mica insulations in general. In severe laboratory tests the newer synthetic bonded mica insulation is able to withstand severe cycling without distress.

Corona and Slot-Discharge Effects

Slot Treatment. Corona prevention in the slot parts of stator coils is accomplished with the use of a low-resistance conducting finish. Varnish-base conducting compounds are in present use. In the past, colloidal graphitic water suspensions have been used. In general, this treatment has successfully eliminated slot corona and has been used by Westinghouse for over 20 years. In a few cases, however, difficulty arising from a loss of electric contact between the conducting coil finish and the core has been encountered. This loss of contact has been limited entirely to top coil sides (those nearest the bore). Under these conditions, at voltages in the range of operating stress, a rather intense capacitive discharge occurs between ungrounded coil sides and the core. This phenomena, which is called a "slot discharge," may be seriously destructive to the coil surface finish and to the basic ground insulation if it continues unchecked.

When this phenomena first was discovered, an investigation of the problem was undertaken. This involved the construction of a core model in which it was possible to study in the laboratory the factors which might lead to the development of surface discharging. The phenomena was reproduced successfully in the laboratory under severe test conditions. The process modifications designed to overcome the tendency for discharge phenomena were subjected to rigorous tests, including high voltage, temperature cycling, and severe vibration. Figure 3 shows coil surface deterioration produced by a slot discharge in the laboratory core model. Figure 4 shows a case of severe coil-surface and filler-strip deterioration observed on a water-wheel generator.

The incidence of this sort of difficulty has been found to be very small. The fact that the possibility (however remote) of trouble from this phenomena exists necessitates the development of suitable testing equipment for detection of discharging and also the development of suitable and economical corrective measures which can be used when difficulty is encountered. Slot-discharge detection equipment has been developed and will be described in a later section of this paper. Corrective treatments have been developed which are effective and economical in suppressing surface discharging.

End-Winding Corona. End-winding corona is minimized effectively in modern windings by stress-relieving semiconducting finishes and by providing suitable spacing between stressed members. Also, the use of inorganic binder tapes, twine, "Micarta" spacers, and synthetic resins with inorganic pigmentation provides surfaces highly resistant to the deteriorating effects of corona. Generally speaking, even a fairly high level of end-winding corona is not a serious hazard and does not limit significantly the usefulness of a machine insulation. In unusual cases, however, attempts have been made to reduce end-winding corona on machines in service. It has been found possible materially to improve conditions by suitable treatments. Reduction in end-winding corona by this means, however, is achieved by some increase in stress on portions of the end-winding insulation. Usually treatments recommended are dictated by observed conditions taking into consideration the design and construction of the machine.

Figure 3. Coil-surface deterioration caused by slot discharge produced in laboratory

Figure 4. Coil-surface and filler-strip deterioration caused by slot discharge on a stator winding in service

Conductor Short Circuits

The design of conductor insulation on multiturn stator coils of large rotating machines usually is very liberal with large factors of safety over anticipated conductor insulation stresses. Also, conductor insulation is subjected to relatively high overpotential tests during manufacture. Nevertheless, an appreciable percentage of winding failures which occur probably originate as turn-to-turn faults. It obviously is desirable, then, to be able to test this insulation at voltages above operating stress. The test equipment de-

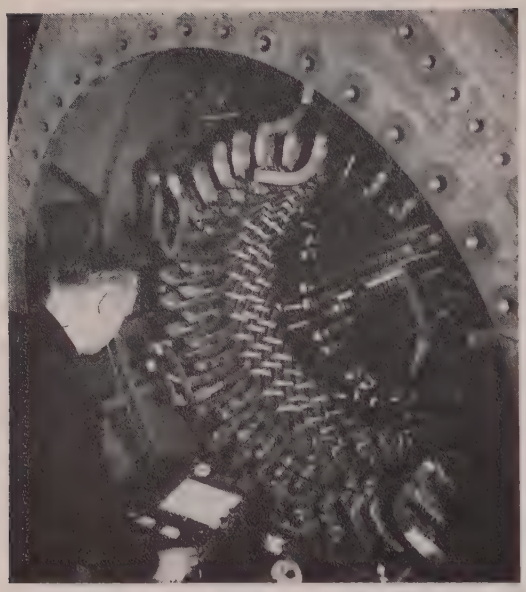

Figure 5 (left). D-c test of a turbine generator stator winding

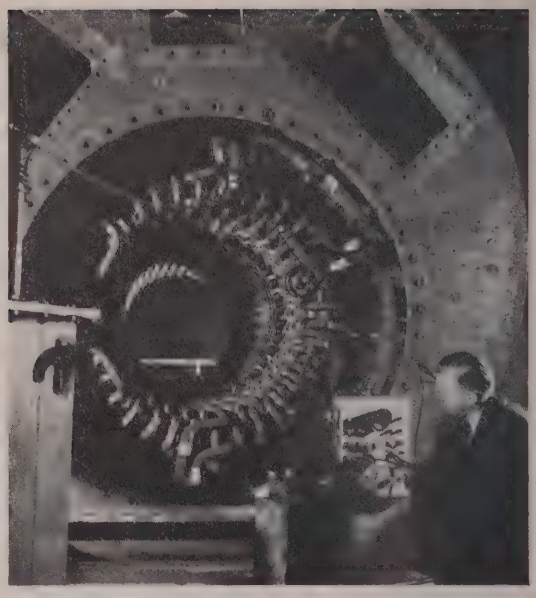

Figure 7 (right). Slot - discharge test on a turbine generator stator

scribed by R. J. Alke and R. M. Sexton[4] is the best means currently available for making tests of this nature on large rotating machines.

Summary of Likely Failure Causes

Modern high-voltage stator windings in general have enjoyed a very high level of service performance. Failures in service have been rare. From the experience which is available, it appears that the following are the nature of likely failure causes.

1. In general, failures do not result directly from the effects of prolonged electrical stress at operating voltages on insulation when the physical integrity remains. In other words, for relatively undisturbed insulation the mechanism that produces failures at high stresses is present at operating stresses to such a minor extent that it does not limit significantly the life expectancy of properly designed insulation.

2. Failures apparently are far more likely where something has occurred to destroy the physical integrity of the insulation. Illustrative of possible causes are:

a. Cracking of the insulation resulting from unusual mechanical stresses.

b. Insulation distress resulting from physical forces incident with thermal expansion effects or from unusual vibration.

c. Operation at temperatures which tend to degrade organic constituents which support and bond the basic mica insulation.

d. Insulation deterioration resulting from surface discharging caused by loss of contact between conducting coil surfaces and core.

e. Eroding effects of foreign magnetic particles embedded or lodged against the coil insulation surface.

f. Contamination by substances which adversely affect insulation strength of all or part of the insulation structure—the most common being moisture contamination.

g. Abnormally high overvoltages resulting from surges on unprotected machines or excessive testing at unnecessarily high overpotentials.

h. Undetected weakness which may have occurred during installation or manufacture.

It appears, then, that maintenance inspection and testing should be directed toward the detection of conditions where the physical integrity of the insulation at some point has been weakened to the extent that failure at operating stress or normal overpotentials may result.

Maintenance Inspection Program

Scope

A knowledge of the design and construction of the machines and over-all field experience with likely causes of distress form the background for this program. The service presently is directed at large turbine generators, water-wheel generators, and synchronous condensers. The inspection includes examination of the machines by engineers with broad experience in this particular field and the application of tests directed toward detecting likely causes of distress. It is not the intention to replace existing maintenance programs, but rather to encourage planned maintenance on the part of users and to supplement these programs with the manufacturer's service to the extent desired by users.

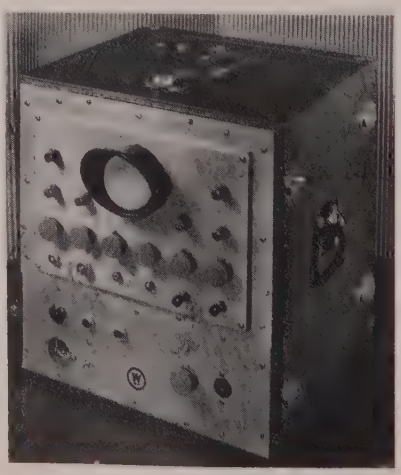

Figure 6. Slot-discharge analyzer

Inspection Periods

It is not practical to establish a definite inspection period for all machines, as operating conditions vary widely. Each case should be considered individually by the user on the basis of the performance and operating history of the machine and its condition at the last inspection.

1. It is recommended that an inspection be made at a convenient time after the first year of operation.

2. Subsequent inspections should be in the range of two to five years.

3. If the first two or three inspections indicate negligible maintenance, the periods between inspections can be lengthened.

4. It is desirable, when possible, to coordinate the generator inspection with the turbine inspection in the case of turbine generators.

Examination

The following are illustrative of the

principal items covered in an inspection of these machines.

Stator Winding

1. General Appearance
a. Coil finish condition
b. General cleanliness

2. Coil Condition in Slots
a. Condition of wedges
b. Checks for wedge movement
c. Checks for loose wedges
d. Checks for evidence of coil looseness

3. Coil Condition in End Winding
a. Condition and tightness of blocks and spacers
b. Condition and tightness of twine lashing
c. Coil surface condition
d. Condition with respect to possible distortion or tape separation

4. Evidence of Corona or Slot-Discharge Distress

5. Tape Separation
a. Extent
b. Nature (superficial or acute)
c. Chart observed conditions for future reference

6. Condition of Core

Rotor Windings

1. Salient Pole
a. Evidence of movement or shifting of coils
b. Evidence of movement or looseness of poles
c. General cleanliness
d. Condition of ground insulation washers, and so forth
e. Connections between coils and to collector
f. Condition of collector insulation

2. Nonsalient Pole
a. Condition of retaining ring fits, wedges, and so forth
b. Condition of end-winding blocking by examination through retaining ring holes and from under side
c. Condition of collector and collector insulation

A thorough visual examination must form the basis of any sound maintenance inspection program. No test methods are available or likely to be developed which will make it unnecessary periodically to examine equipment to determine its physical condition. As outlined, inspections should be directed principally at an evaluation of the mechanical condition of the insulation.

Maintenance Tests

Suitable tests can be useful to supplement visual inspection in determining the suitability of machine insulations for service or to disclose undesirable conditions in need of corrective maintenance. There is no single test which will provide all the desired information relative to insulation condition. Nor is it likely that a test will be developed which will indicate directly the remaining useful life of an insulation. However, there is a sound basis for expecting that the combination of thorough visual inspection and proper interpretation of the available tests will permit a reasonable estimate of probable insulation condition at a given time. Periodic tests and inspections then may be expected to establish conditions of the insulation over a period of time. Reasonable extrapolation of the performance trend thus established would be justified. In this manner it should be possible to exercise better judgment as to when a machine winding is in need of repair or ultimate replacement.

General Nondestructive Tests

The so-called nondestructive tests, such as insulation resistance, power factor, polarization and ionization, are of greatest value when they may be related to physical conditions or changes that may be occurring in the insulation. In many cases the absolute measured values are of themselves of limited significance. It also must be remembered that large insulation areas are involved in machine windings and that discreet areas of weakness would not be expected significantly to affect the characteristics as determined for the entire winding. The greatest significance of such tests then, would be to indicate overall trends.

A sudden drop or a sustained downward trend in insulation resistance might be subject to different interpretation depending on whether it was measured on the stator or the rotor. Different levels of insulation resistance should be expected of different types of machines. Totally enclosed hydrogen-cooled stator windings should have a relatively high level of insulation resistance. A large drop in the normal level of insulation resistance should be regarded seriously as it may be indicative of moisture condensation in the housing, which may lead to failure of creepage surfaces. Open-type machines, particularly with water-spray air cleaners, naturally would be expected to have materially lower values. The same value of insulation resistance which would be indicative of hazardous conditions in the closed machine may not be at all alarming on the open-type machine. Of these nondestructive tests for generator insulation, the insulation-resistance and the dielectric-absorption test appear to have the most merit as indicators of trends with respect to contamination by moisture or other agents which may decrease either the volume or the surface resistivity of the insulation.

Overpotential Tests

Overpotential tests are the only means for providing assurance that the winding insulation has a certain level of insulation strength. Depending on the test value used and the minimum insulation strength of the winding (an unknown quantity), such tests are destructive to a greater or less extent. Because of the steeper slope of the voltage-endurance characteristic as indicated by G. L. Moses,[5] the deterioration with time is much greater for a-c than for d-c test potentials.

A-c tests nevertheless have been and are being used for maintenance overpotential testing. When used, the test value should only be high enough to give assurance of certain minimum required insulation strength. In most cases for relatively infrequent tests a value of $(2E+$

Figure 8. Conductor insulation test on a turbine generator stator

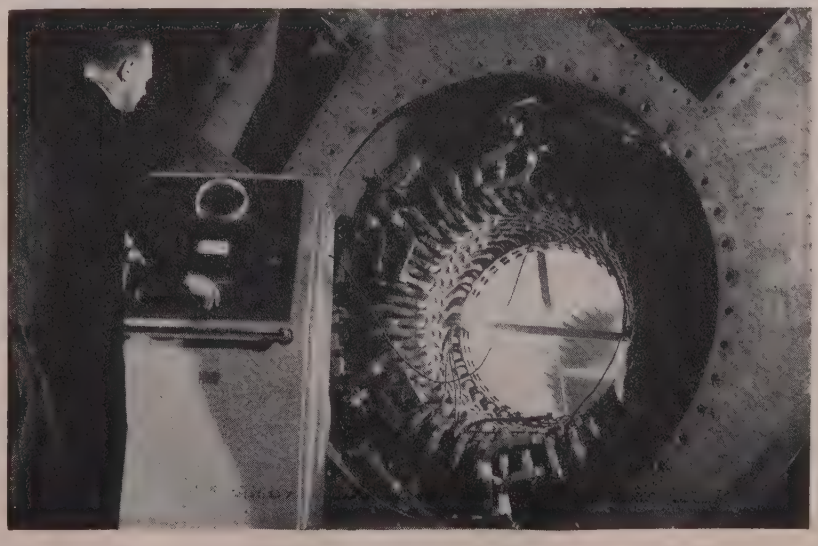

1,000)×65 per cent is believed to be adequate. For relatively frequent tests a somewhat lower value may be desired based on the theory that for shorter times between tests a lower margin over operating stress would be required to give the same over-all safety factor. The application of such a test is a calculated risk which is subject to justification based on the over-all economics of making repairs during scheduled maintenance versus making repairs under emergency conditions.

As indicated in the paper by Mr. Moses,[5] a suitably selected value of d-c overpotential may be equally as searching for likely types of insulation weakness with the expectancy for small or negligible destructive effect on good insulation. There are two reasons for this.

1. An equally searching d-c potential is a smaller percentage of the d-c strength of the insulation than would be the case with comparable a-c stress.

2. Because of the very much flatter voltage-endurance characteristic with d-c potentials the time to failure for an equal percentage of 1-minute strength is far longer with d-c than with a-c potentials.

Accordingly, d-c overpotentials appear to be fundamentally advantageous for maintenance testing. In addition to basic advantages, the required test equipment is much less expensive and far less costly and cumbersome to transport. Also, insulation leakage at high stress may be measured. D-c overpotential maintenance tests therefore are recommended. The risk involved in this test is believed to be very much less than with a comparable a-c test.

A d-c test value 1.6 times the recommended a-c maintenance test of (2E+1,000)×65 per cent has been used and is proposed for general consideration. For convenience, then, this becomes (2E+1,000)×1.04. The tester used in connection with the Westinghouse Maintenance Inspection Service is a multirange Takk Corporation high-voltage d-c tester. The ranges are 1.5, 15, and 45 kv. It is essentially a low-energy device having a maximum output of 2.5 milliamperes. This output is found to be more than adequate. The low-energy feature is considered to be advantageous, since destruction incident with test failure is at a practical minimum. Figure 5 shows this equipment being used to test a stator winding.

Slot-Discharge Analyzer

The slot-discharge analyzer is a single-purpose instrument. It is used for checking the adequacy of the grounding between the low-resistance conducting coil surface in the slot portions and the core. This equipment is effective in detecting and locating the presence of surface discharging from low-resistance areas of coil treatment and core. Detection is accomplished by a simple test from machine terminals. If line-terminal checks indicate existence of discharging, affected coil sides are located by probing coil surfaces at accessible areas such as in vent ducts. Figure 6 shows a slot-discharge analyzer. Figure 7 shows this quipment being used to test a winding.

Surge-Induction Tester

The surge-induction tester is described by R. J. Alke and R. M. Sexton.[4] It provides a means of checking the conductor insulation of wound machines. This equipment is used in the factory for testing multiturn half-coil designs where previously no method was available for testing conductor insulation at half-coil joints. The present equipment induces surges up to approximately twice normal operating stress. Figure 8 shows this equipment being used to test a stator winding.

Summary

During the past decade, the unusually great need for electric power stimulated the power producers to operate generating equipment for long periods at loads well above rated values. In many instances, hydrogen-cooled steam turbine and water-wheel-driven generators have been operated five to ten years without having had a thorough inspection.

There are many parts of generators that are expendable with time and operation, and consequently need periodic inspection and maintenance to be kept in good serviceable condition. The most obvious are commutators, collectors, brushes, bearings, stator iron, end fingers, insulation, coil bracing, and slot wedges. During manufacture, care is exercised by the workers and careful inspection is given to make certain that materials, processes, and assembly procedures are in accordance with the manufacturing specifications. When the unit is completed, recognized commercial tests are made to demonstrate that operation and performance requirements are met. Also, during installation thorough inspection again is exercised and the initial operation of the unit is watched and checked with indicating and recording instruments. Thereafter day-to-day instrument readings supplemented by visual and other observations form the basis for current diagnosis of the general condition of the unit. All large high-voltage rotating machines should be inspected at periodic intervals. Westinghouse is vitally interested in collaborating with users in such a program. In working toward that end trained engineering representatives and specialized equipment and techniques have been made available. It is logical that the first inspection should be made jointly by manufacturer and user after approximately the first year of operation. The time for and the extent of the subsequent inspections could be determined on the basis of conditions found at the time of the first inspection. In the case of steam and hydraulic generators, it is believed that generator inspections can be made at the time normal turbine inspections occur and thus the outages of the complete unit will be reduced to a minimum. The engineering services, test equipment, and inspection techniques now available are of such caliber that the users of large rotating high-voltage equipment should be able to utilize them economically to supplement any inspection and maintenance program now in effect or that may be evolved.

References

1. Field Testing of Generator Insulation, **E.E.I. Committee Report.** *Electrical Engineering* (*AIEE Transactions*), volume 60, December 1941, pages 1003–11.

2. Operation of Synchronous Machines for Continuity of Service on Southern California Edison Company System, **L. F. Hunt, J. H. Vivian.** *Minutes*, Electrical Equipment Committee, Edison Electric Institute (New York, N. Y.), May 3, 1949.

3. A New High-Voltage Insulation for Turbine-Generator Stator Windings, **C. M. Laffoon, C. F. Hill, G. L. Moses, L. J. Berberich.** *AIEE Transactions*, volume 70, part I, 1951, pages 721–30.

4. Detection of Turn-to-Turn Faults in Large High-Voltage Turbine-Generators, **R. J. Alke, R. M. Sexton.** *AIEE Transactions*, volume 70, part I, 1951, pages 270–74.

5. Alternating and Direct Voltage Endurance Studies on Mica Insulation for Electric Machinery, **G. L. Moses.** *AIEE Transactions*, volume 70, part I, 1951, pages 763–69.

6. The Basis for the Nondestructive Testing of Insulation, **R. F. Field.** *Electrical Engineering* (*AIEE Transactions*), volume 60, September 1941, pages 890–95.

7. A Portable Instrument for Measuring Insulation Resistance at High Voltage, **F. W. Atkinson, R. B. Taylor.** *Electrical Engineering* (*AIEE Transactions*), volume 64, April 1945, pages 164–66.

8. Recommended Practice for Testing Insulation Resistance of Rotating Machinery. *AIEE Standard, Number 43*, April 1950.

9. Insulation Tests of Electrical Machinery Before and After Being Placed in Service, **B. L. Barns, C. M. Gilt.** *AIEE Transactions*, volume 48, April Section, 1929, pages 656–65.

10. Generator-Insulation Tests, **B. VanNess.** *Bulletin*, Edison Electric Institute (New York, N. Y.), volume 6, May 1938, pages 204–06 and 231.

11. Maintenance Overpotential Tests for Armature Windings in Service, **R. W. Wieseman.** *General Electric Review* (Schenectady, N. Y.), August 1940, pages 24–28.

Discussion

C. T. Yarbrough (Westinghouse Electric Corporation, East Pittsburgh, Pa.): Planned maintenance programs are not new in industry, as many industrial companies and power companies have good maintenance organization. However, with the new major developments in insulation testing and the new tools available, new concepts of maintenance testing have been created.

The manufacturers of large high-voltage rotating equipment are greatly interested in having this apparatus operate without serious prolonged outages. Thus, the Westinghouse Electric Corporation has made available trained and experienced engineers and special equipment to assist the operating companies in maintaining their equipment.

Until recently, we had only one 45-kv d-c Takk Tester, which was used at the factory for development work and also was shipped by air back and forth across the United States many times to give service on the maintenance inspection program. This would not have been possible with an a-c test unit, as a 300-kva transformer with regulator would have been required on the larger generators tested. We now have four Takk Testers and find them very rugged and portable.

During the last 18 months, a total of 55 large machines were inspected with an aggregate of kilovolt amperes amounting to over 3,000,000. The age of these machines varied from 1 to 30 years of service. Winding repairs varying in extent were made on 15 of the units inspected and tested. Most of the units repaired had been in service over 15 years. Experience has shown that it is more economical to weed out defective coils and repair them during a scheduled outage period, rather than risk a longer and more costly outage caused by a coil failure burning the core iron, necessitating a complete rebuilding job.

The maintenance inspection and nondestructive d-c overpotential test program has been very well accepted by most of the companies using our apparatus. However, there are still some companies who do not want to take the generators out of service long enough for a thorough inspection and thus prefer to take the risk of a long costly outage in case of a coil failure seriously damaging the iron core.

Routine Insulation Testing of Synchronous Machines

L. F. HUNT
FELLOW AIEE

J. H. VIVIAN
FELLOW AIEE

THE OPERATION of all power system equipment for continuity of service is of vital interest to every electric utility company. The Southern California Edison Company has studied this problem, and has accumulated practical field experience in the operation, testing, and maintenance of large synchronous machines during the last eight years that should prove valuable to other electric utilities and to electrical machinery manufacturers. This paper reviews the development, practice, and results of a program of overvoltage testing of large synchronous machines.

The electric power system of the Southern California Edison Company serves the ten central and southern counties of California. There are approximately 900,000 customers in this 18,500 square mile area. There are 59 hydroelectric generators in 24 plants with a total capacity of 1,003,650 kva or 936,000 kw. There are 15 steam electric generators in four plants with a total capacity of 706,269 kva or 675,500 kw and five diesel electric generators in one plant with a total capacity of 37,500 kva or 30,000 kw. In addition to this generating equipment, there are 33 synchronous condensers in 20 stations with a total capacity of 1,050,000 kva, and one frequency changer of 60,000 kva capacity. All together there are 114 machine windings with a total capacity of 3,007,419 kva to be maintained.

The normal operation of a power system of this extent is extremely complicated, and unpredicted failures can seriously affect the operating plan. Power sources are widely separated and involve expedient use of hydro, steam and interconnections with other systems. Predetermined allocation of loads to source is necessary for efficient operation and for conservation of fuel and water. Interconnection with other power systems such as the City of Los Angeles, the Pacific Gas and Electric Company, the San Diego Gas and Electric Company and others requires the long range co-ordination of outages for routine maintenance. Overhaul periods for hydroelectric equipment is scheduled when the runoff is low, and steam electric generator overhauls are scheduled for a time of year when water supply is maximum. Unanticipated outages of either class of generation may be costly not only to the Southern California Edison Company, but also may affect the operations of interconnected companies.

The rapid growth of this area has increased the demand for power to an amount that requires operation of all generating facilities at higher load factors than ever before. The importance of all customers' loads and especially those of major industrial plants, and continuous process plants such as paper mills, rubber mills, steel mills, and glass plants makes it imperative that failures of large units while in service shall not occur.

One of the first steps toward the elimination of winding failures in service was the development of a standard procedure for routine physical inspection. Check charts were prepared so that nothing would be overlooked.

The physical inspection includes careful examination of the stator coils, coil end extensions, coil bracing, spacer blocks, slot wedges, cross connections, and lashing. These items are checked for movement, distortion, rigidity, tightness, strength, and position. The insulation itself is examined for surface condition, dirt, oil, cracks, mechanical damage, outer-tape separation, mechanical strength, solidity, pliability, and elasticity. The stator iron and lamination clamping plates are checked for any looseness, loose laminations, evidence of vibration, iron rust due to fretting, and for signs of local heating.

Inspection of the rotors includes a check of clearance between blowers and coils, check for movement or shifting of field coils, inspection of strap field coils for turn movement and condition of turn-to-turn insulation, check of condition of ground insulation and pole bobbin collars, check of leads and connections from the coils to the collector rings, and a check of all nuts and bolts for loosening. Any defects found are corrected.

In addition to the physical inspection, insulation resistance measurements are made of both stator and rotor.

Records of the conditions found during these inspections are kept for all machines in order that signs of developing troubles will be brought to attention and corrected, or an estimate made of the safety of continuing to operate.

In spite of the careful visual inspections, measurement of winding resistance, and the maintenance program described, some failures in service occurred, and it was decided to supplement the inspections with electrical tests.

Reliable Test Sought

The nature of insulation failures in machine windings makes it practically impossible to predetermine the exact time of failure. This condition has long been recognized in the industry, and a great deal of thought and work has been expended in an effort to discover some simple and reliable nondestructive test to apply that would measure and show the condition of the winding insulation.

The Electrical Equipment Committee

Paper 51-126, recommended by the AIEE Rotating Machinery Committee and approved by the AIEE Technical Program Committee for presentation at the AIEE Winter General Meeting, New York, N. Y., January 22-26, 1951. Manuscript submitted October 23, 1950; made available for printing January 2, 1951.

L. F. HUNT and J. H. VIVIAN are both with the Southern California Edison Company, Los Angeles, Calif.

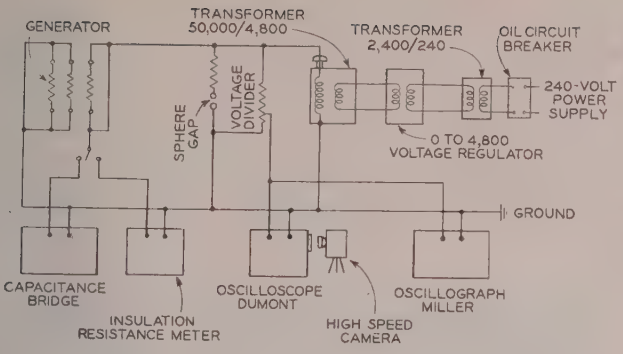

Figure 1 (left). Diagram of connection for overvoltage test

Figure 3 (above). 17,500-kva 6,600-volt generator high-voltage test. Same as Figure 2, except made with cathode ray oscilloscope and high-speed camera

of the Edison Electric Institute undertook active work on this problem in 1935.[1] In 1937, a Special Subject Committee was appointed on Generator Insulation and Testing. This Committee directed the investigations of various member companies and others in the industry, and maintained close contact with the electric machinery manufacturers, with the ultimate objective of developing a reliable test procedure for determining the condition of winding insulation.

The investigation by this Committee resulted in considerably better understanding of the problem, and furnished a useful guide for further work and standardization of insulation testing.

Work on this subject continued, and in December 1946, the Subcommittee on Insulation Resistance of the AIEE Committee on Electric Machinery, published a report on Recommended Practice of Insulation Resistance Testing of A-C Rotating Machinery. The final revision of this report was published April 15, 1950, as AIEE Standard Number 43.[2]

This Standard reviews the factors that affect the insulation resistance characteristics, recommends uniform methods of making insulation resistance tests, and presents a method of determining the approximate minimum insulation resistance values for rotating machines, and is an aid in interpreting the results of insulation tests. However, no correlation between the measured condition of insulation and dielectric breakdown is given.

In spite of all that has been done, it appears that no really reliable nondestructive test is available for predicting the probable remaining life of rotating machine windings in service. No consistent quantitative relation between the insulation resistance and dielectric strength has ever been found.

Local failure can occur in a winding which will appear good by any method of test that does not apply overvoltage to a winding. It, therefore, appears that if failure in service is to be avoided, it is necessary to use overvoltage testing.

Insulation deterioration as well as breakdown depends not only on the magnitude of the applied voltage, but also on the length of time of application. The time of voltage application to cause failure of weak or deteriorated insulation is less than for good insulation. Hence there should be a value of test voltage and length of application for periodic testing that will provide the desired degree of freedom from failure in service. It was with this idea that the engineers of the Southern California Edison Company initiated in 1942 a program of investigation and test in order to develop an overvoltage test procedure that would give the desired results.

Before establishing this procedure of overvoltage testing, or determining the voltage to be used, a review of the existing literature on this subject was made and various manufacturers were requested to furnish information concerning available methods of fixing the Life Expectancy of Windings by nondestructive tests which could be made at the time of overhaul, and to comment on the use of an annual 150 per cent overpotential test.

The comments received in 1944 indicated that the manufacturers did not know of any nondestructive tests that would provide reliable indication that a winding would or would not fail before the next scheduled outage. Repeated overvoltage tests were not generally favored. The main objection to repeated overvoltage testing was not the possible damage due to application of 150 per cent of rated voltage, but rather from accidental sources of misapplication. That is from distorted wave form of test voltage, surge voltages, or high frequency voltages that might result from spark gap breakdown or from arcing if the winding failed during the test.

From the foregoing information and our own studies it was recognized that a reliable method of determining the actual remaining life of a winding was not available.

The windings of the machines on the Edison System vary greatly in age and condition. Some have just been put in service, and some have been operated without rewinding for more than 35 years. Load and service conditions have varied greatly, so that age alone is of no practical value for determining serviceability. However, it was considered necessary to take some action immediately to minimize the possibility of winding failures in operation, and the following program was adopted.

From the case history of each winding, an analysis was made to determine which windings could not reasonably be depended upon to operate without breakdown. In this group were placed all machines whose record showed the windings to be in poor mechanical condition, or whose windings would not carry full load without excessive temperature. These

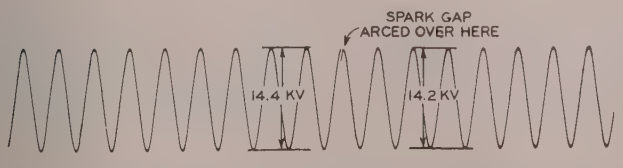

Figure 2. 17,500-kva 6,600-volt generator high-voltage test. Machine winding not connected to test equipment. Test voltage before and after gap breakdown

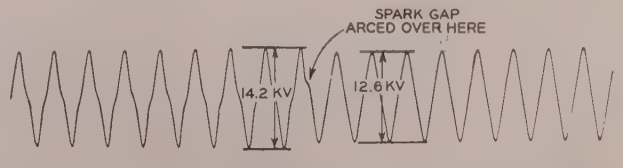

Figure 4. 17,500-kva 6,600-volt generator high-voltage test. Machine winding connected in parallel with spark gap. Test voltage before and after gap breakdown

Table I. Repetitive Overvoltage Tests

28,000-Kva 11,000-Volt Hydroelectric Generator A Phase

Test Number	Test Voltage Applied: Volts	Test Voltage Applied: Per cent of Rated Volts	Excitation Current, Amperes	Duration, Seconds	Megger Reading, Megohms	Capacity to Ground, Microfarads	Dissipation Factor, Per cent
					5 Min. 7,000	0.158	
1	17,500	152		60			
2 to 11	17,250	150	1.1	60 Each	7,000	0.157	4.0
11 to 20	17,250	150	1.1	60 Each	7,000	0.160	4.5
21 to 30	17,250	150	1.1	60 Each	7,000	0.161	4.5
31 to 40	17,250	150	1.1	60 Each	10,000	0.161	4.7
41 to 50	17,250	150	1.1	60 Each	10,000	0.162	5.0
51	20,400	177	1.36	60			
52 to 60	20,150	175	1.34	60 Each	10,000	0.162	5.1
61 to 70	20,150	175	1.34	60 Each	10,000	0.162	5.1
71 to 80	20,150	175	1.34	60 Each	10,000	0.163	5.9
81 to 90	20,150	175	1.34	60 Each	10,000	0.165	5.9
91 to 100	20,150	175	1.34	60 Each	7,000	0.165	6.1
101	24,150	210		6 Sec.	0	Could Not Read	

Table II. Repetitive Overvoltage Tests

28,000-kva 11,000-Volt Hydroelectric Generator B Phase

Test Number	Test Voltage Applied: Volts	Test Voltage Applied: Per cent of Rated Volts	Excitation Current, Amperes	Duration, Seconds	Megger Reading, Megohms	Capacity to Ground, Microfarads	Dissipation Factor, Per cent
					5 Min. 7,000	0.158	5.0
1	17,250	150	1.1	60			
2	20,400	177	1.36	60			
3 to 11	20,150	175	1.33	60 Each		0.162	5.3
12 to 21	20,150	175	1.33	60 Each		0.163	5.3
22 to 31	20,150	175	1.33	60 Each		0.164	5.5
32 to 41	20,150	175	1.33	60 Each		0.165	6.0
42 to 51	20,150	175	1.34	60 Each	7,000	0.165	6.0
52	21,650	188	1.49	60			
53 to 61	21,400	186	1.47	60 Each		0.167	6.5
62 to 71	21,400	186	1.47	60 Each		0.168	6.6
72 to 81	21,400	186	1.47	60 Each		0.168	7.0
82 to 91	21,400	186	1.48	60 Each		0.168	7.0
92 to 101	21,400	186	1.47	60 Each	7,000	0.169	7.5
			After an Interval of One Hour				
102	21,950	191	1.51	60			
103	22,700	197	1.60	60			
104 to 112	22,450	195	1.58	60 Each	7,000	0.168	7.5
113 to 121	22,450	195	1.58	60 Each		0.168	9.0
122	22,450	195	1.58	45 Each	Failed, instantaneous overload relay opened the oil switch		
Failure of back coil in Slot number 36 at top finger plate, fourth coil from line					2,500	0.168	9.0
Endeavored to clear the bad coil in Phase A by cutting clear with bolt cutter							
123	17,250	150	1.08	20	Failed		

windings were to be replaced on the next annual overhaul.

It was planned to make repetitive overvoltage tests on these old windings at the time of removal. The results of these tests were to be used to establish a satisfactory overvoltage test value to be applied to all machines during the annual overhauls and to determine how many times this voltage could be applied without causing measurable deterioration of the windings. A proper voltage for such test should be high enough to cause failure during test if any spot in the winding were seriously deteriorated, but must be low enough not to cause additional deterioration because of its application.

Another object of the tests on these old windings was to determine if high surge voltages or high frequency oscillations would be set up either by flashover of the test sphere gaps or by breakdown of the winding under test.

Experimental Testing for Surge Voltages

Tests were made on a 17,500-kva 6.6-kv generator to study the effect on the test voltage of a spark gap flashover due to breakdown of the calibrating sphere gaps and for study of the effect of repeated application overvoltage. The connections used for these tests are shown by Figure 1.

Figure 2 is an oscillograph of the test voltage taken to show the effect of the spark gap breakdown without the machine connected. It will be observed that the wave form is sinusoidal before and after the point of gap arc over. An interruption can be seen at the peak of the wave where the gap arced over, and beyond this point minute irregularities are found near the zeros of the voltage wave.

Figure 3 was taken at the same time as Figure 2, but was made by photographing the screen of a cathode ray oscilloscope with a high speed camera. This was done to discover any high frequency transients that might not be shown with the magnetic oscillograph.

Figure 4 shows the effect of having the machine winding connected to the high potential test set. Note that the shape of the voltage wave has been distorted and peaked by the machine winding.

Figure 4 also shows the effect of the spark gap arc over. Beyond the point at which the spark gap arced over, there is a reduction in voltage due to the voltage regulation of the test equipment and the wave form is more nearly that of a sine wave. These records show that the breakdown of the gap occurred without impulse voltages and without oscillations.

A test was next made by building up voltage on the machine winding, and with the voltage sustained, the terminal of the phase under test was manually grounded. Figures 5 and 6 show the conditions at the time the ground was applied.

The winding was next tested to failure. The data of this test are shown in Table IV. Figure 7 is a record of the test voltage before, at the time of, and after machine winding failure. At the time the machine winding broke down, the voltage immediately fell to a low value, but some oscillation can be seen on the oscillogram. The winding was not solidly grounded as is evidenced by the voltage building up and breaking down with minor oscillations every one-half cycle.

After the voltage had been removed from the machine for about five minutes, it was reapplied, this time the winding broke down at a lower voltage and there were a few more cycles of oscillations but still no indication of the voltage going higher than it was at the time of breakdown. The oscillogram, Figure 8, shows that the winding was more solidly grounded after this second failure.

A 66,667-kva 11,000-volt steam turbine driven generator was to be rewound in

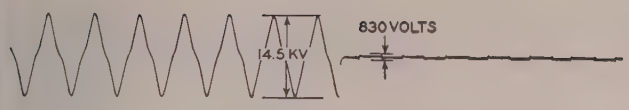

Figure 5. 17,500-kva 6,600-volt generator high-voltage test. Machine winding manually grounded at 14.5 kv. Test voltage before and after grounding

Figure 6. 17,500-kva 6,600-volt generator high-voltage test. Same as Figure 5, except made with cathode-ray oscilloscope and high-speed camera

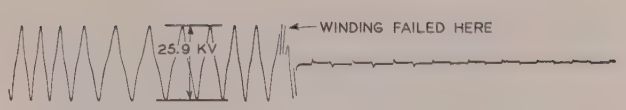

Figure 7. 17,500-kva 6,600-volt generator high-voltage test. Voltage increased until stator winding failed. Test voltage before and after failure

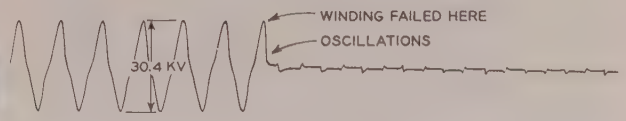

Figure 8. 17,500-kva 6,600-volt generator high-voltage test. Voltage increased until stator winding failed. Test voltage before and after failure. Second breakdown

1949. Again advantage was taken to conduct tests to determine if transient voltages would result from the flashover of a sphere gap connected in parallel with a machine winding.

Conventional high potential test equipment was used, but the record of the test voltage wave at the instant of gap breakdown was made using a cold cathode-ray oscillograph to assure recording high frequency oscillations, if any were present.

Figure 9 shows the arrangement of the equipment used in conducting these tests. The voltage regulator, high potential transformer, voltage divider and miscellaneous equipment are seen in the background, and the cold cathode-ray oscillograph in the right foreground.

Figure 10 shows the flashover of the 6.25 centimeter sphere gap without the generator winding connected to the test equipment. The oscillogram shows a practically smooth voltage wave during the period of gap flashover.

Figure 11 shows the flashover of the 6.25 centimeter sphere gap, this time with the winding connected to the test equipment. This oscillogram shows the same smooth voltage wave as without the machine. There was no evidence of oscillation or high voltage impulse caused by the gap flashover with or without the machine connected.

Our tests indicate that if a suitable noninductive resistance is used in series with the protective spark-gap, no high-voltage transients or high-frequency oscillations of any consequence will result.

Experimental Repetitive Overvoltage Testing

Overvoltage tests were made on the windings of a 28,000-kva, 11.0-kv generator which was to be rewound. Figure 1 shows the arrangement of high-voltage test equipment. The tests were made after the rotor had been removed, but before the windings were stripped from the stator. The line and neutral leads were disconnected at the generator terminals. All voltages shown in the text and tables are rms values. The megger readings shown in the tables are actual readings not corrected for change of temperature. There was no measurable change of winding temperature during any of the repetitive overvoltage tests.

Repeated overvoltage tests were made on each phase to the other two phases and ground. The test procedure consisted of building up the voltage from zero to 17,250 volts rms for 50 successive tests of one minute each. The voltage was decreased to zero between each test and immediately built up again to the test voltage. For the first test in each group, the voltage was raised approximately two per cent above the nominal test voltage to preclude the chance of failure during subsequent tests due to voltage fluctuations.

The insulation resistance was measured by means of a 2,500-volt motor driven megger, and the capacity in microfarads and dissipation factor were measured with a capacitance bridge. These readings were taken at the beginning of each group of tests and after every tenth successive test. The results of this test are shown in Tables I, II, and III.

The reasons for increasing in steps of 25 per cent rated voltage on this first A phase test was to find the approximate insulation level of the winding without spending too much time in numerous

Table III. Repetitive Overvoltage Tests

28,000-kva 11,000-volt Hydroelectric Generator C Phase

Test Number	Test Voltage Applied: Volts	Test Voltage Applied: Per cent of Rated Volts	Excitation Current, Amperes	Duration, Seconds	Megger Reading, Megohms	Capacity to Ground Micro-farads	Dissipation Factor, Per cent
					4,000	0.158	4.0
1	17,250	150	1.12	60		0.159	4.0
2	18,300	159	1.20	60		0.159	4.0
3	19,300	168	1.28	60		0.159	4.5
4	20,350	177	1.38	60		0.158	4.5
5	21,400	186	1.47	60		0.160	4.8
6	22,450	195	1.57	60		0.161	4.8
7	23,500	205	1.67	60		0.159	4.8
8	24,600	214	1.78	60		0.160	5.0
9	25,600	223	1.87	20	Flashed Over at Coil Terminal*		
Built up to 23,500 volts before flashover. After trying to insulate at point of flashover, built up to 25,600 volts and held for 20 seconds before flashover							
Built up again to 25,600 volts, flashover in five seconds							
Made repeated tests at lower voltage							
10–49	22,450	195	1.57	60 Each	Not taken		
50	24,000	209	1.74	60	Not taken		
51	24,000	209	1.74	30	Flashed from puncture in insulation to finger plate		
52	24,000	209	1.74	20	Flashed from puncture in insulation to finger plate		

* Back coil in Slot number 108 about three inches above the iron. Puncture in insulation apparently occurred during the flashover in Test 9 above.

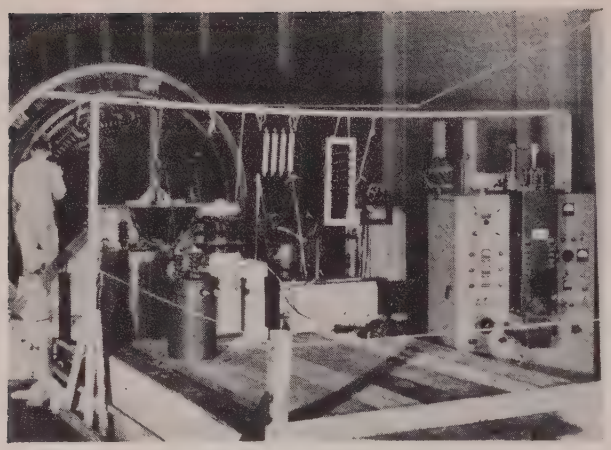

Figure 9. Equipment used for high-voltage tests on 66,667 kva 11,000-volt generator

tests that might be far below the level. After the 175 per cent tests, it was decided to increase to 200 per cent plus 100 volts. This value was used because it was thought to be of interest to see if the winding would stand a series of tests at the voltage applied on a new winding of this rating. On the 101st application of voltage, failure occurred in Slot number 68 at the top finger plate, fourth coil from the line. The megger reading showed zero, and no reading could be obtained with the capacity bridge.

It will be noted by reference to Table I that approximately 150 per cent of rated voltage was imposed on Phase A intermittently for 50 minutes, followed immediately by 175 per cent of rated voltage intermittently for another 50 minutes, not including the time required to build up or to remove the test voltage. Thus, the winding was held at high voltage for a total time of 1 hour and 40 minutes, with only momentary rest periods between each test, with no evidence of injury. If only one 150 per cent voltage 1-minute test had been made each year, the machine would not have been damaged by 100 years of tests.

A change of insulation resistance from 7,000 to 10,000 megohms was measured, but this is not considered significant. The insulation resistance recorded for the 100th test was the same as for the first 30 tests.

The change in winding capacity to ground changed from 0.157 to 0.165 microfarad, or 5.10 per cent.

The greatest measured change was in the dielectric dissipation factor. This increased from 4.0 to 6.1. This progressive increase in dielectric dissipation factor was noted in the subsequent tests on Phases B and C. In the case of Phase B, the dielectric dissipation factor went from 5.0 to 9.0.

It is believed that this increase in dissipation factor was due to a slight increase in winding insulation temperature as a result of the long application of high voltage, and is not indicative of permanent deterioration. Attention is directed to the fact that after the winding had failed, and the megger reading dropped from 7,000 to 2,500 megohms, there was no change in dissipation factor. That means that an insulation power factor measurement taken before and after breakdown would have indicated no change in the condition of the winding. It is considered further significant that with no knowledge other than the final megger reading and insulation power factor reading, anyone would have approved the machine for service. The minimum insulation resistance recommended by the AIEE rules for this machine would be 55.8 megohms at 25 degrees centigrade. No standard has been established for maximum winding power factor.

In the Phase B test, Table II shows that the winding endured the high voltage intermittently for a total time of two hours. Breakdown occurred at 22,450 volts, compared to 24,150 volts in the case of Phase A which had been subjected to the high voltage for 1 hour and 20 minutes intermittently. The over-all time of intermittent high voltage application for Phase C was only nine minutes and the breakdown voltage was 25,600. It might be thought from this series of

Table IV. Repetitive Overvoltage Tests

17,500-kva, 6,600-Volt Hydroelectric Generator

Test No.	Phase	Test Voltage Applied: Volts	Test Voltage Applied: Per cent of Rated Volts	Excitation Current, Amperes	Duration, Seconds	3 Min. Megger Reading, Megohms	Capacity to Ground, Microfarads	Dissipation Factor, Per cent
0	A					3,200	0.840	2.01
1	A	10,000	150		2			
2	A	11,600	176		2			
3	A	14,200	215		2			
4	A	14,000	212		10			
5	A	14,000	212		10			
6	A	14,000	212	0.58	60	3,600	0.840	2.20
7	A	14,000	212	0.58	60			
8	A	19,800	300		1	Winding Broke Down		
						0 Could Not Measure Megohms		
0	B					3,200	0.842	1.96
1	B	14,200	215	0.75	60	4,000	0.842	2.04
2	B	14,200	215	0.75	60	4,800	0.843	2.05
3	B	14,200	215	0.75	60	4,900	0.844	2.01
4	B	14,200	215	0.75	60	5,000	0.845	2.06
5	B	14,200	215	0.75	60	5,000	0.844	2.02
6	B	16,500	250	0.88	60	5,500	0.842	2.05
7	B	16,500	250	0.88	60	5,500	0.842	2.03
8	B	16,500	250	0.88	60	5,000	0.845	2.07
9	B	16,500	250	0.88	60	4,800	0.842	2.05
10	B	16,500	250	0.89	60	4,500	0.845	2.05
11	B	18,500	280	1.01	60	4,500	0.843	2.02
12	B	18,500	280	1.01	60	4,000	0.845	2.05
13	B	18,500	280	1.01	60	4,000	0.845	2.12
14	B	18,500	280	1.01	60	4,000	0.846	2.05
15	B	18,500	280	1.01	60	3,900	0.845	2.09
16	B	19,500	295	1.08	60	3,500	0.852	2.14
17	B					4,000	0.850	2.00
18	B	20,500	311	1.14	60	3,600	0.855	2.07
19	B	21,500	325	1.20	60	3,400	0.855	2.14
20	B	22,500	340	1.26	60	3,000	0.855	2.10
21	B	23,500	356	1.37	60	2,500	0.855	2.11
22	B	24,500	375	1.43	60	2,300	0.855	2.16
23	B	25,500	386		1	1,550	0.855	2.05
24	B	21,000	318		1	0	Could not measure	

NOTE: 1. During Test 18, corona was visible near finger plates.
2. On Test 19, and all subsequent tests, static dischargers in streamers one inch long were jumping from Phase B winding to the rotor.
3. On Test 22, B Phase broke down to C Phase, then to ground.
4. After failure on Test 22, voltage was built up to 21,000 before breakdown. After Test 23, winding showed solid ground.
5. Phase C could not be tested because it was involved in B Phase failure.

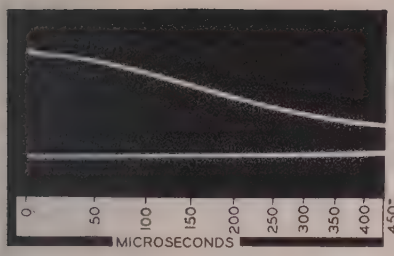

Figure 10. Flashover of sphere gap without generator winding connected. 66,667 kva 11,000-volt generator tests

tests that repeated applications of high voltage had weakened the winding. The evidence from the tests on this one generator however is not adequate to support that conclusion. It is recognized that the failure of insulation under dielectric stress in the range used in these tests is a function of time—shorter times requiring higher voltages. This effect has been attributed to thermal effects. Such effect does not necessarily produce a permanent change in insulation, so that repeated tests separated by time sufficient to allow complete cooling to the initial state might not have shown different final values of breakdown voltage. Furthermore, this is only one machine and some initial difference between the condition of the three phases may have existed. This relation between time and breakdown voltage did not occur in other windings tested. This will be seen by reference to Table IV which gives the results of a similar test on a 17,500 kva 6.6-kv generator.

Table IV shows the results of the repetitive voltage tests on Phase A and Phase B. Phase C could not be tested because it was broken down when the B Phase failed.

After each application of voltage to the B Phase readings of insulation resistance, power factor and dissipation factor were taken. There was no real change in the dissipation factor. The power factor increased from 0.842 to 0.855 which is 1.5 per cent. The greatest change is found in the three minute megger readings. These are shown graphically in Figure 12. The amount of time that elapsed between the successive applications of high voltage was about seven minutes in each case, except between tests 16 and 17. Test 16 was made at 5:09 p.m., and test 17 at 6:15 p.m., before reapplying the high voltage.

The insulation resistance increased after each test up to test 6, which was at 250 per cent of rated voltage. The rise of the megger readings could have been due to a slight increase in the internal temperature of the winding from dielectric losses. There was no measurable change in the surface temperature of the winding.

It appears as if the insulation was beginning to deteriorate after test 7. There was no way to determine whether the change was due to general or localized change in the insulation. However, since there was little change in the capacity and dissipation factor values, which should be affected by the general condition of the insulation, it is believed that localized deterioration was taking place. However, after the 1-hour rest period the insulation resistance increased.

Following test 16, the test voltage, already at 295 per cent of rated voltage, was increased 1,000 volts after each test. Figure 12 shows that the rate of decrease of insulation resistance is slightly greater from Test 17 to 24 than it was between Test 7 to 16. During Test 19 and all subsequent tests, static discharges in great quantity were visible and there was a strong odor of ozone around the generator.

The winding broke down at 25,000 volts which is 386 per cent of the rated voltage. Although the value of the megger readings had been decreasing steadily, the value of 2,300 megohms on the test just preceding the winding failure was still very much higher than the minimum value recommended by the AIEE Standards. For one phase of a machine of this rating, the minimum recommended insulation resistance is 33.5 megohms at 25 degrees centigrade.

Tests were made on the stator winding of a 25,000-kva 11,000-volt hydroelectric generator to determine if the application of 150 per cent of rated voltage for a prolonged period of time would cause an observable decrease of winding insulation strength.

Phase A was tested as follows: 150 per cent of rated voltage, 16.5 kv was applied to Phase A, and held for 30 minutes. The

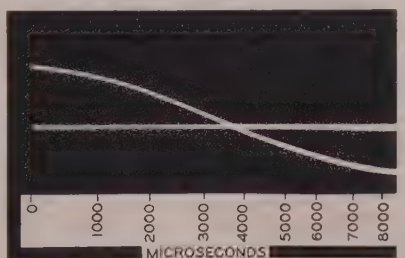

Figure 11. Flashover of sphere gap with generator winding connected in parallel with sphere gap. 66,667 kva 11,000-volt generator tests

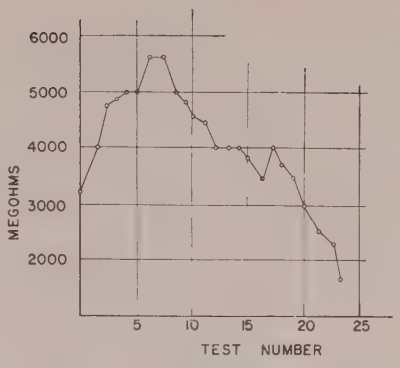

Figure 12. Insulation resistance versus test numbers of Table IV showing change of resistance as a result of overvoltage testing

voltage was then raised 10 per cent to 17.6 kv and held for one minute, then raised 10 per cent again to 18.7 kv. This was continued until the winding failed. Failure occurred at 30.8 kv, which is 280 per cent of rated voltage, or 34 per cent above double voltage plus 1,000. During these tests, several breakdowns occurred from the leads to the generator frame. These points of failure were isolated as required and the test continued.

Phase C was next tested. One hundred and fifty per cent voltage was applied for one minute. Then the test voltage was raised in 10-per cent steps with one minute hold periods until the winding failed at 27.5 kv which is 250 per cent of rated voltage. The duration of the test was ten minutes.

Phase B was next tested by applying 150 per cent of rated voltage for 30 minutes. Then the voltage was raised 15 per cent to 18.1 kv and held for 15 minutes, when the voltage was again increased 15 per cent. This was continued until the winding failed at 28.0 kv at the end of 120 minutes.

The test voltages and time of application are shown in Table V.

The results of these tests indicate that the time of application of the test voltage was not a significant factor affecting the coil breakdown value.

The test on Phase C may be taken as establishing the one minute breakdown value for this insulation as 27.5 kv. If conditioning the insulation by applying 150 per cent of rated voltage for 30 minutes caused any deterioration, it would be expected that the breakdown voltage for the test on Phase A would have been lower than 27.5 kv. Actually, it was higher—30.8 kv.

In the test on Phase B, the test voltage was kept on the winding for 120 minutes, about 12 times as long as the C Phase

Table V. Repetitive Overvoltage Tests

25,000-kva 11,000-Volt Hydroelectric Generator Test Voltages and Time of Application

PHASE A			PHASE C			PHASE B		
Kv	Time Applied*	Remarks	Kv	Time Applied**	Remarks	Kv	Time Applied†	Remarks
16.5	30 Min	OK	16.5	1 Min.	OK	16.5	30 Min.	OK
17.6	1 Min.	OK	17.6	1 Min.	OK	18.15	15 Min.	OK
18.7	1 Min.	OK	18.7	1 Min.	OK	19.8	15 Min.	OK
19.8	1 Min.	OK	19.8	1 Min.	OK	21.45	15 Min	OK
20.9	42 Sec.	Lead Flashover	20.9	1 Min.	OK	23.1	15 Min.	OK
20.9	1 Min.	OK	22.0	1 Min.	OK	24.75	15 Min	OK
22.0	11 Sec.	Lead Flashover	23.1	1 Min	OK	26.4	15 Min.	OK
22.0	1 Min	OK	24.2	1 Min.	OK	28.05	5 Sec.	Winding Failed 6 In. in Slot
23.1	1 Min.	OK	25.3	1 Min.	OK			
24.2	1 Min.	OK	26.4	1 Min.	OK			
25.3	1 Min.	OK	27.5	23 Sec.	Winding Failed 4 In. in Slot			
26.4	1 Min.	OK						
27.5	1 Min.	OK						
28.5	1 Min.	OK						
29.7	1 Min.	OK						
30.8	17 Sec.	Lead Flashover						
30.8	5 Sec.	Lead Flashover						
30.8	27 Sec.	Winding Failed 6 In. in Slot						

* Total time: 44 minutes

** Total time: 10 minutes, 23 seconds.

† Total time: 120 minutes, 5 seconds.

test. However, the breakdown voltage was 28.0 kv.

It should not be considered that only three tests were made. The machine tested had 189 coils, so there were 63 coils per phase. Hence, the results may be considered as the minimum values obtained from testing 63 coils, one at a time, for each procedure.

From these tests it was determined that a value of 150 per cent of rated voltage would be satisfactory for an overvoltage test to be made on each scheduled overhaul. The procedure of routine testing at 150 per cent of rated voltage was put in effect in 1945. Experimental testing was continued as other machines, scheduled to be rewound, became available. The following is a list of four other machines which have been tested to failure to obtain information about the effects of repetitive overvoltage tests:

One 17,500-kva 11.0-kv hydroelectric generator
One 30,000-kva 6.6-kv hydroelectric generator
One 45,000-kva 6.6-kv synchronous condenser
One 15,000-kva 12.0-kv synchronous condenser

The data from the tests on these four machines confirm the results and conclusions of previous testing.

Since the adoption of the overvoltage testing program in 1945, 56 different synchronous machines have been regularly tested at the time of scheduled outages. Twenty-one of these machines have received two or more tests. The maximum number of annual tests on any one machine is six. Winding failures have occurred in seven machines during routine testing. In all cases repairs were made without difficulty and the machinee returned to service after passing the 150 per cent overvoltage test. Up to this time there have been no winding failures while machines have been in operation. It is believed that routine insulation testing as described has no ill effects on a good winding insulation and is effective for eliminating winding failures in service.

References

1. Field Testing of Generator Insulation. **Edison Electric Institute Committee on Generator Insulation.** *Electrical Engineering (AIEE Transactions)*, volume 60, December 1941, pages 1003–11.

2. Recommended Practice for Testing Insulation Resistance of Rotating Machinery. *AIEE Standard Number* 43, April 1950.

No Discussion

Alternating and Direct Voltage Endurance Studies on Mica Insulation for Electric Machinery

GRAHAM LEE MOSES
FELLOW AIEE

Synopsis: A program studying voltage endurance of various mica insulations is reported. This includes dielectric breakdown data with both alternating and direct current on numerous similar samples. Effects of repetitive testing, prolonged a-c (60-cycle) stress and mechanical damage to mica insulation are reported. Detection of insulation faults is described and conclusions are drawn that d-c overpotential maintenance tests can be equally searching but less damaging than a-c overpotential tests for large high-voltage rotating machinery.

THE a-c and d-c dielectric strength of insulations and the time-voltage relation of each to produce dielectric breakdown are questions of considerable interest both to the users and manufacturers of electric equipment. Many investigators have reported results of studies on some phases of these questions; however, there has been no general report of the voltage endurance of mica insulations under both a-c and d-c stress. It was believed that such data would contribute to a better understanding of many insulation phenomena and might aid in explaining some apparently mysterious occurrences during insulation tests. Another reason for undertaking this investigation was to seek a better basis for maintenance testing of insulation.

The Electrical Equipment Committee of the Edison Electric Institute undertook a study of the maintenance testing problem in 1935, and in 1937 a special committee was assigned to the subject of "Generator Insulation and Testing." The report of this committee was presented in 1941.[1] This investigation was confined to the destruction of older windings which constituted large dissimilar samples. This made analysis of the data difficult.

In 1949, L. F. Hunt and J. H. Vivian presented a paper[2] to the Edison Electric Institute outlining an aggressive and comprehensive program of maintenance testing. Here too the windings tested to destruction were older types of insulation and constituted large dissimilar samples. All these overpotential tests were with alternating current (60 cycles).

The Westinghouse program was established to study the problems on modern insulation systems and components of controlled quality in each batch, with a sufficient quantity of samples at each condition of test to establish mean dielectric strength levels and determine deviation by statistical methods. This was intended as a starting point from which could be developed a rational program for testing winding insulation to destruction so that a maintenance testing program could be developed.

It is gratifying to report that this program has developed along these lines to the point that such a maintenance testing program now is available.[3] It is the purpose of this paper to describe the basic investigation of insulation breakdown as carried out by the author and his colleagues in the Westinghouse Research Laboratory and various interested engineering departments and engineering laboratories.

Comprehensive Study of Dielectric Breakdown and Endurance

Realizing the lack of organized data on the dielectric strength and voltage endurance of important machine insulations, an extensive series of tests has been under way for several years. This study has included low-voltage insulations as well as high-voltage insulations, plus the basic mica flakes. Breakdowns have been obtained on sufficiently numerous samples to ensure reasonable accuracy of average values and to permit determination of the deviation by statistical analysis methods. Both a-c (60-cycle) and d-c breakdown data have been obtained over a wide range of time values which in some cases covered the range of one microsecond to several months. Tests included materials separately as well as in coils and

Table 1. Dielectric Strength Tests

One-Minute Step Tests, Using 2-Inch Guarded Electrodes Immersed in Transformer Oil

Description of Material	Nominal Thickness, Inches	No. of A-C Tests	No. of D-C Tests	Max. Ratio D-C to A-C Crest	Min. Ratio D-C to A-C Crest	Aver. Ratio D-C to A-C Crest
Mica slot cell	0.022	15	15	4.64	1.19	2.62
Fishpaper and mica wrapper	0.012	14	14	5.02	1.54	2.90
Fishpaper and mica wrapper	0.010	14	13	5.09	1.13	2.17
Glass backed mica wrapper	0.008	12	12	3.48	1.60	2.26

Paper 51-127, recommended by the AIEE Rotating Machinery Committee and approved by the Technical Program Committee for presentation at the AIEE Winter General Meeting, New York, N. Y., January 22–26, 1951. Manuscript submitted October 16, 1950; made available for printing December 5, 1950.

GRAHAM LEE MOSES is with the Westinghouse Electric Corporation, East Pittsburgh, Pa.

The great assistance of many colleagues is gratefully acknowledged by the author. Those participating through giving counsel and guidance or by accumulating and analyzing vast amounts of data include C. F. Hill, C. M. Laffoon, L. A. Kilgore, J. S. Johnson, W. Schneider, L. J. Berberich, W. W. Pendleton, C. N. Works, H. M. Philofsky, J. G. Wynn, Josephine Garber, R. J. Alke, A. W. Worthington, and others.

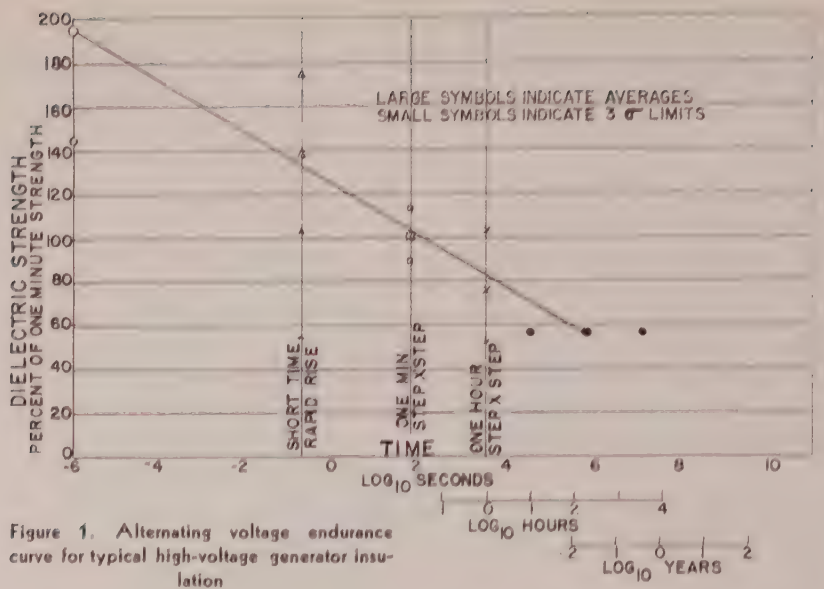

Figure 1. Alternating voltage endurance curve for typical high-voltage generator insulation

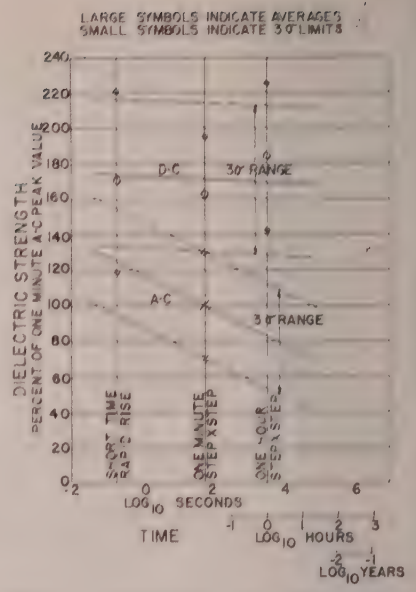

Figure 2. Alternating and direct voltage endurance for high-voltage generator insulation

test bars. Furthermore, substandard insulation on defective coils also was studied. Power factor studies were made on all high voltage insulations studied.

A-C and D-C Tests on Mica Wrappers

Tests were made at Westinghouse Research Laboratories on a variety of mica wrappers and slot cells giving some very interesting information concerning the relative a-c and d-c breakdown of solid mica insulation at one minute time of voltage application. These are shown in Table I. These tests indicate an average ratio of two or more for the d-c to the a-c peak voltage. It is interesting to note that in no case was there a single d-c breakdown at as low a value as the highest peak of an a-c breakdown.

Alternating Voltage Endurance of High-Voltage Insulations

Studies have been in progress for several years evaluating the a-c time-voltage relationship to produce failure on various forms of high-voltage machine insulations. This work formed an important part of the development of Westinghouse Thermalastic insulation as described in a recent AIEE paper.[4] A considerable amount of data has been accumulated concerning the voltage endurance characteristics of asphalt bonded mica tape insulation. Typical behavior of such insulation is shown in Figure 1. This applies to new insulation not subjected to mechanical stresses of winding or operation. From the data it can be concluded that increasing the time under voltage stress reduces the breakdown voltage level of such insulation. While individual samples will vary widely even when made in the same batch, this appears to be a basic phenomena which takes place when insulation is stressed in the range of a-c voltage studies.

Figure 1 indicates that the voltage log time to failure approximates a straight line for a range of almost 12 orders of magnitude in time (10^{-6} seconds to 10^{6} seconds). While times to failure at lower stress have not yet been explored, it is reasonable to expect that the curve may eventually flatten and become parallel to the horizontal axis at some positive stress. Reasonable extrapolation of the present data, however, appears justifiable particularly since possible errors from this assumption would be on the conservative side.

The approximation of the alternating voltage endurance curve which plots a straight line on semilog paper can be expressed as the formula:

$$V = \log T - m + b$$

where

V = applied voltage in kilovolts
T = time in seconds to breakdown
b = voltage in kilovolts to produce failure in one second
m = slope factor which is the voltage increement in kilovolts that reduces the time to failure by a factor of ten

Direct Voltage Endurance Tests on High-Voltage Insulation

Subsequently tests were made on direct voltage endurance of normal insulation similar to that in Figure 1 but made on a different batch of insulation at a different time. Figure 2 plots both a-c and d-c dielectric strengths for a particular batch of insulation.

The flatness of the direct voltage endurance curve is of considerable interest as it indicates that time of direct voltage

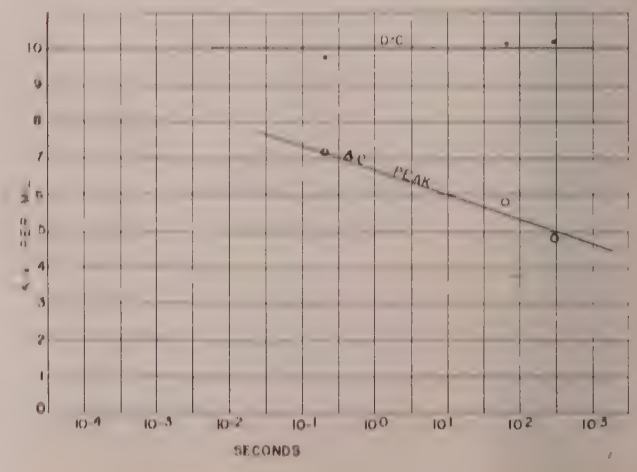

Figure 3. Voltage endurance tests on mica splittings

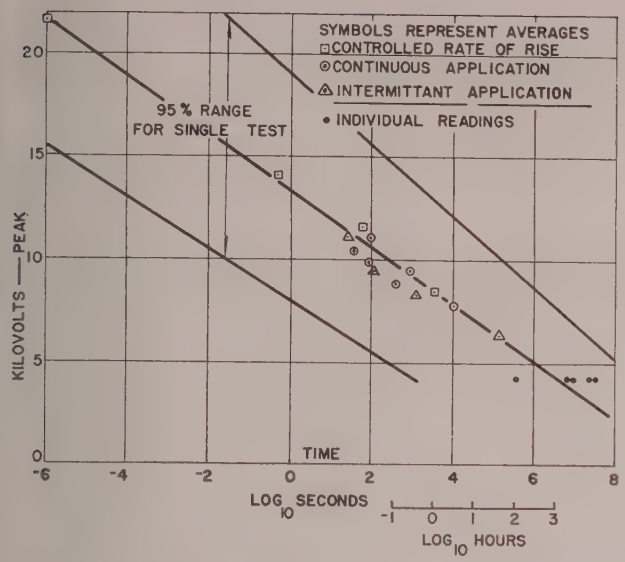

Figure 4. Dielectric strength (a-c 60 cycles) of glass backed mica wrapper (0.010-inch thick) as a function of time and with continuous and repetitively applied voltage

application is far less significant in its effect on failure voltage than when a-c stress is applied. It further indicates that there is no fixed ratio of direct to alternating voltage for equal destructive effect. It is therefore evident that if the concept of a d-c to a-c ratio is to be employed it must be at a specific time of voltage application. For example, one set of samples of high-voltage insulation had a series of average d-c to a-c ratios as follows:

Test Condition	Ratio D-C/A-C Peak
Impulse	1.0
Rapid rise*	1.25
One minute step-by-step*	1.5
One hour step-by-step*	1.8

Note: All A-C tests are 60 cycles.

Tests on Mica Flakes

Studies of the voltage endurance characteristics of muscovite mica splittings (approximately 0.001-inch thick) were made with a-c and d-c stresses. All tests were made in air employing 2-inch diameter electrodes (standard shape prescribed by the American Society for Testing Materials). These results are plotted in Figure 3. It is interesting to note that the slopes for both a-c and d-c stresses agree rather closely with that obtained on the high-voltage insulation (Figures 1 and 2). This suggests that application of relatively high-voltage stress results in deterioration of the mica splittings. Since mica splittings are the basic constituent of major high-voltage machine insulation, it is reasonable to conclude that the time voltage relationships observed for a-c and d-c stresses are basic phenomena. Because of the known thermal endurance of mica, it is unlikely that the voltage-time effect results from thermal instability. It is therefore probable that the action is the result of ionic bombardment by high energy particles mechanically eroding the basic insulation. If this is true it would be expected that no appreciable recovery would occur between test intervals.

Effect of Repetitive Application of Test Voltage

A series of a-c dielectric tests was made on 0.010-inch thick glass backed mica wrapper, such as used on low-voltage coils. This included not only dielectric breakdown at various times of voltage application but repeated 1-minute applications of voltages at various percentages of the average 1-minute dielectric strength of the materials. Test results are shown in Figure 4.

It was found that repeated 1-minute applications of voltage ultimately produced breakdown of the insulation even when the voltage was less than 65 per cent of the average 1-minute step-by-step hold strength. Furthermore, it was observed by these tests that the voltage endurance of this material was essentially the same whether the voltage was applied continuously or intermittently with rest periods between repeated voltage applications. From this it was concluded that for this form of insulation, repeated applications of test voltage are cumulative in effect and that recovery between repeated applications of voltage is not a significant factor in establishing the ultimate time to breakdown.

Figure 5. Effect of pretesting coils and repeated testing on probability of failure on dielectric proof test

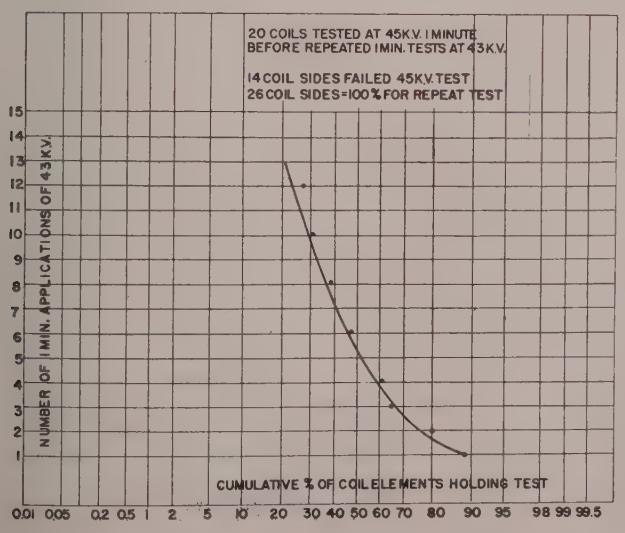
20 COILS TESTED AT 45KV. I MINUTE
BEFORE REPEATED I MIN. TESTS AT 43 KV.
14 COIL SIDES FAILED 45KV. TEST
26 COIL SIDES = 100% FOR REPEAT TEST
NUMBER OF I MIN. APPLICATIONS OF 43 KV.
CUMULATIVE % OF COIL ELEMENTS HOLDING TEST

Figure 6. Effect of repeated dielectric proof tests shown on log probability graph paper

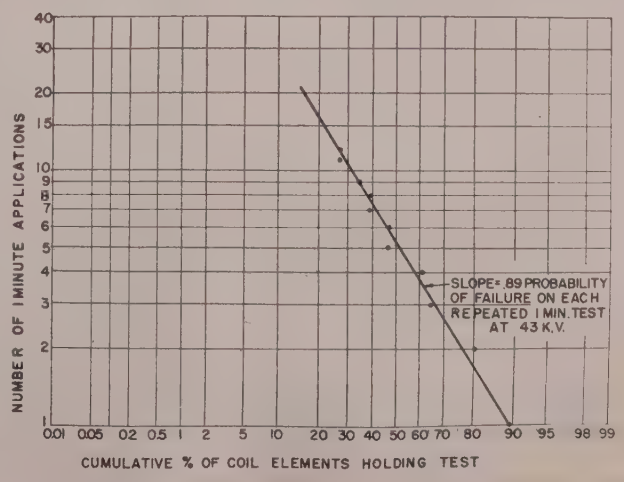
SLOPE = .89 PROBABILITY OF FAILURE ON EACH REPEATED I MIN. TEST AT 43 K.V.
NUMBER OF I MINUTE APPLICATIONS
CUMULATIVE % OF COIL ELEMENTS HOLDING TEST

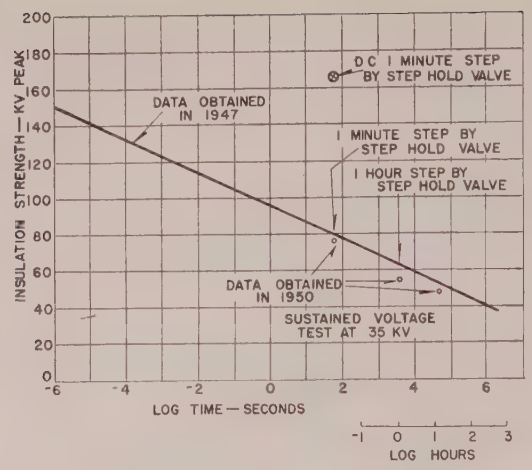
INSULATION STRENGTH — KV PEAK
D.C. 1 MINUTE STEP BY STEP HOLD VALVE
DATA OBTAINED IN 1947
1 MINUTE STEP BY STEP HOLD VALVE
1 HOUR STEP BY STEP HOLD VALVE
DATA OBTAINED IN 1950
SUSTAINED VOLTAGE TEST AT 35 KV
LOG TIME — SECONDS
LOG HOURS

Figure 7. Repeated alternating voltage endurance test data and d-c breakdown versus time for high-voltage insulation

Repetitive Tests on High-Voltage Coil Insulations

Several years ago a large number of high-voltage coils were rejected by the quality control program as having marginal insulation strength. A number of different kinds of tests were made on the ground insulation including: surge tests, rapid rise tests, 1-minute step-by-step tests, and longer time tests. One series of these tests studied the effect of repeated tests at a lower voltage than the original proof test.

Twenty of these coils were selected for repetitive application of voltage. The 20 coils consisting of 40 test specimens (each side being considered a specimen) were first given a 45-kv 1-minute proof test. Fourteen out of 40 coil sides failed this test. Thereafter, the remaining coil sides were tested repeatedly for one minute at a lower voltage (43 kv) than the original 45-kv proof test. The results of this test are shown in Figure 5.

In further analyzing the effects of the repeated tests, the data from Figure 5 was replotted on logarithmic probability paper as Figure 6 wherein the cumulative number of coil elements holding the 43-kv test was plotted as a function of the logarithm of the number of test applications. It is of considerable interest that this curve on logarithmic probability paper becomes a straight line. This indicates that the probability of failure on each repeated test was essentially the same as for the first test.

From this series of tests, it can be seen that the application of a higher proof test than the subsequent repetitive tests did not weed out the weak insulation so as to significantly improve the dielectric level of the batch. The probability of failure on each of the repetitive 1-minute 43-kv tests was unchanged on successive applications of voltage. The conclusion drawn from these tests is that dielectric tests approaching the breakdown level of the insulation are not only damaging but do not change the probability of failure of the batch on subsequent similar tests.

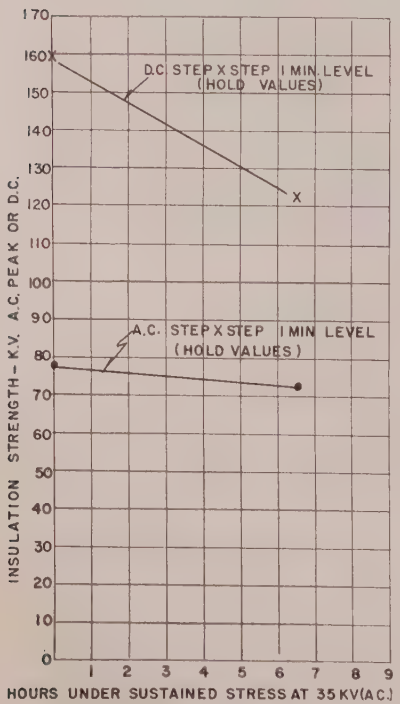
INSULATION STRENGTH — K.V. A.C. PEAK OR D.C.
D.C. STEP X STEP 1 MIN LEVEL (HOLD VALUES)
A.C. STEP X STEP 1 MIN LEVEL (HOLD VALUES)
HOURS UNDER SUSTAINED STRESS AT 35 KV (A.C.)

Figure 8. Effect of sustained a-c stress (6.6 hours at 35 kv) on a-c and d-c step-by-step dielectric strength (1-minute hold values) of high-voltage insulation

Further Testing with Alternating and Direct Current on High-Voltage Insulation

Many months later this work was continued with a new batch of 50 specimens with 13.8-kv insulation. These were divided into seven groups of seven specimens each by random sampling. The groups were tested by several methods with the results shown in Table II.

Figure 7 shows the average a-c held voltages at 1-minute and 1-hour duration on a replot of the earlier test data, Figure 1. This shows excellent agreement. The d-c hold level is shown superimposed on this curve.

Figure 8 presents the data on the reduction in average dielectric level as the result of prolonged a-c stress (6.6 hours at 35 kv) as determined by both a-c and d-c tests to destruction (1-minute step-by-step tests). Here it is evident that the prolonged a-c stress reduces the dielectric strength of the insulation specimens. It is of considerable interest that such degradation is more readily detected by d-c tests than by a-c tests!

Complete power factor data was observed on specimens before dielectric stress was applied and where possible after prestressing before final breakdown. No correlation was observed between power factors and dielectric strength.

A-C and D-C Dielectric Strength of Air

It is well established that in a uniform field such as a sphere gap, the breakdown of gases is the same for direct voltage as the crest of the alternating voltage (AIEE Standard number 4[5]).

Detection of Complete Rupture in Mica Insulation

The extreme form of insulation fault which must be detectable by a maintenance test is a complete rupture in the insulation barrier as a result of mechanical damage. A test not capable of detecting such a fault is not acceptable according to the principles set forth in AIEE Report number 51 Guiding Principles for Dielectric Tests.[6]

Therefore, tests were made on mica insulation with a complete puncture to de-

Table II

1.....	One-minute step-by-step a-c test to breakdown	54.3 kv rms avg. hold $\sigma = 8.6$
2.....	One-minute step-by-step d-c test to breakdown	158.6 kv avg. hold $\sigma = 14.5$
3.....	One-hour step-by-step a-c test to breakdown	38.6 kv avg. hold $\sigma = 5$
4–5–6....	Stressed continuously at 35 kv a-c (rms) until 1/3 of specimens failed	Hours to failure 0.34–1.68–4.1–4.13–4.8–5.9–6.6
1/2 of balance 4–5–6	One-minute step-by-step a-c test to breakdown	51.4 kv avg. rms hold $\sigma = 7.56$
1/2 of balance 4–5–6	One-minute step-by-step d-c test to breakdown	125.7 kv avg. hold $\sigma = 31.3$

termine the relative searching effect of alternating and direct current in the detection of a complete rupture in the ground wall. Mica plate was employed for these tests. Samples selected were 0.063, 0.140, and 0.180 inch thick, each 12-inch square mica plate had nine 1/16-inch holes drilled completely through it. Standard American Society for Testing Materials electrodes were placed on either side of the plate and dielectric breakdowns obtained through the 1/16-inch holes with both alternating and direct current. The results are plotted in Figures 9 and 10. Both curves contain data for the equivalent air spacing breakdown in a uniform field for reference.

From this group of tests, it can be concluded that for the detection of complete ruptures in the ground wall of mica insulation a d-c test voltage of 1.5 to 1.7 times the a-c rms voltage necessary to detect the fault will have equal searching effect.

D-C Tests on Coils with Damaged Insulation

Coils with conventional 11-kv insulation were cut up into short lengths as test specimens. These samples were bent when at room temperature 15 degrees in one direction, then 15 degrees in the opposite direction, and then straightened. Several samples were tested with a special 30-kv d-c tester (Takk model 95). Failure was observed at the voltages given in Table III.

After these tests it was found that approximately the same voltage as before was required to produce failure on subsequent tests. This indicated that the original failures were due to creepage through the torn insulation and that no puncture of solid insulation occurred and that no tracking of creepage surfaces resulted from the test failure.

A complete coil insulated for 11 kv was damaged by severe hammer blows on the corner of the slot insulation. The insulation withstood a d-c test until 30 kv was reached. Failure occurred by current runaway and collapse of the voltage. Reapplication of voltage produced excessive current. This indicated that there was solid insulation in series with crushed insulation at the point of failure.

Table III

Sample No.	Failure Voltage (D-C), Kv.	
1	8	(Slowly rising voltage)
2	12	
3	20	
4	17	
5	15	(After holding 1 minute)

Pros and Cons of D-C Testing

Some limitations and objections to the use of d-c overpotential tests have been as follows:

1. Mechanism of failure is different with alternating and direct current.

2. Voltage distribution over end windings is different with alternating and direct current. With direct current the voltage appears farther out on end windings beyond core. This is aggravated by conducting dirt on insulation surface.

3. Residual charge on windings is persistent and may be hazardous to personnel.

Direct current overpotential testing is desirable as a maintenance procedure because the accumulated evidence indicates that it is searching for insulation defects of the sort that should be detected. Furthermore, these studies have shown that a d-c overpotential test has negligibly small deteriorating influence on good insulation as compared to an a-c test of equal searching effect. The following comments refer to the foregoing objections and limitations:

1. Difference in failure mechanism is not objectionable but is desirable for a nondestructive test if the test is satisfactorily searching for the type of insulation fault to be detected.

2. Differences in voltage distribution exist but have not been found to be a problem on a considerable number of large high-voltage windings tested with direct current. The difference makes the d-c test more searching in the end windings than a corresponding a-c test but has not yet produced a failure on good insulation.

3. Residual charges on windings can be dissipated easily in a relatively short time. Experience has shown that careful operation by the tester can reduce this hazard so that it is practically nonexistent.

For small apparatus which has low capacitance from the windings to ground, a-c test equipment is readily portable as the size of the test transformer is not important. On larger and higher voltage apparatus where the capacitance of the winding to ground is large, the test equipment for overpotential testing with alternating current becomes quite large and maintenance testing presents serious test equipment transportation problems. On the other hand, d-c overpotential test equipment is available which is quite small and readily portable. (Westinghouse uses Takk Corporation equipment of three direct voltage ranges, 15 kv, 45 kv, and 75 kv.) Such test equipment would be desirable in many ways as a voltage source for testing large high-voltage machines, provided the d-c test was satisfactory and accepted by the industry. Alternating current overpotential testing usually involves no current measurement and therefore must be destructive to detect faults. On the other hand, d-c testing makes leakage current measurement easy. Furthermore, the d-c leakage current is not masked by charging current as is the case with a-c testing.

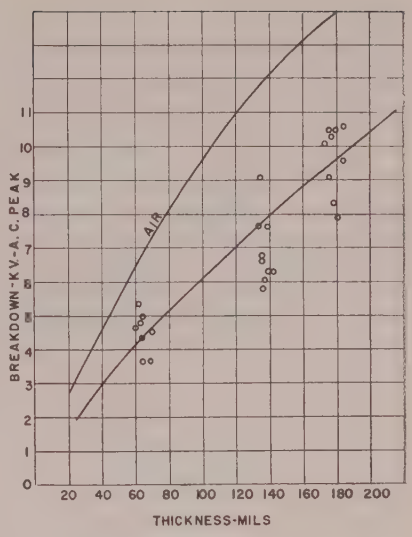

Figure 9. Detection of pin holes in mica plate with a-c test

There has been considerable interest in d-c maintenance testing for many years, especially on large high-voltage equipment, and many engineers have used and

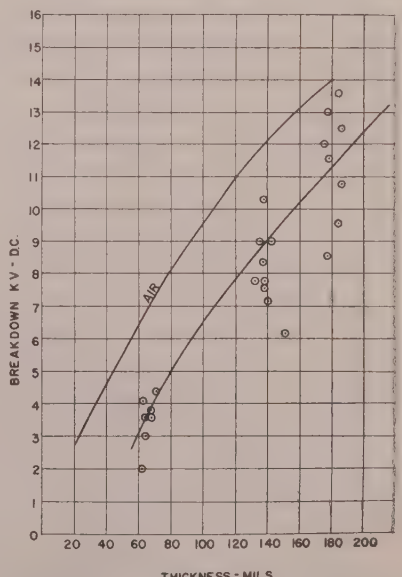

Figure 10. Detection of pin holes in mica plate with d-c test

recommended such tests. No statement in this paper is intended to imply that d-c overpotential testing is new or different from previous concepts except in so far as the relative searching and damaging effects with respect to a-c tests. The data presented herein and the opinions expressed are offered with the hope of providing a rational basis for establishing some standardized basis for d-c overpotential testing, especially as a maintenance procedure on large high-voltage windings.

Conclusions

1. Testing mica insulation with alternating current at voltages near the ultimate dielectric strength of the system is damaging.

2. Repeated a-c testing under such conditions produces cumulative damage with consequent reduction in dielectric strength even at voltages far below the strength of the insulation.

3. Prolonged testing at alternating voltages far below the intrinsic short time dielectric strength of insulation produces an observable reduction in dielectric strength.

4. Repeated testing of insulation does not change the probability of failure on repeated tests, unless the specimens failing the first test are not typical of the batch (such as may be occasioned by mechanical damage).

5. Solid mica insulations such as employed in machinery have a d-c to a-c peak voltage breakdown ratio considerably greater than one except at very short time of voltage application. This ratio is not constant between materials of similar construction and varies with time of voltage application.

6. The searching effect of alternating and direct current through holes in solid insulation is of the same order. However, at the greater spacings (0.100 inch or more), direct current appears to be somewhat less effective than the equivalent a-c peak voltage with an indicated ratio of 1.5 to 1.7 (d-c to a-c rms) for equal searching effect.

7. No significant correlation was observed between power factor and dielectric strength (either alternating or direct current) on high-voltage insulation specimens.

8. Direct current tests can be used as maintenance tests to give assurance of the absence of likely insulation weakness with the possibility of reduced damage to good insulation. For example, a d-c test of appreciably greater voltage than would break down the equivalent gas spacing would give assurance of the presence of intervening solid insulation.

9. Direct current overpotential tests are less damaging than a-c tests when both are the same percentage of the ultimate dielectric strength of the insulation because of the difference in slope of their respective voltage endurance curves.

Recommendations

It is recommended that 1.6 be recognized as a reasonable ratio of d-c to a-c rms voltage (at 1-minute voltage application) for equal searching effect in overpotential testing of solid mica insulations in large electric machinery.

It is further proposed that the following formula for a maintenance overpotential test value for large machine windings be considered and tried out in service.

$$E_{mt} = (2E + 1{,}000)\ 65 \text{ per cent} \times 1.6$$

where

E_{mt} = direct voltage for maintenance test of 1-minute duration

E = rated voltage of machine

References

1. Field Testing of General Insulation, EEI Committee Report. *Electrical Engineering* (*AIEE Transactions*), volume 60, December 1941, pages 1003–11.

2. Operation of Synchronous Machines for Continuity of Service on Southern California Edison Company System, L. F. Hunt, J. H. Vivian. *Minutes*, Electrical Equipment Committee, Edison Electric Institute (New York, N. Y.), May 3, 1949.

3. Inspection and Maintenance Testing of High-Voltage Generator Windings, J. S. Johnson. *AIEE Transactions*, volume 70, part I, 1951, pages 749–55.

4. A New High-Voltage Insulation for Turbine-Generator Stator Windings, C. M. Laffoon, C. F. Hill, Graham Lee Moses, L. J. Berberich. *AIEE Transactions*, volume 70, part I, 1951, pages 721–30.

5. Measurement of Test Voltage in Dielectric Tests. AIEE Standard Number 4, November 1942.

6. Guiding Principles for Dielectric Tests. AIEE Report Number 51, September 1949.

7. Dielectric Strength Ratio Between Alternating and Direct Voltages, J. L. R. Hayden, W. N. Eddy. *AIEE Transactions*, volume 42, 1923, pages 593–99.

8. The Basis for the Nondestructive Testing of Insulation, R. F. Field. *Electrical Engineering* (*AIEE Transactions*), volume 60, September 1941, pages 890–95.

9. Breakdown Curve for Solid Insulation, V. M. Montsinger. *Electrical Engineering* (*AIEE Transactions*), volume 54, December 1935, pages 1300–01.

10. Dielectric Phenomena in High Voltage Engineering, F. W. Peek, Jr. McGraw-Hill Book Company, New York, N. Y., 1929.

11. Mechanism of Dielectric Breakdown, D. T. Hurd. *General Electric Review* (Schenectady, N. Y.), December 1948, pages 26–33.

12. A Portable Instrument for Measuring Insulation Resistance at High Voltage, F. W. Atkinson, R. B. Taylor. *Electrical Engineering* (*AIEE Transactions*), volume 64, April 1945, pages 164–66.

13. Insulation Tests of Electrical Machinery Before and After Being Placed in Service, C. M. Gilt, B. L. Barns. *AIEE Transactions*, volume 49, April section, 1929, pages 656–65.

14. Generator-Insulation Tests, B. Van Ness. *Bulletin*, Edison Electric Institute (New York, N. Y.), volume 6, May 1938, pages 204–06.

15. Maintenance Overpotential Tests for Armature Windings in Service, R. W. Wieseman. *General Electric Review* (Schenectady, N. Y.), August 1950, pages 24–28.

16. Predicting Insulating Performance by Statistical Analysis, Graham L. Moses. *Electrical Manufacturing* (New York. N. Y.), volume 43, April 1949, pages 108–12.

Discussion

L. O. Dorfman (Ebasco Services, Inc., New York, N. Y.): The difficulties encountered in obtaining satisfactory results in the endurance testing of insulating materials of the type discussed in the paper are well known. The author is therefore to be congratulated for selecting such procedure and tests as to bring out the relative searching effects of direct current versus alternating current and to secure a measure of the damaging effect of each type of potential.

Mr. Moses has pointed out that considerable interest has existed for many years in connection with d-c maintenance testing of insulation on large high-voltage equipment. While the general feeling had developed, as a result of much of this testing, that d-c testing is less damaging to coil insulation than a-c testing, nevertheless, the relative influence of the d-c testing compared with a-c testing has not been very well known. No doubt, the final word has not yet been spoken in that connection, but the evidence presented in the paper appears to be much more conclusive than that offered in the past. Perhaps further investigation will lead even more directly to interpretation of the effects of d-c testing in terms of the ability of the insulation successfully to withstand a-c operating potentials.

The operators of large rotating equipment undoubtedly will welcome the information contained in this paper as a further step toward satisfactory testing of coil insulation. It is hoped that maintenance testing data from operating sources will prove out the ratio of direct to alternating voltages for best results in preventing machine outages through insulation failure. The suggested ratio of 1.6 should be tried where testing is indicated as advisable and careful collection of such data and results should prove to be valuable.

E. H. Tovee (Canadian Westinghouse Company, Limited, Hamilton, Ont., Can.): Mr. Moses' paper has provided very valuable and much-needed information on the relationship between a-c and d-c test values. For more than eight years d-c testing has been used by the Canadian Westinghouse Company in the testing of large generator windings.

Early in World War II the demands for

electric power became so great and the production of generator equipment was required so urgently that it became necessary to assemble and wind a large proportion of our generators in the field. In some cases, work was under way on the generators before there was even a roof on the power house. Under these conditions the transportation of testing transformers and the supply of enough power to operate these transformers became very difficult, and in 1942 Mr. H. H. Lang, our service department manager, introduced the use of d-c test equipment which was quite portable and required a very small amount of power. Not having the data which have now been made available by this paper, we used a factor of 1.4 times the alternating test voltage. No subsequent failure of ground insulation on any of these coils has yet been encountered except where mechanical damage or disturbance of the coil also were present.

A majority of the generators installed since 1942 have been tested with direct current; it was found that the direct current was very effective in weeding out any coils which had been damaged mechanically in shipment or assembly, and the excellent service record of these generators has indicated the effectiveness of the test in picking out such damaged coils. Since all coils receive an a-c test during manufacture, the main purpose of the final field test is, of course, to pick out damaged insulation.

We recently had, however, our first indication of the desirability of the factor of 1.6. Mechanical damage of a rather unusual type had been done to two coils in such a way that there apparently was a fair amount of good insulation left coupled with some creepage distance. These coils passed a d-c momentary test when being placed in the stator, but failed at 45 seconds and 50 seconds, respectively, on a final a-c test. Mr. Moses' paper indicates that these coils certainly would have been caught by a higher direct voltage; possibly a full-minute test at the 1.4 value also would have caught the defects.

Direct-current testing also has been found useful in the testing of metal-clad switchgear and other equipment.

Table I. One-Minute Over-Potential Test Voltage for A-C and D-C Armature Windings

	A-C (RMS) Test	D-C Test
New winding	$2E+1{,}000$	$3E+1{,}500$
Winding in service	$1^1/_3E+600$	$2E+1{,}000$

R. W. Wieseman (General Electric Company, Schenectady, N.Y.): This paper gives some interesting a-c and d-c dielectric strength data on several kinds of mica insulation obtained from samples and coils. From these data it is recommended that 1.6 be recognized as the ratio of the d-c and a-c rms 1-minute voltage test for mica windings of large machines. It also is proposed that the direct test voltage for mica windings in service should be 1.04 $(2E + 1{,}000)$.

In Figures 9 and 10 of the paper the ratio of the direct and alternating rms voltage strength of air varies from 1.1 for a 63-mil air space to about 1.66 for a 180-mil air space. Also, it is of interest to note that at an air space of 63 mils, the a-c peak is about 1 kv higher than that of the direct voltage.

The overpotential test for machines in service should be a conservative voltage which can be applied to all types of armature windings. From the viewpoint of surface creepage, an a-c winding with a long end portion is the least vulnerable, whereas a d-c winding is usually the most vulnerable. Since the surface creepage voltage strength depends somewhat on the foreign matter on the winding surface, on the length of the winding end portion, and on the voltage strength of air, the ratio of the direct and alternating rms 1-minute test voltage for all windings should be about 1.5 regardless of the voltage strength of the various components of winding insulation.

Since the 1-minute a-c proof test for new windings is the same for both a-c and d-c armature windings, it should be desirable to have the same test voltage for both a-c and d-c windings in service. On this basis, a simplified table of test voltages is recommended in Table I of this discussion.

The test voltages for windings in service, namely, the a-c rms test of $1^1/_3E + 600$ and the d-c test of $2E + 1{,}000$, have been published,[1] and they have been used for some time. It is of interest to note that the a-c proof test for new windings is the same as the d-c test for windings in service. This should be a desirable feature.

REFERENCE

1. MAINTENANCE OVER-POTENTIAL TESTS FOR ARMATURE WINDINGS IN SERVICE., R. W. Wiesman. *General Electric Review* (Schenectady, N. Y.), volume 53, number 8, August 1950, pages 24–28.

Graham Lee Moses: The response of various discussers is very gratifying. There appears to be reasonable agreement that the data presented contribute to a better understanding of some insulation problems associated with overpotential testing. No serious disagreements are evident in the tentative d-c to a-c test value ratios for equal searching effect. It is hoped that similar data will be reported in the future by others and that such experience will lead to recognition of d-c overpotential tests for certain applications.

Sealed Ignitron Rectifiers for Urban Transit Power Supply

DAVID W. BORST
ASSOCIATE AIEE

Synopsis: Today, the mercury arc rectifier has virtually superseded the older forms of conversion equipment for supplying power to trolley coach and street railway transit systems. The present trend when selecting a rectifier rated 1,000 kw or less is to choose the sealed ignitron type. The sealed ignitron rectifier is metal-enclosed, which makes possible a unit substation type of equipment when it is combined with metal-enclosed switchgear. This gives increased safety to personnel and a reduction in installation cost. A number of substation arrangements are possible, including installation of part or even all of the equipment outdoors in weatherproof enclosures, thus reducing building costs. Operating experience with close to 4,000 sealed ignitron tubes has demonstrated that they can be expected to have an average life of at least six years. Their 1-minute rating of 200 per cent load is more than adequate to handle an urban transit load composed of a number of small increments, where diversity serves to reduce the magnitude of peak swings. In keeping with the smaller equipment ratings possible with sealed ignitrons, light-duty switchgear has been introduced having the necessary current and interrupting ratings at lower initial cost. The high reliability of rectifiers makes it possible in many cases to install a single-unit substation where before two smaller conversion units would have been used. Operators are beginning to recognize this and to take advantage of the savings this accomplishes. Where larger concentrations of power are required than can be provided by a single 1,000-kw rectifier, two or more sealed ignitron rectifiers may be operated in parallel. Heavy-duty drawout metal-enclosed switchgear is available for such installations. If the ultimate bus capacity of the installation exceeds 2,250 kw, high-speed switchgear should be used to protect the rectifier transformers from excessive winding stresses during arc backs.

DURING THE past 20 years the mercury arc rectifier has been chosen more and more often as the conversion equipment for 600-volt urban transit substations, until today it has virtually superseded the motor-generator set and synchronous converter for this service. Higher efficiency at all loads, greater reliability, and adaptability to fully automatic unattended operation, together with lower installation and operating costs, have contributed to the great popularity of mercury arc rectifiers.

The earliest rectifiers used in the United States for transportation substations were the pumped multianode type, where the rectifying action takes place in a vacuum chamber containing 6 or 12 anodes, evacuated by a continuously operating pumping system. Later, the development of the ignitor method of cathode spot excitation made possible the introduction of the pumped ignitron rectifier composed of a number of vacuum chambers, each containing a single anode. This construction makes possible a rectifier which is easier to service, and also permits a significant reduction in the length of the mercury arc, thereby reducing the arc losses and improving the rectification efficiency.

The next logical step in reducing the complexity of the ignitron rectifier was to seal off the vacuum chamber and thereby eliminate the vacuum pumping system and its attendant maintenance problems. Permanently evacuated glass bulb multianode rectifiers have been built since the mercury arc rectifier was developed 50 years ago. However, the permanently evacuated rectifier did not gain popularity in the United States until the introduction in 1936 of the sealed ignitron rectifier tube with metal envelope. Because this tube is far stronger than the fragile glass bulb rectifier, and because each anode is contained in an individual envelope which can be replaced at less cost than a glass bulb with many anodes, the sealed ignitron rectifier has found wide acceptance for rectifiers of moderate size.

Paper 51-131, recommended by the AIEE Electronic Power Converters Committee and approved by the AIEE Technical Program Committee for presentation at the AIEE Winter General Meeting, New York, N. Y., January 22-26, 1951. Manuscript submitted July 12, 1950; made available for printing December 5, 1950.

DAVID W. BORST is with the General Electric Company, Schenectady, N. Y.

Sealed Ignitron Rectifiers

Sealed ignitron rectifiers are now available for use in 600-volt trolley coach and street railway substations in ratings up to 1,000 kw. These rectifiers offer several advantages over pumped ignitron rectifiers for this type of service, some of which are: lower equipment first cost; lower maintenance and operating cost; and metal-enclosed construction.

Metal-enclosed construction results in a unit-substation-type equipment having lower installation cost, reduced floor space requirements, and greater safety to operating and maintenance personnel. Metal-enclosed construction also makes possible the construction of sealed ignitron rectifiers in weatherproof enclosures for out-

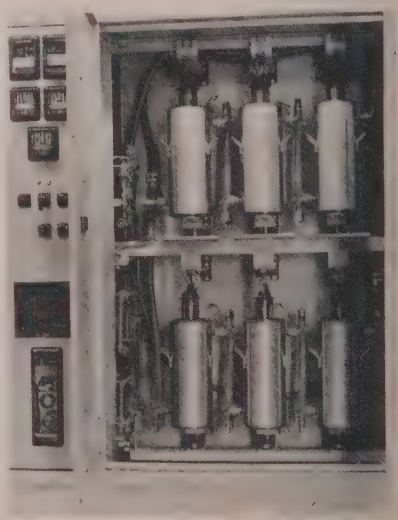

Figure 1. Sealed ignitron rectifier section rated 1,000 kw in 600-volt transportation service

Figure 2 (left). Unit d-c substation rated 500 kw having a-c switchgear, transformer, rectifier, and d-c switchgear

Figure 4 (right). Rear view of substation with two 1,000-kw rectifiers

door installation, thus eliminating entirely the cost of a substation building.

A rectifier unit employing six sealed ignitron tubes and rated 1,000 kw at 600 volts direct current in transportation service is shown in Figure 1. The tubes are installed in a metal enclosure which can be made part of a unit d-c substation. Such substations consist of units completely co-ordinated at the factory, and include all the materials required for interconnecting them during installation. This construction obviously shortens installation time and reduces installation costs.

Substation Arrangements

Of the various possible substation arrangements, the one usually considered basic is shown in Figure 2. This rectifier equipment, rated 500 kw, consists (left to right) of the a-c primary metal-clad switchgear, the rectifier transformer, the rectifier section, and, on the far right, the d-c switchgear and control section. These units are bolted together during installation to form a single metal-enclosed assembly, and all interconnecting power and control conductors are furnished by the manufacturer. The purchaser provides only the power circuits in and out, and the cooling water supply and drain connections.

D-c feeder circuit breakers usually are required, and these can be bolted directly to the d-c switchgear and control section. However, this results in a rather long and narrow assembly which does not always allow an economical building arrangement. A convenient way to rearrange the equipment is to locate the feeder switchgear separately from the rest of the equipment. This arrangement is shown in Figure 2; the feeder switchgear is the separate assembly shown in Figure 3.

Another possibility is to install portions of the equipment outdoors, as this reduces the size of the substation building. Figure 4 shows the rear of a substation that contains two 1,000-kw rectifiers. The rectifier transformers shown are connected to the rectifiers inside the building by bus ducts. One of the rectifiers is shown in Figure 5 and consists (left to right) of two feeder circuit breakers, a cathode circuit breaker, auxiliary control, and the 1,000-kw rectifier section shown in Figure 1. In an installation such as this one the primary a-c switchgear could be installed either inside or outside the substation building; in the particular substation shown an outdoor oil circuit breaker was selected.

Figure 6 shows another substation where both the rectifier transformer and the a-c switchgear are installed outdoors. In this case the alternating voltage is less than 15 kv, permitting the use of outdoor metal-clad switchgear. This is connected directly to the rectifier transformer, and a bus duct connects this to the rectifier. Figures 7 and 8 are photographs taken inside this substation. The rectifier is cooled by a water-to-air heat exchanger instead of by tap water, and the section on the right of the rectifier houses the cathode circuit breaker and control. The feeder circuit breakers are installed by themselves in another part of the building in order to make it of minimum size.

It is but a short step from the substation just shown to a substation employing equipment which is entirely weatherproof, thus eliminating the need for a substation building. Figure 9 shows a 1,000-kw rectifier constructed along this line. The arrangement of equipment here is similar to that in Figure 2. The section to the right of the rectifier is a water-to-air heat exchanger, and the unit on the right end contains most of the rectifier control equipment, including the control for the regenerative power-absorbing resistor mounted on the roof of the substation.

Figure 10 shows another installation of outdoor equipment, this one consisting of two 500-kw rectifier equipments.

Sealed Ignitron Performance

Since the sealed ignitron tube must be discarded when it no longer performs acceptably, tube life has an important

Figure 3 (left). Separate d-c feeder assembly for rectifier unit shown in Figure 2

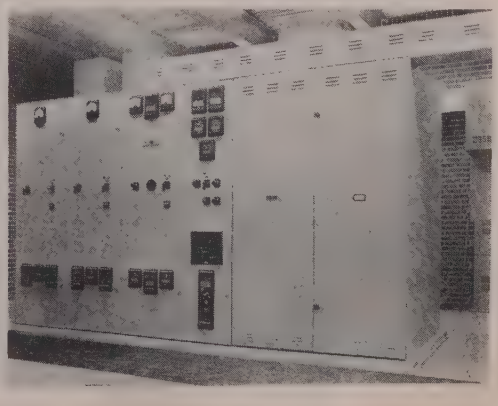

Figure 5 (right). One 1,000-kw rectifier, located in substation shown in Figure 4

Figure 6. Outdoor metal-clad switchgear and transformer for 1,000-kw rectifier

Figure 8 (center). Separate d-c feeder assembly for rectifier shown in Figure 7

Figure 9 (right). Outdoor weatherproof unit d-c substation rated 1,000 kw

bearing on the economy of a sealed ignitron rectifier installation. The tubes are constructed largely of stainless steel, glass being used only for the main anode insulator, and the smaller lead-in insulators for the ignitor and other control elements. Depending upon their rating, the tubes have a 2- or 3-year warranty period, and in addition a warranted 1-year shelf-life period.

Actually, the best indication of tube life expectancy can be obtained from field experience. Field experience with the largest sealed tube which is rated (nominally) 300 amperes now is entering its fourth year, and to date less than two per cent of the nearly 300 of these tubes which have been in service have failed. Tubes rated (nominally) 150 amperes and 75 amperes (at 600 volts direct current) have been used in increasing numbers during the past ten years until at present, in 1950, there are approximately 3,500 in service.

A comprehensive study of tube life conducted in 1948 revealed that of the tubes installed five years previously, more than half were still in service. The percentage of tubes still in service after a given period at that time is shown in Figure 11. Subsequent tube life experience and continual improvements in tube and equipment design now indicate that even better tube performance can be expected.

Based on the evidence so far available, it appears conservative to estimate that the average life of a sealed ignitron tube is in excess of six years.

Early pumped multianode rectifiers had a rating of 150 per cent for two hours and 200 per cent for one minute. Later, pumped rectifiers were improved to where they could be rated 300 per cent for one minute. Sealed ignitron tubes usually are applied so that sealed rectifier units are rated 200 per cent load for one minute. For trolley coach and street railway service this overload capacity is more than sufficient to handle the peak swings encountered, even during periods when the rectifier is carrying its rated 2-hour load of 150 per cent. The reason for this is that the load in urban transit service consists of a considerable number of small increments, only a few of which will be at their peak value at any given time. For example, Figure 12 is a diversity curve for trolley coaches showing the peak swings that are to be expected from various numbers of vehicles.[1] From this curve, which is based on measurements taken on several feeder circuits supplying trolley coaches, it is apparent that, as the number of coaches operating increases, the peak swings approach the average current required by the coaches, assuming the average power consumption of each coach is 55 kw.

Table I is based on these data and shows the maximum current to be expected at various sizes of substations when there is a sufficient number of coaches in operation to represent an average load equal to the 2-hour overload rating of the substation.

Another factor which favors the use of sealed ignitron rectifiers is the duration of these load swings, which usually is less than ten seconds. Thus, a 1-minute rating of 200 per cent load is more than adequate for the service conditions encountered in urban transit work.

Figure 7. Rectifier, heat exchanger, and d-c switchgear in substation shown in Figure 6

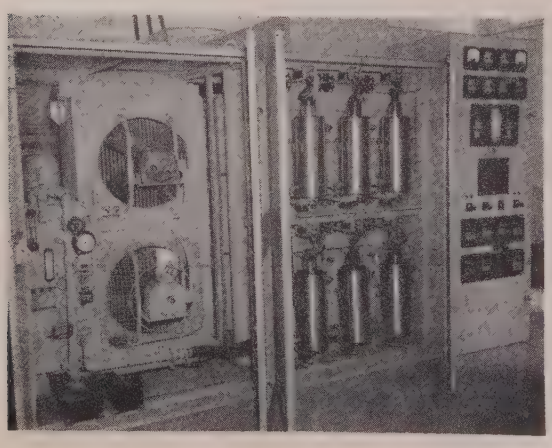

Figure 10. Installation with two 500-kw outdoor rectifiers

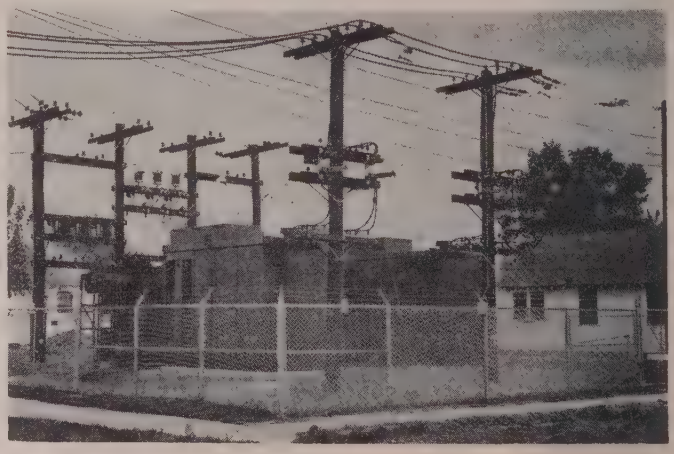

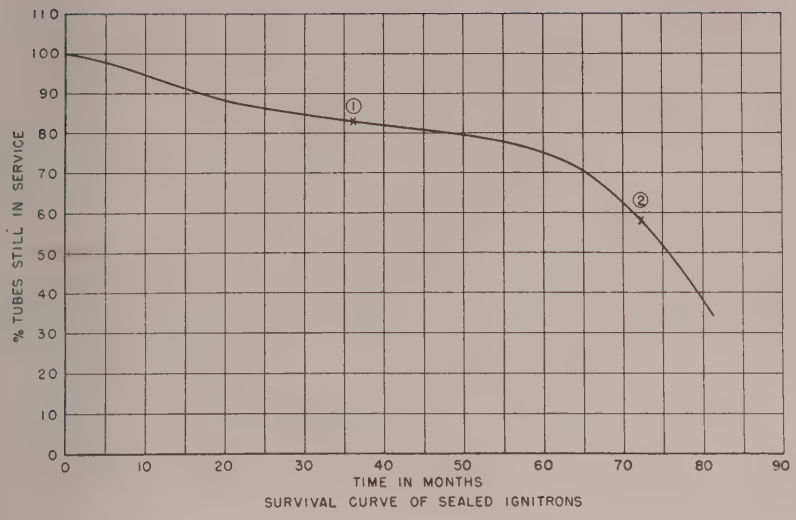

Figure 11 (left). Survival curve of sealed ignitrons

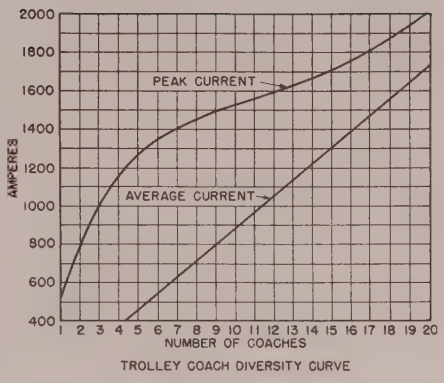

Figure 12 (above). Trolley coach diversity curve

Construction and Selection of D-C Switchgear

Several types of metal-enclosed d-c switchgear seen in the preceding illustrations will now be described more fully. The d-c switchgear shown in Figures 7 and 8 makes use of the familiar 2,000-ampere semi-high-speed d-c circuit breaker mounted in a fixed position in the rear and near the top of each switchgear unit. Recently this circuit breaker has been mounted on a truck, thereby giving it the added feature of drawout construction.

Figure 13 shows such a circuit breaker being inserted in its housing.

Drawout construction facilitates servicing the d-c circuit breaker, since a spare unit may be kept on hand and substituted for a circuit breaker which requires servicing. The d-c switchgear shown in Figure 5 is of the drawout type; the circuit breakers are removed from the side of the equipment opposite that shown in the illustration.

There is a field of application for metal-enclosed d-c switchgear having smaller current ratings and lower interrupting capacity than the heavy-duty switchgear just described, and light-duty switchgear has been developed for this purpose. The d-c switchgear shown in Figures 2 and 3 is of this type.

D-C Switchgear Enclosure Grounding

To minimize the damage from the occurrence of an accidental ground in metal-enclosed d-c switchgear where the negative conductor is grounded, as in most transportation systems, the enclosures for the rectifier and all d-c switchgear are designed to be insulated from ground but grounded through the coil of a ground fault detector relay. In the event of an accidental fault between a positive conductor and the enclosure, this relay is actuated and it instantly opens all d-c and a-c circuit breakers. This action, combined with the resistance of the relay coil, which limits the fault current, effectively prevents more than minor damage.

Single-Unit versus Multiple-Unit Substations

The high order of reliability of rectifiers now makes it possible in many cases to utilize single-unit substations, whereas heretofore two or more smaller conversion units would have been installed at each location. Operators are beginning to recognize this and to take advantage of the saving which results.

Where greater substation capacity than can be provided by a single unit is required, or where the very best reliability is required, two or more sealed ignitron rectifiers may be operated in parallel. In this event the choice of d-c switchgear is influenced by the total d-c bus capacity, heavy-duty switchgear being used in the larger substations, as in Figure 5. When the ultimate substation d-c bus capacity exceeds 2,250 kw (3,750 amperes) high-speed switchgear should be used for the rectifier. High-speed switchgear is required under these conditions to reduce the internal stresses in the rectifier transformers during arc backs, thereby avoiding premature transformer failures. Either high-speed anode or high-speed cathode switchgear may be used to pro-

Table I

Continuous Kilowatts	Substation Rating 150% 2 hours, Amperes	200% 1 minute, Amperes	Number of Coaches	Current Taken by Load Average	Peak
500	1,250	1,667	13	1,193	1,630
750	1,875	2,500	20	1,833	2,000
1,000	2,500	3,333	27	2,435	2,530

Figure 13. Metal-enclosed d-c switchgear with drawout circuit breaker

vide the required protection. In many instances substations larger than 2,000 kw are not required.

Conclusions

This paper has endeavored to show the present-day trend in rectifier substation equipment for urban transit power supply when the unit ratings are 1,000 kw and less. The trend appears to be toward sealed ignitron rectifiers of the unit substation type because of the lower equipment first cost and lower installation and operating costs, and the greater safety to operators and maintainers of this type of equipment. Light-duty, heavy-duty, and high-speed metal-enclosed switchgear is available for use with these rectifiers, the choice depending on the short-circuit capacity of the d-c bus. The high reliability of rectifiers makes feasible single-unit substations where before multiunit substations would have been considered necessary. However, rectifiers may be operated in parallel where larger concentrations of power are necessary. Should the ultimate substation d-c bus capacity exceed 2,250 kw, high-speed switchgear should be used for the rectifiers to minimize internal stresses in the rectifier transformers during arc backs; thereby premature transformer failures can be avoided.

Reference

1. Trolley Coach Distribution System, G. R. McDonald. *AIEE Transactions*, volume 67, part I, 1948, pages 393–402.

No Discussion

Probabilities of Interference Between Resistance Welders

W. K. BOICE
MEMBER AIEE

THIS paper presents calculated data concerning the probabilities that the voltage during a resistance weld will be inadequate because of voltage drops due to other welders. This information is useful for design of power systems for supplying groups of welders.

It is, of course, possible to design a power system so that voltage drop[1] is not excessive even when all machines weld at exactly the same time. However, in many cases, such a system would be more costly than necessary. For most types of welding operations, occasional bad welds are acceptable, if they do not occur too often. Usually, some spoilage is caused by nonelectrical causes, anyway, and a slight contribution to spoilage, as a result of infrequent occurrences of excessive drop, may be acceptable. When the number of welders is fairly large, and their duty cycles are low, simultaneous welding by all welders is extremely infrequent. A power system may be designed so that infrequent combinations of welders will cause excessive drop, but the vast majority of welds will be acceptable. Such a system will usually cost much less than one designed to maintain adequate voltage at all times.

This paper presents methods of checking whether or not there will be an excessive number of welds with inadequate voltage. This will aid in design of the most economical adequate power system for any particular case.

Also, by use of the information presented, the adequacy of existing systems can be ascertained, and proposed modifications evaluated.

This paper does not deal with the problem of light flicker nor with the problem of determining the rms current to a group of welders. As indicated in Appendix V, however, some of the basic probability data calculated for this paper may be used in applying previously presented formulas pertaining to these other problems.

Principal Conclusions

1. The probability of inadequate voltage, for any weld by a selected welder, increases with increases in: number of welders; duty cycle of any other welder on the system; weld time of any other welder on the system; voltage drop due to any other welder on the system.

2. It is important to have the following advance information about each welder, including possible future machines: allowance assigned to voltage drop due to combinations of other welders; proportion of welds which can be permitted to have inadequate voltage; and estimated demand, power factor, duty cycle, and weld time.

3. Cost savings obtainable, by permitting a small number of welds to have inadequate voltage, are particularly substantial when the number of welders is large and their duty cycles are small.

4. Single-phase welders on a single-phase system have a lower probability of interference than the same welders distributed on three phases of a 3-phase system, which has the same per cent impedance on selected base kilovolt-amperes, except when there are only two or three welders, each on a different phase.

5. Increasing the number of welds per welded part does not necessarily reduce the number of defective parts if the same production of parts per hour is maintained.

6. The probability data presented in this paper are applicable to a wide range of welding conditions, even when all welders have differing characteristics.

Effect of System Impedance

The cost of a power system ordinarily increases as the impedance decreases. Hence it is desirable to determine the maximum acceptable system impedance, in order to design for minimum cost. It is usually convenient to express the system impedance in per-unit on selected base kilovolt-amperage.

For preliminary calculations, the system impedance may be assumed to have a resistance-to-impedance ratio equal to the load power factor. In this case, the per-unit voltage drop equals the per-unit value of load current times the per-unit system impedance.

When the resistance-to-impedance ratio differs from the load power factor, voltage drop will be somewhat less, to an extent which may be calculated if necessary.

For preliminary calculations, it may be assumed that the system impedance is a single value common to all welders and that other circuit impedances are associated with individual welders only. When necessary to consider impedances which are common to only some of the welders, those welders which are tapped off at intermediate locations may be considered as being supplied through the entire system impedance, but to have correspondingly smaller demands, so that the circuit considered is simplified, but correct values of drops are used.

Any impedance which is only associated with one welder need not be considered, since allowance for the drop through this impedance can be made by upward adjustment of the welder heat setting.

Of course, it should be ascertained that the total drop will not prevent proper operation of the welder control, and will not reduce the welder maximum (full heat) output below the value needed for welding. However, this can usually be done conveniently after the system impedance has been determined.

Paper 51-137, recommended by the AIEE Electric Welding Committee and approved by the AIEE Technical Program Committee for presentation at the AIEE Winter General Meeting, New York, N. Y., January 22–26, 1951. Manuscript submitted October 24, 1950; made available for printing December 13, 1950.

W. K. Boice is with the General Electric Company, Schenectady, N. Y.

Selected Welder

The maximum acceptable system impedance may be different for different welders on the same system. Except for groups of welders which are exactly alike electrically, and which are similarly located on the system, it is advisable to consider each welder in turn, or at least to be certain that the welder considered is the one which requires the lowest system impedance.

When the probability of having inadequate voltage for any particular weld is being discussed in this paper, the welder making the weld is called the selected welder, and the data presented applies only to drops due to the other welders.

The inverse of the probability of inadequate voltage is the number of welds by the selected welder, for each one of its welds which has inadequate voltage. Hence when the probability of inadequate voltage is 0.001, one weld out of every 1,000 by the selected welder will have inadequate voltage.

It is of interest to note that the possibility of spoilage of several welds at the same time need not be considered. The total spoilage is determined by calculating the spoilage of one welder at a time, without including spoilage of any other welder until its time for consideration.

Welding Voltage

In order to determine the maximum acceptable system impedance, it is necessary to know the assigned allowance for voltage drops due to other welders. This allowance may be determined as follows, if not already established by experience.

1. Estimate the per-unit voltage drop which can be accepted without spoiling a weld of the material considered, under laboratory conditions, with new electrodes, and with current set at the maximum value for an acceptable weld.

2. Subtract an allowance for production welding conditions, such as spreading of electrode diameters after repeated use, inexact heat settings, minor changes in material.

3. Subtract an allowance for expected variations in supply voltage level. For example, a utility supply voltage level might vary appreciably during a day, unless primary line regulating equipment is provided.

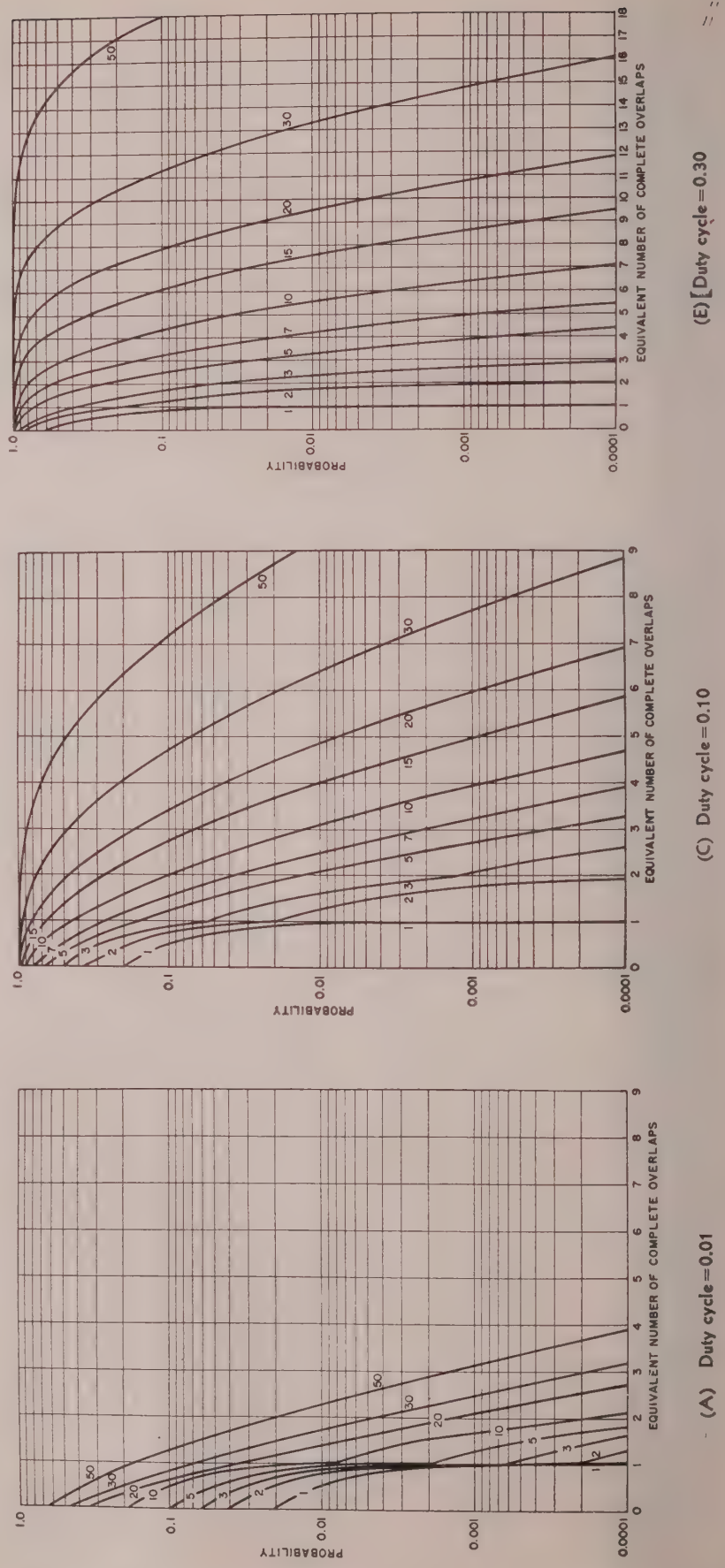

Figures 1(A)-(F). Probability that the sum of all overlaps will exceed a given equivalent number of complete overlaps

All welders have equal weld times of 3 cycles or more (Number on each curve is number of other welders)

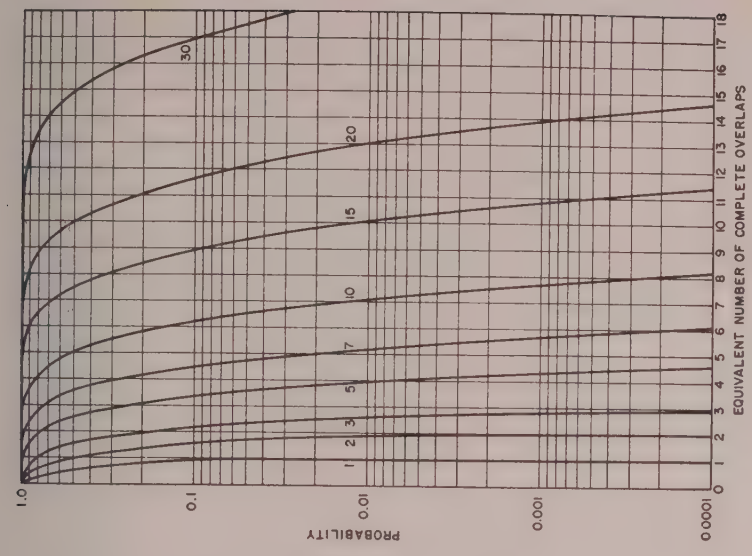

(F) Duty cycle = 0.50

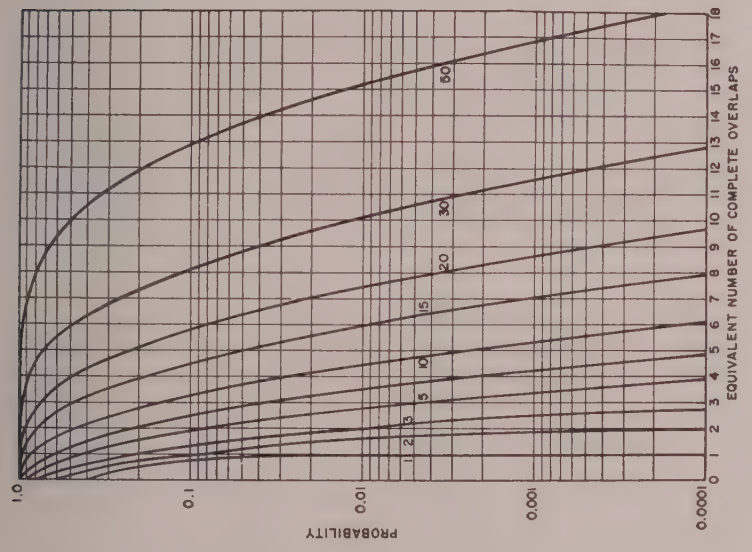

(D) Duty cycle = 0.20

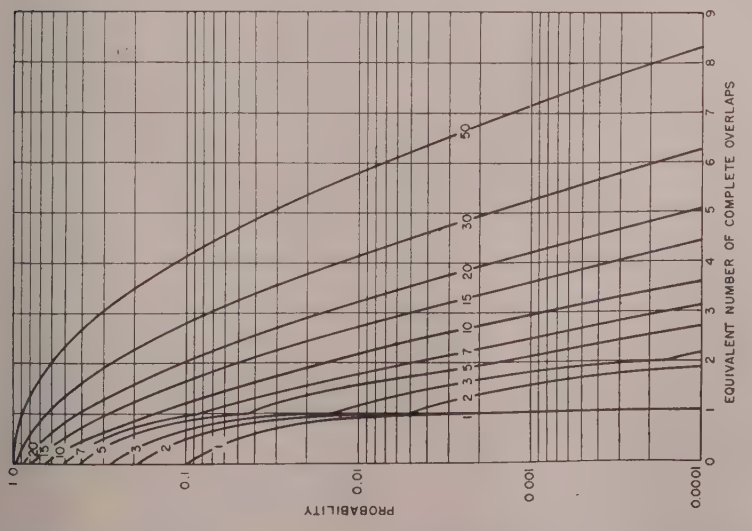

(B) Duty cycle = 0.05

If voltage compensating equipment is included with the welder control, this allowance is unnecessary, since the compensating equipment can easily follow such slow changes as usually occur on a supply system. (For weld times over two or three cycles, it will also partially follow voltage changes due to welders.)

Voltage drops through the system impedance, which are caused by loads other than welders, may be treated as being due to a welder with a high duty cycle, and a very long weld time. If the voltage drop due to these other loads can be estimated, however, using an estimated system impedance, this drop may be considered as another allowance to be subtracted in obtaining the assigned allowance for drops due to welders.

The assigned allowance may be exceeded, but not too frequently. The system should be designed so that it will be exceeded, but only so often that the number of welds with inadequate voltage is not excessive. This number should be somewhat less than the number of bad welds which can be accepted, because some welds will be spoiled by nonelectrical causes. It is apparent that the system designer must know in advance the proportion of welds which may be permitted to have inadequate voltage.

In this paper, the voltage during a weld is considered inadequate if its rms value over the complete weld time is below the minimum voltage for an acceptable weld. However the voltage may dip below this value during portions of a weld, if it is sufficiently above it during the remainder of the weld.

Assumptions

When the voltage drop is a small fraction of the total voltage, the rms voltage over a weld time is nearly equal to the rms no-load voltage minus the average drop (average value, over the weld time of the rms voltage drop). Calculated data presented in this paper are based on average drop, which will be very slightly more than the rms drop.

This practice greatly simplified the calculations and introduced a slight margin of safety.

Any drop in voltage at a welder tends to reduce the current, so that the drop in voltage is slightly less than it would be if the current were maintained. Thus when several welders operate together their total drop is slightly less than the sum of the drops which would be occasioned by each operating separately. The slight difference was neglected, to simplify the calculations made. This introduces an additional margin of safety which is

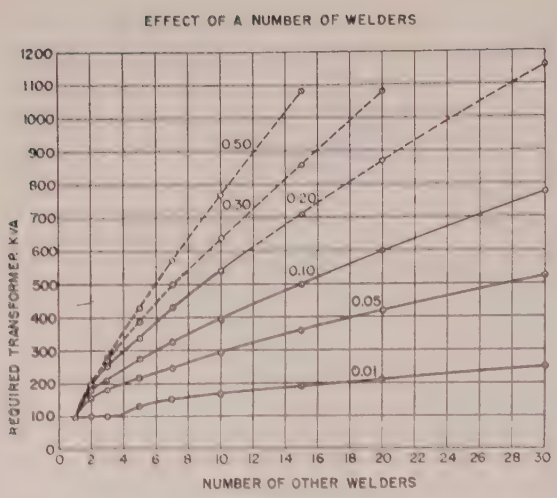

Number on curves are duty cycles

Figure 2 (left). Effect of number of welders

Figure 3 (right). Effect of duty cycle of welders other than the selected welder

Assigned allowance for drops due to other welders = 10% voltage drop. Proportion of welds with greater average drop = 1/1,000; demand of each welder = 200 kva. All welders have equal weld times of 3 cycles or more. System impedance = 5% on transformer kva. System is single-phase.

Note: For case illustrated, kva rating required for continuously carrying rms load of welders exceeds values given on dashed portions of curves

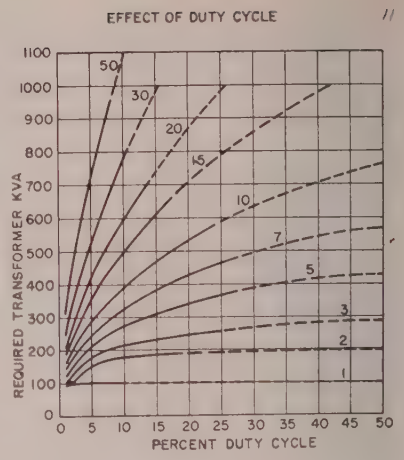

Number on each curve is total number of other welders

roughly proportional to the drop. For example, the margin of safety is in the order of one per cent voltage when the total average drop is 10 per cent. If desired, such an estimate of the margin can be added to the assigned allowance.

The possible spoilage of welds due to incorrect control operation has been neglected. It is considered unlikely that the voltage will fall low enough to cause the control to operate in a seriously wrong manner, without also spoiling the weld due to lack of welding voltage. A voltage drop of more than 10 per cent of rated control voltage if at an unfavorable time during the weld interval might cause a slight variation in weld time. The heat to a weld is proportional to the time, but to the square of the weld voltage. Hence a substantial reduction in weld time would be required to reduce weld heat any more than would an average drop equal to the assigned allowance.

When all welders have the same weld time, and this is three cycles or more, it is assumed that a partial overlap can be any fraction. Actually it can only have certain values (such as a fraction formed by an integral number of cycles divided by

Figure 4. Probability that the sum of all overlaps will exceed a given number of complete overlaps

Selected welder has much shorter weld time than other welders (or all welders have one-cycle weld time). Number on each curve is number of other welders

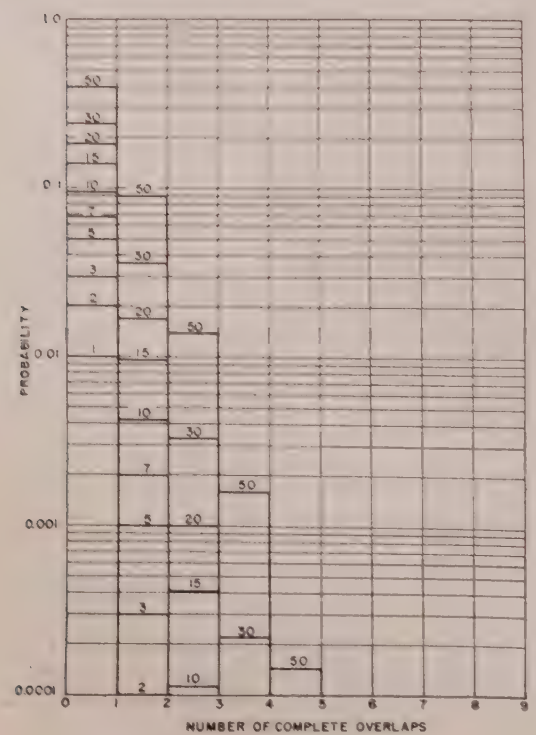

(A) left. Duty cycle = 0.01

(B) right. Duty cycle = 0.05

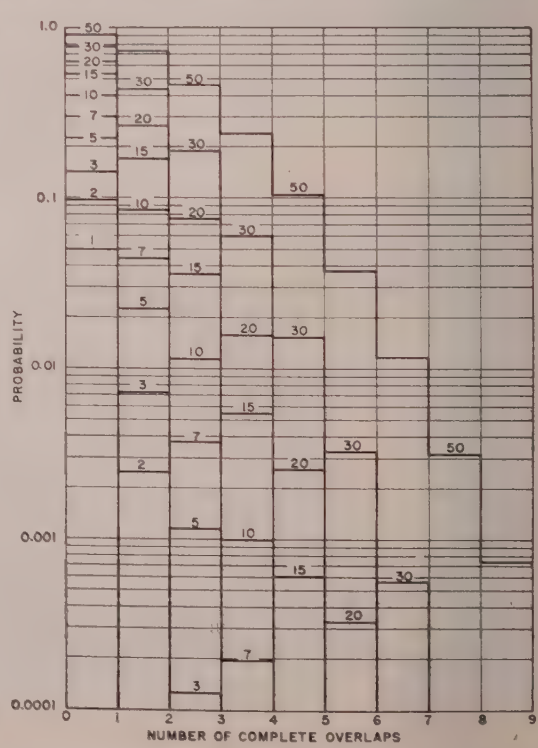

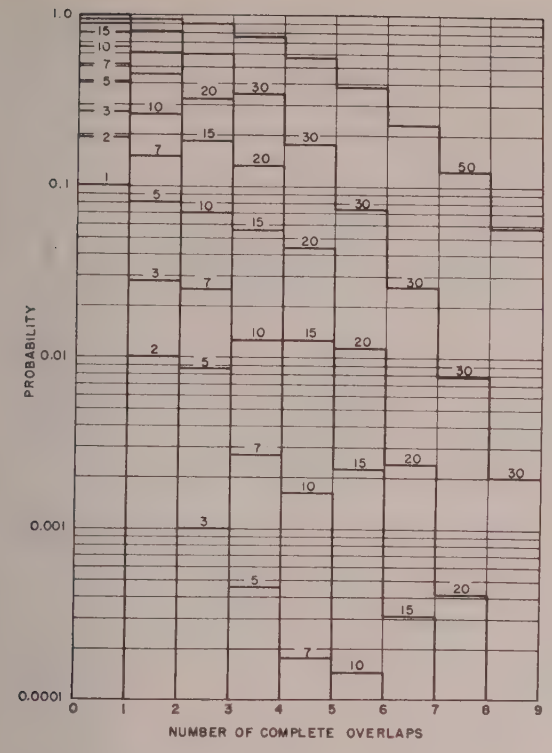

(C) left. Duty cycle = 0.10

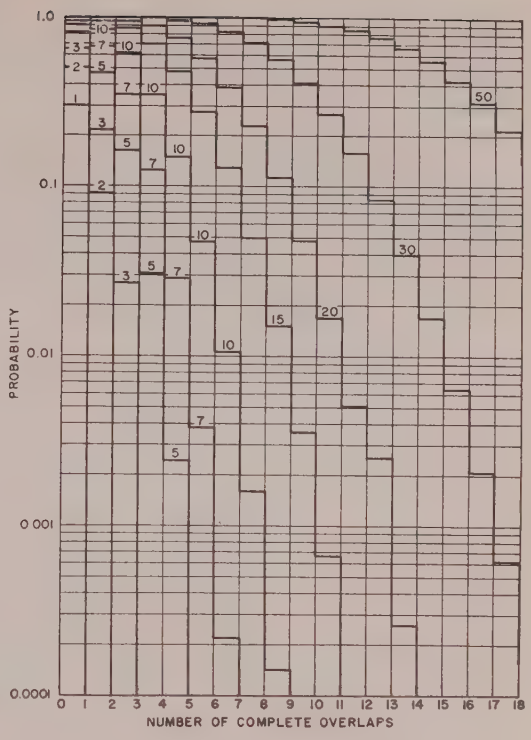

(E) right. Duty cycle = 0.30

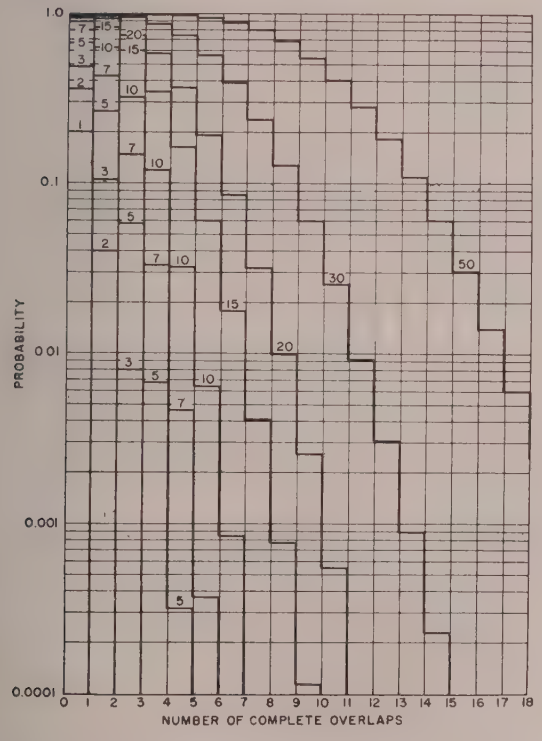

(D) left. Duty cycle = 0.20

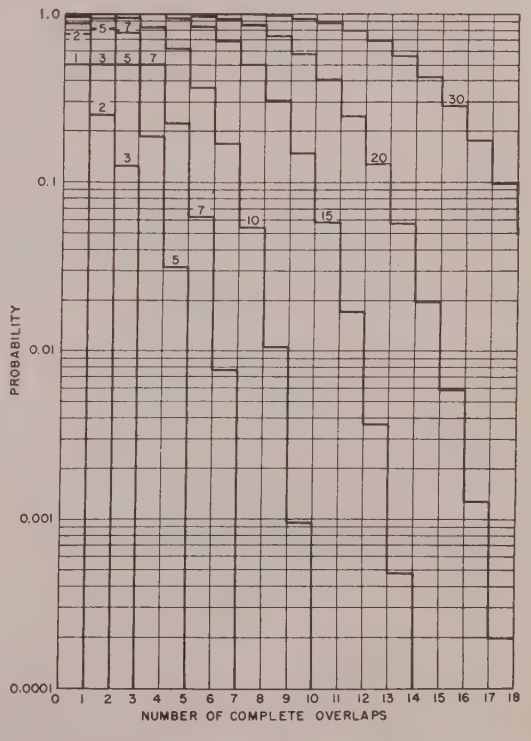

(F) right. Duty cycle = 0.50

Figure 4 (Continued)

the total number of cycles of the weld time). However as explained in Appendix II, this assumption does not introduce serious errors, and does simplify the calculation of the probabilities involved.

It is assumed that interlocking between welders is not used.

Probability Data

When each voltage drop which can be imposed on the selected welder by each other welder is the same, the total drop of a group, averaged over one weld time may be conveniently expressed in units of the drop of one welder. This may be called the equivalent number of complete overlaps. This may vary from zero to the total number of other welders, and may have fractional as well as integer values.

The curves of Figure 1 show probability

of being exceeded plotted against this equivalent number, for several values of duty cycle, and for various numbers of similar welders in a group.

For any selected probability, the equivalent number shown on the curve indicates the number of welders for which allowance must be made in selecting system impedance.

In every particular case, there is a certain equivalent number of complete overlaps for which the probability of being exceeded equals the allowable proportion of welds with inadequate voltage. This equivalent number times the current of one welder will cause a drop just equal to the assigned allowance when the system impedance is at its maximum acceptable value.

For example, if there are 31 identical welders at 0.05 duty cycle on a single-phase system, we may use the curve on Figure 1(B) marked 30 (for 30 other welders). If the allowable proportion of welds with inadequate voltage is 1/200 we may use the point on this curve at a probability of 0.005. This point corresponds to an equivalent number of 4.5 complete overlaps. The system impedance should therefore be sufficiently low so that 4.5 times the current of one welder cannot cause enough drop to spoil a weld.

When the actual system impedance is known in advance, as with an existing system, the probability of inadequate voltage may be determined. This is the probability corresponding to that equivalent number which will just cause the assigned voltage drop to be exceeded.

For example, suppose there are 11 identical welders at 0.01 duty cycle, each of which causes 5 per cent drop on a particular system, and the assigned allowance for drops due to the ten other welders is 10 per cent. From Figure 1(A), at an equivalent number of 2 on the curve marked 10 we find a probability of 0.00016. Hence one in 6,250 welds of each welder will have inadequate voltage.

The probability values for the curves were calculated by methods described in the appendixes of this paper.

Number of Welders

As the number of welders increases, the number for which allowance must be made also increases. However, it does not increase as rapidly as the number of welders. This is illustrated by Figure 2, which shows that with a large number of welders only a small fraction of them need be allowed for in selecting system impedance.

A method described in Appendix IV may be used when the number of welders exceeds 50.

Duty Cycle

A group of welders with high duty cycle requires a lower system impedance than a similar group with a lower duty cycle. This is illustrated by Figure 3. It should be noted, however, that the probabilities are not affected by the duty cycle of the selected welder, since the probabilities calculated apply to any one weld of this welder.

When several welders have equal voltage drops, but different duty cycles, an average duty cycle may be used, with reasonably good accuracy. This may be calculated by means of the following formula.

$$d_{avg} = \frac{d_1 + d_2 + d_3 + \ldots . d_n}{n} \qquad (1)$$

where

d_{avg} = average duty cycle
$d_1, d_2 \ldots d_n$ = duty cycles of each other welder
n = number of other welders

Weld Time

The curves of Figure 1 are for the case when all welders have the same weld time. When the selected machine has a longer weld time than the other machines, no one of them can completely overlap the selected machine. Hence the maximum possible average drop is decreased proportionately; and the probability of exceeding any given equivalent number of complete overlaps also is decreased.

When the weld time of the selected machine is less than that of the others, there are several relative starting times for each other welder, which will result in complete overlap. Hence the probability of a given average drop is increased somewhat.

When the weld times of the other machines are very much longer than that of the selected machine, almost all overlaps are complete ones, and calculation of the associated probabilities is simplified.

The probability of exceeding a given number of overlaps is then as shown in Figure 4.

At points for which the number of overlaps of Figure 4 is an integer, each curve is a vertical line section. The lowest probability on this line is the probability of being exceeded. The highest is the probability of being equalled or exceeded.

Further discussion of weld time is given in Appendix II.

Figure 5 (below). Comparison of single-phase and 3-phase systems

Assigned allowance for drops due to other welders = 10% voltage drop. Proportion of welds with greater average drop = 1/1,000. All welders single-phase, duty cycle = 0.05. Demand of each welder = 200 kva. All welders have equal weld times of 3 cycles or more. System impedance = 5% on total transformer kva. Welders distributed on phases when supply is three-phase. Voltage drop due to any welder on another phase assumed 1/4 the drop due to similar welder on the same phase as the selected welder. Third, sixth, ninth, twelfth, and so forth, other welder is on same phase as selected welder

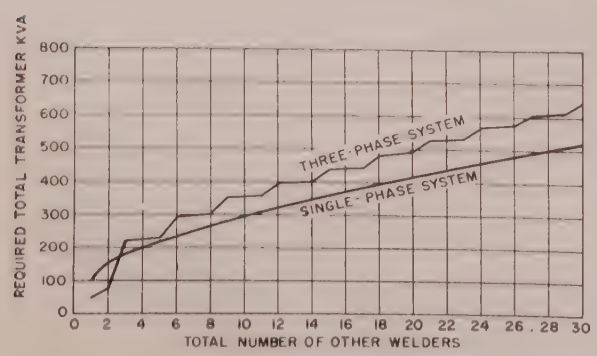

Figure 6 (right). Possible relative operating times of selected welder and one other welder

Weld time = 3 cycles
Duty cycle = 1/3

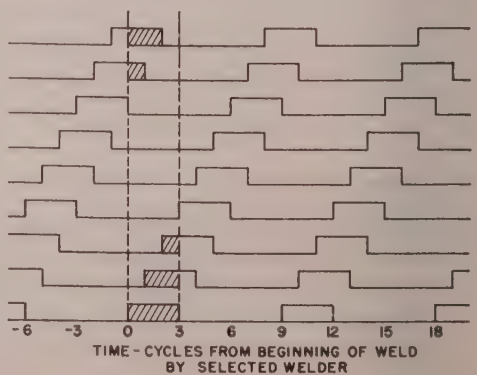

Relative Magnitude of Welder Demands

When the voltage drops due to the other welders are not all alike, calculation of precise probability values tends to become quite complex. However, an approximation may be used which gives satisfactory results in most cases. This consists of using the same assumed voltage drop and assumed duty cycle, for all other welders, these assumed values being chosen in a suitable way. For the actual number of welders involved and the assumed duty cycle, approximate probabilities may be found from Figures 1 or 4. It is suggested that Figure 1 be used unless the weld time of the selected welder is considerably shorter than those of most of the other welders.

For cases for which Figure 1 applies and all duty cycles are 0.5 or less, the assumed voltage drop is:

$$V=\left(\frac{3}{2}\right)\frac{(A^2+B^2)}{B} \tag{2}$$

where

$$A^2=\frac{d_1\left(\frac{2}{3}-d_1\right)V_1^2+\ldots d_n\left(\frac{2}{3}-d_n\right)Vn^2}{n} \tag{3}$$

$$B=\frac{d_1V_1+d_2V_2+\ldots d_nV_n}{n} \tag{4}$$

The subscripts refer to the other welders. As before, n is the number of other welders. The corresponding assumed duty cycle is:

$$d=\left(\frac{2}{3}\right)\frac{B^2}{(A^2+B^2)} \tag{5}$$

When Figure 4 applies, the coefficients (2/3) and (3/2) in the expressions for A^2, V, and d should be replaced by unity. Further discussion of the assumed values is given in Appendix IV.

Number of Phases

The curves of Figures 1 and 4 may be used for 1-phase welders on a 1-phase system, 1-phase welders all on one phase of a 3-phase system, or 3-phase welders on a 3-phase system.

When 1-phase welders are distributed on three phases of a 3-phase system, the voltage drops[1] due to welders on other phases than that of the selected welder will be less than for similar welders on the same phase. In rare cases there will be a voltage rise due to welders on other phases. For preliminary calculations, it is suggested that all welders on other phases be assumed to produce drops equal to one-fourth the values for similar welders on the same phase. By using this suggestion, and the approximate method described in the foregoing, Figure 5 was constructed. This figure compares use of single-phase welders on a single-phase system with the same welders distributed on a 3-phase system.

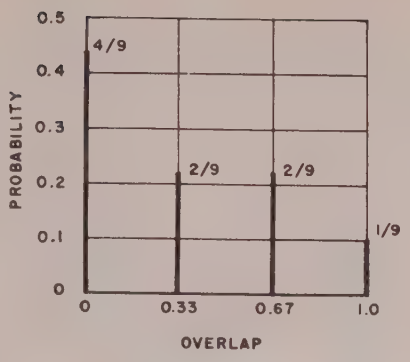

Figure 7. Probability distribution for overlap of selected welder by one other welder

Weld time = 3 cycles
Duty cycle = 1/3

Parts Having Several Welds

When a part to be welded has several welds, one or more of these welds may have inadequate voltage. For some parts, such as gastight seam welded tanks or tubes, one bad weld will spoil the entire part. By making the conservative assumption that every bad weld spoils a different part, the spoilage rate of parts can be estimated. It is then equal to the weld spoilage rate multiplied by the number of welds per part.

If more than one bad weld in succession is required to spoil a part, the number of parts spoiled by a given number of welders at a given duty cycle is greatly reduced. In this case, the spoilage rate (probability of a bad weld) may be multiplied by itself a number of times equal to the number of bad welds required to spoil a part; then this result should be multiplied by the total number of welds per part, as before, to determine the rate of spoilage of parts.

In order to weld so that one bad weld will not spoil a part, the duty cycle must be much higher than otherwise, to maintain the same production of parts per hour. The increased duty cycle increases the probability of overlapping welds so much that little, if any, increase in system impedance is ordinarily permissible. If the increased duty cycle does not, however, affect the spoilage rate due to nonelectrical causes, its use may be found advantageous in particular cases.

Appendix I. Probability Distribution for a Sum

The probability distribution[2] for a variable quantity may be expressed in terms of probability density.

Let u be a variable quantity, and $(y_1)u$ be the probability density of u_1 at $u_1=u$.

By definition, $(y_1)u\,du$ be the probability that u_1 lies between u and $(u+du)$ and $\int_{U_1}^{\infty}(y_1)u\,du$ be the probability that u_1 equals or exceeds U_1.

When there is a finite probability that u_1 exactly equals any certain value U_1, then y_1 is infinite at this point. However, at this same point

$$(y_1)_u du = P_1 = \text{probability that } u_1 = U_1$$

and integration for the probability that u_1 equals or exceeds U_1 is still valid.

Consider an additional variable u_2 with the probability density y_2, and let us determine the probability density y_s applying to the sum u_s of u_1 and u_2.

By definition of u_s

$$u_2=(u_s-u_1) \tag{6}$$

For any selected value of u_1, the probability that u will be between u and $(u+du)$ is[2] the product of the probability $(y_1)_u du$ times the probability $(y_2)_u du$. The total probability $(y_s)_u du$ is the sum of all of such products for all values of u_1.

This sum is

$$(y_s)_u du=[\int_{-\infty}^{\infty}(y_2)_u(y_1)_{(u_s-u)}du]du \tag{7}$$

so the density

$$(y_s)_u=\int^{\infty}(y_1)_u(y_2)_{(u_2-u)}du \tag{8}$$

By analogous reasoning, we also have

$$(y_s)u_s=\int_{-\infty}^{\infty}(y_2)_u(y_1)_{(u_s-u)}du \tag{9}$$

That is, it does not matter in what order the components of the total probability $(y_s)_u du$ are added.

When the probability distribution for the sum of several variables is desired, it may be obtained by successive use of equations 8 or 9. For example, the probability density for the sum u_t of u_1, u_2, and u_3 is

$$(y_t)_u=\int_{-\infty}^{\infty}(y_s)_u(y_3)_{(u_t-u)}\,du \tag{10}$$

Dr. H. Poritsky has pointed out that it is often convenient to express such probability equations in operational form. Let L_1 be the Laplace[3] transform of y_1, and so forth. Then from equation 8 or 9 and a table[3] of transform-function pairs

$$L_s=L_1L_2 \tag{11}$$

Similarly from equation 10

$$L_t=L_1L_2L_3 \text{ and so forth} \tag{12}$$

Another useful characteristic of the probability of the sum of independent variables is that the mean value of the sum is

$$a_s=a_1+a_2+a_3 \tag{13}$$

Also, the standard[2] deviation of such a sum is

$$\sigma_t=\sqrt{\sigma_1^2+\sigma_2^2+\sigma_3^2} \tag{14}$$

Appendix II. Probability Distribution for Overlap by One Welder

Possible relative operating times of one other welder with respect to a selected welder are illustrated by Figure 6. In the case shown, the weld time is 3 cycles and the duty cycle is 1/3.

Figure 7 shows the possible values of equivalent number of welders (a fraction), u, and the probability associated with each value. Figure 8 shows the probability of equalling or exceeding any given value of u. The dashed line shows the form this type of curve approaches as the number of cycles of weld time increases. Figure 9 shows the probability density curve for the dashed line of Figure 8. This curve is used for all cases involving equal weld times of 3 cycles or more.

The operational[3] expression for Figure 9 is

$$L_u=(1-2d)+\frac{2d}{s}(1-\epsilon^{-s}) \qquad (15)$$

where s is the Laplace operator.

When all weld times are 1 cycle, u can only equal one or zero, and the probability of equalling one is equal to the duty cycle d.

If all weld times are 2 cycles, approximate results may be obtained by interpolation between cases for 1 and for 3 or more cycles.

When the weld time of the selected welder is much smaller than those of the other welders, nearly all overlaps are complete,

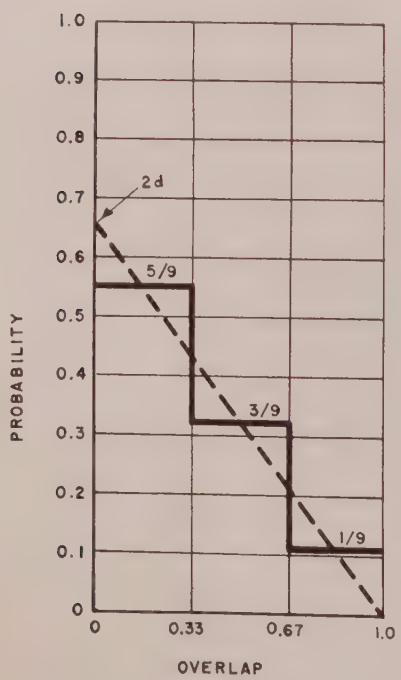

Figure 8. Probability that overlap by one welder will exceed a given amount

Weld time = 3 cycles
Duty cycle = 1/3
Dashed curve is approached as weld time increases

and the probability distribution is similar to the case for all weld times being one cycle. The operational expression for this distribution is

$$L_u=(1-d)+de^{-s} \qquad (16)$$

The preceding discussion assumes that weld times are always in units of one cycle (as with synchronous control) and that both weld times begin with the same polarity of line voltage.

If the weld times are in units of one cycle but begin with different polarities, interference probabilities will be somewhat less than if both welders begin with the same polarity. With half cycle controls (of fixed polarity) interference can occur only between machines connected for the same polarity.

With nonsynchronous control, polarity considerations are not significant, and weld times can be considered to be in units of one half cycle.

The probability distribution for any type or combination of types of control can be developed as shown for equations 15 and 16. In most cases, one or the other of these equations will provide a satisfactory approximation to the actual distribution.

The mean value, a, of deviation, u, for any other welder is equal to its maximum value (unity) times the duty cycle. The standard deviation from this mean is given by the following formulas.

For the distribution of equation 15,

$$\sigma=\sqrt{d\left(\frac{2}{3}-d\right)} \qquad (17)$$

For the distribution of equation 16,

$$\sigma=\sqrt{d(1-d)} \qquad (18)$$

Appendix III. Probability Distribution for Groups of Welders

From Appendix II, the probability distribution for u resulting from a group o several welders is

$$L_g=(L_u)^n \qquad (19)$$

Where n is the number of other welders (in addition to the selected welder)

From equations 15 and 19, for the case of equal weld times of three cycles or more

$$L_g=\left[(1-2d)+\frac{2d}{s}(1-\epsilon^{-s})\right]^n \qquad (20)$$

The transform L_g' for the probability of equalling or exceeding u is obtained by integration of equation 20 from u to infinity. Integration from 0 to u can be accomplished by dividing a Laplace transform by s. The integral from zero to infinity is unity, since this range includes all possible values of u. Hence the probability of equalling or exceeding u is:

$$L_g'=\left(1-\frac{L_g}{s}\right) \qquad (21)$$

The binominal theorem may be applied twice to equation 20. From equations 20 and 21

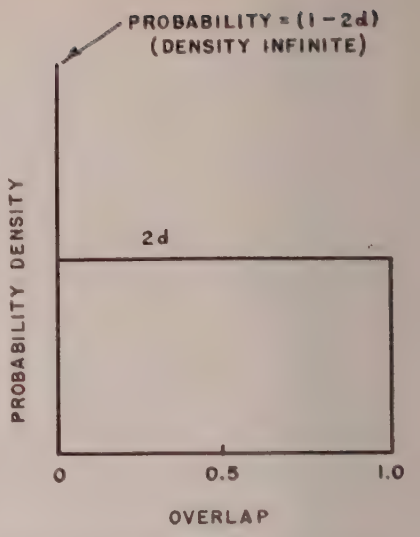

Figure 9. Probability density for overlap by one welder

(Approximate curve for weld times of 3 cycles or more)
Duty cycle = d

$$L_g'=\left[1-\frac{1}{s}\sum_{r=0}^{r=n}P_r\left(\frac{1}{s}\right)^r\times\sum_{v=0}^{v=r}{}_rC_v(-1)^v\epsilon^{-vs}\right] \qquad (22)$$

where

$$P_r={}_nC_n(1-h)^{n-r}(h)^r \qquad (23)$$

$$h=2d \qquad (24)$$

$${}_rC_n=\frac{n!}{r!(n-r)!} \qquad (25)$$

$${}_rC_v=\frac{r!}{v!(r-v)!} \qquad (26)$$

Applying a table of transform-functions airs to equation 22 yields

$$P=1-\sum_{r=0}^{r=n}P_r\left(\frac{1}{r}\right)\times\sum_{v=0}^{v=r}{}_rC_v(-1)^v z^v \qquad (27)$$

where

$$z=(u-v) \text{ for } v\leq u \qquad (28)$$

and $z=0$ for $v\geq u$.

Tabulated values of the binominal coefficients,[4] ${}_nC_r$, and the Bernoullian probability,[5] P_r are available. (The method of finding values of P_r is shown in Appendix V.)

Values of P for Figure 1 were calculated from equation 27 by a punched-card calculating machine.

For the cases for which equation 16 is applicable, we have the following, by similar analysis, for integral values of u (the equivalent number of overlapping welders).

$$P = \sum_{r=u}^{r=n} P_r \qquad (29)$$

where

$$h = d \qquad (30)$$

Calculated values for this case are presented by Figure 4.

Appendix IV. Selection of Approximate Probability Curves

Equations 2 to 5 presented in this paper for the voltage drop and duty cycle which may be assumed to apply to each of a group of welders, which actually have various drops and duty cycles, permit selection of a curve from Figure 1 or Figure 4 which corresponds approximately to the actual probability distribution, because it has the same mean value and the same standard[2] deviation. A slightly closer approximation might be obtained by using a different number of other welders so that the maximum possible deviations of the curves selected correspond to those of the actual case. In this case, an inversely proportionate change in assumed duty cycle should accompany the change in number of other welders. This refinement could be supplemented by modifying the voltage drop and duty cycle of each welder so that the mean and standard deviations of its contribution to voltage drop were unchanged but were based on the assumption of equal weld times for all welders.

The accuracy of the approximations described increase with number of welders and with increases in duty cycles. When more conservative results can be obtained by considering only one complete overlap by the welder with the largest drop, this overlap alone should be used as a preferable basis for estimates.

For a number of welders considerably greater than 50, and duty cycles over 0.05, closely approximate probability data can be obtained by assuming a normal[6] probability distribution having the same mean and standard deviations as for the actual case.

Appendix V. Evaluation of P_r

P_r is the probability[2] of exactly r successes out of n trials, when the probability of success in one trial is h. It is identically equal to the rth coefficient of the MacLaurin (algebraic power) series for

$$[(1-h)+h]^n$$

It has been shown[7] that this coefficient may be obtained from "Tables of the Incomplete Beta Function."[8] The use of these tables was suggested by the Bell Telephone Laboratories.

Values of P_r may be taken from Figure 2 by subtracting the smaller from the larger of the values shown at the extremes of the vertical line at the value of u equal to r for the value of d equal to h.

The probability P_r has many uses. In addition to its use in this paper, it is applicable to formulas for the rms current[9] due to a group of welders, and for study of light flicker[10] due to welders.

References

1. Voltage Changes Due to Resistance Welding Loads, **I. B. Johnson, H. A. Peterson, C. M. Rhoades, Jr.** *AIEE Transactions*, volume 66, 1947, pages 664–73.

2. Introduction to Mathematical Probability (book), **J. V. Upensky.** McGraw-Hill Book Company, New York, N. Y., 1937.

3. Transients in Linear Systems, (book), **M. F. Gardner, J. L. Barnes.** John Wiley and Sons, New York, N. Y., 1942.

4. Probability and Its Engineering Uses (book), **T. C. Fry.** D. Van Nostrand and Company, New York, N. Y., 1928.

5. Higher Mathematics for Engineers and Physicists (book), **I. S. Sokolnikoff.** McGraw-Hill Book Company, New York, N. Y., 1941.

6. Handbook of Engineering Fundamentals (book), **O. W. Eschbach.** John Wiley and Sons, New York, N. Y., 1936.

7. Notes on the Relationship of the Incomplete β-Function to the Sum of the First p Terms of Binominal $(a + b)^n$, **Karl Pearson.** *Biometrika*, University College (London, England), volume XVI, 1924, pages 202–03.

8. Tables of the Incomplete Beta Function, **Karl Pearson** (Editor). Biometrika Office, University College, London, England, 1934.

9. The Design of Low Voltage Welding Power Distribution, **C. A. Adams, J. R. Fetcher, A. C. Johnson.** *AIEE Transactions*, volume 63, 1944, pages 1180–90.

10. A New Approach to Probability Problems in Electrical Engineering, **H. A. Adler, K. W. Miller.** *AIEE Transactions*, volume 65, 1946, pages 630–32.

No Discussion

Welding Calculations—Effect of Conductor Configuration in Overhead Lines

H. WATSON TIETZE
MEMBER AIEE

ELECTRICAL calculations involving open-wire construction with flat conductor configuration on crossarms generally assume triangular spacing of conductors and utilize conductor constants based on the equivalent triangular spacing. In voltage dip problems involving single-phase welders, significant errors can be avoided by using circuit constants which allow for the changes in reactance of conductors due to the interaction of phase currents.

Discussion

Because resistance welding machines have high instantaneous and repetitive demands at low power factor, they raise problems of voltage dip and light flicker. It is necessary, therefore, to determine by calculation in advance of installation the effect of these instantaneous demands upon the electric distribution system.

Once the engineer has a clear understanding of the nature of single-phase load supplied from a 3-phase system, the computations are not difficult. Computation methods have been devised which require application of only the simpler mathematical operations of multiplication and addition once circuit constants have been determined.

It is in this latter element of the computation process, selection of circuit constants, that large errors are possible. Such errors may cause penalty to both the user of the welder and to the power company. The user, because of the magnitude of the voltage flicker or dip calculated, may be required to purchase a series capacitor for the machine, or to finance a costly extension of utility lines, or to radically restrict welding demand and hence the usefulness of the machine. The utility, on the other hand, may lose the prospective customer and the revenue which would be derived from the operation of the customer's supplementary motors and plant lighting, or may find itself faced with an expensive reinforcement not indicated by the erroneously calculated effects of the welding load.

In most voltage regulation computations it is assumed that open-wire circuits are arranged with the conductors at the vertices of an equilateral triangle, and, moreover, that a balanced polyphase load is being supplied. Both assumptions are fallacious when applied to welding loads. Circuits are as a rule arranged with flat configuration on horizontal crossarms, and a single-phase load will not result in balanced currents on a polyphase supply system.

Computation of Constants

The correct solution lies in the application of the general formulas expressing the effect upon the reactance and resistance of a conductor of the presence of adjacent loaded conductors. These formulas are:

$$S_A = S_{AB}^{-i_{BA}} \times S_{AC}^{-i_{CA}} \times S_{AN}^{-i_{NA}} \quad (1)$$

$$S_B = S_{BA}^{-i_{AB}} \times S_{BC}^{-i_{CB}} \times S_{BN}^{-i_{NB}} \quad (2)$$

$$C_C = S_{CA}^{-i_{AC}} \times S_{CB}^{-i_{BC}} \times S_{CN}^{-i_{NC}} \quad (3)$$

$$R_{gA} = R_A + 0.0528 (i_{BA}' \log_{10} S_{AB} + i_{CA}' \log_{10} S_{AC} + i_{NA}' \log_{10} S_{AN}) \quad (4)$$

$$R_{gB} = R_B + 0.0528 (i_{AB}' \log_{10} S_{BA} + i_{CB}' \log_{10} S_{BC} + i_{NB}' \log_{10} S_{BN}) \quad (5)$$

$$R_{gC} = R_C + 0.0528 (i_{AC}' \log_{10} S_{CA} + i_{BC}' \log_{10} S_{CB} + i_{NC}' \log_{10} S_{CN}) \quad (6)$$

where

$$I_B/I_A = i_{BA} + j i_{BA}', \; I_C/I_A = i_{CA} + j i_{CA}', \text{ and so forth} \quad (7)$$

In equations 1, 2, and 3, S_{AB}, S_{AC}, and so forth are the physical separations in inches of phases A and B, phases A and C, and so forth; the exponents, defined by equation 7, are factors expressing the ratios of the appropriate phase currents,

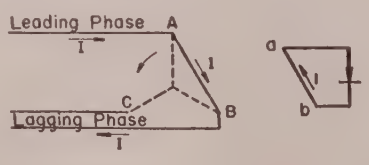

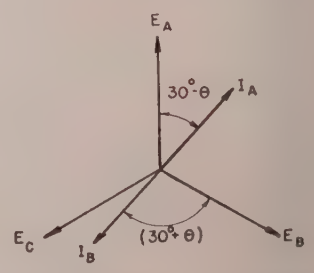

For 30% power factor load $30° - \theta = 42° 30'$ lag
$30° + \theta = 102° 30'$ lag

Figure 1. Vectors for single-phase load connected phase-to-phase

Paper 51-138, recommended by the AIEE Electric Welding Committee and approved by the Technical Program Committee for presentation at the AIEE Winter General Meeting, New York, N. Y., January 22–26, 1951. Manuscript submitted October 24, 1950; made available for printing December 18, 1950.

H. WATSON TIETZE is with Public Service Electric and Gas Company, Newark, N. J.

Table I. True Line Reactance for Open-Wire Circuits

Single-Phase Load on 3-Phase System, Ohms Per Thousand Feet of Conductor

Configuration*	Wire Size	Load Served Through Y-Delta Transformation: Aφ Loaded Aφ	Aφ Loaded Bφ	Aφ Loaded Cφ	Bφ Loaded Aφ	Bφ Loaded Bφ	Bφ Loaded Cφ	Cφ Loaded Aφ	Cφ Loaded Bφ	Cφ Loaded Cφ
1	4	0.1401	0.0809	0.1648	0.0771	0.1379	0.1524	0.2020	0.1947	0.1586
	2/0	0.1257	0.0665	0.1505	0.0627	0.1235	0.1381	0.1862	0.1779	0.1443
	4/0	0.1204	0.0632	0.1452	0.0574	0.1182	0.1328	0.1810	0.1727	0.1390
2	4	0.1479	0.1189	0.1699	0.1098	0.1434	0.1423	0.1869	0.1678	0.1561
	2/0	0.1335	0.1045	0.1555	0.0954	0.1290	0.1280	0.1702	0.1534	0.1418
	4/0	0.1282	0.0992	0.1502	0.0901	0.1237	0.1227	0.1674	0.1481	0.1365
3	4	0.1272	0.1194	0.1511	0.1032	0.1194	0.1032	0.1511	0.1194	0.1272
	2/0	0.1127	0.1049	0.1367	0.0888	0.1049	0.0888	0.1367	0.1049	0.1127
	4/0	0.1077	0.0996	0.1314	0.0835	0.0996	0.0835	0.1314	0.0996	0.1077

Configuration*	Wire Size	Load Served by Phase-to-Phase Transformer: Load A to B Aφ	Load A to B Bφ	Load A to C Aφ	Load A to C Cφ	Load B to C Bφ	Load B to C Cφ
1	4	0.1194	0.1194	0.1606	0.1606	0.1565	0.1565
	2/0	0.1049	0.1049	0.1463	0.1463	0.1422	0.1422
	4/0	0.0996	0.0996	0.1410	0.1410	0.1369	0.1369
2	4	0.1352	0.1352	0.1606	0.1606	0.1515	0.1515
	2/0	0.1208	0.1208	0.1463	0.1463	0.1373	0.1373
	4/0	0.1155	0.1155	0.1410	0.1410	0.1320	0.1320
3	4	0.1194	0.1194	0.1352	0.1352	0.1194	0.1194
	2/0	0.1049	0.1049	0.1208	0.1208	0.1049	0.1049
	4/0	0.0996	0.0996	0.1155	0.1155	0.0996	0.0996

* From Figure 4.

and S_A, S_B, and S_C are the resulting true equivalent spacings in inches from which the true reactance of each phase wire can be determined by referring to standard reactance tables.

In equations 4, 5, and 6 conductor spacings and current ratio factors are similar to those in equations 1, 2, and 3; R_A is the conductor resistance as given in standard resistance tables, and $R_{\varphi A}$ is the resulting true resistance in ohms.

These equations appear formidable, but their application is not difficult. It will be shown that the first three can be greatly simplified, and that the equations for resistance may be neglected when dealing with single-phase loads connected phase-to-phase and Y-delta.

Figures 1 and 2 are vector diagrams of current and voltage relations on the primary supply circuit when feeding a single-phase load respectively from two phases of a 3-phase system and from a 3-phase system through a Y-delta transformer bank. The formulas are applied as follows. Assume a circuit with 2/0 conductor arranged as shown in Figure 3, Configuration 1, with the single-phase load supplied through a Y-delta bank as in Figure 2. Referring to Figure 2, assume $\boldsymbol{I}_A$ as the reference vector and assign arbitrary current values of $\boldsymbol{I}_A=2$ $\boldsymbol{I}_B=\boldsymbol{I}_C=1$ since $\boldsymbol{I}_B$ and $\boldsymbol{I}_C$ are equal to one-half of $\boldsymbol{I}_A$.

$$\frac{\boldsymbol{I}_B}{\boldsymbol{I}_A}=\frac{1/180^\circ}{2/0^\circ}=-0.5+j0=i_{BA}+ji_{BA}'$$

$$\frac{\boldsymbol{I}_C}{\boldsymbol{I}_A}=\frac{1/180^\circ}{2/0^\circ}=-0.5+j0=i_{CA}+ji_{CA}'$$

$$S_A=S_{AB}^{-i_{BA}}\times S_{AC}^{-i_{CA}}$$
$$=(14.5)^{1/2}\times(88)^{1/2}=35.8 \text{ inch true equivalent spacing}$$

$\therefore X_A=0.1257$ ohms/1,000 feet (from standard reactance tables)

$$R_{\varphi A}=R_A+0.0528(i_{BA}'\log_{10}S_{AB}+i_{CA}'\log_{10}S_{AC})$$

but $i_{BA}'=0$ and $i_{CA}'=0$

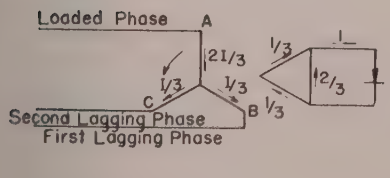

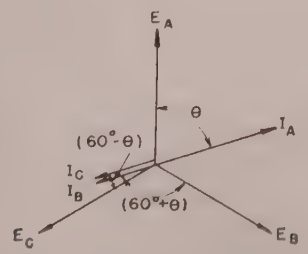

For 30% power factor load $\theta = 72°-30'$ lag

$(60°+\theta) = 132°-30'$ lag

$(60°-\theta) = 12°-30'$ lag

Figure 2. Vectors for single-phase load supplied by Y-delta transformer bank

Table II. Comparative Reactance Constants in Per Cent of Equivalent Triangular Spacing Values Configuration Number 1–2/0 Wire

	Per Cent Ohms Per 1,000 Feet Aφ	Bφ	Cφ
Equivalent triangular spacing (45.4")	100	100	100
Wye-delta connection			
"Loaded" phase—A	95	51	115
"Loaded" phase—B	48	94	105
"Loaded" phase—C	142	136	110
Phase-to-phase connection			
Load between A and B	80	80	
Load between A and C	112		112
Load between B and C		109	109

$\therefore R_{\varphi A}=R_A=0.0821$ ohms/1,000 feet (from standard resistance tables)

It will be noted that the resistance is unchanged from the normal value. This will be found to be true for each phase conductor where the single-phase load is connected phase-to-phase (Figure 1) or Y-delta (Figure 2).

For ready reference and ease of application equations 1, 2, and 3 have been simplified by making the vector substitutions based on Figures 1 and 2. These simplified equations are shown in subsequent paragraphs.

With the load connected phase to phase:

Load A to B:

$$S_A=S_B=S_{AB} \tag{8}$$

Load B to C:

$$S_B=S_C=S_{BC} \tag{9}$$

Load C to A:

$$S_C=S_A=S_{AC} \tag{10}$$

Equations 8, 9, and 10 therefore state in mathematical symbols the fact that for phase-to-phase loads the true equivalent

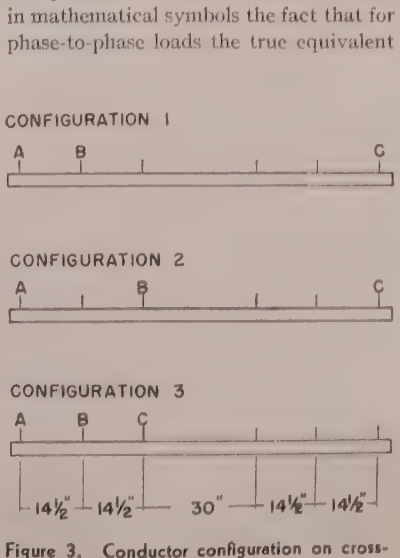

Figure 3. Conductor configuration on crossarm

spacing is equal to the distance between the two phase conductors.

With the load connected through Y-delta bank:

When A is "loaded" phase

$$S_A = (S_{AB})^{1/2} \times (S_{AC})^{1/2} \quad (11)$$

$$S_B = (S_{AB})^{2} \times (S_{CB})^{-1} \quad (12)$$

$$S_C = (S_{AC})^{2} \times (S_{BC})^{-1} \quad (13)$$

When B is "loaded" phase

$$S_A = (S_{AB})^{2} \times (S_{AC})^{-1} \quad (14)$$

$$S_B = (S_{AB})^{1/2} \times (S_{CB})^{1/2} \quad (15)$$

$$S_C = (S_{AC})^{-1} \times (S_{BC})^{2} \quad (16)$$

When C is "loaded" phase

$$S_A = (S_{AB})^{-1} \times (S_{AC})^{2} \quad (17)$$

$$S_B = (S_{AB})^{-1} \times (S_{CB})^{2} \quad (18)$$

$$S_C = (S_{AC})^{1/2} \times (S_{BC})^{1/2} \quad (19)$$

The marked variation in reactance resulting from the application of these equations can be observed in Table I, where there are tabulated the true values for three wire sizes and for the three conductor configurations shown in Figure 3. In the case of the Y-delta connection, values are given assuming in turn each phase as the "loaded" phase. Moreover, the constants given are equally applicable to single-phase loads on 3-phase systems utilizing other transformer connections which result in the primary-current vector relations of Figures 1 and 2.

In Table II there are compared the true reactance values of Table I with the normally-assumed equivalent triangular-spacing constants. This table shows that the error in assuming the latter values may be as great as 52 per cent.

Conclusion

It is not contended that the error in the computed voltage dip will be as great as 52 per cent. That will depend upon the proportion of open-wire reactance to system reactance at the point of connection to the open wire. The conclusion, however, can be drawn that the proper evaluation of the magnitude of the voltage dip in single-phase welding problems requires recognition of the changes in reactance of conductors, disposed on a horizontal crossarm, due to the interaction of the phase currents.

References

1. A Simple Method of Calculating the Voltage Drop in Overhead Lines, **E. S. Seeley.** *The Electric Journal* (East Pittsburgh, Pa.), February 1929, pages 73–76.

2. Transformer Engineering (book), **L. F. Blume, G. Camilli, A. Boyajian, V. M. Montsinger.** John Wiley and Sons, Inc., New York, N. Y., chapter VII, 1938.

3. A Cooperative Approach to Power Supply for Resistance Welding, **H. Watson Tietze.** *Electrical Engineering*, volume 66, July 1947, pages 657–62.

No Discussion

A-C Arc Welders with Saturable Reactor Control

S. OESTREICHER
ASSOCIATE AIEE

A STANDARD transformer is built for nearly constant load voltage for all load currents in its usable, or recommended, output range. A welding transformer must provide a drooping characteristic, as shown in Figure 1. Starting from the open circuit, or no-load voltage, the terminal voltage drops rather fast with increasing load current. The short-circuit current is only slightly higher than the load current for each output setting. In other words, a welding transformer is a limited output device.

Analyzing the load characteristic shows that the starting point, or no-load voltage, of the load characteristic is of importance for the design. A few words about this value, therefore, might be of interest.

Neglecting the magnetizing current, the primary or line current of a transformer can be expressed as:

$$I_1 = I_2 \times \frac{E_{\text{secondary no load}}}{E_{\text{primary}}} \qquad (1)$$

where

I_1 = primary winding current
I_2 = secondary winding or load current
E = voltage

The current in the primary winding is in direct proportion to the value of the open-circuit voltage. The most economical design, as far as the manufacturer is concerned, therefore, is the design with the lowest no-load voltage. A low open-circuit voltage, furthermore, reduces the shock hazard to the operator. These reasons explain the trend of lowering the open-circuit voltage as far as satisfactory welding performance will allow. A picture of the interrelationship of open-circuit voltage, arc voltage, and welding current will help to clarify the importance of the value of the open-circuit voltage on actual welding performance (Figure 2). Between the open-circuit voltage or voltage of the secondary winding of the transformer and the arc voltage exists a considerable phase shift. The arc voltage and the welding current are in phase. For a simple (and simplified) analysis the oscillogram has been redrawn and marked accordingly (Figure 3). The main difference between Figure 2 and Figure 3 is the substitution of a sine wave for the more or less square wave of the arc voltage of the oscillogram.

Whenever the welding current passes through zero the available voltage for restriking the welding arc is given by:

$$E_{\text{restriking}} = 1.41 \times E_{\text{secondary no load}} \times \sin \phi \qquad (2)$$

If we express the desired value of the "restriking voltage" as a multiple K of the amplitude of the arc voltage, we have:

$$1.41 \times E_{\text{secondary no load}} \times \sin \phi = K \times 1.41 \times E_{\text{arc}} \qquad (3)$$

Expressing the kilovolt-ampere input and the kilowatt output of the machine with values of equation 1 we find that:

$$\cos \phi = \frac{E_{\text{arc}} \times I_2}{E_{\text{primary}} \times I_2 \times \frac{E_{\text{secondary no load}}}{E_{\text{primary}}}} = \frac{E_{\text{arc}}}{E_{\text{secondary no load}}} \qquad (4)$$

Consequently, equation 3 can be re written:

$$\sin \phi = K \times \cos \phi \qquad (5)$$

The open-circuit voltage for any desired restriking voltage and arc voltage, therefore, is calculated easily from equations 3 and 5.

The tabulation of Figure 4 gives the corresponding values for $K = 1$, $K = 1.5$, and $K = 2$.

$K = 1$ represents the condition where the restriking voltage is equal to the amplitude of the arc voltage. The designer generally will hesitate before choosing open-circuit voltages below these values.

$K = 1.5$ gives values that provide satisfactory welding performance for most applications.

$K = 2$ or even higher is chosen quite frequently for arc welding machines for automatic welding or "high voltage" electrodes.

These figures should not be used without considering the actual requirements

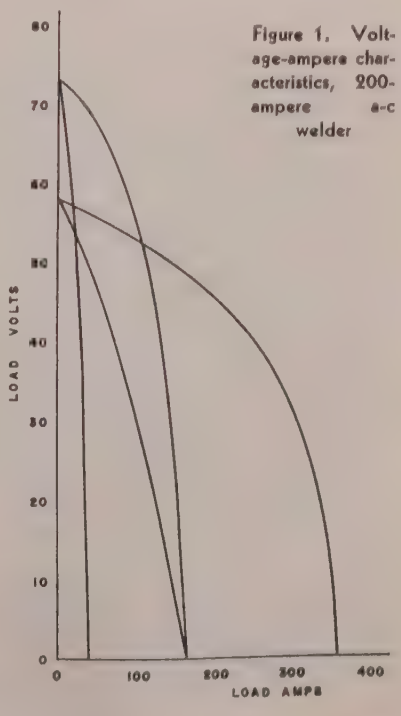

Figure 1. Voltage-ampere characteristics, 200-ampere a-c welder

Paper 51-139, recommended by the AIEE Electric Welding Committee and approved by the AIEE Technical Program Committee for presentation at the AIEE Winter General Meeting, New York, N. Y., January 22–26, 1951. Manuscript submitted October 24, 1950; made available for printing December 13, 1950.

S. OESTREICHER is with the Harnischfeger Corporation, Milwaukee, Wis.

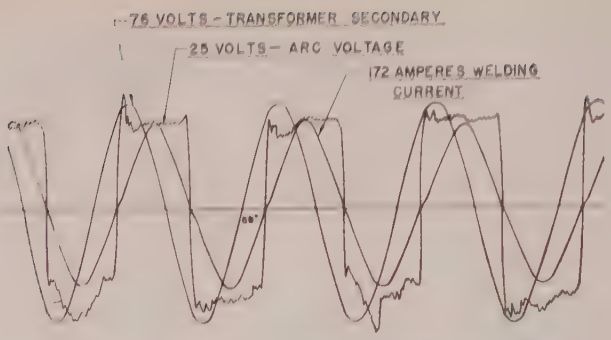

Figure 2. Welding oscillogram, 200-ampere a-c welder

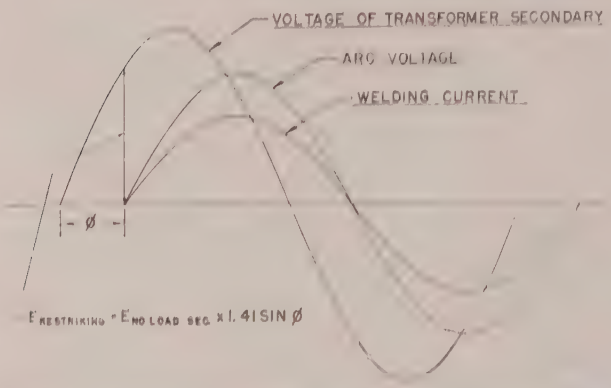

Figure 3. Relationship of secondary voltage to arc voltage and welding current

	K=1		K=1.5		K=2	
E_{ARC} VOLT	30	40	30	40	30	40
$E_{RESTRIK}$ VOLT	424	565	637	846	848	113
$E_{SEC.NL.}$ VOLT	424	565	54	72	67	89.5
Ø	45°		56°		634°	
COS Ø	.707		.55		.447	
SIN Ø	.707		.83		.894	

Figure 4. Relationship between arc voltage, restriking voltage, and no-load voltage for various values of K

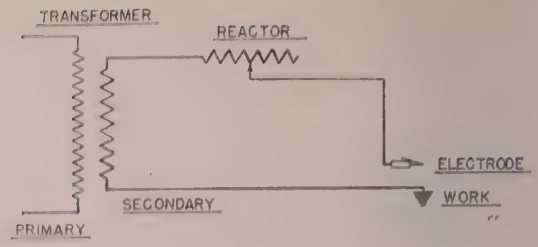

Figure 5. Schematic connection diagram of welder with reactor

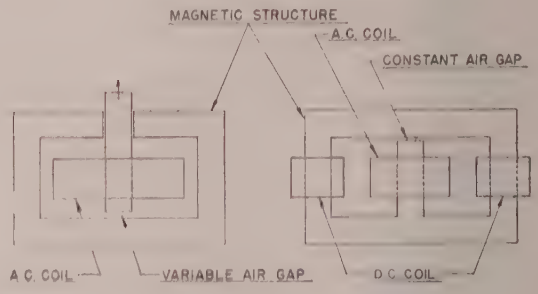

Figure 6. Two types of reactor construction

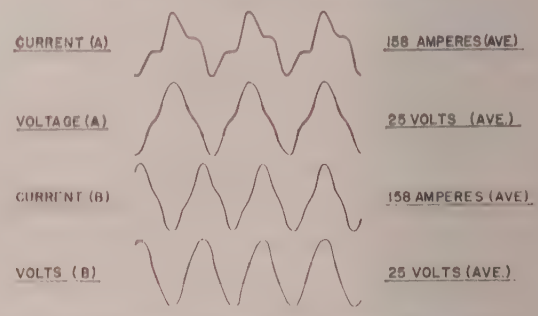

Figure 7. Current and voltage wave forms of 300-ampere welder

A. No air gap in the control reactor
B. 50-mil gap in the control reactor

of different electrodes, applications, and additional design features of the welding machine itself. They are intended mainly as an example of how a design engineer must examine all values that are reflected in the performance and economy of his product.

Many a-c arc welding transformers are built with a loose and variable "magnetic linkage" between the primary and secondary winding. Others use a variable reactor in the output circuit in order to provide the required drooping characteristic and the desired output regulation.

Figure 5 shows the principal connection diagram of a transformer reactor combination. The voltage drop across the reactor coil and the arc voltage add up vectorially to the voltage of the secondary winding of the transformer. Under short-circuit conditions, that is, when striking an arc, the reactor voltage is equal and opposed to the transformer voltage. The reactor voltage can be expressed as:

$$E_{reactor} = C \times T^2 \times S \times \mu \times I$$

where

C = constant value
T = number of turns of the reactor coil
S = cross section of the magnetic core
μ = magnetic conductivity or "permeability"
I = load current in amperes

Equation 6 indicates that any change in the magnetic conductivity, μ, of the structure must be accompanied by a corresponding (inverse) change of the load current to produce the required voltage drop, E reactor. A high value of μ demands a low current value, and vice versa.

Figure 6 shows the principal arrangements of reactors which are used for the purpose of limiting and regulating the output of a-c arc welding machines. The reactor with a mechanically movable center leg varies the permeability of the structure by varying an air gap in the flux path. The reactor with d-c control coils, or saturable reactor, varies the magnetic conductivity of the structure by varying its d-c premagnetization.

The magnetic characteristic, or magnetizing curve, of the structure naturally is reflected in the wave shape of the load current. Figure 7(*A*) shows the load current of a conventional reactor. The pronounced third harmonic creates a prolonged "near zero" current period. The detrimental influence of this current wave shape on welding performance is obvious. The reactors used with a-c welders, therefore, are built with a certain air gap at

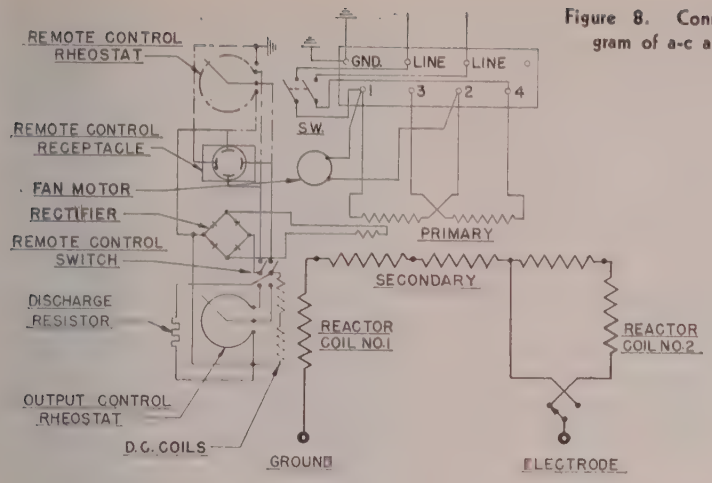

Figure 8. Connection diagram of a-c arc welder

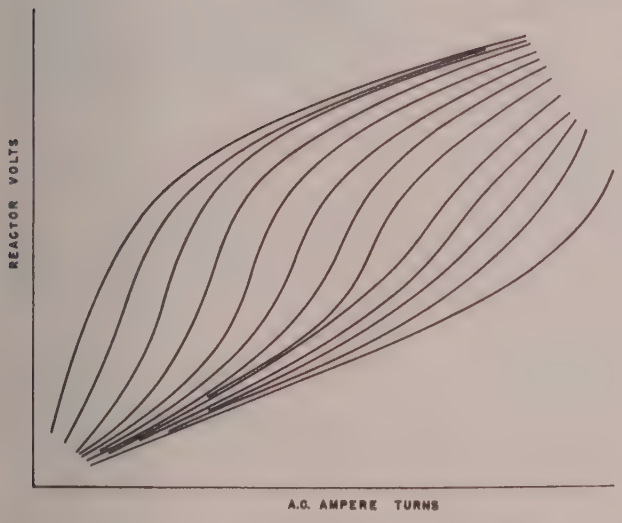

Figure 9 (left). Magnetization curves of saturable reactor for various values of premagnetization

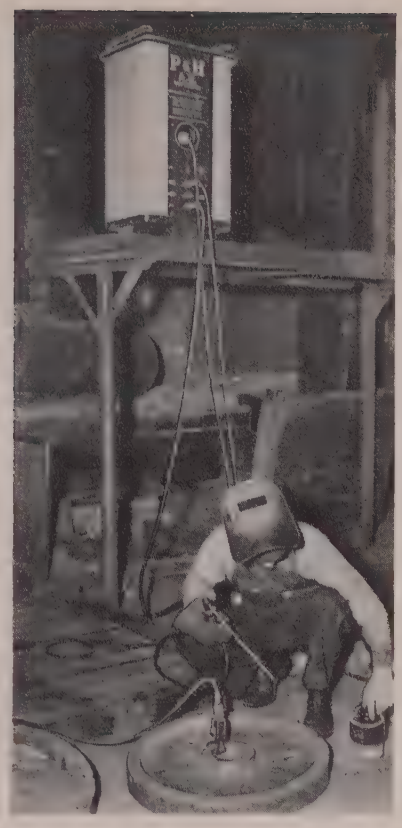

Figure 10 (right). A-c welder with remote hand control

the center leg, as indicated in Figure 6. The oscillogram Figure 7(*B*) shows how the wave shape and the welding performance have been improved by this design feature.

At present most a-c arc welders with saturable reactor control use reactors with the core and coil arrangement shown in Figure 6. The a-c coils surround the center leg of the core, and the d-c control coils are mounted on the outside legs. The air gap interrupts only the flux path of the magnetic lines which are caused by the alternating load current. The path of the lines which are caused by the current in the d-c control coils is not interrupted. The resulting regulation is better than can be achieved by providing the air gap in both flux paths.

Under load the reactor also acts as a transformer, and alternating voltages are induced in the d-c control coils. These voltages add up to zero for the control circuit. The relation of the number of turns of the a-c coils and d-c coils is chosen to give the lowest induced voltage for the individual coils. Splitting each d-c coil into separate smaller coils further reduces the voltage per coil and per layer of winding. Figure 8 gives the connection diagram of an a-c arc welder with saturable reactor control. The potentiometer arrangement of the control rheostat, the discharge resistor, and the disc rectifier effectively prevent the presence of any

Figure 11. A-c welder with remote foot control

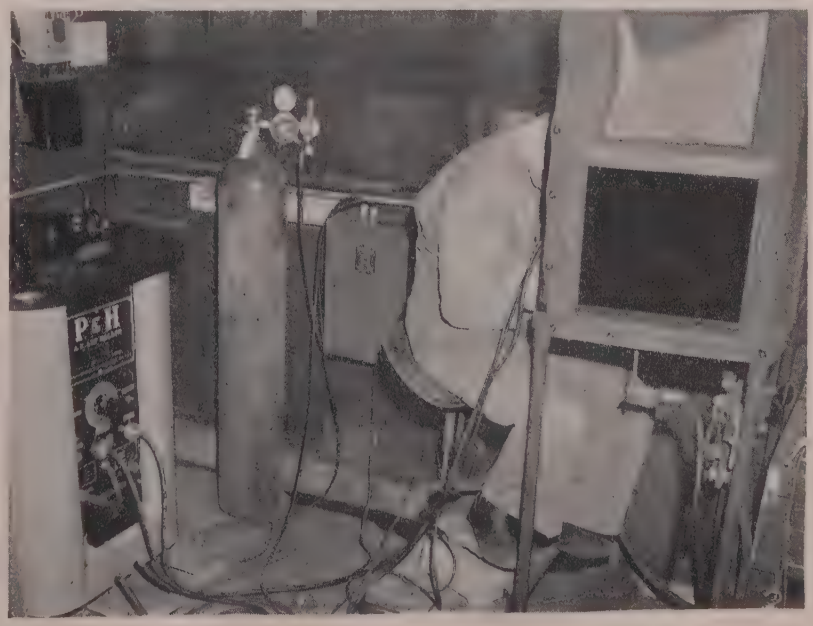

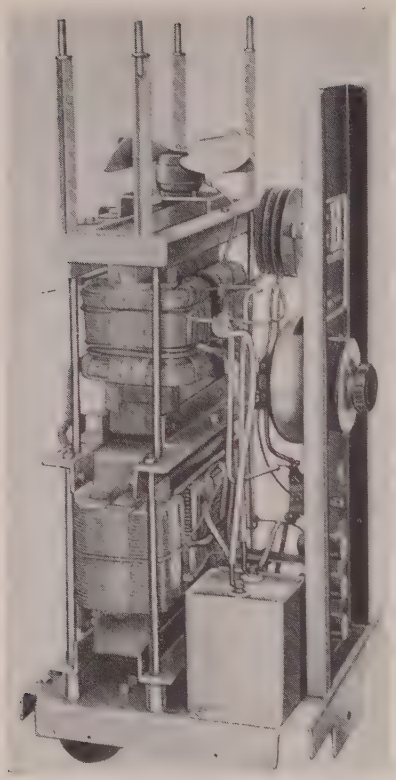

Figure 12. Inside view of a-c welder

appreciable voltage above the operating voltage at the terminals of the control circuit. The direct voltage of the control circuit is in the order of 15 volts.

The output regulation of a saturable reactor of the design used as an example can best be shown by plotting the magnetization curves. Figure 9 presents such a family of curves for different values of d-c magnetization. The output or load current variation for a change in control current can be taken from the spread between the two corresponding curves.

The control circuits of the present models are designed to give approximately 1-kw output variation for a 10-watt change in the control circuits.

A-c welders with saturable reactor control provide a very good "arc striking" characteristic. Each striking operation is reflected in a slight current variation in the control circuit. This variation is enough to reduce the impedance of the a-c coils sufficiently to cause an increased short-circuit current of very short duration. A "hot-start" feature, therefore, is inherent in this design. Other advantages of the design are obvious. The operator has a practically instantaneous means of current adjustment instead of the slower and sometimes tedious mechanical output control. Remote output control is feasible and practical without additional devices. Connecting the control rheostat (potentiometer) to the welding machine by means of an extension cord provides the operator with fingertip or foot control, as illustrated in Figures 10 and 11. The influence on over-all welding time and welding quality, by inducing the operator

Figure 13. Outside view of a-c welder

to use the correct heat, is rather important for many applications.

The simplicity of the electric control also is reflected in the mechanical design features of the welding machines. Cores and coils are assembled and fastened securely in their given positions. Figure 12 presents the inside arrangement, while Figure 13 shows a complete a-c arc welder with control by a saturable reactor.

No Discussion

Contact Resistance—The Contribution of Nonuniform Current Flow

W. B. KOUWENHOVEN
FELLOW AIEE

W. T. SACKETT, JR.
ASSOCIATE AIEE

WHEN two metallic surfaces are brought together, the surfaces never make uniform contact over the entire area. The actual contact occurs only at small subareas. This phenomenon gives rise to what is known as the resistance of contacts. This resistance consists of two parts, (1), a resistance at the contact, R_c, due to adsorbed gases, oxide layers or grease films at the small subareas; and (2), the spreading resistance, R_s, resulting from the nonuniform flow of current in the body of the materials.

This paper presents a study of the contribution that the spreading resistance makes to the total resistance of metals in contact. The spreading resistance was determined experimentally and theoretically for both round rod and flat strip specimens in which a restricted current path or constriction was introduced by machining away part of the material. The influence of the size, location, shape, and number of the constrictions on the spreading resistance was investigated.

The work was made possible by the Resistance Welding Fellowship established at the School of Engineering, The Johns Hopkins University, by the Resistance Welding Committee of the Welding Research Council.

Spreading Resistance

The resistance of a long uniform rod is given by $R=\rho(L/A)$ where ρ is the specific resistance, L the length, and A the cross-sectional area.

When a constriction is introduced in such a rod, the current flow is no longer uniform. Figure 1 shows a plot of the equipotential lines determined experimentally for a flat strip specimen having a sharp constriction. The current flow becomes substantially parallel within a distance equal to the width of the specimen. The spreading resistance is due to the reduction of current density in the corners which results in an increase in resistance.

The spreading resistance is the only resistance that exists between two clean, film-free metal surfaces in contact. The spots where actual contact is made will be of various shapes and sizes randomly located throughout the apparent contact area, and the resistance resulting from the nonuniform current flow will constitute the total contact resistance.

Specimens

The method adopted for the study of the spreading resistance was to measure the increase in resistance produced by making lathe or saw cuts in the central section of a specimen. A typical round rod specimen is shown in Figure 2.

Each specimen was first checked for uniformity of dimensions and resistance and then its resistance between two knife edges eight inches apart was measured in a Kelvin double bridge circuit. Then the central section was machined to the desired constriction. When this was completed, the resistance was again measured between the knife edges.

Paper 51-140, recommended by the AIEE Electric Welding Committee and approved by the AIEE Technical Program Committee for presentation at the AIEE Winter General Meeting, New York, N. Y., January 22–26, 1951. Manuscript submitted October 24, 1950; made available for printing December 26, 1950.

W. B. KOUWENHOVEN is Dean of Engineering and Professor of Electrical Engineering at The Johns Hopkins University, Baltimore, Md. W. T. SACKETT, JR., who was with The Johns Hopkins University at the time this paper was written, now is with Battelle Memorial Institute, Columbus, Ohio.

The spreading resistance, R_s, was determined from these two resistance measurements as follows. From the results of the first measurement the resistance R_A per-unit length and the specific resistance of the sample was calculated. In addition, the resistance R_a per-unit length of the reduced section was determined. If R_o equals the resistance of the rod after the constriction was made, then

$$R_s = R_o - (R_A l_1 + R_a l_2)$$

where l_1 is the rod length of diameter d_1 and l_2 the length of the constricted portion of diameter d_2, see Figure 2.

Experimental Procedure

The measurements were made with direct current using a special Kelvin double bridge constructed for the purpose. During the measurements each sample was immersed in an oil bath. Standards for each different specimen tested were made from the same material in order to simplify the temperature problem. Care was taken to avoid local heating. At all times the accuracy of the measurements was better than one part in 1,000. This was found to be ample as the spreading resistance proved to be larger than anticipated.

Concentric Constrictions: Round Specimens

The spreading resistance for two bronze rods having diameters of 5/8 inch and 1 inch respectively and concentric constrictions of different amounts are plotted in Figure 3. In the figure the abscissa is the ratio of the diameter of the rod to the diameter of the constriction and the

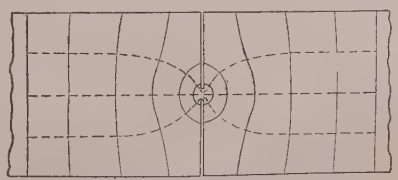

Figure 1. Equipotentials and flow lines on flat strip with constriction

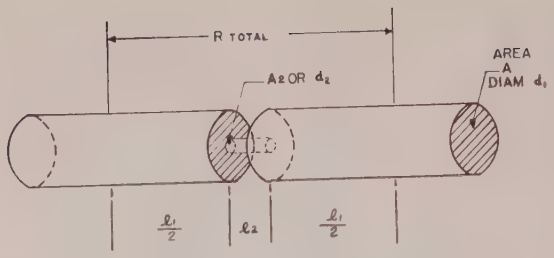

Figure 2 (above). Round rod specimen

Figure 4 (right). Spreading resistance of round rods expressed on a per-unit basis

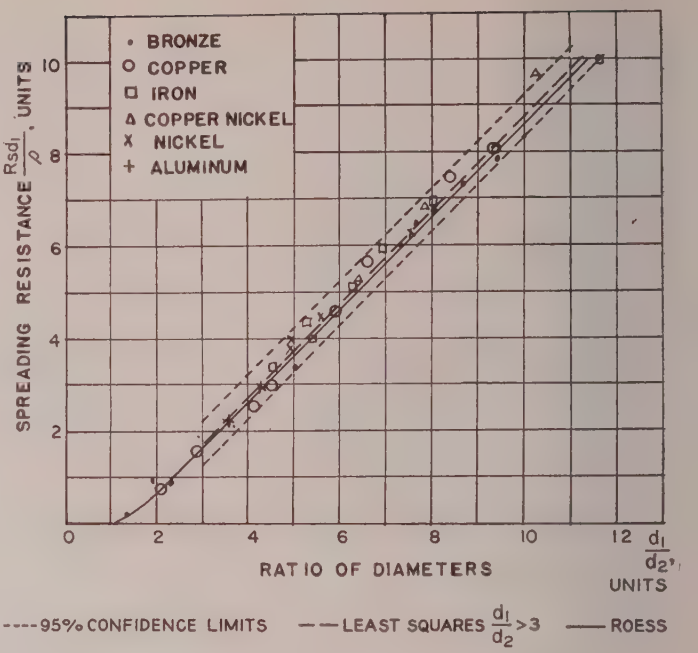

ordinate is the spreading resistance. A study of Figure 3 makes it clear that for each diameter of rod, there is a separate curve when the results are plotted to these coordinates. The results however may be expressed in a per-unit basis[1] by multiplying the spreading resistance by the rod's diameter d_1, and dividing by the specific resistance. Thus when the ordinate of the curve is $R_s d_1/\rho$, it will be found that all of the points lie on the same curve irrespective of diameter and material.

The results found for concentric constrictions on aluminum, bronze, copper, copper-nickel, iron, and nickel rods ranging in diameter from 0.45 inch to 1 inch and with varying size constrictions are plotted in Figure 4. These points when plotted on this per-unit basis all lie on a smooth curve that checks closely with the solution of the Laplace equation for this boundary value problem as given by Dr. L. C. Roess in "Theory of Spreading Conductance" an unpublished report, of the Beacon Laboratories of the Texas Company, Beacon, N. Y.

In the mathematical solution of this problem, certain assumptions were necessary. The validity of these assumptions is confirmed by the experimental measured values. A statistical analysis of the results shows that the least squares line closely coincides with the linear portion of theoretical curve, and that the 95 per cent confidence limits embrace a narrow band. These also are plotted in Figure 4.

Symmetric Constriction: Flat Strip

The spreading resistance was measured on a number of flat strips of brass with a constriction located at the midpoint of the strip. A typical specimen is shown in Figure 5. The results of these measurements are also plotted in Figure 5 where the abcissa is the ratio of the width of the strip to the width of the constriction and the ordinate is on a per-unit basis $R_s w/\rho$. Here w is the thickness of the strip. The solid curve is based on Smythe's mathematical solution.[2] The experimental points check this solution.

Length of Constriction

In practice the length of the constricted path is usually quite small. The question therefore arose: does the length of the constricted path have any effect upon the spreading resistance? Measurements were made on round specimens in which the length of the constricted path varied from 0.163 to 0.007 inch. Within experimental limits the spreading resistance was found to be independent of the length of the constriction, and the points fell on the smooth curve of Figure 4.

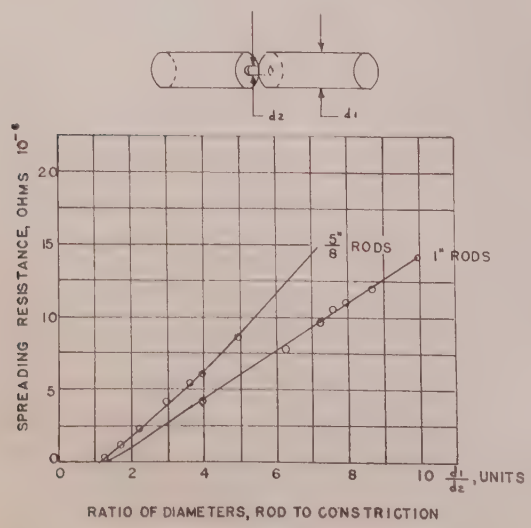

Figure 3 (left). Spreading resistance of round rods for constrictions of varying sizes

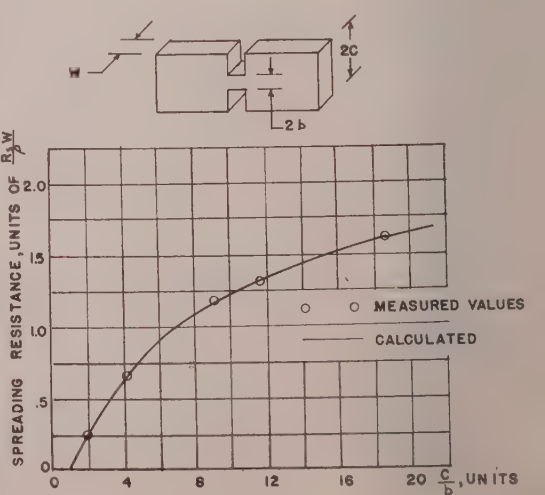

Figure 5 (right). Spreading resistance of flat strips

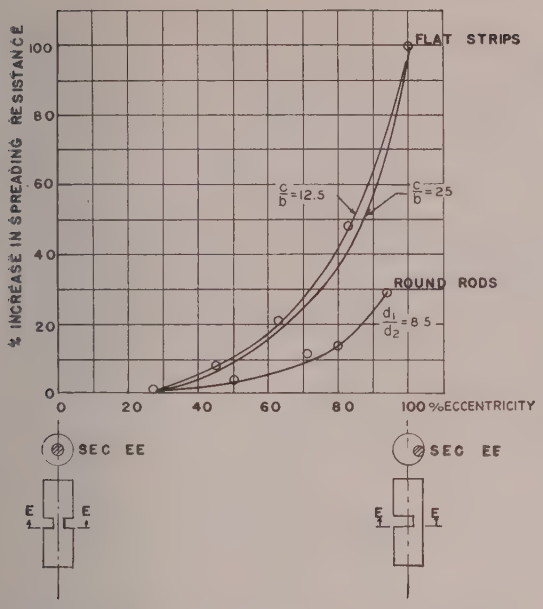

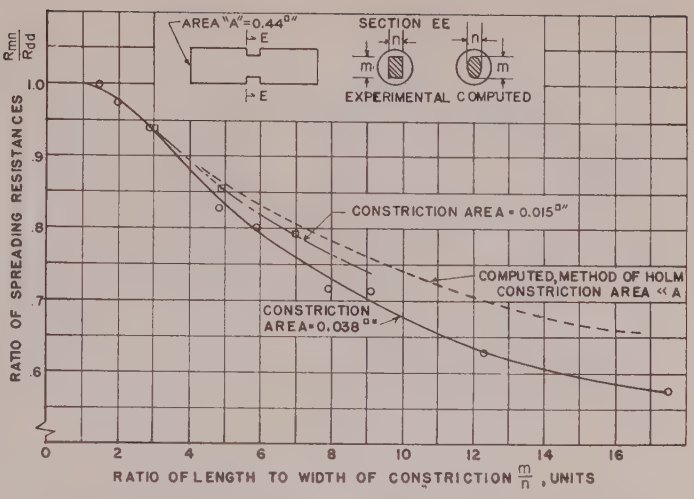
AREA "A" = 0.44 a"
SECTION EE
EXPERIMENTAL COMPUTED
RATIO OF SPREADING RESISTANCES
CONSTRICTION AREA = 0.015 a"
COMPUTED, METHOD OF HOLM CONSTRICTION AREA = A
CONSTRICTION AREA = 0.038 a"
RATIO OF LENGTH TO WIDTH OF CONSTRICTION m/n, UNITS

Figure 6 (left). Effect on spreading resistance of location of contact area

Figure 8 (above). Variation of spreading resistance with the shape of the contact area

Location of the Construction

On actual contacts the constricting area is not symmetrically located, but may be at any point on the surface. The effect on the spreading resistance produced by nonsymmetrically or eccentrically located constrictions was studied for both flat and round specimens. Specimens were made in which the constriction was held to a fixed size and on successive specimens its location was varied from the center to the extreme edge. The results are plotted in Figure 6 for a ratio of $d_1/d_2 = 8.5$ for the round specimens and for the ratios of $c/b = 12.5$ and 25 for the flat samples. The curves for the two types of specimens are similar in shape.

A study of Figure 6 shows that the location of the contact spot does not have much effect on the spreading resistance until the eccentricity exceeds 50 per cent for strip specimens and 60 per cent for round ones. The effect is naturally greater for flat strips because in these the flow lines are more severely restricted than in the round specimens. It was also found that as the area of the constriction was reduced, the effect of nonsymmetrical location was slightly less marked as may also be seen from the figure.

Shape of the Contact Area

It also is true in actual contacts that the shape of the contact area will not be circular. Where contact occurs by virtue of metal being squeezed into fissures made in surface films by high contact pressures, there would be a fairly high degree of "ellipticity" of the contact areas. An experimental study of the influence of the shape of the constriction was therefore made.

The spreading resistance of round rods having square symmetrical constrictions was determined for different constricting areas. A comparison of these measurements with the results for circular constrictions is shown in Figure 7. The dimensionless quantity $R_s d_1/p$ is plotted as ordinate against $\sqrt{A}/a$ as abscissa. A is the cross-sectional area of the round rod, and a that of the constriction. The curve gives the results for round constrictions, while the circled points are measured values found for square constrictions. The points fall above the curve.

The next step in the exploration of the shape effect was to test a series of samples having rectangular constrictions with the same total area, mn = constant. It was then possible to determine the relation of

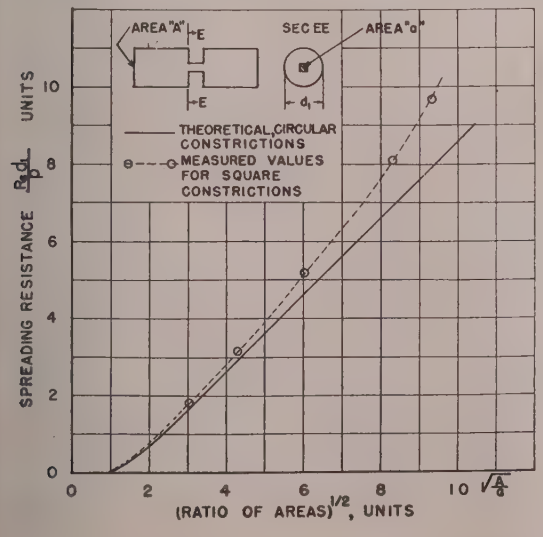

Figure 7 (left). Spreading resistance of round rods with square constrictions

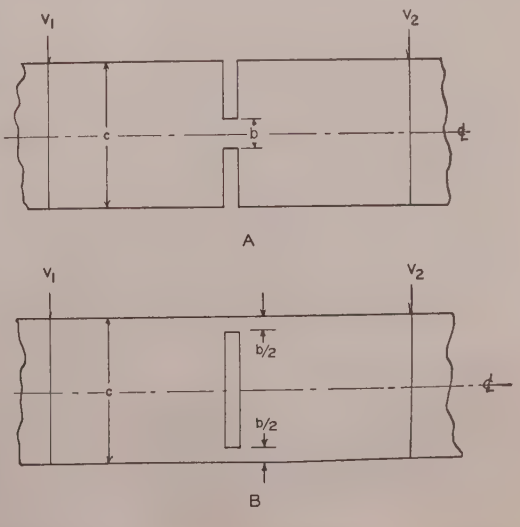

Figure 9 (right). Flat specimens with either one or two connections

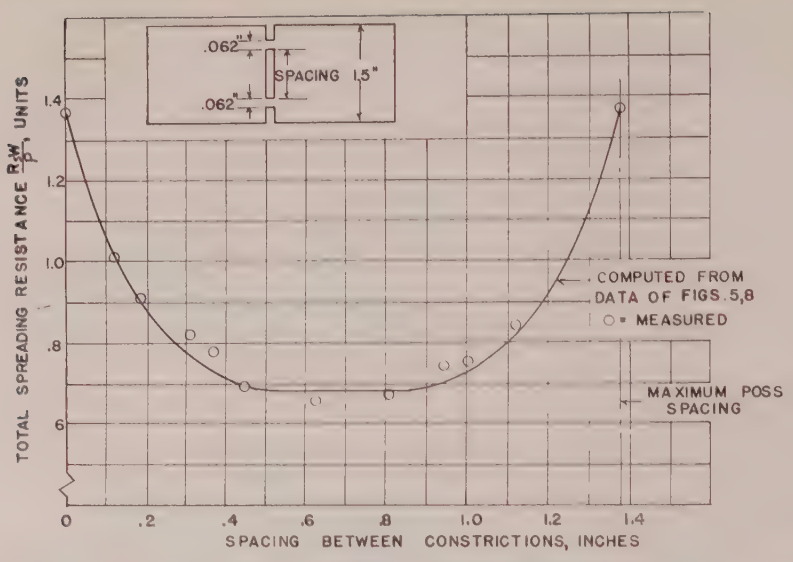

Figure 10. The effect of the location of parallel constriction upon the spreading resistance

spreading resistance to a shape factor, here defined as the ratio of the length, m, to the width, n, of the rectangular constriction.

Holm has shown[3] that the effect of the shape of the constriction can be calculated if one assumes the constricting area to be an ellipse of area much smaller than the cross sectional area of the rod. Then if R_{mn} is the spreading resistance for an elliptical constriction with major axis, m, and minor axis n, and if R_{dd} is the spreading resistance of a circular constriction of diameter d

$$\frac{R_{mn}}{R_{dd}}=\frac{K(k_1)}{\pi}\left(\frac{4d}{m+n}\right), \text{ where } k_1=\frac{m-n}{m+n}$$

K_1 is the modulus of K, a complete elliptical integral of the first kind.

The dotted curve of Figure 8 is a plot of the foregoing equation. In addition there are given in Figure 8 the experimental curves for two rectangular constrictions; one of 0.015 square inch and one of 0.038 square inch. All three curves coincide for an m/n less than 3, where the constriction is well-centered. The curve for the smaller area more nearly fits that of Holm's formula.[3] It is perhaps worth comment that for a given total constricting area, a long thin constriction gives appreciably less spreading resistance than a round constriction, but the magnitude of the decrease would be less than 25 per cent for reasonable shapes.

Parallel Constrictions

Study of the contribution of spreading resistance to contact resistance should involve an inquiry concerning the effect of two or more constricting paths in parallel across the contact surface. When force is applied to the contact members, the yield point of the first contacting areas is quickly reached and flow occurs until enough of the apparent contact area is in load bearing contact to reduce the pressure below the plastic flow limit of the metal. During this process the number of conducting constrictions that form will depend on the surface shape and finish. Holm[4] states that the total load bearing contact area S_b will be relatively constant for a given contact load (P) and contact material, and is of the order of magnitude $S_b=2P/H$, where H is the upper limit of the contact pressure at which plastic flow or splintering occurs.

Windred[6] has stated, "When there is more than one contact point, there may be electromagnetic interactions between the lines of current flow if the contact points are close together, otherwise this may be neglected." Holm[5] uses the phrase "the constricted lines of flow influence each other" if the conducting spots are close together. Both state that if the spots are far apart, the total spreading conductance can be computed by adding the conductances of the individual spots.

The concept of the flow lines of parallel constrictions influencing each other is misleading and that of self or mutual electromagnetic forces on the flow lines under steady flow conditions is probably erroneous. To check this the following experiment was devised. Consider the brass strip with a constriction (two dimensional flow) as shown in Figure 9(A). The flow is symmetrical about the center line; hence, the total resistance of the strip between knife edges V_1 and V_2 should be exactly half that of the individual halves of the strip. Further, if the strip is separated at the center line and put together as in Figure 9(B), exactly the same resistance should be obtained between the knife edges barring disturbance of the flow by electromagnetic forces.

This experiment was performed on several brass strip samples, and each time the spreading resistance of a sample constructed as shown in Figure 9(B) was found to be equal to the corresponding sample Figure 9(A), within the experimental limits. Hence, one can conclude that mutual electromagnetic forces of parallel flow have no practical effect on spreading resistance.

This does not mean, however, that the spreading resistance of parallel constrictions is independent of the spacing between them. It was found that the spreading resistance for single constrictions changes with their location as shown in Figure 6. The influence of the spacing of parallel constrictions on the spreading resistance was studied on thirteen brass strip samples. Each strip was 1.5 inches wide and 1/8 inch thick and each had two symmetrically located parallel constrictions of 0.062 inch wide. All factors were held constant except that the spacing was varied from zero to the maximum possible value. The data is plotted in Figure 10 where the abscissa is the spacing between the constrictions, the ordinate, the dimensionless spreading resistance R_sW/ρ. The solid curve of Figure 10 was computed from the data of Figures 5 and 6 by considering the single strip as consisting of the parallel connection of two separate strips half as wide with eccentrically located constrictions. The circled points are the measured values for the 13 specimens.

It was found that the spreading resistance for two parallel constrictions separated by half the strip width was exactly half that obtained when the spacing was zero (single constriction 0.124 inch wide).

Control of Spreading Resistance

Assuming that Holm is correct in his statement that the total contact area is dependent mainly on the load and the materials in contact,[4] it follows that the total contact area may be concentrated in a single spot or may be distributed randomly in small subareas over the surface. The question arises, "What effect does this have on the resulting spreading resistance and how may this resistance be controlled?" The experimental work in-

dicates that the spreading resistance of two metals in contact may be controlled by varying the number of contact points. For any given total contact area, the lowest spreading resistance will be obtained with the maximum number of symmetrically located constrictions or contact subareas. As the number of contact points is increased, while keeping the total contact area constant, the resulting spreading resistance approaches zero, even though the area of the individual constriction or contact points also approaches zero.

The verification of this statement is based on the following analysis. It has been shown experimentally that the value of the spreading resistance in ohms for a flat strip specimen with a symmetrical constriction varies with the ratio of the width of the strip to the width of the constriction. For a given ratio the spreading resistance is constant provided the thickness of the strip is constant.

Assume that we have a strip of width c and thickness w with a symmetrical constriction of width b and a thickness w. This strip will have a spreading resistance of R_s ohms. Assume now that this strip is replaced by two strips each of width $c/2$ and each with a symmetrical constriction of width $b/2$, both strips having the thickness w. Now each half strip will have a spreading resistance R_s, identical to that of the full sized strip.

If these two strips are joined in parallel, their individual spreading resistance R_s will also be in parallel and the resultant spreading resistance will be $R_s/2$. This is confirmed by the experimental results, Figure 10.

Assume now that each half strip is divided into two strips of width $c/4$ and each with a symmetrical constriction of width $b/4$. Each one of these four strips will have a spreading resistance of R_s equal to that of the original full sized specimen. When these four strips are joined in parallel, the resulting spreading resistance will be one fourth of R_s.

It is evident from the analysis that the resulting spreading resistance of a specimen with a large number of parallel paths approaches zero as the number is increased provided the total constricting area remains constant. The spreading resistance is a maximum for a single contact point of the given area.

A similar analysis may be developed for round or square rod specimens. The analysis is given for a square bar as it has been shown, Figure 7, that in a round bar, a square constriction and a circular constriction of the same area gives very closely the same spreading resistance.

Assume a square bar of W inches on a side and of cross sectional area A_1, having a symmetrical constriction at the center of A_2 square inches. This bar will have a spreading resistance $R_{s1}=Rp/w$, where R is the per-unit spreading resistance.

Now assume that this square bar is divided into quarters each of $W/2$ inches on a side, each of cross sectional area $A_1/4$ and each having a symmetrical constriction of area $A_2/4$. Each one of these quarters will have a spreading resistance of $R_{s2}=R_p/W/2$, or twice that of the original bar. When these four quarters are joined in parallel, the resulting spreading resistance will be one half of that of the original bar with its single symmetrical constriction. This process of subdivision may be repeated indefinitely and so the statement is verified.

From this analysis it is evident that the spreading resistance can be controlled by using the proper surface finish of the contact areas. The maximum spreading resistance will be obtained if there is a single small area of contact as in a projection weld. The spreading resistance may be reduced to a minimum by using a surface finish that provides a large number of contact points or constrictions scattered throughout the area.

Conclusions

The results of this study provide an explanation of spreading resistance, and curves are presented for calculating its magnitude for single and multiple constricting contacts. The study shows that:

1. The spreading resistance forms an important part of the resistance of contacts.
2. The theoretical analysis given by Roess for symmetrical constrictions is confirmed experimentally.
3. Off-center location or eccentricity of the constriction increases the spreading resistance, but the effect is small until the constriction is near the edge of the material.
4. The shape of the constriction effects the spreading resistance.
5. The spreading resistance can be controlled between wide limits by varying the number of parallel conducting spots.

References

1. Electrical Resistance Offered to Nonuniform Current Flow, **W. B. Kouwenhoven, W. T. Sackett.** *Welding Journal* (New York, N. Y.), volume 28, October 1949, page 468.
2. Static and Dynamic Electricity, **W. R. Smythe.** McGraw-Hill Book Company, New York, N. Y., 1939, page 232.
3. Electric Contacts, **Ragnar, Holm.** Gebers, Stockholm, Sweden, 1947, pages 15–17.
4. Op cit, page 2.
5. Op cit, page 19.
6. Electrical Contact Resistance, **G. Windred.** *Journal*, Franklin Institute (Philadelphia, Pa.), volume 231, number 6, page 552.

No Discussion

Selection of Fuses for Resistance Welding Machines

C. B. STADUM
ASSOCIATE AIEE

Synopsis: This paper covers:

1. An analysis of available fuse data with special reference to the data's applicability for resistance welding machines.

2. A proposed method of analysis of fuse characteristics.

3. Discussion of these fuse characteristics.

4. Use of these characteristics in welding applications.

5. The application of fuses as it is practiced in the industry today.

The data that are presented are based only on 250-volt fuses. Six-hundred-volt fuses were checked and found to have characteristics substantially the same as 250-volt fuses. Consequently, any system of rating of 250-volt fuses applies also to other fuses.

CHARACTERISTICS of fuses generally are given by curves in which overload current is plotted against time required to blow the fuse. This relationship is necessary for most applications, but where the fuses are called upon to protect a device which is recurringly overloaded and unloaded, the characteristics are not useful. Examples of a recurring load exist in the resistance welding field, where the welding machine draws up to 4–5 times its thermal rating during the making of a weld. Likewise, for short intervals, the ignitrons switching the welder on and off pass current which may be ten times their thermal rating. Rating sheets for welders and tubes can best be expressed in terms of current and duty cycle, or in terms of current, weld time, and welds per minute. Therefore, the rating sheets for fuses (to be applicable to the welding industry) should be expressed in the same terms, that is, current, weld time, and duty cycle and welds per minute.

The problem considered here is to take the existing fuse rating curves and interpret them in terms which are used by the welding industry.

Paper 51-141, recommended by the AIEE Electric Welding Committee and approved by the AIEE Technical Program Committee for presentation at the AIEE Winter General Meeting, New York, N. Y., January 22-26, 1951. Manuscript submitted October 24, 1950; made available for printing January 2, 1951.

C. B. STADUM is with the Westinghouse Electric Corporation, Buffalo, N. Y.

Protection of Equipment

When fuses are applied to a welding system, they are requested to protect (1) the welding machine, (2) the feeders between the fuses and the machine, and (3) the electronic or magnetic contactor controlling the welding machine. Fuses to protect the system always should be chosen to protect that part of the system which is the most susceptible to burn-out or damage. In most cases, this is the electronic contactor or the contacts on the magnetic control. This is due to the relatively low averaging time of the tubes as compared with the other two circuit elements. The thermal rating of a transformer, cable, and tubes may be 50 amperes, yet it is not unusual for them to operate at 500 amperes for a short period of time, such as 1/2 second. A temporary overload of 500 amperes for 1 second certainly will not damage the transformer or cables since they are slow to heat, that is, they have a long thermal time constant; but it may ruin an ignitron, which has an extremely small time constant and averaging time. Consequently, fuses should be selected to protect that element having the shortest thermal time constant.

Most spot welds are completed in an extremely short time, generally in the range between 5 and 60 cycles. Consequently, in the discussion of fuses, current duration in this range also will be considered. Operation of fuses at 0.1 second (6 cycles) and 1 second (60 cycles) will be considered.

Examination of Data

In order to accumulate data on fuses, inquiries were made of nine major fuse manufacturers in the United States. Information was requested on the current required to blow 250- and 600-volt fuses when the duration of the current was 0.1 – 1.0 seconds. Of the nine manufacturers contacted, only four had data on current required to blow fuses at very short times. Of these four, two had only partial information. One of the fuse manufacturers listed three different types of fuses and had complete information on all three types. In Table I, fuses having Key Numbers II, III, or IV were those made by the same manufacturer.

As can be seen, the data that were available were extremely meager. In addition to that, the data itself are questionable, since no information on accuracy was available to the author.

Data submitted by the manufacturer were of the form given in Figure 1. The data that were obtained gave the blowing characteristics of a fuse within the 0.1-second-300 second range, but in the interest of simplicity only the low time range is reproduced in Figure 1.

Fuse Constants

In order to develop a knowledge of the operation of fuses and their application to resistance welding machines, a theory of operation of fuses is developed in the appendix.

The conclusions reached in the appendix can be summarized by the equation:

$$B = I^A t \qquad (1)$$

where

B = a unit proportional to the temperature at which the fuse will blow
A = a heating constant

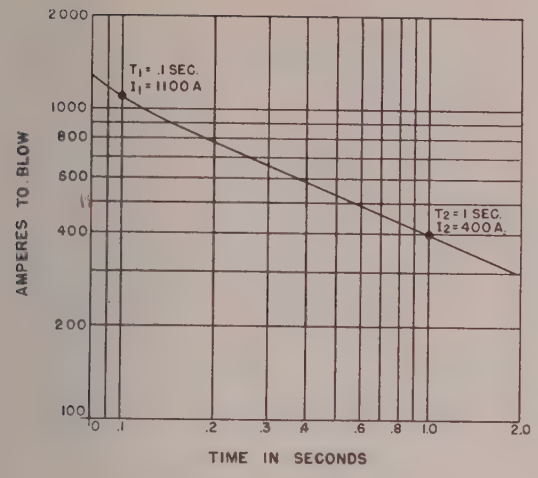

Figure 1 (left). Typical current versus time curve for blowing 250-volt fuses

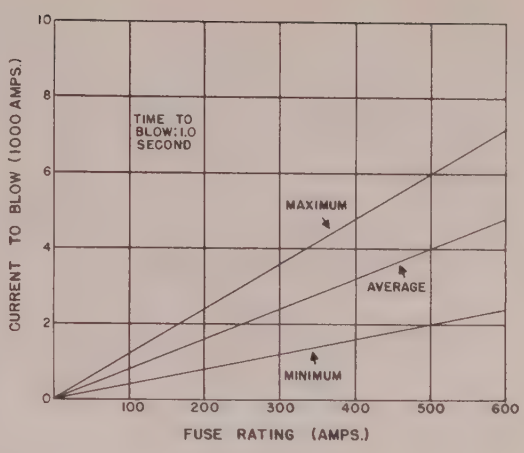

Figure 2 (right). Fuse rating versus blowing current, duration of current impulse 1.0 second

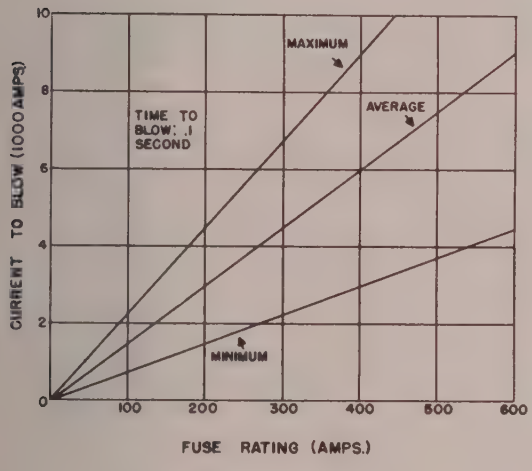

Figure 3 (left). Fuse rating versus blowing current duration of current impulse 0.1 second

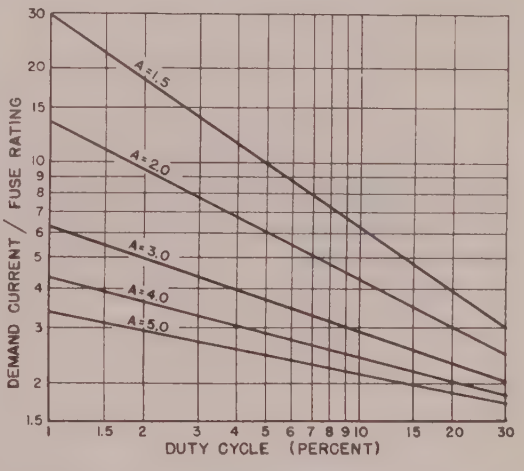

Figure 4 (right). Demand current versus duty cycle for fuses having different constants A

Table I. Data on 250-volt Tubes

Fuse Rating Amperes	Fuse Key Number	Amperes to Blow at t^1 Sec. t^1		Constant A	Constant B	Constant t_c
60	I	260 = I_2	770 = I_1	2.11	9.6×10^4	11.3
60	II	260	430	4.57	8×10^5	152
60	III	560	1,050	3.66	5.5×10^6	1,310
60	IV	340	1,000	2.13	1.36×10^5	21
60	V	260	460	4.03	4.72×10^5	88
60	VI			*3.9	*4.6×10^9	
100	I	400	1,100	2.3	2.43×10^5	12.5
100	II	400	890	2.87	5.3×10^5	73
100	III	900	1,600	4.0	6.5×10^7	5,360
100	IV	640	1,900	2.11	3.9×10^5	26
100	V	460	900	3.33	1.6×10^6	63
100	VI			*3.9	*8.3×10^{10}	
200	I					
200	II	950	2,000	3.1	1.08×10^7	50
200	III	1,800	3,200	4.0	1.05×10^8	1,550
200	IV	1,500	4,500	2.1	2.95×10^6	36.5
200	V	960	2,000	3.13	1.2×10^7	50
200	VI			*3.7	*1.9×10^{11}	
400	I					
400	II	2,300	4,050	4.06	2.95×10^7	390
400	III	4,300	7,800	3.86	2.8×10^8	2,560
400	IV	3,900	8,500	2.95	5.5×10^7	33
400	V	2,300	4,100	3.96	2.7×10^7	340
400	VI			*3.9	*2.5×10^{13}	
600	I					
600	II	3,500	6,400	3.81	3.0×10^{13}	260
600	III	7,200	9,600	8.0	1.6×10^{11}	3,220
600	IV	6,600	9,000	7.45	3.9×10^8	225
600	V	3,500	6,400	3.82	3.0×10^{13}	260
600	VI			*3.5	*8.1×10^{13}	

* Note: Values of A and B calculated from slope of the I versus t curve.

In a normal thermal device, the watts lost is proportional to i^2R, but in the case of a fuse, R is a function of the temperature and consequently, a function of the current. Therefore, in equation 1,

A = a constant which combines the normal I^2R effect plus the effect of the change of resistance
I = the current passing through the fuse
t = the duration of current flow

$$A = \frac{\log t_2/t_1}{\log I_1/I_2} \qquad (2)$$

where

t_1 and t_2 are two "times" to blow corresponding to the currents I_1 and I_2

$$t_c = (I_1/I_0)At_1 \qquad (3)$$

I_0 is the current at which the fuse will blow at an infinite time (135 per cent of the fuse rating).

In any standardized pieces of equipment, constants similar to A, B, and t_c serve as points of comparison between similar products made by different manufacturers and, in general, will be substan-

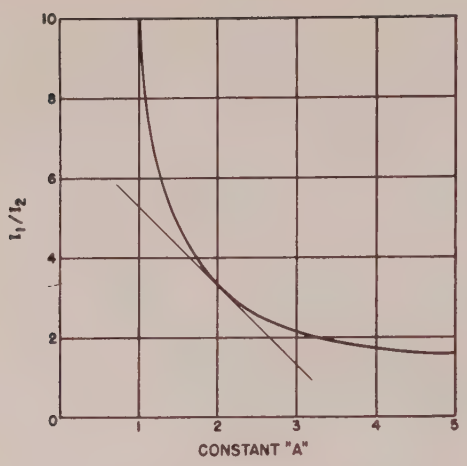

Figure 5. Method of determining constant A. Least "sensitive" combination of A I_1/I_2 is at $A=2$ $A=\frac{\text{Log } 1/0.1}{\text{Log } I_1/I_2}$

Figure 6 (right). Demand current versus duty cycle for $A=2.2$

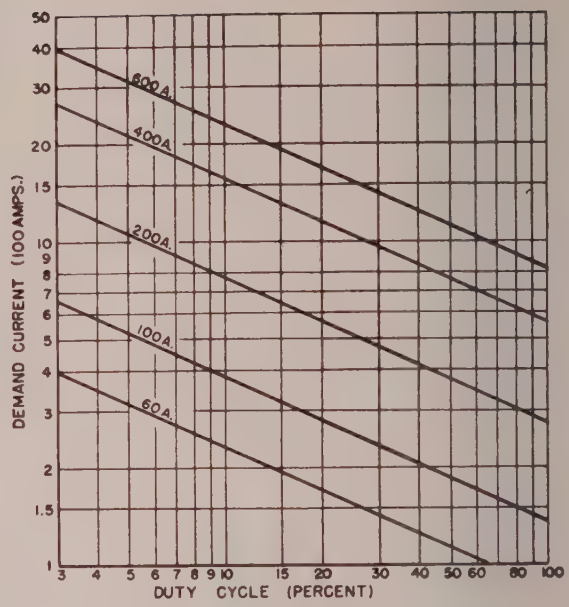

tially constant. By this is meant that electronic tubes, transformers, or resistors made by different manufacturers will have the same maximum operating temperature (proportional to B), the same heat exponent (equal to A), and the same time constant (proportional to t_c). In an effort to see if there is any consistency among fuse manufacturers, the pertinent data, including the constants A, B, and t_c have been presented in Table I. The widespread divergence of all the values lead correctly to the conclusion that it is impossible at this time to write specific rules on application of fuses to resistance welding control.

In order to get a better picture of the importance of the fuse data, the values of currents to blow at 1.0 and 0.1 seconds have been plotted on Figures 2 and 3. The figures show the blowing current ranges from ±50 per cent of the average value. Since this variation precludes any attempt to determine a particular fuse rating for a given welder system, it is necessary to investigate each fuse individually to determine how it shall be applied.

The most convenient method of expressing any rating in a welder system is by a curve giving the relationship between demand current and duty cycle, an expression widely used in the welding industry. In the appendix, the following expression was developed

$$I_0=I(DC)^{1/A}$$

where I_0 is the current at which a fuse will blow as infinite time. This is 135 per cent of fuse rating. I is the demand current, and DC is the duty cycle. A plot of duty cycle versus I/(fuse rating) is shown in Figure 4.

Since it can be seen that the constant A is extremely important in the application of fuses, it must be determined. This can be done from equation 2 when $t_2=1$ and $t_1=0.1$ second. Equation 2 then can be written

$$A=\frac{\log 1/0.1}{\log I_1/I_2}=2.30/\log (I_1/I_2) \qquad (5)$$

This equation is plotted on Figure 5, which gives a convenient way to select A. It should be noted that the best combination of I_1/I_2 and A is at values of A around 2 (where the slope of the curve is 45 degrees), since at this point is the point of "least sensitivity," that is, small changes of either I_1/I_2 or A do not affect

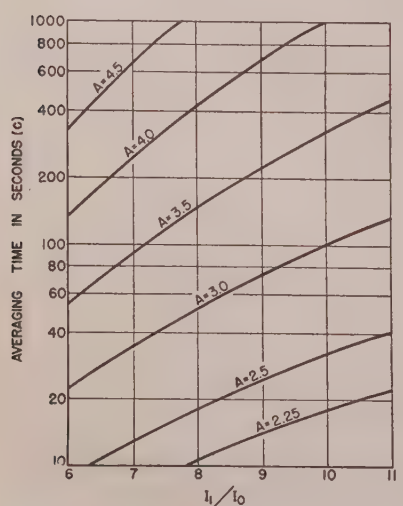

Figure 7. Method of determining averaging time (t_c) of a fuse

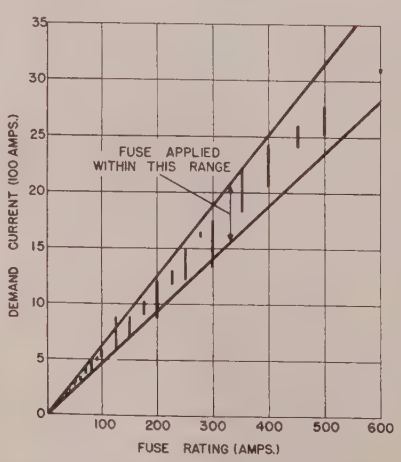

Figure 8. Actual practice of applying fuses to spot, projection, and gun welders. Vertical lines represent range in which fuses have been applied

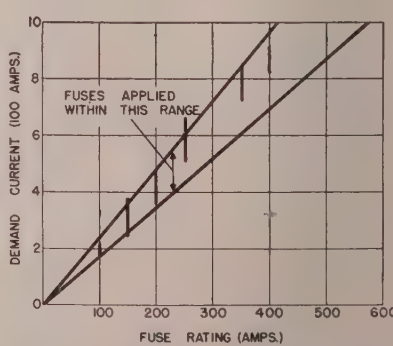

Figure 9. Actual practice of applying fuses to seam welders. Vertical lines represent range in which fuses have been applied

the other variables appreciably. On the other hand, if A is small, small changes in A caused by variations in manufacturing methods will result in large variations in I_1. Large values of A also imply large time constants (see Table I), which result in mismatching of fuses and tubes.

The procedure for obtaining the necessary information for intelligently applying fuses as suggested by the above procedure is:

1. Obtain from the fuse manufacturer I_1 and I_2, which are the currents to blow at 0.1 second and 1 second.

2. From I_1/I_2 determine constant A from Figure 5.

3. With this value of A, use the curve on Figure 4 to apply fuse or

4. Use equation 4 to obtain a specific curve similar to those given in Figure 6.

5. Determine the averaging time of the fuse from equation 3 or

6. Determine the averaging time from Figure 7.

Fuse Practice

In order to check the preceding work with actual fuse practice, data were gathered on "demand current" versus fuse rating for both seam and spot welding. This information is presented on Figures 8 and 9. On seam welders a 100-ampere fuse is used between 170 and 230 amperes. Checking this figure against Figure 6, it can be seen that the duty cycle for a 100-ampere fuse operated at this demand is between 45 and 80 per cent. This is approximately the duty cycle at which seam welders operate. The 100-ampere fuse is used between 475 and 625 amperes for spot welders. Checking this against Figure 6, it can be seen that the duty cycle can be between 4.5 and 8 per cent. This is the duty cycle at which spot welders operate.

Conclusions

1. It has been shown that fuse characteristics are not standardized and, therefore, it is impossible to make specific recommendations on the applications of fuses to resistance welding machines.

2. A method has been proposed whereby it is possible to take the fuse characteristics of a given manufacturer and develop the necessary curve to be able to apply the fuses intelligently to an intermittent load.

3. It has been shown that the results when using the proposed method compare favorably with actual practice.

Appendix

In order to establish ratings for fuses operated on intermittent duty, it is necessary to develop a theory based on a simple model system. The system chosen and the assumptions made are these:

1. The system is one in which heat is lost by conduction and therefore is proportional to the first power of the temperature difference between the fuse and its cooling medium.

2. The model (the fuse) is a small mass in which the temperature at any time is uniform throughout.

The differential equation giving the relationship between the temperature, the energy input, and time during the heating portion of the cycle is:

$$CMd\theta = Wdt - K\theta dt \tag{6}$$

where

C = the specific heat of the model
M = the mass of the model
W = the watts input during the heating period
K = the thermal conduction constant
θ = the temperature difference between the model and the cooling medium
$d\theta$ = the temperature rise of the model in the time dt

Rearranging terms and integrating equation 6 gives

$$\log (W - K\theta) = \text{constant} - Kt/CM \tag{7}$$

assume that at $t=0$, the temperature is 0. This enables the "constant" to be evaluated. Evaluating this constant and solving for θ gives

$$\theta = W/K(1-\epsilon^{-t/t_c}) \tag{8}$$

where

$t_c = MC/K$ = the time constant

If equation 8 is expanded it yields

$$\theta = W/K\left[(t/t_c) - \frac{(t/t_c)^2}{2!} + \frac{(t/t_c)^3}{3!} \cdots\right] \tag{9}$$

when t is small compared with t_c,

$(t/t_c)^2 = 0$ and $(t/t_c)^3 = 0$

Then equation 9 becomes

$$\theta = Wt/Kt_c \tag{10}$$

For ignitrons operated near their thermal rating, $M = k_1 I$ and equation 10 becomes:

$$\theta = k_1 tI/Kt_c \tag{11}$$

where
I is the current passing through the tubes.

For welding transformers

$$W = k_2 I^2$$

and equation 10 becomes

$$\theta = k_2 tI^2/Kt_c \tag{12}$$

Since it is known that the resistance of fuse material is some function of current passing through it, the temperature in a fuse cannot be described as simply as by equations 11 and 12. For a fuse, equation $W = k_3 I^A$ and equation 10 becomes

$$\theta = k_3 tI^A/Kt_c \tag{13}$$

or

$$B = tI^A \tag{14}$$

$$A \log I = \log B/t \tag{15}$$

If it is assumed that θ is a constant temperature at which a fuse will blow, then B also will be a constant. Then, if equation 14 is correct, values of time (t) and current (I) required to blow plotted on a log-log scale will yield a straight line. This is suggested by equation 15, since I and t in this equation plot as a straight line. Plots of I and t for commercial fuses are shown in Figure 1. This figure validates equation 15, since it does yield an approximate straight-line relationship in the time range selected. In the data examined equation 15 is not valid for time ranges greater than 10 seconds.

Constant A can be evaluated from two sets of current and time values as follows:

$$B = t_1 I_1^A = t_2 I_2^A \tag{16}$$

or

$$(I_1/I_2)^A = t_2/t_1 \tag{17}$$

or

$$A = \frac{\log t_2/t_1}{\log I_1/I_2} \tag{18}$$

In order to determine this and the other constants

t_1 has been chosen equal to 0.1 second
t_2 has been chosen equal to 1.0 second
I_1 is the current to blow at 0.1 second
I_2 is the current to blow at 1.0 second

Equation 13 should be expressed in terms of duty cycle to be useful to the resistance welding industry. In order to do this, it is necessary to determine the temperature at which the fuse will blow at an infinite time (equation 8) and equate it to θ in equation 13

$$\theta = W_0/K(1-\epsilon^{-t/t_c}) = W_0/K \tag{19}$$

but

$$W_0 = k_3 I_0^A$$

Therefore equation 19 becomes

$$\theta = k_3 I_0^A/K$$

equating this to equation 13 gives

$$k_3 I_0^A/K = k_3 tI^A/Kt_c$$

or

$$I_0^A = tI^A/t_c$$

or

$$t/t_c = (I_0/I)^A \tag{20}$$

Duty cycle D is defined as

$$D = \frac{t}{t_c}$$

However, since B (equation 14) is linear only for values of t up to 10 seconds for the fuse data examined, values of t in excess of 10 seconds should not be used. For values of t in excess of 10 seconds the continuous rating of the fuse should be used.

In considering other fuses, the range of linearity of B may be determined from the manufacturer's data and the 10 second limit may be altered as required.

For purposes of determining A from equation 20, the continuous rating of a fuse should be taken as 135 per cent of the manufacturer's rating.

No Discussion

The Physical Mechanism of Low- and High-Current Arcs, and Their Relation to the Welding Arc

WOLFGANG FINKELNBURG
NONMEMBER AIEE

RESEARCH on electric arcs at atmospheric (or higher) pressure has become confined more and more to studies of special cases of arcs by specially interested research groups. Typical examples are the old low-current carbon arc, the modern high-current carbon arc, the different types of mercury vapor arcs, the high-power arcs encountered in switching high power loads in electric power houses, the contact arcs of different kinds, and, last but not least, the welding arc. Depending on their different aims, the various research groups concentrated their attention on very different phenomena. The carbon-arc engineer was interested in highest brightness and uniformity of the positive crater and not at all in the inconspicuous arc stream whereas, conversely, the mercury arc development aimed at the highest possible concentration of excited atoms in the arc stream which here forms the source of radiation, without being too much interested in the role of the electrodes or of magnetic fields influencing the arc. The electric power engineer wants to suppress the arc, or extinguish it as quickly as possible, and thus had to study deionization as well as the influence of external magnetic fields and high-velocity gas streams on very long high-current arc streams without being greatly interested in the electrodic mechanism of the arc which, in turn, is of utmost interest to the contact engineer with his generally short contact arcs. The welding engineer, finally, is not interested in the radiation of the arc at all. He strives for a stable, easily directable arc and thus had to study, among other features, the arc's magnetic effects. His main interest, however, had to be concentrated on the complicated phenomena of the material transfer through an arc of variable length, further complicated by restricting requirements concerning chemical and thermal processes at least at one of the electrodes, the work.

It is not the aim of this paper to present any special solutions concerning the welding arc. We rather think it worth while to discuss the problem of electric arcs and their mechanism from a very general point of view, hoping that such a discussion also might shed some light on problems of the welding arc. Particularly it might be of interest to discuss the properties of the so-called high-current arcs, as distinguished from the low-current arcs, because a number of characteristic properties of the welding arc seem to be consequences of what we call the high-current arc mechanism.[1,2]

The Mechanism of Electric Arcs in General

The mechanism of any electric arc depends on the interaction of the three main parts of the discharge: the cathode drop, the anode drop, and the arc stream. The cathode drop is necessary for the production of the electrons, which carry more than 99 per cent of the current, the anode drop for the production of the compensating positive ions, whereas the arc stream is a column of high-temperature plasma which enables the current to bridge the gap between the electrodes.

We stress first the fact that cathode and anode drop both are indispensable for the arc's mechanism: the electron emission from the cathode tip may be either thermionic or may result from any other ionization process at or immediately in front of the cathode surface. If the electron emission is thermionic, the cathode spot has to be kept at a sufficiently high temperature in spite of the fact that it continually loses energy by radiation and electron evaporation. The energy necessary to compensate for this loss can be provided only by the positive ions arriving at the cathode, after they have been accelerated by the cathode drop. In all metal arcs, the cathodic electron emission certainly is not purely thermionic. The mechanism of electron production is not yet precisely known in this case, but there is no doubt that the energy required for the electron production in any case can be provided only by the ions accelerated in the cathode drop. Whatever the mechanism of cathodic electron emission may be in a particular case, a cathode drop therefore is indispensable, and by a detailed discussion it can be shown how in each case positive ions set up a space charge which is observed as cathode drop and which adjusts itself automatically so that the ions, accelerated in the space charge field (cathode drop), carry just the required energy to the cathode spot.

With the anode drop, the situation is quite analogous. Here the electrons are accelerated in the negative space charge field in front of the anode, and thus obtain the energy which is necessary to produce the positive ions which compensate for the electron space charge in the arc stream. Again it is immaterial whether these ions are emitted from the incandescent anode (this is possible only for very high temperature anodes with metal compound surfaces) or by ionization in the gas or vapor in front of the anode. An anode drop is necessary in any case, though the

Paper 51-142, recommended by the AIEE Electric Welding Committee and approved by the AIEE Technical Program Committee for presentation at the AIEE Winter General Meeting, New York, N. Y., January 22-26, 1951. Manuscript submitted October 24, 1950; made available for printing December 13, 1950.

DR. WOLFGANG FINKELNBURG is consultant with the Engineer Research and Development Laboratories, Fort Belvoir, Va.

amount of the potential drop may depend largely on the special mechanism of the ion production. Again we have an automatic adjustment of the anode drop to the required extent of ion production and thus to the externally determined anodic current density.

It is evident from this discussion that a precise knowledge of the cathode and anode drop voltages, as well as the spatial extension of these potential drop regions as functions of the arc parameters, is of tremendous interest for a quantitative understanding (and technological control) of any high-pressure arc. So far only very rough figures for the potential drops near the electrodes are known, and no figures of their spatial extension are available. For that reason we have developed, at the Engineer Research and Development Laboratories, a method of measuring those quantities by shooting thin metal probes into the arc until they touch the anode or cathode surface, respectively. The potential drop between this probe and the respective electrode, as well as the total arc voltage, the arc current, and the distance of the probe's tip from the electrode surface, are recorded simultaneously by a multigalvanometer oscillograph. Absolute figures of the potential drops still are not too certain, because it is difficult to determine the contact potential between such a probe and its surrounding plasma. However, changes of the cathode and anode drop, caused by changed discharge conditions or changed electrode materials, can be determined very accurately by this method. One of the most interesting results of our work with this method so far has been that the spatial extension of the cathode and anode drop regions for carbon arcs at atmospheric pressure can be measured, for the first time, and is found to be of the order of only a few hundredths of a millimeter. This result will help greatly in the development of a more quantitative theory of the electrodic processes of high-pressure arcs. As a variation of the previously described probe method, we used, so to speak, the negative electrode itself as a probe, thus recording the arc voltage and the arc current as functions of the simultaneously recorded distance of the two electrode tips, which in the process of measurement were quickly brought to contact and drawn apart again.

It was a surprising result that also in this experiment cathode and anode drop often could be distinguished and could be compared with the results of the probe measurements proper, thus yielding experimental figures for the unknown contact potential between plasma and metal probe.

Let us now consider the role of the arc stream and its properties. We mentioned already that the arc stream can be regarded as a column of low-resistance high-temperature plasma. The term "plasma" designates that strange physical state of any high-temperature gas or vapor which is distinguished from the normal gaseous state by a high electric and thermal conductivity, an appreciable concentration of dissociated, excited, and ionized atoms and molecules, and a number of optical and magnetic properties quite unusual for an ordinary gas. Because of the high temperature of the arc stream, which ranges from 5,000 to 12,000 degrees Kelvin, depending on the conditions,[2] the gas density in the arc stream is so much lower than that in its cooler surrounding that we may regard this cooler, nonconducting surrounding as a wall which in many respects plays the same role as the glass wall in the conventional low-pressure discharge tubes.

This plasma column which we call the arc stream conducts the current from cathode drop to anode drop. Its field strength (potential drop per centimeter length of the arc stream) is of the order of only 15 volts per centimeter in air and causes the electrons and ions to drift toward their respective electrodes. Some of them get lost continually by diffusing toward the "wall" and recombining to neutral atoms or molecules. The field strength (arc stream gradient) then adjusts itself to such a value that in the average the same number of electrons and ions are formed by ionization as get lost by recombination in the outer regions. The higher the field strength in the arc stream, the higher the energy dissipation (power per centimeter arc stream length = field strength times current) and the higher the axial arc stream temperature. This relation also explains the apparent paradox that an arc stream attains a higher temperature if it is cooled by blowing against it. Blowing reduces the conductivity by removal of charge carriers, so that the field strength increases in order to transport the impressed current, and this increase of the field strength in turn, by more violent collisions, leads to the observed increased temperature. From all this we see that the arc stream gradient is, besides the arc stream diameter, the most important property of the arc stream which must be determined. K. H. Hoecker, P. Schulz, and the author[3,4] have developed a theory from which the axial temperature and its radial distribution in an undisturbed arc stream can be computed, if diameter and gradient are known. Recently we also have used our moving-probe method with oscillographic recording for measuring arc stream gradients, even for axial temperatures up to 12,000 degrees Kelvin. Two probes were flipped through the arc stream at two points one centimeter apart, and the potential difference between each probe and one of the electrodes was recorded. The difference between the two recorded peaks evidently is the potential drop along one centimeter of the arc stream; this method is fairly free of inaccuracies because contact potentials and other causes of errors affect both probes in the same way and thus cancel, the gradient being the difference between the potentials measured at the two points of the arc stream.

Low-Current Arcs and High-Current Arcs

The arc mechanism discussed so far applies to all high-pressure arcs, independent of the amount of the arc current. Systematic studies of the carbon arc[1,2] over a wide range of currents and electrode current densities, however, have led us to the belief that there are two basic phenomena which distinguish arcs of high currents and high electrodic current densities from those operated at currents below 100 amperes and below critical current densities which depend on the electrode material. The critical densities are approximately 100 amperes per centimeter squared for the positive carbon and 5,000 amperes per centimeter squared for the negative carbon. At electrode current densities above these critical values, vapor eruptions occur continually from the electrodes and appreciably influence the mechanism of the arc. The second effect depends on the absolute current (not the current density) and concerns the arc stream. At currents above approximately 100 amperes, the formerly diffuse and structure-free arc stream seems to contract and forms a stiff column, of very high temperature, whose initial direction is always that of the negative electrode. Because of the far-reaching differences in the arc properties which are indicated by these two high-current phenomena, we designate as a low-current arc every electric arc operated at currents below 80 amperes whose electrodic current densities remain below the critical values, so that no vapor eruptions affect the arc mechanism. Conversely, we designate as a high-current arc every electric arc at currents well above 100 amperes whose arc stream exhibits the char-

acteristic contraction and stiffness which we mentioned and shall explain shortly. As an electrodic high-current arc, specifically, we designate every electric arc whose current density at at least one of the electrodes is so high that vapor eruptions, mostly in the form of vapor streams or vapor jets, influence its mechanism and properties. By this terminology, the high-current carbon arc, as used in searchlights and motion picture projection, is an anodic high-current arc with a well-established stationary high-current arc stream. I think, on the other hand, that most welding arcs have to be classified as cathodic or anodic high-current arcs, depending on whether the polarity of the electrode is negative or positive, with a high-current arc stream whose stationary radial temperature equilibrium is disturbed by the material and vapor transfer from the electrode to the work.

The Mechanism of the High-Current Arc Stream

We have studied the mechanism of the stiff, contracted high-current arc stream in some detail in the current range up to 400 amperes and have some scanty knowledge up to 1,000 amperes. The high-current arc stream differs from the low-current arc stream in three main features—its ten times higher current density (1,000 to 3,000 instead of 100 to 300 amperes per centimeter squared), its much higher temperature (10,000 to 12,000 degrees Kelvin compared with 5,000 to 7,000 degrees Kelvin), and its "stiffness," which we mentioned previously. The first two features are related to each other, because a higher current density requires a higher concentration of electrons and ions, and their production, in turn, requires a higher arc stream temperature. The arc, evidently, has two possible choices of reacting on a current increase: it can increase its diameter at constant temperature, or it can increase its temperature at constant diameter. The first possibility is represented in the low-current arc stream, the latter is characteristic of the high-current arc stream. This apparent contraction (or probably more correctly, nonexpansion) of the high-current arc stream seems to be caused, at least partly, by the arc's own magnetic field. It is well known that parallel currents attract each other because of the interaction of their magnetic fields. For this reason, the arc stream, which may be regarded as composed of independently mobile parallel paths of the electrons, tends to contract in diameter as the magnetic field increases, that is, the higher the arc current and the smaller the arc stream diameter.

The magnetic field of the arc has another, even more important, effect on the arc: it exerts a stabilizing influence. The stronger the magnetic field surrounding a current, the stronger is its tendency to remain uniform along the path of the current, that is, to prevent kinks in the current's path. Consequently, the magnetic field of the arc current causes the "stiffness" of the arc stream; it tries to remain in the prolongation of the axis of the electrode, fairly independent of air drafts which fundamentally influence the low-current arc. For this reason, we have called the high-current arc field-stabilized.[5] Being thus stabilized by its own magnetic field, the high-current arc stream also can be deviated from its direction fairly easily by external magnetic fields. This is well known to the welding engineer. He has used guiding magnetic fields to direct the arc stream to the desired spot on the work and has learned how to avoid, by symmetrical current leads, undesired magnetic fields or to compensate for them, if they occur. For special problems, for instance the electric cutting of thick iron plates, a very stiff arc stream at very high temperature seems desirable in order to produce very localized heating. Theoretically, magnetic stiffness and arc stream temperature should increase with increasing current, and actually currents of more than 1,000 amperes have been employed for this purpose. It would be of great interest to study high-current arc stream properties (current density, temperature, potential gradient, and radiation characteristics) in more detail at these high currents. In the normal welding process, the arc stream temperature should be important also, because the welding speed as well as the structure of the bead must depend on the arc stream temperature (sufficient melting, but no bubble formation, and so forth). So far as I know, no temperature measurements have been made for the contracted welding arc stream. Such a study would be of interest, far beyond the circle of the welding engineers, to all gas-discharge physicists.

Electrodic Vapor Eruptions and Their Influence on the Arc Mechanism

As already mentioned, an electrodic high-current arc is characterized by electrode vapor eruptions which influence the arc mechanism. Again the only test case which has been treated, experimentally as well as theoretically, in some detail seems to be the high-current carbon arc, from whose positive crater a steady stream of carbon vapor is emanating with a velocity between 10^3 and 10^4 centimeters per second, depending on the anodic current density. All the details of the interaction of this vapor stream with the space charges in the region adjacent to the positive electrode, and the consequent increase of the potential drop near the positive electrode, have been published in detail elsewhere.[1,2] T. B. Jones, in a most interesting paper,[6] has applied these ideas successfully in explaining the behavior of metal anode spots of a high-current arc which had much more similarity to a welding arc.

A transport of electrode material through the arc also has been studied in the high-current carbon arc. Since the anodic vapor stream mentioned previously consists of carbon vapor (and those materials, vaporized, which we may have mixed into the carbon core), we find a material deposit if we bring the negative electrode (or any other electrode) into the anode vapor stream. If we operate the arc with reasonably pure carbons, we find as deposit, surprisingly enough, a very dense and hard graphite of high purity. Details are published elsewhere.[1] The fact as such is known to the welding engineer. Whenever he uses, for special purposes, a carbon electrode, he uses it with negative polarity, because otherwise he would find an undesired change of the work quality caused by an absorption of carbon vapor by the molten spot of the work.

In the customary welding arc operation, the current density at the work is low; only at the electrode do we have a high current density and, consequently, the typical high-current mechanism. Therefore, we believe that, at least with positive polarity of the electrode, vapor eruptions of the kind studied in our high-current carbon arcs may have considerable bearing on the transport of material (mostly in the form of liquid droplets) from the electrode to the work. For this reason, positive polarity of the electrode should be a decisive advantage. Vapor eruptions are also possible from the negative electrode;[7-9] however, they require much higher current densities. No doubt, besides vapor eruptions and electric forces affecting charged particles, there exist further mechanical forces in the different arc regions which act on larger objects such as metal droplets. Unfortunately, not too much seems to be known about their theory, though the forces themselves are well known to every worker in this field.

Conclusion

In concluding this discussion of the fundamental properties and the mechanism of low- and high-current arcs, I should like to express the hope that the general outline of arc physics may be of some help in studying the complex, nonstationary form of the welding arc, just as every investigation of its properties or behavior is of great interest to the gas-discharge physicist in general.

References

1. Hochstromkohlebogen, **W. Finkelnburg.** Springer-Verlag, Berlin and Heidelberg, Germany, 1948. English presentation (not as complete): The High Current Carbon Arc, *PB-81644*, Office of Technical Services, Department of Commerce, Washington, D. C., 1947.

2. The High Carbon Arc and Its Mechanism, **W. Finkelnburg.** *Journal of Applied Physics* (New York, N. Y.), volume 20, May 1949, page 468.

3. Theory of the High-Current Arc Stream (in German), **K. H. Hoecker, W. Finkelnburg.** *Zeitschrift fur Naturforschung* (Wiesbaden, Germany), volume 1, 1946, page 305.

4. On the Heat Conductivity in the High-Current Arc Stream (in German), **K. H. Hoecker, P. Schulz.** *Zeitschrift fur Naturforschung* (Wiesbaden, Germany), volume 4a, 1948, page 266.

5. Systematics of Electric Arc Types (in German), **W. Finkelnburg, K. H. Hoecker.** *Naturwissenschaften* (Göttingen, Germany), volume 33, 1946, page 55.

6. Formation and Characteristics of Anode Spots in High Current Arcs, **T. B. Jones.** Massachusetts Institute of Technology, Electronics Conference, Cambridge, Mass., April 1949.

7. Production of High Velocity Mercury Vapor Jets by Spark Discharges, **J. R. Haynes.** *Physical Review* (New York, N. Y.), volume 73, April 15, 1948, page 891.

8. Electrode Vapor Jets in Arc and Spark Discharges, **W. Finkelnburg.** *Physical Review* (New York, N. Y.), volume 74, July 15, 1948, page 222.

9. A Theory of the Production of Electrode Vapor Jets by Sparks and Arcs, **W. Finkelnburg.** *Physical Review* (New York, N. Y.), volume 74, November 15, 1948, page 1475.

No Discussion

New Electrodes for Stabilizing Inert-Gas Welding Arcs

J. D. COBINE
MEMBER AIEE

C. J. GALLAGHER
NONMEMBER AIEE

WITH THE increased use of inert-gas arc welding, especially in automatic welding machines, problems of arc ignition and stability become important. It is the purpose of this paper to discuss these problems and to describe new welding electrodes which eliminate some of the difficulties.

The conventional welding electrode is of some nonconsumable material, usually tungsten, and starting is accomplished either by contact or by a high-frequency spark. When spark starting is used, ignition may be quite erratic, depending on the previous history of the tungsten electrode. If the electrode is cold, the arc may not form immediately, or at all, and when formed it may be extremely mobile, with the footpoint moving rapidly over the tungsten surface. In an automatic setup, this type of behavior can lead to losses in both time and material. An example of what may happen is shown in Figure 1. This shows the effect on the work of slow starting and arc wander. In addition, damage may be done to the welding torch.

The fundamental cause of the phenomena described lies in the nature of the current transfer at the tungsten surface. Since the wandering occurs only on straight-polarity welding (that is, the tungsten is cathode), it is clear that we must inquire into the nature of the cathode spot on the electrode. For our purposes, we may consider briefly two types of cathode, namely, the thermionic and the cold cathode. A thermionic cathode is one which operates at a sufficiently high temperature to supply the required current on the basis of the Richardson-Dushman Law.[1] A cold cathode, on the other hand, does not require such a high temperature; the current is supplied by a mechanism which is not fully understood. It does appear that for a cathode spot to exist on a cold cathode, some oxide must be present on the surface.[2,3]

In straight polarity inert-gas arc welding, the tungsten electrode may serve as either type of cathode, depending on the operating conditions. When starting is attempted with a cold electrode, evidently an arc cathode spot cannot be established unless there is some oxide present. If the arc does start, there are two possible conditions, depending on the amount of oxide present and on the electrode current density. If there is sufficient oxide, the cathode spot will stay on the tip and, if the current is great enough, the cathode will become a thermionic emitter as its temperature rises. If there is not enough oxide, the cathode spot will quickly clean the surface at the spot itself and then wander to new oxide-bearing regions. This cleaning action and wandering can take place with great rapidity, before the electrode has become heated to the thermionic condition. If the arc does not start, it is probably because there is no oxide present. The high-frequency spark itself cannot establish a thermionic spot. The condition of no oxide on the electrode can be obtained easily if the electrode has once been operated and then allowed to cool in the inert atmosphere. Cooling in air does not solve the problem, since the oxidation is difficult to control and may produce a dirty weld on the next try.

For straight polarity welding (electrode negative), the solution to the problems discussed previously has been found in the form of specially prepared welding electrodes in which a highly refractory oxide has been supplied by several methods. These electrodes, to be described in the following section, give highly reliable firing on high frequency with little or no delay and subsequent arc wander. They have, in addition, other desirable properties, such as low pickup voltage and greatly extended current range compared to tungsten.

Types of New Electrodes

One group of electrodes uses zirconia (ZrO_2) for the oxide, either as a coating or as a core. When used as a coating, the zirconia is applied to a tungsten rod in a thin coating, 1 to 3 mils thick, with a

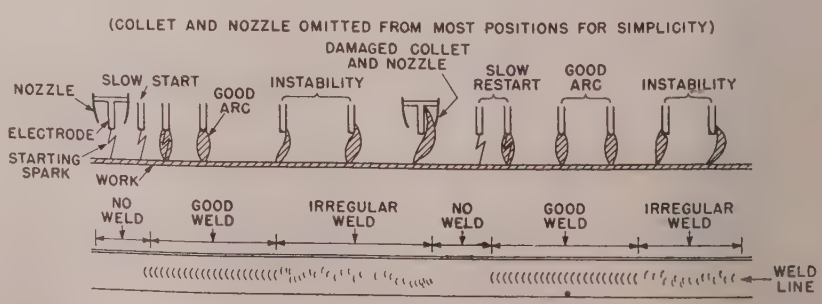

Figure 1. Normal tungsten electrode used in inert-gas arc welding

Paper 51-143, recommended by the AIEE Electric Welding Committee and approved by the AIEE Technical Program Committee for presentation at the AIEE Winter General Meeting, New York, N. Y., January 22-26, 1951. Manuscript submitted August 1, 1950; made available for printing December 7, 1950.

J. D. COBINE and C. J. GALLAGHER are both with the General Electric Research Laboratory, Schenectady, N. Y.

The authors acknowledge with thanks the assistance of M. R. MANY in preparing much of the electrode materials, and also the co-operation of E. F. POTTER, A. E. NEAR, and N. A. CHAPIN in testing them under practical conditions.

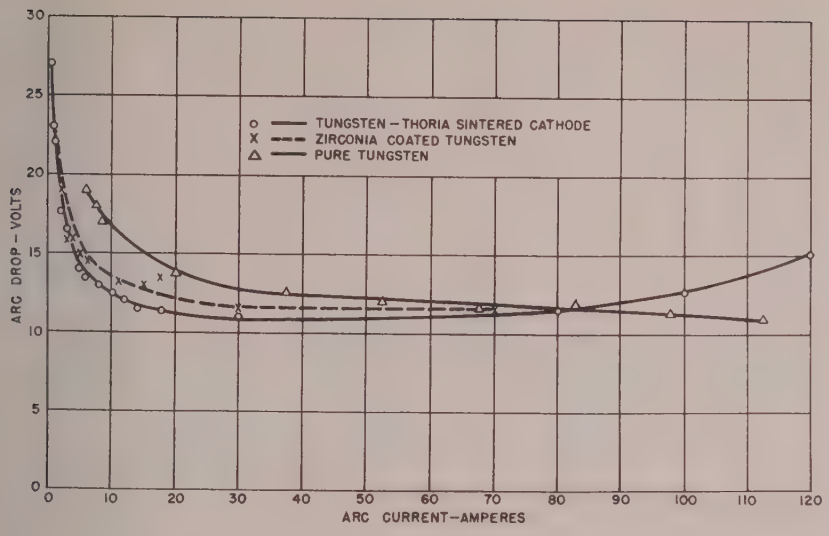

Figure 2. Volt-ampere characteristics of arcs in argon (arc length = 0.1 inch)

suitable binder, such as water glass. Suitable high-temperature firing produces a hard, tenacious coat. As a core, the zirconia may be used in a shell of almost any metal, such as tungsten or tantalum, or the low-melting-point materials, such as copper, aluminum, or stainless steel.

A second group of electrodes makes use of thoria (ThO_2). The thoria may be used as a coating on tungsten, but best results were obtained when used either as a core, again in any of the metals, or as a component in a sintered material. The sintered electrode was made by extruding and firing a ball-milled mixture of thoria and tungsten powder. The optimum proportions appear to be about 15 parts of thoria to 100 parts of tungsten.

Properties of New Electrodes

The important properties of the new electrodes in so far as welding is concerned are:

1. Low open-circuit voltage required for reliable starting
2. Large current-range for a given size of electrode
3. Low arc voltage over the operating range of current
4. Low rate of consumption of electrode material

Items 1 and 2 are summarized in Table I for arcs in argon.

It will be noted that the thoria-tungsten and the zirconia-tungsten electrodes require much lower open-circuit voltages and also that the current range is extended considerably over that of pure tungsten. The minimum current for the thoria-tungsten can be made as low as 0.2 ampere by using a smaller size electrode or pointing a larger one. These low currents may be of interest in special welding applications.

With the low-melting-point metals, the maximum currents are lower than those of the tungsten-base materials. For example, with a copper tube with thoria core, the upper limit is about 150 to 200 amperes. This holds for outside diameters of about 0.125 to 0.1875 inch, with the cross-sectional area of the core about one-half that of the copper. With the use of the low-melting-point metals, some of the metal vapor may appear in the arc, especially at the high end of the current range.

The volt-ampere characteristics of arcs in argon for three types of electrodes are shown in Figure 2. In each case, a water-cooled copper anode was used. Significant differences appear only below about 50 amperes, in which case the drop is highest for tungsten and lowest for the sintered tungsten-thoria. The voltage drop increases at the high-current end of the tungsten-thoria characteristic probably because of the increased voltage drop in the resistor, since the resistivity of the sintered material is about twice that of tungsten at the operating temperature. It was possible to start the arc with zirconia and thoria electrodes at any currents, but the tungsten would start only at higher currents.

The rate of consumption of material for all electrodes is, in general, less than for tungsten. When used in helium, slightly higher rates of loss are observed, due to increased heating, and possibly to less efficient repression of cathode evaporation by the lighter helium atom.

Table I. Electrode Characteristics for Arcs in Argon

	Pure Tungsten	Zirconia-Tungsten	Thoria-Tungsten
Open-circuit voltage for starting with high-frequency spark, volts	190*	40	25
Current range, amperes			
1/16 inch diameter	65-150**	6-200	
3/32 inch diameter approximate	140-280**		6-375

* Approximate.
** Practical Aspects of Inert Gas-Welding, H. A. Huff, Jr., A. N. Kugler. *The Welding Journal* (New York, N. Y.), volume 28, 1949, page 129.

Cathode Spot Phenomena

It is of interest to note some differences in the appearance of the various electrodes under operating conditions which might throw some light on the mechanism of the cathode spot. In Figure 3 are shown some photographs of the cathode spots on the different electrodes operating in argon at 40 amperes. The copper anode was moved slightly to one side to permit end-on viewing of the cathode. A pure tungsten electrode is shown in Figure 3A. The "spot" appears to consist of two zones, a very hot, probably molten, zone in the center, with surrounding highly luminous ring of lower temperature. If the current is divided by the area of the inner zone, a current density of 4,600 amperes per square centimeter is obtained. If one uses instead the total luminous area, the current density is 2,940 amperes per square centimeter. If we assume that the

Figure 3. Cathode spots on various electrodes (1/8-inch in diameter)

A. Pure tungsten
B. Zirconia-coated tungsten
C. Thoria core in sintered tungsten tube
D. Thoria core in copper tube
E. Sintered tungsten thoria electrode

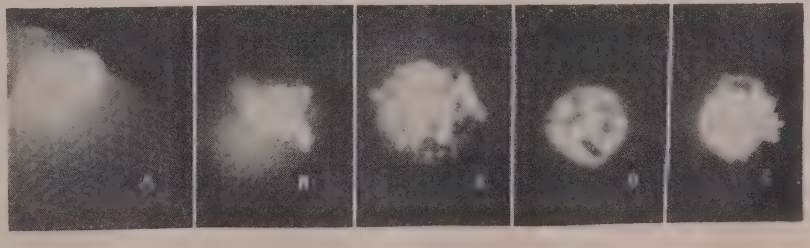

tungsten is a thermionic emitter at 4,000 degrees Kelvin, the Richardson-Dushman equation gives a current density of 3,600 amperes per square centimeter. It thus seems reasonable to assume that the tungsten is a thermionic emitter at a temperature above 4,000 degrees Kelvin.

Figure 3B shows an end-on view of a tungsten rod coated with zirconia. Again two zones appear at the cathode spot. It was observed that the area in the center was not molten, but was covered with an intense blue glow. This is apparently the primary emitting area and corresponds to a current density of greater than 40,000 amperes per square centimeter. It seems highly improbable that such a current density could be supplied by thermionic emission.[3] The zirconia-coated electrode appears to emit electrons by some "cold" cathode mechanism requiring an oxide layer which is not fully understood.

The effect of the thoria is different from that of the zirconia. The thoria-containing electrodes are shown in Figures 3C, D, and E. Measurements of the current density on the thoria-cored copper tube lead to a figure of about 2,700 amperes per square centimeter (Figure 3D). The observed temperature was about 3,300 degrees Kelvin. The thermionic current density calculated for thoria at this temperature is 3,700 amperes per square centimeter, which is in reasonable agreement with the observed value, considering uncertainties in the temperature and thermionic constants.

The cathode spot on the sintered tungsten-thoria electrode is shown in Figure 3E. The measured current density is 2,320 amperes per square centimeter, again in reasonable agreement with the calculated value. Thus, the function of the thoria appears to be that of providing a low work function surface, so that the required current can be supplied by thermionic emission at a temperature much less than would be possible with tungsten.

References

1. Gaseous Conductors (book), **J. D. Cobine.** McGraw-Hill Book Company, New York, N. Y., 1941, page 107.
2. Arc Discharge Not Obtained in Pure Argon Gas, **G. E. Doan, J. L. Myer.** *Physical Review* (New York, N. Y.), volume 40, 1932, pages 36–39.
3. Current Density of the Arc Cathode Spot, **J. D. Cobine, C. J. Gallagher.** *Physical Review* (New York, N. Y.), volume 74, 1948, page 1524.

No Discussion

940–960 Megacycle Communications Equipment for Industrial Applications

FRANK B. GUNTER
MEMBER AIEE

DISCUSSIONS on the reasons for development, the technical details, and the application of microwave communications equipment have been presented previously.[1,2,3] A study of the schematics for these equipments will make it obvious that microwave equipment is made up of arrangements of parts which differ widely from those normally encountered in electronic equipment for industrial applications. The purpose of this paper is to show why this difference exists. For example, it will be shown why a microwave receiver may need 20 or more tubes and a power-line carrier receiver may require only one tube. To illustrate why microwave equipment is different, an analysis will be made of portions of the Westinghouse type *FB* 940–960-megacycle communications equipment.

Frequency

The most obvious difference is in the frequency at which the equipment operates. Generally speaking, frequencies of about 1,000 megacycles and higher are considered microwave frequencies. Certain bands of frequencies have been set aside by the Federal Communications Commission for fixed station operation for industrial applications. These bands are shown in Table I.

The choice of frequency band is dependent on many factors. Among these are availability of components, propagation characteristics, number of signals to be transmitted, and type of modulation. The design of the equipment depends to a large degree on the band chosen.

The Westinghouse type *FB* equipment will operate in the 952–960-megacycle industrial band. Some of the reasons why this band was chosen are:

1. There is adequate spectrum for the services contemplated.
2. The use of many conventional circuits is permitted, giving lower initial cost and cheaper maintenance costs.
3. Availability of suitable components at low cost.
4. Better propagation characteristics.
5. Simpler installations since equipment may be located indoors in convenient positions and connections made to antenna with relatively low cost conductors.

Frequency Control

It is desirable for spectrum economy and mandatory because of governmental regulations that the center or carrier frequency of most radio communications systems be kept constant within very narrow limits. These limits usually are specified as a percentage of center frequency and are met in low-frequency equipment by using crystals or inductance capacitance circuits whose electrical constants do not vary appreciably with temperature, voltage, or loading.

As we go higher in frequency with crystal oscillators, the point is reached where crystals cannot operate at transmitter output frequencies and are forced to add multiplier stages after the crystal oscillator to get the desired output frequency. The multiplier stages have the disadvantage that they multiply the error in center frequency and also give many undesired frequencies which may interfere with other services.

As we go higher in frequency with ordinary inductance capacitance circuits, these circuit elements get so small that the changes due to thermal expansion alone are often sufficient to cause excessive drift in carrier frequencies. It is necessary to make these elements of materials having high dimensional stability or else go to elaborate circuits to compensate for the variations.

When the carrier frequency of a communications transmitter and the local oscillator of a communications receiver vary, there are two ill effects. First, fewer channels can be placed in a given bandwidth and second, the acceptance band of the receiver must be greater, permitting additional noise to be received. To illustrate this point, at several frequencies, Table II was prepared assuming amplitude modulation with maximum modulating frequency of 3 kc, transmitter and receiver local oscillators each with a

Table I. Frequencies for Fixed Industrial Stations

Band, Megacycles	Bandwidth Megacycles	Per Cent
952– 960	8	0.84
1,850– 1,990	140	7.3
2,110– 2,200	90	4.1
2,450– 2,700	250	9.7
6,575– 6,875	300	4.5
12,200–12,700	500	4.0
16,000–18,000	2,000	11.8
26,000–30,000	4,000	14.3

Table II. Poor Use of Frequency Spectrum

Frequency, Megacycles	Transmission Bandwidth Required, Kilocycles	Receiver Bandwidth Required, Kilocycles	Relative Receiver Noise Voltages
0.1	6.005	6.01	1
1.0	6.05	6.10	1.08
30	7.50	9.00	1.22
150	13.5	21.0	1.87
1,000	56.0	106.0	4.20
2,000	106.0	206.0	5.88
6,000	306.0	606.0	10.1

Paper 51-144, recommended by the AIEE Carrier Current Committee and approved by the Technical Program Committee for presentation at the AIEE Southern District Meeting, Miami, Fla., April 11–13, 1951. Manuscript submitted May 18, 1950; made available for printing February 27, 1951.

FRANK B. GUNTER is with Westinghouse Electric Corporation, Baltimore, Md.

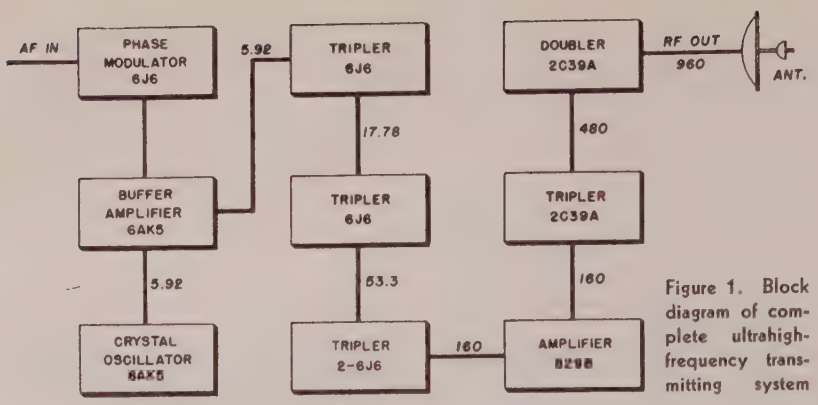

Figure 1. Block diagram of complete ultrahigh-frequency transmitting system

Table III. Frequency Spectrum When Using Four Signals Multiplexed

Frequency, Megacycles	Transmission Bandwidth for Four Signals, Kilocycles	Receiver Bandwidth for Four Signals, Kilocycles	Receiver Bandwidth Per Signal, Kilocycles
0.1	27.005	27.01	6.752
1.0	27.05	27.10	6.775
30	28.5	30.00	7.50
150	34.5	42.00	10.50
1,000	77.5	127.00	31.75
2,000	127.0	227.00	56.75
6,000	327.0	627.00	156.75

frequency stability of 0.005 per cent, and noise of constant amplitude at all frequencies.

Table II demonstrates that even with relatively good frequency control the amount of spectrum used up due to variations in transmitter center frequency gets very large with respect to that required for intelligence transmission and further that the wide receiver bandwidths, necessary to make allowance for these variations, permit excessive noise to be accepted. The poor use of the spectrum illustrated in Table II for single-channel amplitude modulation is one of the reasons why single-channel microwave equipments are seldom used. If several communications circuits are multiplexed and this composite signal used to modulate one microwave carrier, much better use is made of the spectrum. This can be demonstrated by the example of Table III, based on multiplexing four signals (on an amplitude-modulation basis with 2-kc guard bands) and using the same oscillator stability as in Table II.

An analysis of the receiver bandwidth per signal given in the last column of Table III leads to the conclusion that very close frequency control is desirable if the microwave spectrum is to be used efficiently. It is obvious from Table I, however, that at the higher frequency bands there is enough spectrum available to allow for bandwidths per signal which would be prohibitive at lower frequencies.

In the design of the type *FB* Microwave equipment, crystal control was supplied for both transmitter center-frequency control and receiver local-oscillater control. The receiver crystal operates at about 28 megacycles and is followed by multiplier stages particularly designed to minimize the production of spurious signals. The transmitter crystal operates at about six megacycles. This low frequency was necessary because of the type of modulation. To minimize spurious signals, all multiplier stages in the transmitter up to 160 megacycles were made push-pull triplers which have practically no even-order harmonics. At the higher frequencies, the multiplier stages were shielded to reduce spurious output.

The variations in transmitter output and receiver local-oscillator frequencies for a 50-degree variation in ambient temperature are each ±15 kc, giving a total increase in receiver bandwidth to make allowance for frequency variation of ±30 kc or 0.003 per cent of center frequency.

Method of Modulation

As has been shown, the use of amplitude modulation with realizable frequency stabilities results in poor usage of the spectrum and results in reduced signal-to-noise ratios. Frequency modulation, pulse-time modulation, pulse-code modulation, and other systems which give better signal-to-noise ratios at the expense of a not too great percentage increase in bandwidth required per channel normally are used in microwave equipments. The general type of modulation used in a frequency band is determined by available components, techniques, and bandwidth as well as economic considerations.

In present-day microwave systems, phase and frequency modulation are usually used when the number of signal channels to be transmitted over a single microwave equipment is less than ten. This is true whether the signal is a 3-kc-wide voice frequency circuit or a 4-megacycle-wide television circuit. When the number of channels is greater than ten, pulse-type systems usually are used.

In selecting the type of modulation to be used on the type *FB* equipment, it was decided that a maximum of seven voice-frequency channels would meet most of the industrial applications for which it was intended. Crystal control was desirable for the reasons outlined previously. An analysis of methods for obtaining suitable modulation with crystal control led to the conclusion that phase modulating a low frequency crystal output and multiplying its deviation to obtain the desired deviation in the transmitter output would be the simplest and most foolproof system.

Phase modulation has the character-

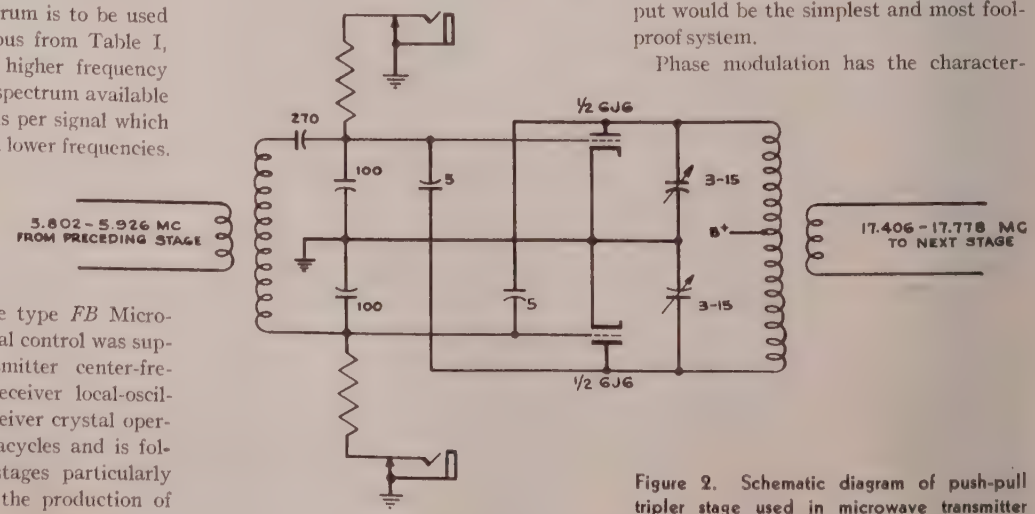

Figure 2. Schematic diagram of push-pull tripler stage used in microwave transmitter

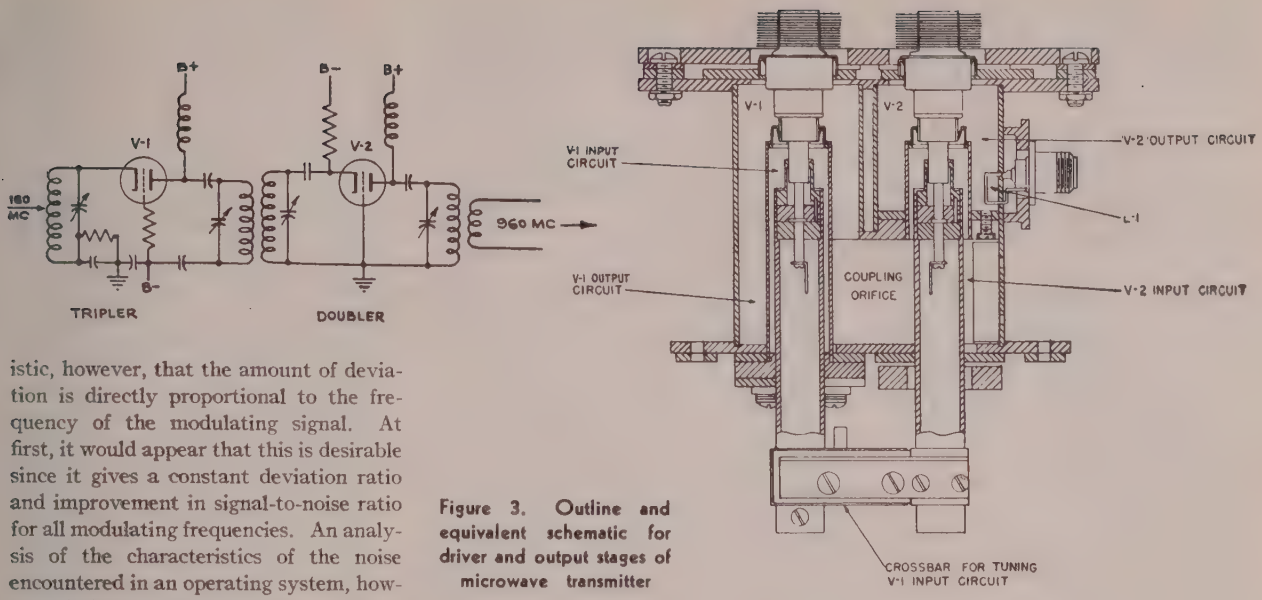

Figure 3. Outline and equivalent schematic for driver and output stages of microwave transmitter

istic, however, that the amount of deviation is directly proportional to the frequency of the modulating signal. At first, it would appear that this is desirable since it gives a constant deviation ratio and improvement in signal-to-noise ratio for all modulating frequencies. An analysis of the characteristics of the noise encountered in an operating system, however, indicates that low frequency noise predominates and that the same signal-to-noise ratios can be obtained at high modulating frequencies with a greatly decreased deviation ratio. Accordingly, it was decided to modulate the transmitter with a signal whose amplitude was inversely proportional to frequency to give essentially constant deviation at all modulating frequencies. Thus, the equivalent of frequency modulation has been obtained indirectly without the excessive cost of center-frequency stabilization required for direct frequency modulation and at the same time a major saving in bandwidth over phase modulation has been made.

To minimize crosstalk and intermodulation in the several signals to be transmitted, it is necessary that the distortion introduced by modulation be very low. Usually, variable reactance circuits are used in phase modulators, and very accurate tuning of the reactance circuit is required to obtain very low distortion with most such circuits. The phase modulator used in the type *FB* equipment is a variable conductance type which is not highly critical in adjustment for distortion percentages less than one per cent. This phase modulator uses a triode-type tube and shifts the phase of the current in a plate tank circuit which is common to the modulator and a buffer amplifier driven by the crystal oscillator. The complete transmitter is shown in block diagram in Figure 1 with the tube types indicated.

Frequency Multiplication

As indicated previously, it is not possible to get oscillator crystals which will operate at frequencies in the microwave spectrum. If crystal control is used in a microwave transmitter, then it is necessary to multiply the output of the crystal oscillator to get the desired output frequency. Also if distortion is to be kept at a minimum in a phase modulator, the range of phase deviation in the modulator must be kept small, necessitating several subsequent multiplier stages if a reasonable deviation ratio is to be obtained in the output signal. In the type *FB* equipment, the transmitter crystal frequency of approximately 6 megacycles is determined by the low-distortion requirements and the required deviation ratio. Tests proved that (1) within the allowable distortion limits, a frequency deviation of about 200 cycles was the maximum permissible, and that (2) an output deviation of approximately 35 kc was required for the desired signal-to-noise ratio. These two factors determine that a multiplication of about 160 times is required in the transmitter.

As mentioned previously, multiplication increases the possibility of spurious radiation and increases the error in crystal frequency. To minimize spurious radiation, push-pull tripler stages similar to those in Figure 2 were used wherever possible in the transmitter. This gave a multiple advantage. First, even-order harmonics are cancelled out by the push-pull action of the tube. Second, the operating frequencies of successive stages are separated enough so that circuit constants can be selected to obviate the possibility of tuning to the wrong harmonic. Third, the use of push-pull circuits with a small amount of positive feedback enables tubes of low rating to operate at high efficiency.

Three tripler stages and a buffer amplifier of conventional design give a multiplication of 27 times to arrive at a frequency of approximately 160 megacycles, as shown in Figure 1; at frequencies much higher than this, conventional circuits have low efficiency and generally are not used. The two final multiplier stages of the transmitter use re-entrant coaxial circuits as tuned elements and utilize tubes that have very low interelectrode spacing and capacity and a mechanical configuration which permits convenient application to coaxial tank circuits. The first of these tubes is a tripler stage with an output frequency of 480 megacycles and the second is a doubler stage having an output in the 940 to 960-megacycle band.

The mechanical construction and a roughly equivalent schematic circuit for the last two stages of the transmitter is shown in Figure 3. Tubes, circuit constants, and operating voltages were selected to give 5 watts' output. Provision was made, however, in the design to permit operation at 15 watts' output where desirable.

Propagation and Antennas

At microwave frequencies, transmission usually is limited to line-of-sight paths. With unity-gain antennas, the transmission losses even with line-of-sight paths are very high and would require very high power transmitters to get even short-range operation. It is possible to get economical transmission over reasonably long distances because of two factors. Because of the short wavelength, it is possible to build relatively small antennas

having high power gain since the gain of an antenna is proportional to the ratio of its area to the square of the operating wavelength. The use of such high-gain antennas both for transmitting and receiving effectively increases the power output of the transmitter. Also, at microwave frequencies there is practically no man-made or natural static which enables satisfactory signal-to-noise ratios to be obtained at signal levels much lower than is practical at lower frequencies. Formulas showing the relation between free space path loss and antenna gain are given in other papers.[1,2] It can be shown that increasing the size of antennas used decreases the apparent path loss between communications terminals.

However, if the path loss were such that extremely large antennas were required and the low experienced over comparable distances with power line carrier it is seen that there is a very great difference. A simple example will illustrate this.

A 960-megacycle microwave system operating over a 25-mile path with 7-foot-diameter antennas will have a total path and coupling loss of about 100 decibels. A power line carrier system operating over a 25-mile long transmission line will have a total path and coupling loss of the order of 25 decibels. If the noise level at the input of the receiver were the same in each case, then the microwave transmitter output voltage would have to be 30 decibels, or 10,000 times as great to give the same signal-to-noise ratio at the input to the receiver. However, there is much more noise at microwave frequencies and the receiving noise is small, that generated in the microwave receiver itself. This enables operation of microwave equipment over considerable distances with transmitter power outputs which are of the same order as power line carrier transmitter outputs. It does mean, however, that the gain of microwave receivers has to be many times as great as that of carrier receivers with a resultant increase in complexity and number of tubes.

The type *FB* microwave equipment is designed to operate with a path loss between transmitter output circuit and receiver input circuit of up to 125 decibels. A wide range of sizes of antennas and types of coaxial cables for interconnection with the equipment is available so that the most economical installation can be worked out for a given application.

Receiver Noise Considerations

As indicated, at microwave frequencies the predominant noise is that generated in the receiver itself. Most of this receiver noise is generated in the first high-gain stage of the receiver. It is important, therefore, to give serious study to the design of these stages. Amplifiers operating at microwave frequencies usually have poor noise characteristics, making it desirable to convert the microwave signal to a lower frequency by means of a low noise converter and then to use amplifiers having better noise characteristics to do the amplification. A synthetic crystal diode is usually used as a mixer in the input circuits of microwave receivers to convert the microwave frequency to a much lower frequency.

In the type *FB* microwave receiver, a type *1N25* crystal having low noise figure and good overload characteristics is used as a mixer. This crystal, which is housed in a cartridge as shown in Figure 4, is fed a signal from the receiver antenna and from a crystal controlled local oscillator multiplier chain, as shown in Figure 5. The local-oscillator signal, which is about 57 megacycles higher in frequency than the incoming signal from the antenna, is mixed with that signal in the crystal detector. The output from this mixer contains the input frequencies, sums, and differences of the input frequencies, and harmonics of the input frequencies. A tuned amplifier, indicated as the high-intermediate-frequency amplifier in Figure 5, amplifies the difference frequency, which is about 57 megacycles.

The first two stages of the high-intermediate-frequency amplifier are connected in a circuit which has the low noise characteristic of a triode and the high gain characteristic of a pentode tube.[6] These two stages effectively act as the first high-gain stage of the receiver and their low noise figure gives the entire receiver a low noise output.

Receiver Spurious Response

Since in most microwave receivers a crystal or other mixer having a very wide frequency response is used in the input circuits, there is danger of undesired signals being accepted by the receiver and producing interference or unsatisfactory operation by saturating the input circuits so that the desired signal is not received.

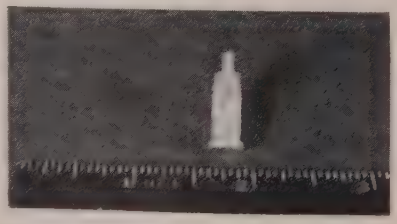

Figure 4. Crystal diode used as mixer in input stage of microwave receiver

In the type *FB* receiver a tuneable-cavity-type preselector is used in front of the mixer crystal. This preselector, together with the last multiplier stage of the local oscillator multiplier chain and the crystal mixer, are shown schematically in Figure 6. The upper portion of Figure 6 enclosed in the heavy lines represents the preselector. The lower portion is the multiplier stage of the local-oscillator source. The incoming and local oscillator signal are fed by *L-4* to the crystal mixer. To give increased protection against the likelihood of undesired signal at frequencies higher than the desired one getting through to the mixer, an additional low pass filter comprising *C-1*, *L-6*, and *C-4* is included in the circuit to the mixer.

Laboratory tests on the type *FB* receivers indicate that the rejection of spurious signals is more than 70 decibels.

Receiver Gain

As pointed out in the foregoing, the high path attenuation and low noise at microwave frequencies make it possible to operate with satisfactory signal-to-noise ratios with very low input signals. In order to get maximum range, these very low input signals must be amplified to a usable level and thus the intermediate frequency amplifiers of microwave receivers must have very high gain. In the design of amplifier for microwave receivers using pulse or other wide band modulation, it is not possible to realize a large gain per stage for two reasons. First, the gain per stage must be kept low enough to prevent oscillation due to feedback through tube interelectrode capacity. Second, for a given tube type and circuit, the product of gain and bandwidth is a constant. For a *6AK5* tube, this gain bandwidth product is approximately 62 megacycles per second, which means that for a bandwidth of 6 megacycles a gain per stage of only 10 could be realized. In any tube, the gain bandwidth product is given by $Gm/2\pi C$, where C is the sum of input and output capacity of the tube and stray capacity of the circuit.

In the type *FB* microwave receiver, a total gain of 90 decibels in the high-intermediate-frequency amplifier and 70 decibels in the low-intermediate-frequency amplifier is obtained. The 67-megacycle strip has a bandwidth of 1.2 megacycles and the 10.7-megacycle strip has a bandwidth of 0.3 megacycle.

In the design of such high-gain amplifiers, extreme caution has to be taken to provide safeguards against oscillation.

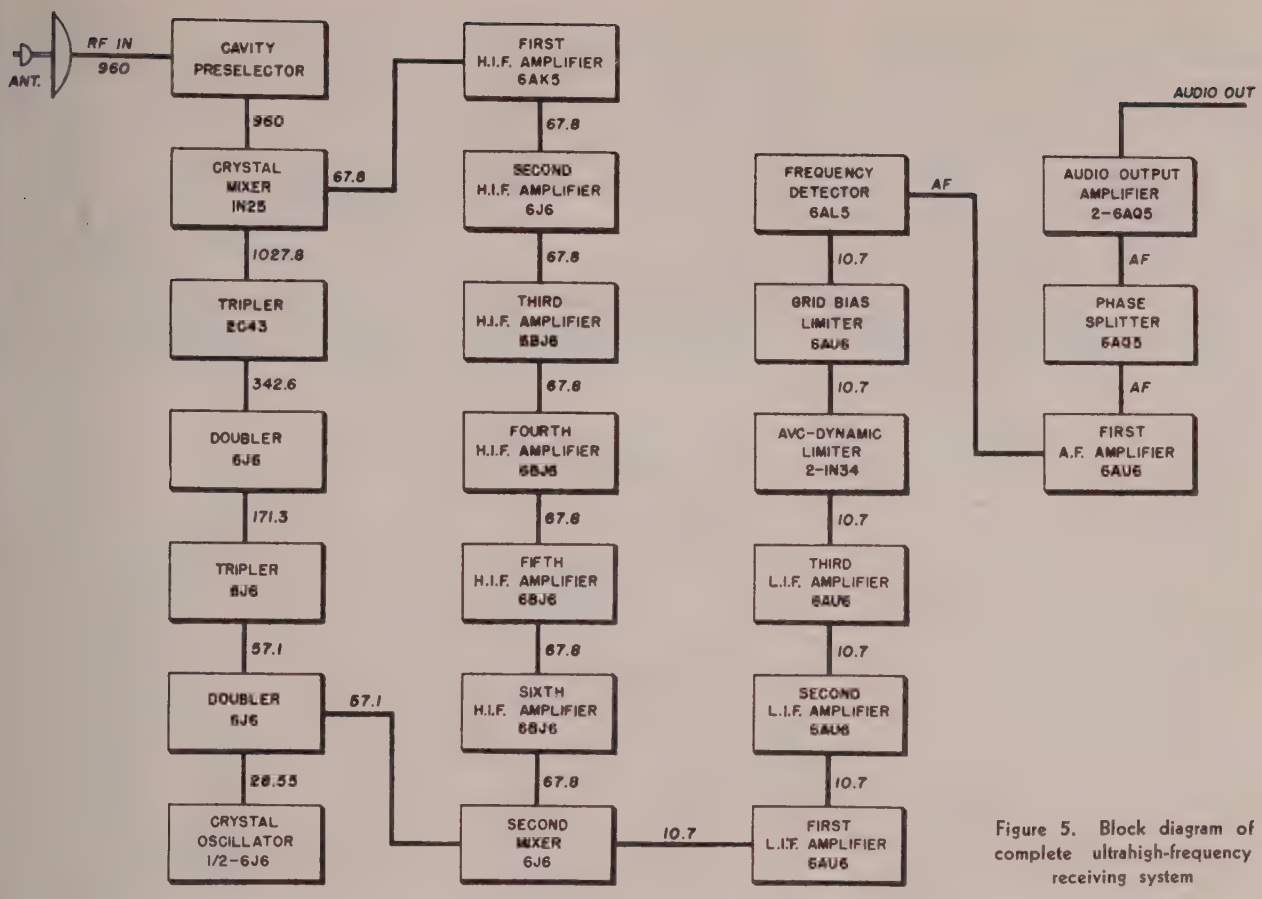

Figure 5. Block diagram of complete ultrahigh-frequency receiving system

Lead lengths must be kept to an absolute minimum. The importance of this is illustrated by the fact that a 1-inch-long length of number 20 wire has a reactance of 8 ohms at 60 megacycles. In the type *FB* receiver each intermediate-frequency amplifier uses a separate subchassis with dimensions designed to keep lead lengths down and to act as a section of waveguide operating below cutoff frequency in order to attenuate feedback which is actually radiated from one circuit to another in the amplifier.

Receiver Input Variations

In microwave systems, there usually are relatively wide variations in receiver input levels due to differences in path lengths, multipath transmission, and other causes. In practically all systems, some device is used to keep the input to the detector of the receiver essentially constant. On frequency-modulated receivers, these amplitude variations could be eliminated completely without any loss of intelligence and, in fact, should be eliminated for low-distortion output from discriminators and other frequency detectors. These amplitude variations are removed in frequency-modulated receivers

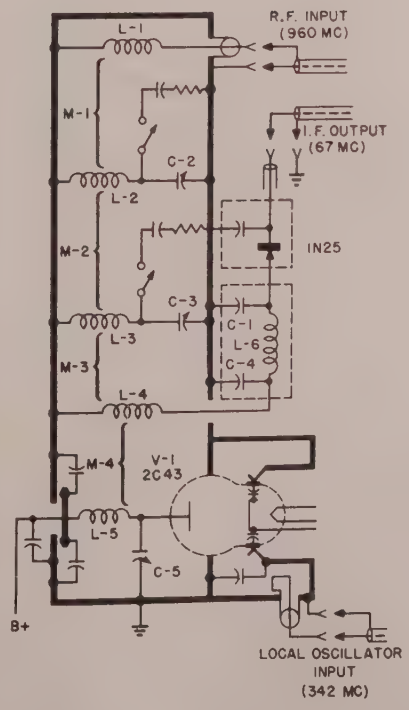

Figure 6. Equivalent schematic of microwave receiver input circuits including tunable preselector and crystal mixer

by a limiter. This limiter can be either one or two stages, with the 2-stage type usually preferred.

In the type *FB* receiver, a 2-stage limiter is used. The first limiter stage utilizes *1N34* crystals and the second is a grid-bias type having a very short time constant to enable it to remove the very-high-frequency amplitude modulation caused by adjacent channel signals.

Detectors

The type of detector used in a microwave system depends, of course, on the type of modulation used. Generally speaking, however, the much greater signal bandwidth used and the necessity for eliminating harmonic products and intermodulation of the multiplicity of signals which may be transmitted over a single channel demand very great care in the design of detectors. System distortions of the order of 4 or 5 per cent which are ordinarily acceptable with low-frequency equipment would cause prohibitive intermodulation and crosstalk on many microwave equipments. Pulse-time, pulse-width, and pulse-code modulation schemes are completely different in philosophy to the schemes normally used in

low-frequency equipment and therefore require completely different types of detectors.

In the type *FB* receiver, the incoming signal is of the frequency-modulation type. The frequency detector is designed to have excellent linearity out to ±400 kc over wide variations in temperature. The distortion in a complete system consisting of a type *FB* transmitter and a type *FB* receiver is less than 1 per cent.

Microwave equipment uses the same kinds of parts applied in the same general manner as in low-frequency equipment. However, because of the wide frequency spectrum available, realizable antenna gains, propagation characteristics, and economic considerations, microwave equipment is widely different from low frequency in design and application.

References

1. 2,000-Megacycle Television Program Chain, **F. M. Deerlake.** *Electronics* (New York, N. Y.), February 1948, pages 94–7.

2. Wide-Band Television Transmission Systems, **Emile Labin.** *Electronics* (New York, N. Y.), May 1949, pages 86–9.

3. 6,000-Mc Television Relay System, **William H. Forster.** *Electronics* (New York, N. Y.), January 1949, pages 80–5.

4. Propagation of Very Short Waves, **D. E. Kerr.** *Electronics* (New York, N. Y.), January 1948, pages 124–8; February 1948, pages 118–23.

5. Field Testing a Microwave Channel for Voice Communication, Relaying, Telemetering, and Supervisory Control, **D. R. Pattison, M. E. Reagan, S. C. Leyland, F. B. Gunter.** *AIEE Transactions*, volume 69, part II, 1950, pages 945–52.

6. A Low Noise Amplifier, **Henry Wallman, Alan B. MacNee, C. P. Godsdon.** *Proceedings*, Institute of Radio Engineers (New York, N. Y.), January 1948, pages 700–08.

No Discussion

Application of Microwave Channels

R. C. CHEEK
MEMBER AIEE

MICROWAVE channels promise to become a vital part of the over-all communication networks on most power systems and in many industrial applications.[1,2] However, very little has been published to date on the practical methods of selecting and applying point-to-point microwave equipment. For this reason, it seems appropriate to present at this time a discussion of some of the problems encountered in applying microwave channels, along with practical data and formulas that have been found useful in microwave application.

The establishment of a microwave channel requires consideration of a number of different factors. Among these is the selection of the frequency band to be used, the selection of the sites for the terminals, the calculation of the free-space loss between the antennas, which in turn influences the selection of the antenna size, and the calculation of other losses, such as the loss between the transmitting and receiving equipment and the antennas.

Selection of Frequency Band

The Federal Communications Commission has assigned various frequency bands in the microwave region from 952 to 30,000 megacycles for commercial point-to-point service. These bands, not including those assigned exclusively for common carrier service, are shown in Figure 1. The bands that will be used initially by power systems and others will probably be the lower-frequency bands, 952 to 960 megacycles, 1,850 to 1,990 megacycles, 2,110 to 2,200 megacycles, 2,450 to 2,700 megacycles, and 6,575 to 6,875 megacycles. This is explained in part by the propagation characteristics of these frequencies as compared with the higher frequencies.

952 to 960 Megacycles. Fading is least severe in this band, but antennas of a given power gain are larger than antennas for higher bands. Several watts of power, more than adequate for good signal-to-noise ratio over most practical line-of-sight distances with antennas of reasonable size, can be generated in transmitters of more or less conventional design using crystal oscillators and frequency-multiplying stages. The only departure from conventional low-frequency practice that is required is the use of tunable cavities or tuned lines instead of lumped-constant resonant circuits in the final multiplying stages. Disk-seal or "lighthouse" tubes, which are similar in their operation to conventional tubes, can be used in the final stages, and therefore the use of klystrons or magnetrons is unnecessary. Solid-dielectric flexible coaxial cable can be used between the transmitter and the antenna with moderate losses for lengths up to several hundred feet, making it possible to install all equipment except the antenna indoors at ground level. This band is narrower than the higher-frequency bands, but its 8-megacycle width can accommodate a large number of channels in a given area, particularly if full advantage is taken of line-of-sight characteristics, antenna directivity, and frequency spacing. This band appears to be the most promising one for immediate use where a small number of multiplexed channels is required.

1,850 to 1,990, 2,110 to 2,200, and 2,450 to 2,700 Megacycles. The relatively greater width of these bands makes them particularly suitable for systems using time-division or wideband frequency-division multiplexing methods, in which a large number of channels per microwave frequency may be used. Many of the advantages of the 952–960-megacycle band are retained, although to a somewhat lesser degree. Tube efficiencies are lower, but disk-seal triodes have been developed for several watts' output at frequencies up to 2,500 megacycles and may be used over most of these three bands. Crystal-controlled transmitters do not appear economically feasible, because of the high order of frequency multiplication required, and frequency stability is an important design and operating factor. Automatic frequency control may be required in receivers, which offsets materially the gains in simplicity made by eliminating crystal control of the transmitters. Only short lengths of flexible coaxial cable can be used, and the rigid coaxial cable or waveguide required for longer distances increases installation expense. An alternative is to mount the transmitter proper close to the antenna, but this usually is undesirable from a maintenance standpoint. Smaller antennas can be used for a given gain in these bands than for the 952 to 960-megacycle band, but large antennas may be required to provide adequate margin for the more severe fading which can be expected in these bands.

In general, these bands appear best suited for trunk-line installations where large numbers of individual voice-frequency channels are required between two points.

6,575 to 6,875 Megacycles. In this band the use of klystrons or magnetrons is practically required, since disc-seal or lighthouse types are not readily applicable. Enormous power gains can be obtained with parabolas of relatively small diameter as compared with those for lower-frequency bands, but the rigidity required of the antenna mountings with the extremely sharp beams obtained is an important consideration. Wave guide must be used between the transmitter-receiver and the antenna unless the distance is extremely short. Alternatively,

Paper 51-145, recommended by the AIEE Carrier Current Committee and approved by the AIEE Technical Program Committee for presentation at the AIEE Southern District Meeting, Miami, Fla., April 11–13, 1951. Manuscript submitted July 6, 1950; made available for printing February 27, 1951.

R. C. CHEEK is with the Westinghouse Electric Corporation, East Pittsburgh, Pa.

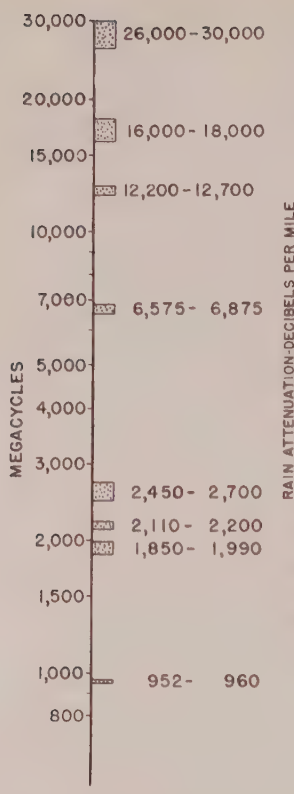

Figure 1. Commercial point-to-point (fixed operational) allocations in the microwave frequency spectrum

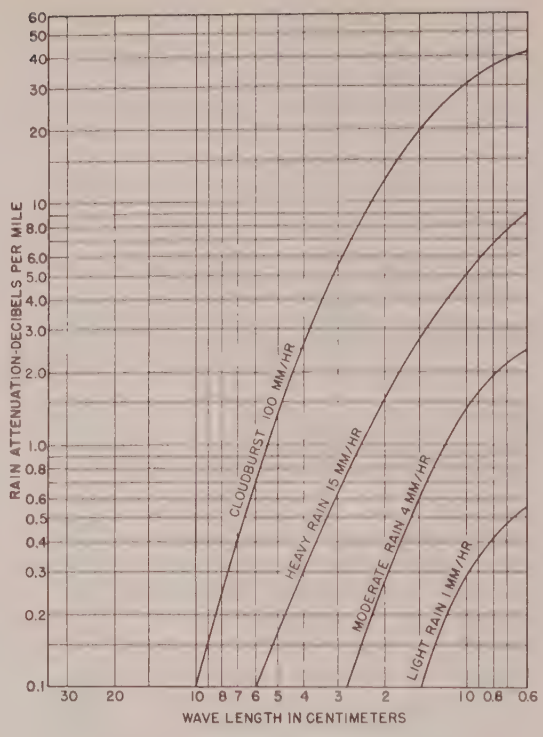

Figure 2. Rain attenuation as a function of wave length

the radiating antenna can be mounted near the ground and directed upward to illuminate a 45-degree plane reflector at the tower top. However, this system also imposes severe requirements with respect to rigidity of mounting. Attenuation caused by rain, sleet, and snow becomes noticeable in this band. For example, as shown by Figure 2, a cloudburst can cause an attenuation of 1.3 decibels per mile at 5 centimeters (6,000 megacycles).[3] Offsetting this, however, is the fact that rain of cloudburst proportions is not likely to be encountered over an appreciable percentage of the total length of a channel. Also, fading caused by multipath propagation and other effects, for which some margin must be provided in establishing the channel, is most severe during calm atmospheric conditions.[4,5] Therefore, some of the fading margin can be applied as a safety factor against rain attenuation.

Selection of Site

Since microwave signals do not follow the curvature of the earth, as do signals in the lower-frequency radio bands, it is necessary to provide a line-of-sight path between the antennas, and, as an additional safety factor, a path clearance of at least 50 feet from all obstructions usually is recommended. It has been reported by a number of observers that fading is considerably more severe when a grazing or near-grazing path is provided than when some clearance is available. Over smooth spherical earth, the formula

$$h=\frac{S^2}{6}+50 \qquad (1)$$

gives with sufficient accuracy the antenna height in feet required at each terminal to give 50-foot clearance for a channel of length S miles. The derivation of equation 1 is given in Appendix I. Table I shows typical antenna heights calculated

Table I. Typical Antenna Heights

Distance, Miles	Antenna Height, Feet
5	54
10	67
15	87
20	116
30	199
40	314
50	462

from this formula for channels of various lengths.

In the practical case, however, smooth spherical earth is rarely encountered, and it usually is necessary to obtain topographical maps of the region in question and to make a profile drawing of the proposed route. The most convenient method of correcting such a drawing for earth curvature probably is to plot the profile directly from the topographical maps, without correcting for curvature, and then, as shown in Figure 3, to correct the height of the most prominent ridges or other obstructions by the equation

$$y=\frac{2}{3}(Sx-x^2) \qquad (2)$$

where y is the correction in feet at a distance x miles from either end along the total path length, S miles (Appendix II). If topographical maps are not available for the region in question, aerial navigations maps sometimes are obtainable, and these provide similar information.

It usually is advisable to consider several alternate locations of the microwave terminals in an effort to find the one which requires the least antenna height. It sometimes will be more economical to locate a microwave terminal at some distance from the actual point of utilization of the transmitted intelligence, using leased or privately owned telephone pairs to carry the information from the microwave equipment to the utilization point, rather than to locate the terminals directly at that point.

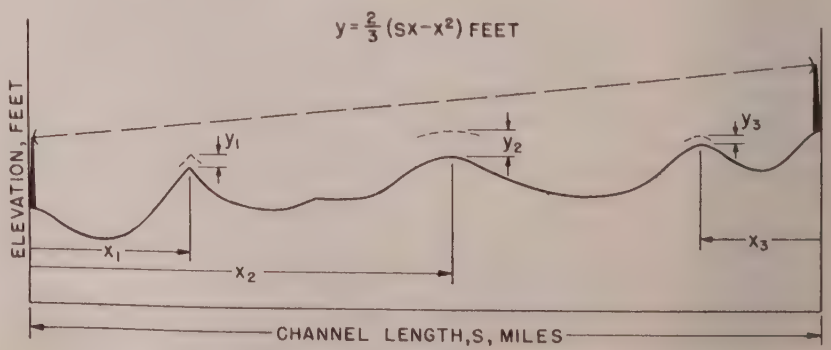

Figure 3. Method of correcting a profile map for earth curvature

In any case, after the sites are tentatively selected, it is advisable to survey the actual locations to make sure a line-of-sight really exists, since there may be some obstruction not shown on the topographical maps.

Calculation of Free-Space Loss

Microwave transmitters and receivers are rated in terms of the maximum decibels of attenuation through which they will operate successfully. This rating is the total attenuation from the transmitter output terminals to the receiver input terminals, and its calculation must include the loss in coaxial cable at both terminals, if such cable is used, as well as the loss of energy in free space. The latter loss usually makes up by far the greater portion of the attenuation of a channel. The derivation of the equations for the calculation of this loss is given in Appendix III. The basic equation is

$$\text{Free-space loss} = 10 \log_{10}\left(\frac{8\lambda}{\pi d^2}\right)^2 s^2 \text{ decibels} \qquad (3)$$

in which λ, d, and s are the wave length, the paraboloid diameter, and the channel length, respectively, all in the same units. An equation better suited for practical use is

$$\text{Free-space loss} = 10 \log_{10} \frac{1.745 S^2}{f^2 D^4} \times 10^{14} \text{ decibels} \qquad (4)$$

in which S is the distance in miles, f is the frequency in megacycles, and D is the antenna diameter in feet. The nomographic chart of Figure 4 solves this equation for a wide range of frequencies, channel lengths, and antenna diameters. If reflectors of different diameters are used at the sending and receiving ends, the equation becomes

$$\text{Free-space loss} \doteq 10 \log_{10} \frac{1.745 S^2}{f^2 D_r^2 D_t^2} \times 10^{14} \text{ decibels} \qquad (5)$$

The chart can be used for problems involving transmitting and receiving antennas of different diameters provided $\sqrt{D_r D_t}$ is used for antenna diameter in reading the scales.

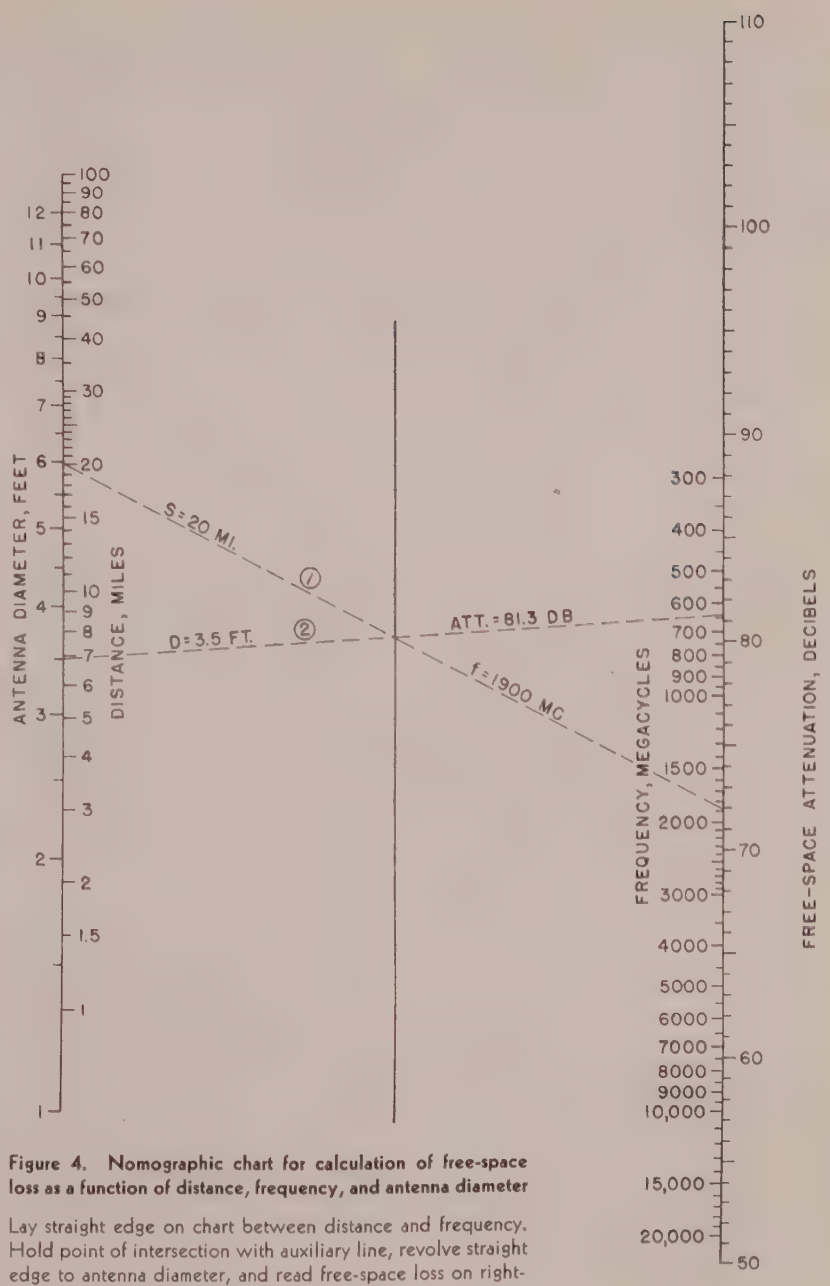

Figure 4. Nomographic chart for calculation of free-space loss as a function of distance, frequency, and antenna diameter

Lay straight edge on chart between distance and frequency. Hold point of intersection with auxiliary line, revolve straight edge to antenna diameter, and read free-space loss on right-hand scale

Beam Width

Beam width is usually defined as the angle between the half-power points of the beam, that is, the angle between the two coplanar lines along which the energy density is half that along the axis of the parabola at the same distance. In terms of wavelength and the diameter of the paraboloid the beam width is given theoretically by

$$\theta = \frac{\lambda}{D} \text{ radians} \qquad (6)$$

or

$$\theta = 57.3 \frac{\lambda}{D} \text{ degrees} \qquad (7)$$

In practical cases, due mainly to uneven illumination of the reflector by the dipole, the actual beam width is about 20 per cent greater, or

$$\theta = 70 \frac{\lambda}{D} \text{ degrees} \qquad (8)$$

If extremely narrow beams are used, the deflection of the antenna supports as a result of wind loading should be checked carefully to make certain that the aiming of the antennas remains correct within half of the beam width under any wind conditions that are likely to be encountered.

Maximum deflection at both ends will result in a loss of a total of 6 decibels, but since deep fading is not likely to occur under turbulent atmospheric conditions, it should not be necessary to include this loss in estimating the maximum attenuation of the channel.

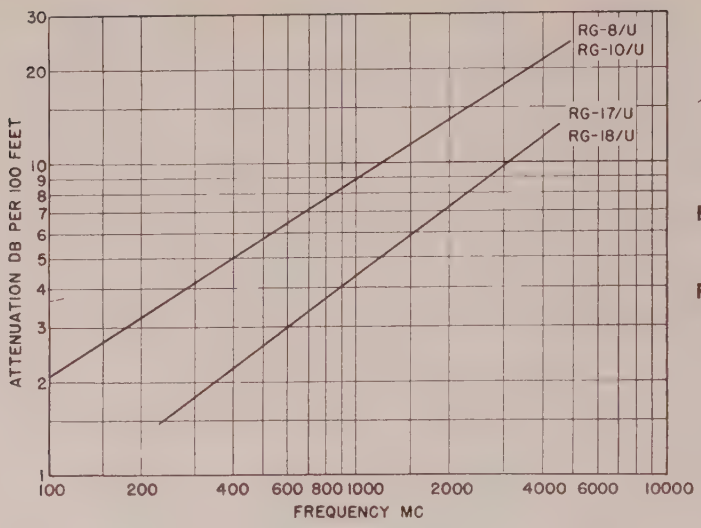

Figure 5 (left). Losses in RG-8/U, RG-10/U, RG-17/U, and RG-18/U coaxial cable as a function of frequency

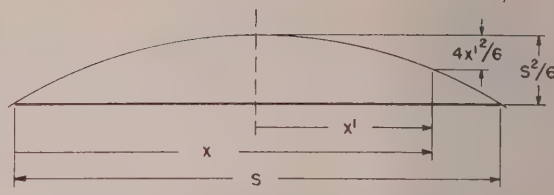

Figure 7 (above). Derivation of formula for correction for earth curvature

Coaxial Cable Loss

The losses in type *RG-8/U* and *RG-17/U* cable at frequencies in the microwave region are shown in Figure 5. Losses in the corresponding armored types, *RG-10/U* and *RG-18/U*, respectively, are the same. An approximate equation for estimating the attenuation of air- or gas-filled coaxial cable is

$$\text{Attenuation} = \frac{0.026\sqrt{f}}{D} \text{ decibels per 100 feet} \qquad (9)$$

where D is the inside diameter of the outer conductor in inches and f is frequency in megacycles. The attenuation of rectangular waveguide at a frequency approximately $\sqrt{2}$ times the cutoff frequency can be estimated by the equation

$$\text{Attenuation} = \frac{0.04\sqrt{f}}{b} \text{ decibels per 100 feet} \qquad (10)$$

where b is the width of the guide in inches. More complete equations can be found in references 6 and 7.

Fading Loss

Some allowance must be made for fading of the signals from free-space values. Experience at 960 megacycles indicates that an allowance of one-half decibel per mile for fading is conservative for a path with 50-foot clearance.[8] Available data on propagation at higher frequencies indicate that an allowance of one decibel per mile should be made at 2,000 and 6,500 megacycles.[4,5] The calculation of the maximum probable attenuation should include this allowance in addition to the free-space loss and the terminal losses at each end.

Example of Calculation of Losses of a Typical 960-Megacycle Channel

The considerations just discussed will be applied in the calculation of the total attenuation of a 960-megacycle channel. Assume that the channel is 32 miles long, and that the terrain is such that antenna elevations of 200 feet are required at each end. From Figure 4, the free-space loss with 42-inch paraboloids at each end is 91.1 decibels. The loss in 400 feet of *RG-17/U* cable (200 feet at each end) is 17 decibels. Including a fading allowance of 0.5 decibel per mile, or 16 decibels, the total attenuation of this channel is 124.1 decibels under maximum fading conditions. This is within the 125-decibel rating of a typical microwave transmitter-receiver for this band. Note that the use of *RG-8/U* cable would have resulted in attenuation in excess of this rating. An alternative would be to use *RG-8/U* cable with parabolas of larger size, but in general it is more economical to use the larger cable, rather than to increase the antenna size, where the necessary reduction in loss can be accomplished in this manner.

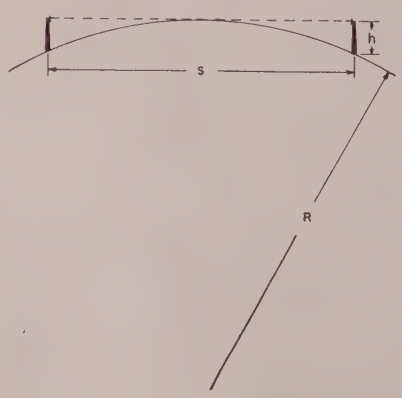

Figure 6. Derivation of formula for required antenna height as a function of distance over smooth spherical earth

Appendix I. Derivation of Formula for Antenna Height Versus Distance Over Smooth Spherical Earth

In Figure 6, h is the antenna height required at each end of a channel of length s for grazing clearance of the earth, R_e is the radius of the earth, and

$$h^2 + 2R_e h = \left(\frac{s}{2}\right)^2 \qquad (11)$$

when all quantities are in the same units. For all practical cases, h^2 is negligible by comparison with the other two terms, and equation 11 becomes

$$h = \frac{s^2}{8R_e} \qquad (12)$$

Expressing h in feet in terms of S in miles, and substituting 3,950 miles for R_e

$$h = \frac{S^2 \times 5{,}280^2}{8 \times 3{,}950 \times 5{,}280} = \frac{S^2}{6} \qquad (13)$$

and adding 50 feet for clearance

$$h = \frac{S^2}{6} + 50 \qquad (14)$$

Appendix II. Derivation of Correction for Earth Curvature

From equation 13, the correction y in feet at a distance $\pm x'$ from the mid-point of a channel S miles in length (Figure 7) is

$$y = \frac{S^2}{6} - \frac{4x'^2}{6} \qquad (15)$$

Translating the left-hand terminal to the origin by substituting $x - d/2$ for x', we get

$$y = \frac{2}{3}(Sx - x^2) \qquad (16)$$

where x is the distance in miles from either terminal along the total path length S in miles.

Appendix III

An isotropic radiator is a point source from which radiation emanates in equal amounts in all directions. If such a source of radiation is surrounded by an imaginary sphere of radius s, the density of the radiation passing through a unit area on the surface of the sphere is inversely proportional to the square of the radius of the sphere. Thus

$$D_i = \frac{P_t}{4\pi s^2} \quad \frac{\text{watts}}{\text{unit of area}} \tag{17}$$

where P_t is the total power being radiated by the point source. In actual practice, since an isotropic radiator is not physically realizable, use is usually made of a simple dipole, of length equal approximately to one-half wavelength of the transmitted frequency. Such a half-wave dipole has a certain amount of directivity, radiating most strongly in a direction perpendicular to its axis. In this direction, it radiates roughly three-halves the power radiated by an isotropic radiator,[9] assuming that the same total power is radiated by each. Thus, the energy flow from a half-wave dipole at any distance s in its favored direction is, applying the three-halves factor to equation 17

$$D_d = \frac{3P_t}{8\pi s^2} \tag{18}$$

At microwave frequencies, it is convenient to think of antennas, especially receiving antennas, in terms of their effective cross section. Actually a simple dipole used as a receiving antenna may have a small physical projected area in the wavefront, but its effective area can be defined in terms of the amount of power that it can intercept and deliver to a load of the proper impedance, when the dipole is mounted perpendicular to the direction of travel of a wavefront with a given energy flow per unit of area. It has been shown that the effective cross section of a dipole, as just defined, can be expressed roughly as[9]

$$A_{eff} = \frac{3\lambda^2}{8\pi} \tag{19}$$

in which λ is the wavelength.

It is the usual practice to use parabolic reflectors with dipoles for both transmitting and receiving, in order to increase the energy density directly at the dipole. The gain provided by such an arrangement over a half-wave dipole without a reflector is equal to the effective cross section of the paraboloid divided by the effective area of the dipole alone. The effective area of a paraboloid is somewhat less than the actual area because a half-wave dipole has physical dimensions and physical dissymmetry which prevent it from illuminating a parabolic reflector as though it were a point source, and conversely this prevents a paraboloid from illuminating it for complete recovery of all the energy intercepted by the paraboloid. For a first approximation, however, it will be assumed that the effective area of a paraboloid is the actual area of its mouth. Then, dividing this area by equation 19, we get

$$G = \frac{\frac{\pi D^2}{4}}{\frac{3\lambda^2}{8\pi}} = 2/3\left(\frac{\pi D}{\lambda}\right)^2 \tag{20}$$

Multiplying this equation by three-halves, the gain due to the dipole, we get the gain of the paraboloid with the dipole over an isotropic radiator as

$$G_i = \left(\frac{\pi D}{\lambda}\right)^2 \tag{21}$$

If we have the usual system with a dipole and a paraboloid at both the transmitting and receiving ends, we can calculate the energy received in terms of the transmitted energy by first determining the energy density at the receiving point and multiplying this by the effective area of the receiving antenna. Thus, multiplying equation 17 by equation 21 to obtain the energy density, and multiplying this by the effective area of the receiving dipole and the gain contributed by the reflector over the dipole, equations 19 and 20, we get

$$P_r = P_t\left(\frac{\pi D^2}{4\lambda s}\right)^2 \tag{22}$$

The free-space loss in decibels then can be calculated from the ratio of the transmitted and received energies as

$$\text{Free-space loss} = 10\log_{10}\left(\frac{4\lambda s}{\pi D^2}\right)^2 \text{ decibels} \tag{23}$$

This is an approximation which still does not take into account the effective area of the reflectors, as compared with the physical area. The effective area depends upon the design of the paraboloid and the location of the dipole, and may vary from 0.5 to 0.8 times the physical area. If in order to be conservative we use a figure of 0.5 for the ratio of effective area to physical area, then equation 23 must be modified to take this factor into account at both ends of the system. Equation 23 then becomes

$$\text{Free-space loss} = 10\log_{10}\left(\frac{8\lambda s}{\pi D^2}\right)^2 \text{ decibels} \tag{24}$$

References

1. Principles and Prospects of Microwave Communication, **F. S. Mabry.** *Westinghouse Engineer* (East Pittsburgh, Pa.), May 1949.

2. Microwave—New Power System Tool, **R. C. Cheek.** *Electrical World* (New York, N. Y.), July 16, 1949.

3. Microwave Repeater Research, **H. T. Friis** et al. *Bell System Technical Journal* (New York, N. Y.), volume 27, number 2, April 1948, pages 183–246.

4. Results of a Microwave Propagation Test on a 40-Mile Overland Path, **A. L. Durkee.** *Proceedings*, Institute of Radio Engineers, (New York, N. Y.), volume 36, number 2, February 1948, pages 197–205.

5. A Microwave Propagation Test, **J. Z. Millar, L. A. Byam, Jr.** *Proceedings*, Institute of Radio Engineers (New York, N. Y.), volume 38, number 6, June 1950, pages 619–26.

6. Reference Data for Radio Engineers (book). Federal Telephone and Radio Corporation, New York, N. Y., 1949.

7. Radio Engineers Handbook (book), **F. E. Terman.** McGraw-Hill Book Company, New York, N. Y., 1943.

8. Field Testing a Microwave Channel for Voice Communication, Relaying, Telemetering and Supervisory Control, **D. R. Pattison, M. E. Reagan, S. C. Leyland, F. B. Gunter.** *AIEE Transactions*, volume 69, part II, 1950, pages 945–52.

9. Transmission Lines, Antennas, and Wave Guides (book), **R. W. P. King, H. R. Mimno, A. H. Wing.** McGraw-Hill Book Company, New York, N. Y., 1945.

No Discussion

Vibracode System of Supervisory Control on a Carrier Communication Channel

T. J. ALLEN
ASSOCIATE AIEE

JOEL DANIEL
NONMEMBER AIEE

THIS paper describes a combined supervisory control and communication system which has been in service on the Georgia Power Company's system for about a year. The vibracode system was selected after study of several proposals because it was the only "package unit" designed to meet the requirements of the particular problem at hand.

In order to understand the problems involved, it will be necessary to describe a portion of the transmission system to which the control was applied (see Figure 1). Plant Arkwright, a 160,000-kw steam plant near Macon, Ga., is the principal generating source for the eastern part of the Georgia Power Company system. This plant is connected through substations at Gordon, Dublin, South Macon, Eastman, and Vidalia to an interconnection with the Savannah Electric and Power Company, and to Brunswick where a generating capacity of 5,500 kw is available. The power flowing 95 miles from Plant Arkwright into Vidalia Substation has exceeded 60,000 kva, and approximately 18,000 kva goes toward Brunswick another 100 miles away.

To provide proper voltage, it was necessary to install a 75,000-kva 110-kv voltage-regulating transformer at Vidalia and three 2,250-kva banks of capacitors (see Figure 2). The substation at Vidalia also supplies the 44-kv transmission system through a 20,000-kva tap-changing-under-load transformer bank, and a 7,500-kva 44/4-kv substation to which the three 2,250-kva capacitor banks are connected. Automatic voltage control of the capacitors, 110/44-kv transformers, and the 110-kv regulator was not practical; however, it was necessary to co-ordinate the operation of the capacitors and regulators to provide proper voltage for each of the 4-kv, 44-kv and 110-kv systems.

South Macon is the trouble-dispatching center for the transmission system and the only full-time attended substation in the area. There is a private telephone circuit between Macon and Vidalia, but an automatic exchange at Dublin and the heavy load on this circuit made it unsuitable for direct control of the equipment at Vidalia; therefore, it was decided to install a system suitable to control the 110-kv regulator and three capacitor banks from South Macon and to make the 110/44-kv transformers automatic voltage control.

Carrier current equipment was specified in order to procure an additional communication circuit to Vidalia. The exposed telephone circuit was chosen as the transmitting medium because of the simplified line coupling and trapping.

Application

The equipment selected had to fulfill the following requirements:

1. System should be suitable for operation by carrier current in the 50-to-100-kc band using the 95-mile exposed telephone line between Macon and Vidalia as the transmitting medium.

2. Provide a high-grade 2-way communication channel between Macon and Vidalia capable of being connected into telephone switching turrets at each end.

3. Be capable of operating the 75,000-kva 110-kv regulating transformer located at the Vidalia 110-kv Substation from the South Macon Substation.

4. To operate indicating lights at South Macon Substation giving a continuous indication of which tap the Vidalia regulating transformer is on.

5. To provide at South Macon a recorded telemetered voltage from the load side of the Vidalia regulating transformer.

6. Include alarm indications at South Macon giving an audible and visual signal when any of the 110-kv oil circuit breakers or 44-kv oil circuit breakers at Vidalia trip and when the three single-phase 110- to 44-kv tap-changing-under-load transformers get out of step.

7. Provide for connecting and disconnecting (one at a time) the three 2,250-kva power-factor corrective capacitor banks to the 4-kv bus at the Vidalia 44- to 4-kv Substation.

8. Be capable of transferring the Vidalia telemeter transmitter from the 110-kv bus voltage to the 4-kv bus voltage.

Description of System

The description of the system will be divided into two parts, the carrier equipment and the supervisory control equipment.

The carrier equipment consists of a terminal containing a transmitter, receiver, line-coupling unit, signalling devices, and telephone termination, installed at South Macon and Vidalia. Carrier frequencies of 55 kc at South Macon and 95 kc at Vidalia were used for the transmitters—the receiver at each location being on the opposite frequency. The South Macon and Vidalia terminals are shown in Figures 3, 4, and 5. A block diagram of the units composing the system is shown in Figure 6.

The carrier current transmitter is a narrow-band frequency-modulated unit designed to operate on a specific frequency with a power output of ten watts. It incorporates a fast-acting automatic modulation control whereby the carrier deviation, due to modulation, is held to a maximum of 2.5 kc. A 2,500-cycle low-pass filter prevents modulation by frequencies outside of the channel. Modulation takes place at a frequency of 455 kc by action of a balanced reactance modulator on a stable oscillator. This 455-kc signal is

Paper 51-146, recommended by the AIEE Carrier Current Committee and approved by the AIEE Technical Program Committee for presentation at the AIEE Southern District Meeting, Miami, Fla., April 11–13, 1951. Manuscript submitted January 12, 1951; made available for printing March 12, 1951.

T. J. ALLEN and JOEL DANIEL both are with the Georgia Power Company, Atlanta, Ga.

mixed with a crystal oscillator to produce a frequency-modulated signal at the carrier frequency.

The carrier current receiver is a narrow-band frequency-modulated superheterodyne unit designed to operate on a specific frequency. The receiver produces a constant audio output for signals varying from 300 microvolts to as high as ten volts. The frequency response is flat over a band width of ±3 kc, while at ±7.5 kc the response is down 100 decibels. The receiver employs a crystal-controlled local oscillator for maximum stability.

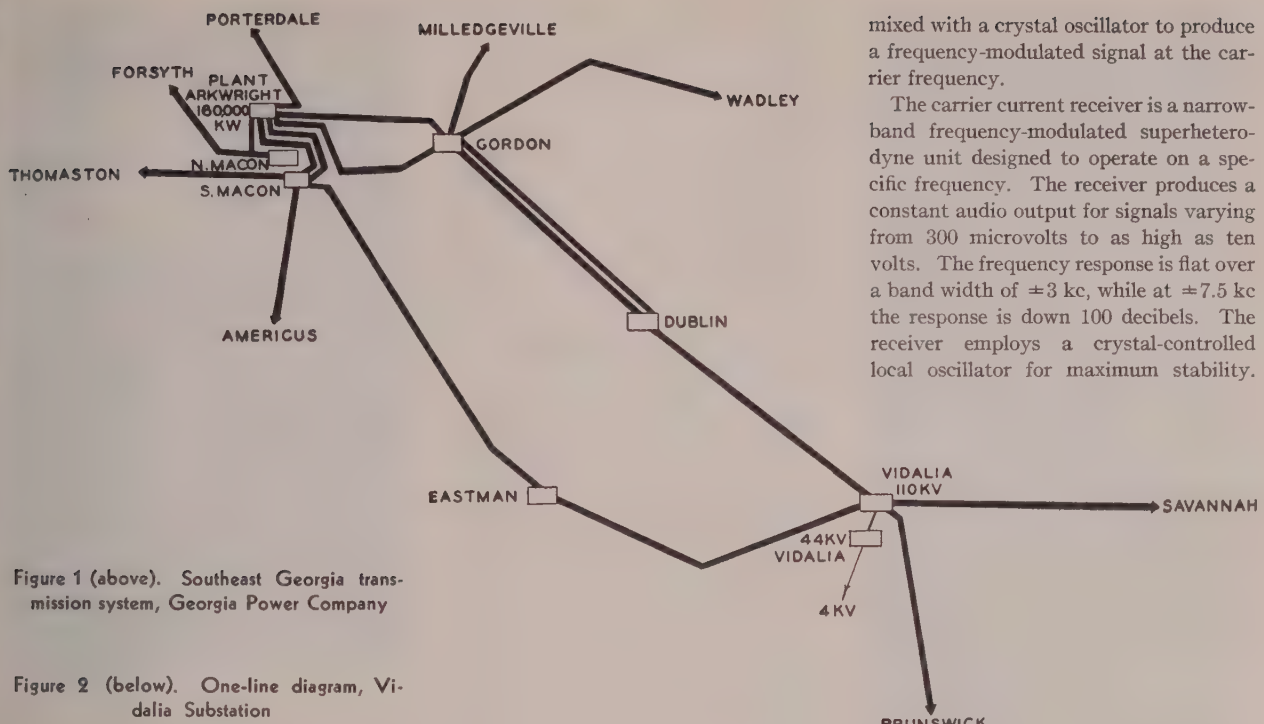

Figure 1 (above). Southeast Georgia transmission system, Georgia Power Company

Figure 2 (below). One-line diagram, Vidalia Substation

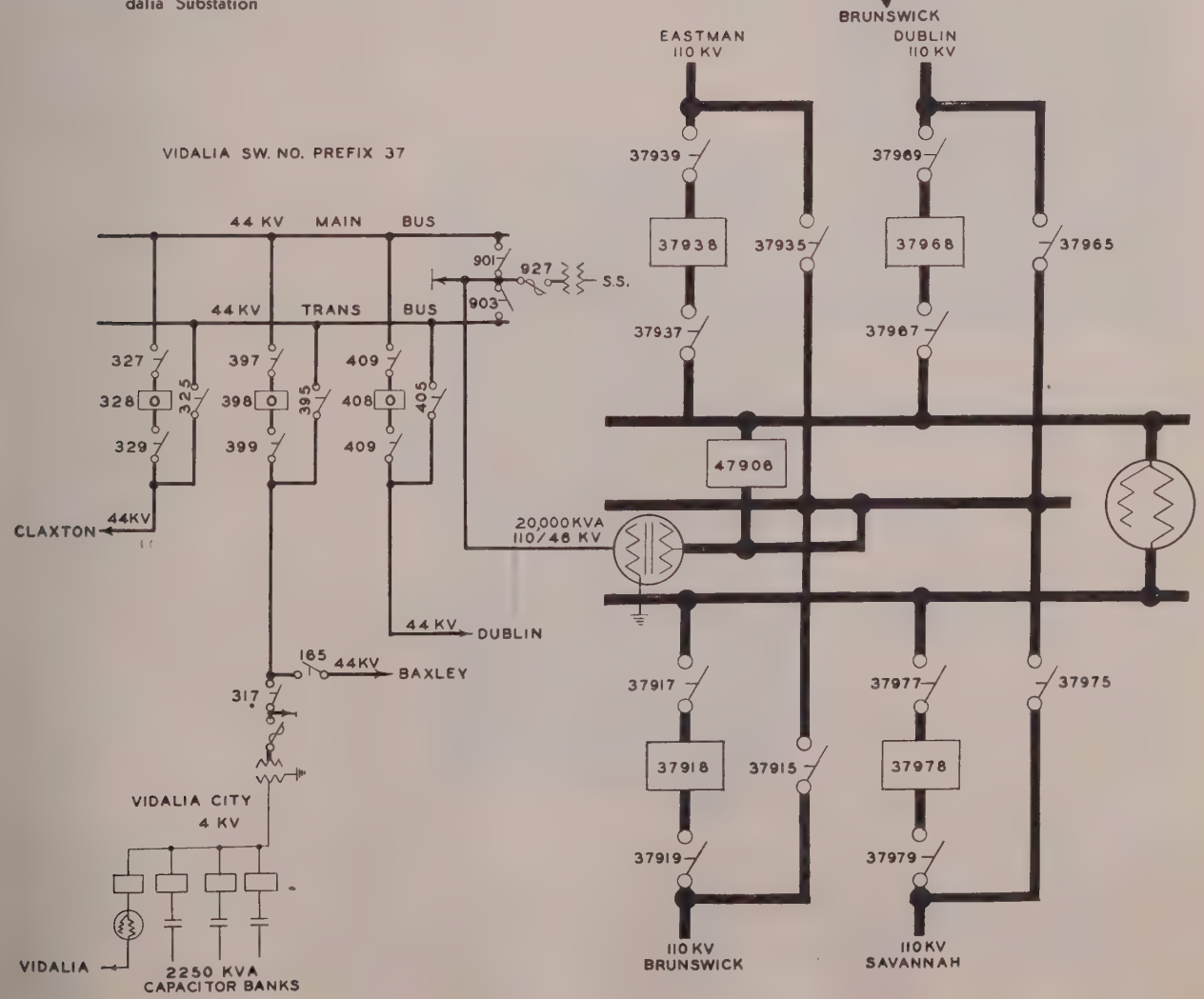

Figure 3. South Macon Substation, front view. Control station for remote operation of tap-changing transformer. Position indicator lights and control escutcheons are shown on the panel at the top of the cabinet

The audio output is one watt with a 2.5-kc deviation of the carrier frequency.

A 15-kv 0.006-microfarad capacitor is used to couple the carrier equipment to the exposed telephone line which is constructed on the transmission-line structures. The tuning unit matches the transmitter and receiver impedances to the line impedance.

Signalling on the communication circuit is accomplished by shifting the transmitter frequency approximately one kc. The telephone termination is designed to permit usage of a 2-wire magneto telephone circuit in duplex transmitter-receiver operation and to provide control circuits for telephone ringing purposes. The balancing networks are adjusted so that the circuit may be extended through the telephone switching turrets.

Built into the transmitter and receiver sections are filters whereby the audio channel is separated into two parts. The first 500 cycles is cut out of the communication channel for supervisory signal tones. This leaves the communication channel operating between 500 and 2,500 cycles with no noticeable impairment in speech quality.

Supervisory Control Equipment

The equipment uses audio frequency tones to provide the control, supervision, telemetering, and alarm signals. The signals are transmitted and received by the frequency-modulated carrier equipment. The particular tone system used is known as the "vibracode" system. The tone source in this system is the "vibrasender" which is essentially a driven tuning fork. It is packaged as a small plug-in unit 1 by 2 by 4 inches and is completely enclosed. A well-regulated power supply, together with a controlled level of oscillation, keeps the output at a constant level and free of harmonics. The vibrasenders

Figure 4. South Macon Substation. Front view with door open. Control station for remote operation of tap-changing transformer. This cabinet contains supervisory control equipment, telephone terminal, carrier transmitter and receiver and telemeter receiving equipment

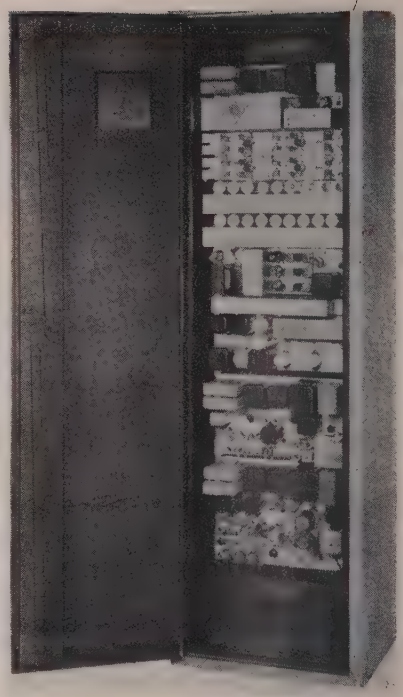

Figure 5. Vidalia Substation. Front view with door open. Remote station of control equipment for remote control of tap-changing transformer. This is an outdoor cabinet and contains from top to bottom supervisory control equipment, telemeter transmitting equipment, telephone voice terminal, carrier receiver and carrier transmitter

maintain the tone frequency within ±0.15 per cent, which includes original setting error and temperature effects from −20 to +80 degrees centigrade. The frequencies of the tones used in this system are 100.0, 110.9, 123.0, 136.5, 154.1, 167.9, 186.2, 206.5, 229.1, 254.1, 281.8, and 312.6 cycles. The tone-responsive element in this system is the "vibrasponder," and is essentially a resonant reed relay. When voltage of the resonant frequency is applied, the reed vibrates readily. The amplitude builds up quickly and reaches the point where a small contact wire on the reed makes contact with a contact screw. This closes a circuit to change the bias on a vacuum tube and operate a relay in its plate circuit. The vibrasponder is packaged in a small 7/8 by 7/8 by $3^3/_{16}$ inch plug-in unit. The vibrasponder maintains its frequency stability within ±0.25 per cent from −20 to +80 degrees centigrade. It has a response curve equivalent to that of a single tuned circuit having a Q of 110. With the basic frequencies being placed approximately 10 per cent apart, the vibrasponder has 25 decibels of selectivity between adjacent channels.

This vibracode system performs the

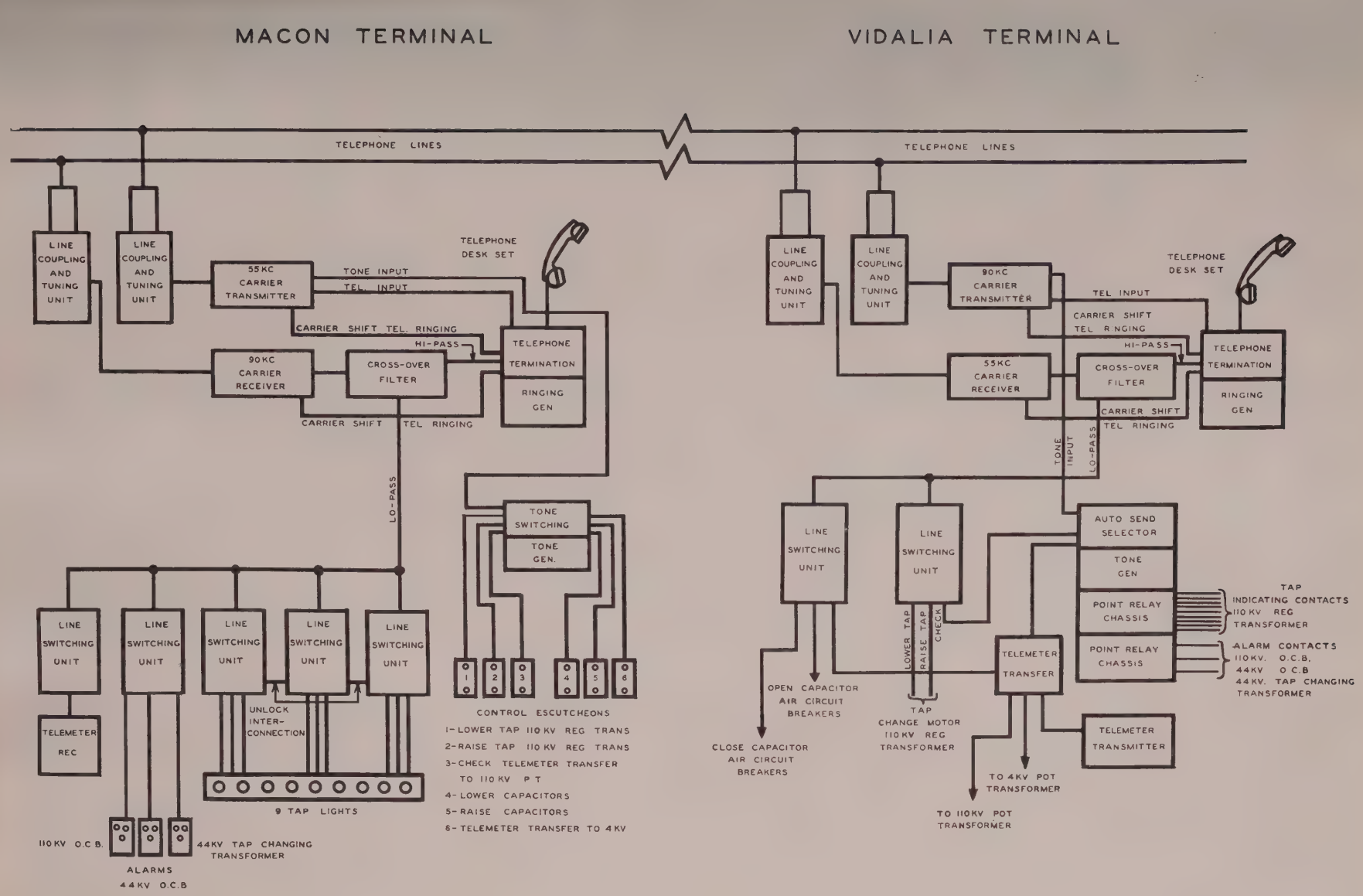

Figure 6. Block diagram of vibracode supervisory control and communication system, Georgia Power Company

various supervisory functions by the selection of two audio tones sent simultaneously. These tones are transmitted over the carrier system being separated from the communication channel by the system of filters which removes the first 500 cycles of the audio channel for use by the supervisory control audio tones. The control function is started by pressing the button on proper control escutcheon at South Macon. A pilot light on the escutcheon gives evidence that the signal is being transmitted. The control button through an auxiliary relay in the "Tone-Switching Panel" selects two tones from the tone generators and feeds them into the tone input of the carrier transmitter where they modulate the transmitter. The tone-switching panel contains an adjustable timing device whereby the time interval of the tone pulse is held to slightly less than one second.

At Vidalia the tone-modulated carrier wave is received and demodulated by the carrier receiver. The output of the receiver is fed into a "crossover filter panel." This filter panel separates the output into two frequency bands. These frequencies from 0 to 500 cycles are passed into the "line switching unit," and frequencies from 500 to 2,500 cycles go from the crossover filter into the telephone termination. The supervisory control tones, being below 500 cycles, are impressed on the input to the line-switching units, which are parallel connected. Each circuit through the line-switching units to a control relay, in effect, has two vibrasponders in series. In order for the control relay to be operated, the proper frequencies to which the vibrasponders are tuned must be impressed upon them. The vibrasponders change the bias on a tube to operate the control relay which is in its plate circuit. The control relay in most instances operates an auxiliary relay which actually performs the desired function. There are six control escutcheons at South Macon which provide for six separate control functions at Vidalia. These control functions are: raise the tap setting on 110-kv regulating transformer, lower the tap setting on 110-kv regulating transformer, check on Macon indications, raise capacitors (adds more capacitors on 4-kv bus), lower capacitors (disconnects capacitors from 4-kv bus), and telemeter transfer (switches telemeter transmitter from 110-kv bus to 4-kv bus).

At Vidalia all the return supervisory signals, consisting of pairs of tones, are initiated by an automatic send selector. This selector contains a 52-point stepping switch which is automatically started whenever a control relay is operated in any of the line-switching units, whenever the check button is pressed at South Macon, or whenever there is a change on any of the alarm indications necessary. This automatic-send selector sends out the pairs of audio tones from vibrasenders at Vidalia for all indications to South Macon in a time interval of approximately ten seconds. The tones on reception at South Macon operate the proper vibrasponders and energize the lights on the panel by operation of the control relays in the various line-switching units.

Telemetering from Vidalia is accomplished by means of a Bristol metameter transmitter keying one of the vibrasender tones at Vidalia which, upon reception at South Macon, operates the control relay in the line-switching unit to supply pulses to the receiving meter. This is the only function which operates on a single audio tone. The telemeter transmitter at Vidalia is arranged so that it can be switched from the 110-kv bus to the 4-kv bus as desired from South Macon.

Conclusion

There are numerous installations of carrier equipment for supervisory control, communication, and telemetering services. The services in most instances have been accomplished by the use of separate carrier transmitting and receiving equipments operating on different frequencies for each service. This system is different in that the same carrier transmitting and receiving equipments operating on one pair of frequencies are used for all three services. This is an economical use of the carrier frequencies, as well as being a lower cost installation to do a complete job.

Experiences to date with this system have been very favorable. The troubles encountered have been mainly relay adjustments. It has been found that relay contacts which operate at infrequent intervals must be adjusted with considerably greater wiping action than those which have a greater frequency of operation. Other troubles have been vacuum-tube failures and telephone line troubles.

The communication circuit is excellent. Only the most trained observer can notice that the first 500 cycles are missing from the audio frequencies.

Discussion

W. A. Derr (Westinghouse Electric Corporation, East Pittsburgh, Pa.): The statement made in the first paragraph of the paper concerning "package unit" design may be misleading. While supervisory control and associated carrier equipment are usually furnished in separate housings, there is no reason why these components cannot be mounted in the same "package."[1]

It is interesting to note that 12 telegraphic-type channels had to be established to provide for the relatively small number of functions required. An average size supervisory control installation would have four or five times as many functions as the one described. There are many installations which provide for ten or 15 times the number of functions discussed. With a multisignal system as described, it would be necessary to provide more than one carrier channel to obtain sufficient telegraphic-type channels for many supervisory control installations. With coded-impulse-type systems of supervisory control, the channel requirements do not change regardless of the number of functions performed.

No information is given concerning the interlocking which is provided to prevent false operations or indications in the event that the receiver relays are operated from any disturbing voltages. A discussion of this interlocking would be of interest.

Since supervisory control has a very low duty cycle, continuous channel supervision is an important consideration. It is desirable that the individual telegraphic-type channels be continuously supervised. With a multisignal system such as described in the paper, it is not possible to continuously supervise all of the telegraphic-type channels employed. However, complete channel supervision can be readily provided with supervisory control systems which require only a single signal responsive element at the controlling and controlled stations.

The conclusion of the paper intimates that the installation described is unique in that the same carrier equipment is used for voice communication, supervisory control and telemetering. Combinations such as this have been made many times for both single station and multistation systems.[1,2,3,4]

References

1. Carrier Supervisory Control of Pumping Station Over Power Cables, **W. A. Derr, W. A. Keller, H. A. W. Hedke.** *Electrical Engineering* (*AIEE Transactions*), volume 65, November 1946, pages 699–705.

2. The Combination of Supervisory Control with Other Functions on Power-Line Carrier Channels, **R. C. Cheek, W. A. Derr.** *Electrical Engineering* (*AIEE Transactions*), volume 64, May 1945, pages 241–46.

3. A Versatile Power-Line-Carrier System, **H. W. Lensner, J. B. Singel.** *Electrical Engineering* (*AIEE Transactions*), volume 63, March 1944, pages 129–33.

4. Multistation Supervisory Control, Telemetering and Communication on Single Frequency Carrier Channel, **W. A. Derr, T. C. Wren, J. V. Kresser.** *AIEE Transactions*, volume 69, part II, 1950, pages 1115–21.

T. J. Allen and **J. Daniel:** The term "package unit" was intended to convey the infor-

mation that all of the components, the supervisory equipment, carrier equipment, and telemetering equipment were furnished by one manufacturer as a custom-made installation to fit the particular application and was not an assembly of a number of components from various manufacturers.

We would like to point out that this system was custom made to cover a particular application. Economics of using standard panels must have prompted the manufacturer to use the 12 tones at one of the terminals. The number of functions from this terminal could be considerably increased without any expenditure other than for auxiliary relays, should the need for them develop. Prevention of false operations is taken care of by the selectivity of the frequency responsive relays and the simultaneous transmission of two tones.

Continuous channel supervision is performed by the recording voltmeter and transformer tap indicating lights at South Macon. The conclusions showed that the system was different, not unique. There have been numbers of other multipurpose carrier channels installed.

An Analysis of Grounding Banks to Balance Distribution Feeder Voltages

LEONARD W. LONG
ASSOCIATE AIEE

GROUNDING banks are ordinarily used for two purposes: (1) on otherwise ungrounded networks to reduce, during single-line-to-ground faults, the voltage rise on the unfaulted phases; (2) at substations, to establish the neutral for 4-wire distribution feeders supplied from delta-connected transformer secondaries. A third purpose has been suggested from time to time: that grounding banks located at one or more points along a distribution feeder can be used to aid in balancing the feeder neutral voltages. In this paper, an analysis will be presented of the contribution which a grounding bank can make to feeder voltage balance and of the grounding current which would flow in the bank. A method will be given for calculating the size, impedance, and effectiveness of the grounding bank.

In general, grounding banks may be either zig-zag or Y-delta banks, but in the applications to distribution feeders, are usually Y-delta. Here, the term grounding bank will be restricted to mean a Y-delta transformer bank, the Y-side tapped from a feeder with the Y-neutral connected to the system neutral, whether the latter be an ungrounded conductor, a multigrounded conductor, or simply the earth itself. In addition, the term will be applied in this paper only to banks located at points other than substations and grounded for the purpose of improving voltage balance. Such a transformer bank is illustrated in Figure 1. The grounding connection is shown dotted and a secondary load is indicated because it is envisioned that existing load-serving banks may be grounded, or that new installations may be expected to perform the dual functions of load-service and grounding duty.

It should be noted that the grounding of load-serving banks is a departure from the usual practice. Wherever the Y-delta step-down transformer combination has been used on a distribution feeder, the ungrounded Y primary has been preferred to the grounded Y primary in spite of the advantage provided by the grounded condition to feeder voltage balance. The reason for this preference is the fear of damage by excessive current to one or more units of the bank when it is grounded. The danger of such damage results from grounding-transformer action, and the common practice is to avoid rather than to impose grounding duty on a Y-delta bank.

This fear of damage is not as well-founded as might at first appear. The very simple practice of placing a fuse in the grounding connection between Y-neutral and system neutral, as shown in Figure 1, is all that is necessary to protect the bank against excessive grounding current. Such fusing is of the utmost importance, and a further treatment will be made near the end of this paper where greater clarity can be achieved.

Although it is hardly necessary to discuss a matter of such common understanding as voltage unbalance, a few brief remarks will help to establish the role which a grounded bank can play. The 3-phase voltages supplied to a substation by a transmission system are usually well-balanced. At almost any point on the primary distribution system, however, the voltages are unsymmetrical to a greater or lesser extent. This effect is, of course, primarily the result of the unsymmetrical voltage drops which occur along the feeder when unbalanced loads are served.

In terms of the symmetrical components of the voltages, the existence of dissymmetry is indicated by the presence of negative-sequence and zero-sequence components, the objectionable features of which are well known. Negative-sequence voltage causes overheating of 3-phase motors, and, for machines having an external neutral connection, zero-sequence voltage has the same effect. The greatest objection, however, is to the unequal magnitudes obtained for service to the separate phases, particularly for lighting loads.

Naturally, the principal method to be employed in balancing voltages is that of distributing loads as equally as possible among the phases. In the case of negative-sequence voltage, this method is the only practicable one available. For the reduction of zero-sequence voltage components, however, additional recourse may be found in the use of grounding banks. Such banks provide low-impedance paths to neutral for zero-sequence current components on the feeder which result from unbalanced load currents. It might be said that the grounded bank acts to drain off the zero-sequence current from the feeder, or that it constitutes a short circuit on zero-sequence voltage.

It should be observed that the grounded Y-delta connection can be only partially successful in balancing voltages since it reduces only the zero-sequence compo-

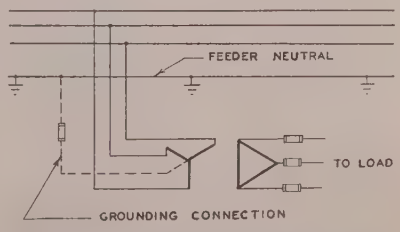

Figure 1. Y-delta transformer bank tapped from distribution feeder. The neutral connection may or may not be made

Paper 51-148, recommended by the AIEE Transformers Committee and approved by the AIEE Technical Program Committee for presentation at the AIEE Southern District Meeting, Miami, Fla., April 11–13, 1951. Manuscript submitted February 1, 1951; made available for printing March 14, 1951.

LEONARD W. LONG is with the North Carolina State College of Agriculture and Engineering of the University of North Carolina, Raleigh, N. C.

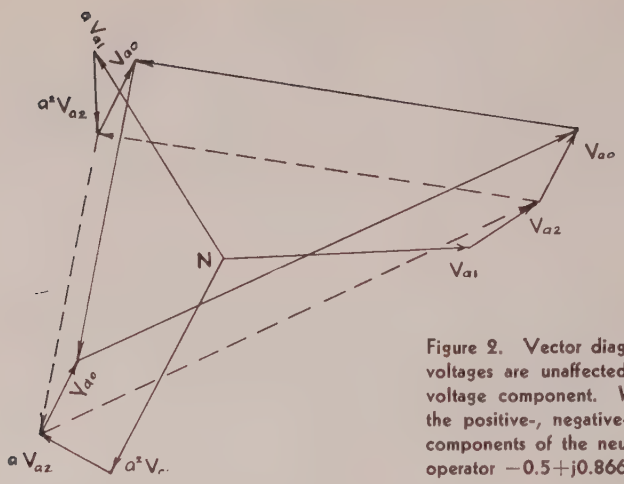

Figure 2. Vector diagram showing that line voltages are unaffected by a zero-sequence voltage component. V_{a1}, V_{a2}, and V_{a0}, are the positive-, negative-, and zero-sequence components of the neutral voltages, a is the operator $-0.5+j0.866$, and N is the neutral point

nent. Both negative- and zero-sequence components produce unequal voltage magnitudes and dissymmetric voltage angles in the line-to-neutral voltages; on the other hand, only the negative-sequence components affect the line voltages. This fact is illustrated for an exaggerated case by the vector diagram of Figure 2. The line voltages indicated by the dotted triangle, which represents a condition of no zero-sequence component, are the same as the line voltages of the solid triangle, which represents the condition that does have a zero-sequence component. Obviously, a grounding bank does nothing to balance line voltages. Consequently, the grounding bank can provide no benefit to the secondary voltages, that is, the actual load voltages, of transformers having no connection to the feeder neutral. These combinations are single-phase line-to-line, delta-delta, delta-Y, Y-Y-ungrounded, and open delta. In addition, the Y-delta connection, whether grounded or not, does not transform zero-sequence voltage to its secondary terminals because of the short-circuiting delta loop. It should be carefully noted that this fact is true even for the grounding bank, itself, and the load voltages it supplies are no better balanced when the bank is grounded than before.

Be that as it may, the balance of voltages for the so-called phase-to-neutral loads, can be much improved. These loads are those supplied by the single-phase-to-neutral, Y-Y-grounded, and open-Y connections. Inspection of Figure 2 reveals that the position of the neutral point N is such that the neutral voltages are more nearly equal for the dotted triangle (no zero-sequence component) than for the solid triangle. For this reason, the grounding bank is sometimes said to stabilize the neutral point; that is, the neutral point is made to remain near the center of the line voltage triangle.

In addition to the beneficial effect on feeder neutral voltages, two minor advantages gained in using a neutral connection where motor loads are served are:

1. Load service is not interrupted by a single open-conductor fault, inasmuch as the bank can then operate as an open-Y bank.

2. Three-phase motors are not subjected to overheating or the failure to start altogether caused by the single-phase service supplied by an ungrounded bank with an open-conductor fault. Even where thermal fusing is employed, 3-phase motors having only 2-legged protection are endangered if the open-conductor fault occurs in a particular leg. Grounding the transformer bank removes this danger.

These advantages, however, are not of much importance. In fact, the first is definitely dubious, since if the three transformers are 100 per cent loaded before the fault, the two remaining active transformers will be approximately 73 per cent overloaded during the fault because of their secondary load alone. As will be pointed out subsequently in this paper, the additional grounding duty imposed by the fault can cause an overload of much higher values than 73 per cent. As for the overheating of 3-phase motors, thermal fusing of motors is so simple and common a practice that it is necessary only to insure the use of 3-legged motor protection where a Y-delta transformer connection is employed. The conclusion is that the only major advantage of grounding the Y neutral is the reduction of zero-sequence voltage on the primary feeder system.

The proposal to make use of this advantage or property of the grounded bank raises several questions. In the case of the bank to be installed solely to stabilize the feeder neutral, these questions are:

1. Where should the bank be located on the feeder?

2. What should be the kilovolt-ampere capacity and the per cent impedance of the transformers used in the grounding bank?

3. What reduction of zero-sequence voltage is thus obtained?

4. What protection is required?

Where consideration is to be given to grounding an existing load-serving bank, the location, size, and impedance of the transformers is already fixed, and the problem becomes one of determining whether grounding is feasible; that is, whether the bank is capable of handling a normal ground current in addition to its load. Accordingly, the determination to be made concerns the ground current that will flow in the bank, and the questions to be settled are:

1. Is grounding feasible?

2. What reduction of zero-sequence voltage is obtained?

3. What protection is required?

In answer to the first question presented, the bank should be placed as near as possible to the location where zero-sequence voltage is normally largest, or at the point where reduction is most needed, for it is at the point where the bank is located that the greatest reduction of zero-sequence voltage is obtained. For example, at a point where a long 4-wire feeder divides into single-phase and open-Y branches of some length themselves, the use of a grounding bank to stabilize the neutral of the feeder may be indicated.

The questions of the capacity and impedance of a bank for neutral-stabilizing duty only and of the feasibility of grounding in the case of the load-serving bank may be treated together. What is needed is some quick method capable of general applicability by which the zero-sequence current flowing in the grounded bank can be calculated as a percentage of transformer current rating. The two quantities, capacity and impedance, are interdependent and their calculation can most easily and practicably be based on an estimate of the unbalance of the feeder and will then itself be in the nature of an estimate. It will be shown later that the method to be outlined is not as inexact as might at first be supposed. The procedure is to assume some reasonable value of per-cent or per-unit unbalance for the given feeder, and further to assume that this entire unbalance is concentrated in a load connected to the feeder at the same location as the grounded bank. With

this simplification, the only factors entering the problem may be listed as follows:

p = per unit unbalance of the feeder expressed as the ratio of neutral current to three times feeder rated current (or three times system base current, if desired),

k = per-unit burden placed on the grounding bank by grounding duty expressed as the ratio of neutral current flowing in the bank to three times the individual transformer current rating,

U_F = 3-phase kilovolt-ampere rating of the feeder (or system 3-phase kva base),

U_T = 3-phase kilovolt-ampere rating of the grounding bank,

$Z_{0/1}$ = the complex value of per unit zero-sequence impedance on feeder (system) base, looking into the feeder at the grounding bank location, but without the grounding bank, and

$Z_{T/1}$ = the complex value of per unit impedance on transformer base of the grounding bank, which may be taken as purely imaginary.

The analysis which leads to the equation now to be presented can be found in Appendix I. The result of this analysis in dimensionless form is:

$$\frac{k}{p} = \left| \frac{1}{\frac{U_T}{U_F} + \frac{Z_{T/1}}{Z_{0/1}}} \right| \qquad (1)$$

The best way to study the meaning of this result is through the medium of the curves shown in Figure 3, which are plotted for real values of the impedance ratio. It is seen that the larger the bank, the less important its per cent impedance, and vice versa. The relative burden of grounding duty, k, thrust on the transformers by a given unbalance on a given feeder increases as the bank size becomes smaller or the transformer impedance decreases.

Obviously, some maximum permissible value of k exists for a particular application. The basis for determining what this value would be is a subject worthy of study in itself, involving as it does the load cycle of the bank if it serves a load, and the diurnal variation of feeder neutral current in both magnitude and phase. Once a maximum permissible value for k is decided, the procedure to be used for a load serving bank is to evaluate the actual grounding current k from equation 1 and compare it to the permissible value. In the case of a bank that does grounding duty only, the procedure is to use the permissible value of k in equation 1 to prepare a table of permissible pairs of capacity and impedance values for the transformers. This latter procedure will be demonstrated in the following problem.

An actual system represented by the 1-line diagram of Figure 4 is used for the calculations. At a point 11 miles from the substation, the 3-phase feeder divides into branches not independently represented in the diagram, and it is desired to have the neutral stabilized at this location for obvious reasons. The problem is to determine what the size and impedance of the bank should be and what its effectiveness will be, but effectiveness will not be dealt with immediately.

The zero-sequence impedance looking into the feeder at the 11-mile point, neglecting loads, on a base of 2,500 kva 3-phase, and 7.2 kv line-to-neutral is found by computation to be $Z_{0/1} = 0.359 + j0.516 = 0.630 \angle 55.2°$. Since the bank is to perform grounding duty only, the value of k permissible is at least 1.0, and could be larger since maximum duty would occur only during peak periods. The value of $k = 1.0$ will be used, however, and for an estimated unbalance of $p = 0.25$, the ratio $k/p = 4.0$. Solving for the desired quantity from equation 1, the minimum permissible value of 3-phase capacity of the bank is:

$$U_T = U_F \left| \frac{1}{k/p} - \frac{Z_{T/1}}{Z_{0/1}} \right| = 2{,}500 \left| \frac{1}{4.0} - \frac{|Z_{T/1}| \angle 90°}{0.630 \angle 55.2°} \right| \qquad (2)$$

$$= |625 - 3{,}970 |Z_{T/1}| \angle 34.8°|$$

See Table I where several values of transformer impedance are tried.

Table I

Per Cent Impedance of Transformers $Z_{T/1} \times 100$	Minimum Size of Bank (3-phase Kva) U_T
3.5	517
5.0	476
7.5	417
10.0	375

Since the results achieved are dependent on the accuracy with which the value of p, the per-unit unbalance, is chosen and on the error involved in the assumption that this unbalance is concentrated at the same location as the Y-delta bank, a further statement about the quantity p is in order. Suppose that measurements are made of the floating neutral voltage at the point where a Y-delta bank is or will be located. Then an application of Thevenin's theorem to the network, neglecting loads, with respect to the Y neutral and the system neutral (ground) as terminals, yields the following equation for the grounded condition. (See Appendix II for proof.)

$$\frac{k}{\frac{V_{N/1}}{Z_{0/1}}} = \frac{1}{\frac{U_T}{U_F} + \frac{Z_{T/1}}{Z_{0/1}}} \qquad (3)$$

where $V_{N/1}$ is the per-unit floating-neutral voltage. But this equation is the same as equation 1 if the value of p is taken to be:

$$p = \left| \frac{V_{N/1}}{Z_{0/1}} \right| \qquad (4)$$

Such a value for per-unit unbalance yields exact results except for the neglected load impedances, which in most cases have a minor influence. It is obvious that the engineer may substitute for the estimate of unbalanced load an estimate of zero-sequence or floating-neutral voltage. Furthermore, the possibility exists of making actual measurements with recording voltmeter equipment and calculating with good accuracy the grounding duty a bank will have to perform.

Now attention is turned to the next question which has been posed, that is, "What is the reduction of zero-sequence

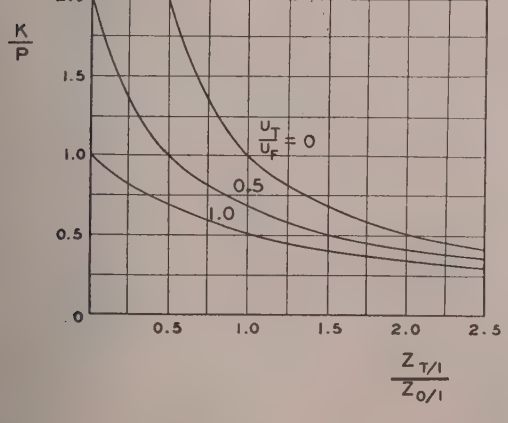

Figure 3 (left). Dimensionless curves showing the ground current flowing in a grounding bank

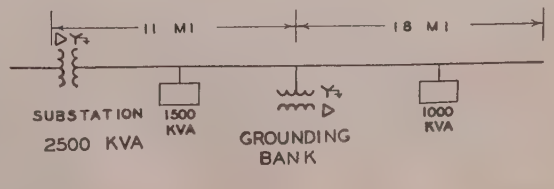

Figure 4 (right). One-line diagram of radial distribution feeder used in numerical problem

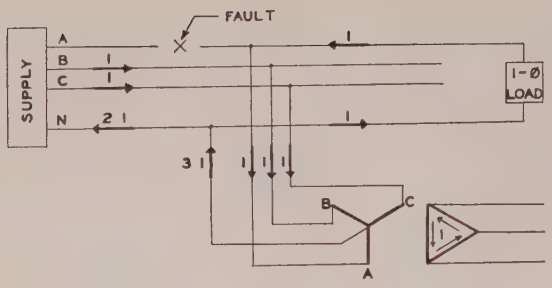

Figure 5. Diagram of open-conductor fault conditions showing that a grounded Y-delta bank must transform current for loads connected to the faulted phase

Table II

Per Cent Impedance of Transformers $Z_T/_1 \times 100$	Minimum Size of Bank (3-phase Kva) U_T	Per Cent Reduction of Zero-Sequence Voltage $e \times 100$
3.5	517	82.8
5.0	476	76.1
7.5	417	66.8
10.0	375	60.0

voltage obtained by grounding?" This question can be answered with generality only for the point on the feeder where the grounding bank is located, but this value of reduction, which is a maximum for the feeder, may be used as an indication of the reduction obtained on the whole feeder. From either the considerations that led to equation 1 or those that led to equation 3, the per-unit reduction, which will be represented by the symbol e for effectiveness, can be shown to be:

$$e = \left| \frac{U_T/U_F}{\frac{U_T}{U_F} + \frac{Z_{T/1}}{Z_{0/1}}} \right| \qquad (5)$$

If the value of the ratio k/p is calculated from equation 1 and is not merely the ratio of two independent estimates, this equation may be written:

$$e = \frac{k}{p} \times \frac{l'_T}{U_F} \qquad (6)$$

By use of this relationship in the problem just considered, the following result is obtained:

$$e = \frac{k}{p} \times \frac{U_T}{U_F} = 4.0 \times \frac{U_T}{2{,}500} = \frac{l'_T}{625} \qquad (7)$$

Addition of this information to that already obtained in the numerical problem gives the result shown in Table II.

The zero-sequence or floating-neutral voltage at the Y-delta bank is 15.7 per cent before grounding for the unbalance assumed in the problem. If a reduction to approximately 5 per cent is desired, any of the first three combinations in Table II would be satisfactory. It is, of course, permissible to use larger banks than the minimum sizes shown, and somewhat larger reductions of zero-sequence voltage are obtained, but it should be noted that effectiveness increases more slowly than size. Therefore, in the interest of economy, banks larger than the minimum required for a given transformer impedance should be avoided.

The last question now remains: "What protection is required?" From the preceding discussion of continuous duty requirements, it is obvious that some protection against overload is needed, since a more than usual degree of load unbalance on the feeder would cause excessive current in a grounding bank with no reserve capacity. Further consideration of the need for protection seems unnecessary. However, it is the business of an engineer to understand the behavior of a system as fully as practicable, and some attention ought to be devoted to the conditions existing during ground faults and open-conductor faults.

In the case of the single-line-to-ground fault, it is apparent that the condition is simply one of a severe unbalance of load, the effect of which has already been studied. As long as relaying occurs at the substation, the bank will be adequately protected, but the danger of sustained faults must be considered. An equivalent load unbalance of 50 per cent is possible on almost any radial feeder without relaying, and this value can be 80 per cent or more on a long rural line. For the numerical problem previously presented, a calculation based on the actual relay settings in use and for the hypothetical 417-kva 7.5 per cent impedance bank gives the maximum unbalance without relaying as 82 per cent. For such an unbalance, the value of k becomes 3.28, representing an overload of 228 per cent.

Even though the sustained ground fault seems a bad condition, the open-conductor fault condition is potentially much worse, particularly for a fault between the substation and the Y-delta bank. The behavior under such a condition is shown for a simplified case in Figure 5. From this diagram it is plain that the duty of supplying the loads beyond the fault which are connected between the faulted phase and neutral falls on the Y-delta bank. The grounded bank must transform this power to the delta side in the two legs tapped from the unfaulted phases and back to the Y side in the remaining leg, all the while supplying its own load as if connected in open Y. Even without more detailed analysis, it is apparent that the fault of this type can impose an intolerably severe condition on all

Figure 6 (below). (A) Diagram showing entire feeder unbalance concentrated at location of grounding bank. (B) Zero-sequence network for (A)

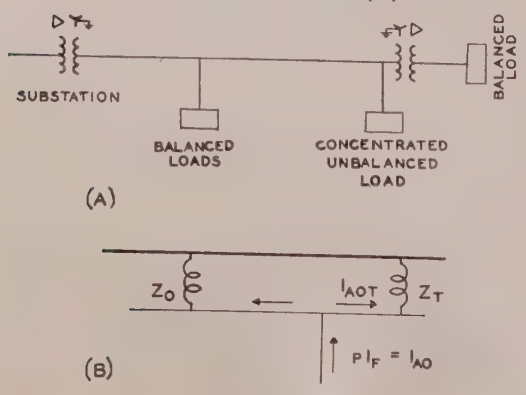

Figure 7 (right). Diagram showing application of Thevenin's theorem to grounding bank problem. The two grounded networks are equivalent

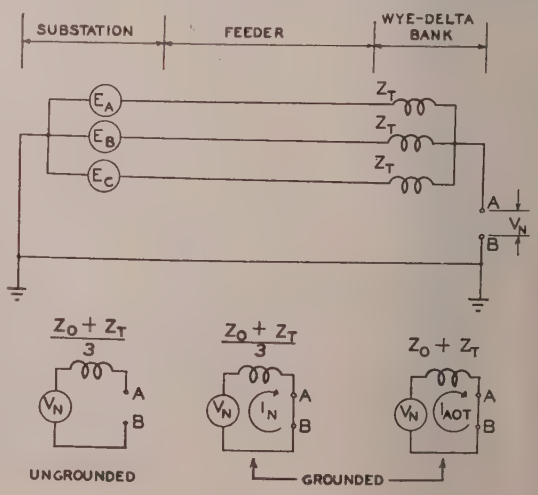

grounded banks. In many instances, the overload during the fault can easily be of the order of 300 per cent. Again, if relaying occurred at the substation, adequate protection would be afforded the bank. However, on most feeders the prefault current at the fault point would have to be about two-thirds of the rated feeder current value to produce action of the neutral relays at the substation. It is absurd, naturally, to expect faults to occur only at points convenient to the engineer, and the necessity for local protection is indicated.

Most transformer banks are protected by fuses placed in the primary phase conductors. If a Y-delta bank which is grounded were to be protected only by primary phase fuses, the arrangement would be most unsatisfactory. Fuse-blowing caused by too high a value of zero-sequence current would then cause an interruption of service to the customer supplied by the Y-delta secondary. On the other hand, if the grounding connection between the Y neutral and the feeder neutral is also fused, the bank would be protected against excessive grounding current, and yet interruption of service would not occur unnecessarily. Fuses rated for full feeder voltage would not be necessary. Furthermore, immediate attention to replacing blown neutral fuses would be entirely unnecessary; the worst that could happen would be that the grounded bank would become an ungrounded bank.

The current rating of the neutral fuse for a bank having no secondary load needs no comment since it poses only the usual problem of transformer duty. For the bank which does serve a load, however, notice should be taken of the fact that the neutral current cannot lie more than 60 degrees from the load current in one transformer leg, and may even be in phase. Since neutral current from unbalanced loads or sustained faults are not unlikely to be constant in phase angle for considerable periods of time, the safest procedure is to allow for the in-phase addition of ground current to load current. Accordingly, the bank should be fused for a neutral current such that, when one third of this value is added in-phase to the load current, the day's duty cycle will not exceed the ability of the individual legs of the bank to handle it. A fuse of this rating insures the blowing of the neutral fuse before that of a primary phase fuse. Since fusing is a waste of time if neutral currents during ordinary service will exceed the fuse rating, grounding of a load-serving bank may not be feasible. However, the calculation of the grounding duty likely to be imposed may be compared to the duty permisssible in order to determine the feasibility.

It is the belief of the writer that the grounded Y-delta connection offers an advantage that has not been fully utilized. Where the Y-delta is to be used for any of the several reasons that might favor this connection, consideration should be given to grounding the Y side for the purpose of helping to stabilize the system neutral. Fear of a bank burn-out can be eliminated by the simple practice of installing a thermal fuse in the grounding connection. Moreover, the installation of grounding banks at points other than at substations ought to be considered for radial feeders with bad voltage unbalance conditions. It is true that the bank sizes required are somewhat large and that the problem of economy is important. There appears to be no technical difficulty, however, that militates against such use of grounded Y-delta transformer banks.

Appendix I

The derivation of equation 1 requires the definition of five quantities in addition to those given in the body of the paper. These factors are:

V = rated line-to-neutral voltage of feeder
I_{a0T} = zero-sequence current flowing in the Y-delta bank, that is, one-third of the neutral current
Z_T = complex value of impedance of transformers in the Y-delta bank based on primary voltage and current
Z_0 = complex value of zero-sequence impedance looking into the feeder from the Y-delta terminals
I_T = primary current rating of the Y-delta bank

In Figure 6(A), the feeder is shown with the entire unbalance concentrated at the Y-delta bank location. The zero-sequence current from this load, pI_F, is shown as flowing into the feeder from the load and thence to ground. This is simply a matter of phase and is permissible. The current from the load will divide between the two paths Z_0 and Z_T according to the following equation:

$$I_{a0T} = pI_F \left| \frac{Z_0}{Z_0 + Z_T} \right| = pI_F \left| \frac{1}{1 + \frac{Z_T}{Z_0}} \right| \tag{8}$$

$$\frac{I_{a0T}}{pI_F} = \frac{I_{a0T}}{pI_T} \times \frac{3VI_T}{3VI_F} = \frac{k}{p} \times \frac{U_T}{U_F} = \left| \frac{1}{1 + \frac{Z_T}{Z_0}} \right| \tag{9}$$

$$\frac{k}{p} = \left| \frac{1}{\frac{U_T}{U_F}\left(1 + \frac{Z_T}{Z_0}\right)} \right| = \left| \frac{1}{\frac{U_T}{U_F} + \frac{U_T Z_T}{U_F Z_0}} \right| \tag{10}$$

In the last expression, a practical advantage is gained by using per-unit impedance values.

Then, since

$$\frac{U_T Z_T}{U_F Z_0} = \frac{U_T Z_T}{3V^2} \div \frac{U_F Z_0}{3V^2} = \frac{Z_{T/1}}{Z_{0/1}} \tag{11}$$

equation 10 becomes the same as equation 1.

Appendix II

This analysis uses symbols from the body of the paper and also Appendix I. In Figure 7, a feeder with loads neglected is shown in a 3-line diagram. The primary windings of the Y-delta bank are labelled Z_T. The floating neutral voltage V_N, which need not be measured with the transformers in place, is the open-circuit voltage for terminals "A" and "B." The impedance looking into these terminals is $^1/_3\ (Z_T + Z_0)$, assuming the line to be symmetrical. Application of Thevenin's theorem as indicated by the three small networks of Figure 7 shows that for the grounded condition, the ground current in any one leg of a Y-delta bank is given as:

$$I_{a0T} = \left| \frac{V_N}{Z_0 + Z_T} \right| = \left| \frac{V_N \times \frac{1}{Z_0}}{1 + \frac{Z_T}{Z_0}} \right| \tag{12}$$

$$k = \frac{I_{a0T}}{I_T} = \frac{I_{a0T} \times 3V}{U_T} = \left| \frac{V_N \times \frac{3V}{Z_0}}{U_T\left(1 + \frac{Z_T}{Z_0}\right)} \right|$$

$$= \left| \frac{\frac{V_N}{V} \times \frac{3V^2}{U_F Z_0}}{\frac{U_T}{U_F}\left(1 + \frac{Z_T}{Z_0}\right)} \right| = \left| \frac{\frac{V_{N/1}}{Z_{0/1}}}{\frac{U_T}{U_F} + \frac{U_T Z_T}{U_F Z_0}} \right| \tag{13}$$

The denominator of the last expression has been dealt with in equations 10 and 11 of Appendix I and is the same as the denominator of equation 1. Comparison of equation 1 and equation 13 shows that these equations are the same provided the per-unit unbalance p takes on the particular value given by equation 4.

References

1. Circuit Analysis of A-C Power Systems, **Edith Clarke,** John Wiley and Sons, New York, N. Y., volume 1, 1943.

2. Distribution Transformer Neutral Grounding, **R. F. Quinn.** *General Electric Review* (Schenectady, N. Y.), volume 48, June 1945.

3. Distribution Transformer Connections, **F. M. Starr.** *Distribution* (Schenectady, N. Y.), volume 1, July 1939.

No Discussion

Electric Home Heating

EARL E. PARKS
NONMEMBER AIEE

THE advantages of electricity for space heating are so obvious that, were it not for the difference in cost, electricity would undoubtedly replace all other fuels for this purpose. The cost of electricity, as compared to other fuels, would depend to a large extent upon the electric rate, but in practically every case, it would be the highest priced fuel.

To offset the higher fuel cost, many savings are possible due to the inherent qualities of electricity. In addition, such factors as comfort, health, and safety, although they may not be valued in terms of money, are none the less, of enormous importance to anyone who is choosing a method of heating his home. On each of these counts, electricity is without an equal.

Since the war other fuels commonly used for heating have increased in cost to such an extent, that the saving in fuel cost which can be made by their use, has not been sufficient to outweigh the benefits of electric heating. As proof of this, since 1945 we have connected over 11,200 electrically heated homes to our lines, and now have a saturation of nearly 15 per cent.

This increase is rather phenomenal, when you consider that we have never promoted it in any way. As a matter of fact, we have been very free to discourage the use of electricity for heating in homes which we consider unsuited to its use; for example, in large homes with little or no insulation. This growth can be attributed to one factor only the recommendation of satisfied users.

This demand for electric heat illustrates a characteristic of the American people, a determination to take advantage of any new method or product which will contribute to their comfort and well being. It also is a characteristic of American business to supply the demand for such products, and at a price the people can afford to pay. For this reason, I am convinced that the use of electricity for heating will continue to grow and that the electrical industry will provide the means for meeting the demand for this type of heat.

At the present time, there are very few locations, where conditions are as favorable for the use of electric heat as in Davidson County in Tennessee. By this I mean favorable for the customer, as it is by no means certain that the heating load is profitable for the Nashville Electric Service. We have a very low residential power rate and a moderate but variable climate, with a 48-year average of 3,613 degree days per year. It is quite certain that neither a low power rate nor a mild climate alone, would insure the widespread use of electricity for heating.

Practically every type of electric heating system has been used in Nashville. By far the largest number of installations have been individual space heaters installed in each room. Second in number, and gaining in popularity, are radiant heating cables installed in the ceiling. There is no great difference in the initial cost between these two methods and so far as we can determine, no difference whatever in the operating cost. Fortunately for the power distributor, both of these systems are controlled by individual thermostats in each room, thus giving considerable diversity to the heating load and its effect upon the distributing system. I might add that the manufacturers of all types have co-operated with us to the fullest extent by using control equipment which will improve the load characteristics of their system.

From the beginning, our company has made every effort to insure that each electrical heating job was a satisfactory one. It was apparent that this type of heating would become very popular. So, to eliminate, as far as possible, all chances for future complaints, we offered a special service for prospective heating customers. At the request of a home owner, architect, builder, contractor, or any interested party, and at no cost to them, we determine the heat loss, make recommendations as to size of heaters required, and give an estimate of the annual heating bill, for old or new houses. These recommendations are made in a letter addressed to the customer. This gives us an opportunity to specify the type of construction on which recommendations were based; for example, the extent of insulation, type of floors, and so forth. It also enables us to point out some of the pitfalls to be avoided, and make other suggestions which may help to insure a satisfactory job.

In no way do we attempt to influence the customer in his choice of methods or in his selection of equipment. We try to answer any question in an unbiased manner. Recommendations are considered confidential. To give you an idea of the extent to which this service is used, our records show that for the year of 1950, we made 2,704 recommendations on new houses, and 458 on old houses—a total of 3,162.

At the time we started this service, we hoped to accomplish four objectives.

First, to prevent the use of electricity for heating in homes which were not suited for its use.

Second, it gave us a chance to explain the means which could be used to reduce heat loss, such as insulation, weatherstrip, and storm sash.

Third, we were able to eliminate the use of large reserve capacity for heating, while at the same time make certain there would be sufficient for the needs.

Fourth, to obtain and keep complete records for most of the electrically heated homes.

Paper 51-150, recommended by the AIEE Domestic and Commercial Applications Committee and approved by the AIEE Technical Program Committee for presentation at the AIEE Southern District Meeting, Miami, Fla., April 11–13, 1951. Manuscript submitted January 15, 1951; made available for printing March 9, 1951.

EARL E. PARKS is with the Electric Power Board of the City of Nashville, Nashville, Tenn.

Table I. Averages for 526 Houses

Cubic feet content	8,720
Connected kw (Heating only)	15.4
Annual kwhr total	19,900
Annual kwhr heating	14,100
Annual kwhr other services	5,800
Kwhr per kw installed	915
Watts installed per cu ft	1.77
Kwhrs per cu ft	1.62

These records contain such information as type of construction, number and size of rooms, heat loss, size heaters recommended, estimated annual heating bill, and space is provided so that if desired, a complete record of the customers' bills may be kept. From these records, it has been possible for us to check our estimates against actual results, and each year, we have taken a representative cross section and made studies whereby we could improve on the accuracy of our estimates. Our last study, which was more complete than any yet made, consisted of 526 houses divided into the following groups:

1. Frame or brick veneer with walls and ceiling insulated and weatherstripped, or with storm sash.
2. Frame or brick veneer with ceiling insulated and weatherstripped.
3. Any house with no insulation.
4. Concrete block house with ceiling insulated and weatherstripped.
5. Insulated homes with central furnace heat.

These houses were segregated into groups so that we could obtain data which would enable us to give accurate estimates for all types of homes. The figures shown in Table I are the averages for the whole 526 homes. These figures must not be considered average for all our heating customers. We could find only 15 homes which had no insulation and all were used in the average. This is certainly a very high percentage of all such homes; whereas, we were able to use only a small percentage of the most common type—the completely insulated home. However, for all practical purposes they may be considered as typical.

It is rather difficult for a customer to tell whether or not his bill is in line with the estimate we gave him. First the amount which would normally be paid for other electrical services must be deducted and then the balance, which represents the amount paid for heating must be corrected to compensate for the number of degree days occurring during the time for which bill was rendered. Actually very few know anything about the degree days and many do not even know the period of time which is covered by the bill and even if they do, have only a hazy recollection of the weather for the whole period. To satisfy the customer we have prepared a chart on which we keep a constant record showing the number of degree days each day and cumulative number for the year starting with July 1. From this we can find out easily the number of degree days for any billing period, and by comparison with the average annual degree days, determine whether or not the bill is in line with our estimate. It is amazing how easy it is to satisfy a customer with such an explanation, and it is surprising how rapidly they can follow your reasoning, especially so, since in most cases, you are talking about something with which they are wholly unfamiliar.

In most cases, where the bill is actually higher than it should be, the cause is due to deficiency in amount of insulation or to a poor installation. In every case where heating was installed in a house with no insulation, it was done without our knowledge or against our recommendations; in either case the customer realizes that it is his responsibility.

In the beginning, our greatest source of trouble regarding high bills was the concrete block house with plaster on the inside and stucco or paint on the outside. In every case that I know of, the bills were higher than our estimates. On investigation we found that in these houses, the heat loss through the walls was so high in cold weather the walls never became warm, and whenever anyone was near any outside walls, the radiation from their warm body to the cold wall gave them a chilling effect. The customer tried to compensate for this by increasing the air temperature. Anyone who maintains a 10-degree higher temperature than the average, automatically increases his heating bill by approximately 50 per cent, so it was not surprising that their bills were high. We learned this the first winter, and from that time on would not recommend the use of electric heat in such houses, or if the customer insisted, we made our estimates accordingly.

It may be surprising to know that with electric heat, generally speaking, a much higher relative humidity is maintained in the house than with any other method of heating. My explanation for this, is the low rate of air change in the house. Most of these houses are well built with complete insulation and weatherstripping, thus cutting down infiltration to a minimum. Moreover with electric heat you eliminate the necessity for bringing in any air to support combustion. To burn a ton of coal, it is necessary to bring in

Table II. Peak Demand for House Heating Customers

No. of Customers	Peak Demand (Per Cent)
1	70
2	64
3	58.3
4	52.6
5	46.9
6	41.2
7	36.1
8	32.4
9	30.6
10	30.1
11	30.0

250,000 cubic feet of air—sufficient to change the entire air in the average house once every day for a month. Whenever cold air is brought in from the outside and the temperature raised, the relative humidity is lowered, unless moisture is added.

Due to the higher relative humidity we have had a great many complaints on account of sweating on the windows. It is generally conceded that this is a healthful condition, and nearly everyone wants to maintain a high relative humidity. Our only solution has been to recommend the use of storm sash or double glass windows. Not only does this eliminate the sweating to a large extent, but it reduces the heat loss, and makes a more comfortable home.

In talking to our customers, it soon became apparent that we were recommending more capacity than needed. In some cases where two heaters were installed in one room, we were told that one was all that was needed. We use a design temperature of 70 degrees and do not allow for any reserve capacity as such. The heat loss is determined from data found in the ASHVE Guide.[1] About the only way to reduce the heat loss in our calculations was to reduce the amount of air change. This has been done and we now use about half the amount which is recommended in the guide. Of the thousands of customers for whom we have made recommendations, not a single one has told us that their heaters were not large enough to keep their house warm. If we were figuring the heat loss as close as we would like for it to be, this would not be the case.

We have sought all possible information which would help us determine the maximum demand which we could expect from heating loads. The experience in other localities would not necessarily apply to our system, but any information of this kind has been of value to us.

We obtained a great deal of information from one group of 73 completely elec-

trified homes which were served by one primary line on which we installed metering equipment. Each of these homes had 13 kw of house heating which added to all other electric equipment, would give a connected load of between 20 and 25 kw. Demand readings at 5:45 p.m. and 7:15 a.m. were made at different times during the year and were plotted on a chart showing the demand versus the temperature. We obtained a curve as shown in Figure 1.

From 76 degrees down to around 12 degrees it is very nearly a straight line curve. Above 76 degrees it levels off to about 1.2 kw per customer, and below 12 degrees it seems to level off, although we do not have sufficient data at the low temperatures to justify any definite conclusion. The average maximum demand was 7 kw per customer, recorded at a temperature of −1 degree.

Information of this kind together with actual experience has enabled our engineering department to set up a chart which is used to determine the transformer capacity necessary to serve the heating load. This is shown in Table II.

The demand is given as a percentage of the total connected load in space heating for 1 to 11 customers served by one transformer. For any number in excess of 11, 30 per cent is used, the assumption being that the diversity will not increase above this number.

The question of demand is one of very great importance to the power company who supplies energy for electric heating. Each kilowatt of demand means that capacity to serve must be provided all along the line from the generators and substations to the distribution transformers, customers service, and meters. To show how serious the added demand of heating customers may become, I can cite the case of our company. The monthly system peak demand for this year jumped from a low of 137,874 kw in July to 269,000 in December. All of this increase can not be attributed to house heating, as the demand in July would normally be one of the lowest for the year. Neither is all of this increase due to the permanently installed house heating load.

A great many of our customers have small portable space heaters which are used for auxiliary heat. During real cold weather many of these are brought into use, especially for rooms which are hard to heat with existing equipment. If the gas pressure is low during cold weather, as is the case in some parts of the city, electric heaters are used to make up the deficiency. During the past four winters at one time or another, both coal and oil have been very scarce. During such periods, portable heaters are always used in great numbers. At one time they were sold in such quantity as to practically exhaust the available supply.

There has been a great deal of talk among power company people, particularly in this area, as to the value of the heating load. The same question was raised when the electric iron was introduced, and again when the electric range started to become popular. These questions can not easily be answered by talk or by figures. I dare say a good man with a pencil could make a case for either side. I thoroughly believe that the electrical heating load will become a profitable load, even if it is not at the present time. To hasten the time, I think the electrical industry should make an intensive effort to learn more about this load and find methods to improve its desirability.

It would be of great benefit, if someone would make thorough studies to determine the minimum capacity required to heat a home electrically with the type of equipment in use today. If we can heat a group of 73 homes, as our tests show, with a maximum peak demand of 7 kw at 0 degree, and our heat loss calculations show the capacity required to be 13 kw, it would appear at first glance that the heat loss figures were too high.

We should encourage in every way the development of heating systems which would improve the load factor. A great deal of experimental work has already been done on the heat pump. Machines which extract the heat from water or the ground have been on the market for a number of years and have proven very satisfactory where conditions are favorable for their use. Unfortunately their use in our territory is very limited, due to the rather peculiar geological formation. Most of Davidson County is underlaid with solid limestone, often times very close to the surface. The insulating character of the limestone prevents the use of the ground as a source of heat. Moreover, it is impossible to get a good well with any degree of certainty, as I understand from geologists, that water is found only where fissures appear in the limestone.

In any event, the initial cost of the heat pump is so high as to limit its use to a very few. On the other hand, the efficiency is such, about 400 per cent, that it is possible to heat in winter and cool in summer, an average size 5-room house with a 3-horsepower unit. The normal operating cost of both heating and cooling would be less than the average cost for heating only. With its low connected load and high load factor, the heat pump is the ideal load for the power distributor.

There now is in production, I understand, a new heat pump using the air-to-air principle of heating. This is being manufactured by the General Electric Company, and their reputation would be sufficient guarantee that it must be practical.

This type of unit has been used more or less experimentally in Texas and other sections of the country where the winters are mild. The greatest handicap for such a unit is that the colder the weather, and a corresponding greater need for heat, the less efficient the unit becomes. There also is a limit as to temperature, below which the unit will not operate. This limit is theoretically the boiling point of the refrigerant and in the case of this particular unit, supposedly −40 degrees.

The advantages of the heat pump are so great and the possible reward for building such a unit at a competitive price is so enormous, that I feel sure it is only a question of time till it will be in widespread use.

During the five months from November through March, to heat an average home of 8,000 cubic foot size would require approximately 11,000 kilowatt-hours of electricity. Three kilowatts used 24 hours per day would be sufficient to heat this home, or 4 kw used 24 hours per day would heat it during the three months of December, January, and February, ordinarily the three coldest months of the year. Using water heated to around 300 degrees Fahrenheit, which would be under 60

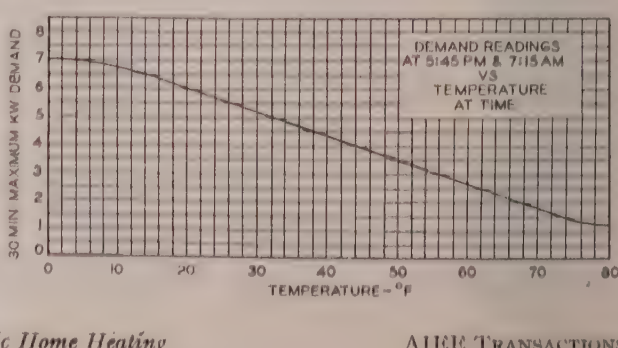

Figure 1. Kilowatt demand per customer versus temperature at time

pounds pressure, a storage tank of 250 cubic foot volume would hold enough hot water so that used in conjunction with a 4.0 kw heater, sufficient heat could be supplied in any one week to take care of twice the normal requirements. Using this principle of stored heat, it may be possible to build a furnace which would be a great deal lower in first cost than the heat pump, and one with just as good a load factor. For if this principle were used, the heating plant could be easily changed to a cooling system by installation of refrigeration coils in the water storage tank.

Our hope for eventual improvement in the characteristics of the electrical space heating load rests primarily on the electrical engineers. Personally, I have every confidence that they will come through with a solution for this just as they have always, in the past, come up with the right answer to our many problems.

Reference

1. Heating, Ventilating, and Air Conditioning Guide. American Society of Heating and Ventilating Engineers (New York, N. Y.).

No Discussion

A New Carrier-Current Frequency-Shift System for Use with Differential Protection of Transformer Banks

R. W. BECKWITH
MEMBER AIEE

WHEN a single transmission line is fed from a transformer, it is economically desirable to omit the high-side circuit breaker. This necessitates transmitting a tripping signal to the remote circuit breaker in the event of a transformer fault as indicated by differential relays.[1] In the past, the available carrier-current systems have not provided the speed of operation or degree of reliability that could be obtained by using a high-side circuit breaker.

The carrier-current system described here has been developed using crystal-controlled frequency-shift techniques to provide high-speed (two cycles) transferred tripping with assurance against undesired tripping due to any combination of power failure, component failure, switching, or other influencing factors. Thus, a degree of reliability is provided which is comparable to the use of a high-side circuit breaker.

This frequency-shift system employs the principles of frequency modulation for the transmission of control impulses. As applied to transferred tripping, a blocking carrier is transmitted normally on one frequency and shifted slightly to a tripping frequency for automatic circuit-breaker operation.

The basic application consists of a single narrow-band frequency-shift carrier-current channel operating on a frequency different from that used for the carrier pilot relaying. In the first application, however, the unusual importance of extreme reliability and simplified testing techniques resulted in the application of two paralleled carrier channels interlocked so that both must operate to cause tripping. Either channel may be tested by itself without causing tripping.

General Objectives

The primary problem of reliability was approached in several ways. First, everything possible was done to reduce the chance of failure of each circuit either due to component failure or due to external influence. Second, the circuits were arranged so that most failures would not cause tripping, and where this was impossible circuits were arranged so that false tripping could not occur except in the extremely rare event of two simultaneous failures.

In view of this, the following performance requirements were established:

1. The equipment should not cause tripping with extreme carrier-frequency disturbances such as is caused by an arcing disconnect switch feeding a short section of bus or line. This condition should be met even with simultaneous failure of the blocking signal.
2. The equipment should trip upon transmission of proper signals even with extreme interference at the receiving end.
3. It should have the greatest possible freedom from the chance of false tripping from a stray signal even with the simultaneous failure of the blocking signal.
4. The over-all operating time should be very short in order to minimize the extent of the fault damage to the protected transformer.
5. The carrier-current equipment should operate from the station battery.
6. The equipment should operate properly with disturbances on the station battery such as are caused by dirty motor commutators, circuit-breaker operation, or battery charging. Tripping should not occur upon failure of the blocking signal with this disturbance on the d-c supply.
7. The number of tubes should be held to a minimum and long-life tubes used wherever possible.
8. The equipment should not cause tripping with the normal emission failure of any tube.
9. There should be some means of indicating at the receiving end the failure of received signal.
10. It should be possible to test the channel completely one part at a time, without depending upon co-ordination of the operators at the two ends to prevent accidental tripping.
11. Preferably equipment for transferred tripping should be independent from carrier-current equipment used for functions other than relaying so that maintenance interruptions can be held to the minimum number necessary for the transferred-trip channel itself.

Frequency-Shift Operation Chosen

Narrow-band frequency-shift equipment, such as was already in use for telemetering,[2] was chosen since it basically fulfilled the most difficult requirements and could be adapted rather easily to fulfill all others. It already had been established that, because of the very narrow bandwidth and the noise balancing characteristics of the crystal-type frequency-shift telemeter equipment, greater distances could be covered and higher noise levels tolerated than with other types of channels used for telemetering.

Each of the requirements was met in a manner which can best be described in the following tabulation which corresponds to the tabulation of requirements.

Paper 51-153, recommended by the AIEE Carrier Current Committee and approved by the Technical Program Committee for presentation at the AIEE North Eastern District Meeting, Syracuse, N. Y., May 2–4, 1951. Manuscript submitted October 24, 1950; made available for printing March 1, 1951.

R. W. BECKWITH is with the General Electric Company, Syracuse, N. Y.

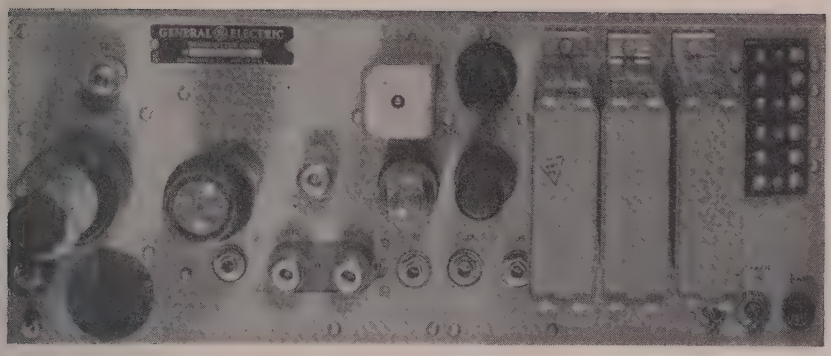

Figure 1. Crystal-controlled frequency-shift carrier-current transmitter used for transmission of transferred tripping signals

1. Random noise, equally distributed over the bandwidth of the receiver, will cancel out in the discriminator.[3] In order to assure that noise will not cause tripping, the crystal filter circuit is unbalanced slightly by means of its balance capacitor. This causes the noise accepted by the receiver to predominate near the blocking frequency and, therefore, to produce a negative discriminator output. In addition, a rectifier and filter circuit in the discriminator output rectifies any fluctuation in the discriminator output and produces further negative blocking voltage. Upon application of the tripping frequency, a positive output operates the relay tube and contacts of the associated relay close the trip circuit.

2. The extreme narrow bandwidth limits the noise energy accepted and permits the desired signal to override it and perform its function.

3. With the use of two channels, the chances of interfering signals occurring at the two precise frequencies necessary at exactly the same time are very remote indeed.

4. Tests show the over-all operating time of the carrier-current equipment to be less than two cycles, not including time of any auxiliary relays.

5. Both transmitter and receiver operate directly from a 125-direct-volt station battery, using tubes with heaters in series.

6. Power supply filters are included in both transmitters and receivers to prevent interference from the power source. The transmitter and receiver operate properly with a 2-second drop to 105 direct volts and with a rise in voltage to 140 direct volts. However, continued operation at voltages more than ±5 per cent away from normal will shorten tube life.

7. The transmitter uses only three tubes and the d-c operated receiver uses four. Tubes designed for long life are used and are operated very conservatively.

8. In the transmitter, the frequency is shifted from one crystal-controlled value to another by means of a reactance tube. Since the most likely failure (loss of emission) of this tube would result in failure to shift frequency, the tube is normally inoperative and is caused to operate and shift frequency for the tripping function. Any other failure is highly unlikely and the simultaneous failure of the tubes in two transmitters, when used, can be disregarded completely. The receiver trip relay normally is dropped out and usual tube failures will not cause current to be drawn. A grid short circuit could cause one tube to pick up the corresponding relay; however, again, the simultaneous failure of relay tubes in two receivers can be disregarded. An alarm is arranged to operate upon closing of either receiver relay so that any possible difficulty can be immediately eliminated.

9. The receiver cathode current of a radio-frequency amplifier tube is fed to an external indicating meter. This serves as an indication of received signal because of automatic volume control action. Also, the blocking frequency is used to operate a signal-alarm relay whose contacts will close an alarm on failure of received blocking signal. This same relay will drop out on failure of supply voltage or on failure of any receiver tube filament. A very complete check is thereby provided on all parts of the channel at all times.

10. With two separate channels, a tripping signal can be sent, first on one and then on the other channel, by means of a switch arranged so that both can never be sent at once.

11. The frequency-shift equipment is fundamentally based on the use of independent equipment for each function.

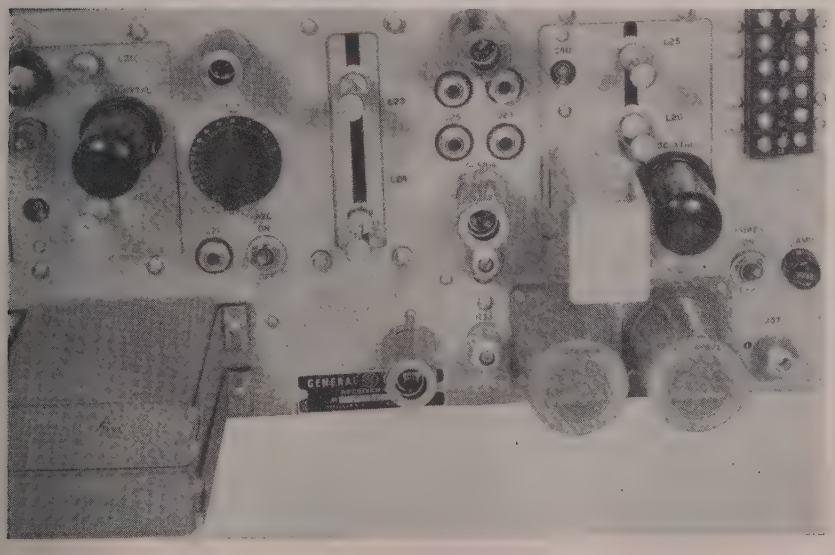

Figure 2. Crystal-controlled frequency-shift carrier-current receiver used for reception of transferred tripping signals

Description of Equipment

Figure 1 shows the transmitter and Figure 2 the receiver of most recent design, both of which are designed for direct operation from 125 or 250 direct volts with external resistor. Figure 3 shows a block diagram of the circuits of the two units. The output power of the transmitter is 1.5 watts which is sufficient for all usual applications. The units are designed for operation with appropriate crystals at any frequency between 70 and 200 kc.

The receiver provides freedom from

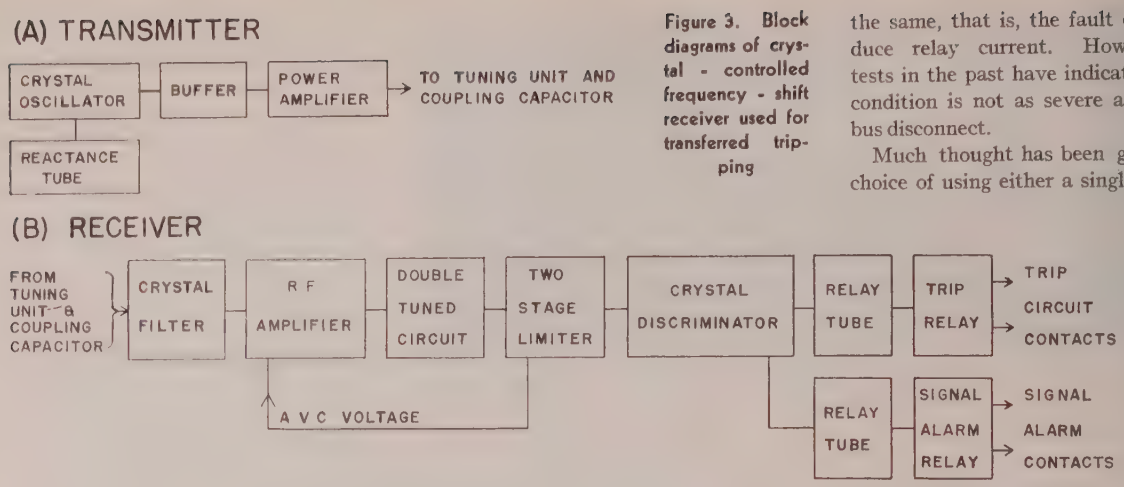

Figure 3. Block diagrams of crystal - controlled frequency - shift receiver used for transferred tripping

effects of random noise and transients, first, by utilizing a crystal filter to accept energy in only the narrowest band possible in order to still pass the necessary desired signals. (It is because of the high Q of this circuit, the crystal discriminator and the crystal oscillator in the transmitter, that a time equal to two cycles is needed to transmit the tripping signal. In other words, these circuits have a high inertia and a definite time is required to change the frequency and thus change from negative blocking to positive tripping output from the discriminator.) Second, an amplitude limiter rejects a large part of the noise effect, as is well known from the use of such a circuit in other frequency-modulation receivers. A third reduction is effected by the balancing effect of the crystal discriminator. Since the blocking frequency is transmitted continuously during fault or test intervals, a negative voltage from the discriminator adds to the fixed bias on the tripping relay tube so that the relay is very effectively prevented from operating. In order to prevent incorrect operation in the event of failure of a blocking signal, several additional steps are taken. A typical discriminator characteristic is shown in Figure 4. If the random noise and transients tend to have frequency components falling both in the region marked A and in region marked B, the net effect over any short period of time will be to cancel out. In order to assure that the trip relay will not pick up upon the simultaneous failure of the blocking signal and the occurrence of a disturbance such as is caused by the opening of a bus disconnect, an adjustment of the crystal filter was found which causes the effect of the transients to fall more largely in region B and therefore will hold the trip relay in the de-energized position. To further distinguish between signal and noise, a rectifier and filter are placed between the discriminator output and relay tube grid. This circuit rectifies variations in discriminator output such as are produced by noise and produces additional negative voltage on the grid of the trip relay tube. When the desired signal is present, the noise variations are suppressed by the limiter, so this latter circuit produces its desirable effect only in the event of carrier failure.

Tests Prove Success of Design

It may seem from the foregoing that afety factors have been added, one on top of another, even to an unnecessary degree. The cost of all of the features is small, however, compared to the cost of the protected equipment. During operating tests of this equipment on a 132-kv line, it was most gratifying to observe proper operation of the equipment even with the blocking signal absent and with so much interfering noise as to continuously ignite a neon bulb connected in the receiver input as a protective device.

These tests were made with noise generated by opening a bus disconnect a small way so that an arc is formed by the charging current to several hundred feet of bus structure, which, of course, had no connected loads. This arc was "tuned" by opening until maximum interfering current was read on some audio-tone transferred-tripping equipment of older design. Observation of current in the tripping relays of the frequency-shift equipment showed zero current on a meter with 100 microamperes' full scale deflection with blocking frequency transmitted or with the transmitter off. When the tripping frequency was transmitted the relay current held steady at the normal operating level.

During a staged arcing fault test an observation of relay current with transmitter off was made and the results were the same, that is, the fault did not produce relay current. However, other tests in the past have indicated that this condition is not as severe as the arcing bus disconnect.

Much thought has been given to the choice of using either a single channel or two channels to perform the operation. In the event that an extraneous signal somehow appeared at the exact tripping frequency at the same time as failure of transmitted signal because of fuse blowing in the power source, tube burnout, and so forth, the use of one channel could result in false tripping. Such a signal might come from another carrier-current transmitter or test oscillator which was being tuned through the tripping frequency for some other reason. As can be seen, this combination of events is quite a remote possibility and may be accepted as a calculated risk. A time-delay relay could be used to open the trip circuit at some fixed time after the signal alarm relay operates, indicating failure of received signal. This would reduce the possible time during which the aforementioned calculated risk could occur. The same feature also can be accomplished by instructing an operator to open the trip circuit manually upon receipt of a carrier failure indication.

A single channel must be tested by first opening the trip circuit at the receiving end and then transmitting a tripping signal. This allows for a human error in coordinating the test and results in divided responsibility in the event of a failure in co-ordination. With two channels, a tripping signal can be transmitted first on one and then the other with a switch

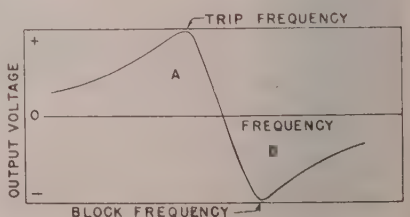

Figure 4. Characteristic of crystal discriminator used in frequency-shift receiver

arranged so that transmission of a simultaneous tripping signal on both channels is impossible. The operator must be present at the receiving end to observe operation but need not perform an operation to prevent actual tripping.

Two channels can be spaced as close as 0.5 per cent in frequency so that common single-frequency line-tuning units, traps, and coupling capacitors may be used. In this way two channels are nearly as easy to fit into a crowded frequency spectrum as a single channel would be.

The use of two channels requires only the addition of a transmitter and receiver unit and small changes in the auxiliary test and tripping circuits. With two channels, switches can be provided for operation on one channel during maintenance work on the other channel.

As can be seen, the choice between single- and double-channel operation depends upon the seriousness of a false circuit-breaker operation and upon whether the additional cost is justified to secure the ultimate in security.

References

1. Carrier-Current Differential Protection for Transformer Banks, **T. A. Cramer.** *Electrical Engineering* (*AIEE Transactions*), volume 62, August 1943, pages 545–48.

2. Characteristics of New Carrier-Current Equipment for Telemetering and Load Control, **R. W. Beckwith.** *AIEE Transactions*, volume 67, part II, 1948, pages 1649–53.

3. Frequency Response Circuits, **R. W. Beckwith.** United States Patent 2,461,956.

Discussion

G. S. Lunge (General Electric Company, Schenectady, N. Y.): The single-shift carrier-current transmitter and receiver combination described in this paper is intended primarily for carrier transferred tripping purposes. However, because the receiver contains two electromechanical relays, one of which responds only to reception of the guard frequency and the other to reception of the shifted frequency only, this type of carrier channel has other uses.

For telemetering kilowatt-hours or kilowatt demand, a carrier channel of this type provides the equivalent of a 3-wire full metallic channel between the transmitter and receiver locations and thereby does the work of two separate carrier channels of on-off type. A 2-position auxiliary relay having operating and reset coils should be interposed between the carrier transmitter and a 3-wire contact device in the watt-hour meter at the transmitting location in order that any chattering of the contact device may not cause over-registration of the impulse-operated distant-dial (kilowatt-hour) mechanism register or demand meter at the receiving location. The latter device should also be of the 3-wire type, so that interruption of a given carrier frequency signal cannot cause an additional advancing impulse to be registered. Advancing impulses, to take effect, must be alternately of the guard and shifted frequencies; hence accidental interruption of reception of a given impulse cannot cause over-registration.

If there is raise-lower control required over a carrier channel, with neither a raise nor a lower function being performed normally but only as required by an automatic load-frequency controller originating impulses of 0.25 second or longer, the single-shift type of carrier transmitter and receiver described in this paper can still be used, with minor additions. In the case of the transmitter, means are added for normally shifting the frequency rapidly from the guard frequency to the shifted frequency and back. In the receiver, a short time delay is introduced in the operation of the two electromechanical relays so that neither will pick up as long as the frequency is being changed rapidly from one frequency to the other. Steady reception of one frequency or the other will pick up the corresponding relay in the carrier receiver, corresponding to a "raise" or "lower" signal. Previously for this type of service it was necessary to use either a double-shift carrier channel without crystal control, or else two separate single-shift carrier channels, as it was not feasible for this extremely narrow-band type of carrier channel to provide a double frequency shift (both above and below a normally transmitted guard frequency) if crystal control was employed.

Thus the availability of the type of carrier channel described in this paper makes possible, for all telemetering or load control uses ordinarily encountered, the saving in carrier spectrum space achieved by the use of single-shift narrow-band crystal-controlled carrier channels.

If a number of functions are to be performed at one location, it will usually be economical to use a single carrier channel in conjunction with supervisory control equipment. The carrier channel can be of the crystal-controlled type, if telephone communication over the supervisory control channel is not required. If the carrier channel is operated on keyed carrier (on-off) basis instead of frequency shift, it is then possible to provide supervisory control or indication, or both, for more than one outlying station by means of the same single-frequency carrier channel, should this feature be necessary initially or at some future time.

Besides requiring only one carrier current transmitter-receiver at the control station, such multistation operation on a single-frequency carrier channel avoids the need for duplicating the common code-sending and receiving equipment of the supervisory control equipment at the control station, with consequent saving in space and equipment there.

The Use of Preferred Orientation Strip Steel in Turbine-Generator Stators

J. W. APPERSON
MEMBER AIEE

C. B. FONTAINE
MEMBER AIEE

Synopsis: Strip steel with preferred grain orientation has been applied successfully to stator punchingsof 2 poleturbine generators. Tests on 16 generators ranging from 1,000 kw to 20,000 kw rating indicate a reduction of 25 to 30 per cent in core losses and 50 per cent in required magnetomotive force in the stator punchings, compared with generators built with present nonoriented hot rolled sheet steels. Use of oriented strip steel permits design of generators of greater efficiency, greater rating for a given size, or both. Effective use is being made of this material in the design of certain 2 pole generators ranging in rating from 1,000 kw, 0.8 power factor, to 125,000 kw, 0.85 power factor.[1] This paper describes the specific application of oriented strip steel to turbine generators in the range of 1,000 kw to 20,000 kw. The advantages of the oriented strip material over the former nonoriented materials are discussed. Test results on 16 generators using oriented strip are presented. The material itself is described, and a brief history of its development given. Special generator manufacturing processes required when using the oriented strip, as well as some of the equipment used, are described. Possible further developments are touched upon.

ORIENTED strip has exceptionally good magnetic properties in the direction of rolling (with grain). This new steel has been used for some years in transformers, but has not been applied previously to large rotating apparatus. Two-pole turbine generators are particularly suited to the advantageous use of these directional properties. Most of the core loss and magnetomotive force drop in the stator core occurs in the yoke behind the stator teeth. By using segmented punchings, 12 or more to a circle, the preferred grain direction of the steel can be made to coincide closely with the direction of the magnetic flux path in this region. This results in appreciable improvement in the over all magnetic properties of the stator core, even though the losses and magnetomotive force in the teeth (across the grain) are about the same as for nonoriented sheet steel.

Active work aimed at testing the performance of oriented strip in a full size turbine generator was begun in 1944 in the company with which the authors are associated. In 1945, a 1,000-kw shop generator was tested with standard nonoriented sheet steel punchings, then restacked with oriented strip punchings and retested. In both cases the generator was given thorough no-load tests on the dynamometer test stand (Figure 1) on which each commercial generator is tested. With this equipment, no-load losses at various speeds, together with saturation characteristics, were measured accurately.

The results of these tests indicated marked advantages for the oriented strip. In 1947, the first commercial generator using the new steel, rated 7,500 kw, was shipped. In 1948, the decision was made to apply oriented strip to all 2-pole hydrogen-cooled generators in the range of 15,000 kw, 0.85 power factor, to 20,000 kw, 0.85 power factor, and eight of these generators have been built and tested to date. All told, the advantages of the oriented strip material have been proved by test on 16 generators. Additional test results are being added at a rapid rate. As each oriented strip generator is tested, its performance is compared with the results of several hundred tests already available on generators using nonoriented sheet steels.

Gain from Use of Oriented Strip

Losses

The reduction in generator core losses through use of oriented strip is best shown by actual test results. Figure 2 shows the comparative generator core

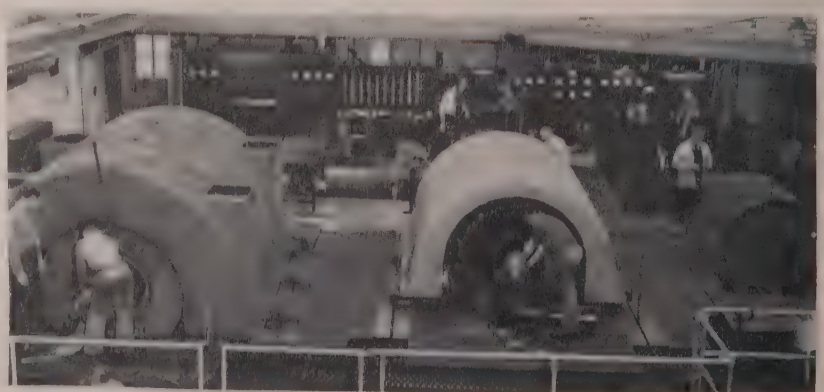

Figure 1. Turbine generators being set up on dynamometer test stand for routine measurement of electrical characteristics and losses

Paper 51-154, recommended by the AIEE Rotating Machinery Committee and approved by the Technical Program Committee for presentation at the AIEE North Eastern District Meeting, Syracuse, N. Y., May 2-4, 1951. Manuscript submitted January 31, 1951, made available for printing March 12, 1951.

J. W. APPERSON and C. B. FONTAINE both are with the General Electric Company, West Lynn, Mass.

The authors gratefully acknowledge their indebtedness to P. L. Alger, W. E. Ruder, and the late M. A. Savage for their foresight in initiating the first test of oriented strip in a full size turbine generator. They acknowledge also the work of a host of their associates at Lynn and Pittsfield, Mass., and Schenectady, N. Y., in contributing the effort and knowledge which made this successful application possible. Finally, they are indebted to J. W. Dougherty and R. E. McVay for accumulating much of the data presented in this paper.

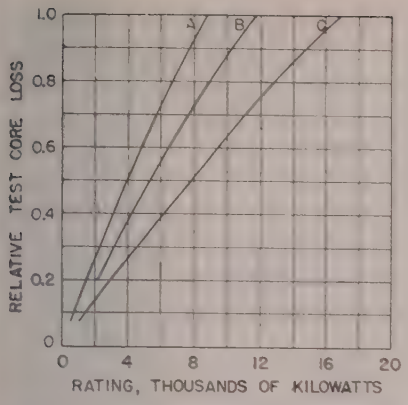

Figure 2. Test core loss versus generator rating

A—0.025-inch nonoriented sheet
B—0.014-inch nonoriented sheet or 0.025-inch oriented strip
C—0.014-inch oriented strip

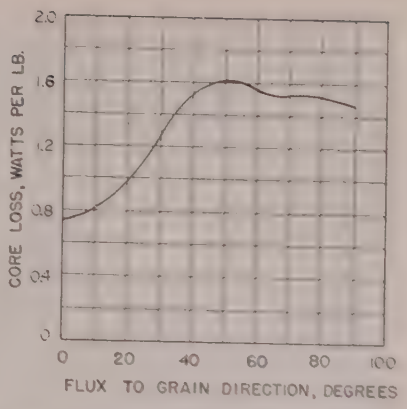

Figure 3. Variation of a-c core loss at 15,000 B, with variation in angle between flux and grain directions

losses for machines built with nonoriented sheet steel and with oriented strip, for two different material thicknesses. The curves represent averages of test results, faired so as to eliminate design differences between generators due to voltage rating, design proportions, and other factors. The curves for the nonoriented steels are based on a large number of test points. The oriented strip curves are based on 16 tests.

These test curves show that core losses in the generator are about 25 to 30 per cent lower for oriented strip than for nonoriented sheet, when punching thickness is the same. The trend is toward greater improvement—that is, machines tested recently show more improvement with oriented strip than those built earlier.

The exact gain for a given generator is of course dependent on the proportions of the generator stator punchings, in addition to other design factors. Epstein tests on samples of the materials used in the generators mentioned show that the oriented strip in the width-grain direction has only about 50 per cent of the loss of the nonoriented sheet. In the cross-grain direction, the losses are about the same. Consequently, the gain from the use of oriented strip is almost entirely in the yoke region of the punchings, behind the teeth. The generators which have the largest ratio of yoke loss to tooth loss thereby will show the greatest improvement through use of oriented strip. Also, use of narrower punching segments with fewer degrees in the segment arc tends to increase the gain with oriented material. The narrower the punching segment, the more nearly the flux direction coincides with the grain directions in the yoke, and the more nearly the flux direction in the teeth will lie directly across the grain. This latter condition is desirable because the highest losses and magnetomotive force drop in the oriented material occur when the flux direction makes an angle of about 50 to 60 degrees with the preferred grain direction. This is shown in Figure 3.

The gain with oriented strip is not confined to reduction in losses in the stator laminations themselves. A portion of the measured core losses are due to flux-linking solid structures outside the stator punchings. Examples are keybars, webplates, and frame wrapper plates. The magnitude of these leakage fluxes, and hence, of the losses they induce, are dependent on the magnetomotive force drop in the stator yoke. Because the magnetomotive force required in the stator yoke is appreciably reduced when using oriented strip, the parasitic losses in the stator steel back of the punchings also are greatly reduced. It should also be pointed out that there are secondary gains when any losses are reduced. For example, less losses mean less ventilating gas required, which in turn means less fan losses. This factor quickly becomes appreciable in air-cooled generators.

Figure 2 shows that the core losses with oriented strip are about 25 to 30 per cent less than with nonoriented sheet for a given generator, when the core is operated at the same flux density level. This means, by the same token, that the flux density in the core may be increased about ten per cent with oriented strip to give the same level of total core loss as with nonoriented sheet. An even greater increase in yoke density can be used for a given total loss, if the tooth density is not changed. This permits generators with a smaller outside diameter for a given rotor diameter, a factor of considerable importance on very large machines. It is thus apparent that the oriented strip material offers the designer new freedom in seeking the optimum generator design consistent with the limitations of size, economics, performance, and other factors.

Magnetomotive Force

The magnetomotive force required to produce magnetic flux in the stator core is reduced appreciably when oriented strip is substituted for nonoriented sheet. However, the magnitude of the reduction cannot be determined accurately by tests on the generator itself. The test quantity that can be measured is the field ampere-turns required to produce a given voltage in the armature windings when the generator is running. Of these measured ampere-turns, perhaps only 5 per cent would be expected to be required by the magnetomotive force drop in the stator teeth and yoke, and this portion cannot be segregated by the test. Therefore measuring any reduction in stator iron ampere-turns for the complete generator through use of oriented strip requires the taking of small differences between large test measurements.

Generator tests to date indicate that on the average the stator iron magnetomotive force when using oriented strip is at least 50 per cent less than with the previous nonoriented sheet. This is about as expected from calculations based on relative magnetization properties of the two materials.

As in the case of the core loss, the gain is concentrated in the yoke. The magnetomotive force required in the teeth is expected to be about the same for either steel. However, the magnetomotive force required at a given density for oriented strip in the with-grain direction is very much less than for the nonoriented

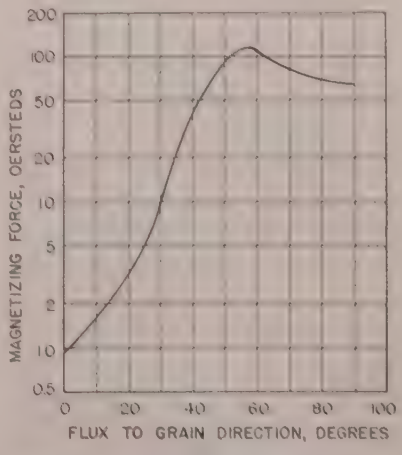

Figure 4. Variation of d-c magnetizing force at 15,000 B, with variation of angle between flux and grain directions

materials, some tests on material samples showing as little as 1 per cent as much magnetomotive force required. Factors other than the inherent properties of the materials reduce this gain; for example the reluctance introduced at the edges of the punching segments, and the fact that the direction of the magnetic flux does not coincide exactly at all points with the preferred grain direction. However, the fact remains that the magnetomotive force in the yoke is very much less with oriented strip than with nonoriented sheet. This allows not only greater flux densities and smaller machines with oriented strip but as pointed out before, greatly reduces the parasitic losses in the solid steel structures outside the stator punchings. Figure 4 gives typical saturation characteristics of the oriented strip material for various angles between direction of magnetic flux and the preferred grain direction.

General Application to Large Rotating Apparatus

The discussion so far has been confined to the use of oriented strip in 2-pole generators, where the properties of the material are best utilized by placing the preferred grain direction parallel to the yoke. This represents one extreme of machine proportions. At the other extreme are slow speed machines such as hydraulic driven generators, which have many poles and relatively shallow yokes. In such machines, the tooth loss predominates. Here the oriented material is best utilized by placing the grain direction parallel to the teeth. A large salient-pole generator is being built in this manner. Use of oriented strip is more difficult to justify economically on machines with intermediate numbers of poles than on the extremes represented by the 2-pole and many-pole designs, but it may well prove to be economical on certain large 4-pole turbine generators.

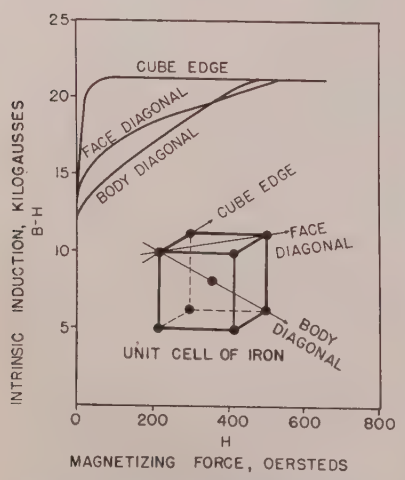

Figure 5. Crystal lattice structure of the iron unit cell, and typical magnetization curves

Table I. Magnetic Properties of Oriented Strip Taken in Direction of Rolling

	0.014 Inch Thick	0.025 Inch Thick
Epstein core loss, 60 cycles, watts per pound:		
10,000 B (Gausses)	0.3 to 0.4	0.5 to 0.6
15,000 B (Gausses)	0.7 to 0.8	1.2 to 1.3
Intrinsic saturation Flux density, B (Gausses)	19,600	19,600
Magnetizing force, H (oersteds)	300	300
Electrical resistivity at 25 degrees Centigrade (micro-ohms per centimeter cubed)	50	50

It may be asked if there does not exist some way to obtain the preferred properties in both the yoke and the teeth. This can be done, of course, by punching both yoke and teeth with-grain, and then mechanically butting, lapping, or welding the teeth to the yoke. A very effective solution would be the development of material with preferred properties in two directions at right angles to each other. None of these solutions has reached the point of general use.

Description of Oriented Strip Material

The material here discussed is a 3 to 3½ per cent silicon steel of comparatively high purity with the crystals or grains oriented so that the best magnetic quality is realized in the rolling direction. The range of magnetic quality of the material, in the rolling direction, as processed for use in generator laminations, is given in Table I.

The properties of the material are basically accounted for by the magnetic anisotropy of the iron crystal. This means that the iron crystal exhibits different magnetic quality and properties in the different crystallographic directions. This also is true of the 3 to 3½ per cent silicon steel here concerned.[2] Figure 5 shows this relation in the unit cell of the iron crystal.

Grains or crystals are each made up of a great multitude of these unit cells. All the unit cells within a grain are identically oriented. To realize similar properties in large pieces, such as laminations, these grains must all be oriented the same way within the piece. Such a condition in material is referred to as an "oriented" structure.

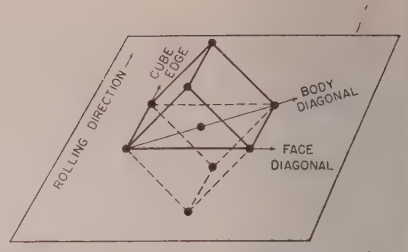

Figure 6. Relation of crystal lattice to orientation developed in oriented silicon steel strip, and showing principal crystal directions in plane of strip

It has been established that by cold-rolling a random structure sufficiently, an oriented structure can be induced.[3] In such a condition the material is of poor magnetic quality, and annealing becomes essential. It has been established further that through proper annealing an oriented structure can be maintained through control of recrystallization, grain nucleation, and subsequent grain growth.[4]

The oriented material being commercially produced has a structure in which the cube direction of the unit cell coincides with the rolling direction, as shown in Figure 6. Also, it is seen that the other principal crystal directions lie in the plane of the strip. This gives rise to considerable change in magnetic quality as the angle from the rolling direction is changed up to 90 degrees, as illustrated in Figures 3 and 4.

The production of high-quality oriented strip requires exceedingly close control in all phases. In the melting practice the control of impurities is essential, and in large measure the control of impurities makes the whole process possible. The ingots are hot-rolled to bands which are then processed through a cold reduction and annealing schedule which results in the final oriented material.

Early Development and Use of Oriented Silicon Strip

The development of oriented silicon strip was founded on the knowledge furnished by many independent investigators. The establishment of the anisotropy of iron and iron-silicon alloy crystals brought the possibility of such a material into sharp focus. X-ray defraction developments supplied an essential tool for subsequent crystal study. The effects of cold deformation on random structure promoting orientation and the subsequent recrystallization and growth orientations produced by annealing thereof were studied. Soon it was realized and demonstrated that it was possible to produce a thin flat material of preferred orientation with the favorable magnetic crystal direc-

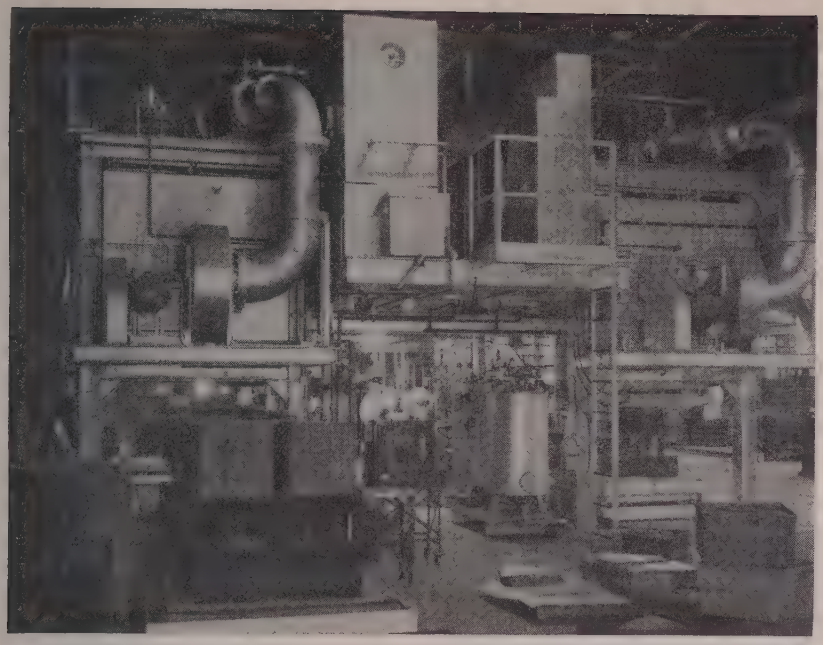

Figure 7. Annealing furnaces. View shows ends of two furnaces, at left and at right, with heat exchangers at tops of furnaces, and circulating blowers at ends. Gas dryers are seen under balcony between the two furnaces. In the left foreground is a car loaded with punchings, and other punchings in boxes are in the right foreground

tion in the plane of the strip.[5] The reduction of the foregoing to reliable mill practice has constituted a major metallurgical accomplishment.

Oriented strip became available in quantity about 1940. By 1942 considerable improvements in quality had been made, with use of the material rapidly expanding in transformer applications. The material is well suited to transformers because of the relative ease of adapting the core structures to its unidirectional character to derive full benefit of its properties. The use of oriented strip in rotating apparatus generally has been limited to a few specialized applications, such as d-c fields where the high-quality properties could be used advantageously.

Manufacture of Oriented Strip Laminations

Today there are two practices in the supply and use of oriented strip. One practice is the mill production of completely finished strip with fully developed magnetic quality, from which the electrical manufacturer produces laminations. The other practice is the mill production of a semifinished strip from which the electrical manufacturer produces laminations, followed by a medium- or high-temperature anneal to develop the final magnetic quality. It is the latter practice which has been followed in the manufacture of the laminations used in the generators discussed in this paper, as being the most economic means of securing punchings of high magnetic quality.

The final annealing of the generator punchings is a carefully controlled process carried out in an electric car-type furnace, equipped with controlled heating and cooling, and supplied with hydrogen for the anneal atmosphere. The loads are control-heated to 980 degrees centigrade and soaked, then control-cooled. Figure 7 shows the furnaces and some of the auxiliary equipment.

In all operations, particularly the anneal, control is exercised to eliminate any out-of-flatness in the laminations. In all operations after the anneal, control is exercised to avoid abuse of the laminations. This is necessitated by the extreme stress sensitivity of high-quality oriented steel, where the level of magnetic quality is appreciably lowered if the material is assembled in a stressed condition.

An additional characteristic of the oriented strip steel is its extremely smooth surface. This gives rise to much higher enamel film resistances for normal film thicknesses, compared to hot-rolled sheet without any cold-rolling treatment. This quality is particularly useful in turbine generators, where good insulation resistance between punchings is essential. The smoothness of the surface also improves the stacking space factor, which in itself contributes to the improvement in losses and magnetomotive force shown by tests on the generators.

Conclusion

The successful application of oriented strip steel material to stator punchings of 2-pole turbine generators has been confirmed by tests on 16 generators. Use of the oriented strip material is economically advantageous in these machines. This material permits the design of machines of greater efficiency, or greater rating from a given size, or both. It is expected that oriented strip ultimately will be used for all 2-pole turbine generators, as well as for many other types of large rotating apparatus.

References

1. Progress in the Development of Large Turbine Generators, **E. D. Huntley, H D. Taylor.** *AIEE Transactions*, volume 70, part I, 1951, pages 580–92.

2. Crystal Orientation in Magnetic Alloys, **Martin Littman.** *Electrical Engineering*, volume 68, number 11, November 1949, pages 977–79.

3. Structure of Metals (book), **Charles S. Barrett,** McGraw-Hill Book Company, Inc., New York, N. Y. First edition, fourth impression, 1943.

4. Oriented Crystals; Their Growth and Their Effects on Magnetic Properties, **Weston Morrill.** *General Electric Review* (Schenectady, N. Y.), volume 53, number 8, August 1950, pages 16–21.

5. New Developments in Electrical Strip Steels Characterized by Fine Grain Structure Approaching the Properties of a Single Crystal, **N. P. Goss.** *Transactions*, American Society for Metals (Cleveland, Ohio), volume 23, 1935, pages 511–37.

Discussion

L. P. Shildneck (General Electric Company, West Lynn, Mass.): The authors are to be congratulated, not only for bringing this important development to a successful conclusion, but also for the strength of their conviction that this project merited expending the necessary time and effort.

Substantial increases in efficiency of turbine-generators are rather rare occurrences, since the efficiency of most generators is already quite close to 100 per cent. Hydrogen cooling caused one such increase by boosting the efficiency of 3,600-rpm turbine generators an amount ranging from one-half to one per cent (a substantial portion of the way to the goal of perfection 100 per cent). The use of preferred orientation strip steel will increase the efficiency of hydrogen-cooled generators another one-quarter of a per cent. This is significant since the amount of increase in efficiency is from one-quarter to one-half the increase in efficiency brought about by hydrogen-cooling, and can be secured at relatively low cost.

In air-cooled generators, this reduction in core loss permits a reduction in cooling air required, which by reducing the fan input, increases the efficiency another one-eighth of a per cent. Thus, the total gain in efficiency, of an air-cooled 3,600-rpm turbine generator, made by using grain-oriented steel is about three-eighths of a per cent, which is half as much as that resulting from using hydrogen cooling alone.

Since the benefit of increased efficiency can be obtained at relatively low cost on both hydrogen-cooled and air-cooled generators, this development of the use of grain oriented steel is bound to have far-reaching effects on the future designs of rotating electrical machinery.

B. M. Cain (General Electric Company, Schenectady, N. Y.): The successful application of grain oriented strip steel to turbine generators, marks an important new step in the field of power generation. This step is significant, not only for the gains to be had in the machine itself, but because it shifts the production of steel from the outmoded hot mill to the modern continuous strip mill.

The advantages, which the authors have shown for this material as a result of its use on medium size generators, are already being extended to larger machines. The first application in a General Electric Company 60,000-kw AIEE preferred standard generator, conforms closely with the results reported in the paper. This application was a direct substitution of grain oriented strip steel in place of hot rolled sheet steel. The measured core loss of the grain oriented steel machine was 68 per cent of that for previous machines made with nonoriented sheet steel, but otherwise of identical design.

Other applications of this steel are giving distinct advantages. For example, new designs, which take full advantage of the greater flux capacity of grain oriented steel, are being made smaller in size. Some very large machines, which would have required a separate core and frame made in several pieces to meet shipping limitations, now are designed for one piece shipment. For example, a generator rated 147,000 kva, 125,000 kw, 0.85 power factor, 3,600 rpm ordered by the Philadelphia Electric Company, which was originally planned for the stator to be shipped disassembled, now is being built as a 1-piece stator by using grain oriented steel. This generator will be completed in about 15 months. Although, as the authors have indicated, the greatest advantages of this steel are gained in 2-pole generators, it is also being used effectively in 4-pole designs.

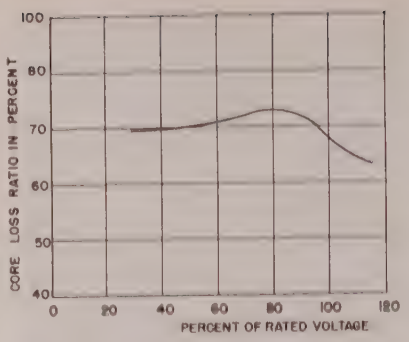

Figure 1. Ratio of core loss for grain oriented strip steel to core loss for hot rolled sheet steel from tests on 60,000-kw AIEE preferred standard turbine generators

An important characteristic of this steel, which the authors have mentioned, is the reduction in extraneous losses resulting from the very large reduction in magnetizing force at flux densities in the range of normal designs. These extraneous losses are caused by flux being forced into the solid steel members of the supporting structure as the core approaches saturation. As a result, the observed core loss increases with increased flux far more rapidly than the fundamental loss in the core iron itself.

Figure 1 of this discussion shows how grain oriented strip steel has reduced this extraneous loss in the 60,000-kw preferred standard generator previously mentioned, which was recently tested. Because of the reduction in extraneous losses, its total core losses do not increase nearly as rapidly as the losses of the sheet steel core when in the region of rated voltage. Consequently, the ratio of losses drops off abruptly in this region as shown by the curve. This important characteristic makes it possible to take full advantage of the lower losses of grain oriented strip steel in designing new machines by using flux densities considerably higher than are possible with nonoriented steels. The use of higher flux density makes an appreciable change in the radial stiffness of the core. This effect is carefully considered in the design of the flexible core mounting for isolating core vibration.

In addition to the above, the authors have pointed out the advantages of the smoothness and flatness of strip steel in making a more compact core. All of these characteristics are being used throughout the entire range of turbine generator sizes to achieve either lower losses, smaller outline dimensions, or greater kilovolt-ampere ratings built with 1-piece stator assemblies.

J. W. Apperson and **C. B. Fontaine:** Mr. Shildneck has presented a clear picture of the increase in efficiency which follows from the reduction in core losses. This approach is a welcome addition to the paper, since the paper touches only generally on the efficiency of the generator itself.

It is of course very gratifying that the first test result on a larger generator, reported by Mr. Cain, should conform closely with the test results on the medium size generators. Figure 1 of Mr. Cain's discussion is an excellent illustration of the reduction in extraneous losses resulting from reduction in magnetizing forces in the stator yoke. The shape of the curve is characteristic of results obtained on the generators tested previously.

System Economics of Extra-High-Voltage Transmission

H. P. ST. CLAIR
FELLOW AIEE

E. L. PETERSON
MEMBER AIEE

AS BROUGHT out in previous and companion papers,[1-11] the program of research and development centering around the Tidd experimental 500-kv Test Project has been devoted to the building up of a sound technical basis for the selection of voltage level and other features of extra-high-voltage transmission, specifically for application to the American Gas and Electric Company system, as well as for the benefit of the transmission art generally. Along with technical and physical requirements, it also was necessary to develop a sound economic basis for the selection and application of the new high-voltage transmission. To this end economic studies have been carried out as described in this paper. Here again, these studies have been made in the light of the specific conditions applicable to the American Gas and Electric Company system, recognizing fully that variations in these conditions, which include type of system, climate, terrain, and so forth, may alter the results and conclusions as applied to other systems and areas. Nevertheless, it is believed that the basic assumptions and procedure used will be of interest and that the results may have some significance for general application.

Although the American Gas and Electric Company system is predominantly of the integrated network type with transmission requirements varying widely as to distance, load factor, and even direction of power flow, it was felt that a general study of the economics of straight bulk power transmission, covering various distances, blocks of power, and voltages, would provide significant data for evaluating different voltage levels in terms of these varying requirements. Such a study, based upon costs for line construction, switchgear, transformer, and other equipment, therefore comprised an important part of the over-all economic investigation as described here.

Economics of Bulk Power Transmission

While exploratory studies were made with voltages as high as 460 kv and serious consideration was given at one stage to the adoption of a 360-kv nominal level (380-kv top), the steeply rising curves of corona and radio influence at 345 kv and above led to the decision to limit these economic studies to the three voltage levels, 230 kv, 287 kv, and 345 kv. As the study progressed it was decided to add an intermediate level at 315 kv.

Although the immediate transmission problem involved only distances under 300 miles, studies were made for line lengths of 100, 200, 300, 400, and 600 miles.

While many factors enter into a study of transmission costs, two basic elements are, first, the load-carrying capability of lines in terms of voltage and distance, and second, the installed cost of lines and associated equipment, particularly transformers and switchgear. Related to both transmission capability and cost is a third factor, an evaluation of the economics of intermediate switching stations. Each of these factors was developed for this study as described here.

Basic Capability of Lines

A practical evaluation of the power-carrying capability of transmission lines cannot be tied down to any single formula but is rather an empirical determination, based largely upon stability limitations for the longer lines, with the emphasis shifting to losses, both real and reactive, for the shorter distances. For very short lines even thermal limitations may be controlling. Because of its underlying importance to the entire study, this question was reviewed very carefully, taking into account operating experience and practices on various types of systems, results of network analyzer studies on both hypothetical and actual systems including that of the American Gas and Electric Service Corporation, and published results of theoretical and practical investigations and conclusions as to stability limitations. The final result of this review has been expressed in the form of a curve, Figure 1, showing capability versus line length in terms of surge impedance loading (SIL), which for all conventional lines using single conductors per phase is substantially 2.5 kv[2]. Thus the curve applies to any line voltage.

For line lengths of 300 miles and above, the load values shown in Figure 1 are based upon reasonable assumptions as to generator and transformer impedances at the sending-end and equivalent receiving-end impedances, together with a reason-

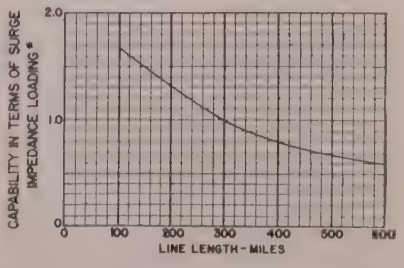

Figure 1. Capability of transmission lines in terms of surge impedance loading (surge impedance loading approximate 2½ kv²)

Paper 51-156, recommended by the AIEE Transmission and Distribution Committee and approved by the Technical Program Committee for presentation at the AIEE North Eastern District Meeting, Syracuse, N. Y., May 2–4, 1951. Manuscript submitted January 30, 1951; made available for printing March 2, 1951.

H. P. St. Clair and E. L. Peterson both are with the American Gas and Electric Service Corporation, New York, N. Y.

The authors wish to acknowledge helpful suggestions and contributions by S. B. Griscom and S. B. Crary in carrying out this economic study. Appreciation also is expressed for the extensive help contributed by W. S. White, Jr., in carrying out calculations and in the preparation of curves and tables used in this paper.

Table I. Severity of Loading

Line Length	Loading in Kilowatt Miles Per Kv[1]
100	420
200	660
300	750
400	800
600	900

Table II. Transmission-Line Physical Design Characteristics

Voltage	230 Kv	287 Kv	315 Kv	345 Kv
Conductor, steel-reinforced aluminum cable	874,500	1,058,900	1,272,000	1,351,500
Conductor, copper equivalent	550,000	666,000	800,000	850,000
Conductor diameter, inches	1.1	1.4	1.6	1.75
Insulator units	14	16	18	20
Single-circuit phase spacing, feet	25.5	27.5	29.5	30.5
Double-circuit phase spacing, feet	20.5	21.5	23.8	

able margin below the actual steady-state stability limit to allow for transient swings. These loadings represent the capability of lines without series capacitor or intermediate synchronous condenser compensation and follow quite closely the conclusions worked out and published by Crary.[12] While such compensation has not been considered in this study, the effect would be to increase the capability of the 400- and 600-mile lines, possibly to the extent of maintaining 2.5 kv[2], or surge impedance loading, up to 600 miles.

Below 300 miles, the loadings shown on Figure 1 have been determined as pointed out in the preceding paragraph, not solely by stability considerations, but to some extent by other considerations such as reactive losses encountered at loads above 2.5 kv[2]. A clear evaluation of the relative severity of loading for the various points on Figure 1 may be made by expressing these loadings in terms of kilowatts × miles per kv[2]. For example, at 300 miles, kilowatts = 1.0 SIL = 2.5 kv[2], and the kilowatt miles per kv[2] = 750. In these terms the severity of loading for each of the points on Figure 1 would be as shown in Table I.

Cost of Lines, Transformers, and Switchgear

To insure that the costs of line and terminal equipment assumed in this study will be not only comparable but reasonably up to date, all of these costs have been based on general price levels and estimates of installation costs prevalent in September 1950.

As pointed out, the estimated transmission line cost figures used in this study were based upon a type of construction which would be considered suitable for the general conditions found in the American Gas system territory and which may vary appreciably from conditions in other areas. For one thing, sleet conditions are generally quite severe and therefore towers have been designed for heavy loading conditions.

To keep the weight of steel as low as possible and still meet these requirements with what is believed to be a necessary factor of safety, nickel alloy steel has been included in the design of tower legs.

Conductor diameters have been selected on the basis of corona and radio-influence requirements, as outlined in companion papers,[8-11] while conductivity has been determined by both thermal limits and economics of losses with sleet-melting a real consideration in the area covered. It may be said that full evaluation of the economics of losses will dictate a conductivity level well above that determined by thermal considerations, while sleet-melting requirements may hold the sizes down somewhat. Taking into account all of these considerations, conductor diameters and equivalent conductivities for each voltage level were chosen as shown in Table II.

The actual conductor was assumed to be an expanded steel-reinforced aluminum cable design as described in a companion paper,[11] which also shows the methods used in determining the number of insulators, clearances to ground, and so forth. Two ground wires were used for single-circuit towers while only one ground wire was used for the double-circuit towers. Table II also shows the number of insulator units and phase spacing for both the single- and double-circuit towers for 230 kv, 287 kv, and 315 kv., and for single-circuit towers only at 345 kv.

The general type of tower design used is illustrated by the 315-kv single- and double-circuit towers shown in Figure 2.

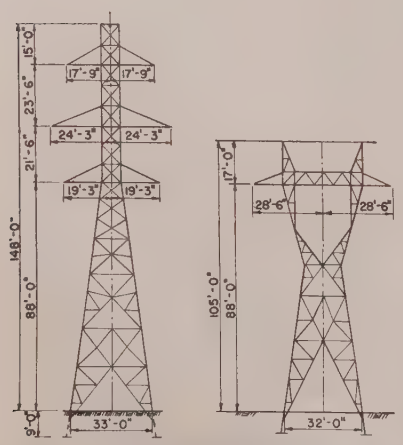

Figure 2. 315-kv single- and double-circuit towers

The final cost figures used in this study for transmission lines are given in Figure 3.

Although step-up transformers generally are considered as an integral part of the generating station, for this study they were included with the transmission system along with high-side switching in order to show the full effect of voltage on total cost. For receiving stations, autotransformers were assumed, stepping down to 138 kv from 345 kv, 315 kv, and 287 kv, and to 115 kv from 230 kv. Total installed costs for step-up transformers of various voltages and in banks of 100,000 kva and 250,000 kva are shown in Figure 4. Similarly, the step-down autotransformer installed costs are shown in Figure 5.

Without going deeply into the subject of switching schemes, it is believed that an average representative cost for high-voltage switching at both sending and receiving stations will be obtained by assuming one circuit breaker for each line and two for each transformer bank. Estimated installed costs for both transformer and line circuit breakers are shown in Figure 6, where it will be noted that a somewhat lower cost per circuit breaker

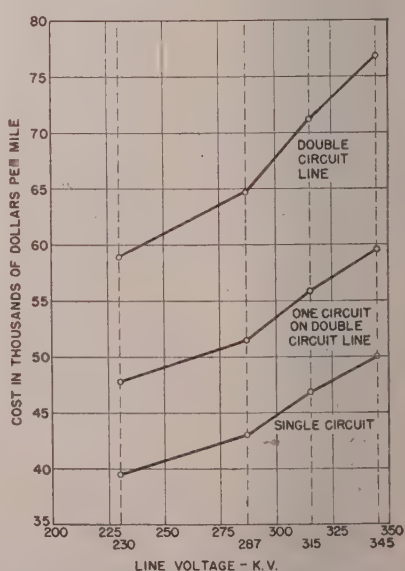

Figure 3. Installed cost of transmission lines at various line voltages

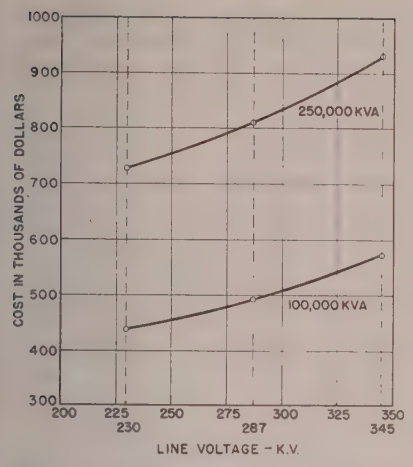

Figure 4. Step-up transformers. Installed cost for banks of three 1-phase units

is obtained for transformers due to a saving in steel requirements for the double circuit-breaker arrangement. While the interrupting capacities were not specifically tied down, the cost estimates assumed ratings of the following order:

230 kv	10,000,000 kva
287 kv	12,000,000 kva
315 kv	15,000,000 kva
345 kv	15,000,000 kva

Economics of Intermediate Switching Stations

A basic assumption followed throughout the entire study was that the useful capability of any line arrangement will be limited to the maximum capability with any one line or line section out of service. For double-circuit line construction, it is true that 2-circuit outages may occur; for the higher voltages, 230 kv and above, however, such outages should be rare. The minimum transmission setup considered, therefore, was two circuits, for

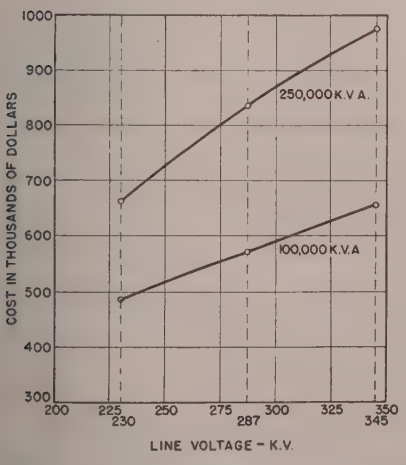

Figure 5. Step-down transformers. Installed cost for banks of three 1-phase units

which the useful capability, without intermediate switching, would be reduced to 1/2 of the normal capability of the two lines as obtained from Figure 1. It is obvious, then, that the introduction of one sectionalizing station will increase the useful capability from 1/2 to 2/3, while two stations will increase it to 3/4 of the normal 2 circuit capability, assuming in each case the loss of only one line section. This, of course, assumes that the rated capacity of terminal equipment, transformers and generators, will be commensurate with the corrected line capability. The reduction factor in terms of the normal capability from Figure 1 and the number of circuits and sectionalizing stations may be expressed as follows:

$$P_s/P_n = \frac{(N-1)(S+1)}{N(S+1)-S}$$

where

P_s = useful capability
P_n = normal capability from Figure 1
N = number of lines in parallel
S = number of sectionalizing stations

For convenient reference, Table III was prepared to show the reduction factors for zero to four sectionalizing stations with two, three, and four circuits in parallel.

It is obvious from all of this that the additional cost of installing intermediate switching stations must be balanced against the resulting gain in useful or effective transmission capability. Such a study was carried out for two, three, and four circuits at each voltage with line distances of 100 to 600 miles and with varying numbers of switching stations. For two circuits, the sectionalizing stations consisted of a ring bus using four circuit breakers, while a double bus with one circuit breaker per line plus a tie circuit breaker was used for three or more circuits.

Using transmission line, terminal equipment, and switching costs as obtained from Figures 3, 4, 5, and 6, and normal line capability as obtained from Figure 1 with the proper reduction factors from Table III for the outage of any one line section, the relation was worked out between over-all investment in dollars per kilowatt mile and the number of intermediate switching stations. The results were plotted in curve form for each voltage, Figures 7 to 12 inclusive, with 287 kv and 345 kv being representative of all the voltages studied.

As a sidelight on Table III, it is interesting to note the effect on useful capability of adding a third and perhaps a fourth circuit to an existing double-circuit arrangement. For example, the reduction factor, which for two circuits and

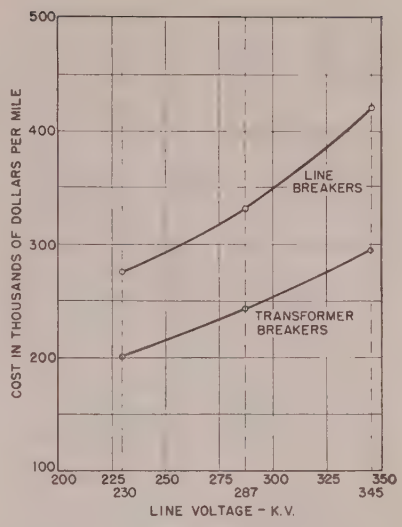

Figure 6. Installed cost of circuit breakers

one sectionalizing station is 2/3, changes to 4/5 when a third circuit is added in parallel with the other two circuits. This means an increase from $2/3 \times 2P_n$ to $4/5 \times 3P_n$, or a net gain of 80 per cent.

An examination of the curves, Figures 7 to 12, shows that fewer sectionalizing stations are justified as the number of circuits in parallel increases. It appears logical for two reasons, therefore, in designing a 2-circuit layout, to stop short of the minimum point on the curve: first, because of the diminishing return where the curve is fairly flat anyway, and second, because of the effect of adding a future third, or even a fourth, circuit. With this in mind, the respective numbers of sectionalizing stations to be used in the study for the various line lengths were chosen from the curves as indicated by points marked with a star.

Transmission Investment Costs, Dollars per Kilowatt Mile

Since the cost of transmission lines themselves is so large a part of the total transmission plant investment, it is evident from the single-circuit and double-circuit line costs shown in Figure 3 that the final results in dollars per kilowatt mile will be appreciably affected by the

Table III. Reduction Factors for Line Section Outages

Number of Sectionalizing Stations	Number of Circuits in Parallel 2	3	4
0	1/2	2/3	3/4
1	2/3	4/5	6/7
2	3/4	6/7	9/10
3	4/5	8/9	12/13
4	5/6	10/11	15/16

Table IV. Transmission Costs, Dollars per Kilowatt Mile

Kilovolts	Distance, Miles	P_c/P_n	P_n, Megawatts	Total Cost in Thousands of Dollars	Unit Cost, Dollars per Kilowatt Mile
		Two Circuits			
230	100	0.75	333	11,920	0.358
	200	0.75	261	18,100	0.347
	300	0.75	198	24,300	0.410
	400	0.80	170	31,000	0.456
	600	0.833	132	43,370	0.548
287	100	0.75	520	15,175	0.292
	200	0.75	408	21,650	0.265
	300	0.75	309	28,330	0.306
	400	0.80	264	35,560	0.336
	600	0.833	206	49,125	0.398
315	100	0.75	625	17,908	0.287
	200	0.75	492	24,806	0.252
	300	0.75	372	31,760	0.284
	400	0.80	319	39,750	0.312
	600	0.833	248	54,950	0.368
345	100	0.75	750	23,584	0.315
	200	0.75	588	33,060	0.281
	300	0.75	446	42,800	0.320
	400	0.80	380	53,580	0.353
	600	0.833	300	74,220	0.412
		Four Circuits			
230	100	0.86	764	24,026	0.315
	200	0.887	617	36,320	0.294
	300	0.90	475	49,050	0.344
	400	0.923	390	62,320	0.399
	600	0.937	297	87,200	0.490
287	100	0.86	1,190	30,647	0.258
	200	0.887	965	43,934	0.227
	300	0.90	740	57,236	0.258
	400	0.923	608	71,658	0.295
	600	0.937	463	98,715	0.356
315	100	0.86	1,435	36,710	0.256
	200	0.887	1,165	50,900	0.218
	300	0.90	892	65,090	0.244
	400	0.923	733	80,640	0.276
	600	0.937	557	109,950	0.329
345	100	0.86	1,720	48,370	0.287
	200	0.887	1,390	67,660	0.243
	300	0.90	1,070	87,150	0.272
	400	0.923	880	108,340	0.308
	600	0.937	670	149,320	0.372
		Six Circuits			
230	100	0.90	1,200	36,100	0.301
	200	0.927	967	54,530	0.282
	300	0.937	744	73,250	0.328
	400	0.952	604	92,700	0.384
	600	0.961	456	130,000	0.475
287	100	0.90	1,870	46,370	0.248
	200	0.927	1,510	65,880	0.218
	300	0.937	1,160	85,430	0.246
	400	0.952	940	106,580	0.284
	600	0.961	710	146,800	0.344
315	100	0.90	2,250	55,520	0.247
	200	0.927	1,825	76,500	0.210
	300	0.937	1,395	97,120	0.232
	400	0.952	1,135	120,230	0.265
	600	0.961	856	164,000	0.320
345	100	0.90	2,700	73,300	0.272
	200	0.927	2,180	99,600	0.229
	300	0.937	1,675	130,200	0.259
	400	0.952	1,358	161,350	0.297
	600	0.961	1,028	222,080	0.360

choice of double-circuit versus single-circuit lines. As indicated in a companion paper,[11] our studies have indicated that double-circuit lines will be quite feasible for voltages as high as 287 and 315 kv, but for a number of reasons were not considered practicable at 345 kv or higher voltages. In line with these conclusions, and using the basic factors of capability and investment costs developed as described previously, we have explored transmission investment cost on the basis of double-circuit lines in units of two, four, and six circuits at each of the voltages 230, 287, and 315 kv, changing to single-circuit lines for the 345-kv class. The results of these studies in dollars per kilowatt mile for line lengths of 100 to 600 miles, and with sectionalizing stations selected in accordance with Figures 7 to 12, are shown in Table IV.

In order to show the comparative economics of single-circuit lines, a similar study has been made, based upon four single-circuit lines for each voltage at line lengths of 200 and 300 miles and the results are shown in Table V. It was believed that such a study would give a basis of comparison which would be representative of other transmission distances and circuit combinations.

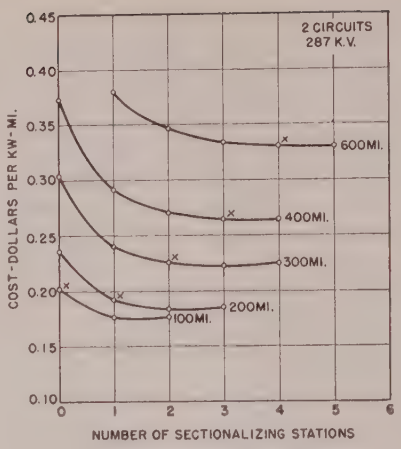

Figure 7. Economics of sectionalizing stations for two circuits at 287 kv

Table V. Transmission Costs, Dollars per Kilowatt Mile—Four Single-Circuit Lines

Kilovolts	Distance, Miles	P_c	Total Cost in Thousands of Dollars	Unit Cost, Dollars per Kilowatt Mile
230	200	617	44,570	0.361
	300	475	61,150	0.429
287	200	965	52,530	0.272
	300	740	70,030	0.316
315	200	1,165	59,820	0.256
	300	892	78,570	0.294
345	200	1,390	67,660	0.243
	300	1,070	87,150	0.272

It will be noted from Table IV that for the 100- and 200-mile lines the reduction factors indicated in Table III have been modified to increase the useful capability. The greatest change made is in the 100-mile 2-circuit line, where the reduction factor with one circuit out has been increased from 50 to 75 per cent. Progressively smaller changes were made for the 4- and 6-circuit 100-mile lines and for the 200-mile lines with one sectionalizing station. This increase in the emergency load capability of 100-mile and 200-mile lines is believed to be justified since reactive loss rather than stability was the important criterion in establishing this portion of the capability curve of Figure 1. With adequate reactive capacity available both in generating stations and in receiving systems, such emergency loadings should be entirely feasible, and, in fact, are believed to be representative of actual practice in loading modern transmission systems.

The data from Tables IV and V have been plotted in Figures 13 to 16 inclusive. It is interesting to note from these curves that, under the assumption of double-

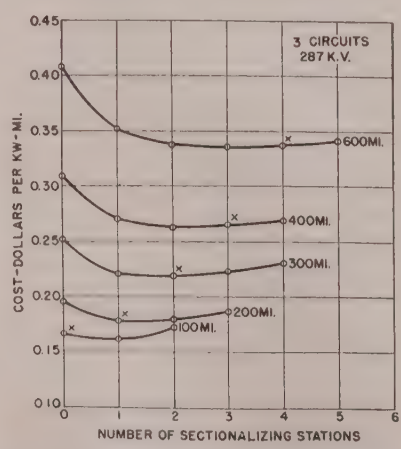

Figure 8. Economics of sectionalizing stations for three circuits at 287 kv

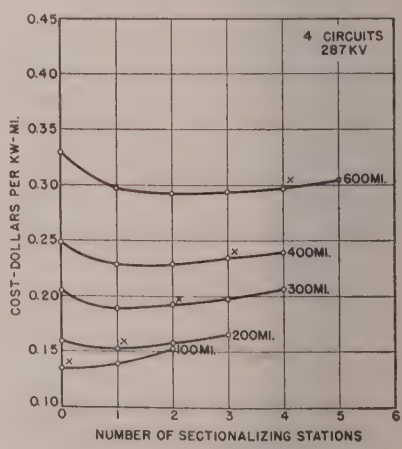

Figure 9. Economics of sectionalizing stations for four circuits at 287 kv

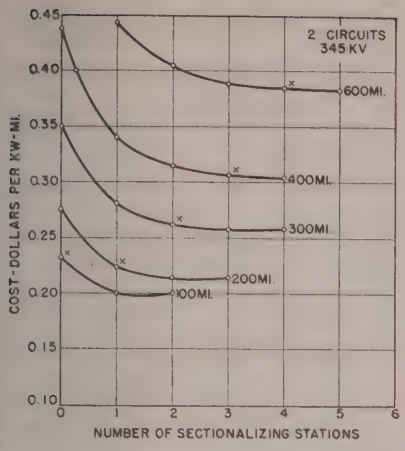

Figure 10. Economics of sectionalizing stations for two circuits at 345 kv

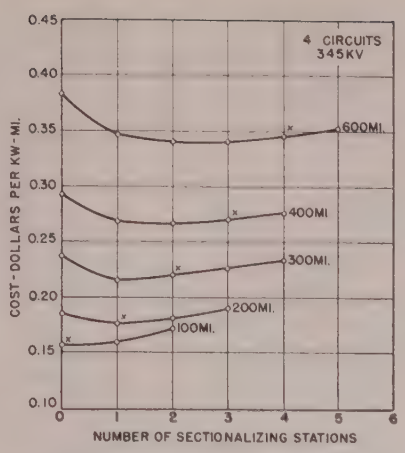

Figure 12. Economics of sectionalizing stations for four circuits at 345 kv

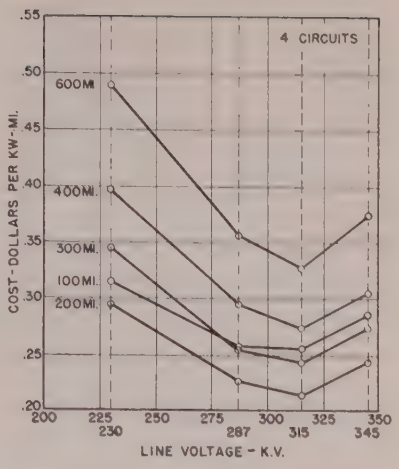

Figure 14. Transmission investment cost in dollars per kilowatt mile for four circuits

circuit construction for all lines below 345 kv, the most economical voltage is 315 kv. This result, of course, is to a large extent attributable to the greater economy of double-circuit construction which was not extended to the 345-kv level. In order to show the direct influence of single-circuit versus double-circuit construction, single-circuit costs in dollars per kilowatt mile for the 200- and 300-mile 4-circuit lines have been superimposed on the curves of Figure 16. This gives a direct comparison of the economics of all four voltages on the same single-circuit basis as that used for 345 kv alone. Here again, it may be observed that the 315-kv level still compares favorably with 345 kv, even on a single-circuit basis.

Transmission Costs, Mills per Kilowatt Hour

In the final analysis the economics of electric power transmission must be measured not only in the investment cost per kilowatt per mile as outlined here, but also in terms of the cost of transmitting energy, that is, mills per kilowatt hour. This introduces several additional factors, including carrying charges on the investment, the cost of losses, and load factor on the lines. In determining these costs the same combinations of line voltages and number of circuits have been followed as in the study of investment costs as shown in Figures 13 to 15. Carrying charges on the investment have been taken as 13.75 per cent, the cost of energy losses at 3.0 mills, and the capacity cost for line losses at $125 per kilowatt. The resistance losses, of course, were calculated on the basis of the line conductors assumed for each of the four voltages from 230 kv to 345 kv.

Since carrying charges on the investment represent by far the largest part of the total cost in terms of mills per kilowatt-hour for transmission, it is obvious that load factor will have a large effect on the result. In these studies the analysis has been carried out for two different load factors, first, a 50 per cent load factor, which for the purpose of loss calculations was assumed to be made up of eight hours use at full load and 16 hours at 25-per cent load, and second, an 80-per cent load factor made up of 16 hours at full load and eight hours at 40-per cent load.

The results of these studies are shown for two, four, and six circuits in Figures 17 to 19 for 50-per cent load factor and Figures 20 to 22 for 80-per cent load factor. Here again, the cost of transmission follows a downward trend as voltages increase from 230 kv to 315 kv, but rises somewhat at 345 kv. This, of course, would be expected from the similar results obtained in the analysis of investment cost.

As previously pointed out, the use of double-circuit construction for the three lower voltages, with single-circuit

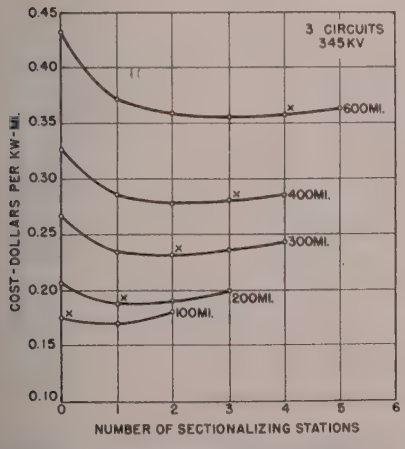

Figure 11. Economics of sectionalizing stations for three circuits at 345 kv

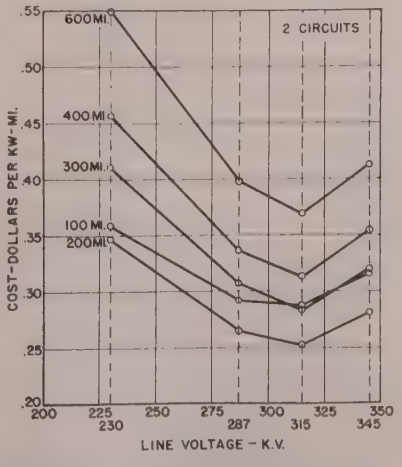

Figure 13. Transmission investment cost in dollars per kilowatt mile for two circuits

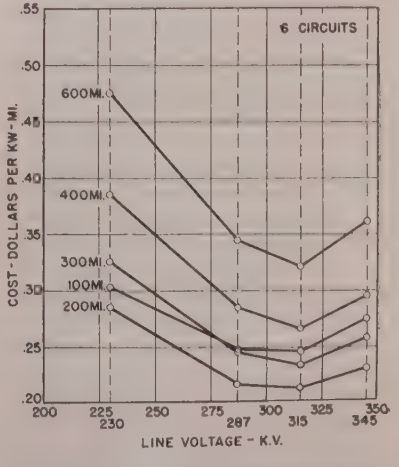

Figure 15. Transmission investment cost in dollars per kilowatt mile for six circuits

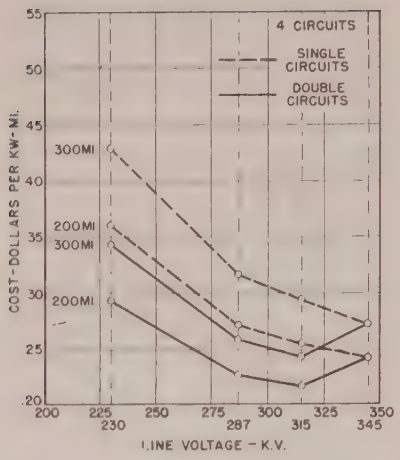

Figure 16. Transmission investment cost in dollars per kilowatt mile for 200-mile and 300-mile distances with single- and double-circuit line construction

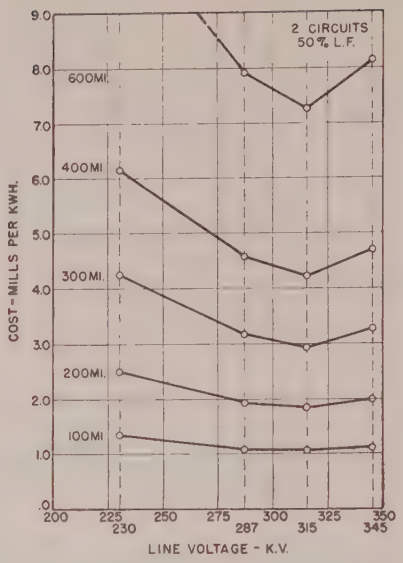

Figure 17. Transmission cost in mills per kilowatt hour for two circuits at 50 per cent load factor

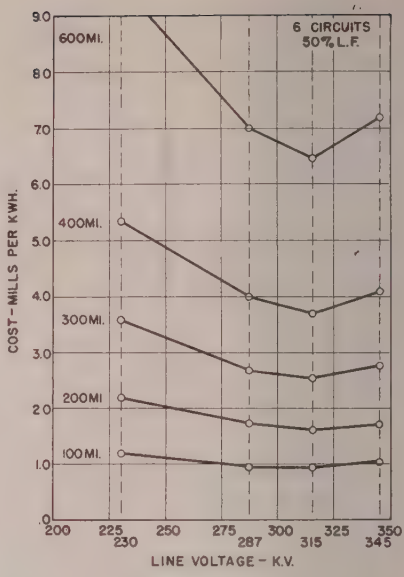

Figure 19. Transmission cost in mills per kilowatt hour for six circuits at 50 per cent load factor

construction only for 345 kv, is largely responsible for the rise in the cost trend above 315 kv.

Figures 23 and 24 have been included to show the effect on transmission cost in mills per kilowatt-hour of single-circuit construction for the three lower voltages with four circuits at transmission distances of 200 and 300 miles. As expected, these curves follow the trend indicated in Figure 16 covering the investment cost with single-circuit construction.

General Considerations in the Application of Extra-High-Voltage Transmission to Existing Systems

As mentioned in the first two paragraphs of the paper, a basic economic study of long-distance bulk transmission was believed to be necessary as a foundation on which to erect various other considerations in the selection of the voltage level and other features of a high-voltage transmission system. One of the most determining considerations is, of course, the type of system on which such transmission is to be applied or superimposed. If the system already involves or requires additional long-distance transmission of bulk power, the economic study here described will have almost a direct application to the problem, particularly if the existing voltage of the system is well below the range of voltages stated. If the existing system is already 230 kv, or perhaps 161 kv, the advantages of superimposing a higher voltage level may be less apparent, particularly in view of the advantages in service continuity and stability characteristics obtainable by adding additional circuits in parallel. In such cases the cost of higher voltage development will have to compete also with possible lower costs obtainable by the use of series capacitors, intermediate switching stations, or intermediate synchronous condensers. If the amount of power to be transmitted is not too large and will increase at only a moderate rate, the addition of circuits at the existing voltage will have the advantage of considerably lower initial cost for the first one or two steps of increase required, not only by reason of the lower cost of the line itself but by the avoidance of the cost of necessary voltage transformation.

On the other hand, extra-high-voltage transmission, even at the disadvantage of a higher initial cost to get it started, may be the more economical and desirable system on a longer time basis. As an extreme example, in Sweden, where a 230-kv system already existed, it was found that the necessary expansion of facilities to bring in the expected development of large hydro resources some 500 to 600 miles north of Stockholm would re-

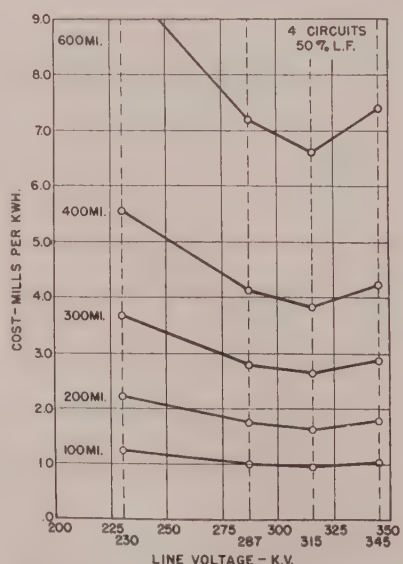

Figure 18. Transmission cost in mills per kilowatt hour for four circuits at 50 per cent load factor

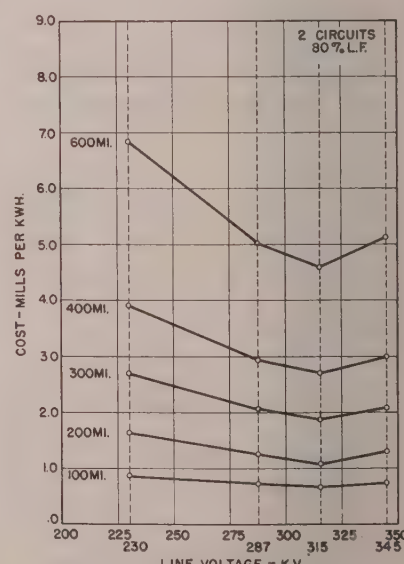

Figure 20. Transmission cost in mills per kilowatt hour for two circuits at 80 per cent load factor

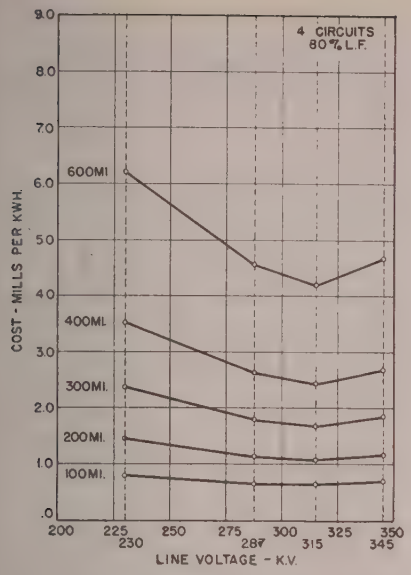

Figure 21. Transmission cost in mills per kilowatt hour for four circuits at 80 per cent load factor

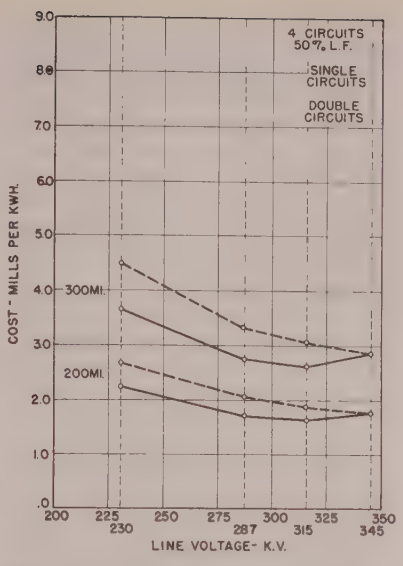

Figure 23. Transmission cost in mills per kilowatt hour for four circuits at 50 per cent load factor, 200-mile and 300-mile distances, single-circuit versus double-circuit construction

quire no less than 20 circuits at the 230-kv level. On this basis the superposition of a higher voltage can hardly fail to give the right answer. With the planned voltage of 380 kv for this project, the number of circuits required obviously can be cut down to one-third of the number required at 230 kv.

In an interconnected network type of system, such as that of the American Gas and Electric Company, the problem, of course, is quite different from that of the long-distance transmission system, but at the same time the need exists for some fairly long-distance transmission of relatively large blocks of power, and, as pointed out in a companion paper,[11] the size of such blocks, if not the necessary transmission distance, will continue to increase as the system continues to grow. Based upon the extent of growth over the past decade, to say nothing of the past 30 years, it seems inevitable that very large increases will take place over the next 30 years. The increase in transmission requirements accompanying such increased load will be very great, even with generating developments distributed as well as they can be on available sites throughout the system. The increase in unit size, coupled with the need for flexibility in transmission to take care of unit outages for maintenance, in itself will require a large increase in interconnecting transmission capacity.

To set forth the various system considerations influencing choice, economic and otherwise, of a transmission system voltage level it may be helpful to summarize on the one hand those considerations which tend toward the selection of a lower voltage level, and on the other hand those which favor the use of the highest possible voltage level.

Considerations Tending to Hold Down Transmission Voltage Levels

1. Heavy initial investment at the higher voltages for the early stages of superposition on an existing transmission system. This is reflected in the cost of establishing the necessary transformation facilities at two or more points on the system, in addition to the cost of the high-voltage line construction.

2. Excessive amounts of transmission capability concentrated in fewer lines or circuits, particularly in the early stages of a superposition program before alternate lines are available for backup in case of a circuit outage. While this defect may be remedied to some extent by the use of ultrahigh-speed reclosing, an appreciable outage possibility will remain, at least with a single-circuit line. It may be said, however, that with a double-circuit extra-high-voltage line of proper coordinated design and equipped with effective high-speed reclosing the probability of a permanent outage of both circuits, that is, failure to reclose at ultrahigh speed, is sufficiently small that it can be neglected in system design. At least it is hoped that this conclusion will be justified by further accumulation of operating experience with extra-high-voltage transmission.

3. Favorable economics of double-circuit lines compared with single-circuit construction, coupled with practical limitations to the voltage level which would be feasible for double-circuit towers and the large transmission capacity which would be concentrated in a single line even if such high-voltage double-circuit towers were attempted.

4. The steeply rising curves of radio influence and corona effects, as pointed out in a companion paper.[10] Information so far obtained from extensive investigations of these effects indicates that this is

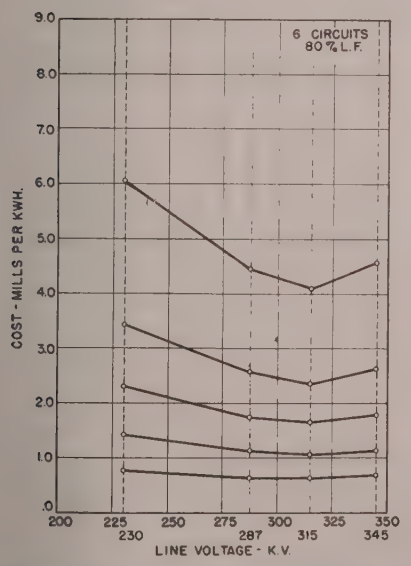

Figure 22. Transmission cost in mills per kilowatt hour for six circuits at 80 per cent load factor

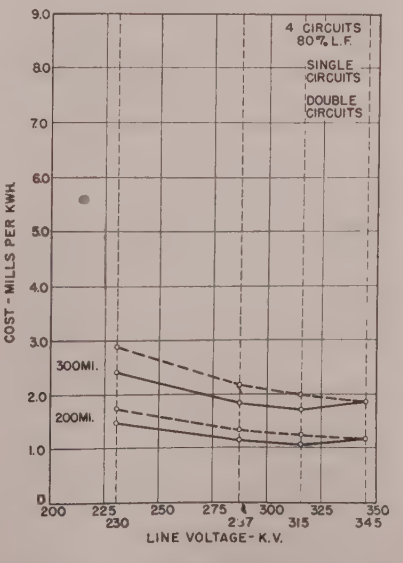

Figure 24. Transmission cost in mills per kilowatt hour for four circuits at 80 per cent load factor, 200-mile and 300-mile distances, single-circuit versus double-circuit construction

perhaps one of the most important considerations in holding down extra-high-voltage transmission levels.

5. Increasing difficulty of sleet-melting for the larger conductors required—both in diameter and conductivity—at higher transmission voltage levels. This consideration, of course, will apply only in areas where sleet formation is a serious problem.

6. Practical limitations in the length of insulator strings for which hot-line maintenance can be used. The limiting voltage beyond which hot-line maintenance ceases to be feasible may be the subject of some difference of opinion throughout the industry, but, at least for the American Gas System, it is believed that this limit coincides rather closely with the limiting voltage level for which double-circuit tower construction was considered feasible, desirable, and practicable.

Considerations Favorable to Higher Voltage Transmission

1. Maximum utilization of available rights of way in areas where available routes are limited in number and costly.

2. Maximum room for future system growth, not only where transmission-line loading is determined mainly by the growth of load in a receiving area but also where emergency maintenance outages on large units and interconnection requirements dictate high transmission capacity for general flexibility and operation.

3. Generally lower transmission losses at the higher voltages for a given system load requirement.

Conclusions

Finally, it is firmly believed that where a choice of transmission voltage is to be made, of all the various considerations brought to bear upon this choice one of the heaviest considerations should be a strong faith not only in the immediate future but in the long-term future growth of power systems generally. It is felt that even a relatively large apparent saving in investment in the immediate future by the choice of a lower transmission voltage may result in even larger losses over a longer term if the voltage proves to be inadequate and uneconomical.

On the basis of the present economic study and in the light of accompanying investigations of radio influence, sleet-melting, hot-line maintenance, and other problems, the 315 to 330-kv transmission level appears to be a logical, practicable, and forward-looking choice. While the various curves described in this study indicate that the downward trend of cost with increasing voltage for double-circuit lines might continue even beyond the 315-kv level, nevertheless it is also apparent that this level is at least not far from a point of maximum economy. Having selected the insulation and other requirements for this nominal level, it may be that further experience and improvement in the art of protection will make it possible to push the upper limit of operating voltage even higher than the present contemplated maximum of 330 kv without making any other changes in the physical design of the equipment and lines, thereby taking advantage of the further economy which this study shows could be realized at such higher levels. This, of course, may not materialize, but it is a possibility which will not be overlooked if experience shows it to be feasible. In any event, even at 315 kv, with a capability for distances up to 300 miles of 250,000 kw per circuit, 500,000 kw per double-circuit line, and with the possibility of maintaining this capability with suitable compensating devices for considerably longer distances, it is believed that transmission at this level will provide an adequate and economical tool for a long time to come.

References

1. Transmission of Electric Power at Extra High Voltages, **Philip Sporn, A. C. Monteith.** *AIEE Transactions*, volume 66, 1947, pages 1571–82.

2. Corona Considerations on High-Voltage Lines and Design Features of Tidd 500-Kv Test Lines, **C. F. Wagner, Anthony Wagner, E. L. Peterson, I. W. Gross.** *AIEE Transactions*, volume 66, 1947, pages 1583–90.

3. Insulators and Line Hardware for Tidd 500-Kv Test Lines, **I. W. Gross, R. L. McCoy, J. M. Sheadel.** *AIEE Transactions*, volume 66, 1947, pages 1592–1602.

4. Line Conductors—Tidd 500-Kv Test Lines, **E. L. Peterson, D. M. Simmons, L. F. Hickernell, M. E. Noyes.** *AIEE Transactions*, volume 66, 1947, pages 1603–11.

5. Transformers and Lightning Arresters—Tidd 500-Kv Test Lines, **F. A. Lane, J. K. Hodnette, P. L. Bellaschi, Edward Beck.** *AIEE Transactions*, volume 66, 1947, pages 1613–18.

6. Switchgear Equipment for Tidd High-Voltage Test Lines, **R. L. Tremaine, G. D. Lippert.** *AIEE Transactions*, volume 66, 1947, pages 1619–21.

7. Instrumentation and Measurement—Tidd 500-Kv Test Lines, **R. L. Tremaine, G. D. Lippert.** *AIEE Transactions*, volume 66, 1947, pages 1624–30.

8. Techniques of Corona Loss Measurement and Analysis—500-Kv Test Project of the American Gas and Electric Company, **O. Naef, R. L. Tremaine, A. R. Jones.** *AIEE Transactions*, volume 70, part I, 1951, pages 496–506.

9. Corona Investigation on Extra-High-Voltage Lines—500-Kv Test Project of the American Gas and Electric Company, **I. W. Gross, C. F. Wagner, O. Naef, R. L. Tremaine.** *AIEE Transactions*, volume 70, part I, 1951, pages 75–94.

10. Radio Influence Tests in Field and Laboratory—500-Kv Test Project of the American Gas and Electric Company, **G. D. Lippert, W. E. Pakala, S. C. Bartlett, C. D. Fahrnkopf.** *AIEE Transactions*, volume 70, part I, 1951, pages 251–69.

11. The 300/315-Kv Extra-High-Voltage Transmission System of the American Gas and Electric Company, **Philip Sporn, E. L. Peterson, I. W. Gross, H. P. St. Clair.** *AIEE Transactions*, volume 70, part I, 1951, pages 64–74.

12. Power System Stability—Volume I (book), **S. B. Crary.** John Wiley and Sons, New York, N. Y., 1945.

Discussion

W. A. Morgan (Bureau of Reclamation, Denver, Colo.): We have looked forward to this paper explaining the reasons for the choice of 315 kv as the nominal voltage of the new American Gas and Electric Company system and the authors are to be congratulated on a very worthwhile presentation. This subject is of considerable interest to us because we are making similar studies at the present time. We have a few questions, the answers to which will be of value to us and perhaps to others of the industry.

It is believed that the question of whether to ignore double-circuit faults is a very important one. It also is noted that you do not intend to provide two overhead ground wires for the double-circuit construction in an effort to minimize double-circuit faults. Relative performance figures of different 230-kv systems have shown 10 to over 50 per cent to be double-circuit faults. We would be interested in knowing what your experience in relative performance of double versus single circuit design has been and what you expect at 315 kv. Do you plan to provide especially low tower footing resistances on the order of 1 to 2 ohms to reduce the total number of faults?

There are some that feel that faults due to causes other than lightning (such as airplanes) may be increasing in percentage. This would be a factor against double-circuit construction in some areas, but perhaps this is not a problem in your area. It is assumed that you have adequately considered the possibility of faults due to galloping conductors caused by wind on ice coated conductors and to jumping conductors in the vertical configuration when the lower conductor loses its ice load.

It is understood that the system considered is one that would be capable of carrying its rated kilowatts with one circuit section out of service. However, it is not clear if this is expected during a 3-phase fault at the worst location. Was a specific criterion of kilowatt loading, type of fault, fault location, and so forth, established for this system?

Since it is stated that high-speed reclosing is to be used, was any consideration given to the fact that reclosing on a sustained fault is worse from a stability standpoint than not reclosing the line back to service? Where reliability is paramount the use of reclosing is not so favorable for this reason. Then, probably the only reason for using high-speed reclosing would be to return to service the faulted line as rapidly as possible in case a second line is tripped

out by a simultaneous multiple-stroke fault due to lightning and the system would not be able to stand the loss of two circuits. Then, it amounts to balancing the possibility of reclosing on a sustained fault against the possibility of two circuits being faulted simultaneously due to lightning. Do you have actual experience which is used as the basis for deciding on high-speed reclosing on what is presumed to be a system requiring a high degree of reliability?

At the risk that this might be covered by a companion paper, I would like to ask whether the choice of 315 kv will introduce a new insulation level for transformers and circuit breakers and what this level would be. While the old 230-kv level now may be considered adequate for 287 kv, it would appear that the old 287 kv would be adequate for higher than 315 kv.

In the studies we have made, quite large conductor sizes have been justified on the basis of economics considering the evaluation of losses. You state that sleet-melting requirements hold down the sizes you have considered over that of a full evaluation of the economics of losses. Is this on the basis of one circuit section being temporarily removed from service so as to provide sufficient current for heating on the remaining second circuit? On one system we are studying there is no sleet problem, and we would be interested in knowing what sizes you would have used if no consideration were given to sleet-melting.

In view of the work done in Sweden, was consideration given to the relative economics of systems utilizing series capacitor compensation and duplex conductors? Either of these features would improve stability by reducing the impedance, and it would appear could be considered as competitive. The duplex conductors would allow greater current carrying capacity and less corona with standard type conductors.

Were variations in required synchronous condenser capacity considered?

Were losses evaluated both by the kilowatt capacity cost as well as on a mill kilowatt-hour basis because of the rates used for selling the power? Or, was one method used for some losses and the other method used for other losses. We agree that the total annual costs should be considered in any comparison including losses, operation and maintenance, replacement, annuity, and amortization of investment.

I wonder if the same results would be obtained if the study were made on the basis of a fixed amount of power to be transmitted over a definite extension to an existing system. The results shown were for a general study. We have found that lines about 300 miles long on our system may be loaded somewhat above the surge impedance loading indicated in Figure 1 of the paper, under transient stability conditions. Was the decision to use 315 kv based on only this general study?

We are quite interested in the background of the decision to use 315 kv in as much as it means pioneering in a new insulation class, and many have been unwilling to go beyond the present highest insulation class in United States of 287 kv. I want to compliment the authors on having the courage to go to this higher voltage because the history in many parts of United States is that the nominal voltages selected are too often just barely adequate for the systems for which they are built and are "undervoltaged" within 10 years. Part of the blame for this is that high-voltage systems cost more and most new additions or systems must be made economically feasible on the basis of more or less immediate future needs.

C. W. Watchorn (Pennsylvania Power and Light Company, Baltimore, Md.): The authors present a very interesting analysis of the relative economics of high-voltage transmission. They have used two standards of measure or indices, the investment cost in dollars per kilowatt-mile, and the annual cost in mills per kilowatt-hour. Both of these standards of measure may appear to lead to the conclusion that 315 kv is the most economical of the four transmission voltages studied. However, as pointed out by the authors, the particular circumstance relating to various characteristics of specific systems may result in quite different conclusions.

Fundamentally, the relative economics of alternative facilities involve primarily the determination of the average annual cost of doing the same job or performing the same function in different ways over a period of years in the future. One factor to be considered is thus the job to be done. If the job is to transmit large blocks of bulk power long distances, as in the case in Sweden cited by the authors, or even of interconnecting two already comparatively large systems, the problem is greatly simplified as compared with that of providing adequate transmission for the growing load of an already existing system. Nevertheless, if it is desired to use more precise methods of evaluation of the relative economics of various alternatives, the fundamental treatment of the various factors involved remains unchanged for all these various conditions, and even for other conditions or functions. However, it is very doubtful if such precise methods of evaluation would at all be justified in the case of transmission of large amounts of power over long distances, as in the Swedish case, for which it is quite possible that either of the indices used by the authors may be entirely satisfactory to indicate the most economical transmission voltage, provided the index chosen is related to the actual amount of power or annual energy to be transmitted rather than to the transmission capability. It is believed that such may very well not be the case in some instances, particularly when the additional transmission is being provided primarily as related to the growing load of an already existing system.

In such a case the annual additional power and energy required to be transmitted by the primary transmission network of the system from year to year is generally relatively small over a long period of years, at present, in many cases, being in the general order of five per cent. The resulting increased transmission capacity requirements can be met usually either by adding relatively small additional transmission capability to the network at rather frequent intervals, possibly on an almost continuous basis; or by adding relatively large additional transmission capability at less frequent intervals. For the first case, which would be the result in the event the additional transmission facilities were provided within the lower voltage range, the additional investment in transmission facilities over a given period of years quite probably would be considerably larger than for the second case, which would be the result in the event the additional facilities were provided within the higher voltage range. It does not necessarily follow, however, that this result is conclusive that the higher voltage is the more economical.

This situation raises the question as to the relative economics of spending smaller amounts of money at frequent intervals, but a larger total amount over a given period of years, to do a given job as compared with spending larger amounts at less frequent intervals, but a smaller total amount over the same period of years to do the same job. This problem involves an application of the time cost of money or present worth concept. This is very important in such cases, because if neglected, it may happen that a less economical alternative may be indicated as being the more economical. To neglect the factor for present worth in such studies is equivalent to maintaining the proposition that a given amount of money as of any number of years hence is worth the same as of today as the same amount of money today. It is believed that no one would agree to such a proposition. Therefore, it would appear that the suggestion, that the effect of the time cost of money is an important factor in such studies merits serious consideration, particularly since to omit it may result in erroneous conclusions.

Such factors should, of course, be applied to all differences in future costs that are the result of the various alternatives being studied.

The differences in energy losses should be with respect to the system as a whole, including those of such various alternatives, and not for the respective alternatives alone. Such differences in losses should be evaluated on the basis of the top incremental generating cost of the system on an annual basis for each of the future years, and then adjusted to an average annual basis in accordance with the present worth concept just discussed.

The transmission losses, as pointed out by the authors, also have a capacity value aspect in addition to that of energy value. In the event the differences in the transmission losses are large, there may be a reduction in the installed capacity for certain of the alternatives, at least from time to time, as compared with others. Such reductions result in decreased fixed charges and possibly other costs, and at the same time may also result in differences in generating costs, which should also be taken into account, but only for those years for which it is estimated there will be differences in installed capacity. On the other hand, however, it may be that the differences in losses may not be large enough to ever result in a reduction in the installed capacity. There are then no differences in the annual costs on this account. This does not mean, however, that there should be no evaluation made on account of the capacity value of the differences in the system transmission losses, as is frequently proposed. Although there is no reduction in annual cost on this account there is quite definitely a difference in the services available, which, since of value to the system, should be evaluated, as was done by the authors. It is believed that it is

reasonable to make the evaluation for this latter condition on the basis of the incremental cost of capacity additions to the system. For the former case, for which there are differences in installed capacity, the differences should be evaluated for those years for which it is estimated such differences will exist, on the basis of the average cost of capacity additions or if such differences are shown as the result of a year to year study, the evaluation should be on the basis of such programmed differences.

One alternative to an extra high-voltage bulk power transmission system, of course, is that of the more widespread location of generating capacity throughout the system. Such a scheme would result in a fairly high degree of balance between the location of load and generation, the result of which quite likely may be that the differences in the transmission losses would be so much smaller than with the system wide bulk power transmission system that the capacity value of such loss differences, together with the effect of the other cost differences, may indicate that such scheme for the location of generating capacity, together with the use of a lower voltage for the system transmission network, is the more desirable basic plan.

S. B. Griscom (Westinghouse Electric Corporation, East Pittsburgh, Pa.): The economics of power transmission is a very involved subject. Before material, equipment, and construction costs can be brought into the picture, many determining factors must be analyzed and specified. Among the most important of these are:

1. Load capabilities of transmission lines as a function of voltage and length.
2. Insulation levels of lines and equipment.
3. Outside diameter of conductors, as dictated by radio influence, sleet melting or corona loss.
4. Conditions affecting tower design such as ty of terrain, wind and ice loading, and isokeraun level.

In assessing economic studies it is well to keep in mind which items are basic and which are subject to change, either because of technical progress, or to altered local conditions.

In the matter of line loading, for example, progress in the last 25 years in high-speed relaying, tripping, and reclosing of circuit breakers plus other improvements, has practically doubled permissible loads. It is of interest to speculate as to whether significant improvement can be expected in the future. The authors' views on the subject of line loadings are contained in Figure 1 and appear to be very realistic with respect to present capabilities. The loadings given are fairly high percentages of theoretical power limits for uncompensated long lines and therefore little increase can reasonably be expected in the future.

The insulation levels given in Table I give effect to the advances made in "lightning proofing" transmission lines, and here again, there appears little prospect of significant reductions in the immediate future. The conductor diameters listed in the same table were based largely on present-day considerations with respect to radio influence. There appears to be no reason for expecting radio influence factors to become worse in the future, but they may possibly improve if in the future FM radio and television, which are comparatively immune, supplant AM radio.

Tower cost is probably the most important single item of transmission expense. Through the years, this item has had the scrutiny of utility engineers and progressive improvements in the economical use of materials have taken place. The expected use of nickel alloy steel for tower legs mentioned by the authors is an example.

The authors' results are summed up by Figures 17 to 24, and justify the selected voltage for use on the system of the American Gas and Electric Company. The study is of great interest to transmission engineers generally, both from the point of view of procedure and from that of quantitative results. Where similar local conditions apply, the conclusions with respect to general level of voltage should apply. With respect to possible changes resulting from future development or from differing local conditions, it would appear that these are most likely to concern factors relating to conductors, towers, and loss evaluations.

The authors have made a noteworthy contribution in the field of power transmission and are to be commended for the clarity of their presentation. The considerations presented in the section on General Considerations in the Application of Extra-High-Voltage Transmission to Existing Systems are particularly valuable to those contemplating extra high-voltage transmission.

S. B. Crary (General Electric Company, Schenectady, N. Y.): The American Gas and Electric Service Corporation and their associates are to be congratulated for the excellent papers they have presented, which give in detail the basis of the selection of a higher voltage and their basic system design philosophy. Probably the most outstanding feature is the selection of as high a voltage as is considered practical for use with double-circuit towers. This is contrasted with the European selection of 380 kv using single-circuit towers and double conductors per phase. One cannot help but be convinced that the selection by the American Gas and Electric Service Corporation is correct for conditions prevailing in the United States, in view of the cost figures presented in the paper. It is quite evident that the double-circuit tower for their conditions provides transmission at the lowest cost per kilowatt mile. This conclusion, which undoubtedly was one of the most determining factors in the selection of the voltage, is substantiated by single-circuit and double-circuit cost comparisons at lower voltage levels, particularly when right-of-way costs are an appreciable factor.

One of the many interesting results of these studies is the decrease in relative importance of line outages caused by lightning as compared with switching surges and normal frequency overvoltages in determining the insulation levels. This certainly appears most reasonable, particularly for interconnected systems of large capacities, where the reclosing procedure can be applied effectively for removal of temporary faults caused by lightning. It also is apparent that further increases in the operating voltage per disk of line insulation may be realized by giving additional attention to means of reducing the switching surge voltages. One of the most obvious and direct methods of accomplishing a further reduction is to use a circuit breaker which has a minimum tendency or no tendency to restrike.

These papers give added emphasis to the trend of high-voltage transmission system design in the United States by:

1. The use of low-resistance conductors.
2. The use of reactive kilovolt-ampere capacity for increasing the transmission line loading.
3. Intermediate switching stations.
4. Stepping up the new generation directly to the high-voltage system.
5. Large capacity transformer ties to the lower voltage (138-kv system).
6. Full use of lightning arresters.
7. Circuit breakers with higher interrupting capacity.

Use of a double-circuit tower line which may carry as much as 800,000 kw in a tower head may present problems of developing operating procedures in case of a double-circuit tower outage. However, there are methods which may be applied to reduce the possibility of severe load interruptions when such an outage does occur. Also, for such a large interconnected system the loss of a fully loaded double-circuit tower line will become less important in the future as the system becomes more fully developed.

In considering this contribution to system design broadly, it will be recognized as giving a most excellent statement of modern American practice. At the same time this paper makes a significant contribution toward the use of double-circuit tower lines of high voltage and holds for the future the possibility of still further reductions in line insulation.

H. P. St. Clair: Mr. Morgan has raised a number of questions regarding expected performance of the proposed 315/330-kv transmission lines and system. Comments on these will be given in order as follows.

As to the large percentage of double-circuit faults, 10 to over 50 per cent, which Mr. Morgan quotes, our experience on several thousand miles of double-circuit 132-kv line equipped with carrier relaying and high-speed reclosing shows a very small percentage of double-circuit faults. We are realizing at least 90 per cent successful high-speed reclosure, which is the real test of our double-circuit line performance. This also is the real answer to the question Mr. Morgan raises as to the desirability of attempting high-speed reclosure against permanent faults which he assumes may be increasing in proportion to transient faults. On our system very nearly all line faults, chiefly lightning, are of a transient nature.

A single ground wire on double-circuit construction is now used on our 132-kv lines and will be used on the 315/330-kv lines for two reasons: first, the center location of the ground wire offers the least danger of contact with phase wires in case of sleet and galloping-conductor phenomena and, second, there is an appreciable saving in cost. In general, it is not planned to take special measures to reduce tower-footing resistances. We intend to rely instead on high-speed reclosing to take care of any additional faults that may result from high-footing resistances

as well as from the use of a single ground wire.

As to the hazard of galloping conductors under wind and ice conditions with conductors in vertical configuration, it is planned, at least in the more complete development of the system, to use the same sleet-melting routine now used on our 132-kv system to remove the ice promptly before it can accumulate heavily on the conductors. In addition, the proposed double-circuit tower design will provide an offset of 5 feet between the center and bottom conductor and 6.5 feet between the center and top conductor. While this will not provide complete protection against trouble, it should take care of many of the less severe conditions.

The economic study described in this paper, as Mr. Morgan states, was based upon line capabilities with any one circuit section out of service. As to the establishment of any "specific criterion of kilowatt loading, type of fault, fault location and so forth," it is assumed that reference is being made to the proposed extra-high-voltage system of the American Gas and Electric Service Corporation described in a previous paper.[1] In this case it is necessary to take into account the type of system we are dealing with and the fact that most if not all of the lines will be fully loaded only on intermittent occasions such as during maintenance outages of large units, heavy interchange with interconnected systems, and emergencies. For this reason no attempt was made to set up specific criteria as to loading or type of fault.

Sleet melting on the proposed system will have to be carried out by actual short circuiting of lines and the application of voltage, probably 132 kv, in the same way that it is carried out on the present system. It would not be possible under most conditions to obtain sufficient current for sleet melting by removing one circuit to increase the loading on another circuit in parallel.

Again, the type of system we are dealing with does not lend itself very readily to a rigorous determination of the most economic conductor size. As pointed out in a previous paper, however, economic considerations would have led to the selection of at least 850,000 or 900,000 circular mils copper equivalent rather than the 800,000 circular mils copper equivalent chosen on account of sleet melting.

For the length of line sections required on the American Gas and Electric Company system, we are convinced that series capacitor compensation would be totally noncompetitive from an economic standpoint. Either series capacitators or duplex conductors at the voltage chosen would have provided what we regard as excessive capability tied up in one transmission line route. Duplex conductors were considered undesirable also from the standpoint of installation and maintenance problems, as well as from the standpoint of sleet-melting difficulties.

Our decision to use 315/330 kv was based not only on the results of the general study described in this paper but also upon various other important considerations outlined in the paper previously mentioned. Radio influence, sleet melting, and the economics of double-circuit construction entered heavily into this decision.

Mr. Watchorn is quite right in pointing out that a strictly correct economic comparison of different transmission voltages should be based upon the actual job to be done in increased transmission loading from year to year, rather than upon the capability of lines at various voltages, since the full capability may not be used. Failure to study the future transmission economics on this basis would be particularly erroneous if annual load growth were as small as 5 per cent and if the present transmission system can be considered fully adequate for present loads and required only small increments of capability to take care of the load increases immediately ahead.

On the American Gas and Electric Company System, however, the annual growth of load has exceeded 5 per cent, even on a long-term basis. In recent years the average growth has been far greater than this, the annual peak having increased from 900,000 kw in 1939 to almost 2,400,000 kw in 1950. The effect of this is not only to increase the average annual increments of transmission required but also to bring about a condition of loading on the present transmission system which is excessive from a loss standpoint and which brings about the need for a relatively large increase in transmission capability in one step, such as that which will be provided by the initiation of the projected extra high-voltage system.

Also, as to the present worth of future savings and the merits of an alternative plan of making less expensive transmission additions as required at lower voltage—perhaps at the existing system voltage—I should like to point out again some of the difficulties involved in expanding the lower-voltage system to keep pace with increases in generation and system load and to maintain the necessary flexibility in system operation. In the middle twenties a modern highly efficient up-to-date plant contained 40,000-kw units and this capacity was nearly commensurate with the surge-impedance loading of a 132-kv line. Today with 150,000-kw units in operation and four 200,000-kw units under construction on the American Gas and Electric Company System, it is obvious that a multiplicity of 132-kv circuits will be required to maintain the necessary flexibility of operation just to take care of normal operating procedures, such as maintenance outages of units, not to mention system emergencies and interconnection schedules. The problem of obtaining rights-of-way for the number of such circuits which the future system would require is certain to be a difficult one, as pointed out by the authors.

Mr. Watchorn's suggestion that savings in transmission requirements may be obtained by locating generating stations closer together and nearer the load centers is a good one and certainly has not been overlooked in our studies. There are limitations, of course, from the standpoint of both availability and cost of fuel and availability of adequate condensing water, although the use of spray ponds or cooling towers is not regarded as necessarily prohibitive. However, even though transmission costs may be reduced in this manner, it is still believed to be a fact that the transmission voltage that was adequate in 1920 and for some years thereafter has become hopelessly inadequate as a tool for taking care of the much greater loads and generator units that are coming on today and will increase even further in the years ahead.

Comments by S. B. Griscom, who contributed materially to the preparation of this paper, are greatly appreciated. While the line loadings given in Figure 1 are close to the limit that can be realized with uncompensated lines, Mr. Griscom voices a welcome note of optimism that radio influence may become a lesser rather than a greater limitation in the future.

Reference

1. See reference 11 of the paper.

An Engineering Approach to Control Room Lighting

V. L. DZWONCZYK
MEMBER AIEE

MODERN control rooms in utility and industrial power stations are nerve centers of multi-million-dollar operations. Like all other engineering projects, lighting for these important work areas can be provided in various ways depending upon what limits are assigned the task. There is no single method to correctly illuminate a control room based on lighting standards alone. The search for a reasonable solution, therefore, suggests a study of the fundamental requirements affecting the problem, and a determination of how best to use the many available new light sources. In essence, the problem synthesizes into the following objectives:

1. The provision of a lighting system consistent with the operators' visual tasks to help them perform their important job efficiently.

2. Refinements in the lighting system should be economically reasonable.

The cost of lighting is often placed in the background on the premise that the portion spent for this item of the power plant entity is very small. Much effort, however, is expended in making a selection from different types of available auxiliary apparatus, different types of usable protective schemes, and so forth, in order to assure the maximum economical advantage from available ways to perform the required job. This method of approach assumes that any part of an engineering project should stand on its own feet, each problem to be solved in the most economical manner. It, therefore, seems reasonable not to discount the cost of a lighting system because, should all small contributions be so treated, the total would not represent the most economical solution, nor would it be necessarily the most efficient. It is with this philosophy in mind that the control room lighting problem was approached.

Several Solutions Possible

Before the advent of fluorescent lamps, power plant control rooms utilized all recognized forms of incandescent lighting systems. The many advantages of fluorescent lamps gradually have made them the preferred sources for control rooms, especially in the following systems:

1. Luminous ceiling systems
   a. Indirectly lighted ceiling
   b. Louvered ceiling
   c. Solid luminous ceiling
2. Direct systems
   a. Ordinary: flush troffers (open, louvered, glass panel, and lens)
   b. Special: ordinary troffers in a speci ally designed ceiling

The relative advantages and disadvantages of each system are not unknown to engineers today, but a short review may be appropriate to complete the story. Table I compares the major advantages and disadvantages of these systems in a general way. A review of the tabulated factors indicates that the luminous ceiling systems minimize shadows on the instrument boards, whereas the ordinary direct system would tend toward harsher shadows. The latter system, however, projects light more efficiently upon specific working surfaces. Special direct systems possess the latter advantage and, in addition, can be designed to make shadows negligible.

Fundamentals Stated

In analyzing the control room lighting problem one observes that its requirements are more particular than most general lighting projects. For instance, the illumination on the horizontal plane is secondary in importance to that on the vertical plane. The matter of specular reflection from the vertical plane gives more concern than in most other lighting problems. Direct and reflected glare, as well as brightness contrasts, require careful attention. We conclude, therefore, that to effectively and economically illuminate a control room the following major fundamentals must be observed.

1. Vertical illumination on the instrument board should be adequate for quick comfortable visibility of the many relatively small scales within glass-faced instruments.

2. The illumination on the vertical plane should be reasonably diffused to minimize shadows on instrument scales.

3. The light sources must not present themselves as images of specular or veiling glare in the glass faces of instruments from operators' usual working positions.

4. The light sources must not present themselves as brightness areas in competition with the object being observed, namely, the instrument scales.

5. The brightness contrasts between various surfaces in the operators' normal fields of view should not cause their visual surrounding to be uncomfortable.

6. The degree of perfection obtained in each category should be balanced by the actual cost of each incremental gain.

If one studies this problem objectively, it also will be realized that since, from the visual standpoint, the operators are the principal parties affected in the matter, their likes and dislikes should be given some, if not prime, consideration. These men are no less diverse in their preferences than illuminating engineers, which makes for a more interesting problem and also lends weight to the hypothesis that there is no one way to light a control room. Some operators prefer a stagelike

Paper 51-157, recommended by the AIEE Power Generation Committee and approved by the AIEE Technical Program Committee for presentation at the AIEE Great Lakes District Meeting, Madison, Wis., May 17–19, 1951. Manuscript submitted November 8, 1950; made available for printing March 30, 1951.

V. L. Dzwonczyk is with the American Gas and Electric Service Corporation, New York, N. Y.

effect wherein the vertical instrument boards are illuminated as the fundamental points of interest and the general room area in which the chief operator's desk is located receives a subdued lighting level. This philosophy introduces a subject containing much argumentative material. Exponents of quality lighting would object to the extreme of such a solution as not conforming to ideal brightness ratios. Others would say that, if the brightness ratios around the room approached the recommended minimum, operators should not be inclined toward a subdued general lighting effect. Let it be considered, however, that a stagelike effect has the major advantage of unconsciously drawing the operator's attention to the control board and that an appreciable number of operators seem to prefer such atmosphere.

From these observations, it is believed that the central portion of the operating room can in most cases be satisfactorily illuminated to a relatively low level, perhaps in the order of 15 to 20 foot-candles. Any higher illumination level appears to be unnecessary for the visual task and need not be the criterion on which the over-all lighting system is selected. If it is assumed that the reflection factor of the horizontal working area is about equal to that of the vertical board surface, then 20 foot-candles on this surface seems reasonable and has been found adequate.

Visual Task Defined

Before attempting a solution to this problem it would be well to define the visual tasks involved. A modern operating room is the heart of a power plant, which today leans toward centralized control, where most major operations required to run the massive turbogenerators, their associated boilers, and numerous auxiliary apparatus are remotely controlled by a relatively small number of operators. These men are located in the control room, which many times is completely out of sight of apparatus being controlled. Their visual tasks, therefore, are as follows:

1. From a centrally located desk (approximately 10 feet from the board face) the chief operator should be able to see, quickly and without visual discomfort, the entire control board with its many glass-faced instruments. Of primary importance is his ability to observe casually the relative position of the indicating pointer with respect to the extremities of the scale. Many of these instruments are small making the scale markings hardly perceptible in the total field of view at any appreciable distance. On the desk the seeing task may be classified as ordinary. The work involves discrimination of moderately fine detail and is performed at intermittent periods of time.

2. From a position adjacent to the board, at approximately arm's length away, the control operator should be able to read clearly indicated readings of instruments. Specular reflections or excessive brightness contrasts in these areas of vision must be reduced to a minimum. For the critical portion of the operation, namely, that concerned with starting up and shutting down turbogenerators, especially during emergency situations, it is of sufficient importance that the position of the pointer be seen in relation to the scale extremities. Under stable conditions, when refinements of operation are being obtained, the operators can choose more favorable positions from which to observe particular instruments and then return to the control position, if remote from instrument, to effect any required adjustment.

Figure 1. Philo control room

Developed Solution

The matter of control room lighting was first studied qualitatively. Thought on the matter suggested that if the fundamental requirements were satisfied in their relative order of importance, the solution should meet good lighting standards. Such a solution also should be relatively inexpensive compared to other systems which may achieve only minor gains through their spectacular elaboration.

Table I. General Characteristics of Control Room Lighting Systems

Factor Considered	Indirect	Luminous Ceilings Louvered	Solid	Direct with Dropped Ceiling	Remarks
Uniform horizontal illumination	Excellent	Excellent	Excellent	Good	A requirement only on operator's desk
Uniform vertical illumination	Good	Good	Good	Good	A requirement especially in the upper half of the control board
Low fixture brightness	Excellent	Good	Good	Good	Desirable
Low ceiling brightness	Fair	Good	Good	Good	Desirable
Ceiling height required	High	High	High	Low	Lower ceilings reduce plant cost
Ceiling specularly reflected from instruments	The higher the illumination level the more reflection	The less evenly luminous the more reflection	Same as louvered plus traces from solid supports	Negligible in most directions	Should be negligible
Fixtures specularly reflected from instruments	Can be made negligible with difficulty	Can be made negligible with difficulty	Can be made negligible with difficulty	Can be made negligible easily	Should be negligible
Relative cost	Low	High	High	Low	Should be low
Shadows, instrument scales and boards	Negligible	Negligible	Negligible	Negligible	Harsh shadows undesirable
Source in field of view	Yes	Yes	Yes	No	Should not be in field of view

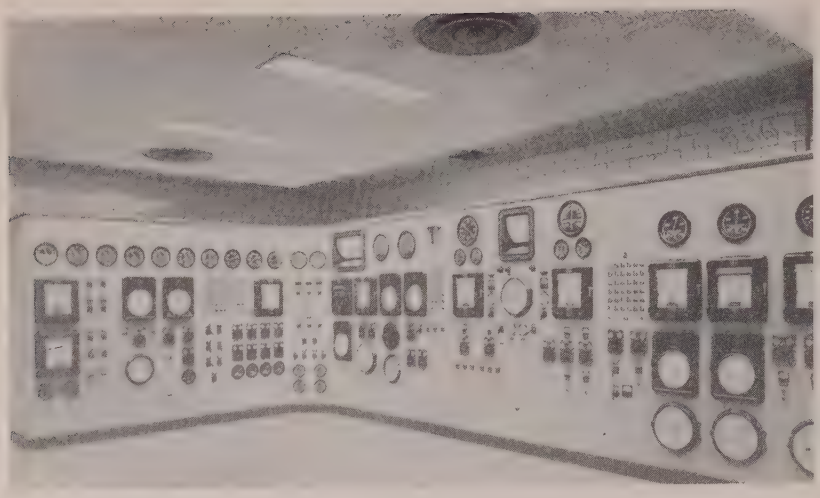

Figure 2. Twin Branch Number 5 control room

The first fundamental requirements, the provision of illumination on the vertical plane, limits the position of the light sources with respect to the major plane of reference. These lights should be as close to the control board as practicable to illuminate it adequately with the least expenditure for the source. Of course, even though the horizontal plane is of secondary importance, it requires sufficient illumination to help the operator tabulate instrument data and read operating instructions. Such illumination also helps reduce excessive brightness contrasts between the horizontal and vertical working planes. Thus, the problem resolves itself into two parts:

1. The provision of light sources to illuminate the vertical plane efficiently and economically with diffuse light.

2. The provision of light sources to illuminate the general area efficiently.

One source to do both jobs is, of course, possible. Such systems have been reported by H. F. Carroll and W. B. Morton,[1] as well as A. A. Brainerd and G. C. Salneu.[2] The former utilize a luminous ceiling of the louvered type, and the latter utilize a luminous ceiling of the total sheet plastic variety. Technical literature records the advantages and disadvantages of these modern lighting techniques. Luminous ceilings tend to produce a general surrounding which inherently characterizes luminosity throughout the room, not the seemingly desirable effect of a more highly illuminated board to attract and help focus the operator's eyes.

The second premise calls for all light sources to be so positioned as to prevent specular reflection toward the operators' usual fields of view. To accomplish this, various degrees of refinement are possible. The simplest solution would be to position the board lights so that for the operators' two active positions the specularly reflected images of the light sources would fall toward the floor out of the fields of view. This source also should be diffused in order to minimize harsh shadows on instrument scales and boards. The source should be low in brightness if it is in the field of view of the operators.

Board Lighting Sources

Following this line of reasoning a practicable solution would be to arrange the board lighting units to follow the contour of the actual control board and in a position relative to it which would direct the specular reflection toward the floor. By obeying the law of specular reflection, this is accomplished, for example, at the Philo Plant Control Room of The Ohio Power Company (see Figure 1). Of course, this solution does not exclude the light sources from the field of view of the operators, nor is it as effective in eliminating shadows as would be a larger source, such as a luminous ceiling.

Figure 3. Twin Branch Number 5 control room, study of direct and reflected light

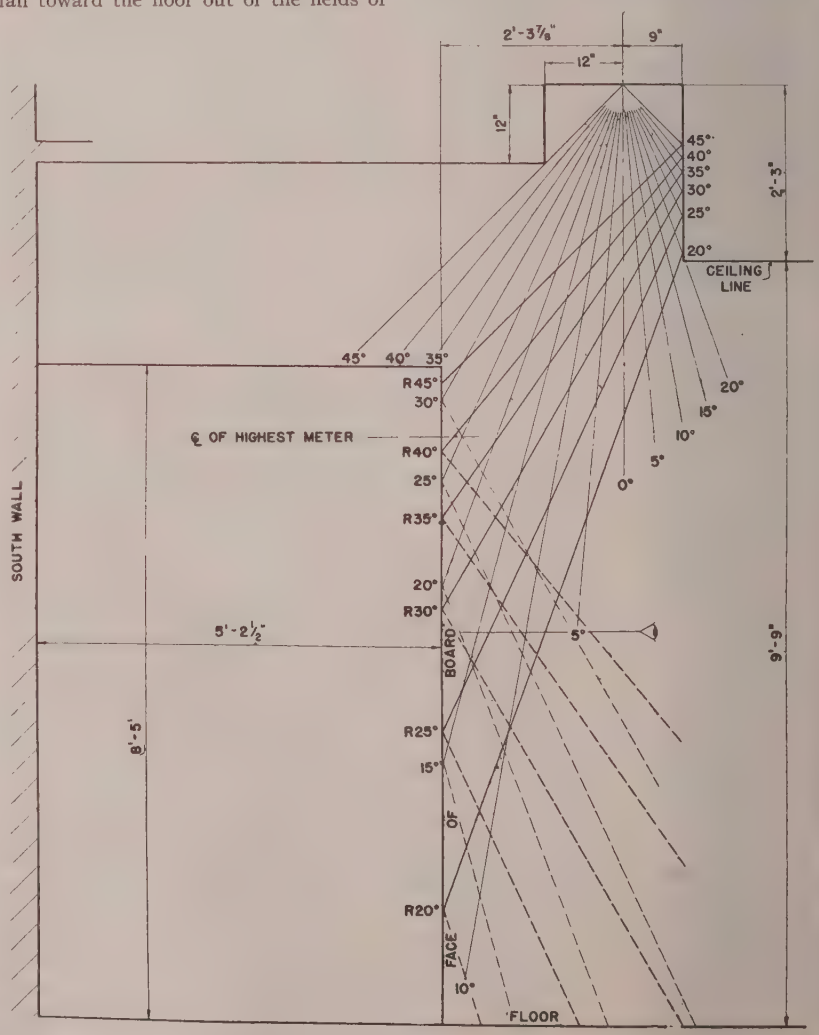

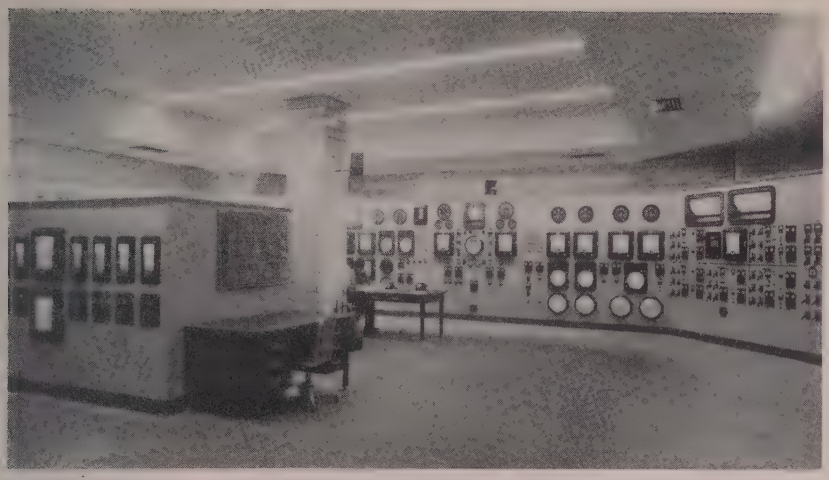

Figure 4. Philip Sporn Control Room Units Number 1 and Number 2, normal lighting

Figure 5. Philip Sporn Control Room Units Number 1 and Number 2, emergency lighting

The elimination of the light source from the field of view of the operator can be accomplished by the following methods:

1. The utilization of shields which would suspend below the ceiling a sufficient amount to hide the fixtures.

2. The utilization of a suitable ceiling contour provided that its use does not incur excessive ceiling construction cost rightfully chargeable to the lighting system.

To appraise the effectiveness of the latter method, an installation was made which allowed the ceiling to drop in the center portion of the room by approximately six inches, enough to hide the fixture from the operators' seated position at the desk. This system was utilized in the control room at the Suburban Plant of The Scranton Electric Company.

The desirable effect and the satisfactory comments from operators proved to be a stimulus, and, as a result, simple unorthodox ceiling contours became no matter of concern, especially since the unorthodox ceiling did not cost any more than a standard flat one. The next logical step, therefore, was not only to utilize the vertical surface of the dropped ceiling to hide the light sources, but also to cause it to become part of a light-reflecting scheme and thus introduce additional diffused illumination on the vertical board at an angle slightly different than from the light source. This involved a simple design, as illustrated in Figure 2, which shows the lighting system in the Unit No. 5 control room at the Twin Branch Plant of The Indiana & Michigan Electric Company. In this scheme the portion of the ceiling toward the walls also was lowered so as to camouflage the dropped center section, thus giving the illusion of a smaller drop than actually utilized. The proportions and relative position of the fixtures in the depressed section were chosen as shown in Figure 3 so as to obtain the maximum lumens on the board directly from the fixtures and also those reflected from the vertical face of the dropped ceiling. This general scheme proved to be satisfactory and has been utilized also in the Tidd No. 2 control room of The Ohio Power Company and the Philip Sporn Plant control room owned by the Appalachian Electric Power Company and The Ohio Power Company (Figure 4).

Table II

Surface	Candles per Square Inch	Brightness Ratio of Adjacent Surfaces	
		Surface	Ratio
Acoustical ceiling above cubicle (a)	0.007		
Tile wall behind board cubicle (b)	0.0034	ab	2.05
Vertical surface of board (8 feet above floor) (c)	0.017	bc	5.0
Vertical surface of board (4 feet above floor) (d)	0.012	cd	1.4
Illuminated air-flow indicator (e)	0.16	de	13
Black frames of instruments (f)	0.001	ef	160

General Area Lighting Source

This phase of the problem deals with the provision of adequate horizontal illumination on the operators' desk and floor area in the center portion of the room. An important factor which should not be overlooked is that this source also must not be specularly reflected from instruments on the vertical board into the operators' principal fields of view. To accomplish this perfectly would involve an unnecessarily elaborate system. Indirect systems do not achieve the desired result entirely because the ceiling of necessity has to be illuminated to a relatively high level. Unless it is properly contoured its brightness would be observed in the instrument faces as a veiling annoyance. Other luminous ceilings have the same tendency. Suspended fixtures themselves become the objects that are reflected from the instruments either as luminous objects against dark backgrounds or dark objects against light backgrounds. A compromise solution, therefore, seemed to be the use of low brightness troffer fixtures so positioned that their effect in this matter is small. The use of *T-17* 40-watt low brightness lamps in parabolic troffer fixtures results in a solution shown in Figure 4. The latter has the additional refinement of utilizing the ceiling contour to shield totally the general lighting fixtures close to the board. Those further away do not present a serious problem because the

Table III. American Gas and Electric Company Modern Control Rooms

Control Room	Total Room Area*	Surface Colors Ceiling	Walls	Floor	Board	Lighting Fixture Data Board Lighting Units	General Lighting Units	Lighting Load, Watts Boards Illumination	General Illumination	Total	Watts per Sq. Ft.	Emergency Lighting, Watts**
Tidd No. 2, The Ohio Power Company	1,160	White	Light buff	75% buff 25% red	Eye rest green	2 40-watt parabolic aluminum troffers	2 40-watt parabolic aluminum troffers	1,200	500	1,700	1.47	1,350
Twin Branch No. 5, Indiana & Michigan Electric Company	1,145	White	Light buff	100% medium green	Eye rest green	2 40-watt parabolic aluminum troffers	2 40-watt parabolic aluminum troffers	1,600	400	2,000	1.75	900
Philip Sporn (1 & 2), Central Operating Company	3,570	White	Light buff	75% tan 25% green	Eye rest green	2 40-watt parabolic aluminum troffers	Center, 1 *T-17* lamp in parabolic aluminum troffers Behind boards, 2 40-watt parabolic aluminum troffers	3,000	1,700	3,700	1.04	1,950
Tanners Creek No. 1, Indiana & Michigan Electric Company	1,565	White	Light buff		Eye rest green	2 40-watt parabolic aluminum troffers	Center, 1 *T-17* lamp in parabolic aluminum troffers Behind boards, 2 40-watt parabolic aluminum troffers	1,800	1,300	3,100	1.98	600

* Area includes space occupied by boards.
** Emergency lights normally kept off.

projected area of luminosity becomes negligibly small.

Emergency Lighting

Since the operating room is the nerve center of the entire plant, it is very desirable that firm service be assured for the lighting system in this area to help operators maneuver quickly during the emergency. For this reason emergency lights in the plants on the American Gas and Electric Company system have been made incandescent and have been arranged so that they are normally out and are switched automatically to the station battery if the a-c source fails. Provision also is made to test these sources periodically.

The emergency lights are strategically placed around the control room and are integrated with the general board lighting scheme. Figure 5 shows the illumination result in the Philip Sporn Plant control room for a hypothetical a-c source failure. This picture was taken with only the incandescent emergency lights on.

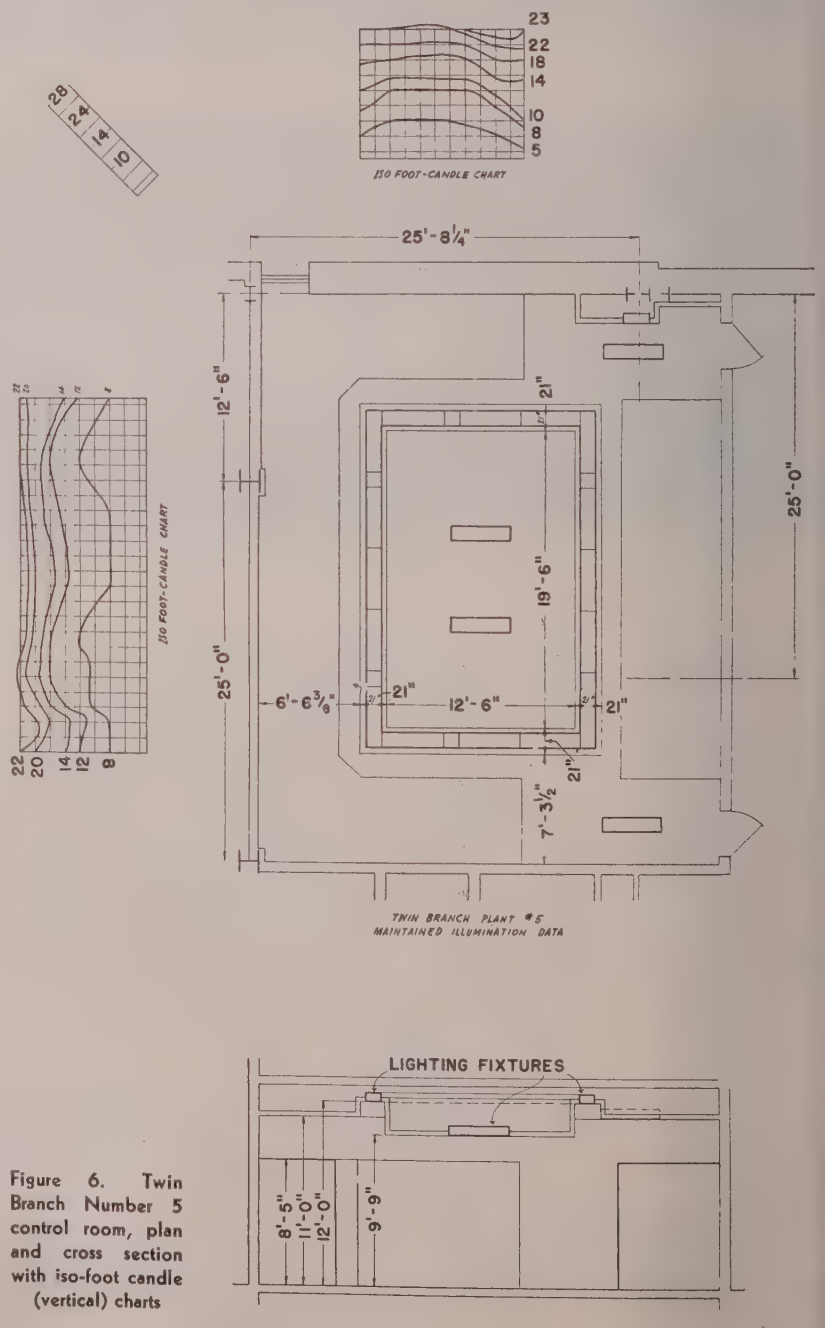

Figure 6. Twin Branch Number 5 control room, plan and cross section with iso-foot candle (vertical) charts

Results

The systems described previously have been found entirely adequate and have been accepted by operators with favorable comments. The boards receive a maintained vertical illumination of 22 foot-candles at the top and 7 foot-candles near the bottom. The measured levels are illustrated in Figure 6 for the Twin Branch No. 5 control room. Typical brightness values for this room are shown in Table II.

Table III shows pertinent data for the three control rooms thus far completed, which utilize the direct lighting system supplemented with drop ceiling design.

It will be noted that the cost of lighting fixtures for these systems averages $0.453 per square foot.

Conclusions

In the foregoing, an effort has been made to set forth major considerations that enter the design of a satisfactory, modern control room lighting system. As indicated herein, there are many possible solutions, each with its own merits based on specialized requirements. This paper considers in detail the direct lighting system using commercially available troffers in conjunction with a special, but not difficult to construct, ceiling design. It is believed that this simple and direct approach accomplishes a good lighting job for a very special problem in a very economical manner.

One point of constant annoyance to the illumination engineer centers around the poor reflection characteristics of the enclosing frames which instrument manufacturers have insisted on supplying. Until recently, these frames were only available in black, which results in extreme brightness contrast between the frames and meter scales, as well as the surface of the board which is the background.

It is noted, however, that some manufacturers recently have introduced instrument frames in pastel shades. This step is commendable and should be considered progressive by engineers involved with control room lighting problems.

References

1. Technique of Lighting Generating Stations, **H. F. Carroll, W. B. Morton.** *Illuminating Engineering* (New York, N. Y.), volume 45, number 2, February 1950, page 83.

2. Lighting a Modern Generating Station, **A. A. Brainerd, G. C. Salneu.** *Illuminating Engineering* (New York, N. Y.), volume 43, February 1948, pages 155–74.

3. Central Control at Sewaren Generating Station, **F. P. Fairchild.** *Electrical Engineering*, volume 69, June 1950, pages 491–92.

4. Design and Operation of Central Control Rooms, **B. F. Borgel.** *AIEE Transactions*, volume 69, part I, 1950, pages 598–602, and *Electrical Engineering*, volume 69, June 1950, pages 487–88.

5. Centralized Control Desirable for Single Boiler-Turbine-Generator Units, **J. A. Lind, J. M. Geiger.** *AIEE Transactions*, volume 69, part II, 1950, pages 1176–79.

6. Single Boiler-Turbine-Generator Units, **J. A. Lind, J. M. Geiger.** *Electrical Engineering*, volume 69, June 1950, pages 489–91.

7. Centralized Control in the Middle West, **J. M. Drabelle.** *Electrical Engineering*, volume 69, June 1950, pages 488–89.

8. Centralized Instrumentation and Controls for Steam Electric Power Stations, **B. C. Mallory.** *AIEE Transactions*, volume 69, part I, 1950, pages 591–96, and *Electrical Engineering*, volume 69, June 1950, pages 485–86.

9. Latest Thinking on Nerve Centers. *Illuminating Engineering* (New York, N. Y.), volume 44, 1949, page 611.

10. The Effects of Luminous Ceiling Elements on Visibility, **B. S. Benson, Jr., E. H. Church.** *Illuminating Engineering* (New York, N. Y.), volume 44, number 12, December 1949, page 715.

11. Louverall Lighting Techniques, **B. S. Benson, Jr.** *Illuminating Engineering* (New York, N. Y.), volume 44, February 1949, page 89.

12. Preliminary Report on Lighting of Instrument Panel Boards. Subcommittee of Illuminating Engineering Society Committee on Lighting Study Projects in Industry, New York, N. Y., 1948.

13. The Fallacy of the Louverall Ceiling, **D. F. Spencer, W. H. Buck, A. A. Wolfson.** *Illuminating Engineering* (New York, N. Y.), volume 44, number 3, March 1949, page 169.

14. Lighting of Control Rooms. Central Station Lighting Committee of Illuminating Engineering Society, New York, N. Y., 1950.

15. The Lighting of Switchboards. *Illuminating Specification Number S-I R-48*, Holophane Company, Inc., (New York, N. Y.).

16. Modern Lighting for Today's Power Plants, **D. H. Tuck.** *Electrical World* (New York, N. Y.), volume 110, December 3, 1938, pages 1594–95.

17. Advanced Methods of Control Room Lighting, **W. B. Morton.** *Electrical World* (New York, N. Y.), volume 110, October 8, 1938, pages 1037–39.

18. Fluorescent Lighting of Gauge Panels, **H. D. Green, W. C. Woodman.** *Electrical World* (New York, N. Y.), volume 116, 1941, pages 2036–38.

19. Glareless Illumination for Instrument Boards, **E. D. Tillson.** *Electrical World* (New York, N. Y.), volume 116, 1941, pages 1715–16.

20. Adequate Lighting for Efficient Load Dispatching, **L. A. Gates.** *Electrical World* (New York, N. Y.), volume 110, 1942, pages 451–53.

21. Sewaren Adopts 1050 Steam. *Electrical World* (New York, N. Y.), volume 132, August 13, 1949, pages 87–91.

22. Built-in Lighting Added to New Benchboard, **L. R. Scott.** *Electrical World* (New York, N. Y.), volume 132, September 24, 1949, page 91.

23. Full Luminous Ceiling for Control Room, **A. A. Brainerd, W. H. Johnson.** *Electrical World* (New York, N. Y.), volume 132, December 3, 1949, pages 102–03.

24. Old Style Control Room Goes Modern, **J. Q. Wray, Jr.** *Electrical World* (New York, N. Y.), volume 131, March 12, 1949, pages 112–14.

25. Security Through Flexibility Marks Mitchell Electrical Design, **H. A. P. Longstaff.** *Electrical World* (New York, N. Y.), volume 132, July 2, 1949, pages 55–58.

26. Compact Board Affords Full Control of Plant Operations. *Electrical World* (New York, N. Y.), volume 133, July 17, 1950, pages 98–99.

27. Systematized Dispatching, **W. C. Foster.** *Electric Light and Power* (Chicago, Ill.), volume 23, September 1945, pages 76–78.

28. Southwork Control Boards Designed for Simplicity and Operating Convenience, **J. T. Branson, E. B. Seymour.** *Electric Light and Power* (Chicago, Ill.), volume 25, October 1947, pages 68–71.

29. Power Plant Lighting Needs Careful Design, **S. L. Chapin, H. E. Wehr.** *Electric Light and Power* (Chicago, Ill.), volume 26, September 1948, pages 110–16.

30. Steam Plant Performance on Fluctuating Loads—Part I, an Operating View, **G. H. McDaniel.** *Electric Light and Power* (Chicago, Ill.), volume 27, April 1949, pages 87–89.

31. Barbadoes Plant Extension Features Economic Design, Reliable Performance, **G. S. Gethen, B. R. Nevins.** *Electric Light and Power* (Chicago, Ill.), volume 27, November 1949, pages 72–76.

32. Warren Station Doubles Capacity, **W. C. Sontum, R. H. Kreismyer.** *Electric Light and Power* (Chicago, Ill.), volume 27, November 1949, pages 90–95.

33. Mitchell Station Augments West Penn Generating Capacity, **G. D. Binlergh.** *Electric Light and Power* (Chicago, Ill.), volume 27, April 1949, pages 76–82.

34. Control Room Lighting System Exemplifies Coordinated Design, **F. A. O'Brien.** *Electric Light and Power* (Chicago, Ill.), volume 27, September 1949, pages 66–67.

35. Sewaren Exemplifies Economic Design, Efficient Operation. *Electric Light and Power* (Chicago, Ill.), volume 27, July 1949, pages 46–51.

36. Illumination of Switchboard Instrument Scales, **H. S. Edgerle, R. N. Rowel.** *General Electric Review* (Schenectady, N. Y.), volume 52, October 1949, pages 28–31.

37. Control Room Lighting and Light Colored Switchboards, **W. B. Morton.** *Electric Journal* (East Pittsburgh, Pa.), volume 32, June 1935, pages 220–23.

Discussion

Walter B. Morton (Pennsylvania Power and Light Company, Allentown, Pa.): The author has adequately covered an analysis of engineering planning of the dropped ceiling direct type of control room lighting design. The point is well made that extravagance should be avoided in lighting design. This is a self-evident requisite for any engineering design whether lighting, switchboards, cables, feed pumps, or any other item in the plant.

Admittedly the type of lighting described in the paper can be designed and installed at lower cost than the more modern luminous ceiling designs. However, the author's claim for equal or greater effectiveness with the dropped ceiling than obtained with some form of luminous ceiling is questioned by many engineers who have designed both types of systems and have made comparisons by means of mock-ups.

Basically, the lighting of a control room should provide adequate illumination on instrument scales, and in addition, should provide maximum eye comfort for the working personnel. Experiments over many years have convinced many engineers that

while satisfactory intensities can be provided on scales of instruments with either direct or luminous ceiling types of light sources, maximum in eye comfort and visual acuity can be achieved only when:

1. There is a minimum of brightness difference throughout the room, without any major bright sources in the field of vision.
2. There is a minimum of shadow on the scales of instruments or nameplates below projections on the board.
3. There is minimum of brightness reflection or veiling glare in the glass covers of instruments.

Mock-ups made by engineers of several utilities have indicated to them that the luminous ceiling type of light source most adequately provides for realizing these basic requirements.

The author's comments on finish of switchboard instrument frames is timely. The Pennsylvania Power and Light Company has conducted experiments with colored instrument frames in one of its large substation control rooms. One 7-panel section of a new 40-foot control switchboard has been equipped with colored instrument frames using seven primary and two additional colors. The results are not yet complete, but a preliminary trial of these colors indicates that bright and varied colors for switchboard devices tend to facilitate accurate reading of instruments and also materially improve the appearance and atmosphere of the control room.

In Table I, the author lists several disadvantages of the luminous ceiling design to which I would take exception. Under ceiling height required, he lists "high" for the louvered ceiling design. Actually, in the Sunbury Station control room of Pennsylvania Power and Light Company, the first of many louver ceiling control room lighting installations that now are in service over the country, the ceiling height is only 9 feet 6 inches. Direct glare and reflection in instruments are negligible and are not "obtained with difficulty," as stated in the paper.

An important advantage of the louver ceiling is that ventilating or air conditioning ducts can be so located above the ceiling with multioutlets that provide very low velocity diffused ventilating air. This not only improves ventilation, but materially reduces cleaning problems. Time between cleaning of louver ceilings at Sunbury has been extended to more than one year.

It is seriously questioned whether shadows on instrument scales and devices can be considered negligible with any direct type of switchboard lighting scheme as indicated in the table. In any direct scheme, the light sources must be placed close to the board to maintain an angle of incidence that will eliminate direct glare in the glass fronts of the instruments. This in itself forces the designer to locate his light sources so close to the switchboard that shadows must result from the low angle with which the light strikes the instrument, unless the instruments are specially designed.

An important premise in switchboard illumination is that if the intensity of light on the scale of the instrument is greater than the intensity of the image reflected in the glass front, no interference with reading of scales will exist. The direct scheme accomplishes this with high concentration of light on the scales requiring an angle of incidence that produces shadows on the scales. The luminous ceiling design accomplishes the result with uniform light source that minimizes reflections by eliminating patterns, and lighting all areas equally.

An important disadvantage of the direct system described by the author is that direct units must be placed in the dropped ceiling area for desk and general illumination. There is no practical method of eliminating direct glare in instruments from these light sources. This veiling glare appears to be quite noticeable in the instruments on the switchboard shown in Figure 2.

It also is noted in Figure 2 that the indicating instruments have dark scales with white lettering. Experiments over many years have convinced the Illuminating Engineering Society (IES) Committees and ASA-AIEE Switchboard Instrument Committees that white scales with black letters are best for visual acuity and quick reading of scales. A mock-up with the two types side by side usually is surprisingly convincing of this fact.

While the paper does not specify the author's recommended illumination levels for control rooms, the inference to be drawn is that he considers 7 to 25 foot-candle vertical illumination entirely adequate. To this I cannot subscribe, and although data on which to base such recommendations are largely empirical, the levels recommended by the IES are much higher. Their recommended values are based on findings of many lighting engineers, and on certain experiments conducted two years ago at Nela Park.

Arthur A. Brainerd (Philadelphia Electric Company, Philadelphia, Pa.): I am glad that Mr. Dzwonczyk has used the expression "An" Engineering Approach rather than "The". It serves to emphasize the fact that engineering is an art as well as a science. The author has described a very satisfactory method of lighting control rooms, but I am sure that he will agree with me that he is not in a position to say that it is the best, since there is seldom one best solution to any engineering problem.

As an individual I agree with the author that 20 foot-candles on the vertical plane of the board is adequate. As Chairman of the IES Committee on Lighting of Central Station Properties, I am forced to agree with the overwhelming majority of the committee members that this value should be much higher. Society standards are achieved by the democratic method.

The use of judging charts is not new. We in Philadelphia have used this system for many years. For example, referring to Table I, let us consider the solid luminous ceiling with which I have had considerable experience. The rating for Uniform Vertical Illumination is "Good." Why not "Excellent"? The same goes for ceiling brightness and fixture brightness. What is his basis of comparison?

Again, he states that the ceiling reflected in the instruments is the "same as louvered plus traces of solid supports." This statement is highly misleading. The reflection of the ceiling is definitely not a disturbing factor. He next states that fixture reflection from instruments "can be made negligible with difficulty." After 18-months operation with an installation of this character we have not been able to detect any drawback of this nature.

In his last item he states that the source of light "should not be in the field of view." For a primary source he may be right, but I find no scientific evidence to justify this statement concerning a secondary source.

This sort of critical analysis might go on indefinitely and at the end Mr. Dzwonczyk would continue to recommend the dropped ceiling, and I would still stick to luminous plastic or luminous indirect. Each of us as engineers is influenced by our cumulative experience and environment. Variety is one of the things that make engineering an interesting occupation.

G. J. Taylor (Day-Brite Lighting, Inc., New York, N. Y.): The premise expressed by the author that "there is no single method to correctly illuminate a control room based on lighting standards alone" is well taken but the conception is not restricted to control room lighting. Most of our lighting problems involving people for the specific purpose of seeing falls into this category of reasoning. Nevertheless, seeing, as associated with the comfort of workers, is the result of certain environmental conditions in any room. Comfortable seeing is accomplished when illumination levels are adequate and brightnesses properly balanced.

The psychological aspects of human behavior are appreciated and the likes and dislikes of people should be given some consideration. The author is a little doubtful on this point in stating ". . . if not prime consideration." It would be better to say ". . . *but* not prime consideration," for the art of lighting has advanced to the point where it is known that engineered illumination provides a high degree of visibility at comfortable ranges. Individual opinions are to be respected but they do not always provide the best solutions for specific lighting jobs when thousands of people are involved in similar seeing tasks. It may be true that a stage-like lighting effect unconsciously draws the operator's attention to the control boards. Yet, such conditions where operators work day in and day out for years on end results in a fatiguing action unconsciously brought about by eye strain. You would not want to work in a room like shown in Figure 5 for long periods of time. The setting is typical stage-like but, as indicated, serves only for "emergency lighting."

The author's approach to "one" solution of control room lighting is indeed a good one. He offers a lighting system that is not only utilitarian in its application and functional but economical as well. Not that economy should be placed high on the list (comfort of vision takes that honor) but when it is attainable with satisfactory lighting as presented by the author the thought is commendable.

There are other elements of human comfort which are used in the jobs described but not stressed by the author. All these elements are of significant importance and have a definite bearing upon visual efficiency and over-all operating efficiency in accomplishing the job to be done. These elements of importance are:

Good lighting—for ease in seeing

Light equipment—for reduced contrasts
Light surrounds—for comfort of vision
Sound proofing—for aid in concentration
Air-conditioning—for combating discomfort due to heat

In spite of the fact that the paper classifies seeing tasks as "ordinary" in control rooms, the levels of illumination above those recommended should be considered. Otherwise, the excellent features explained in dropping the ceiling along the perimeter of control boards and low brightness fluorescent lamps over centrally located operators' desks together with good over-all light colored surrounds in the room the general environment approaches the ideal. Considering the important elements cited above it seems logical to propose higher levels of illumination. This is particularly true today because fluorescent lamps have high efficiencies in light output. A well-lighted room is conducive to increasing the tempo and well-being of operators—it is refreshing, like a cool soft drink on a hot summer day.

In Table II of the paper the following brightness ratios prevail:

Surface of board to ceiling	2.43 to 1
Illuminated indicator to surface of board	9.4 to 1
Surface of board to instrument frames	17 to 1
Illuminated indicator to ceiling	22.9 to 1
Illuminated indicator to instrument frames	160 to 1

The brightnesses are well controlled and within the accepted range for visual comfort at normal fields of view. The exception is with the black frames of instruments. The author recognizes this shortcoming and comments on it interestingly in the concluding paragraph of his paper.

A few brief comments on some of the tables and illustrations presented in the paper may be of interest:

1. Table III. The high reflectances of "surface colors" are commendable. Parabolic aluminum troffers provide low side brightness when viewed crosswise for center room lighting. Low brightness *T-17* fluorescent lamps or the new *T-12* Slimline lamps operating at 200 m.a. (not mentioned) are desirable.

2. Figure 1. Equipment finishes poor. Should have higher reflectance for best seeing conditions.

3. Figure 2. General conditions of over-all room excellent. Instrument frames too dark.

4. Figure 3. Indicates use of parabolic aluminum troffer with reasonable concentration of light. May also be accomplished with certain prismatic lens plates. The vertical surface immediately below the troffer (not shown) at right (in sketch) should be aluminum (preferably specular) for best results in redirecting light rays.

5. Figures 4 and 5. An amazing study in the importance of light colored room finishes and proper distribution of light. For highest comfort brightness engineering is indeed a factor of great importance.

The thoroughness in which the various engineering aspects of control room lighting were studied and presented in this paper is note worthy. Specific problem analysis of this nature is the means toward a better understanding of applied illumination and the ultimate provision of good light for good sight and human comfort.

H. E. D'Andrade (General Electric Company, New York, N. Y.): It has been well stated by Mr. Dzwonczyk that there are several possible solutions to the problem of control room lighting. This is not only true of methods and techniques, but also of foot-candle levels. Only thus can we understand the difference between two schools of thought: namely the 20 foot-candles for vertical surfaces found adequate by Mr. Dzwonczyk, and the 50 (vertical) foot-candles for the type *A* control room recommended in the new report of the IES Committee on Lighting of Central Station Properties.

It would seem that the Type *A* control room is the point of difference. Actually, the IES recognizes a Type *B* control room, for which it recommends 30 (vertical) foot-candles. This is not a wide divergence from the 20 foot-candles found adequate by Mr. Dzwonczyk. At present the Type *A* control room of the IES Committee seems beyond the scope of most utilities, since their control rooms more nearly meet the requirements of the "visual task" defined by the author.

Mr. Dzwonczyk also deserves high praise for his statement that "The operators are the principal parties affected in the matter" and that they should be given "some if not prime, consideration."

My experience confirms these remarks, inasmuch as I have found that most operators prefer a stage-like effect with the vertical boards high-lighted, so to speak, while the areas where they sit have a more subdued lighting level. In one very modern control room, an operator confessed to me that he changes the entire lighting system after "the boss" leaves the room, controlling the system by switches to produce just this stage-lighting effect—the opposite, indeed, of the effect sought by the designers. In many other stations I have found that operators turn half the lights off, and will confess this only to someone who will not tell the story to the "higher-ups." It seems to me, therefore, that illuminating engineers should be factual to that extent, and recognize that the "stage-lighting" effect is legitimate, and perhaps more comfortable.

If another opinion from the point-of-view of the control room operators is permissible, it may be added that many operators consider that a lighting system may be good from the point of view of their superiors, but "spoilt" for the operators by glaring light sources over the board. Such sources should always be concealed, and even "recessing" often proves unsatisfactory. Momentary inspection by a group of executives cannot uncover this fault. Only operators who "live" with the system feel such defects, which are apparent only after a lapse of time, or after habitual work in the room.

The author of the paper is also to be complimented for his use of the *T17* 40-watt low brightness lamps, which have a brightness lower than many glass, or plastic-paneled luminaires with standard 40-watt *T12* lamps. In short, the author's paper indicates that he has experience and engineering knowledge, and that he has combined both to produce satisfactory results which should benefit others who are responsible for the design of lighting in control rooms.

D. J. O'Neill (Holophane Company, Inc., New York, N. Y.): The simplest and most direct way to discuss this paper on control room lighting will be found in the author's approach to the general subject. All plus, or favorable factors are considered; next, some of the unfavorable aspects are reviewed; finally, conclusions are drawn after due consideration of the plus and minus sides of the problem.

Experience in original design and inspection of completed installations must have prompted the author to declare the logical and practical solutions to problems in control room lighting can be found in providing adequate illumination on the principal working planes—the vertical surfaces of the boards themselves, or, in the case of bench boards, vertical planes, and adjacent inclined planes. This thesis differs from the rather widespread advocacy of lighting systems which produce high levels of horizontal illumination for the entire control room and depend on a by-product of this considerable flux in the 0 to 65 degree zone to provide sufficient illumination on the principal work planes noted above. It is noteworthy that the author favors no particular lighting system but includes two general systems with appropriate comments regarding the limitations of the systems.

Several questions are raised as the result of reviewing the illustrations in the paper:

Is the lighting installation, shown in Figure 1, of the Philo Control Room generally satisfactory? Is it not a fact that the old type *H* Thompson meters with their curved window glasses pick up reflected images of every lighting unit on the operators' sides of the meters and in some positions it is virtually impossible to read the meter scales? Is it not true that reverse coves, direct troffers, and luminous ceilings, or any combinations of these systems will fail to overcome the defects in meter design?

Can a lighting result be calculated for the type of installation illustrated in Figure 3, the Twin Branch Number 5 Control Room? If ceiling height, board height, and distance between board and lighting equipment are changed can the lighting results be predicted or will estimates have to be made and checked after the installation is complete?

Referring to the Philip Sporn Control Room shown in Figure 4. Does the author agree that improvements can be made in the case design of Bailey and other type recording meters? Should not the manufacturers restudy these designs and perhaps offer as much improvement in the framing case and cover glass as has been produced recently by manufacturers of voltmeters, ammeters, and similar control board instruments?

What type of instrument was used to take readings of vertical illumination shown in Figure 6 of the Twin Branch Control Room? Does the author agree there is a definite need for a portable instrument that can be relied upon to register true values of vertical illumination?

Finally, commenting on the final paragraph of this paper, has the author observed a control board on which meter frames have been painted to match the color of the board surface? Is it not likley that this condition of no distinction between individual meter frames would produce worse seeing conditions from the standpoint of location of meter scales and ability to read

them than the condition of dark frames on instruments on a light color finished board?

H. A. P. Langstaff (West Penn Power Company, Pittsburgh, Pa.): My one and only comment to the author's very complete story is made from a maintenance point of view. Knowing the importance of control room lighting, its continuity and proper maintenance thereof, I have for the past several years stressed the importance of the elimination of obstructions and maintenance personnel in the control room as far as possible. It is my belief that practically all of the maintenance work for control room lighting should be done from above the ceiling. Practically all recent designs include air ducts above the ceiling and their space requirements can be co-ordinated with the lighting unit installations such as were provided for the Mitchell Station control room of the West Penn Power Company. Plans and photographs of this installation have been included in descriptive periodicals in the Central Station Lighting Committee of IES.

V. L. Dzwonczyk: The value of a technical paper is appreciably enhanced by honest and open discussions, such as have been advanced by Messrs. Brainerd, D'Andrade, Morton, Langstaff, O'Neill and Taylor, each a man of recognized experience with control room lighting problems. It is especially fortunate that comments were received from some members of the IES Committee on Central Station Lighting of which Mr. Brainerd is General Chairman. Mr. Morton is Chairman of the Subcommittee on Control Room Lighting.

It would be a formidable task to answer each of the points raised during discussion. Many of them are adequately discussed by others. A review of the discussions indicate most interest in the following: recommended illumination levels; brightness contrast; instrument frames; and direct versus luminous systems.

Mr. Morton indicates that the writer did not specify an illumination level he would recommend, although it is significant to note that Mr. Brainerd advanced the following as part of his discussion:

"As an individual, I agree with the author that 20 foot-candles on the board is adequate. As Chairman of the IES Committee on Lighting of Central Station Properties; I am forced to agree with the overwhelming majority of members that this value should be much higher." As Mr. Brainerd indicates, I do recommend 20 foot-candles on the vertical plane (66 inches above the floor) and 20 foot-candles on the horizontal plane. The IES Committee will recommend higher levels over my dissenting vote. In all fairness to the committee members, however, I believe their vote was influenced by considering a task more severe than what is found in a centralized control room.

The following is my understanding of the basis on which tests were performed at Nela Park to arrive at the illumination value suggested by the committee, and I quote from the test report:

"The visual task performed in control rooms, reading meters, is a particularly difficult one. This task can normally be divided into two parts: First, critical reading of all meters at distances of about 2 feet at intervals of approximately one hour; and second, approximate reading of all meters at distances between 10 and 20 feet every few minutes. Since critical readings require only a few minutes each hour and are performed at relatively close distances, this is apparently a less difficult visual task than that of the frequent approximate readings at much longer distances.

It would be ideal if it were possible to determine the optimum illumination level for performing the control room tasks. However, at present the variables are too many and intangible to positively determine a universal optimum foot-candle level. The Luckiesh-Moss visibility meter can be used to determine the illumination required for threshold visibility of control room meters, as well as establish the foot-candles necessary to bring the meters up to the visibility as another predetermined task.

Visibility measurements were taken under various conditions for the different visual tasks required. On the *DB-15* meter, a 4-inch meter with 30 point type, the visibility of the numerals as well as the angular position of two different needles, one 5/16-inch thick and the other 1/8-inch thick, was found at various distances. In steam plant gauges the visibility was measured for a more critical task, that of determining the angular position of the needle on a 2-inch meter, number *AD10216*.

Before a foot-candle recommendation can be made, it is necessary to agree upon the visibility level desired. A printed task, such as reading of the Reader's Digest, consisting of 8-point Bodoni type held at 14-inches and illuminated to 50 foot-candles has a visibility of nine. It would appear that the visual task in control rooms should have a visibility at least this high. In choosing the visibility level to recommend, however, it is necessary to take into account the element of quality as well as quantity of illumination. Such factors as brightness contrasts within the entire visual field, the number of meters—and consequently the time involved performing each visual task, and the tolerances permissible in reading the meters, all affect the choice of the visibility level to be recommended."

I suggest that the following points in the above discussion represent a task that is more severe than found in modern centralized control rooms:

1. Approximate reading of all meters at distances between 10 and 20 feet every few minutes. The ability to see the relative position of the pointer, not to read the meter, at a distance of 10 feet would be a maximum seeing task.

2. The selection of 2- and 4-inch instruments for visibility tests between 10 and 20 feet. Any critical instruments that need be seen from such a distance as 10 feet should be at least $8\frac{1}{2}$ inches in diameter.

3. A seeing task such as reading the Reader's Digest at 14 inches under 50 foot-candles.

If the test data is reviewed in light of the above suggestions it is believed that 20 foot-candles becomes more nearly the reasonable illumination level than what the IES Committee recommends. Incidentally, it is also my understanding that the IES Quantity and Quality Committee, using other criteria on which to base its judgment, recommended 20 foot-candles for the vertical and horizontal planes.

The matter of brightness contrast could involve considerable discussion. Let us say that the luminous ceiling, if properly designed, does result in a more uniform brightness contrast throughout the room and that it approaches the ideal limits set for visual surroundings. Do these systems, however, provide surroundings appreciably better for control room operations, than other more efficient lighting systems, to warrant the cost, and to accept illumination levels considerably higher than required on the horizontal plane? I claim that from the standpoint of brightness ratios and shadows on instrument scales the direct lighting system can provide conditions sufficiently close to good practice. Mr. Taylor apparently agrees with this. He comments further, however, by stating that a stage-like effect is one which would not be conducive to good lighting because of improper brightness ratios. As an example let us refer to Figures 4 and 5, the latter of which shows the lighting effect under emergency conditions. The writer agrees wholeheartedly with Mr. Taylor that to work under the extreme conditions simulated by Figure 5 would be very bad. This subject was especially introduced into the paper to bring out such comments as Mr. Taylor raised. It is significant, however, that there are many operators who, in spite of being provided with reasonably good lighting conditions, will resort to the practice of extinguishing the lights in the center portion of the room to achieve a subdued lighting effect. Mr. D'Andrade comments very admirably on this subject with considerable experience.

Instrument manufacturers should take note of the many comments expressing the desire for instrument frames other than black. The writer has endeavored for many years to stimulate such an attitude and recently the first signs of progress became evident. In the Tanners Creek Plant, some electric instruments were purchased with frames finished in a grey color having a reflection factor approximately 20 per cent less than the board surface. This will give some framing effect to the instruments but not such an undesirable extreme as the black. Further tests are being conducted at this plant with other colors. Similar tests being conducted by Mr. Morton should reveal much needed data. It is our aim to equip the Kanawha River and Muskingum River Plant control rooms with instrument frames uniformly colored in some acceptable pastel shade. The above discussion should answer Mr. O'Neill's question pertaining to this subject. It appears that he thought the writer was advocating the frames to be made the same as the panels, which condition would destroy the desirable framing effect.

To be a luminous ceiling enthusiast or not to be one requires many other influencing factors than just lighting consideration. Mr. Morton presents a discussion upholding the merits of the Louverall ceiling type of luminous ceiling. Mr. Brainerd could do the same for a solid luminous ceiling if he chose to do so. Apparently both men have made mock-up installations using various types of lighting systems in control rooms and have concluded that those methods realize their requirements most adequately. There seems to be nothing else that need

be said since both agree that luminous systems cost more and that they are willing to spend an additional amount to obtain this form of lighting. Perhaps some of the cost can be charged off to advertising or public relations, especially if the control room is one of the sightseeing points for guided public tours. The effect of a luminous ceiling is admittedly more awe inspiring.

Let us consider the fundamental aspect of luminous systems which appears to be the fallacy of their use for control rooms. The vertical plane is the principal work plane. The horizontal plane very seldom requires an illumination level higher than what would be adequate for ordinary seeing tasks (IES recommends 30 foot-candles). To get a desired level of lighting on the vertical plane with a luminous ceiling system one must virtually pour between two and three times as many lumens on the horizontal plane. This means that if one wants 50 foot-candles on the vertical plane it is necessary to provide 100 and 150 foot-candles on the horizontal plane whether needed for the task or not. How many office lighting installations are there in this country using such high levels?

The comment concerning the Louverall ceiling as an aid in ventilation, or air-conditioning, is questionable. Heating and air-conditioning men have indicated that this is correct for the cooling cycle, but that if one attempts to introduce heated air into the control room, much higher velocities are required and that difficulty might be experienced. The introduction of air into the control room by the means mentioned should also require a much larger air-conditioning system in the opinion of these men. This again adds to the cost of the installation.

The serious difficulty which Mr. Morton seems to imply with the direct lighting system is that shadows are bound to occur on the board and that specular reflections will occur by installing fixtures in the center of the room for general lighting. These shadows are very very negligible. I should think that Figures 2 and 4 would support this contention. As far as the reflection of the center lights in instruments are concerned, Mr. Morton is correct, but these only occur from very few positions and can be avoided by the operator stepping aside just a trifle. Figure 2 was purposely selected as an exhibit to bring out this point. There is nothing to hide in this respect, since, as mentioned in the paper corrective methods can be devised if the expenditure seems to warrant the result. The next step in this development was to utilize a ceiling as indicated in the Sporn Plant control room, Figures 4 and 5. This system further tends to eliminate the possible positions in which such specular reflections would occur. The use of *T-17* lamps reduces the brightness of the reflected image also.

The comment regarding the black faces of some instruments is very well taken. The writer dislikes black-faced instruments, but as yet has not been able to convince those responsible for purchasing these instruments that white faced units are more easily read.

Mr. Taylor recommends that specular aluminum be used on the vertical surface of the dropped ceiling. This was considered because it would increase the reflected light towards the board but the idea was discarded when the architect claimed exceptionally difficult and costly work of fastening the aluminum to the surface in a good looking manner. Besides it was felt that diffused light from the acoustical tile would help eliminate the shadows on the board.

Mr. O'Neill raises some interesting questions. He asks whether the lighting installation in Figure 1 was considered generally satisfactory. The answer is "no" and that is the reason why further development was undertaken toward dropped ceiling design. The writer feels that no system will be entirely satisfactory in the Philo control room unless the old style type *H* meters are discarded. Mr. O'Neill also questions whether calculations can be made for the system described in this paper which could predict what the level of illumination would be on the vertical plane. Calculations can certainly be devised which would be as accurate as desired. The writer has developed a method which yields results, that are sufficiently accurate to predict the level.

The instrument used to test the illumination at our plants is a Weston model *603* twin-cell paddle-type photocell meter. If better instruments are devised that can be used conveniently we shall use them.

Further development, which was partly forced upon us by inability to purchase aluminum troffers and partly by the desire to reduce further the brightness of the board lighting units in the longitudinal direction, is being introduced into Philip Sporn numbers 3 and 4 control room. In this room shallow troffers utilizing *9015* Holophane Lo-Brightness lens will be used instead of the parabolic aluminum troffers. These fixtures will utilize three lamps per unit so switched that either one, two, or three lamps may be energized, thus affording a means to investigate whether higher vertical illumination levels are desirable.

Mr. Langstaff discussed a very important phase of control room lighting, namely the maintenance problem in relation to interference with operation. Although the approach used in the Mitchell Station design is a commendable one, we did not feel that the added complication and expense of providing for relamping and cleaning fixtures from above the ceiling would be justified in our case. Our approach was to select a fixture which met the prescribed photometric requirements, had features which would tend to keep the depreciation low and would be easy to clean. The two lamp parabolic aluminum troffer manufactured by Daybrite Lighting, Inc., utilizes a wide louver spacing in the plane parallel to the tubes. This feature is an advantage from the maintenance point of view but provides less than desirable shielding in the longitudinal plane—again a compromise. The recent priority restrictions on aluminum forced us to use troffers with Holophane *9015* Lo-Brightness lens' plates. This change will probably make maintenance more difficult but will improve the brightness control longitudinally to the fixture.

A Contribution to the Theory of the Deep-Bar Induction Motor

JOHN F. H. DOUGLAS
FELLOW AIEE

THE deep-bar rotor may be defined as a single-cage rotor in which skin effect plays a prominent part. With rotor slots nearly one inch deep, skin effect reduces starting current and increases starting torque so that in many ratings this type of motor has superseded the older shallow cage motor. Deep bars of various shapes have recently been developed. However, no adequate theory has appeared which enables the designer to predict the characteristics of these newer motors. This paper will provide a theory which will aid in the design of deep-bar rotors.

The earlier deep-bar motors had rectangular slots. The theory for this type of bar was given by A. B. Field[1] in 1905. More recently bars of a T-shape have been used. H. V. Putnam[2] presented the theory for this type of bar in 1927. Typical starting currents for a motor using either of these bars is 5.5 times unit current. With this current a typical starting torque for a motor with rectangular bars is 1.5 times unit torque. When a T-shaped bar is used the corresponding figure may be 1.75 times unit torque.

Motors with bars of trapezoidal shape are in current use, as well as motors with bars having a circular lower part and rectangular upper part. These motors have starting characteristics similar to those of a motor with a T-shaped bar. So far as is known to the author there are no deep-bar motors which compete with the double-cage motor, or meet National Electrical Manufacturers Association design type *C* specifications.

This paper will endeavor to supply the theory of the tapered bar and of bars with a tapered section. It also will endeavor to improve the theory of the round bar. A graphical method for computing the impedance of any shape of bar will be given. The formulas developed indicate that further improvements should result if the bar is somewhat enlarged near the slot opening.

It will be shown that:

1. The tapered bar is superior to the rectangular bar, provided the narrow portion is near the top.
2. Further improvements should be sought among bars of compound shape.
3. The slot constant, for a round slot is close to 0.72 when running.

Statement of the Problem

The problem discussed in this paper is that of finding the impedance of the rotor bars under both starting and running conditions, as the impedance is a major factor in motor performance. The impedance may be found by either graphical or mathematical integration of impedance elements from the bottom of the slot to the slot opening. In previous studies the slot width was assumed constant. In this paper the effect of a varying width of slot will be studied.

Figure 1 shows a slot with lines of force at points x and $(x+dx)$. The current $\boldsymbol{I}$ is that below x. The electric intensity is denoted by $\boldsymbol{E}$. Both $\boldsymbol{I}$ and $\boldsymbol{E}$ vary with x.

The strip of width (dx) in Figure 1 adds an area (dA), contributes a geometric permeance (dP) equal to (dx/W), and carries the current $(d\boldsymbol{I})$. The increase in the voltage $(d\boldsymbol{E})$ is due to the effect of reactance. It is proportional to the current, I, the frequency, and the increment in the permeance (dP). It leads the current 90 degrees. The increase in the current $(d\boldsymbol{I})$ is due to the effect of conductance. It is proportional to the voltage, E, the conductivity, and the increment in area (dA). It is in phase with the voltage.

Figure 2 shows how the bar is represented by an equivalent circuit,[4] and also shows a vector diagram of current and voltage for the layer (dx). The shunted conductance is equal to (dA/ρ). The series reactance is equal to $(2\pi f\mu)dP$. In inch units, with microvolts and amperes, the reactance is $(f/5)(dP)$. If we also allow for the space factor, F, in the copper, a very general form of the basic equations is equations 1.

$$d\boldsymbol{E}=j(f/5)(\boldsymbol{I})(dP);\ d\boldsymbol{I}=(F/\rho)(\boldsymbol{E})(dA) \quad (1)$$

When the lines of force are straight and the slot is narrow, the equation may be written in the more familiar form of equations 2.

$$d\boldsymbol{E}=j(f/5W)(\boldsymbol{I})(dx);\ d\boldsymbol{I}=(FW/\rho)(\boldsymbol{E})(dx) \quad (2)$$

The problem may now be restated more precisely as that of replacing the pair of equations 1 or 2 by a single equation, expressing the variation of the impedance, $\boldsymbol{Z}$, (or admittance $\boldsymbol{Y}$), with x, making due allowance for variations in the width of the slot. This equation must then be integrated to obtain the bar impedance, $\boldsymbol{Z}$, or admittance, $\boldsymbol{Y}$.

Method of Approach: Finding a Single Equation with One Dependent Variable

In taking the derivative of the impedance $\boldsymbol{Z}$, with regard to x, we note that $\boldsymbol{Z}$ is the ratio of $(\boldsymbol{E}/\boldsymbol{I})$, and set,

$$d\boldsymbol{Z}/dx=d(\boldsymbol{E}/\boldsymbol{I})/dx=(1/\boldsymbol{I})(d\boldsymbol{E}/dx)-\boldsymbol{Z}^2(1/\boldsymbol{E})(d\boldsymbol{I}/dx) \quad (3)$$

By the use of equation 2 and substituting

Paper 51-159, recommended by the AIEE Rotating Machinery Committee and approved by the AIEE Technical Program Committee for presentation at the AIEE Great Lakes District Meeting, Madison, Wis., May 17–19, 1951. Manuscript submitted January 23, 1951; made available for printing April 2, 1951.

JOHN F. H. DOUGLAS is with Marquette University, Milwaukee, Wis.

The author wishes to acknowledge the valuable help given by John Kirkish of the Louis Allis Company, Dr. A. B. Drought and J. D. Horgan of Marquette University in the preparation of this paper.

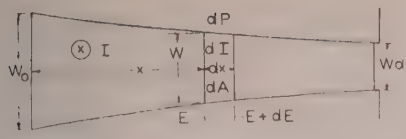

Figure 1. Tapered deep-bar rotor slot

for $(d\boldsymbol{E})$ and $(d\boldsymbol{I})$, equation 4 is obtained. If, however, equation 1 is used, equation 5 results.

$$d\boldsymbol{Z}/dx = j(f/5W) - (\boldsymbol{Z}^2)(F/\rho)(W) \quad (4)$$

$$d\boldsymbol{Z} = j(f/5)(dP) - (\boldsymbol{Z}^2)(F/\rho)(dA) \quad (5)$$

Equation 4 is most useful in analytical work; equation 5 in graphical and tabular integration.

If we write an expression for $(d\boldsymbol{Y})$ similar to equations 3 and 5 then, by proper substitutions, equation 6 will result. This is most useful in graphical integration in the lower portion of the bar.

$$d\boldsymbol{Y} = (F/\rho)(dA) - (\boldsymbol{Y}^2)(j)(f/5)(dP) \quad (6)$$

Equations 5 and 6 are suitable for graphical and tabular integration, with very small increments in permeance, P, and area, A. The number of steps to be taken are a very severe burden, and a modification of the equations is needed to make them suitable for finite increments.

The modification of equations 5 and 6 for finite increments consists in replacing $\boldsymbol{Z}$ or $\boldsymbol{Y}$ by their average values. Thus $\boldsymbol{Z}$ is replaced by $(\boldsymbol{Z}+{}^1/_2\,\Delta\boldsymbol{Z})$ and $\boldsymbol{Y}$ is replaced by $(\boldsymbol{Y}+{}^1/_2\,\Delta\boldsymbol{Y})$. If terms of the third order are neglected, equations 7 and 8 result.

$$\Delta\boldsymbol{Z} = \left(\frac{j(f/5)\,\Delta P - (\boldsymbol{Z}^2)(F/\rho)\,\Delta A}{1+(\boldsymbol{Z})(F/\rho)\,\Delta A}\right) \quad (7)$$

$$\Delta\boldsymbol{Y} = \left(\frac{(F/\rho)\,\Delta A - (\boldsymbol{Y}^2)(jf/5)\,\Delta P}{1+(\boldsymbol{Y})(jf/5)\,\Delta P}\right) \quad (8)$$

The choice of equations 7 or 8 depends on the boundary condition when x is zero. In the bottom section of a bar the boundary value of $\boldsymbol{Y}$ is zero, so that equation 8 is convenient. If a start is made at a point at which the shape of the bar changes, and there is a known initial value of $\boldsymbol{Z}$, then equation 7 is more convenient.

The topics that will be considered are the impedance of a tapered bar, the impedance of two types of compound bar, and the solution of the problem of the round bar. The paper will be concluded with two illustrative examples.

Impedance of a Tapered Bar with a Narrow Slot Opening

While bars of a trapezoidal shape are in current use, the direct solution for the impedance of such a bar will not be considered here. Instead, an equivalent exponentially shaped bar, having the same area, and slot constant will be used. A graphical solution of the trapezoidal bar checks with the analytical solution for the exponentially shaped bar. The advantage of the exponential shape lies in the fact that the differential equation is easily solved. As a matter of fact if the two contours are superimposed on a drawing, the difference is very small. In equation 9, we let the width at the bottom be W_0. At the opening where x is equal to d, the width is W_d. Then at any level,

$$W = W_0\epsilon^{-2ax}; \text{ where } ad = {}^1/_2\log_\epsilon(W_0/W_d) \quad (9)$$

The values of (ad) are shown for convenience in Table I.

When the value of W from equation 9 is substituted into equation 4, the result is that given in equation 10.

$$d\boldsymbol{Z}/dx = (jf/5W_0)(\epsilon^{2ax}) - (\boldsymbol{Z}^2)(F/\rho)(\epsilon^{-2ax}) \quad (10)$$

The detailed work in solving equation 10 is given in Appendix I. The result is

$$\boldsymbol{Z} = (\rho/W_0F)(\epsilon^{2ax})(\boldsymbol{K}\coth(\boldsymbol{K}x) - a); \quad \text{where } \boldsymbol{K}^2 = a^2 + j(fF/5\rho) \quad (11)$$

The correctness of the solution is easily verified by substitution.

Equation 11 gives the impedance of the bar at any level. The impedance of the whole bar is that at level x equal to d. Equation 11 then becomes equation 12.

$$\boldsymbol{Z}_d = (\rho/W_dF)[\boldsymbol{K}\coth(\boldsymbol{K}d) - a] \quad (12)$$

As an additional check on the correctness of the solution, note that if a is zero the bar is rectangular and the solution becomes identical with Field's equation. Since the hyperbolic cotangent of a complex number is not a tabulated function, it is more convenient to use equation 13.

$$\boldsymbol{Z}_d = (\rho/W_dF)\times\left(-a + \boldsymbol{K}\left(\frac{\sinh(2P) - j\sin(2Q)}{\cosh(2P) - \cos(2Q)}\right)\right) \quad (13)$$

where

$$P + jQ = \boldsymbol{K}d \quad (14)$$

In the running range, with small slips, it is more convenient to expand equation 12 as a power series, in which case equation 15 is:

$$\boldsymbol{Z}_d = (\rho/W_dFd)[1 - ad + (\boldsymbol{K}d)^2/3 - (\boldsymbol{K}d)^4/45 - \ldots] \quad (15)$$

The terms in ascending powers of $(\boldsymbol{K}d)$ form a series in powers of the slip frequency. In the running range we need consider only terms that are constant or vary as the first power of the slip. Using the subscript (r) to mark running constants, equations 16 and 17 result.

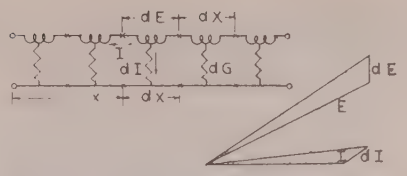

Figure 2. Equivalent circuit and vector diagram for a deep-bar rotor

$$R_r = (\rho/dFW_d)[1 - ad + (ad)^2/3 - (ad)^4/45 \ldots] \quad (16)$$

$$X_r = (d/3W_d)(f/5)[1 - 2(ad)^2/15 + 2(ad)^4/105 \ldots] \quad (17)$$

At starting for a 60-cycle motor, and with bars 1-inch deep, the hyperbolic cotangent is approximately unity. Equation 18 is suggested as convenient for rapid and approximate calculations. The subscript (s) is used to mark starting constants.

$$\boldsymbol{Z}_s = (\rho/FW_d)[-a + (fF/10)({}^1/_2 1 + j1)] \quad (18)$$

P. L. Alger,[3] in an important article points out that motor performance depends on the relations between the starting and running constants. It will, therefore, be of interest to show these relations, for the tapered bar. By combining the above equations, equations 19, 20, and 21 are obtained. In these equations the subscripts r and s are used as above.

$$R_r/X_r = (15\rho/fFd^2)[1 - ad + 7(ad)^2/15 \ldots] \quad (19)$$

$$X_r/X_s = (2d/3)(\rho fF/10)^{1/2}[1 - 2(ad)^2/15 \ldots] \quad (20)$$

$$X_s - R_s = (a\rho/FW_d) \quad (21)$$

The important results are:

1. The ratio of running to starting reactance is controlled by selecting a proper depth of slot.

2. The ratio of resistance to reactance when running is controlled by proper choice of taper.

3. The proper running reactance is controlled by choosing the proper slot opening.

4. The starting resistance is less than the starting reactance.

5. The tapered bar alone cannot meet NEMA design type C specifications, since these require generally that R_s be $> X_s$.

Table I. Slot Constant (ad) for Tapered Slot in Terms of Taper

(W_0/W_d)	1.500	1.600	1.700	1.800	1.900	2.000	2.100	2.200
(ad)	0.204	0.235	0.265	0.295	0.320	0.348	0.370	0.395

Compound Bar with Tapered Section at the Bottom and Enlarged at the Top

Figure 3 shows a bar in which the lower, and major, part is tapered exponentially, and with a minor part at the slot opening of enlarged width. The impedance of the lower part may be computed by equation 13 or by equations 16 and 17. This impedance will be termed ($\boldsymbol{Z}_1$). The upper portion will be considered to consist of a reactance ΔX, and a conductance ΔG arranged as in Figure 2. The problem considered here is that of computing the change in the impedance, $\Delta \boldsymbol{Z}$, caused by the small enlarged section. The computation is made by means of equation 7 which is here rewritten as equation 21.

$$\Delta \boldsymbol{Z} = \left(\frac{j\Delta X - (\boldsymbol{Z}^2)\Delta G}{1 + \boldsymbol{Z}\Delta G} \right) \qquad (21)$$

The increments in X and G may be computed from the width, W_2, and the depth, d_2, of the small upper part. If we take the crude assumption of straight lines of force, ΔG is equal to $(W_2 d_2/\rho)$, and ΔX is equal to $(f/5)\ (W_2/d_2)$. A somewhat better procedure would be to make a flux map for the purpose of estimating ΔP and ΔX.

It is desirable at this point to examine equation 21 in more detail in order to prove that $\Delta \boldsymbol{Z}$ is chiefly a decrease in the reactance of the compound bar. In discussion of equation 21 we first note that the bar is small, and that the denominator of the fraction is nearly unity. In the second place we note that in the phasor $\boldsymbol{Z}$, the resistance component is approximately 85 per cent of the reactance component. Thus when an expression like $(0.85 \pm j1.00)$ is squared, the result is $(-0.28 \pm j1.70)$ and we may say that the numerator consists chiefly of changes in reactance. In the third place we note that in the numerator the first term is considerably smaller than the second term, when there is an increase in the width of the bar, as in this case. If W_2 is twice W_d, then the value of ΔX is one quarter of the value of $(\boldsymbol{Z})^2 \Delta G$, so that the numerator is negative and the change in $\boldsymbol{Z}$ is a decrease in reactance.

Compound Bar with Tapered Section at the Top, Known Impedance at the Bottom of the Slot

Figure 4 shows a bar with a smaller lower part of expanding width, and a larger upper portion with an exponentially tapered shape. Such a bar will not show materially different properties, than

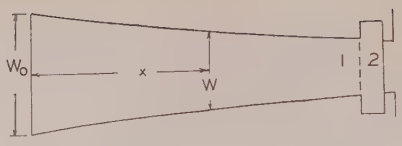

Figure 3. Compound tapered bar with an enlarged slot opening

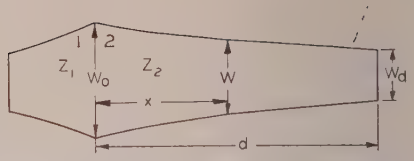

Figure 4. Compound bar with two tapered portions, (1) diverging, (2) converging

that of the simple bar; but it might be useful in avoiding saturation in the rotor teeth. Equation 13 may be used to find the impedances $\boldsymbol{Z}_1$ and $\boldsymbol{Z}_2$ of the two parts of the bar assuming that they are acting independently. The impedance of the whole bar $\boldsymbol{Z}_{12}$ may be found by equation 23.

$$\boldsymbol{Z}_{12} = \left(\frac{\boldsymbol{Z}_1\boldsymbol{Z}_2 + j(f\rho/FW_0W_d)}{\boldsymbol{Z}_1 + \boldsymbol{Z}_2(W_d/W_0) + 2a(\rho/W_0F)} \right) \qquad (23)$$

The extended proof is given in the Appendix I. A simple check on the correctness of equation 23 is to note that it agrees with Putnam's formula when the constant, a, equals zero and W_d equals W_0.

Tabular and Graphical Solution for a Round Bar

The bar shown in Figure 5 was selected as an illustration of the method of tabular and graphical integration using equation 8. The bar in the figure is a compound bar, and the impedance of the whole bar can be found by Putnam's formula if the impedance of the circular portion can be found. The bar chosen had a circular part of 0.5-inch diameter, and a rectangular part of 0.125 inch in width. Copper with a space factor of 0.99 was assumed.

Figure 5 shows a series of lines of force obtained by field methods. Between the points O and P they are orthogonal circles. Between the points P and Q they are nearly circles and straight lines. The several zones were computed or estimated to have permeances of 0.1 geometric unit. Zones 1 and 17 were estimated by special methods to have permeances of 0.16 and 0.13 respectively. The areas of the several zones were computed and are entered in Table II in units of 0.001 square inch.

In computing Y in units of 10^5 mho, (F/ρ) was taken as 12 and $(f/5)$ as 1.2. The complete calculations are given in Table III. The calculations for the 10th zone are shown here. Start with Y_9 of $1.159 - j0.196$.

$$\boldsymbol{Y} = \left(\frac{12(0.0265) - (1.159 - j0.196)^2(j0.12)}{1 + j(0.12)(1.159 - j0.196)} \right)$$
$$= 0.261 - j0.172$$

The tenth value of Y is the sum of this figure and the ninth value of Y. When the value of Y at the end of the 17th zone is converted into an impedance we have;

$\boldsymbol{Z}_{17} = 5.1 + j8.1$ microhms per inch

A similar analysis for running constants disclosed a running reactance of 8.7 microhms per inch of stacking corresponding to a slot constant of 0.72.

Figure 5 also shows the parameters x and θ. In the zones where the lines of force are orthogonal circles, equations 23, 24, and 25 aid in drawing the lines so as to enclose zones of equal permeance and finding the areas.

$$P = 0.319 \log_e (1-x)/(1-x) \qquad (23)$$

$$x = R(\sec\theta - \tan\theta) \qquad (24)$$

$$A = R^2(\theta + (1.57 - \theta)\tan^2\theta - \tan\theta) \qquad (25)$$

A similar calculation was made for a trapezoidal bar confirming the accuracy of the use of an equivalent bar with exponential taper. This method can be used for bars of any shape. It should be used wherever a sudden change in width occurs.

Illustrative Examples

In the numerical examples chosen, it was assumed that the simplified equivalent electric circuit is reliable for computing torque and current, if the proper ratio of transformation is used. It is understood that this includes a term obtained by the use of Thevinin's theorem. It was assumed that by the choice of the number of slots, conductors per slot and other factors the microhm values could be changed into per-unit values, and so that the running reactance of the rotor was made 12 per cent. It was also assumed that the stator impedance was $3 + j9.3$ per cent.

Table II. Areas of Zones of Permeance for a Circular Slot

Zone	1	2	3	4	5	6	7	8	9	14	15	16	17
Zone A	13	12	11	10									
	2.24	1.79	2.98	5.39	8.12	11.9	17.7	21.6	26.5	8.50	5.31	3.44	2.80

Table III. Calculations of the Admittance of a Round Rotor Bar

Zone	ΔX	ΔG	$(1+j+\frac{1}{2}Y\Delta X)$	ΔY	Y
1	0.19	0.027	$1.000+j0.000$	$0.027-j0.0000$	$0.027-j0.0000$
2	0.12	0.021	$1.000+j0.002$	$0.021-j0.0002$	$0.048-j0.0002$
3	0.12	0.036	$1.000+j0.003$	$0.036-j0.0004$	$0.084-j0.0006$
4	0.12	0.065	$1.000+j0.005$	$0.065-j0.0011$	$0.149-j0.0017$
5	0.12	0.098	$1.000+j0.009$	$0.098-j0.0035$	$0.247-j0.0052$
6	0.12	0.143	$1.000+j0.016$	$0.142-j0.010$	$0.389-j0.015$
7	0.12	0.212	$1.000+j0.023$	$0.224-j0.023$	$0.613-j0.038$
8	0.12	0.260	$1.000+j0.037$	$0.252-j0.054$	$0.865-j0.092$
9	0.12	0.318	$1.006+j0.052$	$0.294-j0.104$	$1.159-j0.196$
10	0.12	0.318	$1.012+j0.070$	$0.261-j0.172$	$1.419-j0.362$
11	0.12	0.260	$1.022+j0.085$	$0.114-j0.231$	$1.533-j0.599$
12	0.12	0.212	$1.036+j0.092$	$-0.011-j0.229$	$1.522-j0.828$
13	0.12	0.143	$1.049+j0.091$	$-0.167-j0.173$	$1.355-j1.001$
14	0.12	0.102	$1.060+j0.081$	$-0.216-j0.082$	$1.137-j1.083$
15	0.12	0.064	$1.067+j0.068$	$-0.225+j0.008$	$0.912-j1.075$
16	0.12	0.041	$1.064+j0.055$	$-0.178+j0.044$	$0.734-j1.030$
17	0.16	0.036	$1.061+j0.044$	$-0.177+j0.139$	$0.557-j0.891$

In the table the values of Y are in units of 10^5 mhos. The column marked ΔX is 1.2 times ΔP in these units. The values in the column marked ΔG is 0.012 times the value of ΔA as shown in Table II.

In the first example a bar 0.9 inch deep with a taper of 1.8 and a slot opening of 0.08 inch was chosen. A space factor of 0.93, a frequency of 60 cycles, and a resistivity of 0.83 microhm per inch cube were assumed. Equations 16 and 17 were used to find the running constants, and equation 14 was used to find the starting constants. The constants were computed and entered in Table IV.

In estimating performance an end ring resistance of 0.25 per cent was assumed, and a magnetizing current of 60 per cent was used. On this basis the computed full load slip was 3 per cent, the breakdown torque was 200 per cent, the starting torque 175 per cent with a current of 5.5 times unit current.

In a second numerical example a compound bar similar to Figure 4 was taken. The lower part was of the same depth and taper as in the first example. The width, however, of the slot opening was changed to make the percentage values of running and starting constants 1.08 times as great as those listed in Table IV. The upper part of the bar was assumed to have 40 per cent resistance and 1 per cent reactance.

The end-ring resistance was taken as 0.35 per cent, the magnetizing current as 60 per cent, the stator impedance as $3+j10.1$ per cent. The slip and breakdown torque computed to the same as before, but the computed starting torque was 202 per cent with a starting current of 5.6 times the unit current. The result is so close to NEMA design type c specifications, that the problem is recommended for further study. Without doubt with some other taper, some other slot depth, and other upper portion of the bar, these specifications can be met.

Appendix I. Analysis of the Impedance of Bars with Tapered Section

In the detailed analysis, equation 10 is abbreviated to read

$$d\boldsymbol{Z}/dx = j(f/5W_0)(\epsilon^{2ax}) - \boldsymbol{Z}^2(FW_0/\rho)(\epsilon^{-2ax}) = \boldsymbol{B}\epsilon^{2ax} - A\boldsymbol{Z}^2\epsilon^{-2ax} \quad (26)$$

The substitution of $\boldsymbol{y}\epsilon^{2ax}$ for $\boldsymbol{Z}$ gives the simpler equation 27

$$d\boldsymbol{y}/dx + 2a\boldsymbol{y} + \boldsymbol{y}^2A = \boldsymbol{B} \quad (27)$$

The substitution of $(v-a)/(A)$ for y gives the still simpler equation,

$$d\boldsymbol{v}/dx + \boldsymbol{v}^2 = A\boldsymbol{B} + a^2 = \boldsymbol{K}^2 \quad (28)$$

This equation is of the first order first degree with variables that are easily separated. A very convenient and most general form of the solution is equation 29

$$\boldsymbol{v} = \left(\frac{c\boldsymbol{K}\ \coth\ (\boldsymbol{K}x) + \boldsymbol{K}^2}{\boldsymbol{K}\coth\,(\boldsymbol{K}x) + c}\right) \quad (29)$$

When the variable v is changed back to Z, this equation becomes

$$\boldsymbol{Z} = (\epsilon^{2ax})(1/A)\times \left(\frac{(c-a)(\boldsymbol{K})\coth(\boldsymbol{K}x) + \boldsymbol{K}^2 - ac}{\boldsymbol{K}\coth\,(\boldsymbol{K}x) + c}\right) \quad (30)$$

Table IV. Comparison of Rotor Constants for a Tapered Bar

Constant	Microhms per Inch Running	Starting	Increase	Percentage Values Running	Starting	Ratio of Starting to Running Value
(R)	9.05	24.70	15.65	2.44	6.74	
(X)	44.5	29.2	—15.3	12.0	7.97	0.66
(R/X)				20.3	84.6	

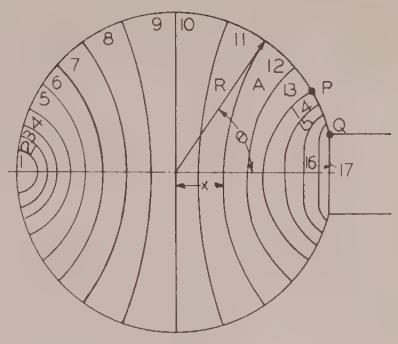

Figure 5. Circular bar divided into zones of equal permeance

The constant c is determined from the boundary conditions. Thus for a simple bar, as x approaches 0, $\boldsymbol{Z}$ approaches infinity, c becomes a very large number and equation 30 becomes

$$\boldsymbol{Z} = (\epsilon^{2ax}/A)(\boldsymbol{K}\coth(\boldsymbol{K}x) - a) \quad (31)$$

On the other hand, with a compound conductor, and an impedance of Z_1 when x approaches zero, we let the term $(c-a)/A$ equal to $\boldsymbol{Z}_1$ obtaining equation (32).

$$\boldsymbol{Z}_{12} = \left(\frac{\boldsymbol{Z}_1\boldsymbol{Z}_2 + (B/A)\epsilon^{2ax}}{\boldsymbol{Z}_1 + \boldsymbol{Z}_2\epsilon^{-2ax} + 2a/A}\right) \quad (32)$$

Next the constants B and A are replaced by the values in equation 26. The expression (ϵ^{2ax}) is replaced by its equivalent (W_0/W_d). These steps result in equation 33.

$$\boldsymbol{Z}_{12} = \left(\frac{\boldsymbol{Z}_1\boldsymbol{Z}_2 + j(f\rho/5FW_0W_d)}{\boldsymbol{Z}_1 + \boldsymbol{Z}_2(W_d/W_0) + 2a\rho/FW_0}\right) \quad (33)$$

Equations 31 and 33 are equations 12 and 22 in the main part of the paper.

Appendix II. A Graphic Interpretation of Skin Effect

At 60 cycles in copper the penetration of current in estimating resistance is 0.38 inch. In estimating reactance the penetration may be taken as 50 per cent greater. Thus in Figure 7 is depicted a tapered slot and conductor in cross section. The trapezoid (A) enclosed by a dotted line, will check equation 18 very closely, as to the resistance. The rectangle (B) will check equation 18 very closely as to the reactance. Actually the current is present all over the slot, but with a density decreasing rapidly toward the bottom of the slot.

Appendix III. Note on the Equivalent Circuit of the Deep Bar Motor

Attention is called to the fact that the "Tee" equivalent circuit used in Figure 2 is substantially the same as that used in reference 4. For an infinitesimal layer it does not matter whether the "Tee," "Pi" or

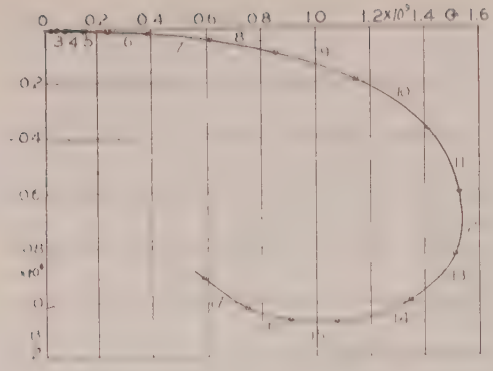

Figure 6 (left). Locus of admittance vector at different levels in a circular slot

Figure 7 (right). Graphic representation of skin effect in a tapered bar, (A) resistance, (B) reactance

"Ell" section is used. For the small finite layer it is to be noted that equations 7 and 8 depend on the calculus of finite differences. Equations 7 and 8 can be used up to 0.1 inch without serious error. It is to be noted further that Putnam's formula can be put into a very useful form that can be used for still larger increments in (dx). This modified Putnam formula is:

$$\Delta Z \left(\frac{j\Delta X - \mathbf{Z}_1^2 \Delta G}{1 + \mathbf{Z}_1 \Delta G + j(1/3)(\Delta X \Delta G) - (1/45)(\Delta X \Delta G)^2 \ldots} \right)$$

It is to be noted that some of the terms in the denominator are the series expansion of $(K\Delta x)\coth(K\Delta x)$. It can, therefore, be carried as far as desired. The series converges rapidly if Δx is 0.2 inch, somewhat more slowly when Δx is 0.4 inch. For depths of 1 inch, it is much easier to use the hyperbolic function.

Appendix IV. List of Symbols Used in the Paper

A = area in square inches
B = an area shown in Figure 7
d = slot depth in inches
E = EMF in micro-volts
f = frequency in cycles per second
F = space factor
G = conductance in mega-mhos
I = current in amperes
K = a constant
P = permeance
P = a constant
Q = a constant
R = a radius in inches
R = resistance in microhms
v = an auxiliary variable
W = width of slot in inches
x = distance of a layer from the origin

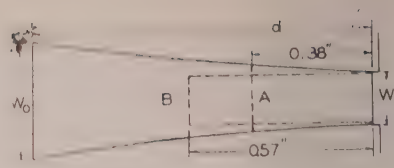

X = reactance in microhms
y = an auxiliary variable
Y = admittance in mega-mhos
Z = impedance in microhms
Δ = finite increment in :
μ = permeability of air 3.19
ρ = resistivity
θ = an angle

Subscripts

o At level, x = 0
d At level, x = d
1 In lower part of conductor
2 In upper part of conductor

References

1. Eddy Currents in Large Slot Wound Conductors, **A. B. Field.** *AIEE Transactions*, volume 24, 1905, pages 761–88.

2. Starting Performance of Synchronous Motors, **H. V. Putnam.** *AIEE Transactions*, volume 46, 1927, pages 39–59.

3. The Development of Low-Starting Current Induction Motors, **P. L. Alger.** *General Electric Review* (Schenectady, N. Y.), July 1925, pages 499–508.

4. Circuit Analysis Method for Determining A-C Impedances of Machine Conductors, **D. S. Babb, J. E. Williams.** *AIEE Transactions*, volume 70, part I, 1951, pages 661–666

No Discussion

Split-Winding Starting of 3-Phase Motors

P. L. ALGER
FELLOW AIEE

H. C. WARD, Jr.
ASSOCIATE AIEE

F. H. WRIGHT
NONMEMBER AIEE

Synopsis: In this paper there is presented a new method of normal voltage reduced current starting for induction motors. The scheme consists in connecting one phase of a 3-phase winding in series during the starting period only, the other phases having circuits in parallel. When full speed is attained, the series connected winding is opened momentarily, and then put back on the line in parallel. This gives the advantages of reduced current without any current surge on reclosing, no external impedance, and a low cost of control. It provides about half torque with two-thirds average current, as compared to full voltage starting; it gives a smooth torque curve on the Y connection, and only a small one-third speed torque dip on delta connection; and it allows about 50 per cent greater stalled time than on full voltage. Although this type of connection will draw unbalanced line currents, this appears unimportant. In most cases there will be other machines on the line to act as phase balancers and absorb the relatively small negative sequence current. Formulas are given for currents and torque with and without external impedances. Formulas are in terms of voltage and forward, backward, and zero phase sequence impedances.

METHODS of reduced current starting fall into two general classifications: (1) those where the stator windings are merely reconnected, and (2) those where part of the stator windings are omitted. The delta-Y method and the use of taps on the stator winding belong to the former classification, while the various "part-winding" methods belong to the latter.

Where starting torque is of minor importance, and it is desired to keep the starting current low, the delta-Y method is often used abroad. Although the starting current is low, one-third normal, the starting torque is also only one-third normal. Also, there is a current surge when the circuits are reclosed on the running connection. In many applications where more starting torque is required and more starting current can be tolerated, this method cannot be used because of the fixed relationship between delta and Y circuits.

Some attempts to circumvent these limitations have been made by putting taps on the stator winding, the winding acting as an autotransformer, but this entails added expense in winding the motor and for control, and also introduces undesirable air gap flux harmonics, with consequent torque dips.

In the usual part-winding scheme, the windings are connected with two or more parallel circuits in each phase on the running connection, one or more of the circuits being left open on the starting connection. If there is a large number of poles, the remaining circuits and their opposing rotor sectors give an approximately normal performance with torque and current proportional to the ratio of the utilized to the total number of circuits. With few poles, and a small air gap, however, as in nearly all induction machines, the "end effects" due to the omitted circuits markedly increase the current and decrease the effective torque. That is, there are large unwanted harmonics in the air gap flux wave, which produce asynchronous crawling, or torque dips. If the windings are arranged to minimize these harmonics, a large unbalanced magnetic pull on the shaft may be created.

Whenever the number of omitted coils is not the same for adjacent poles, even harmonics are introduced. Subharmonic fields also are introduced when successive pairs of poles have different numbers of omitted coils. Thus, when starting motors with small air gaps by these general methods, it is preferable to reconnect, rather than omit, sections of the windings.

The new method that is here proposed has the advantage of using all of the windings throughout the entire starting period, and in addition has no current surge on transferring to the normal run position. It gives about 80 per cent of normal torque per ampere. The proposed starting method may be used for low voltage starting on any dual voltage 3-phase motor, having nine leads brought out, if delta, or 11 leads brought out if wye. The standard Y-connected motor usually has only nine leads brought out and hence cannot be reconnected strictly wye. However, the reconnection can be made without bringing the neutral out in such a manner that the results are almost identical to those had the neutral been brought out. Figure 1 shows the starting connections and the normal run connections for the delta and both Y windings.

Results

For a delta-connected motor, the line currents are:

$$I_1 = \frac{E}{6K^2ZZ_0}[(K+2)^2+Z_0+2(K-1)^2Z+ j3K^2Z_0\sqrt{3}] \quad (1)$$

$$I_2 = \frac{-jE\sqrt{3}}{2} \quad (2)$$

$$I_3 = \frac{-E}{6K+ZZ_0}[(K+2)^2Z_0+2(K-1)^2Z- j3K^2Z_0\sqrt{3}] \quad (3)$$

and the ratio of the locked rotor torque to the torque with the running connection is:

$$T/T_n = \frac{(2+K)}{3K} \quad (4)$$

Paper 51-160, recommended by the AIEE Rotating Machinery committee and approved by the AIEE Technical Program Committee for presentation at the AIEE Great Lakes District Meeting, Madison, Wis., May 17-19, 1951. Manuscript submitted February 16, 1951; made available for printing April 16, 1951.

P. L. ALGER, H. C. WARD, JR., and F. H. WRIGHT are all with the General Electric Company, Schenectady, N. Y.

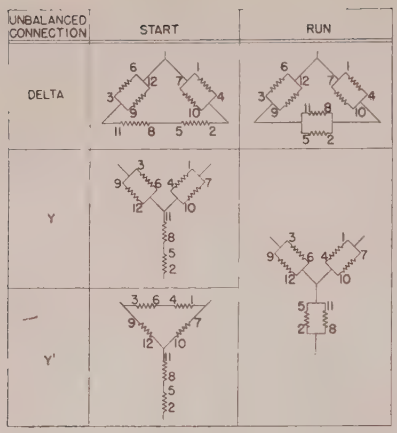

Figure 1. Connections for split winding starting of 3-phase motors

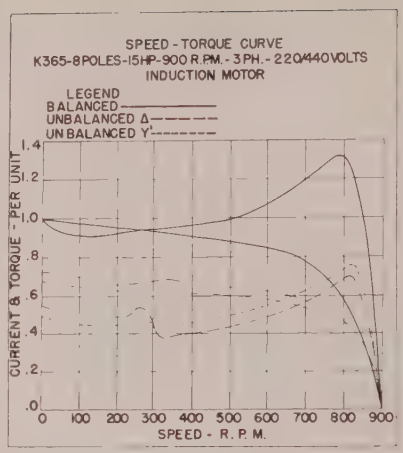

Figure 2. Speed-torque curves with split winding starting

For the Y-connected motor, the line currents are:

$$I_1=\frac{9E}{N} \tag{5}$$

$$I_2=\frac{-9E}{2N}-j\frac{E\sqrt{3}}{2Z} \tag{6}$$

$$I_3=\frac{-9E}{2N}+j\frac{E\sqrt{3}}{2Z} \tag{7}$$

and the torque ratio is:

$$T/T_n=\frac{3(2K+1)Z}{N}$$

where

$N=(2K+1)^2Z+2(K-1)^2Z_0$

E = line voltage

Z = symmetrical stator impedance at standstill per phase, referred to normal turns

Z_0 = zero phase sequence stator impedance at standstill per phase, referred to normal turns

K = ratio of the number of turns in series of the unbalanced phase to the number of turns in series on a normal balanced phase. Normal values of current and torque are obtained by letting $K=1$ in the above expressions. The most usual case is $K=2$, representing a normal 2 circuit winding connected with the two circuits of one phase in series for starting. K is 1.5 for a motor with one phase of the winding divided into two series connected halves, one half consisting of two circuits in series, and the other of two circuits in parallel; while the other two phases have two circuits in parallel throughout

The positive and negative phase sequence line currents for the delta connection are:

$$I_f=\frac{E\sqrt{3}}{9K^2ZZ_0}[(5K^2+2K+2)Z_0+(K-1)^2Z] \tag{8}$$

$$I_b=\frac{E\sqrt{3}}{9K^2ZZ_0}[K-1][2(2K+1)Z_0-(K-1)Z] \tag{9}$$

and, for the Y connection:

$$I_f=\frac{9E}{2N}+\frac{E}{2Z} \tag{10}$$

$$I_b=\frac{9E}{2N}-\frac{E}{2Z} \tag{11}$$

Table I gives the ratios of locked rotor currents and torques on the starting connection to normal (running connection) values, calculated by the foregoing formulas. Table II gives corresponding test values for a number of motors.

Heating

For the delta case, $K=2$, the locked rotor current density in the stator winding is 0.87 of normal in two phases, and is much reduced in the third. Hence, the permissible stalled time is about 1.5 times that for the normal connection so far as the stator is concerned. For the Y case, with $K=2$, the greatest current density is about 0.8 of normal, so that the permissible stalled time is about 1.8 times normal. For both cases, the rotor heating, with $K=2$, is about 75 per cent of normal, giving an allowable stalled time of about 1.5 times normal, so far as the rotor is concerned. This nearly corresponds to the increased starting time required with the 0.6 available starting torque. Thus, the standard thermal overload relays will adequately protect a motor with split winding starting.

On the other hand, the part-winding scheme, using only half of the stator circuits for the starting connection, draws about 0.7 of normal starting current, flowing in half the normal copper section, giving about twice the normal heating rate. Also, the localized rotor heating, at standstill, is not far below normal, while the accelerating torque is greatly reduced. Hence, the standard thermal overload relays will not adequately protect a motor with part-winding starting, unless the motor is thrown over almost immediately to the running connection. The low accelerating torque due to asynchronous crawling tendencies will often require this at any rate. For an induction motor with few poles and a small air gap, therefore, the part-winding scheme is really a step-starting method, drawing the full locked rotor current of the standard motor, but taking it in two steps. A timing relay is required to assure the

Table I. Starting Performance with Split Winding Connection

Turn Ratio of Phase A, K	Current Ratios I_{BC}	I_{AB}	I_{CA}	I_{av}	I_f	I_b	Torque Ratio
Delta Winding $Z_0=Z/2$							
1	1	1.000	1.000	1.000	1.000		1.000
1.5	1	0.755	0.755	0.837	0.827	0.173	0.778
2	1	0.694	0.694	0.796	0.778	0.222	0.667
∞	1	0.680	0.680	0.787	0.778	0.222	0.333
Delta Winding, $Z_0=Z/4$							
1	1	1.000	1.000	1.000	1.000		1.000
1.5	1	0.787	0.787	0.858	0.852	0.148	0.778
2	1	0.764	0.764	0.843	0.833	0.167	0.667
∞	1	1.000	1.000	1.000	1.000		0.333

Turn Ratio of Phase A, K	I_A	I_B	I_C	I_{av}	I_f	I_b	Torque Ratio
Wye Winding, $Z_0=Z/2$							
1	1.000	1.000	1.000	1.000	1.000		1.000
1.5	0.554	0.910	0.910	0.791	0.777	0.223	0.739
2	0.346	0.883	0.883	0.704	0.673	0.327	0.577
∞	0.866	0.866	0.577	0.500	0.500		
Wye Winding, $Z_0=0$							
1	1.000	1.000	1.000	1.000	1.000		1.000
1.5	0.562	0.911	0.911	0.795	0.781	0.219	0.750
2	0.360	0.884	0.884	0.709	0.680	0.320	0.600
∞	0.866	0.866	0.577	0.500	0.500		

Table II. Locked Rotor Test Values with Split Windings

Motor*	Winding Connection	K	Locked Rotor Current Ratio				Locked Rotor Torque Ratio	Relative Torque/Amp
			I_1	I_2	I_3	I_{av}		
A	Delta	2.0	1.02	0.79	0.72	0.85	0.67	0.79
B	Delta	2.0	1.02	0.83	0.68	0.84	0.66	0.78
C	Delta	2.0	0.99	0.79	0.69	0.82	0.69	0.85
E	Delta	2.0	1.01	0.863	0.747	0.845	0.628	0.74
G	Delta	2.0	0.875	0.635	0.63	0.71	0.56	0.79
D	Y	1.5	0.92	0.92	0.53	0.79	0.64	0.81
D	Y	2.0	0.84	0.84	0.33	0.67	0.50	0.75
E	Y	2.0	0.80	0.82	0.36	0.66	0.57	0.87
F	Y	2.0	0.82	0.84	0.34	0.67	0.53	0.79
G	Y	2.0	0.82	0.815	0.337	0.657	0.50	0.76
G	Y'		0.845	0.835	0.338	0.673	0.52	0.775

*Motor A 4 pole, 30 hp, 1,800 rpm, 3-Phase—220/440 v.—Standard
Motor B 4 pole, 30 hp, 1,800 rpm, 3-Phase—220/440 v.—Special Rotor
Motor C 4 pole, 30 hp, 1,800 rpm, 3-Phase—220/440 b—Special Rotor
Motor D 4 pole, 30 hp, 1,800 rpm, 3-Phase—220/440 v.—Special Rotor
Motor E 4 pole, 40 hp, 1,800 rpm, 3-Phase—220/440 v.
Motor F 4 pole, 3 hp, 1,800 rpm, 3-Phase—220/440 v.
Motor G 8 pole, 15 hp 900 rpm, 3-Phase—220/440 v.

prompt execution of the starting sequence.

Control

Figure 3 shows the contactors required for the split winding method. One normally open and two normally closed contactors of reduced capacity are required, in addition to the usual three contactors of full rating. This is not a standard combination, and, therefore, its cost is somewhat higher, and its availability is less than for the standard motor control. The part-winding scheme usually employs two duplicate sets of three contactors of half rating. However, since the motor draws about 0.7 current on the first step, this means that the initially closed contactors must carry 140 per cent of their ostensible rating.

If it is desired to reduce the split winding starting currents below those given, a small impedance may be added in series with the B and C phases, together with two normally closed contactors to short-circuit them in the running connection. In this way, a wide range of starting torque and current values may be obtained, and two or more steps in the starting procedure may be used; corresponding to the use of two or more taps on the autotransformer in the compensator method of starting. Or, very low current can be obtained by initially connecting two of the phases in series, and making the starting sequence consist of two steps.

It should be noted that each of these methods of reducing the locked rotor current will reduce it a little more than indicated by the formulas, because of the reduced magnetic saturation of the leakage flux paths in the motor.

Current Surges

With the split winding method, the transfer to running connection is made by opening, reconnecting, and reclosing one phase, leaving the other two phases on the lines. During the transition, the motor operates on single phase. Since the single-phase torque at full speed is ample to supply any normal load requirement, there will be no drop in speed and no appreciable current surge when the motor is reconnected. With the part-winding scheme, also, the motor is permanently connected to the line, and there is no current surge on transfer. Other schemes, such as the Y-delta or the compensator method normally require that the motor be disconnected during the transfer to running connections, allowing the motor to fall back in speed. Consequently, there may be a high current surge on reclosing, of magnitude comparable to the locked rotor current at full voltage. The resulting momentary voltage dip causes light flicker, and is particularly objectionable where television sets are connected to the circuit.

Unbalance

The split winding method, with $K=2$, draws a negative phase sequence current from the system, equal to 0.2 to 0.3 of the normal full voltage starting current. Other motors (running) on the system have a much lower negative than positive phase sequence impedance, so that they will contribute materially to the supply of this current. Thus, the degree of unbalance in the currents supplied by the power system will be less the larger the proportion of connected live load, and will be small at points distant from the motor being started. Also, the normally balanced impedances in the power lines, when added to the unbalanced motor impedances, will make the total impedance, and, therefore, the actual starting currents, more nearly balanced than for the motor alone. The same cause, high line impedance, that makes voltage flicker objectionable, acts to reduce the unbalance in the line currents, and so makes the flicker more nearly uniform on all phases. Still further improvement can be obtained, as noted above, by adding small series impedances during the starting period, and shorting them out at speed.

It is probable, therefore, that the effective amount of voltage disturbance, or light flicker, will be in proportion to the positive phase sequence currents alone. If there are lights connected on all three phases of the power system, the average rather than the maximum drop in voltage will matter. If only one phase of the system in the vicinity of the motor has connected lights, the motor may be so connected that this particular phase supplies the minimum starting current. Thus, the possibility of connecting the high current motor lead to the power line, whose voltage is least important, ought to fully offset any disadvantage there may be due to the current unbalance.

Comparison with Reactor Starting

Figure 6 shows comparative locked rotor torque and current values for a Y-connected split winding motor ($K = 2$) and for a similar motor with reactor starting. Z_0 is taken equal to $Z/2$. The curves for the split winding motor show the effects of including a reactor in series with each of the normal phases (two reactors in all). The results are summarized in Table III.

The split winding, with no external reactance, gives the same positive sequence current, and about 1.25 times the torque, obtained when reactors are used totalling 2/9 the normal motor locked

Table III

Method	Reactor Impedance/Phase	Ratio to Normal Locked Rotor Values: Positive Phase Sequence Torque	Positive Phase Sequence Current	Torque/Ampere
Split winding	0	0.58	0.67	0.86
Reactor	0.49	0.45	0.67	0.67
Reactor	0.32	0.58	0.76	0.76
Split winding	0.24	0.45	0.57	0.79

rotor kilovolt ampere. The split winding requires the same number of additional contactors, but of smaller size. Thus, the split winding scheme is preferable to the reactor method of starting in all respects except the unbalance of the starting currents, and the requirement for bringing out at least five instead of only three leads.

Conclusions

It is concluded, therefore, that the split winding method of starting with $K = 2$ gives fully comparable performance to the usual compensator method with an 80 to 85 per cent tap. It has the advantages of no current surge on transition from starting to running connection, of requiring less equipment, and an ultimately lower cost. The method may be applied to any dual voltage motor having nine leads brought out. Single voltage motors especially built for this method will require only five leads brought out.

As compared to the part-winding method of starting, it has the important advantages of smooth starting on the first position, no current surge on transfer to running position, and adequate thermal capacity.

The split-winding method is especially adapted to cases where "soft" starting is desired, without any sudden torque peaks.

As compared to the reactor method of starting, the split-winding gives greater torque per ampere and requires less equipment and smaller size auxiliary contactors.

Appendix

Consider a delta-connected 3-phase motor, as shown in Figure 4, having K times as many turns in phase A as in phases B or C.

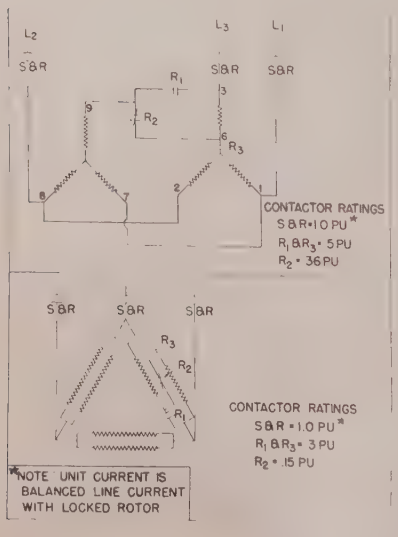

A small impedance, z, is connected in series with each of the B and C phases. Let:

I_A, I_B, I_C = actual phase currents

E_A, E_B, E_C = actual phase voltages

Z_1 = 3-phase impedance of stator per phase, with normal (unit) winding turns

Z_f, Z_b = forward and backward,* 3-phase impedances of rotor and the parallel magnetizing circuit, referred to normal winding turns

z = external impedance in B and C phases

K = ratio of A phase series turns to normal (B and C phase) series turns

Z_0 = zero phase sequence stator impedance per phase, with normal winding turns

Then, the line to neutral impedance of a normal phase, considered alone, is:

$$\frac{2Z_1 + Z_0}{3}$$

and the mutual reactance between any two normal phases is

$$\frac{1}{3}(Z_0 - Z_1)$$

The impressed phase voltages, assumed balanced, are taken to be:

$$E_A = E \tag{12}$$

$$E_B = E/\underline{240} = E(-0.5 - j0.866) \tag{13}$$

$$E_C = E/\underline{120} = E(-0.5 + j0.866) \tag{14}$$

For the winding of Figure 4, the current voltage relations are:

$$3E_A K = K(2Z_1 + Z_0)I_A + (Z_0 - Z_1)I_B + (Z_0 - Z_1)I_C + 3E_A'/K \tag{15}$$

$$3E_B = K(Z_0 - Z_1)I_A + (3z + 2Z_1 + Z_0)I_B + (Z_0 - Z_1)I_C + 3E_B' \tag{16}$$

$$3E_C = K(Z_0 - Z_1)I_A + (Z_0 - Z_1)I_B + (3z + 2Z_1 + Z_0)I_C + 3E_C' \tag{17}$$

where E_A', E_B', E_C' are the voltages induced by the air gap fields.

That is, the first terms of the above equations are the voltages consumed in the stationary and external motor circuits; the final terms are the remaining voltages that are impressed on the rotor.

*Alternatively, positive and negative sequence.

Figure 3 (left). Control diagram for split winding starting of 3-phase motor

Figure 4 (below). Circuit diagram of 3-phase delta-connected motor with external impedance in two phases

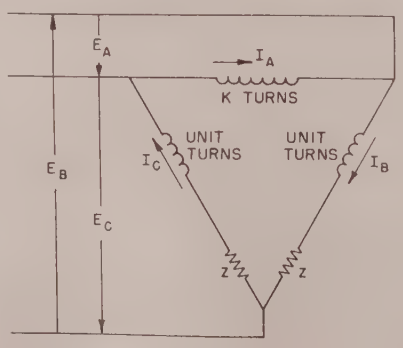

All that the rotor "sees" are the air gap fields due to the stator ampere turns.[7] Since the zero phase sequence stator currents produce no useful air gap fields, only forward and backward fundamental fields exist in the air gap and rotor. Hence, we can substitute:

$$E_A'/K = E_f' + E_b' = I_f Z_f + I_b Z_b \tag{18}$$

$$E_B' = E_f'/\underline{240} + E_b'/\underline{120} = I_f Z_f/\underline{240} + I_b Z_b/\underline{120} \tag{19}$$

$$E_C' = E_f'/\underline{120} + E_B'/\underline{240} = I_f Z_f/\underline{120} + I_b Z_b/\underline{240} \tag{20}$$

The applied (stator) voltages and currents referred to sequence axes, expressed in terms of normal winding turns, are:

$$E_A/K = E_f + E_b + E_0 \tag{21}$$

$$E_B = E_f/\underline{240} + E_b/\underline{120} + E_0 \tag{22}$$

$$E_C = E_f/\underline{120} + E_b/\underline{240} + E_0, \text{ whence} \tag{23}$$

$$3E_f = E_A/K + E_B/\underline{120} + E_C/\underline{240} \tag{24}$$

$$3E_b = E_A/K + E_B/\underline{240} + E_C/\underline{120} \tag{25}$$

$$3E_0 = E_A/K + E_B + E_C \tag{26}$$

$$KI_A = I_f + I_b + I_0 \tag{27}$$

$$I_B = I_f/\underline{240} + I_b/\underline{120} + I_0 \tag{28}$$

$$I_C = I_f/\underline{120} + I_b/\underline{240} + I_0 \tag{29}$$

To transform the 3-phase equations to the sequence axes, we substitute equations 15 to 23 in 24 to 26, giving:

$$3E_f = KZ_1 I_A + (Z_1 + z)I_B/\underline{120} + (Z_1 + z)/\underline{240} + 3I_f Z_f \tag{30}$$

$$3E_b = KZ_1 I_A + (Z_1 + z)I_B/\underline{240} + (Z_1 + z)/\underline{120} + 3I_b Z_b \tag{31}$$

$$3E_0 = KZ_0 I_A + (Z_0 + z)I_B + (Z_0 + z)I_C \tag{32}$$

Substituting equations 27 to 29 in these last equations, and dividing by three throughout:

$$E_f = (Z_1 + Z_f)I_f + z(I_f - I_0)/3 + z(I_f - I_b)/3 \tag{33}$$

$$E_b = (Z_1 + Z_b)I_b + z(I_b - I_0)/3 + z(I_b - I_f)/3 \tag{34}$$

$$E_0 = Z_0 I_0 + z(I_0 - I_f)/3 + z(I_0 - I_b)/3 \tag{35}$$

These three equations are represented by the equivalent circuit of Figure 5. An unusual feature of this circuit is the presence of the outer branches of a mutual impedance, $z/3$, instead of merely a mutual reactance. In practical cases, any external impedance is predominantly a reactance, so that the circuit can be set up on an a-c calculating board by using 1-to-1 ratio insulating transformers to represent the mutual impedances.

If $z = 0$, the circuit breaks down into two independent circuits. One is the normal circuit for a balanced 2-phase motor with unbalanced impressed voltages. The other is the single-phase zero phase sequence circuit. Thus, when there is no external impedance, the motor behaves exactly as if it were a balanced 3-phase motor, with unbalanced voltages, E_A/K, E_B, E_C, impressed on the three phases.

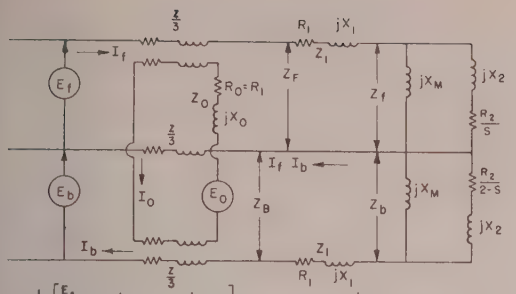

$E_f=\frac{1}{3}\left[\frac{E_A}{K}+E_B\angle 120+E_C\angle 240\right]$ $\quad I_A=\frac{1}{K}(I_f+I_b+I_o)$

$E_b=\frac{1}{3}\left[\frac{E_A}{K}+E_B\angle 240+E_C\angle 120\right]$ $\quad I_B=I_f\angle 240+I_b\angle 120+I_o$

$E_o=\frac{1}{3}\left[\frac{E_A}{K}+E_B+E_C\right]$ $\quad I_C=I_f\angle 120+I_b\angle 240+I_o$

Figure 5 (above). Equivalent circuit of motor connected for split winding starting

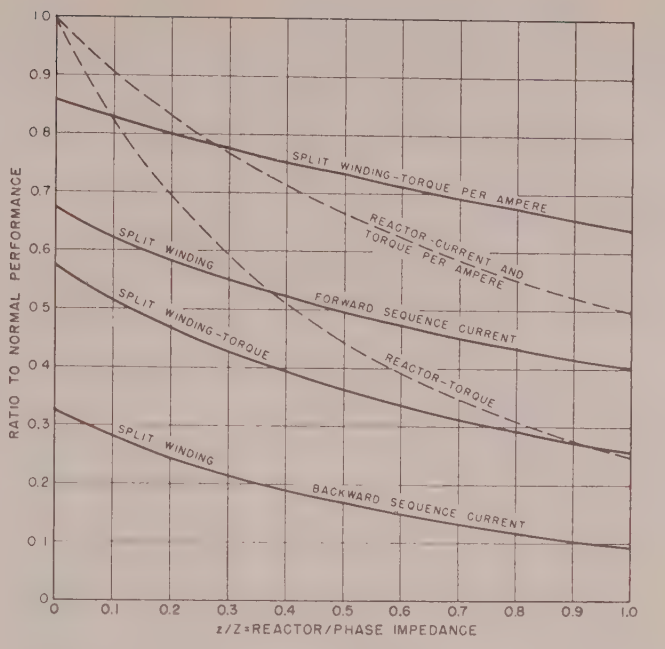
RATIO TO NORMAL PERFORMANCE
z/Z=REACTOR/PHASE IMPEDANCE
SPLIT WINDING-TORQUE PER AMPERE
REACTOR-CURRENT AND TORQUE PER AMPERE
SPLIT WINDING FORWARD SEQUENCE CURRENT
SPLIT WINDING-TORQUE REACTOR-TORQUE
SPLIT WINDING BACKWARD SEQUENCE CURRENT

Figure 6 (right). Three-phase motor performance with reactor starting

REACTOR STARTING OF THREE PHASE MOTORS

SPLIT WINDING (Y CONNECTED, $Z_0=Z/2$, K=2) WITH REACTORS IN 2 LINES ——
NORMAL WINDING WITH REACTORS IN 3 LINES — — —

With balanced impressed voltages, equations 12 to 14, we have, from equations 24 to 26, when $z=0$:

$$E_f=(2K+1)E/3K \tag{36}$$

$$E_b=-(K-1)E/3K \tag{37}$$

$$E_0=-(K-1)E/3K \tag{38}$$

Let, for convenience

$Z_F=Z_1+Z_f=$ total forward field impedance per phase with normal turns (39)

$Z_B=Z_1+Z_b=$ total backward field impedance per phase with normal turns (40)

Substituting in equations 33 to 35, and solving for the currents:

$$I_b=\frac{E(Z_0+z)(Z_F+z-KZ_F)}{K[3Z_FZ_BZ_0+2z(Z_FZ_B+Z_0Z_F+Z_0Z_B)+z^2(Z_F+Z_B+Z_0)]} \tag{41}$$

$$I_f=\frac{E}{Z_F+z}+\frac{(Z_B+z)I_b}{Z_F+z} \tag{42}$$

$$I_0=\frac{(Z_B+z)I_b}{Z_0+z} \tag{43}$$

At standstill, $Z_F=Z_B=Z$, and equations 41 to 43 become:

$$I_b=\frac{E(Z_0+z)(Z+z-KZ)}{K(Z+z)(2Zz+3ZZ_0+Z_0z)} \tag{44}$$

$$I_f=\frac{E[(Z+z)(Z_0+z)+K(Zz+2ZZ_0+Z_0z)]}{K(Z+z)(2Zz+3ZZ_0+Z_0z)} \tag{45}$$

$$I_0=\frac{E(Z+z-KZ)}{K(2Zz+3ZZ_0+Z_0z)} \tag{46}$$

These give, for the phase currents, from equations 27 to 29:

$$KI_A=\frac{E[(K+2)Z_0-(K-1)Z+3z]}{K(2Zz+3ZZ_0+Z_0z)} \tag{47}$$

$$I_B=\frac{-E[(K+2)Z_0+2(K-1)Z]}{2K(2Zz+3ZZ_0+Z_0z)}-\frac{j\sqrt{3}E}{2(Z+z)} \tag{48}$$

$$I_C=\frac{-E[(K+2)Z_0+2(K-1)Z]}{2K(2Zz+3ZZ_0+Z_0z)}+\frac{j\sqrt{3}E}{2(Z+z)} \tag{49}$$

When $z=0$, and these equations are combined, they give the equations for the line currents given in the first part of this paper.

The locked rotor torque is proportional to the difference of the square of the forward and backward sequence currents. Or, from equations 44 and 45:

$$T/T_n=\frac{2(Z_0+z)+KZ_0}{K(Z+z)(2Zz+3ZZ_0+Z_0z)} \tag{50}$$

If $z=0$, this reduces to $(2+K)/3K$.

The zero phase sequence current, as seen by the rotor, which produces a third harmonic air gap field, is given by equation 46. If $z=0$, this reduces to:

$$I_0=\frac{E(1-K)}{2KZ_0} \tag{51}$$

This is not the same as the actual circulating current in the delta of the stator winding, which is $1/3(I_A+I_B+I_C)$ or:

$$I_0'=\frac{-E[(K-1)(K+2)Z_0+(K-1)\times(2K+1)Z-3z]}{K^2(2Zz+3ZZ_0+Z_0z)} \tag{52}$$

If the motor is Y connected, equations 30 to 32 are still true, but we have the new relation that the phase (line) currents must add up to zero:

$$I_A+I_B+I_C=0 \tag{53}$$

whence, from equations 27 to 29, we have:

$$I_0=(K-1)I_A/3 \tag{54}$$

$$(I_f+I_b)=(2K+1)I_A/3 \tag{55}$$

Substituting these values in equations 30 to 32:

$$E_f=(Z_1+Z_f)I_f+z(I_f-I_b)/3+z(I_b-I_0)/3 \tag{33}$$

Hence, equations 33 to 35 are still true, and the equivalent circuit of Figure 5 represents the Y as well as the delta connection. The only difference is in the impressed voltages.

The relations between the unknown Y phase voltages, the known line voltages, and the sequence voltages are, from equations 12 to 14 and 24 to 26:

$$E_C-E_B=E\angle 120-E\angle 240=j\sqrt{3}E=j\sqrt{3}(E_f-E_b)$$

$$2E_A-E_B-E_C=2E-E\angle 120-E\angle 240=3E,$$

giving:

$$E=E_f-E_b \tag{56}$$

$$3E=(2K+1)(E_f+E_b)+2(K-1)E_0 \tag{57}$$

Substituting equations 30 to 32 in these:

$$E=I_f(Z_F+z)-I_b(Z_B+z) \tag{58}$$

$$3E=(2K+1)(Z_FI_f+Z_BI_b)+2(K-1)I_0Z_0+z(I_f-I_0)+z(I_b-I_0) \tag{59}$$

Since there is no neutral connection, the sum of the actual line currents is zero, whence:

$$I_A+I_B+I_C=0 \tag{60}$$

$$I_0=(KI_A+I_B+I_C)/3=(K-1)I_A/3 \quad (61)$$

$$I_f+I_b=KI_A-I_0=(2K+1)I_A/3 =(2K+1)I_0/(K-1) \quad (62)$$

Substituting these in equations 58 and 59, and solving for the currents:

$$I_f=\frac{E}{M}[(K+2)(2K+1)Z_B+3(K+1)z+ (K-1)^2Z_0] \quad (63)$$

$$I_b=\frac{E}{M}[-(K-1)(2K+1)Z_F+ 3Kz-(K-1)^2Z_0] \quad (64)$$

$$I_{II}=\frac{(K-1)E}{M}[(K+2)Z_B-(K-1)Z_F+3z] \quad (65)$$

whence

$$M=(2K+1)^2Z_BZ_F+2(K^2+K+1) (Z_B+Z_F)z+3z^2+(K-1)^2 (Z_B+Z_F+2z)Z_0 \quad (66)$$

These give for the phase currents:

$$I_A=\frac{3E}{M}[(K+2)Z_B-(K-1)Z_F+3z] \quad (67)$$

$$I_B=\frac{\sqrt{3}E}{2M}[\sqrt{3}[(K-1)Z_F-(K+2)Z_B-3z]- j[(2K+1)[(K+2)Z_B+(K-1)Z_F]+ 3z+2(K-1)^2Z_0]] \quad (68)$$

$$I_C=\frac{\sqrt{3}E}{2M}[\sqrt{3}[(K-1)Z_F-(K+2)Z_B-3z]+ j[(2K+1)[(K+2)Z_B+(K-1)Z_F]+ 3z+2(K-1)^2Z_0]] \quad (69)$$

When $z=0$, and $Z_F=Z_B$, these reduce to the values given in the first part of the paper.

From equations 63 and 64, the ratio of locked rotor torque, $Z_F=Z_B=Z$, to its normal value is:

$$T/T_n=(I_f^2-I_b^2)Z^2/E^2 =\frac{3(2K+1)Z^2}{(2K+1)^2Z^2+4Zz(K^2+K+1)+ 2(K-1)^2(Z+z)Z_0+3z^2} \quad (70)$$

When $z=0$, this reduces to the value given in the first part of the paper.

Figure 6 gives the locked rotor current and torque ratios to normal obtained with a Y-connected 2/1 circuit split winding motor ($K=2$), with different values of the external impedance, z, in series with the two high current lines. For comparison, similar ratios are shown for normal reactor starting, with a balanced motor winding and a reactor in each of the three lines.

Discussion

A. F. Ordas (General Electric Company, Fort Wayne, Ind.): Prompted by this paper, we applied the recommended method to a Y-connected synchronous motor; connecting one phase of a 3-phase winding in series during the starting period only, the other phases having circuits in parallel. The rating of this synchronous motor was *TS 975*, 6 pole, 500 horsepower, 500 kilovolt-ampere, 0.8 power factor, 2,300 volts, 3-phase, 60 cycles, 1,200 rpm.

Oscillographic torque tests showing the rate of acceleration were made at quarter voltage and full voltage. The torque curve showed uniform acceleration without harmonic dip from zero to synchronous speed. The line currents also smoothly drop from the starting value to their synchronous value with equal large currents in two legs and smaller current in the third or series leg.

Unfortunately, the power supply used for testing this motor was incapable of supplying full load on the synchronous motor at rated speed, and as a result line impedance was such that the lowest line voltage was 0.8 of the highest line voltage during the starting portion of the torque test. This line impedance distorted our test results slightly from the theoretical values as indicated in Table I of this discussion.

Table I

	Balanced Connection, Calculated	Test 550 V*	Test 2,300 V
Per unit torque	1.44	1.37	
Per unit kva	5.47	5.10	
	Alger Y-Connection, Calculated	**Test 550 V***	**Test 2,300 V**
Per unit current, lines 2 and 3	4.81	3.27	4.40
Per unit current, line 1	1.96	1.57	2.38
Per unit torque	0.86	0.52	0.94
Unbalanced/balanced torque ratio	0.60	0.38	0.69

*Values corrected to 2,300 volts.

There is no doubt that applications exist for this method of starting, and it offers the engineer an additional tool which should help him custom design for specific applications. In this scheme, only one leg is series connected during start. Applications may arise where two legs can be series connected during start with further decrease in kilovolt-ampere and starting torque. Thus, a three step start can be obtained by paralleling one, and then the second of the series phases. Also, if groups of motors are started together, balanced system loading can be obtained even though individual motors took unbalanced current. For best performance, this method requires a Y, 2-circuit winding, or equivalent. For the relatively few motors which have delta-connected windings, the method has the disadvantage that it draws the full voltage starting current from one of the three lines. Also, smaller high-voltage synchronous motors usually require one circuit for construction in minimum frame size. This means that any part winding starting system requiring more than one circuit is disadvantageous on a small synchronous motor. On larger motors this is, of course, not such a large handicap unless the line voltage goes up correspondingly.

One particular disadvantage we did notice with the unbalanced starting connection was that it gave rise to very high induced voltages in the field with the field open-circuited. It is, therefore, very important not to open the field until the motor is operating under the balanced applied voltages in or near synchronism. Even in synchronism with the unbalanced voltages

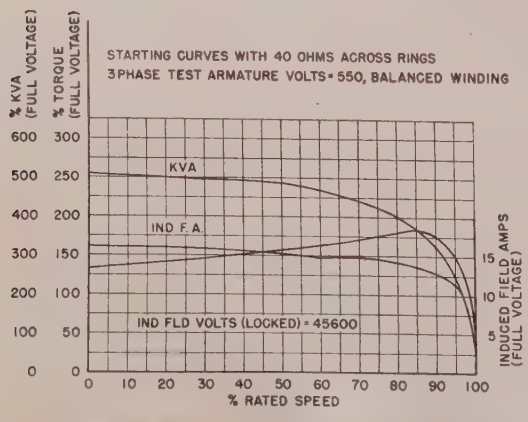
STARTING CURVES WITH 40 OHMS ACROSS RINGS
3PHASE TEST ARMATURE VOLTS=550, BALANCED WINDING
% KVA (FULL VOLTAGE)
% TORQUE (FULL VOLTAGE)
KVA
IND F.A.
IND FLD VOLTS (LOCKED) = 45600
INDUCED FIELD AMPS (FULL VOLTAGE)
% RATED SPEED

Figure 1 (left)

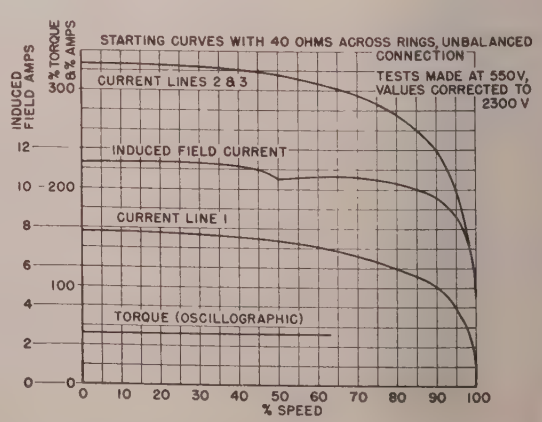
STARTING CURVES WITH 40 OHMS ACROSS RINGS, UNBALANCED CONNECTION
TESTS MADE AT 550V, VALUES CORRECTED TO 2300 V
INDUCED FIELD AMPS & % TORQUE
CURRENT LINES 2 & 3
INDUCED FIELD CURRENT
CURRENT LINE 1
TORQUE (OSCILLOGRAPHIC)
% SPEED

Figure 2 (right)

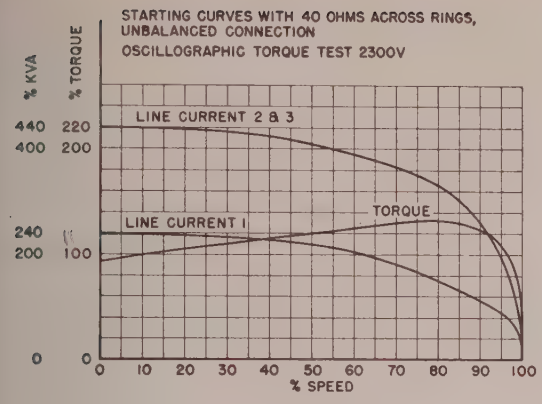

Figure 3

applied, the open field showed sufficient voltage to break down the insulation.

The starting characteristics for the synchronous motor tested are shown in Figures 1, 2, and 3 of this discussion.

John F. H. Douglas (Marquette University, Milwaukee, Wis.): The following data relating to a motor made by Schindler of Lucerne, Switzerland, was furnished by Frank Gutzwiller of the Cutler Hammer Company. This data seems to apply to a split-winding motor: *Construction*—two stator cores, two stator windings, two rotor stackings on one shaft mounted in one housing. Outer cage of each rotor is individual; inner cage runs through both rotor stackings and is common. *Running performance*—11 horsepower, 3 phase, 30 cycles, 2 poles, 380-volts, 16 amperes, torque 2.75 kilogram-meters at 3.3 per cent slip. *Starting performance*—(one stator excited) torque 4.3 kilogram-meters, 56 amperes. *Control*—one contactor is manually operated by a push-button. The other contactor connects in second winding with the aid of a voltage relay. There is no drop in speed or serious inrush at change-over.

P. L. Alger, H. C. Ward, Jr. and **F. H. Wright:** The motor described by Professor Douglas is very interesting, and there is no doubt that it will work satisfactorily, but its cost in this country will be prohibitive. Many such special designs of polyphase motors, using independent cores or windings with electrical or mechanical means for changing conditions between starting and running, have been described by H. M. Hobart.[1]

So far as I know, all these motors have disappeared from American practice. The present-day problem is to find a method of starting that can be used with any standard motor taken directly from stock, for the reason that the extra costs and delays incurred by a special motor design far outweigh the advantages to be gained in nearly all cases.

On the other hand, a scheme requiring special control encounters a similar economic barrier, that is only slightly less serious.

The split-winding method of starting using standard motors and standard control elements, represents an attempt to circumvent these difficulties. Its field of usefulness is in that fringe territory where motors are too large to be started directly and too small to warrant special constructions. The unanswered question is whether this field is extensive enough to warrant development of the packaged control equipment that is necessary.

Reference

1. Modern Polyphase Induction Motors, **F. Punga, O. Raydt.** Isaac Pitman and Sons, Ltd., London, England, 1933.

Shielded Dielectric-Rod Waveguides

ROBERT E. BEAM
MEMBER AIEE

HILLARD M. WACHOWSKI
NONMEMBER AIEE

IF A circular metallic waveguide is filled with a dielectric other than air, the phase velocity and the cutoff frequency are lowered. Such dielectric-filled guides prove useful in such applications as impedance transformation and matching, mode conversion, phase shifting, and as mode exciters for dielectric-rod antennas. Only transverse electric and transverse magnetic modes can exist in such guides under lossless conditions. Dielectric-filled guides have dielectric losses; however, the losses may not be objectionable in many practical cases. Waveguides only partially filled with dielectric should be even more useful in practical applications than those completely filled with dielectric and should have better loss characteristics. They also should have much better characteristics as exciters for dielectric-rod antennas than do the completely filled waveguides.

Studies of dielectric-rod and dielectric-tube waveguides indicate that transverse electric, transverse magnetic, and hybrid modes may exist in such waveguides.[1] Hence, it is reasonable to expect that all three types of modes may exist, at least at high frequencies, in metallic waveguides containing two or more coaxial dielectrics. A dielectric rod surrounded by air and a metal cylinder is here called a "shielded dielectric-rod waveguide" to emphasize the fact that modes of the types associated with dielectric rods may exist as well as those associated with air-filled metallic waveguides.

Special cases of the circular metallic waveguide with two coaxial media have been investigated by Pincherle,[2] Frankel,[3] Buchholz,[4] and by Teasdale and Higgins.[5]

In this paper the boundary value problem posed by a circular metallic waveguide of infinite length containing two coaxial dielectric regions and propagating waves along its axis under steady-state conditions is solved. The conditions under which representative transverse electric, transverse magnetic, and hybrid modes will propagate are given. The cutoff frequencies, guide wave lengths, and transverse field plots are given for the lowest order and lowest rank transverse electric, transverse magnetic, and hybrid modes on such waveguides having polystyrene and air as dielectrics. An approximate theory of attenuation of propagating modes for low-loss dielectrics and small losses in the metal will be outlined. Special emphasis is placed on the shielded dielectric-rod waveguide in which the inner dielectric region is polystyrene and the outer region is air. The method of analysis used is similar to that used by R. E. Beam and his students in treating other waveguide problems.[6,7]

Boundary Value Problem

The system to be investigated and the co-ordinates to be used in the investigation are represented in Figure 1. The metallic cylinder and the dielectric regions are assumed to be lossless. The dielectric constant of region R_1, the inner dielectric region, is represented by ϵ_1, and that of R_2 is represented by ϵ_2. The boundary between R_1 and R_2 is a cylinder of radius a, and the boundary between R_2 and the metal is a cylinder of radius b. Meter-kilogram-second units are assumed.

For a guided wave travelling in the $+z$ or axial direction, the time and z-co-ordinate dependence of the expressions for the field components is accounted for by the factor $e^{j(\omega t-\beta_g z)}$, where $\beta_g=2\pi/\lambda_g$ is the phase constant of the guided wave, λ_g being the wave length. A necessary condition which the expressions for the z components of the electric and the magnetic field intensities must satisfy is that they be solutions of the scalar wave equation in cylindrical co-ordinate form

$$\frac{\partial^2\psi}{\partial r^2}+\frac{1}{r}\frac{\partial\psi}{\partial r}+\frac{1}{r^2}\frac{\partial^2\psi}{\partial\theta^2}=-k^2\psi \qquad (1)$$

where

$$k^2=\omega^2\mu\epsilon-\beta_g^2 \qquad (2)$$

is the separation constant and ψ represents either E_z or H_z. Any solution of equation 1 can be written as linear combinations of the wave functions

$$\psi=[A_n\cos n\theta+B_n\sin n\theta]Z_n(kr)e^{j(\omega t-\beta_g z)} \qquad (3)$$

for different integral values of n, where Z_n represents appropriate Bessel functions or linear combinations thereof.

For the dielectric region R_1, the separation constant is given by

$$k_1^2=\omega^2\mu_0\epsilon_0\epsilon_1-\beta_g^2=(2\pi/\lambda)^2\epsilon_1-(2\pi/\lambda_g)^2 \qquad (4)$$

where μ_0 and ϵ_0 are the free-space values of the permeability and permittivity, respectively. The alternative form of equation 4 is obtained by substituting $(2\pi/\lambda)^2$ for $\omega^2\mu_0\epsilon_0$, where λ is the wave length of free-space plane waves, and $(2\pi/\lambda_g)^2$ for β_g^2.

Similarly for region R_2, the separation

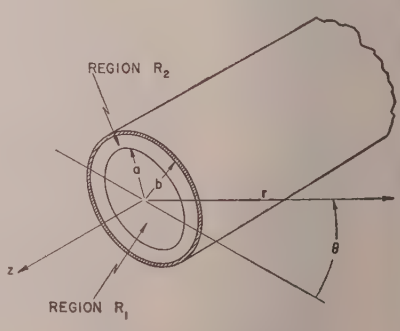

Figure 1. Co-ordinate system

Paper 51-162, recommended by the AIEE Special Communications Applications Committee and approved by the AIEE Technical Program Committee for presentation at the AIEE Great Lakes District Meeting, Madison, Wis., May 17–19, 1951. Manuscript submitted February 15, 1951; made available for printing April 9, 1951.

ROBERT E. BEAM and HILLARD M. WACHOWSKI both are with Northwestern University, Evanston, Ill.

The work reported on in this paper was sponsored by Evans Signal Laboratory under Army Signal Corps, Contract Number *W36-039 sc-38240*, with the Microwave Laboratory, Northwestern University, Evanston, Ill.

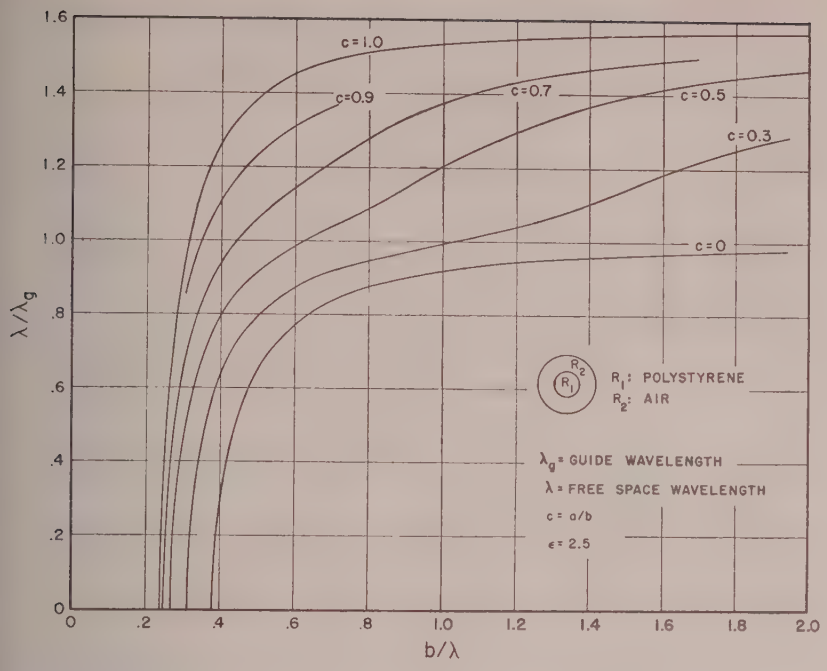

Figure 2. Characteristic curves for TM_{01} mode

constant is given by

$$k_2^2=\omega^2\mu_0\epsilon_0\epsilon_2-\beta_g^2=(2\pi/\lambda)^2\epsilon_2-(2\pi/\lambda_g)^2 \quad (5)$$

The range of variation of λ_g for propagating axial waves can be anticipated from knowledge of the theory of metallic waveguides containing a single dielectric to be between infinity and $\lambda/\sqrt{\epsilon}$ or $\lambda/\sqrt{\epsilon_2}$, whichever is the shorter. Hence, k_1^2 should always be a positive quantity for propagating modes if $\epsilon_1>\epsilon_2$, and k_2^2 should be positive when $\lambda_g>\lambda/\sqrt{\epsilon_2}$ and negative when $\lambda_g<\lambda/\sqrt{\epsilon_2}$. When $\lambda_g=\lambda/\sqrt{\epsilon_2}$, k_2^2 is zero. Similarly, if $\epsilon_1<\epsilon_2$, the separation constant k_2^2 should be a positive quantity for propagating modes, and k_1^2 should be positive when $\lambda_g>\lambda/\sqrt{\epsilon_1}$ and negative when $\lambda_g<\lambda/\sqrt{\epsilon_1}$. This knowledge makes it possible to anticipate the types of Bessel functions required for solutions for each of the two regions for different operating ranges. If the separation constant k^2 is positive, ordinary Bessel functions $J_n(kr)$ and $N_n(kr)$ are required; if k^2 is negative, the modified Bessel functions $I_n(jkr)$ and $K_n(jkr)$ are required.

For region R_1, if the $\theta=0$ line is properly chosen, and if the normalized radial variable $s=r/b$ is introduced, appropriate solutions for the axial field components follow:

When k_1^2 is positive

$$E_{z1}=a_1J_n(V_1s)\cos n\theta$$
$$H_{z1}=b_1J_n(V_1s)\sin n\theta \quad (6A)$$

When k_1^2 is negative

$$E_{z1}=a_1I_n(W_1s)\cos n\theta \quad (6B)$$
$$H_{z1}=b_1I_n(W_1s)\sin n\theta$$

The factor $e^{j(\omega t-\beta_g z)}$ has been omitted for brevity in writing these field expressions and will be omitted hereafter. For a guided steady-state wave, β_g must be the same for both regions R_1 and R_2. In writing equations 6, k_1b has been replaced by V_1 when k_1 is positive real, and by jW_1 when k_1 is positive imaginary.

Similarly, for region R_2 appropriate solutions for the axial field components follow:

When k_2^2 is positive

$$E_{z2}=[a_2J_n(V_2s)+a_3N_n(V_2s)]\cos n\theta$$
$$H_{z2}=[b_2J_n(V_2s)+b_3N_n(V_2s)]\sin n\theta \quad (7A)$$

When k_2^2 is negative

$$E_{z2}=[a_2I_n(W_2s)+a_3K_n(W_2s)]\cos n\theta$$
$$H_{z2}=[b_2I_n(W_2s)+b_3K_n(W_2s)]\sin n\theta \quad (7B)$$

In writing equations 7, k_2b has been replaced by V_2 when k_2 is positive real, and by jW_2 when k_2 is positive imaginary.

The transverse components of the field intensities in the two regions can be obtained from the axial components by utilizing the following equations which were derived from Maxwell's equations:

$$E_\theta=k_i\left[\frac{-j\beta_g}{s}\frac{\partial E_z}{\partial\theta}+j\omega\mu_0\frac{\partial H_z}{\partial s}\right]$$
$$E_r=-k_i\left[j\beta_g\frac{\partial E_z}{\partial s}+\frac{j\omega\mu_0}{s}\frac{\partial H_z}{\partial\theta}\right]$$
$$H_\theta=-k_i\left[j\omega\epsilon_i\frac{\partial E_z}{\partial s}+\frac{j\beta_g}{s}\frac{\partial H_z}{\partial\theta}\right] \quad (8)$$
$$H_r=k_i\left[\frac{j\omega\epsilon_i}{s}\frac{\partial E_z}{\partial\theta}-j\beta_g\frac{\partial H_z}{\partial s}\right]$$

In these relationships $k_i=b/V_1^2$, b/V_2^2, $-b/W_1^2$, or $-b/W_2^2$, depending upon the region to which they are being applied and the sign of the separation constant k^2 for that region. Also, ϵ_i represents the appropriate permittivity for the region under consideration.

In order for equations 6 and 7 and the equations derived therefrom by means of equations 8 to represent solutions to the particular problem under investiga-

Figure 3. Characteristic curves for TM_{01} mode

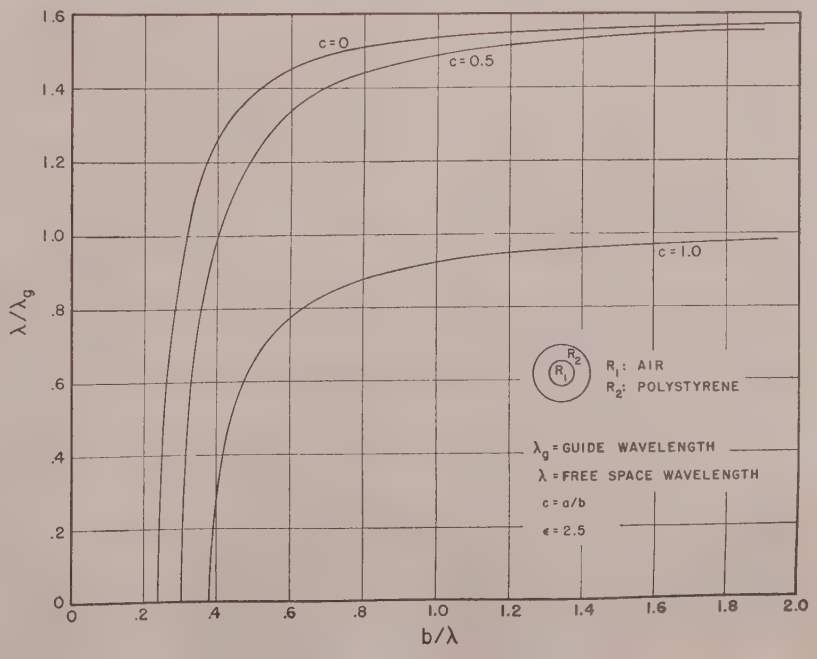

tion, it is necessary that the following boundary conditions be satisfied:

At $s=a/b=c$

$$E_{z1}=E_{z2} \qquad E_{\theta 1}=E_{\theta 2}$$
$$H_{z1}=H_{z2} \qquad H_{\theta 1}=H_{\theta 2}$$

At $s=1$ (9)

$$E_{z2}=0 \qquad E_{\theta 2}=0$$

If these six independent conditions are satisfied, the remaining boundary conditions on the radial field components will automatically be satisfied.

Characteristic Equation

By utilizing the six boundary conditions any five of the six constants a_1 to b_2 in equations 6 and 7 can be expressed in terms of the remaining constant for the appropriate pair of values (V_1, V_2), (V_1, W_2) or (W_1, V_2) which satisfies the following characteristic equation:

$$n^2T^2/Q(\Delta_4-\Delta_3)(\Delta_3\Delta_5-\Delta_2\Delta_4)+[\epsilon_1\Delta_7(\Delta_4-\Delta_3)-\epsilon_2(\Delta_4\Delta_6-\Delta_1\Delta_3]\times[\Delta_2\Delta_4(\Delta_7-\Delta_5)-\Delta_3\Delta_5(\Delta_7-\Delta_1)]=0 \quad (10)$$

where

$$\Delta_1=\frac{J_n'(cV_2)}{cV_2J_n(cV_2)}=\frac{-I_n'(cW_2)}{cW_2I_n(cW_2)}$$

$$\Delta_2=\frac{J_n'(V_2)}{V_2J_n(V_2)}=\frac{-I_n'(W_2)}{W_2I_n(W_2)}$$

$$\Delta_3=\frac{J_n(cV_2)}{N_n(cV_2)}=\frac{I_n(cW_2)}{K_n(cW_2)}$$

$$\Delta_4=\frac{J_n(V_2)}{N_n(V_2)}=\frac{I_n(W_2)}{K_n(W_2)}$$

Figure 4. Characteristic curves for TE_{01} mode

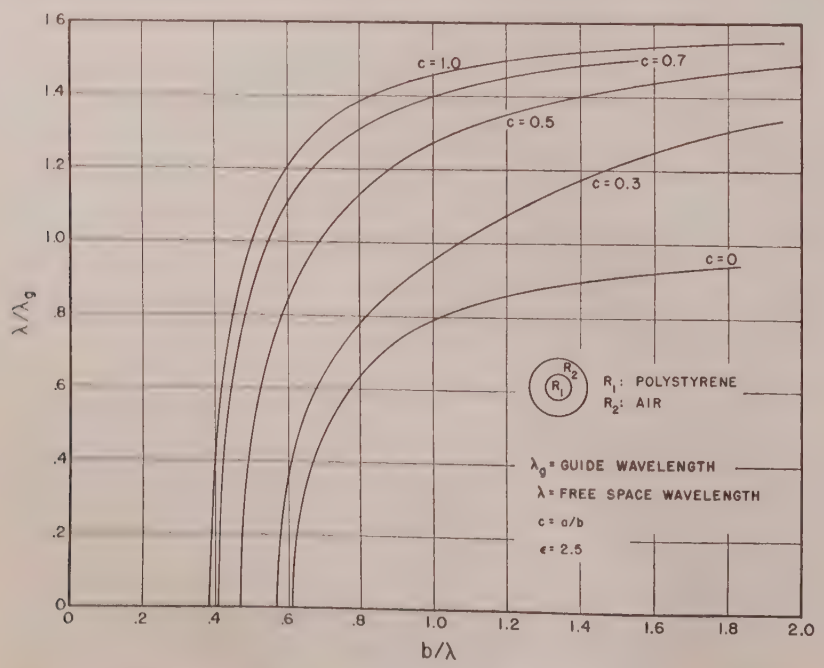

$$\Delta_5=\frac{N_n'(V_2)}{V_2N_n(V_2)}=\frac{-K_n'(W_2)}{W_2K_n(W_2)}$$

$$\Delta_6=\frac{N_n'(cV_2)}{cV_2N_n(cV_2)}=\frac{-K_n'(cW_2)}{cW_2K_n(cW_2)}$$

$$\Delta_7=\frac{J_n'(cV_1)}{cV_1J_n(cV_1)}=\frac{-I_n'(cW_1)}{cW_1I_n(cW_1)} \quad (11)$$

$$T=\frac{1}{c^2}\left[\frac{1}{V_1^2}-\frac{1}{V_2^2}\right] \qquad Q=\left[\frac{\lambda_g}{\lambda}\right]^2=\frac{V_1^2-V_2^2}{\epsilon_2V_1^2-\epsilon_1V_2^2}$$

$$c=a/b \qquad V_1=jW_1 \qquad V_2=jW_2$$

Two expressions are given for each of the Δ's. The one to be used in any case is

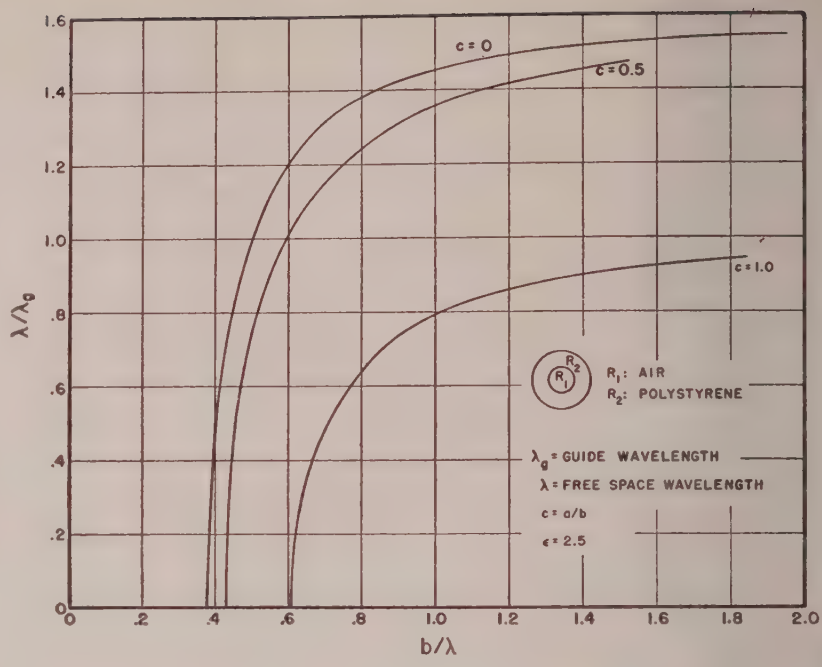

Figure 5. Characteristic curves for TE_{01} mode

the one having a positive real argument. The considerations used in choosing the forms of equations 6 and 7 lead to the appropriate choice of Δ's. To obtain the characteristic equation 10 in the form given it was necessary to divide by the product $N_n(cV_2)\cdot J_n(cV_1)$.

Equations 4 and 5 may be solved simultaneously for $(\lambda_g/\lambda)^2$ and $(b/\lambda)^2$ to yield the following equations after replacing k_1b and k_2b by their equivalents V_1b and V_2b, respectively:

$$(\lambda_g/\lambda)^2=(V_1^2-V_2^2)/(\epsilon_2V_1^2-\epsilon_1V_2^2)$$
$$(b/\lambda)^2=(V_1^2-V_2^2)/(2\pi)^2(\epsilon_1-\epsilon_2) \quad (12)$$

Thus, for given values of n, b, c, ϵ_1 and ϵ_2, equation 10 can be solved for V_1 and V_2, which are then substituted in equations 12 to determine λ_g/λ and b/λ. Equation 10 can be solved for continuous ranges of values of V_1 and V_2 which, when used with equations 12 give λ_g/λ as functions of b/λ.

The limiting forms which the characteristic equation assumes when the radius b becomes infinitely large and when $a=b$ are of interest. The former case is that of a dielectric-rod waveguide if region R_1 is a dielectric rod and region R_2 is air. The latter case is that of a metallic waveguide filled with one dielectric.

The limiting form of equation 10 as b becomes infinitely large is

$$n^2T^2/Q-(\Delta_6-\Delta_7)(\Delta_6-\epsilon_1\Delta_7)=0 \quad (13)$$

This is the characteristic equation of a dielectric-rod waveguide.

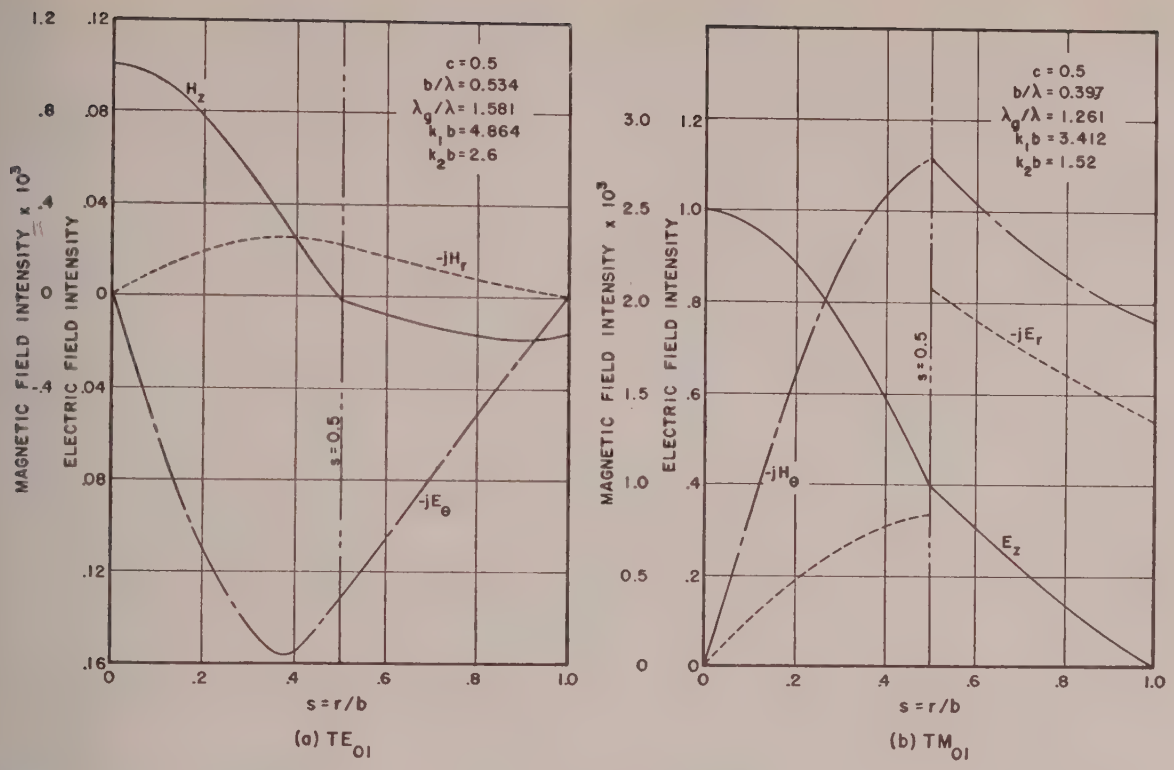

Figure 6. Relative field distributions in shielded polystyrene-rod waveguides

The limiting form of equation 10 as a becomes equal to b is

$$J_n(V_1)\cdot J_n'(V_1)=0 \qquad (14)$$

To obtain this form it is necessary to recall that the characteristic equation was divided by $J_n(cV_1)$ to get it in such a form that Δ_7 could be substituted for $J_n(cV_1)/cV_1J_n(cV_1)$. Equation 14 was obtained from equation 10 multiplied by $J_n(cV_1)$. For $a=0$, the same result as that given in equation 14 with V_1 replaced by V_2 is obtained. This equation is satisfied when either factor is zero. The characteristic equation for transverse electric (TE_{nm}) modes in ordinary metallic waveguides with a single dielectric is given by

$$J_n'(V_1)=0 \qquad (15)$$

The corresponding characteristic equation for transverse magnetic (TM_{nm}) modes is similarly given by

$$J_n(V_1)=0 \qquad (16)$$

For values of V_1 satisfying either equation 15 or 16, the guide wave length can be found by means of equation 4.

Equations for Field Components

For pairs of values satisfying the characteristic equation for given values of n, b, c, ϵ_1 and ϵ_2, the field intensity components are given by equations 6A and 7A and the following expressions which were obtained by means of equations 8:

$$E_{\theta 1}=\frac{j2\pi}{V_1}\frac{b}{\lambda}\left[\frac{n}{V_1 s}\frac{\lambda}{\lambda_g}J_n(V_1 s)a_1+\eta_0 J_n'(V_1 s)b_1\right]\sin n\theta$$

$$E_{r1}=\frac{-j2\pi}{V_1}\frac{b}{\lambda}\left[\frac{\lambda}{\lambda_g}J_n'(V_1 s)a_1+\eta_0\frac{n}{V_1 s}J_n(V_1 s)b_1\right]\cos n\theta$$

$$H_{\theta 1}=\frac{-j2\pi}{V_1}\frac{b}{\lambda}\left[\frac{\epsilon_1}{\eta_0}J_n'(V_1 s)a_1+\frac{n}{V_1 s}\frac{\lambda}{\lambda_g}J_n(V_1 s)b_1\right]\cos n\theta$$

$$H_{r1}=\frac{-j2\pi}{V_1}\frac{b}{\lambda}\left[\frac{\epsilon_1}{\eta_0}\frac{n}{V_1 s}J_n(V_1 s)a_1+\frac{\lambda}{\lambda_g}J_n'(V_1 s)b_1\right]\sin n\theta \qquad (17)$$

$$E_{\theta 2}=\frac{j2\pi}{V_2}\frac{b}{\lambda}\left[\frac{n}{V_2 s}\frac{\lambda}{\lambda_g}[J_n(V_2 s)a_2+N_n(V_2 s)a_3]+\eta_0[J_n'(V_2 s)b_2+N_n'(V_2 s)b_3]\right]\sin n\theta$$

$$E_{r2}=\frac{-j2\pi}{V_2}\frac{b}{\lambda}\left[\frac{\lambda}{\lambda_g}[J_n'(V_2 s)a_2+N_n'(V_2 s)a_3]+\eta_0\frac{n}{V_2 s}[J_n(V_2 s)b_2+N_n(V_2 s)b_3]\right]\cos n\theta$$

$$H_{\theta 2}=\frac{-j2\pi}{V_2}\frac{b}{\lambda}\left[\frac{\epsilon_2}{\eta_0}[J_n'(V_2 s)a_2+N_n'(V_2 s)a_3]+\frac{\lambda}{\lambda_g}\frac{n}{V_2 s}[J_n(V_2 s)b_2+N_n(V_2 s)b_3]\right]\cos n\theta$$

$$H_{r2}=\frac{-j2\pi}{V_2}\frac{b}{\lambda}\left[\frac{\epsilon_2}{\eta_0}\frac{n}{V_2 s}[J_n(V_2 s)a_2+N_n(V_2 s)]+\frac{\lambda}{\lambda_g}[J_n'(V_2 s)b_2+N_n'(V_2 s)b_3]\right]\sin n$$

where $\eta_0=\sqrt{\mu_0/\epsilon_0}$

If k_2^2 is negative and $k_2 b$ is a positive imaginary, equations 7B should be used in equations 8 to determine expressions for the transverse field components in region R_2. The resulting expressions would be identical with those of equations 17 for region R_2 altered in the following ways:

1. $J_n(V_2 s)$ and $N_n(V_2 s)$ replaced by $I_n(W_2 s)$ and $K_n(W_2 s)$, respectively.
2. V_2 replaced by W_2.
3. Each of the four expressions reversed in sign.

Similar changes should be made in the expressions for region R_1 if k_1^2 is negative.

If equations 6, 7, and 17 represent a solution to the boundary value problem, the characteristic equation must be satisfied and the constants must be interrelated as follows as determined by the boundary conditions:

$$a_1=\frac{N_n(cV_2)}{J_n(cV_1)}[\Delta_3-\Delta_4]a_2$$

$$b_1=\frac{N_n(cV_2)}{J_n(cV_1)}\left[\frac{\Delta_3\Delta_5-\Delta_2\Delta_4}{\Delta_5}\right]b_2$$

$$a_3=-\Delta_4 a_2 \qquad b_3=-\frac{\Delta_2\Delta_4}{\Delta_5}b_2 \qquad (18)$$

$$nT/\sqrt{Q}\,\Delta_5(\Delta_4-\Delta_3)a_2+\eta_0[\Delta_2\Delta_4(\Delta_7-\Delta_6)-\Delta_3\Delta_5(\Delta_7-\Delta_1)]b_2=0$$

$$\frac{i}{\eta_0}[e_1\Delta_7(\Delta_{-7}\Delta_3)-e_3(\Delta_4\Delta_6-\Delta_1\Delta_3)]a_2-$$

$$nT/\sqrt{Q}\left[\frac{\Delta_2\Delta_8-\Delta_9\Delta_4}{\Delta_5}\right]b_2=0$$

If k_2^2 is negative instead of positive, $N_n(cV_2)$ in these expressions should be replaced by $K_n(cW_2)$ and the Δ's for region R_2 should be defined in terms of the modified Bessel functions. Similarly if k_1^2 is negative, $J_n(cV_1)$ should be replaced by $I_n(cW_1)$ and the second form of the expression for Δ_7 should be used.

The characteristic equation 10 is the determinant of the coefficients of the last two of equations 18 set equal to zero. For pairs of values V_1, V_2 satisfying the characteristic equation, either of these two equations can be solved for a_2 in terms of b_2 and then any five of the six constants can be expressed in terms of the sixth.

Transverse Modes

If only transverse components of the magnetic field exist, the constants b_1, b_2, and b_3 are zero. If only transverse components of the electric field intensity exist, the constants a_1, a_2, and a_3 are zero. In the former case the resulting modes are called transverse magnetic modes and in the latter case, transverse electric modes. Equations 18 show that the a_1 constants are independent of the b_1 constants when $n=0$. In this case the modes are symmetrical modes in that the expression for the field intensities are independent of the angle θ. For $n \geq 1$, only hybrid modes exist except for the special limiting case of the ordinary metallic waveguide filled with a single dielectric.

For $n=0$, the characteristic equation 10 reduces to the product of two factors either of which may separately equal zero. The first factor set equal to zero yields the following characteristic equation for transverse magnetic modes:

$$e_1\Delta_7(\Delta_4-\Delta_3)-e_2(\Delta_4\Delta_8-\Delta_1\Delta_3)=0 \qquad (19)$$

where the Δ's are evaluated for $n=0$.

Similarly, the second factor yields the following characteristic equation for transverse electric modes:

$$\Delta_2\Delta_4(\Delta_7-\Delta_6)-\Delta_3\Delta_5(\Delta_7-\Delta_1)=0 \qquad (20)$$

Characteristic curves representing solutions to the characteristic equation for a TM_{01} mode in terms of the dimensionless quantities λ/λ_g and b/λ for representative values of c are given in Figures 2 and 3. In Figure 2, polystyrene with a dielectric constant of 2.5 was assumed for region 1 and air was assumed for region 2. In Figure 3, the positions of the dielectric were interchanged. The curves for $c=0$ and $c=1$ are for waveguides with one dielectric. These curves were determined by solving the simplified characteristic equation 16 for its first root and substituting the value of this root into equation 4 or 5, whichever is appropriate. The resulting equation was then plotted in the form of a curve of λ/λ_g versus b/λ. Cutoff occurs in any case when the guide wavelength λ_g is infinite or λ/λ_g is zero. Similarly, characteristic curves for the TE_{01} mode are given in Figures 4 and 5.

Distributions of the field components over the cross section of typical shielded dielectric-rod waveguides are shown in Figures 6 and 7 for both TE_{01} and TM_{01} modes. These distributions were computed using equations 17 and 18. For the TE_{01} mode, the constants a_1, a_2, and a_3 are zero; for the TM_{01} mode, the constants b_1, b_2, and b_3 are zero.

Higher rank modes are determined by higher rank roots of the characteristic equation. Computations of the characteristics of the higher rank TE_{0m} and TM_{0m} modes, m representing the rank, proceed in a manner similar to that used for the first rank modes.

Unsymmetrical or Hybrid Modes

For values of $n \geq 1$ the field distributions are unsymmetrical in that they vary with the angle θ. Also, in general, all six field components exist for $n \geq 1$. Such modes are called hybrid modes. Hybrid modes are ordered according to increasing cutoff frequency and designated as HE_{nm} or EH_{nm} modes, depending upon whether they are more like TE_{nm} or TM_{nm}

Figure 7. Relative field distributions in shielded polystyrene-rod waveguides

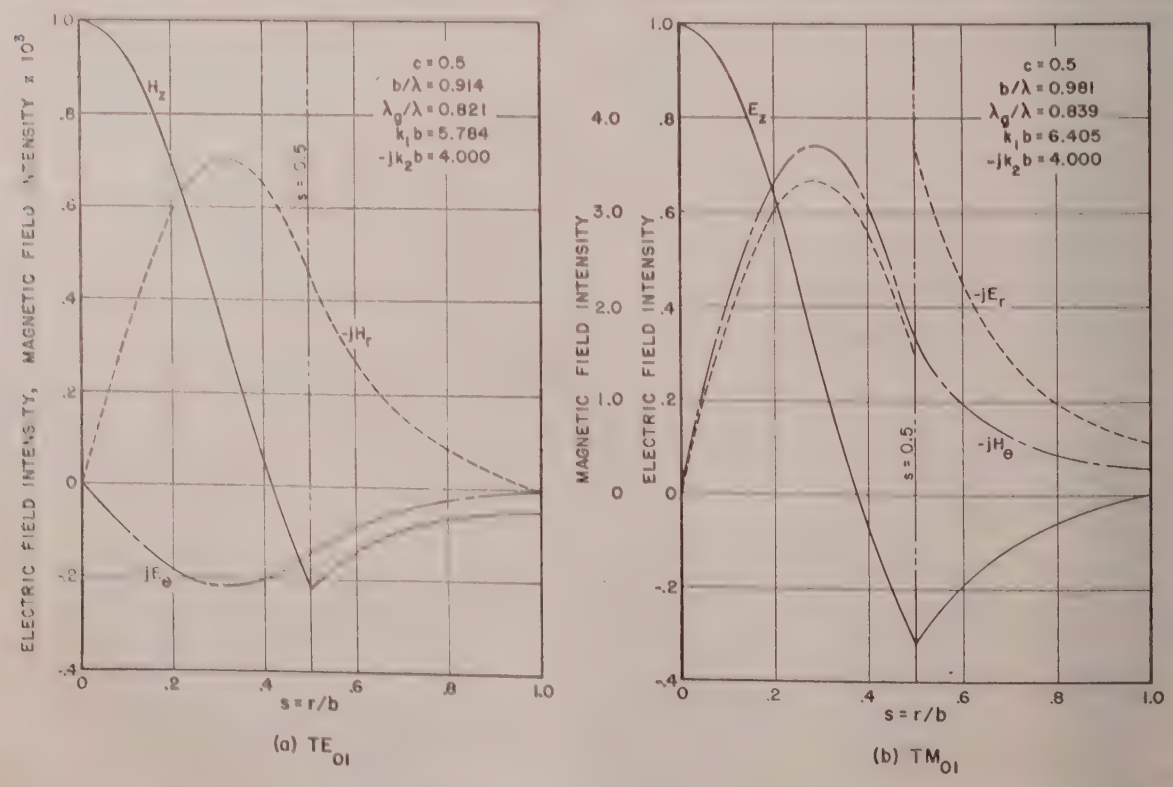

modes, respectively. *TE* modes are sometimes called *H* modes and *TM* modes are sometimes called *E* modes. Hence, the designation *HE* or *EH* to represent hybrid modes.

Hybrid modes are not merely the sum of corresponding order and rank *TE* and *TM* modes but are entirely different modes. However, hybrid modes do not exist in lossless metallic waveguides having a single dielectric. The general characteristic equation 10 reduces to equations 15 and 16 for the case of a single dielectric. These equations are the characteristic equations for either symmetrical or unsymmetrical *TE* and *TM* modes in metallic waveguides with one dielectric.

Characteristic curves for the lowest order and lowest rank *TE*-like hybrid mode, the HE_{11} mode, are given in Figure 8 for a shielded polystyrene-rod waveguide for representative values of the ratio c of the two radii. The curves for $c=0$ and $c=1$ are for a TE_{11} mode in a metallic guide with one dielectric. For $c=0$, the guide is filled with air; for $c=1$, the guide is filled with polystyrene.

Typical curves representing the transverse field distribution for an HE_{11} mode on a shielded polystyrene rod are shown in Figure 9 for a ratio of the radii equal to 0.5. Shielded dielectric rod waveguides excited in the HE_{11} mode have proved quite successful as exciters for polyrod antennas in experimental tests made by members of the staff of the Microwave Laboratory at Northwestern University. Other possible applications of shielded dielectric rod waveguides have been suggested in the opening paragraphs of this paper.

Figure 8. Characteristic curves for HE_{11} mode

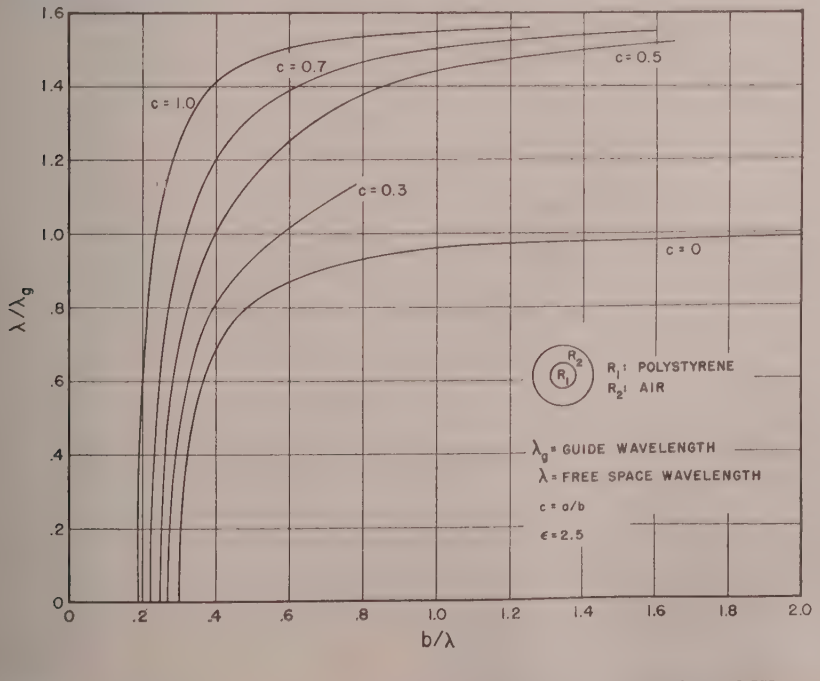

Attenuation

All of the results which have been presented up to this time were based on the assumption of lossless dielectrics and perfectly conducting walls. Since dielectric materials which are suitable for high-frequency operation have small loss tangents and since the walls are good conductors, the theory which has been presented should be adequate for most practical purposes. However, no measure of the attenuation is available from this theory. By introducing complex dielectric constants into the characteristic equation to allow for small losses in the dielectrics, and expanding the resulting characteristic equation about points determined by solutions of the characteristic equation for lossless dielectrics, an approximate expression for the attenuation constant can be derived.[8]

As an example of the method, consider a shielded dielectric rod surrounded by air and a perfectly conducting cylinder. The characteristic equation for such a guide without losses can be symbolized by the equation

$$F(V_1, V_2, \epsilon_1)=0 \tag{21}$$

If a complex dielectric constant $\epsilon_1=\epsilon(1-j\phi)$, where ϕ is the loss tangent of the dielectric, is introduced, the variables V_1 and V_2 will have complex values. If complex values are indicated by bold face type, the characteristic equation for the waveguide with small losses in the dielectric can be approximated by the following terms of a Taylor's series expansion:

$$F(\boldsymbol{V}_1, \boldsymbol{V}_2, \epsilon_1)=F(V_1, V_2, \epsilon_1)+\frac{\partial F}{\partial V_1}(\boldsymbol{V}_1-V_1)+\frac{\partial F}{\partial V_2}(\boldsymbol{V}_2-V_2)+\frac{\partial F}{\phi\epsilon_1}(\epsilon_1-\epsilon_1)+\ldots=0 \tag{22}$$

It is reasonable to assume that to a first order of approximation that the increments in V_1 and V_2 due to the complex dielectric constant are given by

$$\begin{aligned}\boldsymbol{V}_1-V_1&=jb\eta_1\\ \boldsymbol{V}_2-V_2&=jb\eta_2\end{aligned} \tag{23}$$

where η_1 and η_2 have small real values. Since by definition $V_1=k_1b$ and $V_2=k_2b$, it follows that $\boldsymbol{V}_1=\boldsymbol{k}_1b$ and $\boldsymbol{V}_2=\boldsymbol{k}_2b$. For a complex dielectric constant for region R_1, equations 4 and 5 for the separation constants become for ϵ_2 equal to unity

$$\begin{aligned}(\boldsymbol{k}_1)^2&=(\boldsymbol{V}_1/b)^2=(2\pi/\lambda)^2\epsilon_1(1-j\phi)+\Gamma_g^2\\ (\boldsymbol{k}_2)^2&=(\boldsymbol{V}_2/b)^2=(2\pi/\lambda)^2+\Gamma_g^2\end{aligned} \tag{24}$$

In writing these equations $-(2\pi/\lambda_g)^2$ was replaced by Γ_g^2 where $\Gamma_g=\alpha_g+j\beta_g$, in which $\beta_g=2\pi/\lambda_g$ and α_g is the attenuation constant. It is assumed that each component of the field intensities is represented by the same expression as for the case of no losses but with the propagation factor $e^{j(\omega t-\beta_g z)}$ replaced by $e^{j\omega t-\Gamma_g z}$.

By substituting equations 23 into equations 24, making use of equations 4 and 5, and solving for η_1 and η_2, the following expressions are obtained:

$$\begin{aligned}\eta_1&=\frac{\alpha_g\beta_g-(1/2)\phi(2\pi/\lambda)^2\epsilon_1}{V_1/b}\\ \eta_2&=\frac{\alpha_g\beta_g}{V_2/b}\end{aligned} \tag{25}$$

If equations 23 and 25, and $\epsilon_1-\epsilon_1=-j\epsilon_1\phi$ are substituted into equations 22 and the imaginary part is set equal to zero and solved for $\alpha_g\lambda$, the following result is obtained for the attenuation per free space wavelength:

$$\alpha_g\lambda=2\pi\epsilon_1\phi\frac{\lambda_g}{\lambda}\left[\frac{\frac{1}{2}+\frac{V_1}{(2\pi b/\lambda)^2}\frac{\partial F/\partial\epsilon_1}{\partial F/\partial V_1}}{1+\frac{V_1}{V_2}\frac{\partial F/\partial V_2}{\phi F/\partial V_1}}\right] \tag{26}$$

The computation of the attenuation characteristics of a particular mode is a very laborious task. However, Figure 10 represents characteristics for the TM_{01} on shielded polyrod waveguides for various radii ratios and an assumed loss tangent $\phi=3.5\times10^{-4}$. These curves are probably not very accurate for fre-

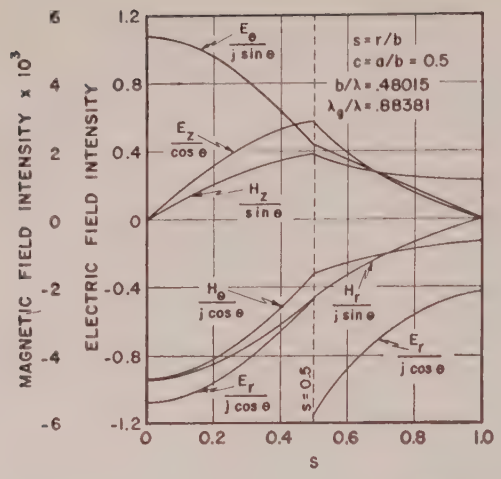

Figure 9 (above). Relative field distributions in shielded polystyrene-rod waveguide for HE_{11} mode

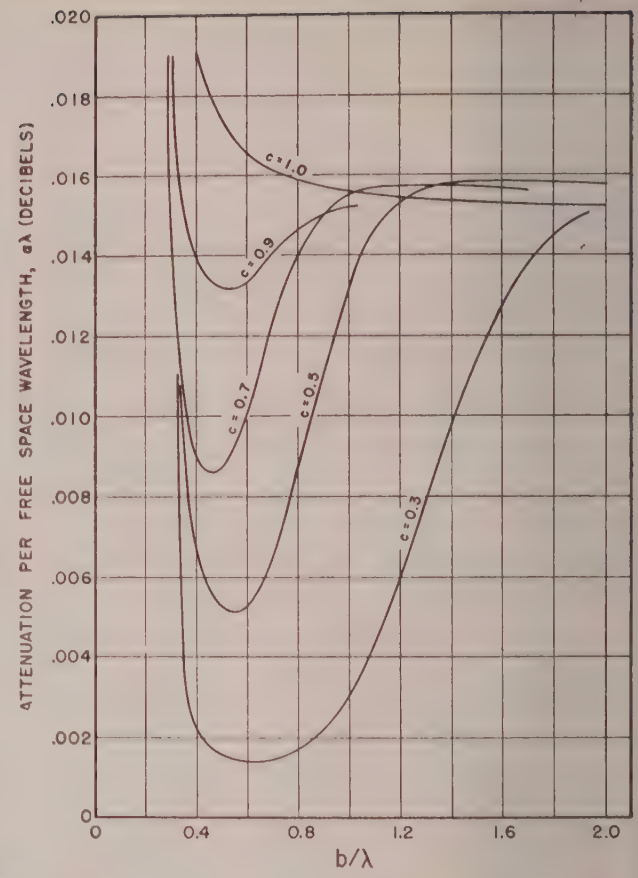

Figure 10 (right). Attenuation due to dielectric losses for TM_{01} mode in shielded dielectric-rod waveguides

quencies near the cutoff frequency of the mode.

Attenuation due to losses in the conductor can be approximated by the customary methods.[9] The quantity $H_t^2 R_s/2$, where R_s is the "skin-depth" resistance and H_t is tangential component of the magnetic field intensity at the surface of the conductor, can be integrated over the surface of a unit length of the guide to determine the losses. The attenuation constant due to these losses can then be approximated by dividing these losses per-unit length by twice the power transmitted through the guide.

References

1. Hyper-frequency Wave Guides, **J. R. Carson, S. P. Mead, S. A. Schelkunoff.** *Bell System Technical Journal* (New York, N. Y.), volume 15, 1936, pages 310–33.

2. Electromagnetic Waves in Metal Tubes Filled Longitudinally with Two Dielectrics, **L. Pincherle.** *Physical Review* (New York, N. Y.), volume 66, September 1 and 15, 1944, pages 118–30.

3. TM_{01} Mode in Circular Wave Guides with Two Coaxial Dielectrics, **S. Frankel.** *Journal of Applied Physics* (New York, N. Y.), volume 18, 1947, pages 650–55.

4. Der Hohlleiter von kreisformigen Querschnitt mit Geschichtetem Dielektrischen Einsatz, **Von Herbert Buchholz.** *Annalen der Physik* (Leipzig, Germany), volume 43, 1943, pages 313–68.

5. Electromagnetic Waves in Circular Wave Guides Containing Two Coaxial Media, **R. D. Teasdale, T. J. Higgins.** *Proceedings*, National Electronics Conference (Chicago, Ill.), volume 5, 1949, pages 427–41.

6. Guided Waves on Hollow Dielectric Tubes, **M. M. Astrahan.** *Thesis*, Northwestern University, Evanston, Ill., 1949.

7. Attenuation and Radiation Characteristics of Dielectric Tube Waveguides, **Wm. C. Jakes, Jr.** *Thesis*, Northwestern University, Evanston, Ill., 1949.

8. Final Report, Army Signal Corps Contract Number W36-039 sc-38240. **R. E. Beam et al.** Microwave Laboratory, Northwestern University, Evanston, Ill., 1950, pages 184–376.

9. Theory and Application of Microwave (book), **A. B. Bronwell, R. E. Beam.** McGraw-Hill Book Company, New York. N. Y., 1947, pages 332–53.

No Discussion

Transient Response of Small 2-Phase Induction Motors

A. M. HOPKIN
ASSOCIATE AIEE

SMALL 2-phase induction motors are frequently used in the construction of servomechanisms in instruments and computers. An analysis of the transient performance of such motors is desirable as an aid in servomechanism design. Furthermore it is desirable to determine whether or not the 2-phase control motor can be considered a linear device over at least a limited operating range, since present-day servomechanism analysis is greatly simplified if only linear devices need be considered.

A set of differential equations for the response of an induction motor has been derived by others.[1] These equations are so complicated that their general solution is very difficult. Solutions have been worked out through special simplifying assumptions,[2] or through the use of the differential analyzer.[3,4] These solutions in general represent special cases. Solutions have been worked out for the specific case of the small 2-phase control motor.[5] The purpose of this paper is to give a form of solution which will permit calculation of motor response in terms of the applied voltages and motor parameters.

In this paper a general solution for the transient response of a 2-phase induction motor will be developed, based on assumptions which are close approximations for many control-type motors. From this general solution the transient response will be derived for the case of a step-voltage input on the control field, and the steady-state response for a sinusoidally-varying amplitude voltage applied to the control field, in both cases with the reference-field voltage amplitude held constant.

Basic Assumptions

In order to simplify the problem so that a general solution can be obtained, the following four assumptions are made:

1. The motors have identical windings or can be made equivalent to a motor having balanced windings by the insertion of an ideal transformer in series with one winding.

2. The electrical time delays due to inductive effects in the rotor and stator circuits are very short in comparison with the mechanical time constant of the rotor. The implication of this assumption is that the steady-state and transient torque-speed relationships are essentially the same. This assumption is generally valid for motors in which the rotor resistance is large compared to the rotor inductance, a condition which frequently holds true for control motors.

3. The steady-state developed torque-speed curves for balanced amplitude sinusoidal voltages applied to the two fields can be approximated by the following straight line relationship:

$$T = KV^2\left(1-\frac{\omega}{\omega_0}\right) \tag{1}$$

where

T = developed torque
K = torque constant
V = balanced line voltage amplitude representing instantaneous voltages of the form $v_a(t)=\sqrt{2}V \sin 2\pi ft$, $v_b(t)=\sqrt{2}V \cos 2\pi ft$ applied to the two fields of the motor
ω = instantaneous shaft speed
ω_0 = synchronous speed

The straight line relationship of the form indicated in equation 1 holds fairly well for usual control motors in which the rotor resistance is large compared to the rotor reactance at line frequency, providing that the impedance of the source is low.[6] This assumption may not hold if one field is excited by a high impedance vacuum tube amplifier.

4. The load and friction and windage torques are of such a form that their sum can be expressed in the form

$$T_L = a+b\omega$$

The Development of the Basic Equation

The reader is referred to Appendix I for the development of the mathematical expressions. All expressions are developed in logical order in Appendix I and are numbered in the order in which they appear there.

The general method of approach utilizes the method of 2-phase symmetrical component analysis[6] to compute the expression for developed steady-state motor torque as a function of shaft velocity and field voltage amplitudes, as given in equation 4. A differential equation of motion, based on the assumption that the steady-state and transient torques for the same voltages and speeds will be identical, is set up as in equation 6. This equation is a linear differential equation with variable coefficients whose formal solution is as follows:

$$\omega = \epsilon^{-\int \frac{K[V_A^2(t)+V_B^2]+2b\omega_0}{2\omega_0 J}} \times \int \frac{K V_A(t) V_B - a}{J} \epsilon^{\int \frac{K[V_A^2(t)+V_B^2]+2b\omega_0}{2\omega_0 J}\,dt}\,dt \tag{7}$$

where J is the combined rotary inertia of the rotor and load.

Equation 7 can be solved for any specific form of time variation of the control field voltage amplitude. However, numerical or graphical integration may be necessary for the solution. For the first

Paper 51-163, recommended by the AIEE Feedback Control Systems Committee and approved by the AIEE Technical Program Committee for presentation at the AIEE Great Lakes District Meeting, Madison, Wis., May 17–19, 1951. Manuscript submitted February 13, 1951; made available for printing April 17, 1951.

A. M. HOPKIN is Assistant Professor in the Electrical Engineering Department of Northwestern Technological Institute, Evanston, Ill.

The author wishes to acknowledge the advice and assistance of Professor Richard W. Jones of the Electrical Engineering Department of Northwestern Technological Institute in the work leading to the preparation of this paper.

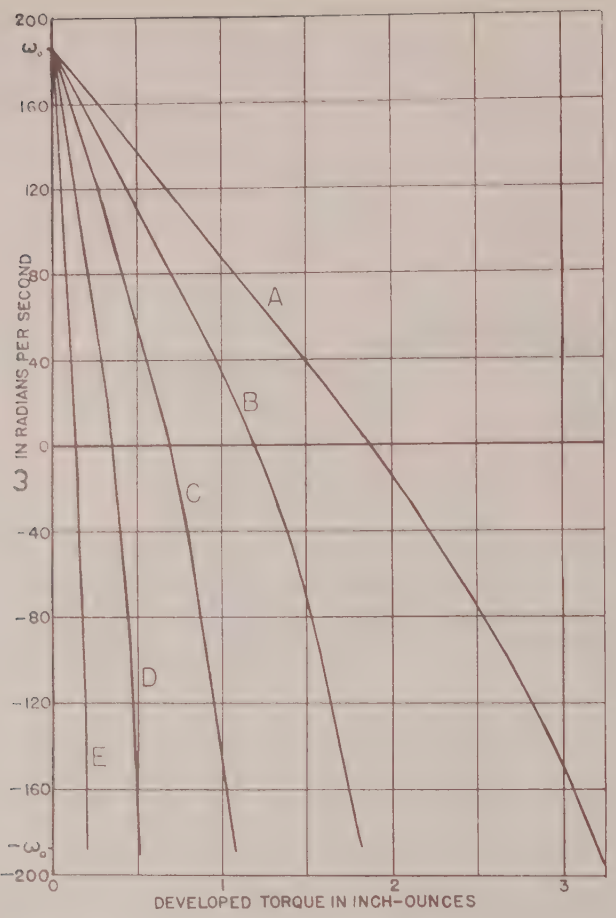

Figure 1. Developed torque-speed curves for a Diehl type *FP-25* 2-phase motor with balanced applied field voltages. Legend: Curve A-20, 20 volts; Curve B-16, 16 volts; Curve C-12, 12 volts; Curve D-8, 8 volts; Curve E-4, 4 volts

case considered in this paper an exact solution is obtained. For the second case considered certain approximations are necessary to avoid numerical graphical integration.

The Response to a Step Change of Control-Voltage Amplitude

For an applied step of control-voltage amplitude in which the instantaneous applied voltage $v_a(t)=\sqrt{2}V_A \sin 2\pi ft$, so that $V_A(t)=V_A=$constant, the solution of equation 7 results in the following expression for instantaneous shaft velocity:

$$\omega=\omega_{ss}\left(1-\epsilon^{-\frac{t}{T}}\right) \tag{12}$$

where

$$\omega_{ss}=\frac{2\omega_0(KV_AV_B-a)}{K(V_A^2+V_B^2)+2b\omega_0} \tag{10}$$

$$T=\frac{2\omega_0 J}{K(V_A^2+V_B^2)+2b\omega_0}$$

$$=\text{effective time constant} \tag{11}$$

where

V_A = control-field voltage amplitude
V_B = constant reference-field voltage amplitude

The response to a step change of control field voltage amplitude is of exponential form with a time constant that is a function of the applied field-voltage amplitude, and that becomes smaller as either the control-field-voltage amplitude V_A or the reference-field-voltage amplitude V_B is increased.

This means that T is not a true time constant.

The Steady-State Response to a Sinusoidal Variation of Control Field Voltage

If the instantaneous voltage applied to the control field is of the form $v_a(t)=V_1 \sin \gamma t \sin 2\pi ft$, representing a sinusoidal modulation of the control field voltage amplitude, the control field voltage amplitude becomes:

$$V_A(t)=V_1 \sin \gamma t \tag{13}$$

where

V_1 = sinusoidally varying amplitude of control-voltage
γ = frequency of variation of the control-voltage amplitude

If V_1 is small, an approximate steady-state solution may be obtained by substituting equation 13 into equation 7 and integrating, neglecting all terms involving higher orders of V_1. This process results in the expression:

$$\omega=\frac{KV_1V_B}{J\sqrt{\gamma^2+\beta^2}} \sin\left(\gamma t-\tan^{-1}\frac{\gamma}{\beta}\right) \tag{19}$$

where

$$\beta=\frac{KV_B^2+2b\omega_0}{2\omega_0 J} \tag{16}$$

These expressions are similar in form to the solution for a single time-constant linear system with a corner frequency at the point

$$\gamma_c=\beta=\frac{KV_B^2+2b\omega_0}{2\omega_0 J}=\frac{1}{T(0)} \text{ where } T(0)=$$

T for case where $V_A=0$

It must be repeated that these solutions hold only for small amplitudes of V_1.

Calculation of Displacement Response from the Velocity Response of the Motor

Integration of the velocity response expressions of equations 12 and 19 leads to expressions for the displacement response. The displacement response for a step input is given in equation 21 and that for a steady-state sinusoidal input is given in equation 23. These equations may be of interest where the motor is used in a position control system.

Application to Servomechanism Problems

It is generally considered desirable that the time constant of the motor-load portion of a servomechanism be kept as small as possible in order to obtain a rapid response. The time constant for the 2-phase motor-load combination is given in Appendix I as

$$T=\frac{2\omega_0 J}{K(V_A^2+V_B^2)+2b\omega_0} \tag{11}$$

T can be considered as a time constant so long as V_A and V_B do not vary time. If V_A or V_B does vary with time, then T is better looked upon as a factor which is an inverse measure of the instantaneous damping in the motor-load combination. If it is desired that a servomechanism give the quickest possible response,

then it is desirable to have the shortest possible time constant for the motor-load combination. This would require that a maximum safe voltage be applied to both control and reference fields to obtain the quickest response to a step input.

For a proportional feedback servomechanism, the voltage applied to the control winding will vary with error, and the damping of the motor will vary accordingly. To obtain the quickest possible response it might be desirable to maintain the control-field voltage at a maximum value to obtain the shortest possible motor time constant. This might be done by inserting some nonlinear compensating element in the feedback path to make the error signal seem large for a longer period of the response time.[7]

Another suggested approach to the compensation of servomechanisms utilizes a variation of the damping factor to give a quicker response without overshoot than could be obtained from a linear system.[8] It is possible that this effect could be obtained by manipulation of one or both field voltages during the transient period of the response.

Since the 2-phase motor transient response cannot be expressed in terms of linear differential equations with constant coefficients, the frequency response of the motor is not particularly meaningful except for the case of small oscillations about some operating point. Then the theory of small oscillations applies, and the resulting linear response can be used for system stability calculations. For this case the expression for the frequency response is that of a single-time constant linear system:

$$\omega = \frac{KV_1V_B}{J\sqrt{\gamma^2+\beta^2}} \sin\left(\gamma t - \tan^{-1}\frac{\gamma}{\beta}\right) \qquad (19)$$

where the corner frequency is given by

$$\gamma_c = \beta = \frac{KV_B{}^2+2b\omega_0}{2\omega_0 J} \qquad (16)$$

The value of γ_c will be greatest when the reference voltage is largest and J is smallest. Equations 16 and 19 apply only to speed oscillations about the zero speed point.

Comparison of Computed Data with Test Data

A Diehl type *FP-25* 2-phase induction motor was used to compare calculated results with actual test results.

This motor was chosen as a typical size and type of 2-phase motor. Motor parameters as obtained from name-plate data and tests on this motor are listed in Appendix II. Torque-speed curves as determined by test are shown for various control- and reference-field voltages in Figures 1 and 2. These curves can be approximated fairly well by straight lines.

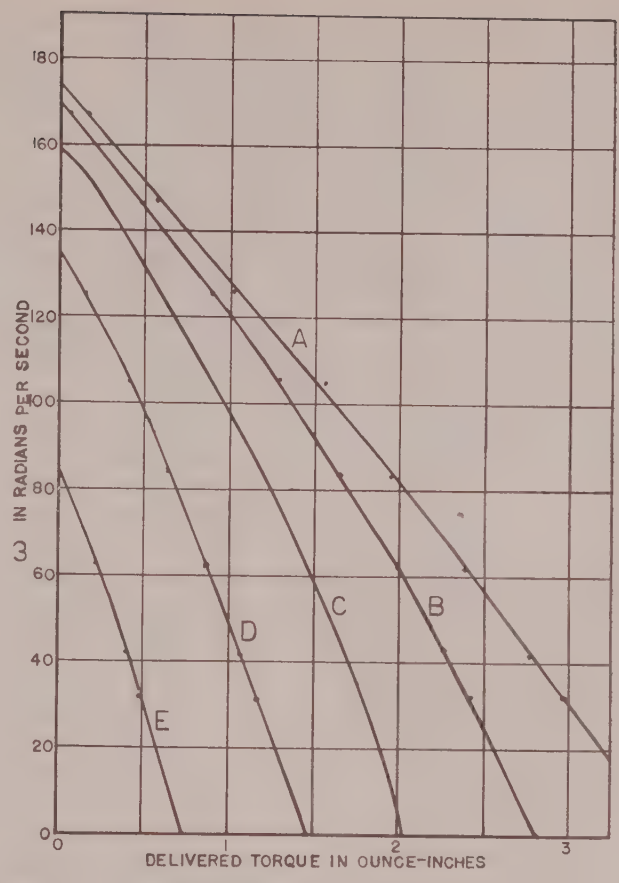

Figure 2. Delivered torque-speed curves for a Diehl type *FP-25* 2 phase motor with 20 volts applied to the reference field. Legend: Curve A-control field volts = 20; Curve B-control field volts = 16; Curve C-control field volts = 12; Curve D-control field volts = 8; Curve E-control field volts = 4

Figure 3 shows experimental transient responses resulting from various step-input voltage amplitudes applied to the control field with various values of reference-field voltages. These responses are plotted as the log of (final velocity minus instantaneous velocity) versus time. These curves are approximately straight lines whose slope is the coefficient of exponential term involved, and hence, the negative reciprocal of the time constant.

The curvature of these responses in the early-time region can be accounted for as being the result of another exponential term of the approximate form $Ce^{-t/0.005}$ caused by electrical time delays in the motor winding which were neglected in the theoretical analysis. This means that the actual system response is of the form:

$$\omega = \omega_{ss}(1 + C_1e^{-t/0.005} - C_2e^{-t/T})$$

instead of the form of equation 12. In most cases T is sufficiently greater than 0.005 to make equation 12 a good approximation. Table I shows a comparison of the values of T and ω_{ss} obtained experimentally and those calculated using equations 10 and 11.

The motor also was oscillated about zero speed by modulating the control-field voltage amplitude at various frequencies. The attenuation and phase shift of the output velocity as a function of frequency was observed. Figure 4 shows a comparison of log-frequency curves of gain and phase for experimental results and results calculated using equations 19 and 21. It will be observed that a very good correlation exists except at the higher frequencies, where the actual attenuation and phase shift becomes greater than the calculated values. Again this effect can be accounted for as being a result of electrical time delays in the windings which were neglected in the calculations.

Summary Conclusion

By making certain assumptions regarding the torque-speed curves of small

2-phase induction motors it is possible to write a first-order differential equation with variable coefficients for the motor speed as a function of time. This equation is solved for the case of a step of voltage applied to the control field and also by approximation for the case of small sinusoidally-varying-amplitude voltages applied to the control winding. The solution for the step input is an exponential rise of shaft velocity similar to that for a linear system except that the coefficient of time in the exponent is a function of the step voltage amplitude, indicating that the motor does not have a true linear response. It is possible to obtain a general solution for the case of sinusoidally varying amplitude only by assuming a very small amplitude of control-field voltage, a case which would fit the theory of small oscillations. For large oscillations of control-field voltage amplitude the response seems quite nonlinear.

The requirements set up in the initial assumptions should be fulfilled sufficiently well by some 2-phase control motors that equations 10, 11, and 12 will be useful in the predicting motor response to step inputs

In the case of other motors these equations may still be useful in predicting general trends in performance, (such as the trend of damping factor change with control voltage changes) which may be important in applications of 2-phase induction motors in servomechanism systems.

Appendix I. Derivation of the Basic Transient Performance Equation

Based on the assumption that the torque-speed curves for the 2-phase motor with balanced applied voltage can be approximated as straight lines as shown in Figure 1, the relationship between the developed torque and the shaft velocity can be approximated as

$$T = KV^2\left(1-\frac{\omega}{\omega_0}\right) \tag{1}$$

where

K = torque constant in $\frac{\text{ounce-inch}}{\text{volt}^2}$

V = balanced line voltage amplitude representing instantaneous voltages of the form $v_a(t)=\sqrt{2}V \sin 2\pi ft$, $v_b(t)=\sqrt{2}V \cos 2\pi$ ft applied to the two fields of the motor

ω = shaft angular velocity

ω_0 = theoretical no-load steady-state angular velocity = synchronous velocity.

The resultant of two unbalanced voltages applied to the motor can be divided into two components—a forward sequence component, and a backward sequence component of voltage by using the method of symmetrical components.[6] The components of motor torque due to these components of voltage can be written

$$T_1 = K\left(\frac{V_A(t)+V_B}{2}\right)^2\left(1-\frac{\omega}{\omega_0}\right) \tag{2}$$

$$T_2 = -K\left(\frac{V_A(t)-V_B}{2}\right)^2\left(1+\frac{\omega}{\omega_0}\right) \tag{3}$$

where

T_1 = forward-sequence component of torque

T_2 = reverse-sequence component of torque

$V_A(t)$ = time-varying control-field voltage amplitude, so that $v_a(t)=\sqrt{2}V_A(t)$ sin $2\pi ft$ is the instantaneous control field voltage

V_B = constant-reference field voltage amplitude, so that $v_b(t)=\sqrt{2}V_B \cos 2\pi ft$ is the instantaneous reference field voltage

The expression for the net torque is then

$$T = T_1+T_2 = K\left(V_A(t)V_B - \frac{V_A^2(t)+V_B^2}{2}\frac{\omega}{\omega_0}\right) \tag{4}$$

By assuming that the friction and load torque function is of the form

$$T_L = a+b\omega$$

where

a = coefficient of coulomb friction

b = coefficient of viscous friction

the differential equation of the motor can be written as

$$T = T_L+J\frac{d\omega}{dt} = a+b\omega+J\frac{d\omega}{dt} \tag{5}$$

where J = effective combined polar moment of inertia of the rotor and load. By substituting equation 4 in equation 5 and rearranging, there is obtained

$$\frac{d\omega}{dt}+\frac{K(V_A^2(t)+V_B^2)+2b\omega_0}{2J\omega_0}\omega = \frac{KV_A(t)V_B-a}{J} \tag{6}$$

Equation 6 can be recognized as a first order linear equation with variable coefficients whose solution is of the form:[9]

$$\omega = \epsilon^{-\int\frac{K[V_A^2(t)+V_B^2]+2b\omega_0}{2\omega_0 J}dt}\times \int\frac{KV_A(t)V_B-a}{J}\epsilon^{\int\frac{K[V_A^2(t)+V_B^2]+2b\omega_0}{2\omega_0 J}dt}dt \tag{7}$$

Evaluation of this integral equation may be difficult in some cases. Graphical or other forms of graphical solution may be necessary. Let us consider two cases.

Case 1. Step Voltage Amplitude Applied to the Control Field

Consider the case where $v_a(t)=\sqrt{2}V_A$ sin $2\pi ft$, so that $V_A(t)=V_A$ = constant.

By substituting $V_A(t)=V_A$ in equation 7 and performing the indicated integrations, there is obtained:

$$\omega = \frac{2\omega_0(KV_AV_B-a)}{K(V_A^2+V_B^2)+2b\omega_0}+C\epsilon^{-\left[\frac{K(V_A^2+V_B^2)+2b\omega_0}{2\omega_0 J}\right]t} \tag{8}$$

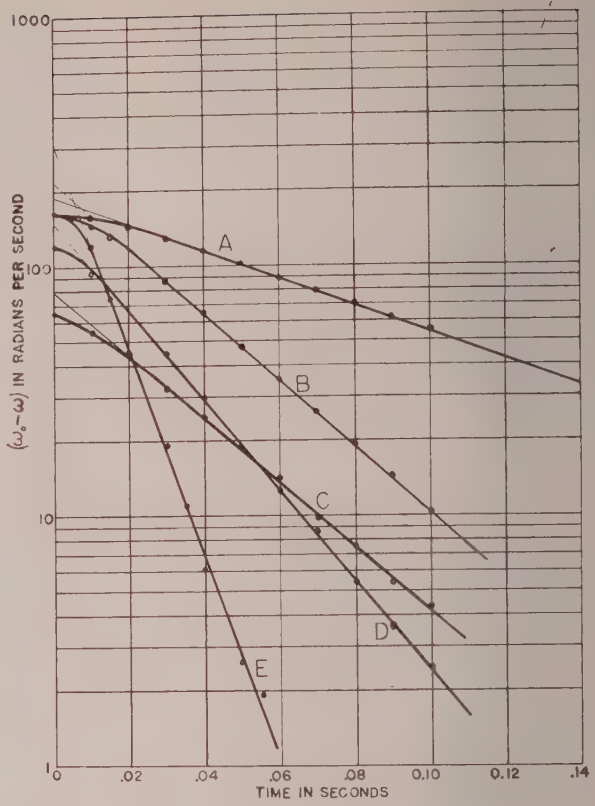

Figure 3. Transient response of a Diehl type FP-35 2-phase motor with various step voltages applied to the control field. Legend: Curve A-reference voltage 8 volts, control field voltage 8 volts; Curve B-reference voltage 12 volts, control field voltage 12 volts; Curve C-reference voltage 20 volts, control field voltage 4 volts; Curve D-reference voltage 20 volts, control field voltage 8 volts; Curve E-reference voltage 20 volts, control-field voltage 20 volts

For the case where $\omega=0$ when $t=0$,

$$\omega=\frac{2\omega_0(KV_AV_B-a)}{K(V_A^2+V_B^2)+2b\omega_0}\times\left(1-\epsilon^{-\left[\frac{K(V_A^2+V_B^2)+2b\omega_0}{2\omega_0 J}\right]t}\right) \quad (9)$$

The steady-state speed of the motor-load system will be

$$\omega_{ss}=\frac{2\omega_0(KV_AV_B-a)}{K(V_A^2+V_B^2)+2b\omega_0} \quad (10)$$

The time constant for the exponential rise of voltage will be the negative reciprocal of the coefficient of t in the exponential term of equation 9:

$$T=\frac{2\omega_0 J}{K(V_A^2+V_B^2)+2b\omega_0} \quad (11)$$

T represents a true time constant only so long as V_A and V_B remain constant. Equation 9 can be rewritten in terms of ω_{ss} and T as defined in equations 10 and 11:

$$\omega=\omega_{ss}\left(1-\epsilon^{-\frac{t}{T}}\right) \quad (12)$$

Case 2. Steady-State Response with a Sinusoidally Varying Amplitude of Voltage Applied to the Control Field

Consider the case where $v_a(t)=\sqrt{2}V_1 \sin \gamma t \sin 2\pi ft$ so that $V_a(t)=V_1 \sin \gamma t$. This process represents modulation of the line frequency voltage applied to the control field. By substituting equation 13 in equation 7 and neglecting coulomb damping, a, there is obtained:

$$\omega=\epsilon^{-\int\frac{K(V_1^2 \sin^2 \gamma t+V_B^2)+2b\omega_0}{2\omega_0 J}dt}\times\int\frac{KV_1V_B \sin \gamma t}{J}\epsilon^{\int\frac{K(V_1^2 \sin^2 \gamma t+V_B^2)+2b\omega_0}{2\omega_0 J}dt}\times dt \quad (14)$$

The parameter β can be determined by integration. However, the exact value of β leads to a form of equation 14 that cannot be integrated by simple means. In order to get a solution for small oscillations, the value of V_1 is taken sufficiently small that all terms involving V_1^2 may be neglected in β. The expression resulting for β is

$$\beta=\frac{KV_B^2+2b\omega_0}{2\omega_0 J} \quad (16)$$

$$\omega=\epsilon^{-\beta t}\int\frac{K_T V_1 V_B \sin \gamma t}{J}\epsilon^{\beta t}dt \quad (17)$$

By integrating equation 17 and multiplying the result by $\epsilon^{-\beta t}$ there is obtained

$$\omega=\frac{KV_1V_B}{J}\frac{\beta \sin \gamma t-\gamma \cos \gamma t}{\gamma^2+\beta^2}+C\epsilon^{-\beta t} \quad (18)$$

For steady-state operation the $C\epsilon^{-\beta t}$ term disappears. Equation 18 can be then rewritten in the following form:

$$\omega=\frac{KV_1V_B}{J\sqrt{\gamma^2+\beta^2}}\sin\left(\gamma t-\tan^{-1}\frac{\gamma}{\beta}\right) \quad (19)$$

Equation 19 represents the form of the frequency response of a single-time-constant linear system.

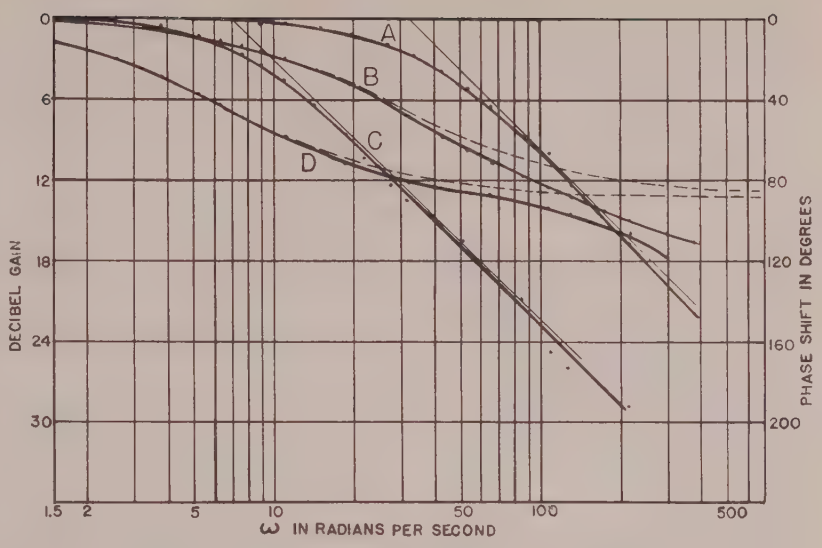

Figure 4. Log-frequency response for a Diehl type *FP-25* 2-phase motor with constant amplitude of 20 volts on the reference field and a sinusoidally varying amplitude of voltage on the control field. Legend: Curves A and B-DB gain and phase curves with a rotor inertia of 0.1 ounce-inch²; Curves C and D-DB gain and phase curves for a rotor inertia of 0.5 ounce-inch². Thin solid lines-theoretical asymptotes for DB curves; Dashed lines-theoretical phase shift curves

Case 3. Calculation of the Displacement Response from the Velocity Response for the Motor

For a step amplitude of control field voltage input the speed response is given by equation 12.

$$\omega=\omega_{ss}\left(1-\epsilon^{-\frac{t}{T}}\right) \quad (12)$$

$$\theta=\int_{t_1}^{t_2}\omega dt=\omega_{ss}\left[t-\frac{1}{T}\epsilon^{-\frac{t}{T}}\right]_{t_1}^{t_2} \quad (20)$$

If $t_1=0$ and $t_2=t$, then

$$\theta=\omega_{ss}\left(t-\frac{1}{T}+\frac{1}{T}\epsilon^{-t}\right) \quad (21)$$

The steady-state displacement response to a sinusoidal variation of control-field voltage amplitude can be obtained by integrating equation 19:

$$\theta=\int_{t_1}^{t_2}\omega dt=\left[\frac{-KV_1V_B}{\gamma J\sqrt{\gamma^2+\beta^2}}\times\cos\left(\gamma t-\tan^{-1}\frac{\gamma}{\beta}\right)\right]_{t_1}^{t_2} \quad (22)$$

if $t_1=0$, $t_2=t$, then

$$\theta=-\frac{KV_1V_B}{\gamma J\sqrt{\gamma^2+\beta^2}}\left[\cos\left(\gamma t-\tan^{-1}\frac{\gamma}{\beta}\right)-\cos\left(\tan^{-1}\frac{\gamma}{\beta}\right)\right] \quad (23)$$

Appendix II. Ratings and Parameters of the Diehl Type FP-25 2-Phase Induction Motor

Rated voltage—20 volts per phase
Rated frequency—60 cycles
Rated speed—1,640 rpm = 173 radians per second
Synchronous speed—1,800 rpm = 188 radians per second
Current—0.7 ampere per phase, practically independent of load
Rated input power—25 watts (12.5 watts per phase)
Maximum delivered power—2 watts
Rated stalled torque—3.6 ounce-inches
Torque constant—0.009 ounce-inch per volt²
Rotor inertia—0.077 ounce-inch² alone
0.10 ounce-inch² coupled to rate generator
0.50 ounce-inch² with added inertia slug

Table I. Response to Step Inputs

Reference Voltage	Control Voltage	Experimental Time Constant T, Seconds	Calculated Time Constant T, Seconds	Experimental ω_{ss}, Radians Per Second	Calculated ω_{ss}, Radians Per Second
20	20	0.011	0.0124	171	169
20	8	0.0243	0.0204	127	104
20	4	0.034	0.022	68	57
12	12	0.033	0.03	170	145
8	8	0.08	0.054	169	118

Coefficient of viscous friction—0.017 ounce-inch second per radian
Coefficient of coulomb friction—0.020 ounce-inch (approximation)

Appendix III. Definition of Symbols

T = developed torque
T_1 = forward-sequence component of developed torque
T_2 = backward-sequence component of developed torque
T_L = load torque
V = balanced line voltage
$v_A(t)$ = time varying control-field voltage amplitude
V_A = constant amplitude of step input of control-field voltage
V_1 = amplitude of sinusoidal modulation of control-field voltage
v_a = instantaneous control field voltage = $\sqrt{2}V_A(t)\sin 2\pi ft$.
v_b = instantaneous reference field voltage = $\sqrt{2}V_B\cos 2\pi ft$.
f = line frequency
ω = instantaneous shaft velocity in radians per second
ω_0 = synchronous shaft velocity in radians per second
ω_{ss} = steady-state shaft velocity in radians per second
K = torque constant in $\frac{\text{ounce-inch}}{\text{volt}^2}$
a = coefficient of coulomb friction
b = coefficient of viscous friction
J = effective combined polar moment of inertia of the motor and load
t = time
T = motor time constant
γ = frequency of modulation of control-field voltage amplitude
β = corner frequency = $\frac{K V_B^2 + 2b\omega_0}{2\omega_0 J}$
θ = angular displacement of the motor shaft in radians

References

1. An Analysis of the Induction Motor, **H. C. Stanley.** *AIEE Transactions*, volume 57, 1938, pages 751–55.

2. Transient Starting Torques in Induction Motors, **A. M. Wahl, L. A. Kilgore.** *Electrical Engineering (AIEE Transactions)*, volume 59, November 1940, pages 603–07.

3. Electro-Mechanical Transient Performances of Induction Motors, **C. N. Weygandt, S. Charp.** *AIEE Transactions*, volume 65, 1946, pages 1000–09.

4. Transient Performance of Induction Motors, **F. J. Maginess, N. R. Schultz.** *AIEE Transactions*, volume 66, 1947, pages 641–46.

5. Stabilization of Carrier Frequency Servomechanisms, **A. Sobczyk.** *Journal*, Franklin Institute (Philadelphia, Pa.), volume 246, pages 21–43.

6. Operating Characteristics of 2 Phase Servomotors, **R. J. W. Koopman.** *AIEE Transactions*, volume 68, part 1, 1949, pages 319–28.

7. A Phase Plank Approach to the Compensation of Saturating Servomechanisms, **A. M. Hopkin.** *AIEE Transactions*, volume 70, part 1, 1951, pages 631–39.

8. Non Linear Techniques for Improving Servo Performance, **Donald McDonald.** *Proceedings*, National Electronics Conference (Chicago, Ill.), volume 6, 1950.

9. Differential Equations (book), **H. B. Phillips.** John Wiley and Sons, New York, N. Y., 1922.

No Discussion

Dielectric Loading for Waveguide Linear Accelerators

GAIL T. FLESHER
STUDENT MEMBER AIEE

GEORGE I. COHN
MEMBER AIEE

WAVEGUIDE linear accelerators have become important as a practical means of producing high energy particles with the development of high power magnetrons and klystrons. They have several important advantages over the circular magnetic accelerators (cyclotron, betatron, and so forth), the chief ones being: elimination of the large, heavy and expensive deflecting magnet and all its associated problems; elimination of the difficulty in extracting the high energy beam at the output; output beams with narrow output energy spectrums; elimination of the radiation loss limitation factor at very high particle energies; and larger beam currents may be produced.

The present practical upper limit in energies attainable from the electrostatic type of linear accelerator is about 12,000,000 electron volts. This limitation is imposed by the direct potential difference which must be maintained by the structure. In the microwave type of linear accelerator the same field is used over and over again, or perhaps a more accurate description would be to say that the same field is used continuously, that is, the particles in the accelerator move along in synchronism with the accelerating field which is propagating as a traveling wave. As a result it appears to the particle that it is falling through a very large potential difference given by the line integral over the path of flight of a practically constant electric field.

Paper 51-164, recommended by the AIEE Nucleonics Committee and approved by the AIEE Technical Program Committee for presentation at the AIEE Great Lakes District Meeting, Madison, Wis., May 17–19, 1951. Manuscript submitted February 14, 1951; made available for printing April 16, 1951.

GAIL T. FLESHER and GEORGE I. COHN are both with the Illinois Institute of Technology, Chicago, Ill.

If the wave is to appear as a static or semistatic field to the particle, the particle must be traveling with substantially the same velocity as the accelerating wave. To accomplish this, the phase velocity of the waves must be slowed from their normal speed in an empty guide, which is greater than the velocity of light, to or below the velocity of light, which is the least upper bound on the speed of material particles. This slowing may be accomplished by loading the waveguide with metal disks as is done in all waveguide linear accelerators under construction or already built which have so far been reported in the available literature.[1] Another method of loading the guide has been suggested by Bruck and Wicher[2] and Frankel[3] and consists of a continuous dielectric loading in the form of a coaxial dielectric cylinder in the guide.

The slowing of the phase velocity by dielectric loading may be explained qualitatively as follows. The phase velocity of radiation in an infinite region of relative dielectric constant ϵ_r is reduced from the velocity in vacuum by the factor

$$\frac{1}{\sqrt{\epsilon_r}}$$

Similarly, the phase velocity can be lowered from the value in the empty guide by filling the guide with dielectric. This calculation would be relatively simple if the guide were to be completely filled with dielectric. However, a hole must be left for the accelerating particles to pass through, thereby complicating the calculations. Thus, the first problem is to find the values of the dimensions and dielectric constants which will allow a given phase velocity at a specified frequency.

Teasdale and Higgins[4] have found the electromagnetic fields in the ideal two coaxial dielectric waveguide. In the lossless traveling-wave type of accelerator the accelerating field intensity adjusts to the value necessary to propagate the input power down the guide. The energy then passes out the far end of the guide and is lost. In the lossless standing-wave type of accelerator the ends of the guide are closed by metal walls so that the energy is reflected and may be used over and over again, thereby enabling much higher field intensities to be obtained. If the losses were neglected, the fields in the guide would build up to indefinitely high values if power were fed in continuously. In the practical case, the fields build up till there is equilibrium between the power being fed in and the power loss in the dielectric and metal parts of the guide. This paper will examine the dielectric loaded case with losses, find the relation between the electric accelerating field and the input power, guide dimensions, frequency, and material characteristics, and examine the predicted performance in comparison with the metal disk loaded accelerator.

Electromagnetic Field Structure

The solution to Maxwell's equation subject to the boundary conditions shown in Figure 1 for perfectly conducting wall and lossless dielectric is, using $E_{z1}=$

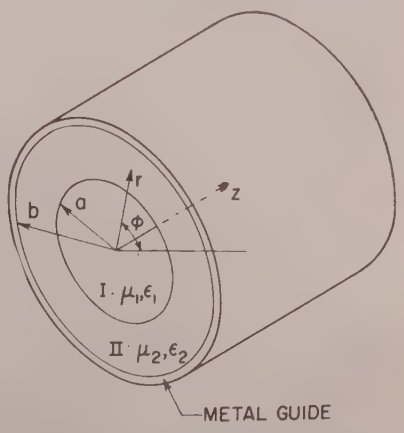

Figure 1. The two coaxial dielectric region waveguide

$E_{z1}{}^0 e^{j(\omega t-\beta z)}$.

REGION I

$$E_{z1}{}^0 = B_1 J_n(K_1 r)\cos(n\phi) \quad (1)$$

$$E_r{}^0 = \left[-\frac{j\beta}{K_1} B_1 J_n'(K_1 r) - \frac{jn\omega\mu_1}{K_1{}^2 r} A_1 J_n(K_1 r)\right]\cos(n\phi) \quad (2)$$

$$E_{\phi 1} = \left[\frac{j\beta n}{K_1{}^2 r} B_1 J_n(K_1 r) + \frac{j\omega\mu_1}{K_1} A_1 J_n'(K_1 r)\right]\sin(n\phi) \quad (3)$$

$$H_{z1}{}^0 = A_1 J_n(K_1 r)\sin(n\phi) \quad (4)$$

$$H_{r1}{}^0 = \left[-\frac{j\omega\epsilon_1 n}{K_1{}^2 r} B_1 J_n(K_1 r) - \frac{j\beta}{K_1} A_1 J_n'(K_1 r)\right]\sin(n\phi) \quad (5)$$

$$H_{\phi 1}{}^0 = \left[-\frac{j\omega\epsilon_1}{K_1} B_1 J_n'(K_1 r) - \frac{j\beta n}{K_1{}^2 r} A_1 J_n(K_1 r)\right]\cos(n\phi) \quad (6)$$

REGION II

$$E_{z2}{}^0 = B_2 F_{nn}(K_2 r)\cos n\phi \quad (7)$$

$$E_{r2}{}^0 = \left[-\frac{j\beta}{K_2} B_2 F_{nn}'(K_2 r) - \frac{jn\omega\mu_2}{K_2{}^2 r} A_2 G_{nn}(K_2 r)\right]\cos(n\phi) \quad (8)$$

$$E_{\phi 2}{}^0 = \left[\frac{j\beta n}{K_2{}^2 r} B_2 F_{nn}(K_2 r) + \frac{j\omega\mu_2}{K_2} A_2 G_{nn}'(K_2 r)\right]\sin(n\phi) \quad (9)$$

$$H_{z2}{}^0 = A_2 G_{nn}(K_2 r)\sin(n\phi) \quad (10)$$

$$H_{r2}{}^0 = \left[-\frac{j\omega\epsilon_2 n}{K_2{}^2 r} B_2 F_{nn}(K_2 r) - \frac{j\beta}{K_2} A_2 G_{nn}'(Kr)\right]\sin(n\phi) \quad (11)$$

$$H_{\phi 2}{}^0 = \left[-\frac{j\omega\epsilon_2}{K_2} B_2 F_{nn}'(K_2 r) - \frac{j\beta n}{K_2{}^2 r} A_2 G_{nn}(K_2 r)\right]\cos(n\phi) \quad (12)$$

where

$$K_1{}^2 = -\beta^2 + \omega^2\mu_1\epsilon_1 \quad (13)$$

$$K_2{}^2 = -\beta^2 + \omega^2\mu_2\epsilon_2 \quad (14)$$

$$F_{nm}(K_2 r) = J_n(K_2 r) - \frac{J_m(K_2 b)}{Y_m(K_2 b)} Y_n(K_2 r) \quad (15)$$

$$G_{nm}(K_2 r) = J_n(K_2 r) - \frac{J_m'(K_2 b)}{Y_m'(K_2 b)} Y_n(K_2 r) \quad (16)$$

$F_{nm}(K_2 r)$ and $G_{nm}(K_2 r)$ are linear combinations of Bessel functions and hence Bessel functions themselves. The first subscript gives the order of the Bessel function as in all Bessel functions. The second subscript has been added to give the order of the Bessel functions comprising the constant coefficient. It has been necessary to add this second subscript rather than letting the first subscript convey all the information because it is desired to use all the standard Bessel function interrelationships in manipulating these new Bessel functions and this introduces combinations in which the two subscripts are not always the same. The constants A_1, A_2, B_1, and B_2 are related by the boundary conditions at the interface between the two regions. Their values are fixed by the power flow or stored energy in the guide. The boundary conditions at the interface require the parameters to satisfy the conditional equation

$$\left[\frac{\mu_1}{K_1 a}\frac{J_{nn}'(K_1 a)}{J_{nn}(K_1 a)} - \frac{\mu_2}{K_2 a}\frac{G_{nn}'(K_2 a)}{G_{nn}(K_2 a)}\right]\times\left[\frac{\epsilon_1}{K_1 a}\frac{J_{nn}'(K_1 a)}{J_{nn}(K_1 a)} - \frac{\epsilon_2}{K_2 a}\frac{F_{nn}'(K_2 a)}{F_{nn}(K_2 a)}\right] = \frac{(\beta n\omega)^2}{(K_1 K_2 a)^4}(\mu_2\epsilon_2 - \mu_1\epsilon_1)^2 \quad (17)$$

Selection of Accelerating Mode

For the purpose of acceleration of particles the most intense z-component of electric field is desired. The mode which provides the maximum accelerating field for a given input power is the $n=0$ mode. Putting n equal to zero in the conditional equation gives

$$\frac{\epsilon_1}{K_1 a}\frac{J_0'(K_1 a)}{J_0(K_1 a)} - \frac{\epsilon_2}{K_2 a}\frac{F_{00}'(K_2 a)}{F_{00}(K_2 a)} = 0 \quad (18)$$

for TM waves or

$$\frac{\mu_1}{K_1 a}\frac{J_0'(K_1 a)}{J_0(K_1 a)} - \frac{\mu_2}{K_2 a}\frac{G_{00}'(K_2 a)}{G_{00}(K_2 a)} = 0 \quad (19)$$

for TE waves. The TE wave is useless for a linear accelerator since by definition $E_z=0$. Thus for a particle accelerator, equation 18 is the simplified conditional equation.

With $n=0$ the field structure simplifies to

REGION I

$$E_{z1}{}^0 = B_1 J_0(K_1 r) \quad (20)$$

$$E_{r1}{}^0 = \frac{j\beta}{K_1} B_1 J_1(K_1 r) \quad (21)$$

$$H_{\phi 1}{}^0 = \frac{j\omega\epsilon_1}{K_1} B_1 J_1(K_1 r) \quad (22)$$

REGION II

$$E_{z2}{}^0 = B_2 F_{00}(K_2 r) \quad (23)$$

$$E_{r2}{}^0 = \frac{j\beta}{K_2} B_2 F_{10}(K_2 r) \quad (24)$$

$$H_{\phi 2}{}^0 = \frac{j\omega\epsilon_2}{K_2} B_2 F_{10}(K_2 r) \quad (25)$$

Specialization of the Conditional Equation

The conditional equation 18 may be rewritten as follows

$$\frac{J_0(K_2 b)}{Y_0(K_2 b)} = \frac{J_1(K_2 a) - \frac{\epsilon_1 K_2 J_1(K_1 a)}{\epsilon_2 K_1 J_0(K_1 a)} J_0(K_2 a)}{Y_1(K_2 a) - \frac{\epsilon_1 K_2 J_1(K_1 a)}{\epsilon_2 K_1 J_0(K_1 a)} Y_0(K_2 a)} \quad (26)$$

Where K_1 and K_2 rewritten are

$$K_1 = \frac{\omega}{C}\sqrt{\mu_{1r}\epsilon_{1r} - \frac{C^2}{V_p{}^2}} \quad (27)$$

$$K_2 = \frac{\omega}{C}\sqrt{\mu_{2r}\epsilon_{2r} - \frac{C^2}{V_p{}^2}} \quad (28)$$

where

$$\mu_n = \mu_{nr}\mu_0 \quad (29)$$

$$\epsilon_n = \epsilon_{nr}\epsilon_0 \quad (30)$$

$$C = \frac{1}{\sqrt{\mu_0\epsilon_0}} \quad (31)$$

Equation 26 relates all the dimensional and material parameters of the guide with the accelerating wave frequency and phase velocity. With only the one conditional relationship to satisfy all the parameters except one may be chosen freely. To reduce computational work the following dimensionless quantities are used:

$$\mu_{1r},\ \mu_{2r},\ \epsilon_{1r},\ \epsilon_{2r},\ \frac{V_p}{C},\ \frac{a\omega}{C},\ \frac{b}{a}$$

Four conditions imposed by available materials and accelerator requirements simplify the conditional equation. These are: Nearly all dielectrics have the permeability of free space, hence

$$\mu_{1r} = \mu_{2r} = 1 \quad (32)$$

Region I must be free space to permit the passage of the particles to be accelerated, thus

$$\epsilon_{1r} = 1 \quad (33)$$

and if the phase velocity of the accelerating wave is less than the velocity of light, the accelerated particles will be limited to finite energies. If the phase velocity is equal to that of light in free space ($v_p = C$) the highest output energies attainable will be limited by the input power and the length of the accelerator. Therefore if the maximum energy is not to be limited by the phase velocity

$$\frac{v_p}{C} = 1 \quad (34)$$

With these conditions

$$K_1 = 0 \quad (35)$$

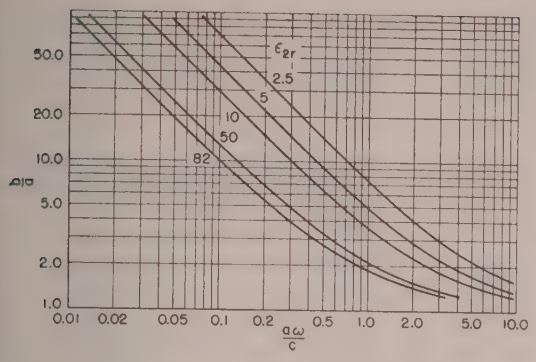

Figure 2 (left). Solution of the conditional equation for the TM_{03} mode

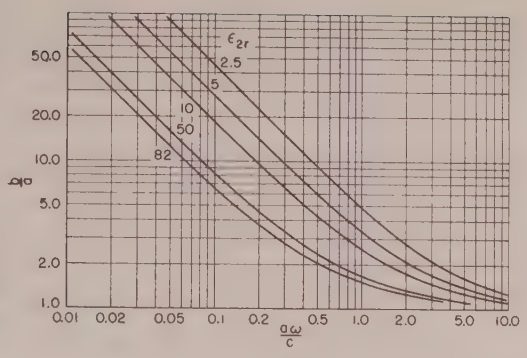

Figure 3 (right). Solution of the conditional equation for the TM_{02} mode

$$K_2 = \frac{\omega}{C}\sqrt{\epsilon_{2r}-1} \tag{36}$$

and the conditional equation simplifies to

$$\frac{J_0(K_2b)}{Y_0(K_2b)} = \frac{J_1(K_2a)-\dfrac{K_2a}{2\epsilon_{2r}}J_0(K_2a)}{Y_1(K_2a)-\dfrac{K_2a}{2\epsilon_{2r}}Y_0(K_2a)} \tag{37}$$

Under these conditions the field in region I simplifies to

$$E_{z1}{}^0 = B_1 \tag{38}$$

$$E_{r1}{}^0 = \frac{j\beta B_1}{2}\,r \tag{39}$$

$$H_{\phi 1}{}^0 = \frac{j\omega\epsilon_1 B_1}{2}\,r \tag{40}$$

In addition to the limitation placed on the particle energies obtainable by phase velocities less than that of light in free space there is another disadvantage. This comes about because when $v_p/C<1$, K_1 becomes imaginary and $J_0(K_1r)$ becomes the modified Bessel function I_0. This has the undesirable feature that it is a minimum on the axis instead of a maximum as is J_0. Furthermore, lower phase velocity means more dielectric,[4] hence greater losses and lower accelerating fields.

Solution of the Conditional Equation

Since every variable occurs in at least one Bessel function argument, the most practical method of solution will be the one which specifies the greatest number of Bessel function arguments. If ϵ_{2r} and $a\omega/C$ are chosen, $K_2\,a$ is known from equation 36 and the right member of equation 37 is completely determined. Thus K_2b, the only unknown in the left member may be found. This method of solution was used. It was found that calculations using curves representing combinations of Bessel functions such as the second term of equation 18, as suggested by Teasdale and Higgins,[4] and Oliner,[5] or the left member of equation 37, as suggested by Frankel[3] were not accurate enough for certain critical field calculations. In Bessel functions, as in all oscillatory functions, a small percentage error in a large argument may mean a large percentage error in the value of the function. Volume VI of the British Association Mathematical Tables[6] was used to obtain the values of the Bessel functions.

The oscillatory nature of J_0 and Y_c provide an infinite number of values of K_2b for each choice of ϵ_{2r} and $a\omega/C$. These solutions are labeled in the usual way followed for transverse eigen values. The smallest value of K_2b determines the TM_{01} mode, the next larger value determines the TM_{02} mode, and so forth.

The results of the solution of equation 37 for the first three modes are shown graphically in Figures 2, 3, and 4. Curves are given for values of $\epsilon_{2r}=2.5$, 5, 10, 50, and 82. If the parameters satisfy the relations shown on the graphs, the guided wave will have a phase velocity $V_p=C$. The following conclusions may be drawn from the curves.

1. For a given ϵ_{2r} and $a\omega/C$, higher modes require larger b/a.
2. For constant $a\omega/C$, the larger ϵ_{2r} is, the lower the necessary b/a.
3. As $a\omega/C$ gets larger, b/a approaches unity for all ϵ_{2r}.
4. For constant ϵ_{2r} the curves asymptotically approach constant values of $b\omega/C$ as $a\omega/C$ becomes small.

Result one indicates that the higher modes should not be used in an accelerator because for a given $a\omega/C$ they require larger values of b/a and hence larger enclosed guide volumes. For a given input power, this means smaller energy density and hence lower accelerating fields. Result two is the manifestation of the greater slowing effect of the higher dielectric constant on the waves in the guide. The third result expresses the fact that very little dielectric is needed for slowing the wave when the cross section of the guide is very large. The fourth result states that the effect of the presence of region I becomes negligible as its radius becomes small.

Method of Determining the Accelerating Field for the Standing Wave Accelerator

There are two schemes with which the waves may be utilized in the linear accelerator. The traveling-wave type allows the accelerating fields to build up to the value necessary to sustain the power flow and losses in the guide. When the wave reaches the end of the guide, its remaining energy is lost in the matched termination. In the standing-wave type of accelerator the wave is reflected at the termination and travels back to the input end of the guide where it is again reflected and combines with the input wave, thereby strengthening the accelerating field, which is the positive traveling wave. For the present, the standing-wave type will be studied; an examination of the traveling-wave accelerator will be given later and a comparison of the two types will be made.

The peak accelerating field on the axis, which is desired as a function of the input power, frequency, and guide parameters, will be designated as E and from equation 20 is

$$E = B_1 \tag{41}$$

The fields in the standing-wave type accelerator are found by adding the fields of the incident and reflected waves. This gives for

REGION I

$$E_{z1} = 2EJ_0(K_1r)\cos(\beta z)e^{j\omega t} \tag{42}$$

$$E_{r1} = \frac{2\beta}{K_1}EJ_1(K_1r)\sin(\beta z)e^{j\omega} \tag{43}$$

$$H_{\phi 1} = j\frac{2\omega\epsilon_1}{K_1}EJ_1(K_1r)\cos(\beta z)e^{j\omega t} \tag{44}$$

REGION II

$$E_{z2} = 2B_2F_{00}(K_2r)\cos(\beta z)e^{j\omega} \tag{45}$$

$$E_{r2}=\frac{2\beta}{K_2}B_2F_{10}(K_2r)\sin(\beta z)e^{j\omega t} \quad (46)$$

$$H_{\phi 2}=j\frac{2\omega\epsilon_2}{K_2}B_2F_{10}(K_2r)\cos(\beta z)e^{j\omega t} \quad (47)$$

For $K_1=0$ the fields in region I reduce to

$$E_{z1}=2E\cos(\beta z)e^{j\omega t} \quad (48)$$

$$E_{r1}=\beta Er\sin(\beta z)e^{j\omega t} \quad (49)$$

$$H_{\phi 1}=j\omega\epsilon_1 Er\cos(\beta z)e^{j\omega t} \quad (50)$$

To satisfy the vanishing of the radial electric field at the reflecting termination of the guide

$$\sin(\beta z_0)=0$$

and hence the length z_0 is required to satisfy the condition

$$z_0=\frac{l\pi}{\beta} \qquad l=0,\ 1,\ 2,\ 3,\ 4,\ 5,\ 6,\ \ldots\ldots$$

The $l=0$ solution means that either $z_0=0$ and hence zero accelerator length, or that $\beta=0$, hence no traveling wave, and, therefore, of no interest here. For accelerators operating in the neighborhood of ten centimeters, values of l between 10 and 20 are of interest. The accelerator is then operating as a resonant cavity in the TM_{01l} mode.

In the interest of generality, the choice of $\epsilon_{1r}=1$ and $v_p/C=1$ and the consequence $K_1=0$, shall not be imposed until after the expressions involving K_1 have been found.

B_2 is found from the boundary condition at the interface of the two dielectric regions and is

$$B_2=E\frac{J_0(K_1a)}{F_{00}(K_2a)} \quad (51)$$

In the steady-state condition the power input to the accelerator is equal to the power dissipated.

$$P_{in}=P_d+P_m \quad (52)$$

where P_{in} is the total input power, P_d is the power dissipated in the dielectric, and P_m is the power dissipated in the metal walls. For low beam currents the power absorbed by the accelerated particles is negligible. P_d and P_m are functions of E and the various parameters. These are substituted into equation 52 which is then solved for E in terms of the various parameters and input power.

Dielectric Losses

Losses similar to hysteresis losses in iron occur in dielectrics at microwave frequencies. For good dielectrics, these losses are small and do not appreciably disturb the fields. Therefore, the dissipation may be found by calculations based on the fields for the lossless case.

Losses for a material are normally accounted for through the use of a finite nonzero conductivity σ which enters the Helmholtz equation for the electric field as follows

$$\nabla^2\boldsymbol{E}=j\omega\mu(\sigma+j\omega\epsilon)\boldsymbol{E} \quad (53)$$

and similarly for the magnetic field. For good insulators the conductivity at very low frequency and direct current is practically zero; however, the losses increase roughly (irregularly so in general) with frequency and hence the material has to be characterized by a variable conductivity. It is most desirable to characterize materials by constants and this desire may be more closely fulfilled by factoring an ω out of the conductivity and using the remaining factor (σ/ω) as the new characteristic parameter. If a j also is factored out, the new factor may be combined with the dielectric constant to form a complex dielectric constant which characterizes both the capacitivity and the losses. The Helmholtz equation then may be written

$$\nabla^2\boldsymbol{E}=-\omega^2\mu\epsilon_c\boldsymbol{E} \quad (54)$$

where

$$\epsilon_c=\epsilon-j\epsilon' \quad (55)$$

and

$$\epsilon'=\frac{\sigma}{\omega} \quad (56)$$

This loss characteristic factor is not normally tabulated but its ratio with the capacitivity and is called the loss tangent

$$\tan\delta=\frac{\epsilon'}{\epsilon} \quad (57)$$

The average density of power loss is given by

$$\frac{\sigma}{2}|\boldsymbol{E}\cdot\boldsymbol{E}^*|$$

which in terms of the loss tangent is

$$\frac{\omega\epsilon\tan\delta\,|\boldsymbol{E}\cdot\boldsymbol{E}^*|}{2}$$

The integral of this over the volume occupied by the dielectric gives as the power dissipated in the dielectric

$$P_d=\int\int\int\frac{\omega\epsilon\tan\delta}{2}|\boldsymbol{E}\cdot\boldsymbol{E}^*|d\tau \quad (58)$$

For the TM_{01} case and dielectric in Region II only, this becomes

$$P_d=\frac{\omega\epsilon_2\tan\delta}{2}\int_0^{2\pi}\int_0^{z_0}\int_a^b\times [E_rE_r^*+E_zE_z^*]rdrd\phi dz \quad (59)$$

Substituting in the field components from equations 45 and 46 gives

$$P_d=2\omega\epsilon_2\tan\delta B_2^2\times \int_0^{2\pi}\int_0^{z_0}\int_a^b\left[F_{00}^2(K_2r)\cos^2(\beta z)+\frac{\beta^2}{K_2^2}F_{10}^2(K_2r)\sin^2(\beta z)\right]rdrd\phi dz \quad (60)$$

Integrating and eliminating B_2 with equation 51

$$P_d=\pi\omega\epsilon_2\tan\delta E^2a^4z_0\frac{\omega^2}{C^2}\times \epsilon_{2r}\left\{\left[\frac{b}{a}\frac{\epsilon_1}{\epsilon_2}\frac{J_1(K_1a)}{K_1a}\frac{F_{10}(K_2b)}{F_{11}(K_2a)}\right]^2-\left[\frac{J_0(K_1a)}{K_2a}\right]^2-\left[\frac{\epsilon_1}{\epsilon_2}\frac{J_1(K_1a)}{K_1a}\right]^2+\frac{2\epsilon_1}{\epsilon_2\epsilon_{2r}}\left[\frac{\beta C}{\omega aK_2}\right]^2\frac{J_1(K_1a)}{K_1a}J_0(K_1a)\right\} \quad (61)$$

Introducing the special case $(v_p=C,$

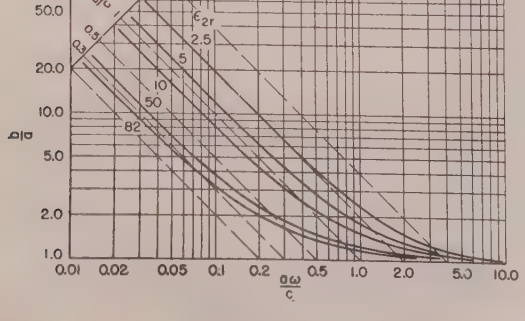

Figure 4 (left). Solution of the conditional equation for the TM_{01} mode

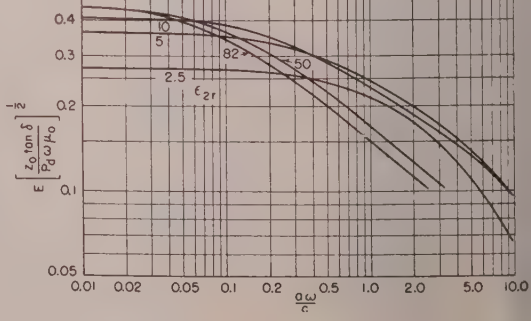

Figure 5 (right). Calculated variation of the dielectric power loss with the electric field strength and the normalized dimensions

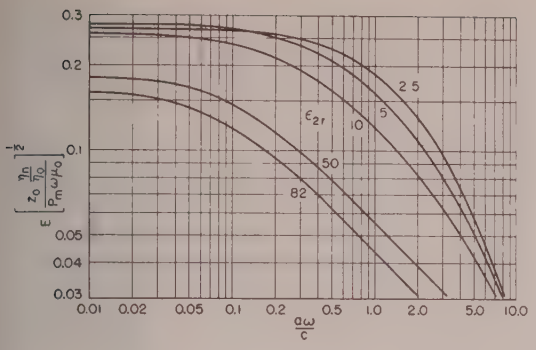

Figure 6 (left). Calculated variation of the metal guide wall power losses with the electric field strength and the normalized dimensions

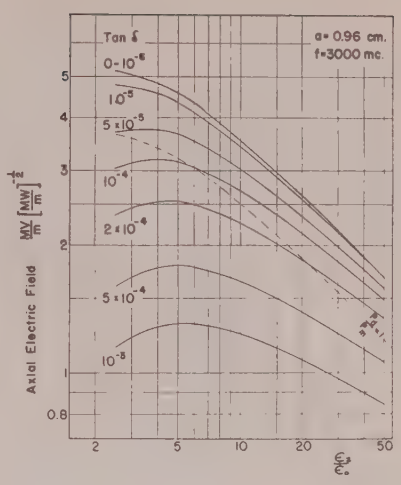

Figure 7 (right). Calculated electric accelerating field strength for a fixed inner radius and frequency

$\epsilon_{1r}=1$, $K_1=0$) and rearranging, equation 61 becomes

$$E\left[\frac{z_0\tan\delta}{P_d\omega\mu_0}\right]^{\frac{1}{2}}=\left\{\frac{\pi}{4}\left(\frac{a\omega}{C}\right)^4\times\left[\left(\frac{b}{a}\frac{F_{10}(K_2b)}{F_{10}(K_2a)}\right)^2-1-4\frac{\epsilon_{2r}+1}{\left(\frac{a\omega}{C}\right)^2}\right]\right\}^{-\frac{1}{2}} \quad (62)$$

The values of Figure 4 are used with equation 62 to obtain Figure 5.

The combination

$$\frac{F_{10}(K_2b)}{F_{10}(K_2a)}=\frac{J_1(K_2b)-\frac{J_0(K_2b)}{Y_0(K_2b)}Y_1(K_2b)}{J_1(K_2a)-\frac{J_0(K_2b)}{Y_0(K_2b)}Y_1(K_2a)} \quad (63)$$

is one that occurs often in the calculations. Since it appears in terms of comparable magnitude which are subtracted from one another, it is necessary to calculate this combination accurately.

For a constant loss tangent and power input per-unit length, the following conclusions can be drawn from Figure 5.

1. As $a\omega/C$ gets small, E asymptotically approaches a constant value for each ϵ_{2r}.

2. For a given ϵ_{2r}, E becomes less as $a\omega/C$ increases.

3. For a given $a\omega/C$, there is a maximum value of E as ϵ_{2r} is varied.

Result two is due to the increase in volume of the guide with increasing "a" thereby reducing the energy density and hence lowering the accelerating field. The third result shows that there is an optimum value of dielectric constant. For a constant $a\omega/C$, a small ϵ_{2r} requires a large value of b/a, and hence large volume, low energy density, and a low accelerating field intensity. As ϵ_{2r} is increased b/a decreases which decreases the volume, increasing the energy density and hence increasing the accelerating field. As the dielectric constant is increased further, more of the energy is concentrated in the dielectric and less in the center region; the losses for a given field intensity thereby go up. Higher ϵ_{2r} nullify the first increases and the accelerating field is decreased, thereby admitting a maximum value of E.

Guide Wall Losses

The finite conductivity of the metal walls of the guide introduce additional losses. For good conductors, these losses are small and do not appreciably disturb the fields. The perturbation of the electric field at the wall can be obtained from the unperturbed magnetic field (magnetic field for the lossless case) at the wall. The perturbation of the magnetic field is negligible but the perturbation of the tangential component of the electric field is the entire tangential component since the unperturbed tangential component at the wall is zero. The tangential electric field at the wall is given by

$$E_z=-Z_sH_\phi \quad (64)$$

where Z_s is the intrinsic surface impedance of the metal and is given by

$$Z_s=R_s+j\omega L_s=(1+j)\sqrt{\frac{\pi f\mu_0}{\sigma}} \quad (65)$$

Complex Poynting's vector giving the average power flow density into the metal wall is

$$P_r=\frac{1}{2}\Re(-E_zH_\phi^*)=\frac{R_s}{2}|H_\phi|^2\Big|_{r=b} \quad (66)$$

Integrating this over the inner surface of the guide gives the average power dissipated in the metal walls as

$$P_m=\frac{R_s}{2}\int\int P_r\,dS \quad (67)$$

Substituting in the field component from equation 47 gives

$$P_m=2\omega^2\frac{\epsilon_2^2B_2^2}{K_2^2}R_sF_{10}^2(K_2b)\times\int_0^{2\pi}\int^{z_0}\cos^2(\beta z)b\,d\phi\,dz \quad (68)$$

Integrating and eliminating B_2 gives for the general K_1

$$P_m=2\pi z_0ba^2R_s\left[\omega\epsilon_1E\frac{F_{10}(K_2b)}{F_{10}(K_2a)}\frac{J_1(K_1a)}{K_1a}\right]^2 \quad (69)$$

For $K_1=0$ this reduces upon rearrangement to

$$E\left[\frac{z_0}{P_m\omega\mu_0}\frac{R_s}{\eta_0}\right]^{\frac{1}{2}}=\left[\frac{\pi}{2}\left(\frac{a\omega}{C}\right)^3\frac{b}{a}\frac{F_{10}^2(K_2b)}{F_{10}^2(K_2a)}\right]^{-\frac{1}{2}} \quad (70)$$

where

$$\eta_0=\sqrt{\frac{\mu_0}{\epsilon_0}}=\mu_0C$$

is the impedance of free space. Equation 70 is presented in Figure 6.

For a given metal, power input per-unit length, and frequency the following observations are made:

1. For a given ϵ_{2r}, E asymptotically approaches a constant value as $a\omega/C$ becomes small.

2. For a given ϵ_{2r}, E decreases as $a\omega/C$ increases.

3. For sufficiently large $a\omega/C$, E decreases as ϵ_{2r} increases.

4. For $a\omega/C<0.15$ there is a maximum E as ϵ_{2r} varies.

When ϵ_{2r} is increased the field strength at the walls is increased sufficiently so that the accelerating field E is actually decreased when $a\omega/C>0.15$. When $a\omega/C<0.15$ a maximum E occurs with variation in ϵ_{2r}. If $a=0$ the maximum accelerating field intensity occurs when $\epsilon_{2r}=4$. From consideration of particle beam size the inner radius must be such that at 3,000 megacycles $a\omega/C>0.3$. Thus, it is desirable to keep the dielectric constant as small as possible in order to keep the metal losses as low as possible.

The losses in the reflecting end plates of the accelerator have been neglected because of their small area compared to the cylindrical wall area.

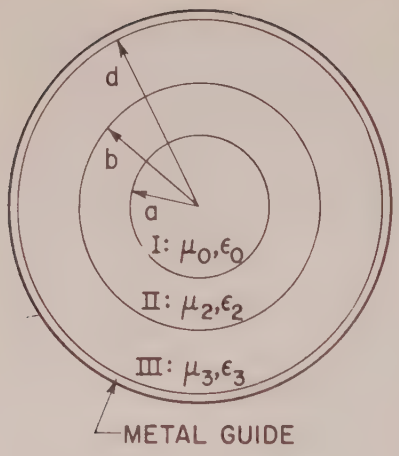

Figure 8. A three region dielectric loaded accelerator waveguide

Axial Accelerating Field

Solving equation 62 for P_d and equation 70 for P_m gives

$$P_d = \frac{E^2 z_0 \tan\delta}{y_d^2 \omega\mu_0} \tag{71}$$

$$P_m = \frac{E^2 z_0 R_s}{y_m^2 \omega\mu_0\eta_0} \tag{72}$$

where

$$y_d = \left\{\frac{\pi}{4}\left(\frac{a\omega}{C}\right)^2\left[\left(\frac{b}{a}\frac{F_{10}(K_2 b)}{F_{10}(K_2 a)}\right)^2 - 1 - 4\frac{\epsilon_{2r}+1}{\left(\frac{a\omega}{C}\right)^2}\right]\right\}^{-\frac{1}{2}} \tag{73}$$

which is plotted in Figure 5, and

$$y_m = \left[\frac{\pi}{2}\left(\frac{a\omega}{C}\right)^3 \frac{b}{a}\frac{F_{10}^2(K_2 b)}{F_{10}^2(K_2 a)}\right]^{-\frac{1}{2}} \tag{74}$$

which is plotted in Figure 6.

Substituting equations 71 and 72 into equation 52 gives for the accelerating field intensity

$$E = \left[\frac{P_{in}\omega\mu_0}{z_0}\right]^{\frac{1}{2}}\left[\frac{\tan\delta}{y_d^2} + \frac{R_s/\eta_0}{y_m^2}\right]^{-\frac{1}{2}} \tag{75}$$

This is the equation we have been looking for and

$$\frac{E}{\sqrt{P_{in}/z_0}}$$

is plotted in Figure 7 as a function of ϵ_{2r} for different values of $\tan\delta$ for the case of the copper guide walls ($R_s = 1.427\times10^{-2}$ ohms), $f = 3\times10^9 \sim$, $a = 0.955$ cm, and $\sqrt{P_{in}/Z_0} = 10^3\,(m\omega/m)^{1/2}$.

Since y_d and y_m are the same order of magnitude over the range of ϵ_{2r} of interest equations 71 and 72 show that the ratio of power lost in the dielectric to power lost in the metal is approximately

$$\frac{P_d}{P_m} \approx \frac{\tan\delta}{R_s/\eta_0} \tag{76}$$

For copper $\sigma = 5.8\times10^7$ mhos/m giving at $f = 3{,}000$ mc.

$$R_s/\eta_0 = 3.79\times10^{-5} \tag{77}$$

This can be compared with $\tan\delta = 3.0\times10^{-4}$ for polystyrene, one of the best low loss dielectrics. Thus, if polystyrene is used for loading, the losses in the dielectric will be about ten times the losses in the metal. From the standpoint of use in a linear accelerator polystyrene is an excessively loss dielectric. Fused quartz with $\tan\delta = 6\times10^{-5}$ is a great deal better but still leaves much to be desired in the way of low loss dielectrics.

Even though the dielectric loss is great, the calculated value of the accelerating field intensity is in the same range as that obtainable from the metal disk loaded linear accelerators as shown in Table 1.

In this table, the disk loaded accelerating fields are calculated from a paper by Slater.[1] Early theoretical work was done by Hahn,[7] Chu and Hansen,[8] and Fry et al.[9]

Traveling Wave Accelerator

The traveling-wave type of accelerator has a third kind of power loss in addition to the metal and dielectric losses. This loss is the power which must flow out the end of the guide to the matched load. For a guide length z_1, the power balance for equilibrium is

$$P_{in} = P_d Z_1 + P_m Z_1 + P_{out} \tag{78}$$

Here it is more convenient to work with the power dissipation per-unit length which in terms of the total dissipations for the standing-wave type are

$$p_d = \frac{P_d}{2Z_0} \tag{79}$$

$$p_m = \frac{P_m}{2Z_0} \tag{80}$$

Therefore, the dissipated powers per-unit length are

$$p_d = \frac{E^2 \tan\delta}{2y_d^2\omega\mu_0} \tag{81}$$

$$p_m = \frac{E^2 R_s/\eta_0}{2y_m^2\omega\mu_0} \tag{82}$$

The power flow down the guide is given by

$$P = v_g \mathrm{u} \tag{83}$$

where v_g is the group velocity and u the stored energy per-unit length. For the case where the microwave power sources are so arranged that the power flow and stored energy per-unit length do not vary over the length of the guide, the power flow out of the end of the guide can be obtained from equation 83 using

$$\mathrm{u} = A\frac{E^2}{2\omega\mu_0} \tag{84}$$

where A depends on the parameters only. Thus, the outflow is

$$P_{out} = v_g \frac{AE^2}{2\omega\mu_0} \tag{85}$$

Substituting equations 81, 82, and 85 into equation 78, gives an accelerating field

$$E = \sqrt{2}\left[\frac{P_{in}}{Z_1}\omega\mu_0\right]^{\frac{1}{2}}\left[\frac{\tan\delta}{y_d^2} + \frac{R_s/\eta_0}{y_m^2} + \frac{v_g A}{Z_1}\right]^{-\frac{1}{2}} \tag{86}$$

The traveling-wave type of accelerator has the disadvantage that the power flow out of the termination reduces the accelerating field intensity as is shown by the presence of $v_g A/Z_1$ in the equation 86. However, the traveling-wave type of accelerator has the advantage that there is no reflected wave to dissipate power in the dielectric and metal walls, and hence the accelerating field intensity is increased by the $\sqrt{2}$ factor. Whether it is most advantageous to use the standing-wave type or the traveling-wave type depends on which gives the greatest accelerating field intensity for a given input power. For a short accelerator the term $v_g A/Z_1$ will be large and cause E to be small, hence the standing-wave type is the best for a short accelerator. For a long accelerator $v_g A/Z_1$ will be small and the accelerating field intensity in the traveling-wave type will be almost $\sqrt{2}$ times as big as that in the standing-wave type, hence the traveling-wave type is best for a long accelerator. Next it is necessary to determine what is long or short.

Table I. Comparison of Calculated Accelerating Fields

Accelerating Structure	Field Structure	Inner and Outer Radius-cm	Accelerating Field $\frac{\mathrm{MV}}{\mathrm{m}}\Big/\sqrt{\frac{\mathrm{MW}}{\mathrm{m}}}$
Stanford disk loaded accelerator	Traveling Wave	$a = 1.58$, $b = 3.8$	3.32
M. I. T. disk loaded accelerator	Standing Wave		3.94
Fused quartz loaded accelerator	Standing Wave	$a = 0.96$, $b = 2.8$	3.5
Lossless dielectric loaded accelerator	Standing Wave		5.2

It is important to point out here that the distribution of power sources along the guide is quite different for the two types of accelerators. In the traveling-wave case there are power sources distributed along the guide which must supply power lost through attenuation in order to keep the field intensity constant over the accelerator length. In the standing-wave type, if the attenuation over the length of the accelerator is small all of the power may be put in at the input.

Standing Wave Versus Traveling Wave

The length of accelerator for which the accelerating field intensity is the same for both traveling and standing wave operation is called l_0. This obtained by equating 75 to 86, which gives

$$l_0 = v_g A \left[\frac{\tan \delta}{y_d^2} + \frac{R_s/\eta_0}{y_m^2} \right]^{-1} \qquad (90)$$

Hence for $z_1 < l_0$ the standing-wave type accelerator gives the greatest field intensities. For $z_1 > l_0$ the traveling-wave type accelerator gives the greatest field intensities. The length of accelerator over which the standing-wave type of accelerator has the advantage is directly proportional to the group velocity.

For polystyrene and $a\omega/C = 1.0$, the length $l_0 = 21.0$ meters. If the loss tangent were zero, the length would become $l_0 = 152.0$ meters.

Heat Dissipation

Tremendous peak power inputs give a large average power input to the small volume of a linear accelerator and hence require that a considerable amount of heat be dissipated. For example, a 2-microsecond pulse of 1 megawatt repeated 500 times a second means an average power dissipation of 1,000 watts. Metal disk loaded guides are capable of conducting the heat away rapidly, but the dielectric lining of the dielectric loaded guide has a very low thermal conductivity and hence the equilibrium temperature will be very high. For the case of polystyrene operated at 1 kw per meter with $a\omega/C = 1.0$ the equilibrium operating temperature will be over 260 degrees centigrade. For the case of fused quartz operating at 1 kw with $a\omega/C = 0.6$ the operating temperature will be over 45 degrees centigrade.

There is an important difference in heating effects between standing and traveling wave operation. The power dissipation is uniform over the length of the dielectric for a traveling wave, but the standing wave causes regions of peak dissipation and high temperature; an important point when considering maximum temperatures. With the dielectrics operating at such temperature ranges it is necessary to know how the loss tangent, dielectric constant, and temperature coefficients vary with temperatures over the operating ranges. At present, very little information of this type is available.

Dissipation of the thermal energy appears to be the principle drawback to the dielectric loaded type of accelerator.

Mode Separation

Unlike the disk loaded accelerator excitation of undesired modes does not seem to be a problem. With the accelerator being fed by pulses a spread of frequencies around the principle frequency will be present. With b and a specified, the frequencies required to excite higher TM modes can be found from Figures 2 and 3. When the frequency is 3,000 megacycles and $a\omega/C = 1.0$ the polystyrene loaded accelerator requires a frequency of 7,400 megacycles to excite the TM_{02} mode. When using a 1-microsecond pulse the amplitude of the TM_{02} mode will be more than 10,000 times smaller than the TM_{01} mode.

Miscellaneous Considerations

Other problems of dielectric loaded linear accelerators are dielectric breakdown from high electric field intensities, dimensional tolerances, absorption of gases in the dielectric, and accumulation of surface charges on the dielectric.

Other Dielectric Configurations

The losses in the metal wall of the guide are influenced by the magnitude of the dielectric constant of the material adjacent to them. Therefore, to minimize losses and still maintain the desired phase velocity an additional region of suitable dielectric material should be introduced. This indicates that the three region guide shown in Figure 8 would have lower losses and hence a higher accelerating field intensity than the two region guide for a given input power.

Conclusions

1. The predicted accelerating field strength of the two region dielectric loaded linear accelerator is shown to be of the same magnitude as obtained with existing metal disk loaded types.

2. A criterion dictating the choice between the standing-wave and traveling-wave type accelerator is presented for the case of uniform fields.

3. Improved dielectric configurations and lower loss dielectrics will allow the dielectric loaded accelerator to give higher accelerating field intensities than the metal disk loaded type.

References

1. Design of Linear Accelerators, **J. C. Slater.** *Reviews of Modern Physics* (New York, N. Y.), 1948, pages 473–518.

2. Slow Transverse Magnetic Waves in Cylindrical Guides, **G. C. Bruck, E. R. Wicher.** *Journal of Applied Physics* (New York, N. Y.), 1947, pages 766–69.

3. TM_{01} Mode in Cylindrical Guide with Two Dielectrics, **Sydney Frankel.** *Journal of Applied Physics* (New York, N. Y.), 1947, pages 650–55.

4. Electromagnetic Waves in Circular Wave Guides Containing Two Coaxial Media, **R. D. Teasdale, T. J. Higgins.** *Proceedings*, National Electronics Conference (Chicago, Ill.), 1949, pages 427–39.

5. Remarks on Slow Waves in Cylindrical Guides, **A. A. Oliner.** *Journal of Applied Physics* (New York, N. Y.), 1949, pages 109–10.

6. Mathematical Tables, Bessel Functions, **British Association for the Advancement of Science.** Cambridge University Press, London, England, 1937.

7. A New Way of Calculating Resonant Cavities, **W. C. Hahn.** *Journal of Applied Physics* (New York, N. Y.), 1941, page 62.

8. Theory of Disc Loaded Waveguides, **L. J. Chu, W. W. Hansen.** *Journal of Applied Physics* (New York, N. Y.), 1947, page 996.

9. Traveling Wave Linear Accelerator for Electrons, **D. W. Fry, et al.** *Nature* (London, England), 1947, page 351.

No Discussion

Effect of the Duration of Voltage Dip on Cyclic Light Flicker

L. BRIEGER
ASSOCIATE AIEE

FLICKER, as considered in this paper, is the sensation of change in the illumination intensity or in the brightness of stationary objects. Only one phase of the flicker problem will be discussed, namely, the cyclic flicker due to the fluctuations of voltage at the terminals of the electric lights which produce the illumination. The performance of 100-watt incandescent and 15-watt "white" fluorescent lamps in particular will be covered.

It is customary to treat flicker in two general groups: cyclic and noncyclic. Cyclic flicker is caused by periodic voltage fluctuations such as may be produced by the operation of a seam welder, while noncyclic flicker is due to occasional voltage dips, such as may be caused by the random operation of a spot welder. A comprehensive report, prepared by the Electrical Testing Laboratories under the direction of Utilities Co-ordinated Research, Inc., in 1937[1] summarized the information available at that time on all types of flicker. With respect to cyclic flicker, which is the primary subject of the present paper, the 1937 report was confined apparently to symmetrical forms of voltage pulsation, Figure 1. Most of the data were obtained with sinusoidally pulsating voltage; some were rectangular in form, that is, both the dip and the recovery of voltage were abrupt. Saw tooth and cusped wave forms also were used in a few instances, but none of the investigations were concerned with the effect of the dip duration on the perceptibility of flicker.

As the flicker produced by nonuniform voltage fluctuations is of practical importance, particularly in problems associated with welder supply, the effect of the duration of the voltage dip on the perceptibility of cyclic flicker was made the subject of a systematic study and the results are given herein. Figure 1(B) illustrates the type of voltage change which was studied and its table outlines the range of the investigation. The tests were made in 1939.

Range of Investigations

The flicker produced by 100-watt incandescent lamps was observed under dips of 1/2, 1, 2, 5, and 10 cycles' duration. In each series, the recurrence of the dips was varied between 0.033 second (in some cases) and ten seconds, which corresponded to a frequency of voltage fluctuations between 30 per second (in some cases) and 1/10 per second. The voltage changes were produced abruptly. Studies on fluorescent flicker were limited to dips of one and five cycles.

Flicker perceptibility varies considerably among apparently normal individuals and it is also greatly affected by the degree of intentness or casualness of the observation. In addition, the wattage of the lamps used, the level of the illumination, and a great many other factors influence the visibility of flicker. An independent study of all of these factors was not necessary as the 1937 report[1] deals adequately with them. The effect of individual variations and the intentness of observations, however, were taken into consideration by using a large number of observers and by segregating the observations into two general categories: intent and casual.

Method of Testing

During intent observations the initiation of each flicker condition was announced and the observers were asked to view the objects best suited individually for the detection of flicker. At the threshold between perceptible and nonvisible flicker, the voltage changes sometimes were impressed and removed without the observers' knowledge and they were asked to call these changes. Votes were taken verbally.

In the series of casual observations, the observers were engaged in some work such as reading, writing, computations, or conversation, and they were unaware of the nature and the time of application of the flicker. After the flicker was removed, the observers voted by secret ballot as to whether the flicker was perceptible and, if so, whether it was considered objectionable.

Figure 2 shows the general arrangement of the six Illuminating Engineering Society luminaires each with one 100-watt inside frosted Mazda lamp, arranged on a table around which were seated the observers. The series of tests for the study of fluorescent flicker was made with one 15-watt white fluorescent lamp with a reactive ballast. Surface illumination at the table varied between 15 and 40 foot-candles during the study of incandescent flicker, while fluorescent flicker was studied under a surface illumination of approximately 16 foot-candles.

Recurrent voltage dips were produced abruptly at the lights by means of electronic timing and control equipment, Figure 3. A vacuum-tube loading circuit, connected in parallel with the lamps, applied additional load on the supply circuit at intervals determined by the operation of the timing circuit. This additional load caused an incremental voltage drop in the resistor (R_{12}) connected in series with the lamps, thus producing a dip at the lamps. Magnitude, duration, and frequency of the dips were measured by means of a cathode-ray oscilloscope with a 9-inch screen. In order to measure the

Paper 51-165, recommended by the AIEE Electric Welding Committee and approved by the Technical Program Committee for presentation at the AIEE Great Lakes District Meeting, Madison, Wis., May 17–19, 1951. Manuscript submitted November 28, 1950; made available for printing March 30, 1951.

L. BRIEGER is with the Consolidated Edison Company of New York, Inc., New York, N. Y.

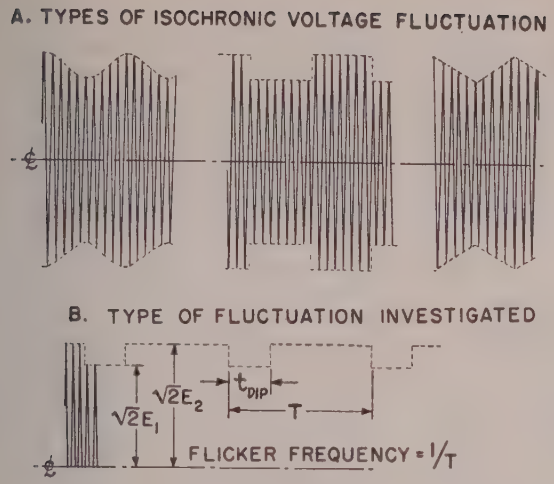

RANGE OF TESTS

	100 WATT INCANDESCENT	15 WATT FLUORESCENT	100 W. INCAND. WITH D.C.
DURATION OF DIP IN CYCLES t_{DIP}	½, 1, 2, 5, 10	1, 5	2, 5
FLICKER FREQUENCY MIN.	.1/SEC.	.1	.1/SEC.
FLICKER FREQUENCY MAX.	30/SEC.	30	15/SEC.
NUMBER OF OBSERVERS	300	8	13
" " OBSERVATIONS	12,000+	200	400
INTENT OBSERVATIONS	✓	✓	✓
CASUAL "	✓	—	—

Figure 1. Type and range of voltage fluctuations investigated

Figure 2. Arrangement of luminaires and observers

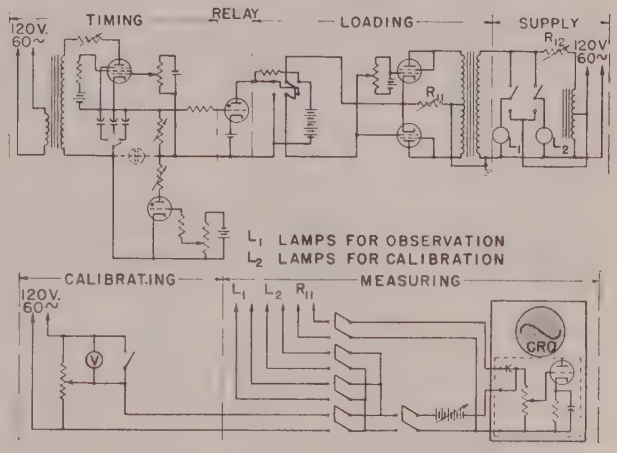

Figure 3. Test equipment for the production of flicker

magnitude of the dip, a biasing battery was connected in series with the amplifier input circuit; thus, only the peaks of the voltage waves appeared on the screen and the oscilloscope functioned as a differential voltmeter of high sensitivity. The duration of the dip was noted from the number of halfway peaks appearing on the screen. Dips were initiated near the zero of the supply voltage wave. Figure 4 shows the appearance on the screen of a 1.5-volt rms voltage dip lasting two cycles.

Results of Observations on 100-Watt Incandescent Lights

A sample of the results is given in Figure 5, which pertains to the perceptibility of flicker under voltage dips of 5-cycle duration under intent and casual observation. Each test condition imposed on the observers is represented by a block, the width of which indicates the size of the observer group. The blocks are divided into an upper (shaded) and lower (unshaded) part in the same proportion as the ratio between affirmative (flicker) and negative (no flicker) votes. Where the flicker was observed by all observers, a totally shaded block is used, while a blank block indicates that none of the observers noticed the flicker. The curves drawn on the figure represent the average of response. The figure illustrates pictorially the variation in the flicker sensitivity of observers and the fact that in investigations of this sort scientific accuracy cannot be expected. A comparison of the two types of observation brings out the appreciable decrease in the perceptibility of flicker when engaged in some activity requiring a measure of concentration. The reduced consistency of response is largely due to different degrees of concentration, and, as is to be expected, the range of response becomes even wider when voting on the objectionableness of flicker. Because of the fact that the observers were acquainted with the nature of the problem, their opinion was probably biased in the direction of considering relatively small variations as objectionable; thus, while the curves indicate trends, the objection thresholds shown below may be lower than experience in actual service would indicate.

Figure 6 is a summary of the results obtained with 100-watt incandescent lamps as illuminants. Each group of curves represents a single dip duration and the three curves in each group are the average thresholds of perception for intent and causal observations and the average threshold of objection.

Under intent observation, flicker seems to be most perceptible when the voltage dip lasts two to five cycles, at all flicker frequencies investigated. The spread between the threshold curves is relatively smaller under casual observation, but the general trend is the same as for intent viewing. It is significant that, on the average, the observers considered the flicker objectionable when the voltage was only slightly above the casual threshold.

The points marked with *X* represent symmetrical pulsations, that is, equal periods of dip and normal voltage. A plot of these points as a function of the flicker frequency, Figure 7, is the type of flicker characteristic heretofore available in the literature. For comparison, data obtained by Lindberg on the most sensitive 10 per cent of his observers[1] and tests reported by Weise[2] also are shown. The general shape of the curves is the same; the disparities are due to differences in

the many factors that influence flicker visibility.

Flicker of 15-Watt Fluorescent Lamp

Intent observations only were made at dips of one and five cycles and the results are shown in Figure 7. The difference between the performance of incandescent and fluorescent lamps is due to fundamental differences in the performance of these illuminants.

1. The change of illumination of a fluorescent lamp under a sustained change of voltage is less than one-half that of an incandescent lamp (1.2 per cent per volt for the fluorescent, and 2.7 per cent per volt for the incandescent lamp).

2. Fluorescent lamps respond much quicker to the change of voltage. The illumination of incandescent lamps changes slowly due to the heat inertia of filament; fluorescent lamps have no similar heat inertia and the relatively slight lag of illumination change is due to the phosphorescent "afterglow" of the coating materials of the tube.

These two factors affect the flicker performance in opposite directions. If the voltage dip lasts for a sufficient length of time so that the filament of the incandescent lamp can attain its new thermal equilibrium, the net change of illumination of the incandescent lamp will be more than that of the fluorescent lamp for the same voltage change. On the other hand, under rapid fluctuations of voltage the incandescent lamp will attain only a fraction of its total illumination change, consequently the incandescent lamp may produce less flicker. Weise's data show that the flicker of incandescent lamps is greater when the frequency is less than 15 per second. Our studies were not sufficiently wide in scope to allow direct comparison with Weise's data at all frequencies but it is significant that at the higher frequencies the threshold was found much lower. At a frequency of 30 per second with dips of 1-cycle duration (symmetrical pulsations), the threshold was established at $1^1/_2$ volts. An extrapolation of Weise's data would give a value considerably greater than two volts. In support of the lower figure, an instance of flicker complaint is cited where the flicker frequency was 30 per second and the voltage drop was approximately 2.5 volts rms. The flicker of 100-watt "Tulamp" units was quite annoying in spite of additional daylight illumination on the premises. On the other hand, a 100-watt incandescent lamp showed no apparent flicker.

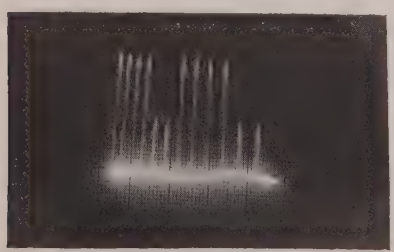

Figure 4. Typical oscillographic view of magnitude and duration of voltage dips

Illumination Pulsations at the Threshold of Perceptibility

It may be interesting to see how the illumination varies at the threshold of perception under the different conditions of flicker frequency and dip duration. Figure 8(A) and (B) show, by way of illustration, the variation of illumination under the same amount of voltage dip but under different duration and frequency. The conditions illustrated are well above the threshold values, and were chosen to indicate clearly that magnitude, duration, and frequency of dips jointly affect the illumination change. The analysis of illumination change may be made with reasonable facility because of the exponential nature of the illumination change as illustrated by Figure 8(C). An exponential curve is a good approximation for both the fall and rise of the illumination, so that for any combination of voltage dip, duration of dip, and total time between repeats, the change in the mean illumination may be simply determined. It is a reasonable assumption that the flicker is not sensibly affected by the inherent pulsation of illumination due to the line frequency variation of voltage but is the result of the much slower change in the mean level of illumination. Previous studies offer evidence in support, and, in addition, independent confirmation was obtained by a series of tests to compare the flicker visibility under the intent observation with a-c and d-c supply. The d-c tests were made with 2- and 5-cycle dips and, as Figure 9 shows, the a-c and d-c perception threshold curves are practically identical.

Typical cases of the mean illumination pulsation at the threshold of intent perception are shown in Figure 10. The curves are grouped to show the illumination flucutation for a fixed flicker frequency. Each curve in a group represents a different dip duration. For example, in the group pertaining to a flicker frequency of 20 per second, the three curves represent dip durations of one-half, one, and two cycles, respectively. Except for the case of three pulsations per second, the net change of illumination within each group is about the same. The group for a flicker frequency of three per second is particularly interesting because the mean illumination change is still approximately constant for dips up to five cycles in length but a much larger pulsation of illumination is required to make a 10-cycle dip visible. It appears then that if the dip is longer than about five cycles, the flicker sensitivity of the eye begins to diminish and a larger net change of illumination is needed for the perception of flicker. That the flicker sensitivity of the eye diminishes at frequencies lower than five cycles is known, of course, but on the basis of Figure 10 it appears that the determining factor is not so much the time between consecutive voltage dip as the time between the fall and rise of illumination.

As a rough first approximation, therefore, it may be assumed that at a fixed frequency and for the same type of illuminant, voltage dips of different duration will produce the same flicker sensation, provided the fluctuations of the mean illumination are the same, and provided that the dip is not longer than five cycles.

Instead of the total net change of illumination, the fundamental harmonic component of the curve representing the fluctuations of mean illumination has been considered, particularly in Europe, as the determining factor in flicker perceptibility. This approach is employed primarily for the evaluation of the inherent flicker of different types of electric illuminants due to the alternations of line voltage at line frequency,[3–5] but it also has been applied to the comparison of incandescent and fluorescent flicker due to low-frequency voltage variations.[6] The attractiveness of the approach on the basis of harmonic analysis would lie in its applicability to flicker produced by voltage variations of any wave form but, of course, it would be restricted to flicker frequency of ten per second or higher. The evidence of the present studies, however, does not lend support to the appropriateness of the method.

Flicker Produced by Frequency-Changer Welders

Published cyclic flicker studies, including the present one, are confined to sustained pulsations. Reciprocating compressors, conventional seam welders, and high-speed automatic spot welders are typical loads to which the available data would apply. Frequency-changer welders[7,8] developed in the last few years also produce cyclic line voltage variations, but in spot welding applications of

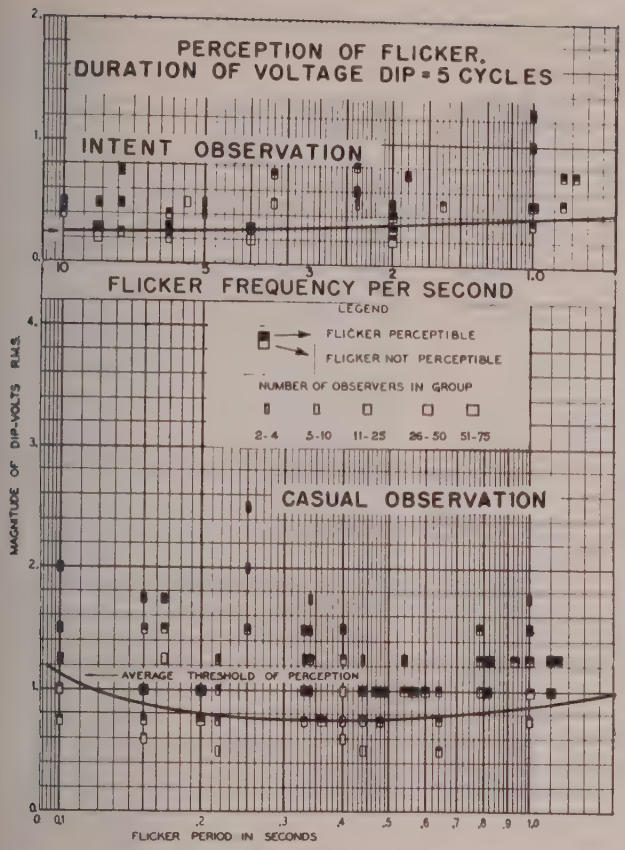

Figure 5. Results of flicker observation for voltage dips of 5-cycle duration

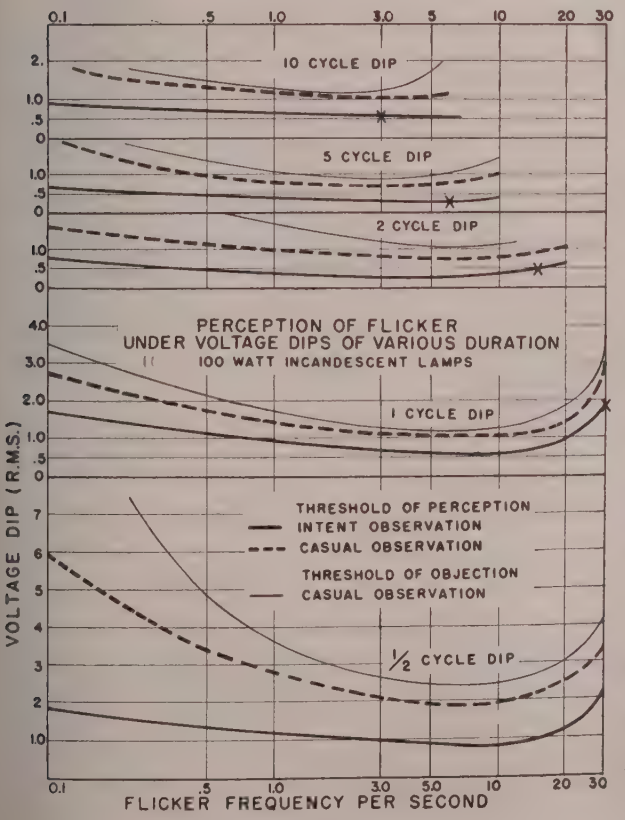

Figure 6. Perception of flicker under voltage dips of various duration

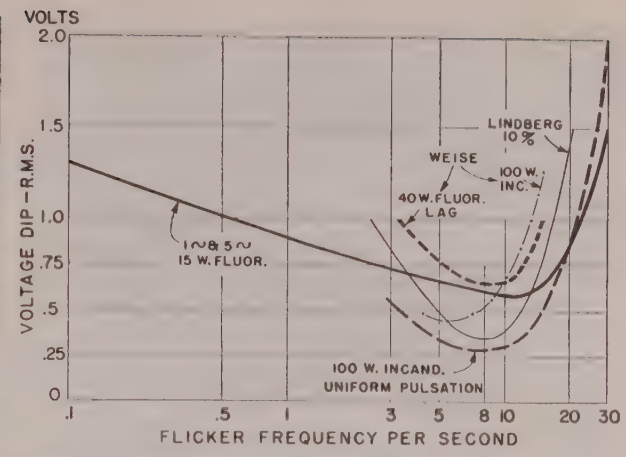

Figure 7. Comparative flicker perceptibility of fluorescent and incandescent lamps

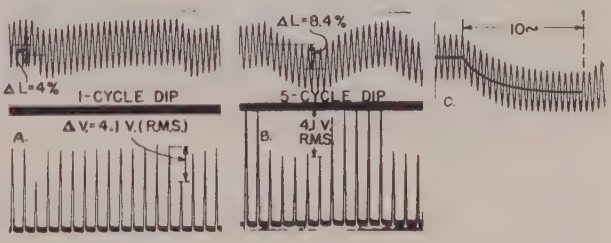

Figure 8. Oscillograms of illumination pulsation

A and B—Upper curve: illumination; Lower curve: voltage
C—Mean illumination varies exponentially

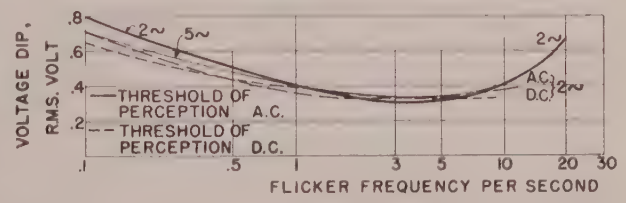

Figure 9. Comparison of perceptibility of flicker with d-c and a-c supply

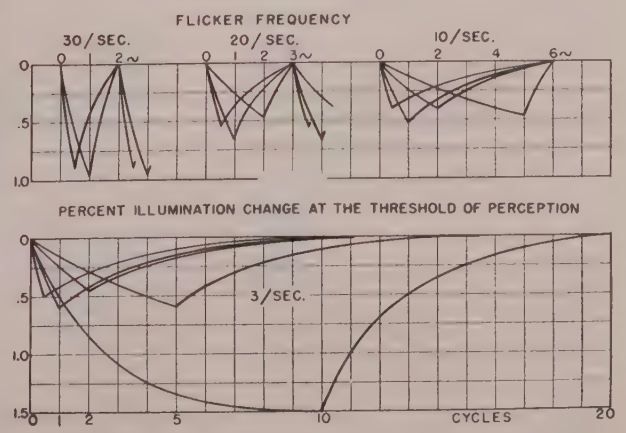

Figure 10. Per cent illumination change at the threshold of perception

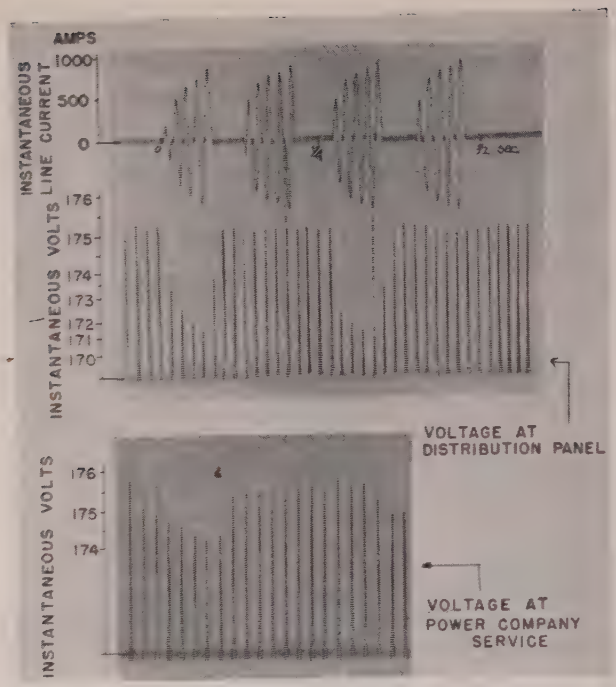

Figure 11. Voltage dip produced by frequency-changer welder

the system the voltage pulsates only briefly, each time a spot is welded. The response of the nervous system to such short-lived pulsations may not be the same as the reaction to a sustained flicker of the same frequency.

While not strictly a part of the studies hereinbefore presented, the increasing importance of frequency-changer welders makes it pertinent to discuss briefly the observations made in one particular application of a 3-phase welder supplied from a 3-phase 4-wire 120/208-volt network system. The welder current in one of the lines is shown in the top oscillogram of Figure 11. The voltage oscillogram in the center of the figure was taken at the light and power distribution panel while the bottom oscillogram shows the voltage at the point of power service to the premises. Because of the distance between the two points, the dip at the service is appreciably lower. Flicker voltage was measured from line to neutral (nominal voltage: 120 volts) by the method of d-c bias and amplification of a-c peaks, described in the section on "Method of Testing."

The oscillogram, taken during routine production, showed a welding time of about 29 cycles (60-cycle basis) in four pulses separated by pauses of $3^1/_2$ cycles. Due to the use of the positive half-cycles of voltage in the measurement of flicker and to the control of the polarities of consecutive current pulses, the voltage dips are recorded for alternate pulses only, as the positive voltage peaks coincide with the periods of zero current during every second group of pulses. Although the current wave shape is nonsinusoidal, the rms voltage drop may be calculated with sufficient accuracy on the basis of a sine wave load equal to the line frequency component of the current.[9] This approach yields for the rms voltage drop approximately 67 per cent of the difference between voltage peaks. Hence, voltage drop at the distribution panel $=0.67\ (175.2-171.0)=2.7$ volts and at the service point $=0.67\ (175.7-174.3)=1.0$ volt.

The user, recognizing that the flicker was produced by his equipment, was willing to put up with a dip of 2.7 volts but in the opinion of the observers the flicker would have been intolerable to others. On the other hand, the dip of 1.0 volts at the power company's service, while noticeable and distinguishable as pulsating flicker, was judged to be just passable.

In the shop, where the 2.7-volt dip was noted, fluorescent and incandescent lamps were available for observation. The flicker of both was judged objectionable. Incandescent lamps only were used in the room where the 1.0-voltage dip was observed.

On a sustained basis, the conditions described represent a flicker frequency of $7^1/_2$ per second, for which the charts on Figure 6 give a threshold of objection of 1.2 volts. Considering the difference in the nature of flicker, the different conditions of observation, and the tapered dip of voltage during each pulse, the good agreement between the observers' judgment and Figure 6 is interesting, but a single observation should not be used as a basis of generalization.

Conclusion

Perceptibility of cyclic flicker was discussed heretofore in terms of the frequency of pulsations. Evidence was offered herein to indicate that the duration of the voltage dip also affects flicker visibility. The new evidence does not imply fundamental changes in the presently used standards, but in borderline cases it may swing the decision as to whether a particular case of flicker is acceptable or not.

The additional information is not sufficient to evaluate the flicker of the frequency-changer welders because the observations were confined to sustained flicker. In view of the increasing use of the new type of welders, a systematic study of their flicker characteristic would be highly desirable.

References

1. The Visual Perception and Tolerance of Flicker. **Electrical Testing Laboratories Report** under the direction and supervision of the Committee for Project Number 10, Utilities Co-ordinated Research, Inc., New York, N. Y., 1937.

2. Cyclic Flicker of Fluorescent Lamps. **W. R. Weise.** *Electrical World* (New York, N. Y.), volume 124, October 27, 1945, page 80.

3. Uber die Welligkeit der Lichtemission bei Wechselstrombetriebenen Leuchtstoff-Entladungsrohren, **E. G. Andresen.** *Das Licht* (Berlin, Germany), 1937, page 235; 1938, page 42.

4. The Flickering of Sources of Electric Light, **P. J. Bouma.** *Philips Technical Review*, Eindhoven, Holland), October 1941, page 295.

5. Papillotage et Phenomenes Stroboscopiques Provenant de Fluctuations de la Lumiere a la Frequence du Reseau, **A Report of the Committee on Flicker.** *Bulletin*, Association Suisse Des Electriciens (Zurich, Switzerland), July 13, 1946, page 367.

6. En Sammenlikning Mellom Lysstoffrer og Glodelamper med Hensyn til Lysblunking som Framkommer ved Korte Spenningsvariasjoner, **Harald Aas.** *Elektroteknisk Tidsskrift* (Oslo, Norway), 1948, number 4, page 43.

7. Three-phase Balanced Load Resistance Welding Machines. **J. L. Solomon.** *The Welding Journal* (New York, N. Y.), May 1947, page 426.

8. Electric Arc and Resistance Welding. *AIEE Special Publication*, May 1949, pages 96–139.

9. Circuit Analysis of Frequency-Changer Welders, **W. K. Boice.** *The Welding Journal* (New York, N. Y.), October 1949, page 946.

Discussion

R. E. Young (Public Service Company of Northern Illinois, Kankakee, Ill.): It is the purpose here to emphasize the importance of the subject "light flicker." It is desired to indicate the difficult circumstances which an individual may encounter in adapting the data contained in this paper.

Light flicker is a continuing problem facing not only the electric utility engineer,

but also the industrial plant engineer. Coincident with the desire of steel producers to use larger electric arc melting furnaces comes the need for more study of possible power system disturbances. In welding-resistance welding, probably the greatest single factor involved in power supply is this matter of what effect will any voltage drop on lighting circuits have on those humans who are using the artificial lighting for seeing tasks at their homes, offices, stores, restaurants, or factories. For those who have not heretofore been concerned with lighting flicker, it may be somewhat difficult to appreciate reasons why voltage drops, particularly for cyclic welding conditions, must be held to such low levels as demonstrated by Mr. Brieger's data. Motor equipment on power circuits in a factory may many times operate satisfactorily with a 10 per cent variation in voltage. Even utility transmission lines designed for steady power and lighting loads are ordinarily satisfactorily operated for voltage variations of 10 per cent. Ordinarily, resistance welding can be accomplished with at least 5 to 10 per cent voltage variation at the welder terminals or if but one welder is involved, a voltage drop of 50 per cent at the welder terminals ordinarily can be compensated by adjustment of welder controls. However, as Mr. Brieger's data shows, such variations for welder loadings cannot be considered for lighting circuits.

Discussion and research on the lighting flicker problem should be stimulated. Although lighting flicker is readily recognized, there has been some neglect of the subject during the last several years. One probable reason for this is the "human factor" involved in flicker studies. As engineers, we deal more with facts and with concrete quantities. Mostly there is little deviation—there can be but one real solution. However, the author has shown in the data presented, that flicker research with humans may produce as many answers as there are individuals being tested. Some respond as the casual observer, others as the intent observer with a much lower tolerance to flicker. In studying all other phases of power supply, one is confronted with facts and mostly a ready solution. But in studying flicker it is particularly difficult to draw conclusions and assign an average condition with a curve to fit all conditions. Also, who is willing to say that complaints of lighting flicker will never arise from the individual who registers objectionable flicker at the lowest voltage level. In other words, are objections liable to arise from the casual or the intent observer level.

It is hoped the author's presentation will stimulate thinking and perhaps additional research on lamp flicker. In view of present day and future use of frequency-conversion-type welders, where the short time loading is not held at sustained values as in most other welding, it is believed that research and evaluation of short time varying intensities of flicker are needed.

L. Brieger: Mr. Young's remarks on the difficulty of assigning an average flicker response curve for use by the distribution system designer are well justified. A survey of flicker voltage limitations in use by utilities throughout the country shows considerable spread, indicating that the response of the relatively few "flicker conscious" observers are given more consideration by some than by others.

It seems to be a reasonable policy in the author's opinion to assign permissible flicker voltage limits on the basis of the number of people affected. Thus, lower limits would be used for the permissible flicker voltage on an entire distribution circuit than in the layout of a local secondary system supplying only a few services.

Ignitrons for Frequency-Changer Welders

RICHARD R. ROTTIER
ASSOCIATE AIEE

IN FREQUENCY-changer resistance welding, 3-phase supply frequency is converted by the control of ignitron tubes to single-phase low-frequency power at the weld. The advantages of this resistance welding circuit have been discussed previously.[1,2] Briefly, the lower weld frequency reduces the input demand kilovolt-amperes of the welding machine and makes possible improved results in the welding of aluminum, magnesium, and their alloys. Furthermore, the power factor is improved and the load is distributed over the 3-phase circuit, which results in less voltage drop than in single-phase welding.

The frequency-changer circuit is basically a 3-phase rectifier circuit. Therefore, the ignitrons are subjected to the requirements of rectifier operation; namely, fast commutation, high-initial-inverse anode voltage after commutation, and high surge currents in the event of tube arc-back. In addition, since the duty is intermittent as required in resistance welding, the tubes must carry high-peak forward currents for short periods of time.

Scope of Paper

This paper gives a brief study of the frequency-changer welder circuit operation from a tube designer's standpoint. Analysis of the circuit has been presented previously.[1] In this paper, however, the effect of the circuit requirements on the tube design and performance are discussed.

Circuit Characteristics Applied to Tubes

Operation of Tubes in Circuit

Figure 1 shows the frequency-changer welder circuit. The power components consist of six ignitron tubes and a welding transformer with three primary windings and one secondary winding. All windings are on the same core. Each primary winding has in series a pair of ignitron tubes connected in inverse parallel. The ignitron tubes act merely as switches allowing current to pass in one direction or the other at the proper time.

The ignitron tubes are controlled in two groups of three tubes each. Tubes A, B, C constitute one group and tubes A', B', C' constitute the other group. Each tube in a group is connected in a direction corresponding to one polarity of induced secondary voltage.

Figure 2 shows the primary windings electrically, that is, each winding 120 degrees out of phase and in delta connection. The control circuit operates tubes A, B, C first while blocking tubes A', B', C'. Current transfers from tube to tube. The current in each winding induces a voltage in the secondary of the same polarity. Current builds up in the secondary as shown in Figure 3 and continues in the same direction for the desired conduction period. Control of the firing of the ignitors blocks all tubes and the current can decay to zero. The other group of tubes is then permitted to operate and current is built up in the transformer in the opposite direction.

Thus, current flows in alternate directions through the secondary. The fundamental frequency of the secondary in present equipments is between 5 and 12 cycles per second. It can be made higher or lower by proper control of the ignitron tubes.

Paper 51-166, recommended by the AIEE Electric Welding Committee and approved by the AIEE Technical Program Committee for presentation at the AIEE Great Lakes District Meeting, Madison, Wis., May 17–19, 1951. Manuscript submitted November 28, 1950; made available for printing April 9, 1951.

Richard R. Rottier is with the General Electric Company, Schenectady, N. Y.

Figure 4 shows the currents through each primary leg of the transformer, while Figure 5 shows the currents in each of the 3-phase lines. Figure 6 is an oscillogram showing the actual circuit action for one cycle of secondary frequency at approximately 60-degree phase retard.

Tube Inverse Voltage

When tubes are not conducting, the anode-to-cathode voltage of each tube is equal to the line-to-line voltage of the phase in which the tube is connected.

When one tube is conducting, the corresponding line to line voltage (less tube drop) is applied to the primary winding. This induces a voltage practically equal to the applied voltage in the other primary windings and in phase with the applied voltage. Figure 7 shows how the induced voltage adds to the line voltage to give the anode-to-cathode voltages across the tubes in the other phases. The result is alternating voltage with a peak value equal to $\sqrt{3}$ times the peak line voltage. Hence,

$$E_t = E\sqrt{6} \tag{1}$$

where E = line to line rms voltage. This also is illustrated in Figure 8.

The wave shape and magnitude of the tube inverse voltage is the same as that for a 3-phase Y rectifier with an applied line-to-line voltage 73 per cent higher than the frequency-changer line voltage.

Tube Commutation Time

When current flows in the primary windings it transfers from one primary winding to another depending on which primary has the highest applied voltage of proper polarity. In Figure 8, the dotted lines show the secondary-voltage corresponding to the primary line voltages. From point 1 to point 2, Figure 8(A) only primary A is carrying current. During this time, the voltage of phase A is inducing also an equivalent voltage in the other two primaries. At point 2, the voltage of phase B begins to exceed that of phase A induced in phase B. Since the ignitor is not phase-retarded, the ignitron tube will begin to conduct as soon as the voltage

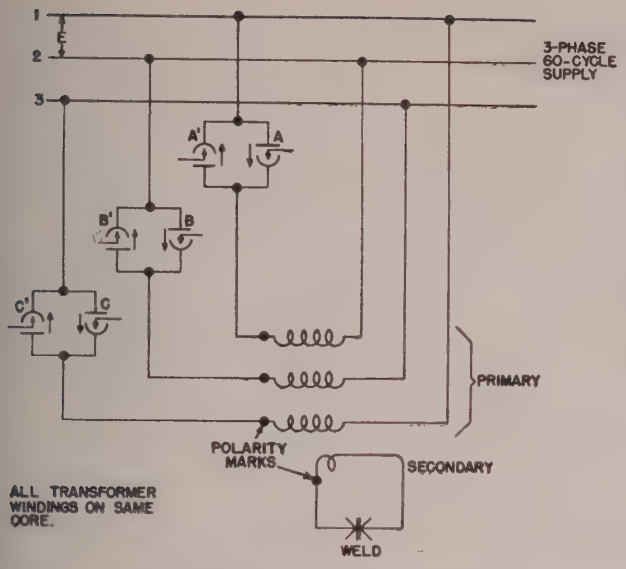

Figure 1. Frequency-changer welder circuit

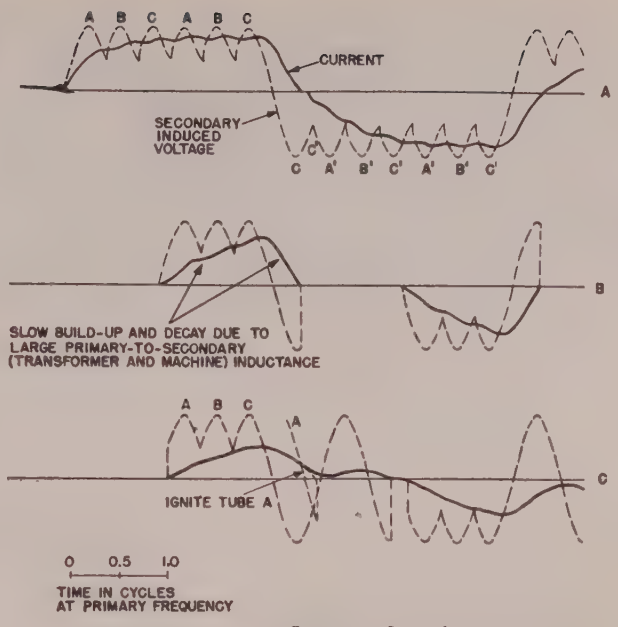

Figure 3. Secondary current

across it exceeds the arc-drop voltage. The arc-drop voltage of approximately 15 volts can be neglected since it is only a small portion of the total voltage available during the current transfer.

Current cannot transfer instantly from one primary winding to another because of the inductance associated with each winding. The time of current transfer is known as the commutation time. It also is called the commutation angle, u, or the angle of overlap because within its duration two tubes, that is, two phases, are carrying current. In the frequency-changer circuit where the three primary windings are on the same core most of the flux of one coil links the other coils. Therefore, during commutation only the leakage flux between the two coils can support the difference in voltage that exists between the two coils.

This voltage difference between the two windings during commutation is known as the commutating voltage, e_c, Figure 9. This commutating voltage divided by the leakage reactance between the two primary windings, X_{pp}, determines the current during commutation, i_c.

In general, the current in one phase at the start of commutation will equal the current in the other phase at the end of commutation. The higher this current to be commutated, the longer the time required to reduce it to zero. Commutation time, therefore, depends upon transformer leakage reactance between primaries, commutating voltage, and current.

It has become the practice to denote the permissible bombardment of the anode by a rating called commutation factor.[3] This factor is designated as the product of rate of change of current immediately preceding the end of the commutation period and the rate of change of inverse anode voltage immediately after the end of the commutation period.

$$di/dt \times de/dt = (\text{amperes/microsecond}) \times (\text{volts/microsecond}) \quad (2)$$

This factor describes the commutating conditions under which the tube will give satisfactory performance.

In the case of ignitrons, this factor can be considered as the commutating conditions that determine a certain probability of arc-back. Reducing the rate of change of current during commutation (that is, increasing commutation time) or decreasing the initial inverse voltage, E_{it}, lessens the probability for tube arc-back. On the other hand, a longer commutation time reduces the average secondary voltage, E_d, and lowers the input power fac-

Figure 2 (below). Primary winding of frequency-changer welder

Figure 4 (right). Current in primary

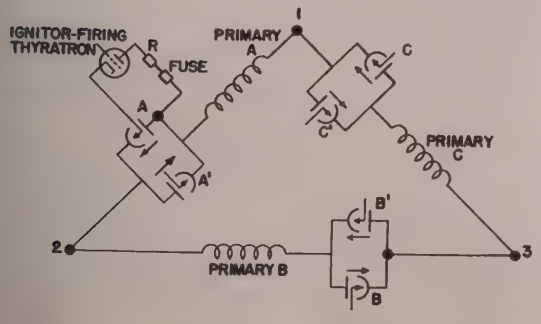

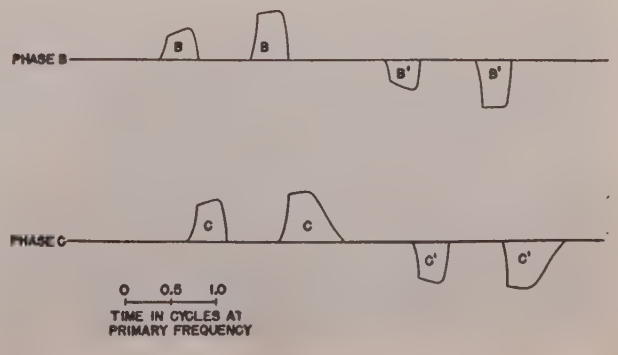

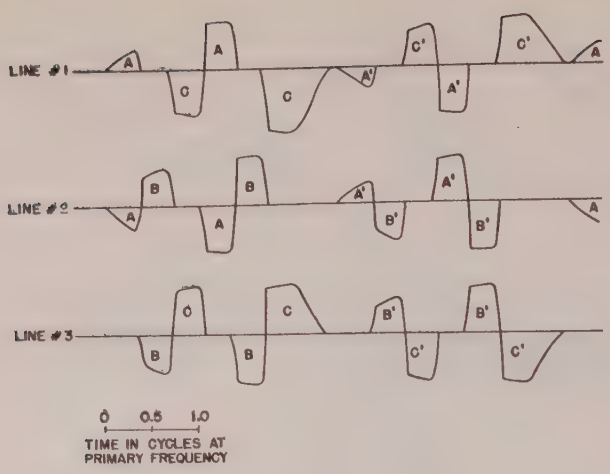

Figure 5 (left). Line current in 60-cycle 3-phase supply

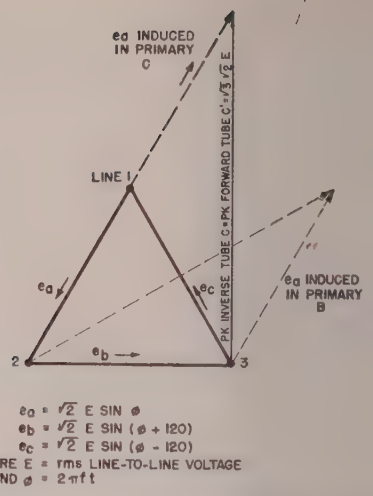
eα INDUCED IN PRIMARY C
LINE 1
eα INDUCED IN PRIMARY B
PK INVERSE TUBE C = PK FORWARD TUBE C = √3/√2 E
eα = √2 E SIN ø
eb = √2 E SIN (ø + 120)
eC = √2 E SIN (ø - 120)
WHERE E = rms LINE-TO-LINE VOLTAGE
AND ø = 2πft

Figure 7 (right). Vector diagram of primary voltage

tor. The shaded areas in Figures 8(A) and 9 graphically show the loss in secondary voltage due to commutation.

An equipment designer should design transformers for this service with as little primary-to-primary reactance as possible in order to improve output voltage and input power-factor, and yet provide reactance enough to obtain satisfactory tube performance. It will be shown later that by limiting the peak arc-back current to a certain maximum value we place a minimum limit on the circuit reactance and commutation time. In this way satisfactory tube performance is assured.

In rectifier circuit analysis[4] the transformer reactance which controls the transfer of current from one phase to another is called the commutating reactance. In a 3-phase Y rectifier, the line-to-neutral commutating reactance is X_c and the complete line-to-line commutating reactance (the reactance involved in commutation) is $2X_c$. To use the equations and curves of rectifier theory for the frequency-changer circuit the term X_c must be replaced by $X_{pp}/2$, where X_{pp} is the leakage reactance.

Current during commutation for a 3-phase Y rectifier with no phase delay is:[4]

$$i_c = \frac{\sqrt{2}E_s \sin \pi/3}{X_c}(1-\cos wt) \qquad (3)$$

where E_s is the line-to-neutral rms voltage. This becomes for the frequency-changer circuit

$$i_c = \frac{\sqrt{2}\,E \sin \pi/3}{X_{pp}/2}(1-\cos wt) \qquad (4)$$

where E is the line-to-line rms voltage. At the end of commutation:

$wt = u$

and $i_c = I_c$, where I_c is current to be commutated. Therefore,

$$I_c = \frac{2\sqrt{2}E \sin \pi/3}{X_{pp}}(1-\cos u)$$

or

Commutation angle $= u = \cos^{-1}\times$

$$\left(1-\frac{I_c X_{pp}}{2\sqrt{2}E \sin \pi/3}\right) =$$

$$\cos^{-1}\left(1-0.408\frac{X_{pp}I_c}{E}\right) \qquad (5)$$

Commutation Time with Phase Retard

Figure 8(B), shows the action with phase retard. Under this condition tube A continues to carry current from points 2 to 3 despite the fact that its voltage is lower than that of tube B. The secondary voltage is reduced by this phase control in addition to the reduction during the commutation period 3 to 4. The commutation angle with phase retard also is reduced because of the increased voltage available for commutation.[4]

With phase retard angle (α) equation 3 becomes:

$$\cos(u+\alpha) = \cos\alpha - 0.408\frac{X_{pp}I_c}{E} \qquad (6)$$

This equation is plotted in Figure 10,

Figure 6 (below). One weld cycle at 40 per cent heat. Weld frequency 8 3/7 cycles per second, 2 cycles conduction 1 1/2 cycles cool time, phase retarded

Curve A—Current, Line 1; curve B—Current, line 2; curve C—Current, line 3; curve D—Voltage, lines 2 and 3; curve E—Secondary voltage; curve F—Ignitor current, tube C'

Figure 8 (right). Frequency-changer welder wave forms

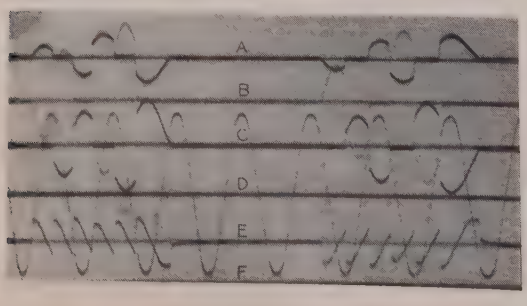

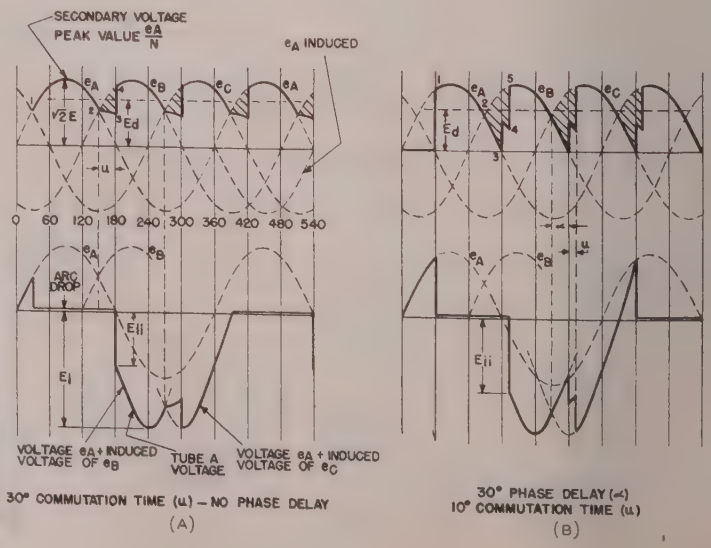

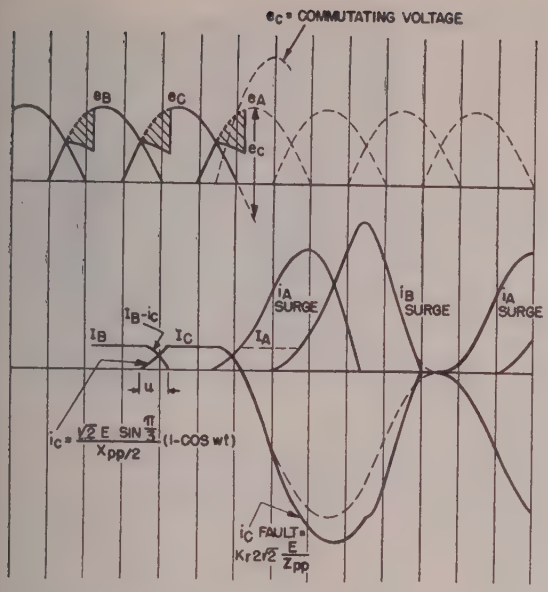

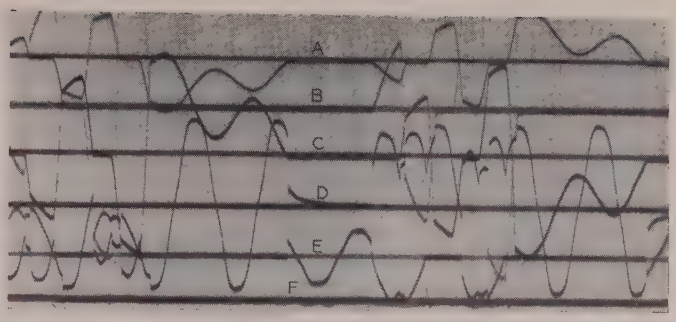

Figure 9 (left). Arc-back on tube C frequency-changer-welder circuit

Figure 11 (above). Long conduction time on last conducting tube. Weld frequency 8 4/7 cycles per second, 2 cycles conduction, 2 1/2 cycles cool time, 100 per cent heat

Curve A—Current, line 1; curve B—Current, line 2; curve C—Current, line 3; curve D—Secondary voltage; curve E—Voltage, tube C'; curve F—Ignitor current, tube C'

showing variation of commutation time with reactance factor, $X_{pp}I_c/E$, and phase retard. By comparing Figure 11 with Figure 6, the shorter commutation time, increase in initial inverse voltage and decrease in secondary current with phase retard can be noted.

Fault Current Through Tubes

Fault current will flow if an arc-back occurs on one of the group of conducting tubes or if an arc-through occurs on one of the group of tubes being held off. An example of such a fault is illustrated in Figure 9, where the fault could be either tube C not holding off the initial inverse voltage or tube C' conducting forward current at the wrong time. This fault current also is equivalent to that obtained when the "cool" time between secondary half-cycles is too short and ignition of the reverse tubes is begun before the current of the last conducting tube reaches zero.

The fault current is limited by the primary resistance, by the leakage reactance between the windings of the transformer, and by the impedance of the supply system. The sum of the forward currents in tube A and B, Figure 9, is essentially the arc-back current in tube C. From the rectifier circuit analysis[5] the peak arc-back current, with a-c supply only, for a 3-phase Y rectifier is:

$$i_{ar} = K_r \frac{\sqrt{2}E_s}{Z_c}$$

where K_r is a function of R_c/X_c. X_c, R_c, and Z_c are line-to-neutral commutating reactance, resistance, and impedance respectively of the rectifier, transformer, tubes, and supply system. Figure 12 is an oscillogram taken of an arc-back on a tube in a 3-phase Y rectifier circuit.

For the frequency changer welder this equation for peak arc-back current be-

Figure 10 (left). Commutation time–frequency-changer-welder circuit

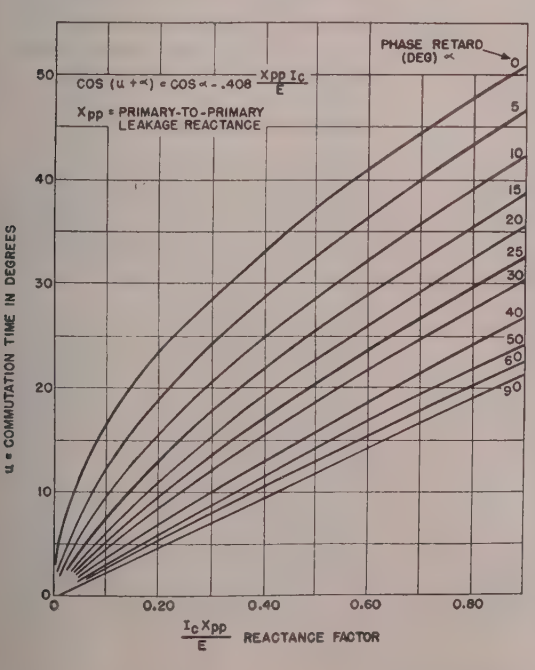

Figure 12 (below). Arc-back on the test circuit. 3-phase Y rectifier operation. Simulating frequency-changer welder circuit. Load—600 volts, 300 amperes, d-c; arc back on tube 3; load L = 26.75 millihenrys; total anode L = 0.19 millihenry; phase retard = 0

Curve A = Timing wave, 60 cycles	
Curve B = Tube voltage, #3	1 mm = 12.5 volts
Curve C = Current, tube 1	1 mm = 304.0 amperes
Curve D = Current, tube 2	1 mm = 267.0 amperes
Curve E = Current, tube 3	1 mm = 377.0 amperes
Curve F = Load current	1 mm = 22.2 amperes
Curve G = Load voltage	1 mm = 43.6 volts

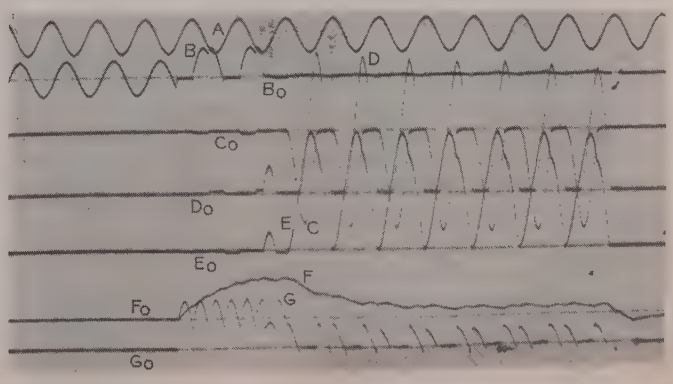

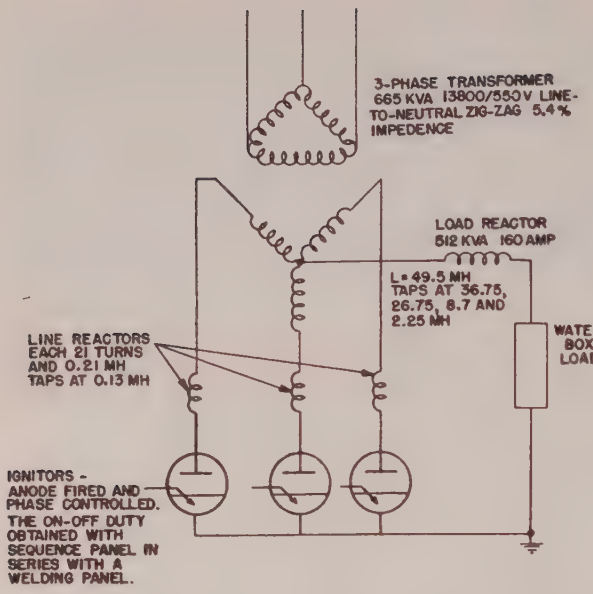
3-PHASE TRANSFORMER
665 KVA 13800/550 V LINE-TO-NEUTRAL ZIG-ZAG 5.4% IMPEDENCE
LOAD REACTOR
512 KVA 160 AMP
L = 49.5 MH
TAPS AT 36.75, 26.75, 8.7 AND 2.25 MH
WATER BOX LOAD
LINE REACTORS EACH 21 TURNS AND 0.21 MH TAPS AT 0.13 MH
IGNITORS - ANODE FIRED AND PHASE CONTROLLED. THE ON-OFF DUTY OBTAINED WITH SEQUENCE PANEL IN SERIES WITH A WELDING PANEL.

Figure 13 (left). Test circuit

Figure 15 (right). Single-phase welder tubes

A (left)—open construction
B (center)—baffles between anode and cathode
C (right)—optimum design

comes,

$$i_{ar} = K_r \frac{\sqrt{2}E}{Z_{pp}/2} = K_r \frac{2\sqrt{2}E}{Z_{pp}} \qquad (7)$$

where K_r is function of R_{pp}/X_{pp} and

$$Z_{pp} = \sqrt{R_{pp}^2 + X}$$

and includes primary resistance, primary to primary leakage reactance, and the impedance of the supply system.

$K_r = 1$ approximately for $R_{pp} = X_{pp}$, and

$K_r = 2$ approximately for $X_{pp} = 10R_{pp}$ (8)

The first portion of the arc-back current in tube C and the forward current of tube A follow the wave-shape of the commutation current. Then when tube B begins to conduct, 90 degrees after the start of the fault, the current wave-shape deviates from that of the commutation current.

The trace of the commutation current equation is shown by dotted line in Figure 9. The arc-back current will be more or less than this current depending on the ratio of R_{pp}/X_{pp}.

Arc-back or arc-through in a tube usually results in a bad weld. It may cause a temporary shutdown, also puts greater stress on the ignitron tubes and associated equipment. Each arc-back is slightly detrimental to the tubes as the reverse current forms a cathode spot on the graphite anode which loosens small particles of the graphite. These small particles of graphite tend to mix with the mercury in the tube and will eventually effect the performance and shorten the life of the tube.

From an equipment design standpoint, the probability of arc-back can be minimized by providing sufficient primary reactance to insure that the current which can flow in the event of fault does not exceed the rated value. The surge current rating is primarily an equipment design rating. It is not intended that the tube should be operated at this current level. The tube, in general, will not be destroyed by conduction of fault currents, but repeated operation may shorten tube life.

Current in Last Conducting Tube

In general, welding control circuits provide a "cool" time which allows a delay between the time of current going to zero on the positive group of tubes and the time for starting of negative groups of tubes.

Figure 3 shows that voltage corresponding to the last conducting primary is generated in the secondary until the current goes to zero. Hence, the secondary voltage may go below zero as shown by Figure 3(B). This slow decay of secondary current is caused by a high ratio of secondary or welder X/R. If this secondary X/R is sufficiently great, the secondary voltage may again return to a positive value, increasing the current in the last conducting tube until after the voltage again goes negative as in Figure 3(C).

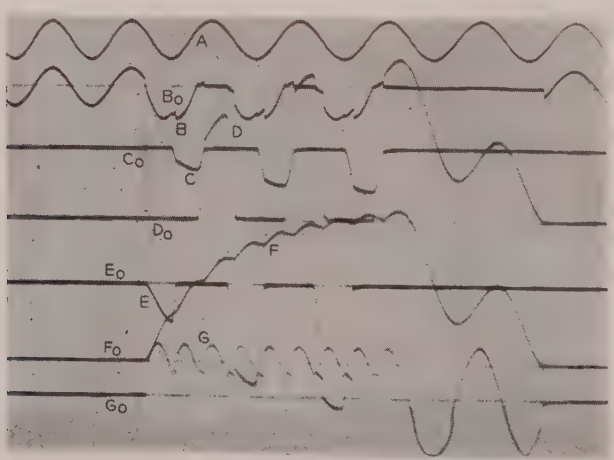

Figure 14. One pulse on test circuit equal to one-half weld on frequency-changer circuit. 3-phase Y rectifier operation. Simulating frequency-changer welder circuit. Load—600 volts, 1,200 amperes, d-c; load $L = 8.7$ millihenrys. Added anode $L = 0.21$ millihenry per leg; phase retard = 0

Curve A = Timing wave, 60 cycles	
Curve B = Tube voltage, #2	1 mm = 16.7 volts
Curve C = Current, tube 1	1 mm = 77.2 amperes
Curve D = Current, tube 2	1 mm = 20.3 amperes
Curve E = Current, tube 3	1 mm = 25.0 amperes
Curve F = Load current	1 mm = 22.2 amperes
Curve G = Load voltage	1 mm = 43.6 volts

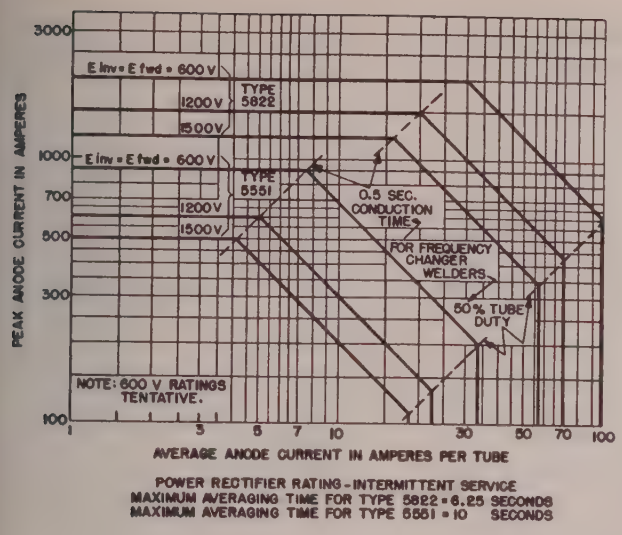

Figure 16. Frequency - changer welder ignitron tube ratings

The secondary current thus will continue to flow for one or more primary cycles after the tube ignition has been cut off and until the energy stored in the system has been dissipated. This imposes extra duty and a long cathode spot on the last conducting tube, and introduces a single-phase, primary-frequency load on the supply line. A longer interval between positive and negative pulses (cool time) will be required which may chill the weld unduly. Also the long cathode spot may travel to the side-wall of the tube and cause wetting of the ignitor. Therefore, extremely high values of welder X/R require special consideration both from tube and equipment standpoint.

As previous circuit analysis has shown[1] the current through the last conducting tube will just decay to zero without again increasing, if the ratio of welder reactance (at supply-frequency) to resistance is less than approximately 3.5. High values of secondary reactance also result in square-wave currents through each tube which means an increase in current to be commutated. This is readily seen from the oscillogram, Figure 12. The higher the current to be commutated, the greater the di/dt during commutation and the greater the probability of tube arc-back.

The long continuous conduction time for the last tube can be minimized by suitable control circuits which transfer the current from tube C to tube A, see Figure 3(C), at the time phase A voltage is still higher than phase C. Since phase A voltage is just starting to go negative, the current will be given 120 degrees longer to decay to zero before the supply voltage of the conducting tube again goes positive. When the welder X/R ratio is large, utilization of such circuits is advisable.

Ignitron Tube Design for the Circuit

In order to determine the adequacy of existing tubes for the frequency-changer service it was necessary to establish test circuit conditions equivalent to that which would be encountered in actual service.

Test Circuit Used

As shown in the foregoing discussion, all the voltage and current conditions that the ignitron tube encounters in the frequency-changer circuit are equivalent to those encountered in the conventional 3-phase Y rectifier circuit with an inductive load. The Y rectifier would, of course, need to operate intermittently to simulate the duty cycle of the welder circuit.

The tubes were tested in a 3-phase rectifier circuit, Figure 13, to establish their ratings for frequency-changer welder service. The ignitor firing could be retarded to provide phase control. The load inductance and size of anode reactors could be varied to provide conditions of operation identical to those experienced in frequency-changer applications. Figure 14 shows a cycle of operation on this test equipment.

Test Procedure

The maximum carrying load ability of a mercury pool tube is generally limited by arc-back, voltage surges, or loss of control.[6] Voltage surges result from current constriction and are considered in the discussion below. Loss of control is prevented by maintaining adequate water flow and temperature.

The tests were conducted under circuit conditions that subjected the tube to the most severe conditions for arc-back: namely, high initial inverse voltage, short commutation time, high temperature, and maximum duty. Tubes were operated under loads each of one hour length, of increasing severity (greater peak and average tube current) until arc-back occurred. Each run was repeated until the maximum load capacity was established.

Test Results

Tests in the rectifier-circuit showed that the single-phase welder tubes were not capable of handling the commutating requirements of the rectifier circuit at their peak and average current single-phase welder ratings. This was due to their slow deionizing ability because of their open construction which is shown in Figure 15(A). Arc-backs were frequent. The power-rectifier ignitrons on the other hand performed very well at low peak currents under the most severe commutating conditions that could be obtained in the test circuit. These tubes contain two baffles between anode and cathode as shown in Figure 15(B). This type of double baffling, however, reduced the cross-section area and thus limits the peak current that can be carried. Experience has shown that wetting of the ignitor results when the arc is constricted too greatly by such baffling.

Therefore, it was necessary to modify the design to provide a compromise between the fast deionization of the rectifier tube and the high peak current capacity of the welder tube. The optimum design is shown in Figure 15(C). The cone-shaped graphite baffle provided sufficient deionizing speed and the more open construction provided the necessary current capacity.

Additional improvement in average current capacity was obtained by the addition of a water spiral in the cooling chamber. This cools the tube more effectively and uniformly and prevents hot spots which have the effect of raising the vapor pressure inside the tube. Higher vapor pressure lessens the ability of the tube to withstand inverse voltage. More arc-backs may be expected at higher temperatures. For this reason nearly all of the tests were conducted at the higher water temperature rating 40 degrees centigrade. Tests also were made at 10 degrees centigrade water temperature to assure that there was no constriction with high peak currents at this lower vapor pressure.

The results of the tests are shown by the rating curves of Figure 16. The capacity of the single baffle tube, which has

the Radio Manufacturers Association (RMA) type designation *5822*, covers the application requirements of the larger frequency-changer welders. For smaller welders, one of the present single-phase welder tubes, RMA type *5551*, had adequate capacity for the lighter duty.

Tube Rating

The basic maximum ratings for the type *5822* frequency-changer tube are given in Table I.

Other requirements, such as the ignitor ratings, are the same as those for the single-phase welder.

The maximum peak inverse and forward anode voltage of 1,200 and 1,500 volts covers frequency-changer line voltages of 440 and 550 volts rms respectively, plus an allowance for a 10 per cent line voltage variation. A 600-volt peak inverse rating (220 volts rms line voltage) now is being considered and a tentative rating is shown on Figure 16. The 1,200 volt and 1,500-volt ratings are related by constant kilovolt-amperes, but the constant kilovolt-amperes relation could not be held at the lower voltage.

Maximum Anode Current

Ratings for maximum anode current are given on the basis of no-phase delay. As the ignition is retarded the anode current will be correspondingly less. Operation with phase retard is more severe on the tubes because of the increase in initial inverse voltage, Figure 8(B); and decrease in commutation time, Figure 10.

Table I. Ratings for Type 5822 Frequency Changer Tube

Maximum peak anode voltage		
Inverse	1,200	1,500 volts
Forward	1,200	1,500 volts
Maximum anode current*		
Peak	1,500	1,200 amperes
Corresponding average	20	16 amperes
Average	70	56 amperes
Corresponding peak	420	336 amperes
Maximum averaging time	6.25	6.25 seconds
Ratio of average to peak current (Maximum averaging time of 0.2 sec)	0.166	0.166
Ratio of surge to peak current, maximum	12.5	12.5
Maximum duration of surge current	0.15	0.15 second
Frequency range	50 to 60	50 to 60 cps

*Straight line interpolation on log-log paper between corresponding points permits determination of other current ratings. Ratings are for zero phase-control angle.

Calculations or readings to check peak or average current ratings must be done at no phase delay (100 per cent heat).

Figure 17 shows the reduction in load with phase retard for a constant rate of arc-back[6] together with a theoretical curve of load reduction with phase retard. It is evident from the curve that the most severe tube condition exists around 30 degrees retard. As mentioned previously, the tests to set up the ratings were made at 30 degrees retard.

Maximum Peak and Corresponding Average Anode Current

For intermittent service, ignitron ratings allow higher peak current at lower average current. For this reason the duty cycle must be lowered if higher peak currents are desired. The *5822* tube was designed to meet a peak current of 1,500 amperes for a 1/2-second weld time. The highest duty cycle, that is, the highest average current, commensurate with satisfactory tube performance at this peak current would then be one point on the rating.

The peak anode current in the frequency-changer circuit is essentially a square wave in shape and may be considered for all six tubes as the peak secondary current divided by the transformer turn ratio. The average current during the weld time can be considered with fair accuracy as the peak tube current divided by number of tubes contributing. The first consideration is more accurate and the latter consideration less accurate with a large primary to secondary reactance. In the latter consideration, the last tube in the sequence would be carrying more, and the first tube less, than the calculated average.

Maximum Averaging Time

Tubes have a comparatively low thermal capacity and, therefore, acquire thermal equilibrium in a few seconds. For this reason, the rated peak currents cannot be carried beyond a certain length of time without having an off period. For a 1/2-second weld time at 1,500 amperes rated peak current in the frequency-changer circuit, it was found necessary to have an off-period of 5.75 seconds.

Maximum Average and Corresponding Peak Anode Current

For the frequency-changer circuit at 100 per cent equipment duty the peak tube current will be six times the average current per tube, each tube carries 1/6 load. The maximum average and corresponding peak anode current commensurate with satisfactory tube performance was established by operating at 100 per cent equipment duty. Tests showed that a straight line variation on log-log paper could be allowed between the maximum peak current rating and the maximum average current rating.

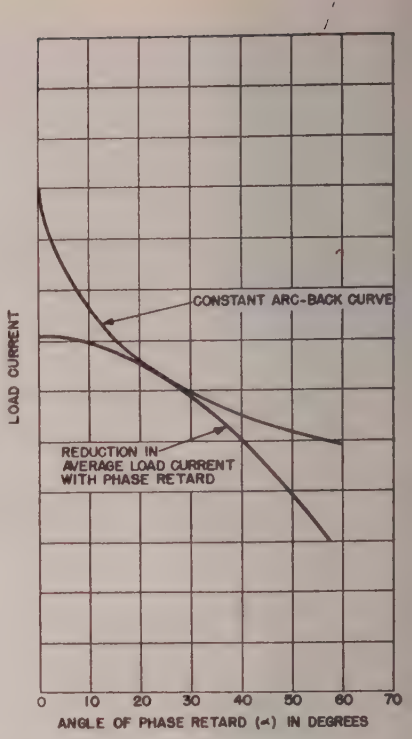

Figure 17. Ignitron tube performance with phase retard for constant load impedance

$I_{avg}/I_{pk}=0.166$ for a Maximum Averaging Time of 0.2 Second

This rating is presented because a half-second conduction time on the frequency-changer circuit is not to be a single weld cycle. A complete cycle of the low-frequency weld must occur in 0.2 second. Actually this does not limit any present equipment or any expected future equipment, for it means that the weld frequency must not be less than 5 cycles per second. Installations today are at weld frequencies of 12 and $8^4/_7$ cycles per second which give a single weld cycle time of 0.0933 and 0.116 second respectively. In terms of 60-cycle power these represent a maximum on-time of one group of tubes of two and three cycles respectively. The 0.2 second averaging time allows a six cycle on-time for one group of tubes.

Since each tube in each cycle of weld frequency (neglecting welder inductance) carries 1/6 of the current, $I_{avg}/I_{pk}=0.166$ as a maximum. As is actually the case, welder inductance will be present, and this ratio will be less. Peak current is

considered the highest current of the inductive build up.

Ratio of Surge to Peak Current=12.5

As mentioned previously the surge current rating is included mainly to assure satisfactory tube performance through the commutating period. Tests determined that at the peak current rating of the tube a 35-degree commutation time was necessary to obtain a certain desired tube performance, that is, a low probability of arc-back.

Commutation time (without phase control) from equation 5 is:

$$u = \cos^{-1}(1 - 0.408 X_{pp} I_c / E)$$

where

I_C = current commutated (peak anode current assuming square wave) = I_{pk}

For $u = 35°$

$X_{pp} = 0.44 E / I_{pk}$

Also the arc-back current from equation 7 will be

$$i_{ar} = K_r \frac{2\sqrt{2}E}{\sqrt{R_{pp}^2 + X_{pp}^2}}$$

For most severe operating conditions where R_{pp} is small in comparison with X_{pp}, K_r has a value of 2. Neglecting

R_{pp}, $I_{ar} = 4\sqrt{2}E / X_{pp}$

Combining, we get

$i_{ar} / I_{pk} = 12.5$

Maximum Duration of Fault Current 0.15 Second

This rating establishes the time for fuses or circuit breakers to operate to minimize damage to the tubes. Most circuit breakers clear in 6 to 8 cycles. This 0.15 second allows a maximum time of 9 cycles.

Conclusions

1. A modified ignitron tube design incorporating a deionization baffle between the anode and the cathode was found necessary to meet the circuit requirements of fast commutation and high initial inverse anode voltage immediately after commutation.

2. The reactance between primaries of the welding transformer has an important influence on the ignitron tube performance. Increasing this reactance increases the commutation time, and decreases the probability of tube arc-back.

3. If the ratio of welder reactance (at supply frequency) to welder resistance exceeds 3.5 special control circuits are advisable, to avoid long conduction time for the last tube.

References

1. Circuit Analysis of Frequency-Changer Welders, **W. K. Boice.** *Welding Journal* (New York, N. Y.), volume 28, October 1949, page 946.

2. Resistance Welding with the Sciaky Three-Phase System, **J. L. Solomon.** AIEE Electric Welding Conference, May 1949.

3. Circuit Cushioning on Gas-Filled Grid Controlled Rectifiers, **D. V. Edwards, E. K. Smith.** *Electrical Engineering* (*AIEE Transactions*), volume 65, October 1946, pages 640–43.

4. Analysis of Rectifier Circuits, **E. F. Christensen, C. H. Willis, C. C. Herskind.** *AIEE Transactions*, volume 63, 1944, pages 1048–58.

5. Rectifier Fault Currents, II, **C. C. Herskind, A. Schmidt, Jr., C. E. Rettig.** *AIEE Transactions*, volume 68, part I, 1949, pages 243–52.

6. Rectifier Capacity, **C. C. Herskind, H. C. Steiner.** *Electrical Engineering* (*AIEE Transactions*), volume 65, October 1946, pages 667–70.

No Discussion

A Gas Tube Inverter with the Supply Voltage Below the Breakdown Voltage

JOHN M. CAGE
MEMBER AIEE

JOHN C. SCHUDER
NONMEMBER AIEE

TO OBTAIN d-c plate-supply voltages for electronic equipment operated by storage batteries, it is customary to use either dynamotors or vibrators. Both devices have been used successfully for automobile radio receivers, for example, but engineers have long been fascinated by the possibility of transforming low d-c voltages to higher voltages without resorting to mechanical motion.

Since a-c voltages can be readily transformed and rectified, a suitable solution to the problem would be to convert low d-c voltages to a-c voltages of the same order of amplitude. The vibrator does this very effectively, but with moving parts. If the initial d-c voltage is high enough, a vacuum-tube oscillator can be used to convert it to alternating voltage. However, the oscillator is not a solution to the present problem, because obtainable vacuum tubes require a great deal more than 6 or 12 or even 24 volts as d-c plate supply, to give reasonable efficiency and power output.

Usually the conventional inverter employing gaseous tubes is not considered applicable when the d-c voltage is lower than 100 volts or thereabouts. However, experimental gas-tube inverters have been made to function by Carl R. Peterson from d-c supplies as low as 6 volts,[1] and the purpose of the present paper is to study some of the characteristics of a simple inverter with plate voltage lower than breakdown voltage. An hypothesis of the special phenomena within the gas tube is presented.

The basic unloaded circuit is shown in Figure 1. The inverter is placed in operation by first closing switch S and then opening it. The current originally flowing through the switch transfers to the capacitor C, charging it until it reaches the breakdown voltage of the tube. The tube then discharges the capacitor and finally stops conducting. This cycle is repeated indefinitely. It is with the detailed study of this apparently simple circuit, together with the possibilities of loading, that this investigation is concerned.

Tube Characteristics

In any circuit investigation, it is desirable to know the characteristics of the elements involved before trying to fit them into the circuit. The tube is usually thought to have the characteristic shown in Figure 2; however, further investigation of this matter is in order.[2]

The circuit usually used for obtaining the volt-ampere characteristic of a gas diode is shown in Figure 3. The data obtained from this circuit are plotted in Figure 4, and this curve is usually considered to represent static values of current and voltage for the tube. This test circuit, however, represents a case where the positive resistance is greater than the negative resistance (of the tube), and a later paper will show that stability is not possible in this case. With this knowledge, an oscillograph was connected across the tube with the result shown in Figure 5. These data show clearly that the results of Figure 4 are not really static values and suggest that a different approach to the problem might be desirable.

In an attempt to gain more information about the tube characteristics, the circuit shown in Figure 6 was constructed. From this circuit the data shown in Table I were obtained. Figure 7 shows a typical waveform of the tube voltage as a function of time for the capacitance values listed in Table I. The unusual fact about the observed waveform is that the tube voltage actually drops to about one-half volt and remains at this value for a considerable time.

At values of capacitance below and above the values listed in Table I, the waveform of tube voltage departs markedly from that shown in Figure 7. For capacitance values less than approximately 0.2 microfarad (mfd) and greater that 0.08 mfd, random frequencies are observed with a maximum amplitude of 13 volts and a minimum amplitude of 0.75 volt. For capacitance values less than 0.08 mfd and greater than 0.01 mfd, sinusoidal oscillations are observed with a maximum instantaneous value of 12 volts and a minimum instantaneous value

Figure 1 (below). The unloaded inverter circuit. Oscillations are started by closing switch S and then opening it

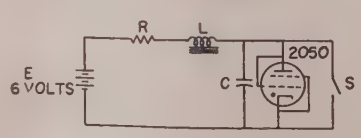

Figure 2 (right). The assumed volt-ampere curve of a gas diode

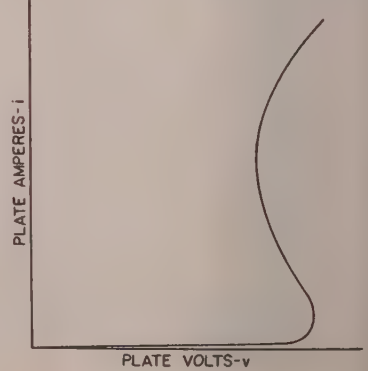

Paper 51-168, recommended by the AIEE Electronics Committee and approved by the AIEE Technical Program Committee for presentation at the AIEE Great Lakes District Meeting, Madison, Wis., May 17–19, 1951. Manuscript submitted February 19, 1951; made available for printing April 18, 1951.

JOHN M. CAGE and JOHN C. SCHUDER are both with Purdue University, Lafayette, Ind.

This paper is a condensation of an unpublished Master's Thesis of the same title by John C. Schuder.

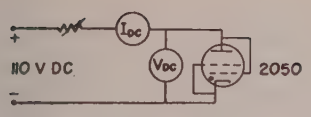

Figure 3. The circuit usually used for obtaining the volt-ampere characteristic of a gas diode

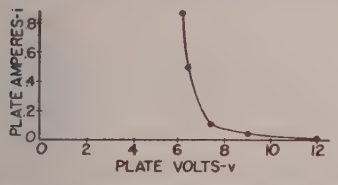

Figure 4. Volt-ampere characteristic of a 2050 tube as determined by circuit of Figure 3

Figure 5. The voltage across the tube, for the circuit of Figure 3, as a function of time

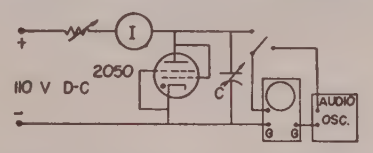

Figure 6. Circuit used to obtain data for tube operation with different values of current and different values of capacitance

of 7 volts. The frequency of oscillation is in the tens of kilocycles per second. This method of operation is probably similar to that of the Poulsen arc oscillator. For capacitance values as near zero as possible, random frequencies were again observed with an apparent maximum of 13 volts and apparent minimum of 3 volts.

For capacitance values above those existing in the table, namely 4 to 10 mfd, oscillations occur with the time A a very small fraction of time T and the voltage B equal to 4 volts. The meaning of A, B, and T is shown in Figure 7. For large capacitance this mode of operation seems to vary each cycle. It is of interest to note that this is the mode of operation usually associated with gas diodes.

The curve of tube voltage as a function of time for the circuit of Figure 6 as shown in Figure 7 suggests the following description of tube operation in this circuit: At time equals zero on the curve of Figure 7, the capacitor C has just been discharged through the tube. The tube remains in a conducting state and continues to conduct current I from the voltage supply. This current cannot, during this interval, be conducted by the capacitor, because the voltage across the capacitor remains constant. After time interval A, the tube stops conducting and the capacitor starts to charge. Since the supply voltage is quite high as compared with the capacitor voltage at any time, the charging current is almost constant; and this results in a linear rise in capacitor voltage. When the capacitor voltage reaches the value V, approximately 13 volts in this case, the tube breaks down and discharges the capacitor in a very short time. The cycle as outlined above repeats indefinitely. The curves of Figure 8 verify the outline of tube operation suggested above.

As noted above, it was found that if a mode of operation is desired where the tube voltage drops almost to zero, a capacitance between 0.2 mfd and 3 mfd should be used. For values of capacitance below and above this range of values the voltage does not drop near zero. The following is a possible simplified explanation of the results observed. First, for low values of capacitance, the peak current caused by capacitor discharge is comparatively low. When the voltage falls below the normal extinction potential, the few remaining ions will quickly be swept to the electrodes or the walls of the tube. For this reason the voltage falls only to a comparatively high value of 2 to 3 volts. Second, for medium values of capacitance, the peak current caused by capacitor discharge is rather high. This creates a large number of ions in the interelectrode space which continue to discharge the capacitor below the normal extinction potential of the tube. The voltage falls almost to zero, but enough ions are still present to continue conduction of supply current for some time. Third, for very high capacitance values, the peak current is even larger. When the tube reaches the normal extinction voltage, there is still a large amount of energy stored in the capacitor. This causes a comparatively heavy current to flow, removing the ions without appreciable reduction in voltage.

Since 1.0 mfd represented a value of capacitance well within the range found to give a period of almost zero voltage, it was used for all further experimental work. Figure 9 shows the average tube voltage as a function of average supply current for the circuit of Figure 6. Figure 9 shows that the voltage approaches 6.5 volts as the supply current approaches zero. As the supply current becomes large, the value of average voltage approaches 4.2 volts in an asymptotic fashion.

If the curve of tube voltage as a function of time, as shown in Figure 7, is idealized to the extent that capacitor discharge time is considered to be zero and the conduction during time A is considered to be at zero voltage, an interesting derivation may be made for the curve of Figure 9. From the geometry of Figure 7,

$$V_{c\,(avg)} = \frac{(T-A)V/2}{T} \qquad (1)$$

Since the charge on the capacitor just be-

Table I. Data for the Circuit of Figure 6*

	I, Milliamperes	Volts B	Volts V	Freq., Cycles Per Second	Time T, Millisecond	Fraction, A/T	Time A, Millisecond
C = 0.3 mfd	20	0.5	13	2,350	0.43	6/20	0.13
	40	0.5	13	3,500	0.29	8/20	0.12
	60	0.5	13	4,300	0.23	9/20	0.10
	80	0.5	13	5,000	0.20	10/20	0.10
	100	0.75	13	5,400	0.19	10/20	0.10
	120	0.75	14	5,900	0.17	10/20	0.09
C = 0.5 mfd	20	0.5	13	1,640	0.61	6/20	0.19
	40	0.5	13	2,590	0.39	8/20	0.16
	60	0.5	13	3,150	0.32	9/20	0.14
	80	0.5	13	3,800	0.26	10/20	0.13
	100	0.75	13	4,250	0.24	11/20	0.13
	120	0.75	13	4,700	0.21	11/20	0.11
C = 1 mfd	20	0.5	13	1,100	0.91	1/4	0.23
	30	0.5	13	1,500	0.67	1/4	0.17
	40	0.5	13	1,810	0.55	3/10	0.17
	50	0.5	13	2,130	0.47	3/10	0.14
	60	0.5	13	2,400	0.42	3/10	0.13
	70	0.5	13	2,620	0.38	7/20	0.13
	80	0.5	13	2,880	0.35	7/20	0.12
	90	0.75	13	3,040	0.33	7/20	0.12
	100	0.75	13	3,300	0.30	4/10	0.12
	120	0.75	13	3,650	0.27	9/20	0.12
C = 3 mfd	20	0.5	13	460	2.2	1/20	0.11
	40	0.5	12.5	900	1.1	2/20	0.11
	60	0.5	12.5	1,260	0.79	3/20	0.12
	80	0.5	12.5	1,590	0.63	3/20	0.09
	100	0.75	13	1,890	0.53	4/20	0.11
	120	0.75	12.5	2,180	0.46	5/20	0.11

*For the significance of A, B, T, and V see Figure 7.

fore the instant of discharge is given by both CV and $I\,(T-A)$,

$$CV=I(T-A) \tag{2}$$

Solving equation 2 for T gives

$$T=\frac{CV}{I}+A \tag{3}$$

Substituting the value of T from equation 3 into equation 1 gives

$$V_{c\,(\text{avg})}=\frac{CV^2/2}{CV+AI} \tag{4}$$

To calculate A let it be supposed that the number of ions in the interelectrode space at the end of capacitor discharge is independent of supply current. Let it further be supposed that the ions may leave in two ways. First, they may leave by ways independent of current and the rate of so leaving will be assumed constant. F will equal the fraction of the total number of ions in the space at the start of the conduction period removed per second by this method. Second, they may go to the electrodes and conduct current, and the rate of so leaving is directly proportional to current. G will equal the fraction of the total number of ions in the space at the start of the conduction period removed per second per ampere of current by this method. Then

$$1=(F+GI)A \tag{5}$$

and substituting the value of A from equation 5 into equation 4 gives

$$V_{c\,(\text{avg})}=\frac{CV^2/2}{CV+\dfrac{I}{F+GI}} \tag{6}$$

That equation 6 will approximately fit the experimental curve of Figure 9 can be seen by noting that equation 6 gives a value of $V/2$ for I equal zero and a value approaching $CV^2/2\times 1/CV+1/G$ which is a constant, for high values of current. Figure 9 shows that the experimental curve gives the same results as predicted by equation 6. While the hypothesis as to how the ions leave the space is probably oversimplified, it nevertheless gives an understandable explanation of the curve of Figure 9.

The problem of deionization is considered in the literature. For a more rigorous analysis of deionization under somewhat different conditions see, for example, reference 3.

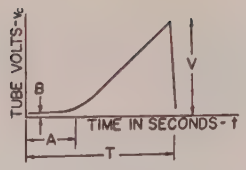

Figure 7. A typical waveform of tube voltage for the circuit of Figure 6. The values of A, B, T, and V for different capacitor and current values are given in Table I

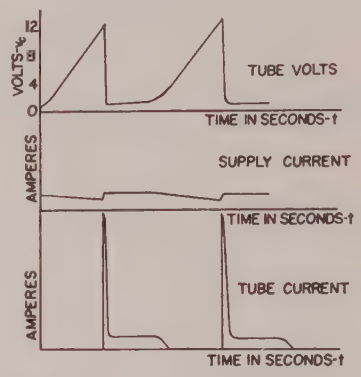

Figure 8. Observed waveforms of tube voltage, supply current, and tube current for the circuit of Figure 6. Supply current is 40 milliampere average

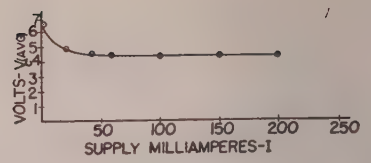

Figure 9. Average tube voltage as a function of supply current

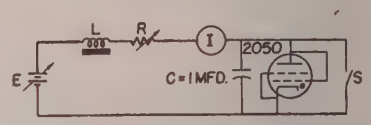

Figure 10. The unloaded inverter circuit

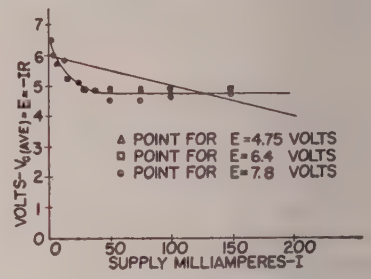

Figure 11. Average tube voltage as a function of supply current. The straight line is the load line for a 6-volt supply and R = 10 ohms

Table II. The Result of Varying R in the Circuit of Figure 10*

	R, including that of coil, ohms	I, Milliamperes	E-IR
$E=4.75$ V	1	100	4.65
	1 ohm is largest that can be used		
$E=6.4$ V	10.5	150	4.8
	16.5	100	4.8
	22.0	75	4.8
	32.0	50	4.8
	39.0	40	4.8
	47.0	30	4.8
	59.0	20	5.2
	74.0	10	5.7
	79.0	8	5.8
	79 ohms is largest that can be used		
$E=7.8$ V	21	150	4.7
	32	100	4.6
	44	75	4.5
	15	50	4.5
	110	25	5.1
	120	15	5.8
	225	10	5.6
	350	5	6.0
	650	2	6.5
	650 ohms is largest that can be used		

*These data appear in curve form in Figure 11.

Experimental Investigation of the Unloaded Inverter

A laboratory study was made of a simple low-voltage inverter circuit, both loaded and unloaded, to check the working hypothesis developed above. In the unloaded circuit of Figure 10 the inductance was made very large. The waveform of voltage across the tube is, then, substantially like that observed in the preceding section. This is so because in both cases the supply current is almost constant with time.

In order to plot average tube voltage versus supply current I, in Figure 10, readings of I were taken as R was varied, for various values of E. The average tube voltage was then computed as $E-IR$, since R included the resistance of the inductance coil. Figure 11 shows that these points fall, within experimental error, along one smooth curve. Furthermore, this curve is substantially the same as Figure 9, the one plotted for Figure 6. It has already been shown that this curve (Figure 9) agrees with equation 6, which was developed from theoretical considerations.

If sustained oscillations are to take place, obviously the voltage given by $E-IR$ must equal that given by Figure

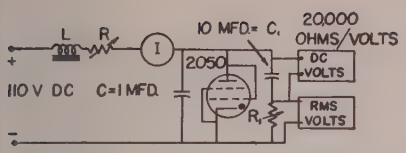

Figure 12. Loaded inverter test circuit

Figure 13. Average tube voltage as a function of supply current for different values of load resistance

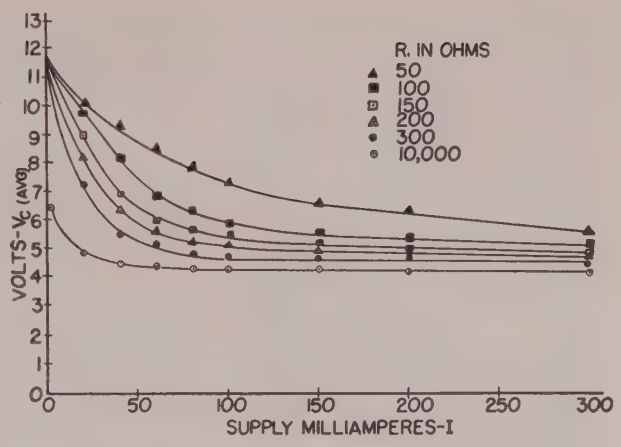

11 or equation 6. The straight line plotted in Figure 11 shows the average tube voltage as a function of current I for a battery voltage of 6 volts, and a resistance of 10 ohms.

This load line crosses the experimental curve at two points. Either of these two points of intersection fulfills the condition of simultaneously satisfying equation 6 and $E-IR=V_{c(avg)}$. Experimentally, however, only the higher current point is observed; that is, the lower current point is a point of instability. It is interesting to notice that if in starting the circuit the switch is closed until the current is between the two points, and then the switch is opened, the current will continue to climb to the higher point. With large inductance, this takes place in a matter of several seconds and is easily observed. If the switch is held closed until current exceeds the high-current point, and then opened, the current will decrease to this point.

As to why the lower current point is not stable, the usual explanation would be something as follows: If for any reason the current should drop below the equilibrium point, the average voltage across the capacitor would exceed that which is supplied by the battery minus the resistance drop. This must mean, then, that the current would drop even further until it finally stopped flowing. Even though this explanation sounds plausible, the analysis of somewhat similar problems makes for skepticism about such simple explanations.

It is believed that the rigorous method of showing this point to be unstable would be to assume a slightly lower current at the start and then to plot this current as a function of time. This would involve the solution of the differential equations of the circuit. The current should go to a slightly lower value at the end of a complete cycle than it had at the start of the cycle. However, since the phenomenon of current dying out is observed to require several seconds and since the frequency is of the order of magnitude of 1,000 cycles per second, the decrease in current over one cycle is very small indeed. This fact makes the mathematical derivation of instability rather difficult. For this reason, it will be taken at present as only an experimental fact that the lower current point is a point of instability.

Suppose that the resistance of the load line in Figure 11 is increased. This causes the load line to swing down and decreases the current. Finally, however, the load line becomes tangent to the curve. It is this condition that represents the maximum permissible circuit resistance for a given battery voltage. It also represents the minimum current.

Figure 11 shows clearly, also, that the circuit cannot operate for supply voltages below approximately 4.6 volts even if zero resistance could be obtained in the inductance.

For supply voltages over approximately $6\frac{1}{2}$ volts, any resistance value could be used; and the current could be made as small as desired. This statement should be limited, however, to the point where the current drops to some 2 milliamperes because at this point the tube is operating on the positive-resistance part of the volt-ampere curve. Under this condition a constant value of current flows through the tube and oscillations do not occur.

The Loaded Inverter

In a sense, the inverter of Figure 10 is loaded by the resistance R, for finite values of L, for some alternating current flows through R. In most cases, however, it would be better to attach the load by means of inductive coupling to the oscillator inductance L or by means of capacitance coupling to the a-c components of voltage across the tube. The latter method of coupling was investigated particularly, and the results and conclusions are given below.

Figure 12 shows the test circuit used for studying the loaded inverter. It will be observed that a higher d-c input voltage was used here rather than the few volts with which we are concerned, but since the supply current I is substantially constant, the inverter operates the same on low supply voltage as it does on high voltage, provided the d-c component of tube voltage is adjusted to be the same in the two cases. The use of higher voltage in the experimental work permitted a greater range of conditions to be obtained conveniently.

Figure 13 plots d-c tube voltage against supply current for various values of load resistance R_1. The curves can be used with load lines to predict whether oscillations are possible under various conditions of load, supply current, and supply voltage. The slope of the load line is determined by R, not by R_1.

Table III gives the experimentally observed output power of the circuit of Figure 12 for various values of load resist-

Table III. Watts Output as a Function of Supply Current and Load Resistance R_1 for the Circuit of Figure 12*

I, Milliamperes	$R_1=300$ Watts Out	$R_1=300$ Eff., Per Cent	$R_1=200$ Watts Out	$R_1=200$ Eff., Per Cent	$R_1=150$ Watts Out	$R_1=150$ Eff., Per Cent	$R_1=100$ Watts Out	$R_1=100$ Eff., Per Cent	$R_1=50$ Watts Out	$R_1=50$ Eff., Per Cent
20	0.06	50	0.08	67	0.10	83	0.12	100	0.13	109
40	0.06	25	0.09	37	0.12	50	0.18	75	0.22	92
60	0.06	17	0.09	25	0.12	33	0.19	53	0.29	80
80	0.06	12	0.09	19	0.12	25	0.19	40	0.34	71
100	0.06	10	0.09	15	0.12	20	0.19	32	0.35	60
150	0.06	7	0.09	10	0.12	13	0.18	20	0.37	41
200	0.06	5	0.08	7	0.12	10	0.18	15	0.37	31
300	0.06	3	0.08	4	0.12	7	0.18	10	0.37	20

*The efficiency values given are those that occur if the circuit will oscillate with a 6-volt supply.

ance and line current. Also listed in Table III are the calculated efficiencies of the circuit on the basis of a 6-volt supply. However, some of these values of efficiency are forbidden because oscillations will not occur. The necessary condition for oscillations is that it be possible to construct a load line in Figure 13 so as to intersect the curve corresponding to the R_1 in question at two points with the highest current point being the I in question. With a 6-volt supply, a maximum efficiency of approximately 21 per cent was calculated from the data of Table III and the curves of Figure 13. Experimental checks with a 6-volt supply substantiated this calculation.

Tube Considerations

As has been shown above, the tube discharges the capacitor once each cycle. After discharging the capacitor, the tube continues to conduct for a period at almost zero-drop. The peak current was observed to be approximately 2 amperes while the average current must, from the circuit arrangement, be the same as the supply current. The anode dissipation of the tube is, to a first approximation, the product of the maximum energy stored in the capacitor and the frequency of oscillation.

Since tubes were operated over long periods of time with peak and average currents that considerably exceeded the published ratings, it is suggested that these ratings be investigated in detail for use in inverters of the type studied. Almost certainly, the average-current ratings could be increased, because the tube voltage remains near zero for a significant part of the current-carrying period. Perhaps the peak-current rating should also be higher for this type of operation.

It seems to be indicated that tubes with lower ignition voltages would give higher efficiencies, and yet the current drawn immediately after ignition must remain as high as possible. Also, it would be important to increase the ability of tubes to pass current at substantially zero tube voltage after a capacitor has been discharged through them. This would seem to be a fertile field for future tube research. Perhaps Tungar techniques could be used since inverse voltages do not exist in this application.

References

1. Tubes at Work, **V. Zeluff.** *Electronics* (New York, N. Y.), volume 22, August 1949, page 140.

2. New Sensitive and Inexpensive Gas Control Tubes, **W. E. Bahles, C. H. Thomas.** *Electronics* (New York, N. Y.), volume 22, September 1941, page 33.

3. Statistical Nature and Physical Concepts of Thyratron Deionization Time, **H. A. Romanowitz, W. G. Dow.** *AIEE Transactions*, volume 69, part I, 1950, pages 368–79.

No Discussion

A Diode Bridge Limiter for Use with Electronic Analogue Computers

RUSSELL J. MEDKEFF
ASSOCIATE AIEE

ROBERT J. PARENT
MEMBER AIEE

Synopsis: A new limiter circuit for use with electronic analogue computers has been developed from the basic diode bridge circuit. This limiter is simple in construction, has only one adjustment and produces an absolute limit. Other useful circuit configurations using the basic diode bridge are given.

AN ALL electronic differential analyzer is often called upon to solve equations which represent nonlinear systems.[1,2] The nonlinearities usually appear as nonconstant coefficients in the differential equations representing the system and very often are functions of only a single variable. Typical nonlinearities to be represented are saturation curves, mechanical limit stops, amplifier overload, backlash, deadband due to static friction, and so forth. Many of these functions can be approximated by the three slope curves shown in Figure 1.

The authors were confronted with the problem of designing devices to produce some of these functions for use with the Philbrick high-speed analogue computer. In this computer all variables are represented as voltages and so voltage sensitive elements must be used. The signal voltages in the computer vary about ground potential and circuits with a symmetrical response are required. After a search of the literature it was decided to try and improve on existing practices.[1,2,3]

Paper 51-170, recommended by the AIEE Computing Devices Committee and approved by the Technical Program Committee for presentation at the AIEE Great Lakes District Meeting, Madison, Wis., May 17–19, 1951. Manuscript submitted February 16, 1951; made available for printing April 9, 1951.

RUSSELL J. MEDKEFF is with the Askania Regulator Company, Chicago, Ill., and ROBERT J. PARENT is with the University of Wisconsin, Madison, Wis.

The adaptation of the diode bridge circuit[4] seemed to hold most promise for improvement. This paper will discuss several adaptations of the bridge circuit to the generation of special functions with emphasis on a limiter circuit which produces an absolute limit.

The most commonly accepted method of obtaining limiter action, Figure1 (A), is to use the basic biased diode circuit[3] of Figure 2(A). This circuit works reasonably well but does not produce an absolute limit due to the resistance of the diodes and bias sources. It also requires the simultaneous adjustment of the two bias voltage sources which is a disadvantage. The circuit may be adapted for the generation of the function of Figure 1(B) by the addition of the resistor R_2 as shown in Figure 2(B). Again the requirement of simultaneous adjustment of the bias sources is a disadvantage.

The diode bridge circuit developed for producing an absolute limit is shown in Figure 3. As can be seen from the diagram the circuit is a simple one and requires only one adjustment, the resistor R_2. The resistors R and the bias sources E are constant for a given design and application. If the e_o versus e_i curve is to be symmetrical the bias sources must be voltages of equal magnitude and opposite polarity. They also should be regulated. These voltage sources may well be available in a computer; for example, the +300 and −300 volt supplies in the Philbrick computer.

Examination of the e_o versus e_i plot shows that $e_o = e_i$ for $e_i < \theta$ and that for $e_i > \theta$ the output voltage e_o is independent of e_i. The circuit thus produces an absolute limit which is controlled by varying R_2. The equations and values given with the e_o versus e_i plot assume the diode resistances to be zero. Due to a finite diode resistance the voltage e_o will be slightly less than e_i for $e_i < \theta$. The limiting value of e_o is not a function of the diode resistance. The effect of diode resistance will be considered in more detail later.

The general principle of operation of the limiter now will be discussed. The currents in the circuit are due to two voltage sources, the d-c bias voltages and the signal e_i. These currents are shown in Figure 4. The currents designated by capital I's are due to the d-c bias voltages and the lower case i's are due to the signal voltage e_i.

All four diodes are made conducting and bilateral by the d-c bias voltages applied through resistors R. If all diodes are conducting and if the diode resistance is assumed zero it can be seen that points D and C are at the same potential and e_o equals e_i. As e_i increases the current i increases and a condition is finally reached where the current $i/2$ flowing through diode CA becomes equal and opposite to the current $I/2$ and diode CA stops conducting and remains nonconducting for all higher values of e_i. After diode CA stops conducting diode BD remains conducting because the signal current through it is less than $I/2$. The output voltage e_o still equals e_i since there is a zero impedance path through diodes CB and BD. As e_i continues to increase a

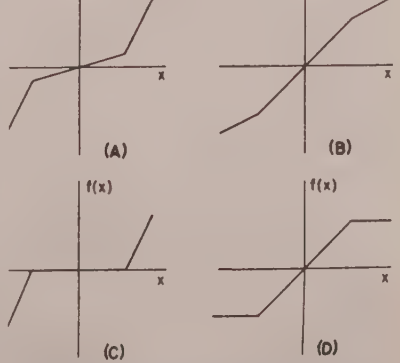

Figure 1. Typical three slope curves which may be used to approximate functions in computation

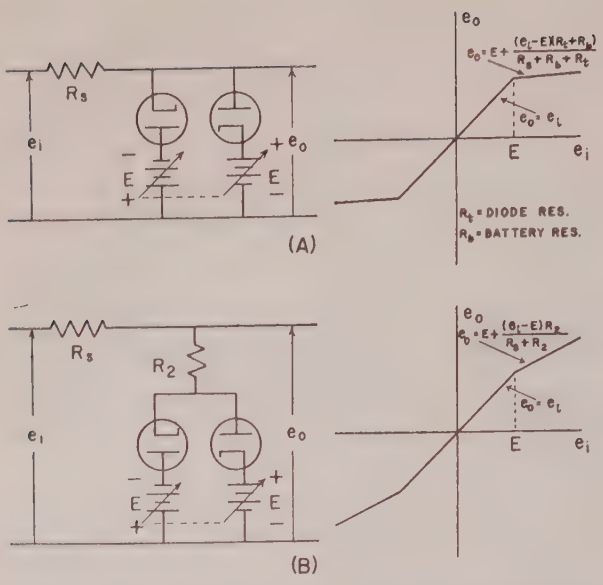

Figure 2. Conventional biased diode limiter circuits and their response curves

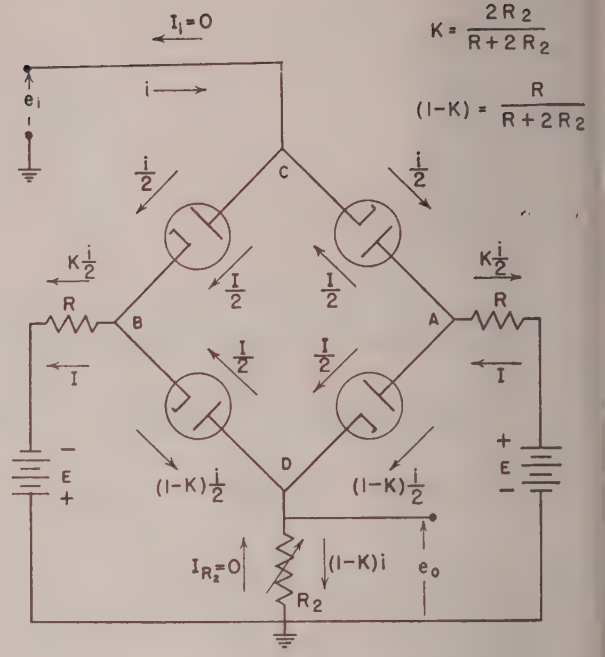

Figure 4. Currents flowing in diode bridge limiter due to the bias sources and the signal e_i

condition is finally reached where $(1-k)i/2$ becomes equal to $I/2$ and diode BD stops conducting, point D becomes isolated from the input and the output voltage e_o becomes independent of any further increase in e_i. The current from the right-hand bias source now flows through R, diode AD and R_2 to ground resulting in a voltage,

$$e_o = ER_2/(R+R_2) \tag{1}$$

The same reasoning with negative e_i will show that the limiting value is

$$e_o = -ER_2/(R+R_2) \tag{2}$$

The value of signal voltage e_i at which limiting takes place, θ of Figure 3(B), may be determined from the equivalent circuits of Figure 5. With the assumption of zero diode resistance the circuit becomes linear in each operating range and superposition may be applied and separate circuits may be drawn for the d-c and a-c components, Figures 5(A) and (B). With all four diodes conducting the currents are

$$I = E/R \tag{3A}$$

and

$$i = e_i(R+2R_2)/RR_2 \tag{3B}$$

Diode CA stops conducting when $i/2 = I/2$ or when $i = I$. Equating the above current expressions and solving for e_i yields,

$$e_i = ER_2/(R+2R_2) \tag{4}$$

As e_i is further increased the current through diode BD decreases and finally goes to zero. This isolates the output from the input and the output voltage is then

$$e_o = ER_2/(R+R_2) \tag{5}$$

as previously determined. The diode BD stops conducting at the instant its cathode potential rises above its plate potential. Since the plate potential at this instant is given by equation 5 and the cathode is at the potential e_i it follows that the value of e_i at which limiting takes place is

$$e_i = \theta = ER_2/(R+R_2) \tag{6}$$

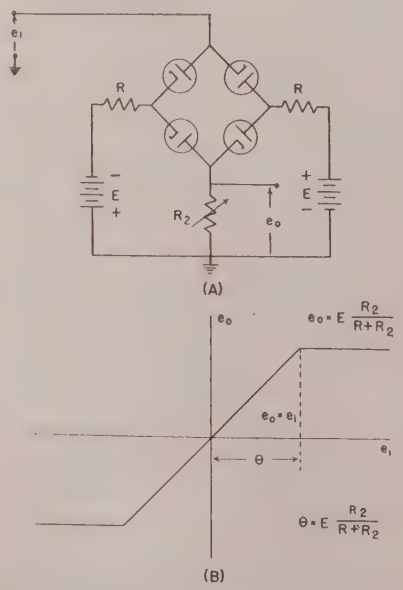

Figure 3. The diode bridge limiter (A) and its response curve (B)

Until this point is reached $e_o = e_i$.

Actually the diode resistance is not zero and its effect should be investigated. In a practical circuit the value of R will be very large compared to the diode resistance R_t and any approximation involving the neglecting of R_t compared with R will be quite valid. The value of R_2, however, may be quite small under certain conditions and approach the order of magnitude of R_t. Terms in the solution of the circuits involving R_t and R_2 should be carried through to investigate the effects of R_t. The analysis of the limiter circuit including R_t is given in the Appendix. Figure 6 shows the result in graphical form and should be compared with Figure 3(B). It is readily seen that if R_t is small compared to R_2 the approximate solution is in negligible error. An example will give some idea of the factors involved.

Example: Assume the following, E = 300 volts, R = 270,000 ohms, the limiting value of e_o = 30 volts and R_t = 200 ohms. From equation 5 $e_o = 30 = 300/(1+R/R_2)$ from which $R/R_2 = 9$ and R_2 = 30,000 ohms. (See Table I). The dif-

Table I

	Approximate Solution $R_t = 0$	More Exact Solution $R_t = 200$
Slope 0 to a	1.0	0.9933
Slope a to b	1.0	0.9866
Value of a	27.27	27.27×1.0033
Value of θ	30.00	30.00×1.0066

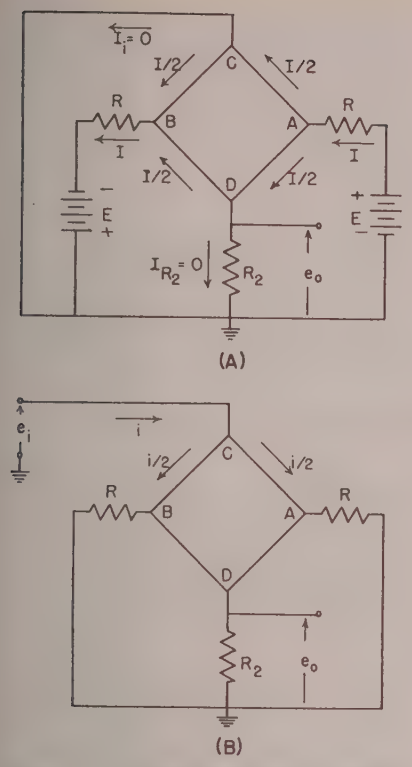

Figure 5. The diode bridge limiter separated into an equivalent circuit for bias currents (A) and signal currents (B)

ferences in this case are hardly measurable and are probably well within the usual accuracy of the physical data of the problem. If necessary the slope error can be corrected by following the limiter with an amplifier of gain slightly greater than one.

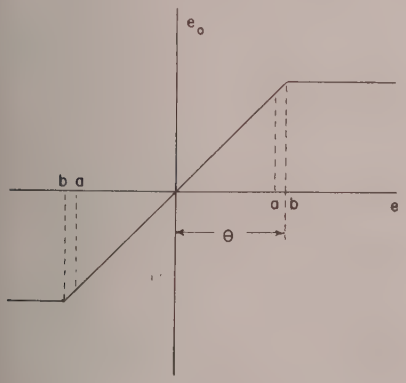

$|e_i| < |a|$ $\quad e_o = e_i \dfrac{R_2}{R_2 + R_t}$

$|a| < |e_i| < |b|$ $\quad e_o = e_i \dfrac{R_2}{R_2 + 2R_t}$

$|e_i| > |b|$ $\quad e_o = \pm E \dfrac{R_2}{R_2 + R}$

$$a = E \frac{R_2}{R + R_2} \left(1 + \frac{R_t}{2R_2}\right)$$

$$b = \theta = E \frac{R_2}{R + R_2} \left(1 + \frac{R_t}{R_2}\right)$$

Figure 6. A plot of the transfer function and expressions for output voltage e_o of the diode bridge with diode resistance considered

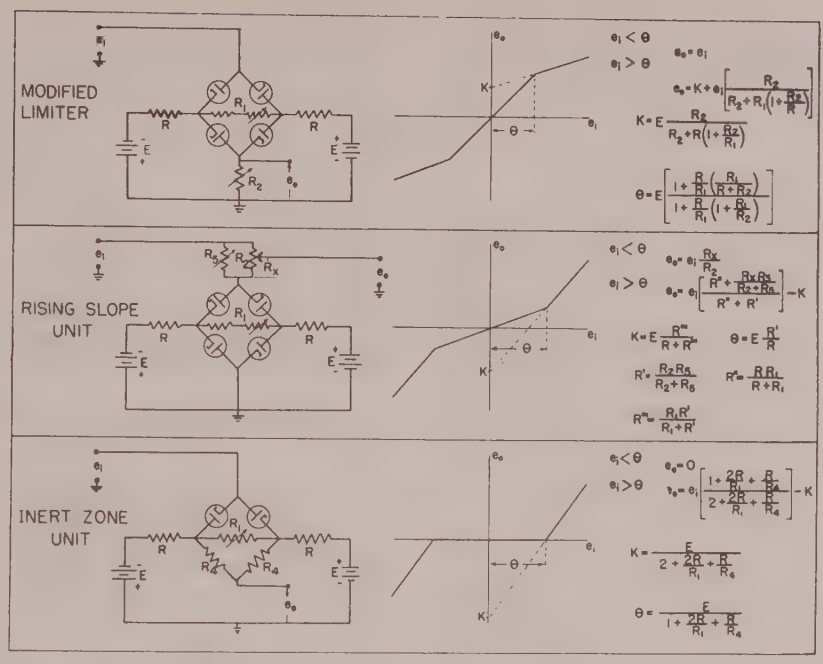
MODIFIED LIMITER
RISING SLOPE UNIT
INERT ZONE UNIT
e_i
e_o
R
E
R_1
R_2
R_3
R_4
R_x
θ
K
$e_i < \theta$
$e_i > \theta$
$e_o = e_i$
$e_o = K + e_i \left[\frac{R_2}{R_2 + R_1\left(1 + \frac{R_2}{R}\right)}\right]$
$K = E \frac{R_2}{R_2 + R\left(1 + \frac{R_2}{R_1}\right)}$
$\theta = E \left[\frac{1 + \frac{R}{R_1}\left(\frac{R_1}{R + R_2}\right)}{1 + \frac{R}{R_1}\left(1 + \frac{R_1}{R_2}\right)}\right]$
$e_o = e_i \frac{R_x}{R_2}$
$e_o = e_i \left[\frac{R' + \frac{R_x R_3}{R_2 + R_3}}{R' + R'}\right] - K$
$K = E \frac{R''}{R + R''}$
$\theta = E \frac{R'}{R}$
$R' = \frac{R_2 R_3}{R_2 + R_3}$
$R' = \frac{R R_1}{R + R_1}$
$R'' = \frac{R_1 R'}{R_1 + R'}$
$e_o = e_i \left[\frac{1 + \frac{2R}{R_1} + \frac{R}{R_4}}{2 + \frac{2R}{R_1} + \frac{R}{R_4}}\right] - K$
$K = \frac{E}{2 + \frac{2R}{R_1} + \frac{R}{R_4}}$
$\theta = \frac{E}{1 + \frac{2R}{R_1} + \frac{R}{R_4}}$

Figure 7 (above). Three adaptations of the diode bridge circuit to produce other transfer functions useful in nonlinear problem solutions

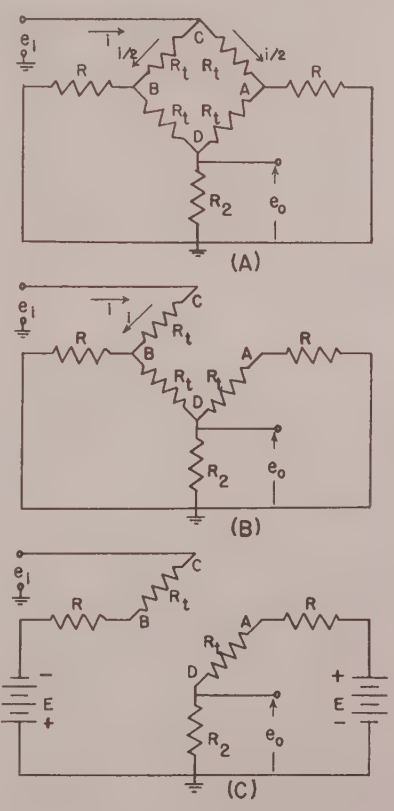

Figure 8 (right). Equivalent circuits used in the more exact analysis of the bridge limiter which includes the effect of diode resistance R_t

Other variations of the diode bridge circuit are possible. Time and space do not permit discussion of them. A number of these circuits and the resulting functions are shown in Figure 7. Most of these circuits have been used successfully by the authors in the solution of nonlinear problems. Arguments and equivalent circuits similar to those outlined in the paper should produce the results tabulated. More complex nonlinear functions may be represented by cascading the proper units to form multiple slope curves.

All of the circuits shown are symmetrical and produce symmetrical functions. If nonsymmetrical functions are desired they can be produced in general by unbalancing the circuit. This might be done by using a somewhat different value for one of the resistors R in series with the bias sources. Other possibilities will become apparent in particular cases.

Zero impedance has been assumed for the source of the signal voltage e_i and the output voltage e_o has been assumed to work into an infinite impedance. In practice these conditions are approached by the use of a cathode follower to drive the bridge circuits and the use of another cathode follower as a buffer between the output terminals of the bridge and the circuit which follows.

A diode bridge limiter has been presented which will produce an absolute limit, is simple in construction, and may be adjusted by means of a single control. The authors feel that this represents an improvement over known circuits. The limiter has worked very satisfactorily in

the solution of several problems involving the need for representing mechanical limit stops in a physical system.

Appendix

A more exact analysis of the bridge limiter circuit which includes the effects of the diode resistance R_t follows. The circuit is shown in Figure 4 with the currents due to the bias sources shown as capital letters and the currents due to the signal voltage e_i shown as lower case letters. Examination of the circuit diagram will reveal that the bias sources produce no current through R_2 with the result that the output voltage e_o is due entirely to the signal voltage e_i.

The equivalent circuit for signal currents can be drawn as in Figure 8(A). Solution of this circuit yields

$$e_o = e_i \frac{R_2}{R_2(1+R_t/R)+R_t(1+R_t/2R)} \approx e_i \frac{R_2}{R_2+R_t} \quad (7)$$

As e_i increases a condition is reached where diode CA becomes nonconducting. This value of e_i is determined by equating the current $i/2$ to $I/2$ $(i=I)$ as shown in equation 8.

$$I = \frac{E}{R+R_t/2} \qquad i = e_i \frac{1}{R_t/2+\dfrac{R(R_2+R_t/2)}{R+R_t+2R_2}} \quad (8)$$

Solving for e_i assuming $R_t << R$

$$e_i \approx E \frac{R_2}{R+2R_2}\left(1+\frac{R_t}{2R_2}\right) \quad (9)$$

This is the quantity a of Figure 6. When diode CA becomes nonconducting the circuit becomes as shown in Figure 8(B). The currents due to the bias source remain virtually unchanged and the contribution to e_o from these sources remains essentially zero. Solution of this circuit for e_o yields.

$$e_o \approx e_i \frac{R_2}{R_2+2R_t} = e_i \frac{1}{1+\dfrac{2R_t}{R_2}} \quad (10)$$

The value of e_i which causes diode BD to become nonconducting can be determined from Figure 8(C). For diode BD to become nonconducting its cathode plate voltage must go to zero which occurs when the potentials of point B and D are equal. This occurs for

$$-E+(e_i+E)\frac{R}{R+R_t} = E\frac{R_2}{R+R_2+R_t} \quad (11)$$

Solving for e_i

$$e_i \approx \frac{ER_2}{R+R_2}\left(1+\frac{R_t}{R_2}\right) \quad (12)$$

This is the quantity θ of Figure 6.[11] After diode BD becomes nonconducting the output voltage remains constant as may be seen from Figure 8(C) which represents the circuit in this condition.

The value of e_o is very nearly shown in the following equation

$$e_o = ER_2/(R+R_2)$$

Note: In all these calculations the resistance R_t has been neglected when it appeared in a sum involving R but not when it appeared added to R_2. R_t will always be small compared to R but may be of the same order of magnitude as R_2.

References

1. Application of the California Institute of Technology Electric Analog Computer to Nonlinear Mechanics and Servomechanisms, **G. D. McCann, C. H. Wilts, B. N. Locanthi.** *AIEE Transactions*, volume 68, 1949, pages 652–60.

2. An Electronic Simulator for Nonlinear Servomechanisms, **C. M. Edwards, E. C. Johnson, Jr.** *AIEE Transactions*, volume 69, part I, 1950, pages 300–06.

3. New Techniques on the Anacom Electric Analog Computer, **E. L. Harder, J. J. Carleton.** *AIEE Transactions*, volume 69, part I, 1950, pages 547–56.

4. Waveforms (book), **B. Chance, et. al.** McGraw-Hill Book Publishing Company, New York, N. Y., 1949, pages 86–92 and 328–35.

No Discussion

Differential Analyzer Study of Harmonic Power Generation with Nonlinear Impedance Element

PAUL E. RUSSELL
ASSOCIATE AIEE

H. A. PETERSON
FELLOW AIEE

Synopsis: Occasionally it is desirable and even necessary to have available sources of voltage supply of harmonic frequencies. Rotating machines with the appropriate number of poles have been used for this purpose. When the power requirements are low, electronic devices may be used. This paper presents results of an analysis of a nonlinear static element circuit which also may be useful as an efficient source of voltage supply of harmonic frequency of good wave form. The circuit is unique in that it uses neither rotating parts nor electronic devices.

NUMEROUS studies of nonlinear electric circuit phenomena have been made in recent years. Progress in this direction has been aided on the purely theoretical side by the work of many individuals, notably Minorsky, Andronow, and Chaikin.[18, 19] Insight into the fundamental physical reason for unusual nonlinear circuit phenomena in specific cases has been greatly aided by the use of some of the new techniques.

There are many practical circuit problems which become impractical of solution by any approach other than that afforded by the availability of special computing machines either of the analogue or digital type.[8,9,11,13,14,15] Many of these may be rather simple circuits. The problem which is to be discussed in this paper is physically simple in that only a few circuit elements are involved. Furthermore, it is somewhat unique in that a steady-state solution is desired rather than a transient solution.

The circuit was studied initially a few years ago by one of the authors. The preliminary results were sufficiently interesting for continuation of the study. This continuation has led to a very detailed investigation and summary which is the basis for a Doctor's thesis now in preparation. Some of these results will be presented in this paper.

The circuit in its simplest and most practical form has the unique ability to receive power at one frequency and deliver it at a frequency exactly three times the input frequency. This it appears possible to accomplish with excellent wave form (approaching that for a good sine wave generator) and with good efficiency. The circuit employs no vacuum tubes and no rotating parts. Methods of obtaining other harmonic frequencies will become obvious to the reader.

A nonlinear reactor is used as a means for requiring the flow of harmonic currents from a constant potential a-c source. These in turn are suppressed by a capacitor and reactor in parallel, suitably proportioned with respect to the harmonic frequency desired, and in series with the nonlinear reactor. The terminals of the parallel capacitor and reactor become the output terminals of the circuit.

Many circuits involving nonlinear reactors have been studied by numerous authors at various times.[7,10,12,16] In some cases theoretical solutions, even though approximate, have sufficed.[6,20] In other cases, step-by-step solutions have been carried out. Linear approximations over restricted ranges of the variables have been employed.[8,12] Differential analyzers[5,17] and other auxiliary devices[1,2,3,4,13] have been used in a number of instances.

The differential analyzer approach seemed to offer the only practical and completely flexible approach to the solution of this circuit problem. The analyzer used is a completely electric high speed device. It has unique characteristics which seem to render it unusually powerful in obtaining solutions to problems of this type. While some of the special components used with the analyzer were developed in the Electrical Engineering Department of the University of Wisconsin, the standard components were built by George Philbrick Researches, Inc.

The study reported here indicates that it is entirely practical to obtain a harmonic voltage power source of good wave form from this static circuit. Possible uses may suggest themselves in view of the excellence of the output wave form and the extreme simplicity of the device.

Theoretical Considerations

When an alternating voltage of sufficient amplitude is impressed on an iron

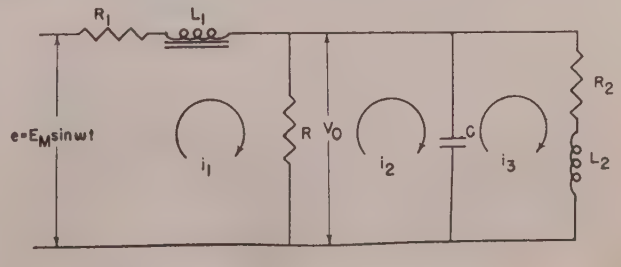

Figure 1. Schematic diagram of the circuit which was studied

Paper 51-172, recommended by the AIEE Computing Devices Committee and approved by the AIEE Technical Program Committee for presentation at the AIEE Great Lakes District Meeting, Madison, Wis., May 17–19, 1951. Manuscript submitted February 20, 1951; made available for printing March 29, 1951.

PAUL E. RUSSELL and H. A. PETERSON both are with the Electrical Engineering Department of the University of Wisconsin, Madison, Wis.

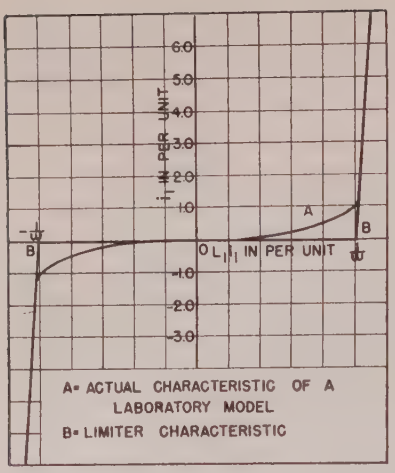

Figure 2 (left). Nonlinear functions generated by the analyzer components

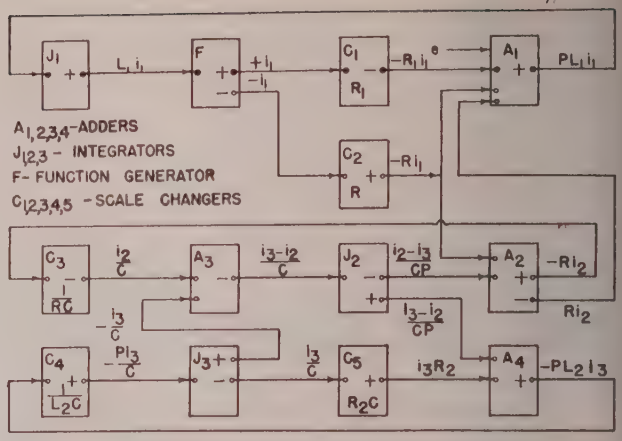

Figure 3 (right). Block diagram of the analyzer arrangement

cored reactor, the resulting current consists not only of currents of the frequency of the impressed voltage, but also of currents which are harmonically related to the frequency of the impressed voltage. The predominant harmonics are usually the third and fifth. If the proper linear components are inserted into the circuit, one harmonic may be amplified, the others suppressed.

One circuit capable of acting in this fashion is shown in Figure 1. In that circuit L_1 is the nonlinear inductor with inherent effective resistance indicated as R_1. L_2 and C tune the circuit to the desired odd harmonic of the impressed voltage $e = E_m \sin \omega t$. R_2 is the effective resistance in L_2. The harmonic power is assumed to be dissipated in the load resistor R. This circuit has been analyzed with an eye toward determining the reactor properties and the values of the other circuit parameters which will permit a reasonable harmonic power generation with a prescribed quality of wave form. In other words, the circuit has been investigated to determine the effect on the quality and magnitude of the output voltage, V_o, of variations in the reactor characteristic, E_m, R_1, R_2, R, L_2, and C. To approach this problem with any tool short of a differential analyzer would either involve approximations which would make the results valueless or else be prohibitively time consuming or both.

The reactor, L_1, is assumed to have a rather abrupt saturation characteristic. The saturation curve for a model which was used for checking purposes is shown in Figure 2, curve A. Since the reactor is saturated over a very large part of the cycle, the curvature in the characteristic below saturation was found to be of small consequence and can be neglected so that for all practical purposes the saturation characteristic may be considered nothing more than two straight lines. The ratio of the slope of the saturation curve before saturation to the slope of the saturation curve after saturation may then be taken as a defining property of the reactor. This ratio of slopes has been given the symbol "δ" in the remainder of this paper.

In order to make the data as general as possible, a per-unit system was adopted. As a base current for this system, the current that flows in the nonlinear inductor at the point of saturation was chosen. For base impedance, the reactance of the nonlinear inductor operating below saturation at fundamental frequency was chosen. These choices are in evidence in Figure 2. The other impedances in the circuit were then calculated at fundamental frequency and reduced to this base. Base volts then became equal to the product of the unsaturated reactance of the nonlinear inductor and the current in the nonlinear inductor at saturation.

In the interest of brevity, analysis of operation of the device as a third harmonic generator ($X_C/X_{L2} = 9$) only is considered in this paper.

Differential Analyzer Arrangement

The differential analyzer available at the University of Wisconsin is a high-speed electronic device. Among the basic components of the analyzer are scale changers, integrators, adders, and various nonlinear units.

The scale changers are essentially d-c amplifiers whose gain can be varied manually from zero to ten so that the output voltage of the device is equal to a constant times the input voltage. This unit contains an inverter stage so that both positive and negative output quantities are available.

The output voltage of an integrator unit is proportional to the time integral of the input voltage. Both positive and negative output quantities are available in this unit also.

With an adder unit, as many as four input voltages are added continuously, the positive sum and the negative sum both being available at the output terminals.

Nonlinear units utilized in the solution of this problem included an arbitrary function generator of the type using a cathode-ray tube with a servo system constraining the beam to follow a mask of the proper shape on the face of the tube.[1,3,4] Also of use was a biased-diode type of limiter unit.[2]

The mesh equations which describe the circuit in Figure 1 are:

$$e = E_m \sin \omega t = R_1 i_1 + pL_1 i_1 + R(i_1 - i_2) \qquad (1)$$

$$0 = R(i_2 - i_1) + \frac{(i_2 - i_3)}{Cp} \qquad (2)$$

$$0 = \frac{i_3 - i_2}{Cp} + R_2 i_3 + L_2 p i_3 \qquad (3)$$

The solution desired was a steady-state solution, with adequate information on the amount and quality of the harmonic power dissipated in R being of prime importance.

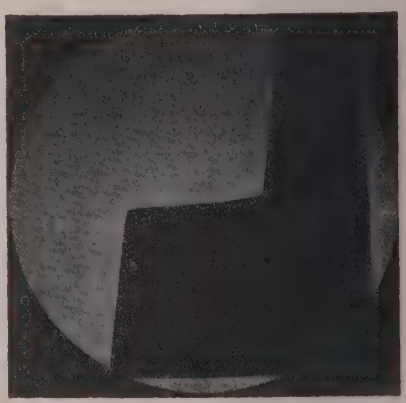

Figure 4. View of the mask for the cathode-ray type of function generator

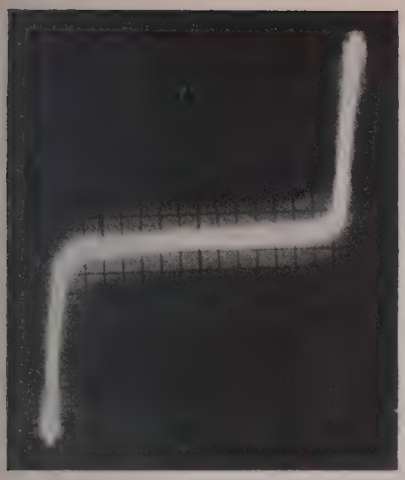

Figure 5. Transfer function effected through the use of the mask in Figure 4 with the function generator

For convenience in setting up the analyzer, the mesh equations were written in this form:

$$pL_1i_1 = Ri_2 - Ri_1 - R_1i_1 + e \tag{4}$$

$$-Ri_2 = -Ri_1 + \frac{i_2 - i_3}{Cp} \tag{5}$$

$$-L_2pi_3 = \frac{i_3 - i_2}{Cp} + R_2i_3 \tag{6}$$

The arrangement of analyzer components shown in Figure 3 satisfies these equations and is the one which was used. The output of the integrator J_2 is proportional to the voltage, V_o, across the load resistor R. This voltage was measured and analyzed with a harmonic analyzer to determine its quality in terms of harmonic content. The power available at the load represented by R was calculated by squaring the effective voltage and dividing by R.

The adders, integrators, and scale changers in the arrangement of Figure 3 have been described briefly though adequately above. However, the function generator may require a little more detailed description. As shown, and as used in this problem, the function generator receives a voltage proportional to L_1i_1 and must deliver a voltage proportional to i_1. In other words the transfer function of the analyzer nonlinear unit must be of the same shape as the saturation curve of the steel in the nonlinear reactor. This characteristic was obtained through the use of the cathode-ray type of function generator developed at the University of Wisconsin. A mask of the shape of the required transfer function was cut and placed on the face of the cathode-ray tube. The horizontal position of the beam is determined by the input voltage to the vertical plates. The beam follows the mask as previously described so that the voltage on the horizontal plates of the tube is proportional to the ordinate prescribed by the mask. Thus, the desired transfer function was obtained. Figure 4 shows a typical mask while Figure 5 shows the transfer function obtained. As can easily be seen, the accuracy and flexibility of such a device are very useful. However, inasmuch as the reactor was working well above saturation for a large portion of the cycle, it was found that equally satisfactory results could be obtained by neglecting that small current that flows before saturation. This allowed the use of a simpler but less powerful tool, the limiter, whose characteristic is shown in Figure 2, curve B. The limiter was used with excellent results.

Discussion of Results

A general idea as to the accuracy of the data from the analyzer may be obtained by referring to Figure 7. For the particular choice of circuit elements indicated there, the maximum error was about 7 per cent, but the average error was considerably less than that amount. It is to be concluded that the accuracy obtainable is well within the limits required for engineering design.

In Figure 8, the effect of varying the load resistance R is shown for various values of R_2, the resistance of the linear inductor. In each case L_2 was selected to give the highest third harmonic voltage at small loads. The ratio of X_C to X_{L2} required for this varied with X_C. As X_C decreases, the X_C to X_{L2} ratio for maximum third harmonic voltages increases and when X_C is very small this ratio approaches 9.0 and becomes very critical. It is apparent from the curves in Figure 8 that a very sizable amount of third harmonic power of very good wave form can be obtained with these parameters. Closer inspection shows that voltage regulation is not a serious difficulty. The dependence of quantity and quality of available power on the resistance of the linear reactor is clearly shown.

The advantages of making Xc small are shown clearly in Figure 9. Here again it is shown that for a given X_C, the wave form and amount of power depend to a large extent on the Q (ratio of reactance to resistance) of the linear reactor. There is a definite advantage in making X_C small. If X_C is very small, then the impedance of the R-L_2-C combination to fundamental frequency is also small. It follows that the fundamental component of the output voltage is less.

It was noted that there is an advantage in not going to an exceedingly high value of E_m for normal operation. As E_m is raised, the fundamental frequency component of input current increases more rapidly than E_m due to saturation in L_1. Consequently, the fundamental frequency

Figure 6. View of the analyzer as arranged for the solution of this problem

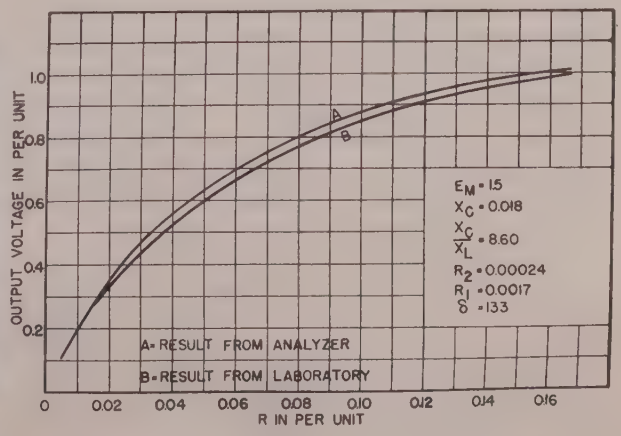

Figure 7. Comparison between laboratory and analyzer results

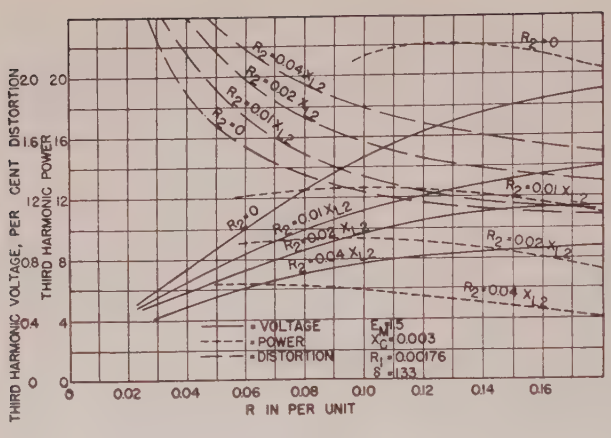

Figure 8. Effect of changes in load and Q of the linear reactor on the harmonic power available

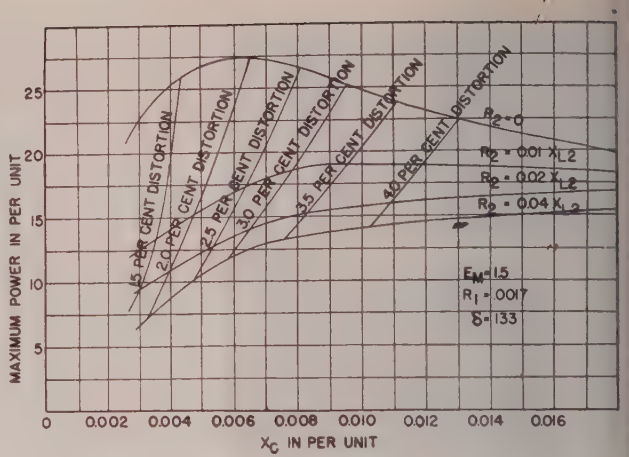

Figure 9. Effect of changes in C and Q of linear reactor on the maximum harmonic power available

component of output voltage may become excessive if E_m is made much greater than 1.5. It was also recognized that if E_m was reduced to values less than 1.2, no appreciable harmonic power was available.

Further, it was noted that a considerable increase in the amount of available power occurred when the abruptness of saturation in the nonlinear reactor was increased. This marked increase in power, however, is attained at the expense of some sacrifice in quality of wave form. That this should be the case is readily appreciated if the increase in the fundamental component of input current is considered.

The least critical parameter in the system was observed to be R_1. Fairly wide variations from the normal had only small effect on the harmonic voltage.

Conclusions

A single-phase nonlinear circuit of the type studied can be used as a third (or other) harmonic power source. The output voltage is sinusoidal with a small amount of fundamental frequency and higher harmonics superimposed. In order to keep the distortion to a minimum and yet maintain an appreciable power capacity, the following suggestions are helpful:

1. Design the nonlinear reactor so that in normal operation, the impressed voltage will not be less than 1.2 nor more than 1.5.

2. Choose a core material for the nonlinear reactor so that the abruptness of saturation is a maximum compatible with wave form requirements.

3. Make C as small as wave form considerations will tolerate. (It will still be large).

4. Critically select L_2 to give maximum third harmonic output at light loads.

5. Make R_2 as small as possible.

6. Let the value of R_1 be small, though its magnitude is not at all critical.

References

1. An Arbitrary Function Generator, **E. H. Fritze.** Thesis, University of Wisconsin, Madison, Wis., 1948.

2. A Diode Bridge Limiter for Use With Electronic Analogue Computers, **R. J. Medkeff, R. J. Parent.** *AIEE Transactions*, volume 70, part I, 1951, pages 913–16.

3. The Application of the Photoelectric Function Generator to Analog Computing, **R. K. Ausbourne.** Thesis, University of Wisconsin, Madison, Wis., 1950.

4. Photoelectric Waveform Generator, **D. E. Sunstein.** *Electronics* (New York, N. Y.), volume 22, February 1949, pages 100–03.

5. An Electronic Differential Analyzer, **A. B. Macnee.** *Proceedings*, Institute of Radio Engineers (New York, N. Y.), volume 37, November 1949, pages 1315–24.

6. Ferroinductance as a Variable Electric Circuit Element, **J. D. Ryder.** *Electrical Engineering* (*AIEE Transactions*), volume 64, October 1945, pages 671–77.

7. Some Aspects of Inductance When Iron is Present, **L. T. Rader, E. C. Litscher.** *Electrical Engineering* (*AIEE Transactions*), volume 63, March 1944, pages 133–39.

8. Abnormal Overvoltages Caused by Transformer Magnetizing Currents in Long Transmission Lines, **H. A. Peterson, T. W. Schroeder.** *Electrical Engineering* (*AIEE Transactions*), volume 62, January 1943, pages 32–40.

9. Criteria for Neutral Stability of Wye-Grounded-Primary Broken-Delta-Secondary Transformer Circuits, **H. S. Shott, H. A. Peterson.** *Electrical Engineering* (*AIEE Transactions*), volume 60, November 1941, pages 997–1002.

10. An Experimental Investigation of Subharmonic Currents, **J. D. McCrumm.** *AIEE Transactions*, volume 60, 1941, pages 533–40.

11. Abnormal Voltage Conditions in Three-Phase Systems Produced by Single-Phase Switching, **Edith Clarke, H. A. Peterson, P. H. Light.** *AIEE Transactions*, volume 60, 1941, pages 329–39.

12. Subharmonics in Circuits Containing Iron-Cored Inductors—II, **Irven Travis.** *AIEE Transactions*, volume 58, 1939, pages 735–42.

13. An Electric Circuit Transient Analyzer, **H. A. Peterson.** *General Electric Review* (Schenectady, N. Y.), September 1939, pages 394–400.

14. Subharmonics in Circuits Containing Iron-Cored Reactors, **Irven Travis, C. N. Weygandt.** *Electrical Engineering* (*AIEE Transactions*), volume 57, August 1938, pages 423–30.

15. Analysis of Series Capacitor Application Problems, **J. W. Butler, C. Concordia.** *Electrical Engineering* (*AIEE Transactions*), volume 56, August 1937, pages 975–88.

16. Mathematics of Modern Engineering, **E. G. Keller.** John Wiley and Sons, Inc., New York, N. Y., volume 2, 1942.

17. A New Differential Analyzer, **H. P. Kuehni, H. A. Peterson.** *Electrical Engineering* (*AIEE Transactions*), volume 63, May 1944, pages 221–28.

18. Introduction to Non-Linear Mechanics, **N. Minorsky.** Edwards Brothers Inc., Ann Arbor, Mich., 1947.

19. Theory of Oscillations, **A. A. Andronow, C. E. Chaikin.** Princeton University Press, Princeton, N. J., 1949.

20. The Generalized Solution for the Critical Conditions of the Ferroresonant Parallel Circuit, **W. T. Thomson.** *AIEE Transactions*, volume 58, 1939, pages 743–46.

No Discussion

Dependence of Direct Sparkover Voltage of Gaps on Humidity and Time

P. B. JACOB, JR.
ASSOCIATE AIEE

G. M. L. SOMMERMAN
MEMBER AIEE

INTEREST in the problem of dependence of direct sparkover voltage arose when it was observed that gaps in equipment operating at high direct voltages exhibited erratic and rather low breakdown strength when the relative humidity was more than 50 per cent. Electrode configuration was indicated as an important variable in the problem.

A negative coefficient of breakdown or sparkover voltage with humidity variation as indicated, is contrary to results obtained with 60-cycle and lightning-like impulse voltages. Thus, in the AIEE Standard[1] the humidity coefficient is indicated as zero for sphere gaps and positive for rod gaps. In this reference there are no data for direct sparkover voltages, but there is a statement that, until data become available, the sphere gap calibrations for 60 cycles may be used for direct voltages.

Much of the early work on the breakdown of gases was done with direct voltages (see, for example, the comprehensive bibliography in the AIEE paper by Howell).[2] In these investigations, however, the humidity was either zero, or very low, or not reported systematically. Peek[3] found that the direct sparkover voltages of sphere gaps were the same as the 60-cycle sparkover voltages. He also found that the direct sparkover voltages of needle gaps were the same as, or slightly less than, the 60-cycle crest values at 34 per cent relative humidity. Lewis and Defandorf,[4] in a study of sphere gaps irradiated with ultraviolet light, found that the 60-cycle sparkover voltage increased slightly with increasing humidity.

In view of our preliminary observations with sustained direct voltages, and the apparent lack of experimental data on the subject, it was decided to conduct a systematic investigation[5] of the effects of humidity and the time of voltage application on the direct-voltage breakdown strength of gaps.

Experimental Procedure

Two electrode configurations were used: (1) 12.5 centimeter diameter spheres; (2) standard rods, one-half inch square cross section, with square edges. This selection permits comparison of the results with those in the Standard[1] for 60-cycle voltages. It provides opportunity to compare the results for gaps with and without corona preceding sparkover. Finally, this selection brackets the electrode configurations existing in commercial d-c equipment.

The sphere shanks and the rods were mounted horizontally. Clearances were in accordance with the Standard.[1] Four spacings were selected for each gap to give sparkover voltages of about 30, 50, 70, and 90 kv.

Direct voltages were obtained from a 100-kv rectifier unit with capacitance output, center-tap grounded, as shown in Figure 1. Voltages were measured by an electrostatic voltmeter V_2, connected across a center section of a corona-free, wire-wound divider of 40 megohms total resistance. The ripple amplitude was found to be less than 0.25 per cent.

Two types of data were taken for both the sphere gap and the rod gap: (1) initial sparkover voltage; (2) time-sparkover characteristics. Eight initial sparkover voltages were read and averaged for each spacing. In order to reduce erratic behavior of the rod gap with direct voltages, it was necessary to apply the voltage to the gap very rapidly. By manual operation of the induction regulator in the a-c supply line, the charging voltage was raised to 90 per cent of the sparkover value in two or three seconds after which it was raised at a rate of about three per cent per second. In order to secure control data, the same procedure was used for the sphere gap. Since the electrostatic voltmeter V_2 could not follow these rapid changes quite accurately, the initial sparkover voltages were read in terms of the input voltmeter V_1. Other output voltage measurements showed that the initial readings so obtained were in error by plus three per cent because of delay in charging the voltage-source capacitor. This error is higher than expected because of high tube drop; however, it becomes very small after two additional seconds of application of con-

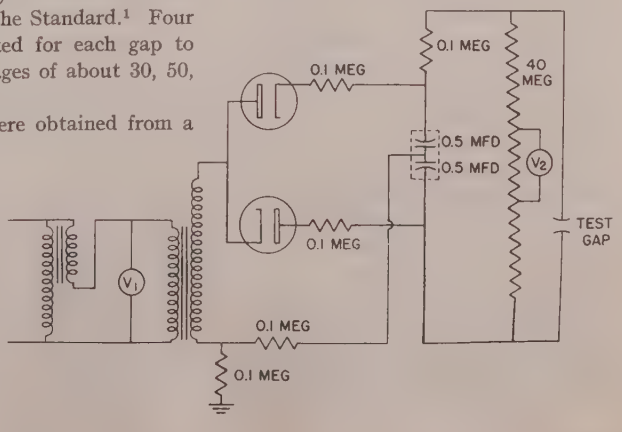

Figure 1. Diagram of connections for the 100-kv direct-voltage source and the voltage measuring circuit

Paper 51-173, recommended by the AIEE Basic Sciences Committee and approved by the AIEE Technical Program Committee for presentation at the AIEE Great Lakes District Meeting, Madison, Wis., May 17–19, 1951. Manuscript submitted February 16, 1951; made available for printing April 17, 1951.

P. B. JACOB, JR., is with Mississippi State College, State College, Miss., and G. M. L. SOMMERMAN is with Northwestern University, Evanston, Ill.

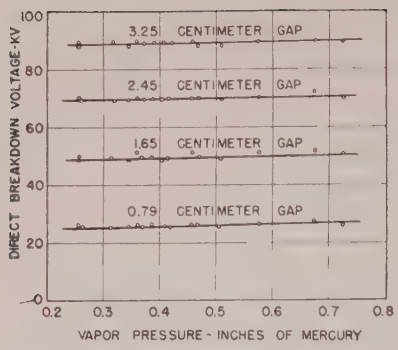

Figure 2. Corrected initial direct sparkover voltage versus humidity, 12.5 centimeters diameter spheres

Values converted to 25 degrees centigrade and 760 mm Hg pressure

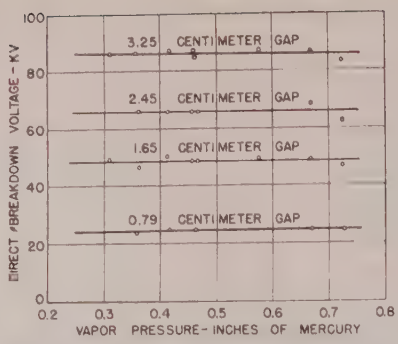

Figure 3. Critical direct withstand voltage versus humidity, 12.5 centimeters diameter spheres

Values converted to 25 degrees centigrade and 760 mm Hg pressure

stant voltage. In compensation for this difficulty, the circuit is insensitive to any rapid fluctuations in line voltage, and there is no evidence that the output voltage was significantly higher than normal during sustained voltage runs.

Time-sparkover characteristics were obtained by setting the voltage at successively lower values and recording the time necessary for sparkover. Tests were run for a duration of 90 seconds. The highest voltage not causing sparkover in three 90-second runs was designated as the critical withstand voltage. It was found that the chance of sparkover occurring after the 90-second limit was small for the rod gap, and even more remote for the sphere gap.

Complete runs on all spacings for the rod gap were paralleled by corresponding runs on the sphere gap within two or three hours. By taking data over a three month period, a wide range of humidity was encountered in the test conditions.

Results for the Sphere Gap

The corrected initial sparkover voltages obtained from a large number of sets of data for the sphere gap are plotted against the humidity in Figure 2. It is seen that these direct sparkover voltages are practically independent of humidity, although there is a suggestion of a slight positive humidity coefficient.

All points in Figure 2 are observed initial sparkover voltages to which a correction of minus three per cent has been applied because of the source-voltage delay mentioned previously. The mean deviation in a set of eight sparkover voltages comprising each point is about one per cent. The mean deviation among initial values in Figure 2, including any humidity effect, is 1.5 per cent (average for four gaps).

Data practically identical to those in Figure 2 were obtained from short-time sparkover voltages measured for each gap at seven different humidities. These short-time values are voltages which were found to produce repeatable sparkovers at closely grouped times averaging two to five seconds after a steady voltage was applied and the output voltage was practically constant and readable. The mean deviation among the seven sets of data is 0.8 per cent (average for four gaps). Comparison of the average short-time direct sparkover voltages for each of the four gaps with corresponding 60-cycle values in the Standard[1] shows a mean deviation of 1.1 per cent, which is within the absolute accuracy of the measurements.

For each of two longest gaps the averages of the short-time sparkover voltages agree with the averages of the corresponding corrected initial sparkover voltages to within 0.5 per cent. For the two shortest gaps the corrected initial values are slightly higher than the short-time values. Accurate measurements of output voltage show that such differences occur for these short gaps on days when the laboratory illumination is mostly from incandescent lamps.

On applying to the sphere gap steady voltages two per cent less than the short-time sparkover voltage, sparkovers were observed at random times averaging 30 seconds in two or three trials in the majority of cases in which three such trials were made. Occasionally such sparkovers occurred at voltages three per cent less than the observed short-time value. The extent of observed voltage reduction possible for random sparkover to occur is about the same as the reduction in sparkover voltage caused by irradiation of such gaps.[4] This behavior merits further study, but a suggested explanation is that cosmic rays are triggering the gap under these conditions. Such a mechanism would lead to time intervals roughly corresponding to the observed times.

In any event the direct critical withstand voltage of sphere gaps is not much less than the short-time sparkover value, and it is essentially independent of humidity as shown in Figure 3. The withstand voltages were determined usually in steps of two per cent. These data are of value for control purposes in considering the rod gap results.

Results for the Rod Gap

A set of curves of rod-gap direct sparkover voltage versus time to sparkover is shown in Figure 4. In contrast with the sphere-gap results there is a marked decrease in sparkover voltage with increasing time for the rod gap. As noted earlier, it was observed that sparkovers practically never occurred beyond 90 seconds at the lower limit voltages.

It should be pointed out that the curves in Figure 4 are presented only to show the general trend of rod gap results as successively lower voltages are applied. In most cases the sparkover times at intermediate voltages are much more erratic than shown in the figure. For the two longest gaps there is often a trend to longer times at lower voltages, then sparkovers at relatively short times at voltages far below the initial sparkover value, and finally a trend again to longer times as the critical withstand voltage is approached. This is an indication of dual sparkover voltages similar to those reported[1] for such gaps for impulse sparkovers, but not indicated for 60-cycle voltages.

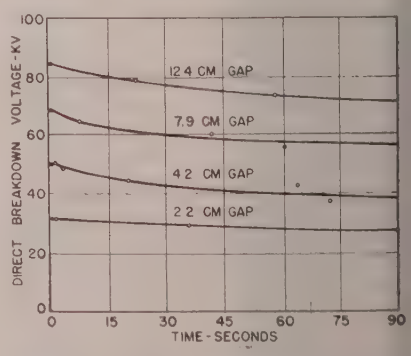

Figure 4. A set of characteristics for direct sparkover voltage versus time of voltage application, standard rod gap

Values converted to 25 degrees centigrade and 760 mm Hg pressure. Actual conditions: 17.8 degrees centigrade, 744.1 mm Hg pressure, 0.335 inch Hg vapor pressure

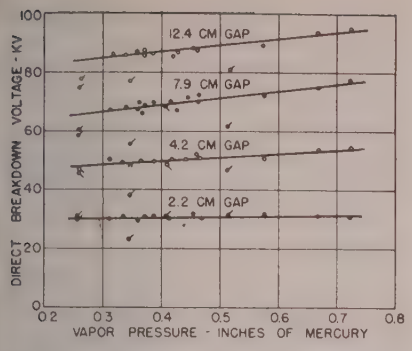

Figure 5. Corrected initial direct sparkover voltage versus humidity, standard rod gap

Values converted to 25 degrees centigrade and 760 mm Hg pressure

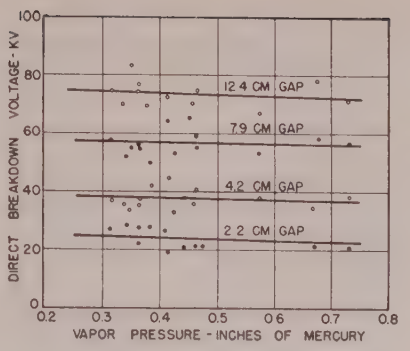

Figure 6. Critical direct withstand voltage versus humidity, standard rod gap

Values converted to 25 degrees centigrade and 760 mm Hg pressure

At the rather well defined lower value of these direct dual sparkover voltages considerable unsteadiness develops in the glow discharges at the rod gap corners, and a brush often lengthens slowly enough to be observed before complete sparkover occurs. On infrequent occasions such a brush may lead to a heavy glow apparently filling the whole gap and drawing an average current of about 1 milliampere. This action occurs with series damping resistors of various sizes in the circuit. It may last for more than 30 seconds and it often ends in a sudden sparkover.

Dual sparkover values are also indicated by some of the initial sparkover results plotted as points with stems in Figure 5. These points were obtained in the first tests made on the rod gap. While some of these points lie on the curves plotted for the other test results, many of them are considerably below the other results. By rapidly raising the voltage through the lower dual value region, sparkover is avoided until the higher sparkover value is reached. Audible indications suggest that a brush often starts to develop at the lower dual voltage and subsides as the voltage is quickly raised above this level.

The points in Figure 5 are initial sparkover values to which the source-voltage delay correction of −3 per cent has been applied. The straight lines showing the average effects of humidity have been drawn without giving weight to the points with stems for reasons described previously. Even neglecting these points it is seen that the amount of scattering of the points is greater than that for the sphere gap sparkover. This is consistent with observations made on such gaps with 60-cycle voltages. The lower order of accuracy of the rod gap is also apparent from the mean deviation of values in a group of eight readings comprising a given point. This varies from day to day and it depends on the gap spacing, but the overall average is about three per cent.

The slopes of the lines in Figure 5 indicate humidity coefficients for the direct sparkover voltages of rod gaps that are appreciably greater than those for corresponding 60-cycle sparkover voltages.[1] Despite this and differences in the methods of grounding, there is general agreement between the values read from the lines in Figure 5 and the 60-cycle rod gap values in the AIEE Standard for vapor pressures between 0.25 inch and 0.61 inch of mercury.*

Figure 6 shows the rod-gap critical direct withstand voltages plotted against humidity. Although the lines drawn in the figure show an average trend to lower values at higher humidities, the scattering in these results is so great that the probable error in the slope is considerable. Therefore, the results do not definitely confirm our comparative observations of a negative humidity coefficient for the direct withstand voltage of other gaps with rough edges. More certain, however, is the indication that the difference between the initial sparkover voltage (Figure 5) and the long-time withstand voltage (Figure 6) increases with increasing humidity. It is interesting to note that the extrapolations of the two sets of curves nearly intersect at zero humidity.

Discussion

The sphere gap, for which the direct sparkover voltage depends but little on humidity, is a gap for which sparkover is not preceded by corona. The rod gap, for which the direct sparkover voltage depends markedly on humidity, is a gap for which sparkover is preceded by corona and brush discharges. Thus, moisture in the air has an appreciable effect on sparkover only if it interacts with pre-breakdown ionization over a period of time. Part of the humidity effect, that of increasing the short-time strength of the rod gap, is an extension of the humidity effect long recognized for such gaps in the subsecond time range. This has been explained by Peek[6] as being caused by the action of the water vapor in smoothing the contour of the pre-breakdown discharges, thus leading to a more uniform field in the space between the discharges and requiring a higher voltage to complete the sparkover.

The results of this investigation suggest that the beneficial effect of humidity on the sparkover voltage of gaps with rough edges disappears under sustained application of direct voltages, or that the ultimate effect might be even to lower the sparkover voltage below that for dry air. Whatever the mechanism, it must be one that proceeds relatively slowly. It is possible that the very fine water droplets that form in sub-second ionization gradually coalesce into larger droplets and migrate to other portions of the gap where the ionization current density is low and the electric field is relatively high. Under these new conditions the field forces could overcome droplet surface tension forces, thus disrupting the droplet into fragments that move into the central regions of the gap. Ionization of the air would then occur around the fragments leading to sudden sparkover.

If water droplets are formed in the gap, recent studies by English[7] may be

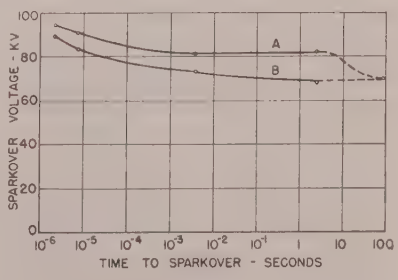

Figure 7. Probable pattern of variation of unidirectional sparkover voltage of a standard rod gap, 10 centimeters spacing, with time to sparkover

Curve A: 0.61 inch Hg vapor pressure

Curve B: zero vapor pressure

Points at less than one second computed from data in reference 1. Points at more than one second computed from present data

*AIEE standard humidity is 0.6085 inch (15.5 millimeters) mercury vapor pressure (13 grams of water per kilogram of dry air at 25 degrees centigrade).

relevant. In this work it was found that with a water drop point in a point-to-plane gap the corona onset voltage at 760 millimeters pressure is no higher than that at about 550 millimeters pressure, and disruption of the drop occurs at the onset voltage under certain conditions.

In order to bring out more strikingly the probable humidity effects on the sparkover-time characteristics, Figure 7 has been drawn. This indicates that the computed zero-humidity sparkover voltage of a rod gap is essentially independent of time of voltage application for times greater than 4 milliseconds. When water vapor is present the direct sparkover voltage decreases to about the zero-humidity level at times above a few seconds. In this figure the scattering of results is not depicted, and relatively small differences in test conditions have not been taken into account. Nevertheless, the main features of the time dependence of humidity effects on unidirectional sparkover voltage seem to follow a pattern as indicated. Additional long-time tests at both very low and moderately high humidities are needed in order to draw the dotted portions of the curves more accurately.

Conclusions

Although directly relevant to the types of gap electrodes and ranges of conditions investigated, the conclusions below may apply rather generally.

1. For air between smooth spherical electrodes, the direct sparkover voltage is practically independent of humidity. Average short-time sparkover values check the 60-cycle crest values in the Standard[1] to within the accuracy of the measurements. Critical direct withstand values are not much less than the short-time sparkover values.

2. For air between standard square-edged rod electrodes, the direct sparkover voltage is erratic partly because of dual values. If direct voltage is applied rapidly to the rod gap, the initial sparkover voltage increases with increasing humidity similar to the 60-cycle behavior. There is a marked decrease in sparkover voltage with time of voltage application, and this decrease appears to become greater with increasing humidity.

3. In the design of electrical equipment to operate in air at high direct voltages, it may be even more important to use electrodes free of sharp edges than it is when only alternating or impulse voltages are applied.

References

1. American Standard for Measurement of Test Voltage in Dielectric Tests, AIEE Standard number 4, 1942.

2. Breakdown Studies in Compressed Gases, **A. H. Howell.** *Electrical Engineering* (*AIEE Transactions*), volume 58, May 1939, pages 193–206.

3. The Effect of High Continuous Voltages on Air, Oil and Solid Insulations, **F. W. Peek, Jr.** *AIEE Transactions*, volume 35, part II, 1916, pages 783–808.

4. Effect of Humidity and Irradiation on 12.5 Centimeter Sphere Gaps, **A. B. Lewis, F. M. Defandorf.** National Bureau of Standards, Laboratory Report No. 460–3, 1935.

5. A Study of Direct Voltage Breakdown of Gaps, **P. B. Jacob, Jr.** *Thesis*, Northwestern University, Evanston, Ill., 1948.

6. Dielectric Phenomena in High-Voltage Engineering (book), **F. W. Peek.** McGraw-Hill Book Co., Inc., New York, N. Y., 1929.

7. Corona from a Water Drop, **W. N. English.** *Physical Review* (New York, N. Y.), volume 74, 1948, pages 179–189.

Discussion

L. C. Aicher, Jr. (Allis-Chalmers Manufacturing Company, Milwaukee, Wis.): The authors have undertaken to provide information for a region not adequately covered in current standards. We in the industry appreciate contributions of this character to our technical storehouse for we have not had the time to justify the diligence required to collect the sort of data presented by these workers.

Several thoughts occur to me, not as criticism, but, because I feel the need for more information that may be available from the data the authors collected.

The sphere gap data contained in AIEE number 4[1] applies to vertically mounted gaps with one sphere grounded. I am wondering if the authors investigated this condition to qualify the insignificance of gap arrangement for small ratios of gap distance to sphere diameter which the Standards infer.

A similar question concerns the rod gap data. The rod gaps used in testing usually have one rod solidly grounded, and are horizontally mounted. Have the authors investigated the effect of the proximity of the ground plane as well as the effect of grounding one electrode?

The data presented in Figures 2 and 3 is interesting. We hardly would have expected the sphere gap sparkover voltage to be so independent of humidity. Each year, during the summer months we experience difficulty with the sphere gaps in our impulse generator. During these months we find it necessary to use larger gap spacings for a given d-c charging voltage than during the remainder of the year. We have always attributed this to humidity for that is the only factor we have been able to associate with it. The condition is most severe about August 10th each year, which corresponds to the peak of median vapor pressure cycle data accumulated over a 12-year period. In order to operate the impulse generators we have found it necessary to increase the gap spacing as much as 16 per cent to prevent premature sparkover. Possibly there are other factors involved. During what part of the year were these authors' data collected? Have any attempts been made to secure similar data with irradiation present? Possibly there is a solar factor that we are not aware of that is affecting sphere gap sparkover.

The authors mention a complete run on all spacings of the rod gap and sphere gap being made within two to three hours. Did the authors check the humidity and relative air density at intervals during this period or did they use a beginning and end determination? When we do similar voltage testing where atmospheric corrections are necessary we have found it necessary to determine the humidity and air density at least each half hour. This may be a condition peculiar to Milwaukee, but I suspect other areas have similar characteristics.

Reference

1. See reference 1 of the paper.

N. W. Richards (Ohio Brass Company, Barberton, Ohio): The paper on the effects of humidity and time on the direct-voltage sparkover of gaps presents additional useful data for determining spacings needed with certain types of air gaps designed to withstand high direct voltages. I am interested in the precautions which should be considered when using air gaps to either measure or withstand high direct voltages. Certainly high direct voltages introduce problems which are not common to high impulse or alternating voltages.

The measurement of high direct voltage by knowing the breakdown strength of air between certain specific electrode configurations has been found erratic especially with certain types of needle and rod gaps. Again, sphere gaps, used as isolating and tripping gaps in high-voltage impulse generators, are temperamental on certain days when the humidity is high. On humid days, the spheres and the gap spacing need additional cleaning and adjusting, especially at the smaller spacings and voltages in the order of 10 to 30 kv. The spheres used approximate 12.5-centimeter sphere and the electrode configuration is similar to isolated horizontally-spaced spheres. Thus, the application of sphere gaps in this case suggests that perhaps certain preliminary precautions also must be observed in direct voltage measurements using gaps before negligible humidity effects on sparkover values can be expected.

Some precautions are mentioned, yet other questions exist, such as the proper care of the spheres themselves. Is there a need for circulating the air in and near the air gap to prevent dust particles from aligning themselves in the field and thereby causing lower sparkover values? Lastly is it likely that humidity has a greater effect on the sparkover values as smaller than 12.5-centimeter spheres are used? For instance, the German Standards have humidity correction factors for 60-cycle sparkover values on the 2.54-centimeter sphere gap.

P. B. Jacob, Jr. and **G. M. L. Sommerman:** Apparently the annual variation of atmospheric conditions in Evanston is similar to that in Milwaukee and in Barberton, for we have observed variations in the performance of isolating and tripping gaps operating under direct voltages similar to those reported by Messrs. Aicher and Richards. The data for the sphere gap and the rod gap reported in Figures 2 to 6, however, were taken in the period from April to July, 1948.

It is likely that some of the variation in the performance of commercial gaps is caused by the presence of dust on the electrodes. As shown by Brooks and Defandorf,[1] dust on electrodes lowers the corona onset voltage more at high humidities than at low humidities. Even when we tried to remove all dust from commercial electrodes, a considerable negative humidity coefficient remained. This we attributed to the presence of rough edges on the electrodes. Such a conclusion is substantiated by the results reported for the sphere gap and the rod gap, although for the latter, the presence of dual values obscures the behavior somewhat. Sphere gap electrodes were polished with crocus cloth, and both sphere gap and rod gap electrodes were cleaned with solvent before tests. The use of preliminary sparkovers before taking data is sometimes helpful in removing the last traces of foreign particles.

Dust in the laboratory air between well-spaced dust-free electrodes appears to have little immediate effect on sparkover. A number of tests were conducted with a fan blowing on the gaps, but since no significant difference could be detected with and without the fan, this practice was not followed for the most part. It should be noted, however, that if direct voltage is applied to gaps with sharp edges, the dust in the air is ionized by the attendant corona, and it is deposited on the electrodes. Thus, over a period of time, dust is deposited on, or by, rough electrodes to a greater extent than is the case where both electrodes are smooth.

It is possible, as Mr. Richards suggests, that the effect of humidity on sphere-gap sparkover is greater for smaller diameter spheres, but we have no quantitative data on this point.

Mr. Aicher has raised certain questions concerning electrode mounting and grounding. In general, no dependence on the type of grounding exists as long as the gap spacing is low enough to lead to no polarity effect with one electrode grounded. The American Standard shows no polarity effect for 12.5-centimeter diameter spheres for spacings up to 3.25 centimeters. The British Standard[2] includes data for spheres connected to center-tap-grounded sources, and for 12.5-centimeter diameter spheres these data agree with those for one sphere grounded to within 0.5 per cent for gap spacings up to 3.25 centimeters. For the grounded rod gap, no polarity effect is observed for spacings up to 4.2 centimeters. For the two largest spacings investigated by us, the results are in between those obtained for two polarities with one rod grounded. The rod gaps were mounted so that the distance to the ground plane was at least five times the gap spacing, but no tests were performed to evaluate the effect of closer proximity of the ground plane.

Irradiation was not used in our direct-voltage tests because it was desired to compare the results with 60-cycle values in the American Standard, and irradiation is not specified for the 12.5-centimeter sphere gap or the rod gap. Analysis of the sphere-gap data indicates that some of the observed scattering of results is caused by lack of natural irradiation on some days. Other data obtained recently indicate that irradiation is beneficial in sphere gap measurements up to 70 kv, at least.

The frequency with which atmospheric measurements should be recorded depends on local operating conditions. The Northwestern laboratory is rather large and it is usually kept closed, resulting in little air leakage. Also, moisture sources are very limited. Under these conditions it is found that humidity changes are quite small in a 3-hour period. The dry-bulb temperature is checked at intervals of about one-half hour; this is important when heat is added intermittently to the laboratory.

References

1. An Experimental Study of the Corona Voltmeter, **H. B. Brooks, F. M. Defandorf.** *Journal of Research*, Bureau of Standards (Washington, D. C.), 1928, pages 589–633.

2. British Standard Rules for the Measurement of Voltage with Sphere Gaps. *Number 358*, British Standards Institution, 1939.

Calculation of the Capacitance of a Circular Annulus by the Method of Subareas

THOMAS JAMES HIGGINS
MEMBER AIEE

DANIEL KINSETH REITAN
STUDENT MEMBER AIEE

THE PURPOSE of this paper is two-fold: to advance the theory of a certain approximate method which enables calculation, to any desired degree of accuracy, of both the charge distribution and the capacitance of a plane area charged to potential V_0 by a charge Q; to illustrate application of this theory by calculation of the charge distribution and capacitance of a certain annular area.

Rigorous determination of the mentioned electrical quantities for a plane area hinges on determination of the potential function V which:

1. Satisfies Laplace's equation $\nabla^2 V = 0$ everywhere;

2. Is of constant value $V = V_0$ over the plane area;

3. Vanishes at infinity except for an arbitrarily chosen constant (usually taken as zero).

The mathematical difficulties associated with determination of V for a specified plane area are of such difficulty that solution has been effected to date for only two plane areas: the elliptical disk and the circular disk (hereafter referred to as the ellipse and the circle), the latter of which is a special case of the former. In consequence, equations for the charge distribution and electrical capacitance are likewise known only for these two areas. However, need of accurate knowledge of one or the other, or both, of these quantities for certain plane shapes occurs in practice, particularly for the circular annulus: for example, in determining the effect of annular guard rings utilized in certain precise measurements of electrical capacitance or in the hydrodynamical problem[1] of determining the normal force* on a thin annular plate moving in a viscous fluid in the direction of its normal. Accordingly, it is most desirable to have a method enabling computation of these electrical quantities to a desired degree of accuracy. Precisely such a method, hereafter termed the method of subareas, is advanced in this paper.

Following sketch of the basic theory, it is applied to effect approximations to the capacitance and charge distribution of a circular annulus and of a circular disk. Comparison of the approximate values for the disk with values computed from the known equations evidence that the values for the annulus are excellent approximations to the exact value.

The Basic Theory

The essential theory is to be epitomized as follows. Let the given area A be considered as comprised of n subareas A_i $(i=1, \ldots, n)$ which are:

1. Of such small area by comparison with the given area that the charge density q_i is essentially constant over each subarea A_i.

2. Of such shape that assumption of uniform charge density enables simple calculation of the potential V_i produced by this uniformly distributed charge.

3. Of such dimensions and shape that if the subarea A_i were alone in space, the potential V_{ij} produced by A_i over that part of space which is actually occupied by another subarea A_j is essentially constant; and similarly for the potential V_{ii} produced by q_i over A_i itself.

Under these assumptions calculation proceeds as follows. By (1), V_{ij} produced over A_j by the uniform charge density q_i on A_i is proportional to q_i whence $V_{ij} = k_{ij} q_i$. Hence by (1) and (3) the total potential over A_j is

$$V_j = \sum_{i=1}^{n} V_{ij} = \sum_{i=1}^{n} k_{ij} q_i$$

a linear equation in the n unknowns q_i $(i=1, \ldots, n)$. Proceeding thus to form the total potential over each subarea yields the set of n equations

$$V_j = \sum_{i=1}^{n} k_{ij} q_i \quad (j=1, \ldots, n)$$

A well-known theorem in electrostatic theory states that the potential is constant, $V = V_0$, over a charged conductor whereon the charge is in equilibrium. Imposing this condition over each of the subareas yields

$$V_0 = \sum_{i=1}^{n} k_{ij} q_i \quad (j=1, \ldots, n)$$

a set of n linear equations in the n unknowns q_i $(i=1, \ldots, n)$. Solution of this set of equations yields a set of values for

* Thus, the normal force R on a thin annular plate moving in the direction of its normal with a velocity V through a liquid of viscosity μ is $R = 8\mu\pi C V$, where C is the capacitance of an annular area of the same radii as the thin plate.

Paper 51-174, recommended by the AIEE Basic Sciences Committee and approved by the AIEE Technical Program Committee for presentation at the AIEE Great Lakes District Meeting, Madison, Wis., May 17–19, 1951. Manuscript submitted February 8, 1950; made available for printing March 30, 1951.

THOMAS JAMES HIGGINS, Professor of Electrical Engineering, and DANIEL KINSETH REITAN are both with the University of Wisconsin, Madison, Wis.

This paper is based in part upon a thesis supervised by Professor Higgins and submitted by Mr. Reitan to the faculty of the University of Wisconsin in June 1949, in partial fulfillment of the requirements for the degree of Master of Science in Electrical Engineering.

We are indebted to one of the reviewers for suggesting calculation of the potential of a uniformly charged ring by use of elliptic functions. Equations 5 and 6 are better suited to rapid calculation of V_1 and V_2 than are the equations in Legendre polynomials given by Ramsey[10] which were used in the first draft of this paper. Recently, one of the discussors furnished a closed form for V_1 of equation 5 similar to that of V_2 of equation 6.

the uniform charge densities q_i over the subareas. Accordingly, the approximate value of the total charge Q is

$$Q=\sum_{i=1}^{n} q_i A_i$$

Finally, the approximate value of the capacitance follows from $C=Q/V_0$ (the q_i, and hence the Q, are expressed in terms of V_0, which cancels out in taking the ratio). Knowledge of the approximate distribution of charge density over the area A is yielded by the known values of the q_i.

Obviously, the capacitance and charge density can be obtained to any desired degree of accuracy by taking subareas sufficiently small in size. Of course, the labor involved in solving the set of n linear equations increases rapidly with n. However, as evidenced by the illustrative examples of this paper, surprisingly accurate values of capacitance and charge distribution can be obtained with use of small n, particularly if the area in question possesses symmetry.

Although the figures of this paper evidence use of circular annular subareas, the general procedure imposes no restriction on the shape of subarea that can be used. In general, however, it is best to use square subareas for plane figures possessing rectilinear symmetry and circular annular subareas for figures possessing angular symmetry.

Finally, it is to be noted that although in this paper attention is confined to plane areas, a similar procedure is applicable to 3-dimensional configurations. In particular, the method of subareas has been employed to solve the long-standing problem of the accurate determination of the capacitance of a cube.[2] Thus, within less than 1 per cent the capacitance of a cube of side a is $C=$

Table I. Capacitance in Micromicrofarads Versus Number of Annular Subareas

Subareas	2 Cm. Disk	4×6 Annulus
1	1.1890	3.7301
2	1.2955	3.8598
4	1.3519	3.9427
∞	1.4147	...

$0.655a$ electrostatic units (esu) $= 0.727a$ micromicrofarad. The best previously published determination[3] is $0.62211a<C<0.71055a$ *esu* or $0.691a<C<0.789a$ micromicrofarad.

Capacitance of a Circular Annulus

With reference to Figure 1, the potential dV at any arbitrary point O in the plane of a uniformly charged ring of inner radius x and width dx can be found by integrating, with respect to θ, the potential $qxdx\ d\theta/p$ contributed at O by the charge $qxdxd\theta$ on an incremental area $xdx\ d\theta$ of the ring. Herein: $q=$ charge density* and $p=$distance from incremental area to point O. Thus,

* The charge density as used here is the sum of the charge densities on the opposite sides of the incremental ring, hence is twice the actual charge density on one side. In view of the nature of the problem under discussion it is convenient to work in unrationalized centimeter-gram-second units. Accordingly, the units of all quantities mentioned are in this system except as specifically noted otherwise.

Table II. Charge Distribution on the Circular Disk of Figure 6

Location	Rigorous Value, Esu	Approx. Value, Esu
$r=0$	$q_0=0.05066\ V_0$	$q_0=$ ...
$r=1/4$	$q_4=0.05106\ V_0$	$q_4=0.05327\ V_0$
$r=3/4$	$q_3=0.05464\ V_0$	$q_3=0.05715\ V_0$
$r=5/4$	$q_2=0.06489\ V_0$	$q_2=0.06559\ V_0$
$r=7/4$	$q_1=0.10463\ V_0$	$q_1=0.14236\ V_0$
$r=15/8$	$q_e=0.14558\ V_0$	$q_e=$ ...

noting that $p^2=(x^2+r^2-2xr\cos\theta)$, we have

$$dV=2qxdx\int_0^{\pi}\frac{d\theta}{(x^2+r^2-2xr\cos\theta)^{1/2}} \quad (1)$$

The potential V at point O produced by a uniformly charged annulus of inner radius b and outer radius a is to be found by integrating this expression for dV with respect to x between $x=b$ and $x=a$. Thus

$$V=2q\int_b^a xdx\int_0^{\pi}\frac{d\theta}{(x^2+r^2-2xr\cos\theta)^{1/2}} \quad (2)$$

Integration of equation 2 hinges on whether $a>r>b$, or $r>a>b$, or $a>b>r$. In consequence, these three cases necessitate the following preliminary computation.

1. Consider an annulus of radii x_1 and r, where $r>x_1$. In this case we have from equation 2

$$V_1=2q\int_{x_1}^{r}xdx\int_0^{\pi}\frac{d\theta}{(x^2+r^2-2xr\cos\theta)^{1/2}} \quad (3)$$

Introducing the substitution $\cos\theta=2\sin^2\phi-1$ gives

$$V_1=4q\int_{x_1}^{r}\frac{x\,dx}{(x+r)}\int_0^{\pi/2}\times\frac{d\phi}{\left[1-\frac{4xr}{(x+r)^2}\sin^2\phi\right]^{1/2}}$$

$$=4q\int_{x_1}^{r}\frac{xK(k)}{x+r}dx \quad (4)$$

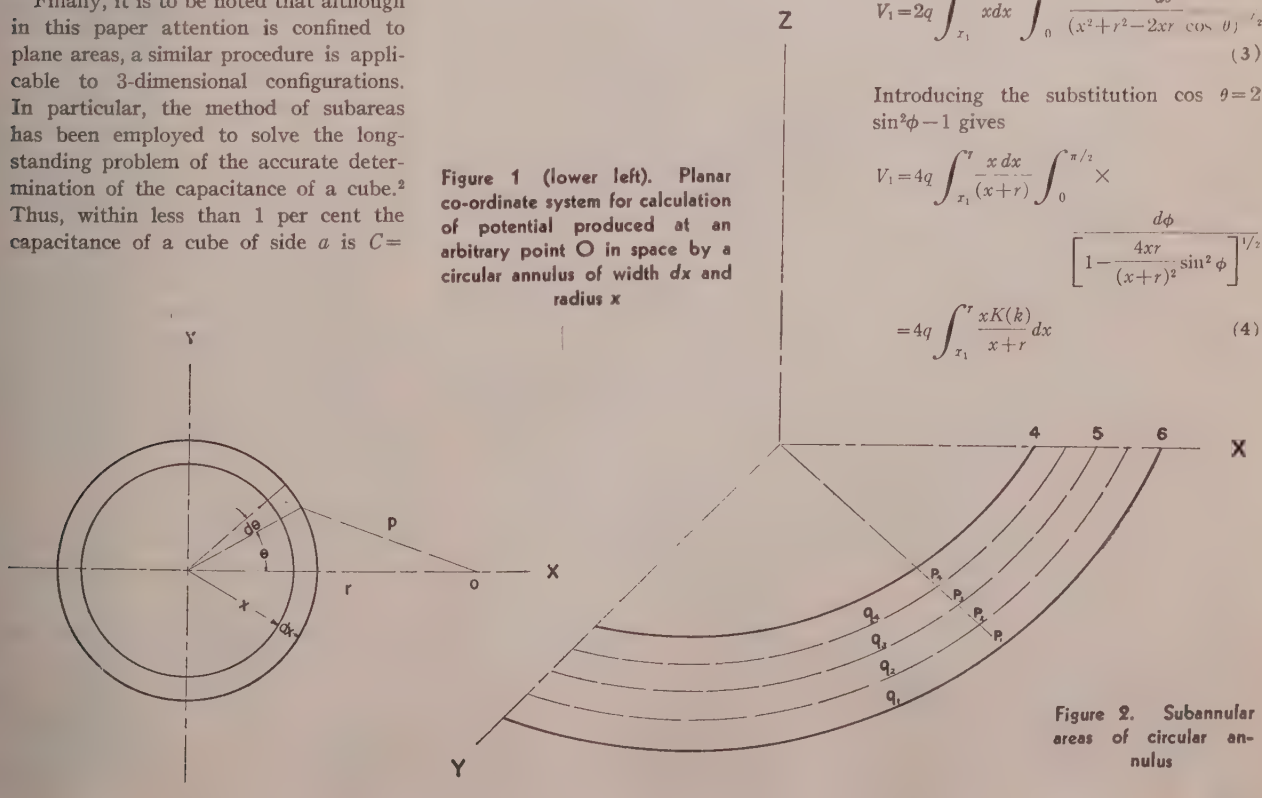

Figure 1 (lower left). Planar co-ordinate system for calculation of potential produced at an arbitrary point O in space by a circular annulus of width dx and radius x

Figure 2. Subannular areas of circular annulus

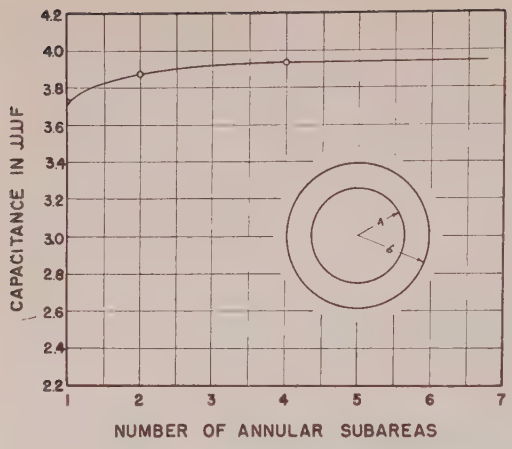

Figure 3. Approximate capacitance of circular annulus as a function of the number of subareas

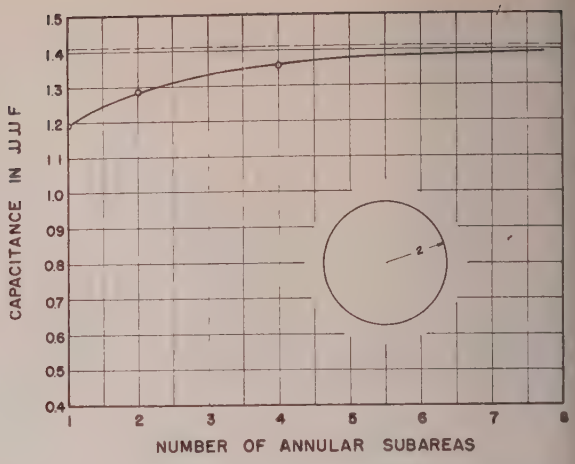

Figure 5. Approximate capacitance of circular disk as a function of the number of subareas

wherein $K(k)$ designates the complete elliptic integral of the first kind with modulus k defined by

$$k=[4xr/(x+r)^2]^{1/2}=2\sqrt{xr}/(x+r)$$

We now introduce the complementary modulus $k'=(1-k^2)^{1/2}$. Then $k'=(r-x)/(r+x)$, $x=r(1-k')/(1+k')$, $x/(x+r)=(1-k')/2$, and $dx=-2r\,dk'/(1+k')^2$. Utilizing the familiar series expansion for $K(k)$ in terms of k' (equation 777.3, page 171 of reference 4)

$$K(k)=\ln\frac{4}{k'}+\frac{1}{2^2}k'^2\left(\ln\frac{4}{k'}-\frac{2}{1\times2}\right)+\frac{1^2\times3^2}{2^2\times4^2}k'^4\left(\ln\frac{4}{k'}-\frac{2}{1\times2}-\frac{2}{3\times4}\right)+\ldots$$

and substituting as indicated in equation 4 gives

$$V_1=-4qr\int_{k_1'}^{0}\frac{(1-k')}{(1+k')^2}\left[\ln\frac{4}{k'}+\frac{1}{4}k'^2\times\left(\ln\frac{4}{k'}-1\right)+\ldots\right]dk'$$

$$=-4qr\int_{k_1'}^{0}(1-3k'+5k'^2+\ldots)\times\left[\ln\frac{4}{k'}+\frac{1}{4}k'^2\left(\ln\frac{4}{k'}-1\right)+\ldots\right]dk'$$

$$=4qr\left[\frac{1}{2}\ln\frac{16}{k_1'^2}\left(k_1'-\frac{3}{2}k_1'^2+\frac{7}{4}k_1'^3-\frac{31}{16}k_1'^4+\frac{665}{320}k_1'^5+\ldots\right)+\left(k_1'-\frac{3}{4}k_1'^2+\frac{1}{2}k_1'^3-\frac{31\cdot19}{16\cdot124}k_1'^4+\ldots\right)\right] \quad (5)$$

where $k_1'=(r-x_1)/(r+x_1)$.

2. Consider an annulus of radii r and x_2, where $x_2>r$. In this case we have from equation 2

$$V_2=2q\int_r^{x_2}x\,dx\int_0^{\pi}\frac{d\theta}{(x^2+r^2-2xr\cos\theta)^{1/2}}$$

$$=2q\int_r^{x_2}dx\int_0^{\pi}\frac{d\theta}{\left(1+\frac{r^2}{x^2}-\frac{2r}{x}\cos\theta\right)^{1/2}}$$

By equation 860.5 of reference 4 we have

$$V_2=4q\int_r^{x_2}dx\int_0^{\pi/2}\frac{d\phi}{\left[1-\left(\frac{r}{x}\right)^2\sin^2\phi\right]^{1/2}}$$

Performing the integration yields

$$V_2=4qr\left[\frac{x_2}{r}E(r/x_2)-1\right] \quad (6)$$

where $E(r/x_2)$ designates an elliptic integral of the second kind of modulus (r/x_2).

With V_1 and V_2 at hand integration of equation 2 reduces to appropriate combination of V_1 and V_2. Three cases occur:

Case 1. $a>r>b$

$$V=V_1|_{x_1=b}+V_2|_{x_2=a} \quad (7)$$

Case 2: $r>a>b$

$$V'=V_1|_{x_1=b}-V_1|_{x_1=a} \quad (8)$$

Case 3: $a>b>r$

$$V''=V_2|_{x_2=a}-V_2|_{x_2=b} \quad (9)$$

With respect to Figure 2 let, typically, $V_{p_1q_1}$ denote the potential at point p_1, due to the charge on the subannulus of charge density q_1. Then the potential of point p_1 where of $r=23/4$ due to the subannulus of charge density q_1 and dimensions $a=6$, $b=11/2$, is, from equation 7,

$$V_{p_1q_1}=V_1|_{x_1=b=11/2}+V_2|_{x_2=a=6}$$
$$=3.07188q_1+3.14341q_1$$
$$=6.21529q_1$$

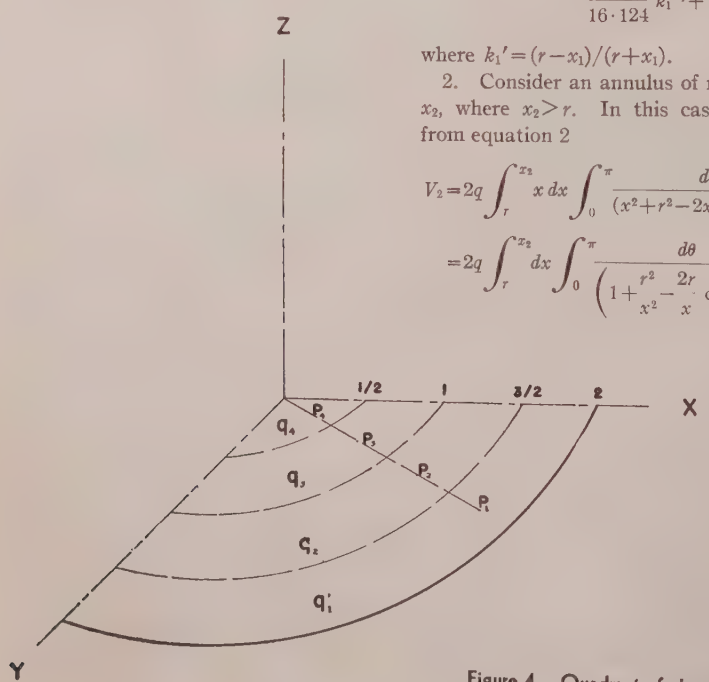

Figure 4. Quadrant of circular disk

Table III. Charge Distribution of the 4 × 6 Annulus of Figure 7

$r=17/4$	$q_4=0.05776\ V_0$ (esu)
$r=19/4$	$q_3=0.03645\ V_0$ (esu)
$r=21/4$	$q_2=0.04042\ V_0$ (esu)
$r=23/4$	$q_1=0.08673\ V_0$ (esu)

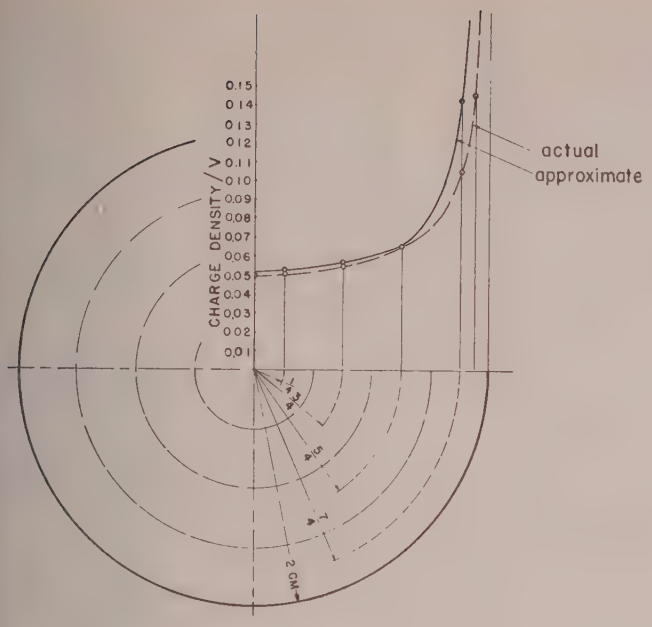

Figure 6. Charge distribution on circular disk

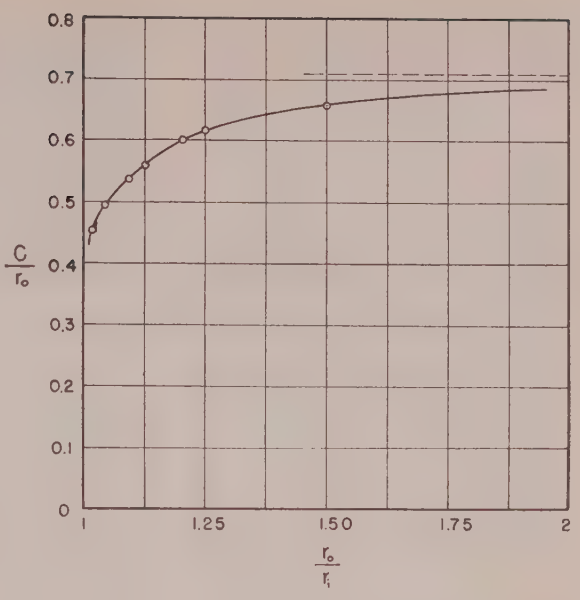

Figure 8. Universal curve: C/r_o versus r_o/r_i

In similar fashion, using the associated a, b, and r values as indicated,

$V_{p_1q_2}=4.32009q_2$ ($a=11/2$, $b=5$, $r=23/4$, in equation 8)

$V_{p_1q_3}=3.40055q_3$ ($a=5$, $b=9/2$, $r=23/4$, in equation 8)

$V_{p_1q_4}=2.81083q_4$ ($a=9/2$, $b=4$, $r=23/4$, in equation 8)

where typically, $V_{p_1q_2}$ designates the potential at point p_1 produced by the sub-annulus of charge density q_2.

Hence for

$$V_{p_1}=V_{p_1q_1}+V_{p_1q_2}+V_{p_1q_3}+V_{p_1q_4}$$

we find

$$V_{p_1}=6.21529q_1+4.32009q_2+3.40055q_3+2.81083q_4$$

Proceeding thus for V_{p_2}, V_{p_3}, and V_{p_4} in turn yields:

$$\begin{aligned}
V_{p_1}&=6.21529q_1+4.32009q_2+3.40055q_3+2.81083q_4\\
V_{p_2}&=4.72563q_1+6.13977q_2+4.19496q_3+3.27285q_4\\
V_{p_3}&=4.10989q_1+4.64588q_2+6.02205q_3+4.08899q_4\\
V_{p_4}&=3.79474q_1+4.03767q_2+4.55923q_3+5.91090q_4
\end{aligned}\qquad (10)$$

Imposing the condition $V_0=V_{p_1}=V_{p_2}=V_{p_3}=V_{p_4}$ and solving the set of equations 10 for the q's yields:

$q_1=0.08673\,V_0$ $\quad q_3=0.03645\,V_0$

$q_2=0.04042\,V_0$ $\quad q_4=0.05776\,V_0$

Accordingly,

$$\begin{aligned}
Q&=\sum_{i=1}^{4}q_i\,\text{area}_i\\
&=(0.08673\,V_0)(18.06397)+(0.04042\,V_0)(16.49319)\\
&\quad+(0.03645\,V_0)(14.92241)+(0.05776\,V_0)(13.35163)\\
&=3.5484\,V_0
\end{aligned}$$

Hence, an approximation to the capacitance of an annulus of inner radius $r=4$ centimeters, outer radius $r=6$ centimeters, and ratio $r_o/r_i=1.5$ is

$C=Q/V_0=3.5484\,V_0/V_0=3.5484$ esu $=$ 3.9427 micromicrofarads

Finally,

$C/r_o=0.6571$ micromicrofarad per centimeter

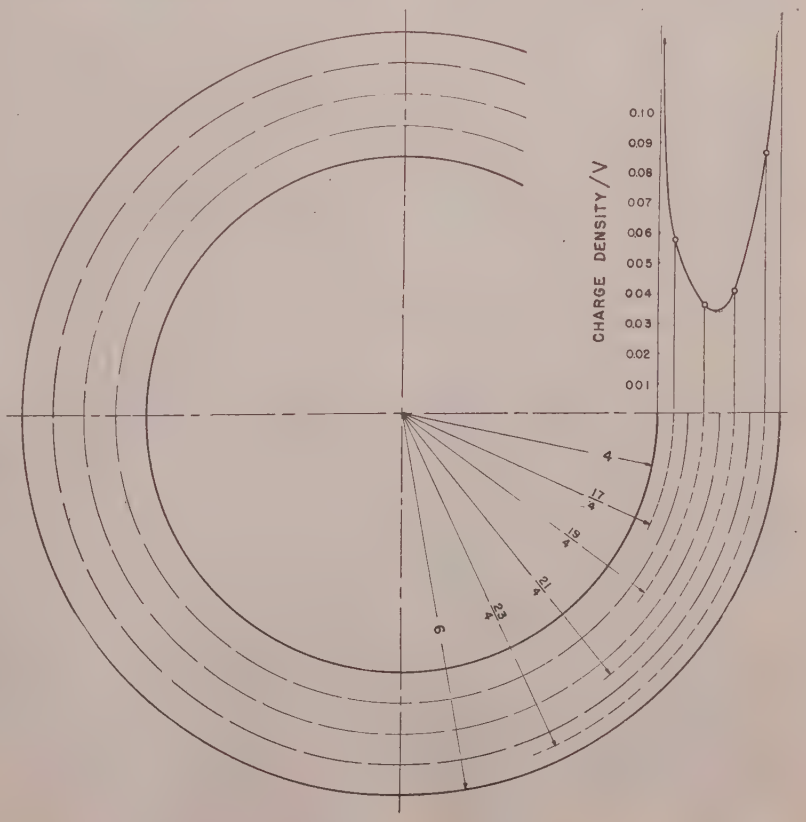

Figure 7. Charge distribution on circular annulus

Table IV. Dimensionless Ratio C/r_0 as a Function of r_0/r_i

r_0/r_i	C(micromicrofarads)/r_0
1.0213	0.4525
1.0435	0.4930
1.0909	0.5382
1.1250	0.5577
1.2000	0.5994
1.2500	0.6197
1.5000	0.6571
∞	0.7073

In that four subannuli have been used in obtaining this approximation, it is appropriate to term it a fourth approximation. Figure 3 and Table I display the various values of C obtained by using one, two, and four subannuli. It is evident from the curve of Figure 3 that the fourth approximation of $C=3.9427$ micromicrofarads is very near to the exact value.

Capacitance of a Circular Disk

Specific insight as to the degree of accuracy to be expected in calculating the capacitance of annuli of various ratios of outer to inner radius r_o/r_i by using four subareas is afforded by similar calculation of the extreme special case ($r_o/r_i=\infty$) of a circular disk of radius $r=2$ centimeters, of which the known exact capacitance is $C=2r/\pi=1.273$ esu $=1.415$ micromicrofarad. Figure 4 indicates the subdivision of the circular disk in effecting the fourth approximation. The details of calculation are the same as for the annulus, hence may well be omitted. Figure 5 displays the values for the first, second, and fourth approximations. The value of the fourth approximation is $C=1.2167$ esu $=1.3519$ micromicrofarad. In this extreme case of $r_o/r_i=2/0=\infty$, the per cent error with only four subareas is about 4.4 per cent. Accordingly, for the annulus of $r_o/r_i=6/4=1.5$ a much smaller error is to be expected, as is indicated by Figure 3.

It is to be noted that the curves of Figures 3 and 5 evidence that as the number of subareas is increased the approximate values of capacitance approach the exact value as a limit from below. This approach from below is a consequence of a well-known theorem in electrostatics: the energy associated with a charged surface is a minimum when the charge is in equilibrium; that is, has distributed itself such that the surface is an equipotential surface. Inasmuch as the method of subareas requires assumption of uniform charge density over each subarea, it follows that the assumed distribution of charge is not that of equilibrium. Accordingly, the energy W associated with the assumed distribution of charge Q is greater than the value W' at equilibrium. Consequently, inasmuch as $C_{exact}=Q^2/2W'$, $C_{approx}=Q^2/2W$ and $W'<W$, it follows that $C_{approx}<C_{xact}$ and C_{approx} approaches C_{exact} as a limit as the number of subareas is increased.

Charge Distribution on the Circular Disk and the Circular Annulus

Use of four subareas for the circular disk yields average charge densities on the four subannuli of Figure 4 as follows:

$$q_1=0.14236\,V_0 \qquad q_3=0.05715\,V_0$$
$$q_2=0.06559\,V_0 \qquad q_4=0.05327\,V_0$$

Assuming these densities at the average radii of the corresponding subareas yields a distribution of charge over the disk as in Figure 6. The marked increase in density toward the outer edge is in accord with the theoretical fact that the charge density at the bounding edge of a plane area is infinite.

The approximate charge distribution is in good agreement with the actual distribution (dashed curve) as plotted from the values of Table II which are calculated from the known equation[5] $q=V/\pi^2(a^2-r^2)^{1/2}=V/\pi^2 a(1-r^2/a^2)^{1/2}$, where r = point under consideration, a = radius of the disk, and q = charge density.*

Figure 7 indicates the charge distribution on the annulus of $r_o/r_i=1.5$ as plotted from the values of Table III, calculated in determining its capacitance. In view of the good agreement between approximate and exact distributions manifest in Figure 6, and having in mind the better accuracy to be expected for the annulus by virtue of the much narrower annular subareas, it is to be inferred that the indicated distribution of Figure 7 is a close approximation to the exact distribution.

A Universal Curve

The primary dimensions of C in centimeter-gram-second units are those of length (whence the terminology of some 19th century texts on electricity and magnetism in stating "a capacitance of 10 centimeters"). Accordingly, the ratio of C to either the inner or outer radius (r_o and r_i) is dimensionless. In that C is a function of its geometry alone, thus of its two radii, and in that C/r_o (say) is dimensionless, it follows that C/r_o must be a function of only the dimensionless ratio r_o/r_i. Thus, any annulus of fixed ratio r_o/r_i has the same value of C/r_o. Thus, a plot of a single curve of C/r_o versus r_o/r_i, where r_o/r_i ranges from 1 to ∞, affords knowledge of the capacitance of an annulus of any desired radii. Figure 8, plotted from the values of Table IV, comprises this universal curve. For convenience of use, C is taken in micromicrofarads.

Previous Solutions for the Circular Annulus

Nicholson[6] has attempted solution for the circular annulus by treating the annulus as the limiting configuration approached by a toroidal ring of elliptical cross section as the semiaxis of the ellipse (which is perpendicular to the plane of the ring) approaches zero. His solutions are invalidated by various incorrect analytical procedures. In substantiation of this remark we need only quote Nicholson's comment based on his solution for the capacitance: "The presence of an inner edge much increases the capacity [over that of a circular disk of the same outer radius]." This remark is directly contrary to the well-known theorem in electrostatics that the capacitance of any portion of a plane area, surface or volume is less than the capacitance of the whole. For example, we found the capacitance of the circular annulus considered above to be slightly greater than 3.94 micromicrofarad; the known exact capacitance of a circular disk of the same external radius is 4.24 micromicrofarad. Thus, the capacitance of the annulus, a part of the disk, is less than the capacitance of the whole disk.

Lebedev[7] also has attempted a solution by considering the annulus as the limiting case of a toroidal ring of certain oval cross section. However, the analysis is extremely complicated and his end result is to express the capacitance in terms of certain harmonic functions associated with the ring which, however, are so complicated in form that they defy calculation. Similar analytic difficulties mark the investigations of Poole[8] and Snow.[9]

In consequence, we have that the solution by subareas, as advanced in this paper, comprises the first numerically-useful solution of the problem of determining the capacitance and charge distribution of a circular annulus.

Summary

1. The basic theory of approximate calculation by the use of subareas of the capacitance of a plane area and of the

* It is to be recalled that the "charge density" under discussion is the sum of the densities on the two sides of the disk at a given point on it.

distribution of charge density over it is outlined.

2. The method of subareas is employed to obtain an accurate value for the capacitance of an annulus of ratio of outer to inner radius of $r_o/r_i = 1.5$.

3. The fourth approximation to the capacitance of a specified circular disk, as calculated by the method of subareas, is found to be in good agreement with the known exact value. As a circular disk is an annulus of ratio of radii $r_o/r_i = \infty$, it is to be concluded that the fourth approximation for the much narrower annulus of ratio 1.5 is very nearly the exact value. This conjecture is substantiated by the curve of Figure 3.

4. Comparison in Figure 6 of the charge distribution on a circular disk as determined both from the known equation and by the method of subareas indicates that calculation of charge distribution by use of subareas affords a good approximation to the actual distribution. Accordingly, the charge distribution of Figure 7 for the much narrower annulus is to be considered as a close approximation to the actual distribution.

5. The universal curve of Figure 8 yields the capacitance of an annulus of any stated ratio of external to internal radii.

References

1. The Flow of Viscous Fluids Round Plane Obstacles, **R. Roscoe.** *Philosophical Magazine* (London, England), series 7, volume 60, 1949, pages 338–51.

2. Calculation of the Capacitance of a Cube by the Method of Subareas, **Thomas James Higgins, Daniel Kinseth Reitan.** *Journal of Applied Physics* (New York, N. Y.), February 1951.

3. Estimating Electrostatic Capacity, **G. Polya.** *American Mathematical Monthly* (New York, N. Y.), volume 54, 1947, pages 201–06.

4. Tables of Integrals and Other Mathematical Data (book), **H. B. Dwight.** The Macmillan Company, New York, N. Y., 1947.

5. A Treatise on Electricity and Magnetism (book), **J. C. Maxwell.** Oxford University Press, Oxford, England, Edition 3, 1893, volume 1, page 239.

6. Problems Relating to a Thin Plane Annulus, **J. W. Nicholson.** *Proceedings*, Royal Society of London (London, England), volume 101A, 1922, pages 195–210.

7. The Functions Associated with a Ring of Oval Cross-Section, **N. Lebedev.** *Journal Technical Physics* (Leningrad, USSR), volume 4, 1937, pages 1–24.

8. Dirichlet's Principle for a Flat Ring, **E. G. C. Poole.** *Proceedings*, London Mathematical Society (London, England), volume 29, 1929, pages 342–54; volume 30, 1930, pages 174–86.

9. The Hypergeometric and Legendre Functions with Applications to Integral Equations of Potential Theory (book), **C. Snow.** National Bureau of Standards (Washington, D. C.), 1942, page 318.

10. An Introduction to the Theory of Newtonian Attraction (book), **A. S. Ramsey.** Cambridge University Press, Cambridge, England, 1940, page 133.

Discussion

H. B. Dwight (Massachusetts Institute of Technology, Cambridge, Mass.): As mentioned in the early part of the paper by T. J. Higgins and D. K. Reitan, there is a formula for the capacitance of only one shape of finite plane area, namely, an elliptical area, which includes the case of a circular disk. There are precise calculations for extremely few shapes of finite conductors. The cases of a finite cylinder, of two parallel plates close together, and of groups of infinitely long wires require certain ratios to be very small.

There are many other shapes for which the calculated capacitance is desired. One of the most common methods to be used is that of a Howe approximation, developed a number of years ago by G. W. O. Howe of England. Uniform charge density is assumed over the metallic surfaces and the calculated average potential of the surfaces is computed. The ratio of charge to average potential gives an approximate value of capacitance.

For groups of infinitely long wires, as in overhead power circuits, the error from using a Howe approximation is of the order of only 1 per cent. This occurs when geometric mean distance is used in calculating capacitance in groups of wires. For a circular disk, the error is about 8 per cent and for a wide annulus it is several per cent. The method of subareas described in this paper can be used where greater accuracy is desired than is available by the Howe approximation. The precision can be made greater and greater by lengthening the calculation.

In view of the various needs for capacitance calculations and for flow calculations of different kinds, such as current flow in the earth, the method of subareas should be of widespread use.

F. W. Grover (Union College, Schenectady, N. Y.): This paper is a clearly written and interesting application of a general method, proposed by the authors, for the solution of problems in electrostatics, where the geometry of the system is such as to render an exact solution very difficult, if not impossible. This general method is one of successive approximations, the accuracy attainable depending upon the number of subareas into which the conductor is supposed to be divided. In the example given, four subareas are assumed and a gratifying degree of precision is attainable. The greater the number chosen, the greater the attainable precision, but the labor of precision goes up as the square of the number of subareas. By applying the method to the solution for the capacitance of a disk, where the exact formula is known, an upper limit to the error of the result in the present problem is obtained and the use of four subareas is proved to be accurate enough for practical purposes. The authors are to be congratulated on their successful method of attack for the solution of such problems.

The accuracy of the solution in the present case depends upon the sufficiency of the equations for the potentials V_1 and V_2. For subareas not very far apart, the series for V_1 in equation 5 will be satisfactorily convergent, since k' will be small. The equation 6 for V_2 is subject to no limitations, since the elliptic integral can be obtained from tables for any modulus. This suggests the possibility that V_1 also may be expressed in elliptic integrals. This proves to be the case. The equation found is

$$V_1 = 4qr[1 - E + k_1'^2 K]$$

where K and E are complete elliptic integrals of the first and second kinds to modulus x_1/r. $k_1'^2 = 1 - (x_1/r)^2$.

As a check on this expression, we find for the case $x_1 = 11/2$ and $r = 23/4$, that is, for the first term of $V_{p_1q_1}$, given in the equation immediately following equation 9.

$$k_1'^2 = 1 - \left(\frac{22}{23}\right)^2 = \frac{45}{529} = 0.0850662,$$
$$K = 2.654443,\ E = 1.092296$$

$$V_1 = 23q_1\left[1 - 1.092296 + \frac{45}{529}(2.654443)\right]$$
$$= 3.07066q$$

This expression applies for annular, concentric, and coplanar subareas at all distances.

For completeness it may be mentioned that, when $k_2' = 1 - [r/x_2]^2$ is small, the expression for V_2 may be expanded to read

$$V_2 = 4qrk_2'\left[\left(\log\frac{4}{k_2'} + 1\right) + \frac{3}{2}k_2' \times \left(\log\frac{4}{k_2'} + \frac{1}{2}\right) + \frac{7}{4}k_2'^2\left(\log\frac{4}{k_2'} + \frac{2}{7}\right) + \ldots\right]$$

For cases where the modulus itself is small, the elliptic integral expressions may be expanded in terms of the well-known expansions of the elliptic integral in powers of the modulus.

It seems likely that the application of the general method to the finding of the capacitance of two coaxial annuli in parallel planes would yield elliptic integral expressions with somewhat more complicated equations for the moduli.

Ernst Weber (Polytechnic Institute of Brooklyn, Brooklyn, N. Y.): The method of subareas represents, without doubt, an excellent contribution to the practical methods of computing capacitance of charge distributions. In principle, the method is an ingenious adaptation of Maxwell's coefficients of potential[1] for a system of electrostatic conductors which system is composed of the subareas into which the given conductor is subdivided. The evaluation of the coefficients of potential still requires considerable detail calculation, but the total amount of effort is incomparably smaller than the complete solution of a boundary value problem would entail. Because the coefficients of potential must be directly computed in this method, it is necessary to choose the subareas of simple geometries as the authors have done for the circular disk and the circular annulus.

I should like to ask a few specific questions:

1. How has the final value been established for Figure 3 giving the capacitance of a circular annulus. Comparison with Figure 5 would indicate that the exact capacitance of the annulus is 5 per cent above the value of the fourth approximation. Should one assume the same degree of accuracy for the fourth approximation of the annulus? It would, of course, be of interest to find the value of the eighth approximation, for example, permitting a better approximation to the exact value.

2. The method is not restricted to uniform subdivision of the conductor area. Nonuniform subdivision towards the edges might lead to a very much better approximation of charge densities. This could be done without undue complication of the computations if the last subarea towards the edge be chosen very narrow.

3. For practical computations the self coefficients of potential for the circular annulus can apparently be taken directly from Figure 8. Would it be possible to substitute for the mutual coefficients between subareas the coefficients of simple circular line charges assuming the lines have very small but finite diameter identical with the thickness of the disk. This might further simplify the detail calculations of the coefficients.

It will be interesting to see further applications of this method to axially symmetrically conductor surfaces for which several rather crude approximation methods have been proposed in the past, as for example by J. C. Maxwell, page 305.[1]

REFERENCE

1. See reference 5 of the paper.

W. R. Smythe (California Institute of Technology, Pasadena, Calif.): The method of subareas presented in this paper is a very powerful one for attacking problems which cannot be solved rigorously by any other means. A striking example is the calculation by these authors of the capacitance of a cube. In the case of the circular annulus it may be of interest to give a formula obtained by another method which, while not quite as accurate as the four subarea approximation when r_o/r_i is 1.5 will be considerably more precise for large values of r_o/r_i and is exact in the limit $r_i = 0$.

First consider a freely charged disk of radius r_o at potential V. Now calculate the charge induced on an infinite sheet at potential zero containing a hole of radius r_i in which there is a fixed charge distribution identical in magnitude but opposite in sign to that on the portion of the disk inside r_i. Superposition of these two systems gives the required annulus at potential V under the influence of a small positive coplanar charge outside it. Removal of this charge will decrease V and hence increase the ratio Q/V so that the capacitance given by this ratio is too low. The original charge on that part of the disk between r_i and r_o is found by integrating equation 3 on page 114 of Static and Dynamic Electricity.[1] The induced charge is found by integration of the result of problem 39 page 203 of the same book. Addition of these charges and division by V gives for the lower limit of the capacitance, in farads,

$$(16\epsilon/\pi)\{r_o\cos^{-1}(r_i/r_o)+(r_o^2-r_i^2)^{1/2}\times \sinh^{-1}[r_i(r_o^2-r_i^2)^{-1/2}]\}$$

where r_o and r_i are in meters and ϵ is 8.855×10^{-12}. In the special case when r_i is 0.04 meter and r_o is 0.06 meter this gives 3.901 micromicrofarads against the 3.9427 micromicrofarads by the four subarea approximation. Although it is 1 per cent less accurate for $r_o/r_i=1.5$ its precision improves rapidly as r_o/r_i increases and when r_i is zero it gives exactly the capacitance $8\epsilon r_o$ of a circular disk.

REFERENCE

1. STATIC AND DYNAMIC ELECTRICITY (book). McGraw-Hill Book Company, New York, N. Y. Second edition, 1950

T. J. Higgins and **D. K. Reitan:** Relative to Professor Dwight's mention of Howe's method for approximating the capacitance of a conductor, it may be remarked that this was originally used by Howe to approximate the capacitance of rectangular plates, in connection with some work on antennas. The authors have pending publication a paper which contains a universal curve for the capacitance of a rectangular plate of length d and breadth b, calculated by the method of subareas. Comparison of this curve with a similar curve stemming from Howe's approximation reveals that the curves are in good agreement for large values of d/b—as is to be expected; but that as d/b decreases the agreement worsens, to the end that the Howe approximation is in error by about 4.8 per cent for the limiting case of the square plate, $d/b = 1$.

In general, if a given conductor is characterized by two appropriately-chosen geometrical parameters, the Howe approximation is good when the value of one parameter is large compared to the other, and worsens as the two approach each other. Thus, in the case of the annulus, if we take r_o and $(r_o - r_i) = t$ as characterizing the annulus, the Howe approximation is excellent when r_o/t is large and—as Professor Dwight remarks—worsens as $r_o/t \to 1$, the limiting case of the circular disk of radius r_o. A similar remark applies to a cylinder of length d and radius r, the error being small for $d \gg r$, the case of a long wire.

On reading Professor Grover's discussion and comparing it with the comments of one of the reviewers, similarity of content *re* discussion of use of elliptic integrals indicated that Professor Grover was probably the mentioned reviewer—a surmise recently confirmed by Professor Grover. The use of elliptic integrals, rather than the series in terms of Legendre polynomials used in the original draft of the paper, very much facilitates numerical computation. The writers are much indebted to Professor Grover for his valuable suggestion.

It is to be remarked that the writers have taken up preparation of a universal curve for the capacitance of a parallel-plate capacitor comprised of two identical coaxial

Figure 1. Charge distribution on circular annulus, using 8 subannuli

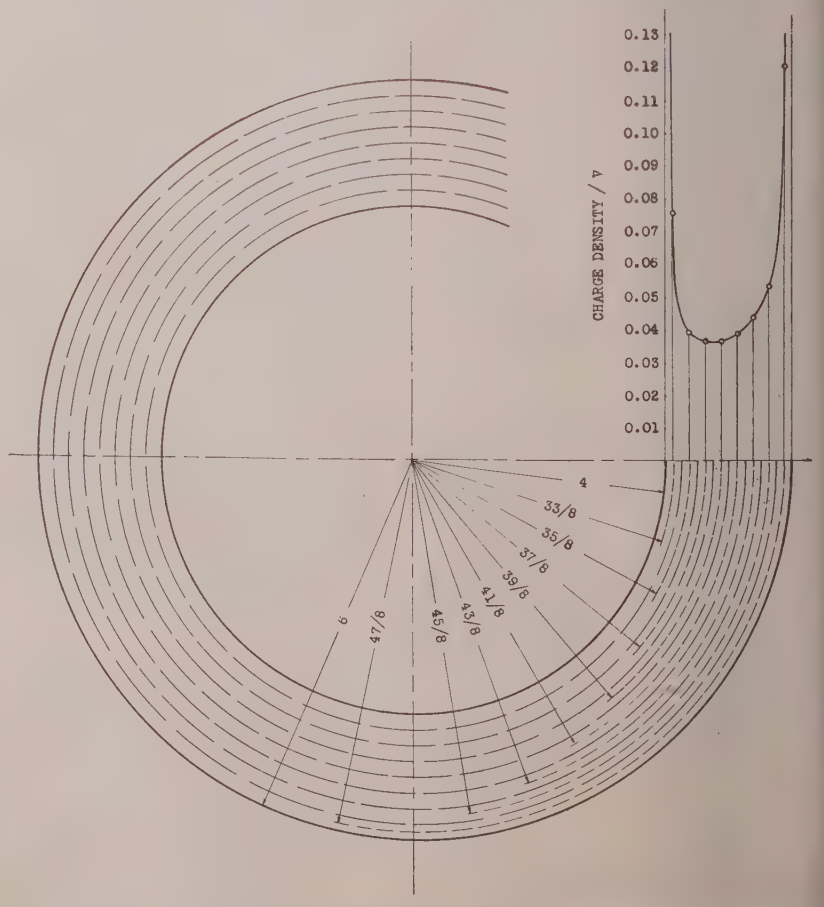

annuli. Professor Grover's conjecture that more complicated elliptic integral expressions would arise proves to be very true! The basic expression required for the mentioned problem is that for the potential of a uniformly charged disk, of unit charge density and of radius r, at any point in space (a, θ, c) and this is found to be

$$V=4\alpha\left\{E_1(k)-k'^2\sin^2\lambda F_1(k)-\frac{k'^2\sin\lambda\cos\lambda}{\sqrt{1-k'^2\sin^2\lambda}}\left[\frac{\pi}{2}+\{F_1(k)-E_1(k)\}\times F(k',\lambda)-E_1(k)\,E(k',\lambda)\right]\right\}$$

wherein

$$k'^2=1-k^2;\quad k=\frac{ar}{r^2+\theta^2};$$

$$\sin^2\lambda=\frac{1}{1+\frac{c^2r^2}{\theta^2}};\quad \alpha^2=r^2+\theta$$

and θ is the positive root of

$$\frac{a^2}{r^2+\theta}+\frac{c^2}{\theta}=1$$

Corroboratively, if the point is on the vertical axis of the disk or in its plane, this expression reduces to known expressions for these two special cases.

We answer Professor Weber's questions in the same order they are advanced:

1. It is to be noted that for four subareas the slope of the curve of Figure 3 (thus, its rate of increase at this point) is much less than that of Figure 5 at the same point. This smaller rate of increase indicates that the curve of Figure 3 is leveling off faster than is the curve of Figure 5 and that the error corresponding to the value of four subareas is smaller for the annulus than for the disk. A confirmation based on the suggested use of 8 annuli has been carried out. The calculated value using 8 annuli is C=3.5875 electrostatic units=3.9861 micromicrofarads. This is only about 1 per cent larger than the value found using 4 subannuli.

2. The suggestion that nonuniform subdivisions be used to increase accuracy of approximation to the charge density is an excellent one. Thus, in that the exact charge distribution on the disk, as indicated in Figure 6, is such that the density is substantially constant from the center up to about $0.5r_o$ suggests that a better agreement of charge distribution is to be obtained by dividing the disk into annuli of radii:

$$r_i=0, r_o=1;\ r_i=1, r_o=1.5;\ r_i=1.5, r_o=1.75;\ r_i=1.75, r_o=2$$

This conjecture is confirmed by calculation with these values. However, it is to be noted that a corresponding increase in the accuracy of the value of the capacitance will not be obtained: the value of this parameter is relatively insensitive to such changes in the radii, being influenced primarily by the number of annuli used. Thus, the charge distribution for the illustrative annulus, as determined through use of 8 subannuli is shown in Figure 1 of the discussion and may be compared with the corresponding distribution of Figure 7 of the paper, based on 4 subannuli.

3. The suggestion advanced was tried but did not prove fruitful.

4. The method of subareas is applicable to the solution of the type of axially-symmetric conductors mentioned. A technically interesting axially-symmetric conductor is the finite cylinder, the capacitance of which has not been calculated accurately to date, except for the limiting cases of the circular disk and the very long cylinder. Calculation of a universal curve by the method of subareas now is under way.

Professor Smythe's method of approximating the capacitance of an annulus is a most interesting one. He is expanding his discussion into a paper which will appear in *The Journal of Applied Physics*.

In conclusion, it is to be emphasized that the method of subareas is not limited to effecting the capacitance and charge distribution of conductors, but is generally applicable to the determination of parameters and variable quantities of numerous problems in electricity, acoustics, heat, fluid flow and aerodynamics which are characterized by a scalar potential function and prescribed boundary conditions. Accordingly, the subarea method enables the rather easy solution of many important problems which have hiterto proved intractable to accurate computation.

The Transient Response of Magnetic Amplifiers—Cases of Negligible Commutation

L. A. FINZI
MEMBER AIEE

D. P. CHANDLER
STUDENT MEMBER AIEE

D. C. BEAUMARIAGE
ASSOCIATE AIEE

Synopsis: Previously developed methods of analysis of magnetic amplifiers with gradually varying incremental permeability are applied to the study of the general transient response of single-stage amplifiers. In the first part of the paper, curves are presented which describe the transient response of magnetic amplifiers without feedback in general dimensionless form. The curves apply for transients in which the alternating voltage at the amplifier terminals is constant, but convey useful information also for other actual operating conditions. In the second part, the analysis is extended to feedback amplifiers with a-c output operating in conditions of negligible commutation. Experimental checks indicate the order of accuracy obtainable.

The General Transient Response of Magnetic Amplifiers Without Feedback

IN A previous paper[1] an analysis has been indicated for the transient response of a magnetic amplifier without feedback upon application of a step signal. The analysis applies to "slow" transients, lasting at least several cycles of the alternating voltage, for which it is acceptable to evaluate instantaneous values of the output current from steady-state expressions on the basis of the value of the d-c component of flux density B_{0t} that exists in the cores at the time considered. B_{0t} is obtained as a function of time during the transient by integration of the first-order circuit differential equations which can be written for the signal circuit and for the various other circuits coupled with it (bias circuits and also loop formed by the output windings, whenever these are parallel-connected) under assumption of negligible leakage fluxes. Graphical solutions are thus obtainable for any specific instance if the steady-state relationship between d-c component of flux density and signal current is known, as shown also by other authors.[2] The integration can be performed also in a straightforward analytical way if the normal magnetization curve of the cores is approximated, for example, by a hyperbolic sine function, whenever the assumption can be made that the alternating component of flux density is constant (or does not vary considerably) during the transients.

The analysis has been developed in reference 1 for the particular case of a step signal voltage applied from initial conditions of zero d-c core magnetization, and curves have been calculated (and checked experimentally) which express the gradual build-up of output currents (crest, or rms or rectified average) towards their final steady state in terms of the data of design of the amplifier. In the first part of the present paper, the study is extended to any more general kind of initial conditions, thus including transients caused by decreases or reversals of the signal. The results of the analysis, performed in Appendix I, are presented concisely in the general dimensionless curves of Figure 1 which have been calculated from equations 18 and 19. The notation used is consistent with the symbols already introduced in a previous analysis in dimensionless form for the steady state.[3] Thus, it is defined

$$\mathfrak{F}_{Lt}=\frac{1}{U}\frac{NI_{Lt}}{l} \tag{1}$$

where I_{Lt} is the output current through the a-c source and load ("rectified average" amperes) at the time t. N is related to the number N_2 of turns per core of the output windings by the relation $N=2N_2$ for the series-connected magnetic amplifier, or $N=N_2$ for the magnetic amplifier with parallel-connected output windings. l is the mean length of the magnetic path of one core (for example, in meters). U is one of the constants appearing in the analytical relationship

$$H=U\sinh uB \tag{2}$$

which approximates the experimental normal magnetization curve of the given cores (H=magnetizing intensity, for example, ampere turns per meter, B=flux density, for example, weber per square meter).

The factor m in Figure 1 is defined in equation 20, reference 3, and is plotted in Figure 2 as a function of $\mathfrak{B}_m$, where

$$\mathfrak{B}_m=uB_m=u\frac{E_{\max}}{N}\frac{1}{2\pi fA} \tag{3}$$

where B_m is the crest of the component of the flux density alternating in the cores at the supply frequency $f=\omega/2\pi$ (for example, cycles per second), $E_{\max}/N$ is the crest value of the corresponding volts per turn, and A is the cross-sectional area of one core (for example, square meters). Furthermore, u is the other constant appearing in equation 2.

For the abscissae of the curves of Figure 1, t represents the time (in seconds) and τ is a time scale factor defined as

$$\tau=\frac{A}{Uuln}\sum_{\nu}\frac{N_\nu^2}{R_\nu} \tag{4}$$

Paper 51-175, recommended by the AIEE Magnetic Amplifiers Committee and approved by the AIEE Technical Program Committee for presentation at the AIEE Great Lakes District Meeting, Madison, Wis., May 17–19, 1951. Manuscript submitted February 20, 1951; made available for printing April 6, 1951.

L. A. FINZI and D. P. CHANDLER both are with the Carnegie Institute of Technology, Pittsburgh, Pa. D. C. BEAUMARIAGE, formerly with Carnegie Institute, now is at Bethpage, N. Y.

This work was done in part under Office of Naval Research Contract *N7 onr*-30306. The comments and advice of Professor D. W. VerPlanck and the skillful co-operation of J. R. Horsch in the execution of the experimental part are hereby acknowledged.

n, as defined in equation 21, reference 3, is the modified Bessel function of first kind and zero order of $\mathfrak{B}_m$ (already defined in equation 3). For easier reference this function also is plotted in Figure 2. The summation of the "turns square per ohm" appearing in equation 4 is extended to include all circuits in which unidirectional currents are induced during the transient. In a magnetic amplifier with series-connected output windings, with a signal circuit having N_1 turns per core and $2R_1$ total signal circuit resistance and with one bias circuit having N_b turns per core and total circuit resistance $2R_b$, it is simply

$$\sum_{\nu} \frac{N_\nu^2}{R_\nu} = \frac{N_1^2}{R_1} + \frac{N_b^2}{R_b}$$

More terms of the same type appear in the summation in cases of more than one bias circuit, and an additional term N_2^2/R_2 appears also for a magnetic amplifier with parallel-connected output windings of N_2 turns and R ohms per core. (It may be also of interest to observe that $1/Uu = (dB/dH)_{H=0}$ for the representation of equation 2 so that τ results evidently as the ratio of an inductance to a resistance.) Every curve of the family plotted in Figure 1 is defined by the steady state of output $\mathfrak{F}_{L\infty}$ reached at the end of the transient, divided by m. This output may be known or may be calculated from the steady-state general dimensionless characteristics presented in Figure 2, reference 3, in terms of the applied a-c voltage and of the steady-state values of signal and bias currents.

It has been found convenient in Figure 1 to express the output $\mathfrak{F}_{Lt}/m$ as a function of t/τ for transients beginning from fictitious initial conditions of infinite d-c component of core magnetization. In any practical instance, of course, the initial conditions of the transient in question will correspond to some finite d-c magnetization to which corresponds also some known finite value of the initial output $\mathfrak{F}_{L0}$. Then, for any such instance, the origin of abscissae needs only to be translated to the right so as to coincide with the abscissa for which, on the proper $\mathfrak{F}_{L\infty}/m$ curve, the output is equal to the given $\mathfrak{F}_{L0}/m$. A justification of this procedure is seen in Appendix I in the fact that the relationship between $\mathfrak{F}_{Lt}$ and t results from the integration of a differential equation which is nonlinear but is still of the first order. Thus the time required during the transient to reach any output $\mathfrak{F}_{Lt}$ from a known initial $\mathfrak{F}_{L0}$ can be evaluated as the time required to reach $\mathfrak{F}_{Lt}$ from an assumed state of infinite d-c magnetization minus the time required to reach $\mathfrak{F}_{L0}$ from the same assumed state of infinite d-c magnetization.

Figure 1. Transient response of magnetic amplifiers without feedback

$$\mathfrak{F}_L = \frac{1}{U}\frac{NI_L}{l} \qquad \tau = \frac{A}{lUun}\sum_{\nu}\frac{N^2_\nu}{R_\nu}$$

For the same reason, it is seen that the use of the curves of Figure 1 is not necessarily limited to the study of transients beginning from a condition of initial steady state. The value of average output current existing at the instant of application of the step signal is sufficient to define the time origin on the graph, regardless of whether this current happened to be constant or rather building up or decaying in other preceding and not yet died-out transients of the same nature. Hence, transients caused by gradual changes of the signal voltage can also be studied under approximate substitution of the given signal with a succession of short step signals of convenient magnitude.

Moreover, transients caused by sudden variations of the resistance of the control circuit are also represented by the curves of Figure 1 on the basis of the values of $\mathfrak{F}_{L0}$ existing before the variation and of $\mathfrak{F}_{L\infty}$ and τ corresponding to the new signal circuit conditions.

The curves given in Figure 1 are of two kinds. Some curves show a continuous decay, that is, $\mathfrak{F}_{Lt}/m$ reaches $\mathfrak{F}_{L\infty}/m$ from the initial value with a constantly negative slope. These curves apply for build-down transients in which the application of the step signal causes a decay but not a reversal of the d-c component of flux density.

Other curves show a decay of $\mathfrak{F}_{Lt}/m$ and a subsequent rise. These curves apply for transients in which the d-c component of flux density decays from its initial value, reaches zero, and builds up again towards its steady state with reversed polarity. These same curves, used in the portion of increasing $\mathfrak{F}_{Lt}/m$, apply also for rising transients, that is, for transients characterized by a continuous increase of the absolute value of d-c component of flux density. (In particular, when the time origin is set at the point of minimum $\mathfrak{F}_{Lt}/m$, these curves yield the same information obtained in reference 1, which was limited to the analysis of rising transients from initial conditions of zero value of initial d-c component of flux density.)

Influence of Loads

The analysis developed is based on the assumption that the alternating component of flux density in the cores varies sinusoidally with constant amplitude throughout. With a-c line voltage constant, the assumption is acceptable when voltage drops in load and output winding resistances are small. Thus, the curves of Figure 1 describe rather well transients, or portions of a transient, in which the output currents are low, as is the case when the d-c component of flux density

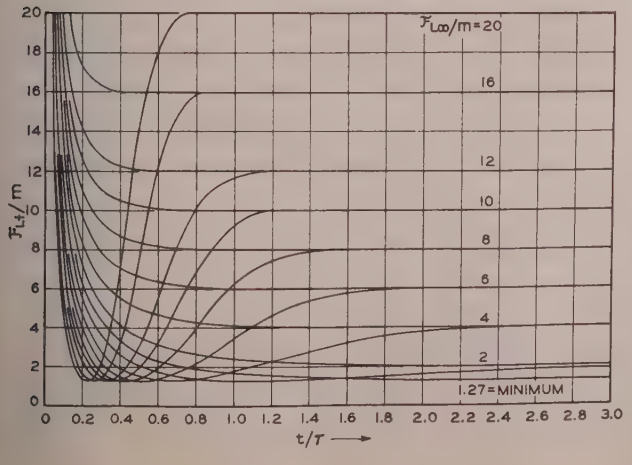

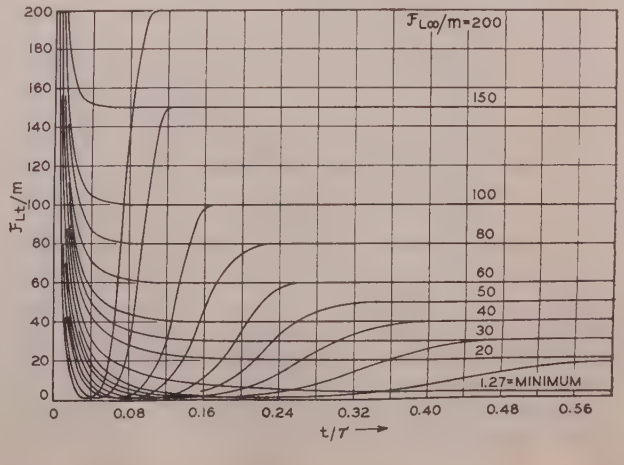

B_{0t} is varying through or around zero. This result of the analysis is already of appreciable practical interest, as it is during these conditions that the amplifier shows a most sluggish response and severe "time lapses" are observed.[4]

A direct extension of the transient analysis presented to conditions of considerable voltage drops in the load is not possible, as the differential equations of the amplifier circuits defy integration rigorously or by any simple numerical procedure. Indeed this difficulty has been recognized already for analyses of steady-state performance and in such cases one resorts to the well-known expediency of using approximate load lines (load ellipses, and so forth) in conjunction with amplifier characteristics that have been measured or calculated under conditions of short-circuited load. Similar procedures can be suggested for the use of the curves of transient response of Figure 1 in actual situations in which loads are present.

Since, for a given a-c supply voltage, $\mathfrak{B}_m$ varies with varying output currents during the transient in a way which is predictable by means of the steady-state load lines, the complete transient conceivably may be subdivided into a number of portions for which different values of an approximately constant $\mathfrak{B}_m$ can be assumed.

A considerably simpler procedure may be adequate providing the variations of $\mathfrak{B}_m$ during the transient are not too extreme. For this, m and τ are evaluated on the basis of the highest value of $\mathfrak{B}_m$ during the transient (which occurs at the lowest $\mathfrak{F}_{Lt}$ and $\mathfrak{B}_{0t}$). The initial and the steady-state value of output currents are known for the given transient and, hence, $\mathfrak{F}_{L0}/m$ and $\mathfrak{F}_{L\infty}/m$ are calculated. The transient in question is represented then fairly well by the curve of Figure 1 defined by such $\mathfrak{F}_{L\infty}/m$, with time origin at $\mathfrak{F}_{L0}/m$. (In this way the given transient with load is approximated by a no-load transient with the same initial and final output currents and with somewhat modified initial and steady-state values of signal.)

A close examination of the influence of $\mathfrak{B}_m$ upon the scale factors and the other parameters defining the curves of Figure 1 supports this procedure qualitatively, although, of course, no quantitative justification can be given for it analytically. An extensive number of experimental investigations, some of which are described here, indicate that the expedient suggested gives results well within the range of accuracy obtainable in problems of this nature.

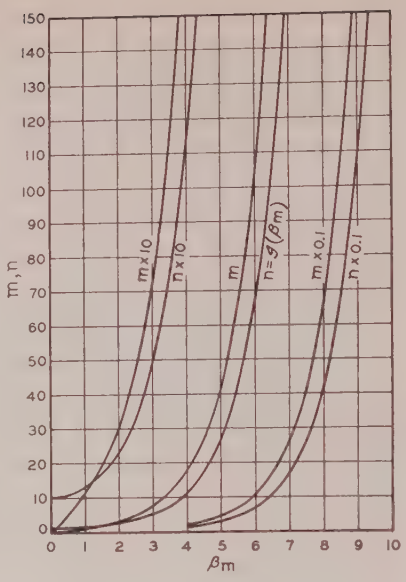

Figure 2. m and n as a function of $\mathfrak{B}_m$

Examples and Experimental Checks

The tests described here have been performed on a magnetic amplifier with the following specifications:

Core material: Hypernik, core cross section $A = 4.2 \cdot 10^{-4}$ square meter, mean length of magnetic path $l = 0.181$ meter, constants of the hyperbolic sine fit $U = 12.7$ ampere turns per meter, $u = 4.6$ square meters per weber.

Signal circuit $N_1 = 2{,}000$ turns per core, total signal circuit resistance $2R_1 = 235$ ohms (in most tests).

Output circuit $N_2 = 2{,}000$ turns per core, resistance per core winding $R_2 = 85$ ohms, output windings connected in series.

Frequency of supply voltage, 60 cycles.

The transient was caused in all cases by a sudden variation of the signal voltage obtained from potentiometric arrangements. The output current was recorded on a calibrated oscilloscope, whose beam initiated its sweep a couple of cycles before the transient, so as to record also the initial pretransient conditions. The time origin of the transient was marked by a pip of increased beam intensity, which is discernible in the oscillograms shown in (A), (B), and (C) of Figure 3.

Since the analysis developed applies to rectified average outputs, while the oscillograms are most easily scanned in terms of peaks of output current, ammeters measuring both quantities were inserted in the output circuit. In this way, ratios between peaks and averages were easily obtained in steady-state measurements over the range of outputs covered in the transient. (Actually, for materials whose magnetization curve can be approximated by a hyperbolic sine, the ratio between peaks and rectified averages is theoretically constant for constant $\mathfrak{B}_m$ and, in fact, good experimental agreements (with errors of no more than 10 per cent) have been found with the upper curve of Figure 12, reference 3, which represents ratios between peak and average outputs as a function of $\mathfrak{B}_m$ only. This, however, no longer applies when loads are present in the output circuits, and in such cases a scaling down from peaks to average values on the basis of steady-state measured ratios is needed.)

Figures 3(a) to 3(f) present some comparison between theoretical transients shown in full lines and experimental values resulting from a reduction of peaks to average values as described previously. These few figures give typical results, chosen from a large variety of tests performed during the preparation of the paper. Some of the tests presented actually are particularly severe as they cover a broad range of outputs with transitions through zero d-c component of flux density.

In Figure 3(a), initial output current $I_{L0} = 85$ milliamperes (ma), steady-state final current $I_{L\infty} = 85$ ma. Crest of the voltage produced by the alternating component of flux density in the $2N_2$ turns $E_m = 387.5$ volts (from rms measurements of voltages induced at the lowest value of output current that occurs during the transient). The corresponding dimensionless quantities $\mathfrak{F}_{L0}$, $\mathfrak{F}_{L\infty}$, and $\mathfrak{B}_m$, calculated per equations 1 and 3, are marked in the figure. Moreover, $\tau = 0.275$ second, and the origin of the abscissae for the theoretical curve of Figure 1 was translated to the point $t_0/\tau = 0.046$. No-load tests, as well as tests with various loads (all with the same I_{L0}, $I_{L\infty}$, and E_m at lowest output) are presented. (Oscillogram A was obtained in this test for the no-load transient.)

In Figure 3(b), I_{L0}, $I_{L\infty}$, and E_m are the same as in Figure 3(a). The transient was speeded up by an increase of 200 ohms in the signal circuit, so as to obtain $\tau = 0.1485$ second. (Oscillogram B was obtained in this test.)

In Figure 3(c), $I_{L0} = 88$ ma, $I_{L\infty} = 5.3$ ma, $E_m = 387.5$ volts (at minimum output). (Oscillogram C was obtained in this test.)

In Figure 3(d), $I_{L0} = 94$ ma, $I_{L\infty} = 94$ ma, $E_m = 225$ volts, $\tau = 0.592$ second, $t_0/\tau = 0.017$.

In Figure 3(e), $I_{L0} = 77$ ma, $I_{L\infty} = 77$ ma, $E_m = 550$ volts, $\tau = 0.120$ second, $t_0/\tau = 0.115$.

In Figure 3(f), $I_{L0} = 94$ ma, $I_{L\infty} = 2.22$ ma, $E_m = 225$ volts, $\tau = 0.592$ second, $t/\tau = 0.024$.

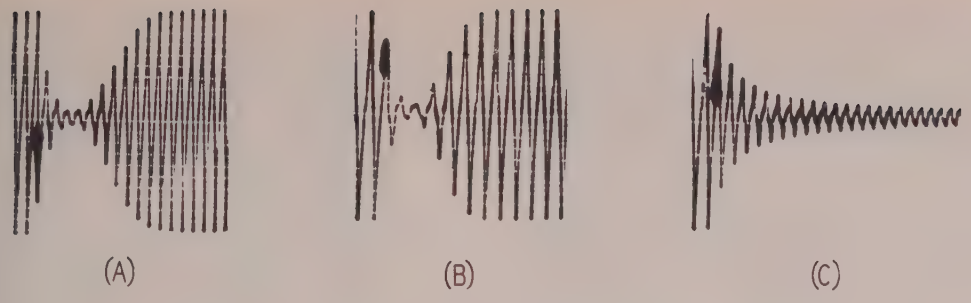

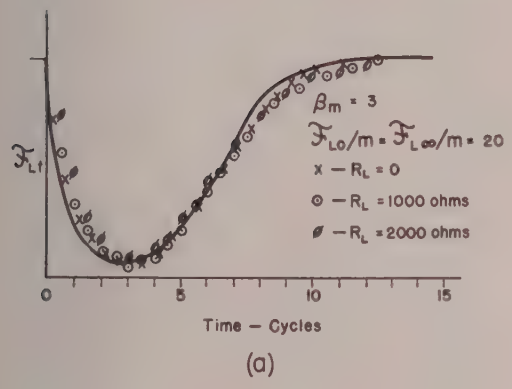

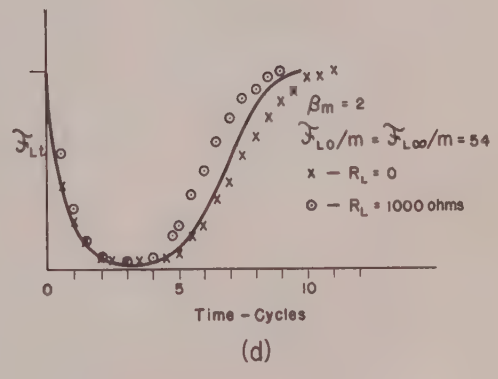

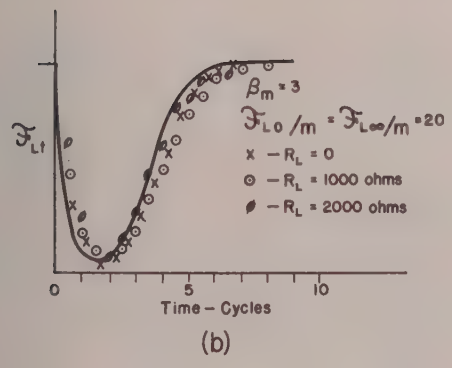

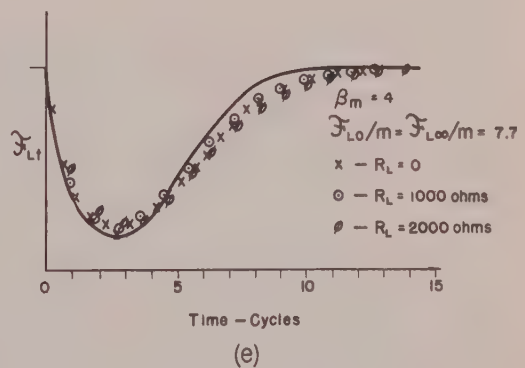

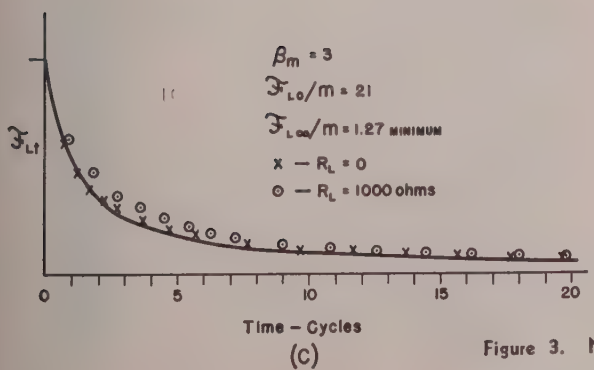

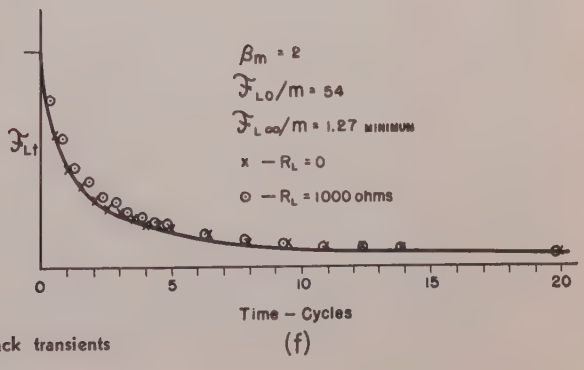

Figure 3. Nonfeedback transients

The Transient Response of Magnetic Amplifiers with Feedback Cases of Negligible Commutation

The presence of feedback circuits (as shown, for example, in Figures 1(C) and 1(D) of reference 3) modified the analysis because the direct component of flux density B_{0t}, which determines the output at any time as per equation 18, Appendix I, depends then not only upon signal and bias currents but also upon the feedback currents.

The direct component of feedback currents may be obtained during the "slow" transient using steady-state relations on the basis of the value of B_{0t}, that exists at any time, but it must be recognized that additional currents of a different kind

(which are not present in any true steady-state operation) also are caused to circulate in feedback turns by voltages that are induced in the feedback windings by the time variations of B_{0t} during the transient. These induced currents may delay the duration of the transient significantly if simultaneous conduction of the feedback rectifiers occurs over large portions of each cycle; in fact, during commutation periods, an easy path is offered directly through the feedback windings on both cores and through the simultaneously conducting rectifiers. On the other hand, when commutation does not occur, or is practically limited to small portions of each cycle only, it can be shown that the over-all response of the amplifier is not affected noticeably. (A justification of this statement is given in Appendix III.)

An extension of the previous transient analysis to amplifiers with feedback circuit is comparatively simple if commutation phenomena are negligible throughout. In such cases, according to the statement in the preceding paragraph, the induced currents mentioned can be neglected. A further simplification is given also by the fact that direct components of feedback currents are equal (or easily related) to rectified averages of output currents, when commutation is negligible. A transient analysis valid for conditions of negligible commutation is given in Appendix II, in which expressions are obtained for the rectified average of output current as a function of time in terms of the crest of alternating flux density and of the initial and steady-state final output current.

On the basis of equations 25 and 28, sets of dimensionless curves can be calculated that apply for a given ratio of feedback turns to output turns and for a chosen value of the dimensionless crest of alternating flux density $\mathfrak{B}_m$. Families of curves of this type are presented in Figures 4(a) and 4 (b) for $\mathfrak{B}_m=2$, and in Figures 4(c) and 4(d) for $\mathfrak{B}_m=4$ for the practically most interesting case of self-feedback (Figure 1(D), reference 3). The same curves apply also for external feedback circuits (Figure 1(C), reference 3) for which the number of feedback turns per core equals the number of turns per core of the output winding.

The symbols used are the same as before (that is, $\mathfrak{F}_{Lt}$ and $\mathfrak{F}_{L\infty}$ are dimensionless rectified average outputs as defined by equation 1 at the time t and in final steady state, respectively; τ is defined by equation 4, although the abscissae are now $t/n\tau$). As in Figure 1, the time origin is established in the curves under assumption of transients starting from initial conditions of infinite d-c magnetization; again the origin of the abscissae shall be translated to the right so as to coincide with the abscissa for which, on the proper $\mathfrak{F}_{L\infty}$ curve, the output is equal to initial $\mathfrak{F}_{L0}$ of the transient considered.

Two additional remarks appear indispensable for the interpretation of the results presented:

(1) Steady-state outputs of magnetic amplifiers without feedback depend only on the absolute value of the resultant magnetomotive forces of signal and bias currents. Sign conventions can be established for one of these currents quite arbitrarily, and the signs to be used for the other currents or magnetomotive forces result rather obviously for any specific situation. Transients in magnetic amplifiers without feedback are defined, in the curves presented in Figure 1, simply by the initial and steady-state final output, with the further information of whether or not the total magnetomotive force of signal and bias remains of the same polarity (no matter whether called positive or negative) throughout the transition from initial to steady-state final conditions; accordingly, two different curves are drawn for each value of $\mathfrak{F}_{L\infty}/m$ in Figure 1 for these two possible situations, and the choice of the appropriate one of the two should present no difficulties.

When magnetomotive forces of feedback are also present, more explicit sign conventions are needed. Since feedback currents can flow only in the direction dictated by the feedback rectifiers, it appears convenient in the following to establish that the magnetomotive force of feedback is inherently positive and to give signs to all other magnetomotive forces accordingly. When in steady state or at any time during a transient the total d-c component of magnetomotive force, obtained by algebraic summation of magnetomotive force of signal, bias, and feedback currents, is positive, positive feedback operation takes place (and, by equation 15, B_{0t} is also positive). This is the case when the magnetomotive force of signal and bias is positive or also negative, but not large enough to overcome the magnetomotive force of feedback. On the other hand, negative feedback operation occurs when the magnetomotive force of signal and bias is negative and large enough to overcome the magnetomotive force of feedback in the algebraic summation (B_{0t} is then negative). The transition between the two types of operation occurs when the d-c components of magnetomotive forces of signal, bias, and feedback cancel. In these conditions, the d-c component of flux density B_{0t} is zero and the output current is minimum by equation 18.

Figures 4(a) and 4(c) apply for transients in which B_{0t} increases algebraically from the initial condition towards the steady state. (On these curves the origin of the time scale corresponds to a fictitious condition of infinite negative d-c magnetization.) On the other hand, Figures 4(b) and 4(d) apply for transients in which B_{t0} decreases algebraically from the initial condition towards the steady state. (On these curves the origin of the time scale corresponds to a fictitious condition of infinite positive d-c magnetization.) Conspicuously different time responses result for the different cases.

(2) The curves presented in Figure 4 have been obtained under the assumption of negligible commutation throughout and therefore, strictly speaking, should be used only when this assumption is justified. One may check whether this is the case for any specific transient extending the considerations given for the commutation phenomena in steady state in reference 3 to the "slow" transient. (In fact, it has been pointed out by others (discussion of reference 2) that the voltages induced in the feedback windings by the time variations of B_{0t} during the transient are not likely to upset noticeably the rhythm of conduction and non-conduction of the single feedback rectifiers.)

Figures 5 or 10 and 11 of reference 3 indicate, for instance, that very short commutation periods may be expected in positive feedback operation for values of the output somewhat larger than minimum. Accordingly, the curves presented in Figure 4 are traced with full lines in portions for which the assumption seems to be valid. On the other hand, the dotted portions represent conditions in which commutation is likely to be considerable. (The information conveyed by the dotted portion may be of some use with the introduction of convenient correction factors, as will be shown in a subsequent paper dealing more specifically with transients under conditions of considerable commutation.)

Examples and Experimental Checks

The tests presented now were obtained using the same reactors described, with the output windings connected for self-feedback operation and a-c output, by use of rectifiers with an approximate forward resistance $R_r=50$ ohms. The tests were made at 60 cycles and in regions of positive feedback, for which assumptions

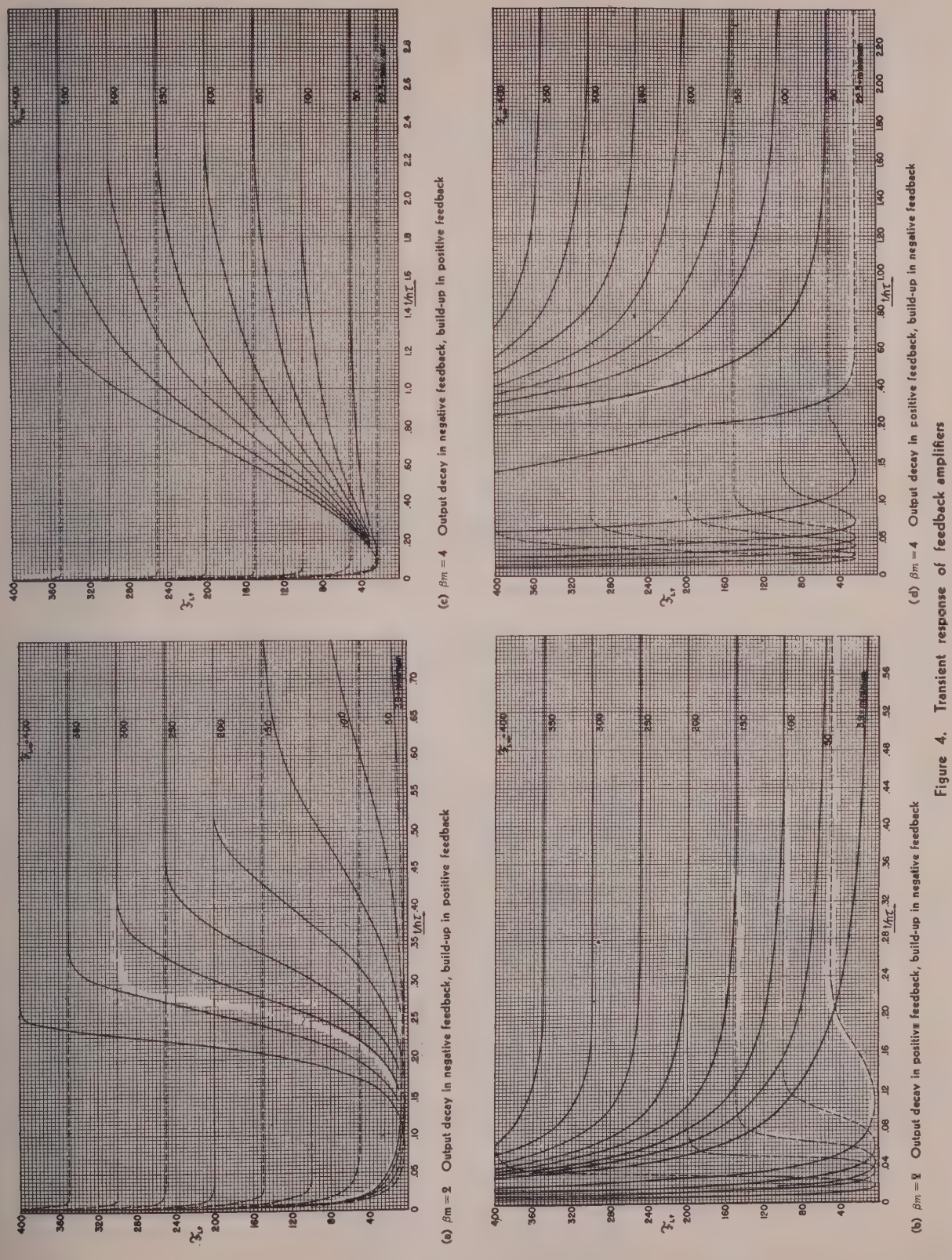
(a) βm = 2 Output decay in negative feedback, build-up in positive feedback
(b) βm = 2 Output decay in positive feedback, build-up in negative feedback
(c) βm = 4 Output decay in negative feedback, build-up in positive feedback
(d) βm = 4 Output decay in positive feedback, build-up in negative feedback

Figure 4. Transient response of feedback amplifiers

of negligible commutation are valid. Comparisons of theoretical transients, (full lines), and experimental values are shown in Figures 5(a), (b), and (c).

In Figure 5(a), initial output current $I_{L0}=42$ milliamperes (ma), steady-state final current $I_{L\infty}=173$ ma. Crest of induced a-c voltage $E_m=225$ volts at minimum (initial) output. Total signal circuit resistance $2R_1=1{,}250$ ohms, $n\tau=0.254$ second, origin of abscissae translated to $t_0/n\tau=0.248$.

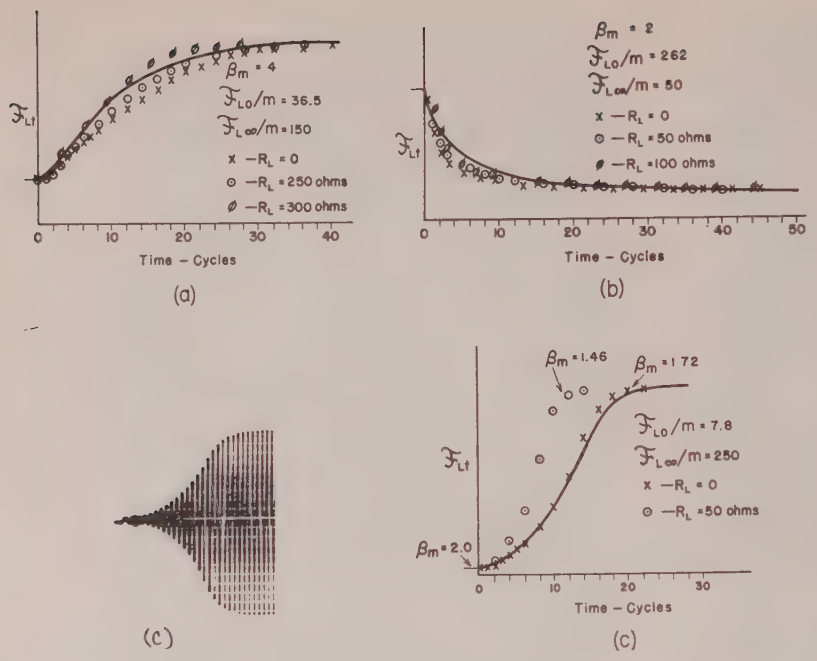

Figure 5. Self-feedback transients

In Figure 5(b), $I_{L0}=300$ ma, $I_{L\infty}=57.5$ ma, $E_m=112.5$ volts at minimum (final) output. Total signal circuit resistance $2R_1=235$ ohms, $n\tau=1.35$ second, $t_0/n\tau=0.048$.

In Figure 5(c), $I_{L0}=9$ ma, $I_{L\infty}=288$ ma, $E_m=112.5$ volts at minimum (initial) output. Total signal circuit resistance $2R_1=235$ ohms, $n\tau=1.35$ second, $t_0/n\tau=0.175$. (Oscillogram of Figure 5(c) was obtained for these conditions at no-load.)

It is seen that, in the presence of loads (R_L's), the transient can be calculated in many cases from the zero load curves of Figure 4 in terms of initial and final outputs and of the value of $\mathcal{B}_m$ that corresponds to the minimum output current. This procedure of expediency, however, has a narrower range of validity than in the case of nonfeedback circuits (as should well be expected). Reasonable accuracy results in Figures 5(a) and 5(b), in which $\mathcal{B}_m$, by varying output current, varied less than 20 per cent from the value at minimum output. On the other hand, considerable departures from the theoretical response were observed in general for load conditions causing larger variations of $\mathcal{B}_m$, the theoretical response resulting is slower than measured in build-up transients and faster in build-down transients. Figure 5(c) indicates results of this kind.

Appendix I. Transient Analysis of Amplifiers Without Feedback

For the magnetic amplifier without feedback and series connected power windings, the following differential equations can be written

$$E_1 = 2R_1 i_1 + N_1 A \frac{d}{dt}(B_\alpha + B_\beta)$$

for the signal circuit (5)

$$E_b = 2R_b i_b + N_b A \frac{d}{dt}(B_\alpha + B_\beta)$$

for the bias circuit (6)

With self-explanatory subscripts and indexes E's are d-c signal or bias voltages, i's are instantaneous values of currents, $2R$'s are total circuit resistances, N's are here number of turns per core. A is the core cross section and B_α and B_β are total instantaneous values of flux densities in the cores α and β at the time t.

For the case of parallel-connected output windings, the additional equation is written for the loop formed by these two windings

$$0 = R_2(i_2 - i_3) + N_2 A \frac{d}{dt}(B_\alpha + B_\beta) \quad (7)$$

where the direction of i_2 is chosen positive when giving magnetomotive force concordant with $N_1 i_1$ and $i_2 + i_3 = i_L$ (current through the load) (see reference 1).

From the assumptions underlying this type of analysis

$$B_\alpha = B_m \sin \omega t + B_{0t}$$
$$B_\beta = -B_m \sin \omega t + B_{0t} \quad (8)$$

That is, an alternating component of flux density, required by the alternating voltage impressed at the amplifier output terminals, is superposed on a direct component B_{0t} which varies gradually in time during the transient considered.

Substituting equation 7 in equations 5 and 6, and considering only the direct components, one obtains

$$E_1 = 2R_1 I_{1t} + 2N_1 A \frac{dB_{0t}}{dt} = 2R_1 I_{1\infty} \quad (9)$$

$$E_b = 2R_b I_{bt} + 2N_b A \frac{dB_{0t}}{dt} = 2R_b I_{b\infty} \quad (10)$$

and also

$$0 = 2R_2(I_{2t} - I_{3t}) + 2N_2 A \frac{dB_{0t}}{dt} \quad (11)$$

for the amplifier with parallel connected output windings. I_{1t} and I_{bt} are instantaneous values of the direct components of currents in the signal and bias circuits, while $I_{1\infty}$ and $I_{b\infty}$, and so forth, are their steady-state values at the end of the transient. (Likewise, I_{2t} and I_{3t} are the instantaneous values of direct components of currents in the output windings. Since no direct component of current flows through the a-c source of the parallel-connected amplifier, $I_{2t} = -I_{3t}$ and moreover $I_2 = -I_3 = 0$ in the final steady-state.) A direct component of magnetomotive force is thus defined as

$$lH_{0t} = N_1 I_{1t} + N_b I_{bt} \quad (12)$$

for the series connected amplifier, or

$$lH_{0t} = N_1 I_{1t} + N_b I_{bt} + N_2 I_{2t} \quad (13)$$

for the parallel connected amplifier. Simultaneous solution of equations 9, 10, and 11 and use of equations 12 or 13 yields

$$t = \sum_\nu \frac{N_\nu^2}{R_\nu} A \int_{B_{0t}}^{B_{0t}} \frac{dB_{0t}}{N_1 I_{1\infty} + N_b I_{b\infty} - lH_{0t}} \quad (14)$$

the summation being extended to the windings considered in equations 9 and 10, and also 11 for the parallel-connected amplifier.

The steady-state relationship of equation 17, reference 3, between direct components of magnetomotive force and of flux density extended here to the "slow" transient is

$$lH_{0t} = lU\mathcal{J}_0(uB_m) \sinh (uB_{0t}) \quad (15)$$

Under assumption of an alternating component of flux density B_m constant throughout the transient, and with the further introduction of dimensionless flux densities of the general form $\mathcal{B} = uB$, equation 14 transforms into

$$t = \tau \int_{\mathcal{B}_{0\infty}}^{\mathcal{B}_{0t}} \frac{d\mathcal{B}_{0t}}{\sinh \mathcal{B}_{0\infty} - \sinh \mathcal{B}_{0t}} \quad (16)$$

where τ is a constant time scale factor, defined in equation 4, and $\mathcal{B}_{00}$, $\mathcal{B}_{0\infty}$, and $\mathcal{B}_{0t}$ are the values of the dimensionless d-c component of flux density initially, in final steady state, and at any generic time t during the transient.

The integration in equation 16 can be performed with this result which is a generalization of equation 12 of reference 1.

$$t = \operatorname{sech} \mathcal{B}_{00} \tanh^{-1} \times$$

$$\frac{\tanh \dfrac{\mathcal{B}_{0t}}{2} - \tanh \dfrac{\mathcal{B}_{00}}{2}}{\left(\tanh \mathcal{B}_{0\infty} - \tanh \mathcal{B}_{0\infty} \tanh \dfrac{\mathcal{B}_\infty}{2} \tanh \dfrac{\mathcal{B}_{0t}}{2} - \operatorname{sech} \mathcal{B}_{0\infty} \left(\tanh \dfrac{\mathcal{B}_{0t}}{2} - \tanh \dfrac{\mathcal{B}_{00}}{2} \right) \right)} \quad (17)$$

Finally, the rectified average value of output current through the load or its corresponding dimensionless quantity $\mathfrak{F}_{Lt}$ defined in equation 1 can be obtained now in terms of $\mathfrak{B}_{0t}$ from the relationship

$$\mathfrak{F}_{Lt}=\frac{4}{\pi}m\cosh\mathfrak{B}_{0t} \tag{18}$$

derived in reference 3 for steady state and extended hereby to any instant of the "slow" transient. To avoid further need for numerical evaluations of equation 17, a number of calculations have been performed during the development of the work covered in this paper. As mentioned in the body of the paper, it has been found particularly convenient to limit the calculations to transients having infinity as initial value of d-c component of flux density as equation 17 simplifies then to

$$\frac{t}{\tau}=2\operatorname{sech}\mathfrak{B}_{0\infty}\tanh^{-1}\frac{\cosh\mathfrak{B}_{0\infty}}{\operatorname{Sinh}\mathfrak{B}_{0\infty}+e^{-\mathfrak{B}_{0t}}} \tag{19}$$

The results of these calculations are presented in the dimensionless curves of Figure 1. The introduction of the concept of an initial infinite core magnetization does not constitute any limitation to the use of these curves for actual transients that actually will be initiated only from finite values of d-c component of flux density. Since

$$\int_{\mathfrak{B}_{00}}^{\mathfrak{B}_{0t}}f(_0\mathfrak{B}_t)d\mathfrak{B}_{0t}=\int_{-\infty}^{\mathfrak{B}_{0t}}f(\mathfrak{B}_{0t})d\mathfrak{B}_{0t}-\int_{-\infty}^{\mathfrak{B}_{00}}f(\mathfrak{B}_{0t})d\mathfrak{B}_{0t}$$

it is seen that only a translation of the origin of the abscissae of the general curves of Figure 1 is required to make them suitable for describing the variation of $\mathfrak{F}_{Lt}$ with time in transients starting from any assigned finite $\mathfrak{B}_{00}$.

Appendix II. Transient Analysis of Feedback Amplifiers

Magnetic Amplifier with Series-Connected Power Windings and External Feedback

The analysis is initiated as in Appendix I by writing the differential equations 5 and 6 of signal and bias circuits and transforming them into equations 9 and 10. The following expression results, however, now for the total direct component of magnetomotive force

$$lH_{0t}=\sum\nolimits_{\nu}N_{\nu}I_{\nu}+N_fI_{ft} \tag{20}$$

where N_f is the number of turns per core of the feedback winding and I_{ft} is the direct component of feedback current at the instant considered and the summation is extended algebraically to signal and bias with signs consistent with the convention established in the body of the paper (that is, magnetomotive forces of feedback are inherently positive).

Simultaneous solution of equations 9 and 10 and use of equation 20 yields

$$t=\sum_{\nu}\frac{N_{\nu}^2}{R_{\nu}}A\int_{B_{00}}^{B_{0t}}\frac{dB_{0t}}{\Sigma_{\nu}N_{\nu}I_{\nu\infty}-(lH_{0t}-N_fI_{ft})} \tag{21}$$

On the other hand, using for the slow transient the steady-state relation, equation 22 of reference 3, for negligible commutation (that is, $\sigma=0$)

$$N_fI_{ft}=\frac{2}{\pi}m\frac{N_f}{N_2}lU\cosh uB_{0t} \tag{22}$$

while again equation 15 applies. Substituting equation 22 into 21 and introducing the general dimensionless notations $\mathfrak{B}=uB$ and also $\mathfrak{F}_c=(1/lU)\Sigma_{\nu}N_{\nu}I_{\nu}$ for the magnetomotive force of "control" (resultant of signal and bias, consistently with the terminology used in reference 3), equation 21 transforms into

$$t=n\tau\int_{\mathfrak{B}_{00}}^{\mathfrak{B}_{0t}}\frac{\mathfrak{B}_{0t}}{\mathfrak{F}_{c\infty}+\frac{2}{\pi}m\frac{N_f}{N_2}\cosh\mathfrak{B}_{0t}-n\sinh\mathfrak{B}_{0t}} \tag{23}$$

where τ is the same as defined in equation 4 and therefore $n\tau=(A/Uul)\Sigma_{\nu}N_{\nu}^2/R_{\nu}$. Equation 23 can be integrated and yields

$$\frac{t}{n\tau}=\frac{2}{\sqrt{\mathfrak{F}_{c\infty}^2-\left(\frac{2}{\pi}m\frac{N_f}{N_2}\right)^2+n^2}}\tanh^{-1}\times\frac{\sqrt{\mathfrak{F}_{c\infty}^2-\left(\frac{2}{\pi}m\frac{N_f}{N_2}\right)^2+n^2}-\left(\tanh\frac{\mathfrak{B}_{0t}}{2}-\tanh\frac{\mathfrak{B}_{00}}{2}\right)}{\left(\mathfrak{F}_{c\infty}+\frac{2}{\pi}m\frac{N_f}{N_2}-\left(\mathfrak{F}_{c\infty}-\frac{2}{\pi}m\frac{N_f}{N_2}\right)\left(\tanh\frac{\mathfrak{B}_{0t}}{2}\tanh\frac{\mathfrak{B}_{00}}{2}\right)-n\left(\tanh\frac{\mathfrak{B}_{0t}}{2}+\tanh\frac{\mathfrak{B}_{00}}{2}\right)\right)} \tag{24}$$

Again a considerable and certainly needed simplification may be introduced if the integral is evaluated from assumed initial conditions of infinite d-c magnetization. Actually for transients leading towards algebraically higher values of B_{0t} an initial condition of $\mathfrak{B}_0=-\infty$ must be taken; while for transients leading towards algebraically smaller B_{0t} an initial condition $\mathfrak{B}_0=+\infty$ must be taken. The first kind of transients are decays of output in negative feedback operation as well as build-ups of output in positive feedback operation; conversely, decays of output in positive feedback operation as well as build-ups of output in negative feedback operation constitute the second kind of transients. The use of a lower limit of integration $=\pm\infty$ yields more simply

$$\frac{t}{n\tau}=\frac{2}{\sqrt{\mathfrak{F}_{c\infty}^2\left(\frac{2}{\pi}m\frac{N_f}{N_2}\right)^2+n^2}}\times\tanh^{-1}\frac{\pm\sqrt{\mathfrak{F}_{c\infty}^2-\left(\frac{2}{\pi}m\frac{N_f}{N_2}\right)^2+n^2}}{\mathfrak{F}_{c\infty}+\left(\frac{2}{\pi}m\frac{N_f}{N_2}\pm n\right)e^{\mp\mathfrak{B}_{0t}}} \tag{25}$$

where the upper signs apply for the first kind of transients while the lower signs apply to the second kind.

For $t=\infty$,

$$\frac{\pm\sqrt{\mathfrak{F}_{c\infty}^2-\left(\frac{2}{\pi}m\frac{N_f}{N_2}\right)^2+n^2}}{\mathfrak{F}_{c\infty}+\left(\frac{2}{\pi}m\frac{N_f}{N_2}\pm n\right)e^{\mp\mathfrak{B}_{0\infty}}}=1 \tag{26}$$

whence the following relation between $\mathfrak{F}_{c\infty}$ and $\mathfrak{B}_{0\infty}$ is found:

$$\mathfrak{F}_{c\infty}=n\sinh\mathfrak{B}_{0\infty}-(2/\pi)m(N_f/N_2)\cosh\mathfrak{B}_{0\infty} \tag{27}$$

On the other hand

$$F_{L\infty}=(4/\pi)m\cosh\mathfrak{B}_{0\infty} \tag{18}$$

and therefore

$$\mathfrak{F}_{c\infty}=(\pm)n\sqrt{\left(\frac{\pi}{4}\frac{\mathfrak{F}_{L\infty}}{m}\right)^2-1}-\frac{N_f}{N_2}\frac{\mathfrak{F}_{L\infty}}{2} \tag{28}$$

The upper or lower sign ($\pm$) applies here depending on whether the final steady-state operation is in the region of positive or negative feedback condition. (In particular minimum steady-state output—which is the point of transition between positive and negative feedback operation—is obtained for

$$\mathfrak{F}_{c\infty}=-\frac{N_f}{N_2}\frac{\mathfrak{F}_{L\infty}}{2}=-\frac{2}{\pi}m\frac{N_f}{N_2}$$

as should be expected.) Using equations 28 and 27 in equation 25, it is finally possible to express by calculations in tabular form the wanted $\mathfrak{F}_{Lt}$ as a function of t in terms of $\mathfrak{F}_{L\infty}$ and $\mathfrak{B}_m$ (which defines the values of m and n). The curves presented in Figure 4 have been evaluated in such a manner. Again, for practical situations in which the transient actually begins from initial conditions of finite d-c magnetization, a simple translation of the time scale origin to the right is needed, so as to coincide with the abscissa for which, on the proper $\mathfrak{F}_{L\infty}$ curve the output coincides with the initial known value $\mathfrak{F}_{L0}$.

The case of the magnetic amplifier with external feedback and parallel-connected power windings could be treated in a quite similar way. This type of connection, however, has limited practical interest when speed of response is important.

Magnetic Amplifier with Self-Feedback

For this amplifier, represented in Figure 1(D) of reference 3, again equations 20 and 21 apply, and equations 23 and 24 are obtained, with t given by equation 4 (with the summation extended to signal and bias circuits only). As the feedback winding on each core actually coincides with the power winding, here $N_f=N_2$.

Appendix III

It has been pointed out in the body of the paper that the d-c component of flux density B_{0t}, varying during the transient, induces noncancelling voltages not only in signal and bias windings but also in feedback windings. Hence, induced currents may flow in such windings and through paths

variously offered in the various types of feedback circuits considered. It has been stated also that delaying effects due to induced currents of this kind can be ignored for transients occurring over ranges of operation of negligible commutation. A justification of this statement is given in the following.

Considering first the case of a self-feedback amplifier, it is seen that currents induced by the time varying B_{0t} in absence of commutation can flow through generator, load, and through the $N_f = N_2$ turns on one core only (core α or β), at the time, depending on which one of the two feedback rectifiers is conducting at the instant considered. Thus, for instance, in the extreme limiting case of negligible resistance for the path of this current, the d-c component of flux density in one core will be prevented from varying during the half-cycle in which the corresponding rectifier is conducting. At the same time, however, the d-c component of flux density in the other core will be forced by the impressed signal voltage to vary twice as fast, as seen in equation 5. In the subsequent half-cycle, the two cores interchange their behavior and so, in a "slow" transient, the net results of such induced feedback currents are cancelled.

A similar situation takes place also in the amplifier with external feedback. Here the induced current flows in both feedback windings in series at all times, but reverses periodically in its further path through the load, generator, and power windings, due to the alternate switching action of the two pairs of feedback rectifiers. Thus, again alternatively in subsequent half-cycles, the d-c component of flux density in one core will be delayed and speeded up in its variation with net over-all results which coincide practically with those of the simplified analysis given. A more accurate study of these phenomena can be given, of course, considering separately the d-c components of flux density in the two cores $B_{\alpha 0t}$ and $B_{\beta 0t}$ and rewriting more properly equations 9 and 10 in the forms

$$E_1 = 2R_1 \cdot I_1 t + N_1 A \frac{d}{dt}(B_{\alpha 0t} + B_{\beta 0t})$$

$$E_b = 2R_b \cdot I_{bt} + N_b A \frac{d}{dt}(B_{\alpha 0t} + B_{\beta 0t})$$

In agreement with the preceding summary reasoning, it is found then that the results of such a more laborious analysis actually coincide with those of the simplified analysis given over any integral number of cycles.

References

1. An Analysis of Transients in Magnetic Amplifiers, **D. W. VerPlanck, L. A. Finzi, D. C. Beaumariage.** *AIEE Transactions*, volume 69, part I, 1950, pages 498–503.

2. An Analysis of Transients and Feedback in Magnetic Amplifiers, **Walter C. Johnson, Frank W. Latson.** *AIEE Transactions*, volume 69, part I, 1950, pages 604–11.

3. General Characteristics of Magnetic Amplifiers, **L. A. Finzi, D. C. Beaumariage.** *AIEE Transactions*, volume 69, part II, 1950, pages 919–27.

4. Response Time of Magnetic Amplifiers, **E. L. Harder, W. F. Horton.** *AIEE Transactions*, volume 69, part II, 1950, pages 1130–41.

Discussion

Ulrik Krabbe (Thomas B. Thrige, Odense, Denmark): It is interesting to see the accuracy it is possible to obtain with the described method of calculation. However, in many cases it is more important to get a simple calculation, and I should like to point out the very simple relation between steady-state curves and time constants for self-saturated magnetic amplifiers.[1] For a self-saturated magnetic amplifier with the same number of turns in the signal winding and the output winding, we have the simple relation that the time constant is equal to the voltage-gain divided by two times the supply voltage frequency.

By means of this formula it is possible to determine the time constant for each working point by drawing a tangent to the curve which indicates signal d-c voltage to output voltage. If the internal voltage drop is large we need to take this into consideration.

Transient in the output winding may increase the value of the time constant, and this influence depends on the connection used.

By means of the formula mentioned it is easy to calculate transients for magnetic amplifiers without feedback, if we regard the self-saturated one as the fundamental and regard the coupling without self-saturation as a magnetic amplifier with negative feed-back.

Reference

1. The Transductor Amplifier, **Ulrik Krabbe.** Munksgaard, Copenhagen, Denmark, 1949, formula 11, 89.

L. A. Finzi, D. P. Chandler and **D. C. Beaumariage:** Dr. Krabbe refers to formulas expressing "time constants" which are derived on the basis of a linearized relationship between mean flux and control current. Indeed, concepts of this kind may be accepted as a matter of expediency, but their limitations should be clearly specified and understood.

The analysis presented in the paper has a somewhat broader aim as it tries to predict the transient response over wide ranges of swing of the direct component of average flux density, rising, falling, or also reversing. As it should be expected, the response curves are by no means simple time exponentials.

Of course, practical needs for "time constants" concepts may be fulfilled to some extent by approximating portions of the curves presented with exponentials of sort. The limits of accuracy obtainable hereby are clearly seen.

Transient Analysis of Rotating Machines and Stationary Networks by Means of Rotating Reference Frames

Y. H. KU
FELLOW AIEE

Synopsis: This paper analyzes the behavior of a-c rotating machines connected to stationary networks or transmission lines and other rotating machines under synchronous or asynchronous operation. Rotating reference frames are introduced. The forward and backward components are correlated to the direct-axis and quadrature-axis components in a simple manner. Part I deals with the interconnection of a rotating machine and a terminal network or a transmission line with lumped or distributed constants. Part II deals with the interconnection of rotating machines. A general network of n machines is analyzed. Part III considers a general machine with n_1 stator phases and n_2 rotor phases under synchronous or asynchronous operation. Concatenation of induction machines and selsyns are studied by means of rotating reference frames.

IN a paper presented before the AIEE Summer Convention, June 1932, the author extended his early analysis of a-c machinery[1] to include the effect of external impedances on salient-pole synchronous machines.[2] In the case of external capacitance, self excitation or negative damping was found to exist. It is gratifying to note that in two important papers on series capacitance and negative damping by Butler and Concordia,[3] and Carter,[4] mention was made to this reference. Extension of Park's Two-Reaction Theory[5,6] was made by Crary[7] to include capacitance load and by Concordia[8] to include any balanced terminal impedance. The correlation of the 2-reaction method and the method of symmetrical vector components was attempted by the author since 1930,[2,9,10] and the extension of the 2-reaction theory to multiphase machines was published in his 1937 AIEE paper.[11] A companion paper[12] analyzed the same problem with symmetrical vector components which are identical to the forward and backward components.

After his important treatise on the tensor analysis of rotating electric machinery,[13] Kron started a series of further studies in setting up the basic equations of stationary networks viewed from uniformly rotating reference frames[14] and in classifying the reference frames from a dynamic and geometric point of view.[15] Under this new light, we can see that the d, q system of the 2-reaction method and the f, b system of the symmetrical vector method belong to the same rotating reference frame. In general, other rotating reference frames can be considered.

I. Synchronous Machine with Stationary Networks and Transmission Lines with Lumped or Distributed Constants

In equations 20 and 21 of reference 1, the author introduced symmetrical vector components of instantaneous values and rotating reference frames to the solution of synchronous machines and reduced the problem to equivalent coupled circuits with stationary windings. As pointed out by Professor Gardner, the principle of superposition was used in the solution of a system which contains a parameter which is not a constant. The use of rotating frames was facilitated by Heaviside's "operand shift" principle. As Laplace Transforms are developed and tensor analysis of rotating machines has been well demonstrated, these transformations from the positive and negative sequence components to the forward and backward components are justified. Notice that the instantaneous symmetrical vector components used in equations 20 and 21 are identical to i_f and i_b mentioned in reference 5.

The fundamental equations for a salient-pole machine with external impedances, amortisseur windings, and excitations in both direct and quadrature axes were given in references 2, 9, 10, and 12. Referring the positive and negative sequence vector components of the stator phase current (Appendix I) to a set of rotating reference axes, we have

$$Z_1^0{}_{(p+jn)}\, i_f + (p+jn)L_1'' i_b + (p+jn)I_f = v_f \quad (1)$$

$$Z_1^0{}_{(p-jn)}\, i_b + (p-jn)L_1'' i_f + (p-jn)I_b = v_b \quad (2)$$

where

$$Z_1^0{}_{(p\pm jn)} = (R_1+R_L)+(L_1^0+L_L)(p\pm jn+\frac{1}{C_1(p\pm jn)}$$

R_1 = resistance of stator, per phase
R_L = resistance of external network, per phase
L_1^0 = constant part of stator synchronous inductance, per phase
L_1'' = maximum value of second harmonic variation of stator synchronous inductance, per phase
L_L = inductance of external network, per phase
C_1 = capacitance of external network, per phase
$i_f = i_+ \epsilon^{-jnt}$, $i_b = i_- \epsilon^{jnt}$
$v_f = v_+ \epsilon^{-jnt}$, $v_b = v_- \epsilon^{jnt}$

Paper 51-176, recommended by the AIEE Rotating Machinery Committee and approved by the AIEE Technical Program Committee for presentation at the AIEE Great Lakes District Meeting, Madison, Wis., May 17-19, 1951. Manuscript submitted January 31, 1951; made available for printing March 30, 1951.

Y. H. Ku is Professor of Electrical Engineering (visiting) at the Massachusetts Institute of Technology, Cambridge, Mass.

The author wishes to acknowledge his indebtedness to Professors H. L. Hazen and W. V. Lyon for inspiration and encouragement, to Professors E. W. Boehne and K. L. Wildes for valuable suggestions and criticism, and to Messrs. P. Y. Tang, M. H. Pai, L. C. King, S. M. Lee, and Y. W. Lee for their kind interest in promoting this research. Grateful thanks are also due to Messrs. P. L. Alger and G. Kron for their encouragement in the preparation of this paper.

i_+, i_- = instantaneous values of positive and negative sequence vector components of stator phase currents

v_+, v_- = instantaneous values of positive and negative sequence vector components of stator phase potentials. For $v_a = V_m \sin nt$, we get $v_+ = \frac{V_m}{2j}\epsilon^{jnt}$,

$v_- = \frac{-V_m}{2j}\epsilon^{-jnt}$

$I_f = \frac{1}{2}(I_d + jI_q)$, $I_b = \frac{1}{2}(I_d - jI_q)$

$I_d = \Sigma M_d i_{dr}$, $I_q = \Sigma M_q i_{qr}$

M_d = maximum value of the mutual inductance between one phase of the stator and one direct axis rotor winding

M_q = maximum value of the mutual inductance between one phase of the stator and one quadrature axis rotor winding

i_{dr} = current in one direct axis rotor winding

i_{qr} = current in one quadrature axis rotor winding

n = relative angular velocity between stator and rotor windings. For synchronous speed, $n = n_0$, and the per unit value is 1. For asynchronous speed, $n = 1 - s$, where s denotes slip

$p = d/dt$, the time differential operator. For per unit values, $p = d/d\theta$, where $\theta = nt$, and $n = 1$ for synchronous speed

In accordance with the conditions mentioned in references 16 and 17 and discussed in connection with reference 11, we have assumed certain ideal conditions for the rotating machine. The essential simplified conditions are

$L_1 = L_1^0 + L_1'' \cos 2\theta$, $M_1 = M_d \cos\theta$, and $M_2 = M_q \sin\theta$

We shall now extend the above results to the general terminal impedance $u(p)/y(p)$ of reference 8. Then, by referring the stationary network to a uniformly rotating reference frame, we have

$$Z_{1(p\pm jn)^0} = R_1 + (p \pm jn)L_1^0 + \frac{u(p \pm jn)}{y(p \pm jn)} \quad (3)$$

The transformation from a stationary frame to a rotating frame can be demonstrated by tensor analysis or matrix analysis. (See Appendix I). By using rotating vectors, the transformations are rather simple. Laplace Transforms have shown that[18]

$$\mathcal{L}\{\epsilon^{-at} f(t)\} = F(p+a)$$

$$\mathcal{L}\{\epsilon^{-at} f(t)\} = F(p-a)$$

where p (or s) is a complex variable In the p-multiplied form,[19] a shift theorem similar to that given in Heaviside's operational calculus also can be demonstrated.[20–23] The shifting idea is the basic viewpoint of relativity, and rotating reference frames will certainly be important tools in the study of rotating mechanical and electrical systems.

The equation for the zero-sequence of stator phase current and voltage is, using the general terminal impedance of reference 8,

$$\left[Z_0 + \frac{u(p)}{y(p)}\right] i_0 = v_0 \quad (4)$$

where Z_0 = zero-sequence impedance = $R_1 + pL_0$, i_0 = zero-sequence stator current, and v_0 = zero-sequence stator potential.

The equations for the rotor currents in the direct and quadrature axes are of the following form:[10,12]

$$Z_{dr} i_{dr} + \Sigma p M_{d\,r(m)} i_{dr(m)} + pM_d'(i_f + i_b) = E_{dr} \text{ or } 0 \quad (5)$$

$$Z_{qr} i_{qr} + \Sigma p M_{q\,r(k)} i_{qr(k)} + pM_q'(i_f - i_b) = E_{qr} \text{ or } 0 \quad (6)$$

where Z_{dr} and Z_{qr} represent the self-impedances of the rotor circuits, M_{dr} and M_{qr} represent the mutual inductances between the rotor circuits of each axis, $M_d' = (3/2)M_d$, and $M_q' = (3/2j)M_q$.

By solving m equations for the direct axis windings simultaneously, we get*

$$i_{dr(m)} = -pA_m(p)(i_f + i_b) + B_m(p)E_{dr(m)}$$

where $B_m(p)$ depends on Z_{dr} and M_{dr}, and $A_m(p)$ depends on M_d', Z_{dr} and M_{dr}. By solving k equations for the quadrature axis windings, we get a similar expression for $i_{qr(k)}$. Then we have

$$I_d = \Sigma M_d i_{dr} = -M_d(p)(i_f + i_b) + G_d(p)E_{dr} \quad (7)$$

$$jI_q = j\Sigma M_q i_{qr} = -M_q(p)(i_f - i_b) + jG_q(p)E_{qr} \quad (8)$$

Substituting equations 3, 7, and 8 into equations 1 and 2, we get

$$\left[R_1 + (p+jn)L_1^0(p) + \frac{u(p+jn)}{y(p+jn)}\right] i_f + [(p+jn)L_1''(p)]i_b = v_f - \frac{1}{2}(p+jn)\times[G_d(p)E_{dr} + jG_q(p)E_{qr}] = e_f \quad (9)$$

$$\left[R_1 + (p-jn)L_1^0(p) + \frac{u(p-jn)}{y(p-jn)}\right] i_b + [(p-jn)L_1''(p)]i_f = v_b - \frac{1}{2}(p-jn)\times[G_d(p)E_{dr} - jG_q(p)E_{qr}] = e_b \quad (10)$$

where $L_1^0(p) = L_1^0 - \frac{1}{2}M_d(p) - \frac{1}{2}M_q(p)$ (11)

$$L_1''(p) = L_1'' - \frac{1}{2}M_d(p) + \frac{1}{2}M_q(p) \quad (12)$$

* For the case of one amortisseur winding in addition to the field winding in the direct rotor axis, we have

$$i_{dr(1)} = -p\frac{[M_{d(1)}' Z_{dr(2)} - M_{d(2)}' pM_{dr}]}{[Z_{dr(1)} Z_{dr(2)} - p^2 M^2_{dr}]}(i_f + i_b) + \frac{Z_{dr(2)} E_{dr(1)}}{[Z_{dr(1)} Z_{dr(2)} - p^2 M^2_{dr}]}$$

where $i_{dr(1)}$ and $E_{dr(1)}$ represent the field current and voltage.

In terms of direct axis and quadrature axis quantities, we have

$$L_d(p) = L_1^0(p) + L_1''(p) = L_d - M_d(p) \quad (13)$$

$$L_q(p) = L_1^0(p) - L_1''(p) = L_q - M_q(p) \quad (14)$$

where $L_d = L_1^0 + L_1''$ and $L_q = L_1^0 - L_1''$.

Transient Solution

For suddenly applied voltages or short circuits on the armature side, we shall consider that all the field windings are short circuited, or E_{dr} and E_{qr} equal to zero. Solving equations 9 and 10 simultaneously, we get

$$i_f = \frac{[R_1 + (p-jn)L_1^0(p) + B]v_f - [(p+jn)L_1''(p)]v_b}{D(p)} \quad (15)$$

$$i_b = \frac{[R_1 + (p+jn)L_1^0(p) + A]v_b - [(p-jn)L_1''(p)]v_f}{D(p)} \quad (16)$$

where

$$D(p) = D_0(p) + (A+B)[R_1 + pL_1^0(p)] + (B-A)[jnL_1^0(p)] + AB \quad (17)$$

$$D_0(p) = Z_{1+}{}^0(p)Z_{1-}{}^0(p) - (p^2+n^2)[L_1''(p)]^2$$

$$Z_{1\pm}{}^0(p) = R_1 + (p \pm jn)L_1^0(p)$$

$$A,\ B = \frac{u(p \pm jn)}{y(p \pm jn)}$$

From equations 9 and 10, we can write down the impedance tensor or matrix of a synchronous machine with a general terminal network as follows:

$$[Z] = \begin{array}{c} \\ v_f \\ v_b \end{array} \begin{array}{c} \begin{array}{cc} i_f & i_b \end{array} \\ \begin{array}{|c|c|} \hline Z_{1+}{}^0(p)+A & X_{1+}{}''(p) \\ \hline X_{1-}{}''(p) & X_{1-}{}^0(p)+B \\ \hline \end{array} \end{array} \quad (18)$$

where $X_{1\pm}{}''(p) = (p \pm jn)L_1''(p)$.

It may be pointed out here that for most cases, the terminal network as referred to a rotating reference frame can be expressed as

$$A,\ B = \frac{u(p \pm jn)}{y(p \pm jn)} = R_e \pm jX_e \quad (19)$$

Let

$$u(p \pm jn) = U_1 \pm jU_2,\ y(p \pm jn) = Y_1 \pm jY_2,$$
$$U^2 = U_1^2 + U_2^2, \text{ and } Y^2 = Y_1^2 + Y_2^2$$

Then

$$R_e = K_1/Y^2,\ X_e = K_2/Y^2,$$
$$Z_e^2 = R_e^2 + X_e^2 = U^2/Y^2$$

where

$$K_1 = U_1Y_1 + U_2Y_2,\ K_2 = U_2Y_1 - U_1Y_2, \text{ and}$$
$$K_1^2 + K_2^2 = U^2Y^2$$

For a transmission line with distributed constants, it can be shown (see Appendix II) that A, B are of the following form

$$A,\ B = \frac{u(p \pm jn)}{y(p \pm jn)} = \frac{Z_\pm \sinh\theta_\pm}{\theta_\pm \cosh\theta_\pm} \quad (19A)$$

where Z represents the total line impedance to the point of fault or the short-circuited end, and $\theta=\sqrt{ZY}$. In this case, it is evident that the more general form A, B should be used instead of $R_e \pm jX_e$.

If A, B can be expressed as given by Equation 19, equations 15 and 16 can be modified to the following:

$$i_f=\frac{Y^2\{[Z_{1-}{}^0(p)+R_e-jX_e]v_f-[X_{1+}{}''(p)]v_b\}}{A(p)} \tag{15A}$$

$$i_b=\frac{Y^2\{[Z_{1+}{}^0(p)+R_e+jX_e]v_b-[X_{1-}{}''(p)]v_f\}}{A(p)} \tag{16A}$$

where

$$A(p)=Y^2D_0(p)+K_1[2R_1+2pL_1{}^0(p)]+K_2[2nL_1{}^0(p)]+U^2 \tag{17A}$$

For asynchronous operation,[24,25] $n=1-s$. Substituting $(1-s)$ for n in equations 15, 16, and 17, we get in general

$$i_f=\frac{\{R_1+[p-j(1-s)]L_1{}^0(p)+B\}v_f-\{[p+j(1-s)]L_1{}''(p)\}v_b}{D(p)} \tag{15B}$$

$$i_b=\frac{\{R_1+[p+j(1-s)]L_1{}^0(p)+A\}v_b-\{[p-j(1-s)]L_1{}''(p)\}v_f}{D(p)} \tag{16B}$$

$$D(p)=D_0(p)+(A+B)[R_1+pL_1{}^0(p)]+(B-A)[j(1-s)L_1{}^0(p)]+AB \tag{17B}$$

We shall consider a simple example where the terminal network has a capacitive reactance x_c and a resistance r_1 in parallel. In this case, $u(p)=x_c$, a constant per-unit value, and $y(p)=(p+a)$, where $a=x_c/r_1$. Then $U_1=x_c$, $U_2=0$, $Y_1=(p+a)$, and $Y_2=n$. (For $r_1=\infty$, $a=0$, $Y_1=p$.) So $Y^2=(p+a)^2+(1-s)^2$, $K_1=x_c(p+a)$, $K_2=-x_c(1-s)$. Substituting these values into equations 15A and 16A, we can check the results of references 2, 7, and 8.

Two-Reaction Components

The basic transformations between i_f, i_b and i_d, i_q are [10-12]

$$i_f+i_b=i_d,\ i_f-i_b=ji_q \tag{20}$$

$$\frac{1}{2}(i_d+ji_q)=i_f,\ \frac{1}{2}(i_d-ji_q)=i_b$$

where

$i_f=i_+\epsilon^{-jnt}$ and $i_b=i_-\epsilon^{jnt}$.

Taking the sum and the difference of equations 15 and 16, we get

$$i_d=\frac{[(R_1+R_e)+pL_q(p)]v_d+[X_e+nL_q(p)]v_q}{D(p)} \tag{21}$$

$$i_q=\frac{[(R_1+R_e)+pL_d(p)]v_q-[X_e+nL_d(p)]v_d}{D(p)} \tag{22}$$

where R_e and X_e will be redefined in a general form as

$$R_e=\frac{A+B}{2},\quad X_e=\frac{A-B}{2j} \tag{23}$$

and

$$D(p)=D_0(p)+2R_eR_1+(R_ep+X_en)\times[L_d(p)+L_q(p)]+Z_e{}^2 \tag{17C}$$

where

$$D_0(p)=Z_d(p)Z_q(p)+x_d(p)x_q(p)$$

$$Z_d(p)=R_1+pL_d(p),\ Z_q(p)=R_1+pL_q(p),\ x_d(p)=nL_d(p),\ x_q(p)=nL_q(p)$$

The impedance tensor or matrix in the d, q system for a synchronous machine with general terminal network will be

$$\boldsymbol{Z'}=\begin{array}{c|c|c} & i_d & i_q \\ \hline v_d & Z_d(p)+R_e & -[x_Q(p)+X_e] \\ \hline v_q & x_d(p)+X_e & Z_q(p)+R_e \end{array} \tag{24}$$

Equation 24 can be obtained from equation 18 by the tensor or matrix transformation:*

$$\boldsymbol{Z'}=\boldsymbol{C}_t{}^*\boldsymbol{ZC} \tag{25}$$

where

$$\boldsymbol{C}=\begin{array}{c|c|c} & d & q \\ \hline f & 1 & j \\ \hline b & 1 & -j \end{array},\qquad \boldsymbol{C}_t{}^*=\begin{array}{c|c|c} & 1 & 1 \\ \hline -j & j \end{array} \tag{20A}$$

Comparing equations 20 and 20A, a factor of 1/2 has been left out in the matrix form. We may follow Kron in adding a factor $1/\sqrt{2}$ to $\boldsymbol{C}$.

Referring to equations 9 and 10 and substituting $(1-s)$ for n, we get

$$i_d=\frac{[Z_q(p)+R_e]e_d+[(1-s)L_q(p)+X_e]e_q}{D(p)} \tag{26}$$

$$i_q=\frac{[Z_d(p)+R_e]e_q-(1-s)L_d(p)+X_e]e_d}{D(p)} \tag{27}$$

For a simple capacitance connected to a synchronous machine, we have $R_e=x_cp/Y^2$, $X_e=-x_cn/Y^2$, $Y^2=p^2+n^2$, $Z_e{}^2=x_c{}^2/Y^2$. Substituting these values into equations 26 and 27, we get Crary's[7] equations 18 and 19:

$$i_d=\frac{[Y^2Z_q(p)+x_cp]e_d+[Y^2(1-s)x_q(p)-(1-s)x_c]e_q}{A(p)} \tag{28}$$

$$i_q=\frac{[Y^2Z_d(p)+x_cp]e_q-[Y^2(1-s)x_d(p)-(1-s)x_c]e_d}{A(p)} \tag{29}$$

* The author is indebted to Mr. Kron for this transformation. The transformation $\boldsymbol{C}^{-1}\boldsymbol{ZC}$ was used originally.

where

$$A(p)=Y^2[Z_d(p)Z_q(p)+(1-s)^2x_d(p)x_q(p)]+x_c\{p[Z_d(p)+Z_q(p)]-(1-s)^2[x_d(p)+x_q(p)]+x_c\} \tag{30}$$

$$Y^2=p^2+(1-s)^2,\ x_d(p)=L_d(p),\ x_q(p)=L_q(p)$$

If a shunt resistance r_1 is connected with the capacitive reactance x_c in parallel, we get the following equations which check with the results of Concordia:[8]

$$i_d=\frac{[Y^2Z_q(p)+x_c(p+a)]e_d+[Y^2nx_q(p)-nx_c]e_q}{A(p)} \tag{31}$$

$$i_q=\frac{[Y^2Z_d(p)+x_c(p+a)]e_q-[Y^2nx_d(p)-nx_c]e_d}{A(p)} \tag{32}$$

where

$a=x_c/r_1$, $n=1-s$, and

$$A(p)=[(p+a)^2+n^2]\{Z_d(p)Z_q(p)+n^2x_d(p)x_q(p)\}+x_c\{(p+a)\times[Z_d(p)+Z_q(p)]-n^2[x_d(p)+x_q(p)]+x_c\} \tag{33}$$

Transient Power and Torque

Let equations 1 and 2 be rewritten as

$$v_f=R_1i_f+Ai_f+p\psi_f+j\psi_f(n) \tag{34}$$

$$v_b=R_1i_b+Bi_b+p\psi_b-j\psi_b(n) \tag{35}$$

where

$$\psi_f=L_1{}^0i_f+L_1{}''i_b+I_f$$

$$\psi_b=L_1{}^0i_b+L_1{}''i_f+I_b$$

If there is no terminal network, or, if R_e and X_e are included in R_1 and $L_1{}^0$, the above expressions simplify to the following:

$$v_f=R_1i_f+p\psi_f+j\psi_f(n) \tag{34A}$$

$$v_b=R_1i_b+p\psi_b-j\psi_b(n) \tag{35A}$$

It is shown in Appendix III that the total instantaneous transient power divided by the number of phases is given by

$$P=i_-v_++i_+v_-=i_bv_f+i_fv_b \tag{36}$$

or

$$P=(1/2)(i_dv_d+i_qv_q) \tag{37}$$

For a 3-phase machine, we have the total transient power given by

$$P=3(i_-v_++i_+v_-)=3(i_bv_f+i_fv_b)=(3/2)(i_dv_d+i_qv_q)$$

This checks with equation 17 of reference 5, as Park used a factor of (2/3) for the per-unit instantaneous power.

The instantaneous transient torque is given in Appendix III as follows:

$$T=i_bj(\psi_f-L_1{}^0i_f)+i_f(-j)(\psi_b-L_1{}^0i_b)=i_bB_f+i_fB_b \tag{38}$$

where

$$B_f = j(\psi_f - L_1{}^0 i_f) = j(I_f + L_1{}'' i_b) = j\psi_{fr}$$
$$B_b = -j(\psi_b - L_1{}^0 i_b) = -j(I_b + L_1{}'' i_f) = -j\psi_{br}$$

So far as the net result is concerned, the total instantaneous value of transient torque divided by the number of phases can be given as

$$T = i_b(j\psi_f) + i_f(-j\psi_b) = (1/2)(i_q\psi_d - i_d\psi_q) \quad (39)$$

From equations 9 and 10, we can rewrite equations 34A and 35A as follows:

$$e_f = R_1 i_f + (p+jn)\psi_f' \quad (34B)$$

$$e_b = R_1 i_b + (p-jn)\psi_b' \quad (35B)$$

where

$$\psi_f' = L_1{}^0(p) i_f + L_1{}''(p) i_b$$
$$\psi_b' = L_1{}^0(p) i_b + L_1{}''(p) i_f$$

By taking the sum and the difference of equations 34 and 35, and using the general transformation of equation 20, we get

$$v_d = R_1 i_d + R_e i_d - X_e i_q + p\psi_d - \psi_q(p\theta) \quad (40)$$

$$v_q = R_1 i_q + R_e i_q + X_e i_d + p\psi_q + \psi_d(p\theta) \quad (41)$$

where

$$\psi_d = \psi_f + \psi_b = I_d + L_d i_d$$
$$j\psi_q = \psi_f - \psi_b = j(I_q + L_q i_q)$$

Without terminal network, equations 40 and 41 simplify to

$$v_d = R_1 i_d + p\psi_d - \psi_q(p\theta) \quad (40A)$$

$$v_q = R_1 i_q + p\psi_q + \psi_d(p\theta) \quad (41A)$$

Classification of Reference Frames

With the foregoing results, we shall follow Kron[15] in a brief discussion of the reference frames which he classified from the dynamic point of view.

Rewriting equations 40A and 41A in tensor form (see equation 7 of reference 15), there is

$$\boldsymbol{v} = \boldsymbol{R}\boldsymbol{i} + p\boldsymbol{\psi} + \boldsymbol{\gamma}\boldsymbol{\psi}p\theta \quad (42)$$

Similarly, the torque expression is given by

$$T = \boldsymbol{i}^* \boldsymbol{\gamma} \boldsymbol{\psi} \quad (43)$$

In equations 42 and 43, $\boldsymbol{\gamma}$ is not a tensor. It is called the "coefficient of rotation" containing ± 1.

When equations 34A and 35A are written in tensor form (see equation 9 of reference 15), there is

$$\boldsymbol{v} = \boldsymbol{R}\boldsymbol{i} + p\boldsymbol{\psi} + \boldsymbol{\gamma}\boldsymbol{\psi}n \quad (44)$$

where

$$\boldsymbol{\gamma} = \begin{array}{c|cc} & f & b \\ \hline f & j & \\ b & & -j \end{array} \quad (45)$$

is a "rotation tensor." As Kron well said: "Since $\boldsymbol{\psi}$ is always a tensor and $\boldsymbol{\gamma}$ became now a tensor (because of the redefinition) their product $\boldsymbol{\gamma\psi}$ must also necessarily be a tensor, a new physical entity, the so-called "flux-density" $\boldsymbol{B}$ of the armature. This is the same physical concept B that occurs in Maxwell's field-equations." The torque expression can now be given as "a generalization of the force equation of Maxwell, namely, of $f = iB$." That is,

$$T = \boldsymbol{i}^* \boldsymbol{B} = \boldsymbol{i}^* \boldsymbol{\gamma} \boldsymbol{\psi} \quad (46)$$

Starting Torque

For the study of starting torque, v_f and v_b are of the form ϵ^{jst} and ϵ^{-jst}. According to the Principle of Superposition, we can consider the effect of the two components separately, and then add the two solutions together. We shall consider v_f first. For $p = js$, $n = 1 - s$, we have, from equations 34A and 35A,

$$\psi_f = \frac{v_f - R_1 i_f}{p+jn} = \frac{v_f - R_1 i_f}{j} \quad (47)$$

$$\psi_b = \frac{-R_1 i_b}{p-jn} = \frac{-R_1 i_b}{-j(1-2s)} \quad (48)$$

or

$$j\psi_f = v_f - R_1 i_f \quad (47A)$$

$$-j\psi_b = (-R_1 i_b)/(1-2s) \quad (48A)$$

So

$$T_1 = i_b(j\psi_f) + i_f(-j\psi_b) = i_b v_f - R_1 i_b i_f \left(1 + \frac{1}{1-2s}\right) \quad (49)$$

where i_f and i_b are given by equations 15B and 16B, for $p = js$.

Similarly, we consider v_b next, where $p = -js$, $n = 1 - s$.

$$\psi_b' = \frac{v_b - R_1 i_b'}{p-jn} = \frac{v_b - R_1 i_b'}{-j} \quad (47B)$$

$$\psi_f' = \frac{-R_1 i_f'}{p+jn} = \frac{-R_1 i_f'}{j(1-2s)} \quad (48B)$$

So

$$T_2 = i_f'(-j\psi_b') + i_b'(j\psi_f') = i_f' v_b - R_1 i_f' i_b' \left(1 + \frac{1}{1-2s}\right) \quad (49A)$$

As v_f and v_b are conjugate, i_f' is conjugate to i_b, and i_b' is conjugate to i_f. Hence T_1 and T_2 are conjugate. The total torque will be

$$T = 2(T_1)_{\text{real}} = P - 2R_1 \left(1 + \frac{1}{1-2s}\right)(i_b i_f)_{\text{real}} \quad (50)$$

where

$$P = 2(i_b v_f)_{\text{real}} = 2(i_b \cdot v_f),$$
$$2(i_b i_f)_{\text{real}} = 2(i_b \cdot i_f)$$

As discussed in Appendix III, equation 50 gives the total torque as divided by the number of armature phases.

Synchronizing and Damping Torques

For hunting problems, equation 39 may be applied to the case of small increments as follows:

$$T = T_0 + \Delta T = (i_{b0} + \Delta i_b)(j\psi_{f0} + j\Delta\psi_f) + (i_{f0} + \Delta i_f)(-j\psi_{b0} - j\Delta\psi_b) \quad (51)$$

Neglecting second-order terms, there is

$$\Delta T = i_{b0}(j\Delta\psi_f) + i_{f0}(-j\Delta\psi_b) + (j\psi_{f0})\Delta i_b - (j\psi_{b0})\Delta i_f \quad (52)$$

From equations 34 and 35, we have

$$\Delta\psi_f = \frac{\Delta v_f - (R_1 + A)\Delta i_f}{p+jn},$$
$$\Delta\psi_b = \frac{\Delta v_b - (R_1 + B)\Delta i_b}{p-jn} \quad (53)$$

Assuming Δv_f and Δv_b are of the form ϵ^{jst} and ϵ^{-jst}, we shall consider the effect of Δv_f first, and get a similar solution for Δv_b. So

$$\Delta T_1 = i_{b0}\left[\frac{\Delta v_f - (R_1 + A)\Delta i_f}{(p+jn)/j}\right] + i_{f0}\left[\frac{-(R_1 + B)\Delta i_b}{(p-jn)/(-j)}\right] + j\psi_{f0}\Delta i_b - j\psi_{b0}\Delta i_f \quad (54)$$

where $p = js$, and $\Delta v_b = 0$. From equations 15 and 16, we get

$$\Delta i_f = \frac{[R_1 + (p-jn)L_1{}^0(p) + B]\Delta v_f}{D(p)},$$
$$\Delta i_b = \frac{[-(p-jn)L_1{}''(p)]\Delta v_f}{D(p)} \quad (55)$$

Substituting equation 55 into equation 54, we get a general expression

$$\Delta T_1 = f(p)\Delta v_f \qquad (p = js) \quad (56)$$

If we assume

$$\Delta T_1 = [T_s + T_d(js)]\Delta v_f \quad (57)$$

then T_s = real part of $f(js)$ and sT_d = imaginary part of $f(js)$, where T_s represents the synchronizing torque coefficient and T_d represents the damping torque coefficient. (See references 5, 6, 7, 26 and 27.)

If Δv_f is considered as suddenly applied, transient solutions can be obtained by considering p as the time differential operator, which has the steady-state value js. Moment of inertia also can be introduced in the solution. Considering the effect of Δv_b similarly, we have

$$\Delta T_2 = i_{f0}'\left[\frac{\Delta v_b - (R_1 + B)\Delta i_b'}{(p-jn)/(-j)}\right] + i_{b0}'\left[\frac{-(R_1 + A)\Delta i_f'}{(p+jn)/j}\right] + j\psi_{f0}'\Delta i_b' - j\psi_{b0}'\Delta i_f' \quad (58)$$

Figure 1. Equivalent single-line diagram

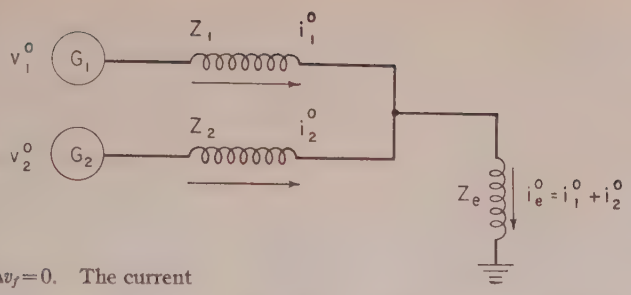

where $p=-js$, and $\Delta v_f=0$. The current expressions are:

$$\Delta i_b' = \frac{[R_1+(p+jn)L_1^0(p)+A]\Delta v_b}{D(p)},$$

$$\Delta i_f' = \frac{[-(p+jn)L_1''(p)]\Delta v_b}{D(p)} \qquad (59)$$

Hence

$$\Delta T_2 = f^*(p)\Delta V_b \quad (p=-js) \qquad (60)$$

Equation 60 is conjugate to equation 56, as $f^*(p)$ is conjugate to $f(p)$, and Δv_f is conjugate to Δv_b. Notice that the steady-state value of p in $f^*(p)$ is $-js$.

II. Interconnection of Rotating Machines—Extension to a General Network of N Machines

It is shown in Appendix IV how machines and networks are interconnected. Let the component systems be denoted by $\boldsymbol{Z}_1$, $\boldsymbol{Z}_2$, ... $\boldsymbol{Z}_e$, etc., where $\boldsymbol{Z}_1$, $\boldsymbol{Z}_2$, ... represent the impedance matrices of the machines, and $\boldsymbol{Z}_e$ represents any terminal impedance. The original impedance matrix $\boldsymbol{Z}$ will be given as

$$\boldsymbol{Z} = \begin{array}{|c|c|c|c|} \hline \boldsymbol{Z}_1 & & & \\ \hline & \boldsymbol{Z}_2 & & \\ \hline & & \cdots & \\ \hline & & & \boldsymbol{Z}_e \\ \hline \end{array} \qquad (61)$$

Let $\boldsymbol{C}$ represent the matrix showing how the systems are connected, or $\boldsymbol{i}=\boldsymbol{C}\boldsymbol{i}'$, where $\boldsymbol{i}$ represents the old currents in the component systems and $\boldsymbol{i}'$ represents the new currents in the resultant system. If $\boldsymbol{C}$ contains no time functions of $\theta=nt$, the impedance matrix of the resultant system after interconnection will be

$$\boldsymbol{Z}' = \boldsymbol{C}_t\boldsymbol{Z}\boldsymbol{C} \qquad (62)$$

Two Machines in Series

From equation 18 the impedance matrix of a synchronous machine can be obtained. In general,

$$\boldsymbol{Z}_1 = \begin{array}{c} \\ v_{1f} \\ v_{1b} \end{array} \begin{array}{c} \begin{array}{cc} i_{1f} & i_{1b} \end{array} \\ \begin{array}{|c|c|} \hline Z_{1+}^0 & X_{1+}'' \\ \hline X_{1-}'' & Z_{1-}^0 \\ \hline \end{array} \end{array}$$

$$\boldsymbol{Z}_2 = \begin{array}{c} \\ v_{2f} \\ v_{2b} \end{array} \begin{array}{c} \begin{array}{cc} i_{2f} & i_{2b} \end{array} \\ \begin{array}{|c|c|} \hline Z_{2+}^0 & X_{2+}'' \\ \hline X_{2-}'' & Z_{2-}^0 \\ \hline \end{array} \end{array} \qquad \boldsymbol{Z}_e = \begin{array}{c} \\ f \\ b \end{array} \begin{array}{c} \begin{array}{cc} f & b \end{array} \\ \begin{array}{|c|c|} \hline A & \\ \hline & B \\ \hline \end{array} \end{array}$$

Referring to Figure 1, if $\boldsymbol{Z}_e$ is infinitely large, we have two machines connected in series.

The transformation matrix between the old currents and the new currents

$$\boldsymbol{Z}' = \begin{array}{c} \\ v_{1f}'-v_{2f}' \\ v_{1b}'-v_{2b}' \end{array} \begin{array}{c} \begin{array}{cc} i_{1f}' & i_{1b}' \end{array} \\ \begin{array}{|c|c|} \hline Z_{1+}^0(p)+Z_{2+}^0(p+js) & X_{1+}''(p)+X_{2+}''(p+js)\epsilon^{-j2\theta} \\ \hline X_{1-}''(p)+X_{2-}''(p-js)\epsilon^{j2\theta} & Z_{1-}^0(p)+Z_{2-}^0(p-js) \\ \hline \end{array} \end{array} \qquad (64A)$$

is given by

$$\boldsymbol{C} = \begin{array}{c} \\ i_{1f} \\ i_{1b} \\ i_{2f} \\ i_{2b} \end{array} \begin{array}{c} \begin{array}{cc} i_{1f}' & i_{1b}' \end{array} \\ \begin{array}{|c|c|} \hline 1 & \\ \hline & 1 \\ \hline -1 & \\ \hline & -1 \\ \hline \end{array} \end{array}$$

$$\boldsymbol{C}_t = \begin{array}{|c|c|} \hline 1 & 1 \\ \hline & \\ \hline -1 & -1 \\ \hline \end{array} \qquad (63)$$

Notice that the minus signs in $\boldsymbol{C}$ and $\boldsymbol{C}_t$ are due to the assumption of the direction of old currents in machine 2 (see Figure 1).

From equations 61, 62 and 63 we get the impedance matrix for two synchronous machines in series: (Appendix IV)

$$\boldsymbol{Z}' = \begin{array}{c} \\ v_{1f}-v_{2f} \\ v_{1b}-v_{2b} \end{array} \begin{array}{c} \begin{array}{cc} i_{1f}' & i_{1b}' \end{array} \\ \begin{array}{|c|c|} \hline Z_{1-}^0+Z_{2+}^0 & X_{1+}''+X_{2+}'' \\ \hline X_{1-}''+X_{2-}'' & Z_{1-}^0+Z_{2-}^0 \\ \hline \end{array} \end{array} \qquad (64)$$

Two Machines Not in Synchronism

We shall examine briefly the case of two machines not in synchronism. Let n_1 and n_2 represent the angular velocities of the two machines, and let $n_1-n_2=s$. If the impedance matrix of the first machine refers to a reference frame rotating at speed n_1, and that of the 2nd machine refers to a reference frame rotating at speed n_2, the two matrices cannot be readily combined. In other words, the transformation matrices given in equation 63 must be duly modified. An alternative way is to investigate first what will be the impedance matrix of machine number 2, if it is referred to a reference frame rotating at speed n_1 instead of n_2. So with n_1 as the common speed for the rotating reference frames, $\boldsymbol{Z}_1$ is the same as given before, and

$$\boldsymbol{Z}_2' = \begin{array}{c} \\ v_{2f}' \\ v_{2b}' \end{array} \begin{array}{c} \begin{array}{cc} i_{2f}' & i_{2b}' \end{array} \\ \begin{array}{|c|c|} \hline Z_{2+}^0(p+js) & X_{2+}''(p+js)\epsilon^{-j2st} \\ \hline X_{2-}''(p-js)\epsilon^{j2st} & Z_{2-}^0(p-js) \\ \hline \end{array} \end{array}$$

Modification of equation 63 gives

$$\boldsymbol{C} = \begin{array}{c} \\ i_{1f} \\ i_{1b} \\ i_{2f} \\ i_{2b} \end{array} \begin{array}{c} \begin{array}{cc} i_{1f}' & i_{1b}' \end{array} \\ \begin{array}{|c|c|} \hline 1 & \\ \hline & 1 \\ \hline -\epsilon^{jst} & \\ \hline & -\epsilon^{jst} \\ \hline \end{array} \end{array}$$

$$\boldsymbol{C}_t^* = \begin{array}{|c|c|} \hline 1 & -\epsilon^{-jst} \\ \hline 1 & -\epsilon^{jst} \\ \hline \end{array} \qquad (63A)$$

The final result is hence given by $\boldsymbol{Z}'=\boldsymbol{C}_t^*\boldsymbol{Z}\boldsymbol{C}$, or

where $\theta=st$. Notice that we can get the same result by adding $\boldsymbol{Z}_1$ and $\boldsymbol{Z}_2'$. For $\theta=\theta_0=$ constant, representing the angular displacement between the rotors, equation 64A also is useful, for $s=0$.

Interconnection of Synchronous and Induction Machines

The impedance tensor or matrix of an induction machine referring to synchronous rotating frame will be given in Part III.[28,29] If we extend example I in Appendix IV, we get

$$\boldsymbol{Z}' = \begin{array}{c} \\ v_{1f} \\ v_{1b} \end{array} \begin{array}{c} \begin{array}{cc} i_{1f}' & i_{1b}' \end{array} \\ \begin{array}{|c|c|} \hline Z_{1+}^0+Z_{s+} & X_{1+}'' \\ \hline X_{1-}'' & Z_{1-}^0+Z_{s-} \\ \hline \end{array} \end{array} \qquad (65)$$

Two Machines in Parallel

Referring to Figure 1 and the results of Example III in Appendix IV, we shall introduce matrix forms for the Maxwell mesh equations as follows:

$$\boldsymbol{v}_1^0 = (\boldsymbol{Z}_1+\boldsymbol{Z}_e)\boldsymbol{i}_1^0+\boldsymbol{Z}_e\boldsymbol{i}_2^0 \qquad (66)$$

$$\boldsymbol{v}_2^0 = (\boldsymbol{Z}_2+\boldsymbol{Z}_e)\boldsymbol{i}_2^0+\boldsymbol{Z}_e\boldsymbol{i}_1^0 \qquad (67)$$

where

$$\boldsymbol{i}_1^0 = \begin{array}{|c|} \hline i_{1f} \\ \hline i_{1b} \\ \hline \end{array} \qquad \boldsymbol{i}_2^0 = \begin{array}{|c|} \hline i_{2f} \\ \hline i_{2b} \\ \hline \end{array}$$

$$\boldsymbol{v}_1^0 = \begin{array}{|c|} \hline v_{1f} \\ \hline v_{1b} \\ \hline \end{array}, \qquad \boldsymbol{v}_2^0 = \begin{array}{|c|} \hline v_{2f} \\ \hline v_{2b} \\ \hline \end{array} \qquad (68)$$

In terms of compound tensors or matrices, we have then

$$\boldsymbol{Z}' = \begin{array}{c} \\ \boldsymbol{v}_1^0 \\ \boldsymbol{v}_2^0 \end{array} \begin{array}{c} \begin{array}{cc} \boldsymbol{i}_1^0 & \boldsymbol{i}_2^0 \end{array} \\ \begin{array}{|c|c|} \hline \boldsymbol{Z}_1+\boldsymbol{Z}_e & \boldsymbol{Z}_e \\ \hline \boldsymbol{Z}_e & \boldsymbol{Z}_2+\boldsymbol{Z}_e \\ \hline \end{array} \end{array} \qquad (69)$$

Expanding equation 69 into its elementary form, we get

$$\boldsymbol{Z}' = \begin{array}{c|cc|cc} & i_{1f} & i_{1b} & i_{2f} & i_{2b} \\ \hline v_{1f} & Z_{1+}{}^{0}+A & X_{1+}{}'' & A & \\ v_{1b} & X_{1-}{}'' & Z_{1-}{}^{0}+B & & B \\ \hline v_{2f} & A & & Z_{2+}{}^{0}+A & X_{2+}{}'' \\ v_{2b} & & B & X_{2-}{}'' & Z_{2-}{}^{0}+B \end{array} \qquad (70)$$

Notice that the above results can be obtained from equations 66 and 67 by substituting in the matrices and making the multiplications.

By using transformations from the f, b system to the d, q system for the 2-machine network, we get

$$\boldsymbol{Z}_d' = \begin{array}{c|cc|cc} & i_{1d} & i_{1q} & i_{2d} & i_{2q} \\ \hline v_{1d} & Z_{1d(p)}+R_e & -[x_{1q(p)}+X_e] & R_e & -X_e \\ v_{1q} & x_{1d(p)}+X_e & Z_{1q(p)}+R_e & X_e & R_e \\ \hline v_{2d} & R_e & -X_e & Z_{2d(p)}+R_e & -[x_{2q(p)}+X_e] \\ v_{2q} & X_e & R_e & x_{2d(p)}+X_e & Z_{2q(p)}+R_e \end{array} \qquad (71)$$

Equation 71 may be considered as another expression of the compound tensor or matrix given by equation 69. In fact, equations 66 and 67 hold for both the f, b and the d, q systems.

The 3-Machine Problem

Referring to Figure 2, we can write down two matrix equations for the two independent meshes similar to equations 66 and 67. Instead of $\boldsymbol{Z}_e$, we have $\boldsymbol{Z}_3+\boldsymbol{Z}_e$.

$$\boldsymbol{v}_1{}^0-\boldsymbol{v}_3{}^0=(\boldsymbol{Z}_1+\boldsymbol{Z}_3+\boldsymbol{Z}_e)\boldsymbol{i}_1{}^0+(\boldsymbol{Z}_3+\boldsymbol{Z}_e)\boldsymbol{i}_2{}^0 \qquad (72)$$

$$\boldsymbol{v}_2{}^0-\boldsymbol{v}_3{}^0=(\boldsymbol{Z}_2+\boldsymbol{Z}_3+\boldsymbol{Z}_e)\boldsymbol{i}_2{}^0+(\boldsymbol{Z}_3+\boldsymbol{Z}_e)\boldsymbol{i}_1{}^0 \qquad (73)$$

The above equations are derived from Kirchhoff's second law as extended to matrix form. From Kirchhoff's first law, we have

$$\boldsymbol{i}_1{}^0+\boldsymbol{i}_2{}^0+\boldsymbol{i}_3{}^0=0 \qquad (74)$$

In fact, equation 74 has been used in writing down equations 72 and 73 according to the mesh method of Maxwell.

The impedance tensor or matrix of the resultant system is hence

$$\boldsymbol{Z}' = \begin{array}{c|cc} & \boldsymbol{i}_1{}^0 & \boldsymbol{i}_2{}^0 \\ \hline \boldsymbol{v}_1{}^0-\boldsymbol{v}_3{}^0 & \boldsymbol{Z}_1+\boldsymbol{Z}_3+\boldsymbol{Z}_e & \boldsymbol{Z}_3+\boldsymbol{Z}_e \\ \boldsymbol{v}_2{}^0-\boldsymbol{v}_3{}^0 & \boldsymbol{Z}_3+\boldsymbol{Z}_e & \boldsymbol{Z}_2+\boldsymbol{Z}_3+\boldsymbol{Z}_e \end{array} \qquad (75)$$

Equation 75 holds for both the f, b system and the d, q system, as both sets belong to the same rotating frame, here designated as the "o" frame. According to Kron's classification (reference 15), d, q belong to "non-holonomic, Riemannian Frame II (a)", and f, b belong to "holonomic, non-Riemannian Frame II(b)." So, in addition to equation 68, we can also define

$$\boldsymbol{i}^0 = \begin{array}{|c|} \hline i_d \\ \hline i_q \\ \hline \end{array} \qquad \boldsymbol{v}^0 = \begin{array}{|c|} \hline v_d \\ \hline v_q \\ \hline \end{array} \qquad (76)$$

$$\boldsymbol{Z}_e = \begin{array}{|c|c|} \hline R_e & -X_e \\ \hline X_e & R_e \\ \hline \end{array} \qquad (77)$$

The impedance tensor or matrix of a synchronous machine is already given by equations 18 and 24 for the f, b and d, q systems respectively. The external impedance network for the f, b system is defined below equation 62, while that for the d, q system is here given by equation 77. In general, for $n_1-n_2=s$, $n_1-n_3=s'$, $\theta=st$ and $\theta'=s't$,

$$\boldsymbol{Z}_2 = \begin{array}{|cc|} \hline Z_{2+}{}^{0}(p+js) & X_{2+}{}''(p+js)\,\epsilon^{j2\theta} \\ X_{2-}{}''(p-js)\,\epsilon^{j2\theta} & Z_{2-}{}^{0}(p-js) \\ \hline \end{array}$$

$$\boldsymbol{Z}_2 = \begin{array}{|cc|} \hline Z_{3+}{}^{0}(p+js') & X_{3+}{}''(p+js')\,\epsilon^{j2\theta'} \\ X_{3-}{}''(p-js')\,\epsilon^{j2\theta'} & Z_{2-}{}^{0}(p-js') \\ \hline \end{array}$$

For synchronous operation, $\theta=\theta_0=\theta_1-\theta_2$, and $\theta'=\theta_0'=\theta_1-\theta_3$.

Three Machines in Parallel

Referring to Figure 3, we have three independent meshes according to Maxwell's method as extended to matrix form. From our previous experiences in getting equations 69 and 75, we can write down the impedance tensor or matrix of the resultant system as follows:

$$[\boldsymbol{Z}'] = \begin{array}{c|ccc} & \boldsymbol{i}_1{}^0 & \boldsymbol{i}_2{}^0 & \boldsymbol{i}_3{}^0 \\ \hline \boldsymbol{v}_1{}^0 & \boldsymbol{Z}_1+\boldsymbol{Z}_e & \boldsymbol{Z}_e & \boldsymbol{Z}_e \\ \boldsymbol{v}_2{}^0 & \boldsymbol{Z}_e & \boldsymbol{Z}_2+\boldsymbol{Z}_e & \boldsymbol{Z}_e \\ \boldsymbol{v}_3{}^0 & \boldsymbol{Z}_e & \boldsymbol{Z}_e & \boldsymbol{Z}_3+\boldsymbol{Z}_e \end{array} \qquad (78)$$

As an illustration, we shall expand equation 78 into its elementary form in the d, q system:

$$\boldsymbol{Z}_d' = \begin{array}{c|cc|cc|cc} & i_{1d} & i_{1q} & i_{2d} & i_{2q} & i_{3d} & i_{4q} \\ \hline v_{1d} & Z_{1d}+R_e & -[x_{1q}+X_e] & R_e & -X_e & R_e & -X_e \\ v_{1q} & x_{1d}+X_e & Z_{1q}+R_e & X_e & R_e & X_e & R_e \\ \hline v_{2d} & R_e & -X_e & Z_{2d}+R_e & -[x_{2q}+X_e] & R_e & -X_e \\ v_{2q} & X_e & R_e & x_{2d}+X_e & Z_{2q}+R_e & X_e & R_e \\ \hline v_{3d} & R_e & -X_e & R_e & -X_e & Z_{3d}+R_e & -[x_{3q}+X_e] \\ v_{3q} & X_e & R_e & X_e & R_e & x_{3d}+X_e & Z_{3q}+R_e \end{array} \qquad (79)$$

For steady-state operation, equation 79 checks with the determinant obtained from the eight simultaneous equations given in Butler and Concordia's paper, Appendix B (reference 3).

The corresponding expression in the f, b system can be similarly obtained. In any case, the tensor or matrix method outlined in Appendix IV can be followed to check the final results. It is believed that after working with many illustrations the simplified procedure may be found to be advantageous, especially as solutions in both the f, b system and the d, q system can be readily obtained.

General Network with N Machines

Let the general network be represented by Figure 4, and let there be n independent meshes. Then we have

$$\boldsymbol{Z}' = \begin{array}{c|cccc} & \boldsymbol{i}_1{}^0 & \boldsymbol{i}_2{}^0 & \cdots & \boldsymbol{i}_n{}^0 \\ \hline \boldsymbol{v}_1{}^0 & \boldsymbol{Z}_{11} & \boldsymbol{Z}_{12} & \cdots & \boldsymbol{Z}_{1n} \\ \boldsymbol{v}_2{}^0 & \boldsymbol{Z}_{21} & \boldsymbol{Z}_{22} & \cdots & \boldsymbol{Z}_{2n} \\ \vdots & \cdots & \cdots & \cdots & \cdots \\ \boldsymbol{v}_n{}^0 & \boldsymbol{Z}_{n1} & \boldsymbol{Z}_{n2} & \cdots & \boldsymbol{Z}_{nn} \end{array} \qquad (80)$$

where $\boldsymbol{i}_1{}^0$, $\boldsymbol{i}_2{}^0$, ... $\boldsymbol{i}_n{}^0$ represent mesh cur-

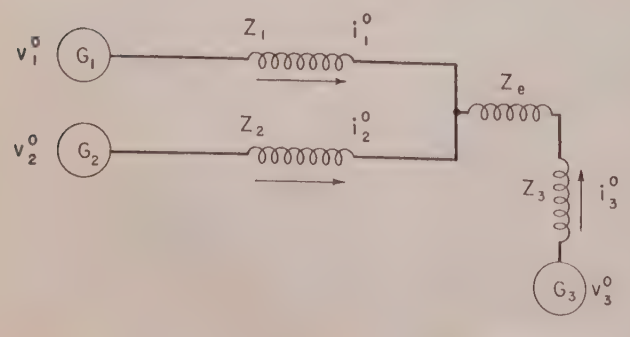

Figure 2. Three machines in series-parallel

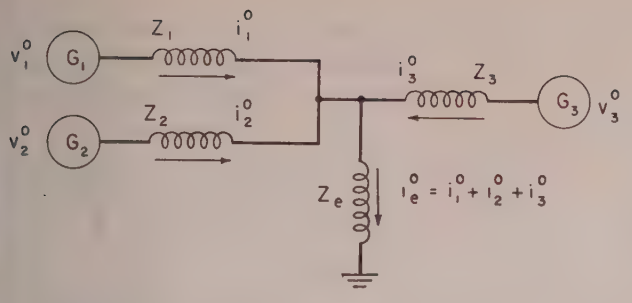

Figure 3. Three machines in parallel

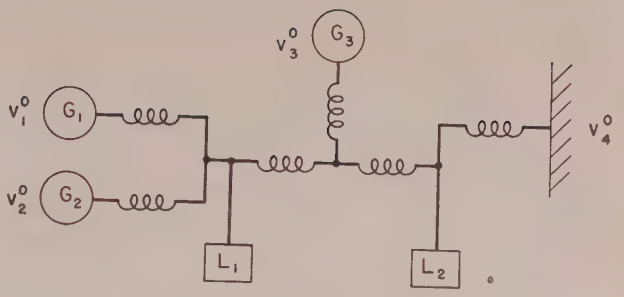

Figure 4. N-machine network

rents, v_1^0, v_2^0, ... v_n^0 represent algebraic sum of potentials around the mesh, Z_{kk} represents the total impedance of the kth mesh, and Z_{kj} represents the component of the impedance in the kth mesh encountered by the jth mesh current.

It is believed that the node method of network analysis also can be extended to matrix form in dealing with rotating machines and stationary networks. A résumé of Maxwell's rules and Kirchhoff's rules has been prepared by the author recently to facilitate such solutions by the node method and the mesh method.

III. General Machine with N_1 Stator Phases and N_2 Rotor Phases for Synchronous and Asynchronous Operation—Concatenation of Induction Motors and Selsyns

In references 11 and 12, the author presented an analysis of multiphase machines for the d, q system and the f, b system respectively. In reference 29, the 2-reaction method was applied to the analysis of an induction motor with 3-phase stator and 3-phase rotor.

For a general machine with n_1 stator phases and n_2 rotor phases, it can be shown that in general we can separate the positive and negative sequence equations from the equations for zero-sequence and other sequences.

Thus we have

$$(R_s+pL_s)i_{s+}+(pM)i_{r+}\epsilon^{jnt}=v_{s+} \quad (81)$$

$$(R_s+pL_s)i_{s-}+(pM)i_{r-}\epsilon^{-jnt}=v_{s-} \quad (82)$$

$$(R_r+pL_r)i_{r+}+(pM')i_{s+}\epsilon^{-jnt}=v_{r+} \text{ or } 0 \quad (83)$$

$$(R_r+pL_r)i_{r-}+(pM')i_{s-}\epsilon^{jnt}=v_{r-} \text{ or } 0 \quad (84)$$

where R, L, M represent resistance, inductance, and mutual inductance (maximum value) between the windings, s and r denote stator and rotor respectively, $M'=(n_1/n_2)M$, and n represents the angular velocity (relative) between the stator and the rotor.

By using suitable rotating reference frames, it is possible to refer the stator to the rotor, or the rotor to the stator, or to some other reference frame. Let equations 81 and 82 be transformed to the following:

$$[R_s+(p+jn)L_s]i_f+[(p+jn)M]i_{r+}=v_f \quad (85)$$

$$[R_s+(p-jn)L_s]i_b+[(p-jn)M]i_{r-}=v_b \quad (86)$$

where the f, b components are related to the $+$, $-$ components as given in Part I and Appendix I. When the rotor windings are short-circuited, v_{r+} and v_{r-} are equal to zero. So we have

$$Z=\begin{array}{c} \\ v_f \\ v_b \end{array}\begin{array}{|c|c|} \multicolumn{1}{c}{i_f} & \multicolumn{1}{c}{i_b} \\ \hline Z_{s+}(p) & \\ \hline & Z_{s-}(p) \end{array} \quad (87)$$

where

$$Z_{s\pm}(p)=R_s+(p\pm jn)L_s(p)$$

$$L_s(p)=L_s-\frac{(n_1/n_2)pM^2}{R_r+pL_r}$$

Suppose we want to refer the stator voltages and currents to a reference frame rotating at synchronous speed n_0 instead of actual speed $n=1-s$. Then equations 85 and 86 have to be changed to the following:

$$[R_s+(p+jn_0)L_s]i_{s+}\epsilon^{-jn_0t}+[(p+jn_0)M]i_{r+}\epsilon^{-jst}=v_{s+}\epsilon^{-jn_0t} \quad (88)$$

$$[R_s+(p-jn_0)L_s]i_{s-}\epsilon^{jn_0t}+[(p-jn_0)M]i_{r-}\epsilon^{jst}=v_{s-}\epsilon^{jn_0t} \quad (89)$$

Referring the rotor voltages and currents to a reference frame rotating at slip speed, s, we have similarly,

$$[R_r+(p+js)L_r]i_{r+}\epsilon^{-jst}+[(p+js)M']i_{s+}\epsilon^{-jn_0t}=0 \quad (90)$$

$$[R_r+(p-js)L_r]i_{r-}\epsilon^{jst}+[(p-js)M']i_{s-}\epsilon^{jn_0t}=0 \quad (91)$$

The impedance tensor or matrix of an induction machine referring to a reference frame rotating at synchronous speed $n_0=1$ is hence

$$Z'=\begin{array}{c} \\ v_f \\ v_b \end{array}\begin{array}{|c|c|} \multicolumn{1}{c}{i_f} & \multicolumn{1}{c}{i_b} \\ \hline Z_{s+}(p+js) & \\ \hline & Z_{s-}(p-js) \end{array} \quad (92)$$

where

$$Z_{s\pm}(p\pm js)=R_s+(p\pm jn_0)L_s(p\pm js)$$

$$L_s(p\pm js)=L_s-\frac{(p\pm js)M^2(n_1/n_2)}{R_r+(p\pm js)L_r}$$

Concatenation of Induction Motors

For the concatenation of induction motors,[32,33] we can make a choice of different rotating frames. In reference 32, all the stator voltages and currents of the first machine are referred to a reference frame rotating at synchronous speed. Here we shall take a reference frame rotating at actual speed, n, first, and then change the frame speed from n to n_0.

As shown in Figure 5, the rotor of the first machine is connected to the stator of the second machine through slip-rings. Referring the first stator to its rotor and referring the second rotor to its stator, we can get the following expression for the concatenation of induction motors:

$$Z=\begin{array}{c} \\ v_{1\pm}{}^0 \\ v_{2\pm} \\ v_{4\pm}{}^0 \end{array}\begin{array}{|c|c|c|} \multicolumn{1}{c}{i_{1\pm}{}^0} & \multicolumn{1}{c}{i_{2\pm}} & \multicolumn{1}{c}{i_{\pm}{}^0} \\ \hline Z_{1(p\pm jn)} & M_{12}(p\pm jn) & \\ \hline M_{12}p & Z_{2(p)}+Z_{3(p)} & -M_{34}p \\ \hline & -M_{34}(p\mp jn) & Z_{4(p\mp jn)} \end{array} \quad (93)$$

where $v_{1\pm}{}^0=v_{1\pm}\epsilon^{\mp jnt}$, $i_{1\pm}{}^0=i_{1\pm}\epsilon^{\mp jnt}$, $v_{4\pm}{}^0=0$, $i_{4\pm}{}^0=i_{4\pm}\epsilon^{\mp jnt}$ $Z_{k(p\pm jn)}=R_k+(p\pm jn)L_k$, and $Z_{k(p)}=R_k+pL_k$, for $k=1, 2, 3, 4$. Notice that the positive sequence and negative sequence components can be separated just as in the balanced operation of a single motor.

Referring to Appendix IV, the transformation matrix between the old cur-

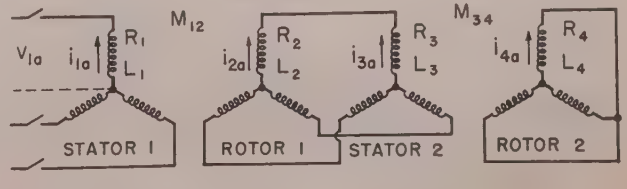

Figure 5. Concatenation of induction motors

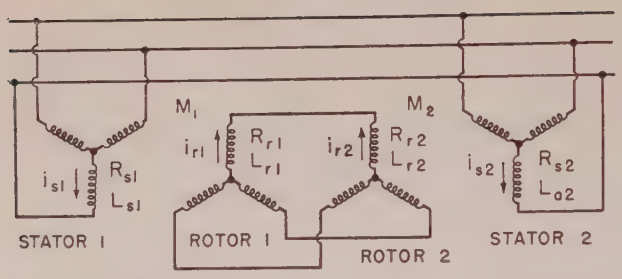

Figure 6. System of selsyns

rents and the new currents is given by

$$C=\begin{array}{c|ccc} & i_1' & i_2' & i_4' \\ \hline i_1 & 1 & & \\ i_2 & & 1 & \\ i_3 & & -1 & \\ i_4 & & & 1 \end{array}$$

$$C_i=\begin{array}{cccc} 1 & & & \\ & 1 & -1 & \\ & & & 1 \end{array}$$

Now if we want to change the speed of the reference frame for the first stator from n to n_0, the synchronous speed, it is only necessary to change p to $(p \pm js_1)$ in equation 93, as we did in getting equation 92 from equation 87. Thus

$$Z'=\begin{array}{c|ccc} & i_{1\pm}{}^0 & i_{2\pm}{}^0 & i_{4\pm}{}^0 \\ \hline v_{1\pm}{}^0 & Z_{1(p\pm jn_0)} & M_{12}(p\pm jn_0) & \\ v_{2\pm}{}^0 & M_{12}(p_\pm js_1) & Z_{2(p\pm js_1)}+Z_{3(p\pm js_1)} & -M_{34}(p\pm js_1) \\ v_{4\pm}{}^0 & & -M_{34}(p\pm js_2) & Z_{4(p\pm js_2)} \end{array} \qquad (94)$$

where

$$n_0=1,\ s_1=n_0-n=1-n,\ s_2=s_1-n=1-2n=-(1-2s_1),$$

$$v_{1\pm}{}^0=v_{1\pm}\epsilon^{\mp jn_0t},\ i_{1\pm}{}^0=i_{1\pm}\epsilon^{\mp jn_0t},$$
$$v_{2\pm}{}^0=0,\ i_{2\pm}{}^0=i_{2\pm}\epsilon^{\mp js_1t},$$
$$v_{4\pm}{}^0=0,\ i_{4\pm}{}^0=i_{4\pm}\epsilon^{\mp js_2t}$$

Equation 94 can be combined to a general system of synchronous machines and external networks all referring to a reference frame rotating at synchronous speed, n_0.

System of Selsyns

For a selsyn system of two slip-ring induction motors, both stators and rotors are connected in parallel as shown in Figure 6. There may be a rheostat between the rotors. In general the rotor impedances may include resistances and reactances connected between the two sets of slip-rings.

Referring the stator voltages and currents of both machines to the same rotating frame and noting that $v_{s1\pm}{}^0=v_{s2\pm}{}^0$ and $i_{r1\pm}=-i_{r2\pm}$, we have

$$Z=\begin{array}{c|ccc} & i_{s1\pm}{}^0 & i_{r1\pm} & i_{s2\pm}{}^0 \\ \hline v_{s1\pm}{}^0 & Z_{s1(p\pm jn)} & M_{1(p\pm jn)} & \\ v_{r1\pm} & M_1p & Z_{r1(p)}+Z_{r2(p)} & -M_2p \\ v_{s2\pm}{}^0 & & -M_{2(p\pm jn)} & Z_{s2(p\pm jn)} \end{array} \qquad (95)$$

The transformation matrix can be given as

$$C=\begin{array}{c|ccc} & i_1' & i_2' & i_3' \\ \hline i_{s1} & 1 & & \\ i_{r1} & & 1 & \\ i_{s2} & & & 1 \\ i_{r2} & & -1 & \end{array}$$

$$C_i=\begin{array}{cccc} 1 & & & \\ & 1 & & -1 \\ & & 1 & \end{array}$$

For a selsyn system of k machines (Figure 7), we have the following expression for the impedance tensor or matrix:

$$Z=\begin{array}{c|ccccc} & i_{s1\pm}{}^0 & \cdots & i_{sk\pm}{}^0 & i_{r1\pm} \cdots\cdots & i_{r(k-1)\pm} \\ \hline v_{s1\pm}{}^0 & Z_{s1(p\pm jn)} & & & M_1(p\pm jn) & \\ \vdots & \cdots\cdots & & \cdots\cdots & \cdots\cdots & \cdots\cdots \\ v_{sk\pm}{}^0 & & & Z_{sk(p\pm jn)} & -M_k(p\pm jn) & -M_k(p\pm jn) \\ v_{r1\pm} & M_1p & & -M_kp & Z_{r1}+Z_{rk} & Z_{rk} \\ \vdots & \cdots\cdots & & \cdots\cdots & \cdots\cdots & \cdots\cdots \\ v_{r(k-1)\pm} & & & -M_kp & Z_{rk} & Z_{r(k-1)}+Z_{rk} \end{array} \qquad (96)$$

The complete equations for $v_{s(k-1)\pm}{}^0$ and $v_{r(k-1)\pm}$ are:

$$v_{s(k-1)\pm}{}^0=[Z_{s(k-1)\pm}]i_{s(k-1)\pm}{}^0+[M_{(k-1)}(p\pm jn)]i_{r(k-1)\pm} \qquad (97)$$

$$v_{r(k-1)\pm}=[M_{(k-1)}p]i_{s(k-1)\pm}{}^0-M_kpi_{sk\pm}{}^0+Z_{rk}i_{r1\pm}+\cdots\cdots+[Z_{r(k-1)}+Z_{rk}]i_{r(k-1)\pm} \qquad (98)$$

Appendix I. Introduction of Rotating Reference Frame to Synchronous Machines and Stationary Networks

Let the equations for the positive- and negative-sequence vector components of the stator currents and voltages be

$$\left[(R_1+R_L)+(L_1{}^0+L_L)p+\frac{1}{pC_1}\right]i_+ + L_1''p(i_-\epsilon^{j2nt})+p(I_f\epsilon^{jnt})=v_+ \qquad (99)$$

$$\left[(R_1+R_L)+(L_1{}^0+L_L)p+\frac{1}{pC_1}\right]i_- + L_1''p(i_+\epsilon^{-j2nt})+p(I_b\epsilon^{-jnt})=v_- \qquad (100)$$

where all the symbols are as defined in Part I of this paper.

Let now the stationary armature axes $+$ and $-$ be transformed to a set of rotating axes f and b, or

$$C=\begin{array}{c|cc} & f & b \\ \hline + & \epsilon^{j\theta} & \\ - & & \epsilon^{-j\theta} \end{array}$$

$$C^{-1}=\begin{array}{c|cc} & + & - \\ \hline f & \epsilon^{-j\theta} & \\ b & & \epsilon^{j\theta} \end{array}=C_i{}^* \qquad (101)$$

where C represents the transformation tensor or matrix and C^{-1} its inverse transformation, $\theta=nt$, $p\theta=n$.

Denoting the old system i_+ and i_- by i and the new system $i_f=i_+\epsilon^{-jnt}$ and $i_b=i_-\epsilon^{jnt}$ by i', we have the following tensor or matrix equation:

$$i=Ci' \qquad (102)$$

For a simple resistance, inductance or capacitance, the impedance tensors or matrices are

$$R=\begin{array}{c|cc} & + & - \\ \hline + & R & \\ - & & R \end{array}$$

$$Lp=p\begin{array}{c|cc} & + & - \\ \hline + & L & \\ - & & L \end{array}$$

$$\frac{S}{p}=\frac{1}{p}\begin{array}{c|cc} & + & - \\ \hline + & S & \\ - & & S \end{array} \qquad (103)$$

where $R=R_1+R_L$, $L=L_1{}^0+L_L$, and $S=1/C_1$.

Let equations 99 and 100 be rewritten as

$$\left(R+Lp+\frac{S}{p}\right)i_+=e_+=v_+-p\psi_+ \qquad (99A)$$

$$\left(R+Lp+\frac{S}{p}\right)i_-=e_-=v_--p\psi_- \qquad (100A)$$

In tensor or matrix form, equations 99A and 100A can be combined into:

$$\left(\boldsymbol{R}+\boldsymbol{L}p+\frac{\boldsymbol{S}}{p}\right)\boldsymbol{i}=\boldsymbol{e}=\boldsymbol{v}-p\boldsymbol{\psi} \qquad (104)$$

where

$$\psi_+=[I_f+L_1''i_-\epsilon^{jnt}]\epsilon^{jnt}=\psi_f\epsilon^{jnt} \qquad (105A)$$

$$\psi_-=[I_b+L_1''i_+\epsilon^{-jnt}]\epsilon^{-jnt}=\psi_b\epsilon^{-jnt} \qquad (105B)$$

Similar to equation 102, we have

$$\boldsymbol{v}=\boldsymbol{C}\boldsymbol{v}',\ \boldsymbol{e}=\boldsymbol{C}\boldsymbol{e}',\ \boldsymbol{\psi}=\boldsymbol{C}\boldsymbol{\psi}' \qquad (102A)$$

Equation 104 can be transformed to the rotating frame as

$$\boldsymbol{R}'\boldsymbol{i}'+\boldsymbol{L}'(\boldsymbol{C}^{-1}p\boldsymbol{C})\boldsymbol{i}'+\boldsymbol{S}'\left(\boldsymbol{C}^{-1}\frac{1}{p}\boldsymbol{C}\right)\boldsymbol{i}'$$

$$=\boldsymbol{e}'=[\boldsymbol{v}'-(\boldsymbol{C}^{-1}p\boldsymbol{C})\boldsymbol{\psi}] \qquad (106)$$

where $\boldsymbol{R}'=\boldsymbol{C}^{-1}\boldsymbol{R}\boldsymbol{C}$, $\boldsymbol{L}'=\boldsymbol{C}^{-1}\boldsymbol{L}\boldsymbol{C}$, and $\boldsymbol{S}'=\boldsymbol{C}^{-1}\boldsymbol{S}\boldsymbol{C}$.

For the particular reference frame chosen, it is readily seen that $\boldsymbol{R}'=\boldsymbol{R}$, $\boldsymbol{L}'=\boldsymbol{L}$, and $\boldsymbol{S}'=\boldsymbol{S}$. It remains to find the values of $\boldsymbol{p}'$ and $\boldsymbol{p}'^{-1}$, where

$$\boldsymbol{p}'\boldsymbol{i}'=(\boldsymbol{C}^{-1}p\boldsymbol{C})\boldsymbol{i}' \qquad (107)$$

$$\boldsymbol{p}'^{-1}\boldsymbol{i}'=\left(\boldsymbol{C}^{-1}\frac{1}{p}\boldsymbol{C}\right)\boldsymbol{i}' \qquad (108)$$

Notice that p and $1/p$ refer to all expressions to the right of them. Now

$$p\boldsymbol{C}\boldsymbol{i}'=(p\boldsymbol{C})\boldsymbol{i}'+\boldsymbol{C}(p\boldsymbol{i}')$$

$$=\frac{\partial\boldsymbol{C}}{\partial\theta}p\theta\boldsymbol{i}'+\boldsymbol{C}p\boldsymbol{i}' \qquad (109)$$

$$\boldsymbol{C}^{-1}(p\boldsymbol{C}\boldsymbol{i}')=\boldsymbol{C}^{-1}\frac{\partial\boldsymbol{C}}{\partial\theta}p\theta\boldsymbol{i}'+\boldsymbol{C}^{-1}\boldsymbol{C}p\boldsymbol{i}' \qquad (109A)$$

or

$$\boldsymbol{p}'\boldsymbol{i}'=(\boldsymbol{\Gamma}p\theta+\boldsymbol{I}p)\boldsymbol{i}' \qquad (110)$$

So we get

$$\boldsymbol{p}'=(\boldsymbol{\Gamma}p\theta+\boldsymbol{I}p) \qquad (110A)$$

where

$$\boldsymbol{\Gamma}=\begin{array}{c|cc} & f & b \\ f & j & \\ b & & -j \end{array}$$

$$\boldsymbol{I}=\begin{array}{c|cc} & f & b \\ f & 1 & \\ b & & 1 \end{array} \qquad (111)$$

Then

$$\boldsymbol{p}'=\begin{array}{c|cc} & f & b \\ f & p+jn & \\ b & & p-jn \end{array} \qquad (112)$$

For the potential across the capacitance, we get from equation 106 as follows:

$$\boldsymbol{S}'(\boldsymbol{C}^{-1}\frac{1}{p}\boldsymbol{C})\boldsymbol{i}'=\boldsymbol{e}_C'=\boldsymbol{e}'-(\boldsymbol{R}'+\boldsymbol{L}'\boldsymbol{p}')\boldsymbol{i}' \qquad (113)$$

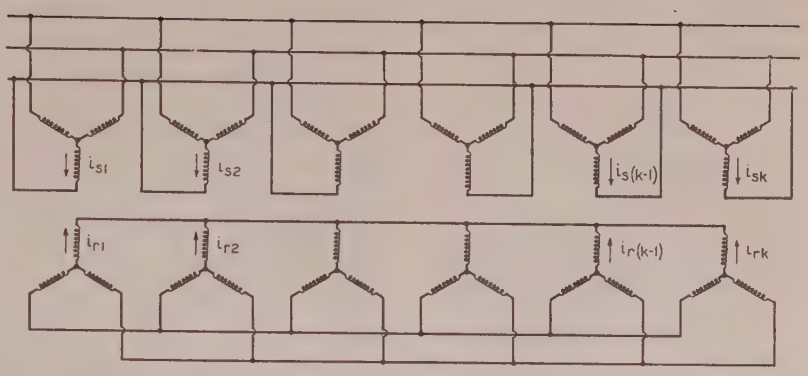

Figure 7. System of selsyns

It can be shown that after suitable manipulations, we get

$$\boldsymbol{p}'\boldsymbol{S}'^{-1}\boldsymbol{e}_C'=\boldsymbol{i}' \qquad (114)$$

Multiplying first by $\boldsymbol{p}'^{-1}$ and then by $\boldsymbol{S}'$, we get

$$\boldsymbol{e}_C'=\boldsymbol{S}'\boldsymbol{p}'^{-1}\boldsymbol{i}' \qquad (115)$$

Substituting equation 115 into equation 113, we get a new expression for equation 106 as

$$\boldsymbol{R}'\boldsymbol{i}'+\boldsymbol{L}'\boldsymbol{p}'\boldsymbol{i}'+\boldsymbol{S}'\boldsymbol{p}'^{-1}\boldsymbol{i}'=\boldsymbol{e}' \qquad (116)$$

which is of the same form as equation 104. The expression for $\boldsymbol{P}'^{-1}$ is

$$\boldsymbol{p}'^{-1}=\frac{1}{p^2+n^2}\begin{array}{c|cc} & f & b \\ f & p-jn & \\ b & & p+jn \end{array}$$

$$=\begin{array}{c|cc} & f & b \\ f & \dfrac{1}{p+jn} & \\ b & & \dfrac{1}{p-jn} \end{array} \qquad (117)$$

From equations 99A, 100A, or 104, the impedance tensor or matrix is given by

$$\boldsymbol{Z}=\begin{array}{c|cc} & + & - \\ + & R+Lp+\dfrac{1}{Cp} & \\ - & & R+Lp+\dfrac{1}{Cp} \end{array} \qquad (118)$$

From equation 116, the new impedance tensor or matrix referring to a new rotating reference frame is hence

$$\boldsymbol{Z}'=\begin{array}{c|cc} & f & b \\ f & R+L(p+jn)+\dfrac{1}{C(p+jn)} & \\ b & & R+L(p-jn)+\dfrac{1}{C(p-jn)} \end{array} \qquad (119)$$

Equation 119 checks with the results of references 2 and 14.

Similar results can be worked out for the general terminal impedance $u(p)/y(p)$. Laplace Transforms and Heaviside's Shifting Theorem can be readily applied as a check on the results obtained by tensor or matrix analysis as outlined above. From the above demonstration, it is evident that the f and b reference frame as used by the author in 1928 at Massachusetts Institute of Technology (reference 1) is to be recommended for the analysis of rotating mechanical and electrical systems. Just as relativity plays an important part in modern science, so rotating reference frames with transformations defined by equation 101 will be a natural view-point for the study of rotating systems.

Appendix II. Synchronous Machine Connected to a Transmission Line with Distributed Constants

Let $z=r+pL$ and $y=g+pC$ represent the series impedance and the shunt admittance of a transmission line per-unit length, $Z=zl$ and $Y=yl$ represent the total impedance and admittance from the sending end to the receiving end or the fault, as the case may be. Also, let $\alpha=\sqrt{zy}$ and $\theta=\sqrt{ZY}=\alpha l$.

The well-known relations between current and electromotive force at any point, distant x from the receiving end, is

$$\frac{\partial i}{\partial x}=(g+pC)e,\qquad \frac{\partial e}{\partial x}=(r+pL)i \qquad (120)$$

$$\frac{\partial^2 e}{\partial x^2}=(r+pL)(g+pC)e=\alpha^2 e \qquad (121)$$

where $p=\partial/\partial t$ is independent of x, $\alpha=\sqrt{zy}$ is a function of p but not of x. The solution of equation 121 is

$$e=A_1\epsilon^{\alpha x}+A_2\epsilon^{-\alpha x}=$$
$$K_1\cosh\alpha x+\sinh\alpha x \qquad (122)$$

For transient studies, we are especially interested in short circuits. So we shall consider the case of short circuits at the receiving end or at some other chosen point on the line. For $x=0$, $e=0$, so $K_1=0$. For $x=l$, $e=Es$, so $K_2=E_s/(\sinh\theta)$, where

$\theta=\sqrt{ZY}$. The general expression for the current is

$$i=\frac{y}{\alpha}(A_1\epsilon^{\alpha x}-A_2\epsilon^{-\alpha x})$$

$$=\frac{Y}{\theta}(K_1\sinh\alpha x+K_2\cosh\alpha x) \quad (123)$$

For a short-circuited end, we get

$$e=\left[\frac{\sinh\alpha x}{\sinh\theta}\right]E_s,\quad i=\frac{Y}{\theta}\left[\frac{\cosh\alpha x}{\sinh\theta}\right]E_s \quad (124)$$

The relation between E_s and I_s can then be expressed as

$$E_s=\frac{u(p)}{y(p)}I_s=\frac{Z}{\theta}\left[\frac{\sinh\theta}{\cosh\theta}\right]I_s \quad (125)$$

where

$$\theta=\sqrt{ZY}=l\sqrt{zy}=l\sqrt{(r+pL)(g+pC)}$$
$$=\theta_0\sqrt{(p+k_1)(p+k_2)} \quad (126)$$

in which

$$\theta_0=\sqrt{LC}l, k_1=r/L, k_2=g/C.$$

The problem now resolves to the evaluation of $u(p\pm jn)/y(p\pm jn)$. From equation 126, we have

$$\theta_\pm=\theta_{(p\pm jn)}=\theta_0\sqrt{(p\pm jn+k_1)(p\pm jn+k_2)}$$
$$=\theta_0\sqrt{p^2+2k_0p-n_0^2\pm j2n(p+k_0)} \quad (127)$$

where

$$k_0=\frac{k_1+k_2}{2},$$

and $n_0^2=n^2-k_1k_2$. For $k_1=k_2=k_0$, the quadratic under the radical will be a perfect square.

From equations 125, 126, and 127 we get

$$\frac{u(p\pm jn)}{y(p\pm jn)}=\frac{Z_\pm}{\theta_\pm}\left[\frac{\sinh\theta_\pm}{\cosh\theta_\pm}\right] \quad (128)$$

The hyperbolic functions in equation 128 also can be expressed as

$$\cosh\theta=1+\frac{\theta^2}{2!}+\frac{\theta^4}{4!}+\frac{\theta^6}{6!}+\cdots\cdots \quad (129)$$

$$\frac{\sinh\theta}{\theta}=1+\frac{\theta^2}{3!}+\frac{\theta^4}{5!}+\frac{\theta^6}{7!}+\cdots\cdots \quad (130)$$

where

$$\theta_\pm^2=\theta_0^2[p^2+2k_0p-n_0^2\pm j2n(p+k_0)] \quad (127A)$$

In actual problems, it may not be necessary to use the infinite series as given by equations 129 and 130. However, the alternate fork to the hyperbolic functions shows that $\theta_\pm^2$ as given by equation 127A are polynomials in p free from fractional powers and that we are justified to derive $F(p\pm jn)$ from $F(p)$, as $F(p)=u(p)/y(p)$ can be expressed in terms of polynomials.

From the above demonstration, we see that a transmission line with distributed constants can be combined with a synchronous machine all referring to the same rotating reference frame. Hence the impedance tensor or matrix can be written as

$$Z=\begin{array}{c|c|c} & i_f & i_b \\ \hline v_f & Z_{1+}{}^0+A & X_{1+}{}'' \\ \hline v_b & X_{1-}{}'' & Z_{1-}{}^0+B \end{array} \quad (131)$$

where

$$A=\frac{Z_+\sinh\theta_+}{\theta_+\cosh\theta_+},\quad B=\frac{Z_-\sinh\theta_-}{\theta_-\cosh\theta_-} \quad (132)$$

The determinant $D(p)$ is given by

$$D(p)=D_0(p)+Z_{1+}{}^0B+Z_{1-}{}^0A+AB \quad (133)$$

where

$Z_{1\pm}{}^0=R_1+(p\pm jn)L_1{}^0(p)$,
$X_{1\pm}{}''=(p\pm jn)L_1{}''(p)$,

and $Z_{\pm\pm}=R_L+(p\pm jn)L_L$, $Z_L=R_L+pL_L=$ total series impedance of the transmission line.

Appendix III. Instantaneous Power and Torque Under Transient Conditions

The fundamental equations of a salient-pole synchronous machine can be given as (see Appendix I):

$$v_+-R_1i_+=p[L_1{}^0i_++L_1{}''(i_-\epsilon^{2j\theta})+I_f\epsilon^{j\theta}]$$
$$=p[\psi_f\epsilon^{j\theta}] \quad (134)$$

$$v_--R_1i_-=p[L_1{}^0i_-+L_1{}''(i_+\epsilon^{-2j\theta})+I_b\epsilon^{-j\theta}]$$
$$=p[\psi_b\epsilon^{-j\theta}] \quad (135)$$

where

$$\psi_f=L_1{}^0i_+{}^0+L_1{}''i_-{}^0+I_f=L_1{}^0i_f+L_1{}''i_b+I_f \quad (136)$$

$$\psi_b=L_1{}^0i_-{}^0+L_1{}''i_+{}^0+I_b=L_1{}^0i_b+L_1{}''i_f+I_b \quad (137)$$

$$i_+{}^0=i_+\epsilon^{-j\theta}=i_f,\ i_-{}^0=i_-\epsilon^{j\theta}=i_b$$

and $\theta=nt$, $p\theta=n$.

The equations for the direct axis and quadrature axis rotor circuits are of the following form (see equations 5 and 6):

$$E_{dr}-R_{dr}i_{dr}=p[L_{dr}i_{dr}+(3/2)M_d(i_f+i_b)] \quad (138)$$

$$E_{qr}-R_{qr}i_{qr}=p[L_{qr}i_{qr}+(3/2j)M_q(i_f-i_b)] \quad (139)$$

The total instantaneous power for a 3-phase machine is

$$P_{3\phi}=i_av_a+i_bv_b+i_cv_c=(i_++i_-)(v_++v_-)+$$
$$(a^2i_++ai_-)(a^2v_++av_-)+$$
$$(ai_++a^2i_-)(av_++a^2v_-)$$
$$=3(i_-v_++i_+v_-) \quad (140)$$

The total instantaneous power divided by the number of phases will be

$$P=i_-v_++i_+v_-=i_-{}^0v_+{}^0+i_+{}^0v_-{}^0$$
$$=i_bv_f+i_fv_b \quad (140A)$$

Multiplying equation 134 by i_- and equation 135 by i_+, we get

$$i_-v_+-i_-R_1i_+=i_-(pL_1{}^0i_+)+$$
$$i_-(pL_1{}''i_-\epsilon^{2j\theta})+i_-(pI_f\epsilon^{j\theta}) \quad (134A)$$

$$i_+v_--i_+R_1i_-=i_+(pL_1{}^0i_-)+$$
$$i_+(pL_1{}''i_+\epsilon^{-2j\theta})+i_+(pI_b\epsilon^{-j\theta}) \quad (135A)$$

Similarly, we have

$$i_{dr}E_{dr}-R_{dr}i_{dr}{}^2=i_{dr}(pL_{dr}i_{dr})+$$
$$(3/2)i_{dr}[pM_d(i_f+i_b)] \quad (138A)$$

$$i_{qr}E_{qr}-R_{qr}i_{qr}{}^2=i_{qr}(pL_{qr}i_{qr})+$$
$$(3/2j)i_{qr}[pM_q(i_f-i_b)] \quad (139A)$$

If the machine runs as a synchronous motor, the total power input will be

$$P_1=3(i_-v_++i_+v_-)+i_{dr}E_{dr}+i_{qr}E_{qr} \quad (141)$$

The total i^2R losses of the armature phases are

$$(i_a{}^2+i_b{}^2+i_c{}^2)R_1=3(i_-i_++i_+i_-) \quad (142)$$

where $i_-i_+=i_+i_-$.

If we subtract all the armature and field i^2R losses from the total instantaneous input power, we get

$$P_2=P_s+P_r=P_1-3(i_-i_++i_+i_-)R_1-$$
$$i_{dr}{}^2R_{dr}-i_{qr}{}^2R_{qr} \quad (143)$$

where P_2 is the sum of P_s, corresponding to the total stored-up energy, and P_r, corresponding to the total rotational energy.

Stored-Up Energy

The stored-up energy in the self-inductances is

$$U_1=\frac{1}{2}L_1{}^0(i_a{}^2+i_b{}^2+i_c{}^2)+\frac{1}{2}L_{dr}i_{dr}{}^2+$$
$$\frac{1}{2}L_{qr}i_{qr}{}^2=3(L_1{}^0)(i_+i_-)+$$
$$\frac{1}{2}L_{dr}i_{dr}{}^2+\frac{1}{2}L_{qr}i_{qr}{}^2 \quad (144)$$

So the corresponding power is

$$P_{s1}=\frac{\partial U_1}{\partial t}=3L_1{}^0[i_-(pi_+)+i_+(pi_-)]+$$
$$L_{dr}i_{dr}(pi_{dr})+L_{qr}i_{qr}(pi_{qr}) \quad (145)$$

The stored-up energy in the mutual inductances between the armature and the field is of the general form (mi_1i_2). In rotating machines, $m=M\cos\theta$, where $\theta=nt$.

For a machine with armature phases a, b and c, and field circuits d and q, we have

$$U_2=m_{da}i_{dr}i_a-m_{qa}i_{qr}i_a+m_{db}i_{dr}i_b-$$
$$m_{qb}i_{qr}i_b+m_{dc}i_{dr}i_c-m_{qc}i_{qr}i_c \quad (146)$$

where

$$m_{da}=M_d\cos\theta,\ m_{db}=M_d\cos\left(\theta-\frac{2\pi}{3}\right),$$
$$m_{dc}=M_d\cos\left(\theta+\frac{2\pi}{3}\right)$$

$$m_{qa}=M_q\sin\theta,\ m_{qb}=M_q\sin\left(\theta-\frac{2\pi}{3}\right),$$
$$m_{qc}=M_q\sin\left(\theta+\frac{2\pi}{3}\right)$$

By substituting in i_+ and i_- components for i_a, i_b and i_c, and combining terms, we get

$$U_2=(3/2)i_{dr}M_d(i_f+i_b)+$$
$$(3/2j)i_{qr}M_q(i_f-i_b) \quad (147)$$

The corresponding power for stored-up energy in the mutual inductances between the armature and field is hence

$$P_{s2}=\frac{\partial U_2}{\partial t}=(3/2)i_{dr}[pM_d(i_f+i_b)]+$$
$$(3/2)(i_f+i_b)[pM_di_{dr}]+$$
$$(3/2j)i_{qr}[pM_q(i_f-i_b)]+$$
$$(3/2j)(i_f-i_b)[pM_qi_{qr}] \quad (148)$$

It can be shown similarly that the stored-up energy in the second harmonic component of the armature self-inductance of a salient-pole synchronous machine is given by

$$U_3=(3/2)L_1''(i_-^2\epsilon^{2j\theta}+i_+^2\epsilon^{-2j\theta})$$
$$=(3/2)L_1''(i_b^2+i_f^2) \quad (149)$$

So the corresponding power for stored-up energy is

$$P_{s3}=\frac{\partial U_3}{\partial t}=3L_1''[i_f(pi_f)+i_b(pi_b)] \quad (150)$$

Rotational Power and Torque

The total instantaneous rotational power will be given by

$$P_r=P_2-P_s=P_2-(P_{s1}+P_{s2}+P_{s3})$$
$$=3[i_b\{j(I_f+L_1''i_b)\}+$$
$$i_f\{(-j)(I_b+L_1''i_f)\}](p\theta)$$
$$=3[i_bj(\psi_f-L_1^0i_f)+$$
$$i_f(-j)(\psi_b-L_1^0i_b)](p\theta) \quad (151)$$

Since $i_b(ji_f)$ and $i_f(-ji_b)$ cancel out, the total instantaneous power (rotational) divided by the number of phases can be given as

$$P_r=[i_b(j\psi_f)+i_f(-j\psi_b)]p\theta \quad (152)$$

The instantaneous torque can be obtained by dividing P_r by $(p\theta)$.

Hence

$$T=i_bj(\psi_f-L_1^0i_f)+i_f(-j)(\psi_b-L_1^0i_b)$$
$$=i_b(j\psi_{fr})+i_f(-j\psi_{br})$$

or

$$T=i_b(j\psi_f)+i_f(-j\psi_b)=i_bB_f+i_fB_b \quad (153)$$

where $B_f=j\psi_f$ and $B_b=-j\psi_b$. As equation 153 holds good so far as the net result is concerned, it may be advisable to define B_f and B_b as

$$B_f=j\psi_{fr}=j(\psi_f-L_1^0i_f)=j(I_f+L_1''i_b) \quad (154)$$

$$B_b=-j\psi_{br}=-j(\psi_b'-L_1^0i_b)$$
$$=-j(I_b+L_1''i_f) \quad (155)$$

It may be pointed out that there are various ways of deriving instantaneous torque.

Professor Lyon's forthcoming book on A-C Machinery will bring out a fundamental approach to this problem. If, instead of equation 152, we express P_r as

$$P_r=i_-(jn\psi_+)+i_+(-jn\psi_-),$$

where

$$\psi_+=\psi_f\epsilon^{j\theta} \text{ and } \psi_-=\psi_b\epsilon^{-j\theta}$$

we see that $\pm jn$ corresponds to $d/dt(\pm j\theta)$. For the similar expression $T=i_-(j\psi_+)+i_+(-j\psi_-)$, $\pm j$ corresponds to $d/d\theta(\pm j\theta)$, and θ may be a constant angle, as we find in starting.

Appendix IV. Interconnection of Machines and Networks in the Same Reference Frame

We shall give a brief outline to show how machines and networks should be connected according to tensorial reasoning. For the theoretical development of the fundamental principles of interconnection, the reader is referred to Mr. Kron's treatise.[13]

If

$$\boldsymbol{Z}_1, \boldsymbol{Z}_2, \boldsymbol{Z}_3 \ldots .$$

represent the impedance matrices of the component systems, and $\boldsymbol{C}$ represents the matrix showing how the systems are connected, then the resultant impedance matrix is

$$\boldsymbol{Z}'=\boldsymbol{C}_t(\boldsymbol{Z}_1+\boldsymbol{Z}_2+\boldsymbol{Z}_3+\ldots\ldots)\boldsymbol{C}=\boldsymbol{C}_t\boldsymbol{Z}\boldsymbol{C} \quad (156)$$

Let the old currents in the component systems be denoted by $\bar{i}$, and the new currents in the resultant system be denoted by $\bar{i}'$. Then

$$\boldsymbol{i}=\boldsymbol{C}\boldsymbol{i}' \quad (157)$$

If the transformation matrix $\boldsymbol{C}$ contains no $\epsilon^{j\theta}$ or $\epsilon^{-j\theta}$ or cos θ terms, where $\theta=nt$, equation 156 holds for the impedance matrix of the group, when machines are interconnected. (See Part VIII of reference 13). It is important to note that if the impedance matrices of the component systems are referred to the same reference frame, they can be connected in a simple manner by a transformation matrix $\boldsymbol{C}$, as $\partial\boldsymbol{C}/\partial\theta=0$. So, when the component systems consist of machines and networks, they must be referred to the same reference frame, whether the frame is stationary or rotating.

We now shall investigate how the impedance matrix of the synchronous machine is combined with the matrix of the terminal network. In a 3-phase synchronous machine, the armature phases a, b, c are actually connected to the terminal impedances. In analytical work, we can use symmetrical components $(+, -, 0)$ or another set known as $(\alpha, \beta, 0)$ components. As α, β components are transformed into d, q components, $+$, $-$ components are transformed into f, b components. Both the d, q components and the f, b components refer to a rotating frame, just as the α, β components and the $+$, $-$ components refer to a stationary frame, which coincides with the physical frame of the stator or armature.

The transformations between the f, b and d, q components are exactly the same as that between the $+$, $-$ and α, β components.

Equation 18 of Part I gives the impedance matrix of the resultant system after the synchronous machine and the terminal impedance are connected. The matrices of the component systems should be referred to the same reference frame before they are interconnected. As the matrix of a synchronous machine refers to a rotating frame, the matrix of the terminal network also must be referred to the same rotating reference frame. We have two choices in a reference system rotating at synchronous speed, namely, the f, b system and the d, q system. We shall take the f, b system as an illustration.

Example I. Interconnection of a Synchronous Machine and a Terminal Network (Stationary)

The matrices of the component systems are:

$$\boldsymbol{Z}_1=\begin{array}{c|cc} & f & b \\ f & Z_{1+}^0(p) & X_{1+}''(p) \\ b & X_{1-}''(p) & Z_{1-}^0(p) \end{array}$$

$$\boldsymbol{Z}_2=\begin{array}{c|cc} & f & b \\ f & A & \\ b & & B \end{array} \quad (158)$$

Let the currents in $\boldsymbol{Z}_1$ and $\boldsymbol{Z}_2$ be i_{1f}, i_{1b}, and i_{2f}, i_{2b} respectively, before the interconnection, and let i_f', i_b' represent the new current in the resultant system.

Then

$$\boldsymbol{C}=\begin{array}{c|cc} & i_f' & i_b' \\ i_{1f} & 1 & \\ i_{1b} & & 1 \\ i_{2f} & 1 & \\ i_{2b} & & 1 \end{array}$$

$$\boldsymbol{C}_t=\begin{array}{c|cccc} & 1 & & 1 & \\ & & 1 & & 1 \end{array} \quad (159)$$

Since $\boldsymbol{Z}_1+\boldsymbol{Z}_2=\boldsymbol{Z}$ is given by (see equation 56, Part II, reference 13):

$$\boldsymbol{Z}=\begin{array}{c|cccc} & 1f & 1b & 2f & 2b \\ 1f & Z_{1+}^0(p) & X_{1+}''(p) & & \\ 1b & X_{1-}''(p) & Z_{1-}^0(p) & & \\ 2f & & & A & \\ 2b & & & & B \end{array} \quad (160)$$

we get by substituting equations 160 and 159 into equation 156,

$$\boldsymbol{Z}'=\begin{array}{c|cc} & f' & b' \\ f' & Z_{1+}^0(p)+A & X_{1+}''(p) \\ b' & X_{1-}''(p) & Z_{1-}^0(p)+B \end{array} \quad (161)$$

which checks with equation 18 of Part I.

Example II. Interconnection of Two Synchronous Machines

Let

$$\boldsymbol{Z}_2=\begin{array}{c|cc} & f & b \\ f & Z_{2+}^0(p) & X_{2+}''(p) \\ b & X_{2-}''(p) & Z_{2-}^0(p) \end{array} \quad (158A)$$

Then equation 160 should be modified such that in the old system there is

$$\boldsymbol{Z}=\begin{array}{c|cc} & Z_1 & \\ & & Z_2 \end{array} \quad (160A)$$

where $\boldsymbol{Z}$ now is expressed as a compound tensor or matrix. We can always check the results by writing down the elementary form from the compound form. The transformations of equation 159 still hold true for the series connection of two machines

and may be expressed in compound matrix form as

$$C = \begin{array}{c|c} & i' \\ i_1 & I \\ i_2 & I \end{array}$$

$$C_t = \left[\begin{array}{c|c} I & I \end{array}\right] \qquad (159A)$$

where

$$I \triangleq \begin{array}{c|cc} & f & b \\ f & 1 & \\ b & & 1 \end{array}$$

Substituting equations 159A and 160A into equation 156, we get in the new system

$$Z' = \left[\begin{array}{c} Z_1 + Z_2 \end{array}\right] \qquad (161A)$$

The elementary matrix for two machines in series will be hence

$$Z' = \begin{array}{c|cc} & f' & b' \\ f' & Z_{1+}{}^{0}(p)+Z_{2+}{}^{0}(p) & X_{1+}{}''(p)+X_{2+}{}''(p) \\ b' & X_{1-}{}''(p)+X_{2}{}''_{-}(p) & Z_{1-}{}^{0}(p)+Z_{2-}{}^{0}(p) \end{array} \qquad (162)$$

Example III. Interconnection of Two Machines and One Terminal Impedance Network

As shown in Figure 1, Z_1 and Z_e are given by equation 158, and Z_2 is defined by equation 158A, in examples I and II above. Let the old currents in the component systems be denoted by i_1, i_2, and i_e. In the resultant system after interconnection, the new currents are i_1', i_2', and $i_e' = i_1' + i_2'$. Hence

$$C = \begin{array}{c|cc} & i_1' & i_2' \\ i & I & \\ i_2 & & I \\ i_e & I & I \end{array}$$

$$C_t = \left[\begin{array}{c|c|c} I & & I \\ & I & I \end{array}\right] \qquad (163)$$

Since

$$Z = \left[\begin{array}{c|c|c} Z_1 & & \\ & Z_2 & \\ & & Z_e \end{array}\right] \qquad (164)$$

we get by substituting equations 163 and 164 into equation 156,

$$Z' = \left[\begin{array}{c|c} Z_1 + Z_e & Z_e \\ Z_e & Z_2 + Z_e \end{array}\right] \qquad (165)$$

This compound matrix form justifies the matrix equations 66 and 67. Expanding into its elementary form, we get equation 70 or

$$Z' = \begin{array}{c|cccc} & 1f' & 1b' & 2f' & 2b' \\ 1f' & Z_{1+}{}^{0}+A & X_{1+}{}'' & A & \\ 1b' & X_{1-}{}'' & Z_{1-}{}^{0}+B & & B \\ 2f' & A & & Z_{2+}{}^{0}+A & X_{2+}{}'' \\ 2b' & & B & X_{2-}{}'' & Z_{2-}{}^{0}+B \end{array} \qquad (165A)$$

By the above examples, we see that tensor or matrix equations for the different meshes of a general network of machines and impedances may be established. "The correctness of the resultant impedance matrix can be checked easily by remembering that each row represents the voltage equation of each closed mesh." So Kirchhoff's second law has been here extended to tensor or matrix analysis of rotating machines.

References

1. Transient Analysis of A-C Machinery, **Y. H. Ku.** *AIEE Transactions*, volume 48, July 1929, pages 707–14.

2. Transient Analysis of A-C Machinery, II, **Y. H. Ku.** *Journal of Electrical Engineering* (Shanghai, China), volume 3, August 1932, pages 179–206 and abstract in *Electrical Engineering*, volume 51, June 1932, page 408.

3. Analysis of Series Capacitor Application Problems, **J. W. Butler, C. Concordia.** *Electrical Engineering* (*AIEE Transactions*), volume 56, August 1937, pages 975–88.

4. Negative Damping of Electrical Machinery, **C. Concordia, G. K. Carter.** *Electrical Engineering* (*AIEE Transactions*), volume 60, March 1941, pages 116–19.

5. Two-Reaction Theory of Synchronous Machines, I, **R. H. Park.** *AIEE Transactions*, volume 48, July 1929, page 716–29.

6. Two-Reaction Theory of Synchronous Machines, II, **R. H. Park.** *AIEE Transactions*, volume 52, June 1933, pages 352–55.

7. Two-Reaction Theory of Synchronous Machines, **S. B. Crary.** *Electrical Engineering* (*AIEE Transactions*), volume 56, January 1937, pages 27–31.

8. Two-Reaction Theory of Synchronous Machines with Any Balanced Terminal Impedance, **C. Concordia.** *Electrical Engineering* (*AIEE Transactions*), volume 56, September 1937, pages 1124–27.

9. Fundamental Equations and Constants of Synchronous Machines, **Y. H. Ku.** *Journal of Electrical Engineering* (Shanghai, China), volume 4, 1933, page 1.

10. Operational Analysis of Synchronous Machines, **Y. H. Ku.** *Science Reports*, Tsing Hua University (Peiping, China), series A, volume 3, 1936, page 477.

11. Extension of 2-Reaction Theory to Multiphase Synchronous Machines, **Y. H. Ku.** *Electrical Engineering* (*AIEE Transactions*), volume 56, September 1937, pages 1197–1201.

12. Generalized Analysis of Multiphase Synchronous Machines, **Y. H. Ku.** *Science Reports*, Tsing Hua University (Peiping, China), series A, volume 4, 1937.

13. The Application of Tensors to the Analysis of Rotating Electrical Machinery (book), **G. Kron.** A serial in *General Electric Review* (Schenectady, N. Y.), beginning in volume 38, April 1935, page 181.

14. Stationary Networks and Transmission Lines Along Uniformly Rotating Reference Frames, **G. Kron.** *AIEE Transactions*, volume 69, 1949, pages 690–96.

15. Classification of the Reference Frames of a Synchronous Machine, **G. Kron.** *AIEE Transactions*, part II, 1950, pages 720–27.

16. Definition of an Ideal Synchronous Machine and Formula of the Armature Flux Linkages, **R. H. Park.** *General Electric Review* (Schenectady, N. Y.), volume 31, 1928, page 332.

17. The Operational Impedances of a Synchronous Machine, **M. L. Waring, S. B. Crary.** *General Electric Review* (Schenectady, N. Y.), volume 35, 1932, page 578.

18. Transients in Linear Systems (book), **M. F. Gardner, J. L. Barnes.** John Wiley and Sons, New York, N. Y., 1942.

19. Modern Operational Calculus (book), **N. W. MacLachlan.** McMillan Company, New York, N. Y., 1948.

20. Operational Circuit Analysis (book), **V. Bush.** John Wiley and Sons, New York, N. Y., 1929.

21. Heaviside's Operational Calculus (book), **E. J. Berg.** McGraw-Hill Book Company, New York, N. Y., 1929.

22. Heaviside's Electric Circuit Theory (book), **H. J. Josephs.** Methuen's Monographs, John Wiley and Sons, New York, N. Y., 1946.

23. A Derivation of Heaviside's Operational Calculus Based on the Generalized Functions of Schwarz, **J. J. Smith, P. L. Alger.** *AIEE Transactions*, volume 68, 1949, pages 939–45.

24. Asynchronous Operation of Synchronous Machines, **Y. H. Ku.** *Journal of Electrical Engineering* (Shanghai, China), volume 2, 1931, page 279.

25. Transient Current and Torque of Synchronous Machines Under Asynchronous Operation, **Y. H. Ku, S. W. Chu, T. S. Chu.** *Science Reports*, Tsing Hua University (Peiping, China), series A, volume 2, 1933 and 1934.

26. Synchronous Machine Damping Torque at Low Speeds, **C. Concordia.** *AIEE Transactions*, volume 69, part II, 1950, pages 1550–53.

27. Synchronous Machine Damping and Synchronizing Torques, **C. Concordia.** *AIEE Transactions*, volume 70, part I, 1951, pages 731–37.

28. Theory and Tensor Analysis of Single-Phase Induction Motors, **M. T. Chang.** *Engineering Quarterly*, Tsing Hua University (Peiping, China), volume 1, 1937.

29. Application of the Two-Reaction Theory to Three-Phase Induction Machines, **Y. H. Ku.** *Engineering Quarterly*, Tsing Hua University (Peiping, China), volume 1, 1937.

30. Transient Analysis of an Alternator, **Y. H. Ku.** *Proceedings*, World Engineering Congress (Tokyo, Japan), 1929 and *Journal of Electrical Engineering* (Shanghai, China), volume 1, 1930, page 1.

31. Operating Characteristics of an Induction Motor with Uniaxial Rotor, **Y. H. Ku, F. Hsu.** *Journal of Electrical Engineering* (Shanghai, China), volume 6, 1935.

32. Studies of Concatenation of Induction Motors, **Y. H. Ku, T. S. Chu, F. Hsu, C. Yen, S. S. Sun.** *Science Reports*, Tsing Hua University (Peiping, China), series A, volume 3, 1935–1936 and volume 4, 1940.

33. Oscillographic Studies on Induction Motors in Concatenation, **Y. H. Ku, T. S. Chu.** *Engineering Quarterly*, Tsing Hua University (Peiping, China), volume 1, 1937.

Discussion

Karl L. Wildes (Massachusetts Institute of Technology, Cambridge, Mass.): The question has been raised as to why Dr. Ku has used symmetrical components or forward and backward components for the analysis of multiphase rotating machines. Two

obvious reasons present themselves for using particular co-ordinates. The first is that the structure of the machine may dictate or suggest the use of certain co-ordinates, as in the resolution of armature reaction along the direct and quadrature axes of the salient-pole rotor before applying a permeance factor to obtain flux or inductance. The second reason for using a special kind of co-ordinate is to simplify the analysis. Some geometrical problems are much more easily solved in terms of cylindrical or spherical than in rectangular co-ordinates. This is the justification for use of symmetrical components or of forward and backward components for special 3-phase problems. Gabriel Kron dealt through tensor reasoning (see reference 15 of paper) with the selection of optimum reference frames for the solution of synchronous machine problems. Dr. Ku has illustrated in the present paper some cases in which rotating reference frames simplify the analysis, and his procedures are straight forward and easy to understand. The Kron "boxes" will scare some readers away, but boxes are not necessary to the understanding of the paper. Incidentally, any reader not familiar with matric methods could profitably spend an evening or two prying into these Kron boxes, because they are an effective aid in the organization of physical and mathematical relationships.

The following physical interpretations should be helpful to the student who reads Dr. Ku's paper.

Currents i_a, i_b, and i_c are instantaneous currents in the stator coils, each coil being distributed in such a way as to give a distribution of magnetic potential at the air gap which may be assumed sinusoidal in space.

Professor Edith Clarke's components defined as

$$i_0=\frac{1}{3}(i_a+i_b+i_c)$$

$$i_\alpha=\frac{1}{3}(2i_a-i_b-i_c)$$

$$i_\beta=\frac{1}{3}(\sqrt{3}i_b-\sqrt{3}i_c)$$

are a set of instantaneous currents conceived to flow in properly positioned coils which would produce the same distribution of magnetic potential as the actual currents in the actual coils. The zero-sequence component i_0 may be considered to flow in all three of the actual coils, and it does not produce any air-gap magnetic potential. The α component i_α flows in a hypothetical coil with its axis coincident with that of the actual phase-a coil and having 3/2 the number of turns of the phase-a coil. The β component flows in a similar hypothetical coil placed 90 electrical degrees ahead (toward phase b) of the α coil. The zero, alpha, and beta axes are therefore stationary axes but are of such nature that, if the rotor were stationary and had its direct axis aligned with the phase-a or α axis, its quadrature axis would be aligned with the β axis. But the rotor is not usually stationary in this position. If the angle by which the direct rotor axis leads the alpha axis is θ a second transformation may be defined as follows:

$$i_0=i_0$$
$$i_d=i_\alpha\cos\theta+i_\beta\sin\theta$$
$$i_q=-i_\alpha\sin\theta+i_\beta\cos\theta$$

The new hypothetical components of current i_d and i_q are instantaneous values which may be considered to flow in coils attached to the direct rotor axis and the quadrature rotor axis respectively, and the magnetic potential distribution is the same as would be produced by the actual a, b, and c currents or by the hypothetical 0-, α-, and β-components. These direct and quadrature components are along rotating axes, and their magnetomotive forces can be combined with those of the field structure to yield the total magnetomotive forces in the two rotor axes. Permeance or other factors can now be applied to give fluxes, linkages, voltages or inductances in each of the axes. Having done this, a return can be made to the stationary axes (0, α and β or a, b, and c) if this seems desirable for the solution of a particular problem, or a new transformation can be made to any other set of useful axes. These considerations or their equivalent have been presented earlier in papers by Ku and Park. Dr. Ku begins in Appendix I with symmetrical components of instantaneous stator currents which are related to the Clarke components as follows:

$$i_0=i_0$$

$$i_+=\frac{1}{2}(i_\alpha+ji_\beta)$$

$$i_-=\frac{1}{2}(i_\alpha-ji_\beta)$$

Up to this point the currents under consideration were actual physical currents which could be considered to circulate in coils properly placed in a physical machine. These symmetrical components are mathematical nonphysical quantities which cannot be conceived to exist in any physical coils. They are nonphysical in the same sense that an alternating current $Ie^{j(\omega t-\theta)}$ is nonphysical; the corresponding physical current is $i=\sqrt{2}I\cos(\omega t-\theta)$. Similarly i_+ is a space vector with components in the α and β directions. It corresponds to a physical current of magnitude

$$|i_+|=\frac{1}{2}\sqrt{i_\alpha^2+i_\beta^2}$$

in a physical coil whose axis is at an angle $\tan^{-1} i_\beta/i_\alpha$ ahead of the α axis. If the factor $1/2$ had not been present, this description would represent the complete physical situation in the machine as far as air-gap magnetomotive force is concerned. Since i_+ is a complex number with respect to clearly defined axes (α and β), the i_- component is in a sense unnecessary; in fact it is always the conjugate of i_+. The i_- component could be interpreted as a physical current in a coil back of the α axis, but such an interpretation does not correspond with the actual physical facts in the machine. It should be noted that the sum of the i_+ effects and the i_- effects does not represent the physical situation.

The i_f and i_b components have exactly the same relation to the i_d and i_q components as do the i_+ and i_- components to the α and β components and may be given the same physical interpretation.

Y. H. Ku: The author is indeed very grateful to the discussion of Professor K. L. Wildes. During the presentation at Madison, Wisconsin, the introductory remarks and comments by Dean W. A. Lewis has been most encouraging to the author and enlightening to the audience. As he wrote to the author after the meeting, he said: "I realize that those who are new to this particular field might have been guided somewhat by my comments.. I had some thought that I might still complete my remarks and ask the AIEE for an extension of time. However, I felt that what I had to say would need some documentation from references, and it was not possible to find time to take care of this within the few days after I received your letter." However, it is the author's privilege to record his appreciation in the closure.

In the final preparation of the paper, the author has been greatly benefited by the comments of the reviewers. One reviewer commented that the paper presents "a fresh point of view," but he brought out the fact that certain derivations of equations cited references which are not generally available. So in this closure, the author feels somewhat obliged to insert in this record certain previous results, especially results of a paper presented before the AIEE in June 1932, but not available to the general reader as only an abstract was published in Electrical Engineering (see reference 2 of the paper).

Extending equations 1 to 4 of reference 1 of the paper to the salient-pole synchronous machine with grounded neutral, there are the following:

$$(R_1+L_1{}^0p)i_A-\frac{1}{3}(L_0{}^0p)(i_A+i_B+i_C)+\frac{2}{3}(L_1{}''p)\left[i_A\cos 2nt+i_B\cos\left(2nt-\frac{2\pi}{3}\right)+i_C\cos\left(2nt-\frac{4\pi}{3}\right)\right]+(M_dp)[i_{dr}\cos nt]-(M_qp)[i_{qr}\sin nt]=v_A \quad (1)$$

$$(R_1+L_1{}^0p)i_B-\frac{1}{3}(L_0{}^0p)(i_A+i_B+i_C)+\frac{2}{3}(L_1{}''p)\left[i_A\cos\left(2nt-\frac{2\pi}{3}\right)+i_B\cos\left(2nt-\frac{4\pi}{3}\right)+i_C\cos 2nt\right]+(M_dp)\left[i_{dr}\cos\left(nt-\frac{2\pi}{3}\right)\right]-(M_qp)\left[i_{qr}\sin\left(nt-\frac{2\pi}{3}\right)\right]=v_B \quad (2)$$

$$(R_1+L_1{}^0p)i_C-\frac{1}{3}(L_0{}^0p)(i_A+i_B+i_C)+\frac{2}{3}(L_1{}''p)\left[i_A\cos\left(2nt-\frac{4\pi}{3}\right)+i_B\cos 2nt+i_C\cos\left(2nt-\frac{2\pi}{3}\right)\right]+(M_dp)\left[i_{de}\cos\left(nt-\frac{4\pi}{3}\right)\right]-(M_qp)\left[i_{qr}\sin\left(nt-\frac{4\pi}{3}\right)\right]=v_C \quad (3)$$

$$(R_{dr}+L_{dr}p)i_{dr}+M_dp\left[i_A\cos nt+i_B\cos\left(nt-\frac{2\pi}{3}\right)+i_C\cos\left(nt-\frac{4\pi}{3}\right)\right]=E_{dr}\text{ or }0 \quad (4)$$

$$(R_{qr}+L_{qr}p)i_{qr}-M_qp\left[i_A\sin nt+i_B\sin\left(nt-\frac{2\pi}{3}\right)+i_C\sin\left(nt-\frac{4\pi}{3}\right)\right]=E_{qr}\text{ or }0 \quad (5)$$

where

i_A, i_B, i_C = instantaneous values of armature currents in phases A, B, C.

v_A, v_B, v_C = instantaneous values of armature terminal potentials in phases A, B, C.

All the other constants are as defined in the paper. Notice that $L_1^0-L_0^0=L_0$ represents the zero-sequence impedance, while L_0^0 is equal to three times the mutual inductance between the armature phases. It may be pointed out that L_1'' is equal to (3/2) the maximum value of the second harmonic of the self-inductance of each armature phase, which is assumed equal to the second harmonic of the mutual inductance between armature phases for an ideal synchronous machine. It should be emphasized that there exist simple relations $L_d=L_1^0+L_1''$ and $L_q=L_1^0-L_1''$, where L_d and L_q are the well-known direct-axis and quadrature-axis inductances of a salient-pole synchronous machine.

Equations 1 to 4 are essentially the same (see reference 2 of the paper). The effect of quadrature-axis winding is here added based on the results given in reference 10 of the paper which treats two additional windings in the direct-axis besides the field winding. The extension of the above equations to multiphase machines is given in reference 12. In all cases, the trigonometric transformations used are essentially the following:

$$\frac{2}{n}[i_A\cos x+i_B\cos(x-\theta_0)+i_C\cos(x-2\theta_0)+\cdots\cdots+i_N\cos(x+\theta_0)]=i_1\epsilon^{-jx}+i_{n-1}\epsilon^{jx}=i_+\epsilon^{-jx}+i_-\epsilon^{jx} \quad (6)$$

$$-\frac{2}{n}[i_A\sin x+i_B\sin(x-\theta_0)+i_C\sin(x-2\theta_0)+\cdots\cdots+i_N\sin(x+\theta_0)]=-ji_1\epsilon^{-jx}+ji_{n-1}\epsilon^{jx}=-j[i_+\epsilon^{-jx}-i_-\epsilon^{jx}] \quad (7)$$

where $\theta_0=2\pi/n$, i_+ and i_- represent the positive- and negative-sequence components of a N-phase system according to the general Fortescue transformation of sequence coordinates in a N-co-ordinate system (see reference 12 and Appendix II of reference 11 of the paper). For a 3-phase system, $n=3$, $n-1=2$, $\theta_0=2\pi/3=120$ degrees. Thus equations 6 and 7 of this discussion reduce to the simple relations:

$$i_d=\frac{2}{3}\left[i_A\cos\theta+i_B\cos\left(\theta-\frac{2\pi}{3}\right)+i_C\cos\left(\theta-\frac{4\pi}{3}\right)\right]=i_1\epsilon^{-j\theta}+i_2\epsilon^{j\theta}=i_f+i_b \quad (6A)$$

$$i_q=-\frac{2}{3}\left[i_A\sin\theta+i_B\sin\left(\theta-\frac{2\pi}{3}\right)+i_C\sin\left(\theta-\frac{4\pi}{3}\right)\right]=-ji_1\epsilon^{-j\theta}+ji_2\epsilon^{j\theta}=-j[i_f-i_b] \quad (7A)$$

where $x=\theta=nt$. For $x=2\theta=2nt$, we have from equation 6

$$\frac{2}{3}\left[i_A\cos 2\theta+i_B\cos\left(2\theta-\frac{2\pi}{3}\right)+i_C\cos\left(2\theta-\frac{4\pi}{3}\right)\right]=i_1\epsilon^{-j2\theta}+i_2\epsilon^{j2\theta} \quad (6B)$$

For $x=x_0=$ constant, equation 6 gives

$$\frac{2}{3}\left[i_A\cos x_0+i_B\cos\left(x_0-\frac{2\pi}{3}\right)+i_C\cos\left(x_0-\frac{4\pi}{3}\right)\right]=i_1\epsilon^{-jx_0}+i_2\epsilon^{jx_0} \quad (6C)$$

Since $i_A=i_0+i_1+i_2$, $i_B=i_0+a^2i_1+ai_2$, $i_C=i_0+ai_1+a^2i_2$, $i_A+i_B+i_C=3i_0$, where $a=\epsilon^{j2\pi/3}$ and $a^2=\epsilon^{j4\pi/3}=\epsilon^{-j2\pi/3}$, we can substitute equation 6 into equations 1, 2, and 3, and separate the sequences to get the following set of equations in terms of symmetrical components:

$$(R_1+L_0p)i_0=v_0 \text{ where } L_0=L_1^0-L_0^0 \quad (7)$$

$$(R_1+L_1^0p)i_1+(L_1''p)[i_2\epsilon^{j2nt}]+\frac{1}{2}p[M_di_{dr}+jM_qi_{qr}]\epsilon^{jnt}=v_1 \quad (8)$$

$$(R_1+L_1^0p)i_2+(L_1''p)[i_1\epsilon^{-j2nt}]+\frac{1}{2}p[M_di_{dr}-jM_qi_{qr}]\epsilon^{-jnt}=v_2 \quad (9)$$

Adding external impedance (R_L+L_Lp+1/pC_1) to these expressions, we get equations 99 and 100 in Appendix I.

From equations 6A and 7A, it is evident that we can write down a new set of equations in terms of i_d and i_q instead of $i_f=i_1\epsilon^{-jnt}$ and $i_b=i_2\epsilon^{jnt}$. These results were given by Park in reference 5. While L_1^0 and L_1'' are convenient constants in the system of symmetrical components, L_d and L_q are better suited to the system of quadrature components. However, in the tensor analysis of 2-phase synchronous machine, Kron found that the transient impedance matrix can be brought to the simpler form by using $A=(L_d+L_q)/2$ and $B=(L_d-L_q)/2$ (see equations 7 and 9, Part VII of reference 13 of the paper).

By substituting equation 6A into equation 4, we get

$$(R_{dr}+L_{dr}p)i_{dr}+\frac{3}{2}M_dp\times(i_1\epsilon^{-jnt}+i_2\epsilon^{jnt})=E_{dr}\text{ or }0 \quad (10)$$

Similarly, by substituting equation 7A into equation 5, we get

$$(R_{qr}+L_{qr}p)i_{qr}+\frac{3}{2j}M_qp\times(i_1\epsilon^{-jnt}-i_2\epsilon^{jnt})=E_{qr}\text{ or }0 \quad (11)$$

These expressions are the same as those given by equations 5 and 6 in the paper and give the following solutions for i_{dr} and i_{qr}.

$$i_{dr}=\frac{E_{dr}}{Z_{dr}}-\frac{3}{2}\frac{M_dp}{Z_{dr}}(i_f+i_b) \quad (12)$$

$$i_{qr}=\frac{E_{qr}}{Z_{qr}}-\frac{3}{2j}\frac{M_qp}{Z_{qr}}(i_f-i_b) \quad (13)$$

By means of Heaviside's "Shifting Formula," equations 8 and 9 were transformed into the following: (see references 2, 10, 12)

$$\left[R_1+(p+jn)L_1^0+\frac{1}{(p+jn)C_1}\right]i_f+(p+jn)L_1''i_b+\frac{1}{2}(p+jn)\times[M_di_{dr}+jM_qi_{qr}]=v_f \quad (14)$$

$$\left[R_1+(p-jn)L_1^0+\frac{1}{(p-jn)C_1}\right]i_b+(p-jn)L_1''i_f+\frac{1}{2}(p-jn)\times[M_di_{dr}-jM_qi_{qr}]=v_b \quad (15)$$

These equations form the starting point of the present paper (compare with equations 1 and 2 in the paper). Solving equations 12, 13, 14, and 15 simultaneously, the instantaneous transient currents i_f, i_b, i_{dr}, and i_{qr} can be readily determined.

The determinant for the transient solution of the above equations was given in reference 2 as:

$$D_s^c(p)=(p^2+n^2)D_s(p)+D_c(p) \quad (16)$$

where $D_s(p)$ is the determinant for a salient-pole synchronous machine without external capacitance, and $D_c(p)$ is a cubic involving C_1 or $x_c=1/C_1$. While $D_s(p)$ has only positive coefficients, $D_c(p)$ may have negative coefficients, "so the combination may give negative coefficients in the expression for $D_s^c(p)$, sufficient to yield positive real roots." So the fifth degree equation (equation 16) did give a quantitative analysis for self-excitation or negative damping of synchronous machines with capacitive loading. In terms of the nomenclature in the present paper, we have for the simple case of an external capacitance the determinant:

$$A(p)=(p^2+n^2)D_0(p)+D_c(p) \quad (17)$$

$$D_c(p)=x_c\{2R_1p+2(p^2-n^2)L_1^0(p)+x_c\} \quad (18)$$

where for the case of one field winding and one amortisseur winding in the quadrature axis,

$$L_1^0(p)=L_1^0-\frac{3}{2}\frac{pM_d^2}{Z_{dr}}-\frac{3}{2}\frac{pM_q^2}{Z_{qr}} \quad (19)$$

Notice that the coefficient $-n^2$ is negative. For asynchronous operation, $n=1-s$, where s represents slip.

In the discussion brought out by Professor Wildes, emphasis has been laid on the instantaneous values of currents and voltages. For instance, the phase currents i_A, i_B, i_C have real instantaneous values. Professor Edith Clarke's components, being real transformations of these instantaneous currents, must have also real values. The relations between i_+, i_- and i_α, i_β components as shown in Professor Wildes' discussion clearly indicate that the positive-sequence and negative-sequence instantaneous component currents are conjugates of each other. As an illustration, if $i_\alpha=$

$\sqrt{2}\cos nt$ and $i_\beta = \sqrt{2}\sin nt$, then $i_+ = 1/2(i_\alpha + ji_\beta) = 0.707\,\epsilon^{jnt}$, $i_- = 1/2(i_\alpha - ji_\beta) = 0.707\,\epsilon^{-jnt}$.

In transient studies, the actual currents may have damped d-c components, damped sinusoids, besides the usual steady-state components. It is important to note that in using different systems of components representing the actual currents, we are dealing with instantaneous values instead of complex representation of sinusoids so that our analysis can be extended from the steady state to the transient problems.

Finally, the author wishes to express his appreciation to Professor T. J. Higgins for co-operation in the presentation of this paper, and takes pleasure in recording the following comments from him: "I find Dr. Ku's paper of the greatest interest. It is certainly a very clear and concise presentation of the essentials of the problem treated. It merits the close attention of all interested in the modern theory of machines and networks.

A Design Method for Polyphase Reluctance Synchronous Motors

C. H. CROUSE
ASSOCIATE AIEE

IT was pointed out by P. H. Trickey[1] that the design of reluctance synchronous motors might be divided into three steps. The three steps are: 1. choose trial dimensions and windings, 2. calculate the motor constants, and 3. calculate the performance of the trial design. Papers have been published which allow the designer to select the optimum rotor punching configuration[2,3] and papers have been published which allow the designer to calculate the constants[4] and the performance.[1] Hence, it is apparent that the selection of stator turns and wire size is still a matter of trial and error. Since such indirect methods exist in the selection of stator turns and wire size, it is then apparent that the calculation of performance will be done by considerable trial and error.

It is intended here to develop an exact method of design, whereby the design is based upon synthesis.[5] This method will allow the designer to calculate directly the number of conductors and the wire size in order to meet a certain value of maximum torque. In addition, an exact method of predicting performance will be developed, which takes into account the voltage drop due to the primary impedance. The equations developed will originate from an equivalent circuit and the equivalent circuit will be based upon the vector diagram which has previously been developed for the unexcited, reluctance synchronous motor using the 2-reaction theory.

Development of the Equivalent Circuit

The vector diagram for the unexcited reluctance synchronous motor was shown by Trickey in Figure 1.

From the vector diagram it can be observed that

$$I_d X_d = E\cos\delta \quad \text{and} \quad I_q X_q = E\sin\delta$$

$$E = \frac{I_d X_d}{\cos\delta} \quad \text{and} \quad E = \frac{I_q X_q}{\sin\delta}$$

or

$$Z_d = \frac{X_d}{\cos\delta} \tag{1}$$

and

$$Z_q = \frac{X_q}{\sin\delta} \tag{1A}$$

Nomenclature

$A = \dfrac{X_d}{X_q} - 1$
C = total series conductors per phase
C_R = voltage correction for stator resistance drop
C_x = voltage correction for stator reactance drop
E = internal voltage per phase
$E' = E + j\dfrac{Ex_1}{Z_e}$
f = frequency, cycles per second
I_L = line amperes
I_d = component of line current in direct axis, amperes
I_q = component of line current in quadrature axis, amperes
K_w = winding factor = distribution factor × pitch coefficient
l_c = one-half average length of conductor, in inches
$M = \dfrac{A}{2}\sin^2\delta$
n = number of phases
P = power output per phase + rotational losses
$\mathcal{P}_L$ = primary leakage permeance
$\mathcal{P}_D$ = magnetizing permeance in direct axis (unsaturated)
r_1 = stator winding resistance per phase, ohms
S_p = stator slots
V = terminal voltage per phase
x_1 = primary leakage reactance, ohms
X_d' = magnetizing reactance in direct axis, unsaturated, ohms
X_d = magnetizing reactance in direct axis, corrected for saturation, ohms
X_q = magnetizing reactance in quadrature axis, corrected for saturation, ohms
$X_{oD} = \dfrac{1}{Y_e} + x_1$ = equivalent open circuit reactance, ohms
Y_e = equivalent admittance, mhos
Z_e = equivalent impedance, ohms
β_R = angle between E' and V, degrees
β_x = angle between E and E', degrees
δ = load torque angle, in degrees
θ' = angle between E and I_L
$\theta = \theta' - (\beta_R - \beta_x)$ = power factor angle
μ = saturation factor
F & W = friction and windage, watts
$\dfrac{C}{\text{slot}}$ = circular mils of copper per slot

The impedances Z_d and Z_q are parallel impedances since

$$I_L = I_d + I_q$$

The impedances developed in equations 1 and 1A can be changed into rectangular co-ordinates by operating with $\cos\alpha + j\sin\alpha$

Let

$$\alpha = -90 - \delta$$

$$Z_d = \frac{X_d}{\cos\delta}(-\sin\delta - j\cos\delta)$$

$$= -X_d\tan\delta - jX_d \tag{2}$$

Let

$$\alpha = -\delta$$

$$Z_q = \frac{X_q}{\sin\delta}(\cos\delta - j\sin\delta)$$

$$= X_q\cot\delta - jX_q \tag{3}$$

If the core loss is represented by R_{Fe},

Paper 51-177, recommended by the AIEE Rotating Machinery Committee and approved by the Technical Program Committee for presentation at the AIEE Great Lakes District Meeting, Madison, Wis., May 17-19, 1951. Manuscript submitted February 15, 1951; made available for printing April 13, 1951.

C. H. CROUSE is with Robbins and Myers Inc., Springfield, Ohio.

The writer wishes to acknowledge the previous work of M. I. Beers, J. H. Karr, and G. V. Mueller in developing the present method. The writer also wishes to express his appreciation to T. C. Lloyd for his suggestions and criticism.

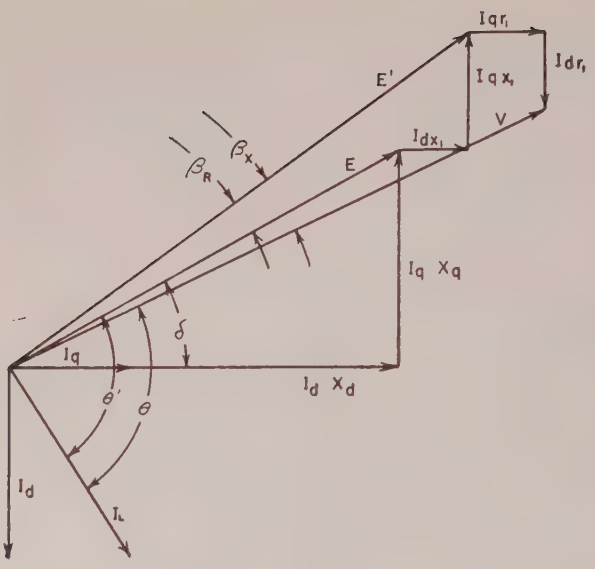

Figure 1 (left). Vector diagram for the unexcited reluctance polyphase synchronous motor

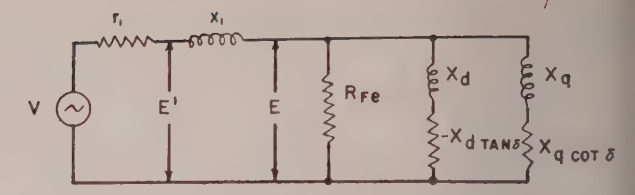

Figure 2. Equivalent circuit for one phase of the unexcited reluctance polyphase synchronous motor

the three elements of the equivalent circuit, which are in parallel, are then R_{Fe}, equation 2, and equation 3.

The equivalent circuit then is constructed with the three parallel branches in series with the primary impedance. The resulting equivalent circuit is shown in Figure 2.

Development of Equations from the Equivalent Circuit

Stator Impedance Drop

In order to develop equations from the equivalent circuit, it will be necessary to derive the equations required to account for the stator impedance drop.

From the equivalent circuit

$$\boldsymbol{I}_L = \boldsymbol{I}_q + \boldsymbol{I}_d + \boldsymbol{I}_{Fe} \tag{4}$$

Therefore

$$Y_e = \frac{1}{Z_d} + \frac{1}{Z_q} + \frac{1}{R_{Fe}}$$

$$= \frac{Z_d}{Z_d^2} + \frac{Z_q}{Z_q^2} + \frac{1}{R_{Fe}}$$

$$= -\frac{X_d \tan\delta - jX_d}{\frac{X_d^2}{\cos^2\delta}} + \frac{X_q \cot\delta - jX_q}{\frac{X_q^2}{\sin^2\delta}} + \frac{1}{R_{Fe}}$$

$$Y_e = \sin\delta\cos\delta\frac{(X_d - X_q)}{X_d X_q} - j\frac{(X_d \sin^2\delta + X_q \cos^2\delta)}{X_d X_q} + \frac{1}{R_{Fe}}$$

$$A = \frac{X_d}{X_q} - 1$$

$$Y_e = \frac{\sin\delta\cos\delta A}{X_d} - \frac{j}{X_d}\left(\frac{X_d}{X_q}\sin^2\delta + \cos^2\delta\right) + \frac{1}{R_{Fe}}$$

$$= \frac{A}{2}\frac{\sin^2\delta}{X_d} - \frac{j}{X_d}(1 + A\sin^2\delta) + \frac{1}{R_{Fe}}$$

$$Y_e = \frac{\frac{X_d}{R_{Fe}} + M - jL}{X_d} \tag{5}$$

where

$$M = \frac{A}{2}\sin^2\delta \tag{5A}$$

and

$$L = 1 + A\sin^2\delta \tag{5B}$$

For voltage correction, it has been found that the term X_d/R_{Fe} can be dropped without undue error. However X_d/R_{Fe} will be used when the line current is to be determined.

Therefore, again from the equivalent circuit

$$E' = E + j\frac{Ex_1}{Ze}$$

$$E = E'\frac{1}{1 + j\frac{x_1}{Z_e}}$$

$$= E'\frac{1}{1 + jx_1 Y_e}$$

$$E = E'\frac{1}{1 + \frac{x_1}{X_d}(L + jM)}$$

$$E = E'(C_x)$$

where

$$C_x = \frac{1}{1 + \frac{x_1}{X_d}(L + jM)} \tag{6A}$$

Also

$$V = E' + \frac{Er_1}{Z_e}$$

$$= E' + E'C_x\frac{r_1}{Z_e}$$

$$E' = V\frac{1}{1 + \frac{r_1 C_x}{Z_e}} = V\frac{1}{1 + \frac{r_1 C_x}{X_d}(M - jL)} = V(Cr)$$

where

$$C_R = \frac{1}{1 + \frac{r_1 C_x}{X_d}(M - jL)} \tag{6B}$$

Thus

$$E = V(C_x)(C_R) \tag{6}$$

The product $(C_x)(C_R)$ is the voltage correction which accounts for the voltage drop of the stator winding. It should be noticed that the voltage correction can be taken at any torque angle, δ, which represents a given load point.

Power Developed

As was pointed out at the beginning of this paper, it is intended that a method be made available by which it is possible to solve directly for the exact stator turns and wire size for a given maximum torque.

From the vector diagram

$$\text{Power developed} = EI_q\cos\delta - EI_d\sin\delta$$

$$= E^2\frac{\sin\delta\cos\delta}{X_d}\left(\frac{X_d}{X_q} - 1\right)$$

$$= \frac{E^2 A\sin^2\delta}{2X_d}$$

Let

$$E^2 = V^2 C_R^2 C_x^2 \tag{7}$$

Therefore

$$P = \frac{V^2 C_R^2 C_x^2 M}{X_d} \text{ per phase}$$

(synchronous watts)

and

Shaft output = P − rotational losses

In order to obtain maximum power or

maximum torque, δ is necessarily 45 degrees, therefore

$$\text{Maximum power output} = \frac{V^2 C_R^2 C_x^2 A}{2X_d} - \text{Rotational losses (synchronous watts per phase)} \quad (8)$$

In order to solve for the stator turns, it is then obvious that the equation be set up in terms of X_d. With X_d known, the stator conductors per phase can be determined from the following relation

$$C = \sqrt{\frac{X_d \mu (10^8)}{2\pi f \wp_D k \omega^2 n}}$$

It also is apparent that the stator turns per phase can be obtained which will produce a given power output at any desired torque angle. Thus, by direct synthesis, it is possible to solve for the stator turns per phase as a direct function of motor performance.

Derivation of Line Current

In order to obtain the line current at a given load point, use will be made of equation 5. Since equation 5 was based on the vector sum of the three currents shown in equation 4, it follows that the line current is

$$I_L = VC_R C_x Y_e \quad (9)$$

The angle θ' is the angle between the internal voltage E and the line current and is obtained from the following relation

$$\theta' = \tan^{-1} \frac{L}{\frac{X_d}{R_{Fe}} + M} \quad (10)$$

Power Input per Phase, Power Factor and Efficiency

In order to obtain the power factor and subsequently the power input per phase, it will be necessary again to return to the following equation

$$E = E' \frac{1}{1 + \frac{x_1}{X_d}(L + jM)}$$

The angle between E and E' is obtained from

$$\beta_x = \tan^{-1} \frac{\frac{x_1}{X_d} M}{1 + \frac{x_1}{X_d} L} \quad (11)$$

Also, the following equation will be used

$$E' = V \frac{1}{1 + \frac{r_1 C_x}{X_d}(M - jL)}$$

The angle between E' and V is obtained from

$$\beta_R = \tan^{-1} \frac{\frac{r_1 C_x}{X_d} L}{1 + \frac{r_1 C_x}{X_d} M} \quad (12)$$

The power factor angle is then

$$\theta = \theta' - (\beta_R - \beta_x) \quad (13)$$

from which the power factor $= \cos \theta$.

The power input per phase is then

$$P = VI_L \cos \theta \quad (14)$$

The efficiency is then

$$\text{Efficiency} = \frac{\text{power output}}{\text{power input}} \text{ (per phase)} \quad (15)$$

Idle Conditions

At no load, the total reactance, X_{OD}, is as follows

$$X_{OD} = \frac{1}{Y_e} + x_1 \quad (16)$$

Therefore

$$I_d = \frac{V}{X_{OD}} \quad (17)$$

$$\text{The primary copper loss} = 3I_d^2 r_1 \quad (18)$$

$$\text{Total idle losses} = \text{Primary Copper loss} + (F\&W) + \text{iron loss}$$

Therefore

$$I_q = \frac{\text{total idle losses}}{3V} \quad (19)$$

From equations 17 and 19, the idle current then can be obtained

$$I_{NL} = Iq - jI_d \quad (20)$$

$$\text{No load power factor angle, } \theta = \tan^{-1} \frac{I_d}{I_q}$$

$$\text{No load power factor} = \cos \theta \quad (21)$$

Summation of Performance Equations

At this point, prior to an example, it might be well to sum up the equations required to determine the motor performance and also emphasize again the equations necessary for design by synthesis.

1. To determine the power output at a given torque angle:

$$\text{Shaft ouput} = \frac{V^2 C_R^2 C_x^2 M}{X_d} - \text{rotational losses, synchronous watts per phase} \quad (7)$$

2. To determine the maximum power output at a torque angle of $\delta = 45$ degrees

$$\text{Maximum output} = \frac{V^2 C_R^2 C_x^2 A}{2X_d} - \text{rotational losses} - \text{synchronous watts per phase} \quad (8)$$

3. To determine the line current I_L at the given torque angle as used above in item 1

$$I_L = VC_R C_x Y_e \quad (9)$$

4. To determine the power factor (same torque angle as in item 1)

$$\beta_x = \tan^{-1} \frac{\frac{x_1}{X_d} M}{1 + \frac{x_1}{X_d} L} \quad (11)$$

$$\beta_R = \tan^{-1} \frac{\frac{r_1 C_x}{X_d} L}{1 + \frac{r_1 C_x}{X_d} M} \quad (12)$$

$$\theta' = \tan^{-1} \frac{L}{\frac{X_d}{R_{Fe}} + M} \quad (10)$$

$$\theta = \theta' - (\beta_R - \beta_x) \quad (13)$$

where power factor $= \cos \theta$.

5. To determine the power input (same torque angle as in item 1)

$$P = VI_L \cos \theta \quad (14)$$

6. To determine the efficiency (same torque angle as in item 1)

$$\text{Efficiency} = \frac{\text{power output}}{\text{power input}} \text{ (per phase)} \quad (15)$$

7. To determine idle conditions

$$I_d = \frac{V}{X_{OD}} \quad (17)$$

$$\text{Primary copper loss} = 3I_d^2 r_1 \quad (18)$$

$$I_q = \frac{\text{total idle losses}}{3V}$$

$$I_{NL} = I_q - jI_d$$

$$\text{No load power factor angle, } \theta = \tan^{-1} \frac{I_d}{I_q}$$

$$\text{No load power factor} = \cos \theta$$

Example

(A). *Design by Synthesis.* As was pointed out in equations 7 or 8, it is possible to design a winding for either of two conditions, for example, (1) on the basis of the maximum torque desired, or (2) on the basis of the full load point at which the motor is to run. In either case equations 7 or 8 can be solved for X_d. It was previously pointed out that the following relation then applies

$$C = \sqrt{\frac{X_d \mu (10^8)}{2\pi f \wp_o K \omega^2 n}}$$

At this point, it would be well to explain that the configuration of the rotor punching along with the stator punching has

been determined. In other words, the stator and rotor punchings have been designed and it is only necessary to determine the constants from the punchings. The stator punching slot constant is determined in the usual manner as well as the slot constant for the rotor. Methods are available for the determination of the direct axis and quadrature axis permeances from the configuration of the rotor punching.

In order to determine C_x and C_R it is necessary to determine r_1/X_d and x_1/X_d. r_1 is set up as follows:

$$r_1 = \frac{(0.88)(l_c)(C^2)(10^{-8})}{\left(\frac{CM}{\text{slot}}\right)\left(\frac{Sp}{n}\right)} \tag{22}$$

Also

$$X_1 = (2\pi f)(C^2)(\mathcal{P}_L)(10^{-8}) \tag{23}$$

And since

$$X_d = \frac{(2\pi f)(C^2)(\mathcal{P}_D)(K\omega^2)(n)}{\mu}$$

Thus

$$\frac{r_1}{X_d} = \frac{(0.88)(l_c)(\mu)((10^{-8})}{\left(\frac{CM}{\text{slot}}\right)\left(\frac{Sp}{n}\right)(2\pi f)(K_w^2)(\mathcal{P}_D)(n)} \tag{24}$$

And

$$\frac{x_1}{X_d} = \frac{(\mathcal{P}_L)(\mu)}{(n)(K_w^2)(\mathcal{P}_D)} \tag{25}$$

In order to determine the full load operating point, it is necessary to decide or know what the full load torque angle, δ, will be. After δ has been chosen, then

$$C_x = \frac{1}{1+\frac{x_1}{X_d}(L+jM)} \tag{6A}$$

and

$$C_R = \frac{1}{1+\frac{r_1 C_x}{X_d}(M-jL)} \tag{6B}$$

Then

$$\text{shaft output} = \frac{V^2 C_R^2 C_x^2 Mn}{X_d} - \text{rotational losses (synchronous watts) from equation 7}$$

from which

$$X_d = \frac{V^2 C_R^2 C_x^2 Mn}{\text{shaft output} + \text{rotational losses}}$$

and

$$C = \sqrt{\frac{X_d \mu (10^8)}{2\pi f \mathcal{P}_D K_w^2 n}}$$

Since from equation 22 the copper slot loading was assumed (CM/slot) and in the actual design the copper slot loading will be held to a value close to the original assumption, the actual full load point will fall very close to the assumed value.

In order to design for a given maximum torque, it was previously pointed out that it is necessary to assume $\delta = 45$ degrees. The procedure can then be followed as outlined in the preceding paragraphs to determine X_d and subsequently C. After the total conductors per phase have been determined, the wire size can be chosen which will result in a slot loading as close as possible to the assumed value.

Example of Design by Synthesis. Assume the requirements of a motor as follows: 1/4 horsepower, 220 volts, 3 phase, 60 cycles, 1,200 rpm.

$$\frac{\text{Maximum torque (synchronous)}}{\text{Synchronous full load torque}} = 1.81$$

The following constants have been determined by calculation or obtained from similar calculations:

$\mathcal{P}_D = 19.8$	$Sp = 36$
$\mathcal{P}_L = 5.17$	$K_w = 0.966$
circuits $= 2Y$	$V = 127$ per phase
coil throw 1–7	$\delta = 45$ degrees
assume $\frac{\text{Cm}}{\text{slot}} = 85{,}000$	$\mu = 1.05$ (assumed)
	$A = 2.03$
$l_c = 8.43$	Pole embrace $= 50$ per cent

Therefore, from equation 24

$$\frac{r_1}{X_d} = \frac{(0.88)(8.43)(1.05)(10^{-8})}{(85{,}000)(12)(377)(0.933)(19.8)(3)}$$

$$= 0.0364 \text{ (hot value} = 0.0412)$$

and from Equation 25

$$\frac{x_1}{X_d} = \frac{(5.17)(1.05)}{(3)(0.933)(19.8)}$$

$$= 0.098$$

Then, from equation 6A

$$C_x = \frac{1}{1+0.098(2.015+j1.015)}$$

$$= \frac{1}{1.221}$$

$$C_x = 0.819$$

From equation 6B

$$C_R = \frac{1}{1+(0.0412)(0.819)(1.015-j2.015)}$$

$$= \frac{1}{1.0744}$$

$$C_R = 0.93$$

From equation 8

$$X_d = \frac{(127)^2(0.819)^2(0.93)^2(1.015)(3)}{337+36}$$

$$= 76.5 \text{ ohms}$$

$$C = \sqrt{\frac{(76.5)(1.05)(10^{+8})}{(377)(19.8)(0.933)(3)}}$$

$$C = 619$$

The nearest turns per coil, which will result in a total number of series conductors per phase, which approaches 619, will be 52 turns per coil. Therefore, 52 turns per coil will be used with a conductor size of number 21. The total series conductors per phase will be 624 and the circular mils of copper per slot will be 84200.

With the above turns per coil and wire size, the following constants result:

$r_1 = 3.21$ (hot) ohms
$x_1 = 7.6$ ohms
$X_d' = 81.3$ (unsaturated) ohms
$\mu = 1.05$
$X_d = 77.4$ (saturated) ohms

Thus,

$$\frac{r_1}{X_d} = 0.0415 \text{ and } \frac{x_1}{X_d} = 0.0983$$

$$C_x = \frac{1}{1+0.0983(2.015+j1.015)}$$

$$= \frac{1}{1.217}$$

$$C_x = 0.824$$

$$C_R = \frac{1}{1+(0.824)(0.0415)(1.015-j2.015)}$$

$$= \frac{1}{1.0756}$$

$$C_R = 0.93$$

$$\text{Maximum output} = \frac{(127)^2(0.824)^2(0.93)^2(1.015)(3)}{77.4} - 36$$

$$= 373 - 36$$

$$= 337 \text{ synchronous watts}$$

$$\text{Maximum torque} = \frac{(112.7)(337)}{1{,}200}$$

$$= 31.6 \text{ ounce feet}$$

The tested value of maximum torque was 33.6 ounce feet. If it is necessary to design the motor for a specified torque angle at full load, the same procedure is followed as shown except that the torque angle δ will be the specified value instead of the value of 45 degrees, as used for the maximum output condition.

(B). *Performance Calculation.* For the second part of the example, a performance prediction will be illustrated. Assume the same motor as illustrated in part (A) of the example.

1/4 horsepower, 3 phase, 220 volts, 60 cycles, 1,200 rpm

As shown in the nomenclature, the

direct axis reactance used is the saturated value, therefore, for each performance point, the direct axis reactance X_d will differ depending on the degree of saturation assumed.

Full load constants:

$X_d = 76$ ohms

$r_1 = 3.21$ ohms

$x_1 = 7.6$ ohms

assumed full load torque angle, $\delta = 13.1$ degrees

Total iron loss = 37 watts

$$A = \frac{X_d}{X_q} - 1 = 2.03$$

$R_{Fe} = 1{,}308$ ohms

From the constants

$$L = 1 + A \sin^2 \delta \qquad (5B)$$

$$= 1 + 2.03 \sin^2 13.1$$

$$= 1.105$$

$$M = \frac{A}{2} \sin^2 \delta \qquad (5A)$$

$$= \frac{2.03}{2} \sin^2 6.2$$

$$= 0.447$$

Then

$$C_x = \frac{1}{1 + \frac{x_1}{X_d}(L + jM)} \qquad (6A)$$

$$= \frac{1}{1 + 0.1(1.105 + j0.447)}$$

$= 0.9$ with the angle between E and E' equal to

$$\beta_x = \tan^{-1} \frac{\frac{x_1}{X_d} M}{1 + \frac{X_1}{X_d} L} = 2.31 \text{ degrees} \qquad (11)$$

$$C_R = \frac{1}{1 + C_x \frac{r_1}{X_d}(M - jL)} \qquad (6B)$$

$$= \frac{1}{1 + (0.9)(0.0422)(0.447 - j1.105)}$$

$$= 0.985$$

with the angle between E' and V equal to

$$\beta_R = \tan^{-1} \frac{\frac{r_1 C_x}{X_d} L}{1 + \frac{r_1 C_x}{X_d} M} = 2.37 \text{ degrees} \qquad (12)$$

$$Y_e = \frac{\frac{X_d}{R_{Fe}} + M - jL}{X_d} \qquad (5)$$

$$= \frac{0.058 + 0.447 - j1.105}{76}$$

$$Y_e = \frac{1.22}{76} = 0.01605 \text{ mhos}$$

with the angle between E and the line current equal to

$$\theta' = \tan^{-1} \frac{L}{\frac{X_d}{R_{Fe}} + M} \qquad (10)$$

$= 65.5$ degrees

Thus, the line current

$$I_L = V C_R C_x Y_e \qquad (9)$$

$$= \frac{(127)(0.985)(0.9)(1.22)}{76}$$

$$I_L = 1.81 \text{ amperes}$$

The power factor then is

$$\theta = \theta' - (\beta_R - \beta_x) \qquad (13)$$

$$= 65.5 - (2.37 - 2.31)$$

$= 65.44$ degrees

power factor = cos 65.44

$= 0.415$

The power input is

$$P = (3)(127)(1.81)(0.415) \qquad (14)$$

$= 286$ watts

The shaft output is then

$$\text{Output} = \frac{V^2 C_x^2 C_R^2 M n}{X_d} - \text{rotational losses} \qquad (7)$$

$$= \frac{(127)^2(0.9)^2(0.985)^2(0.447)(3)}{76} - 36$$

$= 188$ watts or 0.252 horsepower

The efficiency is

$$\text{efficiency} = \frac{188}{286} \times 100 \text{ per cent} = 65.6 \text{ per cent} \qquad (15)$$

The idle conditions are determined as follows:

$X_d = 75.2$ ohms

then

$$X_{OD} = \frac{1}{Y_e} + X_1 \qquad (16)$$

$$= 75 + 7.6$$

$X_{OD} = 82.6$ ohms

$$I_d = \frac{V}{X_{OD}} = \frac{127}{82.6} = 1.535 \text{ amperes} \qquad (17)$$

$$\text{Primary copper loss} = 3 I_d^2 r_1 \qquad (18)$$

$$= (3)(1.535)^2(3.21)$$

$= 22.7$ watts

Total idle losses = primary copper loss + ($F\&W$) + iron loss

$$= 22.7 + 25 + 37$$

$= 84.7$ watts

$$I_q = \frac{\text{total idle losses}}{3V} \qquad (19)$$

$$= \frac{84.7}{(3)(127)}$$

$I_q = 0.222$ ampere

Thus

$$I_{NL} = I_q - jI_d = 0.222 - j1.535 = 1.55 \text{ amperes} \qquad (20)$$

The no-load power factor angle

$$\theta = \tan^{-1} \frac{I_d}{I_q}$$

$$= \frac{1.535}{0.222}$$

$\theta = 81.8$ degrees

power factor = 0.143 (21)

A comparison between the calculated and the tested performance values is shown in Table I.

Conclusion

As was pointed out in the first paragraph of this paper, a gap existed in the three steps of reluctance motor design. The intention of this paper is to provide a means of direct calculation of the stator turns and wire size based on the desired motor performance. This process has been called design by synthesis. In addition to the ability to design directly for the desired performance, a performance method has been presented which takes into account the voltage drop of the stator. This correction provides an accurate method for performance prediction, which has not been available up to the present time. The design method is further supplemented by an equivalent circuit, which is concise in form and which makes use of

Table I

	Calculated	Tested
Full Load Performance Values		
Shaft watts output	188	187
Total watts input	286	288
Line current, amperes	1.81	1.79
Efficiency, per cent	65.6	64.8
Power factor	0.415	0.422
No Load Performance Values		
No load current, amperes	1.55	1.54
No load watts input	84.7	80
No load power factor	0.143	0.136
Maximum torque, ounce feet	31.6	33.6

circuit parameters which are generally known and accepted.

References

1. Performance Calculations on Polyphase Reluctance Motors (Synchronous Motors Without Field Excitation), P. H. Trickey. *AIEE Transactions*, volume 65, April 1946, pages 191–93.

2. Synchronizing Torque of an Unexcited Salient Pole Motor, R. D. Ball. *Electrical Engineering*, volume 52, February 1933, pages 136–37.

3. Graphical Determination of Magnetic Fields—Practical Applications to Salient-Pole Synchronous Machine Design, Robert W. Wieseman. *AIEE Transactions*, volume 46, February 1927, pages 141–54.

4. Calculation of Synchronous Machine Constants, L. A. Kilgore. *AIEE Transactions*, volume 50, December section, 1931, pages 1201–14.

5. Machine Synthesis—An Encounter with an Idea, T. C. Lloyd. *Electrical Engineering*, volume 69, number 11, November 1950, pages 1001–03.

No Discussion

Improved Core Form Transformer Winding

E. J. GRIMMER
MEMBER AIEE

W. L. TEAGUE
FELLOW AIEE

A NEW type of pancake winding for high-voltage core form transformers has been developed to give this important line of electric equipment greatly improved surge distribution characteristics. This improved winding does not depend upon electrostatic shields or other external devices to accomplish this end, but by a simple disposition of turns the series capacitance is increased to such an extent that almost uniform distribution of surge voltages through the winding is achieved. This type of winding was originally developed and patented in England by G. F. Stearn of the English Electric Company. It is the purpose of this paper to describe the winding and show the results of additional development and thorough investigation carried on by the authors. By improving methods of calculating surge distribution, and developing methods of winding these coils as continuous windings the scheme has been adapted to make it thoroughly practical on a commercial scale in this country.

As is well understood, the distribution of surge voltage through conventional pancake core form windings differs greatly from the straight line voltage distribution which exists due to the application of voltages at normal operating frequencies. Figure 1 shows curves of voltage distribution through a conventional pancake winding which must have extra insulation and spacing at the line ends to increase the insulation strength at these points since they are the places of greatest stress. A 1.5 by 38 microsecond negative wave was used for these tests. The straight line indicates the normal operating voltage distribution for the transformer which is directly proportional to the turns.

The lower curve indicates initial distribution of surge voltage through the winding. It shows the instantaneous distribution of voltage when a surge is applied to one end of the winding with the other end grounded. This distribution is entirely determined by the capacitance characteristics of the winding. There are two components of this capacitance. One is the capacitance to ground (C_G). This includes the capacitance between the winding under test and all other windings in the transformer and the capacitance between this same winding and the tank and core. The other component is the series capacitance (C_S). This consists of the capacitance between turns and between sections of the winding.

The expression for the curve of initial voltage distribution is:

$$e = E \frac{\sinh \alpha Y}{\sinh \alpha}$$

where

e = the voltage from ground to any point in the winding
E = the surge voltage applied to the winding
Y = the position of the point in the winding from ground with respect to the total winding
α = the distribution constant $= \sqrt{C_G/C_S}$

As the α factor is decreased in value the curve of initial distribution approaches the straight line of uniform distribution, see Figure 2. Any change in the design of the transformer which decreases the α factor of the winding causes more uniform distribution and reduces the voltage stresses between parts of the winding.

The upper curve of Figure 1 shows the maximum crests of voltages that are obtained in any part of the winding due to oscillations in the winding when surges are impressed on its terminals as described above. The curve shows that parts of the winding as far down as the center may oscillate higher than the impressed voltage on the line terminal. Oscillations within the area between the initial and maximum distribution curves cause voltage stresses between parts of the winding and between parts of the winding and ground. Any factor or factors in the design which decrease this area will reduce the stresses.

The greatest part of the capacitance of a winding-to-ground consists of the capacitance of that winding to other windings on the same leg of the core. For instance, the greater part of the C_G of a single high-voltage winding consists of the capacitance of that winding to the low-voltage winding on the same leg. This capacitance is determined by the circumferential area between the high-voltage and the low-voltage windings, the radial separation between them and the dielectric constants of the insulation between them. These factors are rather firmly fixed by the major insulation and clearances required by the voltage class

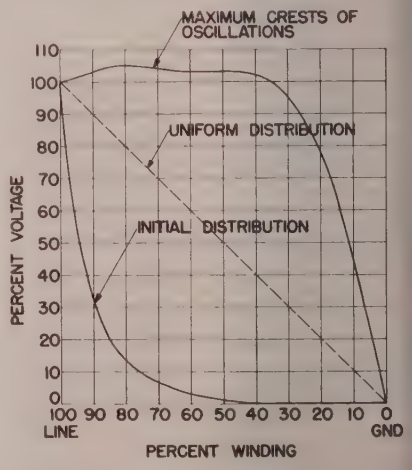

Figure 1. Surge voltage distribution in conventional core form transformer winding

Paper 51-178, recommended by the AIEE Transformers Committee and approved by the Technical Program Committee for presentation at the AIEE Great Lakes District Meeting, Madison, Wis., May 17–19, 1951. Manuscript submitted October 25, 1950; made available for printing March 29, 1951.

E. J. Grimmer and W. L. Teague both are with Westinghouse Electric Corporation, Sharon, Pa.

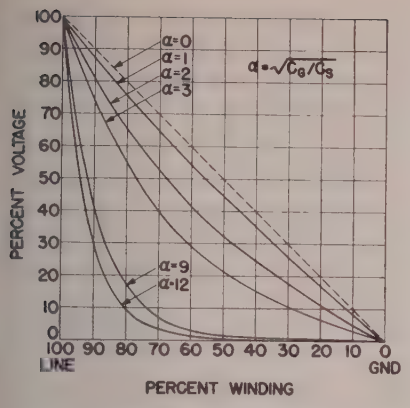

Figure 2. Initial surge voltage distribution for various values of distribution constant

of the high-voltage winding and the impedance and regulation requirements of the transformer. Addition of electrostatic shields in the high-low space may reduce the capacitance to ground but they necessarily introduce more insulation clearance between the high-voltage and low-voltage windings and also penalize the design from an impedance standpoint. The other capacitances from the winding to tank wall, the core, and other phases and leads all add to the capacitance to ground. Any attempt to decrease the α of the winding by decreasing its capacitance to ground is therefore definitely limited.

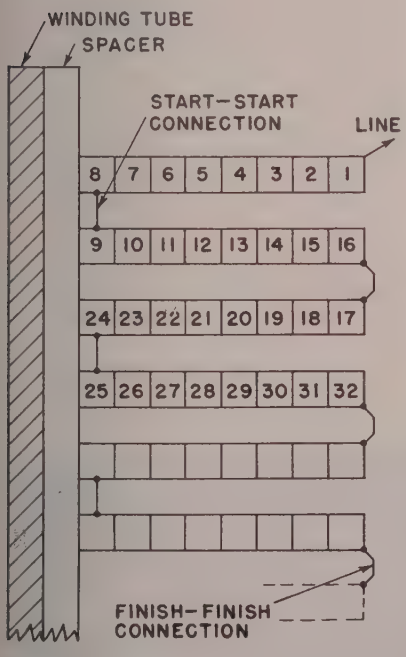
WINDING TUBE
SPACER
START–START CONNECTION
LINE
8 7 6 5 4 3 2 1
9 10 11 12 13 14 15 16
24 23 22 21 20 19 18 17
25 26 27 28 29 30 31 32
FINISH–FINISH CONNECTION

Figure 3. Sectional view of conventional pancake winding showing arrangement of turns. The sections are wound with a single conductor. The turns are numbered from the line

The series capacitance (C_S) of an ordinary pancake winding for core form transformers consists of the turn-to-turn capacitance of all the series turns in the winding and the section-to-section capacitance of all the series sections in the winding. Although the capacitance of one turn to its adjacent turns is considerable, all the turn-to-turn capacitances are in series so the resultant for a complete winding is very small. The capacitances between sections are all in series so that they also add up to a very small value. As coils are designed for higher voltages, or as greater insulation strength is required for nonuniform voltage distribution, additional turn-to-turn insulation and larger ducts between sections further reduce the series capacitance of the winding which results in still higher stresses between winding parts. The total series capacitance of the conventional pancake winding is so small compared to the capacitance to ground that α factors greater than ten are common for high-voltage windings (above 69 kv).

Various methods of winding coils and applying electrostatic shielding to them have been developed in an attempt to overcome this inherent disadvantage of strap wound pancake coils. Some of the methods employed were quite successful but all these devices made the assembly of the transformer more complicated and required more space and material and consequently increased the size and weight of the complete assembly.

Transformer designs employing the shell form construction do not present the same problem because they have fewer coil sections in series and greater surface on the face of each section so that the capacitance to ground is small and the series capacitance is large. These factors result in low values of α, and in long natural periods of oscillation.

The new method of winding core form pancake coils as hereinafter described increases the series capacitance (C_S) very greatly, and reduces the capacitance to ground (C_G) somewhat because of a better space factor in the new winding. Both these factors result in lower values of α and consequently in lower dielectric stress. The coils retain all the advantages of ordinary pancake windings. They are simple in construction and easy to wind. They have excellent ventilation for thermosiphon cooling. They are readily accessible for complete inspection of materials and workmanship thus assuring a uniform quality product. They have great mechanical strength to withstand short circuit stress and can be handled conveniently during manufacture without

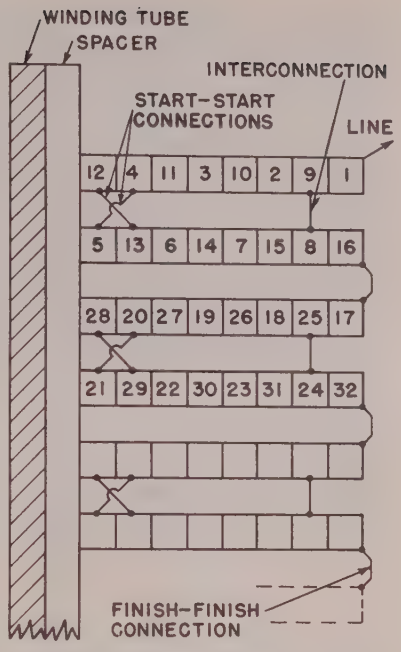
WINDING TUBE
SPACER
INTERCONNECTION
START–START CONNECTIONS
LINE
12 4 11 3 10 2 9 1
5 13 6 14 7 15 8 16
28 20 27 19 26 18 25 17
21 29 22 30 23 31 24 32
FINISH–FINISH CONNECTION

Figure 4. Sectional view of high series capacitance winding. The sections are wound with two conductors in parallel and are interconnected so that turns as numbered from the line are placed as shown

damage. No new manufacturing facilities, processing procedures or maintenance problems are introduced. All these advantages make this new winding most attractive to the purchaser as well as the manufacturer.

Figure 3 shows a conventional pancake winding. Each section consists of eight turns in direct order, one above the other. The pancake sections are wound or assembled on the winding tube. Alternate sections are connected start-start and finish-finish as shown. Only a small part of the winding is illustrated but it is uni-

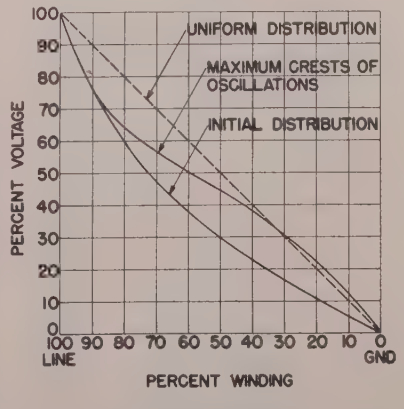

Figure 5. Surge voltage distribution in high series capacitance core form transformer winding

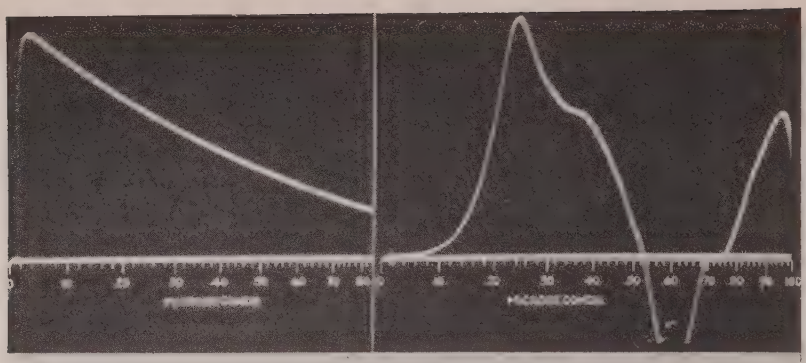

(A) (B)

Figure 6. Typical oscillograms of measured surge voltage in conventional core from winding

(A) Applied wave at line terminal
(B) Voltage at midpoint of winding

form throughout. This winding has a very small value of series capacitance and would have a surge distribution similar to that shown in Figure 1.

Figure 4 shows a similar winding wound by the new method to increase its series capacitance. Because of this character istic it is called the high series capacitance winding. The increase in series capacitance is obtained by the disposition of turns. Turns 1, 2, 3, and 4 are in Section 1 but they are separated from each other by turns 9, 10, and 11, respectively. A start-start connection is made between turn 4 in Section 1 and turn 5 in Section 2. Turns 5, 6, 7, and 8 are wound in Section 2 but they are separated from each other by turns 13, 14, and 15. Interconnection is made between turns 8 of Section 2 and 9 of Section 1. The start-start connection between turn 12 of Section 1 and turn 13 of Section 2 completes the circuit so that the conductor is continuous from turn 1 to turn 16. The two start-start connections are transposed. The rest of the sections in the winding are wound the same way and finish-finish connections are made between pairs of these interconnected sections.

The series capacitance of two of these sections is many times greater than the turn-to-turn capacitance in two of the conventional pancake sections. The two high series capacitance sections are similar to two wound-type capacitors connected in parallel with a voltage between the electrodes equal to half the voltage between sections. There also is some capacitance between the two sections, but since these are connected together at the start-start and at the interconnection this capacitance is negligible. There is series capacitance between the sections which are connected finish-finish. This is in parallel with the turn-to-turn capacitance and adds to it; however, this also is a small part of the total series capacitance.

Calculations indicate, and tests have verified, that the distribution of surge voltage throughout a pair of high series capacitance sections is practically the same as the distribution of turns. The potential at the interconnection between two sections is midway between the potentials of the finishes of those two sections. The turn-to-turn voltage therefore is equal to half the voltage across the pair of interconnected sections, and all turn-to-turn insulation throughout the winding is approximately equally stressed. In the conventional winding, it has long been understood that the turns nearest to the line terminal must withstand the highest surge stress. For this reason sometimes the turn insulation near the line end is increased. More often the turn-to-turn insulation is made strong enough at the line end and then the same thickness of insulation is used throughout the winding. Since the surge does not "pile up" on the line turns of the high series capacitance winding, and all turn-to-turn insulation is essentially uniformly stressed, a more economical use can be made of that insulation. This results in an improved space factor, smaller size, and less weight of the completed assembly.

Figure 5 shows the voltage distribution curves of a high series capacitance winding comparable in size and rating to the winding to which Figure 1 applies. In these tests 0.7 by 58 microsecond negative waves were used. The lower curve for initial distribution is now much nearer the ideal curve for uniform distribution. The distribution of surge voltages in this winding is therefore almost the same as the distribution of the working voltages at normal frequencies. The curve for maximum crest voltage of oscillation coincides with the curve for initial distribution for the first 15 per cent of the winding near the line end since no oscillations are developed in that part of the winding. The reason for this is the close coupling between turns in the sections.

Figure 7. Traces of oscillograms showing voltage to ground at various points in conventional core form winding

1. Applied wave at line terminal
2. Voltage at 87.5 per cent of winding
3. Voltage at 75 per cent of winding
4. Voltage at 50 per cent of winding
5. Voltage at 25 per cent of winding

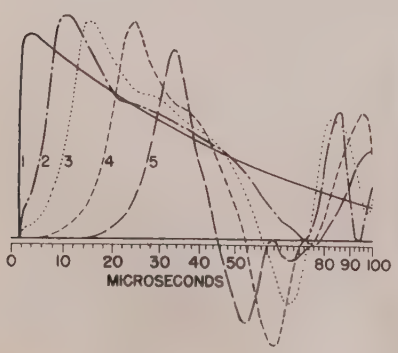

Figure 8. Typical oscillograms of measured surge voltage in high series capacitance core form winding

(A) Applied wave at line terminal
(B) Voltage at midpoint of winding

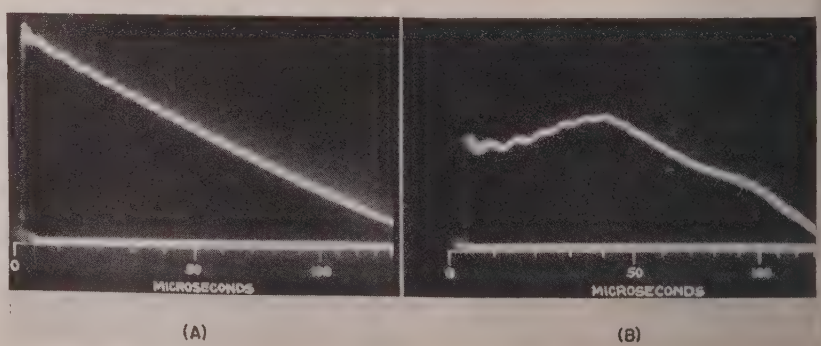

(A) (B)

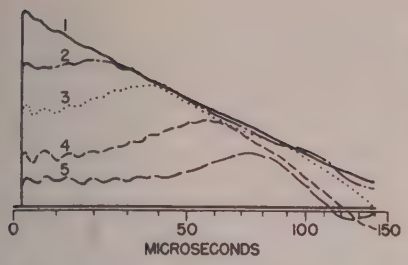

Figure 9. Traces of oscillograms showing voltage to ground at various points in high series capacitance core form winding

1. Applied wave at line terminal
2. Voltage at 87.5 per cent of winding
3. Voltage at 75 per cent of winding
4. Voltage at 50 per cent of winding
5. Voltage at 25 per cent of winding

The curve then gradually rises slightly above the curve for uniform distribution near the grounded end of the winding. The oscillations in the winding are so small that they are of very little importance.

In the conventional pancake winding the normal dynamic turn-to-turn stress is only the normal volts per turn. However, since the line turns have to be insulated for nonuniform distribution of surge voltages, excessive margins are obtained from the standpoint of normal dynamic turn-to-turn stress. At first analysis it appears that since the normal dynamic voltage stress between turns in the high series capacitance winding is equal to volts per turn times the turns per section, great amounts of extra turn insulation would be required to withstand such stress. However, with the more uniform distribution of voltage in the high series capacitance winding, the surge stress between turns is reduced so that the margins for surge strength and for normal dynamic strength can be made more equal. The turn-to-turn insulation is therefore used to better advantage.

The near uniform distribution of impulse voltage in the high series capacitance winding also improves the application of the section-to-section insulation throughout the winding. The impulse voltage stress between adjacent sections is reduced and the stress between all sections which are connected finish-to-finish is practically equal. The stress between the interconnected sections is only twice the turn-to-turn stress. The high localized stresses at the line end, which are common with conventional pancake windings, are eliminated in this new winding and better use is made of the section-to-section insulation.

Figures 6 and 7 show some of the oscillograms of surges applied to a conventional winding. Data from these and similar records are plotted in the curves of Figure 1. Figures 8 and 9 are the oscillograms of surges applied to a high series capacitance winding. These supplied some of the data for the curves of Figure 5.

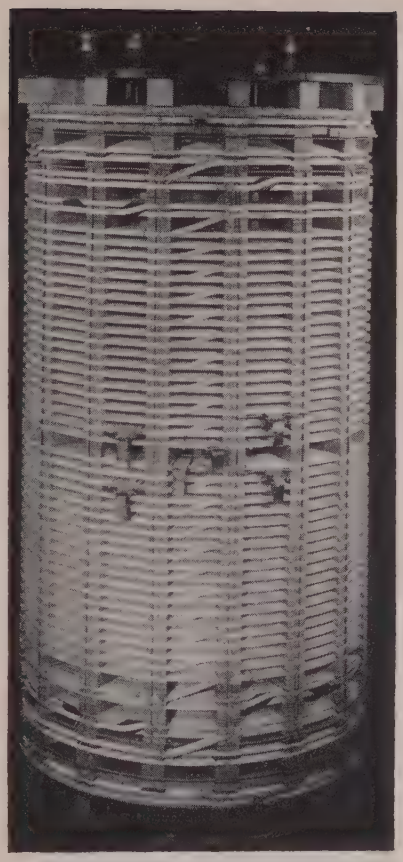

Figure 10. 115-kv conventional core form winding with special sections and insulation at line ends

A conventional core form pancake winding, except for special sections at the line ends, is shown in Figure 10. This picture shows the coil clamped to correct height before it is assembled in the core. The winding is comparable in size and rating to the one to which Figures 1, 6, and 7 apply and shows the general construction of 115-kv coils.

Figure 11 shows a high series capacitance winding before it is assembled on the core. This also is a 115-kv coil and has about the same kilovolt-ampere rating as the coil in Figure 10. The interconnection in each pair of sections, and the finish-finish connection between pairs of sections can be clearly seen. The smaller ducts between sections and the uniformity of the winding throughout the coil are also apparent.

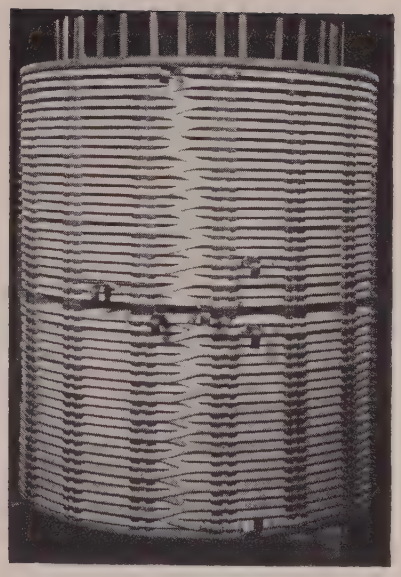

Figure 11. 115-kv high series capacitance winding

This high series capacitance winding has been proved by complete surge investigation and complete surge tests. It has been successfully used in England for $2^1/_2$ years and as a result of the investigations described in this paper has also been applied to commercial use in this country. Its development and use is a great step forward in the art of transformer design. It is progress toward the goal to make core form transformers immune to lightning failure.

References

1. Design of Power Transformers to Withstand Surges Due to Lightning, With Special Reference to a New Type of Winding, **A. T. Chadwick, J. M. Ferguson, D. H. Ryder, G. F. Stearn.** *Paper S-987*, Institution of Electrical Engineers (London, England).

2. Effect of Surges on Transformer Windings, **J. K. Hodnette.** *AIEE Transactions*, volume 49, January 1930, pages 68–75.

3. Abnormal Voltages Within Transformers, **L. F. Blume, A. Boyajian.** *AIEE Transactions*, volume 38, Part 1, 1919, pages 577–614.

4. Analysis of Transient Voltages in Networks, **P. L. Bellaschi, A. J. Palermo.** *AIEE Transactions*, volume 59, 1940, pages 973–81.

5. Transformer Winding, **G. F. Stearn.** British Patent Number 587997. United States Patent Number 2,453,552.

6. Winding Special Continuous Coils, **F. D. Fielder, E. J. Grimmer.** United States Patent Number 2,393,037.

Discussion

J. R. Meador (General Electric Company, Pittsfield, Mass.): The authors have the following to say about core-type concentric disk coil windings:

"The coils retain all the advantages of ordinary pancake windings. They are simple in construction and easy to wind. They have excellent ventilation for thermosiphon cooling. They are readily accessible for complete inspection of materials and workmanship thus assuring a uniform quality product. They have great mechanical strength to withstand short circuit stress and can be handled conveniently during manufacture without damage."

This is a very good appraisal and one with which we heartily agree. From the standpoint of impulse voltage strength there is another major advantage that should be added to the above list. In this construction the ends of the winding are widely separated and the normal voltage per unit of winding height is very low. If a reasonably good voltage distribution is obtained, there is no need for intricate insulation structures between parts of the winding.

Two methods are available for improving the impulse voltage distribution in the winding; namely, electrostatic shielding, and interlacing of turns.

Blume and Boyajian in 1919 presented a pioneering paper[1] that put the impulse voltage distribution problem on an engineering basis. Several years later their coworkers developed the nonresonating transformer, which made the first large scale use of electrostatic shielding. About ten years later a greatly simplified form of shielding, known as cascade rib shielding, was introduced for use in the operating voltage range from 44 kv to 138 kv. These developments permitted the design of a line of core-type transformers provided with shielding consistent with the voltage and size of the transformer, having available the means for obtaining any desired initial impulse voltage distribution. The shields do not detract from the basic advantages of the core-type concentric disk coil winding.

Many schemes have been devised for improving impulse voltage distribution without shielding. In general, they involve some unusual arrangement of the turns in the winding that has the effect of changing the relative series and ground capacitances. The interlaced turn winding described by the authors does this to a marked degree.

Our investigations of this and other somewhat similar winding arrangements have shown that improved voltage distribution is usually achieved at the expense of locating nonconsecutive turns or coils adjacent to one another. This usually limits the field of application to a certain range of transformer proportions. For example, the author's Figure 4 shows that the voltage of one coil section appears between all adjacent turns of the winding. A 115-kv delta-connected winding in a transformer of moderate size may have 30 turns or more per coil section. Thus, 30 times normal voltage appears not only between all adjacent turns of the interlaced winding but also at all connections between sections where conductors bend and cross to the next section. Also, the reduction in impulse voltage between turns must be in the ratio of 30:1 to maintain the same safety factor. Do the authors believe such a case comes within the application range of the winding arrangement they have described? If so, would they care to comment on why it is more attractive than the simple shielding that permits the same winding space factor to be achieved?

REFERENCE

1. ABNORMAL VOLTAGES WITHIN TRANSFORMERS, **Louis F. Blume, A. Boyajian.** *AIEE Transactions*, volume 38, 1919, pages 577–620.

A. Boyajian (General Electric Company, Pittsfield, Mass.): It is interesting that the authors recognize the various intrinsic merits of the core-type concentric transformer construction, such as the superior electrical, mechanical, and thermal characteristics.

Transformers generally require some means of controlling their impulse voltage distribution, and this paper features the Stearn type of shielding, instead of the well-recognized method (the Blume-Lennox type of shielding) used very successfully during the past quarter century on millions of transformer kilovolt-amperes, many of them being among those in the highest voltage and largest kilovolt-ampere class.

The curve of the voltages to ground given by the authors is good, but they have neglected the more important curve, namely, that of the maximum impulse-voltage gradients within the winding.

We may properly ask what price has been paid to secure the improved voltages to ground by the proposed method instead of the usual method. Whereas in the usual method a shield external to the winding is used, in the Stearn method adjacent coils are interwound turn by turn, so as to modify each other's capacitive voltage distributions. The authors admit that this greatly increases the dynamic voltage stresses of the turn-to-turn insulation, even though it is claimed that this is within safe limits. In the customary method of shielding, the normally low dynamic stresses on turn insulation are unaffected by the external shield. Just what the proposed interwinding of the coils does to the turn-insulation stress is shown in Figure 1 of this discussion. The successive turns of the winding are 1, 2, 3, . . . but they are not adjacent. Instead, we see that the adjacent turns are 1, 21, 2, 22, . . ., as a consequence of which the potential progresses along the saw-tooth curve shown. The dynamic voltage across the turn insulation caused by the interwinding is ΔE_W, that corresponding to the normal design (with external shields) is ΔE_G, and the ratio of these two stresses may be of the order of 20–25 to 1. Such intermixing of the turns of different coils, having very different dynamic potentials, must cause the conservative designer to hesitate when a safer alternative is available in the customary external shielding with a long successful experience behind it.

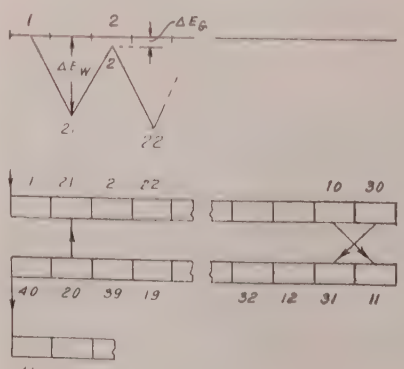

Figure 1. Stearn type interwound disk coils

The authors show their old design, Figure 10, and their new design Figure 11 for comparison, and from those figures one can easily see the reason for their enthusiasm. But their old design is not the customary shielded concentric transformer used extensively during the past quarter century. In the latter, the windings are compact, and the shields—arranged like "ribs" around the disk coils—so simple and unobtrusive. They neither intrude into the winding nor modify the structure and arrangement of the coils in any way, or interfere with the inspection of the coil sections. They can be removed easily without disturbing the windings, and they introduce no criss-cross voltages either into the dynamic or the impulse gradients.

The proposed construction also goes contrary to an important design principle known as the Weed principle.[1] This principle states that a winding will be nonoscillating if the inductive and capacitive voltage distributions are alike, otherwise the difference will set up an oscillation under conditions favorable to it, and such an oscillation may result in gradients much larger than the dynamic gradients.

Now, as in the case of any other principle, if the Weed principle is clearly recognized, it is sometimes permissible to make small departures from it. However, the introduction of such a drastic departure as that shown in Figure 1 of this discussion must cause some concern. Even though the unit tested by the authors may have had permissible gradients, the absence of an avowed aim to approximate the Weed principle incurs in other cases the possibility of unexpectedly large local oscillatory gradients under switching surges, even though no breakdown may be observed during the acceptance tests.

The proposed structure is an interesting novelty.

REFERENCE

1. PREVENTION OF TRANSIENT VOLTAGE IN WINDINGS, **J. M. Weed.** *AIEE Transactions*, volume 41, 1922, pages 145–55.

H. L. Cole (Westinghouse Electric Corporation, Sharon, Pa.): The authors have described a unique method of obtaining a high series capacitance in a transformer winding. It is especially useful in high-voltage core form windings, which have long and narrow stacks of pancake coils. The authors point out that in transformers with shell form construction the problems of obtaining surge strength are different because the series capacitance of the winding is inherently large.

There are some applications of shell form windings, however, in which the use of this new principle can be made to good advantage. Series transformers, used in tap changing under load applications, are exposed to severe impulse voltages across the windings when they are connected in or near

the line terminals of the main transformer. In such cases, the interleaving of the turns within the coils of a shell form series transformer winding will greatly increase the series capacitance of the winding and reduce the concentration of voltage stresses.

Another application of the high series capacitance winding for shell form transformers is in the line end of autotransformers, where the ratio of transformation is at or near unity. For example, an autotransformer for tying in 138-kv and 115-kv transmission lines, with taps to vary the ratio, presents an unusual problem of coil insulation which is greatly simplified by application of the high-series-capacitance principle.

Such an application has already been made to windings on a commercial order. This is pointed out to show that the invention is not strictly limited to windings of the core form although it finds its principal application in such transformers, but also finds applications on other forms of construction where a higher series capacitance is desired than is inherent in the design.

Much development work has been done by the authors to make this idea feasible and practical to apply to transformer design and manufacture. They are to be congratulated for their important contribution to the transformer art.

E. J. Grimmer and W. L. Teague: In their discussions Mr. Meador and Mr. Boyajian agree with our appraisal of the core form of construction. This evaluation should not be a surprise to them, for our many years of experience in manufacturing both core and shell form transformers puts us in a position to know the inherent advantages and limitations of both forms of construction.

With reference to Mr. Meador's questions, the high series capacitance winding can be satisfactorily applied to a 115-kv delta-connected winding of moderate size. It was pointed out in the paper that the normal dynamic voltage stress between turns in the winding is equal to the volts per turn times the turns per section. It is a simple matter to insulate for such voltages. The stresses are definitely known. They come well within the range of values that have been successfully used between adjacent conductors with normal insulation practices for years. Hence, no new insulation problems are involved. The high series capacitance winding is attractive because the improved voltage distribution is obtained by a simple disposition of turns. In the case of shielded windings, the shields are connected to the line where they are subjected to the maximum dynamic and impulse voltages. The shields must be insulated for these high voltages from the windings, from other shields, and from ground.

Referring to Mr. Boyajian's discussion, the voltages at various points in the coil stack are plotted against time in Figure 9. These curves show that the maximum gradient is at the line end of the winding at near zero time. Hence, in the region of the winding adjacent to the line, the maximum voltage between any two points is given by the initial voltage distribution curve.

Mr. Boyajian has questioned the possibility of dangerous oscillations. The voltage oscillograms in Figures 8 and 9 show that no such oscillations occur. The reason that the winding does not oscillate appreciably is that the fundamental principle of having the capacitance and inductance distribution of the winding as a whole approach the same value has been met. This is shown in Figures 5 and 9. The small differences due to the interleaving of the turns are adjusted with negligible oscillations because with their short period these small increments of winding can respond to any practical rates of change to which they are subjected. One familiar with the impulse characteristics of such windings should certainly have no anxiety about their performance on switching surges where the rates of changes are relatively slow.

Mr. Cole has pointed out that this new type of winding has many special applications in both core and shell form transformers. In modern transformer design, it is often advantageous to increase the capacitance across a certain portion of a winding to bring the capacitance and inductance distribution close together to avoid oscillations. This type of winding offers opportunity in this respect for ingenious and clever methods in design. Hence, the high series capacitance winding is much more than an "interesting novelty." It is a valuable tool for designers and represents progress in the art of transformer design.

Piezoelectric Crystals as Sensing Elements of Pressure, Temperature, and Humidity

E. A. ROBERTS
NONMEMBER AIEE

P. GOLDSMITH
ASSOCIATE AIEE

DURING the past 30 years piezoelectric crystals have found increasing use in engineering applications. This class of materials has been used as frequency-stabilizing elements for transmitters and frequency standards, as electromechanical transducers in phonograph pickups and accelerometers, and as elements in wave filters and supersonic delay lines. In these applications care frequently is exercised to prevent the crystal from being affected by atmospheric changes; in many cases hermetic or vacuum sealing and temperature control is used to insure stability of operation.

Methods of using piezoelectric crystals and associated electronic circuits to detect and measure changes in atmospheric pressure, temperature, and humidity have been investigated. Sensing elements of this type display many desirable properties, particularly for telemetering applications. The output of the sensing element is an electrical signal in the form of a frequency or time variation which can be transmitted readily and measured accurately.

Measurement of Pressure

In the measurement of atmospheric pressure two different methods are considered. They are the effect of air pressure on the Q of a low-loss piezoelectric crystal and the change in frequency of a thin quartz oscillating plate produced by differential air loading. The dissipation method will be discussed first.

Air Loading Method

Work done by the oscillating crystal against the surrounding atmosphere may be in the form of energy dissipated as acoustic radiation or as viscous damping depending upon the mode of vibration of this sensing element. The ratio of average stored energy of the crystal to energy dissipated per cycle is a measure of the crystal Q, and varies with the air load the crystal works against. It is therefore necessary to employ a crystal that has a minimum of loss due to internal friction and damping action contributed by the supports to achieve high sensitivity to air loading. If it is assumed that the crystal frequency and the density of the surrounding atmosphere are such that the usual microscopic equations of motion of the viscous gas are applicable, it can be shown that changes in crystal Q produced by air loading are inversely proportional to air pressure for crystals vibrating in extension and flexure, and inversely proportional to the square root of pressure for shear mode elements. Experiments and practical considerations indicate that the most satisfactory type of sensing elements for this application are high-frequency quartz crystals vibrating in the thickness shear mode. These crystals, when properly etched and polished and mounted by pressure clamping, may exhibit Q factors of one-half million or more in vacuum.

Figure 1 is a block diagram of an electronic circuit designed for pressure measuring by detecting changes in air loading of the sensing crystal. The sensing crystal is pulsed at regular intervals, its vibrational amplitude is allowed to decay, and the circuit measures a fixed ratio of decay amplitudes. Since the elapsed time between any two amplitudes, a_0 and a is given by the equation

$$t_1 - t_0 = \frac{2L}{R} \log a_0/a \qquad (1)$$

where L and R are the inductance and the resistance of the equivalent circuit parameters of the crystal, the elapsed time

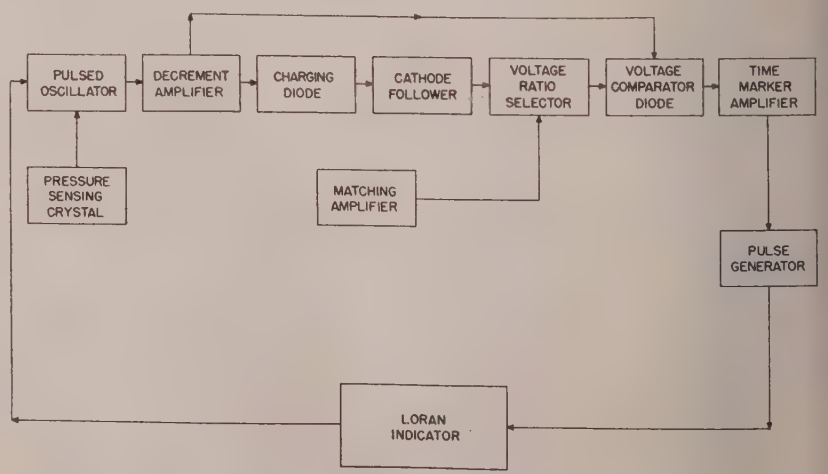

Figure 1. Block diagram of pressure measuring circuit

Paper 51-180, recommended by the AIEE Instruments and Measurements Committee and approved by the AIEE Technical Program Committee for presentation at the AIEE Great Lakes District Meeting, Madison, Wis., May 17–19, 1951. Manuscript submitted February 16, 1951; made available for printing March 30, 1951.

E. A. Roberts and P. Goldsmith are with the Armour Research Foundation, Chicago, Ill.

The authors wish to acknowledge the contributions of H. Ekstein and J. K. Tyson of the Armour Research Foundation, who contributed to the theoretical phases of this work. Scientific personnel of the Meteorological Branch, Evans Signal Laboratory, sponsors of this research program, have been especially helpful with their suggestions.

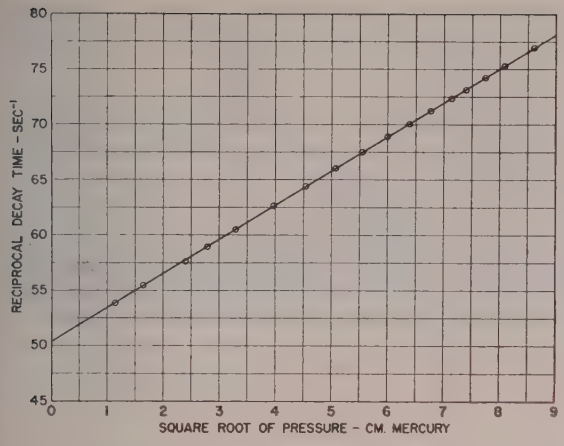

Figure 2 (left). Reciprocal decay time versus square root of pressure

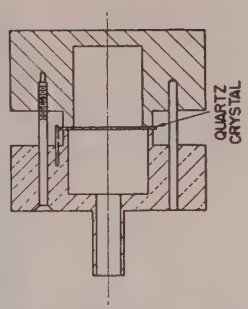

Figure 4 (above). Crystal pressure cup

also is proportional to the Q of the crystal.

A Loran timing indicator has been used for measurement of elapsed time between a predetermined crystal amplitude ratio. This timing device serves the additional purpose of generating a 25-cycle square wave voltage for pulsing the sensing crystal. The pulse is supplied to the plate circuit of a sustaining oscillator associated with the pressure-sensing crystal.

After the square wave voltage pulse has ended, the crystal decay current flows through the circuit elements in parallel with the crystal. These paralleling elements consist of the input impedance of the vacuum tube oscillator and all capacities in parallel with the crystal. The decrement corresponding to the true Q of the crystal is achieved only when the resistance paralleling the crystal is either much greater or less than the reactance of the paralleling capacitance.

The crystal decrement is amplified to approximately 100 volts in the decrement amplifier. The initial amplitude of the decrement is maintained by the action of the charging diode. This voltage is impressed on the grid of a cathode follower, and the output at the cathode closely follows the grid voltage.

A matching amplifier operated at zero grid bias develops a direct plate voltage that equals the plate voltage of the decrement amplifier when the crystal is allowed to decay completely. This voltage is applied to the cathode resistor of the cathode follower, which therefore has the initial value of decay voltage established at the cathode end and the final decay voltage value at the other.

The ratio of peak voltage at the plate of the decrement amplifier to any point on the cathode resistor is not changed by variations in supply voltage or by changes in maximum amplitude of the vibrating crystal. The cathode of the cathode follower therefore serves as a voltage ratio selector for which the elapsed time between the selected amplitudes must be determined accurately.

The function of the voltage comparator diode is to determine the exact time when the crystal amplitude has decayed to the predetermined ratio. When the ratio of decay voltages at the cathode of this diode becomes greater than that selected at the voltage ratio selector, this tube conducts and the steady voltage on the plate decreases exponentially at this time.

The time marker amplifier provides a signal with a steep leading edge to trigger the pulse generator accurately. The rate of change of voltage at the plate of the voltage comparator diode calculated from the time derivative of the decay equation

$$a = A_0 e - \gamma t \qquad (2)$$

is about $-1{,}800$ volts per second after one time constant for an assumed initial decay voltage of 100 volts and a decay time of one-fiftieth of a second, the maximum usable timing period on the indicator. The pentode amplifier has a voltage gain of over 100 and, therefore, produces a wave front with a rise time of approximately two-tenths of a volt per microsecond.

The pulse generator is a "single shot" multivibrator circuit that produces a positive output pulse approximately 100 microseconds in duration for each crystal decrement, occurring at the time when the crystal amplitude has decayed to the predetermined ratio selected at the voltage ratio selector.

The time difference between this pulse and the end of the square wave pulse used to energize the sensing crystal is measured on the timing indicator.

Experimental verification of the relationship between crystal Q and pressure for a shear mode crystal is shown in Figure 2, where the square root of pressure is plotted against the reciprocal of decay time of the pulsed crystal. The pressure-time equation therefore has the form

$$\frac{1}{t} = m\sqrt{P} + b \qquad (3)$$

m and b representing the slope and ordinate axis intercept, respectively. Differentiating this equation and eliminating t

$$\frac{dP}{dt} = \frac{2\sqrt{P}}{m}(b + m\sqrt{P})^2 \qquad (4)$$

It is seen that the accuracy of measurement is greatest at low pressures. The measuring accuracy calculated for a high Q BT-cut 6.4-megacycle thickness shear crystal is shown as a function of pressure in Figure 3.

Atmospheric variations in temperature and humidity will produce responses in these pressure-sensing elements. Since crystal dissipation is a function of the density of the surrounding medium, the necessary corrections for these cross-effects follow the standard relationship between density, temperature, humidity, and pressure for air. An additional temperature cross-effect may result from couplings to spurious modes of vibration. These coupled modes change the internal dissipation of the crystal as a function of temperature. Proper dimensioning of the sensing crystal will minimize this second order effect.

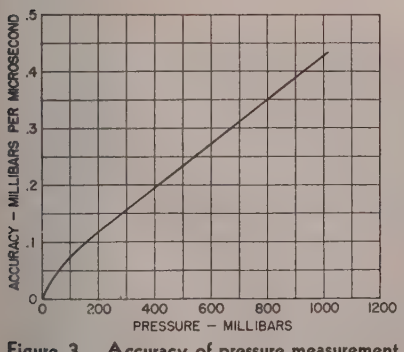

Figure 3. Accuracy of pressure measurement

Decay ratio = one time constant

Bending of a Crystal by Air Pressure

The method of determining pressure by measuring the frequency change produced by the bending of a quartz plate under differential air loading will now be considered. Since the addition of static forces to a linear dynamical system will not change its resonant frequency, this method of sensing pressure does not at first appear promising. A nonlinear elastic theory was developed during the course of this program that accounts for the frequency change that actually occurs when the crystal is bent, and it is shown that this change is proportional to the square of the differential pressure and to

the sixth power of the ratio of bending length to thickness.

The sensing crystal for this application is used as a diaphragm over an evacuated cup as shown in Figure 4. An AT- or BT-cut plated crystal with a low temperature coefficient of frequency may be utilized for pressure sensing. This type of crystal can be clamped at its outer edge without appreciably affecting activity or other performance characteristics. Since the pressure sensitivity of the crystal depends upon the ratio of bending length to crystal thickness, it is important that this ratio is made as high as possible without breaking the crystal from the pressure differential. Experiments have shown that this ratio may be as large as 80 for circularly shaped quartz crystals without exceeding the maximum breaking strain. Frequency changes of 1,400 parts per million per atmosphere can be achieved for these crystals. A typical frequency-pressure characteristic of an AT-cut thickness shear crystal is shown in Figure 5. It is seen that the characteristic very closely approximates the pressure square law.

The over-all accuracy of pressure measurement possible by this method will now be considered. There must be associated with the sensing crystal a negative resistance source, such as a vacuum tube, that supplies energy to the crystal to maintain oscillations. While the crystal with its high Q, and consequently steep reactance characteristic, primarily controls the frequency of oscillation, changes in reactance of other circuit components, or changes in voltage or tube characteristics, will affect the frequency of oscillation of the sensing crystal. Temperature changes will produce the most serious frequency change, affecting both the crystal (since it necessarily has a temperature coefficient of frequency) and circuit components that change their values with temperature.

Figure 6. Electronic pressure indicator

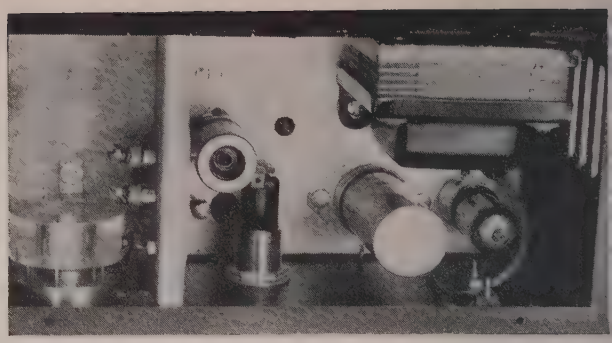

Assuming that the temperature coefficient of the sensing crystal is known, and a stability of one part per million can be maintained in the oscillator circuit, it should be possible to determine pressure to an accuracy of 0.7 millibar with a crystal that changes frequency 1,400 parts per million per atmosphere. Under controlled temperature conditions where much greater oscillator stability is possible, a considerably greater pressure-measuring accuracy may be achieved. This is apparent from the fact that oscillator circuits under controlled temperature conditions may show long time stabilities of 10^{-8} or better. The problem of crystal mounting becomes important under these conditions, since movement of the crystal in the holder will affect the oscillating frequency. The pressure indicator shown in Figure 6 includes power supply, sensing crystal and associated oscillator circuit, a reference oscillator, and a mixer to provide an audio frequency output for pressure indicating.

Measurement of Temperature

An oscillating piezoelectric crystal with a high temperature coefficient of frequency can be employed for temperature sensing. The temperature coefficient of frequency of a vibrating crystal

$$\alpha_f = \frac{1}{f}\frac{df}{dt} \tag{5}$$

is a function of the thermal coefficients of stiffness and expansion. The magnitude of this coefficient of frequency, therefore, depends upon the mode of vibration and the orientation of the crystallographic axis. For quartz the maximum value of the temperature coefficient of frequency is in the order of 10^{-4} per degree centigrade. This value is approached in Y-cut plates oscillating in the thickness shear mode. As the Y-cut crystal is rotated about the X axis, the temperature coefficient decreases through zero, and it is possible to obtain any coefficient between $+90$ and -90 parts per million per degree centigrade by selection of the angle of cut. Crystals designated as AT- and BT-cuts are examples of this type of crystal with the angle of rotation selected to produce a near-zero temperature coefficient. Since the coefficient of stiffness is not constant with temperature, the resulting coefficient of frequency is zero at only one temperature for these cuts. In general, the frequency-temperature characteristic for any crystal is not linear.

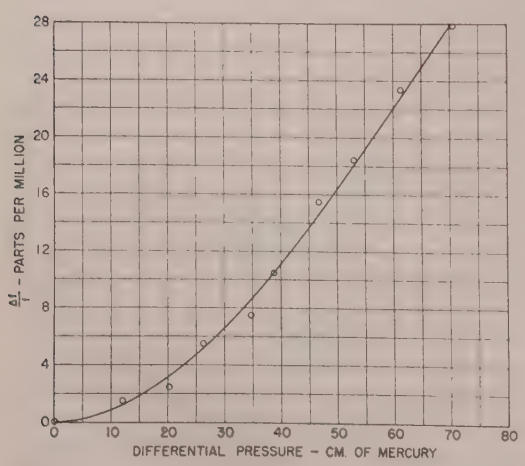

Figure 5 (left). Frequency change produced by the bending of a quartz crystal

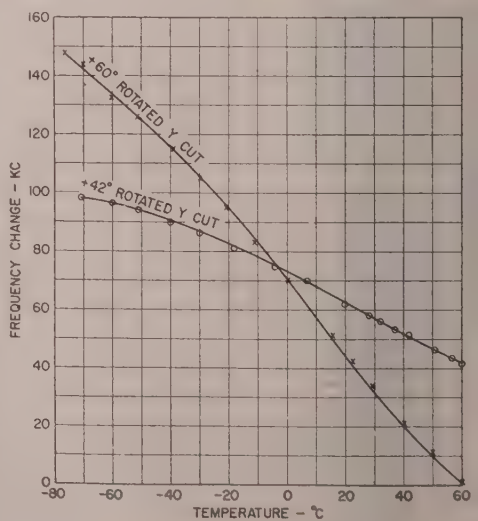

Figure 7 (right). Frequency - temperature characteristics of 16-megacycle rotated Y-cut crystals

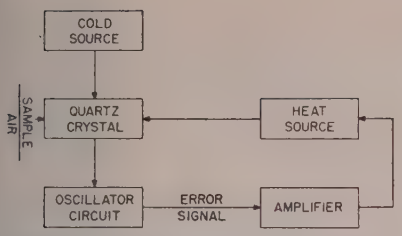

Figure 8. Block diagram of dew point indicating circuit

Coupling between the thickness shear mode and harmonics of lower frequency face shear and flexural vibrations are possible, since all these modes have different temperature coefficients. The elastic constants responsible for the couplings depend upon the crystal orientation, and the problem of coupling becomes most serious for thickness shear elements which have the highest positive temperature coefficients.

Several thickness shear elements with temperature coefficients ranging from $+90$ to -80 parts per million per degree centigrade were used in tests to determine their activity characteristics over a wide temperature range. Y-cut crystals, while having the highest temperature coefficient ($+90 \times 10^{-6}$ per degree centigrade), exhibited a number of frequency discontinuities, while crystals rotated 30 degrees or more about the X axis showed satisfactory frequency spectra over the temperature range from -70 degrees centigrade to $+60$ degrees centigrade. Frequency-temperature characteristics for two of these crystal cuts are shown in Figure 7. The negative temperature coefficients are typical of all thickness shear crystals rotated more than $+35$ degrees from the Y cut. While somewhat larger temperature coefficients could be attained by further rotation about the X axis, the coupling efficiency to the crystal would be reduced, and it would become more difficult to stabilize the associated oscillator circuit.

Thickness shear crystals rotated through a negative angle about the X axis show variations in temperature coefficient similar to those observed for positive angles of rotation. These crystals have a higher frequency constant and a lower coupling efficiency for a corresponding temperature coefficient.

Temperature coefficients of frequency of face shear quartz crystals change with the angle of rotation about the X axis in the same fashion as thickness shear elements. Zero temperature coefficients are obtained for this mode at -52 and $+38$ degrees, and the highest temperature coefficients occur at $+5$ and $+70$ degrees.

The accuracy to which the resonant frequency of a crystal may be measured depends upon the frequency stability coefficient of the crystal, the over-all stability of the circuit that sustains it in oscillation, and the accuracy of the associated frequency-measuring equipment.

Heat generated in the crystal from vibrational losses must be considered as a possible source of temperature error. Calculations and experiments show that this effect can be made insignificantly small by operating the sensing crystal at a low vibrational amplitude.

Another source of temperature error arises from the effects of solar radiation. The temperature rise in the crystal under certain conditions may cause this sensing element to indicate a temperature that is above the ambient air temperature. Since quartz is very nearly transparent to radiated solar energy, and the necessary electrodes can be applied in the form of highly reflecting surfaces, this type of error, which is inherent in all temperature-sensing elements, can be made relatively small for quartz crystals.

Crystal sensing elements can be made very thin, thus reducing thermal lag time. Measurements made on crystals 0.01 centimeter in thickness showed a lag time of approximately five seconds in still air and slightly over two seconds in air moving at a velocity of 10 feet per second.

Of the synthetic crystals available, ethylene diamine tartrate (EDT) appears to be the most suitable for temperature sensing in view of its high physical and chemical stability under all atmospheric conditions. This crystal has a low mechanical dissipation, contains no water of crystallization, and has good long-time stability characteristics. When this crystal is properly orientated it may be made to have a temperature coefficient of nearly -300 parts per million per degree centigrade. Such a crystal with convenient dimensions would oscillate at about 100 kilocycles per second, and would have a total frequency change of nearly 5,000 cycles over a 150-degree temperature range.

From considerations of the various types and cuts of crystals discussed it is apparent that several of them are suitable for temperature sensing. Oscillator circuits similar to those used for measuring pressure by bending of a quartz plate may be used for the temperature-sensing crystals, and over-all accuracies of better than 0.1 degree centigrade can readily be achieved. The sensitivity of the crystals used in this application exceeds 0.001 degree centigrade.

Measurement of Humidity

The method of determining humidity with a piezoelectric crystal involves the deposition of moisture on its vibrating surfaces and the use of the resulting change in oscillating characteristics to

Figure 9 (below). Front view of the electronic dew point indicator

Figure 10 (right). Top view of the electronic dew point indicator

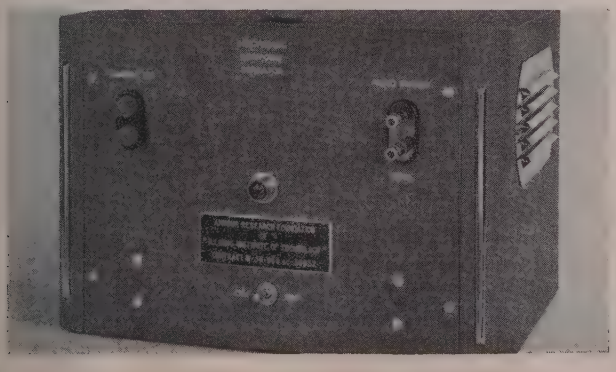

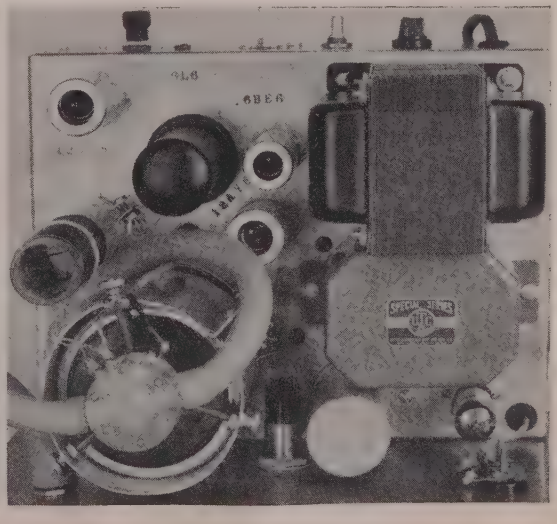

maintain the crystal at the dew point temperature. Calculations and experiment show that a moisture layer thickness of less than one micron is enough to change significantly the oscillating characteristics of a thin crystal in order that the dew point temperature, and hence humidity, can be determined.

During the course of this research program considerable effort was directed toward the development of control circuits that would maintain the crystal at the dew point temperature. Figure 8 is a block diagram representing this general type of circuit. An oscillating crystal is cooled by a cold source which may be dry ice or some other refrigerant, and when the dew point is reached moisture begins to condense on its exposed surfaces. The presence of moisture decreases the amplitude of oscillation of the crystal, which in turn produces a signal that causes the heat source to heat the crystal and dissipate the condensate. The source of heat may be a thin resistance element mounted close to the crystal, or it may be heat generated within the crystal produced by a high level of oscillation, or some other source. Actually, several types of control circuits have been employed successfully for the purpose, but only the most promising one will be discussed.

A dew point indicator using induction heating is shown in Figures 9 and 10. This circuit utilizes the induction of eddy currents into the plated surfaces of a pressure-mounted sensing crystal as the method of maintaining the crystal at the dew point temperature. Since both heating and moisture condensation take place on the same surface, the time lag between the appearance of condensate and the corresponding increase in heating is small and stability of operation is readily achieved.

The sensing crystal is placed on one end of a brass tube several inches in length and the other end of the tube is placed in a refrigerant. The induction coil is located above the sensing crystal. Sample air is passed in through one side of the crystal holder and out the other side after passing over the crystal surface.

The sensing element is a pressure-mounted rotated Y-cut crystal with a large temperature coefficient of frequency, and the dew point temperature is determined by measurement of the crystal frequency. The sensing crystal, therefore, performs the functions of humidity sensing and temperature measuring, as well as acting as an integral part of the temperature control circuit.

Conclusions

Piezoelectric crystals used as sensors of atmospheric pressure, temperature, and humidity display many desirable properties.

These elements can be made small in size and light in weight, and are responsive to rapid changes in atmospheric variations. In utilizing the piezoelectric effect the need of a mechanical linkage to convert a meteorologic change to a useable output signal is eliminated. The output is in the form of an electrical signal, with the intelligence represented by frequency or time. This type of signal can be indicated remotely and measured accurately.

A further advantage of using elements of this class is the simplicity of detecting and measuring parameter changes. For example, the humidity crystal, in addition to collecting moisture and indicating its presence by a decrease in vibrational amplitude, serves as its own thermometer to indicate dew point temperature.

No Discussion

Improvements in Transformer-Loss Compensators for Watt-hour and Var-hour Meters

GEORGE B. SCHLEICHER
MEMBER AIEE

Synopsis: Transformer-loss compensators provide an economical means for metering the loads of utility company customers supplied at transmission voltages on the low-voltage side of the power transformer bank by compensating the watt-hour meter to include the transformer losses in its registration. Improvements have been made in the basic compensator[1] by neutralizing the effect of the flow of meter potential circuit current through the copper-loss compensator. This improves the performance of the compensator, particularly on inductive loads, and makes possible its correct adjustment also for the higher values of losses incurred with var compensation. The burdens imposed by the compensator are sufficiently small to be acceptable in watt-hour metering practice, and for connection to the output side of standard var autotransformers. Under present-day conditions the use of transformer-loss compensators results not only in economies, but also in the conservation of critical materials that would be required for high-voltage instrument transformers on metering installations.

TRANSFORMER-loss compensators connected to watt-hour meters make possible the measurement of energy and demand of high-voltage supply lines from the low-voltage side of the power transformer bank. Their use therefore represents an economy, primarily because of the lower cost of instrument transformer equipment on the low-voltage side as related to the high-voltage side. The basic principles of transformer-loss compensators, and the technique of their application in line with watt-hour meter practice have been described previously.[1] At the time of that presentation, it had been established that the principle of the transformer-loss compensator could be applied also to var-hour meters, but the performance of compensators comprising only the basic components was unsatisfactory for the higher percentages of copper losses incidental to var compensation. Also, in the discussion of the previous paper[1] the need for improvement of low-power-factor performance of the copper-loss compensator was indicated. Extensive tests and analyses have resulted in the improvements which are the subject of this paper. In its improved form, the transformer-loss compensator is suitable for watt-hour and var-hour meter compensation throughout the range of these losses.

Principle of Operation

In Figure 1 the solid lines show the basic transformer-loss compensator and its connections. The iron-loss element (D) consists of a small potential transformer whose primary is connected across the low-voltage output side of the power transformer (G). The 3-volt secondary of the potential transformer is connected across the watt-hour meter current coil through an adjustable resistor, which serves as the iron-loss adjustment. With any given adjustment of the iron-loss resistor the current flow through the meter current coil is proportional to voltage; and within the watt-hour meter (A), by interaction with the potential coil, the torque produced is in accordance with the square of the voltage.

For including the copper-loss increment, a small current transformer has its primary connected in series with the meter current coil, and its secondary is connected to an adjustable resistor which serves as the copper-loss adjustment (C). The output voltage of the current transformer and its resistor is added to the voltage applied to the meter potential coil. As with any given adjustment of the resistor the output voltage of the copper-loss current transformer is proportional to line current; within the meter, by interaction with the current coil, the torque produced is in accordance with the square of the current.

It is apparent from Figure 1 that the meter-potential-coil current also passes through the copper-loss compensator so that its output voltage actually is proportional to $I_L + I_P$, where I_L is the line current, and I_P the potential coil current. Obviously this effect may be made negligible by making I_L large in relation to I_P; however, this would increase the current burden beyond practical limits in watt-hour meter practice. Also, since I_L may vary from zero to the maximum, the effect would remain at the lighter loads. The practical solution was found to be the addition of currents whose vector components neutralize the potential coil current of the meter within the copper-loss compensator. A capacitor having the correct capacitance to neutralize the vars of the potential circuit of the meter may be connected across the meter potential coil; but the wide variation in characteristics of meter potential coils, as shown in Table I, indicates the need for adjustable capacitance compensation. The high-voltage side of the iron-loss transformer is provided with an extended winding having sufficient taps to provide the variation in capacitor current required by the various types of meters. The rating of the capacitor is chosen so that its capacitance is greater than that required for any type of watt-hour meter, and the capacitor current is

Paper 51-182, recommended by the AIEE Instruments and Measurements Committee and approved by the AIEE Technical Program Committee for presentation at the AIEE Summer General Meeting, Toronto, Ont., Canada, June 25–29, 1951. Manuscript submitted March 8, 1951; made available for printing April 20, 1951.

GEORGE B. SCHLEICHER is with the Philadelphia Electric Company, Philadelphia, Pa.

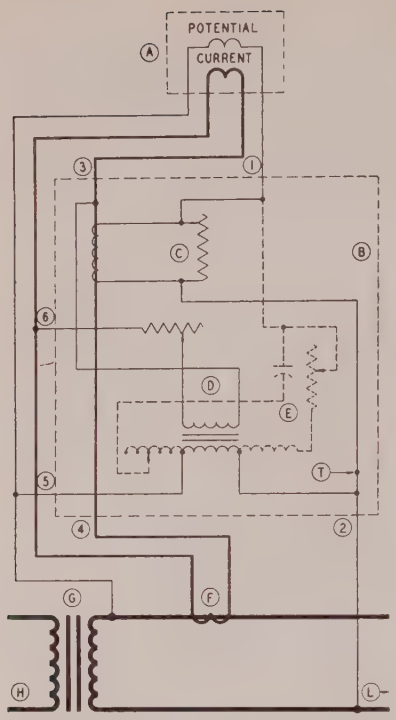

Figure 1. Principle of transformer-loss compensator. Potential circuit compensation shown dotted

A. watt-hour meter, B. transformer-loss compensator, C. copper-loss compensator, D. iron-loss compensator, E. potential circuit compensation, F. metering current transformer, G. power transformer, H. high-voltage supply, L. low-voltage load, T. test point—see text. 1. Numbered terminal designations refer to Figure 3

adjusted by connecting it to a voltage that is less than the available maximum.

When the capacitor has been connected into the circuit, and its current adjusted to the correct value, a small current remains. This is the power component of the meter potential coil current. By providing a voltage proportional to $-E$, a current displaced 180 degrees from the applied voltage may be passed through an adjustable resistor and through the copper-loss compensator secondary to neutralize the power component current of the meter potential coil. The capacitor and resistor connections are shown dotted in Figure 1.

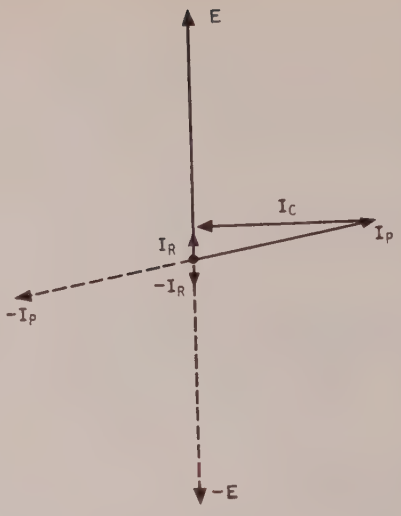

Figure 2. Vector relations of potential circuit current compensation

E line voltage, I_P meter potential circuit current, I_C capacitor current, I_R power component of potential circuit current, $-I_R$ compensating current for I_R, $-I_P$ resultant potential circuit compensating current

Figure 2 shows the vector relations of the potential-circuit compensation. E is the voltage on the low-voltage side of the power transformer, and this voltage is also the voltage that would be applied to the potential coil of a watt-hour meter connected to measure the output of the power transformer. I_P is the current of the highly inductive watt-hour meter potential coil; I_C is the capacitor current, I_R is the power-component current of the meter potential coil, and $-I_R$ is the compensating current obtained from voltage $-E$.

With the voltage $-E$ available, it is apparent that the potential circuit current could also be neutralized by an inductor of the same resistance-reactance characteristics as the meter potential coil. The vector $-I_P$ in Figure 2 applies to this method. The inductor method was eliminated because by omitting the power-factor corrective effect of the capacitor, the resultant potential circuit burdens were increased beyond the capacity of standard var autotransformers.

Practical Application

Potential Circuit Compensation

The characteristics of watt-hour meter potential coils in Table I indicate wide variations, particularly in the values of vars. The required values of capacitance to correct for the lagging vars of potential coils at the line voltage is shown in the last column of Table I. These values are based on 120-volt meters, and for 240-volt meters the values of capacitance are one-fourth of the values given. The required ratings in microfarads are obtained from the formula

$$C=(10^6 V_p)/(2\pi f E^2) \qquad (1)$$

where C is the required capacity in microfarads, V_p is the vars of the meter potential coil, f is the frequency, and E is the voltage rating of the meter potential coil.

In the development of the practical transformer-loss compensator, capacitance required was reduced by applying to the capacitor a voltage greater than that applied to the meter potential coil for 120-volt meters; and by applying a voltage less than the meter potential coil voltage for 240-volt meters. Thus the autotransformer taps shown in Figure 1 are between the 120- and the 240-volt taps. The 240-volt tap serves also for the application of the supply voltage when the circuit to be measured is 240 volts. It is thus possible to produce a universal compensator suitable for use with 120- or 240-volt meters. The maximum required capacitance for service type watt-hour meters becomes 1.5 instead of 3.0 microfarads. By using a 1.0-microfarad and a 0.5-microfarad capacitor, values of 1.5, 1.0, 0.5, and 0.33 microfarads are obtained. The latter is the minimum value required for 240-volt service meters when the capacitor is energized from voltages between 120 and 240.

Table II shows performance characteristics in the measurement of copper loss in terms of meter registration for values of copper-losses of 1.0 per cent and 5.0 per cent at the meter rating. The former value is typical of an adjustment for the measurement of watt losses, and the latter is typical of adjustments that would be made for a var-hour meter. The table includes comparative data at power factors of 0.5 and 1.0 for the basic compensator, with capacitor compensation added, and with capacitor and resis-

Table I. Typical Characteristics of Watt-Hour Meter Potential Coils at 115 Volts 60 Cycles, and Values of Required Compensating Capacitors at Applied Voltage

Make	Type	Volt-Amperes	Watts	Vars lagging	Required μf
Duncan	MG	6.85	1.1	6.75	1.35
	MF	7.73	1.2	7.65	1.54
General Electric	V3	10.1	1.2	10.0	2.01
	DS-19	11.5	2.0	11.4	2.29
Sangamo	HF	4.1	1.3	3.9	0.78
	LC	6.8	1.0	6.7	1.34
Westinghouse	C2	12.7	2.3	12.4	2.49
	OB	6.9	1.1	6.8	1.36

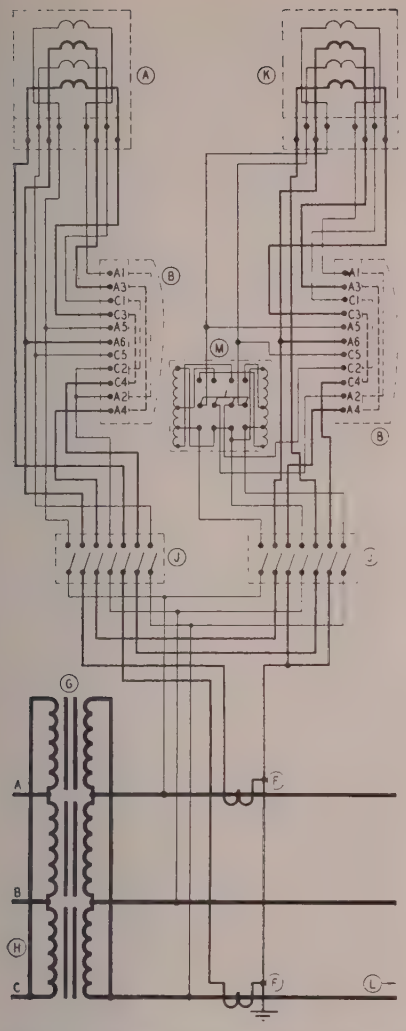

Figure 3. Typical connections of 2-element watt-hour and var-hour meters to transformer-loss compensators

A. watt-hour meter, B. transformer-loss compensators, F. meter current transformers, G. power transformer bank, H. high-voltage supply, J. test switches, K. var-hour meter, L. low-voltage load, M. var autotransformer. For internal connections of compensators, refer to numerical terminal designations in Figure 1

tor compensation properly adjusted. The performance of the compensator thus is satisfactory even for the relatively high percentages of copper loss that are incidental to transformer-loss compensation for var-hour meters.

Burdens

Table III shows the burden characteristics of the transformer-loss compensator. It will be noted that the potential circuit burdens are leading, and when combined with the lagging vars of the meter potential coil the resultant volt-ampere burden is sufficiently small to be connected to the output side of standard var autotransformers. Since a method is now available to neutralize the effect of the meter potential coil current through the copper-loss compensator, it has been possible to reduce the secondary current rating of the copper-loss transformer to 0.25 ampere, thus resulting also in a reduction of current-circuit burdens.

For most watt-hour meter applications, the potential circuit burden values that apply are those in the range from 0 to 1.0 per cent iron loss. For current circuit burdens the usual copper-loss percentages are of the order of 1.0 per cent. These loss percentages are in terms of the meter rating. The higher values of losses and

Table II. Summary of Test Results in Terms of Per Cent Deviation from Desired Values of Load Plus Copper Loss

Tests Made at 120 Volts with Type IB-10 Portable Standard Watt-hour Meters

Load		Desired Loss,	Per Cent Deviation Potential Circuit Compensation		
Amps	Power Factor	Per Cent	None	Capacitor	Complete
		1.0 Per Cent Copper Loss at Meter Rating			
7.5	1.0	1.50	+0.11	+0.11	0
5.0	1.0	1.00	0*	0*	0*
2.5	1.0	0.50	−0.02	0	+0.05
0.5	1.0	0.10	−0.06	+0.01	+0.05
7.5	0.5	3.00	−0.73	+0.37	0
5.0	0.5	2.00	−0.33	+0.24	+0.06
2.5	0.5	1.00	−1.09	+0.09	+0.06
0.5	0.5	0.20	−1.18	−0.09	+0.01
		5.0 Per Cent Copper Loss at Meter Rating			
7.5	1.0	7.50	−0.30	0	−0.14
5.0	1.0	5.00	0*	0*	0*
2.5	1.0	2.50	−0.27	−0.05	0
0.5	1.0	0.50	−0.39	−0.05	−0.07
7.5	0.5	15.00	−4.67	+1.25	+0.10
5.0	0.5	10.00	−4.37	+1.73	+0.10
2.5	0.5	5.00	−5.05	+0.13	−0.07
0.5	0.5	1.00	−1.18	−0.27	+0.03

* Point of adjustment of copper-loss compensation.

Table III. Burden Tests of Transformer-Loss Compensators with Potential Circuit Compensation

Per Cent Iron-Loss Compensation at Meter Rating						
Individual Element Tests	Series Test 2-Element Meter	Series Test 3-Element Meter	Watts	Volt-Amperes	Vars *	Power Factor (Leading)
			Potential Circuit at 115 Volts			
0	0	0	4.50	20.7	−20.2	0.22
1.0	0.50	0.33	4.76	20.7	−20.2	0.23
2.5	1.25	0.83	5.04	20.8	−20.1	0.24
5.0	2.50	1.67	5.50	20.8	−20.0	0.27
10.0	5.00	3.33	6.36	20.9	−19.9	0.30
20.0	10 00	6.67	7.96	21.3	−19.8	0.37
30 0	15.00	10.00	9.81	21.9	−19.6	0.45
40.0	20 00	13.33	11.65	22.7	−19.5	0.51
			Potential Circuit at 230 Volts			
0	0	0	3.12	8.02	−7.4	0.39
1.0	0.50	0.33	3.28	8.02	−7.3	0.41
2.5	1.25	0.83	3.60	8.14	−7.3	0.44
5.0	2.50	1.67	4.08	8.36	−7.3	0.49
10.0	5.00	3.33	4.80	8.82	−7.4	0.54
20.0	10 00	6.67	6.60	9.88	−7.4	0.67
30.0	15.00	10.00	8.46	11.16	−7.3	0.76
40.0	20.00	13.33	10.33	12.57	−7.2	0.82
			Current Circuit at 5 Amperes			
Per Cent Copper-Loss Compensation at Meter Rating						
120-Volt Meter	240-Volt Meter		Watts	Volt-Amperes	Vars	Power Factor (Lagging)
0	0		0.80	1.00	0.6	0.80
1.0	0.5		1.00	1.15	0.5	0.91
2.0	1.0		1.39	1.50	0.6	0.93
3.0	1.5		1.71	1.80	0.6	0.95
5.0	2.5		2.35	2.45	0.7	0.96
10.0	5.0		4.60	4.70	0.9	0.98
15.0	7.5		5.45	5.55	1.0	0.98

* Leading vars are indicated as minus (−).

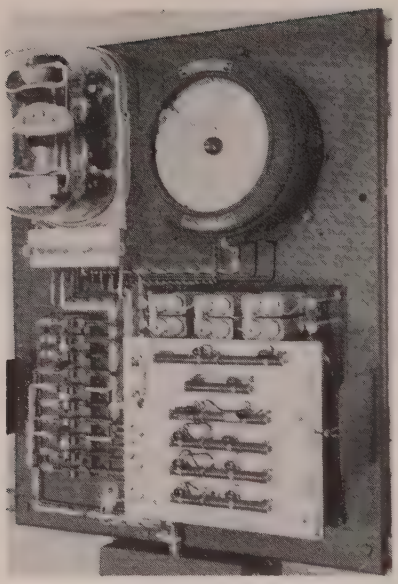

Figure 4. Typical 3-element meter panel with transformer-loss compensator on a 2.3/4.0-kv, 1,500-kva installation compensated to the 33-kv supply, panel cover removed

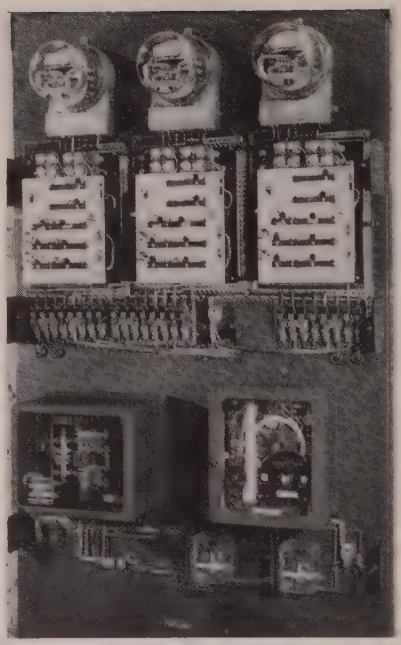

Figure 5. Meter panel for transformer-loss compensators on a 6.6-kv installation with three transformer banks, compensated to the dual 66-kv supply

burdens given in Table III apply in general for var-hour meter compensation.

Polyphase Compensators

The principle of the transformer-loss compensator has been described in the single-phase form. For the usual application to polyphase circuits two-element and three-element compensators are used with two-element and three-element meters respectively. In polyphase compensators it is practical to add the entire iron-loss on one element. This has been established with previous methods.[1,2,5,6,8] As the compensator is fundamentally a single-phase device, a change in phase sequence requires no change in connections.

For customers' installations in general, the loss compensation is added to the registration of the meter. Subtractive compensation may be required for application to tie-lines. This is accomplished by reversing the connections of the iron-loss and the copper-loss transformers within the compensator.

Figure 3 shows the connections of a watt-hour meter and a var-hour meter each connected to a transformer-loss compensator on the low-voltage side of a power transformer bank. The connection is for a 3-phase 3-wire circuit with 2-element meters; but the principle is equally applicable to 3-element meters by using 3-element compensators. In the interest of simplicity, potential transformers on the low-voltage side are not shown.

Figure 4 shows a typical 3-element meter panel with a transformer-loss compensator for the measurement of watt-hours. Such an installation may be made for example on the 2.3/4.0-kv side of a 33:2.3/4.0-kv transformer bank. This installation uses potential and current transformers suitable for 4.0-kv service instead of the more expensive 33-kv instrument transformer equipment required for metering on the high-voltage side.

Figure 5 shows a 2-element transformer-loss compensator installation at 6.6 kv 3-phase 3-wire on three transformer banks connected to a dual 66-kv supply. Combined demand as of the high-voltage side is measured on the demand meter (lower right).

Test Procedure

In the application of transformer-loss compensators three steps are required for their proper calibration:

1. Adjust the compensator to the potential circuit of the meter to be used with it.
2. Adjust the copper-loss element of the compensator to the desired copper-loss percentage.
3. Adjust the iron-loss element of the compensator to the desired iron-loss percentage.

The potential circuits of the compensator may be adjusted to the meter potential coils in several ways. A method suitable for laboratory use consists of connecting the current coil of a low-reading low-power-factor wattmeter at (T) in Figure 1. By means of a double throw switch the potential coil of the wattmeter is connected to be in phase with the voltage applied to the watt-hour meter potential coil in one position for the measurement of watts; and to a voltage displaced by ninety degrees for the measurement of vars. If the compensator and resistor compensation be disconnected, the wattmeter will then measure the watts and vars of the meter potential circuit. For adjustment of the capacitor compensation the wattmeter is connected to measure vars, and the capacitor tap connected to the autotransformer is shifted until the var reading is zero. This is the permanent connection for the capacitor compensation. The wattmeter is then connected to measure watts, and the resistor compensation is adjusted until the wattmeter reading is again zero. This is the permanent adjustment for the resistor compensation. It should be noted that the exact calibration of the wattmeter is not important if the scale range is sufficiently large and the zero is adjusted correctly.

Alternative methods consist of connecting either a milliammeter or a multi-range voltmeter into the circuit at point (T) in Figure 1. With the resistor compensation disconnected, the capacitor

Table IV. Adjustment of Potential Circuit Compensation of Transformer-Loss Compensators with Typical 120-Volt Watt-Hour Meters

Make	Type	Capacitor		Resistor	
		Rating μf	Applied Voltage	Ohms	Applied Voltage
Duncan	MG	1.0	162	12,030	120
	MF	1.0	185	11,100	120
General Electric	V3	1.5	161	11,100	120
	DS-19	1.5	183	6,620	120
Sangamo	HF	0.5	187	10,350	120
	LC	1.0	161	13,100	120
Westinghouse	C2	1.5	199	5,760	120
	OB	1.0	163	12,030	120

connection is made to the tap that results in the minimum reading; the resistor compensation is then adjusted until the reading is again a minimum. The exact calibration of these instruments is not important, because only minimum deflections are used. The voltmeter method is the most practical for field use.

Adjustment of the iron-loss and the copper-loss resistors of the compensator and the loss calculations required to determine the setting points of the compensator have been described in detail in the previous paper.[1] The fundamentals are the calculation of the losses in per cent of load at the normal test points of the meter. The meter itself requires no special adjustments; it remains a standard commercial watt-hour meter adjusted in the usual way. The compensator is adjusted by testing the meter both with and without compensation. A test switch on the compensator provides for both tests. The copper-loss adjustment is conveniently made at the heavy-load test point; the iron-loss adjustment is made at the light-load test point of the meter. It has been established that if the potential balance adjustment of the compensator has been made properly, inductive load performance also will be correct. If inductive load tests are made, it is important that the test power-factor agrees closely with the power-factor for which the calculated loss percentage has been determined, because the loss percentage varies inversely with the power factor.

Conclusions

The transformer-loss compensator provides a companion method to high-voltage billing metering. Frequently the method will result in economies, and under the conditions of today it contributes to the conservation of critical materials required for high-voltage instrument transformer equipment.

Metering on the high-voltage side remains superior for conditions that would involve multiple compensator installations in place of a single high-voltage metering equipment, for those cases where a part of the load is used or distributed at the supply voltage, and for installations where the equipment cost of metering on the high-voltage side is less than for a compensator installation.

In many cases the use of the transformer-loss compensator provides important economies and advantages. Metering costs may be less for supply voltages as low as 13.2 kv, and greater economies are effected for higher supply voltages. Savings in space required for metering equipment frequently are important in metropolitan areas, while for exposed locations on the system metering on the low-voltage side will be less susceptible to lightning and other disturbances. The transformer-loss compensator also makes possible the measurement of losses in those cases where calculated loss factors are now used, and it is of value also for providing measurements as of a remote point. Thus metering may be placed in a terminal substation to provide registration as of a remote billing point, such as a state line. With the inclusion of potential circuit current compensation the transformer-loss compensator is suitable for use with watt-hour and var-hour meters throughout the range of iron and copper losses.

References

1. Metering with Transformer-Loss Compensators, **G. B. Schleicher.** *AIEE Transactions*, volume 66, 1947, pages 851–62.

2. Compensating Metering in Theory and Practice, **G. B. Schleicher.** *AIEE Transactions*, volume 52, 1933, pages 816–23, 829–31.

3. Metering Power on the Low-Voltage Side, **A. J. Petzinger and B. E. Lenehan.** *AIEE Transactions*, volume 62, 1943, pages 159–63, 406–10.

4. United States Patent 1,942,193 (others pending).

5. Application Instructions for Transformer-Loss Compensators. *Bulletin Number 63*, The Eastern Specialty Company (Philadelphia, Pa.), 1951.

6. Primary Energy Measured on Low Side by, Compensating Meter, **George B. Schleicher**, *Electrical World*, New York, N. Y., July 1 , 1933 pages 27–31.

7. Compensating Metering Saves, **Walter C. Wagner.** *Electrical World*, New York, N. Y., September 14, 1935, pages 35, 84.

8. Compensated Transformer Loss, **George B. Schleicher.** *Electrical World*, New York, N. Y., July 14, 1947, pages 95–97.

No Discussion

Power Supply Study and New Rectifier Installation for the United Electric Railways of Providence

W. C. WHITMAN
MEMBER AIEE

F. F. SCHALLER
ASSOCIATE AIEE

Synopsis: A study of the power supply to the United Electric Railways was initiated when new construction necessitated the relocation of rotary converters. Replacement with modern equipment was considered in conjunction with a comprehensive study of the entire power supply. It was evident that the losses on the United Electric Railways feeder and trolley system would be the controlling economic factor. A method of calculating the losses in this d-c supply system was developed, correlated with a measured value of losses, and extended to determine the relative merits of proposed feeder changes and rectifier installations. It is believed that this is the first published study that has made use of available probability methods for calculating losses, voltage drop, flicker, and capacity requirements in a study of the power supply for an electric transportation system. The rotary converters were replaced with 60-cycle rectifiers at two new locations. The design of these substations incorporated certain novel features for the protection of equipment and personnel.

THE United Electric Railways provides transportation for over 500,000 people in Providence and adjacent cities and towns in Rhode Island. The operation of the transportation system which includes both electric and gas-driven vehicles has been described in an earlier paper.[1] The present paper is concerned only with the power supply to the electric vehicles. At the time of this study there were 12 trolley bus routes and five streetcar lines using 205 busses and 93 cars. Since, the trolley cars have been replaced by trolley busses.

The overhead trolley system was supplied at 600-volts direct current from five Narragansett Electric Company substations. The map of Figure 1 shows the geographical location of the trolley feeders and the substations. Except for a 4-kv 60-cycle rectifier installation at Elmwood, the others, Manchester Street, North Main Street, Fountain Street, and Olneyville, were equipped with rotary converters supplied at 11-kv and 25-cycles from the Manchester Street steam station.

An expansion program at this steam plant made it necessary to remove the four rotary converters located there. As these were about 40 years old the question of replacement with more modern equipment was considered in conjunction with a comprehensive study of the entire power supply. This seemed an appropriate time to determine whether to continue the existing 25-cycle supply or to change over to a more modern 60-cycle system.

In commencing the study, it was evident that the d-c transmission losses on the United Electric Railways feeder and trolley system would be the controlling economic factor in determining what kind of 60-cycle system should replace the 25-cycle system, if such replacement worked out to be justified. In order to establish a method of calculating the losses in this d-c trolley supply system and to be able to use this method with con-

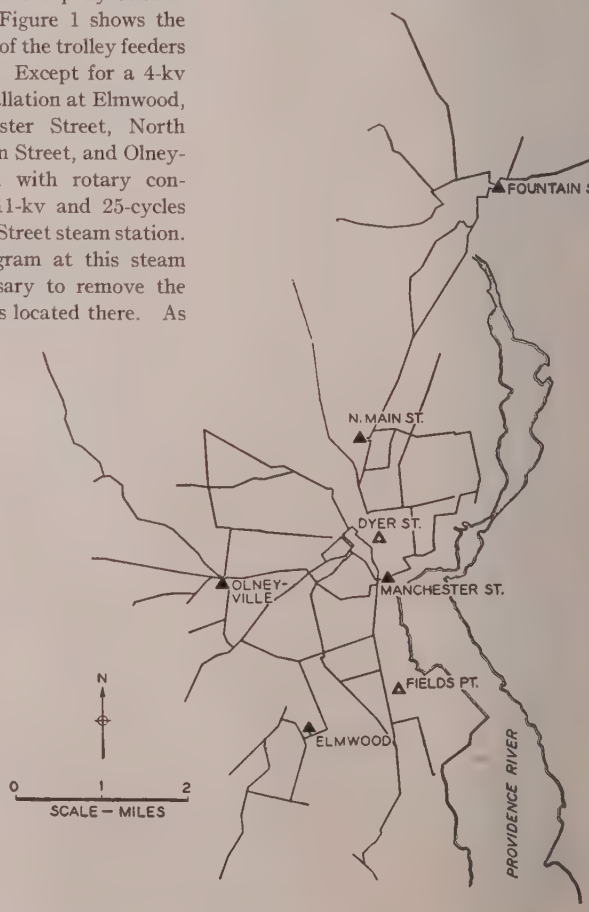

Figure 1. Geographical location of trolley feeders and substations in the Providence area. Solid triangles mark location of original d-c substations. Open triangles show location of new substations that replace the Manchester Street Substation

Paper 51-185, recommended by the AIEE Land Transportation Committee and approved by the AIEE Technical Program Committee for presentation at the AIEE Summer General Meeting, Toronto, Ont., Canada, June 25–29, 1951. Manuscript submitted October 30, 1950; made available for printing April 23, 1951.

W. C. WHITMAN and F. F. SCHALLER are with the New England Power Service Company, Boston, Mass.

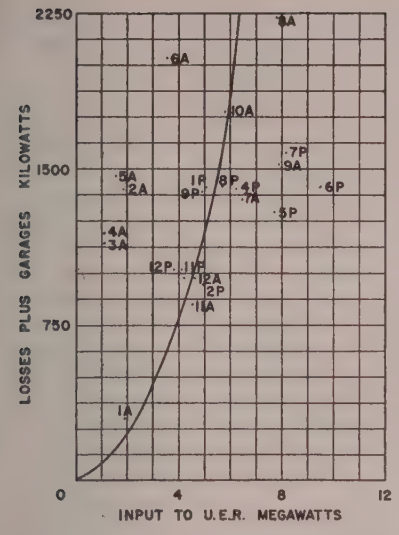

Figure 2. Trolley system losses plus garage use versus d-c input to the United Electric Railways

fidence, it was necessary to obtain a correlation between the calculated and the measured losses. With this accomplished, it was possible to extend the computations to determine the relative merits of various combinations of rectifier installations and feeder changes.

Measurement of Losses on the United Electric Railways

The power input to the United Electric Railways system was obtained from the 25-cycle metering at the Manchester Street station and the 60-cycle metering at the Elmwood rectifier. By averaging the hourly requirements for the months of November and December 1946, the requirements of an average day were determined.

The net input to the d-c trolley system was obtained by subtracting from this metered input the calculated 25-cycle transmission and transformer losses and the calculated losses in conversion equipment. All line and machine loadings were taken from log sheet data.

The power consumption of the trolley busses was determined from a test bus equipped with an ammeter, voltmeter, and watthour meter. During November and December 1946, this test bus was assigned to each scheduled route for one day, excepting Saturdays, Sundays, and holidays. The meters were read at each terminal of the route as well as at some point designated as the dividing line between the congested downtown area and the suburban area of the city. The ammeter and voltmeter were read before and while starting. A note was made of the number of passengers, relative traffic conditions, whether the bus heaters were on or off and the time of reading.

The power use by all the busses on one route was determined by multiplying the test vehicle consumption for each minute of the day by the total number of vehicles scheduled on that line. A minute-by-minute summation gave the hourly power requirements of that route. A minor adjustment was introduced at this point to include the effect of a slight difference in power consumption of two different types of busses. A similar method of calculation was used for the trolley car route.

The test vehicle power measurements were made over a period of two months; to correct these measurements to an average day it seemed reasonable to assume that all variations due to weather, traffic, passengers and bus heaters would be reflected in the a-c input to the system. The hourly test values were therefore multiplied by the ratio of the input for the average day to the input for the test day for each hour.

It was observed that the power requirement of the transportation system varied with the average daily temperature. During the months of November and December the weekday power use for 24 hours exclusive of Saturdays and holidays was 128,600 kilowatt-hours for an average day for this period having an average daily temperature of 45-degrees Fahrenheit. Between the range of 30 and 60 degrees the power-temperature relationship was almost a linear function; the power use varied 2,000 kilowatt-hours per degree change in the average daily temperature, increasing with decrease of temperature.

Loss Determination from Measurements

The losses on the d-c system as determined from measurements were obtained by subtracting the total power use of the trolley busses and cars from the net d-c power input to the trolley system at the United Electric Railways substations. This calculation was made for each hour of an average day. These losses which also included some unmetered use of power at the garages were plotted against the d-c input to the United Electric Railways and beside each point was marked the corresponding time. The plot is shown in Figure 2. The 24-hour totals are given in Table I.

Table I

	Kwhr
Input to system for normal November-December day	128,600
Transmission and substation losses	9,858
Net input to d-c	118,742
Trolley bus consumption	60,186
Trolley car consumption	26,991
D-c circuit losses plus garages	31,565

By looking at Figure 2 it may be seen that most of the points fell reasonably close to a square-law curve. There were two groups that did not: (1) the values corresponding to the five early morning hours between 2:00 a.m. and 6:00 a.m. (2) the values corresponding to the rush hour periods of 7:00 and 9:00 a.m., 5:00, 6:00 and 7:00 p.m. It was readily inferred that during the early morning hours practically all of the input was used at the garages since vehicles on the road could account for only a small part of the total use. The wide divergence of the losses at other hours of the day was the subject of prolonged study. Attempts to correlate the losses with the number of passengers carried, the bus heating use and general traffic conditions were not conclusive.

To explain the lower losses during the "rush hours," it was hypothecated that at these times the busses were concentrated in the downtown area, and because of their being closer to the supply points and because of the better diversity between bus current takings, the feeder losses were not increased in proportion to the number of busses scheduled; furthermore, during the evening rush hours the average bus consumption was less, indicating more waiting time. One explanation of the high losses during the morning rush hours as compared with the afternoon rush hour periods might be that in the morning the busses go to the ends of the line to start their schedules,

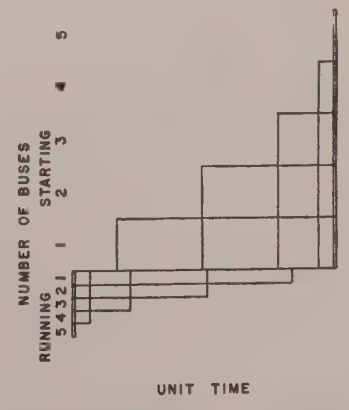

Figure 3. Relative duration and magnitude of current due to simultaneous use of starting and running power for example of 10 busses. Simultaneous starting or running of six or more busses may be neglected. Unit time shown 127 seconds

whereas in the evening the busses go downtown to start their runs.

Calculation of Losses in the D-C Feeders and Trolley System

The losses in the d-c feeders and trolleys caused by the bus power use were determined for the maximum number of busses that would be operating during the peak hour. On a positive feeder map of the d-c supply system the 5:30 p.m. positions of all scheduled vehicles were marked. This network was simplified to equivalent radial networks on which the identity of the bus location was retained. The maximum number of busses on any one radial feeder and trolley was 19. The loss in each section of these radial networks was determined using the rms current equivalent to the intermittent takings of the number of busses drawing power through each section of the resistance network.

A probability method was used to determine the duration of simultaneous use of power by busses on the same feeder. The procedure was adopted from an article by Adler and Miller.[2] The equations used and an example are given in the appendix. The calculations were based on a cycle of bus operation that was assumed to average 10 seconds drawing starting current, ten seconds drawing running current and 40 seconds of no power use in each minute. Manufacturers' data indicated the starting current of a bus would be 300-amperes at 600-volts while the running current would be one-fourth as much. The selection of the time intervals was based on observation of bus operation and checked by comparing the calculated power use for the assumed cycle with measured values.

These calculations were simplified by first considering only the starting current. The results of a calculation of probable duration of simultaneous use of starting current only for an example of ten busses on one feeder are shown by the block steps in the upper part of Figure 3. In this case simultaneous starting of more than five busses need not be considered since simultaneous starting of six busses would be expected to occur for one second out of each 520, while that of seven busses would occur on the average of one second in each hour.

The operation of a bus on the starting, running or stop position are mutually exclusive events. Therefore, it was reasoned that if a bus were not taking starting current there would be a 4-to-1 chance that it would not be taking any current; hence, the probability curve of the running current requirements was assumed to be the inverse of the starting probability steps but of one-fourth the magnitude; it was fitted into the block steps of the starting current overlaps as shown by the placement in the lower part of Figure 3. The maximum number of busses taking running current would be expected to take place at a time when there would be none starting.

The rms current equivalent to the block steps of the starting and running current was readily calculated in terms of the starting current of one bus. Similar calculations were made for other numbers of busses and the results in terms of current factors (k) are shown in Figure 4. For any given number of busses the equivalent rms current can be obtained by reading the current factor value and multiplying by the starting current of a bus. For loss calculations a plot of current factors squared (k^2) was found to be convenient; when multiplied by the square of the bus starting current and the resistance of a feeder section, the power loss was obtained directly. The sum of the losses for all the positive feeder networks was doubled to include the negative feeder losses.

The first calculations were based on a bus starting current of 300 amperes as given by the maker. A comparison of the calculated peak hour feeder losses with the measured value of the peak hour losses as obtained from meter readings showed the calculated losses 45 per cent high. In practice, because of voltage drop, the starting current was observed to be between 200 and 250 amperes. The calculated losses were made equal to the measured losses by changing the assumed value of the bus starting current from 300 to 229 amperes. The 24-hour losses on the average day were 18.15 times the losses on the peak hour. This factor was used later to put the calculated losses on a 24-hour basis. An annual figure was arbitrarily assumed to be 300 times the loss of the average day.

Alternate Methods of Supplying Power to the Trolley System

After developing a method of calculating the losses in the d-c feeder and trolley systems and correlating the calculated values with measured losses, it was possible to use this method to evaluate the relative merit of any proposed change in the power supply.

Preliminary study indicated that replacement of the present 25-cycle system of rotary converters by some type of 60-cycle rectifier installation would offer the most promise. The possibility of using comparatively small rectifiers in numerous places around the trolley system, tapped to existing 60-cycle feeders at either 4-kv or 11-kv, was studied in considerable detail. The proposed plans were examined to insure against the creation of new problems such as undesirable voltage flicker or telephone interference as well as to see if the proposal was economically sound. Three types of 60-cycle rectifier installations were investigated:

1. Rectifiers 500 kw and smaller on the 4-kv feeders.
2. Special locations for rectifiers tapped on the 11-kv feeders.
3. Large rectifier units in existing substations.

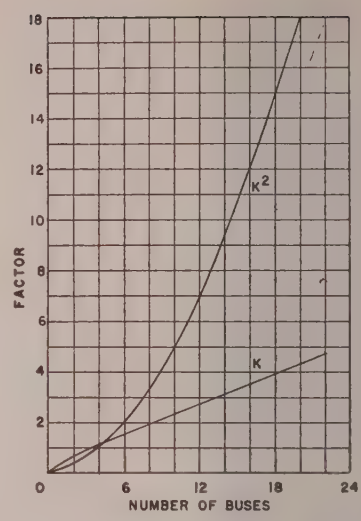

Figure 4. Current factors versus number of busses. To obtain the rms current equivalent for the number of busses indicated by the abscissa, multiply corresponding k value by the starting current of one bus. For loss calculations, use k^2 value and square of starting current of one bus

Small Rectifiers on 4-Kv Feeders

The location selected for the first study of small 60-cycle rectifiers was a high loss radial d-c feeder that extends about $3\frac{1}{2}$ miles beyond the present supply point at Olneyville and has an average of 10 busses scheduled during the rush hours. The load was idealized in that a uniform distance between busses was assumed. Five methods of supplying power were considered for purposes of comparison of losses; namely, a 500-kw rectifier at the supply end, a single 500-kw rectifier at the middle, or smaller units of two 300-kw, or three 200-kw, or four 150-kw units, so spaced as to divide the line in equal

Table II

Number Rectifiers	Annual D-C Losses Kwhr	Cost of Rectifier Installation	Compared with Radial Supply Capitalized Loss Saving	Net Cost Penalty
Radial supply	429,500	$ 33,000*		
1–500 kw rect.	321,000	73,000	$ 9,500	$ 30,500
2–300 kw rect.	219,000	108,000	18,600	56,400
3–200 kw rect.	175,500	140,000	22,300	84,700
4–150 kw rect.	180,000	186,000	21,900	121,000

*Based on the cost of 500 kw of capacity in a substation having 3,000 kw of rectifiers, at 1947 prices.

parts. The rectifier sizes selected were standard units whose total capacity came closest to satisfying the maximum demand anticipated. In all loss calculations the probability method was used. Rectifier conversion losses were assumed to be 7 per cent of the load. The results of these calculations are shown in Table II.

A comparison of these schemes shows that the greatest loss savings would be realized by using the smallest size rectifiers. However, all of these plans involve a net cost penalty when compared with a system at the supply end of the feeder located at an existing substation.

Investigation of 500-Kw Rectifiers on 4-Kv Feeders for Voltage Flicker and Telephone Interference

The economic study of the preceding paragraphs pointed out the uneconomical nature of numerous small rectifiers. The one with the least net cost penalty would be the single large unit in the middle. The voltage flicker and the inductive interference problems were studied only for installations of the 500-kw size as this has the lowest net penalty attached to the small rectifiers.

Voltage Flicker

To estimate voltage flicker that would be caused by trolley bus loads on the 4-kv distribution system, eight possible locations where rectifiers might logically be placed were examined. From the circuit diagram, it was possible to estimate the number of busses on any 4-kv feeder. The probability method was used as a guide in estimating the magnitude and duration of trolley bus loads that would cause voltage dips of more than one second duration.

As a criterion of objectionable flicker 2 per cent was considered just noticeable; 3 per cent was assumed objectionable if recurrent (as would be the case); loads of less than one second duration were neglected. These calculations showed that out of eight possible locations studied, six would have been classified as objectionable and two would have been borderline cases.

Telephone Interference

A rectifier is inherently a prolific harmonic generator. To determine the extent of the inductive interference problem with rectifiers on the 4-kv distribution system, reference was made to the AIEE Committee Report[3] describing a relatively simple analysis that makes it possible to anticipate potential inductive interference problems in rectifier installations.

The three exposures most apt to cause interference are listed as Exposure A, to parallel communication circuits between the supply point and the rectifier, caused by harmonic currents flowing in the supply feeder; Exposure B, to communication circuits that are parallel to extensions of the line that supplies the rectifier, caused by harmonic voltages at the rectifier; Exposure C, to communication circuits that parallel other a-c feeders radiating from the same substation that supplied the rectifier and caused by harmonic voltages at the substation.

The report presents a series of tables and graphs which were used as a guide in classifying a proposed rectifier installation as to the likelihood of the creation of an interference problem. The report classifies an installation in three categories: (I) very unlikely to cause important induction problems, (II) indeterminate, and (III) very likely to cause important inductive problems.

For the proposed installation of a 500-kw rectifier on the 4-kv distribution feeder 9,000 feet from the Olneyville Substation, it was determined that Exposure A would be in Category II, Exposure B in Category III, and Exposure C in Category I. This classification indicated that the Exposure A between the rectifier and the supply would require further study. If the 4-kv distribution were an open wire circuit with the neutral grounded only at the substation and if there were no unbalanced tapped loads in between, there would probably not be any interference with the communication circuits in cables; with open wire communication circuits there might be a problem.

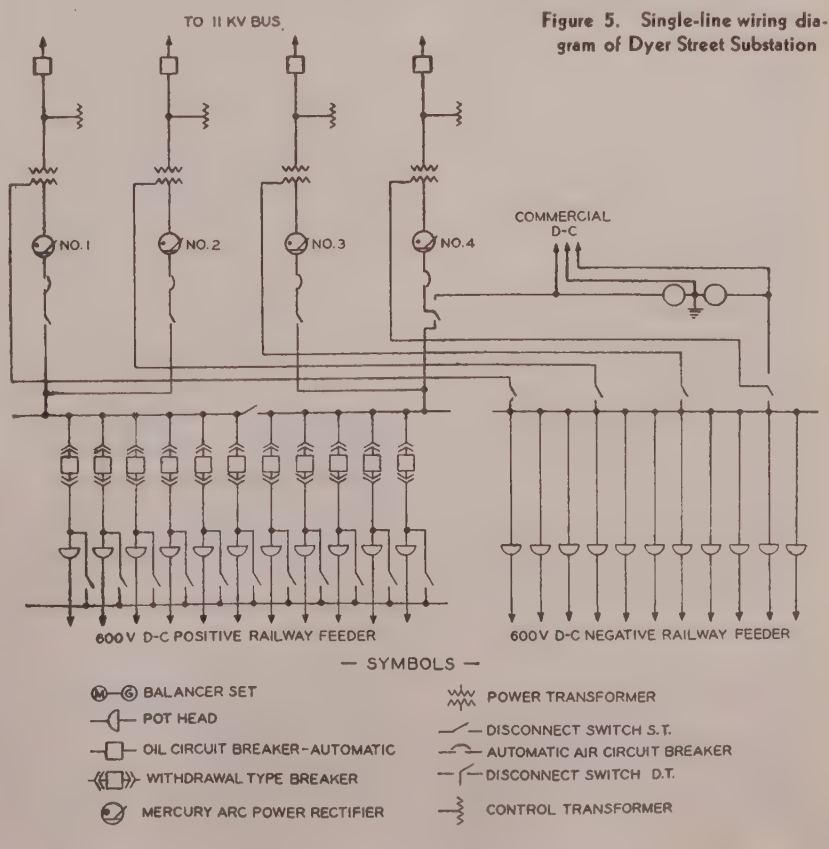

Figure 5. Single-line wiring diagram of Dyer Street Substation

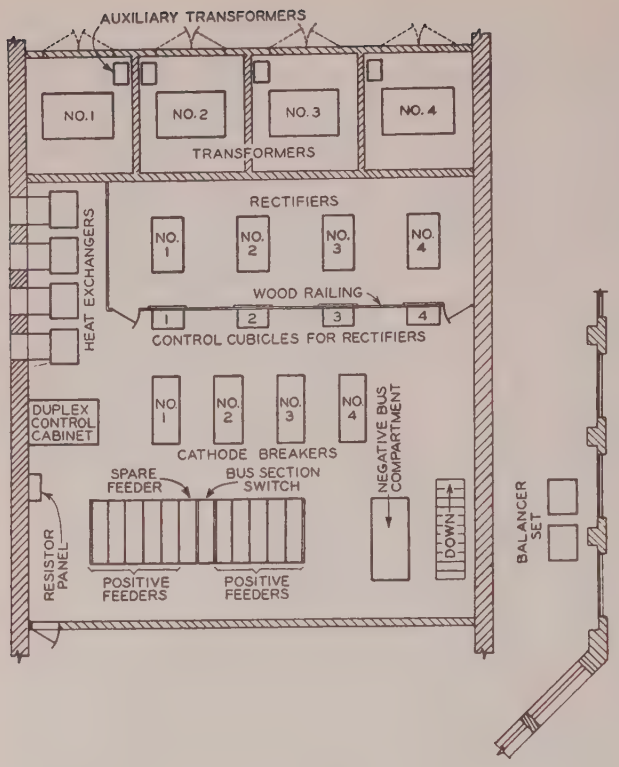

Figure 6 (left). Plan of Dyer Street Substation

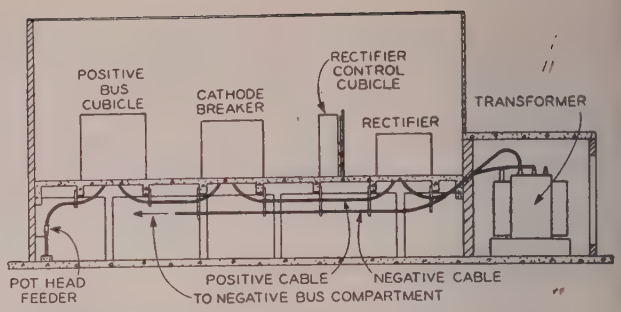

Figure 7 (above). Typical section of Dyer Street Substation

If the 4-kv distribution circuit were multigrounded, the exposure would have been classed as very likely to cause interference with open wire communication circuits; if paralleled by cable circuits it would have been classified as indeterminate. The Exposure B on the feeder beyond the rectifier for this proposed location would have been in the third category and would have caused trouble. The Exposure C on the feeders radiating from the supply station would have been in the first classification and would have offered no problem.

In general, when a preliminary study indicates the need of a more careful specific analysis the presence of capacitors on the distribution system must be checked. Capacitors located relatively close to a rectifier, within several hundred yards, may be beneficial, capacitors located at more remote spots are usually detrimental.

It was concluded that this application of a 500-kw 6-phase rectifier on a 4-kv distribution feeder would cause interference on open wire telephone lines having exposures beyond the rectifier.

Special Location for Rectifier on 11-Kv Feeder—Sprague Street

The preceding analysis showed that the application of small rectifiers on the 4-kv system was not practical. The next logical step was to examine the possibility of installing a single rectifier, tapped on an existing 11 kv industrial or tie line feeder, in an area where comparatively large loss savings in the d-c feeders and trolley system might be realized. A 750-kw rectifier was considered at the Sprague Street Substation located about equidistant from Manchester Street, Olneyville, and Elmwood. The need of having sufficient capacity at this location to be firm was obviated by a plan of operation that contemplated closing feeder ties to adjacent d-c substations in case of failure of the unit.

The probability method was used to determine the number of busses that could be supplied by this station, and feeder changes were planned to take maximum advantage of the closer supply. This installation would have resulted in an annual loss saving of approximately 400,000 kilowatt-hours having a capitalized value of $35,000. The extra cost of this installation over the same amount of capacity as part of a large rectifier substation was estimated to be about twice this sum.

Special Location for Rectifier on 11-Kv Feeder—Prairie Avenue

A modified application of a rectifier supplied from an existing 11-kv 60-cycle feeder was the suggested use of a small unit to supplement the power supply to an area where the d-c feeder losses were high. It was visualized that a 300-kw rectifier could be made completely automatic and installed in a sidewalk vault. By using a reactor in the supply to obtain a drooping voltage characteristic, overloading of the small unit would be prevented.

Such an installation might be located on the so-called Prairie Avenue feeder a half mile west of the Manchester Street Station. The calculations showed that the feeder losses would be approximately halved, thereby saving approximately 200,000 kilowatt-hours of losses annually which would have a capitalized value of approximately $18,000. The estimated extra cost of such an installation over the same amount of capacity, as part of a large rectifier substation, would be approximately twice the value of losses saved.

Large Rectifiers at Present Substations

The proposed installation of rectifiers on 11-kv feeders at special places, while not expected to cause problems of voltage flicker or telephone interference, would have a high net cost per kilowatt as compared with the proportionate cost of the same capacity when considered as part of a larger rectifier installation at an existing substation.

A survey of such possible locations for new rectifiers to replace the rotary converters at the Manchester Street Station showed that Dyer Street and Fields Point would be suitable. Since both are closer to the load than the Manchester Street Station, an incidental loss saving of approximately 6,000 kilowatt-hours per day and a 300-kw reduction of the maximum 15-minute demand at the peak hour was expected. It was calculated that the minimum voltage at the ends of trolleys during bus starting would be improved for practically all feeders in the southeastern section of the city. The feeders with the poorest voltage before

Figure 8. Rectifier installation at Dyer Street

such change would be improved by about 100 volts. In addition to these benefits, the new rectifiers would replace the oldest rotary converters and the elimination of this equipment at the Manchester Street Station would make available necessary space.

Rectifier Station Design at Dyer Street and Fields Point

Dyer Street Substation serves the downtown area of the city and is normally operated without 600-volt d-c ties to other stations. As shown in Figure 5 there are ten railway feeders leaving the station. The positive bus to which they are connected contains a sectionalizing switch in the middle which is normally operated closed and would be opened only in case of a bus fault or for maintenance work. The arrangement of feeders on the bus is such that by closing outside tie switches the entire area served by the station can be carried from either half of the bus. The feeder positives are connected to the bus by semihigh-speed circuit breakers while the negatives are unswitched.

The rectifiers are connected to the positive bus through high speed cathode circuit breakers and to the negative bus through disconnecting switches. In addition number 4 rectifier is equipped with selector disconnecting switches so that it may be used for light and power service on the 3-wire 250/500 volt d-c system. When used in this way the 3-wire neutral is established by means of a balancer set as shown on the wiring diagram.

Consideration was given to use of high speed anode circuit breakers, but the additional cost did not seem justified. The primary sides of the rectifier transformers are connected to an 11-kv 60-cycle bus by means of existing circuit breakers located in the adjacent distribution substation.

All equipment is fully automatic. The positive feeder circuit breakers are equipped with rate-of-rise tripping and load-measuring reclosing control. The rectifiers have load-responsive sequencing control. Voltage controlled light load resistors are provided to limit the voltage rise during the early morning hours when only one or two busses are on the line, and there are regenerative braking resistors to absorb any energy pumped back by dynamic braking equipment on the busses. These latter resistors have a combination voltage and current control.

Figures 6 and 7 show a plan and section of the arrangement of equipment. Figure 8 shows a general view of the equipment at Dyer Street. This arrangement was designed to keep all power leads as short as possible with a minimum number of crossings. Since the building already existed, the freedom in spacing units was somewhat limited. Fortunately there was ample headroom to allow the construction of an elevated floor for all equipment except the transformers. This provided racking space for cables as well as raising the equipment above possible flood damage. The 1938 hurricane raised the salt water of Narragansett Bay to an elevation of seven feet above the original floor. A repetition of this flood would immerse only the lower part of the transformers and the railway feeder potheads which are of the solder seal type. Hence, the equipment would be ready for service soon after the water had receded.

Rectifying Equipment

As shown, the rectifier transformers, which are double-Y with an interphase winding, were installed in vaults due to lack of outdoor space. Ventilation is provided by a fan in the top of each vault which operates whenever the transformer is energized. During the summer months air is drawn from the space under the rectifier equipment floor and exhausted through roof ventilators. In the winter the roof ventilators are closed and the air recirculated to aid in heating the building. The vault ventilating openings are equipped with automatically operated seal-off doors to close in case of fire.

The rectifiers are 1,000 kw 6-tank ignitron type and are cooled with water-to-air heat exchangers. Since the heat exchanger frames are grounded, the first 15 feet of water pipe leaving the rectifiers is made of insulating material and electrolytic targets are used at the rectifier to take the small amount of electrolytic errosion. These targets consist of copper rod which extend from the first metallic pipe fitting at the rectifier into the insulating pipe. It was found by analysis that the resistivity of city water was high enough for use in the cooling system, thus avoiding the necessity of using distilled water.

The heat exchangers, whose fans are controlled by water temperature, normally exhaust air from the room through openings in the north wall. However, dampers are provided so that during the winter the air can be recirculated for heating, and this is the only source of heat provided.

The rectifiers are located within a fenced area which is entered only to make necessary checks, tests or adjustments. In order to protect personnel all grounded metal has been kept out of the area and the spacing is such that greater than an arm span separates the rectifiers. Hence, although the frame of a rectifier (which is at 600-volts positive potential) can be contacted, it is not possible to simultaneously contact the negative or grounded side of the circuit.

The floor of the area was given special treatment to avoid the possibility of shock. It is of concrete construction and all reinforcing and supporting steel was placed well below the surface. In addition a $^{3}/_{16}$-inch insulating layer of sand and bond mixture topped by one quarter inch rubber tile was laid on the concrete. In laboratory test this bonding mixture and rubber tile gave a high potential breakdown in excess of 4,000 volts, 60-cycle rms at the joint between tiles, and also had a high insulation resistance.

The rectifier auxiliary control equipment for the control of ignition, cooling water, and vacuum is mounted in a cabinet located four feet in front of each rectifier. Since this cabinet is grounded, a barrier sheet of insulation board was placed behind it to prevent anyone within the rectifier area from touching it. The

first two feet of each control conduit leaving the rectifiers is made of insulating material and all control wiring has 1,000-volt insulation.

Switchgear

The positive bus structure is of metal-clad type with drawout circuit breakers. The choice of this type of equipment was largely dictated by availability, since delivery promises on other types did not meet the construction schedule. In order to protect the structure, a number of steps were taken against possible damage by arcing faults.

The rating of the four rectifiers together is 6,700 amperes continuously, 10,000 amperes for two hours or 20,000 amperes for one minute. With normal currents of this magnitude at only 600 volts, a small amount of fault resistance will so limit the current in the event of an insulation failure or arc-over, that overcurrent protective relays may fail to recognize the presence of trouble. On the other hand a sustained arc of 1,000 amperes will soon cause serious damage. With an a-c system, differential relaying could be used to provide the required sensitivity but on a d-c system this cannot be done readily. Hence, it was decided to install the switchgear structure on insulating maple sills and ground it only through a 20-ohm resistor. The maximum fault current at the bus structure was thus reduced to 30 amperes. In the event of a fault, a voltage measuring relay connected across the grounding resistor is arranged to trip (after a time delay) all rectifiers supplying the bus and all feeder circuit breakers. The time delay is sufficient to allow fuses on control or instrument circuits to clear any miscellaneous wiring failures.

In order to protect personnel who might be working around the bus structure at the time of a fault, the floor surrounding it was treated the same as that around the rectifiers and grounded metal was kept away from the immediate vicinity.

One of the weakest spots in the insulation of a d-c structure is the ammeters and their connections which really form an extension of the main bus work. There have been cases on other systems where an ammeter insulation failure has started an arc which resulted in serious damage. With fault current limited to 30 amperes for a few seconds, this hazard is eliminated, but it was felt that it would be desirable, if possible, to avoid removing the entire structure from service for such minor trouble. Hence, low resistance 5-ampere fuses were installed in all ammeter leads at the point where they leave the ammeter shunt. Although the fuses chosen were found to have quite uniform resistance it was felt that some type of adjustment should be available to maintain instrument calibration. This was accomplished by using shunts of a higher millivolt drop than the ammeters and installing adjustable calibrating resistors. In order to avoid fuse clip resistance, fuses were obtained with bolted connections.

Another fusing problem arose in the protection of the light load and regeneration braking resistors, which together with their control devices are mounted on a wall panel. These devices require 30- and 200-ampere fuses respectively and, since connection to them comes directly from the negative and positive busses, the fuses must be able to interrupt the maximum bus fault of 75,000 amperes. Such fuses were not in production at the time but were under development; and laboratory models, which were later replaced with production units, were obtained from the manufacturer.

Each high-speed cathode circuit breaker and its bus disconnecting switch are mounted in front of the corresponding rectifier in a steel frame located on insulating maple sills. The frame is then grounded by a relay in parallel with a large red lamp which is mounted at the top of the frame. If the circuit breaker insulation should fail and thus energize the frame, the relay would trip the rectifier 11 kv a-c supply and the cathode circuit breakers. If the insulation failure is on the rectifier side of the circuit breaker this operation will de-energize the frame. If the failure is on the bus side of the circuit breaker the frame will remain energized until the bus side disconnect is opened. In the meantime the red light will be lighted to warn that the frame is alive. As a further safeguard to personnel the frame and circuit breaker are totally enclosed on all sides with doors made of insulating board. In the case of number 4 rectifier which may be connected either to the 600-volt railway system with negative grounded, or the 250/500 volt 3-wire power system with neutral grounded, the calibration of the frame ground relay and the red lamp series resistor, are automatically changed, when going from one system to the other, by means of auxiliary contacts on the positive selector disconnecting switch.

The negative bus structure was designed to contain disconnect switching and at present switches are installed only for the four rectifiers, the outgoing feeders being tied solidly to the bus. If, in the future, the trolley system should be operated ungrounded, disconnect switches for the negative side of each feeder would also be installed. The structure frame was solidly grounded on the basis that with the negative grounded as at present, no fault can occur. If the system should be operated ungrounded, an insulation fault in this structure would be serious only if there were a simultaneous positive fault within the station. This would be a very unlikely coincidence.

Control of the rectifiers is accomplished from the master control panel which contains the instruments, control switches and relays, annunciators, and alarms for all four rectifiers. The sequence in which the rectifiers respond to load changes can be varied in order to equalize the hours of service between them and in addition the selective equipment is arranged to pass over any units which are unavailable for service. This results in a total of some 240 operating setups which the relays must recognize. In addition, any unit may be taken out of the automatic sequence and controlled manually. The load responsive control is set to keep the equipment operating as near maximum efficiency as possible which is between half and full load. Hence, an additional rectifier is brought into operation when the load on the ma-

Table III. Frequency and Duration of Overlap of Simultaneous Starting of 10 Busses

r Number of Buses Starting Simultaneously	t_r Average Duration of Overlap in Seconds	P_r Fraction of Unit Time Occupied by "r" Events	f_r Frequency of Overlap	T_r Average Time Between Simult. Events
0	5.00	0.168	0.0336	29.8
1	3.57	0.315	0.0883	11.3
2	2.78	0.291	0.1045	9.6
3	2.27	0.155	0.0683	14.6
4	1.92	0.054	0.0281	35.6
5	1.66	0.0130	0.0079	127.0
6	1.47	0.002	0.0013	770.0
7	1.32	0.0003	0.00022	4,500.0
8	1.19	0.00004		
9	1.09	0.000005		
10	1.00			

chines in service reaches normal rating and a machine is dropped off when the load per machine decreases to 40 per cent. The equipment may be operated to shut down at night (after load has gone off) and start again in the morning, but since the Dyer Street area is normally isolated from the rest of the system, the control is set up to leave one unit on at all times. The annunciator system provides a record of abnormal operations that occur as well as initiating an alarm in the event that any unit is locked out. The control system was designed by the rectifier manufacturer.

The installation of the two 1,000-kw rectifiers at the Fields Point Substation was similar in general design features, to the Dyer Street Station. The rectifiers are of the excitron type. As there are only two rectifiers semihigh-speed cathode circuit breakers were used and the load responsive sequencing control is considerably less complicated.

Both stations now have been in service a little over two years and, aside from initial shake-down troubles, operation has been very satisfactory. The arc-back rate, so far, has been less than one per machine for the 2-year period and interruptions due to other causes have been few.

When the stations were first put into service, unexpected telephone interference was experienced; this was found to be due to capacitance coupling to ground through the capacitor-type lightning arresters used on the d-c feeders. The trouble was eliminated by the installation of an 0.007-inch gap in series with each lightning arrester.

Summary

1. A method was developed for calculating losses in the d-c feeder and trolley system of an electric transportation company.
2. This method was applied to an investigation of a power supply to the United Electric Railways of Providence where it was necessary to relocate a substation having 40-year old rotary converters.
3. It was determined that this rotary equipment could be most economically replaced by 1,000-kw rectifiers at two existing substations.

Appendix

Where the average rate of occurrence of an event is known, the probability of simultaneous occurrence of multifold events can be determined by the binomial law. The probability of r out of n events occurring simultaneously is given by equation 1. When this expression is used to determine the probability of simultaneous starting of a given r number of busses out of a total number n, all of which have an equal starting cycle, the special case developed in the second reference can be applied.

The average duration of overlap of r simultaneous events in terms of unit time T is given by equation 2.

The average intervals between the overlaps calculated by the second equation are given by equation 3, and the reciprocal of this last gives the frequency of such overlaps, see equation 4.

$$P_r = \frac{n!}{r!(n-r)!} p^r (1-p)^{n-r} \tag{1}$$

$$t_r/T = \frac{(1-p)(p)}{(r+p)(n-2r)} \tag{2}$$

$$T_r = t_r/P_r \tag{3}$$

$$f_r = 1/T_r = P_r/t_r \tag{4}$$

where

P_r = fraction of unit time occupied by r events
n = total number of busses
r = number of busses starting simultaneously. Values 1, 2, 3, —n were substituted in successive calculations
t = duration of starting (10 seconds)
T = unit time (60 seconds)
p = average rate of occurrence of starting $p = t/T$

t_r = average duration of overlap
T_r = average time between simultaneous events
f_r = frequency of overlap

The preceding equations were applied to determine the frequency and duration of simultaneous starting that might be expected with 10 busses on one feeder. With this number of busses r was given values one through ten and the equation solved to obtain the values given in Table III.

References

1. Trackless Trolley Operation in Rhode Island, **H. R. Blomquist.** *AIEE Transactions*, volume 68, part I, 1949, pages 397–402.

2. A New Approach to Probability in Problems of Electrical Engineering, **H. A. Adler and K. W. Miller.** *AIEE Transactions*, volume 65, 1946, pages 630–32.

3. Inductive Coordination Aspects of Rectifier Installations, **AIEE Committee Report.** *AIEE Transactions*, volume 65, 1946, pages 417–36.

Discussion

G. M. Woods (Westinghouse Electric Corporation, East Pittsburgh, Pa.): The city transit industry is peculiar in that its use of electricity has decreased 14 per cent in the last ten years. This decrease is due largely to the greatly increased use of motor buses. While the percentage increase in number of trolley coaches is high, the actual number falls far behind the number of surface cars retired. Generally the investment required for overhead lines and new substations, when they are required, is a powerful deterrent to an industry in almost continuous financial difficulty. This is true in spite of the more favorable economic results of trolley coach operation compared with motor bus operation. The installation in Providence shows that this particular power company has faith in the future of electricity in the city transit business and is willing to back that faith with additional investment. This paper is very timely because a number of transit operators are now faced with the same problem. The questions of number and size of units per substation are continually arising with the first tendency generally to use a large number of small single unit stations. In this case the largest size of rectifier considered proved to have the lowest net cost.

The description of the method of analysis and the description of the installation are most valuable. The paper illustrates that generalizations cannot take the place of a detailed study of existing conditions for each application.

W. C. Whitman and **F. F. Schaller:** The discussion by G. M. Woods highlights some of the major problems which arise in the city transit industry with respect to expenditures for electrification. The authors appreciate his comments as well as the interest shown by others in the field.

Results of a Questionnaire Covering Current Practices in Electrical Tests on Dielectrics in the Field

AIEE COMMITTEE REPORT

THE activities of this Subcommittee, established by its parent committee in 1940, are described in its scope as follows: "to investigate and evaluate the dominant features of instruments and techniques suitable for testing the electrical insulation of power apparatus in the field, to sponsor technical publications and to suggest standard procedures for testing in the field."

As one step towards these objectives, the subcommittee recently sent a questionnaire to the electrical power industry in United States and Canada. The questionnaire consisted of four questions which, in the interests of brevity, are summarized as follows:

QUESTION 1

Do you make electrical tests on dielectrics in the field?

QUESTION 2

What types of a-c insulation tests do you make in the field?

The question consisted of 12 tabular forms, one for each of the common types of power apparatus (see Table II for list). Each form listed the four common types of a-c field tests; dielectric loss and power factor, voltage withstand, voltage distribution, and corona detection; and asked for such data as test voltage and frequency, time of voltage application and electrical characteristics measured, for the tests used. Other spaces in the forms asked for an evaluation of the test results, an estimate of the number of tests and the reasons for which the tests were made.

QUESTION 3

What types of d-c insulation tests do you make in the field?

The third question was the same as the second but listed the four types of d-c field tests; insulation resistance, dielectric absorption, voltage withstand and corona detection; and asked for data similar to that in Question 2.

QUESTION 4

The fourth question asked for information on any other field tests not covered by Questions 2 and 3.

Summary of Returns. The questionnaire was sent to 183 utilities and service companies representing 241 operating systems in the United States and Canada whose combined generating capacity totalled over 65,000,000 kw. (Figures are based on the 1950 McGraw Central Station Directory.)[1] Replies were received from 117 companies covering 129 of the 183 utilities and representing 186 operating systems with a total generating capacity of about 52,000,000 kw, or 80 per cent of the total canvassed. The 54 systems which did not reply represent 13,399,906-kw capacity.

The replies received were distributed fairly broadly and evenly so that the data were secured from a large and very representative cross section of the power industry. The number of systems contacted, classified by generating capacity and geographical location is shown in Table I.

Discussion of Individual Questions

QUESTION 1

"*Do you make electrical tests on dielectrics in the field?*" was answered "Yes" by 169 systems; "No" by 13; "Not in manner described" by two; and "Program not sufficiently developed to answer" by two.

Of the 169 systems doing field testing, two limit their programs to tests on insulating oil only, four to d-c tests and two to a-c tests on rotating machinery, one to tests on oil and rotating machinery, and three to the latter plus d-c tests on power transformers. The balance of 157 systems have programs of field testing which are summarized in Table II. This table lists the different types of test methods reported in the replies tabulated against the 12 common types of power apparatus and shows the number of power systems utilizing each type of test for each type of apparatus. A large number of power systems employ both a-c and d-c tests in various combinations.

Thirteen systems use a-c tests only, nine use d-c tests alone, (of which four test rotating machinery only) and 73 use only a-c tests for the insulation of apparatus other than cables and rotating machinery. The total number of systems using each type of test and the number of apparatus types to which they apply them are shown in Table III. It should be noted that of the 129 systems shown as using the a-c voltage withstand test, 112 use it on insulating oil, 69 of which use it for this purpose alone.

QUESTIONS 2 AND 3

The replies to Questions 2 and 3 have been summarized in Table IV. This

Paper 51-186, recommended by the AIEE Instruments and Measurements Committee and approved by the Technical Program Committee for presentation at the AIEE Summer General Meeting, Toronto, Ont., Canada, June 25–29, 1951. Manuscript submitted March 16, 1951; made available for printing April 23, 1951.

Personnel of the AIEE Subcommittee on Electrical Tests on Dielectrics in the Field: F. C. Doble, *Chairman*, W. G. Amey, D. L. Brown, A. L. Brownlee, E. B. Curdts, C. L. Dawes, W. F. Dunkle, I. G. Easton, W. N. Eddy, J. G. Ford, I. W. Gross, E. S. Lee, W. N. Lindblad, H. C. Marcroft, G. M. L. Sommerman, E. R. Thomas, L. Wetherill.

Table I. Power Systems Contacted, Classified by AIEE Districts Geographically and by Generating Capacity

Generating Capacity kw in Thousands	Reporting Number of Power Systems in AIEE District Number						
	1 Northeastern	2 & 3 Mid-East & N. Y.	4 Southern	5 & 6 Midwest	7 Southwest	8 & 9 Pacific & N. W.	10 Canada
0–49	21	10	7	17	1	2	4
50–99	2	5	4	6	3	1	2
100–499	12	14	8	16	11	7	3
500–999		5	3	5	1	2	3
1,000–up	1	3	2	2		2	1
	36	37	24	46	16	14	13
Not Reporting							
0–49	1	1	1	4	2	2	
50–99	2	1	1	2	2		2
100–499		3	5	8	5	4	2
500–999	1	3	1				
1,000–up				1			1
	4	8	8	15	9	6	5

Table II. Number of Power Systems Using Test Methods Listed on Insulation of Apparatus Shown

Test Method—A-C: Test Voltage Kv	Test Frequency in Cycles per Second	Electrical Characteristics Measured*	Type of Apparatus Insulation Under Test: Line Insulators	Bushings	Potheads	Power Transformers	Distribution Transformers	Instrument Transformers	Lightning Arresters	Insulating Liquids	Carrier Current Capacitors	Cables	Rotating Machinery	Circuit Breakers
			Number of Power Systems											
10	60	I & W	24	99	50	98	24	95	69	77	75	40	22	90
10	60	C & DF		1		1						1		
10	63.5	C & DF		3										
10	70	C & DF		7		3		1	2	1	3			5
2.5	60	I & W		38	4	31	2	31	23	23	20	2	1	29
80–100v	60	C & DF		11	1	2	4	2			3	2	2	1
30 v	60	C & DF		1						1				
Voltage withstand			7	6	13	20	14	15	5	112	3	32	31	9
Voltage distribution			62	3					1				1	
Corona detection			1	4	1		1	1	1				9	1
Test Method D-C														
Insulation resistance			4	20	31	57	16	33	13	2	6	79	91	19
Dielectric absorption					3	27	3	6				25	56	1
Voltage withstand			2	1	32	7	4			1		52	25	
Corona detection													7	

*I & W = current and watts. C & DF = capacitance and dissipation factor.

Table III. Applicability of Various Test Methods

Test Method A-C	Total No. of Systems Using	Cumulative Number of Apparatus Types Tested by No. of Systems*: 1	2	3	4	5	6	7	8	9	10	11	12
10 kv 60 cycle I & W	99	99	99	98	98	94	86	80	54	33	21	1	
10 kv 60 cycle C & DF	1	1	1	1									
10 kv 63.5 cycle C & DF	3	3											
10 kv 70 cycle C & DF	7	7	5	5	2	1	1	1					
2.5 kv 60 cycle I & W	39	39	38	29	25	24	23	22	3	1			
80–110 v 60 cycle C & DF	17	17	9	2									
30 v 60 cycle C & DF	2	2	1	1									
Voltage withstand	129	129	60	38	19	10	6	4	2	1			
Voltage distribution	63	63	3										
Corona detection	13	13	2	1	1	1	1	1					
Test Method D-C													
Insulation resistance	134	134	79	55	43	25	15	12	6	3	1		
Dielectric absorption	70	70	32	15	5								
Voltage withstand	60	60	40	25									
Corona detection	7	7											

*Column number headings do not correlate with Table II. For example: Under "5" the 10 in line 8 means that 10 companies tested at least five of the types of apparatus insulation listed in Table II by the A-C Voltage Withstand method.

I & W = current and watts. C & DF = capacitance and dissipation factor.

table consists of 12 sections, one for each type of power apparatus. In each section are shown the various types of tests reported to be in use on that type of apparatus; the number of repliers using each test method; the range of manufacturer's voltage ratings of apparatus to which the tests are applied; the total of estimated number of tests made by each method classified as "Good", "Fair", "Poor", or "No Rating" according to the evaluation of each test method by each power system reporting; and the reasons for which the tests were made.

It should be noted that the classification of test results refers only to the rating of the test method by each user and not to the physical condition of the test specimen.

Thus the number of tests appearing in the "Good" column indicates the extent to which a test method was considered successful in detecting good, deteriorated, or bad insulation; it does not show the number of good or defective insulations found by that test method.

A noteworthy result was the lack of variation in test method with change in voltage rating of the test specimen. Although space was provided to show such change in method with change in voltage rating on the questionnaire, no significant variations were reported. While test voltages varied with the insulation voltage rating for some d-c insulation resistance tests and all voltage withstands tests, there was not enough unanimity of practice to permit tabulation of these data.

Question 4

This question asked for data on field tests other than those covered by previous questions.

In replying to this question a few companies listed nonelectrical tests on insulation and tests on materials other than insulation. Since these were outside the scope of the questionnaire they are not included in the summary. Answers which omitted significant information such as types of insulation tested or method used are also not included. Only two companies reported the number of tests and their value.

Low-Voltage Cable—600 Volts and Below

Ten companies use d-c insulation resistance on this type of insulation and three companies use withstand tests of 1,000 to 1,100 volts alternating current for one minute.

Two companies reported the use of a continuous ground indicating device.

	Test Method	No. of Users	Voltage Ranges Tested (kv)	Number of Systems and Estimated Number of Tests in Past Year With Value of Results Rated: Good — No. of Systems	Good — No. of Tests	Fair — No. of Systems	Fair — No. of Tests	Poor — No. of Systems	Poor — No. of Tests	No Rating — No. of Systems	No Rating — No. of Tests	Number of Systems Testing to: Prevent Service Failures	Follow Progressive Deterioration	Schedule Maintenance	Accept New Equipment
	Section 1. Tests on Line Insulators														
a-c	10 kv 60 cycle I&W	8	5-230	8	2,908					1	100	7	4	1	3
a-c	Voltage Withstand	6	22-138	3	5,099	1	300			3		1	1	1	4
a-c	Voltage Distribution	30	5-230	23	1,280,352	2	1,000	1	100	4		24	8	10	3
d-c	Insulation Resistance	5	5-230	1	thousands	1	1,150	1		2	21	3	2	2	1
d-c	Voltage Withstand	2		2			22					1		1	2
	Section 2. Tests on Bushings														
a-c	10 kv 60 cycle I&W	44	2.3-220	39	73,401	2	15			6	100	38	38	18	29
a-c	10 kv 70 cycle C&DF	6	12-220	5	3,867	1	300					5	5	4	5
a-c	2.5 kv 60 cycle I&W	12	4-220	11	7,682	1	300					9	8	6	7
a-c	80-100v 60 cycle C&DF	7	5-230	3	163	2	42			2		1	1		2
a-c	Voltage Withstand	6	2.3-220	5	1,010	1						3	3	2	6
a-c	Voltage Distribution	3	5-230	2	3,650	2	12					3	3	1	1
a-c	Corona Detection	4	2.3-220	2	56	1	6			1		3	3	2	2
d-c	Insulation Resistance	19	4-220	7	4,228	10	30,213	1		2		12	5	6	9
	Section 3. Tests on Potheads														
a-c	10 kv 60 cycle I&W	29	4-69	21	2,397	4	124			4	35	25	24	10	10
a-c	2.5 kv 60 cycle I&W	4	2.3-115	3	820	1	140					4	3	4	3
a-c	Voltage Withstand	7	2.4-34	5	46					2		2	1		6
a-c	Corona Detection	2	2.4-15	2	26							1	1	1	1
d-c	Insulation Resistance	24	4-69	8	904	7	851	2	312	7	50	15	10	6	10
d-c	Dielectric Absorption	3	7.5-34.5			3	320					3	2		2
d-c	Voltage Withstand	7	4-115	4	189	2	810			1		4			4
	Section 4. Tests on Power Transformers														
a-c	10 kv 60 cycle I&W	43	2.3-230	38	7,874	3	34			3	3	36	37	20	27
a-c	10 kv 70 cycle C&DF	2	13-132	1	112	1	6					2	2	2	2
a-c	2.5 kv 60 cycle I&W	11	4-220	11	807							10	8	8	8
a-c	Voltage Withstand	12	2.4-220	10	767	1	40			1		6	5	2	10
d-c	Insulation Resistance	39	5-230	18	4,507	9	3,022	3	465	9	34	23	13	9	19
d-c	Dielectric Absorption	14	5-230	7	257	3	22			4	25	9	4	2	12
	Section 5. Tests on Distribution Transformers														
a-c	10 kv 60 cycle I&W	8	2.3-115	7	1,478	3	225					6	6	2	4
a-c	2.5 kv 60 cycle I&W	2	25-66	2	1,512							2	2	1	2
a-c	Voltage Withstand	12	2.4-14.4	6	8,483	2	3,575	2	792	2		4	1	4	4
d-c	Insulation Resistance	12	110v-66 kv	5	5,705	4	1,158			3		5	3	4	4
	Section 6. Tests on Instrument Transformers														
a-c	10 kv 60 cycle I&W	42	2.4-230	37	6,230	1	25			4	27	36	32	19	24
a-c	2.5 kv 60 cycle I&W	8	2.5-140	7	414					1		7	6	7	6
a-c	Voltage Withstand	10	2.4 220	7	1,171	1	10			2		6	2	2	7
d-c	Insulation Resistance	21	110v 220 kv	10	19,895	4	1,722	1	150	6		11	7	5	12
d-c	Dielectric Absorption	4	5 230	1	20	1	2			2			1		3
	Section 7. Tests on Lightning Arresters														
a-c	10 kv 60 cycle I&W	31	3 230	24	3,516	4	646	1	1	3	30	28	19	12	15
a-c	10 kv 70 cycle C&DF	2	34.5-132	1	21	1	3					2	1	1	1
a-c	2.5 kv 60 cycle I&W	6	5-132	1	500	2	51	1	25	2	8	3	3	2	1
a-c	Voltage Withstand	4	3-69	3	1,150					1		4	2	2	3
d-c	Insulation Resistance	7	12-132			3	183	2	1,018	2		5	3	2	4
	Section 8. Tests on Insulating Liquids														
a-c	10 kv 60 cycle I&W	35	All	28	9,850	8	362			3		30	26	18	14
a-c	2.5 kv 60 cycle I&W	7	All	7	1,795							5	4	3	4
a-c	Voltage Withstand	64	All	41	77,800	3	6,175	1	200	19		49	38	35	39
d-c	Insulation Resistance	2	22-132	2	145							1	2	1	1
	Section 9. Tests on Carrier Current Capacitors														
a-c	10 kv 60 cycle I&W	26	15-230	22	648	1	2			3	10	21	16	8	12
a-c	2.5 kv 60 cycle I&W	3	66-132	2	8					1	5	3	2	2	1
a-c	Voltage Withstand	3	0-230	2	25					1		1	1		3
d-c	Insulation Resistance	5	33-161	2	8					3	5	1	1		4
	Section 10. Tests on Cables														
a-c	10 kv 60 cycle I&W	19	4-34.5	10	2,016	8	868			2	6	16	10	5	9
a-c	2.5 kv 60 cycle I&W	2	2.3-19	1	15	1	70					2	2	1	2
a-c	100v 60 cycle C&DF	2	2.4-69	1	1	1	1					1	1		2
a-c	Voltage Withstand	16	2.4-69	7	538	3	17	1	6	6		3	2	1	10
d-c	Insulation Resistance	45	220v 138 kv	19	21,936	12	1,451	4	212	10	48	25	20	9	23
d-c	Dielectric Absorption	13	2.3-34.5	2	236	9	305			2	1	9	8	2	10
d-c	Voltage Withstand	23	600v 138 kv	19	5,029	2	72			2		11	7	6	15
	Section 11. Tests on Rotating Machinery														
a-c	10 kv 60 cycle I&W	9	4-13.8	4	56	3	14			2	5	6	5	3	5
a-c	100-120v 60 cycle C&DF	2	7 13.8			1	8			1		1	1		1
a-c	Voltage Withstand	18	2.3-15.5	11	86		1			6		4	4	3	7
a-c	Corona Detection	4	6.9-13.8	2	16	1	1			1	5	3	3	1	2
d-c	Insulation Resistance	56	125v-22 kv	25	21,347	12	719	1	11	18	15	31	24	15	25
d-c	Dielectric Absorption	32	250v-22 kv	16	873	9	448	2		5	17	23	22	9	19
d-c	Voltage Withstand	4	2.3 kv-15 kv	2	70	1	5			1		3		2	1
	Section 12. Tests on Circuit Breakers														
a-c	10 kv 60 cycle I&W	43	5-230	37	6,343	2	36			4		34	29	17	24
a-c	10 kv 70 cycle C&DF	4	23-161	2	229	1	10			1		4	4	4	2
a-c	2.5 kv 60 cycle I&W	10	5-115	9	1,625					1		7	7	7	7
a-c	Voltage Withstand	7	4.8-220	5	204	1	20			1	20	2	1		5
d-c	Insulation Resistance	15	0-220	10	4,550	2	240			3		9	7	6	8

I&W—Current and Watts. C&DF—Capacitance and Dissipation Factor.

Switch Sticks and Hot Line Tools

Two companies use dielectric loss measurements with watts and current measured at 10 kv, a-c, 60 cycles. One of these reported 70–80 tests per year. Another company uses 2,500-volt insulation resistance at one minute.

Summary of Results

The results of the questionnaire may be briefly summarized as follows:

1. Field testing of high-voltage electrical insulation is done by more than 85 per cent of the reporting power systems.

2. The a-c dielectric loss and power factor test is the most widely accepted test method, 139 systems using equipment operating at 2.5 to 10 kv, 60 cycles, and 29 systems using equipment of lower voltages or different frequencies.

3. This a-c test method is used by most power systems on most types of insulation.

4. There is little difference in test methods because of variation of voltage ratings of apparatus under test.

5. D-c insulation resistance tests are used by most power systems in evaluating cable and rotating machinery insulation.

6. Voltage withstand tests, both alternating and direct current appear to be used primarily for acceptance tests on apparatus. Considerable variation in practice as to test voltages and times of application is found.

7. A-c voltage distribution tests are limited to line insulators and bushings.

8. Corona detection tests, either alternating or direct current, are used on very few systems.

9. Dielectric absorption tests are mainly limited to cable, rotating machinery and transformer insulation.

10. Very few field test methods were reported other than those listed in Questions 2 and 3.

Conclusion

In closing, the members of the Subcommittee wish to express their appreciation for the generous response to the questionnaire. Space limitations made it impossible to include all of the information in the replies and made it necessary to omit from the tabulations any test method not used by more than one company. Nevertheless it is felt that these data will be valuable in the future activities of the Subcommittee and their inclusion in the replies is appreciated, even if they do not appear in this report.

Reference

1. McGraw Central Station Directory. McGraw Hill Book Company, New York, N. Y.

No Discussion

Signal and Supervision Systems Used on Carrier Current Communications Circuits

ROBERT LYON MAYER
ASSOCIATE AIEE

THE past few years have shown us a tremendous growth in the use of carrier-current equipment, to solve a multitude of problems encountered in the operation, construction, and control of power utility equipment.

In many cases the increased use of carrier-current equipment has come about as an economic expedient, with an eye toward more complete utilization of existing plant facilities as well as increasing the ease and efficiency of supervising, operating, and maintaining the modern network of transmission lines, plants, and equipment that make up a complete power system.

In a power system incorporating over 70 electric generating plants, 20 or more gas compressor stations, and the attendant network of transmission lines, consisting of electric conductors, and gas and water pipe-lines, covering in area some two-thirds of the State of California, it is of some importance to utilize not only the voice communications and telemetering advantages of carrier-current systems, but also to give some thought to the supervisory methods that will most efficiently furnish the greatest factor of utilization of these communication channels.

The carrier-current communication system used by the Pacific Gas and Electric Company makes use of special types of supervisory, ringing, and signaling combinations. The network is made up of two general types of carrier-current transmission mediums; namely the power-line carriers, consisting of telephone transmission channels, alarm and supervisory carrier units, all utilizing the power line conductors, as a means of establishing various communications channels. Second, only in sequence, however, we have the telephone-line carrier circuits, consisting of voice, signal, alarm, and control circuits superimposed on the telephone wires, which make up the vast network of the company's telephone system.

These telephone wires vary considerably from commercial telephone lines by the very nature of the duty they perform and their strict co-ordination with the electric transmission system. The matter of inductive co-ordination for the reduction of noise and the protection of personnel and equipment, and matters of protection and co-ordination have in themselves become interesting and complex studies.

The "power-line carriers" as a group vary as to the system of emission of energy conveying intelligence, and the signaling systems, used in the supervision of communications, where circuits are terminated on various plant-telephone switchboards. For the greater part, the emission system used is amplitude modulated (AM) single channel transmission, utilizing two frequency transmission between terminals. These units vary in power output from 5 watts to approximately 50 watts, and are coupled to the power transmission lines through impedance matching radio-frequency networks, capacitive couplers and drainage coils, in the conventional manner.

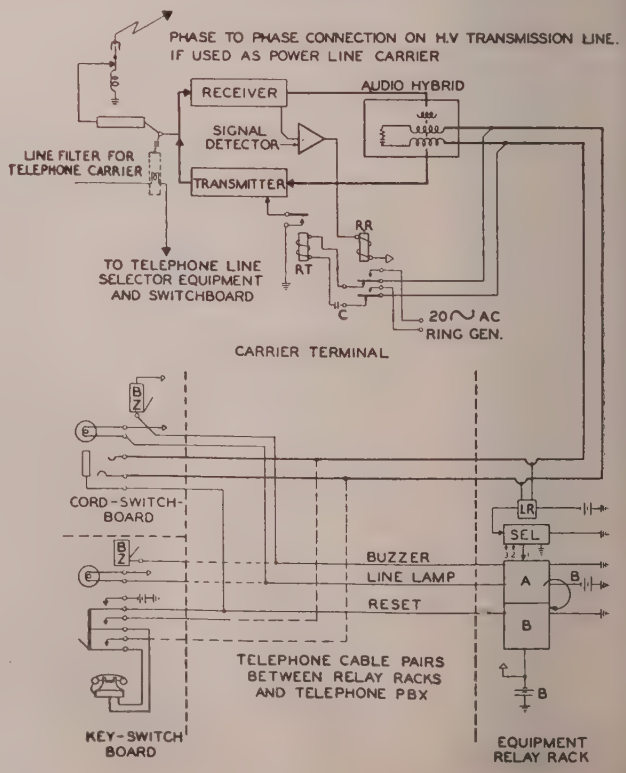

Figure 1. Typical power line and telephone line carrier supervision equipment

Paper 51-188, recommended by the AIEE Carrier Current Committee and approved by the AIEE Technical Program Committee for presentation at the AIEE Summer General Meeting, Toronto, Ont., Canada, June 25–29, 1951. Manuscript submitted June 26, 1950; made available for printing April 23, 1951.

ROBERT LYON MAYER is with the Pacific Gas and Electric Company, San Francisco, Calif.

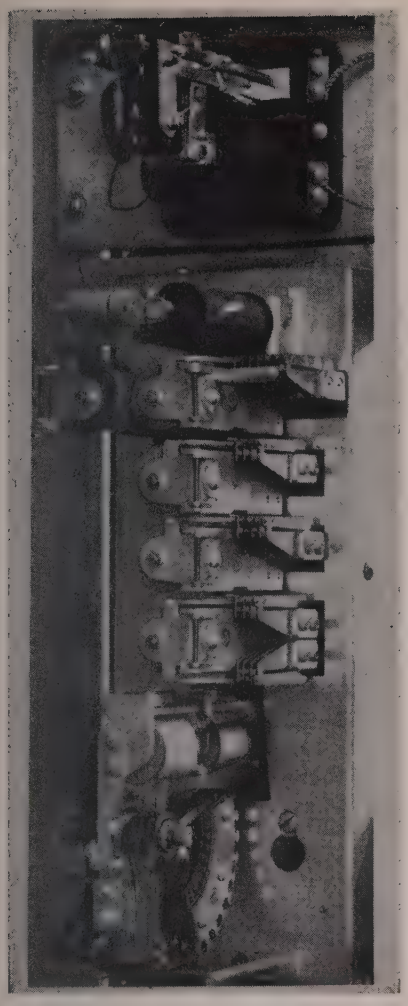

Figure 2. Relay type telephone selector, and associated line-relay

The transmission lines are trapped at most stations to reduce attenuation of the transmitted radio-frequency energy. Traps are installed to reduce losses in the station bus network, circuit breakers, transformer banks, and associated equipment. Radio frequency traps and coaxial by-pass systems are generally provided through intervening transmission substations. In the system under discussion here frequency modulated (FM) and single side-band terminals also are used, in the same frequency ranges, but somewhat less generally than the AM types of equipment.

Ringing and Signaling Systems

The ringing and signal systems of these power-line carrier circuits as a whole are probably somewhat different than in other power utility applications.

Figure 1 shows diagrammatically the general arrangement of a typical power-line carrier-current terminal, with its output and input systems, matched to an audio-frequency hybrid system, and then coupled to a signal supervision system, and terminated on a jack position, of the plant's cord-type telephone switchboard.

Figure 1 also shows the arrangement for coupling the same carrier-current terminal, alternately to a key-type telephone switchboard, commonly used in some plant installations where the necessity for more than three simultaneous conversations originating from the station are not probable.

Other than the channel capacity difference inherent in these key-type switchboards, and the fact that they require the use of line-lamp supervision on their common-battery local circuits within the plant, they are equipped to furnish line-lamp indications of an incoming signal from the carrier terminal and line-busy signals to additional switchboards that might be operated in multiple with the main key-switchboard unit. These switchboards are not required to supply the operator with disconnect, cord-light supervision, as do the majority of the cord-type switchboards used in the larger installations.

Figure 1 also indicates the system used in terminating the greater number of telephone line carrier-current terminals, and illustrates diagrammatically the low and high pass filter assembly, which is inserted in the physical telephone line in order to utilize the frequencies between 4 kc and 40 kc for carrier-frequency communication on the company's telephone lines.

Referring again to Figure 1 we can see that the distant transmitter would transmit energy in its carrier band to the illustrated terminal for ringing or signaling, and also that the signal detector of this receiving terminal would be operated, and would in turn operate a relay in its plate circuit, called a ring-in relay. The function of this relay is to open the drop toward the receive carrier terminal and to apply the drop's tip and ring legs across a local source of 20-cycle ringing power. It appears at this point that the ring-in relay in the signal demodulator's plate circuit might easily apply a d-c potential to a separate circuit in order to operate a selection device, but the use of 20-cycle ringing power allows some degree of standardization in the switchboard and supervision selector equipment, where it is desired to have like supervision and operation of metallic-magneto and carrier-circuits on the same switchboard installation.

Figure 1 indicates that the line-relay (LR) is bridging the drop from the carrier terminal's audio output to the plug-jack on the switchboard. This line relay is shown in Figure 2, mounted above the relay-type code selector, generally associated with it. The line relay is a sensitive unit designed originally for signal use with magneto party telephone lines, and will normally operate over wide limits of 20-cycle voltage, from approximately 12 to 90 volts, and still offer a high impedance to the audio frequencies appearing on the drop, from the carrier terminal's output.

This line relay must respond to coded rings, consisting of a sequence of long pulses of $3\frac{1}{2}$ seconds, and short pulses of 1 second, with a maximum of 3-second and a minimum of 1-second spaces. This system of coded ringing stemmed from the operation of long magneto party lines, where it was desired to ring-in the station code selector from another station, as well as to have a selector that could be operated, by patrolmen and others, using portable telephones, with hand magneto-crank ringers.

The code selector systems used in conjunction with the line relays are shown in

Figure 3. Mechanical type telephone selector

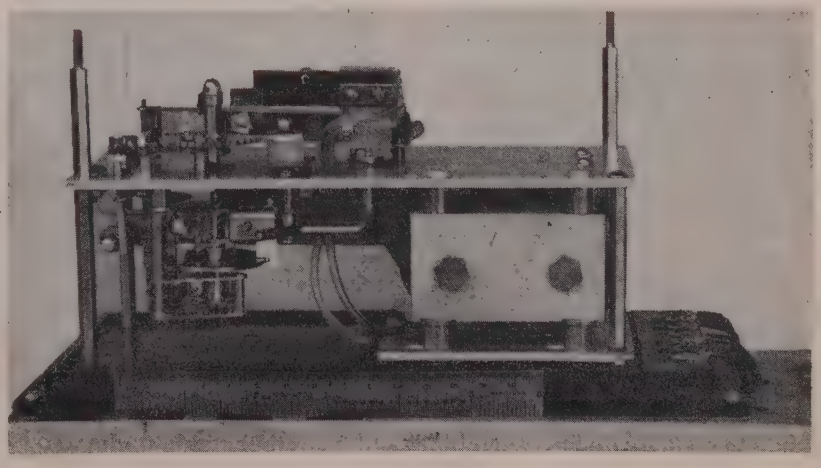

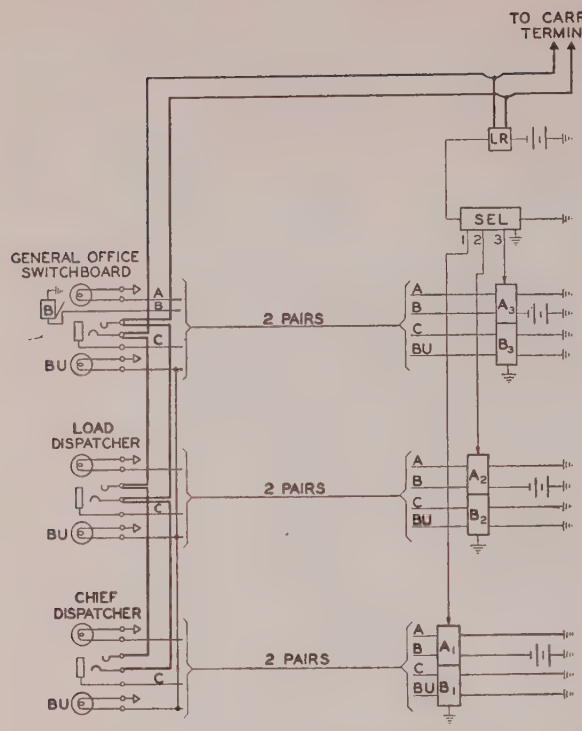

Figure 4. Arrangement of multiple drop supervision from a single carrier-current terminal

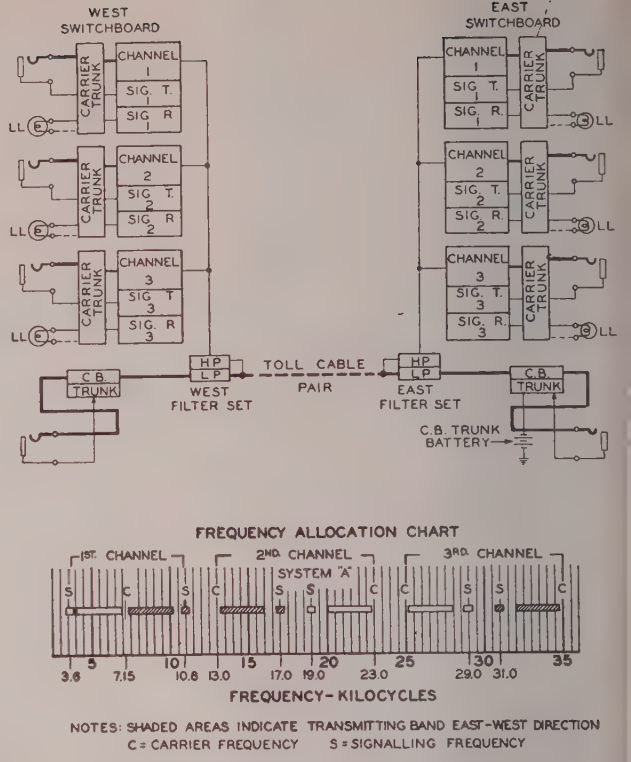

Figure 5. Carrier channels arranged for direct supervision and trunking

Figures 2 and 3. Figure 2 illustrates the typical construction of one of the relay type selectors and its associated line-relay in a rack-mounted assembly. The relay-type selector consists of three slow release slugged telephone relays, one slow-operate relay, a pendulum time delay relay, and a magnetically operated minor switch equipped with two 10-digit banks.

These selector relays are assembled on a base of formed sheet iron and arranged to be jack-mounted on a vertical rack. The strapping on the rack side of the mounting-jack determines which one of 11 possible codes the selector will respond to, with each station in the system having an assigned code.

This arrangement of jack strapping allows any code selector unit to be changed from one station to another without any internal adjustments. Installation in a remote station jack-mounting will therefore establish the proper wiring to the selector and order its response to the proper code.

Improperly coded signals, or signals intended for other stations along a "break-out" carrier installation, are received and followed by the line relay, but any variation in sequence from the proper code will cause the selector to fail and its stepper-switch to lock for $3^1/_2$ seconds after the last pulse of the code, at which time the selector resets automatically under the control of its pendulum time delay relay, and is again ready to respond to any operation of the line relay.

Operation of the selector by its assigned code-sequence causes operation of its line-lamp relay, indicated in Figure 1 as relay "A." This relay locks over its own contacts and holds battery potential on the switchboard line-lamp associated with the circuit. Insertion of a plug or operation of a line key to the signaling line operates relay "B," which in the case of the relay-type selector is also mounted on the same base assembly. Relay "B" energizes the counter coil of relay "A," extinguishing the line-lamp.

The "A," "B," relay combination is so designed, however, to give complete ring-back or "re-ring supervision," that is, with a cord plug inserted in the switchboard and the line-lamp extinguished, should the party at the remote carrier terminal again desire to summon the operator, another coded ring would cause the selector to again operate, and by differential control of the "B" relay, again lock the "A" relay in its operated position, lighting the switchboard line-lamp, which can then be reset, or extinguished by a quick removal and re-insertion of the switchboard plug.

The mechanical-type code selector illustrated in Figure 3 is designed to respond to the same type of codes as the relay-type selector. This mechanical selector, however, offers a 300 per cent greater combination of codes, and somewhat greater ease of field adjustment and maintenance.

The system requires that in using the mechanical selector the relay combinations "A" and "B" (Figure 1) must be supplied in an additional assembly in order to give lock-line lamp and re-ring supervision.

Both types of selectors can be used for multiple switchboard operation as shown in Figure 4, where the system dispatcher, the division distribution operator, and the division office switchboards are all multiple, across some of the same carrier-current terminal outputs. The additional codes required are provided on either type of selector, by making the first code, the basic sequence, and adding pulses for codes two and three. Additional notching also is required in the code wheel of the mechanical selector.

This application of selectors and supervision of carrier-current circuits allow, to a degree, complete magneto supervision on power line carriers and telephone line carriers alike, and is utilized in some cases where the carrier terminal is located some distance from the switchboard. Magneto ringing is utilized on the open wire-line drop to actuate the ring-out relay in the carrier terminal, in order to initiate transmitted signals.

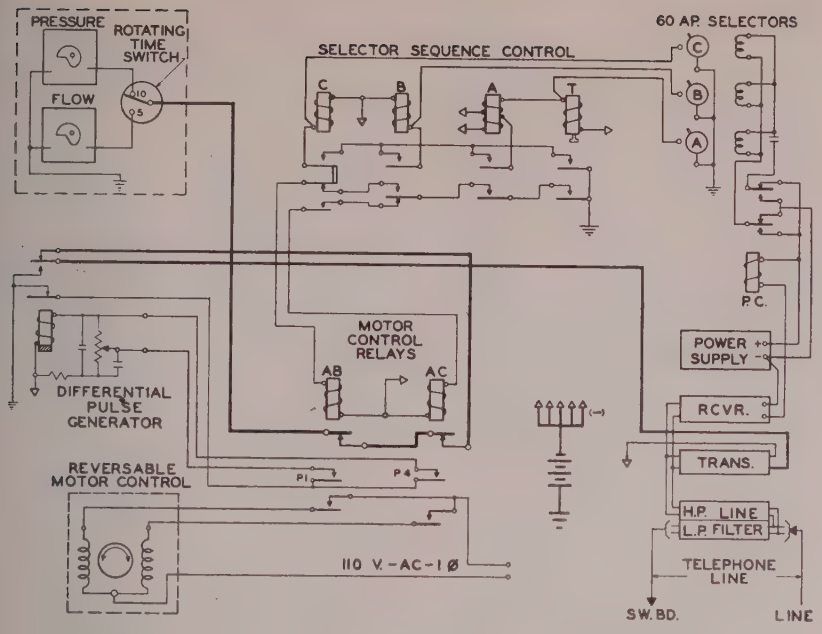

Figure 6. Carrier current system combining telemetering and control

Carrier Channels Arranged for Direct Supervision and Trunking

Up to this point this paper has been concerned with the types of carrier supervision and signaling used with power-line and telephone line carrier, which would fall in a large category of ring down supervision as it would be called in communications parlance.

Figure 5 shows an arrangement for obtaining full common-battery type supervision from a group of carrier-channels. Full supervision must indicate the same conditions of supervision at both switchboard terminations of the carrier circuit. The carrier trunking arrangement illustrated in Figure 5 takes advantage of the fact that, unlike the carrier terminals described before, these units incorporate separate frequencies for signaling and receiving signals, and are designed to incorporate extremely selective band filters, so that the signal frequencies do not interfere with the 2,500-cycle-wide voice channel.

Unlike the carrier units that signal in or near the voice band, these units can signal continuously during use of the voice carrier equipment. The carrier transmitters are equipped with signal oscillators as in the first channel in Figure 5 on 3.6 kc. The insertion of a plug into the switchboard jack associated with this channel operates the relay in the carrier trunk, which in turn applies battery potential to start the signal transmitter of channel number 1 from the West switchboard. The voice circuit, shown only as one side of a tip-ring jack, is connected to the primary of a one to one audio transformer. The secondary of the transformer is coupled to the input of the voice carrier unit. The primary of the one to one transformer in the carrier trunk has its center windings bridging a large condenser, as well as a pair of make contacts in the carrier signal-receiver output relay. This circuit constitutes a d-c block in the primary of the transformer, which holds the West switchboard's cord light energized, and therefore indicates a disconnect to the West operator.

The West signal transmitter, however, causes the East terminal's signal receiver to operate, closing the contacts of its output relay which in turn energize the East switchboard's line-lamp, designated as "LL" in Figure 5.

The East channel's signal receiver relay also closes the d-c block across the capacitor-isolated primary of the one to one audio transformer in the carrier trunk set associated with the East terminal. Upon answering the line-lamp, the East switchboard's operator applies negative battery potential to the carrier trunk relay by inserting a switchboard cord plug, which then operates the East channel's trunk-relay which has two functions and one operation. The series circuit from the East receiver relay which energized the line-lamp is opened by its break contacts, extinguishing the East line-lamp "LL," and its make contacts close to initiate the operation of the East's signal transmitter which in turn causes the West carrier receiver relay to close, shorting the isolating condenser across the center taps of the West carrier's trunks, one to one audio transformer, and this consequent d-c low resistance loop allows the cord circuit relays to operate and extinguish the cord disconnect lamp, thereby indicating to the operator of the West switchboard that the East switchboard has answered the call.

This type of supervision is, of course, equal in an operating sense to the operation of any common battery telephone's manual exchange service, and lends itself admirably to use between stations where large volumes of communications are to be handled on a full-selective basis.

The speed of operation is of prime interest, and the general application of these trunks is one of interconnecting and extending other terminating carrier and line circuits from one main office to another in the power company's communication system. The lower diagram of Figure 5 indicates the frequency allocation and spectrum utilized to operate three such trunks on a single telephone-toll cable pair of wires.

Carrier Current System Combining Telemetering and Control

Figure 6 illustrates schematically a carrier control scheme for combining a conventional carrier-current telemetering and recording channel, with a fail safe valve control system, incorporating a novel control-confirmation indication, transmitted from the remote unattended metering station or a main line valve metering point, to an attended operating station, or compressor station.

The system consists primarily of a telephone-line carrier telemetering transmitter and receiver combination, along with its line filter set and graphic recorder of the conventional type, used for translating and recording pulse information on a rotary chart.

In addition, the controlling terminus of the circuit is equipped with three pulse-signal sending keys. These keys are cam-cut switching devices with coded wheels arranged for various pulse digit keying of the carrier-current transmitter. The three signal keys are each equipped with a different digital combination of 17 pulses and are capable of operating only one selector having a like set of the digital stops, pre-set within the selector mechanism and located at the remote end of the circuit.

The rotary chart recorder is equipped with a signal light in its case, that indicates the pulses being received from the remote end, and functions in accordance with any closure of the telemeter-receiver's relay.

The remote unattended end of the cir-

cuit is equipped with its line filter set, a carrier current telemeter transmitter, and receiver, along with an auxiliary power supply used to energize the "A," "B," and "C" pulse selectors, and a keying pole-changing relay installed along with the carrier-current terminal.

The three railroad-type pulse selectors designated "A", "B", and "C" in Figure 6 are operated in parallel, and simultaneously from the pole-changing relay PC, which receives its operating pulses from the relay supplied in the output of the carrier-current receiver.

Three selector relays, designated "A," "B," and "C," and a gas quenched time delay relay designated "T," make up the selection bank for the a-c operated valve motor-control relays "AB" and "AC". A differential pulse generating relay designated "DIF" is supplied to generate pulses during the operation of the valve motor, from the control of the relays "AB" or "AC".

The remote station is equipped with the conventional pressure and flow telemeter transmitters of the time-division type, and an associated a-c operated selector switch which allows one set of information to be transmitted continuously for 10 minutes, and a second set of information for 5 minutes, in each 15-minute sequence.

Under normal circumstances the control equipment is completely dormant; and the telemetering transmitters, which in turn operate the graph recorder at the control end of the circuit, are telemetering their information continuously. Should the operator at the control station desire to operate the remote valve or switch, he will turn the pulse sending keys "A" and "B" in turn, and should he desire to close the valve or switch he will actuate the "A" and "C" keys.

The full operation of a valve, for example, might require 15 minutes, which is quite common timing for this type of equipment. The gas quenched time delay relay might be set for 2 minutes of operation, which as indicated diagrammatically will sustain the operation of the "A", "B", and "C" selector-relays shown in Figure 6 over a common locking ground contact for the period of its operation only. This of course limits the operation of the valve to 2 minutes, minus the few seconds required for the sending of the "A" and "C" or "A" and "B" codes.

Sending the "A" code and then waiting for possibly a minute and a half before sending the "C" or "B" codes allows a fine degree of valve position adjustment in either direction.

With the idea of failure-safety in mind, the circuit has been arranged so that the operation sequence of all three keys in any sequence, that is, ABC, ACB, or CBA, immediately causes failure of the control relays "AB" or "AC", and therefore furnishes a failure-safe stopping operation.

Contacts are provided on the "AB" and "AC" operating relays to open the operating circuit from the pressure and flow telemetering transmitter to the carrier-current transmitter, and in turn transfer this initiating lead to the differential pulse generator which functions upon the operation of either the "AB" or "AC" relays. This pulse generating relay acts to key the carrier transmitter in a series of four-second marks and alternate one second spaces. The operation of the pulse generator allows the operator at the control end to observe the light in the recorder and confirm the operation of the valve by virtue of the pulse difference.

The railroad type pulse selectors are used in this installation in order to increase the safety factor of operation by transient pulses which might possibly be received by the carrier-current receiver. It would, however, require 34 properly spaced and positive pulses to cause any operation of the control relays. Any operation would immediately be made evident to the operator at the control station by the change in sound and signal of the telemeter recorder's solenoid and the quick pulsing of the light in the recorder's case. This light's normal sequence of four pulses per minute would immediately be changed to the comparatively fast flicker caused by the pulsing of the differential pulse generator.

In Figure 6 a 24-volt battery is indicated for selector relay operation; however, the auxiliary power supply could be used for power if it were found advisable to eliminate the battery plant.

Frequency shift, or pulse-diversity carrier transmission, will lend itself admirably to this system of telemetering and control.

Summary

During the past few years there have been numerous systems of supervisory control and coded digital selectors designed and described in various papers. These systems, as a whole, have been designed for specific use as power-supervisory control units, or as commercial-telephone circuit-switching and trunking assemblies.

The purpose of this paper, however, has been to discuss some signaling and supervisory-trunking systems used in conjunction with the normal operation of a large power utility. It has further been desired to illustrate these systems as they are applied to carrier-current systems and mediums of transmission.

No Discussion

Spiral Arc Chokes Power Flow in New Lightning Arresters

OTTO ACKERMANN
ASSOCIATE AIEE

E. J. DeVAL
ASSOCIATE AIEE

A LIGHTNING arrester is a device which permits a practically unrestricted flow of electric current between its terminals when the terminal voltage exceeds a certain level, and which interrupts the flow of current when the overvoltage ceases. The lightning or surge current establishes an arc path through the device and this is often followed by dynamic power flow. The prompt interruption of power follow current is one of the essential functions of a lightning arrester.

In this respect lightning arresters are comparable to fuses and circuit breakers. All three types of apparatus operate by influencing or modifying the current that would flow if there were a bolted connection instead of the protective device. In d-c interrupters, current modification by the protective device is an absolute necessity. An a-c interrupter could conceivably operate without current modification if it were able to muster enough deionizing action while the current was going through zero in its natural course. Every interrupting device, however, modifies the current which it is to clear, at least by the effect of its arc voltage, no matter how small this may be. Current modification is carried to a rational and well-controlled extreme by the use of resistance materials in certain interrupting devices. This principle is employed in valve-type lightning arresters, circuit breakers with two step switching, and in fuses with fixed series resistors.[1]

Most circuit breakers, fuses, and expulsion-type lightning arresters, however, influence the current only by de-ionizing action in the arc path. De-ionizing action, to be effective at the proper moment, must start before the current becomes zero. It usually manifests itself in rising arc voltage which in turn forces the current to decay faster than it would do in an a-c circuit with linear impedances only.

While limitation of the individual current loops in amplitude as well as in duration with many interrupting devices simply is a phenomenon incidental to their operation, without any significant beneficial effect, this principle is purposely accentuated in other apparatus and is made a feature necessary for their proper functioning.[2] Effective power current limitation is obtained by making the arc voltage about as high as the generated voltage at an early time during the first current loop.[3] This is frequently done in interrupting devices by means of arc transfer or arc switching. With expulsion-type lightning arresters this implies that the arc is forced from its original shortest channel into a longer path. Such action takes place even in open rod gaps due to convection air currents and magnetic effects; it is schematically indicated in Figure 1. It also can be induced in confined spaces such as expulsion arresters which always are contained in a basically tubular structure. However, the gain in arc length cannot be very significant as long as the basic arrangement and principle is that illustrated in Figure 1.

A fundamentally new principle of arc switching in a confined tubular space has been introduced by providing a cylindrical filler with spiral grooves as illustrated in Figure 2. The initial spark from one electrode to the other takes place in a more or less straight line in the space between the spiral filler and the tube wall. The tube wall may touch the ridge of the filler all around or may have a clearance up to 25 mils on the diameter when new. The spark encounters narrow spaces at the land of the spiral and is rather unrestricted where it crosses the grooves. The grooves must furnish adequate absorption space for the gas generated by the surge current since there is no appreciable movement of gas towards the vented end of the tube during a surge lasting only about 100 microseconds. Each tube element essentially must store the gas generated within its confines and sustain the created pressure. If power current should follow the surge discharge, additional gas is produced, all of which gradually moves toward the open end of the arc chamber. Some of it will cross the restricted sections between lands and tube wall, but most will follow the spiral groove. The division of flow is predicated by the respective aerodynamic resistance. Hydraulic flow tests made on

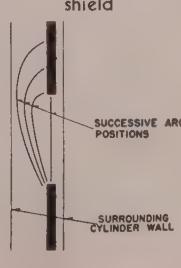

Figure 1 (below). Arc transfer along vertical rod gap space

Figure 2 (right). Basic construction of spiral groove expulsion lightning arrester

1. Upper electrode, 2. Ground electrode, 3. Spiral filler, 4. Static shield

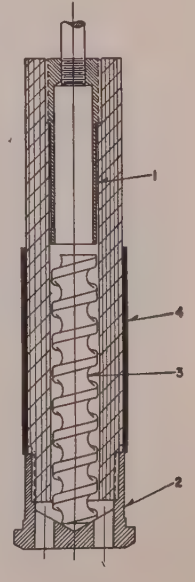

Paper 51-189, recommended by the AIEE Protective Devices Committee and approved by the AIEE Technical Program Committee for presentation at the AIEE Summer General Meeting, Toronto, Ont., Canada, June 25–29, 1951. Manuscript submitted January 31, 1951; made available for printing April 20, 1951.

OTTO ACKERMANN and E. J. DEVAL are both with the Westinghouse Electric Corporation, East Pittsburgh, Pa.

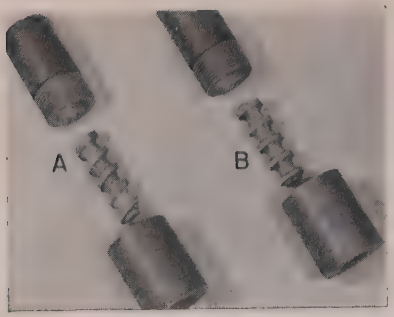

Figure 3. Comparative erosion patterns show effectiveness of spiral groove

(A). Spiral groove sample after ten discharges at 3 kv, 1,000 amperes
(B). Ring groove sample subjected to similar tests

assemblies with tightly fitting fillers and with others having certain clearances, demonstrate that, in the selected design, at 25 mils difference between filler diameter and tube bore, about 33 per cent of the total flow crosses the spiral ridges. Arc current conditions however are vastly more complex than what can be represented by a hydraulic model; the latter merely gives useful indications. Power tests are the only source from which reliable information can be obtained on the mode of operation of such devices.

Figure 3(A) shows the essential parts of a spiral groove expulsion lightning arrester which has undergone a series of tests at a plant setting of 3 kv and 1,000 amperes. It is noted that the periphery of the uppermost turn of the spiral shows a distinct notch. This marks the location where the first surge and power current discharge produced a slight impression on the otherwise uniform periphery of the filler and in the surrounding tube wall. These local changes of dimensions and of electrical characteristics caused all subsequent discharges to take the same path. There can be no doubt that the original surge and the initial portion of the ensuing power current crossed the next lower ridge more or less directly below this notch. However, the absence of a similar notch in the second turn of the spiral or anywhere else farther down is conclusive evidence that the arc gas in the groove quickly begins to travel crosswise to the original arc path and thereby prevents continued current flow in a purely axial direction. The only other pronounced track discernible during the early life of the device is a shallow groove on the inner tube wall, conforming to the spiral channel of the filler. This is convincing proof that the bulk of the arc gases actually flows in the direction of the spiral.

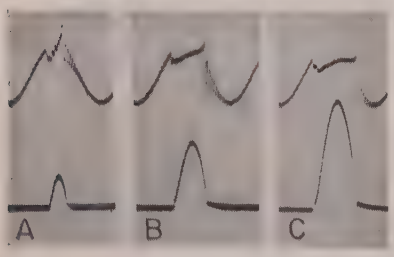

Figure 4. Arc voltage and current produced by different filler types at same power supply (3 kv, 1,000 amperes, rms)

(A). Spiral filler (220 amperes crest)
(B). Ring groove filler with same clearance to tube as spiral filler (470 amperes crest)
(C). Ring groove filler with clearance increased so that total flow resistance is same as with spiral filler (765 amperes crest)

Despite this evidence one still might question whether the current flows in the same direction as the arc gases, for, in general, current need not follow the motion of the conducting medium. It is however, beyond question that wherever the current does flow the results of the expended energy must be evident. In solids, the flow of electricity results in heating; in expulsion arresters, the arc energy converts solids into gaseous form and imparts heat and kinetic energy to gases. As the loss of gas forming material is evident primarily along the walls of the spiral channel one must conclude that the bulk of the current is flowing along this path.

More insight into the functioning of the spiral grooves can be gained from observing the performance of an expulsion lightning arrester having the spiral groove filler replaced by one with ring grooves, as shown in Figure 3(B). This filler, having the same diameter as the spiral type, offers the same gas storage space and the same resistance to gas flow in purely axial direction. It differs from the spiral filler in so far as it does not permit any sustained flow of gas along the grooves and must cause a considerably higher arc gas pressure within the device. For this reason, the arc voltage along a circular groove filler should be higher than that of one with spiral grooves if with the latter the arc current also flowed in an axial direction only. However, exactly the opposite condition is disclosed by measurements as illustrated in Figure 4. The arc voltage of the spiral groove model is higher than that of the one with ring grooves despite the fact that the latter works with higher gas pressures. Furthermore, if the clearance around the ring groove filler is increased so that the internal pressure becomes about the same as that in the spiral groove model, the arc

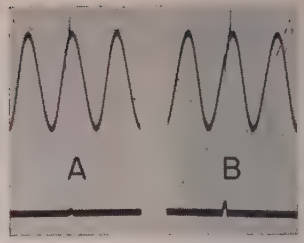

Figure 5. Power follow tests on 3-kv lightning arrester at 3 kv, 22,000 amperes, rms, and maximum severity timing

(A). First operation (850 amperes crest)
(B). Fifth operation (1,500 amperes crest—change of current scale)

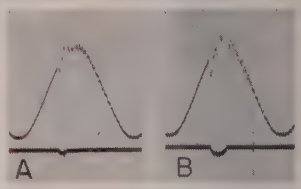

Figure 6. Power follow tests on 9-kv lightning arrester at 8,100 volts, 17,000 amperes, rms, and maximum severity timing

(A). First operation (1,070 amperes crest)
(B). Fifth operation (2,140 amperes crest)

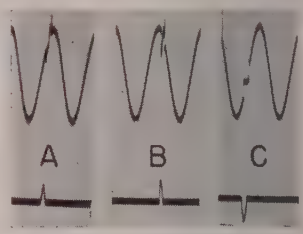

Figure 7. Power follow tests on 3-kv lightning arrester at 3 kv, 22,000 amperes, rms, and cyclicly distributed timing

(A). First operation at maximum severity timing (1,700 amperes crest)
(B). Second operation, timed 80 degrees later (2,100 amperes crest)
(C). Ninth operation (2,100 amperes crest)

voltage of the ring groove assembly becomes decidedly lower, as illustrated in Figure 4(C). The combined evidence strongly points to the conclusion that, with a properly designed spiral filler, the arc current is being switched to the spiral-channel. The ratio between its pitch and its mean length of turn is such that the arc is stretched to about four times its original length.

If this principle is applied to expulsion lightning arrester designs having a relatively long initial sparkover path, the arc length can be increased to dimensions which produce a very decided current limiting effect. This permits the appli-

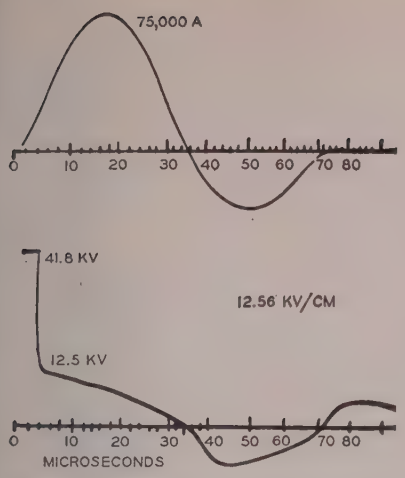

Figure 8. Surge current and arc voltage, 9-kv lightning arrester

cation of such devices at locations where extremely high short-circuit currents so far have been a barrier to the use of expulsion arresters.

Figure 5 shows records of standard duty cycle tests of a 3-kv spiral groove lightning arrester on a 3-kv 22,000-ampere circuit. Figure 6 presents tests of a 9-kv lightning arrester of similar design on a 8,100-volt 17,000-ampere source. The oscillograms illustrate how the arc voltage after very short time rises to values approaching and exceeding the generated voltage, thereby restricting the power follow current to a small fraction of the available supply.

According to the standards, the question of lightning arrester life is satisfactorily answered by the device passing five maximum severity discharges, followed by five operations at minimum current. The tests in Figures 5 and 6 represent maximum severity discharges in accordance with the standards except that they were taken at plant settings much higher than the 10,000 amperes which so far were considered the highest current capacity to be demonstrated for a device suitable for unrestricted application. Both the 3-kv and the 9-kv lightning arresters not only interrupted five additional low current discharges but at the end of the whole test series still were in rather good condition.

While, in the sense of the standards, such tests are sufficient proof of adequate serviceability, the authors feel that service life is even more convincingly demonstrated by a series of tests such as illustrated in Figure 7. This sequence is started with a maximum severity operation as in the standard test series; thereafter however, the timing is shifted 80 electrical degrees for each consecutive operation. This results in a more or less random distribution of the discharges over the whole range of the 60-cycle period not unlike that expected in normal service. During the whole series presented in Figure 7, the supply was maintained at 22,000 amperes; the tests were discontinued with the ninth discharge, after which the lightning arrester still was in very good condition. Similar tests were executed with a 9-kv lightning arrester at 8,100 volts.

These tests demonstrate the long life potential of spiral groove lightning arresters not only by the number of operations performed, but also by the low arc energy recorded. The low arc energy is the product of arc voltage, current and time. It is a good indicator of the consumption rate of the lightning arrester's gas producing material. Examination of the presented records in comparison with those of other types lacking pronounced current limiting ability[4] shows that the average arc energy per discharge through a spiral groove lightning arrester is about one fourth of that of most other expulsion lightning arresters. This means that the consumption of gas generating material in the spiral groove lightning arrester is reduced to a rate which insures exceptionally long arrester life.

It has been general practice to make current interruption duty cycle tests at rated lightning arrester voltage. However, as available fault currents keep on increasing and become more and more the limiting feature in application, the question whether standard performance tests correspond reasonably well to actual service conditions, requires re-examination. The voltage rating of lightning arresters always is higher than normal service line to ground potential. This is done because lightning arresters occasionally must operate at dynamic voltages higher than normal. With grounded systems this may occur because of voltage unbalance at locations far removed from the source of supply; with ungrounded systems a lightning arrester may be called upon to operate while one phase is accidentally grounded. It is to be noted that maximum system fault current cannot flow through the lightning arrester at either of these conditions; in the grounded system, because the source of power is remote; in the ungrounded system, because line-to-line current is always less than the 3-phase fault, the latter being the most severe condition. It is for this reason that tests intended to show maximum current performance have been made at 90 per cent of rated voltage, at least with the 9-kv design.

As the spiral groove lightning arrester operates by generating very high arc

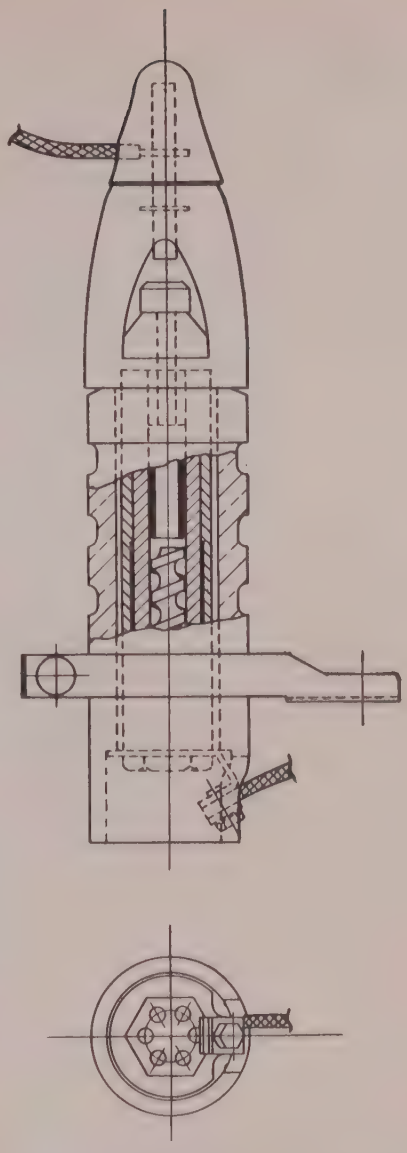

Figure 9. Complete type *LX* expulsion lightning arrester

voltage, the question must be asked whether under certain conditions the arc voltage might not become so high as to defeat the purpose of the protective device. In analyzing this question one will observe that the arc voltage around any one turn of the spiral can never be higher than the insulation strength across the ridge separating the neighboring turns. The sparkover across all the ridges furthermore cannot be more than the initial sparkover of the whole device particularly since during the arcing time most of the space is filled with ionized gas. At best, the ridges of a tightly fitting filler can exclude ionized gas from the width they occupy, which is some 31 per cent of the total electrode spacing. In other words, the arc voltage can hardly be ex-

pected to ever rise above about one third of the critical surge sparkover of the whole device. Figure 8 shows voltage and current oscillograms of a high surge current discharge through a 9-kv spiral groove lightning arrester. It is to be noted on the voltage record that a surge voltage of 41.8 kv, in a fashion characteristic to critical sparkover conditions, was maintained for about 3 microseconds before the lightning arrester started to respond. After sparkover, the highest arc voltage was 12.5 kv, the crest current being 75,000 amperes.

Because of its very pronounced current limiting ability the spiral groove lightning arrester has appreciably widened the range of application of expulsion-type lightning arresters. In other respects the new device also represents a marked advance in the direction of satisfying the power industrys requirements although the latter are by no means uniform. This is true in particular with regard to the location of the series gap and the degree of exposure and mode of grounding of various parts inasmuch as such features often have to conform to existing local safety rules. The type *LX* spiral groove lightning arrester is shown in Figure 9. The series gap is contained in a dome-shaped porcelain with lateral openings. This construction prevents accidental contact of linemen with the electrodes and yet keeps the electrodes open for inspection. The openings furthermore serve the purpose of letting arc gases and electrode material vapors escape freely. The line terminal itself is, or can be, covered by means of an insulating cap. The crossarm bracket is ungrounded which is required by certain power companies. It can on the other hand be grounded by a jumper to the ground terminal. The latter is recessed in the porcelain to prevent accidental contact.

The fiber tube which surrounds the spiral filler is, in turn, sleeved part way into a steel cylinder. One end of the latter is grounded; the other one approaches the upper electrode. Because of this arrangement, very high field stress is produced at the upper electrode when an overvoltage is impressed on it. This results in an electrode spark which, not being able to puncture the wall between electrode and shield will propagate along the wall towards ground. It is sped on its way because at its tip there continues to exist the same high field gradient which caused it to start. By this means a tube length of 6 inches can be made to sparkover internally at a voltage of about 45 kv. This sparkover co-ordinates well with the insulation of apparatus to which 9-kv lightning arresters are applied. In case of power follow, the arc established by the surge is switched into the spiral groove of about four times the original spark length and thereby attains a length of about $2^1/_2$ inches per kilovolt of lightning arrester rating.

The authors feel that they do not risk being presumptuous if they consider this development a major advance in the art. With the everwidening use of expulsion lightning arresters, this development will make this type of protector of increasing utility as distribution systems are growing in power output and concentration.

References

1. A New Three-Element Current-Limiting Power Fuse, **H. L. Rawlins, H. H. Fahnoe.** *Electrical Engineering* (*AIEE Transactions*), volume 63, April 1944, pages 156–159.

2. A New High Interrupting Capacity Low-Voltage Power Fuse, **C. L. Schuck.** *AIEE Transactions*, volume 69, part II, 1950, pages 770–76.

3. Performance Criteria of Current Limiting Fuses, Part II, **E. W. Boehne.** *AIEE Transactions*, volume 65, 1946, pages 1034–1044.

4. The Power Interruption Testing of Lightning Arresters, **O. Ackermann.** *AIEE Transactions*, volume 70, part I, 1951, pages 1–7.

No Discussion

A New Method for Treating Electron Tubes When Used as Oscillators in the Free as Well as in the Synchronized States

ABD EL-SAMIE MOSTAFA
NONMEMBER AIEE

M. EL-SHISHINI BEY
NONMEMBER AIEE

A NEW theoretical analysis, based on treating the electron tube as a periodically varying element is presented. The methods of superposition and successive approximation are applied to the solution of circuits having periodically varying resistances and the results are directly applied to the present nonlinear problem.

The transient and the steady-state oscillations, together with the amount of harmonics, and also the conditions of stability have been determined in the cases of free as well as synchronized oscillators.

Many important problems which can be shown to depend upon nonlinear differential equations are met in practice. The published papers dealing with such problems involve difficult mathematics and are usually limited in application, a fact making the study of nonlinear circuits present great difficulties.

The present analysis is followed from the fact that the electron tube in the oscillatory state can be considered as an element whose admittance varies cyclically and in which the amplitude, phase, and frequency of the periodic variation are self-controlled, that is, it depends on the amplitude, phase, and frequency of the oscillation.

The method of attack presented is general as it can be applied to almost all nonlinear problems. It has been successfully applied by the authors to the cases of superregenerative detectors and harmonic contents in class-C amplifiers where the nonlinear element is again an electron tube. It also has been satisfactorily employed for the evaluation of subharmonic sustained oscillations found in iron-cored reactor oscillatory circuits, in which case, the periodically varying parameter is the inductance instead of the resistance.

Although the present paper is confined to nonlinear circuits where the amount of nonlinearity is small (or what is equivalent to saying that the present work is limited to small signals), yet the same method could be applied, using closer approximations, to any other type of oscillation.

Generation of Oscillation

The phenomena of the generation of oscillation, presumably the simplest, will be treated first. A schematic diagram for a tuned plate oscillator is shown in Figure 1. The losses in the circuit are represented by a shunt conductance G in order to simplify the analysis and the results obtained apply as well to the more usual case where the losses are associated with the inductance.

By applying Kirchhoff's first law for the currents meeting at the point P, we get:

$$i_C+i_G+i_p+i_L=0$$

giving after differentiation,

$$d^2v/dt^2+(1/C)(G+di_p/dv)dv/dt+\omega_0^2v=0 \quad (1)$$

where, i_G and i_L represent the alternating components of the currents in the conductive and inductive branches respectively, i_C is the current in the capacitive branch, i_p = alternating component of plate current, v = alternating component of plate voltage = voltage across the oscillatory circuit, and $\omega_0^2=1/LC$. i_p can be represented as a function of the plate voltage as follows:

$$i_p=f(v)=\alpha v+\beta v^2+\gamma v^3+\eta v^4+\zeta v^5+\ldots.^*$$
$$\text{and } di_p/dv=\alpha+2\beta v+3\gamma v^2+4\eta v^3+ \quad (2)$$

Substitution in equation 1 gives

$$d^2v/dt^2+(1/C)(G+\alpha+2\beta v+3\gamma v^2+4\eta v^3+\ldots)dv/dt+\omega_0^2v=0 \quad (3)$$

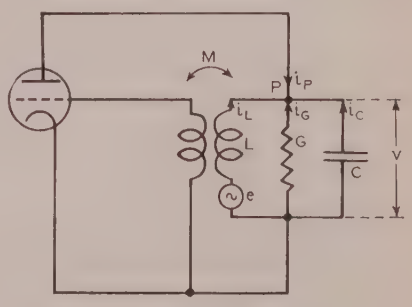

Figure 1. Tuned plate oscillator, polarized potentials omitted

For an oscillatory solution, the voltage v can be assumed to be of the form $V_t \cos \omega_t + V_{t2} \cos (2\omega t+\theta_{t2}) + V_{t3} \cos (3\omega t+\theta_{t3})+\ldots\ldots$, where V_t, being a very slow function of time compared with the frequency of oscillation, is the fundamental amplitude at any instant t, V_{t2}, V_{t3}, ..., θ_{t2}, θ_{t3}, ... are also slow functions of time and represent the amplitudes and phases of the second, third, and so forth

*For very small amplitudes, $i_p=(v/\rho)+gv_g=(v/\rho)(1-\mu M/L)=\alpha v$, and $\alpha=(1/\rho)(1-\mu M/L)$.

Paper 51-191, recommended by the AIEE Basic Sciences Committee and approved by the Technical Program Committee for presentation at the AIEE Summer General Meeting, Toronto, Ont., Canada, June 25–29, 1951. Manuscript submitted December 27, 1949; made available for printing April 24, 1951.

Abd El-Samie Mostafa is Professor of Radio Engineering, Farouk I University, Alexandria, Egypt, and M. El-Shishini Bey is a Member of the Egyptian Senate, Garden City, Cairo, Egypt.

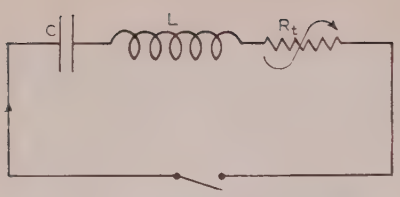

Figure 2. Series oscillatory circuit having a periodically varying resistance

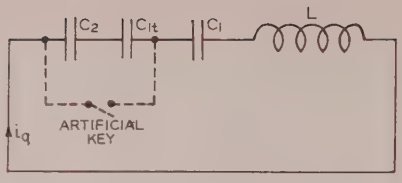

Figure 3. Connection diagram for equation 7

harmonics respectively, $\omega/2\pi$ is the frequency of oscillation (fundamental).

In the following analysis, it is assumed that the amount of nonlinearity is small, that is, each of $(1/\omega C)\beta V_t$, $(1/\omega C)\gamma V_t^2$, $(1/\omega C)\eta V_t^3$, and so forth, is much less than unity, also each of ηV_t^3 and ζV_t^4 is much less than βV_t and γV_t^2 respectively. This is equivalent to saying that the signals are assumed small. In this case, it can be shown that the Fourier series of v is a highly convergent one.

Substituting the Fourier series in equation 2 of di_p/dv, equation 3 becomes:

$$d^2v/dt^2+(G_t/C)(1+h_{1t}\cos\omega t+h_{2t}\times\cos 2\omega t+h_{3t}\cos 3\omega t+\ldots)dv/dt+\omega_0^2v=0 \quad (4)$$

where

$$G_t=G+\alpha+(3/2)\gamma V_t^2+(15/8)\zeta V_t^4+\ldots,$$
$$G_th_{1t}=2\beta V_t+3\eta V_t^3+\ldots,$$
$$G_th_{2t}=(3/2)\gamma V_t^2+(5/2)\zeta V_t^4+\ldots,$$
$$G_th_{3t}=\eta V_t^3+\ldots,$$
$$G_th_{4t}=(5/8)\zeta V_t^4+\ldots, \text{ and so forth}$$

In this way, the nonlinear differential equation 3 has been transformed to a linear one with periodically varying coefficients, in which each of $(G_t/\omega C)$, $(G_t/\omega C)h_{1t}$, $(G_t/\omega C)h_{2t}$, and so forth, is much less than unity, and each of h_{3t} and h_{4t} is much less than h_{1t} and h_{2t} respectively.

For the solution of equation 4, the methods of superposition and successive approximation will be adopted. Consider the series circuit, Figure 2, where R_t is a periodically varying resistance and given by

$$R_t=R_0\left(1+\sum_{n=1}^{\infty}h_n\cos n\omega t\right)$$

while the inductance L and the capacity C are constants.

The differential equation for the charge Q across the capacitor is given by,

$$d^2Q/dt^2+(R_0/L)(1+h_1\cos\omega t+h_2\cos 2\omega t+h_3\cos 3\omega t+\ldots)dQ/dt+\omega_0^2Q=0 \quad (5)$$

where $\omega_0^2=1/LC$.

Although successive approximation can be directly applied to equation 5, yet the amount of work can be reduced by the transformation $Q=q\epsilon^F$, where F is a function of time. Substitution in equation 5 gives

$$d^2q/dt^2+\{2(dF/dt)+R_t/L\}dq/dt+\{(d^2F/dt^2)+(dF/dt)^2+(R_t/L)dF/dt+\omega_0^2\}q=0 \quad (6)$$

F is so chosen that the coefficient of dq/dt in equation 6 vanishes; therefore,

$$F=\int-(R_t/2L)dt=-(R_0/2L)\times\{t+\sum_{n=1}(h_n/n\omega)\sin n\omega t\}$$

Coefficient of q in equation 6 is therefore given by,

$$\omega_0^2\left[1+(R_0/2\omega_0L)(\omega/\omega_0)\sum_{n=1}^{\infty}nh_n\times\sin n\omega t-(R_0/2\omega_0L)^2\times\left(1+\sum_{n=1}^{\infty}h_n\cos n\omega t\right)^2\right]$$

Now, if $(R_0/2\omega_0L)$ is much less than unity and ω is in the vicinity of ω_0, both assumptions being satisfied in the present nonlinear problem, terms containing $(R_0/2\omega_0L)^2$ can be neglected. The coefficient of q will, therefore, approximately equal

$$\omega_0^2L\left\{1+(R_0/2\omega_0L)(\omega/\omega_0)\sum_{n=1}^{\infty}nh_n\sin n\omega t\right\}$$

and equation 6 becomes,

$$di_q/dt+\omega_0^2\{1+(R_0/2\omega_0L)(\omega/\omega_0)\times(h_1\sin\omega t+2h^2\sin 2\omega t+3h_3\times\sin 3\omega t+\ldots\}\int i_qdt=0 \quad (7)$$

where $i_q=dq/dt$.

Let $\omega_0=\omega(1+d)$, and $d=$amount of detune, and it is a small fraction. Therefore, L(coefficient of $\int i_qdt)=(1/C_1)+(1/C_2)+(1/C_{1t})$ where

$$1/C_1=\omega^2L,\ 1/C_2=(2d+d^2)/C_1,$$
$$1/C_{1t}=(1/C_1)(R_0/2\omega L)\sum_{n=1}^{\infty}nh_n\sin n\omega t$$

The connection diagram giving the current i_q of equation 7 will be as shown, Figure 3. The reason for splitting up the capacity C is in order that the natural frequency of the linear circuit having the constant elements L and C_1 would equal fundamental frequency $\omega/2\pi$ of the periodic resistance.

According to the well-known compensation theorem, if short-circuiting C_2 and C_{1t} by closing the artificial key and replacing instead a generator of zero internal impedance and having an electromotive force equals $-\{(1/C_2)+(1/C_{1t})\}\times\int i_qdt$ where i_q is the actual current flowing in the circuit, i_q would be unchanged; but the actual current flowing is unknown, therefore, successive approximations will be adopted as follows.

Closing the artificial key, the current would be given by, $i_1=A\sin(\omega t+\phi)$, where A and ϕ are constants to be determined from initial conditions; the capacitor is assumed to be initially charged. i_1 gives the first approximation for the current i_q.

For a second approximation, replace C_2 and C_{1t} by a generator of zero internal impedance and having an electromotive force

$$v_1=-\{(1/C_2)+(1/C_{1t})\}\int i_1dt=A\{(2d+d^2)/\omega C_1\}\cos(\omega t+\phi)+(A/2\omega C_1)(R_0/2\omega L)[h_1\{\sin(2\omega t+\phi)-\sin\phi\}+2h_2\{\sin(3\omega t+\phi)+\sin(\omega t-\phi)\}+3h_3\{\sin(4\omega t+\phi)+\sin(2\omega t-\phi)\}+\ldots.]=v_{10}+v_{1\omega}+v_{2\omega}+v_{3\omega}+v_{4\omega}+\ldots$$

The voltage v_1 consists of components of frequencies zero (that is, d-c component), $\omega/2\pi$, $2\omega/2\pi$, $3\omega/2\pi$, and so forth.

It should be noted that the voltage component $v_{1\omega}$ is of the same frequency as the natural frequency of the L, C_1 circuit. Therefore, if this component were applied to the L, C_1 circuit, the resulting current would increase indefinitely. In fact, it is this component which has the most important effect in producing current.

To get the effect of $v_{1\omega}$, close the artificial key of Figure 3 and apply such a voltage, other generators being shorted, the current is given by:

$$i_2=-(A/2)\omega^2[2(2d+d^2)\{-(t/2\omega)\times\cos(\omega t+\phi)+(1/4\omega^2)\sin(\omega t+\phi)\}-(R_0/\omega L)h_2\{(t/2\omega)\sin(\omega t-\phi)+(1/4\omega^2)\cos(\omega t-\phi)\}]$$

The components of i_2 which do not contain the time t can be included in $i_1\{=A\sin(\omega t+\phi)\}$ in which case A and ϕ will be different, but yet depend on initial conditions. Therefore, the components which contain the time t will only be considered. The effects of the components of v_1 of frequencies other than $\omega/2\pi$ on the current fundamental can be neglected so long as each of $(R_0/12\omega L)h_1$, $(R_0/16\omega L)h_2$, $(R_0/12\omega L)3h_3$, and so forth, is much less than unity and which is satisfied in the present nonlinear problem.

Therefore, the fundamental component of the current i_q to a second degree of approximation may be given by,

$$i_1+i_2=A\{\sin(\omega t+\phi)+(2(2d+d^2)/4)\omega t\times\cos(\omega t+\phi)+(R_0/\omega L)h_2(\omega/4)t\times\sin(\omega t-\phi)\} \quad (8)$$

Following the same lines, other approximations can be obtained and which may be given by,

$$i_3 = A\left[\left\{(R_0/\omega L)h_2(\omega/4)\right\}^2 - \left\{2(2d+d^2)/4\right\}^2\omega^2\right](t^2/2!)\sin(\omega t+\phi)$$

$$i_4 = A\left[\left\{(R_0/\omega L)h_2(\omega/4)\right\}^2 - \left\{2(2d+d^2)\omega/4\right\}^2](t^3/3!)\times \left\{2(2d+d^2)\omega/4\right)\cos(\omega t+\phi) + (R_0/\omega L)h_2(\omega/4)\sin(\omega t-\phi)\}\Big]$$

$$i_5 = A\left[\left\{(R_0/\omega L)h_2(\omega/4)\right\}^2 - \left\{2(2d+d^2)\omega/4\right\}^2]^2(t^4/4!)\times \sin(\omega t+\phi), \ldots\ldots$$

Therefore, if each of $2(2d+d^2)\omega/4$, $(R_0/\omega L)h_1$, $(R_0/\omega L)h_2$, and $(R_0/\omega L)h_3$, and so forth, is very small compared with unity, the fundamental of the current i_q, to a satisfactory degree of approximation is given by,

$$\begin{aligned} i_{q_{\text{fund}}} &= i_1+i_2+i_3+i_4+i_5+\ldots. \\ &= A\left\{1+(\sqrt{a})^2(t^2/2!)+(\sqrt{a})^4(t^4/4!)+\ldots.\right\}\sin(\omega t+\phi)+ \\ &\quad A\left\{2(2d+d^2)\omega/4\right\}(1/\sqrt{a})\left\{\sqrt{a}t+(\sqrt{a})^3(t^3/3!)+\ldots.\right\}\cos(\omega t+\phi)+ \\ &\quad A\left\{(R_0/\omega L)(h_2\omega/4)(1/\sqrt{a})\right\}\left\{\sqrt{a}t+(\sqrt{a})^3(t^3/3!)+\ldots.\right\}\sin(\omega t-\phi) \\ &= A\left[\cosh(\sqrt{a}t)\sin(\omega t+\phi)+\left\{(\sinh(\sqrt{a}t))/\sqrt{a}\right\}\left\{(2(2d+d^2)\omega/4)\cos(\omega t+\phi)+(R_0/\omega L)\times(h_2\omega/4)\sin(\omega t-\phi)\right\}\right] \quad (9) \end{aligned}$$

where

$$\sqrt{a} = (\omega/4)\sqrt{(h_2R_0/\omega L)^2 - \left\{2(2d+d^2)\right\}^2}$$

a may be positive, zero, or negative depending on whether $(h_2R_0/\omega L)$ is greater than, equal to, or less than $2(2d+d^2)$. The case where a is real and positive and hence $\sqrt{a}$ is the one which is useful in the present nonlinear problem. Therefore, this case will only be considered in the present analysis.

Equation 9 can be written as:

$$i_{q_{\text{fund}}} = B_1\epsilon^{\sqrt{a}t}\sin(\omega t+\phi') + B_2\epsilon^{-\sqrt{a}t}\sin(\omega t+\phi'') \quad (9A)$$

where

$$B_1 = (A/2)\left\{1+(R_0/\omega L)h_2\omega/4\sqrt{a}\right\}\times\left[(\cos\phi/\cos\phi')+\left(\left\{1-(R_0/\omega L)\times(h_2\omega/4\sqrt{a})\right\}/\left\{1+(R_0/\omega L)\times(h_2\omega/4\sqrt{a})\right\}\right)\sin\phi/\sin\phi'\right]$$

$$B_2 = (A/2)\left\{1-(R_0/\omega L)h_2\omega/4\sqrt{a}\right\}\times\left[(\cos\phi/\cos\phi')-\left(\left\{1+(R_0/\omega L)\times(h_2\omega/4\sqrt{a})\right\}/\left\{1-(R_0/\omega L)\times(h_2\omega/4\sqrt{a})\right\}\right)\sin\phi/\sin\phi'\right],$$

$$\tan\phi' = 2(2d+d^2)/\left\{(4\sqrt{a}/\omega)+(R_0h_2/\omega L)\right\},$$

and

$$\tan\phi'' = -2(2d+d^2)/\left\{(4\sqrt{a}/\omega)-(h_2R_0/\omega L)\right\}$$

The angles ϕ' and ϕ'' are independent of the initial conditions, they depend only on the amplitude of variation h_2 and the amount of detune d. However, B_1 and B_2 can be considered as constants depending on initial conditions. As $\sqrt{a}$ is positive, then the term containing $\epsilon^{-\sqrt{a}t}$ in equation 9A can be neglected as it is a highly damped one and $i_{q\text{fund}}$ can be satisfactorily given by,

$$i_{q\,\text{fund}} = B_1\epsilon^{\sqrt{a}t}\sin(\omega t+\phi') \quad (10)$$

The harmonics other than the fundamental as well as the zero-frequency component can be obtained either directly from table term by term or from other predetermined harmonics, using the method of successive approximation, as follows: Replace C_2 and C_{1t} by a generator of zero internal impedance and having an electromotive force

$$\begin{aligned} &= -\left\{(1/C_2)+(1/C_{1t})\right\}\int i_{q\text{fund}}dt = \\ &\quad -\left\{B_1\epsilon^{\sqrt{a}t}/\sqrt{1+(a/\omega^2)}\right\}\times \left[\left\{2(2d+d^2)/2\omega C_1\right\}\sin(\omega t+\phi'-\theta')+(h_1R_0/2\omega L)(1/2\omega C_1)\times \left\{\cos(2\omega t+\phi'-\theta')-\cos(\phi'-\theta')\right\}+(2h_2R_0/2\omega L)(1/2\omega C_1)\times \left\{\cos(3\omega t+\phi'-\theta')-\cos(\omega t-\phi'+\theta')\right\}+(3h_3R_0/2\omega L)\times(1/2\omega C_1)\left\{\cos(4\omega t+\phi'-\theta')-\cos(2\omega t-\phi'+\theta')\right\}+\ldots.\Big] = \\ &\quad v_{0h}+v_{1h}+v_{2h}+v_{3h}+\ldots\ldots \end{aligned}$$

where $\tan\theta' = \omega/\sqrt{a}$.

This voltage consists of components of frequencies zero, $\omega/2\pi$, $2\omega/2\pi$, $3\omega/2\pi$, and so forth, being equal to v_{0h}, v_{1h}, v_{2h}, v_{3h}, and so forth, respectively.

The effect of the component of frequency $\omega/2\pi$ is included in the predetermined fundamental. The effect of components of frequencies zero, $2\omega/2\pi$, $3\omega/2\pi$, and so forth, give the zero frequency, second, third, and so forth, harmonic current components respectively to a good degree of approximation so long as each of $(h_1R_0/\omega L)$, $(h_2R_0/\omega L)$, $(h_3R_0/\omega L)$, and so forth, is much less than unity.

Therefore, the current i_q will be given by,

$$\begin{aligned} i_q &= B_1\epsilon^{\sqrt{a}t}\left[-(R_0/2\omega L)h_1.\cos(\phi'-\theta')/2\times \left\{(\sqrt{a}/\omega)+\omega/\sqrt{a}\right\}\sqrt{1+a/\omega^2}+\sin(\omega t+\phi')-\left\{\sqrt{M_2^2+N_2^2\omega^2}\times\sqrt{4+a/\omega^2}/2\sqrt{a^2+9\omega^4+10a\omega^2}\right\}\times \sin\left(2\omega t+\theta_2+\theta_2'-\psi_2\right)-\left\{\sqrt{M_3^2+N_3^2\omega^2}\sqrt{9+a/\omega^2}/2\times\sqrt{a^2+64\omega^4+20a\omega^2}\right\}\times \sin\left(3\omega t+\theta_3+\theta_3'-\psi_3\right)-\ldots\ldots\ldots\Big] \end{aligned}$$

where

$$M_2 = (1/\sqrt{1+a/\omega^2})(h_1+3h_3)(R_0/2\omega L)\times\sin(\phi'-\theta')$$

$$N_2 = -(1/\sqrt{1+a/\omega^2})(h_1-3h_3)(R_0/2\omega L)\times\cos(\phi'-\theta')$$

$$\tan\theta_2 = N_2/M_2,\ \tan\theta_2' = 2\omega/\sqrt{a},\ \tan\psi_2 = 4\omega\sqrt{a}/(a-3\omega^2)$$

$$M_3 = (1/\sqrt{1+a/\omega^2})(h_2+2h_4)(R_0/\omega L)\times\sin(\phi'-\theta')$$

$$N_3 = -(1/\sqrt{1+a/\omega^2})(h_2-2h_4)(R_0/\omega L)\times\cos(\phi'-\theta')$$

$$\tan\theta_3 = N_3/M_3,\ \tan\theta_3' = 3\omega/\sqrt{a},\ \text{and}\ \tan\psi_3 = 6\omega\sqrt{a}/(a-8\omega^2)$$

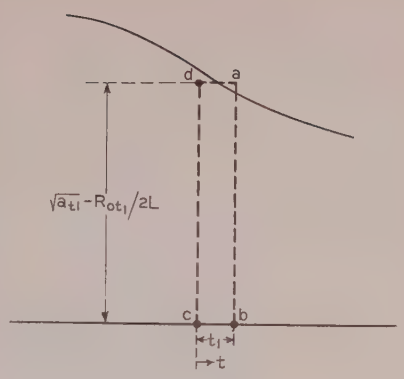

Figure 4. $(\sqrt{a}t - R_{0t}/2L)$ versus time; interval t_1 contains several cycles of oscillations

The charge is given by

$$\begin{aligned} q &= \int i_q dt \doteq (B_1/\omega)\epsilon^{\sqrt{a}t}\left[-\left\{\cos(\phi'-\theta')/2\times(1+a/\omega^2)^{3/2}\right\}(h_1R_0/2\omega L)+\sin(\omega t+\phi'-\theta')/\sqrt{1+a/\omega^2}-\left\{\omega^2\sqrt{M_2^2+N_2^2}/2\sqrt{a^2+9\omega^4+10a\omega^2}\right\}\times \sin(2\omega t+\theta_2-\psi_2)-\left\{\omega^2\sqrt{M_3^2+N_3^2}/2\times\sqrt{a^2+64\omega^4+20a\omega^2}\right\}\times \sin(3\omega t+\theta_3-\psi_3)-\ldots.\Big] \end{aligned}$$

Therefore, the charge Q of equation 5 will be satisfactorily given by,

$$\begin{aligned} Q &= q\epsilon^{\int -(R_t/2L)\,dt} \\ &= q\epsilon^{(-R_0/2L)\left(t+\sum_{n=1}^{\infty}(h_n/n\omega)\sin n\omega t\right)} \quad (11) \end{aligned}$$

Again, in the present nonlinear problem, h_3 and h_4 are small compared with h_1 and h_2 respectively. Also $\sqrt{a}/\omega$ is very small compared with unity. Therefore, the charge Q is approximately given by,

$$\begin{aligned} Q &\cong (B_1/\omega)\epsilon^{\left\{\sqrt{a}-(R_0/2L)\right\}t}\left\{-(h_1R_0/2\omega L)\times\cos(\phi'-\theta')+\sin(\omega t+\phi'-\theta')+(1/3)(h_1R_0/2\omega L)\cos(2\omega t+\phi'-\theta')+(1/8)(h_2R_0/2\omega L)\cos(3\omega t+\phi'-\theta')+\ldots.\right\} \quad (12) \end{aligned}$$

Now, if the coefficients of variation h_1, h_2, h_3, and so forth, the frequency of variation $\omega/2\pi$, as well as the mean value R_0 of the periodically varying resistance, also the capacity C, are not constants but slowly varying functions of time, the analysis will be modified as follows: Let

$$R_t = R_{0t}(1+h_{1t}\cos\omega_t t+h_{2t}\cos 2\omega_t t+h_{3t}\cos 3\omega_t t+\ldots.)$$

and

$$\omega_{0t}^2 = 1/LC_t$$

where R_{0t}, h_{1t}, h_{2t}, h_{3t}, and so forth, ω_t and ω_{0t} are very slow functions, that is, their variation per cycle of $\omega/2\pi$ can be neglected.

Therefore, for a small interval of time t_1, corresponding to several cycles of oscillations, R_{0t}, h_{1t}, h_{2t}, h_{3t}, ..., ω_t and ω_{0t}

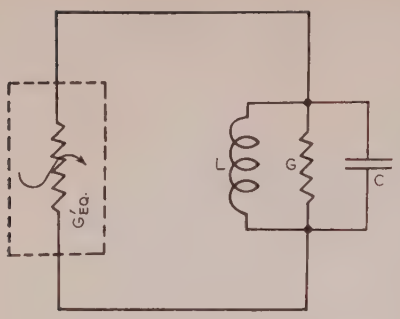

Figure 5. Equivalent circuit of the oscillator

can be considered satisfactorily constants during this interval and equal R_{0t_1}, h_{1t_1}, h_{2t_1}, h_{3t_1}, ..., ω_{t_1} and ω_{0t_1} respectively. The charge Q can therefore be obtained from equation 12 as follows:

$$Q \approx (B_1/\omega_{t1})\epsilon^{(\sqrt{a}_{t1}-R_{0t1}/2L)t}\times \{-(R_{0t_1}/2\omega L)h_{1t_1}\cos(\phi'-\theta')+ \sin(\omega_{t_1}t+\phi'-\theta')+(1/3)\times (R_{0t_1}/2\omega_{t_1}L)h_{1t_1}\cos(2\omega_{t_1}t+\phi'-\theta')+ (1/8)(R_{0t_1}/2\omega_{t_1}L)h_{2t_1}\times \cos(3\omega_{t_1}t+\phi'-\theta')+ \ldots\ldots\}$$

where

$$\sqrt{a}_{t_1}=(\omega_{t_1}/4)\times \sqrt{(h_{2t_1}R_{0t_1}/\omega_{t_1}L)^2-\{2(2d_{t_1}+d_{t_1}^2)\}^2},$$

$$\omega_{0t_1}=\omega_{t_1}(1+d_{t_1}),$$

$$\tan\phi'=2(2d_{t_1}+d_{t_1}^2)/\{(4\sqrt{a}_{t_1}/\omega_{t_1})+ (R_{0t_1}/\omega_{t_1}L)h_{2t_1}\},\text{ and }\tan\theta'=\omega_{t_1}/\sqrt{a}_{t_1}$$

The charge Q given above is true for the time interval t_1 which contains several cycles of oscillations.

Now $\{(\sqrt{a}_{t_1}-R_{0t_1}/2L)t\}$ during the interval t_1 represents the area of the rectangle *abcd* as shown, Figure 4. The actual area under the curve during the interval

$$t_1=\int_{t=c}^{t=b}(\sqrt{a}_t-R_{0t}/2L)dt$$

Similarly, the actual value of $\omega_t t=\int\omega_t dt$. Therefore, at any instant the charge Q would be given by,

$$Q=(B_1/\omega_t)\epsilon^{\int(\sqrt{a}_t-R_{0t}/2L)\,dt}\times [-(R_{0t}/2\omega_t L)h_{1t}\cos(\phi'-\theta')+ \sin\{(\int\omega_t dt)+\phi'-\theta'\}+(1/3)\times (R_{0t}/2\omega_t L)h_{1t}\cos\{(\int 2\omega_t dt)+ \phi'-\theta'\}+(1/8)(R_{0t}/2\omega_t L)h_{2t}\times \cos\{(\int 3\omega_t dt)+\phi'-\theta'\}+\ .....] \quad (13)$$

Now, equation 5, after modification by substituting R_{0t}, h_{1t}, h_{2t}, and so forth, for R_0, h_1, h_2, ..., respectively, is similar to equation 4 with the substitution of Q, R_{0t}, L, and C for v, G_t, C, and L respectively. Also, the assumptions made for the solution of equation 5 are satisfied in equation 4. However, the voltage v must be of the same form as assumed and which is $v=V_t\cos\omega t+\ \ldots$, therefore, a possible solution for equation 4 can be obtained from equation 13 provided $\phi'-\theta'=\pi/2$, giving

$$\tan\phi'=-\cot\theta',\text{ that is, } 2(2d+d^2)/\{(4\sqrt{a}_t/\omega)+(G_t/\omega C)h_{2t}\}=-\sqrt{a}_t/\omega$$

and

$$d=-(1/8)\{(G_t/\omega C)h_{2t}\}^2$$

But, $(G_t/\omega C)h_{2t}$ is very small, and therefore

$$(1/8)\{(G_t/\omega C)h_{2t}\}^2$$

can be neglected, giving, $d\cong 0$, and $\omega\cong\omega_0$, therefore,

$$v=A_s\epsilon^{(1/2C)\int\{\alpha'-G-(3/4)\gamma V_t^2-(5/8)\zeta V_t^4-\ldots\}dt} [\cos\omega t-(1/6\omega C)(2\beta V_t+3\eta V_t^3+....)\times \sin 2\omega t-(1/8\omega C)\{(3/4)\gamma V_t^2+ (5/4)\zeta V_t^4+\ \ldots\}\sin 3\omega t-\ \ldots.] \quad (14)$$

where, $\alpha'=-\alpha$, $\omega\cong\omega_0$ and A_s = a constant depending on initial conditions = amplitude of oscillation at start. Equation 14 shows that the oscillation starts from purely sinusoidal form. As the amplitude V_t increases, the amplitudes of harmonics increase, being functions of the fundamental amplitude.

Building Up of Oscillation

Oscillation builds up according to,

$$V_t=A_s\cdot\epsilon^{\int F_t dt}$$

where

$$F_t=(1/2C)\{\alpha'-G-(3/4)\gamma V_t^2-(5/8)\zeta V_t^4-\ \ldots.\}$$

The rate at which the oscillation builds up is

$$dV_t/dt=\{(\alpha'-G)/2C\}[1-\{(3\gamma/4)/\times (\alpha'-G)\}V_t^2-\{(5\zeta/8)/(\alpha'-G)\}V_t^4-\ \ldots.] \quad (15)$$

Stationary State Oscillation

The amplitude of oscillation at any instant t is given by, $V_t=A_s\epsilon^{\int F_t dt}$. For small values of V_t, F_t is positive and the oscillation builds up from the small starting value A_s. As time goes on, $\int F_t dt$ increases, and hence V_t increases, however, at the same time, F_t reduces. Therefore, $\int F_t dt$ tends towards a constant value, in which case, stationary state takes place and V_t becomes V. Therefore, at stationary state, $\int F_t dt$ = constant $= V/A_s$, and $F_t=F=0$.

Alternatively, at stationary state, $dV_t/dt=0$, but $V_t=A_s\epsilon^{\int F_t dt}$, that is, $\log V_t=\log A_s+\int F_t dt$, differentiation gives, $(1/V_t)(dV_t/dt)=F_t$, and hence at stationary state $F_t=F=0$.

Therefore, stationary state occurs when $F=0$, that is,

$$(3/4)\gamma V^2+(5/8)\zeta V^4+\ \ldots\ldots\ldots=\alpha'-G \quad (16)$$

giving the possible stationary amplitudes.

If three terms in the power series of i_p are only used, the stationary fundamental amplitude will be given by

$$V=\sqrt{(\alpha'-G)/(3\gamma/4)}$$

and equation 15 becomes,

$$dV_t/dt=\{(\alpha'-G)/2C\}(1-V_t^2/V^2)\ldots. \quad (15A)$$

giving

$$V_t=V/\sqrt{[1+\{(V^2/A_s^2)-1\}\epsilon^{-(1/C)\alpha t-G)_t}]^{1/2}}$$

and which are in agreement with those obtained by van der Pol.[4] The voltage v across the oscillatory circuit at the stationary state will be given by:

$$v=V[\cos\omega t-(1/6\omega C)(2\beta V+3\eta V^3+\ \ldots)\times \sin 2\omega t-(1/8\omega C)\{(3\gamma/4)V^2+\ldots\}\times \sin 3\omega t+\ \ldots]$$

The Equivalent Circuit

The differential equation at the stationary state can be obtained from equations 4 and 16 with the substitution of V, h_1, and so forth, for V_t, h_{1t}, and so forth, respectively and which is,

$$Cd^2v/dt^2+\{(3\gamma/4)V^2+(10\zeta/8)V^4+\ldots.\}\times (1+h_1\cos\omega t+2\cos 2\omega t+\ .)\times dv/dt+v/L=0 \quad (17)$$

Therefore, the electron tube when used as an oscillator is equivalent at the stationary state to "a periodically varying conductance", which depends on the amplitude of oscillation, and which is

$$G'_{eq}=-G+\{(3\gamma/4)V^2+(10\zeta/8)V^4+\ldots\}\times (1+h_1\cos\omega t+2\cos 2\omega t+\ .\ .)= -G+G_{stat.}$$

and its average value

$$G'_{eq.\ avg.}=-G+\{(3\gamma/4)V^2+(10\zeta/8)V^4+\ \ldots\}=-G+G_{stat.\ avg.}\ldots. \quad (18)$$

The equivalent circuit at the stationary state is given in Figure 5.

Different Conductances of the Circuit

From the differential equation 4, the

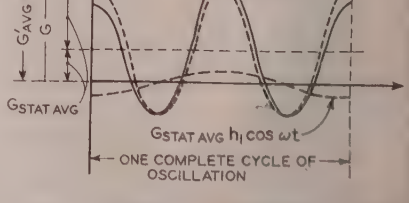

Figure 6. Different conductances of the oscillator at the stationary state

total average conductance of the circuit equals

$$G'_{tot.}=G+\alpha+(3\gamma/2)V^2+(15\zeta/8)V^4+\ldots$$

and which is composed of three parts:

(1) The part due to load $=G$.

(2) The part which remains during stationary self-oscillation $=G_{stat.\ avg.}=(3/4)\gamma V^2+(10/8)\zeta V^4+\ldots$, obtained from equation 18.

(3) The remaining part $=G'_{tot.}-(1)-(2)=G'_{avg.}=-\alpha'+(3/4)\gamma V^2+(5/8)\zeta V^4+\ldots$. From equation 16 $G'_{avg.}=-G$, therefore, $G'_{avg.}$ is negative and consequently it is termed "the average negative conductance". It completely balances the positive load conductance. $G'_{avg.}$ plays an important part in discussing the stability of oscillation.

The different conductances of the circuit at the stationary state are given in Figure 6, where,

$G_{stat.}=$ conductance of the electron tube at the stationary state
$=\{(3/4)\gamma V^2+(10/8)\zeta V^4+\ldots.\}\times(1+h_1\cos\omega t+2\cos 2\omega t)$

and

$h_1=(2\beta V+3\eta V^3+\ldots.)/\{(3/4)\gamma V^2+(10/8)\zeta V^4+\ldots.\}$

$G_{stat.\ avg.}=$ average value of $G_{stat.}$
$=(3/4)\gamma V^2+(10/8)\zeta V^4+\ldots.$

$G_{avg.}{}'=-G$

The full line gives the conductance at the stationary state $G_{stat.}$ it is periodic and has a negative value during a part of the cycle of oscillation.

Condition of Stability of Oscillation

The stationary amplitudes of the Fundamental V can be obtained from equation 16. Whether these amplitudes occur in practice or not depends on their stability.

Now, $v=A_s\epsilon^{\int F_t dt}(\cos\omega t+\ldots.)$. Near the stationary state, $V_t\rightarrow V$ and $F_t\rightarrow F(=0)$ and $\epsilon^{\int F_t dt}\rightarrow V/A_s$. At the stationary state, $V_t=V$, $F_t=F=0$, and $\epsilon^{\int F_t dt}=$constant $=V/A_s$. Therefore, the condition for stability is: If there is a slight increase (δV) in the possible stationary amplitude V, then the increase (δF) in F must be negative, that is, F must be reduced from its stationary value which is zero in this case, to a negative value, otherwise, $\epsilon^{\int F_t dt}$ would increase beyond V/A_s and hence the amplitude would rise indefinitely which is contrary to the fact, and vice versa. Therefore, the condition for stability is $dF/dV<0$.

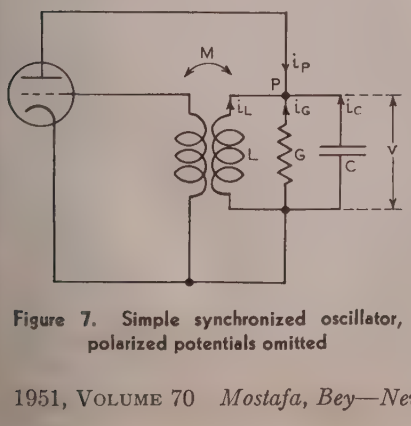

Figure 7. Simple synchronized oscillator, polarized potentials omitted

As

$$F=(1/2C)\{\alpha'-G-(3/4)\gamma V^2-(5/8)\zeta V^4-\ldots.)=(1/2C)(-G'_{avg.}-G)\}$$

Therefore, the condition for stability is:

$$\{(3/2)\gamma V+(5/2)\zeta V^3+\ldots\ldots\ldots\}>0 \text{ or } d(-1/G'_{avg.})/dV>0$$

that is, when the rate of change of the average $-ve$ resistance with respect to time the amplitude is positive.

Synchronization

The second nonlinear problem to be discussed is the behavior of a synchronized oscillator to an external electromotive force. Figure 7 shows a simple triode oscillator acted upon by an external source e, of amplitude E and frequency $\omega/2\pi$, in series with its inductive branch. Near resonance, the amplitude E would be very small compared with the amplitude of the plate voltage v. Therefore, the plate current i_p can be represented as a function of plate voltage only as follows:

$$i_p=\alpha v+\beta v^2+\gamma v^3+\ldots.$$

According to Kirchhoff's 1st law, $\Sigma i=0$ at point P, therefore, $i_C+i_G+i_p+i_L=0$, i_C, i_G, i_p, and i_L have the same indications as before. Now, $v=L(di_L/dt)+e$, and $i_L=(1/L)\int v dt-(1/L)\int e dt$ substitution and differentiation gives:

$$d^2v/dt^2+(-\alpha_1+2\beta_1 v+3\gamma_1 v^2)(dv/dt)+\omega_0^2 v=\omega_0^2\cdot e$$

where $(G+\alpha)/C=-\alpha_1$, $\gamma/C=\gamma_1$ and $\beta/C=\beta_1$.

If synchronized oscillation is only present, whether the system is in the stationary or transient state, the output voltage will generally be of the form $v=b_t\cos\omega t+\ldots.$ and the synchronizing voltage of the form, $e=E\cos(\omega t+\phi_t)$ where both b_t and the instantaneous phase angle ϕ_t are slowly varying functions of time compared with the frequency of oscillation.

Therefore $dv/dt\backsimeq-b_t\omega\sin\omega t$, and $e=E\cos(\omega t+\phi_t)\backsimeq k_t\{v\cos\phi_t+(dv/dt)(1/\omega)\sin\phi_t\}$, where $k_t=E/b_t$, it is also

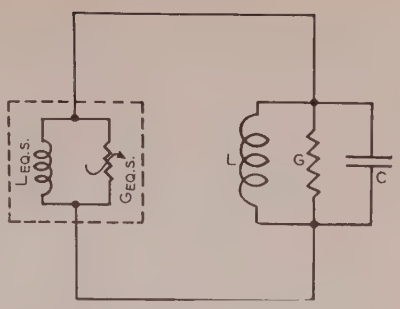

Figure 8. Equivalent circuit of the synchronized oscillator

a slowly varying function of time.

Substitution in the differential equation gives:

$$d^2v/dt^2+(G_t/C)(1+h_{1t}\cos\omega t+h_{2t}\cos 2\omega t)\times dv/dt+\omega_{0t}{}^2v=0 \quad (19)$$

where

$$G_t/C=-\alpha_1-(\omega_0^2/\omega)k_t\sin\phi_t+(3/2)\gamma_1 b_t^2,\quad h_{1t}=2\beta b_t/G_t$$
$$h_{2t}=(3/2)\gamma b_t^2/G_t,\ \omega_{0t}{}^2=\omega_0^2(1-k_t\cos\phi_t)$$

and G_t, h_{1t}, h_{2t}, k_t, ω_{0t}, and ϕ_t are very slow functions of time compared with the frequency of oscillation.

Again, it is assumed that the amount of nonlinearity is small and which is equivalent to saying that the signals are assumed small. Therefore, as in the previous case, the assumptions made for the solution of equation 5, after modification by substituting R_{0t}, h_{1t}, h_{2t}, and so forth, for R_0, h_1, h_2, and so forth, respectively, are satisfied in equation 19. But, the voltage v of equation 19 must be of the same form as assumed and which is $v=b_t\cos\omega t+\ldots.$, therefore a possible solution for equation 19 can be obtained from equation 13 provided $\phi'-\theta'=\pi/2$, that is

$$2(2d+d^2)/\{(4\sqrt{a_t}/\omega)+(G_t/\omega C)h_{2t}\}=-\sqrt{a_t}/\omega,$$

and

$$d\cong-(1/8)(h_{2t}G_t/\omega C)^2$$

But, $(h_{2t}G_t/\omega C)$ is very small, and therefore $(1/8)(h_{2t}G_t/\omega C)^2$ can be neglected, giving

$$d\cong 0 \text{ and } \omega^2=\omega_{0t}{}^2=\omega_0^2(1-k_t\cos\phi_t) \quad (20)$$

and

$$v=A_s\times\epsilon^{(1/2C)\int\{\alpha'-G+(\omega_0^2/\omega)\{Ck_t\sin\phi_t-(3/4)\gamma b_t^2\}\}dt}\times\{\cos\omega t-(1/3)(\beta/\omega C)b_t\sin 2\omega t-(3/32)(\gamma/\omega C)b_t^2\sin 3\omega t-\ldots.\} \quad (21)$$

A_s is a constant depending on initial conditions, and $\alpha'=-\alpha$. Equation 20 shows that $k_t\cos\phi_t=(E/b_t)\cos\phi_t=1-(\omega^2/\omega_0^2)=$constant, showing the form of variation of the phase angle between the output voltage and the synchronizing source.

Stationary State

Stationary state occurs when $db_t/dt=0$. But, $b_t=A_s\epsilon^{\int F_{st}dt}$ and $(1/b_t)(db_t/dt)=F_{st}$, and hence stationary state occurs when $F_{st}=F_s=0$. Therefore, at stationary state, $b_t=b$, $k_t=E/b$, $\phi_t=\phi=$phase angle between the output voltage and the synchronizing source at the stationary state, and

$$F_s=(1/2C)\{\alpha'-G+(\omega_0^2/\omega)(E/b)C\times \sin\phi-(3/4)\gamma b^2\}=0 \quad (22)$$

If $E=0$, the circuit oscillates freely with frequency $\omega_0/2\pi$ and with amplitude b_0 given by $b_0^2=(\alpha'-G)/(3\gamma/4)$, substitution in equation 22 gives,

$$(\omega_0E/b)\sin\phi=-\{(\alpha'-G)/C\}\times\{1-(b^2/b_0^2)\}=-\alpha_1\{1-(b^2/b_0^2)\} \quad (23)$$

and $\alpha_1=(\alpha'-G)/C$. When $(b/b_0)>1$, $\sin\phi$ is positive and vice-versa. Also $\omega_0^2(1-k\cos\phi)=\omega^2$, giving

$$2(\omega_0-\omega)=z=(\omega_0E/b)\cos\phi=\text{amount of detune} \quad (24)$$

Equation 24 shows that as the frequency of the synchronizing source $\omega/2\pi$ is varied, there is a relation between this variation and the phase angle ϕ.

Again, as ω varies from $<\omega_0\rightarrow\omega_0\rightarrow>\omega_0$, ϕ varies from $0\rightarrow\pm\pi/2\rightarrow\pm\pi$. Elimination of ϕ between equations 23 and 24 gives:

$$b^2\{z^2+\alpha_1^2(1-b^2/b_0^2)^2\}=\omega_0^2E^2 \quad (25)$$

Equation 25 gives the ranges and amplitudes of synchronization at the stationary state when only forced oscillations are present, and it is the same as that obtained by van der Pol.[4]

Again, at the stationary state, the voltage v will be given by:

$$v=b\{\cos\omega t-(1/3)(\beta b/\omega C)\sin 2\omega t-(1/8)((\alpha'-G)/\omega C)(b^2/b_0^2)\times\sin 3\omega t-\ldots\} \quad (26)$$

The amplitude b can be obtained from equation 25.

The Equivalent Circuit

The differential equation of the synchronized oscillator at the stationary state can be obtained from equations 19, 22, and 24 with the substitution of b, h_1, and so forth, instead of b_t, h_{1t}, and so forth, respectively, and which is,

$$Cd^2v/dt^2+\{(3\gamma/4)b^2+2\beta b\cos\omega t+(3\gamma/2)b^2\cos 2\omega t\}dv/dt+(1/L)\times(1-z/\omega_0)v=0 \quad (27)$$

Therefore, the electron tube when used as a synchronized oscillator is equivalent at the stationary state to a "periodically varying conductance" $G_{\text{eq.s.}}$ shunted by an inductance $L_{\text{eq.s.}}$, Figure 8, where,

$$G_{\text{eq.s.}}=-G+(3\gamma/4)b^2+2\beta b\times\cos\omega t+(3\gamma/2)b^2\cos 2\omega t, \text{ and}$$
$$L_{\text{eq.s.}}=-\omega_0L/z=\omega_0L/2(\omega-\omega_0)$$

The natural frequency of the circuit composed of L, C, and $L_{\text{eq.s.}}$ is equal to the frequency of oscillation $\omega/2\pi$.

Condition of Stability of Oscillation

From equation 21

$$v=A_s\epsilon^{\int F_{st}dt}\{\cos\omega t-\ldots\ldots\}$$

where

$$F_{st}=(1/2C)\{\alpha'-G+\omega_0Ck_t\times\sin\phi_t-(3\gamma/4)b_t^2\}$$

At the stationary state

$$F_{st}=F_s=0=(1/2C)\{\alpha'-G+\omega_0Ck\times\sin\phi-(3\gamma/4)b^2\} \quad (28)$$

As F_s is responsible for the stability criterion as shown in the case of free oscillation, special consideration will be given to it. At

$b>b_0$, $\sin\phi$ is $+ve$ and $F_s=(1/2Cb^2)\times[\omega_0CEb\sin\phi-b^2C\alpha_1\{(b^2/b_0^2)-1\}]$

but $\omega_0CEb\sin\phi\approx EI_L\sin\phi=2$(power given by the synchronizing source)$=2P_{\text{source}}$, and the source in this case delivers power to the system. $b^2C\alpha_1\{(b^2/b_0^2)-1\}=2$(average power in the rest of the system)$=2P_{\text{system}}$. Therefore,

$$F_s=(1/2Cb^2)2\{P_{\text{source}}-P_{\text{system}}\}=(1/2Cb^2)2P_{\text{net}}$$

where $P_{\text{net}}=$net power in the system.

Now, the stationary amplitudes b of the fundamental can be obtained from equation 25. Whether these amplitudes occur in practice or not depends on their stability. But $b_t=A_s\epsilon^{\int F_{st}dt}$, near the stationary state, $b_t\rightarrow b$ and $F_{st}\rightarrow F_s(=0)$, and $\epsilon^{\int F_{st}dt}\rightarrow b/A_s$.

At the stationary state $b_t=b$, $F_{st}=F_s=0$, and $\epsilon^{\int F_{st}dt}=b/A_s=$constant. Therefore, the condition for stability is: If there is a slight increase δb in the possible* stationary amplitude b, then the increase δF_s in F_s must be negative, that is, F_s must be reduced from its stationary value which is zero in this case to a negative value, otherwise $\epsilon^{\int F_{st}dt}$ would increase beyond b/A_s and hence the amplitude would rise indefinitely which is contrary to the fact, and vice-versa. Therefore, the condition for stability is $\delta F_s/\delta b$ is negative, that is, $(dF_s/db)<0$**, using equations 23, 24, and 28 we get:

$$-\{1/\alpha_1(1-b^2/b_0^2)\}\{z^2+\alpha_1^2(1-b^2/b_0^2)\times(1-3b^2/b_0^2)\}>0$$

and as $b>b_0$, therefore, the condition of stability is:

$$\{z^2+\alpha_1^2(1-b^2/b_0^2)(1-3b^2/b_0^2)\}>0$$

However, at $b<b_0$, $\sin\phi$ is negative, let $\sin\phi=-\sin\phi'$ and $\sin\phi'$ is positive, giving

$$F_s(\sin\phi-ve)=(1/2Cb^2)\times\{b^2\alpha_1C(1-b^2/b_0^2)-\omega CEb\sin\phi'\}=(1/2Cb^2)2\{P_{\text{system}}-P_{\text{source}}\}=-F_s$$
(when $\sin\phi$ is positive)

and the source in this case absorbs power, which is the reverse of the case when $\sin\phi$ is $+ve$.

Therefore, the condition for stability is:

$(dF_s/db)(\sin\phi$ being $-ve)>0$†

and which gives

$$\{z^2+\alpha_1^2(1-b^2/b_0^2)(1-3b^2/b_0^2)\}>0$$

Therefore, the general condition for stability is

$$\{z^2+\alpha_1^2(1-b^2/b_0^2)(1-3b^2/b_0^2)\}>0$$

and which is identical with that obtained by van der Pol.[4]

*By possible is meant a solution for equation 25.

**Alternatively, as $F_s=(1/2Cb^2)2P_{\text{net}}$, therefore $dF_s/db=(1/Cb^2)(dP_{\text{net}}/db)-2(P_{\text{net}}/Cb^2)=(1/Cb^2)(dP_{\text{net}}/db)-(2F_s/b)=(1/Cb^2)(dP_{\text{net}}/db)$, therefore the condition of stability is $(dP_{\text{net}}/db)<0$.

†This means that the condition of stability is till $(dP_{\text{net}}/db)(\sin\phi$ is $-ve)<0$ and $P_{\text{net}}=P_{\text{source}}-P_{\text{system}}=-(P_{\text{system}}-P_{\text{source}})$.

References

1. A Study of Oscillatory Circuits Having Periodically Varying Parameters, **W. L. Barrow, D. B. Smith, F. W. Baumann.** *Journal*, Franklin Institute (Philadelphia, Pa.), volume CCXXI, 1936, pages 403–16.

2. A Further Study of Oscillatory Circuits Having Periodically Varying Parameters, **W. L. Barrow, D. B. Smith, F. W. Baumann.** *Journal*, Franklin Institute (Philadelphia, Pa.), volume CCXXI, 1936, pages 509–29.

3. The Clarification of Average Negative Resistance with Extensions of Its Use, **Brunetti.** *Proceedings*, Institute of Radio Engineers (New York, N. Y.), volume 25, 1937, pages 1595–1616.

4. Non-Linear Theory of Electric Oscillations, **Corbeiller.** Institution of Electrical Engineers (London, England), volume LXXIX, Sept., 1936, pages 361–78.

No Discussion

Measurements and Tests on a Power Line Carrier Relaying System

R. H. MILLER
ASSOCIATE AIEE

A. R. WORTHINGTON
ASSOCIATE AIEE

THE USE of power line carrier controlled relay systems, to provide high speed and simultaneous tripping of faulted transmission lines, has come into general use in the past few years. Incident to the application of carrier to this service, new problems have been encountered, one of which is the fact that the critical time for the operation of the carrier equipment is during the time of the fault. If, as is generally the case, power arcs are a result of the fault, carrier frequency voltage components are produced and propagated along the transmission line to both carrier receiver terminals, and, if these noise voltages are sufficiently great, then the receiver relay tube may be energized and block tripping at a time that the trip circuits should operate. Another factor is that noise components, due to power system distrubances, may be sufficiently high to make it impossible for the relay carrier receiver to determine whether a signal is being received from the remote terminal.

Prior to the placing into service of carrier controlled relay equipment on the 220-kv transmission network of the Pacific Gas and Electric Company, staged fault tests were conducted to determine that the relay equipment, with its associated carrier control, would function satisfactorily under all foreseeable conditions. The conducting of the fault tests presented an opportunity to investigate the amount of noise to be expected under fault conditions, and the effects of such noise on the performance of the relay carrier equipment. This paper discusses the methods used and the results obtained during the staged fault tests.

Staged Fault Tests

The carrier controlled relay system being used on the Pacific Gas and Electric Company 220-kv transmission network uses conventional distance relays, and is arranged for automatic reclosure on ground faults and single-phase faults. The first lines using this equipment are the four parallel transmission lines between Shasta Substation at Cottonwood, Calif., to the Vaca-Dixon Substation near Vacaville, Calif. The distance between these two points is approximately 140 miles, and the four circuits are carried on two twin-circuit steel tower lines, on the same right of way. In order to produce the faults for the tests, a structure was set up adjacent to the first tower north of the Vaca-Dixon Substation, and connected to the Shasta-Vaca 2, 220-kv line. Arrangement was made to produce either ground faults or single-phase faults and equipment was set up to observe the operation of the carrier relays and the automatic reclosing equipment under the two types of fault conditions.

The test work done on carrier noise was of course incidental to the relay and reclosing tests. This paper will be devoted entirely to the carrier noise measurement and results, and the other aspects of the tests will not be discussed at this time.

One problem that immediately presented itself was that of obtaining oscillographic records of the carrier operation, and to distinguish between the remote and local transmitters in order to determine that the equipment was operating in proper sequence. As single frequency equipment is normally used for control of relays, the carrier receivers accept signals from both the local and remote transmitters and, if the signal from the remote transmitter is adequate to saturate the receiver, no indication is available of the actual sequence of operation of the two transmitters.

In order to obtain records of carrier transmission and to distinguish which transmitter terminal was transmitting, as well as to obtain a record of possible interference due to power arcs or the arcing of disconnects, an arrangement was set up to obtain all of this information on a single element of a string oscillograph. In order to distinguish between the local and remote transmitters a carrier frequency voltmeter (tunable vacuum tube voltmeter) was connected across the relay carrier receiver input terminals. The carrier frequency voltmeter is tunable be-

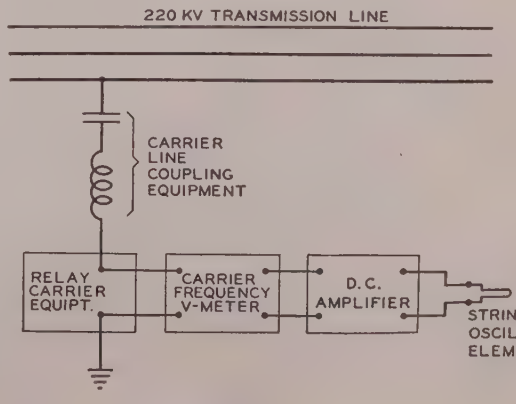

Figure 1. Block diagram of test set up for obtaining oscillographic record of relay carrier operation

Paper 51-192, recommended by the AIEE Carrier Current Committee and approved by the AIEE Technical Program Committee for presentation at the AIEE Summer General Meeting, Toronto, Ont., Canada, June 25–29, 1951. Manuscript submitted November 22, 1950; made available for printing April 24, 1951.

R. H. MILLER and A. R. WORTHINGTON are both with the Pacific Gas and Electric Company, San Francisco, Calif.

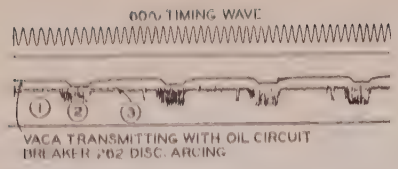

Figure 2. Oscillogram showing noise interference due to arcing of disconnect switch

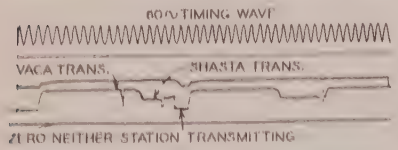

Figure 3. Oscillogram showing difference in level of local and remote carrier transmitters

tween 20 and 500 kc and is sensitive to 80 decibels below one milliwatt, and provides a rectified d-c output. As the d-c output of the carrier frequency voltmeter is insufficient to operate a string oscillograph element, special d-c amplifiers were built and calibrated with the output of the carrier frequency voltmeters. A block diagram of this setup is shown in Figure 1. The d-c amplifier was made linear over a 30-decibel range of signal level into the carrier frequency voltmeter and provided sufficient output to give an adequate deflection of the oscillograph element. The oscillograph was calibrated to give a $\frac{1}{8}$-inch deflection on the trace for local transmission and the remote transmitter then gave approximately $\frac{1}{4}$ inch of deflection. This calibration was well within the linear characteristics of the instruments so that any noise or other interference that might exceed the carrier level would show up as an increased deflection.

Preliminary to the staged fault tests, noise tests were made by arcing 220 kv disconnecting switches, which indicated that under these conditions the noise interference might be as much as 30 decibels above the strongest carrier signal. Figure 2 shows an oscillogram taken with disconnects arcing and with the local carrier transmitter both on and off. The lowest trace on the oscillogram is that of the element connected to the carrier frequency voltmeter. In the section marked (1) the local carrier transmitter was on and the noise peaks extended above the carrier to the dashed line marked (3). In the section marked (2) the carrier transmitter was off and only noise was received.

Figure 3 shows the definite indication obtained for the conditions of local and remote carrier transmission. The oscillograph trace is adequately marked so that it is self-explanatory.

Figure 4 is an oscillogram of the operation of the carrier during the fault tests. On the trace marked Special Receiver the point (1) is at the time of initiation of the power arc at the fault. At this time the local transmitter came on and turned off at point (2) to permit tripping of the oil circuit breaker. At point (3) the remote transmitter came on momentarily; this was a false operation which was later corrected, but for the purposes of this paper the carrier operation is indicated more clearly than in any of the other oscillograms available, so that this picture was selected for discussion. The section of the trace indicated between the bracket (4) shows the noise during the time the power arc was maintained. Due to the false operation mentioned above, the Vaca breaker reclosed into the fault and the local carrier transmitter came on momentarily due to this reclosure. At point (5) the local transmitter went off and tripping of both ends of the line was accomplished as shown at point (6). Of particular interest is the fact that the most severe noise interference occurred after both circuit breakers opened, apparently due to the discharging of the line. This same result was observed during several other tests and would indicate that the most severe noise interference to carrier operation will occur after circuit breaker operation, when relaying has already been accomplished. However, such noise interference might affect relay operation on another line if it was faulted during the persistance of the noise.

Measurement of Carrier Frequency Voltages Due to Power Arcs

In connection with the tests outlined previously, it was considered desirable to obtain a measurement of noise magnitude at carrier frequencies, due to faults on the 220-kv line under test. Preliminary tests were conducted by arcing oil circuit breaker disconnects and measuring the high frequency components of voltage, through a capacitance potential divider, by means of a vacuum tube voltmeter. Such an instrument accepts a very wide band of frequencies, and the results of this preliminary test indicated that the overall summation of high-frequency components of such an arc was in the order of 70,000 volts.

In order to get some idea as to the distribution of noise voltages in the carrier frequency spectrum, due to line faults, and as limited by available measuring equipment, a test setup was made at the Vaca terminal of the Shasta-Vaca number 2 line on which the staged fault tests mentioned were being conducted. The test equipment consisted of a capacitance potential divider, five carrier frequency voltmeters, tuned to 50, 75, 100, 125, and 150 kc and with their detector load resistors connected across the vertical deflection plates of cathode-ray oscilloscopes. Figure 5 shows a block diagram of the test setup. Details of the capacitance poten-

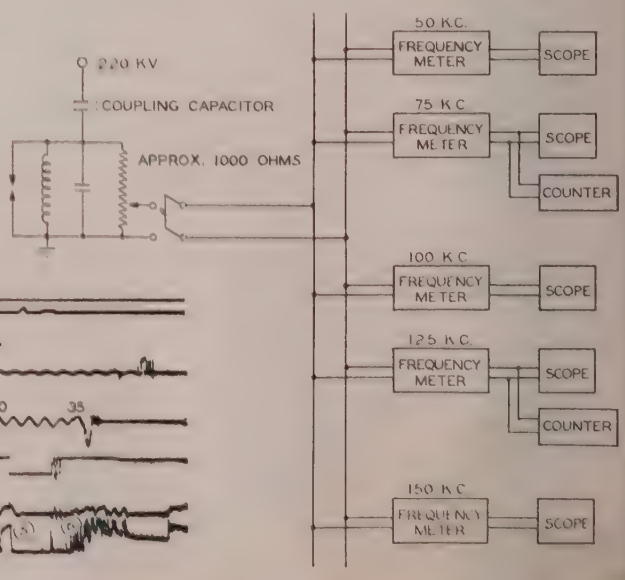

Figure 5 (right). Block diagram of test set up for measuring carrier frequency noise during fault conditions

Figure 4 (below). Oscillographic record of relay carrier operation during staged fault tests

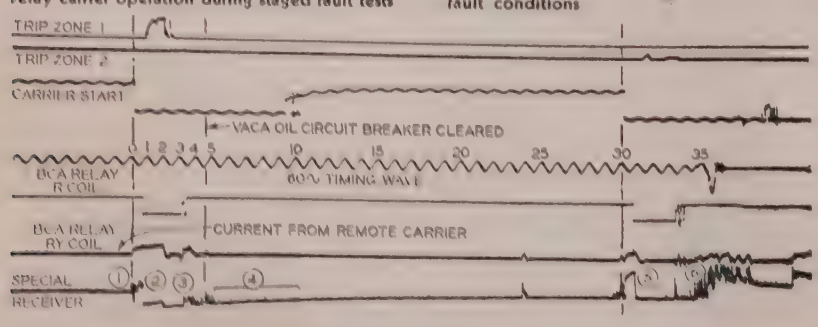

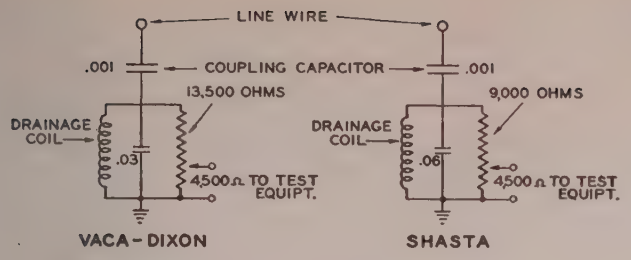

Figure 6 (left). Schematic diagram of capacitance potential dividers used in carrier noise tests

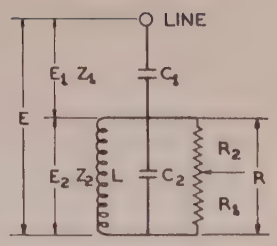

Figure 7

tial dividers used at both ends of the line are given in Figure 6. Prior to conducting the tests the oscilloscopes were calibrated with signal generators and their gain adjustments were then left fixed. No horizontal sweeps were used, so that the deflections due to the noise voltages appeared only as vertical traces, and were visually observed. String oscillograph elements would have been more desirable; however, all available units were in use in other phases of the tests.

From the data collected during the fault tests, it was possible to calculate the voltages appearing on the line in each of the bands accepted by the carrier frequency voltmeters. Calculation of the voltage ratios of the capacitance potential dividers are given in Appendix I, and a tabulation of the results are given in Table I. No noticeable deflection was obtained at 75 kc and, as can be noted from the tabulation, the voltage relations at the various frequencies were rather random. This is probably due to the fact that on the different faults the arc started at different points on the voltage wave, resulting in transients with quite different components.

From the tests described previously, it was possible to determine that all of the relay carrier equipment was operating satisfactorily under conditions simulating actual operation. The results of the tests brought out some difficulties in the carrier equipment which were corrected prior to placing the equipment into service.

The measurements of noise magnitude should not be considered as being exact determinations, but rather are indications of the order of magnitude of voltage that will appear across the input terminals of carrier receivers during fault conditions. It is hoped that further investigations will be made in order that more factual information will be available to engineers responsible for the application of carrier equipment on high-voltage transmission lines.

Appendix I

The calculation of carrier frequency voltages due to line faults on 220-kv fault tests (see Figure 7):

$$E = E_1 + E_2 \tag{1}$$

$$Z_1 = X_{c1}$$

$$Z_2 \cong X_{c2}$$

$$\frac{E_1}{E_2} = \frac{IX_{c1}}{IX_{c2}} = \frac{\dfrac{1}{2\pi f C_1}}{\dfrac{1}{2\pi f C}} = \frac{C_2}{C_1}$$

$$E_1 = E_2 \frac{C_2}{C_1} \tag{2}$$

$$E_2 = I(R_1 + R_2) = IR$$

$$\frac{E_{R1}}{E_{R2}} = \frac{IR_1}{IR_2}$$

$$E_{R2} = E_{R1} \frac{R_2}{R_1}$$

$$E_2 = E_{R1} + \frac{R_2}{R_1} E_{R1} = E_{R1}\left(1 + \frac{R_2}{R_1}\right) \tag{3}$$

from equations 2 and 3

$$E = E_{R1}\left(1 + \frac{R_2}{R_1}\right)\frac{C_2}{C_1} + E_{R1}\left(1 + \frac{R_2}{R_1}\right)$$

$$E = E_{R1}\left(1 + \frac{R_2}{R_1}\right)\left(\frac{C_2}{C_1} + 1\right) \tag{4}$$

For the Vaca-Dixon substation

$$E = E_{R1}\left(1 + \frac{9{,}000}{4{,}500}\right)\left(\frac{0.03}{0.001} + 1\right)$$

$$E = E_{R1}(1+2)(30+1)$$

where

$C_1 = 0.001$ microfarad
$C_2 = 0.03$ microfarad
$R = 13{,}500$ ohms
$R_1 = 4{,}500$ ohms
$R_2 = 9{,}000$ ohms

from equation 4 above

$$E = 93E_{R1}$$

For Shasta Substation

$$E = E_{R1}\left(1 + \frac{4{,}500}{4{,}500}\right)\left(\frac{0.006}{0.001} + 1\right)$$

$$E = E_{R1}(1+1)(6+1)$$

where

$C_1 = 0.001$ microfarad
$C_2 = 0.006$ microfarad
$R_1 = 4{,}500$ ohms
$R_2 = 4{,}500$ ohms

from equation 4

$$E = 14E_{R1}$$

Table I. Tabulation of Carrier Frequency Noise Voltages Due to Staged Faults on 220 Kv Transmission Line

Location	Freq., Kc	Test No. 1 Time 8:40 am	Test No. 2 Time 11:15 am	Test No. 3 Time 2:00 pm	Test No. 4 Time 3:30 pm	Test No. 5
Calibrated Scope Readings in Volts						
Vaca-Dixon	50			3		
	75					
	100		1.5	2		3
	125		3.0	7		3
	150		3.0	3		3
Shasta	75		8	5		0.5
	125		8	6		0.5
Calculated Carrier Frequency Voltages on Power Wires						
Vaca-Dixon	50			279		
	75					
	100		139.5	186		279
	125		279.0	651		279
	150		279.0	279		279
Shasta	75		112	70		7
	125		112	84		7

Action of Line Oil Switches

Vaca-Dixon	Test No.	Shasta	Kind of Arc at Vaca-Dixon
OCO	1	OF	Long
OC	2	OC	Short
OF	3	OC	Short
OF	4	OC	Short

Code: O = Open, C = Closed, F = Failed to close.

No Discussion

The Linascope Transmission Line Fault Locator

K. H. KIDD
ASSOCIATE AIEE

Synopsis: A pulse-type echo ranging fault locator has been developed which is suitable for locating sustained faults on telephone and power transmission lines. A number of these instruments have been in service for several years. They have been used to locate a wide variety of power and telephone line faults with significant reductions in service interruptions and economies in line patrolling.

Before a new circuit is energized it may be tested with the linascope to ensure that all construction grounds have been removed and that all transpositions are correct. Telephone circuits also may be tested to locate sources of mismatch which introduce transmission losses.

An automatic fault locator has been developed, which operates on the same principle and which automatically records the locations of sustained or transient power line faults.

THE Hydro-Electric Power Commission of Ontario operates some 6,000 miles of 230- and 115-kv transmission circuits over an area of 100,000 square miles.

Many of these circuits traverse inaccessible bush in areas where severe sleet and wind conditions often occur in winter and where poor grounding conditions create vulnerability to lightning in summer. Faults are held to a low incidence by adequate design and maintenance and most faults which do occur are due to lightning and are nonsustained. Manual or automatic reclosing is usually successful.

A significant number of sustained faults do occur as a result of various factors.

These faults often occur during adverse weather conditions when patrolling and line-testing is difficult and hazardous and when the power demand is at its peak.

The Commission also operates 7,500 miles of telephone transmission circuits which normally share the power line right-of-ways. These telephone circuits are much more susceptible to faults and service interruptions are frequent in unfavorable weather.

The linascope fault locator has been developed by the Research Division of the Hydro Electric Power Commission for locating sustained faults on long open-wire telephone and transmission lines. It operates on an echo-ranging technique similar to radar, locating a fault by measuring the time taken for a short-duration electrical pulse to travel along the transmission line to the fault, to be reflected from it, and to return to the test terminals. Several years' experience with a number of units has established that the linascope is capable of accurately locating a wide variety of line faults. Significant economies have been effected by the reduction of service interruptions and line-patrolling.

An automatic fault locator working on the same principle also has been developed. This instrument is permanently connected to the transmission line through a carrier coupling capacitor. Transient as well as sustained faults are recorded automatically by obtaining the linascope record while the fault current is still flowing.

Sustained Fault Locator

The sustained fault linascope is about the size of a portable oscilloscope. It may be operated from a 115-volt a-c supply or from a battery-operated vibrapack. A 5-inch diameter cathode-ray tube displays a horizontal trace on which distance is proportional to the distance along the circuit under test. A selection of ranges from 10 to 300 miles is provided.

A vertical pulse at the left side of the trace corresponds to the test location. The fault pulse appears on the sweep at a position corresponding to the fault location. A pulse of opposite polarity to the test-location pulse indicates a short-circuit fault, whereas one of the same polarity indicates an open-circuit fault. The amplitude of the fault pulse depends upon the fault impedance and upon the distance. A pulse also may appear corresponding to the line termination or a junction point. Small pulses also appear which indicate the locations of transposition towers.

An amplitude switch is provided to adjust the fault-pulse amplitude to a convenient size for observation. A dark spot on the horizontal trace can be moved along by means of a precision ranging control. This spot is aligned with the fault pulse and the mileage can then be read off the control to an accuracy of one per cent of full scale. Line and ground output terminals are provided for use on power lines while a balanced line-to-line output is available for use on telephone circuits. Filters are provided to eliminate interference from nearby energized power circuits.

The instrument is shown in Figure 1. Twelve of these units are in use by the Commission and are located at key stations in the various operating regions. The instrument is maintained and operated for both power and telephone line faults by the regional communications maintenance staff.

Operating Procedure

The safety of operator and instrument is an important consideration especially

Paper 51-194, recommended by the AIEE Transmission and Distribution Committee and approved by the AIEE Technical Program Committee for presentation at the AIEE Summer General Meeting, Toronto, Ont., Canada, June 25–29, 1951. Manuscript submitted March 27, 1951; made available for printing May 15, 1951.

K. H. KIDD is with The Hydro-Electric Power Commission of Ontario, Toronto, Ont., Canada.

The author wishes to acknowledge the contributions of J. R. Leslie and D. E. Jones to the development of these instruments.

Figure 1. Portable linascope in use

because the tests are usually made under emergency conditions. Adequate precautions must be taken against the possibility of the line under test becoming energized by such causes as accidental closing of a circuit breaker, contact with another power circuit, induced currents from an adjacent energized circuit, or lightning.

When the linascope is being used the far end of the circuit under test may be left solidly grounded. This ground appears on the linascope trace as a short-circuit pulse and may be used to check the instrument calibration against the total circuit mileage. The linascope output circuit includes a telephone-type carbon block and fuse protector which will operate to ground the test terminals in the event of moderate overvoltages. This protector affords sufficient protection for use on telephone circuits particularly since exposed telephone circuits are normally provided with grounding transformers and short-circuiting protectors which may be left in service while the linascope tests are made.

When a power circuit is under test, however, additional precautions are necessary and a special grounding reactor is provided with the instrument. This reactor has an impedance of less than 5 ohms to the power frequency but is equivalent to an open circuit to the linascope pulse. It is of lightweight construction for portability and measures about one foot square. However it is of adequate size to handle normal induced currents from adjacent power circuits and has been used satisfactorily on a circuit paralleled for several hundred miles by three energized 230-kv circuits. The reactor is bridged by a rugged gap set to a flashover of about 1,000 volts.

In practice the power circuit is handed over for test, isolated, and grounded at both ends. One terminal of the reactor is grounded and the other is connected to one phase of the faulted circuit by using a switch stick. Connection is made from the reactor to the linascope terminals by means of a long flexible extension. When the connections are completed the station grounds are removed at the test terminal and the linascope trace is then examined to identify the fault and to measure the distance to it. Each phase is checked in turn in a similar manner. Best results are obtained when the two phases not under test are left grounded.

Certain types of faults produce a large fault-pulse which can be identified very readily. Other faults may produce low-amplitude fault-pulses which are more difficult to identify from among the small-amplitude pulses always present from transpositions and line irregularities. Some faults cannot be located at all.

Faults which produce large pulses easily identified include broken conductors, parted conductor joints, and phase wires shorted together or touching a steel skywire, tower, or other well-grounded metallic object. A small pulse is produced by a phase conductor down off one or more towers and close to or touching the ground and by a green tree in contact with a conductor. Those faults which can be identified only rarely or not at all include cracked insulators unable to withstand rated voltage, a conductor down on a dry wood cross-arm and a tree within arcing distance of an energized conductor. In general it may be said that to permit a ground fault to be identified with ease, it must have a resistance of less than 1000 ohms as measured at low voltage; an open circuit fault must have a resistance higher than 10 ohms (which rules out the detection of high resistance joints).

The linascope record is shown in Figure 2 of a double phase-to-ground fault which occurred on the 303-mile Leaside-to-Beauharnois 230-kv circuit. An aircraft severed the two skywires which dropped on the phase conductors to produce a white and blue phase-to-ground fault. The aircraft was not damaged! The fault echoes appear at 111 miles on the faulted phases and an induced pulse of lower amplitude also appears on the unfaulted red phase. The closed grounding switches at Beauharnois are indicated clearly on the unfaulted phase and slightly on the faulted phases. Note that the polarity of the transmitted pulse at Leaside is downward. It is of large amplitude but is clipped to the same size as the echo pulses so that the positive overshoot or "tail" is accentuated. The transmitted pulse is reflected from the fault a second time producing a second fault echo at 222 miles. Some transpositions are visible faintly. The fault was located within two spans of the calculated distance.

For the recognition of borderline cases it is of great assistance to have some knowledge of the normal appearance of the circuit. Photographs are taken of the linascope trace when the circuit is in good operating condition. These may be used for reference when one is trying to locate a fault. A conventional oscillograph camera is used for this purpose. Typical records are shown in Figure 3, of the 200-mile Westminster (Buchanan Transformer Station)-to-Minden 230-kv circuit. They were taken with a higher sensitivity than the fault records of Figure 2 so that the transposition echoes appear clearly. An echo also appears at 121.2 miles from the station bus at the Essa Transformer Station.

Once the procedure becomes established the faulted circuits can be made available and checked within half an hour. A topographical map having all circuits marked is kept with the instrument. The mileage is scaled off and the geographical location is given to the repair crew. The accuracy of fault location is within 1 per cent of the line length, which is quite adequate in practice.

It should be noted that the linascope is suitable only on single circuits or on circuits with a limited number of taps. A distribution system or a low-voltage network with a large number of taps and junctions produces a corresponding number of large echo pulses. The fault pulse is then difficult to identify. Since the pulse may have travelled by various paths it would be necessary to do considerable sectionalizing to remove all ambiguities. On telephone circuits the oper-

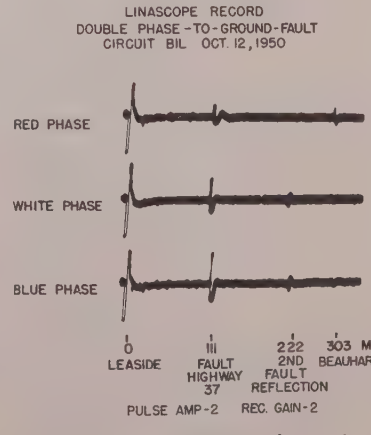

Figure 2. Linascope fault record

ating procedure is much simpler. The Commission's telephone circuits are protected at all terminals with grounding transformers and short-circuiting protectors. The operator simply connects the linascope directly to the line terminals by using rubber gloves. When the repairman is dispatched to the fault he can be "talked in" to the exact location if he has difficulty in locating it. On arriving near the fault the repairman calls the linascope operator, using his test set. They can usually converse with the linascope operating. The test set connection shows up on the linascope and the operator can then direct the repairman closer to the fault. The linascope pulse is of low amplitude and very short duration and is not hazardous.

Operating Experience

Considerable operating experience has been accumulated with the 12 units which have been in service for periods from several months to three years. Several hundred telephone circuit faults have been investigated, with over 90 per cent of the operations successful. Power line faults checked on 44, 115- and 230-kv circuits have totalled over 20 with about 60 per cent of the operations successful.

The power-line faults located have included conductor to skywire, conductor to guy wire, and conductor to conductor contacts; conductor down off one tower; faulty carrier coupling capacitor; and a conductor broken at a strain insulator. These faults were located at distances varying from 0.5 to 111 miles on circuits from 10 to 300 miles in length. Power-line faults not located included trees against the conductors, a tree within arcing distance of the line, and faulty protective relays.

The experience with telephone faults has been better than with power circuits. A ground fault will not cause a telephone interruption unless down to a few hundred ohms, which is readily located with the linascope. On telephone circuits echo pulses appear from transpositions, taps, changes in line spacing or conductor size, and joints. These echo pulses are significant in that they indicate sources of mismatch where signal attenuation is introduced. The instrument has been used extensively to locate such points of mismatch and to reduce losses. High-resistance joints have been located and repaired, reducing circuit loop resistance 30 per cent. A length of several hundred feet of drop wire left tapped to a through circuit after a construction camp had moved away, was identified. In one case a fishing line was entwined in the telephone conductors, producing noise, although it did not completely interrupt service. Numerous cases of multiple faults have been checked. During a heavy wind storm an intermittent short was produced at one point while an intermittent open occurred further along the line.

Both of these faults showed at the proper locations on the linascope trace, appearing and disappearing as the faults came on and off. Some telephone circuit faults are difficult to detect without careful inspection. The "talking-in" technique has proved to be very useful in a number of such cases. In one case a patrolman was guided back and forth over five spans several times before a cunningly concealed short was discovered.

In addition to locating power line faults the linascope has been used to check phasing on nearly a thousand miles of new 115- and 230-kv circuits. Before the circuit is energized each phase is inspected in turn with the instrument. Any construction grounds left on the circuit are located. The terminal-to-terminal phasing is checked by having grounds applied and removed on each phase in turn. Small echo pulses appear from each transposition. A pulse of open-circuit polarity occurs when the phase conductor moves to a position of decreased line-to-ground capacitance, whereas one of short-circuit polarity occurs when the capacitance is increased. Noting the location of each of these pulses enables the correct location of each transposition to be checked and observation of the pulse polarities determines the roll of each phase at each transposition. Thus the one test confirms absence of construction grounds, correct over-all phasing, and correct roll at each transposition tower. The first two tests were formerly made with a Megger, but this involved working with the line open-circuited and introduced the attendant difficulties of induced voltages from adjacent circuits. In one instance a set of construction grounds was located one span from the far end on a 214-mile 230-kv circuit. In another case a phasing error was disclosed and the transposition tower at fault was identified.

It is of theoretical, though of little practical interest, that conductor galloping can be detected and located with the instrument. In a staged test one span at mileage 12 on a 34-mile 115-kv circuit was made to gallop. The point of galloping was located, the amplitude and rate could be measured, and it was also possible to observe the mode.

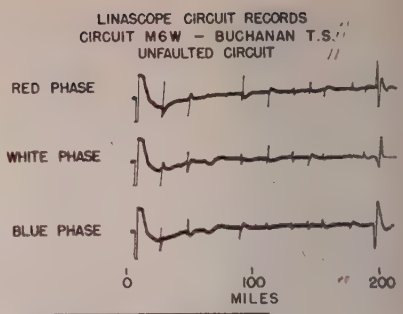

MILEAGE FROM BUCHANAN T.S.	INDENTIFICATION
20.5	TRANSPOSITION
40.6	"
80.9	"
101.0	"
121.2	ESSA T.S
134.4	TRANSPOSITION
146.6	"
171.7	"
184.4	"
196.5	MINDEN S.S.

LINASCOPE LP-1
PULSE AMP = 2
REC. GAIN = 3

Figure 3. Record of unfaulted circuit showing transpositions

Technical Description of Instrument

The linascope generates repetitively a short-duration low-voltage pulse which is connected to the line under test. The return pulses from the line pass through an amplifier to the vertical deflection plates of a cathode ray tube. A linear sweep is generated as each pulse is transmitted. Thus each echo pulse appears along the cathode-ray tube screen at a position proportional to its location along the line. The mileages can be read off the linear sweep with a calibrated scale. Greater accuracy however, is achieved by using the range marker. This circuit produces a short duration pulse at an adjustable time after the transmitted pulse. This pulse is applied to the intensity grid of the cathode ray tube to blank out the trace momentarily. The time interval is adjusted by means of a potentiometer calibrated directly in miles. The dark spot is moved along to align with the fault pulse and the distance is read off the calibrated dial.

A block diagram is shown in Figure 4. The square-wave generator is a free running multivibrator which produces a voltage wave which is alternately zero and 250 volts for equal periods. The repetition rate is adjusted by means of the range switch so that the voltage "on" time is equal to the pulse return time for the particular range (10 microseconds per loop mile). This square wave controls all other circuit functions.

It operates the sweep generator to produce a linearly rising voltage wave which is amplified and connected to the cathode ray tube deflection plates. An "X-Gain" and an "X-Shift" control are provided, so that if desired the sweep can be

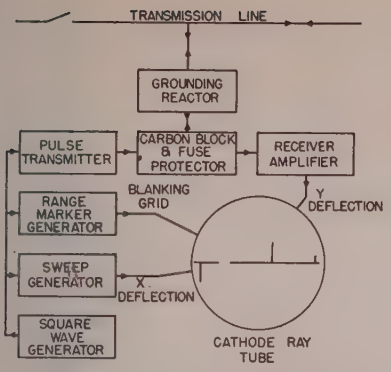

Figure 4. Linascope block diagram

enlarged to several times the cathode-ray diameter and then centered to permit examination of any particular portion of the range in detail.

The front edge of the square wave is used to trigger the transmitted pulse. A short time delay is inserted between the square-wave edge and the pulse initiation so that the pulse is positioned slightly to the right along the sweep. The transmitted pulse is generated by allowing a condenser charged to 300 volts to discharge through a thyratron into the line impedance. Thus the output pulse has a steep front and an exponential tail. An output pulse of 5 microseconds duration is used on the 100- to 300-mile ranges and of half a microsecond duration on the 10-mile range. The attenuation in going along the line is increased as the pulse duration decreases, while the precision of measurement is increased with a short duration pulse. The 5-microsecond pulse, equivalent in duration to half a mile of line, has been found to be a suitable compromise.

A 500-ohm matching resistor is included in the output to match the circuit under test. If the circuit under test is not matched at the transmitting terminal, multiple reflections occur. An echo pulse returning to the transmitting terminal is again reflected, travels to the fault and again returns. Thus a fault echo may appear several times at multiples of the true distance. This effect appears in Figure 2 where a second fault reflection appears. The line impedance may vary from a few hundred to a thousand ohms. Other equipment connected to the terminal contributes to the terminating impedance. On a 3-phase circuit it is impossible to obtain a perfect match without terminating all three phase conductors. Thus the 500-ohm terminating resistor provides only an approximate match and so multiple reflections do occur, in many cases. However, it is not considered necessary to add the complication of an adjustable matching termination.

The return echoes pass through the receiver amplifier and are amplified to a convenient size for observation on the cathode-ray tube. A gain switch provides gains of 1, 30, and 1,000 so that pulses as low as 10 millivolts can be observed. Large echo pulses are limited to a certain maximum amplitude. Thus in Figure 3 the transmitted pulse and the echo from the end of the line appear to be only slightly larger than the transposition echoes although they are actually nearly 100 times greater. In order to reproduce the echo pulses faithfully the receiver amplifier must have a wide band width. To reproduce the 5-microsecond pulse the amplifier must respond to frequencies up to several hundred kilocycles. Since the instrument is connected to a long open-wire line, interfering voltages may appear from various sources. The amplifier includes a bridged-T filter tuned to the power frequency to eliminate interference from induced power-frequency voltage. A radio broadcast station close to the line may create interference. A filter is provided which may be tuned to the frequency of the interfering station. Interference is less with the far terminals grounded than with them open.

The range marker is generated by the leading edge of the square wave in a phantastron circuit. In this circuit a condenser charges at a constant current so that the voltage rise is linear, until the voltage equals the setting on a precision potentiometer. A regenerative action then takes place to produce the marker pulse. A 10-turn helical potentiometer is used which is linear and accurate. Precision components and temperature compensation are provided so that the calibration remains accurate within 1 per cent of full scale despite variations in supply voltage and in ambient temperature. By providing the time delay before the transmitted pulse the lowest portion of the range marker is not used, since in this region it does depart slightly from true linearity. A calibration adjustment is provided so that the range marker can be calibrated from time to time on a circuit of known length.

Theory of Operation

A short-duration voltage pulse travels along a transmission line with little attenuation and distortion and at a speed very nearly that of light (186,000 miles per second or roughly 0.1 loop mile per microsecond). When the pulse reaches an impedance discontinuity an echo pulse is formed which returns at the same speed. The pulse is reflected with reversed polarity from a short circuit and with the same polarity from an open circuit.

In calculating the transmission of a steep-fronted wave along a transmission line it is necessary to take skin effect into account. The problem as applied to lightning surge transmission has been considered in some detail by the British Electrical Research Association.[1] The wavefront is flattened in travelling along the line and the voltage e at a distance x is

$$e = E\left(1 - erf\frac{\sigma x}{2\sqrt{t - x/v}}\right)$$

where

E = initial amplitude of square fronted wave in volts
x = distance in centimeters
t = time in seconds
v = velocity (nearly that of light) centimeters per second
erf = error function
σ = factor for the line construction

The linascope uses a steep-fronted wave with an exponential tail of time constant T seconds. As the wave travels along the line the front is flattened, the tail is lengthened and the peak value is attenuated. By a series of approximations the attenuation for the exponential pulse may be expressed as

$$\frac{29\times10^{6}\sigma}{\sqrt{T}} \text{ decibels per mile}$$

where T is the time to half value for the initial wave.

The value of σ to be used for a single line with line return is

$$\sigma_l = 2.8\times10^{-5}\,\frac{R}{Z}\,\frac{a}{\sqrt{\rho}}$$

where

ρ = resistivity in ohms per cubic centimeter
a = conductor radius in centimeters
R = d-c resistance in ohms/loop centimeter
Z = surge impedance in ohms

For two 795,000 circular mil steel-reinforced aluminum cable conductors spaced 25 feet $\sigma_l = 4.9 \times 10^{-11}$. For a 5-microsecond pulse the attenuation is 0.064 decibel per mile. For a single line with earth return a similar expression for σ is used which gives for the same conductor spaced 60 feet above earth of specific resistivity 10,000

$$\sigma_e = 5.1\times10^{-9}$$

This leads to a value of attenuation of 6.6 decibels per mile.

For a 3-phase circuit in which the linascope pulse is applied to one conductor the attenuation will be between the above two values. The pulse transmission in

this case is best analyzed following the method of Bewley.[2] The main wave travelling down the one phase and the induced waves in the other phases may be considered as composed of components of two types which travel at the same velocity. One component is equal in all three phases, is propagated between the phase conductors and earth, and has the high attenuation factor σ_e. The other component is transmitted between phases, adds to zero for the three phases, and has the low attenuation factor σ_l. For a typical 230-kv circuit the wave on the transmitting phase is made up of about 0.47 of a wave of the first kind plus 0.53 of a wave of the second kind.

The two attenuation factors cannot be added since the maximum values for the two components occur at different times, the first component being rounded more rapidly. It can be seen that the initial attenuation rate is high because the component of the first kind is rapidly attenuated. In three miles the first component has attenuated to one tenth its initial value while the second component has been attenuated only a few per cent. Thus the transmitted wave is down to one half its initial value in the first three miles. Thereafter the rate of attenuation is much lower, being about 3 decibels (one half) for each subsequent 50 miles. For a 1-microsecond pulse an attenuation of 3 decibels occurs in the first mile and thereafter every 20 miles.

At a change in line impedance from Z_1 to Z_2 such as occurs at a transposition a pulse of amplitude E_R is formed

$$E_R = \frac{Z_2 - Z_1}{Z_2 + Z_1} E_I$$

For a 3-phase circuit Z_1 and Z_2 may be calculated using the method of Maxwell Coefficients. For a typical 230-kv circuit of horizontal construction $Z_1 = Z_3 =$ 463 ohms (self impedance of outer conductors) and $Z_2 = 450$ ohms (inner conductor). Hence the reflection on going from an inner to an outer position is

$$E_R = 0.013 E_I (= 40 \text{ decibels})$$

Transposition echoes are of short circuit polarity, open circuit polarity, and almost zero respectively as the conductor goes from outer to inner, inner to outer, and outer to outer positions.

The reflection at a ground fault of resistance R ohms is given by

$$E_R = \frac{-Z}{2R + Z} E_I$$

For the foregoing circuit, a fault of 17,000 ohms resistance will produce a reflection pulse of the same amplitude as a transposition. This is about the limit in sensitivity in practice.

For the two cases described the reflected pulse is of the same waveform as the incident pulse. In the case of a lumped capacitance C and with a steep-fronted incident wave the reflected pulse is

$$E_R = -\exp(-2t/ZC) E_I$$

Thus the reflected pulse is of the same amplitude as the incident wave and of time constant $ZC/2$. Since the incident wave front is rounded in practice the reflected wave front is also rounded and of lower amplitude than the incident wave. A line down off one tower and within one foot of the ground for a distance of 100 feet may be considered to act as a lumped capacity of 0.0005 microfarad. A reflection of time constant 0.1 microsecond will occur at such a fault.

From the foregoing analysis the overall attenuation to the linascope in detecting a borderline fault at the extreme range of 300 miles and using a 5-microsecond pulse is as follows:

	Decibels
Transmission attenuation 3 decibels for first 3 miles and for each 50 miles thereafter	.36
Attenuation at transpositions (complete roll every 25 miles)	1.6
Attenuation at fault (0.013 reflection)	.40
Total attenuation	.78

With a transmitted pulse of 100 volts the received pulse is 10 millivolts.

If the linascope pulse is transmitted on more than one phase of a 3-phase circuit some interesting effects are observed. If there is a single phase-to-ground fault on one phase and if connection is made to that phase an echo pulse $-E_R$ is observed. If connection is made to either one of the other phases the echo pulse observed is $+0.5\,E_R$. If connection is made to one faulted and one unfaulted phase, the echo pulse observed is $-0.5\,E_R$ $(= -E_R + 0.5\,E_R)$. If connection is made to the two unfaulted phases the echo pulse is $E_R (= 0.5\,E_R + 0.5\,E_R)$. If connection is made to all three phases the echo pulse observed is zero $(= -E_R + 0.5\,E_R + 0.5\,E_R)$. This feature is utilized in the automatic linascope.

Automatic Linascope

The pulse-type fault locator may be extended to the automatic recording of the location of sustained and transient faults on important high-voltage transmission lines. Such instruments have been developed by the Bonneville Power Administration and by The Hydro-Electric Power Commission of Ontario and have been described before previous meetings of the Institute.

In this system the instrument is operated and the fault pulse is recorded before the circuit breakers have time to interrupt the power flow to the arcing fault. Connection is made to the energized circuit by using a carrier coupling capacitor and the instrument operation is initiated by means of the station fault relays. This method ensures that the fault location is recorded even if the fault is nonsustained. It has been seen that the sustained-fault linascope is unable to locate sustained ground faults of high impedance. With the automatic instrument this restriction is removed since most faults have an impedance of less than 25 ohms,[3] as long as the fault current is flowing. Thus the reflected pulse at an arcing fault should be 0.9 of the incident pulse.

An automatic linascope has been in service at the Leaside Transformer Station of The Hydro Electric Power Commission for several years. Arcing fault tests have confirmed the operating principles although they indicated the need for minor modifications. No actual fault records have been obtained. The instrument is coupled to the station 230-kv bus at which terminate four 230-kv circuits ranging in length from 50 to 300 miles. When a circuit fault relay operates the linascope transmits five pulses in rapid succession within a period of $^1/_{25}$ second. The cathode-ray tube 300-mile sweep is synchronized to these pulses and the beam is brightened during this period so that the trace is recorded on a camera facing the tube. The instrument must complete its record before the circuit breakers interrupt the fault current.

A train of several pulses is used in preference to a single pulse for two reasons:

1. Better probability of a large fault echo. One pulse may arrive at an instant of fault current zero.

2. Improved discrimination against random pulses and corona noise. A random pulse caused by a lightning or switching surge may be recorded on the film. This may be identified from the true fault echo because the latter, being repetitive, photographs much darker.

The transmitted pulse is shaped to the form of a waveburst, or pulsed oscillation consisting of eight cycles at a frequency of 250 kc. This is chosen in preference to the steep-fronted unidirectional wave used with the sustained fault locator. The burst may be tuned through the coupling capacitor by using a series tuning

coil with little change in amplitude or shape. On the other hand the unidirectional wave is "differentiated" to a pulse of very short duration (1/2 microsecond). This short-duration pulse has given satisfactory service on lines 60 miles long.[4] On longer circuits, however, the longer-duration burst is considered necessary to avoid excessive line attenuation.

The Leaside installation uses a coupling capacitor on each of the white and blue phases of the station 230-kv bus. At this station only the red phases are fitted with power-line carrier equipments and with wave traps isolating each circuit from the bus. By coupling to the bus the pulse should be transmitted uniformly to all four 230-kv circuits although this point has not yet been checked experimentally. In the event of a white or blue phase-to-ground fault the burst is transmitted on the appropriate phase. For a red phase-to-ground fault the burst is transmitted on both the white and blue phases. This arrangement economizes on the use of coupling capacitors and avoids interference with the carrier connections to the red phase. As discussed previously this connection produces a fault echo pulse of the same magnitude but reversed polarity to that which would appear if connection is made to the red phase only.

Cable Linascope

The sustained-fault linascope also has been applied to cable faults with some success. The pulse velocity varies on different cables and is about half that on an open-wire line. Therefore for accurate work it is necessary to calibrate the instrument against a known length of cable (for example, the echo from the far end) or to use the velocity tabulated in handbooks. Since short lengths of cables must be tested and since accuracy within 10 feet is required, the instrument generates a short duration pulse lasting a fraction of a microsecond and utilizes a high-speed sweep of 4 microseconds full scale.

In locating high-impedance cable faults the cable can be charged to a d-c voltage close to the breakdown value. The linascope pulse having an amplitude of 3 to 10 kv is then superimposed on the d-c voltage by using a coupling capacitor. The additional pulse voltage may be sufficient to break down the fault and the echo pulse may then be observed readily.

Conclusions

The pulse reflection technique is finding increasing use in the location of transmission line faults. A portable model suitable for locating sustained faults has found successful application even though it is limited to low-impedance faults. The same principle has been applied to the automatic location of transient as well as sustained power-line arcing faults.

References

1. Surge Phenomena. The British Electrical and Allied Industries Research Association (London, England).

2. Travelling Waves on Transmission Systems, **L. V. Bewley.** John Wiley and Sons, New York, N. Y., page 125.

3. Power System Faults to Ground. *Engineering Report Number 39*, Joint Subcommittee on Development and Research, Edison Electric Institute (New York, N. Y.), 1937.

4. A Transient Fault Locator for High-Voltage Transmission Lines, **L. R. Spaulding, C. C. Diemond.** *AIEE Transactions*, volume 68, 1949, pages 1005–12.

5. New Methods for Locating Cable Faults, **F. F. Roberts.** *Journal*, Institution of Electrical Engineers (London, England), November 1946, part III.

6. Pulse Echo Measurements on Telephone and Power Transmission Facilities, **L. G. Abraham, A. W. Lebert, J. B. Maggio, J. R. Schott.** *AIEE Transactions*, volume 66, 1947, pages 541–48.

7. The "Linascope" An Echo Ranging Type Fault Locator for High Voltage Lines, **J. R. Leslie, K. H. Kidd.** *AIEE Transactions*, volume 67, 1948, pages 1162–66.

8. A Transmission Line Fault Locator Using Fault-Generated Surges, **R. F. Stevens, T. W. Stringfield.** *AIEE Transactions*, volume 67, 1948, pages 1168–79.

No Discussion

Static Magnetic Exciter for Synchronous Alternators

H. F. STORM
MEMBER AIEE

Synopsis: The paper illustrates the application of the theory of electric machinery to the practical design of a static magnetic exciter. The basic exciter circuit is of such nature as to make the alternator (which is energized by the exciter) as much self-regulating as possible. Remaining deviations of the alternator voltage affect a voltage-sensitive circuit which provides a correction signal to the exciter. The energy for the exciter is obtained entirely from the alternator. With this system, no antihunt means are needed, and the steady-state alternator voltage can be easily held within ±0.6 per cent. The transient response is rapid and yet well damped. A short circuit of the alternator will not cause loss of excitation; as a matter of fact, during a short circuit the excitation becomes several times normal, a feature which is desirable for the selective tripping of protective devices.

ONE of the fundamental functions of a voltage regulator is to keep the terminal voltage of the alternator constant at various loads. In order to achieve this end, the excitation of the alternator must be adapted to the alternator line current in magnitude and phase. It has been shown[1] that the line-to-neutral voltage drop $\Delta \boldsymbol{E}$ equals:

$$\Delta \boldsymbol{E} = -jX_s \boldsymbol{I} \tag{1}$$

where X_s is the synchronous reactance of the alternator and $\boldsymbol{I}$ is the line current. Equation 1 assumes a cylindrical rotor, no saturation, and no resistance of the armature winding. It is interesting to note that a typical alternator has a voltage drop $\Delta \boldsymbol{E}$ in the vicinity of rated terminal voltage when loaded with rated line current at zero power factor. This is a very large voltage drop by comparison with a d-c generator which has a typical regulation of only 4 per cent of rated terminal voltage. It follows that the excitation of an alternator has to cover a relatively wide range. As a result, alternators usually require high-gain regulators which often pose stability problems. The excitation system under description, however, avoids the need of a high-gain regulator by attempting inherent compensation for the voltage drop $\Delta \boldsymbol{E}$.

In order to compensate for the voltage drop $\Delta \boldsymbol{E}$, the excitation is required to provide an inner (fictitious) voltage $\boldsymbol{E}_i$:

$$\boldsymbol{E}_i = \boldsymbol{E}_t + jX_s \boldsymbol{I} \tag{2}$$

as shown in Figure 1. This inner voltage $\boldsymbol{E}_i$ is proportional to the field (excitation) ampere turns $I_f N_f$:

$$\boldsymbol{E}_i = k(I_f N_f) \tag{3}$$

where I_f is the field current of the alternator, N_f the number of field turns per pole, k is a factor involving a number of machine constants, such as number of turns in the a-c winding, size of air gap, and so forth.

When saturation is present, or for an a-c winding whose resistance is not negligibly small, or when the alternator is of the salient-pole type, deviations from equation 2 will occur. In order to correct for these deviations, means are provided which are discussed later in the text. Nevertheless, equation 2 remains of fundamental importance for the compensation of the alternator voltage drop $\Delta \boldsymbol{E}$.

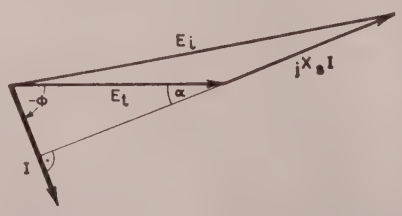

Figure 1. Voltage vector diagram of idealized alternator with cylindrical rotor

Voltage-Drop Compensation

Voltage-drop compensation is obtained by a field current I_f which is proportional to the magnitude of $\boldsymbol{E}_i$, which in turn is determined by the terminal voltage $\boldsymbol{E}_t$ and the alternator current $\boldsymbol{I}$ as shown in Figure 1.

In Figure 2 is shown a 3-phase alternator, connected through three identical current transformers CT to the load. There are also three identical, linear reactors X_1 which are interconnected with the secondaries of the current transformers to three identical resistors R. These resistors symbolize the resistance of the alternator field and it will be shown that the current through the resistors R is proportional to $\boldsymbol{E}_i$.

Assuming a symmetrical 3-phase load, points 7 and 8 of Figure 2 will be at the same potential as the neutral 0 of the alternator. By connecting 7 and 8 to the neutral 0, no changes in the system currents will occur; the system, however, degenerates into three single-phase systems, Figure 3, which are simpler to analyze.

The current transformer CT of Figure 3 is shown by its equivalent circuit in Figure 4 when winding resistances and leakage reactances are neglected.[2] Resistor R is the same as shown in Figure 3 and X_2 is the magnetizing reactance of the secondary of the current transformer CT. Denoting the turn ratio of primary to secondary turns:

$$N_p/N_s = a \tag{4}$$

the alternator current $\boldsymbol{I}$ when referred to the secondary of the current transformer becomes $\boldsymbol{I}'$:

$$\boldsymbol{I}' = a\boldsymbol{I} \tag{5}$$

Paper 51-196, recommended by the AIEE Power Generation Committee and approved by the Technical Program Committee for presentation at the AIEE Summer General Meeting, Toronto, Ont., Canada, June 25–29, 1951. Manuscript submitted February 1, 1951; made available for printing May 1, 1951.

H. F. STORM is with the General Electric Company, Schenectady, N. Y.

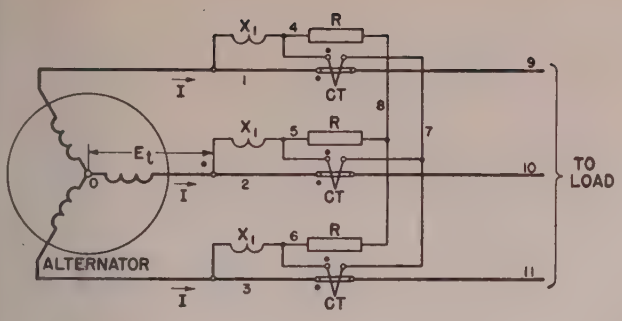

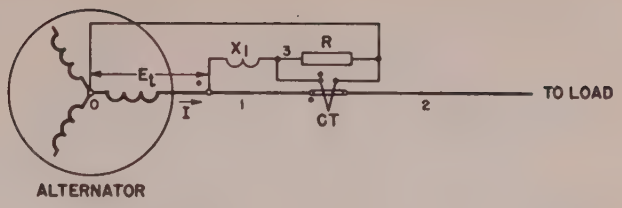

Figure 2 (left). Three-phase network to reconstruct the internal alternator voltage E_t

Figure 3 (above). Single-phase portion of 3-phase network of Figure 2

The equivalent circuit of Figure 3 now is shown in Figure 5. The quantity to be determined is the current I_R which will finally appear to be proportional to the field current I_f.

Acting in the circuit are the terminal voltage E_t and the referred alternator current $I \cdot a$. Accordingly, the current I_R can be seen to consist of two components of which $I_{R,E}$ is derived solely from E_t, and $I_{R,I}$ is derived solely from I:

$$I_R = I_{R,E} + I_{R,I} \tag{6}$$

Determination of $I_{R,E}$

Assume $I = 0$ and apply Thévenin's[3] theorem: with R disconnected, the terminal voltage E_{2-0} between 2 and 0 is:

$$E_{2-0} = E_t \frac{X_2}{X_1 + X_2} \tag{7}$$

The source impedance X, as seen from the terminals 2–0, is equal to X_1 and X_2 in parallel:

$$X = \frac{X_1 X_2}{X_1 + X_2} \tag{8}$$

The current $I_{R,E}$ becomes:

$$I_{R,E} = \frac{E_{2-0}}{R\left(1 + j\frac{X}{R}\right)} \tag{9}$$

and substituting from equation 7:

$$I_{R,E} = E_t \frac{X_2}{X_1 + X_2} \frac{1}{\sqrt{R^2 + X^2}} \underline{/\theta_1} \tag{10}$$

$$\theta_1 = -\tan^{-1}\frac{X}{R} \tag{11}$$

The angle θ_1 is the angle from E_t to $I_{R,E}$, Figure 6.

Determination of $I_{R,I}$

Next, assume $E_t = 0$

$$I_{R,I} = aI \frac{1/R}{(1/R) + (1/jX)} = aI \frac{1}{1 - j\frac{R}{X}} \tag{12}$$

and

$$I_{R,I} = aI \frac{X}{\sqrt{R^2 + X^2}} \underline{/\theta_2} \tag{13}$$

$$\theta_2 = \tan^{-1}\frac{R}{X} \tag{14}$$

The angle θ_2 is from I to $I_{R,I}$.

It follows from equations 11 and 14:

$$\theta_2 = \theta_1 + \frac{\pi}{2} \tag{15}$$

If the current I is lagging the terminal voltage E_t by an angle ϕ, Figure 1, the angle between $jX_s I$ and E_t equals:

$$\alpha = \frac{\pi}{2} - \phi \tag{16}$$

Now let us determine the corresponding angle β between $I_{R,I}$ and $I_{R,E}$. If the line current I lags ϕ radians behind E_t, $I_{R,E}$ lags behind E_t by the angle θ_2':

$$\theta_2' = \theta_2 - \phi = \phi_1 + \frac{\pi}{2} - \phi \tag{17}$$

The angle β between $I_{R,I}$ and $I_{R,E}$, Figure 6, becomes:

$$\beta = \theta_2' - \theta_1 = \frac{\pi}{2} - \phi \tag{18}$$

This proves that:

$$\alpha = \beta \tag{19}$$

which is a necessary condition for the similarity of the triangles OAB and OCD, Figure 6.

By proper selection of X_1, X_2, and a, the ratio of $I_{R,I}/I_{R,E}$ can be made identical to the ratio $X_s I/E_t$: hence the vector diagram OAB becomes similar to OCD. The resultant current I_R, equation 6, will therefore be proportional to the required excitation at any terminal voltage and at any load. By rectifying the current I_R, the alternator field current I_f is obtained.

Correction Circuit

The above field current I_f will compensate for most of the inherent alternator voltage drop, equation 1, but does not produce a perfectly constant alternator voltage, because an actual alternator deviates to some extent from the assumptions previously made; furthermore, the alternator field resistance is subject to

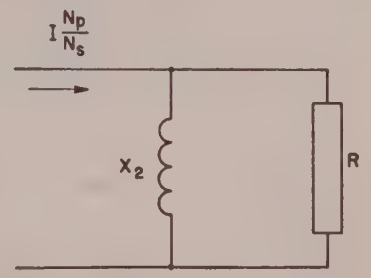

Figure 4. Equivalent circuit for idealized current transformer CT of Figure 3

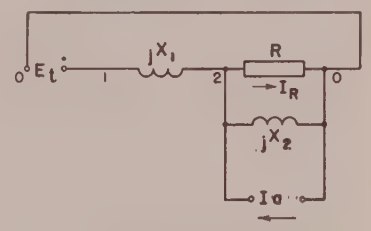

Figure 5. Equivalent circuit for the single-phase network of Figure 3

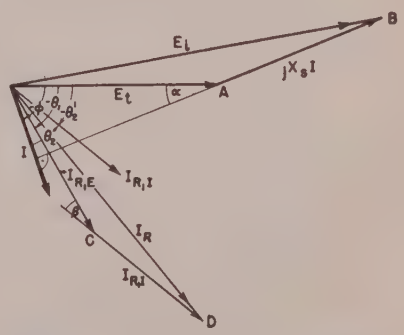

Figure 6. Vector diagram of currents obtained from circuit shown in Figure 3

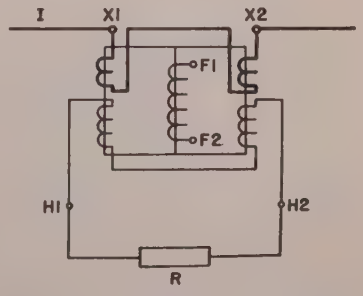

Figure 7. Schematic diagram of saturable current transformer

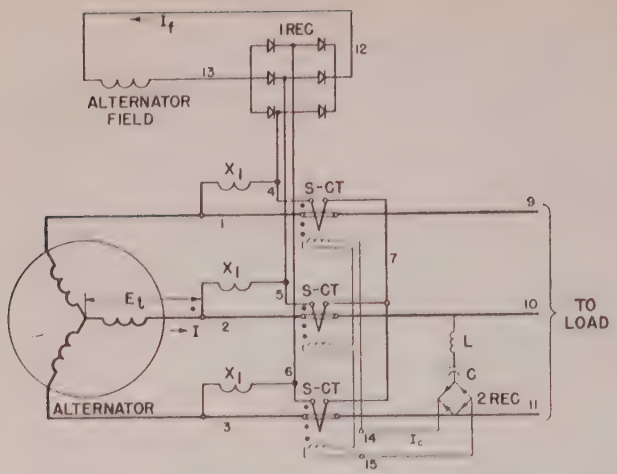

Figure 8 (left). Circuit diagram of static exciter, including correction circuit

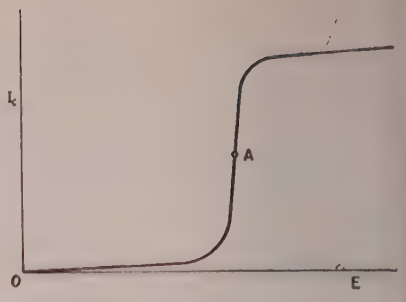

Figure 9 (right). Current I_c of correction circuit as function of alternator terminal voltage E

variation due to temperature changes, which also will affect the alternator terminal voltage. In order to obtain the desirable high degree of alternator voltage constancy, a correction consisting of a voltage-sensitive circuit is superposed on the excitation system.[4] This correction circuit modifies the magnitude of the current I_R and hence, the field current I_f. Because the excitation system (without correction) makes the alternator nearly self-regulating, only a small amount of gain now is necessary for the superposed correction circuit. As a result of this low gain, antihunt means are not necessary.

The magnitude of I_R is determined trigonometrically from equations 6, 10, and 13:

$$I_R^2 = \frac{X_2^2}{R^2(X_1+X_2)^2+X_1^2X_2^2}\left(E_t^2+a^2I^2X_1^2-2E_taIX_1\sin\phi\right) \quad (20)$$

It will be observed that I_R varies with X_2. By applying d-c ampere turns to the current transformer CT of Figures 2 and 3, saturation can be effected in the cores, resulting in a change of X_2 and subsequently a change of I_R.

A schematic diagram of such a transformer, called a saturable current transformer and designated by $S\text{-}CT$, is shown in Figure 7. A 3-legged core structure is used. The primary a-c windings are between terminals $X1$, and $X2$ and the secondary a-c windings are between terminals $H1$ and $H2$. The d-c control winding with its terminals $F1$, $F2$ is wound around the center leg. Because of the polarities of the windings, the a-c fluxes of fundamental frequency and higher, odd harmonics circulate between the outer legs, and no voltage of fundamental or odd frequency is induced in the control winding.[5] A group of three such saturable current transformers is shown in Figure 8.

The excitation circuit including the saturable current transformers is shown in Figure 8. Instead of having points 4, 5, 6 connected to the resistors R, Figure 2, they are now connected to a 3-phase bridge rectifier *1 REC* which energizes the field of the alternator. The control windings of the saturable current transformers are connected in series and terminate at 14 and 15.

In order to superpose corrective action on the excitation system, the control windings of the saturable current transformers are energized from a nonlinear resonant circuit.[6] The single-phase voltage for the energization of this circuit may be taken directly from one phase of the alternator, or it may be obtained from a circuit which produces the average voltage of the three phases of the alternator.

The nonlinear circuit consists essentially of a capacitor C, an iron-core reactor L, a rectifier *2 REC* which energizes the control windings of the saturable current transformers. The current flowing in this nonlinear circuit is shown in Figure 9 as a function of the applied voltage. In the vicinity of A, which is the operating region, a small change in the alternator voltage E causes a very large variation in the current I_c. If, for instance, the alternator voltage E increases, the current I_c in the nonlinear circuit rises sharply. This produces additional saturation in the saturable current transformers, resulting in a reduction of X_2, and hence in the desired reduction of field current I_f, equation 20. In cases where the power output of this nonlinear circuit is not sufficient for its direct application to the saturable current transformers, a magnetic amplifier may be interposed.

Performance

The described static exciter has been tested on a salient-pole alternator of the

Figure 10 (below). Alternator is suddenly loaded with one-half of rated current at a power factor of 0.4 inductive

Figure 11 (right). Same loading as in Figure 10. Oscillogram is taken with suppressed zero line in order to amplify details

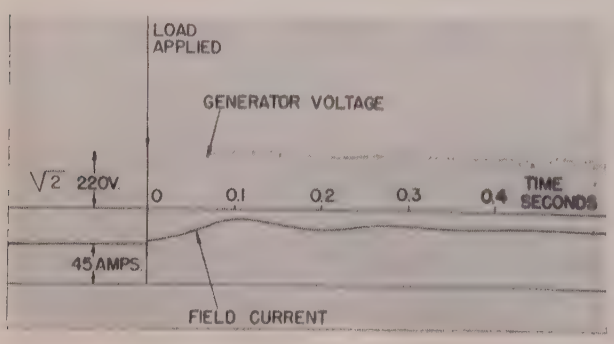

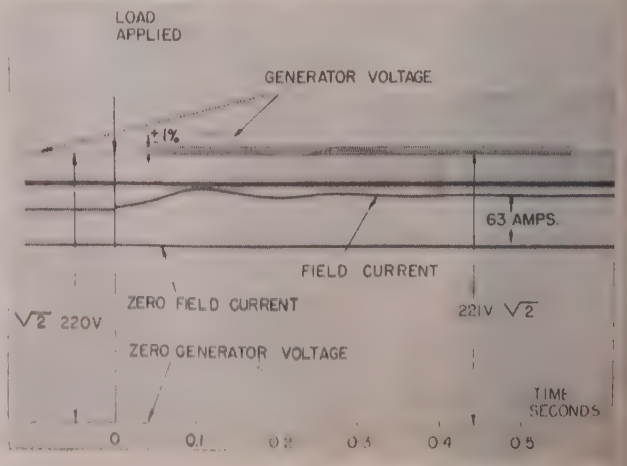

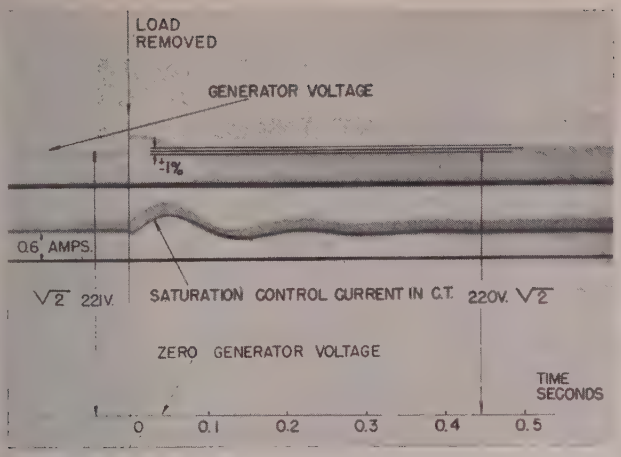

Figure 12. Alternator suddenly loses its load, the load consisted of one-half of rated current at a power factor of 0.4 inductive

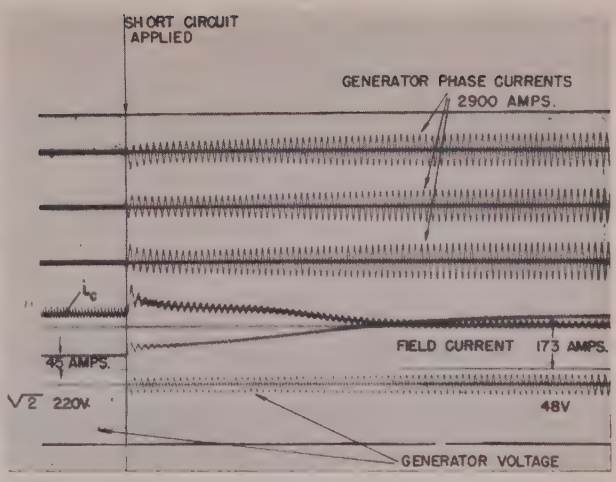

Figure 13. Oscillogram of short circuit test

following description: 3-phase; frequency, 420 cycles per second; line-to-line voltage, 220 volts; rated current, 730 amperes; power factor = 0.8 inductive; synchronous reactance, 0.89 per unit; leakage reactance, 0.22 per unit; open circuit field time constant, 0.25 second; field current for rated alternator current, 80 amperes; field resistance at 25 degrees centigrade, 0.805 ohm; at 90 degrees centigrade, 1.03 ohms; air gap 0.091 inch; speed 1,800 rpm.

Significant for the performance of a voltage regulator are:

1. Steady-state regulation accuracy.
2. Transient response.
3. Alternator current during short circuits.

Steady-State Regulation Accuracy

The voltage drop of the alternator is shown in Table I.

Transient Response

The transient response of the system is demonstrated by the oscillograms shown in Figures 10 to 13. Figure 10 shows the generator voltage and the field current when the alternator is suddenly called on to provide half its rated load current at a power factor of 0.4 inductive. In order to observe more accurately the alternator voltage the same transient was repeated by using a suppressed zero line[7] for the alternator voltage, Figure 11. It will be seen that on application of the load the alternator voltage rapidly recovers and then approaches its sustained value in a highly damped manner. For instance, only 310 milliseconds after the inception of the load, the alternator voltage is already within ± 1 per cent of the final sustained value. Figure 12 shows the case where the previous load was suddenly removed. Here, the recovery to within ± 1 per cent occurs after only 130 milliseconds.

Table I. Steady-state Regulation Accuracy

Type of Load	Alternator Load Current Referred to Rated Current, Per Unit	Power Factor, Inductive, Per Unit	Voltage Drop, Per Cent
Three-phase	1.0	0.75	0.2
Three-phase	1.0	0.06	1.2
Three-phase	0.5	0.4	0.5
Single-phase	0.15	0.96	−0.13

Short Circuit

Another feature of this exciter system consists in its ability to maintain excitation under short-circuit conditions. This feature is important for the selective tripping of protecting devices. An oscillogram of a short-circuit test is shown in Figure 13; it will be observed that the alternator current increases to almost four times of its rated value.

At the point of measurement, the alternator voltage did not quite reach zero because of the impedance in the cables to the short-circuiting breaker. This residual alternator voltage, however, is only coincidental and has no bearing on the basic performance of the system.

Nomenclature

a = turn ratio
E_t = inner (fictitious) line-to-neutral voltage of the alternator, in volts
E_t = line-to-neutral terminal voltage of the alternator, in volts
ΔE = line-to-neutral terminal voltage drop of the alternator, in volts
I = alternator load current, in amperes
I_c = current in correction circuit, in average amperes
I_f = alternator field current, in amperes
I' = alternator load current, referred to secondary of current transformers, in amperes
I_R = current in resistor R, in amperes
$j = \sqrt{-1}$
N_1, N_2 = number of turns of primary, secondary, respectively, of current transformer
N_f = number of turns per pole of alternator field
R = resistance in a-c exciter circuit, representing resistance of alternator field, in ohms
X_1 = reactance of linear reactors, in ohms
X_2 = secondary magnetizing reactance of current transformers, in ohms
X = reactance of X_1 and X_2 in parallel, in ohms
X_s = synchronous reactance of alternator, in ohms
ϕ = phase angle between E_t and I, in radians

References

1. Theoretical Elements of Electrical Engineering, C. P. Steinmetz. McGraw-Hill Book Company, New York, N. Y., 1909, third edition, page 129.

2. Magnetic Circuits and Transformers, Members of Staff of M.I.T. John Wiley and Sons, Inc., New York, N. Y., 1945, page 340.

3. Electric Circuits, Members of Staff of M.I.T. John Wiley and Sons, Inc., New York, N. Y., 1944, page 469.

4. Excitation System for Alternating Current Dynamoelectric Machines, L. W. Thompson, F. E. Crever. United States Patent 2,454,582, November 23, 1948.

5. Some Fundamentals of D-C Controlled Reactors with Resistive Load, H. F. Storm. *AIEE Transactions*, volume 68, part I, 1949, pages 188–94.

6. New Applications of Nonlinear Circuits to Relay and Control Problems, C. G. Suits. *AIEE Transactions*, volume 51, December 1932, pages 914–22.

7. New Method of Expanding the Scale of a Magnetic Oscillograph, R. L. Goetzenberger, Jr. *Instruments* (New York, N. Y.), May 1949, page 405.

No Discussion

Determination of Reserve Capacity by the Probability Method Effect of Interconnections

G. CALABRESE
FELLOW AIEE

THE importance of the allocation of the reserve savings derived from interconnecting two systems does not need any emphasis. Yet this allocation, like most answers to problems dealing with questions of reserve capacity, has been and continues to be based, more or less, on rules of thumb. In a paper presented at the AIEE Convention in Chicago in 1947,[1] the author presented a general method for calculating the effect of interconnecting two systems on their reserve requirements. That method, based on the probability theory, permits evaluating the effect of interconnections on the degree of service reliability of the interconnected systems. It is on this effect that the allocation of the reserve savings, derived from interconnections, should be based. This, in the author's opinion, is the rational approach to the problem.

In the same paper, and in other subsequent publications, the author has introduced the concept of loss of load probability for measuring service reliability. In the general method above referred to, this is calculated on the basis of the actual daily maximum load duration curves of the interconnected systems. Calculations can be simplified if the actual daily maximum load duration curves* of the two interconnected systems are replaced by straight lines or portions of straight lines.

In this paper, the effect of interconnecting two systems on the degree of service reliability of each system is further investigated, assuming straight line daily maximum load duration curves for both systems. In addition, the optimum interconnection capacity is determined on the same assumption.

*See reference 3 for definitions.

Allocation of the Reserve Savings Derived from Interconnecting Two Electric Power Systems

The extensive development of interconnections of electric power systems has been due to the advantages derived from them. On the economic plane these advantages are:

1. Reduction in installed reserve.
2. Reduction in spinning reserve.
3. Economy loading.
4. Staggering of capacity installation.

The evaluation of the savings derived by each system from items 2 and 3 is straightforward and need not be considered here in detail. It consists in computing for each system the annual costs, under each item, with and without interconnection, the difference representing the annual savings.

The same general approach should be used in determining the "value" of the interconnection to each system from the standpoint of installed reserve capacity requirements. A and B are the two systems; L_{am} and L_{bm}, respectively, their maximum loads. The subscripts "a" and "b" are used to indicate quantities pertinent to system A and to system B, respectively.

Let P_{ea} and P_{eb} be the probabilities of loss of load of systems A and B, respectively, without interconnection. P_{ea} and P_{eb} may or may not be equal, depending on the degree of service reliability desired in each system.

Let it be assumed, now, that the two systems are interconnected with an interconnection of capacity R. Evidently, assuming no increase in the loads L_{am} and L_{bm}, the service reliabilities of both systems will increase, that is, P_{ea} and P_{eb} will decrease. Unless, however, the two systems are identical, in general the decrease of the probability of loss of load for the two systems will not be equal. The long range effect, assuming that P_{ea} and P_{eb} obtaining prior to the interconnection are satisfactory, is that the loads L_{am} and L_{bm} can be increased with no additions to the installed capacity of either system.

Starting with no interconnection and increasing the capacity R by small increments, these effects increase with the capacity R of the interconnection and a point of maximum return is reached beyond which any further increase of R will result in smaller and smaller incremental gains or even in no gains at all. From the reserve capacity standpoint there is thus a maximum practical limit for the capacity of the interconnection. It is conceivable for this value of R to be exceeded on considerations other than reserve capacity, such as may arise, for instance, in interconnecting two stations with local loads when one station is completely shut down during part of the day or of the year. Thus, from the reserve standpoint, the following questions arise in interconnecting the two systems:

1. For any given value of R, assuming constant loads, L_{am} and L_{bm}, what is the increase of the degree of service reliability of each system? What is the optimum value of R, the capacity of the interconnection?

Paper 51-198, recommended by the AIEE Power Generation Committee and approved by the AIEE Technical Program Committee for presentation at the AIEE Summer General Meeting, Toronto, Ont., Canada, June 25–29, 1951. Manuscript submitted March 28, 1951; made available for printing May 4, 1951.

G. CALABRESE is Professor of Electrical Engineering with New York University, New York, N. Y.

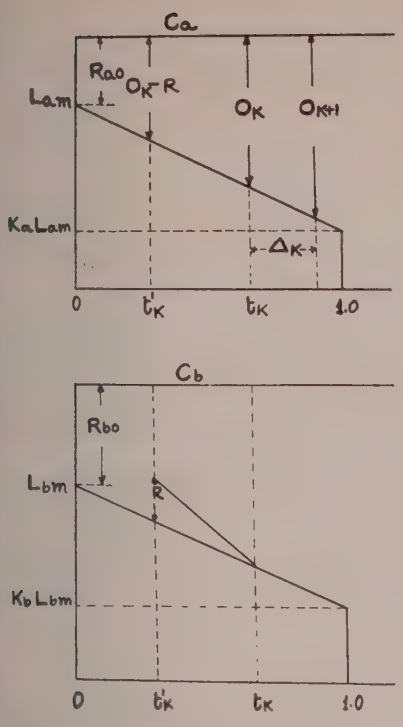

Figure 1. Assumed straight line load duration curves for the two interconnected systems, A and B

2. For any given value of R, assuming constant loss of load probabilities, P_{ea} and P_{eb}, by what amounts can the two loads L_{am} and L_{bm} be increased without increasing the installed capacity of the two systems?

Once these questions have been answered, the determination of the value of the interconnection to each system, from the standpoint of installed reserve capacity, becomes relatively simple.

Under 1, assuming that the loads remain constant, the probability of loss of load of system A decreases from P_{ea} to P_{ea}'. In order to attain the same decrease by installing additional capacity with no interconnection, system A should spend a sum S_a. This sum then represents the investment "value" of the interconnection to system A from the standpoint of reserve requirements.

The total value of the interconnection to system A will be obtained by evaluating, according to conventional engineering economics methods, the savings derived from the installed reserve requirements, as well as those derived from all other sources, such as reduction of spinning reserve, economy loading, and so forth. For system B the value of the interconnection, from the standpoint of installed reserve, and the total value, inclusive of the savings from all other sources, are determined in a similar manner. The total savings for each system, and the grand total for both systems, can be plotted against the capacity R of the interconnection and the optimum value of R thus determined.

If, on the other hand, both or one of the two maximum loads L_{am} and L_{bm} increase, the interconnection will permit staggering the installation of the necessary additional capacity and the savings derived therefrom must be taken into consideration. The installation of additional capacity will affect the "value" of the interconnection to each system, a fact that must be taken into consideration when the effect is appreciable. The determination of the "value" of the interconnection to each system requires a knowledge of their probabilities of loss of load with and without interconnection. The remainder of this paper will be devoted to the calculation of these probabilities

Probabilities of Loss of Load with No Interconnection

Referring to Figure 1, C_a is the total capacity of system A, L_{am} the maximum load, R_{ao} the peak time reserve, and K_aL_{am} the minimum load during the period under consideration, all in kilowatts. C_b, L_{bm}, R_{bo}, and K_bL_{bm} are the corresponding quantities for system B.

In Figure 1 it is assumed that the peaks of the two systems are coincident, that is, there is no diversity between them. This assumption is made to simplify calculations. In the more general case, as previously noted,[1] any diversity between the two systems is taken into consideration by drawing the daily maximum load curves of the two systems in their proper relative position with respect to one another.

The probability of loss of load of system A, with no interconnection (assuming a straight line daily maximum load duration curve and a step outage probability curve) is given by:

$$P_{ea}=\sum p_k t_k=\sum P_k \Delta_k$$

where the summations are extended to all capacity outages O_k in excess of reserve and

p_k = probability of a capacity outage exactly equal to O_k in system A
P_k = probability of a capacity outage in excess of O_k in system A
t_k = time during which the load of system A exceeds C_a-O_k
Δ_k = time interval between two successive capacity outages O_k+1, O_k

The summations are extended to all possible outage values.

If, in addition to using a straight line daily maximum load duration curve, it is assumed that the logarithm of the probability P_k of capacity outages in excess of O_k varies linearly with O_k for all values of $O_k>R_{ao}$, that is, if it is assumed that

$$P_k=A_a\epsilon^{-aO_k}$$

where A_a and a are constants, the probability of loss of load P_{ea} takes the form:

$$P_{ea}=\frac{A_a\epsilon^{-aR_{ao}}}{2a(1-l_a)L_{am}}\left[1-\epsilon^{-2a(1-l_a)L_{am}}\right]$$

where l_a is the daily maximum load ratio of system A.[3] Similar expressions may be written for system B by replacing the subscript a with the subscript b, as already noted.

Probability of Loss of Load with Interconnection

The probabilities of loss of load with interconnection can be calculated according to one of the following three methods:

1. The general method, using the actual daily maximum load duration curves in their proper relative positions. This method was developed in reference 1 and will not be discussed here.

2. The probability of loss of load of either system is calculated, assuming straight line daily maximum load duration curves for both systems and no diversity between the two systems. The actual step curve of the probability of outages, in excess of the various capacity values of each system, is used in the calculations. This method will not be discussed here.

3. The probability of loss of load of either system is calculated assuming straight line daily maximum load duration curves for both systems with no diversity, as under 2. In addition, it is assumed that the probability of capacity outages in excess of O_k in system A is given by $P_k=A_a\epsilon^{-aO_k}$ and the probability of capacity outages in excess of O_b in system B is given by $P_b=A_b\epsilon^{-bO_b}$.

It can be shown that, with this method, the probability of loss of load P of system A is given by:

$$P_{ea}=\frac{A_a\epsilon^{-a(R_{ao}+R)}}{aL_1}[1-\epsilon^{-aL_1}]+$$

$$\frac{C_2}{b(L_1+L_2)}\left[\frac{\epsilon^{(b-a)R}-1}{b-a}+\frac{\epsilon^{-B_1R}-1}{B_1}\right]+$$

$$+\frac{C_2}{(bL_1+L_2)B_1}\left\{\epsilon^{b\left(1+\frac{L_2}{L_1}\right)R}-1\right\}\left\{(1-\epsilon^{B_1L_1})+\right.$$

$$\left.+\frac{C_2\epsilon^{-bL_2+b\left(1+\frac{L_2}{L_1}\right)R-aL_1}}{b(L_1+L_2)(b+B_1)}[1-\epsilon^{(b+B_1)R}]+\right.$$

$$+\frac{C_2\epsilon^{-bL_2-aL_1}}{b(L_1+L_2)a}[\epsilon^{-aR}-1]$$

where for brevity it has been put:

$$L_1=2(1-l_a)L_{am}$$

$$L_2=2(1-l_b)L_{bm}$$

$$C_2=aA_aA_b\epsilon^{-bR_{ao}}\epsilon^{-aR_{bo}}$$

$$B_1=a+b\frac{L_2}{L_1}$$

In actual calculations some of the terms in the above expression can be neglected.

Maximum Value R_{ko} of the Capacity of the Interconnection

Assuming straight line daily maximum load duration curves for both systems and no diversity, the value of R_{ko}, required by different values of capacity outages O_k in system A, is given by:

O_k-R_{ao}, for all outages O_k such that $R_{ao}<O_k\leqslant R_{ao}+R_{bo}$ and by

$$R_{bo}+\frac{(1-l_b)L_{bm}}{(1-l_a)L_{am}}(O_k-R_{ao})\Big/\frac{1+(1-l_b)L_{bm}}{(1-l_a)L_{am}}$$ for all outages $O_k>R_{ao}+R_{bo}$

These relations give the capacity R_{ko} of the interconnection required by any specific outages O_k. The value of R_{ko} increases with O_k. However, as previously noted, from a practical standpoint the capacity R of the interconnection need not be increased above the value for which any further increase would result in a negligible reduction of the probability of loss of load. In other words, in the determination of R only those outages O_k need be considered which have a relatively large outage probability p_k.

References

1. Generating Reserve Capacity Determined by the Probability Method, **G. Calabrese.** *AIEE Transactions*, volume 66, 1947, pages 1439–50.

2. Outage Rates of Steam Turbines and Boilers and of Hydro Units, **AIEE Committee Report.** *AIEE Transactions*, volume 68, part I, 1949, pages 450–57.

3. Determination of Reserve Capacity by the Probability Method, **G. Calabrese.** *AIEE Transactions*, volume 69, 1950, pages 1681–89.

No Discussion

Electrostatic Sources of Ionizing Energy

J. G. TRUMP
MEMBER AIEE

Synopsis: The growing need in science, medicine, and technology for intense sources of high-energy particles and other forms of ionizing energy is being met to an increasing extent by devices which depend upon electrostatic forces and principles. The vitality of these modern uses of ionizing energy and the unique effectiveness of the electrostatic accelerator in meeting their requirements are evident in such diverse activities as experimental nuclear research, the supervoltage X-ray treatment of disease, and the sterilization of biologicals and foods by streams of high-energy electrons.

Nuclear Research

SIR ERNEST RUTHERFORD stated the needs of nuclear science in his presidential address to the Royal Society of London in 1928. "I have long hoped," he said, "for a source of positive particles more energetic than those emitted from naturally radioactive substances." The systematic investigation of nuclear-energy levels and neutron emission thresholds by bombarding elements with streams of protons (Figure 1), deuterons, photons, electrons, and neutrons is now one of the fundamental activities of nuclear physics. For precision work in this field the impinging particles are preferably nearly monoenergetic and must be continuously controllable over a wide range. For nuclear investigations requiring exceedingly high energies, indirect methods of particle acceleration must be employed as in the cyclotron, betatron, and synchrotron. The binding energies of most nuclei, however, lie in the electrostatic accelerator range of a few million and generally below 10,000,000 electron volts, many nuclear resonances appearing at energies less than a few hundred thousand electron volts. Lithium bombarded by protons shows a strong resonance disintegration at the proton energy of 440,000 electron volts where conversion occurs into Beryllium 8 with the emission of gamma rays. The beryllium subsequently disintegrates into two alpha particles. The photodisintegration of beryllium begins sharply at photon energies of 1,630,000 electron volts and that of deuterium at 2,180,000, these representing the energies by which the ejected neutron had been bound to the residual nucleus. Cross-section studies may be made with neutrons of controlled energy produced by bombarding selected light elements with electrostatically accelerated protons or deuterons of appropriate energy. Not only are precise and detailed data on nuclear binding energies and neutron cross-sections of great intrinsic value, but such experimental information will some day provide the basis for a more adequate theory of nuclear structure.

Because of its inherent capabilities in producing streams of monoenergetic positive ions or electrons and the ease of controlling their energy over a wide range, the Van de Graaff electrostatic accelerator[1] has emerged during the last decade as the indicated instrument for precision nuclear research in the binding-energy range. The principal nuclear research laboratories throughout the world have electrostatic generators actively in use—so far, all at energies below 4,000,000 volts. Today at the Atomic Energy Commission laboratory at Los Alamos and at the Massachusetts Institute of Technology two Van de Graaff electrostatic accelerators for nuclear research aimed at the

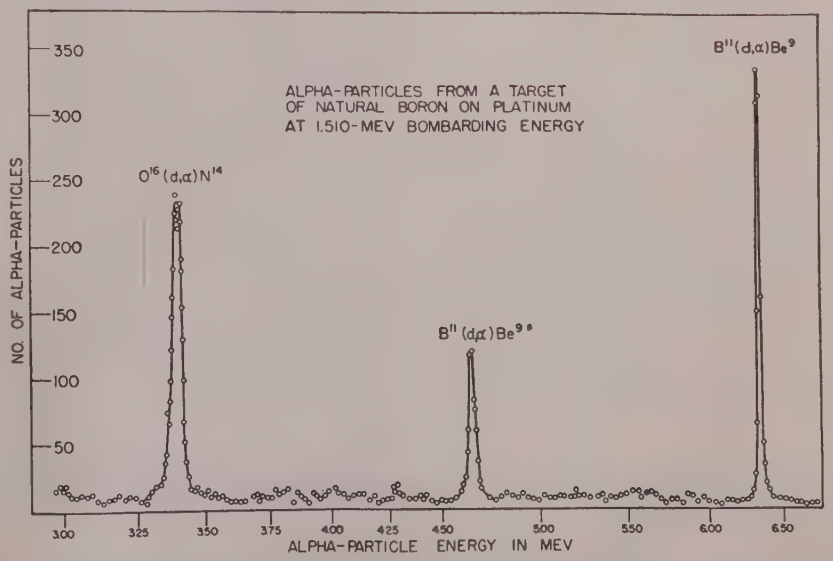

Figure 1. Alpha particles emitted in definite energy groups from Boron 11 and Oxygen 16 bombarded by 1,500,000-volt deuterons from a Van de Graaff accelerator. (Courtesy of Dr. W. W. Buechner, Physics Department, MIT)

Paper 51-199, recommended by the AIEE Electronics Committee and approved by the AIEE Technical Program Committee for presentation at the AIEE Summer General Meeting, Toronto, Ont., Canada, June 25–29, 1951. Manuscript submitted November 1, 1950; made available for printing May 4, 1951.

J. G. TRUMP is with the High Voltage Research Laboratory of the Massachusetts Institute of Technology, Cambridge, Mass.

The author wishes to acknowledge his indebtedness to his associates at the Massachusetts Institute of Technology, including particularly Dr. R. J. Van de Graaff, R. W. Cloud, and K. A. Wright, and to members of the High Voltage Engineering Corporation, Cambridge, Mass. Work described in this paper was supported in part by the American Cancer Society, the Office of Naval Research, and the Atomic Energy Commission.

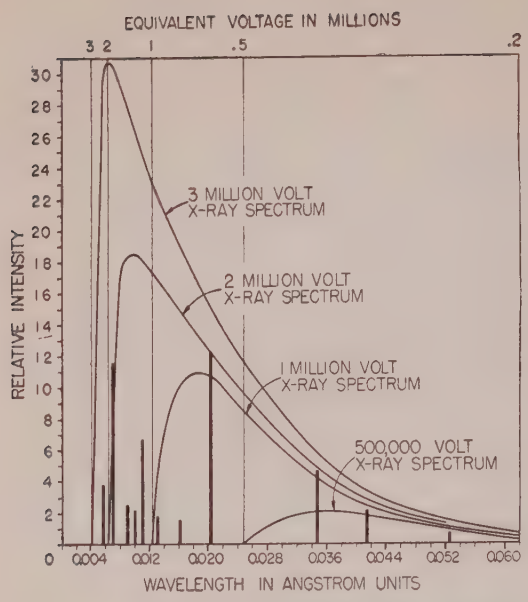
EQUIVALENT VOLTAGE IN MILLIONS
3 2 1 .5 .2
RELATIVE INTENSITY
3 MILLION VOLT X-RAY SPECTRUM
2 MILLION VOLT X-RAY SPECTRUM
1 MILLION VOLT X-RAY SPECTRUM
500,000 VOLT X-RAY SPECTRUM
0 0.004 0.012 0.020 0.028 0.036 0.044 0.052 0.060
WAVELENGTH IN ANGSTROM UNITS

Figure 2. The continuous spectrum of 2,000,000, 1,000,000, and 5,000,000-volt X rays is shown superimposed on the line spectrum of radium gamma rays. X rays of 2,000,000 volts are closely equivalent in physical and biological properties to gamma rays

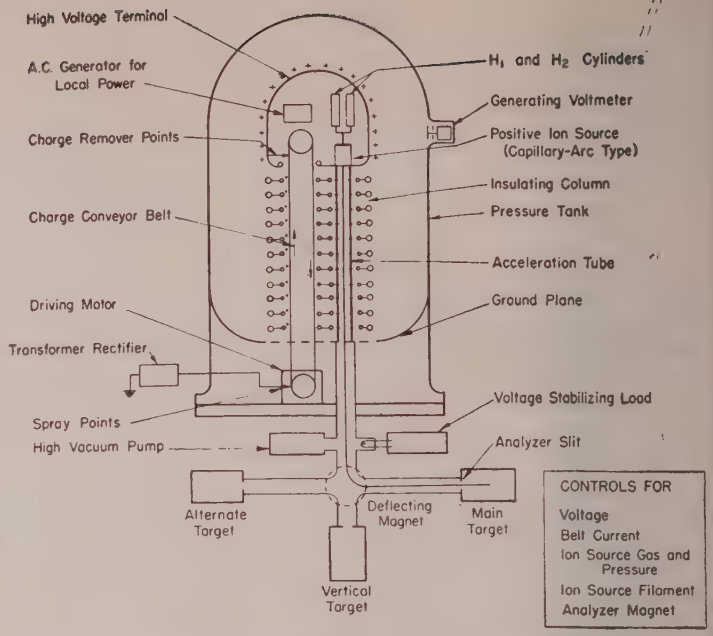

Figure 4. Functional diagram of a Van de Graaff positive-ion accelerator

attainment of 12,000,000 volts are nearing completion.

Supervoltage X-Ray Therapy

An important medical application of ionizing energy lies in the growing recognition of the value of X rays produced at several million volts for the treatment of malignancies. X rays are the penetrating electromagnetic radiation produced by the sudden stopping of high-speed electrons. The effect of increasing the accelerating voltage from the 250,000 volts now in general use for radiation therapy to 2,000,000 volts is to increase the relative penetrating power of the radiation, to reduce its scattering, and to diminish its biological effect in the first layers of tissue at the portal of entry. This last fortuitous fact, the high skin tolerance of supervoltage radiation, is of special value because the skin is an exceedingly radiosensitive organ and has often in the past defined the limit to the dose which could be directed through it toward a deep-seated tumor. X rays produced at 2,000,000 volts appear in a continuous wave-length spectrum which effectively coincides in position with the gamma-ray spectrum of radium in equilibrium with its products. A Van de Graaff X-ray generator operating at 2,000,000 volts produces at the point of electron impact on its water-cooled gold target a source of penetrating electromagnetic radiation physically and biologically identical to the well-studied gamma rays of radium, but with an output intensity greater than that of twice the available world's supply of this precious material.[2] The wise and patient administration of these medically superior rays, guided by accumulated radiological experience of more than 40 years, will undoubtedly advance very significantly the clinical results in the radiation treatment of this difficult disease.[3]

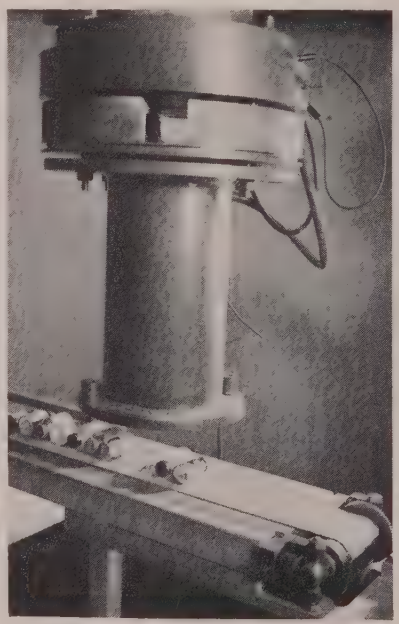

Figure 3. The target end of the 3,000,000-volt electrostatic accelerator showing arrangement for electron sterilization of biologicals, including penicillin and surgical sutures, through their final glass or metal containers

Other sources of supervoltage roentgen rays used for the therapy application are the resonance transformer developed by the General Electric Company and now available in both 1,000,000 and 2,000,000-volt ratings,[4] the betatron developed by Dr. D. W. Kerst[5] at the University of Illinois for radiation therapy at 24,000,000 volts, and the microwave linear accelerator[6] developed in England for the production of 4,000,000-volt roentgen rays. All of these devices have features of special interest for the medical application. The electrostatic generator has advantages of simplicity and compactness and produces a copious source of ionizing radiation at energies which appear to be particularly suitable for clinical therapy.

2,000,000-Volt X Radiography

In industrial radiography, X rays produced at several million volts are also finding increasing application. The greater penetrability and freedom from scatter of such rays makes possible the radiography of heavy metal sections with sensitivity and definition fully equal to that obtained on thin sections at lower voltages. Electrostatic generators developed during the war at the Massachusetts Institute of Technology especially for military radiography produced 2,000,000-volt radiation from a spot on a water-cooled gold target less than 10 mils in

diameter.[7] With an electron current of 300 microamperes, steel sections 8-inches thick could be radiographed with an exposure time of 3 minutes and 4-inch steel plate in 6 seconds. Defects of less than 0.5 per cent of the total plate thickness could be readily discerned on the film complex forgings were found to be readable over a wider thickness range on a single film, and the necessity of packing complex shapes in shot or sand to reduce scatter was eliminated.

An extreme example of the dependence of exposure time on the X-ray voltage was cited in a report of this Massachusetts Institute of Technology group. The measured exposure time on a 14-inch-thick steel submarine forging at 2,000,000 volts and 400 microamperes was 4 hours. Calculations based on experimental data indicated that at 1,000,000 volts and with otherwise similar conditions, the exposure time would have been about 12 weeks, while at 500,000 volts the time would have been about 500 years. With 200 milligrams of radium under these conditions, it was computed that an exposure of about 5 years would be required. On the other hand a careful calculation for 4,000,000-volt X rays showed that the required exposure would be only about 1 minute.

Electron Sterilization

The sterilization of pharmaceuticals and foods by high-energy electrons is a new field for large amounts of ionizing power.[9] All forms of living organisms, including viruses, bacteria, spores, and molds, are destroyed when traversed by high-energy electrons or their lower-energy secondaries. The biological mechanism involves the excitation and ionization of atoms and molecules of the living organism, the breakdown of omnipresent water molecules into activated hydroxyl radicals, the subsequent chemical change within the organism, and—with a sufficient dose—its resultant demise.[8] This is evidently a new and far more efficient means of sterilizing materials than the age-old technique of heating, a process which raises the energy of vibration of the entire molecule until its thermal disintegration is assured. The most radio-resistant organisms, the spore-formers, can be destroyed by a cathode-ray dose of 2,000,000 rep*, an amount of ionizing energy which raises the temperature of the absorber by less than 5 degrees centigrade.[10]

* A rep is that amount of ionizing radiation, whether X rays, cathode rays, or neutrons, which results in an energy absorption of 93 ergs per gram of water or equivalent material.

Many types of heat-sensitive pharmaceuticals, such as penicillin, streptomycin, surgical sutures, and adrenal extracts, can be electron-sterilized in their final glass or plastic container without reduction in potency of the material or other adverse effects, Figure 3. More recently there has been evidence that certain living tissues, such as the aorta and other large blood vessels and the bone and marrow, can be given sterilizing doses, if irradiated at reduced temperature, without impairing their effective use as transplants in surgical procedures. It appears that even relatively complex protein molecules, including those of blood plasma and fractions and of many foods, can often be sterilized to advantage particularly if the irradiation is performed at temperatures as low as that of solid carbon dioxide, at which the diminished ionic mobility markedly reduces unwanted side reactions. The shelf life of cheese is limited by the formation of molds which can be destroyed by a relatively low cathode-ray dose penetrating less than 2 millimeters through the wrapper. Wheat, cereals, meats, and other food materials may be sterilized advantageously by this method.

The Van de Graaff electrostatic accelerator** has proved to be a valuable source of cathode rays of high energy for the scientific research prerequisite to such applications and now is being designed for routine production sterilization of large quantities of materials. Compact cathode-ray units developing 250 microamperes of 2,000,000-volt electrons are now available for fundamental radiobiology, for the research investigation of cathode-ray effects and techniques covering a diversified program, and for routine production sterilization. A unit of this rating, for example, is capable of handling the entire surgical suture sterilization of a large manufacturer. In food applications, however, far larger amounts of ionizing energy are generally required. A basic machine for such purposes now is under construction rated at 3,000,000 volts and 4 milliamperes of electron current, capable of delivering 12 kw of ionizing power in the form of a high-energy electron stream rapidly scanning a product-laden belt.

** In the Van de Graaff electrostatic generator, see Figure 4, electric charge is transferred to the high-voltage terminal at a continuous rate by a belt of insulating material. This charge maintains the terminal at a steady positive potential above ground and supplies the current required by the acceleration tube. Both tube and belt are mounted within the insulating column, which is specially designed to insure a uniform voltage distribution between terminal and ground plane. At the high-voltage end of the tube the positive ions emerge through a small opening in the side of a capillary containing a d-c arc in hydrogen or deuterium. These ions are progressively accelerated and focused as they pass along the acceleration tube and thus acquire the full voltage of the terminal. In precision nuclear research the ion beam is often deflected through a 90 degree angle by a magnetic field. This serves to remove the positive ions of unwanted mass and enables the remaining ions to be selected for energy by means of the analyzer slit system. Thus, steady parallel streams of positive ions accurately homogeneous in energy may be caused to impinge upon any selected target material. The alternate target may be used by reversing the direction of the deflecting magnet current. Although the potential of the Van de Graaff generator is already steady to within 1 per cent, further electronic stabilization may be introduced so as to maintain steadiness to 0.1 per cent or better.

Van de Graaff Operating Principles

The Van de Graaff electrostatic accelerator[11] is essentially a belt conveyor of electric charge designed for the attainment of high constant potentials and provided with a suitably evacuated tube for the acceleration of charged particles. As indicated in Figure 4, electric charge is sprayed onto a moving belt of high dielectric strength and carried into the field-free space of a well-rounded metallic terminal. This high-voltage terminal is supported from ground by an insulating column constructed of spaced metallic equipotential members and glass disk insulators. Both the charge-conveyor belt and acceleration tube are mounted within this column, along which a uniform voltage distribution is secured by the flow of charge from terminal to ground through resistors between the metal sections. Charged particles originating in the terminal end of the tube are progressively accelerated and focused by a succession of electrodes which produce a uniform electric field along the tube. These electrodes obtain their potential by connection to corresponding equipotential planes in the insulating column of the generator.

The steady constant potential of the terminal is maintained by balance between the controllable current brought to the high-voltage terminal by the belt, the voltage distribution current down the generator column, and the current accelerated along the vacuum tube. The generator voltage may be brought to any equilibrium value by regulating the charge sprayed onto the belt. It is common practice to utilize both ascending and descending runs of the belt of an electrostatic generator by causing them to carry charge of opposite polarity.

The current rating of a belt-type electrostatic generator is independent of terminal voltage and depends directly on the area per second of insulating surface entering and leaving the terminal and on the dielectric strength of the gaseous medium in which it is immersed. It can readily be shown that the maximum charge density on a surface in atmospheric

air is 5.3 times 10^{-9} coulombs per square centimeter, assuming 30 kv per centimeter gradient and a uniform electric field normal to the surface in both directions. In practice about half this charge density can be realized. Thus about 4 times 10^5 square centimeters per second of belt surface entering or leaving the terminal is required for each milliampere of current. Consideration of Gauss's law shows that, unless electrically shielded from each other, adjacent runs of belt must run in opposite directions and carry charge of the opposite sign. The effect of an increase in dielectric strength of the surrounding gas is to increase the permissible charge density proportionately or, conversely, to reduce the required belt width for the same current.

In all direct acceleration apparatus operating above 500,000 volts, the charged particles are accelerated in successive increments by fields produced between a series of metal diaphragms spaced between the annular glass sections of the evacuated tube. The particles pass through axial holes in these diaphragms, which serve in part to shield the inner glass surfaces from bombardment of scattered particles and also to maintain a well-focused beam through the focusing action of the slightly fringing electric fields. By this arrangement the cathode and anode ends of the tube may be separated by distances sufficient to insure the insulation of the total terminal voltage, and the insulation problem is reduced to that of a series of relatively low voltage gaps in high vacuum. Only in the limited axial region lengthwise the tube through which the accelerating stream of particles must pass does the possibility of total voltage breakdown in vacuum[12] arise. Nevertheless, it is common experience that the insulating length of direct acceleration tubes must increase more rapidly than their voltages. Much study now is in progress to increase the understanding of high-voltage breakdown in vacuum and of the factors which influence the performance of particle-accelerating tubes. The best performance today permits the reliable insulation and acceleration of particles to 2,000,000 volts in a tube whose insulating length is 33 inches, and the attainment of 6,000,000-volt particles in an insulating length of 12 feet.

Since the particles reaching the grounded end of the tube have been accelerated by a constant potential, they become available as a well-directed stream arriving continuously in time and closely homogeneous in energy. The smooth controllability of this energy over a wide range, together with this homogeneity, is a principal advantage of the Van de Graaff electrostatic accelerator for purposes of scientific research. In a cathode-ray accelerator the high-voltage terminal is charged negatively, and the source of electrons within the acceleration tube is a heated tungsten filament. The high-energy electrons finally pass into the atmosphere through an aluminum window of a few mils thickness, which they traverse with little loss of energy or scattering. Such an electron stream will then continue on through the air and be directly incident upon the biological material or substance to be sterilized. On the other hand the high-energy electron stream may be caused to impinge upon a water-cooled target of high-atomic-number material, such as tungsten or gold, in which case their kinetic energy is converted in part into penetrating electromagnetic radiation. These rays proceed outward in all directions, though with increasing preference for the forward direction at higher voltages. This X-ray source may be defined into a beam by absorbing the unwanted radiation in lead and used in the radiation treatment of malignant diseases or in the examination of heavy metal sections. The substitution of a source of positive ions—a low-voltage d-c discharge in low-pressure hydrogen from which the ions are extracted through a tiny orifice by a probe voltage—for the electron source and the operation of the generator at positive potential transforms it into an instrument for precision nuclear research.

Electrostatics Versus Electromagnetics

Electrostatic processes are inherently more efficient in the production of high constant potentials than electromagnetic methods. The maintenance of an electric potential requires merely the presence of electric charge, and is described by the relation $V = Q/C$, where V is the terminal potential, Q is its isolated charge, and C its capacitance to ground. This equation implies that the attainment of constant potentials of several million volts is primarily an insulation problem and that the terminal and its supporting column should be designed so as to exploit the most advantageous electric field configuration and insulating materials. In an electrostatic belt generator the superior voltage-insulating properties of gases at high pressure and of certain electronegative gas molecules can be fully utilized to reduce the physical size of the terminal and gap for a given voltage, at the same time increasing the charge-carrying capacity of the belt.

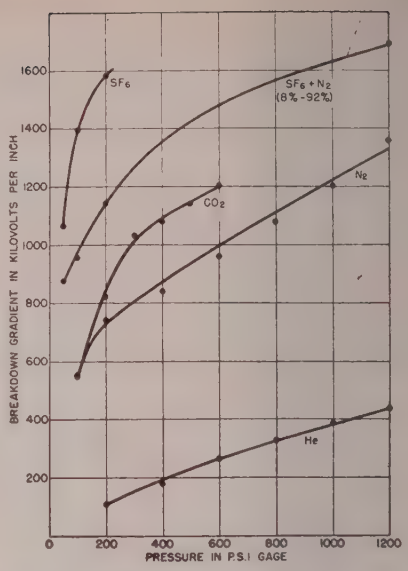

Figure 5. Relative breakdown strength of various gases as a function of pressure up to 80 atmospheres. Uniform field, constant potentials, 0.5-inch gap, polished stainless-steel electrodes 6 inches in diameter

In electromagnetic equipment the attainment of high a-c voltages involves inevitably the continued and cyclical flow of electric charge and the development of large amounts of reactive power. Merely to charge the simple high-voltage terminal of the 2,000,000-volt Van de Graaff accelerator shown in Figure 7 to the same peak value by 60-cycle electromagnetic means would require over 30 kva of reactive power. In the ingenious resonance transformer this reactive power is avoided, as far as the external circuit is concerned, by an air-core transformer design in which an exact balance is achieved between the inductive and capacitive power at 180 cycles per second or higher frequencies. The large internal power circulating between the electric and magnetic fields and the dependence of peak voltage upon considerations of flux and coil ratios tend to limit the advantage attainable with better gaseous insulation in such a-c electromagnetic apparatus. The conversion of a-c power to high constant potential by any of several ingenious circuit arrangements invariably requires a series of electronic rectifiers, filament sources, and capacitors, all of which constitute a formidable technical difficulty.[13]

Compressed-Gas Insulation

The use of gases at high pressure is now an essential feature of compact electro-

static accelerators. By the principle of similarity, a k-fold increase in the dielectric strength of the gas surrounding an electrode system permits a k-fold reduction of all of its physical dimensions without changing its voltage-insulating ability. In the limit the volume occupied by high-voltage electrostatic apparatus varies inversely as the cube of the dielectric strength of its gaseous insulation. These considerations have encouraged research in the field of compressed-gas dielectrics and have led to the use both of progressively higher pressures and of electronegative gas molecules for the insulation of high-voltage devices.

Figure 5 shows the relative dielectric strength of such dissimilar gases as helium, nitrogen, carbon dioxide, and sulfur hexafluoride over a pressure range from 1 to 80 atmospheres and with total applied voltages up to 1,200,000. The gaseous gradients can be observed to be substantially higher than those permitted by typical solid and liquid materials. The curves show the value of electronegative molecules containing oxygen and fluorine in extracting energy from free electrons in the gap and in converting these prolific ionizing agents into innocuous negative ions by attachment. These characteristics of electronegative gases have been recognized in principle since the investigations of Natterer, Paschen, and others at the end of the last century.[14] Two gases, Freon 12 (CCl_2F_2) and sulfur hexafluoride (SF_6), have now emerged as the most practical gases of this character. Both have nearly three times the dielectric strength of nitrogen at the same pressure in a uniform field. At room temperature Freon 12 saturates at about 5 atmospheres of pressure, while sulfur hexafluoride allows over 30 atmospheres. Both show high chemical stability, but dissociate under the influence of corona and sparkover.[15]

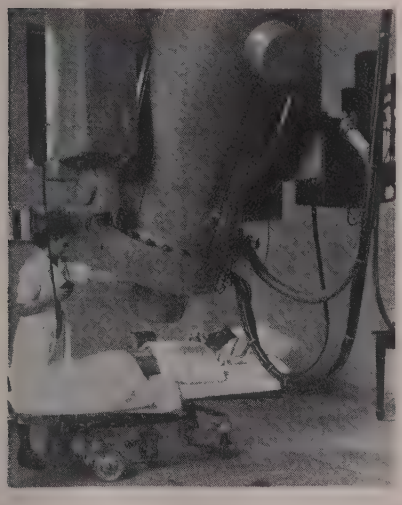

Figure 6. A 2,000,000-volt, 250-microampere Van de Graaff X-ray source used for deep tumor therapy at the Sheffield National Centre for Radiotherapy in England. The X-ray output of this instrument is equivalent to that from 5,000 grams of radium

2,000,000-Volt Electrostatic Accelerators

A powerful source of ionizing radiation which has attained compactness and simplicity through the use of compressed gaseous dielectrics and good electrostatic design is the 2,000,000-volt Van de Graaff accelerator manufactured by the High Voltage Engineering Corporation. This instrument in various forms is used for the production of X rays for medical therapy and industrial radiography, of streams of electrons for biological studies and the sterilization of materials, or of positive ions for nuclear research, Figure 6. Its high-voltage terminal is a hemispherical stainless steel shell 15 inches in diameter, supported on an insulating column of 33-inch active length. This column is built up of metallic equipotential planes separated by glass insulators, and the terminal voltage is divided uniformly along the column by means of high resistors. The charge-conveyor belt is 6 inches wide of multi-ply rubber fabric and travels about 4,000 feet per minute. The acceleration tube also is mounted within the column adjacent to the belt and is likewise divided into over 40 sections by aluminum diaphragms, each of which acquires its proper potential by direct connection to the column. The target end of the acceleration tube extends through the base plate of the pressure tank and terminates in a water-cooled gold target for the production of X rays or an aluminum window when high-energy cathode rays are desired. The entire electrostatic source and acceleration tube is contained within a grounded steel tank 36 inches in diameter and less than 6 feet in over-all length filled with a mixture of nitrogen and carbon dioxide at 27 atmospheres of pressure, see Figure 7.

Since the efficiency of X-ray production is low, maximum output ionizing power from an electrostatic accelerator is realized when the high-energy electrons are permitted to emerge into the atmosphere for direct use as cathode rays. In this case the output power is equal simply to the product of electron current and voltage and is 500 watts in the cited example. The total power input is 2,500 watts, and the over-all efficiency is 20 per cent, a figure higher than that attainable by any other method. Most of the input power is used in overcoming the windage arising from the motion of the belt through the compressed gases. Lesser amounts go into belt flexure, pulley bearing losses, column resistor current, and corona spray power.

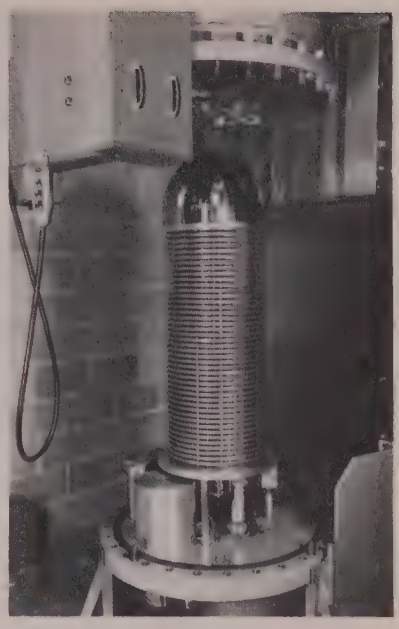

Figure 7. A 2,000,000-volt electrostatic generator with tank removed, showing high-voltage terminal and 33-inch long insulating column

Five hundred watts of electron energy at 2,000,000 volts is capable of profound biological and photochemical activity. This amount of ionizing energy can deliver 1,000,000 rep to over 300 pounds of material per hour and is capable of sterilizing production amounts of pharmaceutical materials on an economic basis. When the electron energy is converted into penetrating X rays by impinging upon a target of high atomic number, even though the efficiency of conversion is only slightly more than 5 per cent at this voltage, the subsequent electromagnetic emission in the continuing X-ray beam corresponds to that of over 5,000 grams of radium.

12,000,000-Volt Positive-Ion Accelerator

The highest-energy apparatus so far attempted by the electrostatic method are the 12,000,000-volt positive-ion accelerators now under construction at the Massachusetts Institute of Technology and Los Alamos. The Massachusetts Institute of Technology unit, which is illustrated in Figure 8, is to be housed in a vertical steel

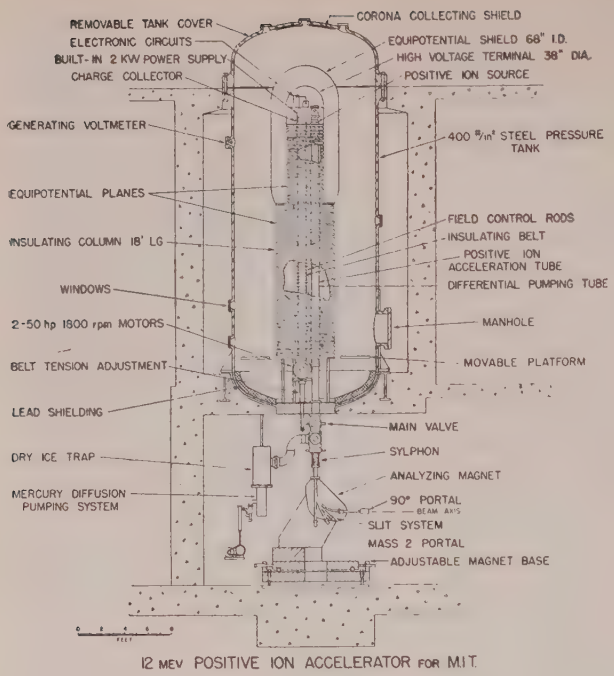

Figure 8. Diagram of 12,000,000-volt electrostatic accelerator now nearing completion at the Massachusetts Institute of Technology. Insulated in compressed nitrogen and carbon dioxide at 27 atmospheres, this accelerator is to produce positive ions or electrons at any selected energy in the range from 2,000,000 volts to maximum with homogeneity of 0.1 per cent. The inside dimensions of the gas-pressure tank are 12 feet diameter and 32 feet high

tank 12 feet in diameter and 32-feet high designed for gas pressures up to 27 atmospheres. The tank is mounted within a concrete silo which forms a part of the special laboratory building, an important feature of which is the large radiation room 40 feet by 60 feet by 16 feet surrounded by 2-foot-thick concrete walls.

The terminal of this electrostatic accelerator is 38 inches in diameter mounted on an insulating column 18 feet high. A 20-inch-wide belt traveling 3,600 feet per minute will supply over 1 milliampere of current to the terminal when required. There are two parallel acceleration tubes within the column, one provided with a positive-ion source in the form of a low-voltage hydrogen arc and the other with an electron source consisting of a spiral tungsten filament. In addition to protons, deuterons, and alpha particles, the accelerator is thus available also as a source of high-energy electrons, X rays, and, through the intermediate process of bombarding light elements, of neutrons.

At a position between the high-voltage terminal and the grounded steel tank an equipotential shield of stainless steel is provided. This shield is mounted on the insulating column at a region one third its total length from the terminal and therefore would be maintained at 8,000,000 volts for the maximum terminal voltage of 12,000,000. The effect of such an equipotential shield is to redistribute the electric field intensity in the air gap between terminal and tank and thus permit the attainment of higher total voltages. The Los Alamos design has many interesting points of difference when compared with that of the Massachusetts Institute of Technology, an important one being the use of five such intermediate equipotential shields arranged for a nearly uniform gradient from terminal to tank.

Future Trends

During the past decade the Van de Graaff electrostatic accelerator, developed initially for precision nuclear research, has proved itself a generic source of high-energy particles meeting the requirements of biologic and physical science, as well as such applications as supervoltage X-ray therapy, the electron sterilization of pharmaceuticals and foods, and X-ray radiography. Important engineering improvements are in progress directed toward increasing the operating voltage, current capacity, and compactness of this electrostatic instrument. Electronegative gases will undoubtedly find an important place in units designed for extreme compactness. The elimination of corona-charging and charge-removing processes in favor of conduction charging of the belt is receiving attention, particularly since this avoids the fundamental conflict of a superior gaseous dielectric which must still at certain points be capable of good conductivity through ionization. Fundamental and engineering studies of the factors upon which depend the voltage-insulating ability of high vacuum are most essential since the capabilities of the acceleration tubes are still the primary design limitation in modern Van de Graaff accelerators. Electronic voltage stabilization now practiced at most research institutions will probably become standard equipment on therapy and radiographic units. In particular, for the sterilization of large amounts of material, attention will be given to the attainment of the maximum charge-conveying capacity of the belt surfaces.

References

1. Electrostatic Production of High Voltages for Nuclear Investigations, **R. J. Van de Graaff, K. T. Compton, L. C. Van Atta.** *Physical Review* (New York, N. Y.), volume 43, 1933, pages 149–57.

2. The Efficient Irradiation of Deep Tumors, **J. G. Trump, C. R. Moster, R. W. Cloud.** *American Journal of Roentgenology and Radium Therapy* (Springfield, Ill.), volume 57, 1947, pages 703–10.

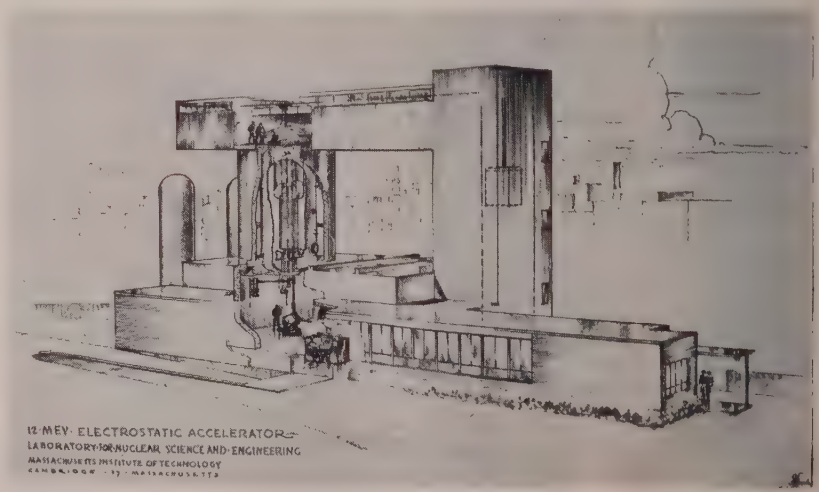
12-MEV ELECTROSTATIC ACCELERATOR
LABORATORY FOR NUCLEAR SCIENCE AND ENGINEERING
MASSACHUSETTS INSTITUTE OF TECHNOLOGY

Figure 9. Electrostatic accelerator laboratory for the Massachusetts Institute of Technology, 12,000,000 volts

3. Two Million Volt X-Ray Therapy Using Rotation, **J. G. Trump, W. W. Evans, H. F. Hare, S. W. Lippincott, Jr.** *American Journal of Roentgenology and Radium Therapy* (Springfield, Ill.), 1951.

4. New Million Volt X-Ray Outfit, **E. E. Charlton, W. F. Westendorp, L. E. Dempster.** *Journal of Applied Physics* (New York, N. Y.), volume 10, 1939, page 374.

5. The Betatron, **D. W. Kerst.** *Radiology* (Syracuse, N. Y.), volume 40, 1943, pages 115–19.

6. Linear Accelerators, **D. W. Fry, W. Walkinshaw.** *Report on Progress in Physics* (Great Britain), volume 12, 1949, pages 102–32.

7. An Investigation of Radiography in the Range from 0.5 to 2.5 Million Volts, **W. W. Buechner, R. J. Van de Graaff, H. Feshbach, E. A. Burrill, A. Sperduto, L. R. McIntosh.** *Bulletin No. 155*, American Society for Testing Materials (Philadelphia, Pa.), December 1948, pages 54–64.

8. Irradiation of Biological Materials by High Energy Roentgen Rays and Cathode Rays, **J. G. Trump, R. J. Van de Graaff.** *Journal of Applied Physics* (New York, N. Y.), volume 19, 1948, pages 599–604.

9. Relationships between Chemical and Biological Effects of Ionizing Radiations, **Raymond Zirkle.** *Radiology* (Syracuse, N. Y.), volume 52, 1949, pages 846–55.

10. Biological and Photo-Chemical Effects of High Energy Electrostatically Produced Roentgen Rays and Cathode Rays, **C. G. Dunn, W. L. Campbell, H. Fram, A. Hutchins.** *Journal of Applied Physics*, (New York, N. Y.), volume 19, 1948, pages 605–16.

11. Electrostatic Generators for the Acceleration of Charged Particles, **R. J. Van de Graaff, J. G. Trump, W. W. Buechner.** *Report on Progress in Physics* (Great Britain), volume 11, 1948, pages 1–18.

12. The Insulation of High Voltages in Vacuum, **J. G. Trump, R. J. Van de Graaff.** *Journal of Applied Physics* (New York, N. Y.), volume 18, 1947, pages 327–32.

13. Standard Handbook for Electrical Engineers (book), **A. E. Knowlton.** McGraw-Hill Book Company, (New York, N. Y.), 8th Edition, 1949, pages 2255–57.

14. D-C Breakdown Strength of Air and of Freon in a Uniform Field at High Pressures, **J. C. Trump, F. J. Safford, R. W. Cloud.** *Electrical Engineering (AIEE Transactions)*, volume 60, March 1941, pages 132–35.

15. Effect of High Voltage Electrical Discharges on Sulfur Hexafluoride, **W. C. Schumb, J. G. Trump, and G. L. Priest.** *Industrial and Engineering Chemistry* (Easton, Pa.), volume 41, 1949, pages 1348–51.

No Discussion

Distribution of Charge in Electrostatic Mineral Separation

FOSTER FRAAS
NONMEMBER AIEE

OLIVER C. RALSTON
NONMEMBER AIEE

CONTRARY to common impressions, there is no one single electrostatic separation process, but there are a number which differ very fundamentally from each other, except that they are carried on in a field between two charged electrodes. One series of them depends on differences in conductance of particles in a mixture, the difference in conductance commonly being important in determining which kind of particles take up the most charge, though the differences in conductance are utilized in other ways. A second series of them depends on the frictional electricity generated when unlike solid surfaces are rubbed together as a means of charging, and in this case at least one must be a poor conductor. This series of processes is handicapped by the necessity of working in atmospheres of relatively low humidity. Other processes depend entirely on differences in dielectric constant of the particles in a mixture. Inductive charging also is known, but the primary phenomenon is formation of dipoles (charged positively on one end and negatively on the other) followed by leakage of some of the charge on the end with the sharpest points or edges, leaving the particle with the excess of electricity of the opposite charge to that which leaked.

This paper deals with the simplest and commonest type of electrostatic separator that has been used in the past, one with a "pure" electrostatic field with negligible leakage between the electrodes. The electrodes are a pair of horizontal cylinders, spaced several inches apart, and one of them "A," Figure 1, rotates so that granular material fed onto its top-most portion will be carried between it and the other cylinder thus passing through an electrostatic field. The potentials commonly used are rarely more than 1/2 the spark over voltage. The electrode carrying the solid particles may be at earth potential. The other electrode may be either positively or negatively charged with respect to earth but is activated from a unidirectional source like rectified alternating current. Often 5,000 to 20,000 volts per inch of gap are used.

When the particles are carried into the electric field between "A" and "B", they acquire charges by a combination of induction and interfacial conduction (1). The amount of charge determines the distance S to which each particle is deflected.

Although all the particles may have the same weight and specific conductivity, the interfacial conduction (electrode "A" to particle), and consequently the deflection distance S is distributed over a range of values. The purpose of this paper is to determine the form of the distribution, the magnitude of the charges on particles, and of the electric work done. The literature is practically void of any measurements of the actual amount of charge on the particles that are of proper size to be effectively deflected by electrostatic forces. By means of data from two independent sources, the quantity of charge on the particles is shown to be distributed as a logarithmic function of the normal probability law. The electrical work done on the particles is shown to be very small.

Correlation of Data

Statistical data, unlike single measurements of high accuracy, must be correlated by some method, one of which is the graph.[2] The procedure in this paper is first to determine the type of distribution directly by charge measurement on a series of individual particles, and then to apply this type to the data derived from electrostatic separator operation. Although all the straight-line plots are not theoretically linear, they are linear within the accuracy of measurement. This is sufficient for determining the type of distribution and for calculating the electrostatic separator performance.

Nomenclature

a_c, a_E, g = centrifugal, electrical, and gravitational acceleration, cm./sec.^{2}
h = length of class interval
F = electric field intensity, statvolts/cm. (1 statvolt = 300 volts)
m = mass of particle, gram
Q = charge on particle, millistatcoulomb or arbitrary
Q_m = mean charge on particle, millistatcoulomb (1 coulomb = 3×10^9 statcoulombs)
v_n, v = nth interval component and resultant velocity, cm./sec.
S_n, S = nth interval component and electrode tangent distance, cm.
t = time—seconds
x = normal law variable
σ = standard deviation
α, θ = Figure 1—degrees

Measurement of Charge

Charges were measured as the particles from the grounded carrier electrode "A" fell through a Faraday cage, which was insulated from ground and connected to an *FP54* thermionic electrometer. The cage, electrometer and 10^5-megohm grid resistor were mounted in a grounded metal box placed close to "A" so that the time of fall through the cage would be long. The cage and grounded guard rings on each end of the cage were cylindrical tubes, 5 centimeters in diameter, with the cage 5 centimeters long and the rings 1.9

Paper 51-202, recommended by the AIEE Electronics Committee and approved by the AIEE Technical Program Committee for presentation at the AIEE Summer General Meeting, Toronto, Ont., Canada, June 25-29, 1951. Manuscript submitted October 2, 1950; made available for printing May 3, 1951.

FOSTER FRAAS is with the Bureau of Mines, College Park, Md., and OLIVER C. RALSTON is with the Bureau of Mines, Washington, D. C.

Acknowledgment is given to P. M. AMBROSE, Chief of the College Park Station, and to F. D. Lamb, in charge of the mineral-dressing unit, for administrative guidance.

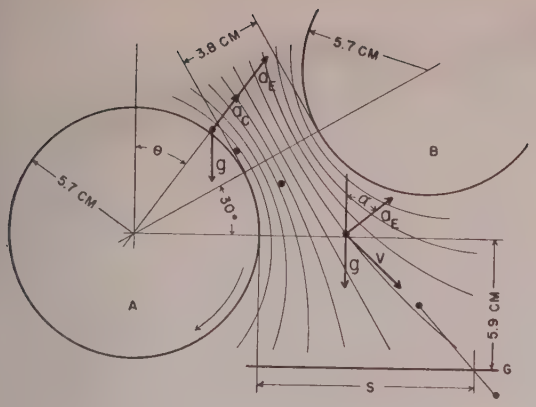

Figure 1 (left). Diagram of separator and particle trajectory

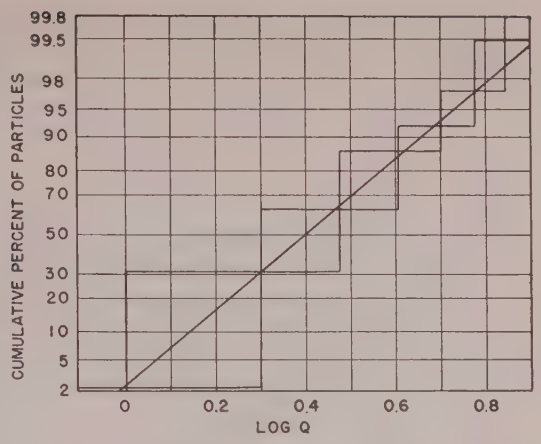

Figure 2 (right). Charge measurement data with cumulative per cent on a probability scale

centimeters long. Electrodes "A" and "B", Figure 1, were of the small diameter of 3.5 centimeters with a 2.6-centimeter gap between them. Electrode "A" was grounded, and electrode "B" was charged negatively to 48 statvolts, (14,400 volts).

The galvanometer and shunt in the electrometer circuit[3] were replaced by the input leads of a Brush *BL-913* amplifier. Differences in ground potential levels were compensated by connecting the amplifier frame to ground through a potentiometer and battery. A vibrating V-shaped feed trough permitted the delivery of one particle at a time over electrode "A." The response for each particle as it fell through the cage was recorded with a Brush *BL-201* recorder, and the particles were thus counted in groups classified according to the deflection on the recorder. The deflection is proportional to the charge Q. Kapteyn and Van Uven, in reference 4, assert that all attributes of growth are distributed according to the normal probability law, either linearly or as some other function.

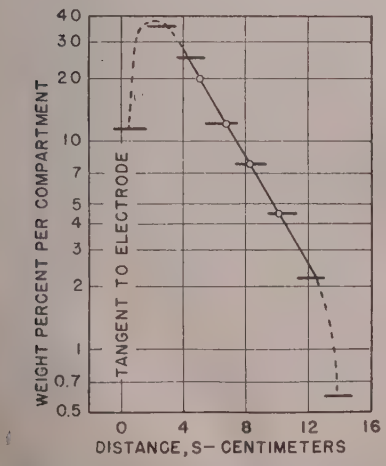

Figure 3. Semilogarithmic plot of deflection data, S

A test for a normal distribution is to plot the data on probability cross section paper with different functions of the attribute. Figure 2 summarizes the counting results with galena particles having a size range so that they passed through a 2.36-millimeter opening screen and were retained on a 1.65-millimeter opening screen. The particles varied in weight from approximately 35 to 100 milligrams each. The rectangles represent a range in percentage for each range in attribute. The unit for Q is arbitrary. In contrast to the curved plot of the linear function, the logarithmic function yields a straight line, and the charges are accordingly distributed as a logarithmic function of the normal probability law. This might be expected, since the charge transferred through interfacial conduction is an exponential function of time.[1]

Graphical Relationship in Deflection Data

A common graphical relationship in electrostatic separation data[1] is the straight line formed when the weight of particles deflected to various horizontal distances during a constant vertical drop is plotted on a logarithmic scale versus the distance on a linear scale. The results with chromite beach sand are shown in Figure 3. The straight line is in the range, $4 < S < 12$. The horizontal lines represent the weight of particles collected in each compartment of a box placed so that the top edges of the compartments are in the horizontal plane G of Figure 1.

The same plot of the data on galena of Figure 2, with Q substituted for S, yields the same shape of curve having a straight line for that portion on the right side of the hump. This similarity indicates that S, the distance a particle is deflected, must be approximately a linear function of Q, the amount of charge on the particle.

Charge Versus Deflection Distance

The accelerations and velocity when a particle is just leaving the carrier electrode, and when it is in flight, are illustrated by the vectors in Figure 1. The string of dots defines the trajectory of an average particle. Because of the dependence on both a_E and α, a theoretical derivation of the expression relating Q and S would be complicated. A simplified procedure is to calculate and plot the trajectory in small time intervals, each plot supplying data for the succeeding calculation.

The horizontal distance from the initial position to the end of the nth interval is,

$$S_n = \int\int a dt^2 = \left[1/2 a_E t^2 \sin \alpha + v_{n-1} t + S_{n-1}\right]_{t=0}^{t=0.05}$$

These are calculated and plotted versus the values calculated from the corresponding equation for the vertical distances.

The initial value of a_E is known from the position of the particle as it leaves the roll, and the subsequent values are determined by the change in field intensity F.

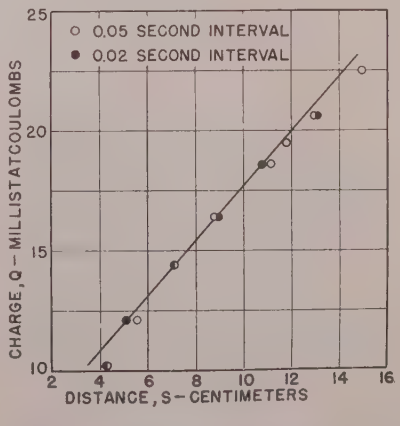

Figure 4. Summary of particle trajectory calculations

The term v_{n-1} is equal to the velocity at the end of the $(n-1)$ th interval.

The charge Q is calculated from the initial value of a_E by the equation,

$$Q=\frac{ma_E}{F}$$

Figure 4 summarizes the calculation for spherical particles having a density of 5 and a diameter of 0.05 centimeter (approximate properties of chromite). The electrode dimensions are those of Figure 1, with a rotation speed of 24 rpm for "A," and a potential of 64 statvolts (19,200 volts) between "A" and "B."

The trajectories for some values of Q were calculated in both 0.02- and 0.05-second intervals. The 0.02- and 0.05-second interval trajectories are superimposed, except for the last interval, when the last 0.05-second interval is unusually long. This is the cause of the deviations shown in Figure 4. A point half white and half black indicates no deviation. The straight line drawn through the 0.02-second data in Figure 4 is therefore a good approximation of a zero interval or continuous trajectory and is represented by the equation,

$$Q=1.15S+6.25 \qquad (1)$$

Q is in millistatcoulombs. The linear range, $5<S<11$, is remarkably close to that of Figure 3.

The calculations were checked by equating for the horizontal component the summation of the electrical work in all the intervals to the final acquired kinetic energy. The actual work is very small and is equivalent to 0.09 watt-hours per ton of particles for the 7.1-centimeter horizontal deflection distance (vertical drop, 10 centimeters during 0.21 second time). This is a surprisingly low amount of energy to produce such a useful effect. A further check could be secured by photographing the particle trajectory.

Deflection Data and the Normal Law

Except for the radius of electrode "B," the dimensions and constants of Figure 1, including the 24-rpm speed, are those of the separator from which the data of Figure 3 were secured. The radius of electrode "B" was 2.5 centimeters. With "A" equal to "B," the plotting of the equipotential lines in the field is simplified.[5] With a compartmented box at ground potential at level G, the lines in this vicinity are distorted. However, the field here is weak and has little influence on the particle. These variations may have some influence on the constants and range of equation 1.

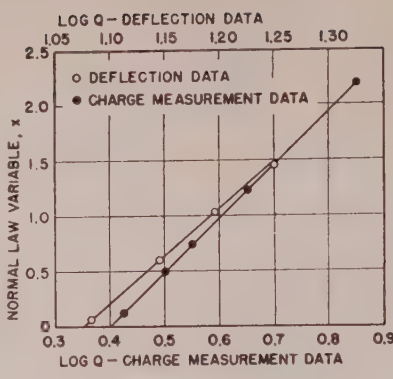

Figure 5. Graphical proof of normal law distribution

The data of Figure 3 are tested for normal law distribution by converting S to Q, and the cumulative percentages to the normal law variable x. The cumulative percentages are summed from the left of Figure 3 and represent the $\Sigma\phi(x)$ of the normal law equation,

$$\phi(x)=\frac{1}{\sqrt{2\pi}}\epsilon^{\frac{-x^2}{2}} \qquad (2)$$

The values for the integral of this equation are given in Table V in a book by T. C. Fry.[6] A plot of log Q, calculated from equation 1 versus x from Table V, is illustrated in the deflection data of Figure 5. Each point is derived from the data on chromite indicated as small circles in Figure 3. A plot also is shown for the charge measurement data. Both are straight lines.

The straight line is proof of a normal law distribution and is represented by the equation,

$$\sigma h=\frac{\log Q-\log Q_m}{x}$$

Q_m and σh are found from the $x=0$ intercept and the slope of the line. For the deflection data, $Q_m=11.9$ millistatcoulombs, and $\sigma h=0.117$. Either σ or h may be assigned arbitrary values, but with $\sigma=1$, as it is in equation 2, log Q must be plotted in class intervals of $h=0.117$. As a comparison to linear functions of the attribute, the constant, $\sigma g=$ antilog σ, is frequently adapted for logarithmic functions.[7] In Figure 3 the peak of the hump is not at Q_m because of the linear function of Q and the accumulation near $S=0$ of particles having a charge less than Q_m.

Although the data of Sun, Morgan, and Wesner[8] are complicated by adhesion of particles to the electrode, some of the straight-line plots which they obtain for particles of very low conductivity, such as fluorite, quartz, and calcite, would indicate that charges generated by the frictional electrical effect also are distributed as a logarithmic function of the normal law.

References

1. Conductance Electrostatic Separation, **F. Fraas.** *Transactions*, American Institute of Mining and Metallurgical Engineers (New York, N. Y.), volume 153, 1943, pages 576–87.

2. An Introduction to Modern Statistical Methods (book), **P. R. Rider.** John Wiley and Sons, Inc., New York, N. Y., 1939.

3. An Improved D-C Amplifying Circuit, **L. A. Du Bridge, H. Brown.** *Review Scientific Instruments* (New York, N. Y.), volume 4, 1933, pages 532–36.

4. Mathematical Methods of Frequency Analysis of Size of Particles, **R. P. Loveland, A. P. H. Trivelli.** *Journal*, Franklin Institute (Philadelphia, Pa.), volume 204, 1927, pages 193–217.

5. Electric and Magnetic Fields (book), **S. S. Attwood.** John Wiley and Sons, Inc., New York, N. Y., 1941.

6. Probability and Its Engineering Uses (book), **T. C. Fry.** D. Van Nostrand Co., Inc., New York, N. Y., 1928.

7. Statistical Description of the Size Properties of Non-Uniform Particulate Substances, **L. Hatch, S. Choate.** *Journal*, Franklin Institute (Philadelphia, Pa.), volume 206, 1929, pages 369–87.

8. Mineral Particles in Electrostatic Separation, **S. C. Sun, J. D. Morgan, R. F. Wesner.** *Transactions*, American Institute of Mining and Metallurgical Engineers (New York, N. Y.), volume 187, 1950, pages 369–73.

No Discussion

The Torsional Damper for Conductors—Service Experience and Further Experimental Work

T. J. BURGESS
MEMBER AIEE

A. D. HOGG
NONMEMBER AIEE

Synopsis: Careful inspection of ACSR (steel-reinforced aluminum cable) conductors operating for ten years equipped with torsional dampers has shown no apparent damage due to aeolian vibration. Type HH copper conductor without dampers has been operating for a similar period without trouble. Further experimental work indicates that there is little tendency for ACSR conductors to vibrate at tensions less than 8 per cent of their ultimate strength.

PRIOR to 1928 the design of the transmission lines of The Hydro-Electric Power Commission of Ontario, Canada, together with the span lengths and tensions used, were such that aeolian vibration was not a serious problem. Subsequently, when longer spans and higher tensions came into greater use, the destructive nature of this vibration was recognized and a program of investigations initiated which lead to the development of the Tebo and Buchanan* torsional damper. The development of this damper, together with considerable related information, has been covered in previous papers by Tebo[1] and Speight.[2]

As an indication of the trend in conductor protection, it may be worthy of note to contrast certain of the changes in high-tension line design between two active periods of the Commission's 220-kv single-circuit construction, that is 1928–30 and 1948–50. Average spans increased from 1,000 feet to 1,100–1,150 feet and 60-degree tension increased from about 11 to 19 per cent. Damping devices changed from armour rods and parallel cable dampers to torsional dampers.

Further Experimental Work

Since the preparation of the Tebo[1] and Speight[2] papers, experimental work has been devoted to the proportioning of torsional dampers for the various sizes of conductors in common use on the Commission's transmission lines, and somewhat to other aspects of conductor vibration and damping. One of the latter which may have a measure of general interest dealt with the relation between conductor tension and vibration characteristics.

Effect of Conductor Tension on Vibration

The tests to investigate this relationship were all made using ACSR conductors. The conductor sizes, span lengths and tensions used, as well as the test dates are given in Table I. It will be noted that each test covered a period of at least three weeks. Figure 1 shows the rocking-type clamp used for the tests. All clamps were the same and fitted the 605,000-circular-mil ACSR (duck) conductor. For the smaller conductors, suitable filler pieces were used. Throughout the tests, records were taken on a 477,000-circular-mil conductor kept substantially at constant tension. This was done to check on the suitability of wind conditions for vibration during each phase of the tests. The vibration records were obtained using the equipment previously described by Tebo,[1] and gave a measure of the deflection relative to the clamp of a point on the conductor $3^1/_2$ inches from the last point of contact between the conductor and the mouth of the clamp.

There are several ways in which the data obtained have been plotted, but it is felt that the co-ordinates shown for Figures 2 and 3 best serve the present purposes. In Figure 2 the maximum deflection in mils for all the conductors is plotted against conductor tension expressed as a percentage of the ultimate strength. The data are insufficient to define the curve completely, but it is seen that with increasing tension the maximum deflection rises rapidly from zero at some tension around 8 per cent to a maximum at around 15 per cent after which it remains substantially unchanged with further increases in tension. The extrapolation to obtain the tension for no vibration may be subject to question. However, the presentation of the data in Figure 3 strongly supports the figure of 8 per cent. In this figure the megacycles of vibration per day are plotted against tension for several deflections covering the range which occurs. Though there is a moderate amount of scatter in the test points, the graphs are rather well defined and when extrapolated meet the axis of zero cycles of vibration at a tension be-

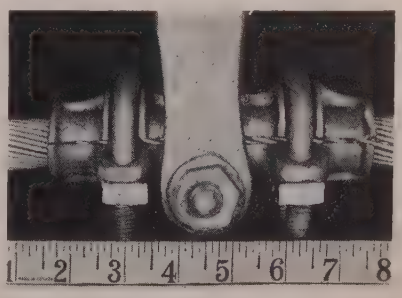

Figure 1. Suspension clamp on 605,000 circular-mil ACSR conductor

Paper 51-205, recommended by the AIEE Transmission and Distribution Committee and approved by the AIEE Technical Program Committee for presentation at the AIEE Summer General Meeting, Toronto, Ont., Canada, June 25–29, 1951. Manuscript submitted March 30, 1951; made available for printing May 1, 1951.

T. J. BURGESS and A. D. HOGG are with The Hydro-Electric Power Commission of Ontario, Toronto, Ont., Canada.

*G. B. Tebo and W. B. Buchanan are with the Electrical Research Department of The Hydro Electric Power Commission of Ontario.

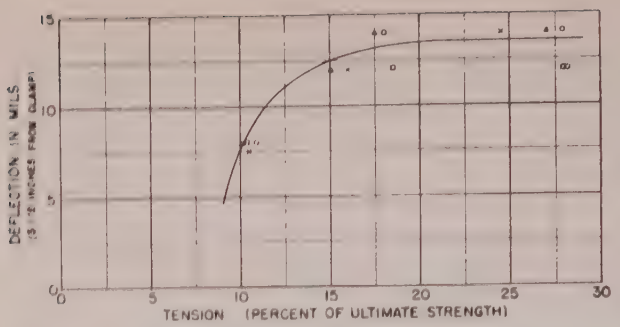

Figure 2 (above). Conductor vibration. Relation between tension and deflection

○ = 336,400 circular mils; 650/644-foot spans
△ = 336,400 circular mils (oriole); 880/1,050-foot spans below 20 per cent, 1,400/1,050-foot spans above 20 per cent
× = 605,000 circular mils (duck) same as △
□ = 3/0 (pigeon); 650/644 foot spans

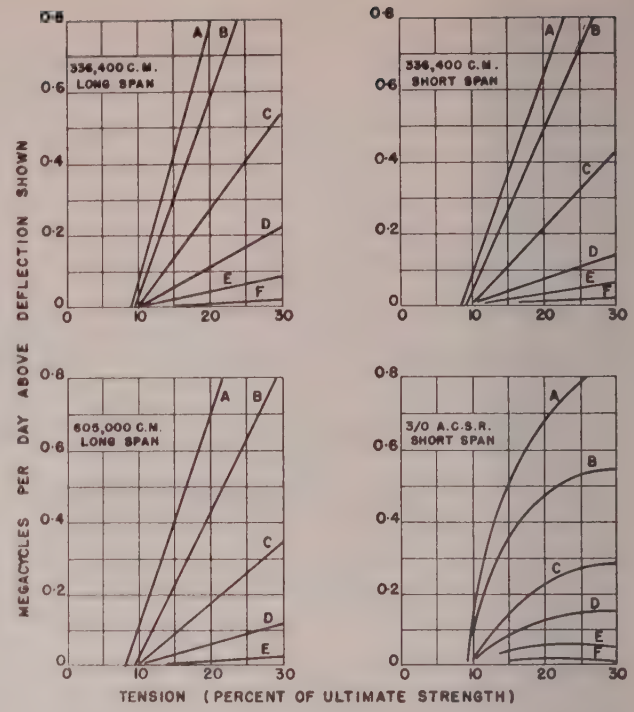
336,400 C.M. LONG SPAN
336,400 C.M. SHORT SPAN
605,000 C.M. LONG SPAN
3/0 A.C.S.R. SHORT SPAN
MEGACYCLES PER DAY ABOVE DEFLECTION SHOWN
TENSION (PERCENT OF ULTIMATE STRENGTH)

Figure 3 (right). Conductor vibration. Relation between megacycles per day and tension

Curve A = 0.001 inch, Curve B = 0.002 inch, Curve C = 0.004 inch, Curve D = 0.006 inch, Curve E = 0.008 inch, Curve F = 0.010 inch

tween 8 and 10 per cent of the ultimate strength.

Summarizing the results of these tests it appears that:

1. There is little tendency to vibrate below a tension of about 8 per cent of the ultimate strength. As the tension increases above this, the maximum deflection or bending at the clamp due to vibration increases rapidly up to 15 per cent tension, after which the maximum deflection remains substantially constant.

2. The number of cycles of vibration per day above any given deflection increases almost linearly with tension.

3. The span length does not seem to be a major factor in vibration. This is at variance with some previous data reported by Tebo.[1]

Vibration Characteristics of Type HH Copper Conductor

In view of some recently reported troubles with type HH copper conductor, the results of our investigations of this conductor may be of interest to some. These dealt with a 500,000-circular-mil conductor for spans of 880 feet and a 60-degree tension of 20 per cent. Tests showed that the fatigue limit of the conductor at this tension corresponded to a deflection of 0.020 inch measured 3.5 inches from the clamp. Field measurement on the naturally vibrating cable gave a maximum deflection of about one-third this value, and also showed that the vibration was very easily damped. A rigid-type torsional damper, shown in Figure 4, was developed for this conductor. This had a weight of 12.4 pounds and a moment of inertia about the conductor of 155 pounds inches squared. One of these dampers was to be used for each span, mounted at alternate towers. Except for a small installation for checking their performance, these dampers have, owing to the relative safety of the undamped conductor, never been used. The trial installation was allowed to remain on the line.

In connection with the rigid torsional damper, it should be understood that it is entirely different and much less effective than the torsional damper as used on the steel-reinforced aluminum conductors. The latter, an example of which is shown in Figure 5, has the dumbbell part attached to the arm through rubber washers. With this arrangement, energy absorption takes place both in these washers and in the conductor, while the rigid damper provides for energy absorption in the conductor only.

Inspection of Field Installations

Torsional Dampers on ACSR Lines

The torsional-type damper has been in service on the Commission's high-tension circuits since 1940. Since then our practice on new high-tension lines has been to omit armour rods and use dampers exclusively to prevent damage by aeolian vibration. Dampers are installed, two per span, one each side of the suspension clamp. The mounting distance is 6 feet for the 795,000-circular-mil ACSR conductor and less for smaller conductors. Completed experimental work covered spans up to 1,200 feet only. An increased number of dampers have been arbitrarily

Table I. Summary of Conditions for Tests on the Effect of Tension on Vibration

Conductor	Period of Test: 31/10/41–21/12/41 Tension Lbs.	Span Ft.	23/12/41–14/1/42 Tension Lbs.	Span Ft.	16/1/42–7/3/42 Tension Lbs.	Span Ft.	9/3/42–30/3/42 Tension Lbs.	Span Ft.
3/0	695	650/644	1,230	650/644	1,180	650/644	1,860	650/644
	10.5%*		18.6%		17.8%		28.1%	
336,400	1,725	650/644	4,790	650/644	2,910	650/644	4,670	650/644
	10.2%		28.2%		17.1%		27.6%	
336,400	1,700	880/1,050	2,650	880/1,050	2,650	880/1,050	4,590	1,400/1,050
	10%		15.6%		15.6%		27%	
477,000	2,500	650/644	2,620	650/644	2,620	650/644	2,600	650/644
	13.3%		13.6%		13.6%		13.5%	
605,000	2,375	880/1,050	3,660	880/1,050	3,660	880/1,050	5,460	1,400/1,050
	10.6%		16.3%		16.3%		24.4%	

*Per cent of the ultimate strength.

Note: The length of span on each side of the test tower is given; the recorder is mounted in the span underlined.

Table II

Type of Damper	Towers	Dampers Opened	Condition of Conductors
Torsional	186	372 (7.5% of total)	No damage
Stockbridge	192	384 (3.5% of total)	No damage

used for spans over this length.

A recent inspection of our earliest damper installation (without armour rods) indicates excellent results. These dampers were installed 10 years ago on: a 110 kv line, 477,000-circular-mil ACSR, average span 1,000 feet, 60-degree tension 15.5 per cent and 103 miles in length; and a 220-kv line, 795,000-circular-mil ACSR, average span 1,150 feet, 60-degree tension 19 per cent and 271 miles in length.

Conductor and damper clamps were opened and the conductor carefully examined for wear or broken strands. Neither wear nor breaks were found, as indicated by the tabulation shown in Table II.

Inspection of HH Copper Conductor

An inspection was made recently of the suspension positions of a 500,000-circular-mil HH copper line, 42 miles in length. This is a double circuit, 220-kv line, average span 880 feet and 60-degree tension of 20 per cent. It has been in service for nine years and the spans are undamped. 876 suspension positions (80 per cent of total) were carefully inspected by opening up the suspension clamp and examining the conductor. No worn or broken segments were located that could be attributed to vibration.

Figure 4. Rigid torsional damper for type HH 500,000 circular-mil copper conductor

Figure 5. Torsional damper for 795,000 circular-mil conductor

Special Installation

As a trial attempt to control galloping conductors in a high-voltage long river span (2,200 feet) which had given trouble on three occasions, torsional dampers were installed, eight per span, per conductor. While no claims are made for this as a cure for galloping, it may be noteworthy that the span has been free of such trouble for approximately 4 years.

Steel Ground Wire

Torsional dampers similar to those in use on ACSR conductors have been designed for $^3/_8$ inch steel ground wire and placed in service on 880 foot spans, 60-degree tension 8.1 per cent. These have been in service 9 years without vibration trouble occurring on the ground wire of a double circuit 220-kv tower line. It is too soon to predict long term results but indications so far are satisfactory.

References

1. Measurement and Control of Conductor Vibration, **Gordon B. Tebo.** *AIEE Transactions*, volume 60, 1941, pages 1188-93.

2. The Theory of Torsional Dampers, **J. W. Speight.** *Electrical Engineering* (*AIEE Transactions*), volume 60, October 1941, pages 907-11

No Discussion

Inductive Co-ordination Aspects of D-C Systems Supplied by Rectifiers

AIEE COMMITTEE REPORT

Synopsis: This report is similar in many respects to the committee report on Inductive Co-ordination Aspects of Rectifier Installations, published in 1946,[1] with the important difference that the latter dealt solely with the a-c side. The present report, which deals with effects associated with d-c systems supplied by rectifiers, can be considered as complementing the 1946 report and material contained in the latter is not generally repeated here. To date, inductive co-ordination problems associated with the output side of rectifiers have involved chiefly d-c traction systems having a single overhead trolley per track (that is, ground-return systems) particularly those having nominal operating voltages of the order of 600 volts direct current. Hence, subsequent to Part II, which describes ways of classifying the d-c sides of proposed installations into three categories, the major part of the more detailed discussion and quantitative information in this report is devoted largely to the 600-volt system with overhead trolley. Summarized technical information, which will serve at least as background material and which will generally be useful in case the inductive co-ordination aspects of a specific rectifier installation require more or less detailed study and analysis also is included.

I. Basic Phenomena Concerned

THE BASIC principle of operation of power rectifiers is such that they produce harmonic voltages on the output side under all load conditions. These voltages will, in turn, cause harmonic currents to flow through the impedances of the d-c system to which the output is connected. In other words, these phenomena are an inherent characteristic of rectifiers, including rectifier equipment of present generally careful design and manufacture.

The magnitudes of the harmonic voltages on the d-c side of a rectifier are affected but little by changes in load impedance. This contrasts with the situation on the a-c side, on which the harmonic currents from a rectifier are usually almost independent of the impedance of the power supply system.

The output voltage of a 6-phase rectifier contains harmonic components having frequencies equal to 6, 12, 18, and so on, times the a-c power supply frequency. For example, when the a-c supply system frequency is 60 cycles, the frequencies of these harmonics on the d-c side are 360, 720, 1,080, 1,440 cycles, and so on. For a 12-phase rectifier, the 12th, 24th, ... harmonics of the supply system frequency are present on the output, and their magnitudes in per cent of the direct voltage are the same as for the corresponding harmonics in the output of a 6-phase rectifier having a corresponding type of transformer connection and impedance. Although the 6th, 18th, 30th, and other harmonics which are odd multiples of the 6th are theoretically zero for the 12-phase rectifier, they are, in practice, actually present in reduced amounts for various reasons such as the unequal division of load between the two groups of six phases composing the 12-phase system.

When phase control[2,4,12] is applied to a rectifier, the "orders" of the harmonics are not changed but considerable changes in their magnitudes (generally upward) can result, and increases of as much as 2 or 3 to 1 can be encountered in certain parts of the load range (Appendix II).

The significant effect of the d-c side from the inductive co-ordination standpoint is that the harmonic currents and voltages produced in the d-c system by the rectifier set up, respectively, magnetic and electric fields of corresponding frequencies about the conductors of that system. These inductive fields will induce voltages of the same frequencies in paralleling telephone circuits which can cause noise in these circuits.

The harmonic currents in the d-c system supplied by a rectifier are a function of the corresponding harmonic voltages in the rectifier, the impedance of the d-c system at the respective harmonic frequencies, the amount of phase control (if used); and, to some extent, the internal impedance of the rectifier unit itself, including the impedance of the rectifier transformer.

The over-all influence of a given balanced or ground-return current is measured by its I·T product while the over-all influence of a given balanced or residual voltage is measured by its KV·T product.

In this report the terms I·T product and voltage TIF are used freely. It may be noted here that I·T product is a measure of the over-all noise influence of a current, including fundamental and harmonics, while voltage TIF (telephone influence factor) is a similar measure for a voltage of known rms value.[27,29]

If the d-c system supplied by the rectifier is well-balanced as, for example, a full-metallic 2-wire d-c system without any grounds, the harmonics start out as balanced components, that is, the currents in the two conductors are equal and opposite, as are the phase-to-ground voltages, and these currents and voltages will remain substantially balanced. This condition can be closely attained on fairly short full-metallic d-c systems.

If the 2-wire d-c system just men-

Paper 51-206, recommended by the AIEE Electronic Power Converters Committee and approved by the AIEE Technical Program Committee for presentation at the AIEE Summer General Meeting, Toronto, Ont., Canada, June 25–29, 1951.

Manuscript submitted April 24, 1951; made available for printing April 30, 1951.

This report was prepared by the AIEE Working Group on Report of Inductive Co-ordination Aspects of D-C Systems Supplied by Rectifiers.

Personnel of the AIEE Working Group on Report of Inductive Co-ordination Aspects of D-C Systems Supplied by Rectifiers; W. E. Bloecker, *Chairman*, J. B. Donnelly, L. E. Dye, C. W. Frick, P. A. Jeanne, R. E. Leonard, W. K. MacAdam, G. W. McCracken, F. A. Overstreet, C. K. Poarch, T. H. Reid, R. E. L. Shirley, S. L. Smith, H. Winograd, R. L. Witzke.

Table I. General Classification of Rectifier Installations— D-C Side

Type of Rectifier Installation	General Characteristics of D-C Side, and So Forth	Category—D-C Side*
1. Rectifier for radio transmitting station	D-c system confined to station itself, with little probability of exposures involving d-c side and commercial telephone circuits.	Category A.
2. Rectifiers for electrochemical processes	Such rectifiers often of considerable size. May have more than 12 phases. D-c system of such an installation confined to a single plant. Little consequent possibility of d-c exposure to commercial telephone circuits (except, perhaps, for small number local telephone circuits located in, or close to the plant). Relocation of a few local pairs, in the chemical plant itself, or other nonextensive co-ordinative measures, may be needed in occasional case.	Category A, except as noted in "Characteristics" column at immediate left.
3. Rectifiers for general industrial service	Will usually have a d-c system which is either confined to a single building or to a plant area of limited extent, with not much probability of important exposures involving the d-c system with wire communications facilities (except, perhaps, within or adjacent to the industrial plant itself). Can generally be considered as in Category A. Possible exception to this classification may be presented by a 2 or 3-wire d-c power distribution system having one of the power conductors multigrounded (which would thus be Category B).	Category A, except as noted in "Characteristics" column at immediate left.
4. Electronic frequency changer	In the two present installations in this country, the d-c link in the electronic frequency changer is very limited in extent. For such installations, having little if any chance of exposure to d-c system—Category A. If the d-c link were fairly long or extensive (with consequent probability of exposure), the link would be—or considered to be—of the nature of d-c transmission and special study would be required. (Item 5.)	Category A, except as noted in "Characteristics" column at left.
5. D-C transmission system	Not beyond the experimental stage in this country but would require study and careful consideration from the inductive co-ordination standpoint. Not treated in further detail herein and not active now.	Special study.
6. Rectifiers for "trolley-coach" systems	(a) If normally operated with one side of the d-c circuit grounded directly at not more than one point, with the positive and negative trolleys carried close together, the positive and negative feeders likewise carried reasonably close together and with no individual feeder located in a position which is widely separated (as, for example, across the street) from that of its opposite-polarity "mate."	Category B.
	(b) If normally operated with one side of the d-c system normally grounded directly at more than one point, or if the positive and negative feeders are not carried close together on their common supporting structure or if, for example, a positive feeder or its corresponding negative "return" feeder were moved (or assigned) to a location across the highway from its opposite-polarity "mate."	Category C (likely). (Much like 600 volt d-c street railway with overhead trolley, Item 7, below.)
	(c) During period of conversion from single-track-per-trolley "ground-return" street railway system to 2-wire metallic system such as referred to in Item 6a.	Category C, if any exposure to speak of.
7. "600-volt" d-c street railway system, with single overhead trolley per track	D-c trolley network is essentially a ground-and-rail return system, apt to be almost entirely unbalanced. Harmonic currents in d-c system are largely ground-return. (See Part III of this Report.)	Category C, if any exposure to speak of.
8. "Third-rail" traction systems		
A. From standpoint of exposures	Harmonic currents existing primarily in a relatively narrow metallic loop, with 3rd rail as one side and the two running rails of same track as the other. Such currents chiefly balanced in nature. With multi-track system, the additional rails provide some shielding.	Category B.
B. From standpoint of "ground-potential" effects at harmonic frequencies	With direct grounding of one side of d-c system at two or more points (as, for example, at rectifier substations), noise effects may arise occasionally from harmonic ground potentials in case telephone equipment having an apparatus ground is located in fairly close proximity (say within several hundred feet) to a point or points of such direct grounding of d-c system.	Category B.
9. Main line railroad electrification with overhead d-c trolley	Likely to involve rectifier units of 1,500–3,000 kw or higher ratings, with operation at direct voltages of 1,500–3,000 volts or more. Harmonic currents largely ground-return. Generally require inductive coordination with communication circuits of railway itself, as well as with the commercial telephone systems involved.	Category C, and requires special study, outside scope of this Report.

* Note particularly that any mention of specific categories in the various parts of this table applies solely to the d-c side of rectifiers. The classification of the a-c side should be carried out in accordance with the 1946 report.[1]

tioned were normally operated with one side of the circuit grounded at but a *single* point, the harmonic voltage of this unigrounded side would tend to approach the potential of the earth, and residual voltages at harmonic frequencies would exist. However, the harmonic currents through the loads and equipment connected between the two metallic sides of the circuit would tend to be essentially balanced.

On the other hand, it should be emphasized that if a 2-wire (+ and −) d-c system supplied by a rectifier is normally operated with grounds on one side of the circuit at more than one point, considerable amounts of harmonic currents can return through the ground, with a resulting relatively large increase in their possible inductive effects per harmonic ampere. Harmonic residual voltages also will exist under this condition.

The importance of such ground-return currents is illustrated by the fact that for roadway separations between the power and communication circuits the ratio of the effect of ground-return current to the effect of an equal magnitude of single-phase balanced current may range from about 10/1 to as much as 80 or 90/1. Similar ratios can be expected with joint-use separations. The corresponding range in the case of residual voltages is smaller, an average value being about 5/1.[30,31,32,38]

II. General Classification of D-C Systems

In so far as practicable, the present report describes ways of classifying the d-c sides of proposed installations into one of the following three categories:

Category A. Very *unlikely* to cause important induction problems.

Category B. Indeterminate.

Category C. Very *likely* to cause important induction problems.

The more important advantages of classifying the d-c side in this manner are substantially the same as those itemized, for the a-c side, in the 1946 report.[1]

In the present report, the three categories are designated as A, B, and C in order to distinguish the classification of the d-c side from the classifications, in accordance with the 1946 report, of the a-c side, which were designated by I, II, and III. An installation would thus be classified by a combined symbol. For example, if the a-c side of a specific rectifier installation were found to be in Category II and the d-c side in Category C, the combined classification would be IIC.

General methods of separating various types of rectifier d-c systems into categories are given in this part of the present

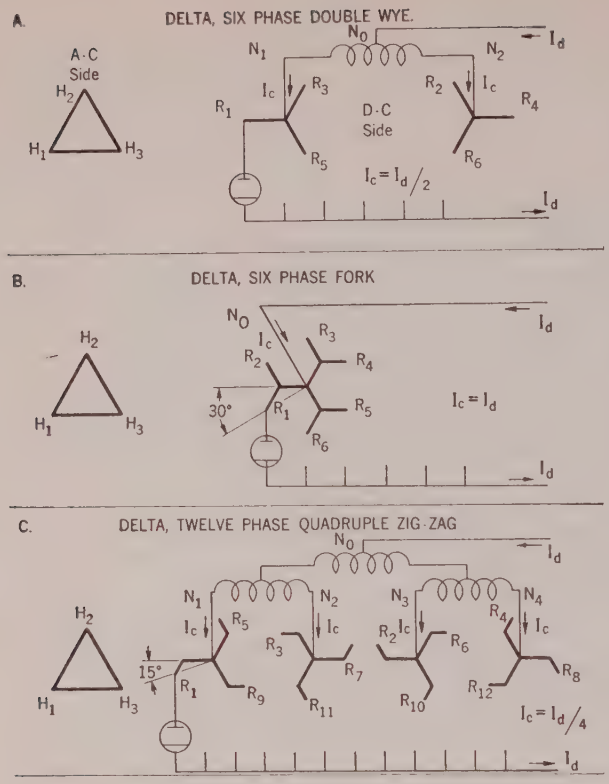

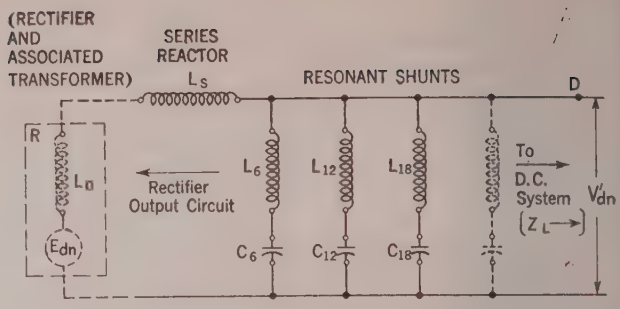

Figure 1 (left). Three rectifier circuits commonly used for 600-volt street railway installations

Figure 2 (above). Filter consisting of series reactor and resonant shunts

report. They are summarized particularly in Table I. By consulting this table first, many situations can be disposed of without going into detailed classification procedures.

In making use of Table I, reliable and adequate information concerning the specific type of d-c system to be supplied by the rectifier, as well as suitable exposure data, will be required.

In a detailed study concerned with the possible inductive effects from the d-c side of a proposed rectifier installation, it is necessary to have rather complete information on exposure conditions. For general classification purposes, however, it usually is sufficient to know the general type and extent of the exposures; for example, the type of d-c system, the extent to which its individual parts are or are likely to be involved in joint-use or other relatively close exposures to telephone open wire, or whether the d-c system will be confined to a single building or a very limited plant area, and so on.

If the rectifier installation is of such a type that any exposures will be confined to a single building or to a limited industrial plant area (possibly involving a very few exchange circuits at the most), a relatively simple sketch of the exposure conditions will usually suffice. On the other hand, if the type of installation is such as to involve communication circuits at joint-use separations or at locations across the highway or in other relatively close exposures with the d-c system, the relative locations of present or proposed telephone circuits with respect to the various parts of the d-c system should be set forth in much the same manner as that illustrated by the exposures shown for various a-c feeders on Figure 5(A) of the 1946 report. With intermeshed d-c networks, a suitable map of the exposures is often helpful.

Rectifier co-ordination problems involve complex phenomena. As a consequence, a few installations which appear to be in Category A may cause important problems. Conversely, a few installations which appear to be in Category C may turn out to be innocuous. Categories A and C have been set up so as to make them as definite as practicable, while Category B covers a wide range of intervening conditions. The chance of a particular case actually falling outside of its indicated category depends to a considerable extent upon its nearness to the "edge" of the range.

Certain additional factors may be considered qualitatively in estimating the likelihood of important induction problems for specific installations, particularly those in Category B. Some of these factors may be favorable and others unfavorable; for example, see the Discussion at the end of the section on Technical Information for Studies.

III. "600-Volt" Overhead Trolley D-C Traction Systems

By far the largest number of inductive co-ordination problems associated with the d-c side of rectifiers and commercial communication circuits, to date, has involved exposures between exchange telephone circuits and single-overhead-trolley-per-track traction systems (such as street railways) having nominal operating voltages of the order of 600 volts supplied by mercury-arc rectifiers.

Experience indicates that in practically all cases involving such 600-volt d-c street railway systems, magnetic induction is controlling and electric induction (Appendix I) can usually be neglected (except, possibly, for some exposures involving open wire telephone circuits).

Similar considerations would apply also in the case of other d-c traction systems of this general nature, including those operating at voltages other than 600 volts.

A. D-C Traction Systems Having Overhead Trolley with Track Return

The more usual 600-volt d-c street railway trolley network supplied by a rectifier is essentially a ground-and-rail return system which, electrically, is almost entirely unbalanced. This means that, with such a system, a large part of the output current usually returns by way of the earth. A given magnitude of harmonic current or voltage in the output circuit is, therefore, generally of considerably more importance from the

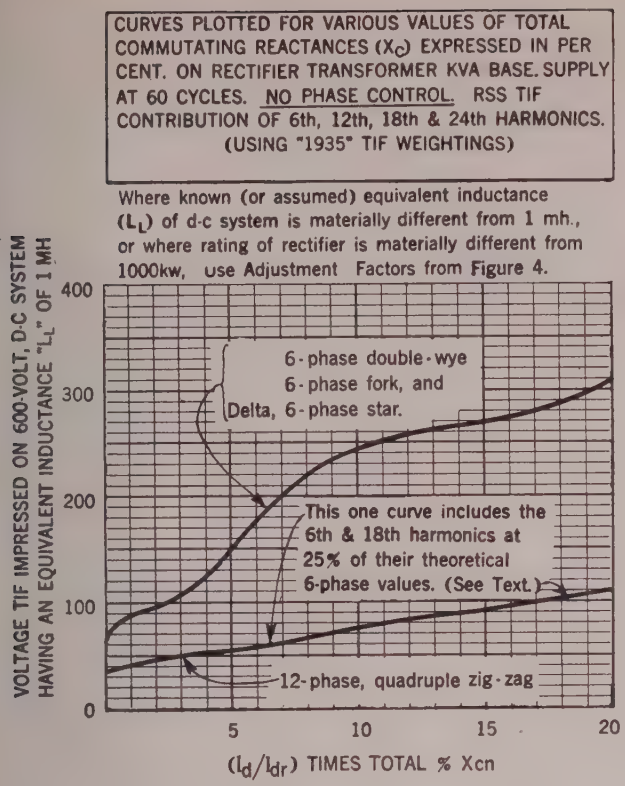
CURVES PLOTTED FOR VARIOUS VALUES OF TOTAL COMMUTATING REACTANCES (X_C) EXPRESSED IN PER CENT. ON RECTIFIER TRANSFORMER KVA BASE. SUPPLY AT 60 CYCLES. NO PHASE CONTROL. RSS TIF CONTRIBUTION OF 6th, 12th, 18th & 24th HARMONICS. (USING "1935" TIF WEIGHTINGS)
Where known (or assumed) equivalent inductance (L_L) of d-c system is materially different from 1 mh., or where rating of rectifier is materially different from 1000kw, use Adjustment Factors from Figure 4.
VOLTAGE TIF IMPRESSED ON 600-VOLT, D-C SYSTEM HAVING AN EQUIVALENT INDUCTANCE "L_L" OF 1 MH
400
300
200
100
0
6-phase double-wye
6-phase fork, and
Delta, 6-phase star.
This one curve includes the 6th & 18th harmonics at 25% of their theoretical 6-phase values. (See Text.)
12-phase, quadruple zig-zag
5
10
15
20
(I_d/I_{dr}) TIMES TOTAL % Xcn

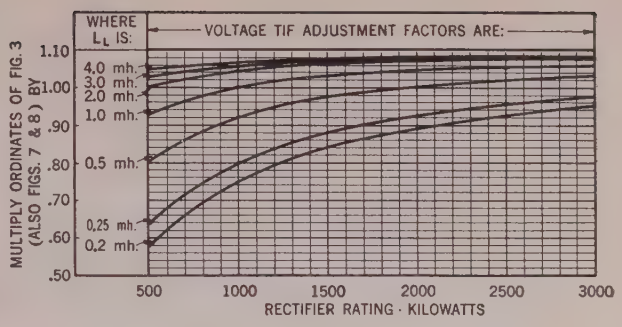

Figure 3 (left). Voltage TIF on d-c side of 600-volt rectifier versus product of (I_d/I_{dr}) times total equivalent per cent commutating reactance ($\%X_{cn}$). For rectifiers supplied by 60-cycle systems. No phase control

Figure 4 (above). Voltage TIF adjustment factors for Figures 3, 7, and 8, to take account of d-c system equivalent inductances (L_L) other than 1 millihenry and rectifier ratings other than 1,000 kw

standpoint of inductive co-ordination than an equal component of the same frequency in an essentially balanced circuit.

It also may be noted here that it has been found that in urban or suburban areas served by commercial telephone circuits, the water pipes, gas pipes or other underground metallic structures, power-circuit multigrounded neutral conductors, telephone cable sheaths and other metallic conductors may serve as return paths for harmonics from the trolley system. While mutual impedance tends to restrict such currents to paths adjacent to the route of the trolley, a part may flow along remote metallic return paths in which overhead conductors of the d-c system are not present. Under this latter condition, inductive effects similar in magnitude (per ampere of inducing current) to those of ground-return harmonic currents can be experienced on communication circuits which closely parallel the path, or paths, of such remote metallic return harmonic currents.

In the majority of exposures between commercial telephone circuits and single-trolley-per-track "600-volt" street railway systems in urban, or even in suburban areas, the telephone circuits are most apt to be in cable. With such cable exposures, electromagnetic induction usually predominates and the I·T product on the d-c trolley-feeders concerned is then of prime importance. The voltage TIF at the rectifier output does, of course, have a certain significance in that it is indicative of the potential ability of the rectifier-output harmonic voltages to produce harmonic currents in the trolley-feeders. In the occasional exposure involving open wire telephone circuits, electric induction from the output harmonic voltages can occur, but here again the predominating induction from such 600-volt trolley systems is generally magnetic.

From these considerations, it follows that with the usual 600-volt d-c traction system with overhead trolley and track return, the over-all inductive influence of each of the respective trolley-feeder circuits is usually controlled by its ground-return I·T. From the practical standpoint, the values of output I·T shown in Figure 5 for rectifiers operating without phase control, or the values of I·T when phase control is used (shown in Figures 9 and 10), are very much greater than the maximum value of I·T *per exposure* which might ordinarily be considered tolerable from the inductive co-ordination standpoint, so that most such d-c traction rectifier installations can be considered to be in Category C without much detailed study. For the "600-volt" street railway system, with track return, this is true even though the ground-return I·T per individual trolley-feeder can be assumed to be of the order of one-fifth of the total output I·T, as discussed later.

B. Trolley-Coach D-C Systems

Where a rectifier supplies a d-c trolley-coach system, output harmonics can likewise exist. If such a 2-wire system is normally operated according to Item 6a of Table I, that is, with one side of the propulsion circuit grounded directly at not more than one point, and so on, some residual harmonic voltages will exist, so that fairly small amounts of ground-return harmonic charging currents can flow. Nevertheless, the harmonic *currents* through the loads and equipment connected between the two metallic sides of the circuit will be essentially balanced in nature (with consequently lessened magnetic inductive effects).

However, if the d-c trolley-coach system is operated with one side multigrounded, as in Items 6b and 6c of Table I, substantial amounts of rectifier output harmonic currents may return through the ground and other grounded metallic structures, such as cable sheaths and various "remote metallic return" paths, referred to previously. Under these conditions a 600-volt d-c trolley-coach system tends to take on the characteristics of the 600-volt d-c street railway system with single overhead trolley, in so far as inductive effects are concerned, and then substantially the same technical considerations will apply. Hence, the two systems are not further differentiated in subsequent parts of this report.

C. Advance Study of Proposed Installation

Experience has demonstrated that the induction co-ordination aspects of a proposed rectifier installation can be handled best by close co-operation between the telephone company (or companies) and the railway company concerned.[37] This would include a joint study of the situation by the *engineering* representatives of the interested companies in the *early* planning stage of the proposed installation. It is helpful, also, to include some consideration of the future conditions which will exist as the d-c system and the telephone facilities may expand, or be rearranged, in addition to the conditions which will exist initially.

In such a study, it should be recognized that, as mentioned earlier, the production of harmonics is an inherent characteristic of a rectifier. Their frequencies are determined largely by the number of phases. The magnitudes of the harmonic vary with load and with the degree of phase control (if used). These harmonics are independent of the type or make of rectifier.

Through such an advance study, the probability and severity of an induction problem can be evaluated, and remedial measures which may be needed in the telephone plant or in the d-c system, either initially or in the near future, can be considered and planned. This might affect the selection of the number of rectifier phases (where there is a reasonable choice). When severe situations may be foreseen, precautions can be taken to provide at least some of the remedial measures in advance of the inception of normal operation of the rectifier.

If the need of filtering equipment should be indicated, space for such equipment can be provided in the installation plans even if such a filter is not installed initially. If filters are not included in the original equipment, advance arrangements might be made to obtain temporary filters without undue delay if a severe induction problem should develop. Such arrangements are particularly helpful in that they tend to prevent any prolonged adverse inductive reactions.

As a part of the engineering study, advance plans also can be made for suitable inductive co-ordination tests to be conducted shortly before and after the rectifier installation is made. Such tests can be considered as necessary for proposed installations of Category B, and particularly so for specific installations of Category C where filters are not included in the original equipment. The primary purpose of such tests is to provide data from which to determine whether remedial measures are required and, if so required, what would be the most suitable measures.

Technical information and other material which will generally assist in the studies just mentioned or in specific test programs are given in the following paragraphs, as well as in Part V and succeeding parts and Appendices.

D. Rectifier Circuits and Transformer Connections

Although lack of reasonably complete information regarding the specific type of transformer connection to be employed is generally not serious in the preliminary consideration of the inductive coordination aspects of a proposed rectifier installation, reliable information on this point is apt to become increasingly useful as the study progresses.

Figure 1 illustrates the three types of rectifier transformer connections which are used most commonly. Other less commonly employed connections can be found in current literature[2] but it is impracticable to cover them here.

In street railway applications in this country, the 6-phase fork connection included on Figure 1 is used infrequently and is at present confined chiefly to rectifiers having power ratings not over about 1,000 kw.

There are two possible rectifier transformer designs for the 12-phase quadruple zigzag circuit illustrated schematically in Figure 1(C). One of these designs is built with a single a-c winding. This

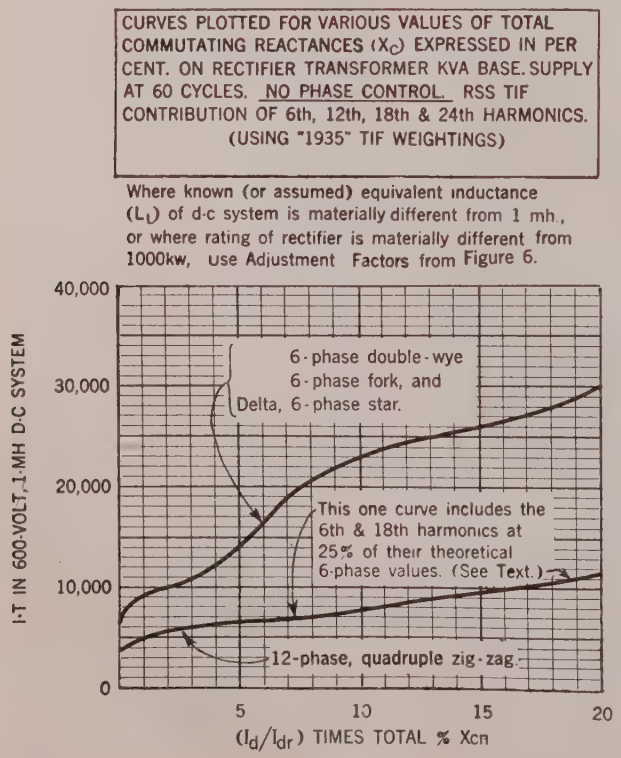
CURVES PLOTTED FOR VARIOUS VALUES OF TOTAL COMMUTATING REACTANCES (X_C) EXPRESSED IN PER CENT. ON RECTIFIER TRANSFORMER KVA BASE. SUPPLY AT 60 CYCLES. NO PHASE CONTROL. RSS TIF CONTRIBUTION OF 6th, 12th, 18th & 24th HARMONICS. (USING "1935" TIF WEIGHTINGS)
Where known (or assumed) equivalent inductance (L_L) of d-c system is materially different from 1 mh., or where rating of rectifier is materially different from 1000kw, use Adjustment Factors from Figure 6.
I·T IN 600-VOLT, 1-MH D-C SYSTEM
40,000
30,000
20,000
10,000
0
6-phase double-wye
6-phase fork, and
Delta, 6-phase star.
This one curve includes the 6th & 18th harmonics at 25% of their theoretical 6-phase values. (See Text.)
12-phase, quadruple zig-zag.
5
10
15
20
(I_d/I_{dr}) TIMES TOTAL % Xcn

Figure 5 (left). I·T produced in d-c system by 600-volt rectifier versus product of (I_d/I_{dr}) times total equivalent per cent commutating reactance ($\%X_{cn}$). For rectifiers supplied by 60-cycle systems. No phase control

Figure 6 (below). I·T adjustment factors for Figures 5, 9, and 10, to take account of d-c system equivalent inductances (L_L) other than 1 millihenry and rectifier ratings other than 1,000 kw

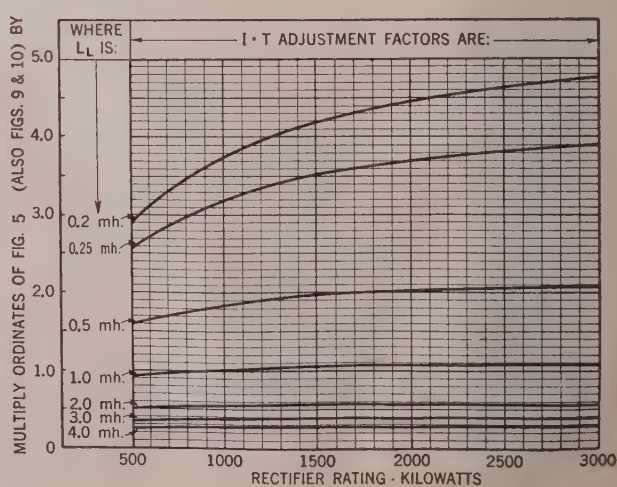

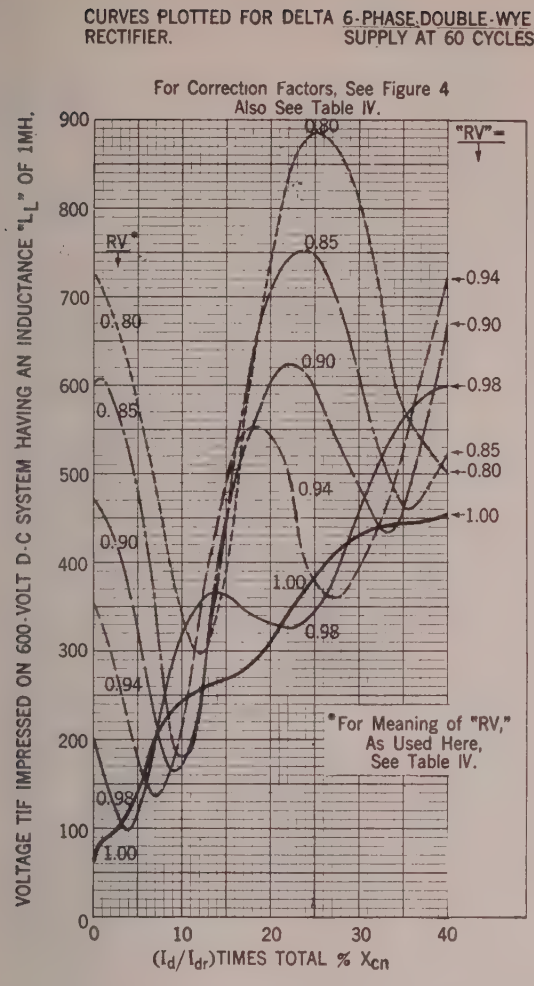

Figure 7 (left). Six-Phase Rectifier. Voltage TIF impressed on 600-volt d-c system. With various amounts of phase control. A-c supply at 60 cycles

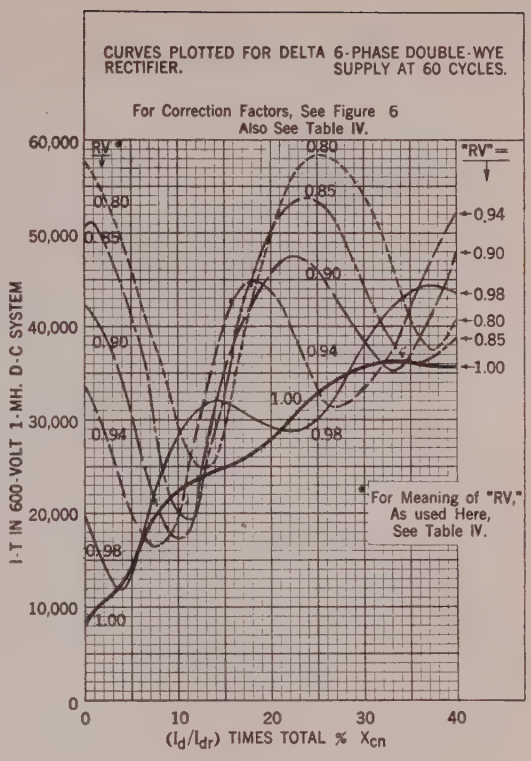

Figure 9 (right). Six-phase rectifier

I·T produced in 600-volt, 1 millihenry, d-c system, with various amounts of phase control, a-c supply at 60 cycles

same basic circuit also is built with a rectifier transformer having two paralleled individual a-c windings, each associated with only two of the four groups of d-c windings (as, for example, 1–5–9 and 3–7–11 or 2–6–10 and 4–8–12). In the latter design, the rectifier transformer is essentially equivalent to two 6-phase transformers having separate cores and a 30-degree displacement between their phase voltages. The Rectifier Standards[2] make no distinction between these two types of construction, both being designated Circuit 53.

Information regarding the orders and magnitudes of the output harmonics produced by the rectifier circuits illustrated in Figure 1 is given in Appendix II.

In general, it may be noted that:

1. Rectifier installations on "600-volt" d-c street railway systems in this country have so far been of various power ratings ranging from 500 to 6,000 kw.

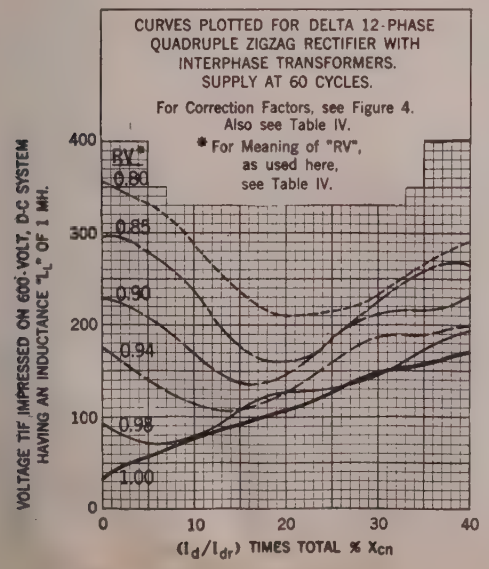
CURVES PLOTTED FOR DELTA 12-PHASE QUADRUPLE ZIGZAG RECTIFIER WITH INTERPHASE TRANSFORMERS. SUPPLY AT 60 CYCLES.
For Correction Factors, see Figure 4.
Also see Table IV.
* For Meaning of "RV", as used here, see Table IV.
RV*
0.80
0.85
0.90
0.94
0.98
1.00
VOLTAGE TIF IMPRESSED ON 600-VOLT, D-C SYSTEM HAVING AN INDUCTANCE "L_L" OF 1 MH.
(I_d/I_{dr}) TIMES TOTAL % X_{cn}

Figure 8 (left). Twelve-phase rectifier

Voltage TIF impressed on 600-volt d-c system, with various amounts of phase control, a-c supply at 60-cycles

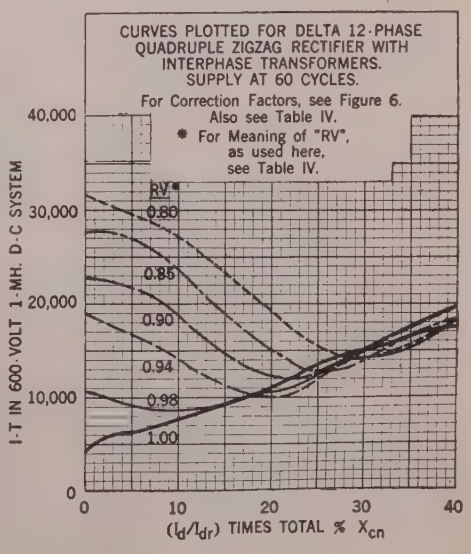
CURVES PLOTTED FOR DELTA 12-PHASE QUADRUPLE ZIGZAG RECTIFIER WITH INTERPHASE TRANSFORMERS. SUPPLY AT 60 CYCLES.
For Correction Factors, see Figure 6.
Also see Table IV.
* For Meaning of "RV", as used here, see Table IV.
RV*
0.80
0.85
0.90
0.94
0.98
1.00
I·T IN 600-VOLT 1-MH. D-C SYSTEM
(I_d/I_{dr}) TIMES TOTAL % X_{cn}

Figure 10 (right). Twelve-phase rectifier

I·T produced in 600-volt, 1 millihenry, d-c system, with various amounts of phase control, a-c supply at 60 cycles

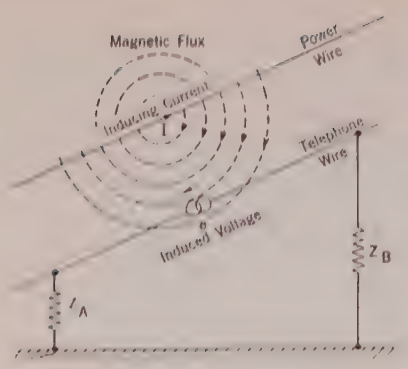

Figure 11. Nature of magnetic induction

2. Many of these have been 6-phase, while some, generally in the upper part of this range of power ratings, have been 12-phase.

3. To date, none of the installations has involved the operation of rectifier connections with more than 12 phases for normal service. In the absence of operating experience, no information on higher-phase installations is included in this report.

IV. Co-ordinative Measures

The solution of problems involving rectifiers, where the application of co-ordinative measures is indicated, is no different from other types of inductive co-ordination problems, in that close co-operation of all interested parties is necessary. Guiding principles and general practices are given in the report on Principles and Practices for Inductive Coordination, by the Edison Electric Institute and the Bell Telephone System,[37] which recognizes that characteristics of both the power and the telephone systems must be taken into account.

The difficulties of applying and maintaining co-ordinative measures on a specific exposure basis have led in recent years to relying more and more on the maintenance of the lowest practicable susceptiveness of telephone circuits in general and of the smallest practicable wave shape distortion on power circuits in general.

Of the various kinds of co-ordinative measures applicable to the power or telephone system, the following are the most important in connection with rectifier problems:

1. Advance planning of the method of supplying the rectifier from the standpoint of minimizing wave shape distortion.[38]

2. Possible phase multiplication of rectifier installation.[10, 19, 38]

3. Frequency selective devices.[24, 38]

4. Avoidance of unnecessarily large amounts of phase control.[4] (Also note Figures 7, 8, 9, and 10 of this report.) This might be accomplished, for example, by the selection of more suitable transformer taps.

5. Shielding of telephone cable circuits,[34] that is, "cable sheath shielding."

6. Reduction of telephone system unbalance to ground,[35] including the application of station sets equipped with ringers of the higher impedance type or, possibly, station sets employing cold cathode tubes in the ringing circuits. (This would also include suitable measures for minimizing leakage unbalance, as for example, on any twisted pair, or at its points of support, or the like which might be used for communication circuits in particularly damp locations, as in mines.)

7. Frequent or co-ordinated transpositions[33] in open wire telephone circuits exposed to the d-c system usually will be helpful. (Of course, transpositions generally cannot be used in the d-c circuits of a traction system.) Twisted pair in a relatively short local telephone circuit when the use of such pair is not precluded from the transmission standpoint embodies, in effect, very frequent transpositions.

It is impracticable within the scope of this report to present a sufficiently detailed discussion of these measures to provide the information required for reaching a solution of an individual situation. However, certain of the material given under this heading in the 1946 report, together with the following additional discussion of some of these measures, may be helpful in a more detailed examination of the material listed in the references.

Improved balance to ground of the newer types of telephone subscriber and central office equipment, which reached the stage of large scale production just prior to the war, has been very helpful from the inductive co-ordination standpoint.

The curves in Figures 3, 5, 7, 8, 9, and 10 afford a general illustration of the effectiveness of phase multiplication in reducing the I·T and voltage TIF on the d-c system, at least in so far as 12- versus 6-phase operation is concerned. This results, to a considerable extent, from a reduction in the number of important harmonics present, as indicated in Table V. Furthermore, where induction problems do arise, remedial measures are usually less expensive than for a smaller number of phases because:

1. The number of important unsuppressed harmonics to be cured for is smaller, and the magnitudes of the additional "normally suppressed harmonics," which remain as a result of unavoidable unbalances in the rectifier installation, are generally much reduced.

2. The size of the shunt elements of devices used for reducing harmonics goes down rapidly as the lowest frequency which they must handle goes up.

While phase multiplication is a powerful tool in the larger capacity installations, the extent to which it can be employed in smaller installations is limited to a considerable degree by the number of rectifier anodes.

A. Frequency Selective Devices

The only presently available method of controlling rectifier output harmonics, other than by phase multiplication, is by some form of frequency selective device, commonly called a filter.

Some form of frequency selective device has been applied on the output side of many rectifier installations on "600-volt" *d-c street railway systems*, (exclusive of subways and third-rail systems). The available information also indicates that in a considerable number of cases where filters were applied, co-ordinated measures were applied to the telephone plant also, as indicated qualitatively in Tables VII and VIII. In some cases there was so little exposure, initially at least, that it was feasible to omit a filter pending operating experience; a certain amount of noise reduction was effected in a number of these cases by the application of co-ordinative measures to the telephone plant alone. However, the available information is not sufficiently comprehensive to provide a quantitative picture regarding such cases.

Selective devices suitable for use on d-c systems may be grouped into three general classes with respect to the manner in which they are applied, as follows:

1. Series devices, including the series reactor and the tuned series reactor

2. Shunt devices, including the capacitor and the resonant shunt

3. Combinations of these series and shunt elements

A comprehensive discussion of these devices is contained in reference 24. The subject is too broad to cover in detail

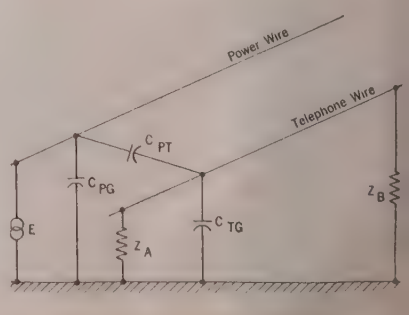

Figure 12. Nature of electric induction

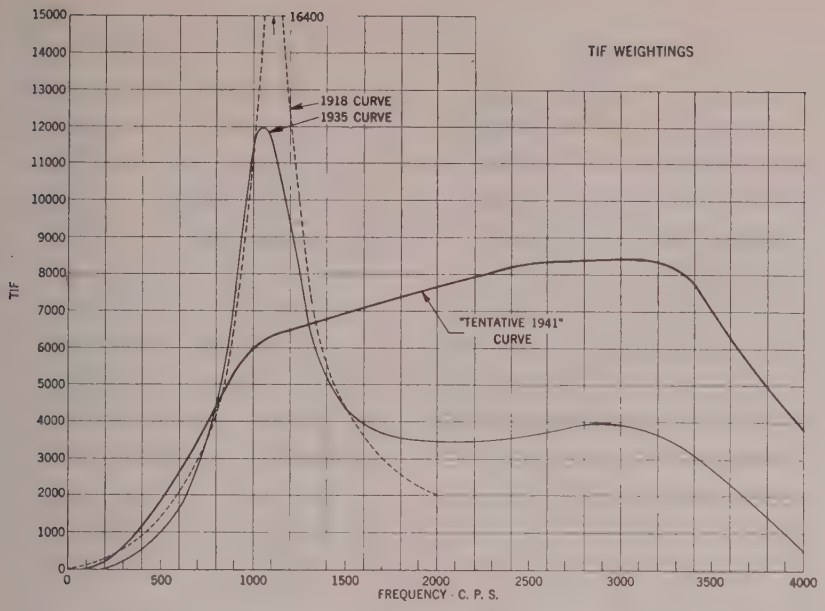

Figure 13. Telephone influence factor weightings at various frequencies

here, but a brief discussion of several important items is included in the following paragraphs.

The applicability of any one of these selective devices will depend to a considerable extent upon the type of d-c system concerned. Resonant shunts involve precision tuning and may require special mounting arrangements. The use of series reactors involves a power loss which has to be considered. The cost of a filter also is an important consideration. A discussion of costs and losses is outside the scope of this report. It should be emphasized, however, that where phase control is used the magnitude of the harmonics, and hence the over-all cost of an effective filter, is apt to be very materially increased.

In general, where it is desired to reduce several harmonic components, a combination of series and shunt elements at the rectifier output, as illustrated in Figure 2, has been found to be more practicable and more economical than either series or shunt elements alone.

The filter of Figure 2 consists of a series reactor L_s and several resonant shunts tuned for the frequencies of the harmonics which are to be reduced. Each shunt consists of a reactor and capacitor connected in series. At the specific frequency for which a shunt is tuned, the reactance of its reactor is equal and opposite to the reactance of the capacitor, so that the net impedance is equal only to the effective resistance of the shunt at the harmonic frequency, and with a properly designed shunt is very low. Each shunt thus provides a low-impedance by-pass for the harmonic current for which it is tuned. The series reactor L_s, together with the internal inductance L_0 of the rectifier unit, limit the harmonic currents in the shunts and largely absorb the harmonic voltages which produce these currents.

With the filter in operation and properly tuned, the voltage V_{dn}' of a specific harmonic frequency *remaining* on the d-c load side of the filter is equal to the product of the harmonic current through and resistance of the resonant shunt provided for that harmonic. The effectiveness or reduction ratio of the filter, for a specific harmonic n, is equal to V_{dn}/V_{dn}', in which V_{dn} is the corresponding harmonic voltage at the output terminals of the rectifier without the filter. This ratio is also equal, approximately, to the over-all reactance $\omega(L_s+L_o)$ of the series reactor and internal inductance at the harmonic frequency divided by the effective resistance of the resonant shunt. There must be a correlation between the constants and ratings of the shunt elements and the inductance of the series reactor to obtain the desired effectiveness of the combined filter (see part 4.3 of reference 24). The series reactor must be capable of carrying the continuous and overload current ratings of the rectifier. There are many possible combinations of constants for the series reactor and shunt elements. The over-all cost and losses in the filter are important considerations in the design.

The leading manufacturers of mercury-arc rectifiers are in a position to furnish d-c filters for rectifier installations. Experience has indicated that local designs of filters generally have not proved sufficiently effective.

The number of resonant shunts and the reduction ratios required for a filter depend largely upon the number of rectifier phases and on whether or not phase control is used. On the basis of experience, and in accordance with the suggestions in previously published literature,[38,40] satisfactory results usually can be expected from filters for rectifier installations on 600-volt street railway service, supplied from a 60-*cycle* a-c system, if the following reduction ratios or greater ones are obtained at full load:

For 6-phase rectifiers, operating without phase control, a reduction ratio of 10 for the 6th, 12th, and 18th harmonics.

For 12-phase rectifiers, operating without phase control, reduction ratios of 10 for the 12th harmonic, and 5 for the 6th and 18th harmonics.

Filters with three resonant shunts will usually provide some incidental reductions also for the 24th and some of the higher harmonics. In some cases, however, a separate shunt may be required for the 24th harmonic of 60 cycles.

The specific numerical reduction ratios mentioned here should be considered as illustrative guides and *not* as any sort of rigid limits.

In Table II are given approximate rms values of the harmonic voltages remaining at full load, without phase control, if filters providing the particular numerical reduction ratios mentioned in the preceding paragraph are used.

The values of remaining (residual) voltages shown in Table II for the 6-phase rectifier may serve as a rough guide in designing a filter for railway rectifiers operating with phase control or for rectifiers using other types of transformer connections.

As can be seen from the curves of Figures 19 to 22, the application of phase control produces an appreciable increase in the magnitudes of the harmonic components of the direct voltage, the increase depending upon the amount of phase control used. It is obvious that larger

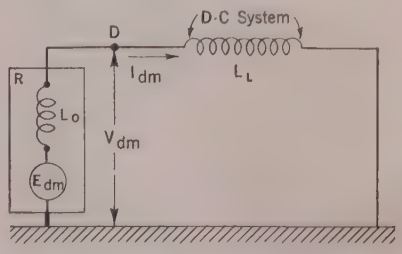

Figure 14. Schematic illustration of output side of a rectifier feeding a d-c street railway

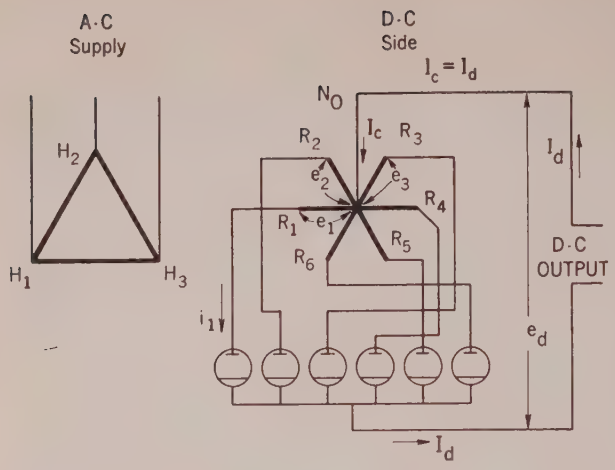

Figure 15 (left). Schematic of simple 6-phase rectifier. (Consists of only one commutating group.)

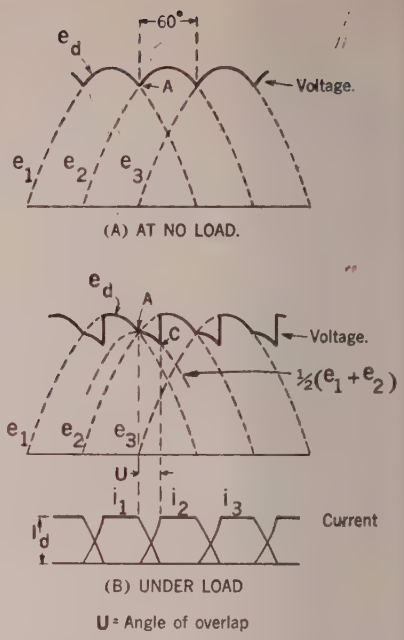

Figure 16 (right). D-c wave shape of 6-phase rectifier without phase control

filters, providing higher reduction ratios, are required in that case to obtain remaining voltages approximating the values of Table II. When phase control is used, there is a greater variation in the magnitudes of the harmonics as the load current is varied. The highest values over the operating load range should be considered in designing the filter, rather than the values at full load.

Care must be taken to avoid overloading the resonant shunts of a rectifier filter. If the filter is designed for a rectifier operating without phase control, it will be overloaded and is likely to be damaged if phase control is applied to the rectifier. Similarly if the filter is designed for a specific amount of phase control, it will be overloaded if that amount is exceeded.

B. Other Measures

The extent to which other remedial measures can be applied in place of control of the rectifier harmonics in a specific case depends on many circumstances which cannot be described in detail here.

Table II. Estimated Harmonic Voltages Remaining, for 600-Volt Rectifiers Supplied from a 60-Cycle System

Transformer Connection	Harmonics 6th (360 Cycles) Volts	12th (720 Cycles) Volts	18th (1,080 Cycles) Volts	24th* (1,440 Cycles)
6-phase, Double-Y or Fork	3.8	1.2	1.1	*
12-phase quadruple zigzag	1.9	1.2	0.6	*

*Note: With the types of filters considered, an incidental reduction of about 4 to 1 can usually be expected for the 24th harmonic of a 6-phase rectifier with 60-cycle a-c supply, a reduction which would result in a corresponding remainder of about 1.8 volts. An incidental reduction of about 2 to 1 can usually be expected in the 24th harmonic of a 12-phase rectifier, giving a remainder of about 3.6 volts.

V. Technical Information for Studies

To provide technical data useful in studies prior to and during a testing program, but not as a substitute for such tests, Figures 3 to 10 and Tables III and IV have been prepared. These and several related matters are discussed in the following Items, A to F.

A. Theoretical Voltage TIF's and I·T Products Without Phase Control

Figures 3 and 5 contain curves of theoretical output voltage TIF and the corresponding total output I·T, for a rectifier operating with zero phase control, supplied from a 60-*cycle* power system, and connected to a 600-volt d-c system of specific assumed equivalent inductance L_L. If phase control is used, or contemplated, reference should be made to the somewhat similar curves of Figures 7, 8, 9, and 10.

For the abscissas of Figures 3 and 5, the product of the total equivalent per cent commutating reactance $\%\ X_{cn}$ and the load ratio (I_d/I_{dr}) is used, in which I_d is the d-c load current considered and I_{dr} is the rated full-load current. The values on the curves represent the combined rss-weighted* contribution of the 6th, 12th, 18th, and 24th harmonics of 60 cycles, which are generally the most important contributors.

The voltage TIF curves in Figure 3 are the same as in Figures 7 and 8 for $RV = 1$. The I·T curves given in Figure 5 would be affected to some extent by the regulation. However, for the commutating reactance values generally used in practice, this effect would be relatively small and could be disregarded for the purposes covered by this report.

In the event that the power system supply frequency is other than 60 cycles, reference can be made to the curves of harmonic voltages shown in Figures 19, 20, 21, and 22, and the information in Appendix II and reference 4 to derive the corresponding influence factors.

In preparing the influence curves of Figures 3 and 5, the following basic assumptions have been used:

1. Rectifier output voltage at full load = 600 volts direct current.

2. Internal inductance L_o of rectifier unit = 0.09 millihenry. (Corresponds approximately to a rectifier power rating of 1,000 kw with a rectifier transformer rating of about 1,150 kva.) (Also see Part V—E.)

3. Total "equivalent inductance" L_L of d-c system = 1.0 millihenry, a value which is fairly representative for a 600-volt d-c street railway system.

4. The impedance of a d-c traction system usually has the characteristics of an inductive reactance throughout the frequency range which is of interest here (although the system impedance has occasionally been found to have the characteristics of a parallel combination of inductance and capacitance). Additional information on this is given in Part V—D.

With these specific values of assumed inductance, the mth harmonic voltage V_{dm} impressed directly upon the d-c system itself would be about 0.92 of the corresponding internally-generated harmonic voltage E_{dm} at any of the frequencies of chief interest, and this has been taken into account in the curves of Figure 3.

* Ratio of the square root of the sum of the squares of the TIF-weighted components in a current or voltage wave to the rms value of the wave. (Appendix I.)

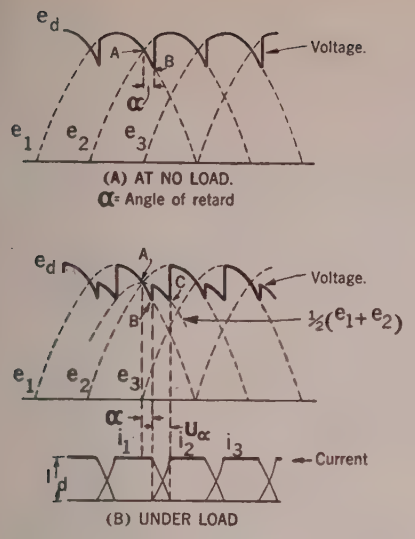

Figure 17. D-c wave shape of 6-phase rectifier with phase control

It is, of course, possible for the equivalent inductance L_L, and the corresponding d-c system harmonic impedances, to vary appreciably with different types of system (Part V—D) and, to some extent, also with load on a particular system. The rectifier-unit internal inductance L_o can also vary for various reasons but generally with much less effect than L_L upon the total impedance.

Estimation of I·T Product Per Trolley-Feeder. For most practical purposes within the ranges of total equivalent inductance L_L generally encountered on 600-volt d-c street railway systems, the I·T product per trolley-feeder without phase control can generally be taken empirically as about 0.2 of the values of *total* output I·T shown in Figure 5, without applying the adjustment factors referred to in a later paragraph of this section.

This approximate relation is based on an assumed inductance of 5 millihenrys for an individual feeder. This is an average value, indicated by available data, for 600-volt street railway feeders having the more usual length of 2 to 3 miles, or about 2 millihenrys per mile. Since the curves of Figure 5 are based on a d-c system inductance of 1 millihenry, the I·T product for a 5-millihenry circuit would be approximately one-fifth, or 0.2 of the values given by the curves. The harmonic output *voltages* of the rectifier are not affected greatly by the variations in the d-c system inductance usually encountered.

If some individual feeder is materially different from the average length of 2 to 3 miles, its inductance can be estimated from the numerical information given in the preceding paragraph and the I·T product for the feeder is equal approximately to the values given in Figure 5 divided by the feeder inductance in millihenrys.

If the kilowatt rating of a rectifier installation is materially different from 1,000 kw or if the inductance L_L of the d-c output circuit differs materially from 1 millihenry, adjustment factors given by the curves of Figures 4 and 6 may be applied to the values of TIF and total I·T obtained from Figures 3 and 5. If the trolley feeders are of the same general type, so that they have approximately the same impedance per mile at the harmonic frequencies, it can be assumed that the total I·T will be distributed among the feeders in about the inverse ratio of their lengths.

B. Estimation of Total Per Cent Commutating Reactance (Total % X_{cn})

When employing Figures 3 or 5, or Figures 7, 8, 9, or 10, use is made of the total commutating reactance of any specific rectifier installation. This reactance is the sum of the individual reactances of the respective parts of the circuit through which power flows to the rectifier, expressed as percentages on the total rectifier transformer kilovolt-ampere base. Methods of estimating or determining this total reactance and its constituent parts, such as the rectifier transformer itself and the a-c supply circuit, are outlined in some detail in the 1946 report[1] as well as in that part of reference 7 which concerns Circuit Constants. These details are not repeated here.

When considering the wave shape on the d-c output, the following items may be helpful:

1. According to the ASA Standard C57.18-1948,[45] the name-plate of a rectifier transformer includes the following data:

   A-c line current and transformer rated kilovolt amperes, which is the kilovolt amperage at the a-c line terminals at full load.

   Per cent impedance, which is the transformer short-circuit impedance determined by factory test with the total d-c winding short-circuited.

   Commutating reactance (X_c), in ohms, referred to the d-c winding. This reactance is determined by factory test, in accordance with Item 5.304 of reference 2.

2. The commutating reactance of a rectifier unit is the important reactance in so far as the wave shape of the d-c output voltage is concerned. (Also see Appendix II.)

3. The total equivalent per cent commutating reactance, for use in connection with Figures 3, 5, 7, 8, 9, and 10, may be determined as follows:

   The commutating reactance X_c (in ohms) of the rectifier transformer is converted into equivalent reactance, in ohms referred to the a-c line, X_{cn}, by equation 1 or 2.

   $X_{cn} = X_c(E_n/E_s)^2$ for the 6-phase double-Y or the 12-phase quadruple zigzag, primary either delta or Y (1)

   $X_{cn} = 3X_c(E_n/E_s)^2$ for the 6-phase fork with primary either delta or Y, and for the 6-phase star, with primary delta (2)

   where

   E_n = a-c system line-to-neutral voltage in rms volts

   E_s = transformer d-c winding line-to-neutral voltage in rms volts

   To the value of X_{cn} for the rectifier transformer, obtained by means of equation 1 or 2, should be added the reactance in ohms of any power circuit element (such as a series reactor on the a-c side) that may be connected ahead of the rectifier transformer, and the reactance in ohms of the a-c supply system.

   The total reactance, in ohms, obtained in the preceding paragraph, should be converted into equivalent total % X_{cn}, on the rectifier transformer kilovolt-ampere base, by means of equation 3 for use in Figures 3, 5, 7, 8, 9, and 10.

   $$\%\ X_{cn} = X_{cn}\left[\frac{\text{kva}}{10\,E_L^2}\right] \quad (3)$$

   in which E_L is the a-c line-to-line voltage in rms kilovolts. This avoids the use of different kilovolt-ampere bases for the two quadruple zigzag connections referred to in Part III—D.

4. If the rectifier transformer kilovolt-amperage is not known, it can be approximated by equation 1 in Table VII of the 1946 report.[1]

5. If the value of the rectifier transformer commutating reactance, or the reactance of any other element in the a-c circuit, is not available, it should preferably be obtained from the manufacturer. If that is not possible, the values of equivalent % X_{cn} given in Table III for the rectifier trans-

Table III. Approximate Equivalent % X_{cn} of Street Railway Rectifier Transformers*

Voltage Class on A-C Side, in Kv	Approximate Equivalent % X_{cn}
Up to 34.5 kv	6
Up to 69.0 kv	8
Up to 115.0 kv	10
Up to 161.0 kv	12

* Refers to transformers for mercury-arc rectifiers Transformers for mechanical rectifiers may have values different from these.

former connections of Figure 1 may be used, for preliminary studies at least.

6. If the reactance of the supply system is not known, it can be approximated from the kilovolt-ampere interrupting capacity rating (kva_R) of the rectifier a-c circuit breaker. The corresponding per cent reactance on the kilovolt-ampere base of the rectifier transformer (kva_R) is (100 kva_R)/kva_S. If the interrupting capacity of the circuit breaker is not known, a value of 1 or 2 per cent can be assumed for the a-c system reactance, and this should be added to the % X_{cm} of the rectifier transformer to obtain the total % X_{cm}. If the per cent reactance is known on a different kilovolt-ampere base from that of the rectifier transformer, it can be converted to the latter by means of equation 4 in Table VII of the 1946 report.

7. For a preliminary study, if the reactances are not known and cannot be estimated, a total % X_{cm} of 8 per cent can be assumed for 6-phase connections and 16 per cent for the 12-phase quadruple-zigzag connection.

C. Output Wave Shape With Phase Control

Certain explanatory material concerning phase control is included in Appendix II. As indicated there, phase control is used on a rectifier for reducing the d-c output voltage to some value below the value obtained without phase control.

The application of phase control to a rectifier may be expected to increase the magnitude of the output harmonic voltages, although it does not change the orders of these harmonics. These effects tend to increase considerably the over-all output voltage THF's and I·T products, except in certain, somewhat critical, operating regions illustrated more specifically by Figures 7, 8, 9, and 10.

As already indicated briefly, Figures 3 and 5 are concerned with the theoretical output voltage THF's and I·T products *without* phase control.

With the aid of Figure 7 or 8, the voltage THF's impressed on a 600-volt 1-millihenry d-c system can be estimated for conditions corresponding to full-load current, fractional-load current or a certain amount of overload current, without phase control or with various amounts of such control. As with Figures 3 and 5, the abscissas on Figures 7-10 are plotted with respect to the product of the load-current ratio I_d/I_{dr} (load current I_d considered with respect to the rated current I_{dr}) and the total equivalent per cent commutating reactance (total % X_{cm}). Here, also, the curves represent the combined rss-weighted contribution of the 6th, 12th, 18th, and 24th harmonics of 60 cycles.

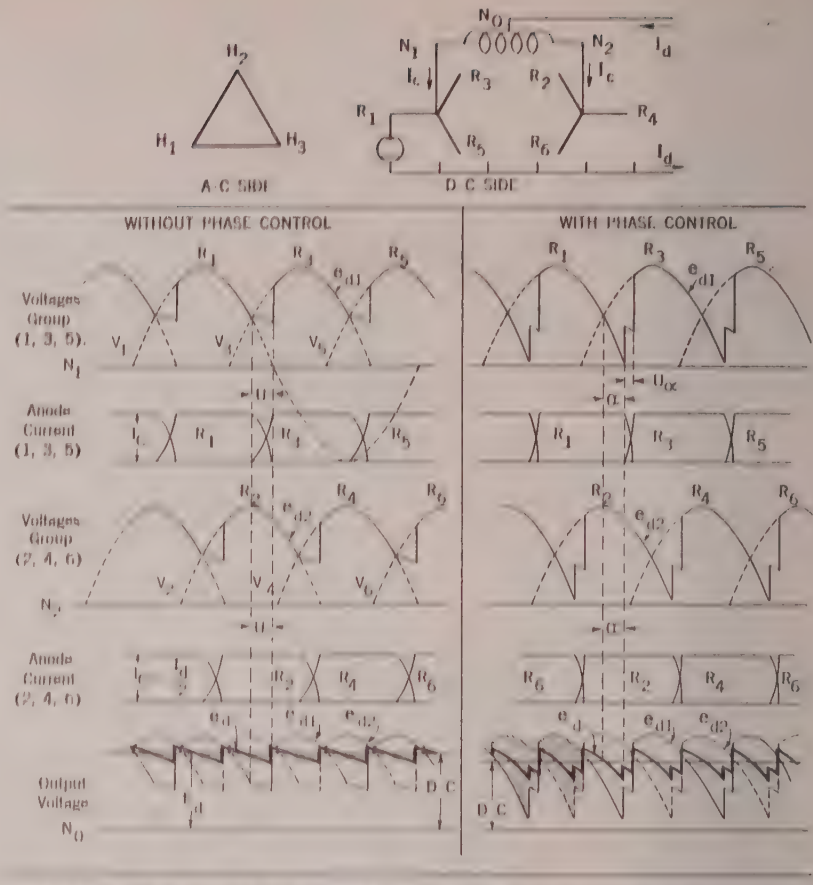

Figure 18. D-c wave shape of 6-phase double-Y rectifier circuit, without and with phase control

In referring to the curves of Figures 3, 5, and 7-10, it should be understood that rectifiers of different types but having the same kilowatt rating and substantially identical ohmic commutating reactance X_c do not necessarily have identical output wave shapes. This can be seen from equations 1-3.

Figures 7 and 8 show the output voltage THF's with various amounts of phase control. These apply to certain rectifier circuits having a total commutating reactance of 8 per cent for the 6-phase circuits and 16 per cent for the 12-phase circuits. Where required, adjustment factors, referred to in Table IV can be obtained from Figure 4.

The I·T's corresponding to the voltage THF's shown on Figures 7 and 8 are indicated on Figures 9 and 10, respectively, for various amounts of phase control. Adjustment factors which can be applied to the ordinates of Figures 9 and 10, under certain conditions referred to in Table IV, are given on Figure 6.

It should be emphasized that the curves of Figures 9 and 10 are based on a total % X_{cm} of 8 per cent for the 6-phase circuits and 16 per cent for the 12-phase circuits and the voltage regulation corresponding to this reactance. Theoretically, supplementary adjustment factors would be required, for these two figures, to take into account the effect (on the I·T's) of the different specific voltage regulation for cases where the total % X_{cm} is other than 8 per cent. For the commutating reactance values generally used in actual practice however, this effect would be reasonably small and can be disregarded for the purposes covered by this report.

It may be noted further that the I·T curves of Figures 9 and 10 are based on a direct output voltage of 600 volts at full load for the non-phase-controlled condition. If this noncontrolled full-load voltage is greater or less than 600, the ordinates of Figures 9 and 10 should be multiplied by the ratio of this actual voltage to 600, in addition to any other adjustment factors which may apply.

Estimation of I·T Product Per Trolley-Feeder. For most practical purposes, the ground-return I·T product per trolley-feeder can generally be estimated empirically as about 0.2 of the respective

Table IV. Notes Concerning Figures 7, 8, 9, and 10

1. *R V* is the ratio of the average direct voltage with phase control to the average direct voltage without phase control at the same load current. This ratio is sometimes called the "voltage control ratio" or the "phase control ratio." For example, if the direct voltage at a given load current were 600 volts without phase control and 15 per cent phase control were then applied (but with the load current staying the same), *R V* would be (1.00—0.15) =0.85 and the "remaining" direct voltage (under the "controlled" condition) would be (0.85) (600) =510 volts.

2. In Figures 7, 8, 9, and 10, the conditions associated with *R V* are:

Amount of Phase Control Near No Load, Per Cent	Remaining Direct Voltage "RV"	Corresponding Angle of Retard α, Degrees
None	1.00	0.0
2.0	0.98	11.5
6.0	0.94	19.9
10.0	0.90	25.8
15.0	0.85	31.8
20.0	0.80	36.9

3. Where known (or assumed) equivalent inductance "L_L" of d-c system is materially different from 1 millihenry, or where rating of rectifier is materially different from 1,000 kw, multiply ordinates of Figures 7, 8, 9, and 10 by adjustment factors as follows: With Figures 7 and 8, use adjustment factors from Figure 4. With Figures 9 and 10, use adjustment factors from Figure 6.

4. Curves on Figures 7, 8, 9, and 10 show *rss* total TIF contribution of 6th, 12th, 18th, and 24th harmonics of 60 cycles. Note also that curves on Figures 8 and 10 (for 12-phase rectifier) include contributions of 6th and 18th harmonics at 25 per cent of their theoretical 6-phase values.

5. Any specific value of I·T on Figure 9 or Figure 10 is a *total* I·T product into a 1-millihenry d-c system. For empirical method of estimating corresponding I·T product *per trolley-feeder*, see text.

Table V. Harmonics Arising in D-C End of Free Rectifiers

Respective Rms Harmonic Voltages Are Expressed in Per Cent of the D-C Voltage, at No Load or at Full Load,* as Indicated

Order of Harmonic	Harmonic Voltages at "No Load" in Per Cent of No Load d-c Voltage**		Rms Harmonic Voltages at Full Load, Expressed in Per Cent of Full Load d-c Voltage**		Harmonic Frequencies with 60-Cycle Source of Supply (Cycles)
	6-Phase Rectifier (Without Phase Control)	12-Phase Rectifier (Without Phase Control)	6-Phase Rectifier	12-Phase Rectifier	
6	4.04	(1.01)‡	0.35	(1.50)‡	360
12	0.980	0.980	2.05	2.10	720
18	0.438	(0.110)‡	1.90	(0.480)‡	1,080
24	0.246	0.246	1.21	1.21	1,440
30	0.157	(0.039)‡	0.94	(0.24)‡	1,800
36	0.109	0.109	0.86	0.87	2,160
42	0.080	(0.020)‡	0.65	(0.16)‡	2,520
48	0.061	0.061	0.62	0.62	2,880
54	0.049	(0.012)‡	0.54	(0.14)‡	3,240
60†	0.039	0.039	0.49	0.50	3,600

* Strictly speaking, the percentage values shown for the full-load condition apply primarily to a 6-phase rectifier having a total commutating reactance of 8 per cent and a 12-phase rectifier with a total commutating reactance of 16 per cent.

** Other harmonics may be present if the rectifier is unbalanced, as by differences in applied voltage or phase control between units, or may come through from the a-c power supply.

† The series continues above these values.

‡ The 6th harmonic and its odd multiples are theoretically eliminated by the 12-phase connection but actually they are found to be present in reduced amounts. The percentage magnitudes shown above, in ( ), for the 12-phase connection are given here as 25 per cent of the theoretical values of the 6th, 18th, 30th, and so on, harmonics for a 6-phase rectifier having a corresponding type of transformer connection.

Note: The percentage magnitudes shown without brackets, for both the 6-phase and the 12-phase rectifiers, are the theoretical values of the unsuppressed harmonics.

values of total output I·T obtained from Figures 9 and 10 and adjusted, where necessary, as just outlined in the preceding paragraphs. The basis for the use of the multiplier of 0.2 was outlined in Part V—A.

If the known or assumed equivalent inductance L_L of the d-c system is materially different from 1 millihenry, or if the rectifier rating is substantially different from 1,000 kw, the adjustment factors given in Figure 6 may be applied to the I·T values obtained from Figures 9 and 10. In that event, the empirical procedure mentioned in the preceding paragraph would not generally apply.

D. Equivalent Inductance of D-C System

For the average city railway substation supplying from five to ten 600-volt d-c feeder sections, it has been found that the system impedance is equivalent to an inductance L_L of about 0.5 to about 1.5 millihenrys, with an average of roughly 1 millihenry.[24] In a concentrated city traffic area, equivalent inductances from about 0.2 to 0.5 millihenry were measured recently. In urban or suburban areas, an empirical average value of about 5 millihenrys per individual feeder of a 600-volt single-trolley-per track street railway might therefore apply, except for feeders less than 2 or 3 miles in length. An equivalent inductance as high as 6 millihenrys has been observed for a single feeder section of a 600-volt interurban system.

If lightning arresters of the electrolytic type (which have appreciable capacitance) are attached to the station bus, or if such lightning arresters are used on the individual trolley cars, a condition of parallel reasonance may sometimes be encountered usually occurring within the range 1,500 to 3,000 cycles and in such occasional cases the d-c system impedance would be capacitive at frequencies above the resonance point.

E. Internal Inductance (L_0) of Rectifier Unit

The equivalent internal inductance L_0 of the rectifier unit, for the harmonic currents in the d-c circuit, is related to the rectifier transformer reactance and depends upon the transformer connection.

The harmonic currents flow through the conducting phases. In general, if p is the number of phases *per commutating group*, and q is the *total* number of rectifier phases, the expression for the equivalent internal inductance of a rectifier having 60-cycle a-c supply is of the following type:

$$L_0 = \frac{p}{q}\frac{X}{377}$$

assuming that the inductance is unaffected by frequency. In the relation just shown, the term X is used in a general, illustrative sense. More specifically, however: For the 6-phase double Y connection, the harmonic current flows through 2 phases in parallel (one phase in each Y) and

$$L_0 = \frac{1}{2}\frac{X_c}{377}, \text{ in henrys} \qquad (4)$$

For the 12-phase quadruple zigzag connection, the harmonic current flows through 4 phases in parallel, and

$$L_0 = \frac{1}{4}\frac{X_c}{377}, \text{ in henrys} \qquad (5)$$

For the 6-phase fork connection,

$$L_0 = \frac{X_s}{377}, \text{ or (approximately) } \frac{2X_c}{377}, \text{ in henrys} \qquad (6)$$

where X_s is the short circuit reactance in ohms, referred to the phase-to-neutral voltage E_s of the d-c side, and X_c is the commutating reactance, in ohms, on the d-c side.

For 600-volt d-c systems, experience indicates that the internal inductance of a rectifier is roughly inversely proportional to the kilovolt amperage rating of

Table VI

Physical Quantity or Relation	Type of Rectifier Transformer Connection: 6-Phase Double-Y or Double-Way. (Circuits 23, 24, 45, and 46[2])	6-Phase Fork or Delta-Star, (Circuits 9, 11, and 12[2])	12-Phase, Quadruple Zigzag (Circuits 53 and 54[2])
A. Some General Relations Applying to Certain Types of Rectifiers—Either Without or With Phase Control			
1. Relationship of the quantity $(I_c X_c / E_s)$ to the total commutating reactance $\%X_{cn}$ at full load current	$\frac{*I_c X_c}{E_s} = 0.0122\ \%X_{cn}$	$\frac{I_c X_c}{E_s} = 0.00707\ \%X_{cn}$	$\frac{*I_c X_c}{E_s} = 0.00632\ \%X_{cn}$
2. I_c = commutated current per secondary phase group, as related to total output current I_d	$I_c* = I_d/2$*	$I_c = I_d$	$I_c* = I_d/4$*
3. p = number of phases per secondary group			
(a) Equivalent, except at no load current and at very light loads:	$p = 3$	$p = 6$	$p = 3$
(b) Actual at no load and very light loads	6	6	12
4. q = total number of rectifier phases	6	6	12
B. Some Relations Which Apply When Rectifier Is Operating Without Phase Control			
5. Angle of overlap u			
(a) At full load current†	$\text{Cos } u = 1 - \%X_{cn}/100$	$\text{Cos } u = 1 - \%X_{cn}/100$	$\text{Cos } u = 1 - 0.516\ (\%X_{cn}/100)$
(b) At any load current I_d	$\text{Cos } u = 1 - 0.816\ I_c X_c / E_s$	$\text{Cos } u = 1 - 1.414\ I_c X_c / E_s$	$\text{Cos } u = 1 - 0.816\ I_c X_c / E_s$
(See Figure 24, curve for $RV = 1.00$)			
6. E_d = direct output voltage with load current of I_d	$E_{do}(1 - 0.408\ I_c X_c / E_s)$	$E_{do}(1 - 0.707\ I_c X_c / E_s)$	$E_{do}(1 - 0.408\ I_c X_c / E_s)$
(See Figure 23, curve corresponding to $RV = 1.00$)			
7. E_{do} = "no-load" direct voltage			
(a) Equivalent, except at actual no load or very light load	$1.17\ E_s$	$1.35\ E_s$	$1.17\ E_s$
(b) Actual at no load or at very light load	$1.35\ E_s$	$1.35\ E_s$	$1.40\ E_s$
C. Some Relations Which Apply When Rectifier Is Operating With Phase Control			
8. Angle of retard: For a given percentage reduction of the output voltage—namely, 100 $(1 - RV)$—the corresponding angle of retard α can be obtained with the aid of Item 10			
9. Total angle of delay $(u_\alpha + \alpha)$ (See Figure 24)	Cosine of $(u_\alpha + \alpha)$ = $(\text{Cos } \alpha - 0.816\ I_c X_c / E_s)$	Cosine of $(u_\alpha + \alpha)$ = $(\text{Cos } \alpha - 1.414\ I_c X_c / E_s)$	Cosine of $(u_\alpha + \alpha)$ = $(\text{Cos } \alpha - 0.816\ I_c X_c / E_s)$
10. RV = ratio of direct output voltage E_d', with retard of α degrees, to output voltage E_d which would exist without retard at same load current I_d	$\frac{2.45 \cos \alpha - I_c X_c / E_s}{2.45 - I_c X_c / E_s}$	$\frac{1.414 \cos \alpha - I_c X_c / E_s}{1.414 - I_c X_c / E_s}$	$\frac{2.45 \cos \alpha - I_c X_c / E_s}{2.45 - I_c X_c / E_s}$
11. Ratio of direct output load voltage E', with retard of α degrees and with specific load current of I_d, to "equivalent" noncontrolled no-load voltage E_{do} (of Item 7a). (Plotted in Figure 23)	$\cos \alpha - 0.408\ (I_c X_c / E_s)$	$\cos \alpha - 0.707\ (I_c X_c / E_s)$	$\cos \alpha - 0.408\ (I_c X_c / E_s)$

* Note carefully the distinction between I_c and I_d for the types of connection indicated by *.

† At other than full-load current, multiply the right-hand part of the equation shown in Line 5 (a)—namely, the part containing $\%X_{cn}$—by the ratio I_d/I_{dr} before determining cos.

the rectifier transformer and, for a number of practical purposes, may be estimated reasonably closely by the approximate formula: L_o, in millihenrys = 110/kva, as mentioned in other literature.[24] In cases where a more accurate determination of L_o might be of value, as possibly, for example, in designing a filter, use can be made of equations 4, 5, or 6.

F. Discussion

Some favorable and some unfavorable factors which may be considered qualitatively in reviewing the inductive coordination aspects of street railway rectifier installations are:

1. Rotary machines normally operating in parallel with the d-c side of rectifiers in the same substation are usually helpful since they offer a shunt path for the rectifier harmonic currents and thus tend to reduce the amount which would otherwise be supplied into the d-c system. The net effect, although appreciable, is seldom a controlling factor.

2. Rotating d-c machines operating on the d-c system in substations adjacent to a rectifier substation are generally unfavorable, since their relatively low impedance will tend to draw increased harmonic currents from the rectifier, over the intervening d-c system; and thus increase the effect of any exposures which exist along the way. Tie feeders between such substations will, of course, tend to increase such currents, particularly if these ties are relatively short.

3. With a radial d-c system, the harmonic currents impressed upon the d-c system as a whole will divide in the several directions from the rectifier. However, the presence of conductors which are not a part of the d-c system may be an unfavorable factor, since such conductors may offer remote metallic-return paths for the rectifier harmonic currents.

4. The capacitance which is, in effect, presented by lightning arresters of the electrolytic type in case they are attached to the station d-c bus, or if they are used on the individual trolley cars, can in some instances affect the inductive co-ordination problem considerably. (See Equivalent Inductance of D-C System, also Appendix III.)

Appendix I. Fundamentals of Noise-Frequency Co-ordination Work and Terms Used

In this Appendix, some of the fundamentals of noise-frequency inductive co-ordination work and the terms used are discussed. For a more complete discussion of this matter, reference should be made to the 1946 report.[1] The following material includes a condensed discussion concerning some of the more important underlying principles and, particularly, certain additional information concerning the significance of the terms balanced, residual, and ground-return currents and voltages as used in connection with d-c circuits in the present report.

Inductive Co-ordination

The practical job of noise-frequency inductive co-ordination is to control coupling influence and susceptiveness within practical limits, so that telephone circuit noise is adequately controlled at minimum cost and maximum satisfaction to both power and telephone customers.

The significance of the terms inductive coupling, inductive influence, and inductive susceptiveness, will be found in reference 37. It is theoretically possible, but usually not practical, to have power circuits with almost zero influence; they would cause very little noise in any telephone circuit regardless of its susceptiveness. It is theoretically possible to have telephone circuits of practically zero susceptiveness (for example, by having perfect balance and transpositions); they would not be noisy regardless of the influence of near-by power circuits. Also, if the power and telephone systems were separated by large distances, the coupling, and hence the noise, would be negligible. However, none of these

The expression "controlled d-c voltage" is used on this curve sheet to denote the product:
"RV" times the d-c voltage which the rectifier would develop at the same specific load current (such as represented by any given value of $I_C X_C/E_S$) without phase control.

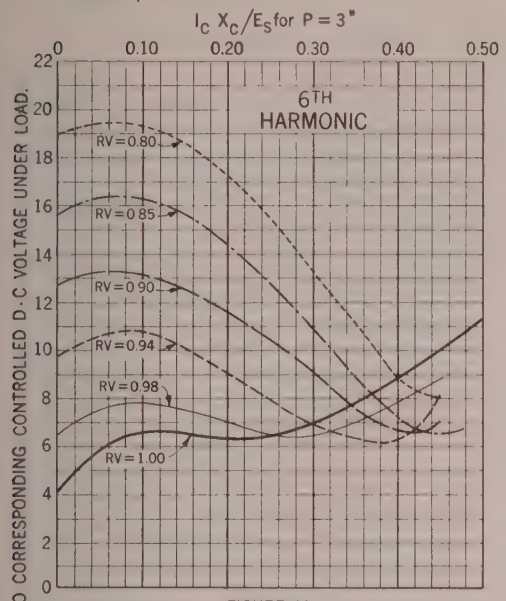

FIGURE 19

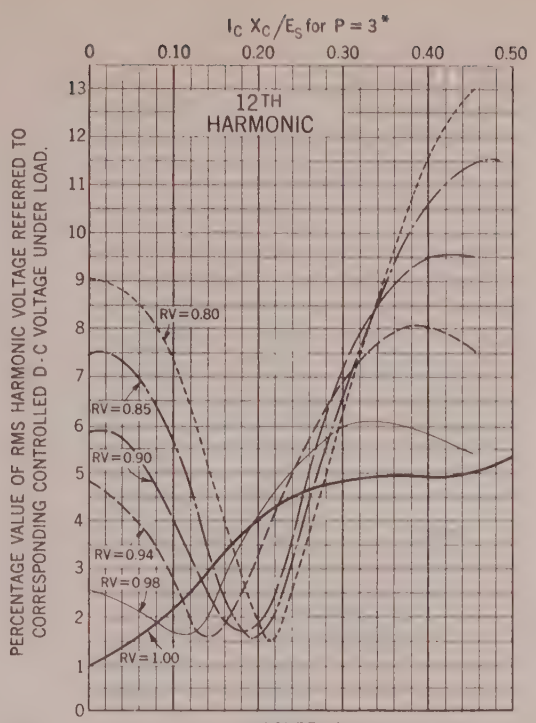

FIGURE 20

Figures 19, 20, 21, and 22. The 6th, 12th, 18th, and 24th harmonic voltages in the output of a phase-controlled rectifier as a function of $I_c X_c/E_s$, for different degrees of phase control. Amount of phase control, in per cent = 100 (1 − RV)

*NOTE: In event that the rectifier circuit is such that "p" = 6 (as, for example, delta 6-phase star):- First (a) multiply the actual value of $I_C X_C/E_S$ by 1.73 and then (b) with this "adjusted" value of $I_C X_C/E_S$ enter directly the scales of abscissae for "p" = 3 shown on the four figures associated herewith.

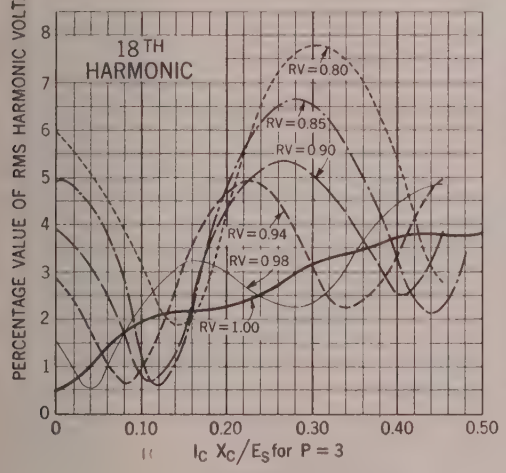

FIGURE 21

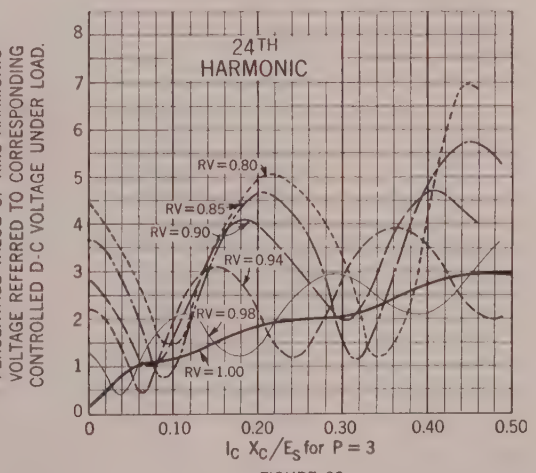

FIGURE 22

theoretical methods is practicable, in general, in the present state of the art.

Magnetic and Electric Induction—Coupling

Voltages induced on telephone circuits by power circuit currents are said to be due to magnetic induction; voltages caused by power circuit voltages are said to be due to electric induction. These forms of induction may be treated as though they exist independently.

The magnetic induction process at harmonic frequencies in its simplest form is illustrated on Figure 11.

1. A mutual reactance, or magnetic coupling, exists between the power wire (of either an a-c or a d-c system) and the near-by telephone wire because the magnetic flux associated with the power-wire current links the telephone wire. The total amount of flux (per unit of power-wire current) which links the telephone wire is proportional to length of exposure and increases as the separation is decreased.

2. The voltage e induced in the telephone wire is proportional to the total flux which links it and to frequency. The current in the telephone wire is this voltage divided by (Z_A+Z_B). The voltage to ground at one end of the exposure is this current times Z_A; at the other, times Z_B.

The electric induction process in its simplest form is illustrated on Figure 12. The power wire has on it an harmonic voltage E to ground.

1. Between the power wire (of either an a-c or a d-c system) and a nearby telephone wire, electric coupling, represented by capacitance C_{PT}, exists. The magnitude of this capacitance is directly proportional to length of exposure and increases as the separation between the wires decreases. Its impedance is inversely proportional to frequency.

2. The telephone wire has finite im-

pedances to ground, Z_A and Z_B, outside the exposure. These impedances are usually much smaller than the impedance of C_{PT}. The current to the telephone wire is therefore controlled by C_{PT}; it is directly proportional to the length of exposure and to frequency and magnitude of E. The corresponding voltage on the telephone wire is approximately equal to the product: current through C_{PT} times the impedance of Z_A and Z_B in parallel, if (as is often the case) the telephone line impedance in the exposure is relatively small in comparison with Z_A and Z_B.

Voltage TIF and I·T Products — Inductive Influence

Each harmonic voltage or current in a power system induces a voltage of the same frequency in a paralleling telephone circuit. This induced voltage may, in turn, actuate a telephone receiver and cause an audible sound. The composite of the sounds of all such frequencies present usually results in a humming sound commonly called noise. Different frequencies in this noise have different interfering effects[27,28] depending on the characteristics of the telephone circuits, receiver, the human ear, and other factors; relative interfering effects are called noise weightings and have been ascertained by extensive tests.

Since the effects of both electric and magnetic coupling are directly proportional to frequency, the relative noise influence of voltages and currents which exist on the (a-c or d-c) power system is proportional to the product of noise weighting and frequency. For any frequency, this product (times a constant) is known as TIF (telephone influence factor). TIF weighting curves as functions of frequency are shown in Figure 13.

There are three different sets of TIF weightings, which reflect changes in transmission-frequency characteristics of telephone circuits and instruments over a long period:

1. The "1918" weightings. These were known as telephone interference factor weightings and this name is still used to distinguish them from the later weightings which are called telephone influence factor weightings.

2. The "1935" weightings.[29] Note that these weightings were used in preparing Figures 3, 5, 7, 8, 9, and 10 of this report.

3. The tentative "1941" weightings. These weightings have not been standardized and they may be out of date soon, since a review of the weighting curves is now in progress. They are shown here chiefly as a matter of information.

The very small weighting of 60 cycles explains why only the harmonics are usually of interest from the noise-frequency induction standpoint.

While much induction work is carried out on the basis of individual harmonics, it frequently is desirable to use an over-all measure of the influence of a current or a voltage in a power circuit. This over-all measure is obtained by multiplying the magnitude of each harmonic present (amperes, for current; kv for voltage) by its TIF weighting, and taking the square root of the sum of the squares of these products. The result is: for current, I·T product; for voltage, KV·T product.

Balanced, Residual and Ground-Return Currents and Voltages

Suppose that in Figure 11 there were another power wire very close to the one shown there and that it carried an harmonic current equal and opposite to the current in the original wire; such a set of currents would be called *balanced*. The flux cutting the telephone wire would then be only the difference between the fluxes at that point arising from the currents in the two power wires. If the separation between the power wires were small, this difference would be small and hence the coupling would be small as compared to that for current which goes out on one or more wires and returns through the earth; that is, *ground-return* current. A similar analysis with respect to the voltages would indicate the same conclusions.

On a railway system with overhead trolley and track return, the harmonic currents are fully unbalanced and largely ground return.

On a trolley-coach system in which the two conductors are adjacent and with one side of the circuit grounded at only one point, the harmonic currents through the loads and equipment are fully balanced and there is practically no ground-return current. If the harmonic currents in the two overhead contact conductors of such a unigrounded d-c system are unequal, due to differences in feeder lengths or unbalanced interconnections between trolley wires on the system, the harmonic currents will still be essentially balanced in nature even through the effective separation d of the conductors constituting, respectively, the going and return paths for a part of this balanced current is greater than that presented by the two (+ and −) trolley conductors.

For the same exposure conditions, any component of balanced harmonic current thus flowing in such a path of greater effective separation would generally produce a greater magnetic coupling, with respect to near-by telephone conductors, than an equal balanced component confined entirely to an overhead trolley conductor and its closely adjacent mate.

On a trolley-coach system having one side of the circuit grounded at *more* than one point, part of the harmonic current will return over the overhead conductor which is connected to the grounded side; the remainder will flow through the earth between the points of grounding. The component of the harmonic current which flows over both overhead conductors is the balanced component. The difference of the harmonic currents in the two conductors is the residual current and is equal to the ground-return current.

Metallic and Longitudinal Telephone Voltages and Currents

With further reference to the voltages induced on the telephone wires (Figures 11 and 12), let it be assumed that in Figure 11 another telephone wire is added parallel and close to the first. The second wire will be linked by nearly the same flux as the first and the difference in the voltages along the two wires will be a small fraction of that along either one. If two telephone wires are thus present and are used as a metallic telephone circuit, there is (a) longitudinal circuit induction, which is the voltage along or to ground on the two telephone conductors in parallel, and (b) direct metallic circuit induction, which is the difference between the voltages along or to ground on the two wires, the direct metallic circuit induction being much the smaller. The same sort of analysis could be carried through for electric induction, with the same conclusions.

Direct metallic circuit induction can be reduced still further by transposing the telephone circuit, that is, interchanging the positions of the conductors periodically so that the voltages on both tend to be equal. In open wire circuits the reduction obtainable, while large, is limited by unavoidable irregularities in exposure conditions. In so-called twisted pair, or in cable circuits, the pairs are twisted so as to be continuously transposed, and direct metallic circuit induction can be neglected. When the telephone circuits are in metal-sheathed cable, the cable sheath provides, in addition, practically perfect shielding against electric induction into the pairs within the cable if the sheath is grounded at one or more points, and it usually provides considerable shielding against magnetic induction if grounded at both ends, the degree of such shielding being limited by the resistance of the sheath and of the grounds.

Susceptiveness

The degree to which a telephone circuit can be affected by given extraneous electric and magnetic fields is called its susceptiveness. Susceptiveness depends on such things as balance, adequacy of transpositions, and on the frequency response of the circuits and instruments and the level (magnitude) of the telephonic current and voltages at the point where the exposure exists.[1,37]

Appendix II. Analysis of Effects of Rectifiers on D-C System Wave Shape

An analysis of any of the output voltage waves of various rectifiers by the Fourier series, as, for example, the waves shown on Figures 16, 17, or 18, shows that it contains, besides the d-c component, harmonic frequencies of various specific orders.[3,4,38,39] An important difference between the a-c systems discussed in the 1946 Report and the d-c systems covered in this report is this: on the d-c side of a multiphase rectifier supplied from a 3-phase system the output voltage has harmonics whose frequencies are integral multiples of six times the fundamental frequency, such as 60 cycles, of the a-c power supply source, whereas the harmonics on the a-c end of such a rectifier are certain odd multiples of the fundamental.[1,8,10,36,38] Such an even or odd integral numerical multiple is commonly referred to as the *order* of the corresponding harmonic.

The orders of the respective output

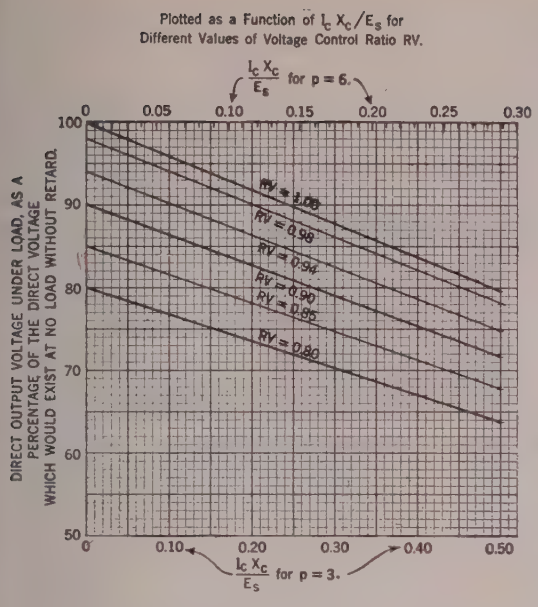
Plotted as a Function of $I_c X_c / E_s$ for Different Values of Voltage Control Ratio RV.
$\frac{I_c X_c}{E_s}$ for p = 6.
DIRECT OUTPUT VOLTAGE UNDER LOAD, AS A PERCENTAGE OF THE DIRECT VOLTAGE WHICH WOULD EXIST AT NO LOAD WITHOUT RETARD.
RV = 1.00
RV = 0.98
RV = 0.94
RV = 0.90
RV = 0.85
RV = 0.80
$\frac{I_c X_c}{E_s}$ for p = 3.

Figure 23 (left). Direct output voltage as a percentage of no-load direct voltage with no retard

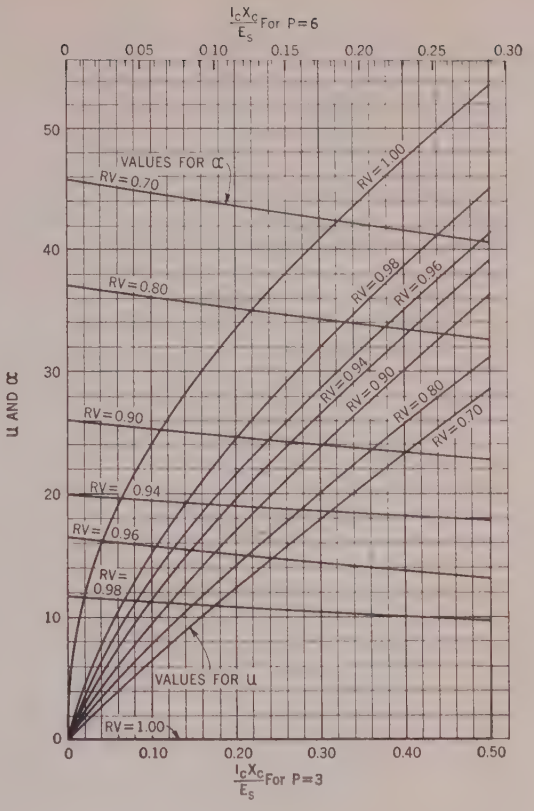

Figure 24 (right). Angle of overlap u, and angle of retard α, as functions of $I_c X_c / E_s$, for different values of voltage control ratio RV

harmonics produced with phase control are not changed by increased phase control but their magnitudes can be changed considerably, generally upward, thereby, as illustrated by Figures 19, 20, 21, and 22.

Output Circuit—Simplified

Figure 14 illustrates, schematically, a d-c system supplied from a rectifier unit R consisting of the rectifier itself and its associated transformer. In addition to a direct voltage, the rectifier can be considered as generating internally a series of individual harmonic voltages, of which any one of them such as the mth harmonic can be represented here by E_{dm}. With no rotary equipment operating in parallel with the rectifier unit at the same substation, the voltage E_{dm} will send a current I_{dm} through the impedance of the d-c system Z_{Lm} in series with the equivalent internal impedance of the rectifier unit Z_{om}. This current will, of course, be $I_{dm}=(E_{dm})/(Z_{Lm}+Z_{om})$ and there will result across the output of the rectifier unit, a location represented by point D—as, for example, the d-c bus—an external voltage $V_{dm}=I_{dm}Z_{Lm}$. This voltage, indicated by V_{dm} on Figure 14, can be considered as representing any individual harmonic voltage, such as the mth or nth, actually impressed upon the d-c system itself.

At harmonic frequencies, the internal impedance Z_o of the rectifier unit can be considered as made up of a substantially pure inductance L_o, namely the equivalent inductance of the rectifier transformer (see Parts V—E, V—D, and V—A of main body). Also, as indicated in Part V—A of the main body of this report, the impedance of a 600-volt d-c traction system usually has the characteristics of an inductance L_L throughout the frequency range of interest here. On this basis, the total nth harmonic current I_{dn} in the d-c circuit becomes $[(E_{dn}/(\omega_n)(L_L+L_o)]$ and the corresponding external harmonic voltage impressed upon the d-c system at point D becomes $[(E_{dn})\times(L_L)/(L_L+L_o)]$.

Harmonics Generated

Table V indicates the harmonic orders, that is, the multiples of the a-c supply fundamental frequency, produced on the d-c side of 6- and 12-phase rectifiers. The theoretical percentage magnitudes of the corresponding harmonic voltages at the respective no-load and full-load conditions specifically indicated on the table are shown by the unbracketed figures in Columns 2–3 and 4–5, respectively. As to the bracketed figures shown there for the 6th, 18th, and so forth, harmonics for a 12-phase rectifier, it may be noted that in comparatively recent operating tests the average reduction in the 6th and 18th harmonics obtained by the use of the 12-phase connection of present design was approximately 3 or 4 to 1 compared with the values which would be obtained with a corresponding 6-phase connection. An assumed suppression ratio of 4 to 1, namely, 25 per cent remaining, in the 6th, 18th, 30th, and so on, harmonics has therefore been incorporated in the bracketed percentage magnitudes shown for those specific harmonics for the 12-phase case.

As illustrated by the columns pertaining to the full-load condition indicated, the specific magnitudes of all of the respective harmonic voltages under load conditions with no phase control will depend to some extent upon the particular type of rectifier connection concerned. Although their respective orders remain unchanged, the magnitudes of the harmonic voltages associated with the output of a free rectifier, particularly harmonics of the higher orders, generally increase as the load current increases and this is further illustrated later by the no-phase-control curves on Figures 19, 20, 21, and 22.

In the relatively occasional case where specific harmonics of fairly large magnitudes are present in the voltage of the a-c supply, the wave shape of the d-c output voltage of the rectifier can be further modified by them. In either the 6-phase or the 12-phase rectifier, such a prominent 5th or 7th harmonic in the supply voltage can of itself contribute some 6th harmonic voltage on the output side; a prominent 11th or 13th can contribute some 12th harmonic, and so on.[4,38] Such possible contributions are in addition to the components normally arising in the d-c side but, for any particular harmonic thus affected, the relative phase angles of these two respective contributions are not usually known. In all of these cases the rms value of a particular harmonic contribution which may thus come through from the a-c side to the d-c side, expressed in per cent of the direct output voltage, is by itself approximately 0.7 times the percentage value of the harmonic on the a-c side which thus produces it.

Principles Underlying Harmonic Generation in Simple 6-Phase Rectifier

The way in which harmonic voltages arise in the output of a simple rectifier is illustrated by the following.

Figure 15 shows the circuit of a simple 6-phase rectifier. Although this delta 6-phase star circuit now is rarely employed in practice, it is useful here in simplifying the explanation of harmonic generation in that it has no interphase transformers. Hence the six windings constitute a single

Table VII. Summary of Studies Made, in a Few Selected Cases, of Output Sides of 600-Volt D-C Traction Rectifier Installations

Case	Direct-Current System*				Output Wave Shape			Exposure Conditions	Co-ordination Problems	Remarks
	Number of Units	Size of Each Unit (in Kw) and Number of Phases	General Arrangement	Type of Area Served	Approx. Total "Equiv. Inductance," Millihenrys	Voltage TIF ("1935" Weighting) Unfiltered	Voltage TIF ("1935" Weighting) Filtered	At D-C Load of (Per Cent or Amperes)			
1	2	1 200–6	Intermeshed	Urban					Chiefly aerial telephone cables on same highway but some effects from harmonic currents in underground cable sheaths	Numerous reports of severe noise immediate with inception of start of rectifier operation	No filter initially. Cable-sheath shielding applied and helped materially but not enough. Rectifier filter applied later. Excellent results
2	1	500–6		Urban and suburban		35			Toll cable with little exposure	None	Frequency of a-c supply was 40 cycles
3	3	1 400–6	Intermeshed	City	6.5/9.0 Exposed feeder only)	40 With series reactor in output)	8 or 9	2,000[a]	Aerial telephone cable for about 2,000 feet mostly at highway separation—to one trolley-feeder	Considerable number of reports of undesirable noise conditions when first unit went into service (with 0.3 mh reactor in series, pending planned addition of resonant shunts	Addition of resonant shunt branches, plus some changes in telephone circuits, eliminated problem
4	2	1 200–6	Straight-away and d-c interconnects with "5"	City "a" plus suburban	1.15	60–70	11	Light	Trunk circuits in underground cable 2½ miles. Exchange circuits mostly in underground cable but several long runs of aerial cable in joint use, for 1/2 mile or so. Reference 5	Serious noise experienced on exchange circuits. Noise increases of order of 10 to 1, some higher. Affected area about 1¼ miles long by 1/2-mile wide	No filter initially. Rectifier filter here and one at "5"—plus some changes in telephone circuits—reduced noise in City "a" by at least 8 or 10 to 1
5	3	1 200–6	Straight-away. Also via 2 routes, to "4"	Suburban plus city "5"		110	35		Moderate in city "b" chiefly underground cable. Relatively small amount of aerial cable. Reference 5	Moderate noise problem in city "b." Rectifier in city "b" also sent harmonic currents, through ties, into "a"	Some changes in telephone circuits, plus filter on "5," remedied noise in city "b." Filter at "5" helped reduce noise in area "a"
6	1	600–6		Suburban and open country	3.5 to 4.7	145	20		Open-wire telephone trunk circuits	Considerable amount of noise resulted from operation of rectifier	No filter initially. Installation of filter provided adequate solution
7	1	1,000[a]–6	Intermeshed	City	Ave. 1.5 1.3 mh at 8 ke.	82 120	18 F, 75 With series reactor only)	30%; 60%; 68%	Six underground telephone cables and five aerial cables affected. Exposures of 1/2 mile or more at highway separation. Some trunks exposed for over 2 miles at 100 to 500-foot separation	Numerous reports of high noise during times when rectifier was in service. (All types of telephone facilities.) Large part of a central office area affected	No filter initially. Changes in telephone circuits insufficient remedy. Then rectifier filter applied. These measures very effective. (Series reactor mentioned at left = about 0.6 mh.) "F" indicates complete filter, with series and shunt elements
8	2	500–6	Intermeshed	City	1.8 to 2.1	180 With One Rectifier Unit Operating	9–10	500[a]		None, with rectifier filtered	Rectifiers and filter installed at same time. Gave adequate reductions at original a-c supply frequency. Changed to 60-cycle supply, and retuned filters, later. Reductions still adequate. Output voltage TIF's shown correspond to 60-cycle operation
9	2	500–12	Mesh 9 has several radiating feeders	Same city as "8"	0.5 to 0.6	55 With One Rectifier Unit Operating	5	1 400[a]	Exchange cable. About 3,000 feet. Separation about 65 feet	None, with rectifier filtered	
10	1	1,000–6	Intermeshed	City	1.10–1.45	95	12	225[a]	Chiefly underground telephone cable. Noise-frequency currents from rectifier existed in these cable sheaths	Undesirable noise conditions without filter resulted over considerable part of a central office area	Initial installation. No filter at start. Co-operatively solved by adequate rectifier filter plus changes in telephone plant
	1	500–6			0.4–0.6	140	20	1 600[a]			
	Total 2	1,500–6			0.3–0.45	170	30	2,600[a]			
11	1	750–6	Intermeshed	City		200		700[a] 55%	Long haul open wire toll line had some exposure. Little exchange exposure	One toll group had severe noise. A few reports of exchange circuit noise	Remedied by changes in telephone plant. No filter on rectifier, pending experience
12	1	1,500–6	Intermeshed	same city as "11"	0.1 to 0.6	190		2 000[a] 80%	Very little direct exposure. Rectifier harmonic currents found to exist in underground sheaths	Undesirable noise. Considerable area. Chiefly at subscriber stations fed from aerial, out of underground cable	No filter initially. Changes in telephone circuits gave reductions but not enough. Rectifier filter installed later, with excellent results
13	1	500–6	Straight-away	City					Railroad company's own telephone dispatch circuits	Serious noise problem on railroad's dispatch circuits	Planned filters plus changes in railroad dispatch circuit
14	1	500–6	Straight-away	Country							
15	1	1,000–12	Straight-away	Country					Railroad's private telephone cable on railroad's right-of-way	No rectifier filter. No noise troubles reported	There are eight other substations. Have converters. Average spacing, about 8.25 miles
16	1	2,500–12		City					About 2,000 feet of aerial telephone cable between "16" and "17"	No rectifier filter. Moderate noise experienced	A-c supply frequency was 25 cycles. Cable sheath shielding was applied and gave
17	1	2,500–12									

commutating group which carries all of the output current I_d. Here, q the total quantity, that is, the total number of rectifier phases and p the number of phases *per commutating group* are, therefore, both equal to 6.[38] These quantities q and p for several types of rectifier are shown in Table VI.

It should be borne in mind that current flow in any individual tube takes place when a positive voltage is impressed on the anode with respect to the cathode after the tube is made conductive. Under the condition of free conduction, each anode is permitted to start firing as soon as its voltage becomes positive with respect to the cathode. If phase control is applied, the start of conduction is further delayed by various means.[2, 4, 11, 12, 39]

The manner in which the corresponding harmonics characteristically arise in the normal operation of the d-c end of a rectifier such as shown in Figure 15 can be visualized from Figure 16, applying to the condition of no phase control, and Figure 17, applying to the phase-controlled condition. It is assumed here that the a-c supply circuit is balanced, with its 3-phase voltages 120 degrees apart and sinusoidal in form.

In these latter two figures e_1, e_2, and e_3 illustrate, symbolically, three of the six phase-to-neutral voltages applied to the respective anodes of a 6-phase rectifier by the rectifier transformer, the crest value of each of these voltages being E_o. The rms value of E_o, namely, 0.707 E_o, is referred to as E_s in various parts of this report. The theoretical output voltage wave shape is indicated by a heavy trace e_d in these figures. With the particular rectifier circuit shown on Figure 15, the equivalent no-load voltage, without phase control, and the actual direct voltage at no load are identical in magnitude and are $E_{do} = 1.35\ E_s$, as indicated in Table VI.

Referring, for simplicity, to two successive anodes, such as R_1 and R_2 of Figure 16, what transpires from the standpoint of wave shape is essentially as follows:

No-Load Conditions

First, assume conditions such that the load on the d-c side is very small, being just sufficient to maintain the arc in the rectifier. Substantially no-load conditions then exist.

Without Phase Control. Refer to Figure 16(A) and consider anode R_1 to be firing, with no phase control. At point A, anode R_2 takes up the firing while anode R_1 ceases to fire.

With Phase Control. Refer to Figure 17(A) and assume that the start of conduction by anode R_2 is delayed beyond point A by phase control applied for a period of time AB represented by the electrical angle α. Under this condition, an anode such as R_1 continues to fire despite the fact that its voltage is lower than that of the next succeeding anode such as R_2. The angle α is known as the angle of retard and the average value of the direct voltage is decreased by increasing this angle.

Under Load

Transfer of load current from anode R_1 to anode R_2 begins at point A on Figure 16(B), without phase control and at point B on Figure 17(B) with phase control. However, this transfer cannot take place instantaneously since it is opposed by the reactance of the two rectifier transformer windings associated with anodes R_1 and R_2 plus that of the a-c supply line, namely by the total commutating reactance. This transfer of current from one anode to the next is called commutation. Its duration in time is represented by the interval AC in Figure 16(B) and BC in Figure 17(B). These time intervals correspond to a so-called angle of overlap, indicated by u on Figure 16(B) without phase control and by u_α on Figure 17(B) with phase control. The subscript α has been added to the symbol u in Figure 17(B) to emphasize the fact that, for any specific magnitude of load current thus commutated, the angle of overlap with phase control on a particular rectifier is smaller than it would be for the same rectifier free-firing. During commutation, the d-c output voltage is the average of the voltages for anodes R_1 and R_2 for the period considered. At the end of the commutating period, namely, at C in Figures 16(B) and 17(B), anode R_1 stops carrying current and the d-c circuit voltage rises to e_3, the value corresponding to anode R_2. The anode current changes during commutation, but the sum (the total commutated current I_c) is at all times equal to the assumed constant d-c output current I_d for the particular rectifier circuit shown on Figure 15. (For rectifiers with interphase transformers, I_c is only a certain part of I_d, as emphasized later.)

The existence of ripples, namely, harmonics, in the output voltage wave is evident from Figures 16 and 17. As already indicated, the presence of these harmonics together with their respective frequencies and theoretical magnitudes can be demonstrated by means of the Fourier series.

In analyzing the wave shapes of the d-c ends of ordinary 6-phase and 12-phase rectifiers it has been found that the assumption of a steady direct current, at any particular load, gives sufficient accuracy for most practical purposes. To facilitate such analysis, it is generally assumed that the d-c system (including the load) supplied by the rectifier is of relatively high inductance.

Harmonic Generation in Rectifier Circuits Having Interphase Transformers

Reference is made, in this Appendix, to the term p, namely, the number of phases per *group* of rectifier transformer secondary windings, that is, on the rectifier side. The significance of this term as contrasted with q (=the *total* number of rectifier phases), for types of connection where this distinction is necessary, is illustrated by Figure 18, which is of itself concerned with the delta 6-phase double-Y connection employing interphase transformers. In the following paragraphs, the interphase transformer exciting current is assumed to be negligible.

6-Phase Double-Y Circuit

In the 6-phase double-Y rectifier circuit shown on Figure 18, the rectifier transformer d-c winding is connected in two individual 3-phase groups, or wyes, with their neutral points interconnected by an interphase transformer, the phase-to-neutral voltages of one group (as 1–3–5) being displaced collectively by 60 degrees from the voltages of the other (as 2–4–6). Also see Principles of Operation, in reference 7. Thus, the respective voltages-to-neutral of the two 3-phase units present, in effect, a synchronous aggregation of six voltages-to-neutral spaced 60 degrees apart in time phase, with a consequent q of 6, while p is 3 over most of the operating range, as indicated in Table VI.

The action of the interphase transformer is such that each Y and the three rectifying elements connected to it constitute a commutating group (hence $p=3$, for this connection) which carries a direct current I_c. The two commutating groups operate in parallel, and each carries substantially one-half of the total direct current I_d.

The direct voltage of the rectifier e_d is shown by the heavy trace in the lower part of Figure 18 and is the average of the direct voltages of the two commutating groups e_{d1} and e_{d2}. The difference between the voltage waves of the two commutating groups is shown by the shaded areas. This voltage appears across the interphase transformer itself, and it is an alternating voltage having a fundamental frequency three times that of the phase voltages.

Except at no load and at very light load currents the rectifier behaves as if E_{do} were 1.17 E_s, that is, a value which corresponds to the use of $p=3$. This is the value of E_{do} which would be used, over most of the operating range, in computing harmonic magnitudes by the methods outlined in other literature.[4] At no load or at very light load currents, the interphase transformer is not fully effective and the corresponding $E_{do} = 1.35\ E_s$ (as if p were 6), but above this relatively narrow lower range of load currents the equivalent E_{do} is 1.17 E_s, as indicated in Table VI and as just shown. (See reference 39, page 139.)

Delta 12-Phase Quadruple Zigzag Circuit

By analogy with the immediately preceding paragraphs, it can be seen that with the 12-phase quadruple zigzag connection having interphase transformers, illustrated in Figure 1(C), the d-c windings are connected into four individual 3-phase groups, with their neutral points interconnected by the interphase transformers. The connections are such that the time phase angles of the phase-to-neutral voltages of each such 3-phase group are collectively displaced with respect to those of the other three individual groups in such a manner that the four 3-phase units present, in effect, a synchronous aggregation of 12 voltages-to-neutral spaced 30 degrees apart in time phase, with a consequent q of 12, while $p=3$ over most of the operating range.

The action of the interphase transformers is such that each Y (3-phase winding group) and the three rectifying elements connected to it constitute a commutating group (hence $p=3$ for this connection) which carries a direct current I_c. The four commutating groups operate in parallel on the output side, dividing the load substantially equally between them, and thus each group carries one-quarter of the total direct current I_d, that is, $I_c = I_d/4$.

Table VIII. Summary of Studies Made of Some "600-Volt" D-C Traction Rectifier Installations with Phase Control[1]

Case	Number of Units	Size of Each Unit (in Kw) and Number of Phases	D-C System: Type of D-c Service	D-C System: Approx. Total Equiv. Inductance, Millihenrys	Output Wave Shape: Voltage TIF ("1935" Weighting) Unfiltered	Output Wave Shape: Voltage TIF ("1935" Weighting) Filtered	Output Wave Shape: At D-C Load of (Per Cent or Amperes)	At Phase Control Angle of Delay of	Exposure Conditions	Co-ordination Problems	Remarks
18.	1	3,000–12,...	Street railway (in... large city	0.4 to 0.2...	50 to 70		3,000 to 2,400.....		..Aerial cable—0.7 mile plus 0.2 mile of joint use .Aerial cable—1/3 mile at 120 140 ft Aerial cable—1/2 mile at 180 ft quately	..Numerous reports of adverse noise started soon as rectifier began operation. Subsequent extensive changes in telephone plant helped but not ade-	..No rectifier filter initially. Filter was installed subsequent to telephone plant changes (which included cable-sheath shielding, et cetera)
						9 to 13	4,850 to 2,400				
19.	.1.....3,125–6		Surface trolleys and el lines	0.3 to 0.45	170 to 260	25 to 40	2,600 to 5,500	15°	Substantial exposure of telephone cables to surface d-c feeders and trolleys	Telephone circuit noise problem resulted when rectifier was 1st operated (no filter)	Filter applied. D-c end of this rectifier was interconnected with other substations (such as 18 and 20) in same city
20.	1	3,125–6	Trolleys and el lines (same city as 18 and 19)	0.15 to 0.3...	65 85	16 20	1,000 to 3,500	30°	..Moderate exposure of telephone cables (500 to 1,000 feet, at 25-foot separation)	..Filter was applied to rectifier.....	..Angle of delay used normally ranged from 30 to 45 degrees; manually controlled to keep the d-c voltage within the range 620 to 625 volts
					135 165	25 35	1,000 to 3,000	45°			
21.	..:.....2,000–12,... (With supply at 50 cycles)		Street railway in large city	1.9 to 0.6	180		3,500	See "Remarks	.Local telephone circuits exposed in both open wire and cable, with several exposures 0.5 to 0.7 mile long at separations of 50 60 feet. Railway company's own telephone circuits were exposed also	..No filter initially. Severe noise then experienced on telephone circuits of both the telephone company and the railway company. Changes in telephone circuits, plus cable sheath shielding, effective but remaining noise not as low as desirable. "Tuned series reactors," plus fairly large shunt capacitor on load side thereof then applied with good results	
					120 140	40 55	2,000	marks			
					200	55 100	1,000				
					230	.....	500				
Same after frequency of a-c supply was changed to 60 cycles				2.5 to 0.15...	265 to 240...	50 to 45...	1/2 to full load	Large (see "Remarks")	.....	..Filter was retuned when supply frequency changed to 60 cycles With either 50 or 60-cycle supply, it was necessary to use relatively high degree of phase control (due to lack of enough transformer taps). (Transformer—formerly used at another location—had been rewound)	
22	.1.....1,000–6		Street railway	0.2 to 0.25... (max. 0.3)	145	50	600	.....	..Rather extensive exposures (cable and some open wire) to aerial d-c feeders radiating from some underground d-c feeders	..No filter initially. Numerous reports of serious noise, immediately following placing in service of the rectifier. Cable sheath shielding and other changes in telephone plant helped but not enough D-c filter installed later	
					210 to 125	42 to 35...	800	...Various			
					170 to 120...	37	1,000	..Various			

At no load or at very light loads, the interphase transformers are not fully effective, as in the 6-phase double-Y connection mentioned previously, and the corresponding $E_{do} = 1.40\ E_s$. Above this relatively narrow extreme lower range, however, the equivalent E_{do} is 1.17 E_s.

Some Uses of the Reactance Factor (I_cX_c/E_s)

In computing certain relations concerned with rectifiers, and in showing these relations graphically, the employment of the so-called reactance factor[2] is often useful, as will be noted from other literature.

For example, as indicated previously in this Appendix, commutation or load current transfer requires a definite time, or commutating angle u, an electrical angle which depends upon the commutating reactance and the commutating voltage. This angle increases with increasing commutating reactance X_c or increasing commutated current I_c and decreases with increasing commutating voltage (which is proportional to E_s), all three of these quantities being expressed with reference to the output side. In other words the angle of overlap without phase control, an electrical angle which is indicated by u on Figure 16(B) and in the left-hand side of Figure 18, is dependent upon the reactance factor, I_cX_c/E_s. On the other hand with an amount of phase control corresponding to an angle of retard of α degrees, the angle of overlap (indicated by u_α on Figure 17(B) and in the right-hand side of Figure 18), is dependent not only upon I_cX_c/E_s but upon the angle α as well.

As mentioned before, for rectifier transformer connections using balanced 3-phase supply, but not employing interphase transformers, I_c is generally the same as the total rms load output current I_d. However, where interphase transformers are present in the rectifier circuit, the current I_c actually commutated in any one group of windings can be one-half, or one-quarter, and so on, of the total rms load current, depending upon the type of rectifier transformer connection concerned. This is illustrated for certain rectifier circuits in Table VI and also by pages 176–186 of reference 39.

Theoretical 6th, 12th, 18th, and 24th Harmonic Voltages

When the circuit constants, the voltage applied to the rectifier, the load current, the type of rectifier circuit, and the desired output voltage with phase control (if used) are known, the angle of retard α and the angle of overlap u_α or u can be estimated by means of the information and equations given in other literature. Corresponding information which applies specifically to the particular rectifier circuits shown in Figures 1 and 15 is included in Table VI, see also Figure 24.

Using values of u and α thus derived, the harmonic voltages can be estimated by information contained in other literature.[4,38] Where it is desired to express such percentage values of rms harmonic voltages with reference to the d-c voltage under load E_d, rather than with respect to the corresponding no load voltage E_{do} without retard, the values determined with reference to E_{do} can be multiplied by the appropriate

Table IX

Section	Number of Tracks	Number of Substations	Rectifiers: Per Substation	Rectifiers: Size in Kw	Rectifiers: Phases	Approx. Spacing
(a)	4	20	1	3000	12	1/2 mile
		1	3	3000	12	
(b)	4	9	1	3000	6	2,000 ft.
(c)	2	5	1	3000	6	3,000 ft.

ratio E_{do}/E_d as obtained, for example, with the aid of Figure 23.

The theoretical 6th, 12th, 18th, and 24th harmonic voltages thus computed, and plotted with respect to the reactance factor, with various degrees of phase control and over a load range, for several types of rectifiers, are shown in the publication listed as reference 4. They, together with certain additional curves corresponding to a voltage control ratio of 0.85 (that is, for $RV=0.85$), are given on Figures 19, 20, 21, and 22, for the convenience of the reader. The harmonic percentage magnitudes shown on these four figures are general rather than applying solely to rectifiers having a 60-cycle a-c supply. The significance of the symbol RV, as used on the figures just mentioned, together with the approximate values of the angle of retard corresponding to the several degrees of phase control thus indicated, are shown in Items 1 and 2, respectively, of Table IV.

Curves of Regulation, Angle of Overlap and Angle of Retard

On Figure 23, the d-c output voltage expressed as a percentage of the equivalent no load voltage with no retard (that is, with no phase control) is plotted as a function of I_cX_c/E_s (for $p=3$) for various different values of voltage control ratio RV. Over the range shown, these regulation curves are substantially straight lines. Figure 24 shows the angle of overlap (u or u_α) and the angle of retard α (for the phase-controlled case) as functions of I_cX_c/E_s for various different values of RV.

On Figures 23 and 24, the angles u and α and so on are, for convenience, plotted with reference to various values of I_cX_c/E_s. It should be understood, however, that the term I_cX_c/E_s does not of itself alone determine these angles and the various harmonic magnitudes but that the term $(\sqrt{2}\sin 180°/p)$ must be included in the denominator of that quantity when computing the theoretical magnitudes of u, u_α and of the harmonics, for any specific rectifier connection. For this basic reason, and in order to make the curves of Figures 23 and 24 applicable to a wider variety of connections than those for which $p=3$, a scale is given on the upper part of each of these figures showing values of I_cX_c/E_s for $p=6$. In the absence of the simpler process mentioned just below, it would be necessary to use this upper scale for a rectifier transformer connection as, for example, a delta 6-phase star, to which this value of p applies.

However, an equivalent but more practical procedure, in the case of a rectifier transformer connection where $p=6$, is to multiply the actual value of I_cX_c/E_s for that specific connection by 1.73 and then to enter directly the (lower) scale of abscissa for $p=3$, Figures 23 and 24, with this adjusted value.

Another simplification in the use of these figures results from the fact that, for each specific type of rectifier transformer connection, there is a direct relation between the total per cent commutating reactance $\%X_{cn}$ and the quantity I_cX_c/E_s. This relation is shown in Table VI, for the several common types of rectifiers specifically treated in this report, thus making it possible to determine the value of I_cX_c/E_s directly from the $\%X_{cn}$ in specific cases involving these particular types of rectifiers, without having to compute X_c, I_c, or E_s separately. This does not obviate the process of further multiplying the actual value of I_cX_c/E_s by 1.73 where it is desired to enter the lower scale of Figure 23 or 24 directly, in cases where $p=6$, referred to in the preceding paragraph.

Appendix III. Examples of Types of Situations Studied

General—Tables VII and VIII

A few of the 600-volt d-c traction rectifier installations where the output side has been studied are summarized in Table VII. Similar information for several such installations known to be equipped for phase control is given in Table VIII. These tables are concerned primarily with rectifiers whose outputs supply d-c overhead trolley-feeder systems having rail return.

The numerical data do not constitute any sort of specification and the order in which the respective items are listed has no significant bearing upon their relative importance. The illustrative material in these two tables concerns only some of the rectifier installations which, in various ways, have come to the attention of the several national headquarters organizations which have participated in the preparation of this report. Hence the data should not be considered as fully statistical in nature.

All of the values of voltage TIF given in Tables VII and VIII are expressed in terms of the "1935" TIF weightings shown in the 1946 report and have been derived from the test results of specific harmonic analyses.

Discussion of Items 1–22

Where the information with a given item indicates that a d-c filter was installed, the filter was of the general type illustrated by Figure 2, except that for Item 21 the filter consisted of two tuned series reactors plus a fairly large shunt capacitor on the load side thereof.

For all items except 2, 16, and 17 the frequency of the a-c power supply system was 60 cycles (with the further exception of the original operating frequency noted under Item 21). Item 2 had a supply frequency of 40 cycles, while for Items 16 and 17 the frequency was 25 cycles.

Item 1 concerns one of the earlier rectifier installations. It required considerable basic study as to remedial measures and so forth. Detailed wave shape data on it are not now available. Several rectifier substations having a total rating of about 14,000 kw were subsequently installed on the same street railway system and, on the basis of the technical and operating experience with Item 1, a d-c filter was included in each of these later installations. Item 2 also was an early installation and it is possible that a series reactor was included in the output when the rectifier was installed.

Items 3, 4, 6–10, and 12 have been chosen to cover, in part, a range of d-c system equivalent inductances L_L but it also must be remembered that with zero phase control the output $I \cdot T$ product generally increases with increased direct load current.

Items 11 and 12 are illustrative of the fact that the specific exposure conditions, namely, conditions external to the rectifier itself, have an important bearing upon the respective inductive co-ordination problems presented by different individual rectifier installations. In these two items, the rectifiers, which are connected to the same d-c system, did not have identical kilowatt ratings but this particular difference had of itself no large bearing on their respective noise coordination problems.

Although noise resulting from inductive effects experienced in direct exposures of aerial communication plant to overhead d-c trolley-feeder systems was of primary importance in many of the situations covered by Items 1 to 12, inclusive, it will be seen that in Items 1, 10, and 12 harmonic currents were found to exist in underground cable sheaths (accompanied by more or less noise). In certain instances, not listed in the tables, noise arising from conductive effects has been experienced in the general vicinity of rectifiers supplying d-c traction systems having ground-rail return.

Items 13, 14, and 15 illustrate instances where the noise experienced on the traction, companies' own communication circuits rather than on commercial telephone circuits, was of primary importance under the unfiltered condition of the rectifiers.

The items shown in Table VIII are indicative of the greater output wave distortion which can occur with rectifiers having phase control, as contrasted with those which are not so equipped. The magnitudes of the voltage TIF's in Items 10, 11, and 12 of Table VII suggest the possibility that the latter rectifiers, too, were phase controlled. On the other hand the relatively low impedance of these three d-c systems could also, of itself, have had an important bearing upon the magnitudes of the $I \cdot T$ products.

In addition to the situations covered by Items 1–22, it is of interest to note that undesirable noise conditions were encountered comparatively recently in a situation involving a rectifier installation supplying a trolley-coach d-c system where capacitance-type lightning arresters

were used on the positive d-c feeders. In that particular instance, the noise difficulty was remedied by the installation of a suitable protective gap in series with each arrester, thus removing the effective capacitance of the latter from the d-c system during normal operation.

Subway Systems

To date, no important noise induction has been experienced from the output ends of rectifiers which supply power to the 600-volt d-c traction circuits associated with extensive sections of subway transportation systems of the types existing in several large cities. Examples of these are given in Table IX.

There were no positive or negative feeders between substations in Items a, b, and c of Table IX. The propulsion circuit for each track consisted of a third rail and one of the running rails.

In Item a, as in Item b, there was an extensive telephone plant in underground cable, in the streets above the subway, along the entire route. In Item c there were from one to several such exposed underground cables along the various parts of the subway route. It seems evident that in these three installations the harmonics from the output of the rectifiers were confined largely to the rails themselves and that, in addition, there was an unknown amount of shielding due to various cable sheaths, water and gas pipes, metallic constituent parts of the subway structure itself, and so forth.

Above-Ground Third-Rail Traction Systems

A number of steam railroads which have electrified considerable parts of their trackage at about 600 volts, direct current, have employed the third-rail system and in several such instances have used rectifiers, aggregating many thousands of kilowatts, as at least a part of their source of d-c supply. While no important noise problems directly ascribable to inductive effects from the d-c end have been reported, there have been a few instances where excess noise attributable to conductive effects in the generally immediate vicinity of points of direct grounding of one side of the d-c system (as might be done, for example, at the individual rectifier stations) has been experienced.

However, severe noise induction problems have been encountered on the a-c side of a number of the rectifiers associated with several of these railroad electrifications. In one such instance, involving something over 100,000 kw of installed rectifier capacity, the problem on the a-c side involves an extensive area and is still under co operative study.

References

1. Inductive Co-ordination Aspects of Rectifier Installations, **AIEE Committee Report.** (*AIEE Transactions*), volume 65, July 1946, pages 417–36.

2. Standard for Pool Cathode Mercury-Arc Power Converters. *C34.1-1949*, American Standards Association (New York, N. Y.), January 1949. (Formerly AIEE Report Number 6).

3. Current and Voltage Wave Shape of Mercury-Arc Rectifiers, **H. D. Brown, J. J. Smith.** *AIEE Transactions*, volume 52, December 1933, pages 973–80.

4. Output Wave Shape of Controlled Rectifiers, **F. O. Stebbins, C. W. Frick.** *Electrical Engineering* (*AIEE Transactions*), September 1934, pages 1259–65.

5. Effect of Street Railway Mercury-Arc Rectifiers on Communication Circuits, **C. J. Daly.** *AIEE Transactions*, volume 47, July 1928, pages 503–6.

6. Measurement of Telephone Noise and Power Wave Shape, **J. M. Barstow, P. W. Blye, H. E. Kent.** *Electrical Engineering* (*AIEE Transactions*), volume 54, December 1935, pages 1307–15.

7. Protection of Electronic Power Converters, **AIEE Committee Report.** *AIEE Transactions*, volume 69, part II, 1950, pages 813–29.

8. Analysis of Rectifier Circuits, **E. F. Christensen, C. H. Willis, C. C. Herskind.** *AIEE Transactions*, volume 63, 1944, pages 1048–58.

9. Mercury Arc Power Converters in North America, **AIEE Committee Report.** *AIEE Transactions*, volume 67, part II, 1948, pages 1031–59.

10. Harmonics and Load Balance of Multiphase Rectifiers; Considerations in the Selection of the Number of Rectifier Phases, **R. D. Evans.** *AIEE Transactions*, volume 62, April 1943, pages 182–87.

11. Voltage Control of Vapor Rectifiers, **D. Journeaux.** *Electrical Engineering* (*AIEE Transactions*), June 1934, pages 976–88.

12. Grid-Controlled Rectifiers and Inverters, **C. C. Herskind.** *Electrical Engineering* (*AIEE Transactions*), 1934, pages 926–35.

13. Ignitron Rectifiers in Industry, **J. H. Cox, G. F. Jones.** *AIEE Transactions*, volume 61, October 1942, pages 713–18.

14. Pentode Ignitrons for Electronic Power Converters, **H. C. Steiner, J. L. Zehner, H. E. Zuvers.** *AIEE Transactions*, volume 63, October 1944, pages 993–97.

15. Development of Excitron-Type Rectifier, **H. Winograd.** *AIEE Transactions*, volume 63, 1944, pages 969–78.

16. The Electronic Converter for Exchange of Power, **F. W. Cramer, L. W. Morton, A. G. Darling.** *AIEE Transactions*, volume 63, 1944, pages 1059–69, 1413.

17. Design of Electronic Frequency Changer, **C. H. Willis, R. W. Kuenning, E. F Christensen, E. D. Bedford.** *AIEE Transactions*, volume 63, 1944, pages 1070–78.

18. Frequency Changers—Characteristics, Applications and Economics, **S. B. Crary, R. M. Easley.** *AIEE Transactions*, volume 64, June 1945, pages 351–58.

19. Electric Equipment for Large Electrochemical Installations, **T. R. Rhea, H. H. Zielinski.** *AIEE Transactions*, volume 61, October 1942, pages 733–41.

20. Group of articles on application of electric conversion equipment to the electrochemical industry, *Electrical Engineering*, October 1947, pages 957–63, November 1947, pages 1063–82.

21. Mercury-Arc Rectifiers for Railroads, **S. S. Watkins.** *AIEE Transactions*, volume 64, February 1945, pages 84–6.

22. High Voltage Ignitron Rectifiers and Inverters for Railroad Service, **J. J. Boyer, C. G. Hagensick.** *AIEE Transactions*, volume 65, July 1946, pages 463–70.

23. Mercury-Arc Rectifiers in the Coal Mining Industry, **D. E. Renshaw.** *AIEE Transactions*, volume 59, April 1940, pages 242–4.

Reports of Joint Subcommittee on Development and Research—Edison Electric Institute and Bell Telephone System

24. Selective Devices for Reducing Harmonics in Power Systems: Part I, D-C Systems, Engineering Report 21.

25. The Impedances of A-C Supply Systems at Harmonic Frequencies to Residual Components, Engineering Report 24.

26. The Impedances of A-C Supply Systems at Harmonic Frequencies to Balanced Components, Engineering Report 23.

27. Relative Interfering Effects of Different Single Frequency Noises in Telephone Circuits, Engineering Report 32.

28. Frequency Weighting for Message Circuit Noise, Engineering Report 45.

29. The Telephone Influence Factor of Supply System Voltages and Currents, Engineering Report 33.

30. A Method of Estimating Noise in Open Wire Toll Circuits, Engineering Report 16.

31. Short-Cut Methods for Estimating Noise in Open Wire Subscriber Circuits Exposed to Power Lines at Roadway Separations, Engineering Report 17.

32. Short-Cut Methods for Calculating Noise in Open Wire Subscriber Circuits Due to Joint-Use Exposures to Power Distribution Circuits, Engineering Report 13.

33. The Use of Power and Telephone Transpositions within Exposure Sections, Engineering Report 36.

34. Effects of Bonding Exchange Aerial Telephone Cable Sheaths to Multi-Grounded Power Neutrals, Engineering Report 43.

35. Susceptiveness of Subscriber Station Sets, Engineering Report 46.

36. Wave Shape of Multiphase Rectifiers, Engineering Report 49.

Other Publications

37. Reports of Joint General Committee of Edison Electric Institute and Bell Telephone System on Physical Relations Between Electrical Supply and Signal Systems. *Publication M5*, Edison Electric Institute (New York, N. Y.), July 1945.

38. Rectifier Wave Shape, *Publication E1*, Edison Electric Institute (New York, N. Y.), April 1937.

39. Mercury-Arc Power Rectifiers (book), **Othmar K. Marti, Harold Winograd.** McGraw-Hill Book Company, Inc., New York, N. Y., 1930.

40. Electrical Transmission and Distribution Reference Book, Westinghouse Electric and Manufacturing Company.

41. Characteristics, Design and Application of Rectifier Transformers, **E. V. DeBlieux.** *General Electric Review* (Schenectady, N. Y.), September 1937, page 412; October 1937, page 481; November 1937, page 539; December 1937, page 568.

42. Mercury-Arc Heating Frequency Converter, **S. R. Durand.** *Electronic Industries* (New York, N. Y.), June 1945.

43. Mercury-Arc Frequency Changer Limits Rolling Mill Demand, **R. W. Holman.** *Electrical World* (New York, N. Y.), volume 125, April 13, 1946, pages 112–16.

44. Current and Voltage Characteristics of Grid-Controlled Rectifiers, **K. Mueller-Luebeck, E. Uhlmann.** *Archiv fuer Elektrotechnik* (Berlin, Germany), volume 27, number 5, May 3, 1933, pages 347–73.

45. Rectifier Transformer Equipment, *C57.18-1948*, American Standards Association (New York, N. Y.), 1948.

No Discussion

Analysis of a 3-Phase Inverter with Resistive Load

ROBERT E. TURKINGTON
NONMEMBER AIEE

Synopsis: Commutation in thyratron or ignitron inverters can be effected with the aid of capacitors connected across the output terminals of the inverter. Since these inverters require no transformers for commutation or coupling, they may be operated over a wide range of frequencies extending down to zero.

In this paper a simplified analysis is made of a 3-phase capacitor-commutated inverter with a resistive load when the inverter is operating with constant input current. Calculated waveforms of the inverter obtained from this analysis are presented for various values of load resistance. Experimental waveforms are included to evaluate the effect of ripple in the input current.

ALTHOUGH gas-tube inverters have had only moderate use in the past, they have potentialities of far wider applications in many fields. Possible applications include (1) use of inverters at the receiving end of a d-c transmission line,[1] (2) use of inverters to supply power to induction and synchronous motors[2,3] and (3) use of inverters in electric railway systems to allow power to flow from the d-c system to the a-c supply.[4] The polyphase inverter circuits described and analyzed in technical publications[2-5] were primarily designed for operation at a fixed frequency or over a limited frequency range. In these circuits transformers have been used frequently as coupling between the inverter and the a-c line, as interphase transformers, and as elements in commutation circuits. The use of transformers prevents these inverters from being operated at very low frequencies, that is, between zero and ten cycles per second. If operation of polyphase inverters can be extended down to zero frequency, inverters may be able to supply variable-frequency power to polyphase induction and synchronous motors, thereby providing continuously variable speed from zero to full speed in either direction. An inverter circuit capable of this type of operation is the 3-phase bridge-type inverter which is commutated by capacitors connected across the output terminals of the inverter.

It is the purpose of this paper (1) to describe the operation of the 3-phase capacitor-commutated bridge-type inverter, (2) to present a method of calculating the voltage wave-forms of the inverter with resistive load, and (3) to compare calculated and experimental waveforms for various load conditions. Also given are a normalized curve of deionization time as a function of load impedance as obtained from calculated output-voltage waveforms, and experimentally determined curves of inverter input and output voltages and output current plotted as functions of the load impedance.

Operation of the Inverter

When thyratron or ignitron tubes are used in a grid-controlled rectifier or in an inverter, conduction in the tubes is initiated when the grid potential is made positive with respect to the cathode. The grid potential is then made negative at or before the end of the tube conducting period. However, the grids alone are ineffective in terminating conduction, and the tubes must be deionized by forcing the anode-to-cathode voltage of the tube negative. In a polyphase rectifier where the anode potentials are determined by the transformer secondary voltages and the cathodes are commonly connected, the start of conduction in an incoming tube raises the cathode potential of all the tubes. Since the anode potential of the outgoing tube is being decreased by the transformer secondary, the anode-to-cathode voltage of the outgoing tube is made negative and the tube is extinguished. This process of transferring conduction from one tube to another is called phase commutation. Phase commutation occurs in inverters when the a-c voltages are determined by the load, as when an inverter is operating into an a-c power system. If the inverter load is not capable of determining the output voltages, phase commutation is not possible. However, the inverter may be commutated by capacitors connected across the output terminals of the inverter. These capacitors act to reverse the anode-to-cathode voltage of the tubes at the proper times, assisting in the transfer of conduction from tube to tube.

The parallel-capacitor method of commutation in a 3-phase full-wave bridge-type inverter can be observed by following one cycle of inverter operation. Consider the inverter shown in Figure 1. Assume that the tubes are fired in the order 1, 6, 3, 2, 5, 4 and that tubes 5 and 4 are conducting. A conducting path exists through the input inductance L, tube 5, the load network, and tube 4. (The term "load network" is used to designate the load resistors and the commutating capacitors. The term "load" is used to designate only the load resistors.) The capacitors are charged with the polarities indicated in Figure 1(A), and if a steady state has been reached for this conduction period, the three output voltages neglecting the tube drops and the resistance of the input inductor are

$$v_{ab} = \frac{1}{2}E_s, v_{bc} = -E_s, v_{ca} = \frac{1}{2}E_s \qquad (1)$$

where E_s is the value of the direct voltage source of the inverter. The potential of

Paper 51-210, recommended by the AIEE Electronic Power Converters Committee and approved by the AIEE Technical Program Committee for presentation at the AIEE Summer General Meeting, Toronto, Ont., Canada, June 25–29, 1951. Manuscript submitted March 22, 1951; made available for printing May 1, 1951.

ROBERT E. TURKINGTON is with the Massachusetts Institute of Technology, Cambridge, Mass.

The author wishes to thank Professor G. C. Newton and Professor A. Kusko for their assistance in preparing this paper.

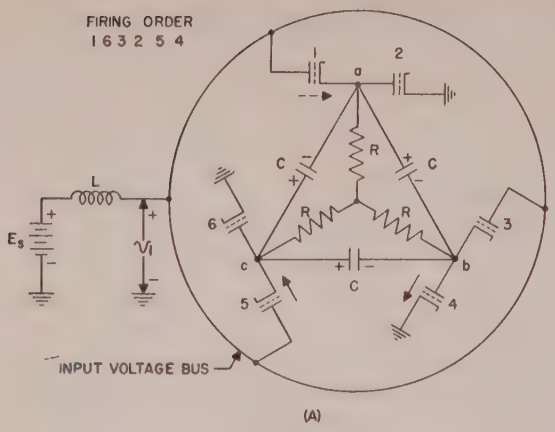

Figure 1 (left). Three-phase inverter with resistive load

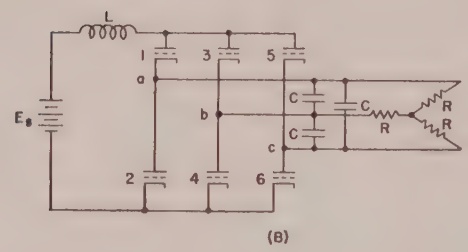

Figure 3 (right). (A) Normalized anode-to-cathode voltage waveforms of tubes 1 and 3 for $\tau f = 0.030$. (B) Normalized waveform of the input voltage for $\tau f = 0.030$

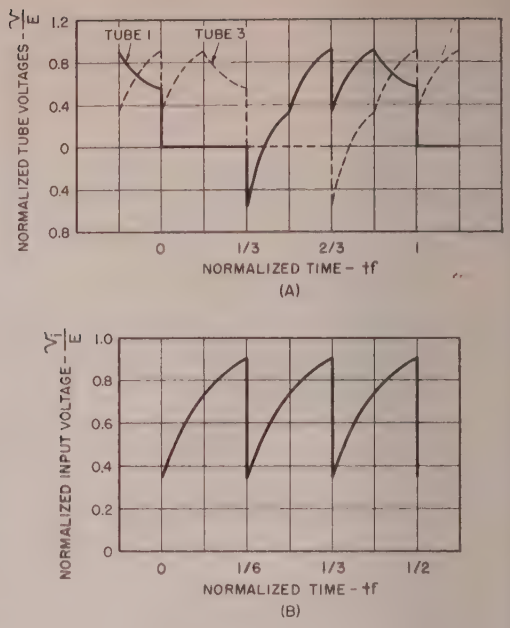

the input bus with respect to ground is E_s and the voltage across tube one is $(1/2)E_s$. (It is assumed that a steady state is reached after each switching operation in order that the various voltages can be easily specified in terms of E_s. During normal operation of the inverter, a steady state is usually not reached.)

Assume that tube one now fires. Node b is held at ground potential, and since the charges on the capacitors cannot change instantaneously, the potential of each node relative to ground remains fixed. The ignition of tube one connects node a to the input voltage bus, and the potential of the bus is immediately dropped by $(1/2)E_s$ volts to the potential of node a. The anode of tube five is also dropped by this amount, forcing it $(1/2)E_s$ volts below the cathode. If the anode potential remains below that of the cathode until deionization takes place in the tube, tube five ceases to conduct. A new conduction path now is established through tubes one and four.

If a steady state is reached for this conduction period, the voltages between the nodes are

$$v_{ab} = E_s, v_{bc} = -\frac{1}{2}E_s, v_{ca} = -\frac{1}{2}E_s \qquad (2)$$

Since tube four is conducting, node b is still at ground potential, and the potential of node c is $(1/2)E_s$. Node c is immediately dropped to ground potential when tube six fires, causing the other two nodes and the input bus to drop by a potential of $(1/2)E_s$. As a result node b and the anode of tube four are forced $(1/2)E_s$ volts below its cathode, and tube 4 ceases to conduct if the tube deionizes. Current now flows through tubes 1 and 6, and if a steady state is again reached, the output voltages are

$$v_{ab} = \frac{1}{2}E_s, v_{bc} = \frac{1}{2}E_s, v_{ca} = -E_s \qquad (3)$$

This process may be continued until tubes 5 and 4 are again conducting, at which time one cycle of operation will have been completed.

The following observations can be made from the foregoing description:

1. The function of the input inductance L is to isolate the input voltage bus from the voltage source, thus allowing the bus voltage to fluctuate.

2. The capacitors are used to extinguish the thyratrons by reversing the anode-to-cathode voltage of the tubes. The capacitors must be large enough to maintain the anode-to-cathode voltage negative until the tubes can deionize.

3. Each tube conducts for one-third of a cycle. There are always two tubes conducting simultaneously except during commutation when three tubes conduct. Commutation takes place every one-sixth of a cycle.

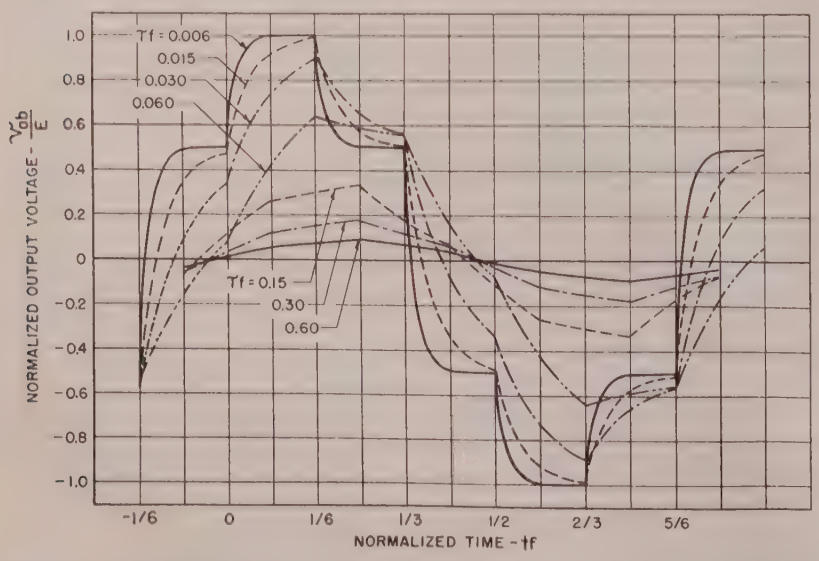

Figure 2. Normalized output-voltage waveforms (v_{ab}/E) for various values of the load-network time constant (τf)

Nomenclature

C = value of delta-connected commutating capacitors
D = constant arc drop of the tubes
$E = 2IR$ = maximum steady-state output voltage
E_s = voltage source of the inverter
I = value of constant input current
I_c = calibrated current in oscillograms
I_o = rms value of output current
L = value of input inductance
R = value of the y-connected load resistors
V_c = calibrated voltage in oscillograms
V_i = average value of input voltage
V_m = peak value of the output voltage
V_o = rms value of output voltage
a, b, c = nodes of load network
ϵ = naperian base
f = frequency of grid excitation
i_a, i_b, i_c = source current flowing into nodes a, b, and c, respectively
i_i = input current
t = time
t_d = inverter deionization time
v_{ab}, v_{bc}, v_{ca} = output voltages of the inverter
$v_{ab}', v_{bc}', v_{ca}'$ = output voltages of the inverter when i_b is zero
$v_{ab}'', v_{bc}'', v_{ca}''$ = output voltages of the inverter when i_a is zero
v_1, v_2 = anode-to-cathode voltages of tubes one and two, respectively
v_i = input voltage to inverter (source voltage minus the input-inductance drop)
$x = 1/(6\tau f)$ = normalized reciprocal time constant
$\tau = 3RC$ = load-network time constant

Calculated Performance

Inverter Waveforms

Determination of the waveforms of the inverter shown in Figure 1 consists of the analysis of a 4-loop network with three independent initial conditions. In order to evaluate the initial conditions, one-half cycle of operation, including four commutation periods, must be considered. The analysis can be greatly simplified by assuming the input inductance to be infinite. The infinite inductance forces the input current i_i to be constant at some value I. This constant input current permits a simplified analysis to be made which was used to calculate various waveforms of the inverter. The analysis is presented in Appendix I.

On the basis of an infinite input inductance, waveforms of the output voltage, two tube voltages, and the input voltage were calculated. Figure 2 shows waveforms of the output voltage of one phase for various values of the load-network time constant. The time reference $t=0$ was chosen as the instant tube one fires. These curves, as well as those shown in Figure 3, are in a dimensionless form: the time scale (t) and the load-network time constant ($\tau = 3RC$) have been normalized with respect to the grid-excitation frequency (f), and the voltages have been normalized with respect to $E = 2IR$, the maximum output voltage that would appear if a steady state were attained between successive commutations. The waveforms of Figure 2 are similar to those calculated by C. F. Wagner for a single-phase inverter.[7]

The following observations can be made from these curves: If a steady state were reached after each commutation, the steady-state voltage would have one of four values, $\pm(1/2)E$ or $\pm E$, depending upon which tubes were conducting. A steady voltage is reached after each switching operation only for the curve $\tau f = 0.006$. If τf were decreased from this value, the capacitor charging time would decrease with respect to the period of the grid excitation, and the voltage would reach its final values more quickly. For the limiting case of $\tau f = 0$, the capacitors would charge in zero time, and the waveform would consist of a series of straight lines. As τf increases from the value 0.006, the capacitors do not have sufficient time to become fully charged, and the steady-state voltage is not reached. As a result the peak value of the voltage waves decreases.

In addition to the peak value of the waves changing as τf varies, the phase also changes. The zero-voltage point for the limiting case of $\tau f = 0$ would be located at $tf = -1/6$. The zero-voltage point of the curve corresponding to $\tau f = 0.60$, the largest value considered in Figure 2, occurs at approximately $tf = 1/12$. This represents a phase shift of about 90 degrees with respect to the previously mentioned limiting case.

Figure 3(A) shows the waveforms of the anode-to-cathode voltage of tubes 1 and 3 for $\tau f = 0.030$. The peak forward and inverse voltages appearing across the tubes are $0.90E$ and $0.57E$, respectively. A comparison of Figures 2 and 3(A) shows that the maximum value of peak forward voltage for varying values of τf is E and occurs when $\tau f < 0.015$; the maximum value of peak inverse voltage is about $0.57E$ and occurs when $\tau f \approx 0.030$.

Since tubes 3 and 5 are fired one-third and two-thirds of a cycle, respectively, after tube 1, the anode-to-cathode voltage waveforms of tubes 3 and 5 are the same as that for tube 1 but are delayed in time by one-third and two-thirds of a period, respectively. A similar relation holds for the voltage waveforms of the even numbered tubes.

The voltages across tubes 1 and 2 were added in order to determine the input voltage, v_i, shown in Figure 3(B). (The constant arc drop of the tubes and the resistance of the input inductor were neglected.) The wave which repeats every one-sixth of a cycle is identical in shape and magnitude to the output-voltage wave during the interval $0 < tf < 1/6$. The average value of the input voltage is $0.695\ E$ and is equal to the value of the

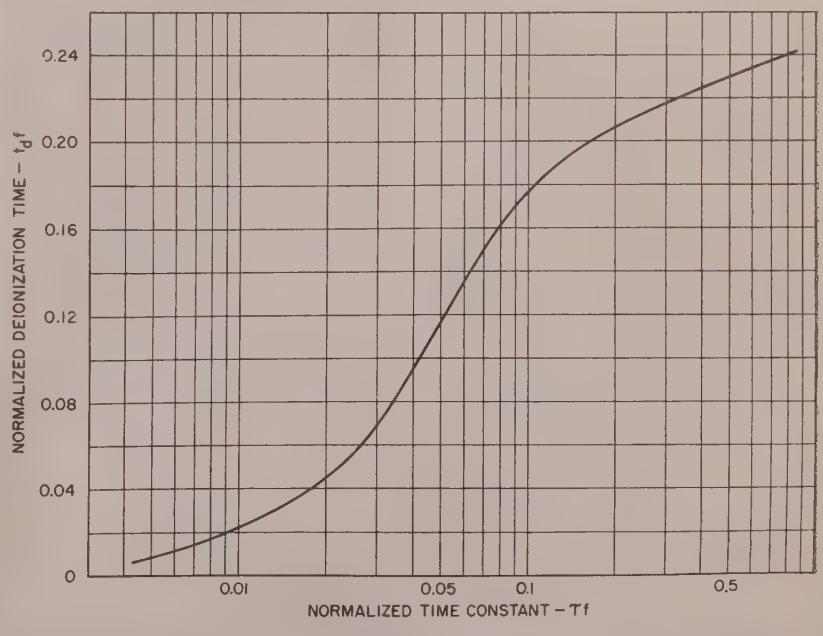

Figure 4. Normalized curve of inverter deionization time ($t_d f$) as a function of the load-network time constant (τf)

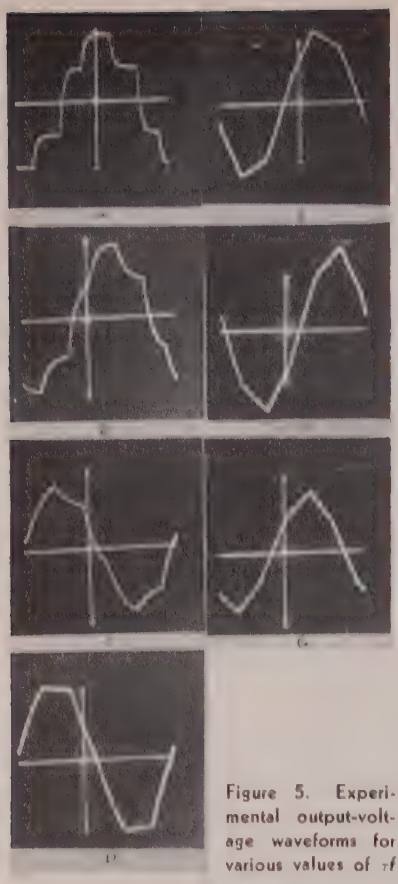

Figure 5. Experimental output-voltage waveforms for various values of τf

(A) $\tau f = 0.006$, $V_c = 1.00E$. (B) $\tau f = 0.015$ $V_c = 1.05E$. (C) $\tau f = 0.030$, $V_c = 1.06I$ (D) $\tau f = 0.060$, $V_c = 0.530E$. (E) $\tau f = 0.150$, $V_c = 0.277E$. (F) $\tau f = 0.300$, $V_c = 0.111E$. (G) $\tau f = 0.600$, $V_c = 0.105I$

direct-voltage source E_s.

If the average value of the input voltage is subtracted from the input-voltage waveform, the induced voltage of the inductor can be obtained

Deionization Time

When conduction is transferred from one tube to another, the outgoing tube will be extinguished if the commutating capacitors can hold the anode-to-cathode voltage negative until the tube deionizes. The length of time during which the tube voltage is negative is frequently called the deionization time of the inverter. This inverter deionization time must be greater than the tube deionization time if commutation is to take place,

The inverter deionization time for various values of the load-network time constant can be obtained from the calculated output-voltage waveforms. It can be seen from Figures 2 and 3(A) that the waveform of the anode-to-cathode voltage of tube 1 during the interval $1/3 < tf < 2/3$ is identical to the output-voltage waveform for $\tau f = 0.030$ during the interval $1/6 < tf < 1/6$. Consequently, the distance in Figure 2 from $tf = -1/6$ to the point where the output voltage first becomes zero is equal to the time the tube voltage is negative, the deionization time of the inverter. (The deionization time is immediately obvious from the anode-to-cathode voltage waveforms. The possibility of determining the time from the set of output-voltage waveforms eliminates the need of plotting a set of tube-voltage waveforms for various values of load.) A normalized curve of the deionization time ($t_d f$) as a function of the normalized load-network time constant (τf) is shown in Figure 4.

Experimental Performance

Inverter Waveforms

The analysis involving an infinite inductance can be applied to a 3-phase bridge-type inverter if the ripple in the input current is small. In order to determine the amount and effect of the ripple present with a finite inductance and to evaluate the assumptions involved in the analysis, waveforms of an experimental inverter operating with an input inductance of about 10 henrys were obtained.

Figure 5 shows oscillograms of the output voltage v_{ab} for various values of τf, while Figure 6 shows oscillograms of the anode-to-cathode voltage of tube 1, the input voltage, and the input current. Each oscillogram includes a calibrated voltage (V_c) or current (I_c), the value of which is expressed as a fraction of E or I. Only one-half cycle of the input-voltage waveform is shown. It may be noted that in several illustrations the waveforms do not exactly repeat each one sixth of a cycle. The cause of this irregularity was inexact timing of the grid voltages, which permitted some tubes to conduct for more than one-third of a cycle and others, for less than one-third

Table I. Comparison of Peak Values of the Calculated and Experimental Waveforms of v_{ab}

τf	$\left(\frac{V_m}{E}\right)$ Measured	$\left(\frac{V_m}{E}\right)$ Calculated
0.000	0.96	1.00
0.015	0.94	0.99
0.030	0.84	0.89
0.060	0.54	0.63
0.150	0.32	0.33
0.300	0.18	0.18
0.600	0.09	0.09

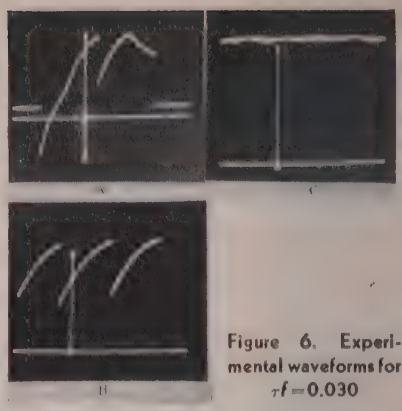

Figure 6. Experimental waveforms for $\tau f = 0.030$

(A) Anode-to-cathode voltage waveform for tube 1. $V_{c1} = +E$, $V_{c2} = -(1/2)E$. (B) Input-voltage waveform. $V_c = (1/2)E$. (C) Input current waveform. $I_c = I$

of a cycle. All of these waveforms were obtained with the inverter operating at a frequency of 10 cycles per second.

A comparison between the experimental and calculated voltage waveforms for corresponding conditions indicates virtually identical waveshapes. The peak values (V_m) of the calculated and experimental output-voltage waveforms for various values of τf are given in Table I. The calculated and experimental values of V_m/E agree within 5.6 per cent for all values of τf except the fourth, $\tau f = 0.060$.

These comparisons indicate that the input-current ripple is small with an input inductance of 10 henrys and has practically no effect upon the voltage waveforms of the inverter.

Average and Rms Values of Voltage and Current

The relations between the average values of the input voltage and current and the rms values of the output voltages and currents for various load conditions cannot be expressed as simply as the corresponding relations for a rectifier since the various waveforms are nonsinusoidal. These relations can be expressed very conveniently in the form of dimensionless curves, obtained either analytically or experimentally. Analytic curves for an inverter with an infinite input inductance could be obtained by integrating the expressions for the input and output voltages given in Appendix I. Experimental curves could be obtained by actual measurements on an experimental inverter.

Figure 7 shows normalized curves of the average input voltage (V_i) and the rms line-to-line output voltage (V_o) and line current (I_o) as functions of the normalized load-network time constant (τf).

The voltage curves have been normalized with respect to $E=2IR$, and the current curve has been normalized with respect to I, the average value of the input current. The measured input voltages were decreased by 32 volts to provide a curve for zero tube drop.

Conclusions

At the present time the future of the gas-tube inverter looks bright. With sufficient refinement it can be used to convert substantial amounts of direct power into alternating power with a fixed or variable frequency. However, commutation remains a major problem in these inverters. Several methods of commutation have been investigated with varying degrees of success, but the desired degree of reliability has not yet been achieved.

A relatively simple analysis of the 3-phase capacitor-commutated inverter with resistive load can be made if the input current is assumed constant. That this analysis can be used when a small amount of ripple is present in the input current is demonstrated by the close agreement between the experimental and the calculated waveforms. The same general method of analysis may be applied to an inverter with an inductive load but the process of determining the various initial conditions is more complicated. With either type of load, however, the analysis is valid only between successive commutations when two tubes are conducting. From the time an incoming tube is fired until the outgoing tube is extinguished, three tubes are conducting. The result is a negative voltage impulse appearing in the anode-to-cathode voltage of certain tubes and in the input voltage. These impulses could not be recorded in the experimental waveforms but could be seen on the oscilloscope.

There are two principal disadvantages to the bridge-type capacitor-commutated inverter described in this paper. The firing system and the commutation system must be very reliable, for the failure of a tube to be fired or extinguished at the proper time may cause two tubes in the same phase to conduct simultaneously and form a short circuit across the d-c source. Quick-acting protective devices in the d-c line must be relied upon to protect the tubes.

Proper operation of the inverter requires that negative reactive power be drawn from the load,[6] necessitating a leading power-factor load. When a resistive load is placed upon a capacitor-commutated inverter, the capacitors supply the required reactive power to the inverter.

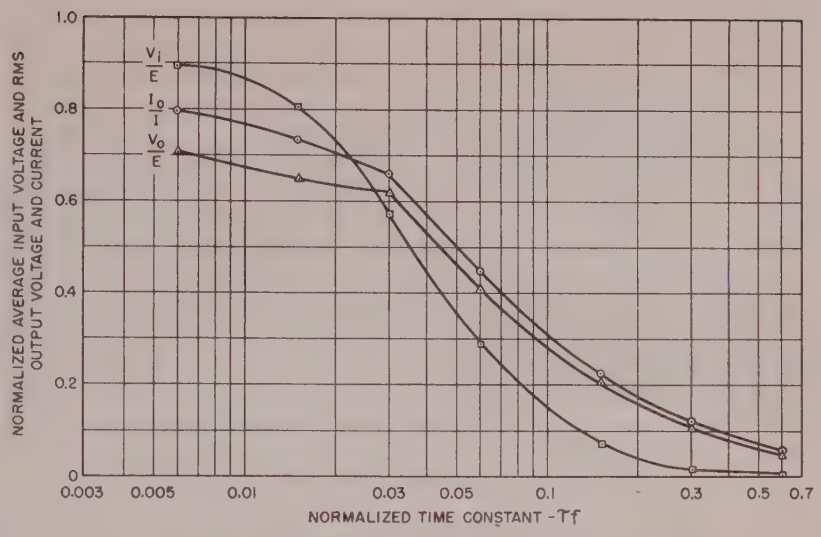

Figure 7. Normalized curves of average input voltage (V_i/E) and rms output voltage (V_o/E) and current (I_o/I) as functions of the load-network time constant (τf)

There is no difficulty in obtaining leading power-factor loads in this case, and the experimental inverter operated properly over a frequency range extending down to zero for various load. When the inverter is supplying an inductive load, however, the capacitors must be large enough to cause the load seen by the inverter to be capacitively reactive. This requirement is difficult to fulfill when low-frequency operation is attempted with inductive loads. Brief experimentation with an induction motor load indicated that satisfactory variable-speed operation could be obtained for frequencies down to about 12 cycles per second. Below this frequency commutation difficulties were frequently encountered caused, in part, by the lack of a leading power-factor load.

Appendix I. Calculation of the Inverter Waveforms

The output voltages of the inverter can be easily found when the input inductance is assumed infinite, thereby causing the input current to be constant. Since the inverter input current must be constant and the firing order of the tubes is known, the source currents flowing into the load network at nodes a and b can be found. The output voltages of the inverter resulting from these node source currents can be found by the principle of superposition.

The Output Voltages

The inverter of Figure 1(A) is assumed to be operating with an infinite input inductance and a tube firing order of 1, 6, 3, 2, 5, 4. The infinite inductance forces the input current to have a constant value I at every instant of time, thus permitting the voltage source and the inductance to be replaced by a current source of value I, as in Figure 8(A). Consequently, the currents flowing into nodes a, b, and c can be determined as functions of time. For example, the source current flowing into node a when tube one is conducting is I; when tube two is conducting, the current is $-I$; and for the remainder of the cycle, it is zero. The waveforms of these currents, i_a, i_b, and i_c, are shown in Figure 8 (B). Since these node input currents are known functions of time, the current source I and the tubes may be replaced by two current sources, one connected from node c to node a with a value of i_a, and another connected from node c to node b with a value of i_b. The output voltages resulting from these current sources can be determined by the principle of superposition.

With node c as a reference, current i_a is applied to the load network while i_b is zero. Since node b is not connected to any source (the impedance of a current source is infinite), the load network may be reduced to the simple RC parallel combinations shown in Figure 8(D). The voltage v_{ac}' resulting from current i_a acting alone consists of a series of exponential curves, as shown in Figure 9(A). Since the time constant of the circuit is

$$\tau=3RC \tag{4}$$

the equations describing the voltage are as follows:

$$0<tf<\frac{1}{3} \quad v_{ac}'(t)=E+[v_{ac}'(0)-E]\epsilon^{-t/\tau} \tag{5}$$

$$\frac{1}{3}<tf<\frac{1}{2} \quad v_{ac}'(t)=v_{ac}'\left(\frac{1}{3f}\right)\epsilon^{-\frac{1}{\tau}(t-1/3f)} \tag{6}$$

where $v_{ac}'(0)$ and $v_{ac}'(1/3f)$ are unknown initial conditions. By symmetry, the voltages for the first and last half of the cycle differ only in sign: thus

$$v_{ac}'\left(\frac{1}{2}<tf<1\right)=-v_{ac}'\left(0<tf<\frac{1}{2}\right) \tag{7}$$

The initial conditions appearing in the preceding equations may be found by con-

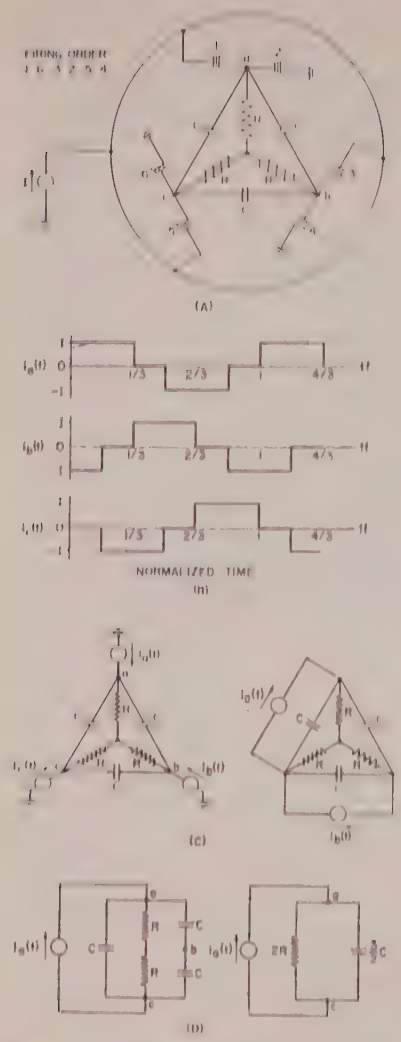

Figure 8. (A) Equivalent circuit for the inverter with an infinite input inductance. (B) Waveforms of the source current flowing into the load network at each node. (C) Simplified equivalent circuits. (D) Equivalent circuits when current-source i_b is inactive

sidering one half cycle of operation. They are

$$v_{ac}'(0) = -E_s \frac{e^{\frac{3}{2}\pi x} - 1}{e^{\frac{3}{2}\pi x} + 1} \tag{8}$$

$$v_{ac}'\left(\frac{1}{3f}\right) = E_s \frac{e^{\frac{3}{2}\pi x} - e^{\frac{\pi}{2}}}{e^{\frac{3}{2}\pi x} + 1} \tag{9}$$

where

$$x = 1/6\tau f.$$

The three node voltages expressed in terms of v_{ac}' are

$$v_{ab}'(t) = \frac{1}{2} v_{ac}'(t) \tag{10A}$$

$$v_{bc}'(t) = \frac{1}{2} v_{ac}'(t) \tag{10B}$$

$$v_{ca}'(t) = -v_{ac}'(t) \tag{10C}$$

The output voltages of the inverter for one complete cycle resulting from current i_a acting alone are given by the preceding equations. The voltages resulting from current i_b acting alone can be found in a similar manner.

When i_a is zero and i_b is the function shown in Figure 8(B), the load network reduces to the same RC combination encountered previously. The voltage v_{bc}'' resulting from i_b has the same shape as v_{ac}' but is delayed in time by one third of a cycle, as shown in Figure 9(B). Consequently, the equations for v_{bc}'' may be formulated directly by making the proper substitutions. Thus

$$v_{bc}''\left(-\frac{1}{6} < tf < \frac{1}{6}\right) = -v_{ac}'\left(0 < tf < \frac{1}{3}\right) \tag{11A}$$

$$v_{bc}''\left(\frac{1}{6} < tf < \frac{1}{3}\right) = -v_{ac}'\left(\frac{1}{3} < tf < \frac{1}{2}\right) \tag{11B}$$

When these relations are used with equations 5–7, one obtains

$$\frac{1}{6} < tf < \frac{1}{6}: \quad v_{bc}''(t) = -E_s$$

$$\frac{1}{6} < tf < \frac{1}{3}: \quad |v_{ac}'(0) - E_s| e^{-\frac{1}{\tau}(t - 1/6f)} \tag{12}$$

$$\frac{1}{6} < tf < \frac{1}{3}: \quad v_{bc}''(t) = -v_{ac}'\left(\frac{1}{3f}\right) e^{-\frac{1}{\tau}(t - 1/3f)} \tag{13}$$

where the initial voltages are given by equations 8 and 9. For the remainder of the cycle

$$v_{bc}''\left(\frac{1}{3} < tf < \frac{5}{6}\right) = -v_{bc}''\left(-\frac{1}{6} < tf < \frac{1}{3}\right) \tag{14}$$

by symmetry. The two remaining output voltages, v_{ab}'' and v_{ca}'', may be expressed in terms of v_{bc}''

$$v_{ab}''(t) = -\frac{1}{2} v_{bc}''(t) \tag{15A}$$

$$v_{ca}''(t) = -\frac{1}{2} v_{bc}''(t) \tag{15B}$$

The node voltages existing when both current sources are active simultaneously the output voltages of the inverter can be obtained by adding the two sets of voltages previously determined.

During the interval of time $0 < tf < 1/6$, the output voltage v_{ab} is

$$v_{ab}(t) = v_{ab}'(t) + v_{ab}''(t)$$

$$= E_s + \frac{1}{2}[(1 + e^{-\frac{\pi}{2}}) v_{ac}'(0) - (1 + e^{-\frac{\pi}{2}}) E_s] e^{-t/\tau}$$

Substituting the expression for $v_{ac}'(0)$, equation 8, into the above equation, the final expression for v_{ab} during the interval $0 < tf < 1/6$ is found to be

$$v_{ab}(t) = E_s - \frac{1}{2} E_s \frac{e^{\frac{3}{2}\pi x} + 2e^{\frac{3}{2}\pi x} + e^{\frac{\pi}{2}}}{e^{\frac{3}{2}\pi x} + 1} e^{-t/\tau} \tag{16A}$$

$$= E_s - \frac{1}{2} E_s A_{1\theta} e^{-t/\tau}$$

The two remaining output voltages, determined in a similar manner, are

$$v_{bc}(t) = -\frac{1}{2} E_s - \frac{1}{2} E_s A_{2\theta} e^{-t/\tau} \tag{16B}$$

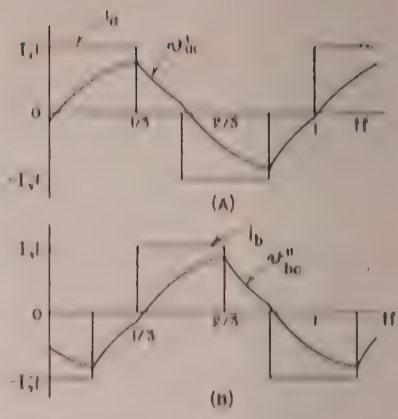

Figure 9. Current excitation and voltage response of network of Figure 8(D)

$$v_{ca}(t) = -\frac{1}{2} E_s + \frac{1}{2} E_s A_{3\theta} e^{-t/\tau} \tag{16C}$$

where A_1, A_2, and A_3 are given as

$$A_1 = \frac{e^{\frac{3}{2}\pi x} + 2e^{\frac{3}{2}\pi x} + e^{\frac{\pi}{2}}}{e^{\frac{3}{2}\pi x} + 1} \tag{17A}$$

$$A_2 = \frac{e^{\frac{3}{2}\pi x} - e^{\frac{3}{2}\pi x} - 2e^{\frac{\pi}{2}}}{e^{\frac{3}{2}\pi x} + 1} \tag{17B}$$

$$A_3 = \frac{2e^{\frac{3}{2}\pi x} + e^{\frac{3}{2}\pi x} - e^{\frac{\pi}{2}}}{e^{\frac{3}{2}\pi x} + 1} \tag{17C}$$

and

$$x = \frac{1}{6\tau f} \tag{18}$$

This procedure may be applied to the output voltages for the remainder of the first half period. The resulting equations are

$$\frac{1}{6} < tf < \frac{1}{3}: \quad v_{ab}(t) = \frac{1}{2} E_s + \frac{1}{2} E_s A_{2\theta} e^{-\frac{1}{\tau}(t - 1/6f)} \tag{19A}$$

$$v_{bc}(t) = -\frac{1}{2} E_s - \frac{1}{2} E_s A_{1\theta} e^{-\frac{1}{\tau}(t - 1/6f)} \tag{19B}$$

$$v_{ca}(t) = -E_s + \frac{1}{2} E_s A_{1\theta} e^{-\frac{1}{\tau}(t - 1/6f)} \tag{19C}$$

$$\frac{1}{3} < tf < \frac{1}{2}: \quad v_{ab}(t) = -\frac{1}{2} E_s + \frac{1}{2} E_s A_{3\theta} e^{-\frac{1}{\tau}(t - 1/6f)} \tag{20A}$$

$$v_{bc}(t) = E_s - \frac{1}{2} E_s A_{1\theta} e^{-\frac{1}{\tau}(t - 1/6f)} \tag{20B}$$

$$v_{ca}(t) = -\frac{1}{2} E_s - \frac{1}{2} E_s A_{2\theta} e^{-\frac{1}{\tau}(t - 1/6f)} \tag{20C}$$

The voltages for the last half period are the negative of the first half period voltages

$$v_{ab}\left(\frac{1}{2} < tf < 1\right) = -v_{ab}\left(0 < tf < \frac{1}{2}\right) \tag{21A}$$

$$v_{bc}\left(\frac{1}{2} < tf < 1\right) = -v_{bc}\left(0 < tf < \frac{1}{2}\right) \tag{21B}$$

$$v_{ca}\left(\frac{1}{2}<tf<1\right)=-v_{ca}\left(0<tf<\frac{1}{2}\right) \qquad (21C)$$

The Tube Voltages

The anode-to-cathode voltages of the tubes can be determined from the above solutions for the output voltages. Consider, for example, the voltages across tubes one and two.

During the time $0<tf<1/3$, tube one is conducting, and the anode-to-cathode voltage is

$$v_1=D \qquad (22A)$$

where D is the arc drop of the tube. During the next one-third of a cycle, tube three is conducting, and if the arc drops of all the tubes are equal, the voltage across tube 1 for this period of time is

$$v_1=D-v_{ab}$$

The expressions for v_{ab} during the second one-third of a period, equations 20A, 21A, and 16A, may be substituted into the preceding expression

$$\frac{1}{3}<tf<\frac{1}{2} \quad v_1=D+\frac{1}{2}E-\frac{1}{2}EA_{3\epsilon}^{-\frac{1}{\tau}(t-1/3f)} \qquad (22B)$$

$$\frac{1}{2}<tf<\frac{2}{3} \quad v_1=D+E-\frac{1}{2}EA_{1\epsilon}^{-\frac{1}{\tau}(t-1/2f)} \qquad (22C)$$

Similarly, the tube voltage for the remainder of the cycle is

$$v_1=D+v_{ca}$$

$$\frac{2}{3}<tf<\frac{5}{6} \quad v_1=D+E-\frac{1}{2}EA_{1\epsilon}^{-\frac{1}{\tau}(t-2/3f)} \qquad (22D)$$

$$\frac{5}{6}<tf<1 \quad v_1=D+\frac{1}{2}E+\frac{1}{2}EA_{2\epsilon}^{-\frac{1}{\tau}(t-5/6f)} \qquad (22E)$$

In a similar manner, the anode-to-cathode voltage of tube two can be found; it is

$$0<tf<\frac{1}{6} \quad v_2=v_{ab}+D$$

$$=D+E-\frac{1}{2}EA_{1\epsilon}^{-\frac{1}{\tau}(t-1/6f)} \qquad (23A)$$

$$\frac{1}{6}<tf<\frac{1}{3} \quad v_2=-v_{ca}+D$$

$$=D+E-\frac{1}{2}EA_{1\epsilon}^{-\frac{1}{\tau}(t-1/6f)} \qquad (23B)$$

$$\frac{1}{3}<tf<\frac{1}{2} \quad v_2=-v_{ca}+D$$

$$=D+\frac{1}{2}E-\frac{1}{2}EA_{2\epsilon}^{-\frac{1}{\tau}(t-1/3f)} \qquad (23C)$$

$$\frac{1}{2}<tf<\frac{5}{6} \quad v_2=D \qquad (23D)$$

$$\frac{5}{6}<tf<1 \quad v_2=v_{ab}+D$$

$$=D+\frac{1}{2}E+\frac{1}{2}EA_{3\epsilon}^{-\frac{1}{\tau}(t-5/6f)} \qquad (23E)$$

The Input Voltage

The input voltage, v_i, may be found from the sum of the voltages across tubes one and two. Performing this addition with equations 22 and 23, the input voltage is found to be

$$0<tf<\frac{1}{6} \quad v_i=v_1+v_2=2D+E-\frac{1}{2}A_{1\epsilon}^{-t/\tau} \qquad (24A)$$

$$\frac{1}{6}<tf<\frac{1}{3} \quad v_i=2D+E-\frac{1}{2}EA_{1\epsilon}^{-\frac{1}{\tau}(t-1/6f)} \qquad (24B)$$

It is seen that the input voltage repeats every one-sixth of a period for the first one-third of a cycle. If the additions had been continued for the remainder of the cycle the waveform would have been the same for each one-sixth of a period.

The above expressions for the output voltages, the tube voltages, and the input voltage were used in calculating the curves of Figures 2 and 3. Several assumptions were made in this analysis; the input inductance was infinite, the resistance of the input inductor was zero, the arc drops of all the tubes were equal, and no more than two tubes were ever conducting simultaneously. (The arc drop was assumed zero for calculating the tube voltages and the input voltage.) It should be noted that the expressions derived in this appendix apply only between commutation times. During commutation when three tubes are conducting, the voltages are unspecified. During commutation the tube voltages and the input voltage are modified as mentioned in the conclusions. The output-voltage waveforms are not affected.

References

1. Some Projects Favourable to Direct-Current Transmission and the Role of the British Electrical Industry in Relation Thereto, **F. J. Erroll.** *Proceedings*, Institution of Electrical Engineers (London, England), volume 96, part I, 1949, pages 49–58.

2. Series-Parallel Type Static Converters, **C. A. Sabbah.** *General Electric Review* (Schenectady, N. Y.), volume 34, 1931, pages 288–301, 580–89, 738–44.

3. The "Ignitron" Type of Inverter, **C. F. Wagner, L. R. Ludwig.** *Electrical Engineering* (*AIEE Transactions*), volume 53, October 1934, pages 1384–88.

4. High Voltage Ignitron Rectifiers and Inverters for Railroad Service, **J. L. Boyer, C. G. Hagensick.** *Electrical Engineering* (*AIEE Transactions*), volume 65, July 1946, pages 463–70.

5. Applications of Harmonic Commutation for Thyratron Inverters and Rectifiers, **C. H. Willis.** *AIEE Transactions*, volume 52, June 1933, pages 701–8.

6. Grid Controlled Rectifiers and Inverters, **C. C. Herskind.** *Electrical Engineering* (*AIEE Transactions*), volume 53, June 1934, pages 926–35.

7. Parallel Inverter with Resistance Load, **C. F. Wagner.** *Electrical Engineering* (*AIEE Transactions*), volume 54, November 1935, pages 1227–35.

No Discussion

Commutating Reactor Control for Mechanical Rectifiers

EDWARD J. DIEBOLD
ASSOCIATE AIEE

THE MECHANICAL rectifier is a synchronous switching device, making a metallic connection between an a-c network and a d-c network. Solid silver contacts, maintained closed by powerful springs, and opened by means of ceramic push rods, perform the switching.

Closed contacts have a resistance of a fraction of 1 milliohm. They are able to carry a very high current without damage.

Open contacts are separated by a substantial distance in clean, dry and nonionized air at atmospheric pressure. They are able to withstand a high voltage without corona or spark-over.

Each contact is opened and closed once each cycle. Being a pure switch, it has no interrupting capacity and cannot be used as a circuit breaker. It is also unable to withstand closing under full power. To use such a switch as a mechanical rectifier, without any protection during the opening and closing periods, will immediately result in its destruction.

During the past 15 years, an increasing number of mechanical rectifiers, using various protective circuits, have been in operation. Experience gathered with them is expressed in the following by four switching conditions. It appears today that these conditions are necessary and sufficient for obtaining a good mechanical rectifier. It is still necessary, however, to clarify and limit these rules, as the knowledge of the art progresses.

Commutating Reactors

A mechanically operated switch with its unavoidable inaccuracy of timing cannot satisfy the switching conditions at all possible loads, voltages, and frequencies. It is possible, however, to satisfy these conditions by the application of essentially nonlinear circuit elements called commutating reactors inserted in series with the switching contacts. These reactors maintain the inrush current after closing and the residual current before opening at a very low value and permit the free flow of current through the contact at any other time of the cycle.

Commutating reactors used in mechanical rectifiers have cores made of vacuum fused high purity 50 per cent nickel-iron. This alloy is cold rolled into a tape of 0.001-inch to 0.002-inch thickness, insulated by powdered magnesium-oxide and wound into a toroidal core. The finished core is annealed at 1,950 degrees Fahrenheit in electrolytic hydrogen and placed into a housing made of insulating material. No other core material has given better performance up to now.

With these cores it is possible to obtain reactors which magnetize at less than one-thousandths of the rated current; at this low current they are magnetized up to 96 per cent of the ultimate intrinsic induction. The increase of the magnetizing force with increasing velocity of magnetization is small and so are the iron losses. While not saturated they have a reactance about 90,000 times the reactance while saturated.

A characteristic of these reactors is their dynamic magnetizing curve, that is, the curve showing the relationship of the magnetizing force and the magnetic induction measured at full speed (sometimes called hysteresis loop). Figure 3 shows the curve measured on a production reactor. The magnetizing force H_c for zero induction (corresponding to the coercive force of the static loop) is more than 1,000 times smaller than the peak magnetization at rated current; Figure 3 therefore shows only about one-thousandths of the widths of the whole curve.

With increasing velocity of magnetization there is an increase in the zero induction magnetizing force H_c, as shown in Figure 4. This increase is a function of the thickness of the tape (due to eddy currents).

Commutation

Without adequate control, the best available commutating reactors do not satisfy the very rigorous switching conditions. There are, however, several known methods to control the operation of the reactors and to compensate for their unwanted properties.

In the following paragraphs, a relatively simple control circuit is described, as an example. It is shown schematically in Figure 1. The operation of the circuit is explained by means of Figure 2. Such a control circuit could be used on a low-voltage high-current rectifier. The explanation is limited to the commutation period which covers the time of the actual switching of two contacts; it is much shorter than the conduction or insulation periods during which the contacts are never subjected to any damage.

Commutation is the transition of the current from one contact to another. In Figure 1 the commutating contacts are assumed to be 1 and 2, they are connected to two different phases *R1* and *R2* of the a-c supply, each contact in series with two commutating reactors, called make coil (*LM1*, *LM2*) and break coil (*LB1*, *LB2*).

Before the commutation, contact 1 carries the current which saturates both reactors *LB1* and *LM1*. The direct voltage is equal to the voltage between *R1* and *R3* (*E13* in Figure 2(A)). Con-

Paper 51-211, recommended by the AIEE Electronic Power Converters Committee and approved by the AIEE Technical Program Committee for presentation at the AIEE Summer General Meeting, Toronto, Ont., Canada, June 25-29, 1951. Manuscript submitted November 8, 1950; made available for printing May 1, 1951.

EDWARD J. DIEBOLD is with the I.T.E. Circuit Breaker Company, Philadelphia, Pa.

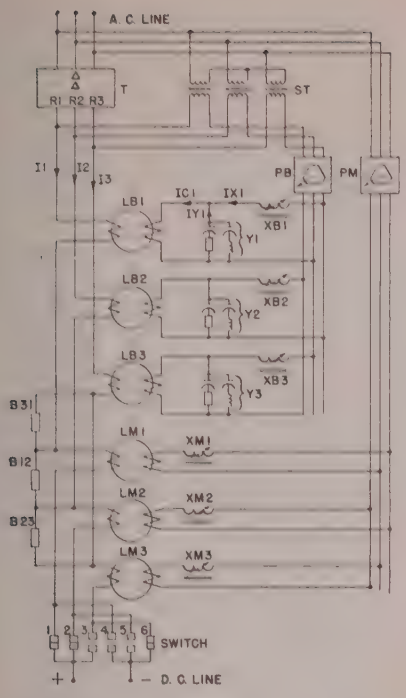

Figure 1 (left). Mechanical rectifier with commutating reactors: schematic diagram of the control circuit

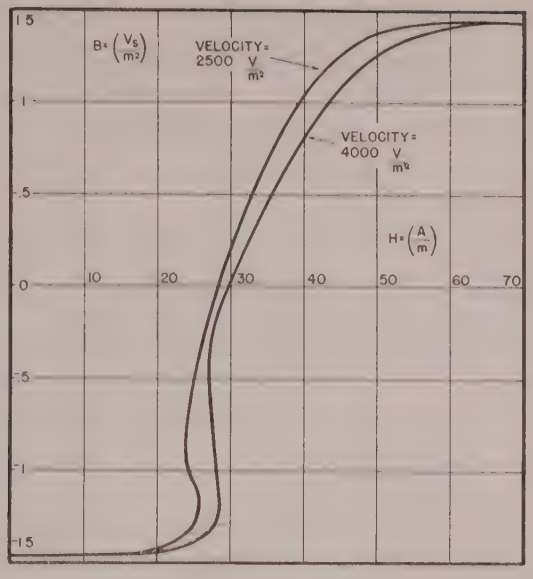

Figure 3 (right). Dynamic magnetizing curve of a commutating reactor at two different velocities

tact 2 is open, its make coil *LM2* is magnetized in the negative direction and its break coil *LB2* in the positive direction of the current to be carried. It is the task of the control circuits to supply this premagnetization of the cores. Without it, the make and break coils would magnetize at the same time and one of them would be useless. The control is accomplished by means of the control currents flowing in auxiliary windings on the commutating reactors.

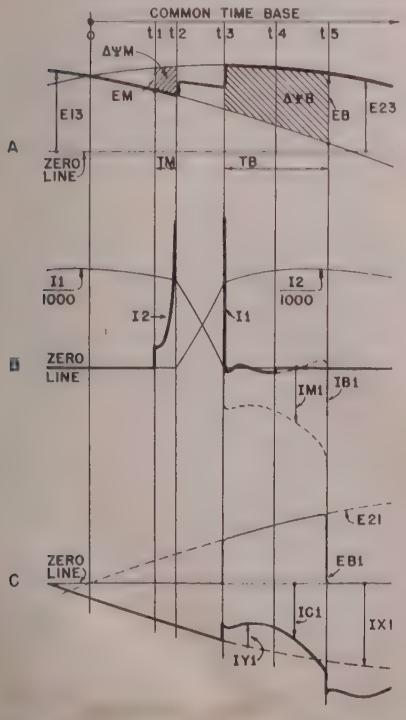

Figure 2. Voltages and currents during one commutation period

Closing the contact 2 parallel to 1, short circuits the two a-c phases *R1* and *R2*. The short-circuit current rises to the value of the magnetizing current of the make coil *LM2*, the full short-circuit voltage now appears on this coil. Therefore the inrush current through the contacts is equal to the magnetizing current of the make coil. Figure 2(B) shows the rise of the current *I2* in contact 2 after closing the contact at the time *t1*, *I2* is kept at a very low value for the time *TM*, which is called the make step. The change of total flux linkage of the make coil is represented by the area $\Delta\Psi M$ in Figure 2(A).

At the time *t2*, the make coil is saturated, *I2* rises and *I1* decreases rapidly, as shown in Figure 2(B) with the currents plotted at a one-thousand times smaller scale. At the time *t3*, *I1* has vanished to zero, and *I2* has reached the full value of the load current.

A control current *IC1* in the auxiliary winding of *LB1* unsaturates this coil at the exact instant that the current *I1* reaches zero (Figure 2(B)). When the *LB1* becomes unsaturated, it blocks any further change of the current *I1* and assumes the full short circuit voltage. This state lasts as long as the flux of the break coil is changing, represented by the area $\Delta\Psi B$ in Figure 2(A); the time *TB* required is called the break step.

A small residual current still flows through contact 1 (shown as a wavy-line in Figure 2(B)). This current must be interrupted by the opening contact 1, at the time *t4*. It is immaterial when this happens, as long as *t4* is after *t3* and before *t5*. After *t4*, the residual current *IB1* is carried by the by-pass resistor *B12*.

During the time *t4* to *t5*, the magnetizing current of the break coil *LB1* is maintained by the auxiliary current *IC1;* hence the short-circuit voltage is maintained on the primary winding of this coil, preventing it from appearing on the opening contact. After this time interval, the contact is separated by a gap large enough to assume the full voltage.

Switching Conditions

In the following paragraphs the experimentally determined switching conditions are stated, and it is explained by means of the simple example shown in Figure 1 how they can be satisfied.

Closing Voltage

Immediately before and while closing a contact, the voltage must not exceed the minimum glow-discharge voltage (normal cathode drop, approximately 280 volts in air). If this voltage is exceeded, a glow discharge develops when the contacts have approached to a favorable distance given by the Law of Paschen. The glow discharge changes into an arc, melting and evaporating some contact matter. After closing, the contacts weld, and the welded parts will be torn apart at the next opening of the contacts. This process is cumulative and, after a few million operations, destructive by transfer and loss of contact matter.

This condition is satisfied for all rectifiers having contacts in open air and operating at a closing voltage of less than 280 volts.

Whenever there is a possibility that the voltage will be higher it is advisable

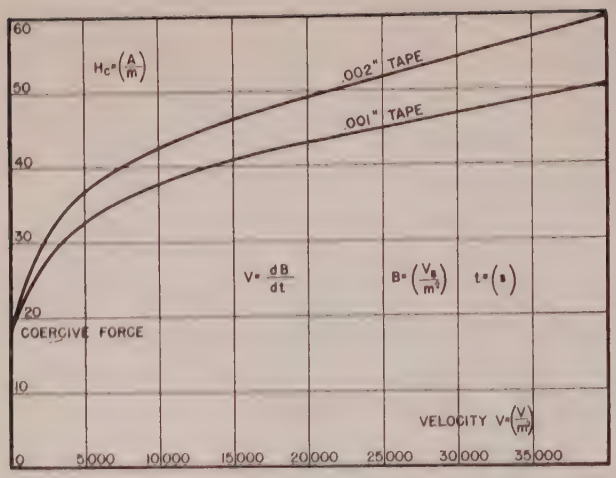

Figure 4. Magnetizing force at zero induction plotted against the velocity of magnetization for two thicknesses of the core material

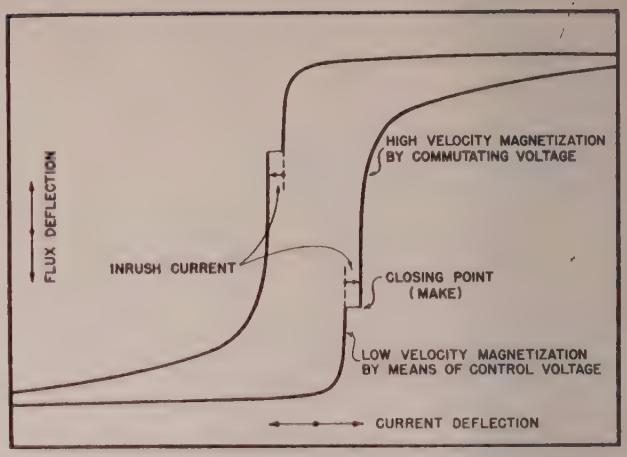

Figure 5. Flux-current oscillograph of a make coil

to have it appear on the make coil, instead of the closing contact. As the duration of the glow discharge is very short, the make step might be initiated shortly ahead of the actual make point without increasing the size of this coil.

To initiate the make step before closing the contact, an electronic by-pass circuit to the contact is used, for example a small mercury-pool cathode rectifier. By means of the grid control of the rectifier, its anodes are fired shortly ahead of the closing time. The grids can be controlled by the bridge contacts of the mechanical rectifier itself. One side of the bridge contacts will always close before the other side, and this unavoidable time delay, due to mechanical inaccuracies, might thus be used to control the grid voltage before the other side closes.

Closing Current

While closing the contact and immediately thereafter (50 to 100 microseconds), the current should be less than the highest tolerable inrush current. When the contacts have approached to a distance small enough to permit transfer of electrons, the resistance is still high. It will decrease rapidly to a very low value if the inrush current is kept small enough. An excessive inrush current produces enough heat to melt and evaporate the first point of contact, leaving an arc discharge. The effects of the arc are the same as described previously. Another cause of damage is the bouncing of the contacts after closing. To cause contact damage, the bouncing does not have to be complete, a reduction of the contact pressure to increase the contact resistance, and thus the heat generated, is enough.

This condition can be satisfied by making the closing circuit highly inductive and limiting the inrush current (1 to 3 amperes) for a time long enough to cover eventual bouncing. In the description of the commutation, the limitation of the make inrush current by means of the make coil is shown.

Without a control circuit, the inrush current is equal to the full magnetizing current of the make coil. For many applications it will be too high and a control or premagnetization current will be applied to an auxiliary winding of the make coil. The auxiliary current will magnetize the make coil at a low velocity of magnetization. When the contact closes, the velocity of magnetization is suddenly increased and hence an inrush current equal to the difference between the high velocity magnetizing current and the low velocity magnetizing current of the make coil will flow through the contact.

Figure 5 shows an oscillographic picture of the flux-current curve of a make coil with premagnetization according to the circuit shown in Figure 1. The inrush current appears as a discontinuity of the curve; it is due to eddy currents in the iron core. It is apparent from Figure 5 that the premagnetization reduces the inrush current to about one-third of the magnetizing current.

Figure 1 shows an example of premagnetization of the make coils *LM1*, *LM2*, *LM3*. The stabilizing reactors, *XM1*, *XM2*, *XM3*, prevent the voltage induced in the auxiliary windings from influencing the control current. *PM* is a phase-shifter permitting the adjustment of a favorable phase position of the control currents such as to cover the whole range of regulation (by means of make delay) with one setting of the elements of the control circuit.

Opening Current

The residual current flowing through the contact, immediately before and during the opening period, should be very small (less than 0.3 ampere).

Magnetic energy, stored by the residual current in the line inductance, will be liberated at the instant of interruption. It appears later as an electrical charge of the capacity of the opening contact, unless the recovery voltage is high enough to produce and/or maintain an arc.

The resistance of the contact increases as the contact pressure is reduced, a too high residual current produces enough heat to melt and evaporate the last bridge of contact matter, leaving an arc fed by the magnetic energy stored in the line inductance.

It is possible to run with a relatively high opening current, but the contacts will not last for more than a few days. Below this limit, however, the transfer of matter disappears altogether.

As an additional safety feature, the residual current (and hence the recovery voltage) is to go through zero by reversing its direction at the end of the break step. If the contacts should draw an arc, its current would be no more than the residual current, low enough to provide very little ionization. At the final reversal of current, the arc will extinguish and not reignite due to the lack of ions.

Without control, the residual current is equal to the magnetizing current of the break coil. In Figure 2(B) this magnetizing current is shown as *IM1*. It is in opposite direction to the line current. The residual current, however, should be smaller, less variable, and positive before

its final rise in the negative direction. By compensating for the magnetizing current of the break coil, this condition will be satisfied.

Figure 3 shows the magnetizing current as a function of the induction of the core material, it increases somewhat irregularly with increasing induction. It shows also that the magnetizing current increases with the velocity of magnetization. Due to the shape of these curves it is not possible to compensate the magnetizing current with a sine-wave shaped alternating current or a direct current.

In order to attain a full compensation over the entire period of magnetization under all conditions of operation, transient control currents are used. These are initiated by the sudden rise of voltage in the winding of the break coil, closed by an oscillating and a nonoscillating circuit. In Figure 1, these circuits are shown as *Y1*, *Y2*, *Y3* and consist of a resistor-capacitor and a capacitor-inductor link.

When the break coil *LB1* demagnetizes (time *t3* in Figure 2), it is subjected to the full commutation voltage *E21*, shown as *EB1* in Figure 2(C). This voltage pulse also appears at the control winding of *LB1*, initiating a transient current *IY1*. By careful adjustment of the circuit elements of *Y1*, *Y2*, and *Y3*, the transient current will compensate for the slope and curvature of the dynamic magnetization curve of the core material.

A sine-wave shaped alternating current *IX1* is added to the transient current. Both currents combined, form the control current *IC1*, shown in Figure 2(C). Comparing *IC1* with the magnetizing current *IM1* in Figure 2(*B*), shows that they are almost identical during the time interval *t3–t5*. The residual current through contact 1 is the difference between *IC1* and *IM1*, it is shown as *I1* and *IB1* in Figure 2(B). By using this method, it is possible to reduce the residual current to less than 1/30,000 of the line current, under all conditions of operation! When contact 1 opens at the time *t4*, the residual current is interrupted, it will thereafter flow through the resistor *B12*.

Figure 2(C) shows that the voltage *EB1* on the break coil *LB1* increases with the phase angle at which the demagnetization occurs. Hence the velocity of magnetization and the magnetizing current also will increase. The transient current is also dependent on the voltage. By carefully adjusting the peak value and the phase angle of the sine-wave current *IX1*, it is possible to have it rise just enough to compensate for the rise of *IY1* and *IM1*, when the phase angle of the break step is delayed. It should be noted that this is true for all causes of delay, such as reduction of d-c voltage by make delay, increase in direct current or increase of frequency. To make these adjustments possible, in Figure 1 a phase shifter *PB* is used, with the adjustable reactors *XB1*, *XB2*, *XB3*. The series-transformers *ST* add a voltage proportional to the primary voltage of the main transformer *T* to the control voltage. When the ratio of *T* is changed by changing taps, the control voltage will have the right value to warrant a satisfactory commutation without readjustment.

Opening Voltage

Immediately after the interruption of the contacts and for a time of approximately 100 microseconds, the recovery voltage across the contacts should be below the smallest voltage required to maintain an arc, which is approximately 10 to 20 volts.

Having satisfied the previous condition of a low residual current, it is easy to satisfy this condition by providing a resistive by-pass with an extremely low inductance for the residual current. As the magnetizing current of the break coil is supplied by the control current and the residual current, the voltage on the break coil remains unchanged at the value of the commutating voltage, preventing it from appearing at the opening contact.

The by-pass resistors are shown as *B12*, *B23*, *B31* in Figure 1, their resistance is determined by the maximum value of residual current and the permissible recovery voltage (50 to 100 ohms).

At the moment of actual interruption, the residual current is displaced from the contact into the by-pass within a very short time. It is essential that the inductance between these paths be extremely small in order to prevent oscillations between this inductance and the capacity of the opening contact. In practical applications these oscillations are always present, they are, however, reduced to a small amplitude by careful design.

Oscillations while breaking and a destructive inrush current while making, are the reasons for which the capacitor cannot be used as an arc suppressor for mechanical rectifiers. A capacitor with a high discharge resistor, connected in series with a dry cell rectifier will form a nonoscillating low inductance by-pass. It can be used whenever the losses of a purely resistive by-pass become prohibitive.

This method is only one of many, the principles outlined are common to all of them.

Conclusion

The rated power of the circuit elements required for the control circuit is small, because the currents they carry are of the order of the magnetizing currents of the commutating reactors. These elements are made adjustable under load. In as much as it is possible to adjust the timing of the switching contacts under load, it becomes possible to do all the adjustments of a mechanical rectifier while it is running.

Experience of the last years has shown that it is relatively easy to interpret the commutation by studying the picture of the voltage across the contacts on a cathode-ray oscilloscope, adjustments if needed can be made by observing this picture.

Readjustments are infrequent and easy to perform. Hence, the mechanical rectifier can be maintained in good operating condition by the operating personnel which greatly reduces the possibility of eventual failure.

References

1. Der Kontaktumformer, **Floris Koppelmann.** *Elektrotechnische Zeitschrift* (Berlin, Germany), volume 62, 1941, pages 3–20, and *Elektrotechnik und Maschinenbau* (Vienna, Austria), volume 59, 1941, pages 253–62, volume 60, 1942, pages 189–94, volume 60, 1942, pages 368–77.

2. Fortschritte auf dem Gebiete des Kontaktumformers, **Erich Rolf.** *Frequenz* (Berlin, Germany), volume 1, 1947, pages 2–15.

3. Der Kontaktumformer mit Schaltdrosseln (book), **Alexander Goldstein.** Leemann (Zurich, Switzerland), 1948.

4. Das Schutzproblem des Kontaktumformers, **Emil Kittl.** *Elektrotechnik und Maschinenbau* (Vienna, Austria), volume 67, 1950, Issues 3 and 4, 15 pages.

5. Das Schaltproblem beim Kontaktumformer, **Alexander Goldstein.** *Brown Boveri Mitteilungen* (Baden, Switzerland), volume 37, 1950, pages 478–88.

No Discussion

Development of a Pumpless Ignitron

C. C. HERSKIND
FELLOW AIEE

E. J. REMSCHEID
MEMBER AIEE

WHEN large rectifiers, using a metal tank, were first built, it was found necessary to provide them with vacuum pumps capable of operating continuously because the techniques were not available for making vacuum tight joints and seals, and for adequately degassing internal parts. This practice has continued up to the present time and many pumped rectifiers are in operation. However, efforts to eliminate the pumps have continued. In this country sealed tubes of the ignitron type have been developed for rectifiers in the smaller sizes. These tubes feature glass-to-metal seals and stainless-steel envelopes. Some tubes have been in successful operation for over 10 years. In Europe, multianode rectifiers, without pumps, have been built for a number of years. These are generally of the air-cooled type featuring soldered metal-to-porcelain or fused metal-and-enamel seals and low carbon steel.

Standard pumped ignitrons have been operated without pumps in both the factory and field. Experience gained in this fashion has shown that even without special techniques the units will operate for considerable periods of time without pumps. On the basis of these observations and with the knowledge of improved techniques recently perfected, it was decided to develop a pumpless rectifier in the larger sizes covered by pumped equipment.

Requirements

Some of the requirements which must be met, if the pumpless rectifier is to successfully supplant the present standard pumped equipment, are as follows:

Ultimate Life. Standard pumped rectifiers have an ultimate life of at least 20 years and pumpless rectifiers must have a similar life.

Service Life. The rectifier must operate for at least five years before reconditioning is necessary.

Reconditioning. The pumpless rectifier must be so constructed that it may be readily reconditioned either at the factory or at the installation.

The final measure of the pumpless tank is, of course, an economic one. To successfully replace the pumped ignitron, it must do the same job at an equal or lower over-all cost. The cost incurred by the greater care to obtain suitable vacuum tightness and the additional degassing required for pumpless operation must be balanced by savings resulting from the elimination of vacuum pumps and manifold connections and the simplification of the rectifier assembly. Likewise the maintenance costs incurred in reconditioning must be of the same order as those met in maintenance of vacuum pumps and systems.

Design Problems

In order that the rectifier operate for long periods of time without vacuum pumps, two simple requirements must be met. First, a very low rate of leakage of gas into the tank must be obtained; that is, all sealed joints must have a very high order of vacuum tightness and, second, the parts within the rectifier must be adequately degassed during the degassing period so that it will not become gassy during operation. These requirements impose a number of design problems.

It is not possible to construct a vacuum chamber with no leakage. If sensitive enough instruments are available, it will be found there is always some leakage, although it can be made very small. To minimize the leakage in welds, the tank construction has been arranged to reduce the length of weld to a practical minimum. All openings are made with spun or pressed flanges instead of fabricated flanges. Welds are eliminated, if possible, by making two parts out of one piece. Where possible, double welds are used. Special precautions are taken to make welds under most favorable conditions by positioning and completing welds in a single pass.

Special measures are necessary to assure the required vacuum tightness at the anode seals, gasketed joints, and seal-off valve. The ignitor seal is demountable and utilizes a gasketed joint. In order to reduce the leakage through this joint to an acceptable value a special gasketed joint was developed. To facilitate reconditioning, the tank is equipped with a vacuum valve which is sealed off after degassing. It was found that a valve is not sufficiently tight for long life. In order to prevent the leakage through the vacuum valve, an arrangement was developed for placing a cap over the valve so as to form a chamber on the atmospheric side of the valve which in turn could be evacuated and sealed off by means of a glass tubulation.

When water cooling is used on pumpless tanks, careful consideration must be given to the prevention of corrosion, as the nascent hydrogen liberated by the corrosive action readily penetrates ordinary steel and enters the vacuum chamber.[1] Several arrangements may be used for avoiding corrosion. If the tank is built of low carbon steel, the corrosive action may be inhibited by treating the water with sodium chromate.[2] A tank of low carbon steel may be cooled with untreated water if it is provided with copper cooling coils soldered in place. Another possibility is to build the tank of stainless steel as are the sealed ignitron tubes.

Except for the modifications necessitated by the above design requirements,

Paper 51-212, recommended by the AIEE Electronic Power Converters Committee and approved by the AIEE Technical Program Committee for presentation at the AIEE Summer General Meeting, Toronto, Ont., Canada, June 25–29, 1951. Manuscript submitted February 13, 1951; made available for printing April 30, 1951.

C. C. HERSKIND and E. J. REMSCHEID are with the General Electric Company, Schenectady, N. Y.

Figure 1. Sectional view of pumpless ig

1 Anode mycalex seal
2 Grid mycalex seal
3 Glass seal—off
4 Anode heater cover
5 Test electrode
6 Anode heater
7 Valve seal guard
8 Vacuum valve seat
9 Valve gasket
10 Vacuum tank cover
11 Cover-tank weld
12 Vacuum tank
13 Water jacket
14 Grid support insulator
15 Heat shield
16 Anode
17 Anode stud
18 Water baffle
19 Splash baffle
20 Starter mycalex seal
21 Ignitor adjusting screw
22 Flexible diaphragm
23 Starter gasket
24 Excitation anode
25 Mercury separator
26 Leg
27 Ignitor
28 Cathode mercury pool

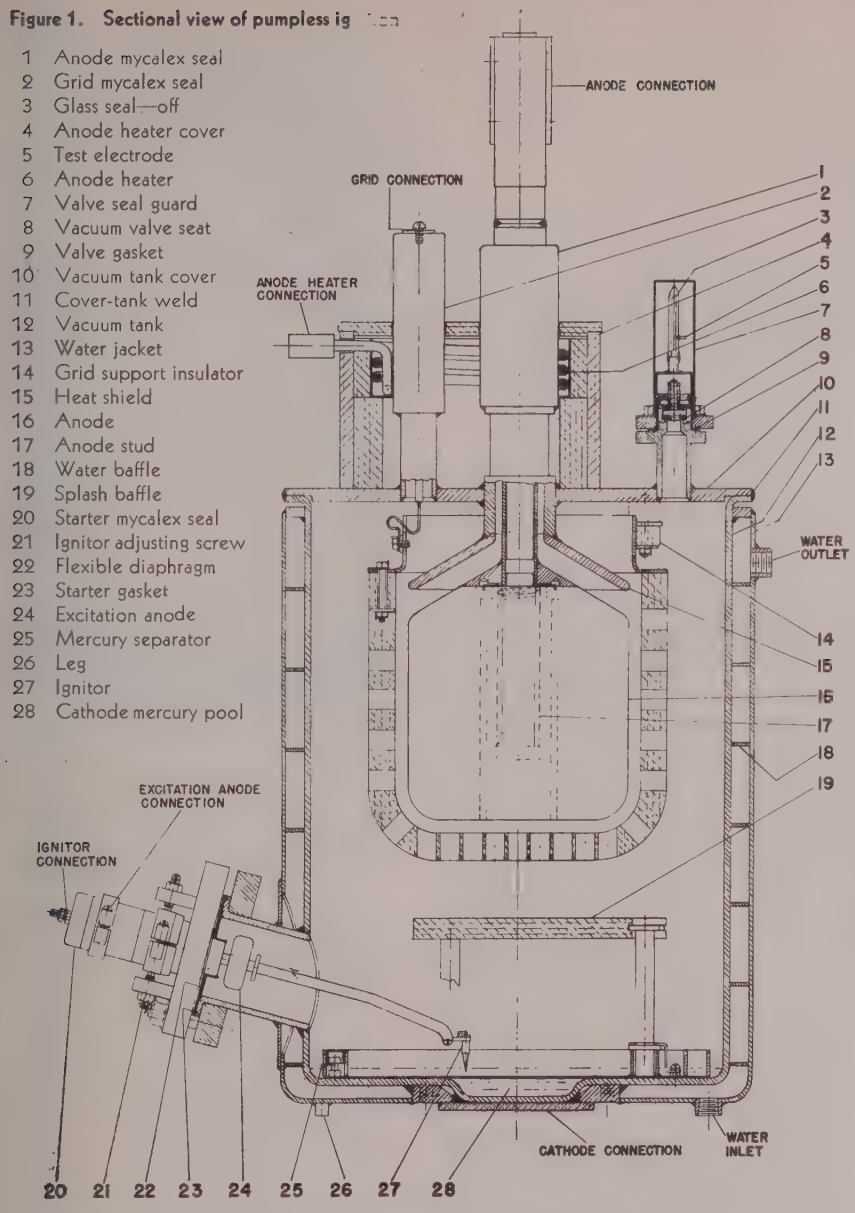
ANODE CONNECTION
GRID CONNECTION
ANODE HEATER CONNECTION
WATER OUTLET
EXCITATION ANODE CONNECTION
IGNITOR CONNECTION
CATHODE CONNECTION
WATER INLET
1 2 3 4 5 6 7 8 9 10 11 12 13 14 15 16 17 18 19
20 21 22 23 24 25 26 27 28

Figure 2. Vacuum valve

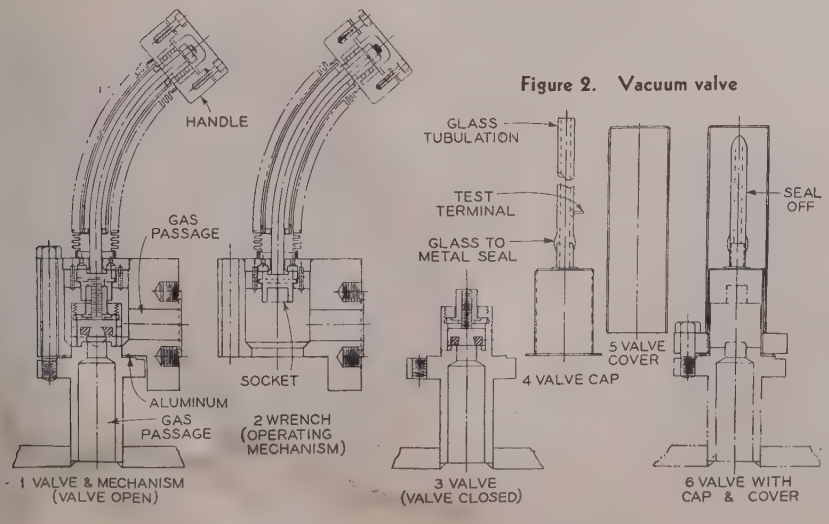

the construction of the pumpless ignitron is similar to that of the pumped rectifier. A sectional view of a 16-inch pumpless ignitron is shown on Figure 1. Referring to this view, it will be noted that the starter assembly is bolted in place so that it may be readily removed for cleaning of the mercury pool, replacement of the ignitor and inspection during normal reconditioning operations. The cover assembly is welded into place and arranged so the weld may be ground off if more extensive maintenance is required during reconditioning. A wide cover flange is provided so the cover may be removed about six times and welded. Anode, grid, and ignitor seals are of mycalex moulded construction. The rectifier tank is of deep drawn low carbon steel and is made by a series of drawing operations. The tank is evacuated through a seal-off valve located on the cover. The valve arrangement is shown in Figure 2. Other features are similar to those employed on standard pumped ignitrons.

Vacuum Testing

The pumpless rectifier must have a high order of vacuum tightness in order to obtain the desired service life before reconditioning. It is not sufficient to have available techniques for obtaining such vacuum tightness. Means for checking the vacuum tightness both during manufacture and operation also must be available. The development of the pumpless tank has been delayed to this late date because of the lack of such means. However, the last ten years has seen the development of the halogen-type leak detector[3] and also the helium leak detector.[4] The availability of these testing means has made the pumpless rectifier practical.

Usual leak testing practice on pumped metal tank rectifiers consists in pressure and seepage tests. The pressure test is made by charging the vessels with compressed air or dry nitrogen, and applying a soap solution to the suspected surfaces and observing the formation of bubbles of escaping gas. The seepage test is made by evacuating the rectifier tank, shutting down the pump and observing the rate of pressure increase on the McLeod vacuum gauge. The minimum size leak which may be detected by these means is limited because of practical considerations of time and labor which may be expended.

The halogen-type leak detector has made it possible to make pressure tests both rapidly and easily, and to locate smaller leaks than could be found with a soap solution. This type of pressure test

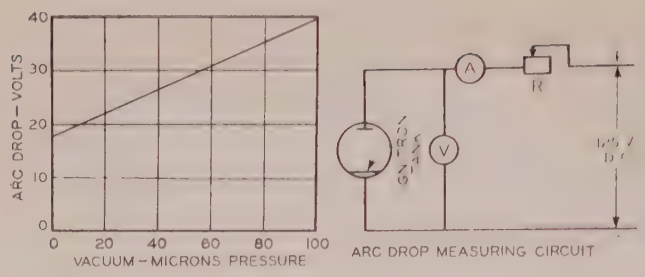

Figure 3 (left). Arc drop versus vacuum in pumpless ignitron

Figure 5 (right). Pumpless ignitron tank

is made by filling the chamber to be tested with compressed air containing a low concentration of halogen vapor, such as ethylene dichloride or carbon tetrachloride. A suction tube which draws air through the sensitive elements of the halogen detector is then passed over the suspected surfaces of the vacuum vessel and indication is obtained on the halogen detector whenever leakage of the halogen vapor mixture occurs. The halogen-type leak detector is especially useful in making factory tests during manufacture in checking vacuum welds, seals, gaskets, and metal parts.

Final vacuum tests are made by means of the helium leak detector which is an adaptation of the mass spectrometer. For these tests, the rectifier tank is evacuated and the exhaust system is connected so that samples of the gas pumped out of the rectifier may be passed through the mass spectrometer. The rectifier tank or any part of it is then enclosed in a bag which is filled with helium. If there is any helium leakage through the rectifier tank, an indication is obtained on the leak detector.

After the rectifier has been placed in service, some method for checking the vacuum without breaking the vacuum seal is desired. From tests it has been found that a rough measure of the vacuum may be obtained by measuring the arc drop with a low value of direct current passing through the tank. Tests have shown that as the foreign gas pressure increases in a range from zero to 250 microns, the arc drop increases likewise as a nearly linear function of pressure. Figure 3 shows the circuit used for making the arc drop measurements and the variation in arc drop with foreign gas pressure for a particular rectifier tank.

Degassing

After a vacuum tight rectifier has been produced and evacuated so that no gases can leak in from the atmosphere, and the mobile gas pumped out from the interior space, it must be degassed before it is operable. That is, the absorbed gases must be removed from the internal parts. It is well known from experience with all types of vacuum discharge devices that after the vacuum chamber has been pumped down, the walls and other parts of the chamber continue to liberate gases, and that this evolution of gas from the internal parts depends upon the temperature of the parts.

If a rectifier is degassed by passing an arc discharge through it, that is, current degassing, it is found that if the degassing current is held constant the liberation of foreign gases will rapidly diminish and apparently cease after a given period of time. If the value of degassing current is then increased, producing higher temperatures of the internal parts, gas will again be liberated for a period of time and then diminish and apparently cease. This process may be continued at successively higher levels of degassing current. From this it is apparent that all the gases are never removed from the internal parts of the rectifiers. What then is the criterion for the adequacy of degassing?

The first requirement for adequacy of degassing is that the degassing process must be carried to levels of temperature equalling those expected in service. This means that the internal parts of the rectifier must be subjected to temperatures approximating those experienced in service for a sufficiently long time to liberate and remove the absorbed gases so that these gases will not be liberated when operating in service, causing a gassy tube.

If it were absolutely necessary that all

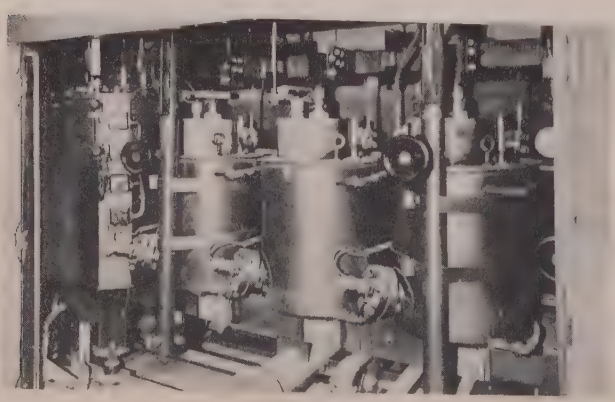

Figure 4 (left) First pumpless ignitron rectifier—front view 6 tank 1,000 kw at 4,000 amperes, 250 volts

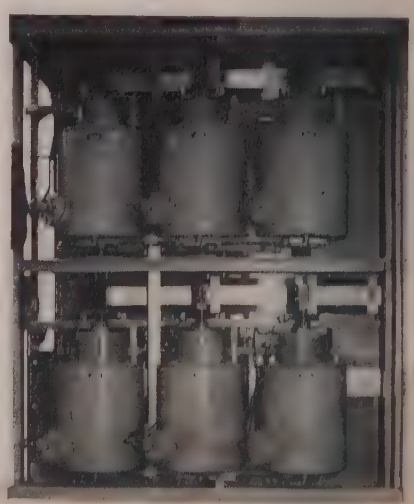

Figure 6 (right). Pumpless ignitron rectifier unit rated 1,000 kw at 4,000 amperes, 250 volts

parts of the rectifiers be carried above the temperature levels experienced in service, so that no gases would be liberated during operation, the construction of a pumpless rectifier would be difficult if not altogether impractical. It would be necessary to employ extreme measures to make sure that all parts have been adequately degassed, not only for the usual temperatures encountered in normal operation, but also for the unusual temperatures that might be rarely experienced during faults, overloads, or other abnormal conditions. Extremely long degassing periods might be required to take care of those parts which degas very slowly and continue to liberate gases for a long time. Also, there would be no provision for the steady deterioration in condition incurred because of the inevitable small leakage which takes place. These difficulties are all removed because of an absorption action exhibited by the rectifier.

Tests have shown that if an arc is established in a rectifier tank which has been degassed but contains a small quantity of foreign gas in mobile state, the gas will disappear.[6] The manner of its disappearance depends upon the nature and amount of the gas and the condition and character of the internal parts of the rectifier. Those gases which are chemically active such as oxygen, nitrogen, et cetera, disappear quite rapidly; the inert gases, such as argon, neon, et cetera, more slowly. The action involves absorption of the gases by the tank walls and electrodes and depends upon the condition of these parts resulting from the degassing treatment.

The second requirement for adequate degassing may therefore be stated; namely, the degassing process must be carried to temperatures sufficient to provide ability to absorb any gases which may be liberated by rectifier parts during operation or which may seep in from the inevitable small leakage.

Various processes may be utilized for degassing.[5] For example, the degassing may be carried out directly by operating the rectifier with a degassing current exceeding the maximum current expected in service. Degassing also may be accomplished by heating the major parts of the rectifier by radiation or induction. Or, again, the various parts, such as anodes or grids may be separately treated before assembly in the rectifier. The choice of degassing procedure becomes then an economic one of finding the simplest and lowest cost methods of providing adequate gas removal.

In an effort to determine the most effective and economical degassing procedure, extensive tests have been made in which both the quality and quantity of gas removed during degassing were measured, with the conditions for liberation determined in terms of temperature, current, and time.

The kind of gases liberated during the degassing process were determined by means of the mass spectrometer. Samples of the gases liberated during degassing were passed through the mass spectrometer at regular intervals during the degassing period. Measurements of gas flow were obtained from the pressure reading during degassing and also by means of a special manometer.

Two general degassing procedures were used during developmental tests: In the first, which was conducted without mercury in the rectifier, the tank walls were heated to various temperatures up to 500 degrees centigrade. Following this wall degassing, the mercury was admitted to the rectifier without breaking vacuum and the rectifier was then given a current degassing in the normal manner used on pumped rectifiers and carried to current levels exceeding those expected in service.

Laboratory tests have shown that zirconium may be used as an effective getter in the presence of mercury vapor. This may prove to be the most economical method for providing the desired absorbing ability in a rectifier. However, tests which have been made so far indicate that the need for a getter is not sufficient to justify the complications introduced by the use of zirconium.

Operating Experience

The first pumpless ignitron was shipped from the factory in August 1948 and put into service about two months later in a steel wire mill. The unit has operated since that time without arc-back at a load factor of approximately 80 per cent. It consists of a 6-tank 1,000-kw unit rated 4,000 amperes at 250 volts. Figure 4 shows the unit taken at the installation.

This unit was degassed and sealed off at the factory prior to shipment and has not been degassed or pumped down since. Periodic readings of vacuum, taken by the arc drop method, give no indication of increasing gas pressure or other deterioration.

Conclusions

On the basis of the very favorable factory and field tests, additional installations of pumpless ignitrons have been undertaken. Figure 5 shows a single pumpless tank, and Figure 6 a 6-tank unit now being installed.

The pumpless rectifier is a logical development extending from the pumped metal tank rectifiers which has long been desired and has finally been made possible and practical by the improvement in vacuum technique and increased knowledge of the physical processes. The pumpless rectifier makes possible a simpler rectifier construction with greater flexibility of arrangement. It is expected that it will eventually supplant the present pumped rectifiers completely.

References

1. Diffusion of Hydrogen From Water Through Steel, **Francis J. Norton.** *Journal of Applied Physics* (New York, N. Y.), volume 11, April 1940, page 262.

2. Water-Cooled Steel-Tank Rectifier Corrosion Problem, **E. J. Remscheid.** *Electrical Engineering* (*AIEE Transactions*), volume 60, April 1941, pages 173–77.

3. Positive Ion Emission, A Neglected Phenomena, **W. C. White.** *Proceedings*, Institute of Radio Engineers (New York, N. Y.), August 1950.

4. High Vacuum Leak Testing With the Mass Spectrometer, **W. G. Worcester, E. G. Doughty.** *AIEE Transactions*, volume 65, 1946, pages 946–55.

5. The Degassing of Metals, **F. J. Norton, A. L. Marshall.** *Transactions*, American Institute of Mining and Metallurgical Engineers (New York, N. Y.), volume 104, 1933, page 136.

6. The Absorption of Gases by the Steel Walls of Vacuum Discharge Apparatus and Its Bearing on the Life of Pumpless Mutators, **W. Deck.** *Brown Boveri Review* (Baden, Switzerland), volume 29, 1942, page 202.

No Discussion

A Servo System for Heterodyne Oscillators

T. SLONCZEWSKI
MEMBER AIEE

Synopsis: A constant rate of progression of frequency of a motor-driven heterodyne oscillator is obtained by comparing its output with a frequency standard. The result is fed into a servo loop which drives the motor at the proper speed. When used in connection with a level recorder a linear frequency scale is obtained which is more accurate than the static calibration of the oscillator.

HETERODYNE oscillators are frequently used in a measuring system in which the oscillator is swept over its frequency range by means of a motor while the characteristic being measured is recorded on a strip of perforated chart paper linked to the frequency control through a toothed chart drive mechanism. The linkage may be purely mechanical or it may be obtained by the use of two synchronous motors, one driving the frequency control of the oscillator, the other the chart advance mechanism on the recorder. One of the advantages of the latter arrangement is that the recording may take place far from the oscillator; for instance, at the end of a long cable whose transmission is being measured, provided the motors are driven from a power source of accurate frequency.

The present paper describes an oscillator driving mechanism which produces a constant time rate of progression of the oscillator frequency independently of the shape of its calibration curve. With such an arrangement, if the synchronous motor at the recording end is driven from a source of constant frequency, the frequency scale is linear and therefore it may be preprinted on the recording paper.

Another use for such an oscillator drive, and incidentally the one for which it was developed, is in measurements where the integral

$$\int_{f_0}^{f} F(f)\,df$$

of the measured characteristic, instead of the characteristic itself, is desired. In such cases $F(f)$ is integrated with respect to time by electronic means, and, since $f = Kt$, when the substitution is made in the above integral

$$\int_{f_0}^{f} F(f)\,df = K\int_{t_0}^{t} F(f)\,dt$$

It is seen that the time integral, when multiplied by a known constant of the system, furnishes the desired frequency integral.

Principle of Operation

In order to obtain the constant time rate of progression of frequency, the oscillator output is fed into a measuring detector (Figure 1) which determines the times t_0, t_1, t_2 . . . at which the oscillator frequency is respectively f_0, f_1, f_2 . . ., the frequencies f_n being separated by a constant frequency interval $\Delta f = f_{n+1} - f_n$. A pacing circuit furnishes a slowly-rising, fast-dropping saw tooth shaped voltage output derived from an accurate frequency standard. The saw tooth wave frequency being constant, the times t_0', t_1', t_2', . . . at which the slowly rising portion of the wave begins, are separated by equal intervals Δt. The values of Δf and Δt are selected so that the ratio $\Delta f/\Delta t$ equals the desired average rate of progression of frequency with time.

A comparison circuit measures the time intervals $t_n - t_n'$. The result of the measurement appears as a control voltage across the grid of a variable gain stage of a power amplifier, which amplifies a 60-cycle signal applied to the motor driving the frequency control of the oscillator.

If the frequency is higher than $t\Delta f/\Delta t$

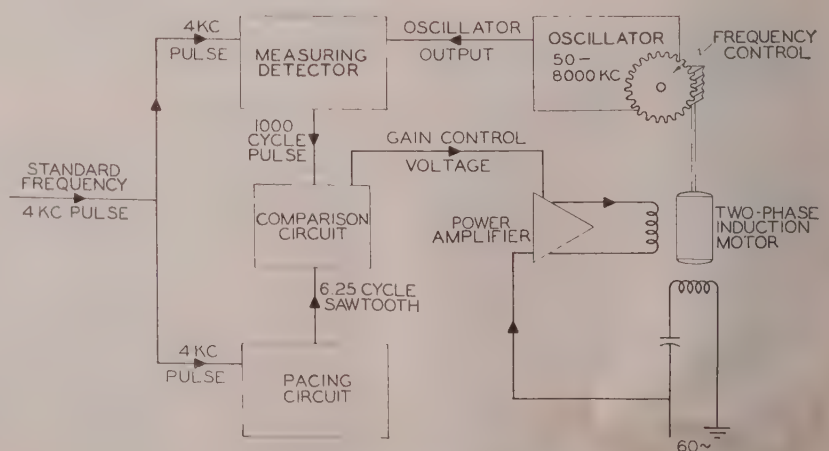

Figure 1. Block diagram of the servo drive

Paper 51-218, recommended by the AIEE Instruments and Measurements Committee and approved by the AIEE Technical Program Committee for presentation at the AIEE Summer General Meeting, Toronto, Ont., Canada, June 25–29, 1951. Manuscript submitted January 23, 1951; made available for printing May 7, 1951.

T. SLONCZEWSKI is with Bell Telephone Laboratories, Inc., Murray Hill, N. J.

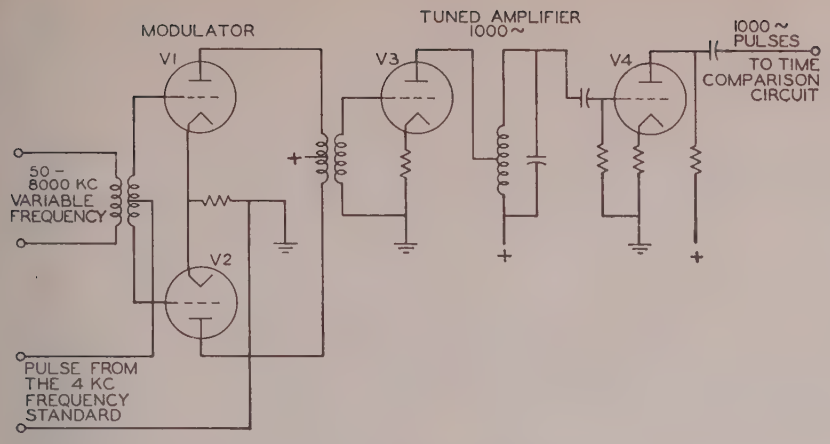

Figure 2. Schematic diagram of the measuring detector

the effect will be to decrease $t_n - t_n'$. The motor voltage will decrease and the motor will slow up. If the frequency is lower, $t_n - t_n'$ will increase and the motor will accelerate.

The Frequency Measuring Detector

The circuit that measures the oscillator frequencies is operated from an accurate 4-kc frequency standard. The 4-kc signal is fed into a harmonic generator which produces a sharp pulse containing all of the harmonics of 4 kc up to 8 megacycles with about the same amplitude. These are fed together with the heterodyne oscillator output, into the grids of the tubes V_1 and V_2 (Figure 2). The result of modulation is shown graphically on Figure 3. There the harmonics of 4-kc pulse, 80, 84, 88 . . . appear as horizontal lines, while the oscillator frequency appears as a line sloping upwards at a rate of approximately 12.5-kc per second. The modulator output of interest here is represented as a series of lines sloping up or down as the oscillator frequency approaches or recedes from a harmonic of 4 kc. The times marked t_0, t_1, t_2, indicate the instant when the modulator output reaches 1,000 cycles. This happens twice for each harmonic of 4 kc; once when f is below and once when it is above. The amplifier stage

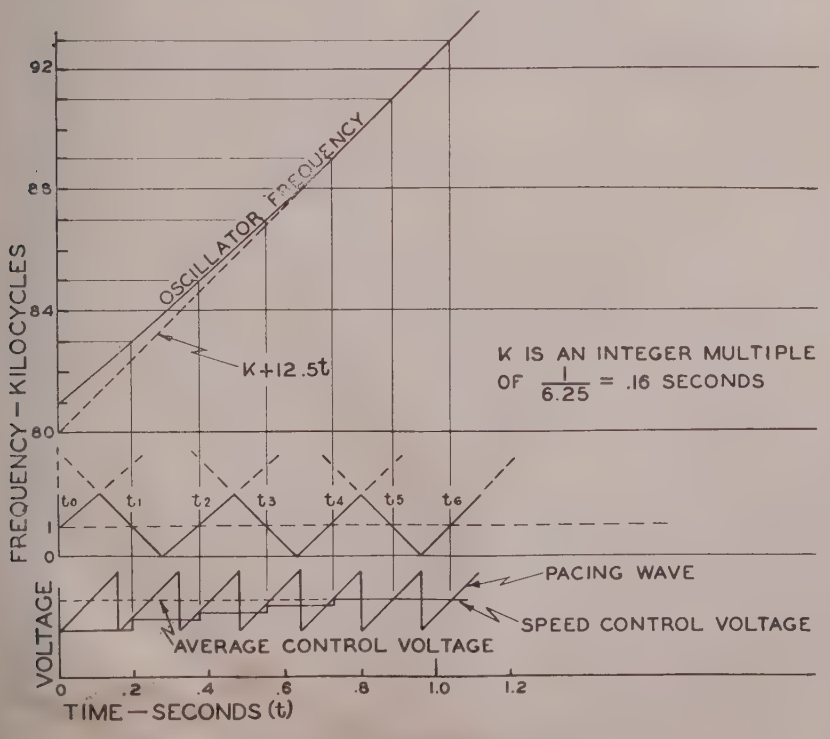

Figure 3. Servo action when the oscillator frequency is too high

V_3 in Figure 2 is tuned to 1,000 cycles so that a large output appears only when the oscillator frequency is $4N+1$ kc, where N is an integer. The value of the 1,000 cycle signal at the peak of the pulse is about 10 volts rms.

The Pacing Circuit

The pacing circuit consists of a conventional 3-stage counter circuit subdividing the 4 kc in a ratio of 640 to one. The output is a 6.25-cycle saw tooth wave rising slowly and dropping rapidly.

The Comparison Circuit

The gain control voltage for the power amplifier is obtained by charging the smoothing capacitor C_1 (Figure 4) to the value of the instantaneous voltage of the pacing wave at the time t_0, t_1 . . . of the arrival of the 1,000 cycle pulse. The voltage is switched on the capacitor only at the times t_0, t_1, t_2 . . . and switched off in between. The capacitor holds the charge it acquired last until the next switching period.

The switching is accomplished by means of the tubes V_1, and V_2, Figure 4. Tube V_1 conveys positive and V_2 negative charges to the smoothing capacitor. Neither tube is conducting normally because the grid leak capacitors C_2 and C_3 have large negative charges, as will be explained below, which bias the tubes beyond the cutoff. When the 1,000 cycle envelope pulse reaches its peak, however, its instantaneous positive peak voltage is at least equal to the capacitor voltage. The tube whose plate is positive with respect to the cathode is not biased beyond cutoff and conveys a charge to the capacitor C_1.

In fact, the instantaneous positive peak voltage is slightly larger than the capacitor voltage. The grid, therefore, draws a positive current which charges the capacitor negatively. The capacitor charge leaks off slowly enough to maintain a negative bias until the next pulse arrives.

The resultant speed control voltage obtaining across the smoothing capacitor is shown on Figure 3 and is seen to be lower at the beginning than the average voltage of the pacing wave because the oscillator frequency used in the example is higher than the required value $K+12.5$ $(t-t_0)$ hence the times t_1, t_2, t_3 . . . occur before the pacing wave reaches its average value. The fact that the control voltage is lower than the average causes the oscillator motor to slow up and the resulting lag in t_4, t_5 . . . brings the control

voltage up, and closer and closer to the average.

Similar reasoning will show that had the oscillator frequency been lower than the required value, the control voltage would have increased.

Thus deviations in frequency from the required value produce a regulating voltage change restoring dynamic equilibrium. Whenever the scale spread of the oscillator is larger than average, the motor has to run faster and the equilibrium point is displaced upwards. Where the scale spread is less than the average the equilibrium point is displaced downwards. The system becomes inoperative when the required control voltage is higher than the peak or lower than the bottom of the pacing wave. The constants of the system are selected so that a 10 per cent variation in the scale spread can be handled.

To prevent rapid leaking off of the charge from the smoothing capacitor the output of the circuit is taken out through a cathode follower.

Power Amplifier

The output of the comparison circuit changes the gain of the variable gain stage of the power amplifier as the grid bias is increased or decreased. The 60-cycle input is fed in from the power line.

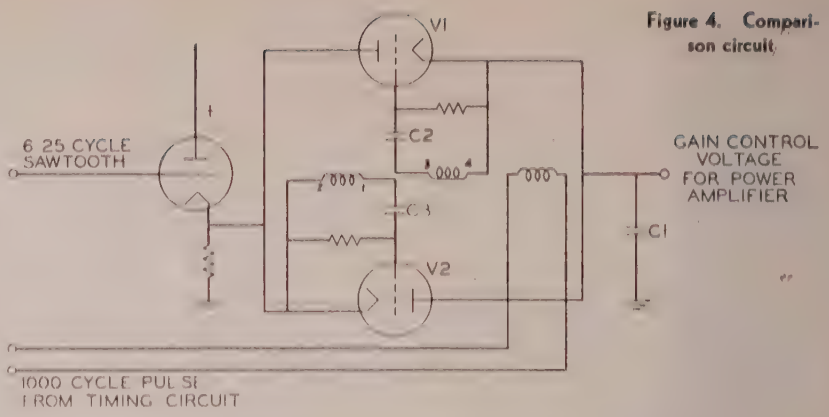

Figure 4. Comparison circuit

Control

The operation of the system is monitored on an oscilloscope where the horizontal deflection is controlled by the 6.25-cycle pacing wave while the vertical shows the envelope of the timing 1,000-cycle pulse. The 60-cycle level and, hence, the average motor speed are adjusted so that the pulse occurs at about 2/3 of the sweep towards the peak. The need for assymmetry arises in the fact that friction hinders acceleration while helping the deceleration of the system.

Results

The accuracy of the oscillator as checked by a monitoring oscilloscope is about ±1 kc over a frequency range of 0.05 to 8 megacycles. This is higher than the reproducibility by manual setting of the oscillator scale.

No Discussion

Line Insulator Loss Under Normal Conditions—500-Kv Test Project of the American Gas and Electric Company

O. NAEF
MEMBER AIEE

R. L. TREMAINE
ASSOCIATE AIEE

A. R. JONES
ASSOCIATE AIEE

MOST of the information in the literature on the performance of line insulators is concerned with conditions which lead to flashover.[1,2,3] Much less information is available on the loss characteristics of insulators under normal conditions, and that available is somewhat contradictory. Information on insulator loss under normal conditions is of considerable interest to corona loss investigators because it is desirable to be able to differentiate between corona and insulator loss. Utility engineers frequently are concerned about normal insulator loss when attempting to evaluate system losses. A summary of published information [4,5,6,10] is presented in Figure 1. These data have been converted to a common base as nearly as possible. Because of extreme sensitivity of the corona instrumentation at Tidd, it was considered desirable to obtain insulator loss data as a function of weather so that accurate records of corona loss could be obtained. To this end, the insulator loss instrumentation can be used for either visual or graphic recording.

Theoretical Considerations

Two methods of measuring insulator loss have been used. One method is to use the current across the grounded insulator unit, and the other is to construct a ground plane in such a manner that it "collects" substantially all of the capacitive current which flows to ground. To evaluate the relative merits of these two methods, it is necessary to understand an insulator string as an electric circuit.

The equivalent circuit representing an insulator string is a complicated series-parallel combination of capacitors and resistors, which has been simplified in Figure 2. The capacitances between insulator units, and from insulator units to conductor have been omitted. These slightly affect the voltage distribution across a string, but do not greatly affect the following discussion. The capacitance of one isolated unit is about 30 micromicrofarads.[4] However, if the capacitance to ground of a string of insulators is measured, it is found to be much greater than 30 micromicrofarads/(number of units) because of distributed capacitance. The capacitance to ground of a 34-unit string at Tidd was 20 micromicrofarads, and of a 30-unit string measured in the Trafford High-Voltage Laboratory of the Westinghouse Electric Corporation, 22 micromicrofarads. Thus it can be seen, that the series capacitance of an insulator unit contributes very little to the capacitance of the string to ground.

Referring to Figure 2 and neglecting resistance, the voltage across the line-end unit, number 1, is given by, $e_1=(i_1+i_2+i_3+i_4)/\omega c_1$. Similarly the voltage across unit 2 is, $e_2=(i_2+i_3+i_4)/\omega c_2$. Thus it becomes evident that the voltage distribution across a string is not uniform, and that the unit at the line end is subjected

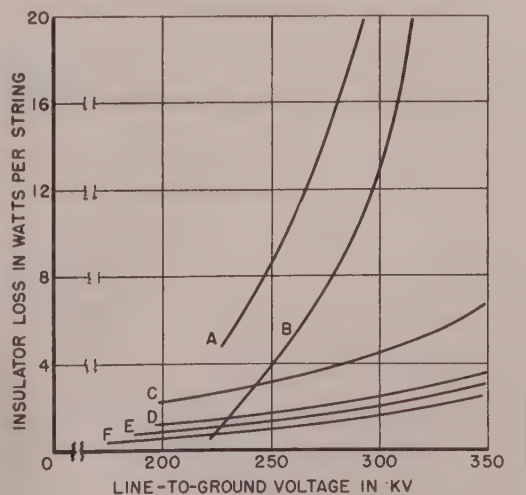

Figure 1 (left). Loss on clean, dry insulators observed by different investigators

A. Vertical string (24 units).[5] B. Horizontal string.[5] C. Vertical string, decreasing voltage (26 units).[4] D. Vertical string, increasing voltage.[4] E. Vertical string (26 units).[6] F. Vertical string (26 units).[10] (Author's measurements indicate fair-weather loss is practically zero, and certainly less than two or three watts up to 289 kv)

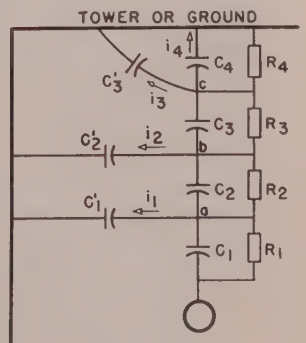

Figure 2 (right, above). Simplified equivalent circuit for an insulator string

Paper 51-224, recommended by the AIEE Transmission and Distribution Committee and approved by the AIEE Technical Program Committee for presentation at the AIEE Summer General Meeting, Toronto, Ont., Canada, June 25–29, 1951. Manuscript submitted March 28, 1951; made available for printing May 15, 1951.

O. NAEF is with the American Gas and Electric Service Corporation, New York, N. Y., and R. L. TREMAINE and A. R. JONES are with the Westinghouse Electric Corporation, East Pittsburgh, Pa.

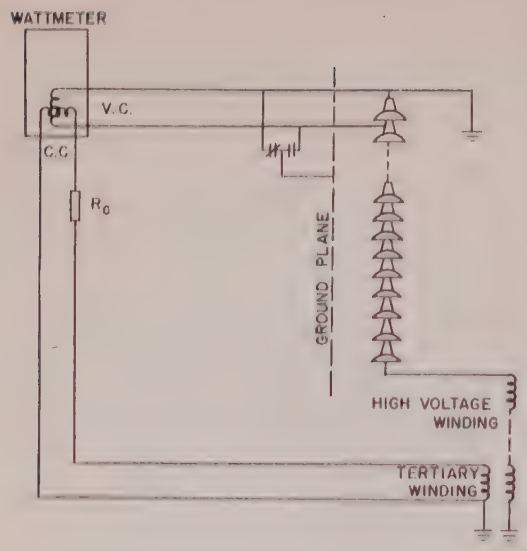

Figure 3 (A) (left). Schematic of the test set-up. (B) (right). Ground plane with stovepipe shielding on plane and bus conductor. The string had been removed

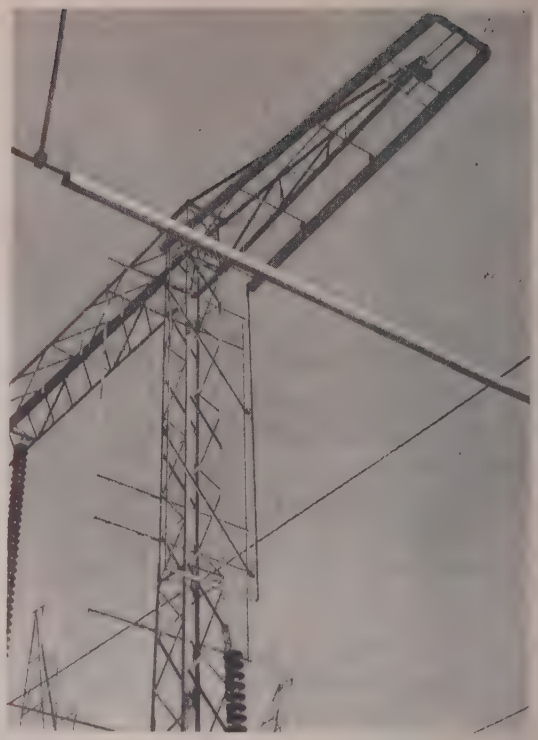

Figure 4 (below and on following page). Sample insulator loss records. (A), (B), and (D) obtained at 216 kv line to ground, (C) at 187 kv line to ground

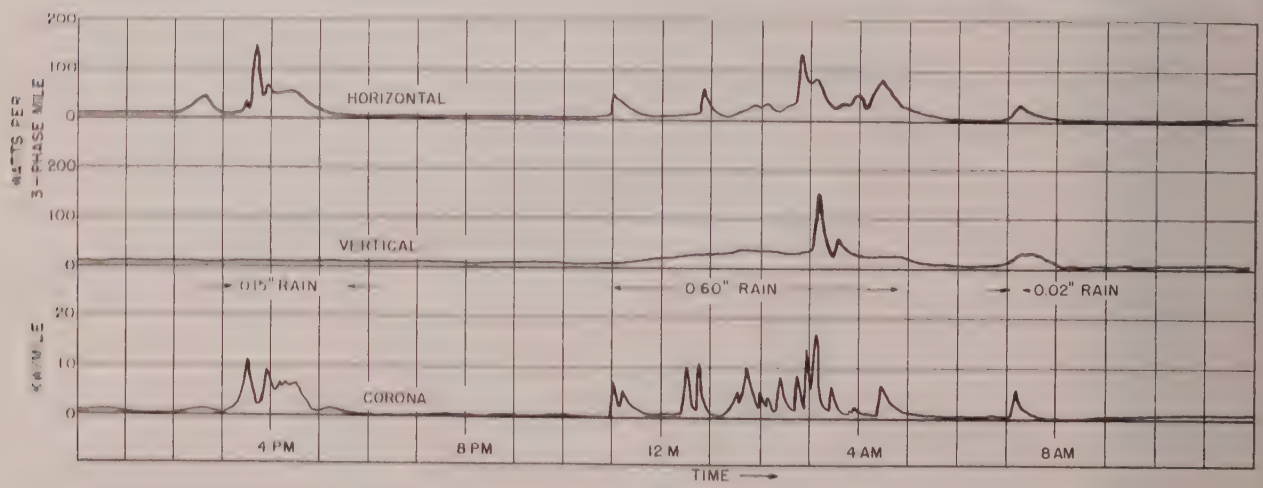

(A)

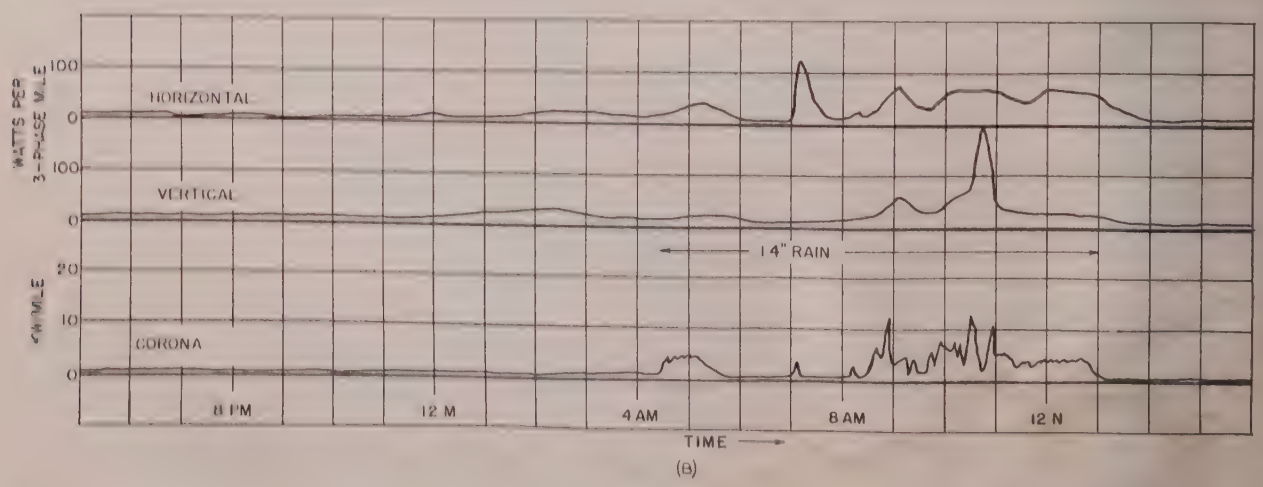

(B)

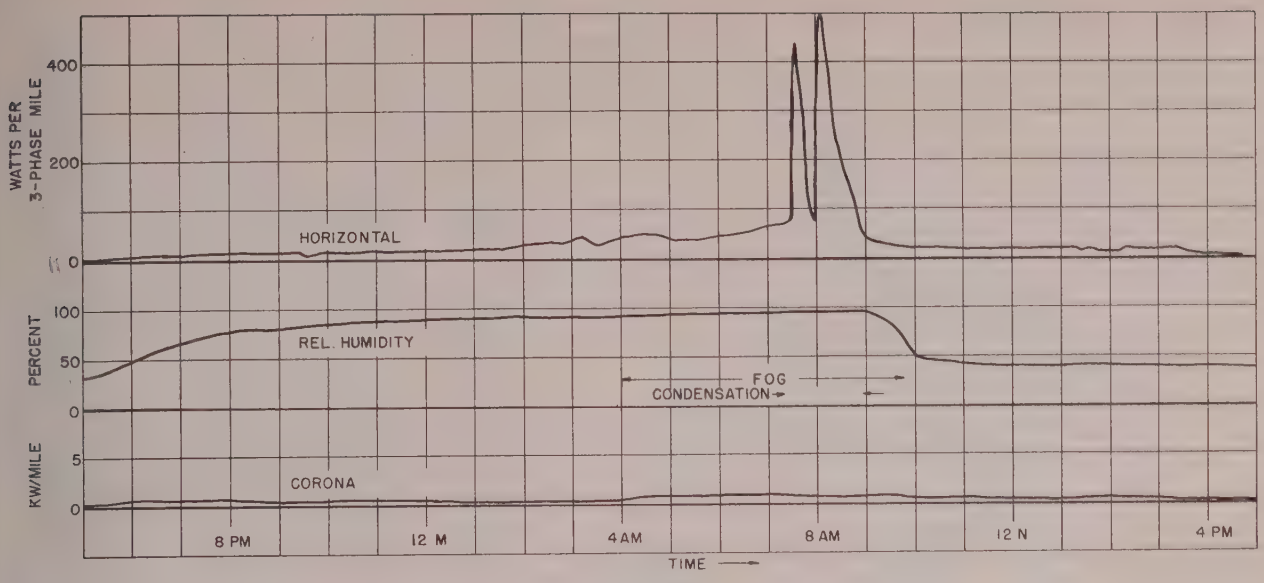

(C)

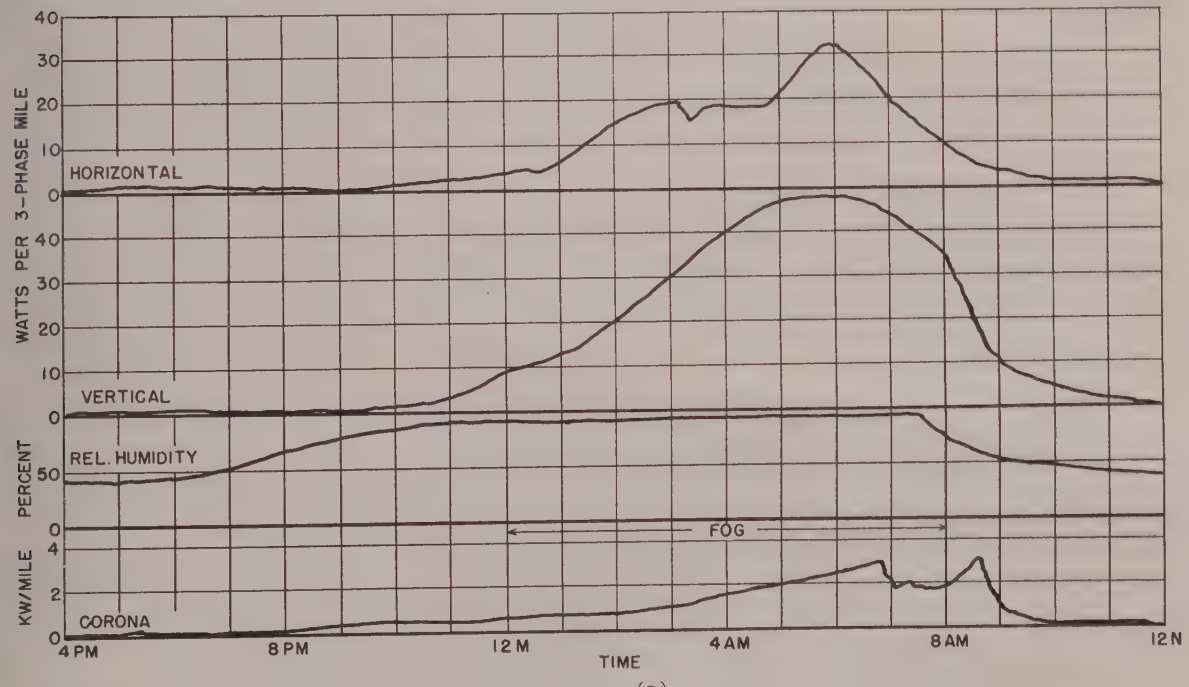

(D)

to the highest stress. (References 7 and 8 show the voltage distribution across insulator strings and the improvement gained by adding a grading ring to a long string.) It should be noted that all currents are in phase if resistance is neglected, regardless of the values of capacitance.

To represent loss on an insulator string, resistance must be introduced into the circuit as shown by resistors R_1 to R_4. The addition of resistance to the circuit not only adds an additional shunt path, but the voltages at points a, b, and c are no longer in phase with the line to neutral voltage, with the result that currents i_1 to i_4 do not lead the applied voltage by 90 degrees. Thus some of the loss component of current on the string can flow to ground through the distributed capacity and will not be recorded by a wattmeter which is supplied with only the current from the grounded unit.

It is logical to assume that the magnitude of the leakage resistance of the individual units is a function not only of contamination and moisture but also of the voltage across the unit. These factors, plus the difficulty of evaluating the magnitudes of the various values of capacitance involved, make an analytical study of an insulator string difficult. If the leakage resistance of an individual unit becomes small compared to the capacitive reactance involved, then the voltage distribution across the string is more nearly uniform and the voltages across individual units are again closely in phase with the applied voltage.

The foregoing discussion, although not conclusive, does indicate the conditions during which accurate measurements can be obtained using only the current from

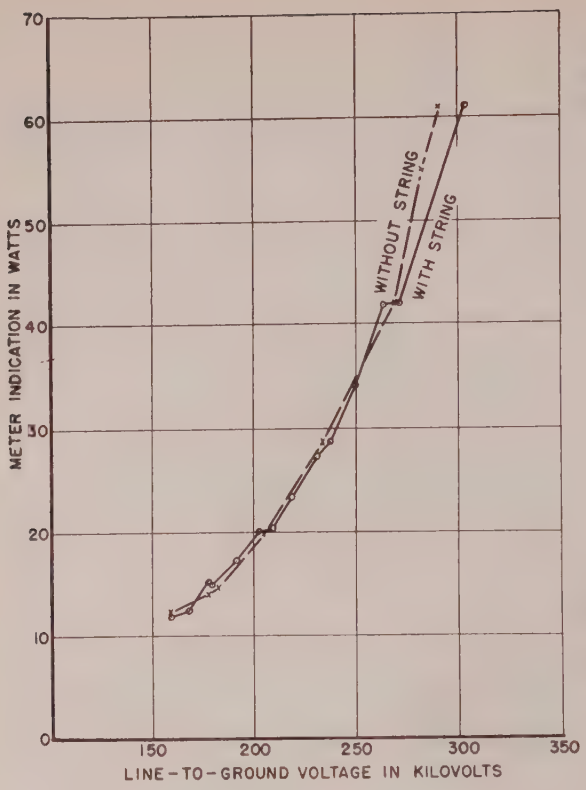

Figure 5 (left). Wattmeter readings with and without the insulator string

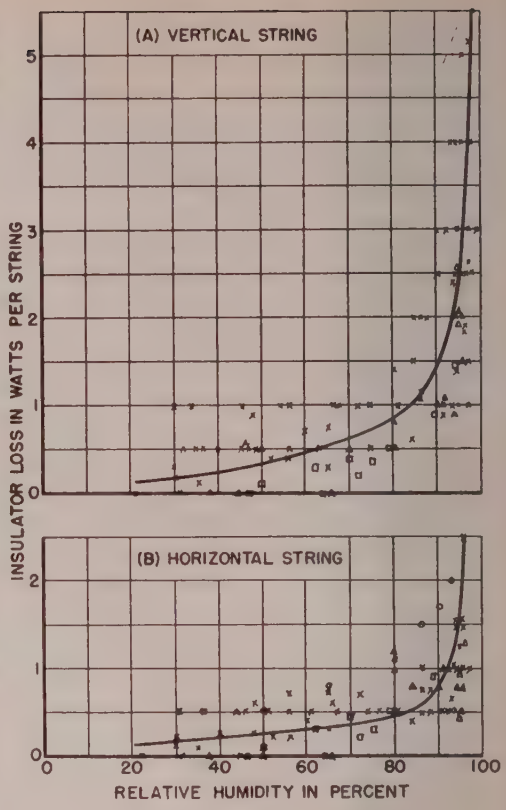

Figure 6 (right). Insulator loss as a function of relative humidity

△ 254 kv L–G
× 222 kv L–G
○ 194 kv L–G
□ 157 kv L–G

the grounded unit. If the actual loss is zero, the wattmeter will indicate this value, and when the loss is extremely high, the meter will indicate closely the correct loss. The most questionable loss values are obtained when the loss is comparable to the charging volt-amperes taken by the string. Thus measurements made using the current from the grounded unit tend to become progressively less accurate at the higher values, since rarely does the loss on an insulator string with reasonable contamination even approach the charging volt-amperes.

Test Setup

The setup used in the study of insulator loss on a vertical string of 34 units is shown schematically in Figure 3(A). By operation of a remotely controlled relay, current from the ground-end unit, or this current plus the current from the ground plane, can be supplied to the wattmeter. Provision also is made to measure the loss on a horizontal string of 26 units, but in this installation there is no ground plane.

Because of the small losses involved, the wattmeter is connected backwards in the sense that the reference current is passed through the current (stationary) coil and the load current through the voltage coil. This allows measurement of extremely low losses at high voltages. The wattmeter is one of the corona-loss meters which was designed especially for the Tidd 500-kv corona tests. Using the most sensitive scale of the wattmeter, a deflection of 2 per cent of full scale is 0.5 watt.

During graphic recording, the losses on the horizontal and on the vertical string are measured alternately for periods of 20 minutes each. In order to distinguish between the loss on the two strings, an auxiliary circuit is used which adds a few watts to the loss on the vertical string. Since it is rather difficult to read these charts without some experience, the data have been replotted so that the loss on horizontal and vertical strings can be readily distinguished. Because the wattmeter records the loss on one string at a time, simultaneous peak values of loss cannot be observed. This fact accounts for some peak losses appearing on one insulator and not on the other. Simultaneous comparisons can be made at each changeover point on the original charts. Sample records replotted to a loss scale based on 15 insulator strings per 3-phase mile are shown in Figure 4.

The insulator strings used in these tests have been in continuous service in the bus of the Tidd 500-kv corona test lines since October 1947. This area is near the Tidd plant of The Ohio Power Company, and is subject to moderate industrial contamination. The test lines are located in a valley and adjacent to a river, hence they are subject to considerable fog. The insulators are not subject to the degree of contamination which would be experienced near a cement or steel mill. Visual examination of the insulators shows their surface to be considerably dulled by the surface deposit, but it is not thick enough to change their color appreciably. Contamination in this area is primarily waste products of soft coal combustion.

Verification of Circuit Accuracy

The initial measurements of loss on the vertical string yielded phenomenonally high values of loss as shown by the curves marked "with string" in Figure 5. However, it was still more amazing when it was found that practically identical values of loss were obtained when voltage runs were made on the setup with the string removed! ! Tests with the string removed are marked "without string" in Figure 5.

From this and other tests, it became apparent that the ground plane picked up corona loss from the bus, and that the insulator string contributed little if any thing to the observed values. The bus is strung with 2.00-inch HH copper conduc-

tors, but for another purpose, a 3/8-inch conductor is spiraled around it. It was found that the phase voltage had to be reduced to 150 kv before the stray loss picked up by the ground plane became zero. The shape of the loss curve obtained was characteristic of a point discharge. Observations at night at voltages slightly above 150 kv revealed no corona discharges in the vicinity of the ground plane. At higher voltages, 200 and 289 kv, corona was visible on the bus and on the ground plane itself.

In an effort to eliminate this stray loss, the bus conductor and the outside edge of the ground plane were shielded with 6-inch stove pipe, as shown in Figure 3(B). Some improvement was noted, but it became apparent that very extensive shielding would be necessary before the ground plane could be used as originally planned.

The ground plane does serve one essential function however, and that is the estimation of fair-weather loss. Comparison of readings taken with and without the insulator string agreed so closely that it was evident that insulator loss was very small. An insulator loss in excess of 2 or 3 watts would have been observed. It was therefore concluded that insulator loss must be less than 2 or 3 watts, and probably close to zero. Fair-weather measurements without the ground plane indicated practically zero, confirming that fair-weather insulator loss is negligible. It was desirable to check one measurement scheme against the other, as it is possible to get an erroneous reading of zero loss using either measurement method. In view of the small magnitude of fair-weather insulator loss, the work necessary to obtain more accurate values was not considered warranted.

A comparison between foul-weather insulator loss measurements made with and without the ground plane is shown in Figure 7. The ground-plane measurements have been corrected for stray loss based on previous measurements. The ground-plane measurements are considered more accurate. It will be noted that there is reasonable agreement except at the higher values, and that even here the agreement is close.

Since statistically the high loss periods contribute little to the long-time average values of loss, a serious error is not introduced by omitting the ground plane for graphic measurements. The method used in Figure 7 does not lend itself readily to graphic measurements. For these reasons, it was decided to make recorded measurements without the ground plane. This method, while not 100 per cent accurate, yields values which are definitely only a function of insulator loss, and do not require detailed corrections.

Figure 7 (right). Typical insulator loss versus voltage curves taken during rain

(Curve a.) Vertical string using ground plane
(Curve b.) Vertical string not using ground plane
(Curve c.) Horizontal string (no ground plane)

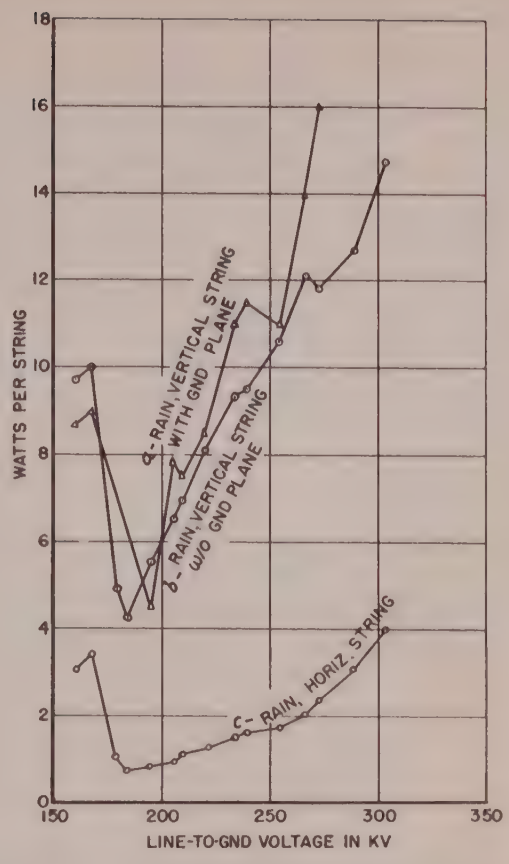

Results

As stated previously, fair-weather insulator loss is apparently negligible and certainly less than 2–3 watts per string at 289 kv. Thus assuming reasonable contamination, fair-weather insulator loss on transmission lines can be neglected.

Insulator loss increases in foul weather, as does corona loss, but not in the same manner. It is possible to have high-corona loss and low-insulator loss as shown in the sample charts of Figure 4.

Insulator loss is a function of the contamination on the surface of an insulator, and the amount of moisture which is present. Heavy rain tends to wash the insulators, thereby reducing the loss. As would be expected, graphic records of insulator loss show that high values of loss are recorded during fog, high humidity, and during the early portions of rain periods. Insulator loss shows less tendency than corona loss to change rapidly with rate of rainfall and is generally moderate or low during prolonged rain periods. Wet snow can also cause fairly high values of insulator loss with peak values being about 12 watts on a horizontal string.

Curiously, insulator loss appears to be more a function of weather than it is of voltage. The highest insulator loss recorded Figure 4(C) occurred during condensation, at the relatively moderate line-to-ground voltage of 187 kv. This fact is borne out by Figure 6 which contains data taken at several voltages. In this figure, insulator loss is shown to be primarily a function of relative humidity and largely independent of voltage.

Corona-loss records obtained during periods of condensation of moisture are distinctly different from records obtained during rain, so that charts of corona loss can be used to determine periods of condensation on the conductors. While admittedly the thermal and radiation characteristics of porcelain are different from those of metals, visual observations indicate that both insulators and conductors are generally subject to condensation at the same time. These observations together with the data from the photographic weather recorder,[9] have enabled the investigators to determine quite accurately the periods of condensation on the insulators. These periods have uniformly yielded high values of insulator loss. During periods of known condensation losses of 10 to 30 watts per string have been recorded. This is two to six times the effect of high humidity alone,

and much higher than average rain losses.

In general the loss on a horizontal string is less than on a vertical string. This is due to the fact that horizontal insulator strings are washed on both sides, whereas a vertical string is washed only on top. The average loss on a horizontal string is about 60 to 70 per cent of that on a vertical string. However, it occasionally happens that the loss on the horizontal string is higher. This condition can be caused by a very fine mist which wets both sides of the horizontal string, but does not wash it. An example of this condition is shown in the sample records, Figure 4.

Conclusions

Insulator loss is not of much economic importance where normal contamination and rain are experienced. A 380-kv line can be expected to have an annual average loss of 2 or 3 watts per string or, assuming 15 strings per mile, of 0.03 to 0.045 kw per 3-phase mile. This value was obtained by integrating the loss on horizontal and vertical strings and dividing by time, assuming the fair-weather loss to be zero.

Insulator loss is a combination of the effects of contamination and moisture. It is highest during periods of condensation, high humidity, and during the initial periods of rainfall. Humidity and condensation of moisture are more important in determining insulator loss than is voltage.

The average loss on horizontal strings is 60 to 70 per cent of that on vertical strings. Fair-weather insulator loss is apparently negligible and certainly less than two or three watts.

References

1. The Characteristics and Performance in Service of High-Voltage Porcelain Insulators, **J. S. Forrest.** *Journal*, Institution of Electrical Engineers (London, England), volume 89, Part II, number 7, February 1942, pages 60–80.

2. Insulators to Withstand Air-Borne Deposits, **J. J. Taylor.** *AIEE Transactions*, volume 67, 1948, pages 1436–41.

3. Insulator Surface Contamination, **H. A. Frey.** *AIEE Transactions*, volume 67, 1948, pages 1420–25.

4. Electrical Characteristics of Suspension-Insulator Units, **C. L. Dawes, R. Reiter.** *AIEE Transactions*, volume 56, 1937, pages 59–66.

5. 500-Kv Experimental Station at Chevilly, Results of a Year's Tests: Use of Bundle Conductors; Corona Effects; Clearance, **P. Ailleret, F. Cahen.** *Paper number 410*, International Conference on Large High Tension Electric Systems (Paris, France), 1948.

6. Comparative Investigations of D-C and A-C Corona on Two-Conductor Transmission Lines, **R. Strigel.** *Wissenschaftliche Veroeffentlichungen Aus Den Siemens-Werken* (Berlin, Germany), volume 15, part 2, 1936, pages 68–91.

7. Insulators and Line Hardware for Tidd 500-Kv Test Lines, **I. W. Gross, R. L. McCoy, J. M. Sheadel.** *AIEE Transactions*, volume 66, 1947, pages 1592–1602.

8. Electrical Transmission and Distribution Reference Book. Westinghouse Electric Corporation (East Pittsburgh, Pa.), 1950, Figure 18, page 619.

9. Techniques of Corona Loss Measurement and Analysis—500-Kv Test Project of the American Gas and Electric Company, **O. Naef, R. L. Tremaine, A. R. Jones.** *AIEE Transactions*, volume 70, part I, pages 496–506.

10. Methods of Controlling Radio Interference, **C. V. Aggers.** *AIEE Transactions*, volume 59, 1940, pages 193–201.

No Discussion

Basic Heat-Transfer Data in Electron Tube Operation

MRS. B. O. BUCKLAND
MEMBER AIEE

SUCCESSFUL operation of an electron tube depends on its heat dissipating characteristics as well as on its electronic characteristics. The tube energy is not all useful, unfortunately, and the part of the total energy that appears as heat must be transferred to the environment. Heat is generated at several sources; the primary sources are at the hottest temperatures, while various structural components assume temperatures intermediate between source temperatures and ambient. All the temperatures are of interest to the tube designer, because of his knowledge of the effect of temperature on the materials with which he works as well as on electron emission.

This paper is primarily concerned with operation of the tube in a known environment, although the topics covered also are of importance in tube design. Evaluation of thermal resistance is the principal topic. The equations and formulas to be presented are available in the literature, which will be cited, but not always in a form convenient for use in electrical problems.

It is possible to estimate the temperature at any location in a tube due to the losses it generates, by means of the well-known device of a thermal circuit. James Clerk Maxwell[1] was the first to point out the analogy between conduction of electricity and conduction of heat. He wrote, in part,

"The analogy between the theory of the conduction of electricity and that of the conduction of heat is at first sight almost complete. If we take two systems geometrically similar, and such that the conductivity for heat at any part of the first is proportional to the conductivity for electricity at the corresponding part of the second, and if we also make the temperature at any part of the first proportional to the electrical potential at the corresponding point of the second, then the flow of heat across any area of the first will be proportional to the flow of electricity across the corresponding area of the second .... Flow of electricity corresponds to flow of heat, the electric potential to temperature, and electricity tends to flow from places of high to places of low potential, exactly as heat tends to flow from places of high to places of low temperature."

The thermal circuit is thus analogous to an electric circuit, with current replaced by heat flow rate, voltage replaced by temperature difference, and resistance replaced by thermal resistance. It is no longer considered necessary to have geometrical similarity, and the procedure may be extended to the case of transient heat flow, by replacing electric capacity with thermal capacity.

The natural mode of heat dissipation from the surface is by free convection and radiation; at room temperature the magnitude of these two effects is about the same. When the tube runs too hot, recourse must be had to forced convection, in which a cooling fluid, usually air or water, is forced over the surface by mechanical means. In some special applications the tube is required to operate in a fixed temperature range, so that sometimes it is cooled and sometimes it is heated.

Thermal Circuit for Steady State

The complete thermal circuit for heat dissipation from a tube consists of a network which is evaluated in the ordinary manner by means of Kirchhoff's laws or similar theorems. However, any element may be evaluated separately if heat flows or temperatures up to the point of consideration are known.

The first circuit to be illustrated gives the temperature of a tube envelope, cooled by radiation and free convection, when the heat generation and the ambient temperature are known, see Figure 1.

The equation of this circuit gives the temperature rise of the surface above ambient air as:

$$t_s - t_a = \frac{q}{A(h_c + h_r)} \qquad (1)$$

which is directly analogous to $E=IR$.

When temperatures t are expressed in degrees centigrade, heat flow q in watts, and area A in square inches, the units of the surface heat-transfer coefficients, h_c for convection and h_r for radiation, are watts, square inches, degrees centigrade. It is to be noted that the coefficients are of the nature of conductances, so that where resistances are more convenient, the reciprocals of the heat transfer coefficients are to be used.

The heat generated in the tube must be known; the losses are the space charge (anode) loss, the filament power and the grid loss. Any other expected losses should be included.

To solve the circuit of Figure 1, a certain amount of cut-and-try is required, because the heat-transfer coefficients are functions of the temperature. This situation is analogous to solving an electric circuit in which the resistances are functions of the voltage. However, three tries should be enough.

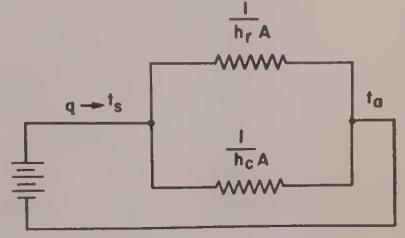

Figure 1. Thermal circuit for tube envelope

Paper 51-227, recommended by the AIEE Electronics Committee and approved by the AIEE Technical Program Committee for presentation at the AIEE Summer General Meeting, Schenectady, N. Y., June 25–29, 1951. Manuscript submitted March 28, 1951; made available for printing May 21, 1951.

MRS. B. O. BUCKLAND is with the General Electric Company, Schenectady, N. Y.

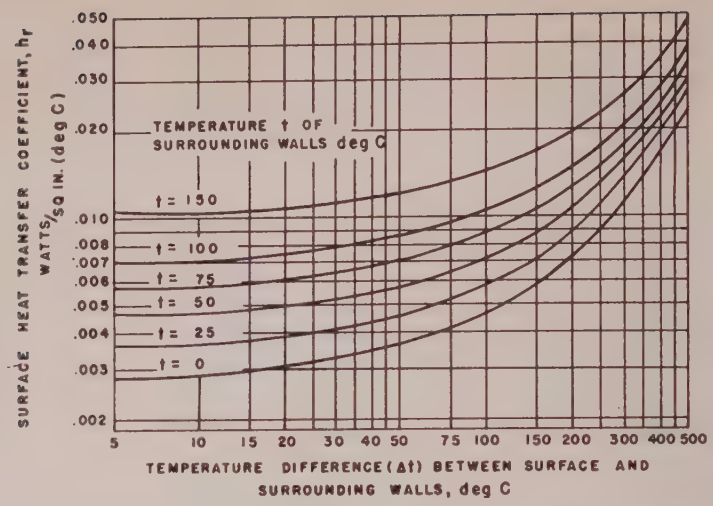

Figure 2. Surface heat-transfer coefficient for radiation, with emissivity 0.9

Radiation

The surface heat-transfer coefficient for radiation h_r is a way of expressing the Stefan-Boltzmann law for the radiation between two bodies at different temperatures. The radiation coefficient given here is a useful tool, rather than a physical constant like the h_c, which can be measured. Heat transferred by radiation is proportional to the fourth power of the temperature; the net radiation between two surfaces, one of which is relatively small and surrounded by the other at a different temperature is given by the expression, with units in watts, inches, and degrees centigrade

$$\frac{q_r}{A} = 37.1\, e_1 \left[\frac{(T_1)^4}{1{,}000} - \frac{(T_2)^4}{1{,}000}\right]$$

where

e_1 = emissivity of surface of small body, dimensionless

T_1, T_2 = absolute temperatures of the two surfaces, degrees Kelvin = 273 + degrees centigrade

In order to get this expression into the form most convenient for natural convection cooling, namely

$$q = (h_c + h_r) A\, \Delta t$$

the radiation coefficient h_r is defined as $q_r/A\,\Delta t$. This is the function plotted in Figure 2. For convenience in the use of this function, it is plotted for $e = 0.9$, a value which is a fair average for glass, for painted surfaces, and for well-oxidized metals. For cases where the surface emissivity is known accurately, the heat-transfer coefficient is adjusted by multiplying by the ratio of the known emissivity to 0.9.

Free Convection

The free convection coefficient for air is plotted in Figure 3. The basic equations, which are to be found in McAdams,[2] are plotted here in electrical units.

The free convection curves are drawn for air at atmospheric pressure with average temperature of surface and ambient 65 degrees centigrade. To correct for other pressures, as in high-altitude operation, the coefficients must be multiplied by the square root of the ratio of the operating pressure to standard atmosphere. To correct for other temperatures, a nearly linear factor is applied, 1.06 for arithmetic mean temperature of surface and ambient equal to zero degrees centigrade, and 0.95 for arithmetic mean of 150 degrees centigrade.

For other fluids, no simple general and precise relation will suffice, because of the wide variation of properties among fluids, and also the variation with temperature of the properties of any one fluid. However, useful correlations are available in the book by W. H. McAdams,[2] page 243 and page 248. An indication of the order of magnitude to be expected is shown by Figure 14, which gives values for water in ducts.

Fins

If calculations on the basis of Figures 2 and 3 indicate that the tube wall will run only a little too hot, some expedients may be tried before forced cooling is resorted to. One possibility is the use of fins, or other extended surfaces, where the tube configuration will allow their construction.

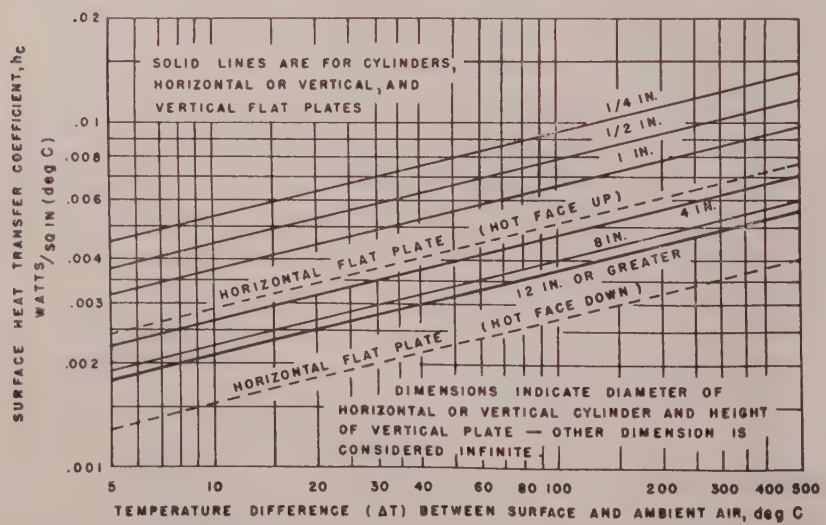

Figure 3. Surface heat-transfer coefficient for free convection in air, cylinders and flat plates

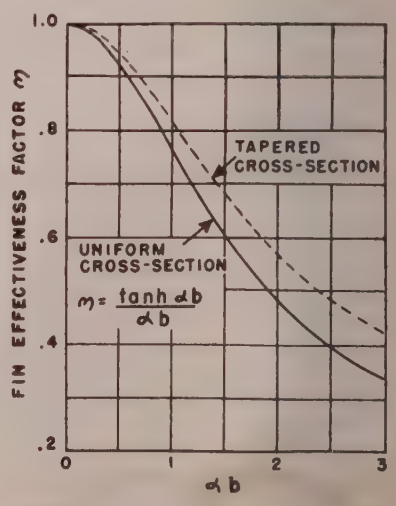

Figure 4. Effectiveness of fins on flat surfaces

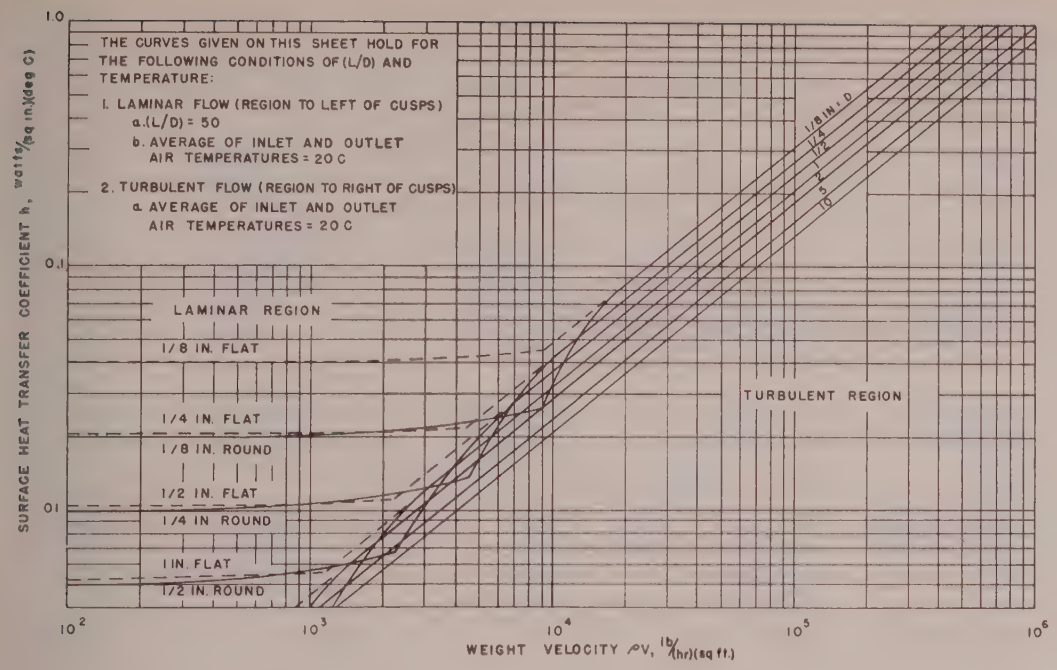

Figure 5. Forced-convection coefficient for air in smooth straight ducts

The additional heat dissipated by fins is given by the relation:

$$q = hA\eta(t_w - t_a) \qquad (2)$$

where η, the fin effectiveness for fins of uniform section, is given by Harper and Brown[3] as:

$$\eta = \frac{\tanh \alpha b}{\alpha b} \qquad (3)$$

where

$$\alpha = \sqrt{\frac{hA_s}{kA_0 b}} \qquad (4)$$

which for flat-sided fins becomes:

$$\alpha = \sqrt{\frac{2h}{k\delta}} \qquad (5)$$

In this case

h = surface heat transfer coefficient
k = thermal conductivity of fin material
δ = fin thickness
A_s = fin surface area
A_0 = fin cross-section area
b = fin height

Figure 4 gives the numerical value of effectiveness for fins of uniform cross-section. It also gives values for tapered fins, where the fin thickness in the above expression for α is the average of base and tip thickness. Effectiveness for a variety of other configurations is given by Gardner.[4]

Several factors must be considered in the use of fins. In the first place, the fin characteristic known as "fin effectiveness" must be high, because this is the quantity that determines how closely the fin surface temperature approaches the fin base temperature. Also, the radiation part h_r of the heat-transfer coefficient applies only to the envelope of the heat-dissipating area. The usual values of free convection coefficient h_c are valid only if the spacing between fins is great enough for free convection to take place effectively. A rule-of-thumb states that free convection tends to be seriously suppressed with spacings less than a quarter of an inch. Recent data[5] give the actual thickness of the boundary layer as a function of the length of a vertical fin; the example of the reference states that for a wall at 93 degrees centigrade in a 20 degree centigrade ambient, 8 inches from the base the thickness is 0.545 inch. In order for the two adjacent boundary layers not to interfere at all, the spacing for fins this height should exceed 1.09 inch. However, somewhat closer spacing is allowable as the temperatures and velocities are dying away rapidly before this value is reached.

Chimneys

Another possibility of increasing the natural convection lies in the use of a shield to introduce a chimney effect. Some tubes are shielded for electronic reasons; the efficacy of the shielding will not be impaired by coating the shield with material of high emissivity, and the heat dissipation will be increased. Moreover, the air space between tube and shield is normally small, so that convection does not take place; opening up the gap to permit air flow will result in further cooling. The same possibility is present in

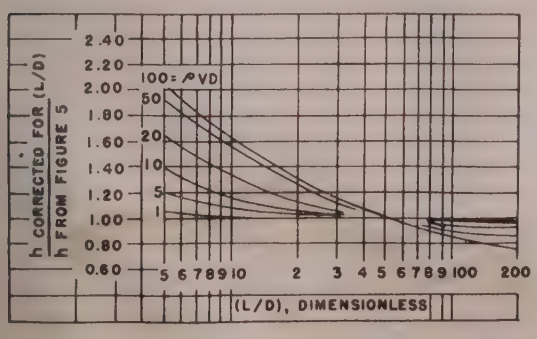

Figure 6 (left). L/D correction factor for laminar flow of air in round ducts

Figure 7 (right). L/D correction factor for laminar flow of air in flat ducts

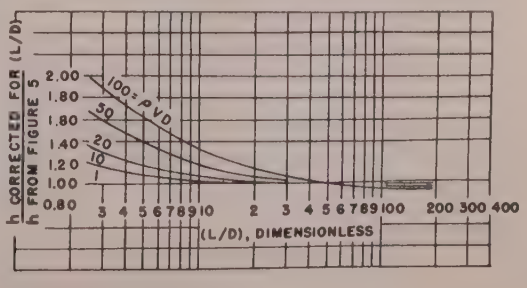

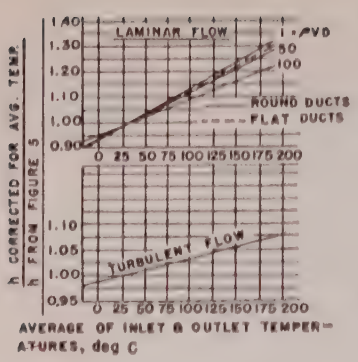

Figure 8 (left). Average-temperature correction factor for flow of air in ducts

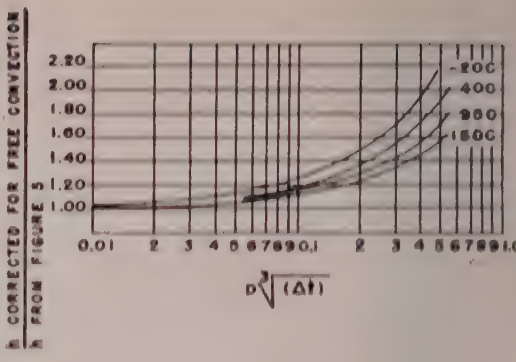

Figure 9 (right). Free-convection correction factor for laminar flow of air in ducts

the case of tubes not usually shielded. Here the spacing is extremely important, as the area for air flow must be large enough so that the head produced by the difference in density is not all used up in overcoming friction, and small enough for the increased air velocity to be effective in increasing heat dissipation.

To evaluate the temperature distribution in a tube enclosed by a shield, refer to Figure 1. An air resistance δ/kA is to be inserted ahead of t_s. This resistance is normally high, because free convection is absent, and the conductivity of still air is very low. Also, for an unpainted metal shield, the h_r is small. If the air space is opened up enough for δ/kA to be replaced by an additional $1/h_c$, and if the shield surface is painted so that h_r increases approximately 5 fold, the temperature rise of the tube will be lower, or for the same tube temperature the losses can be higher.

Forced Convection

The values of forced convection heat transfer coefficients depend on the character of the flow, whether laminar, turbulent, or in the transition region between these two well-defined types. The basic work on character of flow was done by Osborne Reynolds,[6] and the Reynolds number which bears his name gives the criterion for flow. He studied the effect of varying water velocity in a straight glass tube, introducing ink at the center, and photographing the flow pattern. For low velocities the ink proceeded down the tube in a straight line; for high velocities it immediately colored the whole fluid; while for intermediate velocities it produced a wavering pattern. He was able to establish the velocity at which laminar flow ended, and the velocity at which turbulent flow was fully established. The Reynolds number, which is dimensionless, has been a basic parameter in evaluating forced-convection coefficients ever since.

For flow inside ducts laminar flow is usually assumed to be present when the Reynolds number is below 2,100; numbers from 2,100 to 8,000 include the transition region, where the mechanism of heat transfer is uncertain; for numbers above 8,000 the flow is assumed to be turbulent. In the case of flow over planes the critical Reynolds number is much higher, and for flow outside tubes there is no well defined critical.

Three other dimensionless parameters, made up of thermal properties of the fluid, the velocity, and the characteristic dimension, have been found useful in expressing the heat transfer coefficients. These parameters together with the Reynolds number are defined as follows:

Reynolds number: $\rho VD/\mu$
Stanton number: $h/c\rho V$
Prandtl number: $c\mu/k$
Heat transfer factor $\dfrac{h}{c\rho V}\left(\dfrac{c\mu}{k}\right)^{2/3}$

Where, for convenience in using tables of properties, the dimensions are in pounds, feet, Btu, hours, degrees Fahrenheit, so that

D = characteristic dimension, diameter of round ducts, four times the cross-section divided by the perimeter for flats ducts, the difference between outer and inner diameter for annuli and the length along a plane, feet
V = velocity, feet per hour
c = specific heat, Btu per pound-degree Fahrenheit, which is numerically equal to calories per gram-degree centigrade
k = thermal conductivity, Btu per hour-square foot per degree Fahrenheit per foot
ρ = density, pounds per cubic foot
μ = viscosity, pounds per hour foot = 2.42 times centipoises
h = heat transfer coefficient, Btu per hour-square foot-degree Fahrenheit

General correlations of heat-transfer coefficients are available in the litera-

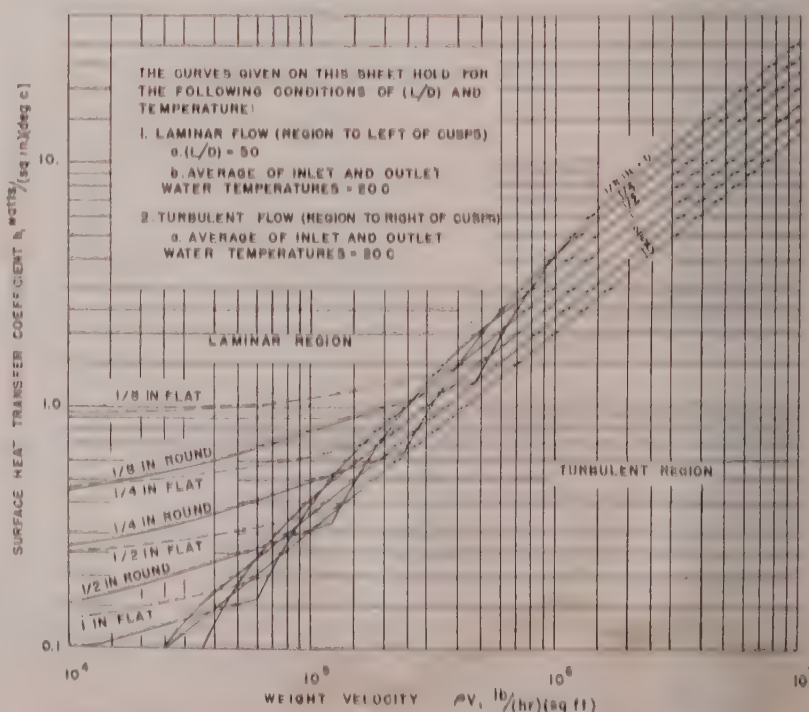

Figure 10. Forced-convection coefficient for water in smooth straight ducts

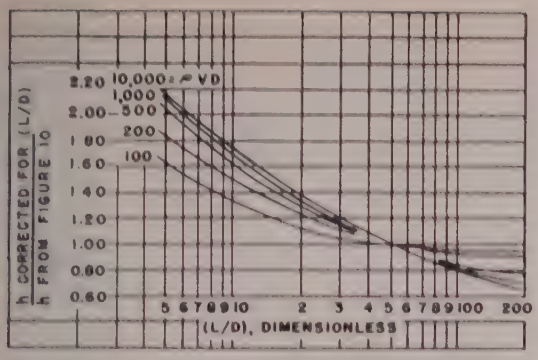

Figure 11 (left). L/D correction factor for laminar flow of water in round ducts

ture[7-10] for gases and for liquids of low viscosity. These correlations make use of the foregoing parameters. The most useful correlation so far proposed is the one due to Colburn,[11] which defines the heat-transfer factor j as:

$$j = \frac{h}{c\rho V}\left(\frac{c\mu}{k}\right)^{2/3}$$

This factor provides a useful means for correlating heat-transfer data on surfaces of different shapes; numerically, for many common shapes, it is approximately equal (within ±20 per cent) to the half friction factor $f/2$, where f is the friction factor in the Fanning equation in hydraulics.

For gases in turbulent flow, there are three values of j in terms of Reynolds number R which have been determined by experiment to be as follows:

Flow in ducts, circular, flat, or annular:

$$j = \frac{0.021}{R^{0.2}}$$

Flow over planes: $j = \dfrac{0.0346}{R^{0.2}}$

Flow over banks of tubes: $j = \dfrac{0.33}{R^{0.4}}$

For liquids of low viscosity in ducts, in the laminar flow region ($R < 2{,}100$) there are two values of j. Both are to be evaluated, and the higher one used:

$$j = \frac{1.615}{(L/D)^{1/3}R^{2/3}}$$

where L/D is the ratio of length to diameter

or $j = \dfrac{3.66}{(c\mu/k)^{1/3}R}$

In the turbulent region

$$j = \frac{0.025}{R^{0.2}}$$

For liquids of high viscosity, and for liquid metals, different relations for j exist. These relations are beyond the scope of this paper.

From the equation for j,

$$h = \frac{jc\rho V}{(c\mu/k)^{2/3}}$$

When h is expressed in watts per square inch-degrees centigrade, the dimensions of the right-hand number must come out in the same units, and this is most easily done by lumping all the conversion factors into a single constant, as follows:

$$h = 0.00366\frac{jc\rho V}{(c\mu/k)^{2/3}}$$

where the units are tabulated in an earlier paragraph of this section.

It is to be expected that a general relationship applying to all fluids will be subject to error, and as a matter of fact heat-transfer coefficients determined from the general equations may be in error by ±30 per cent. However, being in error by ±30 per cent is better than being in error by 2-to-1 or 10-to-1.

Forced Convection for Air and Water in Ducts

Since fluid properties are well known for air and water, it is possible to plot forced-convection heat-transfer coefficients as watts per square inch-degrees centigrade, against weight velocity of the fluid. Figure 5 gives the heat-transfer coefficient for air in smooth straight ducts for the conditions specified on the figure, and is to be used with log-mean temperature difference. Figures 6, 7, and 8 give the correction factors to be applied when the operating conditions differ from those specified in the figure, while Figure 9 gives the free-convection correction factor.

Figure 10 gives the heat-transfer coefficient for water in smooth straight ducts. Figures 11, 12, and 13 give correction factors to be applied as in the case of air, except that the average of inlet and outlet water temperatures is 20 degrees centigrade. Figure 14 gives the curve for free-convection. In case of doubt as to which curve applies, determine h from both and use the higher.

Pressure Drop in Forced Convection

The relation between the half-friction factor $f/2$ and the heat transfer factor has already been discussed. Pressure drop in a pipe is given by the relation:

$$\Delta p = 4f\frac{L}{D}\frac{\rho(V'')^2}{2g}$$

where

p = pressure drop, pound per square foot
f = Fanning friction factor, dimensionless

Figure 12 (below). L/D correction factor for laminar flow of water in flat ducts

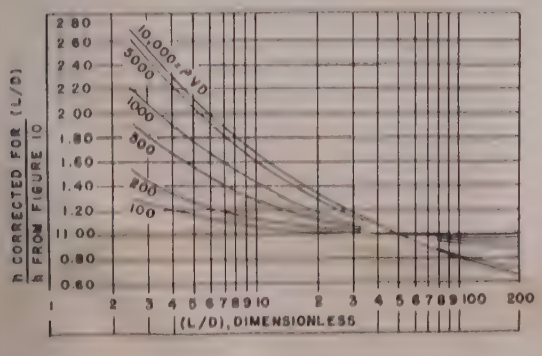

Figure 13. Average-temperature correction factor for flow of water in ducts

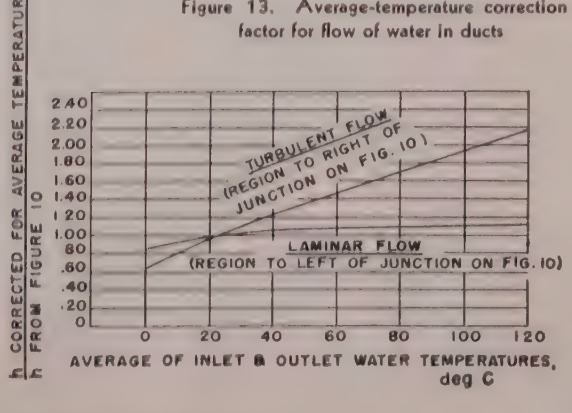

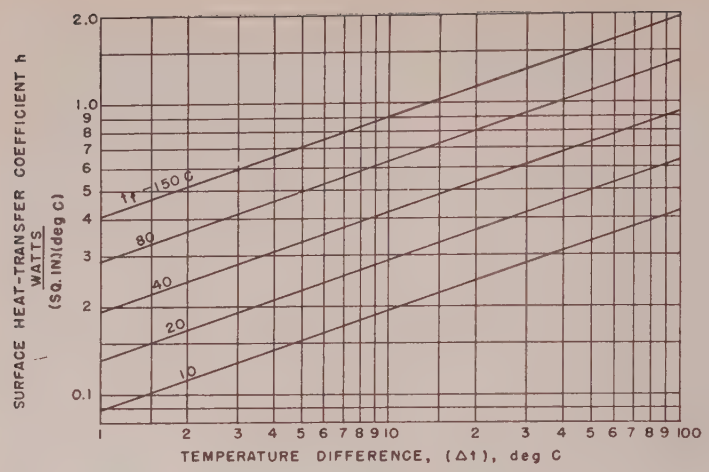

Figure 14 (left). Free-convection heat-transfer coefficient for water in ducts

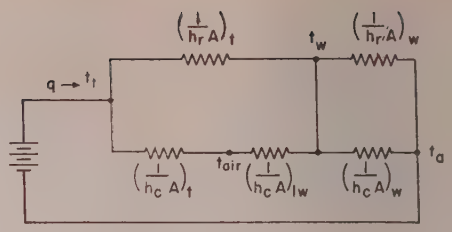

Figure 15 (above). Thermal circuit for tube in enclosure

L/D = length to diameter ratio, dimensionless
ρ = density, pound per cubic foot
V'' = velocity, feet per second
g = 32.2 feet per second per second

For turbulent flow the friction factor is very nearly constant, which means that for a given configuration the pressure drop varies as the square of the velocity. Since the heat-transfer coefficient varies as the 0.8 power of the velocity, it is obvious that high heat transfer can only be obtained at the expense of pressure drop. In deciding what velocities to use, the balance must be economic, that is, the size of blower or pump must be balanced against the gain in heat transfer.

Enclosure Ventilation

In many cases the tube with associated equipment is enclosed in a container. The question then arises as to how much hotter the tube will run. If the container is tightly closed, and dissipating heat by radiation and free convection, the temperature rise may be estimated from Figures 2 and 3. The thermal circuit is shown in Figure 15, where subscript t refers to tube, iw to inner wall, w to outer wall and a to ambient.

The heat from all the sources must be dissipated through the walls of the enclosure. The first step is to evaluate the wall temperature, which is done as before, by cut-and-try. The surface temperature is independent of the sources within the enclosure, except perhaps for local heating due to close proximity of one of the sources. When the surface temperature has been evaluated, the tube temperature and the box air temperature may be calculated. Radiation goes directly from the tube to the wall, while convection heats the air and must, therefore, be evaluated for both surfaces.

This calculation will give the maximum tube temperature. Opening up the box by louvers or holes at top and bottom edges will produce a chimney effect which will lessen the temperatures. The chimney effect is a function of the height of the opening above the heat source, and is, therefore, less effective if holes are punched throughout the walls.

Conversion Factors

Data on heat-transfer coefficients and on fluid properties are to be found in many sources, expressed in a variety of units. Table I gives the principal conversion factors used for heat transfer coefficients.

The numerical value of any dimensionless number is independent of the units employed, as long as the units are self-consistent. Table II gives examples of self-consistent units.

Table I. Surface Heat-Transfer Coefficient h

Multiply	By	To Get
Btu/(hr)(sq ft)/deg F	0.00366	Watts per square inch per degree centigrade
Watts/(sq cm)(deg C)	6.45	
Cal/(sec)(sq cm)/deg C	27.0	
Kg cal/(sq m)(hr)/deg C	0.000750	

The most troublesome unit is viscosity. If its value is given in centipoises, multiply it by 2.42 to get pounds per hour-foot. If it is given in centistokes, it is a kinematic viscosity, and must be multiplied by the specific gravity to get centipoises. If it is given in pounds force-second per square foot, multiply it by 116,000 to get pounds per hour-foot.

Appendix I. The 892-R Triode as an Example

Figure 16 shows the construction of the *892-R* triode. Looked at as a heat-dissipating device rather than as an electron-producing device, the principal source of heat is the anode, with some filament loss. Although the plate dissipation rating is 4 kw, a test was run under the following conditions: plate dissipation 5 kw and filament 1.32 kw, making a total of 6,320 watts to be dissipated by the finned radiator. For this condition, the test air flow was 450 cubic feet per minute. The problem is to determine the temperature which would be read by a thermocouple embedded in the radiator, with inlet air at 27 degrees centigrade.

There are 48 copper fins, 9 inches long, average height 2.44 inches, thickness 0.072 inch, on a core 2.625 inches outside diameter. These dimensions determine the fin spacing to be 0.100 inch at the base and 0.418 inch at the tip.

The quantities to be evaluated are as follows:

1. Air temperature rise.
2. Equivalent diameter of cooling ducts.
3. Surface heat-transfer coefficient.
4. Fin effectiveness.
5. Temperature rise at fin base.
6. Pressure drop.

Table II. Self-Consistent Units for Dimensionless Numbers

h	k	c	μ	ρ	V	D
Btu/(hr)(sq ft)/deg F	Btu/(hr)(sq ft)/deg F/ft	Btu/lb/deg F	lb/(hr)(ft)	lb/cu ft	ft/hr	ft
Cal/(sec)(sq cm)/deg C	cal/(sec)(sq cm)/deg C/cm	cal/gm/deg C	poise	gm/cu cm	cm/sec	cm
Watts/(sq in.)/deg C	watts/(sq in.)/deg C/in.	watt-sec/lb/deg C	lb/(sec) in	lb/cu in.	in./sec	in.

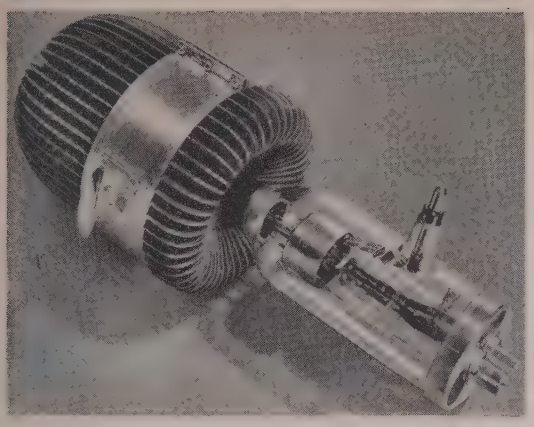

Figure 16. Triode used in heat transfer and pressure drop calculations

To find the air temperature rise Δt, the steady state input is divided by the product of weight and specific heat of the air. The weight flow in pounds per second is $^1/_{60}$ of the flow in cubic feet per minute times the density, where standard air density is 0.075 pounds per cubic foot. The specific heat of air is 0.24 calorie per gram per degree centigrade; to get it in watt seconds per pound per degree centigrade, multiply by 1,899, obtaining 455. The temperature rise is then given by

$$t = \frac{q}{cw} = \frac{6{,}320 \times 60}{455 \times 450 \times 0.075} = 24.7C$$

The area for flow is

$$2.44(0.100 + 0.418)/2 = 0.631 \text{ square inch}$$

Equivalent diameter is

$$4 \times 0.631/(4.88 + 0.518) = 0.467 \text{ inch}$$

Flow velocity V is

$$\frac{450 \times 144 \times 60}{48 \times 0.631} = 128{,}500 \text{ feet per hour}$$

Weight velocity ρV is

$$0.075 \times 128{,}500 = 9{,}650 \text{ pounds per hour per square feet}$$

The heat-transfer coefficient is found from Figure 5, using equivalent diameter 0.467 inch and weight velocity 9,650, to be 0.0360 watt per square inch per degree centigrade.

Fin effectiveness is evaluated from equations 3 and 5, using k of copper as 9.75 watts per square inch-degrees centigrade per inch.

$$\alpha b = b\sqrt{\frac{2h}{k\delta}} = 2.44\sqrt{\frac{2 \times 0.0360}{9.75 \times 0.072}} = 0.783$$

From Figure 4, read fin effectiveness η as 0.84.

The temperature rise at the fin base now is determined from equation 2, with the finned area having an effectiveness of 0.84, and the unfinned area 1.0.

$$\Delta t = \frac{6{,}320}{0.0360[0.84(48 \times 2 \times 2.44 \times 9.0) + 1.0(2.625\pi - 48 \times 0.072)9.0]} = 96.9 \text{ C}$$

The hot spot temperature is then $96.9 + 22.1 + 27 = 146$ degrees centigrade. The measured test value was 128 degrees centigrade rise above 27 degrees centigrade ambient, or 155 degrees. It may seem that the calculated value is thus not conservative. The low value may be explained on the basis that the heat loss is assumed to be uniformly distributed within the core, while in fact it is lower toward the ends and higher toward the center.[12]

A conservative value of pressure drop is obtained by using the friction factor of 0.0137 which is the maximum for turbulent flow in ducts. Substituting in the equation for pressure drop, and converting to inches of water by multiplying by 0.193, the pressure drop is 0.25 inch of water. This value does not include entrance and exit losses, which increase the required head to 0.5 inch of water.

References

1. Treatise on Electricity and Magnetism, **J. C. Maxwell.** Oxford University Press, London, England, 1892, Third Edition, volume I, pages 364–65.

2. Heat Transmission, **W. H. McAdams.** McGraw-Hill Book Company, New York, N. Y., 1942.

3. Mathematical Equations for Heat Conduction in the Fins of Air-Cooled Engines, **Harper, Brown.** *Report 158*, National Advisory Committee for Aeronautics.

4. Efficiency of Extended Surface, **K. A. Gardner.** *Transactions*, The American Society of Mechanical Engineers (New York, N. Y.), volume 67, 1945, Number 8, page 621.

5. Introduction to the Transfer of Heat and Mass, **E. Eckert.** McGraw-Hill Book Company, New York, N. Y., 1950, page 171.

6. Scientific Papers of Osborne Reynolds, **O. Reynolds,** London, England, 1901, page 81.

7. Laminar Heat-Transfer Coefficients for Ducts, **R. H. Norris, D. D. Streid.** *Transactions*, The American Society of Mechanical Engineers (New York, N. Y.), volume 60, 1940, page 525.

8. High Performance Fins for Heat Transfer, **R. H. Norris, W. A. Spofford.** *Transactions*, The American Society of Mechanical Engineers (New York, N. Y.), volume 62, 1942, page 489.

9. Basic Laws and Data of Heat Transmission—Forced Convection, **W. J. King.** *Transactions*, The American Society of Mechanical Engineers (New York, N. Y.), volume 50, 1932, page 410.

10. Surface Heat Transfer Coefficients for Hydrogen-Cooled Rotating Electric Machines, **D. S. Snell, R. H. Norris, Mrs. B. O. Buckland.** *AIEE Transactions*, volume 69, 1950, pages 174–85.

11. A Method of Correlating Forced Convection Data and a Comparison with Fluid Friction, **A. P. Colburn.** *Transactions*, American Institute of Chemical Engineers (New York, N. Y.), volume 29, 1933, page 174.

12. Temperature Distribution in Vacuum Tube Coolers with Forced Air Cooling, **I. E. Mouromtseff.** *Journal of Applied Physics* (New York, N. Y.), volume 12, 1941, page 491.

No Discussion

Choice of Telemetering Systems and Channels for a Power System

C. K. DUFF
MEMBER AIEE

AN ELECTRIC power system consists of the co-ordinated facilities for generation, transformation, and distribution of electric power within a given area. In large, modern power systems this involves the electrical interconnection of many power sources within the area by means of a transmission system which also distributes the power to major load centers. Interconnection often extends to neighboring power systems in adjacent areas, which, in turn, may be connected to others beyond them, thus creating vast interconnected networks or power pools for economic interchange of power. In the operation of such interconnected systems, there are many and varied applications of telemetering, adopted for labor-saving purposes, for improvement of efficiency in plant and system operation, and for the purpose of automatic load and frequency control, without which extensive interconnected operation would not be feasible.

This paper describes typical applications of telemetering in power systems, and points out factors influencing the choice of types. Examples are from practice of the Hydro-Electric Power Commission of Ontario (HEPC).

Interconnected Systems of HEPC of Ontario

The Commission operates four power systems in Ontario. The two largest are the Southern Ontario System and the North-Eastern System which are normally interconnected by a 115-kv tie-line. This integrates some 60 power plants having a capacity of about 2,750,000 kw by means of a network of high-tension transmission lines (115 kv and over) totalling 6,400 circuit-miles, in an area about 500 miles east to west and 500 miles south to north.

Statistics of high-tension line mileage, peak loads, HEPC generating capacity and total interconnected generating capacity are given in Tables I, II, III, and IV respectively.

Ontario also is interconnected at times with systems in New York State, and the chain sometimes extends as far south as Washington, D.C. Future interconnections may include neighboring provinces and states, in a trend which points toward ultimate formation of one great power network blanketing the whole continent, with generators running in synchronism throughout. The control of power distribution in such extensive networks demands continuous, reliable telemetering of power measurements from boundary points of each area to an area control center where automatic equipment regulates the output of generators within the area, thus maintaining the desired transfer of power to or from neighboring areas.

Selection of Telemetering Equipment

Except in a few cases where special equipment was designed and built locally, commercially available equipments have been selected which economically fulfill the physical requirements of the application. Commercial accuracy is usually in the order of 1 per cent of range which is acceptable for most applications. Selection of makes and types is dependent upon the type of transmission channel available, required speed of response, available power supplies at transmitting and receiving ends and other factors. Standardization is desirable, thus permitting a reduction in the supplies of spare parts and meter charts which must be kept in stock, but with rapid development of the art, adherence to standardization is difficult.

Basic Telemetering Types

The five basic types of telemetering systems defined in the 1948 AIEE Telemetering Report[1] are:

1. Current type
2. Voltage type
3. Frequency type
4. Position type (or ratio type)
5. Impulse type (with subtypes)

Fields of application of these types on the Commission's properties are as follows:

Current Type, such as torque balance. For telemetering mechanical motions or electrical quantities over distances up to a few miles on 2-conductor wire circuits.

Voltage Type, such as thermal converters with self-balancing potentiometer recorders. For telemetering electric power measurements over distances up to 20 miles on 2-conductor wire circuit, with or without totalizing, for example: Load of one or more generators, generating stations, transformers or feeders.

Frequency Type. Though not at present used by the Commission, this type is capable of high speed of response, and can be used to telemeter mechanical or electrical quantities over wire circuits or carrier channels which are adapted to pass the desired band of frequencies.

Position Type (ratio type), such as Selsyn or Autosyn, and rectified current system. For telemetering mechanical motions at distances up to a few miles, over wire circuits, for example: Water level, turbine gate position, gate limit setting, governor speed setting, transformer tap-changer position, wind direction indicator.

Paper 51-229, recommended by the AIEE Telemetering Committee and approved by the AIEE Technical Program Committee for presentation at the AIEE Summer General Meeting, Toronto, Ont., Canada, June 25-29, 1951. Manuscript submitted March 26, 1951; made available for printing May 2, 1951.

C. K. Duff is with The Hydro Electric Power Commission of Ontario, Toronto, Ont., Canada.

Table I. High-Tension Line Mileage Data, December, 1950

System	Voltage, Kv	Circuit Miles
S. Ont.	230	2,693
S. Ont.	115	2,638
N. E. Ont	115 to 138	1,069
Total		6,400

Impulse Type, such as Chronoflo, Metameter, Micromax Ballistic. For telemetering mechanical or electrical quantities over wire circuits, carrier on telephone lines, power lines or radio, by channels capable of transmitting a keyed signal.

Examples will be cited to illustrate the application of different types of telemetering in the Commission's power plants, then in regional operation, and finally in system operation.

Telemetering in Hydro Plants

One of the most important factors in the operation of a hydroelectric power plant is head-water level and to a lesser degree tailwater level, since these determine the efficiency, capacity, and stored energy available at a plant. In some plants the levels at more remote points upstream or downstream are also important because of effects on navigation or other interests. To provide an indication in the control room of such quantities requires the aid of telemetering. The two types most commonly used are the well-known position type (Selsyn, or others) and impulse-duration type, operated from a float in a float well. At Sir Adam Beck-Niagara number 1 plant on the Niagara River, both types are in use for forebay level indication in the control room in case either float becomes fouled with ice or debris. Also, the impulse telemeter is used for transmitting to the regional operator's office at Niagara Falls and to the system supervisor's office at Toronto.

Rectified Current, Ratio-Type Telemeter

Conditions at the Chats Falls plant on the Ottawa River led to the choice of the Evershed-Midworth rectified current telemetering system for remote water-level indication. The transmitter is located at a point where no power supply is available. The equipment operates on a-c supply which is passed through the transmitter and receiver in series, using only two line wires. A float-operated rheostat or current-divider and two half-wave rectifiers at the transmitter determine the proportions of positive and negative half-waves of current which are allowed to flow in the circuit. The receiver is a d-c ratio-type indicating instrument with two coils which are supplied through rectifiers so that one is energized by the positive half-waves and the other by the negative half-waves of the alternating current. Operation has been satisfactory except for effects of dampness and ice at the transmitter, in the absence of electric heating. Obstruction of the float or water passages by ice was avoided by the use of oil instead of water in the float well.

Voltage-Type Telemetering and Totalizing

Electrical quantities within a power plant can usually be measured without resort to telemetering, but, for its convenience and adaptability, plant totalizing by means of thermal converters, and a self-balancing potentiometer recorder has recently become standard HEPC practice.

The thermal converter is a device which, with no moving parts, converts an a-c power measurement into a d-c millivoltage proportional to the a-c power. Separate measurements may be added by connecting the d-c outputs of two or more thermal converters in series. Subtraction may be effected by reversing the d-c polarity. Since the d-c output automatically reverses its d-c polarity when the direction of power flow reverses, the thermal converter is useful also for measurement of power in tie lines. A 2-wire circuit is required for connection to a receiving potentiometer, and since this is a sensitive, null-balance instrument, resistance of 1,000 ohms or more can be tolerated in the input circuit. This represents many miles of transmission, even with small wire sizes.

This is an application of voltage-type telemetering, even though the distance of transmission is not great in the case of local plant totalizing. Potentiometer recorders can be purchased which are built to incorporate impulse transmitters for re-transmission of the measurement by impulse-duration telemetering, to more remote regional and system operating centers.

Table II. December 1950, HEPC Peak Loads (Actual Load Carried)

System	Megawatts, 20-Min. Peak 25-Cycle*	60-Cycle	Combined
S. Ont.	1,577	571	2,148
N. E. Ont.	165	74	239
Total			2,386

* Includes Dominion Power 66⅔ cycle load.

Note: 25-cycle and 60-cycle peaks are not necessarily coincident. Loads are given in terms of power generated and purchased.

Table III. HEPC Dependable Generating Capacity, Southern Ontario and Northeastern Systems, December 1950

System	No. of Plants Hydro	Other**	Total Capacity, Megawatts 25 Cy.*	60 Cy.	Total Capacity Mw
S. Ont.	39	6	818.	598.	1,416
N. E. Ont.	18		202.	93.	295
Total	57	6	1,020.	691.	1,711

** Small steam and diesel plants.

* Includes 45 mw of 66⅔ cycle generation.

Telemetering in Regional Operation

For co-ordination of the operation of two or more plants in a local area, telemetering must extend to greater distances. A common case is that of two or more generating stations on one river, where the water passes through each plant in turn, and where the discharges of the plants must be co-ordinated. Frequently one or more such plants are operated as unattended stations by remote control. This usually requires more telemetering than when the plant is attended.

Current-Type Telemeter

A typical example is that of two small plants, one of which, an unattended plant of 7,000 kw capacity, is controlled from a plant about three miles further up the river. Torque-balance telemeters are used to give continuous indications of forebay elevation, gate positions and kilovar outputs of the two generators at the unattended plant, to guide the operators in adjusting load and voltage.

The torque-balance telemeter is one of several makes of current-type telemeters in which a direct current proportional to the measurand is transmitted to an indicating or recording milliammeter at the receiving end. The torque of the primary measuring device is balanced against that of a permanent-magnet moving-coil element which is in series with the transmission circuit. The transmitted current is automatically adjusted to maintain the balance of torques. Totalizing may be accomplished by paralleling the outputs of different transmitters. Accuracy is not affected by changes in circuit resistance or by variations in supply voltage. Transmission distance

in the case cited is 18,000 feet, using pairs of number 19 gauge rubber-insulated conductors in an overhead lead-covered control cable, but the system is usable over much greater distances. The system requires a power supply at the transmitting end only.

Supervision of Niagara Region

A more extensive installation of telemetering for regional supervision exists in the Niagara district, where five large hydroelectric plants discharge water the aggregate amount of which must be limited, as provided by international agreement. In the case of four plants, the water consumption is calculated from the measurement of electric energy output, while in the fifth (De Cew) the water is controlled and measured where it is diverted from the Welland Canal through pipes. Discharge through these pipes is totalized and telemetered by impulse-duration system to De Cew plant where it is recorded and also integrated. Each of the five plants operates at a different head and therefore optimum efficiency in use of the total available water requires careful supervision of the loading of these plants.

At the regional load supervisor's office at Niagara Falls, there are potentiometer recorders operating from thermal converters in the several plants to indicate plant loads; also three impulse-duration type water-level telemeter receivers to show forebay conditions at three of the plants. All these telemetering transmissions are through pairs of wires in lead-covered control or communication cable. The longest run is about 14 miles, in which a pair of number 19 gauge wire of 1,200 ohms loop resistance connects thermal converters at De Cew plant to a potentiometer recorder at the regional office at Niagara Falls. Maximum millivoltage in the measuring circuit is 238 millivolts.

The five load recorders at Niagara supervisor's office are built as impulse transmitters for retransmitting the load readings to the system supervisor's office in Toronto. Two of the water-level indications are also transmitted to Toronto.

Other facilities at Niagara office include a Selsyn-type wind-direction indicator and d-c tachometer-type wind-velocity indicator operated from transmitters on a tower a few hundred yards from the office. One unique facility which is available not only to the Niagara load supervisor but to any plant operator and others who have telephones connected to the HEPC private automatic exchange is an audible indication of water level at any of four water-level gauge stations located on the upper Niagara River and along the 12-mile route of the canal which conveys water from the upper river to the Sir Adam Beck-Niagara number 1 power plant. Although the indication is audible instead of visible, and is "as-called-for" instead of being continuous, the system qualifies as telemetering of the impulse-counting type.

Table IV. Interconnected Generating Capacity, Southern and Northeastern Ontario Systems, December 1950

System	Total Capacity, Megawatts 25 Cy.	60 Cy.	Total Capacity Mw
S. Ont.	1,562	728	2,290
N. E. Ont.	330	120	450
Total	1,892	848	2,740

Note: Includes generating capacity of customers and suppliers, operated in parallel with the Commission's systems. Does not include systems in United States.

Figure 1. HEPC System Interconnections, Southern and Northeastern Ontario as of December 1950

∿∿ = tie line measurements telemetered to control centers

The Toronto load supervisor, in whose office the totalizing recorder is installed, also uses its indications as a guide to operation. In this installation there are now 30 thermal converters connected in series through 20 circuit-miles of small-size conductor in multiconductor communication cable. Total loop resistance is about 1,600 ohms.

Totalizing City Loads

A regional problem which occurs in a municipal load area is that of totalizing the power demand of a municipality which purchases power on a peak demand basis. For example, in the city of Toronto power is delivered at seven stations at each of which graphic meters are installed as the basis of billing. To determine from seven different charts the time when the maximum combined demand occurred is a very onerous task with much risk of error, but a potentiometer-type totalizer, supplied by thermal converters in the various stations, gives the time of the peak, and normally agrees with the total as measured by the seven individual meters within one percent.

Telemetering in System Operation

Supervision of a large interconnected power system aims at the most efficient utilization of all power resources. Provision must be made for meeting all load demands as they change from minute to minute and from hour to hour, and for maintaining suitable voltage levels at load centers. Hence the system supervisor requires an indication of these changing loads as they appear in the output of major generating stations and in the loads of tie-lines and frequency changers interconnecting different systems or divisions within a system. This requires system-wide telemetering, since generating stations and tie lines are likely to be far from the supervisor's office. Figure 1 shows a schematic diagram of the interconnected systems in Ontario and adjacent areas.

Modern practice is to regulate the output of key generating stations in each system or division of an interconnected group so that each area takes care of its own load changes and tie-line loads are maintained at scheduled values. Such regulation is done by automatic con-

Figure 2. Telemeter and control panels in system supervisor's office

trollers which are sensitive to changes in the tie-line loads and also to system frequency, hence called load-frequency control. When deviations occur in either load or frequency the controllers send out raising or lowering impulses which are transmitted to the turbine governors of generators in the selected regulating plants, causing them to change their output to restore scheduled conditions. Other plants tend to hold constant load except when changed by manual control. The variable quantities, regulating plant loads and tie-line loads, are therefore the most important quantities to be telemetered. Tie-line telemetering, being a link in a closed-loop automatic control system, should possess a high degree of reliability and speed of response.

System Supervisor's Office, Toronto

Supervision of the HEPC Southern Ontario System is conducted from an office in Toronto, to which are telemetered, at present, the loads of three 25-cycle generating stations, two 60-cycle generating stations, three frequency-changer stations, one 25-cycle and four 60-cycle tie lines, and two forebay levels. Two load-frequency controllers are located in the Toronto Office, one for control of the 25-cycle division and the other for the 60-cycle division. Niagara plants (Sir Adam Beck-Niagara number 1 or De Cew) are used for 25-cycle system regulation and plants in Eastern Ontario for 60-cycle regulation. Figure 2 shows a metering and control panel in the system supervisor's office, Toronto.

Long-Distance Telemetering

For long distances of transmission over channels of variable attenuation the frequency system or some form of impulse system is most suitable, since the accuracy of the system is not dependent upon the magnitude of the electrical quantity in the transmission circuit, but only upon some time function such as frequency, impulse duration, impulse rate, or impulse spacing. Another advantage is the simplicity of relaying the signal as often as necessary to span any desired distance.

Among impulse systems, the most commonly used in power-system applications is the impulse-duration type in which impulses recur at fixed intervals called the impulse period, and individual impulses have a duration dependent upon the magnitude of the measurand. The ability of this system to follow a rapidly changing variable depends largely upon the impulse period which is usually between two and fifteen seconds, depending upon the make and the application. Short impulse periods give faster response but require more critical adjustments of instruments and also of channel equipment.

With the exception of two local load measurements, which use potentiometer recorders connected by cable circuits to thermal converters at Scarboro, all load telemetering to the Toronto office is impulse-duration type, using almost exclusively Leeds and Northrup "Micromax Ballistic" telemeters. The primary measurement at the transmitting points is by thermal converters and potentiometer recorders, which produce telemetering impulses at 2.4-second intervals. The impulse duration varies between 0.1 and 2.0 seconds in accordance with changes in the load measurement. At the receiver, the incoming impulse applies a slow rate of charge to a capacitor, which at the end of the impulse, retains a voltage proportional to the impulse duration. Mechanically operated contacts then transfer the capacitor to the measuring circuit of the potentiometer recorder by which the voltage is measured, after which the capacitor is discharged and connected again to be charged by the next incoming impulse.

The over-all speed of response of such a load-telemetering system is the combined time delay of the thermal converters and of the telemetering instruments. For tie-line measurements, where automatic control is involved, thermal converters are specified which measure 90 per cent of any load change in one second or less and the over-all speed with 2.4-second impulse period is satisfactory for control purposes under average conditions.

Each load-recording telemeter at Toronto has in it a retransmitting slide-wire or voltage divider. In the case of tie-line load recorders these slide-wires feed into the appropriate system net interchange controller. In the case of generating station load recorders, the retransmitting slide-wires are used for local totalizing. Since some plant outputs are not at present telemetered to Toronto, the loads of these, reported by telephone, are injected into the total by means of manually adjustable voltage dividers, so that an approximate record of total system generation is obtained.

Telemetering and Control Channels

The two principal kinds of channel for telemetering and associated remote control are wire circuits (sometimes called pilot wires) and carrier on existing telephone lines or power lines. The simplest channel is a wire circuit used for no other purpose, in which case any of the five basic types of telemetering may be used up to distances which may be limited by line resistance or leakage or by economic considerations. Open-wire lines are somewhat vulnerable to variable leakage, weather hazards, and inductive inter-

Table V. Channel-Miles of Carrier in Service on Southern Ontario System, April 1951

	Channel Miles	
	Telephone-line Carrier	Power-line Carrier
For load control	642	860
For telemetering	1,023	2,600
Total	1,665	3,460

Figure 3. Signal channels, present and projected, for telemetering and control

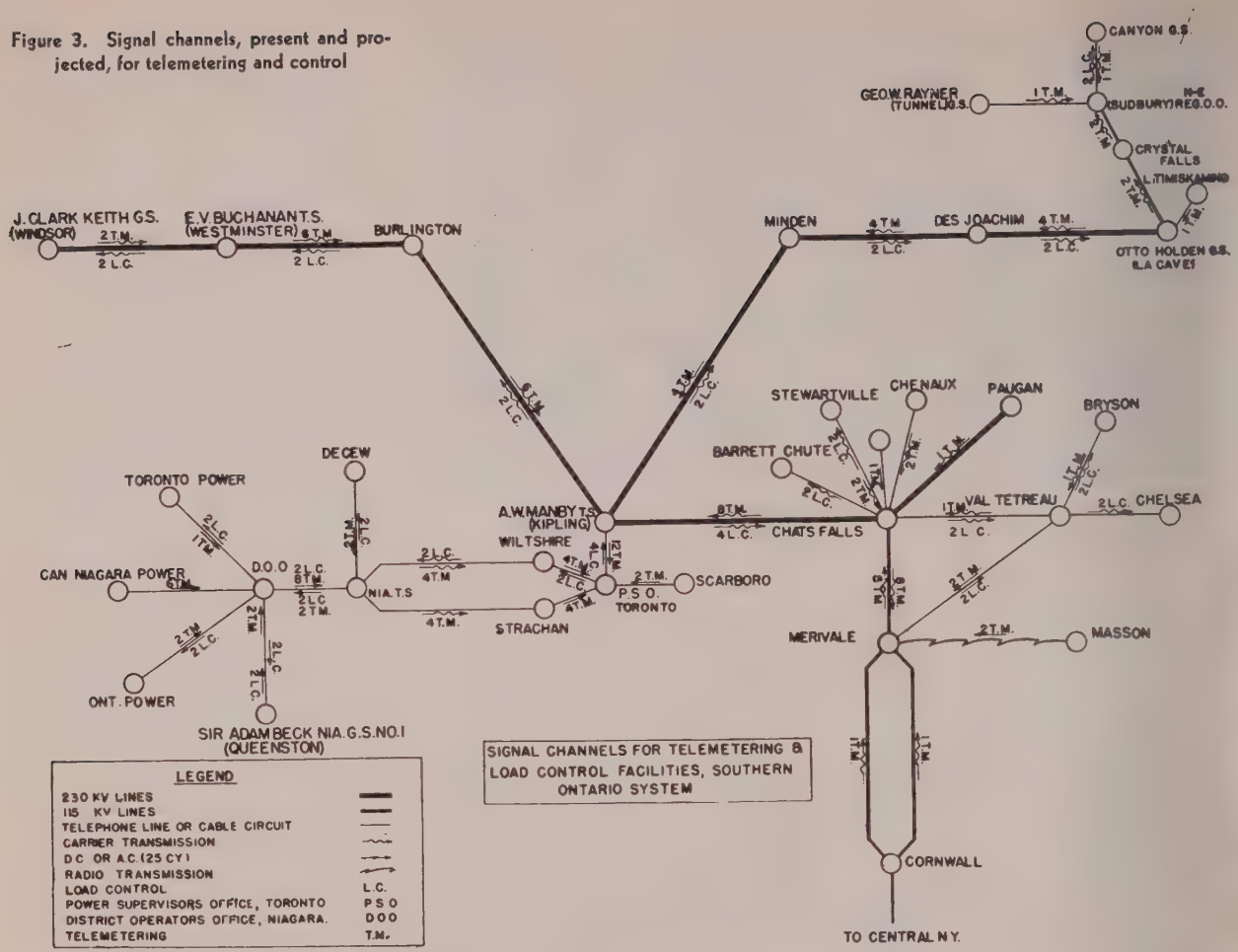

ference. Lead covered cables are more reliable, especially when laid underground in ducts. One pair may be used for two or more channels by using different audio-frequency signals which, of course, are usable only for frequency-type or impulse-type telemetering, though d-c telemetering (current type) may be used simultaneously on the same pair.

Telephone-line carrier is often used as an economical long-distance channel where open-wire telephone lines already exist and where reliability is not of the utmost importance. Frequencies in the range from 12 to 25 kc may be applied for several channels of impulse-type telemetering without interfering with the physical voice channel and one voice carrier in the band between 5 and 10.5 kc. Distances of 100 miles or more can be spanned without repeaters on well-built and properly transposed lines, using by-pass filters at intermediate terminals and blocking filters on tap lines. Attenuation is roughly 0.1 decibel per mile and the input power level is in the order of 16 decibels (above one milliwatt into 600 ohms) on each channel. Coupling to the line at each terminal is through a band-pass filter.

Power-Line Carrier

Greatest reliability is attained in the use of carrier channels on the high-voltage power lines which are built to withstand very severe weather conditions. Coupling is by means of a high-voltage capacitor connected between one line conductor and ground, with a choke coil in the ground lead. A "line trap" is usually connected in series with the line conductor between the terminal station and the point of connection of the coupling capacitor, to prevent dissipation of the carrier within the local station or its transmission into other circuits where it might cause interference with other carriers. A carrier may be connected between one power conductor and ground or between two power conductors each equipped with couplers and traps, or both types of coupling may be used simultaneously with different carrier frequencies, which requires line traps tuned for two frequencies. The carrier frequency is in the band between 50 kc and 300 kc. The simplest use of a carrier is to key it on and off for impulse telemetering of a single quantity, but greater use can be made by modulating it with a number of audio-frequency "tones" each of which can be keyed as a separate telemetering channel. Carrier frequencies and tones must be chosen to suit the line attenuation characteristics and to avoid interference between carriers on different lines in the same area. The tone frequencies also must be selected to avoid mutual interference and interference from harmonics of the power system frequency. Another method of keying a carrier is by the "frequency-shift" system, in which the carrier is shifted by the telemetering signal, between two values, both crystal-controlled, which are close enough together to be passed or blocked by a single filter or choke, but far enough apart for adequate discrimination.

Channels suitable for telemetering are usable also for various other kinds of signalling and control such as raising and lowering load-control signals, for supervisory control of circuit breakers and other equipment, and for the automatic

tripping of faulty lines. Such applications are continually increasing in number so that means of crowding more channels onto the existing power lines are always being sought.

For line-of-sight routes, radio channels, either short wave or microwave, are entering the field as competitors of other means of transmission and they have an economic advantage in some cases.

The HEPC of Ontario in 1950 placed in operation its first power-line carrier telemetering and control channels on a 230-kv power line between Toronto and Chats Falls plant (near Ottawa) a distance of 214 miles, using 71 kc for incoming telemetering and 97 kc for outgoing load control, both coupled to the same two line conductors. Tone frequencies between 200 and 3,000 cycles are used to modulate the carriers to give a maximum number of eight channels each way. Additional tone-modulated carriers and also some frequency-shift carriers are being installed on other lines. Radio channels for telemetering have been tried experimentally between Masson and Merivale in the Ottawa area with encouraging results. The distance is about 23 miles, using high-gain directional antennas at an elevation of 325 feet and 100 feet above ground at the two terminals respectively. Trials to date have been with 1-way transmission at 158.25 megacycles, using frequency modulation for one voice channel, and it is planned to add two tones at frequencies above the voice band for impulse-duration telemetering.

Defining a channel as a path which is suitable for the transmission of any single control or telemetering signal, the number of channel-miles of telephone-line and power-line carrier at present in use for telemetering and control on the Southern Ontario System are summarized in Table V. The diagram of Figure 3 shows schematically the routes of present and projected carrier channels and of wire circuits (mostly in cable) associated with them.

Conclusion

Telemetering has proved itself to be an essential tool in the efficient operation of electric power plants and interconnected systems. The number of applications is continually increasing as systems grow and interconnections are extended, predicated upon the reliability of telemetering instruments and channels, and automatic controls associated therewith.

References

1. Telemetering, Supervisory Control, and Associated Circuits. AIEE, 1948, 39 pages.

2. Principles and Methods of Telemetering (book), **P. A. Borden, G. M. Thynell.** Reinhold Publishing Corporation, New York, N. Y., 1948.

No Discussion

Regeneration with a Mercury Arc Rectifier on the Central Railway of Brazil

A. SCHMIDT, JR.
MEMBER AIEE

THE ESTRADA de Ferro Central do Brasil (Central Railway of Brazil) is one of the most important railway systems in Brazil. It constitutes the only rail link between the two largest cities, Rio de Janeiro and Sao Paulo. It also serves important mineral regions in the State of Minas Geraes, to the north of Rio de Janeiro.

In 1935, electrification of the suburban section about Rio de Janeiro was undertaken,[1] using mercury-arc rectifiers to supply power to an overhead trolley system at 3,000 volts of direct current. This electrification extended to Deodoro, 14 miles from Rio, and was completed in 1938.

Further extension of the electrification was delayed by the incidence of World War II. It was finally undertaken in 1945, and when the present phase is completed, the main line will be electrified as far as Volta Redonda, 88 miles from Rio. The line climbs up to the edge of the coastal incline between Guedes da Costa and H. Antunes. In this interval, there is an average gradient of 1.65 per cent over a distance of 16 miles. Figure 1 shows a map and profile of the electrified section of the main line.

A survey of traffic and load conditions indicated that it would be profitable to install an inverter on this grade to permit power delivered by regenerating locomotives descending the grade to be returned to the primary power-supply system. Accordingly, one of the system substations, consisting of three rectifiers and one inverter, was designed for installation near Scheid, about 7 miles below H. Antunes. The purpose of this paper is to describe the installation at this substation and particularly the regulating system used to control the d-c voltage.

Conversion Apparatus

Rectifiers

Three rectifiers are installed in the substation. Each rectifier has a continuous rating of 2,000 kw at 3,000 volts of direct current with short time ratings of 150 per cent for two hours and 300 per cent for five minutes. These rectifiers are of the multianode continuously-pumped type, having six anodes and control grids. Each rectifier is supplied from a 44-kv 50-cycle system, through a 2,360-kva rectifier transformer having a forked secondary connection.

Each rectifier cathode is connected to the positive bus through a high-speed reverse-current circuit breaker. The transformer neutrals are connected to a negative bus, which, in turn, is connected to the track rails through a filter designed to remove the 6th, 12th, and 18th harmonics from the output of the rectifier.

Inverter

The inverter equipment is rated 1800 kw continuously at 3,000 volts, with short time ratings of 150 per cent for 2 hours and 300 per cent for 5 minutes. The design of the inverter tank is substantially the same as that of the rectifier. The inverter transformer is designed so that when the inverter is operated at 300

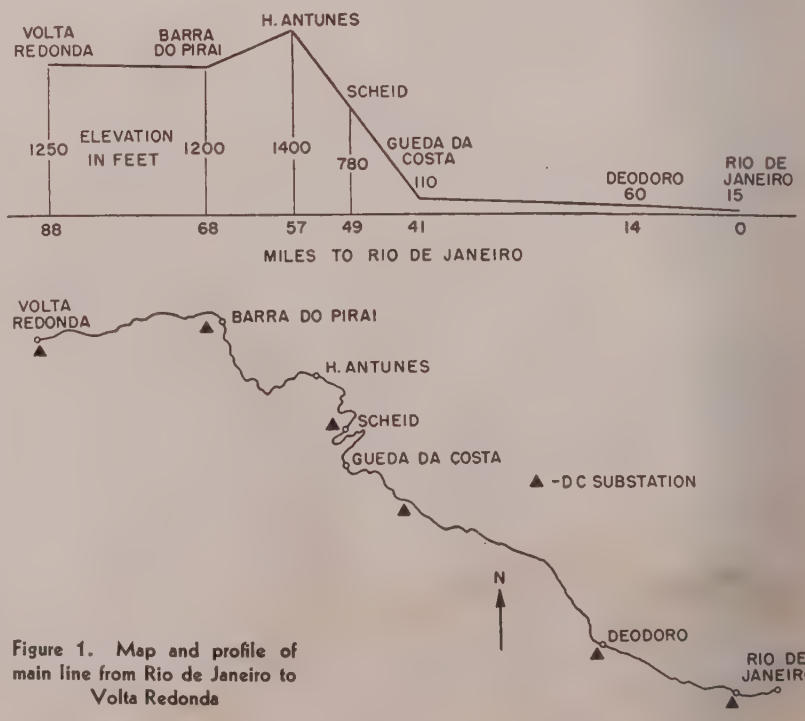

Figure 1. Map and profile of main line from Rio de Janeiro to Volta Redonda

Paper 51-232, recommended by the AIEE Land Transportation Committee and approved by the AIEE Technical Program Committee for presentation at the AIEE Summer General Meeting, Toronto, Ont., Canada, June 25–29, 1951. Manuscript submitted March 26, 1951; made available for printing May 3, 1951.

A. SCHMIDT, JR. is with the General Electric Company, Schenectady, N. Y.

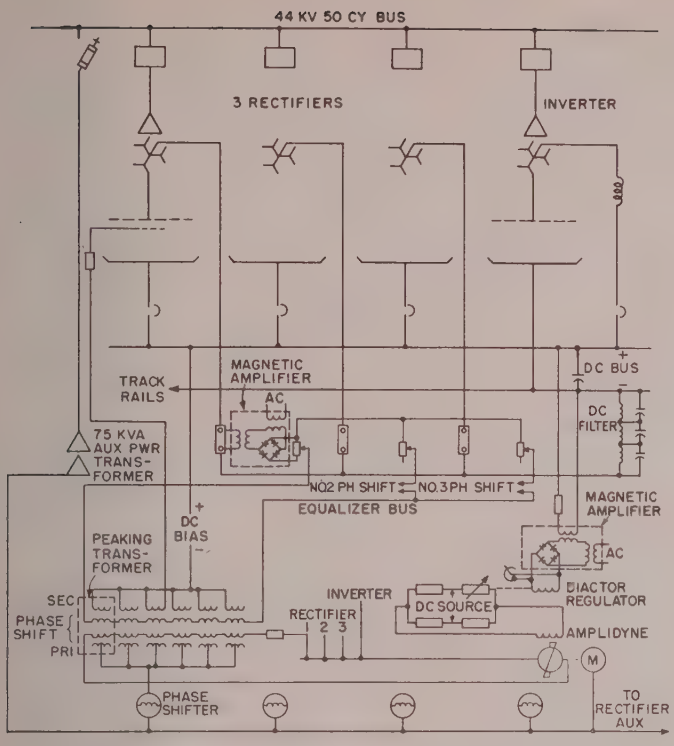

Figure 2. Schematic diagram of power and regulator circuits

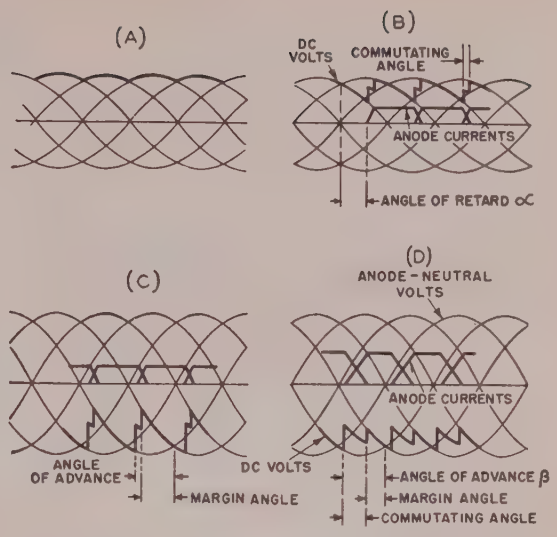

Figure 4. Anode-neutral voltages and anode currents

(A). Rectifier no load
(B). Rectifier with phase retard
(C). Inverter with light load
(D). Inverter with heavy load

per cent load with 90 per cent rated voltage on the a-c bus, there will be an adequate margin angle at the end of commutation. The transformer has a continuous rating of 3,660 kva. This high rating results from the power factor of the inverter which is quite low when the inverter is designed to carry large overloads at reduced alternating voltage.

The neutral of the inverter transformer is connected to the positive bus through an air-core reactor and a high-speed circuit breaker. The cathode of the inverter tank is connected to the station negative bus. The arrangement of power and control connections is shown in Figure 2. Figure 3 is an illustration of the station interior, showing the rectifier and inverter tanks, together with their auxiliaries.

Regulating System

Close control of the station voltage is desirable, particularly when there is heavy regeneration at points remote from the station. In such cases the d-c line-drop increases the voltage at the locomotive and this voltage may become excessive if appreciable voltage rise is permitted at the station.

Figure 3 (below). Interior of substation at Scheid, showing inverter and rectifier tanks and auxiliaries

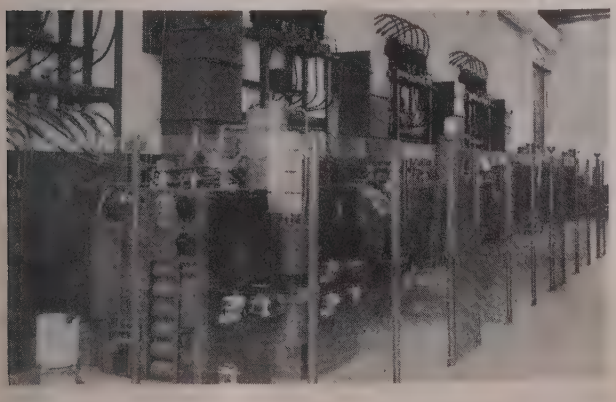

Figure 5 (right). Regulation curves of inverter and two parallel rectifiers

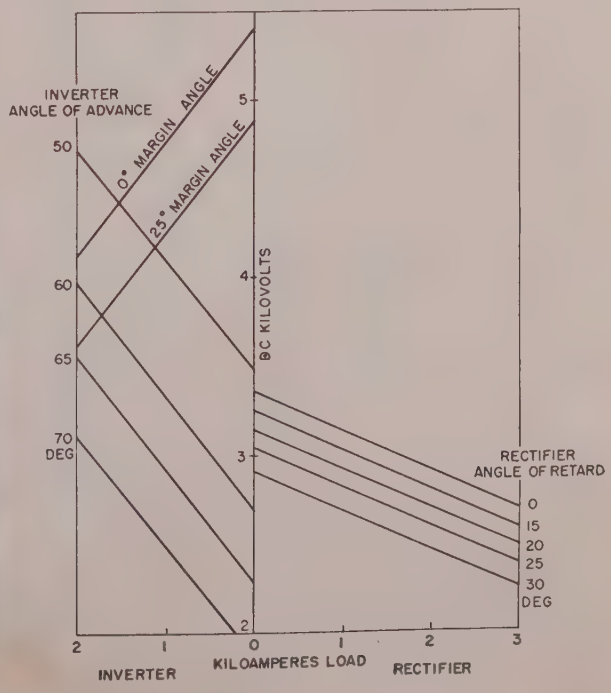

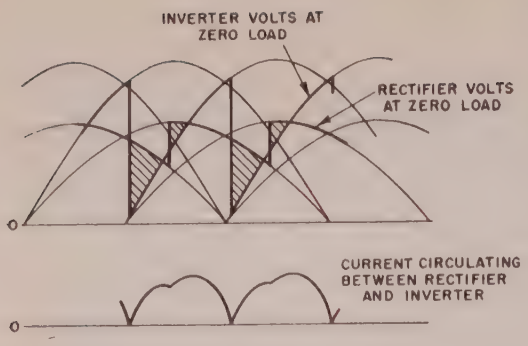

Figure 6 (left). Wave forms of rectifier and inverter adjusted for equal voltages at no load

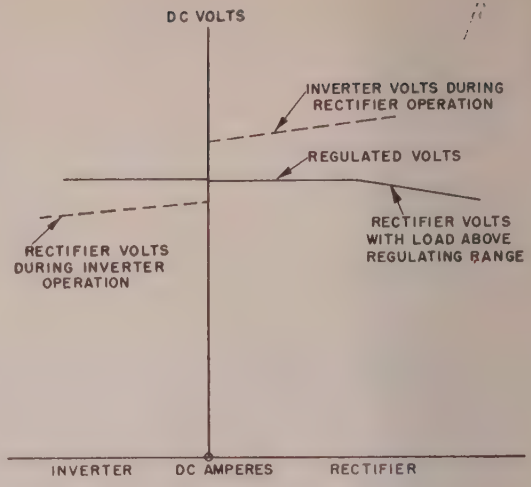

Figure 7 (right). Action of regulator on inverter and rectifier voltages

Grid control of the rectifiers is best achieved with peaking transformers. These transformers have a restricted iron section associated with the secondary winding so that the secondary voltage has a narrow peak with a wavefront which is nearly vertical.

Two important advantages result from the use of peaking transformers.

1. The grid firing time is not affected by distortion of the supply voltage to the excitation circuit. Such distortion becomes pronounced in a long line supplying a large rectifier load where extensive phase multiplication is not employed.

2. By biasing the core of the peaking transformer with a d-c winding and adjusting the current in this winding, the phase of the grid voltage may be varied. D-c voltage control then becomes a matter of controlling current in a d-c circuit where the total power is in the order of dozens of watts.

A separate peaking transformer is employed for each rectifier grid. Negative grid bias is supplied by a dry-plate rectifier. Each peaking transformer has 2-phase-shift windings. One set of phase-shift windings is used to control the station voltage and the other set is used for load balance among the three rectifiers.

The voltage-regulating phase-shift windings are energized by an amplidyne generator, whose field is controlled by a Diactor-type regulator in response to variations in direct voltage. The voltage signal to the voltage regulator is supplied through a magnetic amplifier, which isolates the regulating system from the d-c bus.

The inverter grids are excited from a separate set of peaking transformers, each having a single phase-shifting winding. These phase-shifting windings are energized by the same amplidyne which supplies the rectifier phase-shifting windings.

The grid transformers of the three rectifiers and the inverter are connected to the excitation power-supply through four adjustable phase-shifting devices to permit individual adjustment of the phase of grid excitation at no load.

Circuit Action of Rectifier and Inverter

Figure 2 includes elementary power connections of the rectifier and inverter. Figure 4 shows the wave forms of the anode voltages with respect to the transformer neutral. Figure 4(A) shows rectifier anode voltages and the theoretical no-load voltage, where only the most positive anode is conducting. Voltage control is obtained by using the grids to delay the start of anode conduction. Current is not immediately transferred from one anode to another at the end of a conducting period, but requires an interval of time, or commutating angle, whose value depends on load current, commutating reactance and commutating voltage. Figure 4(B) shows direct voltage and anode currents in a rectifier operating with phase retard.

Since the grid of a vapor rectifier can act only to prevent anode conduction from starting and not to control it after it has started, current transfer between anodes in an inverter circuit must be completed before the outgoing anode becomes more positive than the incoming anode. The period of negative voltage remaining after transfer is completed is called the margin angle. A small margin angle is needed for clean-up of the ionization between grid and anode after current transfer is completed, so that the grid will block the anode when the latter becomes positive.

Increasing commutating time causes the margin angle to become progressively smaller as the load is increased and inverter load limit is reached when the margin angle disappears. Figure 4(C) and 4(D) shows inverter anode-current and d-c voltage wave forms at different loads. The reduced margin angle at increased load is apparent. When the margin angle disappears, current transfer between anodes stops, and the inverter constitutes a short circuit of the d-c system, since its average voltage is zero. The condition is termed "arc-through" and the inverter protective circuit breaker must be arranged to trip on over-current in the forward direction. The inverter d-c reactor limits the rate of rise of current due to arc-through.

Action of Regulating System

Regulation of Rectifier and Inverter

The regulation curves of both the inverter and rectifier[2,3] are linear up to several times rated load. The voltage of the rectifier may be expressed as

$$E_d = E_{rdo} \cos \alpha - K_r I_d - E_a \qquad (1)$$

The voltage of the inverter is

$$E_d = E_{ido} \cos \beta + K_i I_d + E_a \qquad (2)$$

where

E_d = d-c line volts
I_d = d-c amperes
α = angle of retard of rectifier
β = angle of advance of inverter
E_{rdo} = theoretical voltage of rectifier at no load
E_{ido} = theoretical voltage of inverter at no load
E_a = rectifier arc drop

K_r and K_i are constants depending upon the transformer and line reactance and resistance of the rectifier and inverter respectively.

Figure 5 shows the inherent regulation curves of the rectifiers and inverter at Scheid Substation. Figure 5 is drawn for rated a-c system source voltage. If the system voltage varies from this value, E_{rdo} and E_{ido} will vary in direct proportion,

while the other quantities in the above equations will be unchanged.

Requirements of Regulating System

Now let us consider the action in the regulating circuit, where the same amplifier, an amplidyne in this case, operates to shift the phase of both the rectifier and the inverter grids. Reference to Figure 5 shows that if constant voltage is to be maintained, the rectifier grids must be advanced with increasing rectifier load, and the inverter grids must be advanced with increasing inverter load. It is evident from the regulator action that when the rectifier grids are advanced to maintain constant voltage with increasing rectifier load, the inverter grids will be retarded, and the inverter voltage will increase. Similarly, increasing inverter load will be accompanied by decreasing rectifier voltage. Thus, the smallest difference between rectifier and inverter voltages will exist at zero station load.

At zero station load; the rectifier voltage may exceed, equal, or be less than the inverter voltage. In the first case, a continuous current will circulate between the rectifier and inverter, with a value depending on their regulation and their voltage difference.

If the average voltages of the rectifier and inverter are equal, a discontinuous current will circulate because of momentary voltage differences between rectifier and inverter. This is shown in Figure 6, where the shaded areas represent the excess of rectifier over inverter voltage giving rise to circulating current. Such circulating current, while not large compared with the rating of the units, causes unnecessary losses and needless reactive loading of the a-c system.

The value of circulating current is reduced by the d-c reactor in the inverter circuit. It may be further reduced by permitting the inverter voltage to exceed the rectifier voltage at no load. Reference to Figure 6 shows that a shift of a few degrees in the inverter lead angle will result in a material reduction of the shaded area, which is a measure of the peak value of circulating current.

Inspection of Figure 5 shows that a shift of about 6 degrees in inverter angle of advance is sufficient to change the inverter voltage 500 volts. Thus if nonautomatic control of the station voltage were employed, and if the inverter grids were retarded slightly from the position which would give equal rectifier and inverter voltages at no load, there would be a substantial rise in voltage in the event of a regenerative load. The use of a regulating system limits this rise to an amount depending on the loop gain of the regulating system. In the subject case, the regulating system has a gain of more than 50, so that the voltage change at transition from rectifying to inverting is hardly perceptible. Figure 7 shows the nature of the regulated rectifier and inverter voltages over the entire load range.

Calculation of Phase-Shift Settings and Phase-Shift Limits

The regulating system is arranged so that when the system voltage is at rated value, amplidyne voltage of one polarity, which we may term positive, controls the rectifier voltage, while negative amplidyne voltage controls the inverter voltage. At zero amplidyne voltage, the rectifier phase shifter is set in a position such that the output voltage of the rectifiers will have the desired value at the highest a-c system voltage expected to exist-

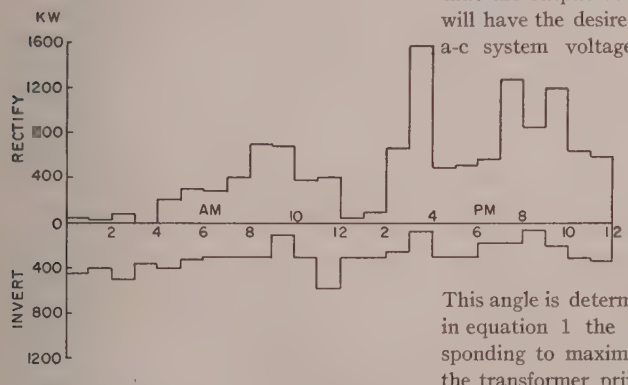

Figure 8. Composite average hourly loading of rectifier and inverter on Scheid Station (averaged over 1 week)

This angle is determined by substituting in equation 1 the value of E_{rdo} corresponding to maximum line voltage and the transformer primary tap selected for operation of the rectifier. Let us suppose that the angle α determined in this way is 31 degrees. The rectifier grid phase shifter is then set in a position such that when there is no phase shift current in the rectifier peaking transformer, grid firing occurs at a point corresponding to 31 degrees phase retard. At large rectifier loads, the angle of phase retard should be zero and the maximum positive amplidyne voltage must be able to shift the rectifier grid excitation at least 31 degrees. It must not advance the phase of grid excitation by as much as 31 degrees plus the width of the peak voltage firing the grids, otherwise the grids will have become negative when the anodes are ready to fire. This condition can be avoided by use of a voltage limiting circuit on the amplidyne.

Turning to the inverter, its grid phase-shifter must be set in such a position that the inverter voltage will have the desired value at or near no-load when the a-c system voltage has its minimum operating value. The angle of advance for this condition is determined from equation 2. When the load reaches its top value of 3 times rated load and the a-c system voltage has its maximum value, the angle of advance will have its maximum value, also determined from equation 2. The maximum negative amplidyne voltage must be sufficient to cover the range between minimum and maximum angles of advance after the phase shifter has been adjusted to give the minimum angle of advance at zero amplidyne volts. With this arrangement, small rectifier loads will result in an amplidyne voltage ranging from zero to a small positive value, depending on the value of a-c line voltage, and small inverter loads will be accompanied by amplidyne voltages ranging from zero to a small negative value.

Rectifier Load Division

Due to differences in the phase-shift characteristics of individual grid transformers and errors in phase-shifter settings, the rectifiers cannot be expected to share load equally over the part of their load range where voltage control is effective. An equalizer circuit, indicated in Figure 2, is employed to compensate for unequal sharing of the load. A magnetic amplifier is connected to a 100-millivolt shunt in the output of each rectifier, and delivers to an equalizer circuit through current-balance phase-shift windings on the peaking transformers a voltage proportional to the output current of the rectifier. If the rectifier currents are all equal, there is no current in these windings. If one rectifier delivers more than its share of current, the equalizer-circuit action retards its grid excitation and advances the other rectifier grids.

The regulating system maintains substantially constant voltage at the station bus under all load conditions within its range. At large station overloads, the bus voltage drops because the rectifier transformer voltage is sufficient to maintain rectifier voltage only to moderate overloads. Large dips in a-c voltage also result in a drop in station voltage when rectifying. Combined with the incidence of heavy inverter loading large dips in a-c voltage can conceivably result in exceeding the commutation limit of the in-

verter. The amount of power handled by the rectifiers and inverter depends on train movements and schedules. Figure 8 shows the average hourly loading of the rectifiers and inverter over a one week period. The integrated inverter load is approximately 60 per cent of the integrated rectifier load. This indicates the power saving achieved with the inverter.

If the d-c traction locomotives are designed for regeneration, it is possible to design mercury arc rectifier substations in hilly terrain so that constant substation voltage is maintained and maximum power economy is achieved.

References

1. Electrification of the Central Railway of Brazil. *The Railway Gazette* (London, England), March 1938, pages 446–50.

2. Grid Controlled Rectifiers and Inverters, C. C. Herskind. *Electrical Engineering* (*AIEE Transactions*), volume 53, 1934, pages 926–35.

3. Analysis of Rectifier Circuits, E. F. Christensen, C. H. Willis, C. C. Herskind. *Electrical Engineering* (*AIEE Transactions*), volume 63, 1944, pages 1048–58.

No Discussion

Carrier Current Supervisory System for Distribution Circuits

L. PODOLSKY
MEMBER AIEE

S. LUBIN
MEMBER AIEE

Synopsis: A new method is described for supervising sectionalizing devices on distribution systems by utilizing a centrally transmitted, unmodulated carrier. This carrier is remotely modulated by equipment located on the load side of the monitored sectionalizing device, and the modulated carrier is received at a conveniently located receiver. A novel indicator gives instantaneous warning of operation of sectionalizing devices or equipment failure. Simplicity and low cost make its use on distribution systems feasible for monitoring of large numbers of sectionalizing devices.

RURAL and suburban distribution and subtransmission lines due both to exposure and usage have relatively high rates of outages. The length of outage time on rural lines is increased by the poor facilities for reporting line failure to service headquarters. Existing supervisory control equipment, such as is used on transmission lines, is economically unfeasible for supervising even a small number of important sectionalizing points on a distribution system. The multiple functions, which make it so useful for transmission line application, are unnecessary on a distribution system. Consequently, there is a need for equipment which will provide instantaneous and unambiguous reporting of the opening of a sectionalizing device and at the same time show its location. This information would considerably reduce the outage time and aid in the location of line faults. When used in conjunction with radio dispatched trouble crews, it can lead to a much improved order of service continuity.

The equipment described in this paper provides this service and indicates, automatically, not only the occurrence and location of an outage, but also the restoration of service to the faulted portions of the system. The equipment is relatively simple and inexpensive, making it possible to monitor a large number of sectionalizing points on a system. It can be used with circuit breakers, reclosers, fuses, air switches, or any other sectionalizing device; it is operated by line power and requires no standby power supply. It is in continuous operating condition, and is self-supervising for faults in the equipment. A minimum of line treatment is required for its operation on distribution lines, and simple auxiliary equipment has been developed for this purpose.

Theory of Operation

The output of a radio frequency generator supplying unmodulated carrier energy to a transmission line may be modulated by changing the impedance of the line. These impedance changes vary the radio frequency current due to variation of the loading of the generator, resulting in the impressing of a modulated carrier current on the line. This modulation may be accomplished by switching a series inductance capacitance circuit tuned to the carrier frequency on and off across the line, Figure 1(A). The result will be an alternately low and high impedance connected to the carrier generator terminals. A modulated (pulsed) signal which can be picked up by a receiver tuned to the carrier frequency will be present on the power line. If the switching is performed mechanically at some definite audio rate, the use of several switched inductance capacitance circuits on the same line will result in a number of audio tones, corresponding to the individual switching rates, which can be detected and separated to identify them. As a more practical method, Figure 1(B), the inductance or capacitance can be varied at an audio frequency rate to produce sinusoidal modulation and avoid harmonics and other difficulties caused by switching of the inductance capacitance circuit. Each of the varying inductance capacitance circuits thereby becomes in effect a remote modulator with a distinctive modulating frequency. The whole complex modulated carrier can be picked up by a carrier receiver, demodulated, and the complex audio signal separated into its components by suitable band pass filters.

If the remote modulators are designed to obtain their operating power directly from the distribution line, the connection of a modulator to the line on the load side of a sectionalizing device will cause the audio signal to be continuously received as long as the line is energized. The opening of the sectionalizing device will

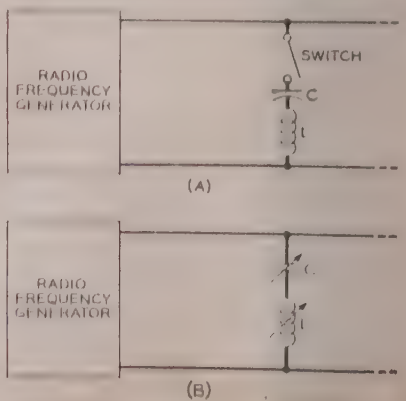

Figure 1(A). Modulation of radio frequency generator by switched series inductance capacitance circuit across line; (B). Modulation of radio frequency generator by sinusoidally variable capacitance or inductance of inductance capacitance circuit

Paper 51-236, recommended by the AIEE Carrier Current Committee and approved by the AIEE Technical Program Committee for presentation at the AIEE Summer General Meeting, Toronto, Ont., Canada, June 25-29, 1951. Manuscript submitted March 21, 1951; made available for printing May 11, 1951.

L. Podolsky and S. Lubin are with the Sprague Electric Company, North Adams, Mass.

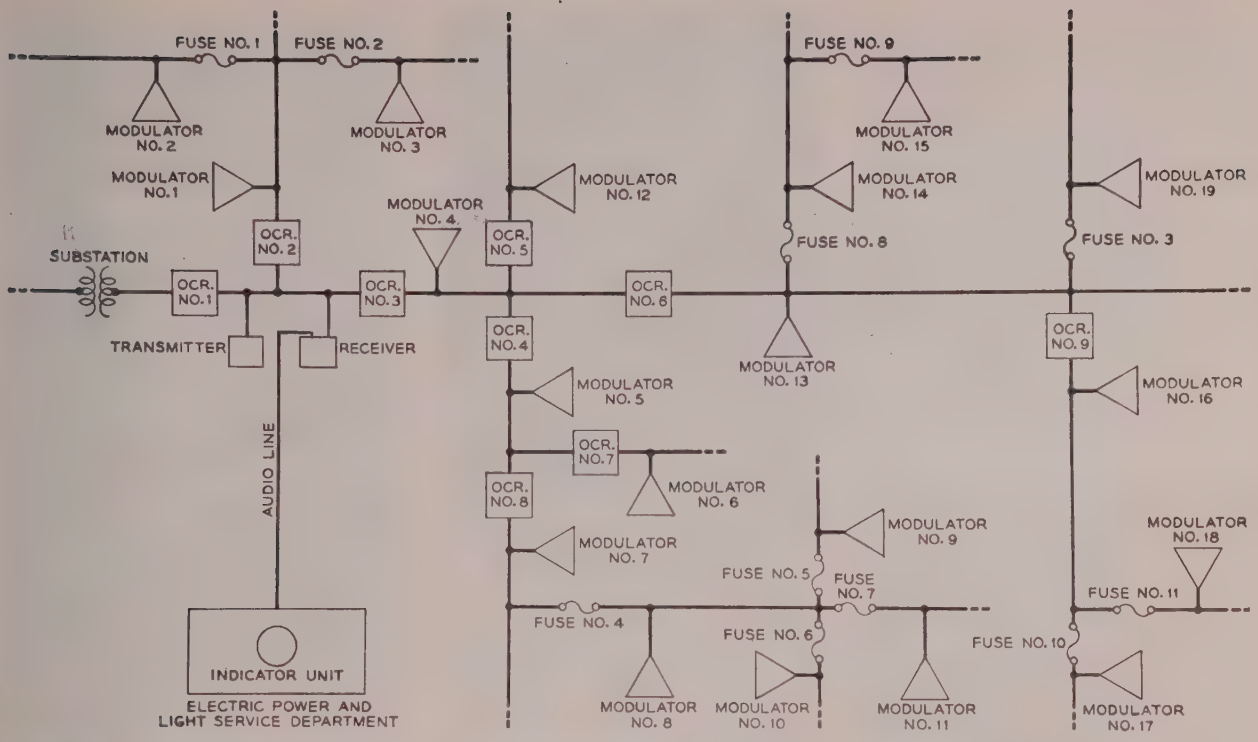

Figure 2. Typical installation of carrier monitor system on distribution circuit

cause interruption of power to the modulator and loss of its characteristic audio tone. The absence of the audio signal actuates an indicator designed to respond only to its audio frequency and gives a visual and audible alarm signal. Since the modulator may be located at almost any point on the load side of the monitored sectionalizing device, it is normally mounted on a distribution transformer pole or on a pole having underbuilt secondary, avoiding the necessity of a separate 115-volt supply. It may, therefore, also be mounted at a location conveniently available for easy inspection and servicing.

The modulated carrier is impressed on the entire power system. The receiver may be coupled to the line at any convenient point. Where the service headquarters are served by the same distribution line, the receiver can be mounted directly at the headquarters and connections made to the indicator unit by a short audio line. In the event that service headquarters are not adjacent to the line, the receiver may be conveniently located on the line with the audio output of the receiver fed to a telephone line of the required length, and the indicator located at service headquarters. A 1-line diagram of a typical installation is shown in Figure 2.

Equipment Details

Transmitter

The transmitter is a conventional carrier transmitter of 25 watts output. The circuit diagram of the engineering model used in field tests is shown in Figure 3. The only unconventional feature in this unit is the power output control circuit consisting of V_3 with variable grid voltage acting as a control on the screen-grid voltage of the final amplifier, V_2. This provides a means of controlling the final amplifier output from full 25 watts output down to a minimum of 2 to 3 watts without requiring retuning of the tank circuit. This control was provided for field test purposes to determine the effects of power output changes on transmission characteristics. To provide for situations where the transmitter and receiver are mounted at the same location and a common coupling capacitor is used, the loading coil L_3 is provided with a small coupling winding to which the receiver may be connected. The transmitter is designed to operate over the frequency range of 50 kc to 150 kc by using plug-in oscillator, tank and loading coils, each tunable over a band of ±3 kc from a nominal center frequency.

Coupling Devices

The transmitter, receiver and remote modulators are coupled line-to-ground through carrier coupling capacitors. For use on systems with line-to-ground voltages up to 8.7 kv, a specially designed 0.002-microfarad coupling capacitor is used. This capacitor, which is pole-

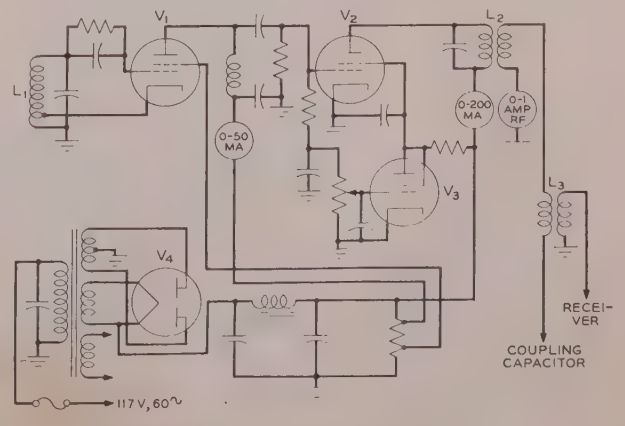

Figure 3. Circuit of engineering model of carrier transmitter

mounted by means of a hanger bracket, is similar to the unit designed for the Bell System Rural Subscriber Telephone Service, Figure 4(A).[1,2] The transmitter and receiver each use a coupling unit, consisting of a drain coil connected from the lower end of the coupling capacitor to ground and protected against surge voltages by a telephone type carbon protector, Figure 4(B). In accordance with standard carrier practice, this drain coil serves to hold the 60-cycle voltage at the transmitter and receiver terminals to a low value while presenting a high impedance to ground at carrier frequencies.

Figure 4(A) (above). Coupling capacitor, 0.002 microfarad, 8,600 volts

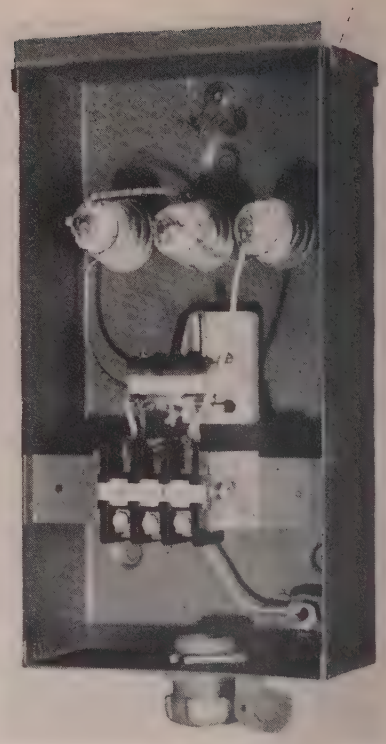

Figure 4(B) (right). Coupling unit for use with transmitter or receiver

Receiver

The receiver, Figure 5, uses a conventional tuned radio frequency front end which feeds into a high gain, high signal to noise ratio audio amplifier with about 1.5 watts undistorted output. The high gain and low noise ratio is necessary to allow for the utilization of signals resulting from the extremely low modulation percentages inherent in the system. This modulation, as seen at the receiver, is in the order of 0.01 per cent to 5 per cent. The receiver output is arranged for coupling to standard 2-wire telephone circuits up to 15 miles in length without the use of additional amplification.

Remote Modulators

The remote modulator is one of the basically novel components of the supervisory system. In consists, essentially, of an inductance capacitance series circuit in which the Q of the inductance is varied at an audio rate, thus varying the carrier impedance across the line at the point of modulation. The circuit diagram of the modulator is shown in Figure 6. The capacitance of the inductance capacitance circuit is provided by the carrier coupling capacitor which is connected to ground through the series coil L_1. This coil is magnetically tuned to resonate with the coupling capacitor at the carrier frequency. The inductance is shunted by diode V_2, which in the nonconducting state constitutes a high resistance shunt and in the conducting stage is a low resistance shunt. The Q of the tuned circuit varies from a value of about 35 down to a very low value, as V_2 goes from a nonconducting to a conducting state. An audio oscillator, utilizing half of double triode V_1 and a specially designed reed controller, is followed by an amplifier stage using the remaining half of V_1. The audio output of this amplifier is fed to the biased diode and causes its impedance to vary sinusoidally in accordance with the audio signal. The carrier voltage appearing across the inductance capacitance circuit is thus sinusoidally modulated, by absorption, at a frequency controlled by the vibrating reed. The audio voltage output of the amplifier can be varied to control the modulation ratio.

The reed controller is a double reed of extremely high-frequency stability and

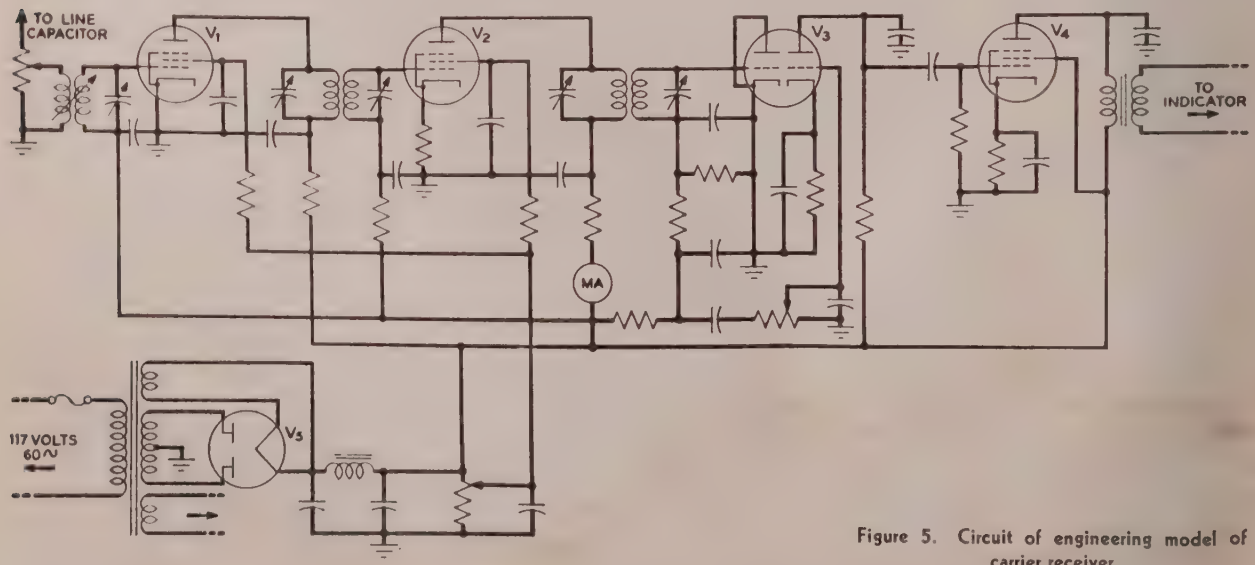

Figure 5. Circuit of engineering model of carrier receiver

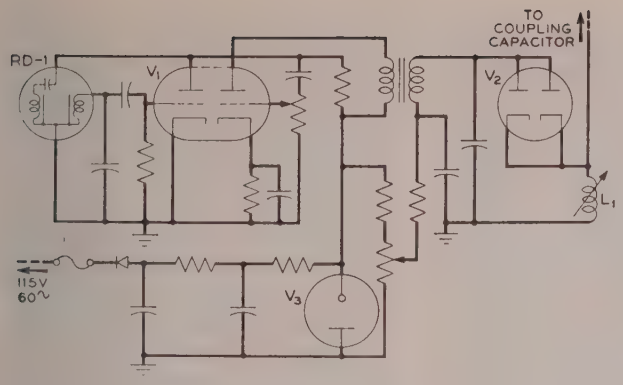

Figure 6. Circuit of remote modulator

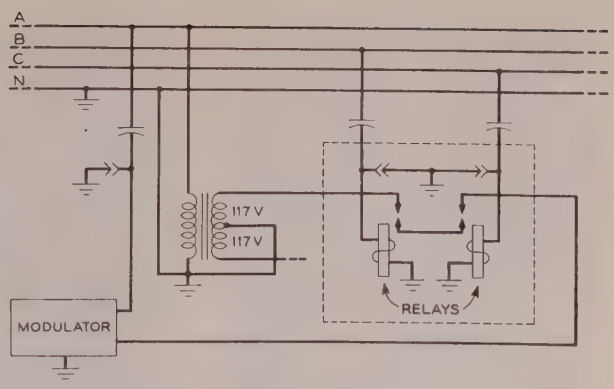

Figure 8. Connection of remote modulator for use in monitoring 3-phase sectionalizing point

very narrow bandwidth. It has a temperature versus frequency stability in the order of 0.1 per cent over the range of −40 degrees centigrade to +55 degrees centigrade, and practically no frequency drift with voltage change. Regulator tube V_3 is used to provide gross voltage regulation for oscillator and amplifier voltages. Radio frequency harmonics generated by the nonlinear operation of the modulator are successfully attenuated by a low-pass filter in the output circuit (not shown in the figure).

The modulator is contained in a standard, weatherproof kilowatt-hour meter housing, and plugs into a meter socket mounted directly to the pole. The socket contact connecting to the coupling capacitor has a built-in grounding switch so arranged that when the modulator housing is pulled out of the socket, the capacitor contact is shorted to ground. This prevents the current through the capacitor from energizing the exposed terminal. It also eliminates the need for a drain coil at each modulator installation. When installed on the pole, a telephone type carbon protector is connected from the low voltage end of the capacitor to ground to protect the modulator inductance against surges, and also to provide protection in the event of the inductance L_1 becoming open circuited.

Indicator

The indicator is another novel component of the system. It consists of an amplifier and power supply and separate channel indicators responsive to each remote modulator frequency. Figure 7(A) shows the circuit diagram of the main amplifier. This is a conventional triode voltage amplifier utilizing one half of double triode V_{1A} feeding cathode follower V_{1B}. The output of V_{1B} is fed to a number of channel indicators in parallel. The individual channel indicator is shown in Figure 7(B). The input from the main amplifier is fed to V_{1A}, operating as a cathode follower, which is coupled into a vibrating reed acting as a band-pass filter. This dual reed responds with a high degree of selectivity to its own resonant frequency, and thus passes a signal to its output circuit only when the remote modulator associated with it is operating. In practice the modulator and indicator reeds are pairs, tuned to the same frequency. The output of the reed band pass filter is amplified in V_{1B}, which is transformer coupled to a biased triode acting as a relay control tube. Triode V_{2A} is biased by voltage from rectifier V_{2B}. The control tube is biased to cut-off and will conduct only when a signal from the vibrating reed is available.

Figure 7(A). Circuit of indicator main amplifier; (B). Circuit of indicator channel

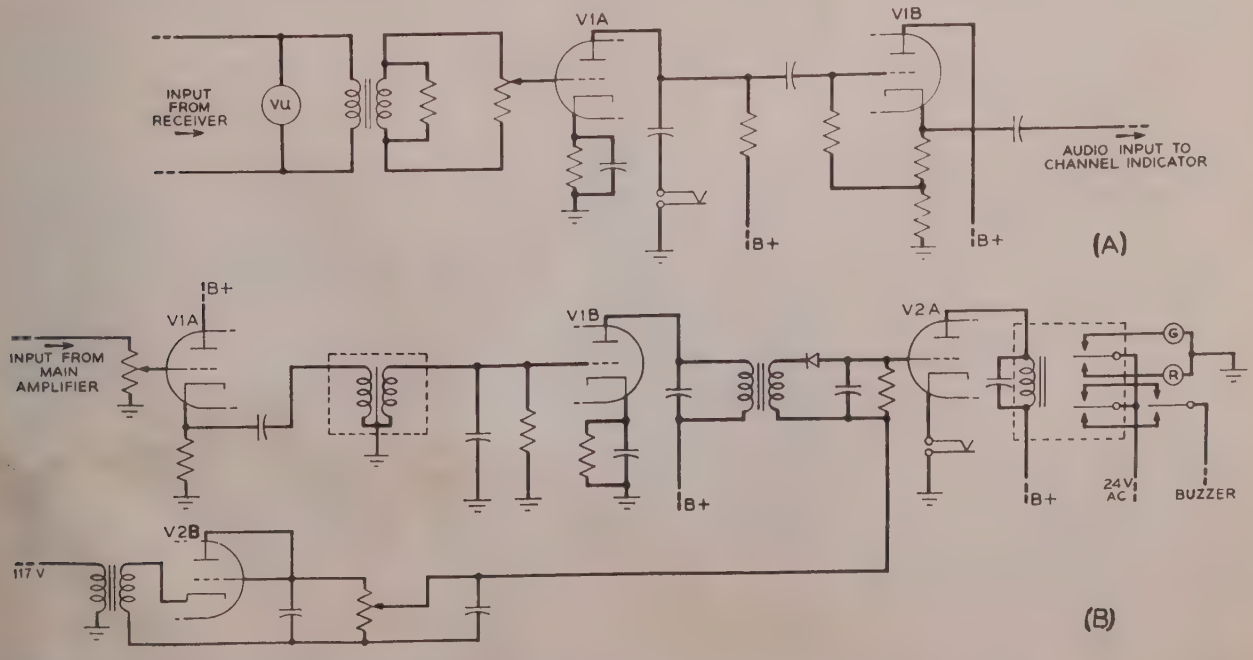

Figure 9(A) (above). Outdoor transmitter installation

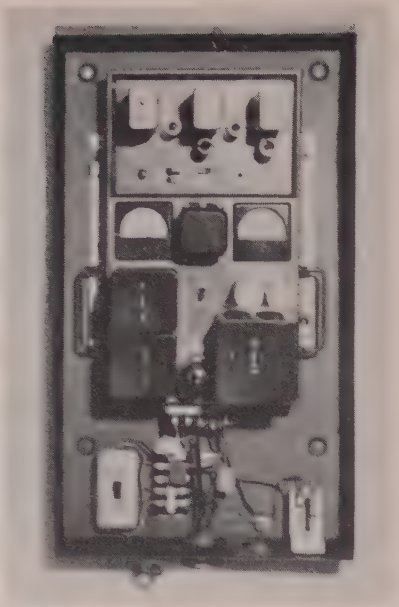

Figure 9(B) (right). Indoor receiver installation

In this condition the relay contacts energize a green panel light to indicate normal operation of the supervised sectionalizing device. Opening of the sectionalizing device, which results in power interruption to the remote modulator, stops vibration of the reed band pass filter and cuts off the relay current in V_{2A}. The relay contacts then switch from a green to a red light indicating opening of the sectionalizing device. Another set of contacts actuates a buzzer or alarm bell to call attention to the outage. A transfer switch on the indicator channel panel allows the alarm to be shut off. It will then sound again when the supervised sectionalizing device is re-energized, signaling the end of the outage. Time delay circuits (not shown in the figure) are used to prevent impulse noise from actuating the indicator.

The filaments of V_{2A} and V_{2B}, which are in one tube envelope, are operated in series to prevent false indication in the event of a filament failure in the bias rectifier. Parallel filament operation would result in unbiasing V_{2A} and a green light would show continually even in the event of an outage. Operating both halves of the filament of V_2 in series gives a trouble indication in the event of either half of the filament becoming inoperative.

The vibrating reed used as a band-pass filter is similar in construction to the oscillator controller reed of the remote modulator. As a band-pass filter, its equivalent Q is in the order of its frequency in cycles, ranging from about 200 at 200 cycles to about 2,000 at 1,000 cycles. Utilizing channels separated at frequency intervals of 3 per cent, it is possible to operate 50 channels in the frequency range of 200 to 1,000 cycles. Adjacent channel discrimination is of the order of 30 decibels. The reed response band width is approximately 0.15 per cent.

Provision is made at the rear of the main amplifier chassis for power take offs from each red and green panel light so that duplicate light signals can be provided on a system map, if desired. While the engineering models used in the field tests are designed for multiples of 5 channels, it is planned in production to have the main amplifier and power supply capable of feeding 50 channels rack mounted in banks of five. In practice it has been demonstrated that up to 50 audio-frequency tones, permitting 50 monitored points, can be conveniently operated on a single carrier. Use of additional carrier frequencies permits multiples of 50 channels to be used.

Monitoring of Multiple Circuit Breaker Installation

The description so far has outlined the method of monitoring a single sectionalizing device. On 3-phase installations where separate single pole reclosers or fuses are used, it would be inconvenient and uneconomical to use a separate remote modulator for each phase. By using the arrangement of Figure 8, one modulator can be used to monitor any multiphase sectionalizing installation. The modulator power is supplied as before from the distribution transformer connected to one phase (phase A in the figure). Additional coupling capacitors on phases B and C are connected in series with relay operating coils to ground. The current through the 0.002-microfarad capacitors is in the order of 5 milliamperes at 7,200 volts and the relays are designed to hold in at 3 milliamperes minimum. The relay contacts are in series with each other and with the modulator power supply. Thus, failure on either phase B or C will cause the relays to drop out and de-energize the modulator.

Installation and Operating Features

On a typical rural distribution system, the transmitter would normally be installed on the source side of the first set of line circuit breakers. It may be installed in the main substation or, if 115-volt service is not available there, at the first distribution transformer beyond the substation.

Where the service headquarters are fed by the same power line, the receiver would be mounted on the office transformer pole and audio leads brought in to the indicator unit. The receiver and transmitter both may be mounted on

Figure 10. Dual transmitter and receive: installation (covers on weatherproof housings)

Figure 11. Modulator installation

Figure 12. Engineering model of 8-channel indicator unit

the same pole and coupled to the line through one capacitor. This procedure is used when the office is located at the power source. Figure 9 shows a typical outdoor transmitter installation and indoor receiver installation. Figure 10 shows a dual transmitter and receiver installation with the weatherproof housings closed.

Modulators are installed on any convenient transformer pole on the load side of the monitored device. Figure 11 shows a typical installation. In general, transmitters, receivers, and modulators are installed in spots conveniently located for easy access, although line impedance considerations may limit the points available for transmitter and modulator installations. In general, best results are obtained when the modulator is located at points on the line corresponding to voltage standing wave maxima. These points can be quickly and easily found by the use of a specially developed survey instrument, which is essentially a portable, battery operated modulator, coupled to the line by means of a coupling capacitor contained in a hotstick. The factors involved are described in a companion paper.[3]

Figure 13(A). Impedance matching network

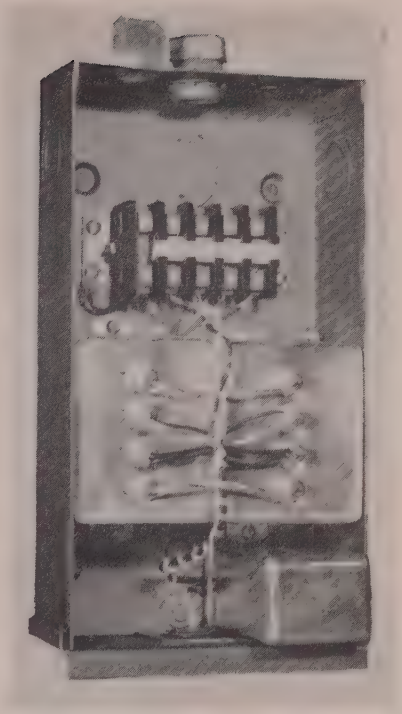

Figure 13(B). Multiphase relay unit with hermetically sealed relays

Indicator units are installed in a convenient spot in the service headquarters, usually at the radio dispatcher's desk. Figure 12 shows an engineering model of the indicator unit. In production models, multiple indicators may be stacked in a relay rack instead of being enclosed in separate cabinets.

Auxiliary components used in the installation consist of impedance matching networks and multiphase relays, Figure 13; capacitors for bypassing voltage regulators; and specially designed chokes for neutralizing the shunting effect of power factor correction capacitors. The use of these auxiliary components as well as a discussion of the effects of series operating coils of oil circuit reclosers are described in the companion paper.[3]

Operating Experience

Two test installations of this type of equipment have been in operation, one for over $2\frac{1}{2}$ years and one for 8 months. The older installation consisted of experimental equipment which was replaced after 18 months by a preproduction model. Extensive work on the problems of operating carrier equipment of this type on distribution lines was carried out over the $2\frac{1}{2}$ year period on this power system and the results are discussed in the companion paper.[3]

The basic operating principles of this system and its design features have been covered by United States patents granted and pending.

References

1. Application of Rural Carrier Telephone System, **E. H. B. Bartelink, L. E. Cook, F. A. Cowan, G. R. Messmer.** *AIEE Transactions*, volume 66, 1947, pages 511–18.

2. A Carrier Telephone System for Rural Service, **J. M. Barstow.** *AIEE Transactions*, volume 66, 1947, pages 501–507.

3. Application of Power Line Outage Monitor, **J. F. Atkinson, J. D. Cooke.** *AIEE Transactions*, volume 70, 1951 (*Proceedings TI-237*).

No Discussion

A Tachometer for Measurement of Instantaneous Variations in Angular Velocity

S. P. BARTLES
MEMBER AIEE

AN ultrasensitive recording tachometer for the measurement of instantaneous and long term speed variations of rotating shafts, rolls, and moving continuous webs is described. The instrument has been designed to operate in a peripheral speed range of 5 to 120 feet per minute and to resolve speed variations occurring at frequencies from 0 to 70 cycles per second. Sensitivity is adjustable in a range from 0.2 to 100 per cent speed variation for full scale deflection. A resolution of 0.005 per cent speed variation is obtained at maximum sensitivity.

Auxiliary equipment has been incorporated in the tachometer for static and dynamic calibration purposes. A frequency analyzer also has been included for determining the frequencies present in the complex wave forms usually encountered. Vibration measuring equipment is sometimes used in conjunction with the tachometer in order to better correlate results.

General Description

The equipment consists of a speed sensing unit $7\frac{1}{2}$ inches long by 3 inches square, and the tachometer proper which is housed in a portable cabinet 4 feet high by 20 inches square. The physical arrangement of the equipment is shown in Figure 1.

A block diagram of the system is shown in Figure 2. The system is composed of a speed sensing unit for generating a frequency signal proportional to angular velocity; an a-c amplifier for amplifying the output signal from the frequency generator; a frequency meter for converting the frequency signal to a direct voltage signal; a bucking circuit for cancelling the major voltage signal, thus leaving only plus or minus variations in voltage; a low-pass filter for eliminating voltages at frequencies above 70 cycles; a d-c amplifier for amplifying the plus or minus variations in voltage; and a direct inking oscillograph recorder capable of recording voltage variations at frequencies up to 100 cycles.

The diagram also shows an audio oscillator equipped with an adjustable modulator which is used in place of the speed sensing unit in making static and dynamic calibration checks of the system response. A displacement-type vibration pickup device and associated amplifier is shown feeding into a second channel of the recorder. A frequency analyzer and associated low-frequency amplifier is shown connected to the output of the low-pass filter.

Speed Sensing Unit

The speed sensing unit is a low inertia photoelectric frequency generator producing 6,000 cycles per revolution of its shaft which is driven at the point being measured by means of a friction drive wheel. A cross section through this signal generator is shown in Figure 3.

The frequency signal is produced by a photographically reproduced shutter disk having 6,000 equally spaced radial lines generated upon it. Conventional projection optics are used to image the disk on a stationary grid which is a copy of a sector of the disk. The light striking the cathode of the phototube is thus alternately shuttered as the disk rotates and produces a frequency signal proportional to angular velocity of the disk.

A cathode follower preamplifier stage is incorporated in the speed sensing unit to reduce the output impedance for transmission of the signal to the tachometer. The speed sensing unit is connected to the tachometer through a shielded cable 25 feet long.

A-C Amplifier and Limiter

The a-c amplifier and limiter has been designed to eliminate the effects of a non-uniform wave shape generated by the speed sensing unit. In general the amplifier raises the voltage of the signal considerably beyond that required to drive the frequency converter and the limiter clips off the tops of the waves thus eliminating the distortion and leaving a square wave signal of good uniformity.

The a-c amplifier consists of a 2-stage capacity-coupled system with a fixed gain of 6,000. The limiter consists of a twin diode clipper stage set to pass a square wave of ± 3 volts amplitude.

Frequency Converter

The frequency converter is a frequency meter having a range of 0 to 50,000 cycles. Basically this unit converts the carrier frequency to a series of pulses of constant amplitude and polarity which are then applied to an inductance-capacitance filter. The relationship between frequency and current through the inductance of this filter is linear over the range used. A shunt diode rectifier is capacity coupled to the filter with a resultant direct voltage developed across the output terminals of 5 volts at 500 cycles and 100 volts at 10,000 cycles.

Paper 51-238, recommended by the AIEE Instruments and Measurements Committee and approved by the AIEE Technical Program Committee for presentation at the AIEE Summer General Meeting, Toronto, Ont., Canada, June 25–29, 1951. Manuscript submitted June 8, 1950; made available for printing May 14, 1951.

S. P. Bartles is with the Eastman Kodak Company, Rochester, N. Y.

The author wishes to acknowledge the contributions of H. J. Emerson, and R. J. O'Connor, of the Eastman Kodak Company, and J. H. Porter formerly of the Eastman Kodak Company, in the development, design, construction, and ultimate operation of the equipment described in the paper.

Figure 1 (left). Ultrasensitive tachometer

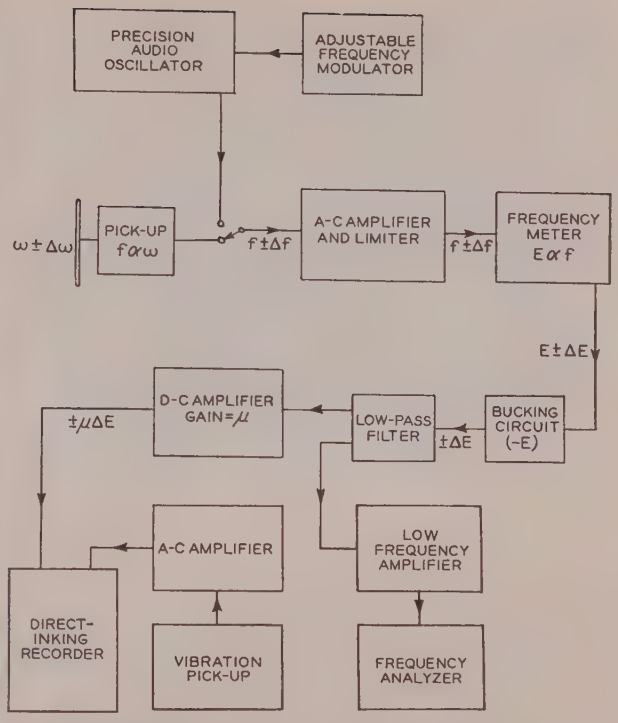

Figure 2 (above). Block diagram

Low-Pass Filter

A multisection resistance-capacitance filter is connected to the output of the frequency converter to suppress any remaining trace of the carrier frequency from the d-c voltage. Since the lowest carrier frequency at which the instrument is applied is 500 cycles, the filter has been designed for cutoff at that frequency. It should be noted that this filter represents a compromise from the standpoint that frequencies considerably below 70 cycles are attenuated to some degree. An inductance-capacitance filter would have a sharper cutoff frequency but would involve undesirable 60-cycle stray field pickup from the power circuits.

Bucking Circuit

A direct voltage bucking circuit is used to cancel out the average voltage signal coming from the frequency converter through the low pass filter, thus leaving only the plus or minus variations in voltage. Since this average voltage signal varies from 5 volts at a carrier frequency of 500 cycles to 100 volts at 10,000 cycles, the bucking circuit is made adjustable over this voltage range for matching to a specific signal.

The bucking circuit consists of a 10,000-ohm 10-turn helical potentiometer connected across a 135-volt radio-type B battery. This combination is inserted in series with and opposing the signal from the frequency converter.

Amplifier and Recorder

A Brush d-c amplifier and dual channel electromagnetic direct inking oscillograph recorder are used to amplify and record the signal passed through the bucking circuit. The dynamic response of this system is practically flat from 0 to 100 cycles. Although the recorder alone has a resonant peak frequency at about 35 cycles and attenuates quite sharply at frequencies above 60 cycles, the amplifier employs feed back frequency compensation for both of these factors thus resulting in a combined response generally flat out to 100 cycles.

The second channel of the recorder is provided to permit the simultaneous measurement of other dependent or influencing variables such as linear vibra-

Figure 3. Speed sensing unit

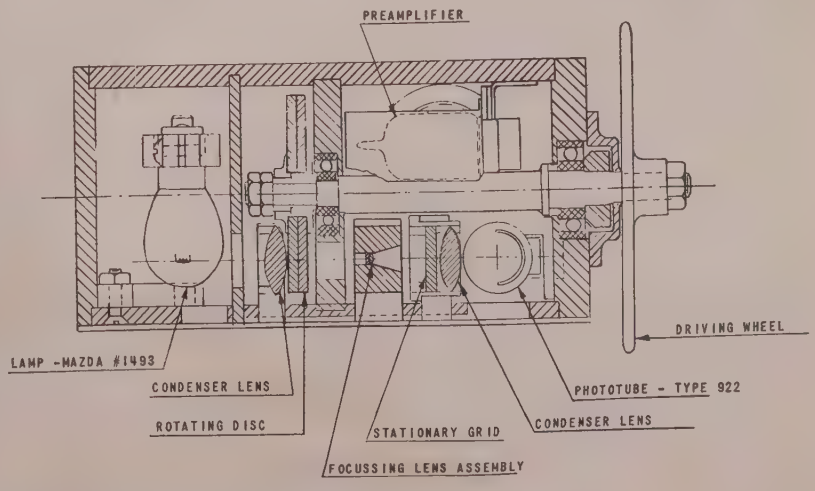

Figure 4. Wave analyzer

Figure 5. Modulator

tion, tension or voltage. A suitable sensing element and amplifier is required for each particular case. The recorder deflection coil has a resistance of 1,500 ohms and requires a potential of 15 volts at 10 milliamperes for full scale deflection.

Wave Analyzer

Because of the complex nature of the record frequently produced by the tachometer, a wave analyzer is provided to permit resolution of the complex wave form into its component frequencies. A Frahm type directly indicating vibrating reed unit has been selected for this purpose. The analyzer consists of 288 magnetically excited reeds covering a spectrum of $12^1/_4$ to 100 cycles. Figure 4 shows the arrangement of this analyzer.

The advantage of this unit over the scanning type lies in the fact that all of the tuned elements are energized continuously and several elements may respond simultaneously to frequencies present in the signal which correspond to the resonance frequency of these elements. A low-frequency amplifier having an impedance output characteristic to match that of the analyzer is used to feed the analyzer from the output of the direct voltage bucking circuit.

Calibration Equipment

Equipment for calibration of over-all static and dynamic response of the tachometer is provided in the form of a beat frequency oscillator and a modulator having an adjustable frequency characteristic in the range from 0 to 70 cycles. The beat frequency oscillator is shown as part of the tachometer proper in Figure 1 and the modulator equipment is shown in Figure 5.

The modulator consists of a 12 to 75 micromicrofarad rotatable air dielectric capacitor driven by an adjustable speed motor having a speed range from 0 to 70 revolutions per second. The motor and speed controller consist of a laboratory-type d-c motor with thyratron field and armature control in order to obtain wide speed range.

The speed sensing unit is replaced by the combination of the oscillator and modulator in calibrating the tachometer response. The oscillator is tuned to produce a frequency signal duplicating that of the speed sensing unit for the particular speed in question. The modulator capacitor is connected into the oscillator tank circuit, and when rotated it produces a small increment variation in oscillator output frequency at a rate corresponding to the motor speed. Thus a signal that can be adjusted for both base speed (carrier frequency) and frequency of variation is produced for feeding into the tachometer. The over-all dynamic response of the tachometer system over a range of 0 to 70 cycles for carrier frequencies of 500, 1,000, 1,500, 5,000, and 10,000 cycles is shown in Figure 6. It is noted that the d-c amplifier feedback compensation is adjusted for optimum response at each carrier frequency.

Auxiliary Equipment

Since linear vibration occurring between the pickup wheel and point of measurement on a roll or moving web is measured as a speed variation, a vibration displacement pickup device is sometimes used along with the speed pickup unit in order to correlate results better. The vibration sensing device consists of either a piezo crystal or a linear differential transformer-type device. The output of the sensing element is fed through a Brush a-c amplifier to the second channel of the recorder.

Figure 6. Over-all tachometer response

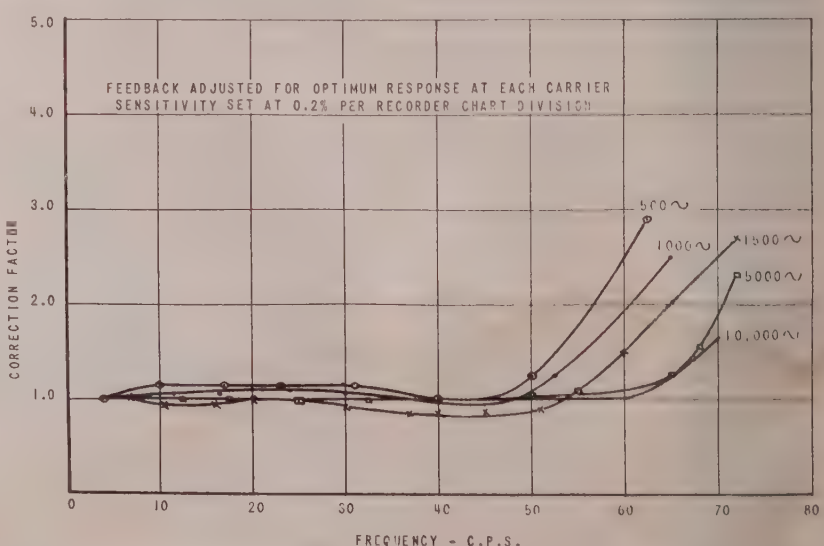

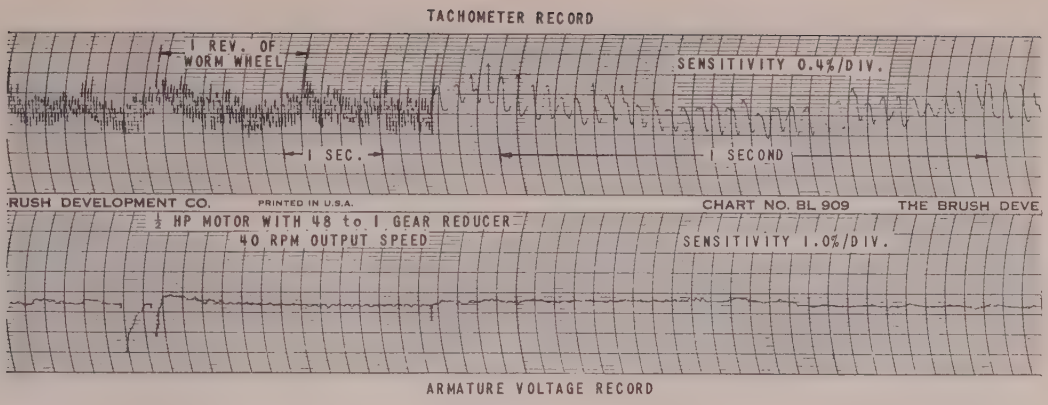

Figure 7. Typical recorder chart

An oscilloscope is incorporated into the tachometer for checking the quality of the incoming signal from the speed sensing unit in respect to wave shape and amplitude variation. The oscilloscope also is used for checking other variables, signal tracing, and on-the-spot maintenance when the equipment is used away from the laboratory.

Application of the Instrument

The speed sensing unit is applied at the rotating member or moving material under consideration. An indicator on the face of the frequency converter shows the carrier frequency generated by the speed sensing unit. This furnishes information for the proper setting of the calibrated feedback compensation potentiometer in the d-c amplifier and also indicates the machine speed at which the readings are being made.

With the gain control of the d-c amplifier set at a low value the output is applied to the recorder and the bucking voltage potentiometer is adjusted to reduce the recorder deflection to zero. The gain then is progressively increased while keeping the recorder on scale with the bucking voltage potentiometer until a conveniently measured modulation is obtained on the recorder. The gain control on the d-c amplifier is calibrated in terms of per cent speed variation per millimeter division on the recorder chart scale.

A section of a typical chart taken from the recorder is shown in Figure 7. This record represents the speed variations on the output shaft of a d-c motor with an integral single stage worm reducer having a ratio of 48 to 1. The motor is operating at a speed of 40 rpm on the output shaft. A speed variation of 3 per cent is clearly shown at a frequency of 32 cycles which corresponds to the gear tooth frequency of the 48-tooth worm wheel.

The second channel on this chart represents variation in direct voltage applied to the armature of the motor simultaneous with the tachometer reading.

Conclusions

The equipment has proved to be very satisfactory in the measurement of speed variations produced by various gear, belt, chain, and other drives. Resonance frequencies of various rotating systems have been established, and such things as torque pulsations, due to dead armature coils incorporated in the design of some d-c motors have been measured.

This equipment combines the desirable features of several instruments, and it is believed that the combination offers many unique features not available in any other form at the present time.

References

1. Electronic Indicator for Low Audio Frequencies, **A. E. Hastings.** *Proceedings*, Institute of Radio Engineers (New York, N. Y.), volume 35, August 1947, pages 821–27.

2. Analysis of a Resistance-Capacitance Parallel T Network and Applications, **A. E. Hastings.** *Proceedings*, Institute of Radio Engineers (New York, N. Y.), volume 34, March 1946, pages 126–29.

3. A New Type of Selective Circuit and Some Applications, **H. H. Scott.** *Proceedings*, Institute of Radio Engineers (New York, N. Y.), volume 26, February 1938, pages 226–36.

4. The Optimum Performance of a Wave Analyzer, **N. F. Barber.** *Electronic Engineering* (London, England), May 1949, pages 175–79.

5. Vibration Testing of Airplanes, **Abner R. Willson.** *Electronics* (New York, N. Y.), volume 22, March 1949, pages 86–91.

6. A Simplified Analysis of the Parallel T Null Network, **M. P. Givens, John S. Saby.** *Review of Scientific Instruments* (New York, N. Y.), volume 18, May 1947, pages 342–46.

7. A Method of Very Rapid Analysis of Sounds, **Erwin Meyer.** *Journal*, Acoustical Society of America (New York, N. Y.), volume 7, October 1935, pages 88–93.

8. A Recording Analyzer for the Audible Frequency Range, **Harry H. Hall.** *Journal*, Acoustical Society of America (New York, N. Y.), volume 7, October 1935, pages 102–10.

9. Photomechanical Wave Analyzer Applied to Inharmonic Analysis, **C. F. Sacia.** *Journal*, Optical Society of America (New York, N. Y.), volume 9, October 1924, pages 487–94.

No Discussion

This section has been established to permit members residing outside of the United States (exclusive of Canada) to submit discussions which could not be received before the closing dates, which are two weeks after the meetings.

Where it was possible to do so, such discussions have been included with the paper, otherwise a footnote has been included at the end of each paper discussed referring to additional discussions in the back of the annual volume.

Thermal Transients on Buried Cable

Discussion of paper 51-9 by F. H. Buller, presented at the AIEE Winter General Meeting, New York, N. Y., January 22–26, 1951, and published in AIEE TRANSACTIONS, 1951, pages 45–55.

H. Lottrup Knudsen (Lecturer at the Royal Technical University of Denmark, Copenhagen, Denmark):

It has been a great pleasure to me to read Mr. Buller's solution to the heat conduction problem connected with a cable buried in earth. The formulas developed in Mr. Buller's paper seem to me to be based on physical assumptions that insure their validity within the limits stated in the paper.

In his paper Mr. Buller refers to an article describing some work made by me a few years ago.[1] However, in Mr. Buller's otherwise correct account of this work a misunderstanding seems to have slipped in, resulting in a misevaluation of the method for solving the heat conduction problem in question, given in my paper. In order to be able to account for this supposed misunderstanding I shall state the main points in my method of calculation.

The mentioned paper describes a single example of the application of a general principle for solving problems of nonstationary heat conduction in unlimited regions in which the heat sources are confined to a finite domain. According to this principle the first thing to do is to demarcate a finite region, containing the heat sources and being so large that the temperature of the bounding, mathematical surface thus introduced, does not vary appreciably during the interval of time to be considered. The simplifying, physical assumption is then introduced that no appreciable error will be committed by setting the temperature of the bounding surface equal to zero. Separating the variables we may then express the temperature field as an infinite series. Retaining only a few terms of this series an approximate expression for the temperature field in the central part of the region is obtained. To sum up, the two simplifying assumptions are

1. A finite region with the surface temperature zero is cut out.
2. Only a finite number of terms in the infinite series expressing the temperature field is retained.

The first assumption will cause the resulting expression for the temperature field to be valid only up to a certain time t_2, whereas the last assumption will cause the expression for the temperature only to be valid after a certain time t_1. By choosing the finite region sufficiently large the upper limit, t_2, of the interval in which the approximate expression applies may be made arbitrarily large; in order to keep the lower limit, t_1, of this interval unchanged we must then usually increase the number of terms in the infinite series expressing the temperature field, thereby increasing considerably the practical difficulties in carrying out the calculation.

a b

Figure 1

An objection was made to the principle used in my paper, in that the temperature field expressed by only a small number of eigen functions is a poor approximation to the actual temperature field at the time $t=0$. However, anybody having even a slight knowledge of the mathematical theory of heat conduction will know that the contribution to the temperature field given by the higher order eigen functions for a sufficiently large value of the time is negligible compared with the contribution given by the first few eigen functions. My paper only aimed at giving an expression for the temperature field for such large values of t that the contribution from the higher order eigen functions was negligible. The objection is therefore unfounded.

Another complaint against the method described above, has been that the choice of the proper magnitude of the finite region depends on an estimate or a rough calculation. However, after having finished the paper referred to by Mr. Buller, I have become aware of an extension of the principle outlined above, that partly eliminates this difficulty and partly involves the advantage that we can calculate the temperature field for an arbitrarily large interval of time, retaining only one or a few terms in the infinite series. The calculation is simply carried out for a number of different sizes of the finite region. Retaining in each of these cases the same small number of terms in the infinite series we choose the magnitudes of the various finite regions so that the curves calculated for the temperature field as a function of time coincide two and two over a certain interval of time.

In my paper a numerical example is worked out with the ratio between the diameter of the finite layer of earth and the diameter of the cable equal to two. How-

Figure 2

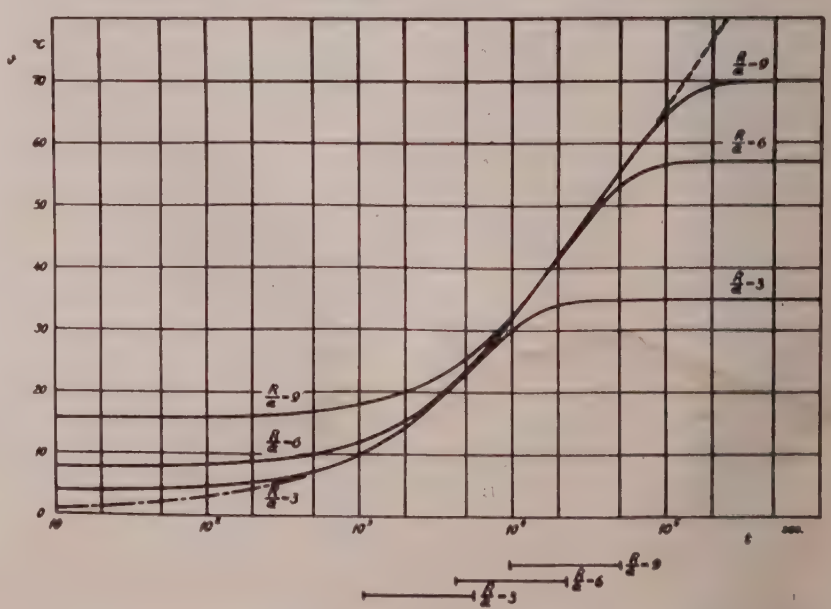

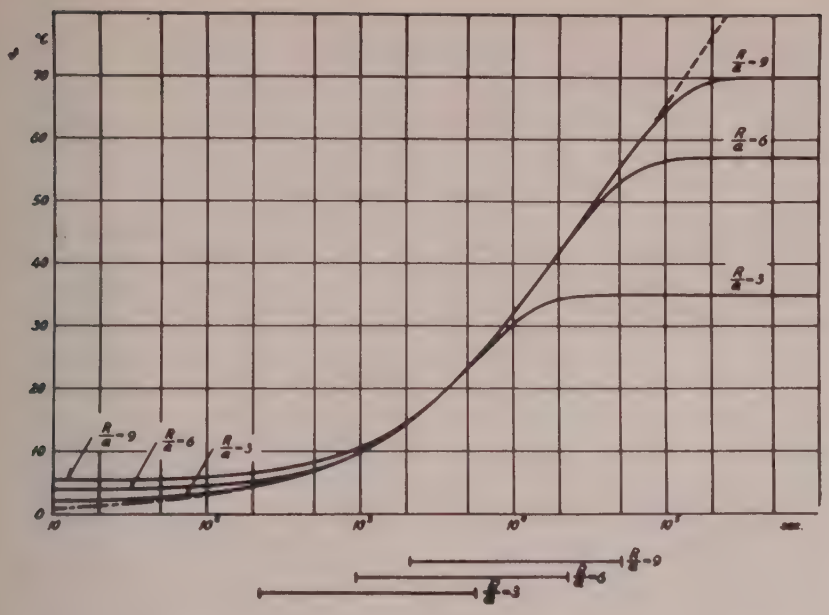

Figure 3

ever, the paper does not contain any recommendation of the specific value of the mentioned ratio as stated by Mr. Buller. On the contrary, curves of auxiliary functions are given for several different values of this ratio.

The above principle will be illustrated by a simpler example than the one occurring in my paper. An infinite, homogeneous medium is heated by sources uniformly distributed over a cylindrical surface with radius a as shown in Figure 1(A) of this discussion. The sources are switched on at the time $t=0$. The medium is supposed to have the specific heat conduction resistance $p=200$ degrees centigrade cm W^{-1} and the specific heat $q=2$ degrees centigrade^{-1} cm^{-3} W second. The radius of the cylinder is supposed to be $a=3$ cm, and the effect of the heat sources per-unit length of the cylinder is assumed to be 1 watt cm^{-1}. Following the principle described above we choose a cylindrical layer of earth with radius R and concentric with the cylindrical surface on which the heat sources are situated as shown in Figure 1(B). Setting the temperature at $r=R$ equal to zero we may easily find an expression for the temperature field by separating the variables. The temperature at the cylindrical surface $r=a$ is calculated for $R/a=3$, 6, and 9. By including only two terms in each of the infinite series we hereby find the temperature curves shown in Figure 2 of this discussion. This figure shows that the intervals in which each of the curves is valid have a lower as well as an upper bound. It is further seen, that the curves coincide two and two over a certain interval of time. On the other hand, if we retain four terms in each of the infinite series, we find for the temperature at $r=a$ the curves shown in Figure 3 of this discussion. The curves in this figure are seen to coincide over larger intervals than those in the preceding figure as a consequence of a diminuation of the lower limits of the intervals in which the various curves are valid.

Approximate expressions for the lower and the upper limits of the intervals in which each of the temperature curves in Figures 2 and 3 applies are given by the time constants in the first and the last term in the mathematical expressions for those curves. The approximate intervals calculated in this way are plotted below the abscissa axes in Figures 2 and 3. With a logarithmic scale for the time axis as used in Figures 2 and 3 a change in R/a is seen to give rise to a translation of the interval in which the approximate expression applies, the length of the interval remaining unchanged. By using only a few different values of R/a it is possible to obtain a temperature curve valid for a very large interval of time.

The reason why the simple example used here was chosen as an illustration of the calculation method in question is that an exact solution exists for this problem. As was shown by Whitehead (reference 4 of the paper) and as was also mentioned in Mr. Buller's paper, the temperature field may in the present case be expressed as an integral, the integrand of which is a product of an exponential function and a modified Bessel function. It is not possible to express this integral in any simple manner by known functions. However, for large values of the time an approximate expression for the integral may be given as shown by Whitehead (reference 5 in Mr. Buller's paper). The temperature at $r=a$ calculated by using this method is plotted in Figures 2 and 3 as the dotted curve. This curve is a good approximation only for large values of the time. For small values of the time an approximate expression for the temperature is obtained most easily by assuming the heat source to be a plane instead of a cylindrical surface and the problem accordingly a 1-dimensional instead of a 2-dimensional one. In this way the dot-and-dashed curve in Figures 2 and 3 is obtained for the temperature at $r=a$. This curve is a good approximation only for small values of the time. It may be shown that both of these approximate expressions give too small values of the temperature. The agreement between the temperature curves valid respectively for small and for large values of the time and the three temperature curves calculated according to the principle described in this note is seen to be good.

In the above a very simple heat conduction problem was used as an illustration of the principle described here. With the heat conduction problem treated in my paper a similar result is obtained. I have had no opportunity of seeing the calculations on which Mr. Buller bases his statement that my method leads for different values of the radius, R, of the layer of earth, to conflicting results. Presumably this conclusion rests on a miscalculation or a misunderstanding of my paper, possibly caused by a misprint, then still unnoticed by me.

The principle outlined here for calculating the temperature field in an infinite region will be discussed in more detail elsewhere.

Reference

1. See reference 20 of the paper.

F. H. Buller: It is very gratifying to learn that Lektor H. L. Knudsen believes that the present solution of this problem is satisfactory, especially since he has given this problem a great deal of study, and has presented a valuable solution of his own.

His solution is based on fundamental assumptions which should be rigorous enough to satisfy the most meticulous; in fact it is hard to see how it could be improved on from this standpoint. However, there are a couple of points in the application of the theory which require elucidation; and this he has provided to a considerable degree in the present discussion.

To be specific these points are:

1. In applying his theory, Lektor Knudsen substitutes a finite Bessel cable for the infinite Bessel cable which should properly represent the earth portion of the circuit.
2. The solution as he has presented it is very difficult to use in practice, involving the roots of a number of complicated equations.

Now there seems to be little doubt that the substitution of a finite Bessel cable for an infinite one should give an acceptable approximation, at any rate for intervals of time which are not too long, provided that the outside radius R of the finite cable thus substituted is large enough. While Lektor Knudsen is, of course, entitled to take any radius he wants in an illustrative example, it is unfortunate that he chose a radius equal to only twice that of the cable in the example which he actually used, and that his presentation left the impression that he felt this should be sufficient in most if not all practical cases. For it turns out that such a radius is not nearly large enough. It is felt that Lektor Knudsen has materially increased the value of his solution by clearing up this point in the present discussion.

Furthermore, he states that, for large values of time, this assumption limits the accuracy of his solution. This statement is correct; but it would seem likely that for such values of time if the radius R is large enough the Knudsen formula will merge into the exponential integral formula (number 3 in my paper). If so, it should be possible to establish the time at which this merging takes place, and to use the simple exponential integral formula for times longer

than this. Such a procedure is probably simpler than the plan which he proposes in his discussion for overcoming this particular difficulty.

As Lektor Knudsen points out, his solution takes the form of an infinite series; and he is quite correct in his statement that it is rarely necessary in practice to use more than the first few terms. For cables in air, experience indicates that three are almost invariably sufficient. Since the number required tends to increase with the insulation thickness, it is possible that four or five might be desirable in the earth portion of the circuit, especially if large values of R are used. Since each term involves a root of a complicated equation, the labor involved in applying the solution is somewhat formidable.

Lektor Knudsen tells us that for small time intervals an approximation is involved because of the omission of all but the first few terms in the series. It is possible that this is the reason why the calculations mentioned in the penultimate paragraph of his discussion fail to agree. All these calculations were made for times of two hours or less from the start of heating. At the end of two hours the heating curves for different values of R show signs of approaching coincidence, though they do not yet coincide in the case calculated.

It would appear that Lektor Knudsen has made a somewhat unfortunate choice in the numerical example he has selected to illustrate his discussion. Here again, of course, he is at liberty to choose any numerical example he pleases to illustrate a point which he has in mind; but it so happens that the example which he has selected is based on the Whitehead assumptions, which are far less accurate from the theoretical standpoint than those on which Knudsen's own technique is based. The limitations of the Whitehead assumptions are brought out in my paper (see comments on equation 5). Those who wish to use Knudsen's method are advised to apply his technique in toto and to avoid the Whitehead assumptions on theoretical grounds.

To sum the matter up—

1. Lektor Knudsen's solution is a perfectly valid one mathematically, and is based on very rigorous fundamental assumptions.

2. To make the substitution of a finite for an infinite Bessel cable work out practically, a large value of R - certainly more than five times the cable diameter and possibly more than ten times - is needed. And even then an additional correction factor is required for long times. Fortunately, such a correction factor is not too difficult to devise.

3. It seems certain that at least three and possibly as many as five terms of the infinite series will be needed to give an accurate answer, the number depending on the degree of accuracy required and whether a thermal transient or an oil demand transient is wanted; also on the degree of precision required for short times.

4. The labor of obtaining such a solution is considerable. Thus Lektor Knudsen's solution also is of value rather as a check on working formulas than as a basis for everyday calculation.

5. It is very gratifying that two different solutions both mathematically sound are now available for this problem. Those who have any doubt about any of the features involved in either one can now check it against the other.

AIEE Transactions Index for Part I, Volume 70, 1951

1. Technical Subject Index

Accelerators, Dielectric Loading for Waveguide Linear. Flesher, Cohn 887–93
Acoustic Models of Transformer Installations. Gettys, Conover . . . . . 333–6; disc. 336
Admittance Functions, Loci of Complex Impedance and. Michaels 299–303
Admittance Remains Constant as Load Varies, Networks for Which Magnitude or Phase Angle of Input Impedance or Transfer. Berkowitz . . 286–91
Aging of Class-B Insulating Material in Nitrogen. Stewart, Whitman . . . . . 436–7; disc. 437
Air Blast Circuit Breaker, A New 69-Kv. Shores, Beatty . . . . . 202–07; disc. 207
Air Circuit Breakers, A Spring Mechanism for Hand Closing of Magnetic Power. Dickinson, Findley . . . . . 189–92; disc. 192
Aircraft D-C Systems, Fault Transients in. Scorgie . . . . . 713–20; disc. 720
Alignment Techniques for Phase-Rotation Single Side-Band Transmitters, Output Analysis and. Whitby, Scheuch 209–12
Alloy Sheaths for Underground Power Cable, Lead-. Halperin, Betzer . . . . . 423–9; disc. 429
Alternating and Direct Voltage Endurance Studies on Mica Insulation for Electric Machinery. Moses . . . . . 763–8; disc. 768
A-C Arc Adjacent to Refractory Surfaces, A Study of Conduction Phenomena Near Current Zero for an. Browne, Strom . . . . . 398–407; disc. 407
A-C Arc Welders with Saturable Reactor Control. Oestreicher 787–90
A-C Generators, Relay Protection of. (Committee Report) . . . . . 275–81; disc. 281
A-C Impedances of Machine Conductors, Circuit Analysis Method for Determination of. Babb, Williams . . . . . 661–5; disc. 665
A-C Instruments, Frequency Compensation of. Miller . . . . . 217–20; disc. 220
A-C Multiple-Car Control for the Pennsylvania Railroad, New. Newhouse . . . . . 645–7; disc. 647
A-C Multiple-Unit Car Control Equipment. O'Kelly 652–6
A-C Multiple-Unit Car Motor. Kreitler . . . . . 648–50; disc. 650
A-C Servomechanisms, Effects of Carrier Shifts on Derivative Networks for. Attura 612–18
A-C Servomechanisms, Network Synthesis by Graphical Methods for. Bjornson 619–25
Alternators, Static Magnetic Exciter for Synchronous. Storm 1014–17
American Gas and Electric Company, Corona Investigation on Extra-High-Voltage Lines—500-Kv Test Project of the. Gross, Wagner, Naef, Tremaine . . . . . 75–91; disc. 91
American Gas and Electric Company, Line Insulator Loss Under Normal Conditions—500-Kv Test Project of the. Naef, Tremaine, Jones 1073–8
American Gas and Electric Company, Radio Influence Tests in Field and Laboratory—500-Kv Test Project of the. Lippert, Pakala, Bartlett, Fahrnkopf . . . . . 251–65; disc. 265
American Gas and Electric Company, Techniques of Corona Loss Measurement and Analysis—500-Kv Test Project of the. Naef, Tremaine, Jones . . . . . 496–505; disc. 505
American Gas and Electric Company, The 300–315 Kv Extra High-Voltage Transmission System of the. Sporn, Peterson, Gross, St. Clair . . . 64–72; disc. 72
Amplifier Subcommittee, Progress Report of the AIEE Magnetic. (Committee Report) . . 445–9; disc. 449
Amplifiers Based on Linear Approximations of the Magnetization Curve, Steady-State Analysis of Self-Saturating Magnetic. Esselman 451–9
Amplifiers—Cases of Negligible Commutation, The Transient Response of Magnetic. Finzi, Chandler, Beaumariage . . . . . 934–42; disc. 942
Analogue Computers, A Diode Bridge Limiter for Use with Electronic. Medkeff, Parent 913–16
Analogue Computing Techniques Applied to Economics. Strotz, Calvert, Morehouse . . . . . 557–62; disc. 562
Analysis and Alignment Techniques for Phase-Rotation Single Side-Band Transmitters, Output. Whitby, Scheuch 209–12
Analysis Method for Determination of A-C Impedances of Machine Conductors, Circuit. Babb, Williams . . . . . 661–5; disc. 665
Analysis of a 3-Phase Inverter with Resistive Load. Turkington 1055–61
Analysis of Grounding Banks to Balance Distribution Feeder Voltages, An. Long 823–7
Analysis of Rotating Machines and Stationary Networks by Means of Rotating Reference Frames. Ku . . . . . 943–54; disc. 954
Analysis of Self-Saturating Magnetic Amplifiers Based on Linear Approximations of the Magnetization Curve, Steady-State. Esselman 451–9
Analyzer Study of Harmonic Power Generation with Nonlinear Impedance Element, Differential. Russell, Peterson 917–20
Angle-Shaped Conductors, Geometric Mean Distances of. Magnusson 121–3
Angular Velocity, A Tachometer for Measurement of Instantaneous Variations in. Bartles 1102–05
Annulus by the Method of Subareas, Calculation of the Capacitance of a Circular. Higgins, Reitan . . . . . 926–31; disc. 931
Apparatus Protection, Some Effects of Lightning Arrester Protective Characteristics and Location upon Station. Kalb . . . . . 379–83; disc. 383
Application, Economics of Power Transformer. Barkle, Witzke . . . . . 440–4; disc. 444
Application of a Series Capacitor to a Synchronous Condenser for Reducing Voltage Flicker, The. Black, Lischer 144–50
Application of Microwave Channels. Cheek . . 813–17
Application of Resonant Grounding in Power Systems in the United States. Gross, Atherton . . . . . 389–93; disc. 393
Application of Shunt Capacitors at Transmission and Distribution Stations. Porter, Zimmerman . . . . . 112–18; disc. 118
Applications, 940–960 Megacycle Communications Equipment for Industrial. Gunter 807–12
Approach to Control Room Lighting, An Engineering. Dzwonczyk . . . . . 852–7; disc. 857
Approach to the Compensation of Saturating Servomechanisms, A Phase-Plane. Hopkin 631–9
Approximations of the Magnetization Curve, Steady-State Analysis of Self-Saturating Magnetic Amplifiers Based on Linear. Esselman 451–9
Arc Adjacent to Refractory Surfaces, A Study of Conduction Phenomena Near Current Zero for an A-C. Browne, Strom . . . . . 398–407; disc. 407
Arc Chokes Power Flow in New Lightning Arresters, Spiral. Ackermann, DeVal 995–8
Arc Rectifier on the Central Railway of Brazil, Regeneration With a Mercury. Schmidt 1092–6
Arc Welders with Saturable Reactor Control, A-C. Oestreicher 787–90
Arcs and Their Relation to the Welding Arc, The Physical Mechanism of Low and High-Current. Finkelnburg 800–03
Arcs, New Electrodes for Stabilizing Inert-Gas Welding. Cobine, Gallagher 804–06
Armatures, Winding Insulation Tester for D-C. Catlin, Rohats 465–8
Arrester Protective Characteristics and Location upon Station Apparatus Protection, Some Effects of Lightning. Kalb . . . . . 379–83; disc. 383
Arresters, Spiral Arc Chokes Power Flow in New Lightning. Ackermann, DeVal 995–8
Arresters, The Power Interruption Testing of Lightning. Ackermann . . . . . 1–5; disc. 5
Audio Noise in Substation Type Transformers, An Investigation of. Vivian, Peck . . . 328–31; disc. 331
Automatic Controls, Some Design Criteria for. Nims 606–11
Automatic Devices, Switching of Distribution Capacitors by Manual and. Hopkins, Schultz . . . 138–43
Automatic Private-Line Teletypewriter Switching System, A Full. Bacon, Locke 473–80
Automatic Trunk Selection in Reperforator Switching. Blanton 481–9

B

Balancing of Large Turbine-Generator Rotors, Modern Practice in the. Laffoon, Hagg, Janthey, Heller . . . . . 593–8; disc. 598
Ballasts, Noise Evaluation of Fluorescent Lamp. Hayes, Gould 573–9
Banks, A New Carrier-Current Frequency-Shift System for Use with Differential Protection of Transformer. Beckwith . . . . . 832–5; disc. 835
Banks, Switching High-Voltage Shunt Capacitor. Funkhouser, VanSickle, Shankle . . . . . 129–33; disc. 134
Banks to Balance Distribution Feeder Voltages, An Analysis of Grounding. Long 823–7
Bar Induction Motor, A Contribution to the Theory of the Deep-. Douglas 862–6
Basic Heat-Transfer Data in Electron Tube Operation. Buckland 1079–85
(Basic Sciences) A New Method for Treating Electron Tubes When Used as Oscillators in the Free as Well as in the Synchronized States. Mostafa, Bey 999–1004
(Basic Sciences) Calculation of Flux Distributions with Saturation. Poritsky . . . . . 309–19; disc. 319
(Basic Sciences) Calculation of the Capacitance of a Circular Annulus by the Method of Subareas. Higgins, Reitan . . . . . 926–31; disc. 931
(Basic Sciences) Contact Transients in Simple Electric Circuits. Martin, Stauss . . . . . 304–07; disc. 307
(Basic Sciences) Dependence of Direct Sparkover Voltage of Gaps on Humidity and Time. Jacob, Sommerman . . . . . 921–4; disc. 924
(Basic Sciences) Loci of Complex Impedance and Admittance Functions. Michaels 299–303
(Basic Sciences) Networks for Which Magnitude or Phase Angle of Input Impedance or Transfer Admittance Remains Constant as Load Varies. Berkowitz 286–91
(Basic Sciences) Tables of Green's Functions, Fourier Series, and Impulse Functions for Rectangular Coordinate Systems. Smith 22–30
(Basic Sciences) The Generalized Transmission Matrix Stability Criterion. Honnell . . . . 292–6; disc. 296
Bibliography of Relay Literature—1947–1949. (Committee Report) 247–50
Blast Circuit Breaker, A New 69-Kv Air. Shores, Beatty . . . . . 202–07; disc. 207
Brazil, Regeneration with a Mercury Arc Rectifier on the Central Railway of. Schmidt 1092–6
Breakdown Voltage, A Gas Tube Inverter with the Supply Voltage Below the. Cage, Schuder 908–12
Breaker, A New 69-Kv Air Blast Circuit. Shores, Beatty . . . . . 202–07; disc. 207
Breakers, A Spring Mechanism for Hand Closing of Magnetic Power Air Circuit. Dickinson, Findley . . . . . 189–92; disc. 192
Bridge Limiter for Use with Electronic Analogue Computers, A Diode. Medkeff, Parent 913–16
Buried Cables, Thermal Transients on. Buller . . . . . 45–52; disc. 52, 1106

C

Cab Signaling and Train Control System for Railroads, A Modern. Allison . . . . . 232–8; disc. 238
Cable, Lead-Alloy Sheaths for Underground Power. Halperin, Betzer . . . . . 423–9; disc. 429
Cable, Washington, D. C., 69-Kv Medium-Pressure Gas-Filled. Clark . . . . . 418–21; disc. 421
Cable with Submerged Repeaters, A Submarine Telephone. Gilbert 564–72
Cables, Thermal Expansion Effects in Power. Schifreen . . . . . 160–8; disc. 168
Cables, Thermal Transients on Buried. Buller . . . . . 45–52; disc. 52, 1106
Calculation of Flux Distributions with Saturation. Poritsky . . . . . 309–19; disc. 319
Calculation of the Capacitance of a Circular Annulus by the Method of Subareas. Higgins, Reitan . . . . . 926–31; disc. 931
Calculations—Effect of Conductor Configuration in Overhead Lines, Welding. Tietze 784–6
Calculator, A New Train Performance. Smith . . 657–60
Capacitance of a Circular Annulus by the Method of Subareas, Calculation of the. Higgins, Reitan . . . . . 926–31; disc. 931
Capacitor Banks, Switching High-Voltage Shunt. Funkhouser, VanSickle, Shankle . . 129–33; disc. 134
Capacitor in Series with a Synchronous Condenser, Technical Problems Associated with the Application of a. Witzke, Michelson 519–25
Capacitor Switching Phenomena. Van Sickle, Zaborszky . . . . . 151–8; disc. 158

Capacitor to a Synchronous Condenser for Reducing Voltage Flicker, The Application of a Series. Black, Lischer....144–50
Capacitors at Transmission and Distribution Stations, Application of Shunt. Porter, Zimmerman....112–18; disc. 118
Capacitors by Manual and Automatic Devices, Switching of Distribution. Hopkins, Schultz....138–43
Capacitors in High-Voltage Transmission Lines, Fundamental Effects of Series. Johnson, Barkle, Povejsil....526–35; disc. 535
Capacity by the Probability Method Effect of Interconnections, Determination of Reserve. Calabrese....1018–20
Car Control Equipment, A-C Multiple-Unit. O'Kelly....652–6
Car Control for the Pennsylvania Railroad, New A-C Multiple-. Newhouse....645–7; disc. 647
Car Equipments?, Why 4-Motor Multiple-Unit. Williamson....240–2
Car Motor, A-C Multiple-Unit. Kreitler....648–50; disc. 650
Car Motor for the Pennsylvania Railroad, A New Multiple-Unit. Jungk....243–5; disc. 245
Carrier Communication Channel, Vibracode System of Supervisory Control on a. Allen, Daniel....818–22; disc. 822
(Carrier Current) Application of Microwave Channels. Cheek....813–17
Carrier Current Communications Circuits, Signal and Supervision Systems Used on. Mayer....990–4
Carrier-Current Frequency-Shift System for Use with Differential Protection of Transformer Banks, A New. Beckwith....832–5; disc. 835
(Carrier Current) 940–960 Megacycle Communications Equipment for Industrial Applications. Gunter....807–12
Carrier Current Supervisory System for Distribution Circuits. Podolsky, Lubin....1096–1101
Carrier Relaying System, Measurements and Tests on a Power Line. Miller, Worthington....1005–07
Carrier Shifts on Derivative Networks for A-C Servomechanisms, Effects of. Attura....612–18
Cars, Electric Equipment and Performance of Lightweight Rapid Transit. Ellis, Sloman....227–30; disc. 230
Cars, Selection of Equipment for Multiple-Unit. Hutchison....640–3; disc. 643
Changer Welders, Ignitrons for Frequency-. Rottier....900–07
Channel Time-Division-Multiplex Telegraph System for Long-Distance Radio Circuits, Four- or Two-. Peterman, Minc....362–72
Channel, Vibracode System of Supervisory Control on a Carrier Communication. Allen, Daniel....818–22; disc. 822
Channels, Application of Microwave. Cheek....813–17
Channels for a Power System, Choice of Telemetering Systems and. Duff....1086–91
Characteristics and Location upon Station Apparatus Protection, Some Effects of Lightning Arrester Protective. Kalb....379–83; disc. 383
Charge in Electrostatic Mineral Separation, Distribution of. Fraas, Ralston....1028–30
Choice of Telemetering Systems and Channels for a Power System. Duff....1086–91
Chokes Power Flow in New Lightning Arresters, Spiral Arc. Ackermann, DeVal....995–8
Circuit Analysis Method for Determination of A-C Impedances of Machine Conductors. Babb, Williams....661–5; disc. 665
Circuit Breaker, A New 69-Kv Air Blast. Shores, Beatty....202–07; disc. 207
Circuit Breakers, A Spring Mechanism for Hand Closing of Magnetic Power Air. Dickinson, Findley....189–92; disc. 192
Circuits and Their Application in Designing Shaded Pole Motors, Equivalent. Chang..690–8; disc. 698
Circuits, Carrier Current Supervisory System for Distribution. Podolsky, Lubin....1096–1101
Circuits, Contact Transients in Simple Electric. Martin, Stauss....304–07; disc. 307
Circuits, Four- or Two-Channel Time-Division-Multiplex Telegraph System for Long-Distance Radio. Peterman, Minc....362–72
Circuits, Signal and Supervision Systems Used on Carrier Current Communications. Mayer....990–4
Circular Annulus by the Method of Subareas, Calculation of the Capacitance of a. Higgins, Reitan....926–31; disc. 931
Class-B Insulating Material in Nitrogen, Aging of. Stewart, Whitman....436–7; disc. 437
Closing of Magnetic Power Air Circuit Breakers, A Spring Mechanism for Hand. Dickinson, Findley....189–92; disc. 192
Coach Power Supply, Economics of Trolley. McDonald, Price....687–9
(Committee Report) Bibliography of Relay Literature—1947-1949. (51-38)....247–50
(Committee Report) Inductive Co-ordination Aspects of D-C Systems Supplied by Rectifiers. (51–206)....1034–54
(Committee Report) Marking of Varmeters. (51–3)....12–14; disc. 14
(Committee Report) Power System Fault Control. (51–66)....410–17
(Committee Report) Progress Report of the AIEE Magnetic Amplifier Subcommittee. (51–71)....445–9; disc. 449
(Committee Report) Relay Protection of A-C Generators. (51–42)....275–81; disc. 281
(Committee Report) Results of a Questionnaire Covering Current Practices in Electrical Tests on Dielectrics in the Field. (51–186)....986–9
(Communication) A Full Automatic Private-Line Teletypewriter Switching System. Bacon, Locke....473–80
(Communication) A Submarine Telephone Cable with Submerged Repeaters. Gilbert....564–72
(Communication) Automatic Trunk Selection in Reperforator Switching. Blanton....481–9
Communication Channel, Vibracode System of Supervisory Control on a Carrier. Allen, Daniel....818–22; disc. 822
(Communication) Operational Study of a Highway Mobile Telephone System. Dorff....31–7
(Communication) Pulse-Time Modulation Telemetering Systems for Rocket Application. Mengel....599–605
(Communication) Shielded Dielectric-Rod Waveguides. Beam, Wachowski....874–80
(Communication) Single-Frequency Signaling System for Supervision and Dialing over Long-Distance Telephone Trunks. Newell, Weaver....489–95
Communications Circuits, Signal and Supervision Systems Used on Carrier Current. Mayer....990–4
Communications Equipment for Industrial Applications, 940–960-Megacycle. Gunter....807–12
Commutating Reactor Control for Mechanical Rectifiers. Diebold....1062–5
Commutation in Universal-Type Motors. Packer....170–6; disc. 176
Commutation, The Transient Response of Magnetic Amplifiers—Cases of Negligible. Finzi, Chandler, Beaumariage....934–42; disc. 942
Compensation of A-C Instruments, Frequency. Miller....217–20; disc. 220
Compensation of Saturating Servomechanisms, A Phase-Plane Approach to the. Hopkin....631–9
Compensators for Watt-hour and Var-hour Meters Improvements in Transformer-Loss. Schleicher....973–7
Complex Impedance and Admittance Functions, Loci of. Michaels....299–303
Computers, A Diode Bridge Limiter for Use with Electronic Analogue. Medkeff, Parent....913–16
Computers, A Method of Gating for Parallel. Ratz, Smith....510–16
Computers, Systematization of Tube Surveillance in Large-Scale. Spence....516–19
(Computing Devices) The Input-Output System of the EDVAC. Snyder....507–09
Computing Techniques Applied to Economics, Analogue. Strotz, Calvert, Morehouse....557–62; disc. 562
Condenser for Reducing Voltage Flicker, The Application of a Series Capacitor to a Synchronous. Black, Lischer....144–50
Condenser, Technical Problems Associated with the Application of a Capacitor in Series with a Synchronous. Witzke, Michelson....519–25
Conditionally Stable Feedback Systems, A Note on the Design of. Travers....626–30
Conduction Phenomena Near Current Zero for an A-C Adjacent to Refractory Surfaces, A Study of. Browne, Strom....398–407; disc. 407
Conductor Configuration in Overhead Lines, Welding Calculations Effect of. Tietze....784–6
Conductors, Circuit Analysis Method for Determination of A-C Impedances of Machine. Babb, Williams....661–5; disc. 665
Conductors, Geometric Mean Distances of Angle-Shaped. Magnusson....121–3
Conductors—Service Experience and Further Experimental Work, The Torsional Damper for. Burgess, Hogg....1031–3
Configuration in Overhead Lines, Welding Calculations—Effect of Conductor. Tietze....784–6
Constant as Load Varies, Networks for Which Magnitude or Phase Angle of Input Impedance or Transfer Admittance Remains. Berkowitz....286–91
Constants, A Per-Unit Interpretation of Transmission Line. Povejsil, Johnson....194–200; disc. 200
Contact Resistance—The Contribution of Non-uniform Current Flow. Kouwenhoven, Sackett....791–5
Contact Testing, An Electronic Power Source for Large D-C. Pettit....320–2
Contact Transients in Simple Electric Circuits. Martin, Stauss....304–07; disc. 307
Contribution of Nonuniform Current Flow, Contact Resistance—The. Kouwenhoven, Sackett....791–5
Contribution to the Theory of the Deep-Bar Induction Motor, A. Douglas....862–6
Control, A-C Arc Welders with Saturable Reactor. Oestreicher....787–90
Control Equipment, A New Lightweight Rapid Transit. Lichtenfels, Moore....224–6
Control Equipment, A-C Multiple-Unit Car. O'Kelly....652–6
Control for Mechanical Rectifiers, Commutating Reactor. Diebold....1062–5
Control for the Pennsylvania Railroad, New A-C Multipe-Car. Newhouse....645–7; disc. 647
Control on a Carrier Communication Channel, Vibracode System of Supervisory. Allen, Daniel....818–22; disc. 822
Control, Power System Fault. (Committee Report)....410–17
Control Room Lighting, An Engineering Approach to. Dzwonczyk....852–7; disc. 857
Control System for Railroads, A Modern Cab Signaling and Train. Allison....232–8; disc. 238
Controllers, The Effects of Loads and Disturbances upon Feedback. Jones....460–4
Controls, Some Design Criteria for Automatic. Nims....606–11
Co-ordination Aspects of D-C Systems Supplied by Rectifiers, Inductive. (Committee Report)....1034–54
Core, A 2,000,000-Kva Transformer. Sealey....8–11
Core Form Transformer Winding, Improved. Grimmer, Teague....962–5; disc. 965
Corona Investigation on Extra-High-Voltage Lines—500-Kv Test Project of the American Gas and Electric Company. Gross, Wagner, Naef, Tremaine....75–91; disc. 91
Corona Loss Measurement and Analysis—500-Kv Test Project of the American Gas and Electric Company, Techniques of. Naef, Tremaine, Jones....496–505; disc. 505
Criteria for Automatic Controls, Some Design. Nims....606–11
Criterion, The Generalized Transmission Matrix Stability. Honnell....292–6; disc. 296
Crystals as Sensing Elements of Pressure, Temperature, and Humidity, Piezoelectric. Roberts, Goldsmith....968–72
Current Flow, Contact Resistance—The Contribution of Nonuniform. Kouwenhoven, Sackett....791–5
Current Supervisory System for Distribution Circuits, Carrier. Podolsky, Lubin....1096–1101
Current, Transformer Magnetizing Inrush. Specht....323–7; disc. 327
Current Zero for an A-C Arc Adjacent to Refractory Surfaces, A Study of Conduction Phenomena Near. Browne, Strom....398–407; disc. 407
Curve, Steady-State Analysis of Self-Saturating Magnetic Amplifiers Based on Linear Approximations of the Magnetization. Esselman....451–9
Cyclic Light Flicker, Effect of the Duration of Voltage Dip on. Brieger....894–8; disc. 899

D

Damper for Conductors—Service Experience and Further Experimental Work, The Torsional. Burgess, Hogg....1031–3
Damping and Synchronizing Torques, Synchronous Machine. Concordia....731–7
Data in Electron Tube Operation, Basic Heat-Transfer. Buckland....1079–85
Deep-Bar Induction Motor, A Contribution to the Theory of the. Douglas....862–6
Delta System, Neutral Inversion of a Single Potential Transformer Connected Line-to-Ground on an Isolated. Gleason....103–10; disc. 110
Dependence of Direct Sparkover Voltage of Gaps on Humidity and Time. Jacob, Sommerman....921–4; disc. 924
Derivative Networks for A-C Servomechanisms, Effects of Carrier Shifts on. Attura....612–18
Design Criteria for Automatic Controls, Some. Nims....606–11
Design, Ice Testing and Its Influence Upon Switch. Heberlein, Field....37–42; disc. 42
Design Method for Polyphase Reluctance Synchronous Motors, A. Crouse....957–62
Design of Conditionally Stable Feedback Systems, A Note on the. Travers....626–30
Designing Frog-Leg Windings of D-C Machines, Rules for. Dwight, Haltmaier....707–11; disc. 711
Detection of Turn-to-Turn Faults in Large High-Voltage Turbine Generators. Sexton, Alke....270–3; disc. 273
Deterioration of Transformer Oil and Paper Insulation by Temperatures. Vogel, Petersen, Matach....18–20; disc. 21
Determination of A-C Impedances of Machine Conductors, Circuit Analysis Method for. Babb, Williams....661–5; disc. 665
Determination of Generator Stand-by Reserve Requirements. Strandrud....179–87; disc. 187

Determination of Reserve Capacity by the Probability Method Effect of Interconnections. Calabrese... 1018-20
Development of a Pumpless Ignitron. Herskind, Remscheid....1066–9
Development of Large Turbine Generators, Progress in the. Huntley, Taylor....580–9; disc. 589
Devices, Switching of Distribution Capacitors by Manual and Automatic. Hopkins, Schultz....138–43
Dialing over Long-Distance Telephone Trunks, Single-Frequency Signaling System for Supervision and. Newell, Weaver....489–95
Dielectric Loading for Waveguide Linear Accelerators. Flesher, Cohn....887–93
Dielectric-Rod Waveguides, Shielded. Beam, Wachowski....874–80
Dielectrics in the Field, Results of a Questionnaire Covering Current Practices in Electrical Tests on. (Committee Report)....986–9
Differential Analyzer Study of Harmonic Power Generation with Nonlinear Impedance Element. Russell, Peterson.... 917–20
Differential Protection of Transformer Banks, A New Carrier-Current Frequency-Shift System for Use with. Beckwith....832–5; disc. 835
Diode Bridge Limiter for Use with Electronic Analogue Computers, A. Medkeff, Parent....913–16
Dip on Cyclic Light Flicker, Effect of the Duration of Voltage. Brieger....894–8; disc. 899
D-C Armatures, Winding Insulation Tester for. Catlin, Rohats.... 465–8
D-C Contact Testing, An Electronic Power Source for Large. Pettit....320–2
D-C Machine Parameters, Measurement of. Saunders....700–05; disc. 705
D-C Machines, Rules for Designing Frog-Leg Windings of. Dwight, Haltmaier....707–11; disc. 711
D-C Power Supplies and Isolation of Faults on Electric Transit Systems. Watkins, Reagan.
Part I. D-C Power Supply....537–42; disc. 542
Part II. Isolation of D-C Faults..543–50; disc. 550
D-C Power Systems, Factors Affecting Minimum Surface Leakage Distances in. Hart, Rosenberry, McClinton....738–42
D-C Systems, Fault Transients in Aircraft. Scorgie....713–20; disc. 720
D-C Systems Supplied by Rectifiers, Inductive Coordination Aspects of. (Committee Report)....1034–54
Direct Sparkover Voltage of Gaps on Humidity and Time, Dependence of. Jacob, Sommerman....921–4; disc. 924
Direct Voltage Endurance Studies on Mica Insulation for Electric Machinery, Alternating and. Moses....763–8; disc. 768
Distances in D-C Power Systems, Factors Affecting Minimum Surface Leakage. Hart, Rosenberry, McClinton.... 738–42
Distances of Angle-Shaped Conductors, Geometric Mean. Magnusson....121–3
Distribution Capacitors by Manual and Automatic Devices, Switching of. Hopkins, Schultz..138–43
Distribution Circuits, Carrier Current Supervisory System for. Podolsky, Lubin....1096–1101
Distribution Feeder Voltages, An Analysis of Grounding Banks to Balance. Long....823–7
Distribution of Charge in Electrostatic Mineral Separation. Fraas, Ralston.... 1028–30
Distribution Stations, Application of Shunt Capacitors at Transmission and. Porter, Zimmerman....112 18; disc. 118
Distributions with Saturation, Calculation of Flux. Poritsky....309–19; disc. 319
Disturbances upon Feedback Controllers, The Effects of Loads and. Jones....460–4
Division Multiplex Telegraph Set, An Electronic Time. Hansen, Slayton....354–61; disc. 361
Division Multiplex Telegraph System for Long-Distance Radio Circuits, Four-or-Two-Channel Time-. Peterman, Minc....362–72
Duration of Voltage Dip on Cyclic Light Flicker, Effect of the. Brieger....894–8; disc. 899

E

Economics, Analogue Computing Techniques Applied to. Strotz, Calvert, Morehouse..557–62; disc. 562
Economics of Extra-High-Voltage Transmission, System. St. Clair, Peterson....841–8; disc. 848
Economics of Power Transformer Application. Barkle, Witzke....440–4; disc. 444
Economics of Trolley Coach Power Supply. McDonald Price....687 9
EDVAC, The Input-Output System of the. Snyder....507–09
Effect of the Duration of Voltage Dip on Cyclic Light Flicker. Brieger....894–8; disc. 899
Effects of Carrier Shifts on Derivative Networks for A-C Servomechanisms. Attura....612–18
Effects of Lightning Arrester Protective Characteristics and Location upon Station Apparatus Protection, Some. Kalb....379–83; disc. 383
Effects of Loads and Disturbances upon Feedback Controllers, The. Jones....460–4
Effects of Series Capacitors in High-Voltage Transmission Lines, Fundamental. Johnson, Barkle, Povejsil....526–35; disc. 535
Efficiency, Transmission Line Load Impedance for Maximum. Lutz....283–5
Electric Circuits, Contact Transients in Simple. Martin, Stauss....304–07; disc. 307
Electric Equipment and Performance of Lightweight Rapid Transit Cars. Ellis, Sloman....227–30; disc. 230
Electric Home Heating. Parks....828–31
(Electric Welding) Effect of the Duration of Voltage Dip on Cyclic Light Flicker. Brieger....894–8; disc. 899
(Electric Welding) Probabilities of Interference Between Resistance Welders. Boice....775–83
Electrodes for Stabilizing Inert-Gas Welding Arcs, New. Cobine, Gallagher....804–06
Electromagnetic Induction Method of Measuring Oscillating Fluid Flow, An. Morris, Chadwick..346–50
Electromechanical Transducer, An. Engelberger, Kretsch.... 213 16
Electron Tube Operation, Basic Heat-Transfer Data in. Buckland....1079–85
Electron Tubes When Used as Oscillators in the Free as Well as in the Synchronized States, A New Method for Treating. Mostafa, Bey....999–1004
Electronic Analogue Computers, A Diode Bridge Limiter for Use with. Medkeff, Parent....913–16
Electronic Power Source for Large D-C Contact Testing, An. Pettit....320–2
Electronic Time Division Multiplex Telegraph Set, An. Hansen, Slayton....354–61; disc. 361
(Electronics) A Gas Tube Inverter with the Supply Voltage Below the Breakdown Voltage. Cage, Schuder....908 12
(Electronics) Analysis of a 3-Phase Inverter with Resistive Load. Turkington....1055–61
(Electronics) Development of a Pumpless Ignitron. Herskind, Remscheid....1066–9
(Electronics) Distribution of Charge in Electrostatic Mineral Separation. Fraas, Ralston....1028–30
(Electronics) Electrostatic Sources of Ionizing Energy. Trump....1021–7
(Electronics) Progress Report of the AIEE Magnetic Amplifier Subcommittee. (Committee Report)....445–9; disc. 449
(Electronics) Steady-State Analysis of Self-Saturating Magnetic Amplifiers Based on Linear Approximations of the Magnetization Curve. Esselman....451–9
Electrostatic Mineral Separation, Distribution of Charge in. Fraas, Ralston....1028–30
Electrostatic Sources of Ionizing Energy. Trump....1021–7
Element, Differential Analyzer Study of Harmonic Power Generation with Nonlinear Impedance. Russell, Peterson.... 917–20
Elements of Pressure, Temperature, and Humidity, Piezoelectric Crystals as Sensing. Roberts, Goldsmith....968–72
Eleven Year Operating Record—Rural Line Sectionalizing by Repeater Fuses. Schahfer, Strout...680–6
Endurance Studies on Mica Insulation for Electric Machinery, Alternating and Direct Voltage. Moses....763–8; disc. 768
Energy, Electrostatic Sources of Ionizing. Trump....1021–7
Engineering Approach to Control Room Lighting, An. Dzwonczyk....852–7; disc. 857
Equipment, A New Lightweight Rapid Transit Control. Lichtenfels, Moore....224–6
Equipment, A-C Multiple-Unit Car Control. O'Kelly....652–6
Equipment and Performance of Lightweight Rapid Transit Cars, Electric. Ellis, Sloman....227–30; disc. 230
Equipment for Industrial Applications, 940–960 Megacycle Communications. Gunter....807–12
Equipment for Multiple-Unit Cars, Selection of. Hutchison....640–3; disc. 643
Equipments?, Why 4-Motor Multiple-Unit Car. Williamson....240–2
Equivalent Circuits and Their Application in Designing Shaded Pole Motors. Chang....690–8; disc. 698
Evaluation of Fluorescent Lamp Ballasts, Noise. Hayes, Gould....573–9
Exciter for Synchronous Alternators, Static Magnetic. Storm....1014 17
Expansion Effects in Power Cables, Thermal. Schifreen....160–8; disc. 168
Experimental Study of Induction Machine End-Turn Leakage Reactance, An. Barnes..671–7; disc. 677
Experimental Work, The Torsional Damper for Conductors—Service Experience and Further. Burgess, Hogg....1031–3

F

Factor in Synchronous Machines, Telephone Influence. Oscarson, Benson....743–8
Factor Meter, A Hook-On Power. Corson, Nylander....468–72
Factors Affecting Minimum Surface Leakage Distances in D-C Power Systems. Hart, Rosenberry, McClinton....738–42
Fault Control, Power System. (Committee Report)....410–17
Fault Locator, The Linascope Transmission Line. Kidd....1008 13
Fault Transients in Aircraft D-C Systems. Scorgie....713–20; disc. 720
Faults in Large High-Voltage Turbine Generators, Detection of Turn-to-Turn. Sexton, Alke....270–3; disc. 273
Faults on Electric Transit Systems, D-C Power Supplies and Isolation of. Watkins, Reagan.
Part I. D-C Power Supply....537–42; disc. 542
Part II. Isolation of D-C Faults...543–50; disc. 550
Feedback Controllers, The Effects of Loads and Disturbances upon. Jones....460–4
Feedback Systems, A Note on the Design of Conditionally Stable. Travers....626–30
Feeder Voltages, An Analysis of Grounding Banks to Balance Distribution. Long....823–7
Feeders, Group Regulation of Urban 4-Kv. Grim, Peck....551–6
Field and Laboratory—500-Kv Test Project of the American Gas and Electric Company, Radio Influence Tests in. Lippert, Pakala, Bartlett, Fahrnkopf....251–65; disc. 265
500-Kv Test Project of the American Gas and Electric Company, Corona Investigation on Extra-High-Voltage Lines—. Gross, Wagner, Naef, Tremaine....75–91; disc. 91
500-Kv Test Project of the American Gas and Electric Company, Line Insulator Loss Under Normal Conditions—. Naef, Tremaine, Jones....1073–8
500-Kv Test Project of the American Gas and Electric Company, Radio Influence Tests in Field and Laboratory—. Lippert, Pakala, Bartlett, Fahrnkopf....251–65; disc. 265
500-Kv Test Project of the American Gas and Electric Company, Techniques of Corona Loss Measurement and Analysis—. Naef, Tremaine, Jones....496–505; disc. 505
Flicker, Effect of the Duration of Voltage Dip on Cyclic Light. Brieger....894–8; disc. 899
Flicker, The Application of a Series Capacitor to a Synchronous Condenser for Reducing Voltage. Black, Lischer....144–50
Flow, An Electromagnetic Induction Method of Measuring Oscillating Fluid. Morris, Chadwick....346–50
Flow, Contact Resistance—The Contribution of Nonuniform Current. Kouwenhoven, Sackett..791–5
Flow in New Lightning Arresters, Spiral Arc Chokes Power. Ackermann, DeVal....995–8
Fluid Flow, An Electromagnetic Induction Method of Measuring Oscillating. Morris, Chadwick..346–50
Fluorescent Lamp Ballasts, Noise Evaluation of. Hayes, Gould....573–9
Flux Distributions with Saturation, Calculation of. Poritsky....309–19; disc. 319
Form Transformer Winding, Improved Core. Grimmer, Teague....962–5; disc. 965
Four-Motor Multiple-Unit Car Equipments?, Why. Williamson....240–2
Four- or Two-Channel Time-Division-Multiplex Telegraph System for Long-Distance Radio Circuits. Peterman, Minc.... 362–72
Fourier Series, and Impulse Functions for Rectangular Co-ordinate Systems, Tables of Green's Functions. Smith....22–30
Frames, Transient Analysis of Rotating Machines and Stationary Networks by Means of Rotating Reference. Ku....943–54; disc. 954
Frequency-Changer Welders, Ignitrons for. Rottier....900–07
Frequency Compensation of A-C Instruments. Miller....217–20; disc. 220
Frequency-Modulation Telegraph Network, A Nationwide. Bramhall, Smith....373–8; disc. 378
Frequency-Shift System for Use with Differential Protection of Transformer Banks, A New Carrier-Current. Beckwith....832–5; disc. 835
Frequency Signaling System for Supervision and Dialing over Long-Distance Telephone Trunks, Single-. Newell, Weaver....489–95
Frog-Leg Windings of D-C Machines, Rules for Designing. Dwight, Haltmaier....707–11; disc. 711
Functions, Fourier Series, and Impulse Functions for Rectangular Co-ordinate Systems, Tables of Green's. Smith....22–30
Functions, Loci of Complex Impedance and Admittance. Michaels....299–303
Fundamental Effects of Series Capacitors in High-Voltage Transmission Lines. Johnson, Barkle, Povejsil....526–35; disc. 535

Fuses, 11-Year Operating Record—Rural Line Sectionalizing by Repeater. Schahfer, Strout..680–6
Fuses for Resistance Welding Machines, Selection of. Stadum..796–9

G

Gaps on Humidity and Time, Dependence of Direct Sparkover Voltage of. Jacob, Sommerman..921–4; disc. 924
Gas-Filled Cable, Washington, D. C., 69-Kv Medium-Pressure. Clark..418–21; disc. 421
Gas Tube Inverter with the Supply Voltage Below the Breakdown Voltage, A. Cage, Schuder..908–12
Gas Welding Arcs, New Electrodes for Stabilizing Inert-. Cobine, Gallagher..804–06
Gating for Parallel Computers, A Method of. Ratz, Smith..510–16
Generalized Transmission Matrix Stability Criterion, The. Honnell..292–6; disc. 296
Generation with Nonlinear Impedance Element, Differential Analyzer Study of Harmonic Power. Russell, Peterson..917–20
Generator Rotors, Modern Practice in the Balancing of Large Turbine-. Laffoon, Hagg, Janthey, Heller..593–8; disc. 598
Generator Standby Reserve Requirements, Determination of. Strandrud..179–87; disc. 187
Generator Stator Windings, A New High-Voltage Insulation for Turbine-. Laffoon, Hill, Moses, Berberich..721–6; disc. 726
Generator Stators, The Use of Preferred Orientation Strip Steel in Turbine-. Apperson, Fontaine..836–9; disc. 839
Generators, Detection of Turn-to-Turn Faults in Large High-Voltage Turbine. Sexton, Alke..270–3; disc. 273
Generators, Progress in the Development of Large Turbine. Huntley, Taylor..580–9; disc. 589
Generators, Relay Protection of A-C. (Committee Report)..275–81; disc. 281
Geometric Mean Distances of Angle-Shaped Conductors. Magnusson..121–3
Graphical Methods for A-C Servomechanisms, Network Synthesis by. Bjornson..619–25
Green's Functions, Fourier Series, and Impulse Functions for Rectangular Co-ordinate Systems, Tables of. Smith..22–30
Ground on an Isolated Delta System, Neutral Inversion of a Single Potential Transformer Connected Line-to-. Gleason..103–10; disc. 110
Grounding Banks to Balance Distribution Feeder Voltages, An Analysis of. Long..823–7
Grounding in Power Systems in the United States, Application of Resonant. Gross, Atherton..389–93; disc. 393
Group Regulation of Urban 4-Kv Feeders. Grim, Peck..551–6

H

Hand Closing of Magnetic Power Air Circuit Breakers, A Spring Mechanism for. Dickinson, Findley..189–92; disc. 192
Harmonic Power Generation with Nonlinear Impedance Element, Differential Analyzer Study of. Russell, Peterson..917–20
Heat-Transfer Data in Electron Tube Operation, Basic. Buckland..1079–85
Heating, Electric Home. Parks..828–31
Hemispherical Radiometers, Total. Gier, Dunkel..339–43; disc. 343
Heterodyne Oscillators, A Servo System for. Slonczewski..1070–2
High-Voltage Insulation for Turbine-Generator Stator Windings, A New. Laffoon, Hill, Moses, Berberich..721–6; disc. 726
High-Voltage Lines—500-Kv Test Project of the American Gas and Electric Company, Corona Investigation on Extra-. Gross, Wagner, Naef, Tremaine..75–91; disc. 91
High-Voltage Shunt Capacitor Banks, Switching. Funkhouser, VanSickle, Shankle..129–33; disc. 134
High-Voltage Transmission Lines, Fundamental Effects of Series Capacitors in. Johnson, Barkle, Povejsil..526–35; disc. 535
High-Voltage Transmission, System Economics of Extra-. St. Clair, Peterson..841–8; disc. 848
High-Voltage Transmission System of the American Gas and Electric Company, The 300–316 Kv Extra-. Sporn, Peterson, Gross, St. Clair..64–72; disc. 72
High-Voltage Turbine Generators, Detection of Turn-to-Turn Faults in Large. Sexton, Alke..270–3; disc. 273
Highway Mobile Telephone System, Operational Study of a. Dorff..31–7
Home Heating, Electric. Parks..828–31
Hook-On Power Factor Meter, A. Corson, Nylander..468–72
Humidity and Time, Dependence of Direct Sparkover Voltage of Gaps on. Jacob, Sommerman..921–4; disc. 924
Humidity, Piezoelectric Crystals as Sensing Elements of Pressure, Temperature, and. Roberts, Goldsmith..968–72

I

Ice Testing and Its Influence Upon Switch Design. Heberlein, Field..37–42; disc. 42
Ignitron, Development of a Pumpless. Herskind, Remscheid..1066–9
Ignitron Rectifiers for Urban Transit Power Supply, Sealed. Borst..770–4
Ignitrons for Frequency-Changer Welders. Rottier..900–07
Impedance and Admittance Functions, Loci of Complex. Michaels..299–303
Impedance Element, Differential Analyzer Study of Harmonic Power Generation with Nonlinear. Russell, Peterson..917–20
Impedance for Maximum Efficency, Transmission Line Load. Lutz..283–5
Impedance or Transfer Admittance Remains Constant as Load Varies, Networks for Which Magnitude or Phase Angle of Input. Berkowitz..286–91
Impedances of Machine Conductors, Circuit Analysis Method for Determination of A-C. Babb, Williams..661–5; disc. 665
Impregnated Paper Insulation, Radial and Tangential Stresses in. Whitehead..56–9; disc. 59
Improved Core Form Transformer Winding. Grimmer, Teague..962–5; disc. 965
Improvements in Transformer-Loss Compensators for Watthour and Var-hour Meters. Schleicher..973–7
Impulse Functions for Rectangular Co-ordinate Systems, Tables of Green's Functions, Fourier Series, and. Smith..22–30
Induction Machine End-Turn Leakage Reactance, An Experimental Study of. Barnes..671–7; disc. 677
Induction Method of Measuring Oscillating Fluid Flow, An Electromagnetic. Morris, Chadwick..346–50
Induction Motor, A Contribution to the Theory of the Deep-Bar. Douglas..862–6
Induction Motor Performance, A Simplified Method for Predicting. Webking..667–70; disc. 671
Induction Motors, Transient Response of Small 2-Phase. Hopkin..881–6
Inductive Co-ordination Aspects of D-C Systems Supplied by Rectifiers. (Committee Report)..1034–54
Industrial Applications, 940–960 Megacycle Communications Equipment for. Gunter..807–12
(Industrial Control) An Electronic Power Source for Large D-C Contact Testing. Pettit..320–2
Inert-Gas Welding Arcs, New Electrodes for Stabilizing. Cobine, Gallagher..804–06
Influence Factor in Synchronous Machines, Telephone. Oscarson, Benson..743–8
Influence Tests in Field and Laboratory—500-Kv Test Project of the American Gas and Electric Company, Radio. Lippert, Pakala, Bartlett, Fahrnkopf..251–65; disc. 265
Input Impedance or Transfer Admittance Remains Constant as Load Varies, Networks for Which Magnitude or Phase Angle of. Berkowitz..286–91
Input-Output System of the EDVAC, The. Snyder..507–09
Inrush Current, Transformer Magnetizing. Specht..323–7; disc. 327
Inspection Program for Large Rotating Machines, A Maintenance. Johnson..749–54; disc. 755
Installations, Acoustic Models of Transformer. Gettys, Conover..333–6; disc. 336
Instantaneous Variations in Angular Velocity, A Tachometer for Measurement of. Bartles..1105–02
(Instruments) A Servo System for Heterodyne Oscillators. Slonczewski..1070–2
(Instruments) An Electromechanical Transducer. Engelberger, Kretsch..213–16
Instruments, Frequency Compensation of A-C. Miller..217–20; disc. 220
(Instruments) Marking of Varmeters. (Committee Report)..12–14; disc. 14
(Instruments) Results of a Questionnaire Covering Current Practices in Electrical Tests on Dielectrics in the Field. (Committee Report)..986–9
(Insulated Conductors) Lead-Alloy Sheaths for Underground Power Cable. Halperin, Betzer..423–9; disc. 429
(Insulated Conductors) 69-Kv Medium-Pressure Gas-Filled Cable, Washington, D. C. Clark..418–21; disc. 421
(Insulated Conductors) Thermal Expansion Effects in Power Cables. Schifreen..160–8; disc. 168
(Insulated Conductors) Thermal Transients on Buried Cables. Buller..45–52; disc. 52, 1107
Insulating Material in Nitrogen, Aging of Class-B. Stewart, Whitman..436–7; disc. 437
Insulation by Temperatures, Deterioration of Transformer Oil and Paper. Vogel, Petersen, Matsch..18–20, disc. 21
Insulation for Electric Machinery, Alternating and Direct Voltage Endurance Studies on Mica. Moses..763–8; disc. 768
Insulation for Turbine-Generator Stator Windings, A New High-Voltage. Laffoon, Hill, Moses, Berberich..721–6; disc. 726
Insulation, Radial and Tangential Stresses in Impregnated Paper. Whitehead..56–9; disc. 59
Insulation Tester for D-C Armatures, Winding. Catlin, Rohats..465–8
Insulation Testing of Synchronous Machines, Routine. Hunt, Vivian..756–62
Insulator Loss Under Normal Conditions—500-Kv Test Project of the American Gas and Electric Company, Line. Naef, Tremaine, Jones..1073–8
Interconnections, Determination of Reserve Capacity by the Probability Method Effect of. Calabrese..1018–20
Interference Between Resistance Welders, Probabilities of. Boice..775–83
Interruption Testing of Lightning Arresters, The Power. Ackermann..1–5; disc. 5
Inversion of a Single Potential Transformer Connected Line-to-Ground on an Isolated Delta System, Neutral. Gleason..103–10; disc. 110
Inverter with Resistive Load, Analysis of a 3-Phase. Turkington..1074–81
Inverter with the Supply Voltage Below the Breakdown Voltage, A Gas Tube. Cage, Schuder..908–12
Investigation of Audio Noise in Substation Type Transformers, An. Vivian, Peck..328–31; disc. 331
Investigation on Extra-High-Voltage Lines—500-Kv Test Project of the American Gas and Electric Company, Corona. Gross, Wagner, Naef, Tremaine..75–91; disc. 91
Ionizing Energy, Electrostatic Sources of. Trump..1071–4
Isolation of Faults on Electric Transit Systems, D-C Power Supplies and. Watkins, Reagan:
Part I. D-C Power Supply..537–42; disc. 542
Part II. Isolation of D-C Faults..543–50; disc. 550

L

Laboratory—500-Kv Test Project of the American Gas and Electric Company, Radio Influence Tests in Field and. Lippert, Pakala, Bartlett, Fahrnkopf..251–65; disc. 265
Lamp Ballasts, Noise Evaluation of Fluorescent. Hayes, Gould..573–9
(Land Transportation) A Modern Cab Signaling and Train Control System for Railroads. Allison..232–8; disc. 238
(Land Transportation) A New Lightweight Rapid Transit Control Equipment. Lichtenfels, Moore..224–6
(Land Transportation) A New Lightweight Rapid Transit Motor. Pettersen..222–3
(Land Transportation) A New Multiple-Unit Car Motor for the Pennsylvania Railroad. Jungk..243–5; disc. 245
(Land Transportation) A New Train Performance Calculator. Smith..657–60
(Land Transportation) A-C Multiple-Unit Car Control Equipment. O'Kelly..639–46
(Land Transportation) A-C Multiple-Unit Car Motor. Kreitler..648–50; disc. 650
(Land Transportation) Economics of Trolley Coach Power Supply. McDonald, Price..687–9
(Land Transportation) Electric Equipment and Performance of Lightweight Rapid Transit Cars. Ellis, Sloman..227–30; disc. 230
(Land Transportation) New A-C Multiple-Car Control for the Pennsylvania Railroad. Newhouse..645–7; disc. 647
(Land Transportation) Regeneration With a Mercury Arc Rectifier on the Central Railway of Brazil. Schmidt..1092–6
(Land Transportation) Why 4-Motor Multiple-Unit Car Equipments? Williamson..240–2
Lead-Alloy Sheaths for Underground Power Cable. Halperin, Betzer..423–9; disc. 429
Leakage Distances in D-C Power Systems, Factors Affecting Minimum Surface. Hart, Rosenberry, McClinton..738–42
Leakage Reactance, An Experimental Study of Induction Machine End-Turn. Barnes..671–7; disc. 677
Light Flicker, Effect of the Duration of Voltage Dip on Cyclic. Brieger..894–8; disc. 899
Lighting, An Engineering Approach to Control Room. Dzwonczyk..852–7; disc. 857
Lightning Arrester Protective Characteristics and Location upon Station Apparatus Protection, Some Effects of. Kalb..379–83; disc. 383
Lightning Arresters, Spiral Arc Chokes Power Flow in New. Ackermann, DeVal..995–8
Lightning Arresters, The Power Interruption Testing of. Ackermann..1–5; disc. 5

Lightning Incidence Is High, Protection of Transmission Lines Over Mountainous Region Where. Housley, Harper....124–6; disc. 126
Lightweight Rapid Transit Cars, Electric Equipment and Performance of. Ellis, Sloman....227–30; disc. 230
Lightweight Rapid Transit Control Equipment, A New. Lichtenfels, Moore....224–6
Lightweight Rapid Transit Motor, A New. Pettersen....222–3
Limiter for Use with Electronic Analogue Computers, A Diode Bridge. Medkeff, Parent....913–16
Linascope Transmission Line Fault Locator, The. Kidd....1008–13
Line Carrier Relaying System, Measurements and Tests on a Power. Miller, Worthington....1005–07
Line Constants, A Per-Unit Interpretation of Transmission. Povejsil, Johnson....194–200; disc. 200
Line Fault Locator, The Linascope Transmission. Kidd....1008–13
Line Insulator Loss Under Normal Conditions—500-Kv Test Project of the American Gas and Electric Company. Naef, Tremaine, Jones....1073–8
Line Load Impedance for Maximum Efficiency, Transmission. Lutz....283–5
Line Sectionalizing by Repeater Fuses, 11-Year Operating Record—Rural. Schahfer, Strout....680–6
Linear Accelerators, Dielectric Loading for Waveguide. Flesher, Cohn....887–93
Linear Approximations of the Magnetization Curve, Steady-State Analysis of Self-Saturating Magnetic Amplifiers Based on. Esselman....451–9
Lines—500-Kv Test Project of the American Gas and Electric Company, Corona Investigation on Extra-High-Voltage. Gross, Wagner, Naef, Tremaine....75–91; disc. 91
Lines, Fundamental Effects of Series Capacitors in High-Voltage Transmission. Johnson, Barkle, Povejsil....526–35; disc. 535
Lines Over Mountainous Region Where Lightning Incidence Is High, Protection of Transmission. Housley, Harper....124–6; disc. 126
Lines, Welding Calculations—Effect of Conductor Configuration in Overhead. Tietze....784–6
Load, Analysis of a 3-Phase Inverter with Resistive. Turkington....1059–61
Load Impedance for Maximum Efficiency, Transmission Line. Lutz....283–5
Load, Transient Response of Saturable Reactors with Resistive. Storm....95–102
Load Varies, Networks for Which Magnitude or Phase Angle of Input Impedance or Transfer Admittance Remains Constant as. Berkowitz....286–91
Loading for Waveguide Linear Accelerators, Dielectric. Flesher, Cohn....887–93
Loads and Disturbances upon Feedback Controllers, The Effects of. Jones....460–4
Locator, The Linascope Transmission Line Fault. Kidd....1008–13
Loci of Complex Impedance and Admittance Functions. Michaels....299–305
Long-Distance Radio Circuits, Four- or Two-Channel Time-Division-Multiplex Telegraph System for. Peterman, Minc....362–72
Long-Distance Telephone Trunks, Single-Frequency Signaling System for Supervision and Dialing over. Newell, Weaver....489–95
Loss Compensators for Watt-hour and Var-hour Meters, Improvements in Transformer-. Schleicher....973–7
Loss Measurement and Analysis—500-Kv Test Project of the American Gas and Electric Company, Techniques of Corona. Naef, Tremaine, Jones....496–505; disc. 505
Loss Under Normal Conditions—500-Kv Test Project of the American Gas and Electric Company, Line Insulator. Naef, Tremaine, Jones....1073–8

M

Machine Conductors, Circuit Analysis Method for Determination of A-C Impedances of. Babb, Williams....661–5; disc. 665
Machine Damping and Synchronizing Torques, Synchronous. Concordia....731–7
Machine End-Turn Leakage Reactance, An Experimental Study of Induction. Barnes....671–7; disc. 677
Machine Parameters, Measurement of D-C. Saunders....700–05; disc. 705
Machinery, Alternating and Direct Voltage Endurance Studies on Mica Insulation for Electric. Moses....763–8; disc. 768
Machines, A Maintenance Inspection Program for Large Rotating. Johnson....749–54; disc. 755
Machines and Stationary Networks by Means of Rotating Reference Frames, Transient Analysis of Rotating. Ku....943–54; disc. 954
Machines, Routine Insulation Testing of Synchronous Hunt, Vivian....756–62
Machines, Rules for Designing Frog-Leg Windings of D-C. Dwight, Haltmaier....707–11; disc. 711
Machines, Selection of Fuses for Resistance Welding. Stadum....796–9
Machines, Telephone Influence Factor in Synchronous. Oscarson, Benson....43–8
Magnetic Amplifier Subcommittee, Progress Report of the AIEE. (Committee Report)....445–9; disc. 449
Magnetic Amplifiers Based on Linear Approximations of the Magnetization Curve, Steady-State Analysis of Self-Saturating. Esselman....451–9
Magnetic Amplifiers—Cases of Negligible Commutation, The Transient Response of. Finzi, Chandler, Beaumariage....934–42; disc. 942
Magnetic Exciter for Synchronous Alternators, Static. Storm....1014–17
Magnetic Power Air Circuit Breakers, A Spring Mechanism for Hand Closing of. Dickinson, Findley....189–92; disc. 192
Magnetizing Inrush Current, Transformer. Specht....323–7; disc. 327
Magnitude or Phase Angle of Input Impedance or Transfer Admittance Remains Constant as Load Varies, Networks for Which. Berkowitz....286–91
Maintenance Inspection Program for Large Rotating Machines, A. Johnson....749–54; disc. 755
Manual and Automatic Devices, Switching of Distribution Capacitors by. Hopkins, Schultz....138–43
Marking of Varmeters. (Committee Report)....12–14; disc. 14
Material in Nitrogen, Aging of Class-B Insulating. Stewart, Whitman....436–7; disc. 437
Matrix Stability Criterion, The Generalized Transmission. Hornell....292–6; disc. 296
Maximum Efficiency, Transmission Line Load Impedance for. Lutz....283–5
Mean Distances of Angle-Shaped Conductors, Geometric. Magnuson....121–3
Measurement and Analysis—500-Kv Test Project of the American Gas and Electric Company, Techniques of Corona Loss. Naef, Tremaine, Jones....496–505; disc. 505
Measurement of D-C Machine Parameters. Saunders....700–05; disc. 705
Measurement of Instantaneous Variations in Angular Velocity, A Tachometer for. Bartles....1102–05
(Measurements) A Hook-On Power Factor Meter. Corson, Nylander....468–72
Measurements and Tests on a Power Line Carrier Relaying System. Miller, Worthington....1005–07
Measurements of Resistance, Three-Phase. Matsch, Bass, Horcher....350–2; disc. 352
(Measurements) Total Hemispherical Radiometers. Gier, Dunkle....339–43; disc. 343
Measuring Oscillating Fluid Flow, An Electromagnetic Induction Method of. Morris, Chadwick....346–50
Mechanical Rectifiers, Commutating Reactor Control for. Diebold....1062–5
Mechanism for Hand Closing of Magnetic Power Air Circuit Breakers, A Spring. Dickinson, Findley....189–92; disc. 192
Mechanism of Low and High Current Arcs and Their Relation to the Welding Arc, The Physical. Finkelnburg....899–903
Megacycle Communications Equipment for Industrial Applications, 940–960. Gunter....807–12
Mercury Arc Rectifier on the Central Railway of Brazil, Regeneration with a. Schmidt....1092–6
Meter, A Hook-On Power Factor. Corson, Nylander....468–72
Meters, Improvements in Transformer-Loss Compensators for Watt-hour and Var-hour. Schleicher....973–7
Method Effect of Interconnections, Determination of Reserve Capacity by the Probability. Calabrese....1018–20
Method for Determination of A-C Impedances of Machine Conductors, Circuit Analysis. Babb, Williams....661–5; disc. 665
Method for Polyphase Reluctance Synchronous Motors, A Design. Crouse....957–62
Method for Predicting Induction Motor Performance, A Simplified. Webking....667–70; disc. 671
Method for Treating Electron Tubes When Used as Oscillators in the Free as Well as in the Synchronized States, A New. Mostafa, Bey....999–1004
Method of Gating for Parallel Computers, A. Rutz, Smith....510–16
Method of Measuring Oscillating Fluid Flow, An Electromagnetic Induction. Morris, Chadwick....346–50
Methods for A-C Servomechanisms, Network Synthesis by Graphical. Bjornson....619–25
Mica Insulation for Electric Machinery, Alternating and Direct Voltage Endurance Studies on. Moses....763–8; disc. 768
Microwave Channels, Application of. Check....813–17
Mineral Separation, Distribution of Charge in Electrostatic. Franz, Ralston....1026–30
Mobile Telephone System, Operational Study of a Highway. Dorfi....31–7
Models of Transformer Installations, Acoustic. Gerrys, Conover....333–6; disc. 336
Modern Cab Signaling and Train Control System for Railroads. Allison....232–8; disc. 238
Modern Practice in the Balancing of Large Turbine Generator Rotors. Lathan, Hagg, Janthey, Heller....593–8; disc. 598
Modulation Telegraph Network, A Nationwide Frequency. Bramhall, Smith....[illegible]
Modulation Telemetering Systems for Rocket Application, Pulse-Time. Mengel....599–605
Motor, A Contribution to the Theory of the Deep Bar Induction. Domke....[illegible]
Motor, A New Lightweight Rapid Transit. Pettersen....[illegible]
Motor, A-C Multiple-Unit Car. Kreith....648–50; disc. 650
Motor for the Pennsylvania Railroad, A New Multiple Unit Car. Jungk....343–5; disc. 345
Motor Multiple-Unit Car Equipments?, Why Four. Williamson....340–2
Motor Performance, A Simplified Method for Predicting Induction. Webking....667–70; disc. 671
Motors, A Design Method for Polyphase Reluctance Synchronous. Crouse....[illegible]
Motors, Commutation in Universal-Type. Packer....170–6; disc. 176
Motors, Equivalent Circuits and Their Application in Designing Shaded-Pole. Chang....690–8; disc. 698
Motors, Split-Winding Starting of 3-Phase. Alger, Ward, Wright....867–73; disc. 872
Motors, Transient Response of Small Servo. Hopkin....881–6
Mountainous Region Where Lightning Incidence Is High, Protection of Transmission Lines Over. Housley, Harper....124–6; disc. 126
Multiple-Car Control for the Pennsylvania Railroad, New A-C. Newhouse....645–7; disc. 647
Multiple-Car Control Equipment for [illegible]....[illegible]
Multiple-Unit Car Equipments?, Why 4 Motor. Williamson....[illegible]
Multiple-Unit Car Motor, A-C. Lemke....648–50; disc. 650
Multiple-Unit Car Motor for the Pennsylvania Railroad, A New. Jungk....343–5; disc. 345
Multiple-Unit Cars, Selection of Equipment for. Hutchison....640–3; disc. 643
Multiplex Telegraph Set, An Electronic Time-Division. Hansen, Slayton....354–61; disc. 361
Multiplex Telegraph System for Long-Distance Radio Circuits, Four- or Two-Channel Time-Division. Peterman, Minc....362–72

N

Nationwide Frequency-Modulation Telegraph Network, A. Bramhall, Smith....373–8; disc. 378
Network, A Nationwide Frequency-Modulation Telegraph. Bramhall, Smith....373–8; disc. 378
Network Synthesis by Graphical Methods for A-C Servomechanisms. Bjornson....[illegible]
Networks by Means of Rotating Reference Frames, Transient Analysis of Rotating Machines and Stationary. Ku....943–54; disc. 954
Networks for A-C Servomechanisms, Effects of Carrier Shifts on Derivative. Attina....612–18
Networks for Which Magnitude or Phase Angle of Input Impedance or Transfer Admittance Remains Constant as Load Varies. Berkowitz....286–91
Neutral Inversion of a Single Potential Transformer Connected Line-to-Ground on an Isolated Delta System. Gleason....105–10; disc. 110
New Lightweight Rapid Transit Control Equipment, A. Lichtenfels, Moore....224–6
New Lightweight Rapid Transit Motor, A. Pettersen....222–3
New 69-Kv Air Blast Circuit Breaker, A. Shores, Beatty....202–07; disc. 207
Nitrogen, Aging of Class-B Insulating Material in. Stewart, Whitman....436–7; disc. 437
Noise Evaluation of Fluorescent Lamp Ballasts. Hayes, Combs....[illegible]
Noise in Substation-Type Transformers, An Investigation of Audio. Vivian, Peck....328–41; disc. 341
Nonlinear Impedance Element Differential Analyzer Study of Harmonic Power Generation with. Russell, Peterson....917–20
Nonuniform Current Line Current Responses, The Contribution of. Kuwanoboshi, Sackett....791–5
Note on the Design of Conditionally Stable Feedback Systems, A. Travers....626–30
(Nuclemeters) Dielectric Loading for Waveguide Linear Accelerators. Flesher, Cohn....887–93

O

Oil and Paper Insulation by Temperatures, Deterioration of Transformer. Vogel, Peterson, Matsch....18–20; disc. 21
Operating Record—Rural Line Sectionalizing by Repeater Fuses, 11-Year. Schahfer, Strout....680–6
Operation, Basic Heat-Transfer Data in Electron Tube. Buchanan....[illegible]

Operational Study of a Highway Mobile Telephone System. Dorff....31-7
Orientation Strip Steel in Turbine-Generator Stators, The Use of Preferred. Apperson, Fontaine....836-9; disc. 839
Oscillating Fluid Flow, An Electromagnetic Induction Method of Measuring. Morris, Chadwick....346-50
Oscillators, A Servo System for Heterodyne. Slonczewski....1070-2
Oscillators in the Free as Well as in the Synchronized States, A New Method for Treating Electron Tubes When Used as. Mostafa, Bey....999-1004
Output Analysis and Alignment Techniques for Phase-Rotation Single Side-Band Transmitters. Whitby, Schenck....209-12
Output System of the FDVAC, The Input. Snyder....507-09
Overhead Lines, Welding Calculations Effect of Conductor Configuration in. Tietze....784-6

P

Paper Insulation by Temperatures, Deterioration of Transformer Oil and. Vogel, Petersen, Matsch....18-20; disc. 21
Paper Insulation, Radial and Tangential Stresses in Impregnated. Whitehead....56-9; disc. 59
Parallel Computers, A Method of Gating for. Ratz, Smith....510-16
Parameters, Measurement of D-C Machine. Saunders....700-6; disc. 706
Pennsylvania Railroad, A New Multiple-Unit Car Motor for the. Jungk....243-5; disc. 245
Pennsylvania Railroad, New A-C Multiple-Car Control for the. Newhouse....645-7; disc. 647
Per-Unit Interpretation of Transmission Line Constants, A. Povejsil, Johnson....194-200; disc. 200
Performance, A Simplified Method for Predicting Induction Motor. Webking....667-70; disc. 671
Performance Calculator, A New Train. Smith....657-60
Performance of Lightweight Rapid Transit Cars, Electric Equipment and. Ellis, Sloman....227-30; disc. 230
Phase Angle of Input Impedance or Transfer Admittance Remains Constant as Load Varies, Networks for Which Magnitude or. Berkowitz....286-91
Phase-Plane Approach to the Compensation of Saturating Servomechanisms, A. Hopkin....631-9
Phase-Rotation Single Side-Band Transmitters, Output Analysis and Alignment Techniques for. Whitby, Schenck....209-12
Phenomena, Capacitor Switching. VanSickle, Zaborszky....151-8; disc. 158
Phenomena Near Current Zero for an A-C Arc Adjacent to Refractory Surfaces, A Study of Conduction. Browne, Strom....398-407; disc. 407
Physical Mechanism of Low and High-Current Arcs, and Their Relation to the Welding Arc, The. Finkelnburg....800-03
Piezoelectric Crystals as Sensing Elements of Pressure, Temperature, and Humidity. Roberts, Goldsmith....968-72
Plane Approach to the Compensation of Saturating Servomechanisms, A Phase-. Hopkin....631-9
Pole Motors, Equivalent Circuits and Their Application in Designing Shaded. Chang....690-8; disc. 698
Polyphase Reluctance Synchronous Motors, A Design Method for. Crouse....957-62
Potential Transformer Connected Line-to-Ground on an Isolated Delta System, Neutral Inversion of a Single. Gleason....103-10; disc. 110
Power Air Circuit Breakers, A Spring Mechanism for Hand Closing of Magnetic. Dickinson, Findley....189-92; disc. 192
Power Cable, Lead-Alloy Sheaths for Underground. Halperin, Betzer....423-9; disc. 429
Power Cables, Thermal Expansion Effects in. Schifreen....160-8; disc. 168
Power Factor Meter, A Hook-On. Corson, Nylander....468-72
Power Flow in New Lightning Arresters, Spiral Arc Chokes. Ackermann, DeVal....995-8
(Power Generation) An Engineering Approach to Control Room Lighting. Dewonezyk....852-7; disc. 857
(Power Generation) Progress in the Development of Large Turbine Generators. Huntley, Taylor....580-9; disc. 589
Power Generation with Nonlinear Impedance Element, Differential Analyzer Study of Harmonic. Russell, Peterson....917-20
Power Interruption Testing of Lightning Arresters, The. Ackermann....1-5; disc. 5
Power Line Carrier Relaying System, Measurements and Tests on a. Miller, Worthington....1005-07
Power Source for Large D-C Contact Testing. An Electronic. Pettit....320-2
Power Supplies and Isolation of Faults on Electric Transit Systems, D-C. Watkins, Reagan:
Part I. D-C Power Supply....537-42; disc. 542
Part II. Isolation of D-C Faults....543-50; disc. 550
Power Supply, Economics of Trolley Coach. McDonald, Price....687-9
Power Supply, Sealed Ignitron Rectifiers for Urban Transit. Borst....770-4
Power Supply Study and New Rectifier Installation for the United Electric Railways of Providence. Whitman, Schaller....978-85; disc. 985
Power System, Choice of Telemetering Systems and Channels for a. Duff....1086-91
Power System Fault Control. (Committee Report)....410-17
Power Systems, Factors Affecting Minimum Surface Leakage Distances in D-C. Hart, Rosenberry, McClinton....748-52
Power Systems in the United States, Application of Resonant Grounding in. Gross, Atherton....389-93; disc. 393
Power Transformer Application, Economics of. Barkle, Witake....440-4; disc. 444
Practice in the Balancing of Large Turbine-Generator Rotors, Modern. Lattson, Hagg, Janthey, Heller....593-8; disc. 598
Preferred Orientation Strip Steel in Turbine-Generator Stators, The Use of. Apperson, Fontaine....836-9; disc. 839
Pressure Gas-Filled Cable, Washington, D. C., 69-Kv Medium-. Clark....418-21; disc. 421
Pressure, Temperature, and Humidity, Piezoelectric Crystals as Sensing Elements of. Roberts, Goldsmith....968-72
Private-Line Teletypewriter Switching System, A Full Automatic. Bacon, Lacke....473-80
Probabilities of Interference Between Resistance Welders. Boice....775-83
Probability Method Effect of Interconnections, Determination of Reserve Capacity by the. Calabrese....1018-20
Problems Associated with the Application of a Capacitor in Series with a Synchronous Condenser, Technical. Witzke, Michelson....519-25
Program for Large Rotating Machines, A Maintenance. Johnson....[illegible]; disc. 785
Progress in the Development of Large Turbine Generators. Huntley, Taylor....580-9; disc. 589
Progress Report of the AIEE Magnetic Amplifier Subcommittee. (Committee Report)....445-9; disc. 449
Project of the American Gas and Electric Company, Techniques of Corona Loss Measurement and Analysis—500-Kv Test. Nacf, Tremaine, Jones....496-505; disc. 505
Protection of A-C Generators, Relay. (Committee Report)....275-81; disc. 281
Protection of Transformer Banks, A New Carrier-Current Frequency-Shift System for Use with Differential. Beckwith....833-8; disc. 838
Protection of Transmission Lines Over Mountainous Region Where Lightning Incidence is High. Housley, Harper....124-6; disc. 126
Protection, Some Effects of Lightning Arrester Protective Characteristics and Location upon Station Apparatus. Kalb....379-83; disc. 383
Protective Characteristics and Location upon Station Apparatus Protection, Some Effects of Lightning Arrester. Kalb....379-83; disc. 383
(Protective Devices) Application of Resonant Grounding in Power Systems in the United States. Gross, Atherton....389-93; disc. 393
(Protective Devices) 11-Year Operating Record—Rural Line Sectionalising by Repeater Fuses. Schahfer, Strout....680-6
(Protective Devices) Power System Fault Control. (Committee Report)....410-17
(Protective Devices) Spiral Arc Chokes Power Flow in New Lightning Arresters. Ackermann, DeVal....995-8
Providence, Power Supply Study and New Rectifier Installation for the United Electric Railways of. Whitman, Schaller....978-85; disc. 985
Pulse-Time Modulation Telemetering Systems for Rocket Application. Mengel....599-605
Pumpless Ignitron, Development of a. Herskind, Rensheid....1066-9

Q

Questionnaire Covering Current Practices in Electrical Tests on Dielectrics in the Field, Results of a. (Committee Report)....986-9

R

Radial and Tangential Stresses in Impregnated Paper Insulation. Whitehead....56-9; disc. 59
Radio Circuits, Four- or Two-Channel Time-Division-Multiplex Telegraph System for Long-Distance. Peterman, Minc....362-72
Radio Influence Tests in Field and Laboratory—500-Kv Test Project of the American Gas and Electric Company. Lippert, Pakala, Bartlett, Fahrnkopf....251-65; disc. 265
(Radio) Operational Study of a Highway Mobile Telephone System. Dorff....31-7
Radiometers, Total Hemispherical. Gier, Dunkle....339-43; disc. 344
Railroad, New A-C Multiple-Car Control for the Pennsylvania. Newhouse....645-7; disc. 647
Railroads, A Modern Cab Signaling and Train Control System for. Allison....232-8; disc. 238
Railway of Brazil, Regeneration with a Mercury Arc Rectifier on the Central. Schmidt....1092-6
Railways of Providence, Power Supply Study and New Rectifier Installation for the United Electric. Whitman, Schaller....978-85; disc. 985
Rapid Transit Cars, Electric Equipment and Performance of Lightweight. Ellis, Sloman....227-30; disc. 230
Rapid Transit Control Equipment, A New Lightweight Lichtenfels, Moore....224-6
Rapid Transit Motor, A New Lightweight. Pettersen....222-4
Reactance, An Experimental Study of Induction Machine End-Turn Leakage. Barnes....671-7; disc. 677
Reactor Control, A-C Arc Welders with Saturable. Oestreicher....87-90
Reactor Control for Mechanical Rectifiers, Commutating. Diebold....1063-5
Reactors with Resistive Load, Transient Response of Saturable. Storm....95-102
Record—Rural Line Sectionalising by Repeater Fuses, 11-Year Operating. Schahfer, Strout....680-6
Rectangular Co-ordinate Systems, Tables of Green's Functions, Fourier Series, and Impulse Functions for. Smith....22-30
Rectifier Installation for the United Electric Railways of Providence, Power Supply Study and New. Whitman, Schaller....978-85; disc. 985
Rectifier on the Central Railway of Brazil, Regeneration with a Mercury Arc. Schmidt....1092-6
Rectifiers, Commutating Reactor Control for Mechanical. Diebold....1063-5
Rectifiers for Urban Transit Power Supply, Sealed Ignitron. Borst....770-4
Rectifiers, Inductive Co-ordination Aspects of D-C Systems Supplied by. (Committee Report)....1004-54
Reference Frames, Transient Analysis of Rotating Machines and Stationary Networks by Means of Rotating. Ku....944-54; disc. 954
Refractory Surfaces, A Study of Conduction Phenomena Near Current Zero for an A-C Arc Adjacent to. Browne, Strom....398-407; disc. 407
Regeneration with a Mercury Arc Rectifier on the Central Railway of Brazil. Schmidt....1092-6
Regulation of Urban 4-Kv Feeders, Group. Grim, Peck....551-6
Relay Literature-1947-1949, Bibliography of. (Committee Report)....247-50
Relay Protection of A-C Generators. (Committee Report)....275-81; disc. 281
Relaying System, Measurements and Tests on a Power Line Carrier. Miller, Worthington....1005-07
Reluctance Synchronous Motors, A Design Method for Polyphase. Crouse....957-62
Repeater Fuses, 11-Year Operating Record—Rural Line Sectionalizing by. Schahfer, Strout....680-6
Repeaters, A Submarine Telephone Cable with Submerged. Gilbert....564-72
Reperforator Switching, Automatic Trunk Selection by. Blanton....481-9
Report of the AIEE Magnetic Amplifier Subcommittee, Progress. (Committee Report)....445-9; disc. 449
Requirements, Determination of Generator Stand-by Reserve. Strandrud....179-87; disc. 187
Reserve Capacity by the Probability Method Effect of Interconnections, Determination of. Calabrese....1018-20
Reserve Requirements, Determination of Generator Stand-by. Strandrud....179-87; disc. 187
Resistance, The Contribution of Nonuniform Current Flow, Contact. Kouwenhoven, Sackett....791-8
Resistance, Three-Phase Measurements of. Matsch, Basu, Horchor....350-2; disc. 352
Resistance Welders, Probabilities of Interference Between. Boice....775-83
Resistance Welding Machines, Selection of Fuses for. Stadum....796-9
Resistive Load, Analysis of a 3-Phase Inverter with. Turkington....1055-61
Resistive Load, Transient Response of Saturable Reactors with. Storm....95-102
Resonant Grounding in Power Systems in the United States, Application of. Gross, Atherton....389-93; disc. 393
Response of Magnetic Amplifiers—Cases of Negligible Commutation, The Transient. Feiza, Chandler, Beaumariage....944-53; disc. 953
Response of Saturable Reactors with Resistive Load, Transient. Storm....95-102
Response of Small 2-Phase Induction Motors, Transient. Hopkin....884-6
Results of a Questionnaire Covering Current Practices in Electrical Tests on Dielectrics in the Field. (Committee Report)....986-9

Rocket Application, Pulse-Time Modulation Telemetering Systems for. Mengel.....599–605
Rod Waveguides, Shielded Dielectric-. Beam, Wachowski.....874–80
Room Lighting, An Engineering Approach to Control. Dzwonczyk.....852–7; disc. 857
(Rotating Machinery) A New High-Voltage Insulation for Turbine Generator Stator Windings. Laffoon, Hill, Moses, Berberich.....721–6; disc. 726
(Rotating Machinery) Aging of Class-B Insulating Material in Nitrogen. Stewart, Whitman.....436–7; disc. 437
Rotating Machines, A Maintenance Inspection Program for Large. Johnson.....749–54; disc. 755
Rotating Machines and Stationary Networks by Means of Rotating Reference Frames, Transient Analysis of. Ku.....943–54; disc. 954
Rotation Single Side-Band Transmitters, Output Analysis and Alignment Techniques for Phase-. Whitby, Scheuch.....209–12
Rotors, Modern Practice in the Balancing of Large Turbine-Generator. Laffoon, Hagg, Janthey, Heller.....593–8; disc. 598
Routine Insulation Testing of Synchronous Machines. Hunt, Vivian.....756–62
Rules for Designing Frog-Leg Windings of D-C Machines. Dwight, Haltmaier.....707–11; disc. 711
Rural Line Sectionalizing by Repeater Fuses, 11-Year Operating Record—. Schahfer, Strout.....680–6

S

Saturable Reactor Control, A-C Arc Welders with. Oestreicher.....787–90
Saturable Reactors with Resistive Load, Transient Response of. Storm.....95–102
Saturating Magnetic Amplifiers Based on Linear Approximations of the Magnetization Curve, Steady-State Analysis of Self-. Esselman.....451–9
Saturating Servomechanisms, A Phase-Plane Approach to the Compensation of. Hopkin.....631–9
Saturation, Calculation of Flux Distributions with. Poritsky.....309–19; disc. 319
Scale Computers, Systematization of Tube Surveillance in Large-. Spence.....516–19
Sealed Ignitron Rectifiers for Urban Transit Power Supply. Borst.....770–4
Sectionalizing by Repeater Fuses, 11-Year Operating Record—Rural Line. Schahfer, Strout.....680–6
Selection in Reperforator Switching, Automatic Trunk. Blanton.....481–9
Selection of Equipment for Multiple-Unit Cars. Hutchison.....640–3; disc. 643
Selection of Fuses for Resistance Welding Machines. Stadum.....796–9
Self-Saturating Magnetic Amplifiers Based on Linear Approximations of the Magnetization Curve, Steady-State Analysis of. Esselman.....451–9
Sensing Elements of Pressure, Temperature, and Humidity, Piezoelectric Crystals as. Roberts, Goldsmith.....968–72
Separation, Distribution of Charge in Electrostatic Mineral. Fraas, Ralston.....1028–30
Series, and Impulse Functions for Rectangular Coordinate Systems, Tables of Green's Functions, Fourier. Smith.....22–30
Series Capacitor to a Synchronous Condenser for Reducing Voltage Flicker, The Application of a. Black, Lischer.....144–50
Series Capacitors in High-Voltage Transmission Lines, Fundamental Effects of. Johnson, Barkle, Povejsil.....526–35; disc. 535
Series with a Synchronous Condenser, Technical Problems Associated with the Application of a Capacitor in. Witzke, Michelson.....519–25
Service Experience and Further Experimental Work, The Torsional Damper for Conductors—. Burgess, Hogg.....1031–5
Servo System for Heterodyne Oscillators, A. Sloczewski.....1070–2
Servomechanisms, A Phase-Plane Approach to the Compensation of Saturating. Hopkin.....631–9
Servomechanisms, Effects of Carrier Shifts on Derivative Networks for A-C. Attura.....612–18
Servomechanisms, Network Synthesis by Graphical Methods for A-C. Bjornson.....619–25
Shaded Pole Motors, Equivalent Circuits and Their Application in Designing. Chang.....690–8; disc. 698
Sheaths for Underground Power Cable, Lead-Alloy. Halperin, Betzer.....423–9; disc. 429
Shielded Dielectric-Rod Waveguides. Beam, Wachowski.....874–80
Shift System for Use with Differential Protection of Transformer Banks, A New Carrier-Current Frequency. Beckwith.....832–5; disc. 835
Shifts on Derivative Networks for A-C Servomechanisms, Effects of Carrier. Attura.....612–18
Shunt Capacitor Banks, Switching High-Voltage. Funkhouser, VanSickle, Shankle.....129–33; disc. 134
Shunt Capacitors at Transmission and Distribution Stations, Application of. Porter, Zimmerman.....112–18; disc. 118
Side-Band Transmitters, Output Analysis and Alignment Techniques for Phase-Rotation Single. Whitby, Scheuch.....209–12
Signal and Supervision Systems Used on Carrier Current Communications Circuits. Mayer.....990–4
Signaling and Train Control System for Railroads, A Modern Cab. Allison.....232–8; disc. 238
Signaling System for Supervision and Dialing over Long-Distance Telephone Trunks, Single-Frequency. Newell, Weaver.....489–95
Simplified Method for Predicting Induction Motor Performance, A. Wehking.....667–70; disc. 671
Single-Frequency Signaling System for Supervision and Dialing over Long-Distance Telephone Trunks. Newell, Weaver.....489–95
69-Kv Air Blast Circuit Breaker, A New. Shores, Beatty.....202–07; disc. 207
69-Kv Medium-Pressure Gas-Filled Cable, Washington, D. C. Clark.....418–21; disc. 421
Some Design Criteria for Automatic Controls. Nims.....606–11
Some Effects of Lightning Arrester Protective Characteristics and Location upon Station Apparatus Protection. Kalb.....379–83; disc. 383
Source for Large D-C Contact Testing, An Electronic Power. Petit.....520–2
Sources of Ionizing Energy, Electrostatic. Trump.....1021–7
Sparkover Voltage of Gaps on Humidity and Time, Dependence of Direct. Jacob, Sommerman.....921–4; disc. 924
Spiral Arc Chokes Power Flow in New Lightning Arresters. Ackermann, DeVal.....995–8
Split-Winding Starting of 3-Phase Motors. Alger, Ward, Wright.....867–72; disc. 872
Spring Mechanism for Hand Closing of Magnetic Power Air Circuit Breakers. Dickinson, Findley.....189–92; disc. 192
Stability Criterion, The Generalized Transmission Matrix. Honnell.....292–6; disc. 296
Stabilizing Inert-Gas Welding Arcs, New Electrodes for Cobine, Gallagher.....804–06
Stable Feedback Systems, A Note on the Design of Conditionally. Travers.....626–30
Stand-by Reserve Requirements, Determination of Generator. Strandrud.....179–87; disc. 187
Starting of 3-Phase Motors, Split-Winding. Alger, Ward, Wright.....867–72; disc. 872
State Analysis of Self-Saturating Magnetic Amplifiers Based on Linear Approximations of the Magnetization Curve, Steady-. Esselman.....451–9
States, A New Method for Treating Electron Tubes When Used as Oscillators in the Free as Well as in the Synchronized. Mostafa, Bey.....999–1004
Static Magnetic Exciter for Synchronous Alternators. Storm.....1014–17
Station Apparatus Protection, Some Effects of Lightning Arrester Protective Characteristics and Location upon. Kalb.....379–83; disc. 383
Stationary Networks by Means of Rotating Reference Frames, Transient Analysis of Rotating Machines and. Ku.....943–54; disc. 954
Stations, Application of Shunt Capacitors at Transmission and Distribution. Porter, Zimmerman.....112–18; disc. 118
Stator Windings, A New High-Voltage Insulation for Turbine-Generator. Laffoon, Hill, Moses, Berberich.....721–6; disc. 726
Stators, The Use of Preferred Orientation Strip Steel in Turbine-Generator. Apperson, Fontaine.....836–9; disc. 839
Steady-State Analysis of Self-Saturating Magnetic Amplifiers Based on Linear Approximations of the Magnetization Curve. Esselman.....451–9
Steel in Turbine-Generator Stators, The Use of Preferred Orientation Strip. Apperson, Fontaine.....836–9; disc. 839
Stresses in Impregnated Paper Insulation, Radial and Tangential. Whitehead.....56–9; disc. 59
Strip Steel in Turbine-Generator Stators, The Use of Preferred Orientation. Apperson, Fontaine.....836–9; disc. 839
Studies on Mica Insulation for Electric Machinery, Alternating and Direct Voltage Endurance. Moses.....763–8; disc. 768
Study of a Highway Mobile Telephone System, Operational. Dorff.....31–7
Study of Conduction Phenomena Near Current Zero for an A-C Arc Adjacent to Refractory Surfaces, A. Browne, Strom.....398–407; disc. 407
Study of Harmonic Power Generation with Nonlinear Impedance Element, Differential Analyzer. Russell, Peterson.....917–20
Study of Induction Machine End-Turn Leakage Reactance, An Experimental. Barnes.....671–7; disc. 677
Subareas, Calculation of the Capacitance of a Circular Annulus by the Method of. Higgins, Reitan.....926–31; disc. 931
Subcommittee, Progress Report of the AIEE Magnetic Amplifier. (Committee Report).....445–9; disc. 449
Submarine Telephone Cable with Submerged Repeaters, A. Gilbert.....564–72
Substation Type Transformers, An Investigation of Audio Noise in. Vivian, Peck.....328–31; disc. 331
(Substations) Group Regulation of Urban 4-Kv Feeders. Grim, Peck.....951–6
Supervision Systems Used on Carrier Current Communications Circuits, Signal and. Mayer.....990–4
Supervisory Control on a Carrier Communication Channel, Vibracode System of. Allen, Daniel.....818–22; disc. 822
Supervisory System for Distribution Circuits, Carrier Current. Podolsky, Lubin.....1096–1101
Supply, Economics of Trolley Coach Power. McDonald, Price.....687–9
Supply Study and New Rectifier Installation for the United Electric Railways of Providence, Power. Whitman, Schaller.....978–85; disc. 985
Supply Voltage Below the Breakdown Voltage, A Gas Tube Inverter with the. Cage, Schuder.....908–12
Surface Leakage Distances in D-C Power Systems, Factors Affecting Minimum. Hart, Rosenberry, McClinton.....738–42
Surfaces, A Study of Conduction Phenomena Near Current Zero for an A-C Arc Adjacent to Refractory. Browne, Strom.....398–407; disc. 407
Surveillance in Large-Scale Computers, Systematization of Tube. Spence.....516–19
Switch Design, Ice Testing and Its Influence Upon. Heberlein, Field.....37–42; disc. 42
(Switchgear) A New 69-Kv Air Blast Circuit Breaker. Shores, Beatty.....202–07; disc. 207
Switching, Automatic Trunk Selection in Reperforator. Blanton.....481–9
Switching High-Voltage Shunt Capacitor Banks. Funkhouser, VanSickle, Shankle.....129–33; disc. 134
Switching of Distribution Capacitors by Manual and Automatic Devices. Hopkins, Schultz.....138–43
Switching Phenomena, Capacitor. VanSickle, Zaborszky.....151–8; disc. 158
Switching System, A Full Automatic Private-Line Teletypewriter. Bacon, Locke.....473–80
Synchronous Alternators, Static Magnetic Exciter for. Storm.....1014–17
Synchronous Condenser for Reducing Voltage Flicker, The Application of a Series Capacitor to a. Black, Lischer.....144–50
Synchronous Condenser, Technical Problems Associated with the Application of a Capacitor in Series with a. Witzke, Michelson.....519–25
Synchronous Machine Damping and Synchronizing Torques. Concordia.....731–7
Synchronous Machines, Routine Insulation Testing of. Hunt, Vivian.....756–62
Synchronous Machines, Telephone Influence Factor in. Oscarson, Benson.....743–8
Synchronous Motors, A Design Method for Polyphase Reluctance. Crouse.....957–62
Synthesis by Graphical Methods for A-C Servomechanisms. Bjornson.....619–25
System, A Full Automatic Private-Line Teletypewriter Switching. Bacon, Locke.....473–80
System Economics of Extra-High-Voltage Transmission. St. Clair, Peterson.....841–8; disc. 848
System Fault Control, Power. (Committee Report).....410–17
System for Heterodyne Oscillators, A Servo. Sloczewski.....1070–2
System for Supervision and Dialing over Long-Distance Telephone Trunks, Single-Frequency Signaling. Newell, Weaver.....489–95
System, Measurements and Tests on a Power Line Carrier Relaying. Miller, Worthington.....1005–07
System, Neutral Inversion of a Single Potential Transformer Connected Line-to-Ground on an Isolated Delta. Gleason.....103–10; disc. 110
System of Supervisory Control on a Carrier Communication Channel, Vibracode. Allen, Daniel.....818–22; disc. 822
System of the American Gas and Electric Company, The 300–315 Kv Extra-High-Voltage Transmission. Sporn, Peterson, Gross, St.Clair.....64–72; disc. 72
System of the EDVAC, The Input-Output. Snyder.....507–09
System, Operational Study of a Highway Mobile Telephone. Dorff.....31–7
Systematization of Tube Surveillance in Large-Scale Computers. Spence.....516–19
Systems, A Note on the Design of Conditionally Stable Feedback. Travers.....626–30
Systems, Factors Affecting Minimum Surface Leakage Distances in D-C Power. Hart, Rosenberry, McClinton.....738–42
Systems, Fault Transients in Aircraft D-C. Scorgie.....713–20; disc. 720
Systems in the United States, Application of Resonant Grounding in Power. Gross, Atherton.....389–93; disc. 393
Systems Supplied by Rectifiers, Inductive Co-ordination Aspects of D-C. (Committee Report).....1034–54
Systems Used on Carrier Current Communications Circuits, Signal and Supervision. Mayer.....990–4

T

Tables of Green's Functions, Fourier Series, and Impulse Functions for Rectangular Co-ordinate Systems. Smith....22–30

Tachometer for Measurement of Instantaneous Variations in Angular Velocity, A. Bartles....1102–05

Tangential Stresses in Impregnated Paper Insulation, Radial and. Whitehead....56–9; disc. 59

Technical Problems Associated with the Application of a Capacitor in Series with a Synchronous Condenser. Witzke, Michelson....519–25

Techniques Applied to Economics, Analogue Computing. Strotz, Calvert, Morehouse..557–62; disc. 562

Techniques of Corona Loss Measurement and Analysis—500-Kv Test Project of the American Gas and Electric Company. Naef, Tremaine, Jones....496–505; disc. 505

Telegraph Network, A Nationwide Frequency-Modulation. Bramhall, Smith....373–8; disc. 378

Telegraph Set, An Electronic Time Division Multiplex. Hansen, Slayton....354–61; disc. 361

Telegraph System for Long-Distance Radio Circuits, Four- or Two-Channel Time-Division-Multiplex. Peterman, Minc....362–72

Telemetering Systems and Channels for a Power System, Choice of. Duff....1086–91

Telemetering Systems for Rocket Application, Pulse-Time Modulation. Mengel....599–605

Telephone Cable with Submerged Repeaters, A Submarine. Gilbert....564–72

Telephone Influence Factor in Synchronous Machines. Oscanson, Benson....743–8

Telephone System, Operational Study of a Highway Mobile. Dorff....31–7

Telephone Trunks, Single-Frequency Signaling System for Supervision and Dialing over Long-Distance. Newell, Weaver....489–95

Teletypewriter Switching System, A Full Automatic Private-Line. Bacon, Locke....473–80

Temperature, and Humidity, Piezoelectric Crystals as Sensing Elements of Pressure. Roberts, Goldsmith....968–72

Temperatures, Deterioration of Transformer Oil and Paper Insulation by. Vogel, Petersen, Matsch....18–20; disc. 21

Test Project of the American Gas and Electric Company, Corona Investigation on Extra-High-Voltage Lines—500-Kv. Gross, Wagner, Naef, Tremaine....75–91; disc. 91

Test Project of the American Gas and Electric Company, Line Insulator Loss Under Normal Conditions—500-Kv. Naef, Tremaine, Jones....1073–8

Test Project of the American Gas and Electric Company, Techniques of Corona Loss Measurement and Analysis—500-Kv. Naef, Tremaine, Jones....496–505; disc. 505

Tester for D-C Armatures, Winding Insulation. Catlin, Rohats....465–8

Testing, An Electronic Power Source for Large D-C Contact. Pettit....320–2

Testing and Its Influence Upon Switch Design, Ice. Heberlein, Field....37–42; disc. 42

Testing of Lightning Arresters, The Power Interruption. Ackermann....1–5; disc. 5

Testing of Synchronous Machines, Routine Insulation. Hunt, Vivian....756–62

Tests in Field and Laboratory—500-Kv Test Project of the American Gas and Electric Company, Radio Influence. Lippert, Pakala, Bartlett, Fahrnkopf....251–65; disc. 265

Tests on a Power Line Carrier Relaying System, Measurements and. Miller, Worthington....1005–07

Tests on Dielectrics in the Field, Results of a Questionnaire Covering Current Practices in Electrical. (Committee Report)....986–9

Theory of the Deep-Bar Induction Motor, A Contribution to the. Douglas....862–6

Thermal Expansion Effects in Power Cables. Schifreen....160–8; disc. 168

Thermal Transients on Buried Cables. Buller....45–52; disc. 52, 1106

300–315 Kv Extra-High-Voltage Transmission System of the American Gas and Electric Company, The. Sporn, Peterson, Gross, St.Clair....64–72; disc. 72

Three-Phase Inverter with Resistive Load, Analysis of a. Turkington....1055–61

Three-Phase Measurements of Resistance. Matsch, Basu, Horcher....350–2; disc. 352

Three-Phase Motors, Split-Winding Starting of. Alger, Ward, Wright....867–72; disc. 872

Time, Dependence of Direct Sparkover Voltage of Gaps on Humidity and. Jacob, Sommerman....921–4; disc. 924

Time Division Multiplex Telegraph Set, An Electronic. Hansen, Slayton....354–61; disc. 361

Time-Division-Multiplex Telegraph System for Long-Distance Radio Circuits, Four- or Two-Channel. Peterman, Minc....362–72

Time Modulation Telemetering Systems for Rocket Application, Pulse-. Mengel....599–605

Torques, Synchronous Machine Damping and Synchronizing. Concordia....731–7

Torsional Damper for Conductors—Service Experience and Further Experimental Work, The. Burgess, Hogg....1031–3

Total Hemispherical Radiometers. Gier, Dunkle....339–43; disc. 343

Train Control System for Railroads, A Modern Cab Signaling and. Allison....232–8; disc. 238

Train Performance Calculator, A New. Smith..657–60

Transducer, An Electromechanical. Engelberger, Kretsch....213–16

Transfer Admittance Remains Constant as Load Varies, Networks for Which Magnitude or Phase Angle of Input Impedance or. Berkowitz....286–91

Transfer Data in Electron Tube Operation, Basic Heat-. Buckland....1079–85

Transformer Application, Economics of Power. Barkle, Witzke....440–4; disc. 444

Transformer Banks, A New Carrier-Current Frequency-Shift System for Use with Differential Protection of. Beckwith....832–5; disc. 835

Transformer Connected Line-to-Ground on an Isolated Delta System, Neutral Inversion of a Single Potential. Gleason....103–10; disc. 110

Transformer Core, A 2,000,000-Kva. Sealey....8–11

Transformer Installations, Acoustic Models of. Gettys, Conover....333–6; disc. 336

Transformer-Loss Compensators for Watt-hour and Var-hour Meters, Improvements in. Schleicher....973–7

Transformer Magnetizing Inrush Current. Specht....323–7; disc. 327

Transformer Oil and Paper Insulation by Temperatures, Deterioration of. Vogel, Petersen, Matsch....18–20; disc. 21

Transformer Winding, Improved Core Form. Grimmer, Teague....962–5; disc. 965

(Transformers) An Analysis of Grounding Banks to Balance Distribution Feeder Voltages. Long,....823–7

Transformers, An Investigation of Audio Noise in Substation-Type. Vivian, Peck....328–31; disc. 331

Transient Analysis of Rotating Machines and Stationary Networks by Means of Rotating Reference Frames. Ku....943–54; disc. 954

Transient Response of Magnetic Amplifiers—Cases of Negligible Commutation, The. Finzi, Chandler, Beaumariage....934–42; disc. 942

Transient Response of Saturable Reactors with Resistive Load. Storm....95–102

Transient Response of Small 2-Phase Induction Motors. Hopkin....881–6

Transients in Aircraft D-C Systems, Fault. Scorgie....713–20; disc. 720

Transients in Simple Electric Circuits, Contact. Martin, Stauss....304–07; disc. 307

Transients on Buried Cables, Thermal. Buller....45–52; disc. 52, 1106

Transit Cars, Electric Equipment and Performance of Lightweight Rapid. Ellis, Sloman....227–30; disc. 230

Transit Control Equipment, A New Lightweight Rapid. Lichtenfels, Moore....224–6

Transit Motor, A New Lightweight Rapid. Pettersen....222–3

Transit Power Supply, Sealed Ignitron Rectifiers for Urban. Borst....770–4

Transit Systems, D-C Power Supplies and Isolation of Faults on Electric. Watkins, Reagan.
Part I. D-C Power Supply....537–42; disc. 542
Part II. Isolation of D-C Faults..543–50; disc. 550

Transmission and Distribution Stations, Application of Shunt Capacitors at. Porter, Zimmerman....112–18; disc. 118

(Transmission) Corona Investigation on Extra-High-Voltage Lines—500-Kv Test Project of the American Gas and Electric Company. Gross, Wagner, Naef, Tremaine....75–91; disc. 91

Transmission Line Constants, A Per-Unit Interpretation of. Povejsil, Johnson....194–200; disc. 200

Transmission Line Fault Locator, The Linascope. Kidd....1008–13

(Transmission) Line Insulator Loss Under Normal Conditions—500-Kv Test Project of the American Gas and Electric Company. Naef, Tremaine, Jones....1073–8

Transmission Line Load Impedance for Maximum Efficiency. Lutz....283–5

Transmission Lines, Fundamental Effects of Series Capacitors in High-Voltage. Johnson, Barkle, Witzke....526–35; disc. 535

Transmission Lines Over Mountainous Region Where Lightning Incidence is High, Protection of. Housley, Harper....124–6; disc. 126

Transmission Matrix Stability Criterion, The Generalized. Honnell....292–6; disc. 296

(Transmission) Radio Influence Tests in Field and Laboratory—500-Kv Test Project of the American Gas and Electric Company. Lippert, Pakala, Bartlett, Fahrnkopf....251–65; disc. 265

Transmission, System Economics of Extra-High-Voltage. St.Clair, Peterson....841–8; disc. 848

Transmission System of the American Gas and Electric Company, The 300–315 Kv Extra-High-Voltage. Sporn, Peterson, Gross, St.Clair....64–72; disc. 72

(Transmission) Techniques of Corona Loss Measurement and Analysis—500-Kv Test Project of the American Gas and Electric Company. Naef, Tremaine, Jones....496–505; disc. 505

Transmitters, Output Analysis and Alignment Techniques for Phase-Rotation Single Side-Band. Whitby, Scheuch....209–12

(Transportation, Air) Fault Transients in Aircraft D-C Systems. Scorgie....713–20; disc. 720

(Transportation, Land) A Modern Cab Signaling and Train Control System for Railroads. Allison....232–8; disc. 238

(Transportation, Land) A New Lightweight Rapid Transit Control Equipment. Lichtenfels, Moore....224–6

(Transportation, Land) A New Lightweight Rapid Transit Motor. Pettersen....222–3

(Transportation, Land) A New Multiple-Unit Car Motor for the Pennsylvania Railroad. Jungk....243–5; disc. 245

(Transportation, Land) A New Train Performance Calculator. Smith....657–60

(Transportation, Land) A-C Multiple-Unit Car Control Equipment. O'Kelly....652–6

(Transportation, Land) A-C Multiple-Unit Car Motor. Kreitler....648–50; disc. 650

(Transportation, Land) Economics of Trolley Coach Power Supply. McDonald, Price....687–9

(Transportation, Land) Electric Equipment and Performance of Lightweight Rapid Transit Cars. Ellis, Sloman....227–30; disc. 230

(Transportation, Land) New A-C Multiple-Car Control for the Pennsylvania Railroad. Newhouse....645–7; disc. 647

(Transportation, Land) Regeneration with a Mercury Arc Rectifier on the Central Railway of Brazil. Schmidt....1092–6

(Transportation, Land) Why 4-Motor Multiple-Unit Car Equipments? Williamson....240–2

Trolley Coach Power Supply, Economics of. McDonald, Price....687–9

Trunk Selection in Reperforator Switching, Automatic. Blanton....481–9

Trunks, Single-Frequency Signaling System for Supervision and Dialing over Long-Distance Telephone. Newell, Weaver....489–95

Tube Inverter with the Supply Voltage Below the Breakdown Voltage, A Gas. Cage, Schuder....908–12

Tube Operation, Basic Heat-Transfer Data in Electron. Buckland....1079–85

Tube Surveillance in Large-Scale Computers, Systematization of. Spence....516–19

Tubes When Used as Oscillators in the Free As Well as in the Synchronized States, A New Method for Treating Electron. Mostafa, Bey....999–1004

Turbine-Generator Rotors, Modern Practice in the Balancing of Large. Laffoon, Hagg, Janthey, Heller....593–8; disc. 598

Turbine-Generator Stator Windings, A New High-Voltage Insulation for. Laffoon, Hill, Moses, Berberich....721–6; disc. 726

Turbine-Generator Stators, The Use of Preferred Orientation Strip Steel in. Apperson, Fontaine....836–9; disc. 839

Turbine Generators, Detection of Turn-to-Turn Faults in Large High-Voltage. Sexton, Alke....270–3; disc. 273

Turbine Generators, Progress in the Development of Large. Huntley, Taylor....580–9; disc. 589

Turn-to-Turn Faults in Large High-Voltage Turbine Generators, Detection of. Sexton, Alke....270–3; disc. 273

Two-Channel Time-Division-Multiplex Telegraph System for Long-Distance Radio Circuits, Four or. Peterman, Minc....362–72

2,000,000-Kva Transformer Core, A. Sealey....8–11

Two-Phase Induction Motors, Transient Response of Small. Hopkin....881–6

U

Underground Power Cable, Lead-Alloy Sheaths for. Halperin, Betzer....423–9; disc. 429

Unit Car Control Equipment, A-C Multiple-. O'Kelly....652–6

Unit Car Equipments?, Why 4-Motor Multiple-. Williamson....240–2

Unit Car Motor, A-C Multiple-. Kreitler....648–50; disc. 650

Unit Car Motor for the Pennsylvania Railroad, A New Multiple-. Jungk....243–5; disc. 245

Unit Cars, Selection of Equipment for Multiple-. Hutchison....640–3; disc. 643

Unit Interpretation of Transmission Line Constants, A Per-. Povejsil, Johnson....194–200; disc. 200

United Electric Railways of Providence, Power Supply Study and New Rectifier Installation for the. Whitman, Schaller....978–85; disc. 985

United States, Application of Resonant Grounding in Power Systems in the. Gross, Atherton.....389–93; disc. 393
Universal-Type Motors, Commutation in. Packer.....170–6; disc. 176
Urban 4-Kv Feeders, Group Regulation of. Grim, Peck.....551–5
Urban Transit Power Supply, Sealed Ignitron Rectifiers for. Borst.....770–4
Use of Preferred Orientation Strip Steel in Turbine-Generator Stators, The. Apperson, Fontaine.....836–9; disc. 839

V

Variations in Angular Velocity, A Tachometer for Measurement of Instantaneous. Bartles..1102–05
Var-hour Meters, Improvements in Transformer Loss Compensators for Watt-hour and. Schleicher.....973–7
Varmeters, Marking of. (Committee Report).....12–14; disc. 14
Velocity, A Tachometer for Measurement of Instantaneous Variations in Angular. Bartles..1102–05
Vibracode System of Supervisory Control on a Carrier Communication Channel. Allen, Daniel.....818–22; disc. 822
Voltage Below the Breakdown Voltage, A Gas Tube Inverter with the Supply. Cage, Schuder..908–12
Voltage Dip on Cyclic Light Flicker, Effect of the Duration of. Brieger.....894–8; disc. 899
Voltage Endurance Studies on Mica Insulation for Electric Machinery, Alternating and Direct. Moses.....763–8; disc. 768
Voltage Flicker, The Application of a Series Capacitor to a Synchronous Condenser for Reducing. Black, Lischer.....144–50
Voltage of Gaps on Humidity and Time, Dependence of Direct Sparkover. Jacob, Sommerman.....921–4; disc. 924
Voltage Transmission, System Economics of Extra-High-. St.Clair, Peterson.....841–8; disc. 848
Voltages, An Analysis of Grounding Banks to Balance Distribution Feeder. Long.....823–7

W

Washington, D. C., 69-Kv Medium-Pressure Gas-Filled Cable. Clark.....418–21; disc. 421
Watt-hour and Var-hour Meters, Improvements in Transformer-Loss Compensators for. Schleicher..973–7
Waveguide Linear Accelerators, Dielectric Loading for. Flesher, Cohn.....887–93
Waveguides, Shielded Dielectric-Rod. Beam, Wachowski.....874–80
Welders, Ignitrons for Frequency-Changer. Rottier..900–07
Welders, Probabilities of Interference Between Resistance. Boice.....775–83
Welders with Saturable Reactor Control, A-C Arc. Oestreicher.....787–90
Welding Arc, The Physical Mechanism of Low and High Current Arcs and Their Relation to the. Finkelnburg.....800–03
Welding Arcs, New Electrodes for Stabilizing Inert-Gas. Cobine, Gallagher.....804–06
Welding Calculations—Effect of Conductor Configuration in Overhead Lines. Tietze.....784–6
Welding Machines, Selection of Fuses for Resistance. Stadum.....796–9
Winding, Improved Core Form Transformer. Grimmer, Teague.....962–5; disc. 965
Winding Insulation Tester for D-C Armatures. Catlin, Rohats.....465–8
Winding Starting of 3-Phase Motors, Split-. Alger, Ward, Wright.....867–72; disc. 872
Windings, A New High-Voltage Insulation for Turbine-Generator Stator. Laffoon, Hill, Moses, Berberich.....721–6; disc. 726
Windings of D-C Machines, Rules for Designing Frog-Leg. Dwight, Haltmaier.....707–11; disc. 711

Z

Zero for an A-C Arc Adjacent to Refractory Surfaces, A Study of Conduction Phenomena Near Current. Browne, Strom.....398–407; disc. 407

2. Author Index

Ackermann, Otto. The Power Interruption Testing of Lightning Arresters. (51–1).....1–5; disc. 7
Ackermann, Otto; E. J. DeVal. Spiral Arc Chokes Power Flow in New Lightning Arresters. (51–189).....995–8
Aicher, L. C., Jr. Disc.....924
Alger, P. L., Disc.....665, 678
Alger, P. L.; H. C. Ward, Jr.; F. H. Wright. Split-Winding Starting of 3-Phase Motors. (51–160).....867–72; disc. 872
Alke, Roger J.; R. M. Sexton. Detection of Turn-to-Turn Faults in Large High-Voltage Turbine Generators. (51–41).....270–3; disc. 274
Allen, T. J. Disc.....126
Allen, T. J.; J. Daniel. Vibracode System of Supervisory Control on a Carrier Communication Channel. (51–146).....818–22; disc. 822
Allison, L. R. A Modern Cab Signaling and Train Control System for Railroads. (51–34).....232–8; disc. 239
Amchin, Howard K. Disc.....394
Anderson, E. R.; L. J. Anderson. Disc.....344
Anderson, L. J.; E. R. Anderson. Disc.....344
Apperson, J. W.; C. B. Fontaine. The Use of Preferred Orientation Strip Steel in Turbine-Generator Stators. (51–154).....836–9; disc. 840
Arnold, G. W. Disc.....711
Atherton, Edward W.; E. T. B. Gross. Application of Resonant Grounding in Power Systems in the United States. (51–64).....389–93; disc. 396
Atkinson, R. W. Disc.....60, 168, 353, 429
Attura, George M. Effects of Carrier Shifts on Derivative Networks for A-C Servomechanisms. (51–100).....612–18

B

Babb, D. S.; J. E. Williams. Circuit Analysis Method for Determination of A-C Impedances of Machine Conductors. (51–109).....661–5; disc. 665
Bacon, W. M.; G. A. Locke. A Full Automatic Private-Line Teletypewriter Switching System. (51–76).....473–80
Balentine, C. J.; E. B. Rietz. Disc.....118, 135, 159
Bany, H. Disc.....14
Barkle, J. E.; A. A. Johnson, D. J. Povejsil. Fundamental Effects of Series Capacitors in High-Voltage Transmission Lines. (51–89).....526–35; disc. 535
Barkle, J. E.; R. L. Witzke. Economics of Power Transformer Application. (51–70).....440–4
Barnes, E. C. An Experimental Study of Induction Machine End-Turn Leakage Reactance. (51–111).....671–7; disc. 678
Barnes, H. C.; J. H. Kinghorn. Disc.....282
Bartles, S. P. A Tachometer for Measurement of Instantaneous Variations in Angular Velocity. (51–238).....1102–05
Bartlett, S. C.; G. D. Lippert, W. E. Pakala, C. D. Fahrnkopf. Radio Influence Tests in Field and Laboratory—500-Kv Test Project of the American Gas and Electric Company. (51–40).....251–65; disc. 269
Basu, N. C.; L. W. Matsch, G. R. Horcher. Three-Phase Measurements of Resistance. (51–59).....350–2; disc. 352
Beam, Robert E.; H. M. Wachowski. Shielded Dielectric-Rod Waveguides. (51–162).....874–80
Beatty, J. W.; R. B. Shores. A New 69-Kv Air Blast Circuit Breaker. (51–27).....202–07; disc. 208
Beaumariage, D. C.; L. A. Finzi, D. P. Chandler. The Transient Response of Magnetic Amplifiers—Cases of Negligible Commutation. (51–175).....934–42; disc. 942
Beck, Edward. Disc.....134
Beckwith, R. W. A New Carrier-Current Frequency-Shift System for Use with Differential Protection of Transformer Banks. (51–153).....832–5; disc. 835
Beckwith, Sterling. Disc.....591
Beeman, D. L. Disc.....444
Bellaschi, P. L. Disc.....21, 72
Benson, Ikel C.; G. L. Oscarson. Telephone Influence Factor in Synchronous Machines. (51–124).....743–8
Berberich, L. J.; C. M. Laffoon, C. F. Hill, G. L. Moses. A New High-Voltage Insulation for Turbine-Generator Stator Windings. (51–121).....721–6; disc. 730
Berkowitz, Raymond S. Networks for Which Magnitude or Phase Angle of Input Impedance or Transfer Admittance Remains Constant as Load Varies. (51–45).....286–91
Betzer, C. E.; H. Halperin. Lead-Alloy Sheaths for Underground Power Cable. (51–68).....423–9; disc. 434
Bewley, L. V. Disc.....386
Bey, M.El-Shishini; Abd El-Samie Mostafa. A New Method for Treating Electron Tubes When Used as Oscillators in the Free as Well as in the Synchronized States. (51–191).....999–1004
Bjornson, George A. Network Synthesis by Graphical Methods for A-C Servomechanisms. (51–101).....619–25
Black, P. M.; L. F. Lischer. The Application of a Series Capacitor to a Synchronous Condenser for Reducing Voltage Flicker. (51–20).....144–50
Blanton, W. B. Automatic Trunk Selection in Reperforator Switching. (51–78).....481–9
Bliss, T. J.; R. L. Witzke. Disc.....386
Boice, W. K. Probabilities of Interference Between Resistance Welders. (51–137).....775–83
Borst, David W. Sealed Ignitron Rectifiers for Urban Transit Power Supply. (51–131).....770–4
Boyajian, A. Disc.....966
Brainerd, Arthur A. Disc.....858
Bramhall, F. B.; L. A. Smith. A Nationwide Frequency-Modulation Telegraph Network. (51–62).....373–8; disc. 378
Brancato, E. L. Disc.....438
Brazier, L. G. Disc.....421
Brieger, L. Effect of the Duration of Voltage Dip on Cyclic Light Flicker. (51–165)...894–8; disc. 899
Brown, H. F. Disc.....542, 550, 643
Browne, T. E., Jr.; A. P. Strom. A Study of Conduction Phenomena Near Current Zero for an A-C Arc Adjacent to Refractory Surfaces. (51–65).....398–407; disc. 409
Buchanan, L. W. Disc.....678
Buckland, Mrs. B. O. Basic Heat-Transfer Data in Electron Tube Operation. (51–227)....1079–85
Buller, F. H. Thermal Transients on Buried Cables. (51–9).....45–52; disc. 54, 1107
Buller, R. M. Disc.....200
Burgess, T. J.; A. D. Hogg. The Torsional Damper for Conductors—Service Experience and Further Experimental Work. (51–205).....1031–3
Burrell, R. W. Disc.....430
Butler, R. M. Disc.....535

C

Cage, John M.; J. C. Schuder. A Gas Tube Inverter with the Supply Voltage Below the Breakdown Voltage. (51–168).....908–12
Cain, B. M. Disc.....840
Calabrese, G. Determination of Reserve Capacity by the Probability Method Effect of Interconnections. (51–198).....1018–20
Calvert, J. F.; R. H. Strotz, N. F. Morehouse. Analogue Computing Techniques Applied to Economics. (51–93).....557–62; disc. 562
Camilli, G. Disc.....327
Carfrae, W. J. Disc.....589
Carpenter, T. J. Disc.....6
Carroll, Joseph S. Disc.....93, 506
Catlin, F. H.; N. Rohats. Winding Insulation Tester for D-C Armatures. (51–74).....465–8
Chadwick, Joseph H.; A. J. Morris. An Electromagnetic Induction Method of Measuring Oscillating Fluid Flow. (51–58).....346–50
Chandler, D. P.; L. A. Finzi, D. C. Beaumariage. The Transient Response of Magnetic Amplifiers—Cases of Negligible Commutation. (51–175).....934–42; disc. 942
Chang, S. S. L. Equivalent Circuits and Their Application in Designing Shaded Pole Motors. (51–116).....690–8; disc. 699
Cheek, R. C. Application of Microwave Channels. (51–145).....813–17
Clark, H. W. 69-Kv Medium-Pressure Gas-Filled Cable, Washington, D. C. (51–67).....418–21; disc. 422
Cobine, J. D.; C. J. Gallagher. New Electrodes for Stabilizing Inert-Gas Welding Arcs. (51–143).....804–06
Coggeshall, I. S. Disc.....378
Cohn, George I.; G. T. Flesher. Dielectric Loading for Waveguide Linear Accelerators. (51–164).....887–93
Cole, H. L. Disc.....966
Concordia, Charles. Synchronous Machine Damping and Synchronizing Torques. (51–122)....731–7
Conover, William B.; B. Gettys. Acoustic Models of Transformer Installations. (51–56).....333–6; disc. 337
Cook, S. S. Disc.....394
Corson, A. J.; A. L. Nylander. A Hook-On Power Factor Meter. (51–75).....468–72
Cowles, Laurence G. Disc.....297
Craig, A. B. Disc.....17, 118
Crary, S. B. Disc.....73, 850
Crouse, C. H. A Design Method for Polyphase Reluctance Synchronous Motors. (51–177)..957–62
Crowdes, G. J. Disc.....168
Cybulski, John; J. O'Connor. Disc.....705

D

D'Andrade, H. E. Disc.....859
Dana, George. Disc.....395
Daniel, Joel; T. J. Allen. Vibracode System of Supervisory Control on a Carrier Communication Channel. (51–146).....818–22; disc. 822
Darrow, K. G. Disc.....193
de Bellis, A. M. Disc.....207
Del Mar, William A. Disc.....52, 61, 168, 421
Derr, W. A. Disc.....822

DeVal, E. J.; O. Ackermann. Spiral Arc Chokes Power Flow in New Lightning Arresters. (51–189) 995–8
DeWeese, Fred C. Disc. 127
Dickinson, R. C.; J. D. Findley. A Spring Mechanism for Hand Closing of Magnetic Power Air Circuit Breakers. (51–25) ..... 189–92; disc. 192
Diebold, Edward J. Commutating Reactor Control for Mechanical Rectifiers. (51–211) 1062–5
Dillow, N. E. Disc. 135
Doggett, L. A. Disc. 698
Dorff, Louis A. Operational Study of a Highway Mobile Telephone System. (51–7) 31–7
Dorfman, L. O. Disc. 768
Douglas, John F. H. A Contribution to the Theory of the Deep-Bar Induction Motor. (51–159) ..862–6
Douglas, John F. H. Disc. 665, 873
Dovjikov, Alexander. Disc. 135
Duff, C. K. Choice of Telemetering Systems and Channels for a Power System. (51–229) 1086–91
Dunkle, R. V.; J. T. Gier. Total Hemispherical Radiometers. (51–57) ..... 339–43; disc. 345
Dwight, H. B. Disc. 931
Dwight, H. B.; R. G. Haltmaier. Rules for Designing Frog-Leg Windings of D-C Machines. (51–119) ..... 707–11; disc. 712
Dzwonczyk, V. L. An Engineering Approach to Control Room Lighting. (51–157) ...852–7; disc. 860

E

Ebel, L. C.; L. F. Roehmann. Disc. 59
Eckel, John F. Disc. 431
Ellis, W. R.; M. L. Sloman. Electric Equipment and Performance of Lightweight Rapid Transit Cars. (51–33) ..... 227–30; disc. 231
El Samie Mostafa, Abd; M.El-Shishini Bey. A New Method for Treating Electron Tubes When Used as Oscillators in the Free as Well as in the Synchronized States. (51–191) 999–1004
El-Shishini Bey, M.; Abd El-Samie Mostafa. A New Method for Treating Electron Tubes When Used as Oscillators in the Free as Well as in the Synchronized States. (51–191) 999–1004
Engelberger, J. F.; H. W. Kretsch. An Electromechanical Transducer. (51–29) 213–16
Espenschied, Lloyd. Disc. 361
Esselman, Walter H. Steady-State Analysis of Self-Saturating Magnetic Amplifiers Based on Linear Approximations of the Magnetization Curve. (51–72) 451–9
Estoppey, R. F. Disc. 221
Evans, Byron. Disc. 393

F

Fahrnkopf, C. D.; G. D. Lippert, W. E. Pakala, S. C. Bartlett. Radio Influence Tests in Field and Laboratory—500-Kv Test Project of the American Gas and Electric Company. (51–40) ..251–65; disc. 269
Ferri, Louis F. Disc. 110
Field, E. J.; G. E. Heberlein. Ice Testing and Its Influence Upon Switch Design. (51–8) ..... 37–42; disc. 43
Findley, J. D.; R. C. Dickinson. A Spring Mechanism for Hand Closing of Magnetic Power Air Circuit Breakers. (51–25) ..... 189–92; disc. 192
Fink, L. H. Disc. 169
Finkelnburg, Wolfgang. The Physical Mechanism of Low- and High-Current Arcs, and Their Relation to the Welding Arc. (51–142) 800–03
Finzi, L. A.; D. P. Chandler, D. C. Beaumariage. The Transient Response of Magnetic Amplifiers—Cases of Negligible Commutation. (51–175) ..... 934–42; disc. 942
Flesher, Gail T.; G. I. Cohn. Dielectric Loading for Waveguide Linear Accelerators. (51–164) 887–93
Fontaine, C. B.; J. W. Apperson. The Use of Preferred Orientation Strip Steel in Turbine-Generator Stators. (51–154) ..... 836–9; disc. 840
Fowler, C. J.; R. M. Showers. Disc. 267
Fraas, Foster; O. C. Ralston. Distribution of Charge in Electrostatic Mineral Separation. (51–202) 1028–30
Frick, C. W. Disc. 265
Funkhouser, A. W.; R. C. Van Sickle, D. F. Shankle. Switching High-Voltage Shunt Capacitor Banks. (51–18) ..... 129–33; disc. 137

G

Gallagher, C. J.; J. D. Cobine. New Electrodes for Stabilizing Inert-Gas Welding Arcs. (51–143) 804–06
Gault, J. S. Disc. 671, 677
Gerdel, R. W. Disc. 344
Gettys, Briggs; W. B. Conover. Acoustic Models of Transformer Installations. (51–56) ..... 333–6; disc. 337
Gier, J. T.; R. V. Dunkle. Total Hemispherical Radiometers. (51–57) ..... 339–43; disc. 345
Gilbert, J. J. A Submarine Telephone Cable with Submerged Repeaters. (51–94) 564–72
Gleason, Lyle L. Neutral Inversion of a Single Potential Transformer Connected Line-to-Ground on an Isolated Delta System. (51–14) ..103–10; disc. 110
Goldsmith, P.; E. A. Roberts. Piezoelectric Crystals as Sensing Elements of Pressure, Temperature, and Humidity. (51–180) 968–72
Goodrich, R. D., Jr. Disc. 200
Gordy, T. D. Disc. 319, 331, 337
Gould, H. R.; C. P. Hayes. Noise Evaluation of Fluorescent Lamp Ballasts. (51–95) 573–9
Grim, C. L.; H. B. Peck. Group Regulation of Urban 4-kv Feeders. (51–92) 551–6
Grimmer, E. J.; W. L. Teague. Improved Core Form Transformer Winding. (51–178) ..962–5; disc. 967
Griscom, S. B. Disc. 850
Grobel, L. P. Disc. 598
Gross, Eric T. B.; E. W. Atherton. Application of Resonant Grounding in Power Systems in the United States. (51–64) ..... 389–93; disc. 396
Gross, I. W. Disc. 384
Gross, I. W.; P. Sporn, E. L. Peterson, H. P. St. Clair. The 300–315 Kv Extra-High-Voltage Transmission System of the American Gas and Electric Company. (51–11) ..... 64–72; disc. 73
Gross, I. W.; C. F. Wagner, O. Naef, R. L. Tremaine. Corona Investigation on Extra-High-Voltage Lines—500-Kv Test Project of the American Gas and Electric Company. (51–12) ..... 75–91; disc. 94
Grover, F. W. Disc. 931
Gunter, Frank B. 940–960 Megacycle Communications Equipment for Industrial Applications. (51–144) 807–12

H

Hagg, A. C.; C. M. Laffoon, C. H. Janthey, P. R. Heller. Modern Practice in the Balancing of Large Turbine-Generator Rotors. (51–97) ..... 593–8; disc. 598
Halperin, Herman; C. E. Betzer. Lead-Alloy Sheaths for Underground Power Cable. (51–68) ..... 423–9; disc. 434
Halperin, Herman. Disc. 729
Haltmaier, R. G.; H. B. Dwight. Rules for Designing Frog-Leg Windings of D-C Machines. (51–119) ..... 707–11; disc. 712
Hamilton, W. S. H. Disc. 650
Hansen, T. A.; R. D. Slayton. An Electronic Time Division Multiplex Telegraph Set. (51–60) 354–61
Harder, E. L. Disc. 450
Harper, John D.; J. E. Housley. Protection of Transmission Lines Over Mountainous Region Where Lightning Incidence is High. (51–17) ..... 124–6; disc. 126
Harrison, H. R.; A. H. Powell. Disc. 43
Hart, J. E.; W. W. Rosenberry, A. T. McClinton. Factors Affecting Minimum Surface Leakage Distances on D-C Power Systems. (51–123) ..738–42
Hayes, C. P.; H. R. Gould. Noise Evaluation of Fluorescent Lamp Ballasts. (51–95) 573–9
Heberlein, G. E.; E. J. Field. Ice Testing and Its Influence Upon Switch Design. (51–8) ..... 37–42; disc. 43
Heil, V. E.; F. Spayth. Disc. 307
Heller, P. R.; C. M. Laffoon, A. C. Hagg, C. H. Janthey. Modern Practice in the Balancing of Large Turbine-Generator Rotors. (51–97) ..... 593–8; disc. 598
Herskind, C. C.; E. J. Remscheid. Development of a Pumpless Ignitron. (51–212) 1066–9
Herzog, E. Disc. 396
Hickernell, L. F.; C. J. Snyder. Disc. 433
Higgins, Thomas James; D. K. Reitan. Calculation of the Capacitance of a Circular Annulus by the Method of Subareas. (51–174) ..926–31; disc. 932
Hill, C. F.; C. M. Laffoon, G. L. Moses, L. J. Berberich. A New High-Voltage Insulation for Turbine-Generator Stator Windings. (51–121) ..721–6; disc. 730
Hoffmann, Banesh. Disc. 296
Hogg, A. D.; T. J. Burgess. The Torsional Damper for Conductors—Service Experience and Further Experimental Work. (51–205) 1031–3
Honnell, Pierre M. The Generalized Transmission Matrix Stability Criterion. (51–46) ..... 292–6; disc. 298
Hopkin, Arthur M. A Phase-Plane Approach to the Compensation of Saturating Servomechanisms. (51–103) 631–9
Hopkin, A. M. Transient Response of Small 2-Phase Induction Motors. (51–163) 881–6
Hopkins, R. J.; N. R. Schultz. Switching of Distribution Capacitors by Manual and Automatic Devices. (51–19) 138–43
Horcher, G. R.; L. W. Matsch, N. C. Basu. Three-Phase Measurements of Resistance. (51–59) ..... 350–2; disc. 352
Housley, J. Elmer; J. D. Harper. Protection of Transmission Lines Over Mountainous Region Where Lightning Incidence is High. (51–17) ..... 124–6; disc. 126
Howard, S. B. Disc. 385
Hunt, L. F.; J. H. Vivian. Routine Insulation Testing of Synchronous Machines (51–126) 756–62
Huntley, E. D.; H. D. Taylor. Progress in the Development of Large Turbine Generators. (51–96) ..... 580–9; disc. 591
Hutchison, W. M. Selection of Equipment for Multiple-Unit Cars. (51–104) ..... 640–3; disc. 643

I

Ingersoll, L. R. Disc. 53

J

Jacob, P. B., Jr.; G. M. L. Sommerman. Dependence of Direct Sparkover Voltage of Gaps on Humidity and Time. (51–173) ..... 921–4; disc. 925
Janthey, C. H.; C. M. Laffoon, A. C. Hagg, P. R. Heller. Modern Practice in the Balancing of Large Turbine-Generator Rotors. (51–97) ..... 593–8; disc. 598
Johnson, A. A.; J. E. Barkle, D. J. Povejsil. Fundamental Effects of Series Capacitors in High-Voltage Transmission Lines. (51–89) ....526–35; disc. 535
Johnson, A. A.; D. J. Povejsil. A Per-Unit Interpretation of Transmission Line Constants. (51–26) ..... 194–200; disc. 201
Johnson, I. B.; L. E. Saline. Disc. 127, 384
Johnson, I. B.; J. R. Stevenson. Disc. 136
Johnson, John S. A Maintenance Inspection Program for Large Rotating Machines. (51–125) ..749–54
Jones, A. R. Disc. 92
Jones, A. R.; O. Naef, R. L. Tremaine. Line Insulator Loss Under Normal Conditions—500-Kv Test Project of the American Gas and Electric Company. (51–224) 1073–8
Jones, A. R.; O. Naef, R. L. Tremaine. Techniques of Corona Loss Measurement and Analysis—500-Kv Test Project of the American Gas and Electric Company. (51–80) ..... 496–505; disc. 506
Jones, R. W. The Effects of Loads and Disturbances upon Feedback Controllers. (51–73) 460–4
Jungk, H. G. A New Multiple-Unit Car Motor for the Pennsylvania Railroad. (51–36) ..243–5; disc. 245

K

Kalb, J. W. Some Effects of Lightning Arrester Protective Characteristics and Location upon Station Apparatus Protection. (51–63) ..379–83; disc. 387
Karr, J. H. Disc. 177
Kelham, W. O. Disc. 408
Kelly, C. F. Disc. 344
Kidd, K. H. The Linascope Transmission Line Fault Locator. (51–194) 1008–13
Kilbourne, C. E. Disc. 726
Killian, S. C. Disc. 43
Kinghorn, J. H.; H. C. Barnes. Disc. 282
Knight, M. H. Disc. 72
Knowlton, A. E. Disc. 16
Knudsen, H. Lottrup. Disc. 1106
Komives, L. I. Disc. 61, 421, 433
Kouwenhoven, W. B.; W. T. Sackett, Jr. Contact Resistance—The Contribution of Nonuniform Current Flow. (51–140) 791–5
Krabbe, Ulrik. Disc. 449, 942
Kreitler, F. C., Jr. A-C Multiple-Unit Car Motor. (51–106) ..... 648–50; disc. 651
Kretsch, H. W.; J. F. Engelberger. An Electromechanical Transducer. (51–29) 213–16
Ku, Y. H. Transient Analysis of Rotating Machines and Stationary Networks by Means of Rotating Reference Frames. (51–176) ... 943–4; disc. 955

L

Laffoon, C. M.; A. C. Hagg, C. H. Janthey, P. R. Heller. Modern Practice in the Balancing of Large Turbine-Generator Rotors. (51–97) ..... 593–8; disc. 598
Laffoon, C. M.; C. F. Hill, G. L. Moses, L. J. Berberich. A New High-Voltage Insulation for Turbine-Generator Stator Windings. (51–121) ..721–6; disc. 730
Lamborn, R. Disc. 245
Lane, Frederic A. Disc. 589
Langstaff, H. A. P. Disc. 134, 273, 860
Lenehan, B. E. Disc. 220
Leonard, M. G. Disc. 5
LeVesconte, Lester B. Disc. 444
Lichtenfels, I. W.; H. G. Moore. A New Lightweight Rapid Transit Control Equipment. (51–32) 224–6

Lippert, G. D.; W. E. Pakala, S. C. Bartlett, C. D. Fahrnkopf. Radio Influence Tests in Field and Laboratory—500-Kv Test Project of the American Gas and Electric Company. (51-40).....251-65; disc. 269
Lischer, L. F. Disc.....281
Lischer, L. F.; P. M. Black. The Application of a Series Capacitor to a Synchronous Condenser for Reducing Voltage Flicker. (51-20).....144-50
Locke, G. A.; W. M. Bacon. A Full Automatic Private-Line Teletypewriter Switching System. (51-76).....473-80
Long, Leonard W. An Analysis of Grounding Banks to Balance Distribution Feeder Voltages. (51-148).....823-7
Lubin, S.; L. Podolsky. Carrier Current Supervisory System for Distribution Circuits. (51-236).....1096-1101
Lunge, G. S. Disc.....835
Lutz, S. G. Transmission Line Load Impedance for Maximum Efficiency. (51-44).....283-5

M

MacLeod, D. R. Disc.....643
Magnusson, P. C. Geometric Mean Distances of Angle-Shaped Conductors. (51-16).....121-3
Manning, M. L. Disc.....438
Martin, E. R. Disc.....711
Martin, Frank E.; H. E. Stauss. Contact Transients in Simple Electric Circuits. (51-48).....304-07; disc. 308
Matsch, L. W.; N. C. Basu, G. R. Horcher. Three-Phase Measurements of Resistance. (51-59).....350-2; disc. 352
Matsch, L. W.; F. J. Vogel, C. C. Petersen. Deterioration of Transformer Oil and Paper Insulation by Temperatures. (51-4).....18-20; disc. 21
Maust, Charles I. Disc.....119
Mayer, Robert Lyon. Signal and Supervision Systems Used on Carrier Current Communications Circuits. (51-188).....990-4
McClinton, A. T.; J. E. Hart, W. W. Rosenberry. Factors Affecting Minimum Surface Leakage Distances on D-C Power Systems. (51-123)...738-42
McCoy, R. L. Disc.....266
McDonald, G. R.; J. C. Price. Economics of Trolley Coach Power Supply. (51-115).....687-9
Meador, J. R. Disc.....965
Medkeff, Russell J.; R. J. Parent. A Diode Bridge Limiter for Use with Electronic Analogue Computers. (51-170).....913-16
Mengel, John T. Pulse-Time Modulation Telemetering Systems for Rocket Application. (51-98).....599-605
Merrell, Edwin J. Disc.....61, 433
Meyerhoff, L. Disc.....60
Michaels, Edward L. Loci of Complex Impedance and Admittance Functions. (51-47).....299-303
Michelson, E. L.; R. L. Witzke. Technical Problems Associated with the Application of a Capacitor in Series with a Synchronous Condenser. (51-88).....519-25
Miller, C. J., Jr. Disc.....267
Miller, John H. Frequency Compensation of A-C Instruments. (51-30).....217-20
Miller, R. H.; A. R. Worthington. Measurements and Tests on a Power Line Carrier Relaying System. (51-192).....1005-07
Minc, A.; W. C. Peterman. Four- or Two-Channel Time-Division-Multiplex Telegraph System for Long-Distance Radio Circuits. (51-61)...362-72
Moore, H. G. Disc.....240
Moore, H. G.; I. W. Lichtenfels. A New Lightweight Rapid Transit Control Equipment. (51-32).224-6
Morehouse, N. F.; R. H. Strotz, J. F. Calvert. Analogue Computing Techniques Applied to Economics. (51-93).....557-62; disc. 562
Morgan, W. A. Disc.....535, 848
Morris, Albert J.; J. H. Chadwick. An Electromagnetic Induction Method of Measuring Oscillating Fluid Flow. (51-58).....346-50
Morton, W. B. Disc.....42, 857
Moses, Graham Lee. Alternating and Direct Voltage Endurance Studies on Mica Insulation for Electric Machinery. (51-127).....763-8; disc. 769
Moses, Graham Lee; C. M. Laffoon, C. F. Hill, L. J. Berberich. A New High-Voltage Insulation for Turbine-Generator Stator Windings. (51-121).....721-6; disc. 730
Mostafa, Abd El-Samie; M. El-Shishini Bey. A New Method for Treating Electron Tubes When Used as Oscillators in the Free as Well as in the Synchronized States. (51-191).....999-1004
Murray, C. S. Disc.....337

N

Naef, O.; I. W. Gross, C. F. Wagner, R. L. Tremaine. Corona Investigation on Extra-High-Voltage Lines—500-Kv Test Project of the American Gas and Electric Company. (51-12).....75-91; disc. 94
Naef, O.; R. L. Tremaine, A. R. Jones. Line Insulator Loss Under Normal Conditions 500-Kv Test Project of the American Gas and Electric Company. (51-224).....1073-8
Naef, O.; R. L. Tremaine, A. R. Jones. Techniques of Corona Loss Measurement and Analysis—500-Kv Test Project of the American Gas and Electric Company. (51-80).....496-505; disc. 506
Nau, Robert H. Disc.....407
Nebel, J. H. Disc.....52
Nevins, B. R. Disc.....14
Newell, N. A.; A. Weaver. Single-Frequency Signaling System for Supervision and Dialing over Long-Distance Telephone Trunks. (51-79).....489-95
Newhouse, S. E. New A-C Multiple-Car Control for the Pennsylvania Railroad. (51-105).....645-7; disc. 647
Nims, Paul T. Some Design Criteria for Automatic Controls. (51-99).....606-14
Noest, John G. Disc.....590
Nylander, A. L.; A. J. Corson. A Hook-On Power Factor Meter. (51-75).....468-72

O

O'Connor, John; J. Cybulski. Disc.....705
Oestreicher, S. A-C Arc Welders with Saturable Reactor Control. (51-139).....787-90
Ogden, H. S. Disc.....647
O'Kelly, W. S. A-C Multiple-Unit Car Control Equipment. (51-107).....652-6
O'Neill, D. J. Disc.....859
Opsahl, A. M. Disc.....383
Ordas, A. F. Disc.....872
Oscarson, G. L.; I. C. Benson. Telephone Influence Factor in Synchronous Machines. (51-124).743-8
Owens, J. B. Disc.....42

P

Packer, L. C. Commutation in Universal-Type Motors. (51-24).....170-6; disc. 178
Packer, L. C. Disc.....698
Pakala, W. E.; G. D. Lippert, S. C. Bartlett, C. D. Fahrnkopf. Radio Influence Tests in Field and Laboratory—500-Kv Test Project of the American Gas and Electric Company. (51-40).....251-65; disc. 269
Parent, Robert J.; R. J. Medkeff. A Diode Bridge Limiter for Use with Electronic Analogue Computers. (51-170).....913-16
Parks, Earl E. Electric Home Heating. (51-150).....828-41
Parmelee, George V. Disc.....343
Peck, H. B.; C. L. Grim. Group Regulation of Urban 4-Kv Feeders. (51-92).....551-6
Peck, R. R.; J. H. Vivian. An Investigation of Audio Noise in Substation Type Transformers. (51-55).....328-31; disc. 332
Peterman, W. C.; A. Minc. Four- or Two-Channel Time-Division-Multiplex Telegraph System for Long-Distance Radio Circuits. (51-61)...362-72
Petersen, C. C.; F. J. Vogel, L. W. Matsch. Deterioration of Transformer Oil and Paper Insulation by Temperatures. (51-4).....18-20; disc. 21
Peterson, E. L.; H. P. St. Clair. System Economics of Extra-High-Voltage Transmission. (51-156).....841-8; disc. 850
Peterson, E. L.; P. Sporn, I. W. Gross, H. P. St. Clair. The 300-315 Kv-Extra-High-Voltage Transmission System of the American Gas and Electric Company. (51-11).....64-72; disc. 73
Peterson, H. A.; P. E. Russell. Differential Analyzer Study of Harmonic Power Generation with Nonlinear Impedance Element. (51-172).....917-20
Peterson, Thomas F. Disc.....93
Pettersen, R. A. A New Lightweight Rapid Transit Motor. (51-31).....222-3
Petit, D. L. An Electronic Power Source for Large D-C Contact Testing. (51-51).....320-2
Podolsky, L.; S. Lubin. Carrier Current Supervisory System for Distribution Circuits. (51-236).....1096-1101
Poritsky, H. Calculation of Flux Distributions with Saturation. (51-50).....309-19; disc. 319
Porter, F. M.; C. P. Zimmerman. Application of Shunt Capacitors at Transmission and Distribution Stations. (51-15).....112-18; disc. 119
Porter, F. M.; C. P. Zimmerman. Disc.....134, 159
Povejsil, D. J.; A. A. Johnson. A Per-Unit Interpretation of Transmission Line Constants. (51-26).....194-200; disc. 201
Povejsil, D. J.; A. A. Johnson, J. E. Barkle. Fundamental Effects of Series Capacitors in High-Voltage Transmission Lines. (51-89)....526-35; disc. 535
Powell, A. H.; H. R. Harrison. Disc.....43
Price, J. C.; G. R. McDonald. Economics of Trolley Coach Power Supply. (51-115).....687-9
Puchstein, A. F. Disc.....176

R

Ralston, Oliver C.; F. Fraas. Distribution of Charge in Electrostatic Mineral Separation. (51-202).....1028-30
Ratz, A. G.; V. G. Smith. A Method of Gating for Parallel Computers. (51-83).....510-16
Reagan, M. E.; S. S. Watkins. D-C Power Supplies and Isolation of Faults on Electric Transit Systems Part I—D-C Power Supply. (51-90).....537-42; disc. 542
Part II—Isolation of D-C Faults. (51-91).....544-50; disc. 550
Reitan, Daniel Kinseth; T. J. Higgins. Calculation of the Capacitance of a Circular Annulus by the Method of Subareas. (51-174)..926-31; disc. 932
Remscheid, E. J.; C. C. Herskind. Development of a Pumpless Ignitron. (51-212).....1066-9
Richards, N. W. Disc.....924
Rietz, E. B.; C. J. Balentine. Disc.....118, 135, 159
Robert, J. R. Disc.....91, 119, 267, 505
Roberts, E. A.; P. Goldsmith. Piezoelectric Crystals as Sensing Elements of Pressure, Temperature, and Humidity. (51-180).....968-72
Robertson, Lawrence M. Disc.....394
Roehmann, L. F.; L. C. Ebel. Disc.....59
Rohats, N.; F. H. Catlin. Winding Insulation Tester for D-C Armatures. (51-74).....465-8
Rorden, H. L. Disc.....268, 387
Rosenberg, L. T. Disc.....591
Rosenberry, W. W.; J. E. Hart, A. T. McClinton. Factors Affecting Minimum Surface Leakage Distances on D-C Power Systems. (51-123)..738-42
Ross, M. D. Disc.....590
Rottler, Richard R. Ignitrons for Frequency-Changer Welders. (51-166).....900-07
Rowell, Ralph M. Disc.....14, 221
Runciman, A. S. Disc.....127
Russ, J. C. Disc.....395
Russell, Paul E.; H. A. Peterson. Differential Analyzer Study of Harmonic Power Generation with Nonlinear Impedance Element. (51-172).....917-20

S

Sackett, W. T., Jr.; W. B. Kouwenhoven. Contact Resistance—The Contribution of Nonuniform Current Flow. (51-140).....791-5
St. Clair, H. P.; E. L. Peterson. System Economics of Extra-High-Voltage Transmission. (51-156).....841-8; disc. 850
St. Clair, H. P.; P. Sporn, E. L. Peterson, I. W. Gross. The 300-315 Kv Extra-High-Voltage Transmission System of the American Gas and Electric Company. (51-11).....64-72; disc. 73
Saline, L. E.; I. B. Johnson. Disc.....127, 384
Salmonson, W. G. Disc.....238
Salter, E. H. Disc.....352
Satterlee, W. W. Disc.....21, 438
Saunders, Robert M. Measurement of D-C Machine Parameters. (51-118).....700-05; disc. 705
Saunders, R. M.; Otto J. M. Smith. Disc.....562
Schahfer, R. M.; F. H. Strout. 11-Year Operating Record—Rural Line Sectionalizing by Repeater Fuses. (51-112).....680-6
Schaller, F. F.; W. C. Whitman. Power Supply Study and New Rectifier Installation for the United Electric Railways of Providence. (51-185).....978-85; disc. 985
Scheuch, Donald R.; O. Whitby. Output Analysis and Alignment Techniques for Phase-Rotation Single Side-Band Transmitters. (51-28).....209-12
Schifreen, C. S. Thermal Expansion Effects in Power Cables. (51-22).....160-8; disc. 169
Schleicher, George B. Improvements in Transformer-Loss Compensators for Watt-hour and Var-hour Meters. (51-182).....973-7
Schmidt, A., Jr. Regeneration with a Mercury Arc Rectifier on the Central Railway of Brazil. (51-232).....1092-6
Schroeder, T. W. Disc.....394
Schuder, John C.; J. M. Cage. A Gas Tube Inverter with the Supply Voltage Below the Breakdown Voltage. (51-168).....908-12
Schultz, N. R. Disc.....158
Schultz, N. R.; R. J. Hopkins. Switching of Distribution Capacitors by Manual and Automatic Devices. (51-19).....138-43
Scorgie, Donald G. Fault Transients in Aircraft D-C Systems.....713-20; disc. 720
Sealey, W. C. A 2,000,000-Kva Transformer Core. (51-2).....8-11
Sexton, Robert M.; R. J. Alke. Detection of Turn-to-Turn Faults in Large High-Voltage Turbine Generators. (51-41).....270-3; disc. 274
Shanck, R. B. Disc.....378
Shankle, D. F.; A. W. Funkhouser, R. C. VanSickle. Switching High-Voltage Shunt Capacitor Banks. (51-18).....129-33; disc. 137
Shildneck, L. P. Disc.....839

Shores, R. B.; J. W. Beatty. A New 69-Kv Air Blast Circuit Breaker. (51–27).....202–07; disc. 208
Short, H. D. Disc.....429
Showers, R. M.; C. J. Fowler. Disc.....267
Slayton, R. D.; T. A. Hansen. An Electronic Time Division Multiplex Telegraph Set. (51–60).....354–61
Sloman, M. L.; W. R. Ellis. Electric Equipment and Performance of Lightweight Rapid Transit Cars. (51–33).....227–30; disc. 231
Slonczewski, T. A Servo System for Heterodyne Oscillators. (51–218).....1070–2
Smith, Arthur Bessey. Disc.....268
Smith, H. B. Disc.....15
Smith, J. J. Tables of Green's Functions, Fourier Series, and Impulse Functions for Rectangular Coordinate Systems. (51–6).....22–30
Smith, L. A.; F. B. Bramhall. A Nationwide Frequency-Modulation Telegraph Network. (51–62).....373–8; disc. 378
Smith, Otto J. M.; R. M. Saunders. Disc.....562
Smith, S. V. A New Train Performance Calculator. (51–108).....657–60
Smith, V. G.; A. G. Ratz. A Method of Gating for Parallel Computers. (51–83).....510–16
Smythe, W. R. Disc.....932
Snyder, R. L., Jr. The Input-Output System of the EDVAC. (51–82).....507–09
Sommerman, G. M. L.; P. B. Jacob, Jr. Dependence of Direct Sparkover Voltage of Gaps on Humidity and Time. (51–173).....921–4; disc. 925
Spayth, Frank; V. E. Heil. Disc.....307
Specht, T. Transformer Magnetizing Inrush Current. (51–53).....323–7; disc. 327
Specht, T. R. Disc.....331, 336
Spence, Homer W. Systematization of Tube Surveillance in Large-Scale Computers. (51–84)..516–19
Sporn, Phillip; E. L. Peterson, I. W. Gross, H. P. St. Clair. The 300–315 Kv Extra-High-Voltage Transmission System of the American Gas and Electric Company. (51–11).....64–72; disc. 73
Stadum, C. B. Selection of Fuses for Resistance Welding Machines. (51–141).....796–9
Stauss, Henry E.; F. E. Martin. Contact Transients in Simple Electric Circuits. (51–48).....304–07; disc. 308
Stevenson, J. R.; I. B. Johnson. Disc.....136
Stewart, H. C.; L. C. Whitman. Aging of Class-B Insulating Material in Nitrogen. (51–69).....436–7; disc. 438
Storm, H. F. Static Magnetic Exciter for Synchronous Alternators. (51–196).....1014–17
Storm, H. F. Transient Response of Saturable Reactors with Resistive Load. (51–13).....95–102
Strandrud, H. T. Determination of Generator Standby Reserve Requirements. (51–23).....179–87
Strom, A. P.; T. E. Browne, Jr. A Study of Conduction Phenomena Near Current Zero for an A-C Arc Adjacent to Refractory Surfaces. (51–65).....398–407; disc. 409
Strotz, R. H.; J. F. Calvert, N. F. Morehouse. Analogue Computing Techniques Applied to Economics. (51–93).....557–62; disc. 562
Strout, F. H.; R. M. Schahfer. 11-Year Operating Record—Rural Line Sectionalizing by Repeater Fuses. (51–112).....680–

T

Taylor, G. J. Disc.....858
Taylor, H. D.; E. D. Huntley. Progress in the Development of Large Turbine Generators. (51–96).....580–9; disc. 591
Taylor, P. L. Disc.....208
Teague, W. L.; E. J. Grimmer. Improved Core Form Transformer Winding. (51–178)..962–5; disc. 967
Tietze, H. Watson. Welding Calculations—Effect of Conductor Configuration in Overhead Lines. (51–138).....784–6
Tovee, E. H. Disc.....768
Travers, Paul. A Note on the Design of Conditionally Stable Feedback Systems. (51–102).....626–30
Tremaine, R. L.; I. W. Gross, C. F. Wagner, O. Naef. Corona Investigation on Extra-High-Voltage Lines—500-Kv Test Project of the American Gas and Electric Company. (51–12).....75–91; disc. 94
Tremaine, R. L.; O. Naef, A. R. Jones. Line Insulator Loss Under Normal Conditions—500-Kv Test Project of the American Gas and Electric Company. (51–224).....1073–8
Tremaine, R. L.; O. Naef, A. R. Jones. Techniques of Corona Loss Measurement and Analysis—500-Kv Test Project of the American Gas and Electric Company. (51–80).....496–505; disc. 506
Trump, J. G. Electrostatic Sources of Ionizing Energy. (51–199).....1021–7
Turkington, Robert E. Analysis of a 3-Phase Inverter with Resistive Load. (51–210).....1055–61

V

Van Sickle, R. C. Disc.....407
Van Sickle, R. C.; A. W. Funkhouser, D. F. Shankle. Switching High-Voltage Shunt Capacitor Banks. (51–18).....129–33; disc. 137
Van Sickle, R. C.; J. Zaborszky. Capacitor Switching Phenomena. (51–21).....151–8; disc. 158
Vikoren, O. B. Disc.....193
Vivian, J. H.; L. F. Hunt. Routine Insulation Testing of Synchronous Machines. (51–126).....756–62
Vivian, J. H.; R. R. Peck. An Investigation of Audio Noise in Substation Type Transformers. (51–55).....328–31; disc. 332
Vogel, F. J.; C. C. Petersen, L. W. Matsch. Deterioration of Transformer Oil and Paper Insulation by Temperatures. (51–4).....18–20; disc. 21

W

Wachowski, Hillard M.; R. E. Beam. Shielded Dielectric-Rod Waveguides. (51–162).....874–80
Wagner, C. F.; I. W. Gross, O. Naef, R. L. Tremaine. Corona Investigation on Extra-High-Voltage Lines—500-Kv Test Project of the American Gas and Electric Company. (51–12)...75–91; disc. 94
Walters, T. R. Disc.....437
Ward, H. C., Jr.; P. L. Alger, F. H. Wright. Split-Winding Starting of 3-Phase Motors. (51–160)..867–72; disc. 872
Watchorn, C. W. Disc.....187, 849
Watkins, S. S.; M. E. Reagen. D-C Power Supplies and Isolation of Faults on Electric Transit Systems. Part I—D-C Power Supply. (51–90).....537–42; disc. 542
Part II—Isolation of D-C Faults. (51–91).....543–50; disc. 550
Weaver, A.; N. A. Newell. Single-Frequency Signaling System for Supervision and Dialing over Long-Distance Telephone Trunks. (51–79).....489–95
Webb, R. L. Disc.....192
Weber, Ernst. Disc.....931
Webking, Henry E. A Simplified Method for Predicting Induction Motor Performance. (51–110).....667–70
Wentz, E. C. Disc.....111
Whitby, Oliver; D. R. Scheuch. Output Analysis and Alignment Techniques for Phase-Rotation Single Side-Band Transmitters. (51–28).....209–12
Whitehead, J. B. Radial and Tangential Stresses in Impregnated Paper Insulation. (51–10).....56–9; disc. 62
Whitman, L. C.; H. C. Stewart. Aging of Class-B Insulating Material in Nitrogen. (51–69).....436–7; disc. 438
Whitman, W. C.; F. F. Schaller. Power Supply Study and New Rectifier Installation for the United Electric Railways of Providence. (51–185).....978–85; disc. 985
Wieseman, R. W. Disc.....769
Wildes, Karl L. Disc.....954
Williams, J. E.; D. S. Babb. Circuit Analysis Method for Determination of A-C Impedance of Machine Conductors. (51–109).....661–5; disc. 665
Williamson, R. A. Why 4-Motor Multiple-Unit Car Equipments? (51–35).....240–2
Wiseman, Robert J. Disc.....431
Witzke, R. L.; J. E. Barkle. Economics of Power Transformer Application. (51–70).....440–4
Witzke, R. L.; T. J. Bliss. Disc.....386
Witzke, R. L.; E. L. Michelson. Technical Problems Associated with the Application of a Capacitor in Series with a Synchronous Condenser. (51–88).....519–25
Woods, G. M. Disc.....985
Worthington, A. R.; R. H. Miller. Measurements and Tests on a Power Line Carrier Relaying System. (51–192).....1005–07
Wright, F. H.; P. L. Alger, H. C. Ward, Jr. Split-Winding Starting of 3-Phase Motors. (51–160)..867–72; disc. 872

Y

Yarbrough, C. T. Disc.....755
Young, R. E. Disc.....898

Z

Zaborszky, J.; R. C. Van Sickle. Capacitor Switching Phenomena. (51–21).....151–8; disc. 158
Zimmerman, C. P.; F. M. Porter. Application of Shunt Capacitors at Transmission and Distribution Stations. (51–15).....112–18; disc. 119
Zimmerman, C. P.; F. M. Porter. Disc.....134,159

DATE DUE

UIC REC'D JUN 04 '98

GAYLORD PRINTED IN U.S.A.

3 8198 306 810 118
THE UNIVERSITY OF ILLINOIS AT CHICAGO